



# EUROPEAN AEROSOL CONFERENCE

**EAC 2017**

August 27 – September 1, 2017  
University of Zurich  
Campus Irchel, Switzerland

[eac2017@gaef.de](mailto:eac2017@gaef.de)  
[www.gaef.de/EAC2017](http://www.gaef.de/EAC2017)



## Conference Venue

University of Zurich  
Campus Irchel  
Winterthurerstrasse 190  
8057 Zurich  
Switzerland

**[www.gaef.de/EAC2017](http://www.gaef.de/EAC2017)**

## Deadlines

1-page abstract final form	January 31, 2017
Notification to Authors	May 31, 2017
Early registration ends	July 1, 2017
Conference dates	August 27 – September 1, 2017

## Conference Secretary

Dr. Gunthard Metzger  
Karlsruher Institut für Technologie (KIT)  
FTU – GAeF  
Postfach 36 40  
76021 Karlsruhe, Germany  
Fon: +49 721 608-24800  
Fax: +49 721 608-24857  
E-mail: [treasurer@gaef.de](mailto:treasurer@gaef.de)

## Conference Organisers

European Aerosol Assembly (EAA)



Gesellschaft für Aerosolforschung

PAUL SCHERRER INSTITUT



---

---

---

---

# European Aerosol Conference 2017

Zürich, Switzerland, August 27 to September 1, 2017

Organized by Gesellschaft für Aerosolforschung, Conference Chair: Prof. Martin Gysel

## Table of contents

Foreword	p. 5
Committees, General Information, Awards	pp. 6-13
Program	pp. 14-145
Abstracts:	
SPS1	pp. 146-151
SPS2	pp. 152-158
SPS3	pp. 159-170
SPS4	pp. 171-181
SPS5	pp. 182-195
SPS6	pp. 196-215
T101	pp. 216-240
T102	pp. 241-252
T103	pp. 253-266
T104	pp. 267-277
T105	pp. 278-280
T106	pp. 281-290
T107	pp. 291-293
T108	pp. 294-307
T109	pp. 308-311
T110	pp. 312-316
T111	pp. 317-321
T112	pp. 322-324
T114	pp. 325-326
T115	pp. 327-331
T116	pp. 332-342
T117	pp. 343-348
T118	pp. 349-352

T119	pp. 353-367
T120	pp. 368-379
T201	pp. 380-406
T202	pp. 407-416
T203	pp. 417-440
T204	pp. 441-467
T205	pp. 468-507
T206	pp. 508-521
T207	pp. 522-546
T208	pp. 547-557
T209	pp. 558-580
T210	pp. 581-603
T211	pp. 604-624
T212	pp. 625-632
T213	pp. 633-641
T214	pp. 642-683
T215	pp. 684-733
T216	pp. 734-749
T217	pp. 750-760
T302	pp. 761-782
T303	pp. 783-790
T304	pp. 791-800
T305	pp. 801-807
T306	pp. 808-818
T307	pp. 819-830
T308	pp. 831-836
T309	pp. 837-838
T310	pp. 839-852
T311	pp. 853-863
T312	pp. 864-869
T313	pp. 870-876
T314	pp. 877-878
T315	pp. 879-883
T401	pp. 884-890
T402	pp. 891-909
T403	pp. 910-916
T404	pp. 917-921
T406	pp. 922-947

T407	pp. 948-953
T408	pp. 954-960
T409	pp. 961-968
T410	pp. 969-983
T411	pp. 984-988
T412	pp. 989-993
T413	pp. 994-1003
T414	pp. 1004-1005
T417	pp. 1006-1009
T501	pp. 1010-1011
T502	pp. 1012-1027
T503	pp. 1028-1030
T504	pp. 1031-1042
T505	pp. 1043-1046
T506	pp. 1047-1050
T507	pp. 1051-1058
T508	pp. 1059-1062

## PREFACE

The European Aerosol Conference (EAC) is the meeting place in Europe for the international research community working in the field of aerosol science and technology. These conferences are organized annually under the auspices of the European Aerosol Assembly (EAA), which decides on the date and venue. The 2017 conference takes place in Zurich, Switzerland. It is organized by the “Gesellschaft für Aerosolforschung” (GAeF), jointly with the Paul Scherrer Institute as local organizer.

The EAC2017, which received 879 abstract submissions in total, follows a well-established format: 267 talks will be presented in 41 oral sessions, preceded by a daily plenary lecture in one of the key areas of active aerosol research, and 566 posters presented in 3 poster sessions. Following numerous requests, it was also possible to accommodate 6 special session topics. Wednesday afternoon leaves ample room for individual discussions, laboratory visits, workshops, user group meetings or just sightseeing and leisure.

The organizers of the EAC2017 gratefully acknowledge the efforts of the EAA Working Groups, reviewers and other committee members, who all played a major role in the process of shaping the conference structure, reviewing and selecting the abstracts, suggesting plenary speakers, setting up the various special sessions and implementing the best poster award. A very special Thank-You goes to all sponsors and exhibitors for their financial support.

Martin Gysel  
Paul Scherrer Institute  
Conference Chairman

## COMMITTEES

The Organising Committee and Committee responsible for the scientific program of EAC 2017 comprise the following individuals:

**Chairman:** Gunthard Metzиг (Germany)

### Organising Committee

Sibylle Mann (Germany)  
 Gunthard Metzиг (Germany), Chairman  
 Torsten Neck (Germany)  
 Beate Wernick (Germany)

### Local Organisation

Nicolas Bukowiecki (Switzerland)  
 Martin Gysel (Switzerland)  
 Hannelore Krüger (Switzerland)

### Committee responsible for the scientific program

Lucas Alados Arboledas (Spain)	Stavos Kassinos (Cyprus)
Luewton Agostinho (The Netherlands)	Ana Kroflic (Slovenia)
Christof Asbach (Germany)	Einar Kruis (Germany)
George Biskos (The Netherlands)	Arkadiusz Kuczai (Switzerland)
Andrei Bologna (Germany)	Antti Lauri (Finland)
Michael Boy (Finland)	Risto Makkonen (Finland)
Giorgio Buonanno (Italy)	John McAughey (UK)
Yannis Drossinos (Italy)	Willy Maenhaut (Belgium)
Lukas Durdina (Switzerland)	Attila Nagy (Hungary)
Annica Ekman (Sweden)	François-Xavier Ouf (France)
Luca Ferrero (Italy)	Zoran Ristovski (Australia)
Bernard J. Geurts (The Netherlands)	Joan Rosell Llompart (Spain)
Martin Gysel (Switzerland), Chairman	Julia Schmale (Switzerland)
Otto Hänninen (Finland)	Martin Sommerfeld (Germany)
Andreas Held (Germany)	Mar Viana (Spain)
Werner Hofmann (Austria)	Michal Vojtisek (Czech Repblik)
Ulas Im (Denmark)	Birgit Wehner (Germany)
Christina Isaxon (Sweden)	Aneta Wierzbicka (Sweden)
Christopher Kampf (Germany)	Oliver Witschger (France)

### Supporting Reviewers

Darrel Baumgardner (USA)	Sanja Frka Milosavljevic (Croatia)
Irena Grgic (Slovenia)	Peter Molnar (Sweden)
Thorsten Hoffmann (Germany)	Anke Mutzel (Germany)
Christoph Hüglin (Switzerland)	Laurent Poulain (Germany)
Yoshiteru Iinuma (Japan)	Isabell Rumrich (Finland)
Niku Kivekäs (Finland)	Johannes Schneider (Germany)
Otto Klemm (Germany)	

### Conference Organizer

The EAC 2017 is organized by Gesellschaft für Aerosolforschung e.V. (GAeF).

## GENERAL INFORMATION

### Venue and Dates

August 27 – September 1, 2017

University of Zurich, Campus Irchel  
Winterthurerstrasse 190  
8057 Zurich, Switzerland

### Public Transportation

From Sunday, 27 August to Friday, 1 September 2017 your conference name badge will serve as a ticket to all public tram and bus lines within the Zurich central area “ZONE 110” (Zürcher Verkehrsverbund). Tickets only valid for second class.

The conference site can be reached by trams no 9 and 10 (stop “Zürich Universität Irchel”), and trams no 7, 9, 10, 11, 14 (stop “Zürich Milchbuck”). It is located within walking distance (about 5 - 10 minutes) from these tram stops.

### Mobile Phone Policy

Delegates are advised that, in accordance with EAC policy, mobile phones have to be switched off in the meeting rooms.

### Language

The official language of the Conference is English.

### Registration Desk, Information Desk and Conference Secretariat

OPENING HOURS:

Sunday, 27 August	17:00-19:30
Monday, 28 August	08:00-16:15
Tuesday, 29 August	08:00-17:00
Wednesday, 30 August	08:15-13:00
Thursday, 31 August	08:15-16:15
Friday, 1 September	08:30-13:00

Information on Social Events and Tours are available at the registration and information desks. Tickets to the Conference Dinner and Tours can be booked there as well.

### Lost and Found

For lost or found personal belongings, please contact the Information Desk.

## **Name Badge**

Your personal badge is your entrance ticket to all sessions and the exhibition. Please remember always to wear your badge. Your name badge will also serve as a ticket to all lines of the public transportation system within the Zurich central area “ZONE 110” (Zürcher Verkehrsverbund).

## **Lunch at the Canteen of the University**

Lunch is available either at the canteen (“Mensa”) or at the university cafeteria, which are located in the same building complex as the lecture halls. Several menus including vegetarian options will be available at a special price of 10.50 CHF (cash payment only, name badge needed to get the special price). Additionally, snacks and beverages are available at the cafeteria.

## **First Aid**

In an emergency, please contact the Information Desk.

## **Climate and Dress**

The weather in Zurich at this time of the year is usually sunny, cloudy or rainy with daily mean temperatures around 12–20 °C and peak temperatures of 20–28 °C.

Dress code will be informal throughout the conference.

## **Time Zone**

The time zone in Zurich is GMT + 2 hours (daylight saving time).

## **Electricity**

The voltage in Switzerland is 230 V at a frequency of 50 Hz.

### **Swiss power socket**

Make sure you bring a plug adapter for Switzerland – a picture of the Swiss power socket is shown on the right. Please note that the European “Schuko” plug does not fit into the Swiss power socket, whereas the two-pin unearthened Europlug does fit.



## **Currency**

The Swiss Franc (CHF) is the standard currency used in Switzerland. The Euro (€) is often accepted for cash payments, though the exchange rates may not be favorable and change will be in CHF. All major credit cards are accepted in most places.

## Exhibition

The Exhibition is held in the “Atrium” and is continuously open from Monday noon until Friday 10:30 a.m. during the conference hours. Time slots have been allocated specifically for your visit:

Monday, 28 August	13:45 - 15:30
Tuesday, 29 August	13:30 - 15:15
Thursday, 31 August	13:45 - 15:30

## YOUNG INVESTIGATOR NETWORK

The Gesellschaft für Aerosolforschung e.V. (GAeF) invites all young investigators (Students, PhDs & early PostDocs) for a special session on:

### - Networking vs. Excellence -

### How to boost your individual career path

Meet professionals from both academia and business covering different fields of aerosol research and learn more about their individual career paths. After a 45 minutes panel discussion you will have the opportunity to ask your questions. Get in contact with the experts and other young investigators while enjoying free drinks and food.

Join this event and boost your conference network at the first day of the conference!

**Monday, 28<sup>th</sup> 18:15 – 20:00 Room 04G40**

**This event is supported by**



## SOCIAL PROGRAM

### Welcome Reception

**Sunday, 27 August 2017 (17:30 - 20:00)**

During this welcome reception, everybody will have the opportunity to meet old friends and make new ones.

### Conference Dinner

**Thursday, 31 August 2017, (19:30 - 23:00)**

The conference dinner takes place at the Schützenhaus Albisgütli in South-West of Zurich (20 minutes from the city centre by tram). The Albisgütli is a historic restaurant built in 1839. It can be reached by trams no 13 and 17, stop "Albisgütli" (terminal stop). The best transfer option to reach lines 13 and 17 is via the stop "Paradeplatz".

For remaining tickets please contact the registration desk by Wednesday noon at the latest.

### Sightseeing

Several tours are offered:

**Wednesday, 30 August 2017 (14:00 - 19:00)**

Half-day trip to the Rhine Falls – the largest plain waterfall in Europe – near the town of Schaffhausen

**Wednesday, 30 August 2017 (14:00 - 16:00)**

2 h guided walking tour: Stories of the Old Town – Discover Zurich's Historic Center

**Saturday, 2 September (07:00 - 21:00)**

A combined touristic/scientific excursion to the Jungfrauoch including a visit of the high-alpine research station. The excursion will start and end in Zurich.

For all tours the number of participants is limited. For remaining tickets please contact the registration desk.

## LABORATORY VISIT

Laboratory visits are possible on Wednesday, 30 August, in the afternoon. A first option is visiting the aerosol research facilities of the Paul Scherrer Institute. This will require transfer to Villigen by coach, organized by the conference, and it will last for the entire afternoon. A second option is visiting several aerosol research laboratories at ETH Zurich, which is located in the town center.

Please sign up for the laboratory visits at the registration desk as early as possible, as the number of participants is limited.

## AWARDS

### **Smoluchowski Award**

The Smoluchowski Award, named after the physicist Marian Smoluchowski, is intended to recognize significant research contributions to aerosol science. The award is given to a young researcher (as a rule under 40 years of age) who has achieved and published new results in aerosol science in the preceding 3 years. It may be shared by two individuals judged to be equally meritorious. The award is conferred by the Gesellschaft für Aerosolforschung (GAeF) during the annual European Aerosol Conference.

The Award committee is composed of at least four members of the GAeF. The committee invites nominations of candidates from members of GAeF and other scientists working in the field of aerosol science according to the regulations issued by the Committee and posted at the home page of GAeF and by public announcement in the Journal of Aerosol Science and/or other scientific publications.

Marian Smoluchowski was born on 28 May 1872 in Vorderbühl, Austria, and died on 5 September 1917 in Kraków, Poland. He was a Polish physicist. Smoluchowski described Brownian motion and worked on the kinetic theory at the same time as Albert Einstein. In his work, he presented an equation which became the basis of the theory of stochastic processes. Smoluchowski did research at several places, such as Paris, Glasgow, Berlin and Cambridge (UK).

The first recipient of the Smoluchowski Award was Paul E. Wagner (in 1986). In the past 3 years the Award was given to Ilona Riipinen (2014), Andreas Kürten (2015), and Alexandra Teleki (2016).

The award ceremony follows the plenary session on Wednesday morning, 30 August at 9:30.

### **Best Poster Awards (BPA)**

Up to fifteen poster prizes will be awarded in total. The poster prizes are presented by the BPA committee chair Nønne Prisle. The award consists of a certificate signed by the conference chair and the BPA committee chair and a prize money of 100 €. The organising committee of the European Aerosol Conference will provide the prize money out of the conference budget.

The award ceremony follows the plenary session on Friday morning, 1 September at 9:30.

## SCIENTIFIC INFORMATION

### Abstract Book

All abstracts are published on the EAC 2017 Abstract USB-stick, handed out during registration.

### Certificate of Attendance

A certificate of attendance is handed out during registration (included in your personal registration envelope).

### Posters

Posters are displayed in the poster area in three different sessions:

- Poster Session I on Monday 28 August 2017, 13:45-15:30  
Posters to be mounted on Monday morning and left on display till Tuesday evening. Please remove your poster by this time.
- Poster Session II on Tuesday 29 August 2017, 13:30-15:15  
Posters to be mounted on Monday morning and left on display till Tuesday evening. Please remove your poster by this time.
- Poster Session III on Thursday 31 August 2017, 13:45-15:30  
Posters to be mounted on Wednesday morning beginning with the coffee break at 10:00 a.m. and left on display till Friday noon.  
Please remove your poster by the end of the conference.

Presenting authors are asked to attend their poster during their poster sessions.

Use only the special fixing material provided by the organizer. Please do not use any of your own fixing material!!

### Instructions for Oral Presenters

Please hand in your presentation (Powerpoint or PDF) on USB-stick one day before your talk at the Speaker Ready Room Y22G74 (next to the registration). You can briefly browse through your slides to make sure everything is displayed correctly. Your presentation will then be transferred to the computer in the lecture hall where your session will take place.

Please note that for organizational reasons, you may not use your own notebook for presentation.

Speakers are requested to be present at their oral session at least 5 minutes before it starts and identify themselves to the session chair.

A total time of 20 minutes has been allocated for regular talks, 15 minutes for presentation and 5 minutes for discussion.

### Opening hours speakers ready room:

Sunday, 27.8:	17:00 – 19:00
Monday, 28.8:	08:00 – 18:00
Tuesday, 29.8:	08:00 – 18:00
Wednesday, 30.8:	08:00 – 13:00
Thursday, 31.8:	08:00 – 18:00
Friday, 1.9:	08:00 – 10:00

**SUNDAY 27 AUGUST 2017**

<b>17:00- 19:30</b>	<b>Pre-Registration</b>
-------------------------	-------------------------

<b>17:30- 20:00</b>	<b>Welcome Party</b>
-------------------------	----------------------

# MONDAY 28 AUGUST 2017

<b>08:00</b>	<b>Registration</b>
--------------	---------------------

	<b>Room 04G30</b>
<b>08:30</b>	<b>Opening Ceremony</b>
<b>09:00</b>	<b>Plenary Lecture I</b>

<b>10:00</b>	<b>Coffee Break</b>
--------------	---------------------

	<b>Room 04G30</b>	<b>Room 24G45</b>	<b>Room 15G20</b>
<b>10:30</b>	Source Apportionment Studies I	Aerosol-Cloud Interaction: The Role of Organic Aerosol	Special Session #1: Education, Careers, and Outreach in Aerosol Science
	<b>Room 15G40</b>	<b>Room15G60</b>	
	Numerical and Experimental Methods in Particle-Lung Interaction	Instrumentation for Ambient Aerosols	

<b>12:30</b>	<b>Lunch Break</b>
--------------	--------------------

<b>12:30</b>	<b>GAeF Board Meeting</b>	<b>Room Y13L11/13</b>
--------------	---------------------------	-----------------------

<b>13:45</b>	<b>Poster Session Part I and Exhibition</b>
--------------	---

<b>15:30</b>	<b>Coffee Break and Exhibition</b>
--------------	------------------------------------

	<b>Room 04G30</b>	<b>Room 24G45</b>	<b>Room 15G20</b>
<b>16:00</b>	Source Apportionment Studies II	Aerosol/Cloud/Climate Interaction	Special Session #6: Emissions from Aircraft and Ships
	<b>Room 15G40</b>	<b>Room15G60</b>	
	Special Session #4: Targeted Generation and Delivery of Aerosolized Medicines	Aerosol Transport and Transformation	

<b>18:00</b>	<b>End of Conference Day</b>
--------------	------------------------------

<b>18:15</b>	<b>General Assembly of GAeF</b>	<b>Room 04G20</b>
--------------	---------------------------------	-------------------

<b>18:15</b>	<b>GAeF Young Investigator Network</b>	<b>Room 04G40</b>
--------------	--	-------------------

<b>18:15</b>	<b>Journal of Aerosol Science - Editorial Board Meeting</b>	<b>Room Y13L11/13</b>
--------------	---	-----------------------

<b>18:15</b>	<b>Meeting of Hellenic Association for Aerosol Research</b>	<b>Room 04G60</b>
--------------	---	-------------------

## TUESDAY 29 AUGUST 2017

<b>08:00</b>	<b>Registration</b>
--------------	---------------------

	<b>Room 04G30</b>
<b>08:30</b>	<b>Plenary Lecture II</b>

<b>09:30</b>	<b>Coffee Break</b>
--------------	---------------------

	<b>Room 04G30</b>	<b>Room 24G45</b>	<b>Room 15G20</b>
<b>10:00</b>	New Particle Formation: Lab and Field Studies	Biomass Burning Aerosol	Stationary Sources of Combustion Aerosol
	<b>Room 15G40</b>	<b>Room15G60</b>	<b>Room 24G55</b>
	Toxicological Characterization of Ambient and Engineered Particles	New Instrumentation	Special Session #5: Electrohydrodynamic Atomization (EHDA) Technologies: from Fundamentals to Application

<b>12:20</b>	<b>Lunch Break</b>
--------------	--------------------

<b>12:20</b>	<b>IARA Committee Meeting</b>	<b>Room Y13L11/13</b>
--------------	-------------------------------	-----------------------

<b>13:30</b>	<b>Poster Session Part II and Exhibition</b>
--------------	--

<b>15:15</b>	<b>Coffee Break and Exhibition</b>
--------------	------------------------------------

	<b>Room 04G30</b>	<b>Room 24G45</b>	<b>Room 15G20</b>
<b>15:45</b>	<b>Atmospheric Aerosol</b> Working Group Meeting	<b>PMx</b> Working Group Meeting	<b>Aerosol Based Nanotechnology</b> Working Group Meeting
	<b>Room 15G40</b>	<b>Room15G60</b>	<b>Room 24G55</b>
	<b>Inhalation, Exposure and Health</b> Working Group Meeting	<b>Fundamentals</b> Working Group Meeting	<b>Instrumentation</b> Working Group Meeting

	<b>Room 04G30</b>	<b>Room 24G45</b>	<b>Room 15G20</b>
<b>16:20</b>	<b>Atmospheric Chemistry</b> Working Group Meeting	<b>Aerosol Modelling</b> Working Group Meeting	<b>Combustion Aerosols</b> Working Group Meeting
	<b>Room 15G40</b>	<b>Room15G60</b>	
	<b>Indoor and Working Place Aerosols</b> Working Group Meeting	<b>Electrical Effects</b> Working Group Meeting	

<b>16:50</b>	<b>Break</b>
--------------	--------------

	<b>Room 04G30</b>	<b>Room 24G45</b>	<b>Room 15G20</b>
<b>17:00</b>	New Particle Formation and PM Sources	Aerosol Chemical Composition, Tracers and Trends	Electrical Effects: from Fundamental Study to Application
	<b>Room 15G40</b>	<b>Room15G60</b>	
	Airborne Pathogens and Microbes and their Viability	Aerosol Dynamics: from Particle Removal to Morphology	
<b>19:00</b>	<b>End of Conference Day</b>		

## WEDNESDAY 30 AUGUST 2017

<b>08:15</b>	<b>Registration</b>		
	<b>Room 04G30</b>		
<b>08:30</b>	<b>Plenary Lecture III</b>		
<b>09:30</b>	<b>Presentation of the Smoluchowski Award</b>		
<b>10:00</b>	<b>Coffee Break and Exhibition</b>		
	<b>Room 04G30</b>	<b>Room 24G45</b>	<b>Room 15G20</b>
<b>10:30</b>	Secondary Organic Aerosol	Exposures and Health Impacts of Aerosols	Mobile Sources of Combustion Aerosol
	<b>Room 15G40</b>	<b>Room 15G60</b>	
	Synthesis and Structuring of Functional Nanoparticles	Aerosol Optical Properties	
<b>12:50</b>	<b>Lunch Break and Exhibition</b>		
<b>12:50</b>	<b>EAA Board Meeting</b>		<b>Room Y13L11/13</b>
<b>13:45</b>	<b>End of Conference Day</b>		
<b>14:00</b>	<b>Workshop on Urban Air Pollution Mitigation Tools</b>		<b>Room 04G20</b>
<b>14:00</b>	<b>Magee Scientific User Group Workshop</b>		<b>Room 24G45</b>
<b>14:00</b>	<b>Stories of the Old Town – Rediscover Zurich’s Historic Center Guided walking tour</b>		
<b>14:00</b>	<b>Bus Tour to Rhine Falls near Schaffhausen Europe’s Biggest Water Falls</b>		
<b>14:30</b>	<b>Tour A: Laboratory visits at ETH</b>		
<b>13:30</b>	<b>Tour B: Laboratory visits at Paul Scherrer Institute (Villigen)</b>		

## THURSDAY 31 August 2017

<b>08:15</b>	<b>Registration</b>
--------------	---------------------

	<b>Room 04G30</b>
<b>08:30</b>	<b>Plenary Lecture IV</b>
<b>09:30</b>	<b>IAC2018 and EAC2019 Launch</b>

<b>09:40</b>	<b>Coffee Break and Exhibition</b>
--------------	------------------------------------

	<b>Room 04G30</b>	<b>Room 24G45</b>	<b>Room 15G20</b>
<b>10:10</b>	Atmospheric Aerosols: Physical and Chemical Properties	Nanoparticle Coating and Functionalization	Molecular Characterization & Marine Aerosols
	<b>Room 15G40</b>	<b>Room15G60</b>	
	Workplace Aerosols: from Source to Exposure	Miniaturized Instrumentation and Low Cost Sensors	

<b>12:30</b>	<b>Lunch Break</b>
--------------	--------------------

<b>12:30</b>	<b>Working Group Chairs Meeting</b>	<b>Room Y13L11/13</b>
--------------	-------------------------------------	-----------------------

<b>13:45</b>	<b>Poster Session Part III and Exhibition</b>
--------------	---

<b>15:30</b>	<b>Coffee Break and Exhibition</b>
--------------	------------------------------------

	<b>Room 04G30</b>	<b>Room 24G45</b>	<b>Room 15G20</b>
<b>16:00</b>	Properties and Dynamics of Atmospheric Aerosols	Special Session #3: Electronic Cigarettes - Scientific Evidence	Multiphase Chemistry & Bioaerosols
	<b>Room 15G40</b>	<b>Room15G60</b>	
	Special Session #2: Aerosols in Earth System Models	Particle Formation and Growth: Simulations and Experiments	

<b>18:00</b>	<b>End of Conference Day</b>
--------------	------------------------------

<b>19:30</b>	<b>Conference Dinner</b>
--------------	--------------------------

## FRIDAY 1 SEPTEMBER 2017

<b>08:30</b>	<b>Registration</b>
--------------	---------------------

	<b>Room 04G30</b>
<b>08:30</b>	<b>Plenary Lecture V</b>
<b>09:30</b>	<b>Presentation of the Poster Awards</b>

<b>09:45</b>	<b>Coffee Break and Exhibition</b>
--------------	------------------------------------

	<b>Room 04G30</b>	<b>Room 24G45</b>	<b>Room 15G20</b>
<b>10:15</b>	Aerosol Optical Properties and Remote Sensing	Carbonaceous Aerosol	Nanoparticles: Electrical Discharges and Modeling
	<b>Room 15G40</b>	<b>Room15G60</b>	
	Non-Industrial Indoor Aerosols	Instrumentation for Chemical Aerosol Characterization	

	<b>Room 04G30</b>
<b>12:40</b>	<b>Closing Remarks</b>

<b>13:00</b>	<b>End of Conference</b>
--------------	--------------------------

## SATURDAY 2 SEPTEMBER 2017

<b>07:00</b>	<b>Excursion to the Jungfrauoch including a visit to the high-alpine research station</b>
--------------	---

**MONDAY 28 AUGUST 2017****MEETINGS**

<b>12:30 - 13:45</b>	<b>GAeF Board Meeting</b>	<b>Room Y13L11/13</b>
----------------------	---------------------------	-----------------------

<b>18:15 - 19:00</b>	<b>General Assembly of GAeF</b>	<b>Room 04G20</b>
----------------------	---------------------------------	-------------------

<b>18:15 - 20:00</b>	<b>GAeF Young Investigator Network</b>	<b>Room 04G40</b>
----------------------	--	-------------------

<b>18:15 - 19:00</b>	<b>Meeting of Hellenic Association for Aerosol Research (HAAR)</b>	<b>Room 04G60</b>
----------------------	--	-------------------

<b>18:15 - 19:00</b>	<b>Journal of Aerosol Science Editorial Board Meeting</b>	<b>Room Y13L11/13</b>
----------------------	---	-----------------------

## MONDAY 28 AUGUST 2017

<b>Monday 28 August 2017</b>	<b>08:00 - 16:15</b>	<b>Registration</b>
------------------------------	----------------------	---------------------

<b>Monday 28 August 2017</b>	<b>08:30 - 09:00</b>	<b>Room 04G30</b>
------------------------------	----------------------	-------------------

### OPENING CEREMONY

***Roberta Vecchi***

**President of the European Aerosol Assembly (EAA)**

***Michael Hengartner***

**President of the University of Zurich**

***Helmuth Horvath***

**President of the Gesellschaft für Aerosolforschung (GAeF)**

***Martin Gysel***

**Chairman of the European Aerosol Conference 2017**

<b>Monday 28 August 2017</b>	<b>09:00 - 10:00</b>	<b>Room 04G30</b>
------------------------------	----------------------	-------------------

### PLENARY LECTURE I

**Chair: Sotiris Pratsinis and Jyrki Mäkelä**

<b>09:00</b>	Plenary Lecture	<b><i>In situ</i> diagnostics in the gas-phase synthesis of functional nanomaterials</b> <b><i>Christof Schulz</i></b>
--------------	--------------------	---

<b>Monday 28 August 2017</b>	<b>10:00 - 10:30</b>	<b>Coffee Break</b>
------------------------------	----------------------	---------------------

Monday 28 August 2017

10:30 - 12:30

Room 04G30

**SOURCE APPORTIONMENT STUDIES I**Chairs: **Willy Maenhaut and Giulia Stefenelli**

- 10:30** T215N236 **Near real time measurements and source apportionment of aerosol trace elements in Härkingen, Switzerland**  
*P. Raj, M. Furger, J.G. Slowik, F. Canonaco, R. Fröhlich, A.S.H. Prevot, and U. Baltensperger*
- 10:50** T215N04c **A PMF source apportionment study of redox-active metals in atmospheric fine particulate matter (PM<sub>2.5</sub>) in Central Los Angeles using highly time-resolved measurements**  
*M.H. Sowlat, A.H. Mousavi, and C. Sioutas*
- 11:10** T215N390 **Organic aerosol source apportionment on long-term, spatially dense observation networks using 3 mass spectrometry techniques**  
*K. R. Daellenbach, I. El-Haddad, I. Kourtchev, G. Stefenelli, C. Bozzetti, A. Vlachou, P. Fermo, R. Gonzalez, A. Piazzalunga, J. G. Slowik, S.M. Luedin, V. Pflueger, G. Vogel, J.-L. Jaffrezo, M. Kalberer, U. Baltensperger, and A.S.H. Prévôt*
- 11:30** T215N10c **A synergic approach to perform source apportionment of organic aerosol using offline and online measurements in positive matrix factorization**  
*D. Srivastava, O. Favez, N. Bonnaire, E. Perraudin, V. Gros, F. Lucarelli, E. Villenave, and A. Albinet*
- 11:50** T215N197 **Aerosol source apportionment in a European air pollution hot spot with both aerosol chemical composition and number size distribution**  
*C. Leoni, P. Pokorná, M. Masiol, J. Hovorka, K. Krupal, Y. Zhao, S. Cliff, and P.K. Hopke*
- 12:10** T215N202 **Size-segregated aerosol source apportionment by multistage cascade impactor samples collected at a pollution hot-spot area (Milan, Italy)**  
*V. Bernardoni, A. Bigi, P. Fermo, A. Piazzalunga, G. Valli, and R. Vecchi*
- Back-up Paper** T215N3bb **Source apportionment of ambient organic aerosol by online extractive electrospray ionization time-of-flight mass spectrometry (EESI-TOF)**  
*G. Stefenelli, F. D. Lopez-Hilfiker, V. Pospisilova, A. Vogel, C. Hüglin, U. Baltensperger, A.S.H. Prévôt, and J.G. Slowik*

Monday 28 August 2017

12:30 - 13:45

Lunch Break

Monday 28 August 2017

10:30 - 12:30

Room 24G45

**AEROSOL-CLOUD INTERACTION: THE ROLE OF ORGANIC AEROSOL****Chairs: Karoline Diehl and Luca Ferrero**

- 10:30** T201N499 **The impact of photochemistry on the cloud condensation nuclei (CCN) activity of organic aerosols**  
*N. Borduas, R. Ossola, Z.A. Kanji, and K. McNeill*
- 10:50** T201N156 **Hygroscopic properties and surface activity of pollenkitt and its importance for cloud activation of pollen particles**  
*J.J. Lin, S.K. Purdue, H. Lin, J.C. Meredith, A. Nenes, and N.L. Prisle*
- 11:10** T201N0fa **The first data on size segregated surfactants in atmospheric aerosols: Reconsideration of their impact on cloud droplet formation**  
*S. Frka, M. Simmel, H. Wex, I. Grgic, and A. Kroflic*
- 11:30** T201A174 **The effects of heterogeneous ice formation on precipitation in a deep convective cloud: Model simulations with COSMO-SPECS**  
*K. Diehl, M. Simmel, and V. Grützun*
- 11:50** T201N190 **Inferring cloud super-saturations by combining below-cloud cloud condensation nuclei and in-cloud cloud droplet residual and interstitial particle measurements**  
*S. Mertes, S. Henning, W. Birmili, A. Beyer, R. Otto, D. van Pinxteren, K. Dieckmann, A. Wiedensohler, F. Stratmann, and H. Herrmann*
- 12:10** T201A111 **Impact of heat treatment and cloud cycling on single particle chemical composition of soil dust**  
*X. Shen, R. Ramisetty, H. Saathoff, T. Schiebel, K. Höhler, O. Möhler, and C. Mohr*
- Back-up Paper** T201N2f8 **Pre-activation of aerosol particles by ice preserved in pores**  
*C. Marcolli*

Monday 28 August 2017

12:30 - 13:45

Lunch Break

**Monday 28 August 2017****10:30 - 12:30****Room 15G20****SPECIAL SESSION #1:  
EDUCATION, CAREERS, AND OUTREACH IN AEROSOL SCIENCE****Chairs: Antti Lauri and Julia Schmale**

- Talk 1**    SPS1N210    **Climate.now – online learning material about basics of climate change**  
*L. Riuttanen and Climate.now team*
- Talk 2**    SPS1N2a1    **Educating future aerosol scientists: a pedagogical model for multidisciplinary research-oriented learning**  
*A. Lauri, T.M. Ruuskanen, L. Riuttanen, P. Hari, and M. Kulmala*
- Talk 3**    SPS1N3ac    **Popularization of science using graphic novels**  
*T. Mielonen*
- Talk 4**    SPS1N3ed    **Horizontal learning as one of the key pedagogical approaches in multidisciplinary research-oriented studies and intensive courses**  
*M. Paramonov, A. Lauri, V. Sylvius, and M. Kulmala*
- Talk 5**    SPS1N457    **Science: a dance, a story, a picture**  
*S.B. Mazon*

**Monday 28 August 2017****12:30 - 13:45****Lunch Break**

<b>Monday 28 August 2017</b>	<b>10:30 - 12:30</b>	<b>Room 15G40</b>
<b>NUMERICAL AND EXPERIMENTAL METHODS IN PARTICLE-LUNG INTERACTION</b>		
<b>Chairs: Otmar Schmid and Otto Hänninen</b>		

- 10:30** T407N478 **Anthropometry and anatomy based tools for generation of personalized human respiratory model for aerosol inhalation exposure simulations**  
*A. Przekwas, A. Zhou, R. Kannan, and P. Segars*
- 10:50** T401N044 **Numerical analysis of the effect of pulsating airflow on the nebulized aerosols in a patient-specific human nasal cavity**  
*A. Farnoud, X.G. Cui, I. Baumann, and E. Gutheil*
- 11:10** T407N38c **Computational modeling to predict regional deposition of inhaled e-cigarette aerosols within the respiratory tract**  
*A.A. Rostami, B. Asgharian, O. Price, and Y.B. Pithawalla*
- 11:30** T408N416 **Dosimetric considerations for designing toxicological studies with aerosolized nanoparticles: On the role of dose metric and tissue-delivered dose**  
*O. Schmid*
- 11:50** T401N19e **Charting the human airways with airborne nanoparticles, AiDA**  
*J. Jakobsson, H.L. Aaltonen, P. Wollmer, and J. Löndahl*
- 12:10** T407N361 **Particle deposition in the lung of mothers and their children in residential environments**  
*A. Stamatelopoulou, M. Pilou, C. Housiadas, D.N. Asimakopoulos, D. Sarigiannis, and T. Maggos*
- Back-up Paper** T409N231 **Aerosol emission and human health effects from cleaning spray use studied in an exposure chamber**  
*K. Lovén, C. Isaxon, J. Nielsen, E. Assarsson, P. Tallving, and A. Gudmundsson*

<b>Monday 28 August 2017</b>	<b>12:30 - 13:45</b>	<b>Lunch Break</b>
------------------------------	----------------------	--------------------

Monday 28 August 2017

10:30 - 12:30

Room 15G60

**INSTRUMENTATION FOR AMBIENT AEROSOLS****Chairs: Aladár Czitrovsky and Attila Nagy**

- 10:30** T310N2ee **A new on-line single particle laser mass spectrometer for detection of both, polyaromatic hydrocarbons and inorganic constituents from the same individual particles**  
*J. Passig, J. Schade, M. Fuchs, M. Oster, C. Jäger, M. Sklorz, and R. Zimmermann*
- 10:50** T303N37c **Comparison of aerosol chemical characterization techniques utilizing a PTR-ToF-MS: A study of biogenic SOA formation and aging**  
*G. Gkatzelis, P. Eichler, T. Hohaus, M. Müller, P. Schlag, S. Schmitt, R. Tillmann, Kang-Ming Xu, R. Holzinger, A. Wisthaler, and A. Kiendler-Scharr*
- 11:10** T310N0bc **Fate of atmospheric clusters inside a mass spectrometer (CI-API-TOF)**  
*M. Passananti, M.P. Rissanen, C. Yan, X.C. He, J. Kangasluoma, F. Bianchi, H. Junninen, M. Ehn, and H. Vehkamäki*
- 11:30** T307N28e **Helmos Hellenic Atmospheric Aerosol and Climate Change station first measurements of saharan dust events**  
*P. Fefatzis, S. Vratolis, V. Vasilatou, and K. Eleftheriadis*
- 11:50** T307N1fa **Multi-instrument intercomparison of aerosol light absorption coefficient measurements**  
*D. Massabò, J. Perim de Faria, V. Bernardoni, U. Bundke, P. Prati, G. Valli, R. Vecchi, and A. Petzold*
- 12:10** T302N3ab **Smart Air Quality Network, the measurement network for the future**  
*V. Ziegler, M. Beigl, M. Budde, J. Cyrys, St. Emeis, Th. Gratza, H. Grimm, M. Pesch, A. Philipp, T. Riedel, K. Schäfer, and J. Schnelle-Kreis*
- Back-up Paper** T304N4b4 **A miniature particle counter (LOAC) under meteorological balloons for the study of the temporal and spatial variability of stratospheric aerosols**  
*D. Vignelles, J.-B. Renard, G. Berthet, F. Dulac, F. Jégou, L. Rieger, A. Bourassa, J.-P. Vernier, G. Taha, S. Khaykin, T. Lurton, B. Couté, and V. Duverger*

Monday 28 August 2017

12:30 - 13:45

Lunch Break

**Monday 28 August 2017****13:45 - 15:30****Poster Area****POSTER SESSION PART I AND EXHIBITION****AEROSOL/CLOUD/CLIMATE INTERACTION**

- T201N00b **Self-match sampling of Geophysica exhaust in ice saturated conditions: jet fuel combustion aerosol and the microphysics of emission induced, freshly formed ice particles**  
*R. Weigel, C. Mahnke, M. Port, M. Krämer, C. Rolf, A. Afchine, J.-U. Grooss, and S. Borrmann*
- T201N0a6 **Ice nucleating particles in the Yucatan Peninsula: concentration, composition, and variability**  
*L.A. Ladino, G.B. Raga, H. Alvarez, M. Andino, I. Rosas, L. Martinez, B. Figueroa, A. Garcia, C. Chou, and A. Bertram*
- T201N12c **The effect of aerosol on cloud properties and precipitation in KIAPS integrated model with simplified chemistry module**  
*S. Y. Bae, J.-Y. Kang, and R. Park*
- T201N160 **The Lille Ice Nucleation Chamber (LINC). Reproducing in laboratory conditions the heterogeneous nucleation of ice on aircraft soot**  
*J. Wu, A. Faccinetto, S. Batut, D. Petitprez, and P. Desgroux*
- T201N1ce **Formation of methane under aerobic conditions**  
*A.C Saydam and A.H.A. Ghandi*
- T201N213 **Observational evidence for aerosols increasing upper tropospheric humidity**  
*L. Riuttanen, M. Bister, V.-M. Kerminen, V.O. John, A.-M. Sundström, M. Dal Maso, J. Räisänen, V.A. Sinclair, R. Makkonen, F. Xausa, G. de Leeuw, and M. Kulmala*
- T201N2f8 **Pre-activation of aerosol particles by ice preserved in pores**  
*C. Marcolli*
- T201N35c **The effect of aerosol-cloud interactions on shallow marine clouds**  
*T. Raatikainen, J. Ahola, J. Tonttila, S. Romakkaniemi, A. Laaksonen, and H. Korhonen*
- T201N3b2 **Microphysical cloud properties in sub-arctic environment during three Cloud Pallas Experiments**  
*K.M. Doulgeris and D. Brus*
- T201N3cb **Aerosol PSD and occurrence frequencies of clouds for temperate areas**  
*I. Marsli, M. Diouri, H. Steli, and A. Ben-Tayeb*
- T201N3ef **Pollen cytoplasmic granules induce heterogeneous nucleation of water droplets at low supersaturation**  
*S. Grimonprez, N. Visez, M. Choël, and D. Petitprez*

- T201N418 **Sampling arctic clouds with a new automated ground-based cloud sampling system**  
*R. Krejci, P. Zieger, J. Ström, H.C. Hansson, P. Tunved, C. Ritter, R. Neuber, Y.J. Yoon, M. Ramstrom, and F.J. Brechtel*
- T201N483 **Occurrence frequencies of clouds and aerosol PSD in the equatorial area**  
*H. Stelj, M. Diouri, I. Marsli, and A. El khabbouti*
- T201N4a2 **Results of laboratory studies of immersion mode heterogeneous ice nucleation by kaolin and quartz aerosols**  
*V.V. Chukin, A.F. Sadykova, and V.N. Nikulin*
- T201N4d5 **Role of cloud parameterization scheme on pollutants concentration over Indian domain**  
*N. Srivastava and N. Blond*

<b>Monday 28 August 2017</b>	<b>15:30 - 16:00</b>	<b>Coffee Break and Exhibition</b>
------------------------------	----------------------	------------------------------------

**Monday 28 August 2017****13:45 - 15:30****Poster Area****POSTER SESSION PART I AND EXHIBITION****AEROSOL TRANSPORT AND FORMATION**

- T207N07e **Multivariate analysis of upwind SO<sub>2</sub> emission influences on air pollution in Rochester, NY**  
*F. Emami, M. Masiol, and P.K. Hopke*
- T207N107 **Long-term trends and spatio-temporal changes in atmospheric aerosols at Zugspitze**  
*J. Sun, M. Herrmann, L. Ries, W. Birmili, and A. Wiedensohler*
- T207N1f8 **Aerosol particle dry deposition velocities above environmental substrates according to the diameter and the micrometeorological parameters: for the first time the "V" curve between 1.5 nm and 1 µm**  
*G. Pellerin, D. Maro, E. Gehin, D. Boulaud, P. Laguionie, D. Hébert, O. Connan, and L. Solier*
- T207N208 **Comprehensive analysis of HYSPLIT model sensitivity to different meteorological input data**  
*M. Reizer, J.A.G. Orza, and K. Juda-Rezler*
- T207N21d **Changes of <sup>7</sup>Be concentrations in air observed during dust episodes, 2009-2015**  
*J. Kusmierczyk-Michulec*
- T1207N2b0 **Long-term monitoring of atmospheric radioactive aerosols in Prague, Czech Republic**  
*M. Hýža, P. Rulík, H. Malá, V. Bečková, Z. Hölggye, and E. Schlesingerová*
- T207N321 **Rapid nitrate-induced atmospheric ageing of diesel soot in wintertime urban plumes**  
*A.C. Eriksson, C. Wittbom, P. Roldin, M. Sporre, E. Öström, P. Nilsson, J. Martinsson, J. Rissler, E.Z. Nordin, B. Svenningsson, J. H. Pagels, and E. Swietlicki*
- T207N323 **Tracking and tracing of aerosols using encapsulated DNA nanoparticles**  
*R.N. Grass, J. Koch, C. Mora, and W.J. Stark*
- T207N39c **Size resolved aerosols by the different regional influences in the West coastal Korea during KORUS-AQ campaign**  
*M.S. Bae, Z.H. Shon, S.H. Oh, T.H. Lee, S.S. Park, and G.T. Park*
- T207N3f7 **Changes in sub-micron number size distributions at Czech rural and urban background stations in the last ten years**  
*N. Zíková, J. Ondráček, Z. Wagner, and V. Ždímal*

- T207N3f9 **Seasonal variation of organic compounds in PM<sub>2.5</sub> measured at Anmyeon Island, a background site in South Korea and major factors affecting their levels**  
*J.S. Lee, E.S. Kim, Y.P. Kim, C.H. Jung, J.Y. Lee*
- T207N4a6 **Potential impacts of electric vehicles on air quality in Taiwan**  
*N. Li, J.-P. Chen, and I.-C. Tsai*
- T211N1e9 **Atmospheric evolution of primary and secondary organic aerosols: an explicit modeling of organic compound sources and sinks**  
*M. Camredon, G. Siour, R. Valorso, V. Lannuque, and B. Aumont*

**Monday 28 August 2017**

**15:30 - 16:00**

**Coffee Break and  
Exhibition**

**Monday 28 August 2017****13:45 - 15:30****Poster Area****POSTER SESSION PART I AND EXHIBITION****ELECTRICAL MEASUREMENT TECHNIQUES,  
INCLUDING ELECTRICAL MOBILITY ANALYSIS**

T308N2aa **Development and characterization of a 3D printed precipitator for aerosol nanoparticle segregation**

*A.A. Floutsi, S. Bezantakos, N. Surawski, and G. Biskos*

T308N2e3 **Approaching the resolving power of SEADM's DMA P5 to its theoretical limit**

*M. Amo-Gonzalez and J. Fernandez de la Mora*

T308N3e2 **Measurement of atmospheric charged particle during a lightning event by AEMSAp**

*H.-K. Lee and K.-H. Ahn*

T308N49e **Expanded size range of high-resolution nanoDMAs by improving the sample flow injection at the aerosol inlet slit**

*J. Fernandez de la Mora*

**Monday 28 August 2017****15:30 - 16:00****Coffee Break and  
Exhibition**

Monday 28 August 2017

13:45 - 15:30

Poster Area

**POSTER SESSION PART I AND EXHIBITION****INSTRUMENTATION FOR AMBIENT AEROSOLS**

- T303N203 **Quantification of black carbon on filters of different station types in Austria via transmissiometer measurements**  
*M. Greiling, L. Drinovec, G. Močnik, G. Schauer, and A. Kasper-Giebl*
- T303N368 **Evaluation of semi-continuous OCEC analyzer performance with the EUSAAR2 protocol**  
*A. Karanasiou, P. Panteliadis, M.C. Minguillón, M. Pandolfi, N. Perez, G. Titos, and A. Alastuey*
- T303N4b1 **Field comparison of instruments for measurement of air pollutants**  
*F. Borghi, A. Spinazze, G. Fanti, L. Del Buono, D. Campagnolo, S. Rovelli, A. Cattaneo, and D.M. Cavallo*
- T304N4b4 **A miniature particle counter (LOAC) under meteorological balloons for the study of the temporal and spatial variability of stratospheric aerosols**  
*D.Vignelles, J.-B. Renard, G. Berthet, F. Dulac, F. Jégou, L. Rieger, A. Bourassa, J.-P. Vernier, G. Taha, S. Khaykin, T. Lurton, B. Couté, and V. Duverger*
- T305N305 **Performance evaluation of the sizing capabilities of a new diffusion charging based particle sensor**  
*L. Salo, J. Gao, S. Saari, E. Saukko, K. Janka, T. Rönkkö, and J. Keskinen*
- T306N01d **Development of carbonaceous particulate matter analyser**  
*Y.D. Kim, J.H. Kang, M.E. Kim, J.Y. Lee, J.S. Jung, and S. Lee*
- T309N0a5 **Real-time measurement of PM<sub>2.5</sub> size distribution using a lab-made 11-stage electrical low pressure impactor**  
*J. Han, J. Seo, J. Hyun, and J. Hwang*
- T312N0d5 **How to measure volatile substances in various size classes of UFP**  
*H. Plachá, M. Bitter, P. Goll, and J. Kufel*
- T312N155 **Setup of an interface for operation of IAGOS (In-service Aircraft Global Observing System) CORE instruments onboard the IAGOS CARIBIC platform**  
*U. Bundke, M. Berg, H. Franke, A. Zahn, H.Boenisch, J. Perim de Faria, F. Berkes, and A. Petzold*
- T312N169 **Identification and quantification of ambient cigarette-related aerosol using online aerosol mass spectrometry**  
*C. Struckmeier, P. Faber, F. Fachinger, F. Drewnick, and S. Borrmann*
- T312N3fe **Determining the connection between hygroscopicity and semi-volatile composition**  
*J. Alroe, Z. Ristovski, B. Miljevic, L. Cravigan, and G. Johnson*

Monday 28 August 2017

15:30 - 16:00

Coffee Break and  
Exhibition

Monday 28 August 2017

13:45 - 15:30

Poster Area

## POSTER SESSION PART I AND EXHIBITION

## NEW PARTICLE FORMATION I

- T203N02C **One-year air ion observation at Dome C, Antarctica**  
*X. Chen, A. Virkkula, V.-M. Kerminen, H.E. Manninen, M. Busetto, C. Lanconelli, A. Lupi, V. Vitale, M. Del Guasta, R. Väänänen, E.-M. Duplissy, and M. Kulmala*
- T203N0d7 **Features of new particle formation in Central European background air**  
*Á. Molnár, K. Imre, and P. Aalto*
- T203N10d **New particle formation studied by PSM at rural background site Košetice**  
*A. Holubová Šmejkalová, N. Zíková, and V. Ždímal*
- T203N15c **Automated method for identifying NPF types using characteristic nucleation-mode particles and air ions**  
*L. Dada, R. Chellapermal, S. Buenrostro Mazon, J. Sulo, H. Junninen, V.M. Kerminen P. Paasonen, and M. Kulmala*
- T203N27e **Ultrafine particle events during anticyclonic and advection conditions in Madrid**  
*N. Perez, A. Alastuey, C. Reche, M. Ealo, G. Titos, A. Ripoll, M.C. Minguillon, F.J. Gómez-Moreno, E. Alonso-Blanco, E. Coz, E. Diaz, B. Artinano, Saúl García dos Santos, R. Fernández-Patier, A. Saiz-Lopez, F. Serranía, M. Anguas-Ballesteros, B. Temime-Roussel, N. Marchand, D.C.S. Beddows, R.M. Harrison, and X. Querol*
- T203N296 **The effect of NO on the formation of condensable vapours in the oxidation of  $\alpha$ -pinene/p**  
*O. Peräkylä, O. Garmash, M. Riva, L. Heikkinen, L. Quéléver, M. Äijälä, L. Fischer, E. Canaval, A. Hansel, T. Petäjä, and M. Ehn*
- T203N29f **Anthropogenic nanoparticle formation in the Vienna industrial region**  
*S. Brilke, A. Kropf, and P.M. Winkler*
- T203N2af **Secondary aerosol formation in a traffic influenced coastal desert environment**  
*B. Alfoldy and M. Kotob*
- T203N316 **A Monte Carlo approach to nucleation**  
*C. Köhn, M.B. Enghoff, and H. Svensmark*
- T214N407 **What is the mechanism behind new particle formation in highly polluted urban environments?**  
*F. Bianchi, L. Yao, O. Garmash, C. Yan, J. Kontkanen, H. Junninen, S. Buenrostro Mazon, M. Ehn, M. Sipilä, T. Petäjä, M. Kulmala, D.R. Worsnop, and L. Wang*

Monday 28 August 2017

15:30 - 16:00

Coffee Break and  
Exhibition

Monday 28 August 2017

13:45 - 15:30

Poster Area

POSTER SESSION PART I AND EXHIBITION

**NUMERICAL AND EXPERIMENTAL METHODS IN PARTICLE-LUNG INTERACTION**

- T214N371 **Nitro-monoaromatic compounds in urban aerosols of Central and Southeastern Europe: mass size distribution and solubility in simulated lung fluids**  
*Z. Kitanovski, G. Lammel, R. Prokeš, C. Samara, P. Shahpoury, and A. Voliotis*
- T315N347 **Aerosol trapping, optimization and characterization for comparative in-vitro assessment of combustible and heat-non burn platforms**  
*D. Goedertier, I. Gonzalez Suarez, G. Vuillaume, J. Hoeng, and M.C. Peitsch*
- T401N010 **Aerosol-made E-nose for selective formaldehyde detection in breath screening of lung cancer and air quality monitoring**  
*A.T. Guentner, V. Koren, K. Chikkadi, M. Righettoni, and S.E. Pratsinis*
- T401N3e3 **Rapid disease screening and monitoring from exhaled breath with portable sensor arrays**  
*N.J Pineau, A.T. Güntner, and S.E. Pratsinis*
- T401N4db **Investigation of electrostatic behaviour of dry powder inhaled formulations**  
*M. Jetzer and B. Morrical*
- T404N219 **In vitro dosimetry and bioimaging with aerosol-made  $YVO_4:Eu^{3+},Bi^{3+}$  nanophosphors**  
*A. Spyrogianni, P.G. Tiefenboeck, F. Krumeich, J.-C. Leroux, S.E. Pratsinis, G.A. Sotiriou*
- T406N172 **Development of eye exposure characteristic chamber for the identification of environmental disease caused by fine particles**  
*S.Yoon, S. Han, K.-J. Jeon, and S. Kwon*
- T406N20f **Estimation of pulmonary toxicity of nanomaterials following subacute inhalation**  
*Y. Morimoto, H. Izumi, Y. Yoshiura, Y. Fujisawa, T. Tomonaga, T. Oyabu, T. Okada, T. Myojo, M. Shimada, and M. Kubo*
- T406N283 **Development of eye exposure characteristic chamber for the identification of environmental disease caused by fine particles**  
*S. Han, J.-S. Yi, J.-S. Youn, H.-S. Lee, J. Seo, and K.-J. Jeon*
- T407N11a **Lung deposition model of airborne multi-walled carbon nanotubes for inhalation exposure assessment**  
*Y.K. Bahk, P. Sachinidou, E. Gitsis, and J. Wang*

- T407N488 **Method for processing cascade impactor data to estimate activity of radioactive aerosol particles deposited in different regions of human respiratory tract**  
*A.E. Karev, A.G. Tsovyanov, and S.M. Shinkarev*
- T408N312 **Pulmonary effects of silver nanowires with different length in instillation study**  
*T. Oyabu, Y. Morimoto, Y. Yoshiura, and T. Myojo*
- T409N02a **Particle deposition efficiency in respiratory tract cast models**  
*D.J. Hsu, H.Y. Lin, and Y.M. Sun*
- T409N231 **Aerosol emission and human health effects from cleaning spray use studied in an exposure chamber**  
*K. Lovén, C. Isaxon, J. Nielsen, E. Assarsson, P. Tallving, and A. Gudmundsson*

**Monday 28 August 2017**

**15:30 - 16:00**

**Coffee Break and  
Exhibition**

Monday 28 August 2017

13:45 - 15:30

Poster Area

**POSTER SESSION PART I AND EXHIBITION****OPTICAL MEASUREMENT TECHNIQUES**

- T307N04d **Enhanced particle size analysis using polarization scattering method**  
*Q. Xie, N. Zeng, S. Chen, H. Ma*
- T307N07c **Characterisation of the filter loading effect in various filter materials**  
*L. Drinovec, T. Müller, A. Wiedensohler, and G. Močnik*
- T307N0f2 **Mapping aerosol concentrations in the port of Newcastle with a scanning lidar**  
*Y. Zheng, J. Fisher, and H. Bridgman*
- T307N1e8 **Measurements of vapour pressure using the Union College Electrodynamic Balance**  
*P. Kotowitz, U.K. Krieger, U. Weers, A.T. Novak, C. Porat, and A.J. Huisman*
- T307N34e **A sensor for reliable in-situ detection of volcanic ash in the presence of cloud particles**  
*E. Weingartner, Z. Jurányi, D. Egli, B. Neininger, and H. Burtscher*
- T307N315 **Revival of an old method with new techniques: In-situ measurement of aerosol light absorption using photothermal interferometry**  
*B. Visser, A. Meier, S. Sjogren, D. Egli, P. Steigmeier, H. Burtscher and E. Weingartner*
- T307N402 **Study of the wavelength dependence of the optical depth for estimation of the aerosol contamination of the atmosphere**  
*A. Nagy, A. Czitrovsky, A. Kerekes, Sz. Kugler*
- T307N41b **Measurement of physical and optical properties of aerosol particles in urban environment**  
*A. Nagy, A. Czitrovsky, A. Kerekes, and W.W. Szymanski*

Monday 28 August 2017

15:30 - 16:00

Coffee Break and  
Exhibition

Monday 28 August 2017

13:45 - 15:30

Poster Area

POSTER SESSION PART I AND EXHIBITION

**STATIONARY SOURCES AND INDUSTRIAL COMBUSTION AEROSOL**

- T117N306 **Characterization of oil shale combustion emissions by SP-AMS and CI-API-TOF-MS**  
*M. Aurela, F. Mylläri, M. Bloss, P. Simonen, A. Konist, D. Neshumayev, M. Maasikmets, L. Salo, S. Saarikoski, H. Timonen, M. Sipilä, M. Dal Maso, J. Keskinen, and T. Rönkkö*
- T117N31c **Particle sampling under extreme conditions: An analysis of the corrosion-relevant aerosol in boilers of waste incineration plants**  
*S. Schumacher, J. Lindermann, B. Stahlmecke, D. Jarzyna, A. Khot, T. van der Zwaag, H. Nordsieck, J. Harpeng, R. Warnecke, and C. Asbach*
- T117N348 **Characterization of nanoparticles and polymer nanocomposites in flames for subsequent studies on health effects**  
*N. Teuscher, W. Baumann, M. Hauser, S. Müllhopt, M. Hufnagel, A. Hartwig, M. Garcia-Käufer, R. Gminski, M. Berger, T. Krebs, H.-R. Paur, and D. Stapf*
- T118N1af **Numerical simulation of cyclone separator comparison between CFD-DEM and DDPM**  
*I. Hwang, S. Kim, and J. Hwang*
- T118N33f **Particle characteristics from wood pellet-coal-mixture combustion in a large combined heat and power plant**  
*F. Mylläri, L. Pirjola, H. Lihavainen, E. Asmi, E. Saukko, V. Vakkari, E. O'Connor, J. Rautiainen, A. Häyriinen, V. Niemelä, J. Maunula, R. Hillamo, J. Keskinen, and T. Rönkkö*
- T119N16f **Novel electrical charging condensing heat exchanger for particle emission reduction in small boilers**  
*O. Sippula, J. Grigonyte, H. Suhonen, A. Laitinen, M. Kortelainen, J. Tissari, P. Tiitta, A. Lähde, J. Keskinen, and J. Jokiniemi*
- T119N17f **Determination of indoor pollutants from coal combustion in a controlled setting**  
*M.L.M. Barabad, M.E. Versoza, W.S. Junf, and D.S. Park*
- T119N2fc **Influence of wood quality on reduction of particle emissions from biomass combustion boiler**  
*A. Bologna, W. Aich, M. Ecker, U. Frei, K. Woletz, H.-P. Rheinheimer, and H.-R. Paur*
- T119N3d9 **Emission reduction of PCDD/Fs from a diesel generator fueled with water-containing butanol and waste cooking oil-based biodiesel blends**  
*J.-H. Tsai, S.-J. Chen, K.-L. Huang, G.-P. Chang-Chien, W.-Y. Lin, B.-C. Jheng, and Y.-C. Hsieh*

- T119N3dc **Emissions of PAHs and particulate metals from a diesel engine generator fueled with blends of waste cooking oil-based biodiesel and fossil diesel**  
*J.-H. Tsai, S.-J. Chen, K.-L. Huang, C.-C. Lin, W.-Y. Lin, H.-T. Huang, and J.-T. Lee*
- T119N450 **On-line, size-resolved elemental analysis of ZnO nanoparticles during wood combustion processes**  
*D. Foppiano, M. Tarik, E. Müller, and C. Ludwig*
- T119N4c5 **Trace metal and PAH enrichment within the penetration window of an ESP**  
*I. Ibarra, I. Gomez, J. Gonzalez, D. Sanz, E. Rojas, J. J. Rodríguez-Maroto, R. Ramos, E. Borjabad, R. Escalada, I. Celades, S. Gomar, V. Sanfelix, and C. Gutierrez-Canas*
- T120N228 **Atmospheric Hg-g and Hg-p concentrations in the surroundings of a clinker plant**  
*A. Carratalá, F.A. Santos, E. Yubero, and M. Santacatalina*
- T120N3d0 **On-field measurement of PM<sub>2.5</sub> and carbonaceous aerosol emissions from biomass fuel combustion in traditional Indian cookstoves**  
*G. Habib, A. Padhi, and I. Husain*
- T120N438 **Emissions from wood and catalytic tar removal combustion in household stoves**  
*H-L. Kupri, M. Maasikmets, R. Rebane, K. Vainumäe, R. Titova, E. Teinemaa, and V. Voronova*
- T120N4b7 **V<sub>2</sub>O<sub>5</sub> / TiO<sub>2</sub> catalysts for VOC removal analysis**  
*J.-T. Lee and H.-C. Chen*
- T214N2c3 **Very low emissions of airborne particulate pollutants measured from two municipal solid waste incineration plants in Switzerland**  
*A. Setyan, M. Patrick, and J. Wang*

<b>Monday 28 August 2017</b>	<b>15:30 - 16:00</b>	<b>Coffee Break and Exhibition</b>
------------------------------	----------------------	------------------------------------

**Monday 28 August 2017****13:45 - 15:30****Poster Area****POSTER SESSION PART I AND EXHIBITION****SOURCE APPORTIONMENT STUDIES I**

- T215N051 **Source apportionment of water-soluble organic aerosols measured at an urban site**  
*G.-H. Yu and S. Park*
- T215N056 **Estimation of source apportionment for semi-continuous PM<sub>2.5</sub> data using the EPA-PMF at various air pollution monitoring supersites in Korea**  
*I. Hwang, T.-J. Lee, H.-J. Lim, and S.-M. Yi*
- T215N0f5 **Seasonal aerosol characteristics and sources at a rural site south in Beijing, China**  
*Y. Hua, S. Wang, J. Jiang, F. Canonaco, A.S.H. Prévôt, W. Zhou, Q. Xu, X. Li, and B. Liu*
- T215N122 **Organic aerosol in urban air of China: chemical composition, sources and atmospheric processes**  
*R.-J. Huang, Y.C. Wang, Y. He, R. Fröhliche, F. Canonaco, M. Elser, K.R. Daellenbach, I. El Haddad, J. Slowik, M.R. Canagaratna, D.R. Worsnop, A.S.H. Prévôt, and J.J. Cao*
- T215N128 **Long-term measurements of the chemistry and sources of submicron aerosols at SIRTA in Paris area, France**  
*Y. Zhang, O. Favez, A. Albinet, F. Canonaco, F. Truong, T. Amodeo, A. Prevot, J. Sciare, and V. Gros*
- T215N19b **Stable carbon isotope composition, sources and chemical processing of aerosol particles**  
*A. Masalaite, R. Holzinger, A. Garbaras, V. Remeikis, T. Röckmann, and U. Dusek*
- T215N1e3 **Source apportionment of the organic fraction in the forest area**  
*S. Byčėnkiene, L. Krikšėikas, G. Mordas, V. Dudoitis, and V. Ulevicius*
- T215N1f3 **Source apportionment of atmospheric particulate matter (PM<sub>10</sub>) using a constrained US-EPA-PMF<sub>5.0</sub> model on different urban environments in France**  
*D. Salameh, O. Favez, B. Golly, J.L. Besombes, L. Alleman, A. Albinet, and J.L. Jaffrezo*
- T215N20d **Composition, sources and long range contribution for PM<sub>2.5</sub> in Po valley urban background**  
*A. Bigi, A. Piazzalunga, L. Pontoni, G. Calzolari, M. Giannoni, F. Pirozzi, G. Ghermandi, and S. Teggi*
- T215N25a **PM<sub>10</sub> chemical composition and sources in the Central Mediterranean**  
*G. Calzolari, S. Becagli, S. Nava, F. Lucarelli, M. Chiari, M. Giannoni, R. Traversi, M. Severi, M. Marconi, R. Udisti, A. di Sarra, G. Pace, D. Meloni, C. Bommarito, F. Monteleone, F. Anello, and D. Sferlazzo*

- T215N25d **Source apportionment of Arctic aerosol collected at Ny Alesund – Svalbard Islands: Results from the 2015 campaign**  
*G. Calzolari, S. Nava, M. Chiari, F. Lucarelli, M. Giannoni, S. Becagli, R. Traversi, L. Caiazzo, F. Giardi, M. Severi, M. Mazzola, and R. Udisti*
- T215N263 **Review on source apportionment of fine aerosol using carbonaceous constituents and organic molecular markers: case studies from India and South East Asia**  
*L. Gupta, G. Habib, and R.S. Raman*
- T215N26a **Quantifying the sources of air pollution in the Danube macro-region to support the development of abatement strategies**  
*C.A. Belis, E. Pisoni, and P. Thunis*
- T215N277 **A new approach for classifying airborne particles: A case study on the quantification of PM10 from railway and road traffic in the Reuss valley (Canton of Uri, Switzerland)**  
*J. Rausch, T. Zünd, D. Jaramillo Vogel, R. Locher, M. Meier, and K. Kammer*
- T215N3bb **Source apportionment of ambient organic aerosol by online extractive electrospray ionization time-of-flight mass spectrometry (EESI-TOF)**  
*G. Stefenelli, F. D. Lopez-Hilfiker, V. Pospisilova, A. Vogel, C. Hüglin, U. Baltensperger, A.S.H. Prévôt, and J.G. Slowik*
- T215N3a5 **Extensive full-year source apportionment data analysis of organic aerosols**  
*A. Tobler, Y. Sosedova, F. Canonaco, R. Fröhlich, K. Dällenbach, A. Vlachou, A. Prévôt, and U. Baltensperger*
- T215N3d5 **Sources of PM10 at an urban air monitoring site in New South Wales, Australia**  
*K. Larcombe, R. Jayaratne, and G. A. Ayoko*

**Monday 28 August 2017****15:30 - 16:00****Coffee Break and  
Exhibition**

Monday 28 August 2017

13:45 - 15:30

Poster Area

POSTER SESSION PART I AND EXHIBITION

**TOXICOLOGICAL CHARACTERIZATION OF AMBIENT AND ENGINEERED PARTICLES**

- T214N257 **On-line measurements of particle-bound reactive oxygen species (ROS) in Beijing**  
*S.S. Steimer, F.P.H. Wragg, and M. Kalberer*
- T403N15e **Ecotoxicological assessment of guaiacol and its nitrated derivatives**  
*A. Kroflič, M. Pflieger, M. Debeljak, and K. Vogel-Mikuš*
- T403N2e8 **In vitro dosimetric and cytotoxic assessment of a commercially available tobacco heating product (THP) versus a reference cigarette**  
*J. Adamson, T. Jaunky, S. Santopietro, A. Terry, D. Thorne, D. Breheny, and M. Gaça*
- T404N302 **Particle mass monitoring by Quartz Crystal Microbalance using electrostatic deposition enhancement**  
*S. Mülhopt, C. Schlager, T. Krebs, M. Berger, and H.-R. Paur*
- T404N446 **Efficiency, variability and control of aerosol sampling and deposition in the Vitrocell® 24/48 trumpet unit**  
*A.K. Kuczaj and F. Lucci*
- T404N44e **A temperature and humidity controlled air-liquid interface for cell culture exposition based on high-efficiency electrostatic deposition**  
*H. Wiegand, K. Fetsch, J. Meyer, and G. Kasper*
- T406N0b8 **Oxidative potential of water-soluble fractions of PM<sub>2.5</sub> and PM<sub>10</sub> in South-Eastern Italy during advection of African dust**  
*D. Chirizzi, D. Cesari, M.R. Guascito, A. Dinoi, L. Giotta, A. Donateo, and D. Contini*
- T406N200 **The oxidative potential of subway PM<sub>2.5</sub>**  
*T. Moreno, F. Kelly, C. Dunster, A. Oliete, V. Martins, C. Reche, M.C. Minguillón, F. Amato, M. Capdevila, E. de Miguel, and X. Querol*
- T406N374 **Toxicity of wood smoke particles in human lung epithelial cells: the role of PAHs, soot and zinc**  
*M. Dilger, J. Orasche, C. Schlager, S. Mülhopt, R. Zimmermann, H.-R. Paur, S. Diabaté, and C. Weiss*

- T406N43f **Investigation of spatial and temporal and genotoxicity and cytotoxicity of atmospheric particles collected from Kutahya**  
*G. Cakmak Demircigil, E. Emerce, P. Erturk, A. Ari, R. Schins, S. Burgaz, and E.O. Gaga*
- T408N18a **Nanoparticle stability and size as important factors in nano-TiO<sub>2</sub> toxicity in macrophage-like cells**  
*J. Sikorova, T. Brzicova, A. Milcova, K. Vrbova, J. Klema, P. Pikal, J. Topinka, and P. Rossner*
- T408N359 **Characterization of the air-liquid interface cell exposure (ALICE-CLOUD) system for in-vitro toxicological studies of engineered nanomaterials (ENMs)**  
*Y.o Ding, P. Weindl, C. Wimmer, P. Mayer, T. Krebs, and O. Schmid*
- T409N0d9 **Generation of copper and copper oxide nanoparticles for exposure studies by MOCVD**  
*P. Moravec, J. Schwarz, P. Vodička, J. Kupčík, and J. Švehla*
- T409N1cd **Comparison of four acellular methods for measuring the Oxidative Potential of PM collected in five French cities**  
*A. Calas, G. Uzu, A. Oliete, C. Dunster, F.J. Kelly, J.M.F. Martins, S. Houdier, C. Begorre, S. Weber, and J.-L. Jaffrezo*
- T409N27a **Effect of inhaled PbO nanoparticles on mice organs after long-term exposition**  
*P. Mikuška, Z. Večeřa, M. Buchtová, J. Dumková, B. Putnová, B. Dočekal, L. Čapka, P. Coufalík, K. Křůmal, P. Fictum, and A. Hampl*

**Monday 28 August 2017****15:30 - 16:00****Coffee Break and  
Exhibition**

Monday 28 August 2017

13:45 - 15:30

Poster Area

**POSTER SESSION PART I AND EXHIBITION****URBAN AEROSOLS**

- T214N068 **Air pollution by nanoparticles in 5D diagrams**  
*L. Hejkrlik, H. Plachá, and D. Richterová*
- T214N0d2 **Calibration of shortwave radiometers in Brussels with an AOD rejection channel**  
*S. Nevens, A. Chevalier, C. Conscience, and J. Amand*
- T214N0db **Bias caused by water adsorption in hourly PM measurements**  
*K. Imre, Á. Molnár, and G. Kiss*
- T214N0fc **Oxidative potential of atmospheric aerosols collected at high air pollution site related to chemical composition: Krakow case study**  
*K. Styszko, M. Kistler, L. Samek, K. Szramowiat, K. Kubisty, A. Korzeniewska, R. Rakoczy, and A. Kasper-Giebl*
- T214N145 **Estimation of airborne PM to total tire wear fraction under constant speed driving condition using a tire simulator**  
*S.H. Lee, K.B. Kim, and Y.R. Kim*
- T214N153 **Daytime and nighttime concentrations of PM10 and water-soluble ions at a traffic site in the Western Mediterranean**  
*N. Galindo, E. Yubero, J.F. Nicolás, M. Varea, R. Castaner, S. Caballero, J. Gil-Moltó, C. Pastor, and J. Crespo*
- T214N158 **Metal concentrations in aerosols at a traffic site in Elche, Southeastern Spain**  
*N. Galindo, E. Yubero, J.F. Nicolás, M. Varea, R. Castaner, S. Caballero, J. Gil-Moltó, C. Pastor, and J. Crespo*
- T214N183 **PM10 and black carbon exposure during bicycle commuting: the effect of route selection**  
*T. Siponen, P. Tiittanen, P. Taimisto, A. Pulkkinen, P. Aarnio, A. Kousa, T. Yli-Tuomi, J. Niemi, and T. Lanki*
- T214N1b9 **Spatial distribution of particulate matter and its temporal evolution in a complex hot spot with influence in an urban park**  
*F. J. Gómez-Moreno, B. Artínano, E. Díaz Ramiro, M. Barreiro, S. Vardoulakis, C. Dimitroulopoulou, C. Yagüe, G. Maqueda, C. Román-Cascón, M. Sastre, and R. Borge*
- T214N1c9 **One year of aerosol size and black carbon measurements in Nanjing, China**  
*A. Leskinen, A. Ruuskanen, D. Fang, K. Kuusalo, P. Jalava, Q. Wang, C. Gu, J. Jokiniemi, M.-R. Hirvonen, K.E.J. Lehtinen, S. Romakkaniemi, and M. Komppula*

- T214N273 **Seasonal and spatial differences of size-segregated trace elements in Turkey**  
*P. Ertürk Ari, A. Ari, and E.O. Gaga*
- T214N279 **Determination of carbonaceous aerosol levels at two different stations in the capital of Turkey, Ankara**  
*P. Faramarzi, S.Y. Aslanoglu, F. Ozturk, A.C. Saydam, and G. Gullu*
- T214N289 **Variability of traffic generated urban aerosols (PM10) in city street canyon: Riga (Latvia) case study**  
*I. Steinberga, A. Kanisceva, L. Sustere, J. Bikše Jr., and J. Kleperis*
- T214N294 **Concentrations and gradients of traffic-derived metals in PM10 and PM2.5 near a major road**  
*T. Yli-Tuomi, P. Taimisto, A. Pulkkinen, J.V. Niemi, A. Kousa, and T. Lanki*
- T214N297 **Study of Particulate Matter (PM) levels in Sao José dos Campos using a Generalized Linear Model (GLM)**  
*D.C. Nogarotto and S.A. Pozza*
- T214N2b3 **PM emissions by electric cars**  
*H. Horvath*
- T214N2cb **Summer-autumn air pollution in León (Spain): changes in the aerosol size distribution and effects on the respiratory tract**  
*F. Oduber, A. Castro, A.I. Calvo, C. Blanco-Alegre, E. Alonso-Blanco, P. Belmonte, E. Coz, A.S.H. Prévôt, G. Močnik, and R. Fraile*
- T214N2cf **Aerosol concentration during a thermal inversion followed by rain in Northwestern Iberia**  
*C. Blanco-Alegre, A. Castro, A.I. Calvo, E. Alonso-Blanco, F. Oduber, E. Coz, A.S.H. Prévôt, G. Močnik, and R. Fraile*
- T214N42f **Aerosol PSD and optical depth of mega-agglomerations**  
*R. Meziane and M. Diouri*
- T214N493 **Seasonal variation of urban coarse particles in Amman – Jordan**  
*T. Hussein, H. Juwhari, and M. Qaisi*
- T214N494 **Measurements of the vertical distribution of the pollution in Paris (France) by the light aerosol counter LOAC on-board the tethered touristic balloon “OAG”**  
*J.-B. Renard, K. Léger, Amélie Fritz, J. Giacomoni, B. Couté, V. Duverger, and M. Jeannot*
- T214N4a7 **Climate effects of urban aerosols**  
*M. Zoran, R. Savastru, D. Savastru, and A. Dida*
- T214N4d8 **Highly resolved spatiotemporal variability of fine particle concentrations in an urban neighborhood**  
*Y. Etzion and D.M. Broday*

**Monday 28 August 2017****13:45 - 15:30****Poster Area****POSTER SESSION PART I AND EXHIBITION****SPECIAL SESSION #4: TARGETED GENERATION AND DELIVERY OF AEROSOLIZED MEDICINES**

SPS4N0b3 **Large Eddy simulations of laryngeal air flow in three-dimensional patient-specific geometry models**

*S. Voß, G. Janiga, C. Arens, S. Voigt-Zimmermann, and D. Thévenin*

SPS4N322 **Aerodynamic deposition of amikacin dry powder for inhalation**

*L. Mašková, J. Kozáková, F. Buttini, and V. Ždímal*

SPS4N3bf **Modeling of aerosolized drugs targeting in the lung - Parametric study in a PRB**

*M. Pilou, A. Skiadopoulos, P. Neofytou, and C. Housiadas*

SPS4N4ae **Regional targeting of aerosolized drugs in murine lungs**

*O. Schmid, R. Winkler-Heil, G. Eder, W. Möller, and W. Hofmann*

**Monday 28 August 2017****15:30 - 16:00****Coffee Break and  
Exhibition**

Monday 28 August 2017

13:45 - 15:30

Poster Area

POSTER SESSION PART I AND EXHIBITION

**SPECIAL SESSION #6: EMISSIONS FROM AIRCRAFT AND SHIPS**

- SPS6N161 **Contamination induced by the use of PTFE lines in aeronautic soot sampling**  
*I.K. Ortega, C. Irimiea, D. Delhaye, and C. Focsa*
- SPS6N1ba **Chemical, physical and optical properties of ship plumes catching by MEGA-chamber**  
*X. Pei, R.K. Pathak, A.C. Eriksson, K. Salo, and M. Hallquist*
- SPS6N1f0 **Ship plume aerosol characterization and contribution to inland air quality**  
*S. Ausmeel, K. Kling, E. Ahlberg, M. Spanne, A. Eriksson, and A. Kristensson*
- SPS6N235 **Mass and size resolved optical properties of black carbon particles in aircraft engine exhaust**  
*M. Elser, B.T. Brem, L. Durdina, and J. Wang*
- SPS6N24c **Correlations of nonvolatile PM mass and number emissions with smoke number determined for commercial aircraft jet engines**  
*L. Durdina, B.T. Brem, and J. Wang*
- SPS6N24d **Aircraft-based single particle measurements in the Baltic Sea marine boundary layer**  
*F. Köllner, J. Schneider, H. Bozem, P. Hoor, M. Zanatta, H. Schulz, A. Herber, U. Bundke, J. de Faria, A. Petzold, R. Brauner, and S. Borrmann*
- SPS6N2bb **Effects of the fuel chemical composition on volatile organic compounds emitted by aircraft engines**  
*A. Setyan, Y.-Y. Kuo, B.T. Brem, L. Durdina, A.C. Gerecke, N.V. Heeb, R. Haag, and J. Wang*
- SPS6N379 **Brown carbon in ship-engine exhaust: imaginary refractive index and mass absorption cross-section retrieval**  
*J. C. Corbin, A. A. Mensah, M. Zanatta, S. Pieber, G. Jakobi, J. Orasche, J. G. Slowik, N. Kumar, I. El Haddad, F. Klein, B. Stengel, R. Zimmermann, A.S.H. Prévôt, U. Baltensperger, and M. Gysel*
- SPS6N3b5 **An effect of fuel on composition specific volatility of marine engine exhaust particles**  
*M. Isotalo, N. Kuittinen, P. Karjalainen, P. Aakko-Saksa, P. Simonen, F. Mylläri, H. Wihersaari, J. Keskinen, T. Rönkkö, and H. Timonen*
- SPS6N3de **Impact of alternative fuels on the non-volatile particulate matter mass and number emissions of an in-production aero gas turbine**  
*B.T. Brem, L. Durdina, M. Elser, A. Setyan, D. Schönenberger, S. Wyss, K Zeyer, F. Siegerist, M. Munoz, R. Haag, D. Rentsch, J. Mohn, N.V. Heeb, and J. Wang*

SPS6N3fa **On-board measurements of particle and gaseous emissions from a large cargo vessel at different operating conditions**

*T. Chu Van, Z.D. Ristovski, and R. Brown*

SPS6N400 **Black carbon from shipping over the Baltic Sea**

*M. Zanatta, H. Schulz, F. Köllner, J. Schneider, H. Bozem, P. Hoor, U. Bundke, J. de Faria, A. Petzold, R. Brauner and S. Borrmann, and A. Herber*

T116N3a1 **A study on the geometry of pre-treatment device for removal of particulate matter**

*B.H. Park, J.Y. Lee, H.G. Kim, and J.S. Choi*

**Monday 28 August 2017**

**15:30 - 16:00**

**Coffee Break and  
Exhibition**

Monday 28 August 2017

16:00 - 18:00

Room 04G30

**SOURCE APPORTIONMENT STUDIES II**

Chairs: Mar Viana and Otto Klemm

- 16:00** T215N211 **Distinguishing source specific black carbon production from meteorologically driven temporal variability by means of  $^{222}\text{Rn}$  tracer**  
*A. Gregoric, L. Drinovec, I. Ježek, J. Vaupotic, L. Wang, M. Mole, S. Stanic, and G. Mocnik*
- 16:20** T215N3ad **Source apportionment of PM in Leipzig, Germany: From coarse to ultrafine particle size ranges**  
*D. van Pinxteren, K. Wadinga Fomba, K. Müller, G. Spindler, G. Löschau, A. Hausmann, and H. Herrmann*
- 16:40** T215N3a7 **Seasonal characterization of organic aerosol sources and composition using extractive electrospray ionization time-of-flight mass spectrometry (EESI-TOF)**  
*L. Qi, A.L. Vogel, S. Esmaeilrad, M. Chen, X. Ge, U. Baltensperger, A.S.H. Prevot, and J.G. Slowik*
- 17:00** T215N046 **Assessment of the primary and secondary contributions from wood burning to the PM<sub>10</sub> OC for a rural site in Belgium by making use of molecular markers and PMF**  
*W. Maenhaut, M. Claeys, R. Vermeylen, A. Kahnt, and J. Vercauteren*
- 17:20** T211N26f **Source apportionment of PM<sub>2.5</sub> by using organic and inorganic tracers in a suburban site of Turkey**  
*A. Ari, P. Ertürk Ari, and E.O. Gaga*
- 17:40** T215N42c **Source Apportionment of Organic Aerosols in Lithuania using thermal desorption proton-transfer reaction mass spectrometry (TD-PTRMS)**  
*Y. Tong, D. Steinfeld, C. Bozzetti, R. Holzinger, I. El Haddad, J.G. Slowik, A.S.H. Prévôt, and U. Baltensperger*
- Back-up Paper** T215N3a5 **Extensive full-year source apportionment data analysis of organic aerosols**  
*A. Tobler, Y. Sosedova, F. Canonaco, R. Fröhlich, K. Dällenbach, A. Vlachou, A. Prévôt, and U. Baltensperger*

Monday 28 August 2017

18:00

End of Conference Day

Monday 28 August 2017

16:00 - 18:00

Room 24G45

**AEROSOL/CLOUD/CLIMATE INTERACTION****Chairs: Michael Boy and Sabine Wurzler**

- 16:00** T201N01c **What do we learn from long-term CCN observations?**  
*J. Schmale, S. Henning, B. Henzing, H. Keskinen, K. Sellegri, J. Ovadnevaite, A. Bougiatioti, A. Jefferson, S.S. Yum, P. Schlag, A. Kristensson, A. Matsuki, M. Pöhlker, J. Brito, F. Stratmann, M. Gysel, and the CCN Team*
- 16:20** T201N404 **Cloud condensation nuclei (CCN)-activation behaviour of atmospheric black carbon particles in relation to their size and mixing state**  
*G. Motos, J. Schmale, J.C. Corbin, M. Zanatta, U. Baltensperger, and M. Gysel*
- 16:40** T201N4a0 **Ice nucleation abilities of atmospheric soot particles**  
*F. Mahrt, R.O. David, U. Lohmann, Z. Wu, C. Stopford, and Z.A. Kanji*
- 17:00** T201N426 **Single particle analysis of residues from cloud droplets and ice crystals**  
*J. Schneider, S. Mertes, A. Roth, S. Schmidt, H. Clemen, T. Klimach, O. Eppers, F. Köllner, and S. Borrmann*
- 17:20** T202N448 **Heating rate of black carbon. Experimentally determination of traffic contribution over a large conurbation**  
*L. Ferrero, G. Mocnik, S. Cogliati, R. Colombo, C. Rizzi, and E. Bolzacchini*
- 17:40** T203N1b4 **Formation and evolution of aerosol nanoparticles within volcanic plumes**  
*M. Sahyoun, E. Freney, R. Dupuy, A. Colomb, D. Picard, J. Brito, J. Duplissy, T. Bourianne, C. Denjean, A. Schwarzenboeck, C. Planche and K. Sellegri*
- Back-up Paper** T201N213 **Observational evidence for aerosols increasing upper tropospheric humidity**  
*L. Riuttanen, M. Bister, V.-M. Kerminen, V. O. John, A.-M. Sundström, M. Dal Maso, J. Räisänen, V. A. Sinclair, R. Makkonen, F. Xausa, G. de Leeuw, and M. Kulmala*

Monday 28 August 2017

18:00

End of Conference Day

Monday 28 August 2017

16:00 - 18:00

Room 15G20

**SPECIAL SESSION #6: EMISSIONS FROM AIRCRAFT AND SHIPS**

Chairs: Lucas Durdina and Prem Lobo

- 16:00**    SPS6N205    **EXPLIC Program: Impact of aromatic content in different alternative aeronautic fuel emissions**  
*D. Delhaye, J. Ancelle, M. Sicard, L. Jing, and I.K. Ortega*
- 16:20**    T119N071    **Impact of alternative fuels on particle emission from an aircraft jet engine in a test rig**  
*T. Schripp, F. Herrmann, P. Oßwald, M. Köhler, A. Zschocke, D. Weigelt, C. Werner-Spatz, and M. Mroch*
- 16:40**    SPS6N3df    **Metallic elements in aero gas turbine exhaust**  
*B.T. Brem, C. Schreiner, R. Figi, L. Durdina, A. Setyan, M. Elser, D. Schönenberger, and J. Wang*
- 17:00**    SPS6N46b    **Marine BC measurements from two large engine test facilities**  
*K.A. Thomson, J. Pedersen, S. Gagne, and J.-P.Hansen*
- 17:20**    SPS6N458    **Airborne characterization of particle emission rates from ships**  
*T.F. Villa, R. Jayaratne, F. Gonzalez, L. Morawska, R. Schofield, C.L. Vincent, S. Fiddes, R. Ryan, M. Harvey, T. Bromley, S. Gray, and Z. Ristovski*
- 17:40**    SPS6N3fb    **Primary and secondary particles from ship emissions in port cities**  
*A. Aulinger, M. Ramacher, M. Karl, and V. Matthias*
- Back-up Paper**    SPS6N24c    **Correlations of nonvolatile PM mass and number emissions with smoke number determined for commercial aircraft jet engines**  
*L. Durdina, B.T. Brem, and J. Wang*

Monday 28 August 2017

18:00

End of Conference Day

Monday 28 August 2017

16:00 - 18:00

Room 15G40

**SPECIAL SESSION #4: TARGETED GENERATION AND DELIVERY OF AEROSOLIZED MEDICINES****Chairs: Bernard Geurts and Stavros Kassinos**

- 16:00** SPS4N349 **An efficient in silico method for deposition studies in the deep lung**  
*P.G. Koullapis, P. Hofemeier, J. Sznitman, and S.C. Kassinos*
- 16:20** SPS4N07d **Targeted delivery in upper airways using inhaled magnetic particles**  
*Y. Ostrovski and J. Sznitman*
- 16:40** SPS4N217 **Experimental data for validation of particle transport simulations in human lungs**  
*F. Janke, F. Lizal, M. Belka, J. Jedelsky, M. Jicha, and K. Bauer*
- 17:00** SPS4N05d **Comparison of Lagrangian and Eulerian modeling for predicting aerosol deposition in the human upper airways**  
*P.G. Koullapis, E.M.A. Frederix, S.C. Kassinos, B.J. Geurts, A. Kuczaj, and M. Nordlund*
- 17:20** SPS4N440 **Comparison of two inhaler devices including wall collision detachment**  
*Y. Cui and M. Sommerfeld*
- 17:40** SPS4N15d **Experimental study of particle deposition in a physical model of human respiratory tract**  
*M. Belka, F. Lizal, J. Jedelsky, and M. Jicha*
- Back-up Paper** SPS4N4ae **Regional targeting of aerosolized drugs in murine lungs**  
*O. Schmid, R. Winkler-Heil, G. Eder, W. Möller, and W. Hofmann*

Monday 28 August 2017

18:00

End of Conference Day

Monday 28 August 2017

16:00 - 18:00

Room 15G60

**AEROSOL TRANSPORT AND TRANSFORMATION**Chairs: **Mona Kurppa and Andreas Held**

- 16:00** T207N076 **Assessing ventilation and air quality in real city blocks using LES**  
*M. Kurppa, A. Hellsten, M. Auvinen, and L. Järvi*
- 16:20** T207N079 **The topography contribution to the influence of the planetary boundary layer at high altitude stations**  
*M. Collaud Coen, E. Andrews, and D. Ruffieux*
- 16:40** T207N1c0 **Seasonal variation of aerosol size distributions at the Puy de Dôme station with emphasis on free tropospheric conditions**  
*A. Farah, E. Freney, A. Chauvigné, J.L. Baray, A. Colomb, D. Hadad, M. Abboud, W. Farah, and K. Sellegri*
- 17:00** T207N3c2 **Melpitz Column Campaigns 2015 and 2017 – Detailed studies to characterize the vertical structure of the aerosol concentration and properties in the continental boundary layer under different conditions**  
*B. Wehner, S. Düsing, T. Müller, H. Baars, J. Corbin, M. Gysel, N. Bukowiecki, R. Käthner, H. Siebert, and the Melpitz Teamz*
- 17:20** T207N0ef **Modelling of SOA markers: simulation through detailed mechanisms and validation by comparison with measurements. A new approach to understand SOA formation**  
*G.M. Lanzafame, D. Srivastava, N. Bonnaire, F. Couvidat, O. Favez, B. Bessagnet, and A. Albinet*
- 17:40** T207N3c0 **Improving CAMx with volatility basis set scheme for organic aerosol modelling: From chamber data to chemical transport model**  
*J. Jiang, S. Aksoyoglu, G. Stefenelli, G. Ciarelli, U. Baltensperger, I.El. Haddad, and A.S.H. Prevot*

Monday 28 August 2017

18:00

End of Conference Day

## **TUESDAY 29 AUGUST 2017**

### **MEETINGS**

**12:20 - 13:30**

**IARA Committee Meeting**

**Room Y13L11/13**

**TUESDAY 29 AUGUST 2017**

<b>Tuesday 29 August 2017</b>	<b>08:00 - 17:00</b>	<b>Registration</b>
-------------------------------	----------------------	---------------------

<b>Tuesday 29 August 2017</b>	<b>08:30 - 09:30</b>	<b>Room 04G30</b>
-------------------------------	----------------------	-------------------

**PLENARY LECTURE II****Chair: Jonathan Reid and Robera Vecchi**

<b>08:30</b>	Plenary Lecture	<b>Submicron molecular aggregates: Formation, structure, photochemistry</b> <i>Ruth Signorell</i>
--------------	--------------------	--

<b>Tuesday 29 August 2017</b>	<b>09:30 - 10:00</b>	<b>Coffee Break and Exhibition</b>
-------------------------------	----------------------	--

Tuesday 29 August 2017

10:00 - 12:20

Room 04G30

**NEW PARTICLE FORMATION: LAB AND FIELD STUDIES**Chairs: **Birgit Wehner and Michael Boy**

- 10:00** T203N06b **The impact of NO<sub>x</sub> on oxidation products of monoterpenes and the subsequent nano-particle formation and growth**  
*C. Yan, W. Nie, A.L. Vogel, L. Dada, K. Lehtipalo, D. Stolzenburg, F. Bianchi, M.P. Rissanen, R. Wagner, M. Simon, M. Heinritzi, L. Ahonen, M. Sipilä, J. Curtius, J. Kirkby, U. Baltensperger, N.M. Donahue, M. Ehn, D.R. Worsnop, M. Kulmala, and the CLOUD Collaboration*
- 10:20** T203B0fe **Influence of atmospheric conditions on pure biogenic nucleation in the CLOUD chamber**  
*L. Dada, D. Stolzenburg, L. Ahonen, F. Bianchi, L. Fischer, H. Gordon, M. Heinritzi, K. Lehtipalo, H.E. Manninen, C. Rose, M. Simon, C. Yan, J. Curtius, M. Kulmala, and J. Kirkby*
- 10:40** T203N103 **Atmospheric evidence for pure biogenic nucleation**  
*C. Rose, Q. Zha, F. Bianchi, S. Buenrostro Mazon, L. Dada, H. Junninen, T. Petäjä, and M. Kulmala*
- 11:00** T203N117 **Freshly formed boundary layer aerosol under different weather conditions during 'Melpitz Column 2015'**  
*B. Altstädter, A. Lampert, A. Platš, M. Jähn, H. Baars, J. Lücknerath, A. Held, M. Hermann, J. Bange, and B. Wehner*
- 11:20** T203N135 **Nucleation of sulfuric acid and dimethylamine: Results from the CLOUD experiment and possible atmospheric implications**  
*A. Kürten and P.H. McMurry*
- 11:40** T203N3fc **Investigation of the role of aromatic hydrocarbons in new particle formation under urban atmospheric condition in the CLOUD chamber**  
*M. Xiao, C.R. Hoyle, L. Dada, O. Garmash, D. Stolzenburg, U. Molteni, K. Lehtipalo, I. El Haddad, J. Dommen, U. Baltensperger, and the CLOUD Collaboration*
- 12:00** T203N406 **The Himalayan aerosol factory: the chemistry of new particle formation**  
*F. Bianchi, H. Junninen, A. Bigi, P. Bonasoni, S. Buenrostro Mazon, L. Dada, J. Dommen, C. Frege, C.R. Hoyle, P. Laj, K. Lehtipalo, J. Kontkanen, A. Marinoni, U. Molteni, M. Riva, V. Sinclair, K. Sellegri, C. Yan, D.R. Worsnop, U. Baltensperger, and M. Kulmala*

Tuesday 29 August 2017

12:20 - 13:30

Lunch Break

Tuesday 29 August 2017

10:00 - 12:20

Room 24G45

**BIOMASS BURNING AEROSOL**

Chairs: Christoph Hüglin and Irena Grgic

- 10:00** T209N36c **Atmospheric lifetime of biomass burning organic markers: influence of vapor wall losses in smog chamber experiments**  
*A. Bertrand, G. Stefenelli, E. Bruns, S. Pieber, B. Temime-Roussel, A.S.H. Prevot, J. Dommen, J. Slowick, H. Wortham, I. El Haddad, and N. Marchand*
- 10:20** T209N2e2 **Regional influence of wildfires on atmospheric aerosol in the western US and insights into emission and aging of biomass burning organic aerosol**  
*Q. Zhang, S. Zhou, S. Collier, D. Jaffe, J. Hee, N. Wigder, T. Onasch, L. Kleinman, and A. Sedlacek*
- 10:40** T209N0f3 **Morphochemical characteristics and mixing state of long range transported wildfire particles at Ny-Ålesund (Svalbard Islands)**  
*B. Moroni, S. Crocchianti, S. Becagli, L. Caiazzo, R. Traversi, R. Udisti, M. Mazzola, K. Markowicz, C. Ritter, T. Zielinski, and D. Cappelletti*
- 11:00** T209N1d2 **High PM1 emissions from savannah and grassland fires in southern Africa**  
*V. Vakkari, J.P. Beukes, K. Jaars, M. Josipovic, A.D. Venter, and P.G. van Zyl*
- 11:20** T209N2c0 **SOA formation and particle characteristics in the emissions from biomass cook stoves used in the developing countries**  
*C. Andersen, R. Lindgren, R.L. Carvalho, V.B. Malmborg, E. Ahlberg, N.G. López, A.C. Eriksson, T.B. Kristensen, B. Svenningsson, C. Boman, and J. Pagels*
- 11:40** T209N27b **Identification of volatile organic compounds from small-scale wood combustion and their potential as secondary organic aerosol precursors**  
*A. Hartikainen, P. Tiitta, P. Yli-Pirilä, A. Leskinen, M. Kortelainen, J. Orasche, R. Zimmermann, J. Jokiniemi, and O. Sippula*
- 12:00** T209N241 **Organic speciation of gas and particle phase emissions from residential wood combustion**  
*D. Bhattu, G. Stefenelli, P. Zotter, J. Zhou, T. Nussbaumer, A. Bertrand, N. Marchand, B. Temime-Roussel, U. Baltensperger, J. G. Slowik, A.S.H. Prevot, I. El Haddad, and J. Dommen*
- Back-up Paper** T209N2ba **The contributions of coal, peat and wood burning to ambient PM2.5**  
*J. Arndt, P.C. Buckley, I.P. O'Connor, E.J. McGillicuddy, P.C. Buckley, S. Hellebust, J.R. Sodeau, and J.C. Wenger*

Tuesday 29 August 2017

12:20 - 13:30

Lunch Break

Tuesday 29 August 2017

10:00 - 12:20

Room 15G20

**STATIONARY SOURCES OF COMBUSTION AEROSOL****Chairs: Zoran Ristovski and Mattias Hallquist**

- 10:00** T115N3e8 **High-temperature porous tube sampling of combustion aerosols**  
*J. Jokiniemi, W. Baumann, M. Hauser, N. Teuscher, H. Suhonen, J. Ruusunen, M. Ihalainen, H.-R. Paur, and O. Sippula*
- 10:20** T119N0f9 **Particle-bound PAH trends during combustion of biomass in small stoves**  
*M. Kistler, M. Flasch, C. Schmidl, and A. Kasper-Giebl*
- 10:40** T119N166 **Characterization of particulate emissions from a variety of developing-world cookstoves**  
*Y. Ting, E.J.S. Mitchell, J. Allan, D. Liu, D.V. Spracklen, A. Williams, J.M. Jones, A.R. Lea-Langton, G. McFiggans, and H. Coe*
- 11:00** T119N1f4 **Formation of SOA from logwood combustion upon photochemical aging in PEAR flow tube reactor**  
*P. Tiitta, A. Hartikainen, M. Ihalainen, P. Yli-Pirilä, M. Kortelainen, J. Tissari, H. Lamberg, A. Leskinen, J. Jokiniemi, and O. Sippula*
- 11:20** T115N265 **Mobility size and effective density of soot nanoparticles**  
*G.A. Kelesidis, E. Goudeli, and S.E. Pratsinis*
- 11:40** T120N2c1 **Studying the optical and physiochemical properties of soot of various maturity from a mini-CAST using different measurement techniques**  
*S. Török, V. Malmberg, J. Simonsson, K. Kling, A. Eriksson, M. Mannazhi, J. Martinsson, A. Karlsson, J. Pagels, and P-E. Bengtsson*
- 12:00** T115N2c6 **Relating refractory soot mass spectra with nanostructure and combustion conditions**  
*V.B. Malmberg, A. Eriksson, S. Török, K. Kling, M. Novakovic, S. Shamun, M. Shen, M. Tuner, P-E. Bengtsson, and J. Pagels*
- Back-up Paper** T119N16f **Novel electrical charging condensing heat exchanger for particle emission reduction in small boilers**  
*O. Sippula, J. Grigonyte, H. Suhonen, A. Laitinen, M. Kortelainen, J. Tissari, P. Tiitta, A. Lähde, J. Keskinen, and J. Jokiniemi*

Tuesday 29 August 2017

12:20 - 13:30

Lunch Break

Tuesday 29 August 2017

10:00 - 12:20

Room 15G40

## TOXICOLOGICAL CHARACTERIZATION OF AMBIENT AND ENGINEERED PARTICLES

Chairs: Christina Isaxon and Ralf Zimmermann

- 10:00** T406N1ef **Ultrafine particles from biomass burning: Chemical composition and biological effects from a laboratory study and ambient air measurements in northern Italy**  
*R. Vecchi, S. Becagli, V. Bernardoni, D. Caruso, L. Corbella, E. Corsini, M. Dell'Acqua, P. Fermo, C.L. Galli, G. Lonati, L. Marabini, M. Marinovich, S. Ozgen, A. Papale, S. Signorini, R. Tardivo, and G. Valli*
- 10:20** T406N1c2 **Ambient sources and health effects of reactive oxygen species - PM 2.5 characteristics and effects to normal and diseased airway epithelia**  
*Z. Leni, L.E. Cassagnes, J. Dommen, I. El Haddad, and M. Geiser*
- 10:40** T406N26e **Reactive oxygen species (ROS) formation mechanism: links between in situ ambient measurements and laboratory aging experiments of different emission sources**  
*J. Zhou, M. Elser, G. Stefanelli, P. Zotter, M. Krapf, E.A. Bruns, R. Fröhlich, J.G. Slowik, T. Nussbaumer, M. Geiser, U. Baltensperger, R. Huang, A.S.H. Prevot, I. El Haddad, and J. Dommen*
- 11:00** T409N3e9 **A novel device based on thermophoresis for cell exposure at the air-liquid interface**  
*M. Ihalainen, P. Jalava, T. Ihtola, K. Kuusalo, M.-R. Hirvonen, and J. Jokiniemi*
- 11:20** T406N38e **Molecular biological effects and toxicity of combustion aerosol emissions on air/liquid-interface exposed human and murine lung cells**  
*R Zimmermann, T.G. Dittmar, T. Kanashova, J. Buters, S. Öder, A. Huber, H. Paur, S. Mülhopt, M. Dilger, C. Weiß, B. Buchholz, B. Stengel, K. Hiller, S.C. Sapccariu, K.A. Berube, A.J. Włodarczyk, B. Michalke, T. Krebs, M. Kelbg, J. Tiggesbäumker, T. Streibel, E. Karg, S. Scholtes, J. Schnelle-Kreis, J. Lintelmann, M. Sklorz, S. Klingbeil, J. Orasche, L. Müller, A. Rheda, J. Passig, T. Gröger, G. Abbaszade, S. Smita, J. Orasche, O. Uski, P. Jalava, M. Hoppo, A. Hartikainen, H. Lamberg, M.-R. Hirvonen, S. Kasurinen, O. Sippula, and J. Jokiniemi*
- 11:40** T403N28d **Mechanisms of toxicity of particulate emissions produced by different gasoline and alternative fuels in human lung cells**  
*H. Libalova, M. Vojtisek-Lom, J. Klema, M. Machala, and J. Topinka*
- 12:00** T408N090 **Effect of nanoparticles on oxidative stress and intracellular calcium signaling in pulmonary artery endothelial cells in physiological and pathological conditions**  
*J. Deweirdt, J.F. Quignard, C. Guibert, J.P. Savineau, and I. Baudrimont*

**Tuesday 29 August 2017**

**12:20 - 13:30**

**Lunch Break**

Tuesday 29 August 2017

10:00 - 12:20

Room 15G60

**NEW INSTRUMENTATION****Chairs: Martin Fierz and Oliver Bischof**

- 10:00** T203N2da **Design and performance of a commercially available tandem drift tube ion mobility spectrometer and fast response condensation particle counter**  
*D.R. Oberreit, D.T. Buckley, and C.J. Hogan*
- 10:20** T204N2a6 **A miniature curved plate mobility classifier**  
*D.-R. Chen and Q. Liu*
- 10:40** T306N070 **Intercomparison of condensation particle counters challenged by various nanoaerosols in the range 6 - 460 nm**  
*S. Bau, R. Payet, and O. Witschger*
- 11:00** T305N30f **Characterization of the boosted 3776 butanol TSI CPC as detector in the sub 2 nm range. Activation of sub 2 nm with butanol vapors**  
*M. Attoui*
- 11:20** T305N2f0 **Dekati Diluter characterization in the 1-20 nm particle size range**  
*J. Vanhanen, M. Svedberg, E. Miettinen, J.-P. Salo, and M. Väkevä*
- 11:40** T106N27c **High resolution measurement of aerodynamic focusing behaviour of nanoparticles in different gases and gas-mixtures using a Differential Aerodynamic Particle Sizer (DAPS)**  
*D. Kiesler and F.E. Kruis*
- 12:00** T307N0ca **Direct measurement of the dependence of photoacoustic signal upon droplet size**  
*J.W. Cremer, P.A. Covert, E. Parmentier, and R. Signorell*
- Back-up Paper** T106N0d6 **Surface normalised aerosol photo emission sensor**  
*J. Röhrbein and A.P. Weber*

Tuesday 29 August 2017

12:20 - 13:30

Lunch Break

Tuesday 29 August 2017	10:00 - 12:20	Room 24G55
<b>SPECIAL SESSION #5: ELECTROHYDRODYNAMIC ATOMIZATION (EHDA) TECHNOLOGIES: FROM FUNDAMENTALS TO APPLICATION</b>		
<b>Chairs: Luewton Agostinho and Joan Rosell-Llompart</b>		

- 10:00** SPS5N188 **Solid-state electrolytes for lithium ion batteries: Application of electrospray technique**  
*S.W. Karuga, M.J. Gatari, E.M. Kelder, and J.C.M. Marijnissen*
- 10:20** SPS5N392 **Aerosol deposits from electrospraying liquid suspensions**  
*S. Martin, D. Rodriguez-Perez, P.L. Garcia-Ybarra, and J.L. Castillo*
- 10:40** SPS5N46d **Mass transfer between a Taylor-cone and the surrounding gas phase**  
*C. Lübbert and W. Peukert*
- 11:00** SPS5N49d **A bipolar electrospray source of singly charged salt clusters of precisely controlled composition**  
*J. Fernandez de la Mora and C. Barrios-Collado*
- 11:20** SPS5N1b6 **Investigating the electrohydrodynamic atomization of highly conductive metallic salt precursors**  
*V.A. Ganesan, M. Gensch, and A.P. Weber*
- 11:40** SPS5N3ea **Extractor-free one-dimensional arrays of electrosprays**  
*N. Sochorakis, J. Rosell-Llompart, and J. Grifoll*
- 12:00** SPS5N391 **Electrohydrodynamic atomization of a non-Newtonian solution with high solid content**  
*C.W. Gachara, I. Kapasi, I. Hausz, J.C.M. Marijnissen, M.J. Gatari, and L.L.F. Agostinho*
- Back-up Paper** SPS5N387 **Nanoparticle synthesis using an electrohydrodynamic atomizer integrated flame spray pyrolysis system**  
*V.A. Ganesan, M. Gensch, and A.P. Weber*

Tuesday 29 August 2017	12:20 - 13:30	Lunch Break
------------------------	---------------	-------------

**Tuesday 29 August 2017****13:30 - 15:15****Poster Area****POSTER SESSION PART II AND EXHIBITION****AEROSOL CHEMICAL COMPOSITION, TRACERS AND TRENDS**

- T215N04b **Exposure trends of PM<sub>2.5</sub> and black carbon sources in Gothenburg 1990-2011**  
*P. Molnár, D. Segersson, L. Stockfelt, and G. Sallsten*
- T215N23e **Biogenic secondary organic aerosol relation to temperature depending tree stress emissions**  
*K. Plauškaite, J. Pauraitė, S. Byčėnkiene, A. Augustaitis, V. Marozas, and V. Ulevičius*
- T215N24a **Levels and spatial distribution of metals in a heavily industrialized region (Dilovasi, Kocaeli) of Turkey**  
*M. Keles, B. Cetin, S. Yurdakul, and F. Ozturk*
- T215N278 **Source apportionment of particulate matter in a coal fired power plant area in Turkey**  
*E. Can, A. Ari, G. Tuncel, and E.O. Gaga*
- T313N242 **Spatial variability of PM<sub>2.5</sub> in New Delhi, India**  
*P. Pant, S. Guttikunda, M. Kumar, J.L. Matawle, S. Kushwaha, S. Pervez, and R.E. Peltier*
- T313N46a **Spatial and temporal variation of haze in the Yangtze River Delta region from 1961 to 2015**  
*R. Han, S. Wang, and J. Wang*

**Tuesday 29 August 2017****15:15 - 15:45****Coffee Break and  
Exhibition**

Tuesday 29 August 2017

13:30 - 15:15

Poster Area

**POSTER SESSION PART II AND EXHIBITION****AIRBORNE PATHOGENS AND MICROBES AND THEIR VIABILITY**

- T116N16c **Efficiency of Non-conductive Ultrasonic Transducers (NCUT) for inactivation of airborne virus**  
*M. Versoza, W. Jung, Y. Lee, M.L. Barabad, J. Hwang, and D. Park*
- T402N007 **Automatic pollen monitoring: towards an operational system**  
*B. Crouzy, B. Clot, T. Konzelmann, and B. Calpini*
- T402N084 **Characteristics of aerosol suspension in a rotating drum**  
*W.R. Ke, C.W. Lin, S.H. Huang, W.C. Lee, Y.M. Kou, and C.C. Chen*
- T402N0cf **Generation of a fungal consortium: impact of analytic tools on biodiversity analysis**  
*J. Degois, X. Simon, C. Bontemps, P. Leblond, and P. Duquenne*
- T402N1b0 **Inactivation of bacterial activity in the circulation water of wet electrostatic precipitator as home air purifier**  
*C.G. Woo, B. Han, H.-J. Kim, and Y.-J. Kim*
- T402N1ee **Aerobiological study in Southeast Spain: Olea vs Ole e1**  
*M. Varea, S. Martinez-Perez, E. Flores, V. Soriano, J. Fernández, J. Gil-Moltó, N. Galindo, E. Yubero, J.F. Nicolás, S. Caballero, R. Castaner, C. Pastor, and J. Crespo*
- T402N1fc **Commuters exposure to airborne microorganisms in the Barcelona subway system**  
*T. Moreno, X. Triadó-Margarit, M. Veillette, C. Duchaine, M. Talbot, M. C. Minguillón, V. Martins, F. Amato, E. de Miguel, and E.O. Casamayor*
- T402N285 **Bioaerosol capture via passive technique: design and performance of Rutgers Electrostatic Passive Sampler (REPS)**  
*J. Therkorn, J. Scheinbeim, and G. Mainelis*
- T402N299 **Continuing development of electrostatic precipitator for bioaerosols with high concentration rate**  
*T. Han and G. Mainelis*
- T402N2ea **Pollen calendar: Airborne pollen in Southeastern Spain (Alicante)**  
*D. Liu, R. Mariman, M.E. Gerlofs-Nijland, G. Folkerts, J.F. Boere, J.J.E. Reijnders, F.R. Cassee, and E. Pinelli*
- T402N3a8 **Ambient air BioPMs originated from different sources and their effects on innate immune responses**  
*D. Liu, R. Mariman, M.E. Gerlofs-Nijland, G. Folkerts, J.F. Boere, J.J.E. Reijnders, F.R. Cassee, and E. Pinelli*

- T402N45d **A novel co-culture model of alveolar macrophage and epithelial cells to investigate immune responses to bioaerosol components**  
*S. Khera, V. Sharma, S.F. Tyrrel, Z.A. Nasir, T.L. Gladding, C.A. Rolph, E.T. Hayes, B. Williams, A. Bennett, G. Fejer, and S.K. Jackson*
- T402N4a4 **The effect of passive air sampling parameters on determining the aerosol microbial composition and abundance**  
*N. Grydaki, C. Whitby, and I. Colbeck*
- T402N4a9 **Investigation of bioaerosol characterization on a global scale using automobile air conditioning filter**  
*J. Li and M.S. Yao*
- T403N08d **Neutralization of aerosolized spores by combustion products of powdered materials: effect of exposure time**  
*S.A. Grinshpun, W. Nakpan, M. Yermakov, R. Indugula, T. Reponen, E. L. Dreizin, and M. Schoenitz*
- T406N3ca **Water disinfection by antimicrobial fibrous material produced by aerosol filtration**  
*M. Bhamidipati, S. Adam, M. Valenti, P. Kooyman, and A. Schmidt-Ott*

<b>Tuesday 29 August 2017</b>	<b>15:15 - 15:45</b>	<b>Coffee Break and Exhibition</b>
-------------------------------	----------------------	------------------------------------

Tuesday 29 August 2017

13:30 - 15:15

Poster Area

**POSTER SESSION PART II AND EXHIBITION****BIOMASS BURNING**

- T209N064 **Extreme fire event over Siberia in summer 2012: radiative characteristics of aerosol**  
*T.B. Zhuravleva, D.M. Kabanov, I.M. Nasrtdinov, T.V. Russkova, S.M. Sakerin, A. Smirnov, and B.N. Holben*
- T209N0b7 **Development of compound-specific carbon isotopic analysis for levoglucosan and its isomers, biomarkers of biomass burning**  
*W. Wang and D.W. Han*
- T209N0f7 **Evaluation of a residential wood heating emissions abatement policy at local scale in a complex area, the Arve valley, France**  
*J. Allard, F. Chevrier, I. Ježek, G. Močnik, J.L. Besombes, G. Brulfert, J.P. Laurent, and J.L. Jaffrezo*
- T209N123 **Analysis of brown carbon organic species in primary and aged biomass-burning emissions under controlled conditions**  
*V. Samburova, D. Sengupta, C. Bhattarai, R.K. Chakrabarty, A. Watts, J. Connolly, A. Khlystov, and H. Moosmüller*
- T209N12e **Near-field changes to the optical and chemical properties of biomass burning particles**  
*T. B. Onasch, J. Wormhoudt, A. Sedlacek, L. Kleinman, E. Fortner, J. Shilling, M. Pekour, D. Chand, S. Collier, Q. Zhang, R. Yokelson, K. Adachi, P. Buseck, L. Williams, and A. Freedman*
- T209N151 **Influence of biomass burning from residential and district heating on local air quality assessed by mobile air pollutant measurements**  
*F. Fachinger, F. Drewnick, and S. Borrmann*
- T209N24e **Particle pollution from wood burning in mainland UK: a six-year national assessment**  
*A. Font, D. Green, D. Butterfield, and G.W. Fuller*
- T209N2a8 **Emissions and short time scale processing of biomass burning examined at the FIREX lab intensive campaign**  
*E. Fortner, T. Onasch, L. Williams, M. Canagaratna, W. Xu, P. Croteau, S. Herndon, R. Roscioli, T. Yacovitch, C. Daube, B. Werden, E. Wood, B. Knighton, J. Shantanu, L. Lewane, A. Galang, S. Tarun, A. Sedlacek, J. Jayne, and D. Worsnop*
- T209N2ba **The contributions of coal, peat and wood burning to ambient PM<sub>2.5</sub>**  
*J. Arndt, P.C. Buckley, I.P. O'Connor, E.J. McGillicuddy, P.C. Buckley, S. Hellebust, J.R. Sodeau, and J.C. Wenger*

- T209N34b **Chemical composition of emissions originating from biomass and municipal solid waste burning in a masonry heater**  
*M. Bloss, F. Mylläri, M. Aurela, M. Maasikmets, H.-L. Kupri, K. Vainumäe, P. Simonen, L. Salo, V. Niemelä, T. Rönkkö, and H. Timonen*
- T209N377 **Influence of the renewal of residential wood stoves on the PM biomass burning contribution in a French Alps valley**  
*A. Sylvestre, B. Golly, J.C. Francony, C. Piot, J.L. Jaffrezo, A. Provent, R. Vidaud, H. Chanut, G. Brulfert, and J.L. Besombes*
- T209N3e6 **Biomass burning fingerprint in Spain using ACSM**  
*M.C. Minguillón, A. Ripoll, X. Querol, and A. Alastuey*
- T209N495 **Water-soluble dicarboxylic acids, oxocarboxylic acids and alpha-dicarbonyls in atmospheric aerosols during summer in Central Alaska: an influence of biomass burning and biogenic sources**  
*D.K. Deshmukh, K. Kawamura, M.M. Haque, and Y. Kim*
- T214N168 **Impact of residential wood combustion on benzo(a)pyrene and black carbon concentrations in the Helsinki metropolitan area, Finland**  
*J.V. Niemi, H. Hellén, L. Kangas, A. Kousa, M. Vestenius, K. Teinilä, A. Karppinen, J. Kukkonen, H. Timonen, T. Rönkkö, and L. Pirjola*
- T216N0f8 **Sugar patterns in biomass burning emission samples – a link between burned and living biomass**  
*M. Kistler and A. Kasper-Giebl*

<b>Tuesday 29 August 2017</b>	<b>15:15 - 15:45</b>	<b>Coffee Break and Exhibition</b>
-------------------------------	----------------------	------------------------------------

Tuesday 29 August 2017

13:30 - 15:15

Poster Area

**POSTER SESSION PART II AND EXHIBITION****ELECTRICAL EFFECTS: FROM FUNDAMENTAL STUDY TO APPLICATION**

- T107N479 **A study of a needle-plate corona charger to reduce agglomeration during synthesis of aerosol nanoparticles by spark discharge**  
*A.A. Efimov, P.V. Arsenov, and V.V. Ivanov*
- T109N039 **Improving inactivation effect for microorganisms in an electrostatic precipitator operated under low ozone concentration by humidification**  
*A. Zukeran, I. Kobayashi, W. Risei, and J. Sawai*
- T109N05a **The effect of Na<sub>2</sub>CO<sub>3</sub> on inactivation of zygosaccharomyces rouxii in seawater using pulsed electric field**  
*Y. Nakada, Y. Komatsu, A. Zukeran R. Wada, J. Sawai, and T. Inui*
- T109N065 **Investigation of inactivation process in an electrostatic precipitator by estimating protein quantitation**  
*S. Toguchi, R. Oi, M. Shiraishi, A. Zukeran, R. Wada, and J. Sawai*
- T110N089 **Continuous separation of similar size distribution of atomized bacteria and PSL particles using corona discharge mechanisms**  
*A.M. Nasrabadi, J. Han, M.M. Farid, S.-G. Lee, and J. Hwang*
- T110N21e **Impact of surface roughness, dielectric constant and resistivity of wall on the deposition of submicron particles driven by the negative air ionizer**  
*K.P. Yu, W.M. Lee, and C.J. Peng*
- T110N2df **Performance evaluation of a charged micro-size particle generator**  
*Y.-H. Joe, J. Shim, and H.-S. Park*
- T111N0a8 **Study of collection mechanism on hole-type electrostatic precipitator by particle behaviour and fluid flow**  
*H. Miyashita, S. Ibaraki, Y. Ehara, T. Inui, and T. Sawada*
- T111N0a9 **Simulation analysis of particle behavior in hole type electrostatic precipitator**  
*M. Shimoda, Y. Ehara, T. Inui, and T. Sawada*
- T111N13d **Improved collection efficiency of fine particles by ESP combined with electropray**  
*M.-J. Oh and M.-H. Lee*
- T111N409 **Analysis of different liquid-liquid combinations and conditions for the formation of a stable cone-jet mode in electropray emulsification processes**  
*A.W. Kamau, M.J. Gatari, J.C.M. Marijnissen, and L.L.F. Agostinho*

Tuesday 29 August 2017

15:15 - 15:45

Coffee Break and  
Exhibition

Tuesday 29 August 2017

13:30 - 15:15

Poster Area

**POSTER SESSION PART II AND EXHIBITION****EXPOSURES AND HEALTH IMPACTS OF AEROSOLS**

- T214N0d3 **Evaluation of bioaccessible trace metal fractions in urban PM10 samples collected near a ferroalloy plant**  
*A. Hernández-Pellón, S. Lanza, C. Lasa, and I. Fernández-Olmo*
- T314N49a **Development of an integrated exposure - dose management tool for reduction of particulate matter in air: overview of the LIFE index-air project**  
*S.M. Almeida, M. Almeida-Silva, N. Canha, T. Faria, K. Eleftheriadis, E. Diapouli, V. Galifianakis, A. Miranda, J. Ferreira, O. Hänninen, and M. Lazaridis*
- T406N15f **Development of a multilevel regression model to analyze the association between eye diseases and air pollutants (PM10, PM2.5, NO<sub>2</sub>, SO<sub>2</sub>, O<sub>3</sub>)**  
*S.-J. Park, S. Han, J.-S. Youn, J. Seo, and K.-J. Jeon*
- T406N1ed **Important sources and chemical species of ambient fine particles related to adverse health effects**  
*J. Heo and S.-M. Yi*
- T406N389 **Multi-model assessment of health impacts of air pollution in Europe in frame of the AQMEII model intercomparison project**  
*U. Im, J. Brandt, C. Geels, K.M. Hansen, J.H. Christensen, M.S. Andersen, E. Solazzo, U. Alyuz, A. Balzarini, R. Baro, R. Bellasio, R. Bianconi, J. Bieser, A. Colette, G. Curci, A. Farrow, J. Flemming, A. Fraser, P. Jimenez-Guerrero, N. Kitwiroon, G. Pirovano, L. Pozzoli, M. Prank, R. Rose, R. Sokhi, P. Tuccella, A. Unal, M.G. Vivanco, G. Yardwood, C. Hogrefe, and S. Galmarini*
- T406N4da **Winter smog in Poland, is it a real hazard to health?**  
*M. Kowalska and J.E. Zejda*
- T406N4e4 **Association between reactive oxygen species formation with environmental persistent free radicals and transition metals in PM2.5 in Beijing**  
*F. Liu, F. Shen, M. Yao, X. Zhang, J. Li, T. Zhang, K. Lucas, M. Shiraiwa, U. Pöschl, and H. Tong*
- T408N1d0 **Combined source and health risk apportionment approach to develop an emission reduction plan for PM2.5 in the Sha-Lu area, Taiwan**  
*H.T. Hsu, L.H. Young, B.F. Hwang, M.Y. Lin, C.N. Chen, Y.C. Chen, and P.J. Tsai*
- T409N23c **Wood-smoke inhalation exposures from traditional hunting practices in a First Nations community**  
*P. Pant, R. J. Moriarity, M. Wilton, E.N. Liberda, L.J. Tsuji, and R.E. Peltier*

Tuesday 29 August 2017

15:15 - 15:45

Coffee Break and  
Exhibition

Tuesday 29 August 2017

13:30 - 15:15

Poster Area

**POSTER SESSION PART II AND EXHIBITION****FUNDAMENTALS I**

- T502N08a **Using dynamic meshes to evaluate transparent electrode performance**  
*A.M. Nasrabadi, J. Han, and J. Hwang*
- T502N0bf **Multilayer particle resuspension in a turbulent boundary layer**  
*S.E. Chatoutsidou, Y. Drossinos, and M. Lazaridis*
- T502N0df **Sedimentation effect of finely dispersed aerosol in tubes in shock-wave and shock-free modes**  
*D.A. Gubaidullin, R.G. Zaripov, and L.A. Tkachenko*
- T502N106 **Features of reflection of acoustic waves from the boundary or layer of aerosol**  
*D.A. Gubaidullin, D.D. Gubaidullina, and Yu.V. Fedorov*
- T502N141 **Acoustic waves in multifractional aerosols with heat and mass transfer**  
*D.A. Gubaidullin and E.A. Teregulova*
- T502N437 **Temporally resolved measurements of heavy, rigid fibre translation and rotation in nearly homogeneous isotropic turbulence**  
*L. Sabban, A. Cohen, and R. van Hout*
- T502N4df **The liquid phase aerosol particle evaporation under the dry gas blow**  
*M.P. Anisimov, V.I. Terekhov, P.K. Hopke, and N.E. Shishkin*
- T502N4e2 **Semiempirical design of the nucleation rate surfaces**  
*M.P. Anisimov and O.O. Petrova-Bogdanova*
- T504N142 **Collection of polyamide nanofibers on PTFE foam coated filter**  
*H.-B. Kim, K.B. Lee, S.-J. Cho, and M.-H. Lee*
- T504N17c **Simultaneous removal of soot and NO<sub>x</sub> from biomass boiler fumes over catalytic sintered filter**  
*G. Tesquet, A. Villot, A. Guyon, F. Tresse, and L. Le Coq*
- T504N1a5 **Stokes-Brinkman model of fluid flow through porous body of arbitrary shape**  
*R.F. Mardanov, S.K. Zaripov, V.F. Sharafutdinov, and S.J. Dunnett*
- T504N1dc **Study on the penetration of silver nanowires passing through polyester filters**  
*S. Lim, H. Lee, H. Park, and W.G. Shin*
- T504N2c2 **Nanodroplets oil separation in fibrous filters modified by aerogel**  
*Ł. Werner, A. Jackiewicz, J. Gac, B. Nowak, and M. Bojarska*

- T504N31d **Cleaning efficiency and aging of electret filters in mobile air purifiers**  
*S. Schumacher, D. Spiegelhoff, U. Schneiderwind, H. Finger, and C. Asbach*
- T504N341 **Efficiency of air filters for general ventilation and gas turbines in humid environments**  
*F. Schmidt, T. Engelke, C. König, E. Däuber, C. Asbach, and S. Haep*
- T504N342 **Filtration performance of particle filters for general ventilation aged in real life or loaded with ASHRAE or A2 test dust in the lab**  
*F. Schmidt, T. Engelke, A. Breidenbach, and C. Asbach*

<b>Tuesday 29 August 2017</b>	<b>15:15 - 15:45</b>	<b>Coffee Break and Exhibition</b>
-------------------------------	----------------------	------------------------------------

Tuesday 29 August 2017

13:30 - 15:15

Poster Area

**POSTER SESSION PART II AND EXHIBITION****MEASUREMENT TECHNIQUES FOR COMBUSTION AEROSOLS**

- T303N1bd **Influence of dilution stage on measurements of particle emissions of a small scale biomass boiler**  
*I.V Dyakov, B. Bergmans, F. Idczak, and H. Breulet*
- T303N4a3 **Characterizations of black carbon produced from a miniCAST soot generator over a wide range of setpoints**  
*F. Liu, M. Saffaripour, K.A. Thomson, and G.J. Smallwood*
- T311N1a0 **Measurements of size distribution and mass concentration of fine particles from a stack of a coal-fired power plant in Korea**  
*B. Han, H.-J. Kim, C.G. Woo, Y.-J. Kim, and S.-N. Chun*
- T311N1da **Raman microspectroscopic analysis of soot samples from wood combustion: Influences of aging**  
*A.C. Wiesheu, A. Hartikainen, O. Sippula, M. Ihalainen, H. Lamberg, J. Jokiniemi, R. Niessner, and N.P. Ivleva*
- T311N223 **Ambient pressure particle mass spectrometry for inline detection of nanoparticle growth in flame reactors**  
*S. Suleiman, S. Kluge, Ch. Schulz, and H. Wiggers*
- T311N274 **Laser-based techniques applicability for soot particles detection and analyses: soot particles nucleation into laboratory flames**  
*C. Irimiea, A. Faccinnetto, Y. Carpentier, I.K. Ortega, E. Therssen, and C. Focsa*
- T311N282 **Chemical characterisation of particulate matter from different emission sources with thermal and laser desorption atmospheric pressure photo ionisation ultra-high resolution mass spectrometry**  
*C.P. Rüger, A. Neumann, M. Sklorz, and R. Zimmermann*
- T311N30d **FATCAT: a new characterization method for particulate emissions from wood burning appliances**  
*A. Keller, D. Egli, P. Steigmeier, and H. Burtscher*
- T311N330 **Variation of nanostructure of laboratory generated soot aerosols with particle size**  
*R. Dastanpour, S. Rogak, K. Thomson, and J. Olfert*
- T311N3ff **Assessment of a propane diffusion flame generator (CAST) as a reference aerosol generator in the sub-23 nm range**  
*E. Daskalos, A.D. Melas, P. Baltzopoulou, A.G. Konstandopoulos*

Tuesday 29 August 2017

15:15 - 15:45

Coffee Break and  
Exhibition

Tuesday 29 August 2017

13:30 - 15:15

Poster Area

## POSTER SESSION PART II AND EXHIBITION

## MOBILE SOURCES OF COMBUSTION AEROSOL

- T116N295 **Regulated and unregulated emissions of three way catalyst Euro 6 G-DI gasoline vehicle over chassis dynamometer**  
*A. Martinez Valiente, C. Louis, B. R'Mili, P. Tassel, P. Perret, M. André, Y. Liu, and B. D'Anna*
- T116N2be **Chemical composition discrimination of soot particles emitted by a heavy-duty engine: impact of operating regime and fuel biodiesel content**  
*Y. Carpentier, C. Irimiea, O. Popovicheva, E. Kireeva, I.K. Ortega, J. Schwarz, M. Vojtisek, and C. Focsa*
- T116N35e **Chasing measurements for real-world emissions of city buses**  
*A. Järvinen, P. Karjalainen, M. Bloss, O. Potila, P. Simonen, H. Kuuluvainen, H. Timonen, S. Saarikoski, J.V. Niemi, J. Keskinen, and T. Rönkkö*
- T116N447 **Chemical characterisation of the particulate matter emitted by automobile motors: the PEMs4Nano project**  
*J. A. Noble, Y. Carpentier, M. Vojkovic, B. Chazallon, C. Pirim, M. Ziskind, and C. Focsa*
- T117N4c4 **High-efficiency simultaneous removal of trace HM and organic pollutants from an iron ore sintering plant**  
*J. Gonzalez, B. Gonzalez, I. Ibarra, K. Datta, I. Gomez, V. García, F. J. Gonzalez, and C. Gutierrez-Canas*
- T119N2ce **Engine out PM emissions from RME biodiesel and conventional diesel combustion with exhaust gas recirculation**  
*V.B. Malmberg, M. Novakovic, S. Shamun, M. Shen, K. Kling, A. Eriksson, M. Tuner, and J. Pagels*
- T119N4bd **The impact of different blending ratios of waste cooking oil-based biodiesel on the emissions of PAHs, PCDD/Fs and PCBs from diesel engine**  
*C.Y. Chen, W.J. Lee, L.C. Wang, and C.H. Tsai*
- T120N477 **DownToTen: key particle properties, emission and measurement conditions, instruments and sampling setup**  
*M. Bainschab, A. Bergmann, P. Karjalainen, J. Keskinen, J. Anderson, B. Giechaskiel, C. Haisch, A. Gerini, L. Ntziachristos, and Z. Samaras*

Tuesday 29 August 2017

15:15 - 15:45

Coffee Break and  
Exhibition

Tuesday 29 August 2017

13:30 - 15:15

Poster Area

**POSTER SESSION PART II AND EXHIBITION****NEW INSTRUMENTATION**

- T106N0d6 **Surface normalised aerosol photo emission sensor**  
*J. Röhrbein and A.P. Weber*
- T302N024 **Improved understanding of HGPMS collection of airborne particles**  
*M.-D. Cheng, P. Cable-Dunlap, and S.L. Allman*
- T302N1b8 **Estimation of the ratio of aerosol to molecular backscattering by two closely disposed wavelengths using CuBr LIDAR sounding (510.6nm, 578.2nm)**  
*I. V. Grigorov, D. V. Stoyanov, and G. V. Kolarov*
- T302N1d5 **The effect of sheath flow rate on the particle trajectory inside an optical cavity with direct flow configuration**  
*H. Lee, Y.-S. Jeong, K. Choi and W. G. Shin*
- T302N1dd **Generation of monodisperse particles using inkjet aerosol generator**  
*W.J. Shin, H. Lee, Y.-S. Jeong, K. Choi, and W.G. Shin*
- T302N1ea **Coupling of an electrodynamic balance with mass spectrometry as a platform for atmospheric chemistry research**  
*A.W. Birdsall, U.K. Krieger, and F.N. Keutsch*
- T302N262 **Extending the use of 1nm-growth enhancers to a wider range of CPCs**  
*A.F. Zerrath, J.H.T. Scheckman, J. Spielvogel, and A.J. Tiwari*
- T302N33a **The effect of temperature and humidity on the performance of low-cost PM sensors**  
*X. Liu, A. Mabon, A.B. Asumadusakyi, M. Mazaheri, R. Jayaratne, M. Dunbabin, and L. Morawska*
- T302N3af **A state of the art device for continuous unattended measurements of ultrafine particles**  
*M. Pesch, V. Ziegler, F. Tettich, and W. Frenzel*
- T302N3d1 **New developments in single particle measurements of black carbon and bioaerosols**  
*A.R. Attwood, H Schulz, G. Granger, M. Zanatta, A.B. Herber, M. Mahin, D. Baker, G.L. Kok, and R. Gerdes*
- T302N428 **Offline validation of the new 'Total Carbon Analyzer'**  
*M. Rigler, L. Drinovec, A. Vlachou, A.S H. Prévôt, C. Hüglin, A. D. A. Hansen, J.-L. Jaffrezo, and G. Močnik*

T302N480 **Formation of the new approaches for detection and radiation control of technogenic aerosols in conditions of improvement of cleaning technologies of a radioactive gas-aerosol emissions**

*A.G. Tsovianov, A.E. Karev, D.E. Fertman, N.V. Tsoy, and C.B. Chebushov*

T302N4d2 **Applications of individual ion counting**

*B. Gorbunov, G. Hyatt-Gipson, M. Burton, B. Steer, and R. Muir*

T312N1e0 **Development of a dual-wavelength thermo-optical transmittance analyser: characterization and first results**

*D. Massabo, A. Altomari, V. Bernardoni, G. Valli, R. Vecchi, and P. Prati*

**Tuesday 29 August 2017**

**15:15 - 15:45**

**Coffee Break and  
Exhibition**

<b>Tuesday 29 August 2017</b>	<b>13:30 - 15:15</b>	<b>Poster Area</b>
<b>POSTER SESSION PART II AND EXHIBITION</b>		

<b>NEW PARTICLE FORMATION II</b>
----------------------------------

- T203N334 **Relative formation times of charged and neutral particles in an urban environment**  
*R. Jayaratne, B. Pushpawela, and L. Morawska*
- T203N36e **Study of new particle formation events in Southern Italy**  
*A. Dinoi, K. Weinhold, W. Birmili, A. Wiedensohler, A. Donato, and D. Contini*
- T203N3c6 **Long term study of new particle formation and shrinkage events in a coastal environment: Meteorology, gas phase and solar radiation implications**  
*A. del Águila, M. Sorribas, J.A. Adame, J.M. Vilaplana, J.A. Bogeat, C. Córdoba-Jabonero, and M. Yela*
- T203N442 **Development of a near-explicit model of HOMs formation from  $\alpha$ -pinene ozonolysis**  
*U. Molteni, U. Baltensperger, J. Curtius, M. Heinritzi, C.R. Hoyle, M. Simon, C. Yan, J. Dommen, and the CLOUD collaboration*
- T203N453 **Long-term declining trend in new particle formation observed at San Pietro Capofiume, Italy**  
*T. Nieminen, J. Joutsensaari, A. Laaksonen, A. Virtanen, S. Decesari, L. Tarozzi, and M.C. Facchini*

<b>Tuesday 29 August 2017</b>	<b>15:15 - 15:45</b>	<b>Coffee Break and Exhibition</b>
-------------------------------	----------------------	------------------------------------

Tuesday 29 August 2017

13:30 - 15:15

Poster Area

POSTER SESSION PART II AND EXHIBITION

**OPTICAL PROPERTIES OF ATMOSPHERIC AEROSOLS**

- T204N050 **Light absorption characteristics of brown carbon in PM<sub>2.5</sub> at an urban site during KORUS-AQ campaign**  
*G.-H. Yu, J.-M. Yu, and S. Park*
- T204N092 **Black carbon vertical profiles measured by a micro-aethalometer in North China Plain**  
*L. Ran, Z.Z. Deng, X.B. Xu, P. Yan, W.L. Lin, Y. Wang, P. Tian, P.C. Wang, W.L. Pan, and D.R. Lu*
- T204N093 **Study on polarization characterization for aerosol morphology**  
*S. Chen, N. Zeng, Y. Chen, and H. Ma*
- T204N095 **Approximated expression of the mass extinction efficiency as a function of particle size for polydispersed accumulation mode aerosols**  
*C.H. Jung, J. Um, J. Lee, and Y.P. Kim*
- T204N129 **Aerosol optical properties and carbon isotope analysis during Gosan Pollution Experiment (GoPoEx) 2014**  
*S.-W. Kim, C. Cho, P. Sheridan, Ö. Gustafsson, A. Andersson, W. Fang, R. J. Park, and M. Lee*
- T204N132 **Estimating contribution of brown carbon from multi-wavelength absorption measurements during summer and winter at an urban site**  
*J.-M. Yu, Y. Zhang, and S.S. Park*
- T204N1b2 **Measurements of aerosol optical properties at a suburban site in Belgium**  
*V. De Bock, A. Mangold, A. Delcloo, C. Hermans, and H. De Backer*
- T204N1e4 **Long term studies of aerosol optical properties and scavenging into clouds: Puijo semi-urban site**  
*A. Ruuskanen, S. Romakkaniemi, A. Arola, A. Virtanen, K. E. J. Lehtinen, M. Komppula, and A. Leskinen*
- T204N26b **Morphology and optical properties of nascent and mature soot**  
*G.A. Kelesidis and S.E. Pratsinis*

- T204N298 **Optical properties and PM concentration in air masses arriving at a high altitude location in the Mediterranean coast**  
*R. Castaner, J.F. Nicolás, M. Pandolfi, M. Ealo, S. Caballero, N. Galindo, J. Gil-Moltó, C. Pastor, M. Varea, E. Yubero, A. Alastuey, and J. Crespo*
- T204N29e **The first multi-year observation-based study of aerosol direct radiative forcing, its sensitivities and uncertainties in the Southeast US**  
*J.P. Sherman, N. Hall, and C. Holt*
- T204N3c8 **11-years continuous monitoring of the in-situ aerosol optical properties at El Arenosillo Observatory: emphasis on an extreme Saharan dust event in February 2016**  
*M. Sorribas, E. Andrews, J.A. Adame, A. del Águila, M. Yela, P. Sheridan, and J.A. Ogren*
- T204N3cc **Attenuation of solar radiation by aerosols near Ouarzazate solar farm**  
*A. Ben-Tayeb, M. Diouro, and I. Marsli*
- T204N3cd **Optical properties of aerosols observed in desert area**  
*A. Tahiri and M. Diouri*
- T204N455 **Cirrus clouds observations at the Atmospheric Observatory 'El Arenosillo' (SW Iberian Peninsula) and their effects on the surface solar radiation**  
*A. del Águila, L. Gómez, J.M. Vilaplana, J.A. Adame, M. Sorribas, and C. Córdoba-Jabonero*
- T204N4ad **Aerosol microphysical properties at different relative BC content in Beijing region**  
*M.A. Sviridenkov, A.S. Emilenko, V.M. Kopeikin, and W. Gengchen*
- T208N220 **UV-Vis absorption properties of water soluble HULIS in ambient aerosols: a study for IGP**  
*V. Kumar and A. Goel*

Tuesday 29 August 2017

15:15 - 15:45

Coffee Break and  
Exhibition

Tuesday 29 August 2017

13:30 - 15:15

Poster Area

POSTER SESSION PART II AND EXHIBITION

**PROPERTIES AND DYNAMICS OF ATMOSPHERIC AEROSOLS I**

- T205N075 **Multistep phase transition in single optically-trapped aqueous aerosol particles**  
*K. Esat, G. David, T. Poulkas, M. Shein, and R. Signorell*
- T205N0e4 **Seasonal variations of mass size distribution of carbon in atmospheric HULIS and WSOC for an urban background environment of Ljubljana, Slovenia**  
*S. Frka, I. Grgić, J. Turšič, M.I. Gini, and K. Eleftheriadis*
- T205N1be **Black carbon and particle number concentrations from a large and uncontrolled combustion of a tire landfill**  
*F. J. Gómez-Moreno, B. Artinano, E. Díaz, E. Alonso-Blanco, E. Coz, M. Becerril-Valle, and B. L. van Drooge*
- T205N1ca **One year of on-line chemistry measurements of the non-refractory submicron aerosol at the Puy de Dome with an emphasis on air mass transport, free troposphere / boundary layer conditions, and organic aerosol sources**  
*A. Farah, E. Freney, J. Nicolas, M. Abboud, W. Farah, and K. Sellegri*
- T205N1f2 **Light extinction estimates using the IMPROVE algorithm: The relevance of site-specific coefficients**  
*S. Valentini, V. Bernardoni, D. Massabo, P. Prati, G. Valli, and R. Vecchi*
- T205N1fd **Combined measurements of the physicochemical, optical and dynamic properties of single secondary organic aerosol (SOA) particles**  
*J. P. Reid, G. Rovelli, Y. C. Song, K.L. Pereira, J.F. Hamilton, and D.O. Topping*
- T205N21c **Characterising semivolatile evaporation and condensation to understand the partitioning of secondary organic matter**  
*S. Ingram, Y. Chul-Song, D.R. Glowacki, D.O. Topping, and J.P. Reid*
- T205N230 **Long-term observations of aerosol and cloud condensation nuclei concentrations in the Amazon rain forest and at a continental site with urban and rural influences**  
*O. Lauer, M.L. Pöhlker, C. Pöhlker, F. Ditas, T. Klimach, I. Hrabě de Angelis, A. Araújo, H.G. Bingemer, J. Brito, S. Carbone, Y. Cheng, R. Ditz, S.S. Gunthe, J. Kesselmeier, T. Könnemann, J.V. Lavrič, S.T. Martin, E. Mikhailov, D. Moran-Zuloaga, D. Rose, J. Saturno, C. Schulz, H. Su, D. Walter, J. Wang, S. Wolff, H.M.J. Barbosa, P. Artaxo, Jo. Curtius, M.O. Andreae, and U. Pöschl*
- T205N258 **Hygroscopic properties of different aerosol types at a suburban site (Madrid) in the Iberian Peninsula**  
*E. Alonso-Blanco, F.J. Gómez-Moreno, M. Becerril-Valle, E. Coz, E. Díaz, and B. Artinano*

- T205N29b **Characterization of secondary aerosols by cryo-TSEM-EDS: methodological development**  
*S. Guilbaud, K. Deboudt, P. Flament, and M. Fourmentin*
- T205N2a2 **Atmospheric aerosol and CCN properties in Dronning Maud Land, East Antarctica**  
*A. Mangold, Q. Laffineur, H. De Backer, V. De Bock, A. Delcloo, C. Hermans, C. Gielen, P. Herenz, and H. Wex*
- T205N2b5 **Mass closure for particle size distribution measurements**  
*H. Flentje and B. Briel*
- T205N2b9 **Probing structure and chemical properties of freestanding clusters with synchrotron radiation**  
*N.L. Prisle, J. Malila, K. Jänkälä, M. Patanen, and M. Huttula*
- T205N31b **Measured saturation vapour pressures of phenolic and nitro-aromatic compounds**  
*T.J. Bannan, M. Booth, B.T. Jones, S. O'Meara, M.H. Barley, I. Riipinen, C.J. Percival, and D. Topping*
- T205N39b **Relationship between reactive oxygen species and benzene carboxylic acids in the coastal area during KORUS-AQ campaign**  
*M.S. Bae, Z.H. Shon, T.H. Lee, J.H. Jeong, and J.J. Schauer*
- T205N3c1 **Heterogeneous ice nucleation from MD simulations**  
*M. Lbadapoui-Darvas and S. Takahama*

**Tuesday 29 August 2017**

**15:15 - 15:45**

**Coffee Break and  
Exhibition**

Tuesday 29 August 2017

13:30 - 15:15

Poster Area

**POSTER SESSION PART II AND EXHIBITION****SECONDARY ORGANIC AEROSOL**

- T211N047 **Regional SOA modeling under consideration of HOMs**  
*K. Gatzsche, Y. Iinuma, A. Tilgner, T. Berndt, L. Poulain, and R. Wolke*
- T211N0ac **Characterization of biogenic secondary organic aerosols in Malaysia affected by Indonesian peatland fires**  
*Y. Fujii, S. Tohno, and M. Mahmud*
- T211N105 **Comparison of different methodologies used for the estimation of secondary organic carbon (SOC)**  
*D. Srivastava, O. Favez, N. Bonnaire, E. Perraudin, V. Gros, J.-L. Jaffrezo, E. Villenave, and A. Albinet*
- T211N137 **Influence of NH<sub>3</sub> on secondary organic aerosols from the ozonolysis and photooxidation of  $\alpha$ -pinene in a flow reactor**  
*Z.B. Babar, J.-H. Park, I.-J. Hwang, and H.-J. Lim*
- T211N360 **Secondary aerosol formation from shipping emissions**  
*P. Simonen, E. Saukko, L. Ntziachristos, K. Lehtoranta, H. Timonen, F. Mylläri, T. Rönkkö, P. Karjalainen, J. Keskinen, and M. Dal Maso*
- T211N3a2 **Using factor analysis methods in the analysis of PTR-MS data from herbivore induced plant volatile measurements**  
*S. Mikkonen, S. Isokääntä, E. Kari, A. Buchholz, L.Q. Hao, A. Virtanen, and C.L Faiola*
- T211N3ec **Investigation of traffic related secondary aerosol formation in Helsinki city centre**  
*K. Teinilä, M. Aurela, J. Niemi, A. Kousa, S. Saarikoski, S. Carbone, L. Kangas, R. Hillamo, and H. Timonen*
- T211N420 **Molecular characterization of biogenic SOA using online extractive electrospray ionization mass spectrometry: on the fate of condensed phase ELVOC**  
*F. D. Lopez-Hilfiker, V. Pospisilova, M. Xiao, J. Dommen, A. Prévôt, U. Baltensperger, and J. G. Slowik*

Tuesday 29 August 2017

15:15 - 15:45

Coffee Break and  
Exhibition

Tuesday 29 August 2017

13:30 - 15:15

Poster Area

## POSTER SESSION PART II AND EXHIBITION

## SOURCE APPORTIONMENT STUDIES II

- T215N303 **Source apportionment of PM<sub>2.5</sub> observed at Daebu Island, Korea using air quality receptor models**  
*S.H. Kim, T.Y. Kim, D.G. Park, S.M. Yi, and J.B. Heo*
- T215N310 **Chemical composition and source apportionment of PM<sub>2.5</sub> in Pohang, Korea**  
*M.K Kim*
- T215N32d **Source apportionment of PM<sub>2.5</sub> mass and optical attenuation over an ecologically sensitive zone in Central India by positive matrix factorization**  
*J. Nirmalkar and R. Sunder Raman, and S. Kumar*
- T215N369 **Identification of main PM<sub>2.5</sub> sources at a suburban site in Douai, Northern France**  
*R. Roig, E. Perdrix, A. Chakraborty, L.Y. Alleman, B. Malet, B. Herbin, E. Tison, and V. Riffault*
- T215N385 **PM<sub>10</sub> characterization and source apportionment in Mt. Aitana**  
*E. Yubero, N. Galindo, J.F. Nicolás, M. Varea, J. Gil-Molto, R. Castaner, S. Caballero, C. Pastor, and J. Crespo*
- T215N3d8 **Aerosol chemical composition and spatial distribution in industrial areas using mobile aerosol mass spectrometry**  
*M. Maasikmets, M. Elser, C. Bozzetti, H. Keernik, E. Teinemaa, I. El-Haddad, R. Richter, J.G. Slowik, U. Baltensperger, and A.S.H. Prévôt*
- T215N489 **Source apportionment analysis of rural background AMS data**  
*O. Makeš, P. Vodička, J. Schwarz, and V. Ždímal*
- T215N491 **Source apportionment of trace metals in a respirable size fraction of PM<sub>10</sub>, at an urban site of a South Asian Mega City**  
*I. Shahid, M.U. Alvi, K. Alam, M.Z. Shahid, and F. Chishtie*
- T215N40a **Comprehensive source apportionment of long-term ACSM data**  
*F. Canonaco, A. Tobler, K. Dällenbach, C. Bozzetti, J. G. Slowik, I. El Haddad, U. Baltensperger, and A.S.H. Prévôt*
- T215N49f **Air quality in a street canyon: particles and traffic composition**  
*M. Almeida-Silva, P. Baptista, N. Canha, T. Faria, J. Lage, A.V. Faria, G. Duarte, C. Alves, and S.M. Almeida*

**T313N178 Predicting indoor PM10 using artificial neural network at subway station, Seoul, Korea**

*S. Park, M. Kim, H.-G. Namgung, S.-J. Bae, and S.-B. Kwon*

**Tuesday 29 August 2017**

**15:15 - 15:45**

**Coffee Break and  
Exhibition**

Tuesday 29 August 2017

13:30 - 15:15

Poster Area

POSTER SESSION PART II AND EXHIBITION

**SPECIAL SESSION #5: ELECTROHYDRODYNAMIC ATOMIZATION (EHDA) TECHNOLOGIES: FROM FUNDAMENTALS TO APPLICATION**

SPS5N188 **Solid-state electrolytes for lithium ion batteries: Application of electrospray technique**

*S.W. Karuga, M.J. Gatari, E.M. Kelder, and J.C.M. Marijnissen*

SPS5N1cb **Effect of EHDA in the simple-jet mode with whipping break-up on the evaporation ratio in thermal desalination system**

*L.K. Kiriinya, N. Nyambane, M.J. Gatari, L.L.F. Agostinho, and J.C.M. Marijnissen*

SPS5N387 **Nanoparticle synthesis using an electrohydrodynamic atomizer integrated flame spray pyrolysis system**

*V.A. Ganesan, M. Gensch, and A.P. Weber*

SPS5N3ba **Modeling the effect of lateral forces in the trajectories of droplets electrosprayed in the simple-jet mode**

*O.M. Ondimu, V. A. Ganesan, M. J. Gatari, J.C.M. Marijnissen, and L.L.M. Agostinho*

SPS5N45b **Long-term testing of catalytic layers deposited by electrospray for PEM fuel cell electrodes**

*S. Martin, J.L. Castillo, and P.L. Garcia-Ybarra*

SPS5N46e **Experimental investigation of the liquid-to-gas-phase-transfer of macro-ions**

*C. Lübbert and W. Peukert*

SPS5N46f **Ion specific effects in electro-spraying measured in an electrochemistry free setup**

*C. Lübbert and W. Peukert*

Tuesday 29 August 2017

15:15 - 15:45

Coffee Break and  
Exhibition

**Tuesday 29 August 2017** **15:45 - 16:50**

**WORKING GROUP SESSIONS**

**Tuesday 29 August 2017** **15:45 - 16:15** **Room 04G30**

**WORKING GROUP: ATMOSPHERIC AEROSOLS**

**Chair: Birigit Wehner**

**Tuesday 29 August 2017** **15:45 - 16:15** **Room 24G45**

**WORKING GROUP: PM<sub>x</sub>**

**Chair: Willy Maenhaut**

**Tuesday 29 August 2017** **15:45 - 16:15** **Room 15G20**

**WORKING GROUP: AEROSOL BASED NANOTECHNOLOGY**

**Chair: Einar Krus**

**Tuesday 29 August 2017** **15:45 - 16:15** **Room 15G40**

**WORKING GROUP: INHALATION, EXPOSURE AND HEALTH**

**Chair: Otto Hänninen**

**Tuesday 29 August 2017** **15:45 - 16:15** **Room 15G60**

**WORKING GROUP: FUNDAMENTALS**

**Chair: Yannis Drossinos**

**Tuesday 29 August 2017** **15:45 - 16:15** **Room 24G55**

**WORKING GROUP: INSTRUMENTATION**

**Chair: Aladar Czitrovski**

**Tuesday 29 August 2017** **16:20 - 16:50** **Room 04G30**

**WORKING GROUP: AEROSOL CHEMISTRY**

**Chair: Ana Kroflic**

**Tuesday 29 August 2017** **16:20 - 16:50** **Room 24G45**

**WORKING GROUP: AEROSOL MODELLING**

**Chair: Michael Boy**

**Tuesday 29 August 2017** **16:20 - 16:50** **Room 15G20**

**WORKING GROUP: COMBUSTION AEROSOLS**

**Chair: Zoran Ristovski**

**Tuesday 29 August 2017** **16:20 - 16:50** **Room 15G40**

**WORKING GROUP: INDOOR AND WORKING PLACE AEROSOLS**

**Chair: Aneta Wierzbicka**

**Tuesday 29 August 2017** **16:20 - 16:50** **Room 15G60**

**WORKING GROUP: ELECTRICAL EFFECTS**

**Chair: Andrei Bologna**

**Tuesday 29 August 2017** **16:50 - 17:00** **Break**

Tuesday 29 August 2017

17:00 - 19:00

Room 04G30

**NEW PARTICLE FORMATION AND PM SOURCES****Chairs: Mihkail Paramonov and Gary Fuller**

- 17:00** T214N32f **Aerosols Over Auckland**  
*G. Coulson, G. Olivares, S. Gray, and O. Wilson*
- 17:20** T214N20a **Online molecular-level characterization of submicrometer particulate organic matter in urban atmospheres and its application to source apportionment**  
*M. Müller, P. Eichler, B. D'Anna, W. Tan, and A. Wisthaler*
- 17:40** T214N403 **Insights into PM1 during haze episodes in Beijing, China, using an aerosol mass spectrometer in a two-month winter field campaign 2016**  
*S.H. Schmitt, P. Schlag, G. Gkatzelis, T. Hohaus, Y. Wang, D. Shang, M. Hu, K. Lu, A. Wahner, and A. Kiendler-Scharr*
- 18:00** T214N207 **PM10, PM2.5, and PM10-2.5 in the Po valley: variability, pattern and trend since 1998**  
*A. Bigi and G. Ghermandi*
- 18:20** T214N4b3 **Mass concentration and health risk assessment of toxic trace metals in size-segregated airborne particulate in Como, Northern Italy**  
*S. Rovelli, A. Cattaneo, F. Borghi, W. Nischkauer, A. Limbeck, and D.M. Cavallo*
- 18:40** T214N244 **Land-use regression modelling of ultrafine particles, soot, PM2.5, PM10, PMcoarse, and nitrogen oxides in the Augsburg region, Germany**  
*J. Cyrys, K. Wolf, T. Hrciniková, A. Schneider, J. Gu, T. Kusch, and A. Peters*
- Back-up Paper** T214N407 **What is the mechanism behind new particle formation in highly polluted urban environments?**  
*F. Bianchi, L. Yao, O. Garmash, C. Yan, J. Kontkanen, H. Junninen, S. Buenrostro Mazon, M. Ehn, M. Sipilä, T. Petäjä, M. Kulmala, D.R. Worsnop, and L. Wang*

Tuesday 29 August 2017

19:00

End of Conference Day

Tuesday 29 August 2017	17:00 - 19:00	Room 24G45
------------------------	---------------	------------

## AEROSOL CHEMICAL COMPOSITION, TRACERS AND TRENDS

**Chairs: Peter Molnar and Giulia Calzolai**

- |                      |          |  |
|----------------------|----------|--|
| <b>17:00</b>         | T215N25b | <p><b>Chemical Composition and source apportionment of PM10 in Port Talbot</b><br/> <i>D.C. Green, A. Font, A.H. Tremper, M. Priestman, and F. Canonaco</i></p>  |
| <b>17:20</b>         | T215N0ba | <p><b>Air quality planning and diesel vehicles: some surprises</b><br/> <i>T. Retny, O. Klemm, H. Hebbinghaus, and S. Wurzler</i></p>  |
| <b>17:40</b>         | T215N033 | <p><b>Spatial and temporal aerosol elemental composition trends over Auckland, New Zealand</b><br/> <i>P. Davy, N. Talbot, T. Ancelet, W. Trompetter, A. Markwitz</i></p>  |
| <b>18:00</b>         | T215N0b5 | <p><b>Air quality in Ecuador: PM10 characterization from 3 sites in the Amazon and Pacific Coast regions impacted by oil activities</b><br/> <i>F. Barraza, G. Uzu, E. Schreck, H. Guyard, A. Calas, J-L. Jaffrezo, and L. Maurice</i></p> |
| <b>18:20</b>         | T215N1b5 | <p><b>A chemometric approach to predict the contribution of ships to air pollution</b><br/> <i>H. Czech, T.W. Adam, B. Stengel, M. Sklorz, T. Streibel, and R. Zimmermann</i></p>  |
| <b>18:40</b>         | T313N09e | <p><b>Factors influenced and variable interactions of particulate matter (PM10) concentrations at an industrial cities in Peninsular Malaysia</b><br/> <i>N.Z. Yahaya and Z.F. Ibrahim</i></p>   |
| <b>Back-up Paper</b> | T215N0b4 | <p><b>Exposure trends of PM2.5 and black carbon sources in Gothenburg 1990-2011</b><br/> <i>P. Molnár, D. Segersson, L. Stockfelt, and G. Sallsten</i></p>   |

Tuesday 29 August 2017	19:00	End of Conference Day
------------------------	-------	-----------------------

**Tuesday 29 August 2017**

**17:00 - 19:00**

**Room 15G20**

**ELECTRICAL EFFECTS: FROM FUNDAMENTAL STUDY TO APPLICATION**

**Chairs: Andrei Bologna and Caner Yurteri**

- 17:00**    T111N409    **Analysis of different liquid-liquid combinations and conditions for the formation of a stable cone-jet mode in electrospray emulsification processes**  
*A.W. Kamau, M.J. Gatari, J.C.M. Marijnissen, and L.L.F. Agostinho*
- 17:20**    T107N43c    **Key parameters to control the mean charge in post-DBD aerosol neutralization**  
*N. Jidenko, R. Mathon, and J.-P. Borra*
- 17:40**    T112N2f9    **Electrostatic precipitation of particulate matter from syngas**  
*A. Bologna, K. Woletz, H.-R.Paur, and D.Stapf*
- 18:00**    T112N164    **Gas and PM removal performance of a wet scrubber system combined with a water-film ESP for IT manufacturing industries**  
*H.J. Kim, Y.J. Kim, B. Han, and C.G. Woo*
- 18:20**    T110N335    **Efficiency of an ionizer in removing airborne particles**  
*B. Pushpawela, A. Nguy, R. Jayaratne, and L. Morawska*
- 18:40**    T114N07a    **Mechanism of organic solvent induced charge degradation of electret filters**  
*P. Sachinidou, C. Heuschling, and J. Wang*

**Tuesday 29 August 2017**

**19:00**

**End of Conference Day**

Tuesday 29 August 2017	17:00 - 19:00	Room 15G40
------------------------	---------------	------------

## AIRBORNE PATHOGENS AND MICROBES AND THEIR VIABILITY

**Chairs:** Otto Hänninen and Jacob Löndahl

- |              |          |   |
|--------------|----------|---|
| <b>17:00</b> | T402N06f | <p><b>The bioaerosol bacterial microbiome at urban, agricultural, and industrial sites: Exposure, size fraction and composition</b><br/> <i>R.M.W. Ferguson, A.J. Dumbrell, C. Whitby, and I. Colbeck</i></p>                       |
| <b>17:20</b> | T402N049 | <p><b>Biophysical characterisation of pathogen containing aerosols</b><br/> <i>E. Pfrommer, T. Gutschmann, C. Dreier, R. Reimer, C. Schneider, G. Gabriel, K. Schepanski, and U.E. Schaible</i></p>                                 |
| <b>17:40</b> | T402N1d6 | <p><b>Accurately assessing the viability dynamics of infectious species in aerosol using next generation technology</b><br/> <i>M. Otero-Fernandez, A.E. Haddrell, and J.P. Reid</i></p>  |
| <b>18:00</b> | T402N226 | <p><b>Experimental set-up for studies of viability of aerosolized model organisms for infectious diseases</b><br/> <i>M. Alsved, T. Šantl-Temkiv, S. Holm, T. Svensson, P. Medstrand, A. Widell, M. Bohgard, and J. Löndahl</i></p> |
| <b>18:20</b> | T116N16c | <p><b>Efficiency of non-conductive ultrasonic transducers (NCUT) for inactivation of airborne virus</b><br/> <i>M. Versoza, W. Jung, Y. Lee, M.L. Barabad, J. Hwang, and D. Park</i></p>  |
| <b>18:40</b> | T402N4ac | <p><b>Dominant pathogens detected in exhaled breath using a novel Loop-Mediated Isothermal Amplification based protocol</b><br/> <i>Y. Zheng, X. Li, M. Yao, and J. Xu</i></p>  |

Tuesday 29 August 2017	19:00	End of Conference Day
------------------------	-------	-----------------------

Tuesday 29 August 2017

17:00 - 19:00

Room 15G60

**AEROSOL DYNAMICS: FROM PARTICLE REMOVAL TO MORPHOLOGY****Chairs: Abdelouahab Dehbi and Yannis Drossinos**

- 17:00** T502N05f **A large Eddy simulation of particle removal in a room-sized differentially heat cavity**  
*A. Dehbi, J. Kalilainen, and T. Lind*
- 17:20** T505N281 **Towards a coarse-grained model of nano-particle agglomeration**  
*M. Smiljanic, A. Kronenburg, R. Weeber, and C. Holm*
- 17:40** T504N343 **Nanoparticle filtration efficiency of HVAC filters and their media**  
*C. Asbach, W. Mölter-Siemens, A. Schmitz, F. Schmidt, and A.M. Todea*
- 18:00** T504N0e0 **Modeling and simulation of electrostatically charged particle dynamics in the inflow and transition area of cabin air filter media**  
*C. Schober, D. Keerl, M. Lehmann, and M. Mehl*
- 18:20** T508N405 **Morphology and optical properties of mixed aerosol particles**  
*M.M. Fard, U. Krieger, Y. Rudich, C. Marcolli, and T. Peter*
- 18:40** T501N102 **Long term aerosol aging under atmospherically relevant conditions in a CSTR-like aerosol tank**  
*F. Friebe, P. Lobo, S. Drossaert van Dusseldorp, E. Mühlhofer, and A.A. Mensah*
- Back-up Paper** T502N0df **Sedimentation effect of finely dispersed aerosol in tubes in shock-wave and shock-free modes**  
*D.A. Gubaidullin, R.G. Zaripov, and L.A. Tkachenko*

Tuesday 29 August 2017

19:00

End of Conference Day

## WEDNESDAY 30 AUGUST 2017

### MEETINGS AND WORKSHOPS

<b>12:50 -13:45</b>	<b>EAA Board Meeting</b>	<b>Room 13L11/13</b>
---------------------	--------------------------	----------------------

<b>14:00 - 15:30</b>	<b>Workshop on Urban Air Pollution Mitigation Tools</b>	<b>Room 04G20</b>
----------------------	---	-------------------

<b>14:00 - 17:00</b>	<b>Magee Scientific User Group Workshop</b>	<b>Room 24G45</b>
----------------------	---	-------------------

### SIGHTSEEING AND LAB TOURS

<b>14:00</b>	<b>Stories of the Old Town - Rediscover Zurich's Historic Center guided walking tour</b>
--------------	--

<b>14:00</b>	<b>Bus Tour to Rhine Falls near Schaffhausen Europe's Biggest Water Falls</b>
--------------	---

<b>14:30</b>	<b>Tour A: Laboratory visits at ETH</b>
--------------	---

<b>13:30</b>	<b>Tour B: Laboratory visits at Paul Scherer Institute (Villigen)</b>
--------------	---

**WEDNESDAY 30 AUGUST 2017**

<b>Wednesday 30 August 2017</b>	<b>08:15 - 13:00</b>	<b>Registration</b>
---------------------------------	----------------------	---------------------

<b>Wednesday 30 August 2017</b>	<b>08:30 - 10:00</b>	<b>Room 04G30</b>
---------------------------------	----------------------	-------------------

**PLENARY LECTURE III****Chair: Aneta Wierzbicka and Otto Hänninen**

**08:30** Plenary Lecture **Health effects of atmospheric particulate matter**  
*Bert Brunekreef*

**09:30** Award Ceremony **Presentation of the Smoluchowski Award**  
*Alfred P. Weber*

<b>Wednesday 30 August 2017</b>	<b>10:00 - 10:30</b>	<b>Coffee Break and Exhibition</b>
---------------------------------	----------------------	------------------------------------

<b>Wednesday 30 August 2017</b>	<b>10:30 - 12:50</b>	<b>Room 04G30</b>
<b>SECONDARY ORGANIC AEROSOL</b>		
<b>Chairs: Johannes Schneider and Jay Slowik</b>		

- 10:30** T211N09f  **$\alpha$ -pinene SOA at low temperature: Influence of formation conditions on chemical composition and viscosity**  
*W. Huang, H. Saathoff, K.-H. Naumann, A. Pajunoja, A. Virtanen, and C. Mohr*
- 10:50** T211N1ab **Modelling the impact of viscosity on Secondary Organic Aerosols formation with the SOAP thermodynamic model inside a 3D air quality model**  
*F. Couvidat, Y. Kim, and K. Sartelet*
- 11:10** T211N2a7 **Chemical ionization mass spectrometry as a probe for peroxy radical chemistry and SOA formation pathways**  
*M. Ehn, C. Yan, O. Peräkylä, L. Quéléver, Q. Zha, M.P. Rissanen, and M. Riva*
- 11:30** T211N42d **Formation and contribution of highly oxidized organic molecules to the growth of new particles over the boreal forest**  
*P. Roldin, E. Öström, D. Taipale, N. Kivekäs, M. Kulmala, T. Kurtén, M. Rissanen, E. Swietlicki, M. Ehn, and M. Boy*
- 11:50** T211N3b3 **Molecular composition of secondary organic aerosol during new particle formation and growth experiments at the CLOUD chamber**  
*A.L. Vogel, C. Zuth, C. Yan, J.B. Nowak, J. Kirkby, T. Hoffmann, D.R. Worsnop, and the CLOUD collaboration*
- 12:10** T211N435 **Gas phase composition and secondary organic aerosol formation from gasoline direct injection vehicles investigated in batch and flow reactors: cold-start emissions and the effect of a gasoline particle filter**  
*S.M. Pieber, U. Baltensperger, D. Bhattu, E.A. Bruns, P. Comte, J. Czerwinski, J. Dommen, N. Heeb, A. Keller, F. Klein, N.K. Kumar, A.S.H. Prévôt, and J.G. Slowik*
- 12:30** T211N427 **Partitioning of SOA components during photochemical smog in Beijing and Hong Kong**  
*M. Hallquist, M. Le Breton, A. Lutz, S. Guo, J.Z. Yu, Å.M. Hallquist, R.K. Pathak, Q. Liu, C.K. Chan, Y. Wang, Z. Wu, and M. Hu*
- Back-up Paper** T211N105 **Comparison of different methodologies used for the estimation of secondary organic carbon (SOC)**  
*D. Srivastava, O. Favez, N. Bonnaire, E. Perraudin, V. Gros, J.-L. Jaffrezo, E. Villenave, and A. Albinet*

<b>Wednesday 30 August 2017</b>	<b>12:50 - 13:45</b>	<b>Lunch Break</b>
---------------------------------	----------------------	--------------------

<b>Wednesday 30 August 2017</b>	<b>13:45</b>	<b>End of Conference Day</b>
---------------------------------	--------------	------------------------------

Wednesday 30 August 2017

10:30 - 12:50

Room 24G45

**EXPOSURES AND HEALTH IMPACTS OF AEROSOLS****Chairs: Aneta Wierzbicka and Christina Isaxon**

- 10:30** T413N337 **Comparative personal exposure assessment of school children to particle number concentrations in Australia, Italy and Bhutan**  
*L. Morawska, M. Mazaheri, G. Buonanno, S. Clifford, F. Fuoco, and T. Wangchuk*
- 10:50** T406N062 **A statistical analysis of brown haze events, surface air pollutants, and hospital admissions in Auckland, New Zealand**  
*N.P. Talbot, J. Scarfe, K.N. Dirks, J.A. Salmond, and R. Marshall*
- 11:10** T414N086 **Hourly land-use regression model using data collected with low-cost PM monitors**  
*M. Masiol, N. Ziková, A.R. Ferro, P.K. Hopke, D.C. Chalupa, and D.Q. Rich*
- 11:30** T406N3b1 **Detection of air pollution-related biomarkers of exposure and harm in urine of travellers between Germany and China**  
*X. Wu, J. Lintelmann, S. Klingbeil, J. Li, and R. Zimmermann*
- 11:50** T406N3d3 **A study of aerosol concentration and composition on cardiovascular illness at a semi urban site in Delhi**  
*A. Bhardawaj, N.A. Baig, G. Habib, and S. Singh*
- 12:10** T412N466 **Indoor to outdoor ratio of black carbon concentrations in occupied residences**  
*A. Wierzbicka, S. Lucciola, Y. Omelekhina, P.T Nilsson, and A. Gudmundsson*
- 12:30** T406N31f **Air pollution epidemiology and regional differences in concentration-response relationships**  
*O. Hänninen, I. Rumrich, and A. Asikainen*
- Back-up Paper** T406N15f **Development of a multilevel regression model to analyze the association between eye diseases and air pollutants (PM10, PM2.5, NO<sub>2</sub>, SO<sub>2</sub>, O<sub>3</sub>)**  
*S.-J. Park, S. Han, J.-S. Youn, J. Seo, and K.-J. Jeon*

Wednesday 30 August 2017

12:50 - 13:45

Lunch Break

Wednesday 30 August 2017

13:45

End of Conference Day

<b>Wednesday 30 August 2017</b>	<b>10:30 - 12:50</b>	<b>Room 15G20</b>
<b>MOBILE SOURCES OF COMBUSTION AEROSOL</b>		
<b>Chairs: Michal Vojtisek-Lom and Joakim Pagels</b>		

- 10:30** T116N375 **Towards standardizable measurements of passenger car brake dust emissions**  
*Chr. Asbach, H. Kaminski, J. Lindermann, A.M. Todea, M. Zessinger, R.-J. Conhoff, G. Frentz, D. Schneider, and S. Schumacher*
- 10:50** T116N43e **Characterisation of fresh and aged particle and gaseous emissions from in-use diesel, RME and CNG buses**  
*Å.M. Hallquist, M. Psichoudaki, M. Le Breton, Å. Watne, M. Jerksjö, H. Fallgren, and M. Hallquist*
- 11:10** T118N352 **Secondary aerosol formation potential reduction from a non-road diesel engine with exhaust aftertreatment systems**  
*P. Karjalainen, L. Ntziachristos, P. Simonen, K. Teinilä, H. Timonen, H. Saveljeff, M. Lauren, M. Happonen, P. Matilainen, T. Maunula, J. Nuottimäki, T. Rönkkö, and J. Keskinen*
- 11:30** T120N00c **The catalytic effect of potassium compounds in soot oxidation**  
*A. Rinkenburger, K. Yasuda, and R. Niessner*
- 11:50** T120N2f2 **Role of oxidative exhaust after-treatment in the partition of sulphuric species**  
*J. Alanen, P. Karjalainen, K. Teinilä, S. Saarikoski, H. Timonen, J. Keskinen, and T. Rönkkö*
- 12:10** T116N382 **Measurement of particulate matter emissions from diesel locomotives and rail vehicles during real-world line-haul operation**  
*M. Vojtisek-Lom, M. Pechout, V. Beránek, and J. Jirku*
- 12:30** T116N253 **Implementation of a population balance model utilizing the sectional method within a stochastic reactor engine model**  
*N.A. Eaves, J. Akroyd, S. Mosbach, and M. Kraft*
- Back-up Paper** T117N4c4 **High-efficiency simultaneous removal of trace HM and organic pollutants from an iron ore sintering plant**  
*J. Gonzalez, B. Gonzalez, I. Ibarra, K. Datta, I. Gomez, V. Garcia, F. J. Gonzalez, and C. Gutierrez-Canas*

<b>Wednesday 30 August 2017</b>	<b>12:50 - 13:45</b>	<b>Lunch Break</b>
---------------------------------	----------------------	--------------------

<b>Wednesday 30 August 2017</b>	<b>13:45</b>	<b>End of Conference Day</b>
---------------------------------	--------------	------------------------------

Wednesday 30 August 2017

10:30 - 12:50

Room 15G40

**SYNTHESIS AND STRUCTURING OF FUNCTIONAL NANOPARTICLES****Chairs: Andreas Schmidt-Ott and Sotoris Pratsinis**

- 10:30** T101N022 **Numerical and experimental investigation of the buoyancy effect on iron-oxide nanoparticle formation in a down-firing flat flame reactor**  
*J. Sellmann, S. Kluge, A. Fomin, S. Cheskis, A. Pilipody, P. Fiodorow, H. Wiggers, C. Schulz, I. Rahinov, A. Kempf, and I. Wlokas*
- 10:50** T101N0c5 **The impact of lanthanum loading on alumina-supported cobalt catalysts synthesised via double flame spray pyrolysis**  
*J. Horlyck, S. Pokhrel, E. Lovell, L. Mädler, and J. Scott*
- 11:10** T101N0d4 **Biomimetic luminescent antioxidant nanoparticles for H<sub>2</sub>O<sub>2</sub> biosensings**  
*A. Pratsinis, G.A. Kelesidis, F. Krumeich, J.-Ch. Leroux, and G.A. Sotiriou*
- 11:30** T101N177 **Superparamagnetic nanoparticles for triggered drug release from alginate hydrogels**  
*A. Teleki, F.L. Haufe, A.M. Hirt, S.E. Pratsinis, and G.A. Sotiriou*
- 11:50** T101N247 **Spray-flame synthesis of barium titanate nanoparticles for electro- and photochemical applications**  
*A. Tarasov, Y. Xiong, F. Marlow, C. Schulz, and H. Wiggers*
- 12:10** T101N36a **Fabrication of slippery, liquid-infused porous surfaces by flame based aerosol synthesis**  
*P. Juuti, J. Haapanen, C. Stenroos, H. Niemelä-Anttonen, J. Harra, H. Koivuluoto, H. Teisala, J. Lahti, M. Tuominen, J. Kuusipalo, P. Vuoristo, and J.M. Mäkelä*
- 12:30** T102N074 **Gas-phase carbon nanostructures for energy storage device microfabrication via supersonic cluster beam deposition**  
*L.G. Bettini, P. Piseri, and P. Milani*
- Back-up Paper** T101N167 **Single-step fabrication of nanocatalyst microarrays by coupling flame spray pyrolysis with supersonic expansion**  
*S. Vinati, E. Barborini, K. Wegner, and P. Milani*

Wednesday 30 August 2017

12:50 - 13:45

Lunch Break

Wednesday 30 August 2017

13:45

End of Conference Day

<b>Wednesday 30 August 2017</b>	<b>10:30 - 12:50</b>	<b>Room 15G60</b>
<b>AEROSOL OPTICAL PROPERTIES</b>		
<b>Chairs: Andreas Petzold and Martine Collaud Coen</b>		

- 10:30** T204N113 **Angular scattering of the Sahara dust aerosol**  
*H. Horvath, L. Alados Arboledas, and F.J. Olmo Reyes*
- 10:50** T204N189 **Measurements of the real and imaginary components of the refractive index of single aerosol particles**  
*R.E. Willoughby, M.I. Cotterell, A. Valenzuela, B.R. Bzdek, H. Lin, A.J. Orr-Ewing, and J.P. Reid*
- 11:10** T204N11f **Aerosol climatology and trends at Mauna Loa Observatory**  
*P. Sheridan, E. Andrews, J. Barnes, and N. Hyslop*
- 11:30** T204N150 **A long-term study of suburban aerosol optical properties based on CAPS PM<sub>2.5</sub> monitor measurements**  
*M.I. Gini, P. Fefatzis, S. Vratolis, and K. Eleftheriadis*
- 11:50** T204N2ae **Optical closure study for background aerosol from helicopter-borne in-situ and ground-based lidar measurements**  
*S. Düsing, B. Wehner, P. Seifert, N. Ma, L. Poulain, S. Henning, H. Baars, H. Siebert, and A. Wiedensohler*
- 12:10** T204N34d **Optical and radiative properties of atmospheric brown carbon aerosols from Kanpur-India**  
*P.M. Shamjad, R.V. Satish, N.M. Thamban, N. Rastogi, and S.N. Tripathi*
- 12:30** T204N3da **Explaining variation in light absorption by black carbon aerosols observed in Cabauw, the Netherlands**  
*R.L. Modini, N. Bukowiecki, J.S. Henzing, M. M. Moerman, M. Ealo, P. Fefatzis, K. Eleftheriadis, A. Apituley, P. Laj, and M. Gysel*
- Back-up Paper** T213N018 **Relevance of wildfires on dust emissions via interaction with near-surface wind pattern**  
*R. Wagner, M. Jähn, and K. Schepanski*

<b>Wednesday 30 August 2017</b>	<b>12:50 - 13:45</b>	<b>Lunch Break</b>
---------------------------------	----------------------	--------------------

<b>Wednesday 30 August 2017</b>	<b>13:45</b>	<b>End of Conference Day</b>
---------------------------------	--------------	------------------------------

## THURSDAY 31 AUGUST 2017

### MEETINGS

<b>12:30 - 13:45</b>	<b>Working Group Chairs Meeting</b>	<b>Room Y13L11/13</b>
----------------------	-------------------------------------	-----------------------

### SOCIAL EVENTS

<b>19:30</b>	<b>Conference Dinner</b>
--------------	--------------------------

**THURSDAY 31 AUGUST 2017**

Thursday 30 August 2017	08:15 – 16:15	Registration
-------------------------	---------------	--------------

Thursday 30 August 2017	08:30 - 09:40	Room 04G30
-------------------------	---------------	------------

**PLENARY LECTURE IV****Chair: Yannis Drossinos and Mattias Hallquist**

**08:30** Plenary Lecture      **Nucleation theory: Are we nearly there yet?**  
*Ian Ford*

**09:30** Next Conferences      **IAC2018 and EAC2019 Launch**  
*Pratim Biswas and Mattias Hallquist*

Thursday 31 August 2017	09:40 - 10:10	Coffee Break and Exhibition
-------------------------	---------------	-----------------------------

Thursday 31 August 2017

10:10 - 12:30

Room 04G30

**ATMOSPHERIC AEROSOLS: PHYSICAL AND CHEMICAL PROPERTIES**

Chairs: Anne Kasper-Giebl and Claudia Marcolli

- 10:10** T205N05e **Aerosol characterisation results from the South West Asian Aerosol-Monsoon Interactions (SWAAMI) aircraft experiment**  
*J. Brooks, H. Coe, W. Morgan, P. Williams, J. Allan, D. Liu, S. Haslett, S.K. Satheesh, S. Suresh Babu, and A. Turner*
- 10:30** T205N429 **Driving factors for aerosol variability in the foothills of Central Himalayas**  
*R.K. Hooda, N. Kivekäs, E. O'Connor, M. Collaud-Coen, J-P. Pietikäinen, V. Vakkari, J. Backman, A.-P. Hyvärinen, and H. Lihavainen*
- 10:50** T205N423 **On-road measurements of primary and secondary aerosol on European highways from the Baltic Sea to the Mediterranean**  
*M. Dal Maso, M. Olin, J. Heikkilä, P. Simonen, A. Rostedt, E. Saukko, H. Kuuluvainen, J. Kalliokoski, O. Potila, A. Järvinen, M. Poikkimäki, T. Rönkkö, and J. Keskinen*
- 11:10** T205N40e **Cloud droplet activation of black carbon particles containing organic coating**  
*M. Dalirian, A. Ylisirniö, A. Buchholz, A. Virtanen, and I. Riipinen*
- 11:30** T205N3f3 **Identifying the main sources of brown carbon in the atmosphere**  
*I. El Haddad, N. Kumar, K. Daellenbach, C. Bozzetti, J. Corbin, D. Massabò, E. Bruns, A. Vlachou, J.G. Slowik, P. Prati, U. Baltensperger, J.-L. Jaffrezo, G. Mocnik, M. Gysel, and A.S.H. Prevot*
- 11:50** T205N324 **Volatility distribution of organic aerosol components using ambient and laboratory measurements**  
*E. Karnezi, E. Louvaris, E. Kostenidou, K. Florou, and S. N. Pandis*
- 12:10** T205N35f **Comparison of atmospheric aerosol volatility at a rural site in Central Europe**  
*L. Kubelová, P. Vodicka, O. Makeš, N. Zíková, J. Ondráček, J. Schwarz, and V. Ždímal*
- Back-up Paper** T205N22b **The effect of relative humidity and chemical composition on the evaporation of secondary organic aerosol particles**  
*A. Buchholz, C. Mohr, A. Lambe, C. Faiola, E. Kari, S.A. Nizkorodov, A. Pajunoja, O.-P. Tikkanen, A. Ylisirniö, D. Worsnop, T. Yli-Juuti, and A. Virtanen*

Thursday 31 August 2017

12:30 - 13:45

Lunch Break

Thursday 31 August 2017 10:10 - 12:30 Room 24G45

## NANOPARTICLE COATING AND FUNCTIONALIZATION

Chairs: Alfred Weber and Janne Haapanen

- 10:10** T102N1c4 **The spark ablation as a perspective method for the solvent-free aerosol jet printing**  
*A.A. Efimov, A.A. Lizunova, P.V. Arsenov, and V.V. Ivanov*
- 11:30** T103N0da **PECVD process for the continuous coating of aerosol nanoparticles with silica at ambient temperature**  
*P. Post, J.-P. Borra, and A.P. Weber*
- 10:50** T103N1db **Synthesis and photoelectrochemical property of monodisperse hollow metal oxide microspheres**  
*H. Lee, W.J. Shin, Y. Sohn, and W.G. Shin*
- 11:10** T103N1ec **Mesoporous carbon nitride as an efficient photocatalyst for aerosol- photopolymerization**  
*J. Poostforooshan, M. Shaban, and A.P. Weber*
- 11:30** T103N256 **One step aerosol synthesis of various supported metal catalyst particles with tuneable pore sizes, defined metal crystallite sizes and different loadings**  
*A. Martínez and A.P. Weber*
- 11:50** T103N17b **Comparison of catalyst immobilization techniques onto filter media for airborne VOCs decomposition**  
*S. Drdova, X. He, and J. Wang*
- 12:10** T103N020 **Coating and functionalization of ultra-fine powders by fluidized bed chemical vapour deposition (FB-CVD)**  
*M. Seipenbusch, F. Weis, and G. Kasper*
- Back-up Paper** T101N35a **Antibacterial nanocoatings by liquid flame spray**  
*J. Haapanen, P. Juuti, M. Gunnell, K. Brobbey, E. Eerola, J.J. Saarinen, M. Toivakka, P. Huovinen, and JM. Mäkelä*

Thursday 31 August 2017

12:30 - 13:45

Lunch Break

Thursday 31 August 2017

10:10 - 12:30

Room 15G20

**MOLECULAR CHARACTERIZATION & MARINE AEROSOLS**

Chairs: Alexander Vogel and Magda Claeys

- 10:10** T216N255 **Development of online Orbitrap mass spectrometry of organic aerosols: Applications for the identification of VOCs and SOA particle phase composition**  
*C. Zuth, A. Vogel, S. Ockenfeld, R. Huesmann, and T. Hoffmann*
- 10:30** T216N165 **Observation of synergies in secondary brown carbon formation from a monoterpene oxidation intermediate and dicarbonyls in aerosol mimicry experiments**  
*C.J. Kampf, S. Wittemann, F. Kunkler, A. Filippi, and T. Hoffmann*
- 10:50** T216N0f6 **On abundance and potential sources of nitroaromatic compounds in size resolved ambient water soluble organic aerosols**  
*S. Frka, M. Šala, J. Turšič, and I. Grgić*
- 11:10** T216N434 **Characterization of secondary organic aerosol sources using extractive electrospray time-of-flight mass spectrometry**  
*J.G. Slowik, F.D. Lopez-Hilfiker, V. Pospisilova, L. Qi, G. Stefenelli, Y. Tong, A. Vogel, U. Baltensperger, and A.S.H. Prévôt*
- 11:30** T216N28a **Organosulfates and other molecular tracers of secondary organic aerosols in Xi'an, China during summer and winter**  
*M. Glasius, L.S. Iversen, A.M.K. Hansen, and R.-J. Huang*
- 11:50** T212N1a2 **Marine bio-chemical variabilities and secondary organic aerosols over the Middle Adriatic area: Insight into organosulfur prevalence**  
*A. Cvitešić, A. Kroflic, Z. Ljubešić, M. Šala, I. Grgić, I. Ciglenecki, and S. Frka*
- 12:10** T212N46c **Sources of cloud condensation nuclei over the Southern Ocean inferred from water uptake and volatility**  
*L. Cravigan, J. Alroe, B. Miljevic, R. Humphries, M. Keywood, P. Selleck, J. Ward, A. Protat, and Z. Ristovski*
- Back-up Paper** T216N41f **Molecular characterization of nanoparticles using extractive electrospray ionisation time-of-flight mass spectrometry**  
*V. Pospisilova, F. D. Lopez-Hilfiker, M. Xiao, O. Garmash, A. Baccharini, C.R. Hoyle, A.S.H. Prévôt, U. Baltensperger, J.G. Slowik, and the CLOUD collaboration*

Thursday 31 August 2017

12:30 - 13:45

Lunch Break

Thursday 31 August 2017 10:10 - 12:30 Room 15G40

## WORKPLACE AEROSOLS: FROM SOURCE TO EXPOSURE

Chairs: Olivier Witschger and Sergey Grinshpun

- 10:10** T410N10b **On the equivalence between mass-specific surface area of powders and their aerosols and proposal of a new dustiness index for bulk nanomaterials**  
*C. Dazon, O. Witschger, S. Bau, R. Payet, V. Fierro, K.A. Jensen, E. Jankowska, D. Bard, I. Tuinman, and P. Llewellyn*
- 10:30** T413N2b8 **Prediction and quantification of emissions and workers exposure during ceramic industrial processes**  
*C. Ribalta, M. Viana, M.C. Minguillón, A. López-Lilao, S. Estupiñá, and E. Monfort*
- 10:50** T410N249 **Characterization of fine and ultrafine particles emitted from hardwood processing**  
*J. Gu, I. Kirsch, T. Schripp F. Froning, D. Berthold, and T. Salthammer*
- 11:10** T413N08f **Aerosol monitoring for a rapid detection of the respirator performance failure**  
*S.A. Grinshpun, J. Corey, B. Wu, M. Yermakov, and Y. Liu*
- 11:30** T413N232 **Source measurements directional and distance evaluation**  
*A.C.Ø. Jensen, A.B. Blume, M. Dal Maso, O.J. Nielsen, T. Rosenørn, and I.K.K. Koponen*
- 11:50** T417N48c **Effect of the supply air supporting the shaping of exhaust air during processing of nanomaterials**  
*T. Jankowski*
- 12:10** T411N259 **Exposure estimation by propagation modelling based on experimental determined airborne particle release data from nanostructured materials**  
*D. Göhler, R. Gritzki, M. Rösler, C. Felsmann, and M. Stintz*
- Back-up Paper** T410N0be **Aerosol particles (0.3-10 µm) inside a workshop area**  
*A. Maragkidou, O. Jaghbeir, K. Hämeri, and T. Hussein*

Thursday 31 August 2017 12:30 - 13:45 Lunch Break

Thursday 31 August 2017

10:10 - 12:30

Room 15G60

**MINIATURIZED INSTRUMENTATION AND LOW COST SENSORS****Chairs: Christof Asbach and Markus Pesch**

- 10:10** T304N462 **Low-cost and lightweight instruments for probing physicochemical properties of aerosol particles**  
*G. Biskos, K. Barmounis, S. Bezantakos, and A. Maisser*
- 10:30** T306N234 **Evaluation of cost effective and lightweight optical particle counters for measuring the size of atmospheric particles with unmanned aerial vehicles**  
*F. Schmidt-Ott, S. Bezantakos, N. Surawski, and G. Biskos*
- 10:50** T303N401 **Comparison between remote sensing and airborne in-situ measurements using drones**  
*D. Mamali, E. Marinou, M. Pikridas, I. Binietoglou, P. Kokkalis, A. Tsekeri, M. Kottas, V. Amiridis, J. Sciare, C. Keleshis, R. Engelmann, A. Ansmann, H.W.J. Russchenberg, and G. Biskos*
- 11:10** T311N2e5 **Half-mini DMA modification for high temperature aerosols and evaluation on various combustion exhausts**  
*M. Amo, C. Barrios, J.C. del Castillo, J.F. de la Mora, A.G. Konstandopoulos, P. Baltzopoulou, and N.D. Vlachos*
- 11:30** T302N42e **Photoionization sensor: method for detecting ultrafine particle surface area, size and concentration in continuous flow**  
*R. T. Nishida, A. M. Boies, and S. Hochgreb*
- 11:50** T304N4b2 **Developments in personal and mobile monitors: a survey**  
*F. Borghi, A. Spinazzè, D. Campagnolo, L. Del Buono, S. Rovelli, A. Cattaneo, and D.M. Cavallo*
- 12:10** T306N344 **Intercomparison of a personal CPC and different conventional CPCs**  
*C. Asbach, A. Schmitz, F. Schmidt, C. Monz, and A.M. Todea*
- Back-up Paper** T304N44a **Miniaturized aerosol instruments for unmanned aerial vehicles**  
*F.J. Brechtel, M. Ramstrom, A.B. Corless, and T.S. Bates*

Thursday 31 August 2017

12:30 - 13:45

Lunch Break

Thursday 31 August 2017

13:45 - 15:30

Poster Area

**POSTER SESSION PART III AND EXHIBITION****BIOAEROSOLS I**

- T208N030 **An inquiry on the potential uses of UV fluorescence for the detection of microorganisms in air, in suspension and on surface**  
*M. Skulinova, G. Marchand, J.-F. Gravel, J. Lavoie, and Y. Cloutier*
- T208N0bb **Fungal compositions in dry and wet deposition samples in Seoul, South Korea**  
*C. An, C. Woo, S. Xu, and N. Yamamoto*
- T208N138 **Potential pathogenicity of psychrotolerant yeasts isolated from atmospheric aerosols of Southwestern Siberia**  
*I.S. Andreeva, A.S. Safatov, V.V. Morozova, N.V. Tikunova, I.V. Babkin, G.A. Buryak, E.K. Emelyanova, and E.N. Gorina*
- T208N332 **Re-aerosolisation of biological aerosols from hot surfaces**  
*K. Mirskaya and I.E. Agranovski*
- T208N3b0 **Assessment of total airborne microbes on hazy days in a typical semi-arid city of Northwest China**  
*Y. Li, Z. Xie, R. Lu, W. Li, and Y. Song*
- T208N425 **Characterization of the Chambre atmospheric simulation chamber**  
*P. Prati, E. Gatta, P. Brotto, D. Massabñ, F. Parodi, A. Comite, C. Costa, J. F. Doussin, and P. Formenti*
- T208N4af **Real time characterization of bioaerosols emissions from green waste composting**  
*Z.A. Nasir and S. Tyrrel*

Thursday 31 August 2017

15:30 - 16:00

Coffee Break and  
Exhibition

Thursday 31 August 2017

13:45 - 15:30

Poster Area

POSTER SESSION PART III AND EXHIBITION

**CARBONACEOUS AEROSOLS**

- T204N104 **Contribution and potential sources of nitroaromatic compounds in water soluble brown carbon of size-resolved ambient aerosols**  
*S. Frka, A. Kroflic, J. Turšic, M. Šala, and I. Grgic*
- T204N1c6 **Size distribution of submicron aerosol absorptive properties in the North China Plain**  
*Z.Z. Deng, L. Ran, and P.C. Wang*
- T210N06e **Sector analysis of elemental and organic carbon (EC-OC) data from the Košetice Observatory (ACTRIS and EMEP site, Czech Republic)**  
*M.Vana, A. Holubová Šmejkalová, and E. Chalupnicková*
- T210N073 **Seasonal variability of carbonaceous aerosols in South-East Italy**  
*D. Cesari, E. Merico, A. Dinoi, A. Marinoni, P. Bonasoni, and D. Contini*
- T210N082 **Highly time resolved measurement of atmospheric elemental and organic carbon at a typical background site in Central Europe**  
*S. Mbengue, M. Fusek, J. Schwarz, and I. Holoubek*
- T210N0c9 **Black carbon, carbon monoxide and carbon dioxide in the free troposphere at Helmos Hellenic Atmospheric Aerosol and Climate Change (HAC2) station in Greece**  
*A.-C. Kalogridis, P. Fetfatzis, O. Hermansen, and K. Eleftheriadis*
- T210N144 **Photophoresis of fractal-like soot aggregates: new microphysical model and atmospheric applications**  
*S.A. Beresnev, L.B. Kochneva, V.I. Gryazin, and M.S. Vasiljeva*
- T210N1c5 **Black carbon and brown carbon aerosols in Ireland**  
*P.C. Buckley, S. Hellebust, J. Arndt, I.P. O'Connor, E.J. McGillicuddy, E. Nicolosi, G. Fuller, and J. Wenger*
- T210N2b1 **Correlation between black, elemental and organic carbon in urban and rural areas in the Iberian Peninsula**  
*M. Becerril-Valle, E. Coz, A.S.H. Prévôt, G. Mocnik, S.N. Pandis, A.M. Sánchez de la Campa, A. Alastuey, and B. Artíñano*
- T210N2b2 **Calculation of photophoretic motion characteristics of fractal-like soot aggregates using the specialized aerosol solver**  
*V.I. Gryazin and S.A. Beresnev*
- T210N2b4 **Spatial and seasonal distribution of light absorbing carbonaceous aerosol**  
*S. Gilardoni, A. Marinoni, P. Massoli, S. Deilulis, F. Migliorini, V. Gianelle, G. Lonati, A. Malandrino, S. Ozgen, and A. Freedman*

- T210N325 **Temporal variability and implications to estimates of black carbon radiative forcing over an ecologically sensitive zone in Central India**  
*A.K. Paswan, A. Singh, S. Kumar, and R.S. Raman*
- T210N355 **Radiocarbon and AMS coupled source apportionment of carbonaceous aerosols in the Baltic region**  
*A. Vlachou, C. Bozzetti, K.R. Daellenbach, G.A. Salazar, S. Szidat, J.-L. Jaffrezo, M. Elser, M. Maasikmets, V. Ulevicius, U. Baltensperger, I. El Haddad, and A.S.H. Prévôt*
- T210N396 **The mixing state of black carbon in Beijing during wintertime**  
*D. Liu, R. Joshi, J. Allan, H. Coe, M. Flynn, J. Olfert, K. Broda, M. Irwin, P. Fu, Y. Sun, X. Ge, and J. Wang*
- T210N3db **Annual behavior of EBC size distribution in submicron aerosol in West Siberia**  
*V. S. Kozlov, D.G. Chernov, and M.V. Panchenko*
- T210N3eb **Correlation of temperature-resolved carbon fractions with individual organic compounds in PM<sub>2.5</sub> measured at a background site in South Korea**  
*Y.W. Chang, J.S. Lee, E.S. Kim, Y.P. Kim, C.H. Jung, and J.Y. Lee*

Thursday 31 August 2017

15:30 - 16:00

Coffee Break and  
Exhibition

**Thursday 31 August 2017****13:45 - 15:30****Poster Area****POSTER SESSION PART III AND EXHIBITION****CHARACTERIZATION AND NOVEL MEASUREMENT TECHNIQUES OF AEROSOL-BASED NANOMATERIALS**

- T106N017 **Physicochemical characterization of nanoparticles-containing spray coating generated by atomization process**  
*O. Fichera, J. Mejia, J. Laloy, L. Alpan, S. Lucas, and J-M. Dogné*
- T106N094 **Study on photocatalytic hydrogen production and photodegradation of oxytetracycline using Pt/TiO<sub>2</sub> composite**  
*J. Tian and C.T. Chang*
- T106N116 **Characterisation of aerosol release from the combustion of epoxy/graphene nanoplatelet/DOPO nanocomposites**  
*W. Netkueakul, F. Nüesch, B. Fischer, S. Gaan, M. Jovic, and J. Wang*
- T106N27d **Sintering of Fe-nanoparticles in a well-defined model flow reactor**  
*T. Rosenberger and F.E. Kruis*
- T106N386 **Ethanol and hexamethyldisilazane removal with composites of zeolite and molecular sieve**  
*H.W. Huang and C.T. Chang*
- T106N39a **Distribution of radioactive admixtures on aerosol particles**  
*V.A. Zagaynov, M.E. Masyanovich, M.V. Zhukovsky, V.V. Maksimenko, A.A. Lushnikov, and I.E. Agranovski*

**Thursday 31 August 2017****15:30 - 16:00****Coffee Break and Exhibition**

Thursday 31 August 2017

13:45 - 15:30

Poster Area

**POSTER SESSION PART III AND EXHIBITION****CLIMATE EFFECTS OF AEROSOLS AND GLOBAL MODELLING**

- T104N441 **Effective BVOCs exchange of boreal forests: emissions versus in-canopy sinks**  
*P. Zhou, L. Ganzeveld, D. Taipale, Ü. Rannik, M.P. Rissanen, P. Rantala, and M. Boy*
- T202N0ff **Trends in fog occurrence in Czechia – association with air pollution and climate**  
*I. Hůnová, M. Brabec, M. Malý, and A. Valeriánová*
- T202N126 **Impacts of carbonaceous aerosol on hydrological cycle over the Northern Africa**  
*J.-H. Yoon, P.J. Rasch, H. Wang, V. Vinoj, and D. Ganguly*
- T202N130 **Implementation of simplified chemistry module in KIAPS integrated model**  
*J.-Y. Kang, S.Y. Bae, and R. Park*
- T202N245 **Robust signals of regional climate impact on antropogenic aerosols**  
*K. Nordling, J. Merikanto, D. O'Donnel, J. Räisänen, and H. Korhonen*
- T202N33e **On connection between remote dust aerosol and Indian summer monsoon**  
*S. Kumar and A. Arora*
- T202N42a **Influence of clouds on black carbon direct radiative effect and heating rate over Milan**  
*A. Gregorič, L. Ferrero, G. Močnik, S. Cogliati, F. Barnaba, L. Di Liberto, G.P. Gobbi, and E. Bolzacchini*
- T202N4c2 **Radiative forcing from CALIPSO measurements: method and comparison to state-of-the-art forcing estimations from ground**  
*N. Papagiannopoulos, M. Sicard, L. Mona, A. Comeron*
- T207N496 **Current state and future of aerosol process parameterizations in air quality models**  
*K. Semeniuk, A. Dastoor, and K. Toyota*

Thursday 31 August 2017

15:30 - 16:00

Coffee Break and  
Exhibition

Thursday 31 August 2017

13:45 - 15:30

Poster Area

POSTER SESSION PART III AND EXHIBITION

**FILTRATION FOR FUNCTIONAL MATERIALS, COMBUSTION AND INDUSTRIAL AEROSOLS**

- T108N016 **Nanoparticle filtration by multilayer meltblown depth filters**  
*Y.-O. Park, K.-S. Lee, N. Hasolli, S.-M. Jeon, J.-R. Lee, K.-D. Kim, and J. Hwang*
- T108N036 **Reduction of PCDD/F emission by employing catalytic ceramic fiber filter**  
*S.-L. Lin, R. Aniza, S.-I Shih, and Y.-M. Kuo*
- T108N03a **Diesel PM combustion using non-thermal plasma and catalyst**  
*H. Kawakami, T. Inui, Y. Nozaki, H. Miyashita, and Y. Ehara*
- T108N05c **Removal efficiency for PAHs emitted from diesel engine using an electrostatic precipitator**  
*K. Ito, Y. Nanjo, A. Zukeran, and T. Inui*
- T108N0aa **Discharge current characteristic on hole-type electrostatic precipitator**  
*S. Suzuki, S. Yokoyama, H. Miyashita, Y. Ehara, T. Inui, and T. Sawada*
- T108N0ab **PIV analysis of re-entrainment phenomenon in the electrostatic precipitator**  
*K. Yanagawa, H. Miyashita, Y. Ehara, T. Inui, and T. Sawado*
- T108N0ae **Relationship between back corona discharge current and elapsed time in an electrostatic precipitator**  
*T. Mitsui, S. Ito, K. Yasumoto, and A. Zukeran*
- T108N0c8 **Effect of electrode length on collection efficiency for nano-particles emitted from diesel engine with residual fuel oil in an electrostatic precipitator**  
*H. Sawano, K. Yasumoto, and A. Zukeran*
- T108N2de **Effect of vortex finder's geometric dimensions on the performance of Stairmand cyclone**  
*J. Shim, Y.-H. Joe, and H.-S. Park*
- T108N2e1 **Effect of pulsing valves on bag filter cleaning and dust emission**  
*H.-S. Park, J. Shim, and Y.-H. Joe*
- T108N304 **Tests for thermal, chemical and mechanical degradation characteristics of cleanable filter media**  
*J. Weimann, F. Schmidt, A. Hugo, S. Kreckel, and T. Mayer-Gall*

T108N367 **Fly-ash PM emissions and filtration from combustion of different biomass materials and preparations**

*D. Sanz, E. Rojas, J.J. Rodríguez-Maroto, R. Ramos, E. Borjabad, R. Escalada, S. García Alonso, C. Gutiérrez-Canas, G Aragon, I. Mugica, I. Ibarra, I. Celades, and V. Sanfelix*

T108N3e1 **Study on the production and filtration of electret filters**

*C.T. Wang, T.M. Tu, Y.Y. Kao, L.Y. Li, B.L. Hong, S.H. Huang, C.C. Chen, and W.Y. Lin*

**Thursday 31 August 2017**

**15:30 - 16:00**

**Coffee Break and  
Exhibition**

Thursday 31 August 2017

13:45 - 15:30

Poster Area

**POSTER SESSION PART III AND EXHIBITION****FUNDAMENTALS II**

- T503N331 **Effective dielectric permeability of a monolayer of precipitated metal aerosol**  
*V.V. Maksimenko, V.A. Zagaynov, A.S. Smoliyanskiy, and I.E. Agranovski*
- T503N373 **Absorption efficiency of particulate and gaseous aerosol constituents at aqueous surfaces**  
*S. Steiner, P. Diana, E. Dossin, P. Guy, G. Vuillaume, A. Kondylis, S. Majeed, S. Frentzel, and J. Hoeng*
- T505N209 **Random fragmentation of linear chains**  
*L. Isella, A.D. Melas, A.G. Konstandopoulos, and Y. Drossinos*
- T505N339 **A new mechanism of ultrafine particle generation during concrete fracture**  
*L. Morawska, P. Kumar, N. Jabbour, R. Jayaratne, G. Johnson, J. Alroe, E. Uhde, T. Salthammer, L. Cravigan, and E. Faghihi*
- T506N0eb **Electron scattering in water clusters, water droplets, and liquid bulk water**  
*S. Hartweg, B. L. Yoder, D. Luckhaus, and R. Signorell*
- T506N22e **Settling rate of nanosized fractal-like agglomerates by Brownian dynamic simulations accounting for rotational dynamics**  
*A. Spyrogiani, K.S. Karadima, E. Goudeli, V.G. Mavrantzas, S.E. Pratsinis*
- T506N4bf **Liquid-liquid phase separation in several types of secondary organic materials free of inorganic salts**  
*M. Song, P.F. Liu, S.T. Martin, and A.K. Bertram*
- T507N06c **Direct observation of cluster size distributions during nucleation and growth in laval expansions**  
*M. Lippe, S. Chakrabarty, J.J. Ferreiro, and R. Signorell*
- T507N121 **First results from the Antarctic circumnavigation expedition: New particle formation and its chemistry over the sub Antarctic ocean**  
*A. Baccarini, J. Schmale, S. Henning, F. Tummon, M. Hartmann, A. Welti, F. Stratmann, N. Harris, A. Prévôt, M. Gysel, U. Baltensperger, and J. Dommen*
- T507N12f **Determination of the cesium chloride nanodrops surface tension from experiments on the vapor nucleation**  
*S.A. Trubachev, S.V. Valiulin, A.M. Baklanov, V.V. Karasev, A.A. Onischuk, and S.V. Vosel*

Thursday 31 August 2017

15:30 - 16:00

Coffee Break and  
Exhibition

Thursday 31 August 2017

13:45 - 15:30

Poster Area

## POSTER SESSION PART III AND EXHIBITION

## INDOOR AND WORKING PLACE AEROSOLS

- T313N456 **Mineral-oil-spread agar plates do not enhance the efficiency of the viable Andersen cascade impactor for measurement of size distribution of airborne fungi**  
*P. Duquenne, X. Simon, V. Koehler, and C. Coulais*
- T410N072 **Combining NSAM and CPC concentrations to determine airborne nanoparticle count mode diameter: application to a set of six workplace aerosols**  
*S. Bau and O. Witschger*
- T410N0be **Aerosol Particles (0.3-10  $\mu\text{m}$ ) inside a workshop area**  
*A. Maragkidou, O. Jaghbeir, K. Håmeri, and T. Hussein*
- T410N13e **Characteristics of nanoparticle and hazardous air pollutants (HAPs) in three-dimensional (3D) printing center**  
*J. Youn, E. Han, S. Han, Y. Jung, and K.J. Jeon*
- T410N18c **Characteristics of nano-sized wear particles in subway tunnels**  
*Y.I. Lee, K.M. Choi, D.G. Kim, W.D. Kim, S.J. Bae, T.S. Kim, and D.S. Park*
- T410N1f9 **Investigating indoor air quality of a shooting range**  
*S.Y. Aslanoglu, F. Ozturk, and G. Gullu*
- T410N3a0 **Ultrafine particle emissions in the ceramic industry: determinants of release and impact on worker exposure**  
*M. Viana, C. Ribalta, A. Salmatonidis, M.C. Minguillón, X. Querol, A. S. Fonseca, A. López-Lilao, V. Sanfélix, P. Carpio, E. Monfort, C. Estepa, C. Borrell, and G.F. de la Fuente*
- T410N41c **Aerosol particle release at finishing of dental composites**  
*L. Ondrackova, P. Bradna, V. Zdimal, and D. Pelclova*
- T410N4c6 **Unit operations at WEEE plastics recycling line as sources of ultrafine particles and microparticles**  
*E. Hroncová and J. Ladomerský*
- T410N267 **Analysis of incense burning in a temple and its health impacts: A study of Kanpur**  
*A.Goel, O.P. Choudhary, and R. Mundra*
- T411N1ff **Fate of aerosolized nanoparticles: The influence of surface active substances on lung deposition and respiratory effects (NANOaers)**  
*L. Hillemann, D. Göhler, S. Wagener, C. Cascio, J. Tentschert, E. Visileanu, H. Steiner, G. Brenn, B. Suarez, J.D. Brain, and M. Stintz*

- T413N159 **Sampling and analysis of bitumen fumes: comparison of German and French methods**  
*B. Sutter, E. Pelletier, M. Blaskowitz, C. Ravera, C. Stolze, C. Reim, E. Langlois, and D. Breuer*
- T413N185 **Inhaled particle number concentration of subway users in Seoul, Korea**  
*M. Kim, S. Park, H.-G. Namgung, S. Ryu, C. Heo, M. Jung, and S.-B. Kwon*
- T413N3e5 **Application of secondary nanoelectrospray ionization ultrahigh resolution mass spectrometry (nanoSESI-UHRMS) for detecting exhaled particles in real time**  
*X. Li, D.D. Jin, and L. Huang*
- T413N49b **Energy efficiency, comfort and indoor air quality in ClimACT schools**  
*S. M. Almeida, V. Manteigas, J. Lage, M. Almeida-Silva, N. Canha, C. Pina, C. Mafra, and R. Rato*
- T417N080 **Development of cool and clean air motorcycle helmets**  
*A.L. Jian, S.H. Huang, W.C. Lee, Y.M. Kou, and C.C. Chen*
- T417N459 **Investigation of nano-particle exposure by spray coating processes**  
*U. Uhrner, Q. Ye, T. Nöst, O. Tiedje, P.J. Sturm, and J. Laloy*

<b>Thursday 31 August 2017</b>	<b>15:30 - 16:00</b>	<b>Coffee Break and Exhibition</b>
--------------------------------	----------------------	------------------------------------

**Thursday 31 August 2017****13:45 - 15:30****Poster Area****POSTER SESSION PART III AND EXHIBITION****INSTRUMENT CALIBRATION, ACCURACY OR IMPROVEMENT OF EXISTING METHODS**

- T305N131 **How to compare the efficiency of different air disinfection devices**  
*A.S. Safatov, V.G. Akimkin, G.A. Buryak, A.V. Nagolkin, G.V. Shuvalov, D.A. Trubitsin, and V.A. Vechkanov*
- T306N194 **An improved Well Impactor Ninety-Six (WINS) as the PM2.5 sampling inlet**  
*T.C. Le and C.J. Tsai*
- T306N268 **Evaluation of atomic force microscopy measurements of small regular and non-regular particles using Gwyddion software**  
*J. Šperka, M. Havlíček, M. Valtr, D. Nečas, and P. Klapetek*
- T306N2c7 **Measurement of the number concentration of nanoparticles in suspensions using electrospray sources**  
*G. B. Baur, F. Lüönd, and K. Vasilatou*
- T306N370 **Calculation model to simulate the performance of a diffusion size classifier sensor for nanoparticle characterisation**  
*S. Gerken and L. Cachón*
- T315N33c **Development of an isokinetic sampling probe appropriate for high-speed flow conditions**  
*N.G. Heo, J.H. Lim, K.H. Ahn, and S.J. Yook*

**Thursday 31 August 2017****15:30 - 16:00****Coffee Break and  
Exhibition**

Thursday 31 August 2017

13:45 - 15:30

Poster Area

POSTER SESSION PART III AND EXHIBITION

**INSTRUMENTATION FOR CHEMICAL AEROSOL CHARACTERIZATION**

- T211N421 **Characterization of an online Extractive Electrospray Ionization Time of Flight Mass Spectrometer (EESI-TOF): application to atmospheric aerosol**  
*F. D. Lopez-Hilfiker, V. Pospisilova J. Dommen, A. Prévôt, U. Baltensperger, and J. G. Slowik*
- T305N193 **A mass-based calibration technique for the high time resolution XACT 625 X-ray fluorescence monitor**  
*A.H. Tremper, T.-C. Chung, and D.C. Green*
- T305N327 **Quantitative feature extraction for calibration of aerosol FT-IR spectra**  
*S. Takahama, M. Reggente, G. Ruggeri, A. T. Weakley, and A. M. Dillner*
- T310N087 **Bipolar reference spectra of atmospherically relevant single particles by laser ablation aerosol particle time-of-flight mass spectrometry**  
*X. Shen, R. Ramisetty, W. Huang, C. Mohr, and H. Saathoff*
- T310N0c3 **Time-resolved characterization of organic nitrogen in particulate matter: An investigation into Beijing's air quality**  
*S.J. Swift, W. Dixon, R.E. Dunmore, N.J. Farren, F. Squires, K.L. Pereira, J.D. Lee, and J.F. Hamilton*
- T310N2ab **Chemical image-based determination of particle size and chemical composition – Towards image-based particle quantification**  
*J. Ofner, E. Eitenberger, G. Friedbacher, H. Lohninger, B. Lendl, and A. Kasper-Giebl*
- T310N206 **Novel FTIR online method for e-cigarette aerosol characterization**  
*F. Radtke, R. Monni, A. Susz, A. Stoop, J. Verbeeck, and S. Maeder*
- T310N2c4 **Development of a mobile observation platform for air quality monitoring**  
*X.G. Chi, Z. Xu, L.F. Zheng, C.J. Zhu, and A.J. Ding*
- T310N2f6 **An Aerosol-icpTOF: direct measurement of trace multi-elements for ambient aerosol**  
*H. Hagino, M. Tanner, O. Borovinskaya, H. Hikita, A. Shimono, and Y. Mizuno*
- T310N37b **Can chemical biomarkers help discriminating environmental microbial species?**  
*S. García-Alcega, S. Tyrrel, and F. Coulon*
- T310N3b7 **Highly selective formaldehyde detection with microporous membranes for indoor air quality monitoring**  
*A.T. Güntner, S. Abegg, K. Wegner, and S.E. Pratsinis*
- T310N43d **A novel field reversal - surface ionization detector for characterization of biomass burning and sea salt aerosols**  
*D. Gall, C. Nejman, and J.B.C. Pettersson*

- T310N4e6 **Development of a detection method to determine alcohols and carboxylic acids in aerosol particles using in-situ silylation and aerosol mass spectrometry**  
*M. Weloe, S. Morat, and T. Hoffmann*
- T315N031 **Sampling artefacts from biomass burning aerosol collected at three sites in Indochina**  
*C.-T. Lee, C.C.-K. Chou, S.-E. Sun, Z.-T. Chuang, and N.-H. Lin*
- T315N35b **Atmospheric cluster analysis by tandem DMA-MS**  
*M. Passananti, J. Kangasluoma, M. Attoui, and H. Vehkamäki*

**Thursday 31 August 2017**

**15:30 - 16:00**

**Coffee Break and  
Exhibition**

Thursday 31 August 2017

13:45 - 15:30

Poster Area

**POSTER SESSION PART III AND EXHIBITIONS****MARINE AEROSOLS****T212N01b Overview of aerosol and trace gases measurements during the Antarctic Circumnavigation Expeditions 2016 - 2017**

*J. Schmale, S. Henning, A. Baccharini, F. Tummon, M. Hartman, A. Welti, J. Dommen, F. Stratmann, C. Bolas, N. Harris, D. Rosenfeld, K. Carslaw, M. Schnaiter, A. Prévôt, U. Baltensperger, and M. Gysel*

**T212N0a7 Wind dependence of sea-salt and non-sea-salt components in ambient aerosol in Niigata Plain during winter seasons**

*S. Ohara, N. Kihara, and N. Murao*

**T212N180 Investigation of aerosol optical and microphysical characteristics in the atmosphere of Kara and Barents Seas in summer and autumn of 2016**

*S.A. Terpugova, P.N. Zenkova, M.V. Panchenko, V.V. Polkin, D.G. Chernov, D.M. Kabanov, V.S. Kozlov, V.P. Shmargunov, S.M. Sakerin, A.P. Lisitzin, V.P. Shevchenko, and N.V. Politova*

**T212N398 Characteristics of high aerosol concentration cases measured at vessel Gisang 1 over Yellow Sea during KORUS-AQ campaign**

*J.W. Cha, S.-B. Ryoo, B. Shin, H.C. Lee, H.-J. Ko, Y.K. Lim, and S.S. Lee*

**T212N39d Latitudinal distribution of particulate MSA and MSA:nssSO<sub>4</sub> over the Atlantic using a validated quantification method with HR-ToF-AMS**

*S. Huang, L. Poulain, D. van Pinxteren, M. van Pinxteren, Z.J. Wu, H. Herrmann, and A. Wiedensohler*

Thursday 31 August 2017

15:30 - 16:00

Coffee Break and  
Exhibition

<b>Thursday 31 August 2017</b>	<b>13:45 - 15:30</b>	<b>Poster Area</b>
<b>POSTER SESSION PART III AND EXHIBITION</b>		

<b>MINERAL DUST</b>
---------------------

- T207N3dd **The simulation of the dust emission rate from Jhuoshuei River**  
*C.T. Wang, T.H. Chiu, Y.Y. Kao, Y.H. Tseng, S.J. Chen, K.H. Chang, and W.Y. Lin*
- T213N018 **Relevance of wildfires on dust emissions via interaction with near-surface wind pattern**  
*R. Wagner, M. Jähn, and K. Schepanski*
- T213N077 **Road dust of Venice (Italy) international airport: characterization and risk assessment**  
*G. Valotto, D. Zannoni, G. Rampazzo, F. Visin, G. Formenton, A. Gasparello, D. Bassano, and S. Sollecito*
- T213N0d0 **The 40K used as tracer of Saharan dust contributions**  
*C. Dueñas, E. Gordo, E. Liger, M. Cabello, S. Cañete, and M. Pérez*
- T213N196 **New approach in airborne asbestos fibres identification, monitoring and source apportionment**  
*P. Pokorná, M. Klán, D. Havlíček, J. Plocek, M. Racek, and J. Hovorka*
- T213N290 **Estimation and dispersion modelling of particulate matter (PM10) emissions from the ceramics industry**  
*J.B. Sousa, A.J. Rossini, and S.A. Pozza*
- T213N2ad **Physico-chemical transformation of Saharan dust particles by the city of Vienna – A combined chemical imaging approach**  
*J. Ofner, E. Eitenberger, G. Friedbacher, G. Schauer, M. Greiling, H. Lohninger, B. Lendl, and A. Kasper-Giebl*
- T213N32a **Anomalous Si/Al ratios in PM10 and PM2.5 road dust at several locations in India**  
*S. Samiksha and R.S. Raman*

<b>Thursday 31 August 2017</b>	<b>15:30 - 16:00</b>	<b>Coffee Break and Exhibition</b>
--------------------------------	----------------------	------------------------------------

**Thursday 31 August 2017****13:45 - 15:30****Poster Area****POSTER SESSION PART III AND EXHIBITION****MINIATURIZED INSTRUMENTATION AND LOW COST SENSORS**

**T304N14e Optofluidic surface-enhanced raman spectroscopy (SERS) platform for airborne bacteria particles**

*J.H. Jung*

**T304N2ec PoCAMon – “All in one“ personal online continuous air monitor , gamma dose meter and gas warner**

*T. Streil and V. Oeser*

**T304N37a A new PAHs and BC monitor for automatic routine monitoring of urban ambient aerosol**

*C. Carbone, E. Cozzani, S. Zampolli, M.G. Pietrogrande, A. Poggi, S. Fuzzi, and S. Decesari*

**T304N44a Miniaturized aerosol instruments for unmanned aerial vehicles**

*F.J. Brechtel, M. Ramstrom, A.B. Corless, and T.S. Bates*

**T304N487 A low-cost optical instrument for estimating the contribution of waste-to-energy plants to the local PM2.5**

*M. Del Guasta*

**Thursday 31 August 2017****15:30 - 16:00****Coffee Break and  
Exhibition**

Thursday 31 August 2017

13:45 - 15:30

Poster Area

POSTER SESSION PART III AND EXHIBITION

**MOLECULAR CHARACTERISATION AND IDENTIFICATION OF AEROSOL CONSTITUENTS AND MARKERS**

**T211N221 Characterization of gas phase emissions from residential coal combustion using proton transfer reaction time-of-flight mass spectrometry**

*F. Klein, S.M. Pieber, A. Bertrand, H. Li, G. Stefenelli, B. Temime-Roussel, N. Marchand, I. El-Haddad, J.G. Slowik, U. Baltensperger, R. Huang, and A.S.H. Prévôt*

**T216N1e5 Iron speciation of natural and anthropogenic atmospheric aerosols by X-ray absorption spectroscopy and selective leaching experiments**

*C. Petroselli, B. Moroni, S. Crocchianti, R. Selvaggi, F. Soggia, M. Grotti, F. d'Acapito, and D. Cappelletti*

**T216N20e Probing the chemical composition of fine ambient aerosol, rainwater and hailstone with UHPLC-MS technique. Is there anything in common?**

*P. Wach, G. Spólnik, K.J. Rudziński, W. Danikiewicz, K. Skotak, and R. Szmigielski*

**T216N280 Improving LC-MS methods for a detailed SOA characterization**

*G. Spolnik, P. Wach, K. Rudzinski, K. Nestorowicz, K. Skotak, W. Danikiewicz, and R. Szmigielski*

**T216N29c Organic markers and compounds in PM1 aerosol in urban and rural area in winter 2017**

*K. Křůmal, P. Mikuška, and Z. Večeřa*

**T216N2b7 Quantification of aliphatic amines in the aerosol particulate matter**

*A. Tinti, L. Corbella, P. Fermo, C. Colombi, E. Cuccia, V. Gianelle, S. Takahama, and S. Gilardoni*

**T216N2d0 Synthesis and high resolution mass spectrometry characterisation of peroxydic acids as a potential SOA markers**

*S.S. Steimer, D. Pitton, T. Hoffmann, and M. Kalberer*

**T216N41f Molecular characterization of nanoparticles using extractive electrospray ionisation time-of-flight mass spectrometry**

*V. Pospisilova, F. D. Lopez-Hilfiker, M. Xiao, O. Garmash, A. Baccharini, C. R. Hoyle, A.S.H. Prévôt, U. Baltensperger, J. G. Slowik, and the CLOUD collaboration*

**T216N4ba Submicron organic nitrate particles in a subtropical forest**

*Chr.M. Salvador, C.C.-K. Chou, H.-C. Cheung, T.-T. Ho, and C.-Y. Tsai*

Thursday 31 August 2017

15:30 - 16:00

Coffee Break and Exhibition

**Thursday 31 August 2017****13:45 - 15:30****Poster Area****POSTER SESSION PART III AND EXHIBITION****MULTIPHASE CHEMISTRY**

- T211N470 **Carboxylic acid oxidation products from limonene ozonolysis and their role in SOA formation**  
*J. Hammes, C. Faxon, A. Lutz, R. Kant Pathak, T. Mentel, and M. Hallquist*
- T211N476 **High-Nox photooxidation of n-dodecane: Influence of temperature and relative humidity on secondary organic aerosol formation**  
*A. Gratien, H. Lamkaddam, E. Pangui, M. Cazaunau, M. David, J.-M. Polienor, M. Jerome, C. Gaimoz, B. Picquet-Varault, and J.-F. Doussin*
- T217N10a **Feedbacks between microphysics and photochemical aging in viscous aerosol**  
*J. Dou, P. Corral Arroyo, P.A. Alpert, M. Ammann, T. Peter, and U.K. Krieger*
- T217N1fe **Studies of enhanced chemical reaction rates and photochemical reactions in dry aerosol droplets**  
*A. Marsh and J.P. Reid*
- T217N233 **Heterogeneous reactivity of pesticide-coated silica particles with OH radicals: influence of the humidity and the nature of particles**  
*C. Mattei, J. Socorro, E. Quivet, N. Marchand, and H. Wortham*
- T217N270 **Effects of particle phase water on the heterogeneous OH oxidation of aqueous organic droplets**  
*M.M. Chim, C.Y. Chow, J.F. Davies, M.N. Chan*
- T217N3f8 **Condensed phase diffusivity measurements of volatile organics in levitated viscous aerosol particles**  
*S. Bastelberger, U. Krieger, B. Luo, and T. Peter*

**Thursday 31 August 2017****15:30 - 16:00****Coffee Break and  
Exhibition**

Thursday 31 August 2017

13:45 - 15:30

Poster Area

POSTER SESSION PART III AND EXHIBITION

**NANOPARTICLE COATING AND FUNCTIONALIZATION**

- T101N30c **Multilayered omniphobic coating on stainless steel based on aerosol nanoparticle synthesis**  
*M. Sorvali, J. Haapanen, L. Vuori, M. Pudas, M. Valden, and J.M. Mäkelä*
- T101N35a **Antibacterial nanocoatings by liquid flame spray**  
*J. Haapanen, P. Juuti, M. Gunell, K. Brobbey, E. Eerola, J.J. Saarinen, M. Toivakka, P. Huovinen, and J.M. Mäkelä*
- T101N41a **Highly active Au clusters on ceria for water-gas shift reaction**  
*N.A. Wahab, K. Fujiwara, and S.E. Pratsinis*
- T102N21f **Passivation and magnetic properties of core-shell aerosol Fe(Cr,Mn) alloy nanoparticles**  
*C. Preger, L. Ludvigsson, B.O. Mueller, R. Westerström, and M.E. Messing*
- T102N224 **Gas-phase synthesis of inline coated silicon nanoparticles in a microwave plasma reactor**  
*A. Münzer, J. Sellmann, A. Kempf, C. Schulz, and H. Wiggers*
- T102N412 **Study on removal of bacteria and particles by nylon 6 nanofibers with electrospinning different salts components**  
*M.-H. Lin and C.-T. Chang*
- T103N057 **Ag/Au-doped graphene sheets and carbon nanoflowers for thin film applications**  
*A. Meščeriakovas, J. Jokiniemi, and A. Lähde*
- T103N1a9 **Aerosol based fabrication of polymer-coated semiconductor nanoparticles**  
*M. Shaban, J. Poostforooshan, and A.P. Weber*
- T103N3e7 **A new furnace with molten polymer and a condenser for coating of magnetic moment markers**  
*L. Boskovic and I.E. Agranovski*

Thursday 31 August 2017

15:30 - 16:00

Coffee Break and  
Exhibition

Thursday 31 August 2017

13:45 - 15:30

Poster Area

**POSTER SESSION PART III AND EXHIBITION****NANOPARTICLES: ELECTRICAL DISCHARGES AND MODELING**

- T101N2a4 **Evolution of Au nanoparticle XRD by molecular dynamics**  
*E. Goudeli and S.E. Pratsinis*
- T102N432 **Applying spark mixing to produce Au-Pd alloy nanoparticle catalysts for CO<sub>2</sub> electro-reduction**  
*M. Valenti, W. A. Smith, and A. Schmidt-Ott*
- T104N11d **Investigation of the early stages of growth of zirconia nanostructures produced by supersonic cluster beam deposition: from the sub-monolayer to the thin film regime**  
*F. Borghi, C. Piazzoni, P. Milani, and A. Podesta*
- T104N124 **Atomistic Monte Carlo simulation of the fractal dimensions of nanoparticle agglomerates**  
*E.N. Skountzos, V.G. Mavrantzas, and S.E. Pratsinis*
- T104N254 **NanoDome software platform for multi-scale modelling of gas-phase nanoparticle synthesis**  
*F. Strappaveccia, F. Galleni, P. Wollny, and E. Ghedini*
- T104N293 **Modelling of transport processes of biological aerosol impurity in a ground boundary layer of industrial centers**  
*L.G. Voskressensky, S.L. Rychkov, V.V. Sablin, and A.V. Shatrov*
- T104N388 **Sensitivity analysis of a model characterizing nanoparticle agglomeration, dispersion and deposition processes in the atmosphere**  
*M. Poikkimäki, P. Juuti, J. Kalliokoski, and M. Dal Maso*

Thursday 31 August 2017

15:30 - 16:00

**Coffee Break and  
Exhibition**

Thursday 31 August 2017

13:45 - 15:30

Poster Area

**POSTER SESSION PART III AND EXHIBITION****PROPERTIES AND DYNAMICS OF ATMOSPHERIC AEROSOLS II**

- T205N22b **The effect of relative humidity and chemical composition on the evaporation of secondary organic aerosol particles**  
*A. Buchholz, C. Mohr, A. Lambe, C. Faiola, E. Kari, S.A. Nizkorodov, A. Pajunoja, O.-P. Tikkanen, A. Ylisirniö, D. Worsnop, T. Yli-Juuti, and A. Virtanen*
- T205N3f6 **Particle number and elemental concentrations at Mount Kenya Global Atmospheric Watch Station in Kenya**  
*S.M. Gaita, E.S. Thomson, J.B.C. Pettersson, J. Boman, M.J. Gatari, and A. Andersson*
- T205N40b **Seasonal variability of submicronic aerosols in Romania**  
*C. Marin, L. Marmureanu, and J. Vasilescu*
- T205N40d **Environmental molecular beam studies of water interactions with condensed nopinone surface**  
*S.M. Johansson, X. Kong, E.S. Thomson, and J.B.C. Pettersson*
- T205N414 **Hygroscopicity of dimethylamine-sulfuric acid nanoparticles**  
*O.-P. Tikkanen, O. Väisänen, H. Wang, E. Holopainen, L. Hao, A. Buchholz, A. Pajunoja, A. Virtanen, and T. Yli-Juuti*
- T205N43b **Could the diesel thermal power generators be a sulfate source of fine aerosol particles in the Central Amazonian basin (ATTO)?**  
*S. Carbone, F. Coelho, D. Moran, J. Saturno, B. Holanda, C. Pöhlker, W. Qiaoqiao, M.O. Andreae, A. Medeiros, R.A.F. de Souza, S. Martin, J. Brito, L. Rizzo, P. Schlag, J.H. Barbosa, and P. Artaxo*
- T205N445 **Characterisation of propane-based CAST soot samples by combined vibrational spectroscopic and mass spectrometric studies**  
*J. A. Noble, L. Ngo, A. R. Ikhenazene, C. Irimiea, G. Lefevre, M. Vojkovic, D. Duca, S. Kenny, C. Pirim, Y. Carpentier, B. Chazallon, N. Nuns, J. Yon, E. Therssen, and C. Focsa*
- T205N452 **Characterization of the aging process of smoke observed over Austria using organic carbon mixing ratio**  
*C. Talianu*
- T205N47b **Stable carbon and nitrogen isotopic composition in fine aerosol at a Central European background station**  
*P. Vodička, K. Kawamura, B. Kunwar, and J. Schwarz*
- T207N32c **Investigating the nature and sources of non-water soluble sulfate sulfur in fine particles over a National Park in Central India**  
*S. Kumar, D. Shah, and R. Sunder Raman*

Thursday 31 August 2017

15:30 - 16:00

Coffee Break and  
Exhibition

Thursday 31 August 2017

13:45 - 15:30

Poster Area

**POSTER SESSION PART III AND EXHIBITION****REMOTE SENSING OF AEROSOL PROPERTIES**

- T206N0af **Tropospheric aerosol layers: homogeneity in vertical distribution of optical and microphysical characteristics**  
*S.V. Samoilova, I.E. Penner, G.P. Kokhanenko, and Yu.S. Balin*
- T206N0ec **Remote sensing of atmospheric aerosol components based on sun-sky radiometer measurements**  
*Y.S. Xie, Z.Q. Li, Y. Zhang, and D.H. Lior*
- T206N238 **Analysis of aerosol optical and microphysical properties and radiative forcing estimates based on AERONET measurements at two sites of the Iberian Peninsula**  
*A.J. Fernández, F. Molero, M.A. Revuelta, P. Salvador, M. Becerril-Valle, E. Alonso-Blanco, M. Barreiro, E. Coz, E. Díaz, F.J. Gómez-Moreno, L. Núñez, M. Palacios, B. Artinano and M. Pujadas*
- T206N286 **Ground-level PM<sub>2.5</sub> prediction using 3 km MODIS AOD over Tehran megacity**  
*S. Sotoudeheian, M. Arhami, and F. Azarmi*
- T206N2c5 **Planetary boundary layer height influence on ground base aerosol concentrations**  
*L. Marmureanu, J. Vasilescu, S. Andrei, F. Toanca, A. Dandocsi, and C. Marin*
- T206N3b4 **Comparison of commercial lidars and ceilometers with advanced Raman lidars in the frame of INTERACT-II ACTRIS campaign**  
*M. Rosoldi, F. Madonna, G. Pappalardo, J. Vande Hey, Y. Zheng, and VAISALA Team*
- T206N47e **Mathematical simulation of brightness fields of reflected solar radiation: Influence of 3D cloud effects**  
*T.B. Zhuravleva, I.M. Nasrtdinov, T.V. Russkova, A.V. Artyushina, and A.N. Duchko*
- T206N48b **Technique for remote sensing of droplets of sulfuric acid in the stratosphere**  
*W. Sun, G. Videen, Y. Hu, and R.R. Baize*

Thursday 31 August 2017

15:30 - 16:00

**Coffee Break and  
Exhibition**

**Thursday 31 August 2017****13:45 - 15:30****Poster Area****POSTER SESSION PART III AND EXHIBITION****SPECIAL SESSION #3: ELECTRONIC CIGARETTES - SCIENTIFIC EVIDENCE****SPS3N067 E-cigarettes and in vitro pulmonary health effects***M. Delaval, D. Egli, H. Burtscher, and M. Geiser***SPS3N2b6 The properties of aerosols released from electronic cigarettes (ECs) at different formation conditions***M. Odziomek, Ł. Kwiatkowski, and T.R. Sosnowski***SPS3N300 Novel nicotine aerosol delivery devices - the impact of a tobacco heating product and e-cigarettes on indoor air quality***M. Forster, J. Margham, C.U. Yurteri, C. Liu, J. Murphy, Chr. Proctor, and J. McAughey***SPS3N36f The continuous characterisation of aerosol droplets in simulated inhalation conditions***J.S. Walker, J.M. Clark, and P.D. Smith***SPS3N47a Novel aerosol exposure devices for in-vitro testing of e-cigarettes at the air/liquid interface***T. Krebs***Thursday 31 August 2017****15:30 - 16:00****Coffee Break and  
Exhibition**

Thursday 31 August 2017

13:45 - 15:30

Poster Area

POSTER SESSION PART III AND EXHIBITION

**SYNTHESIS AND STRUCTURING OF FUNCTIONAL NANOPARTICLES**

- T101N011 **Flame-made Si-doped MoO<sub>3</sub> for selective breath NH<sub>3</sub> sensing to detect kidney failure**  
*A.T. Guentner, M. Righettoni, S.E. Pratsinis*
- T101N012 **Easy cholesterol monitoring from breath by isoprene-selective and flame-made Ti-doped ZnO nanoparticles**  
*A.T. Guentner, N.J. Pineau, D. Chie, F. Krumeich, and S.E. Pratsinis*
- T101N040 **Deep tissue imaging with highly fluorescent NIR nanocrystals after systematic host screening**  
*F.H.L. Starsich, P.M. Gschwend, A. Sergeyev, R. Grange, and S.E. Pratsinis*
- T101N058 **Synthesis and characterization of perovskite nanoparticles for oxygen evolution catalysis**  
*B. Alkan, H. Wiggers, M. Muhler, W. Schuhmann, and C. Schulz*
- T101N059 **Nanothermometry by fluorescent Nd<sup>3+</sup>-doped nanocrystals**  
*P.M. Gschwend and S.E. Pratsinis*
- T101N167 **Single-step fabrication of nanocatalyst microarrays by coupling flame spray pyrolysis with supersonic expansion**  
*S. Vinati, E. Barborini, K. Wegner, and P. Milani*
- T101N1d3 **Spray-flame synthesis of nanoscale LaCoO<sub>3</sub> perovskite catalyst**  
*S. Angel, H. Wiggers, and C. Schulz*
- T101N23f **Flame enthalpy influences silanol content and cytolytic activity of silicas made by flame spray pyrolysis**  
*A. Spyrogianni, I.K. Herrmann, S.E. Pratsinis, and K. Wegner*
- T101N269 **Control of particle morphology and size distribution by relative humidity**  
*G.A. Kelesidis, F. Furrer, E. Goudeli, M.L. Eggersdorfer, K. Wegner, and S.E. Pratsinis*
- T101N28b **Synthesis of pure and doped ceria nanomaterials on the pilot plant scale**  
*S. Schnurre, M. Spree, B. Hellack, and T. Hülser*
- T101N2ca **Quantifying isolated Pd site in FSP-made Pd/TiO<sub>2</sub> for photocatalytic NO removal**  
*K. Fujiwara and S.E. Pratsinis*
- T101N2cd **Highly active atomically dispersed Pt on CeO<sub>2</sub> for reverse water-gas shift reaction**  
*K. Fujiwara and S.E. Pratsinis*

- T101N3cf **Porous SnO<sub>2</sub> nanospheres with three-dimensionally interconnected trimodal pores for ultrasensitive detection of ethanol**  
*J.-W. Yoon, S. H. Choi, J.-S. Kim, H. W. Jang, Y. C. Kang, and J.-H. Lee*
- T102N0ce **Polyacrylonitrile microfiber modified with sodium hydroxide and glycol and its adsorption behavior for Cu(II) removal**  
*L.-Y. Liu, A. Yu, and C.-T. Chang*
- T103N0b1 **Diethylenetriamine modified magnetic biochar on removal of Cr(VI) from aqueous solution**  
*F. Wang, T. Ouyang, and C.T. Chang*
- T103N0b2 **Chromium adsorption from wastewater by modifying carbon material**  
*S.-Y. Lee and Ch.-T. Chang*
- T103N100 **CCN-activation of soot particles after long term exposure to atmospherically relevant ozone concentrations**  
*F. Friebel, P. Lobo, S. Drossaart van Dusseldorp, E. Mülhofer, and A.A. Mensah*
- T103N176 **Synthesis of Ag/ZnO particles by aerosol techniques for enhanced visible light photocatalysis**  
*X. He and J. Wang*
- T105N2e7 **Catalytic reaction of reproducible oxide-free copper nanoparticles with gaseous oxides**  
*H. Tanaka, M. Miyagawa, and J. Hirokawa*
- T105N365 **Synthesis and evaluation of doped LiNi<sub>0.5</sub>Mn<sub>1.5</sub>O<sub>4</sub> particles by aerosol spray pyrolysis for next -generation Li-ion cathode materials**  
*G. A. Ganas, G. Kastrinaki, D. Zarvalis, A.G. Konstandopoulos, D. Versaci, N. Penazzi, S. Bodoardo, M. Bengoechea, and I. de Meaza*

Thursday 31 August 2017

15:30 - 16:00

Coffee Break and  
Exhibition

Thursday 31 August 2017

13:45 - 15:30

Poster Area

**POSTER SESSION PART III AND EXHIBITION****LATE POSTERS**

- T207N1bf **Using unmanned air vehicle to verify the air quality space distribution simulation at Toucheng Interchange near national road No.5**  
*S. Yu, R.C. Jhuang, and C.T. Chang*
- T308N1d8 **Electrochemical oxidation of RBk5 with using graphene/TiO<sub>2</sub> composite electrode**  
*J.Y. Li, J.M. Hong, and C.T. Chang*
- T410N501 **Real-time number size distributions of particles released from stick incense burning**  
*Y.I. Tsai, N. Chantrawichaikun, and S.-C. Kuo*
- T410N502 **Chemical characterization of fine particulate matter emitted from incense stick burning**  
*S.-C. Kuo, Y.I. Tsai, and N. Chantrawichaikun*
- T120N4f8 **Comparison of emission factors of air pollutants from CNG and gasoline vehicles**  
*Y. Wang, X. Huang, Z. Xing, and K. Du*
- T302N50d **Towards accurate determination of aerosol transport parameters in microgravity**  
*A. Vedernikov, D. Balapanov, and S. Beresnev*
- T204N50c **Study of the effect of sampling artefacts in multi-lambda measurements of the absorption coefficient of atmospheric aerosol**  
*R.E. Pileci, V. Bernardoni, G. Valli, and R. Vecchi*
- T209N4fe **Measurement of the volatility distribution of emission factor from biomass burning**  
*Y. Fujitani, K. Sato, A. Fushimi, K. Tanabe, Y. Kondo, Y. Morino, S. Kobayashi, and A. Takami*
- T205N4f4 **Composition, sources apportionment and risk assessment of particulate organic matter at industrial, urban and forest areas of Northern Algeria**  
*S. Khedidji, C. Balducci, A. Cecinato, M. Perilli, and N. Yassaa*
- T215N50a **Influence of intense secondary aerosol formation and long range transport on aerosol chemistry and properties in the Seoul Metropolitan Area during spring time: Results from KORUS-AQ**  
*H. Kim and Q. Zhang*
- T102N510 **Synthesis of GaAs quantum dots via hydrogen-assisted spark discharge**  
*K. Lee, D. Lee, and M. Choi*

- T214N523 **Determination of elemental composition of particulates in Antalya urban atmosphere**  
*A.M. Tepe, A. Zararsiz, and G. Doğan*
- T502N51f **Experimental study on effect of external disturbance on a carbon fiber particle**  
*J. Lin and L. Jiang*
- T406N517 **On lung anti-oxidant depletion as a measure of oxidative potential for ambient fine particles: predictive indicator of cellular stress**  
*B. Crobeddu, J. Sciare, J. Deweirdt, I. Baudrimont, and A. Baeza-Squiban*
- T403N518 **Brake wear (nano)particles: physico-chemical characterization and effects on airway epithelial cells**  
*C. Puisney, E. Oikonomou, S. Nowak, A. Chevillot-Biraud, JF. Berret, and A. Baeza-Squiban*
- T201N515 **Effect of sea ice on aerosols in Eastern Lapland, Finland**  
*E.-M. Duplissy, R. Väänänen, S. Hakala, T. Petäjä, V.-M. Kerminen, and M. Kulmala*
- T214N535 **Seasonal characteristics of fine and coarse mode aerosol particles over an urban region**  
*A. S. Pipal, T. A. Rajesh, and S. Ramachandran*
- T406N52a **In-vitro cytotoxicity of nanoparticles and condensable compounds from biomass combustion determined by a simple sampling method**  
*P. Zotter, S. Richard, M. Egli, and T. Nussbaumer*
- T406N528 **Comparison of the pro-inflammatory effects of size-segregated particles sampled in different sites in Africa (Abidjan in Cote D'Ivoire and Cotonou in Benin)**  
*M. Tran, J. Adon, C. Liousse, A. Baeza-Squiban, V. Yoboué, A. Akpo, C. Galy-Loeaux, C. Chiron, E. Gardrat, and J.F. Léon*
- T205N53f **Characteristics and formation of typical winter haze in Handan, one of the most polluted cities in China**  
*S. Yang, F. Duan, and K. B. He*
- T205N542 **Typical winter haze pollution in Zibo, an industrial city in China: Characteristics, secondary formation, and regional contribution**  
*H. Li, F. Duan, and K. He*
- T306N549 **Accuracy and reproducibility of fast mobility size spectrometers over 10 years**  
*J.P.R. Symonds and M. Irwin*
- T214N54c **Urban air quality monitoring in relation with <sup>222</sup>Radon at the surface level**  
*M. Zoran, R. Savastrun, and D. Savastru*
- T120N551 **Investigation of the organics nanodrop influence on the explosion hazard of the methaneair**  
*S.V. Valiulin, V.V. Zamaschikov, A.A Onischuk, and A.M. Baklanov*

- T216N553 **Molecular characterization of organosulfates in organic aerosol from European and Chinese cities by ultrahigh resolution mass spectrometry**  
*K. Wang, R. Huang, C. Kampf, Y. Cheng, U. Pöschl, and T. Hoffmann*
- T403N555 **Pro-inflammatory effects of PM<sub>2.6</sub> from Beijing winter haze: Revealing the role of individual external and internal microbiome**  
*F. Shen, F. Liu, X. Zhang, J. Li, K. Ziegler, T. Zhang, T. Zhu, M. Shiraiwa, M. Yao, H. Tong, K. Lucas, and U. Pöschl,*
- T208N55b **Sticking of particulate matter on airborne pollen**  
*A. Ivanovsky, N. Visez, A. Roose, and M. Choël*
- SPS2N55e **Viscosity model for mixtures of propylene glycol, glycerol, water, and nicotine**  
*A.P. Spann, M.J. Hancock, R.S. Sundar, M. Rusyniak, R.W. Lau, Y.B. Pithawalla, and A.A. Rostmii*
- T508N562 **Absorption coefficient spectral behavior of laser-heated carbonaceous nanoparticles**  
*F. Migliorini, S. De Iuliis, R. Dondè, and G. Zizak*
- T311N567 **Characterization of brake wear particle emitted from passenger car brake system**  
*H. Hagino*
- T310N56a **ACMCC (Aerosol Chemical Monitor Calibration Center): Results from the 2016 ACTRIS**  
*E. Freney, O. Favez, V. Gros, J. Sciare, T. Amedeo, F. Trong, J. Jayne, P. Croteau, L. Williams, S. Canagaratna, A.S. Lambe, M. Cubison, and all intercomparison participants*
- T302N56d **Use of the Aerodynamic Aerosol Classifier (AAC) for evaluation of aerosol microphysical and optical properties**  
*J.D. Allan, D. Liu, M.R. Alfarra, and P.I. Williams*
- SPS6N572 **Aircraft black carbon particle number emissions - A new predictive method and uncertainty analysis**  
*R. Teoh, M.E.J. Stettler, A. Majumdar, and U. Schumann*
- T101N573 **Single-step aerosol synthesis of ratiometric hydrogen peroxide biosensors**  
*D.F. Henning and G.A. Sotiriou*
- T215N576 **The relationship between black carbon and lung deposited surface area in different urban environments in London**  
*E. Abdollahei, T. Zhu, and M. Stettler*
- T120N577 **A study on the reduction of fine particulate contaminants in textile manufacturing process**  
*B.H. Park, J.Y. Lee, H.G. Kim, and J.S. Choi*
- T406N578 **Effects of short term exposure to particulate matter on cognitive performance**  
*M.A. Shehab and F.D. Pope*

- T313N57a **Multivariate study for examining influence of physical and operational properties of urban railway system on subway air quality**  
*M.J. Kim, J.W. Park, J.S. Sim, D.S. Moon, and D.S. Park*
- T209N57b **The effects of biomass burning on fine aerosol acidity, liquid water content and nitrogen partitioning**  
*A. Bougiatioti, D. Paraskevopoulou, I. Stavroulas, R. Weber, A. Nenes, M. Kanakidou, and N. Mihalopoulo*
- T203N57c **Airborne observations of high altitude sub-10 nm aerosol particle layers**  
*J. Lampilahti, K. Leino, R. Väänänen, A. Manninen, S. Buenrostro Mazon, H.E. Manninen, T. Petäjä, and M. Kulmala*
- T117N57d **Investigation of nano particles during additive manufacturing processes**  
*St. Blei and R. Heidenreich*
- T205N57e **Local vitrification of water in secondary organic aerosol**  
*M.Lbadaoui-Darva, S. Takahama, and M.N.D.S. Cordeiro*
- T210N57f **Ecotoxicity of humic-like substances**  
*G. Kiss, M. Gángó, E. Horváth, K. Imre, and N. Kováts*
- T502N580 **AeroSolved: Eulerian computational platform for polydisperse aerosol transport, evolution and deposition**  
*E.M.A. Frederix, F. Lucci, M. Nordlund, B.J. Geruts, and A.K. Kuczaj*
- SPS3N587 **Solid particle investigations in the mainstream of 3R4F reference cigarettes, and the Tobacco Heating System THS2.2 and commercial cigarettes**  
*P. Pratte, St. Cosandey, and C. Ginglinger*
- T401N589 **Aerosol-assisted synthesis of large-pore mesoporous silica nanoparticles as drug carriers for controlled release**  
*M. Shaba, J. Poostforooshan, S. Reiser, M. Türk, and A.P. Weber*
- T214N58c **Association between surface temperature inversion and high PM<sub>2.5</sub> measured with an unmanned aerial vehicle**  
*E. Gramsch, C. Ayala, and A. Arellano*

Thursday 31 August 2017	15:30 - 16:00	Coffee Break and Exhibition
-------------------------	---------------	-----------------------------

Thursday 31 August 2017

16:00 - 18:00

Room 04G30

**PROPERTIES AND DYNAMICS OF ATMOSPHERIC AEROSOLS****Chairs: Sebastian Schmitt and Stefania Gilardoni**

- 16:00** T205N171 **Imaging molecular diffusion and iron oxidation reaction in organic aerosol particles**  
*P.A. Alpert, P. Corral Arroyo, M. Ammann, J. Dou, U. Krieger, S.S. Steimer, J.-D. Förster, F. Ditas, C. Pöhlker, S. Rossignol, M. Passananti, C. George, B. Wang, S. Zhang, S. China, and A. Laskin*
- 16:20** T205N118 **Molecular dynamics simulation of the local structure and morphology of atmospheric nanoparticles**  
*K.S. Karadima, V.G. Mavrantzas, and S.N. Pandis*
- 16:40** T205N0b9 **Dynamics of single submicron aerosol particles measured by UV broadband light scattering and Raman spectroscopy**  
*G. David, K. Esat, and R. Signorell*
- 17:00** T214N214 **Characterization of PM<sub>2.5</sub> sources at Central European urban background site**  
*K. Juda-Rezler, M. Reizer, J.A.G. Orza, K. Maciejewska, K. Klejnowski, and B. Blaszcak*
- 17:20** T214N15b **Understanding of the chemical processes involving nitro- and oxy-PAHs in ambient air and evaluation of SOA PAH contribution on PM via annual and intensive field campaigns**  
*A. Albinet, S. Tomaz, D. Srivastava, G.M. Lanzafame, O. Favez, J.-L. Jaffrezo, N. Bonnaire, V. Gros, L.Y. Alleman, F. Lucarelli, E. Perraudin, and E. Villenave*
- 17:40** T207N25e **Network analysis of PM<sub>2.5</sub> monitoring data and model output for Alberta using KZ filtering and hierarchical clustering**  
*J. Soares, P.A. Makar, A. Akingunola, and Y. Aklilu*
- Back-up Paper** T205N445 **Characterisation of propane-based CAST soot samples by combined vibrational spectroscopic and mass spectrometric studies**  
*J.A. Noble, L. Ngo, A.R. Ikhenazene, C. Irimiea, G. Lefevre, M. Vojkovic, D. Duca, S. Kenny, C. Pirim, Y. Carpentier, B. Chazallon, N. Nuns, J. Yon, E. Therssen, and C. Focsa*

Thursday 31 August 2017

18:00

End of Conference Day

Thursday 31 August 2017

16:00 - 18:00

Room 24G45

**SPECIAL SESSION #3: ELECTRONIC CIGARETTES – SCIENTIFIC EVIDENCE****Chairs** Arkadiusz Kuczaj and Caner Yurteri

- 16:00** SPS3N2ff **Physical and chemical properties of e-cigarette aerosol**  
*J. Margham, K. McAdam, M. Forster, C. Liu, C. Wright, D. Mariner, C. Proctor, C.U. Yurteri, and J. McAughey*
- 16:20** SPS6N1fb **Online aerosol analysis using FTIR: Assessing carbonyl yields in e-cigarette aerosol**  
*F. Radtke, R. Monni, A. Susz, A. Stoop, J. Verbeeck, and S. Maeder*
- 16:40** SPS3N38b **Computational modeling for characterizing performance of Electronic Nicotine Delivery Systems (ENDS)**  
*A.A. Rostami, N.D. Castro, J.H. Miller, G.D. Karles, and Y.B. Pithawalla*
- 17:00** SPS3N308 **Comparison of deposition patterns of stable aerosol particles and evolving e-cigarette droplets**  
*R. Winkler-Heil, L. Pichelstorfer, and W. Hofmann*
- 17:20** SPS3N411 **In vitro testing of aerosolized substances with PRIMARY 3D Human Airway Epithelia: Application of ALICE-Cloud technology to eLiquids (e-cigarettes)**  
*S. Constant, A. Stelzl, K. Wieland, and O. Schmid*
- 17:40** SPS3N358 **Aerosol from electronic cigarettes: lung cancer risk estimation for direct vaping and second-hand exposure**  
*M. Scungio, V. Rizza, A. Pacitto, L. Stabile, G. Cortellessa, and G. Buonanno*
- Back-up Paper** SPS3N067 **E-cigarettes and in vitro pulmonary health effects**  
*M. Delaval, D. Egli, H. Burtcher, and M. Geiser*

Thursday 31 August 2017

18:00

End of Conference Day

Thursday 31 August 2017

16:00 - 18:00

Room 15G20

**MULTIPHASE CHEMISTRY & BIOAEROSOLS****Chairs: Claudia Mohr and Hang Su**

- 16:00** T217N198 **Biogenic SOA: Chemistry, morphology, and cloud activation at lower to upper tropospheric conditions**  
*C. Mohr, W. Huang, A. Pajunoja, H. Saathoff, A. Virtanen, and R. Wagner*
- 16:20** T217N21b **Impact of aerosol acidity and liquid water content on nitrogen containing SOA species formed from  $\alpha$ -pinene ozonolysis**  
*L. Heikkinen, M. Riva, O. Peräkylä, O. Garmash, M. Äijälä, E. Canaval, L. Fischer, A. Hansel, L. Quéléver, T. Petäjä, D. Worsnop, and M. Ehn*
- 16:40** T217N109 **Impact of particle phase chemistry on nanoparticle composition and growth rate**  
*M. Johnston, P. Tu, Y. Wu, M. Apsokardu, Ch. Stangl, and J. Krasmonowitz*
- 17:00** T217N14c **Aqueous-phase reactivity of 1,2-dihydroxybenzenes (catechol) under nighttime atmospheric conditions**  
*K. Vidović, D. Lašić Jurković, A. Kroflic, S. Frka, M. Šala, and I. Grgić*
- 17:20** T217N1d1 **Photochemistry of iron citrate in aerosol particles**  
*P. Corral Arroyo, P.A. Alpert, J. Dou, U. Krieger, and M. Ammann*
- 17:40** T208N3f0 **Uptake of ozone on birch pollen grains**  
*N. Visez, C. Zhu, J. Farah, S. Gosselin, M. Choël, and D. Petitprez*
- Back-up Paper** T208N425 **Characterization of the Chambre atmospheric simulation chamber**  
*P. Prati, E. Gatta, P. Brotto, D. Massabò, F. Parodi, A. Comite, C. Costa, J.F. Doussin, and P. Formenti*

Thursday 31 August 2017

18:00

End of Conference Day

Thursday 31 August 2017	16:00 - 18:00	Room 15G40
-------------------------	---------------	------------

**SPECIAL SESSION #2: AEROSOLS IN EARTH SYSTEM MODELS**

**Chairs** Annica Ekman, Ulas Im, and Risto Makkonen

- |              |          |   |
|--------------|----------|---|
| <b>16:00</b> | SPS2N271 | <b>Landscape fires dominate terrestrial natural aerosol – climate feedbacks</b><br><i>C.E. Scott, S.R. Arnold, S.A. Monks, A. Asmi, P. Paasonen, and D.V. Spracklen</i>   |
| <b>16:20</b> | T202N346 | <b>Bisosphere-aerosol-cloud-climate interactions investigated using NorESM</b><br><i>M.K. Sporre, A. Grini, T.K. Berntsen, S.M. Blichner, and R. Makkonen</i>   |
| <b>16:40</b> | SPS2N2bc | <b>Global trends of cloud condensation nuclei concentrations</b><br><i>R. Makkonen and O. Krüger</i>  |
| <b>17:00</b> | SPS2N36b | <b>Improving the simulation of global aerosol with size-segregated anthropogenic number emissions</b><br><i>F. Xausa, P. Paasonen, R. Makkonen, M. Arshinov, A. Ding, H.D. Van Der Gon, V-M. Kerminen, and M. Kulmala</i> |
| <b>17:20</b> | SPS2N301 | <b>Impact of reductions in present day model biases on the anthropogenic aerosol effect</b><br><i>D. Neubauer and U. Lohmann</i>  |
| <b>17:40</b> | SPS2N229 | <b>First evaluation of ECMWF C-IFS model with E-PROFILE ALC network</b><br><i>M. Hervo, I. Mattis, A.L. Borg, H. Diemoz, J. Letertre-Danczak, A. Benedetti, and A. Haefele</i>  |

Thursday 31 August 2017	18:00	End of Conference Day
-------------------------	-------	-----------------------

Thursday 31 August 2017

16:00 - 18:00

Room 15G60

## PARTICLE FORMATION AND GROWTH: SIMULATIONS AND EXPERIMENTS

Chairs: Donguk Suh and Jonas Elm

- 16:00** T507N3c7 **Water vapour nucleation on solid aerosol particles by molecular dynamics**  
*B.R. Keijzers, J. Feng, M. Valenti, G. Biskos, and A. Schmidt-Ott*
- 16:20** T115N3bd **Liquid atomization by Flow Blurring® (FB) in a high-pressure environment for combustion applications**  
*L.B. Modesto-López and A.M. Gañán-Calvo*
- 16:40** T507N4bb **Water vapour nucleation on solid aerosol particles by molecular dynamics**  
*D. Suh and K. Yasuoka*
- 17:00** T507N02d **Formation rate of charged nanoparticles and ion balance**  
*X. Chen, V.-M. Kerminen, J. Paatero, P. Paasonen, H.E. Manninen, T. Petäjä, and M. Kulmala*
- 17:20** T508N44f **Formation and light absorption properties of black and brown carbon aerosol particles co-emitted from combustion in flames**  
*R. Kant Pathak, X. Pei, M. Hallquist, E. Ljungström, S. Guo, J.H. Pagels, N.M. Donahue, B. Svenningsson, and A.C. Eriksson*
- 17:40** T507N21a **Molecular understanding of atmospheric new particle formation from sulfuric acid and diamines**  
*J. Elm*
- Back-up Paper** T505N339 **A new mechanism of ultrafine particle generation during concrete fracture**  
*L. Morawska, P. Kumar, N. Jabbour, R. Jayaratne, G. Johnson, J. Alroe, E. Uhde, T. Salthammer, L. Cravigan, and E. Faghghi*

Thursday 31 August 2017

18:00

End of Conference Day

**FRIDAY 1 SEPTEMBER 2017**

Friday 1 September 2017	08:30 - 13:00	Registration
-------------------------	---------------	--------------

Friday 1 September 2017	08:30 - 09:45	Room 04G30
<b>PLENARY LECTURE V</b>		
Chair: Urs Baltensperger and Nønne Prisle		

<b>08:30</b>	Plenary Lecture	<b>How do changes in regional aerosol particle emissions affect climate in other regions of the world</b> <i>Annica Ekman</i>
<b>09:30</b>	Award Ceremony	<b>Presentation of the Poster Awards</b> <i>Nønne Prisle</i>

Friday 1 September 2017	09:45 - 10:15	Coffee Break and Exhibition
-------------------------	---------------	--------------------------------

Friday 1 September 2017

10:15 - 12:35

Room 04G30

**AEROSOL OPTICAL PROPERTIES AND REMOTE SENSING**

Chairs: Patrick Sheridan and Helmuth Horvath

- 10:15** T206N02b **A European ceilometer and lidar network for aerosol profiling**  
*W. Thomas, I. Mattis, F. Wagner, M. Pattantyus-Abraham, and H. Flentje*
- 10:35** T206N353 **Information content of lidar backscattering and extinction profiles with respect to the chemical composition of atmospheric aerosol**  
*M. Kahnert and E. Andersson*
- 10:55** T206N0e9 **A new model to estimate aerosol optical depth from surface solar global and diffuse irradiance data**  
*F. Filipitsch, K. Behrens, and L. Doppler*
- 11:15** T206N1a4 **Trends in MODIS and AERONET derived aerosol optical thickness over Northern Europe**  
*P. Glantz, E. Freud, Chr. Johansson, and M. Tesche*
- 11:35** T207N3ae **Data assimilation on dust forecast model using nighttime AOT retrieved from artificial neural network**  
*S.-S. Lee, B.J. Sohn, H.C. Lee, and S.B. Ryoo*
- 11:55** T206N215 **PathfinderTURB: an automatic boundary layer algorithm. Development, validation and application to study the impact on in-situ measurements at the Jungfraujoch**  
*Y. Poltera, G. Martucci, M. Collaud Coen, M. Hervo, L. Emmenegger, S. Henne, D. Brunner, and A. Haeefe*
- 12:15** T213N291 **Long term flux of Saharan Dust to the Attica Region, Greece**  
*K. Eleftheriadis, V. Vasilatou, M. Manousakas, M. Gini, and E. Diapouli*
- Back-up Paper** T204N112 **Aerosol optical properties over Europe: an evaluation of the AQMEII3 simulations against satellite observations**  
*L. Palacios-Peña, P. Jiménez-Guerrero, A. Balzarini, R. Baró, R. Bianconi, G. Curci, U. Im, G. Pirovano, M. Prank, P. Tuccella, and S. Galmarini*

Friday 1 September 2017

12:40 - 13:00

Room 04G30

**CLOSING REMARKS**

Friday 1 September 2017

13:00

End of Conference

Friday 1 September 2017	10:15 - 12:35	Room 24G45
<b>CARBONACEOUS AEROSOL</b>		
Chairs: Gary Fuller and Sanja Frka		

- 10:15** T210N1a8 **A new method and instrument for the measurement of carbonaceous aerosols**  
*M. Rigler, L. Drinovec, A. Vlachou, G. Stefenelli, J.G. Slowik, A.S.H. Prévôt, C. Hüglin, A.D.A. Hansen, and G. Mocnik*
- 10:35** T210N24b **Long-term trend of equivalent black carbon at different site types in Switzerland**  
*Ch. Hueglin, A. Fischer, B. Schwarzenbach, and L. Emmenegger*
- 10:55** T210N16b **Characterizing the vertical presence of atmospheric black carbon in the Arctic during spring and summer**  
*H. Schulz, M. Zanatta, A. Herber and R. Gerdes*
- 11:15** T210N227 **Calculating mass absorption cross-sections from elemental and organic carbon analysis**  
*E.M.G. Nicolosi, P. Quincey, and G.W. Fuller*
- 11:35** T210N3ee **Combined 14C/AMS-PMF source apportionment during SOAS field campaign**  
*M. Vonwiller, G. Salazar, W.W. Hu, J.-L. Jimenez, E. Edgerton, S.L. Shaw, A.S.H. Prevot, and S. Szidat*
- 11:55** T210N37d **Multi seasonal functional group analysis by FT-IR spectroscopy of atmospheric aerosol in Zurich**  
*M. Reggente, G. Ruggeri, C. Hüglin, and S. Takahama*
- 12:15** T210N0de **Elucidating the composition of humic-like substances in the atmospheric aerosol via 2D liquid chromatographic fractionation and ultra-high resolution mass spectrometry**  
*T. Spranger, D. van Pinxteren, O. Lechtenfeld, T. Reemtsma, and H. Herrmann*
- Back-up Paper** T210N0c9 **Black carbon, carbon monoxide and carbon dioxide in the free troposphere at Helmos Hellenic Atmospheric Aerosol and Climate Change (HAC2) station in Greece**  
*A.-C. Kalogridis, P. Fefatzis, O. Hermansen, and K. Eleftheriadis*

Friday 1 September 2017	12:40 - 13:00	Room 04G30
<b>CLOSING REMARKS</b>		

Friday 1 September 2017	13:00	End of Conference
-------------------------	-------	-------------------

Friday 1 September 2017	10:15 - 12:35	Room 15G20
-------------------------	---------------	------------

## NANOPARTICLES: ELECTRICAL DISCHARGES AND MODELING

**Chairs:** Einar Kruis and George Biskos

- |               |          |   |
|---------------|----------|---|
| 10:15         | T102N1a7 | <b>Stability control of spark discharge generated metal nanoparticle synthesis via air ion injection</b><br><i>D.H. Park, Y.H. Joe, J.H. Byeon, and J. Hwang</i>  |
| 10:35         | T102N436 | <b>Effect of flow configuration on size distributions in a VSP-G1 spark generator</b><br><i>J. Breeman, T.V. Pfeiffer, and A. Schmidt-Ott</i>   |
| 10:55         | T102N34c | <b>Continuous synthesis of silicon nanoparticles in a low pressure microwave plasma reactor on the pilot-plant scale</b><br><i>F. Kunze, M. Spree, T. Hülser, H. Wiggers, and S.M. Schnurre</i>               |
| 11:15         | T104N0cb | <b>Sorting silicon microspheres in a hot-wall chemical vapour deposition reactor</b><br><i>M. Garin, R. Fenollosa, and L. Kowalski</i>  |
| 11:35         | T104N026 | <b>The crystal structure of coalescing Ag-Au nanoparticles by molecular dynamics simulations</b><br><i>E. Goudeli and S.E. Pratsinis</i>  |
| 11:55         | T104N163 | <b>A Monte Carlo simulation of nucleation, coagulation, growth and evaporation</b><br><i>G. Kotalczyk, I. Skenderovic, and F.E. Kruis</i>   |
| 12:15         | T104N25c | <b>Multiscale simulation of gas-phase nanoparticle formation and dynamics in a hot wall reactor applying the NanoDome platform</b><br><i>P. Wollny, F. Strappaveccia, A. Kempf, E. Ghedini, and I. Wlokas</i> |
| Back-up Paper | T104N124 | <b>Atomistic Monte Carlo simulation of the fractal dimensions of nanoparticle agglomerates</b><br><i>E.N. Skountzos, V.G. Mavrantzas, and S.E. Pratsinis</i>  |

Friday 1 September 2017	12:40 - 13:00	Room 04G30
-------------------------	---------------	------------

**CLOSING REMARKS**

Friday 1 September 2017	13:00	End of Conference
-------------------------	-------	-------------------

Friday 1 September 2017	10:15 - 12:35	Room 15G40
<b>NON-INDUSTRIAL INDOOR AEROSOLS</b>		
Chairs: Aneta Wierzbicka and Lidia Morawska		

- 10:15** T412N439 **O/I aerosol particle transformation**  
*J. Ondráček, N. Talbot, L. Kubelová, O. Makeš, M. Cusack, J. Schwarz, P. Vodicka, N. Ziková, and V. Ždímal*
- 10:35** T412N26c **Particle indoor to outdoor ratio separated into chemical components in an occupied residence**  
*Y. Omelekhina, A. Eriksson, P.T. Nilsson, J. Pagels, and A. Wierzbicka*
- 10:55** T413N338 **Assessment of traffic-related emissions on exposure to particles at schools**  
*M. Mazaheri, C. Reche, I. Rivas, M. Álvarez-Pedrero, M. Viana, A. Alastuey, J. Sunyer, L. Crilley, X. Querol, and L. Morawska*
- 11:15** T412N17e **Advanced air ventilation strategy based on predicted indoor particulate matter level for underground subway station**  
*S.-B. Kwon, M. Kim, S. Park, H.-G. Namgung, and T.-S. Oh*
- 11:35** T411N31e **Evaluation of mobile air purifiers under real conditions**  
*S. Schumacher, M. Küpper, D. Spiegelhoff, U. Schneiderwind, H. Finger, and C. Asbach*
- 11:55** T410N44c **Aerosol behavior at the Museum of “Last Supper” of Leonardo Da Vinci: secondary formation and volatilization**  
*L. Ferrero, G. Mocnik, C. Rostagno, A. Proto, C. Pironti, R. Cucciniello, O. Motta, C. Rizzi, and E. Bolzacchini*
- 12:15** T411N276 **Experimental determination of the air and surfaces transfer coefficients of exhaled droplets in a classroom**  
*G. Da, E. Géhin, S. Delaby, S. Ritoux, T.L. Ha, and E. Robine*
- Back-up Paper** T410N267 **Analysis of incense burning in a temple and its health impacts: A study of Kanpur**  
*A. Goel, O.P. Choudhary, and R. Mundra*

Friday 1 September 2017	12:40 - 13:00	Room 04G30
<b>CLOSING REMARKS</b>		

Friday 1 September 2017	13:00	End of Conference
-------------------------	-------	-------------------

Friday 1 September 2017 10:15 - 12:35 Room 15G60

## INSTRUMENTATION FOR CHEMICAL AEROSOL CHARACTERIZATION

Chairs: Olivier Witschger and Frederik Weis

- 10:15** T306N3c3 **The accuracy of commercial pulsed LII compared with reference rBC mass in laboratory and field measurements**  
*J.-F. Yuan, J. C. Corbin, R. L. Modini, M. Zanatta, T. Müller, and M. Gysel*
- 10:35** T302N1bb **In-situ characterization of aerosol nanoparticles at close-to-ambient conditions by small angle x-ray scattering (SAXS)**  
*P.S. Bauer, H. Amenitsch, and P.M. Winkler*
- 10:55** T302N3a3 **The PINQ: A novel instrument for the rapid quantification of PM oxidative potential**  
*R.A. Brown, S. Stevanovic, N.K. Gali, Z. Ning, and Z. Ristovski*
- 11:15** T106N2dd **Aerosol multielement spectrometer for near real-time measurement of aerosol elemental concentration**  
*P. Kulkarni, L. Zheng, G. Deye, and M.E. Birch*
- 11:35** T302N01a **A novel fully automated aerosol particle mass spectrometer combining laser ablation and flash vaporization techniques: Design and first aircraft measurements**  
*A. Hünig, O. Appel, A.M. Batenburg, A. Dragoneas, S. Molleker, and S. Borrmann*
- 11:55** T302N1ea **Coupling of an electrodynamic balance with mass spectrometry as a platform for atmospheric chemistry research**  
*A.W. Birdsall, U.K. Krieger, and F.N. Keutsch*
- 12:15** T302N4d1 **Novel concept of ion counting based upon aerosol technology**  
*B. Gorbunov*

Friday 1 September 2017 12:40 - 13:00 Room 04G30

CLOSING REMARKS

Friday 1 September 2017 13:00 End of Conference

# **Abstracts SPS1**

## Educating future aerosol scientists: a pedagogical model for multidisciplinary research-oriented learning

A. Lauri<sup>1</sup>, T.M. Ruuskanen<sup>1</sup>, L. Riuttanen<sup>1</sup>, P. Hari<sup>2</sup> and M. Kulmala<sup>1</sup>

<sup>1</sup>Department of Physics, University of Helsinki, Helsinki, FI-00014, Finland

<sup>2</sup>Department of Forest Sciences, University of Helsinki, Helsinki, FI-00014, Finland

Keywords: multidisciplinary learning, pedagogy, research training, scientific outreach.

Presenting author email: antti.lauri@helsinki.fi

Atmospheric aerosol research involves several fields of science such as chemistry, physics, meteorology, mathematics, biology, agricultural and forest sciences, technology, and geosciences, combining observations, experimentation and modelling. The shift from discipline-tied fundamental education towards multidisciplinary is imperative for a successful career in climate and global change science (Nordic Climate Change Research, 2009).

Based on our experiences in educating several generations of students during the past 20 years, we have developed a model to improve the learning outcomes in multidisciplinary atmospheric science. The model is a result of work including pedagogical experiments, workshops for teachers and supervisors, and most importantly organizing a long series of multidisciplinary hands-on research-intensive short courses for graduate students.

Let us consider four disciplines – in our case typically physics, chemistry, meteorology and biology. On an average short atmospheric (aerosol) science course, we have participants and other contributors from each of these disciplines. In Figure 1, each triangle represents one discipline. Each one of the triangles can be seen as a pyramid representing the learning of the methodologies and concepts of that particular discipline – the paradigm. During a research-intensive short course the learning happens and new ideas arise in the shaded centre, where the tops of the pyramids meet.

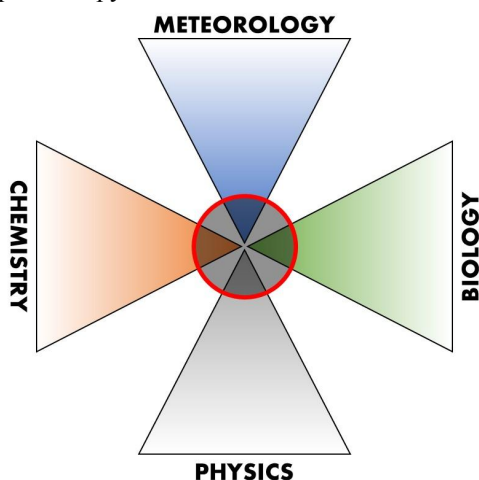


Figure 1. Where the tops of the pyramids meet – an example from a research-intensive short course.

The pedagogical approaches on the short courses include e.g. horizontal learning, participatory action research, problem-based learning, and active

development and utilization of modern technologies supporting learning (Paramonov et al., 2011; Hennessy and Murphy, 1999; Duch et al., 2001; Junninen et al., 2009).

A recent successful example of such short course was a two-week course about the effects of climate change on Arctic ecosystems and societies. It was given in July 2016 in two locations in Greenland and Iceland. The scope of the course was scientific, including familiarization with atmospheric and ecosystem measurements in different locations in Greenland and Iceland, and a series of lectures introducing the special features of Arctic ecosystems and societies. However, the emphasis was on intensive group work. The 26 students on the course, most of them in their PhD phase, were divided into groups each having 3-5 students and 1-3 supervisors. Two projects to work with during the course were given to each group. One of the projects included analysis of atmospheric and environmental observations in the Arctic, and the other one involved a strong social science component, studying the local communities' perception of climate change in their region. As a new component in our research-intensive courses we provided training and practice in scientific outreach. The groups reported their progress in Twitter, and prepared blog posts about their conclusions in the end of the course. The course was organized by a companionship of nine European universities, research institutes and research infrastructures.

Part of this work was supported by NordForsk under project number 79618, which is gratefully acknowledged.

Duch, B. J., Groh, S. E. and Allen, D. E. (2001) *The Power of Problem-Based Learning*, Stylus Publishing, Sterling, VA, U.S.A.

Hennessy, S. and Murphy, P. (1999) *International Journal of Technology and Design Education* **9**(1), 1–36.

Junninen, H., Lauri, A., Keronen, P., Aalto, P., Hiltunen, V., Hari, P. and Kulmala, M. (2009) *Boreal Env. Res.* **14**, 447–457.

Nordic Climate Change Research (2009) *NordForsk Policy Briefs 2009-8*, Mandag Morgen.

Paramonov, M., Lauri, A., Sylvius, V. and Kulmala, M. (2011) *Proc. of Int. Symposium on Integrating Research, Education, and Problem Solving (IREPS)*, Orlando, FL, U.S.A., 231-235.

## Popularization of science using graphic novels

T. Mielonen<sup>1</sup>

<sup>1</sup>Atmospheric Research Centre of Eastern Finland, Finnish Meteorological Institute, Kuopio, 70211, Finland

Keywords: popular science, outreach, graphic novel.

Presenting author email: [tero.mielonen@fmi.fi](mailto:tero.mielonen@fmi.fi)

Popularization of science is challenging, especially if you are doing it based on your own research. It is quite difficult to assess which are the most interesting topics in the eyes of the general public, how detailed information to include and how to generalize the scientific concepts and findings without oversimplifying them. When you are deep inside your field, it is surprisingly easy to forget that the general public does not necessarily know the principles and basic theories of your discipline and they are not familiar with the jargon you use every day. Therefore, real effort is needed to popularize science in an accessible and interesting way. There are several ways to popularize science and the most suitable media depends on the audience you want to reach. Probably the most traditional way is to write a book but it might not be the best media for engaging teenagers or young adults. For them, Youtube (dance) videos, TV shows, animations, web comics, podcasts, songs or blogs could be more accessible. However, you can write a book on your own using the same tools you use in your everyday research but for example, videos and animations usually require skills not typically needed in scientific work. Therefore, there is a smaller threshold for using books in outreach than modern online media. However, this will most likely change in the future as the younger generations, more accustomed to making online content, are taking the lead in the field of science. One medium that lies between books and moving pictures is comics. It combines words and pictures almost seamlessly thus; it is an ideal medium for popularizing science as graphics and text can be used to describe complicated concepts accessibly. In Finland, comics discussing marginal topics such as science have a long history: several scientific disciplines (such as history, archeology, linguistics, pedagogy, philosophy, mathematics, astronomy, and physics) have been covered in comics/graphic novels published in Finnish in the 21<sup>st</sup> century.

Despite the above mentioned challenges, popularization of science is an important task and scientist should put effort into it. After all, we are the experts in our field and we are mainly paid by public funds thus, we are obligated to inform the public how their money has been spent and disseminate the knowledge we have attained. Scientific knowledge should be shared as widely as possible and people should have an easy access to it so that they can make knowledge-based decisions in their own life and improve the state of the world.

My personal contribution to popular science is a graphic novel called *Otsonipäiväkirjat* (Ozone diaries in English, cover shown in Figure 1). It was illustrated by a Finnish comic book artist, Pentti Otsamo and it was

published by Ursa Astronomical Association in 2016. The book tells about a Finnish scientist who moves to the Netherlands to study ozone with satellite measurements. The story describes how science is made in practice but it is also a travelogue describing the main characters life in the Netherlands and his trips around Europe. All these topics are bound together with a touch of humour. The slice of life story is a mix of fact and fiction: all things related to science are described accurately but the characters are fictional in order to have a more interesting story. The motivation for writing the book was to tell the general public how contemporary science is made and give a short introduction to the remote sensing of the atmosphere focusing on ozone and atmospheric aerosols.

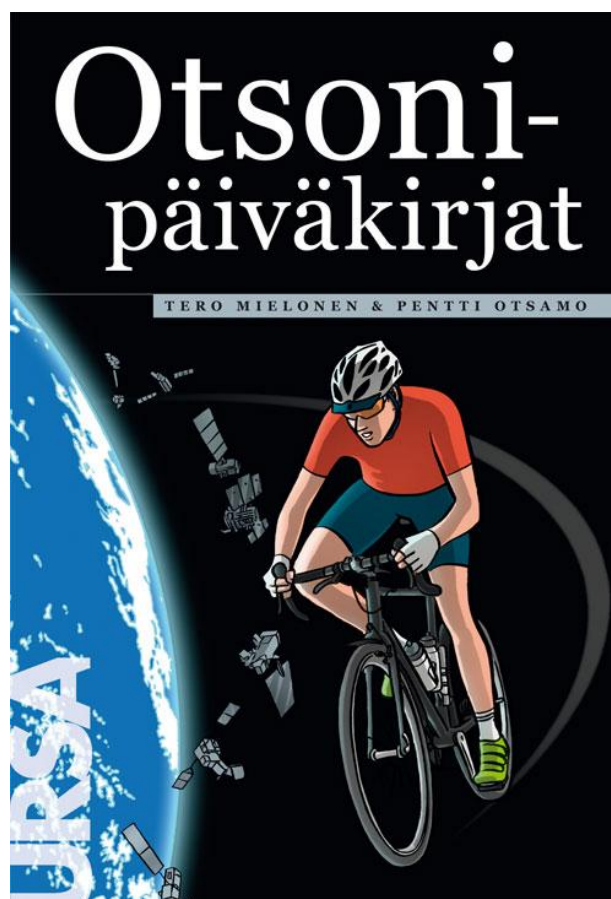


Figure 1. The cover of the graphic novel *Ozone diaries*.

This work was supported by the Kone Foundation and Arts Promotion Centre Finland.

## Horizontal learning as one of the key pedagogical approaches in multidisciplinary research-oriented studies and intensive courses

M. Paramonov<sup>1</sup>, A. Lauri<sup>2</sup>, V. Sylvius<sup>3</sup> and M. Kulmala<sup>2</sup>

<sup>1</sup>Institute for Atmospheric and Climate Science, ETH Zürich, Zürich, CH-8092, Switzerland

<sup>2</sup>Department of Physics, University of Helsinki, Helsinki, FI-00014, Finland

<sup>3</sup>Space Systems Finland, Kappelitie 6B, Espoo, FI-02200, Finland

Keywords: horizontal learning, multidisciplinary atmospheric research, participatory action research.

Presenting author email: mikhail.paramonov@env.ethz.ch

The shift from discipline-tied fundamental education towards multidisciplinary is imperative for a successful career in climate and global change science (Nordic Climate Change Research, 2009). Therefore, adopting the education of the next generation of scientists in a truly multidisciplinary way of thinking as the chief educational and knowledge transfer goal is important for any educational institution. Participatory action research has been acknowledged as the main tool to achieve this goal. It is also important to emphasize the recognition of the research career as a whole, ranging from master-level studies to postdoctoral researcher level.

Current atmospheric research spans several different disciplines and, at least to a certain degree, requires knowledge of all of them. Basics of meteorology, physics, mathematics, biology and programming, among others, are all necessary for a successful education of future atmospheric researchers, deeming multidisciplinary an essential element of educational programmes and requiring effective approaches towards its implementation. Paramonov et al. (2011) have described several such approaches, including horizontal learning, e-learning and joint programmes.

Intensive field courses, such as those given by the University of Helsinki, have proven to be of great interest to both students and researchers. The forms of working during intensive courses include lectures, exercise sessions, seminars, discussion sessions, field work as well as social activities. Very often the emphasis is placed on intensive work in small student groups. From the pedagogical point of view, the intensive courses often represent a form of problem-based learning (PBL; e.g. Duch et al. (2001)). The goals for the course are often set by the students in the beginning of the course, after a few introductory lectures. Teachers take the role of facilitators rather than lecturers. Collaborative learning is carried out throughout the courses. This allows for the social construction, sharing of information and cognition, and finally improves the metacognitive skills of the students, which, in turn, enhance self-directed learning and creative problem-solving skills.

Horizontal learning is a key pedagogical approach during the implementation of intensive field courses. The course participants typically come from very different backgrounds and are specialized in very different topics. Thus, traditional “vertical” training approach would not be very efficient. Instead, horizontal learning takes place, taking a broader approach, addressing a cross-section of

knowledge from different fields and blending the information to reach new levels of understanding (Fig. 1). Students work in small groups and take the responsibility to find the best ways to reach the previously set goals in a short time. Often the solution has been horizontal: students from different fields of study give small lectures to each other in the groups, and several times it has occurred that students wanted to present their ideas to the whole audience for a common discussion. This horizontal learning principle has been shown to be a good example of participatory action research, and the experiences on intensive courses have been very encouraging, both from the teachers’ and students’ points of view. Comparing to traditional classroom courses, intensive field courses and the applied pedagogical approaches, such as horizontal learning, greatly improve the students’ overall learning.

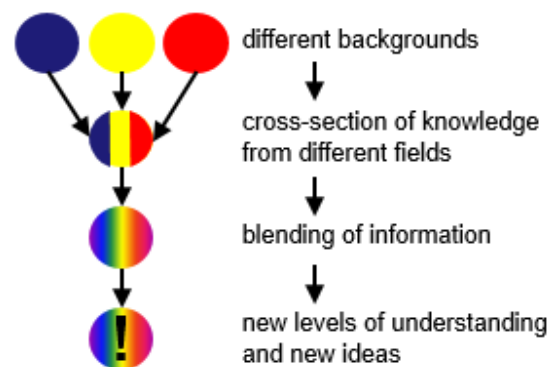


Figure 1. Principles of horizontal learning during intensive courses.

Duch, B. J., Groh, S. E. and Allen, D. E. (2001) *The Power of Problem-Based Learning*, Stylus Publishing, Sterling, VA, U.S.A.

Nordic Climate Change Research (2009) *NordForsk Policy Briefs 2009-8*, Mandag Morgen.

Paramonov, M., Lauri, A., Sylvius, V. and Kulmala, M. (2011) *Proc. of Int. Symposium on Integrating Research, Education, and Problem Solving (IREPS)*, Orlando, FL, U.S.A., 231-235.

## **Climate.now – online learning material about basics of climate change**

L. Riuttanen<sup>1</sup> and Climate.now team<sup>2</sup>

<sup>1</sup>Department of Physics, University of Helsinki, Helsinki, P.O. Box 64 00014 University of Helsinki, Finland

<sup>2</sup>see full list of Climate.now team members and collaborators at [www.climatenow.fi/people.html](http://www.climatenow.fi/people.html)

Keywords: climate change, higher education, MOOC, blended learning.

Presenting author email: [laura.riuttanen@helsinki.fi](mailto:laura.riuttanen@helsinki.fi)

Climate change expertise is urgently needed in all fields of the society. In Finland, however, there has been severe shortcomings in teaching the basics of climate change in many universities and study fields, although, at least to some extent, climate change has been included in teaching in all universities (Liljeström and Monni, 2015).

Climate.now is a multidisciplinary learning material about basics of climate change published online in Autumn 2016 at [www.climatenow.fi](http://www.climatenow.fi). It is meant for higher education and is available online for anyone to use. Climate.now has been done in collaboration with multidisciplinary experts from University of Helsinki, Lappeenranta University of Technology, Metropolia University of Applied Sciences and Finnish Innovation Fund Sitra. Experts of natural sciences, technology, pedagogy as well as arts have been included.

Climate.now material is located at the University of Helsinki MOOC platform ([www.mooc.helsinki.fi](http://www.mooc.helsinki.fi)). Material consists of text, figures, video and assignments. It covers the topic of climate change from different perspectives: from physical background to ecological and societal effects as well as adaptation. All material is available both in English as well as in Finnish. Climate.now learning material can be freely used by any universities or other institutions, like companies, as a study material for a climate change course.

The Climate.now material includes a detailed plan for a climate change course that can be easily applied by a university teacher when starting a new course. By answering to multiple choice questions, student gets an automatic certificate. To get credit points, student needs to register to one of the university courses organized based on the material. Currently there are courses going on at the University of Helsinki, Lappeenranta University of Technology and Aalto University in Finland.

Experiences from the first courses have been inspiring. Students have found multidisciplinary courses challenging. On the other hand, multidisciplinary applied projects were found as best learning methods during the courses. Climate change has been found both as a motivating and depressing topic to study.

This work was supported by the Finnish Innovation Fund Sitra.

Liljeström, E. and Monni, S. (2015) Ilmastoalan yliopisto-opetuksen nykytila Suomessa, Sitra report series 2015.

## Science: a dance, a story, a picture

S. B. Mazon

Department of Physics, University of Helsinki

Keywords: science communication, outreach, social media.

Presenting author email: Stephan.mazon@helsinki.fi

If great science is done in a forest, and no one is there to hear it, will it make a sound?

The implications of aerosol science are strongly relevant to society, be it their involvement in the climate system, or in air quality. Many of our careers are funded by society. But how much effort are we investing to report back to this important stakeholder?

We are returning to a time when story-telling is a valued resource. Infographics and short videos have successfully overflowed social media, making them efficient methods of communication. In order to give our research more exposure, we need to explore alternative platforms to present our science, with our target audience in mind. Early career scientists are having the advantageous opportunity to receive training in science communication in addition to scientific writing. But how do we translate our science –the physics, the chemistry and the numbers– to a compelling story someone outside our field will want to listen? There is a fierce competition for attention in the internet, so it's time to get creative: from blogs, games, design and YouTube channels, to public speaking.

But science communication is not only public engagement; it is also communicating with our colleagues. This is particularly important in large, multidisciplinary research groups. The division of Atmospheric Sciences of the University of Helsinki has its own e-newsletter that includes announcements, introduces new researchers and students, recent publications, and interviews centred on ongoing research projects. The tools are freely available online to start such a newsletter, and they will be presented in more detail (Fig. 1).

I focus on three examples of science outreach from my work: a dance video, a newsletter, and a “scicomm” blog (Fig. 2).

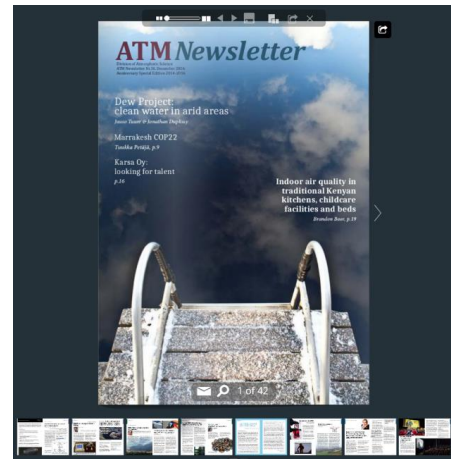


Figure 1. ATM Newsletter aims to foster multidisciplinary science communication. Tools for communication are freely available online.

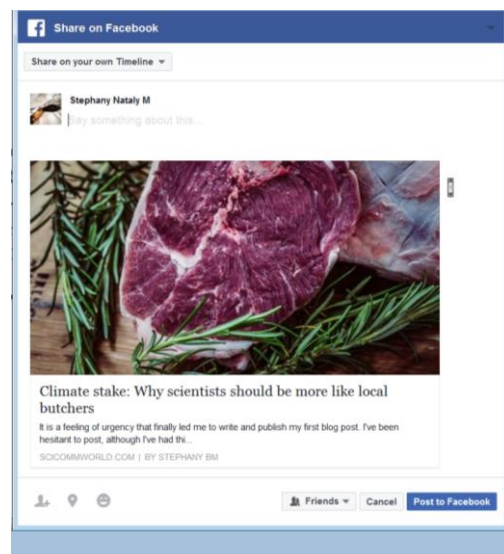


Figure 2. Example of a personal blog. Communicating science in alternative ways.

## **Abstracts SPS2**

## Global trends of cloud condensation nuclei concentrations

R. Makkonen<sup>1</sup> and O. Krüger<sup>1</sup>

<sup>1</sup>Department of Physics, University of Helsinki, Helsinki, FI-00014, Finland

Keywords: aerosol-cloud interactions, CCN, climate modeling

Presenting author email: risto.makkonen@helsinki.fi

Atmospheric aerosols can influence cloud optical and dynamical processes by acting as cloud condensation nuclei (CCN). While historically many global climate models have fixed CCN concentrations to a certain level, most state-of-the-art models calculate aerosol-cloud interactions with sophisticated methodologies based on interactively simulated aerosol size distributions (Ekman, 2014). However, due to scarcity of atmospheric observations simulated global CCN concentrations remain poorly constrained. Here we assess global CCN variability with a climate model, and attribute potential trends during 2000-2010 to changes in emissions and meteorological fields.

We have used ECHAM5.5-HAM2 model with M7 microphysical aerosol model (Stier et al., 2005; Zhang et al., 2012). Dust and sea salt emissions are calculated online, based on wind speed and hydrology. We calculate CCN at 0.2% supersaturation from the aerosol size distribution. Each experiment is 11 years, analysed after a 6-month spin-up period. The MODIS CCN product (Terra platform) is used to evaluate model performance throughout 2000-2010. While passive optical remote observation of CCN could include deficiencies (e.g. Shinozuka et al., 2015), the product serves as a proxy for changes during the simulation period. In our analysis we utilize the observed and simulated vertical column integrated CCN concentration ( $\text{cm}^{-2}$ ), and limit our analysis only over marine regions.

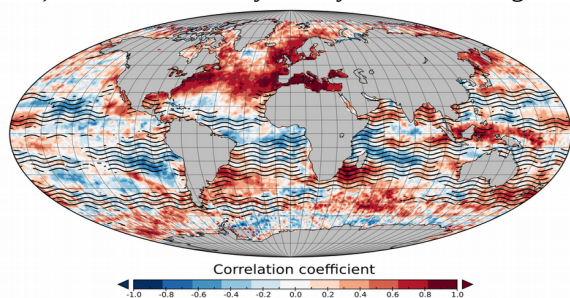


Figure 1. Correlation of simulated CCN (*Control*) and MODIS CCN calculated over annual averages during 2001-2010. Waved lines indicate areas where simulated intra-annual sea salt concentration correlates ( $R^2 > 0.1$ ) with monthly MODIS CCN.

Figure 1 shows the correlation of annual-average CCN from MODIS and ECHAM-HAM during 2000-2010. Most evident pattern of high correlation is found over North Atlantic Ocean, extending throughout Europe and up to Gulf of Mexico. All of these regions show a generally decreasing trend throughout the decade in

simulations (*Control*) and MODIS CCN, and the simulations including the emission trends clearly improve the simulations with climatological emissions (*FixedEmission*). In regions where the observed intra-annual cycle correlates well with sea-spray emissions (Figure 1), the long-term annual correlation usually remains poor. This could indicate that the model is unable to capture the natural variability in aerosol emissions.

We have analyzed trends in CCN(0.2%) during 2001-2010. The CCN over North America shows a declining trend throughout seasons, caused by both decreasing anthropogenic emissions (*FixedMeteo*) and decrease in natural background CCN (*FixedEmis*). While western Europe shows a significant decrease specifically during summer months, the eastern sector indicates some CCN increase due to changes in natural emissions. In Eastern China, simulated natural CCN formation seems to decrease, while anthropogenic perturbations cause a positive trend of a few percent per year. The simulated trends are in good agreement with MODIS data around North America, Europe and Eastern Siberian outflow. However, the MODIS CCN decrease over outflow from China can not be fully captured in model simulations. The model experiments allow to isolate CCN variability and trends caused by anthropogenic and natural emissions, as well as meteorological conditions.

### ACKNOWLEDGEMENTS

This work was supported by the Academy of Finland Centre of Excellence (grant no. 272041) and EU FP7 project BACCHUS (FP7-ENV-2013-603445).

### REFERENCES

- Ekman, A. (2014). *J. Geophys. Res.*, **119**, 817 – 832.  
 IPCC Climate Change 2013: The Physical Science Basis (eds Stocker, T. F. et al.) (Cambridge Univ. Press, 2013).  
 Shinozuka, Y. et al. (2015) *Atmos. Chem. Phys.*, **15**, 7585-7604.  
 Stier, P. et al. (2005) *Atmos. Chem. Phys.* **5(4)**: 1125-1156.  
 Zhang, K. et al. (2012) *Atmos. Chem. Phys.* **12**, 8911-8949.

## Improving the simulation of global aerosol with size-segregated anthropogenic number emissions

F. Xausa<sup>1</sup>, P. Paasonen<sup>1</sup>, R. Makkonen<sup>1</sup>, M. Arshinov<sup>2</sup>, A. Ding<sup>3</sup>, H. D. Van Der Gon<sup>4</sup>, V-M. Kerminen<sup>1</sup> and M. Kulmala<sup>1</sup>

<sup>1</sup>Division of Atmospheric Sciences, University of Helsinki, Helsinki, 00650, Finland

<sup>2</sup>Institute of Atmospheric Optics, SB RAS, 634055, Tomsk, Russia.

<sup>3</sup>Joint International Research Laboratory of Atmospheric and Earth System Sciences, School of Atmospheric Sciences, Nanjing University, Nanjing 210023, China.

<sup>4</sup>TNO, the Netherlands Organisation for Applied Scientific Research, Utrecht, the Netherlands.

Keywords: aerosol, number size distribution, gains, global climate model

Presenting author email: [risto.makkonen@helsinki.fi](mailto:risto.makkonen@helsinki.fi)

Climate models are important tools that are used for generating climate change projections, in which aerosol-climate interactions are one of the main sources of uncertainties. In order to quantify aerosol-radiation and aerosol-cloud interactions, detailed input of anthropogenic aerosol number emissions is necessary. However, the anthropogenic aerosol number emissions are usually converted from the corresponding mass emissions in pre-compiled emission inventories through a very simplistic method depending uniquely on chemical composition, particle size and density, which are defined for a few very wide main source sectors.

In this work, the mass-based anthropogenic emissions converted from the AeroCom in the ECHAM-HAM climate model were replaced with the recently-formulated number emissions from the Greenhouse Gas and Air Pollution Interactions and Synergies (GAINS) -model, where the emission number size distributions vary, for example, with respect to the source sector, fuel and technology. A special attention in our analysis was put on accumulation mode particles (particle > 100 nm) because of (i) their capability of acting as cloud condensation nuclei (CCN), thus forming cloud droplets and affecting Earth's radiation budget, and (ii) their dominant role in forming the coagulation sink and thus limiting the concentration of sub-100 nanometers particles. In addition, the estimates of anthropogenic CCN formation, and thus the forcing from aerosol-climate interactions are expected to be affected.

Analysis of global particle number concentrations and size distributions reveal that GAINS implementation increases CCN concentration compared with AeroCom (Fig. 1), with regional enhancement factors reaching values as high as 10. A comparison between modeled and observed concentrations shows that the increase in number concentration for accumulation mode particle agrees well with measurements, but it leads to a consistent underestimation of both nucleation and Aitken mode (particle diameter < 100 nm) particle number concentrations. This suggests that revisions are needed in the new particle formation and growth schemes currently applied in global modeling frameworks.

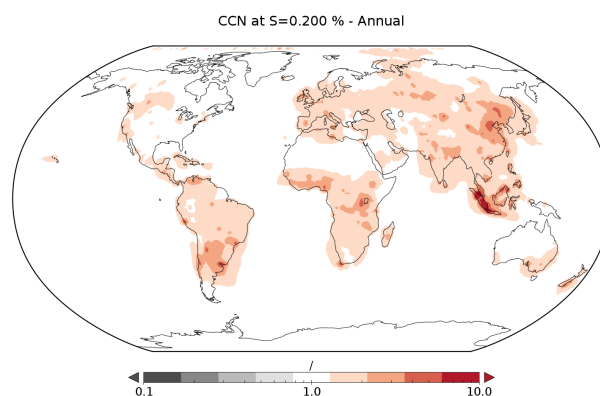


Figure 1. GAINS/AEROCOM annual ratio of CCN at 0.2% supersaturation.

This work was supported by the MAJ and TOR NESSLING Grant n. 201600369 and the Division of Atmospheric Sciences at University of Helsinki, Finland.

- Paasonen, P., Kupiainen, K., Klimont, Z., Visschedijk, A., Denier van der Gon, H. A. C., and Amann, M. (2016) Continental anthropogenic primary particle number emissions, *Atmos. Chem. Phys.*, 16, 6823-6840, doi:10.5194/acp-16-6823-2016.
- Stier, P., Feichter, J., Kinne, S., Kloster, S., Vignati, E., Wilson, J., Ganzeveld, L., Tegen, I., Werner, M., Balkanski, Y., Schulz, M., Boucher, O., Minikin, A., and Petzold, A. (2005) The aerosol-climate model ECHAM5-HAM, *Atmos. Chem. Phys.*, 5, 1125-1156, doi:10.5194/acp-5-1125-2005.

## Viscosity Model for Mixtures of Propylene Glycol, Glycerol, Water, and Nicotine

A. P. Spann<sup>1</sup>, M. J. Hancock<sup>1</sup>, R. S. Sundar<sup>2</sup>, M. Rusyniak<sup>2</sup>, R. W. Lau<sup>2</sup>, Y. B. Pithawalla<sup>2</sup> and A. A. Rostami<sup>2</sup>

<sup>1</sup>Veryst Engineering, LLC, Needham, MA, 02461, USA

<sup>2</sup>Altria Client Services LLC, Research, Development & Regulatory Affairs, 601 East Jackson Street, Richmond VA 23219

Keywords: e-liquids, mixture model, viscosity, propylene glycol, glycerol, nicotine, water

Predicting the performance (e.g. aerosol characteristics) of Electronic Nicotine Delivery Systems (ENDS) is an important step in their design and development. In particular, prediction of e-liquid (a liquid used in an ENDS) flow through channels and porous media such as wicks within the devices is important to controlling flow, ensuring adequate e-liquid replenishment during vaporization, and mitigating potential leakage. These quantities are all affected by viscosity, which, among all the thermophysical properties of e-liquid mixtures, is subject to the highest variability with mixture composition and temperature. Hence an accurate model for e-liquid mixture viscosity is needed, with dependence on mixture composition and temperature. Propylene glycol (PG), glycerol (GL), water (W), and nicotine (NIC) are commonly found in e-liquid mixtures. Here we use publicly available binary liquid data and newly reported PG-GL-W-NIC quaternary mixture data to calibrate a viscosity model for PG-GL-W-NIC quaternary mixtures. The model is validated by additional measurements of the viscosities of various e-liquid formulations at different temperatures.

We seek to create a mixture viscosity model with fitted parameters that have an intuitive physical meaning. Such mixture model should also reduce to known models for one-, two- and three- component mixtures when the mass fractions of the absent components are set to zero. Cheng (2008) developed a two-coefficient model for binary suspensions of W-GL, where the fitted coefficients represent the effect of adding a small amount of one component to the other. When the mass fraction of either component is zero, Cheng's model reduces to the temperature-dependent viscosity of the remaining pure component.

We generalize the technique of Cheng (2008) to a quaternary mixture of PG-GL-W-NIC with six fitted coefficients, each pair of coefficients representing a binary interaction between two of the component liquids PG, GL, and W. Nicotine, present in small amounts, is added as a log-linear component. We fit our model to data from Segur and Oberstar (1951) (Figure 1), Curme and Johnston (1952), and new PG-GL-W-NIC mixture data from Altria Client Services (Figure 2). We validate our model by predicting the viscosities of different e-liquid formulations as well as by comparing predicted viscosities with additional literature data from Sun and Teja (2004) and Khattab *et al.* (2012).

Our model demonstrates the ability to make accurate viscosity predictions for e-liquids across a variety of temperatures. The model may be extended to

incorporate different or additional component liquids or a wider temperature range given additional fitting data.

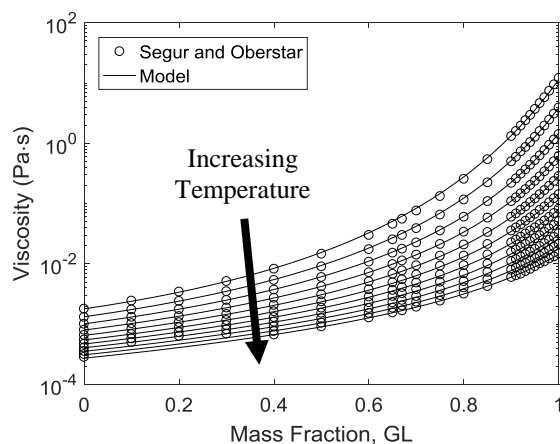


Figure 1. Comparison of model fit calibrated to data of Segur and Oberstar (1951) for W-GL binary mixtures at temperatures from 0 to 100°C in 10°C increments.

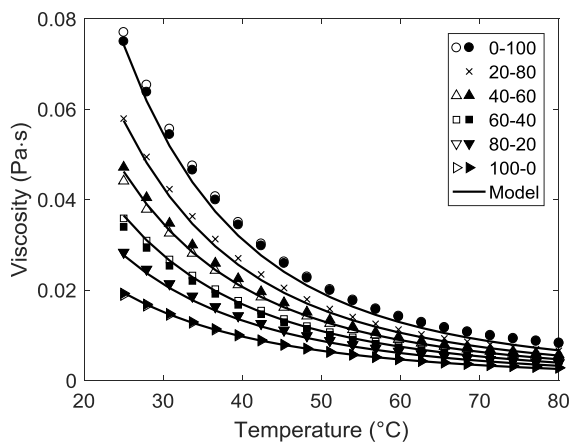


Figure 2. Comparison of model fit to viscosity measurements of quaternary solutions comprising 15% water, 1.5% nicotine, plus a mixture of PG-GL at ratio shown. Middle 4 lines of data used in calibration. Open and filled symbols represent different experimental runs.

Cheng, N. S. (2008) *Ind. & Eng. Chem. Res.* **47**, 3285–3288

Curme, G. O., and Johnston, F. (1952) *Glycols*. Reinhold.

Khattab, I.S. *et al.* (2012) *Arab. J. Chem.*

<https://doi.org/10.1016/j.arabjc.2012.07.012>

Segur, J. B., and Oberstar, H. E. (1951) *Ind. & Eng. Chem.* **43**, 2117–2120.

Sun, T., and Teja, A. S. (2004) *J. Chem. Eng. Data* **49**, 1311–1317.

**First evaluation of ECMWF C-IFS model with E-PROFILE ALC network.**M.Hervo<sup>1</sup>, I. Mattis<sup>2</sup>, A. L. Borg<sup>3</sup>, H. Diemoz<sup>4</sup>, J. Letertre-Danczak<sup>5</sup>, Angela Benedetti<sup>5</sup> and A. Haeefe<sup>2</sup><sup>1</sup> MeteoSwiss, Payerne, Switzerland,<sup>2</sup> Deutsche Wetterdienst, Hohenpeissenberg, Germany,<sup>3</sup> Norwegian Meteorological Institute, Oslo, Norway<sup>4</sup> ARPA Aosta, Aosta, Italy,<sup>5</sup> ECMWF, Reading, United Kingdom.

Keywords: Aerosol, Model, Ceilometer.

Presenting author email: maxime.hervo@meteoswiss.ch

E-PROFILE is a EUMETNET observation programme regrouping measurements of Automatic Lidars and Ceilometers (ALC). Twenty National Weather Services are funding E-PROFILE and more than 10 universities are contributing to the network. At the beginning of 2017, 68 ALCs were sending data operationally. Several hundreds of instruments are expected in the next years. ALCs have a strong potential for models evaluations and assimilation: they measure 24/7 and the high number of instruments can compensate for their limited power.

ALC measurements from 8 countries were compared with ECMWF Composition Integrated Forecasting System (C-IFS) model. To our knowledge, it is the first time that this kind of comparison is realised on a continental scale. Two forward operators were used to convert aerosol concentration in simulated Lidar profile. First, the methodology used by the Copernicus Atmosphere Monitoring Service (CAMS) was used. Secondly, the experimental forward operator implemented at ECMWF was tested.

On a 3-month period, the average difference between ALC measurements and CAMS forward operator was less than 50% (Figure 1), suggesting the good agreement between model and measurements. However, the sea-salt concentration forecasted at Lindenberg is clearly overestimated (Figure 2). As Lindenberg is located at more than 150km from the closest sea, only a very punctual Sea-salt contribution would be expected. The concentration of Sulphate aerosol in the free troposphere was also clearly overestimated by the model. The same observations were realised at other sites. Similar results were found with ECMWF experimental forward operator.

The comparison between measured and simulated profiles also highlights instrumental limitations like overlap artefacts. (Figure 1): the constant decrease in the measured signal at 400m is not consistent with the hypothesis of dynamical boundary layer. This artefact can be corrected using the method proposed by Hervo et al. (2016).

These results show the potential of ALC in constraining aerosols forecast. After the evaluation, assimilation test will be performed to integrate the E-PROFILE

observation in the ECMWF global assimilation procedure.

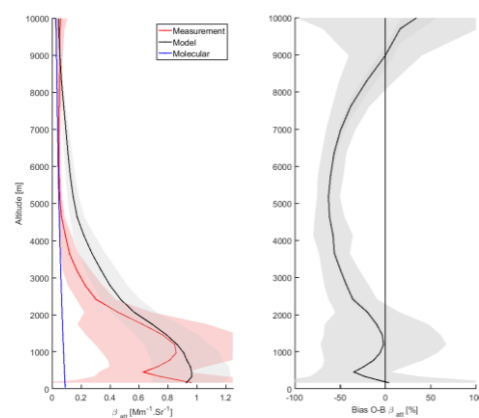


Figure 1. Left panel: Attenuated Backscatter forecasted (black) and measured (red) at Lindenberg from June to August 2016. Right Panel: Average bias in percent.

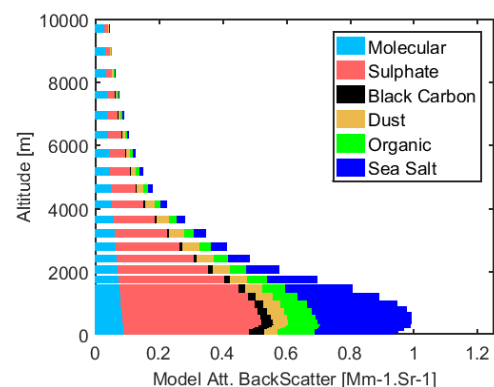


Figure 2. Average chemical composition forecasted at Lindenberg from June to August 2016

Acknowledgement: This study was realised in the frame of the COST Action TOPROF (ES1303). The authors would like to acknowledge all the participants for their fruitful collaboration.

Data kindly provided by the Norwegian Meteorological Institute, MeteoSwiss, Deutsche Wetterdienst, ARPA Aosta and ECMWF.

## Landscape fires dominate terrestrial natural aerosol – climate feedbacks

C. E. Scott<sup>1</sup>, S. R. Arnold<sup>1</sup>, S. A. Monks<sup>2,3</sup>, A. Asmi<sup>4</sup>, P. Paasonen<sup>4</sup>, D. V. Spracklen<sup>1</sup>

<sup>1</sup>School of Earth and Environment, University of Leeds, LS2 9JT, UK

<sup>2</sup>Cooperative Institute for Research in Environmental Sciences, University of Colorado, Boulder, Colorado, USA

<sup>3</sup>Chemical Sciences Division, NOAA Earth System Research Laboratory, Boulder, Colorado, USA

<sup>4</sup>Department of Physics, University of Helsinki, P.O. Box 64, 00014, Finland

Keywords: biogenic secondary organic aerosol, fire, earth system modelling

Presenting author email: c.e.scott@leeds.ac.uk

The terrestrial biosphere is an important source of natural aerosol including landscape fire emissions, dust and secondary organic aerosol (SOA) formed from biogenic volatile organic compounds (BVOCs). Atmospheric aerosol alters the Earth's climate by absorbing and scattering radiation (direct radiative effect; DRE) and by perturbing the properties of clouds (aerosol indirect effect; AIE).

Natural aerosol sources are strongly controlled by climate as well as altering climate meaning that there is the potential for natural aerosol climate feedbacks. One proposed feedback involves increased temperature driving an increase in BVOC emissions and therefore SOA formation, with a negative radiative effect and cooling on climate (Kulmala *et al.*, 2004).

Earth System Models (ESMs) include a description of some of these natural aerosol – climate feedbacks, predicting substantial changes in natural aerosol over the coming century with global mean radiative perturbations as large as  $1 \text{ W m}^{-2}$  (Carslaw *et al.*, 2010). Despite this, the sensitivity of natural aerosols simulated by ESMs to changes in climate or emissions has not been robustly tested against observations.

Here we combine long-term observations of aerosol number (Paasonen *et al.*, 2013) and a global aerosol microphysics model (Mann *et al.*, 2010) to make the first global assessment of terrestrial natural aerosol climate feedbacks constrained against observations.

We find a strong positive relationship between the summertime anomaly in observed concentration of particles greater than 100 nm diameter and the anomaly in local air temperature. This relationship is well reproduced by the model and is driven by variability in dynamics and meteorology as well as natural sources of biogenic and landscape fire aerosol.

We use an offline radiative transfer model (Edwards and Slingo 1996) to determine the radiative effects (DRE and AIE) due to changes in two important natural aerosol sources: biogenic SOA and landscape fire. Interannual variability in simulated global natural aerosol radiative effect (RE) is negatively related to the global temperature anomaly. We find that the interannual RE from biogenic secondary organic aerosol (SOA) is more strongly related to temperature compared to fire aerosol, driven by the strong link between temperature and biogenic emissions.

For both natural aerosol sources the direct radiative feedbacks are stronger than the indirect feedbacks (Figure 1); for biogenic SOA the direct

feedback is more than three times greater than the indirect feedback.

The magnitude of global aerosol climate feedback (sum of direct and indirect effects) is estimated to be  $-0.15 \text{ W m}^{-2} \text{ K}^{-1}$  for wildfire aerosol, greater than the  $-0.06 \text{ W m}^{-2} \text{ K}^{-1}$  estimated for biogenic SOA. These feedbacks are comparable in magnitude, but opposite in sign to the snow albedo feedback, highlighting the need for natural aerosol feedbacks to be included in climate simulations.

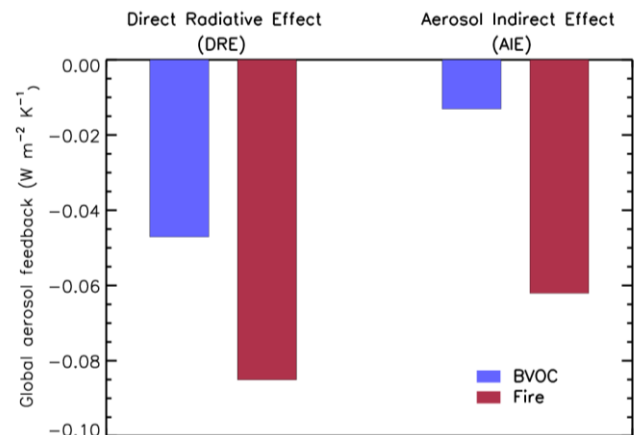


Figure 1. Simulated global aerosol feedback; values are shown for biogenic volatile organic compounds (BVOCs; blue) and landscape fires (red).

This work was supported by the Natural Environment Research Council under grant NE/K015966/1.

Carslaw, K. S. et al., (2010) *A review of natural aerosol interactions and feedbacks within the Earth system*, Atmos. Chem. Phys., 10, 1701-1737.

Edwards, J. M. and Slingo, A. (1996) *Studies with a flexible new radiation code .1. Choosing a configuration for a large-scale model*, Q. J. R. Meteorol. Soc., 122, 689-719.

Mann, G. W. et al., (2010) *Description and evaluation of GLOMAP-mode: a modal global aerosol microphysics model for the UKCA composition-climate model*, Geoscientific Model Development, 3, 519-551.

Kulmala, M. et al., (2004) *A new feedback mechanism linking forests, aerosols, and climate*, Atmos. Chem. Phys., 4, 557-562.

Paasonen, P., Asmi, A. et al., (2013) *Warming-induced increase in aerosol number concentration likely to moderate climate change*, Nat. Geosci., 6, 438-442.

## Impact of reductions in present day model biases on the anthropogenic aerosol effect

D. Neubauer<sup>1</sup> and U. Lohmann<sup>1</sup>

<sup>1</sup>Institute for Atmospheric and Climate Science, ETH Zürich, Zürich, 8092, Switzerland

Keywords: model development, model tuning, anthropogenic aerosol effect

Presenting author email: david.neubauer@env.ethz.ch

Climate models are continuously improved by developing new parameterizations based on physical understanding, by adjusting uncertain parameter values to improve simulation of observable (predominantly present day) climate metrics (referred to as model tuning; Hourdin et al., 2016) or by using new input datasets that become available.

The anthropogenic aerosol effect is rather an emerging quantity that will be affected by all these changes throughout the model development.

Recently the impact of parametric uncertainty on the anthropogenic aerosol effect has been studied systematically within one model by Lee et al. (2016). They found that many combinations of parameters can agree with observations (due to compensation of parameter effects), leading to a large range of possible aerosol radiative forcings. One way to reduce uncertainty is to isolate single processes.

Hourdin et al. (2016) argue that estimating uncertain parameters in model development is an important process that should be made transparent by documenting tuning strategies and targets. Tuning could hide or reveal structural errors if an unrealistic parameter value is necessary for agreement with observations. Documentation of tuning also allows assessing if a model can be used for a particular task.

We show here for the recent model development of the ECHAM6-HAM (Stevens et al., 2013; Zhang et al., 2012; Neubauer et al., 2014) global aerosol-climate model (GCM) how modelling uncertainty (structural and parametric) and emission uncertainty (aerosol emission datasets and parameterizations) impact the simulated anthropogenic aerosol effect.

Several model configurations were tested by only changing one parameter (tuning, parameterization or input dataset) at a time. For each of these configurations the anthropogenic aerosol effect was computed. The changes leading to the anthropogenic aerosol effect of the final model version can therefore be retraced.

All changes made reduce model biases of present day climate, cloud or aerosol metrics or make the ECHAM6-HAM GCM more physically realistic. While the changes for the natural aerosol emission parameterizations only weakly impact the aerosol forcing, changes of the anthropogenic aerosol emissions datasets, in particular wildfire emissions, change the anthropogenic aerosol effect by up to  $-1 \text{ W/m}^2$ . Some corrections in model parameterizations also have a noticeable impact on the anthropogenic aerosol effect. The tuning of ECHAM6-HAM to agree with observed climate and cloud quantities leads to rather small variations in the anthropogenic aerosol effect.

The ECHAM-HAMMOZ model is developed by a consortium composed of ETH Zurich, Max Planck Institut für Meteorologie, Forschungszentrum Jülich, University of Oxford, the Finnish Meteorological Institute and the Leibniz Institute for Tropospheric Research, and managed by the Center for Climate Systems Modeling (C2SM) at ETH Zurich.

Hourdin, F., Mauritsen, T., Gettelman, A., Golaz, J., Balaji, V., Duan, Q., Folini, D., Ji, D., Klocke, D., Qian, Y., Rauser, F., Rio, C., Tomassini, L., Watanabe, M. and Williamson, D. (2016) *Bull. Amer. Meteor. Soc.*, **0**, doi: 10.1175/BAMS-D-15-00135.1.

Lee, L.A., Reddington, C.L. and Carslaw, K.S. (2016) *Proc. Natl. Acad. Sci. USA*, **113**, 5820–5827, 10.1073/pnas.1507050113.

Neubauer, D., Lohmann, U., Hoose, C. and Frontoso, M. G. (2014) *Atmos. Chem. Phys.*, **14**, 11997–12022, doi:10.5194/acp-14-11997-2014.

Stevens, B., Giorgetta, M., Esch, M., Mauritsen, T., Crueger, T., Rast, S., Salzmann, M., Schmidt, H., Bader, J., Block, K., Brokopf, R., Fast, I., Kinne, S., Kornblueh, L., Lohmann, U., Pincus, R., Reichler, T., and Roeckner, E. (2013) *J. Adv. Model. Earth Syst.*, **5**, 146–172, doi:10.1002/jame.20015.

Zhang, K., O'Donnel, D., Kazil, J., Stier, P., Kinne, S., Lohmann, U., Ferrachat, S., Croft, B., Quaas, J., Wan, H., Rast, S. and Feichter, J. (2012) *Atmos. Chem. Phys.*, **12**, 8911–8949, doi:10.5194/acp-12-8911-2012.

## **Abstratcs SPS3**

## The properties of aerosols released from electronic cigarettes (ECs) at different formation conditions

M. Odziomek, Ł. Kwiatkowski, T. R. Sosnowski

Faculty of Chemical and Process Engineering, Warsaw University of Technology, Warsaw, 00-645, Poland

Keywords: aerosols, e-cigarettes, e-liquids, size distribution measurements,

Presenting author email: m.odziomek@ichip.pw.edu.pl

Electronic cigarettes (e-cigarettes, ECs), which are new technical devices for nicotine delivery through the respiratory system, are still poorly characterized regarding the quality and dynamic behavior of inhalable aerosol they release. Both, generation and penetration of aerosol released from e-cigarettes into the respiratory system depend on droplets nucleation dynamics, but at the same time they are strictly related to the processes of aerosol dilution and hygroscopic growth inside the respiratory tract.

The role of conditions in which aerosol was formulated, i.e. conditions of mixing vapor produced by heating e-liquid with external air during inhalation was imperceptible so far. Therefore, the main goal of this work is to clarify the influence of the dynamic of inhalation (puffing flow rate) on properties of aerosol released from e-cigarettes.

We characterized aerosol properties (e.g. mass median diameter - MMD, mass concentration) released from several available on the polish market e-cigarette models (e.g. White – Volish, Venture 3 Pulse – Provog, eBox – Vype, eGrip – Joyetech) at different flow rates (from 2 to 6 dm<sup>3</sup>/min). ECs were filled up with several e-liquids with different content of glycerin (VG), propylene glycol (PG) and nicotine. The viscosity of e-liquids was measured with rotational viscometer (Smart, Fungilab). The measurements of aerosol properties were done with Spraytec (Malvern) spectrometer (equipped with inhalation cell) which was successfully used in our previous measurements (Sosnowski, 2015, Sosnowski and Kramek-Romanowska, 2015). Spraytec gives concentration-independent results using a multiple scattering analysis and not requiring dilution of analyzed aerosols. It has great importance because the majority of published data have been achieved with instruments which require a high degree of aerosol dilution to lower aerosol concentrations down to the operational range. This significantly affects obtained results and makes that some of the processes (e.g. coagulation in the original dense suspensions) are diminished. However, the major problem is that high dilution required for measurements almost certainly causes the significant droplet evaporation Alderman et al. (2015) and Ingebretsen et al. (2012).

The exemplary results are shown in Figure 1A and 1B. Tested e-cigarettes were filled up with two e-liquids with equal PG/VG content (1:1) but different concentration of nicotine: A – 0 mg/ml, B – 12 mg/ml. The measured viscosity of e-liquid with nicotine (B) was only slightly higher than viscosity of sample A (140, 1 and 133,41 mPas respectively). In this case, the potential influence of e-liquid viscosity on MMD calculated for

aerosols released from e-cigarettes is not clearly observed. To observe this relationship we analyzed also e-liquids with different PG/VG ratio. Simultaneously we noted high differences in MMD value between analyzed e-cigarettes models but only at low flow rate – 2 dm<sup>3</sup>/min (Figure 1).

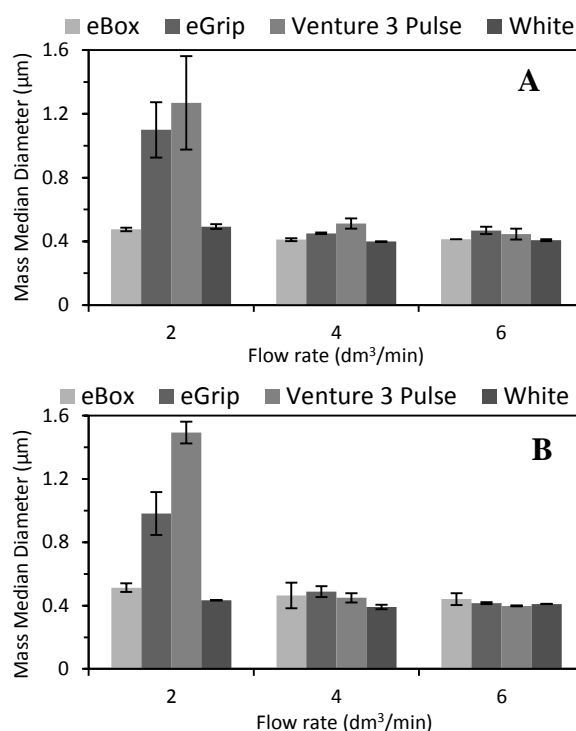


Figure 1. The mass median diameter of aerosols released from e-cigarettes at different flow rates. E-liquids composition: PG/VG – 1:1, nicotine content: A – 0 mg/ml, B - 12 mg/ml

The analysis of the influence of aerosol formation conditions in e-cigarettes will be helpful for assessment of safety and dangers related to EC mists inhalation.

This work was supported by the Polish National Science Center under grant no. DEC-2015/19/D/ST8/00822

Alderman, S.L., Song, C., Moldoveanu, S.C. and Cole, S.K. (2015) *Contributions to Tobacco Research*, **26** (4), 183-190.

Ingebretsen, B.J., Cole, S.K. and Alderman, S.L. (2012) *Inhal. Toxicol.*, **24**(14), 976-984.

Sosnowski, T. R. (2015) *J. Aerosol Med. Pulm. Drug Deliv.*, **28**(3), A28-A29.

Sosnowski, T.R. and Kramek-Romanowska, K. (2015) *J. Aerosol Med. Pulm. Drug Deliv.* **29**(3), 299-309

## Physical and chemical properties of e-cigarette aerosol

Jennifer Margham, Kevin McAdam, Mark Forster, Chuan Liu, Christopher Wright, Derek Mariner, Christopher Proctor, Caner U. Yurteri and John McAughey

British American Tobacco, R&D Centre, Southampton, SO15 8TL, UK

Keywords: e-cigarette, aerosol chemistry, aerosol physics.

Presenting author email: john\_mcaughey@bat.com

Electronic cigarettes (e-cigarettes) have emerged as a significant consumer product category world-wide and have been adopted by many tobacco cigarette users as a product to reduce or replace cigarette use or as a potential cessation aid. The degree of regulatory oversight of these products varies widely around the world, from no regulation to prohibition, and variously as consumer, tobacco or pharmaceutical products. There is significant ongoing debate on issues as diverse as:-

- harm reduction for existing tobacco smokers,
- use of flavours and their inhalation toxicity
- smoking cessation support
- a 'gateway' product to tobacco use
- indoor air exposure to bystanders
- electrical and battery safety

The first two bullet points need an assessment of user exposure and dose, as determined by the chemical composition and physical behaviour of the aerosol generated. This further needs an appropriate approach to product stewardship and toxicological assessment of bulk components of the e-liquid, namely glycerol, propylene glycol, nicotine, water and flavours. Costigan and Meredith, 2015 have proposed screenings for purity requirements, a consideration of thermal breakdown products, and avoiding ingredients that are carcinogenic, mutagenic, toxic to reproduction or respiratory sensitizers.

### Chemical composition

There is interest in the relative toxicities of emissions from electronic cigarettes and tobacco cigarettes. Lists of cigarette smoke priority toxicants have been developed to focus regulatory initiatives. We examined 150 chemical emissions from an e-cigarette (Vype ePen), a reference tobacco cigarette (Ky3R4F), and laboratory air/method blanks (Margham *et al*, 2016). All measurements were conducted by a contract research laboratory using ISO 17025 accredited methods.

Of the 150 measurands examined in the e-cigarette aerosol, 104 were not detected and 21 were present due to laboratory background. Of the 25 detected aerosol constituents, 9 were present at levels too low to be quantified and 16 were generated in whole or in part by the e-cigarette. These comprised major e-liquid constituents (nicotine, propylene glycol, and glycerol), recognized impurities in Pharmacopoeia-quality nicotine, and eight thermal decomposition products of propylene glycol or glycerol. By contrast, approximately 100 measurands were detected in mainstream cigarette smoke.

Depending on the regulatory list considered and the puffing regime used, the per-puff emissions of toxicants identified for regulation were from 82 to >99% lower than Ky3R4F cigarette smoke.

### Physical aerosol properties, inhalation and deposition

Dose is also determined by the site and magnitude of aerosol deposition in the airways and aerosol droplet diameter and concentration may influence this. Both types are condensation aerosols and typically can achieve concentrations of  $1e9.cm^{-3}$ . Size measurement has been conducted typically by electrical mobility, laser diffraction and impaction-type methods. Although both are sub-micron, cigarette smoke aerosols are typically smaller in the range of 150-250 nm mass median diameter, depending on design, particularly ventilation, which influences coagulation time. E-cigarette aerosol droplets are typically 400-600 nm mass median diameter.

The principal factors controlling growth and deposition of the two aerosols are similar, but occur at different rates and degrees of magnitude (Pichelstorfer *et al*, 2016). The principal mechanisms are coagulation in the mouth and hygroscopic growth in the lung; the latter being particularly influenced by chemical composition, and particularly by high glycerol content in e-cigarette aerosol. In practice, aerosol deposition fraction is high for both; 0.6-0.8 for cigarette smoke as reviewed by Baker & Dixon, 2006 and > 0.9 for the principal components of e-cigarette aerosol as measured by St Helen *et al*, 2015.

These data demonstrate that e-cigarettes can be developed that offer the potential for substantially reduced dose relative to cigarette toxicants. Further studies are required to establish whether the potential lower consumer exposure to these toxicants will result in tangible public health benefits.

Baker, R. & Dixon, M *Inhal Toxicol*, 2006, **17**, 255–299.  
Costigan, S. & Meredith, C. *Reg. Tox. Pharmacol.*, 2015, **72**, 361-369.

Margham, J., McAdam, K., Forster, M., Liu, C., Wright, C., Mariner, D. and Proctor, C. *Chemical Research in Toxicology* 2016 **29**, 1662-1678.

Pichelstorfer, L., Hofmann, W., Winkler-Heil, R., Yurteri, C.U., McAughey, J. J. *Aerosol Sci.*, 2016, **99**, 125-132.

St.Helen, G., Havel, C., Dempsey, DA., Jacob III, P. & Benowitz, NL. *Addiction*, 2015, **111**, 535–544

## The continuous characterisation of aerosol droplets in simulated inhalation conditions

Jim S. Walker, James M. Clark, Paul D. Smith

Biral, PO Box2, Portishead, Bristol BS20 7JB

Keywords: aerosol optical tweezers, inhalation, droplet, characterisation

Presenting author email: JWalker@biral.com

Aerosols are dynamic systems and the characteristics of individual particles can change, sometimes radically, in response to changes in the surrounding environment. Inhalation of droplets generated by electronic cigarettes or “vaping” equipment subjects them to a very rapid environmental change and so, potentially, a similarly rapid change to the droplet properties. The kinetics of these changes are such that attempting to study them using conventional aerosol analysis techniques is very difficult indeed. What is required is a technique that can continuously monitor changes to the droplet characteristics in response to simulation of the environment of the respiratory system and to do so with very good time resolution.

### Aerosol Optical Tweezers

Trapping a single droplet in the focus of a laser beam, using a technique known as aerosol optical tweezers, enables the physical and chemical characteristics of the droplet to be monitored continuously. Such a technique uses the trapping beam as an excitation source for Raman spectroscopy which can be used to characterise the droplets both physically and chemically. By separately illuminating the droplet with a different single wavelength source the visible changes to the droplet, including any phase changes, can be observed microscopically.

### Monitoring Particle Size and Refractive Index

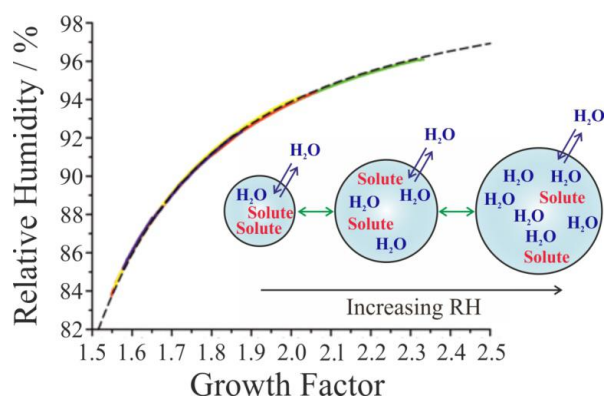
Cavity enhanced Raman spectroscopy of trapped, spherical droplets provides a technique to measure and monitor changes in particle size. This is achieved by tracking the movements of resonant peaks in the Raman spectrum generated by whispering gallery modes in the spherical droplet. The technique delivers exceptional sensitivity ( $<1\text{nm}$ ) and time resolution ( $<1\text{s}$ ) that is not achievable by any other method. The same technique also enables the refractive index of particles to be measured with an accuracy of 0.05% and with a similar time resolution.

### Chemical and Physical Characterisation

In addition to monitoring the physical characteristics of the droplet, changes to its chemical composition can be followed either by observing changes to features in the Raman spectrum or by monitoring the refractive index. In the humid environment of the lung, changes are most likely to be

initiated by the uptake of water. This can be very easily simulated in the aerosol optical tweezers by controlling the humidity of a stream of air passing over the trapped droplet. Changes caused by the uptake of reactive gases or vapours can be similarly observed.

Uptake of water by inhaled particles is very likely to occur in the humid conditions of the lung and the resultant changes to physical parameters of the droplet, such as viscosity and surface tension may affect its fate following deposition. These parameters can be accurately measured by bringing together two droplets trapped in neighbouring laser foci and observing the dynamics of the resultant controlled coalescence.



### Experimental Results

The potential of the aerosol optical tweezers technique for making a wide range of measurements appropriate to the characterisation of inhalable droplets will be illustrated by results obtained in related projects.

Cal, C., Stewart, D.J., Preston, T.C., Walker, J.S., Yang, Y. -H. and Reid, J.P. (2014) *Phys. Chem. Chem. Phys.* 16 3162 - 3171

## Computational Modeling for Characterizing Performance of Electronic Nicotine Delivery Systems (ENDS)

A. A. Rostami, N.D. Castro, J.H. Miller, G.D. Karles and Y.B. Pithawalla

Altria Client Services LLC, Center for Research and Technology, East Jackson Street, Richmond VA 23219, USA

Keywords: Electronic nicotine delivery, ENDS, e-cigarette, computational model, performance characterization  
Presenting author email: ali.a.rostami@altria.com

In order to better characterize the impact of design and use conditions on electronic nicotine delivery systems (ENDS) devices, it is important to be able to produce scientific information about the performance of the system including aerosol delivery, energy distribution and temperature profiles, under a wide range of use conditions and operating specifications.

We have developed a physics-based computational model that can be used to evaluate the performance of cigalike ENDS devices. The three dimensional computational fluid dynamic (CFD) model takes into account the geometric and electro-thermo-physical properties of the device and predicts the device performance under a variety of use conditions, such as puff duration and volume. Among the performance parameters predicted by the model are aerosol mass and composition, maximum and transient device temperatures, aerosol temperature, and the energy distribution, air flow and pressure drop in the system.

The model performs an energy analysis on the system and produces an energy distribution map that shows the various heat losses and most importantly the net energy available for vaporization. Such analyses indicate that in a cigalike configuration, there are several energy losses that do not directly contribute to aerosol formation, including the loss to device structures, convection heat transfer to air and heat losses to the e-liquid without vaporization. Such energy distribution maps may be used to evaluate the energy efficiency of different systems in terms of their performance for aerosol generation. Figure 1 shows a typical energy distribution map of a prototype ENDS device.

Another important performance parameter is the average heater temperature. Figure 2 shows the evolution of the average heater temperature during a five second puff, drawn on a prototype cigalike ENDS device. The temperature rises during the puff and declines afterwards due to dissipation of heat from the heater to the device structure and to the e-liquid. This model can also predict the heater maximum temperature under dry conditions, wherein the system may have run out of e-liquid supply. The model can be used to predict the heater temperature under different puffing regimes, such as CORESTA recommended conditions, etc. In this presentation, modeling results will be compared to experimental measurements performed under selected conditions.

The aerosol delivery predictions from the model were validated with the experimental data for three devices.

Figure 3 shows the model predictions and experimental data for aerosol delivery vs. power input to the system for three devices. The agreement is remarkably good.

The validated model can be used to predict the aerosol mass delivery under a variety of ENDS use conditions such as puff volume, duration and rate, battery charge level over use time, etc.

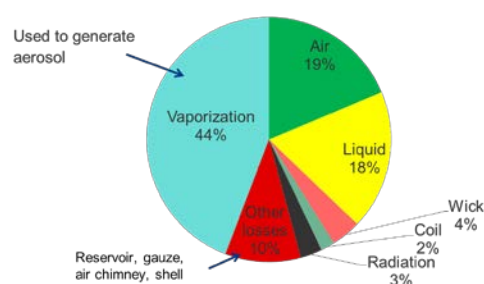


Figure 1. Energy distribution map of a prototype cigalike ENDS device

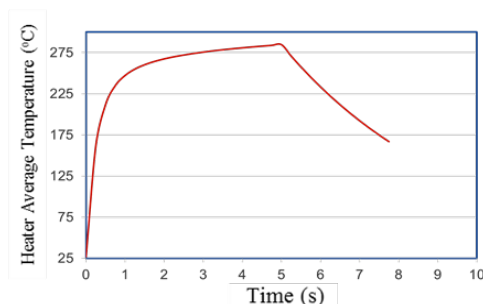


Figure 2. Average heater temperature for a five second puff, drawn on a prototype cigalike ENDS device.

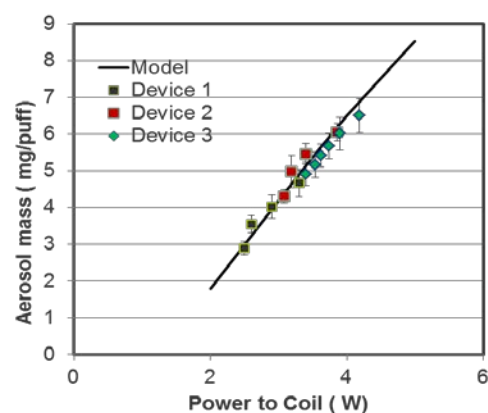


Figure 3: Comparison of modeling predictions to experimental data for aerosol delivery from three prototype cigalike ENDS devices.

## Novel Aerosol exposure devices for in-vitro testing of e-cigarettes at the air/liquid interface

Tobias Krebs

VITROCELL Systems GmbH, Waldkirch, 79183, Germany  
Keywords: air/liquid interface, exposure systems, e-cigarettes  
Presenting author email: [t.krebs@vitrocell.com](mailto:t.krebs@vitrocell.com)

### Abstract

In state-of-the-art health risk assessment, it is becoming increasingly important to accurately characterize the biological activities of active airborne substances, gases and complex mixtures in the human respiratory system. This can be achieved by using in vitro exposure technologies for mammalian cellular systems from the respiratory tract. The exposure of mammalian cells or tissues to airborne substances is frequently performed under submerged conditions. In doing so, the test substances are dosed into the culture medium. This procedure results in an undesired interaction of the formerly airborne substances with the medium, causing limitations for authentic analysis. Furthermore, assessment of the applied dose proves to be difficult using this technique.

In response to the scientific need to expose in physiologically relevant conditions, cutting-edge exposure systems have been specifically designed and engineered to enable direct exposure of mammalian cells or tissue at the air/liquid interface. For this purpose the cell systems are cultivated on microporous membranes and later exposed while not being covered with culture medium. This approach allows for more credible and authentic results than achieved by submerged exposure due to a closer replication of the human physiology.

A typical in vitro exposure system for testing of e-cigarettes consists of 4 major component groups: the smoking machine, dilution system, exposure modules and dosimetry tools.

For a reliable product assessment it is essential that all components match the requirements of exposure the air/liquid interface.

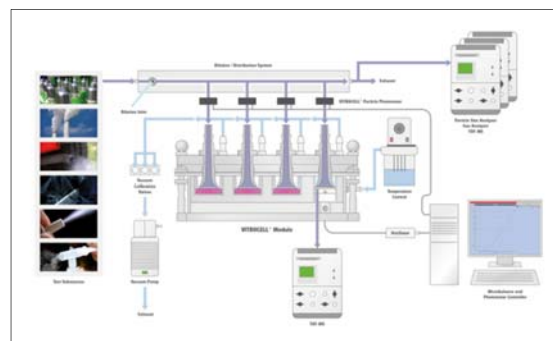


Figure 1: In vitro exposure system with dosimetry tools

The author explains the key components and solutions for smaller to higher throughput.

Arkadiusz K. Kuczaj, Markus Nordlund, Santhosh Jayaraju, Ed Komen, Tobias Krebs, Manuel C. Peitsch, Julia Hoeng

*Aerosol Flow in the Vitrocell 24/48 Exposure System: Flow Mixing and Aerosol Coalescence*  
Applied In Vitro Toxicology. (2016), Vol. 2, No. 3: 165-174

Filippo Zanetti, Alain Sewer, Carole Mathis, Anita R. Iskandar, Radina Kostadinova, Walter K. Schlage, Patrice Leroy, Shoaib Majeed, Emmanuel Guedj, Keyur Trivedi, Florian Martin, Ashraf Elamin, Celine Merg, Nikolai V. Ivanov, Stefan Frentzel, Manuel C. Peitsch, Julia Hoeng  
*Systems Toxicology Assessment of the Biological Impact of a Candidate Modified Risk Tobacco Product on Human Organotypic Oral Epithelial Cultures*  
Chem. Res. Toxicol. (2016) 29, 1252–1269

Louise Neilson, Courtney Mankusb, David Thornea, George Jacksonb, Jason DeBayb, Clive Meredith

*Development of an in vitro cytotoxicity model for aerosol exposure using 3D reconstructed human airway tissue; application for assessment of e-cigarette aerosol*  
Toxicology in vitro (2015), Volume 29, Issue 7

## E-cigarettes and *in vitro* pulmonary health effects

M. Delaval<sup>1</sup>, D. Egli<sup>2</sup>, H. Burtscher<sup>2</sup> and M. Geiser<sup>1</sup>

<sup>1</sup>Institute of Anatomy, Baltzerstrasse 2, University of Bern, 3012 Bern, Switzerland

<sup>2</sup>Institut für Aerosol - und Sensortechnologie Fachhochschule Nordwestschweiz, Klosterzelgstrasse 2, 5210 Windisch, Switzerland

Keywords: electronic cigarettes, *in vitro* pulmonary toxicity, respiratory epithelium.

Presenting author email: mathilde.delaval@ana.unibe.ch

**Background:** The use of “electronic cigarettes” (e-cigs), battery-operated products which deliver a vapour containing nicotine, flavour and/or other chemicals, has exponentially increased during the last decade. The drastic growth has not only been observed in smokers but also in never smokers, women and teenagers. There are indicators for adverse effects not only by nicotine, but also by the e-liquid and vapour components. E-liquids have often tempting labelling, are flavoured and thus easily mistaken for drinks or syrups, especially by children. Therefore, viscosity of e-liquids may also represent a risk of aspiration toxicology, in addition to inhalation.

**Objectives:** This project aims to elucidate the adverse effects of aspired e-liquids or inhaled vapours generated from e-cigarettes to normal and vulnerable human airway epithelia at the cellular and molecular levels.

**Methods:** The physicochemical properties of e-liquids and vapours generated by e-cigs are characterized (particle size distribution, carbonyls, nicotine and nicotine-related impurities, tobacco-specific nitrosamines, volatile organic compounds, metals). Differentiated human bronchial epithelial cells (HBEC) are treated at the air-liquid interface (ALI) by either (i) direct application of the e-liquids onto cells cultures with a micropipette for aspiration exposure or (ii) using a realistic *in vitro* test system allowing direct exposure to e-cigarette vapour (NACIVT, <http://www.nacivt.ch>, Jeannot, 2015) for inhalation exposure. Cells are exposed to the selected e-liquids for 4 hours. Biological endpoints are measured at 24 hours after the exposure. The induction of cell death (LDH release by damaged or dead cells for necrosis and caspase-3 activity for apoptosis), as well as oxidative stress markers (expression of HMOX-1 and COX-2 by qPCR) and (pro-)inflammatory responses (qPCR and release of cytokines) are determined.

**Results:** We developed a system to generate realistic vapours from e-cigs. The instrument allows mimicking the puff topography, whose parameters were deduced from the available literature and cigarette studies. Three e-devices and five e-liquids were chosen based on the device design, mode of operation and their availability and popularity on the Swiss market. The particle size distributions of e-cig vapours are in the range of nanometer scale (Figure 1).

**Conclusion:** Our first results confirmed the generation of particles in the nanoscale in the vapours generated by different e-cigs. Our study will provide

new toxicological evidences for the e-cig risk assessment on the human pulmonary health. Our interdisciplinary approach combining aerosol technology and biology offers a unique approach in identifying adverse effects of e-liquids and e-cigs using both a unique experimental setup and a realistic *in vitro* pulmonary model.

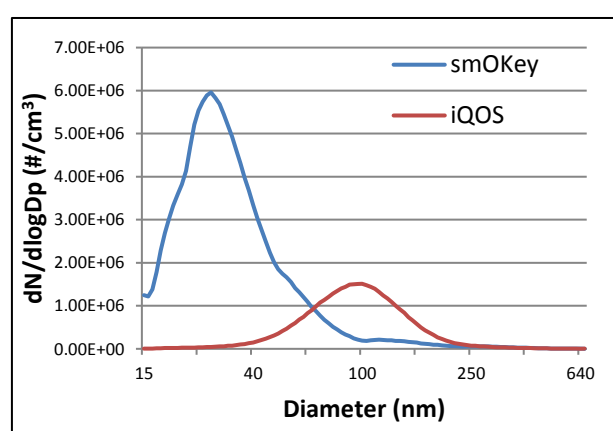


Figure 1. Particle size distributions of two vapours generated by a first generation e-device (smOKey) and a heat-not-burn smoking device (iQOS).

This work was supported by the Federal Office of Public Health FOPH Switzerland.

Jeannot N., Fierz M., Kalberer M., Burtscher H., Geiser M. (2015) *Nanotoxicology*, 9(1):34-42.

## Novel nicotine aerosol delivery devices – the impact of a tobacco heating product and e-cigarettes on indoor air quality

Mark Forster, Jennifer Margham, Caner U. Yurteri, Chuan Liu, James Murphy, Christopher Proctor and John McAughey

British American Tobacco, R&D Centre, Southampton, SO15 8TL, UK

Keywords: tobacco smoke, second hand smoke, ETS, e-cigarette  
Presenting author email: john\_mcaughey@bat.com

Novel nicotine inhalation devices such as e-cigarettes (EC) and more recent tobacco-heating products (THPs), which heat and not burn tobacco, have the potential to significantly reduce levels of combustion-derived toxicants in the aerosol compared with cigarette smoke (CS), and thereby reduce harm to both users and bystanders. The levels of mainstream emissions, and by implication exhaled aerosol emissions are significantly reduced. Furthermore, owing to its enclosed heat not burn design (THP), and wicking and evaporation of simple glycerol and propylene glycol liquids (EC); these novel delivery systems produce little so-called “sidestream emissions” between puffs. In contrast, in cigarettes, combustion of the tobacco continues with smouldering between puffs.

In this study an environmentally controlled room of 37.8 m<sup>3</sup> volume was used to simulate ventilation conditions corresponding to residential and hospitality environments as stipulated by EN 15251: 2007 Standard. Indoor air quality (IAQ) based on chemicals in the air and aerosol characterisation was compared for the novel products and conventional cigarettes over 4 hours, with room occupied and unoccupied blank exposures. Four smoking volunteers, from whom informed consent had been obtained, consumed a total of 20 cigarettes or 20 THP consumables, or  $\geq 160$  e-cigarette puffs in the least ventilated scenario (1.2 air changes per hour (ACH)).

Data for the THP versus CS are used for illustration as tobacco remains an aerosol source for both products. In an analysis of known tobacco smoke markers, Volatile Organic Compounds (VOCs) measured in air sampled around the novel THP did not exceed those measured in background (occupied) room samples for Total VOCs (TVOC) and 7 specific VOCs; isoprene, benzene and toluene which were quantifiable, and 1,3-butadiene, acrylonitrile, acrylamide and propylene glycol which were below levels of detection (LoD). For THP carbonyls, formaldehyde and acetaldehyde were greater than background but significantly lower (> 95%) than equivalent cigarette smoke data; acrolein and crotonaldehyde were not raised over background levels. Analyses for 15 polycyclic aromatic hydrocarbons (PAHs) and 4 tobacco specific nitrosamines (NNK, NNN, NAT and NAB) were below LoD for both the THP and CS; this was also the case for glycerol and carbon monoxide. Nicotine was measured for the cigarette exposure but below LoD for the novel THP.

Aerosol concentration and diameter were measured directly by electrical mobility in the range of 5-1000 nm using the Cambustion DMS-500 spectrometer set at 10s frequency. Aerosol concentrations were significantly reduced for THP versus CS for both particle number concentration (> 95 % - Figure 1) and mass (> 95 %).

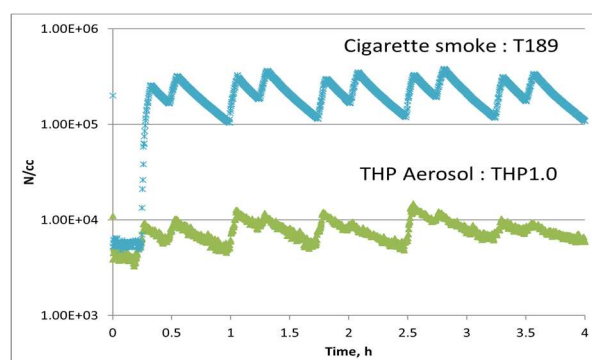


Figure 1 – Aerosol number concentration (log scale)

Aerosol diameters were sub-micron with median diameters from 150-250 nm (Figure 2). The absence of larger droplets was confirmed by light scattering (TSI Dusttrak). Aerosol accumulation was observed during the number concentration decay periods.

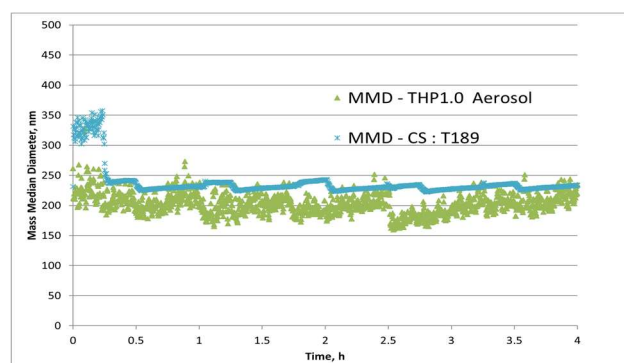


Figure 2 – Aerosol diameter

In conclusion, these data show that the novel nicotine delivery systems where electrical heating either of tobacco or an e-liquid is used rather than combustion, significantly reduces exposure, and has the potential to considerably reduce the risk of harm caused by environmental “second-hand” tobacco smoke.

## Comparison of deposition patterns of stable aerosol particles and evolving e-cigarette droplets

R. Winkler-Heil, L. Pichelstorfer and W. Hofmann

Department of Chemistry and Physics of Materials, University of Salzburg, Salzburg, 5020, Austria

Keywords: lung, deposition, stable aerosols, e-cigarette droplets.

Presenting author email: Werner.Hofmann@sbg.ac.at

Current lung deposition models refer to the inhalation of stable aerosols, i.e. solid particles which do not change their size in the lungs, and normal breathing conditions, i.e. for a constant flow rate (Hofmann, 2011). In contrast, inhalation of e-cigarette droplets is characterized by a continuous modification of droplet diameters due to coagulation, condensation, evaporation, and chemical changes and smoker-specific inhalation conditions, i.e. puffing, mouth-hold and bolus inhalation (Pichelstorfer *et al.*, 2016). In addition, droplet deposition is accompanied by the production of volatile compounds and resulting vapour phase deposition.

The dynamic changes of inhaled e-cigarette droplets in the lungs due to coagulation, phase transition, conductive heat and diffusive/convective vapor transport are described by the Aerosol Dynamics in Containment (ADiC) model (Pichelstorfer *et al.*, 2016). For the calculation of particle and droplet deposition, this model is coupled with the IDEAL Monte Carlo code (Koblinger and Hofmann, 1990; Hofmann, 2011), based on a stochastic, asymmetric airway model of the human lung.

Simulations of deposition patterns are based on the following input parameters: (1) Normal inhalation:  $Q = 800 \text{ cm}^3 \text{ s}^{-1}$  ( $V_T = 1200 \text{ cm}^3$  and  $t_{in} = 1.5 \text{ s}$ ), while smoker-specific inhalation parameters are: 2.0 s puffing time, 1 s mouth-hold and bolus inhalation with  $Q = 800 \text{ cm}^3 \text{ s}^{-1}$ , where a  $50 \text{ cm}^3$  bolus (volume of the oral cavity) is inhaled during the first 0.094 s, followed by aerosol free air during next 1.406 s ( $t_{in} = 1.5 \text{ s}$ ). (2) The number size distribution of the e-cigarette droplets is described by a median diameter of 163 nm with a GSD of 1.44, a number concentration of  $1.54 \times 10^9 \text{ cm}^{-3}$  (Pichelstorfer *et al.*, 2016) and the droplets consist of 9% water, 88.5% glycerol and 2.5% nicotine.

To illustrate the effect of breathing conditions on particle deposition patterns, Figure 1 presents a comparison between normal inhalation and smoker-specific inhalation conditions for stable aerosol particles. Since particles entrained in the bolus are inhaled at the onset of inhalation, they can reach the peripheral region of the lung, where deposition efficiencies are much higher than those in proximal airways. In the case of normal inhalation, where particles are continuously inhaled, particles inhaled towards the end of inhalation reach only the proximal airways before they are exhaled. As a result, deposition fractions are significantly higher for bolus inhalation conditions (22.4% vs. 8.6%).

The effect of aerosol dynamics on particle deposition patterns is illustrated in Figure 2, comparing nicotine particles and nicotine in evolving e-cigarette droplets for smoker-specific inhalation conditions.

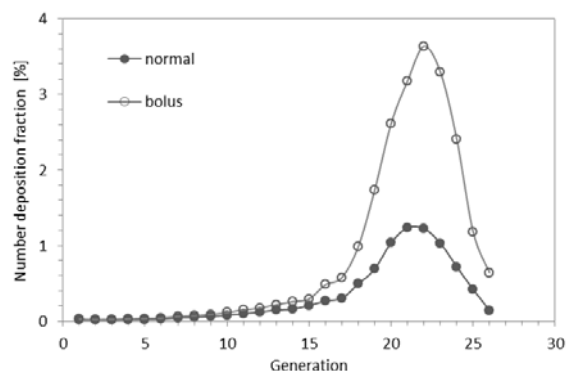


Figure 1. Comparison of generational number deposition fractions between normal and smoker-specific inhalation conditions for stable particles.

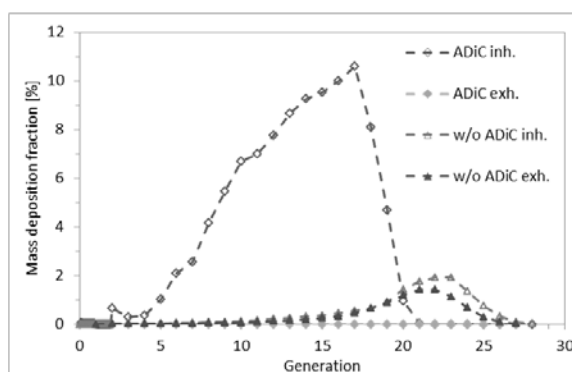


Figure 2. Comparison of generational nicotine mass deposition fractions between stable particles and evolving e-cigarette droplets for smoker-specific inhalation conditions.

If aerosol dynamics are considered, nicotine is completely deposited in vapour form already during the inhalation phase within the first 20 airway generations, with only a very small fraction in particle form, while only 24% of the inhaled nicotine mass is deposited in particle form during inhalation and exhalation if aerosol dynamics mechanisms are neglected.

This work was supported in part by British American Tobacco (Investments) Limited, Southampton, UK.

Hofmann, W. (2011) *J. Aerosol Sci.* **42**, 693-724.

Koblinger, L. and Hofmann, W. (1990) *J. Aerosol Sci.* **21**, 661-674.

Pichelstorfer, L. *et al.* (2016) *J. Aerosol Sci.* **99**, 125-132.

## Aerosol from electronic cigarettes: lung cancer risk estimation for direct vaping and second-hand exposure

M. Scungio<sup>1</sup>, V. Rizza<sup>1</sup>, A. Pacitto<sup>1</sup>, L. Stabile<sup>1</sup>, G. Cortellessa<sup>1</sup>, G. Buonanno<sup>2</sup>

<sup>1</sup>Department of Civil and Mechanical Engineering, University of Cassino and Southern Lazio, Cassino (FR), 03043, Italy

<sup>2</sup>Department of Engineering, University of Naples "Parthenope", Naples, 80133, Italy

Keywords: ELCR, Electronic cigarettes, Ultrafine particles, Lung cancer.

Presenting author email: [m.scungio@unicas.it](mailto:m.scungio@unicas.it)

Electronic cigarettes (ECs) are perceived to be safer than traditional tobacco cigarettes since the absence of combustion processes. The use of these devices, anyway, expose the users (vapers) to high concentrations of fine and ultrafine particles (UFPs) that could deliver toxic and carcinogenic compounds. In the present work, the Excess Lifetime Cancer Risk (ELCR) model developed by Sze-To et al. (2012) was applied to evaluate the potential carcinogenic effects of ECs by estimating the probability of lung cancer incidence.

The risk model adopted in the present work requires the following data: (i) surface area and mass concentration as well as particle size distribution of the emitted particulate matter; (ii) nature and quantity of the hazardous compounds deposited on the emitted particles; (iii) dose-response characteristics for each compound.

In order to characterize the emitted EC aerosol, an experimental campaign was carried out at the Laboratory of Industrial Measurements (LAMI) of the University of Cassino and Southern Lazio (Cassino, Italy), using dedicated instrumentation. The hazardous compounds deposited onto particles were obtained through literature analysis, while the relationship between dose and response is defined by the U.S. Environmental Protection Agency as cancer slope factor (SF). The ELCR equation for each pollutant for 70 years is:

$$ELCR_i = \frac{SF_i}{BW} \cdot \frac{m_{i-EC}}{PM_{10-EC}} \cdot \left( c_f \cdot \delta_S + \delta_{PM_{10}} \right)$$

where  $ELCR_i$  is the excess lifetime cancer risk of the  $i$ -th pollutant,  $SF_i$  is the inhalation slope factor used to describe the mass-based cancer potency of the  $i$ -th pollutant,  $BW$  is the body weight,  $m_{i-EC}$  is the mass concentration of the  $i$ -th pollutant condensed on the aerosol particles,  $PM_{10-EC}$  is the  $PM_{10}$  concentration,  $\delta_S$  and  $\delta_{PM_{10}}$  are the particle surface area and  $PM_{10}$  deposited doses and  $c_f$  is a coefficient determined experimentally.

Two different scenarios were modelled: direct vaping and second-hand exposure; the corresponding ELCR values, for male and female, were evaluated on the basis of particle characteristics and deposited toxic compounds measured in emission or in exposure, respectively, and for ECs with and without nicotine.

In Figure 1, typical particle size distributions for EC aerosols with and without nicotine are reported, while Table 1 and 2 report the ELCR as most probable values (mpv) obtained through a Monte Carlo method

applied on the input data of the model, for male and female.

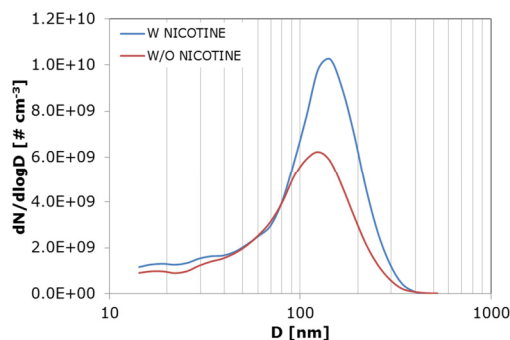


Figure 1. Particle size distributions measured for EC aerosols with and without nicotine.

The ELCR for ECs results lower than traditional cigarettes (approximately  $10^{-1}$ ). The presence of tobacco-specific nitrosamines (NNN-NNK) for ECs with nicotine leads to higher ELCR for direct vaping, while these substances were not detected in second-hand exposure. The higher values of ELCR for second-hand exposure for ECs without nicotine is due to the higher  $PM_{10}$  concentration measured for these ECs.

Table 1. Total ELCR values per average Italian vapers (male and female), for direct vaping.

	Male	Female
W nicotine (mpv)	$8.3 \times 10^{-4}$	$7.0 \times 10^{-4}$
W/O nicotine (mpv)	$3.8 \times 10^{-4}$	$3.3 \times 10^{-4}$

Table 2. Total ELCR values per average Italian vapers (male and female), for second-hand exposure.

	Male	Female
W nicotine (mpv)	$4.8 \times 10^{-5}$	$4.1 \times 10^{-5}$
W/O nicotine (mpv)	$5.9 \times 10^{-5}$	$5.1 \times 10^{-5}$

As a comparison, the ELCR for people living 24 hours a day in the point of maximum risk around an incinerator is equal to  $7 \times 10^{-7}$  (Scungio et al., 2016).

Sze-To GN, Wu CL, Chao CYH, Wan MP, Chan TC. *Exposure and cancer risk toward cooking-generated ultrafine and coarse particles in Hong Kong homes.* HVAC and R Research 2012; 18: 204-216.

Scungio, M., Buonanno, G., Stabile, L., Ficco, G. *Lung cancer risk assessment at receptor site of a waste-to-energy plant.* Waste Management 2016; DOI: 10.1016/j.wasman.2016.07.027.

## ***In vitro* testing of aerosolized substances with PRIMARY 3D Human Airway Epithelia: Application of ALICE-Cloud technology to eLiquids (e-cigarettes)**

Samuel Constant<sup>1</sup>, Andreas Stelzl<sup>2,3</sup>, Katharina Wieland<sup>2,3</sup>, Otmar Schmid<sup>2,3</sup>

<sup>1</sup>Epithelix, CH-1228 Genève, Switzerland

<sup>2</sup>Institute of Lung Biology and Disease, Helmholtz Zentrum München, 85764 Neuherberg, Germany

<sup>3</sup>Comprehensive Pneumology Center - Member of the German Center for Lung Research (DZL), 81377 Munich, Germany

Keywords: aerosol-cell exposure, air-liquid interface, *in vitro*, toxicology.

Presenting author email: otmar.schmid@helmholtz-muenchen.de

Reliable *in vitro* assessment of the toxicity of inhaled substances such as eLiquids (charging liquid of electronic cigarettes) requires cell-based testing under physiologically relevant conditions. The objective of this study was to 1) characterize the performance of the ALICE-CLOUD technology for rapid, efficient and dose-controlled delivery of aerosolized eLiquids to cells and 2) investigate if the ALICE-CLOUD system can be used to deliver aerosolized substances to primary human lung cells (MucilAir<sup>TM</sup>) cultured at air-liquid interface conditions for physiologically realistic biological response analysis.

Aerosol-to-cell delivery using a VITROCELL-CLOUD-12/9 system (Vitrocell Systems, Germany), the commercial version of the ALICE-CLOUD technology introduced by Lenz et al., 2014, was tested by quantitative fluorescence analysis using a fluorescein (15 µg/ml in PBS) and a generic eLiquid solution (75% propylene glycol, 15% vegetal glycerin, 10% water, no nicotine or artificial flavors). A primary pseudostratified 3D cell model of the human airways (MucilAir<sup>TM</sup>, Epithelix, Switzerland) was cultured at the air-liquid interface in 12-well inserts and exposed to various amounts of nebulized eLiquid using the VITROCELL-CLOUD system (1×, 3× or 6×200µl of eLiquid (1:4 dilution in PBS) nebulized by Aeroneb vibrating mesh nebulizers (Aerogen Inc., Ireland)). After a 24h incubation period six biological endpoints (see below) were evaluated for assessment of the pulmonary toxicity of e-liquids. Saline exposure was used as sham control and for each endpoint a positive control substance was included.

Pure eLiquid cannot be nebulized with Aeroneb nebulizers, but dilutions of eLiquid in saline can. With increasing concentration of the eLiquid solution in saline (0-40% was nebulizable) the aerosol output rate of the Aeroneb nebulizer was reduced from 0.3 to 0.8 ml/min for pure saline (depending on nebulizer) to ca. 0.02 ml/min. In spite of this large range of output rates the performance of the VITROCELL-CLOUD system was relatively invariant. For instance the area-scaled aerosol-cell deposition efficiency (referred to as deposition factor) varied between 0.7 and 1.05 (fit curve in Figure 1). For output rates below 0.3 ml/min the deposition factor was close to the ideal value of unity. Due to limited cell coverage in the VITROCELL-CLOUD system this translates into an aerosol-to-cell delivery efficiency of 7.5% (for nine 12-well inserts).

For cell experiments the lowest applied eLiquid dose corresponds to smoking of about 500 e-cigarettes (within 7 min of exposure time). In spite of this high dose and dose rate, eLiquid exposure did neither impair tissue integrity (TEER ~ 350 ohm·cm<sup>2</sup>) nor induce release of proinflammatory cytokines such as IL-8. However, eLiquid exposure adversely affected cell morphology (cells turned round), cilia beating frequency (15% reduction) and mucin secretion (<2-fold reduction).

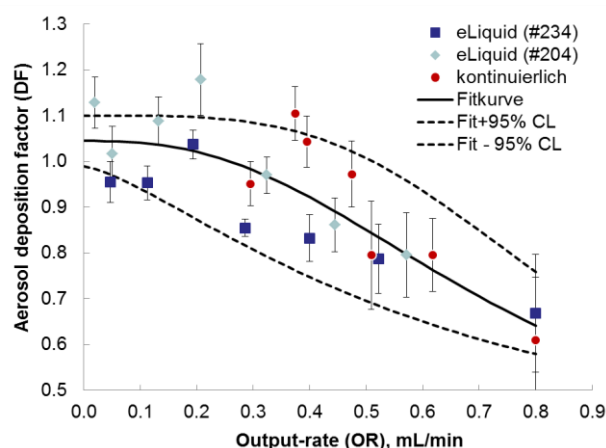


Figure 1. Deposition factor (area-scaled deposition efficiency) of eLiquid-saline mixtures in VITROCELL-CLOUD system

Considering the extremely high tissue specific dose, this *in vitro* study suggests that the generic components of eLiquids (without additives) are not very toxic - at least not in their original, not thermally treated state as investigated here. This study also demonstrates that the VITROCELL-CLOUD system is suitable for reliable, easy-to-handle, and efficient delivery of aerosolized liquid substances to primary *in vitro* cells cultured under physiologic conditions.

Lenz, A.-G., Stoeger, T., Cei, D., Schmidmeir, M., Semren, N., Burgstaller, G., Lentner, B., Eickelberg, O., Meiners, S., Schmid O., *Am. J. Resp. Cell Mol. Biol.*, 51, 526–535, 2014.



## **Abstracts SPS4**

## Large Eddy simulations of laryngeal air flow in three-dimensional patient-specific geometry models

S. Voß<sup>1</sup>, G. Janiga<sup>1</sup>, C. Arens<sup>2</sup>, S. Voigt-Zimmermann<sup>2</sup> and D. Thévenin<sup>1</sup>

<sup>1</sup>Laboratory of Fluid Dynamics and Technical Flows, University of Magdeburg “Otto von Guericke”, Magdeburg, 39106, Germany

<sup>2</sup>Department of Otorhinolaryngology, Head and Neck Surgery, University Hospital, Magdeburg, 39120, Germany

Keywords: Larynx, Respiration, Large Eddy Simulation (LES), Computational Fluid Dynamics (CFD)  
Presenting author email: samuel.voss@ovgu.de

Investigations of fluid dynamics and flow interactions related to phonation and speech might be a key factor on the way toward an improved treatment of voice disorders. The phenomenon of sound production is a complex interplay between fluid dynamics, structural dynamics and acoustics inside the larynx. Many aspects analysed by experimental setups or computer simulations over the last years helped to understand underlying mechanisms (Mittal et al., 2013). The detailed description of the laryngeal airflow is one of the key challenges. Cui and Gutheil (2011) used Large Eddy Simulation (LES) to investigate the airflow through a simplified geometry, revealing effects that are highly varying in space and time and, therefore, difficult to capture properly.

The present study focuses instead on clinical data sets. In accordance to local ethics committee two CT data sets of patients with no pathological events in the region of interest underwent careful geometry segmentation to obtain a surface mesh. This contains the respiratory tract from the trachea to the pharynx with open vocal folds. The generated volume mesh consists of approx. 6 mio. cells. Inside the glottis the cell size limit is 0.18 mm. As inlet, a constant velocity of 27.5 l/min (normal human respiration) is defined. Further, no-slip wall condition and a zero-pressure outlet are used. The temporal discretization of the transient simulation is 10  $\mu$ s. Air is modelled according to Suh and Frankel (2008). All simulations are performed using STAR-CCM+ (Siemens AG, Berlin, Germany). First initialization is done using a Reynolds-averaged Navier-Stokes simulation; the actual simulation during several flow-through times are based on LES using the WALE subgrid-scale model. Post-processing includes comprehensive Proper Orthogonal Decomposition (POD) analysis of several sampling planes. Based on the POD analysis an additional technique is derived in order to find a reduced representation of the spatial and temporal flow domain.

The solved flow field reveals local velocity magnitudes up to 6 m/s. Figure 1 visualizes the velocity field using iso-surfaces. In a) an instantaneous snapshot of the velocity magnitude ( $v = 4$  m/s) is shown, while b) depicts the temporal average. Comparing both, almost the same flow structure is observed below the vocal folds,

indicating locally a steady flow behaviour. On the contrary, in the glottis and the upper part, high fluctuations occur, showing transitional or even turbulent conditions (see Figure 1c). These different flow regimes can be quantified based on the POD analysis. Therefore, a classification of the flow domain into four sections (laminar flow, transition, turbulence, relaminarization) is performed, enabling an easy separation of the locally dominant flow characteristics during respiration.

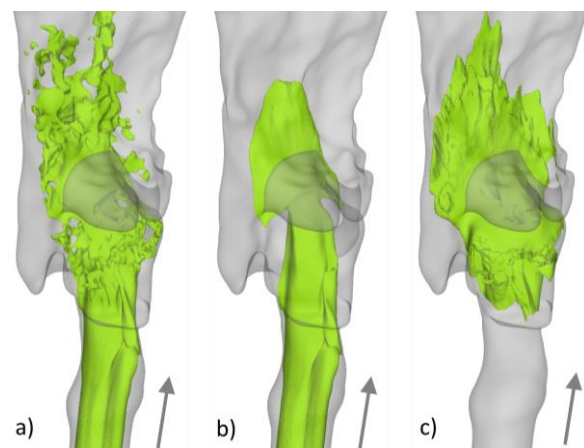


Figure 1. Iso-surface of air velocity inside a patient-specific larynx model during respiration, a) instantaneous velocity magnitude ( $v = 4$  m/s), b) temporally-averaged velocity magnitude ( $v = 4$  m/s) and c) temporal variance of velocity ( $v' = 1$  m/s).

- Cui, X.G. and Gutheil, E. (2011) *Journal of Biomechanics* **44**, 2768–2774.  
Mittal, R., Erath, B. D. and Plesniak, M. W. (2013) *Annual Review of Fluid Mechanics* **45**, 437–467.  
Suh, J. and Frankel, S. H. (2008) *Journal of the Acoustical Society of America* **123** (3), 1237–1240.

## Modeling of aerosolized drugs targeting in the lung – Parametric study in a PRB

M. Pilou, A. Skiadopoulos, P. Neofytou and C. Housiadas

Thermal Hydraulics & Multiphase Flow Laboratory, INRASTES,  
National Centre for Scientific Research “Demokritos”, 15310 Agia Paraskevi, Greece

Keywords: Aerosol modelling, active targeting, CFD, PRB.

Presenting author email: pilou@ipta.demokritos.gr

Among the various proposed biomedical uses of inhaled micro- and nano-particles, there are applications related to cancer diagnosis and therapy, stem cell therapy, advanced drug delivery systems and medical imaging (Ali et al. 2015, In and Nieva 2015, Kuzmov et al. 2015). The effectiveness of particles designed for targeted delivery is mainly regulated by their ability to adhere as needed on specific sites of the respiratory system. The strength of adhesion depends on a variety of parameters: local fluid shear rate, size, shape and ligand surface decoration of particles, and availability of corresponding receptors at the site of interest. Therefore the design of particles for targeted delivery is not a straight-forward process. Computational modeling can serve as an alternative to experiments for multi-parametric studies in more complex and realistic geometries and/or fluid flows, at least at a first screening investigation of the designed particles efficiency.

In the present work, the transport and deposition of ligand decorated particles dispersed in air that flow over the adhesive walls of a physiologically realistic bifurcation (PRB) is numerically investigated in a breathing cycle (Figure 1).

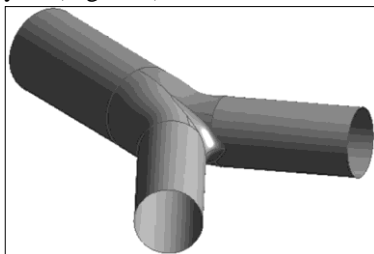


Figure 1. PRB based on the third and fourth generation (G3-G4) of the human lung.

A multiblock structured grid with the adoption of the “butterfly” topology representing the PRB is used (Makris et al. 2014). The airflow velocity and pressure fields in the PRB during a breathing cycle are calculated using in-house computational fluid dynamics (CFD) software (Neofytou & Tsangaris 2006).

The mass conservation equation of the particles is described by the extended time-dependent convection-diffusion equation, which in differential form is written as (Pilou et al. 2011, Makris et al. 2014):

$$\frac{\partial c}{\partial t} + \nabla \cdot (c\vec{v}_c) = \nabla \cdot (D\nabla c) \quad (1)$$

where  $c$  is the particle volume mass concentration, and  $D$  is the particles Einstein-Stokes diffusion coefficient. In Eq.(1),  $\vec{v}_c$  is the particle convective velocity:

$$\vec{v}_c = \vec{u} + \vec{v}_{ext} - \tau_p \left( \frac{\partial u}{\partial t} + \vec{u} \cdot \nabla \vec{u} \right) \quad (2)$$

where  $\vec{u}$  is the air velocity,  $\vec{v}_{ext}$  is the velocity that a particle acquires due to the influence of an external force field (if present), and  $\tau_p$  the particle relaxation time (inertial effects). Equation (1), thus, describes particle convective diffusion taking also into consideration the effects of particle inertia, and external force fields in an Eulerian formulation. The following boundary conditions are applied for the solution of Eq.(1): a) constant inlet NPs concentration at the PRB inlet during inhalation and zero during exhalation, b) zero diffusive flux boundary condition at the outlet, and c) the interaction of the particles with the wall is described by a Robin type boundary condition. In particular, the diffusive flux of particles towards the wall is related directly to the particle binding on the wall and, in turn, to the increase in mass of bound particles per unit surface:

$$-D \frac{\partial c}{\partial n} \Big|_{wall} = k_A c_{wall} = \frac{\partial B}{\partial t} \quad (3)$$

where  $c_{wall}$  is the NPs volume concentration of free particles at the wall,  $B$  is the surface concentration of bound particles and  $k_A$  the kinetic rate constant for particle attachment.

The wall boundary condition of Eq.(3) is incorporated in the CFD-based code of Pilou et al. (2011, 2013) and the total deposition fraction, particle concentration profiles and deposition sites are obtained under different conditions. The effect of flow shear rate, particle diameter and ligand density on particles adhesion is studied.

- Ali, M.E., McConville, J.T. and Lamprecht, A. (2015) *Expert Opin. Drug Deliv.* **12**, 929-945.
- In, G.K. and Nieva, J. (2015) *Transl Cancer Res* **4**, 340-355.
- Kuzmov, A. and Minko, T. (2015) *J. Control. Release* **219**, 500-518.
- Makris, E., Pilou, M., Neofytou, P., Tsangaris, S. and Housiadas C. (2014) *Aerosol Sci. Technol.* **48**,150-162.
- Neofytou, P. and Tsangaris S. (2006) *Int. J. Num. Methods Fluids* **51**, 489-510.
- Pilou, M., Antonopoulos, V., Makris, E., Neofytou, P., Tsangaris, S. and Housiadas C. (2013) *Appl. Math. Model.* **37**, 5591-5605.
- Pilou, M., Tsangaris, S., Neofytou, P., Housiadas, C. and Drossinos, Y. (2011) *Aerosol. Sci. Technol.* **45**,1376-1387.

## Regional targeting of aerosolized drugs in murine lungs

Otmar Schmid<sup>1,2</sup>, Renate Winkler-Heil<sup>3</sup>, Gunter Eder<sup>1,2</sup>, Winfried Möller<sup>1,2</sup>, Werner Hofmann<sup>3</sup>

<sup>1</sup>Institute of Lung Biology and Disease, Helmholtz Zentrum München, 85764 Neuherberg, Germany

<sup>2</sup>Comprehensive Pneumology Center - Member of the German Center for Lung Research (DZL), 81377 Munich, Germany

<sup>3</sup>Department of Chemistry and Physics of Materials, University of Salzburg, 5020 Salzburg, Austria

Keywords: drug delivery, aerosol bolus, inhalation therapy, lung deposition model

Presenting author email: otmar.schmid@helmholtz-muenchen.de

Targeting of inhaled drugs into specific regions of the lung is desirable, since it offers improved treatment options for lung diseases and may provide new insights into fundamental biological questions. For instance specific targeting of inhaled drugs to the bronchial and alveolar region may improve the therapeutic index of drugs (higher efficacy and less side effects) for asthma and emphysema, respectively. Moreover, regional drug targeting would allow investigation of fundamental biological questions such as the localization of drug-specific receptors. Regional targeting of inhaled drugs mainly depends on aerosol size and inhalation manoeuvre. There is also convincing evidence that aerosol bolus application, i.e. non-continuous aerosol delivery during allows for regional targeting. In this study, we investigate the possibility of regional drug targeting in mice by combining the effects of respiratory parameters and bolus application using the IDEAL computational model for aerosol deposition in mice (Winkler-Heil and Hofmann, 2016). The IDEAL model is a Monte Carlo deposition model based on a stochastic, asymmetric lung structure of the Balb/c mouse.

The Flexivent system for lung function measurement in mice (EMKA/Scireq, France/Canada) is introduced here for regional drug targeting. Mice are intubated and mechanically ventilated, which allows for exact control of the respirator parameters. Moreover, aerosol is generated by a vibrating mesh nebulizer (Aerogen, Ireland; inhaled aerosol: MMAD = 2.8  $\mu$ m; GSD = 1.75), which can be triggered at any given time during the inhalation phase. The profile of the aerosol bolus was measured with a custom-designed aerosol photometer and pneumotachograph. Here, first results on pulmonary aerosol deposition are presented for a shallow aerosol bolus where the first 145  $\mu$ l of inhaled air is aerosol-free. We hypothesize that the length and position of the aerosol bolus provided by the Flexivent system can be adjusted and used for regional targeting of inhaled drugs.

Aerosol deposition in healthy C57BL/6 mice (n = 5) receiving a shallow bolus (145  $\mu$ l delay volume) with a slow and deep inhalation pattern (120 breath/min; tidal volume 0.4 ml; Inh./Exh-time = 2:1) was measured with quantitative fluorescence spectrometry (Barapatre et al., 2015). This yielded an aerosol deposition fraction of  $0.258 \pm 0.048$  (mean  $\pm$  2SEM), which is in good agreement with predictions by the IDEAL model, but only if the bolus type application is considered (Fig. 1). Model predictions for continuous aerosol application are significantly higher than the measured values (Fig. 1). Investi-

gation of regional targeting with the IDEAL model shows that increasing the tidal volume from 0.2 to 0.8 ml decreases the bronchial-to-acinar aerosol dose ratio from 2.3 to 1.1 (Fig. 2). Interestingly, for continuous aerosol application an inverse trend is observed ranging from 0.5 to 0.9 (Fig. 2).

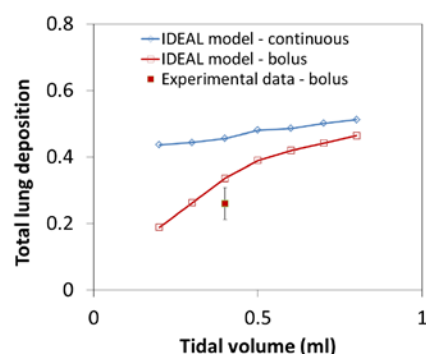


Figure 1: Total pulmonary aerosol deposition fraction for intubated-ventilated mice with continuous and shallow bolus (145  $\mu$ l) aerosol application (120 breath per minute, Inh./Exh-time = 2:1; MMAD=2.8  $\mu$ m; GSD=1.75).

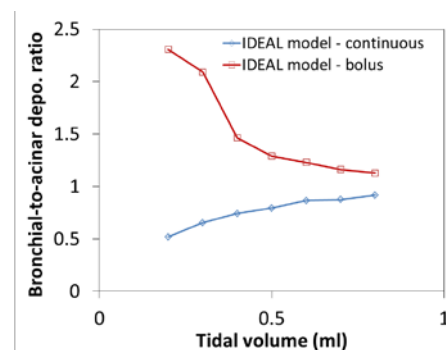


Figure 2: Bronchial targeting fraction for same conditions as in Figure 1

Thus, the Flexivent system is a promising tool for region-specific targeting of inhaled drugs in mice based on aerosol bolus application.

This work was supported by the German Federal Ministry of Education and Research within the Leading-Edge Cluster "m4-Personalized Medicine" in Munich.

Barapatre, N., et al., Schmid, O., (2015), *J. Pharm. Biomed. Anal.*, 102: 129-136.

Winkler-Heil R., Hofmann W., (2016), *Inhal. Toxicol.*, 28:180-191.

## Comparison of Lagrangian and Eulerian modeling for predicting aerosol deposition in the human upper airways

P.G. Koullapis<sup>1</sup>, E.M.A. Frederix<sup>2</sup>, S. C. Kassinos<sup>1</sup>, B.J. Geurts<sup>2,3</sup>, A. Kuczaj<sup>4</sup> and M. Nordlund<sup>4</sup>

<sup>1</sup>Department of Mechanical and Manufacturing Engineering, University of Cyprus, Cyprus

<sup>2</sup>Multiscale Modeling and Simulation, Applied Mathematics, University of Twente, The Netherlands

<sup>3</sup>Anisotropic Turbulence, Applied Physics, Eindhoven University of Technology, The Netherlands

<sup>4</sup>Philip Morris International R&D, Philip Morris Products S.A., Quai Jeanrenaud 5, 2000 Neuchatel, Switzerland

Keywords: CFD, upper airways, Deposition, Eulerian/Lagrangian modeling.

Presenting author email: pkoull01@ucy.ac.cy

Drug delivery via the pulmonary route is becoming a promising method for the treatment of both lung and systemic diseases. Computational methods offer a valuable approach for predicting deposition and due to their increasing accuracy can nowadays more and more replace complex and expensive in-vivo/in-vitro tests. An advantage of these in silico methods is that they can provide detailed information of local deposition patterns inside the lung geometry and independently identify the dominant transport and deposition mechanisms.

Transport and deposition of aerosol drug formulations can be simulated using either a Lagrangian point-particle approach, where the aerosol particles are represented as discrete entities, or the Eulerian approach in which the aerosol is considered as a continuous phase. Both approaches have their pros and cons: equations of motion in the Lagrangian framework can be derived quite thoroughly and a variety of forces can be considered directly, but the simulation can become computationally expensive in the case of dense aerosol suspensions. On the other hand, Eulerian approaches have the potential to reduce the computational cost, but the formulation of the transport equations becomes increasingly heuristic as more physical details are included in the model.

The purpose of this work is to compare the performance of both a Eulerian and a Lagrangian approach in predicting regional aerosol deposition in a model of the human upper airways. The model includes the oral cavity and the first seven generations of the tracheobronchial tree. Computational deposition predictions by both methods are compared with deposition data obtained from in vitro measurements that also include regional deposition information.

Figure 1 shows the geometry of the upper airways along with the segments and their numbering as used in the in-vitro deposition measurements of Lizal et al. (2015). Figure 2 shows the Deposition Fractions per segment of spherical particles with a diameter of 4.3  $\mu\text{m}$  during steady inhalation at an inlet flowrate of 15 lt/min. This corresponds to flow conditions in the sedentary regime. The LES-Lagrangian predicted deposition results are compared to the in-vitro results of Lizal et al. (2015). The CFD toolbox OpenFOAM was used to solve the incompressible filtered Navier-Stokes equations using the dynamic Smagorinsky subgrid model and to track the particle trajectories. Good agreement is

observed between CFD and measurements. Eulerian modeling results will be included in the final conference contribution.

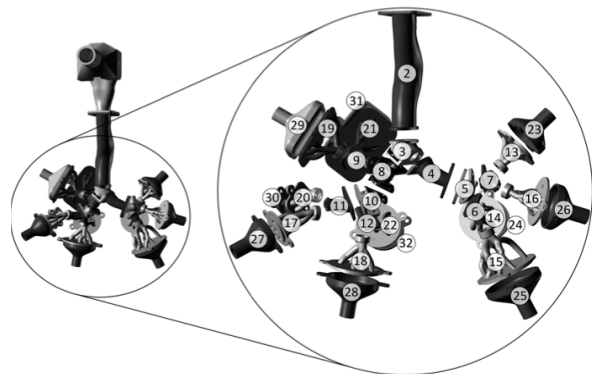


Figure 1. Geometry of the human upper airways (left) and segments with their numbering as used in the experiment (right).

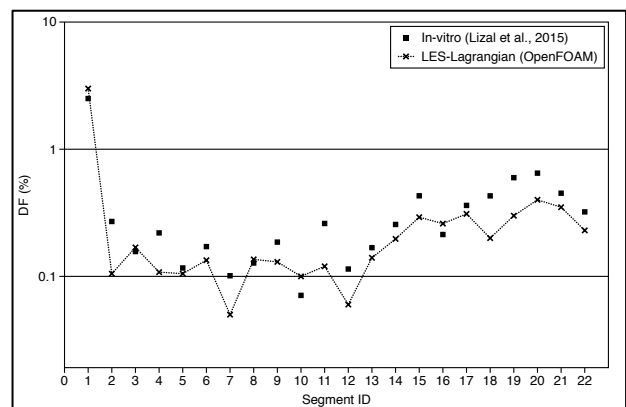


Figure 2. Deposition fraction per segment comparing LES-Lagrangian and in-vitro measurement deposition data of Lizal et al. (2015) for spherical particles with a diameter of 4.3  $\mu\text{m}$ .

This work was supported by COST Action MP1404: Simulation and pharmaceutical technologies for advanced patient-tailored inhaled medicines (SimInhale).

Lizal F., Belka M., Adam J., Jedelsky J., and Jicha M. (2015) A method for in-vitro regional aerosol deposition measurement in a model of the human tracheobronchial tree by the positron emission tomography. *Proc IMechE Part H: J Engineering in Medicine*, 229 (10), 750-757.

## Targeted delivery in upper airways using inhaled magnetic particles

Y. Ostrovski<sup>1</sup>, J. Sznitman<sup>1</sup>

<sup>1</sup>Department of Biomedical Engineering, Technion – Israel Institute of Technology, Haifa, Israel

Keywords: Targeted delivery, aerosols, Inhalation medicine, SPIONs.  
Presenting author email: yanost@gmail.com

The pulmonary route presents an attractive delivery pathway for topical treatment of lung diseases. While significant progress has been achieved in understanding the physical underpinnings of respiratory flows and aerosol deposition in the lungs, our ability to deliver inhalable drugs to specific lung targets, or even particular lung regions, remains to date disappointingly poor (Kleinstreuer, Zhang, & Donohue, 2008).

To overcome such challenges, it has been hypothesized that magnetically-loaded inhaled drug particles could locally increase deposition outcomes in the presence of an external magnetic field (Dames et al., 2007). Yet such conjecture has faced a number of hurdles including importantly, that in most instances the magnet could not overcome the drag forces imposed on the particles during the inhalation maneuver (e.g. Pourmehran et al. 2015). In addition, substantial deposition occurred in undesired locations regardless of the magnetic field, while only a relatively small increase in deposition was witnessed in the targeted regions.

Here, we discuss the feasibility of a novel pulmonary targeting technique to overcome past hurdles. To examine our new method we first implement CFD simulations on a physiologically-accurate airway tree model. These simulations are coupled with an in-house DEM (Discrete element method) code to track the intricate motion of the magnetized aerosol particles under the influence of an external magnetic field. In parallel, an *in vitro* system is devised based on the insights acquired from the CFD results. Briefly, the system incorporates a model molded from a 3D printed upper airway tree. A computer-controlled “smart inhaler” device delivers a short pulsed aerosol bolus, and a custom-designed ventilation machine carries the pulse along the airway tree to its target, where it is then deposited under the action of a magnetic field.

By carefully selecting particle sizing and the magnetic field, in conjunction with tuning the breathing maneuver with the “smart” computer-controlled inhaler and ventilation machine, our method could allow for the first time site-specific targeting of inhaled therapeutics (see Fig. 1). Such advancements may pave the way for specialized topical lung treatments including tumor targeting in cancer patients (Ostrovski, Hofemeier, & Sznitman, 2016).

This work was supported by the European Research Council (ERC Starting Grant, Grant Agreement nr. 677772).

Dames, P., Gleich, B., Flemmer, A., Hajek, K., Seidl, N.,

Wiekhorst, F., ... Rudolph, C. (2007). Targeted delivery of magnetic aerosol droplets to the lung. *Nature Nanotechnology*, 2(8), 495–9.

Kleinstreuer, C., Zhang, Z., & Donohue, J. F. (2008). Targeted drug-aerosol delivery in the human respiratory system. *Annual Review of Biomedical Engineering*, 10, 195–220.

Ostrovski, Y., Hofemeier, P., & Sznitman, J. (2016). Augmenting Regional and Targeted Delivery in the Pulmonary Acinus using Magnetic Particles. *International Journal of Nanomedicine*, 11, 3385–3395.

Pourmehran, O., Rahimi-Gorji, M., Gorji-Bandpy, M., & Gorji, T. B. (2015). Simulation of magnetic drug targeting through tracheobronchial airways in the presence of an external non-uniform magnetic field using Lagrangian magnetic particle tracking. *Journal of Magnetism and Magnetic Materials*, 393, 380–393.

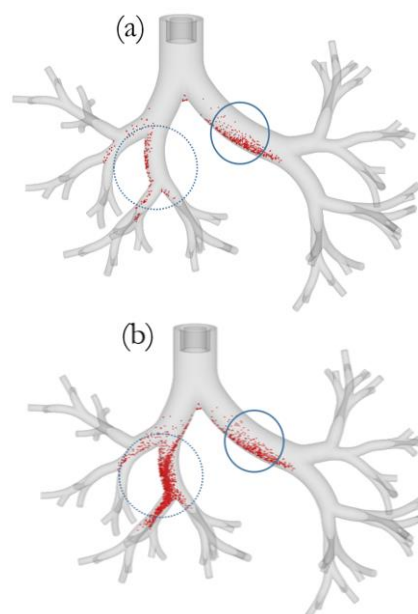


Figure 1. Preliminary results of the targeted delivery simulations. (a) Targeted delivery with our magnetic targeting method. (b) Targeted delivery using the most advanced method in the market (in development). The targeted region is circled with a solid line. Untargeted region where deposition was drastically reduced is marked with a dotted line.

## Experimental study of particle deposition in a physical model of human respiratory tract

M. Belka<sup>1</sup>, F. Lizal<sup>1</sup>, J. Jedelsky<sup>1</sup>, and M. Jicha<sup>1</sup>

<sup>1</sup>Department of Thermodynamics and Environmental Engineering, Energy Institute, Brno University of Technology, Brno 616 69, Czech Republic

Keywords: particle transport, deposition, physical cast, respiratory airways.  
Presenting author email: belka@fme.vutbr.cz

Nowadays, inhalation of aerosolized medicines is commonly used for treatment of respiratory diseases, such as chronic obstruction pulmonary disease (COPD). However, it can also provide a systemic drug delivery of various therapeutic peptides and proteins via air-blood barrier (Pirozynski and Sosnowski 2016). The success of this treatment goes hand in hand with the ability of the medicine to deposit in the targeted region of lungs. Failure to do so increase the treatment costs and can cause unwanted side effects. Therefore, targeted delivery in patient specific respiratory airways is important objective nowadays.

Understanding particle transport and deposition is one of essential factors for effective and localized aerosol delivery. Computational fluid particle dynamics (CFPD) methods are very strong tools for prediction of aerosol deposition within respiratory airways. However, it is necessary to validate these methods by either *in vivo* or *in vitro* measurements (Longest and Holbrook 2012). One way of doing this is the use of physical airway casts as a benchmark for initial CFPD simulations.

That is why we performed deposition experiments using a physical model of respiratory airway tract which encompasses respiratory airways from the oral cavity to the 7th generation of bronchial branching (Lizal et al. 2012). Deposition was studied for steady inhalation and the flow rates used were 15, 30 and 60 LPM. Several types of liquid or solid particles were used and the effect of particles shape on deposition was analysed.

The deposition quantities for specific regions of the model were acquired by various methods depending on the particles used. Di-ethyl-hexyl-sebacate (DEHS) particles were tagged with radioactive fluorine and the model was analysed by positron emission tomography after the exposure (Lizal et al. 2015). After the exposure to glycerol or glass fibrous particles, the model was disassembled and the particles were extracted from predefined model regions. Deposition of glycerol was analysed by gas chromatography-mass spectrometry method. Glass fibers were detected by phase-contrast microscopy (Belka et al. 2013).

The regional deposition was quantified as deposition fraction and deposition efficiency. Deposition efficiency expresses an ability of given airway to collect or filter passing particles. It is usually correlated with Stokes number which represents particle's ability to follow the streamlines within respiratory airways. Deposition efficiency of various particles as a function of Stokes number is depicted in Figure 1.

Deposition efficiency increased with increasing Stokes number. This indicates that the larger particles during high flow inhalation were more likely to deposit in the model and that the impaction mechanism was a key deposition mechanism.

Comparing the particle shape, the deposition of spherical particles was higher than that of fibrous particles having the same aerodynamic diameter. This can be caused by the fiber ability to align with the flow and thus better react to the air flow direction changes.

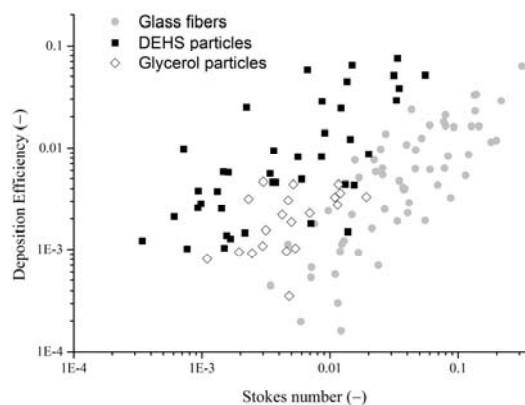


Figure 1. Deposition efficiency in the tracheobronchial tree of various particles as a function of Stokes number

Next step will be to analyze particle deposition during cyclic inhalation and to study effect of respiratory diseases, such as airway constriction in one of the lung lobes, on deposition.

Authors greatly acknowledge support from the projects FSI-S-17-4444 funded by the Ministry of Education, Youth and Sports of the Czech Republic, the grant no. GA16-23675S funded by the Czech Science Foundation, and the project MP1404 - SimInhale.

Belka, M., Lizal, F., Jedelsky, J., Jicha, M. (2013). Epj Web Conf 45.

Lizal, F., Belka, M., Adam, J., Jedelsky, J., Jicha, M. (2015). Proceedings of the Institution of Mechanical Engineers Part H-Journal of Engineering in Medicine 229:750-757.

Lizal, F., Elcner, J., Hopke, P. K., Jedelsky, J., Jicha, M. (2012). Proceedings of the Institution of Mechanical Engineers Part H-Journal of Engineering in Medicine 226:197-207.

Longest, P. W. and Holbrook, L. T. (2012). Advanced drug delivery reviews 64:296-311.

Pirozynski, M. and Sosnowski, T. R. (2016). Expert Opin Drug Del 13:1559-1571.

## Experimental data for validation of particle transport simulations in human lungs

T. Janke<sup>1</sup>, F. Lizal<sup>2</sup>, M. Belka<sup>2</sup>, J. Jedelsky<sup>2</sup>, M. Jicha<sup>2</sup> and K. Bauer<sup>1</sup>

<sup>1</sup>Institute of Mechanics and Fluid Dynamics, TU Bergakademie Freiberg, 09599, Germany

<sup>2</sup>Faculty of Mechanical Engineering, Brno University of Technology, Brno, 616 69, Czech Republic

Keywords: PIV, human airways, flow patterns, particle transport, deposition

Presenting author email: katrin.bauer@imfd.tu-freiberg.de

Information about distribution of aerosols and their deposition in the human lung airways is of growing interest. The aim is on the one hand to estimate the adverse effects of air pollutants and on the other hand to improve targeted drug delivery. Up to date a large number of numerical simulations of particle transport and deposition behaviour already exist (e.g. Kleinstreuer, 2008). However, they critically lack experimental validation. Due to limited accessibility, in vivo data hardly are available. Hence, we generated an in-vitro model which allows both, numerical simulation as well as experimental measurements. The model is based on human CT data incorporating geometry information from the mouth down to the 7<sup>th</sup> bifurcating generation.

For optical flow measurements a transparent model is required. Therefore, the internal core was first 3D printed and in a next step transparent silicone was casted with the core inside. After dissolving the core in acetone a transparent silicone model with hollow branches is received.

Here, we employ Particle Image Velocimetry (PIV) as well as Particle Tracking Velocity (PTV) measurements to visualize the flow (Janke, 2016). The set-up of the flow visualization measurement in the lung model is shown in Fig. 1.



Figure 1. Transparent lung model made from silicone in test rig for PIV measurement.

Flow measurements need to be carried out in a refractive index matching box in order to achieve an unobstructed view in the lung model. Here, a liquid is used as working fluid instead of air. Flow similarity is considered by keeping typical similarity numbers such as Reynolds- and Womersley number constant. PTV measurements reveal typical pathways of mass transport including local velocity information, thus providing information about preferred deposition regions. The pathline pattern during

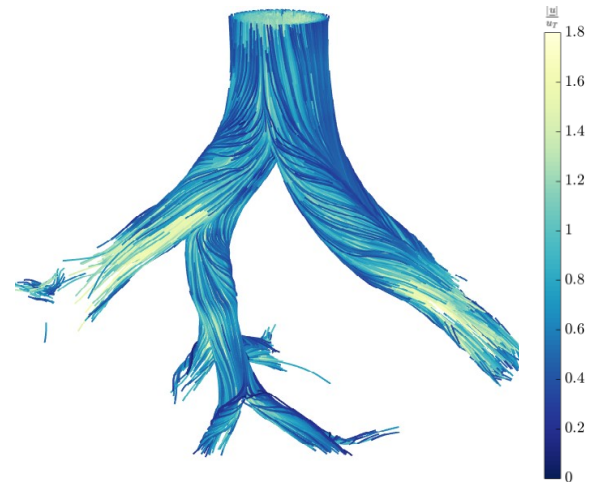


Figure 2. Pathline pattern from PTV measurements, colour coded with local relative velocity from the main bifurcation down to the 4<sup>th</sup> generation.

inspiration for the case of normal breathing is presented in Fig. 2.

In parallel, particle deposition behaviour is investigated experimentally at the same geometry but different model. Here, deposition efficiency in distinctive segments of the geometry is measured by positron emission tomography (PET) (Lizal, 2015). This is done for different flow rates of 15, 30 and 60 l/min. Both data will be used to validate numerical simulations which can be carried out again at the same geometry.

This work is supported by the Germany Research Council (DFG) under grant no. BA 4995/2-1 and by the Czech Science Foundation no. 16-23675S.

Janke, T., Bauer, K. (2016) *Development of a 3D-PTV algorithm for the investigation of turbulent flow structures in the upper human bronchial tree*. Proc. of 18th Int. Symp. on Appl. of Laser Techniques to Fluid Mechanics, Lisbon, Portugal.

Kleinstreuer, C., Zhang, Z., Donohue, J. F. (2008) *Targeted drug-aerosol delivery in the human respiratory system*. Annual Review of Biomedical Engineering, **10**, 195-220.

Lizal, F., Belka, M., Adam, J., Jedelsky, J., Jicha, M. (2015) *A method for in vitro regional aerosol deposition measurement in a model of the human tracheobronchial tree by the positron emission tomograph*. Proc. of the Inst. of Mech. Eng., Part H: Journal of Engineering in Medicine, **229**(10), 750-757

## Aerodynamic deposition of amikacin dry powder for inhalation

L. Mašková<sup>1</sup>, J. Kozáková<sup>1</sup>, F. Buttini<sup>2</sup>, V. Ždímal<sup>1</sup>

<sup>1</sup>Laboratory of Aerosol Chemistry and Physics, Institute of Chemical Process Fundamentals of the CAS, Prague, 165 02, Czech Republic

<sup>2</sup>Department of Pharmacy, University of Parma, Parma, 43124, Italy

Keywords: number/mass size distribution, amikacin, ICRP model

Presenting author email: kozakova@icpf.cas.cz

Treatment of lung infections in cystic fibrosis patients requires high doses of antibiotics. Dry powder inhaler (DPI) formulations are able to deliver high payloads of drug in a shorter time, offering a convenient alternative to solutions for nebulization (Buttini *et al.*, 2012). The aim of this study was to characterise in detail the aerodynamic particle size distribution of an amikacin dry powder for inhalation.

The formulation of the amikacin dry powder which was found as the most respirable in the previous studies (Belotti *et al.*, 2014; 2015) was characterised. The particle number size distribution was determined by an Aerodynamic Particle Sizer (APS, TSI, USA, 0.5-20  $\mu\text{m}$ , 52 size bins) and the particle mass size distribution was measured by a Berner Low Pressure Impactor (BLPI, Hauke, Austria, 0.025-10  $\mu\text{m}$ , 10 size fractions). The main modes were used to estimate the region of the particle deposition in the human respiratory tract using the deposition model of the International Commission on Radiological Protection (ICRP, 1994).

The preliminary results revealed that the number size distribution of the amikacin dry powder determined by the APS (N=10) were constant with the number mode at 1.6  $\mu\text{m}$  (Figure 1).

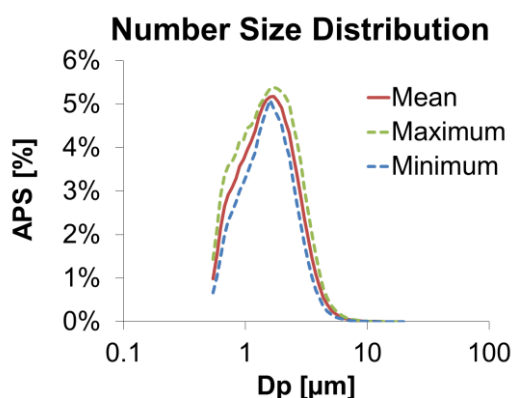


Figure 1. The aerodynamic diameter of mean, maximum and minimum values of number size distribution for amikacin dry powder.

The comparison of the mass size distribution data measured by the spectrometer APS and the cascade impactor BLPI showed a good agreement. The APS main mass mode was found at 3.3  $\mu\text{m}$  (Figure 2).

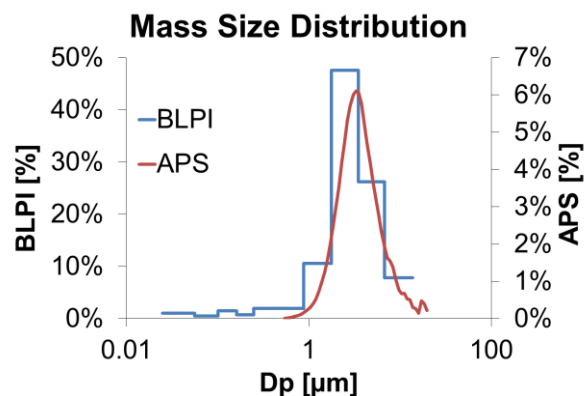


Figure 2. The mass size distribution of the amikacin dry powder measured by the APS and the BLPI.

The ICRP model showed that approximately 5% of the number and 6% of the mass concentrations will be deposited in the target tracheobronchial region of the respiratory tract. The fraction seems to be low, however, according to the model the powder has an optimal size distribution which allows the maximal possible deposition in the target region.

This work was supported by the COST-European Cooperation in Science and Technology, to the COST Action MP1404: Simulation and pharmaceutical technologies for advanced patient-tailored inhaled medicines (SimInhale).

Belotti S, Rossi A, Colombo P, Bettini R, Rekkas D, Politis S, *et al.* (2014) *Int. J. Pharm.* **471(1-2)**, 507-515.

Belotti S, Rossi A, Colombo P, Bettini R, Rekkas D, Politis S, *et al.* (2015) *Eur. J. Pharm. Biopharm.* **93**, 165-172.

Buttini F, Colombo P, Rossi A, Sonvico F, Colombo G. (2012) *J. Control Release* **161**, 693-702.

ICRP, Publication 66: Human Respiratory Tract Model for Radiological Protection. Oxford (1994).

## An efficient in silico method for deposition studies in the deep lung

P.G. Koullapis<sup>1</sup>, P. Hofemeier<sup>2</sup>, J. Sznitman<sup>2</sup> and S. C. Kassinos<sup>1</sup>

<sup>1</sup>Department of Mechanical and Manufacturing Engineering, University of Cyprus, Cyprus

<sup>2</sup>Biofluids Laboratory, Department of Biomedical Engineering, Technion – Israel Institute of Technology, Israel

Keywords: Computational fluid-particle dynamics, Deep human airways, Particle deposition.

Presenting author email: pkoull01@ucy.ac.cy

High-fidelity simulations of the complete airway tree are still beyond the capabilities of the current computers. Most of the existing studies focus either in the upper extrathoracic regions or in the terminal alveolar regions. Few studies to date have tackled the intermediate central conducting airways, that are thought to play a significant role on the characteristics of the particle phase entering the alveoli region. An example would be the size as well as spatial distribution of particles exiting the central airways into the alveolar region, which are expected to deviate from the simple uniform spatial distribution. As a result, deposition in the deeper alveoli regions will also be likely to be altered. Moreover, current studies in the literature related to deposition in the central bronchial airways, consider particle deposition only during the inhalation phase since particles that escaped the geometry cannot be tracked back during the exhalation phase. In order to take into account the impact of exhalation phase on particle deposition in the human lung, coupled simulations of bronchial and alveoli regions are required to “close” the system.

The objective of the current work is the prediction of deposition during a full breathing cycle in a simplified approximation of the deep lung. The geometry of the simplified model consists of an idealised 10-generation bifurcating tree (figure 1a), that represents the central to terminal bronchial airways (generations 10 to 19) and a sub-acinus model that represents the alveoli regions (figure 1b). The bronchial tree is generated starting from an idealised bifurcation unit with a branching angle of  $70^\circ$ , parent to daughter diameter ratio ( $D_p/D_d$ ) equal to 1.2445 and length to diameter ratio ( $L/D_d$ ) equal to 3. The bifurcation unit is repeatedly scaled, translated and rotated to build the final 10-generation tree. The nonplanarity of the tree is taken into account by randomly selected out-of plane angles between  $0-180^\circ$ . The overall dimensions of the tree are in fair agreement with morphometry measurements (Yeh and Schum, 1980). The resulting tree consists of 511 bifurcations, 1023 branches and 512 outlets. The sub-acinus model is created using the mathematical model of Koshiyama and Wada (2015) for generating a heterogeneous acinus structure model. It includes 493 alveoli and has an average of 4.85 generations.

Simulation of the 10-generation bronchial tree coupled to 512 sub-acinus units (a sub-acinus at each of the 512 outlets of the bronchial tree) is computationally infeasible. An efficient methodology is developed in order to overcome constraints related to computational resources. The low Reynolds number in the bronchial

tree in conjunction with the simplified geometry result in flow similarity in the various bifurcations of a certain generation. Consequently, the bronchial tree can be decomposed and the airflow in one representative bifurcation at a certain generation would need to be simulated. Regarding the particle phase, gravitational sedimentation is the dominant deposition mechanism in these airways for particles greater than  $1\mu\text{m}$ . Since the various bifurcations at a certain generation are oriented differently with regards to gravity, the deposition can differ greatly from bifurcation to bifurcation. Therefore, if the tracking of the particles at a certain generation is done in the representative bifurcation, which is oriented arbitrary in space, the direction of the gravity forces acting on these particles should take into account their exact positions in the bronchial tree. In this manner, particles are transported by the same flow in the representative bifurcation and they “feel” gravity as they were moving in the bronchial tree. Ultimately, instead of simulating the complete airway tree, one representative bifurcation is simulated for a certain generation, resulting in great savings in computational cost. The same procedure is applied in the alveoli region, resulting in the simulation of one sub-acinus unit. At the time of the conference the developed method as well as deposition results will be presented.

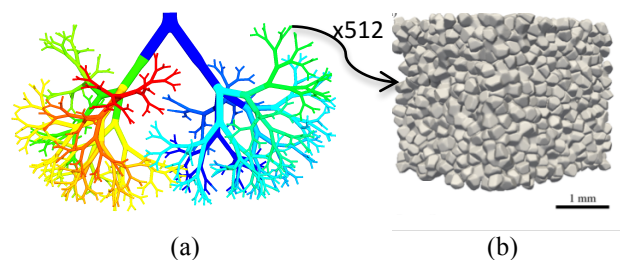


Figure 1. Geometries used for the simplified deep lung model: (a) Idealised 10-generation bifurcating tree; (b) sub-acinus model.

This work was supported by COST Action MP1404: Simulation and pharmaceutical technologies for advanced patient-tailored inhaled medicines (SimInhale).

Yeh H. & Schum G. (1980) Models of human lung airways and application to inhaled particle deposition. *Bulletin of Mathematical Biology* 42, 461-480.

Koshiyama K. & Wada S. (2015) Mathematical model of a heterogeneous pulmonary acinus structure. *Computers in Biology and Medicine* 62, 25-32.

## Comparison of Two Inhaler Devices including Wall Collision Detachment

Y. Cui<sup>1</sup> and M. Sommerfeld<sup>2</sup>

<sup>1</sup>Chair of Applied Mechanics, University of Erlangen-Nuremberg, Erlangen, D-91052, Germany

<sup>2</sup>Multi-Phase Flow Group, University of Magdeburg, Halle (Saale), D-06130, Germany

Keywords: Dry powder inhaler; Particle detachment model; Particle-wall collision.

Presenting author email: yan.cui@fau.de

Pulmonary drug delivery of dry powders is increasingly being used for medical treatment because of a number of benefits associated with an inhalation therapy. Essential for an efficient use of dry powder inhalers is the pressure drop and consequently the achievable breathing flow rate as well as the fine powder delivery to the patient's lung. Therefore, numerous geometrical designs of inhalers are available on the market (Fig. 1a). Such small drug particles (i.e. in the range between 1 and 5  $\mu\text{m}$ ) are very cohesive and are mostly blended with a larger carrier particle as one particle cluster for better dispersion by the breathing airstream. The inhaler must insure the detachment of drug powder from the carrier. This detachment is brought about by different fluid dynamic stresses (Fig. 2) and carrier particle wall impacts. Today's efficiency of drug powder delivery is typically between 30% and 40% depending on the design of the inhaler.

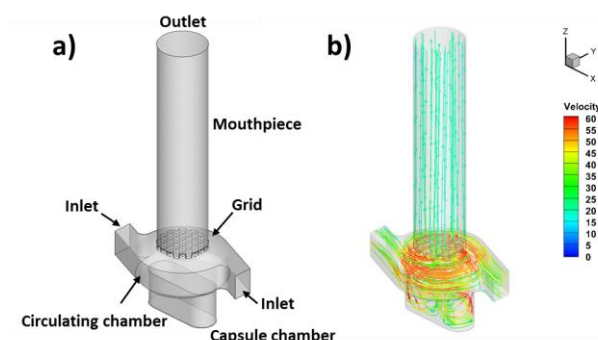


Figure 1. a) Flow domain and b) streamlines of Cyclohaler<sup>®</sup> (pressure drop: 4 kPa).

In order to improve the efficiency of inhalers a multi-scale numerical analysis is adopted. First the flow field through the inhaler is numerically calculated and the flow stresses experienced by the carrier particles are recorded (Cui *et al.*, 2014). This information is used for micro-scale simulations using the Lattice-Boltzmann method (LBM) where only one carrier particle covered with drug powder is placed in cubic flow domain and exposed to the relevant flow situations, e.g. plug flow, shear flow, turbulent flow with different particle Reynolds numbers as well as surface roughness (Cui and Sommerfeld, 2015). Furthermore, a new and efficient numerical particle-wall collision model for simulating the instantaneous forces and velocities on particles during wall collision process is developed. The most important feature of the new model is the accurate prediction of the disappearance of friction force when particles stop sliding in the compression phase; in

addition the changes of translational and rotational velocities of the carrier during collision are calculated (Cui, 2016).

The purpose of present study is twofold: (a) to compare the drug delivery efficiency of two different DPIs, i.e. the commercial Cyclohaler<sup>®</sup> and Unihaler designed by University of Kiel, with application of above detachment models; and (b) to perform a stochastic study on the measured drug size distribution and van der Waals force (i.e. adhesion force between drug and carrier). The results show that both types of inhalers considered showed extremely high wall collision rates, whereby drug particles are effectively detached by inertial effects. The stochastic distribution of measured drug size is more effective than the stochastic van der Waals force on the lift-off detachment of drug powders as shown in Fig. 2.

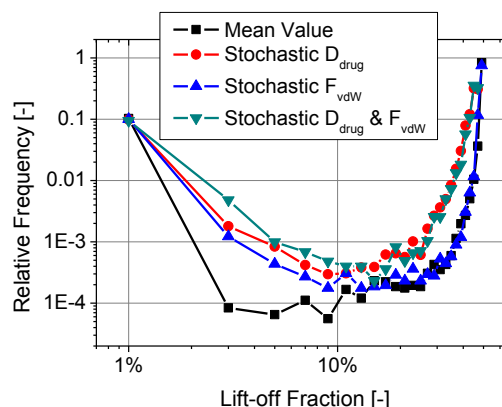


Figure 2. The relative frequency of lift-off fraction of drugs in dependent of measured stochastic values (Cyclohaler<sup>®</sup>, pressure drop: 4 kPa,  $D_{\text{drug, mean}} = 2.45 \mu\text{m}$ ,  $D_{\text{carrier}} = 100 \mu\text{m}$ , surface treatment: TC8h).

This work was supported by DFG SPP 1486 (PiKo) under contract No. SO 204/38-1 to 3.

- Cui, Y., Schmalfuß, S., Zellnitz, S., Sommerfeld, M. and Urbanetz, N. (2014) Towards the optimisation and adaptation of dry powder inhalers. *Int. J. Pharm.*, 470, 120-132.
- Cui, Y. and Sommerfeld, M. (2015) Forces on micron-sized particles randomly distributed on the surface of larger particles and possibility of detachment. *Int. J. Multiphase Flow*, 72, 39-52.
- Cui, Y. (2016) Application of the Lattice Boltzmann method for analysing the detachment of micro-sized drug particles from a carrier particle. *Doctoral Dissertation*, urn:nbn:de:gbv:3:4-18052.

## **Abstracts SPS5**

## Investigating the electrohydrodynamic atomization of highly conductive metallic salt precursors

V.A. Ganesan, M. Gensch and A.P. Weber

Institute of Particle Technology, Technical University of Clausthal, Clausthal, 38678, Germany

Keywords: EHDA, metal salts, conductivity, cone-jet mode

Presenting author email: varun.aiyar.ganesan@tu-clausthal.de

Electro hydrodynamic Atomization (EHDA) is a process that uses strong electric fields to influence the break-up of a liquid dispersed through a capillary nozzle (Agostinho, 2013). EHDA operates in different modes based on the flow parameters, electric field strength and the characteristics of the liquid.

In the dripping regime, cone-jet mode operation of an EHDA system mostly results in monodispersed droplets that are  $< 100 \mu\text{m}$  in diameter, achieved mainly with liquids that have low conductivity ( $1\text{-}100 \mu\text{S}\cdot\text{cm}^{-1}$ ). (Tang & Gomez, 1996). Many authors have reported successful electrospray in the cone-jet mode with significantly higher conductivities in the range of  $10 - 1000 \text{mS}\cdot\text{cm}^{-1}$  (Singh, et al., 2016) (Borra, et al., 1999). Simple-jet mode operation, conversely results in electrospray and atomization of droplets even with higher conductivity liquids. There is however the dependence of the droplet diameter on the inner diameter of the nozzle in the case of simple-jet mode operation. (Agostinho, 2013)

With the intention to use EHDA system to atomize liquid with higher conductivity in the range of  $100 - 10000 \text{mS}\cdot\text{cm}^{-1}$ , it was required to study the effects of these liquids in both the jetting regime and dripping regime and optimize operational parameters. In this work, the production of electrospray droplets that could be used as a feeder for a Flame Spray Pyrolysis (FSP) system has been discussed. In fact, first experiments with small droplets (Fig.1) generated from high salt content solutions (water/ethanol mixtures) with a pneumatic nebulizer and introduced into a FSP flame showed that even at moderate flame temperatures homogeneous nanoparticles could be produced (Fig.2).

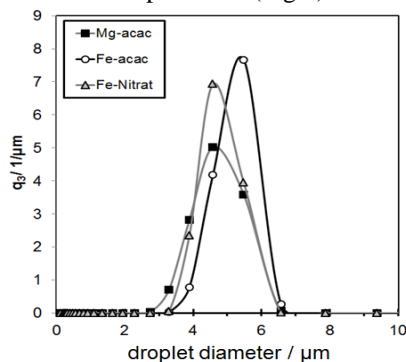


**Fig.1:** Droplet size distribution for various precursor solutions measured with laser diffraction

This observation is in contrast to the usual conception that explosion-promoting species such as

carboxylate precursors are needed for the formation of homogeneous nanoparticles in FSP.

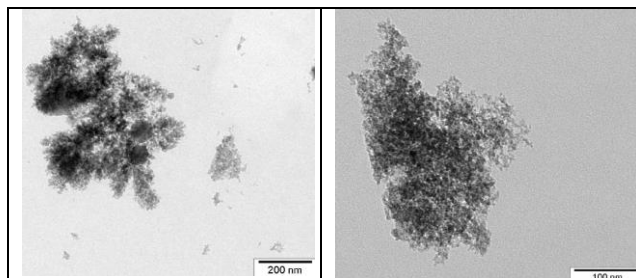


**Fig.2:** FSP-generated nanoparticles: (left) iron oxide from Fe-acac precursor solution (1.3wt%) and (right) iron oxide from Fe-nitrate solution (6.5wt%)

The electrosprayed droplets were produced from precursor liquids consisting of a mixture of water, ethanol and different metallic salts. The salts used for the experiments were Magnesium Acetate, Iron Nitrate, Magnesium Nitrate and Aluminium Nitrate.

Precursor solutions with different concentrations of salt and varying ratios of Ethanol-water mixture were used for the experiments. The electrosprayed droplet's size was measured using a Laser Diffraction apparatus and a High Speed Camera with back light illumination. The average droplet size was measured and represented for varying flow rates, applied potential, conductivity and surface tension of the precursor liquid.

It was observed from the experiments that the concentration of the salts in the precursor liquid was detrimental in determining the stability of the different modes that were obtained in the dripping regime. In some cases, a stable cone-jet mode was not achieved.

The results from the experiments conducted in this phase of the research shall be used to consider the introduction of EHDA as a direct liquid feed-in method for a FSP system used to synthesize nanoparticles extending the variety of solvent and precursors in FSP.

### References

- Agostinho, L., 2013. *Electrohydrodynamic Atomization in the Simple-Jet mode*, Delft: Delft University of Technology.
- Borra, J., Tombette, Y. & Ehouarn, P., 1999. Influence of electric field profile and polarity on the mode of EHDA related electric discharge regimes. *Journal of Aerosol Sciences*, Volume 30, pp. 913-926.
- Singh, S. et al., 2016. Electrodynamic atomization of high-conductivity pure solvent. *Particle Science Technology*, Volume 34, pp. 608-615.
- Tang, K. & Gomez, A., 1996. Monodisperse Electrosprays of Low Electric Conductivity Liquids in the Cone-Jet mode. *Journal of Colloid and Interface Science*, 184(2), pp. 500-511.



## MODELING THE EFFECT OF LATERAL FORCES IN THE TRAJECTORIES OF DROPLETS ELECTROSPRAYED IN THE SIMPLE-JET MODE

O.M. Ondimu<sup>1,2,5</sup>, V. A. Ganesan<sup>5</sup>, M. J. Gatari<sup>1</sup>, J.C.M. Marijnissen<sup>1,3,4</sup>, L.L.M. Agostinho<sup>2,4,5</sup>,

<sup>1</sup>Institute of Nuclear Science and Technology, University of Nairobi, Nairobi, Kenya,

<sup>2</sup>Centre of Expertise Water Technology, Leeuwarden, 8934CJ, The Netherlands,

<sup>3</sup>University of Florida, Gainesville, FL 32611, United States,

<sup>4</sup>Wetsus, Leeuwarden, 8911MA, The Netherlands,

<sup>5</sup>NHL University of Applied Sciences, Leeuwarden, 8917DD, The Netherlands,

Keywords: Electro Hydrodynamic Atomization (EHDA), Electro spraying, Simple-Jet Mode, Modelling, Droplet Trajectories, Packing Factor

Presenting author email: obedmarube@gmail.com

Electrohydrodynamic atomization, or simply Electro spraying is the process of influencing the breakup of a liquid using a strong electric field ( $\text{kV}\cdot\text{cm}^{-1}$ )<sup>1</sup>. Some research has been carried out on this phenomenon and various models for spraying in the cone-jet mode have been presented<sup>1,2</sup>. However, not much has been published concerning modelling of the simple-jet mode<sup>5</sup>.

In this work the effect of a lateral force (wind) on the trajectories of electro sprayed droplets in the simple-jet mode has been carried out theoretically and experimentally. The experiments were done using a nozzle to ring electro spray setup, as described in the work of *Agostinho 2012*. An imaging system comprising of a High speed camera (Photron ASX-2) and backlight illumination (Dedocool® light) was used to obtain the images, which were then processed using ImageJ® software. The lateral force on the droplets was created using a wind tunnel with controllable direction and intensity (Leybold-Heraeus® pump model number 373-04). This effect of lateral wind was introduced to a two-dimensional model, which solves the force balance equation for each droplet breaking up from the jet. The model took into consideration; the initial droplet velocity, the forces of gravity, electric field, inter-droplet coulombic and drag<sup>5</sup>.

The lateral force (wind) was applied perpendicularly to the spray axis at a distance of 40 mm down from the breakup point, where it could not interfere with the droplet formation mechanism, and where the packing factor was less than 0.2 (measured and determined via analysis of the spray images) to decrease inter-particle interference.

The tests were performed on electro sprays in the simple-jet mode for different liquid flow rates and applied electric potentials. After that, the theoretical and experimental spray shapes of the manipulated droplets' trajectories were compared.

The obtained results showed a good agreement between the experimentally observed spray shapes and the theoretically simulated droplet trajectories.

Support by the Centre of Expertise Water Technology (CEW) and the International Science Program (ISP) are acknowledged.

1. L. L. F. Agostinho, G. Taminga, C. U. Yurteri, S. Brouwer, E. C. Fuchs en J. C. M. Marijnissen, „Morphology of water Electro sprays in the Simple-jet mode,” *Phy. Rev. E*, vol. 066, nr. 86, pp. 317-326, 2012.
2. C. Yurteri, R. Hartman and J. Marijnissen, "Production of Pharmaceuticals Particles via Electro spraying with an Emphasis on Nano and Nano Structured Particles-A Review," *KONA Powder and Particle Journal No. 18*, pp. 91-115, 2010.
3. W. C. Hinds, *Aerosol Technology; Properties, behaviour, and measurement of airborne particles*, New York: John Wiley & Sons, Inc., 1999.
4. N. Fuchs, *The mechanics of Aerosols*, Toronto, Canada: Pergamon Press Ltd., 1964.
5. O. M. Ondimu, V. A. Ganesan, M. J. Gatari, J. C. M. Marijnissen and L. L. F. Agostinho “Modeling simple-jet mode electrohydrodynamic-atomization droplets' trajectories and spray pattern for a single nozzle system” *European Aerosol Conference, 2016*.

## Extractor-free one-dimensional arrays of electrosprays

N. Sochorakis<sup>1</sup>, J. Rosell-Llompart<sup>1,2</sup> and J. Grifoll<sup>1</sup>

<sup>1</sup>Chemical Engineering Department, Universitat Rovira i Virgili, Tarragona, E-43007, Spain

<sup>2</sup>ICREA – the Catalan Institution for Research and Advanced Studies, Barcelona, E-08010, Spain

Keywords: electro spray scale up, space charge, sprays, droplets.

Presenting author email: nikolas.sochorakis@urv.cat

Multiplexing of emitters is necessary in order to achieve industrially relevant production of monodisperse micro/nano-droplets from electro spray sources, for making micro/nano-particles or coatings. The collection density is lower for emitters arranged as 1D arrays than as 2D-arrays (in principle). However, extractor-type electrodes are not needed in 1D-arrays, simplifying the design (unlike in 2D-arrays; Bocanegra et al, 2005; Deng et al, 2006). On the other hand, the greater number of electrostatic interactions between sprays and emitters existing in extractor-free 1D-arrays leads to more complex physics.

We have studied the stability behaviour of linear arrays of extractor-free electro sprays in order to learn whether and how they are capable of robust operation, and which role is played by the electrostatic interactions just mentioned. Using current-vs-time data, we have determined the moment at which each sprayer goes stable or unstable as the applied voltage is scanned at constant liquid flow rate. End electrodes are located at the ends of our arrays (Rulison and Flagan, 1993, Hubacz and Marijnissen, 2003, and Quang Tran *et al*, 2010), while the sprayers protrude from a back plate.

Figure 1 shows an array of 11 operating emitters with centre-to-centre distance of 2.5 mm. For this configuration, Figure 2(a) shows the minimum and maximum operating voltages as a function of the number of operating sprayers  $N$ , which was varied from  $N=1$  (centre sprayer), subsequently turning on neighbouring sprayers ( $N=3, 5$ , etc.) to the maximum of 11. The increases of  $V_{\min}$  and  $V_{\max}$  with  $N$  are consistent with the (expected) increase in electrical space charge associated with the sprays, which weaken the electric field strength at the Taylor cone-jet regions. Figure 2(b) shows the minimum operating voltage  $V_{\min}$  vs.  $N$  for different liquid electrical conductivities. Raising the electrical conductivity causes the  $V_{\min}$  to increase, again consistently with increased space charge, and reduced electric field strength on the Taylor cone-jets.

These data are supplemented with deposition patterns on the collector created by spraying polymer solutions, and with numerical analysis of the electric field.

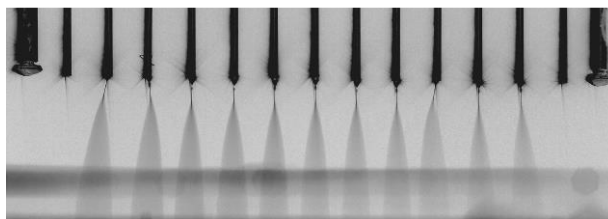


Figure 1 – Example image of 11 operating sprayers (negative photograph).

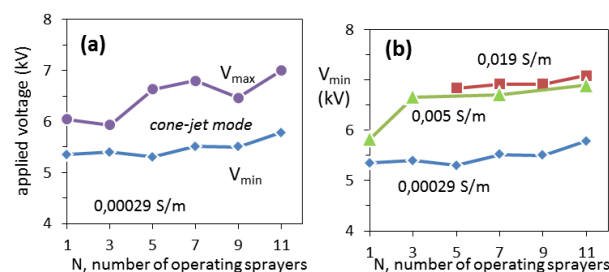


Figure 2 – (a) Maximum and minimum operating applied voltages ( $V_{\max}$  and  $V_{\min}$ ) vs. number of sprayers ( $N$ ), and (b)  $V_{\min}$  vs.  $N$  for liquids of different electrical conductivity (shown).

This work has been supported by the Spanish MINECO under grants DPI2015-68969-P and DPI2012-35687, and the Catalan government under grant 2014 SGR 1640. Nikolas Sochorakis, acknowledges BES-2013-064098 Spanish fellowship.

- Bocanegra, R., Galán, D., Márquez, M., Loscertales, I. G., and Barrero, A. (2005) *J. Aerosol Sci.* 36, 1387-1399.
- Deng, W., Klemic, J.F., Li, X., Reed, M.A., and Gomez, A. (2006) *J. Aerosol Sci.* 37, 696-714.
- Hubacz, A.N. and Marijnissen, J.C.M. (2003) *J. Aerosol Sci.* 34(Suppl.2), S1269-1270.
- Quang Tran, S.B., Byun, D., Nguyen, V.D., Yudistira, H.T., Yu, M.J., Lee, K.H., Kim, J.U. (2010) *J. Electrostatics* 68, 138-144.
- Rulison, A.J. and Flagan, R.C. (1993) *Rev. Sci. Instrum.* 64, 683-686.

## Long-term testing of catalytic layers deposited by electrospray for PEM fuel cell electrodes

S. Martin, J.L. Castillo and P.L. Garcia-Ybarra

Departamento de Fisica Matematica y de Fluidos, Facultad de Ciencias, Universidad Nacional de Educacion a Distancia (UNED). Madrid 28040, Spain

Keywords: electrospray, catalytic deposits, nanotechnology, fuel cell

Presenting author email: jcastillo@ccia.uned.es

Electrospraying of suspensions made of catalytic particles dispersed in a volatile alcohol allows to build nanostructured layers with large active areas, suitable to support catalytic processes (Castillo *et al.*, 2014). In particular, Pt on carbon nanoparticles dispersed in ethanol have been electrosprayed in the cone-jet mode (Martin *et al.*, 2012) on substrates to prepare electrodes for polymeric fuel cells (PEMFC). These electrodes have shown a large performance compared to catalytic layers prepared by other techniques (Martin *et al.*, 2013).

For practical purposes, fuel cells must be able to work in stable regimes for long times, on the order of thousands of hours, depending on the specific application. However, electrochemical and transport phenomena in the catalytic layer of the PEMFC deteriorate the catalytic activity and the deposited nanostructures leading to a continuous degradation of performance until useless values are reached.

To test the reliability of the electrosprayed catalytic layers, long-term runs of PEMFC's with electrodes prepared by this technique have been performed.

In the electrospraying process, a flow rate of  $0.2 \text{ ml h}^{-1}$  was selected to obtain a catalytic deposit made of small clusters, each cluster formed by aggregation of a few Pt/C catalyst and Nafion<sup>®</sup> particles. The voltage drop was set at 9 kV to get a stable operation of the electrospray in the cone-jet mode during the whole deposition time and a needle-substrate distance of 7 cm was chosen to ensure the complete evaporation of the ethanol in the catalytic ink droplets ejected by the needle throughout its flight-time.

Pairs of identical electrodes were assembled with Nafion XL membranes (27  $\mu\text{m}$  thickness, Electrochem Inc.) sandwiched between them (Figure 1) and inserted in the fuel cell hardware (FC05-01SP Electrochem, Inc.). All the measurements were carried out at ambient pressure and 40 °C cell temperature.

Tests were carried out in a 5  $\text{cm}^2$  active area single-cell configuration under non-humidifying regime fed from dry H<sub>2</sub> and dry air. Runs of 1000 hours were achieved for electrodes prepared from Pt/C catalysts with Pt percentage on the carbon support in the range: 10 – 60 wt.% and with a Pt loading of  $0.2 \text{ mg}_{\text{Pt}}\text{cm}^{-2}$  on each electrode. Commercial gas diffusion layers (GDL) based on non-woven carbon cloth coated with a carbon microporous layer (MPL, Freudenberg H24C3) were used as substrate to deposit the catalyst.

The fuel cells attained steady-state voltages in the approximate range 500 – 600 mV, at  $200 \text{ mA cm}^{-2}$ ,

ambient pressure and 40°C cell temperature and exhibited almost no net performance loss.

An even longer durability test conducted with electrodes prepared from 20 wt.% Pt/C demonstrated the feasibility of the non-humidifying regime for these electrosprayed electrodes. This fuel cell worked uninterruptedly for 5000 hours with a performance loss of 10 % and 20 % after 2200 and 3800 hours, respectively (Martin *et al.*, 2016).

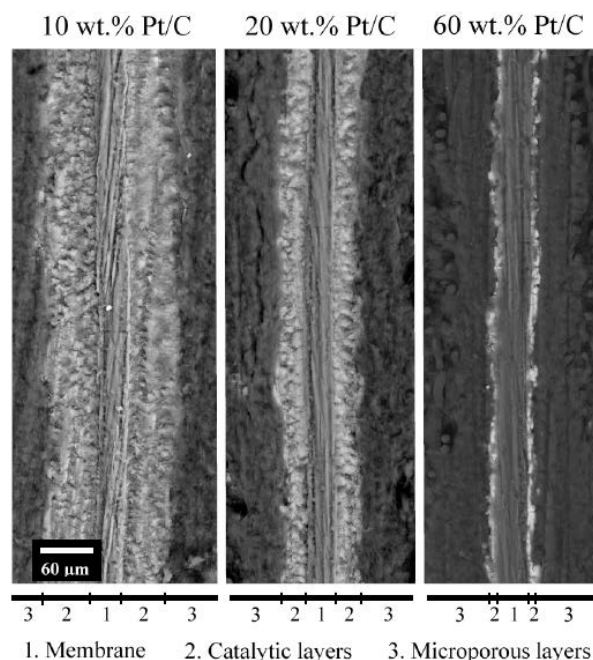


Figure 1. Backscattered SEM micrographs of the cross-section of membrane-electrode assemblies prepared from catalysts with different Pt/C ratio.

Work supported by Ministerio de Economia y Competitividad (Spain), grant no. ENE2015-67635-R.

- Castillo, J.L., Martin, S., Rodriguez-Perez, D., Perea, A., Garcia-Ybarra, P.L. (2014) *KONA Powder and Particle Journal*. **31**, 214-233.
- Martin, S., Garcia-Ybarra, P.L., Castillo, J.L. (2017) *Applied Energy*. Submitted December 2016.
- Martin, S., Martinez-Vazquez, B., Garcia-Ybarra, P.L., Castillo, J.L. (2013) *J. Power Sources*. **229**, 179-184.
- Martin, S., Perea, A., Garcia-Ybarra, P.L., Castillo, J.L. (2012) *J. Aerosol Sci.* **46**, 53-63.

## Mass Transfer between a Taylor-Cone and the Surrounding Gas Phase

C. Lübbert<sup>1</sup> and W. Peukert<sup>1</sup>

<sup>1</sup>Department of Particle Technology, University of Erlangen-Nuremberg, Erlangen, 91058, Germany

Keywords: Taylor-Cones, Mass-Transfer, Evaporation, Condensation, Conductivity.

Presenting author email: christian.luebbert@fau.de

### Introduction

The mass transfer between a Taylor cone and the surrounding gas phase is an important aspect in electro spraying, especially with small flow rates. "Small" can in general be quantified as a function of liquid properties and the capillary dimensions of the electro spray setup. A theoretical correlation between capillary dimensions and solvent properties is derived which allows to estimate the relevance of the mass transfer processes.

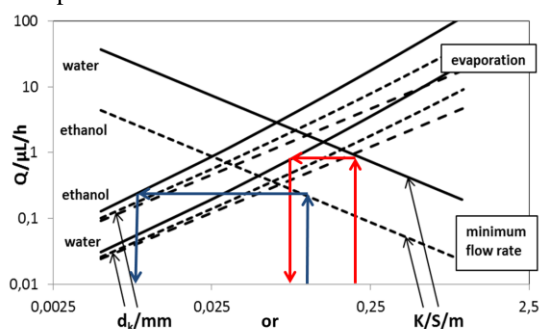


Fig. 1: Minimum feed flow rate as function of the liquid conductivity and evaporating flux as function of the capillary diameter in a vapour free gas phase at ambient conditions for ethanol and water. A maximum capillary diameter to spray a liquid at the minimum flow rate in a vapour free gas phase can easily be found as indicated by the red (water) and blue (ethanol) arrows.

Using large capillary dimensions and high conductivity considerable liquid evaporating solvent fluxes are reached and liquid composition and temperature in the cone may change significantly (or the whole liquid feed may even evaporate).

Changes in the liquid composition have in general an impact on surface tension, relative permittivity and viscosity. The latter is directly correlated to the specific conductivity and is influenced by the changes of temperature due to evaporation, too. In most application relevant situations the liquid which is actually sprayed from the tip of a Taylor cone will differ significantly from that fed into the capillary.

This problem can be significantly reduced by spraying under vapour enriched/saturated gas phase conditions which reduces the amount of evaporating solvent and the change in composition largely. Realizing the importance of the mass transfer at the Taylor cone a virtue is easily made of the necessity. Particularly interesting is the case when liquids are sprayed in a gas phase saturated by vapours which are in equilibrium with other solvents or solvent mixtures.

### Experimental validation

It is well known, that water cannot be sprayed under air atmosphere at ambient conditions. Due to its high surface tension gas discharges occur prior to stable Taylor cone development. Spraying water under vapour saturated atmospheres, whereby the vapours are in equilibrium with alcohol water mixtures, the composition of the liquid in the Taylor cone is very close to the equilibrium liquid composition which corresponds to the vapour phase. We have validated this by feeding water-sodium chloride solutions into the spray capillary and comparing surface tensions of the liquid in the Taylor cone to that of the liquid used to saturate the gas atmosphere. The saturated gas phase is fed as a sheath flow around the spray capillary at a flow rate of 1...2 mL/s. Results are shown in Fig. 2.

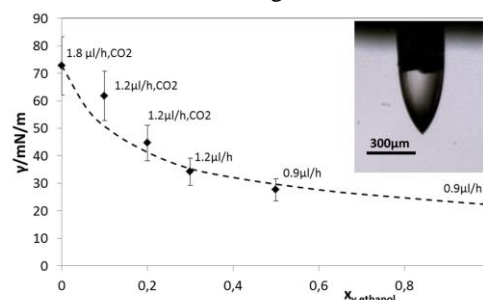


Fig. 2: Surface tension of sodium chloride in water sprayed under gas atmospheres which are in equilibrium with water ethanol mixtures of different ethanol volume fractions. Surface tension values are derived from the voltage applied to the spray to obtain equal Taylor cone tip position using pure water and the corresponding operation voltage as calibration point. Surface tension values were calculated as  $\gamma_{cone} = \gamma_{water} (U/U_{water})^2$ .

Changing the liquid composition by the surrounding gas phase allows not only switching fast between different solvent compositions. Manipulation of other parameters such as conductivity and pH are possible as well using volatile acids or bases in the vapour phase. Spraying water acetic acid solutions under vapours containing ammonium, results in a strong increase of conductivity due to improved dissociation of the acetic acid (formation of ammonium acetate). The same effect is obtained when solutions of weak bases are sprayed under CO<sub>2</sub>.

And finally electro sprays can be established from hygroscopic solutions fed with liquid only via condensation from the gas phase - a method which allows adjusting very small flow rates. Experimental results on the latter statements will be part of the presentation.

## Experimental Investigation of the Liquid-to-Gas-Phase-Transfer of Macro-Ions

C. Lübbert<sup>1</sup> and W. Peukert<sup>1</sup>

<sup>1</sup>Department of Particle Technology, University of Erlangen-Nuremberg, Erlangen, 91058, Germany

Keywords: Charged residue model, Macro molecules, SMPS, Spray polarity, Escape probability.

Presenting author email: christian.luebbert@fau.de

The mechanism by which large ions are transferred from electrosprayed drops into the gas phase is still not understood well. The probability that large ions such as ionic polymers or proteins escape from the drops by ion evaporation is practically excluded. Fernandez de la Mora argued based on molecule charge states that the transfer mechanism for such species can be explained only by the charged residue model.

We have measured size spectra of evaporation residues from drops containing significantly more than a single macro-ion in the positive and the negative ion mode by SMPS. As macro-ions we used two proteins BSA (PI 4.7) and lysozyme (PI 11.3), respectively, and Nafion, a sulfonated fluor-polymer,  $PI < 1$ . These molecules were dissolved in water containing 5% acetic acid for acidic spray conditions and 1.5% pyrrolidin under alkaline conditions. The gas phase in the spray chamber was enriched with vapours in equilibrium with a 50%<sub>v</sub> water 50%<sub>v</sub> 2-propanol mixture to allow spraying the solutions in the negative and positive ion mode. In the experiments under alkaline conditions nitrogen was used as carrier gas for the vapours to ensure that the pH is not changed by CO<sub>2</sub> absorption from the air.

The measured size spectra reveal that large amounts of the dispersed macro-ions escape from the drops during the evaporation process if the spray polarity equals the surface charge polarity of the macro molecules. In the opposite case the macro-ions remain quantitatively inside the parent drop and form a single solid residue per drop (see Fig. 1).

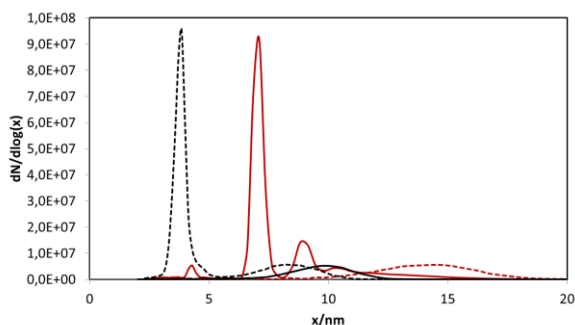


Fig. 1: Evaporation residues of BSA (red) and Nafion (black) when sprayed in the negative ion mode (dashed lines) and in the positive ion mode (solid lines). All sprays are performed from acetic acid 5%<sub>v</sub> in water under 2-propanol, water vapour atmosphere. The Nafion (a monomer of 3nm in diameter,  $pI < pH$ ) escapes in the negative ion mode only while the BSA (monomer at 6,8nm,  $pI > pH$ ) escapes only in the positive ion mode.

Close to the isoelectric point (e.g. for lysozyme sprayed under alkaline conditions) roughly equal escape probabilities in the positive and negative ion mode were observed. However, the escaping fractions are lower compared to those under acidic conditions in the positive ion mode. Therefore, the probability for the drop-to-gas phase transfer cannot be explained from the charged residue model alone or intrinsic surface activity of the molecules.

An explanation for this behaviour is found from a characterisation of the electric states of the drops. Solving the Poisson-Boltzmann equation inside the drop at the drop surface reveals that the “inner” electric potential (drop centre to surface – but practically over a few Debye length only) for weak bases or acids used as electrolyte is typically in the range 1.5...2.5kT/e. With 2...3 elementary charges at the shear plane as relevant charges on the macro-ions (estimated from the  $\zeta$ -potentials of the macro-ions) a significant enrichment/depletion of the macro-ions at the drop surface is predicted under equilibrium conditions dependent on the spray polarity. Results from numerical calculations for positively charged molecules (charge at  $\zeta$ -potential: +3e) are shown in fig. 2.

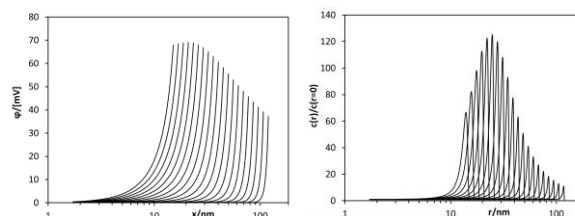


Fig. 2: Simulated inner potentials and corresponding surface enrichment factors of a macro ion with +3 elementary charges in a positively charged drop containing a dissociation limited electrolyte (e.g. acetic acid at sufficiently high concentration). Different curves represent different drop sizes during the evaporation process.

Assuming the escape probability to be proportional to the close-to-surface concentration under consideration of the inner electric state allows predicting the measured size spectra almost quantitatively.

Fernandez de la Mora, J. F. (2000), *Analytica Chimica Acta* **406**, 93–104.

## Ion specific Effects in Electro spraying measured in an Electrochemistry free Setup

C. Lübbert<sup>1</sup> and W. Peukert<sup>1</sup>

<sup>1</sup>Department of Particle Technology, University of Erlangen-Nuremberg, Erlangen, 91058, Germany

Keywords: Scaling laws, spray current, acids, residue size spectra.

Presenting author email: christian.luebbert@fau.de

Scaling laws for prediction of electro spray properties correlate the current uptake and the generated particle size to the flow rate and the liquid properties. Liquid properties considered are conductivity, surface tension, viscosity, density and relative permittivity. Differences caused by the choice of the electrolyte are therefore in general not expected based on the scaling laws.

Especially with low viscosity liquids scaling laws predict high ionization efficiencies. This efficiency can be expressed in terms of excess ions in the spray with respect to the total ion flux which is given by the liquid flow rate and the ion concentration in the sprayed liquid. The conductivity (which is used in scaling laws) is correlated to the ion concentration by the ion specific conductivity. Comparing acids and salts one typically finds differences in the specific conductivities as high as a factor of 3. And while the ionization efficiency for a liquid having a viscosity of 1mPas is predicted to be around 25% when a salt is used as electrolyte, one finds roughly 70% for acids from scaling laws at low flow rates. With efficiencies that high the question arises whether electrochemical processes have an impact on the ion composition and concentration in the liquid inside the Taylor-cone on the one hand. On the other hand the Debye-length is significant in these cases and will be a function of the specific conductivities of the electrolyte.

We have developed a simple electro spray setup which electrochemical processes are excluded. Flow-rate, current curves were measured with this setup where the composition of the electrolyte is well known. The data are represented the dimensionless plot suggested by Ganan-Calvo and show indeed significant differences for different electrolytes used to establish conductivity. Fig.1 shows a comparison between potassium chloride and hydrochloric acid used as electrolyte in a mixture of 33.3%<sub>v</sub> Methanol in water.

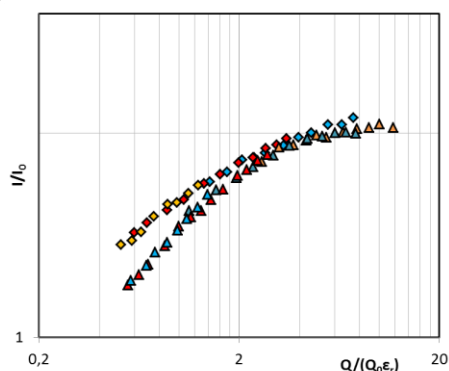


Fig.1 : Influence of electrolyte on flowrate current uptake curves. Diamonds: potassium chloride, triangles: hydrochloric acid.

While the current uptake is a function of the electrolyte but not of the spray polarity we find the outcome of fission products to be polarity dependent when acids are used as electrolytes. This has been found by spraying sucrose solutions 0.1%<sub>v</sub> in positive and negative ion mode. Results are shown in figures 2 and 3.

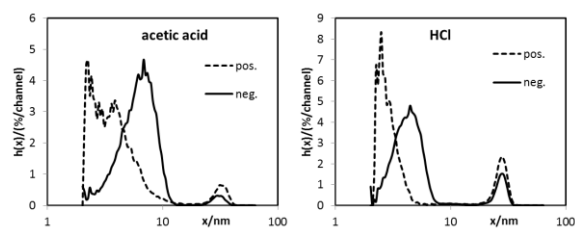


Fig. 2: Size spectra of evaporation residues for a weak and a strong acid in positive and negative spray polarity.

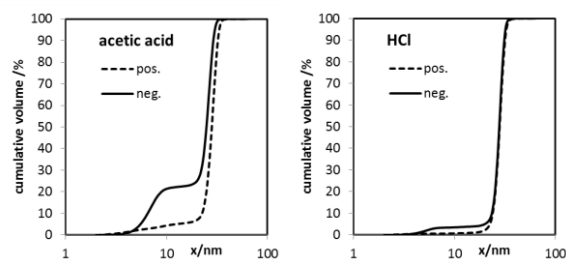


Fig. 3: cumulative volume distribution corresponding to size spectra in Fig. 2.

Large polarity dependent asymmetries in the emitted mass are found in case that acids are used as electrolyte. The asymmetry is in general a function of the strength of the acid used. This can be explained by the dissociation limited amount of ions in the evaporation process for weak acids. While the conductivity (and Debye-length) are limited with weak acids at an early point in the evaporation process this happens much later with strong electrolytes.

Concerning the polarity dependent asymmetry it must be mentioned that with electrolytes of close to equal limiting conductivities of positive and negative ions, such as NaCl or KCl, the emitted masses in fission processes and the size of the off-spring drop residues are perfectly polarity independent. Therefore, the asymmetry must be caused by the difference in the limiting conductivities of the ions involved. We explain this behaviour by a non-stationary Debye-length approach adapted from plasma physics.

Ganan-Calvo, A. M. (2004), *Journal of Fluid Mechanics* **507**, 203-212.

## A Bipolar electro spray source of singly charged salt clusters of precisely controlled composition

J. Fernandez de la Mora<sup>2</sup> and C. Barrios-Collado<sup>1</sup>

<sup>1</sup> SEADM, Parque tecnológico de Boecillo 205, 47151 Valladolid, Spain

<sup>2</sup>Yale University, Mechanical Engineering Department, New Haven, CT 06420

Keywords: Electro spray, charge reduction, neutralization, cluster.

Presenting author email: juan.delamora@yale.edu

We combine two oppositely charged electro sprays to convert initially electro sprayed multiply charged particles into primarily singly charged particles. Excellent independent stable control of the positive and the negative sprays brought very close to each other is achieved by isolating them electrostatically with a symmetrically interposed metallic screen (Figure 1), similarly as in Fernandez de la Mora (2016)



Fig. 1: Image of the bipolar ES chamber with 2 windows, 2 connectors oriented at 90° bringing in 2 capillary emitters. A metallic grid isolates the capillaries

A first set of tests combines two oppositely charged electro sprays of solutions of the same salt  $B^+A^-$ , including:  $(C_nH_{2n+1})_4N^+Br^-$  ( $n=4,7,12,16$ ), the large phosphonium cation  $(C_6H_{13})(C_{16}H_{33})P^+$  paired with the anions  $Im^- [(CF_3SO_2)_2N^-]$  or  $FAP^- [(C_2F_5)_3PF_3^-]$ , and the asymmetric pair [*1-Methyl-3-pentylimidazolium*<sup>+</sup>*FAP*<sup>-</sup>].

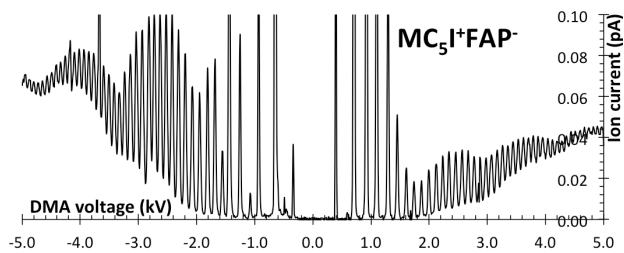


Figure 2: Bipolar mobility spectrum of *1-Methyl-3-pentylimidazolium*<sup>+</sup>*FAP*<sup>-</sup> showing up to 43 resolved clusters in each polarity.

As shown in the mobility spectra of Figure 2, both polarities are simultaneously produced by this source in comparable abundances, primarily as singly charged  $A^+B^-_{n±1}$ , with tiny contributions from higher charge states. Some but not all of these clusters produce narrow mobility peaks typical of pure ions (Figure 3).

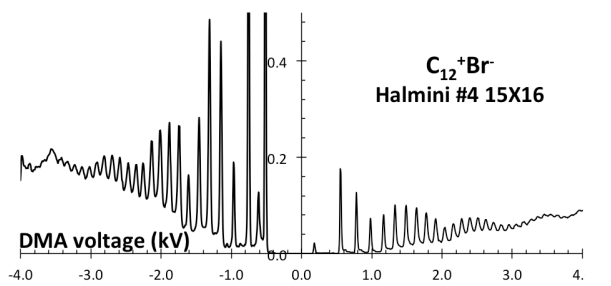


Figure 3: Bipolar mobility spectra of  $(C_nH_{2n+1})_4N^+Br^-$  with  $n=12$ , showing peaks broader than in Figure 2

Two nanoDMAs covering the size range up to 30 nm (Halfmini and Herrmann DMAs, with classification lengths of 2 and 10 cm) are characterized with these standards, revealing resolving powers considerably higher than previously seen with unipolar electro spray sources.

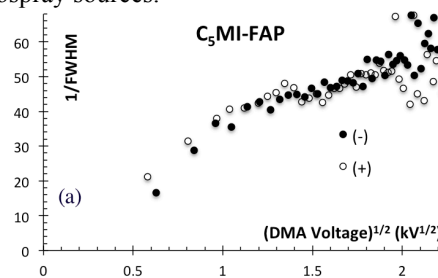


Figure 4: Resolution ( $1/FWHM$ ) for the Halfmini DMA challenged with  $MC_5I^+FAP^-$  clusters, demonstrating resolving powers  $>50$  with sufficiently large particles.

This bipolar source of *pure* and chemically homogeneous clusters described permits studying size and charge effects in a variety of aerosol instruments in the 1-4 nm size range.

In a second set of experiments to be described, an aqueous protein solution is electro sprayed from the positive capillary, and an alcohol solution of a volatile salt is electro sprayed from the negative capillary. This results similarly in charge-reduced protein ions.

Conclusions: The bipolar source is an excellent substitute for radioactive neutralizers.

Fernandez de la Mora, J. (2015) High-Resolution Mobility Analysis of Charge-Reduced Electro sprayed Protein Ions, *Anal. Chem.*, 87, 3729–3735

## Solid-state electrolytes for lithium ion batteries: Application of electro spray technique

S.W. Karuga<sup>1</sup>, M.J. Gatari<sup>1</sup>, E.M. Kelder<sup>2</sup> and J.C.M Marijnissen<sup>1,3</sup>

<sup>1</sup>Institute of Nuclear Science and Technology, University of Nairobi, Nairobi, Kenya

<sup>2</sup>Faculty of Applied Sciences, Delft University of Technology, Delft, 2600 GA, The Netherlands

<sup>3</sup>University of Florida, Gainesville, FL 32611, United States

Keywords: Aerosol, Electrostatic spray deposition, Cone-jet, Pyrolysis

Presenting author email: swkaruga@yahoo.com

Li-ion batteries have shown high energy densities for wide applications but they use organic liquids as electrolytes. This poses a safety concern because of their flammability and it explains the recently reported accidents with Tesla, Samsung Galaxy and the Dreamliner; therefore, different studies to improve on their safety are ongoing. The most recent is on how to replace the organic liquids with solid-state (inorganic) electrolytes of either ceramic or glassy origin. Success of this replacement is based on the exemplary performance of Li-ion conductivity exhibited by glassy electrolyte materials of lithium-sulfur-phosphorus (Li-S-P) compounds. In view of these findings, it is possible to make a completely safe solid-state lithium ion battery system. However, the major drawback of the solid-state Li-ion batteries has been the poor solid contacts between the electrolyte and the electrodes thus limiting their commercial applications. Several techniques of increasing contact area at the interface have been explored and coating the electrodes with the solid electrolyte has attracted attention.

The standard thickness of a commercial Li-ion battery electrolyte is about 10  $\mu\text{m}$  and a layer thinner than 1  $\mu\text{m}$  would significantly lower the battery's internal resistance hence boosting its ionic conductivity. However, the challenge here is to deposit thin layers based on Li-S-P with a thickness of about 100 nm and to deposit these layers homogeneously over the complete electrode surface thus preventing any electrical short circuits. Therefore, this study reports on the optimisation of the solid interface using electrostatic spray deposition (electrospray) which is an aerosol particle deposition technique. It stands out because of its ability to generate charged droplets hence higher deposition efficiency is expected compared to other methods (Leeuwenburgh *et al.*, 2006).

In electro spray, different spraying modes can be achieved by changing the applied electric field strength and the flow rate of the liquid precursor. For this work, cone-jet mode is preferred since it generates spherical monodisperse droplets that are in the nano/micrometer range and model equations are available for estimation of the droplet size (Yurteri *et al.*, 2010). Using a selected solvent, an electrolyte liquid precursor is prepared and by applying electro spray, aerosol particles are generated and directed towards a heated substrate/electrode to form a thin film. During this process, highly electrically charged droplets are generated and the mutual Coulomb repulsion among them causes self-dispersion hence formation of thin films with uniform thickness. Usually, the temperature

of the substrate/electrode is set such that a combination of pyrolysis, reduction and/or oxidation takes place to form the final desired compound. This method allows the formation of thin films with different surface morphologies depending on the physical and chemical properties of the electrolyte liquid precursor like density, surface tension, conductivity, concentration and viscosity.

Experimental parameters like liquid flow rate and the applied voltage also play an important role in achieving the desired film. Consequently, homogeneous coatings with a thickness of 100 nm or less will be achieved. Eventually, a solid-state battery will be fabricated by alternating electro spray steps for electrode and electrolyte layers (Figure 1). This will simplify the battery design and improve its handling safety and cell durability. The latest results on this study will be presented at the conference.

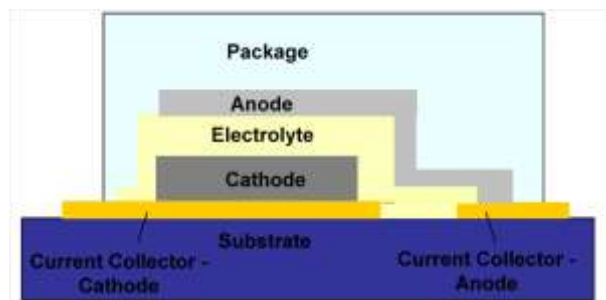


Figure 1. Schematic representation of a thin film solid-state Li-ion battery in 2-D (Adapted from Garcia, 2014).

This work is supported by the International Science Programme, Uppsala University, Sweden and Delft University of Technology, Netherlands.

Leeuwenburgh, S. C. G., Heine, M. C., Wolke, J. G. C., Pratsinis, S. E., Schoonman, J. and Jansen, J. A. (2006). Morphology of calcium phosphate coatings for biomedical applications deposited using Electrostatic Spray Deposition. *Thin Solid Films*, **503**, 1 - 2.

Garcia, T. E. (2014) Advanced Thin Layer Deposition of Materials for Li-ion Batteries via Electro spray. *Ph.D thesis*, Delft University of Technology, pp 14.

Yurteri, C. U., Hartman, R. P. A., and Marijnissen J. C. M. (2010). Producing Pharmaceutical Particles via Electro spraying with an emphasis on Nano and Nano structured Particles - A Review. *KONA Powder and Particle Journal*, **28**, 91 - 115.

## Nanoparticle synthesis using an Electrohydrodynamic Atomizer integrated Flame Spray Pyrolysis system

V.A. Ganesan, M. Gensch and A.P. Weber

Institute of Particle Technology, Technical University of Clausthal, Clausthal, 38678, Germany

Keywords: EHDA, FSP, nanoparticles, cone-jet mode

Presenting author email: varun.aiyar.ganesan@tu-clausthal.de

Electrohydrodynamic Atomization (EHDA) or electrospray is a technique used to generate fine droplets with mono-disperse size distribution from a liquid under the influence of electrostatic forces (Yurteri, et al., 2010). The atomized droplet's size depends on parameters like flow rate, electric field strength, conductivity & viscosity of liquid among others (Agostinho, 2013).

Flame spray pyrolysis (FSP) is a process that assists in rapid and scalable synthesis of nanoparticle using appropriate precursors that are fed as liquid to a flame (Teoh, et al., 2010). Liquid feed is generally established with pneumatic atomizers at increased expense of carrier gases or feeding methods requiring use of precursors with additive mixtures.

In this work, the use of an EHDA system to atomize and spray liquid precursor droplets directly on to the flames generated from a flat flame burner is discussed. Tetraethyl orthosilicate mixed with 20 vol % of 2-propanol was used as the precursor. The EHDA system consisted of a nozzle assembly, a high voltage source for energizing the nozzle and in this case, the flame itself was acting as a counter electrode, and a high-speed camera with rear illumination. The precursor liquid's characteristics were determined and mode analysis tests were conducted. The cone-jet mode was determined as the appropriate mode of operation. The droplets had a mean diameter of 24.8  $\mu\text{m}$  and 0.22 RSD.

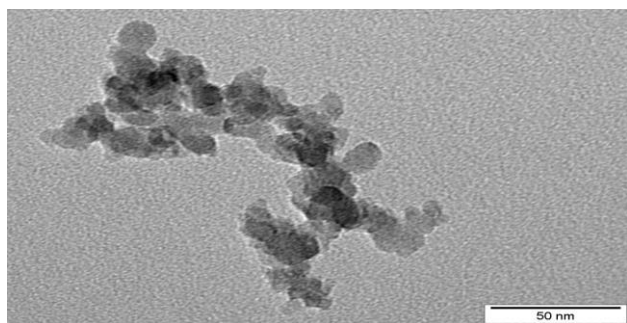


Figure 1 EHDA assisted FSP generated nanoparticle agglomerate of SiO<sub>2</sub> from Tetraethyl orthosilicate and 2-propanol (20% vol.) precursor solution

The placement of the nozzle and the burner was optimized in a manner such that the fine droplets would precisely enter the flame at a pre-determined target region. The system was run for a period of 30 minutes and the particles produced were collected in a filter. Subsequently the particles were analysed using TEM images (fig 1) and an EDX measurement (fig 2).

The TEM images were used for image analysis to determine the primary particle size of the synthesized SiO<sub>2</sub> nanoparticles. The average diameter was 32 nm with a standard deviation of 17.16 nm. This observation is in contrast to the usual conception that explosion-promoting species such as carboxylate precursors are needed for the formation of homogeneous nanoparticles in FSP.

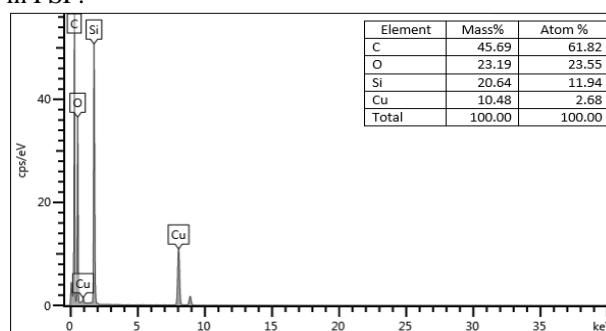


Figure 2 Energy-dispersive X-ray spectroscopy measurements of the nanoparticle with the elemental composition of the different substances. (Note: Cu and C are from the TEM grid)

The results from the EDX tests show that the particle seen in the TEM image is SiO<sub>2</sub>.

The advantage of using this system is the monodisperse droplet size that allows studying the influence of the droplet diameter on the resulting nanoparticle morphology. In addition, there are indications that for small enough droplets a new route will open to extend the variety of simple solvent that can be used in FSP. The EHD atomizer acts as an add-on equipment and does not require any modification of the burner or its assembly. This makes it a viable option for nanoparticle synthesis.

The results obtained in this experiment shall be important in providing better understanding of the use of an EHDA feeding system for particle synthesis using the liquid fed FSP route for metallic salts with higher conductivity.

### References

- Agostinho, L., 2013. *Electrohydrodynamic Atomization in the Simple-Jet mode*, Delft: Delft University of Technology.
- Teoh, W., Amal, R. & Madler, L., 2010. Flame spray pyrolysis: An enabling technology for nanoparticles design and fabrication. *Nanoscale*, 2(8), pp. 1324-1347.
- Yurteri, C., Hartman, R. & Marijnissen, J., 2010. Producing Pharmaceutical particles via Electro spraying with an emphasis on nano and nano structured particles - A review. *KONA Powder and Particle Journal*, Issue 28, pp. 91-115.

## Electrohydrodynamic Atomization of a non-Newtonian solution with high solid content

C.W.Gachara<sup>1</sup>, I. Kapasi<sup>2</sup>, I. Hausz<sup>2</sup>, J.C.M.Marijnissen<sup>1,4</sup>, M.J Gatari<sup>1</sup> and L.L.F.Agostinho<sup>3</sup>

<sup>1</sup>Institute of Nuclear Science & Technology, University of Nairobi, P.o Box 30197-00100 Nairobi, Kenya.

<sup>2</sup>Department of Agricultural & Environmental Sciences, Szent István University, Páter Károly 1, 2100 Hungary.

<sup>3</sup>NHL University of Applied Sciences, Agora 1, 8934 CJ, Leeuwarden, The Netherlands.

<sup>4</sup>University of Florida, Gainesville, FL 32611, USA

Keywords: Electro hydrodynamic Atomization (EHDA), High-solid content, non-Newtonian, spray mode.

Presenting author email: waigachara@yahoo.com

Electrohydrodynamic atomization (EHDA) has been used as a versatile tool to produce well dispersed droplets with defined size and different morphologies (Yurteri *et al* 2010). Some examples of applications are medicine encapsulation (Orlu-Gul *et al* 2014), nanofibers production (Reneker and Yarin, 2008) and metal recovery in liquid media (Parmentier *et al* 2016). More recently some authors have also reported the characteristics and functioning of EHDA with non-Newtonian liquids. Some examples are the work of Zang *et al* (2006) who used high viscous silicone oil with viscosity ( $\sim 58,200\text{mPa}\cdot\text{s}$ ) and electrical conductivity ( $\sim 10^{-9}\text{Sm}^{-1}$ ) to produce micro threads (i.e.  $130 \leq d \leq 170 \mu\text{m}$ ), the work of Pancholi *et al* (2009) who electrospayed chitosan a suspension in a stable cone jet and reported about the effects of liquid viscosity and surface tension on particle diameter, and the work of Watanabe *et al* (2003) who used different high viscous, non-Newtonian polymer solutions and derived scaling laws relating the produced droplet size with the Weber and Reynolds numbers and the electric field intensity. Such interest is justified by the fact that many industrial/commercial processes are based on the atomization of non-Newtonian liquids, e.g. milk drying processes, spray painting, etc.

In this work, the behavior of a non-Newtonian emulsion with more than 50%w/w solid content (carbohydrate, protein, oil) electrospayed at different flow rate regimes, i.e. dripping regime ( $We < 4$ ) and jetting regime ( $We > 4$ ), and different electric field intensities, was studied. Main objective was to study the droplet formation mechanism and electrospay and compare it to what is in the literature for low viscous Newtonian liquids (Cloupeau and Prunet-Foch, 1990). The experiments were conducted using a nozzle to plate configuration, with the nozzle set at ground and the plate at negative (high) potential. A high speed camera (Photron SAX2<sup>®</sup>) with a microscopic lens was used to capture the images during the atomization process. Further, the obtained images were analyzed using ImageJ<sup>®</sup> to provide the data about droplet size and size distribution.

Results have shown that the characteristics of the studied liquid, strongly influences its break up mechanism which consequently influences the formation of the electrospay modes. Such effect can be specially observed with the high flow experiments (Figure 1c), where the formation of the Rayleigh instabilities is strongly damped by the viscous drag. The low flow

experiments (figure 1 a and b) allowed the formation of an unstable meniscus where small and big parcels formation takes place. High flow experiments (figures 1 c and d) provided the formation of a simple-jet mode with whipping breakup (figure 1d), however with frequent big parcels detachments.

Droplet size analyses have shown a big dispersion ( $RSD > 0.6$ ) for all the tested configurations.

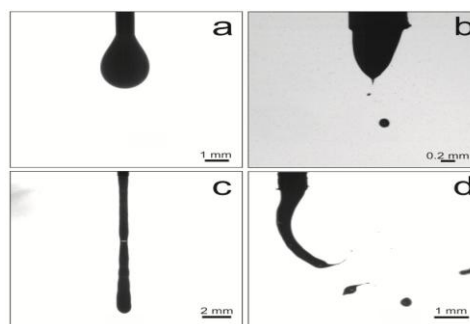


Figure 1. Obtained EHDA modes with  $We < 4$  (a and b) with no potential (1a) and 13kV (1b) and  $We > 4$  (c and d) with no potential (1c) and 20kV (1d). Nozzle to plate distance is 2cm (a and b) and 5cm (c and d).

The authors would like to kindly thank the technical and financial support of The Centre of Expertise Water Technology (CEW) and FB Oranjewoud Foundation.

- Cloupeau, M., & Prunet-Foch, B. (1989) *Journal of Electrostatics*. **25**(2), 165-184.
- Orlu-Gul, M., Topcu, A. A., Shams, T., Mahalingam, S., & Edirisinghe, M. (2014) *Current opinion in pharmacology*. **18**, 28-34.
- Parmentier, D., Rybałtowska, A., van Smeden, J., Kroon, M. C., Marijnissen, J. C., & Lemos, L. (2016) *Journal of Electrostatics*. **80**, 1-7.
- Pancholi, K., Ahras, N., Stride, E., & Edirisinghe, M. (2009) *Journal of Materials Science: Materials in Medicine*. **20** (4), 917-923.
- Reneker, D. H., & Yarin, A. L. (2008) *Polymer*. **49**(10), 2387-2425.
- Watanabe, H., Matsuyama, T., & Yamamoto, H. (2003) *Journal of Electrostatics*. **57**(2), 183-197.
- Yurteri, C. U., Hartman, R. P., and Marijnissen, J. C. (2010) *KONA Powder and Particle Journal*. **28**, 91-115.
- Zhang, H. B., Jayasinghe, S. N., and Edirisinghe, M. J. (2006) *Journal of electrostatics*. **64**(6), 355-360.

## Aerosol deposits from electro spraying liquid suspensions

S. Martin, D. Rodriguez-Perez, P.L. Garcia-Ybarra and J.L. Castillo

Departamento de Fisica Matemática y de Fluidos, Facultad de Ciencias, Universidad Nacional de Educacion a Distancia (UNED). Madrid 28040, Spain

Keywords: electro spray, aerosol deposits, nanotechnology

Presenting author email: jcastillo@ccia.uned.es

In this experimental work, a suspension of carbon nanoparticles in ethanol was steadily electro sprayed in the cone-jet mode with the resulting charged droplets driven towards a collecting surface. Ethanol evaporates during the droplet flight and the particles emitted at the electro spray tip are collected on the substrate building up a granular deposit of nanoparticles. As it was reported earlier, changes in the liquid composition and in the electro spray working parameters (needle voltage, collector voltage and flow rate) affect the stability of the cone-jet mode (Martin *et al.*, 2012) and also have a strong influence on the particle arrival to the collecting surface which indeed determine the deposit structure (Rodriguez-Perez *et al.*, 2007).

In many practical applications which make use of porous materials suitable values of surface roughness and bulk porosity may be required. Thus for instance, these structural properties have a strong influence on the performance (Martin *et al.*, 2013, Castillo *et al.*, 2014) and long-term durability (Martin *et al.*, 2017) of highly porous catalytic enhancers. Therefore, a broad study of deposit features as a function of electro spray working conditions was needed.

The aim of this work is to analyse the aerosol deposit morphology depending on the electro spray flow rate ( $Q$ ). The enclosed figures depict SEM images of carbon deposits formed with different values of  $Q$  but the same total collected mass.

Image processing analysis of these images allows to determine the main deposit features. The deposit mean porosity is rather high but decreases with the flow rate showing a transition from dry deposition to wet deposition probably due to incomplete evaporation of ethanol at large enough flow rates.

Work supported by Ministerio de Economía y Competitividad (Spain), project ENE2015-67635-R.

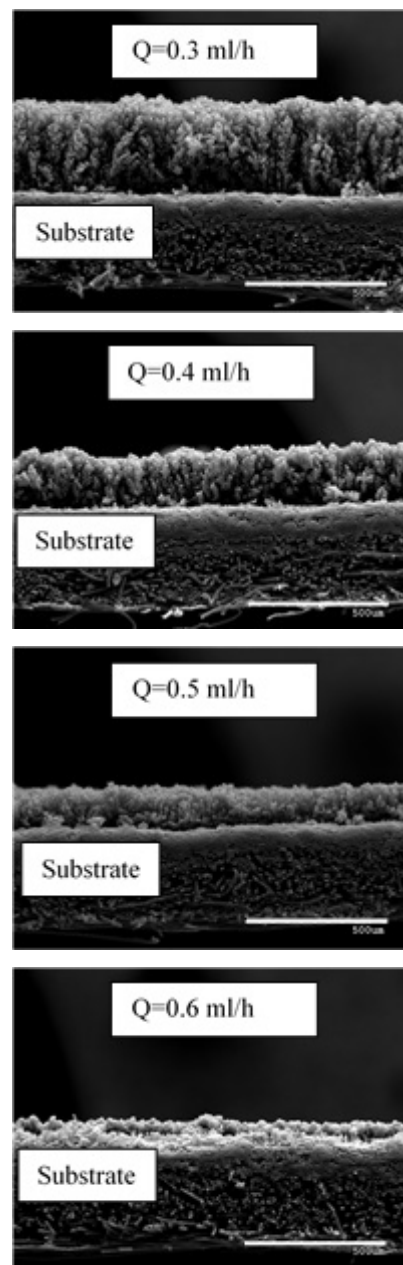
Castillo, J.L., Martin, S., Rodriguez-Perez, D., Perea, A., Garcia-Ybarra, P.L. (2014) *KONA Powder and Particle Journal*. **31**, 214-233.

Martin, S., Martinez-Vazquez, B., Garcia-Ybarra, P.L., Castillo, J.L. (2013) *J. Power Sources*. **229**, 179-184.

Martin, S., Garcia-Ybarra, P.L., Castillo, J.L. (2017) *Applied Energy*. Submitted December 2016.

Martin, S., Perea, A., Garcia-Ybarra, P.L., Castillo, J.L. (2012) *J. Aerosol Sci.* **46**, 53-63.

Rodriguez-Perez, D., Castillo, J.L., Antoranz, J.C. (2007) *Phys. Rev. E*, **76**, 011407.



**Figures.** SEM images of granular deposits formed on a collecting substrate from electro sprayed suspensions of carbon nanoparticles in ethanol. Same deposited total mass in all cases but at different electro spray flow rates ( $Q$ ). The scale bar at the bottom is 500  $\mu\text{m}$  in all figures.

## **Abstracts SPS6**

## Chemical, physical and optical properties of ship plumes catching by MEGA-chamber

Xiangyu Pei<sup>1</sup>, Ravi Kant Pathak<sup>1</sup>, Axel C. Eriksson<sup>2</sup>, Kent Salo<sup>3</sup>, Mattias Hallquist<sup>1</sup>

<sup>1</sup>Department of Chemistry and Molecular Biology, University of Gothenburg, Gothenburg, 41296, Sweden

<sup>2</sup>Division of nuclear physics, Department of Physics, Lund University, Lund, 22100, Sweden

<sup>3</sup>Earth and Space Sciences, Chalmers University of Technology, Gothenburg, 41296, Sweden

Keywords: shipping emission, exhaust plume, black carbon, MEGA-chamber

Presenting author email: xiangyu.pei@chem.gu.se

The shipping activities can significantly contribute to the anthropogenic emissions, including sulphur, nitrogen species and particulate matter (PM). Emissions of these pollutants can have serious effects on environment, climate and health on both regional and global scales. About 70% of ship emissions occur within 400 km of coastlines, and about 60,000 premature deaths per year is assumed to be caused by ship emissions (Corbett *et al.*, 2007). Emissions from ships contain black carbon (BC) and brown carbon (BrC), which are important climate forcing agents warming the atmosphere. After emitted from ships, properties of BC and BrC including absorption, scattering and hygroscopicity can change significantly during ageing processes. The emission of SO<sub>x</sub> from ships is controlled by regional and global caps on the allowed fuel sulphur content (FSC) in marine bunker fuels. In the sulphur emission controlled areas (SECA) the allowed maximal FSC was reduced to 1% in July 2010 and to 0.1% since January 2015. Prior to January 2015, the ship used a heavy fuel oil (HFO) but switched to a lowsulfur residual marine fuel oil (RMB30) after the implementation of the new FSC limit.

Multiple Exhaust Gas Analysis (MEGA)-chamber was developed in order to preserve the ship plume for a long enough extraction time for measuring the both physical and chemical properties of particles. The MEGA-chamber consists of a steel duct pipe with a diameter of 600 mm and has a volume of 450 l. The tube has butterfly duct valves mounted in both ends and a high flow of 300 l s<sup>-1</sup> is continuously drawn through the chamber using an axial duct fan. Air samples are taken from the centre of the chamber to minimize wall effects. Particle number size distribution was measured with a Scanning Mobility Particle Sizer (SMPS). Optical properties including absorption and scattering were measured with Photo-Acoustic Soot Spectrometer at three wavelengths of 405, 532, 781 nm (PASS-3), while the cloud droplet formation was measured by a Cloud Condensation Nuclei Counter (CCNC). Soot Particle-Aerosol Mass Spectrometer (SP-AMS) was used to measure the chemical composition of particles. Thermo-denuder at 400°C was used to characterise volatility of particles.

During the measurement campaign, in total 23 different types of individual ship plumes were captured and analysed. In this study, absorption and scattering properties of particles with and without

thermo-denuder are studied to quantify the optical properties of fresh BC and overall particles of each ship plume. Single Scattering Albedo (SSA) was 0.85 for undenuded particles, whereas 0.6 for denuded particles at wavelength of 405 nm, indicating the scattering nature of shipping emission particles. Absorption Ångström exponent (AAE) between 405 nm and 781 nm for undenuded particles was ~1.5, whereas AAE for denuded particles was ~1, indicating the BrC existed in the ship plume. Mass concentration of chemical species including BC, organic matter, sulphate, nitrate and ammonium measured with SP-AMS indicated that coatings will enhance the absorption and hygroscopicity of BC particles.

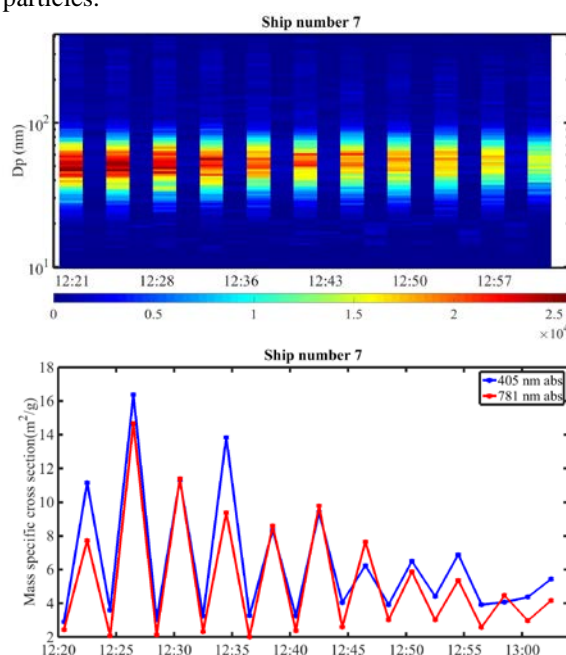


Figure 1. Particle number size distribution and mass absorption cross-section (MAC) of ship number 7 (cement carrier) in the MEGA-chamber; thermo-denuder was used or bypassed every 2 min alternatively.

This work was supported by the Swedish Research Council FORMAS, Modelling the Regional and Global Earth system (MERGE) and Climate, Biodiversity and Ecosystem services (ClimBEco).

Corbett, J. J. et al. (2007). *Environ. Sci. Technol.* 41, 8512-8518.

## Ship plume aerosol characterization and contribution to inland air quality

Stina Ausmeel<sup>1</sup>, Kirsten Kling<sup>2</sup>, Erik Ahlberg<sup>1</sup>, Mårten Spanne<sup>3</sup>, Axel Eriksson<sup>4</sup>, Adam Kristensson<sup>1</sup>

<sup>1</sup>Nuclear Physics, Lund University, PO Box 118, Lund, SE-221 00, Sweden

<sup>2</sup>National Research Centre for the Working Environment, Copenhagen, DK-2100, Denmark

<sup>3</sup>Malmö Environmental Department, Malmö, SE-205 80, Sweden

<sup>4</sup>Ergonomics and Aerosol Technology, Lund University, Box 118, Lund, SE-22100, Sweden

Keywords: ship plumes, atmospheric measurements, physicochemical properties

Presenting author email: stina.ausmeel@nuclear.lu.se

Near coastal areas, emissions from maritime shipping influence air quality and consequently the health of the population (González *et al.*, 2011). Depending on the distance travelled, the aerosol reaching populated areas can either be fresh or have changed properties during atmospheric ageing.

During 2016 two measurement campaigns were carried out at a coastal location (Falsterbo) in southern Sweden, roughly 5-10 km from a shipping route within a Sulphur Emission Control Area. The main tasks have been to quantify the size dependent chemical composition of particles in ship plumes with an atmospheric age of up to 1 hour, and to study the contribution from ship emissions to the inland particle concentrations in southern Sweden. Chemical analysis of filter samples will be used to look for ship emission tracers for use in modelling of the ship contribution to inland air pollution.

The aerosol properties measured in Falsterbo were number concentration, size distribution, physicochemical properties and light absorption. Further atmospheric aging was simulated using a Potential Aerosol Mass (PAM) reactor. The gaseous compounds CO<sub>2</sub>, NO<sub>x</sub> and SO<sub>2</sub> were also monitored. Several markers can be used to identify the ship plumes from the background pollution levels. An example of the particle increase and change in particle size distribution over time due to ship plumes can be seen in Fig. 1 (upper panel) as well as the total number concentration over the same time period (lower panel).

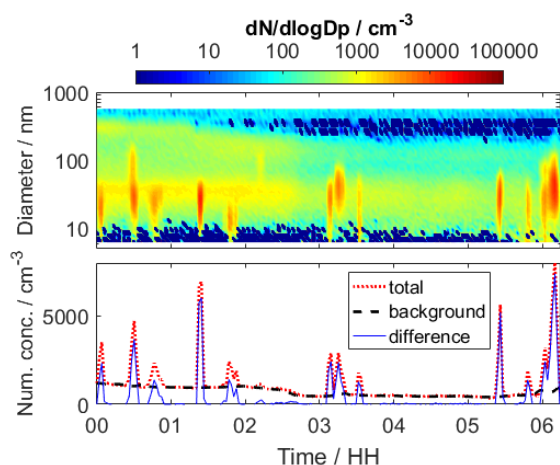


Figure 1. Sampled SMPS size distribution (upper) and total particle number concentration together with calculated background level (lower) over six hours during January 28, 2016. Ships plumes are distinguishable from background concentrations.

Background concentrations prior the shipping lane were not measured but extracted from the total concentration by using a percentile based method (Kivekäs *et al.*, 2014) for smoothing of the data (Fig. 1, lower panel). The ships' contribution to the particle number concentration during different seasons can be seen in Table 1 and compared to the results of Kivekäs *et al.* (2014).

Table 1. Local contribution from ships to particle number concentration. The season and SMPS size intervals are given within parenthesis. The absolute and relative contribution refers to days when the wind was passing over the shipping route. The yearly contribution includes all wind directions.

Increase in particle number concentration due to ships			
	Absolute (cm <sup>-3</sup> )	Relative (%)	Yearly (%)
This study (6-570 nm, Jan-Mar)	240	17	13
This study (6-570 nm, May-Jul)	270	11	8
Kivekäs <i>et al.</i> (2014) (12-490 nm, Mar-Jul)	170	11-19	5-8

From the preliminary analysis the PAM reactor appears to have no large effect on ageing of the aerosol. A fraction of the plumes were visible in the instruments detecting chemical species, indicating a large fraction of the total pollution being caused by a few of the emitters. Further, the contributions from individual ships will also be studied using AIS (Automatic Identification System) data which is a tracking system for vessels.

The project is a collaboration between Lund University, Chalmers University of Technology, Malmö Environmental Department, the National Research Centre for the Working Environment (Denmark), the Swedish Meteorological and Hydrological institute and the Swedish Environmental Protection Agency and is funded by the Swedish Research Council FORMAS (project no. 2014-951).

González, Y., Rodríguez, S., Guerra García, J. C., Trujillo, J. L., & García, R. (2011). *Atmospheric Environment*, **45**(28), 4907-4914.

Kivekäs, N., Massling, A., Grythe, H., Lange, R., Rusnak, V., Carreno, S., Skov, H., Swietlicki, E., Nguyen, Q. T., Glasius, M., Kristensson, A. (2014). *Atmos. Chem. Phys.*, **14**(16), 8255-8267.

## ONLINE AEROSOL ANALYSIS USING FTIR: ASSESSING CARBONYL YIELDS IN E-CIGARETTE AEROSOL

F. Radtke<sup>1</sup>, R. Monni<sup>1</sup>, A. Susz<sup>1</sup>, A. Stoop<sup>1</sup>, J. Verbeek<sup>1</sup> and S. Maeder<sup>1</sup>

<sup>1</sup>PMI R&D, Philip Morris Products S.A., CH-2000 Neuchâtel, Switzerland  
(Part of Philip Morris International group of companies)

Keywords: Infrared Spectroscopy, Puff-by-Puff Aerosol Characterization, Online Chemical Quantification.  
Presenting author email: Falk.Radtke@pmi.com

The global electronic cigarettes (e-cig) market and product variety has been steeply increasing, counting more than 2 million users worldwide (Cressey, 2014). Together with the questions related to the continuous inhaling of main constituents of e-liquids, e.g. glycerol and 1,2-propanediol (PG), the regulatory authorities and producers are focusing on harmful aerosol constituents like carbonyls such as formaldehyde, acetaldehyde and acrolein (NAS, 2010). The latter are mainly observed during End of Liquid (EoL) operating conditions and identified as markers for thermal degradation of the e-liquid constituents, e.g. glycerol and PG (Kosmider et al., 2014).

Standard methods used for carbonyl quantification in smoke or aerosol rely on aerosol trapping in an impinger filled with a liquid solution of 2,4-dinitrophenylhydrazine (2,4-DNPH) (CORESTA-N° 74, 2014). This method is offline, averages several puffs (a minimum of 20) and does not allow parallel analysis of other aerosol constituents. As an alternative we developed an online puff-by-puff analysis method using a Fourier Transform Infrared (FTIR) spectrometer (Radtke, 2016). This method allows a carbonyl analysis e.g. during EoL, different device power settings, and heat control algorithm. Moreover, the main e-liquid constituents were simultaneously analyzed, in order to monitor their ratios in the generated aerosol and to determine their concentration at the moment of carbonyl generation.

The experimental setup is composed of three main parts: 1) a programmable single syringe aerosol generation pump, 2) a transfer section with a heated pump and heated tubes, and 3) a Gasmeter™ FTIR spectrometer.

For the presented investigations the aerosol was generated in accordance with two different smoking regimes: i) the Coresta recommended e-cig smoking protocol, namely 55 mL drawn with a rectangular puff profile during 3 seconds and drawing one puff every 30 seconds (CORESTA-N° 81, 2015); and ii) a more intense smoking regime, namely 55 mL drawn with a rectangular puff profile during 5 seconds and drawing one puff every 30 seconds. The latter smoking regime was defined on the basis of topography studies. (Evans & Hoffman, 2014)

Figure 1 shows a direct comparison of glycerol and formaldehyde concentrations on puff-by-puff basis obtained from a test device without heat control algorithm. With this method it is possible to define the concentration of glycerol at which the formaldehyde is generated and link it e.g. to the remaining liquid in the device, applied power or heating temperature. As all of the aerosol analysis results are obtained online during the

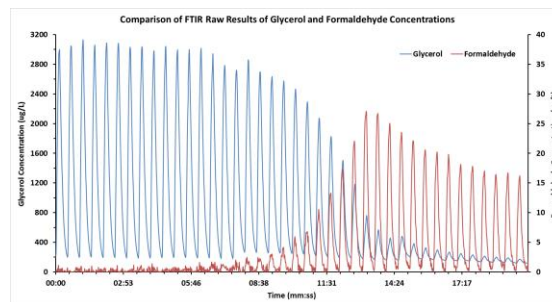


Figure 1. Comparison between the glycerol (solid blue) and formaldehyde (solid red) concentrations in the aerosol generated by a test device without heat control algorithm. The concentrations shown refer to diluted samples.

aerosol generation the user will gain further information and reduce analysis time and effort compared to the classical trapping, sample preparation and off-line carbonyl analysis method.

CORESTA-No. 74 - Determination of Selected Carbonyls in Mainstream Cigarette Smoke by High Performance Liquid Chromatography (HPLC) (2014).

CORESTA-No. 81 - Routine Analytical Machine for E-Cigarette Aerosol Generation and Collection - Definitions and Standard Conditions (2015).

Cressey, D. (2014). E-cigarettes: The lingering questions. *Nature*, 513, 24-26. doi: 10.1038/513024a

Evans, S. E., & Hoffman, A. C. (2014). Electronic cigarettes: abuse liability, topography and subjective effects. *Tobacco Control*, 23(suppl 2), ii23-ii29. doi: 10.1136/tobaccocontrol-2013-051489

Kosmider, L., Sobczak, A., Fik, M., Knysak, J., Zaciera, M., Kurek, J., & Goniewicz, M. L. (2014). Carbonyl Compounds in Electronic Cigarette Vapors—Effects of Nicotine Solvent and Battery Output Voltage. *Nicotine & Tobacco Research*. doi: 10.1093/ntr/ntu078

NAS. (2010). Acute Exposure Guideline Levels *Acute Exposure Guideline Levels for Selected Airborne Chemicals: Volume 8* (Vol. 8): National Academy of Sciences.

Radtke, F. (2016). *FTIR method for e-cigarette aerosol characterization*. Paper presented at the Tobacco Science Research Conference, U.S.A.

## Effects of the fuel chemical composition on volatile organic compounds emitted by aircraft engines

A. Setyan<sup>1,2</sup>, Y.-Y. Kuo<sup>1,2</sup>, B.T. Brem<sup>1,2</sup>, L. Durdina<sup>1,2</sup>, A.C. Gerecke<sup>1</sup>, N.V. Heeb<sup>1</sup>, R. Haag<sup>1</sup>, and J. Wang<sup>1,2</sup>

<sup>1</sup>Empa, Laboratory for Advanced Analytical Technologies, 8600 Dübendorf, Switzerland

<sup>2</sup>ETH Zürich, Institute of Environmental Engineering, 8093 Zürich, Switzerland

Keywords: aircraft emissions, volatile organic compounds, fuel composition, gas chromatography/mass spectrometry.

Presenting author email: ari.setyan@empa.ch

Aircraft emissions received increased attention recently because of the steady growth of aviation transport in the last decades. Aircraft engines substantially contribute to emissions of particulate matter and gaseous pollutants in the upper and lower troposphere. Among all the pollutants emitted by aircrafts, volatile organic compounds (VOCs) are particularly important because they are mainly emitted at ground level, posing a serious health risk for people living or working near airports.

A series of measurements was performed at the aircraft engine testing facility of SR Technics (Zürich airport, Switzerland). Engine exhausts were sampled at the engine exit plane by a multi-point sampling probe. A wide range of instruments was connected to the common sampling line to determine physico-chemical characteristics of non-volatile particulate matter (nv-PM) (Durdina *et al.*, 2014; Brem *et al.*, 2015) and gaseous pollutants. An in-service turbofan engine was tested during this study. Conventional Jet A-1 fuel was used as the base fuel, and measurements were performed with the base fuel doped with two different mixtures of aromatic compounds (Solvesso 150 and naphthalene-depleted Solvesso 150) and an alternative fuel (hydro-processed esters and fatty acids [HEFA] jet fuel).

During this presentation, we will show results obtained for VOCs. These compounds were sampled with 3 different adsorbing cartridges, and analyzed by thermal desorption gas chromatography/mass spectrometry (TD-GC/MS, for Tenax TA and Carboxen 569) and by ultra-performance liquid chromatography/mass spectrometry (UPLC/MS, for DNPH). The total VOC concentration was also measured with a flame ionization detector (FID). In addition, fuel samples were also analyzed by GC/MS, and their chemical compositions were compared to the VOCs emitted via engine exhaust.

Total VOCs concentrations were highest at ground idle (>200 ppm C at 4-7% thrust). Those at high thrust were substantially lower (<3 ppm C during take-off, 100% thrust). These results may be due to lower temperature and poorer air/fuel mixing in the primary combustion zone, and lower fuel/air equivalence ratios at low thrust. The VOCs identified with the Tenax TA and Carboxen 569 cartridges were alkanes, aromatics, and oxygenated compounds. Most concentrated were small molecules (C<sub>3</sub>-C<sub>7</sub>).

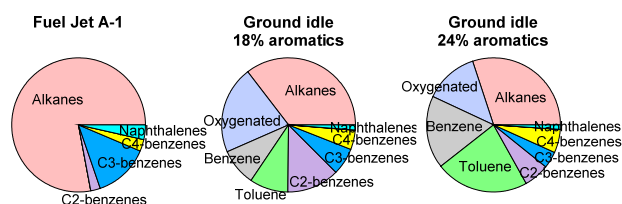


Figure 1. Left: composition of the Jet A-1 fuel. Middle: VOC composition at ground idle with base fuel (18% aromatics). Right: VOC composition at ground idle with base fuel doped with Solvesso 150 (24% aromatics).

Figure 1 compares the chemical composition of fuel samples and VOCs emitted by the aircraft engine. Fuel samples were dominated by alkanes (Figure 1, left), whereas VOCs emitted by the aircraft engine were mainly constituted of alkanes, oxygenated compounds, and benzene derivatives (Figure 1, middle). Approximately 50 % of the compounds identified in the exhaust were not present in the fuel (in particular benzene, toluene, and oxygenated compounds), and thus were formed during combustion. The effects of the alternative fuel (Jet A-1 fuel doped with HEFA) on the VOCs emitted by the engine will also be discussed.

This work was supported by the Swiss Federal Office of Civil Aviation (FOCA), projects “Particulate matter and gas phase emission measurement of aircraft engine exhaust” and “Emissions of particulate and gaseous pollutants in aircraft engine exhaust” (EMPAIREX), and by the Swiss National Science Foundation.

Brem, B.T., Durdina, L., Siegerist, F., Beyerle, P., Bruderer, K., Rindlisbacher, T., Rocci-Denis, S., Andac, M.G., Zelina, J., Penanhoat, O., Wang, J. (2015) *Environ. Sci. Technol.* **49**, 13149–13157.

Durdina, L., Brem, B.T., Abegglen, M., Lobo, P., Rindlisbacher, T., Thomson, K.A., Smallwood, G.J., Hagen, D.E., Sierau, B., and Wang, J. (2014) *Atmos. Environ.* **99**, 500-507.

## An effect of fuel on composition specific volatility of marine engine exhaust particles

M. Isotalo<sup>1</sup>, N. Kuittinen<sup>1</sup>, P. Karjalainen<sup>1</sup>, P. Aakko-Saksa<sup>2</sup>, P. Simonen<sup>1</sup>, F. Mylläri<sup>1</sup>, H. Wihersaari<sup>1</sup>, J. Keskinen<sup>1</sup>, T. Rönkkö<sup>1</sup>, H. Timonen<sup>3</sup>

<sup>1</sup>Aerosol Physics, Faculty of Natural Sciences, Tampere University of Technology, Tampere, 33101, Finland

<sup>2</sup>VTT Technical Research Centre of Finland, Espoo, 02044, Finland

<sup>3</sup>Finnish Meteorological Institute, Helsinki, 00101, Finland

Keywords: marine engine, volatility, chemical composition, exhaust particles.

Presenting author email: mia.isotalo@tut.fi

Recently volatilities of ambient and laboratory-generated aerosol particles have been studied quite widely (e.g. Huffman et al., 2009). Nevertheless, more scientific research information is required about the volatilities of different chemical species in ambient aerosols and especially in engine exhaust gas. The volatility of aerosol particles is an important physical property, which provides information of the chemical composition of the aerosol and may also reveal a chemical history of the particles (Jonsson et al., 2007).

Huffman et al. (2009) connected a rapid temperature-stepping thermodenuder with a High-Resolution Time-of-Flight Aerosol Mass Spectrometer (HR-ToF-AMS) and measured chemically-resolved urban particle volatility from two megacities. The results show that ambient nitrate as having the highest volatility while sulfate showed the lowest volatility. The volatility of total organic aerosol was between nitrate and sulfate.

In this study, volatility and composition of marine engine exhaust particles were studied with four different fuels. The test engine was a 1.6 MW medium-speed test-bed engine equipped with mechanical injection system. Tested fuels were Marine Diesel Oil (MDO, 0.1 % S), High Sulphur Fuel Oil (HFO, 2.5 % S), Intermediate Fuel Oil (IFO, 0.5 % S) and a blend of biofuel (30%) and distillate fuel (70%). Used load conditions were 25% and 75%. Both primary and secondary emissions were studied during the campaign. In secondary measurements the exhaust gas was aged by using a PAM chamber (Kang et al., 2007).

Two different dilution systems were used in this study. In primary measurements the sample went through a porous tube diluter (dilution ratio, DR=12) followed by a residence time chamber. In secondary measurements a combination of a hot ejector (DR=4.5) and an ejector diluter (DR=8) was used. In both cases the sample was further diluted by using an ejector diluter (DR=8). The volatility of the particles was studied by directing the sample flow through a thermodenuder or a catalytic stripper (Amanatidis et al., 2013). The thermodenuder was heated up to 265 °C and kept in constant temperature. Furthermore temperature ramps were conducted by heating the thermodenuder up to 300 °C and allowing it to cool down to room temperature. The catalytic stripper was used at 350 °C temperature. The chemical composition of the exhaust particles was measured with a Soot-Particle Aerosol Mass Spectrometer (SP-AMS, Aerodyne Research Inc.). Also particle size distributions

were measured using an SMPS (TSI Inc.) and a Nano-SMPS (TSI Inc.).

The results showed that the size distributions shifted left to the lower particle sizes at higher thermodenuder temperatures (Figure 1). Also the shape of the size distributions and number of separate modes depend on thermodenuder temperature and used fuel. Our primary aim is to determine at which temperatures each chemical species in marine engine exhaust particles are starting to evaporate and how strong the evaporation process is.

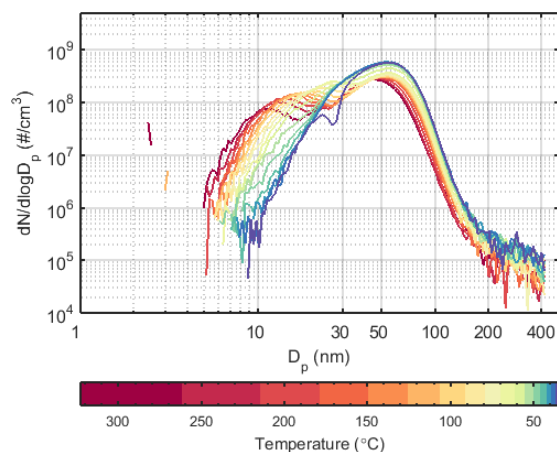


Figure 1. The size distributions measured during the temperature ramp with High Sulphur Fuel Oil at 75 % load.

The financial support from Tekes (40356/14) and from industrial partners, Wärtsilä, Pegasor, Spectral Engines, Gasmot, VG-Shipping, HaminaKotka Satama Oy, Oiltanking Finland Oy and Kine Robotics, is gratefully acknowledged.

Amanatidis, S. et al. (2013) *Journal of Aerosol Science*, **57**, 144-155.

Huffman, J. A. et al. (2009) *Atmospheric Chemistry and Physics*, **9**, 7161-7182.

Jonsson, A. M. et al. (2007) *Journal of Aerosol Science*, **38**, 843-852.

Kang, E. et al. (2007) *Atmospheric Chemistry and Physics*, **7**, 5727-5744.

## Impact of alternative fuels on the non-volatile particulate matter mass and number emissions of an in-production aero gas turbine

B.T. Brem<sup>1,2</sup>, L. Durdina<sup>1,2</sup>, M. Elser<sup>1,2</sup>, A. Setyan<sup>1,2</sup>, D. Schönenberger<sup>1,2</sup>, S. Wyss<sup>5</sup>, K Zeyer<sup>5</sup>, F. Siegerist<sup>3</sup>,  
M. Munoz<sup>1</sup>, R. Haag<sup>1</sup>, D. Rentsch<sup>4</sup>, J. Mohn<sup>5</sup>, N.V. Heeb<sup>1</sup>, and J. Wang<sup>1,2</sup>

<sup>1</sup>Empa, Laboratory for Advanced Analytical Technologies, 8600 Dübendorf, Switzerland

<sup>2</sup>ETH Zürich, Institute of Environmental Engineering, 8093 Zürich, Switzerland

<sup>3</sup>SR Technics Switzerland AG, 8302 Kloten, Switzerland

<sup>4</sup>Empa, Laboratory for Functional Polymers, 8600 Dübendorf, Switzerland

<sup>5</sup>Empa, Laboratory for Air Pollution and Environmental Technology, 8600 Dübendorf, Switzerland

Keywords: aircraft emissions, soot, non-volatile particulate matter mass and number

Presenting author email: benjamin.brem@empa.ch

While alternative less carbon intensive propulsion and powertrain systems have advanced in other areas of mobility, aviation will likely rely on the combustion of hydrocarbon fuels for decades to come. Currently, alternative aviation fuels from non-fossil feedstocks are considered the most viable way to reduce the carbon intensity of the aviation sector, and several airlines and airports are already using low quantities of blended alternative fuels originating from various feedstocks. Understanding the carbon intensity and the sustainability of the feedstocks of these fuels is of utmost importance and currently a topic of much political debate. In addition, the combustion products of these fuels also need careful evaluation.

Complex interactions between fuel chemistry and engine operating conditions determine the non-volatile particulate matter (nvPM) mass and number emissions of aero gas turbines. The link between the chemistry and the sooting propensity of fuels has long been the focus of research, and decreased levels of mono-aromatic and naphthenic hydrocarbons in the fuel have been associated with lower soot emissions. Aromatic compounds promote the formation of large polycyclic aromatic hydrocarbons (PAH) and the subsequent soot nucleation and growth in fuel-rich pockets in the combustion zone. A constant oxidation of these newly formed species takes place in parallel in lean zones; therefore, the engine operating conditions, in particular air to fuel equivalence ratio (AFR) and engine combustor temperature and pressure, are critical for the understanding of fuel effects.

A few datasets indicate a clear thrust dependence of the fuel chemistry effects on nvPM or BC emissions. Under low AFR conditions, which concur with high temperatures and pressures in the combustor, fuel chemistry seems to play a minor role. At high AFR conditions, on the other hand, fuel effects on nvPM emissions are clearly visible.

In this work, we conduct a fuel sensitivity study using Jet A-1 fuel blended with three ratios (5, 10 and 44% by volume) of alternative HEFA (hydro-processed esters and fatty acids). These experiments known as the EMPAIREX 1 campaign will be conducted in March

2017. Table 1 provides fuel composition data relevant for the nvPM emissions. The experiments are conducted on an in-service turbofan engine in the test cell of SR Technics at Zurich airport. The nvPM sampling system and system operation correspond to the recommended practice (SAE International, 2013). In addition to the nvPM mass and number measurements, particle size distributions will be measured with a scanning mobility particle sizer.

Table 1. Fuel specifications

Fuel	Tot. Aromatics Content (% v)	Smoke Point (mm)
Jet A-1 (ZRH)	18.0	21
Pure HEFA	0.5	>40
44 % HEFA-Blend	9.4	33

The work we present here extends our previous findings from A-PRIDE 7 (Brem *et al.*, 2015) and A-PRIDE 8 to lower levels of fuel aromatics contents of the HEFA fuels used. It will be determined if the correlation of relative change in emissions with the change in fuel hydrogen mass content, found previously, still holds for these fuels. Furthermore, the impact on regulatory issues, such as fuel composition corrections for nvPM measurements, will be discussed.

We thank SR Technics Switzerland AG for their help and support. This work is financially supported by the Swiss Federal Office of Civil Aviation (FOCA).

SAE International (2013) E-31, AIR 6241, 2013-11-18

Brem, B.T., Durdina, L., Siegerist, F., Beyerle, P., Bruderer, K., Rindlisbacher, T., Rocci-Denis, S., Andac, M.G., Zelina, J., Penanhoat, O., Wang, J. (2015) *Environ. Sci. Technol.* **49**, 13149–13157.

## Metallic elements in aero gas turbine exhaust

B.T. Brem<sup>1,2</sup>, C. Schreiner<sup>1</sup>, R. Figi<sup>1</sup>, L. Durdina<sup>1,2</sup>, A. Setyan<sup>1,2</sup>, M. Elser<sup>1,2</sup>, D. Schönenberger<sup>1,2</sup>  
and J. Wang<sup>1,2</sup>

<sup>1</sup>Empa, Laboratory for Advanced Analytical Technologies, 8600 Dübendorf, Switzerland

<sup>2</sup>ETH Zürich, Institute of Environmental Engineering, 8093 Zürich, Switzerland

Keywords: aircraft emissions, metals, metallic ash, trace elements

Presenting author email: benjamin.brem@empa.ch

Particulate matter (PM) emissions from aircraft gas turbines are a concern for human health, environmental pollution, and climate change. Non-volatile aircraft PM consists primarily of soot but further includes trace amounts of non-combustible, inorganic material referred to as metal PM or ash. Due to the small size (nuclei mode) these particulate trace element emissions potentially cause adverse health effects and have been the focus of increasingly stringent emission standards in the automotive industry (Utell and Frampton, 2000). Their sources have been identified as metallic lube oil additives and engine wear metals (*e.g.* Higgings *et al.*, 2002, Apple *et al.* 2009). However, the origin, physical and chemical properties and emission rates of these types of particles are not well characterized in aircraft gas turbine emissions.

This work presents preliminary results on the composition and concentrations of trace metals emitted by current technology high bypass turbofan engine sources. All samples were collected in the aircraft engine testing facility of SR Technics, Zürich airport where a permanent PM sampling system is installed. Two types of samples were collected: (i) swab wipe samples of thermophoretically deposited soot PM on the inner walls of engine exhaust nozzles and (ii) heated quartz fiber filter samples of raw engine exhaust. The filter measurements were performed at five selected engine thrust levels ranging from idle (< 7%) to take-off (~100%). In addition to the swab and filters samples, engine fuel and lubrication oil samples were taken at the testing facility.

After a sample digestion procedure which included a hydrofluoric acid treatment, the metal content in all the samples was analyzed by inductively coupled plasma mass spectrometry (8800 ICP-QQQ, Agilent). All agents used had the highest grade of purity and blanks of agents and filters were analyzed for quality control.

As an example result, the composition of the major metallic elements in two engine exhaust nozzle swab samples is provided in Table 1. Besides sulfur which originates from the fuel, wearing of engine components can be considered the dominant source of metallic emissions in these samples. The collected soot in the nozzle of Engine 1 which is late 80's technology contained also significantly more metals than the one of Engine 2 which is a newer model. Interesting is also the high amount of zirconium in both samples which is used

in thermal barrier coatings (TBCs) of engine combustor chambers and might be able to serve as a metallic tracer for aircraft PM.

Table 1. Metallic elements in a swab sample from soot deposited on the inner walls of an engine exhaust nozzle.

Element	Engine 1 (µg/g)	Engine 2 (µg/g)	Likely Origin
S	26000	5800	Fuel
Ni	22000	7900	Wear
Ca	18000	1900	Oil
Zr	14000	900	Wear TBC
Cr	12000	4000	Wear
Al	8200	22000	Wear
Fe	7800	5100	Wear
Mo	5200	1800	Wear
Na	3700	700	Oil/ Fuel
K	2900	500	Oil/ Fuel

This work will further analyze these results and present quantified metal emission indices linked to engine thrust which is currently being carried out in the Empairex 1 campaign. Finally, an estimate of the contribution of metals to the total non-volatile PM mass in aircraft engine exhaust will be provided.

We thank Frithjof Siegerist and SR Technics AG for their help and support. This work is financially supported by the Swiss Federal Office of Civil Aviation (FOCA).

Utell, M.J., Frampton, M.W. (2000), Acute health effects of ambient air pollution: The ultra-fine particle hypothesis, *J. Aerosol Med.*, 13, pp. 355–359

Higgings, K., Jung, H., Kittelson, D.B., Roberts J.T., Zachariah, M.R. (2002), Size-selected nanoparticle chemistry: Kinetics of soot oxidation, *J. Phys. Chem.*, 106 (1), pp. 96–103

Apple, J., Gladis D., Watts, W., Kittelson, D.B. (2009), Measuring diesel ash emissions and estimating lube oil consumption using a high temperature oxidation method *SAE Int. J. Fuels Lubr.* 2(1): 850-859

## On-Board Measurements of Particle and Gaseous Emissions from a Large Cargo Vessel at different operating conditions

T. Chu Van<sup>1,2,3</sup>, Z.D. Ristovski<sup>1,2</sup> and R. Brown<sup>1,2</sup>

<sup>1</sup>Biofuel Engine Research Facility, QUT, Brisbane, QLD 4000, Australia

<sup>2</sup>International Laboratory for Air Quality and Health, QUT, Brisbane, QLD 4000, Australia

<sup>3</sup>Vietnam Maritime University (VMU), Haiphong 180000, Vietnam

Presenting author email: z.ristovski@qut.edu.au

Shipping-related emissions are one of the major contributors to global air pollution, especially in coastal areas (Viana et al 2014). An assessment published in 2010 (Eyring, et al 2010) found that over 70% of ship emissions have been detected up to 400 km inland and significantly contribute to air pollution in the vicinity of harbours. Moreover, shipping activities also significantly contribute to ocean acidification. Quantitative and qualitative estimation of pollutant emissions from ships and their dispersion are thus becoming more important.

The measurements were performed in October and November 2015 on a large cargo vessel at Port of Brisbane, Gladstone, and Newcastle. All measurements have been carried out on both main and auxiliary engines of the vessel for different operating conditions, experienced at berth, manoeuvring, and at sea. Instruments were placed on a deck high up in the machinery room where the exhaust gas was sampled and measured continuously from two holes cut in the exhaust channel after the turbocharger of the main engine. From the first sampling point, the raw hot-exhaust gas was directed to a DMS 500MKII – Fast Particulate Spectrometer with a heated sample line, and two dilution system. The second sampling point was used for measurements by a Testo 350XL gas meter, and by a DustTrak II Aerosol Monitor (8530 TSI) and Sable CO<sub>2</sub> monitor connected after a Dekati ejector dilutor. Data on engine power, engine revolution, fuel oil consumption, and exhaust gas temperature were measured by the ship's instrumentation. The ship used HFO for both her main and auxiliary diesel engines. All of the measurements were grouped into 3 categories: Ocean-going, Manoeuvring and at Berth.

Particle number size distributions were measured in the size range of 5nm – 1.0µm with a sample frequency of 1 Hz. The particle mass emission factor (EF<sub>PM</sub>), in the size range <1.0 µm, was calculated from the number concentrations measured with the DMS 500 assuming spherical particles with different densities for nucleation and accommodation mode. In addition, mass concentrations of PM<sub>10</sub>, PM<sub>2.5</sub>, and PM<sub>1.0</sub> were also measured with a DustTrak.

The top figure shows the average particle number and mass size distributions for particles measured with the DMS500. The particle number size distributions observed only one mode for different operating conditions of the ship, with a peak at around 40 – 50 nm, which was dominant by nano-particles. The highest particle number concentrations were observed at berth while the largest particle mass emissions were observed

during manoeuvring (see bottom graph). The PM<sub>1</sub> emission factors measured with the DustTrak and DMS500 were in good agreement. It is also interesting to observe that all of the mass emitted even with HFO is carried by the particles in the size range below 1µm.

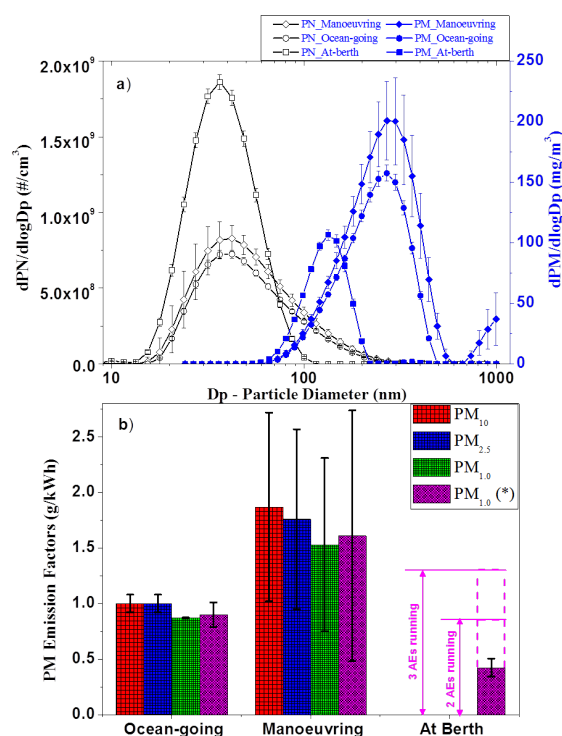


Figure 1. Top: Particle number and mass size distributions and Bottom: Particle mass concentrations at different operating conditions of the ship.

In addition to the average emission factors results on the real time (second by second) data on both particle and gasses for the whole voyage will be presented.

The authors would like to acknowledge the outstanding support received from all employees and crew of CSL Group Inc. This work was supported by the International Association of Maritime Universities (IAMU) and the Nippon Foundation in Japan.

Viana, M. et al. (2014) *Atmos. Environ.* **90**, 96-105.

Eyring, V. et al. (2010) *Atmos. Environ.* **44**(37), 4735-4771.

## Primary and secondary particles from ship emissions in port cities

A. Aulinger, M. Ramacher, M. Karl and V. Matthias

Institute for Coastal Research, Helmholtz-Zentrum Geesthacht, Geestacht, 21502, Germany

Keywords: ship emissions, emission modeling, urban air quality, dispersion modeling, particle formation

Presenting author email: armin.aulinger@hzg.de

Ships emit considerable amounts of pollutants, not only when sailing, but also during their stay at berth. This is of particular importance for port cities hosting large vessels. Ships contribute to the particulate concentration levels both by directly emitting particles like black carbon or sulfates and by emitting nitrogen and sulfur oxides which are the most important precursor substances for secondary particles.

To estimate the emissions from ships in ports both the technical specifications of the ships and their emission factors specific to the different ship activities, sailing, maneuvering and berthing need to be known. At our institute, we combined a line source model approach for moving ships (Aulinger et al. 2016, Matthias et al. 2016) and a point source model for ships at berth following an approach by Hulskotte and Denier van der Gon (2010). For moving ships, emission factors depend on the ship size and type and the load of the engines during sailing. For berthing ships, functional relationships between ship size and fuel use per hour at berth for different ship types have been derived. These functions have been combined with ship activities derived from AIS data and tables of port calls to calculate the energy use, fuel consumption and emissions of the most important gaseous and particulate pollutants.

As a first example, ship emissions for the port of Hamburg were calculated with this model. The resulting emission inventory served as input for the Chemical Transport Model systems TAPM and Citychem. To investigate the impact of ship emissions on air pollution in the Hamburg area two different model runs for January and July 2013 were performed; one model run including land-based emissions and the ship emissions and another model run just including the land-based emissions. The model results were evaluated with air quality data and resulted in dispersion maps of pollutants from harbor related ships in the Hamburg metropolitan area.

Due to the strict regulations for the fuel sulfur content in ports the sulfur dioxide and sulfate emissions are low compared to the emissions of nitrogen oxides. In 2013, the total  $\text{NO}_x$  emissions from ships amounted to more than 5000 tons while  $\text{SO}_2$  emissions were about 650 tons. Primary aerosol emissions comprising sulfates, black carbon and other primary organic aerosols were about 280 tons according to the model results.

Evaluating the results of the dispersion modeling both with and without ship emissions revealed that the influence of ship emissions on  $\text{NO}_2$ , which is in absence of  $\text{SO}_2$  the most relevant precursor for secondary particles, can reach up to 5% and more even in areas not adjacent to the port. Figure 1 shows the relative increase of

$\text{NO}_2$  concentrations in July 2013 resulting from ship emissions.

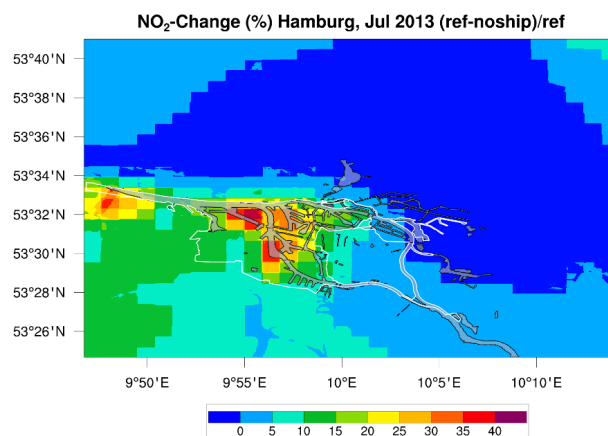


Figure 1. Relative increase of  $\text{NO}_2$  concentrations resulting from ship emissions ( $\text{NO}_x$ ).

The largest influence of ship emissions can of course be seen in the port area. As an example, the average  $\text{PM}_{25}$  concentration in January 2013 measured at the air quality monitor (Hamburger Luftmessnetz) Wilhelmsburg is met when including ship emissions and significantly underestimated otherwise (Figure 2) - tested with a paired t-test.

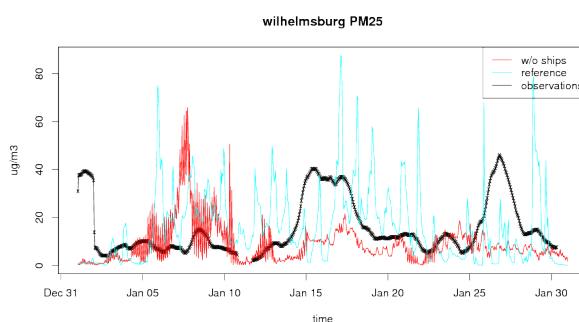


Figure 2. Daily average concentrations of  $\text{PM}_{25}$  in January 2013 at the AQ monitor Wilhelmsburg.

Aulinger, A., Matthias, V., Zeretzke, M., Bieser, J., Quante, M. and Backes, A. (2016) *Atmos. Chem. Phys.* **16**, 739–758.

Matthias, V., Aulinger, A., Backes, A., Bieser, J., Geyer, B., Quante, M. and Zeretzke, M. (2016) *Atmos. Chem. Phys.* **16**, 759–776.

Denier van der Gon, H. and Hulskotte, J. (2010) *Methodologies for estimating shipping emissions in the Netherlands*, Netherlands Environmental Assessment Agency (TNO)

## Correlations of nonvolatile PM mass and number emissions with smoke number determined for commercial aircraft jet engines

L. Durdina<sup>1,2</sup>, B.T. Brem<sup>1,2</sup>, and J. Wang<sup>1,2</sup>

<sup>1</sup>Laboratory for Advanced Analytical Technologies, Empa, Dübendorf, 8600, Switzerland

<sup>2</sup>Institute of Environmental Engineering, ETH Zürich, Zürich, 8093, Switzerland

Keywords: aircraft emissions, soot, smoke number, air quality

Presenting author email: lukas.durdina@empa.ch

For over 30 years, aircraft jet engines have been certified for visible exhaust smoke using the smoke number (SN). SN is the relative change of reflectance of a filter paper after drawing a given mass of raw exhaust through it. This qualitative method does not readily provide any useful characteristics of the PM emitted, such as particle number and mass concentrations. In the light of the steadily growing air travel, researchers and regulatory agencies need accurate methods to estimate PM emissions from jet engines to assess their effects on the local air quality and climate.

In the near future, the assessments might become more accurate owing to the new regulatory standard for non-volatile PM (nvPM) emissions from commercial gas turbine engines. This standard will come into force in 2020 and will require engine manufacturers to report both the nvPM mass and number-based emissions. However, this standard will only concern in-production engines. Since the service life of jet engines spans up to 30 years, nvPM emissions of many in-service engines will never be reported. Therefore, the nvPM emissions will need to be estimated from the certification SN data.

The recommended method for estimating nvPM emissions from airport operations has been the first order approximation version 3 (FOA3, Wayson et al. 2009). Recently, alternative correlations have been developed that predict up to a factor of 4 higher PM mass emissions than FOA3, but none of them uses standardized measurements of SN and nvPM emissions of in-service turbofan engines (Stettler et al. 2013a, 2013b).

Here, we present the correlations of nvPM mass and number emissions with SN determined for in-service turbofan engines. The engine tests were done in the test cell of SR Technics, Zurich airport, Switzerland. Data were collected on various engines during post-maintenance test runs burning standard Jet A-1 fuel as well as during a dedicated measurement campaign using various blends of Jet A-1 with HEFA (hydro-processed esters and fatty acids). The nvPM emissions and SN were sampled and measured according to the regulatory standards and using state-of-the-art instrumentation.

Preliminary results show good agreement of the measurement data with FOA3 for SN > 5 (Figure 1). However, since the maximum SN of modern engines can be < 1, we focus also on the correlations with ultra-low SN for both the nvPM mass and number emissions. Moreover, none of the correlations previously developed address particle loss, which is a significant artifact associated with gas turbine exhaust sampling (Durdina et al. 2014). We address the particle loss in the

standardized sampling system to provide the best estimates of engine-out emissions relevant for the environmental impact assessment.

The updated correlations of nvPM concentrations and emission indices (amount of pollutant / kg fuel burned) with SN can be implemented in air quality models as well as in methods to estimate aircraft cruise emissions.

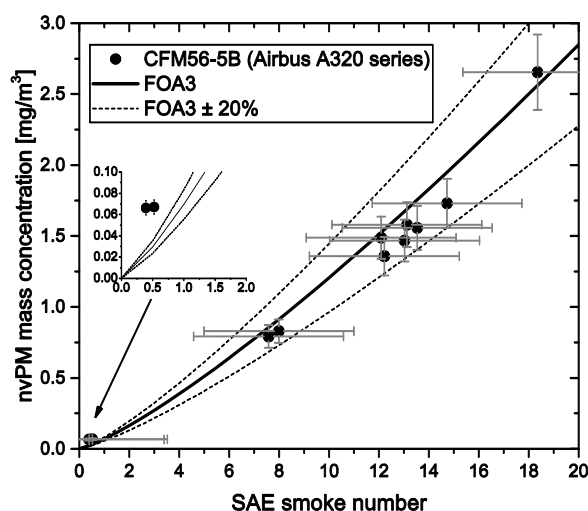


Figure 1. NvPM mass concentration (without particle loss correction) and SN determined during one run of a CFM56-5B engine.

This work was supported by the Swiss Federal Office of Civil Aviation (FOCA). The exhaust sampling probe was partially funded by the Swiss National Science Foundation. We further acknowledge SR Technics AG for operating the engine testing facility.

Wayson, R. L., Fleming, G. G., & Iovinelli, R. (2009). *J. Air Waste Manag. Assoc.*, **59**(1), 91–100.

Stettler, M. E. J., Swanson, J. J., Barrett, S. R. H., & Boies, A. M. (2013). *Aerosol Sci. Technol.*, **47**(11), 1205–1214.

Stettler, M. E. J., Boies, A. M., Petzold, A., & Barrett, S. R. H. (2013). *Environ. Sci. Technol.*, **47**(18), 10397–404.

Durdina, L. et al. (2014). *Atmos. Environ.*, **99**, 500–507.

## Aircraft-based single particle measurements in the Baltic Sea marine boundary layer

F. Köllner<sup>1,2</sup>, J. Schneider<sup>1</sup>, H. Bozem<sup>2</sup>, P. Hoor<sup>2</sup>, M. Zanatta<sup>3</sup>, H. Schulz<sup>3</sup>, A. Herber<sup>3</sup>, U. Bundke<sup>4</sup>, J. de Faria<sup>4</sup>, A. Petzold<sup>4</sup>, R. Brauner<sup>5</sup> and S. Borrmann<sup>1,2</sup>

<sup>1</sup>Particle Chemistry Department, Max Planck Institute for Chemistry, Mainz, 55128, Germany

<sup>2</sup>Institute for Atmospheric Physics, Johannes Gutenberg University, Mainz, 55128, Germany

<sup>3</sup>Alfred Wegener Institute for Polar and Marine Research, Bremerhaven, 27570, Germany

<sup>4</sup>Institute of Energy and Climate Research, Forschungszentrum Jülich GmbH, Jülich, 52428, Germany

<sup>5</sup>Seefahrt und Logistik, Jade Hochschule, 26931, Elsfleth, Germany

Keywords: single particle mass spectrometry, aircraft measurements, ship emissions, marine boundary layer.

Presenting author email: f.koellner@mpic.de

Air quality in the Baltic Sea marine boundary layer is strongly influenced by gaseous and particulate emissions from numerous cargo and passenger ships (Jalkanen *et al.*, 2016). Besides the air quality aspects, these emitted particles might modify the Earth's radiation budget directly and indirectly by acting as cloud condensation nuclei (Durkee *et al.*, 2000).

To study the atmospheric composition in this specific area, the airborne measurement campaign BALTIC2015 was conducted with the research aircraft Polar 5 (operated by the Alfred Wegener Institute for Polar and Marine Research) in the Baltic Sea Region between Fehmarn and Gotland during August 26-30, 2015. We operated in altitudes between 50 and 1300 m covering the marine boundary layer and the transition to the free troposphere.

The aircraft was equipped with instruments for physico-chemical aerosol analysis, several trace gases, and meteorological parameters. In particular, direct reading chemical composition measurements on single aerosol particles were performed by means of the Aircraft-based Laser Ablation Aerosol Mass Spectrometer (ALABAMA; Brands *et al.*, 2011). The instrument covers a size range from approximately 200 to 2000 nm. Furthermore, aerosol size distributions and number concentrations were obtained from an Optical Particle Counter (Grimm 1.129 (size range 250 nm – 30 µm)).

Based on a single particle clustering algorithm (Roth *et al.*, 2016), approximately 3 % of all measured particles (in total: around 7400) include different metals. As can be seen in Figure 1, vanadium ( $m/z +51$  and  $m/z +67$ ), iron ( $m/z +54/56$ ), nickel ( $m/z +58/60$ ) and sodium ( $m/z +23$ ) dominate the positive mean spectrum of this metal-containing particle type. Furthermore, these particles are coated with nitrate and sulfate as evident from the negative ion spectrum. Healy *et al.* (2009) observed a similar particle type attributed to several ship emission plumes close to the port in Cork, Ireland.

Some longer flight segments of about 15 minutes with increased relative fraction of this particle type are accompanied by enhancements of CO and CO<sub>2</sub> mixing ratios as well as higher particle number concentration (Figure 2). This indicates a significant influence of ship emissions on the undisturbed background composition of the atmosphere.

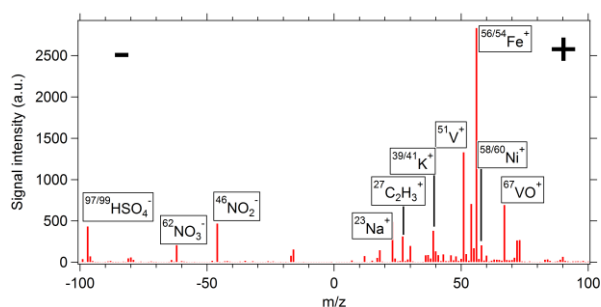


Figure 1. Bipolar mean mass spectrum of the metal-containing particle type.

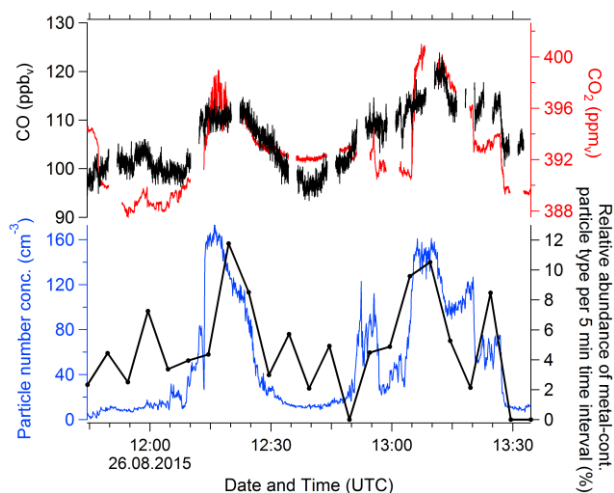


Figure 2. Time series of a specific measurement leg during the flight on August 26, 2015 of CO (upper panel, black), CO<sub>2</sub> (upper panel, red), particle number concentration (lower panel, blue) and relative abundance of metal-containing particles (lower panel, black).

Jalkanen, J.-P., et al. (2016) *Atmos. Chem. Phys.* **16**, 71–84.

Durkee, P. A., et al. (2000) *J. Atmos. Sci.*, **57**, 2523–2541.

Brands, M., et al. (2011) *Aerosol Sci. Technol.* **45**, 46–64.

Roth, A., et al. (2016) *Atmos. Chem. Phys.* **16**, 500–524

Healy, R. M., et al. (2009) *Atmos. Environ.* **43**, 6408–6414.

## Marine BC measurements from two large engine test facilities

K.A. Thomson<sup>1</sup>, J. Pedersen<sup>2</sup>, S. Gagne<sup>1</sup>, J.-P.Hansen<sup>3</sup>

<sup>1</sup>Measurement Science and Standard, National Research Council, Ottawa, K1A 0R6, Canada

<sup>2</sup>MAN Diesel and Turbo, Copenhagen, DK-2450, Denmark

<sup>3</sup>Alfa Laval Aalborg A/S, Marine & Offshore System, Marine Boilers & Heaters, Aalborg, 9100, Denmark

Keywords: Marine, Black Carbon, Scrubber, Diagnostics

Presenting author email: kevin.thomson@nrc-cnrc.gc.ca

As part of assessing the impact of shipping on the Arctic, the International Maritime Organization (IMO) has requested research to support the selection of measurement method(s) to characterize Black Carbon (BC) emissions from marine engines and to investigate possible control strategies.

In November 2016, a two-part measurement campaign was performed at MAN Diesel and Turbo, Copenhagen, and Alfa Laval, Aalborg. At MAN, a 2-stroke, slow speed, 7 MW engine and at Alfa Laval, a 4-stroke, medium speed, 2 MW engine were tested using marine distillate and heavy fuel oil (HFO). For the 4-stroke engine, samples were acquired upstream and downstream of an exhaust scrubber system.

Measurements of total PM were performed using gravimetric filter analysis of a ~10:1 diluted exhaust as well as in-stack hot exhaust. BC was analysed from the raw exhaust at MAN using a smoke meter (AVL 415S). Dilute BC was measured from both engines using thermal optical analysis (TOA, Sunset Labs Model 4 and 5 analyzers) and photo acoustic spectroscopy (PAS, Droplet Measurement Technologies, PAX870). Laser Induced Incandescence measurement (LII, Artium LII300) of the dilute exhaust was also performed for some conditions of the 4-stroke engine. Samples were acquired for transmission electron microscopy (TEM) and Raman analysis.

As a pre-test instrument comparison, the smoke meter, PAS, and TOA filters were connected on a common tunnel and sampled BC particles generated by a miniCAST burner operating at SP1 and diluted using a variable diluter. Smoke meter filter smoke number (FSN) readings were converted to equivalent Black Carbon (eBC) using the manufacturer specified relationship:

$$C \left[ \frac{mg}{m^3} \right] = \frac{1}{0.405} \times 5.32 \times FSN^{0.3062 * FSN}$$

A comparison of the smoke meter and PAS readings are included in Figure 1. Linearity agreement with a small intercept and slope near one was observed over the measured concentration range. Conversely, preliminary comparison of smoke meter and dilution corrected PAS on the 2-stroke engine running HFO show smoke meter readings exceeding PAS by greater than a factor of 2. This difference may in part be explained by line losses which have not been accounted for with the PAS measurements but have with the smoke meter readings. Further investigation is needed to validate these readings.

TOA filters are being analysed and EC results will be added to the comparison.

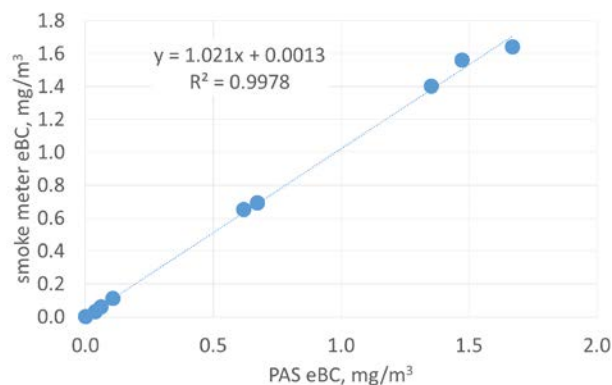


Figure 1 – Comparison of smoke meter and PAS on miniCAST burner SP1 with variable aerosol dilution.

Preliminary TOA analysis of filters from the 2-stroke engine operated with HFO suggest that organic carbon (OC) dominates the total carbon (TC) content of the filter with OC/TC > 90%. Due to concerns about the accuracy of the split point between OC and elemental carbon (EC), various TOA protocols (NIOSH, EUSAAR-2, IMPROVE-A, and variants of these) were tested. In all cases, significant charring was observed, with 45 to 65% of the OC readings attributable to charred OC which evolved during the EC phase. Charring may be enhanced by the presence of sulphates on the filters.

Filter analysis is ongoing and the finds of the two engine studies, including the pre and post exhaust treatment with scrubber system, will be presented.

This work was supported by the Danish Maritime Fund - Blue INNOShip program and Transport Canada - Clean Transportation Initiative.

## Contamination induced by the use of PTFE lines in aeronautic soot sampling

I.K. Ortega<sup>1</sup>, C. Irimiea<sup>2</sup>, D. Delhay<sup>1</sup> and C. Focsa<sup>2</sup><sup>1</sup>Onera-The French Aerospace Lab, F-91761 Palaiseau, France<sup>2</sup>Laboratoire de Physique des Lasers, Atomes et Molécules (UMR CNRS 8523), Université de Lille 1 Sciences et Technologies, 59655 Villeneuve d'Ascq, France

Keywords: Sampling line, airplane emissions, mass spectrometry, soot.

Presenting author email: Ismael.ortega@onera.fr

Measurements campaigns focused on combustion aerosol particles characterization are technically challenging. Exhaust particles must be cooled down and diluted prior to reaching the measurements instruments. The sampling lines used are often heated between 60°C and 160°C to avoid formation of volatile particles. The material used in these lines should minimize line losses and assure the cleanliness of the sample. In addition, in many tests it is desirable that these lines are flexible.

Conductive silicone lines have been widely used due to their low particle losses and their flexibility. On the other hand, they have been shown to be responsible of sample contamination in airplane engine emission studies (Timko et al., 2009). Poly-dimethyl siloxane (PDMS) was found in the soot samples collected through conductive silicon tubing. The PDMS uptake by soot particles was found to be up to 30%.

In the last years, the use of antistatic PTFE lines has become more and more popular. They present low particle losses, are flexible, there are commercial versions including as all-in-one solution the temperature control and, in principle, they should be free of siloxane.

In the present work we have used Time of Flight Secondary Ion Mass Spectrometry (ToF-SIMS) to characterize air and soot samples collected on filters through a two meter long, antistatic PTFE line (Winkler GmbH).

In a first experiment we flow HEPA filtered air through the line heated at different temperatures. At the beginning of the experiment the line was kept at 60°C. Then we increase the line temperature up to 160°C. Finally we let the line cool down to 30°. The filter holder used to take the samples was kept at 160°C.

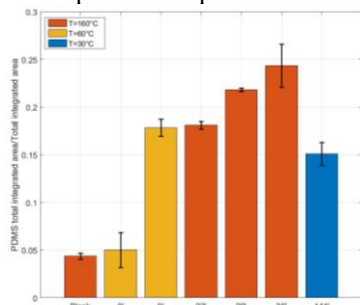


Figure 1. PDMS fragments integrated area normalized to total area for different samples studied.

Our results show the presence of PDMS in the blank sample from the filter holder at 160°C. We suspect that this is linked to the silicon O-ring used in it. We also confirmed the presence of PDMS in the samples

obtained through the line. This contamination was more important when the temperature of the line was set to 160°C.

For the second experiment, soot was produced using a liquid Combustion Aerosol Standard generator (CAST, Jing GmbH) burning standard JetA1 kerosene. The sample flow passed through a catalytic stripper coupled with a Dekati Engine Exhaust Diluter (DEED, Dekati OY) just before entering the line to avoid the presence of volatile particulate matter. The filter holder was kept at room temperature to avoid PDMS contamination

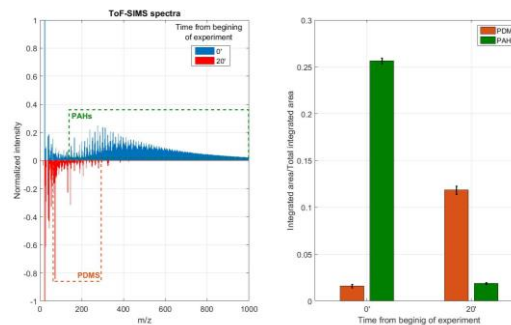


Figure 2. Left panel: ToF-SIMS spectra for two soot samples taken at different times. Right panel: Total integrated area for PDMS and PAH peaks normalized to total area

The results for soot samples are similar to those obtained for air samples. In the case of soot we can see how the presence of PDMS alters the detection of PAHs adsorbed on the soot, suggesting that the PDMS is adsorbed in the surface of soot.

Our results point to a potential problem when using PTFE lines in the temperature conditions imposed by the current normative for certification. The source of this contamination is unclear, thus further work is needed to isolate the cause of this problem and guarantee a contamination free sampling system.

This work was supported by ONERA projects EMPIRE and PROMETE and the French National Research Agency (ANR) through the PIA (Programme d'Investissement d'Avenir) under contract ANR-10-LABX-005 (LABEX CaPPA - Chemical and Physical Properties of the Atmosphere).

Timko, M.T., Yu, Z., Kroll, J., Jayne, J.T., Worsnop D.R., et al. (2009) *Aerosol Sci. Technol.* **43**, 855-865.

## EXPLIC Program: Impact of aromatic content in different alternative aeronautic fuel emissions

D. Delhay<sup>1</sup>, J. Ancelle<sup>1</sup>, M. Sicard<sup>1</sup>, L. Jing<sup>2</sup>, and I.K. Ortega<sup>1</sup>

<sup>1</sup>Onera-The French Aerospace Lab, F-91761 Palaiseau, France

<sup>2</sup>Jing Ltd., Im Park 4, CH-3052 Zollikofen, Switzerland

Keywords: Bio-fuel, emissions, soot.

Presenting author email: Ismael.ortega@onera.fr

Aviation is actually one of the strongest growing transport sectors, and this trend is predicted to continue. In the period up to 2030, global aviation is expected to grow by 5 % annually according to International Air Transport Association IATA (Lee et al. 2010). Currently, aviation represents 2 % of global CO<sub>2</sub> emissions, but is expected to grow to 3 % by 2050. While solar and electric aircrafts are being researched, it is not expected they will be feasible in the near or medium term. Therefore, the aviation industry has identified the development of biofuels as one of the major ways it can reduce its emissions from fossil origin.

With an increasing number of alternative fuels available, currently there are five biofuel production pathways technically certified and many more certifications are in preparation, there is a need for a systematic method to evaluate how the chemical composition of different fuels affects their emissions. Complete engine tests are technically and economically challenging. In addition, the high fuel consumption (~600 lpm) and the low availability of biofuels impose strict time limits for these tests, thus systematic experiments beyond the standard certification purposes are rarely available.

In this work, we have used a novel Combustion Aerosol STANDar (CAST) Generator especially designed to work with liquid fuel (Jing et al. 2003) to study the emission generated by up to 15 different fuels: JetA-1, Synthetic Paraffinic Kerosene (SPK), Aromatic Fluid (AF) 450 (a mixture of 3 aromatic representative cuts found in a jet fuel, AF 100, 150 and 200), SPK/JetA-1 blends (4 and 8 % aromatic contents (AC)), SPK/Jet A-1 blends (4, 6, 8 and 20.6 % AC), SPK/AF 450 blends (8 and 20.6 % AC), SPK/AF 100 blends (8 and 20.6 % AC), SPK/AF 150 blends (8 and 20.6 % AC) SPK/AF 200 blends (8 and 20.6 % AC) and SPK/1-Methyl-naphthalene blends (8 and 20.6 % AC).

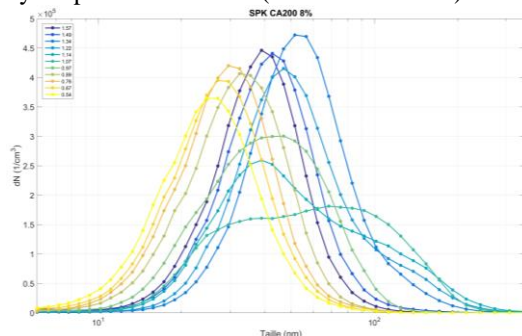


Figure 1. Example of particle size distributions obtained for different flame richness using a SPK/AF 200 8 % AC fuel

We have measured the total number and size distribution of particles produced by these fuels at different flame richness (between 0.5-1.6), both at the raw exhaust (Fig.1) and after treatment by a catalytic stripper coupled with a Dekati Engine Exhaust Diluter (DEED, Dekati oy) to remove the volatile fraction.

We have focused our study on the impact of fuel aromatic content on particle size distributions.

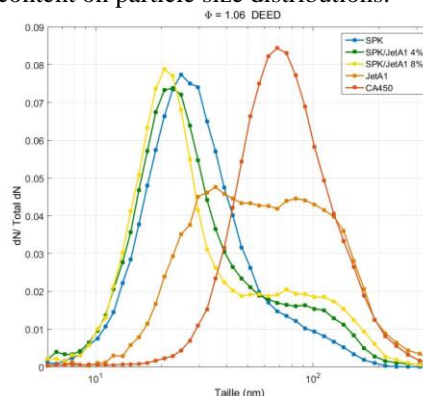


Figure 2. Size distributions obtained with a flame richness of 1.06 for JetA-1 (20.6 % AC), SPK (2.5 % AC), SPK/Jet A-1 blends of 4 and 8 % AC and AF 450 (100 % AC).

As can be seen in Fig. 2, the main differences between SPK and the blends with an increasing AC percentage, is the second mode around 100 nm, which increase with the AC. If we compare to the size distribution obtained with the fuel with 100 % AC, we can see how the aromatic compounds seems to be linked to this second mode.

During the conference, we will present the results on all fuels, showing the role of not only the fuel AC on particle size and number, but also the nature of these aromatic compounds.

This work was supported by ONERA project EXPLIC.

Lee, D. S., Pitari, G., Grewe, V., Gierens, K., Penner, J.E., Petzold, A., Prather, M.J., Schumann, U., Bais, A., Bernsten, T., Lachetti, D., Lim, L.L., Sausen R. (2010) *Atmos. Environ.*, **44**, 4678-4734.

Jing, L. (2003) *7th ETH Conference on Nanoparticle Measurement*, ETH Höggerberg Zürich.

## Mass and size resolved optical properties of black carbon particles in aircraft engine exhaust

M. Elser<sup>1,2</sup>, B.T. Brem<sup>1,2</sup>, L. Durdina<sup>1,2</sup> and J. Wang<sup>1,2</sup>

<sup>1</sup>Laboratory for Advanced Analytical Technologies, Empa, Dübendorf, 8600, Switzerland

<sup>2</sup>Institute of Environmental Engineering, ETH Zürich, Zürich, 8093, Switzerland

Keywords: aircraft emissions, optical properties, CAPS PM<sub>ssa</sub>, PAX.

Presenting author email: miriam.elser@empa.ch

The steady growth of aviation transport in the last decades and the predicted 4.5% global annual air traffic growth for the next 20 years (Leahy J., 2016), have raised the interest of the scientific community regarding gaseous and particulate emissions from aircraft engines. Aircraft emissions are a concern for local air quality in the vicinity of airports and have significant impacts on radiative forcing and climate. Although the contribution of aviation to global black carbon (BC) is low in comparison to other sources, this is a unique source contributing to the particulate mass in the upper troposphere. A detailed understanding of the optical properties of BC is essential to estimate its related climate effects.

A Cavity Attenuated Phase Shift-based single scattering albedo monitor (CAPS PM<sub>ssa</sub>) was used to measure scattering and extinction coefficients ( $b_{\text{scat}}$  and  $b_{\text{ext}}$ ) of aircraft emissions during the A-PRIDE 8 campaign. Two engine types were tested at various thrust levels using Jet A-1 fuel doped with an aromatic solvent. Figure 1a shows the absorption coefficient ( $b_{\text{abs}} = b_{\text{ext}} - b_{\text{scat}}$ ) as a function of thrust level for two engine tests. Very low  $b_{\text{abs}}$  (0 to 50  $\text{Mm}^{-1}$ ) were determined for both engines at thrust levels below 40 %, while a linear increase up to 1400  $\text{Mm}^{-1}$  was observed for higher thrust levels. Moreover, at thrust levels above 40 %, the PW4168A engine was characterized by smaller  $b_{\text{abs}}$  (and BC emissions) than the CFM56-7B26 engine type. A similar trend is observed for  $b_{\text{abs}}$  with the particle size. As shown in Fig. 1b, the low  $b_{\text{abs}}$  values at low thrusts were related to particles with size distributions peaking below 30 nm, while a linear increase in  $b_{\text{abs}}$  was observed for larger particles. Note that no dependence with the engine type was observed in this case. This could relate to particles of different sizes having different morphologies and thus different scattering properties.

In order to further investigate the effect of the particle size and mass on the optical properties of aircraft BC emissions, size resolved measurements of the optical properties are planned during the upcoming Empairex1 campaign. In addition to the CAPS PM<sub>ssa</sub> instrument at a wavelength of 532nm a Photoacoustic Extinctionmeter (PAX) at 870 nm wavelength is used to study the wavelength-dependence of the optical properties. A Centrifugal Particle Mass Analyzer (CPMA) will be deployed in parallel to the optical instruments to retrieve the particle mass distribution at the selected size. The effects of alternative fuel blends on the optical properties will also be investigated in this campaign. For this

purpose the various blends of Jet A-1 fuels with an HEFA (Hydro-processed Esters and Fatty Acids) will be studied.

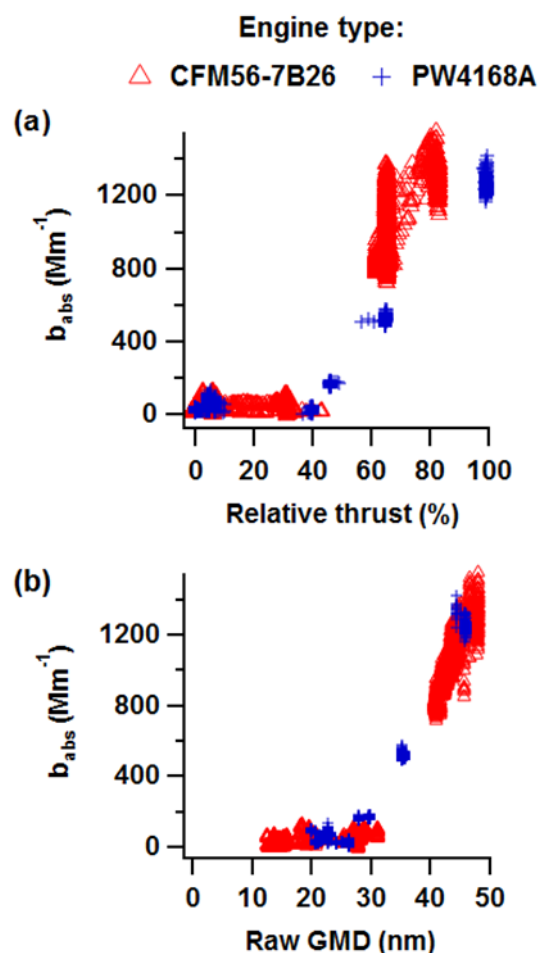


Figure 1. (a) Absorption coefficient ( $b_{\text{abs}}$ ) as a function of the thrust level; (b)  $b_{\text{abs}}$  as a function of the raw (not line-loss corrected) geometric mean diameter (GMD) of the particle size distribution.

This work was supported by the Swiss Federal Office of Civil Aviation (FOCA): The exhaust sampling probe has been partially funded by the Swiss National Science Foundation. We further acknowledge SR Technics AG for operating the engine testing facility and AVL GmbH for loaning the PAX instrument.

Leahy, J. (2016) *Airbus Global Market Forecast 2016-2035*.

## Brown carbon in ship-engine exhaust: imaginary refractive index and mass absorption cross-section retrieval

J. C. Corbin<sup>1</sup>, A. A. Mensah<sup>2</sup>, M. Zanatta<sup>1</sup>, S. Pieber<sup>1</sup>, G. Jakobi<sup>3,4</sup>, J. Orasche<sup>3,4</sup>, J. G. Slowik<sup>1</sup>, N. Kumar<sup>1</sup>, I. El Haddad<sup>1</sup>, F. Klein<sup>1</sup>, B. Stengel<sup>3</sup>, R. Zimmermann<sup>3,4</sup>, A. S. H. Prévôt<sup>1</sup>, U. Baltensperger<sup>1</sup>, and M. Gysel<sup>1</sup>

<sup>1</sup> Laboratory of Atmospheric Chemistry, Paul Scherrer Institute, 5232 Villigen PSI, Switzerland

<sup>2</sup> Institute for Atmospheric and Climate Science, ETH Zurich, 8092 Zurich, Switzerland

<sup>3</sup> University of Rostock, 18051 Rostock, Germany

<sup>4</sup> Helmholtzzentrum Munich, Ingolstädter Landstrasse 1, 85764 Oberschleissheim, Germany

Keywords: ship emissions, HFO, refractive index, brown carbon.

Presenting author email: martin.gysel@psi.ch

Shipping emissions represent a rare source of aerosol pollution in the relatively-clean marine atmosphere. The radiation and cloud interactions of these polluting aerosols are influenced by their content of light-absorbing carbon, which includes both black carbon (BC) and light-absorbing organic particulate matter (BrC) (Mueller et al., 2015). The production and emission of these species by a ship engine depends on the composition of the fuel, which has traditionally been the sulfur-rich residual fuel “Heavy Fuel Oil” (HFO), and on operation conditions.

Since 2010, European regulations have required low-sulfur distillate fuels like “Marine Gas Oil” (MGO) or diesel fuel (DF) to be used in and around European ports (Jonson et al., 2015). Whereas traditional HFO contains very large aromatics, these distillate fuels consist of lighter hydrocarbons. This should lead to fundamentally different Mass Absorption Cross-sections (MACs) for organic PM from these different fuels. In addition, distillate fuels emit a significantly higher BC mass fraction.

We will present MACs evaluated for three different fuels in a four-stroke ship diesel research engine, derived from in situ measurements. The in-situ measurements were made using a CAPS-PM<sub>SSA</sub> monitor for the 780 nm absorption coefficient (Aerodyne, USA), laser-induced incandescence for BC (SP2, DMT, USA), aerosol mass spectrometry for organic matter (OM; Aerodyne HR-AMS) and dual-spot aethalometer for Absorption Ångström exponents (AAEs) (AE33, Aerosol d.o.o., Slovenia). Example measurements are shown in Figure 1C.

In addition to the MACs, we derive the wavelength-dependent imaginary refractive index  $k_{OM,\lambda}$  by fitting a Mie model to the data. Empirical constraint of the Mie model using time-resolved SP2 light-scattering data will be discussed. We find that BrC absorption from HFO exhaust can be as important as BC absorption in the shorter visible wavelengths, while BrC emissions are negligible for MGO and DF.

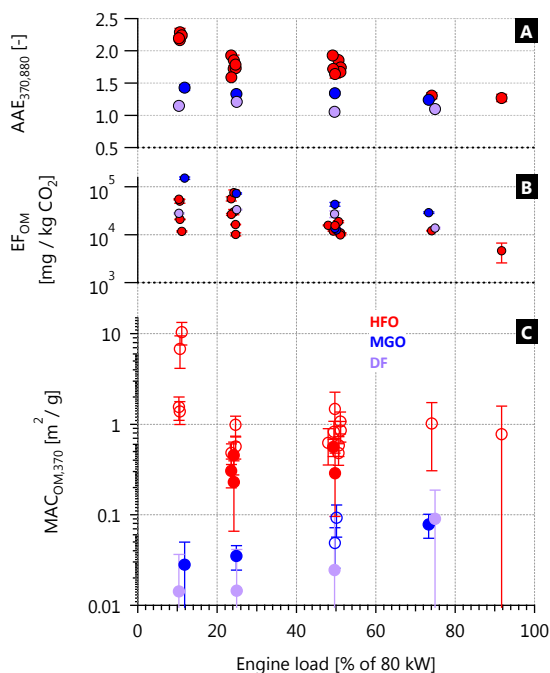


Figure 1. (A) Absorption Ångström exponents, (B) organic aerosol emission factors, and (C) mass-absorption cross-sections of OM from heavy fuel oil (HFO), marine gas oil (MGO), and diesel fuel (DF). Closed symbols:  $b_{\text{abs}}$  by CAPS-PM<sub>SSA</sub>. Open symbols:  $b_{\text{abs}}$  by CAPS-calibrated AE33.

This work was supported by an European Research Council grant (ERC-CoG 615922-BLACARAT) and by the SNF and DFG grants “WOOSHI”.

Mueller et al., Applied Energy 155, 204–217, 2015.

Jonson et al., Atmos. Chem. Phys. 15, 783–798, 2015.

## Black carbon from shipping over the Baltic Sea

M. Zanatta<sup>1</sup>, H. Schulz<sup>1</sup>, F. Köllner<sup>2,3</sup>, J. Schneider<sup>2</sup>, H. Bozem<sup>3</sup>, P. Hoor<sup>3</sup>, U. Bundke<sup>4</sup>,  
J. de Faria<sup>4</sup>, A. Petzold<sup>4</sup>, R. Brauner<sup>5</sup> and S. Borrmann<sup>1,2</sup> and A. Herber<sup>1</sup>

<sup>1</sup>Alfred Wegener Institute for Polar and Marine Research, Bremerhaven, 27570, Germany

<sup>2</sup>Particle Chemistry Department, Max Planck Institute for Chemistry, Mainz, 55128, Germany

<sup>3</sup>Institute for Atmospheric Physics, Johannes Gutenberg University, Mainz, 55128, Germany

<sup>4</sup>Institute of Energy and Climate Research, Forschungszentrum Jülich GmbH, Jülich, 52428, Germany

<sup>5</sup>Seefahrt und Logistik, Jade Hochschule, 26931, Elsfleth, Germany

Keywords: black carbon; aerosol; airborne, ship emissions, marine background.

Presenting author email: marco.zanatta@awi.de

While black carbon (BC) particles are recognized to have a global impact on climate warming and human health, the contribution of the shipping sector is rather uncertain (Aardenne et al., 2013). This is due, in first instance, to a missing regulation for BC shipping emissions and scarcity of observations. Nevertheless, the scientific and maritime communities are collaborating in order to quantify and estimate the potential impacts of BC emission from shipping and various abatement technologies (IMO, 2016). Within this work we aim to better quantify the impact of ship traffic on BC levels in marine background environment.

The southern Baltic Sea is one of the most frequented European shipping routes, with more than 2000 vessels operating every day (HELCOM, 2016). The present study is based on the airborne campaign BALTIC2015, conducted with the research aircraft Polar 5 (operated by the Alfred Wegener Institute for Polar and Marine Research) between 26<sup>th</sup> and 30<sup>th</sup> August 2015 in the Baltic Sea Region between Fehmarn and Gotland (Figure 1). Refractory black carbon (rBC) was detected on-board with the Single Particle Soot Photometer (SP2; Droplets Measurement Technologies, USA). The SP2 provides number and mass concentration, and size distribution of rBC (between 80-550 nm). Total aerosol number concentration and size distribution (between 60-1000 nm) was monitored with the Ultra High Sensitivity Aerosol Spectrometer (UHSAS; Droplets Measurement Technologies, USA). Additional properties as aerosol chemical composition and gas trace presence were monitored.

Background conditions were identified as low altitude observations far from the main trading corridor. For the 28<sup>th</sup> of August background number concentration of BC and total aerosol were quantified as 13 and 395 #/cm<sup>3</sup> respectively, while background mass concentration of rBC was quantified as 0.029 µg/sm<sup>3</sup>. In the vicinity of shipping transects the aerosol concentration increased consistently, with number concentration of total and rBC aerosol enhanced by 79% and 81% respectively, while rBC mass concentration reached 0.054 µg/sm<sup>3</sup>. Surprisingly, the number fraction of rBC particles does not change, suggesting a rather well mixed polluted layer. On the contrary, the fraction of particles smaller than 150 nm in-

creased within the shipping corridor, suggesting the presence of freshly emitted particles. The spikes in the time series in Figure 2 show multiple encounters with the exhaust plume of the container ship MV Thetis D.

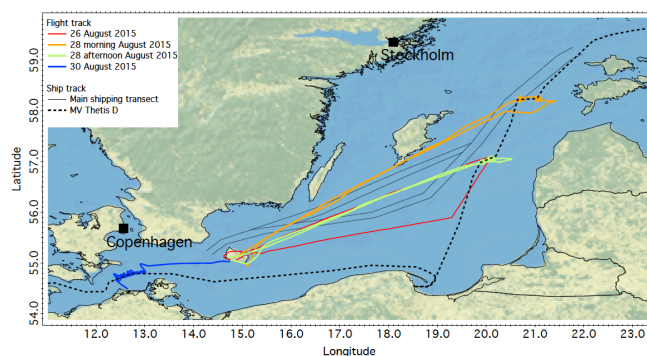


Figure 1. Operational of Polar 5 aircraft, main shipping corridors and track of the container ship MV Thetis D.

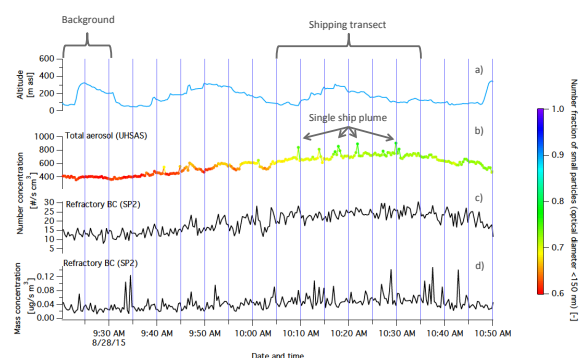


Figure 2. Time series of a specific measurements taken on August 28, 2015: a) airplane altitude; b) number concentration of total aerosol; c-d) Number and mass concentration of refractory black carbon.

Aardenne (2013); *The impact of international shipping on European air quality and climate forcing*. HELCOM (2016); *Baltic Sea clean shipping guide*. IMO (2016); *Investigation of appropriate control measures to reduce black carbon emissions from international shipping*.

## Airborne Characterization of Particle Emission Rates from Ships

T.F. Villa<sup>1</sup>, R. Jayaratne<sup>1</sup>, F. Gonzalez<sup>2</sup>, L. Morawska<sup>1</sup>, R Schofield<sup>3</sup>, C.L. Vincent<sup>3</sup>, S. Fiddes<sup>3</sup>, R. Ryan<sup>3</sup>, M. Harvey<sup>4</sup>, T. Bromley<sup>4</sup>, S. Gray<sup>4</sup> and Z. Ristovski<sup>1</sup>

<sup>1</sup>International Laboratory for Air Quality and Health (ILAQH), QUT, Brisbane, Australia

<sup>2</sup>Australian Research Centre for Aerospace Automation (ARCAA), QUT, Brisbane, Australia

<sup>3</sup>School of Earth Sciences, University of Melbourne, Melbourne, Australia

<sup>4</sup>National Institute for Water and Air (NIWA), Wellington, New Zealand

Presenting author email: [z.ristovski@qut.edu.au](mailto:z.ristovski@qut.edu.au)

Quantifying ship emitted pollutants, in particular ultrafine particles in terms of particle number (PN) concentration, is critical to improve our understanding of shipping impact on climate and health (Corbett et al 2007, Lack et al 2011). To achieve this, a large scale quantification of ship emission factors (EFs) is necessary and different methods have been used to investigate emissions from ships namely: test-bench, ship plume-based and on-board measurements. Test-bench studies (Reda et al 2015) have been used to characterize emissions from different engines at various loads. However, engine performance and its emissions are different if the engine is tested in a laboratory rather than during real operations. This calls for measurements of ship emissions in-situ, to collect more significant data for EF calculation, but only a few of on-board ship studies to calculate real emission factors have been undertaken (Blasco et al 2015). Airborne, ship plume-based measurements (Beecken et al 2014) offered important insight regarding ship generated pollution. However, it is the cost and challenges such as difficulties to deploy the systems which limit the applicability and wide use of these measurements.

Recent advances in hexacopter unmanned aerial vehicle (UAV) technology enable to measure ship generated pollutants inside the ship plume, overcoming cost, safety and time issues. To date, no studies have reported the use of a UAV system capable to measure PN concentrations, for EF calculations, under real world condition, in open waters.

This research demonstrated the capability of a UAV system to characterize the emissions from the research vessel Investigator while operating at sea. Data collected with the UAV were compared to those collected by a tethered balloon. The two airborne systems measured the ship plume flying autonomously at varying altitudes and distances, downwind, behind the Investigator or, in the case of the balloon, floating at a fixed altitude, motionless in the air.

The UAV that was carrying the scientific payload was a DJI S800 hexacopter. The S800 weighing 3.7 kg with minimum and maximum take-off weights of 6.7 kg and 8 kg respectively. The UAV uses a 16000 mAh LiPo 6 cell battery, with a hover time of approximately 20 min and no additional payload. The payload of the S800 consisted of a Mini Diffusion Size Classifier (DISCmini). The DISCmini is a portable monitor used to measure concentration of particles ranging in diameter size from 10-500 nm and a time resolution of up to 1s (1

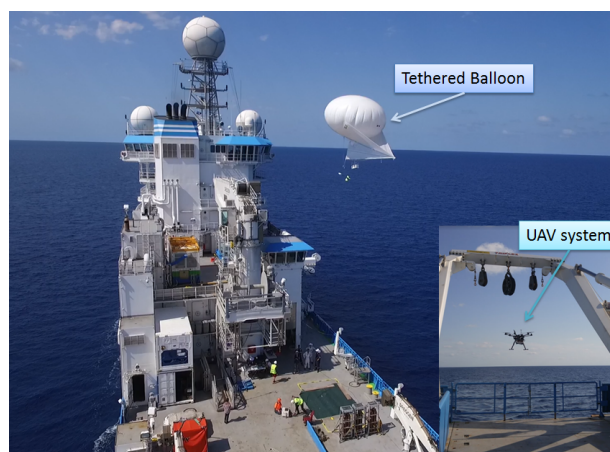


Figure 1. The UAV and the Tethered Balloon used on board the RV Investigator

Hz). A TSI IAQ-calc 7545 model was used as monitor to measure CO<sub>2</sub>.

The tethered balloon was a 9 m<sup>3</sup> helium filled balloon with a kite for stability. A Light Optical Particle Counter (LOAC) was used in addition to the DISCmini and Q-trak on the tethered balloon. The LOAC measured the particle size distribution in 19 channels from 0.2 to 100 μm.

EFs were calculated relative to the fuel consumption, using the fuel combustion derived plume CO<sub>2</sub>. Calculated particle number EFs for the RV Investigator were between  $9.19 \times 10^{+14}$  and  $5.15 \times 10^{+15}$  # (kg fuel)<sup>-1</sup>. The average of the RV Investigator EF<sub>PN</sub> are in line with literature plume data, ranging from 0.2 to 6.2  $\times 10^{+16}$  # (kg fuel)<sup>-1</sup>.

The authors would like to acknowledge the ARCAA Operations Team (Dirk Lessner, Gavin Broadbent) who operated the Unmanned Aerial Vehicle (S800) as well as the crew and MNF support staff on the RV Investigator.

Beecken, J., et al. (2014) *Atmos. Measur. Tech.* **7**, 1957-1968.

Blasco, J., et al. (2014) *Environ. Int.* **66**, 44-7.

Corbett, J.J., et al. (2007) *Environ. Sci. Tech.*, **41**, 8512-8518.

Lack, D.A., et al. (2011) *Environ. Sci. Tech.*, **45**, 9052-9060.

Reda, A.A., et al. (2015) *Atmos. Environ.* **112**, 370-380.

## Aircraft Black Carbon Particle Number Emissions – A New Predictive Method and Uncertainty Analysis

Roger Teoh<sup>1</sup>, Marc E.J. Stettler<sup>1</sup>, Arnab Majumdar<sup>1</sup> and Ulrich Schumann<sup>2</sup>

<sup>1</sup>Department of Civil and Environmental Engineering, Imperial College London, London, SW7 2AZ, UK

<sup>2</sup>Deutsches Zentrum für Luft- und Raumfahrt, Institute of Atmospheric Physics, 82234 Oberpfaffenhofen, Germany

Keywords: Aviation, Black Carbon, Particle Number Emissions, Contrails.

Presenting author email: rt415@ic.ac.uk

### Abstract

Black Carbon (BC) particle number emissions from aircraft jet engines contribute to anthropogenic climate change and the deterioration of air quality. BC emitted by aircraft is associated with direct and indirect climate forcing. Possibly the largest uncertainty in civil aviation's climate impact is the indirect forcing due to the formation of contrails (Lee et al., 2010), which have a significant and short-lived climate impact. Previous studies have shown that the number of contrail ice particles is dependent on the number of BC particles emitted by aircraft (Kärcher & Yu, 2009).

Existing methods to estimate BC particle number emissions per mass of fuel ( $EI_n$ ) rely on simplified assumptions. This research proposes a new method to estimate  $EI_n$  for global civil aviation based on theory of the morphology of fractal aggregates. Equation 1 represents the new  $EI_n$  predictive model, named as the Fractal Aggregates (FA) approach.

$$EI_n = \frac{EI_m}{\rho_0 \left(\frac{\pi}{6}\right) (a)^{3-D_{fm}} GMD^\varphi \exp\left(\frac{\varphi^2 \ln(GSD)^2}{2}\right)} \quad (1)$$

where:  $\varphi = 3b + (1 - b)D_{fm}$   
 $EI_m$  = BC mass emissions index  
 $\rho_0$  = Material density of BC primary particles  
 $D_{fm}$  = Mass-mobility exponent  
 $GMD$  = Geometric Mean Diameter  
 $GSD$  = Geometric Standard Deviation

Most BC  $EI_n$  estimates from the new method agree within a factor of 2 relative to experimental measurements. Uncertainty analysis suggests a  $\pm 62\%$  uncertainty for the  $EI_n$  outputs calculated from the new model. A variance-based sensitivity analysis identified GMD as the most critical parameter for  $EI_n$  outputs.

The new  $EI_n$  model is subsequently applied to an aircraft activity dataset. The average cruise BC  $EI_n$  is estimated to be around  $1.2 \times 10^{15} \text{ kg}^{-1}$  [ $4.4 \times 10^{14} - 1.9 \times 10^{15} \text{ kg}^{-1}$ ], 40% higher than previous estimates. Modelling results for an example transatlantic flight is presented in figure 1. When the usage of alternative fuel is assumed for the entire fleet, average BC  $EI_n$  is reduced by around 29% to 60%.

A higher BC  $EI_n$  estimate relative to previous methodologies implies that young contrail properties will have a smaller ice particle diameter (Schumann, Jeßberger & Voigt, 2013) and larger optical depth (Kärcher, 2016). As a result, contrail lifetime and its magnitude of radiative forcing is expected to increase (Schumann & Heymsfield, 2017).

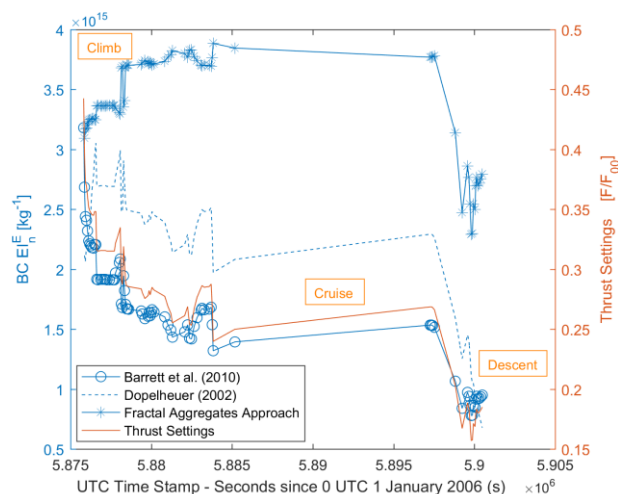


Figure 1: Changes in BC  $EI_n$  from different estimation methodologies and thrust settings across a transatlantic flight profile made by an A330-300 aircraft.

This research recommends the incorporation of the new BC  $EI_n$  estimation methodology into a contrail model. While the new BC  $EI_n$  estimation methodology might not necessarily reduce the output uncertainties of a contrail model, its accuracy on the modelling of initial contrail characteristics and its subsequent climate impacts can certainly be improved.

### Acknowledgements

Funding for this research was received from The Lloyds Register Foundation, and the Skempton Scholarship from the Department of Civil and Environmental Engineering, Imperial College London.

### References

- Kärcher, B. (2016) The importance of contrail ice formation for mitigating the climate impact of aviation. *Journal of Geophysical Research: Atmospheres*. 121 (7), 3497-3505.
- Kärcher, B. & Yu, F. (2009) Role of aircraft soot emissions in contrail formation. *Geophysical Research Letters*. 36 (1), .
- Lee, D., Pitari, G., Grewe, V., Gierens, K., Penner, J., Petzold, A., Prather, M., Schumann, U., Bais, A. & Bertsen, T. (2010) Transport impacts on atmosphere and climate: Aviation. *Atmospheric Environment*. 44 (37), 4678-4734.
- Schumann, U. & Heymsfield, A. J. (2017) On the lifecycle of individual contrails and contrail cirrus. *Meteorological Monographs*. 58 (1), .
- Schumann, U., Jeßberger, P. & Voigt, C. (2013) Contrail ice particles in aircraft wakes and their climatic importance. *Geophysical Research Letters*. 40 (11), 2867-2872.

## **Abstracts T101**

## The impact of lanthanum loading on alumina-supported cobalt catalysts synthesised via double flame spray pyrolysis

J. Horlyck<sup>1</sup>, S. Pokhrel<sup>2</sup>, E. Lovell<sup>1</sup>, L.Mädler<sup>2</sup> and J. Scott<sup>1</sup>

<sup>1</sup>Department of Chemical Engineering, University of New South Wales, Sydney, 2033, Australia

<sup>2</sup>Foundation Institute of Materials Science (IWT), Department of Production Engineering, University of Bremen, 28359 Bremen, Germany

Keywords: flame synthesis, gas phase nanoparticles, combustion process, particle formation.

Presenting author email: j.horlyck@unsw.edu.au

The active and stable catalysis of methane dry reforming relies upon the ability of the material to inhibit carbon formation. Central to this is the ability of a catalyst support to remove oxygen from the acidic carbon dioxide gas, storing or transporting this oxygen, before releasing it to oxidise an adsorbed  $\text{CH}_x$  intermediate species (Djinović et al., 2012). For the first time, an aerosol method was used to mix lanthanum with cobalt/alumina materials to improve support basicity.

Double flame spray pyrolysis was used to synthesise heterogeneous mixtures of cobalt oxide, alumina and lanthanum oxide. In order to inhibit the formation of complex cobalt-aluminate ( $\text{CoAl}_2\text{O}_4$ ) spinels during synthesis, lanthanum loadings of up to 15 wt% were investigated at two separate nozzle distances (11 and 18cm). The lanthanum content in the materials and the nozzle distance separating the flames were both found to have a key influence over material composition and properties.

The structure of the supported cobalt catalysts was characterised by hydrogen temperature programmed reduction, X-ray diffraction spectroscopy, carbon dioxide temperature programmed desorption, X-ray photoelectron spectroscopy and transmission electron microscopy. Catalytic activity and stability for methane dry reforming was determined via testing in a fixed bed reactor over a temperature range of 500-800 °C.

The basicity of the flame sprayed materials was found to increase with higher lanthanum content. Furthermore, the strength of the basic sites within the support materials was improved. The same pattern was observed for both the 11 and 18 cm nozzle distances.

The lanthanum content and nozzle distance were both observed to impact the formation of  $\text{CoAl}_2\text{O}_4$  spinels. The hydrogen temperature reduction profile and Rietveld refinement of the X-ray diffraction patterns indicate that the catalyst mixtures without lanthanum content readily form the spinel structures at a nozzle distance of 11 cm. Introducing even small quantities of lanthanum to the support material is sufficient to promote the formation of the more favourable  $\text{Co}_3\text{O}_4$  phase. Additionally, increasing the nozzle distance to 18 cm was found to inhibit spinel formation.

Performance testing of the catalyst materials showed that lanthanum content has a strong influence on catalytic activity at the 11 cm nozzle distance (Figure 1), with the methane and carbon dioxide conversion of materials increasing on the inclusion of lanthanum in the support structure. Lanthanum content had less of an

impact on the performance of the materials synthesised with an 18 cm nozzle distance (Figure 2). This was attributed to the promotion of Co into the  $\text{Co}_3\text{O}_4$  phase which resulted from the greater nozzle separation.

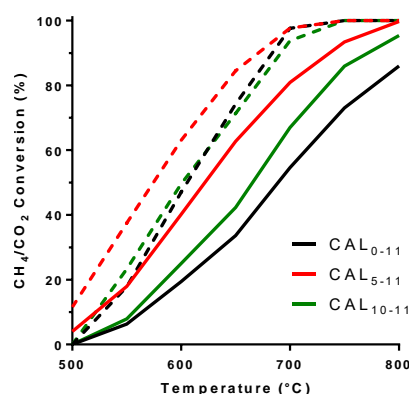


Figure 1.  $\text{CH}_4$  (—) and  $\text{CO}_2$  (--) conversion during methane dry reforming by cobalt-alumina-lanthanum ( $\text{CAL}_{x-11}$ ) catalysts prepared via double flame spray pyrolysis with a nozzle distance of 11 cm, where  $x$  represents La loading (wt%)

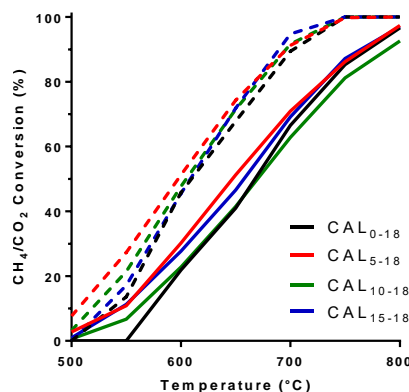


Figure 2.  $\text{CH}_4$  (—) and  $\text{CO}_2$  (--) conversion during methane dry reforming by cobalt-alumina-lanthanum ( $\text{CAL}_{x-18}$ ) catalysts prepared via double flame spray pyrolysis with a nozzle distance of 18 cm, where  $x$  represents La loading (wt%)

The Australian Research Council and the Faculty of Engineering, UNSW is acknowledged for their support of the project.

Djinović, P., Črnivec, I.G.O., Erjavec, B. and Pintar, A. (2012). *Applied Catalysis B: Environmental*, **125**, 259-270.

## Biomimetic luminescent antioxidant nanoparticles for H<sub>2</sub>O<sub>2</sub> biosensing

Anna Pratsinis<sup>1</sup>, Georgios A. Kelesidis<sup>2</sup>, Frank Krumeich<sup>2</sup>, Jean-Christophe Leroux<sup>1</sup> and Georgios A. Sotiriou<sup>1,3</sup>

<sup>1</sup>Drug Formulation and Delivery, Institute of Pharmaceutical Sciences, Department of Chemistry and Applied Biosciences, ETH Zurich, 8093, Zurich, Switzerland.

<sup>2</sup>Particle Technology Laboratory, Institute of Process Engineering, Department of Mechanical and Process Engineering, ETH Zurich, 8092 Zurich, Switzerland.

<sup>3</sup>Department of Microbiology, Tumor and Cell Biology, Karolinska Institutet, 17177 Stockholm, Sweden.

Keywords: nanotechnology, biosensors, hydrogen peroxide.

Presenting author email: georgios.sotiriou@ki.se

Cerium oxide nanomaterials have received a lot of attention recently due to their antioxidant *enzyme-like* (nanozyme) properties (Wei *et al* 2013). Here, europium doped cerium oxide (CeO<sub>2</sub>:Eu<sup>3+</sup>) nanoparticles with well-defined size ( $d_{XRD}$ : 4 – 16 nm) were prepared by flame aerosol technology and characterized in regards to H<sub>2</sub>O<sub>2</sub> sensor response in physiologically-relevant solutions. Temporal stability was compared to a commercially available fluorescent dye in a peroxidase coupled reaction.

CeO<sub>2</sub> nanoparticles containing 5 at% europium were prepared by flame spray pyrolysis. The particle size was controlled by tuning the flow rate of the liquid precursor solution ( $x$ ) and the flow rate of the O<sub>2</sub> dispersion gas ( $y$ ) (Madler *et al* 2002). Crystallinity and crystal size was characterized by X-ray diffraction.

Particles were dispersed in deionized water (diH<sub>2</sub>O) or a phosphate based buffer by vigorous vortexing and sonication. For all sensing measurements 75  $\mu$ L of 0.25 mg/mL CeO<sub>2</sub>:Eu<sup>3+</sup> were added to 75  $\mu$ L blank or H<sub>2</sub>O<sub>2</sub> and kept at room temperature (RT) for 30 min prior to measuring the signal intensity by phosphorescence ( $\lambda_{Ex/Em}$ : 330/590). Applied H<sub>2</sub>O<sub>2</sub> concentration ranged from 0.05 to 1000  $\mu$ M, a blank sample without substrate was included for each measurement. The sensor response (SR) was derived as follows from the sample intensity ( $I_S$ ) and blank intensity ( $I_0$ ):

$$SR = 1 - I_S/I_0 \quad (1)$$

For stability testing a H<sub>2</sub>O<sub>2</sub> sensitive probe, Amplex Ultra Red (AUR) was employed in a peroxidase (HRP) coupled reaction. 50  $\mu$ L AUR/HRP were added to 50  $\mu$ L H<sub>2</sub>O<sub>2</sub> and the signal measured directly by fluorescence ( $\lambda_{Ex/Em}$ : 490/585). CeO<sub>2</sub>:Eu<sup>3+</sup> particles and AUR/HRP were kept for 8 h at RT, unprotected from light and the signal intensity for 2  $\mu$ M H<sub>2</sub>O<sub>2</sub> monitored over time.

While largest CeO<sub>2</sub>:Eu<sup>3+</sup> particles showed highest signal intensity in the absence of substrate, smallest nanoceria ( $d_{XRD}$ : 4.4 nm) showed highest sensor response and were therefore selected for subsequent H<sub>2</sub>O<sub>2</sub> sensing. A clear substrate concentration signal dependency could be observed (Fig. 1). A limit of quantitation of 0.4  $\mu$ M for PBS and 1.16  $\mu$ M for 100 mM KPi (both at pH 7.4) was observed with linearity up to 5  $\mu$ M. When the concentration and sensor response reciprocals were plotted, as this is typically done for

enzymatic reactions, a broader linear range could be observed.

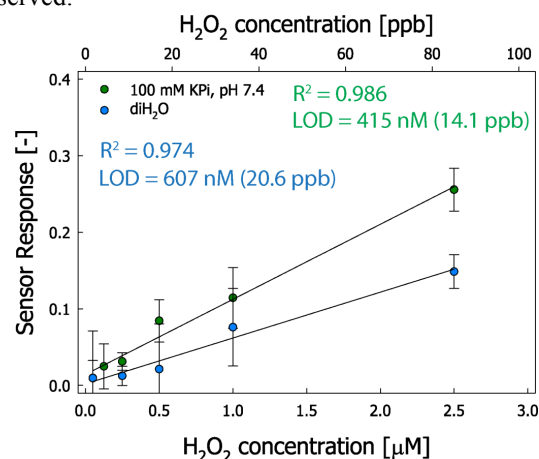


**Fig. 1:** Hydrogen peroxide sensor response of smallest CeO<sub>2</sub>:Eu<sup>3+</sup> nanoparticles in KPi and diH<sub>2</sub>O.

In contrast to AUR/HRP, nanoceria particles were able to maintain their H<sub>2</sub>O<sub>2</sub> detection properties after 8 h demonstrating superior stability and reduced susceptibility to photobleaching.

Fine-tuning the particle size revealed higher substrate sensitivity for smallest particles. CeO<sub>2</sub>:Eu<sup>3+</sup> demonstrated signal linearity in both diH<sub>2</sub>O and phosphate-based solutions enabling H<sub>2</sub>O<sub>2</sub> quantitation in biological systems using standard fluorimetric approaches (e.g. plate reader). Finally, improved stability over currently available H<sub>2</sub>O<sub>2</sub> detection systems highlight the potential of the robust and inexpensive CeO<sub>2</sub>:Eu<sup>3+</sup>.

Financial support from the research grant ETH-10 13-1 and the Phospholipid Research Center is acknowledged. GAS acknowledges the Swiss National Science Foundation for an *Advanced Researcher* fellowship.

Wei, H., Wang, E. K. Nanomaterials with enzyme-like characteristics (nanozymes): next-generation artificial enzymes. *Chem. Soc. Rev.*, **42**, 6060-6093 (2013).

Madler, L., Stark, W. J., Pratsinis, S. E. Flame-made ceria nanoparticles. *J. Mater. Res.*, **17**, 1356-1362 (2002).

## Spray-flame synthesis of nanoscale LaCoO<sub>3</sub> perovskite catalyst

S. Angel<sup>1</sup>, H. Wiggers<sup>1,2</sup> and C. Schulz<sup>1,2</sup>

<sup>1</sup>IVG, Institute for Combustion and Gas Dynamics – Reactive Fluids

<sup>2</sup>CENIDE, Center for Nanointegration, University of Duisburg-Essen

Keywords: LaCoO<sub>3</sub>, nanoparticle synthesis, micro-explosions, complexation.

Presenting author email: steven.angel-canas@uni-due.de

The versatile properties of the LaCoO<sub>3</sub> perovskite nanomaterial have led to the utilization of this material in multiple applications such as gas sensing, reforming of methane using CO<sub>2</sub>, and catalytic oxidation of hydrocarbons, alcohols, and CO. The synthesis of the respective materials is usually done in batch processes using wet chemical routes with subsequent treatments as filtration, washing, drying and calcination. Aiming to prepare a functional LaCoO<sub>3</sub> nanomaterial in a single step and in a cost-effective way, spray-flame synthesis (SFS) is investigated as a synthesis route. This continuous gas-phase technology allows to synthesize mixed oxides in large quantities with improved structural and catalytic properties and enables the formation of materials with a broad range in composition.

The spray-flame synthesis of LaCoO<sub>3</sub> has been investigated by a small number of research groups using mainly nitrates and acetates as precursors for the metal ions (Lu et al., 2013; Purwanto, Wang, Lenggoro, & Okuyama, 2007). When nitrates (La(NO<sub>3</sub>)<sub>3</sub>·6H<sub>2</sub>O and Co(NO<sub>3</sub>)<sub>2</sub>·6H<sub>2</sub>O) are employed, the challenges concerning a functional material with specific properties include the formation of a homogeneous material and the avoidance of secondary phases such as La<sub>2</sub>O<sub>3</sub> and La<sub>2</sub>CoO<sub>4</sub>.

For improving the particle size homogeneity, micro-explosions based on solvents such as 2-ethylhexanoic acid (2-EHA) were successfully employed in this work. As a requirement for the synthesis of homogeneous nanoparticle sizes made from nitrate precursors, it has been suggested to use a selection of solvents in a way that micro-explosions in the droplets are generated during droplet combustion. In case of the samples that contain 2-EHA, this solvent reacts with the nitrates to create 2-hexanoates (Rosebrock, Wriedt, & Mädler, 2016) that should facilitate micro-explosions. Nevertheless, the presence of this compound is not a guarantee for the synthesis of mixed oxides without secondary phases.

To effectively avoid the formation of secondary phases, we have used polymeric solvents. The intention is to create metal complexes of lanthanum and cobalt by combining chelating agents such as acetic acid (AA) or citric acid (CA) and a polyol e.g. ethylene glycol (EG). It is supposed that this combination undergoes an intermediate esterification reaction when heated during the combustion process of the droplets in the SFS reactor. It was identified that besides the addition of the chelating agents and the polyol, a low content of ethanol is required to both decrease the viscosity of the mixtures, and to readily dissolve the nitrates. We observed that a high molar ratio of ethylene glycol to the metal ions present in the solution (above 40) is needed for improving the purity

and crystallinity of the synthesized LaCoO<sub>3</sub> compounds as presented in the Figure 1.

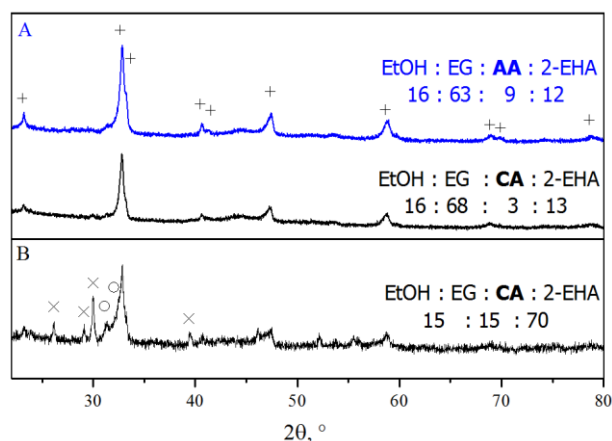


Figure 1. X-ray diffractograms of the synthesized LaCoO<sub>3</sub> perovskites with the concentration of the solvents expressed in volume percentage for EG/metals ratios of 42 (A) and 3 (B). Phases: (+) LaCoO<sub>3</sub>, (o) La<sub>2</sub>CoO<sub>4</sub>, (x) La<sub>2</sub>O<sub>3</sub>.

S.A. acknowledges the support from the German Academic Exchange Service (DAAD) Research Scholarship 2016/2017 “Promotionen in Deutschland” (57214224) and from the IMPRS RECHARGE from the Max-Planck Institute of Chemical Energy Conversion.

Lu, Y., Eyssler, A., Otal, E. H., Matam, S. K., Brunko, O., Weidenkaff, A., & Ferri, D. (2013). *Catalysis Today*, 208, 42–47.

Purwanto, A., Wang, W.-N., Lenggoro, I. W., & Okuyama, K. (2007). *Journal of the European Ceramic Society*, 27(16), 4489–4497.

Rosebrock, C., Wriedt, T., & Mädler, L. (2016). *American Institute of Chemical Engineers*, 62(2), 381–391. <http://doi.org/10.1002/aic.15056>

## Evolution of Au nanoparticle XRD by Molecular Dynamics

E. Goudeli and S.E. Pratsinis

Department of Mechanical and Process Engineering, ETH Zürich, CH-8092 Zürich, Switzerland

Keywords: gold, nanocrystallinity, molecular dynamics.

Presenting author email: [goude005@umn.edu](mailto:goude005@umn.edu)

Gold nanoparticles find a score of applications including electronics, catalysis, sensors, plasmonic biosensing, target-specific drug delivery, nanolithography and ion detection. Their physical properties depend on the particle size, shape, composition as well as crystal structure and surface facet orientation affecting eventually the end-product performance, especially for particles below 10 nm where their behavior differs both from that of the bulk metal and the Au molecules. The particle crystal structure at the nanoscale is important in electronics as it affects ion/electron transport properties, in catalysis where atomic steps and kicks enhance catalytic activity and molecular sensing devices where single-crystalline nanoparticles can optimize performance. Experimental investigation of particle nanocrystallinity with electron microscopy leads to incomplete characterization as it is based on the analysis of 2D projections of nanoparticles. However, Molecular Dynamics (MD) simulations can be used to provide physical insight in crystal structure changes and dynamics with atomistic detail (Buesser and Pratsinis, 2015) and can complement the above experiments, especially for very small nanoparticles.

Here, MD simulations are used to investigate the crystallinity of Au nanoparticles at the nanoscale during their coalescence or sintering at different temperatures. The method has been validated in Goudeli and Pratsinis (2016) by the attainment of the melting temperature,  $T_m$ , that increases with increasing particle size approaching the bulk melting point of Au, in excellent agreement with theoretical (Lewis et al., 1997; Shim et al., 2002; Arcidiacono et al., 2004) and experimental data (Buffat and Borel, 1976; Sambles, 1971). Furthermore, the X-ray diffraction (XRD) patterns quantifying the crystallinity of single or pair Au nanoparticles of various sizes (2 - 7 nm) equilibrating or coalescing at 300 - 1000 K are extracted and compared to experimentally-obtained XRD spectra of colloidal gold agglomerates (Uppal et al., 2013).

Figure 1 shows the effect of temperature,  $T$ , on the XRD patterns of two Au nanoparticles with initial diameter,  $d_{p,0} = 4$  nm, having coalesced at (a) 800 and (b) 600 K for 10 ns. The cross-section snapshots of the Au nanoparticles are colored based on the local disorder variable indicating the degree of crystallinity (Fig. 1: insets). Blue atoms are highly crystalline while green and red ones are amorphous. Higher temperature results in highly amorphous coalesced nanoparticles (Fig. 1a: inset) and broadening of their XRD peaks. This peak broadening is related to smaller XRD sizes as can be obtained by the Scherrer equation. Regardless of sintering temperature the XRD patterns of coalescing

nanoparticles exhibit the four characteristic peaks of bulk Au planes (triangles).

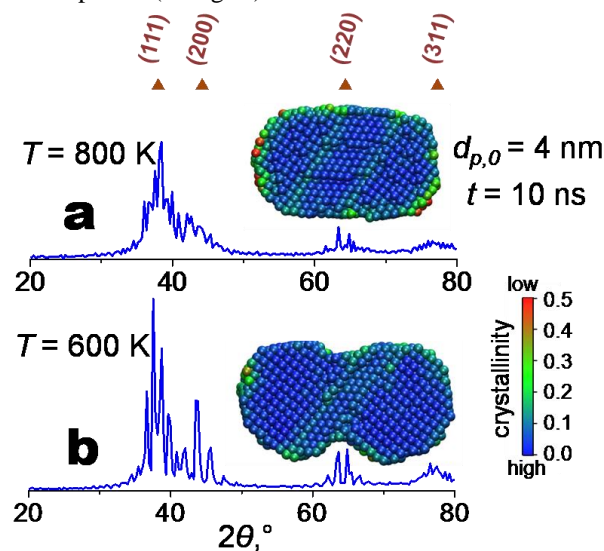


Figure 1. XRD patterns of two Au nanoparticles with initial diameter,  $d_{p,0} = 4$  nm, having coalesced at (a) 800 and (b) 600 K after 10 ns.

Furthermore, the crystallite size is calculated by the first peak of the XRD spectra based on the Scherrer equation and the effect of nanoparticle size, polydispersity, temperature and sintering on the resulting pattern is quantified by MD for the first time to our knowledge. Increasing the temperature results in the formation of a layer of amorphous atoms on the nanoparticle surface, broadening of the XRD peaks and reduction of the crystallite size.

- Arcidiacono, S., Bieri, N.R., Poulikakos, D., Grigoropoulos, C.P. (2004) *Int. J. Multiphas. Flow* **30**, 979-994.
- Buffat, P., Borel, J-P. (1976) *Phys. Rev. A* **13**, 2287-2298.
- Goudeli, E, Pratsinis, S. E. (2016) *AIChE J.* **62**, 589-598.
- Lewis, L. J., Jensen, P., Barrat, J-L. (1997) *Phys. Rev. B.* **56**, 2248-2257.
- Sambles, J.R. (1971) *Proc. R. Soc. Lond. A* **324**, 339-351.
- Shim, J-H., Lee, B-L., Cho, Y.W. (2002) *Surf. Sci.* **512**, 262-268.
- Uppal, M. A., Kafizas, A., Ewing, M.B., Parkin, I.P. (2013) *J. Mat. Chem. A.* **1**, 7351-7359.

## Quantifying isolated Pd site in FSP-made Pd/TiO<sub>2</sub> for photocatalytic NO removal

K. Fujiwara\* and S.E. Pratsinis

Particle Technology Laboratory, ETH Zurich, Sonneggstrasse 3, 8092 Zurich, Switzerland  
 Keywords: flame spray pyrolysis, atomically dispersed noble metal, NO removal, photocatalyst  
 Presenting author email: fujiwara@ptl.mavt.ethz.ch

Identification of an active site is critical for designing optimal heterogeneous catalysts. Recently, isolated platinum group metal sites have been proposed as an active site for various reactions.<sup>1</sup> Such isolated Pd atoms on TiO<sub>2</sub> prepared by flame spray pyrolysis (FSP) exhibits superior photocatalytic activity for NO removal and the isolated Pd sites seems to be the dominant active site.<sup>2</sup>

Here, the number of isolated Pd sites in different FSP-made Pd/TiO<sub>2</sub> catalysts is quantitatively compared by diffuse reflectance infrared Fourier transform spectroscopy using NO as a probing molecule and BaSO<sub>4</sub> powder as an internal standard. The photocatalytic NO (1 ppm) removal by FSP-made Pd/TiO<sub>2</sub> under solar light (100 mW/cm<sup>2</sup>) was evaluated based on ISO 22197-1:2007. The average NO<sub>x</sub> removal<sup>2</sup> ( $\eta_{\text{NO}_x}$ ) for 5 h is

$$\eta_{\text{NO}_x} [\%] = \int_0^{5h} \frac{c_{\text{NO}_{in}} - c_{\text{NO}_{out}} + c_{\text{NO}_{2out}}}{c_{\text{NO}_{in}}} dt \cdot 100.$$

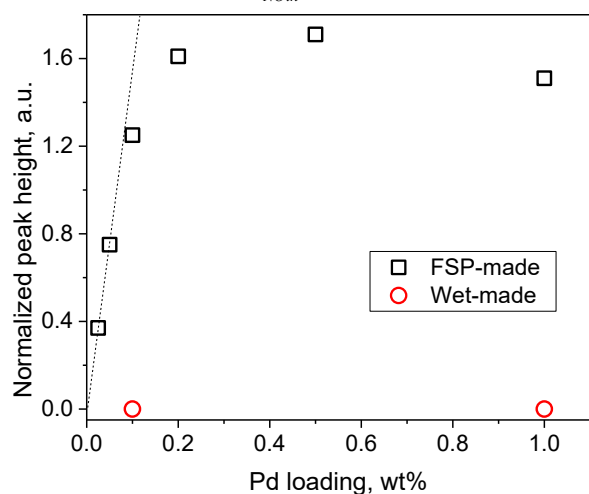


**Figure 1** DRIFTS peak height of NO adsorption on isolated Pd atoms (1845 cm<sup>-1</sup>)<sup>2</sup> normalized by the S-O bond peak (1967 cm<sup>-1</sup>) of BaSO<sub>4</sub> (50 wt%) in FSP-made Pd/TiO<sub>2</sub> (squares) and photodeposited Pd on FSP-made pure TiO<sub>2</sub> (circles) as a function of the Pd loading.

Figure 1 shows the normalized peak height of the NO adsorption on isolated Pd sites in FSP-made Pd/TiO<sub>2</sub> (squares) and photodeposited Pd on FSP-made TiO<sub>2</sub> (circles) as a function of the Pd loading. The peak height is normalized by the S-O bond peak at 1967 cm<sup>-1</sup> of BaSO<sub>4</sub> (50 wt%) as an internal standard and thus, the higher peak height indicates the larger number of isolated Pd sites on the surface. The peak height of FSP-made Pd/TiO<sub>2</sub> linearly increases up to 0.1 wt.% of the Pd loading as indicated by the broken line while, above that loading, it reaches a plateau. This implies the dominant

presence of isolated Pd sites below 0.1 wt.% of Pd and the formation of Pd particles above 0.2 wt.% of Pd that is consistent with our previous report.<sup>2</sup> In case of photodeposited Pd (circles), there is no detectable peak of the NO adsorption.

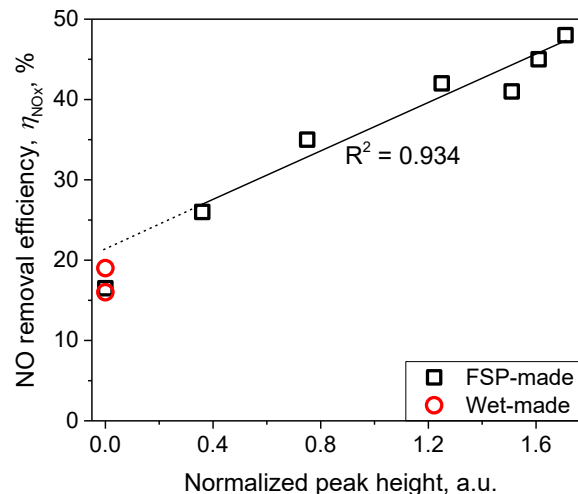


**Figure 2.** Relation between the normalized peak height of the NO adsorption in Fig 1 and solar-photocatalytic NO<sub>x</sub> removal efficiency by FSP-made Pd/TiO<sub>2</sub> (squares) and photodeposited Pd on FSP-made TiO<sub>2</sub> (circles). 1. The approximate straight line (solid line) is calculated by the least-squares method using the data at 0.025-1 wt% of Pd loading.

Figure 2 shows relation between the normalized peak height of the NO adsorption in Fig. 1 and solar-photocatalytic NO<sub>x</sub> removal efficiency by FSP-made Pd/TiO<sub>2</sub> (squares) and photodeposited Pd on FSP-made TiO<sub>2</sub> (circles). The NO<sub>x</sub> removal efficiency predominantly depends on the peak height of the NO adsorption on isolated Pd atoms that corresponds to the number of isolated Pd sites. The approximate straight line (solid line) obtained from the values at 0.025-1 wt% of Pd loading results in R<sup>2</sup> = 0.934. The approximated intercept is 21.4 that is close to the NO<sub>x</sub> removal efficiency by FSP-made pure TiO<sub>2</sub>. Thus, isolated Pd atoms on TiO<sub>2</sub> are the dominant active sites for solar photocatalytic NO<sub>x</sub> removal. Indeed, photodeposited Pd nanoparticles (circles) does not improve the NO<sub>x</sub> removal efficiency regardless of the loading (0.1 or 1 wt%). Therefore, even if both Pd clusters and isolated atoms exist, the activity primarily originates from isolated Pd atoms.

1. Flytzani-Stephanopoulos, M.; Gates, B. C., *Annu. Rev. Chem. Biomol. Eng.* **2012**, 3, 545-574.
2. Fujiwara K, Pratsinis SE. *AIChE J.* 2017;63(1):139-146.

## Highly active atomically dispersed Pt on CeO<sub>2</sub> for reverse water-gas shift reaction

K. Fujiwara\* and S.E. Pratsinis

Particle Technology Laboratory, ETH Zurich, Sonneggstrasse 3, 8092 Zurich, Switzerland  
 Keywords: flame spray pyrolysis, atomically dispersed noble metal, reverse water-gas shift reaction  
 Presenting author email: fujiwara@ptl.mavt.ethz.ch

CO<sub>2</sub> is a major greenhouse gas and thus, reducing its emissions is an extensive task. Catalytic CO<sub>2</sub> conversion to CO by reverse water-gas shift (RWGS) reaction is an attractive approach.

Size reduction of platinum-group metal (PGM) catalysts down to atomic-scale is a promising way to enhance their activity with minimizing the use of expensive PGMs although the optimal cluster size varies for different reactions.<sup>1</sup> To investigate such size effect, preparing catalysts by flame spray pyrolysis (FSP) is a suitable as it allows to control the PGM size from a few nanometers to that of single atoms on metal oxide supports.<sup>2</sup>

Here, CeO<sub>2</sub> with different Pt loading (0-2 wt.%) were prepared by FSP to attain differently sized Pt clusters from a few nanometers to that of single atoms. The size of Pt clusters was investigated by a scanning transmission electron microscope (STEM). The activity of the FSP-made catalysts (50 mg) for RWGS reaction was investigated at 200-300 °C and 60 mL/min of 5% CO<sub>2</sub> + 15% H<sub>2</sub> + 80% Ar. The CO<sub>2</sub> and CO concentrations at the outlet of the reactor were measured by a mass spectrometer (Pfeiffer Vacuum, ThermoStar).

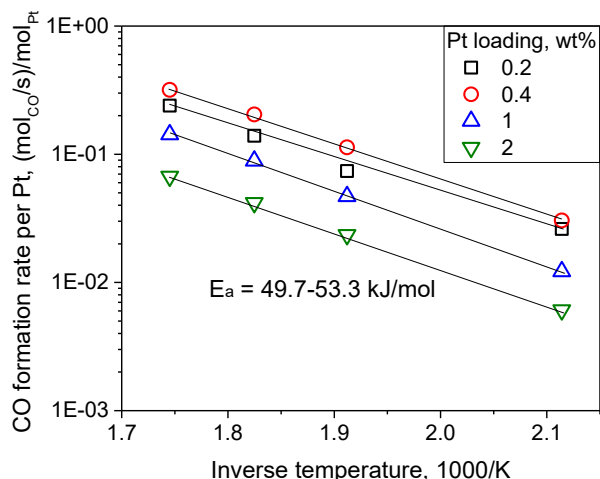


**Figure 1** Arrhenius plot of the CO formation rate via RWGS reaction per Pt (in mol) at 5% CO<sub>2</sub> and 15% H<sub>2</sub> by FSP-made Pt/CeO<sub>2</sub>.

Figure 1 shows Arrhenius plot of CO formation rate via RWGS reaction per Pt at 5% CO<sub>2</sub> and 15% H<sub>2</sub> by FSP-made Pt/CeO<sub>2</sub>. Note that no by-products such as CH<sub>4</sub> are detected. At 0.2-0.4 wt% of Pt, the CO formation rate per mole of Pt are comparable level while above that loading (1-2 wt.%), the rate decreases by the increase of the loading. The activation energy of the reaction calculated from the slope of the Arrhenius plot is 49.7-53.3 kJ/mol for all the catalysts, which is

consistent with the values of Pt catalysts in literature.<sup>3</sup> Thus, the reaction pathway is the same for all Pt loading.

Figure 2 shows STEM images of FSP-made CeO<sub>2</sub> prepared with (A) 1 and (B) 0.4 wt% of Pd. At 1 wt.% of Pt, some Pt subnano-clusters (in red circles) are present. On the other hand, at 0.4 wt.% of Pt (B), such clusters hardly appear. This indicates the presence of atomically dispersed Pt that is the active site for RWGS reaction.<sup>4</sup> Notably, the CO formation rate per Pt by FSP-made Pt/CeO<sub>2</sub> (0.31(mol/s)/mol<sub>Pt</sub>) is 10 times higher than that by atomically dispersed Pd on La-doped Al<sub>2</sub>O<sub>3</sub> in literature (0.03 (mol/s)/mol<sub>Pd</sub>)<sup>4</sup>.

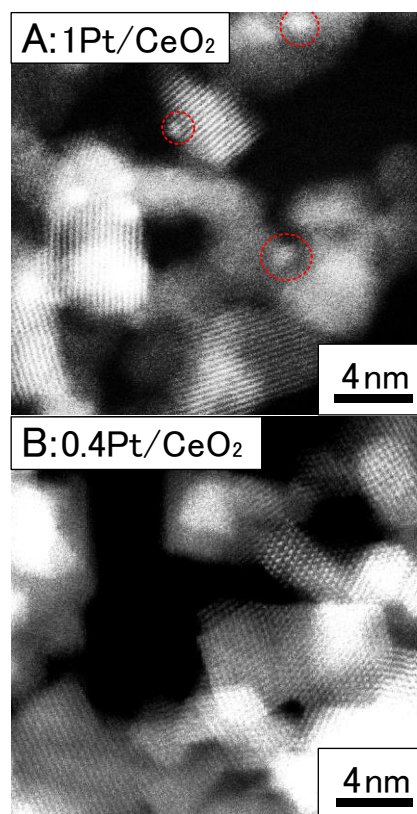


**Figure 2.** STEM images of FSP-made CeO<sub>2</sub> prepared with (A) 1 and (B) 0.4 wt% of Pd. The red circles in (B) indicate Pt clusters.

1. Flytzani-Stephanopoulos, M.; Gates, B. C., *Annu. Rev. Chem. Biomol. Eng.* **2012**, *3*, 545-574.
2. Fujiwara K, Pratsinis SE. *AIChE J.* 2017;63(1):139-146.
3. Román-Martínez MC, Cazorla-Amorós D, Linares-Solano A, de Lecea CS-M. *Appl. Catal. A-Gen.* 1994; 116(1-2): 187-204.
4. Kwak JH, Kovarik L, Szanyi Jn. *ACS Catal.* 2013; 3(9):2094-2100.

## Porous SnO<sub>2</sub> nanospheres with three-dimensionally interconnected trimodal pores for ultrasensitive detection of ethanol

J.-W. Yoon<sup>1</sup>, S. H. Choi<sup>1</sup>, J.-S. Kim<sup>1</sup>, H. W. Jang<sup>2</sup>, Y. C. Kang<sup>1</sup>, and J.-H. Lee<sup>1</sup>

<sup>1</sup>Department of Materials Science and Engineering, Korea University, Seoul, 02841, Republic of Korea

<sup>2</sup>Department of Materials Science and Engineering, Seoul National University, Seoul, 02841, Republic of Korea

Keywords: Trimodal pores, spray pyrolysis, nanostructures, gas sensors.

Presenting author email: uhpupu@korea.ac.kr

Porous solids consisting of, or assembled from, nanostructures are excellent nanoarchitectures that can significantly enhance the mass transfer of gases to reaction surfaces with minimal sacrifice of the active surfaces in the nanostructures [1]. In general, the gases diffuse towards the reactive surfaces via macro-, meso-, and micro-pores, and mass transfer through porous structures depends upon the pore size. For instance, different gas diffusion mechanisms, such as normal, Knudsen, and surface diffusion, are predominant in macro-, meso-, and micro-pores, respectively. Therefore, to take best advantage of the benefits of porous nanostructures for gas sensor applications, multimodal porous structures that contain macro-, meso-, and micro-pores are considered a promising platform. For this, the size, volume, distribution, and interconnectivity of the different pores should be controlled precisely and independently. In this study, highly gas-accessible SnO<sub>2</sub> spheres with three-dimensionally interconnected, size-tunable, trimodal pores were prepared for the first time with a facile, one-pot, spray pyrolysis method. Trimodally porous SnO<sub>2</sub> spheres exhibited ultrahigh gas response, even for ppb level of ethanol.

Trimodally porous SnO<sub>2</sub> (3M-SnO<sub>2</sub>) spheres were obtained via the spray pyrolysis of an aqueous solution, and the subsequent heat treatment of the precursor powders. A spray solution was prepared by dissolving 1.7 g of SnC<sub>2</sub>O<sub>4</sub> in 250 mL of distilled water containing the well-dispersed MWCNTs (1 mg mL<sup>-1</sup>) and PS spheres (3.0 g). The droplets of the spray solutions were generated with 5 ultrasonic transducers (1.7 MHz), which were subsequently transported to a high-temperature (700 °C) tubular reactor by a flow of Ar gas (5 L min<sup>-1</sup>). The as-prepared precursor powders were collected in a Teflon bag filter in the particle-collecting chamber. The precursor powders were converted into the trimodally porous SnO<sub>2</sub> spheres via a heat treatment at 600 °C for 3 h. The heating rate was 10 °C min<sup>-1</sup>. For the comparison, bimodally porous (2M-SnO<sub>2</sub>) and dense SnO<sub>2</sub> (D-SnO<sub>2</sub>) spheres were prepared by spray pyrolysis of the solution without the MWCNTs and without both the MWCNTs and PS spheres, respectively.

To investigate the effects of multimodal porosity on the gas accessibility of the nanoparticles, the ethanol-sensing characteristics of the D-, 2M-, and 3M-SnO<sub>2</sub> spheres were measured between 350 and 450 °C (Fig. 1). The D-SnO<sub>2</sub> spheres exhibit the lowest response ( $S = R_a/R_g$ , where  $R_a$  and  $R_g$  are the resistances in air and the analyte gas, respectively) and relatively slow response and recovery kinetics (Fig. 1a). The maximum response

to 5 ppm of ethanol is 34.2 at 450 °C (Fig. 1a1) and the times taken to reach a 90% variation in the resistance upon exposure to ethanol and air ( $\tau_{res}$  and  $\tau_{recov}$ , respectively) are 6 and 1485 s, respectively (Figs. 1a2,a3). The maximum ethanol response of the 2M-SnO<sub>2</sub> spheres (117.6) occurs at 350 °C (Fig. 1b1), which is 3.4 times higher than that of the D-SnO<sub>2</sub> spheres. In addition, the  $\tau_{res}$  and  $\tau_{recov}$  values have significantly decreased to 2 and 550 s, respectively (Figs. 1b2,b3). The 3M-SnO<sub>2</sub>-based sensor exhibits an ultrahigh gas response of 316.5 at 400 °C (Fig. 1c1), as well as fast  $\tau_{res}$  and  $\tau_{recov}$  values of 1 and 416 s, respectively (Figs. 1c2,c3), showing a further enhancement of the gas sensing properties. The response of the 3M-SnO<sub>2</sub> sensor to 5 ppm of ethanol (316.5) is one of the highest values ever reported in the literature for undoped SnO<sub>2</sub>-based gas sensors. An unprecedentedly high response to ethanol of 3M-SnO<sub>2</sub> sensor can be understood by the increased pore-size-dependent Knudsen gas diffusion and enhanced gas accessibility by introducing highly connected one-dimensional pores via MWCNT templates.

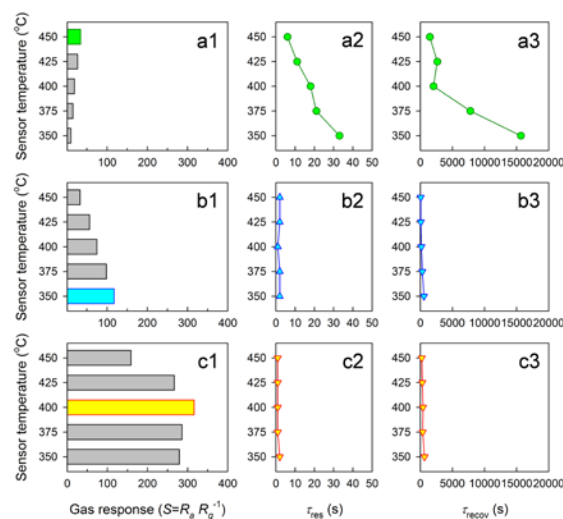


Figure 1. Gas sensing characteristics of the (a) D-, (b) 2M-, and (c) 3M-SnO<sub>2</sub> spheres to 5 ppm ethanol at 350 – 450 °C.

This work was supported by the National Research Foundation of Korea (NRF), which was funded by the Korean government (Ministry of Education, Science, and Technology (MEST), No. 2013RIA2A1A01006545).

[1] Tiemann, M. (2007) *Chem. Eur. -J.* **13**, 8376-8388.

## Flame-made Si-doped MoO<sub>3</sub> for selective breath NH<sub>3</sub> sensing to detect kidney failure

A.T. Güntner, M. Righettoni, S.E. Pratsinis

Department of Mechanical and Process Engineering, ETH Zurich, CH-8092 Zurich, Switzerland  
 Keywords: NH<sub>3</sub>, breath analysis, kidney failure & hemodialysis, gas sensor, flame spray pyrolysis, MoO<sub>3</sub>  
 Presenting author email: Andreas.Guentner@ptl.mavt.ethz.ch

Around 3 million patients worldwide suffer from kidney failure, a number that increases at ~7% annually. (Fresenius Medical Care 2012) Early detection and real-time monitoring of its progression may improve medical treatment to a point-of-care therapy with higher chance for patient recovery and drastic reduction of expenses. Breath analysis represents a promising non-invasive, fast and cost-effective method to detect kidney failure in an early stage. In specific, exhaled breath NH<sub>3</sub> increases from 400 - 1800 ppb for healthy people to 820 - 14700 ppb for kidney failure patients. (Davies 1997)

Especially when done with portable breath analyzers, easy screening of populations would be possible. For this purpose, metal-oxide (chemo-resistive) gas sensors are especially attractive since they offer a simple operation and low power consumption in a compact design. Furthermore, analyte selectivity can be obtained by exploring unique material compositions, e.g. Ti-doped ZnO for isoprene (Güntner 2016a) or by combining several sensors to an electronic nose as demonstrated for formaldehyde (Güntner 2016b).

Here, a chemo-resistive gas sensor is presented consisting of flame-made nanostructured  $\alpha$ -MoO<sub>3</sub>. (Güntner, 2016c) A key novelty is the thermal stabilization of  $\alpha$ -MoO<sub>3</sub> by Si-doping inhibiting sintering and crystal growth at high operational conditions (~400 °C). When directly deposited onto sensor substrates, such nanoparticles form highly porous films. While pure MoO<sub>3</sub> forms belt-like structures (Figure 1a), Si-doping significantly refines the network towards nanoparticle/needle-like morphology. (Figure 1b)

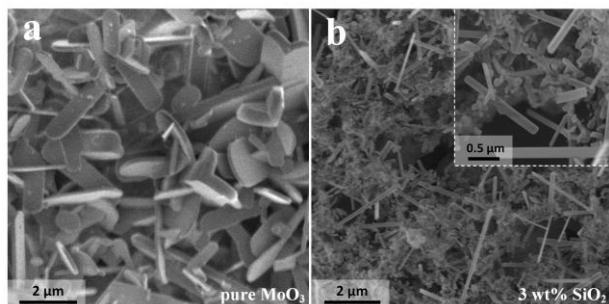


Figure 1. SEM image (top view) of pure (a) and 3 wt% Si-doped (b) MoO<sub>3</sub> films. MoO<sub>3</sub> has grown to thin belts with dimensions of several  $\mu$ m (a). The Si-doping alters drastically that morphology to increased porosity (b) by a finer network of agglomerated nanoparticles and needle-like structures (inset).

Si-doped MoO<sub>3</sub> sensors (1.5 - 3.5 wt% SiO<sub>2</sub>) showed enhanced response and superior selectivity for NH<sub>3</sub> towards other breath-relevant gases (acetone, NO,

CO) than pure MoO<sub>3</sub>. Optimal dopant level and sensor operational temperature were identified at 3 wt% SiO<sub>2</sub> and 400 °C, respectively. This sensor could clearly distinguish breath-relevant NH<sub>3</sub> levels down to 400 ppb at realistic conditions (90% relative humidity) with fast response and recovery times (< 1 min) and operational stability. (Figure 2)

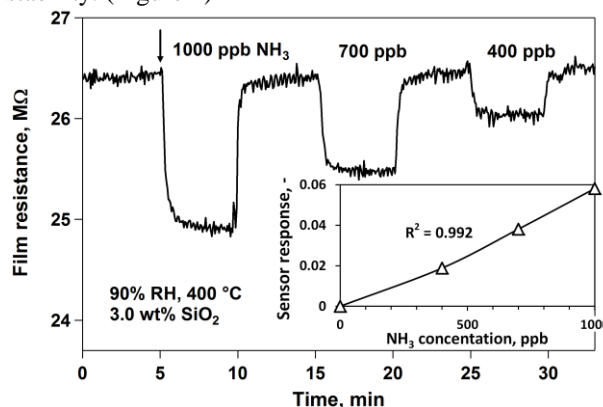


Figure 2. The resistance of the optimally Si-doped (3 wt%) MoO<sub>3</sub> sensor upon exposure to 1000, 700 and 400 ppb of ammonia at 90% RH and 400 °C. These breath-relevant NH<sub>3</sub> concentrations are detected with high signal-to-noise ratio (>15) and can be clearly distinguished. The inset shows the calibration curve.

Such sensors can be readily incorporated into portable devices (Righettoni 2015) indicating their high potential as hand-held breath NH<sub>3</sub> detector for easy kidney failure detection.

This work was supported by the European Union's Seventh Framework Program (FP7/2007-2013, ERC Nr. 247283) and the Swiss National Science Foundation (Nr. 200021\_159763/1)

Davies, S., Spanel, P. and Smith, D. (1997) *Kidney Int.* **52**, 223-228.

Fresenius Medical Care (2013), *ESRD Patients in 2012: A Global Perspective*, Bad Homburg.

Güntner, A.T., Pineau, N. J., Chie, D., Krumeich, F. and Pratsinis, S.E. (2016a) *J. Mater. Chem. B* **4**, 5358-5366.

Güntner, A.T., Koren, V., Chikkadi, K., Righettoni, M. and Pratsinis, S.E. (2016b) *ACS Sens.* **1**, 528-535.

Güntner, A.T., Righettoni, M. and Pratsinis, S.E. (2016c) *Sens. Actuators B* **223**, 266-273.

Righettoni, M., Ragnoni, A., Güntner, A.T., Loccioni, C., Pratsinis, S.E. and Risby, T.H., (2015) *J. Breath Res.* **9**, 047101.

## Easy cholesterol monitoring from breath by isoprene-selective and flame-made Ti-doped ZnO nanoparticles

A.T. Güntner, N.J Pineau, D. Chie, F. Krumeich and S.E. Pratsinis

Particle Technology Laboratory, Department of Mechanical and Process Engineering, ETH Zürich, Sonneggstrasse 3, CH-8092 Zürich, Switzerland

Keywords: Isoprene, breath analysis, cholesterol monitoring, Ti-doped ZnO, flame spray pyrolysis  
Presenting author email: Andreas.Guentner@ptl.mavt.ethz.ch

Approximately 39% of the world population has high blood cholesterol that might be responsible for a third of ischaemic heart diseases and strokes leading to over 2.6 million estimated deaths per year. (WHO 2015) Breath isoprene detection could provide a non-invasive method for easy and rapid assessment of high blood cholesterol synthesis rates and enable real-time monitoring of its therapy. (Salerno-Kennedy 2005)

Breath isoprene sensors based on nanostructured metal oxides are rather promising due to their fast response times (Güntner 2016a), low fabrication cost, simple applicability and compact size (Güntner 2016b) that can be easily integrated into a portable breath sampler (Righettoni 2015). However for isoprene, no suitable materials are available that possess sufficiently low detection limit at breath-realistic, high relative humidity and selectivity against other breath compounds (e.g.  $\text{NH}_3$  and acetone).

Here, we present for the first time (to our knowledge) an *isoprene-selective* chemoresistive gas sensor consisting of Ti-doped ZnO. (Güntner 2016c) These nanostructured particles are made by flame spray pyrolysis (FSP) and directly deposited onto sensor substrates (Figure 1a). At 2.5 mol% Ti-doped ZnO, the particles are ultra-fine and most are smaller than 20 nm (Figure 1b). Elemental mapping indicates that Zn (red) and Ti atoms (green) are distributed over the particles (Figure 1c) suggesting that metastable solid solutions and no segregated ZnO and  $\text{TiO}_2$ . Furthermore, Ti seems more present at the particle surface which might indicate the formation of nanoclusters.

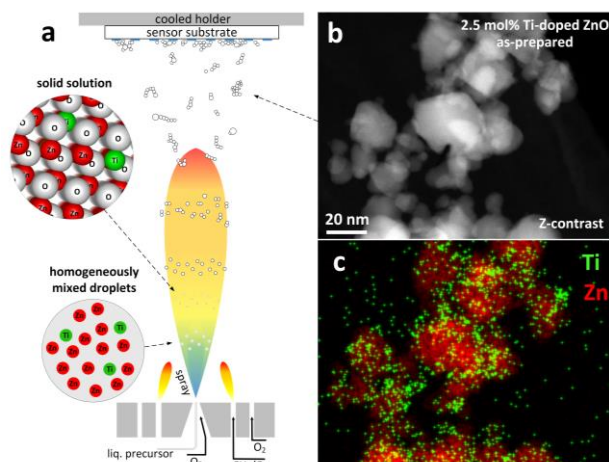


Figure 1. Synthesis of flame aerosol-made Ti-doped ZnO nanoparticles and deposition onto sensor substrates.

Doping with Ti turns the ZnO sensors *isoprene-selective*. In fact, increasing the Ti content to 2.5 mol% enhances the isoprene response more than 15 times compared to pure ZnO (Figure 2) while it increases only moderately for other analytes. That way and most notably, breath-relevant isoprene concentrations can be detected accurately down to 5 ppb with high (> 10) signal-to-noise ratio. As a result, an inexpensive isoprene detector has been developed that could be easily incorporated into a portable breath analyzer for non-invasive monitoring of high blood cholesterol concentrations.

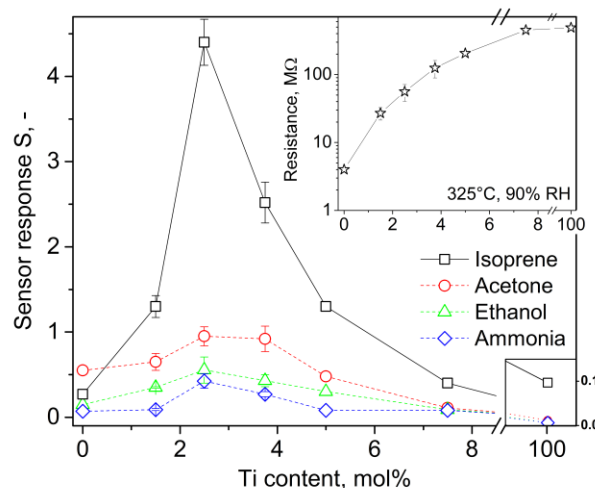


Figure 1. Ti-doped ZnO sensor response as a function of Ti content to 500 ppb of various analytes 500 ppb at 90% RH. Ti-doping turns ZnO *isoprene-selective*.

This work was supported by the Swiss National Science Foundation (grant Nr. 200021\_159763/1).

Güntner, A. T., Righettoni, M. and Pratsinis, S. E. (2016a) *Sens. Actuators B.* **223**, 266-273.

Güntner, A.T., Koren, V., Chikkadi, K., Righettoni, M. and Pratsinis, S.E. (2016b) *ACS Sens.* **1**, 528-535.

Güntner, A. T., Pineau, N. J., Chie, D., Krumeich, F. and Pratsinis, S. E. (2016c) *J. Mater. Chem. B.* **4**, 5358-5366.

Righettoni, M., Ragnoni, A., Güntner, A.T., Loccioni, C., Pratsinis, S.E. and Risby, T.H., (2015) *J. Breath Res.* **9**, 047101.

Salerno-Kennedy, R. and Cashman, K., (2005) *Klin. Wochenschr.* **117**, 180-186.

WHO., (2015) *Global Health Observatory (GHO) data..*

## Numerical and Experimental Investigation of the Buoyancy Effect on Iron-Oxide Nanoparticle Formation in a Down-Firing Flat Flame Reactor

J. Sellmann<sup>1</sup>, S. Kluge<sup>2</sup>, A. Fomin<sup>4</sup>, S. Cheskis<sup>3</sup>, A. Pilipody<sup>3</sup>, P. Fjodorow<sup>2</sup>, H. Wiggers<sup>2</sup>, C. Schulz<sup>2</sup>, I. Rahinov<sup>3</sup>, A. Kempf<sup>1</sup> and I. Wlokas<sup>1</sup>

<sup>1</sup>Department of Fluid Dynamics, University of Duisburg-Essen, Duisburg, 47057, Germany

<sup>2</sup>Department for Reactive Fluids, University of Duisburg-Essen, Duisburg, 47057, Germany

<sup>3</sup>School of Chemistry, Tel Aviv University, Tel Aviv, Israel

<sup>4</sup>Department of Natural Sciences, The Open University of Israel, Raanana, Israel

Keywords: iron oxide, iron pentacarbonyl, flat flame.

Presenting author email: johannes.sellmann@uni-due.de

The iron oxide particle formation from laminar pre-mixed, low-pressure flat flames with an iron pentacarbonyl precursor was investigated numerically and experimentally. The burner operated at 30 mbar, burning either a hydrogen/oxygen mixture or a hydrogen/methane/oxygen mixture, diluted with argon. The burner fires in downward direction, causing a strong effect of buoyancy on the flowfield. Together with the invasive probing applied, a complex flow field results, so that simulations of the reacting, particle forming flow must be conducted in at least 2D to interpret the findings from the experiments.

Table 1. Inflow conditions of the investigated flames; the operating pressure was 3000Pa in all cases.

Flame #	H <sub>2</sub> / sccm	O <sub>2</sub> / sccm	Ar/s ccm	CH <sub>4</sub> / sccm	Fe(CO) <sub>5</sub> / ppm
Flame 1	400	400	600	-	-
Flame 2	400	400	600	-	50.71
Flame 3	234	430	682	50	50.85
Flame 4	234	430	682	50	-
Flame 5	400	400	600	-	200

A total of five different flames was studied, for the inflow conditions summarized in Table 1. The flame temperature was measured along the burner axis by laser induced fluorescence (OH-LIF), and intra-cavity laser absorption spectroscopy was used to monitor the formation of the intermediate species FeO. The formation of particulate matter was observed by a quartz-crystal microbalance (QCM), while the particle sizes were determined by mass spectrometry (PMS). Further detail on the diagnostics has been published by Kluge et al. [1].

The simulations were performed with finite rate chemistry and detailed transport models for species diffusion and the mixture properties [2]. The reaction kinetics of the fuel/oxygen/precursor system was based on a reduced, skeletal version of the iron pentacarbonyl combustion mechanism proposed by Feroughi et al. [3] combined with a reduced version of the C1 mechanism by Li et al. [4] for the H<sub>2</sub>/O<sub>2</sub> system or the DRM-19 mechanism [5] for the cases with CH<sub>4</sub>. The formation, coagulation and coalescence of the nanoparticles from the flame

was described using the monodisperse model by Kruis [6], extended for nucleation, diffusion and convection.

The simulations revealed a strong impact of the reactor orientation on the velocity field. The buoyancy decelerates the flow on the centreline, causing a stagnation point below the burner. Compared to the experimental results, the 2D simulations show a good agreement with the temperature and intermediate species (FeO) profiles. The simulations show particle growth downstream of the flat flame but also during the particle transport in radial direction, tangential to the stagnation plane. Compared to the experimental data, the mean particle diameter is underestimated by a factor of two – possibly due to deficiencies of the kinetic model and its coupling to the population balance model, which does not account for the (possible) formation of iron oxide from iron clusters. (The existing reaction mechanisms were optimized for flames where this formation route plays no major role.)

Based on the flow field data computed by 2D simulation, it is now possible to conduct one-dimensional simulations along the stagnation streamline, applying detailed reaction kinetics to further improve the reaction mechanism and the models for the formation of iron and iron-oxide particle.

The authors gratefully acknowledge the financial support by DFG through FOR2284.

- [1] Kluge, S., Deng, L., Feroughi, O., Schneider, F., Poliak, M., Fomin, A., and Dreier, T. (2015) *CrystrEngComm*, 17(36), 6930-6939.
- [2] L. Deng, A. Kempf, O. Hasemann, O. P. Korobeinichev and I. Wlokas, *Combust. Flame*, 2014.
- [3] O. M. Feroughi, S. Hardt, I. Wlokas, T. Hülser, H. Wiggers, T. Dreier and C. Schulz, *Proc. Combust. Inst.*, 2015, **35**, 2299–2306
- [4] J. Li, Z. Zhao, A. Kazakov, M. Chaos, F. L. Dryer and J. J. Scire, *Int. J. Chem. Kinet.*, 2007, **39**, 109–136
- [5] A. Kazakov and M. Frenklach, *Reduced Reaction Sets based on GRI-Mech 1.2*, <http://combustion.berkeley.edu/drm/>, 2014
- [6] Kruis, F. E., Kusters, K. A., Pratsinis, S. E., and Scarlett, B. (1993) *Aerosol Science and Technology*, 19(4), 514-526.

## Flame enthalpy influences silanol content and cytolytic activity of silicas made by flame spray pyrolysis

Anastasia Spyrogianni<sup>1</sup>, Inge K. Herrmann<sup>2</sup>, Sotiris E. Pratsinis,<sup>1</sup> Karsten Wegner<sup>1,3</sup>

<sup>1</sup>Department of Mechanical and Process Engineering, ETH Zurich, Zurich, CH-8092, Switzerland

<sup>2</sup>Department of Materials Meet Life, Swiss Federal Laboratories for Materials Science and Technology (Empa), St. Gallen, CH-9014, Switzerland

<sup>3</sup>ParteQ GmbH, D-76456 Kuppenheim, Germany

Keywords: silica, surface chemistry, flame conditions, *in vitro*.

Presenting author email: spyrogianni@ptl.mavt.ethz.ch

The properties of amorphous silicas with high specific surface areas largely depend on their surface chemistry (Iler, 1979). This not only determines their numerous applications, *e.g.* as catalyst supports or adsorbents, but can also influence their biological activity (Gazzano *et al.*, 2012; Sun *et al.*, 2015). The surface silanol groups are the main determinants of its surface chemistry (Iler, 1979) and their population varies between flame- and wet-made silicas (Burneau *et al.*, 1990). This can influence the silica nanoparticle interactions with cells *in vitro* (Gazzano *et al.*, 2012) and *in vivo* (Sun *et al.*, 2015).

Here, the effect of the employed process parameters on the silanol content of silica nanoparticles made by flame spray pyrolysis is investigated. The silanol content is determined semi-quantitatively by Raman spectroscopy and quantitatively by thermogravimetric analysis (Mueller *et al.*, 2003) and the lithium alanate method (Chertov *et al.*, 1966). Human monocytes are selected as representative of the first line of defense upon systemic exposure (Oberdörster *et al.*, 2005). The effect of the varying silanol content on the cell membrane damage is evaluated, maintaining the cells and silica nanoparticles in suspension to prevent any sedimentation effects (Spyrogianni *et al.*, 2016).

Silicas made in flames with high enthalpy density that have long high temperature residence times show a surface silanol density of  $\sim 4$  OH/nm<sup>2</sup>. This is slightly higher than observed for commercial fumed silica (2 - 3 OH/nm<sup>2</sup>). Decreasing the flame enthalpy density leading to shorter and colder flames increases the surface silanol density up to  $\sim 8$  OH/nm<sup>2</sup>. Such high silanol surface densities are typically observed for wet-phase processes. Comparing the effect of two silica nanopowders with the same specific surface area but different surface silanol density on human monocytes (Figure 1) shows that silicas with 8 OH/nm<sup>2</sup> made in colder flames induce lower cell membrane damage than those with 4 OH/nm<sup>2</sup> made in hotter flames.

Varying process parameters and flame enthalpy densities in flame spray synthesis of silica does not only allow to control the specific surface area but also the surface chemistry of product silica nanoparticles. This can broaden the range of applications for flame-made silica and may also reduce their toxicity.

This work was supported by the Swiss National Science Foundation (no. 200020-146176) and the European Research Council (FP7/2007–2013, no. 247283).

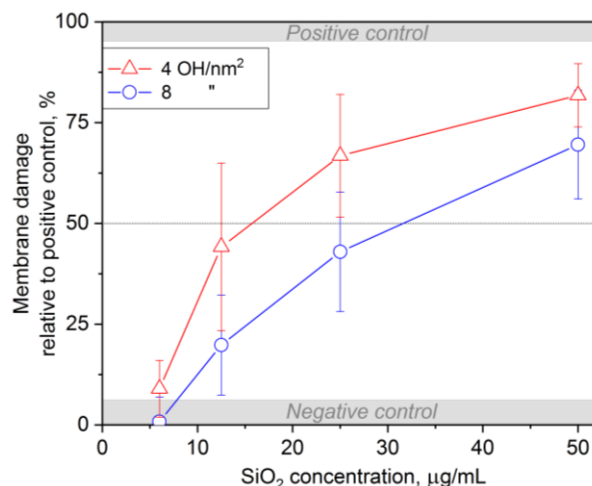


Figure 1. Membrane damage in human monocytes relative to positive control as a function of SiO<sub>2</sub> concentration for two silicas of identical specific surface area but different silanol surface density, of 4 (triangles) and 8 OH/nm<sup>2</sup> (circles) flame.

- Burneau, A., Barres, O., Gallas, J.P., & Lavalley, J.C. (1990) *Langmuir* **6**, 1364-1372.
- Chertov, V.M., Dzhambaeva, D.B., Plachinda, A.S., & Neimark, I.E. (1966) *Russ. J. Phys. Ch. USSR* **40**, 282-&.
- Gazzano, E., Ghiazza, M., Polimeni, M., Bolis, V., Fenoglio, I., Attanasio, A., Mazzucco, G., Fubini, B., & Ghigo, D. (2012) *Toxicol. Sci.* **128**, 158-170.
- Iler, R.K. (1979). *The chemistry of silica: Solubility, polymerization, colloid and surface properties and biochemistry of silica*: John Wiley & Sons.
- Mueller, R., Kammler, H.K., Wegner, K., & Pratsinis, S.E. (2003) *Langmuir* **19**, 160-165.
- Oberdörster, G., Maynard, A., Donaldson, K., Castranova, V., Fitzpatrick, J., Ausman, K., Carter, J., Karn, B., Kreyling, W., Lai, D., Olin, S., Monteiro-Riviere, N., Warheit, D., & Yang, H. (2005) *Part. Fibre Toxicol.* **2**, 8.
- Spyrogianni, A., Herrmann, I.K., Lucas, M.S., Leroux, J.C., & Sotiriou, G.A. (2016) *Nanomedicine (Lond.)* **11**, 2483-2496.
- Sun, B.B., Pokhrel, S., Dunphy, D.R., Zhang, H.Y., Ji, Z.X., Wang, X., Wang, M.Y., Liao, Y.P., Chang, C.H., Dong, J.Y., Li, R.B., Madler, L., Brinker, C.J., Nel, A.E., & Xia, T. (2015) *ACS Nano* **9**, 9357-9372.

## Synthesis of pure and doped ceria nano materials on the pilot plant scale

S. Schnurre<sup>1</sup>, M. Spree<sup>1</sup>, B. Hellack<sup>1</sup> and T. Hülser<sup>1</sup>

<sup>1</sup>Institute of Energy and Environmental Technology e.V. (IUTA), Duisburg, 47229, Duisburg

Keywords: Gas-Phase Synthesis, Combustion, Ceria Nanomaterials, Doping

Presenting author email: huelser@iuta.de

### Introduction

Ceria-based oxides have gained a major position in the list of active co-catalysts and advanced materials, mainly for environmental and energy conversion applications (Fornasiero and Trovarelli, 2015). Ceria exhibits structure sensitivity for numerous processes and its catalytic activity can be enhanced by doping with lanthanides (Capdevila-Cortada et al., 2016). However, cerium oxide nanoparticles (NP) have already been shown their tremendous potential and impact on catalysis (Fornasiero and Trovarelli, 2015). Recent research is for example focused on highly specific mixed oxide doped (e.g.  $Ce_xZr_{1-x}O_2$ ) NP to enhance the catalytic activity. Typically, these materials result from wet-chemical processes, hardly applicable for industrial and continuous production processes. Therefore, only a few materials have found their way into practical applications up to now. To investigate sustainable and cost effective production of doped ceria on the pre industrial scale we set-up a pilot plant, which allows the synthesis of complex oxide materials using efficient gas-phase synthesis by spray flame technology.

### Material Synthesis

As a step towards mixed oxides, highly specific  $CeO_2$ -NPs (pure/doped/small size distribution) are produced by pilot scale gas phase reactors to understand fundamental formation and proof the up-scale options, respectively. Therefore, ceria-nitrate in 2-propanol (0.5 molar) was used as an initial precursor material and a production rate of 40 g/h was successfully established to verify the ability of pre-industrial scale-up. An Eu-doping of ceria was realized by the addition of Eu-nitrate into the precursor liquid. To vary material properties the precursor concentration of ceria was varied from 0.1 molar to 0.5 molar resulting into production capacities from 8 g/h to 40g/h.

Additionally, the influence of the fuel/air-ratio of the spray flame on the particle size and morphology of the powder material was investigated. For this purpose, three different operating states were set within the test series. Furthermore, 10% of the fuel was replaced by water to analyse the modification on particle morphology due to the presence of  $H_2O$ .

### Characterization

The material characterization revealed a homogeneous size distribution of the particles, while the specific surface area of pure and doped ceria particles is depending on the process conditions between 39  $m^2/g$  and 81  $m^2/g$  corresponding to particle size between ~ 10 nm and 20 nm. The specific emission spectrum of  $Eu^{3+}$  received by luminescence investigation accounts for efficient Eu doping of ceria NPs (see Fig. 1). The

position of the peaks are in good agreement with literature (Kunimi and Fujihara, 2012). It is well known that metal oxides show a decrease of the optical band gap with increasing oxygen vacancies. Therefore, the high capability of oxygen diffusion within doped particles is optically proven by a thermal treatment leading to a colour shifting from grey-white to bright blue under ambient atmosphere.

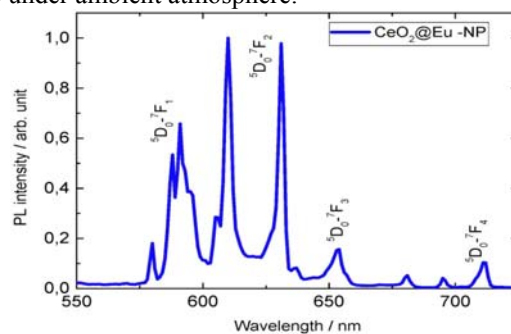


Figure 1. Emission spectrum of Eu doped ceria.

Transmission Electron Microscopy (TEM) as well as BET measurements were used to analyze the influence of fuel/air-ratio and the presence of water during synthesis.

Electron microscopy on particle ensembles generated under fuel/air ratios between 0.8 and 1 and the absence of water in the precursor material reveal the synthesis of small particles of ~10 nm, which is in good agreement with BET value. However, the sporadic formation of particle bigger than 100 nm was detected. Morphological characterization of particles ensembles generated under the presence of water reveal higher specific surface areas in combination with a significant reduction of the formation of particles in the 100 nm size regime.

The catalytic activity of the doped material is successfully proven during the conversion of CO into  $CO_2$ .

### Acknowledgement

This work was supported by Bundesministerium für Bildung und Forschung (BMBF), Germany under grant of DENANA - Design criteria for sustainable nanomaterials

### Literature

- Fornasiero, P. and Trovarelli, A. (2015) *Catalysis Today* **253**, 1–2.  
 Capdevila-Cortada, M.; Vilé, G.; Teschner, D.; Pérez-Ramírez, J.; Lópeza, N. (2016) *Applied Catalysis B: Environmental* **197**, 299-312  
 Kunimi S. and Fujihara S. (2012) *ECS J. Solid State Sci. Technol.* **1**, R32-R36;

## Multilayered omniphobic coating on stainless steel based on aerosol nanoparticle synthesis

M. Sorvali<sup>1</sup>, J. Haapanen<sup>1</sup>, L. Vuori<sup>2</sup>, M. Pudas<sup>3</sup>, M. Valden<sup>2</sup>, J.M. Mäkelä<sup>1</sup>

<sup>1</sup> Aerosol Physics, Faculty of Natural Sciences, Tampere Univ. of Technology, P.O.Box 692, FI-33101, Finland

<sup>2</sup> Surface Science Laboratory, Photonics, Tampere Univ. of Technology, FI-33101, Finland

<sup>3</sup> Picosun Oy, Espoo, Finland

Keywords: Omniphobic, Liquid flame spray, Aerosol synthesis, Nanoparticles, Coatings, ALD  
Presenting author email: miika.sorvali@tut.fi

### Introduction

Omniphobic coatings have attracted a lot of attention during the last decade due to their potential in various applications. The poor mechanical stability of such surfaces is generally the biggest problem. Also, hard and resistant materials, like stainless steel, present challenges for the fabrication process (Chen *et al.* 2016). Combination of three superimposed layers was studied to solve this problem. The three layers were produced as follows: a nanoparticle layer was synthesized via aerosol route with Liquid Flame Spray (LFS) to produce a necessary nanostructure for omniphobicity, Atomic Layer Deposition (ALD) was used to enhance the stability of the coating, and silanization tuned the surface chemistry for lower surface energy value.

### Methods

LFS is an aerosol synthesis method for fabricating nanoparticles and –coatings. A liquid precursor solution is fed into a turbulent H<sub>2</sub>/O<sub>2</sub> flame and nanomaterial is produced through aerosol processes (Tikkanen *et al.* 1997). The coated steel samples were then burned in oxygen atmosphere in order to dispose of possible impurities. In ALD, the substrate is exposed to sequential pulses of gaseous precursors to form a very thin and conformal coating. The thickness can be controlled with the number of coating cycles. Silanization was performed by dip coating the substrate into a prepared solution in order to modify the surface chemistry to a specific form.

The coatings were characterized with contact angle measurements along with SEM and XPS imaging. Contact angle measurements were used to evaluate the repellency of liquids. The imaging methods revealed details of the structure, elemental composition and the bonding states of the coating. SEM will still be used to study the cross-sectional structure of the final coating. In addition, durability testing will be performed. A simple scotch tape test was used to study the adhesion of the particle layer quickly during the research process.

### Results

A suitable combination of process parameters was found for producing good repellency against various liquids. Super repellency, i.e. contact angle at least 150°, was achieved for deionized water, diiodomethane, ethylene glycol and olive oil. Too thin nanoparticle layer wouldn't form the necessary surface structure and a too thick ALD layer would start to cover it.

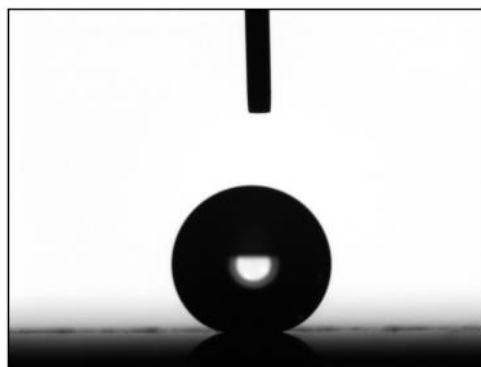


Figure 1. A droplet of water sitting on the coated stainless steel surface. The contact angle is ~169°.

### Conclusions

An omniphobic multilayer coating was fabricated on a stainless steel substrate. The coating consists of a nanoparticle layer synthesized with a flame aerosol method, a thin ALD layer and a silane layer. Parameters were found for a good repellency.

### Acknowledgements

This work was performed under the project No. 2105/31/2013, HYBRIDS (2014-2017) funded by Finnish Metals and Engineering Competence Cluster, FIMECC-SHOK.

### References

- Chen, K., Wu, Y., Zhou, S. & Wu, L. (2016). *Macromol. Rapid Commun.* 37, pp. 463-485.
- Tikkanen, J., Gross, K.A., Berndt, C.C., Pitkänen, V., Keskinen, J., Raghu, S., Rajala, M & Karthikeyan, J. (1997). *Surf. Coat. Tech.* 90, pp. 210-216.

## Antibacterial nanocoatings by Liquid Flame Spray

J. Haapanen<sup>1\*</sup>, P. Juuti<sup>1</sup>, M. Gunell<sup>2</sup>, K. Brobbey<sup>3</sup>, E. Eerola<sup>2</sup>, J.J. Saarinen<sup>3</sup>, M. Toivakka<sup>3</sup>, P. Huovinen<sup>2</sup>, J.M. Mäkelä<sup>1</sup>

<sup>1</sup>Aerosol Physics, Faculty of Natural Sciences, Tampere University of Technology, Tampere, Finland

<sup>2</sup>Department of Medical Microbiology and Immunology, University of Turku, Turku, Finland

<sup>3</sup>Laboratory of Paper Coating and Converting, Center for Functional Materials, Abo Akademi University, Turku, Finland

Keywords: nanocoating, aerosol synthesis, Liquid Flame Spray, antibacterial

\*presenting author: janne.haapanen@tut.fi

Aim of this study is to evaluate antibacterial activity of nanocoatings, made by Liquid Flame Spray (LFS) aerosol synthesis method (Tikkanen et al.). Produced nanoparticles are deposited onto substrate directly from the flame or indirectly, using specially designed deposition tube. In both deposition methods, substrate is covered with nanoparticles from the aerosol. However, when using metal nitrates as precursors, larger residual particles are often observed. To minimize the residual particle formation, process parameters and precursor solvents can be tuned. Process can be monitored in real-time with aerosol instruments, such as ELPI+ and DENSMO (Juuti et al.) and LFS parameters optimized accordingly.

Microscopic glass slides were chosen as the primary substrate material, but other (even heat-sensitive) substrates can be used as well, such as LDPE and PET films. LFS nanocoatings have been previously applied also in roll-to-roll process (Haapanen et al.), which would be beneficial for developing cost-effective antibacterial surfaces for various applications.

Liquid precursor solutions for ZnO and Ag nanoparticles were prepared by diluting zinc and silver nitrate into ethanol and mixture of deionized water and ethanol, respectively. Nanocoatings were done by depositing nanoparticles onto substrate surface directly from the flame by sweeping substrate through the flame or “indirectly” by using specially designed flow tube prior to deposition. Produced nanoparticles were analyzed in aerosol phase by SMPS, ELPI+ and DENSMO for process optimization. Deposited nanoparticles (primary particle size ~30 nm) were analyzed by TEM and SEM. Antibacterial activity was tested with Falcon tube method where o/n growth bacteria (*E. coli* / *S. aureus*) was diluted into phosphate buffer saline (PBS). Nanocoated samples were put into Falcon tube containing 1ml PBS and incubated at room temperature (RT) or 37°C for 6 to 24 hours. Given values for bacterial growth (Figure 1) are related to logarithm of the counted number of colony forming units (CFU) on the nutrition rich analyte film.

Results of the antibacterial testing show a clear decrease in bacterial growth activity as the amount of the nanocoating increases (Figure 1). Coating thickness increases as number of coating sweeps

increase. LFS-made Ag and ZnO nanocoatings are highly antibacterial according to preliminary antibacterial tests. Further study will focus on combining antibacterial and photocatalytic properties to one nanocoating. Amount of undesired residual particles were minimized by optimizing precursor solvents and other process parameters.

The authors would like to acknowledge Academy of Finland for funding this research, project “Nanostructured large-area antibacterial surfaces” (nLABS, grant no 278 846)

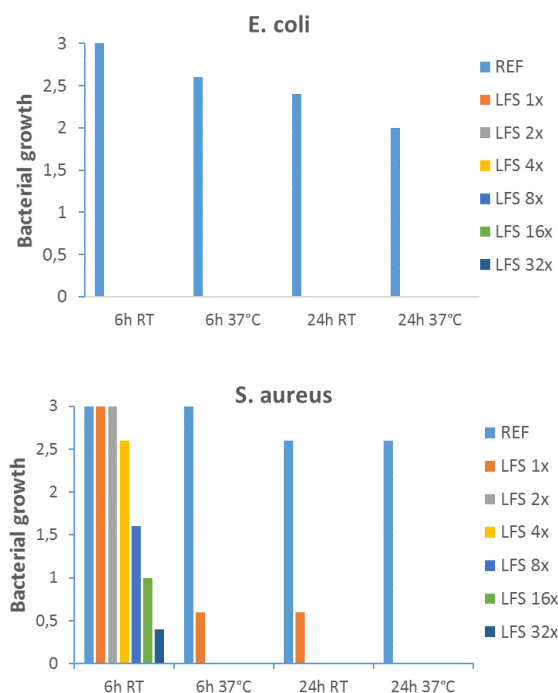


**Figure 1:** Antibacterial activity of Ag nanocoatings (lower bar better) with different thicknesses (number of sweeps), tested with *E. coli* and *S. aureus*.

Tikkanen et al. (1997). *Surf. Coat. Tech.* 90 (3), 210–216

Juuti et al. (2016). *Aerosol Sci. Tech.*, 50(5), pp. 487-496

Haapanen et al. (2015). *Mater. Chem. Phys.* 149-150, pp. 230-237

## Fabrication of slippery, liquid-infused porous surfaces by flame based aerosol synthesis

P. Juuti<sup>1</sup>, J. Haapanen<sup>1</sup>, C. Stenroos<sup>2</sup>, H. Niemelä-Anttonen<sup>2</sup>, J. Harra<sup>1</sup>, H. Koivuluoto<sup>2</sup>, H. Teisala<sup>3</sup>, J. Lahti<sup>3</sup>, M. Tuominen<sup>4</sup>, J. Kuusipalo<sup>3</sup>, P. Vuoristo<sup>2</sup> and J. M. Mäkelä<sup>1</sup>

<sup>1</sup>Aerosol Physics, Faculty of Natural Sciences, Tampere University of Technology, Tampere, 33720, Finland

<sup>2</sup>Surface Engineering RT, Faculty of Engineering Sciences, Tampere University of Technology, 33720 Tampere, Finland

<sup>3</sup>Packaging Technology RT, Faculty of Engineering Sciences, Tampere University of Technology, 33720 Tampere, Finland

<sup>4</sup>SP Technical Research Institute of Sweden, 11428 Stockholm, Sweden

Keywords: Liquid Flame Spray, titania nanoparticles, SLIPS, icephobicity

Presenting author email: paxton.juuti@tut.fi

In colder climates, ice accretion is a serious problem with seasonal or even year-round consequences. Accumulated ice can hinder the operation of moving infrastructure, such as bridges and wind turbines, and obscure the view of surfaces and through windows. Ideally this problem should be solved by completely preventing the ice accretion on surfaces, for example through surface functionalization.

One promising way to significantly improve the icephobicity of a surface is to convert it to slippery, liquid-infused porous surface (SLIPS). SLIPS is a composite structure that utilizes the interactive properties of lubricants and a porous matrix that can hold the liquid in place. Most surfaces can be made porous with mechanical and wet-chemical methods, which create for example nanoposts that support the lubricant layer. However, especially wet-chemical methods are material specific and thus require multiple process routes to functionalize materials ranging from wood and plastics to metals and glasses.

In this work, we show a novel aerosol route for producing the porous structure required by the SLIPS. Titania (TiO<sub>2</sub>) nanoparticles created with a flame-based aerosol synthesis method, Liquid Flame Spray (LFS) (Mäkelä et al., 2017), are deposited *in-situ* on a low-density polyethylene (LDPE) film to create a nanoporous sub-micron thick layer to hold the applied lubricant on the surface. This layer is subsequently impregnated with silicon oil to complete the SLIPS structure. (Juuti et al., 2017) This process is depicted in Figure 1.

Ice adhesion strength of the LFS-SLIPS structure on LDPE was tested against a plain LDPE surface and PTFE-tape (typical reference material). First ice was grown on the samples within an icing wind tunnel, and then the samples were centrifuged with increasing angular velocity until a sufficient force detached the ice from the surface. These results are shown in Figure 2. Based on these results, the ice adhesion strength of the initial LDPE film was reduced from 110 kPa to 12 kPa after surface functionalization, which is also a quarter of the value measured for the PTFE.

This work presents a novel approach for preparing an icephobic lubricant-impregnated surface by utilizing nanoparticles made with the aerosol synthesis method, LFS. This kind of sample was tested for ice adhesion strength against references and was shown to have improved by an order of magnitude, thus proving the capability of the LFS as a method for producing porous surfaces for SLIPS.

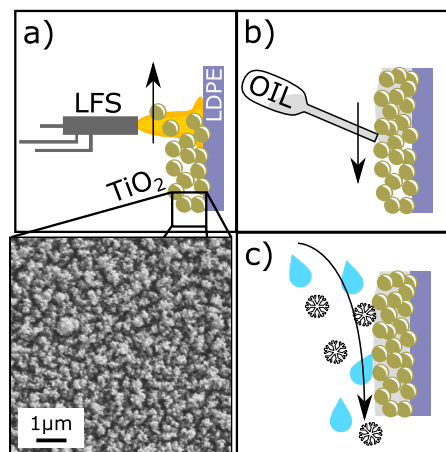


Figure 1. Creating an icephobic lubricant-impregnated surface: a) aerosol nanoparticle coating with the LFS, b) oil application into the porous structure and c) functionalized surface repelling water and ice accretion. The FESEM micrograph shows the top view of porous titania layer on top of a LDPE film.

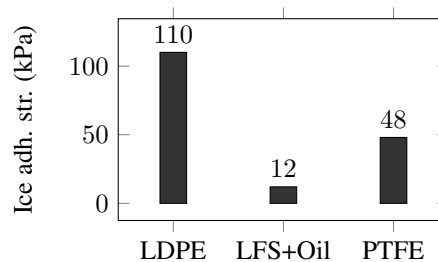


Figure 2. Ice adhesion strength values for plain LDPE, oil impregnated LFS made nanostructure and PTFE-tape surfaces.

The authors would like to acknowledge Tekes for funding this research (grant n° 40365/14, ROLLIPS). P.J. acknowledges the TUT's graduate school and H.T. acknowledges Walter Ahlström -foundation for financial support.

Mäkelä, J.M., Haapanen, J., Harra, J., Juuti, P. and Kuusipalo, S. (2017). *KONA Powder and Particle Journal*, **34**:141-154.

Juuti, P., Haapanen, J., Stenroos, C., Niemelä-Anttonen, H., Harra, J., Koivuluoto, H., Teisala, H., Lahti, J., Tuominen, M., Kuusipalo, J., Vuoristo, P. and Mäkelä J.M. (2017). *Applied Physics Letters*, **Submitted**.

## Deep tissue imaging with highly fluorescent NIR nanocrystals after systematic host screening

F.H.L. Starsich<sup>1</sup>, P.M. Gschwend<sup>1</sup>, A. Sergeev<sup>2</sup>, R. Grange<sup>2</sup> and S.E. Pratsinis<sup>1</sup>

<sup>1</sup>Department of Mechanical and Process Engineering, ETH Zürich, Zürich, 8092, Switzerland

<sup>2</sup>Department of Physics, ETH Zürich, Zürich, 8093, Switzerland

Keywords: fluorescence, flame spray pyrolysis, near-infrared

Presenting author email: gschwend@ptl.mavt.ethz.ch

Photoluminescent inorganic nanoparticles are attractive as bio-imaging contrast agents because they do not degrade or suffer from photobleaching and concentration quenching, such as clinically applied organic dyes. Neodymium ( $\text{Nd}^{3+}$ ) is the dopant of choice for such *in vivo* diagnostics since both of its excitation and emission spectra peak between 700 and 900 nm, the near-infrared (NIR) window. There, absorption and scattering by human tissue are reduced significantly. Here, for the first time, oxide, phosphate and vanadate nanocrystals doped with  $\text{Nd}^{3+}$  are examined systematically as down-converting photoluminescent contrast agents for bio-imaging. Through close control of their crystal size, the resulting fluorescence properties are investigated quantitatively under NIR excitation revealing that  $\text{BiVO}_4$  doped with  $\text{Nd}^{3+}$  is the most efficient composition. Its application as photoluminescent NIR imaging contrast agent is demonstrated *ex vivo* with chicken skeletal muscle and bovine liver tissues. Under harmless laser power density ( $0.2 \text{ W/cm}^2$ ), fluorescent  $\text{BiVO}_4$  particles could be clearly detected at an injection depth of up to 20 mm by a commercial camera.

## Highly active Au clusters on ceria for water-gas shift reaction

N. A.Wahab, K. Fujiwara and S.E. Pratsinis

Particle Technology Laboratory, ETH Zurich, Sonneggstrasse 3, 8092 Zurich, Switzerland

Keywords: flame spray pyrolysis, supported noble metal catalysts, low temperature water-gas shift reaction

Presenting author email: pratsinis@ptl.mavt.ethz.ch

NO<sub>x</sub> and VOCs are major air pollutants mainly emitted from internal combustion systems in vehicles. Such internal combustion engines can potentially be replaced by fuel cells that operate vehicles without the emission of NO<sub>x</sub> and VOCs. Fuel cells require CO-free H<sub>2</sub> as a fuel. In practice, H<sub>2</sub> is produced by coal gasification but it also forms significant CO. To remove CO in H<sub>2</sub>, the water gas shift (WGS) reaction (H<sub>2</sub>O + CO => H<sub>2</sub> + CO<sub>2</sub>) can be employed at low temperature as an onboard fuel purification step.

Supported platinum-group metal (PGM) catalysts have been employed for the low temperature WGS reaction. Size reduction of such PGM catalysts is a classic way to enhance their activity with minimizing the use of expensive noble metals. Especially, single PGM atom catalysts are currently receiving renewed interest.<sup>1</sup> To control the PGM size from a few nanometers to that of single atoms on metal oxide supports, flame spray pyrolysis (FSP) is a promising technology.<sup>2</sup>

Here, subnano-sized Au (0.2-1 wt.%) supported on CeO<sub>2</sub> catalysts were prepared by FSP and calcined in air at 400 °C for 2 hours to remove any incomplete combustion products. Their catalytic activity for WGS reaction was investigated with 50 mg of FSP-made Au/CeO<sub>2</sub> at 150-250 °C and 15 mL/min of 10% CO in He + 3% H<sub>2</sub>O. The products produced by the catalysts were measured by a mass spectrometer.

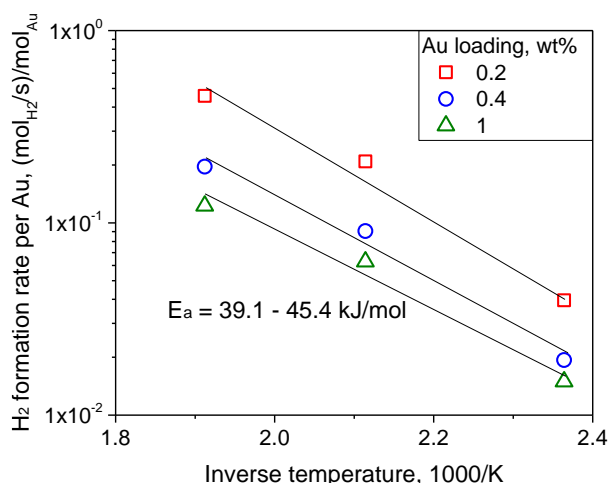


**Figure 1.** Arrhenius plots of the H<sub>2</sub> production rate via WGS reaction per mol of Au at 10% CO and 3% H<sub>2</sub>O by FSP-made Au/CeO<sub>2</sub>.

Figure 1 shows Arrhenius plots of the H<sub>2</sub> production rate via WGS reaction per mol of Au at 10% CO and 3% H<sub>2</sub>O by FSP-made Au/CeO<sub>2</sub>. All catalysts exhibit an activation energy of 39.1 – 45.4 kJ/mol.

Thus, the reaction pathway is the same for all Au loading. For flame made catalysts the activity is increased with decreasing Au loading with the 0.2 wt.% Au/CeO<sub>2</sub> catalyst showing highest reaction rate. This could be attributed to the smaller Au clusters at the lower Au loading. Interestingly, the rate at 200 °C by CeO<sub>2</sub> with 0.2 wt.% of Au (0.21 s<sup>-1</sup>) is higher than that by single Au atoms on TiO<sub>2</sub> (0.09 s<sup>-1</sup>) tested under the same conditions.<sup>3</sup>

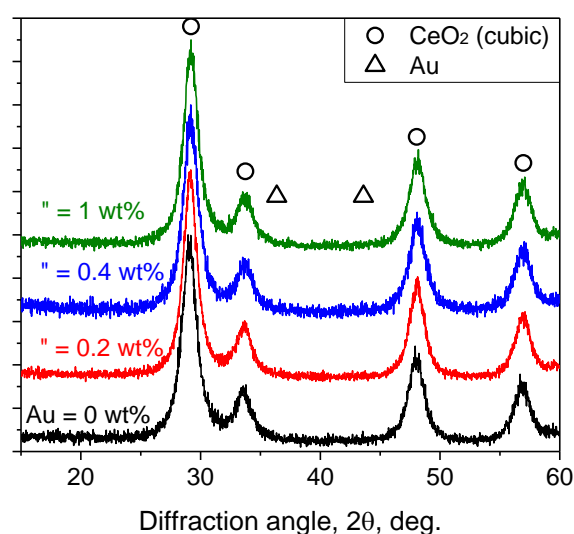


**Figure 2.** XRD patterns of FSP-made Au/CeO<sub>2</sub>. Peak positions of CeO<sub>2</sub> (cubic) and Au are indicated by circles and triangles, respectively.

Figure 2 shows XRD patterns of FSP-made CeO<sub>2</sub> with 0-1 wt.% of Au. The XRD patterns show cubic CeO<sub>2</sub> for all catalysts and the crystal size is 6.1-6.4 nm. Such small CeO<sub>2</sub> could be attributed to high catalytic activity.<sup>4</sup> There is no distinguishable Au peaks (triangles) in these patterns indicating the presence of small Au clusters. In conclusion, highly active Au clusters on CeO<sub>2</sub> for WGS reaction have been successfully synthesized in one-step by FSP.

1. Flytzani-Stephanopoulos, M.; Gates, B. C., *Annu. Rev. Chem. Biomol. Eng.* **2012**, *3*, 545-574.
2. Fujiwara K, Pratsinis SE. *AIChE J.* 2017;63(1):139-146.
3. Yang M, Allard LF, Flytzani-Stephanopoulos M. *J. Am. Chem. Soc.* 2013;135(10):3768-3771.
4. Xu J, Harmer J, Li G, Chapman T, Collier P, Longworth S, Tsang SC. *Chem. Commun.* 2010; 46(11):1887-1889.

## Synthesis and Characterization of Perovskite Nanoparticles for Oxygen Evolution Catalysis

B. Alkan<sup>1</sup>, H. Wiggers<sup>1</sup>, M. Muhler<sup>2</sup>, W. Schuhmann<sup>3</sup>, C. Schulz<sup>1</sup>

<sup>1</sup> IVG and CENIDE, University of Duisburg-Essen, Duisburg, 47057, Germany

<sup>2</sup> Laboratory of Industrial Chemistry, Ruhr-University Bochum, Bochum, 44801, Germany

<sup>3</sup> Analytical Chemistry–Center for Electrochemical Sciences (CES), Ruhr-University Bochum, Bochum, 44780, Germany

Keywords: Oxygen Evolution Catalysts, Perovskites, Spray-flame Synthesis.

Presenting author email: baris.alkan@uni-due.de

Enhancing the large-scale use of electrochemical energy storage and conversion technologies through water splitting requires low-cost, efficient, and robust electrode materials for the oxygen evolution reaction (OER). The development of non-precious metal-based materials is a promising way to synthesize new catalysts for the OER. One main challenge is to increase the kinetics of this reaction that is slow due to high overpotentials. Cobalt-based nanoscale perovskite structures are promising catalysts and have recently demonstrated high catalytic activity towards OER (Suntivich et al. (2014)).

Spray-flame synthesis allows tuning materials characteristics such as composition, particle size, and morphology over a wide range. So far, spray-flame synthesized  $\text{LaCoO}_3$  nanoparticles and the influence of partial substitution of Co by other transition metals on the OER has not been studied in detail.

250°C. This post-treatment improves the phase purity and the catalytic activity of the nanoparticles for the OER. The materials are processed by spin coating on an electrode support and characterized by TEM, XPS and a variety of electrochemical techniques.

B.A. acknowledges the IMPRS-SurMat of the Max Planck Society for financial support.

Suntivich, J., May, K.J., Gasteiger, H. A., Goodenough, J. B. and Shao-Horn, Y. S. (2014) *Science* **334**, 1383-1384.

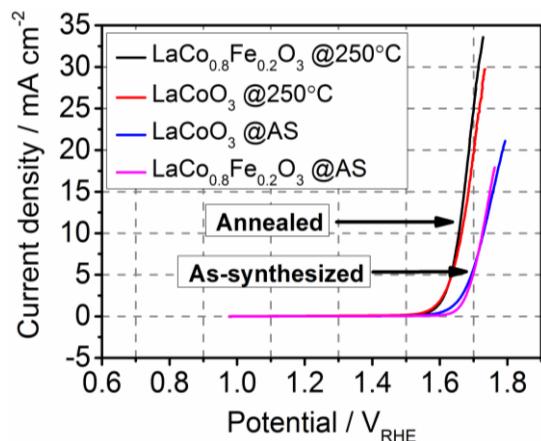


Figure 1. Comparison of OER activities of the as-synthesized and annealed catalyst materials.

The motivation of this study is to synthesize and optimize the tailored formation of  $\text{LaCoO}_3$  and  $\text{LaCo}_{1-x}\text{Fe}_x\text{O}_3$ -based nanoparticles by spray-flame synthesis. Using this technology, we are able to vary the particle size as well as the elemental composition. Particles with a size down to 10 nm in diameter could be obtained. Fe is homogeneously incorporated into the  $\text{LaCoO}_3$  phase during the synthesis with variable concentration. We identified that residuals of the combustion products partly cover the nanoparticles' surface, which can be removed by heat treatment at

## Nanothermometry by fluorescent $\text{Nd}^{3+}$ -doped nanocrystals

P.M. Gschwend and S.E. Pratsinis

Department of Mechanical and Process Engineering, ETH Zurich, Zurich, 8092, Switzerland

Keywords: flame spray pyrolysis, neodymium, near-infrared, thermometry, luminescence.

Presenting author email: [gschwend@ptl.mavt.ethz.ch](mailto:gschwend@ptl.mavt.ethz.ch)

Temperature is one of the most fundamental properties and its measurement is crucial in our daily life as well as for scientific investigations. For example, local temperature changes in cells can give valuable information about undergoing dynamics and mechanism, such as cell division and metabolism. It is known that cellular pathogenesis of cancer and other diseases leads to heat production (Kuruganti and Qi, 2002). Therefore, being able to measure temperature with a high resolution could provide means of understanding cellular events and therefore detection of diseases (Jaque et al., 2014). However, measuring the temperature at the nanoscale in biological systems is not an easy task: Conventional thermography can only accurately measure the surface temperature and thermocouple-based methods are invasive (Usamentiaga et al., 2014). Additionally, both lack the required spatial resolution (Brites et al., 2012).

A very promising alternative is luminescence thermometry, where distinct features of the luminescence are used to detect alterations in the surroundings. It is a non-invasive method allowing high spatial and temporal resolutions (Jaque et al., 2014). Most work for thermometers at the nanoscale employed luminescence in the visible wavelength region, where absorption and scattering of biological tissue is much higher compared to the near-infrared region (NIR). Thus, there is a need for luminescent nanothermometers working in the NIR.

Here, inorganic rare-earth doped nanocrystals made by flame spray pyrolysis (Camenzind et al., 2005) are investigated as nanothermometers. Specifically, Neodymium ( $\text{Nd}^{3+}$ ) is the most promising dopant due to its excitation and emission peaks in the NIR. The effect of particle characteristics such as size and crystallinity on the thermal sensitivity is investigated. Furthermore, the influence of dopant concentration as well as thermal treatment is studied.

Figure 1 shows the fluorescence emission spectrum of  $\text{BiVO}_4:\text{Nd}^{3+}$  nanocrystals at different temperatures. The thermal sensitivity here could be increased ~1 order of magnitude compared to previously reported values of  $\text{Nd}^{3+}$ -doped nanocrystals (Benayas et al., 2015).

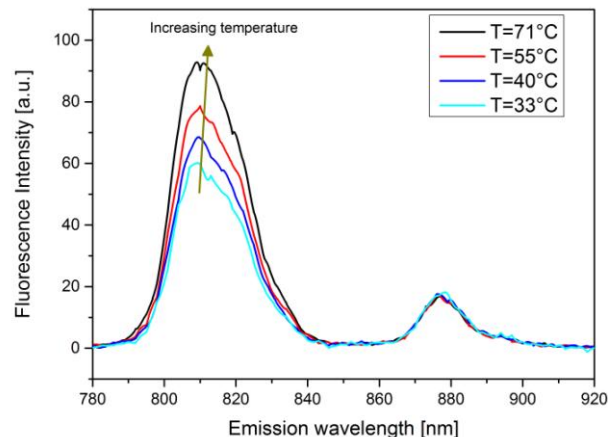


Figure 1. Fluorescence emission spectrum of  $\text{BiVO}_4:\text{Nd}^{3+}$  at different temperatures revealing its potential for nanothermometry.

- Kuruganti, P.T. and Qi, H.R. (2002) *P Ann Int Ieee Embs*, 1155-1156.
- Jaque, D., del Rosal, B., Rodriguez, E.M., Maestro, L.M., Haro-Gonzalez, P., Solé, J.G. (2014) *Nanomedicine*, **9**,1047-1062.
- Usamentiaga, R., Venegas, P., Guerediaga, J., Vega, L., Molleda, J., Bulnes, F.G. (2014) *Sensors-Basel*, **14**, 12305-12348.
- Brites, C.D.S., Lima, P.P., Silva, N.J.O., Millan, A., Amaral, V.S., Palacio, F., Carlos, L.D. (2012) *Nanoscale*, **4**, 4799-4829.
- Camenzind, A., Strobel, R., Pratsinis, S.E. (2005) *Chem Phys Lett*, **4**, 193-197
- Benayas, A., del Rosal, B., Perez-Delgado, A., Santacruz-Gomez, K., Jaque, D., Hirata, G.A., Vetrone, F. (2015) *Adv Opt Mater*, **3**, 687-694.

## Single-step fabrication of nanocatalyst microarrays by coupling flame spray pyrolysis with supersonic expansion

S. Vinati<sup>1</sup>, E.Barborini<sup>1</sup>, K. Wegner<sup>2,3</sup> and P. Milani<sup>4</sup>

<sup>1</sup>Tethis S.p.A., Milan, 20143, Italy

<sup>2</sup>Department of Mechanical and Process Engineering, ETH Zurich, Zurich, CH-8092, Switzerland

<sup>3</sup>ParteQ GmbH, Kuppenheim, D-76456, Germany

<sup>4</sup>CIMAINA-Department of Physics, University of Study of Milan, Milan, 20133, Italy

Keywords: nanoparticle beam deposition, flame spray pyrolysis, microcatalyst

Presenting author email: simone.vinati@tethis-lab.com

FlameBeam (FB) is a powerful technique that enables the synthesis of a wide class of nanoparticles and their direct deposition and integration onto planar devices (Wegner, 2012). Basically, the technique consists of coupling flame spray pyrolysis (FSP) (Strobel, 2007), with supersonic expansion (SE). This approach merges the advantages of both techniques: the high versatility of FSP to synthesize nanoparticles offers the possibility to obtain complex nano-composites in a single-step process; the SE allows to generate a collimated beam by gas expansion through a critical flow nozzle into a vacuum chamber. If nanoparticles are seeded in the expanding gas, the beam becomes a nanoparticle beam. This allows the deposition of nanoparticles with high precision permitting the integration/functionalization of devices and micro-devices (Tolstosheeva, 2014).

Here we report the synthesis of Pt/Ce.5Zr.5O<sub>2</sub> 1%wt (PCZ), an automotive catalyst (Stark, 2005), and its deposition in form of micrometric patches on a planar substrate, forming an array of catalysts (Figure 1).

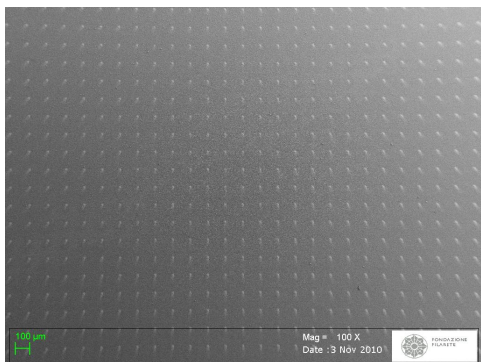


Figure 1. SEM image of the array of the micro-catalysts grown in a single fabrication step with FB. The substrate used here is a wafer silicon.

A solution containing the appropriate quantities of Pt-acetylacetonate, Ce-2-ethylhexanoate and Zr-2-ethylhexanoate in acetic acid and 2-ethylhexanoic acid was sprayed in the FB burner. The subsequent combustion process leads to the formation of PCZ nanoparticles. Because FB is interfaced to a vacuum chamber through a sonic nozzle, the flame is quenched and cooled before it expands into the chamber generating a supersonic nanoparticle beam. Exploiting the collimation of the beam, the deposition of the catalyst

array can be patterned with high lateral resolution on extended areas by a stencil mask (Barborini, 2008).

The PCZ has been characterized by XRD, HRTEM and SEM in order to depict the structural and morphological properties of the material. Figure 2 reports a TEM image that shows how the obtained highly crystalline nanoparticles of 5-15 nm size are assembled. This gives to the material a high specific area and makes it potentially highly reactive. XRD demonstrates that a solid solution of Zr and Ce oxides is formed.

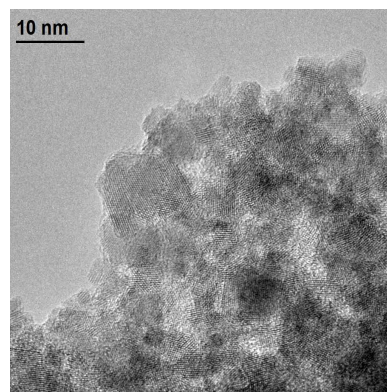


Figure 2. TEM image of crystalline PCZ.

These results suggest the potential use of FlameBeam for the fabrication of micro-devices by direct integration of nanomaterials on platforms.

Wegner, K., Vinati, S., Piseri, P., Antonini, A., Zelioli, A., Barborini, E., Ducati, C. and Milani, P. (2012) *Nanotech.*, **23**, 185603

Strobel, R. and Pratsinis, S.E. (2007) *J. Mater. Chem.*, **17**, 4743

Tolstosheeva, E., Barborini, E., Meyer, E.M., Shafi, M., Vinati, S., Lang, W. (2014) *J. Micromech. Microeng.*, **24**, 015001

Stark, W.J., Grunwaldt, J., Maciejewski, M., Pratsinis, S.E. and Baiker A. (2005) *Chem.Mater.*, **17**, 3352

Barborini, E., Vinati, S., Leccardi, M., Repetto, P., Bertolini, G., Rorato, O., Lorenzelli, L., Decarli, M., Guarnieri, V., Ducati, C. and Milani, P. (2008) *J. Micromech. Microeng.*, **18**, 055015

## Superparamagnetic nanoparticles for triggered drug release from alginate hydrogels

Alexandra Teleki<sup>1,2</sup>, Florian L. Haufe<sup>1</sup>, Ann M. Hirt<sup>3</sup>, Sotiris E. Pratsinis<sup>1</sup> and Georgios A. Sotiriou<sup>4,5</sup>

<sup>1</sup>Particle Technology Laboratory, Institute of Process Engineering, Department of Mechanical and Process Engineering, ETH Zurich, 8092 Zurich, Switzerland.

<sup>2</sup>Department of Pharmacy, Uppsala University, 75123 Uppsala, Sweden.

<sup>3</sup>Department of Earth Sciences, ETH Zurich, 8092 Zurich, Switzerland.

<sup>4</sup>Drug Formulation and Delivery, Institute of Pharmaceutical Sciences, Department of Chemistry and Applied Biosciences, ETH Zurich, 8093, Zurich, Switzerland.

<sup>5</sup>Department of Microbiology, Tumor and Cell Biology, Karolinska Institutet, 17177 Stockholm, Sweden.

Keywords: nanotechnology, drug release, stimuli-responsive.

Presenting author email: alexandra.teleki@farmaci.uu.se

While magnetic nanomaterials have already been used in clinics for contrast enhancement in magnetic resonance imaging (MRI) (Singh and Sahoo, 2014), there has been no clinical approval for a drug delivery system containing such nanoparticles, yet. Magnetic nanoparticles currently investigated for their possible application in biomedicine are predominantly different crystalline polymorphs of iron oxides. For small enough crystal sizes, iron oxides exhibit the so-called “superparamagnetic” behavior, a feature combining high magnetization with very low coercive forces. Such superparamagnetic nanoparticles show great potential in therapeutic applications due to their ability to transform the energy of an alternating magnetic field to thermal energy in what is often called magnetic fluid hyperthermia (Jordan *et al.*, 1999). These particles dissipate thermal energy by magnetic relaxation through the Brownian and Neel mechanisms. Therefore, aqueous suspensions at relatively higher nanoparticle concentrations (g/L), the so-called “ferrofluids”, also increase their temperature in the presence of an alternating magnetic field (Sotiriou *et al.*, 2013).

In this work, a composite multi-scale structure consisting of the biopolymer alginate, functional nanoparticles and a model drug is fabricated and analyzed. We demonstrate the highly scalable and reproducible synthesis of uniformly SiO<sub>2</sub>-coated superparamagnetic Fe<sub>2</sub>O<sub>3</sub> nanoparticles (Teleki *et al.*, 2009), and evaluate their suitability as stimuli-responsive nanofillers in a drug-loaded biopolymer alginate matrix. The superior colloidal stability of the SiO<sub>2</sub>-coated Fe<sub>2</sub>O<sub>3</sub> nanoparticles over their uncoated counterparts and their dispersibility in aqueous suspensions facilitates their incorporation in alginate hydrogel microbeads. We perform detailed physicochemical and magnetic characterization on the hybrid alginate hydrogel beads and evaluate their potential in magnetic fluid hyperthermia and enhanced biomolecule release in the presence of an external alternating magnetic fields. We examine the hyperthermia performance of such multiscale particle structures in the presence of alternating magnetic fields and compare the release of dextran (a model biomolecule) in the presence and absence of external stimuli. The enhanced triggered release of dextran in the presence of magnetic fields

further highlights the potential of such superparamagnetic SiO<sub>2</sub>-coated Fe<sub>2</sub>O<sub>3</sub> nanoparticles as a functional transducer in such systems.

The possibility to externally stimulate drug release will open up new possibilities in intelligent, on-demand drug administration (Teleki *et al.*, 2016).

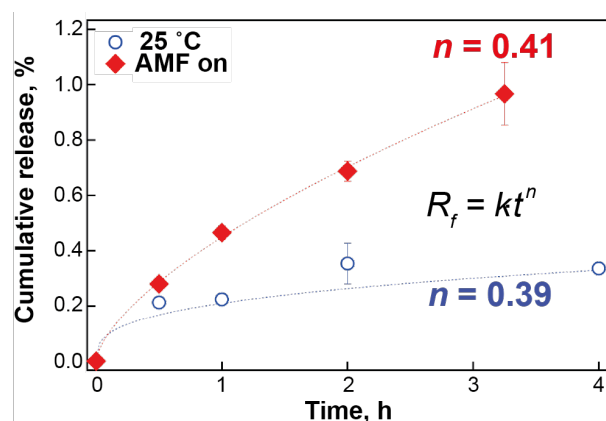


**Fig. 1:** Cumulative release of dextran (model drug) from alginate hydrogels with superparamagnetic nanoparticles in the presence (red diamonds) and absence (blue circles) of an external magnetic field (AMF).

This research was supported by the European Research Council under the European Union's Seventh Framework Program (FP7/ 2007-2013, ERC grant agreement no. 247283). Georgios A. Sotiriou was supported by a Swiss National Science Foundation *Advanced Researcher* fellowship (grant no. 145392).

Jordan A., R. Scholz, P. Wust, H. Fahling, R. Felix, *J. Magn. Magn. Mater.*, **201**, 413-419 (1999).

Singh, A., S. K. Sahoo, *Drug Discov. Today*, **19**, 474-481 (2014).

Sotiriou G.A., M. A. Visbal-Onufrak, A. Teleki, E. J. Juan, A. M. Hirt, S. E. Pratsinis, C. Rinaldi, *Chem. Mater.*, **25**, 4603-4612 (2013).

Teleki A., M. Suter, P. R. Kidambi, O. Ergeneman, F. Krumeich, B. J. Nelson, S. E. Pratsinis, *Chem. Mater.*, **21**, 2094-2100 (2009).

Teleki A., F. L. Haufe, A. M. Hirt, S. E. Pratsinis, G. A. Sotiriou, *RSC Adv.* **6**, 21503-21510 (2016).

## Spray-flame synthesis of barium titanate nanoparticles for electro- and photochemical applications

A. Tarasov<sup>1</sup>, Y. Xiong<sup>2</sup>, F. Marlow<sup>2</sup>, C. Schulz<sup>1</sup>, H. Wiggers<sup>1</sup>

<sup>1</sup>IVG – Reactive Fluids and CENIDE, University of Duisburg-Essen, Germany

<sup>2</sup>Max-Planck-Institut für Kohlenforschung, Mülheim

Keywords: barium titanate, spray-flame synthesis, nanoparticles  
alexander.tarasov@uni-due.de

Barium titanate BaTiO<sub>3</sub> is known as a ferroelectric material with a high dielectric constant, which finds its applications mostly as a multilayer ceramic capacitor in microelectronics. At the same time, it is of a particular interest for photocatalytic applications as its ability to create spontaneous polarization has a significant influence on the surface photochemistry, thus enhancing the effectiveness of surface-based reactions (Cui et al., 2013). High-purity BaTiO<sub>3</sub> powders in the nanometer range with clean surfaces and without secondary phases show higher photocatalytic performance with respect to e.g. water splitting compared to commercially available barium titanate.

As of today, conventional methods for barium titanate production such as a number of sol-gel processes and solid-state reactions are being used. While in the first case high temperature post-treatment procedures are required to remove solvents and stabilizers and coarse sizes of the particles are obtained in the second case, there are compelling enough arguments to investigate new production methods. Therefore, a closer analysis of alternative production processes regarding the applications named above is very much needed.

As known from many metal oxide formation processes, flame synthesis is an easy scalable production method. From the variety of flame synthesis methods, spray-flame synthesis (SFS) has been particularly gaining popularity in the last couple of decades as an established lab-scale gas-phase based combustion synthesis method. Main advantages of this method are production of crystalline particles with well-defined morphology in the nanometer range and the possibility to adjust chemical composition of the intended product by mixing the desired amounts of precursors in a combustible solvent.

Here, we report on the SFS of barium titanate nanoparticles in a continuous process. Due to the presence of large quantities of CO<sub>2</sub> in the off gas, avoiding the formation of thermally stable BaCO<sub>3</sub> as a byproduct is a challenge. We observed that a careful choice of solvents, precursors, and process conditions has a decisive impact on the final powder quality. In order to compare powders produced from solvents with different energetical inputs, the combustion enthalpy density, which is the ratio of combustion enthalpies of all components divided by the O<sub>2</sub> dispersion gas mass value, was used as a criteria during the synthesis (Josson et al., 2005).

X-ray diffraction analysis indicated that energetically capable solvents result in a highly crystalline powder with two different crystal phases present (Fig. 1). That is a ferroelectric tetragonal phase

and a high-temperature hexagonal phase, which should not be present at room temperature and is a consequence of rapid cooling of a particle flow within the reactor. Solutions with lower enthalpy density values show almost pure-phase particles but with a lower degree of crystallinity, which can be amended by heat treatment at 450°C. The count median diameter (CMD) obtained from transmission electron microscopy (TEM) suggests for all cases particle sizes of around 10 nm.

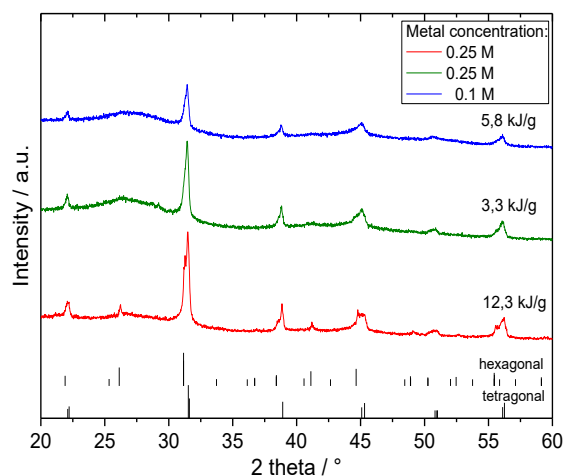


Figure 1. X-ray diffraction data of the as-synthesized BaTiO<sub>3</sub> powders with different enthalpy densities.

Independent of the combustion enthalpy density, the surface of the pristine particles contains adsorbed moieties of combustion products as revealed by IR analysis. However, a mild subsequent heat treatment at 250°C is sufficient for any BaTiO<sub>3</sub> powder from SFS to clean the surface without leading to coarsening or sintering effects.

A.T. acknowledges the IMPRS-SurMat of the Max Planck Society for financial support.

Cui, Y., Briscoe, J., and Dunn, S. (2013) *Chemistry of Materials* **25** (21): 4215–4223.

Josson, R., Pratsinis S., Stark W. and Mädler L. (2005) *J. Am. Ceram. Soc.*, **88** [6] 1388-1393

## Control of Particle Morphology and Size Distribution by Relative Humidity

G.A. Kelesidis<sup>1</sup>, F. Furrer<sup>1</sup>, E. Goudeli<sup>2</sup>, M.L. Eggersdorfer<sup>1</sup>, K. Wegner<sup>1</sup> and S.E. Pratsinis<sup>1</sup>

<sup>1</sup>Department of Mechanical and Process Engineering, ETH Zürich, Zürich, CH-8092, Switzerland

<sup>2</sup>Department of Mechanical and Process Engineering, University of Minnesota, Minneapolis, MN-55455, U.S.A.

Keywords: water condensation, mass-mobility exponent, agglomerate density, relative humidity

Presenting author email: gkelesidis@ptl.mavt.ethz.ch

Nanoparticles with compact structure are attractive for biomedical applications, such as drug delivery and theranostics, due to enhanced bioavailability and light absorption in the near infrared spectrum (Sotiriou *et al.*, 2014). Flame-made nanoparticles, however, typically are ramified agglomerates of primary particles with open structure and mass-mobility exponent,  $D_{fm}$ , of about 2.17 (Sorensen, 2011). Such agglomerates can restructure in the presence of humidity to smaller and more compact entities, as has been observed for soot (Ma *et al.*, 2013). Here, this effect of agglomerate restructuring is investigated for flame-made silica aiming at small and compact nanoparticles with well-defined size distributions.

Water vapor produced by an evaporator is introduced into a diluted aerosol stream sampled above the flame, resulting in controlled saturation ratios,  $S$ , of 1.15 to 1.55. Water initially condenses on the particle surface and then is largely removed, as the humid aerosol flow passes through a series of two diffusion dryers. Combined Differential Mobility Analyser and Aerosol Particle Mass measurements are employed to determine particle structure and anisotropy by the  $D_{fm}$  and the mass-mobility prefactor,  $k_m$ , respectively.

Silica agglomerates restructure more with increasing  $S$  resulting in more spherical and compact structures, corresponding to larger  $D_{fm}$  and smaller  $k_m$ , respectively. The asymptotic morphology obtained after complete agglomerate collapse for  $S = 1.55$  is characterized by a  $D_{fm}$  of  $3.02 \pm 0.11$  and a  $k_m$  of  $0.26 \pm 0.06$ , in good agreement with the  $D_{fm}$  of 2.79 and  $k_m$  of 0.63 measured from soot agglomerates restructured after water condensation and evaporation (Ma *et al.*, 2013).

Figure 1 shows the packing density,  $\theta$ , defined by the effective density,  $\rho_{eff}$ , normalized by the bulk silica density,  $\rho_{bulk}$ , of silica agglomerates processed with  $S = 0.25$  (circles), 1.15 (triangles), 1.35 (squares) and 1.55 (diamonds) as function of their mobility diameter,  $d_m$ , normalized by the primary particle diameter,  $d_p$ . The  $\theta$  of silica particles processed with  $S = 0.25$  (circles, blue inset) decreases with  $d_m/d_p$  as larger agglomerates become more ramified and porous. As  $S$  increases to 1.15 (triangles) and 1.35 (squares), water condensation and evaporation make silica agglomerates slightly more compact, increasing  $\theta$  up to 19 % for  $d_m/d_p = 10$  and  $S = 1.35$ . Further increase of  $S$  up to 1.55 results in silica agglomerate restructuring into compact, spherical entities (red inset) with average  $\theta = 0.28 \pm 0.01$  (broken line), invariant of mobility diameter. The average  $\theta$  is lower compared to that of soot (dotted line, light blue inset: Zangmeister *et al.*, 2014) due to the larger

polydispersity of silica primary particles attained by sintering.

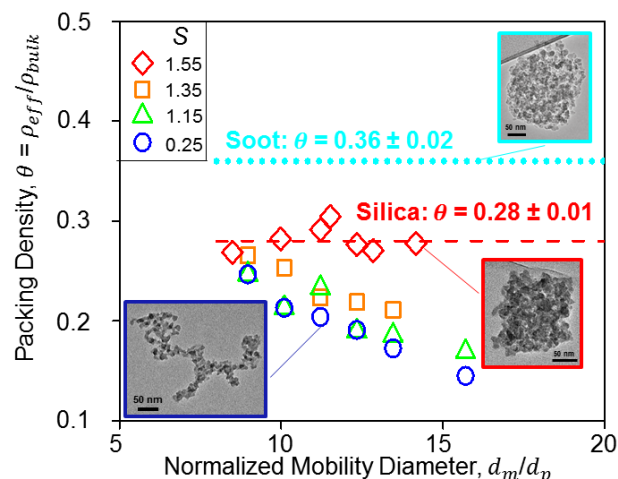


Figure 1. Packing density,  $\theta$ , of silica agglomerates processed with  $S = 0.25$  (circles, blue inset), 1.15 (triangles), 1.35 (squares) and 1.55 (diamonds, red inset) as function of the normalized mobility diameter,  $d_m/d_p$ . The average  $\theta$  of restructured silica agglomerates (broken line) is lower than that of soot (dotted line, light blue inset: Zangmeister *et al.*, 2014).

The compact structures attained with increasing  $S$  have smaller size, decreasing the average  $d_m$  from 107.6 nm in ambient conditions to 91.4 nm for  $S = 1.55$ . Larger agglomerates restructure more than smaller ones, resulting in narrower size distributions with smaller mobility-based geometric standard deviation,  $\sigma_{g,m}$ . A gradual  $\sigma_{g,m}$  reduction is obtained for increasing  $S$ , reaching a maximum 22.4 % decrease for  $S = 1.55$ . Thus, particle processing with humidity is a promising method to finely tune their morphology and size distribution.

Ma, X.F., Zangmeister, C.D., Gigault, J., Mulholland, G.W., Zachariah, M.R., (2013) *J. Aerosol Sci.* **66** 209-219.

Sorensen, C.M. (2011) *Aerosol Sci. Technol.* **45**, 765-779.

Sotiriou, G.A., Starsich, F., Dasargyri, A., Wurnig, M.C., Krumeich, F., Boss, A., Leroux, J.C., Pratsinis, S.E. (2014) *Adv. Funct. Mater.* **24**, 2818-2827.

Zangmeister, C.D., Radney, J.G., Dockery, L.T., Young, J.T., Ma, X.F., You, R.A., Zachariah, M.R. (2014) *PNAS* **111**, 9037-9041.

## Single-Step Aerosol Synthesis of Ratiometric Hydrogen Peroxide Biosensors

D.F. Henning<sup>1,2</sup>, G.A. Sotiriou<sup>1</sup>

<sup>1</sup>Department of Microbiology, Tumour and Cell Biology, Karolinska Institutet, Solna, 171 77, Sweden

<sup>2</sup>Department of Mechanical and Process Engineering, ETH Zürich, Zürich, 8092, Switzerland

Keywords: biosensing, hydrogen peroxide, flame spray pyrolysis

Presenting author email: dorian.henning@ki.se

Hydrogen peroxide (H<sub>2</sub>O<sub>2</sub>) is an important (bio)molecule in a variety of bioprocesses and is often decomposed in vivo using the enzyme catalase. Growing interest in quantification of H<sub>2</sub>O<sub>2</sub> exists particularly in pharmaceutical and biological applications, since it is not only a potential biomarker for inflammations and infections, but also an intermediate molecule in enzyme-based assays such as the plasmonic ELISA. However, a label-free and calibration free assay has yet to be developed.

In this work, we propose a nanoparticle-based ratiometric optical biosensor to detect  $\mu\text{M}$  quantities of H<sub>2</sub>O<sub>2</sub> in physiological relevant solutions. For this goal, we combine luminescent enzyme-mimetic CeO<sub>2</sub>:Eu<sup>3+</sup> nanoparticles with optically stable Y<sub>2</sub>O<sub>3</sub>:Tb<sup>3+</sup> nanophosphors (Sotiriou et al., 2011 & Sotiriou et al., 2012) that serve as concentration-independent reference value.

Both nanoparticles are synthesized by flame aerosol technology simultaneously in a single-step, allowing for a highly scalable and reproducible production as well as facilitating direct deposition of this material on glass substrates for fabrication of H<sub>2</sub>O<sub>2</sub> biosensing surfaces. It is shown, that the luminescence properties of the CeO<sub>2</sub>:Eu<sup>3+</sup> nanoparticles vary dramatically for different concentrations of H<sub>2</sub>O<sub>2</sub>, while the Y<sub>2</sub>O<sub>3</sub>:Tb<sup>3+</sup> phosphors are highly utilizable as reference material. The sensing performance of the nanoparticles was evaluated with hydrogen peroxide producing bacteria in biological media. Our results show, the presented material can be used for selective, label-, and calibration-free H<sub>2</sub>O<sub>2</sub> sensing with smaller variance than conventional methods (Syk et al., 2014) as well as be synthesized in a highly scalable fashion.

Sotiriou, G.A., Schneider, M. and Pratsinis, S.E. (2011) *J. Phys. Chem. C* **115**, 1084-1089.

Sotiriou, G.A., Franco, D., Poulidakos, D. and Ferrari, A. (2012) *ACS Nano* **6**, 3888-3897.

Syk, A., Norman, M., Fernebro, J., Gallotta, M., Farmand, S., Sandgren, A., Normark, S., Henriques-Normark, B. (2014) *J. Infect. Dis.* **210**, 4-13.

## **Abstracts T102**

## Polyacrylonitrile microfiber modified with sodium hydroxide and glycol and its adsorption behavior for Cu(II) removal

Lan-Yao Liu<sup>1</sup>, Ang Yu<sup>2</sup>, Chang-Tang Chang<sup>1,\*</sup>

<sup>1</sup>Department of Environmental Engineering, National I-Lan University, I-Lan, 26047, Taiwan

<sup>2</sup>College of the Environment & Ecology, XiaMen University, Xia-Men, 361121, China

Keywords: PAN microfiber; modification; adsorption behavior

Presenting author email: ctchang@niu.edu.tw

Nowadays, the industrial polluted effluent containing heavy metal ions, such as chromium, copper, lead, mercury, and cadmium, is a worldwide environmental issue. It will contaminate potable water and cause serious toxic effects to living organisms, including human beings. Therefore, it is an important issue to remove superfluous heavy metal ions from water.

Numerous techniques, including liquid partition, chemical precipitation, membrane separation, adsorption, and ion exchange, have been used to solve the problem of heavy metal pollution. Among these methods, people pay more attention to adsorption due to its high removal efficiency and cost effectiveness.

Many studies have been investigated about the removal of Cu(II) ions from aqueous solutions using different adsorbents (Hong et al., 2015). These adsorbents can be derived from many materials including high polymer. Particularly, polyacrylonitrile (PAN), as a common high polymer material, can be easily made into micro fibers by electrospinning and modified into chelating fibers. PANs can be easily modified into various chelating groups with the functional group of the nitrile ( $C\equiv N$ ). Electrospinning is a versatile method to tune and control the morphology and chemical composition of microfibers. Because of the micro diameter, electrospun microfibers have large specific surface areas (Pei and Leung, 2013). Herewith, modified micro fibers can be a good adsorbent for adsorption of heavy metal ions.

In this study, the microfiber are prepared through an electrospinning solution system. The surface of the electrospun PAN fibers was reacted with a series of different concentration sodium hydroxide glycol solution at 65-75°C for modification. The function groups of modified PAN microfibers (C-gPAN) were determined by Fourier-transform Infrared Spectroscopy (FT-IR). The ability to absorb metal ions was then evaluated against Cu(II) ions under different pH and initial Cu(II) concentration. Furthermore, its concentration was analyzed by 2,9-Dimethyl-1,10-

phenanthroline spectrophotometric method (HJ 486—2009, China).

The amounts of the Cu(II) ions adsorbed by C-gPAN microfiber were influenced by the initial pH and the initial concentration of the metal ion solutions. At the pH of 5.0, the amounts of the Cu(II) ions adsorbed by the C-gPAN reached a maximum, 15.0 mg g<sup>-1</sup>. In addition, the adsorption capacity is increased with increasing initial concentration. Furthermore, the adsorption isotherms fits Langmuir model better. According to the Langmuir fitting, the maximum adsorption capacity was 33.2 mg g<sup>-1</sup>.

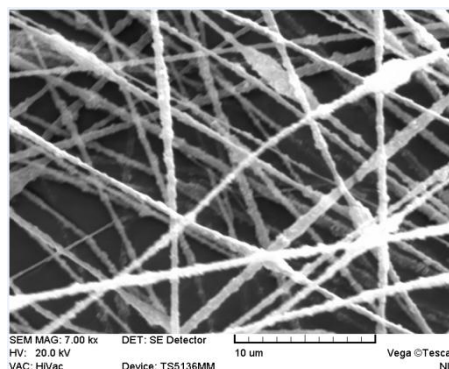


Fig.1 SEM images of PAN microfiber prepared through electrospinning

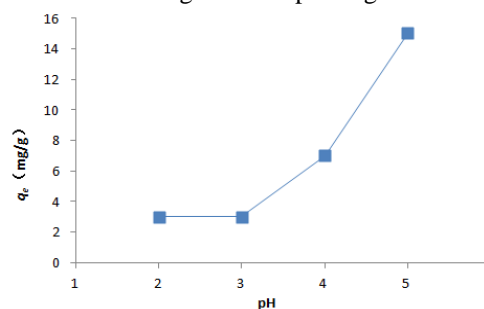


Fig.2 Effect of pH on the adsorption capacity with C-gPAN for Cu(II) at 293K

G. Hong, X. Li, L. Shen, M. Wang, C. Wang, X. Yu, X. Wang, *Journal of Hazardous Materials*, 295 (2015) 161-169.

C.C. Pei and W.W.-F. Leung, *Separation and Purification Technology*, 114 (2013) 108-116.

## Stability control of spark discharge generated metal nanoparticle synthesis via air ion injection

Dae Hoon Park<sup>1</sup>, Yun Haeng Joe<sup>2</sup>, Jeong Hoon Byeon<sup>3</sup> and Jungho Hwang<sup>1</sup>

<sup>1</sup>Department of Mechanical Engineering, Yonsei University, Seoul, 03722, Republic of Korea

<sup>2</sup>Climate Change Research Division, Korea Institute of Energy Research, Daejeon, 34152, Republic of Korea

<sup>3</sup>School of Mechanical Engineering, Yeungnam University, Gyeongsan, 38541, Republic of Korea

Keywords : Air ion, spark discharge, nanoparticles, synthesis, particle generation

Presenting author email: dhoonpark@yonsei.ac.kr

Today, researches and industrial applications of nanoparticles are increasing. There are several methods of synthesis of nanoparticles. Among those methods, we focus on the spark discharge generation (SDG) method, which has been recognized as a powerful technique for producing metallic nanoparticles from bulk materials with high surface purity (Roth *et al* (2004), Tabrizi *et al* (2009)). This method has been widely studied and applied for synthesis of various kinds of aerosols (Anastasopol *et al* (2013), Byeon *et al* (2014)).

Recently, many researchers focus on the stability of nanoparticle generation from SDG system. In this study, when air ions were injected to the spark region, the effect of air ion on the stability of spark discharge was observed. In order to control the repetition of a spark, a personal switching circuit was used. The voltages between two electrodes and across the capacitor were measured with different ion concentration. The characteristics of generated particles, such as mass and number concentrations and mode diameter were measured.

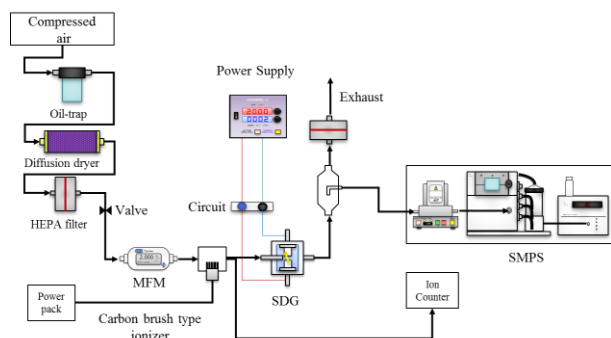


Figure 1. Schematic of the lab-made SDG system.

The experimental system consisted of a clean air supply system, a lab-made SDG system including test circuit fabricated with the concept of switching circuit which is suggested from Pfeiffer *et al* (2014), an ionizer, and a particle measurement system (Fig. 1). The mass concentrations and mode diameter of the generated nanoparticles were measured using a scanning mobility particle sizer (SMPS, TSI Inc.).

To verify the stability of the characteristics of generated particles via air ion injection, we applied particles for fabricating anti-viral air filters with same coating areal density. The stability of the anti-viral ability of the fabricated filters was evaluated against aerosolized bacteriophage MS2.

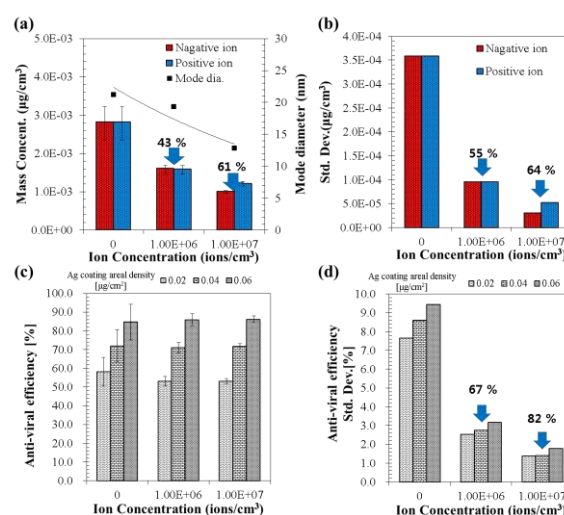


Figure 2. (a) Mass concentration and mode diameter, (b) standard deviation of mass concentrations, (c) anti-viral efficiency and (d) standard deviation of anti-viral efficiencies with various air ion concentrations

The results were shown in Fig. 2. The standard deviation of mass concentrations was evidently decreased with increasing air ion concentration but there was no significant difference as ion polarity. And the anti-viral efficiencies of the fabricated filters were similar, but standard deviation of anti-viral efficiencies was evidently decreased with increasing air ion concentration and same coating areal density.

This research was supported by Korea Ministry of Environment (MOE) as “Advanced Technology Program for Environmental Industry”.

Roth, C., Ferron, G. A., Karg, E., Lentner, B., Schumann, G., Takenaka, S., and Heyder, J. (2004) *Aerosol Sci. Tech.* **38**(3), 228-235.

Tabrizi, N. S., Ullmann, M., Vons, V. A., Lafont, U., and Schmidt-Ott, A. (2009) *J. Nanopart. Res.* **11**(2), 315-332.

Anastasopol, A., Pfeiffer, T. V., Middelkoop, J., Lafont, U., Canales-Perez, R. J., Schmidt-Ott, A., Mulder, F. M., and Eijt, S. W. H. (2013) *J. Am. Chem. Soc.* **135**, 7891-7900.

Byeon, J. H., and Kim, Y.-W. (2014) *ACS Macro Lett.* **3**, 205-210.

Pfeiffer, T. V., Feng, J., and Schmidt-Ott, A. (2014) *Adv. Powder Technol.* **25**, 56-70.

## The spark ablation as a perspective method for the solvent-free aerosol jet printing

A.A. Efimov, A.A. Lizunova, P.V. Arsenov and V.V. Ivanov

Department of Physical and Quantum Electronics, Moscow Institute of Physics and Technology, Dolgoprudny, 141700, Russia

Keywords: aerosol jet printing, spark discharge generator, focusing nanoparticles.

Presenting author email: [efimov.aa@mipt.ru](mailto:efimov.aa@mipt.ru)

Currently, there is active development of technology for production of electronic devices at low cost. These technologies will be in demand for the production of flexible displays, RFID tags, active coatings, and other (Nisato *et al*, 2016). Aerosol jet printing is one such technology (Hoey *et al*, 2012).

Conventional aerosol jet printing is based on the use of nanoink that are sprayed and deposited onto the substrate through a focusing nozzle. The use of nano-ink causes some significant problems:

- environmental pollution due to the use of organic solvents;
- requirements to the conditions and terms for storage of the inks;
- necessity of removing and recycling solvent and surfactant after deposition.

In this regard, researchers are developing and investigating the new environmentally friendly and versatile source of nanoparticles for aerosol jet printing, which does not require the use of inks with solvents. It is known that spark ablation is a promising method for generating the dry aerosol nanoparticles with size less than 10 nm. This work presents the results of experiments on the use of spark ablation for dry aerosol jet printing.

The experimental setup consisted of a multi-spark discharge generator (m-SDG) (Efimov *et al*, 2016) and a commercial system for the particle deposition AJ 15XE with coaxial nozzle 100  $\mu\text{m}$  in outlet diameter (Fig. 1a). Aerosol nanoparticles were synthesized by the m-SDG as a result of electrical erosion of silver electrodes in air. The aerosol flow  $Q_a$  entered the coaxial nozzle through the inner cylindrical channel, while the sheath flow  $Q_{sh}$  was inserted through the outer conically converging axisymmetrical channel. Then the focused aerosol beam was directed to the glass substrate for deposition. In the process of moving the substrate relatively to the focused aerosol beam at speed of motion about 10 mm/min, we formed the line of deposited silver nanoparticles on the substrate. Printed lines were annealed in a muffle furnace at 450°C for 1 hour at air atmosphere. The width of formed lines was measured by using the optical microscope. The microstructure, cross-sectional profile and thickness of the line were studied using scanning electron microscope (SEM). Electrical resistivity of the printed and sintered lines was measured by four-probe method.

The result of the experiments show that by controlling the flow of a sheath gas, it is possible to change the width of the printed lines is more than 2.5 times. This result demonstrates the realization of the

aerodynamic focusing of the nanoparticles beam in the coaxial nozzle. The minimum width of the printed lines was about 60  $\mu\text{m}$  (Fig. 1b). The analysis of the microstructure of formed lines in SEM has shown that the typical sized of the deposited agglomerates of nanoparticles are in the range of 50-100 nm. The cross-section profile of the line has a bell-shaped form with maximum thickness and width equal to  $13\pm 2$  and  $64\pm 6$   $\mu\text{m}$ , respectively (Fig. 1c).

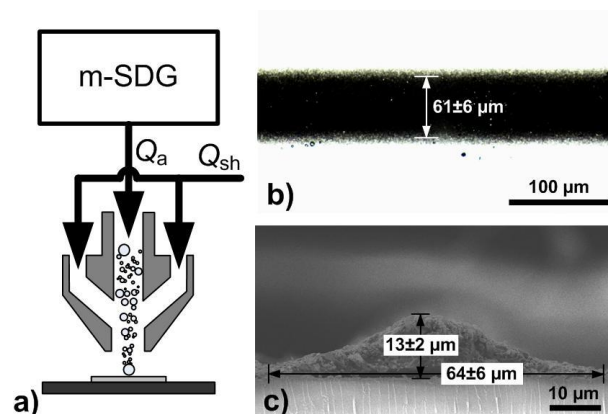


Figure 1. (a) The scheme of the experiment of solvent-free aerosol jet printing using the multi-spark discharge generator; (b) optical image and (c) SEM-image of line of deposited silver nanoparticles.

Printed microstructures showed low electrical resistivity equal to 7.5  $\mu\Omega\cdot\text{cm}$ , which is five times greater than the resistivity of bulk silver. The same microstructures can be used in printed electronics devices. The proposed solvent-free method is a promising alternative to the conventional method of «wet» aerosol jet printing.

This work was supported by the Russian Science Foundation (project # 15-19-00190).

Nisato, G., Lupo, D., & Ganz, S. (Eds.). (2016) *Organic and Printed Electronics: Fundamentals and Applications*. Pan Stanford.

Efimov, A., Lizunova, A., Sukharev, V. and Ivanov, V. (2016) *Korean J. Mater. Res.*, **26** (3), 123-129.

Hoey, J. M., Lutfurakhmanov, A., Schulz, D. L. and Akhatov, I. S. (2012) *J. Nanotechnol.*, **2012**, e324380.

## Passivation and magnetic properties of core-shell aerosol Fe(Cr,Mn) alloy nanoparticles

C. Preger<sup>1</sup>, L. Ludvigsson<sup>1</sup>, B. O. Mueller<sup>1</sup>, R. Westerström<sup>2</sup> and M. E. Messing<sup>1</sup>

Solid State Physics, Lund University, Box 118, 221 00 Lund, Sweden

<sup>2</sup>Division of Synchrotron Radiation Research, Lund University, Box 118, 221 00 Lund, Sweden

Keywords: Alloyed nanoparticles, core-shell, spark discharge,

Presenting author email: [calle.preger@ff.lth.se](mailto:calle.preger@ff.lth.se)

Stainless steel is an Fe/Cr alloy that obtains its corrosion resistive properties by forming a thin passivation layer when exposed to oxygen. This layer is 3-4 nm thick and does not affect the bulk composition. However, when forming nanoparticles this passivation layer becomes a substantial and the particle will separate into a core-shell structure where the passivation layer becomes the shell. The formation of this passivation layer for alloyed nanoparticles is important to understand in order to both optimize the properties of the passivation layer as well as the core composition of these easily oxidized nanoparticles. By tuning the composition, desirable magnetic properties such as exchange bias can be obtained (Bins, 2013).

The aim of this work is to demonstrate how the formation and passivation of a bimetal alloyed nanoparticle can be tuned by varying input material and gas environment and also how this will change the magnetic property of these different nanoparticles.

### Method

The generation of the nanoparticles is performed in a closed system with a continuous aerosol flow. Primary particles are formed by spark discharge, agglomerates consisting of primary particles are size selected and reshaped with a tandem DMA and furnace setup (Messing, 2009). As the particle source, four different types of alloyed electrodes have been used Fe<sub>82.5</sub>Cr<sub>17.5</sub>, Fe<sub>60</sub>Cr<sub>40</sub>, Fe<sub>95</sub>Cr<sub>5</sub> and Fe<sub>85</sub>Mn<sub>15</sub>. Both Cr and Mn have similar lattice structure as Fe and can therefore occupy the same lattice sites and also form similar oxides. Mn and Cr are more easily oxidized than Fe, which will affect the composition of passivation layer. The nanoparticles have also been produced in different kind of carrier gas environment; one without oxygen and one where oxygen exists in small amount. The shape and composition of the deposited nanoparticles has been analysed with TEM, XEDS and XPS. The magnetic properties were obtained from SQUID measurements.

### Conclusions

When using the carrier gas with low oxygen amount, single crystal oxidized nanoparticles will be formed with the same metallic ratio as the bulk alloy electrode. When particles are formed in an environment without oxygen a core-shell structured particle is formed with a single crystal metallic core and an amorphous oxide layer, acting as shell. This shell is formed after the

deposition when the particles are exposed to air. Disregarding the size of the core the shell thickness will always become 3-4 nm which is the same as the bulk passivation layer, see Figure 1

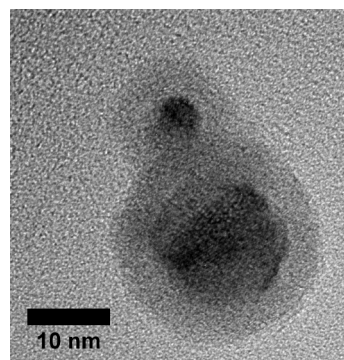


Figure 1. Two differently sized core-shell particles with a crystalline core and a 3-4 nm thick amorphous shell

When Fe<sub>82.5</sub>Cr<sub>17.5</sub> electrodes were used as particle source the core-shell particles consisted of oxidized iron and chromium as well as a metallic  $\alpha$ -Fe phase. No signal from Cr(0) was detected, indicating that all or almost all chromium has migrated into the amorphous shell during passivation. Based on this, this work will continue to investigate and will present how the core-shell composition varies with different electrodes composition and how the magnetic properties of these core-shell nanoparticles varies with different amount of Cr or Mn in the core.

The research leading to these results received funding from the Swedish Research Council. XPS measurements were performed at PEARL beamline at Swiss Lightsource (SLS). This work was performed within NanoLund at Lunds University with financial support from Myfab.

Bins, C. (2013). *Nano Lett.*, 13, 3334-3339 Cambridge, U.K.: Cambridge University Press.

Messing, M. E. (2009), *Gold Bulletin*, 42, 20-26

## Continuous synthesis of silicon nanoparticles in a low pressure microwave plasma reactor on the pilot-plant scale

F. Kunze<sup>1</sup>, M. Spree<sup>1</sup>, Tim Hülser<sup>1</sup>, H. Wiggers<sup>2</sup> and S. M. Schnurre<sup>1</sup>

<sup>1</sup>IUTA, Institute of Energy and Environmental Technology e.V., Duisburg, Germany

<sup>2</sup>IVG, Institute for Combustion and Gas Dynamics, University of Duisburg-Essen, Germany

Keywords: silicon, nanoparticles, plasma, pilot scale.

Presenting author email: kunze@iuta.de

Within the last years, numerous research results have indicated that nano-sized silicon can be used for a multitude of different applications. Especially its size-dependent properties such as limited phonon transport (in thermoelectric devices), structural flexibility (for battery applications) or quantum-confined optical properties (for optical applications) are of high interest.

Gas phase synthesis is a suitable method for the continuous production of high amounts of specific nanoparticles, which enables applications based on highly-pure nanostructured materials. Up to now, microwave plasma reactor processes have mainly been investigated on the laboratory scale and only a very few approaches were dealing with scaling to higher production rates. Therefore, microwave supported plasma reactors are not yet regarded as a competitive manufacturing method to produce high amounts of nanoparticles with consistent high quality.

We show that microwave plasma reactors can be used for the generation of silicon nanoparticles from silane ( $\text{SiH}_4$ ) at the pilot scale. Our reactor uses a microwave frequency of 915 MHz and a microwave power up to 50 kW in contrast to 2.45 GHz and 3 kW on the laboratory scale.

We will show the influence of different process conditions on nanoparticle properties such as particle size and morphology. Figure 1 shows a typical silicon nanoparticles synthesized with the microwave plasma reactor. The particles are spherical, highly crystalline and typically don't show any hard agglomerates due to Coulomb repulsion during particle formation.

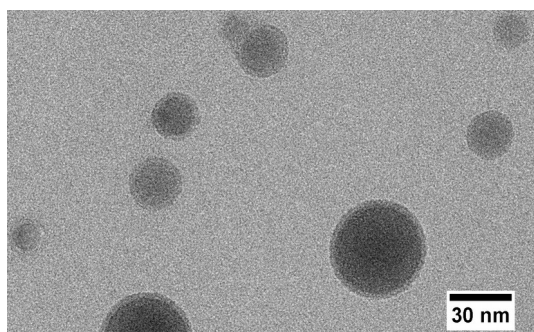


Figure 1. TEM image of synthesized silicon nanoparticles.

Furthermore, the nanoparticle size can be precisely adjusted within a certain limit ranging from a few up to about 100 nanometer in diameter. Figure 2 shows, that a higher outlet velocity of the nozzle feeding the silane results in a reduced residence time, thus leading to shorter growth time and smaller particles.

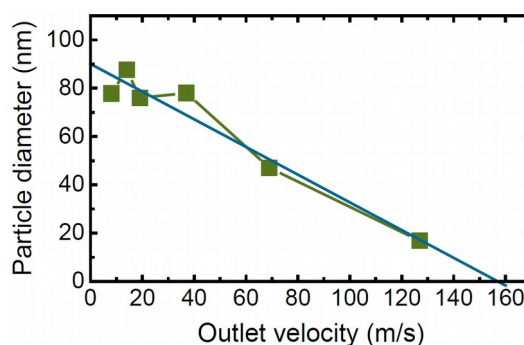


Figure 2. Particle diameter (calculated from BET measurements) depending on outlet velocity of the nozzle feeding silane into the reactor.

It will be shown that we are able to run a production process with consistently good quality of the silicon nanoparticles at high production rates of up to 200 g/h. Therefore, a full-day synthesis of silicon nanoparticles was performed. Nanoparticles were collected at fixed time intervals during the synthesis period and characterized via BET measurements and TEM images. This continuous sampling allows to detect unwanted changes of the particle properties during the synthesis and gives an indication of the long-term stability of the plasma process. The results indicate a stable process for many hours.

The authors gratefully acknowledge the support by the German research foundation (DFG) in scope of the research group 2284 "Model-based scalable gas-phase synthesis of complex nanoparticles".

## Gas-phase carbon nanostructures for energy storage device microfabrication via Supersonic Cluster Beam Deposition

L.G. Bettini<sup>1</sup>, P. Piseri<sup>1</sup> and P. Milani<sup>1</sup>

<sup>1</sup>CIMaNa and Physics Department, University of Milano, Milano, 20133, Italy

Keywords: carbon, nanoparticles, gas phase, supercapacitors, supersonic cluster beam deposition.

Presenting author email: lucagiacomo.bettini@unimi.it

Supercapacitors are energy storage devices that store energy in the electric double layer formed at the interface between a polarizable nanostructured electrode and an electrolyte. Supercapacitors are currently used in a variety of applications, such as electric vehicles and grid storage, and hold great potential in complementing energy harvesters for self-sustaining autonomous microelectronic devices. The fabrication of microsupercapacitors is challenging and requires the development of techniques enabling the synthesis and deposition of nanostructured electrodes with controlled morphological and structural properties. The compatibility of these techniques with standard microelectronic fabrication approaches is another issue to be addressed to integrate microsupercapacitors into more complex platforms.

Gas-phase routes for the production of nanoparticles are promising technologies for the integration of nanomaterials with controlled physico-chemical properties into functional devices. Supersonic Cluster Beam Deposition (SCBD) is a gas-phase technology based on the production of intense and highly collimated nanoparticle beams that enables the high throughput deposition, in clean high vacuum conditions, of nanostructured materials on a wide variety of substrates, including microfabricated platforms, smart nanocomposites and fragile materials. The manipulation of neutral nanoparticles through supersonic expansions and aerodynamic focusing offers the capability to deposit thin films with controlled nanostructure (Wegner 2006).

The assembling of gas-phase carbon nanoparticles produced in a Pulsed Microplasma Cluster Source (PMCS) and deposited by SCBD is an effective approach for the growth of nanostructured carbon (nsC) thin films (Figure 1a). nsC produced by SCBD typically exhibits a high surface roughness and a large porosity that have been demonstrated to be beneficial for electrochemical applications (Figure 1b).

Here we present the integration, via SCBD, of nsC-based electrodes into planar and flexible microsupercapacitors. Microsupercapacitors fabricated by SCBD consist of two coplanar nsC electrodes deposited by the use of stencil masks and soaked in an ionic liquid serving as electrolyte (Figure 1c). So prepared devices exhibit a specific capacitance of about 10 F cm<sup>-3</sup> and were demonstrated to operate, in a flat and bent configuration, at 3 V with long cycling stability over more than 10<sup>4</sup> cycles even at temperatures up to 80°C. The measured volumetric specific power

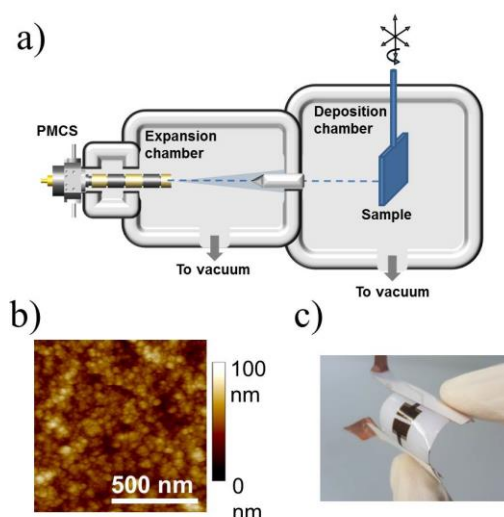


Figure 1. (a) Schematic representation of a PMCS/SCBD apparatus, (b) typical surface morphology of a nsC thin film and (c) picture of a nsC-based microsupercapacitor fabricated by SCBD.

and energy are of 10÷14 W cm<sup>-3</sup> and 2.5÷10 mWh cm<sup>-3</sup>, respectively (Bettini 2015, Soavi 2016). Although being non optimized prototypes, the energy storage performances of these microsupercapacitors are of interest for different devices, that, if properly designed and connected, could bring about miniaturized autonomous systems (Soavi 2016). To this end, we also present the use of SCBD to integrate nsC thin films, serving as gate electrodes, into PEDOT:PSS-based organic electrochemical transistors, enabling the use of the charge storage properties of the nsC to operate the transistors without power supply (Yi 2017).

- Wegner, K., Piseri, P., Vahedi Tafreshi, H. and Milani, P. (2006) *J. Phys. D: Appl. Phys.* **39**, R439
- Bettini, L.G., Piseri, P., De Giorgio, F., Arbizzani, C., Milani, P. and Soavi, F. (2015) *Electrochim. Acta* **170**, 57-62
- Soavi, F., Bettini, L.G., Piseri, P., Milani, P., Santoro, C., Atanassov, P. and Arbizzani, C. (2016) *J. Power Sources* **326**, 717-725.
- Yi, Z., Bettini, L.G., Tomasello, G., Kumar, P., Piseri, P., Valitova, I., Milani, P., Soavi, F. and Cicoira, F. (2017) *J. Poly. Sci. Pol. Phys.* **55**, 96-103.

## Gas-phase synthesis of inline coated silicon nanoparticles in a microwave plasma reactor

Adrian Münzer<sup>1</sup>, Johannes Sellmann<sup>2</sup>, Andreas Kempf<sup>2,3</sup>, Christof Schulz<sup>1,3</sup>, Hartmut Wiggers<sup>1,3</sup>

<sup>1</sup>IVG, Institute for Combustion and Gas Dynamics – Reactive Fluids

<sup>2</sup>IVG, Institute for Combustion and Gas Dynamics – Fluid Dynamics

<sup>3</sup>Center for Nanointegration Duisburg-Essen (CENIDE), University of Duisburg-Essen, Duisburg, Germany

Keywords: Gas-phase synthesis, silicon nanoparticles, inline coating, microwave plasma

Presenting author email: adrian.muenzer@uni-due.de

Gas phase synthesis of nanoparticles (NPs) in plasma reactors is an established approach to produce pure, highly specific and complex nanomaterials in large quantities. As particle surface properties are strongly related to their further processing and application, post-processing by particle coating, embedding, or surface functionalization is often required to adjust the materials' properties with respect to their further utilization. In this regard, single-step processes for direct surface treatment of as-synthesized nanoparticles are highly attractive, especially for industrial production.

We report on a scalable and continuous gas-phase synthesis with subsequent inline coating of silicon nanoparticles by a single-step microwave plasma process. It is based on a two-stage supply of particle precursor ( $\text{SiH}_4$ ) and coating precursor, respectively (see Figure 1).

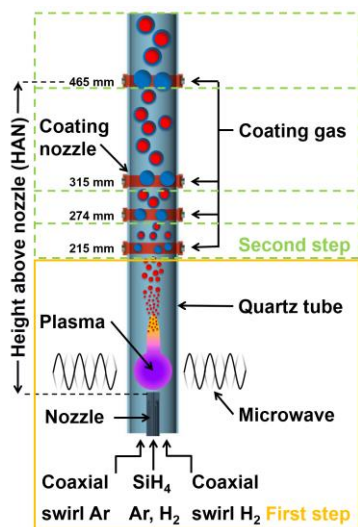


Figure 1: Experimental setup indicating the quartz tube, the plasma zone, and the nozzles to inject plasma and coating gas

We are using hydrocarbons (e.g. ethylene) and silica precursors (e.g. HMDSO ( $((\text{CH}_3)_3\text{Si})_2\text{O}$ ), TMOS ( $\text{Si}(\text{OCH}_3)_4$ ) or TMSO ( $((\text{CH}_3)_2\text{HSi})_2\text{O}$ )) to form either a carbonaceous or a silica shell directly after particle formation. The modular experimental setup enables to investigate multiple process conditions and different distances between plasma zone and coating nozzle to investigate the influence of reactor geometry and residence time on particle size, morphology and core/shell structure. To facilitate a fast and homogeneous intermixing of the coating gas and the hot, nanoparticle-

laden exhaust gas downstream the plasma zone, laminar flow simulations were performed to design and optimize the coating nozzle mass flow and geometry (number, direction, angle, and diameter of the bores).

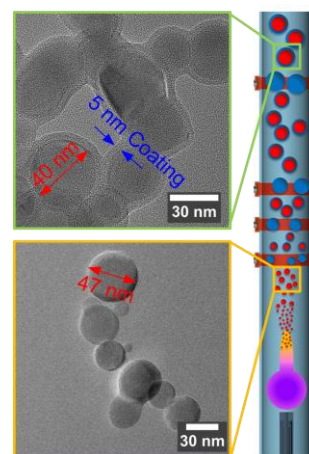


Figure 2: TEM images of silicon nanoparticles with coating or without coating

Using ethylene as a coating gas we observed the formation of a silicon carbide shell in case of close distances between plasma zone and coating nozzle while a polyethylene shell is formed (see Figure 2) in case of large distances as revealed by Raman, FTIR and XPS measurements. We attribute the formation of silicon carbide close to the plasma zone to the presence of free radicals, ions and electrons thus resulting in high reactivity at the pristine nanoparticles' surface while the formation of polyethylene is most probably driven by thermal polymerization of ethylene. As an outlook, the paper will also present the characterization results of the silica coating using the named precursors.

This work was supported by the German research foundation (DFG) in scope of the research unit 2284 "Model-based scalable gas-phase synthesis of complex nanoparticles".

## Study on Removal of Bacteria and particles by Nylon 6 Nanofibers with Electrospinning Different Salts Components

Ming-Han Lin<sup>1</sup> and Chang-Tang Chang<sup>1,\*</sup>

<sup>1</sup> Department of Environmental Engineering, National I-Lan University, I-Lan, 26047, Taiwan

Keywords: Electrospinning, Nylon 6, Bacteria, Particles

Presenting author email: a0987289073@gmail.com

Particles and bacterial are formed closely related to human activities. Particles are generated by combustion processes or vehicle emissions. In addition, human activities will produce a large number of bacteria. It is important to remove bacteria and particles to keep human safe. Fine particles, as one of the most serious sources of air pollution, have been shown to be a major cause of adverse health effects from human respiratory tract to extra pulmonary organs. These free radicals undergo a series of reactions with contaminants which can be suppressed and eliminated. Presently, conventional fiber-based nonwoven filtration media often have a number of performance disadvantages, such as relatively low filtration efficiency and high energy consumption, and are not suitable for capturing fine particles due to micron-sized fiber diameters. Cho et al. (2013) reported that excellent air filtration efficiency and low pressure drop are achieved by covering the substrate with polymer nanofibers containing metal oxide nanoparticles. It can strongly affect the electrostatic interaction between the dust particles and the nanofibers.

In this study, titanium dioxide and triangular nano-silver, photosensitive semiconductor, can absorb ultraviolet light to form reactive free radicals for promoting bacterial inhibition. In addition, nylon 6 fibers (T-Ag/TiO<sub>2</sub>-N6) containing different salts were prepared. The physical and chemical properties of the photocatalyst were determined by a spectrophotometer (UV-vis), X-ray diffraction (XRD), Fourier transform infrared spectroscopy (FTIR) and scanning electron microscopy (SEM) were used.

The results show that the photocatalytic activity with T-Ag/TiO<sub>2</sub>-N6 is better than that with electrospun N6. The effects of operation condition on particle and

bacteria removal performance with adding different salts (NaCl, KCl, KBr) into nanofibers were investigated using single factor experiments. The particle removal efficiency of N6 nanofibers is about 95%. Furthermore, the maximum particle removal efficiency of Nylon 6 nanofibers containing 10%NaCl, 15%KCl and 15%KBr is 98.5%, 96.9% and 96.5%, respectively, as shown in Figure 1.

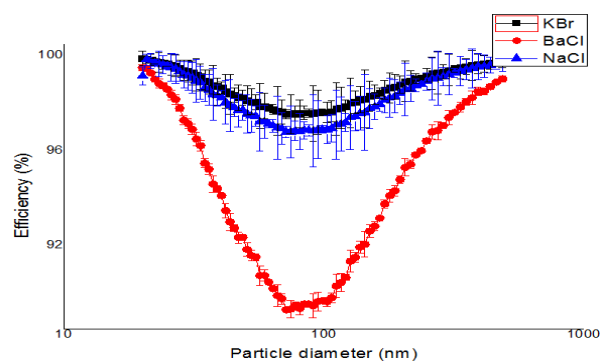


Figure 1. Removal efficiency with different additives.

The bacteria removal performance of nano-silver Nylon 6 nanofibers is also better than that of pure Nylon 6 nanofibers.

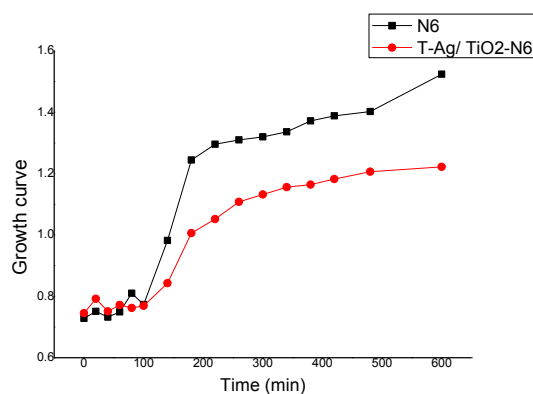


Figure 2. The Nylon 6 and T-Ag / TiO<sub>2</sub>-N6 Bacteria growth curve.

Cho, D., Naydich, A., Frey, M. W., and Joo, Y. L. (2013), *Polymer*, 54(9), 2364-2372.

## Applying spark mixing to produce Au-Pd alloy nanoparticle catalysts for CO<sub>2</sub> electro-reduction

M. Valenti, W. A. Smith, A. Schmidt-Ott

Faculty of Applied Sciences, Delft University of Technology, NL-2600GA Delft, Netherlands

Keywords: alloy nanoparticles, CO<sub>2</sub> electro-reduction, solar fuels

m.valenti@tudelft.nl

CO<sub>2</sub> electro-reduction coupled with renewable electricity sources (e.g., solar cells), is a promising technology for the production of sustainable fuels. However, new catalysts need to be developed in order to achieve higher reaction selectivities towards desirable products (e.g., CO and Methane). In transition metals the binding energy to the CO<sub>2</sub> reduction intermediates (e.g., COOH and CO) significantly affects the CO<sub>2</sub> reduction products and selectivities. By alloying transition metals, the binding energy of the CO<sub>2</sub>-reduction adsorbate intermediates can be tuned, which allows to systematically understand the relationship between the binding energy of intermediates and the synthesis of desired products. A significant challenge to undertake this study is the synthesis of pure transition metal alloy nanoparticles with predefined compositions.

In transition metals, the way the d-band interacts with the adsorbates determines the intermediate binding energy. The lower the energy of the d-band relatively to the metal Fermi level, the weaker the binding energy to the adsorbate intermediates. Au has an ideal binding energy to COOH and CO intermediates for the production of CO among the transition metals. Alloying Au with Pd can bring the d-band of Au closer to its Fermi level, which will increase the interaction with both intermediates COOH and CO. Alloying Au with transition metals that bind the intermediate strongly (e.g., Pd) facilitates the protonation of the intermediate CO to HCO or COH before it desorbs (Kortlever et al., 2016), which promotes the production of Methane. The objective of this work is to systematically study the CO<sub>2</sub> electro-reduction on Au, Pd and Au/Pd alloy nanoparticles.

Aerosol spark mixing (Tabrizi et al. 2010) is, from its principle, an extremely versatile method. In the present study we demonstrate its practical usefulness, namely to produce alloyed nanoparticulate electrodes and show that it is very suitable for tuning the band structure of catalysts for CO<sub>2</sub> electro-reduction to optimize their performance.

**Methodology:** Pd/Au alloy electrodes were used as feedstock in the spark-discharge particle generator (SDG) (Schwyn et al., 1988) to produce alloyed nanoparticles with the same composition. An electrostatic precipitator is used to deposit the particles on glassy carbon substrates.

**Results:** The valence band X-ray photoelectron spectroscopy (XPS) spectra of the Au, Pd and alloy nanoparticles are shown in Figure 1. The steep increase in the density of states revealed by XPS corresponds to the d-band energies of the transition metals. As expected, the d-band of Pd is close to the Fermi energy of the metal (0

eV), while the d-band of Au lies ~ 2.3 eV away from the Fermi level. Since XPS probes the surface of the metal, the measured d-band energies with respect to the Fermi level give a direct indication of how strongly the nanoparticle-based electrode will bind with the intermediates. A clear shift in the d-band is obtained with the alloy nanoparticles. Such a shift indicates an increase in the binding energy when compared to Au and a decrease when compared to Pd. Accordingly, preliminary gas chromatography (GC) measurements show that the faradaic efficiency for the production of CO decreases with increasing composition of Pd.

**Conclusions and outlook:** Spark mixing synthesizes arbitrarily composed nanoparticulate electrodes, allowing to tune the binding energy for the CO<sub>2</sub> reduction intermediates. Our preliminary studies indicate a direct effect on the CO<sub>2</sub> reduction selectivity due to alloying. Within this work we will test five different Au/Pd compositions and will analyse the gas and liquid products in order to shed light on the mechanism pathways for the production of CO.

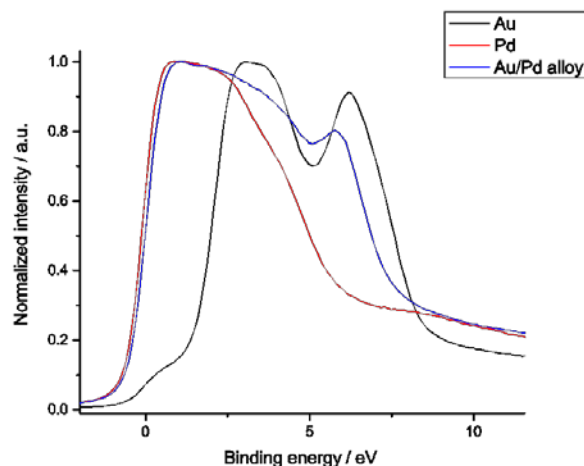


Figure 1 XPS valence band spectra of the synthesized nanoparticles.

Kortlever, R.; Peters, I.; Balemans, C.; Kas, R.; Kwon, Y.; Mul, G.; Koper, M. T. M., *Chemical Communications.*, 52, 10229-10232 (2016).

Schwyn, S., Garwin, E. & Schmidt-Ott, A., *J. AerosolSci.*, 19(5), 639-642 (1998).

Tabrizi, N. S., Xu, Q., Pers, N. M. & Schmidt-Ott, A. Generation of mixed metallic nanoparticles from immiscible metals by spark discharge. *J. Nanoparticle Res.* 12, 247–259 (2010).

## Effect of flow configuration on size distributions in a VSP-G1 spark generator

J. Breeman<sup>1</sup>, T.V. Pfeiffer<sup>2</sup> and A. Schmidt-Ott<sup>1,2</sup>

<sup>1</sup>Faculty of Applied Sciences, Delft University of Technology, Delft, 2629 HZ, the Netherlands

<sup>2</sup>VSParticle B.V., Delft, 2629 JD, the Netherlands

Keywords: spark ablation, nanoparticle source, coagulation, flow configuration.

Presenting author email: t.pfeiffer@vsparticle.com

Spark generators are used to produce aerosols of small nanoparticles (Meuller *et al.*, 2012). Their main advantage is flexibility in terms of composition and dynamic size range. Particles have the same composition as the ablated electrodes, e.g. two metal rods, which are easily replaced by another conductive material. Particle size and concentration are controlled by electrical input power  $P$  and the gas flow rate  $Q$ , with almost immediate response.

Because ablated mass  $\dot{m}$  increases proportionally with spark power, basic Smoluchowski coagulation theory, using  $P/Q$  for the number concentration  $N$  and the residence time  $\tau$  (system volume  $V$  divided by  $Q$ ), allows quick and remarkably accurate approximation as long as coalescence occurs, i.e. for mean (singlet) particle diameter up to about 5 nm (Feng 2016). At larger sizes the approximation represents agglomerate mass, which can be converted to diameter when the fractal dimension is known. To obtain meaningful estimates for size distribution, mixing effects such as dilution and distributions in residence time need to be considered. In practice, one either assumes self-preservation ( $\sigma_g \sim 1.3$ – $1.4$ ), or ends up ‘calibrating’ their spark generator.

Various flow configurations have been reported on in literature: radial, axial (Meuller, 2012), wire-to-hole, pin-to plate (Chae *et al.*, 2015), hollow electrodes, and several more. While various benefits are claimed for each configuration, it can be difficult to distinguish whether the results are caused by e.g. the different electrode shapes, electrode size, reactor housing geometry or the spark generating circuit itself. This information gap on the impact of flow in/around the spark gap particularly presents challenges when scaling up production.

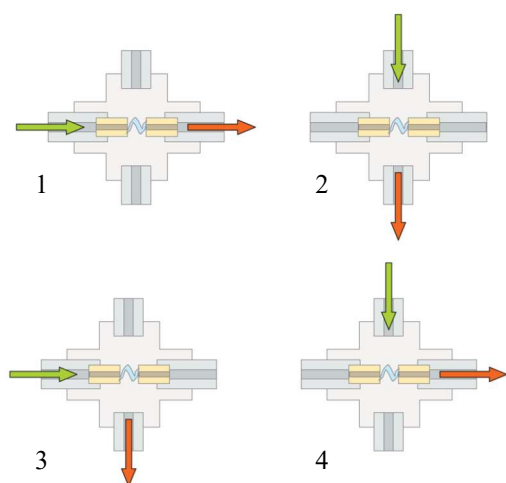


Figure 1. Flow configurations: (1) hollow in- and outlet, (2) cross-flow, (3) hollow inlet, and (4) hollow outlet.

Here, we look at dilution and residence time using a VSP-G1 spark generator fitted with a standard DN40KF cross and 8 mm O.D./3mm I.D. tubular electrodes. We varied flow configurations in the reactor without changing the reactor geometry. Flow was controlled via mass flow controller to achieve the four basic flow configurations shown in figure 1. They are characterized by residence volume ( $\tau_1 = \tau_4 \ll \tau_2 \sim \tau_3$ ), and the presence (config. 3, 4) or absence (config. 1, 2) of forced flow through the gap.

Figure 2 shows typical size distributions, obtained by DMA+AEM without neutralizer. As residence time decreases, particle size shrinks as expected. The total concentration of negatively charged particles at the AEM drops from  $4 \times 10^7 \text{ cm}^{-3}$  to  $1 \times 10^7 \text{ cm}^{-3}$ . Forced flow through the gap increases yield for a hollow outlet, but lowers yield and size for an ‘open’ outlet.

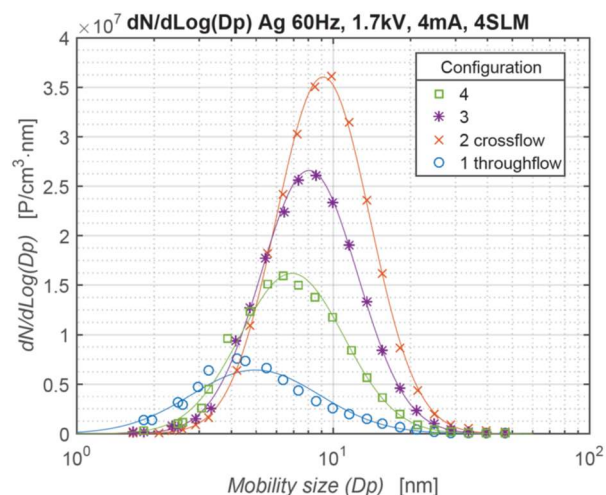


Figure 2. Size distributions for Ag at 6.8W, 4 SLM. Small to large: (1) throughflow, (4) hollow outlet, (3) hollow inlet, (2) cross-flow.

We compare these and similar experiments with coagulation theory, and discuss how and to what extent flow configuration experiments help us understand early particle formation stages in spark generators, with the aim of getting closer to a generalizable spark generator model.

Chae, S., Lee, D., Kim, M.-C., Kim, D.S., and Choi, M. (2015) *Aerosol Sci. Technol.* **49**, 463–471.

Feng, J., Huang, L., Ludvigsson, L., Messing, M.E., Maisser, A., Biskos, G. and Schmidt-Ott, A. (2016) *J. Phys. Chem. C* **120**, 621–630.

Meuller, B.O., Messing, M.E., Engberg, D.L.J., Jansson, A.M., Johansson, L.I.M., Norlén, S.M., Tureson, N., and Deppert, K. (2012) *Aerosol Sci. Technol.* **46**, 1256–1270.

## Synthesis of GaAs quantum dots via hydrogen-assisted spark discharge

K. Lee<sup>1†</sup>, D. Lee<sup>2†</sup> and M. Choi<sup>1,2</sup>

<sup>1</sup>A Global Frontier Center for Multiscale Energy Systems, Seoul National University, Seoul, 08826, Republic of Korea

<sup>2</sup>Department of Mechanical & Aerospace Engineering, Seoul National University, Seoul, 08826, Republic of Korea

Keywords: Spark discharge, Gallium Arsenide, Quantum dots.

Presenting author email: bluewings96@snu.ac.kr

<sup>†</sup>These authors contributed equally on this work

GaAs has been considered as one of the most prominent III-V semiconductors because of its excellent electronic and photonic properties, such as high electron mobility and direct band gap. Also, due to its large Bohr radius and strong quantum confinement effect, there have been intense effort to synthesize GaAs nanocrystals (NCs) with radius of under 10 nm. However, despite these advantages of GaAs NCs, there has been inherent difficulties of synthesizing GaAs NCs restricting its overall explorations and applications.

Recently, our group demonstrated that silicon nanocrystals with high purity and crystallinity can be generated through hydrogen assisted spark discharge. (D. Lee et al, 2016) This work was based on the thought that Si nanoparticles become highly crystalline by hydrogen atom's insertion into and desorption from Si bonds. (S. Sriraman, 2002) However, GaAs NCs are hardly obtained by hydrogen introduced spark discharge since unlike Si NCs, in the case of GaAs, spark discharge energy is not sufficient for the desorption of hydrogen gas from GaAs matrix. This amorphousness and embedded hydrogen atoms in GaAs matrix can be identified by transmission electron microscopy (TEM) and Fourier transform infrared spectroscopy (FTIR). In order to extract these embedded hydrogen and obtain crystalline GaAs nanoparticles, we add heating procedure. After generation of hydrogen-inserted GaAs nanoparticles via hydrogen-assisted spark discharge, these GaAs aerosols pass through tube furnace with temperature of 950°C for the desorption of inserted hydrogen atoms and crystallization of GaAs nanoparticles. As represented in Figure 1, we confirm that fabricated GaAs NCs exhibit high crystallinity from TEM and X-ray diffraction (XRD).

Additionally, we demonstrate that these GaAs NCs exhibit quantum confinement effects from photoluminescence measurement. We generate GaAs NCs with various size by varying the capacitance of spark discharge circuit from 0.5nF to 6nF, and observe that these GaAs NCs exhibit different photoluminescence peaks according to its size.

Even though there are several other methods for fabricating GaAs quantum dots such as chemical synthesis, chemical vapour deposition (CVD), and molecular beam epitaxy (MBE), these methods inherently possess drawbacks, such as undesirable by-products, toxic materials and bad controllability. Since our aerosol-based technique is free from these obstacles, our GaAs quantum dots (QDs) are considered to be utilized in various

applications, such as solar cell, LED, and transistor. In addition, our fabricating GaAs QDs technique is expected to provide an additional degree of freedom in synthesizing various semiconductor quantum dots with high crystallinity.

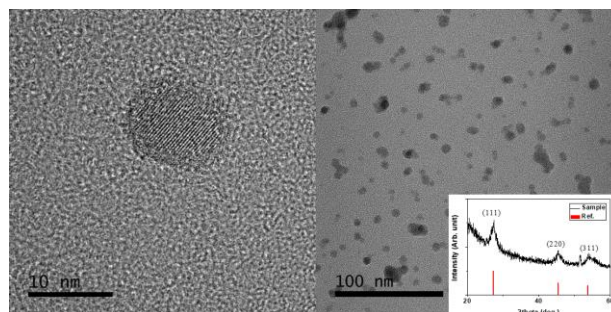


Figure 1. Transmission electron microscopy (TEM) images of GaAs NCs. The inset image represents X-ray diffraction (XRD) spectrum of GaAs NCs.

This work was supported by Global Frontier R&D Program on Center for Multiscale Energy System by National Research Foundation (NRF) under the Ministry of Science, ICT and Future Planning, Korea (Grant no.2012M3A6A7054855).

Lee, D., Lee, K., Kim, D.S., Lee, J.-K., Park, S.J., and Choi, M. (2016) *American Association for Aerosol Research* 2016.

Sriraman, S., Agarwal, S., Aydil, E.S., and Maroudas, M. (2002) *Nature* **418**, 62-65.

## **Abstratcs T103**

## Diethylenetriamine modified magnetic biochar on removal of Cr (VI) from aqueous solution

F. Wang<sup>1</sup>, T. Ouyang<sup>1</sup> and C.T. Chang<sup>2</sup>

<sup>1</sup>Department of Environmental Science and Technology, Xiamen University, Xiamen 361102, China

<sup>2</sup>Department of Environmental Engineering, National IAN University, I-Lan 26047, Taiwan

Keywords: biochar, modification, chromium.

Presenting author email: wangfei@stu.xmu.edu.cn

### Abstract

In recent years, mining, smelting, processing and commercial manufacturing activities of heavy metal increased to result in lots of heavy metals (such as arsenic, copper, chromium) emitted into atmosphere, water and soil, which caused serious environmental pollution (Lin, 2017). With heavy metal ions enriched in organisms through food chain, unrepairable harm will be caused to human health and ecological environment eventually. Therefore, the effective treatment technology of heavy metals has attracted the attention of the whole society.

In that case, adsorption was used to treat heavy metals of wastewater for heavy metals and adsorbents recycling. Magnetic biochar, easy to be separated from solution, was modified to improve adsorption and recycling capacity for heavy metals removal. The biochar characterization was analysed with XRD, SEM and BET. In addition, the best conditions for removing heavy metals among different concentration, temperature, pH and dosage were also studied. In order to establish bonding mechanism of heavy metals from internal or external materials, various valances of heavy metals and the distribution states inside or outside materials were analysed.

Biochar, prepared from biomass waste, can not only solve the problem of environmental protection, high efficiency and sustainable development about waste reused, but also be benefit to improve water quality of polluted water. Then, the dual proposes of saving the cost and maintaining ecological safety would be achieved.

### Methods

The magnetic biochar was prepared with waste bamboo as the raw biomass material and pyrolysis method referring to Yang et al (2016). Before pyrolysis, the waste bamboo was dried, crushed, washed and sieved to 200 mesh. 5 g bamboo was then soaked in FeCl<sub>3</sub> aqueous solution for 1.5 h under magnetic stirring, with the mass ratio between FeCl<sub>3</sub> and bamboo is 1.5:1.0. After that, different amount of diethylenetriamine (1.25 - 10 μmol) was added into the combined solution. Thirty minutes later, the samples were filtered and pyrolyzed at 600 °C for 1 h under N<sub>2</sub> flow. After cooling to room temperature, the materials were washed to pH = 7 ± 0.1 and named as xNMBC, where x represents the amount of diethylenetriamine (DETA). For comparison, magnetic biochar was pyrolyzed without DETA, which was named as MBC.

### Results

More DETA modified MBC was considered that there would be more adsorption sites existing in the surface of the materials. Fig. 1 shows different amount DETA modified MBC. As DETA increased, 5NMBC has harsher surface than 1.25NMBC and 2.5NMBC. But 10NMBC has a relatively smooth surface. In addition, Fig. 2 provides that 5NMBC has the best adsorption capacity compared with other materials.

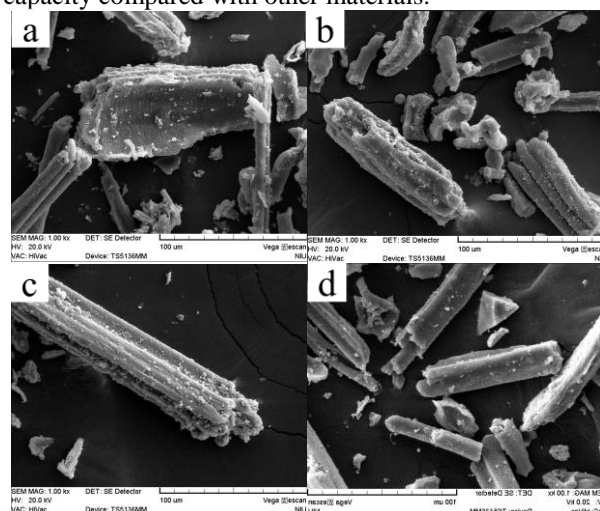


Fig. 1 SEM images of 1.25NMBC (a), 2.5NMBC (b), 5NMBC (c) and 10NMBC (d).

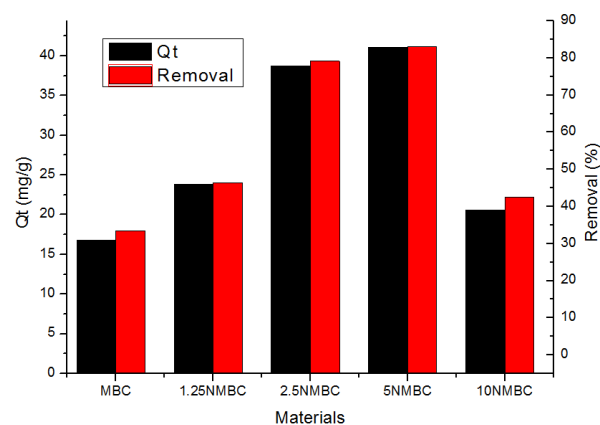


Fig. 2 Adsorption capacity and removal efficiency of Cr(VI) on materials (dosage = 1 g/L, C<sub>0</sub> = 50 ppm, initial pH = 5.00 ± 0.01, t = 36 h and temperature = 25 ± 1 °C).

Lin, Y., Cao, W. and Ouyang T. et al (2017). J. Taiwan. Inst. Cheme. 70, 311-318.

Yang, J., Zhao, Y. and Ma S. et al (2016). Environ. Sci. Technol. 50, 12040-12047.

## Chromium adsorption from wastewater by modifying carbon material

Sung-Ying Lee<sup>1\*</sup>, Chang-Tang Chang<sup>1</sup>

<sup>1\*</sup>Department of Environmental Engineering, National I-Lan University, Taiwan, [presenting author](#),

Keywords: biochar, chemical activation, chromium.

Presenting author email: nps80001@gmail.com

### INTRODUCTION

The recent years, environmental protection consciousness have been noted gradually. The people also pay more attention to the quality of tap water, particularly the content of heavy metals in water. If there is no appropriate processing method for heavy metals in water, it will destroy the whole eco-system. The chromium in water mostly comes from the industrial waste water. In addition, the hexavalent chromium has stronger toxicities Budinova *et al* (2006). If the concentration of hexavalent chromes in water is higher than 0.1 mg L<sup>-1</sup>, it will be harmful to human body. Therefore, it must reduce the concentration of hexavalent chromium to less than 0.1 mg L<sup>-1</sup> to avoid causing the pollution of the environment.

At present, most people use the adsorbing method to remove the heavy metals in water. But this technique often needs to change adsorbent and the follow-up processes are complicated, therefore the cost have been increased. To reduce the cost effectively, this research makes use of the combustion products of the rice hull ash as a carbon material source, and changes it to new and composite material with holes and cavities to catch the chromium ion in the waste water effectively Zhou *et al* (2016).

### EXPERIMENTAL/THEORETICAL STUDY

The activated carbon was prepared according to the following procedure. The carbonization includes the hot processes under the appropriate temperature. The stable environment temperature are between 700-750 °C. The forerunner material have been changed to the carbon with low surface with pyrolysis method. The purpose of the activation phase is to produce porous carbon structure with more holes. This phase need oxidant to resolve oxide which blocking the pores. The activation of the product with higher hole physical volume and surface at this stage, can improve the pollutant removal capacity.

In this study, activate carbon (Activated carbon) and carbonization rice hull (Rice husk) without modification, activate carbons (Activated carbon EDTA) and carbonization rice hull (Rice husk EDTA) after modification were used to adsorb the chromium ion in water. Nitrogen spirit/take off and attach the instrument (N<sub>2</sub> adsorptions/desorptions system, BET) and other instruments ware used to analyze the characteristic of materials to identification of material physical and chemical properties.

### RESULTS AND DISCUSSION

In this study, 0.2 g/L activated carbon and carbonization rice the hull were used to resolve 4 kinds of different concentration hexavalent chromium in water. By comparing the adsorption efficiency (figure 1a and b), it can be seen that the activated carbon is obviously better. Although there is no obvious effect in the 120 ppm, activated carbon is better in the 15 ppm, 30 ppm and 60 ppm. This is because the adsorbing activating area of the materials are limited, so hexavalent chromium need to compete to rob the activating area when its concentration is higher. Therefore, the concentration is higher, the efficiency is lower.

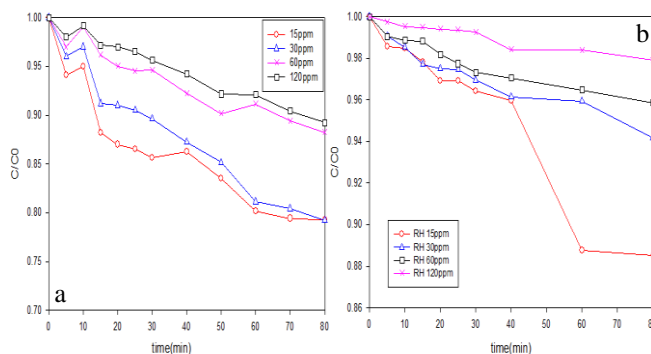


Fig. 1 Variety of concentrations uses 0.2 g/L and adsorbs the material, it adsorbs the effect (a) activate carbon (b) carbonization rice hull.

### CONCLUSION

By the results of preliminary study, with the increase of the chromium concentration in the waste water, the ability of adsorbent increased. When the concentrations of chromium are 15, 30, 60 and 120 ppm, the adsorb ability of the activate carbon material are 1.67, 8.93, 9.01 and 11.19 mg/g. The adsorption capacities of activated carbon adsorbent with (contain the an radicle's percentage as 30%) or without are 0.05 and 1.67 mg g<sup>-1</sup>. So the adsorption capacity of activated carbon adsorbent with amino is better.

### REFERENCES

1. T. Budinova et. al. (2006) *Fuel Process. Technol.* **87**, 899-905.
2. J. Zhou et. Al. J. (2016) *Colloid Interface Sci.* **462**, 200-207.

## PECVD process for the continuous coating of aerosol nanoparticles with silica at ambient temperature

Patrick Post<sup>1</sup>, Jean-Pascal Borra<sup>2</sup> and Alfred P. Weber<sup>1</sup>

<sup>1</sup>Institute of Particle Technology, Clausthal University of Technology, Leibnizstrasse 19, 38678 Clausthal-Zellerfeld, Germany

<sup>2</sup>Laboratoire de Physique des Gaz et des Plasmas, CNRS, Univ. Paris Sud F-91405, CentraleSupélec, Université Paris-Saclay, 3 Rue Joliot Curie, 91192 Gif-sur-Yvette, France

Keywords: aerosol coating, silica, TEOS, PECVD

Presenting author email: patrick.post@tu-clausthal.de

There are many applications where silica coatings of nanoparticles are desirable, but not many processes that allow the coating of an aerosol in a continuous way at ambient temperature. The presented method uses a Plasma Enhanced CVD process for this purpose. A non-thermal dielectric barrier discharge (DBD) plasma at atmospheric pressure is used for the production of active species, making the method flexible in its combination with other processing steps. The precursor is not in contact with the DBD plasma itself, which enables a more stable process without the risk of changing the discharge behaviour as a result of deposition of material in the discharge zone. Tetraethyl orthosilicate (TEOS) is used since it reacts more slowly compared to other common silica precursors, which facilitates the control of the process. Two variations of this process will be shown, one in which the reaction takes place at room temperature, and another where elevated temperatures are used.

In both cases active species are generated with a DBD discharge to facilitate the reaction. Since the mixing of the gas flowing through the discharge with the precursor and aerosol flows occurs a few seconds after the discharge, many reactive but short-living species from the discharge do not participate in the reactions. However, more stable species such as ozone and nitrogen oxides are present and play important roles. Even so the only differences in the setup between the two process variants are the temperature at which the reaction takes place and the residence time, different plasma species act as reaction partners. While at higher temperatures this seems to be the atomic oxygen produced from the thermal dissociation of ozone, ozone does not facilitate the reaction at room temperature and instead  $\text{HNO}_3$  seems to have a significant role.

In both process variants, but especially the one at room temperature, a liquid-like behaviour of the coatings can be observed on agglomerates where the coating is concentrated in the interparticle spaces between branches which suggests a liquid intermediate that condenses on the aerosol prior to the formation of the solid silica coatings. TEOS itself does not condense on the particles at these conditions. A residence time of at least a few minutes between mixing of the precursor with the plasma species and the sampling is required for the hardening of the shell at room temperature. The control of both the reaction time and precursor concentration allows a variation of the coating thickness on spherical

particles as well as on agglomerates. Since the process is relatively slow it enables a good homogeneity (Fig. 1). In contrast, the process at elevated temperatures (up to  $300^\circ\text{C}$ ) is faster ( $< \text{min}$ ) but often results in less homogeneous coatings.

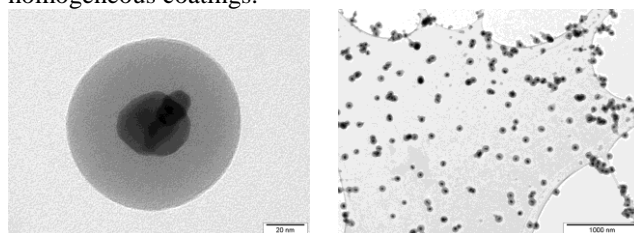


Figure 1. TEM micrographs of coated Pt particles showing the homogeneity of the coating in regard to individual particles (left) and over many particles at a lower magnification (right).

The coating process also allows the creation of different silica structures. Beside the complete coating of individual particles shown in Fig. 1, hollow “inflated bag” structures can be produced when a core material is removed after coating (Fig. 2 left) or silica in which the core particles are located with a certain distance to each other (Fig. 2 right). The process can be used for the thermal stabilization of agglomerates, where silica is applied in the interparticle spaces between branches and so impedes a restructuring as has been shown in our recent paper (Post et al., 2016).

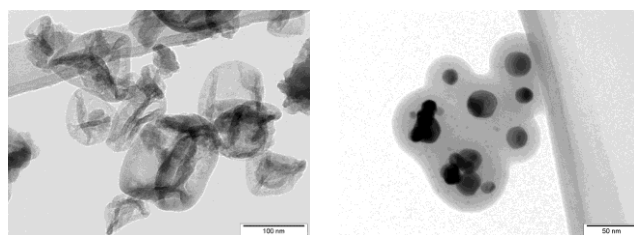


Figure 2. Examples of silica morphologies created with the process at room temperature. Left: Hollow “inflated bags” of silica, right: “matrix” of metal particles in silica.

This work was supported by the German Research Foundation under grant WE 2331/18-1.

Post, P., Jidenko, N., Weber, A. P. and Borra, J.-P. (2016) *Nanomaterials* 6(5), 91.

## Aerosol Based Fabrication of Polymer-Coated Semiconductors Nanoparticles

Masoom Shaban, Jalal Poostforooshan and Alfred P. Weber

Institute of Particle Technology, Technical University of Clausthal, Clausthal-Zellerfeld, Germany

Keywords: aerosol-photopolymerization, polymer-coated nanoparticles, semiconductor nanoparticles

Presenting author email: masoom.shaban@tu-clausthal.de

The study of core-shell nanoparticles, consisting of an inorganic semiconductor core and polymeric shell, has received much attention due to their promising applications (Wang *et al.*, 2015). These nanoparticles have the potential to combine different properties of the semiconductor nanoparticle (SNP) and polymer shell into a single particle. Generally, encapsulation of inorganic SNPs with a polymer shell may prevent particle-particle aggregation and offer excellent compatibility in a polymer matrix. Moreover, special shells such as conducting polymers donate the core nanoparticles with versatile properties.

The coating of polymer shell onto the inorganic SNP is normally done in the liquid phase via emulsion polymerization, where the use of surfactants and appropriate solvent is required and surface modification of inorganic nanoparticles is usually necessary before polymerization. To overcome the drawbacks of liquid process routes, processes based on aerosols have been investigated. In contrast to conventional wet methods, continuous aerosol-photopolymerization is simpler and requires fewer unit operations. It also allows for a direct collection of particles (Shaban *et al.*, 2016).

In this work, we report for the first time a general and facile approach to produce various inorganic semiconductor-polymer core-shell nanostructures in a continuous aerosol-photopolymerization. This technique is based on heterogeneous condensation of monomer vapor around the surface of gas-born inorganic SNPs, which is then polymerized under UV light irradiation, within the average aerosol residence time of 90 s in the flow-through photoreactor (Figure 1).

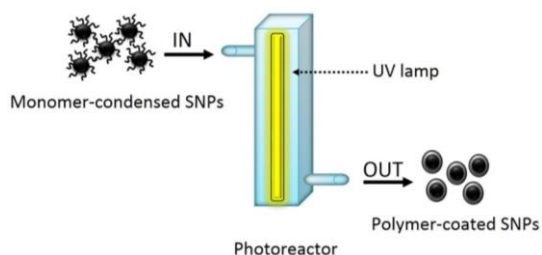


Figure 1. Schematic diagram of continuous experimental setup for aerosol based fabrication of core-shell materials.

As an example of inorganic SNPs, ZnO nanoparticles have been used in aerosol based fabrication of core-shell materials. As illustrated in Figure 2, our novel method shows excellent performance in the encapsulation of ZnO nanoparticles with polybutyl acrylate (PBUA) shell. In this method, isolated polymer particles were not observed in TEM investigations.

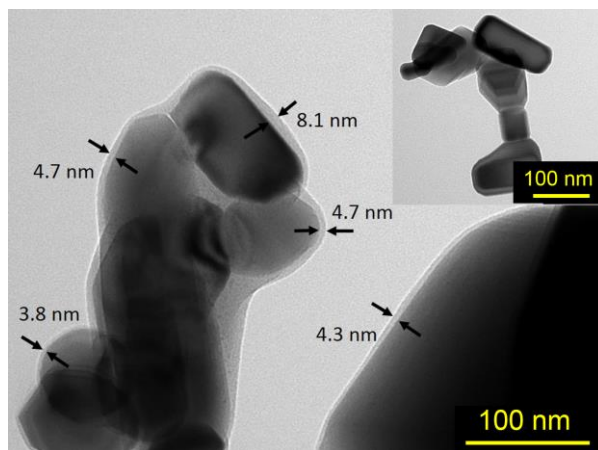


Figure 2. TEM images of ZnO-PBuA core-shell synthesized by aerosol-photopolymerization. The inset shows a TEM of the unmodified ZnO nanoparticles.

Evidence for the conversion of condensed BuA monomer into polybutylacrylate (PBUA) on the surface of ZnO nanoparticles is brought by FTIR spectroscopy (Figure 3). The strong band at  $1733\text{ cm}^{-1}$  arise from C=O vibrations in PBUA. Moreover, the C=C stretching band at  $1640\text{ cm}^{-1}$  from the BuA monomer disappeared after polymerization. These results indicated that the polymerization has successfully occurred and no unreacted BuA monomer residue remained after aerosol-photopolymerization.

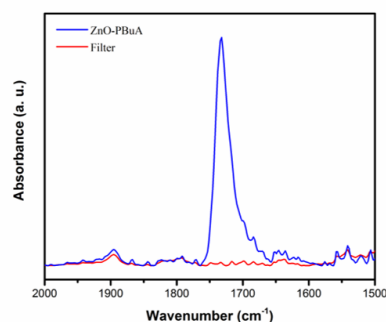


Figure 3. FTIR spectra of ZnO-PBuA core-shell nanoparticles synthesized by aerosol- photopolymerization.

This work was supported by German Science Foundation (DFG) under grant WE 2331/19-1.

Shaban, M., Ramazani, A., Ahadian, M. M., Tamsilian, Y., Weber, A. P., (2016) *Eur. Polym. J.*, **83**, 323-336.  
Wang, X., Lu, Q., Wang, X., Joo, J., Dahl, M., Liu, B., Gao, C., Yin, Y., (2015) *ACS Appl. Mater. Interfaces* **8**, 538-546.

## Synthesis and photoelectrochemical property of monodisperse hollow metal oxide microspheres

Haneol Lee<sup>1</sup>, Woo Jin Shin<sup>1</sup>, Youngku Sohn<sup>2</sup> and Weon Gyu Shin<sup>1</sup>

<sup>1</sup>Department of Mechanical Engineering, Chungnam National University, Daejeon, 34134, South Korea

<sup>2</sup>Department of Chemistry, Chungnam National University, Daejeon, 34134, South Korea

Keywords: hollow sphere, inkjet aerosol generator, metal oxide nanoparticle, photoelectrochemistry

Presenting author email: wgshin@cnu.ac.kr

Hollow micro/nano structures are of great interest in many current and emerging areas of technology. The large fraction of void space in hollow structures has been successfully used to encapsulate and control release of sensitive materials such as drugs (Zhu et al., 2010), and DNA (Zhu et al., 2009). Especially, hollow and porous TiO<sub>2</sub> particles are known to have good photovoltaic, and photocatalytic properties.

Synthetic strategies for hollow structure particles are broadly categorized into hard templating method (Zeng et al., 2010), soft templating method (Xu and Wang, 2007), sacrificial templating method (Zhang et al., 2010) and template free method (Li et al., 2007). However, using those methods may be time consuming to generate hollow particles. Therefore, there is a need for a new method that can produce hollow particle rapidly and simply.

In this study, we present a new method to generate hollow TiO<sub>2</sub>, SnO<sub>2</sub> and ZnO microspheres by using droplet generation system followed by a drying module (Shin et al. 2016). The droplet generation system can generate micron sized drops in a controlled manner. And the drying module helps to evaporate solvent and to form the agglomeration of template material quickly.

Water droplets generated from an inkjet nozzle containing clusters of polystyrene latex (PSL) particles covered with metal oxide nanoparticles and were continuously dried up forming PSL clusters decorated with metal oxide nanoparticles. By heating the clusters up to 400 °C, the PSL particles are evaporated forming hollow spheres. Monodisperse hollow TiO<sub>2</sub>, SnO<sub>2</sub> and ZnO spheres in the size range of 5.1–8.6 μm were consequently generated with a narrow particle size distribution. Fig. 1 shows the Scanning Electron Microscope (SEM) image of a hollow TiO<sub>2</sub> particle with the diameter of 5.1 μm.

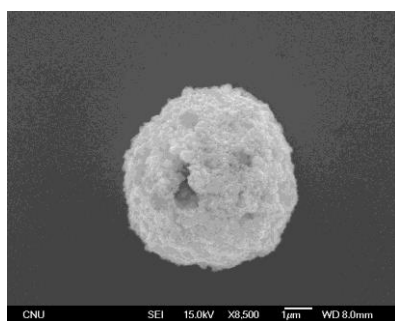


Figure 1. SEM image of hollow TiO<sub>2</sub> particle.

And the hollow TiO<sub>2</sub>, SnO<sub>2</sub> and ZnO spheres have 41.0, 30.0 and 85.3 nm sized pores, respectively. The size of hollow particles can be controlled by controlling the droplet size.

Also we demonstrate the potential applicability of the prepared samples to a photoelectrochemical cell. Hollow TiO<sub>2</sub> grown a Si substrate was selected to preliminarily examine the UV-light photoelectrochemical properties. The result of linear sweep voltammograms in the dark and under UV light irradiation from -0.5 to +1.0 V shows the photocurrent of TiO<sub>2</sub> was increased under UV-light condition. Also, the light ON-OFF photocurrent response was measured. Result shows photocurrents were generated by UV light absorption of TiO<sub>2</sub>.

In summary, a simple and easily scalable template approach using InkJet Aerosol Generator has been demonstrated for synthesizing size controllable hollow TiO<sub>2</sub>, SnO<sub>2</sub> and ZnO particles. Droplet size ejected from inkjet nozzle can be controlled by adjusting waveform parameters. Also, size of synthesized hollow/porous microsphere can be controlled adjusting droplet size. Hollow TiO<sub>2</sub> grown a Si substrate was demonstrated to be used as a photoelectrochemical catalyst. This method could be extended to prepare other hollow spheres with a variety of industrial applications.

This research was supported by the Basic Science Research Program through the National Research Foundation of Korea (NRF) funded by the Ministry of Science, ICT and Future Planning (2014-008356).

- L. Li, Y. Chu, Y. Liu, L. Dong (2007), *J. Phys. Chem.*, **111**, 2123-2127.  
W. J. Shin, H. Lee, Y. Sohn, W. G. Shin (2016) *Chem. Eng. J.* **292**, 139-146.  
H. Xu, W. Wang (2007), *Angewandte Chemie*, **46**, 1489-1492.  
Y. Zeng, X. Wang, H. Wang, Y. Dong, Y. Ma, J. Yao (2010), *Chem. Commun.*, **46**, 4312-4314.  
L. Zhang, G. Jia, H. You, K. Liu, M. Yang, Y. Song, Y. Zheng, Y. Huang, N. Guo, H. Zhang (2010), *Inorg. Chem.*, **49**, 3305-3309.  
Y. Zhu, T. Ikoma, N. Hanagata, S. Kaskel (2010), *Small*, **6**, 471-478.  
H. Zhu, J. Wang, G. Xu (2009), *Cryst. Growth Des.*, **9**, 633-638.

## Mesoporous carbon nitride as an efficient photocatalyst for aerosol-photopolymerization

J. Poostforooshan, M. Shaban and A.P. Weber

Institute of Particle Technology, Technical University of Clausthal, Clausthal-Zellerfeld, D-38678, Germany  
 Keywords: Aerosol-photopolymerization, Mesoporous carbon nitride, Spray drying, Nanoporous silica particles.  
 Corresponding and presenting author email: weber@mvt.tu-clausthal.de

A continuous aerosol-based process is employed to produce submicron spherical polymer particles using semiconductor mesoporous carbon nitride as photocatalyst and template. Initially, spherical silica particles were synthesized by spray drying of nanocolloidal SiO<sub>2</sub>, using polyvinylpyrrolidone (PVP) as pore template. After removal of the PVP by calcination, spherical mesoporous silica (SMS) particles were obtained. Then, mesoporous carbon nitride spheres (MCNSs) with relatively high surface area and pore volume have been successfully synthesized via a nanocasting approach by using SMS as a hard template through a simple polymerization reaction between ethylenediamine (EDA) and carbon tetrachloride (CCl<sub>4</sub>) as precursors (Poostforooshan *et al.* 2016). It was observed that the specific surface area (A<sub>BET</sub>), pore volume (V<sub>P</sub>) and pore diameter (D) of MCNS are significantly higher as compared to the SMS template (Table 1).

Table 1. Textural parameters of SMS and MCNS.

Sample	A <sub>BET</sub> (m <sup>2</sup> g <sup>-1</sup> )	V <sub>P</sub> (cm <sup>3</sup> g <sup>-1</sup> )	D (nm)
SMS	138	0.31	8
MCNS	718	1.22	23

Finally, by ultraviolet (UV) irradiation of the aerosol butyl acrylate monomer solution droplets contained MCNS as photocatalyst and template, produced with the help of an atomizer, polymerization is initiated “in flight” within the average aerosol residence time of 2 min in the photoreactor (Figure 1).

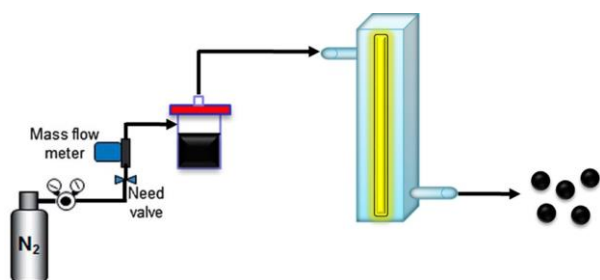


Figure 1. Scheme of the continuous aerosol-photopolymerization process of the butyl acrylate monomer contained MCNS.

Highlights of this aerosol-photopolymerization procedure are the continuous, simple and requires few unit operations, setup with a flow-through photoreactor operated at ambient temperature and without any solvent and surfactant required.

Figure 2 summarizes the complete synthesis details of submicron spherical polymer particles using mesoporous carbon nitride.

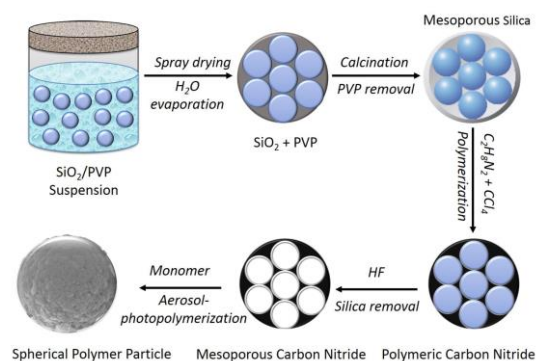


Figure 2. Synthesis procedure of polymer particle.

The resulting materials have been characterized by various techniques.

TEM and SEM images of the spherical mesoporous silica template and resulting mesoporous carbon nitride and poly(butyl acrylate) particles show that the spherical morphology is well replicated and the diameter of spheres is submicron in size (Figure 3).

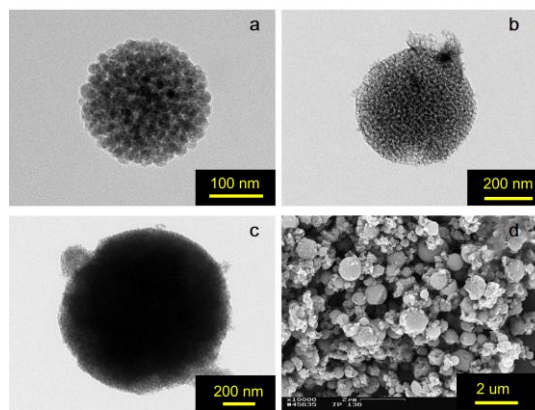


Figure 3. TEM images of (a) spherical mesoporous silica, (b) mesoporous carbon nitride, (c) poly(butyl acrylate) particle, and (d) SEM image of poly(butyl acrylate) particles produced by aerosol-photopolymerization.

This work was supported by German Science Foundation (DFG) under grant WE 2331/12-2.

Poostforooshan *et al.* (2016) *ACS Appl. Mater. Interfaces*. **8**, 21731–21741.

## A new furnace with molten polymer and a condenser for coating of magnetic moment markers

L. Boskovic<sup>1</sup> and I.E. Agranovski<sup>2</sup>

<sup>1,2</sup>School of Engineering, Griffith University, Brisbane, 4111, Australia

Keywords: nanoparticles, magnetic properties, gas-phase, coating.

Presenting author email: lucija.boskovic@griffithcollege.edu.au

A constant problem associated with magnetic nanoparticles is their intrinsic instability over longer period of time. The particles tend to form agglomerates, and are easily oxidized in air, resulting in loss of magnetism and dispersibility Lu et al (2007). For many applications including magnetic fluids, catalysis, biotechnology/biomedicine, magnetic resonance imaging, data storage, environmental remediation it is crucial to develop protection strategies to chemically stabilize the magnetic nanoparticles against degradation during or after the synthesis.

While most research has involved wet-chemistry synthesis, gas-phase nanoparticle production offers a distinct advantage over wet-chemistry synthesis techniques by allowing particle synthesis to occur in environments where the surrounding gas is either inert or non-reacting, allow greater purity and do not require management and disposal of environmentally hazardous solvents. They also have an advantage when multilayer composites are to be prepared (Gubin, 2009). The gas-phase methods are more compatible with systems in which the particles have been synthesised in the gas phase. They allow greater purity, can be run as continuous rather than batch processes, and do not require management and disposal of environmentally hazardous solvents.

Some of the gas-phase methods could not be used as they utilize high temperature processes capable of changing a desired structure of produced nanoparticles (for ex. flames and plasma based methods), and others produce a coating which is very thick and could not be suitable for the desired application. To help solving these problems a new furnace with molten polymer and a condenser for coating has been designed and tested. The size distribution and concentration of uncoated and coated nanoparticles was simultaneously monitored by two Diffusion Aerosol Spectrometers (DAS), Model 2702, AeroNanoTech, Moscow, Russia (Figure 1). A Scanning Electron Microscope (SEM) (JEOL, 1010) was used for microscopic study of the particle morphology and quality of coating. A glowing wire generator (GWG) Model 3709, AeroNanoTech, Moscow, Russia was used for production of Nickel (Ni) and chromium (Cr) nanoparticles by passing a current through the nichrome wire (length 5cm and diameter 0.75mm), suspended in flowing nitrogen gas at 2 lpm flow rate. It should be noted that instead of nichrome wire any other electrically conductive material that has a vapour pressure higher than  $5 \times 10^{-3}$  Pa at its melting point can be used to produce nanoparticles, Peineke et al (2006).

By mixing with the gas, the vapour was quenched, reaching supersaturation almost immediately upon

leaving the wire surface, and thus quickly nucleates homogeneously to form nanoparticles.

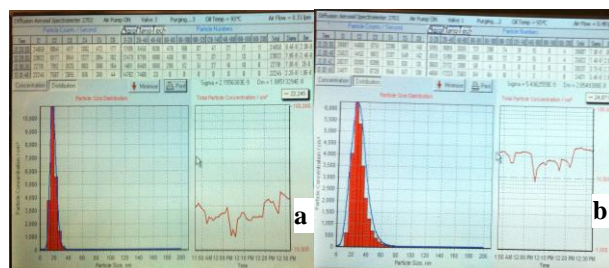


Figure 1. The concentration and size distribution of uncoated and coated nanoparticles at 72°C simultaneously monitored by the two DAS instruments.

The aerosol stream was further forced through the particle coating stage which consists of a furnace with molten polymer (polypropylene) and a condenser. The temperature of the furnace and an amount of loaded polymer were carefully adjusted to create the required vapour pressure and temperature of the evaporated polymer. The last stage of the process was collection and analysis of the coated nanoparticles. The particles were collected by thermophoretic precipitator (TP) for subsequent microscopic analysis by the SEM. The Figures 2a and 2b confirm that the coating thickness can be conveniently varied from a few nanometers to hundreds of nanometer by controlling temperature of the furnace, an amount of loaded polymer in order to create the required vapour pressure and temperature of the evaporated polymer.

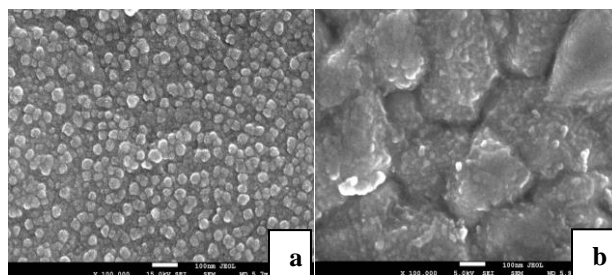


Figure 2. Scanning electron micrograph of Ni-Cr particles encapsulated inside of the polymer at a) 72°C and b) 140°C.

Gubin, S.P. (2009) *Introduction, in Magnetic Nanoparticles*, Weinheim, Germany Wiley-VCH.

Lu, A-H., Salabas, E.L., and Schuth, F. (2007) *Angew. Chem. Int. Ed.* **46**, 1222-1244

Peineke, C., Attoui, M.B., and Schmidt-Ott, A. (2006) *Aerosol Science* **37**, 1651-1661.

## Comparison of Catalyst Immobilization Techniques onto Filter Media for Airborne VOCs Decomposition

Sarka Drdova<sup>1,2</sup>, Xu He<sup>1,2</sup> and Jing Wang<sup>1,2</sup>

<sup>1</sup>Institute of Environmental Engineering, ETHZ, Zürich, CH-8083, Switzerland

<sup>2</sup>Lab of advanced analytical technologies, Group of air and particle analysis, EMPA, Dübendorf, CH-8600, Switzerland

Keywords: photocatalysis, spray-coating, dip-coating, electrospinning.  
Presenting author email: sarka.drdova@empa.ch

Volatile organic carbon compounds (VOCs) represent the main source of indoor air contamination and may result in a number of chronic health effects. For their degradation to harmless products (CO<sub>2</sub> and H<sub>2</sub>O), semiconductor photocatalysts, such as titanium dioxide (TiO<sub>2</sub>) or zinc oxide (ZnO), have been widely investigated. They are popular due to their non-toxicity, low price, chemical stability and photocatalytic activity. However, they have wide band gaps in ultraviolet (UV) light region (Mo *et al.*, 2009). A novel synthesized material, Ramsdellite MnO<sub>2</sub> nanoparticles, has revealed its photothermal activity in full solar spectrum, visible-infrared and even infrared light. It demonstrated more than 200 times higher catalytic activity than TiO<sub>2</sub> (Yang *et al.*, 2017).

The photocatalytic oxidation has been beneficially coupled with filtration by the immobilization of catalyst onto filtration media, which results in both VOCs and particles removal (Denny *et al.*, 2010). For immobilization of catalysts onto substrates, methods such as dip-coating, spray (Han *et al.*, 2012) and electrospinning have been used.

This study provides a comparison of the simple immobilization techniques and evaluates their efficiency for VOCs degradation in gas phase. Different catalysts and filters were also compared. TiO<sub>2</sub>, ZnO and MnO<sub>2</sub> were immobilized onto glass fibre filters usually used in air filtration and fabricated nylon mesh. The amount of coated catalyst was determined by filter weighting before and after coating. For electrospinning, Nylon-6 polymer was used. The immobilization performance was characterised with SEM. Furthermore, catalytic activity was tested by VOCs decomposition in gas phase. The decomposition was carried out in a stainless steel photocatalytic filter reactor. The reactor was fitted with a borosilicate glass cover enabling irradiation and it was cooled by a fan. GC/FID was used for the characterization of degradation level.

The preliminary results showed that TiO<sub>2</sub> sprayed onto the nylon mesh provided the highest degradation activity with respect to the VOC concentration decrease by a unit mass of the coated catalyst. In 5 minutes, TiO<sub>2</sub> sprayed onto nylon mesh removed 5 times more concentration of VOCs compared to other coating methods. It can be explained by the distribution of thin and uniform film on the surface of nylon mesh (Figure 1-a) and good accessibility of irradiation. SEM images showed that the dip-coated nylon mesh provided non-

uniform film (Figure 1-b). TiO<sub>2</sub> sprayed onto glass fibre filter showed 25% higher degradation compared to dip-coated.

TiO<sub>2</sub> immobilized by electrospinning onto the nylon fibres provided no photocatalytic reaction, which could be caused by blockage by the polymer.

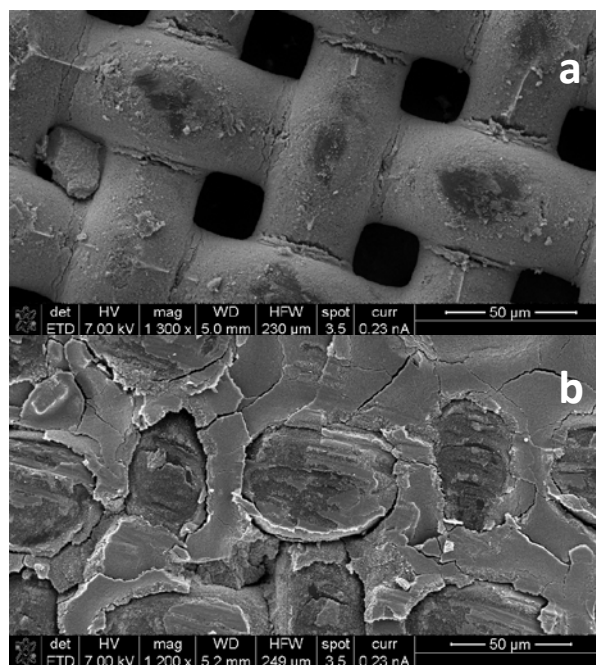


Figure 1 SEM images of TiO<sub>2</sub> coated onto nylon mesh by spraying (a) and dip-coating (b)

This study shows the applicability of simple coatings methods for air pollutant degradation coupled with filtration and enables comparison of these methods performed under similar conditions.

- Denny, F., Permana, E., Scott, J., Wang, J., Y. H. Pui, D., and Amal R. (2010) *Environmental Science & Technology* **44** (14), 5558-5563
- Han, Z., Chang, V., Zhang, L., Tse, M., Tan, O., and Hildemann, L. (2012) *Aerosol and Air Quality Research*, **12**, 1327-1335
- Mo, J., Zhang, Y., Xu, Q., Lamson, J., and Zhao, R. (2009) *Atmospheric Environment* **43**, 2229-2246
- Yang, Y., Li, Y., Mao, M., Zeng, M., and Zhao, X (2017) *ACS Applied Materials & Interface* **9** (3), 2350-2357

## Coating and functionalization of ultra-fine powders by fluidized bed chemical vapour deposition (FB-CVD)

M. Seipenbusch<sup>1</sup>, F. Weis<sup>2\*</sup> and G. Kasper<sup>2</sup>

<sup>1</sup>Parteq GmbH, 76456 Kuppenheim, Germany

<sup>2</sup>Institute of Mechanical Process Engineering and Mechanics, Karlsruhe Institute of Technology, 76131 Karlsruhe, Germany

\*current address: Palas GmbH, 76229 Karlsruhe

Keywords: fluidized bed, chemical vapour deposition, coating, core-shell

Presenting author email: seipenbusch@parteq.net

The need for scale up of an aerosol process for the functionalization of nano-scaled oxide particles (led to the development of a fluidized bed reactor.

Fluidization of nanopowders is not trivial and requires special measures to overcome the dominating interparticle forces. We used two established approaches to this problem. One is the use of a secondary high velocity flow in addition to the primary fluidization gas (see fig. 1). The second approach is a vibration activated fluidized bed, which was used for Geldart C-type powders, such as TiO<sub>2</sub>.

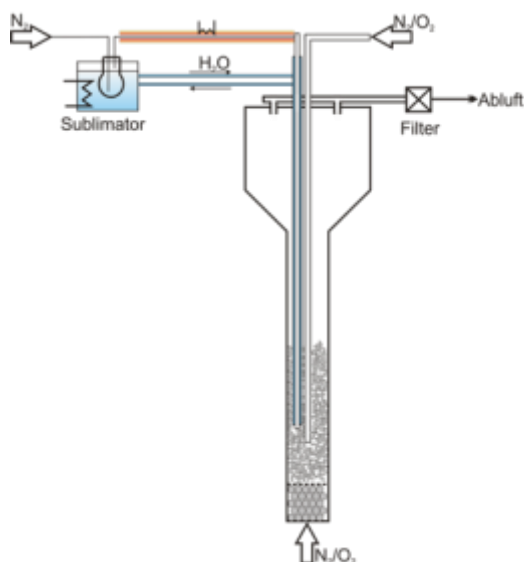


Figure 1. Fluidized bed reactor

Several oxide materials were successfully fluidized using these systems.

Precursors for functionalization are vaporized and introduced into the fluidized bed using a heated lance to prevent condensation or resublimation. The reactor is equipped with electrical heating and can be heated up to 200°C.

Coating experiments were carried out with Molybdenum hexacarbonyl and TEOS as precursors to generate core-shell structures of alumina-, silica and TiO<sub>2</sub> particles. Figure 2 exemplarily shows the course of a coating experiment of MoOx/SiO<sub>2</sub>. The reactor temperature was kept at 130°C, images were taken every 30 minutes.

The characterization of the coatings in the electron microscope and by zeta-potential measurements showed very thin but closed films of MoOx on alumina.

The functional properties of the nanocomposites produced by FB-CVD were analysed by means of their photocatalytic properties.

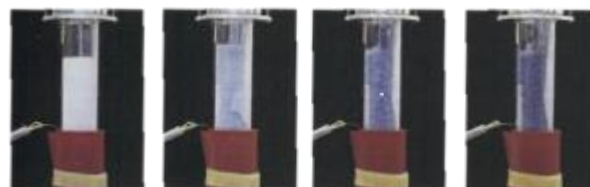


Figure 2. FB-CVD coating of silica NP with MoOx.  
Total duration: 90 min.

This work was supported JointLab IP<sup>3</sup>, a collaboration of KIT and BASF.

Weis, F., Schneider, R., Seipenbusch, M., Kasper, G. (2013) *Surface & Coatings Technology* **230**, 93-100.

**Ag/Au-doped graphene sheets and carbon nanoflowers for thin film applications**A. Meščeriakovas<sup>1</sup>, J. Jokiniemi<sup>1</sup>, A. Lähde<sup>1</sup><sup>1</sup>Department of Environmental Science, University of Eastern Finland, Kuopio, 70211, Finland

Keywords: graphene, doping, gold nanoparticles, transparent films

Presenting author email: arunas.mesceriakovas@uef.fi

Graphene is an atomically thin layer of sp<sup>2</sup>-bonded carbon atoms, stacked in a two-dimensional (2D) honeycomb lattice. It has attracted interest due to its potential application in e.g., supercapacitors, biosensors, photovoltaics and touch panels [Konios *et al* 2014]. When doped and stacked thin enough, graphene becomes a viable candidate for transparent electrodes in display applications [De *et al* 2010].

Graphene materials used in this study were previously produced by aerosol assisted induction annealing from pre-ceramic silicon carbide nanoparticles [Miettinen *et al* 2014]. The produced interconnected hybrid material consists of a crystalline SiC core with graphene (G) sheets growing vertically outwards. The tips of graphene sheets are decorated by multilayered carbon nanoflowers (CNF). These components can be separated with a series of ultrasonication /centrifugation/ re-suspension steps in organic solvents [Modesto *et al* 2015].

The stabilized suspensions of graphene/CNF were prepared by dispersing the particles in organic solvent mixtures e.g., toluene/N-Methyl-2-pyrrolidone (NMP) and 1-butanol/hexane by ultrasonication in a low-power bath sonicator. The ratios of solvents were tuned to achieve stable suspensions using Hansen solubility parameters. Doping was done to increase DC conductivity by addition of organometallic precursors containing dodecanethiol coated Au, Ag nanoparticles (NP) and subsequent sonication.

The properties of Au-doped graphene suspensions were characterized with UV-vis and transmission electron microscopy (Fig. 1).

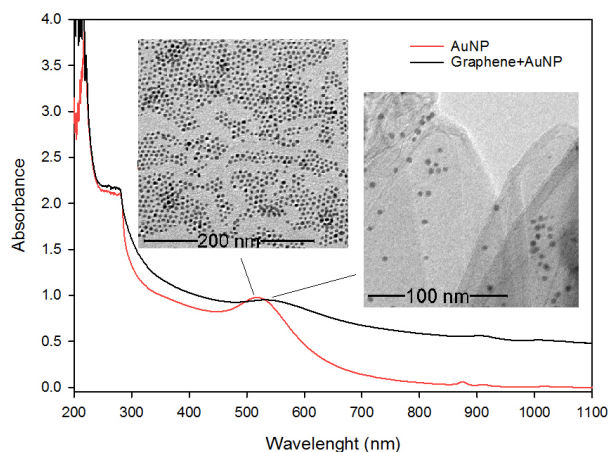


Figure 1. UV-Vis spectra and TEM images of gold nanoparticles (AuNP) and graphene doped with AuNP

The peak at 532 nm in the graphene+AuNP sample is ascribed to the surface plasmon resonance of AuNP. The morphology of the prepared sample is

observed by TEM, revealing a unimodal distribution of spherical AuNP particles having a diameter of 5 nm and situated between the graphene sheets.

Thin films of the prepared suspensions were deposited via (1) aerosol spraying by atomizing the suspensions to submicron droplets, drying, collecting downstream on membrane filters and (2) vacuum filtration. Properties of the deposited films were controlled by varied spraying time, graphene and doping agent concentrations in the suspensions.

Deposited films were transferred onto flexible transparent polymers by sandwiching the target substrate with the filter membrane and using elevated/room temperature press/roll transfer methods (Fig. 2)

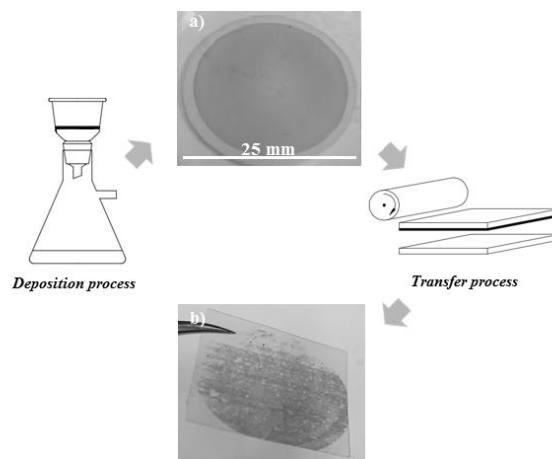


Figure 2. Schematic illustration of graphene deposition and transfer processes; (a) deposited film, (b) transferred film

This work was supported by the Finnish Funding Agency for Innovation (Tekes/EAKR), the project Fine-g (3096/31/2015).

De, S., Coleman, J. (2010) *J. Am. Chem. Soc.*, **4**(5), 2713-2720.

Konios, D., Stylianakis, M., Stratakis, E., Kymakis, E. (2014) *J. Colloid Interface Sci.*, **430**, 108-112.

Miettinen, M., Hokkinen, J., Karhunen, T., Torvela, T., Pfu, C., Ramsteiner, I., Tapper, U., Auvinen, A., Jokiniemi, J., Lähde, A. (2014) *J Nanopart Res.*, **16**, 2168-2180.

Modesto, L., Miettinen, M., Torvela, T., Lähde, A., Jokiniemi, J. (2015) *Thin Solid Films*, **578**, 45-52.

## **CCN-Activation of soot particles after long term exposure to atmospherically relevant ozone concentrations**

F. Friebel<sup>1</sup>, P. Lobo<sup>2</sup>, S.D. van Dusseldorp<sup>1</sup>, E. Mühlhofer<sup>1</sup>, and A. A. Mensah<sup>1</sup>

<sup>1</sup> ETH Zurich, Institute for Atmospheric and Climate Science, Zurich, Switzerland

<sup>2</sup> Center of Excellence for Aerospace Particulate Emissions Reduction Research, Missouri University of Science and Technology, Rolla, Missouri, USA

Keywords: soot particle aging, CCN-activation, ambient conditions, long term aging

Presenting author email: franz.friebel@env.ethz.ch

Freshly emitted soot particles are known to be poor cloud condensation nuclei (CCN), but from atmospheric measurements it can be deduced that a significant fraction of soot particles act as CCNs. One process which might contribute to this discrepancy is the heterogeneous oxidation of soot particles. Soot particles have an average atmospheric lifetime of one week. During this time, they are exposed to different oxidants which might change how the soot particles interact with water.

The investigation of those processes is an experimentally challenging task, due to the long time span which should be covered. Many studies were conducted in which soot was treated with oxidants at concentrations exceeding the atmospheric average by a factor of 1000. This approach reduces the needed observation time, but also bears the risk of not representing chemical processes well.

In summer 2016 we conducted a lab campaign at ETH Zurich where we exposed soot particles to atmospherically relevant ozone concentrations for 12 h in an CSTR-like aerosol tank. We observed that 100 nm size selected soot particles showed significant CCN-activity at a supersaturation of 0.4 % after they were exposed for 8 h to 200 ppb Ozone at 80 % humidity. Additionally, a linear correlation between exposure time and critical supersaturation was observed

The soot aerosol was produced with a propane flame burner and had a high organic carbon content. 100 nm particle were size selected and diluted with particle free and VOC-filtered wall air. To investigate the impact of oxidation and deposition of VOCs in the surrounding gas phase onto the soot particles, a charcoal denuder was used. The aerosol flow was filled continuously into a 3 m<sup>3</sup> stainless steel tank at a rate of 25 liter per minute (CSTR-like aerosol tank). Inside the tank the soot particles were exposed to different levels of humidity (0-80 %) and ozone concentrations (0-200 ppb). The fresh and the modified aerosol was characterized by following properties: CCN-activity, ice nucleation activity, size distribution, single particle mass, and hygroscopicity.

## Synthesis of Ag/ZnO Particles by Aerosol Techniques for Enhanced Visible Light Photocatalysis

Xu He<sup>1,2</sup> and Jing Wang<sup>1,2</sup>

<sup>1</sup>Institute of Environmental Engineering, ETHZ, Zürich, CH-8083, Switzerland

<sup>2</sup>Lab of advanced analytical technologies, Group of air and particle analysis, EMPA, Dübendorf, CH-8600, Switzerland

Keywords: Aerosol technique, visible light photocatalysis, Ag/ZnO particles.

Presenting author email: xu.he@empa.ch

Doping the catalysts by specific metallic particles could enhance their catalytic performance, for example loading Ag particles on the surface of ZnO enables the catalyst to work in the spectrum of visible light (Saravanan, R., *et al.* (2013)), while the size of the loaded Ag particles could not be control precisely. In this study, the aerosol techniques were utilized to generate the doping particles (Ag) with different specific sizes. By controlling the experimental conditions, influences of the properties of the doping particles such as size and doping amount on the performance of the catalyst are studied systematically.

The schematic of the experimental setup is shown in Figure 1. Airborne Ag nanoparticles were generated by a tube furnace. By adjusting the temperature of the furnace, the size distribution and concentration of the produced Ag nanoparticles can be controlled. Following the tube furnace, a DMA was utilized to choose the Ag particles with a specific size. Then the chosen Ag nanoparticles were dispersed into the prepared suspension of ZnO particles. In order to control the mass of the loaded Ag nanoparticles, after the size classification by DMA, the mass distribution of the chosen particles was also measured by the combination of CPMA (Couette Centrifugal Particle Mass Analyzer) and CPC (Condensation Particle Counter).

After centrifugation and drying processes, the catalytic performance of the obtained Ag/ZnO catalysts under the visible light was tested by the degradation of pollutants such as methylene blue. The performance of the obtained catalysts was also compared with the catalysts synthesized by the hydrothermal method (Gu, Changdong., *et al.* (2009)) in which the commercial Ag particles were utilized.

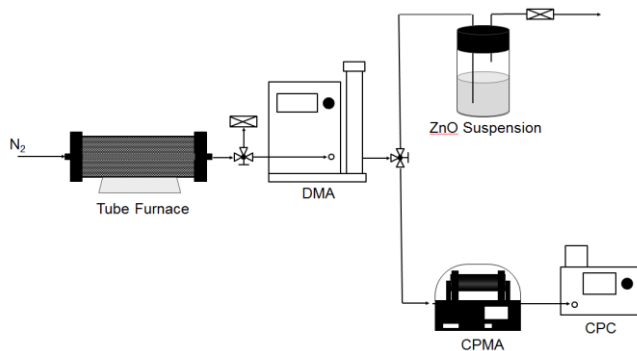


Figure 1. Schematic of the experimental setup.

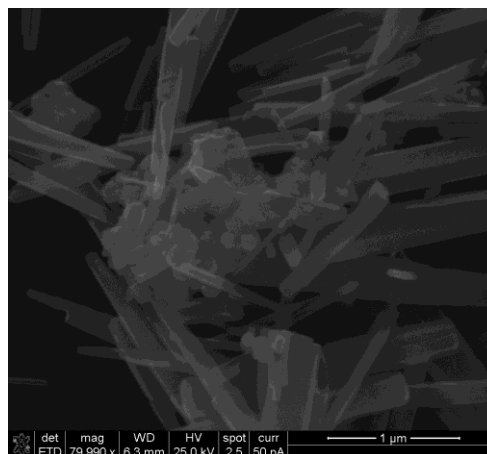


Figure 2. SEM image of Ag/ZnO particles synthesized by hydrothermal method.

The SEM image shown in Figure 2 indicated that the Ag nanoparticles could not be loaded uniformly on the surface of the rod-shaped ZnO particles. The experimental results also indicated that the loaded amount of the Ag particles did not influence the degradation efficiency of methylene blue significantly when the Ag/ZnO catalysts were synthesized by hydrothermal method (mass ratio of Zn to Ag varied among 10:1; 20:1 and 40:1), which was possibly due to the uneven loading of the Ag particles. The obtained mass distribution of the 10 nm Ag particles indicated that the mode of the mass of the particles was  $6.15 \times 10^{-3}$  fg. So the loaded mass of Ag particles can be controlled based on the obtained data during the synthesise process by the aerosol techniques. Through controlling the size and the loaded mass of Ag particles precisely by the aerosol techniques, the influence of particle size and loaded mass of Ag particles can be studied in the following experiments.

### Reference

- Saravanan, R., *et al.* (2013) *Materials Science and Engineering: C* 33.4: 2235-2244.  
 Gu, Changdong., *et al.* (2009) *Crystal Growth and Design* 9.7: 3278-3285.

## One step aerosol synthesis of various supported metal catalyst particles with tuneable pore sizes, defined metal crystallite sizes and different loadings.

A. Martínez, A.P. Weber

Institute of Particle Technology, Technical University of Clausthal, 38678 Clausthal-Zellerfeld, Germany

Keywords: Aerosol synthesis, catalyst particles, different metals, tuneable pore size distribution, defined crystallite size

Presenting author email: aurina.martinez.arias@tu-clausthal.de

Porous particles with well-defined pore structures are of interest for applications involving catalyst due to their unique properties (Rytter et al., 2007). Catalyst particles are employed for different application when the appropriate metals are used. Moreover, the efficiency of the final product strongly depends on the catalyst properties such as pore size, crystallite size and metal loading, herein for the production of the desired catalyst particles these parameters needs to be defined.

The aim of this contribution is to introduce a “one-step” aerosol synthesis method for porous catalyst particles with SiO<sub>2</sub> as a support and different metals like cobalt oxide, nickel oxide, copper oxide and iron oxide, with tuneable pore size and defined metal crystallite size. While during the synthesis process the metal crystallites are encountered as oxides, they may be reduced to the metals state in a finishing step. Furthermore, a model of the mechanics of growing of the metal particles inside this SiO<sub>2</sub> matrix will be outlined for SiO<sub>2</sub>-Co<sub>3</sub>O<sub>4</sub> catalyst particles as a function of calcination time and temperature, metal loading and surface area.

For the production of these catalyst particles the metal component was directly dissolved as nitrate into the silica suspension and spray-dried. The metal particles formed directly during the drying and calcination process within the porous silica matrix.

In this one step aerosol synthesis of porous catalyst particles the metal crystallite size can be controlled through the calcination characteristics (duration and temperature). A comparison of the Co<sub>3</sub>O<sub>4</sub> particles size before and after the calcination shows that the initial Co<sub>3</sub>O<sub>4</sub> particles grow during the calcination as it is illustrated in Fig 1. The same behavior was observed for the other metals.

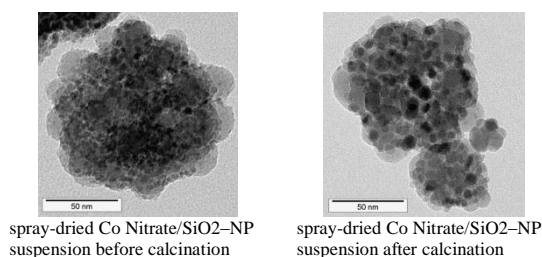


Figure 1. TEM micrographs of spray-dried Co Nitrate/SiO<sub>2</sub>-NP before calcination (left), and after calcination (right).

Regarding to the pore size, it is possible to adjust it in broader steps by varying the primary particles size of the silica suspension (Fig.2) and in smaller steps by changing the pH of the final suspension before the spray drying.

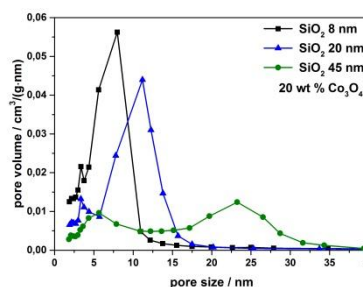


Figure 2. Pore size distributions for various silica primary particle sizes obtained from sorption isotherms according to BJJ evaluation.

The advantage of this method is the formation of catalyst particles with defined pore size, crystallite particle size and metal loading in the same synthesis step. Moreover, it is a flexible method which can be used with different metals and different supports.

### Acknowledgment

The authors like to thank the German Science Foundation (DFG) for the financial support within the program SPP 1570 under the grant no. WE 2331/13-1-2-3.

-Rytter, E., Eri, S., Skagseth, T.H., Schanke, D., Bergene, E., Myrstad, R., & Lindvag, A.; (2007) *Industrial and Engineering Chemistry Research*. 46, 9032-9036.

## **Abstracts T104**

## Sorting silicon microspheres in a hot-wall chemical vapour deposition reactor

M. Garín<sup>1</sup>, R. Fenollosa<sup>2</sup> and L. Kowalski<sup>1</sup>

<sup>1</sup>Grup de recerca en Micro i Nanotecnologies, Departament d'Enginyeria Electrònica, Universitat Politècnica de Catalunya, Jordi Girona Pacual 1-3, Barcelona 08034, Spain

<sup>2</sup>Instituto de Tecnología Química (CSIC-UPV), Universitat Politécnica de Valencia, Av. Tarongers s/n, 46022, Valencia, Spain

Keywords: Silicon, Hot Wall CVD, Microspheres, Thermophoresis.

Presenting author email: rfenollo@ter.upv.es

Silicon microspheres, with size in the micrometer and sub-micrometer range, constitute a base material that provides important properties in different fields of technology, such as photonics, optoelectronics and medicine, to name a few. Different applications impose different requirements in terms of particle size, dispersion and spherical perfection (Kuznesov, 2012), (Shi, 2013), (Garín, 2014). The Hot Wall Chemical Vapor Deposition (HWCVD) route, based on the decomposition of disilane in a closed reactor, provides silicon particles with high sphericity and surface smoothness. However the control of particle size and dispersion are particularly challenging goals because of the complex physical and chemical aerosol phenomena (Körmer, 2010) that occur inside the reactor at the same time, namely nucleation and coalescence of particles, gas convection, thermophoresis, etc.

We have found that under several conditions, that include reactor geometry and heating strategy (Fig. 1), two important processes related with particle size sorting can be realized. The first one consists of preventing particles with size below a certain value from depositing onto the supporting substrate, the second one is a particle size sorting effect where microspheres are deposited in different substrate zones depending on their diameter (Fig. 2). We have analysed quantitatively these effects and we provide a qualitative explanation in terms of the equilibrium between convection, gravitational and thermophoretic forces acting on the particles (Garín, 2016).

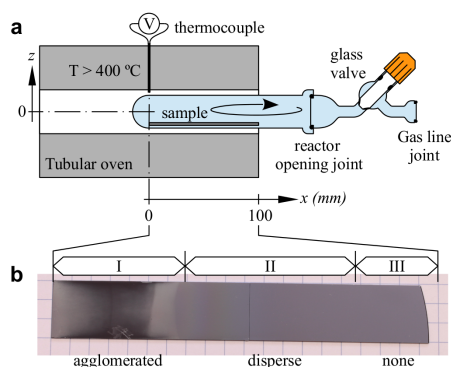


Figure 1. (a) Schematic of the HWCVD set up. (b) Photograph of a typical as-synthesized sample indicating three main areas where particles deposit differently.

Simulations of the convection process reveal that a strong temperature gradient appears at the bottom of the reactor, which produces a thermophoretic force lifting the particles upwards. At the same time, the gravitational force pushes them downwards. Therefore, the minimum particle size can be determined by equating these two opposite forces. The variation of the temperature gradient and thus its associated thermophoretic force along the reactor produces the sorting effect.

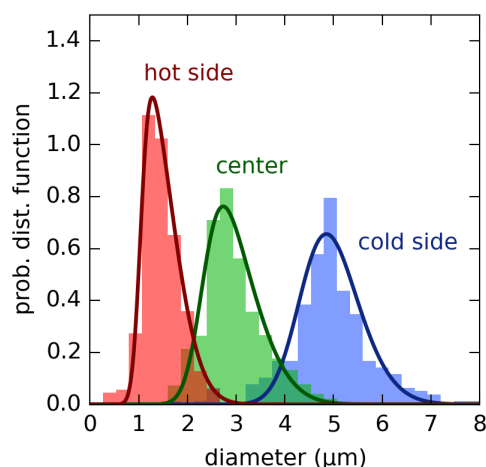


Figure 2. Particle size distribution at different sample locations.

This work was supported by ENE2013-49984-EXP, MAT2012-35040, MAT2015-69669-P and ESP2014-54256-C4-2-R of the Spanish Ministry of Economy and Competitiveness (MINECO), and PROMETEO II/2014/026 of the Regional Valencian Government.

Garín, M., Fenollosa, R., Alcubilla, R., Shi, L., Marsal, F., Meseguer, F. (2014) *Nat. Commun.* 5:3440.

Garín, M., Fenollosa, R., Kowalski, L. (2016) *Sci. Reports* 6:38719.

Körmer, R., Schmid, H.-J., Peukert, W. (2010) *J. Aerosol Sci.* 41, 1008-1019.

Kuznetsov, A.I., Miroshinchenko, A.E., Fu, Y.H., Zhang, J., Luk'yanchuk, B. (2012) *Sci. Rep.*

Shi L., Harris J. T., Fenollosa R., Rodriguez I. Lu X. Korgel B. A. Meseguer F. (2013) *Nat. Commun.* 4:1904.

## Investigation of the early stages of growth of zirconia nanostructures produced by supersonic cluster beam deposition: from the sub-monolayer to the thin film regime

F. Borghi<sup>1</sup>, C. Piazzoni<sup>1</sup>, P. Milani<sup>1</sup>, A. Podestà<sup>1</sup>

<sup>1</sup>CIMaIna and Department of Physics, University of Milano, Milano, 20133, Italy

Keywords: clusters, low-energy deposition, ballistic deposition, AFM.

Presenting author email: francesca.borghi@unimi.it

One of the main advantage of using nanostructured materials in catalytic, biomedical or energy conversion devices is that their structural and functional properties can be controlled by a precise choice and assembling of their nanoscale elemental building blocks. In particular, the deposition of pre-formed clusters on a substrate offers the possibility of carefully controlling the dimensions of building blocks, and hence to tune the structural and functional properties of the resulting systems (Schulte et al., 2017)

Supersonic Cluster Beam Deposition (SCBD) (Wegner et al., 2006) is a bottom-up approach for the fabrication of nanostructured systems, since it allows the deposition on a variety of substrates of neutral clusters produced in the gas phase, preserving their properties after deposition. The survival of the nanoscale building blocks during the assembly process is the basis of the so-called ‘memory effect’ (Podestà et al., 2015).

SCBD presents several advantages in terms of deposition rate, lateral resolution compatible with planar microfabrication technologies, and mass selection of neutral particles, by exploiting aerodynamic focusing effects (Tafreshi et al. 2002; Piseri et al. 2001). All these features make SCBD a superior tool for the production of nanostructured films with controlled structural and functional properties.

We here describe the early stages of growth of zirconia nanostructured thin films (ns-ZrO<sub>2</sub>) (Borghi et al. 2016), produced by SCBD. In particular, we present the results of an Atomic Force Microscopy study of the aggregation mechanisms of incident primeval clusters (see Figure 1), from the sub-monolayer to the thin film regime.

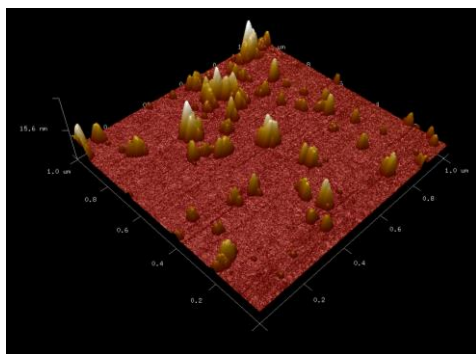


Figure 1. AFM 3D map of ns-ZrO<sub>x</sub> clusters and islands for low coverage (coverage  $\theta \sim 5\%$ ):

We discuss the influence of the building-blocks dimensions on the growth mechanisms, and on the scaling of surface RMS roughness. The size distribution of the incident clusters affects the growth dynamics in the sub-monolayer

regime (see Figure 2). The diffusion on the surface and nucleation events are favored for smaller clusters, which form islands on the surface, and promote a 2D growth. Larger clusters in turn act as static nucleation sites, where a 3D growth-mode is favored. A marked increase in the roughening rate is observed at a critical coverage of 70%. The evolution of surface roughness is compatible with the ballistic deposition regime across the whole coverage range, included the thin film regime.

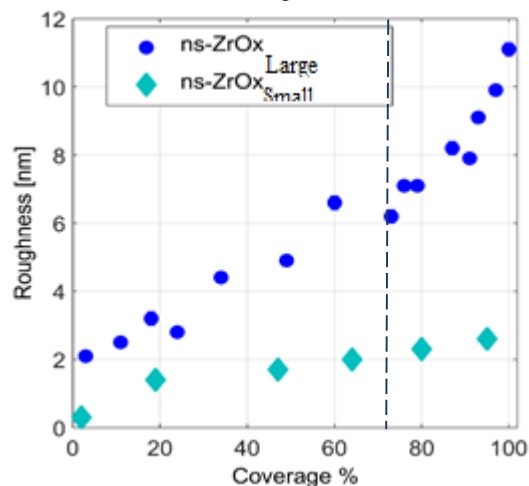


Figure 2. Evolution of surface roughness with coverage in sub-monolayer regime.

The results of our study provide relevant insights on the growth mechanisms of cluster-assembled nanostructures, as well as quantitative cues to control their morphological properties.

- Schulte, C., Podestà, A., Lenardi, C., Tedeschi, G., Milani, P. (2017) *Acc. Chem. Res.* DOI: 10.1021/acs.accounts.6b00433
- Wegner, K., Piseri P., Vahedi Tafreshi, H., Milani, P. (2006) *J. Phys. D: Appl. Phys.* **39** R439-R459.
- Podestà, A., Borghi, F., Indrieri, M., Bovio, S., Piazzoni, C., Milani, P. (2015) *J. App. Phys.* **118** 234309.
- Vahedi Tafreshi, H., Benedek, G., Piseri, P., Vinati, S., Barborini, E., Milani P. (2002) *Aerosol Sci. Technol.* **36** 593–606.
- Piseri, P., Podestà, A., Barborini, E., Milani P. (2001) *Rev. Sci. Instrum.* **72** 2261.
- Borghi, F., Sogne, E., Lenardi, C., Podestà, A., Merlini, M., Ducati, C., Milani P. (2016) *J. Appl. Phys.* **120** 055302.

## Multiscale Simulation of Gas-Phase Nanoparticle Formation and Dynamics in a Hot Wall Reactor applying the NanoDome Platform

P. Wollny<sup>1</sup>, F. Strappaveccia<sup>2</sup>, A. Kempf<sup>1</sup>, E. Ghedini<sup>2</sup> and I. Wlokas<sup>1</sup>

<sup>1</sup>Department of Fluid Dynamics, University of Duisburg-Essen, Duisburg, Germany

<sup>2</sup>Department of Industrial Engineering, University of Bologna, Italy

Keywords: nanoparticles, synthesis, multiscale, CFD

Presenting author email: [patrick.wollny@uni-due.de](mailto:patrick.wollny@uni-due.de)

Synthesis of nano-sized materials via the gas phase route is a well-established process realized at lab and industrial scales. For the prediction of the product properties like size distribution or particle morphology, a coupled modelling of the transport process and of the particle aerosol dynamics is essential. Furthermore, the product particle properties depend on their growth history, beginning with gas phase reaction kinetics, first formation steps from particle monomers, and the succeeding coagulation process accompanied by coalescence and surface growth. Thus, the model description of the process requires coverage of all scales involved.

We present a mesoscopic model, which is being developed in the scope of the NanoDome H2020 project. It is coupled to a finite volume calculation of a pilot-scale hot wall reactor. The mesoscopic model is encapsulated in the numerical Lagrangian particle (parcel) and calculates the nanoparticle formation and growth dynamics using interpolated thermochemical and flow field data from the underlying finite volume simulation. In order to capture stochastic effects, which have a strong impact on the particle motion, the diffusive drift is considered applying a random walk model. Temperature gradients in hot wall reactors cause strong thermophoretic forces on particles, which are considered following the model by Li and Wang (2004). The thermochemical state is calculated using finite rate chemistry. The individual species mass diffusion follows the mixture averaged model. The viscosity and heat conductivity of the mixture is calculated using the formulas proposed by Wilke (1950), while the pure species transport properties are pre-calculated using kinetic theory models. Particle nucleation is assumed to follow the classical nucleation theory.

The NanoDome platform is capable of predicting nanoparticle dynamics offering three different models, a classical method of moments approach (MM, Pratsinis et al., 1988), a multivariate population balance method (MPBM, Shekar et al., 2012) and a Coarse Grained Molecular Dynamics (CGMD) approach, which resolves the particle phase by solving the Langevin equations within the physical space.

The models are applied using a one-way coupling. The continuum mechanical simulation is conducted as a first step, for a steady state solution of the laminar, reacting flow. In the succeeding step, the Lagrangian particles are released into the flow field, transported and tracked, approximating their mass diffusion coefficient and mean particle diameter by applying a simple monodisperse population balance model (Kruis et al, 1993). Due to the ran-

dom walk model, every particle history is unique and statistically independent. The models are applied using a sample of different trajectories for the coupling procedure. Additionally, a calculation is performed using an artificial trajectory, which represents an average particle history and is calculated from a mean of unique trajectories.

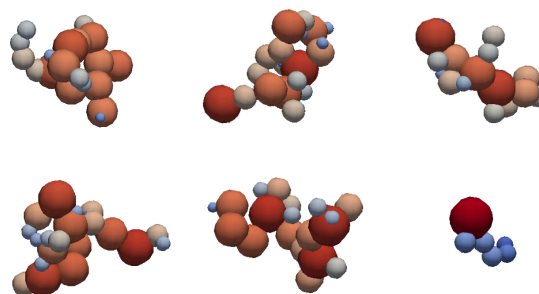


Figure 1: Particle morphology of different aggregates from a test case based on hot wall reactor conditions. Test case was performed using the CGMD algorithm of the NanoDome mesoscopic model.

The results obtained by the different methods of the mesoscopic model (MM, MPBM, CGMD) are compared with TEM and SMPS measurements from Si-particle synthesis from Silane pyrolysis in a wall-heated reactor. Particle size distributions, time histories of nanoparticle properties like surface, volume and aggregate diameter are shown. Furthermore, the capability of the CGMD model to predict realistic particle morphologies is shown by comparing with TEM pictures and proves the advantage of this model.

The work is supported by the European commission in the Horizon 2020 framework, project NanoDome (reference: 646121).

Li, Z., Wang, H. (2004) *Physical Review E*, 70(2), 021205.

Wilke, C. R. (1950) *The journal of chemical physics*, 18(4), 517-519.

Pratsinis, S.E. (1988) *Journal of Colloid and Interface Science* 142 2, 416-427

Shekar, S. et al (2012) *Computers and Chemical Engineering* 43, 130-147

F. E. Kruis, K. A. Kusters, S. E. Pratsinis, B. Scarett, (1993) *Aerosol Science and Technology* 19 514–526.

## The Crystal Structure of Coalescing Ag-Au Nanoparticles by Molecular Dynamics Simulations

E. Goudeli and S.E. Pratsinis

Department of Mechanical and Process Engineering, ETH Zurich, Zurich, 8092, Switzerland

Keywords: alloys, silver, gold, molecular dynamics.

Presenting author email: [goude005@umn.edu](mailto:goude005@umn.edu)

Bimetallic nanoparticles have gained significant commercial interest because of their superior or even novel electronic, chemical and plasmonic properties compared to the monometallic counterparts making them excellent candidates for many biomedical, sensory or catalytic applications. For example, gold nanoparticles that are used extensively in catalysis exhibit reduced electron transfer on Au(111) surface, hindering the adsorption of O<sub>2</sub>. However, formation of gold-based bimetallic nanoparticles (e.g. with Ag) can enhance the affinity with O<sub>2</sub> compared to pure gold nanocatalysts. Furthermore, Ag nanoparticles exhibit remarkable antibacterial properties but are highly cytotoxic rendering their use as therapeutic agents challenging. Alloyed Ag-Au is an interesting example in biomedicine with potential in theranostic applications since addition of Au in Ag nanoparticles improves biocompatibility without destroying the antibacterial activity of nano-silver (Sotiriou et al., 2014).

Here, the evolution of surface composition of free-standing but coalescing Ag-Au nanoparticles is investigated for different particle sizes and temperatures by atomistic molecular dynamics (MD) simulations. The MD method is validated by the attainment of the melting point of Ag-Au core-shell nanoparticles that increases with increasing particle size and follows closely the trend of the size-dependent melting temperature of pure Au (Goudeli et al., 2016) and Ag nanoparticles (Buesser and Pratsinis, 2015). Silver atoms exhibit increased mobility upon coalescence and occupy gradually the surface of the segregated particle, consistent with experiments. When Ag nanoparticles are sufficiently smaller than Au ones, a patchy Ag layer forms at the Au particle surface. Sintering of equally-sized Ag and Au nanoparticles results in the formation of segregated nano-alloys with Ag-enriched surface, consistent with the literature. The initial particle morphology affects the sintering rate but also the particle crystallinity. The X-ray diffraction patterns of Ag-Au nanoparticles are calculated during sintering, revealing that even though segregated structures exhibit the characteristic peaks of pure Ag and Au, the alloyed nanoparticles exhibit only the (111) and (200) peaks.

Figure 1 shows XRD patterns of (a) nano-alloyed and (b) segregated nanoparticles with  $d_{p,0} = 4$  nm that had coalesced for  $t = 50$  ns at 600 (blue patterns) and 800 K (red patterns). The particle snapshots (insets) are colored based on the local disorder variable (Steinhart et al., 1983; Lechner and Dellago, 2008; Kawasaki and Onuki, 2011) that indicates the local crystalline structure. FCC-like structured atoms are blue (high crystalline order) while disordered ones are red (low

crystalline order). The nanoparticles are crystalline (blue atoms) in the bulk while most of the surface atoms tend to be amorphous (green to red atoms), especially at  $T = 800$  K.

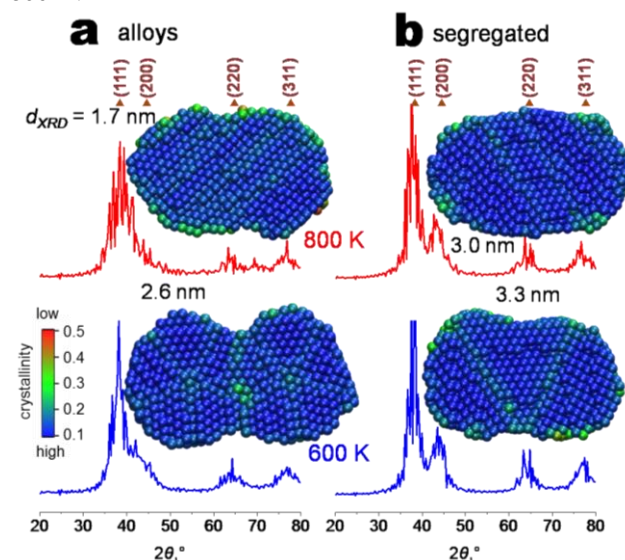


Figure 1. XRD patterns of (a) alloyed and (b) segregated nanoparticles with  $d_{p,0} = 4$  nm having coalesced for  $t = 50$  ns at 600 (blue patterns) and 800 K (red patterns).

Both Au and Ag nanoparticles exhibit four characteristic peaks (triangles) corresponding to (100), (200), (220) and (311), respectively of bulk Au and Ag atomic planes. The XRD patterns of alloyed nanoparticles exhibit the (111), (200) and (311) characteristic peaks of Au and Ag but the (200) peak at  $2\theta = 44.4^\circ$  is not distinguishable, especially at 800 K. In contrast, the (220) and (311) peaks hardly appear in the XRD pattern of the segregated and alloyed nanoparticles. Therefore, the XRD pattern could give an indication of the structure of bimetals as it distinguishes segregated nanoparticles from alloyed ones at a given temperature.

- Buesser, B. and Pratsinis, S. E. (2015) *J. Phys. Chem. C*, **119**, 10116-10122.
- Goudeli, E. and Pratsinis, S. E. (2016) *AIChE J.* **62**, 589-598.
- Kawasaki, T. and Onuki, A. (2011) *J. Chem. Phys.* **135**, 174109-1-174109-8.
- Lechner, W. and Dellago, C. *J. Chem. Phys.* 2008; **129**, 114707-1-114707-5.
- Sotiriou, G. A., Etterlin, G. D., Spyrogianni, A., Krumeich, F., Leroux, J-C. and Pratsinis, S. E. (2014) *Chem. Commun.* **50**, 13559-13562.
- Steinhart, P. J., Nelson, D. R. and Ronchetti, M. (1983) *Phys. Rev. B* **28**, 784-805.

## Atomistic Monte Carlo simulation the fractal dimensions of nanoparticle agglomerates

E.N. Skountzos<sup>1,2</sup>, V.G. Mavrantzas<sup>1,2,3</sup> and S.E. Pratsinis<sup>3</sup>

<sup>1</sup>Department of Chemical Engineering, University of Patras, Patras, 26504, Greece

<sup>2</sup>Institute of Chemical Engineering Sciences, FORTH/ICE-HT, Patras, 26504, Greece

<sup>3</sup>Particle Technology Laboratory, Department of Mechanical and Process Engineering, ETH-Zurich, Zurich, CH-8092, Switzerland

Keywords: Monte Carlo, atomistic simulation, nanoparticles, agglomeration, fractal dimensions.

Presenting author email: skountzos@chemeng.upatras.gr

An outstanding issue in the field of nanoparticle science and technology is the prediction of the complex morphological properties of nanoparticle agglomerates and their fractal structure directly from the chemical constitution of the primary particles and their inter-atomic interactions (including those with the bath molecules). Such a problem is not easy to address through a brute-force application of the atomistic molecular dynamics (MD) method because the longest times that can be simulated today even with the most powerful supercomputers and the use of thousands of graphics processing units (GPUs) are still on the order of a few hundreds of nanoseconds (up to a few microseconds in some cases) while typical agglomeration processes in the gas phase take place on time scales the order of milliseconds ( $10^{-3}$  sec).

However, if one is not interested in the dynamic properties of the system but only in its final structural and morphological properties, one can resort to a non-dynamic method which is inherently free of any such long time restrictions. Such a method is the Metropolis Monte Carlo (MC) method of importance sampling which is based on the generation of a Markov chain of states, i.e., a sequence of states in which the outcome of a trial state depends only on the state that immediately precedes it (Allen and Tildesley (1987)). The MC technique has been used with exceptional success in simulating the thermodynamic and morphological properties (conformation and self-assembly) of many Soft Matter Physics systems (Mavrantzas *et al.* (1999), Alexiadis *et al.* (2008)).

We extend it here to the case of nanoparticle (NP) agglomeration using as test primary particles amorphous silica ( $\text{SiO}_2$ ) and fullerenes ( $\text{C}_{60}$ ). Our Monte Carlo algorithm is based on the design and efficient implementation of a set artificial (sometimes even unphysical) but very drastic moves that help the system sample configurational space ergodically, thereby quickly driving it to the state of thermodynamic equilibrium. Six different such moves have been designed here to model NP agglomeration: a) NP displacement, b) NP rotation, c) agglomerate displacement, d) agglomerate rotation, e) NP

incorporation in an agglomerate, and f) NP scission from an agglomerate. For the needs of the current project, two different versions of the MC algorithm have been developed: a fully atomistic one (Demiralp *et al.* (1999), Girifalco *et al.* (2000)) and a coarse-grained one based on the computed effective potential (the potential of mean force) between a pair of NPs.

Results will be presented from both types of simulations (which are typically completed within a few hours of CPU time) and will be compared with each other. They will also be compared with other (typically mesoscopic or coarse-grained) simulation methods in the literature (Goudeli *et al.* (2015)). We will see that the new method can provide accurate predictions of the fractal dimensions of the agglomerated nanoparticles in the gas phase starting solely from their chemical structure. Typical configurations of the initial and final configurations are shown in Figure 1 (obtained from the Coarse-Grained MC simulations).

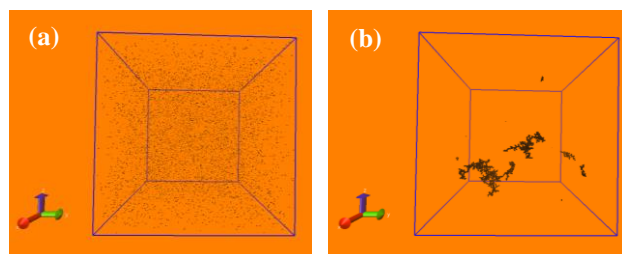


Figure 1. Typical snapshot of the initial (a) and final (b) configurations of a system containing 20,000  $\text{C}_{60}$  primary particles from our NVT MC simulation at  $T = 298.15\text{K}$  and volume fraction  $\phi = 10^{-4}$ .

Allen, M.P., Tildesley, D.J. (1987) *Computer Simulation of Liquids*, Oxford University Press.

Mavrantzas, V.G., Boone, T., Zervopoulou E. and Theodorou, D.N. (1999) *Macromolecules* **32**, 5072-5096.

Alexiadis, O., Daoulas, K.Ch. and Mavrantzas, V.G. (2008) *J. Phys. Chem. B* **112**, 1198-1211.

Demiralp, E., Cagin, T. and Goddard, W.A. (1999) *Phys. Rev. Lett.* **82**, 1708-1711.

Girifalco, L.A., Hodak, M. and Lee, R.S. (2000) *Phys. Rev. B* **62**, 13104-13110.

Goudeli, E., Eggersdorfer, M.L. and Pratsinis, S.E. (2015) *Langmuir* **31**, 1320-1327.

## A Monte Carlo simulation of nucleation, coagulation, growth and evaporation

G. Kotalczyk<sup>1</sup>, I. Skenderovic<sup>1</sup> and F.E. Kruis<sup>1</sup>

<sup>1</sup> Institute of Technology for Nanostructures (NST) and Center for Nanointegration Duisburg-Essen (CENIDE),  
University Duisburg-Essen, Duisburg, D-47057, Germany  
Presenting author email: gregor.kotalczyk@uni-due.de

In the early stages of particle formation, many concurring physical processes are encountered, such as nucleation, condensation, evaporation and coagulation. We present a parallel algorithm, based on the low-cost graphics processing unit (GPU), which allows the fast Monte Carlo (MC) simulation of all these simultaneous processes and report a self-preserving particle size distribution (PSD), which is attained for specific materials, and can be described by the competing mechanisms of evaporation and coagulation.

### Simulation method

The presented simulation approach resorts to weighted MC particles (Zhao *et al* (2009)). This allows the modelling of the nucleation of novel particles in the framework of a constant-number scheme, by the merging of existent MC particles with similar properties. The low-weight merging scheme is described as an efficient algorithm, which helps to minimize the computational costs and introduced systematic errors caused by the ‘merging’.

The coagulation of weighted MC particles is treated by the concept of the ‘stochastic resolution’, which virtually transforms the given weighted MC particle population to an ensemble of equally weighted MC particles in order to describe the coagulation event and, finally, transforms the gained results back to a population consisting of weighted MC particles, again.

The continuous processes of condensation (resp. evaporation) are coupled in a hybrid way to the discrete MC-events for the coagulation and nucleation, using the operator-splitting technique (e.g. Celnik *et al* (2007)). Due to the discrete nature of the resulting differential equation for each weighted MC particle, numerical diffusion is per se avoided during the simulation. Simple test-cases are provided, which underline this assumption.

### Simulation results

The simulated system converges into a self-preserving PSD for longer simulation times, which is broader than the self-preserving PSD attained for simulations describing the coagulation only, as can be seen in figure 1.

The simulations indicate further, that systems which describe the coagulation coupled to condensation (evaporation) and nucleation lead for longer simulation times to more reliable PSDs than systems which neglect the nucleation process completely and assume that the only depletion of the saturation takes place in the form of

a continuous growth/evaporation mechanism, as shown in figure 2.

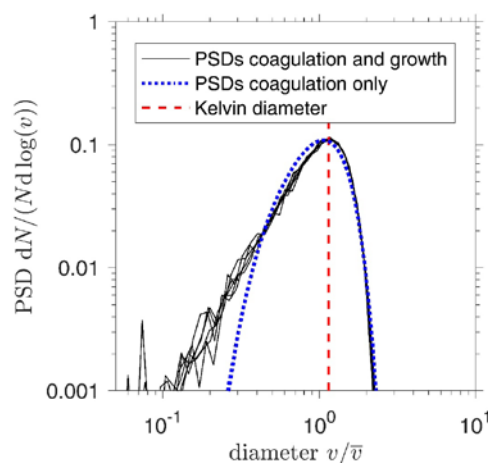


Figure 1. The PSDs resulting from the combined simulations for coagulation and growth/evaporation differ from the self-preserving PSD for coagulation only.

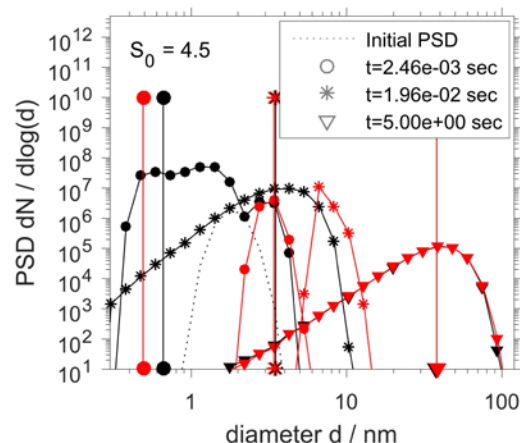


Figure 2. The PSDs describing the coagulation, growth/evaporation and nucleation (black) compared with simulations describing the same system without nucleation (red), the vertical lines describe the Kelvin diameter of the systems.

This work was supported by the Deutsche Forschungsgemeinschaft in the scope of the priority program SPP 1679.

Celnik, M., Patterson, R., Kraft, M. and Wagner, W. (2007), *Combust Flame*, **148**(3), 158–176.  
Zhao, H., Kruis, F. E. and Zheng, C. (2009), *Aerosol Sci Tech*, **43**(8), pp. 781–793.

## NanoDome Software Platform for Multi-Scale Modelling of Gas-Phase Nanoparticle Synthesis

F. Strappaveccia<sup>1</sup>, F. Galleni<sup>1</sup>, P. Wollny<sup>2</sup> and E. Ghedini<sup>1</sup>

<sup>1</sup>Department of Industrial Engineering, Alma Mater Studiorum - Università di Bologna, Bologna, Italy

<sup>2</sup>Department of Fluid Dynamics, University of Duisburg-Essen, Duisburg, Germany

Keywords: Modelling, Synthesis, Nanoparticle, Multiscale, Plasma.

Presenting author email: emanuele.ghedini@unibo.it

Nanoparticle Gas-Phase (GP) synthesis is an industrial scalable bottom-up approach to nanoparticle production that can ensure a high level of control on the product properties. GP synthesis approach starts from the thermal decomposition and/or chemical reaction of solid, liquid or gaseous precursor materials leading to the formation of a supersaturated vapour. Nucleation from the vapour phase can be tuned via reactor design (e.g. quenching, gas circulation, stoichiometry control) in order to achieve the desired primary particle properties. The formation of aggregates of partially sintered primary particles occurs if the sintering time exceeds the collision time during the cooling phase while degree of aggregation can be tuned by the adjustment of parameters such as temperature gradients, precursor concentration and vapour density.

High quality nanoparticles with tuneable particle size and morphology can be obtained via GP synthesis by plasma, hot wall or flame reactors that can ensure the use of a wide range of precursors, high temperatures and energy density, high cooling rates and controlled atmosphere. However, because of the several degrees of freedom provided by such technology, optimization of existing processes or the design of synthesis routes for new materials can be a long and expensive process, so that an accurate control of particle properties still remains a big challenge.

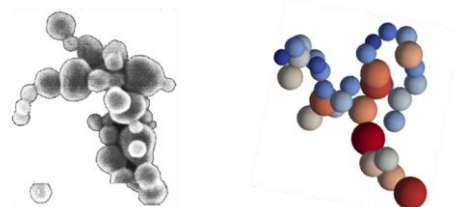
The NanoDome H2020 project is aimed to the development of an open platform for GP synthesis processes modelling in order to speed up design and optimization of nanoparticles production by providing the users with insights into the mechanisms of nanoparticles formation, growth and functionalization. Nanoparticle formation and evolution is predicted at mesoscopic level using a Coarse Grained Molecular Dynamics (CGMD) approach for primary particles and aggregates dynamics and formation, including sintering and interparticle forces. The model is expected to describe the lifecycle of a nanoparticles ensemble inside a control volume with side length between 1nm ~ 10 $\mu$ m, predicting the size of discrete primary nanoparticles, together with the morphology of the aggregates (i.e. partially sintered nanoparticles) and agglomerates (i.e. softly bounded larger structure of nanoparticles). Less computational expensive methods, such as moments (MM) (Pratsinis, 1988) and population balanced (PBM) (Shradda, 2012) methods, have been developed using the same mesoscopic framework and user interface, in order to provide the users with some computational effort scalability options.

A multiscale approach is used in order to connect the mesoscopic model to a reactor scale continuum CFD

model, enabling the user to integrate the mesoscopic approach to existing reactor modelling tools (e.g. plasma torch, flame or heated reactor tube). This is achieved by providing methods for interfacing and communication between the different scales via coupling or linking (simultaneous or sequential solution, respectively).

In this work, simulation results for the synthesis of Si nanoparticles in an Inductively Coupled Plasma Torch reactor are presented. The plasma torch and the full-scale reactor have been modelled using a CFD approach, including solid Si precursors evaporation and vapour diffusion, under the assumption of LTE for the plasma composition and properties (Colombo, 2012). Flow data from CFD simulation have been used to predict the evolution of volume parcels within the reactor in terms of temperature, pressure and species concentrations, following velocity streamlines. The NanoDome mesoscopic model has been applied to each streamline in order to predict the properties of the nanoparticles generated within each single volume parcel.

Results obtained by applying MM, PBM and CGMD methods at mesoscopic level are compared with the results obtained by applying the moments method at CFD level, together with an analysis of the computational efforts.



TEM image of a nanoparticle  
J. Guo et al., *Plasma Sci. Tech.* 12 2  
(2010), 188-199

Nanoparticle computed by  
NanoDome

Figure 1. Qualitative comparison between experimental and simulated nanoparticle morphologies.

The NanoDome project has received funding from the European Union's Horizon 2020 Research and Innovation Programme, under Grant Agreement n. 646121 ([www.nanodome.eu](http://www.nanodome.eu))

Pratsinis, S.E. (1988) *Journal of Colloid and Interface Science* **142** 2, 416-427

Shradda, S. et al (2012) *Computers and Chemical Engineering* **43**, 130-147

Colombo, V et al (2012) *Plasma Sources Science and Technology* **21**, 055007

## Modelling of transport processes of biological aerosol impurity in a ground boundary layer of industrial centers

L.G. Voskressensky<sup>1</sup>, S.L. Rychkov<sup>2</sup>, V.V. Sablin<sup>3</sup>, A.V. Shatrov<sup>2</sup>

<sup>1</sup> Department of Mathematics and Physics, The Peoples Friendship University of Russia, 117198, 6, Miklukho-Maklaya Str., Moscow, Russia

<sup>2</sup> Department of Mathematical Modeling, Vyatka State University, 610000, 36, Moskovskaya Str., 36, Kirov, Russia

<sup>3</sup> Science Research Laboratory “AlphaNanoTech”, 610000, 36, Moskovskaya Str., Kirov, Russia

Keywords: aerosol allergenic pollen, ground boundary layer, heat and mass transfer, numerical simulation, parallel programming.

Presenting author email: avshatrov1@yandex.ru

The new quasi two-dimensional model of mesoscale processes of transport and diffusion of an impurity in under layer of atmosphere with allowance of its temperature non-uniformity is submitted. Its conclusion is based on a technique described by [1-3]. The model represents development of the theory of “shallow water” on baroclinic atmosphere. With the help of a designed numerical scheme was calculated the structure of an impurity cloud from a distributed source of allergenic pollen arranged in large town with allowance for a thermal-uniformity of an underlying surface and an advection. The site by the sizes 100 km on 100 km in neighborhood of city Kirov (Russia) undertook is demonstrated that at a rather gentle south - western wind (speed of 2 m/s) the horizontal temperature non-uniformity introduces essential change to a current of traffic of a plume of an impurity (see Figure 1,2).

calculation is executed on the programming language Intel Fortran in Packet Intel Cluster Studio for Linux under control OS Linux Red Hat 7.0, established on the cluster supercomputer HP HPC Enigma X000 of Vyatka state University.

Also the approach given in this work helps to organize on-line monitoring of intensifying of allergenic pollen emission into the ground boundary layer of atmosphere for above industrial town.

This work was supported by the Education and Science Ministry project № 2014/66, title of project 1281 “New information technology in data analysis and modelling of developing economy and ecology with means HPC in cluster system”

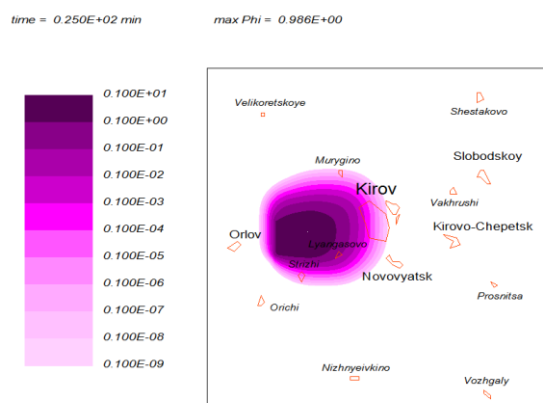


Figure 1. Distribution of concentration of an Impurity in lobes of marginal concentration in 25 minutes

The count of interplay of an aerosol pollen with an underlying surface of ground was made with condition of non-uniformity of distribution of a coupling coefficient, which calculated with the help of the information of a map of land of computational area. The parallel implementation of algorithm of

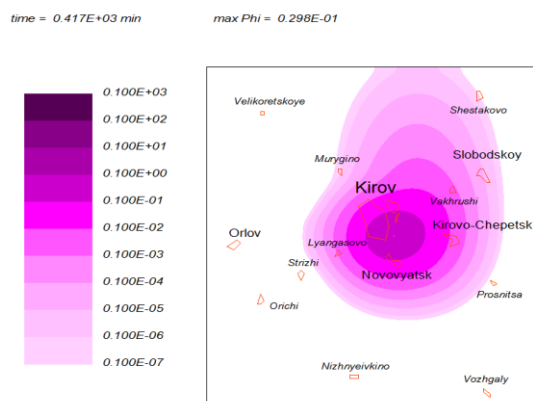


Figure 2. Distribution of concentration of an Impurity in lobes of marginal concentration in 417 minutes

Aristov, S.N., Frik, P.G. (1988) *Fluid Dynamics*, 4, 48-55.

Schwarz, K.G.(1998) *AIAA Progr. Ser.* 182, .271-279.

Shatrov, A.V., Shvarts, K.G.(2009) *European Aerosols Conf., Karlsruhe,6-11 Septmber*, Abstract T031A1

Shatrov, A.V., Shvarts, K.G.(2011) *Fluid Dynamics*, 2. 333-339.

## Sensitivity analysis of a model characterizing nanoparticle agglomeration, dispersion and deposition processes in the atmosphere

M. Poikkimäki<sup>1</sup>, P. Juuti<sup>1</sup>, J. Kalliokoski<sup>1</sup> and M. Dal Maso<sup>1</sup>

<sup>1</sup>Aerosol Physics, Faculty of Natural Sciences, Tampere University of Technology, Tampere, Finland  
Keywords: Nanomaterial, Risk assessment, Environment, Atmospheric dispersion, Sensitivity analysis.

Presenting author email: mikko.poikkimaki@tut.fi

An increasing amount of nanoscale materials such as engineered nanoparticles (ENP) are produced for various industrial applications and everyday products. Recent studies have shown that some ENPs may cause adverse effects on human health (De Jong *et al.*, 2008; Geiser and Kreyling, 2010) and the environment (Handy *et al.*, 2008; Kahru and Dobourguier, 2010). Therefore, a need to assess and govern risks resulting from their production, use and disposal has arisen. However, present risk assessment models include dynamic microphysical processes affecting ENPs after they are released into the atmosphere only superficially. In addition, current models are still lacking testing and calibrating, which can result in uncertain risk estimates (Hristozov *et al.*, 2016). As an answer to this problem, the reliability and accuracy of the models could be increased by means of sensitivity analysis.

In this study, the nanoparticle Agglomeration, Dispersion and Deposition model (ADD, Anttila and Dal Maso, 2015) is further developed to be used in risk assessment of an atmospheric release of ENPs. It is based on the Gaussian dispersion equation (Stockie, 2011), which introduces a non-recurring point source. The spatial and temporal evolution of airborne particle number concentration is modeled by taking into account atmospheric dispersion, deposition to the ground and agglomeration of the aerosol population. However, the particle concentration in the air does not directly illustrate the risks on, e.g., soil microorganisms or a human respiratory system. For this reason, the ADD-model has been improved to compute exposure and dose estimates to be used in risk assessment. The deposited amount of particles at a certain point is integrated over the whole simulation time in order to estimate the particle concentration in soil due to deposition and the respirable number of particles.

A sensitivity analysis, using the one-at-a-time method (Saltelli *et al.*, 2008), is executed on the ADD-model. The input parameter values are varied over the whole range of considered realistic values by changing one value at the time, while keeping the other values unaltered. The change in number and mass concentrations in soil (exposure) are mapped along with the lung deposited number and mass of particles (dose). The main goal of this sensitivity analysis is to acquire information on how the values of output parameters change when the values of the input parameters are varied.

The results show that number concentration in soil (Fig. 1) is most sensitive for variations in the total particle material mass released to the air  $M$ , the size of the released particle plume  $d_{lim}$ , particle size  $d_0$ , wind

speed  $U$  and Pasquill stability class  $Sta$  (Gifford, 1961). Contrarily, varying the atmospheric boundary layer height  $B_{lh}$ , particle fractal dimension  $D_f$ , particle density  $\rho$ , shape factor  $\chi$ , dispersion parametrization  $Di$  or air temperature  $T$  did not cause significant changes on the concentrations in soil. The same outcomes apply similarly for lung deposited number with an exception that varying the particle density causes notable change in the lung deposition.

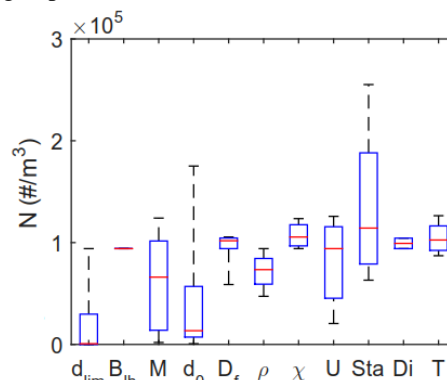


Figure 1. Particle number concentration in soil 200 meters from the particle source for different input parameter values. Red lines represent median values, the edges of blue boxes are 25 and 75 percentiles and the tails point out min and max values.

Information acquired from sensitivity analysis acts as a guide for generation of new exposure and hazard data. Hence, it also increases the accuracy and reliability of risk assessment models. The methodology used here can be applied to all currently available nano-specific environmental and human risk assessment models.

We thank Dr. T. Anttila for developing the ADD-model. M. P. was supported by the European Union's Horizon 2020 research and innovation programme (caLIBRAte project - Grant Agreement No. 686239). M. P. also acknowledges TUT Grad school for financial support.

- Anttila, T. and Dal Maso, M. (2015) *Aerosol Technology 2015 –conference*, Tampere, Finland.  
De Jong, W. H. *et al.* (2008) *Biomat.* **29**(12), 1912-1919.  
Geiser, M. and Kreyling, W. G. (2010) *Particle and fibre toxicology* **7**(1), 2.  
Gifford, F. A. (1961) *Nucl. Safety* **2**, 47-51.  
Handy, R. D. *et al.* (2008) *Ecotoxicology* **17**(5), 315-325.  
Hristozov, D. *et al.* (2016) *Env. International* **95**, 36-53.  
Kahru, A. and Dobourguier, H.-C. (2010) *Toxicology* **269**(2-3), 105-119.  
Saltelli, A. *et al.* (2008) *Global sensitivity analysis: the primer*, John Wiley & Sons.  
Stockie, J. M. (2011) *SIAM Review* **53**(2), 349-372.

## Effective BVOCs exchange of boreal forests: emissions versus in-canopy sinks

P. Zhou<sup>1</sup>, L. Ganzeveld<sup>2</sup>, D. Taipale<sup>3,4</sup>, Ü. Rannik<sup>1</sup>, M. P. Rissanen<sup>1</sup>, P. Rantala<sup>1</sup> And M. Boy<sup>1</sup>

<sup>1</sup>Department of Physics, University of Helsinki, P.O. Box 64, FI-00014, Helsinki, Finland

<sup>2</sup>Meteorology and Air Quality (MAQ), Department of Environmental Sciences, Wageningen University and Research Centre, Wageningen, Netherlands

<sup>3</sup>Department of Forest Sciences, University of Helsinki, P.O. Box 27, FI-00014, Helsinki, Finland

<sup>4</sup>Estonian University of Life Sciences, Department of Plant Physiology, Kreutzwaldi 1, EE-51014, Estonia

Keywords: BVOC, dry deposition model, boreal canopy, emissions

Presenting author email: michael.boy@helsinki.fi

### Introduction

A multi-layer BVOCs dry deposition model has been implemented into a 1-dimensional chemical transport model SOSAA (Boy et al., 2011) to investigate the in-canopy sources and sinks of BVOCs. The deposition model for BVOCs was proposed two decades ago (e.g., Wesely, 1989). However, only until recently the detailed single-layer deposition model of BVOCs have been applied to investigate the BVOCs fluxes (Nguyen et al., 2015) and the loss of secondary organic aerosol (SOA) (Hodzic et al., 2014). Therefore the newly implemented multi-layer BVOCs deposition model in this study can provide a new insight on the BVOCs exchange of boreal forest, which is also useful for estimating BVOCs fluxes at the canopy top. The new model can also be applied in large-scale models.

### Methods

The gas dry deposition model was based on the ozone dry deposition model described in Zhou et al. (2017). For BVOCs, the parametrisation method for mesophyll resistance, cuticular resistance, soil resistance and wet skin resistance were extended from Wesely (1989) and Nguyen et al. (2015). The Henry's law constant values of all species included in current model were obtained from the measurement data if available (Sander, 2015), otherwise they were computed with the software EPI Suite v4.11. The reactivity factors were taken from three values 0 (non-reactive), 0.1 (semi-reactive) and 1 (reactive), which were proposed according to the functional groups of organic compounds (Wesely, 1989; Karl et al., 2010). BVOC emissions were calculated by MEGAN (Guenther et al., 2006) with the emission potentials derived from measurement data in previous studies.

### Conclusions

The model was set up to simulate a whole month from July 1st to 31st in 2010. The normalized relative contributions of sources and sinks for individual species during the whole month are shown in Fig. 1. Here Qturb represents the in-canopy concentration change of BVOCs due to turbulent transport, which can be positive (downward) as a source term or negative (upward) as a sink term. Qemis is the emission source. Qdepo is the deposition sink. Qchem is the total chemical gain and loss.

For those compounds emitted from vegetation, e.g., isoprene (C5H8) and monoterpenes (MT), Qemis is the

dominant source. The net chemical production is significant for sesquiterpenes and isoprene oxidation products ISOP34OOH and ISOP34NO3. Deposition is the main sink for most compounds except MT, SQT, C5H8 and MBO. For the very reactive compounds, e.g., sesquiterpenes, Qchem is the main removal mechanism. The emitted isoprene and monoterpenes inside the canopy are lost via turbulent transport to the air above the canopy.

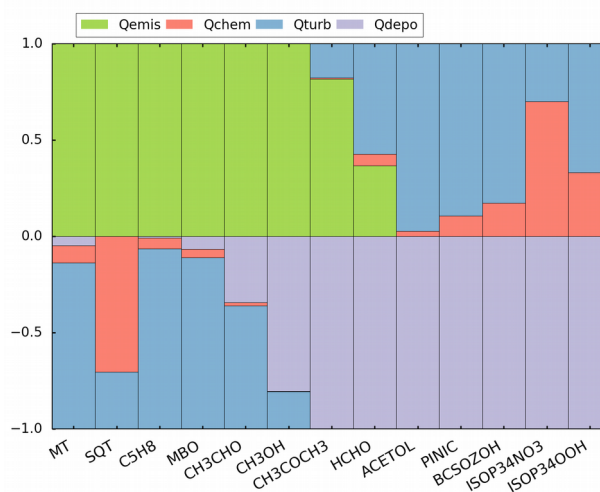


Figure 1. Modelled relative contributions of sources and sinks for individual compounds within the canopy.

This work was supported by Maj ja Tor Nessling funding, the Academy of Finland, CRAICC, eSTICC, FcoE, IUT20-11 and the European Regional Development Fund. The authors also wish to acknowledge CSC - IT Center for Science, Finland, for computational resources.

Boy, M., et al. (2011). *Atmos. Phys. Chem.*, **11**, 43-51. Zhou, P., et al. (2017). *Atmos. Phys. Chem.*, **17**, 1361-1379.

Guenther, A., et al. (2006). *Atmos. Phys. Chem.*, **6**, 3181-3210.

Hodzic, A., et al. (2014). *Geophys. Res. Lett.*, **41**, 4795-4804.

Karl, T., et al. (2010). *Science*, **330**, 816-819.

Nguyen, T. B., et al. (2015). *PNAS*, **112**, E392-E401.

Sander, R. (2015). *Atmos. Phys. Chem.*, **15**, 4399-4981.

Wesely, M. L. (1989). *Atmos. Env.*, **23**, 1293-1304.

## **Abstracts T105**

## Catalytic reaction of reproducible oxide-free copper nanoparticles with gaseous oxides

H. Tanaka<sup>1</sup>, M. Miyagawa<sup>1</sup> and J. Hirokawa<sup>2</sup>

<sup>1</sup>Department of Applied Chemistry, Chuo University, Tokyo, 112-8551, Japan

<sup>2</sup>Faculty of Environmental Earth Science, Hokkaido University, Sapporo, 060-0610, Japan

Keywords: Cu nanoparticle, catalytic reaction, reproduction, oxide-free.

Presenting author email: htanaka@kc.chuo-u.ac.jp

Since gaseous oxides including nitrogen oxides are often harmful to the environment, extensive catalysts converting them as safe have been developed. Actually, many useful catalysts were discovered and developed, but most of them were expensive and limited resources containing noble metals such as platinum. From this point of view, it is strongly desired to substitute them by copper, which is inexpensive and abundant materials. In fact, the copper nanoparticles have been synthesized using a reducing agent such as hydrazine. However, since the oxidation potential of copper is higher than that of typical noble metals, radical and hazardous reagents were usually used in order to reduce copper ions. In addition, the obtained copper nanoparticles are usually oxidized readily because of their high reactivity. In this study, we have examined to establish eco-friendly synthesis method of oxide-free copper nanoparticles using photoreduction method. For these nanoparticles, their stability and reactivity with air and nitrogen oxides have been also examined.

Copper nanoparticles were synthesized by photoreduction with help of titanium oxide as a photocatalyst. In brief, copper acetate was dissolved in ethanol solution which was diluted 10-fold with water, and TiO<sub>2</sub> nanoparticles dispersion was added to this solution without any degassing processes. The mixed solution was photoirradiated by LED light of which irradiation wavelength was 365 nm at room temperature.

The obtained dispersion was analyzed by optical spectrum, HRTEM and XRD. The stability and reactivity for the nanoparticles were also analysed by these methods.

When the initial dispersion was irradiated by the light, its color started to change light blue to dark red rapidly. In its optical spectrum, a peak ascribed to surface plasmon resonance band (SPR) for copper nanoparticles was observed. The nanoparticle formation was also confirmed by HRTEM observation. In addition, XRD pattern was suggested that the obtained nanoparticles were composed of only metallic copper without any oxides. On the other hand, when the photoirradiated dispersion was exposed to air, its color changed dark red to light blue rapidly. Actually, the SPR peak was vanished and a peak ascribed to copper ions appeared in optical spectrum. Furthermore, this faded dispersion was irradiated by the light again, its color turned to dark red again and the SPR peak also re-appeared. These indicate

that the copper nanoparticles synthesized by present method are reproducible.

When the copper nanoparticle dispersion thus prepared was exposed to gaseous nitric oxide, color fading was also observed. The increase of the concentration of nitrogen dioxide was also detected in the gas passed through the dispersion. This indicates that the copper nanoparticles work as a catalyst for the conversion of nitrogen oxides. Furthermore, this faded dispersion was found to be able to convert to copper nanoparticle dispersion by the light irradiation again. This indicates that the present nanoparticles have a potential for the application as a catalyst for a new type of nitrogen oxides harmless.

Miyagawa, M., Maeda, T., Tokuda, R., Shibusawa, A., Aoki, T., Okumura, K. and Tanaka, H. (2016) *RSC Adv.* **6**, 104560-104565.

Miyagawa, M., Yonemura, M. and Tanaka, H. (2016) *Chem. Phys. Lett.* **665**, 95-99.

Nishida, N., Miyagshita, A., Hashimoto, S., Murayama, H. and Tanaka, H. (2011) *Eur. Phys. J. D*, **63**, 307-310.

Tanaka, H., Aoki, T., Yonemura, M., Miyagawa, M. and Okumura, K. (2016) *J. Phys.* **712**, 012120/1-4.

## Synthesis and Evaluation of doped $\text{LiNi}_{0.5}\text{Mn}_{1.5}\text{O}_4$ Particles by Aerosol Spray Pyrolysis for Next -generation Li-ion Cathode Materials

G. A. Ganas<sup>1</sup>, G. Kastrinaki<sup>1</sup>, D. Zarvalis<sup>1</sup>, A.G. Konstandopoulos<sup>1,2</sup>, D. Versaci<sup>3</sup>, N. Penazzi<sup>3</sup>, S. Bodoardo<sup>3</sup>, M. Bengoechea<sup>4</sup>, I. de Meatza<sup>4</sup>

<sup>1</sup>Aerosol & Particle Technology Laboratory, CERTH/CPERI, P.O. Box 60361, 57001, Thessaloniki, Greece

<sup>2</sup>Department of Chemical Engineering, Aristotle University, PO. Box 1517, 54006, Thessaloniki, Greece

<sup>3</sup>Applied Science and Technology Department, Politecnico di Torino, C.so Duca degli Abruzzi 24, 10129 Torino, Italy

<sup>4</sup>IK4-CIDETEC, Parque Tecnológico de San Sebastián, Paseo Miramón 196, 20014, Donostia-San Sebastián, Spain

Keywords: aerosol spray pyrolysis, LNMO, particle size distribution

Presenting author email: georgiak@certh.gr

The development of high voltage (5V) cathode materials for Li-ion cells is one of the key issues to develop batteries with improved performances in terms of energy density (Goodenough et al), power density and cycle life, suitable for EVs (Electric Vehicles) and PHEVs (Plug-in Hybrid Electric Vehicles).  $\text{LiMn}_{1.5}\text{Ni}_{0.5}\text{O}_4$  (LMNO) and its variants is a top candidate due to the its access to a rare two-electron transition from  $\text{Ni}^{2+}$  to  $\text{Ni}^{4+}$  at two voltage plateaus near 4.7 V vs  $\text{Li}^+/\text{Li}$ , a theoretical capacity of  $147 \text{ mAhg}^{-1}$  and fast three-dimensional lithium-ion diffusion paths within the cubic lattice. A study concerning the synthesis and evaluation of LNMO particles via Aerosol Spray Pyrolysis (ASP) has already been implemented (Gkanas et al) regarding the materials crystal structure, particle size, morphology, surface area and pore size distribution while in the current paper a further optimization of the candidate materials has been performed regarding the doping of the LNMO lattice with Fe, Al and Mg.

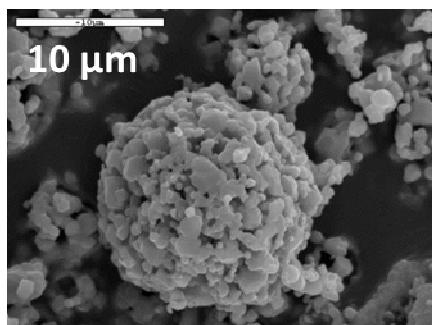


Figure 1. SEM image of the  $\text{LiNi}_{0.5}\text{Mn}_{1.5}\text{O}_4$  particles synthesized by the pilot scale reactor

In the previous work a primary study was developed in order to tune the synthesis conditions in a lab scale aerosol spray pyrolysis reactor for the evaluation of the materials in a T-cell battery system and electrochemically evaluate them for their specific capacity and cyclic voltammetry under numerous cycle numbers at low and high C-rates. The precursor solution chemistry and reactor operating conditions were adjusted in order to obtain the  $\text{LiNi}_{0.5}\text{Mn}_{1.5}\text{O}_4$  structure, while the post-calcination profile conditions of the collected powder were studied in a view order to obtain the two

most important spinel phases: the ordered ( $P4_332$ ) and the disordered ( $Fd3m$ ). The temperature profiles which have been studied vary from  $700\text{-}900^\circ\text{C}$ , with the temperatures over  $700^\circ\text{C}$  leading to the disordered phase and larger crystallite sizes, while a second calcination step below  $700^\circ\text{C}$  formed the ordered structure again. The  $\text{LiNi}_{0.5}\text{Mn}_{1.5}\text{O}_4$  phase was determined by micro-Raman spectroscopy. Dense materials with the disordered structure showed the best electrochemically activity towards EV requirements and their material characteristics were transmitted at a pilot scale aerosol spray reactor for large scale synthesis.

Current work presents the synthesis study of  $\text{LiNi}_{0.5}\text{Mn}_{1.5}\text{O}_4$  particles at pilot scale reactor system for the production of sufficient powder for electrode processing, half and full cell assembly, evaluation and optimization of the scaling up protocol for cathode electrode preparation, full Graphite/LNMO cell harmonization and real HEV driving conditions requirements. The  $\text{LiNi}_{0.5}\text{Mn}_{1.5}\text{O}_4$  material was further doped with Fe, Al and Mg in order to study the materials specific capacity and cycling activity. Doping of the lattice led to decrease in the particle size distribution which affected the tapped density of the material leading to enhanced activity in the Fe case.

This work was supported by the Horizon 2020 eCAIMAN project under the grand GV-01-2014 - 653331.

Goodenough, J. B., and Kim, Y. (2010) *Chem. Mater.* **22**, 587

Gkanas, G., Kastrinaki, G., Zarvalis, D., Konstandopoulos, A.G., Versaci, D., Penazzi, N., and Bodoardo, S., (2016), *In Proc. European Aerosol Conference*, Tours

## **Abstracts T106**

## Surface Normalised Aerosol Photo Emission Sensor

J. Röhrbein<sup>1</sup>, A.P. Weber<sup>1</sup>

<sup>1</sup>Institute of Particle Technology, Technical University of Clausthal, 38678 Clausthal-Zellerfeld, Germany

Keywords: photo emission, aerosol, particle characterization

Presenting author email: jannis.roehrbein@tu-clausthal.de

The surface properties of particulate material are influencing various powder properties. For instance flowability, dispersibility or compressibility might be noticed here. These properties are from huge interest for handling and characterization of those materials. The surfaces of gas-borne particles can be modified in various ways: Beside a chemical oxidation, a condensation process might be used, to deposit material in their surface. If these condensation processes are to be investigated, it is very important not to change the particle environment during probing.

Nowadays there are a lot of different systems, to determine the surface properties of particles, like electron-spectroscopy or laser-induced-fluorescence. Unfortunately these methods have some slight disadvantages when it comes to the measurement environment or requirements towards the material. For electron-spectroscopy it is required to obtain a vacuum environment to analyse the gas-borne particles. If it is from interest to investigate the effect of condensating material on the surface of the particles, a vacuum would heavily disturb this state of the particle, because the material would evaporate and could not be determined.

For the Laser-induced fluorescence for example, a non-fluorescent particle material and a fluorescent adsorbate-material is needed, to show an effect.

In this work, a new system is presented, which operates at ambient pressure and does not require a vacuum. It is based on the photoelectric effect, while the particle-surface will be measured with diffusion charging. Therefore gas-borne particles are being charged with light of different wavelengths coming from an adjustable monochromatic light source. The photoelectric effect leads to a charging of the particles, which means that an electron is removed from the particle and an uncharged particle will remain with a positive charge. This effect can be described by the Fowler-Nordheim equation as follows [1]:

$$Y = K_c \cdot (h\nu - \phi_p)^m$$

Here Y describes the yield of electrons, which means a charging rate.  $K_c$  is a factor which can be neglected, if only the work function  $\phi_p$  is from interest. The exponent  $m$  is material specific and is found to be 2 for metallic materials. In the experiments used here, the particles are pre-charged with a negative charge and when they emit an electron due to photoelectric charging, they will become neutral. This is then measured by a CPC with and without an electro-filter before the CPC to remove any charged particles. With this setup, the concentration of all particles and the concentration of the uncharged particles is being measured for each wavelength, from which  $h\nu$  is derived. By rewriting the equation to

$$\sqrt{Y} = \sqrt{K_c} \cdot (h\nu - \phi_p)$$

the work function can be obtained by the x-axis intercept. Using this simple equation, the work function of silver particles can be measured in various different environments. The silver particles are generated by a spark-

discharge generator under atmospheric pressured air and afterwards sintered in an oven at different temperatures and then classified by a DMA.

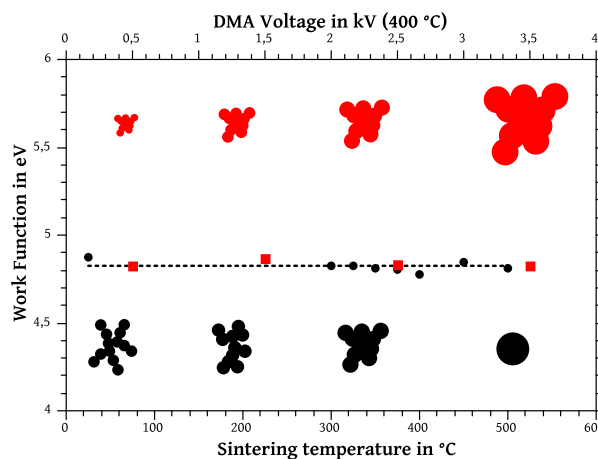


Figure 1: Work function of oxidised silver particles for different sintering temperatures at the same classification voltage (3kV, round points) and different classification voltages at the same temperature (400°C, square points).

As it can be seen in fig. 1, neither a change of the morphology of the particles due to sintering in an oven or a classification by different DMA voltages will change the work function, because of the fact, that the surface material of the particles will be always be the same. The changes of the particle morphology will be measured with diffusion charging, what is not implemented yet and will create the ability to measure surface normalised properties. When the particle material is changed, the work function will vary, as it is been shown in table 1.

Table 1: Work functions for different metal(oxides) measured by photoemission.

Material	Measured work function in eV
Iron	5.9
Aluminium	5.4
Silver	4.8
Titanium	5.6

The goal of this project is the development of a characterization method, which gives reliable information about the surface state of gas-borne particles, without being influenced by any changes in the morphology.

This work was supported by the DFG (Deutsche Forschungs Gesellschaft) what is hugely appreciated.

Müller, U., Ammann, M., Burtscher, H. Schmidt-Ott, A. Photoemission from clean and oxygen-covered ultrafine nickel particles, *Phys. Rev. B* 44 (1991), 8284-8287

## Aerosol Multielement Spectrometer for Near Real-Time Measurement of Aerosol Elemental Concentration

Pramod Kulkarni, Lina Zheng, Gregory Deye, M. Eileen Birch

<sup>1</sup>Centers for Disease Control and Prevention, National Institute for Occupational Safety and Health, Cincinnati, OH 45213, USA

Keywords: portable instrument, real-time elemental analysis, nanoparticle measurement  
Presenting author email: PSKulkarni@cdc.gov

Compact, field-portable sensors that can provide real-time information about chemical and physical properties of aerosols are valuable tools for exposure measurement. A hand-portable Aerosol Multielement Spectrometer (AMS) has been developed for near real-time measurement of elemental concentration of aerosols and airborne nanomaterials. The instrument employs atomic emission spectroscopy using pulsed spark microplasma as the excitation source (Diwakar and Kulkarni, 2012). Particles are collected on the tip of an electrode and then subject to ablation and excitation by the microplasma, which leads to significant improvement in measurement precision, limits of detection, and time resolution of measurement (Diwakar and Kulkarni, 2012; Zheng et al., 2016). The compact instrument can simultaneously measure most elements in the periodic table at a time resolution of few seconds to few minutes, including carbon (Zheng et al., 2016). Algorithms were developed for real-time spectral analysis to obtain quantitative elemental information. The instrument was calibrated for various elements, including carbon, and their detection limits were determined and were found to be in the range of few tens to hundreds ng/m<sup>3</sup>. Its performance was evaluated using parallel samples collected using filters and analyzed using mass spectrometry. Field measurements were conducted to characterize aerosols in the breathing zone of a mobile person and compared with those from the filter samples. Overall design, development, and analytical figures-of-merit of the instrument will be presented.

The instrument was tested in several field studies and its performance was evaluated using filter measurements.

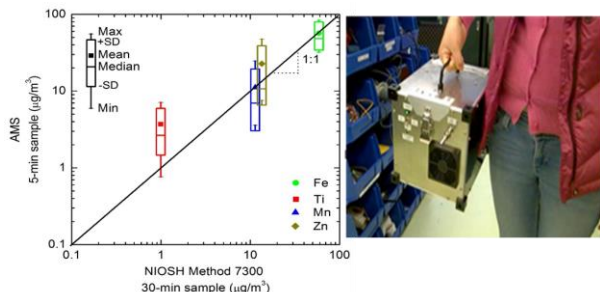


Figure 1: Comparison of 5-min AMS measurements with filter measurements (NIOSH 7300; 30-min samples).

Figure 1 shows a comparison of elemental concentrations measured in the workplace by AMS (in the worker's breathing zone during welding operation) to those from the filter measurements using NIOSH Method 7300, showing consistent results for the two methods. The time

required to obtain one measurement, i.e., time resolution of the instrument, can be adjusted from several seconds to few minutes depending on the aerosol concentration and the detection limits of target analytes. Figure 2 demonstrates the near real-time, continuous monitoring capability of the AMS for simulated transient aerosols (aerosol concentration changing continuously) containing various metals. This demonstrates the ability of the

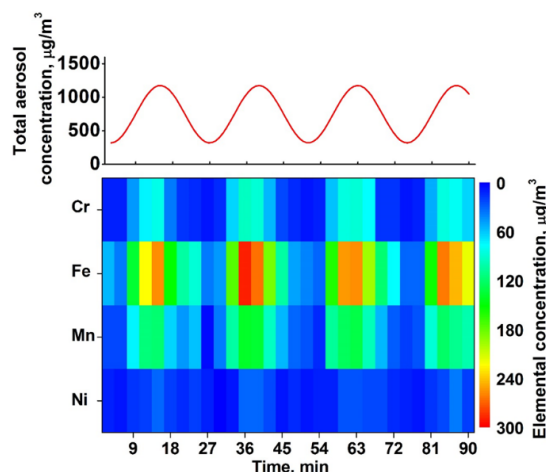


Figure 2: Continuous monitoring of multiple elements in a simulated transient exposure

instrument to effectively capture short-term, acute exposures typical in many industrial atmospheres involving combustion processes and nanomaterials.

### References

1. Diwakar, P. and P. Kulkarni, *Measurement of Elemental Concentration of Aerosols Using Spark Emission Spectroscopy*. *J. Anal. At. Spectrom.*, 2012. **27**(7): p. 1101-1109.
2. Zheng, L., Kulkarni, P., Birch, M. E., Deye, G. and Dionysiou, D. D. (2016). Near Real-Time Measurement of Carbonaceous Aerosol Using Microplasma Spectroscopy: Application to Measurement of Carbon Nanomaterials. *Aerosol Science and Technology* 50:1155-1166.
3. Zheng, L., Kulkarni, P., Zavvos, K., Liang, H., Birch, M. E. and Dionysiou, D. D. (2017). Characterization of an Aerosol Microconcentrator for Analysis Using Microscale Optical Spectroscopies. *Journal of Aerosol Science* 104:66-78.

## Physicochemical characterization of nanoparticles-containing spray coating generated by atomization process

O.Fichera<sup>1</sup>, J. Mejia<sup>1</sup>, J. Laloy<sup>2</sup>, L. Alpan<sup>2</sup>, S. Lucas<sup>1</sup> and J-M. Dogné<sup>2</sup>

<sup>1</sup>Department of Physics (PMR-LARN), <sup>2</sup>Department of pharmacy

All of University of Namur, Namur Nanosafety Centre (NNC), Namur, Belgium.

### Abstract:

Nanomaterials are nowadays the great concern of scientists. They are used in a wide range of industrial applications and incorporated into many common products (cosmetic, foods, consumer electronics, textiles...). Paints and coatings are part of these products and nanoparticles (NPs) are increasingly been added to their formulations to improve mechanical, physicochemical and antimicrobial properties. Spray painting is known to cause harmful effects (workers exposure to small paint aerosol) due to the generation of nano-size particles during the spraying process. Inhalation is the major route of exposure to airborne NPs and their potential effects on the human health (in particular on the deep lungs) remains unclear. In this work, we report the characterization of the non-volatile fraction of paint overspray created by air spray guns. Different techniques were used as Centrifugal Liquid Sedimentation (CLS), Transmission Electron Microscopy (TEM), Scanning Electron Microscopy (SEM), Energy-dispersive X-ray spectroscopy (EDX) and Electrical Low Pressure Impactor (ELPI). Paints containing titanium dioxide (TiO<sub>2</sub>) or carbon black (CB) NPs were studied and aerosols were produced by using IWATA 1,3 mm gun (flow rate: 20 g /min). TEM confirms the presence of two kinds of droplets in the aerosol spray: microdroplets (1 μm to 10 μm) and nanodroplets (100 nm to 1 μm). TiO<sub>2</sub> NPs appear only in the form of agglomerates (average size: 460 nm) while individualized C NPs are observed. In both cases, NPs are preferentially located inside microdroplets. Characterizations show also that NPs seems strongly embedded into the polymer matrix, this means that different interactions as hydrogens bonds, electrostatic and Van Der Waals interactions may take place between the NPs and the polymer. In parallel to this study, the acute potential toxicity of the paint aerosol in a whole-body exposure model will be evaluated on rats. For this, hispathological examinations of mains organs, and evaluation of the

biopersistence using Particles Induced X-ray Emission (PIXE) will be performed.

**Keywords:** engineered nanoparticles, paints, coatings, spray can aerosol, spray painting process, airborne particles and automotive industry.

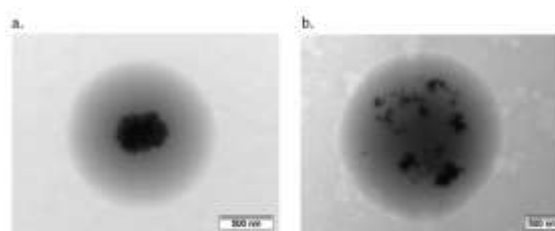


**Figure 1:** TEM images of a paint droplet containing a. titanium dioxide (TiO<sub>2</sub>) NPs, b. Carbon black (CB) NPs. Samples were analyzed with a Philips Tecnai 10 operating at 100 keV and in bright-field mode.

### References:

1. Lövestam, G. and al. (2010) Considerations on a definition of nanomaterial for regulatory purposes, *Joint Research Centre (JRC) Reference Reports*, 80004-1.
2. Hagedorfer, H. and al. (2010) Size-fractionated characterization and quantification of nanoparticle release rates from a consumer spray product containing engineered nanoparticles, *Journal of nanoparticle research*, 2481-2494.
3. Chen, B. T. and al. (2010) Nanoparticles-containing spray can aerosol: characterization, exposure assessment, and generator design, *Inhalation toxicology*, 1072-1082.
4. Yang, W. and al. (2008) Inhaled nanoparticles—a current review, *International Journal of Pharmaceutics*, 239-247.

## High resolution measurement of aerodynamic focusing behaviour of nanoparticles in different gases and gas-mixtures using a Differential Aerodynamic Particle Sizer (DAPS)

D. Kiesler<sup>1</sup> and F.E. Kruijs<sup>1</sup>

<sup>1</sup>Institute of Technology for Nanostructures (NST) and Center for Nanointegration Duisburg-Essen (CENIDE), University Duisburg-Essen, Duisburg, D-47057, Germany

Keywords: aerodynamic focusing, particle relaxation time, gas dependency, online measurement, Presenting author email: dennis.kiesler@uni-due.de

### Motivation

Gas properties play an important role for aerosol dynamics and transport. In this work, the transport properties of nanoparticles in pure gases and mixtures are studied based on the particles relaxation time  $\tau$ . The instrument used, is the Differential Aerodynamic Particle Sizer (DAPS), which is designed to separate particles according to their relaxation time  $\tau$  with a high resolution differential transfer characteristic (Kiesler and Kruijs, 2016, Huber *et.al.*, 2016). The measurement method is based on aerodynamic focusing at a thin plate orifice (Liu *et al.*, 1995). The typical pressure range of the instrument is 1 mBar to 10 mBar, which is comparable to nano-impactors, and the results are valid for Knudsen-numbers  $Kn \gg 1$ . The online measurement capability of the DAPS is well suited for this task.

### Experimental setup

The DAPS consists of an aerodynamic lens which is combined with a central sheath gas inlet in front of the orifice to keep the axis particle free before focusing. After the focusing, particles on the axis are sampled and counted in an electrometer. The selected diameter can be changed by scanning the pressure in the system, allowing the online measurement of a full particle number-size-distribution.

The full setup is shown in figure 1. To count the particles selected by the DAPS, the system is combined with a corona charger and a faraday-cup-electrometer. Gas mixtures can be created easily by exchanging the particle free sheath gas in the system. Thus a parallel measurement with already established measurement systems (SMPS, ELPI) is possible.

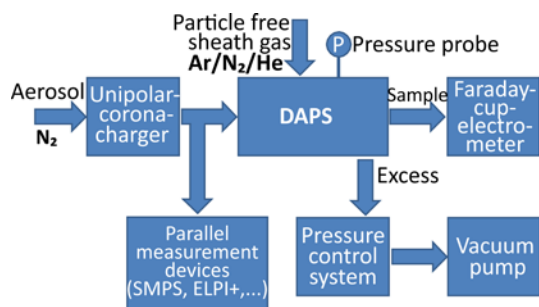


Figure 1. Experimental Setup. Gas mixtures are created by adding different gases as sheath gas.

### Results

First results are shown in figure 2, where a silver nanoparticle aerosol was generated, sintered and a monodisperse fraction was selected by a DMA. The Helium content was altered by changing the sheath and aerosol gas flowrate keeping the total flowrate constant. Gas viscosity and mean free path have been calculated as averages for the mixtures. The focused diameter predicted (lines) by theory corresponds to a Stokes-number  $Stk = 1$ . The measured values (dots) agree well with the predictions.

The addition of a light gas helps to focus smaller particles at the same system pressure and flowrate.

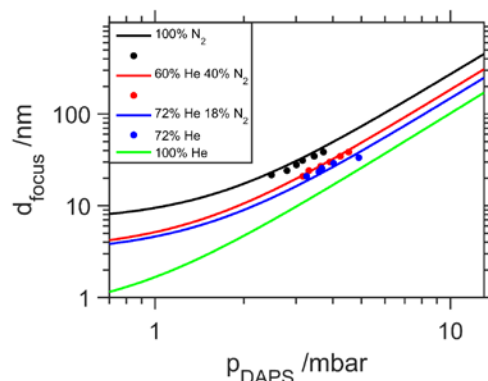


Figure 2. Comparison between  $Stk = 1$  focused diameter prediction for averaged gas properties (lines) in comparison to the measured focused diameter (dots).

### Acknowledgement

The research leading to these results has received funding from the Deutsche Forschungsgemeinschaft (DFG) in the framework of the joint research program “multi-parameter characterization of particle-based functional materials by innovative online measurement technology” (PAK688).

Kiesler, D. and Kruijs, F.E. (2016) *European Aerosol Conference, Presentation*, Tours, France.

Huber, F., Pitz, M., Kiesler, D. (2016), Partec 2016 - International Congress on Particle Technology (Proceedings), Nuremberg, 19.-21.04.2016, paper 4.34

Liu, P. Ziermann, P.J., Kittelson, D.B. and McMurry, P.H. (1995) *Aerosol Sci. Technol.* **22**, 293 .

## Sintering of Fe-Nanoparticles in a Well-defined Model Flow Reactor

T. Rosenberger<sup>1</sup>, F.E. Kruis<sup>1</sup>

<sup>1</sup>Institute of Technology for Nanostructures (NST) and Center for Nanointegration Duisburg-Essen (CENIDE), University of Duisburg-Essen, Duisburg, D-47057, Germany

Keywords: sintering, laminar flow, instrumentation

Presenting author email: thore.rosenberger@uni-due.de

Formation of particle structure during sintering is complex process due to their dependency of various particle properties, for example size, shape, agglomerate structure as well as the dependency of the process parameters like temperature and residence time in the reactor. Precise experimental data are needed to validate sinter models (Kruis *et al.* 1993).

This precision can be increased by a model flow reactor, where the process parameters can be simplified by using a laminar flow field with well-defined particle trajectories and a narrow resident time distribution. CFD simulations can be used to calculate the temperature and resident time of the particles in the reaction zone.

The model flow reactor is based on a vertical tube furnace with water cooled gas in- and outlets. Particles are entering at the bottom of the reactor flow covered by a preheated sheath gas in the centre. Therefore, a small variation in residence time of the particle can be achieved. The water cooled in- and outlet are used to restrict the structure changes to the heated area. A setup for very short residence times around 100 ms in turbulent flows was presented by Kirchhof *et al.* (2004). In contrast our new setup is designed for resident times of at least 1 s.

### CFD-Simulation and validation

The construction of the model flow reactor is supported by CFD-Simulations, which are verified by measurements in the final setup (Figure 1). The reactor is optimised and a laminar flow field is assured in the temperature range from 773K to 1273K. A main problem in the design phase was a negative gas velocity in axial direction caused by convection. This is solved by adjusting the heating zone and providing a preheated sheath gas. As a result, the heating and cooling rate on the centre line are increased.

The simulations have been validated by a 2D temperature measurement with 9 thermocouples type K for three different temperatures, 1273K, 1023K and 773K. The thermocouples were positioned in the reactor with a radial resolution of 2 mm and 10 mm in axial direction (Figure 2).

### Sinter experiments

An aerosol consisting of monodispersed iron agglomerates, classified by its electrical mobility, is sintered in the model flow reactor for different temperatures ranging from 1373K to 573K. The particle mass and size distribution are measured by online instrumentation to detected structural changes of the particles. By using different particle sizes, the sinter kinetic can be determined.

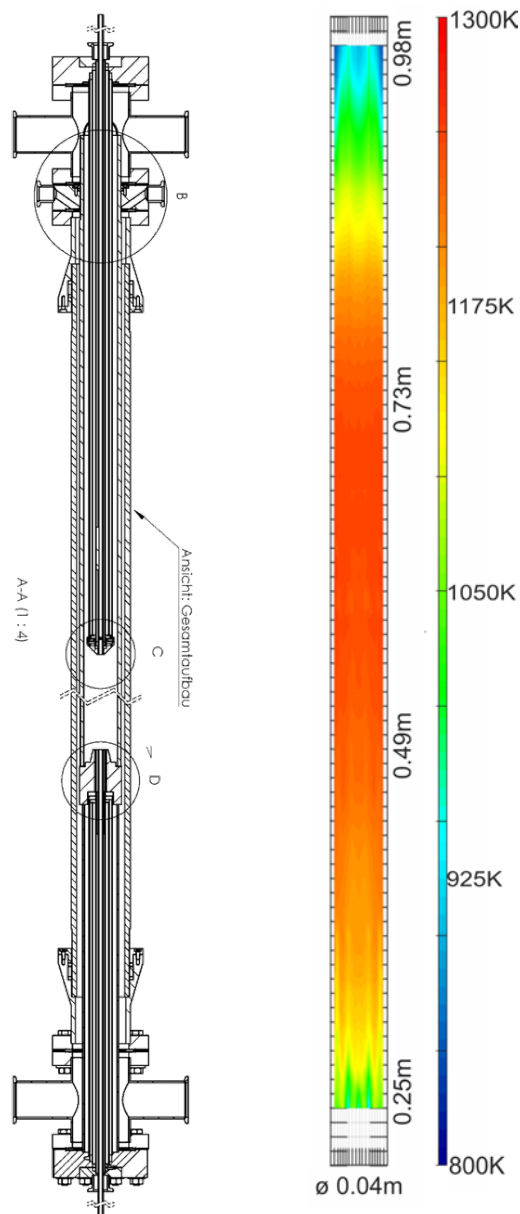


Figure 1. Construction drawing of the model flow reactor.

Figure 2. 2D measured temperature profile for 1273K.

### Acknowledgement

The research leading to these results received funding from the Deutsche Forschungsgemeinschaft (FOR 2284).

Kirchhof, M.J., Schmid, H.-J., Peukert, W. (2004) *Review of Scientific Instruments*, 75 (11), pp. 4833-4840.

Kruis, F.E., Kusters, K.A., Pratsinis, S.E. (1993) *Aerosol Science and Technology*, 19 (4), pp. 514-526.

## Distribution of radioactive admixtures on aerosol particles

V.A. Zagaynov<sup>1,2</sup>, M.E. Masyanovich<sup>3,4</sup>, M.V. Zhukovsky<sup>3,4</sup>, V.V. Maksimenko<sup>1,2</sup>, A.A. Lushnikov<sup>1,2</sup>,  
I.E. Agranovski<sup>5</sup>

<sup>1</sup>National Research Nuclear University MEPhI (Moscow Engineering Physics Institute), 31, Kashirskoe shosse, 115409, Moscow, Russia

<sup>2</sup>Karpov Institute of Physical Chemistry, Vorontsovo Pole, 10, 105064, Moscow, Russia

<sup>3</sup>Institute of Industrial Ecology UrB RAS, Yekaterinburg

<sup>4</sup>Ural Federal University by President Eltsyn, Yekaterinburg

<sup>5</sup>School of Engineering, Griffith University, Brisbane, 4111 QLD, Australia

Keywords: radioactivity, distribution, nanoparticles, coagulation.

Presenting author email: vzagaynov@yandex.ru

It is well known, that aerosol particles in atmosphere are vehicle for transport of radioactivity and other air admixtures in the ambient air. At the same time, one of the main sources of radioactivity in the atmosphere is natural radon. Transport properties of the aerosol particles depend on the particle size distribution. It is known that Radon is an inert gas producing  $^{222}\text{Rn} \rightarrow ^{218}\text{Po} \rightarrow ^{214}\text{Pb} \rightarrow$  as the result of radioactive decay. These radioactive metallic products could potentially collide with aerosol particles and remain on their surfaces turning neutral aerosols into radioactive ones. Such alteration enables one characterizing aerosol parameters by monitoring radioactivity of particles. To measure distribution of radioactivity on aerosol particles diffusion batteries were used. At the same time, a Diffusion Aerosol Spectrometer was used to get particle size distribution. The measurements were carried out in a radon box equipped with the air booster and gas analyzer. Aerosol particles were generated from natural glycerin and polypropylene glycol by evaporative generator. The screen-type diffusion battery consisting of 20 stages was used for measuring radioactive aerosol size distribution in the range from 1 to 200 nm. Consecutive arrangement of capturing elements of this cascade-type diffusion battery allows assessment of the aerosol size distribution in a single sampling run. Two types of capture elements with different physical parameters were used in this research. The first type, made out of brass wire mesh (Cu-Zn) with a density of  $8.5 \text{ g/cm}^3$ , wire thickness of  $65 \mu\text{m}$  and opening of  $100 \times 100 \mu\text{m}$ , has  $d_{50}$  in a range from 1.5 to 16.5 nm. The second type with  $d_{50}$  in a range from 3.0 to 32 nm was made out of stainless steel wire mesh with the density of  $7.8 \text{ g/cm}^3$ , wire thickness -  $30 \mu\text{m}$ , and opening of  $40 \times 40 \mu\text{m}$ . The air sample was made to pass through the diffusion battery and deposited radioactive radon decay products on 20 capturing elements of diffusion battery were consequently measured with scintillation alpha-radiometer. Method of expectation maximization, as suggested by Maher and Laird (1985), was used to evaluate the results of the indirect measurement data inversion in terms of accuracy. To convert obtained measured data into particle size distribution the method of transformation integral equation into nonlinear algebraic equation was used (Zagaynov, 2006). The

penetration  $P(n)$  of particles throughout screen type diffusion batteries with  $n$  screens was calculated as:

$$P(n) = \left(1 + \frac{An}{\lambda}\right)^{-\gamma}$$

where  $A=4.52$ ;  $\lambda$  and  $\gamma$  are parameters of gamma distribution. As the result, the distribution of radioactivity on the aerosol particles was obtained as presented in Fig. 1.

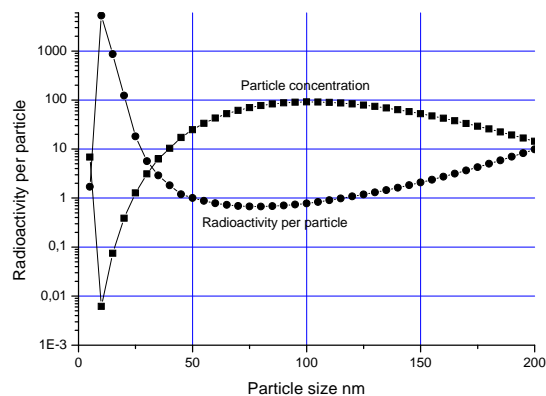


Figure 1. Measured distribution of radioactive admixture on aerosol particles. Cubes – activity distribution, rounds – particle size distribution

As is seen, the activity distribution is not monotonic with size. To get corrected information on this distribution the model calculations are required and the results will be presented at EAC-2017

Acknowledgments. The work was supported by RSCF (project # 14-03-00507 and # 14-07-00025)

Maher, E. F. and Laird, N. M. EM algorithm reconstruction of particle size distributions from diffusion battery data. *J. Aerosol Sci.* 16(6), 557–570, 1985

Zagaynov V.A. Diffusion aerosol spectrometer for nanoparticle diagnostics in gas phase – *Nanotechnics*, №1, c. 141 – 146, 2006

## Study on photocatalytic hydrogen production and photodegradation of oxytetracycline using Pt/TiO<sub>2</sub> composites

Jingjing Tian<sup>1</sup>, ChangTang Chang<sup>2</sup>

<sup>1</sup>Department of Environment Engineering, National Ilan University, Ilan City260, Taiwan

<sup>2</sup>Department of Environment Engineering, National Ilan University, Ilan City260, Taiwan

Keywords: hydrogen production, photodegradation of OTC, photocatalyst

Presenting author email: jjtian0522@gmail.com

Hydrogen is considered as a promising energy source with its high energy yield, renewable, environment friendly properties. TiO<sub>2</sub> modified with noble metal is widely used for solar photocatalytic decomposition of water to produce hydrogen. In this study, Pt was used to modify TiO<sub>2</sub> nanoparticles and it was successfully synthesized by photodeposition method. The characterizations of the synthesized catalysts by UV-vis, XRD, FTIR, SEM and TEM analysis were also conducted.

Oxytetracycline (OTC) is popularly used in humans and a toxic threat to the ecosystem. However, it is hardly degraded by conventional biological treatment methods because of its antibiotic property and chemical stability. Therefore, the object of this study is to use metal modified TiO<sub>2</sub> photocatalysts for OTC removal.

The maximum hydrogen production rate was approximately 6.33 mmol h<sup>-1</sup> g<sup>-1</sup> when the Pt content was 0.5 wt.%. Higher and lower than 0.5 wt.% of Pt loading content both result in low efficiency of hydrogen production. The mechanism of Pt /TiO<sub>2</sub> for improving photocatalytic activity is proposed. The results showed that 0.1 g L<sup>-1</sup> is found to be the optimum catalyst concentration for optimal hydrogen production. Excess catalyst may result in opacity of the reaction solution and the light intensity is decreased.

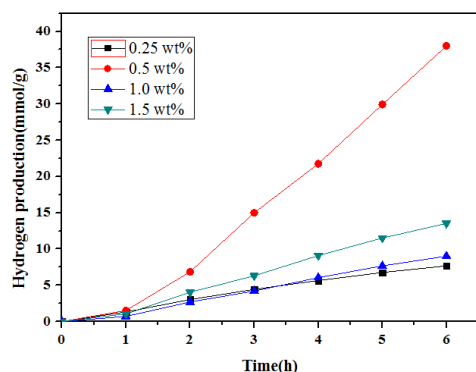


Figure1. Effects of Pt loading content on hydrogen production (catalyst concentration 0.1g L<sup>-1</sup>; sacrificial agent 10 vol.% methanol; a 500 W Xenon lamp)

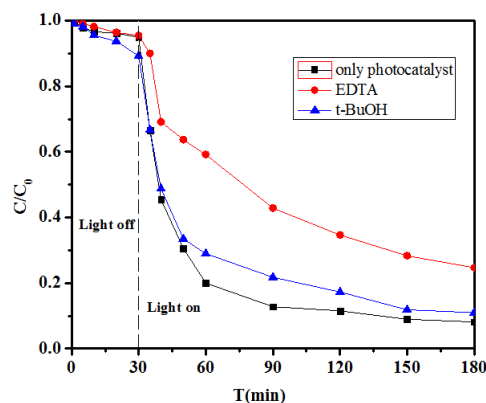


Fig.2. Effect of EDTA and t-BuOH on the photocatalytic degradation of oxytetracycline (10 mg L<sup>-1</sup>oxytetracycline, 0.1 g L<sup>-1</sup> 0.5 wt.% Pt/TiO<sub>2</sub>, a 500 W Xenon lamp)

In addition, the results showed that 0.5 wt.% Pt/TiO<sub>2</sub> had a higher degradation capacity of approximately 92 % OTC removal than other contents of Pt. Besides, the hole scavengers and radical scavengers (Hu et al, 2016) were added (with 10 mM of EDTA or t-BuOH, respectively) into the reaction for understanding whether the photogenerated holes and electrons is the main oxidant during the photocatalytic process. The poorest performance was found by supplementation of EDTA, which could capture hole to inhibit oxidation, to indicate the holes involved in the reaction were the major active oxidant.

Hu, X. Y., Zhou, K. F., Chen, B. Y., & Chang, T. C. (2016) *Graphene/TiO<sub>2</sub>/ZSM-5 composites synthesized by mixture design were used for photocatalytic degradation of oxytetracycline under visible light: Mechanism and biotoxicity*. Applied Surface Science.

## Characterisation of aerosol release from the combustion of epoxy/graphene nanoplatelet/DOPO nanocomposites

W. Netkueakul<sup>1,2</sup>, F. Nüesch<sup>3</sup>, B. Fischer<sup>3</sup>, S. Gaan<sup>4</sup>, M. Jovic<sup>4</sup> and J. Wang<sup>1,2</sup>

<sup>1</sup>Institute of Environmental Engineering, ETH Zürich, Switzerland, <sup>2</sup>Department of Advanced Analytical Chemistry, Empa, Switzerland, <sup>3</sup>Department of Functional Polymer, Empa, Switzerland, <sup>4</sup>Department of Advanced Fibers, Empa, Switzerland

Keywords: Nanocomposite, Particle release, Graphene, Organophosphorous flame retardant.

Presenting author email: woranan.netkueakul@empa.ch

Novel classes of flame retardants have gained more interests due to the banishment of toxic halogen-containing flame retardants. DOPO (9,10-dihydro-9-oxa-10-phosphaphenanthrene-10-oxide) is a widely used organophosphorous flame retardant because of its outstanding thermal stability. However, some studies reported that DOPO could deteriorate certain mechanical properties of polymer materials (Wang *et al.*, 2013). Graphene nanoplatelet (GnP) has been studied as a nanofiller to enhance the performance of polymers such as mechanical properties (Chatterjee *et al.*, 2012), flame retardancy (Hu *et al.*, 2014), and electrical properties (Tang *et al.*, 2013). So far, there have been a few studies investigating the combination of GnP and DOPO in polymer composites (Wang *et al.*, 2013; Liu *et al.*, 2016; Yang *et al.*, 2016). Although DOPO is an effective flame retardant, it has neurotoxicity concerns. However, the release of this compound from nanocomposites was still unknown. To our best knowledge, the characterization of particle emissions from the combustion of epoxy/GnP/DOPO nanocomposites was performed for the first time in this study.

The aim of this study is i) to investigate the mechanical property and thermal stability of manufactured epoxy/GnP/DOPO nanocomposites, and ii) to characterise the release of aerosol particles during the combustion of the nanocomposites. Epoxy matrix was Araldite GY-250 from Huntsman, USA. Jeffamine D-230 (Huntsman, USA) was used as a curing agent with the resin/hardener ratio of 100:32. DOPO (TCI, Japan) was incorporated into an epoxy matrix with various amounts at 0 wt%, 3 wt%, and 10 wt%. The concentrations of 25 µm GnP (XG Company, USA) in either epoxy matrix or epoxy/DOPO were 0 wt%, 0.1 wt%, 0.5 wt%, and 1.0 wt%. The dispersion of GnP in an epoxy matrix or epoxy/DOPO was conducted using three-roll milling (SDY200, Buhler AG, Switzerland).

The flexural modulus of nanocomposites was determined according to ISO178:2001 using Zwick roell (model Z10). The thermal properties of nanocomposites were determined using thermogravimetric analysis, TGA (Netzch TG 209 F1 instrument). A large set of instruments was employed to characterize the size distribution, morphology, and elemental composition of the particles released (adapted from Schlagenhauf *et al.*, 2015) as shown in Figure 1. The FTT cone colorimeter was used for testing the flame retardancy properties of nanocomposites. During the combustion, the emissions were sampled and characterised as followed. The

aerosol-sampling probe was placed above flame. The emissions were diluted and cooled with the filtered air in a 10-litre chamber. A thermal denuder could be applied for the differentiation of volatile compounds from soot particles. The particle size distributions were measured using scanning mobility particle sizer (SMPS). The nanometer aerosol sampler (NAS, model 3089, TSI, USA) was used to collect samples for further SEM analysis.

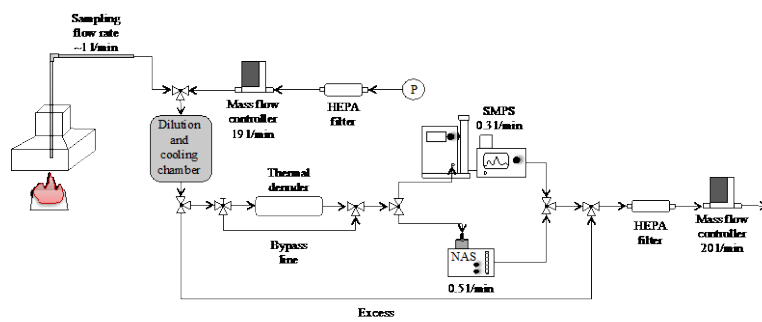


Figure 1: A schematic experimental set up.

The preliminary results showed that an increase in percentage of GnP resulted in a gradual increase in flexural modulus of epoxy/GnP nanocomposites. The addition of DOPO showed a significantly increase in flexural modulus. On the other hand, an increase in GnP content in the presence of DOPO reduced the flexural modulus of the composites. The TGA results showed that the addition of either GnP or DOPO resulted in a decrease in the decomposition temperatures of nanocomposites.

- Chatterjee, S., Nafezarefi, F., Tai, N.H., Schlagenhauf, L., Nüesch, F.A. and Chu, B.T.T. (2012) *Carbon* **50**, 15, 5380–5386.
- Hu, W., Song, L., Wang, L., Hu, Y. and Zhang, P. (2014) *Fire Safety Sci* **11**, 895–904.
- Liu, S., Fang, Z., Yan, H. and Wang, H. (2016) *RSC Adv.* **6**, 5288–5295.
- Schlagenhauf, L., Kuo, Y.Y., Bahk, Y.K., Nüesch, F. and Wang, J. (2015) *J Nanopart Res* **17** (11).
- Tang, L.C., Wan, Y.J., Yan, D., Pei, Y.B., Zhao, L., Li, Y.B., Wu, L.B., Jiang, J.X., and Lai, G.Q. (2013) *Carbon* **60**, 16–27.
- Wang, X., Song, L., Pornwannchai, W., Hu, Y., and Kandola, B. (2013) *Composites* **53**, 88–96.
- Yang, S., Wang, J., Huo, S., Wang, M., Wang, J. and Zhang, B. (2016) *Polym Degrad Stab* **128**, 89–98.

## Ethanol and hexamethyldisilazane removal with composites of zeolite and molecular sieve

H.W. Huang<sup>1</sup> and C.T. Chang<sup>2</sup>

<sup>2</sup>Department of Environmental Engineering, National ILAN University, I-Lan 26047, Taiwan

Keywords: VOCs, HMDS, Zeolite.

Presenting author email: littleyellow39@yahoo.com.tw

### Abstract

The semiconductor industry often discharges VOCs containing high concentrations of HMDS (Hexamethyldisilazane) and ethanol. Thermal decomposition of the HMDS causes solid silica to deactivate the catalyst and therefore requires pretreatment to separate HMDS from VOCs. HMDS contains Si components in high temperature incineration and generates silicon dioxide powder. It is noteworthy that if RTO (Regenerative Thermal Oxider) was used as the final incineration system without removing HMDS, the generated silica powder would block the RTO of the thermal storage material. As a result, the pressure loss would be increased and the function of RTO will be failed. Therefore, the aim of this research is to develop a novel selective adsorbent to remove HMDS from flue gas before entering catalyst reaction.

Domestic and foreign research shows adsorption treatment is the best method to remove HMDS. The granulated mixture of 4A molecular sieve (M) and zeolite (Z) with different proportion was used to assess the adsorption performance. The adsorption experiments were carried out at room temperature under different C<sub>2</sub>H<sub>5</sub>OH and HMDS concentration, material dose and gas flow rate.

The results show that the adsorption capacity of HMDS was decreased with increasing the ratio of molecular sieve. It demonstrated that component of zeolite is more important than that of molecular sieve. The adsorption capacity of HMDS is ranged from 0.5 to 1.2 mg g<sup>-1</sup>, as shown in Figure 1. The highest adsorption capacity of HMDS is 1.2 mg g<sup>-1</sup> with using the ratio of M and Z as 2:3 due to contribution of zeolite. The size of HMDS is suitable by using the composite of M and Z with the ratio as 2:3. In contrast, adsorption capacity of HMDS is only 0.5 mg g<sup>-1</sup> with M.

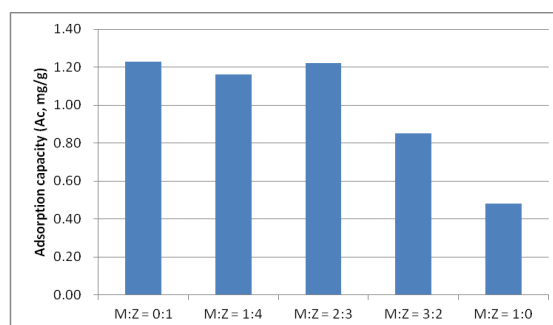


Fig.1 Adsorption capacity with different adsorbents

In addition, the breakthrough time was increased with the zeolite content. The largest breakthrough time happens with using pure zeolite due to its high surface area and small pore volume. In contrast, the breakthrough time is very small with using pure 4A molecular sieve due to its small pore volume.

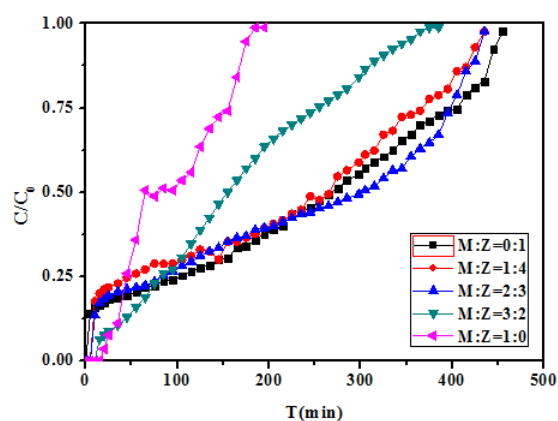


Fig.2 Breakthrough time with different adsorbents  
Tsai, Hsiao-Hsin (2015) Acetone and Hexamethyldisilazane Removal with Mesoporous Materials and Catalysts prepared from Calcium Fluoride Sludge, ILAN University

## **Abstracts T107**

## Key parameters to control the mean charge in post-DBD aerosol neutralization

N. Jidenko, R. Mathon and J.-P. Borra

Laboratoire de Physique des Gaz et des Plasmas, CNRS, Univ. Paris Sud, CentraleSupélec, Université Paris-Saclay, 3 Rue Joliot Curie, F-91192 Gif-sur-Yvette, France

Keywords: bipolar diffusion charging, electrical discharges, charge distribution, dielectric barrier discharge.

Presenting author email: nicolas.jidenko@u-psud.fr

Aerosol neutralization is required to limit losses of charged aerosol by self-electrostatics repulsion or to control aerosol charge distribution for submicron particles size distributions measurements with a differential mobility analysis (DMA). Diffusion of bipolar ions leads to well-defined charge distributions (Fuchs, 1963; Wiedensohler, 1988) when aerosol reaches a stationary charge distribution. The conditions to reach the steady state are defined in (de la Verpilliere et al. 2015). The aim is here to confirm the key parameters of post-DBD neutralizer that control the mean charge per particle for the measurement of aerosol size distribution in the range from 15 to 730 nm. We have already confirmed, as predicted by Gunn's law, that the mean charge and the squared standard deviation are proportional to particle diameter and constant whatever the aerosol concentration is (Mathon et al.). Gunn's law also predicts that, in constant ion densities, the mean charge depends on the  $N_i^+ \cdot Z_i^+ / (N_i^- \cdot Z_i^-)$  ratio with  $N_i$  and  $Z_i$  the ion density and the electrical mobility of ions. In decreasing ion densities, we define an equivalent  $N_i \cdot Z_i$  ratio leading to the measured mean charge.

Bipolar chargers, based on post-Dielectric Barrier Discharge (DBD), have been characterized in terms of post-discharge ion densities and aerosol charge distribution. Positive and negative post-DBD ion currents have been measured downstream the DBD to estimate the ion fluxes and the ratio of positive to negative ion density at the inlet and the outlet of the charging volume.

Plane-to-plane DBD arrangements produce bipolar ions. Ions are blown from the discharge using airflow rate from 0.3 up to 4 L.min<sup>-1</sup>. Then, aerosols and ions are mixed in a charging chamber. Aerosol is injected in post-DBD to avoid aerosol precipitation in the discharge gap and the related discharge destabilization. Two planes of alumina (thickness of 0.5 mm) are separated by a gap of 1.6 mm and polarized by metal cylinder electrodes with 4 mm diameter and 30 mm length. The flow section is 1.6 mm height × 50 mm length. The discharge occurs as thin and brief filamentary discharges (100 μm diameter and 20 ns duration) that can be used for aerosol or ion production (Borra 2006). Each filament is a transient and localised source of positive and negative ions initially located at the cathode and anode side of the filament respectively (Xu et al. 2000). During the 100 ms transport from the discharge to the charging chamber, ions are mixed to reach homogeneous bipolar cloud.

As example, the mean charge per particle versus DBD overvoltage  $\Delta V$  (from extinction voltage) is presented in Fig. 1 for two DBD arrangements at  $F=60$  kHz and 0.3 L.min<sup>-1</sup> for both aerosol and post-DBD ion flows.

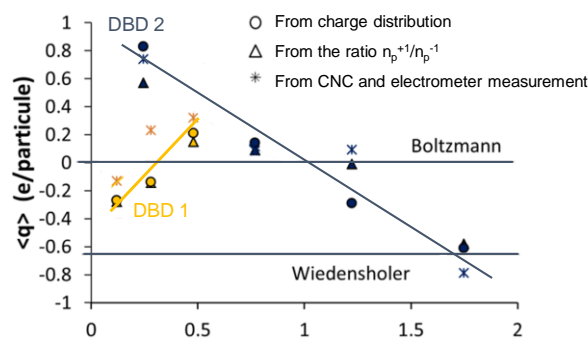


Fig. 1. mean charge per particle for 440 nm monodispersed aerosol neutralized by 2 DBD neutralizers with air flow versus discharge overvoltage.

Post-DBD ions densities and mobilities can be controlled by flow rates, DBD voltage (cf. Fig. 1), and post-discharge arrangement (cf. Fig. 1). Thus, charge distribution could be adjusted for aerosol neutralization.

In the charging volume, the equivalent  $N_i \cdot Z_i$  ratio is controlled by recombination and diffusion of ions, which depend on charging time and initial  $N_i \cdot Z_i$  ratio at the entrance of the charging volume. The  $N_i \cdot Z_i$  ratio at the entrance of the charging volume is controlled by electro-collection of ion on the walls and recombination, which depend on electric field (including Laplace, surface and space charge electric fields) and the transit time from the discharge to the entrance of the charging volume.

Whatever the condition of neutralisation, the size distributions are similar with <sup>85</sup>Kr and post-DBD neutralizer, for aerosol with diameters from 20 to 730 nm and concentration up to  $6 \times 10^{12}$  m<sup>-3</sup> with a total concentration of the size distribution only affected within less than 10 %. The differences arise from the slightly different mean charge in post-DBD than in <sup>85</sup>Kr that could be corrected using the proper charge distribution in the data inversion.

This post-DBD bipolar charger can neutralizer submicron aerosol and is suitable for SMPS size distribution measurements, with air or nitrogen injection in the DBD to suppress ozone production from air DBD.

Fundings: The authors would like to thank Palas GmbH for their funding of this research.

### References

- Borra J.-P. (2006). *J Phys.D.: Appl. Phys.* **39**(2), R19-R54.  
 de La Verpilliere JL, Swanson, JJ & Boies, AM (2015) *JAS* **86**,56-68.  
 Fuchs, N. A. (1963). *Geofisica Pura e Applicata*, **56**, 185-193.  
 Gunn, R. (1955). *J. Coll Sci*, **10**(1), 107-119.  
 Mathon R., Jidenko N. and J-P Borra (2017) *JAST* on line  
 Wiedensohler, A. (1988). *JAS*, **19**(3), 387-389.  
 Xu X. & Kushner, MJ (1998). *J. of Appl. Phys.*, **83**(12), 7522-32.

## A study of a needle-plate corona charger to reduce agglomeration during synthesis of aerosol nanoparticles by spark discharge

A.A. Efimov, P.V. Arsenov and V.V. Ivanov

Department of Physical and Quantum Electronics, Moscow Institute of Physics and Technology, Dolgoprudny, 141700, Russia

Keywords: agglomeration, aerosol nanoparticles, needle-plate corona charger.

Presenting author email: [efimov.aa@mipt.ru](mailto:efimov.aa@mipt.ru)

In recent years there has been growing interest in using aerosol nanoparticles to create new materials and devices (Kortshagen *et al.*, 2016). It is known that the properties of aerosol nanoparticles significantly depend on their size. It is also known that the size of aerosol nanoparticles is increased in the process of their synthesis as a result of agglomeration of nanoparticles. In this regard, researchers are developing methods and devices to reduce the agglomeration of nanoparticles. The most effective method to reduce the agglomeration of nanoparticles is a dilution. However, this method is not always realized in practice, since there are physical limitations to increase dilution ratio during the synthesis of nanoparticles. Charging of the particles is an alternative method to reduce agglomeration of nanoparticles. Device for charging of aerosol nanoparticles are called the chargers. In this work, we investigate the needle-plate unipolar charger to reduce agglomeration of aerosol nanoparticles of  $\text{Al}_2\text{O}_3$  obtained by multi-spark discharge generator (Efimov *et al.*, 2016).

The studied unipolar charger was a discharge gap in the form of a steel needle and a plate, which was mounted in a plastic tube with a diameter of 45 mm, see Fig. 1a. The needle is placed in the center of the plate at a distance of about 10 mm.

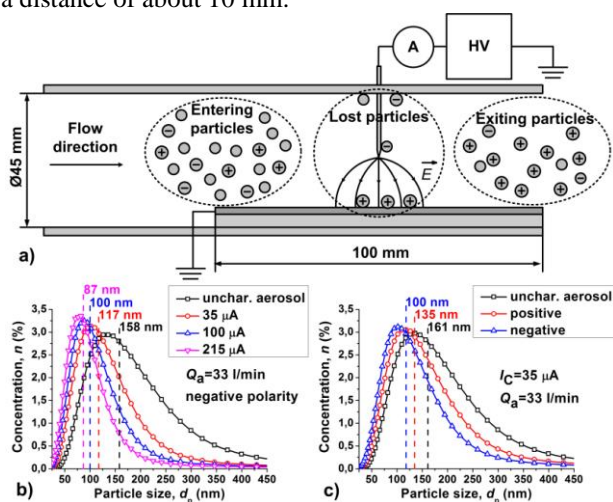


Figure 1. The scheme of the needle-plate corona charger (a); Particle size distribution depending on the value of ion current (b) and polarity (c) of the charger.

The radius of curvature of the needle was about 200  $\mu\text{m}$ . The plate had the dimensions of 100x30  $\text{mm}^2$ . A corona discharge was observed by applying a high voltage between the needle and the plate. Aerosol nanoparticles

that have passed through the corona discharge region become charged particles. The polarity of the charged particles depended on the polarity of the voltage on the needle. The test of charger is performed by varying the values of corona discharge current and the polarity of the charger.

It is found that the size of agglomerates decreases more than in 2 times from 161 to 70 nm when the value of the corona current increases from 35 to 215  $\mu\text{A}$ , respectively (see Fig. 1b). Also found that the charged aerosol passes through the charger has an exit charging efficiency of about 50-83%. The obtained results show that agglomeration of the nanoparticles is reduced probably due to the Coulomb repulsion of same charged particles. In addition, it is found that the charger works as an electrostatic precipitator. Moreover, the efficiency of deposition of large agglomerates is higher than for small particles. This result is explained by the fact that large agglomerates have higher electrical mobility than the smaller particles due to the high number of charges on the particles.

It is also established that the size of agglomerates is less, if the charger operates at negative polarity electrodes (see Fig. 1c). This result is due to the fact that the electrical mobility of the electrons is higher than mobility of positive ions. As a result, the charging efficiency of particles in the negative corona is higher than in the positive.

The results of the study showed that to reduce agglomeration of the particles it is necessary to use high values of corona current and a negative polarity of the charger. In this case, reduction of particle agglomeration is a result of Coulomb repulsion of the charged particles and the electric filtration large agglomerates in an electric field. Thus, the obtained result demonstrates the ability to use the needle-plate corona charger for controlling particle size, which can be important for a number of applications in electronics.

This work was supported by the grant of the President of Russian Federation for young scientists MK-2302.2017.8.

Kortshagen, U. R., Sankaran, R. M., Pereira, R. N., Girshick, S. L., Wu, J. J., and Aydil, E. S. (2016). *Chemical Reviews*, **116** (18), 11061-11127.

Efimov, A., Lizunova, A., Sukharev, V. and Ivanov, V. (2016) *Korean J. Mater. Res.*, **26** (3), 123-129.

## **Abstracts T108**

## Discharge current characteristic on Hole-type Electrostatic Precipitator

Shohei Suzuki<sup>1</sup>, Shun Yokoyama<sup>1</sup>, Hiroataka Miyashita<sup>1</sup>, Yoshiyasu Ehara<sup>1</sup>, Takashi Inui<sup>2</sup>, Tomoyuki Sawada<sup>2</sup>

<sup>1</sup>Department of Technology, Tokyo City University, Tokyo, 158-8557, Japan

<sup>2</sup>Fuji Electric Co., Ltd., Tokyo, 141-0032, Japan

Keywords: electrostatic precipitator, re-entrainment, corona discharge, collection efficiency.

Presenting author email: g1315076@tcu.ac.jp

In recent years, air pollution by ships' diesel engines has been regarded as a problem. SO<sub>x</sub>, NO<sub>x</sub>, PM are cited as main causes of air pollution, which adversely affect human body and the environment. The electrostatic precipitator (ESP) has a simpler structure, a smaller pressure loss than other exhaust gas purification devices, and a high collection efficiency for high-concentration particles (wang *et al* 2013). However, there is a problem that re-entrainment occurs due to passage of time. Therefore, as a method to solve the re-entrainment, we developed a hole-type ESP (Ehara *et al* 2014). Hole-type ESP is an ESP with a hole in the collecting electrode. Particles are influenced by ionic wind generated by corona discharge and are induced in the holes. At this time, suppression of re-entrainment can be expected by inducing particles in the collection space where the electric field is 0. In this research, discharge current characteristics on hole-type ESP were investigated.

A diesel engine using light oil as a fuel was used. A 75% load was applied to the engine, and the exhaust gas was allowed to flow directly into the hole-type ESP. Particle size distribution was measured using a particle counter (PC: Rion, measuring range 300 to 5000nm) and a scanning mobility particle sizer (SMPS: TSI, measuring range 20 to 1000nm). Fig.1 shows the electrode structure of a hole-type ESP. The electrode configuration consists of a high-voltage needle electrode and a flat-plate hole ground electrode. The hole shape of the ground electrode has a diameter of 20 mm and an aperture ratio of 16%.

Fig.2 shows the result of collecting for each discharge current value in the hole-type ESP. The collection efficiency for particle size of 40~700nm increased with increasing the discharge current. It is considered that the particles are more easily charged by increasing the current and a strong Coulomb force is generated. On the other hand, the collection efficiency for particle size of 1000nm or more decreased with increasing the discharge current. When the discharge current is high, the electric field is high. Therefore, the electrostatic repulsion force due to induction charge becomes strong in high electric field. In particular, it is considered that particles with large sizes tend to re-entrainment due to large saturated charge amount and susceptibility to wind.

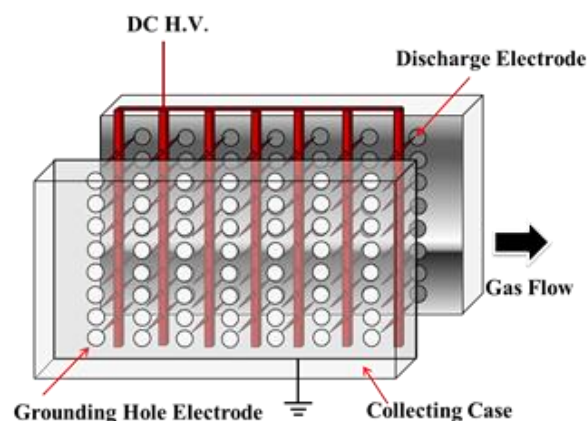


Figure 1. Hole-type ESP

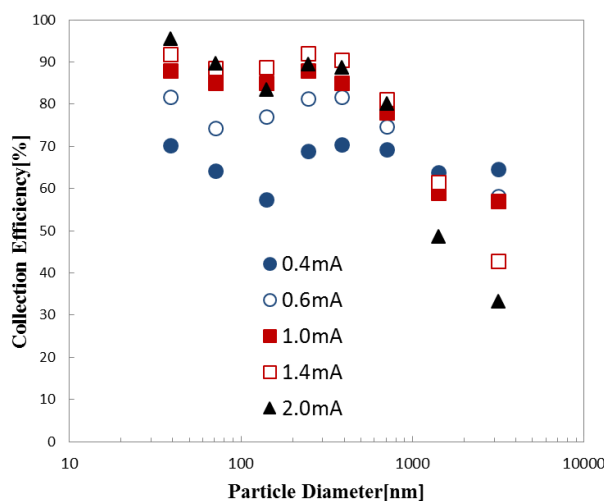


Figure 2. Collection efficiencies for the discharge current

This work was supported by JSPS Grant-in-Aid for Scientific Research, JP16H04606.

Xiaohua Wang , Changfu You (2013) *Effect of Humidity on Negative Corona Discharge of Electrostatic Precipitators*, IEEE Transactions on Dielectrics and Electrical Insulation Vol. 20, No. 5.

Y. Ehara, A. Osako, A. Zukeran, K. Kawakami T. Inui (2014), *Diesel PM collection for marine emission using hole-type electrostatic precipitators*, AIR POLLUTION 2014, Vol. 183

## PIV Analysis of Re-entrainment Phenomenon in the Electrostatic Precipitator

Kota Yanagawa<sup>1</sup>, Hiroataka Miyashita<sup>1</sup>, Yoshiyasu Ehara<sup>1</sup>, Takashi Inui<sup>2</sup>, Tomoyuki Sawado<sup>2</sup>  
<sup>1</sup>Dept. of Electrical and Electronic Engineering, Tokyo City University, Tokyo, 158-8557, Japan  
 Fuji Electric Co., Ltd, Tokyo, Japan

Keywords: Electrostatic Precipitator, Particle Image Velocimetry, Ionic Wind.  
 Corresponding author email: g1681346@tcu.ac.jp

In recent years, environmental problems are getting worse and become an important problem to be solved. An electrostatic precipitator (ESP), one of the air purification devices, has advantages such as high collection efficiency and low pressure loss. However, on the contrary, a re-entrainment phenomenon when collecting low resistance particles is regarded as a problem. In a previous study, clear photograph and moving image have not been reported about re-entrainment phenomenon. In this study, The re-entrainment phenomenon was visualized and determine the characteristics by particle image velocimetry (PIV) analysis.

The experimental system is shown in Fig. 1. The system consists of ESP, high speed camera (Photron FASTCAM SA 4), PC, power supply, laser irradiation part (Japan Laser, DPGL-2W), and PIV analysis software (Kato Koken, Flow Expert). The laser is irradiated parallel to the gas flow in the ESP, and particles inside the ESP are visualized by irradiating the laser from above. The visualized particles were photographed with a high-speed camera placed on the side of the ESP and analyzed by transmitting the image to the PC. ESP has a structure of needle-to-plate electrode. For the experimental conditions, the main fluid velocity was 0.5 m/s, the discharge current value was 3  $\mu$ A, the tracer particles were a talc, and the particles were collected for 10 minutes. After that, the surface of the electrode was photographed while the discharge state was maintained.

The experimental results are shown in Fig. 2. This image is a position behind 16mm from the needle electrode, 7.2mm in height and 12.5mm in width. The white area shows the PM collecting electrode, and the white dot shows the tracer particle. The image (a) is shown the particles are towards the collection electrode. The image (b) is shown the large particles are popping out from the collecting electrode. It was confirmed that the size of the re-entrainment particle is larger than the average particle diameter of ordinary talc. It is considered that the re-entrainment particles aggregated due to induced charging. The Coulomb force and the fluid resistance force became strong, so it was thought that they fly again. The white large dot in the image (b) is re-entrainment particle. This speed is 1.8m/s. Also, the angle is 23 ° from the collecting electrode. The velocity of the re-entrainment particles became faster than the main fluid velocity. It is considered that this reason because the Coulomb force from the counter electrode acts re-entrainment particles by induction-charge.

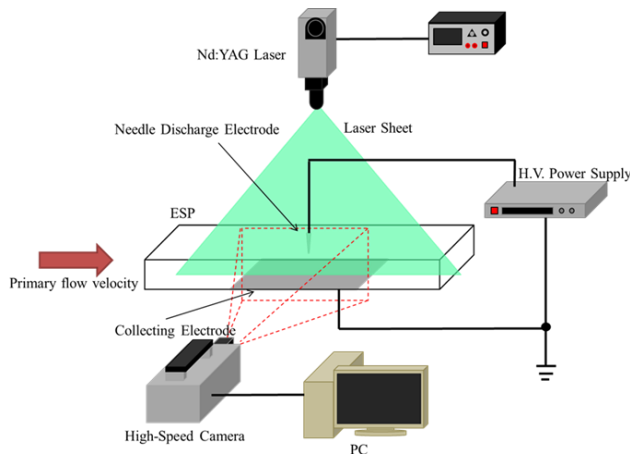
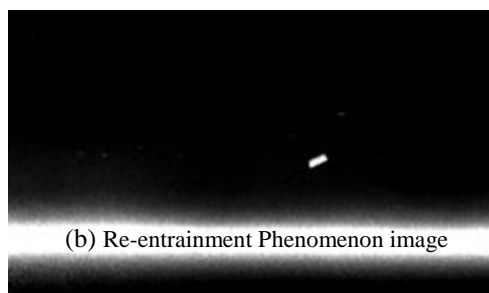


Fig1. PIV experiment system



(a) Collecting Particle image



(b) Re-entrainment Phenomenon image

Fig2. Particle Image

This work was supported by JSPS KAKENHI Grant Number JP16H04606

## Relationship between back corona discharge current and elapsed time in an electrostatic precipitator

Tomoya Mitsui<sup>1</sup>, Shoichi Ito<sup>1</sup>, Koji Yasumoto<sup>1</sup>, Akinori Zukeran<sup>1</sup>

<sup>1</sup>Dept. of Electrical and Electronic Engineering, Kanagawa Institute of Technology, Kanagawa, 242-0292, Japan

Keywords: back corona, electrostatic precipitator

Corresponding author e-mail: zukeran-akinori@ele.kanagawa-it.ac.jp

Particulate matter included in exhaust gas emitted from a factory or a power station become a problem for the air environment. Therefore, an electrostatic precipitator (ESP) has been extensively used for removal particulate matter. However, when particles, which has high resistivity, deposit on dust-collection electrodes, back corona discharge is generated, and the dust-collection performance decreases.

In this study, relationship between back corona discharge current and elapsed time was measured to investigate the process.

The schematic diagram of the experimental equipment is shown in Figure 1. ESP consisted of a high-voltage application electrode (tungsten,  $\Phi 0.26$ ) and a grounded plate electrode ( $90 \times 150$  mm) with the gap of 15 mm. Resistance ( $10 \text{ k}\Omega$ ) was connected to grounded plate electrodes for measuring corona discharge current. The ESP was located in an incubator at the temperature of  $80 \text{ }^\circ\text{C}$ . Calcium carbonate dust (1 g) was located on the grounded plate electrode.

The rectangular AC high voltage was supplied to the wire electrode to generate corona discharge. The voltage was  $\pm 8.5 \text{ kV}$ , and the frequency was  $10 \text{ Hz}$ . The high voltage waveform and the discharge current waveform were measured.

The high voltage waveform is shown in Figure 2. It is rectangular waveform at the maximum voltage of  $\pm 8.5 \text{ kV}$  and the frequency of  $10 \text{ Hz}$ . The voltage polarity at the time between 0 and 50 ms is positive, and that between 50 and 100 ms is negative.

The discharge current waveform is shown in Figure 3. Pulses at 50 ms and 100 ms are current induced due to changing the voltage. The polarity of current during positive voltage is plus, and that during negative voltage is minus. During positive voltage, the current for the time between 0 and 23.5 ms was approximately  $0.02 \text{ mA}$  due to corona discharge. However, the current increased with elapsing the time after 23.5 ms, and reached  $0.18 \text{ mA}$ . This is due to back corona discharge. During negatively voltage, the current for the time between 50 ms and 52 ms was approximately  $-0.07 \text{ mA}$ . The current after 52 ms increased with increasing the time and became constant at approximately  $-0.5 \text{ mA}$  after 57.5 ms.

This result indicates that negative voltage is easy to generate back corona discharge. This may be due to the discharge current value in the negative corona is greater than that in the positive corona at same applied voltage.

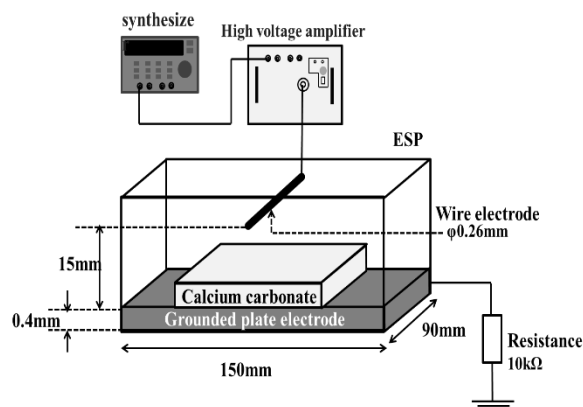


Figure 1. Schematic diagram of experimental equipment.

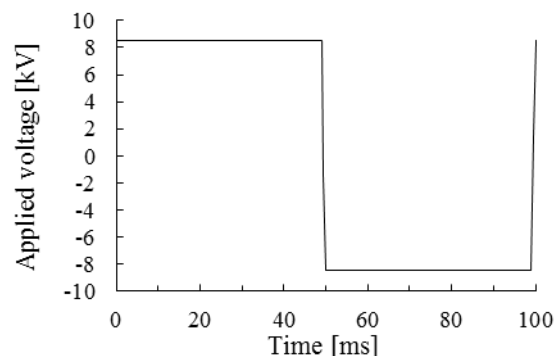


Figure 2. High voltage waveform.

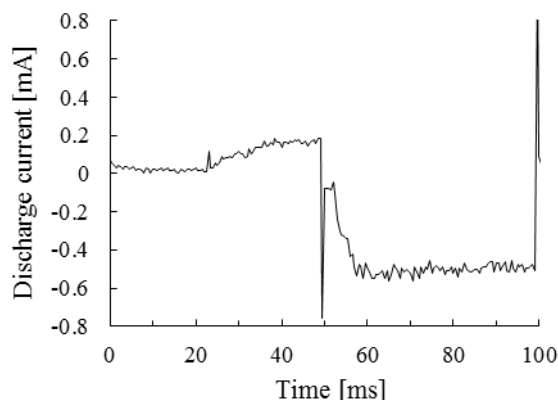


Figure 3. Discharge current waveform.

## Effect of electrode length on collection efficiency for nano-particles emitted from diesel engine with residual fuel oil in an electrostatic precipitator

Hidetoshi Sawano<sup>1</sup>, Koji Yasumoto<sup>1</sup>, Akinori Zukeran<sup>1</sup>

<sup>1</sup>Dept. of Electrical and Electronic Engineering, Kanagawa Institute of Technology, Kanagawa, 243-0292, Japan

Keywords: diesel engine, ion-induced nucleation, collection efficiency, nano-particle, electrostatic precipitator

Corresponding author email: zukeran-akinori@ele.kanagawa-it.ac.jp

Diesel engines has been extensively used as a generator, an automobile or an agrimotor due to low CO<sub>2</sub> emission. However, their exhaust gas contains air pollutants, such as NO<sub>x</sub> and particulate matter (PM). It is known that nano-particles are included in PM. SO<sub>x</sub> is also included in exhaust gas, when residual fuel oil is used.

The purpose of this study is to remove PM using an electrostatic precipitator (ESP). In particular, the relationship between nano-particle collection efficiency and the electrode length was investigated for emission gas from diesel engine with residual fuel oil.

The schematic diagram of experimental system is shown in Fig.1. Emission gas at the gas temperature of 160 °C from diesel engine with residual fuel oil (S:0.61%) was used for experiment. ESP is a coaxial cylinder structure consisted of a grounded cylinder electrode (SUS303, inside diameter: 58 mm) and a high voltage application wire electrode (tungsten, Φ0.26 mm). The electrode length was between 80 and 230 mm. DC +8 kV was supplied to the wire electrode to generate corona discharge. The diesel exhaust emission was sampled at the downstream side of the ESP, and diluted to 10 times with the air at the same temperature. The size distribution for the particle size between 5.94 nm and 216.7 nm was measured using a scanning mobility particle sizer (TSI, Model 3936) after cooling the sample gas to normal temperature. The collection efficiency  $\eta$  was calculated by equation (1).

$$\eta = (1 - (N/N_0)) \times 100 \quad (1)$$

where, N is particle density after applying the voltage, and N<sub>0</sub> is particle density before applying the voltage.

The collection efficiency as a function of particle diameter for various electrode lengths is shown in Fig.2. Negative collection efficiency indicates that the particle concentration at applying high voltage is greater than that at the voltage of 0 kV. The collection efficiency at the electrode length of 80 mm has a negative peak value of -359 % at the particle size of 10.6 nm, which means that the particle concentration at applying voltage increased by approximately 4.6 times comparison with that at 0 kV. This is most likely because nano-particles were generated

due to corona discharge in the exhaust gas included SO<sub>x</sub>, which phenomena was ion-induced nucleation.

The collection efficiency for the particle larger than 10.6 nm increased with increasing the particle diameter. And, the collection efficiency increased as the electrode length increased. Negative peak value was also improved. Thus, increasing nano-particle concentration was prevented due to collection effect of ESP.

These results indicated that particle concentration smaller than approximately 20 nm increased, and that larger than approximately 20 nm decreased, when particles emitted from the diesel engine with residual fuel oil were collected using the ESP. However, it was also clear that increasing the particle concentration was prevented with increasing the electrode length of the ESP. Furthermore, the collection efficiencies for the total number of particles at the electrode lengths of 80, 130 and 230 mm were 67, 82 and 88%. Therefore, the collection efficiency for nano-particle hardly affect that for the total number of particles.

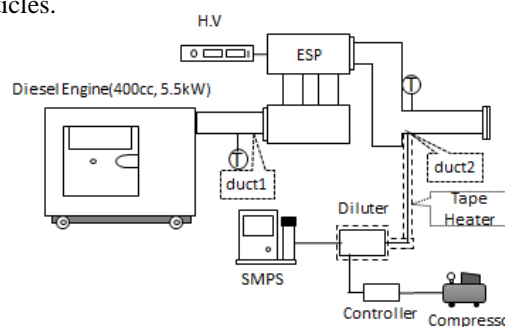


Fig.1. Schematic diagram of experimental system.

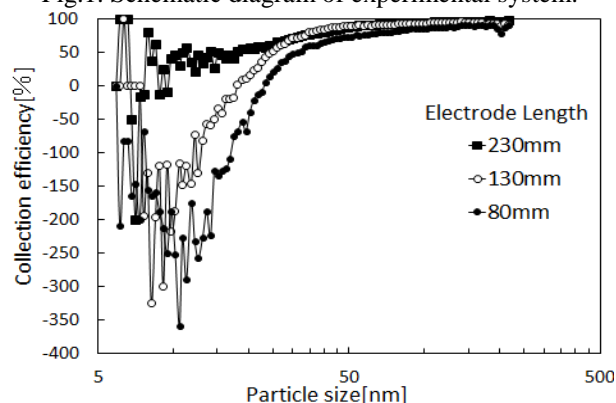


Fig.2. Collection efficiency as a function of particle diameter for various electrode lengths.

## Effect of vortex finder's geometric dimensions on the performance of Stairmand cyclone

J. Shim, Y.-H. Joe and H.-S. Park

Korea Institute of Energy Research, Daejeon, 34129, Korea

Keywords: Stairmand cyclone, Vortex finder, Geometric effect

Presenting author email: jmshim@kier.re.kr

Cyclone is widely used in industry related to air pollution control for removing particulate matter (PM) from flue gases due primarily to its easy construction and installation as well as low costs of operation and maintenance. It is a dust collector which uses centrifugal forces for capturing particles with high inertia. In detail, the centrifugal forces are formed at every point inside the cyclone, therefore the discrete phase starts to separate out and move towards the cyclone walls. These particles with the influence of axial velocity move down to the bottom of the cyclone. The clean air then spins and rises up. After which, it is emitted from the cyclone through the vortex finder.

In this study, we investigated the effect of the length and diameter of vortex finder on the performance of a Stairmand type cyclone. To that end, vortex finders were installed in an in-house designed cyclone and experimental examinations have been conducted. The geometric configuration of the Stairmand cyclone can be generally normalized by the cyclone body diameter. The body diameter of the testing cyclone was fixed at 50 mm. A schematic diagram of the experimental setup for the cyclone performance tests is shown in Figure 1. An aerosol generator was used to generate potassium chloride (KCl) particles for the experiments. For the PM concentration measurements, an optical particle counter (GRIMM 1109) was used to sample aerosol flow upstream and downstream of the testing cyclone. The pressure drop between the inlet and the outlet of the testing unit was measured by a pressure gage at five different gas velocity (5, 10, 15, 20, and 25 m/s). Nine vortex finders with three different diameters (tube diameter = 15, 20, 25 mm) and three different lengths (tube length = 25, 30, and 50 mm) were used in the experiments. The assemblies with the various vortex finders were modifications of the Stairmand type cyclones.

Figure 2 shows the collection efficiencies of cyclones having tube diameter 25 mm with the tube length 25, 35, and 50 mm. As the results, there was no great difference about the variation of the vortex finder's length in the geometric aspect for the PM collection efficiencies. We also investigated the effects of the diameter on the cyclone performances, i.e. pressure drop and collection efficiency.

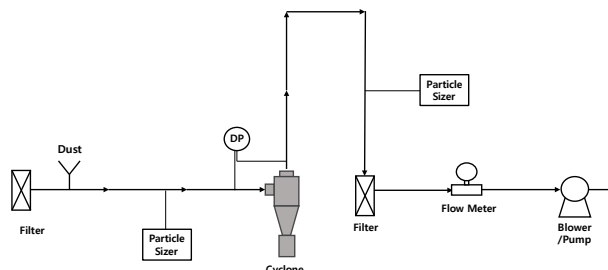


Figure 1. Schematic diagram of the experimental setup.

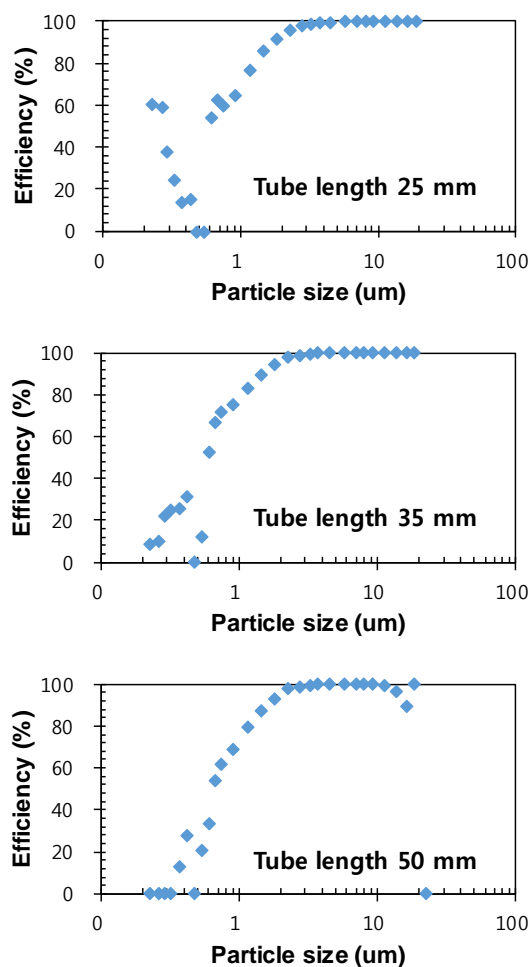


Figure 2. Collection efficiencies of cyclones (tube diameter 25 mm) at velocity 10 m/s with the tube length 25 mm (upper), 35 mm (middle), and 50 mm (lower)

This work was supported by the National Research Council of Science & Technology (NST) grant by the Korea government (MSIP) (No. CRC-15-07-KIER).

## Effect of Pulsing Valves on Bag Filter Cleaning and Dust Emission

Hyun-Seol Park\*, Joonmok Shim and Yun-Haeng Joe

Korea Institute of Energy Research, Daejeon, 34129, Korea

Keywords: Bag filter, Pulse jet, Pulsing valve, Pressure drop

Presenting author email: phs@kier.re.kr

In order to remove the particulate matter emitted from middle and large establishments, such as power plant, factory, and iron works, bag houses have been widely used in industry. In the bag house, suspended particles in a gas are deposited and formed dust cake on the filter surface during filtration. The dust cake blocks the gas flow and leads to increase of a pressure drop across the filter medium, finally it causes instability of the bag house. By this reason, filter cleaning devices such as a pulse-jet cleaning system are installed to remove the dust cake from the filter surface. The bag filters installed in the bag house are periodically cleaned and re-generated by a compressed clean air blasted from the pulse-jet cleaning system. Generally, 10 or 12 bag filters are arranged in a row, and a blow pipe is located above of the bags. Since performance of the pulse-jet cleaning system is depended on various factors, such as filtration velocity, pressure of pulsing air, amount of air flow blasted from the system, and pulsing nozzle type, the effect of each parameter should be examined.

In this study we investigated the effects of the pressure of pulsing air and filtration velocity on the pulsing-jet cleaning performance. Moreover, two diaphragm valves of 40A and 80A as pulsing valve were selected to investigate the effect of amount of blasting air flow. Three bag filters which have 15m length and 156 mm diameter were installed in a test unit of bag house equipped with a modified pulse-jet cleaning system. Fly ash from coal fired power plant was used as test dust and concentration of inlet dust was fixed as  $20 \text{ g/m}^3$ . 1.5 m/min and 2.0 m/min of filtration velocities were used in this test, and three cases of pulsing air pressure, 2, 3 and 5  $\text{kgf/cm}^2$  were used. The mass concentration of emitted dust particles was measured by an optical particle counter (GRIMM 1109), and filter cleaning performance was monitored by measuring pressure drop of bags. Filter cleaning was triggered when the pressure drop of bag filter reached  $100 \text{ mmH}_2\text{O}$ .

The pressure drop across the filter bag was increased during filtration and sharply decreased by operation of pulse-jet cleaning system. The frequency of pulse jet operation was increased with pulsing-air pressure. The size of pulsing valve did not lead to significant difference at 1.5 m/min of filtration velocity. However, 80A pulsing valve was more effective under 2  $\text{kgf/cm}^2$  of pulsing air pressure and 2.0 m/min of filtration velocity than 40A valve. The concentration of dust emission was increased with pulsing air pressure and diaphragm valve size.

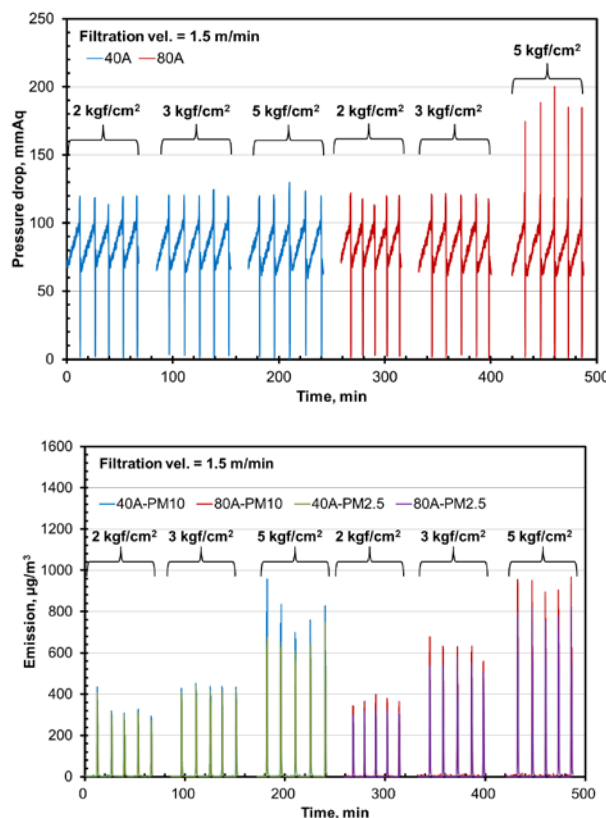


Figure 1. (a) Pressure drop and (b) dust emission characteristics for different size of pulsing valve @ filtration velocity of 1.5 m/min.

This work was supported by the National Research Council of Science & Technology (NST) grant by the Korea government (MSIP) (No. CRC-15-07-KIER).

## Diesel PM Combustion using Non-thermal Plasma and Catalyst

Hitomi Kawakami<sup>1</sup>, Takashi Inui<sup>1</sup>, Yusuke Nozaki<sup>2</sup>, Hiroataka Miyasita<sup>2</sup>, Yoshiyasu Ehara<sup>2</sup>

<sup>1</sup>Industrial Infrastructure Business Group, Fuji Electric Co., Japan

<sup>2</sup>Department of Electrical and Electronic Engineering, Tokyo City University, Tokyo, Japan

Keywords: non-thermal plasma, catalyst, Particulate Matter

Presenting author email: kawakami-hitomi@fujielectric.com

The particulate matters (PMs) emitted from marine diesel engine exhaust during the combustion process have low resistivity and extremely small in the range of 70-120nm. These particles cause a various human health and environment impacts. International standards limiting NO<sub>x</sub>, SO<sub>x</sub>, and PM emissions from ships are established through Annex VI of the international convention for the prevention of pollution from ships, otherwise known as MARPOL.

Authors have been developed non-thermal plasma (NTP) reactor for removal of PM emissions from a diesel engine (Ehara *et al* (2012, 2013). In the NTP reactor, the air is activated by discharge and produces ozone, oxygen radical and nitrogen radical, resulting the diesel particulates are oxidized under low temperature condition. Diesel PMs combusted by ozone produced in NTP. When the gas temperature is higher than 250°C, NO in the flue gas is oxidized to form NO<sub>2</sub> by ozone and O radical, then carbon particles combusted.

This research has been developed an after treatment system for removal of diesel PM from the ship exhaust. The PM was collected by electrostatic precipitator using corona discharge. The NTP reactor used for this experiment was shown in Fig. 1. The reactor had a coaxial double tube structure. The pellets as a catalysts or glass beads are packed between the inner and outer tubes. The air is flowed from inlet of the inner tube, and the air passes the pellets in the reactor, enters the inner tube again, and is exhausted. The catalysts and glass beads surfaces depositing the PM were filled into the reactor. PM is taken from the diesel generator was operated with light oil. The catalyst used was NS-1A (Nikki-Universal., LTD.). It is spherical and the diameter is about 4mm.

Fig. 2 shows the discharge power with the catalysts and glass beads as a function of the applied voltage. The discharge power was measured by Lissajous method. The discharge power increased with increasing the applied voltage, these value at 300°C are higher than achieved at 200°C. Additionally, the discharge power with catalysts is higher than glass in the same voltage.

The weight of PM combustion as a function of injected discharge power is shown in Fig. 3. The injected discharge power is a product of the discharge power and the elapsed time. The weights of PM combustion with the catalysts increased with increasing the injected discharge power. However, the weights of PM combustion with the glass beads are the saturated tendency. These results show that the synergistic effect by the plasma and the catalyst can be expected.

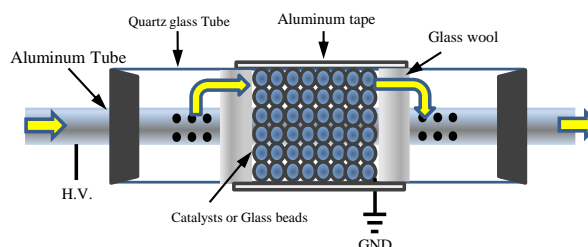


Fig. 1. Non-thermal plasma reactor.

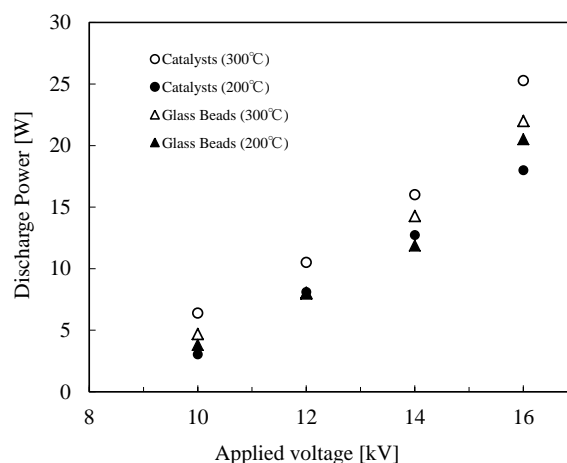


Fig. 2. Discharge power for applied voltage.

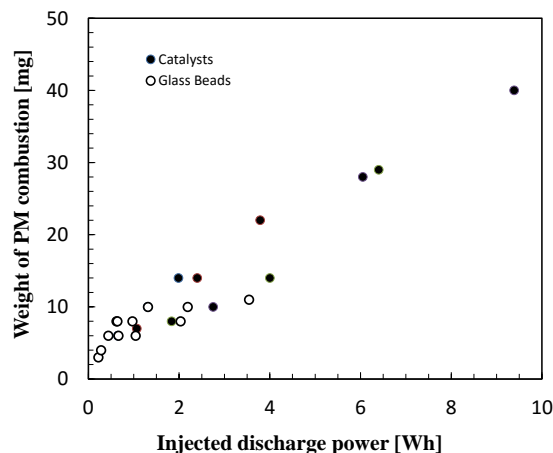


Fig. 3. Weight of PM combustion.

- Y. Ehara, M. Kobayashi, T. Yamamoto, A. Zukeran, H. Kawakami, "Development of dielectric barrier discharge system for continuous removal of diesel particulate matter", ISNTP-8, SP-11, 2012
- Y. Ehara, M. Kobayashi, H. Muramatsu, A. Zukeran, H. Kawakami, T. Inui "Diesel PM Incineration for Marine Emissions Using Dielectric Barrier Discharge Type Electrostatic Precipitator", Proc. ESA Annual Meeting on Electrostatics, F3, 2013

### Study on the production and filtration of eletret filters

C.T. Wang<sup>1</sup>, T.M. Tu<sup>1</sup>, Y.Y. Kao<sup>1</sup>, L.Y. Li<sup>1</sup>, B.L. Hong<sup>1</sup>, S.H. Huang<sup>2</sup>, C.C. Chen<sup>2</sup> and W.Y. Lin<sup>1\*</sup>

<sup>1</sup>Institute of Environmental Engineering and Management, National Taipei University of Technology, Taipei, 10608, Taiwan

<sup>2</sup>Institute of Occupational Medicine and Industrial Hygiene, National Taiwan University, Taipei, 10608, Taiwan  
 Keywords: Electrostatic, Charged fibers, filtration efficiency.

Presenting author email: wylin@ntut.edu.tw

Electrostatic attraction is a kind of basic mechanisms by with an aerosol particle can be collected onto a fiber (Hinds, 1999). Charged fibers can greatly enhance filter collection. High removal efficiency can be achieved without incurring large pressure drop (Nifuku et al., 2001). The objective of this study was to investigate the filtration properties of electrostatic filter.

This study used an electrospinning system to produce filter as shown in Fig. 1 (a), and use the filtration system Fig. 1 (b) to test filter particle filtration efficiency. The solutions for electrospinning were prepared by different amounts of PMMA ( poly methyl methacrylate) powders and DMF (dimethyl formamide) solutions. Fiber producing was related with solution concentration, working distance, feed rate and supply voltage. The operational parameters in electrospinning and the parameters of filtration test were shown in table 1.

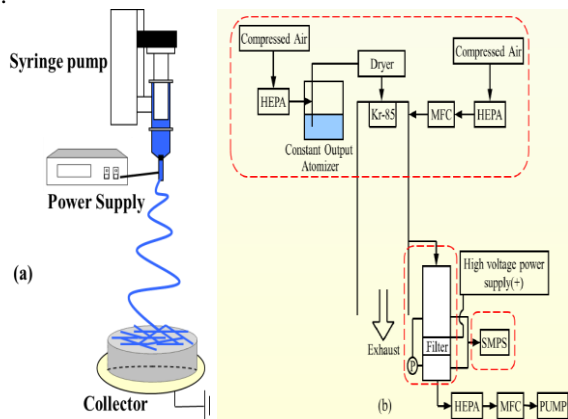


Figure 1. (a) The electrospinning system(b) Filtration system

Table 1. The operational parameters of electrospinning

Produced Parameters	
Concentration	100, 120, 180 mg/ml
Working distance	15, 20 cm
Feed rate	1, 2 ml/hr
Supply voltage	12 Kv
Needle size	0.41 mm
Filtration test	
Test particles	NaCl
Fiber diameter	500, 1000, 2000 nm
Test flow rate	5, 10, 15 cm/s
Applied voltage	10, 12 Kv

The product elements from electrospinning depended on different characteristics. Besides, Fig.2 the pressure drop of test filters were increased as the surface velocity increasing, and as the fiber diameter decreasing..

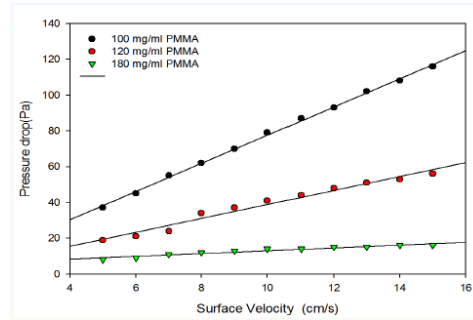


Figure 2. The effect of various filtration velocities on pressure drop

Figure 3, 4 and 5 shows that the charged filters have better penetration than uncharged filters, moreover, slower surface velocity is, greater filtration is.

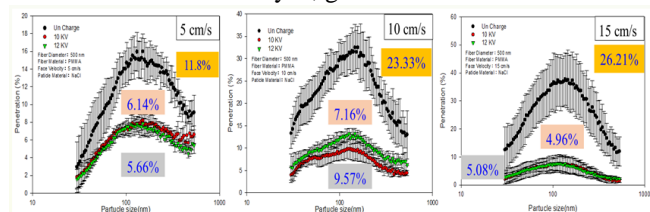


Figure 3 Particle penetration of filter — 500 nm.

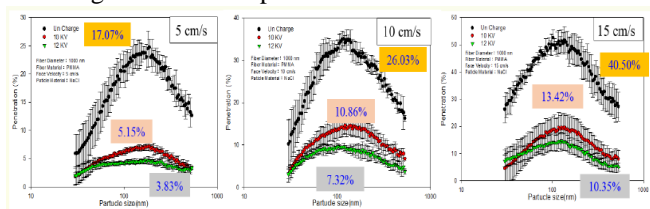


Figure 4 Particle penetration of filter — 1000 nm

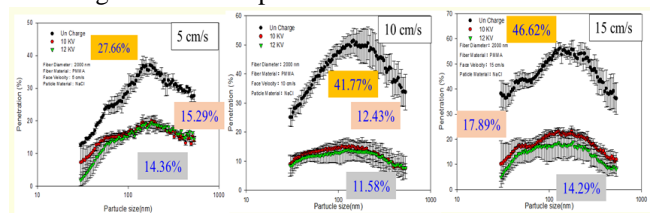


Figure 5 Particle penetration of filter — 2000 nm.

The results suggested that the penetration increased with decreasing the fiber diameter of fiber filters. Besides, the filter quality of fine fiber filter was greater than coarse fiber filter; however, the greater filter quality was also related with higher pressure drop.

Hanley, J.T., Ensor, D.S., Foarde, K.K. and Sparks, L.E. (1999). Proceedings of Indoor Air '99, Edinburgh, Scotland.

Nifuku, M., Zhou, Y., Kisiel, A., Kobayashi, T. and Katoh, H. (2001) J. Electrostat. 51–52: 200-205.

## Removal efficiency for PAHs emitted from diesel engine using an electrostatic precipitator

Kohei Ito<sup>1</sup>, Yuki Nanjo<sup>1</sup>, Akinori Zukeran<sup>1</sup>, Takashi Inui<sup>2</sup>

<sup>1</sup>Dept. of Electrical and Electronic Engineering, Kanagawa Institute of Technology, Kanagawa, 243-0292, Japan

<sup>2</sup>Facility Engineering Dept. Fuji Electric Co., Ltd., Tokyo, 191-8502, Japan

Keywords: PAHs, corona discharge, electrostatic precipitator.

Corresponding author e-mail: zukeran-akinori@ele.kanagawa-it.ac.jp

### 1. Introduction

Environmental Protection Agency (EPA) regulated Polycyclic Aromatic Hydrocarbons (PAHs), which have carcinogenicity, mutagenesis and strong toxicity, to protect the air, water and soil. Diesel emission includes PAHs which are generated due to incomplete combustion of the fuel. Therefore, PAHs emitted from diesel engine may be regulated in the future.

The aim of this study is to remove PAHs in a diesel emission using an electrostatic precipitator and a heat exchanger.

### 2. Experimental method

The experimental system<sup>1)</sup> consisted of a diesel engine (DA-3100SS-IV, Denyo), a heat exchanger (HE) and an electrostatic precipitator (ESP). Heavy oil A (S:0.61 %) was used as a fuel. The HE can cool the exhaust gas from 160°C to 20°C. The ESP has a parallel plate electrode structure composed of high-voltage electrode and grounded plate electrode alternately arranged with a gap of 9.5 mm. The high-voltage electrode have saw-tooth edges on their upper part and under part, however the grounded electrodes have no such edges<sup>2)</sup>. The high-voltage electrode was supplied with DC voltage of between 0 and -9.5 kV to generate corona discharge and collect charged particles.

PAHs in the exhaust gas have two phases, which are particulate and gaseous matters. Particulate PAHs were collected by a Teflon coated glass filter, and gaseous PAHs were sampled to a resin absorbent. The filter and the absorbent sampled PAHs were extracted using a soxhlet extraction with dichloromethane. PAHs concentration in the extraction liquid was measured using a gas chromatograph mass spectrometer (GCMS).

### 3. Result and Discussion

Relationships between gaseous PAHs removal rate and applied voltage is shown in Figure 1. The gaseous removal rate increased with increasing the applied voltage. The removal rate at the voltage of -6.0 kV was 32 % and reached 77 % at -9.5 kV. Generally, it is difficult for ESP to remove gaseous matter. This may be due to reactive oxygen species produced by corona discharge. It is necessary to investigate the process in the future.

Relationships between particulate PAHs removal rate and applied voltage is shown in Figure 2. The particulate removal rate increased with increasing the applied voltage. The removal rate at the voltage of -6.0

kV was 90 % and exceeded 95 % at -9.5 kV. PAHs is attached on surfaces of soluble organic fraction (SOF), sulphate and dry soot. These are collected on the ESP at the voltage greater than -4 kV due to generating corona discharge<sup>2)</sup>. Therefore, PAHs attached on these particles were removed by the ESP.

### 4. Conclusion

The effect of the ESP on removing PAHs in the exhaust gas was investigated. As a result,

- 1) Gaseous and Particulate PAHs removal rates were achieved to 77 % and 95 %, respectively.
- 2) It is indicated that PAHs emitted from a diesel engine are removed using an ESP.

This work was supported by JSPS KAKENHI Grant Number 15H04216.

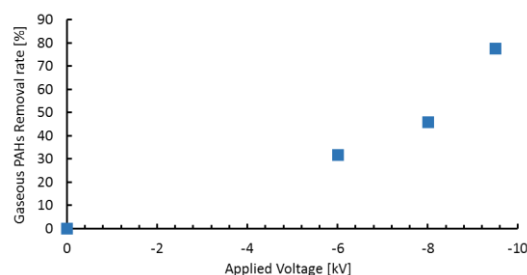


Figure 1. Relationships between gaseous PAHs removal rate and applied voltage.

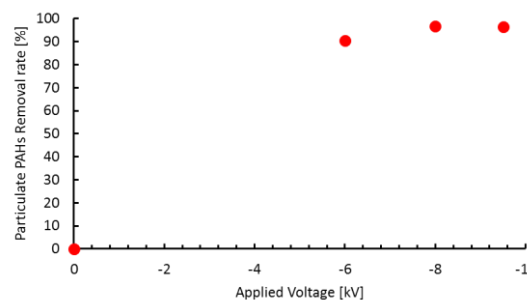


Figure 2. Relationships between particulate PAHs removal rate and applied voltage.

### References

- 1) Yuki Nanjo et al., EAC 2016.
- 2) .A.Zukeran et al., *WIT Transaction on Ecology and The Environment*, Vol.183, pp.165-176, 2014.

## Nanoparticle filtration by multilayer meltblown depth filters

Young-Ok Park<sup>1\*</sup>, Kang-San Lee<sup>1,2</sup>, Naim Hasolli<sup>1</sup>, Seong-Min Jeon<sup>1</sup>, Jae-Rang Lee<sup>1,3</sup>, Kwang-Deuk Kim<sup>1</sup>,  
Jungho Hwang<sup>2</sup>

<sup>1</sup>Climate Change Research Division, Korea Institute of Energy Research, Daejeon, Korea

<sup>2</sup>Department of Mechanical Engineering, Yonsei University, Seoul, Korea

<sup>3</sup>Department of Chemical & Biological Engineering, Korea University, Seoul, Korea

Keywords: meltblown depth filter, nanoparticle, filtration, penetration.

Presenting author email: yopark@kier.re.kr

Fibrous filters can be effectively used for removal of fine solid particles. Efficient removal of nanoparticles though can be a challenge. Due to the toxic nature and large specific area of nanoparticles, only high efficiency filters with multilayer and fine fiber structures can be used for their removal.

Practically, the filter media can remove solid particles using the fibrous assembly structure, which has great air permeability and flexibility. Among them, the complex capturing mechanism of meltblown filter media, characterized by microporosity, are interception, inertial impaction, Brownian diffusion, gravitational settling, and etc. Especially, the meltblown filter is widely used as light-weighted filter utilizing its large surface area that forms reticular structure of microfiber assembly. Polypropylene is a thermoplastic material, used as a base material for melt blown nonwoven fabric.

Furthermore, polypropylene can be used for high efficiency filtration in combination with electrostatic charging. The corona charging is a typical method of electrostatic treatment.

The quality of filter is defined as a function of pressure drop and filtration efficiency, meaning that a filter with low pressure drop and high filtration efficiency is characterized as a high performance filter and its performance can be easily compare with other filter samples. To develop a filter with high quality factor, the multi-layer meltblown filter is being used to increase the filtration efficiency and thermalbond layer (TB) is used as supporting layer and to increase the stiffness of pleated filter.

In this study, we observed the filtration performance of KCl particles within 17-600 nm range, and have conducted a comparative analysis of filter layer effect on filter performance based on number of layers by designing 3 types of 2-4 multilayer meltblown filters.

The particles were generated from the diffusion dryer filled with silica gels, by spraying and passing 1.0wt% KCl solution using the pressure atomizer. Table 1 shows the experimental conditions.

Table 1. Experimental conditions.

Conditions	Value
Filter media	Meltblown filters
Sample dimension	42mm
Particle density	1.98g/cc
Mean particle diameter	75nm
Test aerosol	1% KCl
Filtration velocity	5.3cm/s

Based on the thickness of each layer of filter samples, the pressure drop appeared to be different for same test conditions at filtration velocity of 5.3cm/s. For particle size in the range between 40nm to 200nm, the nanoparticle penetration is almost similar. MB1 layer has the great effect on the nanoparticle collection efficiency. Furthermore, the nanoparticle collection efficiency of the 2-layer filter was the most superior.

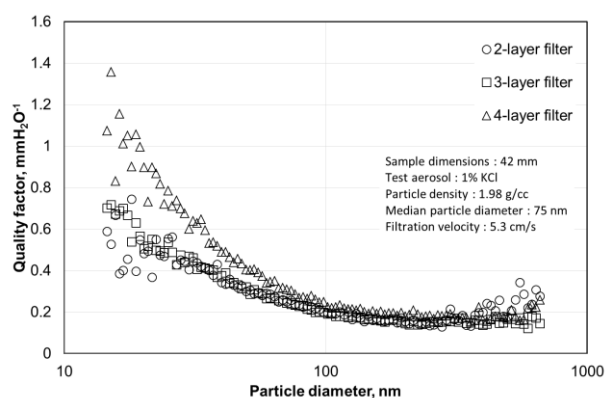


Figure 1. Quality factor of multilayer depth filters

If we consider the quality factor, the performance of 4-layer filter was the best for nanoparticles smaller than 100nm. As a result, the filter has high dust collection efficiency with low pressure drop for particles smaller than 70nm.

This work was supported by Korea Ministry of Environment (MOE) as “Advanced Technology Program for Environmental Industry:.

Lokis, B., Motyl, E. (2001) *Journal of Electrostatics*, 51-52, 232-238.

Zhang, D., Sun, C. Q., and Song, H. (2004). *Journal of applied polymer science*, 94, 1218-1226.

Brunig, H., Zhandarov, S., Beyreuther, R. (2000). *Advances in Polymer Technology*, 19(4), 312-316.

Cheung, C. S., Cao, Y. H., Yan, Z. D. (2005). *Computational Mechanics*, 35(6), 449-458.

ISO/TS 21220. (2009). 1<sup>st</sup> Ed.

Lee, K. W., Liu, B. Y. H. (1982). *Journal of Aerosol Science and Technology*, 1(2), 147-161.

## Reduction of PCDD/F Emission by Employing Catalytic Ceramic Fiber Filter

Sheng-Lun Lin<sup>1,2\*</sup>, Ria Aniza<sup>3</sup>, Shun-I Shih<sup>4</sup>, and Yi-Ming Kuo<sup>5</sup>

<sup>1</sup> Department of Civil Engineering and Geomatics, Cheng Shiu University, Kaohsiung 83347, Taiwan

<sup>2</sup> Super Micro Mass Research and Technology Center, Cheng Shiu University, Kaohsiung 83347, Taiwan

<sup>3</sup> Department of Environmental Engineering, National Cheng Kung University, Tainan 70101, Taiwan

<sup>4</sup> Department of Environmental Engineering, Kun Shan University, Tainan 71003, Taiwan

<sup>5</sup> Department of Safety Health and Environmental Engineering, Chung Hwa University of Medical Technology, Tainan 71703, Taiwan

Keywords: dioxins, catalytic ceramic fiber filter, removal efficiency, engine generator

Presenting author email: cbmsgml@gmail.com

Several conventional devices were designed for treating the Polychlorinated Dibenzo-*p*-dioxin and Dibenzofurans (PCDD/Fs) in the flue gases. The most widely used is activated carbon injection-baghouse filtration (ACI-BF), while it has high removal efficiencies (RE) but only removes instead of destroys pollutants. Another popular series is electrostatic precipitator-selective catalytic reduction (ESP-SCR), which captures PM and oxidizes PCDD/Fs. Unfortunately, the catalyst was easily poisoned by sulfur and metals during long-term operation. Nowadays, the selective catalyst reduction (SCR) became popular and promising technique to deal with multi-pollution, while the catalytic filter (CF) were developed to both reduce gaseous and particulate pollutants. It caused less secondary problems, while the PCDD/Fs and PM were reduced in flue gas by various way, including adsorption and oxidation and produce harmless small molecules (CO<sub>2</sub>, H<sub>2</sub>O and HCl) However, it has poisoned problem after a long-term continuous operation.

In this study, an PCDD/F removal efficiencies from flue gas was investigated by using catalytic ceramic fiber filter (CCFF) as the abatement techniques. CCFF is a material that designed to distribute the catalyst inter the ceramic fibers. It was designed in such way for both preventing the poisoning from the undesired species like a shield and removing the particulate matter at the same time. The main purpose of this study is to test the CCFF removal efficiencies of traditional pollutants and PCDD/Fs those existed in the flue gas.

The samples in this study was collected from the flue gases of a heavy-duty diesel engine generator, operated at 3.2 kW (80% of max. load). A ceramic material that distributed the V<sub>2</sub>O<sub>5</sub>/TiO<sub>2</sub> powders inter its fiber structures by impregnation to form a 2-cm (thickness) catalytic ceramic fiber filter (CCFF), while the catalysts could be protected by the outer Nano-scale fiber structure. The fiber structure was produced by sol-gel process, which would be not discussed in detail since the patent of CCFF production is still not opened to the public. The CCFF was installed in a heating system, which the temperature could be controlled up to 800°C by heating units (as shown in Figure 1). There were seven operation temperatures (150–350°C) to investigate the dioxin removal efficiencies (RE).

The sampling and analysis procedures in this study referred to the USEPA modified method 23 and NIEA 808.75B (Taiwan EPA certified for the stationary sources).

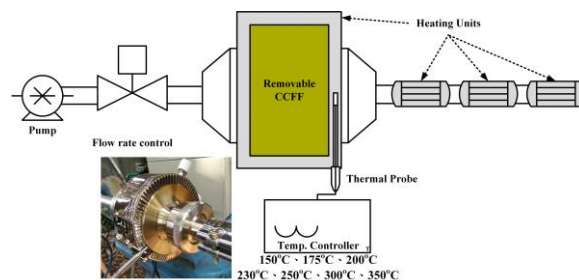


Figure 1. The CCFF unit employed in this study.

The highest RE of PCDD/F I-TEQ were 99.4% at 175°C. However, the *de novo* synthesis occurred within 250–350°C and drew back the removal efficiency. The particle removal dominated the overall removal mechanism, when the gaseous RE even occurred minus values at 300°C. Consequently, the CCFF could be effective to inhibit traditional and PCDD/F emissions at certain operation conditions.

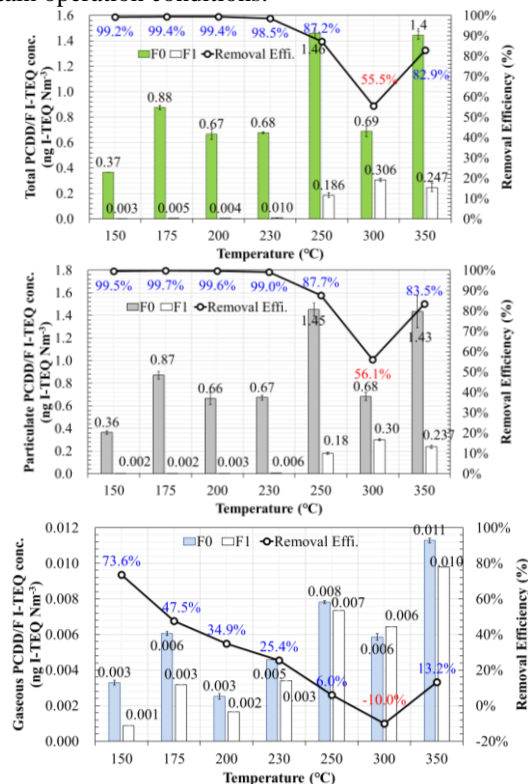


Figure 2. PCDD/F I-TEQ levels.

### References

- Wang, H.C., Hwang, J.F., Chi, K.H., Chang, M.B. (2007) *Chemosphere*. **67**, S177–S184.
- Ji, S., Ren, Y., Buekens, A., Chen, T., Lu, S., Cen, K., Li, X.-D. (2014) *Environ. Sci. Pollut. Res.* **22**, 14621–14628

## Tests for thermal, chemical and mechanical degradation characteristics of cleanable filter media

Johannes Weimann<sup>1\*</sup>, Frank Schmidt<sup>1</sup>, Achim Hugo<sup>2</sup>, Sabine Kreckel<sup>2</sup>, Thomas Mayer-Gall<sup>3</sup>

<sup>1</sup> University Duisburg-Essen, Duisburg, Germany

<sup>2</sup> Institut für Energie- und Umwelttechnik e.V. (IUTA), Duisburg, Germany

<sup>3</sup> (DTNW), Krefeld, Germany

Keywords: filtration, filter test, degradation, non-woven fabrics

\*Presenting author email: johannes.weimann@uni-due.de

Cleanable surface-loading bag filters are commonly used for industrial air and gas cleaning processes, e.g. dedusting of cement grinding plants, recycling of pharmaceutical products and flue gas cleaning of waste incineration plants. The steady exposure to severe conditions like high temperatures, presence of moisture and acid gases like NO<sub>x</sub> and SO<sub>2</sub>, as well as the high mechanical burden caused by high filter surface loads and the pulse-jet systems can lead to property changes of the filter fabric and thus a degradation of the filters and their performance with operating time. The changes in chemical and physical properties of filter media can be differentiated into *thermal*, *chemical* and *mechanical* degradation.

EN ISO 16891:2016-05 defines a systematic reference test method in order to determine the extent of thermal and chemical degradation mechanism on tensile strength of filter media. Standardized simulated test conditions for exposing non-woven filter fabrics to hot and/or corrosive gas atmospheres are given in the standard, based on basic studies of Tanaka (2004). Standard test procedures for filtration characterization of cleanable filter media at room temperature are described in ISO 11057:2011 and VDI 3926-1:2004.

However, the requirements for comprehensive investigations of cleanable filter media under conditions of industrial use and in reasonable time, are not clearly defined yet. For example, considerations regarding the effect of thermal or chemical degradation mechanisms on the separation efficiency are lacking.

In the present study we developed a conceptual design for an interacting test method, composed of a long-term filter test rig (LTC) according to the EN ISO 16891:2016-05 and an upgraded VDI 3926 filter test rig with heating sleeves, acid gas supply and humidifier (MCT) as shown in Fig. 1.

For degradation tests of different synthetic fibre types, five common non-woven filter fabrics from different materials (PAN, PPS, Aramid, PES, PE) were investigated. The newly designed LTC enables simultaneous accelerated ageing of up to 10 filter specimens under identical conditions. Before and after treatment, the tensile strengths of the specimens and the filtration efficiencies are measured. A set of test conditions and durations has been chosen in order to derive guidance towards standardizable ageing tests. Alternatively, raw filter samples are exposed to corrosive gas and high temperature conditions in the modified VDI 3926 (MCT) test rig. The comparison of the different

degrees of degradation is expected to provide information on the mechanical degradation and whether the simultaneous ageing method is suitable.

The reference test method and results for different filter media will be presented on the poster (i.e. separation efficiency and tensile strength as a function of ageing treatment) and discussed in view of reproducibility and standardizability of the test procedures.

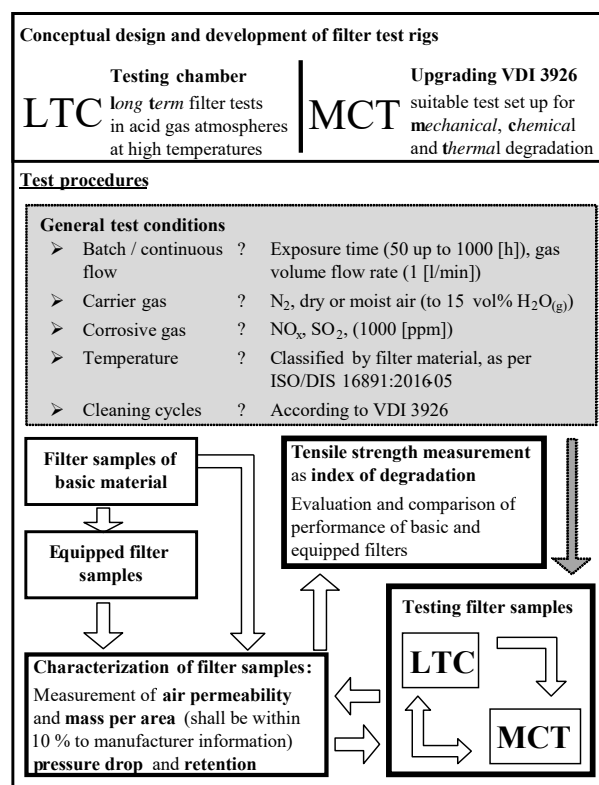


Fig. 1: Interacting test method scheme LTC as per EN ISO 16891 and modified VDI 3926 test rig MCT

The IGF-project 18307N of the research association "DECHEMA" is funded by the German Federal Ministry for Economy and Energy (BMWi) via AiF within the framework of the program for the promotion of industrial cooperative research and development (IGF) based on a decision by the German Bundestag.

Tanaka, S., Kanaoka, C: *Durability Validation of synthetic filter bags*, *Filtration* 4(4), 2004

## Fly-ash PM emissions and filtration from combustion of different biomass materials and preparations

D Sanz<sup>1</sup>, E Rojas<sup>1</sup>, J J Rodríguez-Maroto<sup>1</sup>, R Ramos<sup>2</sup>, E Borjabad<sup>2</sup>,  
R Escalada<sup>2</sup>, S García Alonso<sup>1</sup>, C Gutierrez-Canas<sup>3</sup>, G Aragon<sup>3</sup>,  
I Mugica<sup>3</sup>, I Ibarra<sup>3</sup>, I Celades<sup>4</sup> and V Sanfelix<sup>4</sup>

1 CIEMAT Avda Complutense 40, 28040 Madrid, Spain

2 CEDER-CIEMAT Autovía A-15 salida 56, 42290 Lubia (Soria), Spain

3 Universidad del País Vasco UPV-EHU Alameda Urquijo s/n, 48013 Bilbao, Spain

4 Instituto de Tecnología Cerámica Avda Vicent Sos Baynat s/n, 12006 Castellon, Spain

Keywords: biomass, emissions, filtration.

Presenting author email: david.sanz@ciemat.es

CLEANBIOM research project is aimed at the investigation of the sustainability of combustion valorisation of Mediterranean residual biomass materials in medium-size plants. As part of the project, various test runs have been carried out in a semi-industrial fluidised bed combustion plant (1 MWth). Some results regarding the influence of biomass material and preparation on fly-ash characteristics and filtration are presented in this work.

Two different biomass materials were tested, olive wood (sieved and non-sieved chips and pellets) and wheat straw pellets.

### Facility and methods

The facility consists of a bubbling fluidized bed combustion plant (1 MW nominal output) and a hybrid filter (HF) that integrates electrostatic precipitation (ESP) (dry, wire-plate) and fabric filter (BF) modules.

Pseudo isokinetic aerosol sampling was undertaken both upstream and downstream of the HF. The aerosol sample was passed through a cyclone and then collected on 47mm filter for mass concentration determination. In addition, a low pressure cascade impactor was used to assess mass size distribution. Also, CNC and DMA were used for determination of number concentration and size distribution.

Table 1. Fly-ash mass concentration as a function of fuel and combustion conditions.

Test	Excess Oxygen	Secondary air	Fly-ash conc. (mg/Nm <sup>3</sup> )
CB3.1(olive)	30%	69%	194
CB3.2 (olive)	22%	46%	808
CB3.3 (straw)	14%	49%	162
CB3.4 (straw)	28%	45%	14

### Results

Results on the comparison between sieved (tests CB2.3, 2.4 and 2.5) and non-sieved (tests CB2.1 and 2.2) olive wood chips were already presented previously (Sanz et al, 2016).

Wheat straw pellets combustion (tests CB3.3 and 3.4) produces lower mass concentration of fly-ash than olive wood pellets (CB3.1 and 3.2). Lower excess of

oxygen seems to result in higher fly-ash mass concentration for both fuels.

Regarding mass size distribution of fly-ash, as determined using low pressure cascade impactor, olive wood pellets and chips produced coarser fly-ash (MMAD 1µm) than wheat straw pellets (MMAD 0.2 µm).

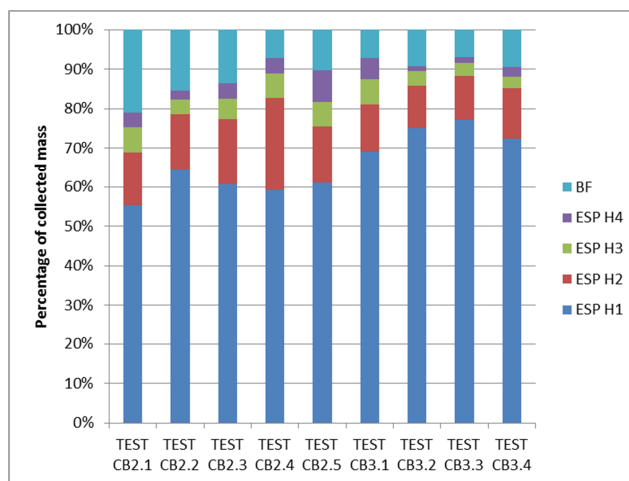


Figure 1. Distribution of collected fly-ash in different sections of HF.

The HF achieved high collection efficiencies (98.7 – 99.7% by mass) in all olive wood tests, except for test CB2.4 (92.3%). Most of the collected fly-ash was captured in the ESP module of the HF (figure 1). Fly-ash mass concentration in clean gas ranged between 1.17 and 3.31 mg/Nm<sup>3</sup> in all olive wood tests except CB2.4. It could not be determined during straw pellets combustion tests, but number concentration was found to be particularly low, in the range 100 – 200 #/cm<sup>3</sup> roughly one order of magnitude lower than in most olive wood tests.

The authors are grateful to Ministerio de Economía, Industria y Competitividad for supporting CLEANBIOM project.

Sanz, et al (2016) *Proc. 22<sup>nd</sup> European Aerosol Conference*

## **Abstracts T109**

## The effect of Na<sub>2</sub>CO<sub>3</sub> on inactivation of *Zygosaccharomyces rouxii* in seawater using pulsed electric field

Yuta Nakada<sup>1</sup>, Yorihiro Komatsu<sup>1</sup>, Akinori Zukeran<sup>1</sup>  
Risei Wada<sup>2</sup>, Jun Sawai<sup>3</sup>, Takashi Inui<sup>4</sup>

<sup>1</sup>Dept. of Electrical and Electronic Engineering, Kanagawa Institute of Technology, Kanagawa, 243-0292, Japan

<sup>2</sup>Dept. of Applied Bioscience, Kanagawa Institute of Technology, Kanagawa, 243-0292, Japan

<sup>3</sup>Dept. of Nutrition and Life Science, Kanagawa Institute of Technology, Kanagawa, 243-0292, Japan

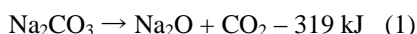
<sup>4</sup>Facility Engineering Dept., Fuji Electric Co., Ltd., Tokyo, 191-8502, Japan

Keywords: inactivation, pulsed electric field, microbubble, ballast water, scanning electron microscope,

Corresponding author email: zukeran-akinori@ele.kanagawa-it.ac.jp

Ballast water is used as weights for balancing ships. The ballast water is discharged at a distinction port where is different from a source port country, whereby that may cause problem in a marine ecosystem. The purpose of this study is to inactivate microorganisms in seawater using pulsed electric field and microbubbles.

The schematic diagram of the experimental system is shown in Fig. 1. Simulated seawater was poured into a beaker and installed needle electrodes which the electrode gap was 1 mm. Na<sub>2</sub>CO<sub>3</sub> or NaHCO<sub>3</sub> were added in seawater. Na<sub>2</sub>CO<sub>3</sub> and NaHCO<sub>3</sub> concentration were 10 %. Microorganism concentration, which was *Zygosaccharomyces rouxii* (*Z. rouxii*), in simulated seawater was 10<sup>4</sup>~10<sup>5</sup> CFU/ml. The pulsed electric field was generated in the seawater due to applying the pulse high voltage to between electrodes. The voltage and the current were measured using a high voltage probe and a current probe. The peak value, the rising time and the frequency of the pulse voltage were 13 ~ 15 kV, 75 ns and 50 Hz, respectively. The chemical reaction formula of Na<sub>2</sub>CO<sub>3</sub> and NaHCO<sub>3</sub>, when the pulse electric field was generated in seawater, is shown by equation (1), (2). CO<sub>2</sub> was generated as microbubbles in seawater.



Seawater of 1 mL was sampled periodically, and then incubated for 72 hours at 25 °C. The survival ratio  $\eta$  was calculated by equation (3):

$$\eta = \log (N / N_0) \quad (3)$$

where N is the number of colony count after treatment, and N<sub>0</sub> is the initial number of colony count.

The survival ratio as a function of the number of pulses is shown in Fig. 2. Decreasing the survival ratio means improving the inactivation effect. The survival ratio at the seawater decreased with increasing the number of pulses, and reached lower than 10<sup>-4</sup> at the number of pulses of 20000 or higher. This is most likely due to electroporation or increasing the seawater temperature. SEM images which *Z. rouxii* after treatment was destroyed were also obtained<sup>1)</sup>. The survival ratio in the seawater with Na<sub>2</sub>CO<sub>3</sub> decreased as the number of

pulses increased, and that lower than 10<sup>-4</sup> were achieved at the number of pulses of 10000. The effect of seawater with Na<sub>2</sub>CO<sub>3</sub> was higher 100 times than that without Na<sub>2</sub>CO<sub>3</sub>. This is may be due to CO<sub>2</sub> microbubbles generated by equation (1). However, the survival ratio the seawater with NaHCO<sub>3</sub> was almost equal to that without NaHCO<sub>3</sub>. It is necessary to investigate this reason in the future.

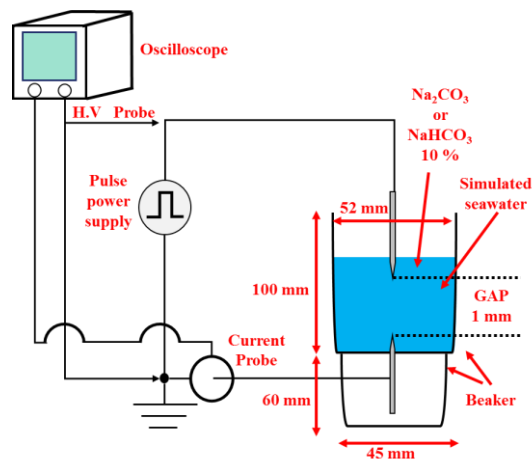


Fig. 1 Schematic diagram of experimental system.

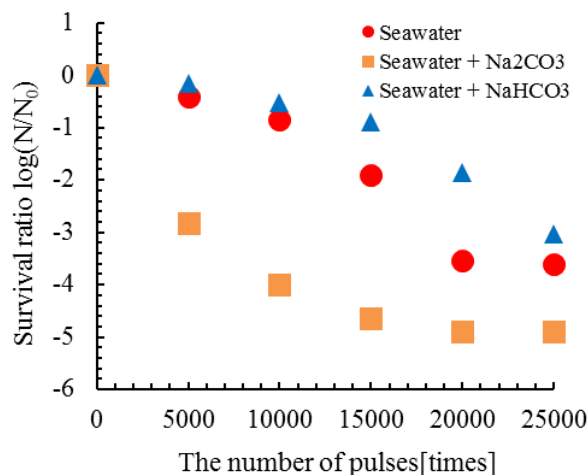


Fig. 2 The survival ratio as a function of the number of pulses.

### References

- 1) Yuta Nakada, et al., European aerosol conference 2016.

## Improving inactivation effect for microorganisms in an electrostatic precipitator operated under low ozone concentration by humidification

Koji Yasumoto<sup>1</sup>, Akinori Zukeran<sup>1</sup>, Iori Kobayashi<sup>1</sup>, Wada Risei<sup>2</sup>, Jun Sawai<sup>3</sup>

<sup>1</sup>Dept. of Electrical and Electronic Engineering, Kanagawa Institute of Technology, Kanagawa, 243-0292, Japan

<sup>2</sup>Dept. of Applied Bioscience, Kanagawa Institute of Technology, Kanagawa, 243-0292, Japan

<sup>3</sup>Dept. of Nutrition and Life Science, Kanagawa Institute of Technology, Kanagawa, 243-0292, Japan

Keywords: Keywords— inactivation, electrostatic precipitator, corona discharge, humidification

Corresponding author e-mail: zukeran-akinori@ele.kanagawa-it.ac.jp

Electrostatic Precipitators (ESPs) have been extensively used for the cleaning of industrial process flue gases, combustion flue gases and ventilation flue gases for road tunnels, etc. A home air cleaner of ESP is also one application. Such air cleaners must be capable of eliminating and inactivating airborne microorganisms to improve indoor air quality. An ESP using corona discharge is expected to be effective for such purposes.

Authors investigated the inactivation characteristic, and improved the effect of inactivating microorganisms collected on a plate electrode in an ESP by humidification. The influence of the location of collection, ozone concentration, elapsed time and relative humidity (RH) on inactivation of microorganisms was experimentally investigated. As a result, it was obtained that the inactivation effects were improved with increasing RH to 60 % or higher by humidification at an ozone concentration of 1 ppm<sup>1</sup>. However, ozone concentration was very high for a home air cleaner.

The aim of this study is to investigate the inactivation effect of humidification in an ESP operated under low ozone concentration of 0.06 ppm. *Staphylococcus aureus* was used for the experiment.

The schematic diagram of the experimental apparatus is shown in Fig. 1. The apparatus consisted of a discharge section and an electrostatic section. The discharging section has a wire-and-plates configuration composed of a high-voltage application wire electrode placed between grounded plate electrodes. The discharging section was supplied with DC voltage of approximately -6.4 kV, whereby the discharge current was adjusted to between 2 and 4 μA, which ozone concentration was approximately 0.06 ppm. The electrostatic section had a parallel-plate electrode structure composed of a high-voltage application electrode sandwiched between grounded plate electrodes. The electrostatic section was supplied with DC voltage of -5 kV. The wind velocity was 0.5 m/s, the temperature was approximately 20 °C, RH in the gas was controlled between 33 % and 90 % using a humidifier. The operating time was for 60 min.

The survival as a function of relative humidity at location 6 is shown in Fig.2. The survival decreased with increasing RH, and reached to approximately 20 % or lower at RH greater than 80 %. The comparison of the survival rate at six locations is shown in Fig.3. The rate at all location with the humidifier is lower than that

without the humidifier. It is clear that inactivation effects are significantly improved at low ozone concentration due to humidification.

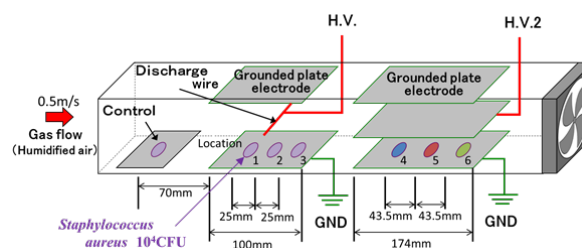


Fig.1 Schematic diagram of the experimental apparatus.

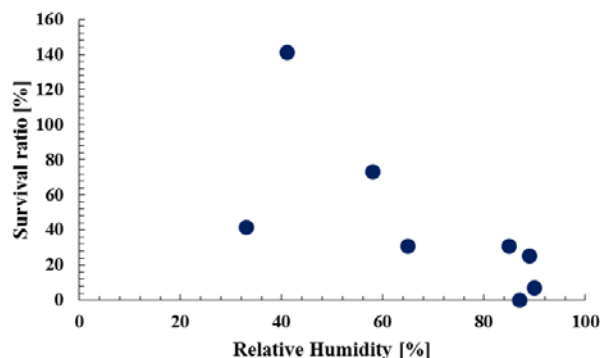


Fig.2 Survival as a function of relative humidity at location 6.

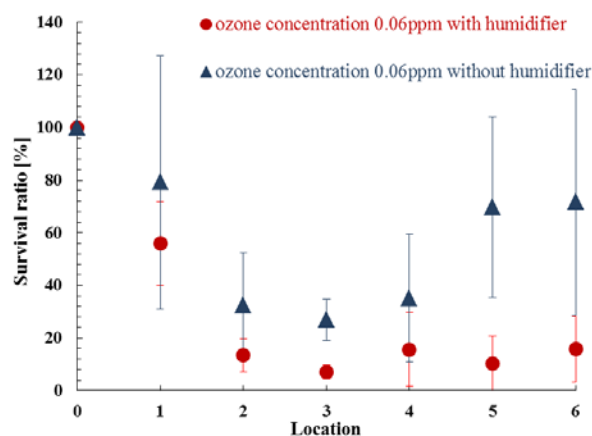


Fig.3 The comparison of the survival rate at six locations

### References

- 1) A. Zukeran et al, "Humidification effect on inactivation of *Staphylococcus aureus* in an electrostatic precipitator", *International Journal of Plasma Environmental Science & Technology*, Vol. 10, No.2, pp. 181-185, 2016.

## Investigation of inactivation process in an electrostatic precipitator by estimating protein quantitation

Soma Toguchi<sup>1</sup>, Ryo Oi<sup>1</sup>, Munehiro Shiraishi<sup>1</sup>, Akinori Zukeran<sup>1</sup>, Risei Wada<sup>2</sup>, Jun Sawai<sup>3</sup>

<sup>1</sup>Dept. of Electrical and Electronic Engineering, Kanagawa Institute of Technology, Kanagawa, 243-0292, Japan

<sup>2</sup>Dept. of Applied Bioscience, Kanagawa Institute of Technology, Kanagawa, 243-0292, Japan

<sup>3</sup>Dept. of Nutrition and Life Science, Kanagawa Institute of Technology, Kanagawa, 243-0292, Japan

Keywords: inactivation, electrostatic precipitator, corona discharge, protein quantitation

Corresponding author email: zukeran-akinori@ele.kanagawa-it.ac.jp

### 1. Introduction

An electrostatic precipitator (ESP) using corona discharge is expected to be effective for eliminating and inactivating airborne microorganisms to improve indoor air quality.

Authors investigated the effect and the process in an EPS. As a result, inactivation effect by the corona discharge was obtained. From observations of the distribution of reactive oxygen species (ROS), using a scanning electron microscope and a fluorescence microscope, it was revealed that cell walls were destroyed due to ROS generated in the corona discharge, whereby they were sterilized<sup>1)</sup>.

The aim of this study is to measure the protein quantitation for investigating inactivation process of microorganisms collected on a collection electrode in an ESP.

### 2. Experimental Method

The schematic diagram of the experimental system is shown in Fig. 1. The system consists of discharge wire and grounded plate electrodes. *Staphylococcus aureus* NBRC13276 (*S. aureus*) was used as model airborne microorganisms. *S. aureus* diluted with pure water was put on the grounded plate electrode under the discharge wire. A control was located at the outside for estimating natural decrement of *S. aureus*. After natural drying for 0.5 hours, microorganisms were exposed to corona discharge. The applied voltage was controlled between DC -8.5 kV and -9.5 kV, whereby the discharge current was adjusted to approximately 22  $\mu$ A, which maintain the ozone concentration at approximately 1 ppm. The wind velocity was 0.5 m/s, the temperature was approximately 27 °C. The relative humidity was approximately 70 %.

After corona discharge treatment, *S. aureus* on the electrode was wiped off using RASPER CHECK™, which was a wiping swab, and the absorbance at 260 nm of the rinse solution was measured using a spectrophotometer (GE, SimpliNano).

### 3. Result and Discussion

The absorbance measured by the spectrophotometer is shown in Fig. 2. The increase in absorbance indicates the leakage of 260 nm absorbing substances, such as protein and minerals, from the bacterial cells on the electrode. Values on the Ctrl and the electrode were 0.052 and 0.147, respectively. Standard deviations on the Ctrl and the electrode were

0.013 and 0.010. It is clear that the 260 nm absorbing substances on the electrode was significantly greater than that on the Ctrl. This result shows that cell content flowed out from microorganisms exposed in corona discharge.

### 4. Conclusion

The inactivation process in an EPS was investigated. As a result, it was revealed that cell content flowed out due to exposing microorganisms in the corona discharge. Thus, cell walls were destroyed due to ROS generated in the corona discharge, whereby they were sterilized due to cell content flowing out in an ESP.

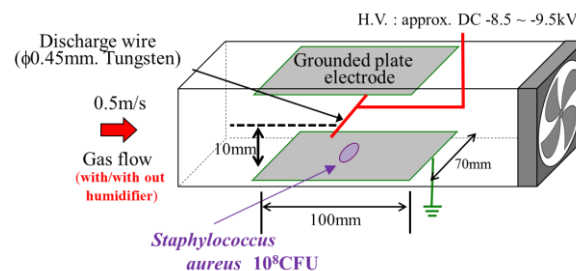


Fig. 1 Schematic diagram of experimental system.

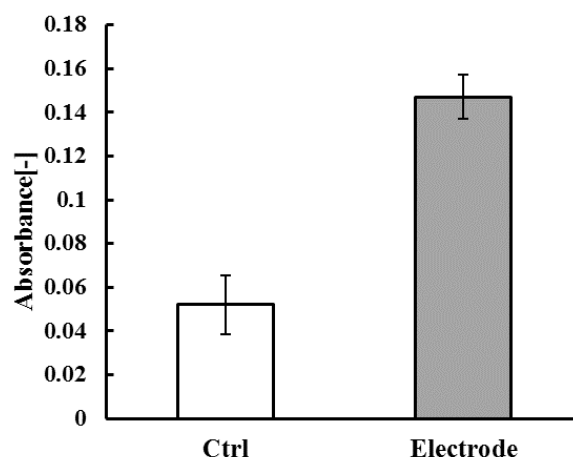


Fig. 2 Comparison of absorbance on Ctrl and Electrode.

### References

1) Akinori Zukeran, et al., *Proceedings of the 21st International Conference on Gas Discharge and their Applications*, Vol.2, pp.509 - 512, 2016.

## **Abstracts T110**

## Performance Evaluation of a Charged Micro-size Particle Generator

Y.-H. Joe, J. Shim and H.-S. Park\*

Korea Institute of Energy Research, Daejeon, 34129, Korea

Keywords: Particle generator, Corona charger, micro-size particle.

Presenting author email: YHJoe@kier.re.kr

Various particle generators have been used to generate test particles. Generally, an atomizer is widely used to generate test particles, such as NaCl and KCl particles in a Lab.-scale experiment. The size of particles generated from the atomizer is normally under one micro-meter, since there is an impaction plate right-after atomizing nozzle for which increases generation rate of nano-size particles and maintains its stability during particle generation. By this reason, it is hard to conduct Lab.-scale experiment using micro-size particles using the atomizer. Charging of particles is an important process in aerosol sizing, measuring, and removing. Various types of unipolar chargers have been studied and used in Lab.-scale experiment. However, almost applications are focused on the charging of nano-size particles. Thus, there is a lack of research on generating and charging of the micro-size particles, even though the particles, such as PM2.5 and PM10, also important factors in indoor and outdoor environmental research.

In this study, we fabricated a charged micro-size particle generator and evaluated its performance. A spray nozzle was installed on the top of a reactor having 400 mm of height in 150 mm diameter. KCl solution was atomized by the nozzle and the sprayed droplets were dried by high temperature sheath air which was injected from the bottom of the reactor. Then the particles were entered to a corona charger installed right-after the reactor, finally, charged micro-size particles are generated.

In order to evaluate performance of the generator, the generated and charged micro-size particles were entered to the test chamber (made from acryl, cross-sectional area:  $100 \times 100 \text{ mm}^2$ ) and concentrations of particles and current of the charged particles were measured by an optical particle counter and an aerosol electrometer, respectively. 2 wt.% of KCl solution was used in this study, and 0 to 4 kV DC voltage was applied to the corona charger to generated air ions. Total number and mass concentrations of generated particles decreased with increasing of applied voltage (particle loss in the charger), and these values were approximately  $2.4 \times 10^5$  particles/cm<sup>3</sup> and  $817 \mu\text{g}/\text{m}^3$ , respectively, when 3 kV of high voltage was applied on the corona charger. The charge number at each size of particle was calculated using measured number concentration and current of the charged particles, and the charge number was reached to the saturation value when applied voltage to the charger was over than 4 kV.

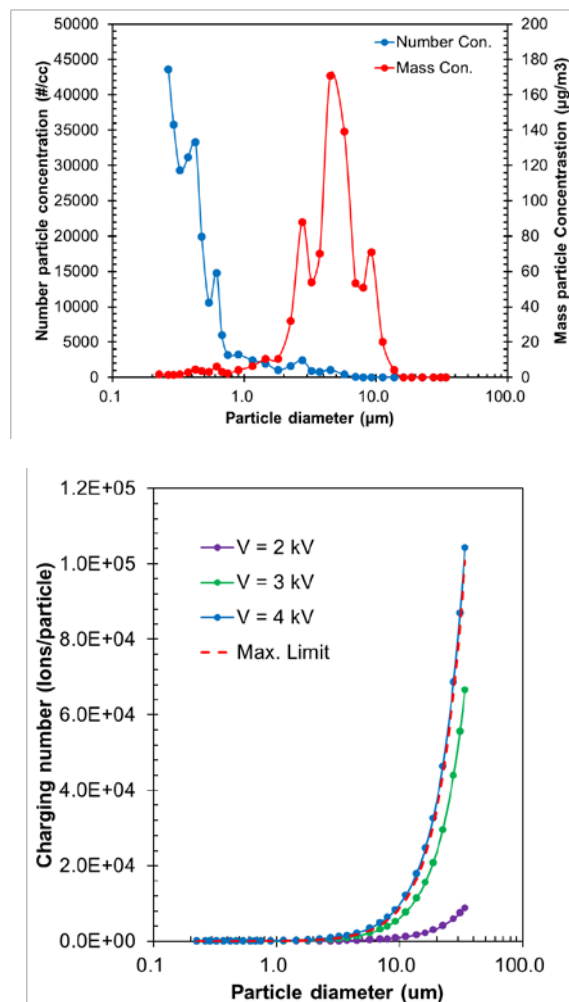


Figure 1. (a) number and mass concentration of generated particles and (b) charging number of particles with various applied voltage.

This work was conducted under framework of the research and development program of the Korea Institute of Energy Research (B7-2435-01).

## Impact of surface roughness, dielectric constant and resistivity of wall on the deposition of submicron particles driven by the negative air ionizer

K.P. Yu<sup>1</sup>, W.M. Lee<sup>2</sup> and C.J. Peng<sup>2</sup>

<sup>1</sup>Institute of Environmental and Occupational Health Sciences, National Yang-Ming University, Taipei, 11221, Taiwan (ROC)

<sup>2</sup>Graduate Institute of Environmental Engineering, National Taiwan University, Taipei 106, Taiwan (ROC)

Keywords: submicron particles, surface roughness, dielectric constant, resistivity, ionic air purifier

Presenting author email: kpyu@ym.edu.tw

Many previous studies have proven that the surface characteristic of the wall materials plays an important role in the deposition rate of submicron particles in a room. However, there were only very few studies investigating the effects of wall materials on the performance of the ionic air purifier (IAP) on the deposition of submicron particles. This study aims to evaluate the effects of surface characteristics of wall materials, including roughness, dielectric constant, and electrical resistivity on the deposition of submicron particles driven by the IAP.

The experiments were conducted in a 1-m<sup>3</sup> stainless steel chamber, which equipped with a negative air ionizer (an IAP). The surfaces of chamber wall were covered by six different wall materials, including cement paint, latex paint, walnut, white oak, and two kinds of wallpaper, for testing. In the experiment, the NaCl<sub>(s)</sub> monodisperse submicron particles in the range of 50 to 300 nm (50, 80, 100, 200 and 300 nm) were introduced into the chamber, and then the decay of particle number concentration was monitored continuously with a Condensation Particle Counter (CPC). In general, the particle concentration in the test chamber could be expressed as the following equation:

$$C(t) = C_0 \exp(-kt), \quad k = k_n \text{ or } k_a \quad (1)$$

where  $C(t)$  is the particle number concentration at the time,  $t$ ;  $C_0$  is the initial particle number concentration;  $k_a$  and  $k_n$  are the decay constant of particle number concentration with and without IAP operating. The effectiveness of IAP on the deposition of aerosol particles can be evaluated by the Effective Cleaning Rate (ECR) (Yu et al. 2017):

$$ECR = (k_a - k_n)V \quad (2)$$

where  $V$  is the volume of the test chamber.

Surface roughness would diminish the thickness of particle-concentration boundary layer and change the air flow pattern near the walls (Thatcher et al. 2002; Zhao and Wu 2007), and hence beneficial to the effectiveness of IAP on the deposition of particles smaller than 200 nm, as shown in Table 1. Besides, the wall materials with the higher dielectric constant could acquire more electrostatic charges, and thus, a "back corona" develops more likely on these materials. As a result, the performance of IAP was negatively correlated with the dielectric constants. Also, the "back corona" arises more probably on the material with higher electrical resistivity. However, when the resistivity is very low, the electrostatic charges on the deposited particles would be drained off very fast, and the particle

might be re-entrained into the air. According to our experimental result, when the resistivity of wall material was within  $3 \times 10^{10} \sim 9 \times 10^{10} \Omega \text{ cm}$ , the IAP performed better.

Conclusively, our result provides a systematic conception on how for the surface characteristics influence the deposition of submicron particles driven by the IAP

Table 1. Spearman's rho correlation between the characteristics of wall materials and Effective cleaning rate (ECR)

	Spearman's rho				
	50 nm	80 nm	100 nm	200 nm	300 nm
Roughness vs. ECR	0.714	0.886*	0.771	0.371	-0.257
Dielectric constant vs. ECR	-0.429	-0.714	-0.486	-0.657	0.257
Resistivity vs. ECR	-0.029	-0.371	0.029	0.429	0.771

This work was supported by the Ministry of Science and Technology of Taiwan (ROC) under grant MOST 105-2221-E-010-002-MY3.

Thatcher, T.L., Lai, A.C., Moreno-Jackson, R., Sextro, R.G. and Nazaroff, W.W. (2002) *Atmospheric Environment* **36**,1811-1819.

Yu, K.-P., Shih, H.-C., Chen, Y.-C. and Yang, X.-E. (2017) *Building and Environment* **114**,166-177.

Zhao, B. and Wu, J. (2007) *J. Hazard. Mater.* **147**, 439-448.

## Continuous Separation of similar size distribution of atomized bacteria and PSL particles using corona discharge mechanisms

Ali Mohamadi Nasrabadi, Jangseop Han, Milad Massoudi Farid, Sang-Gu Lee and Jungho Hwang\*

Department of Mechanical Engineering, Yonsei University, Seoul, 03722, Republic of Korea

Keywords: bioaerosol, corona discharge, electrical mobility

\*Corresponding author: hwangjh@yonsei.ac.kr

Presenting author email: a.mohamadi@yonsei.ac.kr

For rapid and effective detection, various biological and chemical techniques have been developed such as immunoassay, UV-Vis spectroscopy, polymerase chain reaction (PCR), and biosensors. However, each of them still suffers from some deficiencies. Non-target particles and dust are one of these problems that can affect accuracy of measurements and detection, especially in the case of PCR and biosensors.

In the following, we introduced a methodology to separate bacterial and non-bacterial aerosols of the same mean size due to the difference in their electrical mobilities. In this sense,  $0.9 \mu\text{m}$  *Staphylococcus epidermidis* (*S. epidermidis*) and polystyrene latex (PSL) particles were chosen, respectively, as target and non-target particles. By passing these particles through a corona region, *S. epidermidis* and PSL particles gained different electrical charge values (88 and 65, respectively) since the number of charges obtained by aerosol particles depends on their relative permittivity. The PSL particles and *S. epidermidis* were separated from each other when an external electric field was applied to the direction perpendicular to the flow. For this purpose, a mobility analyzer developed by Mainelis et al. (2002) was used.

The schematic of the rectangular-shaped separator is shown in Fig. 1. The separator consisted of two parallel plates and had two inlets and two outlets. Air flow containing charged PSL and *S. epidermidis* particles entered through one inlet (0.3 LPM) while clean sheath air that entered through another inlet (0.9 LPM). Then the external electrical field in the direction of Y-axis caused the negative charged bacteria to be deflected toward the anode so that they could exit through the 'Outlet 1'. The PSL particles were also deflected toward the anode. However, their charge number (57) was much lower than that of *S. epidermidis* (88). Therefore, the PSL particles were supposed to exit through the other outlet, 'Outlet 2'. A rectangular pin was embedded at the end of the separator to increase the separation efficiency.

The aerosol number concentrations were measured at the inlet and outlet to determine the separation performance. The recovery is defined as the fraction of particular species exiting the separator to the species injected to the separator. The purity is defined as the

fraction of particular species to the total species exiting through an outlet.

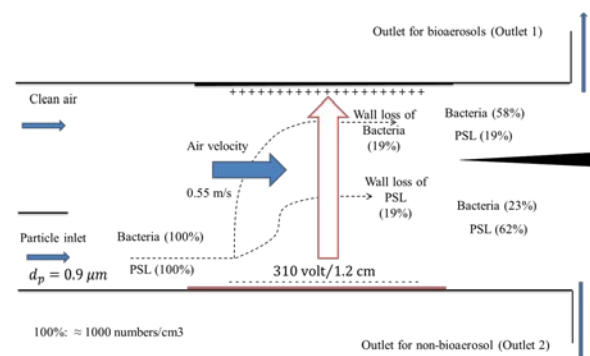


Figure 1. Fates of PSL and *S. epidermidis* through the analyzer

Figure 1 shows that the recovery for *S. epidermidis* was 58% while the recovery of PSL was 62%. Meanwhile, 23% of *S. epidermidis* exited through outlet 2 and 19% of PSL exited through outlet 1. The purity of *S. epidermidis* for outlet 1 was 79.1% ( $= 58 / (58+19)$ ) and the purity of the PSL in outlet 2 was 69% ( $= 62 / (62+23)$ ). The wall losses for bacteria and PSL were 19% and 19%, respectively. Although the purities for both *S. epidermidis* and PSL are acceptable, more investigation would be needed for increasing recovery and decreasing wall loss. Nonetheless, this methodology can give a fast and simple solution for increasing the detection accuracy of bacterial agents in air.

This research was supported by Basic Science Research Program through the National Research Foundation of Korea (NRF) funded by the Ministry of Science, ICT and future Planning (NRF-2015R1A2A1A01003890).

Mainelis, G., Willeke, K., Baron, P., Grinshpun, S. A., & Reponen, T. (2002). *Aerosol Science & Technology*, 36(4), 479-491.

## Efficiency of an Ionizer in Removing Airborne Particles

Buddhi Pushpawela, Aline Nguy, Rohan Jayaratne and Lidia Morawska

International Laboratory for Air Quality and Health,  
Queensland University of Technology, Brisbane 4001, QLD, Australia

Keywords: Atmospheric Ions, Aerosols, Air Ionizer, Air Cleaner

Presenting author email: buddhi.pushpawela@hdr.qut.edu.au

It is known that air ions clean indoor environments by the removal of aerosol particles (Grabarczyk, 2001; Grinshpun et al., 2005). Although, the precise mechanism is as yet unknown, negative ions (generally oxygen molecules with an excess of electrons) are believed to have beneficial effects on human health by enhancing our well-being. These ions cause particles of pollution (mostly positively charged) suspended in the air to aggregate or clump together and deposit on the floor and other surfaces. Negative ions are naturally found in areas like the beach, in the mountains, in forests and near waterfalls. Further, these ions can be artificially generated by electrical devices such as air ionizers (also known as negative ion generators).

Several types of air ionizers are commercially available to clean indoor environments. In this study, we tested the efficiency of a small negative ion generator (Aironic AH-202) in removing ultrafine particles (diameter smaller than  $0.1 \mu\text{m}$ ) in three enclosures of different volumes - a closed chamber of volume  $0.9 \text{ m}^3$ , in a small unventilated room of volume  $20 \text{ m}^3$  and in a large ventilated room of volume  $132 \text{ m}^3$ . This device is mains-powered, contains four corona needles and emits approximately  $1 \times 10^6$  negative ions  $\text{s}^{-1}$ . An air cleaner fitted with a HEPA filter was used to compare the removal efficiencies. A TSI P-trak (model 8525) was used to measure the number concentration of ultrafine particles.

In the closed chamber, 70% of ambient air particles, initially at a concentration of about  $5000 \text{ cm}^{-3}$ , were removed in a period of 15 min. The air cleaner was able to remove all the particles in the chamber within 2 min. The comparison of the results is shown in figure 1. The percentages of particles that were removed by the ionizer in 15 min in the small unventilated room and in the large ventilated room were 50% and 25% respectively (figure 2).

The results of this study showed that, although not as effective as an air cleaner fitted with a HEPA filter, ionizers can effectively remove a significant fraction of airborne particles in closed and unventilated indoor environments. Its efficiency reduces to about 25% in ventilated rooms.

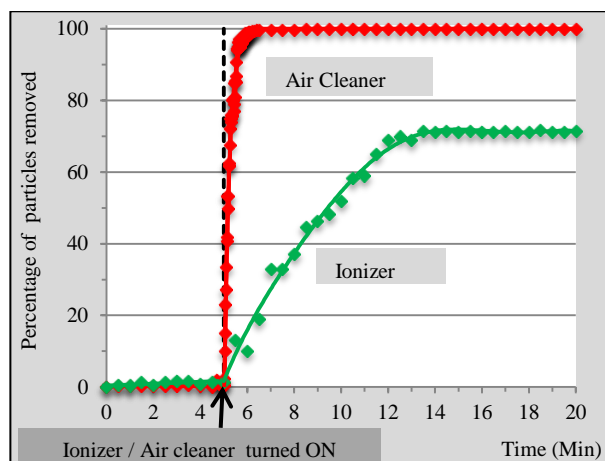


Figure 1. Percentage of particles removed in a closed chamber using the ionizer (in green) and the air cleaner (in red). Both instruments were turned on at 5 min.

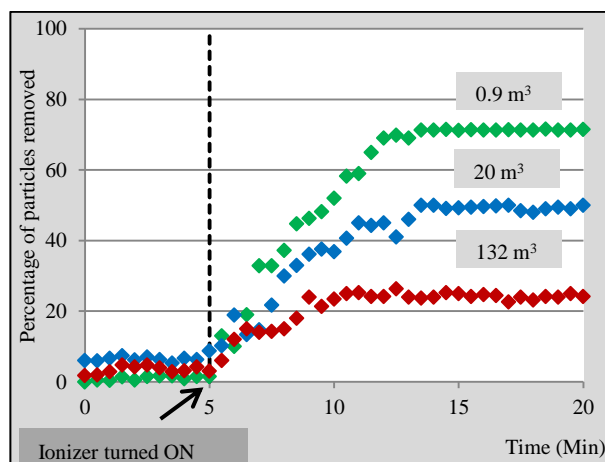


Figure 2. Percentage of particles removed in a closed chamber (in green), in a small unventilated room (in blue) and in a large ventilated room (in red) using the ionizer. The ionizer was turned on at 5 min.

Grabarczyk,Z (2001). Effective of indoor air cleaning with corona ionizers. *Journal of Electrostatics*, 51, 278-283.

Grinshpun, S., Mainelis, G., Trunov, M., Adhikari ,A., Reponen, T., & Willeke, K., (2005). Evaluation of ionic air purifiers for reducing aerosol exposure in confined indoor spaces. *Indoor air* , 15 (4), 235-245.

## **Abstracts T111**

## Study of Collection Mechanism on Hole-type Electrostatic Precipitator by Particle Behaviour and Fluid Flow

Hiroataka Miyashita<sup>1</sup>, Shumpei Ibaraki<sup>1</sup>, Yoshiyasu Ehara<sup>1</sup>, Takashi Inui<sup>2</sup>, Tomoyuki Sawada<sup>2</sup>

<sup>1</sup>Dept. of Electrical and Electronic Engineering, Tokyo City University, Tokyo, 158-8557, Japan

<sup>2</sup> Fuji Electric Co., Ltd, Tokyo, Japan

Keywords: Electrostatic Precipitator, Particle Image Velocimetry, Ionic Wind.

Presenting author email: g1691302@tcu.ac.jp

The electrostatic precipitator (ESP) is a means to collect PM. They are characterized by a high particle collection efficiency with low pressure drop. However, re-entrainment phenomenon is caused according to the condition. The new hole-type ESP was developed to overcome the re-entrainment in the ESP. The hole-type ESP utilizes the ionic wind. The ionic wind is caused by the corona discharge. The particle flow into the hole by ionic wind. The Electric field of a collecting zone in the hole is zero. It can be expected that suppression of the re-entrainment. However, it has not been clarified how the particle flow into the hole. Therefore, an investigation of the ionic wind is necessary to improve the performance of ESP. Particle image velocimetry (PIV) was used to analyze the ionic wind and particle behaviour in hole-type ESP. In this paper, results of PIV of the particle flow velocity fields and simulation analysis of the ionic wind in a hole-type ESP model are presented.

The experimental system is shown in Fig. 1. The electrodes are composed of a needle discharge and a plate. The needle discharge electrode was installed above the hole. The hole of 20 mm in diameter was opened to the plate electrode. The tracer particles of talc flowed in ESP. The particles were visible to irradiate with the laser sheet. The movement velocity distribution of particle was requested by analysing the image acquired with a high-speed camera.

The averaged particle flow velocity field in ESP is shown in Fig. 2. Primary flow velocity is 0.3 m/s. Primary flow velocity is an average speed when the particle flows from the upstream to the downstream. The particle blows from the needle discharge electrode toward the hole. The particle velocity right under of the needle discharge electrode was the fastest.

The analysis results of the fluid affected by the ionic wind is shown in Fig. 3. This study was used COMSOL Multiphysics® (simulation software based Finite Element Method). By coupling of Poisson's equation and the positive ion continuous, it was analyzed electric field and space charge density. The flow velocity of the ionic wind was around 1m/s at just below the needle. In addition, the obtained analysis result is quantitatively in good agreement with experimental results (PIV). In the simulation, when the flow rate became faster, the main stream didn't into the hole. It is considered to show the same result in PIV.

This work supported by The Japanese Society for the Promotion of Science. Grant number JP16H04606.

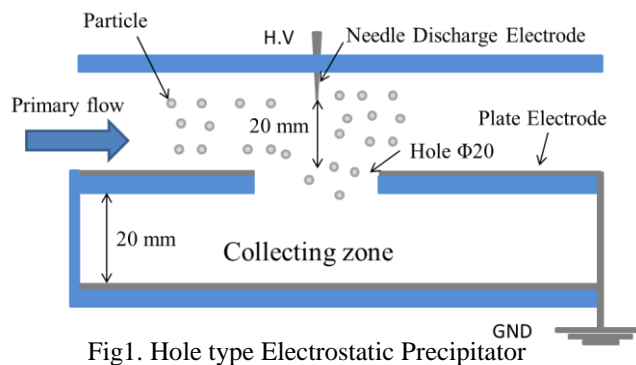


Fig1. Hole type Electrostatic Precipitator

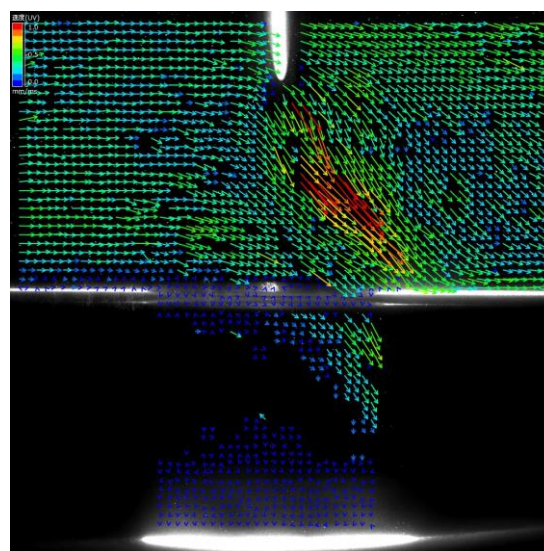


Fig2. Particle velocity field (Talc, 1 $\mu$ A, 0.3 m/s)

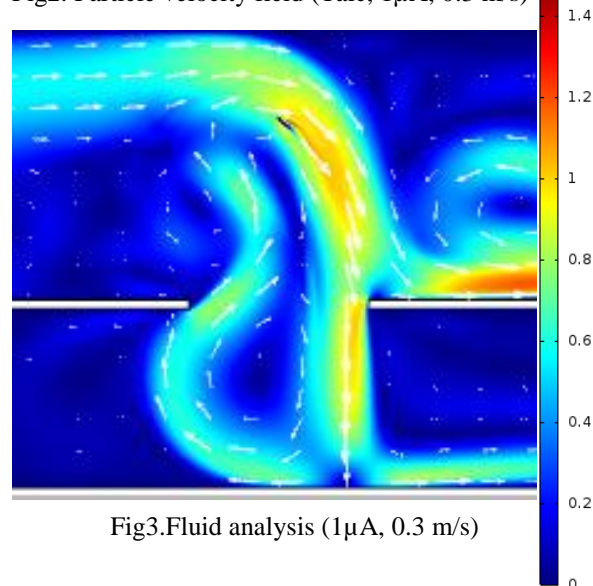


Fig3. Fluid analysis (1 $\mu$ A, 0.3 m/s)

## Simulation analysis of particle behavior in hole type Electrostatic precipitator

Masaya Shimoda<sup>1</sup>, Yoshiyasu Ehara<sup>1</sup>, Takashi Inui<sup>2</sup>, Tomoyuki Sawada<sup>2</sup>

<sup>1</sup> Department of Electrical and Electronic Engineering, Tokyo City University, Tokyo, 158-8557, Japan

<sup>2</sup> Industrial Infrastructure Business Group, Fuji Electric CO. LTD, Japan

Keywords: electrostatic precipitator, corona discharge, simulation, particle behavior.

Presenting author email:Shimodmas@gmail.com

As a cause of air pollution, the reduction of particulate matter contained in the exhaust gas of marine diesel engines is a problem all over the world. If particulate matter enters the human body, especially respiratory organs, it may cause serious health problems, such as bronchitis, lung cancer, and allergic diseases. Electrostatic precipitators (ESP) have attracted attention in order to reduce PM. However a re-entrainment of collected PM in ESP is a problem. As a device for preventing this phenomenon, hole type ESP was developed. In this study, the results of simulation analysis in hole type ESP were reported.

We used COMSOL Multiphysics simulation software using finite element method in this research.

A simulation model is shown in Fig 1. This model is a two-dimensional representation of a hole type ESP. The main fluid gas blows from the left to the right, and line of electric force extend mainly from the needle electrode to the edge of the grounded electrode. Normally, gas flows straight from the left to the right. However corona discharge is generated from the needle electrode, so that ionic wind blows from the electrode toward the edge of the grounded electrode, and fluid is blown into the hole.

As an expression used for analysis, Poisson equation

$$-\nabla \cdot \epsilon_r \epsilon_0 \nabla V = \rho \quad (1)$$

Equation of positive ion continuity

$$\frac{\partial N_p}{\partial t} + \nabla \cdot (-D_p \nabla N_p + \mu_p E N_p) = 0 \quad (2)$$

$$\rho = e(-N_e + N_p - N_n) \quad (3)$$

Electric field and positive ion charge density analysis were carried out. Coulomb force derived from analysis is incorporated into Navier-Stokes equation

$$\rho_g \frac{\partial U}{\partial t} + \rho_g (U \cdot \nabla) U = -P + \mu_g \nabla^2 U + F \quad (4)$$

Analysis of ion wind was carried out by calculating as external force term of equation (4). In addition, as an equation for analyzing particle behavior, a particle charging formula was given and particle behavior was analyzed.

$$Z = \frac{3\pi\epsilon_0\epsilon_s d^2 E}{(\epsilon_s + 2)} \quad (5)$$

Fig.2 shows the analysis results of the fluid flow. (a) shows a image of fluid flow from 0.5 second after the start of discharge, (b) shows 2 seconds later. Primary flow velocity is 0.3m/s. It can be confirmed that the wind blows into the hall because of the ion wind both (a) and (b).

In order to simplify the simulation, the particle behavior analysis was carried out by disposing saturated charged PMs. Simulation model of particle behaviour is

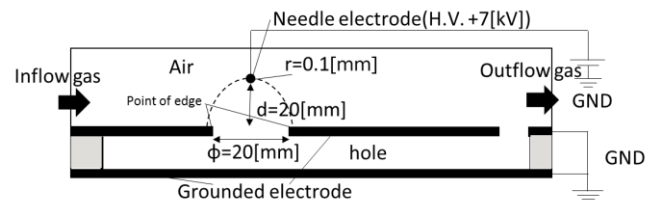
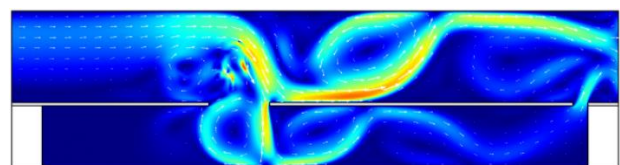
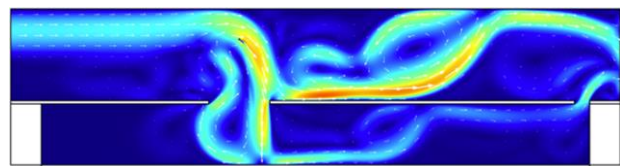


Fig.1.Simulation model



(a) t = 0.5 second



(b) t = 2.0 second

Fig.2. Fluid flow analysis

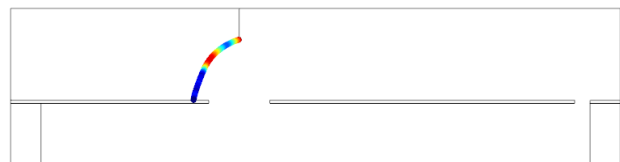


Fig.3. Particle behavior analysis (t = 0.5[s])

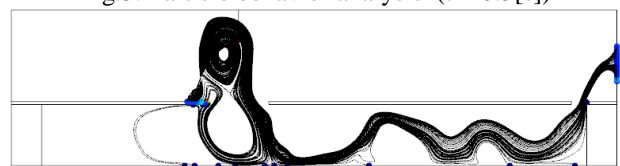


Fig.4. Particle behavior analysis (t = 2.0[s])

shown in Fig.3. 100 particles were placed on the line of electric force in which an electric field is strongest. Simulation of particle behavior was analysed from 0.5 second after the start of discharge. The particle diameter is 6.2 μm.

Fig.4 shows analysis result of the particle behavior. The almost particles penetrated into the hole. However a part of the particles did not adhere to the grounded electrode and went off the hole. These problem are the future work.

This work was supported by JSPS KAKENHI Grant Number JP, 16H04606.

## Improved collection efficiency of fine particles by ESP combined with electro spray

Min-Jeong Oh and Myong-Hwa Lee\*

Thermochemical Energy System R&D Group, Korea Institute of Industrial Technology, Republic of Korea

Keywords: Electro spray, Electrostatic precipitator, Particle charging, Fine particles.

Presenting author email: myonghwa@kitech.re.kr

Although the ESP has a high collection efficiency at low pressure drop, it has relatively lower collection efficiency for the particle size range of 0.1~1  $\mu\text{m}$  due to the low charging efficiency by both diffusion charging and field charging. Moreover, the particle collection efficiency decreases due to the particle re-entrainment by rapping. This problem can be solved by employing a wet electrostatic precipitator, which uses a flow of water to collect particles on the collecting electrodes. However, the system requires an additional wastewater treatment facility. Therefore, an ESP combined with an electro spray device is a potential system that can be used to minimize water consumption and increase the collection efficiency, and developed in this study. The effect of the operating parameters, such as the water feedrate, water conductivity, electric field and internal pressure in the electro spray system, on the droplet size were investigated. In addition, the collection efficiency of the electro spray based ESP was compared with that of an individual ESP.

Figure 1 shows the experimental setup used to measure the particle collection efficiencies in the electrostatic precipitator combined with the electro spray device. The system consists of a charged droplet generation zone, a particle generation zone, a particle collection zone and a particle measurement zone. Charged droplets were electro sprayed under an electric field between a nozzle and an induced ring. Positive potential from a high voltage power supply was applied to the induced ring in order to generate negatively charged droplets. The generated charged droplets and test particles collided together upstream of the ESP and were charged negatively. Negatively charged particles effectively migrated to the collecting electrode when negative potential was applied to the discharging electrode.

In terms of results, we found that, due to the decreased electrostatic repulsion inside of the droplets, the droplet size increased with increasing water feedrate under identical electric field. However, the droplet size decreased with increasing electric field, water conductivity and internal pressure in the chamber because the increased electrostatic repulsive force increased compared to the surface tension of water. In addition, compared to the ESP only, the collection efficiency of the ESP combined with the electro spray device showed an increase of about 10~15 % in the electric field of -0.11~-0.28 kV/cm; this increase was due to the increased collision frequency between particles and charged droplets.

### Acknowledgement

This work was supported financially by the Creative convergence research project of National Research Council of Science & Technology, Republic of Korea.

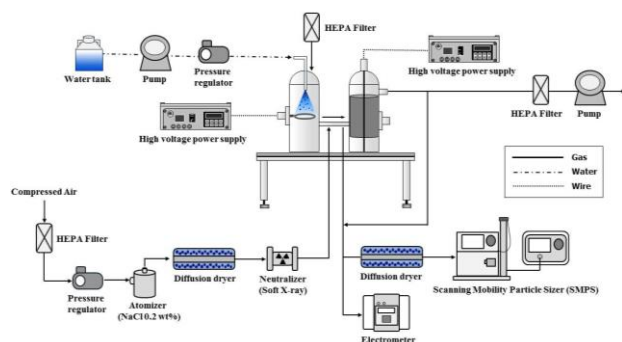


Figure 1. Schematic diagram of ESP combined with electro spray device.

## Analysis of different liquid-liquid combinations and conditions for the formation of a stable cone-jet mode in electrospray emulsification processes

A.W. Kamau<sup>1</sup>, Gatari M. J.<sup>1</sup>, J.C. M. Marijnissen<sup>1,2</sup> and L.L.F. Agostinho<sup>3</sup>

<sup>1</sup>Institute of Nuclear Science and Technology, University of Nairobi, Nairobi, 30197-00100, Kenya

<sup>2</sup>University of Florida, Gainesville, FL 32611, United States

<sup>3</sup>NHL University of Applied Sciences, Rengerslaan 10 Leeuwarden, The Netherlands

Keywords: ethylene glycol-hexane, liquid properties, charged droplets, monodisperse distribution.

Presenting author email: annwairimuk@gmail.com

Electrohydrodynamic atomization (EHDA) is the breaking up of a liquid into droplets under the influence of a strong electric field (kV/cm). Cloupeau and Prunet-Foch (1994) have shown that there are different modes generated depending mainly on the electric field characteristics and flow rate for the same liquid. Barrero *et al* (2004) have afterwards mentioned some electrospray characteristics when the continuous media is another liquid i.e. electrospray emulsification process. Later, Jaworek (2008) published some applications of the electrospray under similar conditions. In this work the conditions necessary to obtain cone-jet mode in electrospray emulsification different liquid-liquid combinations i.e. water-hexane, water-paraffin oil, ethylene glycol-hexane and glycerol-hexane were studied. Additionally, the liquid combination which allowed electrospraying in a stable cone-jet mode, was further analyzed regarding produced droplet size, size dispersion and the stability of the generated emulsion.

For the experiments, the dispersed phase was pumped through a nozzle into the continuous phase. A high voltage difference was applied to the nozzle while a counter electrode (ring), placed at 1cm below it, was kept grounded. A high-speed digital camera coupled with a microscopic lens was used to capture the images of the electrospray. Among all the tested combinations, ethylene-glycol-hexane and glycerol-hexane systems generated stable cone-jet mode. For ethylene glycol-hexane, the cone jet was obtained when the electric potential was set between 6 and 8 kV and the flow rate at 0.5 mLh<sup>-1</sup>. Other modes were observed for this same flow rate at different potentials i.e. dripping and micro-dripping modes between 0 and 2kV, an intermittent cone-jet mode between 3 and 5kV, and a multi-jet mode (two steady cone-jets) for potentials bigger than 8kV. At the onset of the cone-jet mode, the tip of the jet manifested 'whipping instabilities'.

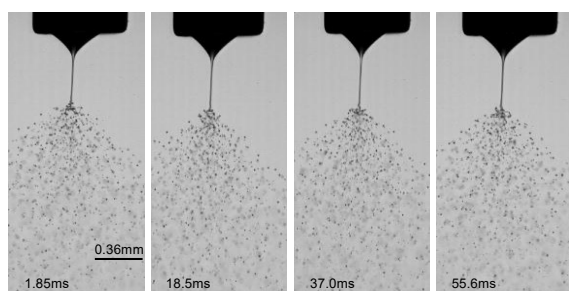


Figure 1. A steady cone jet mode observed over time (ethylene glycol-hexane system at 0.5mL/h and 6kV)

After recording, the images of the droplets were analyzed with an imaging software (ImageJ). Results indicated that between 3 and 5 kV, the spray was rather polydisperse. For the stable cone-jet mode (potentials 7kV and 8kV), a bimodal distribution with average diameters of ~4 $\mu$ m and 8 $\mu$ m was observed. Theoretical calculations using the same approach suggested by Hartman *et al* (1999) indicated that the average droplet size (d) varied with the flow rate (Q) as  $d \sim Q^{0.33}$ . The spray electric current scaled with the flow rate by  $I/I_0 \sim (Q/Q_0)^{0.5}$ , where  $Q_0$  and  $I_0$  are the characteristic values of flow rate and its respective current.

During the experiment, the droplet dispersion into the continuous phase was observed to be enhanced in the presence of the electric field. The analysis done with different liquid-liquid combinations indicated that the liquids properties interfacial tension, the ratio between the liquids electrical permittivity and the viscosity ratio can be used as important parameters to determine whether a stable cone-jet could be generated.

Support by Wetsus Academy, NHL University of Applied Sciences, International Science Programme and the University of Nairobi is acknowledged.

Cloupeau and B. Prunet-Foch (1994), *Electrohydrodynamic spraying functioning modes: A critical review*. Journal of Aerosol Science, **25** (6): 1021-1036

Barrero, J.M. López-Herrera, A. Boucard, I.G. Loscertales and M. Márquez (2004), *Steady cone-jet electrosprays in liquid insulator baths*. Journal of Colloid and Interface Science. **272**: 104-108

Jaworek (2008), *Electrostatic micro- and nanoencapsulation and electroemulsification: A brief review*. Journal of Microencapsulation **25**(7): 443-468

Hartman, Brunner D.J., Camelot D.M.A., Marijnissen J.C.M., and Scarlett B. (1999), *Electrohydrodynamic atomization in the cone-jet mode physical modelling of the liquid cone and jet*. Journal of Aerosol Science. **30** (7): 823-849

## **Abstracts T112**

## Electrostatic precipitation of particulate matter from syngas

A. Bologna, K. Woletz, H.-R. Paur and D. Stapf

Karlsruhe Institute of Technology, D-76344 Eggenstein - Leopoldshafen, Germany

Keywords: corona discharge, high pressure, helium, current-voltage characteristics

Presenting author email: andrei.bologa@kit.edu

The combustion of biomass is a direct way for use of biofuel for generation of heat. Another way is the production of so-called second generation biofuels, from which the syngas is the most one. The syngas from the gasification facility usually contains particulate and gaseous contaminants. If they are not removed, this could result in damage of the equipment and in decrease of final product quality.

In (Villot, 2012) the results of the tests of a wire-cylinder electrostatic precipitator (ESP) with syngas at  $T_{\text{gas}}$  up to 680°C and  $P_{\text{gas}}$  up to 0,2 MPa are discussed. The ESP mean mass collection efficiency was  $\eta \approx 95\%$ . The syngas contained fine particles with diameter  $< 1 \mu\text{m}$  and large particles with diameter up to 100  $\mu\text{m}$ . It is shown that the control of corona discharge characteristics of the ionizer is a key-point for effective particle charging in electric field. To ensure stable operation, the ESP should be cleaned and should be equipped with a high voltage (HV) insulator suitable for operation in HT-conditions.

The scope of the current study is the development of a compact and effective electrostatic precipitator for collection of particulate matter from dry high temperature high pressure (HT-HP) syngas.

The designed HT-HP ESP is a space charge electrostatic precipitator, in which particles are charged in the corona discharge ionizer and are further precipitated in a grounded external electric free collector stage. The ESP is equipped with a system for cleaning of both the ionizer and collector. The collected material is joined in the bottom part of the precipitator and should be periodically evacuated from the precipitator.

The study of the characteristics of a corona discharge ionizer in the syngas was carried out for various operation conditions. The ionizer was installed inside of the batch HT-HP reactor. The HV unit with  $U_{\text{max}}=20 \text{ kV}$  and  $I_{\text{max}}=10 \text{ mA}$  was used during the tests. The measurements were carried at  $T_{\text{gas}}$  up to 500°C and  $P_{\text{gas}}$  up to 0,1 MPa. The tests were carried out in a mixture of two ( $\text{H}_2+\text{CO}$ ) and five gases ( $\text{H}_2, \text{CO}, \text{CO}_2, \text{CH}_4, \text{N}_2$ ). The current-voltage characteristics (CVCs) were measured for positive and negative polarity corona discharge. The  $I=f(U)$  dependences (so-called “direct” CVCs) were measured by increase of voltage up to the value  $U$ , which corresponded to  $I_{\text{max}}$  (Fig.1) or up to  $U_{\text{max}}$  when current  $I$  was  $I < I_{\text{max}}$ . Then the voltage was decreased to the value  $U$  when the current was  $I=0\text{mA}$  (so-called “indirect” CVCs). Among the measurements of the CVCs, the long-term stability of the corona discharge in the syngas was investigated.

The results confirm that the negative corona discharge ensures higher corona currents than the positive one. So, the negative corona discharge is used for particle charging in the HT-HP ESP.

A loop between the “direct” and “indirect” CVCs was observed and it is similar to a hysteresis one. This effect was observed in both of syngas mixtures. The surface of the loop strongly depends on syngas temperature and pressure. The nature of the observed phenomenon needs further study.

At certain operation conditions the particulate matter was formed (Fig.2) inside of the ionizer. This disturbed the corona discharge stability and required the periodical cleaning of the HT-HP ionizer. A series of laboratory studies was carried out to prove the design of a HV insulator suitable for operation at HT-conditions. The results were used for the design of the pilot ESP.

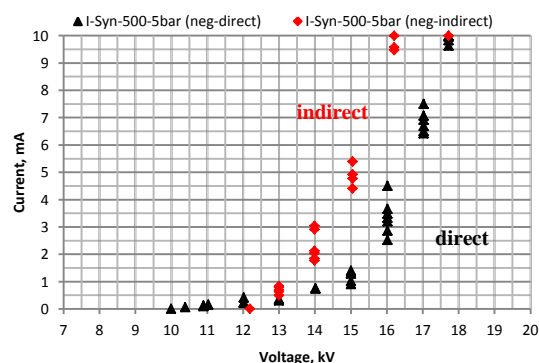


Figure 1. CVCs in the 5-gas mixture syngas,  $T=500^\circ\text{C}$ , over pressure  $P=5 \text{ bar}$

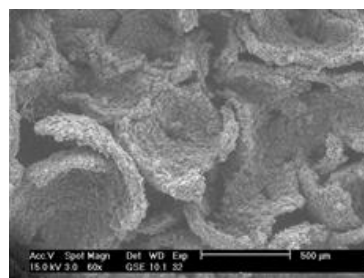


Figure 2. Particulate matter inside of the ionizer

Currently it is planned to study the operation of the HT-HP ESP at various gas temperatures and pressure and particle mass concentrations in the syngas flow at the laboratory set-up and at the Research Entrained Flow Gasifier.

Villot, A, etc., (2012), *Separation and Purification Technology* **92**, 181-190.

## Gas and PM removal performance of a wet scrubber system combined with a water-film ESP for IT manufacturing industries

H.J. Kim, Y.J. Kim, B. Han, and C.G. Woo

Environmental and Energy Systems Research Division, Korea Institute of Machinery and Materials, Daejeon, Korea, Republic of

Keywords: Gas, PM, removal, ESP, IT manufacturing

Presenting author email: diayolk@kimm.re.kr

A novel wet scrubber system combined with a water-film ESP to remove fine particles and gaseous pollutants such as NO<sub>x</sub>, SO<sub>x</sub>, HCl from IT manufacturing industries has been developed that uses a dry oxidation method to change NO to NO<sub>2</sub>, a wet scrubber absorbing soluble gases with basic solutions, finally a wet ESP to remove all particles and mists from the wet scrubbing system. In this study, an ozone generator (30 g/hr, 500W) was used to generate sufficient ozone to oxidize NO, and a packed-bed type scrubber (300 x 150 x 1440 mm, 2 inch packing balls) to remove NO<sub>2</sub>, SO<sub>2</sub>, HCl and coarse particles, and a cylindrical type ESP (2 cylinders, diameter 155 mm, height 600 mm) with water film to collect all the fine particles including mists from the scrubber.

The flow rate in this study was maintained at 1 m<sup>3</sup>/min, and gas concentration was kept at a range between 200-300 ppm. Liquid to gas ratio in the scrubber was varied from 5-10 L/min, NaOH was supplied to maintain pH as 12 to remove soluble gases such as SO<sub>2</sub> and HCl, and Na<sub>2</sub>S was also supplied to maintain ORP as -300 mV to absorb NO<sub>2</sub>. SiO<sub>2</sub> dusts and water mists were used to measure particle collection efficiency. Photochemical and FTIR type measurement systems for NO<sub>x</sub>, SO<sub>x</sub> and HCl, and an optical particle counter for particles were used.

Figure 1 shows the NO<sub>x</sub> removal efficiency of the scrubber system with various Na<sub>2</sub>S solutions and 0.1% NaOH solution during continuous operation time for approximate 3 hours. 1:1 ratio of NO/O<sub>3</sub> was necessary to convert NO to NO<sub>2</sub> which is soluble, and NO<sub>x</sub> removal efficiency was dependent on Na<sub>2</sub>S concentration and 80% NO<sub>x</sub> was removed with 0.1% Na<sub>2</sub>S and NaOH 0.1% solution.

Figure 2 shows the particle collection efficiency as a function of particle size with different applied voltages from -5 to -17 kV. The collection efficiency increased with applied voltage, and it reached over 90% with applied voltage of -13 kV and 1.5 mA, corresponding specific corona density of 2.5 mA/m<sup>2</sup>.

In this study, we conclude that a novel wet scrubber system combined with a water-film ESP could be an efficient exhaust gas treatment system for gas cleaning from IT manufacturing industries.

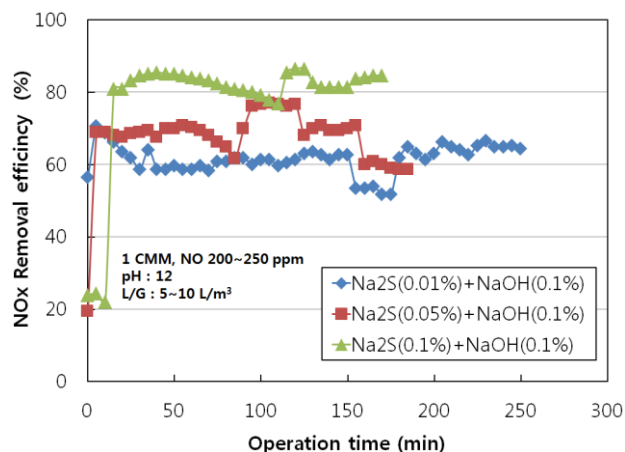


Figure 1. NO<sub>x</sub> removal efficiency of the wet type gas cleaning system in this study with different Na<sub>2</sub>S solutions for 3 hours of continuous operation.

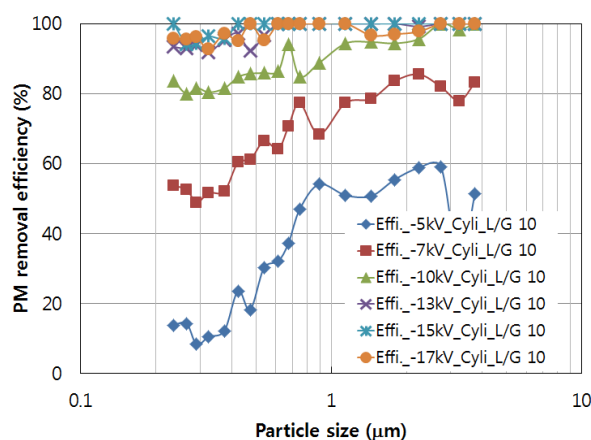


Figure 2. Size-dependent collection efficiency of the ESP with change of applied voltage.

This work was partially supported by the Eco-Innovation project (GG2790) and also by the R&D center for Reduction of Non-CO<sub>2</sub> Greenhouse gases (GG2740), funded by the Ministry of the Environment, Republic of Korea.

## **Abstracts T114**

## Mechanism of organic solvent induced charge degradation of electret filters

Panagiota Sachinidou<sup>1,2</sup>, Claire Heuschling<sup>1</sup>, Jing Wang<sup>1,2</sup>

<sup>1</sup>Analytical Chemistry Laboratory, Empa, Dübendorf, 8600, Switzerland, <sup>2</sup>Institute of Environmental Engineering, ETH Zurich, Zurich, 8093, Switzerland,

Keywords: filter discharge, discharge mechanism, solvent induced charge degradation.

Presenting author email: psachini@ethz.ch

Large quantities of nanoparticles are produced from material synthesis and combustion, thus high efficiency filters should be tailored for their applications. However, the pressure drop usually increases together with enhanced filter performance with respect to mechanical filtration mechanisms.

An option to increase filtration efficiency, maintaining the pressure drop low, is to produce electrostatically charged filters. However, it is very important to accurately determine the minimum filtration efficiency after charge deterioration. Thus, filters should be completely discharged in standardized efficiency tests. Filtration performance can deteriorate due to the exposure in organic solvents such as IPA (isopropyl alcohol), ethanol etc. ISO 29461-1 describes a procedure to discharge the filter media by exposing it to isopropanol vapour or liquid. However, the mechanism which contributes to the discharge is not completely understood.

Researchers (Cantaloube et al. (1979), Kim et al. (2007)) proposed several mechanisms which could contribute to the filter discharge by exposure to organic solvents. The most plausible explanation is the charge liberation by the penetration of the solvent into the polymer network. This procedure depends on the affinity of the solvent and the filter material.

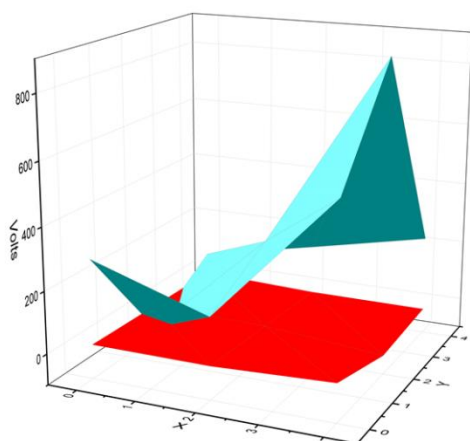


Figure 1 Filter discharge after exposure to liquid ethanol (blue surface shows the initial charge distribution on the filter surface and red shows the final charge).

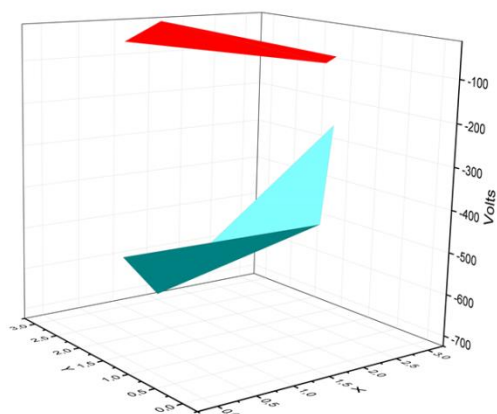


Figure 2 Filter discharge after exposure to ethanol vapour (blue surface shows the initial charge distribution on the filter surface and red shows the final charge).

Experiments are being performed to investigate the aforementioned mechanism. Different polymer filters are exposed to the liquid and vapour phase of different organic solvents such as IPA, ethanol, butanol and the electrostatic charge is measured with a voltmeter. Indicative results presented in Figure 1 and Figure 2 show that the PET filter media is almost completely discharged when it is either immerse in the liquid or exposed to ethanol vapour. The results will facilitate the understanding of the discharge mechanism.

Cantaloube, B., Dreyfus, G. and Lewiner, J. (1979)  
*Vapor-induced depolarization currents in electrets.*  
*J. Polym. Sci. Polym.Phys.Ed.*,**17**: 95–101.

International Organization for Standardization ISO 29461-1 (2013) “*Air intake filter systems for rotary machinery — Test methods — Part 1: Static filter elements*”.

KIM, J., JASPER, W. and HINESTROZA, J. (2007)  
*Direct probing of solvent-induced charge degradation in polypropylene electret fibres via electrostatic force microscopy.* *Journal of Microscopy*, **225**: 72–79

## **Abstracts T115**

## Relating refractory soot mass spectra with nanostructure and combustion conditions

V.B. Malmberg<sup>1</sup>, A. Eriksson<sup>1,2</sup>, S. Török<sup>3</sup>, K. Kling<sup>4</sup>, M. Novakovic<sup>5</sup>, S. Shamun<sup>5</sup>, M. Shen<sup>5</sup>, M. Tuner<sup>5</sup>, P-E. Bengtsson<sup>3</sup>, and J. Pagels<sup>1</sup>

<sup>1</sup>Division of Ergonomics and Aerosol Technology, Lund University, Box 118, SE-22100, Lund, Sweden

<sup>2</sup>Division of Nuclear Physics, Lund University, Box 118, SE-22100, Lund, Sweden

<sup>3</sup>Department of Combustion Physics, Lund University, Box 118, SE-22100, Lund, Sweden

<sup>4</sup>National Research Centre for the Working Environment, 2100 Copenhagen, Denmark

<sup>5</sup>Division of Combustion Engines, Lund University, Box 118, SE-221 00, Lund, Sweden

Keywords: Soot, mass spectra, nanostructure, low temperature combustion

Presenting author email: Vilhelm.malmberg@design.lth.se

The soot particle aerosol mass spectrometer (SP-AMS) can detect infrared-light absorbing refractory aerosol particles. Vaporization occurs when a focused beam of particles enters a cavity ring down laser (Nd:YAG 1064nm) and the two beams overlap. Refractory mass spectra of soot have previously been used mostly to characterise the ratio of organic to refractory black carbon in soot particles. However, recent studies highlight the information contained in the carbon cluster ( $C_x^+$ ) distribution of soot particle refractory mass spectra (Malmberg et al., 2017; Onasch et al., 2015).

Soot mass spectra show strikingly different  $C_x^+$  distributions depending on the source and combustion condition. Soot in fuel-rich flames at high temperatures and with well-organized nanostructures, typically traditional diesel combustion soot, have mass spectra completely dominated by a few carbon cluster ions with low carbon number ( $C_1^+$ - $C_5^+$ ) of which  $C_3^+$  has the strongest signal. On the other hand, soot with less organized nanostructure, for example soot from advanced diesel combustion, show a wider distribution of carbon clusters. Soot from these latter types of combustion processes have elevated signals at  $C_{10}^+$ - $C_{15}^+$  and  $C_{30}^+$ - $C_{70}^+$ . The highest signal intensities from carbon clusters with large carbon numbers (i.e.,  $C_{30}^+$ - $C_{70}^+$ ) are found at carbon numbers of stable fullerenes (e.g.,  $C_{36}$ ,  $C_{44}$ ,  $C_{50}$ ,  $C_{60}$ ,  $C_{70}$ )

Refractory mass spectra of soot produced in a large number of different combustion processes were collected with the SP-AMS (Aerodyne Research Inc.). The soot nanostructure was analysed using high-resolution transmission electron microscopy (HR-TEM) for a selection of the soot samples. A thermodenuder (Aerodyne Research Inc.) was used, for a subset of the soot samples, to evaporate semi-volatile components.

The  $C_x^+$  distribution of mini-CAST (Jing Ltd.) OP1 soot with well-organized nanostructures and long lamellas was confined to low carbon numbers. Such distributions were also present for soot from conventional diesel and biodiesel (rape seed methyl esters) combustion in a heavy duty diesel engine without exhaust gas recirculation (EGR). With increased nitrogen flow and decreased oxidation airflow, the  $C_x^+$  distribution of mini-CAST OP5, OP6 and OP7 soot had increasing signal from large carbon clusters. The mini-CAST soot at OP5-OP7 have decreasing degree of ordered nanostructures and much shorter lamellas than OP1 soot. Similar types of  $C_x^+$

distributions were found in low temperature diesel combustion at very high EGR (Figure 1).

Fuel composition (i.e., diesel vs biodiesel) influenced the soot nanostructure. However, The  $C_x^+$  distribution of soot mass spectra from the two fuels was similar, although combustion with conventional diesel had higher fullerene signal. This could indicate that combustion temperatures (which are reduced by EGR) are more important in determining the soot properties that will form large carbon clusters, than fuel composition.

A first analysis between the tortuosity and fullerene signal did not show a correlation. However, it should be noted that short lamellas and highly disordered nanostructure may influence the determination of the tortuosity. Our analysis shows that a higher degree of disorder and shorter lamellas are associated with larger carbon clusters and a wider  $C_x^+$  distribution. With the large set of refractory mass spectra collected from different soot, our aim is to determine the relationship between soot nanostructure and refractory mass spectra, and the combustion conditions that form the various soot properties.

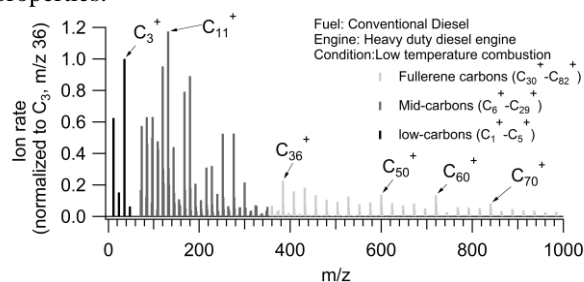


Figure 1. SP-AMS refractory mass spectrum of soot from low temperature diesel combustion. The spectrum has been normalized to the  $C_3^+$  intensity.

This work was supported by the Swedish research councils VR and FORMAS, the Swedish energy agency and the Danish centre for Nanosafety.

Malmberg, V. B., Eriksson, A. C., Shen, M., Nilsson, P., Gallo, Y., Waldheim, B., Martinsson J., Andersson, Ö. & Pagels, J. (2017). *Environ. Sci. Technol.*

Onasch, T. B., Fortner, E. C., Trimborn, A. M., Lambe, A. T., Tiwari, A. J., & Worsnop, D. R. (2015). *Aerosol Sci. Technol.*, 49 (6), 409–422

## Liquid atomization by Flow Blurring® (FB) in a high-pressure environment for combustion applications

L.B. Modesto-López and A.M. Gañán-Calvo

Department of Aerospace Engineering and Fluid Mechanics, University of Seville, Seville, E-41092, Spain

Keywords: flow blurring, liquid atomization, droplets, high-pressure.

Presenting author email: lmodesto@us.es

Liquid atomization requires conversion of a fraction of an energy input into surface energy. In pneumatic atomization, the interaction of a gas flow with a liquid flow is typically accompanied by turbulent motions that result in the generation of droplets of relatively small size. An efficient atomization is achieved by maximizing the surface area of the liquid flow and preventing droplet coalescence simultaneously minimizing the gas expense.

Gañán-Calvo (2005) proposed the so-called flow blurring (FB) mechanism for efficient atomization of liquids. In flow blurring, an unexpected back-flow pattern produces small scale perturbations, thus resulting in an efficient mixing between the gas and liquid phases (Figure 1). FB atomizers use a simple yet robust design in which the interaction of the liquid and gas flows is controlled by a geometrical parameter ( $\phi$ ), that is, the ratio of the distance from the exit of the feeding tube ( $H$ ) to the discharge orifice ( $D$ ), as depicted in Figure 1. Gañán-Calvo (2005; Rosell-Llompart and Gañán-Calvo, 2008) has shown that flow blurring is more efficient than other existing atomization techniques.

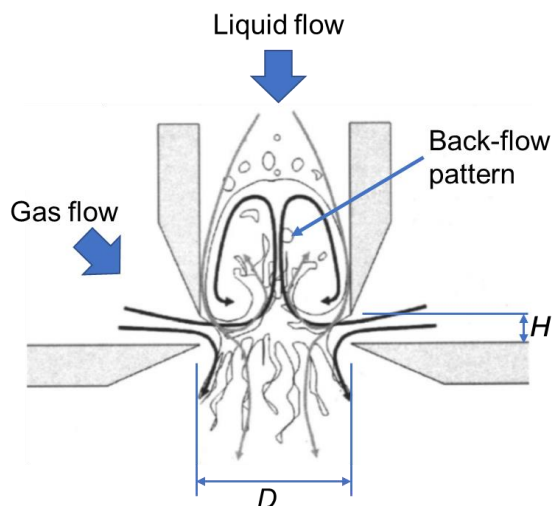


Figure 1. Description of the flow blurring mechanism.

Because of its high efficiency, FB finds use in a number of applications ranging from atomic spectrometry (Almagro *et al.*, 2006) to combustion of biofuels (Simmons and Agrawal, 2012).

In this work, we report the characterization of droplets generated by a flow blurring device into a high-pressure environment ( $> 20$  bar), using water and ethanol. Typically, the reported combustion applications of the FB technology are performed at ambient or moderate pressures. We have used an ultra-high-speed camera, capable of recording up to  $10^6$  frames per

second to observe the dynamics of the droplets *in situ*, in a pressurized chamber (up to 50 bar) with an in-house design. Furthermore, we have coupled an automated droplet measurement (ADM) software used in microfluidics (Chong *et al.*, 2016) with ultra-high-speed videos to estimate the velocity profile and the size distribution of the droplets (see Figure 2). Such approach may be useful in the development of on-line real-time aerosol characterization techniques (Modesto-López and Gañán-Calvo). In addition, we have applied a light-scattering measurement system (Malvern® Spraytec) to obtain droplet size distributions and compare them with those obtained with the ADM software. The aerosols produced thereby were then applied to a combustion system where a relatively high-throughput and small droplets are required.

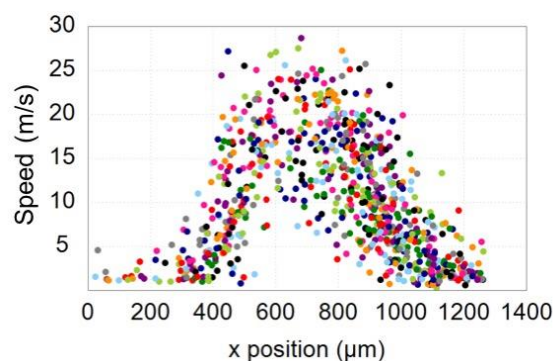


Figure 2. Typical droplet velocity profile obtained with ADM.

This work was supported by the Juan de la Cierva Program of the Ministry of Economy and Competitiveness of Spain (grant JCI-2012-12037) and by the Physics of Fluids and Microfluidics Research Group of the University of Seville.

Gañán-Calvo, A.M. (2005) *Appl. Phys. Lett.* **86**, 214101 (3pp).

Rosell-Llompart J. and Gañán-Calvo A.M. (2008) *Phys. Rev. E* **77**, 036321 (10pp).

Almagro B., Gañán-Calvo A.M., Monserrat H., and Canals A. (2006) *J. Anal. At. Spectrom.*, **21**, 770-777.

Simmons B.M. and Agrawal A.K. (2012) *Combust. Sci. Technol.* **184**, 660-675.

Chong Z.Z., Tor S.B., Gañán-Calvo A.M., Chong Z.J., Loh N.H., Nguyen N.-T., Tan S.H. (2016) *Microfluid. Nanofluid.* **66**, 1-14.

Modesto-López L.B. and Gañán-Calvo A.M. (2017, to be submitted to *Aerosol Sci. Technol.*)

## High-temperature porous tube sampling of combustion aerosols

J. Jokiniemi<sup>1</sup>, W. Baumann<sup>2</sup>, M. Hauser<sup>2</sup>, N. Teuscher<sup>2</sup>, H. Suhonen<sup>1</sup>, J. Ruusunen<sup>3</sup>, M. Ihalainen<sup>1</sup>, H.-R. Paur<sup>2</sup> and O. Sippula<sup>1</sup>

<sup>1</sup> Fine Particle and Aerosol Technology Laboratory, University of Eastern Finland, P.O. Box 1627, FI-70211, Kuopio, Finland

<sup>2</sup> Institute for Technical Chemistry, Karlsruhe Institute of Technology, 76021 Karlsruhe, Germany

<sup>3</sup>Venacontra Ltd, P.O. Box 1188, FI-70211, Kuopio, Finland

Keywords: Sampling, combustion aerosol, high temperature aerosol, biomass, boiler

Presenting author email: [jorma.jokiniemi@uef.fi](mailto:jorma.jokiniemi@uef.fi)

Sampling of aerosols from high temperatures is needed in order to get experimental data on aerosol formation and transformation in combustion systems or other high temperature processes. However, sampling from high temperature processes is usually very challenging due to high particle concentrations and/or condensable vapors in the sample and usually high temperature gradients occurring in the sampling system. In this work a quench-diluting sampling system, based on porous tube dilution, was developed and tested. The aim of the sampling system is to quench the sample, by decreasing temperature and concentrations rapidly, to freeze the chemical reactions and coagulation. We present the high-T sampling probe during its utilization in several biomass-fired units under different temperature regions.

The High Temperature Diluting Aerosol Sampling System (HDAS) consists of a porous tube diluter in which dilution gas (usually air or N<sub>2</sub>) is supplied through a porous wall and mixed with the sample. The diluter is surrounded by a cooling jacket in which various cooling agents can be used (Figure 1). The porous tube diluter is followed by a large-orifice ejector diluter after which the sample is stabilized and conditioned to be divided for selected aerosol analyzers.

The measurements were carried out at the University of Eastern Finland with a 40 kW grate combustion reactor and at the Karlsruhe Institute of Technology with a 100 kW wood boiler and in the KLEAA batch combustion reactor. All units were fired with wood chips. The samplings were carried out after the heat exchanger ( $T < 200$  °C), before heat exchanger ( $T \approx 600$  °C) and directly from the combustion chamber ( $T = 800$ - $1000$  °C). The diluting probe was water cooled and operated with varying dilution ratios, ranging from 14 to 120. The diluted sample was measured using a Scanning Mobility Particle Sizer and an Electrical Low Pressure Impactor. In addition, samples for electron microscopy and chemical analyses were collected. Multicomponent thermodynamic equilibrium models (Factsage and HSC softwares) were used for interpreting the experimental results.

PM1 of the wood chip fired grate combustion reactor was analysed to consist mainly of potassium sulfate, potassium chloride and smaller amounts of zinc oxide, sodium salts, EC and OC (Kortelainen et al., 2015). The particle size distributions (PSD) measured after the heat exchanger of the wood-fired grate combustion reactor ( $T < 200$  °C) were unimodal and stable towards changes in the dilution ratio (Figure 2).

The dilution corrected number concentrations varied in the range  $1$ - $3 \times 10^8$  particles/cm<sup>3</sup>. In contrast, the

PSDs measured directly from the combustion chamber at about 800-900 °C were very sensitive to dilution ratio, indicating that aerosol dynamic processes (condensation, coagulation, nucleation) were still ongoing in the sampling position and continued in the probe. The very high number concentration and small particle size (Figure 2) is consistent with thermodynamic considerations, indicating that from the major chemical species only zinc oxide and possibly alkali sulfate is in the condensed phase and should exist as freshly formed seed particles at this temperature. The difference between hot and cold sampling agrees well with coagulation expected within the residence time between the sampling points. The PSDs measured before the heat exchanger at the 100 kW wood boiler ( $T \approx 600$  °C) showed a bimodal size distribution. The larger mode was similar to measurements after the heat exchanger but there was an additional nucleation mode below the mobility size of 30 nm. According to thermodynamic equilibrium alkali metal chlorides are mainly still in the gas-phase at 600 °C and the nucleation mode is evidently formed from alkali metal chlorides inside the probe (Sippula et al., 2012).

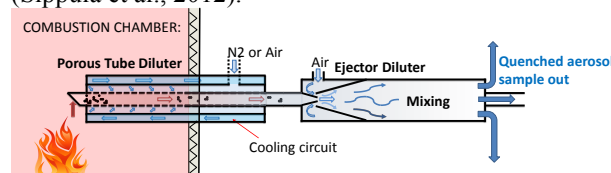


Figure 1. Principle of operation in the high-temperature sampling system.

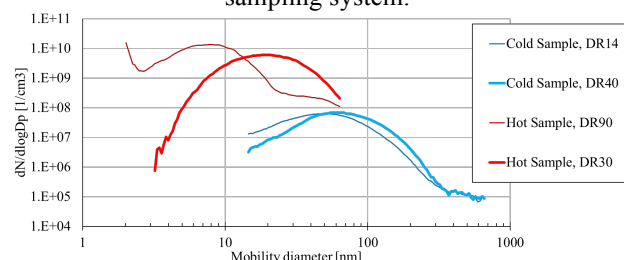


Figure 2. Particle number size distributions (SMPS) measured after the heat exchanger ( $T < 200$  °C) and directly from the combustion chamber ( $T = 800$ - $900$  °C).

The results show that the HDAS high-temperature sampling system can be used for obtaining detailed and valuable information on the formation and dynamics of aerosols at high temperatures.

Kortelainen, M. et al. (2015) *Fuel*, **143**, 80-88.

Sippula, O., Koponen, T. and Jokiniemi, J. (2012) *Aerosol Sci. Technol.* **46**, 1151-1162.

## Mobility Size and Effective Density of Soot Nanoparticles

G.A. Kelesidis<sup>1</sup>, E. Goudeli<sup>2</sup> and S.E. Pratsinis<sup>1</sup>

<sup>1</sup>Department of Mechanical and Process Engineering, ETH Zürich, Zürich, CH-8092, Switzerland

<sup>2</sup>Department of Mechanical and Process Engineering, University of Minnesota, Minneapolis, MN-55455, U.S.A.

Keywords: soot morphology, aggregation, mobility size, effective density

Presenting author email: gkelesidis@ptl.mavt.ethz.ch

Soot impact on health strongly depends on its effective density and mobility size (Rissler *et al.*, 2012). As nascent soot nanoparticles evolve to their mature well-developed fractal-like structures by agglomeration and surface growth, their effective density decreases up to an order of magnitude lower than bulk soot (Rissler *et al.*, 2013; Yon *et al.*, 2015).

The mobility size estimation of such evolving fractal-like aggregates is not trivial, as it depends on their structure as well as the number and size of their constituent primary particles. A scaling law describing the mobility size of agglomerates consisting of monodisperse primary particles in point contact (Sorensen, 2011) overestimates the mobility diameter of mature soot aggregates from diffusion flames for a given number of primary particles (Rissler *et al.*, 2013). Rissler *et al.* (2013) attributed this difference to the primary particle polydispersity and chemical bonding induced by surface growth (aggregation), neglected in the above scaling law (Sorensen, 2011). Typically population balance models for soot formation estimate the mobility diameter assuming it is equal to the gyration diameter (Yapp *et al.*, 2015).

Here, the Discrete Element Model (DEM) of nascent soot agglomeration and surface growth by acetylene pyrolysis (Kelesidis *et al.*, 2017) is extended to investigate the dynamics of mature soot formation at longer residence times and different flow regimes than nascent soot in the absence of soot oxidation. The evolution of soot mean gyration, mobility and primary particle diameters as function of the mean number of primary particles per aggregate,  $n_p$ , are elucidated.

Figure 1 shows the evolution of the DEM-derived (solid line) ratio of the mean mobility diameter to the diameter of gyration,  $d_m/d_g$ , of soot particles growing by agglomeration and surface growth as function of their  $n_p$ . The DEM-derived  $d_m$  and  $d_g$  are quite different for  $n_p = 1$ , where  $d_m/d_g = 1.29$ , consistent with theory (Sorensen, 2011). When surface growth take place, compact aggregates with strong chemical bonding are formed (starting from dimers,  $n_p = 1.5$ ), having  $d_m$  40 % larger than their  $d_g$ . For  $n_p > 1.5$ , the  $d_m/d_g$  ratio starts to decrease as surface growth progressively stops. For  $n_p > 10$ , the soot aggregate  $d_g$  becomes larger than  $d_m$ . The common assumption that the mobility is equal to the gyration diameter (dotted line) leads to 40% underestimation of the nascent soot mobility size and 30% overestimation of the mature soot aggregate mobility diameter.

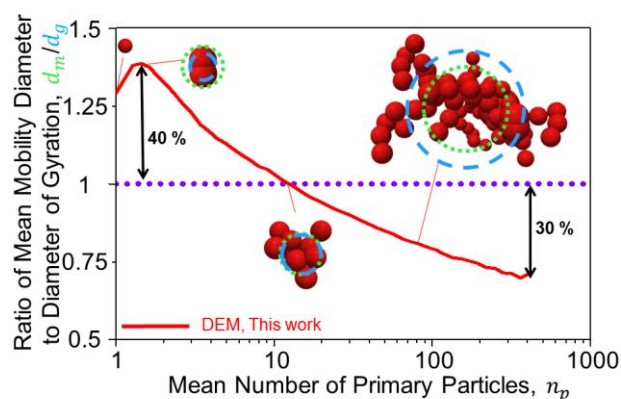


Figure 1. DEM-derived evolution of  $d_m/d_g$  as function of  $n_p$  of soot particles formed by agglomeration and surface growth (solid line) compared to the common assumption by population balance models of  $d_m = d_g$  (dotted line).

Relationships for the soot mobility size and effective density are derived by following the evolution from nascent to mature soot morphology and compared to the correlation of Sorensen (2011) and mass-mobility measurements in quenched diffusion flames (Rissler *et al.*, 2013; Yon *et al.*, 2015). The scaling law for agglomeration in the absence of surface growth (Sorensen, 2011) overestimates the measured mature soot aggregate mobility size by 37 % and underestimates its effective density by 44 %. Accounting, however, for the primary particle polydispersity and chemical bonding or aggregation induced by surface growth reduces the deviation from the mass-mobility measurements down to 7 and 11 % for the mobility size and the effective density, respectively.

- Kelesidis, G.A., Goudeli, E., Pratsinis, S.E. (2017) *Proc. Combust. Inst.* **36**, in press.
- Rissler, J., Swietlicki, E., Bengtsson, A., Boman, C., Pagels, J., Sandström, T., Blomberg, A., Löndahl, J. (2012) *J. Aerosol Sci.* **48**, 18-33.
- Rissler, J., Messing, M.E., Malik, A.I., Nilsson, P.T., Nordin, E.Z., Bohgard, M., Sanati, M., Pagels, J.H. (2013) *Aerosol Sci. Technol.* **47**, 792-805.
- Sorensen, C.M. (2011) *Aerosol Sci. Technol.* **45**, 765-779.
- Yapp, E.K.Y., Chen, D., Akroyd, J., Mosbach, S., Kraft, M., Camacho, J., Wang, H. (2015) *Combust. Flame* **162**, 2569-2581.
- Yon, J., Bescond, A., Ouf, F.X. (2015) *J. Aerosol Sci.* **87** (2015) 28-37.

## **Abstracts T116**

## Chemical composition discrimination of soot particles emitted by a heavy-duty engine: impact of operating regime and fuel biodiesel content

Y. Carpentier<sup>1</sup>, C. Irimiea<sup>1,2</sup>, O. Popovicheva<sup>3</sup>, E. Kireeva<sup>3</sup>, I. K. Ortega<sup>4</sup>, J. Schwarz<sup>5</sup>, M. Vojtisek<sup>6</sup>, C. Focsa<sup>1</sup>

<sup>1</sup>Univ. Lille, CNRS, UMR 8523 - PhLAM - Physique des Lasers Atomes et Molécules, F-59000 Lille, France

<sup>2</sup>Univ. Lille, CNRS, UMR 8522 - PC2A - Physicochimie des Processus de Combustion et de l'Atmosphère, F-59000 Lille, France

<sup>3</sup>Skobeltsyn Institute of Nuclear Physics, Lomonosov Moscow State University, Moscow 119991, Russia

<sup>4</sup>Onera-The French Aerospace Lab, F-91761 Palaiseau, France

<sup>5</sup>Institute of Chemical Process Fundamentals CAS, Prague, CZ-16502, Czech Republic

<sup>6</sup>Center for Sustainable Mobility, Czech Technical University in Prague, CZ-16607, Czech Republic

Keywords: biodiesel, soot, mass spectrometry, multivariate analyses.

Presenting author email: yvain.carpentier@univ-lille1.fr

The global consumption of biodiesel fuels in the European countries increased rapidly in the past several decades. Control of diesel particulate emissions became an important issue, attracting the attention on their evolution with the fuel composition and the engine operating regime. In this context, a sampling campaign has been performed on an engine dynamometer aiming at characterizing particulate emissions from on-road heavy diesel engines running on diesel (B0), 30% biodiesel with diesel (B30), and 100% biodiesel (B100). An Iveco Tector engine was operated under transient and steady-state conditions.

Soot particles collected on quartz fiber filters have been characterized using thermo-optic analysis, capillary electrophoresis, FTIR spectroscopy, and two surface mass spectrometry techniques: Two-step Laser Mass Spectrometry (L2MS) with different ionization schemes (single photon ionization (SPI) and resonant photon ionization (R2PI)) and Secondary Ion Mass Spectrometry (SIMS). Bulk measurements provide the differences in organic carbon (OC) to elemental carbon (EC) ratio, and water-soluble ionic content, while surface techniques supply comprehensive characterization of the organic/inorganic functionalities.

The OC has a constant trend irrespective of the fuel and working regime, while the EC decreases from B0 to B100. This observation is demonstrated to be in good agreement with the relative abundance of  $C_n^-$  fragments in mass spectrometry. FTIR and MS techniques suggest that particles coming from the analyzed fuels emissions contain aromatic and aliphatic components, and the addition of biodiesel changes the emitted particles chemistry into a more oxygenated and nitrogenized component. Additionally, a much lower concentration of aromatic, with respect to aliphatic compounds is observed for biodiesel emissions. R2PI-L2MS mass spectra show that the alkylated PAH content decreases when adding biodiesel. This observation helps at the identification of the polyaromatic compounds origin (pyrogenic vs petrogenic).

Because it is not straightforward to attribute molecules detected with MS (which sometimes exhibits significant fragmentation) to functionalities detected with FTIR, multivariate analyses methods as principal component analysis (PCA) and correlation clustering

were applied to the mass spectrometry dataset. Correlation clustering groups families of molecules that are coming from the same combustion sources. In this way, it is possible to associate chemical compounds or their fragments detected with MS to FTIR functionalities. Fragments as  $CH_3O^+$ ,  $C_2H_5O^+$ ,  $C_2H_3O_2^+$ ,  $C_3H_7O^+$  detected with MS are attributed to oxygenated functionalities identified with FTIR. PCA inferred from SIMS mass spectra suggests that PM emission composition is influenced by the fuel and slightly by the working regime as it can be seen in Fig. 1.

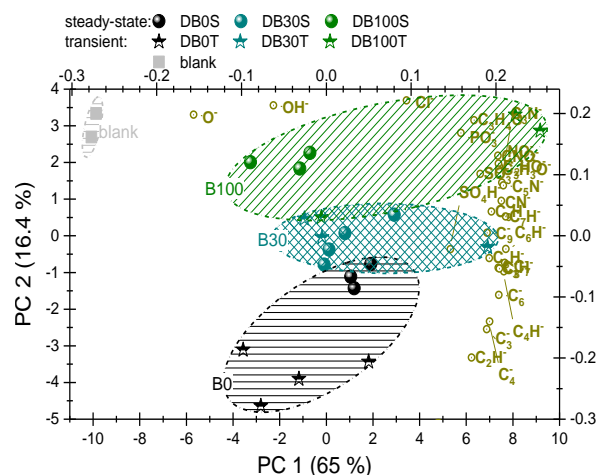


Figure 1. Biplot representing the first two components obtained for SIMS data (negative polarity). Scores (samples) correspond to the left/bottom scales, and loadings (molecules) to the right/top ones.

The analytical methods applied in this work elucidate the main parameters responsible for the speciation of diesel engine emissions.

This work was supported by the LABEX CaPPA (Chemical and Physical Properties of the Atmosphere) under the contract ANR-10-LBX-005 and by the CPER CLIMIBIO (Hauts-de-France Region and European Funds for Regional Economic Development).

## A Study on the Geometry of Pre-treatment device for Removal of Particulate Matter

B.H. Park<sup>1</sup>, J.Y. Lee<sup>1</sup>, H.G. Kim<sup>1</sup> and J.S. Choi<sup>1,2</sup>

<sup>1</sup>Technology Institute, Anytech Co., Ltd, Suwon, 16690, Republic of Korea

<sup>2</sup>Department of Environmental Science & Engineering, Kyung Hee University, Suwon, 17104, Republic of Korea

Keywords: particulate matters, geometry, inertial force, pre-treatment first, second, third, fourth.

Presenting author email: grapeman77@hanmail.net

The International Maritime Organization (IMO) implements regulations on the emission of pollutants from marine vessels in order to protect the marine environment. The International Maritime Organization (IMO) implements regulations on the emission of pollutants from marine vessels in order to protect the marine environment. In recent years, the existing Tier-2 standards have been strengthened by applying the Tier-3 standard. In order to comply with the Tier-3 standard, it is impossible to reduce pollutants by ship technology such as navigation technology or fuel policy. Therefore, in order to respond to regulations, additional pollution control facilities should be installed and operated inside the vessel.

In order to effectively treat the exhaust gas discharged from the ship in such a situation, it is necessary to develop a pretreatment process for removing a large amount of particulate matter generated in the engine before entering the reduction apparatus in order to increase the efficiency of the process. In order to apply the abatement device on the ship, it is necessary to consider the space limitation and the load generating condition of the engine. Therefore, it is not possible to apply an apparatus which generates kinetic energy by power as in the case of a conventional particulate reduction apparatus or a process in which a differential pressure is generated to increase the efficiency.

In order to solve this problem, this study experimented on the performance of various types of particle preprocessing devices.

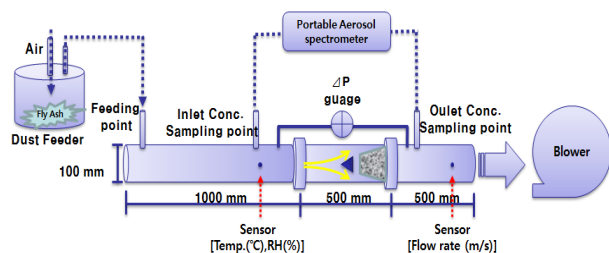


Figure 1. Schematic drawing of the experimental setup.

In order to optimize the device through reviewing various shapes, we tried to evaluate the characteristics according to the number of spirals by fabricating three types of cone shaped inflow part with the same length. Also, we tried to compare the performance of the device with the spacing between the inflow and outflow parts under different conditions.

The number of blades designed at the front end of the cone shape, the separation distance between the inlet and outlet, and the mesh type of the filtration part were evaluated by A-D. First, the differential pressure generated by each shape is measured at the inflow flow rate of 3 CMM and is summarized in the table below. Experimental results show that the pressure difference in the pretreatment system was measured to be less than 20 mmAq. Therefore, it is considered that there is no great influence on the load of the engine when the apparatus is mounted on the ship.

Table 1. Comparison of differential pressure drop with various shapes of pre-treatment devices.

Support	Cone	Pressuredrop (mmAq)			
		A [MLMF]	B [152 um]	C [279 um]	D [508 um]
L-1	C-1	15	23	21	19
	C-2	15	23	21	19
	C-3	16	24	22	20
L-3	C-3	-	20	-	-
L-5	C-3	-	19	-	-

This work was supported by Ministry of Land, Infrastructure and Transport of Korean government for research (Project no. 16RTRP-B082501-03).

Fridell, E., Steen, E., and Peterson, K. (2008) *Atmospheric Environment*, 42, pp. 1160–1168.

## Efficiency of Non-conductive Ultrasonic Transducers (NCUT) for Inactivation of Airborne Virus

Michael Versoza<sup>1,3</sup>, Wonseok Jung<sup>1,2</sup>, Yongil Lee<sup>1,2</sup>, Mona Loraine Barabad<sup>1,3</sup>  
Jeongho Hwang<sup>4</sup>, Duckshin Park<sup>1,3</sup>

<sup>1</sup>Transportation Environmental Research Team, Korea Railroad Research Institute, Uiwang City, South Korea

<sup>2</sup>Mechanical Engineering Department, Sungkyunkwan University, Suwon, South Korea

<sup>3</sup>Railway System Engineering Department, University of Science and Technology, Daejeon City, South Korea

<sup>4</sup>Mechanical Engineering Department, Yonsei University, South Korea

Keywords: Inactivation, Airborne virus, Non-conductive Ultrasound, Ultrasonic technology  
versozamichael23@gmail.com

Airborne viruses are a serious threat to the human health and can be in the air for a long periods of time (Nazaroo, 2004; Qian, 2012). Airborne droplets that contained viruses can travel in the air at relative distances (1 – 2 meters) which can be inhaled. Also, viruses on the contaminated surfaces could still be infectious from hours to even days which could re-suspended due to dispersion displacement in the air, increasing the concerns to have better treatments or conditions for its inactivation (La Rosa, 2013).

Ultrasound technology were used for inactivation of microorganisms for its ability to propagate sound waves in the medium that create pressure alternately compressing and expanding and collapsing violently which generates shock waves and causes cavitation to the microorganisms. But these other studies used liquid mediums which are not ideal for airborne viruses (Joyce, 2003).

Air attenuation hinders the propagation of intensive ultrasound waves but this was successfully addressed by Non-conductive Ultrasound Transducers (NCUT) (Hoover, 2002). The aim of this study was to determine the efficiency of the NCUT at frequencies of 28.39, and 29.1 kHz, for inactivation of airborne viruses in relation to distance and applied voltage.

MS2 bacteriophages were used for it is common for virus experiment in other studies (Fang, 2014) which was aerosolized through a closed duct system with a HEPA filter H14 (99.995%) and been exposed with NCUT. These samples were then diluted and plate count

was done with *E. coli* C300 host after 24hours of culture.

In the results, higher inactivated efficiencies were 60.22±14.45% (5mm) and 81.95±9.79% (8.5mm) for 28.39, and 29.1 kHz respectively. The frequency of 29.1 kHz were then change its applied voltage from 100V to 50V and 200V but the inactivated efficiencies were 38.28±11.18% and 17.98±1.23% which is lower compared to the previous results (Fig.1). In conclusion, the NCUT were seen for its potential to inactivate airborne viruses with relation to closer distance and specific applied voltage.

**Acknowledgements:** This subject is supported by Ministry of Environment as "Korea Environmental industry & Technology institute (KEITI) (NO.2015000120002)

Nazaroo W. W. (2004) *Indoor Air*, **14**, 175 – 183.

Qian, J., Hospodsky, D., Yamamoto, N. et al., (2012) *Indoor Air*, **22**, 339 – 351.

La Rosa, G., Fratini, M., Della Libera, S., Iaconelli, M., Muscillo M. (2013) *Viruses and Indoor Environments*, **49**, 124 – 132.

Joyce, E., Phull, S. S., Lorimer, J. P. Mason, T.J. (2003) *Ultrasonic sonochemistry*, **10**, 315 – 318.

Hoover, K., Bhardwaj, M., Ostiguy, N. (2002) *Mat Res Innovat.* **6**, 291 – 295.

Fang, J., Lui, H., Shang, C., Zeng, M., Ni, M., Liu, W. (2014) *Front. Environ. Sci. Eng.*, **8**, 547 – 552.

## Chasing measurements for real-world emissions of city buses

A. Järvinen<sup>1</sup>, P. Karjalainen<sup>1</sup>, M. Bloss<sup>2</sup>, O. Potila<sup>1</sup>, P. Simonen<sup>1</sup>, H. Kuuluvainen<sup>1</sup>, H. Timonen<sup>2</sup>, S. Saarikoski<sup>2</sup>, J. V. Niemi<sup>3</sup>, J. Keskinen<sup>1</sup> and T. Rönkkö<sup>1</sup>

<sup>1</sup>Aerosol Physics, Faculty of Natural Sciences, Tampere University of Technology, Tampere, FI33720, Finland

<sup>2</sup>Atmospheric Composition Research, Finnish Meteorological Institute, Helsinki, FI00101, Finland

<sup>3</sup>Helsinki Region Environmental Services Authority (HSY), FI00066 HSY, Finland

Keywords: vehicle emissions, bus emissions, air quality, PM emissions.

Presenting author email: anssi.jarvinen@tut.fi

Diesel engine powered city buses are known to be emitters of particulate matter (PM) and gaseous pollutants. These emissions are generated in a close proximity of people, especially in densely populated areas, which increases their potential effects on the health of population in urban areas. On the other hand, vehicle technologies are continuously developed aiming to decrease emissions, especially the emissions of particulate mass, soot particle number and some gaseous compounds such as NO<sub>x</sub>. Thus, investments on new buses can be assumed to decrease the impact of public transport on air quality. In principle, similar effects can also be achieved by retrofitting existing bus fleets by advanced emission control technologies.

Vehicle emissions are regulatory tested in laboratory conditions in specific driving cycles. However, both the conditions and driving cycles can differ from real world situations thus possibly causing real-world emissions to significantly differ from the emissions measured for regulatory purposes. The newest vehicles utilize several means to reduce emissions, including filtration and catalytic processes. This complexity may even increase the need for real-world emission studies.

In this study, a mobile laboratory was used for chasing measurements to characterize diesel bus emissions in a part of the Helsinki region bus route 550 (Jokerilinja), see Figure 1. Measured buses consisted of EEV and EuroVI emission levels as well as an EEV level retrofitted with a particle filter and an SCR-system. Each measurement period lasted 10 min and included 6 bus stops. Average speed was approximately 25 km/h. The mobile laboratory was equipped with several real-time aerosol instruments, including CPC, PSM, ELPI, aethalometer, and gas analysers for CO<sub>2</sub> and NO<sub>x</sub>. The chemical composition of particles was analysed using a soot-particle aerosol mass spectrometer (SP-AMS), also installed inside the mobile laboratory. The aerosol sample was taken through an inlet above the windshield.

The bus emissions were analysed as an average over the measurement route taking the background aerosol concentrations into account. The exhaust plume CO<sub>2</sub> concentrations were used to calculate the emission factors in the same way as in study of Pirjola *et al.* (2016). According to preliminary results, the particle number emission were mostly in the order of  $1 \cdot 10^{15}$  1/kg<sub>fuel</sub> for Euro VI and retrofitted buses. The EEV buses produced slightly more particle number emissions. The black carbon (BC) emissions were approximately 0.13 g/kg<sub>fuel</sub> for the EEV buses and reduced down to 0.06 g/kg<sub>fuel</sub> for

the retrofitted and the Euro VI buses. This reduction in emissions is shown in Figure 1, which represents the BC concentration along the measurement route in the cases of a single EEV and a single Euro VI bus. The largest differences between the technology levels were observed in PM<sub>1</sub> and lung deposited surface area (LDSA) concentrations calculated from the ELPI data. The PM<sub>1</sub> reduced from approximately 0.25 to 0.08 g/kg<sub>fuel</sub> and the LDSA from 0.8 to 0.2 m<sup>2</sup>/kg<sub>fuel</sub>. The NO<sub>x</sub> emissions were approximately 20 g/kg<sub>fuel</sub> for the EEV and in the limits of measurement accuracy, below 2 g/kg<sub>fuel</sub>, for the Euro VI buses. Two of the retrofitted buses were found to produce the same level of NO<sub>x</sub> as the normal EEV buses, while the other retrofitted buses emitted similar NO<sub>x</sub> emissions as the Euro VI buses.

In general, the emissions of the EEV buses are in line with the previous study of Pirjola *et al.* (2016). Here we also studied the newest Euro VI buses in real traffic. The Euro VI level buses were observed to generate significantly lower BC, NO<sub>x</sub> and PM<sub>1</sub> emissions than the older EEV level buses.

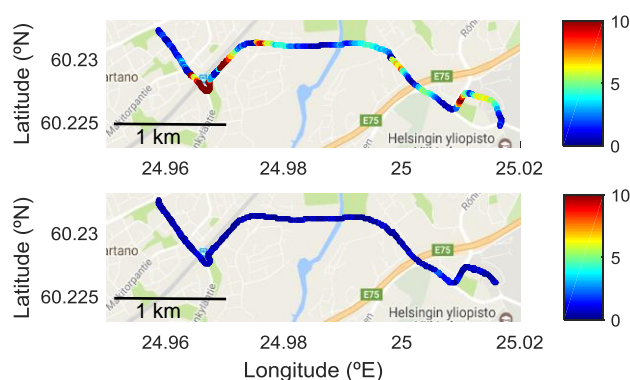


Figure 1. BC concentrations measured by chasing an EEV (above) and Euro VI bus (below), color scale unit ( $\mu\text{g}/\text{m}^3$ ). The map is courtesy of Google Inc. and created using a `plot_google_map` function for Matlab.

This study was funded by Tekes (the Finnish Funding Agency for Innovation), HSY and Pegasor Oy as a part of Cityzer project. Helsingin Bussiliikenne Oy is acknowledged for providing assistance during measurements.

Pirjola L., Dittrich A., Niemi J.V., Saarikoski S., Timonen H., Kuuluvainen H., Järvinen A., Kousa A., Rönkkö T., Hillamo R. (2016) *Environ. Sci. Technol.*, **50**, 294-304.

## Characterisation of fresh and aged particle and gaseous emissions from in-use diesel, RME and CNG buses

Å. M. Hallquist<sup>1</sup>, M. Psychoudaki<sup>2</sup>, M. Le Breton<sup>2</sup>, Å. Watne<sup>2</sup>, M. Jerksjö<sup>1</sup>, H. Fallgren<sup>1</sup> and M. Hallquist<sup>2</sup>

<sup>1</sup>IVL Swedish Environmental Research Institute, Gothenburg, Sweden

<sup>2</sup>Department of Chemistry and Molecular Biology, University of Gothenburg, Gothenburg, Sweden

Keywords: Bus emissions, Mass spectrometry, Secondary Organic Aerosols (SOA), PAM

It is well known that traffic is a large contributor to particles and gaseous pollutants in the urban atmosphere. In the atmosphere primary vehicle emissions can further oxidize leading to the formation of secondary pollution, e.g. secondary organic aerosol (SOA), which is very important on a regional and global scale (Hallquist et al., 2009). In order to meet the challenges with increased transportation and enhanced greenhouse gas emissions, the European Union has decided to replace 10% of conventional road fuels by alternative fuels in 2020.

In this work the emissions from in-use transit buses running on diesel (MK1, <10 ppm S), rapeseed methyl ester (RME) and compressed natural gas (CNG) were thoroughly investigated both regarding the primary emissions as well as the potential to form secondary mass from the co-emitted gaseous fraction using state-of-the-art instrumentation.

To enable detailed characterisation of primary emissions and secondary formation regarding particles and gaseous compounds our newly developed method for characterising individual emission sources (Fig. 1) (Hallquist et al., 2013) was used together with a high resolution time of flight chemical ionisation mass spectrometer (HR-ToF-CIMS) and a PAM-chamber (Go:PAM).

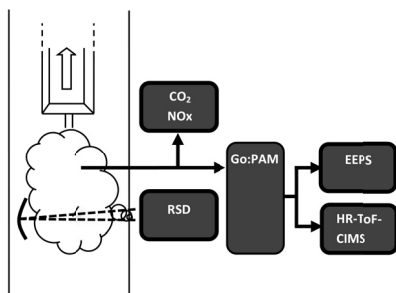


Figure 1. Schematic of the measurement set-up.

The CIMS was configured with a FIGAERO inlet, enabling characterisation of the gas and condensed phase. Go:PAM is an oxidation chamber which simulates several days of ageing of the exhaust sample via exposure to high hydroxyl radical concentrations. By this method emission factors (EF) of different constituents can be determined by relating the change in concentration of a specific constituent in the diluted exhaust plume to the change in CO<sub>2</sub> concentration, comparing to background concentrations.

In total 29 buses were studied: 5 diesel, 11 RME (of which 5 were electrical hybrids (RME<sub>ELH</sub>)) and 13

CNG. The sampling of the emissions was conducted according to Hallquist et al., 2013 which involves extractive sampling of a passing bus plume during acceleration from stand still. Prior the measurements a warm-up route was driven to prevent cold engines. A minimum of three accelerations were studied for each individual bus and setting (i.e. fresh and aged), but often more repetitions were performed.

Particle size, number and mass data compared between fuel types and fresh and aged emissions will be presented as well as the chemical composition of the gas and the condensed phase.

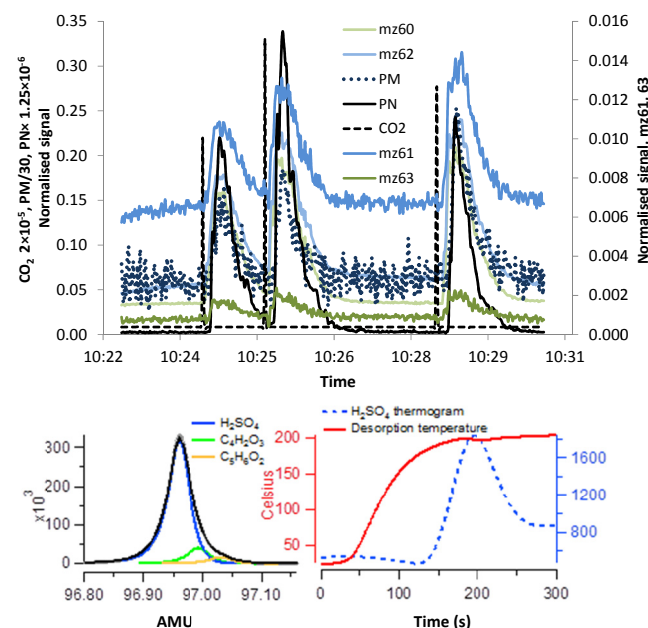


Figure 2. Examples of emission signals measured.

This work was financed by Vinnova, Sweden's Innovation Agency and Formas. The support from Västrafik, responsible for the public transport in all of Västra Götaland, Sweden, is gratefully acknowledged. The drivers and the personnel at the measurement sites are also gratefully acknowledged for their assistance and hospitality.

Hallquist Å.M. et al. (2013) *Particle and gaseous emissions from individual diesel and CNG buses*, Atmos. Chem. Phys., 3, 5337-5350.

Hallquist M. et al., (2009) *The formation, properties and impact of secondary organic aerosol: current and emerging issues*, Atmos. Chem. Phys., 9, 5155-5236.

## Implementation of a population balance model utilizing the sectional method within a stochastic reactor engine model

N.A. Eaves<sup>1</sup>, J. Akroyd<sup>1</sup>, S. Mosbach<sup>1</sup>, and M. Kraft<sup>1,2</sup>

<sup>1</sup>Department of Chemical Engineering and Biotechnology, University of Cambridge, Cambridge, CB2 3RA United Kingdom

<sup>2</sup>School of Chemical and Biomedical Engineering, Nanyang Technological University, 637459, Singapore

Keywords: particulate, IC engine, emissions, sectional method.

Presenting author email: nae28@cam.ac.uk

Combustion processes are heavily utilized for energy production, currently accounting for 90% of global energy production and rising. This reliance is of concern, as nanoparticle emissions from combustion have negative effects on climate change and human health. Nanoparticles emitted from combustion processes can be classified as soot particles, organic and inorganic ash, and volatile organic compounds. These nanoparticles can be absorbed deeply into the lungs, causing respiratory diseases, such as lung cancer, asthma, bronchitis, and heat attacks. Polycyclic Aromatic Hydrocarbons (PAHs), which are pre-cursors to soot formation, and soot have been classified as known carcinogens by the International Agency for Research on Cancer (IARC). Additionally, soot is the second largest contributor to global warming, as it can deposit on glaciers and accelerate the rate at which glaciers melt due enhanced radiation absorption. Due to these negative effects, there is a strong need to reduce particulate emissions from combustion devices, such as internal combustion (IC) engines. In order to achieve this, detailed particulate population balanced models (PBMs) with predictive capability must be developed. Subsequently, these detailed must be integrated into engine combustion simulation software to provide design engineers with the insights required to develop engines with lower particulate emissions, while still maintaining computational tractability. Given the recent EURO 6 standards, understand how to influence the particle size distribution (PSD) of particulate emissions is of strong importance.

Engine simulation software utilizing stochastic reactor models (SRMs) can provide a computationally efficient means to model a combustion engine. Such an engine model has been coupled to a detailed PBM in Wang *et al* (2016). The detailed PBM described individual aggregates, which contained poly-disperse primary particles composed of PAH molecules. However, due to the complexity of the utilized PBM, a Monte Carlo solution method was required. The level of complexity in a PBM places constraints on the numerical methods that can be utilized to solve them. Reduction of the model complexity can allow for less computationally demanding methods such as the sectional method, while retaining the ability to predict the particle size distribution. In this work, a detailed PBM utilizing the sectional method is implemented within an engine SRM.

An SRM is a spatially zero-dimensional model of the contents of the combustion chamber based on PDF

transport methods. Being a PDF method, an SRM describes distributions of temperature and species concentrations within the engine cylinder. These distributions are represented by an ensemble of stochastic particles, each of which can be thought of as a fluid parcel in the cylinder with its own temperature and composition. The time-evolution of the stochastic particles and hence the distributions as a consequence of processes such as turbulent mixing, heat transfer, direct injection, and flame propagation is described by appropriate sub-models. The number of particles governs the precision of predictions.

The soot formation model and sectional method utilized in the CoFlame code, a 2D axisymmetric diffusion flame computational fluid dynamics (CFD) code is coupled to a stochastic reactor model. Soot particle dynamics are described using a fixed sectional method, in which soot particle mass ranges are divided logarithmically into thirty-five discrete sections. Soot particles are assumed to be aggregates composed of spherical primary particles of equal size with a constant fractal dimension of 1.8. Two transport equations are solved for each section; those being aggregate number density ( $N_A$ ) and primary particle number density ( $N_P$ ). The model includes several processes, those being nucleation, PAH condensation and HACA surface growth, surface oxidation, coagulation, fragmentation, particle diffusion, and thermophoresis. This model has been successfully applied to study soot formation in diffusion flames under conditions relevant to engines, such as diluted, high pressure, and gasoline flames. The Coflame code is described in detail in Eaves *et al* (2016).

The newly implemented model is validated against experimental engine data. Parametric studies are performed to investigate the influence of model parameters on predicted engine emissions.

This work was supported by the Horizon 2020 GV-02-2016 program under grant agreement number 724145.

Eaves, N., Zhang, Q., Liu, F., Guo, H., Dworkin, S., Thomson, M. (2016) *Comput. Phys. Commun.* **207** 464-477

Wang, B., Mosbach, S., Schmutzhard, S., Shuai, S., Huang, Y. and Kraft, M. (2016) *Appl. Energy* **163**, 154-166

## Regulated and unregulated emissions of three way catalyst Euro 6 G-DI gasoline vehicle over chassis dynamometer

A. Martinez Valiente<sup>1</sup>, C. Louis<sup>2</sup>, S. Martinet<sup>2</sup>, B. R'Mili<sup>1</sup>, P.Tassel<sup>2</sup>, P.Perret<sup>2</sup>, M.André<sup>2</sup>, Y.Liu<sup>2</sup> and B. D'Anna<sup>1</sup>

<sup>1</sup>IRCELYON - UMR 5256 CNRS - Université Claude Bernard Lyon 1, 69626 Villeurbanne, France

<sup>2</sup>IFSTTAR, AME, LTE, Lyon, 69675, France

Keywords: Gasoline, Euro 6, Emissions, Chassis dynamometer

Presenting author email: [Alvaro.martinez-valiente@ircelyon.univ-lyon1.fr](mailto:Alvaro.martinez-valiente@ircelyon.univ-lyon1.fr)

Corresponding author: [barbara.danna@ircelyon.univ-lyon1.fr](mailto:barbara.danna@ircelyon.univ-lyon1.fr)

Exposure to particulate matter (PM) poses serious public concerns related to both health risk and air quality (HEI, 2013). Vehicle exhaust emissions have been the subject to numerous scientific reviews by international organizations due to these emissions can promote health concerns as lung and heart diseases (IARC, 2013). Increasingly restrictive regulations have been introduced to reduce harmful gas and particle emissions from passenger cars in Europe.

In the frame of the CAPVEREA project, regulated and unregulated exhaust emissions of Euro 6 gasoline vehicles were investigated at a chassis dynamometer test bench. Exhaust emissions were evaluated under representative driving cycles as Artemis and WLTC. Exhaust gases were sampled using a two-stage dilution system, a FPS-4000 Dekati<sup>®</sup> and a Constant Volume Sampler (CVS). A scheme of the experimental setup is shown in figure 1.

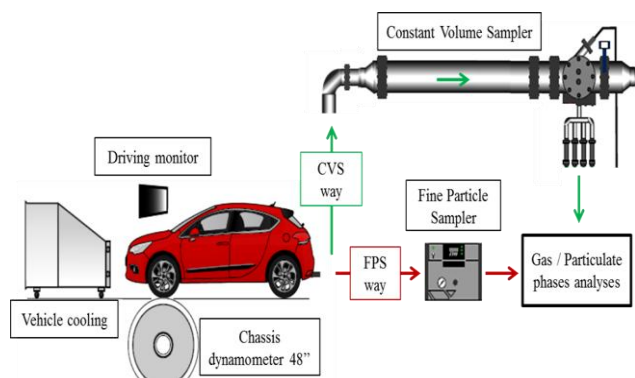


Figure 1. Experimental setup

Particle monitoring was assured by several dedicated instruments (FMPS, SMPS, SMPS+E and CPC). Black Carbon was measured by aethalometer. Samples were also collected on TEM-porous grids for morphology studies. Regulated and non-regulated gaseous compounds were measured with an Industrial Gas System working under FTIR principle and a Horiba emission measurement system.

The study suggest that large amount of particles (including black carbon) are emitted mainly during cold start as well as during high speed driving conditions (ex motorways) a similar pattern is observed for hydrocarbons.

### Abstract review

A Chassis dynamometer test bench was deployed to evaluate exhaust emissions from a Euro 6 Gasoline passenger car under transient conditions (WLTC and CADC cycles). Gas and particle phase characterization indicate that high particle number concentration and gas phase pollutants (as HCHO, hydrocabons, NH<sub>3</sub>, etc) are emitted during cold start and high speed driving conditions. Figure 2 shows BC emission factors calculated for Artemis and WLTC cycles.

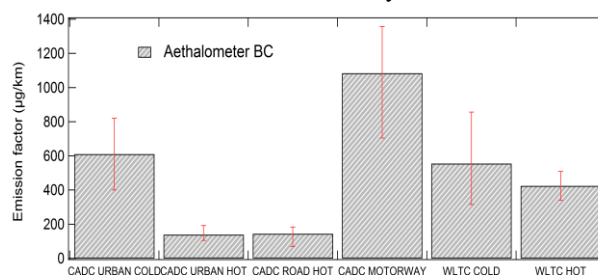


Figure 2: BC emission factor calculated for Artemis and WLTC cycles.

### References

- HEI, *review panel on ultrafine particles. Understanding the health effects of ambient ultrafine particles* (HEI Perspectives 3, Health Effects Institute, Boston, MA),2013,<http://pubs.healtheffects.org/getfile.php?u=893>
- IARC, *Diesel and gasoline engine exhausts and some nitroarenes*, Volume 105. 2013

Acknowledgments: the authors would like to thank the ADEME agency for financial support of the CORTEA project CaPVeREA (N° 1466C0001) and the Auvergne Rhône-Alpes region.

## Towards standardizable measurements of passenger car brake dust emissions

Christof Asbach<sup>1\*</sup>, Heinz Kaminski<sup>1</sup>, Jörg Lindermann<sup>1</sup>, Ana Maria Todea<sup>1</sup>, Marco Zessinger<sup>2</sup>, Ralf-Joachim Conhoff<sup>3</sup>, Georg Frentz<sup>3</sup>, David Schneider<sup>3</sup>, Stefan Schumacher<sup>1</sup>

<sup>1</sup> Institut für Energie- und Umwelttechnik e.V. (IUTA), Duisburg, Germany

<sup>2</sup> Link Engineering, Limburg, Germany

<sup>3</sup> Daimler AG, Sindelfingen, Germany

Keywords: Brake dust, emissions, nucleation particles, standardization

\*Presenting author email: [asbach@iuta.de](mailto:asbach@iuta.de)

Particulate emissions from vehicles including passenger cars and their potential effect on environmental pollution and public health have been under debate for several decades. While over the years tailpipe emissions have been strongly reduced by engine improvements and exhaust gas after treatments like diesel particulate filters, the emissions of brake dust get more and more into the focus. Grigoratus and Martini (2015) recently estimated that brake wear can contribute up to 21% to the total traffic-related PM<sub>10</sub> emissions. A large fraction of these emissions are metallic particles, which may be highly reactive and thus toxic. Brake wear particles can span a very wide range of particle sizes, ranging from approximately 1 nm (Nosko et al., 2017) to several tens of micrometers (Thorpe and Harrison, 2008).

Despite the increasing interest in brake dust emissions, there is currently no standardized test method to assess them. However, in view of a planned future regulation of brake dust emissions, such a test method is urgently needed.

In preparation for a proper design of a measurement test rig to reproducibly sample and measure brake wear particles on a dynamometer, we initially thoroughly studied the aerosols released from an SUV brake with two different brake pads, one non-asbestos organic (NAO) and one according to ECE regulation 90 (ECE). Online measurements were carried out with 1 s time resolution, using a combination of a Fast Mobility Particle Sizer (FMPS) and an Aerodynamic Particle Sizer (APS) to cover a size range from 5.6 nm to >10 µm. The brake was installed on a dynamometer and the aerosols produced during different types of brake actions were studied. These brake actions included urban, motorway and fade, where fade mimics downhill braking.

Urban and motorway braking typically produced bimodal size distributions with a fine mode around 150-200 nm and a coarse mode around 1.8 µm. The onset of an additional nucleation mode at around 10 nm was observed, whenever the brake disc temperature exceeded a critical limit (180-200°C for NAO, see figure 1, and around 220°C for ECE). This temperature was mainly reached during fade and sometimes during motorway brake actions. The number concentration of the nucleation mode was several orders of magnitude higher than the concentration of the larger particles and could reach values of >10<sup>9</sup> 1/cm<sup>3</sup>, whereas the total number concentrations during urban braking were typically only between 10,000 and 15,000 1/cm<sup>3</sup>. Measurements with a

thermodenuder revealed that the measured particles were non-volatile.

Based on the preliminary measurements, a brake dust sampling test rig was designed based on computational fluid dynamics simulations and constructed. The test rig consists of an enclosure for the brake while installed in a dynamometer. The enclosure is continuously flushed with the required cooling air with flow rates between 500 and 4,200 m<sup>3</sup>/h. The enclosure is designed such that at least all PM<sub>10</sub> particles are carried away with the flow. An isokinetic probe is used to sample the aerosol at a flow rate of 2.3 m<sup>3</sup>/h from the flow leaving the enclosure. The sampled flow first passes a PM<sub>10</sub> impactor, before it is split to the measurement instruments. A variety of measurement and sampling instruments can be used, including FMPS/EEPS, APS, OPS, as well as electrostatic, filter or (cascade) impactor samplers. This new set up allows for reproducible measurement and sampling of brake dust emissions and hence eventually for deriving emission factors from the measured concentrations that will be needed for future legislation.

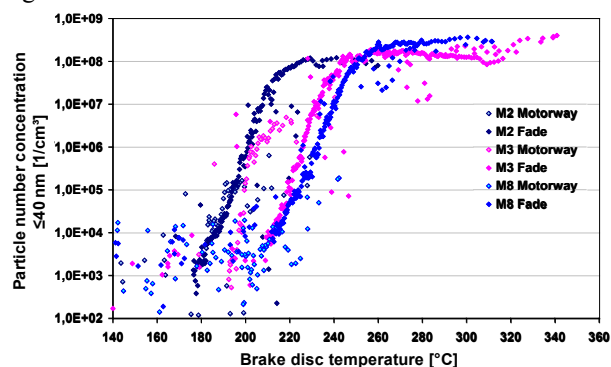


Figure 1: Dependence of particle number concentration on brake disc temperature with NAO brakes

The results from the preliminary measurements as well as first results with the new test rig will be presented and discussed in view of future standardization.

### References

- Grigoratos, T. and Martini, G. (2015), *Environ. Sci. Pollut. Res.* **22**: 2491-2504  
 Nosko, O.; Vanhanen, J.; Olofsson, U. (2017), *Aerosol Sci. Technol.* **51**: 91-96  
 Thorpe, A. and Harrison, R.M. (2008), *Sci. Total Environ.* **400**: 270-282

## Measurement of particulate matter emissions from diesel locomotives and rail vehicles during real-world line-haul operation

M. Vojtisek-Lom<sup>1,2</sup>, M. Pechout<sup>3</sup>, V. Beránek<sup>1</sup>, J. Jirků<sup>4</sup>

<sup>1</sup> Center for Sustainable Mobility, Fac. Mech. Eng., Czech Tech. Univ. Prague, CZ-16607, Czech Republic

<sup>2</sup> Department of Vehicles and Engines, Technical University of Liberec, CZ-46117, Czech Republic

<sup>3</sup> Dept. of Vehicles and Ground Transportation, Czech University of Life Sciences Prague, CZ-16500

<sup>4</sup> Dept. of Logistics and Management of Transport, Fac. Transp. Sciences, Czech Tech. Univ. Prague, CZ-11000

Keywords: non-road diesel, locomotive, emissions, real-world, particulate matter, nanoparticles

Presenting author email: michal.vojtisek@fs.cvut.cz

Particulate matter from local heating appliances and internal combustion engines is one of the leading causes of premature deaths in many urban areas, as particles are small, carcinogenic, and are distributed at nearly the ground level. Particle emissions from on-road vehicles have been successfully reduced, at least in wealthier regions, by the widespread introduction of particle filters. Legislation targeting especially very small and very large non-road engines has been lagging. Targeting of large - over 560 kW – engines has been also difficult due to longevity of the engines and due to very limited and rather expensive options for laboratory testing.

In this study, a line-haul diesel-electric locomotive has been fitted with portable on-board monitoring instrumentation and its emissions were measured during its regular scheduled operation on passenger train service to demonstrate the feasibility of such approach and to establish a baseline.

The locomotive was a 1979 754-series Czech Railways engine with a ČKD model K 12 V 230 DR 12-cylinder, 129-liter, 1460 kW turbocharged direct injection diesel engine with mechanically driven unit injectors. The engine powers a DC traction generator providing power for traction motors at each axle, a DC generator for heating passenger carriages, air compressor, and various auxiliary loads.



Fig. 1: On-board instrumentation installation

The exhaust gases were extracted from the stack by a stainless steel line leading into a 6 m conductive heated sample line running at 150 C and divided into a portable electric-charge based nanoparticle analyzer (NanoMet3, Testo), a portable Fourier Transform Infra Red spectrometer (in-house production, 6 m cell running at 121 C, MCT detector, 0.5 cm<sup>-1</sup> optical resolution), and a miniature gas analyzer (in-house production, NDIR bench for CO and CO<sub>2</sub>, electrochemical cells for NO and NO<sub>2</sub>). NanoMet3 data provides the total particulate mass (PM), particle mean diameter and total number of non-volatile particles (PN) correlated with the PN measured

per the EU Particle Measurement Program. The FTIR spectra were resolved for CO, CO<sub>2</sub>, NO, NO<sub>2</sub>, methane, N<sub>2</sub>O, ammonia, ethane, ethylene, formaldehyde and acetaldehyde. The exhaust flow was calculated from measured engine rpm, intake air temperature and pressure, engine displacement, and engine technical data. Additional data including traction generator and heating generator loads were logged by the locomotive electronic system. The instrumentation installation was subject to several constraints: presence of overhead 3 kV DC traction lines during portion of the run, presence of vegetation outside of the minimum clearance outline, usage of both engineer's cabins at locomotive ends, absence of openings connecting engine compartment with engineer's cabin, exclusion of test staff in the engine compartment during the run, and relatively narrow locomotive access doors.

The measurement took place on a 140 km Prague to Tanvald run, which was run three times round trip, with four to six cars depending on the trip.

The overall emissions rates were 0.4-0.5 g PM, 6x10<sup>13</sup> particles and 65 g NO<sub>x</sub> per kg fuel, or about 0.5-0.6 g PM 7x10<sup>13</sup> particles and 79 g NO<sub>x</sub> per km, with both fuel consumption and emissions varying with the load. Virtually all NO<sub>x</sub> was emitted as NO, which is typical for engines with no oxidation catalyst. Little hydrocarbons or CO was produced. Idling of the engine consumed 10-36 kg/h fuel and has produced 1.5-5 g/h PM and 0.6-3 kg/h NO<sub>x</sub> depending on the usage of car heating (up to 110 kW) and other accessories; regardless of car heating, the PN emissions were around 10<sup>15</sup> #/h.

The results are consistent with previous studies on a diesel-hydraulic motorized unit and another diesel-electric locomotive, where particle emissions were on the order of tenths of grams per kg of fuel and NO<sub>x</sub> emissions were similar and typical for a diesel engine without any type of NO<sub>x</sub> controls. The particle emissions were relatively low, not dissimilar from high-emitting diesel cars on a per km basis, suggesting that large engines can have relatively low emissions deterioration rates. NO<sub>x</sub> and PM emissions per passenger are not out of line with newer in-use diesel cars.

Supported by the Czech Technical University Student Grant 16/106/OHK2/1T/16. Equipment was financed by the EU LIFE project LIFE10 ENV/CZ/651 and by the Czech Ministry of Education projects LO1311 and CZ.1.05/2.1.00/19.04.08.

## Chemical characterisation of the particulate matter emitted by automobile motors: the PEMs4Nano project

J. A. Noble, Y. Carpentier, M. Vojkovic, B. Chazallon, C. Pirim, M. Ziskind, and C. Focsa

Laboratoire de Physique des Lasers, Atomes et Molécules (PhLAM, UMR 8523 CNRS), Université de Lille, Lille F-59000, France

Keywords: particulate emission, mass spectrometry.

Presenting author email: jennifer.noble@univ-lille1.fr

Particulate emission from vehicles is fast becoming a prominent societal concern due to the toxicity of particles released from motors. There is a critical lack of certification procedures under real driving conditions and for the smallest particles down to 10 nm. The development of such measurement procedures would provide an important contribution towards both the future regulation of particle emissions and the development of new engine technologies. In the framework of the PEMs4Nano project (H2020), particle characteristics, including their size-dependent chemical composition, will be investigated at various locations in the tailpipe. The overall objective of the PEMs4Nano project is to develop/achieve measurement procedures down to 10 nm, providing a contribution to future regulation on particle emissions, in particular in real driving conditions.

The contribution of the PhLAM laboratory at the University of Lille will be the determination of size-dependent particulate composition of aerosol particles sampled from a cylinder engine reactor operated in various operating regimes (i.e. engine load conditions and fuels). In particular, the determination of particle surface composition will allow us to discern, in the context of measurements on engines or vehicles, the different sources of particles (e.g. combustion, fuel additives, lubricating oil, mechanical wear, etc). Sampling is performed at two different position in the exhaust line, where particles are deposited on gold-coated silicon substrates using a nanometer aerosol sampler (TSI), allowing us to study size-selected particles.

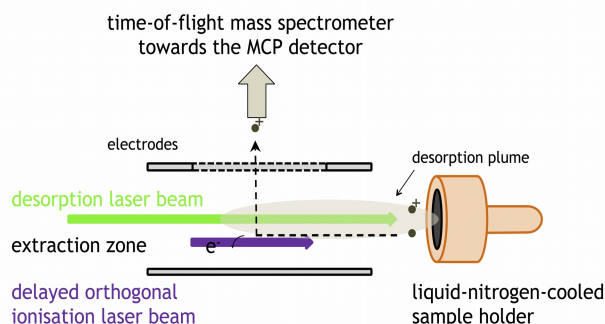


Figure 1. A schematic view of the L2MS technique.

The chemical characterisation of the collected particulate matter is performed using a custom built

Time-of-Flight Mass Spectrometer (ToF-MS) instrument coupled to a laser desorption/ionisation technique (L2MS), as illustrated in Figure 1. Various ionisation methods developed in our laboratory are used, including VUV sources. This permits the selective detection of aliphatic and aromatic species. Complementary high-resolution information is obtained on particular classes of molecules identified in the samples, including organosulfates, oxygenated hydrocarbons, nitrogenated hydrocarbons, polycyclic aromatic hydrocarbons (PAHs) and heavy metals. In particular, the degree of aromaticity, determined by the relative abundance of PAHs in the soot, will determine its physicochemical properties. PAHs are targeted because they are considered to be the main precursors of soot particles. L2MS is especially well adapted for PAH detection as it is possible to achieve a smooth desorption/ionisation step, thus avoiding post-ionisation fragmentation (Faccinnetto *et al.* 2011).

Further chemical mapping is performed using a Secondary Ion Mass Spectrometry (SIMS) instrument available on campus. In contrast to the L2MS technique, ToF-SIMS provides high sensitivity for both inorganic and organic species. Nevertheless, this technique has not, so far, been widely used in atmospheric environmental science (Cheng *et al.* 2014). Sulfates and metals are particularly targeted as well as  $C_n^-$  ions representing elemental carbon. These compounds are useful in determining the sources of PM in the tailpipe. The combination of L2MS and SIMS spectroscopic studies on size-selected particulate matter will provide critical physicochemical data necessary to develop measurement procedures down to 10 nm in the PEMs4Nano project.

This work has received funding from the European Union's Horizon2020 Programme for research, technological development and demonstration under Grant Agreement no. 724145 (H2020-GV-2016), the French National Research Agency (ANR) through the PIA Programme d'Investissement d'Avenir under contract ANR-10-LABX-005 (LABEX CaPPA – Chemical and Physical Properties of the Atmosphere), and the CLIMIBIO project via the Contrat de Plan Etat-Région of the Haute-France region.

Cheng, W. J., Weng, L. T., Li, Y. J., Lau, A., Chan, C., and Chan, C. M. (2014) *Surf. Interface Anal.* 46, 480-488.

Faccinnetto, A., Desgroux, P., Ziskind, M., Therssen, E., and Focsa, C. (2011) *Combust. Flame* 158, 227-239.

## **Abstracts T117**

## High-efficiency simultaneous removal of trace HM and organic pollutants from an Iron Ore Sintering Plant.

J. Gonzalez<sup>1\*</sup>, B. Gonzalez<sup>2</sup>, I. Ibarra<sup>1</sup>, K. Datta<sup>2</sup>, I. Gomez<sup>1</sup>, V. García<sup>2</sup>, F. J. Gonzalez<sup>2</sup> and C Gutierrez-Canas<sup>1</sup>

<sup>1</sup>University of the Basque Country UPV-EHU Alameda Urquijo s/n, 48013 Bilbao, Spain

<sup>2</sup>ArcelorMittal Global R&D Asturias. P.O. Box 90 Aviles 33400, Spain

Keywords: hybrid filtration, trace pollutants, iron ore sintering

\*Presenting author email: jgonzalez077@ikasle.ehu.es

Iron ore sintering is basically a pre-treatment process step to produce the main metallic burden for the blast furnace. In this context, sintering refers basically to an agglomeration process through combustion. Sintering involves the heating of iron ore fines along with flux and coke fines to produce a semi-molten mass that solidifies into porous pieces of sinter with the size, chemical composition and strength characteristics necessary for blast furnace processing.

The emission control strategy includes specific measures for both gases and particulate matter, specifically, for trace metals and organic pollutants enriched therein of sinter strand. Thus, the process line usually consist of a combination of adsorption and filtration blocks. A broad range of process alternatives have been proposed aiming at a maximization of PCDD/Fs aerosol removal efficiency (Guerriero, 2009) presents the performance of a line consisting of an electrostatic precipitator and a wetfine scrubber in an iron ore sintering plant. However, most of the research has been conducted at lab scale.

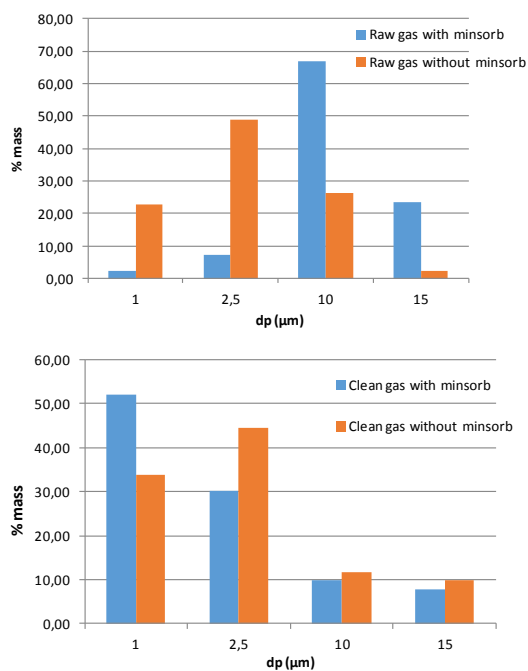


Figure 1. The shape of gravimetric size distribution of the aerosol directly upstream (above) and downstream of the pilot plant, with (blue) and without (red) previous adsorption using MINSORB.

Here are presented the preliminary results of a pilot plant installed as a bypass in a full-scale sinter consisting of a hybrid filter (electrostatic precipitator and fabric filter), allowing the use of catalytic media (Finocchio,2006). The project aims at a complete assessment of minimization methods for sinter strand emissions (Menad, 2006). Although the adsorption using activated carbon is widely considered as BAT (Ooi, 2011), in this case, a mineral adsorbent –MINSORB™– is used, due to its characteristics(Leroy, 2004) –non-flammable, among others- and to its performance.

The experimental setup includes simultaneous measurements for dynamic characterization of both process and clean aerosol. Results include the determination of the intrinsic variability of raw aerosol (Figure 1) and the assessment of the best HF operation (mode ESP, mode HF, filtration media, operating conditions). Further physicochemical analysis highlights the chemical efficiency for aptricular trace pollutants.

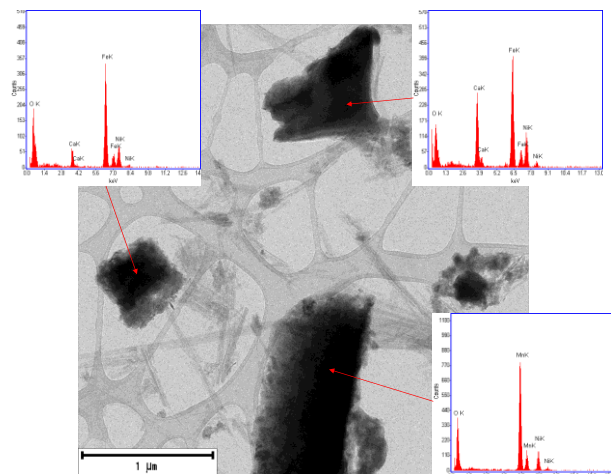


Figure 2. Adsorbed material on the micronic fraction. Trace pollutants burden displaced out of the penetration window.

Guerriero E. et al. *J. Haz. Mat.* 2009, **172** (2-3), 1498–1504

Finocchio E. et al. *App. Catalysis B: Environmental*. 2006, **62** (1-2), 12–20

Menad N. et al. *J. Cleaner Prod.*, 2006, **14** (8), 740– 747

Ooi T.C. et al. *Chemosphere*, 2011, **85** (3), 291– 299

Leroy G. et al, *Annual International Conference on Incineration and Thermal Treatment Technologies*, **23**; 2004

## Particle sampling under extreme conditions: An analysis of the corrosion-relevant aerosol in boilers of waste incineration plants

S. Schumacher<sup>1</sup>, J. Lindermann<sup>1</sup>, B. Stahlmecke<sup>1</sup>, D. Jarzyna<sup>1</sup>, A. Khot<sup>1</sup>,  
T. van der Zwaag<sup>1</sup>, H. Nordsieck<sup>2</sup>, J. Harpeng<sup>3</sup>, R. Warnecke<sup>4</sup>, and C. Asbach<sup>1</sup>

<sup>1</sup>Institut für Energie- und Umwelttechnik e.V. (IUTA), 47229 Duisburg, Germany

<sup>2</sup>bifa Umweltinstitut GmbH, 86167 Augsburg, Germany

<sup>3</sup>Abfallentsorgungszentrum Asdonkshof, 47475 Kamp-Lintfort, Germany

<sup>4</sup>GKS Gemeinschaftskraftwerk Schweinfurt GmbH, 97424 Schweinfurt, Germany

Keywords: waste incineration, particle sampling, size distributions, chemical analysis

Presenting author email: schumacher@iuta.de

Although the particulate phase in the boilers of waste incineration plants has for a long time been under suspicion to essentially drive the corrosion of the superheater tubes, it has not been comprehensively characterized to the present. This is mainly attributed to the extreme conditions present in the boilers such as very high temperatures, concentrations of condensable vapours and dust loads. These cause tremendous artefacts when using conventional measurement techniques that extract the aerosol from the boiler (Deuerling, 2010).

Therefore, we developed within the frame of the project VOKos a novel two stage sampling probe, which allows the collection of particles in the interesting size range and largely suppresses condensation artefacts (Schumacher, 2016).

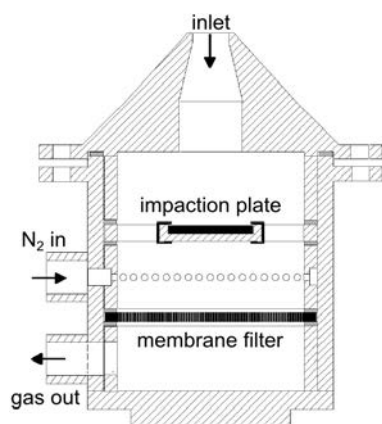


Figure 1: Cross section of the sampling probe.

Larger particles are sampled on an impaction plate, whereas the remaining smaller particles are collected on a nickel membrane filter with well-defined pore size and pattern. Together, a broad particle size range from a few 10 nm up to several 100  $\mu\text{m}$  is covered. Before and after sampling, the probe is flushed with an excess of clean nitrogen until the probe and the nitrogen flow are in thermal equilibrium with the sampling environment in order to avoid condensation of salts and chemical post-reactions.

The substrates are well-suited for scanning electron microscopy (SEM), which provides a comprehensive investigation of the size distribution, morphology and chemical properties of individual particles. Using computational fluid dynamics (CFD), the collection

efficiencies of the impactor as well as of the membrane filter have been studied in detail, which allows to deduce the airborne particle number and mass size distributions from counting the collected particles in SEM images. Furthermore, the probe can easily be adapted for total dust sampling and analysis (Schumacher, 2017).

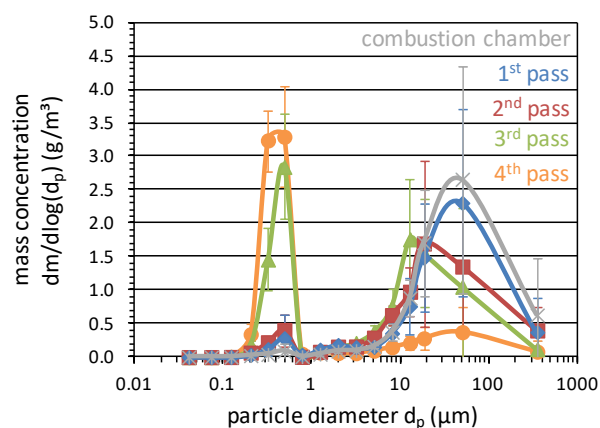


Figure 2: Evolution of the airborne particle mass size distribution in the course of the boiler for one plant.

The probe has been successfully employed for measurements in the combustion chamber (1250°C) and the four passes (250 - 950°C) of two waste incineration plants with strongly different corrosion rates to characterize the evolution of the aerosol on its way through the boilers. As shown in Fig. 2 for one plant, the concentration of particles with sizes between 0.1 and 1  $\mu\text{m}$  grows by condensation of salt vapours during cooling, whereas the concentration of larger particles decreases due to deposition losses. We show that especially particles with sizes of several micrometers, which have been difficult to measure up to now, contain high chlorine fractions. Finally, we discuss, based on our results, possible reasons for the different corrosion rates of the plants.

This work has been supported by the Federal Ministry of Education and Research (BMBF) within the project VOKos (Grant No 03X3589).

Deuerling, C. F. et al. (2010): *Aerosol Sci. Technol.* **44** 1.  
Schumacher, S. et al. (2016): *Corros. Sci.* **110** 82.  
Schumacher, S. et al. (2017): submitted to *Aerosol Sci. Technol.*

## Investigation of nano particles during additive manufacturing processes

S. Blei<sup>1</sup>, R. Heidenreich<sup>1</sup>

<sup>1</sup>Department of Air Pollution Control, Institute of Air Handling and Refrigeration, Bertolt-Brecht-Allee 20, 01309, Dresden, Germany

Keywords: nano particles, additive manufacturing, selective laser melting

Conventional production is based on established process chains that have been refined over several decades. In this context, design is adapted to the manufacturing technology. Additive manufacturing offers high potential for the production of components with highly complex geometries and integrated functionalities. Due to the layer-like production, the material is only installed where it is necessary. This allows the optimization of products to their functionality and to make production more flexible.

A generative manufacturing method to directly produce three-dimensional components is Selective Laser Melting (SLM) by using a powder bed.

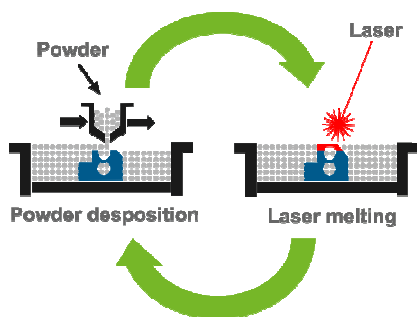


Figure 1. selective laser melting [www.mosttech.at]

The SLM process is a stratiform construction consisting of the repetition of two steps up to the necessary component height. The first step is the application of a thin layer of metal powder (thickness 30 microns). In the second step a high-performance laser melts and welds the metal powder at these locations, where a solid component is to be produced. The process has to be repeated until the component height is reached. Although the metal powder has grain sizes of 20-30  $\mu\text{m}$  nanoparticles are formed during laser melting.

This paper gives an overview about measurements of aerosols from additive manufacturing processes esp. selective laser melting with metal powder. Particle size distributions were measured by an SMPS (Model 3910, TSI, USA, Particle-Range: 0.01–0.36  $\mu\text{m}$ ) and OPS (Model 3330, TSI, USA, Particle-Range: 0.3–5  $\mu\text{m}$ ).

In initial studies the influence of the process on the generation of nanoparticles were investigated. During the laser melting process a very high concentration of particles of  $10^6$  particles/ $\text{cm}^3$  is generated (figure 2). This results in a periodic pattern with low and high particle concentration. It can be assumed that the

high concentration is generated at the laser melting process, while the low concentration is generated by further dilution with a purge gas during the metal powder application.

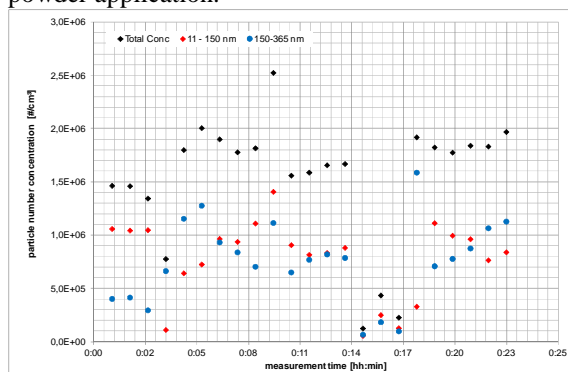


Figure 2. particle number concentration at selective laser melting process at 0.01-0.36  $\mu\text{m}$

The particle spectrum during laser melting shows a modal value of approx. 90-200 nm. This spectrum is similar to the laser processing of silica wafers or stainless steel surfaces. It is important to note that there is a temporary bi-modality of the particle distribution. The size distribution has 2 peaks at about 90 and 200 nm.

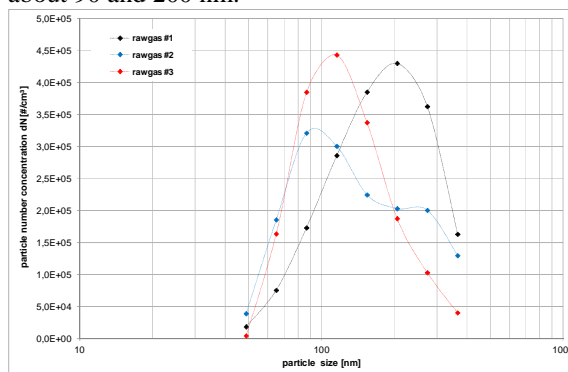


Figure 3. particle size distribution at process

The peaks do not occur simultaneously in the respective strongest expression. The temporal sequence of the occurrence of the 90 nm or 200 nm peak remains unexplained. The most plausible reason is an agglomeration process from small particles (90 nm) to larger particles (200 nm), which is superimposed by the sequence of powder application and laser melting process in the process chamber.

The results show that the process of selective laser melting needs to be further investigated and that special action has to be taken in the field of occupational health and safety.

**Characterization of oil shale combustion emissions by SP-AMS and CI-APi-TOF-MS**M. Aurela<sup>1,2</sup>, F. Mylläri<sup>2</sup>, M. Bloss<sup>1</sup>, P. Simonen<sup>2</sup>, A. Konist<sup>3</sup>, D. Neshumayev<sup>3</sup>, M. Maasikmets<sup>4</sup>, L. Salo<sup>2</sup>, S. Saarikoski<sup>1</sup>, H. Timonen<sup>1</sup>, M. Sipilä<sup>5</sup>, M. Dal Maso<sup>2</sup>, J. Keskinen<sup>2</sup> and T. Rönkkö<sup>2</sup><sup>1</sup>Atmospheric Composition Research, Finnish Meteorological Institute, Helsinki, Finland<sup>2</sup>Aerosol Physics, Faculty of Natural Sciences, Tampere University of Technology, Finland<sup>3</sup>Tallinn University of Technology, Tallinn, Estonia<sup>4</sup>Estonian Environmental Research Centre, Tallinn, Estonia<sup>5</sup>Department of Physics, University of Helsinki, Finland

Keywords: SP-AMS, secondary aerosol, CI-APi-ToF-MS, oil shale  
 Presenting author email: Minna.Aurela@fmi.fi

Oil shale is sedimentary rock containing up to 50% organic matter. Once extracted from the ground, the rock can either be used directly as a power plant resource, or be processed to produce shale oil and other chemicals and materials. Considerable quantities of oil shale are mined in Estonia, Russia, China, Brazil, Australia, and Germany. Estonia's oil shale industry is currently the most developed in the world and oil shales is mainly used for electricity and thermal energy generation. Estonia generates over 90% of its power from oil shale.

Oil shale has high mineral content; around 40-50% of the original mass remains after combustion. Oil shale operations result in emissions of sulphur, nitrogen oxides, particulates, ozone precursors, and carbon monoxide and dioxide. Estonian oil shale (kerogen) contains up to 2% sulphur. (Konist *et al.*, 2013)

In this study the physico-chemical properties and aging behaviour of emissions originating from oil shale combustion were investigated. Measurements were conducted in the 60 kW circulating fluidized bed (CFB) combustion test facility in Tallinn, Estonia.

Aerosol chemical composition (inorganic ions, organics, BC and metals) was measured with a Soot-Particle Aerosol Mass Spectrometer (SP-AMS, Onasch *et al.*, 2015). Together with chemical composition, physical properties (e.g. size distribution, number concentration) of submicron particles and trace gas concentrations were measured with a large variety of instruments. In addition, a nitrate ion based Chemical Ionization Atmospheric Pressure interface Time-Of-Flight Mass Spectrometer (CI-APi-TOF-MS, Jokinen *et al.*, 2012) was used for measuring sulphuric acid molecules and clusters. A potential aerosol mass (PAM, Kang *et al.*, 2007) chamber was used to simulate secondary aerosol formation potential of precursor gases in the atmosphere. Primary or secondary particles were measured alternately in approximately 30 min time intervals. Double-ejector system (hot and cold) was used for diluting the flue gas. Dilution ratio was calculated based on the ratio between trace gas concentrations at raw emissions and after the ejectors. The flue gas was cleaned with a fabric filter and the water vapour at the final stage was condensed.

At the beginning of the campaign, no primary particles were detected with the SP-AMS in its size range of 50-700 nm (Figure 1). However, small amounts of sulphuric acid monomer and dimer were detected with the

CI-APi-TOF-MS together with a maximum in particles number at the nucleation mode measured with the Scanning Mobility Particle Sizers (SPMS). The sulphuric acid monomer signal was clearly higher than for its dimer.

Large amounts of secondary organic and sulphate aerosols were formed, when flue gas was passed through the PAM chamber. Also, concentration of sulphuric acid measured with the CI-APi-TOF-MS increased significantly, when flue gas was oxidized in the PAM chamber compared to the primary emissions.

Due to variation in burning conditions, the concentrations of particles and sulphuric acid clusters varied a lot during the experiment (Figure 1).

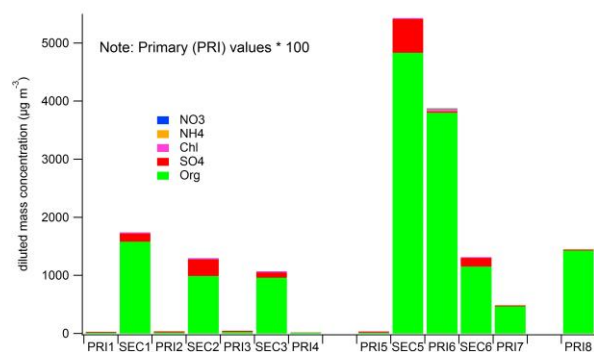


Figure 1. Average concentrations of primary (PRI) and secondary (SEC) aerosols after dilution during oil-shale combustion experiment measured with SP-AMS. PRI1 was measured just before SEC1 etc. The concentrations of primary aerosols were multiplied by 100.

This work was supported by the Estonian Environmental Investment Centre project no. 10627.

Jokinen, T., Sipilä, M., Junninen, H., Ehn, M., Lönn, G., Hakala, J., Petäjä, T., Mauldin III, R., Kulmala, M., and Worsnop, D. (2012) *Atmos. Chem. Phys.*, **12**, 4117–4125.

Kang, E., Root, M., Toohey, D. and Brune W. (2007) *Atmos. Chem. Phys.*, **7**, 5727–5744.

Konist, A., Pihu, T., Neshumayev, D. and Külaots, I. (2013) *Oil Shale*, **30**, 294–304.

Onasch, T., Trimborn, A., Fortner, E., Jayne, J., Kok, G., Williams, L., Davidovits, P. and Worsnop, D. (2012) *Aerosol Sci. Technol.* **46**, 804-817.

## Characterization of nanoparticles and polymer nanocomposites in flames for subsequent studies on health effects

N. Teuscher<sup>1</sup>, W. Baumann<sup>1</sup>, M. Hauser<sup>1</sup>, S. Mülhopt<sup>1</sup>, M. Hufnagel<sup>2</sup>, A. Hartwig<sup>2</sup>, M. Garcia-Käufer<sup>3</sup>, R. Gminski<sup>3</sup>, M. Berger<sup>4</sup>, T. Krebs<sup>4</sup>, H.-R. Paur<sup>1</sup> and D. Stapf<sup>1</sup>

<sup>1</sup>Institute for Technical Chemistry, Karlsruhe Institute of Technology, Karlsruhe, 76021, Germany

<sup>2</sup>Institute for Applied Biosciences, Karlsruhe Institute of Technology, Karlsruhe, 76021, Germany

<sup>3</sup>Environmental Health Sciences and Hospital Infection Control, Universitätsklinikum Freiburg, Freiburg, 79106, Germany

<sup>4</sup>Vitrocell Systems GmbH, Waldkirch, 79183, Germany

Keywords: nanoparticles, flames, polymer nanocomposites, thermal waste treatment

Presenting author email: [nadine.teuscher@kit.edu](mailto:nadine.teuscher@kit.edu)

Nanoparticles are used in everyday products like cosmetics, wall colours, textiles or polymer composites. As the products reach their end of life they usually will be disposed. Since the untreated deposition of waste is prohibited in Germany and many other countries, it's quite usual to use a thermal treatment (municipal and hazardous waste incineration) on certain types of waste. Few work has been published on the behaviour and possible release of these nanoparticles during incineration (Lang et al., 2015). In the project 'ProCycle' the possible risk on health and environment of aerosols produced during grinding or thermal treatment of polymer nanocomposites is investigated. Basic investigations on the thermal stability of the pure nanoagglomerates are executed as well as the combustion behaviour of nanoparticles embedded in polymer matrices.

The basic investigations are carried out at a tube burner where nanoparticles or the grinded polymer nanocomposites are added to the flame (Ethylene/Air, Propane/Air). The temperature of the flame can be changed via addition of inert gases and the influence on morphology, size distribution, sintering behaviour, or new particle formation is investigated in different heights above the burner.

SMPS measurements of TiO<sub>2</sub>-nanoparticles (Figure 1) were carried out with and without flame under varying argon fractions and therefore varying temperatures.

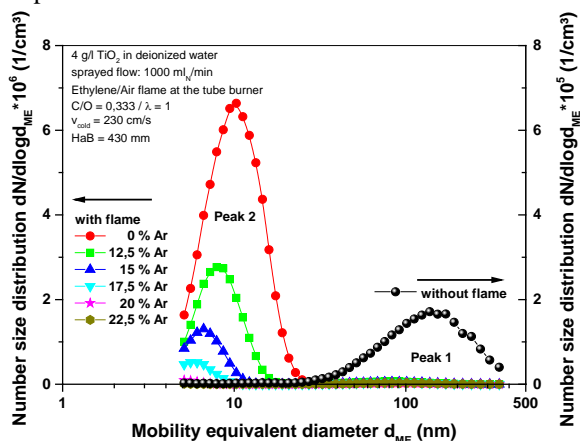


Figure 1. SMPS measurements of a Titania suspension added to the tube burner. The black dotted line belongs to the right axis and the other curves to the left axis.

The original aerosol (black dotted curve) consists of agglomerates with a modal diameter of 140 nm (Peak 1). When the flame is ignited a new particle mode starts to form in the size region around 10 nm (Peak 2).

The starting temperature for this effect is material dependent and metal oxides react to hydroxides or oxyhydroxides in the presence of water vapour (Golden & Opila, 2016).

With the Vitrocell® Automated Exposure Station at the Air Liquid Interface the toxicity of nanoparticles from polymer nanocomposite combustion on human lung cells can be tested (Figure 2).

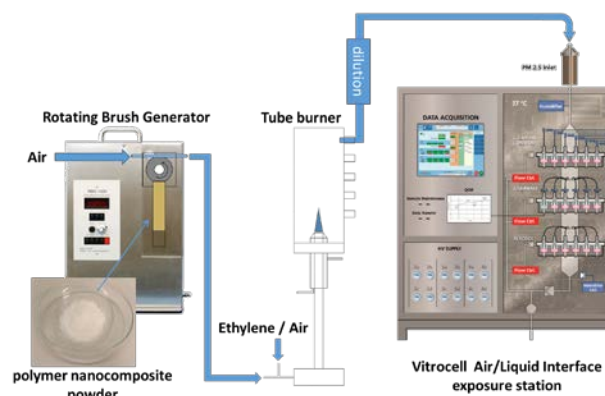


Figure 2. Experimental setup for the exposure of human lung cells to nanoparticles from the combustion of polymer nanocomposites.

This work was supported by the Federal Ministry of Education and Research under grant 03XP0009F within the project 'ProCycle'.

Golden, R.A., and Opila, E.J. (2016). A method for assessing the volatility of oxides in high-temperature high-velocity water vapor. *Journal of the European Ceramic Society*, 36, pp. 1135–1147.

Lang, I.-M. et al. (2015). Untersuchungen zur Freisetzung von synthetischen Nanopartikeln bei der Abfallverbrennung. In: K.J. Thomé-Kozmiensky, and M. Beckmann (Eds.), *Energie aus Abfall*, Band 12. TK-Vlg: Nietwerder, pp. 347–370.

## **Abstracts T118**

## Numerical simulation of cyclone separator comparison between CFD-DEM and DDPM

InSik Hwang<sup>1</sup>, Sangwoo Kim<sup>1</sup> and Jungho Hwang<sup>1</sup>

<sup>1</sup>Department of Mechanical Engineering, Yonsei University, Seoul, 03722, Republic of Korea

Keywords : CFD, Cyclone separator, DDPM

Presenting author email: ngari@yonsei.ac.kr

Cyclone separator is the most widely used device which controls the particle separation. Because of its simple design, low maintenance cost, and adaptability to a wide range of operating conditions, cyclone separator has become one of the most common particle removal devices (Chuah et al.,2006). Cyclone separator can easily remove high concentration of dust flowing along with fluid (air) and does not require frequent maintenance and replacement because aerodynamic separation of dust particles from an air stream does not pass through a physical filtration medium. Cyclone separator is particle separation device that uses centrifugal force generated from the spinning airflow to separate suspended particulate matter in the air stream.

Discrete phase model (DPM) was usually used to simulate cyclone separation in FLUENT. In DPM, one of the models for the Eulerian-Lagrangian approach, a fundamental assumption is that the solid phase occupies a low volume fraction, which is ignored in the Navier-Stokes equations for the gas phase. Additionally, the interaction between particles is neglected when solving the equation of motion for particle. Therefore, DPM is inappropriate for modelling system with particle of a high volume fraction (Ansys Fluent 14.0). The ways to extend DPM for high particle volume fraction are discrete element method (DEM) and dense discrete phase model (DDPM).

DEM was introduced by Cundall and Strack(1979). In the frame of the DEM, all particles in the computational domain are tracked in a Lagrangian way, explicitly solving each particle's trajectory, based on corresponding momentum balances for translational and angular accelerations. In recent years DEM approach has proven to be effective in modelling various particle fluid flow systems (Chu et al., 2011).

DDPM consider the volume fraction of the solid phase in the Navier-Stokes equation for the gas phase. The volume fraction and velocity field of the solid phase come from the Lagrangian tracking solution, and the interaction between the solid particles is calculated at the Eulerian grid using solid stress-strain tensor, which is calculated using the kinetic theory granular flow approach.

DEM and DDPM regard fluid as Eulerian frame and particle as Lagrangian frame. Also Both method of particle fluid interaction use empirical models for sub-grid particles to simulate particle fluid interaction. DEM can predict accurate determination of particle particle interactions, but DDPM can only predict approximate particle particle interactions determined by granular models. This difference makes results and time of simulation. In general, DEM leads to massive CPU effort.

Therefore, in this work DDPM was used to simulate cyclone separator and compared to DEM results.

The cyclone considered is a typical Lapple cyclone which is coming from Chu et al (2011).

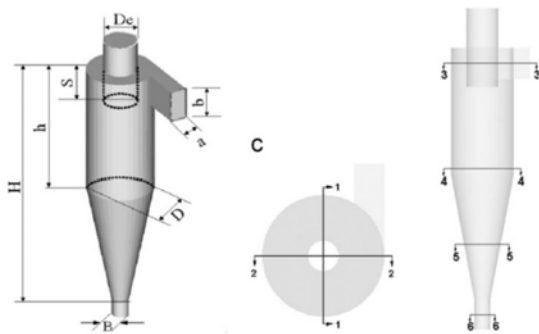


Figure 1. Schematic of the cyclone considered

Table 1. Geometry of the cyclone considered(D=0.2m)

a/D	b/D	De/D	S/D	h/D	H/D	B/D
0.25	0.5	0.5	0.625	2.0	4.0	0.25

The results showed that at high solid loading ratio, pressure drop was similar with experimental data and DEM results.

This subject is supported by Korea Ministry of Environment (MOE) as "the Technologies for Responding to Atmospheric Environment Policies Program".

T. Chuah, J. Gimbin, T.S.Y. Choong, *A CFD study of the effect of cone dimensions on sampling aerocyclones performance and hydrodynamics*, Powder Technology 162 (2) (2006) 126–132

ANSYS FLUENT 14.0. Canonsburg, U.S.: ANSYS Inc.; 2011.

P. A. Cundall and O. D. L. Strack, *A Discrete Numerical Model for Granular Assemblies*, Geotechnique 29 (1979) 47-65

K.W. Chu, B. Wang, D.L. Xu, A.B. Yu, *CFD-DEM simulation of the gas-solid flow in a cyclone separator*, Chemical Engineering Science 66 (2011) 834–847

## Particle characteristics from wood pellet-coal-mixture combustion in a large combined heat and power plant

F. Mylläri<sup>1</sup>, L. Pirjola<sup>2</sup>, H. Lihavainen<sup>3</sup>, E. Asmi<sup>3</sup>, E. Saukko<sup>1</sup>, V. Vakkari<sup>3</sup>, E. O'Connor<sup>3</sup>, J. Rautiainen<sup>4</sup>, A. Häyriäinen<sup>4</sup>, V. Niemelä<sup>5</sup>, J. Maunula<sup>6</sup>, R. Hillamo<sup>3</sup>, J. Keskinen<sup>1</sup>, and T. Rönkkö<sup>1</sup>

<sup>1</sup>Aerosol Physics, Faculty of Natural Sciences, Tampere University of Technology, FI-33101 Tampere, Finland

<sup>2</sup>Department of Technology, Metropolia University of Applied Sciences, FI-00180, Helsinki, Finland

<sup>3</sup>Finnish Meteorological Institute, FI-00560, Helsinki, Finland.

<sup>4</sup>Helen Oy, FI-00090 Helen, Helsinki, Finland

<sup>5</sup>Dekati Ltd., Tykkitie 1, FI-36240 Kangasala, Finland

<sup>6</sup>Valmet Technologies Oy, FI-33101 Tampere, Finland

Keywords: coal, wood pellet, black carbon, power plant.

Presenting author email: fanni.myllari@tut.fi

To minimize CO<sub>2</sub> emissions the energy companies have to develop new ways to increase their renewable fuel based energy production. In coal-fired power plants, one possibility is to substitute part of the coal with wood pellets. In principle, this kind of change has potential to affect also the characteristics of particle emissions of power production. Only few studies have reported how pellet addition effects on flue gas emissions (Frey et al. 2014; Saarnio et al. 2014). This experimental study focuses on the effects of co-combustion of wood pellets and coal to the number concentration and mean diameter of particles and black carbon concentrations in the stack of large CHP power plant.

Two different flue-gas cleaning situations were studied during the measurement; when electrostatic precipitators (ESP) were used together with desulphurization (FGD) unit and fabric filters (FF) or without them. The flue gas sample from the stack was diluted using a Fine Particle Sampler (FPS, Dekati Ltd.) before the particle measurement equipment (SMPS and ELPI). An aethalometer (AE33, Magee Scientific) was used to measure the light absorbing particulate mass concentrations. The morphology of the particles was studied by utilizing TEM for particles sampled from flue gas.

As expected, the flue gas cleaning strongly affected the particle emissions, see Figure 1 (Mylläri et al. 2016). The FGD and the FF reduced the particle concentrations in the flue gas as well as changed the chemical composition of the particles (e.g. existence of CaSO<sub>4</sub> particles during the “FGD+FF on”). The light absorbing mass concentration was determined for particles <1 μm. The mass concentration of light absorbing particulate matter, like BC, was close to zero with “FGD+FF on”. Instead, for the “FGD+FF off” situation the light absorbing mass values were on average 2.5·10<sup>4</sup> μg/m<sup>3</sup> when wood pellets were combusted with coal, but 0.5·10<sup>4</sup> μg/m<sup>3</sup> for coal. This result highlights the importance of high-efficiency flue-gas cleaning technologies when wood-based fuels are combusted in power plants.

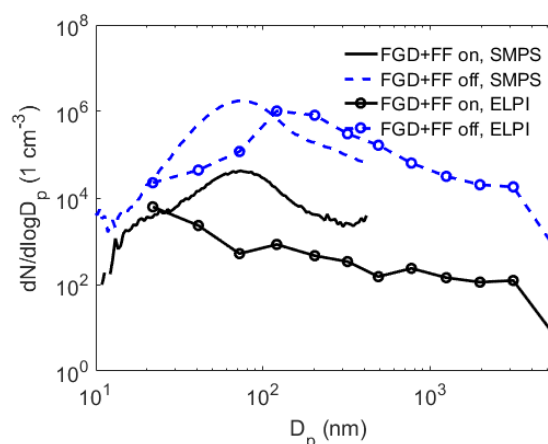


Figure 1. Particle number size distribution measured at the stack with ELPI and SMPS when the power plant was fuelled with coal. See Mylläri et al., 2016.

This work was made in the MMEA research program (work package 4.5.2.), supported by Tekes. TR and FM acknowledges also the financial support from the Academy of Finland (grant number 293437)

Frey, A., et al. (2014) *Optical and Chemical Characterization of Aerosols Emitted from Coal, Heavy and Light Fuel Oil, and Small-Scale Wood Combustion*, Environmental Science & Technology.

Mylläri, F. et al. (2016) *New particle formation in the fresh flue-gas plume from a coal-fired power plant: effect of flue-gas cleaning*, Atmospheric Chemistry and Physics.

Saarnio et al. (2014) *Chemical composition and size of particles in emissions of a coal-fired power plant with flue gas desulfurization*, Journal of Aerosol Science.

## Secondary aerosol formation potential reduction from a non-road diesel engine with exhaust aftertreatment systems

P. Karjalainen<sup>1,2</sup>, L. Ntziachristos<sup>1</sup>, P. Simonen<sup>1</sup>, K. Teinilä<sup>2</sup>, H. Timonen<sup>2</sup>, H. Saveljeff<sup>3</sup>, M. Lauren<sup>3</sup>, M. Happonen<sup>4</sup>, P. Matilainen<sup>5</sup>, T. Maunula<sup>5</sup>, J. Nuottimäki<sup>6</sup>, T. Rönkkö<sup>1</sup>, J. Keskinen<sup>1</sup>

<sup>1</sup>Aerosol Physics, Faculty of Natural Sciences, Tampere University of Technology, Tampere, Finland

<sup>2</sup>Atmospheric Composition Research, Finnish Meteorological Institute, Helsinki, Finland

<sup>3</sup>Turku University of Applied Sciences, Turku, Finland

<sup>4</sup>Agco Power Oy, Nokia, Finland

<sup>5</sup>Dinex Ecocat Oy, Laukaa, Finland

<sup>6</sup>Neste Oyj, Porvoo, Finland

Keywords: exhaust particle, particle emissions, secondary particles, PAM, exhaust aftertreatment

Presenting author email: panu.karjalainen@tut.fi

The new Stage V for non-road mobile machinery (NRMM) was introduced with Regulation (EU) 2016/1628. Stage V extends the scope of emission control including engines >560 kW. It also clarifies engine categories and streamlines emission limits per category. On the technological front, the new regulation calls for the introduction of diesel particle filters (DPFs) on most diesel engine categories as a result of the decision to regulate particle number on top of particle mass. In addition, the engine performance will be examined by in-use tests, using portable emission measurement equipment (PEMS), similar to the ones used for road transport. Stage V goes several steps forward that Stage IV, for which deNO<sub>x</sub> specific aftertreatment seemed adequate to reach demanded emission levels.

Therefore, understanding the potential of different aftertreatment technologies to bring real world reductions in the emissions of NO<sub>x</sub> and PM is required.

Recent research activities suggest that vehicles contribute to atmospheric PM concentrations not just through their direct (primary) PM emissions, measured at the tailpipe but, even more significantly, through photo-oxidation and gas-to-particle processes of initially gaseous exhaust components (secondary PM). To understand the health and environmental effects of exhaust emissions, both primary (direct) particulate emission and secondary particle formation (from gaseous precursors in the exhaust emissions) need to be therefore characterized. In this study we used a comprehensive set of measurements to characterize both primary and secondary particulate emissions of a modern heavy-duty nonroad engine with the most relevant exhaust aftertreatment systems in use.

The test engine used was a late technology medium-duty engine typically used in non-road applications (Stage IV, 100 kW). Two fuel grades, one typical diesel fuel oil (DFO) and one so-called renewable diesel – hydro-treated vegetable oil (HVO) were used in the testing. Primary emissions were measured following raw exhaust sampling with a porous tube dilutor. Secondary particle formation was initiated using a Potential Aerosol Mass (PAM) chamber to simulate secondary aerosol formation in the atmosphere.

Figure 1 shows impacts of different exhaust aftertreatment devices on primary and secondary PM emissions, estimated from PM size distributions. Results are shown for the two different fuels with 50% load at intermediate speed. Advanced aftertreatment seems to satisfactorily decrease both primary and secondary PM emissions. In particular DPF efficiency is above 90% for both particle types. A well operating selective catalytic reduction (SCR), combined with a diesel oxidation catalyst, also leads to significant PM and NO<sub>x</sub> reductions. Excess ammonia events (NH<sub>3</sub> slip) may lead to disproportional increase of secondary PM and have to be carefully controlled and avoided.

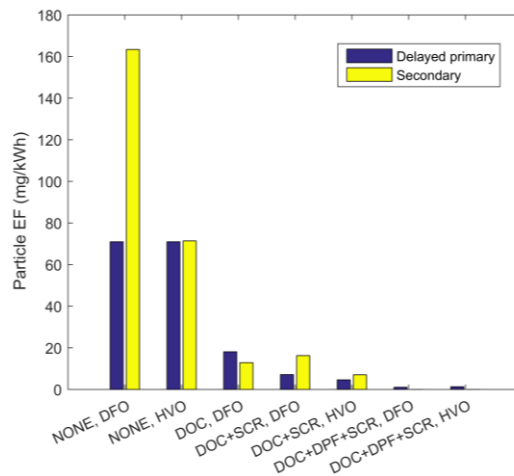


Figure 1. Delayed primary particle and formed total particle (including secondary) emission factors measured by two ELPIs with 50% load at intermediate speed.

We acknowledge HERE projected financed by Tekes (the Finnish Funding Agency for Technology and Innovation), Dekati, Dinex, Neste, Pegasor and Wärtsilä.

Tkacik, D. S., et al., *Environ. Sci. Technol.*, 48(19), 11235–11242, doi:10.1021/es502239v, 2014.

Kang, E. et al., *Atmos. Chem. Phys.*, 7(22), 5727–5744, doi:10.5194/acp-7-5727-2007, 2007.

Kang, E., et al., *Atmos. Chem. Phys.*, 11(4), 1837–1852, doi:10.5194/acp-11-1837-2011, 2011.

## **Abstracts T119**

## Particle-bound PAH trends during combustion of biomass in small stoves.

M. Kistler<sup>1</sup>, M. Flasch<sup>1</sup>, C. Schmidl<sup>1,2</sup> and A. Kasper-Giebl<sup>1</sup>

<sup>1</sup> Institute of Chemical Technologies and Analytics, TU Wien, Vienna, 1060, Austria

<sup>2</sup>Bioenergy 2020+, Wieselburg, Austria

Keywords: particle-bound PAHs, small scale biomass combustion, time resolved emissions.

Presenting author email: magdalena.kistler@tuwien.ac.at

Residential biomass heating systems, especially the manually operated ones are known to be responsible for significant emissions of polycyclic aromatic hydrocarbons (PAH). Kortelainen et al., (2015) showed for one stove and fuel type, using real-time aerosol measurements, that particle-bound PAHs are predominantly formed in phases when the combustion is not stable.

Here, the variation of particle-bound PAH emission from modern small scale heating devices for different fuels was described by filter measurements conducted with 5 min resolution (details in Kistler et al., 2015). The PAH trends were compared with particulate matter mass (PM10), carbon parameters (EC, OC) and volatile organic compound emissions (VOC).

Two different manually operated log wood stoves (called here 1 and 2) with power output under 10 kW, and different combustion air supply technology were tested. Spruce logs (S), beech logs (B) and commercial softwood briquettes (R) were burned. The measurements lasted over two or three full-load cycles including the cold start-up phase. PM10 was collected after 1:10 dilution (at ambient temperature) on quartz fiber filters each 5 min during whole burning cycle. Gas emissions (O<sub>2</sub>, CO<sub>2</sub>, CO, NO<sub>x</sub>, VOCs) were monitored continuously. Various combustion phases: SUP (Start-up), SOP1 (Steady-operation 1), BOP1 (Burn-out 1), RLP (Reload), SOP2 (Steady-operation 2) and BOP2 (Burn-out 2) were defined according to changes in temperature and CO<sub>2</sub> in flue gas.

The trends for PM10 and OC were similar to PAHs. Other than expected PAH trends were not clearly correlated with VOC or EC emissions, although these groups are PAH precursors or are formed at the same pathway. This was in line with observations of Meier et al., (2016) for wood chip/pellet boilers.

The most dominant feature for all tests was the high emission peak after reloading of the stove. This increase occurred for all components, although while for gaseous components (VOC) it was seen immediately (in RLP) for particulate emissions it was sometimes a few minutes shifted (beginning of SOP2) as showed in **Figure 1**. This was independent to fuel and stove. The emission increase during RLP was in all cases higher than emissions observed during start-up (SUP) with cold stove, which can be a hint that fuel loaded into high stove was not placed in the correct way. Lowest emissions were found during stable combustion phases, but the values in steady- and burn-out phases after reloading, were always a bit higher, with increase of lighter PAHs in the end visible for briquettes.

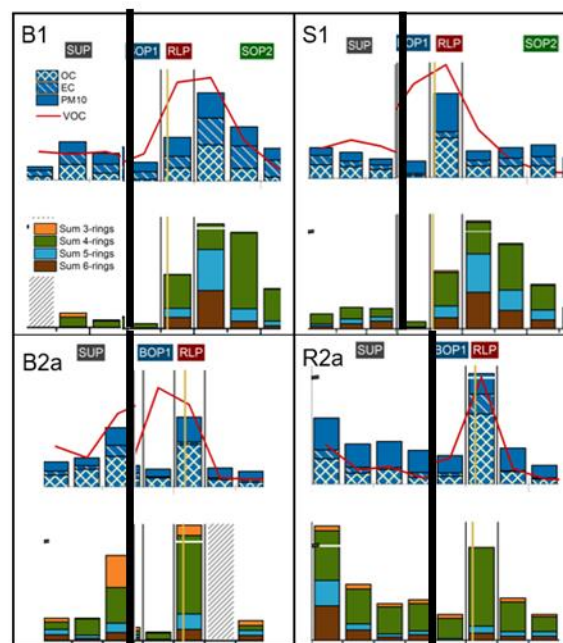


Figure 1. Start phase (SUP, left to the thick black line) and measurements around the stove reload process (RLP, right to the thick black line) for test with three different fuels (Beech (B), Spruce (S) and R (Softwood briquettes) and two different stoves (1 and 2).

Although no clear differences were observed between stove types and the fuels in the time resolution, the average total emissions for stove with automatic air supply regulation showed lower emissions than the other one and PAH levels observed for beech were higher than for spruce and briquettes.

Kortelainen A., Joutsensaari J., Tiitta P., Jaatinen A., Miettinen P., Hao L., Leskinen J., Viren A., Torvela T., Tissari J., Jokiniemi J., Worsnop D.R., Laaksonen A., Virtanen A. (2015) *Energy & Fuels* **29**, 1143-1150.

Kistler, M., Schmidl, C., Cetintas, E.C., Padouvas, E., Bauer, H., Puxbaum, H., Kasper-Giebl, A. (2015) *Papers of the 23th European Biomass Conference*, 457-463.

Meier, F., Schwabl M., Sedlmayer I., Kistler M., Schmidl C., Weissinger A., Haslinger W. (2016) *Papers of the 24th European Biomass Conference*, 429-432.

## Formation of SOA from logwood combustion upon photochemical aging in PEAR flow tube reactor

P. Tiitta<sup>1</sup>, A. Hartikainen<sup>1</sup>, M. Ihalainen<sup>1</sup>, P. Yli-Pirilä<sup>1</sup>, M. Kortelainen<sup>1</sup>, J. Tissari<sup>1</sup>, H. Lamberg<sup>1</sup>, A. Leskinen<sup>2,3</sup>, J. Jokiniemi<sup>1</sup>, and O. Sippula<sup>1</sup>

<sup>1</sup>Fine Particle and Aerosol Technology Laboratory, Department of Environmental and Biological Sciences, University of Eastern Finland, P.O. Box 1627, Kuopio, FI-70211, Finland

<sup>2</sup>Department of Applied Physics, University of Eastern Finland, Kuopio, FI-70211, Finland

<sup>3</sup>Finnish Meteorological Institute, P.O. Box 1627, 70211 Kuopio, Finland

Keywords: aerosols, photochemical aging, flow tube, wood combustion

Presenting author email: petri.tiitta@uef.fi

A comprehensive understanding of the formation processes of aerosol during aging is necessary for assessing atmospheric influence of combustion aerosol and their health effects. Transformation of wood combustion aerosols can be studied in controlled conditions in a smog chamber (Tiitta *et al.*, 2016) wherein time-steps of SOA evolution are observable whereas flow tube experiments are achieved for a wider degree of oxidant exposure times and a continuous aging process which follow combustion cycle. In this work, the photochemical emissions aging flow tube reactor (PEAR), developed at the University of Eastern Finland, was applied to study the aging of logwood combustion under different atmospheric oxidant exposures as time-resolved analysis over the cyclic combustion process.

A modern heat-storing masonry heater was used as the combustion source and both dry (moisture content of 5%) and wet (moisture content of 22%) spruce wood logs (*Picea abies*) was burned including ignition, flaming combustion and residual char burning phases (Leskinen *et al.*, 2014), totally five cycles / experiment. The OH exposure times were estimated by measuring D9-butanol gas decay with HR-PTR-ToF-MS (Ionicon) during the experiments. Ozone concentration and lamp intensities were varied to achieve the desired OH exposure times from 21 h (short aging) to 5.5 days (long aging) corresponding to total OH exposures of  $7.4 \times 10^{10}$  and  $4.9 \times 10^{11}$  molec.  $\text{cm}^3$ , respectively. In addition to photochemical aging, dark aging (UV Off) and POA (UV and ozone off) investigations were conducted.

Aged combustion aerosols were measured by the soot particle aerosol mass spectrometer (SP-HR-ToF-AMS, Aerodyne Research, Inc.) to determine changes in mass concentrations and composition of submicron particles focusing on SOA formation.

Analysis of spring 2016 measurements campaign results showed significant SOA formation during aging in PEAR flow tube, resulting OA increase by factor of 3 for dry spruce wood logs and even higher for wet logs. Composition of aged OA (PEAR) agreed well with OA aged in a ILMARI smog chamber (Figure 1; Tiitta *et al.*, 2016) with the same wood combustion source and comparable OH exposures indicating that photochemical emissions aging reactor (PEAR) simulates well polluted boundary-layer conditions.

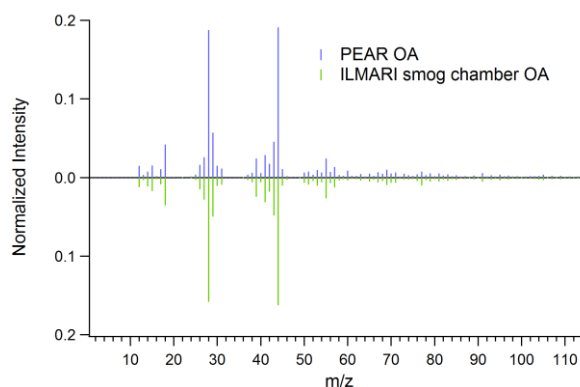


Figure 1. Comparison of OA spectra from spruce logwood combustion emissions aged in PEAR flow tube (upper) and in ILMARI smog chamber (lower). OH exposure times were 21 h and 18 h and corresponding total OH exposures were  $7.4 \times 10^{10}$  and  $6.6 \times 10^{10}$  molec.  $\text{cm}^3$  for PEAR and ILMARI (Leskinen *et al.*, 2015), respectively.

In the PEAR setup the time-resolved analysis of both primary and aged emission reveals the most important combustion phases for SOA formation. It was observed that particularly an insertion of new wood batch on glowing embers leads to a very high momentary SOA emission.

This work was supported by the Academy of Finland (Grants: 304459 & 296645).

Leskinen, A., *et al.* (2015) Characterization and testing of a new environmental chamber, *Atmos. Meas. Tech.* **8**, 2267-2278.

Leskinen, J., *et al.* (2014) Effective density and morphology of particles emitted from small-scale combustion of various fuel types, *Environ. Sci. Technol.* **48**, 13298-13306.

Tiitta P. *et al.* (2016) Transformation of logwood combustion emissions in a smog chamber: formation of secondary organic aerosol and changes in the primary organic aerosol upon daytime and nighttime aging, *Atmos. Chem. Phys.* **16**, 13251-13269.

## Engine out PM emissions from RME biodiesel and conventional diesel combustion with exhaust gas recirculation

V.B. Malmberg<sup>1</sup>, M. Novakovic<sup>2</sup>, S. Shamun<sup>2</sup>, M. Shen<sup>2</sup>, K. Kling<sup>3</sup>, A. Eriksson<sup>1,4</sup>, M. Tuner<sup>2</sup>, and J. Pagels<sup>1</sup>

<sup>1</sup>Division of Ergonomics and Aerosol Technology, Lund University, Box 118, SE-22100, Lund, Sweden

<sup>2</sup>Division of Combustion Engines, Lund University, Box 118, SE-221 00, Lund, Sweden

<sup>3</sup>National Research Centre for the Working Environment, 2100 Copenhagen, Denmark

<sup>4</sup>Division of Nuclear Physics, Lund University, Box 118, SE-22100, Lund, Sweden

Keywords: Biodiesel, Exhaust Gas Recirculation, Black Carbon, Diesel Exhaust

Presenting author email: Vilhelm.malmberg@design.lth.se

### INTRODUCTION

Low level blending of rapeseed oil methyl esters (RME) and other fatty acid methyl esters (FAME) in diesel (e.g., 10% biodiesel and 90% diesel) are widely used to reduce CO<sub>2</sub> emissions. Higher blends and 100% RME can be used in diesel engines for much stronger reductions of the fossil CO<sub>2</sub> emissions. The particulate emissions are altered by biodiesels. Reduced soot (black carbon; BC) and increased organic emissions are commonly observed for both low and high level blends of FAME biodiesels in diesel (Stevanovic et al., 2013). Associated with FAME biodiesels are also smaller primary BC particles, increases in the fractal dimension of the agglomerates, a greater disorder of the soot nanostructure (Savic et al., 2016), and increased in-vitro toxicity (Hedayat et al., 2016). Although FAME biodiesels are expected to have similar effects on the particle emissions, few studies have been conducted on RME. In addition to new biodiesel-fuels, modern engine concepts that reduce NO<sub>x</sub> emissions by using exhaust gas recirculation (EGR) influence particle emissions and properties. The combined effect of biodiesel blends and modern engine concepts on the particle characteristics are largely unknown. In this research, particulate emissions from a modern heavy-duty diesel engine with varying EGR and fueled with diesel or 100% RME were analyzed. Mass spectrometric signatures, BC mass emissions, particle size distributions and the BC nanostructure will be disseminated.

### METHODS

Particles were sampled from the exhaust of a modern heavy duty diesel engine at low load and 1200 rpm. Two fuels were used, petroleum-based MK1 diesel and 100% RME biodiesel. The EGR level was varied, corresponding to inlet O<sub>2</sub> concentration from ambient (no EGR) to <8% (very high EGR). A Soot particle aerosol mass spectrometer (SP-AMS), an AVL micro soot sensor (MSS), a fast mobility analyzer (DMS500), and sampling for transmission electron microscopy (TEM) were used to characterize the emissions.

### CONCLUSIONS

RME biodiesel reduced soot emissions in comparison to diesel. The reduction was observed for all EGR levels (Figure 1) and becomes very important for low temperature combustion at low inlet O<sub>2</sub>. Both EGR and RME influence the chemical composition of the exhaust particles. At high inlet O<sub>2</sub>, diesel and RME had organic mass spectra resembling that of lubrication oil. At

low inlet O<sub>2</sub>, PAHs increased significantly. The organic fraction of the exhaust particles was consistently much higher for RME combustion (Figure 1, ion signals normalized to C<sub>3</sub>, 36 m/z). Further evaluation of mass spectra and soot properties will investigate if these variations also apply to known markers of soot toxicity.

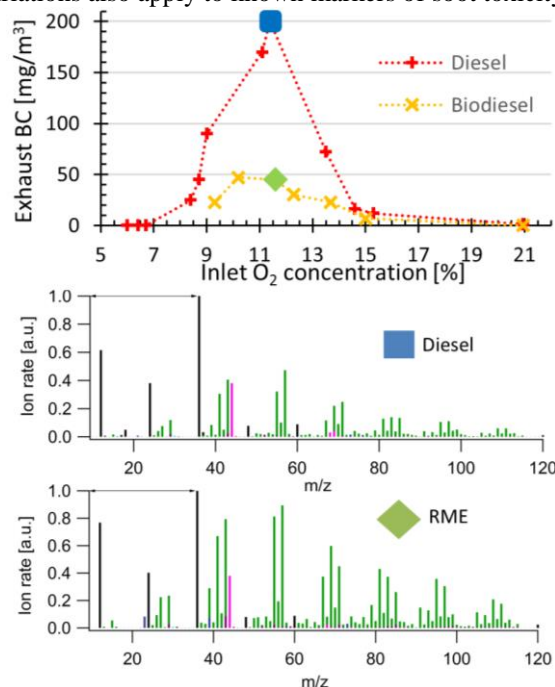


Figure 1. Exhaust BC mass concentrations (MSS) with declining inlet O<sub>2</sub> concentration (top). SP-AMS mass spectra normalized to C<sub>3</sub> of exhaust particles at 11.4% O<sub>2</sub> (Diesel) and 11.6% O<sub>2</sub> (RME).

This work was supported by the FORTE Centre METALUND, the Swedish research council FORMAS and the Swedish Energy Agency.

Stevanovic, S.; Miljevic, B.; Surawski, N. C.; Fairfull-Smith, K. E.; Bottle, S. E.; Brown, R., & Ristovski, Z. D. (2013). *Environ. Sci. Technol*, 47(14), 7655-7662.

Savic, N.; Rahman, M.; Miljevic, B.; Saathoff, H.; Naumann, K.; Leisner, T.; Riches, J.; Gupta, B.; Motta, N.; Ristovski, Z. (2016). *Carbon*, 104, 179-189.

Hedayat, F.; Stevanovic, S.; Milic, A.; Miljevic, B.; Nabi, M. N.; Zare, A.; Bottle, S.; Brown, R. J.; Ristovski, Z. D.. (2016). *Sci. Total Environ*. 545, 381-388.

## Influence of wood quality on reduction of particle emissions from biomass combustion boiler

A. Bologna<sup>1</sup>, W. Aich<sup>2</sup>, M. Ecker<sup>2</sup>, U.Frei<sup>1</sup>, K. Woletz<sup>1</sup>, H.-P. Rheinheimer<sup>3</sup> and H.-R. Paur<sup>1</sup>

<sup>1</sup>Karlsruhe Institute of Technology, D-76344 Eggenstein - Leopoldshafen, Germany

<sup>2</sup>HDG Bavaria GmbH; D- 84323 Massing, Germany

<sup>3</sup>CCA-Carola Clean Air GmbH, D-76344 Eggenstein – Leopoldshafen, Germany

Keywords: combustion aerosol, particle charging, electrostatic precipitation

Presenting author email: andrei.bologa@kit.edu

The biomass combustion boilers are widely used for domestic heat power generation. In spite of the progress achieved in the enhancement of the combustion technology and boiler design, there is still a range of problems which need their solution. One of the problems is the reduction of particle emissions from the exhaust gas formed during the biomass combustion. Usually fine particles in the exhaust gases are high in number concentration and contribute to PM-burden in many locations, especially during winter heating period.

The scope of the current work was to study the reduction of fine particles emissions from a wood-chips combustion boiler equipped with compact electrostatic precipitators (ESP).

The scientific innovation of the development relates to the investigation of the boiler and ESP operation stability. The tests were devoted to optimisation of ESP operation parameters and development of the effective algorithm for their control. This allows the enhancement of precipitation of fine particles from exhaust gases by various combustion conditions.

The technological innovation of the study relates to the development of cost-effective ESPs. The development trends to use of “stand-alone” ESPs; electrostatic precipitators which are electronically adopted to the boilers and the boilers with integrated ESPs.

The experiments were done at the KIT test set-up equipped with a HDG Compact 100 wood chips boiler and the space charge electrostatic precipitator type CCA-100. The study was carried out during the measuring campaigns when the wood-chips from leaf-trees (mixture from poplar, willow, beech, birch and alder), needle-trees (mixture from spruce, fir and pine) and the mixed wood-chips were burnt. During the campaigns the simultaneous gravimetric measurements of particle mass concentration in the gas flow upstream and downstream the ESP were carried out using the analyser SM 500 (Fa. Wöhler).

The conditions and the results of the tests are summarized in the Table 1. The diagram which illustrates the distribution of the mass of collected ash in the boiler and ESP is presented in the Fig.1. The combustion of wood-chips from leaf-trees shows the highest particle mass concentrations in the exhaust gas (the reason could be that 35% of wood

was poplar). The combustion of needle-tree wood-chips is characterized by high gas temperatures. ESP mass collection efficiency achieves its maximum during combustion of mixed and needle-tree wood chips. In spite of the fact, that the power consumption for particle charging in the ESP is rather constant, the quality of wood and combustion conditions show to be responsible for particles mass and of cause number concentrations in the exhaust gas and the ESP collection efficiency.

Table 1. Operation conditions

Conditions	Measuring campaign (MC)		
	MC1	MC2	MC3
Wood-chips	mixed	leaf-tree	needle-tree
Mass of dry wood, kg	3267	3027	3377
Ash content, %	1,1	1,8	1,1
Operation time, h	216	212	221
<b>Collected ash</b>			
Boiler bottom ash, kg	30,688	38,806	36394
Boiler heat exchanger, kg	1,691	4,187	3,095
ESP, kg	1,808	2,510	2,245
Penetration, kg	0,403	0,798	0,557
<b>Mass of ash</b>			
Calculated, kg	35,937	54,477	37,147
Experiment, kg	34,590	46,301	42,291
Mass balance, %	96,25	84,99	113,85
<b>Particle mass concentration and ESP collection efficiency</b>			
Gas temperature, °C	151±11	167±7	183±8
Raw gas, mg/m <sup>3</sup>	77,6±11	100,8±3	90,1±11
Clean gas, mg/m <sup>3</sup>	16,2±3,3	33,5±6	22,1±4
Power consumption for particle charging, W	42,9±1,2	42,7±3,4	44±0,8
Collection efficiency, %	78,9±4,0	66,3±7	75,1±5

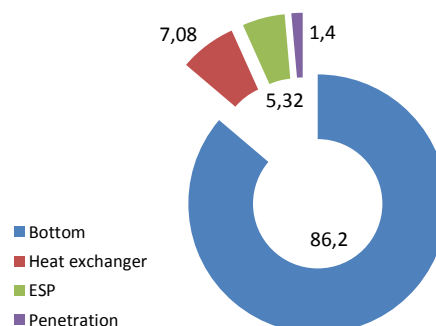


Figure 1. Distribution of the mass of the collected ash in the boiler and ESP (mean % values)

Acknowledgement: The project is funded by the Fachagentur Nachwachsende Rohstoffe e.V. (FNR), Germany (FKZ 22017814)

## Emission reduction of PCDD/Fs from a diesel generator fueled with water-containing butanol and waste cooking oil-based biodiesel blends

Jen-Hsiung Tsai<sup>1</sup>, Shui-Jen Chen<sup>1,\*</sup>, Kuo-Lin Huang<sup>1</sup>, Guo-Ping Chang-Chien<sup>2,3</sup>, Wen-Yinn Lin<sup>4</sup>, Bo-Cheng Jheng<sup>1</sup>, Yi-Chin Hsieh<sup>1</sup>

<sup>1</sup>Department of Environmental Science and Engineering, National Pingtung University of Science and Technology, Pingtung County, 91201, Taiwan

<sup>2</sup>Supermicro Mass Research and Technology Center, Cheng Shiu University, Kaohsiung City, 83347, Taiwan

<sup>3</sup>Department of Cosmetics and Fashion Styling, Cheng Shiu University, Kaohsiung City, 83347, Taiwan

<sup>4</sup>Institute of Environmental Engineering and Management, National Taipei University of Technology, Taipei City, 10608, Taiwan

Keywords: PCDD/F, butanol, water-containing, waste cooking oil-based biodiesel, generator.

Presenting author email: chensj@mail.npust.edu.tw

Recently, several studies have reported the emissions of chlorine or bromine substituted pollutants (e.g., PCDD/Fs, PCBs, PBDD/Fs, PBBs and PBDEs) from diesel engines (Popovicheva *et al.*, 2014; Wang *et al.*, 2010a). Chang *et al.* (2014) found that the use of water-containing acetone-butanol-ethanol (ABE) solution blended biodiesel could simultaneously reduce PM, NO<sub>x</sub>, and PAH by 4.30–30.7%, 10.9–63.1%, and 26.7–67.6%, respectively. In this study, blends of water-containing butanol (5% water content), waste cooking oil-based biodiesel (WCO-biodiesel), and pure diesel fuel were tested for decreasing the PCDD/F emissions from diesel engines.

The fuel blends, consisted of pure diesel oil with 30 vol% pure/water-containing acetone (denoted as B/B'), 20 vol% WCO-biodiesel (denoted as W), were tested at the stable energy output (110 V/60 Hz, 1800 rpm) of a generator under 1.5 and 3.0 kW loadings. An auto-detector flow sampling system was installed on the downstream side of the diesel generator exhaust to determine particulate phase PCDD/F (equipped with quartz fiber filters) and gas phase PCDD/F (collected by two connected cartridges (filled with XAD-2 resins)) samples. The detailed analytical procedures and instrumental analytical parameters of PCDD/Fs were presented in our previous works (Wang *et al.*, 2010b).

At the 1.5 and 3.0 kW loads, the emitted PCDD/F mass and toxic equivalent (WHO-TEQ) concentrations decreased as the added WCO-biodiesel and butanol increased, when compared with D100 (Fig. 1). In comparison to W20, the fuel blends which contained 30 vol% pure or water-containing butanol (i.e. W20B30 and W20B'30) further reduced the emission of PCDD/Fs; moreover, the reductions of PCDD mass and toxicity concentrations (47–53% and 67–77%, respectively) were higher than those of PCDFs (47–53% and 67–77%, respectively). This phenomenon was probably resulted from the addition of WCO-biodiesel (approximately 11 wt% oxygen) and butanol (C<sub>4</sub>H<sub>10</sub>O; 21.6 wt% oxygen) in pure petroleum diesel to increase oxygen content of the fuel blends, enhance the combustion efficiency of the engine, and reduce pollutant emissions. Additionally, water content in oil droplets will be vaporized or boiled first during the tests because diesel had a higher boiling point than the blends. The rapid expansion of water

vapor might induce micro-explosions or secondary atomization of oil droplets (Tsai *et al.*, 2014). This phenomenon increased the contact surface area of oil droplets with air and enhanced fuel combustion. It is also possibly related to the fact that the amounts of PCDD/Fs precursors (such as aromatic compounds and C<sub>2</sub> radicals) of biodiesel were few, and thus the *de novo* synthesis of PCDD/Fs were inhibited (Weber and Kuch, 2003).

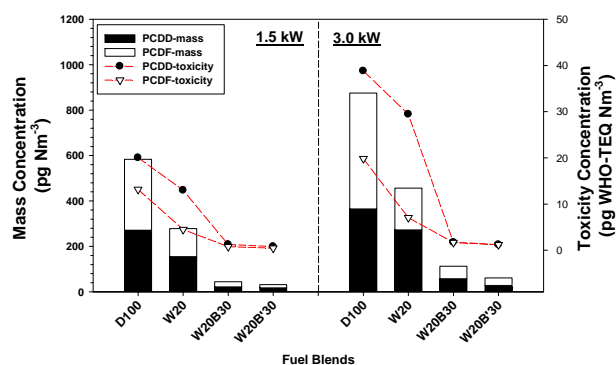


Figure 1. The mass and toxicity concentrations of PCDD/Fs emitted from the diesel-generator under 1.5 and 3.0 kW loads.

This work was supported by the Ministry of Science and Technology, Taiwan, under grant MOST 104-2221-E-020-003-MY3.

Chang, Y.C., Lee, W.J., Wu, T.S., Wu, C.Y. and Chen, S.J. (2014) *Energy* **64**, 678–687.

Popovicheva, O.B., Kireeva, E.D., Steiner, S., Rothen-Rutishauser, B., Persiantseva, N.M., Timofeev, M.A., Shonija, N.K., Comte, P., Czerwinski, J. (2014) *Aerosol Air Qual. Res.* **14**, 1392–1401.

Tsai, J.H., Chen, S.J., Huang, K.L., Lin, W.Y., Lee, W.J., Chao, H.R., Lin, C.C. and Hsieh, L.T. (2014) *J. Hazard. Mater.* **274**, 349–359

Wang, L.C., Lee, W.J., Lee, W.S., Chang-Chien, G.P., (2010a) *Environ. Pollut.* **158**, 3108–3115.

Wang, M.S., Chen, S.J., Huang, K.L., Lai, Y.C., Chang-Chien, G.-P., Tsai, J.-H., Lin, W.-Y., Chang, K.C., Lee, J.T. (2010b) *Chemosphere* **80**, 1220–1226.

Weber, R., Kuch, B. (2003) *Environ Int* **29**, 699–710.

## Emissions of PAHs and particulate metals from a diesel engine generator fueled with blends of waste cooking oil-based biodiesel and fossil diesel

Jen-Hsiung Tsai<sup>1</sup>, Shui-Jen Chen<sup>1\*</sup>, Kuo-Lin Huang<sup>1</sup>, Chih-Chung Lin<sup>1</sup>, Wen-Yinn Lin<sup>2</sup>,  
Ho-Tsang Huang<sup>1</sup>, Jia-Twu Lee<sup>1</sup>

<sup>1</sup>Department of Environmental Science and Engineering, National Pingtung University of Science and Technology, Pingtung County, 91201, Taiwan

<sup>2</sup>Institute of Environmental Engineering and Management, National Taipei University of Technology, Taipei City, 10608, Taiwan

Keywords: Biodiesel, waste cooking oil, metal, PAHs, generator.

\*Corresponding author email: chensj@mail.npust.edu.tw

Diesel engine exhausts (DEEs) may cause adverse health effects because of their varied chemical compositions (IARC, 2012), including carbonaceous matters, polycyclic aromatic hydrocarbons (PAHs), and trace metals (Lin *et al.*, 2005; Lin *et al.*, 2008). In urban atmosphere, the main contributors to environmental PAH level are mobile sources. These PAHs may be from products of incomplete combustion and pyrolysis of fossil fuels and other organic materials from natural and anthropogenic sources. It was nearly no doubt that use of biodiesel can help reduce diesel engine emissions, such as HC, CO, CO<sub>2</sub>, and PM (Kalam *et al.*, 2003; Dorado *et al.*, 2003). However, the characteristics of particulate metals and PAHs in the exhausts of off-road diesel engines which use waste cooking oil-based (WCO) biodiesels are seldom addressed.

To understand the impacts of using fossil diesel (D100) and WCO-biodiesel blends (W) on the emissions of particle-bound metals and PAHs from a generator at different loadings, this study utilized traditional fossil diesel added with 20% and 40% WCO-biodiesel blends (W20 and W40) as the fuels of generator at 1.5 and 3.0 kW loads to investigate the emission characteristics of PM metals and PAHs.

The results showed that the HMW-PAHs (emission) reduction in Total-PAHs (emission) reduction was relatively small (1.6% on average), but that of HMW-BaP<sub>eq</sub> was high (71.2 % on average) (Fig. 1). The Total-BaP<sub>eq</sub> reduction was contributed mainly from the

reduction of HMW-BaP<sub>eq</sub> (88% on average). The 21 analyzed PM metals were mainly consisted of Na, Mg, Al, K, Ca, Fe and Zn, accounting for 90% of ΣMetal. Mn, Cu, Sr and Pb were the main species of the other 14 trace metals (Fig. 2). To consider the impacts of DEEs on the environment and human health, using biodiesels (W20 and W40) as the generator fuel could effectively reduce the emissions of Total-PAHs (44% on average) and Total-BaP<sub>eq</sub> (80% on average) of DEEs. Therefore, WCO-biodiesel is a good candidate of clean alternative fuels.

This work was supported by the Ministry of Science and Technology, Taiwan, under grant MOST 104-2221-E-020-003-MY3.

Dorado, M.P., Ballesteros, E., Arnal, J.M., Gomez, J. and Lopez, F.J. (2003) *Fuel* **82**, 1311–1315.

IARC (2012) Press Release, available at: [http://www.iarc.fr/en/media-centre/pr/2012/pdfs/pr213\\_E.pdf](http://www.iarc.fr/en/media-centre/pr/2012/pdfs/pr213_E.pdf)

Kalam, M.A., Husnawan, M. and Masjuki, H.H. (2003) *Renew Energy* **28**, 2405–2415.

Lin, C.C., Chen, S.J., Huang, K.L., Hwang, W.I., Chang-Chien, G.P. and Lin, W.Y. (2005) *Environ. Sci. Technol.*, **39**, 8113–8122.

Lin, C.C., Chen, S.J., Huang, K.L., Lee, W.J., Lin, W.Y., Tsai, J.H. and Chaung, H.C. (2008) *Environ. Sci. Technol.*, **42**, 4229–4235.

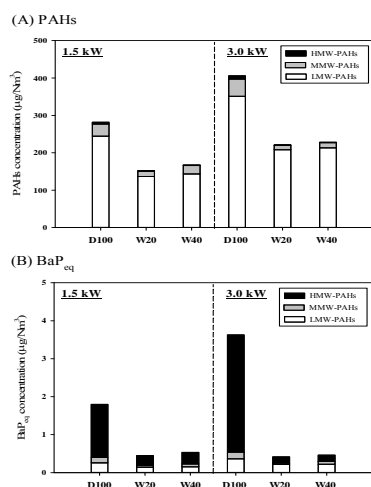


Figure 1. Concentrations of PAH and BaP<sub>eq</sub> in the exhausts of generator fueled with WCO-biodiesels at two loads.

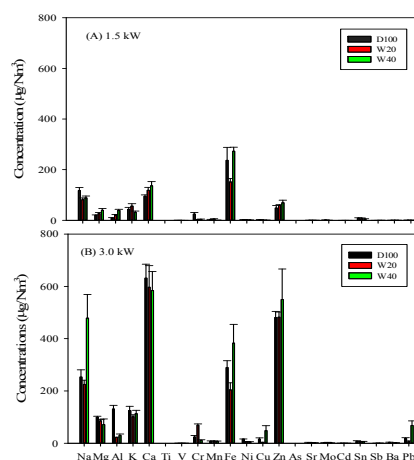


Figure 2. Concentrations of particle-bound metals in the exhausts of generator fueled with WCO-biodiesels at two loads.

## ***The impact of different blending ratios of waste cooking oil-based biodiesel on the emissions of PAHs, PCDD/Fs and PCBs from diesel engine***

C.Y. Chen<sup>1</sup>, W.J. Lee<sup>1</sup>, L.C. Wang<sup>2</sup> and C.H. Tsai<sup>3</sup>

<sup>1</sup>Department of Environmental Engineering, National Cheng Kung University, 70101, Taiwan

<sup>2</sup>Department of Civil Engineering and Geomatics, Cheng Shiu University, 83347, Taiwan

<sup>3</sup>Department of Chemical and Materials Engineering, 807, Taiwan

Keywords: diesel engine, WCO-based biodiesel, POPs.

Presenting author email: [lcwang@csu.edu.tw](mailto:lcwang@csu.edu.tw)

Biodiesel, with higher oxygen content than petroleum diesel, can create more complete combustion and reduce the incomplete combustion byproducts from diesel engine. The impact on emission from diesel engine by using biodiesel have been concluded that carbon monoxide (CO), PM and unburned hydrocarbon (HC) would be reduced compared to diesel (Kulkarni et al., 2006). However, the higher viscosity of biodiesel may worsen fuel spray property. Furthermore, the chlorine content in waste cooking oil-based (WCO-based) biodiesel is about five times higher than that in diesel, having potential to increase the chlorinated persistent organic pollutants (POPs) concentration in exhaust. Therefore, this study measured the emissions of PAHs, PCDD/Fs and PCBs from one diesel engine fueled by from low to high blend ratios of WCO-based biodiesel to investigate the optima ratio of using WCO-based biodiesel blends.

The ratio of WCO-based biodiesel used in this study were 0% (D100), 20% (B20), 40% (B40), 60% (B60), 80% (B80) and 100% (B100). The tested engine is compliant to the EURO Phase 4 emission regulations. The dynamometer used in this study was provided from the Environmental Protection & Energy Test Lab of Automotive Research & Test Center, which is fully accredited by Taiwan EPA for executing emission tests of diesel engines. The diesel engine was tested following the US Federal Test Procedure (FTP-75). Sampling procedure was the same as our previous study (Chang et al., 2014).

The results (Table 1) showed that POP emission factors were reduced along with the increase of blend ratio of WCO-based biodiesel until B60. It can achieve the highest reduction rates (37% for PM, 73% for PAHs, 64% for PCDD/Fs, and 41% for PCBs based on mass concentration) at B60. The extra oxygen provided by biodiesel could promote more complete oxidation of aromatic rings and their precursors (C2 radical). Together with the lower levels of precursors (i.e., aromatic contents) in the WCO-based biodiesel, this could explain the decrease in PM, PAHs, PCDD/Fs and PCBs.

When the blending ratios of WCO-based biodiesel were at 80%, the PM and POP emission factors increased, although these pollutant emissions were still lower than those of D100 trial. The increase on the PM and POP emission factors may be resulted from the incomplete combustion caused by worsened fuel spray because of the higher viscosity of high biodiesel blend ratio.

Table 1. The POP emission factors of the EURO IV diesel engine fueled with different ratios of WCO-based biodiesel

Emission factor		D100	B20	B40	B60	B80	B100
PM	Mass (mg/bhp hr)	722	548	524	453	651	512
PAHs	BaP <sub>eq</sub> (μg/bhp hr)	33.0	19.1	10.7	9.04	15.7	11.7
PCDD/Fs	WHO-TEQ (pg/bhp hr)	35.2	29.9	26.2	12.7	35.8	22.1
PCBs	WHO-TEQ (pg/bhp hr)	8.03	6.55	5.88	4.72	6.85	6.34

Kulkarni, M.G. and Dalai, A.K. (2006). *Industrial & Engineering Chemistry Research* 45: 2901–2913.  
Chang, Y.-C., Lee, W.-J., Wang, L.-C., Yang, H.-H., Cheng, M.-T., Lu, J.-H., Tsai, Y.I. and Young, L.-H. (2014). *Applied Energy* 113: 631-638.

## Trace metal and PAH enrichment within the penetration window of an ESP

I. Ibarra<sup>1\*</sup>, I. Gomez<sup>1</sup>, J. Gonzalez<sup>1</sup>, D. Sanz<sup>2</sup>, E. Rojas<sup>2</sup>, J. J. Rodríguez-Maroto<sup>2</sup>, R. Ramos<sup>3</sup>, E. Borjabad<sup>3</sup>, R. Escalada<sup>3</sup>, I. Celades<sup>4</sup>, S. Gomar<sup>4</sup>, V. Sanfelix<sup>4</sup> and C Gutierrez-Canas<sup>1</sup>

<sup>1</sup>Universidad del País Vasco UPV-EHU Alameda Urquijo s/n, 48013 Bilbao, Spain

<sup>2</sup>CIEMAT Avda Complutense 40, 28040 Madrid, Spain

<sup>3</sup>CEDER-CIEMAT Autovía A-15 salida 56, 42290 Lubia (Soria), Spain

<sup>4</sup>Instituto de Tecnología Cerámica Avda Vicent Sos Baynat s/n, 12006 Castellon, Spain

Keywords: biomass, combustion, heavy metals, thermodynamic

\*Presenting author email: iibarra011@ikasle.ehu.es

Medium-scale Combustion Plants (MCPs) are a feasible alternative for agricultural or forestry waste management. In this work a MCP is equipped with a Hybrid Filter (HF), which integrates electrostatic precipitator (ESP) with 4 collected hoppers and bag filter (BF), as described in detail by Aragon et al (2015).

The experimental campaigns were performed using olive tree pruning and wheat straw pellets, with 30% of excess air for combustion and a bed temperature of 840°C. In order to study the trace metal and PAH presence in the ESP penetration window, emission measurements (mass and number size distributions) and the composition of ashes collected along the HF were made.

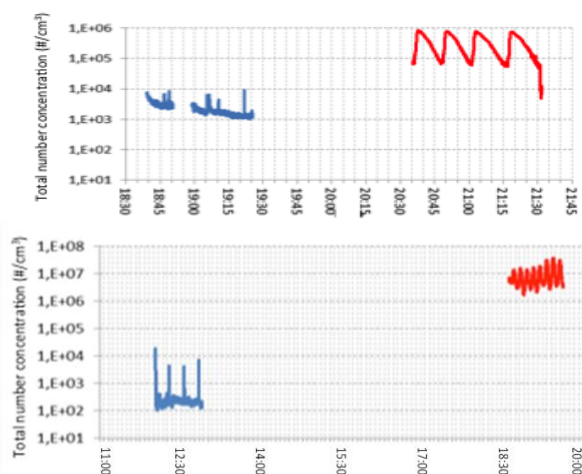


Figure 1. Total number concentration (red: raw and blue: clean gas) firing olive tree pruning pellets (above) and wheat straw pellets.

The HF is able to deal with different raw gas concentrations depending on the fuel, as it is observed in Figure 1. In the Figure 2 is shown the mass distribution before and after de HF using both fuels. In this case the mass distribution over size depends strongly on the fuel and the air-to-fuel ratio. The residence time is roughly the same along the process line.

The PAHs are distributed unevenly within the penetration window of the ESP (Figure 3). The bag filter downstream ensures the removal of this fraction.

For multiproduct biomass boilers, the HF ensures not only the performance when challenged with different aerosol loads, but also an enough efficient control of the trace pollutants mainly present in the near-micronic size range.

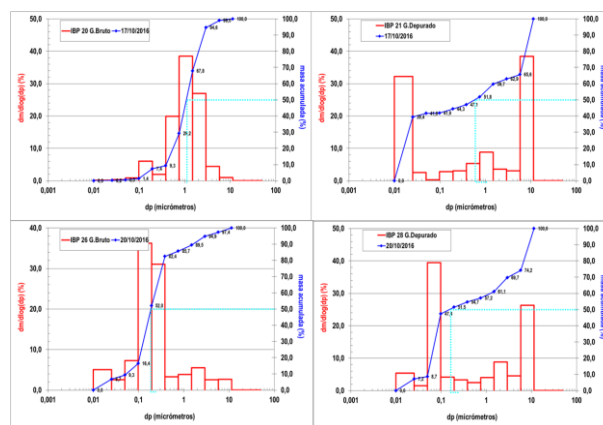


Figure 2. Mass relative distribution in raw (left) and clean (right) gas firing olive tree pruning pellets (above) and wheat straw pellets (below).

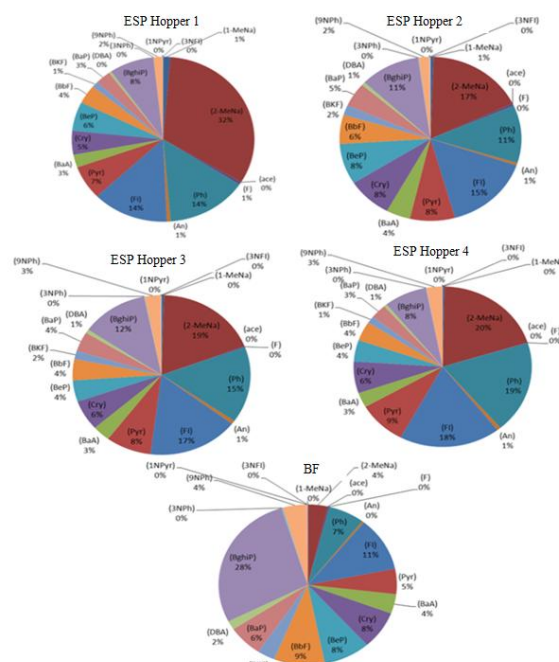


Figure 3. PAHs distribution (%) in the ashes collected along de HF firing olive tree pruning.

This work was supported by the Spanish MINECO under grant CLEANBIOM (2014-2017).

Aragon, G. et al. *Energy & Fuels* 2015, **29** (4), 2358–2371.

## Novel electrical charging condensing heat exchanger for particle emission reduction in small boilers

O. Sippula<sup>1</sup>, J. Grigonyte<sup>1</sup>, H. Suhonen<sup>1</sup>, A. Laitinen<sup>2</sup>, M. Kortelainen<sup>1</sup>, J. Tissari<sup>1</sup>, P. Tiitta<sup>1</sup>, A. Lähde<sup>1</sup>, J. Keskinen<sup>2</sup> and J. Jokiniemi<sup>1</sup>

<sup>1</sup>Fine Particle and Aerosol Technology Laboratory, Department of Environmental and Biological Sciences, University of Eastern Finland, P.O Box 1627, FI-70211, Kuopio, Finland

<sup>2</sup>Aerosol Physics Laboratory, Department of Physics, Tampere University of Technology, Tampere, Finland

Keywords: biomass, boiler, combustion aerosol, cleaning technology

Presenting author email: [olli.sippula@uef.fi](mailto:olli.sippula@uef.fi)

There is an urgent need to develop cost-efficient particle emission reduction technologies for small to medium scale biofuel-fired boilers in order to reduce adverse health and environmental effects of fine particulate matter and to comply the small boilers with the forthcoming European Ecodesign directive. We have recently demonstrated the usage of two novel approaches for cost-efficient separation of fine particle emission from combustion gases. First, a condensing heat exchanger (CHX) system was developed, in which the thermophoretic and diffusiphoretic particle precipitation was optimized, leading to approximately 50% fine PM reduction in a small biomass boiler (Grigonyte et al., 2014). The setup was designed to be integrated in a boiler system and to replace the conventional heat exchanger. It is especially beneficial for boilers operating with moist fuels, such as forest residues or pyrolysis oil. Second, a shielded corona charger (TassuESP) was recently demonstrated, as an inexpensive system for electrical precipitation of particles from pellet boiler flue gases (Laitinen et al. 2016). In the present work, we have combined these technologies and demonstrate a CHX system, in which particle charging is carried out upstream of the heat exchanger and the charged particles are collected in the heat exchanger surfaces, and finally removed with the flowing condense film, formed at the heat exchanger tube surface.

The pilot heat exchanger system was installed in the grate combustion reactor of the ILMARI research facility of the University of Eastern Finland. In the heat exchanger the flue gas flow is divided into several tubes which are cooled with water circulation. The heat exchanger was set up vertically, with combustion aerosol flowing from top to down. The combustion reactor was fired with wood chips (30% moisture content) with an output of 9 kW. The shielded corona charging electrode was installed upstream the condensing heat exchanger, at about 600 °C flue gas temperature. Aerosol sampling was carried out downstream the CHX with diluting sampling system consisting of a porous tube diluter and two sequential ejector diluters. Particle emissions were measured online using SMPS, CPC, ELPI and TEOM. Offline samples were collected on filters for gravimetric and thermal-optical carbon analyses as well as for imaging with electron microscopy. Gas-phase composition was measured both upstream and downstream the CHX using the FTIR multicomponent analyser. In addition, reference experiments with a

conventional firetube boiler heat exchanger with the same combustion settings were conducted.

The flue gas temperature decreased on average to 43 °C in the CHX. The condense water flow was 30 g/MJ, resulting in a thermal efficiency of 105%, based on the conventional efficiency calculation method. The mean PM1 emissions were 23 mg/MJ, 13 mg/MJ and 4 mg/MJ with the reference heat exchanger, CHX and corona charger assisted CHX, respectively (Figure 1a). Thus, the usage of CHX only, resulted in 40% decrease in PM1 emissions. Particle charging upstream the CHX increased the particle collection to 82%. Particle number emissions (PN) were 1.2 and 1.3 × 10<sup>13</sup>/MJ for CHX and reference heat exchanger, respectively, while the usage of corona charger decreased the particle number emission to 7.6 × 10<sup>12</sup>, leading to 42% PN reduction efficiency. Interestingly, the usage of charger resulted in a bimodal particle size distribution with a nucleation mode below particle size of 30 nm (Figure 1b).

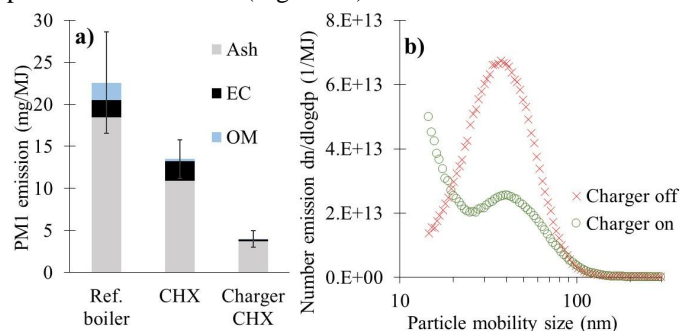


Figure 1. PM1 emissions with different heat exchanger setups (a) and particle size distributions (b)

The particle charging condensing heat exchanger was confirmed to have a high reduction efficiency for fine particles with simultaneous high thermal efficiency under conditions representing automatic biofuel boilers. The system replaces the conventional heat exchanger in boilers, making it a cost-efficient and compact solution, when compared to traditional flue gas cleaning devices.

This work was funded by the European Regional Development Fund, within the Pyreus project.

Grigonyte, J., Nuutinen, I. Koponen T., Lamberg H., Tissari, J., Jokiniemi, J. and Sippula O. (2014) *Energy Fuels* **28**, 6058-6065.

Laitinen, A., Keskinen, J. (2016) *J Electrostat* **83**, 1-6.

## Determination of indoor pollutants from coal combustion in a controlled setting

M.L.M. BARABAD<sup>1,2</sup>, M. E. VERSOZA<sup>1,2</sup>, W.S. JUNG<sup>1</sup> and D.S. PARK<sup>1</sup>

<sup>1</sup>Transportation Environmental Research Team, Korea Railroad Research Institute,  
176, Woramdong, Cheoldo-Bakmulgwan-ro, Uiwang City, Gyeonggi Province, 16105 South Korea

<sup>2</sup>Railway System Engineering, University of Science and Technology, Daejeon City, South Korea

Keywords: PM. Heavy metals, coal, combustion.

Presenting author email: mlmbarabad@gmail.com

Biomass burning is a significant source of PM and a great percentage of total carbonaceous aerosol mass in the atmosphere (Bond et al., 2004). Burned biomass also accounts for more than one-half of domestic energy mostly in developing countries and about 95% in lower income countries (Smith et al., 2004). Coal is a biomass fuel that has been commonly used for cooking and eating, however, studies reported that exposure from coal burning have linked to several health problems (Fullerton et al., (2008), Desia et al., (2004)). The aim of this study is to determine pm and heavy metal emission from coal combustion using a dual cone calorimeter. The experimental set-up applied control temperature to achieve burning status of the coal samples. Three bituminous coals were pulverized and burned. The results from the process showed that total percentages of the PM emission have values of 93.8, 93.4, and 99.8% were collected from coal a, b and c, respectively. The highest concentration were collected from the pm range of 0.35-0.45  $\mu\text{m}$  from all coals. Heavy metals, such as calcium (Ca), boron (B) and iron (Fe) have significant values that were collected from the combustion. High level of PM concentrations and hazardous heavy metals were identified, hence indicated an assumption that exposure of burned coal may lead to health risks from indoor pollutants. Furthermore, the analysis from a controlled experiment can be a useful comparison to actual field setting.

Desia, M.A., Mehta, S., Smith, K.R. (2004) *Indoor smoke from solid fuels: Assessing the environmental burden of disease at national and local levels. Environmental Burden of Disease Series. 4.* WHO.

This work was supported by a grant from the Railway Technology Research Project of the Ministry of Land Infrastructure and Transport (16RTRP-B082486-03).

Bond, T.C., Streets, D.G., Yarber, K.F., Nelson, S.M., Woo, J.-H., and Klimont, Z. (2004). *A technology-based global inventory of black and organic carbon emissions from combustion.* J. Geophys. Res., **109**.

Smith, K.R., Mehta, S., Maeusezahl-Feuz, M. (2004). *Indoor air pollution from solid fuel use, in : Ezzatti, M., Lopez, A.D., Rodgers, A., Murray, C.J.L., (eds), Comparative Quantification of Health risks: Global Regional Burden of Disease Attributable to Selected Major Risk Factors.* World Health Organization. Geneva. 1435-1493.

Fullerton, D.G., Bruce, N., Gordon, S.B. (2008). *Review: Indoor air pollution from biomass fuel smoke is a major health concern in the developing world.* Transactions of the Royal Society of Tropical Medicine and Hygiene. **102**. 843-851.

## Impact of Alternative Fuels on Particle Emission from an Aircraft Jet Engine in a Test Rig

T. Schripp<sup>1</sup>, F. Herrmann<sup>1</sup>, P. Oßwald<sup>1</sup>, M. Köhler<sup>1</sup>, A. Zschocke<sup>2</sup>, D. Weigelt,  
C. Werner-Spatz<sup>3</sup> and M. Mroch<sup>3</sup>

<sup>1</sup>Institute of Combustion Technology, German Aerospace Center, Stuttgart, 70569, Germany

<sup>2</sup>Deutsche Lufthansa AG, Köln, 50679, Germany

<sup>3</sup>Deutsche Lufthansa Technik AG, Hamburg, Germany

Keywords: Combustion, Alcohol-to-Jet, EEPS, CPC.

Presenting author email: tobias.schripp@dlr.de

The application of fuels from alternative sources is an expected future market in the field of aviation. Currently, most of the fuel used in public transport is Jet A-1. Available alternative fuels are mostly a blend of regular Jet A-1 and fuel from renewable sources. This approach is necessary since – until now - no alternative fuel has been approved for aviation use as an unblended fuel. The maximum permitted blend ratio is 50%. Overall, fuel substitution is handled very conservatively due to enhanced safety requirements in aviation.

Performing experiments at jet engines with variable fuel composition is complicated by the upper mentioned restrictions. Furthermore, emissions are influenced by the fossil fuel used for blending. This limits the number of related scientific studies.

This study used the test engine EVE at the Lufthansa Technik engine test cell in Hamburg. This system is a regular CFM56 engine that has been withdrawn from operational service, and hence can use even unapproved fuel. The engine was operated with three different fuels (Table 1) at different speed levels ranging from 900 RPM (“ground idle”) to 4500 RPM (“take off”). For the first time, a jet engine was operated with a pure synthetic jet fuel from a bioprocess route (“alcohol-to-jet”-type). The results of this study illustrate the impact of severe changes of the fuel composition on the release of gases and particles at a real jet engine.

Table 1. Jet fuels applied in the EVE test rig

Short	Description	C/H ratio
Ref1/Ref2	Regular Jet A-1	1.956
ARA	CH kerosene	1.896
Gevo ATJ	Alcohol-to-Jet	2.196

The emissions were monitored in a flow tunnel attached to the test rig using a Scanning Mobility Particle Sizer (SMPS), an Engine Exhaust Particle Sizer (EEPS), a Condensation Particle Counter (CPC), an Optical Particle Counter (OPC) and a mobile Infrared Spectrometer (FT-IR) to quantify the combustion gases. The emission indices - i.e. the emission per mass of burned fuel - of the exhaust gases carbon monoxide, nitrogen monoxide and nitrogen dioxide showed no significant difference between the tested fuels. The release of carbon dioxide slightly differed in correspondence with the C/H ratio. The release of particles corresponded with the speed setting of the engine (Figure 1). In relation to the fuel combustion, the

emission index of particles decreased for the reference fuels and the ARA fuel from the lowest speed setting to the highest setting. The ATJ fuel, however, featured very low particle emission at the lowest setting and increased to the level of the other fuels at the highest engine speed. In the range of 3000 RPM, which roughly corresponds to the aircrafts cruise speed, the fuels featured low particle emission. The minimum deviation between the different fuels is given for take-off conditions.

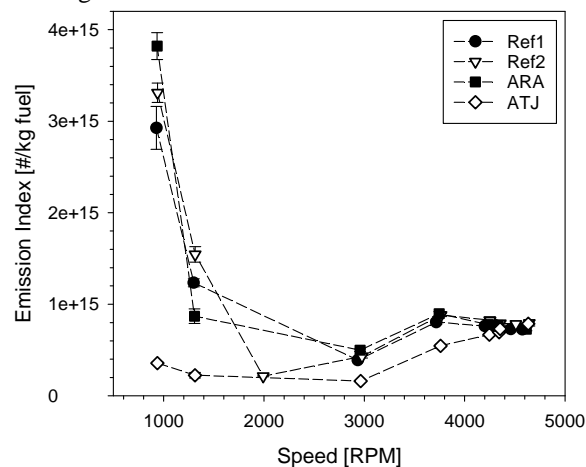


Figure 1. Emission index for (ultra)fine particles (CPC) for the applied fuels in dependence of the engine thrust.

Regarding the chemical composition, one noticeable difference between the fuels is the content of aromatics. The reference kerosenes and the ARA featured aromatic contents of 15.1% and 20.9% respectively. In contrast, the content was less than 1% for the ATJ fuel. The vast difference at low thrust settings illustrates the particle reduction potential associated with the use of alternative fuels. However, it must be considered that the tested ATJ fuel is not intended for 100% usage in regular jet engines due to technical limitations (e.g. insufficient swelling properties for sealing rings). Blending with other fuels that contain aromatic compounds is, thus, a mandatory approach. Nevertheless, the present investigation indicated that alternative fuel from renewable resources is not only applicable in current jet engines designs, but has the potential of beneficiary environmental effects. Further optimization of jet fuels with regard to particle release will depend on several complex parameters, such as economic efficiency, and will be a huge challenge for further research.

## Characterization of particulate emissions from a variety of developing-world cookstoves.

Y. Ting<sup>1</sup>, E. J. S. Mitchell<sup>2</sup>, J. Allan<sup>1,3</sup>, D. Liu<sup>1</sup>, D. V. Spracklen<sup>4</sup>, A. Williams<sup>2</sup>, J.M. Jones<sup>2</sup>, A.R. Lea-Langton<sup>5</sup>, G. McFiggans<sup>1</sup>, H. Coe<sup>1</sup>

<sup>1</sup>School of Earth and Environmental Science, University of Manchester, Manchester, M13 9PL, UK

<sup>2</sup>School of Chemical and Process Engineering, University of Leeds, Leeds, LS2 9JT, UK

<sup>3</sup>National Centre for Atmospheric Science, Manchester, M13 9PL, UK

<sup>4</sup>School of Earth and Environment, University of Leeds, Leeds, LS2 9JT, UK

<sup>5</sup>Department of Mechanical, Aero and Civil Engineering, University of Manchester, Manchester, M13 9PL, UK

Keywords: Solid fuel, combustion, black carbon, organic matter.

Presenting author email: yu-chieh.ting@postgrad.manchester.ac.uk

Solid fuels such as wood and charcoal are widely used as the primary sources for cooking and heating especially in the developing countries, with severe impacts on human health, air quality and climate (Dickau et al., 2016). The source profiles are important for initializing models to investigate their subsequent impact on air quality and climate, however such information for residential solid fuel burning is scant and introduce one of largest uncertainties.

In this study, the characterization of the emissions from residential solid fuel burnings was provided by simulating combustion conditions in a dilution tunnel using real-world cooking stoves that are used in the developing world with a range of solid fuels, providing fundamental information that will underpin future mitigation strategies.

A series of solid fuel combustion experiments were conducted at the combustion test facility (Mitchell et al., 2016) with a heating stove (willow logs, pine and coal), two optimised cook stoves (dry willow sticks, dry/wet oaks and charcoal) commonly used in Western Africa and a small-scale pyrolytic wood stove (wood pellets) used in Ethiopia and Zambia. The sub-micrometer non-refractory aerosol compositions and concentrations were determined by an aerosol mass spectrometer (AMS), and physical and optical properties of individual refractory black carbon (rBC) particles were characterised using a single particle soot photometer (SP2). A Dekati diluter was deployed before the inlet of the AMS and SP2. The number concentrations and size distribution in PM<sub>1</sub> were measured by Fast Particle Spectrometer DMS500 and filter samples for gravimetric analysis were taken. Trace gases, flows, mass consumption and temperature were also simultaneously measured using a variety of instruments.

Results obtained showed that the compositions of emitted aerosols largely depend on the burn conditions and phases. The burning phases are identified using the modified combustion efficiency ( $\text{CO}_2 / (\text{CO} + \text{CO}_2)$ ) and temperature in the flue. Over 90% of the BC was emitted during the flaming phase and OM dominates during the smouldering phase. The relative contribution of OM and BC in different phases rely significantly on the fuel conditions such as moisture and volatility content. It is the first time that the mixing state of the OM and BC components has been characterized for these sources.

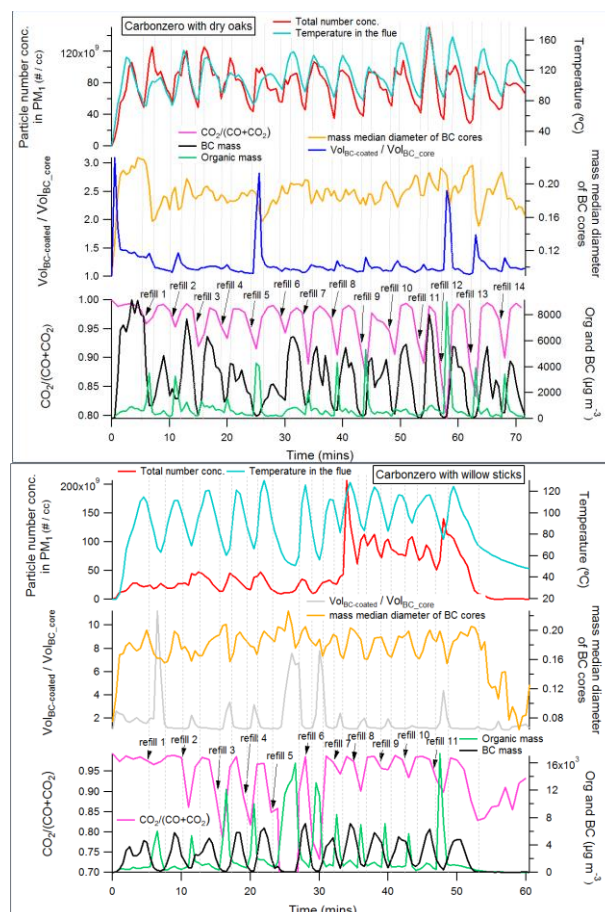


Figure 1. The OM and BC mass loadings, combustion efficiency ( $\text{CO}_2 / (\text{CO} + \text{CO}_2)$ ), mass median diameter of BC cores, ratios of volume<sub>BC\_coated</sub> and volume<sub>BC\_core</sub>, total particle number concentrations and temperature of two solid fuel combustion experiments with carbon zero stove.

This work was supported by EPSRC (Engineering and Physical Science Research Council) in the University of Leeds.

Anenberg et al. (2013) *Environmental Science & Technology*, 47, 3944-3952.

Dickau et al. (2016) *Aerosol Science & Technology*, 50, 759-772.

Mitchell et al. (2016) *Fuel Processing Technology*, 142, 115-123.

## KCl and NaCl condensation in a high temperature biomass gasification facility

A-K. Froment<sup>1</sup>, G. Ratel<sup>1</sup>, L. Jimenez<sup>1</sup>, M. Petit<sup>3</sup>, F. Patisson<sup>2</sup> and J.M. Seiler<sup>1</sup>

<sup>1</sup>LITEN/DTBH/LPB, CEA, 17, rue des Martyrs, 38054 Grenoble Cedex 9, France

<sup>2</sup>Institut Jean Lamour, Labex DAMAS, Université de Lorraine, CS 50840, 54011 Nancy, France

<sup>3</sup>IFP Energies nouvelles Lyon-Solaize, 69360 Solaize, France

Keywords: Aerosol, gasification, agglomeration, modelling.

Presenting author email: gilles.ratel@cea.fr

Biomass may contain up to 10-wt% of inorganic species in the ash-forming materials, sometimes more. These may cause many difficulties when condensation takes place from their gaseous form, especially after gasification at very high temperatures (above 1000°C): corrosion, deactivation of the catalysts, and deposition under several forms on the heat exchange surfaces. These problems have to be managed to optimize industrial processes (e.g., the entrained flow reactor (EFR) for biomass gasification).

For this purpose, condensation tests of vapours of model inorganic species (KCl and NaCl) usually formed during biomass gasification were carried out in an analytical test facility (ANACONDA). A gaseous inert flow containing both solid salt particles and solid carbon particles (simulating soot) was first heated to (partially) vaporize the salts and then cooled down at a controlled rate. The cooling rates (1000 or 300 K/s) were chosen as representative of those encountered in EFRs.

Results focussed on the morphology, the number-size distribution of the condensed particles collected at the outlet, as well as on the particle deposits on the inner wall of the facility.

The results show that the aerodynamic diameters of the condensed particles lie in the range 0.4 to 0.7 µm. The wall deposit represents from 50 to 80 wt% of the initial inorganic amount and it decreases in the presence of carbon particles, of about 10% absolute (Figure 1).

Experiments carried out at room temperature, with neither vaporization nor condensation mechanisms, lead to wall deposit between 15 and 20 wt%, mainly resulting from the gravity settling. Due to our experimental facility, some parameters could not be investigated separately: the condensation rate and length, and the salt initial amount and the initial solid particle size. The influence of these coupled parameters was nevertheless analysed.

The measurement of the aerodynamic diameter evolution (using Electrical Low Pressure Impactor, ELPI) revealed that NaCl and KCl exhibit the same behaviour. The presence of carbon particles makes the aerodynamic diameter of the condensed particles increase. It was also found that the carbon particles could agglomerate during their flow through the oven at 963 K.

The aerosol behaviour was modelled using SOPHAEROS, a IRSN software (Cousin 2008) dedicated to fission products transport in nuclear power plants. SOPHAEROS included all the necessary sub-models for transport, agglomeration, vaporization, condensation, etc., but it was necessary to modify the thermodynamic data in order to introduce potassium and sodium chlorides in the code instead of fission products. The agreement between the calculated and the experimental results is so far only qualitative, but the trends are correctly predicted (Table 1): the increase in the deposit when the cooling rate decreases for both salts, the decrease in the deposit when using NaCl salt with a lower concentration instead of KCl salt.

Table 1. Comparison between SOPHAEROS predictions and experimental measurements for the wall deposit in the ANACONDA experiment.

	Cooling rate 1000K/s		Cooling rate 300K/s	
	Exp. deposit	Calc. deposit	Exp. deposit	Calc. deposit
T= 700°C				
KCl (1 wt%)	59%	31%	79%	53%
NaCl (0.5wt%)	54%	25%	63%	36%

The particle size distribution shapes are also well reproduced even if the particle diameters are larger in the calculations than in the experiments.

Although additional work is necessary to reduce the gap between calculation and experiments, the correct trends observed shows the interest of using a tool like SOPHAEROS in the experiment interpretation and in the transposition to the aerosol behaviour in the EFR gasification process.

Cousin, F., K. Dieschbourg, and F. Jacq. 2008. "New Capabilities of Simulating Fission Product Transport in Circuits with ASTEC/SOPHAEROS v.1.3." Nuclear Engineering and Design 238 (9): 2430 – 2438.

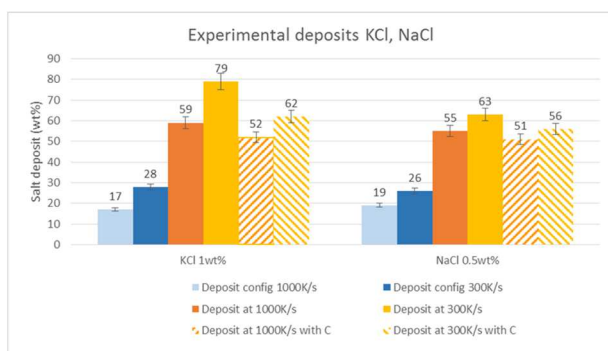


Figure 1. Experimental deposits calculated from inlet-outlet measured mass flowrates.

## On-line, size-resolved elemental analysis of ZnO nanoparticles during wood combustion processes

D.Foppiano<sup>1,2</sup>, M.Tarik<sup>2</sup>, E.Müller<sup>2</sup> and C.Ludwig<sup>1,2</sup>

<sup>1</sup>Department of ENAC-IIE, EPFL – École Polytechnique Fédérale de Lausanne, Lausanne, 1015, CH

<sup>2</sup>Division of ENE-LBK, PSI – Paul Scherrer Institute, Villigen PSI, 5232, CH

Keywords: On-line, size-resolved elemental analysis, wood combustion, ZnO NPs.

Presenting author email: debora.foppiano@psi.ch

Increasingly with the interest in reduction of atmospheric particle emissions, the release of fine particles from combustion processes is of great importance.

ZnO is one of the relevant metallic nanoparticles (NPs) since it is widely used in many applications like coatings and adhesives, paints, impregnation and waterproofing sprays, and may contribute to significant amount of inflammatory responses after high exposure (Uski et al. 2015).

In this work we aim to study the behaviour of ZnO during wood combustion as model for a waste biomass, and hence to understand the influence of the different generated species on the redox-sensitive Zn (Ludwig, 2001).

The physical and chemical behaviour of Zn is studied during the combustion of a wood sample impregnated with polyacrylic acid-stabilized (PAA) ZnO NPs suspensions. A standard combustion procedure was applied to simulate the combustion processes in an industrial plant (drying step, fast pyrolysis from 300°C to 900°C and afterburning from 900°C to 400°C).

The experimental setup consist on a tubular furnace used as lab-scale incinerator, connected to an SMPS-ICP-MS, a recently developed and validated analytical method to determine on-line the particle size distribution and elemental composition in aerosols and process gases. The method couples a modified SMPS (scanning mobility particle sizer) operating with argon instead of air with an ICP-MS (inductively coupled plasma mass spectrometer) (Hess et al. 2016). A well-defined flow of the aerosol is introduced into the SMPS with a rotating disk diluter (RDD) and a heating tube allowing an adjustable dilution ratio.

The results (Fig. 1a) show that during wood combustion Zn is released and reform as ZnO nanoparticles, confirmed by the correspondence between the PSD (particle size distribution) and the ICP-MS signal in the emission gas measured (Fig. 1b). Further characterization was performed with TEM-EDS (transmission electron microscopy- energy-dispersive X-ray spectroscopy) analysis on the size-selected samples collected after the DMA (differential mobility analyser), with particle size and chemical composition in agreement with the results shown in Fig. 1.

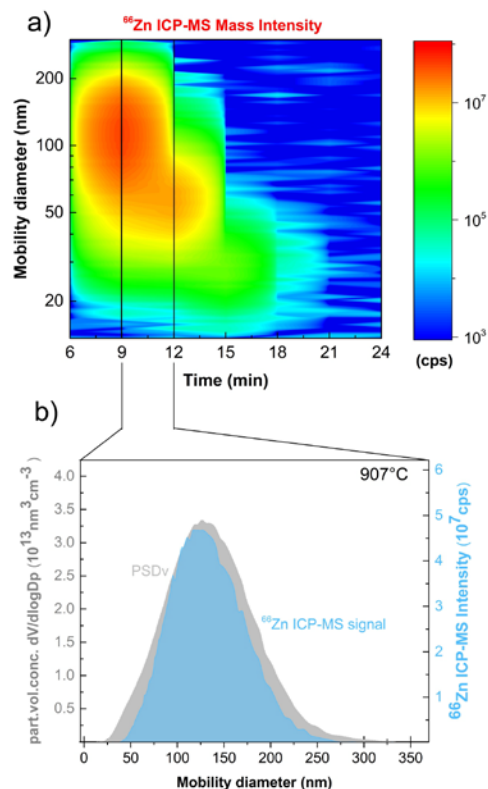


Figure 1. Corrected ICP-MS mass intensity of <sup>66</sup>Zn (a); Comparison between PSDv (volume related particle size distribution) and <sup>66</sup>Zn ICP-MS signal in the selected range of 3 min (b)

Uski, O. et al., (2015). *Science of the Total Environment*, **511**, 331–340.

Ludwig, C., Lutz, H., Wochele, J. (2001) *J. Anal. Chem.*, **371**, 1057-1062.

Hess, A. Tarik, M., Foppiano, D. et al., (2016). *Energy and Fuels*, **30(5)**, 4072–4084.

## **Abstracts T120**

## The catalytic effect of potassium compounds in soot oxidation

A. Rinckenburger<sup>1</sup>, K. Yasuda<sup>2</sup> and R. Niessner<sup>1</sup>

<sup>1</sup>Chair of Analytical Chemistry, Institute of Hydrochemistry, Technical University of Munich, Munich, D-81377, Germany

<sup>2</sup>Department of Applied Quantum Physics and Nuclear Engineering, Kyushu University, Fukuoka, 819-0395, Japan

Keywords: combustion aerosols, soot structure, alkali metal catalysis, Diesel.  
Presenting author email: alexander.rinckenburger@tum.de

Diesel soot is one of the major pollutants in the world and is classified as carcinogenic by the WHO's International Agency for Research on Cancer (Benbrahim-Tallaa *et al.*, 2012). Soot/black carbon is also theorized to have the second largest impact on global warming after CO<sub>2</sub> (Bond *et al.*, 2013). In North America and Europe, soot is mainly emitted by diesel engines (Ramanathan and Carmichael, 2008), which are mostly equipped with particulate filters to minimize emissions.

Regeneration of these filters is done by oxidation (combustion) of the soot. Uncatalyzed oxidation requires temperatures >600 °C in O<sub>2</sub> (5 Vol.-% in N<sub>2</sub>), which result in poor fuel efficiencies. Additives can enhance soot reactivities during soot formation, leading to internally-mixed soot and possible oxidation temperatures under 400 °C. Besides oxidic additives, salts are also able to lower the temperatures for soot oxidation significantly. Nevertheless, combustion processes are still not fully understood and require further research.

Therefore, a custom-built propane/air diffusion burner was used to produce different soot internally-mixed with potassium salts. The soot were collected either thermophoretically or on quartz fiber filters. Atomic absorption spectroscopy (AAS) was applied to characterize the salt content of the soot; soot reactivity was studied using Temperature-programmed Oxidation (TPO). Soot aerosols were characterized regarding their particle number concentrations by using a scanning mobility particle sizer (SMPS) setup. Structural parameters of the different soot were derived from Raman Microspectroscopy, BET analysis, scanning electron microscopy (SEM) and high resolution transmission electron microscopy (HRTEM). The electronic structure was investigated closer by using electron paramagnetic resonance spectroscopy (EPR).

Combustion in a Diesel Particulate Filter (DPF) was simulated by applying Temperature-programmed Oxidation (TPO). Soot samples were combusted in a defined atmosphere (5 Vol.-% O<sub>2</sub> in N<sub>2</sub>) and temperature range (100 °C - 700 °C; 5 °C/min). Combustion products were detected in an FTIR spectrometer. All salts lead to a pronounced decrease of the TPO temperatures of maximum CO + CO<sub>2</sub> emissions (T<sub>max</sub>) with K<sub>2</sub>CO<sub>3</sub> leading to a decrease of up to 300 °C compared to uncatalyzed soot. Increased salt contents also lead to lower ratios of CO/CO<sub>2</sub> at T<sub>max</sub>. Structural parameters of the different soot, derived from Raman Micro-

spectroscopy, SEM and SMPS measurements did not vary significantly compared to uncatalyzed soot, BET areas only showed slight trends to lower areas with higher salt content.

On the contrary, the oxidation reactivity could be correlated to parameters derived from HRTEM and EPR measurements. Our study presents a detailed view of the catalytic potential of potassium compounds for all kinds of soot oxidation and carbon gasification and gives new indications towards a more complete understanding of the catalyzed soot oxidation. It also shows the need for a fast and on-line method to fully characterize soot oxidation reactivities.

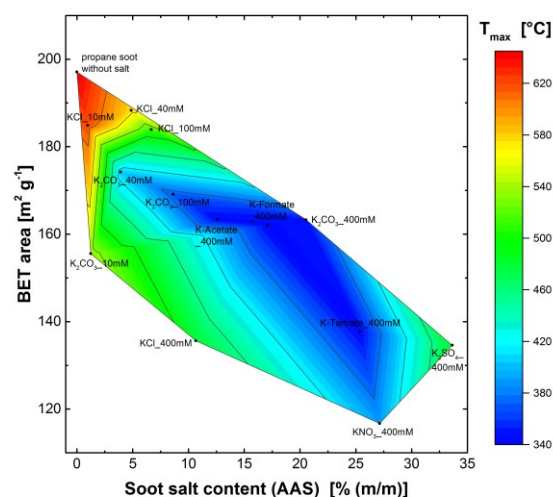


Figure 1. Contour plot of T<sub>max</sub> vs. BET areas and soot salt contents.

This work was supported by the Institute of Hydrochemistry, Technical University of Munich, Germany, and the Ultramicroscopy Research Center at Kyushu University, Fukuoka, Japan.

Benbrahim-Tallaa, L. *et al.* (2012) *Lancet Oncol.* **13**, 663-664.

Bond, T. C. *et al.* (2013) *J. Geophys. Res-Atmos.* **118**, 5380-5552.

Ramanathan, V. and Carmichael, G. (2008) *Nat. Geosci.* **1**, 221-227.

## Studying the optical and physiochemical properties of soot of various maturity from a mini-CAST using different measurement techniques

S. Török<sup>1</sup>, V. Malmberg<sup>2</sup>, J. Simonsson<sup>1</sup>, K. Kling<sup>3</sup>, A. Eriksson<sup>2</sup>, M. Mannazhi<sup>1</sup>, J. Martinsson<sup>4</sup>, A. Karlsson<sup>5</sup>, J. Pagels<sup>2</sup>, P-E. Bengtsson<sup>1</sup>

<sup>1</sup>Department of Combustion Physics, Lund University, Box 118, SE-22100, Lund, Sweden

<sup>2</sup>Division of Ergonomics and Aerosol Technology, Lund University, Box 118, SE-22100, Lund, Sweden

<sup>3</sup>National Research Centre for the Working Environment, 2100 Copenhagen, Denmark

<sup>4</sup>Department of Nuclear Physics, Lund University, Box 118, SE-22100, Lund, Sweden

<sup>5</sup>Department of Electrical and Information Technology, Lund University, Box 118, SE-22100, Lund, Sweden

Keywords: soot, optical properties, maturity

Presenting author email: sandra.torok@forbrf.lth.se

### Introduction

Soot is an un-wanted byproduct formed during incomplete combustion. Depending on the type of combustion, the soot can have various properties related to how mature they have become during formation, Wang (2011). Further, soot is believed to be the second largest contributor to climate forcing, IPCC (2013), but as there are still large uncertainties, extensive research on the matter is needed.

### Methods

We studied the optical and physiochemical properties of various types of soot from a mini-CAST soot generator (model 5201C; Jing Ltd, Zollikofen, Switzerland) using a set of diagnostic instruments. The optical properties were studied with multi-wavelength laser diode extinction, an aethalometer, laser induced incandescence and with a nephelometer. A scanning mobility particle sizer, a soot particle aerosol mass spectrometer, high resolution transmission electron microscopy and an aerosol particle mass analyzer was used to obtain physiochemical information about the various soot types produced. Additionally, a thermodenuder and an oven was used to heat the particles for the possibility of studying the refractory soot core separate from the organic coatings.

### Results

Our results show that the mini-CAST can generate soot particles originating both from the early and the later soot formation process, generating soot particles of different maturity. Large mature graphitized aggregates with a low absorption Ångström exponent (AAE) around 1.2 in the VIS-NIR spectral region, see figure 1, following the theoretical relationship for small particles in the Rayleigh regime, Bohren and Hoffman (2008). While the smallest clusters of nascent primary particles were generated with a large fraction of organic aerosol (~30%) and a large AAE around 3.5. The various types of soot studied were either studied as they were generated or after heating to 250 °C or sequentially to 250 °C and 500 °C and thereby allowing us to study the remaining soot when the volatile organic compounds were evaporated. It was found that the most mature particles were not affected by heating in any way, while for the nascent soot a large fraction of organic

compounds were evaporated, still the AAE did not decrease to that of the mature soot, indicating that the soot core of the nascent soot itself was responsible for most of the absorption at wavelengths below 650 nm (as no PAHs remained on the soot after heating to 500 °C).

We conclude that soot particles do not always have an AAE = 1 which is indicated by theory as it is strongly dependent on level of soot maturity.

Further on the mass absorption cross sections (MAC) for soot of different maturity will be evaluated. Extinction measurements will be combined with scattering measurements and numerical evaluations based on nephelometer measurements and HR-TEM results.

This work was supported by the Swedish research council Formas and VR.

Bohren, C. F., & Huffman, D. R. (2008). *Absorption and scattering of light by small particles*. John Wiley & Sons.

IPCC (2013). *Summary for Policymakers*. Cambridge, United Kingdom and New York, NY, USA: Cambridge University Press: 1–30.

Wang, H. (2011). Proceedings of the Combustion Institute 33, 41-67.

## Role of oxidative exhaust after-treatment in the partition of sulphuric species

J. Alanen<sup>1</sup>, P. Karjalainen<sup>1,2</sup>, K. Teinilä<sup>2</sup>, S. Saarikoski<sup>2</sup>, H. Timonen<sup>2</sup>, J. Keskinen and T. Rönkkö<sup>1</sup>

<sup>1</sup>Aerosol Physics, Faculty of Natural Science, Tampere University of Technology, Tampere, 33720, Finland

<sup>2</sup>Atmospheric Composition Research, Finnish Meteorological Institute, 00101, Helsinki, Finland

Keywords: sulphur partition, oxidative exhaust after-treatment, particulate emission, secondary aerosol formation.

Presenting author email: jenni.e.alanen@tut.fi

Sulphuric compounds originated from fuel and lubricant oil are a significant part of vehicle emissions. They may exist in gaseous phase but also in nucleation particles and on surfaces of larger soot particles. It is highly possible that vehicle technologies have an effect on which phase they exist in high temperature exhaust, freshly emitted exhaust and in aged atmospheric aerosol.

Partition of sulphuric species was studied with a laboratory setup build to replicate the gaseous and particulate matter concentrations from vehicles. Measurements were conducted in the hot exhaust, after dilution and cooling process (delayed primary) and after simulated aging in the atmosphere.

The targeted exhaust composition was a simplified diesel exhaust or e.g. natural gas engine exhaust with very little soot formation. The exhaust flow was generated as a mixture of SO<sub>2</sub> (6 ppm), air (50%) and N<sub>2</sub> (50%) that was led through a heated oxidation catalyst (oxicat). The second reference exhaust composition was generated by adding also soot particles in the flow. The soot particles were generated with a flat flame burner (acetylene as fuel) and mixed in with the exhaust flow in an ejector system (Dekati Ltd.).

The sampling and dilution was done with a porous tube diluter (PTD) with dilution ratio of ca. 12, followed by an ejector diluter with dilution ratio of ca. 10. A potential aerosol mass (PAM) oxidation flow reactor at a constant UV-light voltage was used to imitate the atmospheric aging of the aerosol sample. An ELPI+ (Dekati Ltd.), Nano- and Long-SMPS (TSI Inc.), an Aethalometer (Andersen Instruments Inc.) and a Soot-Particle Aerosol Mass Spectrometer (SP-AMS, Aerodyne Research Inc.) were used to characterize the formed particulate matter.

In this experiment, the oxicat was heated to 3–5 different temperatures between 235–344 °C enabling different SO<sub>2</sub> oxidation rates. The delayed primary and secondary aerosol formation in these varying oxicat temperatures is presented in Fig. 1.

According to preliminary results, the delayed primary particulate formation depended strongly on the oxicat temperature (see also Rönkkö et al., 2013). With the lowest oxicat temperatures, no sulphur-driven nucleation particles were formed. With the increasing oxicat temperature, the delayed primary particulate mass concentration was at maximum  $1.8 \times 10^5 \mu\text{g m}^{-3}$  (calculated to the volume of raw exhaust). With the soot addition, the dependence of delayed primary particulate mass concentration on the oxicat temperature was also

strong. Furthermore, the soot addition offered the sulphuric species a condensation sink and decreased the lowest oxicat temperature where sulphuric particle formation could happen.

Nevertheless, the secondary particulate matter formation did not depend strongly on the oxicat temperature (Fig. 1). In all the measured oxicat temperatures, with both exhaust compositions, the formed secondary particulate mass was  $0.8\text{--}1.2 \times 10^5 \mu\text{g m}^{-3}$ .

In conclusion, the sulphuric species are in gaseous form in the exhaust. The phase of the sulphuric species in freshly emitted exhaust depends on their oxidative state, i.e. for instance on the performance of the oxidation catalyst. According to our PAM study, the sulphuric species finally end up in particulate phase in the atmosphere almost independent on the oxidative catalyst exhaust after-treatment.

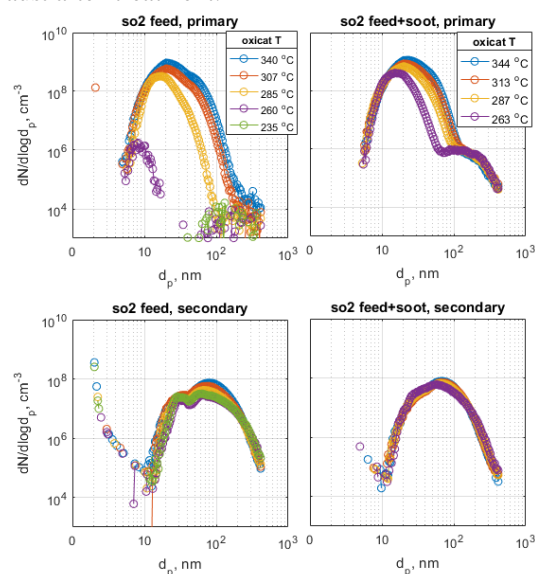


Figure 1. The number distributions of delayed primary and secondary particles measured with the SMPS. The concentrations have been corrected with the dilution ratios.

This work was supported by the project NewGas, funded by Tekes, Neste Oyj, Airmodus Oy, Dekati Oy, Wärtsilä Finland Oy, Dinex Ecocat Oy and Oilon Technology Oy. Jenni Alanen acknowledges Gasum kaasurahasto for financial support.

Rönkkö, T., Lähde, T., Heikkilä, J., Pirjola, L., Bauschke, U., Arnold, F., Schlager, H., Rothe, D., Yli-Ojanperä, J., Keskinen, J. (2013) *Env. Sci. Tech.* **47**, 11882-11889.

## On-Field Measurement of PM<sub>2.5</sub> and Carbonaceous Aerosol Emissions from Biomass Fuel Combustion in Traditional Indian Cookstoves

Gazala Habib\*, Annada Padhi, and Imam Husain

Department of Civil Engineering, Indian Institute of Technology, New Delhi, 110016, India

Keywords: Biomass, Traditional cookstove, EC/OC

Presenting author email: [gazala.civil@iitd.ac.in](mailto:gazala.civil@iitd.ac.in)

Biomass fuel combustion is a widespread source for cooking mostly in the rural households of South Asian countries. Further, laboratory based aerosol emission measurement from combustion of solid biomass fuel (i.e. wood, agricultural residue, and dried cattle manure) in cooking stoves have established this source as one of the major sources of fine particulate matter (PM<sub>2.5</sub>) and carbonaceous aerosol emissions in South Asia. Additionally, recent studies have also indicated that the climate forcing emissions from residential cook stoves are not well characterized due to limited knowledge on aerosol emission factor (gram of pollutant emitted/kg of fuel burned) and regional activity (fuel use). Present study aimed to monitor the PM<sub>2.5</sub> and characterized for carbonaceous constituents [elemental carbon (EC) and organic carbon (OC)] from the on-field evaluation of cook stove emissions during daily meal preparation in villages of North India. The emissions due to the burning of mixed biomass fuels consisting of fuelwood, dungcake, and crop waste together in the traditional mud stoves are captured for the first time in the field. A cyclone was operated at 10 lpm for cut size 2.5 μm and PM<sub>2.5</sub> was collected on Teflon, front quartz, and backup quartz filters for artifact correction. The particle collected during meal preparation which consists of boiling, steaming and frying. The emission factors were calculated using the carbon balance approach and compared with literature (Table 1).

**Table 1.** Emission factors of PM<sub>2.5</sub> for various cooking cycle using a mixture of fuel in traditional mud-cookstove

Cooking type (no. of exp.)	Fuel mix (FW: DC: CW)	PM <sub>2.5</sub> emission factors (gkg <sup>-1</sup> )		Fuel type
		Present study Field	Literature Lab <sup>#</sup> /Field*	
BS <sup>§</sup> (3)	0.5:0.9:0.1	4.8±0.9	1.9 <sup>a</sup> , 3.8 <sup>b</sup> , 3.7±2.2 <sup>c</sup> , 8.5±1.6 <sup>*d</sup>	FW
FS <sup>§</sup> (3)	0.6:1.1:0.1	9.8 ± 1.4	5.4±2.9 <sup>e</sup> , 7.5±3.3 <sup>f</sup> , 9.3±4.1 <sup>f</sup> , 9.1±5.7 <sup>g</sup>	CW
BB <sup>§</sup> (3)	0.5:0.8:0.2	7.8 ± 1.0	5.4±2.4 <sup>f</sup>	DC

<sup>§</sup>BS=Baking+steaming; <sup>§</sup>FS=Frying+steaming; <sup>§</sup>BB=Boiling;

<sup>#</sup>Standard WBT; **References:** <sup>a</sup>Ahuja et al (1987); <sup>b</sup>Zhang et al. (2000); <sup>c</sup>Johnson et al. (2007); <sup>d</sup>Roden et al. (2006);

<sup>e</sup>Shen et al. (2014); <sup>f</sup>Habib et al. (2008); <sup>g</sup>Wei et al. (2013)

The comparison of the PM<sub>2.5</sub> emission factor (EF<sub>mix</sub>, g/kg) calculated for the different cooking cycles have been shown in the fig. 1. It is observed that the cooking cycle with frying and steaming (FS) has the higher emission factor than those from boiling and baking, and only boiling (BB, BS). The mixture of fuel used for all the cooking cycle is same which consists mainly of regional fuel wood, dungcakes and crop wastes.

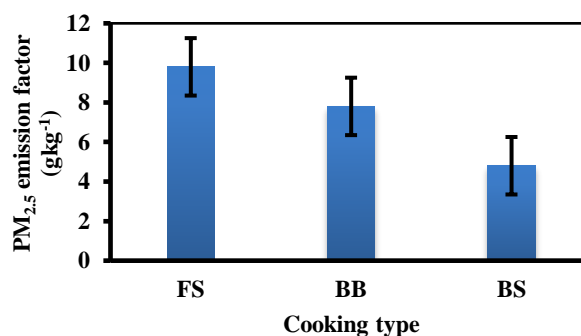


**Figure 1.** PM<sub>2.5</sub> emission factors as per cooking type. Error bars are standard deviation around mean from 3 set of experiments

This study will discuss the emissions of aerosol and its carbonaceous constituents from combustion of prevailing biomass fuel in traditional mud stove in North India. The study will discuss the implications of emission in regional climate change.

**Acknowledgment:** We thanks Prof. Ramya S. Raman for OC/EC analysis. This work was supported by MOEF, IIT Delhi and UGC grant for JRF.

### References

- Ahuja, D. R., Joshi, V., Smith, K. R., Venkataraman, C. (1987), *12*, 247–270.
- Habib, G., Venkataraman, C., Bond, T. C., Schauer, J. J. (2008). *Environmental Science and Technology*, 42(23),8829–8834.
- Johnson, M., Edwards, R., Alatorre F. C., Masera, O. (2008). *Atmospheric Environment*, 42(6), 1206–1222.
- Zhang, J., Smith, K., Ma, Y., Ye, S., Jiang, F., Qi, W., Thorneloe, S. (2000). *Atmospheric Environment*, 34(26), 4537–4549.
- Roden, C. a, Bond, T. C., Conway, S., and Pinel, A. B. O. (2006). *Environmental science & technology*, 40(21), 6750–7.
- Shen, G., Xue, M., Chen, Y., Yang, C., Li, W., Shen, H., Huang, Y., Zhang, Y., Chen, H., Zhu, Y., Wu, H., Ding, A., and Tao, S. (2014). *Atmospheric Environment*, Elsevier Ltd, 89, 337–345.
- Wei, S., Shen, G., Zhang, Y., Xue, M., Xie, H., Lin, P., Chen, Y., Wang, X., and Tao, S. (2014). *Environmental Pollution*, Elsevier Ltd, 184, 18–24.

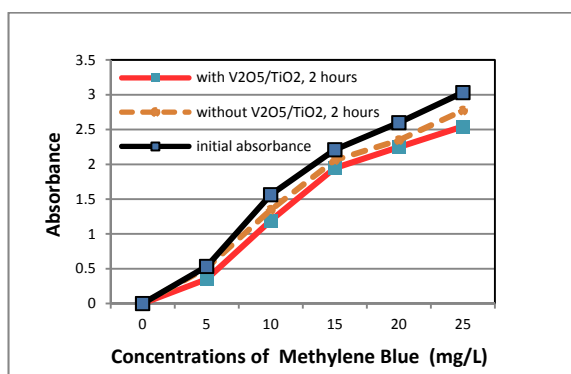
**V<sub>2</sub>O<sub>5</sub>/TiO<sub>2</sub> catalysts for VOC removal analysis**Jia-Twu Lee<sup>1,\*</sup> and Hua-Chun Chen<sup>1</sup><sup>1</sup>Department of Environmental Science and Engineering, National Pingtung University of Science and Technology, Pingtung County, 91201, TaiwanKeywords: VOC, photocatalyst, degradation, V<sub>2</sub>O<sub>5</sub>, TiO<sub>2</sub>.

Presenting author email: leejia@mail.npust.edu.tw

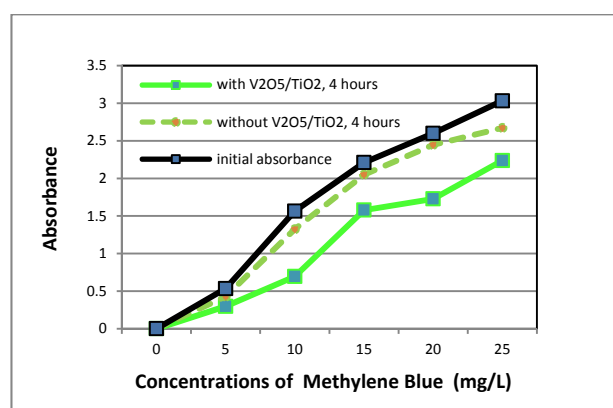
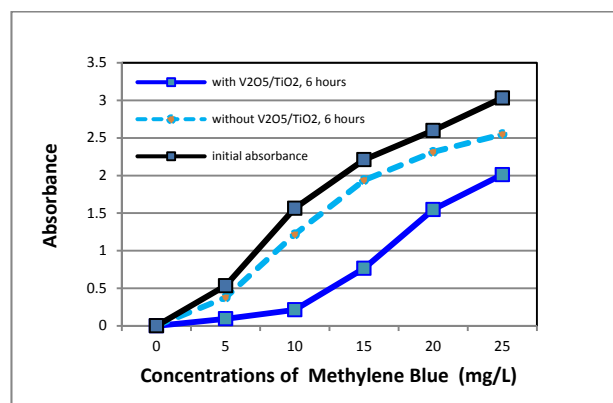
Many studies have found that VOC pollution can cause harm to human health (Paschalidou *et al.*, 2015), industry is well known as a source of VOC emissions. Temperature control and tail gas treatment (e.g. activated carbon adsorption, scrubbing tower) can reduce VOC emissions. However, VOCs captured from exhaust require costly additional processing facilities with rising costs and a risk of secondary pollution. Photocatalysts are widely adopted in processing VOCs. The V<sub>2</sub>O<sub>5</sub>/TiO<sub>2</sub> catalyst has good resistance to fly ash clogging and toxic components in flue gas.

This study adopted experimental method described in Shen *et al.* (2016) and Zhao *et al.* (2014). The catalysts were prepared using a sol-gel method. Solutions "A" and "B" was prepared, and solution A was added drop-wise to solution B under vigorous stirring. The glass fiber was impregnated in the solution under 40°C for 5 hour. Subsequently, the fiber was dried at 70°C for 8 hour and calcined at 400°C for 5 hour to obtain the glass fiber support V<sub>2</sub>O<sub>5</sub>/TiO<sub>2</sub> catalysts. The effects of different concentrations of methylene blue on the photocatalytic degradation were measured by UV-Vis spectrophotometer. The experiments were performed using a control group (without catalyst) and an experimental group (with catalyst).

Results of preliminary experiments indicate that methylene blue removal rates after 2, 4 and 6 hours of illumination with visible light were 20%, 38% and 62%, respectively (Figs. 1–3). The reductions of methylene blue for V<sub>2</sub>O<sub>5</sub>/TiO<sub>2</sub> catalysts increased as the degradation time increased in spite of the initial methylene blue concentrations.

Figure 1. Methylene blue degradation with V<sub>2</sub>O<sub>5</sub>/TiO<sub>2</sub> for 2 hour.

Compared to the initial absorbance of various methylene blue concentrations, the levels of methylene blue of control group were slightly decreased regardless of degradation times. Moreover, the levels of methylene blue decreased significantly in the experimental group (with V<sub>2</sub>O<sub>5</sub>/TiO<sub>2</sub> catalyst) for all tested conditions, showing that the V<sub>2</sub>O<sub>5</sub>/TiO<sub>2</sub> catalyst was effective in degrading the methylene blue.

Figure 2. Methylene blue degradation with V<sub>2</sub>O<sub>5</sub>/TiO<sub>2</sub> for 4 hour.Figure 3. Methylene blue degradation with V<sub>2</sub>O<sub>5</sub>/TiO<sub>2</sub> for 6 hour.

- Paschalidou, A.K., Kassomenos, P. and Karanikola, P. (2015) *Sci. Total Environ.* **527-528**, 119–125.  
 Shen, B., Wang, F., Zhao, B., Li, Y. and Wang, Y. (2016) *J. Ind. Eng. Chem.* **33**, 262–269.  
 Zhao, B., Liu, X., Zhou, Z., Shao, H., Wang, C., Si, J. and Xu, M. (2014) *Chem. Eng. J.* **253**, 508–517.

## Comparison of emission factors of air pollutants from CNG and gasoline vehicles

Yang Wang<sup>1</sup>, Xiaoyan Huang<sup>2</sup>, Zhenyu Xing<sup>2</sup> and Ke Du<sup>2</sup>

<sup>1</sup>College of Resources and Environmental Science, Hebei Normal University, Shijiazhuang, 050024, China

<sup>2</sup>Department of Mechanical and Manufacturing Engineering, University of Calgary, Calgary, T2N 1N4, Canada

Keywords: emission factors, black carbon, gasoline, CNG.

Presenting author email: wangy@pkusz.edu.cn

The rapid growth of road traffic in China leading to a plethora of vehicles increases the pressure for environmental protection. China's government has issued a series of strict vehicle emission standards and all these standards have motivated researchers to develop clean fuels. The use of compressed natural gas (CNG) as vehicle fuel is increasing due to its lower emissions and better fuel economy. To quantify "how clean" burning CNG is compared to burning gasoline, accurately measure the vehicles emissions when burning different fuels and under various operating conditions is needed.

In this study, a fleet of bi-fuel vehicles was selected to measure the emissions of black carbon (BC), carbon monoxide (CO), hydrocarbon (HC) and nitrogen oxide (NO<sub>x</sub>) for driving in CNG mode and gasoline mode respectively under the same driving conditions. We quantify emission factors (EFs) using in-situ method, which would reduce the uncertainty if the exhaust concentration is not significantly higher than ambient values (Wang et al., 2016).

Figure 1 shows the average mileage-based BC EFs of all the test vehicles fuelled by CNG and gasoline respectively under different speeds. The reduction of BC EFs by burning CNG comparing to burning gasoline under different speeds ranges from 54% to 83%. The average BC EF fuelled by CNG under the speed of 70 km/h is 0.0253±0.0265 mg/km, while the average BC EF fuelled by gasoline is 0.1474±0.1315 mg/km, resulting in the maximum reduction of BC EF.

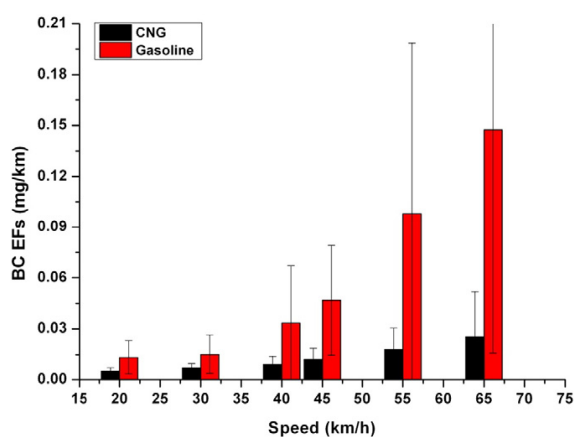


Figure 1. BC EFs under different speeds for the test vehicles fuelled by CNG or gasoline.

As shown in Table 1, vehicles emit more HC when burning gasoline than CNG by a factor of 2.39-12.59. CNG vehicles emit more NO<sub>x</sub> than gasoline vehicles, the range of factor is 1-1.2, which is very small.

Vehicles of brand 1 emit 40-80% lower CO when burning CNG compared to gasoline for all the constant speed conditions. However, the results from vehicles of brand 2 are opposite. At all the operating conditions except 40 km/h, the average CO emission of burning CNG is 1.1-2.0 times higher than gasoline. This relatively lower CO emission from vehicles of brand 2 burning gasoline is possibly due to the 50% lower accumulated mileage than vehicles of brand 1. Ntziachristos et al. has proven that vehicle age, as reflected by vehicle mileage, is responsible for increases in the average level of emissions of all non-CO<sub>2</sub> major pollutants like CO, HC and NO<sub>x</sub>.

Table 1. EFs of CO, HC and NO<sub>x</sub> under different speeds for the test vehicles fuelled by CNG or gasoline.

	Speed km/h	CO mg/km	HC mg/km	NO <sub>x</sub> mg/km
Vehicle1 gasoline	19	2693.1	149.1	9.4
	38	5249.8	140.5	9.2
	63	5302.6	66.2	9.6
Vehicle1 CNG	19	789.8	27.6	11.8
	38	1020.4	23.2	11.7
	63	2990.7	24.1	11.9
Vehicle2 gasoline	19	2149.3	164.7	10.1
	38	2435.7	190.0	9.7
	63	2845.5	272.3	8.8
Vehicle2 CNG	19	2396.2	26.3	11.4
	38	2268.8	20.4	12.2
	63	5820.4	38.8	11.0

It can be concluded that CNG vehicles produce less BC emissions than gasoline vehicles. This may account for the lower carbon emissions of CNG vehicles when compared with gasoline vehicles. CNG is a more environmentally friendly fuel for motor vehicles in terms of CO and HC emissions. Accurate determination of EFs will be helpful in understanding and controlling air pollutants from motor vehicles as transportation.

This work was supported by the Natural Science Foundation of Guangdong Province (2014A030310290), Knowledge Innovation Program of the Chinese Academy of Sciences (KZCX2-EW-408).

Yang, W., Zhenyu, X., Shuhui, Z., Mei, Z., Chao, M., Ke, D. (2016) *Sci. Total Environ.* **547**, 422-428.

Ntziachristos, L., Samaras, Z. (2000) *Atmos. Environ.* **34**, 4611-4619.

## Atmospheric Hg<sub>g</sub> and Hg<sub>p</sub> concentrations in the surroundings of a clinker plant

A. Carratalá<sup>1</sup>, F.A. Santos<sup>1</sup>, E. Yubero<sup>2</sup> and M. Santacatalina<sup>3</sup>

<sup>1</sup>Department of Chemical Engineering, University of Alicante, P.O. Box 99, 03080 Alicante, Spain

<sup>2</sup>Laboratory of Atmospheric Pollution (LCA), Miguel Hernández University, Av. de la Universidad s/n, Edif. Alcudia, 03202 Elche, Spain

<sup>3</sup>University Institute of Engineering of Chemical Processes., University of Alicante, P.O. Box 99, 03080 Alicante, Spain

Keywords: mercury, clinker, active carbon, PM10.

Presenting author email: a.carratala@ua.es

In this study, the direct mercury analyser DMA 80 Milestone has been used to elucidate the range of atmospheric mercury levels (gas and particulate) around a clinker plant using residues derived combustibles. The industrialization has led an increase of the emissions of mercury in its different forms into the atmosphere, whose speciation depends on the burned fuel (charcoal solid waste, sewage sludge...), the treatment of cleaning of gases and the temperature of the industrial processes Liu *et al* (2007).

In 2014, in the Valencian Community, the mineral industries generate 0.083 t/year of mercury and compounds (PRTR) while in 2011 were 0.016 t/year. Total Hg emissions from the cement and clinker facility located in the surroundings of the University of Alicante, ranked from 11.2 kg in 2011 to 22.28 kg in 2014. Due to that, people are aware of the importance of the detection and control of the emission mercury levels into the atmosphere.

In the University of Alicante there is an air quality surveillance program with special target on PM10 that are measured and chemically characterized since 2005. Several heavy metals including regulatory ones are measured by microwave acid digestion and the subsequent analysis by ICP-MS. However, Hg appears frequently under detection limits and when detected is in the range of ng/m<sup>3</sup>. Therefore, an effort to improve the knowledge about atmospheric levels has been done with the available techniques.

### Abstract review

Several forms mercury could be into the atmosphere: in gas fraction, Hg<sub>g</sub> (Hg<sup>0</sup> and reactive Hg) and particulate fraction, Hg<sub>p</sub>.

To estimate the gas fraction filtered air was fluxed active carbon cartridges and Hg<sub>g</sub> was adsorbed. Carbon cartridges were desorbed by DMA 80 and determined by FAAS. Several flux rates and sampling periods were essayed to determine the better conditions to obtain confident estimations.

In the case of Hg<sub>p</sub>, a portion of PM10 filters from the High Volume Sampler (HVS Digital DL80) have been introduced directly in the DMA 80. It was thermally desorbed, concentrated in the amalgam and analysed (FAAS). In the case of Hg<sub>g</sub>, the reanalysis of samples, with levels above the detection limit (acid digestion + ICP-MS) conducted in 2014, shows a good correlation

between both techniques. However, the levels of ICP-MS are much higher than the ones measured by DMA.

In the year 2015, all samples have Hg<sub>p</sub> below ICP-MS detection limit. The reanalysis of the samples shows that values were between 1.85 and 19.65 pg/m<sup>3</sup> and a better sensibility of this technique compared with ICP-MS after acid digestion. The rank of values of Hg<sub>g</sub> and Hg<sub>p</sub> are shown in Table 1. The Hg<sub>g</sub> rank, from 0.79 to 12.87 ng/m<sup>3</sup>, is much higher than particulate one. This is in agreement with literature and remarks the relevance of measuring Hg<sub>g</sub> better than Hg<sub>p</sub>.

Table 1. Rank of Hg<sub>g</sub> and Hg<sub>p</sub> values.

Data	Hg <sub>g</sub> (ng/m <sup>3</sup> )	Hg <sub>p</sub> (pg/m <sup>3</sup> )
Nº of samples	11	19
Max	12.87	19.65
Min	0.79	1.85
Average	7.03	8.32

Figure 1 shows month average values, Hg<sub>p</sub> (pg/m<sup>3</sup>), rainfall (l/m<sup>2</sup>) and temperature (°C) in 2015. The concentrations of particulate mercury are lower in winter months, in a period of lower temperatures and scarce rainfall. It could be related to higher emissions and stagnant atmospheric conditions.

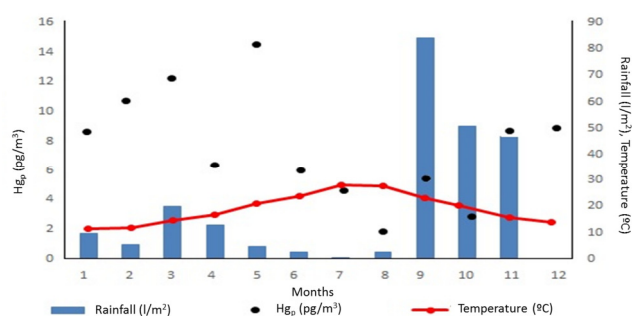


Figure 1. Month average values in 2015.

This work was supported by The University of Alicante.

Liu B., Keeler G.J., Dvonch J.T., Barres J.A., Lynam M.M., Marsik F.J., Morgan J.T. (2007). *Temporal variability of mercury speciation in urban air*. Atmospheric Environment 41, 1911–1923.

PRTR, Registro Estatal de Emisiones y Fuentes Contaminantes de España.

## Emissions from wood and catalytic tar removal combustion in household stoves

H-L. Kupri<sup>1,2</sup>, M. Maasikmets<sup>1,3</sup>, R. Rebane<sup>1,4</sup>, K. Vainumäe<sup>1</sup>, R. Titova<sup>1</sup>, E. Teinemaa<sup>1</sup> and V. Voronova<sup>2</sup>

<sup>1</sup>Estonian Environmental Research Centre, Tallinn, 10617, Estonia

<sup>2</sup>Department of Environmental Engineering, Tallinn University of Technology, Tallinn, 19086, Estonia

<sup>3</sup>Institute of Agricultural and Environmental Sciences, Estonian University of Life Science, Tartu, 51014, Estonia

<sup>4</sup>Chair of Analytical Chemistry, University of Tartu, Tartu, 50411, Estonia

Keywords: wood combustion, catalytic tar removal emissions

Presenting author email: hanna-lii.kupri@klab.ee

Estonia's health impact assessment study showed that due to fine particulate matter in an ambient air, the life expectancy has shortened up to 13 months, with the highest decrease in city centres or areas with extensive domestic heating (Orru *et al*, 2011). Estonians have been stable users of stoves for heating purposes (in 2015, 36% of Estonians were using stoves for heating purposes) (SE, 2015) and therefore the emissions from residential wood combustion (RWC) is a topic of concern.

It is well known that polychlorinated dibenzo-p-dioxins (PCDDs), polychlorinated dibenzo-furans (PCDFs) and hexachlorobenzene (HCB) can be formed as an undesirable side product in case of favourable combustion conditions (Hedman *et al*, 2006, Wielgosiński, 2010). PCDD/F formation can be connected with the synthesis from various types of organic precursors and incomplete combustion where precursors may react both in gaseous phase and on the surface of metals being present in the composition of volatile ash from the combustion (Karasek *et al*, 1987). RWC in stoves and fireplaces is estimated to account for 53% of PCDD/F and 70% of HCB emissions in Estonia in 2010 (Kohv *et al*, 2012).

According to the Fire Safety Act, Estonians need to request certified chimney sweeper services at least once during a period of five years. However, it has emerged that during the five year period some people have started to use uncertified means in a form of burning tar removal catalytic powder and -bricks in order to maintain the oven and chimney. These means do not have a composition list on the package to inform the users, but they probably consist mainly different kind of metal salts and copper, which is known to favour PCDD/F formation. The environmental impact of such catalytic tar removing means has not been analysed thoroughly and usage is not regulated at the EU level.

In this research we have measured emissions from the modern masonry heater that occur during catalytic tar removing powder and -brick combustion. 3 types of experiments were conducted in the Estonian Environmental Research Centre's stove laboratory. First experiments included combusting pure conifer and hardwood logwood. Conifer, hardwood logwood and tar removing powder experiments were conducted in two ways: 1. burning conifer, hardwood logwood and including weighted tar removing powder in three stages throughout the incineration process; 2. burning conifer, hardwood logwood and sprinkling the tar removing

powder over the wood before the ignition. During the conifer, hardwood logwood and tar removing brick experiments, the brick was placed inside the oven before the ignition.

All samples were taken from the hot flue gas. For the particle size distribution and number concentration measurements ELPI+ (10 l/min, (Dekati Ltd) was used. Gas samples (O<sub>2</sub>, SO<sub>2</sub>, NO, NO<sub>2</sub>, CO, CO<sub>2</sub>, HCl, HF, VOCs), temperature (°C), RH (%) and gas flow (m/s) were measured simultaneously during the whole burning process. Samples for the gas analyses were taken through an insulated, externally heated (180 °C) sample line and through the filter units to the FT-IR gas analyser (DX-4000, Gasmeter Oy). PCDD/F and HCB samples were collected from the hot flue gas, with an Eva dioxin sampler (Metlab) into filter, XAD-2 adsorbent and pre-afterwash. Samples were analysed with the GC/HRMS.

In this research we have found that the combustion of catalytic tar removing means have a significant effect on RWC air emission increasing the levels of PCDD/F and HCB. Using such tar removal means are a point of concern, because there is limited research on the environmental impact. It is currently not known if such means are legal or generally available in all EU member states.

This work was supported by Estonian Environmental Investment fund.

Hedman, B., Näslund, M., Marklund, S. (2006) *Science & Technology* **40**, 4968-4975.

Karasek, F. W., Dickson, L. C., (1987) *Science*, vol. 237, 754-756

Kohv, N., Heintalu, H., Mandel, E., Link, A. (2012) *Estonian Informative Inventory Report 1990-2010*.

Orru, H., Maasikmets, M., Lai, T., Tamm, T., Kaasik, M., Kimmel, V., Orru, K., Merisalu, E., Forsberg, B. (2011) *Air Qual, Atmos Health* **4**, 247-258.

SE database LER26 (2015) [www] <http://pub.stat.ee/px-web.2001/dialog/statfile1.asp>

Wielgosiński, G., (2010) *Int J Chem Eng Appl*. 2010, Article ID 392175

## DownToTen: Key Particle Properties, Emission and Measurement Conditions, Instruments and Sampling Setup

M. Bainschab<sup>1</sup>, A. Bergmann<sup>1</sup>, P. Karjalainen<sup>2</sup>, J. Keskinen<sup>2</sup>, J. Anderson<sup>3</sup>, A. Mamakos<sup>4</sup>, B. Giechaskiel<sup>5</sup>,  
C. Haisch<sup>6</sup>, A. Gerini<sup>7</sup>, L. Ntziachristos<sup>8</sup>, and Z. Samaras<sup>8</sup>

<sup>1</sup>Institute of Electronic Sensor Systems, Graz University of Technology, Graz, 8010, Austria

<sup>2</sup>Aerosol Physics, Department of Natural Sciences, Tampere University of Technology, Tampere, 33720, Finland

<sup>3</sup>Ricardo UK, Limited, Shoreham-by-Sea, BN43 5FG, United Kingdom

<sup>4</sup>AVL List GmbH, Graz, 8020, Austria

<sup>5</sup>Sustainable Transport Unit, Institute for Energy, Transport and Climate, Joint Research Centre, European Commission, Ispra, 21027 Italy

<sup>6</sup>Chair of Analytical Chemistry, Institute of Hydrochemistry, Technische Universität München, Munich, 81377, Germany

<sup>7</sup>Centro Ricerche Fiat SCPA, Orbassano, 10043, Italy

<sup>8</sup>Laboratory of Applied Thermodynamics, Aristotle University of Thessaloniki, Thessaloniki, 541 24, Greece

Keywords: emission, particle number, sub-23 nm,

Presenting author email: m.bainschab@tugraz.at

We present the objectives, the impacts and first results of the Horizon 2020 Green Vehicle project “DownToTen”.

This project is developing a robust methodology that will enhance the regulatory approach towards particle number (PN) emissions in the sub-23 nm region. The focus is on the newest generations of direct injection gasoline and diesel engines under real world conditions.

Based on detailed investigations of the nature and characteristics of these particles, DownToTen is evaluating a variety of sub-23 nm PN measurement instruments and sampling approaches, using rigorous criteria under conditions of challenging aerosol from a variety of sources. The objective is a PN-Portable Emission Measurement System (PEMS) demonstrator with high efficiency in determining PN emissions of current and future engine technologies in the real world (Giechaskiel, 2017).

DownToTen also aims to assess the fraction of particles left out of control and assist the better understanding of exhaust particle impacts on air pollution. Furthermore, the particle and sampling dynamics that lead to a bias between PEMS and CVS measurements are modelled.

We present the first results on the iterative way to the PN-PEMS demonstrator. Important factors like robustness against artefacts (re-nucleation, growth of sub-cut particles), losses of (solid) particles, storage/release effects of gas phase compounds are assessed in detail by multiphysical simulations and experiments. Special attention is drawn to losses of secondary aerosol precursors within the primary dilution stage. A scheme of the preliminary sampling setup for testing in the synthetic aerosol laboratory is shown in Figure 1.

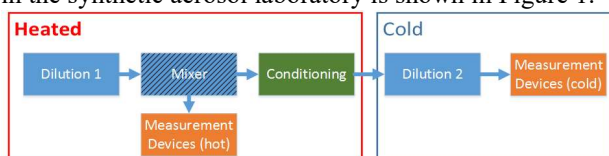


Figure 1: Schematic illustration of the preliminary sampling setup

This setup was designed to maximize the penetration of non-volatile particles below 23 nm while limiting the effects of gaseous artefacts. The selection of the setup's components (primary and secondary dilution stage, conditioning system, mixing elements, measurement devices) in order to meet the aforementioned criteria are based on experimental and theoretical data. The success in meeting these criteria is evaluated by comparing the sampling setup to a PMP reference system. Critical components are discussed in detail. CFD simulations and particle penetration optimizations based on the simulation results are presented.

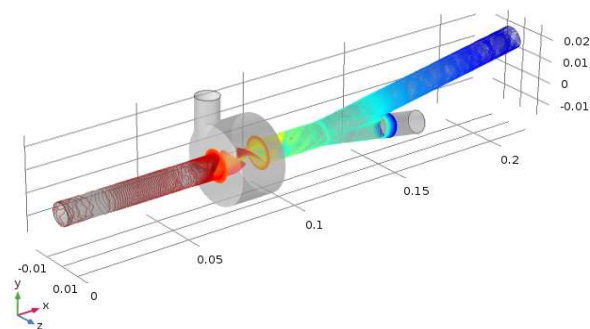


Figure 2: CFD simulation of a porous tube diluter including a static mixer and a flow splitter.

The suppression of artefacts is emphasized. This is achieved by a systematic multi-step modification process which results in the presented setup.

This work is conducted in the framework of the H2020 DownToTen project, funded by the Innovation and Networks Executive Agency of the European Commission, Grant Agreement No 724085

## Investigation of the organics nanodrop influence on the explosion hazard of the methane-air gas mixtures

S.V. Valiulin<sup>1</sup>, V.V. Zamaschikov<sup>1,2</sup>, A.A Onischuk<sup>1,2</sup>, A.M. Baklanov<sup>1</sup>

<sup>1</sup>Voevodsky Institute of Chemical Kinetics and Combustion SB RAS, Novosibirsk, 630090, Russia

<sup>2</sup>Novosibirsk State University, Novosibirsk, 630090, Russia

Key words: coal, nanodrop, explosion hazard.

Presenting author email: [valiulin@kinetics.nsc.ru](mailto:valiulin@kinetics.nsc.ru)

In recent decades, high-performance heading-and-winning machines of a new generation have been developed, whose operation produces nanosized organic coal dust. In this connection, it is very important to study the influence of nanosized aerosol particles on the combustion of dust-gas mixtures.

In the present work the detailed study of the effect of organic aerosol on the explosion hazard of methane-air mixture was carried out. For this, in the course of this study, a method for generating an organic aerosol from a coal tar with its physicochemical properties (size, morphology, chemical composition), similar to the aerosol, formed in a coal mine was developed.

To investigate the coal aerosol influence on the combustion of gaseous mixtures the 10 l the standard "constant volume combustion bomb" was used. As result the dependences of the maximum pressure and the rate of pressure buildup during the explosion as function mass concentration of organic aerosol in a methane-air mixture with methane content from 2 to 6.5 vol. % was measured. It is proved that the addition of an organic aerosol creates an explosive methane-air mixture. Has been determined the minimally necessary mass concentration of organic nanoaerosol to convert poor air - methane mixture to explosion hazard mixture.

The reported study was funded by RFBR according to the research project №16-33-00012 mol\_a.

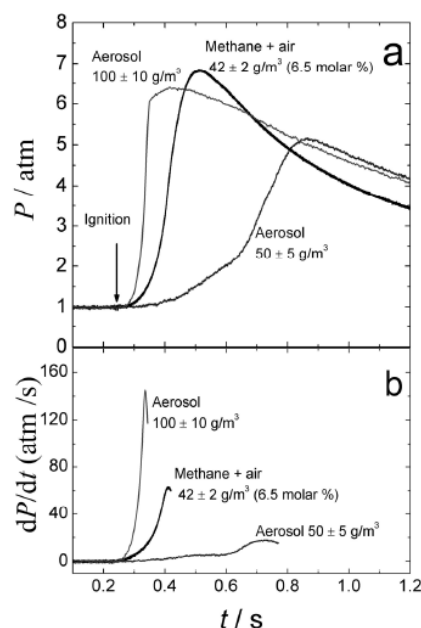


Figure 1. Pressure (a) and time derivative (b) vs. time dependences for the combustion of aerosol in air and air-methane mixtures. Mass concentrations are shown in the graph.

## A Study on the Reduction of Fine Particulate Contaminants in Textile Manufacturing Process

B.H. Park<sup>1</sup>, J.Y. Lee<sup>1</sup>, H.G. Kim<sup>1</sup> and J.S. Choi<sup>1,2</sup>

<sup>1</sup>Technology Institute, Anytech Co., Ltd, Suwon, 16690, Republic of Korea

<sup>2</sup>Department of Environmental Science & Engineering, Kyung Hee University, Suwon, 17104, Republic of Korea

Keywords: particulate matters, electro spray, pre-treatment, textile manufacturing.

Presenting author email: grapeman77@hanmail.net

Most of the facilities that produce air pollutants (odors) in the dyeing industry are largely tenter facilities and coating facilities. In particular, tenter facilities produce a large amount of oil mist, which is a high concentration odor inducing substance. The number of companies operating coating facilities is less than 10% of all dyeing companies, but more than 70% of dyeing companies have tenter facilities, and the biggest source of odor problems in the dyeing industrial complexes in each region is the tenter facility. The tenter process is a process of drying and ironing (heat-treating) a dyed fabric to improve the quality of the fiber, and a medicine such as a fabric softener, an antistatic agent or a water repellent agent is used. In addition, lubricants are used to prevent wear of tenter devices at high temperatures, and these chemicals are vaporized due to high temperatures during the tenter process. It is discharged in the form of gaseous odor substances such as vaporized fine oil mist and causes civil complaints. However, there is no clear solution at present.

In the conventional electrostatic dust collecting system, the load and the dust collecting unit are located in one system, and in some cases, they can act as obstacles to efficient dust collecting. (Significant reduction of dust collection efficiency in case of reverse corona phenomenon) In order to solve the above problem, another research has been conducted to construct an electrostatic precipitator with a two-stage system by installing another load on the front end of the electrostatic precipitator. However, the improvement of the dust collecting efficiency has not been achieved. Although a wet electrostatic precipitator is used to prevent the dust from being scattered again, this dust collector has a problem that a wastewater treatment facility is additionally required.

Therefore, a methodology capable of achieving a high dust collection efficiency while solving all of these problems is to install the electrostatic atomizing device on the upstream side of the electrostatic precipitator. It can be installed in a narrow space and it is expected that it will achieve a high dust collecting efficiency in an electrostatic dust precipitator because fine dust particles can be supplied and supplied with a small amount of water to effectively charge the fine dust.

In this study, we propose a dry electrostatic precipitator using electrostatic spray to reduce the aerosol generated in the tentative process, which is the main odor generation process in the textile industry.

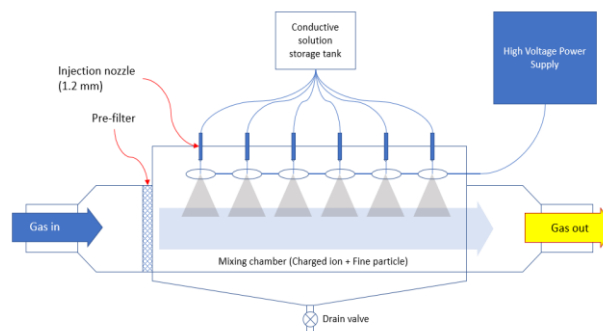


Figure 1. Schematic drawing of the experimental setup.

In this study, we applied electrostatic spraying technique using induction electrode to generate charged droplet at the front of electrostatic precipitator. Figure 1. is a conceptual diagram of the charged droplet generator using electrostatic spray. In this device, when a high voltage is applied to the induction electrode while the nozzle is grounded, the conductive liquid gradually injected by the gravity in the nozzle and passes through the induction electrode, and simultaneously the droplet is injected by the electric force. Finally, the charged droplets are mixed with the contaminated exhaust gas in the chamber to charge the mist-shaped aerosol, thereby improving the efficiency of the reduction in the electrostatic precipitator.

This work was financially supported by Ministry of Environment(MOE), Republic of Korea (Project no. RE201703026).

Lucia, M., Di Natale, F., Carotenuto, C. and Lancia, A. (2016) *Chemical Engineering Transactions*, 52, pp. 421–426.

## **Abstracts T201**

## Self-match sampling of *Geophysica* exhaust in ice saturated conditions: jet fuel combustion aerosol and the microphysics of emission induced, freshly formed ice particles

R. Weigel<sup>1</sup>, C. Mahnke<sup>1,2</sup>, M. Port<sup>2</sup>, M. Krämer<sup>3</sup>, C. Rolf<sup>3</sup>, A. Afchine<sup>3</sup>, J.-U. Grooss<sup>3</sup>, S. Borrmann<sup>1,2</sup>

<sup>1</sup>Institute for Physics of the Atmosphere, University of Mainz, D-55128 Mainz, Germany

<sup>2</sup>Particle Chemistry Department, Max Planck Institute for Chemistry, D-55128 Mainz, Germany

<sup>3</sup>IEK-7, Research Centre Jülich, D-52425 Jülich, Germany

Keywords: self-match, exhaust, fuel combustion aerosol, contrail, ice particle formation  
contact: weigelr@uni-mainz.de

During the 2016 StratoClim field mission with the Russian high altitude research aircraft *M-55 Geophysica*, conducted from Kalamata, Greece, a particular flight manoeuvre (flight on 01 Sept.) was dedicated for an intentional in-flight crossing of the *Geophysica*'s own exhaust plume (cf. Figure 1, main view). The emissions of *Geophysica*'s twin-jet engine in cruising mode (consumption: ~850 kg fuel per hour) were released under conditions very close to ice saturation at ~224 K ambient air temperature and at an altitude of about 10.4 km followed by a left-turning loop manoeuvre at fairly constant flight altitude of 10.2-10.3 km (cf. Figure 1, close-up view). After approximately 10 minutes the loop manoeuvre was accomplished. During the loop the *Geophysica* exhaust was encountered, very likely at the plume's edge.

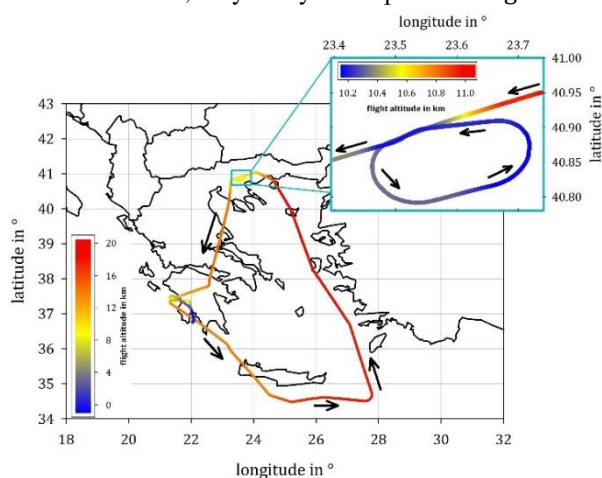


Figure 1: Main view of the flight pattern of the StratoClim flight on 01. Sept. and close-up view – note the individual altitude scales. Black arrows indicate flight course.

Parts of the *Geophysica*'s instrumental equipment allow for investigating:

- aerosol total number concentration with different lower detection size in the ultra-fine aerosol mode (diameter  $D_p$  of 6, 10 and 15 nm with the four-channel COndensation PArticle counting System, COPAS, one sample line is heated to 270°C upstream of the detector discriminating refractory aerosol of  $D_p > 10$  nm) up to a few micrometres in size,
- aerosol size distributions (in the size range of  $60 \text{ nm} < D_p < 1 \mu\text{m}$ ; with the Ultra High Sensitivity Aerosol Spectrometer, UHSAS) and

- (ice) cloud particle microphysical parameters (Cloud Combination Probe, CCP) such as number concentration, size distribution and particles' shape, overall covering the detection of particle sizes ranging from a few nanometres up to about one millimetre in diameter.

The accomplished self-match is indicated by a significant increase (at ~09:19 UTC) of aerosol number (detected by the UHSAS). Aerosol number concentrations of up to almost the double of corresponding background concentrations were observed over about 80 seconds in the second part of the loop manoeuvre (cf. Figure 2).

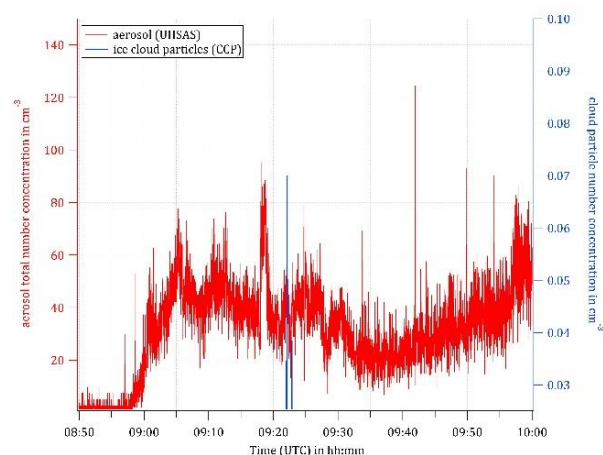


Figure 2: Section of the measurement times series during the exhaust encounter for aerosol (red, UHSAS) and the ice cloud particles (blue, CCP).

Time-delayed, by about 2 minutes, a thin layer of ice cloud particles ( $D_p \approx 30 \mu\text{m}$ ) was encountered (at ~09:21 UTC) in concentrations of up to  $7 \cdot 10^{-2} \text{ cm}^{-3}$  which sets apart from the background of zero. Very likely, the detected ice particles formed on the surfaces provided by the jet exhaust aerosols and subsequently were horizontally displaced by the winds. The presentation provides an analysis of this self-match event concerning the various aerosol and cloud particle parameters detected during this flight section.

This work received funding by the BMBF within ROMIC/SPITFIRE (01LG1205A) and under the EC 7<sup>th</sup> Framework Program (FP/2007-2013)/ERC Grant Agreement No. 321040 (EXCATRO) as well as by StratoClim (Grant Agreement no. 603557).

## Ice Nucleating Particles in the Yucatan Peninsula: Concentration, Composition, and Variability

Luis A. Ladino<sup>1</sup>, Graciela B. Raga<sup>1</sup>, Harry Alvarez<sup>2</sup>, Manuel Andino<sup>3</sup>, Irma Rosas<sup>1</sup>, Leticia Martinez<sup>1</sup>, Bernardo Figueroa<sup>4</sup>, Agustín Garcia<sup>1</sup>, Cedric Chou<sup>5</sup>, and Allan Bertram<sup>5</sup>

<sup>1</sup>Centro de Ciencias de la Atmósfera, Universidad Nacional Autónoma de México, México City, México

<sup>2</sup>Departamento de Física, Facultad de Ciencias, Universidad Nacional Autónoma de México, México

<sup>3</sup>Departamento de Química, Universidad de Investigación de Tecnología Experimental Yachay Tech, Ecuador

<sup>4</sup>Laboratorio de Ingeniería y Procesos Costeros, Instituto de Ingeniería, UNAM, Sisal, Yucatán, México

<sup>5</sup>Chemistry Department, University of British Columbia, Vancouver, Canada

*Keywords:* Ice nucleating particles, Marine aerosol, Bioaerosol, Mixed-phase clouds

[luis.ladino@atmosfera.unam.mx](mailto:luis.ladino@atmosfera.unam.mx)

Although oceans cover 70% of the planet, most the regional and global climate and numerical models do not consider the oceans as a source of ice nucleating particles (INPs). This is in part due to the lack of robust experimental evidence of the relative importance and the spatial distribution of their sources in the marine environment. However, recent studies have demonstrated that oceans can emit aerosol particles with the capability to nucleate ice in clouds (e.g., Wilson and Ladino et al., 2015; Mason et al., 2015; DeMott et al., 2016; Ladino et al., 2016; and McCluskey, et al., 2017). Obtaining this information about the INPs is very important and could be included in climate and weather models to predict the formation of ice in clouds. For this reason, there is a need to conduct field measurements in tropical latitudes, since most of the past and recent studies have been conducted in mid- and high latitudes, to understand the role that marine aerosol play in the hydrological cycle and climate of tropical regions.

The present study shows the results obtained in a field campaign conducted in the village of Sisal, located on the coast of the Yucatan peninsula in Mexico (21°09'55"N 90°01'50"O) in January 2017, the first measurements obtained at this tropical site and one of the few data sets at similar latitudes. The objective of the study is to evaluate the potential sources of INPs measured at this coastal location on the Gulf of Mexico. The concentration of INPs in eight different size-bins are compared with the total and coarse mode aerosol particle concentrations, the chemical composition, meteorological variables, and the bacterial and fungal spore concentrations. The measured INP concentrations will be compared with INP concentrations obtained at different locations around the planet and the available INP

parametrizations will be validated with the present observations.

Measured variable	Used Instrument
INP concentration	MOUDI-DFT (MSP)
Aerosol concentration	Condensation particle counter (CPC, TSI)
Coarse aerosol size distribution	LasAir optical particle counter (PMS)
Chemical Composition	GC-MS
Bacterial and Fungal spore concentrations	Biostage Impactor (SKC)
Meteorology	Vaisala weather station

### References

- DeMott, P.J., et al. (2016) Sea spray aerosol as a unique source of ice nucleating particles. *Proc. Natl. Acad. Sci.*, 113(21), 5797-5803.
- Ladino, L.A., et al. (2016) Addressing the ice nucleating abilities of marine aerosol: A combination of deposition mode laboratory and field measurements. *Atmos. Environ.*, 132, 1-10.
- Mason, R.H., et al. (2015) Ice nucleating particles at a coastal marine boundary layer site: correlations with aerosol type and meteorological conditions. *Atmos. Chem. Phys.*, 15(21), 12547-12566.
- McCluskey, C.S., et al. (2017) A Dynamic Link between Ice Nucleating Particles Released in Nascent Sea Spray Aerosol and Oceanic Biological Activity during Two Mesocosm Experiments. *J. Atmos. Sci.*, 74(1), 151-166.
- Wilson, T.W., and Ladino, L. A., et al. (2015) A marine biogenic source of atmospheric ice-nucleating particles. *Nature*, 525(7568), 234-238.

## The first data on size segregated surfactants in atmospheric aerosols: Reconsideration of their impact on cloud droplet formation

S. Frka<sup>1,2</sup>, M. Simmel<sup>2</sup>, H. Wex<sup>3</sup>, I. Grgić<sup>1</sup> and A. Kroflič<sup>1,5</sup>

<sup>1</sup>Department of Analytical Chemistry, National Institute of Chemistry, Ljubljana, 1000, Slovenia

<sup>2</sup>Division for Marine and Environmental Research, Ruđer Bošković Institute, Zagreb, 10000, Croatia

<sup>3</sup>Modelling of Atmospheric Processes, Leibniz Institute for Tropospheric Research (TROPOS), Leipzig, 04318, Germany

<sup>4</sup>Experimental Aerosol and Cloud Microphysics, TROPOS, Leipzig, 04318, Germany

<sup>5</sup>Atmospheric Chemistry, TROPOS, Leipzig, 04318, Germany

Keywords: surfactants, surface tension, CCN, water soluble organic carbon

Presenting author email: frka@irb.hr

Indirect impact of aerosol particles on global energy budget by changing the microphysical properties, lifetime, and coverage of clouds has been identified as fundamental climate variable, but also the one containing the largest uncertainties. These mainly result from the limited understanding of aerosol-cloud interactions during cloud condensation processes, in particular of the hygroscopic growth and cloud condensation nuclei (CCN) activity of atmospheric aerosol organic matter. The latter is described by the Köhler's theory which describes the interplay between the Kelvin term, depending on the surface tension (ST) of the nuclei, and the solute effect linking the bulk composition of the particle with the surrounding water vapor (Köhler, 1936).

Numerous works report on the effect of surfactants or surface active substances (SAS) on the ST of atmospheric cloud and fog water and aqueous extracts of atmospheric aerosols from a wide variety of sources (e.g. Facchini *et al.*, 2000). Although organic SAS are often cited as a cause of discrepancy in CCN closure, current models largely ignore the effect of SAS on the ST reduction by assuming that the ST of growing droplets is that of pure water. The progress in discarding of the model assumptions has been recently made by linking the presence of SAS and the CCN properties of aerosol particles by proving that SAS considerably enlarge droplet activation diameters (Ruehl *et al.*, 2016). Moreover, the fact that the majority of the existing instruments designed to study the cloud droplet formation are unable to detect ST effects on CCN imply that SAS could have a significant effect on the global climate (Nozière *et al.*, 2014). Concentrations of SAS have been determined in a variety of bulk aerosol water extracts. However, data on a size-resolved SAS content in submicron or smaller aerosol particles is necessary.

We report on a seasonal variability of surfactant size distribution among atmospheric particles and their effect on the droplet growth for the first time. Two different cases were considered: 1) SAS is dissolved within the water shell of the corresponding size segregated particles and 2) SAS material is accumulated on the particle surface and compared to the estimated ST data according to Gérard and coworkers (Gérard *et al.*, 2016) assuming their even distribution within PM<sub>2.5</sub>.

Cloud parcel model was used to investigate the influence of a lower ST due to the presence of the measured SAS on the kinetics of drop activation. We showed that the ST decrease influences the drop number to about the same extent as increase in CCN by a factor of two.

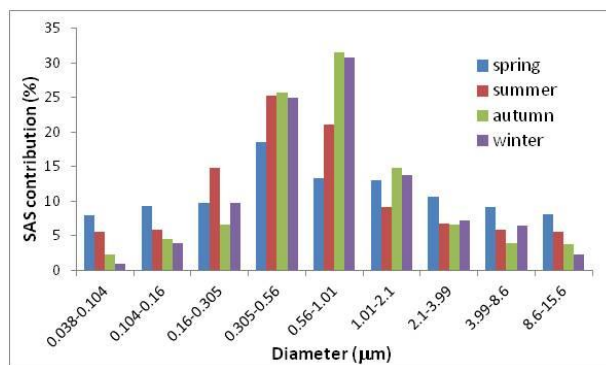


Figure 1. Contributions of the individual-stage surfactant (SAS) concentrations to the overall SAS obtained after summing up over all impactor stages.

This work was supported by the European Commission and the Croatian Ministry of Science, Education and Sports through Marie Curie FP7-PEOPLE-2011-COFUND, project NEWFELPRO and by the Slovenian Research Agency (Contract no. P1-0034-0140).

Köhler, H. (1936) *Trans. Faraday Soc.* **32**(0) 1152-1161.  
Facchini, C., et al. (2000) *Atmos. Environ.* **34**(28) 4853.  
Ruehl, C. R., et al. (2016) *Science* **351** 1447.  
Nozière, B., et al. (2014) *Nat. Commun.* **5**, 4335.  
Gérard, V. et al. (2016) *Environ. Sci. Technol.*, **50** 2974-2982.

## What do we learn from long-term CCN observations?

J. Schmale<sup>1</sup>, S. Henning<sup>2</sup>, B. Henzing<sup>3</sup>, H. Keskinen<sup>4,5</sup>, K. Sellegri<sup>6</sup>, J. Ovadnevaite<sup>7</sup>, A. Bougiatioti<sup>8,9</sup>, A. Jefferson<sup>10</sup>, S.S. Yum<sup>11</sup>, P. Schlag<sup>12,13</sup>, A. Kristensson<sup>14</sup>, A. Matsuki<sup>15</sup>, M. Pöhlker<sup>15</sup>, J. Brito<sup>16</sup>, F. Stratmann<sup>2</sup>, M. Gysel<sup>1</sup> and the CCN Team

<sup>1</sup>Laboratory of Atmospheric Chemistry, Paul Scherrer Institute, 5232 Villigen, Switzerland; <sup>2</sup>Experimental Aerosol & Cloud Microphysics, Leibniz Institute for Tropospheric Research, Permoserstrasse 15, 04318 Leipzig, Germany; <sup>3</sup>Netherlands Organisation for Applied Scientific Research, Princetonlaan 6, 3584 Utrecht, The Netherlands; <sup>4</sup>Department of Physics, University of Helsinki, Gustaf Hällströmin katu 2, Helsinki, Finland; <sup>5</sup>Hyytiälä Forestry Field Station, Hyytiäläntie 124, Korkeakoski, Finland; <sup>6</sup>Laboratoire de Météorologie Physique, 4 Avenue Blaise Pascal, 63178 Aubiere Cedex, France; <sup>7</sup>School of Physics and CCAPS, National University of Ireland Galway, University Road, Galsway, Ireland; <sup>8</sup>Department of Chemistry, University of Crete, Voutes, 71003 Heraklion, Greece; <sup>9</sup>National Observatory of Athens, P. Penteli 15236, Athens, Greece; <sup>10</sup>Earth System Research Laboratory, National Oceanic and Atmospheric Administration, 325 Broadway, Boulder, CO 80305, USA; <sup>11</sup>Department of Atmospheric Science, Yonsei University, Seoul, South Korea; <sup>12</sup>Institute for Marine and Atmospheric Research, University of Utrecht, Utrecht, The Netherlands; <sup>13</sup>Institute for Energy and Climate Research (IEK-8): Troposphere, Forschungszentrum Jülich, Jülich, Germany; <sup>14</sup>Department of Physics, Lund University, 221 00 Lund, Sweden; <sup>15</sup>Multiphase Chemistry and Biogeochemistry Departments, Max Planck Institute for Chemistry, Mainz, Germany; <sup>16</sup>Instituto de Física, Universidade de São Paulo, Rua do Matão 1371, CEP 05508-090, São Paulo, SP, Brazil

Keywords: cloud condensation nuclei, ACTRIS, chemical composition, size distribution  
Presenting author email: julia.schmale@psi.ch

Cloud condensation nuclei (CCN) influence the microphysical and optical properties of clouds. To predict cloud radiative properties, understanding the spatial and temporal variability of CCN concentrations in different environments is important. However, currently, the effects of atmospheric particles on changes in cloud radiative forcing are still the largest contribution to uncertainty in climate forcing prediction.

Numerous field campaigns have explored detailed characteristics of CCN in many locations around the world. However, these short-term observations can generally not address seasonal or inter-annual variations, and comparison between sites is difficult. Here we present results of multi-year CCN number concentrations, as well as size distribution and chemical composition data covering at least one full year between 2006 and 2014. The 12 locations include ACTRIS stations (<http://www.actris.net/>) in Europe, and further sites in the Americas and Asia. The observatories represent various environments as provided in Table 1.

Figure 1 shows the seasonal cycles of CCN number concentrations at 0.2 % supersaturation ( $CCN_{0.2}$ ), the geometric mean diameter of the size distribution and the activation diameter ( $D_{crit}$ ). Characteristic features for each site are evident. For example, at the high-altitude station JFJ,  $CCN_{0.2}$  increase in summer due to boundary layer air mass injections. In the rainforest (ATT) concentrations are higher in the dry season, July to December, than in the wet season, and in the Arctic (BRW) the haze season from January to May shows higher  $CCN_{0.2}$ .

Additional analyses on the data include frequency distributions of various CCN and size distribution parameters, comparison of CCN activation curve slopes over a spectrum of supersaturations, seasonal cycles of aerosol chemical composition and therefrom derived kappa values for a subset of the sites, autocorrelation of CCN concentration time series (persistence) and closure studies based on the kappa-Köhler theory.

Table 1. Overview of observatories and the environments they represent

Station name	Abbreviation	Country	site category
Atto	ATT	Brazil	rainforest
Barrow	BRW	Alaska, USA	Arctic maritime
Cesar Tower	Cesar Tower	The Netherlands	near coast, rural back-ground
Finokalia	FIK	Crete, Greece	coastal
Jungfraujoch	JFJ	Switzerland	high alpine, back-ground
Melpitz	MEL	Germany	continental back-ground
Mace Head	MHD	Ireland	coastal back-ground
Noto	NOT	Japan	coastal back-ground
Peninsula Puy de Dôme	PUY	France	mountain, continental back-ground
Seoul	SEO	South Korea	urban, monsoon influence
Smear	SMR	Finland	rural back-ground, boreal forest
Vavihill	VAV	Sweden	rural back-ground

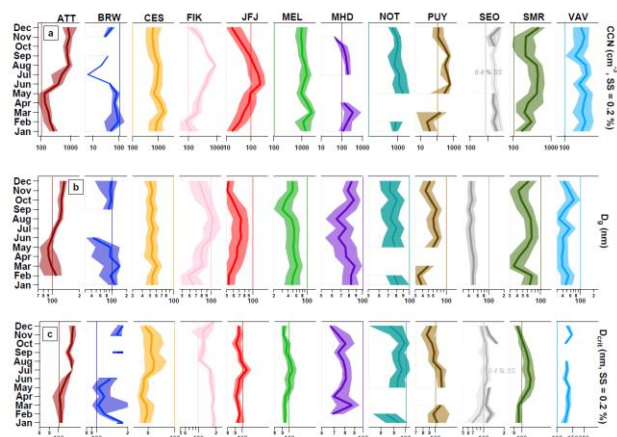


Figure 1: Seasonal cycles of (a) CCN number concentrations at 0.2 % supersaturation (SS), (b) the geometric mean diameter, and (c) the activation diameter at SS = 0.2 %.

Acknowledgement: FP7 projects ACTRIS (grant agreement no. 262254) and BACCHUS (grant agreement no. 603445).

## Formation of methane under aerobic conditions

A.C Saydam and A.H.A. Ghandi

Department of Environmental Engineering, University of Hacettepe, Ankara, 06800, Turkey

Keywords: dust, decarboxylation, methane, chitin.

Presenting author email: saydam@hacettepe.edu.tr

One of the unanimously accepted fact is the necessity of anoxic conditions for the production of methane. Despite this fact the observations of the co-variations of both methane and carbon dioxide by atmospheric monitoring stations is simply ignored. Such co-variations are also observed at Mace Head station as a part of the ICOS Atmospheric Measurement Network but have not been addressed up to know.

Saydam and Senyuva(2002) have shown that the during the course of the long range transport of desert dust the photochemical production of reduced iron as well as carbon dioxide takes place through decarboxylation reaction by the action of oxalate released by the fungus. The results obtained at Mace Head atmospheric measurement network or any other station on worldwide further suggested that methane should also be formed within the cloud along with carbon dioxide under “aerobic” conditions. Despite these discouraging preliminary assumptions, we have proceeded with our hypothesis and found out that the chitin is an essential part of the carbohydrate skeleton of the fungal cell wall Lenardon *et al* (2010). The close inspection of chitin molecular structure reveals the presence of acetyl groups that may lead to the formation of methane by the action of acid as to support our hypothesis.

Thus, we have tested this hypothesis by using the desert soil that have been selected and imported by us from southern Tunisia near city of Tozeur. 8 grams of Saharan dust and 250 ml of distilled water have been encapsulated within the headspace cups and analysed for possible methane formation. One set kept in dark as well as covered by aluminium foil as to test the possible impact of light on the methane formation. Composition of gas formation has been investigated by Agilent 6890N GC/FID system by using Porapak column and the results were presented in Figure 1.

It can be seen that methane is formed under aerobic conditions simply by using desert dust and water mixture most possible by the action of oxalate released by the bacteria and fungus that present within the dust veil. To our knowledge, apart from the results published by Keppler *et al* (2006) this is the first mechanistic approach that addresses methane formation under aerobic conditions. Keppler *et al* (2008) identified methoxyl groups of plant pectin as a precursor of atmospheric methane. Instead, we have concentrated on chitin and further postulated that upon deacetylation

further decomposition of chitin by oxalate and solar light by a hitherto unrecognized process may lead to the formation of much required amine groups.

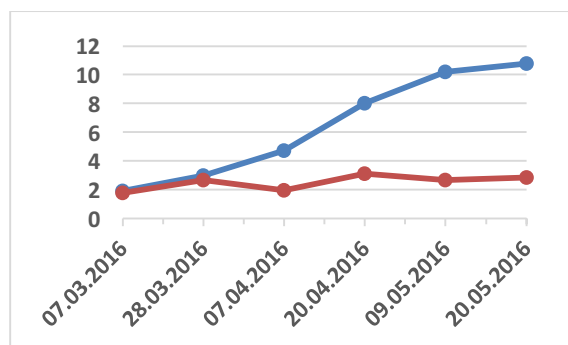


Figure 1. The formation of methane (ppm) in light and dark conditions.

This may also address the results published by Mace *et al* (2003) where they have observed all essential amino acids within the rain samples originated from Sahara. Of course, this iconoclastic approach will not only help us to explain the co variance of methane and carbon dioxide during the course of air masses that have been affected by desert dust but will also force us to reconsider the formation mechanisms of this essential greenhouse gas under aerobic conditions.

Keppler, F., Hamilton, J. T., Braß, M., & Röckmann, T. (2006). Methane emissions from terrestrial plants under aerobic conditions. *Nature*, 439(7073), 187-191.

Keppler, F., Hamilton, J. T., McRoberts, W. C., Vigano, I., Braß, M., & Röckmann, T. (2008). Methoxyl groups of plant pectin as a precursor of atmospheric methane: evidence from deuterium labelling studies. *New Phytologist*, 178(4), 808-814.

Lenardon, M. D., Munro, C. A., & Gow, N. A. (2010). Chitin synthesis and fungal pathogenesis. *Current opinion in microbiology*, 13(4), 416-423.

Mace, K. A., Kubilay, N., & Duce, R. A. (2003). Organic nitrogen in rain and aerosol in the eastern Mediterranean atmosphere: An association with atmospheric dust. *Journal of Geophysical Research: Atmospheres*, 108(D10).

Saydam, A. C., & Senyuva, H. Z. (2002). Deserts: Can they be the potential suppliers of bioavailable iron?. *Geophysical research letters*, 29(11).

## Pre-activation of aerosol particles by ice preserved in pores

C. Marcolli

Institute for Atmospheric and Climate Science, ETH Zurich, Switzerland

Keywords: cloud condensation and freezing, ice nucleation, clouds, mineral dust

Presenting author email: claudia.marcolli@env.ethz.ch

Pre-activation denotes the capability of particles or materials to nucleate ice at lower relative humidities or higher temperatures compared to their intrinsic ice nucleation efficiency after having experienced an ice nucleation event or low temperature before. It was first reported by Fournier d'Albe (1949). A number of studies followed using different pre-activation setups and protocols to investigate various materials for their susceptibility to pre-activation. Ice preserved in pores is only one explanation put forward for pre-activation, other ones being a surface phase change (Edwards and Evans, 1971) or a surface ice film (Mason, 1950). Research on pre-activation ceased in the early 1970s with no consensus achieved regarding its microphysical explanation. It was taken up again by Knopf and Koop (2006), who clearly favored the survival of ice in pores and capillaries as explanation. Also in a very recent study by Wagner et al. (2016) the pre-activation behavior of the investigated particles was analyzed under the presumption that pre-activation is due to capillary condensation of supercooled water and subsequent homogeneous freezing (Marcolli, 2014). Here, I focus on ice preserved in pores as the reason for pre-activation. I use idealized trajectories of air parcels to discuss the ability of pores of different shape and size to show pre-activation.

The pore width needed to keep pores filled with water decreases with decreasing relative humidity as described by the inverse Kelvin equation. Thus, narrow pores remain filled with ice well below ice saturation. However, the smaller the pore width, the larger the melting and freezing point depressions within the pores. Therefore, pre-activation due to pore ice is constrained by the melting of ice in narrow pores and the sublimation of ice from wide pores imposing restrictions on the temperature and relative humidity range of pre-activation for cylindrical pores. Ice is better protected in ink-bottle-shaped pores with a narrow opening leading to a large cavity. However, whether pre-activation is efficient also depends on the capability of ice to grow macroscopically, i.e. out of the pore. A strong effect of pre-activation is expected for swelling pores, because at low relative humidity their openings narrow and protect the ice within them against sublimation. At high relative humidity, they open up and the ice can grow to macroscopic size and form an ice crystal. Ice protected in pockets is perfectly sheltered against sublimation but needs the dissolution of the surrounding matrix to be effective. Pores partially filled with condensable material may also show pre-activation. In this case, complete filling occurs at lower relative humidity than for empty pores and freezing shifts to lower temperatures.

A literature review of pre-activation experiments confirms that materials susceptible to pre-activation are indeed porous. Pre-activation was observed for clay minerals like illite, kaolinite and montmorillonite with inherent porosity. The largest effect was observed for the swelling clay mineral montmorillonite. Materials that may acquire porosity depending on the formation conditions are  $\text{CaCO}_3$ , meteoritic material and volcanic ash, which showed pre-activation for some samples or in some studies but not in other ones. Some materials like quartz and AgI always failed to show pre-activation.

Different atmospheric scenarios can be identified for which pre-activation by ice preserved in pores may be relevant. Lower-level clouds may be seeded by pre-activated particles released from high-level clouds. Porous particles may be recycled in wave clouds and show pre-activation with subsequent ice growth as soon as ice saturation is exceeded after having passed a first cloud event. Volcanic ash particles and meteoritic material likely influence ice cloud formation by pre-activation. Therefore, the possibility of pre-activation should be considered when ice crystal number densities in clouds exceed the number of ice-nucleating particles measured at the cloud forming temperature.

Edwards, G. R. and Evans, L. F. (1971) *J. Atmos. Sci.* **28**, 1443-1447.

Fournier D'Albe, E. M. (1949) *Q. J. Roy. Meteor. Soc.* **75**, 1-14.

Knopf, D. A. and Koop, T. (2006) *J. Geophys. Res.* **111**, D12201.

Marcolli, C. (2014) *Atmos. Chem. Phys.* **14**, 2071-2104.

Mason, B. J. (1950) *Q. J. Roy. Meteor. Soc.* **76**, 59-74.

Wagner, R., Kiselev, A., Möhler, O., Saathoff, H., and Steinke, I. (2016) *Atmos. Chem. Phys.* **16**, 2025-2042.

## Microphysical cloud properties in sub-arctic environment during three Cloud Pallas Experiments

K.M. Doulgeris and D. Brus

Finnish Meteorological institute, PO Box 503, FI-00101, Helsinki, Finland

Keywords: clouds, Pallas, in situ, cloud probes.

Presenting author email: Konstantinos.doulgeris@fmi.fi

Atmospheric clouds are complicated systems which are key elements of the hydrological cycle. Cloud properties (e.g. albedo, precipitation rate and lifetime) depend, amongst other factors, on the number concentration of aerosol particles and on their chemical composition (Lohmann and Feichter, 2005; Lihavainen *et al.*, 2008).

Continuous, semi-long term, ground based, in-situ cloud measurements were conducted during the autumn intensive Pallas Cloud Experiments (PaCE) in years 2012, 2013 and 2015. PaCE 2012 lasted from September 13<sup>th</sup> till October 30<sup>nd</sup>, PaCE2013 lasted from September 14<sup>th</sup> till November 28<sup>nd</sup> and PaCE 2015 lasted from October 6<sup>th</sup> till December 2<sup>nd</sup>. The measuring station - Sammaltunturi station (67°58'N, 24°07'E) - resides on a top of a round topped treeless hill, in a 50-km-long north and south chain of fields at an elevation of 565 m a.s.l and is a part of Pallas-Sodankyla- Global Atmosphere Watch (GAW) programme. Sammaltunturi station is, due to topography of the surrounding terrain, a great place for ground-based observations of low level clouds.

Instrumentation that was used to measure the cloud properties were the Cloud, Aerosol and Precipitation Spectrometer probe (CAPS, DMT) (0.51-930  $\mu\text{m}$ ) and the Forward Scattering Spectrometer Probe (FSSP-100, DMT) (1.2-47  $\mu\text{m}$ ). The CAPS probe includes two instruments for droplet size measurements: the Cloud and Aerosol Spectrometer (CAS) (0.51-50  $\mu\text{m}$ ), and the Cloud Imaging Probe (CIP) (12.5-930  $\mu\text{m}$ ). Both probes were installed at the roof of the station (Figure1).

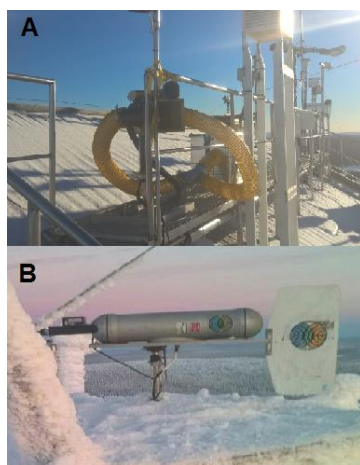


Figure 1. A) CAPS and B) FSSP-100 probes as they were installed on Sammaltunturi measurement site during PaCE 2015.

In this work, a detailed analysis of all measured cloud microphysical properties was made and how they were influenced by meteorology was thoroughly investigated. To estimate the presence of a cloud at the measurement site we used the cloud droplet count measured with the cloud probes. In addition, this was crosschecked against the visibility measurements. We considered that the station was inside a cloud while the horizontal visibility was less than 1000 meters.

Table 1 summarizes an example for the averaged data for effective diameter ( $ED_{CAS}$ ) and median volume diameter ( $MVD_{CAS}$ ) as they were derived from CAS size distribution when the station was inside a cloud.

Table 1. Example averaged data of effective diameter and median volume diameter as they were counted from CAS probe.

Campaign	$ED_{CAS}$ ( $\mu\text{m}$ )	$MVD_{CAS}$ ( $\mu\text{m}$ )
PaCE 2012	14.10 (5.21)	15.39 (5.46)
PaCE 2013	13.38 (2.35)	14.86 (4.25)
PaCE 2015	12.28 (5.10)	13.38 (5.38)

This work was supported by KONE foundation, Nordforsk Contract number 26060, CRAICC Amendment on CRAICC-PEEX Collaboration, Academy of Finland project: Greenhouse gas, aerosol and albedo variations in the changing Arctic (project number 269095), Academy of Finland Center of Excellence program (project number 272041), BACCHUS (EU 7th Framework program), Natural Environment Research Council (NERC), grant number NE-L011514-1 and ACTRIS-2, the European Research Infrastructure for the observation of Aerosol, Clouds, and Trace gases. This project has received funding from the European Union's Horizon 2020 research and innovation programme under grant agreement No 654109.

Lihavainen, H., Kerminen, V.-M., Komppula, M., Hyvarinen A.-P., Laakia J., Saarikoski S., Makkonen, U. Kivekas, N., Hillamo, R., Kulmala, M. and Viisanen, Y. (2008) *Atmos. Chem. Phys.*, **8**, 6925-6938.

Lohmann, U. and Feichter, J. (2005) *Atmos. Chem. Phys.*, **5**, 715-737.

## Aerosol PSD and occurrence frequencies of clouds for temperate areas

I. Marsli, M. Diouri, H. Steli and A. Ben-Tayeb

Atmospheric Physic Laboratory, University Mohammed 1st, Oujda, 6020, Morocco

Keywords: AERONET<sup>(\*)</sup>, Particle size distribution, Cloud optical depths, sun photometer, temperate areas.

Presenting author email dyourim@gmail.com

This study focus on aerosol particle size distribution (PSD), Cloud optical depths (COD) and occurrence frequencies of cloud relative to six cities in the temperate area. (Table 1). Concerning PSD, results show that the coarse mode size ranges higher than  $2\mu\text{m}$  and seems more important for Zanzan (Iran) and CEILAP-Neuquen (Argentina) with an average radius around  $3\mu\text{m}$ . The fine mode size ranges lower than  $0.4\mu\text{m}$  is important for New York with an average radius around  $0.15\mu\text{m}$  that indicate more influence of anthropogenic aerosol. Time series of COD indicate a dominant variation in the interval (8,100) that implies the importance of Stratus and Altostratus occurrence frequencies. COD values are higher in winter and spring, but with a decline in summer and autumn.

Sites	Lat.	Long.	Alt.
Oujda	34.6N	1.8W	620
Zanzan	36.70N	48.50E	1805
New York	40.82N	73.94W	100
CEILAP-Neuquen	38.93S	68.13W	271
OHP_Observatoire	43.93N	5.71E	680
Graciosa Island	39.09N	28.02W	15

Table 1. Site Coordinates and Elevation

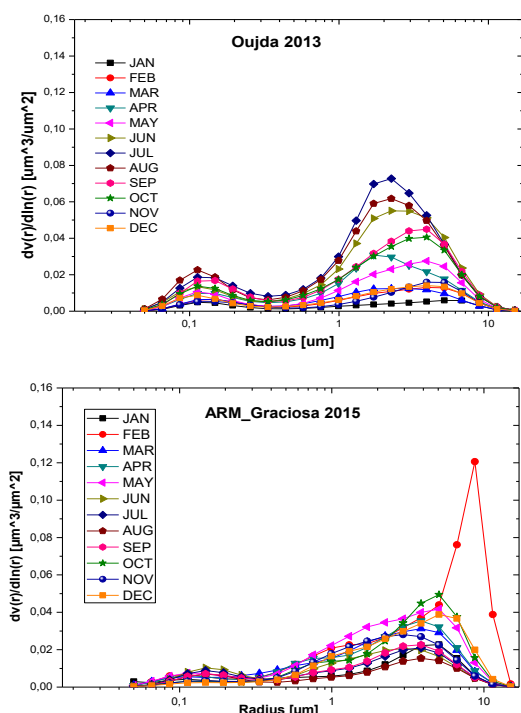


Figure 1. Monthly mean PSD

Oujda and Graciosa histogram samples (Fig.2) show a variety of cloud frequencies which imply an important effect on global terrestrial radiative forcing. The Figure 1 shows that the coarse mode is important for both sites, but with different origins: Mineral dust in Oujda and mineral salt in Graciosa.

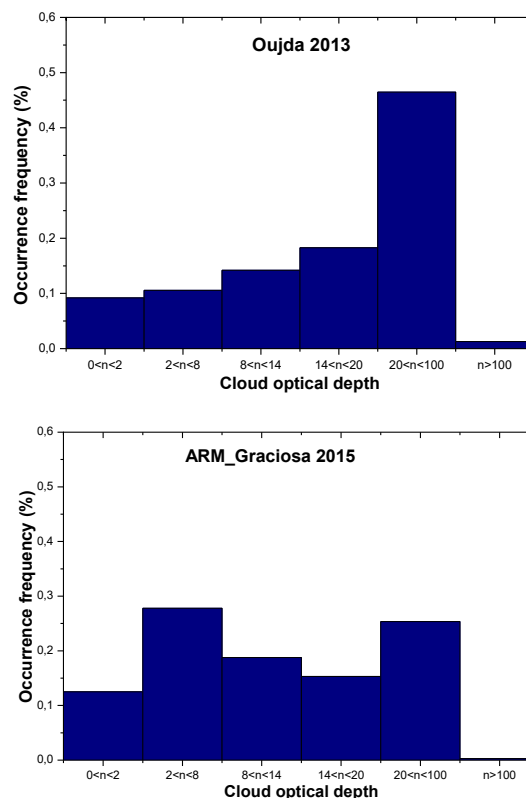


Figure 2. Occurrence frequency of cloud

(\*) <http://aeronet.gsfc.nasa.gov/>

Natalie Mahowald and al. (2013), The size distribution of desert dust aerosols and its impact on the Earth system Aeolian Research.

D.M. Giles and al. (2012), An analysis of AERONET aerosol absorption properties and classifications representative of aerosol source region, Journal of geophysical research.

### Acknowledgements

Kindly thanks to the AERONET/PHOTONS PI: Rick Wagener, Philippe Goloub, Brent Holben, Barry Gross and Hamid Khalesifard

## Pollen Cytoplasmic Granules Induce Heterogeneous Nucleation of Water Droplets at Low Supersaturation

S. Grimonprez<sup>1</sup>, N. Visez<sup>1</sup>, M. Choël<sup>2</sup> and D. Petitprez<sup>1</sup>

<sup>1</sup>Univ. Lille, CNRS, UMR 8522, PC2A, F-59000 Lille, France

<sup>2</sup>Univ. Lille, CNRS, UMR 8516, LASIR, F-59000 Lille, France

Keywords: hygroscopicity, heterogeneous condensation, CCNC, clouds.

Presenting author email: symphorien.grimonprez@univ-lille1.fr

Pollen grains are important contributors to the primary biological aerosols. During pollination, pollen grains can travel up to several thousand kilometers. During dispersal, pollen undergoes chemical and physical transformations, including rupture of the grains.

Rupture of pollen envelope may occur from several mechanisms: difference in osmotic pressure, abortive germination or wind-induced mechanical release. Rupture of pollen could release inner sub-particles including pollen cytoplasmic granules. A pollen grain can generate up to several hundreds of sub-particles (Suphioglu et al., 1992), with sizes comprised between 0.5 and 4.5  $\mu\text{m}$ .

Pollen, with size in the order of a few tens of micrometers, has the ability to act as giant cloud condensation nuclei (GCCN) (Johnson, 1982). Inner pollen sub-particles may act also as CCN (Steiner et al., 2015).

In this work, we aim to gain better insight on the ability of the pollen cytoplasmic granules to act as CCN. Our approach was to generate pollen sub-particles by mechanical rupture which prevents the use of water.

In order to simulate wind-induced subparticles dispersion, pollen grains were manually crushed and introduced in a glass vessel. Using mechanical stirring, pollen granules were dispersed within a constant flow of nitrogen.

Pollen sub-particles were exposed to water vapor in supersaturated conditions within a commercial Cloud Condensation Nuclei Counter (DMT-CCNc) to initiate heterogeneous condensation of water droplets. The activated fraction is calculated as the ratio of nucleated water droplets to the total number of particles entering the CCNc measured by a Condensation Particle Counter (CPC). Size distribution of pollen subparticles was measured with an Aerodynamic Particle Sizer; the main mode is centered on 2  $\mu\text{m}$  diameter.

The activate ratio reaches a plateau for supersaturation higher than 0.6. The critical supersaturation ( $S_c$ ) was determined by fitting with Boltzmann function.  $S_c = 0.08\%$  has been determined in this work for birch pollen sub-particles.

For comparison, Steiner showed that the supersaturation measured for sub-particles was between 0.8 and 0.12%, for particles size between 50 and 200 nm. These values are higher than our measurements. This difference can be explained by the Kelvin effect: the size

of the particle studied in this work is larger compare to those used by Steiner.

Moreover our measurements were made with initially dry particles. The use of filtered suspension of pollen in water may create artifacts in hygroscopic properties as some organics compounds may migrate on existing particles or condense to create new particles.

Considering that the median supersaturation reported within small or moderate cumulus is approximately 0.1 % (Pruppacher et al., 1998), our value shows that the pollen cytoplasmic granules could act as CCN at low supersaturation and have a significant effect on cloud precipitation.

This work is a contribution to the CPER research project CLIMIBIO. The authors thank the French Ministère de l'Enseignement Supérieur et de la Recherche, the Hauts de France Region and the European Funds for Regional Economical Development for their financial support to this project. The CaPPA project (Chemical and Physical Properties of the Atmosphere) is funded by the French National Research Agency (ANR) through the PIA (Programme d'Investissement d'Avenir) under contract ANR-11-LABX-005-01

Johnson, D.B., 1982. *J. Atmospheric Sci.* 39, 448–460.  
Pruppacher, H.R., Klett, J.D., Wang, P.K., 1998. *Microphysics of clouds and precipitation.*  
Steiner, A.L., Brooks, S.D., Deng, C., Thornton, D.C., Pendleton, M.W., Bryant, V., 2015. *Geophys. Res. Lett.* 42, 3596–3602.  
Suphioglu, C., Singh, M.B., Taylor, P., Knox, R.B., Bellomo, R., Holmes, P., Puy, R., 1992. *The Lancet* 339, 569–572.

## Ice nucleation abilities of atmospheric soot particles

F. Mahrt<sup>1</sup>, R. O. David<sup>1</sup>, U. Lohmann<sup>1</sup>, Z. Wu<sup>2</sup>, C. Stopford<sup>3</sup> and Z. A. Kanji<sup>1</sup>

<sup>1</sup>Institute for Atmospheric and Climate Science, ETH Zurich, Zurich, 8092, Switzerland

<sup>2</sup>Peking University, Beijing, China

<sup>3</sup>Centre for Atmospheric and Instrumentation Research, University of Hertfordshire, Hatfield, Hertfordshire, United Kingdom

Keywords: ice nucleation, black carbon, cirrus clouds, soot.

Presenting author email: fabian.mahrt@env.ethz.ch

Soot particles are primary particles produced by incomplete combustion of both biomass and/or fossil fuels. Thus, soot constitutes a major anthropogenic pollutant. Emission sources include combustion related processes in transport vehicles, industrial and residential uses. Particles emitted in these processes are generally complex internal mixtures of black carbon (BC) and organic matter (OM) (Bond et al., 2013; Petzold et al., 2013). While these properties strongly depend on the emission sources, they can be altered during atmospheric cycling of these particles, including interactions of the primary particles with other atmospheric matter and/or gases.

The total climate impact of these particles is still not well understood. While BC generally absorbs solar radiation, thus contributing to a warming effect on global climate it can also act as a heterogeneous ice nucleating particle (INP) and impacting cloud-radiation interactions, potentially cooling the climate (Lohmann, 2002). The overall estimates of the net radiative forcing associated with BC are therefore still associated with large uncertainties, even though being one of the most important climate forcing agents (Bond et al., 2013).

Our abilities to predict the ice nucleation behavior of soot particles is partly impeded by conflicting results between laboratory studies and field observations.

In this study, we present a systematic laboratory-based investigation of the ice nucleation behavior of different soot particles. Different commercial soot samples are used, including an amorphous, industrial carbon black frequently used in coatings and coloring (FW 200, Orion Engineered Carbons) a fullerene soot (572497 Aldrich), e.g. used as catalyst, as well as a Lamp Black carbon (Orion Engineered Carbons), that has previously been used in ice nucleation studies. Besides we use soot generated from a propane flame Combustion Aerosol Standard Generator (miniCAST, JING AG), frequently used as proxy for atmospheric soot particles. Ice nucleation ability of these soot types is tested on size-selected particles for a wide temperature range from 253 K to 218 K, using the Horizontal Ice Nucleation Chamber (HINC), a Continuous Flow Diffusion Chamber (CFDC) (Kanji and Abbatt, 2009).

Besides, chemically more complex real world samples, collected on filters, will be tested and compared to the commercial carbon blacks. Filters were collected during winter haze periods in Beijing, China during 2016/2017 and represent atmospheric soot particles stemming from both industrial and residential emissions.

Particles collected on filters will be re-suspended and aerosolized using an atomizer (TSI, model 3076) and dried by a diffusion drier prior to ice nucleation experiments.

Ice nucleation experiments using HINC are complemented by auxiliary measurements including BET-surface determination and thermogravimetric analysis, in order to characterize the physio-chemical properties of the tested aerosol particles. Finally, usage of a Particle Phase Discriminator (PPD) coupled in series to HINC allows discrimination of size-resolved liquid and ice hydrometeors formed on injected particles and thus allows to more precisely quantify the microphysical properties of these particles in cloud processes.

Results show different activation behavior of the soot over the temperature range investigated. While the commercial soot samples show heterogeneous freezing well below water saturation in the cirrus regime, CAST-brown soot needs conditions above water saturation to show any activation. For the mixed-phase cloud conditions all soot types show droplet activation for high supersaturations w.r.t water.

Bond, T. C., Doherty, S. J., Fahey, D. W., Forster, P. M., Bernsten, T., DeAngelo, B. J., . . . Zender, C. S. (2013). Bounding the role of black carbon in the climate system: A scientific assessment. *Journal of Geophysical Research-Atmospheres*, 118(11), 5380-5552. doi:10.1002/jgrd.50171

Kanji, Z. A., & Abbatt, J. P. D. (2009). The University of Toronto Continuous Flow Diffusion Chamber (UT-CFDC): A Simple Design for Ice Nucleation Studies. *Aerosol Science and Technology*, 43(7), 730-738. doi:10.1080/02786820902889861

Lohmann, U. (2002). A glaciation indirect aerosol effect caused by soot aerosols. *Geophysical Research Letters*, 29(4), 11-11-11-14. doi:10.1029/2001GL014357

Petzold, A., Ogren, J. A., Fiebig, M., Laj, P., Li, S. M., Baltensperger, U., . . . Zhang, X. Y. (2013). Recommendations for reporting "black carbon" measurements. *Atmos. Chem. Phys.*, 13(16), 8365-8379. doi:10.5194/acp-13-8365-2013

## Results of laboratory studies of immersion mode heterogeneous ice nucleation by kaolin and quartz aerosols

V.V. Chukin<sup>1</sup>, A.F. Sadykova<sup>1</sup> and V.N. Nikulin<sup>1</sup>

<sup>1</sup>Department of Experimental Atmospheric Physics, Russian State Hydrometeorological University, Saint-Petersburg, 195196, Russia

Keywords: ice nucleation, immersion mode, aqueous solution, laboratory experiments

Presenting author email: chukin@meteolab.ru

Aerosols affect the climate system not only by changing the opacity of the air, but also due to the formation of water droplets and ice crystals in the clouds (Sadykova, 2014). Ice crystals play a significant role in the formation of radiation properties of clouds and precipitation processes. To build a model of the phase state of the clouds we carried out laboratory experiments on immersion mode heterogeneous ice nucleation in aqueous solutions.

### Methods

The experimental setup LINC for investigation of the ice nucleation was created in Laboratory of Meteotehnology, RSHU (Nikulin, 2015). The experimental installation consists of an optical microscope, digital microscope, temperature sensors, freezer and Peltier module. The optical microscope is used for the preparation of substrates and drops. The temperature of Peltier module is controlled by a programmable power supply. The images of freezing droplets are obtained with the help of the digital microscope. Moment of droplet freezing is determined automatically by computer vision system. The experimental installation allow one to carry out experiments at 243 K and below.

The particles of kaolin and quartz were used in laboratory experiments. According to the experience, the surface area of the substrate plays an important role in the ice nucleation. The substrate properties of ice nuclei formation are described by the parameter, named specific linear energy (SLE) (Chukin, 2009). In the theory of ice nucleation by Chukin-Platonova this parameter characterizes the properties of substrates: the less SLE, the easier the formation of ice crystals on a substrate.

### Data and Analysis

The amount of experiments on the crystallization of supercooled droplets of aqueous solution with the water activity in range from 0.97 to 1.00 equals 359.

Example comparison of the experimental data and the model is shown in Figure 1. Analysis of the experimental data showed that the average values of the SLE of kaolin and quartz particles are  $16.1 \pm 1.8$  and  $17.8 \pm 0.9$  pJ/m, respectively. The temperature dependence of SLE was found.

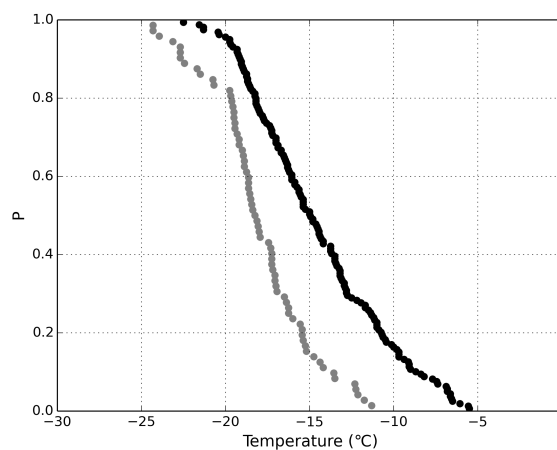


Figure 1. Experimental dependence of droplet freezing probability on temperature for kaolin (black dots) and quartz (grey dots) aerosols.

### Conclusions

The phase state of cloud can be determined on the basis of the obtained results as a function of temperature and concentration of aerosols. This will not only allow to simulate the effect of aerosols on the radiative properties of clouds, but also to determine the crystallizing properties of the aerosols from satellite data.

Sadykova, A.F., Nikulin, V.N. and Chukin, V.V. (2014) *Modern High Technologies* **5-2**, 235.

Nikulin, V.N., Chukin, V.V. and Sadykova, A.F. (2015) *Scientific Notes of RSHU* **8**, 102-112.

Chukin, V.V. and Platonova, A.S. (2009) *Natural and Technical Sciences* **4**, 231-236.

## Role of cloud parameterization scheme on pollutants concentration over Indian domain

Nishi Srivastava<sup>1,2</sup> and Nadège Blond<sup>2</sup>

<sup>1</sup>Department of Physics, B.I.T.-Mesra, Ranchi, India

<sup>2</sup>Université de Strasbourg, CNRS, Laboratoire Image Ville Environnement (LIVE) UMR 7362, F-67000 Strasbourg, France.

Keywords: aerosol, chemical transport modeling, parameterization scheme, pollutants

Presenting author email: nishi.bhu@gmail.com

Recent investigations, both national and international campaigns, have shown that anthropogenic aerosols have significant impact on climate forcing, health effects (respiratory and cardiovascular diseases), pollution, eutrophication/acidification of aquatic and terrestrial ecosystems. In recent assessment report of IPCC, it has been stated that radiative forcing due to aerosols involves high uncertainty. For proper estimation and understanding of radiative forcing accurate spatial distribution of aerosol is need of the day. Though several national and international efforts are made to generate a spatial distribution of aerosols still there exists a large gap in its understanding. Over Indian domain, this is due to complex terrain structure and meteorological condition.

In the framework of previous studies, the chemical transport model CHIMERE (Menut et al., 2013) was used over Indian domain to generate spatial distribution of pollutants concentration. Comparisons with several types of observations show that main model errors appear on urban areas during summer monsoon (Srivastava et al., 2016a), where the CHIMERE model significantly underestimates the aerosol concentrations (Srivastava et al., 2016b,c). Primary cause for this underestimation of pollutants could be overestimation of rain in model during the monsoon season.

To check this hypothesis, in present work we perform CHIMERE simulations driving the model with a meteorological driver with different cloud parameterization

schemes to evaluate the impact of parameterization schemes on spatial distribution of aerosol/pollutants. Sensitivity runs with different cloud/cumulus schemes show that cloud parameterization scheme have strong control on rain simulated by model, and lead to significant changes in the pollutants concentrations. This results guide us to find the most efficient cloud/cumulus parameterization scheme over the Indian continent.

### Reference:

- Srivastava, N., S. Satheesh, N. Blond, K. Krishna Moorthy (2016a) *Anthropogenic Aerosol Fraction over Indian Region: Simulations versus Multi-Satellite Data Analysis*, *International Journal of Remote Sensing* 37, 782-804.
- Srivastava N., S.K. Satheesh, Nadege Blond and K. Krishna Moorthy (2016b) *Simulation of aerosol fields over South Asia using CHIMERE – Part-I: Spatio-temporal characteristics and heterogeneity*, *CURRENT SCIENCE, SPECIAL SECTION, RAWEX-GVAX, VOL. 111, NO. 1, 10 JULY* (pp. 76-82), 2016b,
- Srivastava N., S.K. Satheesh, Nadege Blond and K. Krishna Moorthy (2016c) *Simulation of aerosol fields over South Asia using CHIMERE – Part-II: Performance evaluation*, *CURRENT SCIENCE, SPECIAL SECTION, RAWEX-GVAX, VOL. 111, NO. 1, 10 JULY 2016* (pp. 83-92)
- Menut L., B. Bessagnet, D. Khvorostyanov, M. Beekmann, N. Blond, A. Colette, I. Coll, G. Curci, G. Foret, A. Hodzic, S. Mailler, F. Meleux, J.-L. Monge, I. Pison, G. Siour, S. Turquety, M. Valari, R. Vautard, and M. G. Vivanco (2013) *CHIMERE 2013: a model for regional atmospheric composition modelling*, *Geosci. Model Dev.*, 6, 981-1028, doi:10.5194/gmd-6-981-2013

## The effect of aerosol on cloud properties and precipitation in KIAPS integrated model with simplified chemistry module

S. Y. Bae<sup>1</sup>, J.-Y. Kang<sup>1</sup> and R Park<sup>1</sup>

<sup>1</sup>Korea Institute of Atmospheric Prediction Systems (KIAPS), Seoul, 07071, Republic of Korea

Keywords: CCN, global numerical model, microphysics scheme

Presenting author email: sy.bae@kiaps.org

Atmospheric aerosols play an important role in cloud formation by acting as cloud condensation nuclei (CCN). Their chemical composition and number size distribution significantly modify cloud microphysical properties and precipitation amount by altering cloud droplet number concentration, droplet effective radius, cloud albedo, cloud liquid water content, and cloud lifetime (Twomey 1974). These microphysical changes exert a significant cooling effect at the Earth's surface to partially offset a warming effect by greenhouse gases (Lohmann and Feichter 2005).

KIAPS has been developing a next generation of global operational model for Korea Meteorological Administration (KMA) since 2011. We are updating KIAPS integrated model in every quarter since July 2015 and beta version will be released soon. Dynamic core is developed based on nonhydrostatic equations. Prognostic cloudiness scheme is developed in KIAPS and orography gravity wave drag scheme is improved widely. Size-aware method in the deep convection and vertical diffusion schemes are considered to prepare for shift to high-resolution grid model. KIAPS global model does not include chemistry module yet owing to increase computational burden. Therefore, it needs to develop a simplified chemistry model for simulation of the effect of aerosols on properties of cloud and hydrometeors and precipitation.

The model is developed based on GOCART (Goddard Chemistry Aerosol Radiation and Transport) chemistry module (Chin *et al.*, 2000) in WRF-Chem (Weather Research and Forecasting model coupled with Chemistry) model by reducing number of chemistry species and reactions (see the details of a new simplified chemistry module in J.-Y. Kang's presentation).

We modified the physics schemes to calculate CCN number concentration (NCCN) in microphysics scheme and precipitation rate with the NCCN in deep convection scheme. The equation of NCCN from Morcrette *et al.* (2011) is applied in WDM6 (WRF Double Moment 6-class) microphysics scheme. The NCCN equation is as a function of only aerosol mass concentration. The chemical species considered are sulfate (SO<sub>4</sub>), organic carbon (OC), and sea salt. NCCN is largely increased with higher OC and SO<sub>4</sub>. For example, NCCN is more than 10000 cm<sup>-3</sup> when both OC and SO<sub>4</sub> are 100 μg m<sup>-3</sup> (figure 1). CCN is activated to cloud droplet according to the ratio of relative humidity to maximum supersaturation. Precipitation conversion parameter is changed from constant to a function of NCCN in deep convection scheme. The convective precipitation rate decreases as increasing of NCCN

(figure 1) while non-convective rainfall dose not decreased linearly owing to interaction between hydrometeors and change of temperature. The sensitivity analysis will be executed for several real cases to explain the effect of aerosol on precipitation.

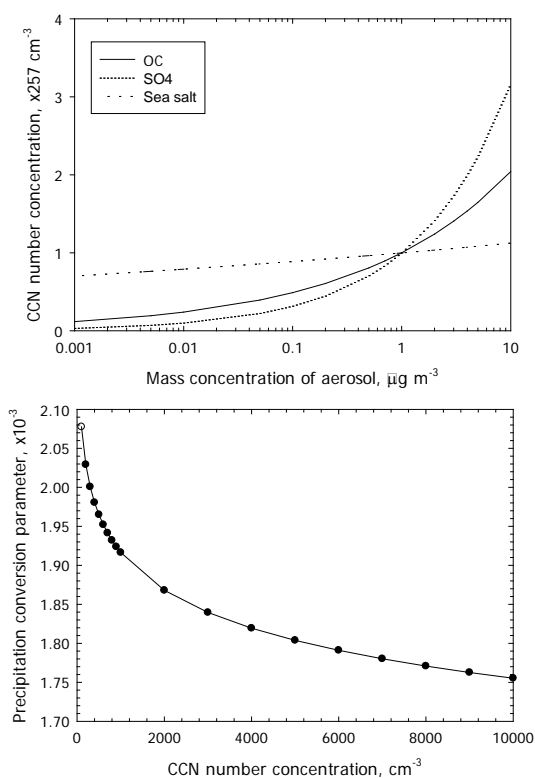


Figure 1. CCN number concentration (NCCN) calculated with mass concentration of aerosol species (top) and the change of precipitation conversion parameter for NCCN (bottom).

This work has been carried out through the R&D project on the development of global numerical weather prediction systems of Korea Institute of Atmospheric Prediction Systems (KIAPS) funded by Korea Meteorological Administration (KMA).

Chin, M., Rood R. B., Lin S.-J., Muller J. F., and Thompson A. M. (2000) *J. Geophys. Res.* **105**, 24671-24687.

Lohmann, U. and Feichter, J. (2005) *Atmos. Chem. Phys.* **5**, 715-737.

Morcrette, J.-J., Benedetti, A., Ghelli, A., Kaiser, J. W., and Tompkins, A. M. (2011) *ECMWF Technical memorandum* 660.

Twomey, S. (1974) *Atmos. Environ.* **8**, 1251-1256.

## The effect of aerosol-cloud interactions on shallow marine clouds

T. Raatikainen<sup>1</sup>, J. Ahola<sup>1</sup>, J. Tonttila<sup>2,3</sup>, S. Romakkaniemi<sup>2</sup>, A. Laaksonen<sup>1</sup> and H. Korhonen<sup>1</sup>

<sup>1</sup>Climate Research, Finnish Meteorological Institute, P.O. Box 503, 00101 Helsinki, Finland

<sup>2</sup>Atmospheric Research Centre of Eastern Finland, Finnish Meteorological Institute, P.O. Box 1627, 70211 Kuopio, Finland

<sup>3</sup>Karlsruhe Institute of Technology, Karlsruhe, Germany

Keywords: LES, modelling, precipitation, climate.

Presenting author email: tomi.raatikainen@fmi.fi

Shallow clouds dominate subtropical and polar oceans, which makes these clouds important for the Earth's radiation budget. Dynamics of these shallow clouds is driven largely by radiative cooling from cloud tops and turbulent transport of moisture and heat from the sea surface. Moreover, cloud formation requires aerosol that act as cloud condensation nuclei (CCN). Because availability of CCN is often limited in remote marine regions, aerosol can have significant effect on cloud dynamics. Understanding aerosol effects requires models that are applicable to shallow clouds and contain aerosol that can interact with water vapour and cloud species. Here we use recently developed UCLALES-SALSA model (Tonttila *et al.*, 2017) to examine interactions between shallow marine clouds and aerosol.

UCLALES-SALSA is based on a well-known Large Eddy Simulation (LES) model UCLALES (Stevens *et al.*, 1999 & 2005) which was coupled with a sectional aerosol module SALSA (Kokkola *et al.*, 2008). The LES model solves the turbulent transport equations and takes care of the transport of scalar variables from the SALSA module. SALSA module takes care of aerosol and cloud microphysics including cloud activation and rain formation.

UCLALES-SALSA was initialized using meteorological boundary conditions from the Arctic Summer Cloud Ocean Study (ASCOS) described by Tjernström *et al.* (2014). Two different initial aerosol concentrations (30 and 80 cm<sup>-3</sup>) were selected, but these were allowed to change after 3 hour spin-up. Observations have shown that a continuous cloud layer can break-up when CCN concentration is less than ~10 cm<sup>-3</sup>. One of our aims is to see if this behaviour can be captured by UCLALES-SALSA simulations.

Figure 1 shows the average cloud properties from the two simulation cases (high and low CCN concentrations). These are quite similar during the first six hours, but then the differences become clear. Cloud layer starts to descend in the low CCN simulation due to the formation of precipitation and its evaporation below cloud base. When precipitation reaches the surface after about 10 hours, some CCNs are permanently lost. This leads to a rapid decrease in cloud droplet number concentration (CDNC) and break-up of the continuous cloud layer. The remaining clouds are optically thin containing low concentrations of large cloud drops and small drizzle drops. When the initial CCN concentration is higher (80 cm<sup>-3</sup>), steady cloud layer is observed throughout the simulation.

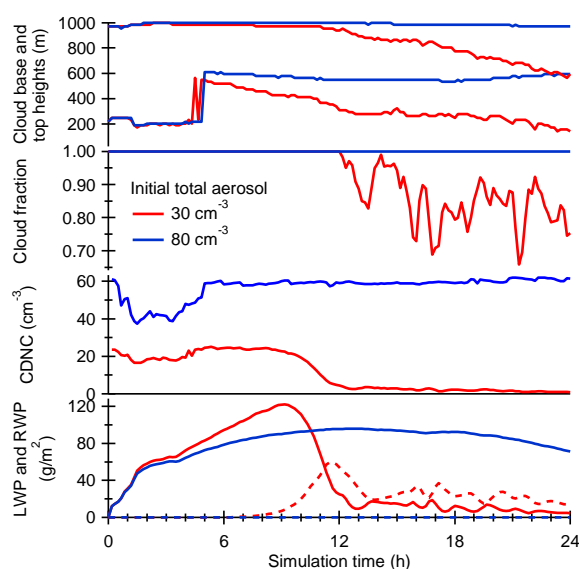


Figure 1. Mean cloud properties (cloud layer altitude, cloud fraction, cloud droplet number concentration, and liquid (solid line) and rain (dashed line) water paths) from simulations where the initial aerosol concentrations are 30 and 80 cm<sup>-3</sup>.

UCLALES-SALSA model was able to simulate a case where a continuous cloud layer broke-up due to the lack of potential CCN, which were removed by wet deposition. Such cases can be seen when the initial aerosol concentration is sufficiently low.

This work was supported by the European FP7 project BACCHUS (Grant agreement no: 603445) and European Research Council project ECLAIR (grant no: 646857).

- Kokkola, H., Korhonen, H., Lehtinen, K. E. J., Makkonen, R., Asmi, A., Järvenoja, S., Anttila, T., Partanen, A.-I., Kulmala, M., Järvinen, H., Laaksonen, A., and Kerminen, V.-M. (2008) *Atmos. Chem. Phys.*, **8**, 2469-2483.
- Stevens, B., Moeng, C.-H., and Sullivan, P.P. (1999) *J. Atmos. Sci.*, **56**, 3963-3984.
- Stevens, B., et al. (2005) *Mon. Wea. Rev.*, **133**, 1443-1462.
- Tjernström, M., et al (2014) *Atmos. Chem. Phys.*, **14**, 2823-2869.
- Tonttila, J., Maalick, Z., Raatikainen, T., Kokkola, H., Kühn, T., and Romakkaniemi, S. (2017) *Geosci. Model Dev.*, **10**, 169-188.

## Impact of heat treatment and cloud cycling on single particle chemical composition of soil dust

X. Shen, R. Ramisetty, H. Saathoff, T. Schiebel, K. Höhler, O. Möhler, and C. Mohr  
Institute of Meteorology and Climate Research, Karlsruhe Institute of Technology, Hermann-von-Helmholtz-Platz 1, 76344 Eggenstein-Leopoldshafen, Germany

Keywords: soil dust particles, chemical composition, ice nucleation, single particle mass spectrometry  
Presenting author email: xiaoli.shen@kit.edu

Soil dust particles are considered to be the second largest primary atmospheric particle source globally (Silva et al., 2000). The major inorganic components, e.g. minerals, and organic species of soil dust particles may play a yet unclear but potentially crucial role in atmospheric ice nucleation (O'Sullivan et al., 2014; Tobo et al. 2014; Hill et al., 2016). Large knowledge gaps still exist related to the chemical composition of the organic and inorganic components, their mutual interaction, and the influence of the organic components on the propensity of soil dust particles to act as ice nucleating particles (INPs).

We deployed a Laser Ablation Aerosol Particle Time-of-Flight Mass Spectrometer (LAAPTOF, Aeromegt GmbH) at the Aerosol Interaction and Dynamics in the Atmosphere (AIDA) simulation chamber during the SOIL02 campaign, aiming to compare the chemical composition of different soil dust particles with their ice nucleating behaviour. Four different soil dusts sampled at two sites in Germany (SDGe01 and SDPA01), Argentina (SDAr08), and Wyoming (USA) (SDWY01) were studied with and without heat treatment (2 hours at 300°C in air), as well as before and after cloud expansion. The LAAPTOF, capable of measuring the chemical composition and mixing state of individual aerosol particles on line (Gemayel et al., 2016), typically recorded positive and negative ion mass spectra of several hundred individual particles of each soil dust type before and after cloud expansion experiments in the temperature range 228–260 K.

The characteristics of the size dependent chemical composition of the differently treated soil dust particles before and after cloud expansion experiments are: 1) the mass spectral peak patterns are similar for all soil dust particle types studied and are dominated by mineral components (c.f. Fig. 1). 2) We found more elemental carbon (EC) in the heated samples than in the untreated ones, especially for smaller particles. 3) Compared to the untreated samples, the peaks related to nitrogen-containing organic compounds ( $m/z$  26  $CN^-$ ) and EC are much more pronounced for heat treated samples, while the peaks indicative of organic acids ( $m/z$  45  $COOH^-$ ) are substantially reduced. Our experiments show that heated particles are less ice-active than untreated ones. 4) After cloud cycling of the soil dust particles, less hydrocarbon signatures were visible. This might be caused by their preferred cloud activation and subsequent loss by settling.

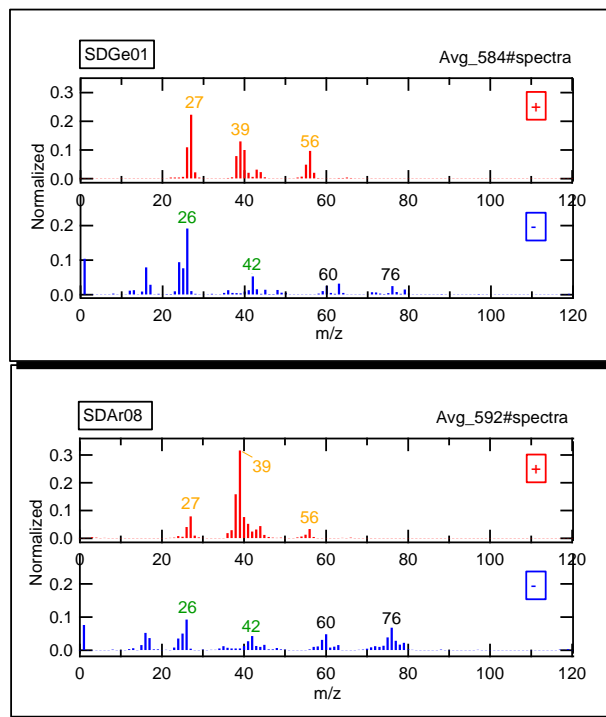


Figure 1. Average mass spectra for German (SDGe01) and Argentinian (SDAr08) soil dust particles. Black tags represent inorganic fragments; green tags represent organic fragments; orange tags represent fragments resulting from inorganic and organic species.

The changes of both the ice nucleation activity and the single particle composition with heat treatment will be discussed.

- Gemayel et al. (2016) *Atmos. Meas. Tech.* **9**, 1947–1959.  
Hill et al. (2016) *Atmos. Chem. Phys.* **16**, 7195–7211.  
O'Sullivan et al. (2014) *Atmos. Chem. Phys.* **14**, 1853–1867.  
Silva et al. (2000) *Atmos. Environ.* **34**, 1811–1820.  
Tobo et al. (2014) *Atmos. Chem. Phys.* **14**, 8521–8531.

## Hygroscopic properties and surface activity of pollenkitt and its importance for cloud activation of pollen particles

J.J. Lin<sup>1,6</sup>, S.K. Purdue<sup>1</sup>, H. Lin<sup>2</sup>, J.C. Meredith<sup>2</sup>, A. Nenes<sup>1,2,3,4</sup>, and N.L. Prisle<sup>1,2,5,6</sup>

<sup>1</sup>School of Earth & Atmospheric Sciences, Georgia Institute of Technology, Atlanta, 30332, USA

<sup>2</sup>School of Chemical & Biomolecular Engineering, Georgia Institute of Technology, Atlanta, 30332, USA

<sup>3</sup>Institute of Chemical Engineering Sciences (ICE-HT), FORTH, Patras, GR-26504, Greece

<sup>4</sup>Institute for Environmental Research and Sustainable Development, NOA, Athens, GR-15236, Greece

<sup>5</sup>Department of Physics, University of Helsinki, Helsinki, 00014, Finland

<sup>6</sup>Nano and Molecular Systems Research Unit, University of Oulu, Oulu, 90014, Finland

Keywords: bioaerosols, pollenkitt, surface activity, cloud activation.

Presenting author email: Nonne.Prisle@oulu.fi

Bioaerosols are atmospheric particles that are released directly into the atmosphere from the biosphere. They can serve as nuclei for water droplets and ice crystals and can therefore potentially impact Earth's hydrological cycle and radiative balance (Fröhlich-Nowoisky *et al.*, 2016). Pollen is an important class of bioaerosol that exhibits a remarkable breadth of complex solid surface features. In addition, many pollen grains are coated with a viscous, hydrophobic liquid, pollenkitt, thought to play important roles in pollen dispersion and adhesion (Lin *et al.*, 2013). The composition of pollenkitt is likely distinct between different plant species, but generally a hydrophobic mixture of saturated and unsaturated lipids, carotenoids, flavonoids, and proteins and carbohydrates (Pacini and Hesse, 2005). Hydration at high humidity has been found to change pollenkitt properties and its capillary adhesion that may in turn affect its atmospheric lifetime of pollen and ability of pollen to act as atmospheric condensation nuclei (Lin *et al.*, 2015). The molecular and functional composition of pollenkitt suggest that they may be surface active in aqueous solution, as is also the case for many other environmental organics. Surface activity may affect pollenkitt response to hydration in ways analogous to e.g. marine fatty acids (Prisle *et al.* 2008; 2010).

In this work, we present measurements of supersaturated hygroscopicity and surface tension of pollenkitt extracted from the pollen of six different species. Scanning Mobility CCN Analysis (SMCA) is used to make rapid measurements of size-resolved CCN distributions of the pollenkitt extract for supersaturations between 0.1-1.4%.

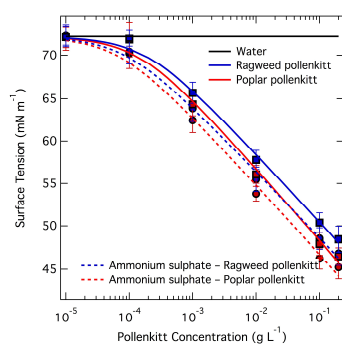


Figure 1. Surface tension depression as a function of pollenkitt aqueous concentration.

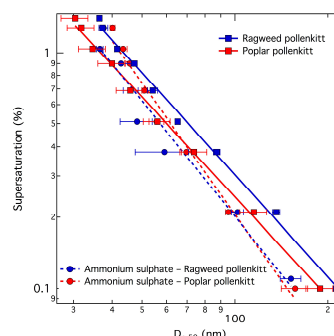


Figure 2. Critical supersaturation as a function of dry diameter two pollenkitts and their mixtures with ammonium sulfate.

A video contact angle system was used to systematically characterize surface activity of aqueous pollenkitts and their mixtures with ammonium sulfate at a wide range of concentrations, confirming the surface activity of pollenkitt in water. This is used for detailed thermodynamic characterization of the impact of surface activity on warm cloud activation potential (Prisle *et al.*, 2011).

This work was supported by the Finnish Academy of Sciences (257411) and a Georgia Power Faculty chair and a Cullen-Peck Fellowship from the Georgia Institute of Technology. This project has received funding from the European Research Council (ERC) under the European Union's Horizon 2020 research and innovation programme (grant agreement No 717022).

Fröhlich-Nowoisky, J. *et al.* (2016) *Atmos. Res.*, **182**, 346-376.

Lin, H., Gomez, I. and Meredith, J.C. (2013) *Langmuir*, **29**, 3012-3023.

Lin, H. *et al.* (2015) *J. Colloid Interface Sci.*, **442**, 133-139.

Paccini, E. and Hesse, M. (2005) *Flora*, **200**, 399-415.

Prisle, N.L. *et al.* (2008), *Tellus*, **60B**, 416-431.

Prisle, N.L. *et al.* (2010), *Atmos. Chem. Phys.*, **10**, 5663-5683.

Prisle, N.L., Dal Maso, M., and Kokkola, H. (2011) *Atmos. Chem. Phys.*, **11**, 4073-4083.

## The Lille Ice Nucleation Chamber (LINC). Reproducing in laboratory conditions the heterogeneous nucleation of ice on aircraft soot.

J. Wu, A. Faccinnetto, S. Batut, D. Petitprez and P. Desgroux

<sup>1</sup>PC2A UMR8522, University of Lille1, Villeneuve d'Ascq, 59655, France

Keywords: condensation trails, soot, aviation, heterogeneous nucleation, ice nucleation chamber

Presenting author email: alessandro.faccinnetto@univ-lille1.fr

Within this project we aim to a better understanding of the indirect role of aircraft soot on persistent cloud formation. Aircraft jet engines release in the high troposphere soot aerosols that potentially act as condensation nuclei for water and ice. The nucleated ice particles and water droplets form the so called condensation trails (*contrails*) that may evolve in persistent cirrus-like clouds when the conditions are favorable and therefore impact the local radiative balance of the atmosphere especially in high density air traffic regions. In order to provide information on the onset of thermodynamic condition at which heterogeneous nucleation of ice occurs, a dedicated experiment, the *Lille ice nucleation chamber* (LINC), has been built at PC2A laboratory and it is currently in early testing stage. The LINC is a continuous flow diffusion chamber based on the system first developed at the Colorado State University (CSU-CFDC)<sup>1</sup> which then evolved in the *Zurich ice nucleation chamber* (ZINC) built at the Swiss Federal Institute of Technology<sup>2</sup>. Temperature as low as  $-50^{\circ}\text{C}$  and ice supersaturation as high as 140% can be reached. A short timescale, up to 10 s, is chosen in order to simulate the early steps of the formation of contrails.

The main goal of this work in progress is to validate the experimental protocol to operate the LINC and nucleate ice particles under reproducible conditions. The measurements on the efficiency of soot particles as ice nuclei are still subject to large uncertainty, it is therefore our opinion that experiments aiming to reproduce ice nucleation at laboratory scale should detail the experimental conditions as thoroughly as possible. Hence, we present a first complete characterization of the onset of conditions in which ice particles are nucleated inside the LINC. Since the methodology behind the operation of ice nucleation chambers is not yet fully validated, this approach will help creating a common measurement protocol, possibly at international level. The investigated variables include the ice layer thickness, the iced walls temperature map, the flow conditions and a detailed characterization of the seeding aerosols. In particular, soot aerosols are generated in laboratory flames and have morphology close to that of aeronautics soot<sup>3</sup>. In a typical experiment, soot aerosols are sampled by means of a quartz microprobe, size selected, dried and finally injected into the LINC at controlled temperature, pressure and ice supersaturation. The comparison of the data obtained from different measurements is expected to provide original and useful information on the interaction between soot aerosols and water.

This work is supported by Labex CaPPA and by project MERMOSE.

<sup>1</sup>D.C. Rogers, *Atmos. Res.* **22** (1988) 149-181.

<sup>2</sup>O. Stetzer, B. Baschek, F. Lüönd, U. Lohmann, *Aerosol Sci. Technol.* **42** (2008) 64-74.

<sup>3</sup>C. Irimiea, Y. Carpentier, I.K. Ortega, M. Ziskind, A. Faccinnetto, F.X. Ouf, F. Salm, D. Delhayé, D. Gaffié, A. Bescond, J. Yon, E. Therssen, C. Focsa, *Proceedings of the European Combustion Meeting 2015*, P5-04.

## The effects of heterogeneous ice formation on precipitation in a deep convective cloud: Model simulations with COSMO-SPECS

K. Diehl<sup>1</sup>, M. Simmel<sup>2</sup>, and V. Grützun<sup>3</sup>

<sup>1</sup>Institute of Atmospheric Physics, University of Mainz, 55099, Germany

<sup>2</sup>Leibniz Institute for Tropospheric Research, Leipzig, 04318, Germany

<sup>3</sup>Meteorological Institute, University of Hamburg, 20146, Germany

Keywords: model simulations, heterogeneous freezing, ice nucleating particles.

Presenting author email: kdiehl@uni-mainz.de

In deep convective clouds reaching 14 km altitudes with temperatures below  $-40^{\circ}\text{C}$  a large fraction of ice is formed by homogeneous drop freezing. However, additional effects of heterogeneous freezing processes taking place already at higher temperatures at lower altitudes may modify the ice particle spectra in a way that eventually precipitation is affected.

Model simulations are performed with the 3D cloud-resolving model COSMO-SPECS which provides a link between aerosol particles, cloud properties, and precipitation (Grützun *et al.*, 2008). It contains a spectral microphysical scheme for aerosols and hydrometeors. Idealized test cases are investigated by using vertical profiles of temperature and dew point from Weisman and Klemp (1982) and an initial particle number size distribution from Kreidenweis *et al.* (2003). The complete model domain includes  $80 \times 80 \text{ km}^2$  with an altitude of 18 km. A deep convective cloud of 20 km diameter is initialized by a temperature disturbance of 1.5K.

Homogeneous freezing may occur at temperatures below  $-37^{\circ}\text{C}$  according to volume and molality of the drops (Diehl and Wurzler, 2004). Immersion, contact, and deposition freezing are described particle-type dependant (Diehl and Mitra, 2015). Simulated ice nucleating particle types (INP) are mineral dust and biological particles. Active INPs are defined as part of the initial particle spectrum with variable fractions  $F_{INP}$ . The reference case is with homogeneous freezing only. More cases are simulated with additional heterogeneous freezing, with varying contributions from the different freezing modes and with varying fractions of different INP types.

The results indicate significant differences in the temporal development of precipitation but less deviations in the total precipitation amounts which are determined by the INP type and by the contributing freezing processes. An example is shown in Figure 1 for ice-active fractions of 0.1% mineral dust particles (feldspar, illite, and kaolinite).

Most cases given in Figure 1 indicate a similar behavior as the reference case but with reduced precipitation during early cloud stages. In contrast, kaolinite in the immersion mode only (light blue line) affects an enhancement of precipitation during early cloud stages. Additional deposition freezing (yellow line) leads to a reduction during early cloud stages while additional both deposition and contact freezing (rose line) result in an enhancement at later cloud stages and an increased total precipitation after 3 h model run time.

Evaluating ice water mixing ratios and ice particle spectra of different cases illustrates how ice formation influences precipitation. In cases with more primary ice formation by direct drop freezing high numbers of small ice particles are formed. As a result, more condensed water stays in the cloud. In contrast, in cases with less primary ice formation more ice is formed via growth and riming processes, i.e. the ice mass increases and larger ice particles are formed. As a result more condensed water is removed from the cloud.

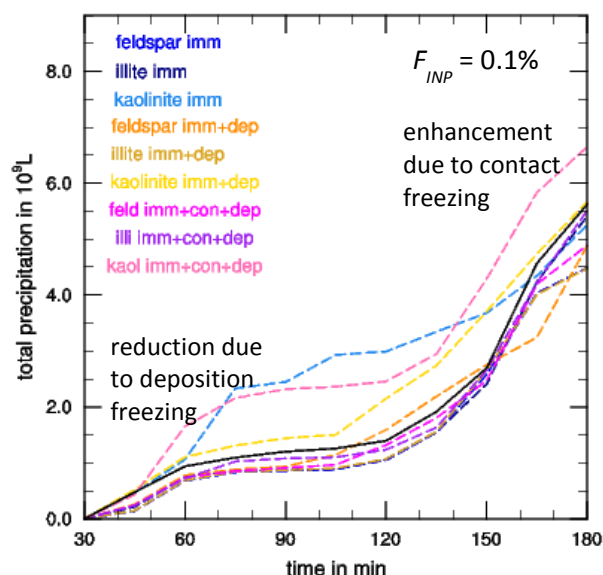


Figure 1. Temporal development of total precipitation.

Black line: reference case homogeneous freezing.

Coloured lines: INP types and active freezing modes.

This work is part of the research group INUIT and is supported by the Deutsche Forschungsgemeinschaft under grant DI 1539/1-2.

Diehl, K., and Wurzler, S. (2004) *J. Atmos. Sci.* **61**, 2063-2072.

Diehl, K., and Mitra, S.K. (2015) *Atm. Chem. Phys.* **15**, 12741-12763.

Grützun, V., Knöth, O., and Simmel, M. (2008) *Atm. Res.* **90**, 233-242.

Kreidenweis, S., et al. (2003) *J. Geophys. Res.* **D7**, 4213.

Weisman, M., and Klemp, J. (1982) *Mon. Weather Rev.* **110**, 504-520.

## Inferring cloud super-saturations by combining below-cloud cloud condensation nuclei and in-cloud cloud droplet residual and interstitial particle measurements

S. Mertes<sup>1</sup>, S. Henning<sup>1</sup>, W. Birmili<sup>1,2</sup>, A. Beyer<sup>1</sup>, R. Otto<sup>1</sup>, D. van Pinxteren<sup>1</sup>, K. Dieckmann<sup>1</sup>,  
A. Wiedensohler<sup>1</sup>, F. Stratmann<sup>1</sup> and H. Herrmann<sup>1</sup>

<sup>1</sup> Leibniz Institute for Tropospheric Research, Leipzig, 04318, Germany

<sup>2</sup> now at Umweltbundesamt, Berlin, 14195, Germany

Keywords: cloud super-saturation, activation diameter, cloud condensation nuclei, cloud droplet residuals.

Presenting author email: Stephan.mertes@tropos.de

In 2010 the Hill Cap Cloud Thuringia (HCCT2010) cloud field experiment was conducted in a low mountain range in the centre of Germany (Tilgner *et al.*, 2014) deploying three measurement sites (Fig.1). At southwesterly winds air masses had to pass the Schmücke (SM) mountain ridge while Goldlauter (GL) is located upwind.

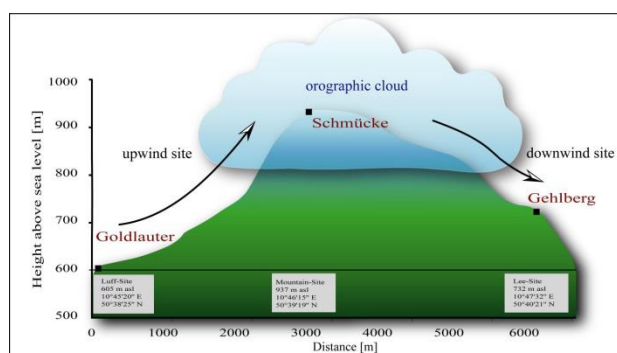


Figure 1. Sketch of the experimental methodology of HCCT2010 with three measurement sites

In this study, measurements are taken into account when a connected flow between the stations existed and the summit station was engulfed in a cloud. Thus, particles measured at GL are considered as the below cloud aerosol that become potentially activated at the cloud base and thereby forming and maintaining the cloud.

In GL, aerosol particles are characterized for their cloud condensation nuclei (CCN) capabilities by size-resolved drop activation measurements at four different super-saturations (SS) by means of a CCN counter (Henning *et al.*, 2014). The 50 % activation diameter  $D_{50\%}$ , and the hygroscopicity parameter  $\kappa$ , are derived for each adjusted SS.

At SM an interstitial inlet (INT) and a counterflow virtual impactor (CVI) were operated side by side in order to separately collect interstitial particles (IP) and drops inside cloud (Mertes *et al.*, 2005). Inside the CVI system collected cloud drops are evaporated releasing dry cloud drop residual particles (CDR), which are expected to be closely related to the original cloud condensation nuclei forming the clouds. Downstream both inlets, the particle number size distribution of IP and CDR were simultaneously determined by two mobility particle size spectrometers. From the particle number size distributions, size-dependent fractions of activated particles

can be derived, similar to the ones obtained by the CCNC measurements in GL.

For the cloud period FCE\_1.1-4 the activation fractions determined inside (from CVI and INT) and below cloud (CCNC) are given in Fig.2.

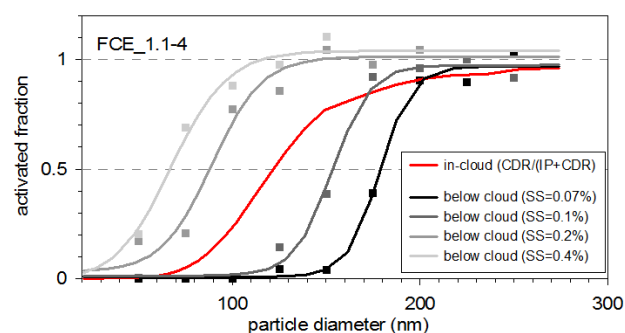


Figure 2. Activated particle fractions as a function of particle diameter measured below cloud for different SS and in-cloud

Obviously the cloud SS was between 0.1 and 0.2 %. In order to further constrain this value,  $\kappa$  from the below cloud measurements and the  $D_{50\%}$  from the in-cloud measurement are used to infer the actual SS in the prevailing cloud. This is an alternative approach to Krüger *et al.* (2014), who deployed a CCNC behind an interstitial inlet. With the presented approach, the absolute level and the course of the super-saturation in different cloud events of HCCT2010 are tracked. This offers a new empirical approach to infer cloud SS, which is not directly measurable.

This work was supported by the German Research Foundation DFG-SPP 1294, grants HE 939/25-1 and ME 3534/1-2.

Henning, S., Dieckmann, K., *et al.* (2014) *Atmos. Chem. Phys.* **14**, 7859-7868.

Krüger, M. L., Mertes, S., *et al.* (2014) *Atmos. Meas. Tech.* **7**, 2615-2629.

Mertes, S., Lehmann, K., *et al.* (2005) *Atmos. Environ.* **39**, 4247-4256.

Tilgner, A., Schöne, L., *et al.* (2014), *Atmos. Chem. Phys.*, **14**, 9105-9128.

## Observational evidence for aerosols increasing upper tropospheric humidity

L. Riuttanen<sup>1</sup>, M. Bister<sup>1</sup>, V.-M. Kerminen<sup>1</sup>, V. O. John<sup>2,3</sup>, A.-M. Sundström<sup>1,a</sup>, M. Dal Maso<sup>4</sup>, J. Räisänen<sup>1</sup>, V. A. Sinclair<sup>1</sup>, R. Makkonen<sup>1</sup>, F. Xausa<sup>1</sup>, G. de Leeuw<sup>1,5</sup> and M. Kulmala<sup>1</sup>

<sup>1</sup>Department of Physics, University of Helsinki, P.O. Box 64, 00014 Helsinki, Finland.

<sup>2</sup>Met Office Hadley Centre, FitzRoy Road, Exeter, Devon, EX1 3PB, UK.

<sup>3</sup>EUMETSAT, Eumetsat Allee 1, 64295 Darmstadt, Germany.

<sup>4</sup>Tampere University of Technology, P.O. Box 692, 33101 Tampere, Finland.

<sup>5</sup>Finnish Meteorological Institute, P.O. Box 503, 00101 Helsinki, Finland.

<sup>a</sup>now at: EMPA, Swiss Federal Laboratories for Materials Science and Technology, Überlandstrasse 129, 8600 Dübendorf, Switzerland.

Keywords: aerosol-cloud interactions, deep convection, upper tropospheric humidity, aerosol optical depth.

Presenting author email: laura.riuttanen@helsinki.fi

Aerosol-cloud interactions are the largest source of uncertainty in the current radiative forcing estimates of the global climate (Boucher et al., 2013). Especially processes related to deep convective clouds are yet poorly understood (Tao et al., 2012). A recent study by Riuttanen et al. (2016) shows strong observational evidence that aerosols are increasing upper tropospheric humidity (UTH). As the radiative transfer is highly sensitive to UTH (Held and Soden, 2000), this means aerosols may have a more positive radiative forcing on climate than currently taken into account in the estimates of the anthropogenic climate change.

Ramanathan et al. (2001) suggested that aerosol-induced suppression of precipitation in the updrafts of deep clouds can transport more water into the upper troposphere. But even without changes in the total amount of precipitation, changes in cloud microphysics, namely sublimation of the increased amount of hydrometeors in the upper troposphere, can increase the UTH (Bister and Kulmala, 2011).

In this study we used satellite data from June, July and August in years 2007-2013. The China outflow region was chosen for a more detailed study (25-45 °N, 120-149 °E). UTH, i.e. the relative humidity with respect to water, in a layer between approximately 200 and 500 hPa, was obtained from the microwave humidity sounder (MHS, Bonsignori; 2007) onboard the MetOp-A satellite. A microwave method developed by Buehler et al. (2008) enabled us to detect relative humidities also in the areas of anvil clouds. We used AOD from the Moderate Resolution Imaging Spectroradiometer (MODIS) instrument onboard the Terra satellite (Remer et al., 2005) and the daily rainfall product, 3B42, from the Tropical Rainfall Measuring Mission (TRMM) multisatellite analysis (Huffman et al., 2007) in this study.

The UTH data were binned according to daily precipitation in the same 1°x1° grid. The applied data were restricted to those cases when the daily precipitation was more than 1 mm.

ERA-Interim reanalysis data (Dee et al., 2011) were used to study the possible meteorological covariation of AOD and UTH in the study area. The sensitivity of the radiative transfer to perturbations in the

UTH was tested by using the libRadtran radiative transfer code (Mayer and Kylling, 2005).

Higher values of UTH were observed in association with high AOD. AOD was observed to increase almost linearly as a function of cirrus fraction. Linear regression was applied to AOD data in order to remove any possible data contamination by cirrus.

Considerable efforts were made to study the effect of meteorological covariation or other possible causes behind the observations. We conclude that any other causes but aerosols behind the increase in UTH are very unlikely.

This work was supported by the Academy of Finland Center of Excellence program (project number 272041) and the COST Action / M. B.

Bister, M. and Kulmala, M. (2011). *Atmos. Chem. Phys.*, 11(9):4577-4586.

Bonsignori, R. (2007). *Proc. SPIE* 6744, Sensors, Systems, and Next-Generation Satellites XI, 67440A.

Boucher, O., et al. (2013). Clouds and Aerosols, book section 7, p. 571-658. In: *Climate Change 2013: The Physical Science Basis*. Cambridge University Press, Cambridge, United Kingdom and New York, NY, USA.

Buehler, S. A., et al. (2008). *J. Geophys. Res.*, 113(D14):D14110.

Dee, D., et al. (2011). *Q. J. R. Met. Soc.*, 137(656):553-597.

Huffman, G. J., et al. (2007). *J. Hydrometeorol.*, 8(1):38-55.

Mayer, B. and Kylling, A. (2005). *Atmos. Chem. Phys.*, 5:1855-1877.

Ramanathan, V., Crutzen, P., Kiehl, J., and Rosenfeld, D. (2001). *Science*, 294(5549):2119-2124.

Remer, L., et al. (2005). *J. Atmos. Sci.*, 62(4):947-973.

Riuttanen, L., et al. (2016). *Atmos. Chem. Phys.*, 16(22):14331-14342.

Tao, W.-K., Chen, J.-P., Li, Z., Wang, C., and Zhang, C. (2012). *Rev. Geophys.*, 50:RG2001.

## Cloud condensation nuclei (CCN)-activation behaviour of atmospheric black carbon particles in relation to their size and mixing state

G. Motos<sup>1</sup>, J. Schmale<sup>1</sup>, J.C. Corbin<sup>1</sup>, M. Zanatta<sup>1,2</sup>, U. Baltensperger<sup>1</sup> and M. Gysel<sup>1</sup>

<sup>1</sup>Laboratory of Atmospheric Chemistry, Paul Scherrer Institute, 5232 Villigen PSI, Switzerland

<sup>2</sup>Now at Alfred Wegener Institute, Helmholtz Centre for Polar and Marine Research, Bremerhaven, Germany

Keywords: black carbon, coating, fog, CCN  
Presenting author email: [ghislain.motos@psi.ch](mailto:ghislain.motos@psi.ch)

Black carbon (BC) is formed during the combustion of fossil and biogenic fuels. It is most often emitted bare, thus non hygroscopic, or internally mixed with non-hygroscopic material, but its hygroscopicity can be enhanced by the acquisition of water-soluble coatings (by condensation or coagulation of organic and inorganic materials, see Figure 1). Accurately predicting the rate of this increase in hygroscopicity is a major challenge for current climate models, as it has direct implications on the life-cycle of BC and thus its climate impacts.

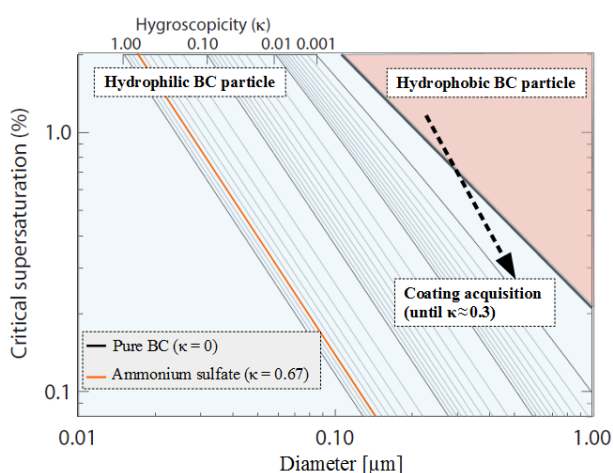


Figure 1. Theoretical CCN-activation as a function of particle hygroscopicity  $\kappa$  and critical supersaturation. The arrow qualitatively represents the modifications of the BC particles properties with acquisition of a water-soluble coating. This figure is modified from Petters and Kreidenweis (2007).

While clouds mainly form above the planetary boundary layer, where the great majority of BC-containing particles are already aged, the presence of fog at low altitudes, close to the sources of BC, enables potential interactions with BC at any aging level.

Furthermore, the significant occurrence of fog on a world scale (mainly subpolar seas, subtropical and middle-latitude coastal areas) justifies the importance of studying its peculiar conditions of CCN-activation, with very low supersaturations compared to clouds. Nonetheless, very few studies have focused on that topic so far. Schroder et al. (2015) showed that BC particles of 95 nm volume-equivalent diameter with median coating thicknesses of at least 65nm were incorporated into low-

altitude cloud droplets with supersaturations similar to the ones found in fog.

In this study, we investigated the droplet activation behavior of BC-containing and BC-free particles in fog conditions in Zurich, Switzerland. We used a total and an interstitial inlet to sample air into a single particle soot photometer (SP2) and two scanning mobility particle sizers (SMPS). A cloud condensation nuclei counter (CCNC) and an aerosol chemical speciation monitor (ACSM) were run in parallel. We were able to identify size-dependent CCN-activation of BC-containing particles (Figure 2). We found that, besides BC core size, also the mixing state with water-soluble coatings, plays a key role for their CCN activity. These results will be discussed in detail and compared with the behavior of BC-free particles.

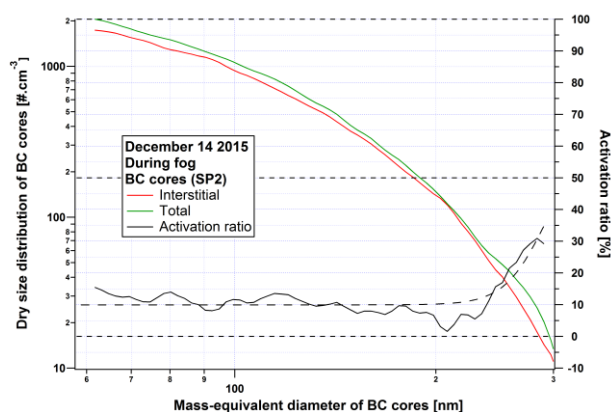


Figure 2. Activation behavior of BC cores during a fog event on December 14, 2015. 10% of cores smaller than around 220 nm activate to fog droplets, while the largest cores have an even higher activation ratio.

This work is supported by the ERC under grant ERC-CoG-615922-BLACARAT and the EU FP7 project BACCHUS (grant no. 603445).

Petters M. D. and Kreidenweis S. M. (2007) A single parameter representation of hygroscopic growth and cloud condensation nucleus activity, *Atmos. Chem. Phys.*, 7, 1961–1971.

J. C. Schroder et al. (2015) Size-resolved observations of refractory black carbon particles in cloud droplets at a marine boundary layer site, *Atmos. Chem. Phys.*, 15, 1367–1383.

## Sampling Arctic Clouds with a New Automated Ground-based Cloud Sampling System

R. Krejci<sup>1</sup>, P. Zieger<sup>1</sup>, J. Ström<sup>1</sup>, H.C. Hansson<sup>1</sup>, P. Tunved<sup>1</sup>, C. Ritter<sup>2</sup>, R. Neuber<sup>2</sup>, Y.J. Yoon<sup>3</sup>, M. Ramstrom<sup>4</sup>, and F.J. Brechtel<sup>5</sup>

<sup>1</sup>Department of Environmental Science and Analytical Chemistry, Stockholm University, Stockholm, Sweden

<sup>2</sup>Alfred Wegener Institute, Potsdam, Germany

<sup>3</sup>Korea Polar Research Institute, Incheon, Korea

<sup>4</sup>Hugo Tillquist AB, 164 22 Kista, Sweden

<sup>5</sup>Brechtel Manufacturing Incorporated, Hayward, CA, 94544, USA

Keywords: Arctic, cloud, GCVI, CCN.

Presenting author email: fredj@brechtel.com

A ground-based Counterflow Virtual Impactor cloud sampling system (GCVI, Brechtel Mfg. Model 1205) has been deployed at mountain-top stations in China, Halifax, Sweden and at the Ny-Alesund Arctic research station. The system automatically detects the presence of cloud and activates a small wind tunnel, all pumps and other components to initiate size-selective cloud droplet sampling over the 6 to 50  $\mu\text{m}$  diameter range. The droplet cut size diameter of the system can be controlled between 6 and 15  $\mu\text{m}$  by varying system air flow rates. All unactivated particles are rejected by the inlet, only droplets larger than the cut size enter the warmed evaporation zone eventually to become residual particles representative of the CCN that originally formed the drops. The GCVI provides up to 15 lpm of sample flow to aerosol instruments and also has an easy-to-clean and replaceable porous tip assembly. An automated inlet switching feature allows the sample flow delivered to instruments to be switched from the GCVI to a clear-sky inlet when the sampling site is no longer in cloud.

Results from validation studies (Shingler et al, 2012) of the performance of the CVI indicate that the measured droplet cut sizes over a range of operating conditions agree with theoretically predicted values within 13%. The number concentration sampling efficiency performance was tested on-board a research aircraft and good agreement found between simultaneous cloud droplet number concentration measurements and CCN residue concentrations measured downstream of the GCVI.

The GCVI has been continuously deployed since November 2015 in the Arctic at the Zeppelin station at Ny-Alesund, Svalbard to study cloud residual microphysical properties on a seasonal basis. Using the GCVI inlet, the cloud residual total particle number concentration, number size distribution, and black carbon content were measured. In addition, the water vapor mixing ratio was measured so that the cloud liquid water content could be estimated. A cloud condensation nuclei counter (CCNC) sampling from the GCVI inlet allowed an estimate to be made of the ambient cloud supersaturation at which particles were activated. Compared to ambient aerosol properties, the size dependent fraction of aerosol particles activated into cloud droplets and ice crystals was derived.

Differences between observed cloud residual properties under different air mass source regions are

explored with the goal of better understanding aerosol-cloud interactions in the Arctic and the potential anthropogenic influence on Arctic clouds.

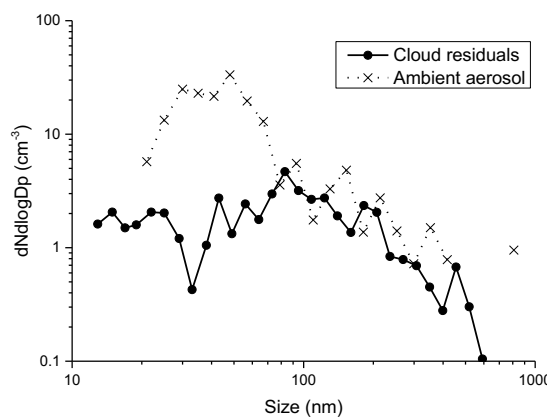


Figure 1. Observed ambient aerosol size distribution (interstitial and cloud activated aerosol) and cloud residual size distribution observed at Zeppelin station on 22 January 2016. For this cloud event, activation diameter is around 0.07  $\mu\text{m}$ .

This work was supported by Swedish Environmental Protection Agency (Naturvårdsverket), The Swedish research Council FORMAS and the Norwegian Polar Institute.

Shingler et al. (2012) Characterisation and airborne deployment of a new counterflow virtual impactor, *Atmos. Meas. Tech.*, **5**, 1259-1269.

Coggon, M. M., A. Sorooshian, Z. Wang, J. S. Craven, A. R. Metcalf, J. J. Lin, A. Nenes, H. H. Jonsson, R. C. Flagan, and J. H. Seinfeld. (2014) Observations of continental biogenic impacts on marine aerosol and clouds off the coast of California. *Journal of Geophysical Research: Atmospheres*, **119**, 6724-6748.

## Single particle analysis of residues from cloud droplets and ice crystals

J. Schneider<sup>1</sup>, S. Mertes<sup>2</sup>, A. Roth<sup>1</sup>, S. Schmidt<sup>1</sup>, H. Clemen<sup>1</sup>,  
T. Klimach<sup>1</sup>, O. Eppers<sup>3,1</sup>, F. Köllner<sup>1</sup>, and S. Borrmann<sup>3,1</sup>

<sup>1</sup>Particle Chemistry Department, Max Planck Institute for Chemistry, Mainz, 55128, Germany

<sup>2</sup>Leibniz Institute for Tropospheric Research, Leipzig, 04318, Germany

<sup>3</sup>Institute for Atmospheric Physics, Johannes Gutenberg University, Mainz, 55128, Germany

Keywords: aerosol-cloud interactions, aerosol mass spectrometry, single particle analysis.

Presenting author email: johannes.schneider@mpic.de

Aerosol-cloud interaction has several aspects: Aerosol particles can act as cloud condensation nuclei (CCN), forming liquid cloud droplets, and as ice nucleating particles (INP) triggering heterogeneous freezing. Both processes are a function of the chemical composition and size of the aerosol particles. Furthermore, cloud processing of aerosols in clouds, i.e., uptake of gas-phase species by cloud droplets, possibly followed by subsequent reversible or irreversible aqueous-phase reactions and the subsequent release of the aerosol particles upon cloud evaporation, alters their chemical composition and size after cloud passage and changes the mixing state and the hygroscopicity of the aerosol particles.

We present the results of various studies conducted between 2010 and 2014 that focused on the analysis of cloud residuals. The studies are: HCCT-2010 (Roth et al., 2016), ACRIDICON-Zugspitze 2012, INUIT-JFJ 2013 (Schmidt et al., 2017), and ML-CIRRUS 2014 (Voigt et al., 2016), including ground based (mountain top experiments) and aircraft based measurements.

The cloud elements (liquid cloud droplets and ice crystals) were sampled by means of a counterflow virtual impactor (CVI), which in addition evaporated the water/ice so that the residuals were analysed by single particle mass spectrometry. The instrument employed was the Aircraft-based Laser Ablation Aerosol Mass Spectrometer ALABAMA (Brands et al., 2011). Different CVI systems were used, dependent on the measurement platform and the type of clouds that were probed: A wind tunnel CVI for ground based liquid cloud sampling (Mertes et al., 2005), the Ice-CVI for ice crystal sampling (Mertes et al., 2007), and the HALO-CVI for aircraft-based sampling.

The residual particle size range that can be sampled and analysed by ALABAMA (approx. 150 - 2000 nm) is not suited for activation studies of CCN, because typically the activation diameter for liquid clouds is in the size range of the lower cut-off diameter of the ALABAMA. However, cloud processing can be studied by comparing the composition of cloud residuals with out-of-cloud aerosol particles. Our results show that uptake of gaseous species leads to a more uniform distribution of inorganic compounds (Roth et al., 2016): The fraction of particles containing nitrate is higher in cloud droplets than in out-of-cloud aerosol, and the same finding holds for sulfate.

The analysis of ice particle residuals (IPR) extracted from mixed-phase clouds showed significant

differences to the out-of-cloud aerosol, thereby giving information on heterogeneous INP (Schmidt et al., 2017). We found that primary particles like minerals and soil dust, but to a larger degree also anthropogenic, metal-containing particles are markedly enhanced in the IPR population, see Table 1.

Table 1. Enhancement factors of particle types in IPR in comparison to out-of-cloud aerosol particles, observed at the mountain station Jungfraujoch in January-February 2013 (Schmidt et al., 2017).

Particle type	Enhancement factor in IPR
biological/amine	1.5 ( $\pm$ 0.7)
biomass burning	--
soil dust	5.5 ( $\pm$ 2.5)
minerals	30 ( $\pm$ 14)
sea salt/cooking emissions	--
aged material	0.09 ( $\pm$ 0.04)
engine exhaust	560 ( $\pm$ 320)
PAH/soot	1.0 ( $\pm$ 0.4)
lead-containing	140 ( $\pm$ 70)
industrial metals	6.2 ( $\pm$ 1.9)
K dominated	0.02 ( $\pm$ 0.02)
Na + K	0.6 ( $\pm$ 0.2)
others	0.9 ( $\pm$ 0.4)

Cirrus cloud residuals studied during ML-CIRRUS onboard the research aircraft HALO showed that the residuals from in-situ cirrus ice crystals resemble the background aerosol to a large degree (Voigt et al., 2016), while residuals from a liquid-origin cirrus showed features of typical CCN (sea salt, nitrate). This observation indicates that different formation and freezing processes are relevant for different types of cirrus clouds.

This work was supported by the DFG (FOR 1525, SPP 1294), and the Max Planck Society.

Brands, M. et al., (2011) *Aerosol Sci. Tech.*, **45**, 46-64 2011.

Mertes, S. et al. (2005) *Atmos. Environ.*, **39**, 4247-4256.

Mertes, S. et al. (2007) *Aerosol Sci. Tech.*, **41**, 848-864.

Roth, A. et al. (2016) *Atm. Chem. Phys.*, **16**, 505-524.

Schmidt, S. et al. (2017) *Atm. Chem. Phys.*, **17**, 575-594.

Voigt, C. et al. (2016) *Bull. Amer. Met. Soc.*, doi:10.1175/BAMS-D-15-00213.1

## Occurrence frequencies of clouds and aerosol PSD in the equatorial area

H. Steli, M. Diouri\*, I. Marsli and A. El khabbouti

Atmospheric Physic Laboratory, University Mohammed 1st, Oujda, 60020, Morocco

Keywords: AERONET, Aerosol optical depth, Cloud optical depth, Sun photometer, Particle size distribution.

Presenting author email: dyourim@gmail.com

This study is based on analysis of the optical properties of atmospheric aerosols using a year available AERONET data (<http://aeronet.gsfc.nasa.gov/>), over five sites that have continuous and representative measurements. We focus our work on cloud and aerosol optical depth, specially their monthly mean values which characterize every site. Other key parameter we studied here is the aerosol particle size distribution APSD determined from the registered spectral AOD and sky brightness measurements. The monthly mean volume APSD variations at the studied sites are analyzed; their statistical characteristics are of course linked to cloud formation and evolution.

Table 1: Location characteristics of the selected stations.

Site	Latitude	Longitude	Altitude
Nauru (1)	0.52S	166.90E	7
Manus (2)	2.06S	147.40E	4
Manaus (3)	2.89S	59.96W	115
CRPSM-Malindi (4)	2.99S	40.19E	12
ARM-Manacapuru (5)	3.21S	60.59W	50

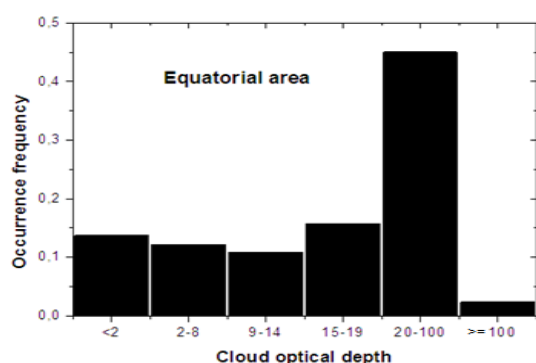


Figure 1: Histogram obtained for the indicated 5 sites. The COD occurrence frequencies of the five studied sites, built on the same histogram (Figure 1), expresses the appearance of different types of clouds provide a comprehensive characterization of the equatorial zone with respect to the appearance of different types of clouds. The clouds optical depth observed in the five sites equatorial have a maximum (> 54%) Recorded in Manus corresponding to the COD in the interval [20-100].

The volume mean distributions of the aerosol are characterized by a coarse mode in the vicinity of 3.02  $\mu\text{m}$  and a fine mode of lesser importance at 0.19 $\mu\text{m}$ .

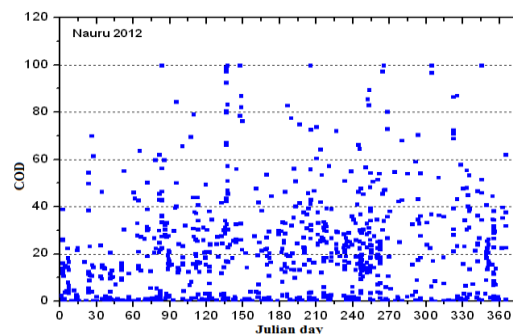


Figure 2. Time series of the COD in the Nauru.

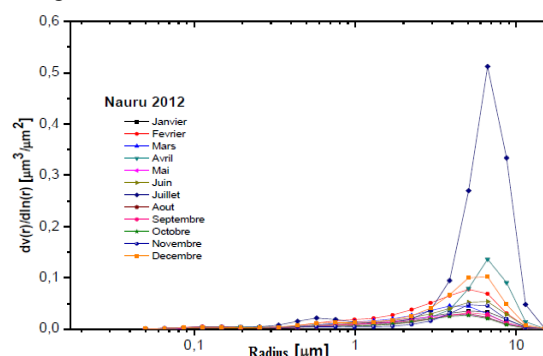


Figure 3: Monthly means of volume PSD at Nauru.

The maximum amplitude of the total volume are recorded in Manus (0.191  $\mu\text{m}^3 / \mu\text{m}^2$ ) which is in the same time, the site where we record a higher occurrence frequency of dense clouds (COD>20 and >100).

Table 2: Monthly means of volume PSD Characteristics

Sites	Fine mode			Coarse mode		
	$r_m$ ( $\mu\text{m}$ )	$\sigma$	$C_v$ ( $\mu\text{m}^3/\mu\text{m}^2$ )	$r_m$ ( $\mu\text{m}$ )	$\sigma$	$C_v$ ( $\mu\text{m}^3/\mu\text{m}^2$ )
(1)	0.20	0.50	0.008	3.21	0.58	0.097
(2)	0.23	0.56	0.012	3.86	0.47	0.179
(3)	0.17	0.49	0.038	2.58	0.72	0.088
(4)	0.16	0.48	0.017	2.62	0.60	0.100
(5)	0.17	0.51	0.037	2.83	0.71	0.089

### References

- John Seinfeld H., Spyros Pandis N., Atmospheric Chemistry and Physics: From Air Pollution to Climate Change, John Wiley & Sons. Inc. 1998.
- El Aouadi I. and Diouri M., Size distributions of aerosol and total atmospheric water vapour content over NE Morocco, J. Aerosol Sci. (2004) 507-508.

### Acknowledgments

Authors want to thank all PI of the AERONET studied sites: Mr. Rick Wagener, Nguyen Xuan Anh, Rick, Jack Molinie, Brent N. Holben and Serm Janjai.

## The impact of photochemistry on the cloud condensation nuclei activity of organic aerosols

N. Borduas<sup>1</sup>, R. Ossola<sup>1</sup>, Z. A. Kanji<sup>2</sup>, K. P. McNeill<sup>1</sup>

<sup>1</sup>Institute for Biogeochemistry and Pollutant Dynamics, ETH Zurich, 8092, Switzerland

<sup>2</sup>Institute for Atmosphere and Climate, ETH Zurich, 8092, Switzerland

Keywords: dissolved organic matter, photochemistry, cloud condensation nuclei, organic aerosol.

Presenting author email: nadine.borduas@usys.ethz.ch

Surface waters, such as marine or freshwater, are the source of a large portion of biogenic atmospheric aerosols globally (Andreae and Rosenfeld, 2008). These aerosols are generated through bubble bursting mechanisms and contain a mixture of inorganic salts and dissolved organic matter (DOM) (Quinn et al., 2015). Lake spray aerosols are a recently recognized source of aerosols, and have been identified to have high organic content compared to sea spray aerosol (Axson et al., 2016).

Aerosols are impacted by photochemistry during their one-week lifetime in the atmosphere, altering their chemical and physical compositions. Hygroscopicity, and thus cloud condensation nuclei (CCN) activity, of organic aerosol is thought to increase with atmospheric aging, but the chemical processes leading to this change are not well characterized (Farmer et al., 2015).

Our research project aims to better understand how photolysis and oxidation reactions impact the hygroscopicity of organic matter found in lake spray aerosol for example (Figure 1). DOM samples from the Dismal Swamp in Virginia were subjected to photochemical reactions in a Rayonet photoreactor and subsequently aerosolized and analyzed using a cloud condensation nuclei counter for their ability to activate clouds. We correlate changes in hygroscopicity, using the kappa parameter (Petters and Kreidenweis, 2007), with changes in chemical composition including, total organic carbon (TOC), pH, UV/Vis absorbance, and CO, CO<sub>2</sub>, acetic acid, pyruvic acid and formic acid production. Importantly, we find that the kappa of DOM increases substantially upon photo-oxidation to above 0.40. This results cannot be explained by organic functional groups and suggests a significant conversion of organic matter into inorganic matter, supported by decreasing TOC values.

Furthermore, we compare the results to authentic cloud water samples. We then attempt to understand the chemical changes using single organic molecule probes. The hygroscopicity parameters determined in these laboratory experiments will help to better characterize the interaction between surface water, biogenic aerosols and cloud activation with the goal of improving climate model predictions.

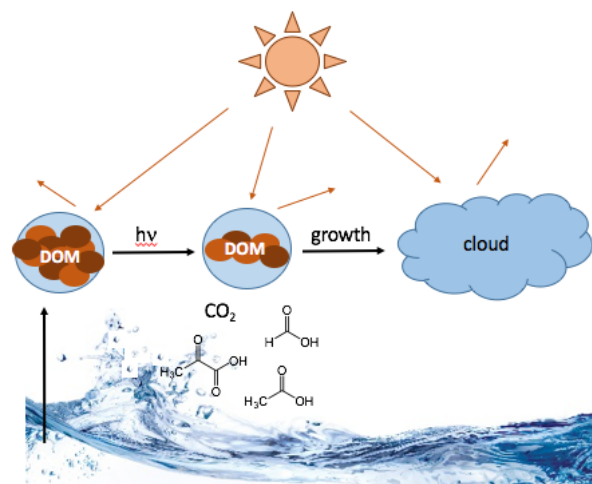


Figure 1: DOM can be present in organic aerosols emitted from surface waters. In the atmosphere, it is exposed to sunlight radiation and gets oxidized to form by-products while change the CCN ability of the aerosol.

This work was supported by ETH and N.B is grateful for a NSERC postdoctoral fellowship.

- Andreae, M.O., Rosenfeld, D., 2008. Aerosol–cloud–precipitation interactions. Part 1. The nature and sources of cloud-active aerosols. *Earth-Sci. Rev.* 89, 13–41. doi:10.1016/j.earscirev.2008.03.001
- Axson, J.L., May, N.W., Colón-Bernal, I.D., Pratt, K.A., Ault, A.P., 2016. Lake Spray Aerosol: A Chemical Signature from Individual Ambient Particles. *Environ. Sci. Technol.* 50, 9835–9845. doi:10.1021/acs.est.6b01661
- Farmer, D.K., Cappa, C.D., Kreidenweis, S.M., 2015. Atmospheric Processes and Their Controlling Influence on Cloud Condensation Nuclei Activity. *Chem. Rev.* 115, 4199–4217. doi:10.1021/cr5006292
- Petters, M.D., Kreidenweis, S.M., 2007. A single parameter representation of hygroscopic growth and cloud condensation nucleus activity. *Atmos Chem Phys* 7, 1961–1971. doi:10.5194/acp-7-1961-2007
- Quinn, P.K., Collins, D.B., Grassian, V.H., Prather, K.A., Bates, T.S., 2015. Chemistry and related properties of freshly emitted sea spray aerosol. *Chem. Rev.* 115, 4383–4399. doi:10.1021/cr500713g

## Effect of sea ice on aerosols in eastern Lapland, Finland

E.-M. Duplissy, R. Väänänen, S. Hakala, T. Petäjä, V.-M. Kerminen and M. Kulmala

Department of Physics, University of Helsinki, 00014 Helsinki, Finland

Keywords: Aerosol concentration, Aerosol size distribution, Sea ice, aerosol-cloud interaction

Presenting author email: ella-maria.duplissy@helsinki.fi

Arctic sea ice is declining rapidly (Stroeve, 2007), which will inevitably have influences on aerosol properties around the Arctic due to the different aerosol sources and sinks over sea ice and open sea. Also, the decreasing sea ice is expected to change the atmospheric circulation patterns (Vihma, 2014). Here we show results how the aerosol concentrations and size distributions change in eastern Lapland, Finland, as a function of the time that the air mass has spent over sea ice or as a function of sea ice area. We also briefly look at the differences during positive or negative phase of North Atlantic Oscillation and Arctic Oscillation.

We calculated daily median size spectrums and aerosol total and modal concentrations for days with at least 15 DMPS spectra and binned those according to how many hours the air mass had spent over sea ice with >80% sea ice concentration (SIC), >15% SIC, open sea and land. Only trajectories which had spent >90% of their travel time north of SMEAR I and where time over land (TOL) was less than 40 hours, were considered. We also excluded all data with SO<sub>2</sub> above 75th percentile. This way we could neglect the effect of high sulphur to aerosol concentrations (Kyrö, 2014). We calculated linear regressions to the modal and total aerosol number concentrations and mode peak diameters as a function of trajectory's travel time over sea ice (TOSI80, TOSI15), time over open sea (TOOS), and TOL. We also looked at the sea ice area (SIA) in different sea areas in the Arctic and compared it to the aerosol concentrations during negative or positive phase of NAO and AO. Since the aerosol concentration is strongly dependent on temperature (Paasonen, 2013), we only looked at temperature range -10-0°C. Within this range, the median accumulation mode concentration is not dependent on temperature at SMEAR I.

During summer, the total aerosol number, Aitken mode and accumulation mode concentrations were decreasing with increasing time the air mass spent over the sea ice (TOSI80, time over sea ice with >80% SIC) by -8.9, -5.3 and -1.6 cm<sup>3</sup>/h, respectively. The Aitken mode diameter was decreasing -0.3 nm/h and the accumulation mode diameter -0.5 nm/h. During winter there was a decrease in total, nucleation mode and Aitken mode concentrations (-1.3, -0.3, -0.6 cm<sup>3</sup>/h, respectively). During winter the Aitken mode did not change but the accumulation mode diameter was increasing 0.5 nm/h. Since the accumulation mode concentration and mean diameter both decrease with increasing time over sea ice in summer, the concentrations of potential CCN could be higher in air masses arriving to continental Arctic from north in the future, as the sea ice continues to decrease. This can affect the cloud properties and radiative balance.

Contrary to the trends in concentrations as a function of TOSI, the aerosol concentrations were increasing with increasing SIA in most of the cases. Statistically most of these trends were not significant, but in many of the trends the R<sup>2</sup> was fairly large. SIA and TOSI, however, are not correlated with each other – majority of SIA values are observed with low TOSI values and on the other hand, there is a large variation of TOSI for high SIA values. For accumulation mode particles, the largest correlation was with SIA in Kara and Barents seas. This sea area is closest to SMEAR I. The trends were smaller during negative NAO or AO and bigger with positive NAO or AO. The largest trends were found with SIA in Greenland Sea. This sea area is located west to northwest of SMEAR I and air masses arrive often at the station through that region.

Both the time that the air mass travels over sea ice or open sea, as well as the sea ice area affect aerosols in Eastern Lapland. However, it is hard to interpret what is the overall effect on clouds and climate when those two exhibit contrasting trends. Further investigations are needed.

This work was supported by the Nordic Centre of Excellence CRAICC (Cryosphere-atmosphere interactions in a changing Arctic climate), Academy of Finland Centre of Excellence program (project no. 1118615) and the European Research Council (project no. 227463).

Kyrö, E.-M., Väänänen, R., Kerminen, V.-M., Virkkula, A., Petäjä, T., Asmi, A., Dal Maso, M., Nieminen, T., Juhola, S., Shcherbinin, A., Riipinen, I., Lehtipalo, K., Keronen, P., Aalto, P. P., Hari, P., and Kulmala, M. (2014). *Atmos. Chem. Phys.* **14**, 4383-4396.

Paasonen, P., Asmi, A., Petäjä, T., Kajos, M. K., Äijälä, M., Junninen, H., Holst, T., Abbatt, J. P. D., van der Gon, H. D., Hamed, A., Hoffer, A., Laakso, L., Laaksonen, A., Leaitch, W. R., Plass-Dülmer, C., Pryor, S. C., Räisänen, P., Swietlicki, E., Wiedensohler, A., Worsnop, D. R., Kerminen, V.-M. and Kulmala, M. (2013). *Nature Geoscience*. **6**, 438-442.

Stroeve, J., M.M. Holland, W. Meier, T. Scambos and M. Serreze (2007). *GRL*. **34**, L09501.

Vihma, T (2014). *Surv. Geophys.* **35**, 1175-1214.

## **Abstracts T202**

## Trends in fog occurrence in Czechia – association with air pollution and climate

I. Hůnová<sup>1</sup>, M. Brabec<sup>2,3,4</sup>, M. Malý<sup>2,3,4</sup> and A. Valeriánová<sup>5</sup>

<sup>1</sup>Ambient Air Quality Department, Czech Hydrometeorological Institute, Prague, Czechia

<sup>2</sup>National Institute of Public Health, Prague, Czechia

<sup>3</sup>Institute of Computer Science, Academy of Sciences of the Czech Republic, Prague, Czechia

<sup>4</sup>Czech Institute of Informatics, Robotics, and Cybernetics, Czech Technical University in Prague, Prague, Czechia

<sup>5</sup>Meteorology and Climatology Department, Czech Hydrometeorological Institute, Prague, Czechia

Keywords: fog, sulphur dioxide, temperature, generalized additive model.

Presenting author email: hunova@chmi.cz

Fog is an obscuration in the surface layer of the atmosphere, which is caused by a suspension of water droplets reducing visibility to less than 1000 m (Meteorological glossary of UK Met Office). Fog has numerous practical connotations, and therefore is recorded on a regular basis at meteorological stations.

Fog is a very complex phenomenon. Its formation, development, and dissipation are related to complex interactions among numerous factors: local microphysical, dynamical, radiative and chemical processes, boundary layer conditions, and large-scale meteorological processes, such as frontal systems (Gultepe et al., 2007). Fog plays a crucial role in atmospheric chemistry. It scavenges aerosol particles and gases from the air, and is a medium for different aqueous phase reactions. Fog may contribute substantially to atmospheric deposition, both in term of water and ion input, in particular in mountain areas (Zimmermann and Zimmermann, 2002), which was documented also for Czechia (Bridges et al., 2002; Hůnová et al., 2011).

For fog formation, the presence in air of hygroscopic particles absorbing water is very important. These are often sulphates and nitrates, fine secondary particles formed via oxidation and condensation of gaseous species. The vast majority of  $\text{SO}_4^{2-}$  and  $\text{NO}_3^-$  particles found in the atmosphere are formed through the oxidation of  $\text{SO}_2$  and  $\text{NO}_x$ , the major source of which is combustion of fossil fuels (Hyslop, 2009).

The fog frequency has been changing in the long run. Analysis of daily observations of horizontal visibility in 1976–2006 showed a significant decrease in number of days with fog, in large portions of Europe the number of days with fog has halved (van Oldenborgh et al., 2010). The fog decline is speculated to occur due to either climate change or improvement of ambient air quality (Maalick et al., 2016; Vautard et al., 2009). Klemm and Lin (2016) presented the first physical evidence that both climate change and improvement of air quality can contribute to the reduction of fog.

The aim of our study was to examine fog events occurrence in Central Europe, specifically in the Czech Republic, the region with a history of heavy air pollution (Bridgman et al., 2002). We have investigated the association between fog occurrence (in terms of

frequency of events, their duration, and intensity), and ambient air pollution and meteorology, using a generalized additive model. As a proxy for ambient air pollution we considered  $\text{SO}_2$  concentrations, as proxies for the climate change, we considered temperature and relative humidity records. For our analysis we use high quality data measured on daily basis in the long run (1970–2015) by the Czech Hydrometeorological Institute.

- Bridges, K., Jickells, T., Davies, T.D., Zeman, Z., Hůnová, I. (2002) *Atmos Environ* **36**, 353–360.
- Bridgman, H.A., Davies, T.D., Jickells, T., Hůnová, I., Tovey, K., Bridges, K., Surapipith, V. (2002) *Atmos Environ* **36**, 3375–3389.
- Gultepe, I., Tardif, R., Michaelidis, S.C., Cermak, J., Bott, A. et al. (2007) *Pure Appl Geophys* **164**, 1121–1159.
- Hůnová, I., Kurfurst, P., Maznová, J., Coňková, M. (2011) *Erdkunde* **65**, 247–259.
- Hyslop, N.P. (2009). *Atmos Environ* **43**, 182–195.
- Klemm, O., Lin, N-H. (2016) *Aerosol Air Qual Res* **16**, 1131–1142.
- Maalick, Z., Kuhn, T., Korhonen, H., Kokkola, H., Laaksonen A., Romakkaniemi, S. (2016) *Atmos Environ* **133**, 26–33.
- van Oldenborgh, G.J., Yiou P., Vautard, R. (2010) *Atmos Chem Phys* **10**, 4597–4609.
- Vautard, R., Yiou P., van Oldenborough, G.J. (2009) *Nat Geosci* **2**, 115–119.
- Zimmermann, L., Zimmermann, F. (2002) *J Hydrol* **256**, 166–175.

## Radiative forcing using CALIPSO measurements: method and comparison to state-of-the-art forcing estimations from ground

N. Papagiannopoulos<sup>1</sup>, M. Sicard<sup>2,3</sup>, L. Mona<sup>1</sup> and A. Comeron<sup>2</sup>

<sup>1</sup>Consiglio Nazionale delle Ricerche, Istituto di Metodologie per l'Analisi Ambientale (CNR-IMAA), C. da S. Loja, Tito Scalo (PZ), 85050, Italy

<sup>2</sup>Remote Sensing Laboratory, Universitat Politècnica de Catalunya, Barcelona, Spain

<sup>3</sup>Ciències i Tecnologies de l'Espai - Centre de Recerca de l'Aeronàutica i de l'Espai /Institut d'Estudis Espacials de Catalunya (CTE-CRAE /IEEC), Universitat Politècnica de Catalunya, Barcelona, Spain

Keywords: aerosol, radiative forcing, global scale, CALIPSO, EARLINET.

Presenting author email: nikolaos.papagiannopoulos@imaa.cnr.it

Cloud-Aerosol Lidar and Infrared Pathfinder Satellite Observations (CALIPSO) mission provides aerosol extinction and typing profiles at a global scale in near-real time (Winker et al., 2009). Composite maps of CALIPSO products (AOD, etc.) are routinely delivered by NASA. How far are we from producing radiative forcing products from CALIPSO stand-alone measurements? In this study we test the reliability of radiative forcing calculations from CALIPSO stand-alone measurements for three types of particles, defined in the classification scheme of CALIPSO, with a potentially strong forcing effect: dust, smoke and sea-salt. CALIPSO forcings are compared to state-of-the-art forcing estimations parameterized with ground-based aerosol extinction profiles, columnar single scattering albedo and asymmetry factor, satellite-based surface albedo, thermodynamic profiles from radiosoundings and so forth. Barragan *et al* (2016) showed radiative forcing estimations taking profit of the ground-based European Aerosol Research Network (EARLINET) measurements.

The performance of CALIPSO retrieval is given for the three aerosol types considered. Results of the comparison to an extensive aerosol dataset (Papagiannopoulos *et al*, 2016) will be presented.

This work is supported by the ACTRIS (Aerosols, Clouds, and Trace Gases Research Infrastructure Network) Research Infrastructure Project funded by the European Union's Horizon 2020 research and innovation programme under grant agreement n. 654169; by the Spanish Ministry of Economy and Competitiveness (MinECo, project TEC2015-63832-P) and of Science and Innovation (project UNPC10-4E-442) and EFRD (European Fund for Regional Development) and by the Department of Economy and Knowledge of the Catalan autonomous government (grant 2014 SGR 583). The authors would also like to acknowledge the CALIPSO mission scientists and associated NASA personnel for the production of the data used in this research.

Barragan, R., Romano, S., Sicard, M., Burlizzi, P., Perrone, M. R., and Comeron, A. (2016) *J. Geophys. Res. Atmos.* **121**, 10237–10261.

Papagiannopoulos, N., Mona, L., Alados-Arboledas, L., Amiridis, V., Baars, H., Biniotoglou, I., Bortoli, D., D'Amico, G., Giunta, A., Guerrero-Rascado, J. L., Schwarz, A., Pereira, S., Spinelli, N., Wandinger, U., Wang, X., and Pappalardo, G. (2016) *Atmos. Chem. Phys.* **16**, 2341-2357.

Winker, D. M., Vaughan, M. A., Omar, A. H., Hu, Y., Powell, K. A., Liu, Z., Hunt, W. H., and Young, S. A. (2009) *J. Atmos. Oceanic Technol.* **26**, 2310-2323.

## On connection between remote dust aerosol and Indian summer monsoon

1 1  
Siddharth Kumar , Anika Arora

1  
Indian Institute of Tropical Meteorology, Pune, 411008, India

Keywords: Indian summer monsoon, remote dust aerosol, direct radiative forcing  
Presenting author's email: siddharth.cat@tropmet.res.in

Understanding of interaction between remote dust aerosol and Indian summer monsoon (ISM) remains dubious in literature because of wide disagreement among previous studies. Using a recent version of Modern Era Retrospective Analysis for Research and Application (MERRA-2), this problem is revisited. A new hypothesis is proposed to explain covariability of dust over Arabian Sea and ISM circulation. Findings of the present study provide a new insight into remote dust-ISM connection problem and the hypothesis proposed differs considerably from previously proposed hypotheses (Vinoj et al., 2014; Jin et al., 2014, 2015)

Dust extinction aerosol optical thickness from MERRA-2 (Bosilovich et al., 2015) is used to quantify dust loading over south Asian monsoon region. Temperature tendency from shortwave radiation assuming clear sky is used as a measure of heating produced from solar absorption by dust aerosol. Other parameters such as horizontal components of wind, temperature etc. is also taken from MERRA-2. West Asian region considered in this study is one of the driest regions in the world and therefore indirect aerosol effect is of least importance. Only direct radiative effects of aerosol are considered in this work. Analogous to the definition of active spells of monsoon, all those events when dust loading is anomalously very high is identified and circulation anomaly composites are constructed accordingly.

ISM variability is not constrained by changes in dust aerosol over most parts of west Asia/north Africa. The new proposed hypothesis explains relationship between dust variability over Arabian Sea and monsoon circulation. Largescale forcing modulates monsoon intraseasonal oscillations (ISOs) and creates active-like condition

over Indian landmass extending up to Arabian Sea/Arabian peninsula. Organized convection induces anomalous southwesterly and northwesterly circulation through latent heating feedback. Enhanced northwesterly winds strengthen transport of dust over Arabian Sea. Augmented dust forcing and associated warming over Arabian Sea is unlikely to create a positive feedback because of its limited spatial extent.

Interaction between aerosol radiative forcing and atmospheric circulation is an active area of study in global science community and there has been ongoing research since last few decades, but the quantum of uncertainty involved has not improved significantly. Part of this problem is related to the fact that modelling studies based on aerosol-circulation interaction is difficult to be validated with the real observations. Present study is an effort to reduce the involved uncertainty amidst the complexity of the system.

Indian Institute of Tropical Meteorology is an autonomous institute under the ministry of earth sciences, Govt. of India.

Bosilovich, M. G., and Coauthors (2015) *Series on Global Modeling and Data Assimilation Tech. Rep.* NASA/TM-2015-104606, Vol. 43, 145 pp.

Jin, Q., Wei, J. & Yang, Z. L. *Geophys Res Lett* 41,4068–4074 (2014).

Jin, Q., Wei, J., Yang, Z. L., Pu, B. & Huang, J. *Atmos Chem Phys* 15, 9897–9915 (2015).

Vinoj, V., P. J. Rasch, H. Wang, J.-H. Yoon, P.-L. Ma, K. Landu, and B. Singh (2014) *Nat. Geosci.*, doi:[10.1038/ngeo2107](https://doi.org/10.1038/ngeo2107).

## Influence of clouds on black carbon direct radiative effect and heating rate over Milan

A. Gregorič<sup>1</sup>, L. Ferrero<sup>2</sup>, G. Močnik<sup>3,4</sup>, S. Cogliati<sup>2</sup>, F. Barnaba<sup>5</sup>, L. Di Liberto<sup>5</sup>, G. P. Gobbi<sup>5</sup>, E. Bolzacchini<sup>2</sup>

<sup>1</sup>University of Nova Gorica, 5000 Nova Gorica, Slovenia

<sup>2</sup>University of Milano-Bicocca, DISAT, 20126 Milan, Italy

<sup>3</sup>Aerosol d.o.o., 1000 Ljubljana, Slovenia

<sup>4</sup>Jožef Stefan Institute, 1000 Ljubljana, Slovenia

<sup>5</sup>Institute for Atmospheric Sciences and Climate, National Research Council, 00133 Rome, Italy

Keywords: black carbon, direct radiative effect, heating rate, clouds

Presenting author email: asta.gregoric@ung.si

Atmospheric black carbon (BC) absorbs solar radiation and warms the atmosphere. However, its effective climate forcing is highly uncertain, since the induced heating reflects in different semi-direct and indirect effects (Bond *et al.*, 2013). The relative cloud-aerosol location influences the magnitude of radiative forcing. Modelling studies confirmed the highest impact on radiative forcing by BC layers located above reflective clouds, however studies of the influence of different cloudy sky conditions on the BC induced heating rate (HR) in the atmospheric layer below clouds are still very scarce. This contribution presents the analyses of the influence of clouds and their properties on the BC direct radiative effect and induced HR in a ground based atmospheric layer due to changes in the magnitude of direct, diffuse and reflected solar irradiance.

Radiative power density absorbed into a ground-based atmospheric layer (ADRE), as well as the consequent HR induced by the aerosol absorptive component, were experimentally determined in high time resolution for more than one year period (from March 2015 – November 2016) over Milan (Italy) (Ferrero *et al.*, 2016). BC from traffic or biomass burning emissions is considered as the main absorptive aerosol component in an urban environment. The ADRE and HR have been determined by coupling spectral aerosol absorption measurements with the spectrally resolved measurements of the direct, diffuse downward radiation and the surface reflected radiance components. Additionally, ceilometer data from the same site were used for the determination of cloud base height and its vertical depth.

To better understand the importance of sky condition on direct, diffuse and reflected component of ADRE and HR, the fraction of sky covered by clouds and the cloud type were considered. The cloud cover (opaqueness) was evaluated based on the ratio between observed global irradiance and solar irradiance at the top of the atmosphere. Cloud types were classified into several classes: stratus (low level), cumulus and cirrus (low and high), cirrus clouds (high) and clear sky cases (the order with increasing opaqueness). Low cumulus clouds in the presence of cirrus clouds are characterised by high deviation of observed solar irradiance and short periods of higher global irradiance than expected for clear sky condition, which happens due to the scattering of the solar radiation by clouds.

In order to analyse the effect of different sky conditions, ADRE and its direct (ADRE<sub>dir</sub>), diffuse (ADRE<sub>dif</sub>) and reflected (ADRE<sub>ref</sub>) component were

normalised to BC mass concentration and expressed in mW  $\mu\text{g}^{-1}$  of BC. Normalised ADRE thus increases with solar irradiance and Ångström exponent, due to the higher absorption in the lower wavelengths of the spectrum. The mean normalised ADRE was  $12.0 \pm 6.5 \text{ mW } \mu\text{g}^{-1}$  and normalised HR:  $0.88 \pm 0.49 \text{ K } \mu\text{g}^{-1} \text{ day}^{-1}$ , 36 % attributed to direct, 40 % to diffuse and 24 % to reflected radiation. The highest direct irradiance in the clear sky conditions is leading also to the highest normalised ADRE<sub>dir</sub> ( $8.9 \text{ mW } \mu\text{g}^{-1}$ ) which decreases with cloud cover and thus changes with the type of clouds (Figure 1). On the other hand, normalised diffuse ADRE fraction increases with cloud cover up to opaqueness of about 50 % and is the highest in the case of cumulus and in the combination of cumulus and cirrus clouds, when it can reach even higher values than the direct fraction in clear sky condition. The highest normalised ADRE<sub>dir</sub> was found during the periods of cumulus clouds ( $7.9 \pm 3.4 \text{ mW } \mu\text{g}^{-1}$ ) with the highest values observed in May, reaching up to  $24.7 \text{ mW } \mu\text{g}^{-1}$ . The normalised ADRE<sub>ref</sub> follows similar pattern as ADRE<sub>dir</sub>.

The results show the strongest impact on ADRE by low level cumulus clouds, which (according to lidar data) form on the top of the mixing layer in late spring. Scattering of sun radiation by clouds increases the diffuse irradiance and leads to the highest values of normalised ADRE. Therefore, the highest normalised ADRE is observed in May and not during the period of summer solstice.

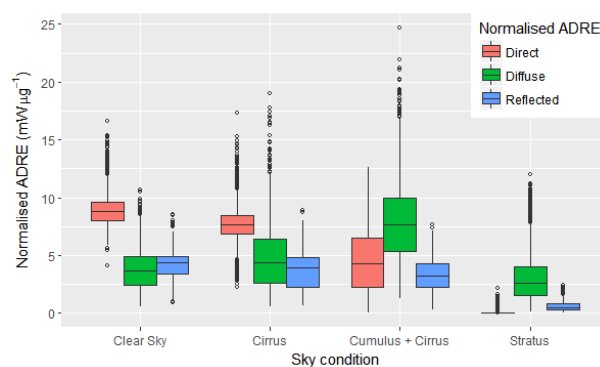


Figure 1. ADRE normalised to BC concentration for direct, diffuse and reflected fraction of solar irradiance and different sky condition.

Bond, T. C., *et al* (2013) *J. Geophys. Res. - Atmos.* **118**(11), 5380–5552.

Ferrero, L., *et al* (2016) *Geophys. Res. Abstr.*, EGU 2016, **18**, 16473.

## **Impacts of carbonaceous aerosol on hydrological cycle over the Northern Africa**

Jin-Ho Yoon<sup>1</sup>, Philip J. Rasch<sup>2</sup>, Hailong Wang<sup>2</sup>, V. Vinoj<sup>3</sup>, and Dilip Ganguly<sup>4</sup>

<sup>1</sup>School of Earth Sciences and Environmental Engineering, Gwangju Institute of Science and Technology, Gwangju, South Korea

<sup>2</sup>Pacific Northwest National Laboratory, Richland, WA, USA

<sup>3</sup>Indian Institute of School of Earth, Ocean and Climate Sciences, Indian Institute of Technology Bhubaneswar, Odisha, India

<sup>4</sup>Center for Atmospheric Sciences, Indian Institute of Technology Delhi, New Delhi, India

Keywords: Aerosol-Cloud interaction, African rainfall, Carbonaceous Aerosol

Presenting author email: [yjinho@gist.ac.kr](mailto:yjinho@gist.ac.kr)

The Northern Africa has exhibited extensive drought in the late 20<sup>th</sup> century. Most of the variability in rainfall has been attributed to change in the Sea Surface Temperature (SST) in both the Atlantic and Indian Oceans. However, most of the climate models have difficulty in reproducing magnitude of rainfall reduction. Various climate feedback processes such as Vegetation-Albedo feedback were suggested as amplifying mechanisms which are typically missing in most of current climate models. In this study, aerosol indirect effects (AIE) are analyzed with a focus on its impact on hydrological cycle over the Northern Africa. Previously various pathways were suggested to explain how aerosols can affect the hydrological cycle and climate. However, most of them were based on climate models with capability of simulating only the aerosol direct effect through changes in radiative properties of the atmosphere.

The Community Atmosphere Model (CAM) version 5 has fully predictive aerosol life cycle, which actively interacts with both radiative property and cloud microphysics. Therefore, we can investigate how the carbonaceous aerosols from biomass burning can affect rainfall over the Northern Africa due to aerosol indirect and direct effects using sets of sensitivity experiments. Our goal is to explore how the AIE may alter the atmospheric hydrological cycle over the Northern Africa.

This work was supported by the KOPRI, the GIST, and the Office of Science and the United States Department of Energy.

Yoon, J.-H., and coauthors, 2016: The role of carbonaceous aerosols on short-term variations of precipitation over North Africa, *ASL*, 17, 407-414, doi:10.1002/asl.672

## Implementation of simplified chemistry module in KIAPS integrated model

Jung-Yoon Kang, Soo Ya Bae, and Raeseol Park

Korea Institute of Atmospheric Prediction Systems, Seoul, 07071, Republic of Korea

Keywords: Aerosol modelling, NWP

Presenting author email: jy.kang@kiaps.org

Aerosol affects atmospheric radiation budget by scattering and/or absorbing radiation, and modifying cloud properties. Feedbacks between meteorology and aerosol, however, have not been included in Numerical Weather Prediction (NWP) because of the scientific complexities and lack of computational power. In recent years, online coupled meteorology chemistry models are developed rapidly by the air quality modelling community due to dramatic increase in computer power, and these models are also of interest for the NWP community as they can consider the potentially important effects of atmospheric composition on weather (Baklanov *et al.*, 2014).

Online meteorology chemistry models for short-term applications like NWP do not require full comprehensive chemistry which would increase the computational cost tremendously. Baklanov *et al.* (2014) pointed out that NWP should benefit from including such feedbacks as aerosol-cloud-radiation interactions with simplified chemistry (e.g., sulfur chemistry).

A simplified chemistry module which is based on the GOCART (Goddard Chemistry Aerosol Radiation and Transport) scheme (Chin *et al.*, 2000) of WRF-Chem (Weather Research and Forecasting with Chemistry) was implemented in KIAPS (Korea Institute of Atmospheric Prediction Systems) integrated model to include the effects of aerosol on weather. The KIAPS integrated model is a 3D global forecast system on a cubed-sphere grid with a non-hydrostatic dynamical core.

Five tracers ( $\text{SO}_2$ ,  $\text{SO}_4$ , hydrophobic organic carbon (OC), hydrophilic OC, and sea salt) are considered in the simplified chemistry module and their source/sink terms are summarized in Table 1. MACC/City (MACC/CityZEN EU projects) anthropogenic and biomass burning emission data are used for  $\text{SO}_2$  and hydrophobic OC emissions. For sulfur chemistry, oxidation of  $\text{SO}_2$  is calculated by prescribed  $\text{H}_2\text{O}_2$  and OH fields. Sea salt particles ranging from 0.5 to 5  $\mu\text{m}$  in radius are considered in the model with one size bin.

Table 1. Source and sink terms for five considering species.

Source		Sink
$\text{SO}_2$	Emission	$\text{SO}_2 + \text{OH} \rightarrow \text{SO}_4$
		$\text{SO}_2 + \text{H}_2\text{O}_2(\text{aq}) \rightarrow \text{SO}_4$ Dry/Wet deposition
$\text{SO}_4$	$\text{SO}_2 + \text{OH} \rightarrow \text{SO}_4$ $\text{SO}_2 + \text{H}_2\text{O}_2(\text{aq}) \rightarrow \text{SO}_4$	Dry/Wet deposition
OC (hydro- phobic)	Emission	$\text{OC}_{\text{phobic}} \rightarrow \text{OC}_{\text{philic}}$ Dry deposition

OC (hydro- philic)	$\text{OC}_{\text{phobic}} \rightarrow \text{OC}_{\text{philic}}$	Dry/Wet deposition
Sea salt (2 $\mu\text{m}$ )	Emission	Settling Dry/Wet deposition

The simulated aerosol mass concentrations through the online coupled simplified chemistry module are used in the calculation of CCN (Cloud Condensation Nuclei) concentration for MPS (Microphysics Parameterization Scheme) and CPS (Cumulus Parameterization Scheme).

The aerosol concentrations are compared with other global model results and global budget analysis is carried out for each species.

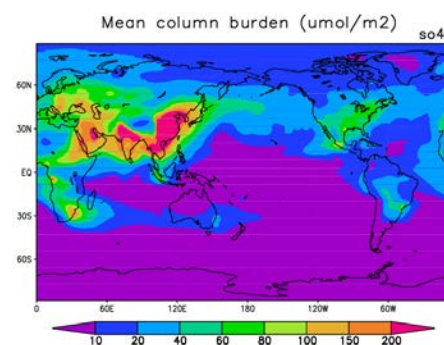


Figure 1. 30-day averaged column burden of  $\text{SO}_4$ .

This work has been carried out through the R&D project on the development of global numerical weather prediction systems of the Korea Institute of Atmospheric Prediction Systems (KIAPS) funded by Korea Meteorological Administration (KMA).

Baklanov, A., Schlünzen, K., Suppan, P., Baldasano, J., Brunner, D., Aksoyoglu, S., Carmichael, G., Douros, J., Flemming, J., Forkel, R., Galmarini, S., Gauss, M., Grell, G., Hirtl, M., Joffre, S., Jorba, O., Kaas, E., Kaasik, M., Kallos, G., Kong, X., Korsholm, U., Kurganskiy, A., Kushta, J., Lohmann, U., Mahura, A., Manders-Groot, A., Maurizi, A., Moussiopoulos, N., Rao, S. T., Savage, N., Seigneur, C., Sokhi, R. S., Solazzo, E., Solomos, S., Sørensen, B., Tsegas, G., Vignati, E., Vogel, B., and Zhang, Y. (2014) *Atmos. Chem. Phys.* **14**, 317-398.

Chin, M., Rood R. B., Lin S.-J., Muller J. F., and Thompson A. M. (2000) *J. Geophys. Res.* **105**, 24671-24687.

## Robust signals of regional climate impact on antropogenic aerosols

K. Nordling<sup>1</sup>, J. Merikanto<sup>1</sup>, D. O'Donnell<sup>1</sup>, J. Räisänen<sup>1</sup> and H. Korhonen<sup>1</sup>

<sup>1</sup>Finnish Meteorological Institute, PL 503 00101 Helsinki, Finland

Keywords: Climate modelling, Climate change, aerosols

Presenting author email: kalle.nordling@fmi.fi

Regional changes in climate have significant impacts on people's lives. One of the key drivers of climate change are aerosols, which can strongly affect the atmospheric radiation budgets by scattering and absorbing solar radiation and by modifying cloud properties. Since the aerosol concentrations have large spatial variations, aerosol radiative effects can be the dominant climate forcers on a regional scale. Besides these local effects, aerosols can also affect large scale weather patterns, leading to remote regional effects (e.g. Guo et al., 2016). The combination of these effects can be best studied via large scale circulation models. Previous studies have shown that while some common regional signals exist between different models, the scatter in modelled regional impacts of aerosols has been large (e.g. Rotstayn, 2014). In previous studies typically only aerosol emissions were harmonized, and model-to-model differences in the simulated aerosol radiative effects have been significant due to differences in modelled aerosol microphysics (Myhre et al., 2012). Therefore, it is unclear to what extent the differences in the modelled regional aerosol effects have been driven via the differences in radiative forcing fields, or via the differences in modelled atmospheric dynamics.

Our ongoing project RECIA will carry out a systematic investigation of the local and remote regional climate impacts of aerosols. To achieve this, we use a standardized anthropogenic aerosol representation, MACv2-SP (Stevens, 2016), which provides a simple representation of the changes in aerosol optical properties and cloud droplet number concentrations due to anthropogenic aerosols. This enables us to focus on the differences and similarities in the regional aerosol effects that arise solely from the modelled atmospheric dynamics. The MACv2-SP scheme is now implanted to

three independent climate models (NorESM, EC-earth and ECHAM-HAM).

Here, we will present our first results from the simulations with systematic perturbations to regional aerosol fields (for example, South East Asia and Africa). We will discuss the similarities and variability in modelled regional temperature and pressure fields, circulation features and other meteorological parameters. Our results will further our knowledge on the consistency of modelled regional climate signals when the differences in aerosol properties and loadings are minimized.

Guo, L., Turner, A. G., & Highwood, E. J. (2016).

*Local and remote impacts of aerosol species on Indian summer monsoon rainfall in a GCM. Journal of Climate*, 29(19), 6937-6955.

Myhre, G. et al. (2013). *Radiative forcing of the direct aerosol effect from AeroCom Phase II simulations.*

*Atmospheric Chemistry and Physics*, 13(4), 1853.

Rotstayn, L. D., et al. (2014). *Declining aerosols in CMIP5 projections: Effects on atmospheric temperature structure and midlatitude jets.* *Journal of Climate*, 27(18).

Stevens, B., et al. (2016). *Simple Plumes: A parameterization of anthropogenic aerosol optical properties and an associated Twomey effect for climate studies.* *Geosci. Model Dev. Discuss. Model Dev. Discuss.*, doi: <http://dx.doi.org/10.5194/gmd-2016-189>

## Biosphere-aerosol-cloud-climate interactions investigated using NorESM

M.K. Sporre<sup>1</sup>, A. Grini<sup>1,2</sup>, T.K. Berntsen<sup>1</sup>, S.M. Blichner<sup>1</sup> and R. Makkonen<sup>3</sup>

<sup>1</sup>Department of Geosciences, University of Oslo, Oslo, 0315, Norway

<sup>2</sup>Norwegian Meteorological Institute, Oslo, 0310, Norway

<sup>3</sup>Department of Physics, University of Helsinki, Helsinki, 00014, Finland

Keywords: Earth System Modelling, climate feedbacks, aerosol, cloud.

Presenting author email: m.k.sporre@geo.uio.no

### Introduction

Climate feedbacks can either enhance or suppress the ongoing warming of the climate on Earth. One proposed feedback involves the terrestrial biosphere (Kulmala *et al*, 2014), which emits biogenic volatile organic compounds (BVOC) to the atmosphere. Enhanced levels of CO<sub>2</sub> in the air are expected to increase gross primary production (GPP) and temperatures, which will increase the emissions of BVOC. Some of the BVOC condense and form secondary organic aerosol particles (SOA) in the atmosphere, while a fraction of organic vapors can also participate in nucleation and early growth of particles. More aerosol mass in the atmosphere leads more aerosol scattering which results in more diffuse radiation reaching the terrestrial biosphere. This can enhance the (GPP) which leads to more BVOC produced and a positive feedback. More aerosol particles in the atmosphere can, on the other hand, also lead to an enhanced first indirect aerosol effect on clouds which would reduce temperatures. It is thus possible that climate and CO<sub>2</sub> induced changes in BVOC emissions could reduce the warming in the future.

### Method

To investigate the BVOC feedback on the climate, we use the community atmospheric model (CAM5.3) configured with an alternative aerosol-scheme which is documented in Kirkevåg *et al* 2013 (CAM5.3-Oslo). In this setup, CAM5.3-Oslo is coupled to the Community Land model (CLM4.5) which includes the Model of Emissions of Gases and Aerosols from Nature (MEGAN) version 2.1. MEGAN interactively calculates the emissions of isoprene and monoterpenes. In the atmospheric model, oxidation of isoprene and monoterpenes by O<sub>3</sub>, OH and NO<sub>3</sub> results in SOA. The yield is 5% for isoprene and 15% for monoterpenes. Only the oxidation products from the monoterpene-O<sub>3</sub> reaction are involved in the formation of new particles, and the rest of the oxidation products condense onto existing particles.

Some short model simulations have been run to test how sensitive the emissions of BVOC are to changing CO<sub>2</sub> levels and temperature. The simulations are run with fixed sea surface temperatures (SST) and fixed vegetation in CLM. The simulations were run for 7 years, where the first 2 are considered spin-up years. The simulations were run with emissions for the year 2000 (control run), and a simulation with the CO<sub>2</sub> doubled. However, since SST are constant, the temperatures do not increase by much in the 2xCO<sub>2</sub> run. Therefore,

another simulation where the SST were increased by 2 degrees everywhere was run.

### Results

The preliminary results from the model simulations show that isoprene emissions decreases with increasing CO<sub>2</sub> levels (Table 1), due to an inhibiting effect of CO<sub>2</sub> in isoprene emissions. For land areas in the northern hemisphere, where there is a temperature increase in the 2xCO<sub>2</sub> simulation, the inhibition is overcome by the positive response of the emissions to temperature. Moreover, in the SST+2 simulations the global isoprene emissions increase by approximately 19 %. There is no CO<sub>2</sub> inhibition for monoterpene in the model, and these emissions increase with 4.3 % in the 2xCO<sub>2</sub> simulation and 16 % in the SST+2 simulations. The changes in the BVOC emissions could be seen to affect the amount of SOA condensate, which was found to increase by on average 7.2 % and 9.6% in the 2xCO<sub>2</sub> and SST+2 simulations respectively. Both the numbers for the BVOC emissions and SOA formation are expected to be larger when simulations with changing vegetation density are run.

Table 1. Surface emissions of BVOCs.

Simulations	Isoprene (Tg/yr)	Monoterpene (Tg/yr)
1xCO <sub>2</sub>	422	116
2xCO <sub>2</sub>	414	121
SST+2	504	134

### Future plans

The plan over the next few months is to run longer simulations with increased CO<sub>2</sub> or SSTs where GPP is allowed to change to better capture the feedback. The same simulations will then be run but with the feedbacks turned off (fixed emissions of the BVOC), to estimate the effect of the feedbacks. The study will include a stepwise investigation along the feedback loop including: the effects of the BVOC on aerosol scattering, cloud condensation nuclei, cloud droplet number concentration and cloud forcing. This will enable us to estimate the magnitude of the feedback loop.

This work was funded by the EU FP7 Bacchus project (grant agreement 603445).

Kulmala, M., *et al* (2014) *Boreal. Environ. Res.* **19(suppl. B)**, 2-19.

Kirkevåg, A., *et al* (2013) *Geosci. Model Dev.* **6**, 207-244.

## Heating Rate of black carbon: experimental determination of traffic contribution over a large conurbation

L. Ferrero<sup>1,\*</sup>, G. Močnik<sup>2,3</sup>, S. Cogliati<sup>1</sup>, R. Colombo<sup>1</sup>, C. Rizzi<sup>1</sup> and E. Bolzacchini<sup>1</sup>

<sup>1</sup>Department of Earth and Environmental Sciences, University of Milano-Bicocca, Piazza della Scienza 1, 20126, Milan, Italy.

<sup>2</sup>Aerosol d.o.o., Kamniška 41, SI-1000 Ljubljana, Slovenia.

<sup>3</sup>Department of Condensed Matter Physics, Jozef Stefan Institute, SI-1000 Ljubljana, Slovenia

Keywords: Black Carbon, heating rate, source, low emission zone.

Presenting author email: [luca.ferrero@unimib.it](mailto:luca.ferrero@unimib.it)

Black carbon (BC) absorbs sunlight in the atmosphere heating it<sup>[1]</sup>. The heating rate (HR) can be determined from the divergence of the net radiative flux with altitude (vertical profiles) or from the modelling activity; however, its determination is, up to now, too sparse<sup>[2,3]</sup>. This work applies a new method<sup>[4]</sup> to experimentally determine the HR induced by the absorptive component of aerosol in an atmospheric layer close to the ground. In an urban context, it is essentially related to BC. The methodology is based on the direct determination of the radiative power density absorbed into a ground-based atmospheric layer (determined coupling spectral aerosol absorption measurements with the spectrally resolved measurements of the direct, diffuse and reflected radiation; the spectral absorption of BC aerosol allows its source apportionment (traffic and biomass burning (BB)<sup>[5]</sup>) allowing the same apportionment on HR.

Experimentally the HR was determined using: 1) Aethalometer (AE-31, Magee Scientific, 7- $\lambda$ ), 2) Multiplexer-Radiometer-Irradiometer (diffuse, direct and reflected radiance: 350-1000 nm in 3648 spectral bands), 3) a meteorological station (LSI-Lastem) including a full set of radiometers, 4) condensation and optical particle counters (TSI 3775 and Grimm 1.107), 5) low volume sampler (FAI Hydra, PM<sub>2.5</sub> and PM<sub>10</sub>).

Six months of data (March-October 2015) of high-time resolution measurements (5 min) of HR were measured in Milan inside the Low Emission Zone (LEZ; Villa Necchi) area and outside in a background monitoring site (U9, University of Milano-Bicocca).

Results allowed to determine first that on average in the background site of Milan the mean monthly values of HR along one year was  $1.0 \pm 0.1$  K/day. The traffic source contributed to this HR value with 70% of radiative effect, while the remaining 30% was due to the radiative effect of BB sources of BC.

Apart the average values over Milan, the experimental set-up allowed to experimentally determine the magnitude of changes in aerosol sources on the induced atmospheric HR.

Particularly, within the LEZ an averaged reduction of BC of  $-19.3 \pm 1.1\%$  was observed. This observation is in agreement with literature studies<sup>[5]</sup>.

Interestingly the BB contribution to BC within the LEZ was the same of that in the background U9 Milan site. This resulted in an identical diurnal BB HR behaviour within and outside the LEZ (Figure 1, upper panel). Conversely, the traffic BC experienced a reduction which resulted in a diurnal HR decrease of  $-10.8 \pm 0.9\%$  within LEZ. This difference originated during the morning rush hour as shown in Figure 1 (lower panel). A deeper investigation will be presented using the full dataset.

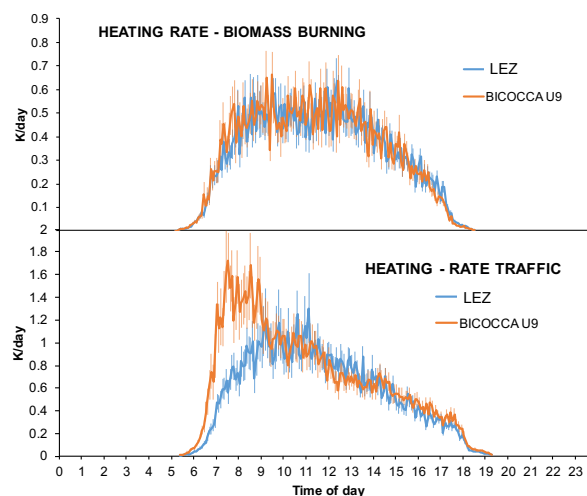


Figure 1. Diurnal behaviour of the heating rate within the Milan LEZ and outside at high time resolution from March to October 2015. Upper panel: biomass burning induced HR; lower panel: traffic induced HR.

### References:

- [1] Bond et al., J. Geophys. Res., VOL. 118, 1–173, doi:10.1002/jgrd.50171, 2013.
- [2] Samset et al., Atmos. Chem. Phys., 14, 12465–12477, 2014.
- [3] Ferrero et al., Atmos. Chem. Phys., 14, 9641–9664, 2014.
- [4] Ferrero, L., et al (2016) Geophys. Res. Abstr., EGU 2016, 18, 16473.
- [5] Holman, C., et al (2015) Atmos. Environ., 111, 161–69.

## **Abstracts T203**

## Features of new particle formation in Central European background air

Molnár, A.<sup>1</sup>, Imre, K.<sup>1</sup>, Aalto, P.<sup>2</sup>

<sup>1</sup>MTA-PE Air Chemistry Research Group, University of Pannonia, Veszprém, H-8201, Hungary

<sup>2</sup>Department of Physics, University of Helsinki, Helsinki, FI-00014, Finland

Keywords: new particle formation, nucleation, DMPS  
Presenting author email: kornelia@almos.uni-pannon.hu

### Introduction

Formation of new secondary aerosol particles has been observed all over the world from the tropics to polar regions, from megacities to remote places, over oceans and continents as well as at ground level and in the free troposphere. The growing scientific interest in these very small aerosol particles is mainly due to their role in atmospheric processes and their diverse effects that ranges from the climate system to human health.

Particles above 50 nm in diameter can serve as active cloud condensation nuclei, and the number of these particles can effectively control the planetary albedo (indirect aerosol climate effect). When particles grow above 100 nm into the optically active size range, they significantly contribute to the light extinction (direct aerosol effect). Despite their important effects on the radiation transfer there are still high uncertainties in global climate models, largely because of our limited understanding of aerosols and clouds. In this work the characteristics of new particle formation events are presented on the basis of continuous 8-years long monitoring data measured by DMPS. The measurements were carried out from 2008 to 2015 at K-pusztá Hungarian background air pollution monitoring station.

### Sampling

K-pusztá, operated by the Hungarian Meteorological Service is a background air pollution monitoring station referred as a rural measurement site located in Hungary (46°58'N, 19°35'E, 125 m a.s.l.) on the Great Hungarian Plain. The station is a part of the GAW and EMEP networks and one of the EUSAAR supersites. The sampling site is 15 km northwest from the nearest town Kecskemét and 80 km southeast from Budapest. The surroundings of the measurement site are dominated by mixed forest (62% coniferous, 28% deciduous) and grassland (10%), while the soil around the site is sandy.

Sampling has been carried out from 2008 to 2015 with a Differential Mobility Particle Sizer. Particles with an electrical mobility diameter from 6 to 800 nm are recorded in their dry state in 30 channels. The aerosol classifier was a copy of a Hauke-type differential mobility analyzer. The sample and sheath flow rates were 1 and 5 LPM, respectively. Time resolution of the measurement was approximately 10 min. The particle counter was a TSI model 3010 condensation particle counter.

### Results and discussion

In this work the average and seasonal characteristics of new particle formation (NPF) events is summarized. During eight years 2125 days could be classified. The overall data show that at K-pusztá the frequency of NPF events is 27% of the classified days (without missing days and bad data), undefined days and non-event days represent 20% and 54% of the days, respectively.

The intra-year study of the data revealed that the occurrence of event and non-event days has definite seasonal variation. Event days are characterized by spring and fall maxima. Evidently winter is the most inactive season in the NPF however; it is notable that summer months also seem rather low activity in secondary particle formation. Non-event days have inverse seasonal variation compared to NPF events, while undefined days have maximum in June. Seasonal variation of NPF event types shows that generally Ia events dominate throughout the year except summer. From June to August the number of Ia events considerably decreases, while the importance of Ib and II types in the NPF events significantly increases. This clearly indicates that in summer the formation processes of new particles become more disturbed.

The nucleation (type Ia) generally begins before noon, on the average at 9:10. In spring when the occurrence of NPF events is the highest, the start time is shifted to earlier (at 8:20). The latest time of beginning of nucleation is found in fall.

The formation and growth rates of the particles were also studied.

- The annual average formation ( $J_0$ ) and growth rates are  $2.2 \text{ cm}^{-3}\text{s}^{-1}$  and  $7.0 \text{ nm s}^{-1}$ , respectively.
- The growth of the particles represents seasonal variation it ranges from 5.4 (winter) to  $10.0 \text{ nm s}^{-1}$  (summer) while  $J_0$  varies between 1.1 and  $3.3 \text{ cm}^{-3}\text{s}^{-1}$ .

The average duration of the nucleation episodes at K-pusztá is 3h 11min. We found that the nucleation events are the longest in spring and shortest in summer. Finally, an average NPF event (including nucleation and subsequent particle growth) lasts 7h 54min, somewhat shorter duration is found only in summer.

## Influence of atmospheric conditions on pure biogenic nucleation in the CLOUD chamber

L. Dada<sup>1</sup>, D. Stolzenburg<sup>2</sup>, L. Ahonen<sup>1</sup>, F. Bianchi<sup>1,3</sup>, L. Fischer<sup>4</sup>, H. Gordon<sup>5,6</sup>, M. Heinritzi<sup>4,7</sup>, K. Lehtipalo<sup>1,3</sup>, H. E. Manninen<sup>5</sup>, C. Rose<sup>1</sup>, M. Simon<sup>7</sup>, C. Yan<sup>1</sup>, J. Curtius<sup>7</sup>, M. Kulmala<sup>1</sup>, J. Kirkby<sup>5,7</sup> and the CLOUD Collaboration

<sup>1</sup>Department of Physics, University of Helsinki, Helsinki, Finland

<sup>2</sup>Faculty of Physics, University of Vienna, Vienna, Austria

<sup>3</sup>Laboratory of Atmospheric Chemistry, Paul Scherrer Institute, Villigen, Switzerland

<sup>4</sup>University of Innsbruck, Institute for Ion and Applied Physics, Innsbruck, Austria

<sup>5</sup>CERN, Geneva, Switzerland

<sup>6</sup>School of Earth and Environment, University of Leeds, Leeds, United Kingdom

<sup>7</sup>Institute for Atmospheric and Environmental Sciences, Goethe-University of Frankfurt, Frankfurt, Germany

Keywords: New Particle Formation, CLOUD Experiment, Ozonolysis

Presenting author email: Lubna.Dada@helsinki.fi

Atmospheric aerosols affect Earth's radiative energy (IPCC, 2013). New particle formation (NPF) by gas-to-particle conversion is estimated to contribute to a substantial fraction of global cloud condensation nuclei (Merikanto et al., 2009). Originally, it was thought that NPF can only occur in the presence of sulfuric acid vapour and that ions do not play a major role in particle formations. However, chamber and laboratory experiments have shown that particles can form from organic precursors in the absence of sulfuric acid.

The discovery of pure biogenic nucleation reported by Kirkby *et al.* (2016) resulted from ozonolysis of a single monoterpene at 5°C and in the absence of other vapours. Here we report pure biogenic nucleation rates measured in the CLOUD (Cosmics Leaving Outdoor Droplets) chamber in 2015 and 2016, and extend the original study to include several biogenic under a range of environmental conditions. Studying pure biogenic nucleation helps understand night-time NPF which occurs in the absence of sulfuric acid, and also NPF in very clean environments such as rain forests or at high altitudes as well as in the pristine pre-industrial climate. Our aim is to study the influence of realistic atmospheric conditions on pure biogenic nucleation.

The CLOUD experiment at CERN (Duplissy et al., 2016; Kirkby et al., 2016) is designed to study NPF and under extremely low contamination levels as well as precisely controlled conditions. Moreover, the chamber allows studying particle formation under different ion-pair concentrations which can mimics “neutral” nucleation or ion-induced nucleation for which the formation rates can be determined.

The new measurements to be reported here were made during the CLOUD10 (Fall 2015) and 11 (Fall 2016) campaigns started using different concentrations of pure monoterpenes at temperatures (-25, 5, 25 °C). Followings, a sesquiterpene and isoprene were added to from a pure biogenic “soup” An example of pure biogenic particle formation from a soup of  $\alpha$ -pinene, isoprene and  $\beta$ -caryophyllene at 5 °C is shown in Figure 1. Upon

increasing the concentrations of the individual components of the mixture, an increase in nucleation and growth rates is evident. The size distribution was measured with three instruments, a scanning PSM (Vanhanen et al. 2011), a DMA-train (Stolzenburg et al. 2016) and a TSI nano-SMPS (Wang and Flagan 1990).

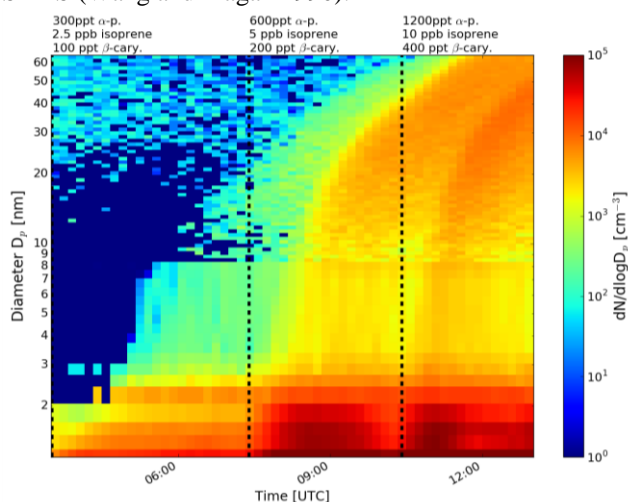


Figure 1. The time evolution of the number size distribution during a typical pure biogenic NPF experiment in the CERN CLOUD chamber.

Duplissy, J et al.(2016) *J. Geophys. Res. Atmos.*, **121**, 1752-1775.

IPCC: (2013). *Cambridge University Press*, **1**, 535-531.

Kirkby, J et al (2016). *Nature*, **533**, 521-526.

Merikanto, J.,(2009). *Atmos Chem Phys*, **9**, 8601-8616.

Stolzenburg, D. et al (2016) *Atmos. Meas. Tech. Discuss.*, doi:10.5194/amt-2016-346.

Vanhanen, J et al. (2011). *Aerosol Sci. Tech.*, **45**:533–542

Wang, S. C., and Flagan, R. C. (1990): *Aerosol Sci Tech*, **13**, 230-240.

We thank the European Organization for Nuclear Research (CERN) for supporting CLOUD with important technical and financial resources and for providing a particle beam from the CERN Proton Synchrotron as well as all the research academies and institutes for providing the financial support for the CLOUD experiment.

## Formation and evolution of aerosol nanoparticles within volcanic plumes

M. Sahyoun<sup>1</sup>, E. Freney<sup>1</sup>, R. Dupuy<sup>1</sup>, A. Colomb<sup>1</sup>, D. Picard<sup>1</sup>, J. Brito<sup>1</sup>, J. Duplissy<sup>2</sup>, T. Bourianne<sup>3</sup>, C. Denjean<sup>3</sup>, A. Schwarzenboeck<sup>1</sup>, C. Planche<sup>1</sup> and K. Sellegri<sup>1</sup>

<sup>1</sup> Université Clermont Auvergne, Laboratoire de Météorologie Physique, UMR-CNRS 6016, Clermont-Ferrand, 63000, France

<sup>2</sup> Department of Physics, University of Helsinki, Helsinki, Finland

<sup>3</sup> Centre National de Recherches Météorologiques, Météo-France, Toulouse, URA1357, France

Keywords: new particle formation, aerosol nucleation, volcanic particles

Presenting author email: m.sahyoun@opgc.univ-bpclermont.fr

Volcanic emissions are one of the major natural sources of particles in the atmosphere. Volcanic particles injected in the atmosphere can act as cloud condensation nuclei (CCN) (Hobbs et al., 1982) or ice nuclei (IN) (Hoyle et al., 2011) affecting the cloud physical and microphysical properties and, consequently, the Earth's radiation budget causing significant impact on weather and climate. They are also important components for air quality degradation (Schäfer et al., 2011). Different measurement techniques have been adopted to study tropospheric volcanic aerosols including in-situ sampling techniques and remote sensing either from ground, from airborne measurements or from satellite. To date only few in-situ measurements of volcanic emissions have been carried out, largely due to difficulties associated with coordinating the measurements in space and time with volcanic eruptions, as well as due to the relatively harsh environment in the vicinity of volcanic plumes.

Previous in-situ measurement studies have reported: a) the occurrence of nucleation and new secondary particle formation (NPF) events within the volcanic plume (Boulon et al., 2011) and b) the presence of larger particles in the range of 2-3  $\mu\text{m}$  in locations far from the respective volcano. The phenomenon is attributed to particle growth and transport processes (Hervo et al., 2012). The latter result of growth process was also confirmed by LIDAR observations (Bukowiecki et al., 2011).

In 2016, as part of the CLERVOLC/STRAP project, a series of ground based and airborne based (French research aircraft, ATR-42) measurements were performed around Etna and Stromboli volcanos in Italy. A total of five flights took place over and around Etna and Stromboli on the 14-16<sup>th</sup> of June. The ATR-42 was equipped with a number of instruments, including: Scanning Mobility Particle Sizer (SMPS) and two Condensation Particle Counters (CPCs) to measure aerosol physical properties. This combination of instruments covered a wide particle size range (3 nm up to 450 nm) allowing the detection of freshly nucleated particles as well as their growth process within the plume.

In this work, we present an overview of the aerosol and gas phase measurements made aboard the ATR-42. Evidence of NPF was observed within the volcanic plume for both Etna and Stromboli. The NPF events coincided with increases in  $\text{SO}_2$  concentrations. In particular, the performed measurements contribute to a

better understanding of the gas to particle conversion within the volcanic plume, and how the conversion process evolves with time. Finally, the airborne in-situ measurements performed within the Etna and Stromboli passive plumes are used to improve nucleation parametrizations to be incorporated into models. The presented relationship between nanoparticles and their gas-phase precursors in the vicinity of passive plumes was never experimentally evidenced in the past.

This work was supported by Labex ClerVolc (programme 1) and ANR STRAP projects.

Boulon, J., Sellegri, K., Hervo, M., Laj, P., 2011. Observations of nucleation of new particles in a volcanic plume. *Proc. Natl. Acad. Sci. U. S. A.* 108, 12223–6. doi:10.1073/pnas.1104923108

Bukowiecki, N., Zieger, P., et al., 2011. Ground-based and airborne in-situ measurements of the Eyjafjallajökull volcanic aerosol plume in Switzerland in spring 2010. *Atmos. Chem. Phys.* 11, 10011–10030. doi:10.5194/acp-11-10011-2011

Hervo, M., Quennehen, B., et al., 2012. Physical and optical properties of 2010 Eyjafjallajökull volcanic eruption aerosol: ground-based, Lidar and airborne measurements in France. *Atmos. Chem. Phys.* 12, 1721–1736. doi:10.5194/acp-12-1721-2012

Hobbs, P. V., Tuell, J.P., et al., 1982. Particles and gases in the emissions from the 1980–1981 volcanic eruptions of Mt. St. Helens. *J. Geophys. Res.* 87, 11062. doi:10.1029/JC087iC13p11062

Hoyle, C.R., Pinti, V., et al., 2011. Ice nucleation properties of volcanic ash from Eyjafjallajökull. *Atmos. Chem. Phys.* 11, 9911–9926. doi:10.5194/acp-11-9911-2011

Schäfer, K., Thomas, W., et al., 2011. Influences of the 2010 Eyjafjallajökull volcanic plume on air quality in the northern Alpine region. *Atmos. Chem. Phys.* doi:10.5194/acp-11-8555-2011

## One-year air ion observation at Dome C, Antarctica

X. Chen<sup>1</sup>, A. Virkkula<sup>2</sup>, V.-M. Kerminen<sup>1</sup>, H. E. Manninen<sup>1,3</sup>, M. Busetto<sup>4</sup>, C. Lanconelli<sup>4</sup>, A. Lupi<sup>4</sup>, V. Vitale<sup>4</sup>, M. Del Guasta<sup>5</sup>, R. Väänänen<sup>1</sup>, E.-M. Duplissy<sup>1</sup>, and M. Kulmala<sup>1</sup>

<sup>1</sup>Department of Physics, University of Helsinki, P.O. Box 64, FI-00014 Helsinki, Finland

<sup>2</sup>Finnish Meteorological Institute, Air Quality Research, P.O. Box 503, FI-00101 Helsinki, Finland

<sup>3</sup>CERN, CH-1211 Geneva, Switzerland

<sup>4</sup>Institute of Atmospheric Sciences and Climate, Italian National Research Council, 40129 Bologna, Italy

<sup>5</sup>Istituto Nazionale di Ottica, INO-CNR, 50019 Sesto Fiorentino (FI), Italy

Keywords: air ions, AIS, NPF, Antarctica

Presenting author email: xuemeng.chen@helsinki.fi

Air ions are known to participate in new particle formation (NPF) (Kulmala and Kerminen, 2008), which are charge carriers in the atmosphere. As part of the atmospheric aerosol formation study, air ion observations have been carried out at many sites around the world (Hirsikko et al., 2011). The involvement of air ions in NPF has also been reported at Aboa, Antarctica (Virkkula et al., 2007). At Dome C, however, though NPF events were observed (Järvinen et al., 2013), no investigation connected to air ions was conducted. In this work, we analysed the first air ion dataset collected at Dome C Station Concordia (75°06' S, 123°23' E, 3220 m above sea level) during 22 December 2010 –16 November 2011, aiming to characterise key features in air ions at this Antarctic site and to identify the air ion seasonality and analyse the variability in relation to NPF.

Air ions measured by an Air Ion Spectrometer (AIS (Mirme et al., 2007)) were studied together with atmospheric aerosol particle and meteorological data. A Differential Mobility Particle Sizer (DMPS (Järvinen et al., 2013)) was used to collect aerosol data and meteorological data were from the routine meteorological observation at Station Concordia (www.climantartide.it). Growth rates (GRs) were determined using the appearance time method (Lehtipalo et al., 2014) and the mode fitting method (Dal Maso et al., 2005) to study NPF.

Table 1. Summary of different types of features in the observed air ions at Dome-C.

NPF (days)	Wind-induced ion formation (days)	Cloud activation (days)	Event-free (days)
32	36	7	85

We identified features in air ions related to NPF, wind-induced ion formation and cloud activation, based on the one-year measurement (Table 1). NPF events were classified as suppressed NPF events, in which no clear growth exceeding 10 nm was observed, and multi-mode NPF events, where two or more separate NPF events and subsequent growths existed. 0.9 - 1.9 nm ions exhibited a clear seasonal variation on days without foregoing events or other anomaly that alter the ion concentration in this size range. Notably, higher 0.9 - 1.9 nm ion concentrations were found on NPF event

days than on the event-free days (Figure 1). It seems that GRs derived using the appearance time method could better characterise the fast particle growth in NPF whereas those based on the mode fitting method worked better for slow growth.

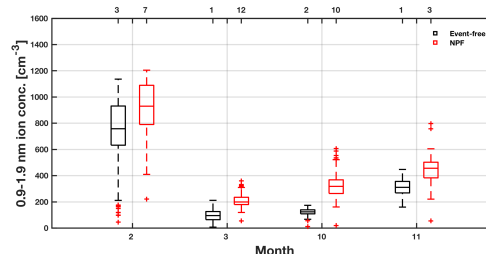


Figure 1. A comparison between ion concentrations in the 0.9-1.9 nm size range on event-free days and on NPF days. The numbers of days classified as either event-free or NPF are displayed on the top of the panel.

This work was supported by the Academy of Finland (projects no. 264375 and 264390), the Nordic Centre of Excellence CRAICC (Cryosphere-atmosphere interactions in a changing Arctic climate), and the Academy of Finland's Centre of Excellence program (Centre of Excellence in Atmospheric Science – From Molecular and Biological processes to the Global Climate, project no. 272041). Valuable advice from Dr. Sander Mirme is appreciated.

Dal Maso, M., M. Kulmala, I. Riipinen, R. Wagner, T. Hussein, P. P. Aalto, and K. E. J. Lehtinen (2005), *Boreal Env. Res.*, **10**, 323 - 336.

Hirsikko, A., et al. (2011), *Atmos. Chem. Phys.*, **11**(2), 767-798, doi:10.5194/acp-11-767-2011.

Järvinen, E., et al. (2013), *Atmospheric Chemistry and Physics*, **13**(15), 7473-7487, doi:10.5194/acp-13-7473-2013.

Kulmala, M., and V.-M. Kerminen (2008), *Atmospheric Research*, **90**(2-4), 132-150, doi:10.1016/j.atmosres.2008.01.005.

Lehtipalo, K., et al. (2014), *Boreal Environ. Res.*, **19** (suppl. B), 215-236.

Mirme, A., E. Tamm, G. Mordas, M. Vana, H. Uin, S. Mirme, T. Bernotas, L. Laakso, A. Hirsikko, and M. Kulmala (2007), *Boreal Env. Res.*, **12**, 247-264.

Virkkula, A., A. Hirsikko, M. Vana, P. P. Aalto, R. Hillamo, and M. Kulmala (2007), *Boreal Env. Res.*, **12**, 397-408.

## Secondary aerosol formation in a traffic influenced coastal desert environment

B. Alföldy, M. Kotob

Environmental Science Center, Qatar University, Doha, 2713, Qatar

Keywords: nucleation burst, diurnal variation, particle growth rate, urban air pollution

Presenting author email: balint@qu.edu.qa

Secondary particle formation is a significant contributor to the ultrafine particle budget that can occur at various conditions and locations (remote locations, urban or rural areas, industrial or agricultural regions, continental or coastal environments, Vu *et al.*, 2015). The precursor molecules of nucleation processes show also variability involved sulfuric acid (from industry and traffic), several volatile organic compounds (from traffic), and iodine molecules (biogenic marine emission).

It was believed previously that clean atmosphere favors nucleation since presence of particle surface is an important condensational sink. Recently, it was proven that presence of mineral dust can catalyze the nucleation by surface chemistry on mineral particles (Dupart *et al.*, 2012; Nie *et al.*, 2014).

Qatar is a coastal desert country with strong solar radiation, high mineral aerosol load, heavy traffic and industrial emissions. In addition, the Qatari atmosphere is influenced by biogenic emission from the sea (as the major biogenic source there). Based on the above literature summary we expected intensive secondary particle formation activity there.

The Atmospheric Laboratory of Qatar University is conducting real-time monitoring of ultrafine particles by a TSI SMPS system. In this paper, recent results are presented regarding the size distribution of the ultrafine particles measuring in the course of five month monitoring period (January-May, 2016). Several cases of new particle formation events have been observed and demonstrated in the paper, however, the precursors of the secondary aerosol particles are still unknown.

### Results

Different types of nucleation events (banana, apple and hump) have been registered during the five months monitoring. The new particle formation events were detected under 10 nm particle diameter and number concentration can reach up to  $2 \times 10^5 \text{ cm}^{-3}$  during severe events.

Figure 1 shows the averaged diurnal variation of particle number (PN) concentration in the 3-120 nm size interval. In the figure, the CO mixing ratio is also presented as an indicator for traffic emission. It is seen that following a deterministic traffic emission related peak at 7h the CO mixing ratio starts to decrease due to the broking up of the nocturnal inversion layer. In the same time, the PN concentration slightly decreases and stays constant until 13h indicating the gas-to-particle conversion of the traffic emitted gaseous precursors.

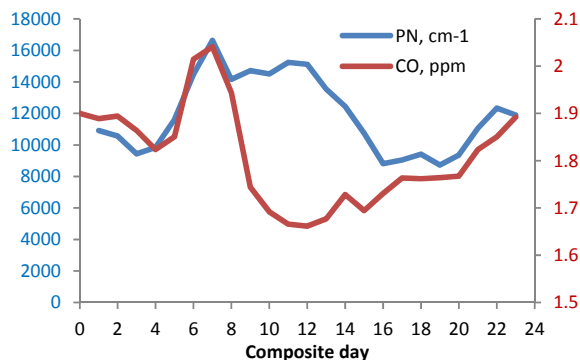


Figure 1. Averaged diurnal variations of particle number and CO concentrations, January-May, 2016.

Figure 2 demonstrates two nucleation burst events happened in 10<sup>th</sup> February (red) and 2<sup>nd</sup> April (green), 2016. The time variation of the PN concentration in the two cases is similar during the whole day, what indicates the same determinant conditions behind the events.

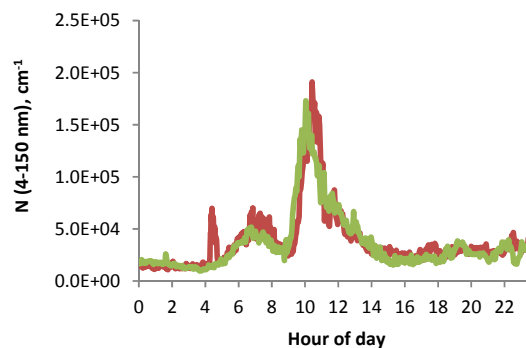


Figure 2. Diurnal variation of particle number concentration during severe nucleation bursting events (10<sup>th</sup> February and 2<sup>nd</sup> April, 2016).

The results demonstrate the significant natural and anthropogenic contribution of ultrafine particles to the total aerosol budget in coastal desert environment.

Dupart, Y. *et al.* (2012) *Proc. Natl. Acad. Sci.* **109** (51), 20842–20847.

Nie, W. *et al.* (2014) *Nature Scientific Reports* **4** (6634), DOI: 10.1038/srep06634.

Vu, TV., Delgado-Saborit, JM., Harrison, RM. (2015) *Atm. Env.* **122**, 114-132.

## Long term study of new particle formation and shrinkage events in a coastal environment: Meteorology, gas phase and solar radiation implications

A. del Águila<sup>1</sup>, M. Sorribas<sup>1</sup>, J.A. Adame<sup>1</sup>, J.M. Vilaplana<sup>1</sup>, J.A. Bogeat<sup>1</sup>, C. Córdoba-Jabonero<sup>1</sup> and M. Yela<sup>1</sup>

<sup>1</sup>National Institute for Aerospace Technology (INTA), El Arenosillo Atmospheric Observatory, Mazagón, Huelva, 21130, Spain

Keywords: New particle formation, shrinkage, size distribution, particle number concentration.

Presenting author email: aguilapa@inta.es

Atmospheric aerosol particles contribute to light absorption and scattering affecting the total radiation budget, the climate change process as well as they contribute to cloud formation (IPCC, 2013). The nucleation plays an important role in the atmospheric particle number concentration. Freshly nucleated particles eventually grow to larger particles that can affect the light-particles interactions as they interfere in the total radiation budget and consequently, they can affect the climate change and also the cloud formation. For some grown particles, it has been observed a particle size decrease, whose consequences are not clear at present and the studies concerning these events are scarce. The new particle formation (NPF) process and the subsequent size decrease, is called as shrinkage event (SE). A comparison between both processes, NPF and SE has been carried out for a 4-years data available period, over a long term period between 2004 and 2012. The aim of the study was to characterise the SE by comparison with the previous NPF by means of correlating the meteorology, gas phase ( $O_3$ ,  $SO_2$ , CO and  $NO_2$ ) and solar radiation (UVA, UVB and global).

The study took place at 'El Arenosillo' (ARN) atmospheric observatory, which is located in the southwestern part of Spain ( $37.1^\circ$  N,  $6.7^\circ$  W, 40 m a.s.l.), which is inside of a natural protected environment near Doñana National Park and less than 1 km from the Atlantic coastline. ARN is managed by the Spanish Institute for Aerospace Technology (INTA). The sub-micrometric particle number size distribution in the range 14.3-675.3 nm, was monitored with a Scanning Mobility Particle Sizer (SMPS) (Electrostatic Classifier TSI Model 3080). A particle counter (TSI Model 3022A) was used until May 2008 and was later replaced with an ultrafine particle counter (TSI Model 3776).

In a previous work of Sorribas *et al* (2015), NPF processes were classified depending on the wind direction over ARN in three main groups: Non-breeze (NB), Sea-breeze (SB) and land-breeze (LB). From this classification, the shrinkage processes after the NB nucleation events (type I, NB-I, due to its clear 'banana' shape) have been studied, and these events are called as SE or NB-I SE. In order to consider if there was a SE event, the classification has been done according to the geometrical diameter ( $D_g$ ): if there is a decrease of  $D_g$  for more than two hours after a NPF event, it can be considered as SE event. These processes have occurred the 36% of the total number of NB-I, which is 20. In Table 1, it is shown the start and end averaged times of the NPF processes, followed by a shrinkage process. The SE

are nocturnal events, starting normally at midnight. In Figure 1, the maxima  $D_g$  reached by the NPF are coloured in black, and the minima  $D_g$  reached by the SE are coloured in red. It is observed that during the shrinkage process, the lowest values reached are never as low as the nucleation starting diameters of 14.3 nm.

This first classification of SE from clear NPF (NB-I) is a preliminary study at ARN station about these kind of processes and it will be used for a long-term classification for the remaining nucleation cases.

NB-I	$T_{start}$ (hh:mm)	$T_{end}$ (hh:mm)	$D_g$ (nm)
NPF	11:30±01:20	23:10±02:40	52±12
SE	23:50±03:00	05:00±04:00	32±9

Table 1. Comparison between NPF and SE with  $T_{start}$ ,  $T_{end}$  and  $D_g$  maximum (NPF) and minimum (SE) reached respectively. (value±SD)

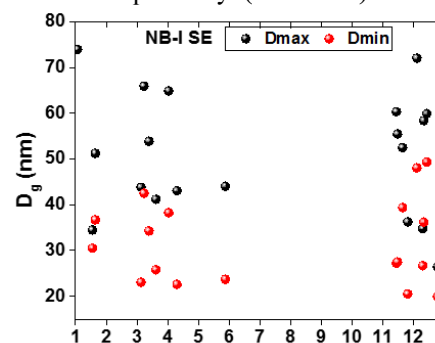


Figure 1. Daily means of  $D_{g,max}$  and  $D_{g,min}$  for NB-I SE in a monthly basis.

This work was supported by the Spanish Ministerio de Economía y Competitividad (MINECO) under grants CGL2014-55230-R (AVATAR) and CGL2014-56255-C2-2-R (ICARO).

Myhre *et al.* (2013) *Anthropogenic and natural radiative forcing*. In: Stocker, T.F., Qin, D., Plattner, G.-K., Tignor, M. Allen, S.K., Boschung, J., Nauels, A., Xia, Y., Bex, V., Midgley, P.M. (Eds.), *Climate Change 2013: The Physical Science Basis. Contribution of Working Group I to the Fifth Assessment Report of the Intergovernmental Panel on Climate Change*. Cambridge University Press, Cambridge, NY, USA.

Sorribas, M., Adame, J.A., Olmo, F.J., Vilaplana, J.M., Gil-Ojeda, M. and Alados-Arboledas, L. (2015) *A long-term study of new particle formation in a coastal environment: Meteorology, gas phase and solar radiation implications*, *Sci. Total Environ.* **511**, 723-737.

## Investigation of the role of aromatic hydrocarbons in new particle formation under urban atmospheric condition in the CLOUD chamber

M. Xiao<sup>1</sup>, C.R. Hoyle<sup>1</sup>, L. Dada<sup>2</sup>, O. Garmash<sup>2</sup>, D. Stolzenburg<sup>3</sup>, U. Molteni<sup>1</sup>, K. Lehtipalo<sup>1,2</sup>, I. El Haddad<sup>1</sup>, J. Dommen<sup>1</sup>, U. Baltensperger<sup>1</sup> and the CLOUD Collaboration

<sup>1</sup>Laboratory of Atmospheric Chemistry, Paul Scherrer Institute, Villigen, 5232, Switzerland

<sup>2</sup>Department of Physics, University of Helsinki, Helsinki, 00014, Finland

<sup>3</sup>Faculty of Physics, University of Vienna, Vienna, 1090, Austria

Keywords: new particle formation, chamber, aromatic, nucleation.

Presenting author email: mao.xiao@psi.ch

Atmospheric aerosols play an important role on climate by affecting radiative forcing via direct interaction with radiation and indirect effect on cloud formation (IPCC 2013). Aerosols can also adversely impact visibility and human health. New particle formation (NPF) has a great effect on the particle number concentration and size distribution. The physical and chemical mechanisms behind the NPF process are still under investigation.

Great advancements were made in resolving chemical and physical mechanisms of NPF with a series of experiments conducted at the CLOUD (Cosmic Leaving Outdoor Droplets) chamber facility at CERN (Geneva, Switzerland). Binary nucleation of sulfuric acid-water (Kirkby *et al.*, 2011; Duplissy *et al.*, 2016) as well as ternary nucleation of sulfuric acid-water with ammonia (Kirkby *et al.*, 2011; Kürten *et al.*, 2016), dimethylamine (Almeida *et al.*, 2013) and oxidation products from biogenic precursors (Riccobono *et al.*, 2014) were investigated systematically. Recently it has been shown how highly oxygenated molecules (HOMs) from terpenes ozonolysis are leading to pure biogenic nucleation (Kirkby *et al.* 2016; Tröstl *et al.* 2016). However, studies on NPF under conditions of urban atmospheres, where huge populations are exposed to high aerosol concentrations, are still missing and are urgently needed.

Urban atmospheres are highly polluted with high concentrations of SO<sub>2</sub>, ammonia, NO<sub>x</sub> and volatile organic vapors from anthropogenic activity as well as with high particle concentrations, which provide a high condensation sink for condensable gases. Aromatic hydrocarbons from industrial activities, traffic and residential combustion are present at high concentrations and contribute significantly to photochemical smog in the urban environment. HOMs formation from aromatic hydrocarbons precursors has been observed in a recent study (Molteni *et al.*, 2016). In this study, we investigated whether HOMs from aromatic hydrocarbons could contribute to NPF events detected in urban areas.

The experiments were conducted at the CLOUD chamber facility during CLOUD11 campaign in fall 2016. Three aromatic hydrocarbons were selected in this study: toluene, 1,2,4-trimethylbenzene and naphthalene. Experiments were also conducted with mixtures of the three aromatic hydrocarbons to better represent the urban atmosphere. All the experiments were conducted in the presence of sulfuric acid concentrations between  $1 \times 10^7$

$\text{m}^{-3}$  to  $2 \times 10^8 \text{ cm}^{-3}$  with or without the addition of ammonia (> 500 ppt) and NO<sub>x</sub> (from 0 to 25 ppb). HOMs formation is observed with all three compounds. Their concentration and composition was influenced by the NO<sub>x</sub> concentration. New particle formation rates and early growth rates derived for each precursor and their mixture, together with sulfuric acid and with or without the addition of ammonia and NO<sub>x</sub> will be reported.

The research is supported by the Swiss National Science Foundation. We thank CERN for supporting CLOUD with important technical and financial resources, and for providing a particle beam from the Proton Synchrotron. OG acknowledges European Research Council (Grant 638703-COALA) and tofTools software for mass spectrometry analysis.

Almeida, J., *et al.* (2013) *Nature*, **502**, 359-363.

IPCC (2013) *The Physical Science Basis: Working Group I Contribution to the Fifth Assessment Report of the Intergovernmental Panel on Climate Change*, Cambridge University Press

Duplissy, J., *et al.* (2016) *J. Geophys. Res. Atmos.*, **121**, 1752-1775

Kirkby, J., *et al.* (2011) *Nature*, **476**, 429-433.

Kirkby, J., *et al.* (2016) *Nature*, **533**, 521-526.

Kürten, A., *et al.* (2016) *J. Geophys. Res. Atmos.*, **121**, 12,377-12,400.

Molteni, U., *et al.* (2016) *Atmos. Chem. Phys. Discuss.*, doi:10.5194/acp-2016-1126

Riccobono, F., *et al.* (2014) *Science*, **344**, 717-721.

Tröstl, J., *et al.* (2016) *Nature*, **533**, 527-531.

## THE IMPACT OF NO<sub>x</sub> ON OXIDATION PRODUCTS OF MONOTERPENES AND THE SUBSEQUENT NANO-PARTICLE FORMATION AND GROWTH

C. Yan<sup>1</sup>, W. Nie<sup>2,1</sup>, A. L. Vogel<sup>3</sup>, L. Dada<sup>1</sup>, K. Lehtipalo<sup>1,3</sup>, D. Stolzenburg<sup>4</sup>, F. Bianchi<sup>1</sup>, M.P. Rissanen<sup>1</sup>, R. Wagner<sup>1</sup>, M. Simon<sup>5</sup>, M. Heinritzi<sup>5</sup>, L. Ahonen<sup>1</sup>, M. Sipilä<sup>1</sup>, J. Curtius<sup>5</sup>, J. Kirkby<sup>6</sup>, U. Baltensperger<sup>3</sup>, N. M. Donahue<sup>7</sup>, M. Ehn<sup>1</sup>, D. R. Worsnop<sup>8,1</sup>, M. Kulmala<sup>1</sup> and the CLOUD Collaboration

<sup>1</sup>Department of Physics, University of Helsinki, Helsinki, 00140, Finland

<sup>2</sup>School of Atmospheric Sciences, Nanjing University, Nanjing, 210046, China

<sup>3</sup>Laboratory of Atmospheric Chemistry, Paul Scherrer Institute, Villigen, 5232, Switzerland

<sup>4</sup>Faculty of Physics, University of Vienna, Vienna, 1090, Austria

<sup>5</sup>Institute for Atmospheric and Environmental Sciences, Goethe-University of Frankfurt, Frankfurt, 60438, Germany.

<sup>6</sup>CERN, Geneva, 1211, Switzerland

<sup>7</sup>Center for Atmospheric Particle Studies, Carnegie Mellon University, Pittsburgh, Pennsylvania, 15213, USA.

<sup>8</sup>Aerodyne Research, Inc., Billerica, MA, 01821, USA

Keywords: NO<sub>x</sub>, HOMs, nano-particle formation, CLOUD chamber

The new particle formation and subsequent growth is potentially a large source for cloud condensation nuclei (CCN) (Merikanto et al., 2009) thus may exert significant impact on climate (IPCC 2013).

Recent studies have highlighted the important roles of various highly oxidized multifunctional compounds (HOMs) in the new particle formation process through condensing onto freshly nucleated particles (Ehn et al., 2014; Tröstl et al., 2016) and even triggering the particle nucleation (Kirkby et al., 2016). These studies were conducted in NO<sub>x</sub>-free conditions, which well represented the pre-industrial atmosphere.

The ubiquitous nitrogen oxides (NO<sub>x</sub>) in the present-day atmosphere are known to significantly influence the HOM formation, through reacting with peroxy radicals or initiating the oxidation by NO<sub>3</sub> (Hallquist et al., 2009). Such influences have been observed even in remote or rural areas with the scarce emissions (Yan et al., 2016). Thus, a better understanding of the extent to which NO<sub>x</sub> would affect the HOM production pathways and detailed information about the properties of HOMs are essential for modelling the aerosol budget and its climate impact in present days.

We conducted dedicated experiments at the CERN CLOUD chamber to study the HOM production and nano-particle formation under atmospherically relevant levels of sulphuric acid (SA), monoterpenes, and NO<sub>x</sub>. Fig. 1 exhibits an example of how HOMs and nano-particle formation were modified when NO<sub>x</sub> were involved. We will present more detailed information on the identities of various NO<sub>x</sub>-relevant HOMs and their plausible formation pathways that are deduced based on their elemental compositions as well as their responses to NO<sub>x</sub> variation. We will show the degree to which such chemistry under the chamber conditions mimic the present-day atmosphere. By characterizing the properties of such NO<sub>x</sub>-relevant products, we will attempt to explain the negative effect of NO<sub>x</sub> on nano-particle formation.

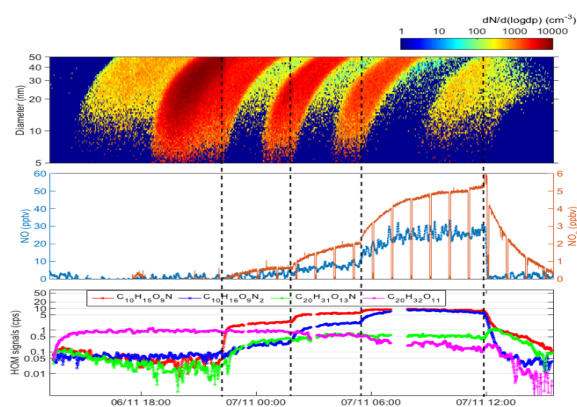


Fig. 1. Response of HOMs and particle formation to NO<sub>x</sub> and ions.

### ACKNOWLEDGEMENTS

We thank CERN for supporting CLOUD with important technical and financial resources. Research received funding from the EC Seventh Framework Programme (Marie Curie Initial Training Network "CLOUD-ITN" no. 215072, MC-ITN "CLOUD-TRAIN" no. 316662, and ERC-Advanced "ATMNUCLE" grant no. 227463), the Academy of Finland (Center of Excellence project no. 1118615, projects 135054, 133872, 251427, 139656, 139995, 137749, 141217, 141451), and several other project fundings.

### REFERENCES

- Ehn, M., et al. (2014). *Nature* **506**: 476-479.  
 Hallquist, M., et al., (2009). *Atmos. Chem. Phys.* **9**(14): 5155-5236.  
 IPCC (2013): *Climate Change*. Cambridge University Press.  
 Kirkby, J., et al. (2016). *Nature* **533**: 521-526.  
 Merikanto, J., et al. (2009). *Atmos. Chem. Phys.* **9**(21): 8601-8616.  
 Tröstl, J., et al. (2016). *Nature* **533**: 527-531.  
 Yan C., et al (2016). *Atmos. Chem. Phys.* **16**: 12715-12731.

## New particle formation studied by PSM at rural background site Košetice

A. Holubová Šmejkalová<sup>1,2,4</sup>, N. Žíková<sup>3</sup> and V. Ždímal<sup>3</sup>

<sup>1</sup>Institute for Environmental Studies, Faculty of Science, Charles University, Prague

<sup>2</sup>Czech Hydrometeorological Institute, Prague

<sup>3</sup>Institute of Chemical Process Fundamentals, CAS, Prague

<sup>4</sup>Global change research institute, CAS, Brno

adela.holubova@chmi.cz

New particle formation (NPF) as a key process of atmospheric aerosol dynamic influences particle concentration and particle size distribution (Kulmala et al. 2013, Spracklen et al. 2006). NPF events cover a diversity of nucleation mechanisms, and a better understanding of processes leading to NPF and their transformations are valuable for climate studies (Birmili and Wiedensohler 2000, Kulmala et al. 2001, Kulmala et al. 2004). Currently available measuring technologies enable us to detect particles even below 3 nm. One of the first studies utilizing the parallel aerosol monitoring by PSM and SMPS was published by Kulmala et al. in 2012. This work is focused on differences in cluster formation below and over 3 nm in rural environment. We'll try to detect patterns of clustering which lead to formation new particles in comparison to variability of meteorological elements.

Experimental data were measured from 5<sup>th</sup> August to 30<sup>th</sup> September 2016 at rural background station - National Atmospheric Observatory Košetice (NAO Košetice). NAO Košetice is located in one of the cleanest regions in the Czech Republic (534 m a. s. l., 49° 34' 24.2'' N, 15° 4' 49.0'' E). Freshly nucleated aerosol particles were recorded by particle size magnifier (PSM, model A11, Airmodus) in the scanning mode in the size range from 1.2 to 3 nm every 4 minutes. Aerosol size distributions from 10 to 800 nm were monitored by scanning mobility particle sizer (SMPS, IfT Tropos) in 5-minute time resolution.

SMPS data were used for determining days with NPF events, Non-event and undefined days according to the Dal Maso et al. (2005) method. Due to calibrations and unexpected faults, only 44 days when both instruments measured simultaneously were available. From the 44 days, 16 days were analyzed as NPF event days, 17 days as Non-event days and rest (11) as undefined days that were not evaluated further.

Fig. 1 shows NPF event and Non-event days median of diurnal variation of cluster concentrations in different size classes. In both types of events, cluster concentrations decreased with larger cluster size. NPF event days diurnal patterns are typical of higher variation during the day with clear maximum in midday hours. The lowest variability in 1.17 to 1.26 nm clusters is probably connected to their slow growth and instability of products of chemical reactions (Kulmala et al. 2013). Cluster concentrations are less variable during Non-event days.

Differences between clusters formation during NPF and Non-event days will be also evaluated with regard to meteorological conditions, with special focus on diurnal temperature variation, amount of global radiation, and variability of air pressure and relative humidity.

This project has received funding from the European Union's Horizon 2020 research and innovation programme under grant agreement No 654109 and is supported by Ministry of Education, Youth and Sports of the Czech Republic within project for support of national research infrastructure ACTRIS – participation of the Czech Republic (ACTRIS-CZ - LM2015037).

Dal Maso et al., (2005). *Boreal Environment Research*, 10(5), 323.

Birmili, W., Wiedensohler, A. (2000). *Geophysical Research Letters*, 27(20), 3325-3328.

Kulmala, M. et al. (2001). *Tellus B*, 53(4), 479-490.

Kulmala, M., et al. (2004). *Journal of Aerosol Science*, 35(2), 143-176.

Kulmala, M., et al. (2012). *Nature protocols*, 7(9), 1651-1667.

Kulmala, M. et al. (2013). *Science*, 339(6122), 943-946.

Spracklen, D. V., et al. (2006). *Atmospheric Chemistry and Physics*, 6(12), 5631-5648.

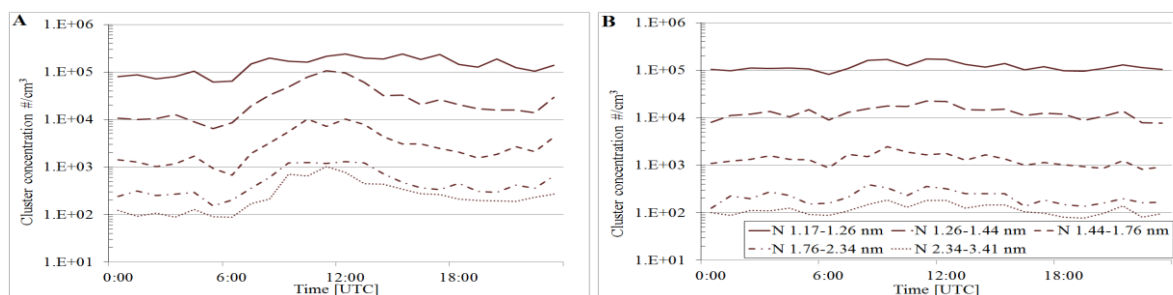


Figure. 1 Median of diurnal variations of the cluster concentrations in 5 PSM size levels measured during NPF event days (A) and Non-event days (B) evaluated according to the dal Maso et al. (2005).

## Automated method for identifying NPF types using characteristic nucleation-mode particles and air ions

L. Dada, R. Chellapermal, S. Buenrostro Mazon, J. Sulo, H. Junninen, V.M. Kerminen  
P. Paasonen and M. Kulmala

Department Of Physics, University Of Helsinki, P.O. Box 64, Fin-00014 Helsinki, Finland

Keywords: NAIS, Transported Events, Intermediate Ions  
Presenting Author Email: Lubna.Dada@helsinki.fi

New particle formation (NPF) is a phenomenon which occurs in many places around the globe (Kulmala et al., 2004). Particles formed are shown to result in global cooling indirectly by modifying cloud properties (IPCC, 2013). Previously, in order to determine whether a burst of particles is classified as a NPF event, we followed the method proposed by Dal Maso *et al.* (2005). It classifies the days into three main categories based on the appearance of a new persisting mode of particles within diameter range from 3 to 25 nm. The classes defined are event days, during which such mode appears, non-events days and undefined days. Sub-classes of event days are also defined depending on the analyzability of the event.

However, with improved instrumentation, e.g. NAIS (Neutral and Air Ions Spectrometer, Mirme and Mirme (2013)) we are now capable to detect particles and ions < 3 nm diameter, those which represent the initial steps of NPF. Here, we modify the classification of events by applying the information whether the measurement site is within the NPF area (< 3 nm particles are detected) or the air masses from the NPF area have been transported to the site (only 3-25 nm particles are detected). Additionally, we determine the exact start-time and end-time for those events that are observed in < 3 nm size range. This method allows, for the first time, to form a time series which defines the active time window of NPF enabling us to study the properties and variables involved in particle formation.

Table 1. Event classification in Hyytiälä based on the intermediate ion and large particle concentration. The 'X' marks represent the occurrence of a concentration of the ions or particles above the assigned peak value.

Classification	Intermediate ions (2.25-4nm)	Large particles (7-25nm)
Events in Hyytiälä	X	X
Transported		X
Ion Burst	X	
Non-event		

We apply our method for a dataset including 11 years of continuous aerosol observations recorded at the SMEARII station in Hyytiälä, which is a boreal forest site located in southern Finland defined by low pollution and thus acts as a background semi-clean location. Later on, our proposed method can be applied to other locations.

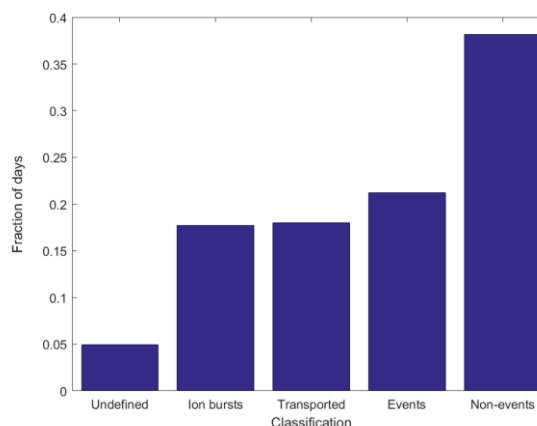


Figure 1: New classification: Fraction of ion-bursts, transported events, events in Hyytiälä, and non-events.

Days in Hyytiälä were classified into five different classes. While less than 5% of the data points were unclassified due to missing NAIS data, the remaining four classes were divided based on whether either of the concentrations of intermediate ions or large particles reached the assigned peak value, or both. The classification is shown in Table 1. Our results (Events in Hyytiälä + Transported Event frequency) fall in agreement up to 88% (Events) with the old classification method proposed by Dal Maso *et al.* (2005). Using the 11 years of available data from NAIS, results show the fraction of days included in each class (Figure 1). Also, we are able to extract the yearly trends, seasonal trends and each class NPF frequency in Hyytiälä. We found that events occurring in Hyytiälä are more frequent in the spring while the transported ones events are most frequent in summer.

This work was funded by the Doctoral Programme in Atmospheric Sciences (ATM-DP, University of Helsinki and the Academy of Finland Centre of Excellence program (grant no. 272041).

Dal Maso, M. et al (2005). *Boreal Environment Research*, **10**, 323.

IPCC: Boucher, O. et al. (2013). *Cambridge University Press*, **1**, 535-531.

Kulmala, M. et al. (2004) *Journal of Aerosol Science*, **35**, 143-176.

Mirme, S., and Mirme, A. (2013) *Atmospheric Measurement Techniques*, **6**, 1061-1071.

## Ultrafine particle events during anticyclonic and advection conditions in Madrid

N. Perez<sup>1</sup>, A. Alastuey<sup>1</sup>, C. Reche<sup>1</sup>, M. Ealo<sup>1</sup>, G. Titos<sup>1</sup>, A. Ripoll<sup>1</sup>, M.C. Minguillon<sup>1</sup>, F. J. Gómez-Moreno<sup>2</sup>, E. Alonso-Blanco<sup>2</sup>, E. Coz<sup>2</sup>, E. Diaz<sup>2</sup>, B. Artiñano<sup>2</sup>, Saúl García dos Santos<sup>3</sup>, R. Fernández-Patier<sup>3</sup>, A. Saiz-Lopez<sup>4</sup>, F. Serranía<sup>4</sup>, M. Anguas-Ballesteros<sup>4</sup>, B. Temime-Roussel<sup>5</sup>, N. Marchand<sup>5</sup>, D. C. S. Beddows<sup>6</sup>, R. M. Harrison<sup>6</sup> and X. Querol<sup>1</sup>

<sup>1</sup>Institute of Environmental Assessment and Water Research (IDAEA-CSIC), Barcelona, 08034 Spain

<sup>2</sup>Department of Environment, Joint Research Unit Atmospheric Pollution CIEMAT-CSIC, Madrid, 28040 Spain

<sup>3</sup>Instituto de Salud Carlos III (ISCIII), Madrid, 28222 Spain

<sup>4</sup>Department of Atmospheric Chemistry and Climate, IQFR-CSIC, Madrid 28006, Spain

<sup>5</sup>Aix Marseille Université, CNRS, LCE UMR 7376, 13331 Marseille, France

<sup>6</sup>National Centre for Atmospheric Science, University of Birmingham, B15 2TT United Kingdom

Keywords: nucleation, photochemistry, urban aerosol, ultrafine particles.

Presenting author email: noemi.perez@idaea.csic.es

The study of ultrafine (UF) particles in urban environments is complex, due to the wide variety of sources, precursors and processes involved in their emission or formation. In addition, measurement techniques are sometimes not reaching the lower size ranges. Successful nucleation and growth of particles is markedly influenced by atmospheric conditions, which may favour the occurrence of nucleation events even at the regional scale.

In this work, ultrafine particle measurements starting at a size of 1nm were carried out during a monitoring campaign devised to study O<sub>3</sub> events, its precursors and photochemical pollution in the Madrid region, central Spain, during 7-19th July 2016. Measurements of particle number concentrations and size distributions covering a wide size range (1nm to 1µm) were carried out using similar equipment at one urban (CSIC) and two suburban (ISCIII and CIEMAT) monitoring sites at a maximum distance of 20km. Particles under 4nm were measured at all sites by means of Airmodus-PSM and TSI 1 nm-SMPS. Supporting measurements such as BC, gaseous pollutants or meteorological parameters were also carried out.

During the campaign a transition between two different atmospheric scenarios affected markedly the variability of all pollutants. The regional accumulation of air masses during 7-10th July was replaced by a strong advection from the North-western Atlantic during 11-14th July. After this, the recirculation of air masses favoured the accumulation of pollutants again until the end of the campaign.

During the first accumulation period, pollutants with a local origin, mainly related to traffic emissions, such as BC, NO<sub>x</sub>, and also UF particle number concentrations presented higher concentrations at all sites. Parameters related to vehicle emissions presented a daily pattern characterized by maxima during morning and evening traffic peak hours.

During advection days, lower levels of pollutants were measured in general, reflecting the renovation of air masses. Concentrations of parameters related to traffic emissions, such as BC, NO and NO<sub>2</sub> were reduced by around 60, 35 and 50% at all sites, with respect to working days during the accumulation period. In the case of particle number concentration (over 2.5 or 7 nm)

the reduction was around 20-30%. Nevertheless, the entrance of Atlantic air masses cleaned the atmosphere and favoured the formation and growth of new particles from gaseous precursors and very clear events of particle nucleation, growth and shrinkage were observed during these days (Figure 1).

Regarding particles under 4nm concentrations were markedly higher at ISCIII, where building works were carried out at the moment of the campaign, whereas at CSIC, the measurement height (6th floor) is probably related to the lower levels measured.

It is interesting to highlight that during the advection period nucleation and growth events were registered simultaneously at the three monitoring stations, suggesting that this process is occurring at a regional extent. Therefore the conditions required for the formation of new particles are taking place over a scale of at least 20km, regardless the different characteristics of the monitoring sites in terms of proximity to sources or monitoring height, although differences were observed in terms of number concentration and the temporal evolution of the particle size ranges studied.

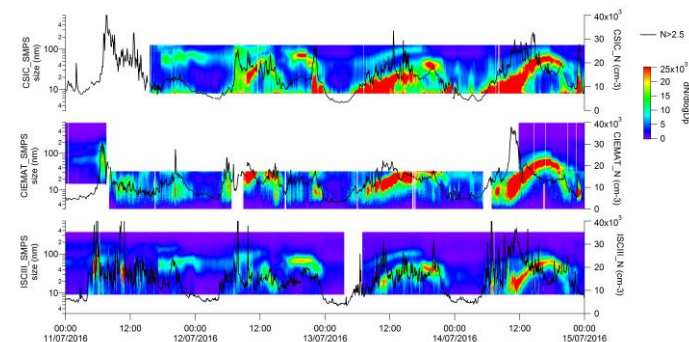


Figure 1. UF particle size distributions and number concentrations measured at the three monitoring sites during the advection period

This work was funded by the Spanish ministry of the Environment, Madrid Regional Government and Madrid City Council. We thank Alava Ingenieros, TSI, Solma Environmental Solutions, and Airmodus for their participation and support. CIEMAT participation was funded by PROACLIM (CGL2014- 52877-R) and TECNAIRE (P2013/MAE-2972) projects.

## Anthropogenic nanoparticle formation in the Vienna industrial region

Sophia Brilke<sup>1</sup>, Andreas Kropf<sup>1</sup> and Paul M. Winkler<sup>1</sup>

Faculty of Physics & VDSP, University of Vienna, 1090 Vienna, Austria

Keywords: urban aerosol, anthropogenic, new particle formation, sulphuric acid.

Presenting author email: sophia.brilke@univie.ac.at

New particle formation from trace gases emitted by anthropogenic sources is of scientific interest since atmospheric aerosols influence global climate and strongly affect human health. Particulate mass (PM) measurements of sizes below 2.5 and 10  $\mu\text{m}$  are routinely carried out in air quality measurements. However, PM<sub>2.5</sub> and PM<sub>10</sub> cannot serve as a measure of particles in the low nanometer range since the mass of particles of that size is comparably negligible.

Vienna is a typical European metropolitan area including distinct source areas such as a large industrial park including an oil refinery. In May 2016, we measured nanoparticle size distributions during a short test campaign in a suburb of Vienna, Schwechat. Different patterns of the nanoparticle population for air masses originating from different source areas were found.

A recent study (Sarnela et al., 2015) measured sulphuric acid and nano-particles in the direct vicinity of an oil refinery during a short intensive campaign. The study shows that the measurement site has to be chosen carefully and that continuous measurements are needed. We improved our setup by building up a set of measurement sites located such that air masses from the main source areas are covered. The sites are equipped with instrumentation for continuous measurement of particle size distribution and total particle concentration. Meteorological, trace gas and PM measurement data of the region are obtained from meteorological and environmental agencies.

The main source areas in the Vienna metropolitan area are (see figure 1) the city of Vienna, a suburban area, a rural and agricultural area and an industrial area including Austria's largest oil refinery and the Vienna International Airport. The continuous measurements are carried out at three measurement sites (see figure 1). The roof-top laboratory of the Faculty of Physics (1) serves as a reference point in the city centre. A second measurement site (2) is established in Schwechat, located 12 km downstream Vienna and at 2 km distance of the oil refinery followed by the Vienna International Airport. The third measurement site at the airport completes the setup. Wind from North-West following the Danube River is the prevailing wind direction. The carefully chosen measurement locations allow to discriminate the influence of air masses from different sources on particle production with a focus on emissions from distinct anthropogenic sources.

This long-term study will provide a large data set of continuous size distribution measurements and will contribute to the understanding of the mechanisms leading to nanoparticle production in a typical European metropolitan area.

This work was supported by the European Research Council under the European Community's Seventh Framework Programme (FP7/2007-2013) / ERC grant agreement No. 616075.

Sarnela, N., et al. "Sulphuric acid and aerosol particle production in the vicinity of an oil refinery." *Atmospheric Environment* 119 (2015): 156-166.

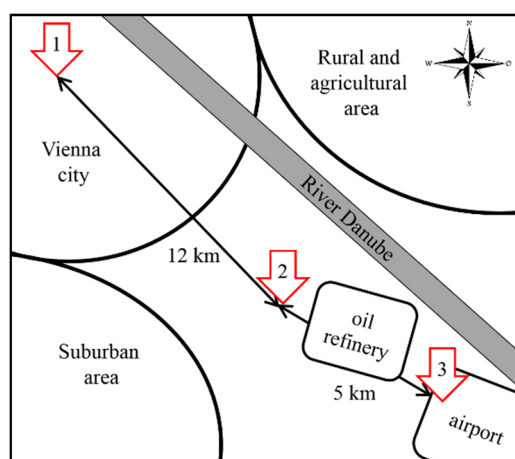


Figure 1. Three measurement sites located along the main wind direction in Vienna at the Faculty of Physics (1), suburban Schwechat (2) and the Vienna airport (3).

## Study of new particle formation events in Southern Italy

A. Dinoi<sup>1</sup>, K. Weinhold<sup>2</sup>, W. Birmili<sup>2</sup>, A. Wiedensohler<sup>2</sup>, A. Donateo<sup>1</sup>, D. Contini<sup>1</sup>

<sup>1</sup>Institute of Atmospheric Sciences and Climate, ISAC-CNR, S. P. Lecce-Monteroni km 1.2, 73100 Lecce, Italy

<sup>2</sup>Leibniz Institute for Tropospheric Research, 04318 Leipzig, Germany

Keywords: ultrafine particles, new particle formation, aerosol size distributions, meteorological conditions

Presenting author email: [a.dinoi@le.isac.cnr.it](mailto:a.dinoi@le.isac.cnr.it)

New particle formation (NPF) from gas precursors can be considered one of the most important sources of atmospheric particle (Kulmala et al., 2004). This process is a global phenomenon and it might control the total particle number and condensation nuclei concentration over continental areas largely. The probability of the occurrence of NPF events at a given location and time depends on various factors including emissions strength of precursors, meteorological parameters and photochemical processes (Kulmala et al., 2001). Intensive research has been carried out over several decades and recently substantial progress has been made in revealing the mechanisms leading to the formation and growth of new particles but there are still many gaps to be filled (Yu et al., 2016; Kulmala et al., 2014).

In this work, we analyzed a comprehensive data set of simultaneous measurements of particle number size distributions in an urban background station in the Apulia Region (South East of Italy) to identify and characterize NPF events. Measurements of PM<sub>2.5</sub> mass concentration and gaseous pollutants (NO<sub>x</sub>, SO<sub>2</sub>) have been also taken into account. Meteorological parameters (temperature, relative humidity (RH), wind speed, wind direction, and solar radiation fluxes) together with HYSPLIT (Hybrid Single-Particle Lagrangian Integrated Trajectory) air mass back-trajectory analysis were used to interpret the impact of the air masses origin on the frequency and intensity of observed nucleation events. The data evaluated in this work were taken from January 2015 to July 2016 at the Environmental Climate Observatory (GAW-WMO regional station), built in an urban background area in Lecce (40°20'8"N-18°07'28"E, 37 m asl). Particle number size distributions, in the size range of 10-800 nm, were measured using a TROPOS-type mobility particle size spectrometer.

The identification of NPF events was done using the method introduced by Dal Maso et al. (2005) with day-by-day approach. Daily aerosol size distributions have been analyzed visually and then classified into event, non-event and undefined days. During the whole measurement period, 107 clear NPF events have been identified out of 520 observation days. On average, NPF bursts were detected with high particle number concentrations in the size range between 10 and 20 nm between late morning and midday, followed by a subsequent and gradual shift of the new nucleation mode towards larger particle sizes. Fig.1 shows contour plot of a typical NPF event observed on a winter day and the hourly time evolution of particle number concentrations of nucleation ( $D_p < 20$  nm) and Aitken ( $20 \text{ nm} < D_p < 100$  nm) modes. The event starts at about 10:00 AM, showing the typical “banana” shape, and continues to

grow throughout the course of the day until 06:00 PM reaching about 40 nm size. The classification of event days showed a significant seasonal trend with higher frequencies of NPF events in spring and summer with a maximum in September (43%).

Meteorological parameters have highlighted that NPF events occur almost exclusively on days with low RH values (~40% between 9:00 AM and 04:00 PM) and daily average radiation of more than 400 Wm<sup>-2</sup>. The fraction of event days generally increased with an increasing value of solar radiation. HYSPLIT back trajectories analysis demonstrated that the probability of NPF occurrence is higher when the air masses, usually cooler, drier and relatively clean, originate from the North-Northeast. No significant differences were found in PM<sub>2.5</sub>, NO<sub>x</sub> and SO<sub>2</sub> concentrations between event and non-event days.

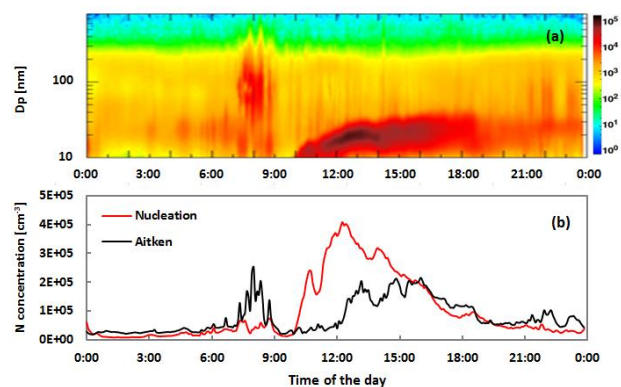


Figure 1. The time series of nucleation event observed at Lecce on February 5, 2015; (a) contour plot of size distribution, the color axis  $dN/d\log D_p$  ( $\text{cm}^{-3}$ ); (b) particle number concentration of nucleation and Aitken mode particles.

Work supported by I-AMICA (Infrastructure of High Technology for Environmental and Climate Monitoring - PONa3\_00363) project funded by National Operational Program (PON) for "Research and Competitiveness 2007-2013" co-funded with European Regional Development Fund (ERDF) and National resources.

Kulmala, M., Vehkamäki, H., Petäjä, T., Dal Maso, M., et al. (2004) *J. Aerosol. Sci.*, **35**(2), 143–176.

Kulmala, M., Dal Maso, M., Mäkelä, J. M., Pirjola, L., et al. (2001) *Tellus*, **53B**, 479–490.

Yu, H., Zhou, L., Dai, L., Shen, W., et al. (2016) *Atmos. Chem. Phys.*, **16**, 2641–2657.

Kulmala, M., Petäjä, T., Ehn, M., Thornton, J., et al. (2014) *Annu. Rev. Phys. Chem.*, **65**, 21–37.

Dal Maso, M., Kulmala, M., Riipinen, I., et al. (2005) *Boreal Environ. Res.* **10**, 323–336.

## Airborne observations of high altitude sub-10 nm aerosol particle layers

J. Lampilahti<sup>1</sup>, K. Leino<sup>1</sup>, R. Väänänen, A. Manninen<sup>1</sup>, S. Buenrostro Mazon<sup>1</sup>, H. E. Manninen<sup>2</sup>, T. Petäjä<sup>1</sup> and M. Kulmala<sup>1</sup>

<sup>1</sup>Department of Physics, University of Helsinki, Helsinki, 00560, Finland

<sup>2</sup>CERN, CH-1211 Geneva 23, Switzerland

Keywords: new particle formation, planetary boundary layer, airborne measurements

Presenting author email: [janne.lampilahti@helsinki.fi](mailto:janne.lampilahti@helsinki.fi)

Atmospheric new particle formation (NPF) has important implications for health, environment and climate (e.g. Kulmala et al. 2013). While NPF has been studied extensively from ground-based measurements it is still unclear what happens aloft. In order to gain a more complete picture of NPF in the lower troposphere we have analyzed vertical profile measurements of aerosol particles and meteorological variables from roughly 100 m up to 3000 m above ground.

The measurements were done using an instrumented Cessna 172 aircraft. A total of seven intensive measurement campaigns were conducted over a rural boreal forest region in southern Finland between the years 2013-2017 (Väänänen et al. 2016). Key aerosol instruments onboard were a TSI 3776 CPC that measured particles larger than 3 nm, Airmodus PSM that measured particles larger than ~1.5 nm and a homemade SMPS that measured 10-400 nm particle number-size distribution.

On multiple days we found elevated sub-10 nm particle concentrations near the interface between the residual layer and the free troposphere (capping inversion). The small size of the particles and the lack of surface influence suggests that the particles were freshly formed *in situ*.

Our results suggest that separate NPF may happen above the convective boundary layer, specifically

in the capping inversion where the conditions for nucleation may be particularly favourable. This is supported by some previous observations (Wehner et al., 2010) and modeling studies (Nilsson and Kulmala, 1998). Further work is being done in order to assess the prevalence and impact of the phenomenon.

This work was supported by the Office of Science (BER), U.S. Department of Energy. This research has been funded by the ERC-Advanced "ATM- NUCLE" (grant no. 227463), the Academy of Finland (Center of Excellence project no. 272041), the Eurostars Programme under contract no. E!6911 and the European Commission under the Framework Programme 7 (FP7-ENV-2010-265148), and the European Union's FP7 capacities programme under ACTRIS (grant no. 262254), and Horizon 2020 research and innovation programme under ACTRIS-2 (grant no. 654109). In addition, this work was supported by CRAICC and the Swedish Research Councils.

Kulmala, M. et al. (2013) *Science* **339**, 943-946.

Väänänen R. et al. (2016) *Atmos. Chem. Phys. Discuss.*

Wehner B. et al. (2010) *Atmos. Chem. Phys.* **10**, 4319-4330.

Nilsson E. D. and Kulmala M. (1998) *J. Geophys. Res. Atmos.* **103**, 1381-1389.

## Atmospheric evidence for pure biogenic nucleation

C. Rose<sup>1</sup>, Q. Zha<sup>1</sup>, F. Bianchi<sup>1</sup>, S. Buenrostro Mazon<sup>1</sup>, L. Dada<sup>1</sup>, H. Junninen<sup>1</sup>, T. Petäjä<sup>1</sup> and M. Kulmala<sup>1</sup>

<sup>1</sup>Department of Physics, University of Helsinki, P.O. Box 64, FIN-00014 Helsinki, Finland

Keywords: new particle formation, ion, mass spectrometry

Presenting author email: clemence.rose@helsinki.fi

Atmospheric formation of nanometer sized particles is a frequent phenomenon which significantly contributes to global aerosol particle number concentration throughout the troposphere (Merikanto et al., 2009). Besides their effect on human health, these newly formed particles can, after they grow to larger sizes, act as cloud condensation nuclei (CCN), and impact the climate through cloud related radiative processes (Kerminen et al., 2012).

Benefiting from the continuous advancement of measurement techniques, our understanding of NPF has significantly improved during the last decade. For instance, state-of-the-art mass spectrometers, namely APi-TOF (Atmospheric Pressure interface Time-Of-Flight; Junninen et al., 2010) and CI-APi-TOF (Chemical Ionization Atmospheric Pressure interface Time-Of-Flight; Jokinen et al., 2012), have provided new insights into the identification of the gaseous precursors involved in the process. Using such techniques, evidence for the role of oxidized organic compounds (referred as HOMs, *Highly Oxidized Multifunctional organic compounds*) together with sulfuric acid already in the early stages of the NPF process was highlighted in several studies (eg. Bianchi et al., 2016; Ehn et al., 2014; Schobesberger et al., 2013). More recently, Kirkby et al. (2016) reported ion induced cluster formation solely from  $\alpha$ -pinene oxidation products under atmospheric conditions in the CERN CLOUD (Cosmics Leaving OUTdoor Droplets) chamber.

Although organic nucleation at extremely low sulphuric acid concentration has been already observed in the free troposphere (Bianchi et al., 2016), the aforementioned mechanism, in which highly oxidized biogenic molecules form new particles, has never been clearly evidenced in the real atmosphere.

The formation of negatively charged clusters was frequently observed in Hyytiälä, Finland (Hari and Kulmala, 2005), during spring time before the sunset, as illustrated on Figure 1. In addition to low sulfuric acid concentrations, the simultaneous appearance of HOM dimers and their subsequent “growth” up to tetramers, which is not observed in the absence of cluster ion formation event, suggests a strong involvement of these biogenic compounds in the formation of the negatively charged clusters, as previously shown by Kirkby et al. (2016). Moreover, the cluster formation rates measured in Hyytiälä are similar to those reported from the CLOUD experiment in comparable conditions, supporting the fact that the mechanism evidenced in the chamber might also occur in the real atmosphere. However, since the newly formed clusters do not grow beyond 3 nm in Hyytiälä, the relevance of the ion induced pure biogenic nucleation

with respect to climate might be very limited, at least in the boreal forest.

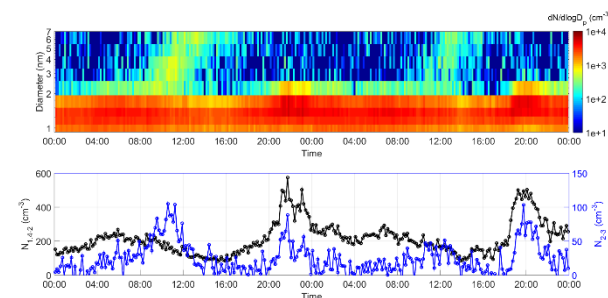


Figure 1. Identification of “evening” negative cluster ion formation events on 20 – 21 April 2013.

This work was funded by the Academy of Finland Centre of Excellence program (grant no. 272041). Part of this work is supported by the Doctoral Programme in Atmospheric Sciences (ATM-DP, University of Helsinki). We thank the tofTools team for providing tools for mass spectrometry analysis.

Bianchi, F., et al., (2016). *Science*, **352**, 1109–1112.

Ehn, M., et al., (2014). *Nature*, **506**, 476–479.

Hari P. and Kulmala M., (2005). *Bor. Environ. Res.*, **10**, 315–322.

Jokinen, T., et al., (2012). *Atmos Chem Phys*, **9**, 4117–4125.

Junninen, H., et al., (2010). *Atmospheric Meas. Tech.*, **3**, 1039–1053.

Kerminen, V.-M., et al., (2012). *Atmos Chem Phys*, **12**, 12037–12059.

Kirkby, J., et al., (2016). *Nature*, **533**, 521–526.

Merikanto, J., et al., (2009). *Atmos Chem Phys*, **9**, 8601–8616.

Schobesberger, S., et al., (2013). *Proc. Natl. Acad. Sci.*, **110**, 17223–17228.

## Freshly formed boundary layer aerosol under different weather conditions during ‘Melpitz Column 2015’

B. Altstädter<sup>1\*</sup>, A. Lampert<sup>1</sup>, A. Platis<sup>2</sup>, M. Jähn<sup>3</sup>, H. Baars<sup>3</sup>, J. Lückerrath<sup>4</sup>, A. Held<sup>4</sup>, M. Hermann<sup>3</sup>, J. Bange<sup>2</sup> and B. Wehner<sup>3</sup>

<sup>1</sup>Institute of Flight Guidance, Technische Universität Braunschweig, 38108 Braunschweig, Germany

<sup>2</sup>Center for Applied Geoscience, Eberhard Karls University Tübingen, 72074 Tübingen, Germany

<sup>3</sup>Leibniz Institute for Tropospheric Research, 04318 Leipzig, Germany

<sup>4</sup>Atmospheric Chemistry, University of Bayreuth, 95440 Bayreuth, Germany

Keywords: Melpitz Column 2015, airborne measurements, new particle formation, boundary layer

\*Presenting author email: b.altstaedter@tu-braunschweig.de

This study focuses on formation of boundary layer (BL) aerosol under different weather conditions and shows the variability of occurrence in the vertical distribution and the temporal development of freshly formed aerosol. For three case studies, new particle formation (NPF) appeared at various altitudes: at ground level, within the inversion layer and during short intervals between cloud parcels.

Airborne measurements were performed at the global atmosphere watch station in Melpitz, 40 km NE of Leipzig in Germany, as part of the extensive field campaign ‘Melpitz Column 2015’. More than 150 vertical profiles were obtained with the unmanned aerial system (UAS) ALADINA (Altstädter *et al.*, 2015) from June 16 until July 1, 2015. Boundary layer evolution, total aerosol number concentration and aerosol size distribution were measured from ground level up to 1200 m in altitude. For a complete analysis, the airborne data was validated with an expanded LES model (Jähn *et al.*, 2015), instrumentation on-site, remote-sensing and additional airborne platforms that were partially operated at the same site in order to investigate further information of BL parameters, gas concentration and optical properties of airborne aerosols.

Taken from ground observations, at 06:30 UTC on July 1, NPF occurred at ground level in relation to a significant growth rate and high deposition fluxes, spread out through the BL as consequence of updraft in the growing inversion height and was observed by profiling with ALADINA. Besides, in the early morning a low level jet appeared that may favour formation processes in the BL as assumed by Siebert *et al.* (2007). On the measurement day, NE wind was prevalent and high incoming solar radiation led to pronounced surface fluxes of latent and sensible heat. In addition, two distinct layers of enhanced aerosol load existed during the day and were captured with ALADINA.

Figure 1 represents from left to right vertical profiles of water vapour mixing ratio  $q$  and  $w'\theta'$  taken from LES model in an 1 h interval (solid lines). In addition, total aerosol number concentration in the particle diameter of 7 nm to 2  $\mu\text{m}$  ( $N_7$ ) and 390 nm ( $N_{390}$ ) were detected with ALADINA are shown on four ascents at 04:43 (blue), 07:34 (green), 09:01 (black) and 09:23 (red) UTC. The vertical distribution of the total aerosol number concentration of ultrafine particles

depended on the BL height. Starting with NPF at ground,  $N_7$  increased during the day as result of updraft to a maximum of  $6.3 \times 10^4 \text{ cm}^{-3}$  in 500 m at 09:01 UTC. At 09:23 UTC, the BL was well-mixed and the ultrafine particles were evenly dispersed. Besides, the amount of accumulation mode particles was rather low and behaved controversial to ultrafine particles in the vertical distribution.

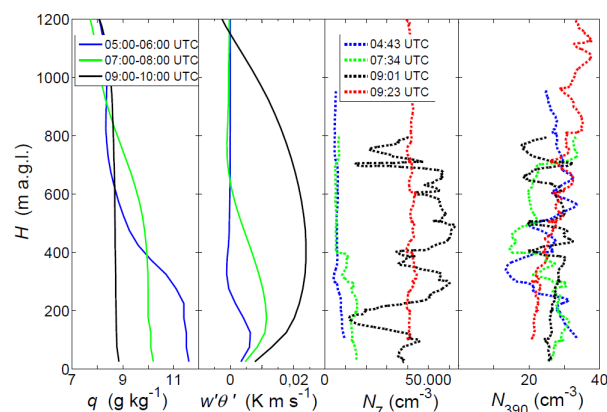


Figure 1. Vertical profiles of  $q$ ,  $w'\theta'$  and total aerosol number concentration measured in Melpitz on July 1, 2015 (see explanations in text).

The authors acknowledge the funding of this project with the number ‘LA2907/5-2, WI1449/22-2, BA1988/14-2’ by the German Research Foundation (DFG).

Altstädter, B., Platis, A., Wehner, B., Scholtz, A., Lampert, A., Wildmann, N., Hermann, M., Käthner, R., Bange, J. and Baars, H. (2015), ALADINA – an unmanned research aircraft for observing vertical and horizontal distributions of ultrafine particles within the atmospheric boundary layer, *Atmos. Meas. Tech.*, **8**, 1627-1639, doi:10.5194/amt-8-1627-2015.

Jähn, M., Knoth, O., König, M. and Vogelsberg, U. (2015), ASAM v2.7: a compressible atmospheric model with a Cartesian cut cell approach, *Geosci. Model Dev.*, **8**, 317-340, doi:10.5194/gmd-8-317-2015.

Siebert, H., Wehner, B., Hellmuth, O., Stratmann, F., Boy, M. and Kulmala, M. (2007), New-particle formation in connection with a nocturnal low-level jet: Observations and modeling results, *Geoph. Res. Lett.*, **34**, L16822, doi:10.1029/2007GL029891.

## Nucleation of sulfuric acid and dimethylamine: Results from the CLOUD experiment and possible atmospheric implications

A. Kürten<sup>1</sup>, P.H. McMurry<sup>2</sup>, and the CLOUD collaboration

<sup>1</sup>Institute for Atmospheric and Environmental Sciences, Goethe University Frankfurt, Frankfurt am Main, 60438, Germany

<sup>2</sup>Department of Mechanical Engineering, University of Minnesota, Twin Cities, MN 55455, USA

Keywords: new particle formation.

Presenting author email: kuerten@iau.uni-frankfurt.de

The exact particle formation mechanisms in the boundary layer are still mostly unresolved. However, a CLOUD (Cosmics Leaving Outdoor Droplets) experiment at CERN showed that sulfuric acid and dimethylamine (DMA) produce new particles very efficiently at a temperature of 278 K and 38% RH (Almeida *et al.*, 2013). This was the case even at relatively low DMA mixing ratios in the pptv range and at atmospherically relevant sulfuric acid concentrations. Further analysis of the chamber measurements revealed that the particle formation even proceeds at the highest possible rate, i.e. at the kinetic limit, meaning that the cluster evaporation rates are essentially zero for the conditions of the experiment (Kürten *et al.*, 2014). The possibility that new particle formation could be kinetically controlled was, however, suggested already many years before (McMurry, 1980), although the relevant (amine) molecules were not identified at that time.

The finding that new particle formation can essentially be kinetically controlled, even at amine mixing ratios in the pptv range, is quite puzzling when comparing the chamber results to the atmospheric observations. Many studies reported relatively high atmospheric amine mixing ratios above several pptv (e.g. Freshour *et al.*, 2014). However, there have been relatively few field experiments so far with sufficient instrumentation to identify sulfuric acid-amine nucleation (Zhao *et al.*, 2011). Furthermore, the atmospheric new particle formation rates do not seem to reach the high values that would be expected for kinetic nucleation. Therefore, this leads to two questions: (1) How important is sulfuric acid amine nucleation in the atmosphere? (2) And additionally, how representative are the atmospheric amine measurements?

Based on further analysis of the previously collected CLOUD data, this work is revisiting the question, if sulfuric acid amine nucleation is proceeding at the kinetic limit. In this context it is, however, reasonable to expect that the cluster evaporation rates are not exactly zero but are effectively zero, i.e. at the conditions of the experiment, the very small evaporation rates can be neglected. Comparison between measurements and modelled cluster/particle concentrations yields an upper limit for the evaporation rate of the smallest sulfuric acid-dimethylamine cluster. Using this information a model taking into account cluster coagulation and evaporation of the smallest cluster can be used to estimate the new particle formation rates for different amine mixing ratios. These results will be

compared to atmospheric new particle formation rates in order to estimate, to what extent sulfuric acid-amine nucleation could explain the atmospheric observations.

Lastly, a new method for extrapolating particle formation rates from particle size distribution measurements (starting at ~4 nm) to a small diameter (e.g. 1.7 nm) is tested for the sulfuric acid-dimethylamine system in CLOUD (Kürten *et al.*, 2015). This method takes into account the effect of self-coagulation.

We would like to thank CERN for supporting CLOUD with important technical and financial resources, and for providing a particle beam from the CERN Proton Synchrotron. This research was funded by the European Commission Seventh Framework Programme (Marie Curie Initial Training Network “CLOUD-ITN”, grant no. 215072), the German Federal Ministry of Education and Research (project nos. 01LK0902A and 01LK1222A), the European Research Council Advanced Grant “ATMNUCLE” (project no. 227463), the Academy of Finland (project nos. 1133872, 1118615, and 272041), the Swiss National Science Foundation (project nos. 200020\_135307 and 206620\_141278), the US National Science Foundation (grants AGS-1439551 and AGS-1447056), the Austrian Science Fund (project nos. P19546 and L593), and the Davidow foundation.

Almeida, J. *et al.* (2013) *Nature* **502**, 359–363.

Freshour, N. A. *et al.* (2014) *Atmos. Meas. Tech.* **7**, 3611–3621.

Kürten, A. *et al.* (2014) *P. Natl. Acad. Sci. USA* **111**, 15019–15024.

Kürten, A. *et al.* (2015) *Atmos. Chem. Phys.* **15**, 4063–4075.

McMurry, P.H. (1980) *J. Colloid. Interf. Sci.* **78**, 513–527.

Zhao, J. *et al.* (2011) *Atmos. Chem. Phys.* **11**, 10823–10836.

## The effect of NO on the formation of condensable vapours in the oxidation of $\alpha$ -pinene

O. Peräkylä<sup>1</sup>, O. Garmash<sup>1</sup>, M. Riva<sup>1</sup>, L. Heikkinen<sup>1</sup>, L. Quéléver<sup>1</sup>, M. Äijälä<sup>1</sup>, L. Fischer<sup>2</sup>, E. Canaval<sup>2</sup>, A. Hansel<sup>2</sup>, T. Petäjä<sup>1</sup> and M. Ehn<sup>1</sup>

<sup>1</sup>Department of Physics, University of Helsinki, Helsinki, 00140, Finland

<sup>2</sup>Institute of Ion Physics and Applied Physics, Innsbruck University, Innsbruck, 6020, Austria

Keywords: HOM, SOA, Anthropogenic enhancement, NPF.

Presenting author email: otso.perakyla@helsinki.fi

Organic compounds play a key role in the formation of atmospheric aerosol around the globe (Zhang *et al* 2007, Jimenez *et al* 2009). Most of the organics are originally emitted into the atmosphere in the gas phase. These volatile organic compounds (VOCs) can get oxidized, forming compounds of lower volatility, which may condense onto pre-existing aerosol particles or nucleate to form secondary organic aerosol (SOA). The VOCs can be either anthropogenic or biogenic in origin. Even with purely biogenic VOCs, anthropogenic emissions, such as those of nitrogen oxides (NO<sub>x</sub>), may alter their oxidation process, and thus affect SOA formation. Our current knowledge on SOA formation, especially the interplay between biogenic and anthropogenic effects, remains poor, which contributes to the uncertainty in climate simulations (Hallquist *et al* 2009).

There is a discrepancy between SOA formation observed in the atmosphere, and that predicted by process models (Hallquist *et al* 2009). A promising candidate to explain this discrepancy is the condensation of a newly found class of VOC oxidation products, highly oxidized multifunctional organic compounds (HOMs) (Ehn *et al* 2014). HOMs form rapidly in the oxidation of many VOCs, and generally have a very low volatility. As a result, they contribute significantly to SOA formation (Ehn *et al* 2014). HOMs arise from the autoxidation of peroxy radicals (RO<sub>2</sub>) formed in the oxidation reaction. This autoxidation reaction is sensitive to the presence of free radicals in the atmosphere. Different radicals, such as nitric oxide (NO), can thus alter the reaction pathways and influence the yields and properties of HOMs formed, and therefore SOA formation. This could, in turn, potentially impact the observed enhancement of biogenic SOA formation in the presence of anthropogenic emissions (Hallquist *et al* 2009). Therefore, unravelling the effect of NO on HOM formation could significantly enhance our understanding of SOA, and improve the predictive capability of models, in both the current and future climates.

To resolve how the presence of NO affects the formation of HOMs, we performed chamber measurements where we oxidized  $\alpha$ -pinene, a VOC emitted in large quantities from boreal forests, with ozone. Among other parameters, we varied the NO concentration. We conducted the measurements in a 2 m<sup>3</sup> Teflon chamber operated in a continuous flow mode. The gas- and particle phase oxidation products were measured using wide range of instruments, including the chemical ionization atmospheric pressure interface time-of-flight mass spectrometer (CI-API-TOF, Jokinen *et al*

2012) utilizing nitrate ionization for the detection of gas-phase HOMs. In conjunction with the CI-API-TOF, the particle phase instrumentation allows us to ascertain the effect of the HOMs on SOA formation.

We observed a decrease of total HOMs detected with increasing NO concentration. There was a clear shift from HOMs consisting purely of carbon, hydrogen and oxygen towards HOMs containing nitrogen as well, while HOM dimers were suppressed. Additionally, we observed various highly oxidized HOMs with a lower carbon number appearing with the addition of NO. At high NO concentrations these changes contribute to a shift of the HOMs to a higher volatility, and lowered potential for the formation of SOA and new particle formation. However, there are indications that, at low to moderate concentrations of NO, the effect is to enhance SOA formation. We are targeting this range of low NO concentrations with currently ongoing measurements. Along with a better control of NO concentrations, we are using a CI-API-TOF equipped with a long TOF mass analyser (LTOF). The LTOF has a greatly enhanced mass resolution compared to the ordinary high resolution TOF, enabling a much better separation of nitrogen-containing HOMs from RO<sub>2</sub> radicals, which normally cannot be readily distinguished. These improvements will allow us to explore the effect of NO on HOM formation in unprecedented detail.

This work was supported by the European Research Council (Grant 638703-COALA). We thank the tofTools team for providing tools for mass spectrometry data analysis.

Ehn, M., *et al* (2014). A large source of low-volatility secondary organic aerosol. *Nature*, **506**, 476-479.

Hallquist, M., *et al* (2009). The formation, properties and impact of secondary organic aerosol: current and emerging issues. *Atmospheric Chemistry and Physics*, **9**.

Jimenez, J. L., *et al* (2009). Evolution of organic aerosols in the atmosphere. *Science*, **326**, 1525-1529.

Jokinen, T., *et al* (2012). Atmospheric sulphuric acid and neutral cluster measurements using CI-API-TOF. *Atmospheric Chemistry and Physics*, **12**.

Zhang, Q., *et al* (2007). Ubiquity and dominance of oxygenated species in organic aerosols in anthropogenically-influenced Northern Hemisphere midlatitudes. *Geophysical Research Letters*, **34**.

## A Monte Carlo approach to nucleation

C. Köhn<sup>1</sup>, M.B. Enghoff<sup>1</sup> and H. Svensmark<sup>1</sup>

<sup>1</sup>DTU Space, Danish Technical University, Kgs. Lyngby, 2800, Denmark

Keywords: Nucleation, Modelling, Monte Carlo

Presenting author email: enghoff@space.dtu.dk

The nucleation of molecular clusters is estimated to contribute about half of all cloud condensation nuclei globally. Thus an understanding of the nucleation process is central for describing atmospheric aerosols accurately. A central molecule in nucleation is sulfuric acid which can nucleate by itself or with various other molecules.

In this work we present a particle Monte Carlo code to study the formation and growth of sulfuric acid clusters as well as its dependence on the ambient temperature. In contrast to common density models, we here trace individual sulfuric acid molecules as they collide and evaporate.

We initiate a swarm of sulfuric acid molecules with a radius of 0.15 nm with densities between  $10^7$  and  $10^8$   $\text{cm}^{-3}$  at temperatures between 200 and 300 K. After every time step, we update the position and velocity of particles as a function of size-dependent diffusion coefficients. If two particles encounter, we merge them and add their volumes and masses. Inversely, we check after every time step whether molecules evaporate from each cluster based on evaporation coefficients from literature (Yu 2005, Yu 2006).

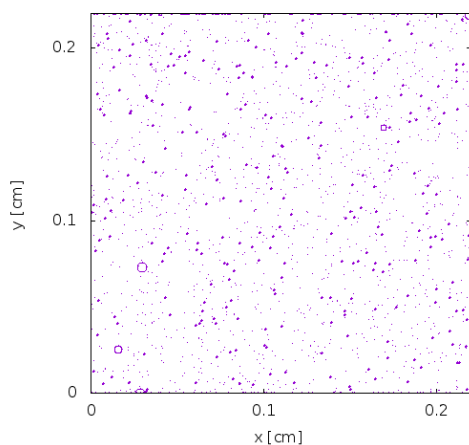


**Figure 1.** The spatial distribution of all particles (monomers and clusters) after 0.19 ms projected onto the xy plane for a run with 1000 sulphuric acid molecules in a  $0.01 \text{ cm}^3$  box. The size of each circle represents the size of each particle, scaled for visibility.

This approach allows us to track the evolution of the spatial distribution of all the molecules in 3D along with the development of the size distribution. The

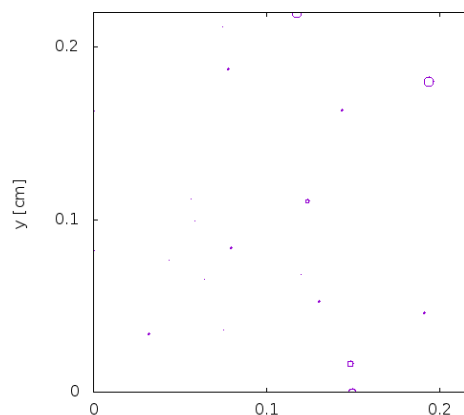


**Figure 2.** The same simulation as in Fig. 1 at  $t = 1.0$  ms, where most of the initial sulfuric acid has condensed into clusters.

nucleation rate of clusters with a diameter of 1.7 nm is also calculated as a function of time and we determine how the nucleation rate depends on the initial molecule density and the temperature. It is a goal to also implement ions in the simulations to model ion induced nucleation.

The research leading to these results has received funding from the People Programme (Marie Curie Actions) of the European Union's Seventh Framework Programme (FP7/2007–2013) under REA grant agreement no 609405 (COFUNDPostdocDTU).

Yu, F. (2005), *J. Chem. Phys.* **122**, 074501

Yu, F. (2006), *Atmos. Chem. Phys.* **6**, 5193-5211

## Relative Formation Times of Charged and Neutral Particles in an Urban Environment

Rohan Jayaratne, Buddhi Pushpawela and Lidia Morawska

International laboratory for Air Quality and Health,  
Queensland University of Technology, Brisbane 4001, QLD, Australia

Keywords: Atmospheric Ions, Aerosols, New Particle Formation

Presenting author email: r.jayaratne@qut.edu.au

A neutral cluster and air ion spectrometer (NAIS) was used to determine the characteristics of over 100 new particle formation (NPF) events in the urban environment of Brisbane, Australia (Jayaratne et al., 2016). The aim of this study was to assess the effectiveness of ion-induced nucleation by determining the initial formation times of charged and neutral particles in these events. An NPF event was defined as an event where the rate of increase of particles in the size range below 10 nm achieved a value greater than  $15,000 \text{ cm}^{-3} \text{ h}^{-1}$ . As the formation rates were most obvious in the smallest size bin of the NAIS, 1.8-3.2 nm, we determined the times at which the concentrations of charged and neutral particles in this size bin reached their peak values during each event.

Of the 108 NPF events that were investigated, we identified 79 events where the formation times of charged and neutral particles were different. Out of these, in 29 events the difference was less than 5 min. In 42 of the remaining 50 events, charged particles clearly formed before the neutral particles. The mean time lag in these events was 24 min with a standard deviation of 12 min. Our observations are in agreement with two other previous studies carried out in forest environments in Europe (Manninen et al., 2010; Gonser et al., 2014) where the main gaseous precursors of NPF are generally biogenic organics. This is the first study to show the same observation in an urban environment where it is known that new particles are mainly produced by motor vehicle emissions with the gaseous precursors being mainly sulphuric acid and organic hydrocarbons. It is also the first such study in the Southern Hemisphere.

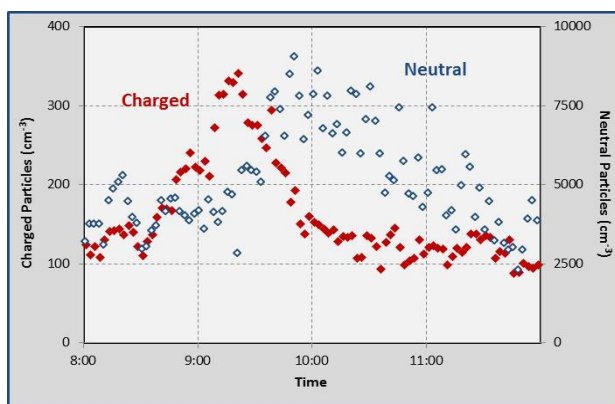


Figure 1. Time series of the charged and neutral particle concentrations in the NAIS size bin 1.8-3.2 nm during a typical NPF event, showing a peak concentration time lag of about 35 min.

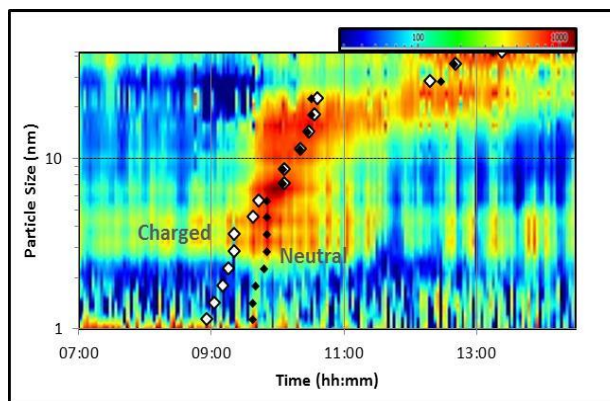


Figure 2. NAIS spectrogram overlaid with markers showing the times at which the charged and neutral particle concentrations in each size bin attained their maximum values.

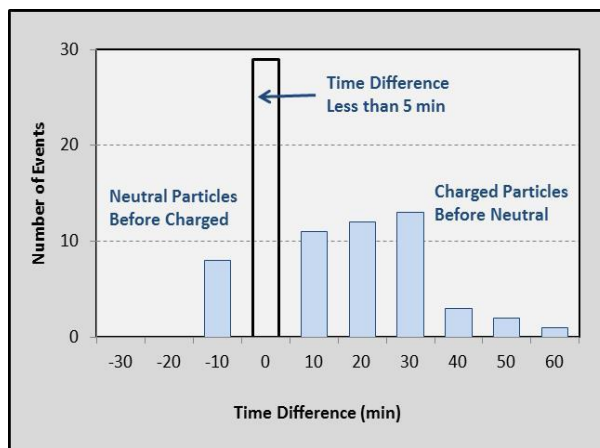


Figure 3. Number of NPF events arranged according to the time delay between the initial formation times of charged and neutral particles. Charged particles appeared before neutral particles in 42 of the 50 events in which the difference was clear (greater than 5 min).

Gonser S, Klein F, Birmili W et al. (2014). *Atmospheric Chemistry and Physics*, 14(19), 10547-10563.

Jayaratne, E.R., Pushpawela, B., Morawska, L. (2016) *Frontiers Environ Sci Eng.* 10(5), 13, 2016.

Manninen H, Nieminen T, Asmi E et al. (2010). *Atmospheric Chemistry and Physics*, 10(16), 7907-7927.

## The Himalayan aerosol factory: the chemistry of new particle formation

F. Bianchi<sup>1,2</sup>, H. Junninen<sup>1</sup>, A. Bigi<sup>3</sup>, P. Bonasoni<sup>4</sup>, S. Buenrostro Mazon<sup>1</sup>, L. Dada<sup>1</sup>, J. Dommen<sup>2</sup>, C. Frege<sup>2</sup>, C.R. Hoyle<sup>2</sup>, P. Laj<sup>1,5</sup>, K. Lehtipalo<sup>1,2</sup>, J. Kontkanen<sup>1</sup>, A. Marinoni<sup>4</sup>, U. Molteni<sup>2</sup>, M. Riva<sup>1</sup>, V. Sinclair<sup>1</sup>, K. Sellegrì<sup>6</sup>, C. Yan<sup>1</sup>, D.R. Worsnop<sup>1,7</sup>, U. Baltensperger<sup>2</sup>, M. Kulmala<sup>1</sup>

<sup>1</sup>Department of Physics, University of Helsinki, Helsinki, 00014, Finland

<sup>2</sup>Laboratory of Atmospheric Chemistry, Paul Scherrer Institute, Villigen, 5232, Switzerland

<sup>3</sup>Department of Engineering “Enzo Ferrari”, Università degli studi di Modena e Reggio Emilia, Modena, 41125, Italy

<sup>4</sup>Institute of Atmospheric Sciences and Climate, National Research Council of Italy, Bologna, 40129, Italy

<sup>5</sup>Univ. Grenoble-Alpes, UGA, CNRS, IGE, F-38000, France

<sup>6</sup>Laboratoire de Météorologie Physique, Observatoire de Physique du Globe de Clermont-Ferrand, Université Blaise Pascal, Aubière, 63171, France

<sup>7</sup>Aerodyne Research, Inc., 45 Manning Road, Billerica, MA 01821, USA

Keywords: Nucleation, Free Troposphere, Mass Spectrometry, Ions.

Presenting author email: Federico.bianchi@helsinki.fi

A substantial fraction (> 50%) of cloud condensation nuclei (CCN) in the atmosphere arises from new particle formation (NPF) (Merikanto et al., 2009) where 35% are directly formed in the free troposphere. While NPF has been observed in many places around the world, the mechanisms governing this process are still poorly understood, especially at high altitude. So far, only few studies have shown that NPF can frequently take place at high altitudes (Venzac et al., 2008). However, none of these have identified the chemical composition of the growing clusters.

In the last few years, we have focused our studies on further characterizing NPF processes at high altitudes performing measurements with advanced mass spectrometers, in order to gain a better understanding on the chemical cluster composition and therefore the nucleation precursors. Our first measurements were performed at the Jungfraujoch station (Switzerland) and have been described in recent publications (Bianchi et al., 2016, Tröstl et al., 2016, Frege et al., 2017).

In November and December 2014, we conducted measurements with state-of-the-art instrumentation, including an Atmospheric Pressure interface Time-Of-Flight (APi-TOF), Particle Size Magnifier (PSM), a Neutral clusters and Air Ion Spectrometer (NAIS), and a Scanning Mobility Particle Sizer (SMPS) at the Himalayan Nepal Climate Observatory Pyramid (NCO-P, 5079 meters asl), close to the Everest Base Camp. Here we present results from this campaign with a special focus on the mechanism driving NPF at high altitude in the Himalayan region.

During the measurement period (23 days of good measurements), we observed and characterized 18 NPF events at the NCO-P station. NPF was characterized from the combined PSM, NAIS and SMPS data within a size range from 1.1 nm to 80 nm. All NPF events occurred during clear-sky conditions, and they were observed right after the establishment of the valley breeze. Figure 1 confirms the ion size distribution found in a previous study (Venzac et al., 2008) and, for the first time, we were able to follow also the growth of neutral clusters from 1.1 nm (with the PSM) up to 42 nm (with

the NAIS). Figure 1 shows that every nucleation event is observed in the ion mode as well as in the neutral clusters. At the same time, thanks to the mass spectrometer, we were able, for the first time, to determine the chemical composition of the growing clusters at such a location.

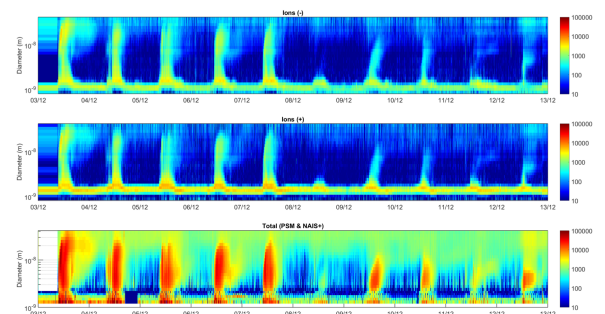


Figure 1. Series of nucleation events observed with a NAIS and a PSM at NCO-P, Nepal, 5079 m asl. The top two panels present the ion size distributions and the bottom one the particle size distribution.

This work was supported by the Swiss National Science Foundation (grant no. P2EZP2\_168787, 20020\_152907/1 and 206021\_144947/1) and the Academy of Finland Center of Excellence (grant no. 272041). The Nepal study was carried out within the framework of ABC-UNEP and SHARE-Evk2CNR Projects in collaboration with the Nepal Academy of Science and Technology as foreseen by the Memorandum of Understanding between Nepal and Italy.

Bianchi, F., et al., (2016) *Science* 6289, 1109-1112.

Frege, C., et al., (2017) *Atmos. Chem. Phys. In press*.

Merikanto, J., et al., (2009) *Atmos. Chem. Phys.* 9 (21), 8601–8616.

Tröstl, J., et al., (2016) *J. Geophys. Res.-Atmos.* 121, 11,692–11,711.

Venzac H., et al., (2008) *Proc. Natl. Acad. Sci. USA*, 105 (41), 15666–15671.

## Development of a near-explicit model of HOMs formation from $\alpha$ -pinene ozonolysis

U. Molteni<sup>1</sup>, U. Baltensperger<sup>1</sup>, J. Curtius<sup>2</sup>, M. Heinritzi<sup>2</sup>, C. R. Hoyle<sup>1</sup>, M. Simon<sup>2</sup>, C. Yan<sup>3</sup>, J. Dommen<sup>1</sup> and the CLOUD collaboration

<sup>1</sup>Laboratory of Atmospheric Chemistry, Paul Scherrer Institute, CH-5232 Villigen, Switzerland

<sup>2</sup>Goethe University Frankfurt, Institute for Atmospheric and Environmental Sciences, 60438 Frankfurt am Main, Germany

<sup>3</sup>Department of Physics, University of Helsinki, FI-00014 Helsinki, Finland

Keywords:  $\alpha$ -pinene, ozonolysis, CLOUD, HOMs, mass spectrometers,

Presenting author email: [josef.dommen@psi.ch](mailto:josef.dommen@psi.ch)

Recently it was found that  $\alpha$ -pinene (AP) ozonolysis leads to the formation of highly oxygenated molecules (HOMs) of extremely low saturation vapour pressure which can induce new particle formation (NPF) in the absence of sulfuric acid (SA) (Ehn et al., 2014, Kirkby et al., 2016). HOMs are generated via an autoxidation process, where peroxy radicals abstract internally a hydrogen atom with subsequent addition of molecular oxygen to the newly formed carbon centred radical (Crouse et al., 2013). This cycle is repeated a few times thus greatly enhancing the O:C ratio and introduces several hydroperoxide groups into the molecular structure. Various laboratory and theoretical studies have been performed so far on the autoxidation of terpenes and proxy molecules, but the mechanism giving rise to HOMs is still far from being understood.

In this work we report results from the CLOUD 8 campaign (autumn 2013) at the CLOUD (Cosmics Leaving Outdoor Droplets) chamber at CERN (Geneva, Switzerland). Ozonolysis experiments were performed in the virtual absence of SA ( $< 5 \times 10^4 \text{ cm}^{-3}$ ) over a range of AP concentrations. Measurements were done with a nitrate chemical ionization atmospheric pressure interface time of flight mass spectrometer (CI-APi-TOF) which has been shown to be highly selective in detecting gas phase sulfuric acid and HOMs at extremely low concentration (ppq).

A generalized mechanism including radical chain propagation, auto-termination and radical-radical recombination reactions is set-up to describe the observed HOM monomers and dimers. These reactions were then implemented into the  $\alpha$ -pinene mechanism of the MCM 3.3.1 (Saunders et al. 2003). Reaction rate constants and branching ratios were varied to fit the model to the measured time trends and concentration levels of HOMs. Possible solutions and implications with regard to the mechanism are presented.

This work was supported by the Swiss National Science Foundation (20020\_152907) as well as the Marie Curie Initial Training Network 'CLOUD-TRAIN', no. 316662.

Crouse, J. D. et al. (2013). Autoxidation of organic compounds in the atmosphere, *The Journal of Physical Chemistry Letters*, 4(20), 3513-3520.

Ehn, M. et al. (2014). A large source of low-volatility secondary organic aerosol, *Nature*, 506(7489), 476-479.

Kirkby, J. et al. (2016). Ion-induced nucleation of pure biogenic particles, *Nature*, 533(7604), 521-526.

Saunders, S. M. et al. (2003). Protocol for the development of the Master Chemical Mechanism, MCM v3 (Part A): tropospheric degradation of non-aromatic volatile organic compounds. *Atmos. Chem. Phys.*, 3, 161-180.

## Long-term declining trend in new particle formation observed at San Pietro Capofiume, Italy

T. Nieminen<sup>1</sup>, J. Joutsensaari<sup>1</sup>, A. Laaksonen<sup>1,2</sup>, A. Virtanen<sup>1</sup>, S. Decesari<sup>3</sup>, L. Tarozzi<sup>3</sup> and M. C. Facchini<sup>3</sup>

<sup>1</sup>Department of Applied Physics, University of Eastern Finland, Kuopio, Finland

<sup>2</sup>Finnish Meteorological Institute, Helsinki, Finland

<sup>3</sup>Institute of Atmospheric Sciences and Climate (ISAC) of the Italian National Research Council (CNR), Bologna, Italy

Keywords: new particle formation and growth, long-term trends.

Presenting author email: tuomo.nieminen@uef.fi

Atmospheric aerosols have a large impact on air quality, human health and even the global climate. One of the largest uncertainties related to climate change is the magnitude of the cooling effect of aerosols that counteracts the warming caused by greenhouse gases (IPCC, 2013). Formation of secondary aerosol particles is a major source of atmospheric aerosols (Merikanto *et al.*, 2009), and has been a subject of active research during the past two decades. However, only few long-term datasets (over 10 years of measurements) of atmospheric new particle formation (NPF) exist. Observations in the Finnish boreal forest and at two Arctic sites indicate very small changes in NPF over the past twenty years (Asmi *et al.*, 2011; Kyrö *et al.*, 2014; Nieminen *et al.*, 2014), whereas in Central Europe a clear decrease in NPF occurrence has been reported (Hamed *et al.*, 2010).

In this work, we characterize the NPF occurrence at the San Pietro Capofiume meteorological station in Po Valley, northern Italy. The number size distributions of 3-630 nm particles have been measured at the station continuously since March 2002. The station is influenced by emissions of local anthropogenic pollutants as well as long-range transport from Central and Eastern Europe (Sogacheva *et al.*, 2007), and thus can provide important information on the impact of anthropogenic activity on atmospheric NPF.

The particle number size distribution data was classified into NPF event, non-event and undefined days according to the guidelines presented by Kulmala *et al.* (2012). To quantify the NPF events, the formation rates of nucleation mode particles (defined here as particles of 3–25 nm in diameter) were calculated based on the measured number size-distribution data, taking into account the losses due to coagulation and the condensational growth of particles out from the nucleation mode. The particle growth rates were calculated by fitting log-normal modes to the measured size-distribution data and following the time evolution of the geometric mean size of the fitted nucleation mode.

Figure 1 shows the hourly averaged number concentration of 3-25 nm particles measured from 2002 until end of 2015. A statistically significant decreasing linear trend of  $-4.2\%$ /year is observed. At the same time, also the particulate matter concentrations (PM<sub>2.5</sub>) have been observed to decrease at a similar rate throughout Northern Italy (Bigi and Ghermandi, 2016). This would indicate that eventhough the sink for the

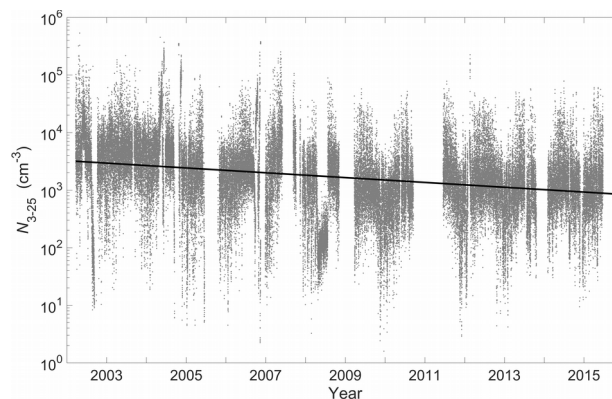


Figure 1. Number concentration of 3-25 nm particles measured at SPC in 2002–2015 (grey points), and the fitted linear trend (black line).

newly formed particles has decreased, a simultaneous decrease in precursor vapour emissions (sulphur dioxide, ammonia, amines, organics) has also occurred.

This work was supported by the Academy of Finland Centre of Excellence (grant no. 272041).

- Asmi, E., Kivekäs, N., Kerminen, V.-M., *et al.* (2011) *Atmos. Chem. Phys.* **11**, 12959-12972.
- Bigi, A. and Ghermandi, G. (2016) *Atmos. Chem. Phys.* **16**, 15777-15788.
- Hamed, A., Birmili, W., Joutsensaari, J., *et al.* (2010) *Atmos. Chem. Phys.* **10**, 1071-1091.
- IPCC (2013) *Climate Change 2013: The Physical Science Basis*. Cambridge University Press, Cambridge, UK and New York, NY, USA.
- Kulmala, M., Petäjä, T., Nieminen, T., *et al.* (2012) *Nat. Protocols* **7**, 1651-1667.
- Kyrö, E.-M., Väänänen, R., Kerminen, V.-M., *et al.* (2014) *Atmos. Chem. Phys.* **14**, 4383-4396.
- Merikanto, J., Spracklen, D. V., Mann, *et al.* (2009). *Atmos. Chem. Phys.* **9**, 8601-8616.
- Nieminen, T., Asmi, A., Dal Maso, M., *et al.* (2014) *Boreal Env. Res.* **19** (suppl. B), 191-214.
- Sogacheva, L., Hamed, A., Facchini, M. C., *et al.* (2007) *Atmos. Chem. Phys.* **7**, 839-853.

## **Abstracts T204**

## Measurements of aerosol optical properties at a suburban site in Belgium

V. De Bock<sup>1</sup>, A. Mangold<sup>1</sup>, A. Delcloo<sup>1</sup>, C. Hermans<sup>2</sup> and H. De Backer<sup>1</sup>

<sup>1</sup>Department of Observations, Royal Meteorological Institute of Belgium, Uccle, B-1180, Belgium

<sup>2</sup>Royal Belgian Institute for Space Aeronomy, Uccle, B-1180, Belgium

Keywords: Absorption coefficient, Scattering coefficient, Aerosol Optical Depth, Single Scattering Albedo

Presenting author email: Veerle.DeBock@meteo.be

Since a few years, the Royal Meteorological Institute of Belgium (RMIB) has several instruments at its disposal that are able to measure aerosol optical properties simultaneously. The instruments are located at Uccle, Belgium (50°48'N, 4°21'E, 100m a.s.l.), a residential suburb of Brussels about 100km from the shore of the North Sea. The dataset consists of aethalometer, nephelometer and Brewer measurements, collected over a period from March 2014 to January 2017. Also, measurements from a collocated Cimel sunphotometer (owned by the Belgian Institute for Space Aeronomy (BISA)), will be used to improve our insights into the optical properties of aerosols over Uccle. A detailed analysis was performed and the results of this analysis will be presented.

The aethalometer (Magee Sci.; AE31) measures the light absorption of aerosol particles at wavelengths covering the UV and the near-InfraRed (370, 470, 520, 590, 660, 880 and 950nm). From the instrument, the absorption coefficient ( $\sigma_a$ ) (in  $Mm^{-1}$ ) and the mass concentration of light-absorbing particles ( $ng/m^3$ ) can be derived (Weingartner et al. 2003).

From March 2014 to October 2014, the Aurora 3000 nephelometer (Ecotech) provided the scattering ( $\sigma_s$ ) and backscattering coefficient ( $\sigma_{bs}$ ) (both in  $Mm^{-1}$ ) of particles at 450, 525 and 635nm. Afterwards, the instrument was moved to the Princess Elisabeth Station Antarctica and it was replaced by a new nephelometer (TSI, 3563) at Uccle. This instrument also measures  $\sigma_s$  and  $\sigma_{bs}$ , but at slightly different wavelengths (450, 550 and 700nm).

Combining the absorption measurements of the aethalometer and the scattering measurements of the nephelometer enables us to determine the Single Scattering Albedo (SSA).

The Brewer spectrophotometer (Kipp&Zonen, #178), which was originally designed to measure ozone in the atmosphere from UVB radiation, can also be used to retrieve the AOD in the UVB region (De Bock et al. 2010). Brewer#178, a double monochromator, was installed in 2001 and provides AOD at the five ozone wavelengths (303.3, 310.1, 313.5, 316.8 and 320.1nm). However, in addition to the standard observation routines, a routine (i.e. an adapted sun scan routine) was developed to allow the determination of AOD at 340nm from the double monochromator instrument (De Bock et al. 2010, 2014). These AOD measurements at 340nm are used for the present study.

Preliminary results from simultaneous data from March 2015 to January 2017 indicate that special events

distinguish themselves clearly from days with normal conditions. This is shown in Figures 1 and 2. The values in the orange rectangles were measured on three days: 17<sup>th</sup> March 2015, 11<sup>th</sup> March 2016 and 12<sup>th</sup> March 2016. These days were characterized by higher PM amounts (higher than  $\sim 50\mu g/m^3$ ) and higher BC concentrations in contrast to the other days for which these values were distinctly lower (according to measurements from www.irceline.be).  $\sigma_a$  and  $\sigma_s$  were also clearly higher for these days. The calculated SSA values for the three days ranged from 0.98 and 1.00 and did not differ significantly from the other values. The relation between AOD and  $\sigma_a$  and  $\sigma_s$  is clearly not straightforward. For the same AOD value, a large spread in  $\sigma_a$  and  $\sigma_s$  values could be observed.

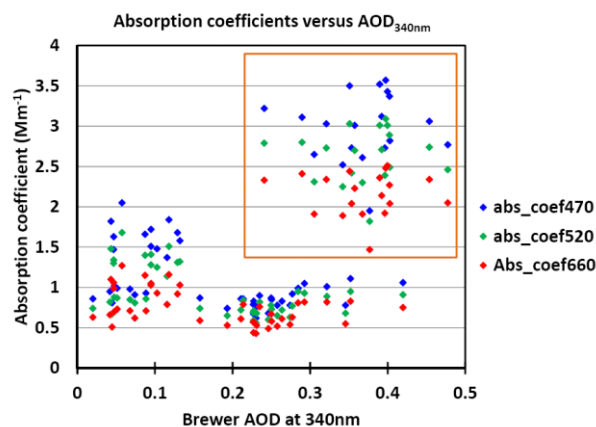


Figure 1. Absorption coefficients versus AOD at 340nm

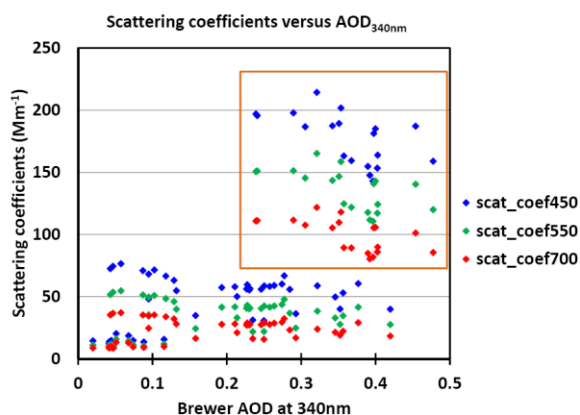


Figure 2. Scattering coefficients versus AOD at 340nm

De Bock, V., De Backer, H., Mangold, A. and Delcloo, A. (2010), *Atmos. Meas. Tech.* **3**, 1577-1588.

Weingartner, E., Saathoff, H., Schnaiter, M., Streit, N., Bitnar, B. and Baltensperger, U. (2003), *J. Aero. Sci.*, **34**, 1445-1463.

## Size distribution of submicron aerosol absorptive properties in the North China Plain

Z.Z. Deng<sup>1</sup>, L. Ran<sup>1</sup>, and P.C. Wang<sup>1</sup>

<sup>1</sup>LAGEO, Institute of Atmospheric Physics, Chinese Academy of Sciences, Beijing, 100029, China

Keywords: Aerosol Absorption, Size Distribution, micro-Aethalometer, North China Plain.

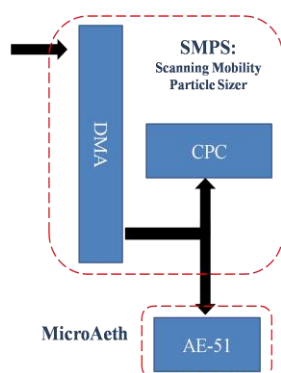
Presenting author email: dengzz@mail.iap.ac.cn

Black carbon (BC) aerosols exert an important impact on the radiative balance by imposing a positive radiative forcing (Stier et al., 2007). Influenced by emission sources and aging processes, the composition and size distribution of light-absorbing aerosols continuously change (Zhang et al., 2008). Size-resolved aerosol absorption is important to understanding aerosol aging as well as estimating aerosol optical properties and thereby aerosol radiative forcing, yet observational studies on this topic are currently still scarce.

Previously, the size distribution of absorptive components was usually obtained by chemical analytical method, which is quite laborious and costly, also suffers a compromised size and temporal resolution. The setup of a micro-aethalometer (Model AE-51) in combination with a scanning mobility particle sizer (SMPS) as shown in Fig.1, allows the direct and continuous determination of size-resolved aerosol absorption by an optical method (Ning et al., 2013).



Figure 1. The micro-aethalometer (AE-51) and the instrument setup.



Measurements were conducted during 2014/11/04 and 12/03 at an urban site Beijing and a rural site Xianghe in the North China Plain (NCP). SMPS measured particle number size distribution (PNSD) with a range of 20-750 nm. Using a density of  $1.7 \text{ g cm}^{-3}$ , particle mass concentration distribution (PMSD) was calculated (Fig. 2(Top)). The size distribution of absorption at 880 nm was directly measured by the operating system and represented by equivalent BC mass concentration (Fig. 2(Middle)). Thus, size-resolved BC mass fraction could be determined (Fig. 2(Bottom)).

Generally, aerosol mass concentrations were mostly contributed by particles within the size range of 200-600 nm in the NCP. The situation was similar for BC, which composed about 10% of total mass concentrations of submicron aerosols. The average size distribution of BC mass fraction displayed a peak around 500 nm in Beijing, while showed a plateau across 200-500 nm in Xianghe, suggesting BC aerosols to be more aged in the

urban area. Diurnally, BC mass fraction reached the highest level at midnight in Beijing. High BC mass fractions were often encountered in the morning and evening rush hours in Xianghe. The comparative study covered strict emission control period for the APEC (11/05-11/11) and the heating period (since 11/15). It was found that the emission control strategy was effective in Beijing, leading to a lower level of aerosol mass concentrations and BC mass fractions. However in Xianghe, the difference between the emission control period and the heating period was negligible.

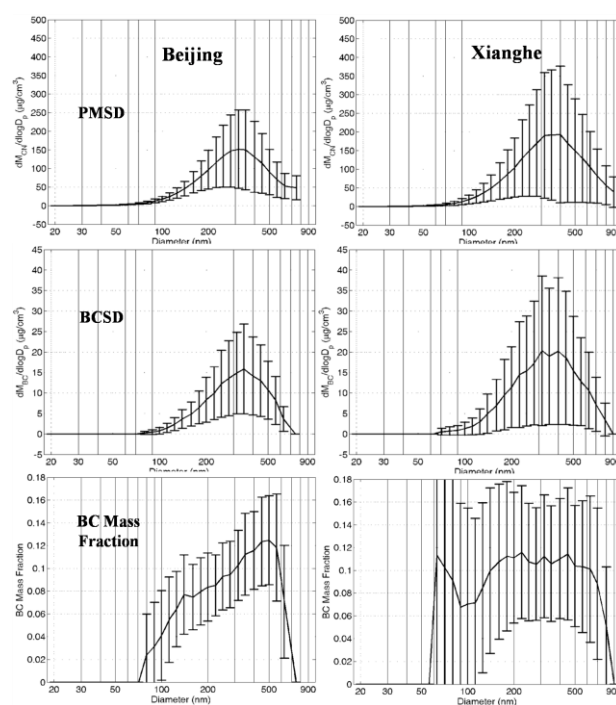


Figure 2. Average size distributions of (Top) Aerosol mass concentrations measured during 2014/11/04-12/03 in Beijing(Left) and Xianghe (right); (Middle) BC mass concentrations; (Bottom) BC mass fractions.

This work was supported by the National Natural Science Foundation of China (NSFC) under grant no. 41205098 and 41675037, and the “Strategic Priority Research Program” of the Chinese Academy of Sciences (Grant No. XDA05100000).

Ning, Z., Chan, K. L., Wong, K. C., and et al. (2013) *Atmos. Environ.* **80**, 31-40.

Stier, P., Seinfeld, J. H., Kinne, S., and et al. (2007) *Atmos. Chem. Phys.* **7**, 5237-5261.

Zhang, R. Y., Khalizov, A. F., Pagels, J., and et al. (2008) *Proc. Natl. Acad. Sci.* **105**, 10291-10296.

## Long term studies of aerosol optical properties and scavenging into clouds: Puijo semi-urban site

A. Ruuskanen<sup>1</sup>, S. Romakkaniemi<sup>1</sup>, A. Arola<sup>1</sup>, A. Virtanen<sup>2</sup>, K. E. J. Lehtinen<sup>1,2</sup>, M. Komppula<sup>1</sup> and A. Leskinen<sup>1,2</sup>

<sup>1</sup>Finnish Meteorological Institute, P.O.Box 1627, FI-70211, Kuopio, Finland

<sup>2</sup>University of Eastern Finland, Department of Applied Physics, P.O.Box 1627, FI-70211, Kuopio, Finland

Keywords: cloud activation, aerosol optical properties, aerosol-cloud interaction

Presenting author email: antti.ruuskanen@fmi.fi

We have studied optical properties and particle size distributions of semi urban aerosol for a period of four years (2010 – 2014). In the studies we have focused on cloud activation, and, differences between cloud activation and non-activation events.

Measurement site of Puijo is located in Kuopio, Eastern Finland, surrounded by lake Kallavesi. The measurement station is located on top of the Puijo observation tower (306 m a.s.l, 224 m above the surrounding lake level). A more detailed overview of the station and the surrounding area can be found in e.g. Leskinen et al. (2009).

Two inlets with different cut-off sizes (1  $\mu\text{m}$  and 40  $\mu\text{m}$ , referred as interstitial and total) were used for sampling to retrieve information about differences in activated and non-activated particle populations. We measured scattering coefficient (intergrating nephelometer), absorption coefficient (multi-angle absorption photometer) and particle number size distributions (twin-DMPS) from both samples, total and interstitial. In addition, to study cloud activation events we had to define cloud events. In our study, we have used visibility of less or equal than 200 m as a definition. Visibility was measured with FD12P present weather sensor. More detailed information about measurement site and setup can be found from Leskinen et al. (2009) and Portin et al. (2014).

We have observed that light scattering (wavelength of 550 nm) of dry aerosol is, on average, 36.7% smaller in interstitial sample than total sample without any cloud events. Similar value for absorption is only 20.0%. Since there are no cloud events and relative humidity is below 50% we have concluded that difference is caused by coarse particles. This is backed up by Aeronet size distributions from Kuopio.

Time series of scattering coefficient values from both lines are presented in Fig. 1. Additionally, scattering coefficients calculated from Aeronet size distributions are presented. The Aeronet data is used to verify the effect of larger ( $>1 \mu\text{m}$ ) particles and estimate, how optical properties would change with smaller particles with same distribution shape.

Additionally, we have studied how cloud events affect scattering and absorption of dry aerosol in interstitial and total lines. The difference between these two lines is defined as scavenged fraction i.e. particles scavenged into the cloud as cloud droplets. We have found out that scavenged fraction of scattering and absorption both have increasing trend as a function of ambient temperature. The trends are  $0.005 \text{ }^\circ\text{C}^{-1}$  and  $0.001 \text{ }^\circ\text{C}^{-1}$  for scavenged scattering and absorption

coefficients, respectively. Thus the scavenged absorption fraction is almost constant while scattering is more clearly temperature dependent. Similar analyses have been done also with wind direction and scavenged volume fraction of aerosol.

Our long term studies indicate scattering being affected relatively more than absorption during cloud events when considering dry conditions of particles. We observed temperature and scavenged volume dependencies while wind direction had little effect.

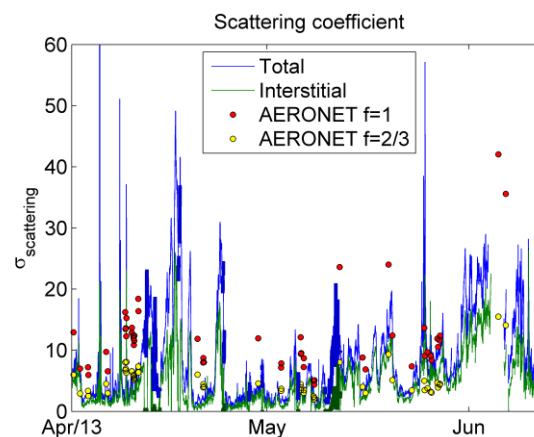


Figure 1. Example timeseries of total and interstitial line scattering coefficients. In addition scattering coefficients calculated from AERONET size distributions multiplied with size factor  $f$ . Size factor is used to move distribution from higher sizes to smaller ones while preserving the shape of distribution. Cloud events are marked with slightly wider and darker lines.

This work has been supported by Maj and Tor Nessling Foundation (201500134, 201600105, 201700418) for PhD thesis work, Academy of Finland (259005, 272041) and European Research Council (Starting Grant 335478).

Leskinen, A.; Portin, H.; Komppula, M.; Miettinen, P.; Arola, A.; Lihavainen, H.; Hatakka, J.; Laaksonen, A.; Lehtinen, K. E. J. (2009), *Boreal Env. Res.*, 14, 576–590

Portin, H.; Leskinen, A.; Hao, L.; Kortelainen, A.; Miettinen, P.; Jaatinen, A.; Laaksonen, A.; Lehtinen, K. E. J.; Romakkaniemi, S.; Komppula, M. (2014), *Atmos. Chem. Phys.*, 14, 6021-6034

## Optical closure study for background aerosol from helicopter-borne in-situ and ground-based lidar measurements

S. Düsing<sup>1</sup>, B. Wehner<sup>1</sup>, P. Seifert, N. Ma<sup>1</sup>, L. Poulain<sup>1</sup>, S. Henning<sup>1</sup>, H. Baars<sup>1</sup>, H. Siebert and A. Wiedensohler<sup>1</sup>  
<sup>1</sup>Leibniz Institute for Tropospheric Research (TROPOS), 04318 Leipzig, Germany

Keywords: optical properties, profiling, boundary layer, closure study  
 Presenting author email: duesing@tropos.de

The “HD(CP)<sup>2</sup> Observational Prototype Experiment” in Melpitz (HOPE-Melpitz) was performed between 12 and 28 September 2013. This study provides a holistic data-set of in-situ measurements on ground complemented by in-situ measurements from the helicopter-borne platform ACTOS (Airborne Cloud and Turbulence Observation System; Siebert et al., 2013) and by ground-based lidar measurements of TROPOS. A comparison of modeled aerosol optical properties with lidar measurements is discussed in this study.

### Measurements

During the campaign 8 measurement flights, each with a duration of up to two hours, were performed around the continental ACTRIS (Aerosols, Clouds, and Trace gases Research InfraStructure Network) site of Melpitz, Germany (51.5° N, 12.9° E, 90 m above sea level, 40 km NE of Leipzig) up to an altitude of 2.3 km.

On ACTOS, the particle number size distribution (PNSD) in dry state ( $rH < 40\%$ ) was derived within a size-range from 8 nm to 2.8  $\mu\text{m}$ . Furthermore, the total particle number concentration  $N_{\text{tot}}$  as well as the number concentration of cloud condensation nuclei (CCN)  $N_{\text{CCN}}$  at 0.2% super-saturation were measured.

On ground, measurements of particle composition, CCN concentration at different supersaturations, and dry-state PNSD were performed.

The in-situ measurements were complemented by a continuously running ground-based 3+2 multiwavelength polarization Raman lidar system Polly<sup>XT</sup> (Engelmann et al., 2016) measuring profiles of  $\sigma_{\text{bsc}}$ . With a height-constant backscatter-to-extinction ratio (lidar ratio) we derived profiles of  $\sigma_{\text{ext}}$ . Aerosol optical properties in ambient state were calculated using the airborne in-situ PNSD measurements with a Monte-Carlo simulation based on the Mie code of Bohren and Huffman (1983) assuming spherical, coated particles. Further input information like the refractive index  $m$  and particle hygroscopicity  $\kappa$  was derived with ground-based measurements of the aerosol chemical composition and were used for calculations in all investigated heights. Finally, the ambient state modeled optical coefficients were compared with the lidar measurements.

### Results

An overview of the correlation of the modeled ( $\sigma_{\text{ext,mie}}$ ) and with the lidar measured extinction coefficients ( $\sigma_{\text{ext,lid}}$ ) is given in Fig. 1. Here, 13 data points derived for different altitudes and conditions on 14 and 17 Sept. 2013 are included. For 355 nm 54% of all cases agree within the uncertainties and for 532 nm

55% of the cases. On average, the model underestimates the measured extinction coefficients for 355 nm by 3.5% and overestimates the measurements by 7.9% at a wavelength of 532 nm. Correlation coefficients are 0.944 and 0.947, respectively.

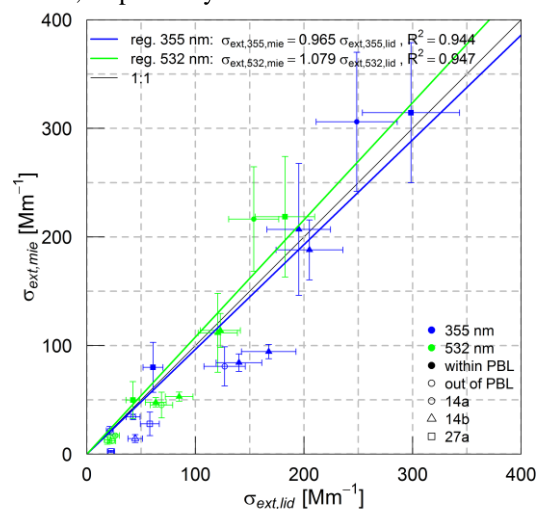


Figure 1: Correlation of  $\sigma_{\text{ext}}$  in ambient state derived with a Mie model from helicopter measurements and measured by the lidar for different altitudes and conditions. Filled symbols mark measurements within the planetary boundary layer while open symbols represent measurements above.

### Conclusions

This study presents a closure study between in-situ airborne and ground-based lidar measurements. The complex instrumentation with ACTOS and the multi-wavelength lidar system provided a unique data-set, which allows to investigate the aerosol optical properties under ambient conditions within the planetary boundary layer with a high spatio-temporal resolution. The planned MelCol-winter campaign in Melpitz (February 2017) will be performed to provide data under more polluted conditions.

### Acknowledgements

This work was supported by the HOPE campaign (01LK1212 C).

Siebert, H. et al., The fine-scale structure of the trade wind regime over Barbados - An introduction to the CARRIBA project, *Atmos. Chem. Phys.*, **13**, 10061–10077, 2013.

Bohren, Craig F., and Donald R. Huffman. *Absorption and scattering of light by small particles*. John Wiley & Sons, 2008.

Engelmann, R. et al., The automated multiwavelength Raman polarization and water-vapor lidar Polly<sup>XT</sup>: the neXT generation, *AMT*, **9**, 1767–1784, 2016.

## 11-years continuous monitoring of the in-situ aerosol optical properties at El Arenosillo Observatory: emphasis on an extreme Saharan dust event in February 2016

M. Sorribas<sup>1</sup>, E. Andrews<sup>2</sup>, J.A. Adame<sup>1</sup>, A. del Águila<sup>1</sup>, M. Yela<sup>1</sup>, P. Sheridan<sup>3</sup>, and J.A. Ogren<sup>3</sup>

<sup>1</sup>El Arenosillo Atmospheric Observatory, AIIA, INTA, Mazagón, Huelva, 21130, Spain

<sup>2</sup>University of Colorado, CIRES, Boulder, CO 80309, USA

<sup>3</sup>Earth System Research Laboratory, NOAA, Boulder, CO 80305, USA

Keywords: aerosol optical properties, climate change, Saharan desert dust, extreme meteorological event.

Presenting author email: sorribasm@inta.es

### Introduction

Aerosols are emitted into the troposphere and their optical, chemical and microphysical properties influence their direct radiative forcing. In order to characterize the means, variability and trends of the absorbing and scattering aerosol processes, the collaboration between National Institute for Aerospace Technology (INTA-Spain) and National Oceanic & Atmospheric Administration (NOAA-USA) established a long-term monitoring site for aerosol optical properties at southwestern Spain. This work shows the climatological values of several aerosol optical properties. It is also explored the radiative and atmospheric impacts of a February 2016 desert dust (DD) episode.

### Sampling site

El Arenosillo Observatory is located on the coast of the Atlantic Ocean (37.1°N, 6.7°W, 40 m a.s.l.), and close to the Mediterranean Sea and the North African coast. This observatory contributes data to the World Data Centers of the WMO Global Atmosphere Watch. It is also running under the framework of the NOAA/ESRL Federated Aerosol Network. ([www.esrl.noaa.gov/gmd/aero/net/arn/index.html](http://www.esrl.noaa.gov/gmd/aero/net/arn/index.html)).

### Climatological analysis (all referenced to 550 nm)

The scattering coefficient showed a mean value of  $40.8 \pm 9.2 \text{ Mm}^{-1}$ . The mean aerosol light absorption coefficient was  $3.70 \pm 0.42 \text{ Mm}^{-1}$  and was observed to be highest in late autumn. The mean value for single scattering albedo was  $0.90 \pm 0.02$  with the lowest values during November. Mean scattering and absorption Ångström exponents were  $1.37 \pm 0.06$  and  $1.30 \pm 0.06$ , respectively, both with lower values during summer time. Major light scattering and absorption events were identified in the aerosol record and were attributed to long-range transport of mineral aerosol from Sahara desert and smoke from the North Spain.

### Extreme Saharan desert dust episode

It had its origin in North Africa and occurred on the 20th–23rd of February 2016. The dust transport phenomenon was exceptional because of its unusual intensity during the coldest season (Sorribas *et al.*,

2017). Associated with a low-pressure system in western North Africa, flows transported air from the Sahel to Algeria and consequently increased temperatures from the surface to 700 hPa by up to 7–9 °C relative to the last decade. These conditions favoured the formation of a Saharan air layer. The arrival of the DD event at ARN did not affect the surface weather conditions or O<sub>3</sub> but did impact the aerosol radiative forcing at the top of atmosphere (RF<sub>TOA</sub>). Some aerosol radiative properties did change relative to historical; the particle size and the amount of the aerosol were significantly higher. The DD event caused an increase (in absolute terms) of the mean aerosol RF<sub>TOA</sub> to a value of  $-8.1 \text{ W m}^{-2}$  (long-term climatological value  $\sim -1.5 \text{ W m}^{-2}$ ).

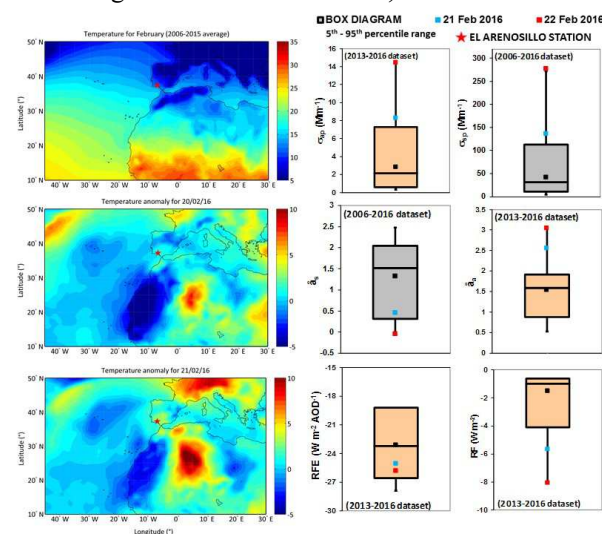


Figure 1. (Left) Temperature at 2 m for February (2006-2015 average) and anomalies for the 20<sup>th</sup> and 21<sup>st</sup> of February 2016. (Right) February climatology of aerosol optical properties and surface O<sub>3</sub>. Daily means during 21 and 22 February 2016 are also shown.

This work was supported by the MINECO through the AVATAR project (CGL2014-55230-R) and the European Union's Horizon 2020 research and innovation programme under grant N° 654109 (ACTRIS-2).

Sorribas, M., Adame, J.A., Andrews, E. and Yela, M. (2017) *An anomalous African dust event and its impact on aerosol radiative forcing on the Southwest Atlantic coast of Europe in February 2016*, Sci Total Environ, DOI: 10.1016/j.scitotenv.2017.01.064.

## Attenuation of solar radiation by aerosols near Ouarzazate solar farm

Abdelmoula BEN-TAYEB, Mohammed DIOURI\*, Ibtissam MARSLI

Atmospheric Physic Laboratory, FSO, Mohammed First University, 60020 Oujda, Morocco  
 Keywords: AERONET, aerosol optical thickness, atmospheric aerosol, insolation, sun photometer.

\*Corresponding author: [dyourim@gmail.com](mailto:dyourim@gmail.com)

### Abstract

The precise knowledge of the insolation of a given region is a key factor for the use of solar energy as an energy source adapted to the chosen site. The solar irradiance depends on geographical and astronomical parameters (length of sunshine and the angular height of the sun above the horizon) and variable factors which depend on the type of the atmosphere as aerosol load (Natural or anthropogenic) and cloud cover.

This study is devoted to the estimation of annual insolation at Ouarzazate (30,92°N; 6,91°W; 1136 m) near Noor solar farm with determination of the attenuation of solar irradiance by aerosols. The insolation is obtained from our calculation model basis on Iqbal formula and with the introduction of aerosol optical thickness data provided by AERONET (Aerosol Robotic Network).

Desert aerosol contributes significantly to the attenuation of regional incident solar radiation. The results show that its reduce about 12% of annual incident solar irradiance for 2013, 17,5% for 2014 and 17% for 2015, While the cloudless atmosphere reduce respectively about 22%, 26% and 25,5% for 2013, 2014 and 2015.



Sun photometer at Ouarzazate (Morocco)

### Effect of the atmosphere on solar irradiance:

The attenuation of irradiance may be expressed with the Beer-Lambert law on the wavelength  $\lambda$  by:

$$I(\lambda) = I_0(\lambda) \cdot \exp[-m_{\text{air}} \cdot \tau(\lambda)]$$

$I_0$ : solar irradiance regardless of the atmosphere.

$m_{\text{air}}$  is the relative air mass

$\tau(\lambda)$  is the total atmospheric optical thickness (AOT) (the sum of the contributions of Rayleigh interactions  $\tau_R$ , aerosols  $\tau_a$  and gas  $\tau_g$ ).

$$\tau(\lambda) = \tau_{\text{Ray}}(\lambda) + \tau_{\text{aer}}(\lambda) + \tau_{\text{gaz}}(\lambda)$$

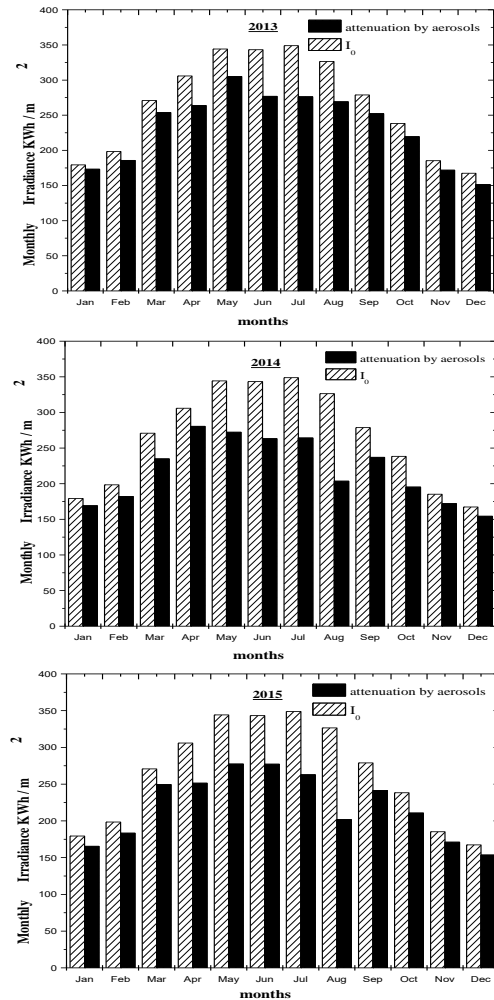


Figure 1. Monthly variation of solar irradiance through the atmosphere with and without aerosols

- A. Ben-tayeb, M. Diouri, R. Meziane *Determination of insolation in the northern earth hemisphere, International Aerosol Conference 2014*
- T. Diner, W. von Hoyningen-Huene, J.P. Burrows, A. Kokhanovsky, . Bierwirth, M. Wendisch, D. Muller, R. Kahn and M. Diouri *Retrieval of aerosol optical thickness for desert conditions using MERIS observations during the SAMUM campaign J. Tellus (2009), 61B, 229-238*
- Kasten F. and A. T. Young, 1989. *Revised optical air mass and approximation formula. Appl. Opt., 28, 4735-4738*
- M. Iqbal, *An Introduction to solar Radiation, Academic Press, Toronto (1983)*
- Aerosol robotic network <http://aeronet.gsfc.nasa.gov>

## Optical properties of aerosols observed in desert area

A. Tahiri and M. Diouri

Atmospheric Physics Laboratory, Faculty of science, Mohammed First University, Oujda, 60020 Morocco

Keywords: Sun-photometer, Aerosol Optical Depth, Aerosol Radiative Forcing, AERONET.  
Presenting author email: sath2006@hotmail.com

### Abstract

The desert aerosol has an important role in the atmospheric evolution as well as the climatic changes. In this study, we present the results of the Aerosol Optical Depth (AOD) and Aerosol Radiative Forcing (ARF) of desert aerosol at Kuwait-University (29.32N, 47.97E, 42m) and Seville (34.35N, 106.88W, 1477m). All these optical parameters are determined from sun-photometer recorded data of AERONET/PHOTONS network.

The annual cycle of the AOD daily averages shows variable values due to the changeable weather. High AOD at 0.5  $\mu\text{m}$  reaching 1.7 are clearly more recorded at Kuwait site due to mineral dust and salt particles (Fig.1a). The lower values which characterize continental particles are observed at Seville (Fig.1b).

The ARF values at surface (BOA) ranged from -10  $\text{W}/\text{m}^2$  to -85  $\text{W}/\text{m}^2$  recorded at Kuwait (Fig.2) reveals that the desert dust aerosol reduce significantly the solar radiation reaching the ground level and thus producing a large surface cooling. The ARF at top of the atmosphere (TOA) changed from -18.89  $\text{W}/\text{m}^2$  to 03.60  $\text{W}/\text{m}^2$  where negative values indicates that desert dust aerosol causes an increase of light scattered back to space inducing a significant Earth-atmosphere cooling and the positive values may indicate a greater amount of radiative energy reflected by passenger's cirrus.

### Method

#### Aerosol Optical Depth (AOD)

The aerosol optical Depth ( $\tau_{Aer}$ ) is defined by:

$$\tau_{Aer}(\lambda) = \frac{1}{m_{air}} \ln \left( \frac{I_0(\lambda)}{I(\lambda)} \right) - \tau_{Ray}(\lambda) - \tau_{gaz(\lambda)}(\lambda)$$

With  $\tau_{gaz}$ : Optical depth of gaseous absorbers

$\tau_{Ray}$ : Optical depth of Rayleigh scattering.

$I(\lambda)$ : Solar flux measured by the sun photometer

$I_0(\lambda)$ : Solar flux extra-terrestrial;  $m_{air}$ : Air mass

#### Aerosol Radiative Forcing (ARF)

Aerosol radiative forcing is defined as the increase or decrease of the net radiation flux at the altitude  $z$  due to an instantaneous change of aerosol atmospheric content. The atmosphere free of aerosols is the reference case. Thus, the ARF values can be derived from the following expression:

$$ARF_{(z)} = (F^{\downarrow} - F^{\uparrow})_{(z)} - (F^{\downarrow}_0 - F^{\uparrow}_0)_{(z)}$$

$F$  and  $F_0$  denote respectively the global irradiances with and without aerosol. The arrows indicate the direction of the global irradiances,  $\downarrow$  indicating downward irradiance and  $\uparrow$  indicating upward irradiance.

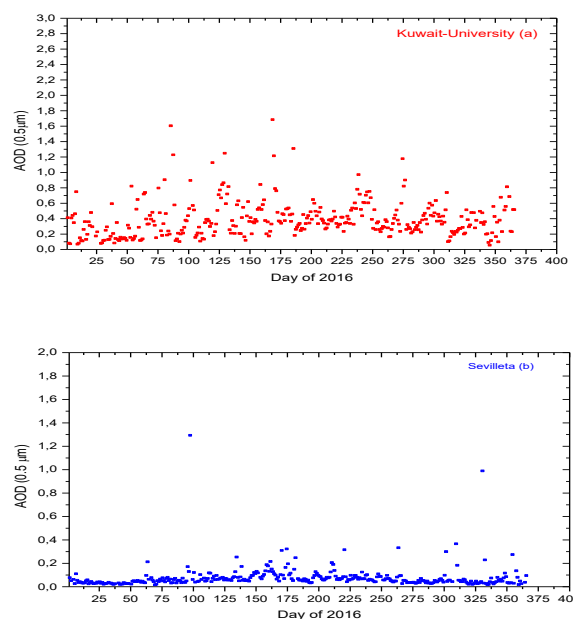


Figure 1. Daily averages of AOD (0.5 $\mu\text{m}$ ) at Kuwait-University (a) and Seville (b) in 2016.

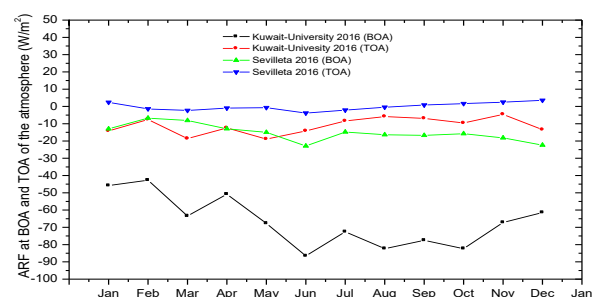


Figure 2. Monthly means of ARF at Bottom of the atmosphere (BOA) and Top of the atmosphere (TOA).

### References

Abdelouahid Tahiri and Mohammed Diouri. Aerosol Radiative Forcing of Desert Regions. Environmental Sciences, Vol. 3, 2015, no. 1, 17-29. <http://dx.doi.org/10.12988/es.2015.4118>.

Abdelouahid Tahiri and Mohammed Diouri. Desert aerosol optical properties in Morocco. Environmental Sciences, Vol. 4, 2016, no. 1, 63-78. <http://dx.doi.org/10.12988/es.2016.631>

### Acknowledgements

Kindly thanks to the AERONET/PHOTONS PI at Seville and Kuwait-University Ms: D. Moore, H. Al-Jassar.

## Explaining variation in light absorption by black carbon aerosols observed in Cabauw, the Netherlands

R.L. Modini<sup>1</sup>, N. Bukowiecki<sup>1</sup>, J.S. Henzing<sup>2</sup>, M. M. Moerman<sup>2</sup>, M. Ealo<sup>3</sup>, P. Fetfatzis<sup>4</sup>, K. Eleftheriadis<sup>4</sup>, A. Apituley<sup>5</sup>, P. Laj<sup>6</sup>, and M. Gysel<sup>1</sup>

<sup>1</sup>Laboratory of Atmospheric Chemistry, Paul Scherrer Institute, Villigen, CH-5232, Switzerland

<sup>2</sup>Netherlands Organization for Applied Scientific Research (TNO), Utrecht, the Netherlands

<sup>3</sup>Institute of Environmental Assessment and Water Research (IDAEA-CSIC), Barcelona, Spain

<sup>4</sup>National Centre of Scientific Research “DEMOKRITOS”, Athens, Greece

<sup>5</sup>Royal Netherlands Meteorological Institute (KNMI), Utrechtseweg 297, 3731 GA De Bilt, the Netherlands

<sup>6</sup>Université Grenoble-Alpes, CNRS, Institut des Geosciences pour l'Environnement (IGE), Grenoble, France

Keywords: absorption, mass absorption coefficient, black carbon

Presenting author email: robin.modini@psi.ch

Black carbon (BC) particles warm the Earth's atmosphere by absorbing light. As BC particles age, their absorption per unit mass (mass absorption coefficient, MAC) increases due to *lensing* through condensed or attached non-BC material. Modelled and observed estimates of BC absorption enhancements due to ageing can vary by up to 40% (Cappa et al., 2013). Further observations are required to resolve this discrepancy and to accurately model climate warming due to BC.

A field campaign was conducted at the Cabauw Experimental Site for Atmospheric Research (CESAR) in the Netherlands from 10 September to 20 October 2016 as part of the ACTRIS-2 JRA1 program. Comprehensive measurements of refractory BC (rBC) mass concentrations (SP2: single particle soot photometer, EC), aerosol optical properties (MAAP, CAPS PM<sub>ss</sub>, Aetholometer, Nephelometer), size distributions (SMPS, APS, OPC) and chemical composition (OC, HPLC, XRF) were performed from the base of the CESAR tall tower

Black carbon mass concentrations ranged from 0.14 to 1.07  $\mu\text{g m}^{-3}$  (rBC, 5<sup>th</sup> – 95<sup>th</sup> percentile) during the campaign period. MAC values at 637 nm derived from MAAP and SP2 measurements ranged from 9.8 to 19.5  $\text{m}^2 \text{g}^{-1}$ , which is towards the upper end of the range of thermo-optical EC-based MAC values observed across Europe (Zanatta et al., 2016). This comparison suggests that the BC reaching Cabauw had aged considerably, or that there are potential systematic differences between thermo-optical EC and SP2 rBC measurements.

BC mixing state was derived from a coating analysis of the SP2 measurements. MAC values at 637 nm depended positively on the ratio of coated to uncoated rBC particles observed by the SP2 (Fig. 1). This observation indicates a BC lensing effect. Air mass back trajectories reaching the site were clustered to demonstrate that air arriving from the west and north-east generally contained lower BC mass concentrations, lower MAC values, and lower BC coating ratios. Air masses from the south-west and particularly the east and south-east contained higher BC mass concentrations, higher MAC values, and larger BC coating ratios.

Mie calculations of aerosol absorption are currently being conducted to determine if the BC mixing state information provided by the SP2 is sufficient to

predict the observed MAC values and/or their variation. This process provides a unique opportunity to test the core-shell approximation typically used in SP2 coating analyses, and to search for a parsimonious means of quantifying MAC value variability. The results of these model-observation closure studies will be discussed during the presentation

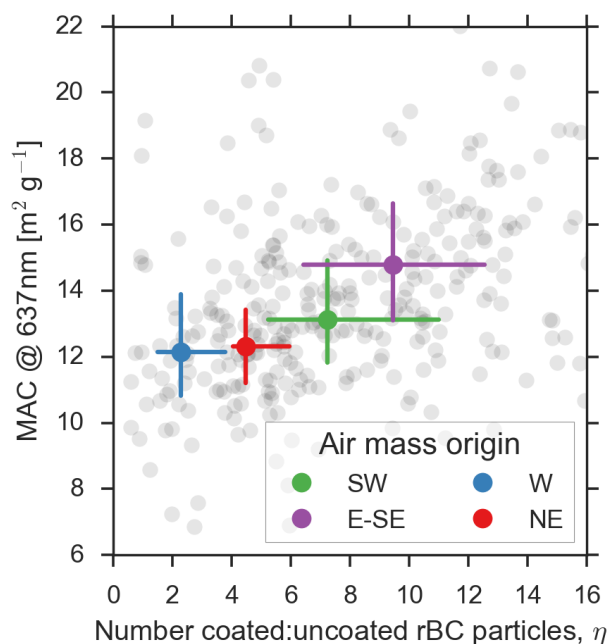


Figure 1. MAC values at 637 nm versus the ratio of coated to uncoated particles, grouped by air mass origin.

This work is part of the ACTRIS-2 project that has received funding from the European Union's Horizon 2020 research and innovation program under grant agreement No 654109.

Cappa, C. D., Onasch, T. B., et al., (2013) *Science*, 339(6118), 393–39, 10.1126/science.1230260.  
Zanatta, M., Gysel, M., et al., (2016) *Atmos. Env.*, 145, 346–364, 10.1016/j.atmosenv.2016.09.035.

## Aerosol microphysical properties at different relative BC content in Beijing region

M.A. Sviridenkov<sup>1</sup>, A.S. Emilenko<sup>1</sup>, V.M. Kopeikin<sup>1</sup> and Wang Gengchen<sup>2</sup>

<sup>1</sup>A.M. Obukhov Institute of Atmospheric Physics, Russian Academy of Sciences, Moscow, 119017, Russia

<sup>2</sup>Institute of Atmospheric Physics, Chinese Academy of Sciences, Beijing, 100029, China

Keywords: atmospheric aerosols, optical properties, microstructure, black carbon.

Presenting author email: sviridenkovt@ifaran.ru

Earlier, in Sviridenkov *et al.*, 2006 we analyzed transformation of the aerosol optical and microphysical properties during one smog episode in Beijing. It was found that in the process of aerosol accumulation in the ground layer, its parameters undergo matched variations: the particle's effective radius increases, while the refractive index, and relative BC content decrease with aerosol concentration growth. In the present paper, we consider all the data obtained during 2003-2004 measurement campaigns from the point of view of searching the regularities in fine aerosol properties at different relative content of black carbon (BC).

Measurements were carried out in fall seasons in Beijing and at Mountain Observatory Xinglong, located at 150 km to the north-east from Beijing at the height of 1 km. Aerosol optical properties were measured with PhAN nephelometer-polarimeter. The set of parameters, measured by PhAN, is sufficient for solving the inverse problem and retrieving both aerosol size spectra and the particle refractive index  $n$ . Inversion results are most reliable in the size range of 0.05 – 0.6  $\mu\text{m}$  (Panchenko *et al.*, 2008). In parallel with optical measurements, aerosol probes were sampled to quartz fibre filters for further determination of mass BC content ( $M_{\text{BC}}$ ) using extinction method. Relative BC content, or BC volume fraction (BCf) was determined as the ratio of volume BC content to the aerosol volume concentration  $V$  in the size interval 0.05 – 0.6  $\mu\text{m}$  (the BC density was assumed to be equal to 1.8  $\text{g}/\text{cm}^3$ ).

Both data arrays (for Beijing and Xinglong) were divided into several sub-arrays, corresponding to different intervals of BCf values. The following intervals of BCf were chosen:  $\text{BCf} < 0.07(0.05)$ ;  $0.07(0.05) \leq \text{BCf} < 0.09(0.06)$ ;  $0.09(0.06) \leq \text{BCf} < 0.11(0.07)$ ;  $0.11(0.07) \leq \text{BCf} < 0.13(0.08)$ ;  $0.13(0.08) \leq \text{BCf} < 0.15(0.10)$ ;  $0.15(0.10) \leq \text{BCf}$  (numbers in brackets correspond to Xinglong). Further, for all the sub-arrays the average size distributions and values of  $M_{\text{BC}}$ ,  $V$ ,  $n$ , effective radius  $r_{\text{eff}}$  were calculated.

It was found that tendencies, revealed in analysis of the single smog formation and decay, are general for aerosol transformation both in Beijing and at the regional background observational site. Less values of BCf correspond on the average to bigger values of  $M_{\text{BC}}$ ,  $V$  and  $r_{\text{eff}}$  and less values of  $n$ , and vice versa. Mean aerosol volume size distributions from the data of observations in Beijing are presented in Figure 1. It can be seen in Figure 1 that there is a significant difference between size distributions for BCf less and more than 0.13. Changes in  $n$ ,  $V$ ,  $M_{\text{BC}}$  with average BCf in Xinglong are shown in Figure 2. Qualitatively they are

similar to those in Beijing, except for the more than two times less average level of the aerosol and BC pollution at mountain station.

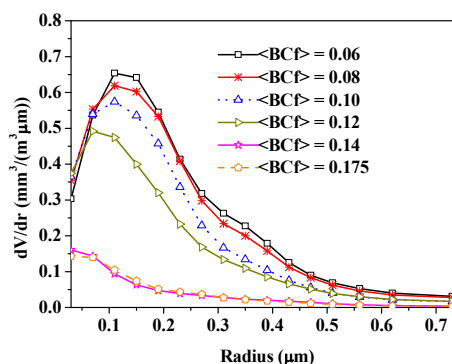


Figure 1. Average volume size distributions for different intervals of BCf values in Beijing.

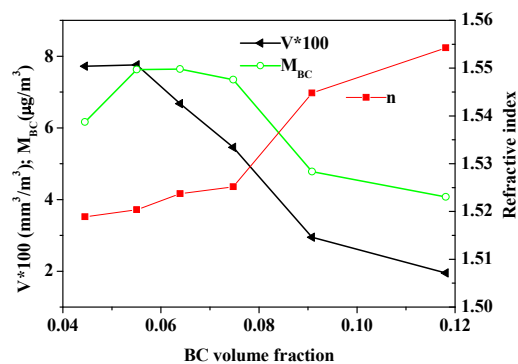


Figure 2. Average BC mass concentration, fine aerosol volume concentration and refractive index for sub-arrays, corresponding to different intervals of BCf in Xinglong.

This work was supported in part by the Russian Foundation for Basic Research under Project 16-05-00985a.

Panchenko, M.V., Sviridenkov, M.A., Terpigova, S.A. and Kozlov, V.S (2008) *Int. J. Rem. Sens.* **29**, 2567-2583.

Sviridenkov, M.A., Emilenko, A.S., Kopeikin, V.M. and Wang Gengchen. (2006) *Atmospheric and oceanic optics.* **19**. 469-472.

## Aerosol climatology and trends at Mauna Loa Observatory

Patrick Sheridan<sup>1</sup>, Elisabeth Andrews<sup>1,2</sup>, John Barnes<sup>1,2</sup>, Nicole Hyslop<sup>3</sup>

<sup>1</sup>Global Monitoring Division, National Oceanic and Atmospheric Administration, Boulder, 80305, USA

<sup>2</sup>Cooperative Institute for Research in Environmental Sciences, University of Colorado, Boulder, 80309, USA

<sup>3</sup>Crocker Nuclear Laboratory, University of California, Davis, 95616, USA

Keywords: aerosol, climatology, trends, optical properties.

Presenting author email: Patrick.Sheridan@noaa.gov

The National Oceanic and Atmospheric Administration has made in-situ surface aerosol measurements at the Mauna Loa Observatory (MLO) since 1974. The measurements include spectral aerosol light scattering and light absorption as well as aerosol number concentration. In addition, the National Park Service through their IMPROVE network has made aerosol chemistry measurements at the site since 1988. Here, we update and expand the aerosol optical property climatology and trend information presented in Andrews *et al* (2011), Coen Collaud *et al* (2013) and Asmi *et al* (2013). Additionally, we connect the IMPROVE aerosol elemental chemistry measurements (e.g., Hyslop *et al*, 2013) with the aerosol optical observations to further explicate observed trends and temporal patterns.

Figure 1 shows contour plots (based on 11 years of data) showing temporal patterns for both aerosol light scattering (Fig. 1a) and aerosol light absorption (Fig. 1b). These plots exhibit several interesting phenomena. First, the scattering contour plot shows the effect of upslope/downslope flow at MLO with the highest aerosol scattering being observed from mid-morning to early evening. Second, there is a large influx of aerosol to MLO in the late winter and early spring which is associated with the well-known Asian outflow of both dust and pollution (e.g., Bodhaine, 1983). Lastly, the aerosol absorption starts sooner in the year than aerosol scattering and does not show a strong diurnal cycle, suggesting contributions from different sources. While elemental analysis shows that most elements exhibit an annual cycle similar to that observed for aerosol light scattering, a small subset of the elements appear to track more closely to aerosol absorption. Unlike the aerosol optical properties and most of the chemical elements, aerosol number concentration (not shown) exhibits a small broad peak in the late summer and early fall. The particles contributing to the peak in number concentration must be very small, optically insignificant and account for only a minor fraction of the aerosol volume distribution, as they do not correspond to the observed aerosol scattering, absorption or elemental mass concentrations.

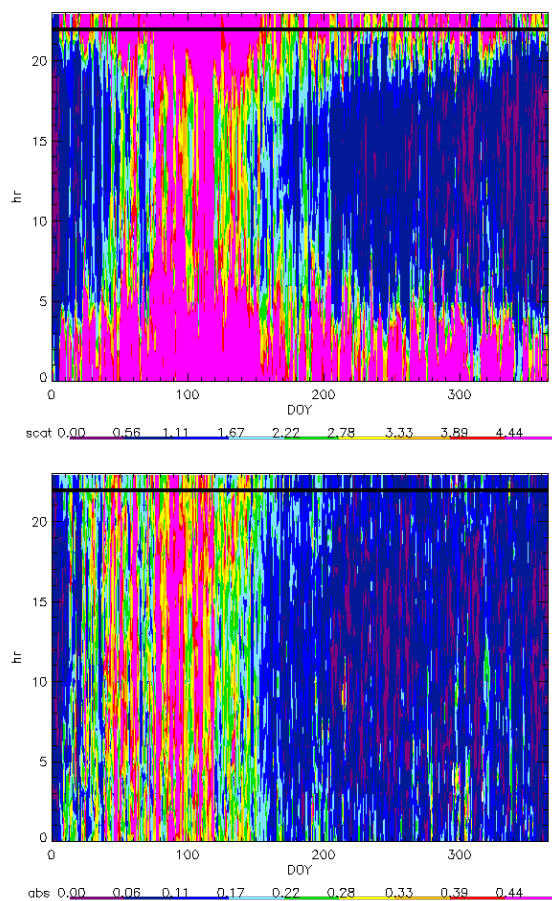


Figure 1. Temporal patterns in (a) aerosol light scattering and (b) aerosol light absorption. Horizontal black line represents local noon.

Andrews *et al* (2011) *Atmos. Res.* **102**, 365-393.

Asmi *et al* (2013) *Atmos. Chem Phys.* **13**, 895-916.

Bodhaine *et al* (1983) *J. Geophys Res.* **88**, 10753-10768.

Coen Collaud *et al* (2013) *Atmos. Chem Phys.* **13**, 869-894.

Hyslop *et al* (2013) *Atmos. Environ.* **80**, 259-263.

## Morphology and Optical Properties of Nascent and Mature Soot

G.A. Kelesidis and S.E. Pratsinis

Department of Mechanical and Process Engineering, ETH Zürich, Zürich, CH-8092, Switzerland

Keywords: soot morphology, aggregation, mobility size, effective density

Presenting author email: gkelesidis@ptl.mavt.ethz.ch

Soot optical properties are typically approximated with the well-known and relatively easy-to-use Mie theory for spheres, neglecting the fractal-like nature of soot. The Rayleigh-Debye-Gans (RDG) theory for agglomerates consisting of primary particles in point contact has been applied alternatively, resulting in better agreement with optical measurements (Loepfe *et al.*, 2014). However, it is unable to resolve the effect of overlapping soot primary particles typically observed in microscopic images of soot. The robust Discrete Dipole Approximation (DDA) has been validated against RDG for the case of agglomerates (Liu *et al.*, 2008) and can also be used for aggregates of chemically-bonded primary particles.

Here, the Discrete Element Model (DEM) for agglomeration and surface growth by acetylene pyrolysis in the absence of oxidation (Kelesidis *et al.*, 2017) is used to derive the evolution from nascent to mature soot morphology, quantified by the fractal dimension,  $D_f$ , and mass-mobility exponent,  $D_{fm}$ . Figure 1 shows the evolution of  $D_f$  (broken line) and  $D_{fm}$  (solid line) of soot particles growing by agglomeration and surface growth as function of  $n_p$ . The DEM-derived evolution of  $D_f$  is in agreement with microscopic measurements of nascent soot in premixed flames (squares, blue insets; Schenk *et al.*, 2013) having  $n_p < 8$ , indicating that aggregation and surface growth are the major processes involved in nascent soot formation. For  $n_p > 8$ , surface growth stops and the formed aggregates further coagulate increasing their  $n_p$  up to 40. The  $D_{fm}$  decreases until a quasi-asymptotic value of about  $2.45 \pm 0.05$  is attained. Further agglomeration leads to the formation of mature soot with  $n_p > 400$  and  $D_{fm}$  of about 2.2, in good agreement with the asymptotic  $D_{fm} = 2.17 \pm 0.1$  for agglomerates of spheres. In contrast,  $D_f$  decreases constantly with increasing  $n_p$  until the attainment of its asymptotic  $1.91 \pm 0.03$  for  $n_p > 20$ , in good agreement with theory. The good agreement found between the DEM-derived evolution of  $D_{fm}$  and mass-mobility measurements in quenched diffusion flames (Rissler *et al.*, 2013) and the Cast soot generator (Yon *et al.*, 2015) indicates that the present DEM for agglomeration and surface growth accurately captures the transition from nascent to mature soot morphology by agglomeration and surface growth, before oxidation takes over.

The DEM-derived soot aggregate optical properties are quantified by the absorption,  $C_{abs}$ , and scattering cross-sections,  $C_{sca}$ , calculated by DDA and compared to those of agglomerates having monodisperse primary particles. The DDA calculations for agglomerates are validated against those of Liu *et al.* (2008). Nascent soot aggregates formed in the early

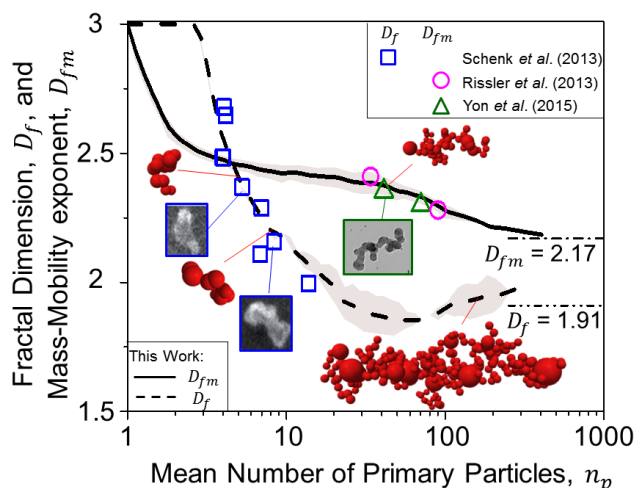


Figure 1. DEM-derived evolution of  $D_f$  (broken line) and  $D_{fm}$  (solid) as function of  $n_p$  compared to microscopic (squares, blue insets; Schenk *et al.*, 2013) and mass-mobility measurements (circles: Rissler *et al.*, 2013; triangles, green inset: Yon *et al.*, 2015) of nascent and mature soot, respectively.

stages of soot formation, when surface growth is dominant, have to 86 % larger  $C_{sca}$  and  $C_{abs}$  for mass,  $m = 0.002$  fg compared to agglomerates formed at the same residence time in the absence of surface growth. At longer residence times, however, when surface growth has stopped and mature soot grows primarily by agglomeration, the difference between aggregates and agglomerates decreases to about 1 % for both  $C_{sca}$  and  $C_{abs}$ . The mature soot aggregate and agglomerate  $C_{sca}$  and  $C_{abs}$  find good agreement with optical measurements in quenched diffusion flames (Zhang *et al.*, 2008).

Kelesidis, G.A., Goudeli, E., Pratsinis, S.E. (2017) *Proc. Combust. Inst.* **36**, in press.

Liu, L., Mishchenko, M.I., Arnott, W.P., (2008) *J. Quant. Spectrosc. Radiat. Transfer* **109**, 2656-2663.

Loepfe, M., Juranyi, Z., Nenkov, M., Burtscher, H., Allemann, M., Duric, A., Lauber, S., Schmid, B. (2014) *AUBE14*.

Rissler, J., Messing, M.E., Malik, A.I., Nilsson, P.T., Nordin, E.Z., Bohgard, M., Sanati, M., Pagels, J.H. (2013) *Aerosol Sci. Technol.* **47**, 792-805.

Schenk, M., Lieb, S., Vieker, H., Beyer, A., Götzhauser, A., Wang, H., Kohse-Höinghaus, K. (2013) *PhysChemPhys* (2013) **14**, 3248-3254.

Yon, J., Bescond, A., Ouf, F.X. (2015) *J. Aerosol Sci.* **87** (2015) 28-37.

Zhang R., Khalizov, A.F., Pagels, J.H., Zhang, D., Xue, H. McMurry P.H. (2008) *PNAS* **105**, 10291-10296.

## The first multi-year observation-based study of aerosol direct radiative forcing, its sensitivities and uncertainties in the southeast US

James Patrick Sherman<sup>1</sup>, Nicholas Hall<sup>2</sup> and Chastity Holt<sup>1</sup>

<sup>1</sup>Department of Physics and Astronomy, Appalachian State University, Boone, NC, USA 28608

<sup>2</sup>Department of Chemistry, Appalachian State University, Boone, NC, USA 28608

Keywords: aerosol optical properties, aerosol-climate interactions, aerosol measurements

Presenting author email: shermanjp@appstate.edu

The southeastern United States (SE US) is home to high warm-season concentrations of biogenic secondary organic aerosols and sulfate aerosols, whose radiative effects may have played a role in the region's lack of warming during the 20<sup>th</sup> century (Goldstein *et al.*, 2009). Large reductions in sulfates and overall particulate matter in the eastern US in recent decades may potentially reduce the cooling effect of aerosols but aerosol-climate interactions are still poorly constrained in models.

The Global Aerosol Watch (GAW) site at the semi-rural, mountainous Appalachian State University in Boone, NC (36.21°N, 81.69°W, 1050m asl) is home to the only co-located NOAA-ESRL, NASA AERONET, and NASA MPLNET aerosol monitoring sites in the eastern US and is uniquely positioned to improve our understanding of aerosol optical properties (AOPs) and direct radiative forcing (DRF) in the SE US. The current study examines seasonal variability in diurnally-averaged DRF and AOPs influencing DRF above the Appalachian State site over a nearly 4-year period (June 2012-Feb 2016). The study also examines DRF sensitivity to AOPs and surface albedo, along with uncertainties in DRF. It represents (to the best of our knowledge) the first such study in the SE US.

Spectral aerosol optical depth (AOD) is used along with single-scattering albedo (SSA), and scattering asymmetry parameter ( $g$ ) as aerosol inputs to the Santa Barbara DISORT radiative transfer code (SBDART; Ricchiazzi *et al.*, 1998) to calculate diurnally-averaged DRF and direct radiative forcing efficiency (DRFE; equal to the DRF per unit AOD). MODIS 8-day surface reflectance products are also used as inputs to SBDART, along with model meteorological profiles. Seasonal variability in DRF and DRFE are examined, along with their sensitivity to AOD, SSA,  $g$ , and surface albedo. DRF sensitivity factors and measurement uncertainty of the AOPs are then used to estimate the uncertainties in DRF.

Aerosol DRF at top-of-atmosphere and surface are most negative during summer months, when AOD is highest and DRFE is least negative. DRF is most sensitive to AOD, followed by (in order) SSA,  $g$ , and surface reflectance. While the DRF sensitivity to AOD only varies by ~25% with season, DRF sensitivity to SSA,  $g$ , and surface reflectance demonstrate much higher seasonal variability. Measurement uncertainties in the AOPs and surface reflectance lead to DRF uncertainties of 10-20% for all seasons except winter,

when the uncertainty is close to 50%. Aerosol optical depth measured by satellite-based platforms such as MODIS possesses higher uncertainty than AERONET-measured AOD, which would lead to higher DRF uncertainty when using MODIS AOD.

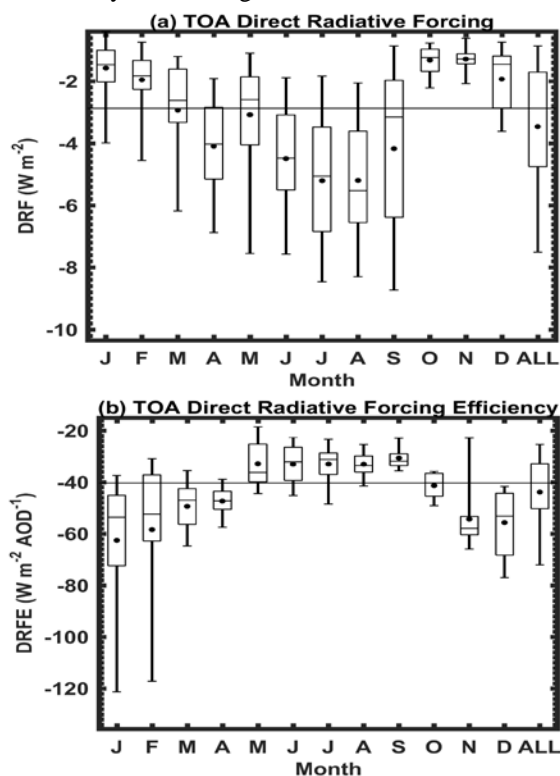


Figure 1. Boxplots of calculated monthly-binned aerosol direct radiative forcing (DRF) and direct radiative forcing efficiency (DRFE) at top of atmosphere. The 'ALL' box provides the statistics for all days. The mean for each month is denoted by the dot while the horizontal bar represents the median. The top and bottom of the box represent 75<sup>th</sup> and 25<sup>th</sup> percentiles while the top and bottom whisker extend to the 95<sup>th</sup> and 5<sup>th</sup> percentiles, respectively. The horizontal line drawn through all boxes of each plot represents the median value over the entire period (all months).

Goldstein, A.H., Koven, C.D., Heald, C.L., and Fung, I.Y. (2009). *P. Natl. Acad. Sci. USA*, **106**, 8835-8840.

Ricchiazzi, P., Yang, S., Gautier, C., and Sowle, D. (1998). *Bull. Am. Meteorol. Soc.* **79**, 2101-2114.

## Optical and radiative properties of atmospheric brown carbon aerosols from Kanpur-India

P. M. Shamjad<sup>1</sup>, R.V. Satish<sup>2</sup>, Navaneeth M. Thamban.<sup>1</sup>, N. Rastogi<sup>2</sup>, S.N. Tripathi<sup>1</sup>

<sup>1</sup>Department of Civil Engineering, Indian Institute of Technology, Kanpur, India

<sup>2</sup>Physical Research Laboratory, Ahmedabad, India

Keywords: Brown carbon, absorption, refractive index, radiative forcing

Presenting author email: pmshamjad@gmail.com

Atmospheric aerosols influence Earth's radiative balance by absorbing and scattering light. Among various aerosol species present in the atmosphere, carbonaceous aerosols are of particular interest in climate studies due to their large mass fraction and high light absorbing capacity. Black carbon (BC) and organic carbon (OC) constitutes the carbonaceous aerosol group, in which BC is known to absorb light highly throughout the spectra compared to any other species. The OC fraction mainly scatters light, but recent studies report a subset of OC known as brown carbon (BrC), with a capacity to absorb light in the UV-visible wavelengths. The bulk aerosol light absorption in the atmosphere is mainly contributed by BC, BrC, dust and a process known as lensing effect, which increases the absorption when internal mixing between aerosols form a core-shell type structure. Optical properties of BC is well characterized and reported from around the globe, but the same for BrC shows large scale variations due to its various primary and secondary sources and involvement in photochemical reactions.

We present spectral imaginary refractive indices of water-soluble organic carbon (WSOC) and total organic carbon (OC) during a winter season, where copious amount of aerosols are emitted into the atmosphere due to biomass and trash burning. Measurements were made from the city of Kanpur, India located in the Indo-Gangetic Plain (IGP). Absorption and mass concentration of WSOC is measured using a combination of Particles into Liquid (PILS), Liquid Waveguide Capillary Cell (LWCC) and Total Organic Carbon (TOC) analyzer system. Same for OC is measured using an offline method, where samples were collected over quartz filter and then analyzed in LWCC and OC-EC analyzer. Our results show that BrC in the IGP is highly absorbing, with an imaginary refractive index 4 to 5 times higher than similar values from other parts of the world (Shamjad et al., 2016). The WSOC shows more absorbing capacity compared to OC at 365 nm but reduces drastically at higher wavelengths. Spectral nature of the refractive indices shows WSOC with a

higher wavelength dependence compared to OC. The absorption capacity of WSOC is negligible above 470 nm, but absorbance from OC is visible till 565 nm.

Using atmospheric and thermally denuded (heated at 300 °C) absorption measurements, the contribution of volatile species to total absorption is calculated. The analysis shows that ~70% of absorption is contributed by BC alone and the remaining is from externally mixed BrC and lensing effect. Using Mie theory, the diurnal variation of this absorption attribution is calculated, which indicates that BrC has less absorption capacity during the daytime.

Two cases of radiative forcing calculations are performed by keeping BrC as scattering (case 1) and absorbing (case 2) conditions. The case 2 shows a warming trend compared to case 1. Similar forcing is also calculated for a core-shell assumption, by varying the thickness and absorbing capacity of the shell. The analysis shows that thin absorbing shell warms the atmosphere compared to thick shells. Incorporating the measured refractive index and shell thickness values in global models might reduce the current cooling effect by OC or can create warming in regions dominated by biomass burning events.

### Acknowledgements

We gratefully acknowledge the financial support by Indo-UK Monsoon project, Ministry of Earth Sciences, Government of India (MoES/NERC/16/ 02 110 PC) to conduct this research work. We also acknowledge the support of IIT Kanpur for providing us HR-ToF-AMS for PG research and teaching.

### Reference

Shamjad, P.M., Tripathi, S.N., Thamban, N.M., Vreeland, H., (2016). *Refractive Index and Absorption Attribution of Highly Absorbing Brown Carbon Aerosols from an Urban Indian City-Kanpur*. Scientific Reports 6, 37735.

## Light absorption characteristics of brown carbon in PM<sub>2.5</sub> at an urban site during KORUS-AQ campaign

Geun-Hye Yu, Jae-Myeong Yu and Seungshik Park

Department of Environment and Energy Engineering, Chonnam National University, 77 Yongbong-Ro, Buk-ku, Gwangju 61186, Republic of Korea

Keywords: brown carbon, light absorption, HULIS, mass absorption efficiency.

Presenting author email: fanygh@naver.com, park8162@chonnam.ac.kr

Radiative impact of organic aerosols (OAs) has a large uncertainty in estimating the global direct radiative forcing of aerosols. This large uncertainty could arise from the light absorption from a subclass of OA referred to as brown carbon (BrC). However, the absorption properties of BrC are poorly understood. Examples of BrC include water-soluble humic-like substances (HULIS) (Hoffer *et al.* 2006), and water and organic solvent extracts of ambient aerosols (Cheng *et al.* 2016; Zhang *et al.* 2013) or biomass burning aerosol (Park and Yu, 2016). This study examines the absorption characteristics of BrC from water and methanol extracts of fine particulate matter measured at an urban site of Korea during KORUS-AQ (Korea U.S. – Air Quality) campaign.

In this study 24-hr PM<sub>2.5</sub> samples were collected using a hi-vol sampler between May 2 and June 11, 2016 at an urban site of Gwangju, Korea and analyzed for organic carbon (OC), elemental carbon (EC), water-soluble OC (WSOC), HULIS, and ionic species. HULIS was separated using HLB solid phase extraction method and quantified by total organic carbon analyzer. In addition, the absorption Ångström exponent (AAE), absorption coefficient, and the mass absorption efficiency (MAE) were calculated using a UV-vis spectrophotometer (300–700 nm) to investigate the light absorption properties of water, HULIS, and methanol extracts.

During the study period, WSOC concentration was  $2.76 \pm 1.15 \mu\text{g C/m}^3$  (1.05–5.99), accounting for approximately 52% (30–65%) of particulate OC. HULIS concentration ranged from 0.41 to  $3.60 \mu\text{g C/m}^3$  with an average of  $1.38 \pm 0.70 \mu\text{g C/m}^3$ , accounting for on average 49% of the WSOC (27–64%). Strong correlations of WSOC with OC ( $R^2=0.88$ ) and HULIS ( $R^2=0.9$ ) indicate their similar chemical characteristics. Light absorption by the water (WSOC), HULIS, and methanol (MSOC) extracts from fine aerosol samples exhibited strong wavelength dependence with a sharply increasing absorption as the wavelength decreases. The average AAE values of three extracts fitted between 300 and 410 nm wavelengths were 6.5, 7.0, and 4.2, respectively. The WSOC and HULIS AAE values were comparable to those reported from previous studies. However, the AAE of MSOC was considerably lower than that (7.1) measured during winter in Beijing (Cheng *et al.*, 2016). The average MAE values of WSOC and HULIS measured at 365 nm ( $\text{MAE}_{365}$ ) were  $0.94 \pm 0.36$  and  $0.79 \pm 0.29 \text{ m}^2/\text{g}$ ,

respectively. Moreover, for methanol extracts, normalizing the absorption coefficient measured at 365 nm to MSOC concentration, which was not quantified in this study and assumed as total OC, yielded an average  $\text{MAE}_{365}$  of  $1.16 \pm 0.35 \text{ m}^2/\text{g}$ , which was a little lower than that (1.45) from a previous study (Cheng *et al.*, 2016).

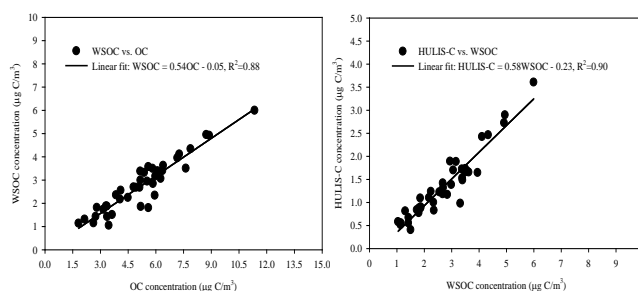


Figure 1. Relationships between WSOC, OC, and HULIS concentrations over the study period.

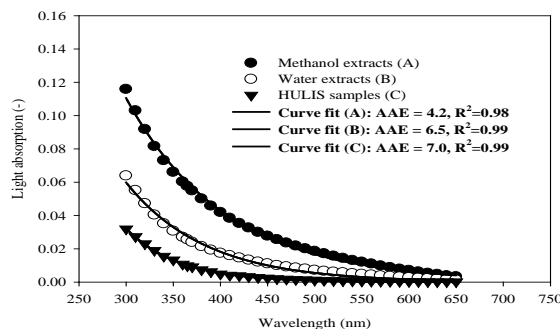


Figure 2. Wavelength dependence of light absorption by methanol extracts, water extracts, and HULIS samples

This research was supported by Basic Science Research Programs through the National Research Foundation of Korea (NRF) funded by the Ministry of Education (NRF-2017R1A1A4A03000511).

Cheng, Y. *et al.* (2016) *Atmos. Environ.* **127**, 355–364.

Hoffer A. *et al.* (2006) *Atmos. Chem. Phys.* **6**, 3563–3570.

Park, S.S. and Yu, J.M. (2016) *Atmos. Environ.* **136**, 114–122.

Zhang, X., Lin, Y.H., Surratt, J.D. and Weber, R.J. (2013) *Environ. Sci. Technol.* **47**, 3685–3693.

## Study of the effect of sampling artefacts in multi-lambda measurements of the absorption coefficient of atmospheric aerosol

R. Pileci<sup>1,2</sup>, V. Bernardoni<sup>1</sup>, G. Valli<sup>1</sup>, R. Vecchi<sup>1</sup>

<sup>1</sup>Department of Physics, University of Milan and INFN-Milan, via Celoria 16, 20133, Milan, Italy

<sup>2</sup>Now at: Laboratory of Atmospheric Chemistry, Paul Scherrer Institute, Villigen, CH-5232, Switzerland

Keywords: aerosol optical properties, sampling artefacts, MAC, brown carbon.

Presenting author email: rosariaerika.pileci@gmail.com

Atmospheric aerosol plays an important role in the atmospheric radiative processes. It acts both directly by absorbing and scattering solar radiation and indirectly through aerosol-cloud interactions. Light absorption is dominated by two minor components: black carbon (BC) and brown carbon (BrC). Both are characterized by a non-null imaginary part of refractive index which is wavelength independent for BC whereas it increases with the decrease of wavelength for BrC.

It is well known that there are drawbacks in filter-based optical instruments. Recently, the role of organic sampling artefacts in filter-based light absorption measurements has been investigated for  $\lambda = 635$  nm (Vecchi et al., 2014).

The purposes of the current study were:

- An investigation of organic sampling artefacts in filter-based light absorption measurements at four wavelengths:  $\lambda = 405$  nm, 532 nm, 635 nm and 780 nm.
- An evaluation of a robust and reliable Mass Absorption Coefficient (MAC) for the urban area of Milan, with the changing of seasons and wavelengths.

To these aims, two sampling campaigns of PM<sub>10</sub> were carried out in Milan both in summer and winter 2016 with four parallel sampling lines (Teflon filters, undened quartz fiber filters, denuded quartz fiber filters and quartz fiber filters to be washed).

The measurements of the aerosol absorption coefficient at different wavelengths was carried out by a polar photometer (PP\_UNIMI) developed by the Environmental Physics Research Group of the University of Milan (Vecchi et al., 2014; Bernardoni et al., 2017). In PP\_UNIMI, the beam produced by a laser source hits the filter and the transmitted and scattered radiation is measured for angles between 0° and 173°. The atmospheric aerosol absorption coefficient is determined by applying a radiative transfer algorithm (Hanel, 1987; Petzold and Schönlinner, 2004). Laser sources at 405 nm, 532 nm, 635 nm and 780 nm are available. Furthermore, additional measurements for the evaluation of the mass concentration and the chemical characterization were performed on the collected samples.

The results confirmed that the organic compounds adsorbed on the sample produce a coating on the fibers affecting the measurements of light absorption coefficient (up to 30% in summer and up to 39% in winter). Different behaviors depending both on season and wavelength variations were observed, possibly due

to the different nature of the organic compounds present in the atmosphere and to the presence of other chemical components. The MAC value was estimated for both seasons and with the variation of wavelength. It was found that the difference between the MAC calculated in the winter samples and that calculated in the summer samples increases with the decreasing of wavelength.

Table 1. Comparison of MAC values for summer and winter samples with the varying of wavelength.

	$\lambda = 405$ nm	$\lambda = 532$ nm	$\lambda = 635$ nm	$\lambda = 780$ nm
Summer	12.2 ± 0.5	12.9 ± 0.5	10.9 ± 0.4	9.8 ± 0.4
Winter	21.3 ± 0.8	15.2 ± 0.5	13.3 ± 0.5	10.2 ± 0.4
Both seasons	20.9 ± 0.6	15.2 ± 0.4	13.2 ± 0.3	10.2 ± 0.3

This behavior could be likely explained by the absorption contribution that comes from BrC, which is not considered in MAC determination. The BrC contribution during summer is small, whereas it grows in winter due to the presence of sources such as wood combustion processes. The presence of BrC can introduce significant bias in the measurements of BC. When BC is determined by optical measurements in the spectral range of the near IR, it is measured only its contribution, while that of the BrC remains negligible. With decreasing of wavelengths, when the absorption contribution of BrC begins to be important, the gap between the summer and winter MAC values increases.

- V. Bernardoni, G. Valli, R. Vecchi (2017), *Set-up of a multi-wavelength polar photometer for off-line absorption coefficient measurement on 1-hour resolved aerosol samples*, *Journal of Aerosol Science* 107.
- G. Hanel, (1987), *Radiation budget of the boundary layer. Part 2: Simultaneous measurement of mean solar volume absorption and extinction coefficients of particles*, *Applied optics*, Vol. 27, No. 11.
- A. Petzold, M. Schönlinner, (2004), *Multi-angle absorption photometry – new method for the measurement of aerosol light absorption and atmospheric black carbon*, *Aerosol Science* 35 421-441 123-126.
- R. Vecchi, V. Bernardoni, C. Paganelli, G. Valli (2014), *A filter-based light-absorption measurement with polar photometer: Effects of sampling artefacts from organic carbon*, *Journal of Aerosol Science* 70 15–25.

**Black carbon vertical profiles measured by a micro-aethalometer in North China Plain**L. Ran<sup>1</sup>, Z.Z. Deng<sup>1</sup>, X.B. Xu<sup>2</sup>, P. Yan<sup>3</sup>, W.L. Lin<sup>3</sup>, Y. Wang<sup>2</sup>, P. Tian<sup>4</sup>, P.C. Wang<sup>1</sup>, W.L. Pan<sup>1</sup> and D.R. Lu<sup>1</sup><sup>1</sup>LAGEO, Institute of Atmospheric Physics, Chinese Academy of Sciences, Beijing, 100029, China<sup>2</sup>Institute of Atmospheric Composition, Chinese Academy of Meteorological Sciences, Beijing, 100081, China<sup>3</sup>Meteorological Observation Center, China Meteorological Administration, Beijing, 100081, China<sup>4</sup>Beijing Weather Modification Office, Beijing, 100089, China

Keywords: Black Carbon, Vertical Distribution, micro-Aethalometer, North China Plain.

Presenting author email: shirleyrl@mail.iap.ac.cn

Black carbon (BC), produced mainly from incomplete combustion processes, is a dominant absorber in the visible spectrum and a potent factor in climatic effects. Despite the significance of radiative forcing imposed by BC, large uncertainties remain in the quantitative assessment (IPCC, 2013). Among affecting factors, one critical aspect is the high sensitivity of BC radiative impact to its vertical distributions (Samset et al., 2013). However, in-situ measurements of vertical profiles of BC or aerosol absorption were currently rather limited (e.g., Ferrero et al., 2014), especially in China (e.g., Zhang et al., 2012; Li et al., 2015), where the challenge to reliably estimate regional climatic effects of BC under severe air pollution due to rapid economic growth and urbanization is urgent (Liao and Shang, 2015 and references therein).

In summer 2014, an intensive field campaign VOGA (Vertical Observations of trace Gases and Aerosols) was carried out at a semirural site in the North China Plain (NCP), one of the most polluted regions in the world. Vertical profiles of BC mass concentrations (absorption equivalent at 880 nm) within 1 km above the ground were measured using a lightweight (about 280 g) and small-sized (117 mm×66 mm×38 mm) micro-aethalometer (microAeth® Model AE-51, Magee Scientific, USA) attached to a tethered balloon system.

The diurnal cycle of BC vertical distributions following the evolution of the mixing layer was investigated for the first time in the NCP region (Fig. 1)(Ran et al., 2016). Statistical parameters including identified mixing height ( $H_m$ ) and average BC mass concentrations within the mixing layer ( $C_m$ ) and in free troposphere ( $C_f$ ) were obtained for a selected dataset of 67 vertical profiles.  $H_m$  was usually lower than 0.2 km in the early morning and rapidly rose thereafter due to strengthened turbulence. The maximum height of the ML was reached in late afternoon. The top of a full developed ML exceeded 1 km on sunny days in summer, while stayed much lower on cloudy days. The sunset triggered the collapse of the ML and a stable nocturnal boundary layer (NBL) gradually formed. Accordingly, the highest level  $C_m$  was found in the early morning and the lowest in the afternoon. In the daytime, BC almost uniformly distributed within the ML and significantly decreased above the ML. During the field campaign,  $C_m$  averaged about  $5.16 \pm 2.49 \mu\text{g m}^{-3}$ , or as  $\sigma_{BC}$  of about  $21.64 \pm 10.45 \text{ Mm}^{-1}$ , with a range of  $1.12$  to  $14.49 \mu\text{g m}^{-3}$ , comparable with observational results in many polluted urban areas such as Milan in Italy and Shanghai in China.

As evening approached, BC gradually built up near the surface and exponentially declined with height. In contrast to the large variability found both in  $H_m$  and  $C_m$ ,  $C_f$  stayed relatively unaffected through the day.  $C_f$  was less than 10% of the ground level under clean conditions, while amounted to half of the ground level in some polluted cases.

Hopefully, in-situ measurements of BC vertical profiles would have an important implication for accurately estimating direct radiative forcing by BC and improving the retrieval of aerosol optical properties by remote sensing in this region.

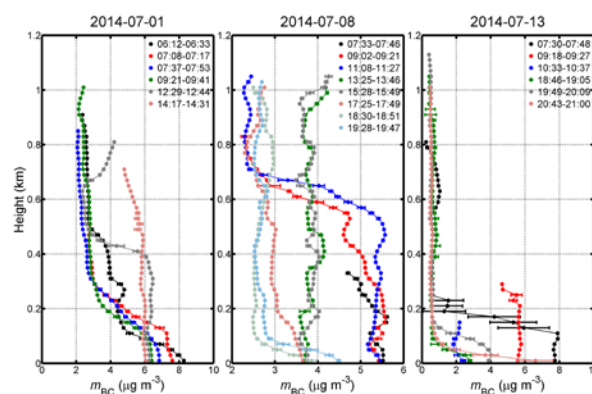


Figure 1. BC vertical profiles on July 1, 8, and 13, 2014 (different colors for different time). Dots represent 20-m averaged  $m_{BC}$ , with standard deviations as error bars.

This work was supported by the National Natural Science Foundation of China (NSFC) under grant no. 41305114, 41205098, 41330442, and 41127901.

- Ferrero, L., Castelli, M., Ferrini, B. S. and et al. (2014) *Atmos. Chem. Phys.* **14**, 9641-9664.  
 IPCC (2013) *Climate change 2013: the physical science basis*, Cambridge University Press.  
 Li, J., Fu, Q. Y., Huo, J. T. and et al. (2015) *Atmos. Environ.* **123**, 327-338.  
 Liao, H. and Shang, J. J. (2015) *J. Meteor. Res.* **29**, 525-545.  
 Ran, L., Deng, Z. Z., Xu, X. B. and et al. (2016) *Atmos. Chem. Phys.* **16**, 10441-10454.  
 Samset, B. H., Myhre, G., Schulz, M. and et al. (2013) *Atmos. Chem. Phys.* **13**, 2423-2434.  
 Zhang, D. Z., Chen, B., Yamada, M. and et al. (2012) *J. Meteorol. Soc. Japan* **90**, 361-375.

## Study on Polarization Characterization for Aerosol Morphology

Sirui Chen<sup>1,2</sup>, Nan Zeng<sup>1,2</sup>, Yuerong Chen<sup>1,2</sup>, Hui Ma<sup>1,2</sup>

<sup>1</sup>Shenzhen Key Laboratory for Minimal Invasive Medical Technologies, Institute of Optical Imaging and Sensing, Graduate School at Shenzhen, Tsinghua University, Shenzhen 518055, China

<sup>2</sup>Department of Physics, Tsinghua University, Beijing 100084, China

Keywords: aerosol morphology, polarization scattering, Mueller matrix

Presenting author email: threechen@aliyun.com

Due to its convenience, real-time, and in-situ, light scattering method is a promising way to analyse the suspended air pollutants in the atmosphere [1]. By extracting polarization features during scattering, we can obtain more details on the individual composition and microstructure of the measured aerosols [2].

Morphology analysis plays an important role of particle characterization in the field of cell classification, atmosphere optics, and oceanography. Compared with homogeneous spheres, the scattering Mueller matrix elements of anisotropic particles like cylinders or spheroids have different symmetry and distribution, which can be a potential indicator to identify various particle morphology [3]. The purpose of this paper is to extract some possible polarization indexes to describe the aerosol morphology and then discuss their efficiency by theoretical simulation and experimental ways.

By simulations and comparison of the scattering Mueller matrixes of suspended particles with three typical shape. We extract a polarization character K2, which can be detected easily by a horizontal linear incident polarized light and two orthogonal linear polarization analysers (parallel and vertical). For an approximately centrosymmetric particle, the linear polarized light parallel to the detection plane is difficult to be depolarized, meaning a constant K2 value theoretically. Once the aerosol morphology is non-centrosymmetric, the mean value, the probability and the angular distribution will be changed correspondingly. In addition, using our synchronous four channel polarization analysers, the K2 index can be detected and analysed in real time, suitable for the field test of our polarization optical air quality monitoring system.

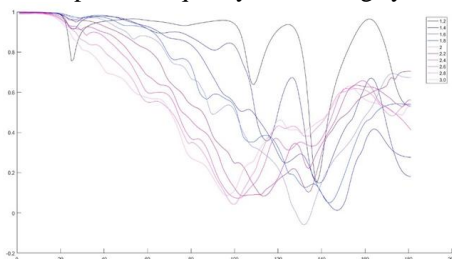


Figure 1. The simulated angular distribution of K2 index for various anisotropy degree of particles

We employ a polarization sensitive Monte Carlo simulation program to simulate the scattering process and the corresponding polarization change by sphere, cylinder, and spheroids. Fig.1 shows the angular distribution of K2 index for spheroids with different

aspect ratio. The value gradient of K2 at forward scattering is sensitive to the anisotropy of degree of aerosol shape. Fig.2 presents the histogram analysis of K2 at three forward scattering angles, and further confirms the potential of the probability spectrum of K2 to evaluate the aerosol morphology. Fig.3 show three type samples used in our experiments corresponding to sphere, cylinder, and spheroids.

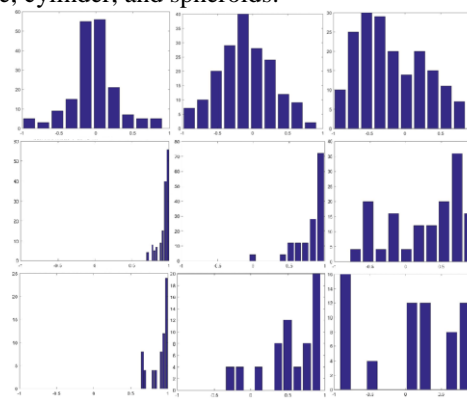


Figure 2. The histogram analysis of K2 index at three forward scattering angles for different particle morphology

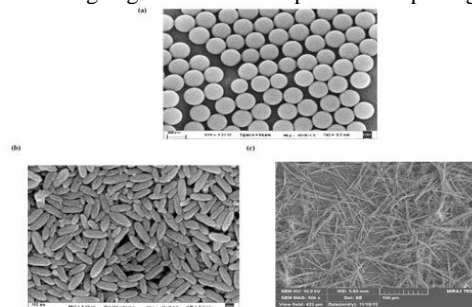


Figure 3. SEM images of experimental samples of aerosol morphology (a) spheres, (b) the spheroids and (c) chains.

This work was supported by National Natural Science Foundation of China (NSFC) (41475125); and The National Key Research and Development Program of China (2016YFC0208600, 2016YFF0103000).

- [1] C. F. Bohren and D. R. Huffman, *Absorption and Scattering of Light by Small Particles* (Wiley, 1983).
- [2] Bronk, "Light scattering calculations exploring sensitivity of depolarization ratio to shape changes. I. Single spores in air", *Appl. Opt.* **48**, 716(2009).
- [3] M.I. Mishchenko, L.D. Travis and Macke A, "Scattering of light by polydisperse, randomly oriented, finite circular cylinders," *Appl. Opt.* **35**, 4927-4940 (1996).

## Approximated expression of the mass extinction efficiency as a function of particle size for polydispersed accumulation mode aerosols

Chang H. Jung<sup>1</sup>, Junshik Um<sup>2</sup>, JiYi Lee<sup>3</sup>, Yong Pyo Kim<sup>4</sup>

<sup>1</sup>Department of Health Management, Kyungin Women's University, Korea-South

<sup>2</sup> Department of Atmospheric Sciences, University of Illinois at Urbana-Champaign, USA

<sup>3</sup> Department of Environmental Engineering, Chosun University, Korea-South

<sup>4</sup> Department of Environmental Science and Engineering, Ewha Womans University, Korea-South

Keywords: analytical approach, polydispersed aerosol, mass extinction efficiency, aerosol size distribution

Presenting author email: jch@kiwu.ac.kr

Among the many physical and optical parameters that characterize atmospheric aerosol properties, aerosol mass extinction efficiency (MEE) is most important in understanding aerosol optical properties.

In general, aerosol MEE is a function of the refractive index and size distribution of aerosol particles. However, because of its complexity, MEE is often regarded as a size-independent parameter and, as a result, it is assumed to be dependent on only the chemical compositions of aerosol particles. For example, the Interagency Monitoring of Protected Visual Environments (IMPROVE) network measured light scattering coefficients using a nephelometer with an assumption of constant MEE. According to Hand and Malm (2007), for example, the scattering coefficient can be expressed using the following formula:

$$b_{scat} = (3.0)(C_{[(NH_4)_2SO_4]} + C_{[NH_4NO_3]})f_{AS}(RH) + (4)C_{[OMC]} + (1)C_{[SOIL]} + 0.6 C_{[CM]} + 1.37f_{SS}(RH) C_{[SS]}$$

$$b_{abs} = (10.0)C_{[LAC]} \quad (1)$$

Here,  $b_{scat}$  and  $b_{abs}$  are the reconstructed scattering and absorption coefficients. The ratio between dry and wet scattering as a function of RH is referred to as the relative humidity scattering enhancement factor,  $f(RH)$ . The factors  $f_{AS}(RH)$  and  $f_{SS}(RH)$  refer to the enhancement factors for ammonium sulfate  $[(NH_4)_2(SO)_4]$ , and sea salt (NaCl), respectively.  $C_{[(NH_4)_2SO_4]}$  and  $C_{[NH_4NO_3]}$  are the fully neutralized ammonium sulfate and ammonium nitrate ( $NH_4NO_3$ ) mass concentration, respectively; and  $C_{[OMC]}$ ,  $C_{[SOIL]}$ ,  $C_{[CM]}$  and  $C_{[SS]}$  are the mass concentrations of organic carbon, soil, coarse mass (CM) and fine sea salt (SS), respectively.

The physical relationship between light extinction and atmospheric particulate constituents can be established if both the particulate concentration and the size distribution of each chemical species are known. Theoretically, the overall extinction coefficient,  $b_{ext}$ , can be calculated using Mie's theory as follows:

$$b_{ext} = \sum_i b_{ext,i} \quad (2) \text{ and}$$

$$b_{ext,i} = \int_0^{d_p^{max}} \frac{\pi d_p^2}{4} Q_{ext,i}(d_p, \lambda, m) n(d_p) dd_p, \quad (3)$$

where the total extinction coefficient,  $b_{ext,i}$ , can be expressed as a summation of the extinction coefficients for each chemical composition of multi-compositional external mixtures. For simplicity the estimates above have assumed aerosol particles to be spherical in shape.

Here,  $n(d_p)$  is the size distribution, and  $Q_{ext}(d_p, \lambda, m)$  is the extinction efficiency of a particle with diameter ( $d_p$ )

and refractive index  $m$  at a wavelength ( $\lambda$ ) of light.

Under the given mass concentration, the resulting aerosol MEE is defined as the ratio of aerosol extinction coefficient to aerosol mass concentration in a unit volume of air (Malm et al., 2000; Hand and Malm, 2007).

Subsequently, the overall extinction coefficient can be simplified as follows:

$$b_{ext} = \sum_i b_{ext,i} = \sum_i [C_i \times MEE_i] \quad (4)$$

$$b_{ext,i} \cong C_i \times MEE_i, \text{ and } MEE_i = \frac{b_{ext,i}}{C_i}, \quad (5)$$

where  $MEE_i$  is the specific mass extinction efficiency in  $m^2/g$ , and  $C_i$  is the mass concentration of the individual chemical species (in  $gm^{-3}$ ). In this study, mass extinction, scattering and absorption efficiencies of polydispersed aerosol particles were estimated analytically. Geometric mean diameter ranges of 0.3–2.5 $\mu m$  were considered assuming lognormal size distribution for all aerosol species. An analytical approach to the approximated formula for the MEE of each aerosol chemical composition was estimated by fitting the formula results to the results from Mie. Finally, a comparison between the mass efficiencies of different mixtures is made, and water content is calculated using the Aerosol Thermodynamic model (SCAPE2, Kim et al., 1993a, b). Throughout the manuscript, obtained results are compared with the results from the Mie-theory-based calculations.

Hand, J. L., & Malm, W. C. (2007). Review of aerosol mass scattering efficiencies from ground-based measurements since 1990. *Journal of Geophysical Research*, 112, D16203

Jung, C. H., Lee, J. Y., & Kim, Y. P. (2015). Estimation of aerosol optical properties considering hygroscopicity and light absorption. *Atmospheric Environment*, 105, 191–201.

## Contribution and potential sources of nitroaromatic compounds in water soluble brown carbon of size-resolved ambient aerosols

S. Frka<sup>1,2</sup>, A. Kroflič<sup>1</sup>, J. Turšič<sup>3</sup>, M. Šala<sup>1</sup> and I. Grgić<sup>1</sup>

<sup>1</sup>Department of Analytical Chemistry, National Institute of Chemistry, Ljubljana, 1000, Slovenia

<sup>2</sup>Division for marine and environmental research, Ruđer Bošković Institute, Zagreb, 10000, Croatia

<sup>3</sup>Environmental Agency of the Republic of Slovenia, Ljubljana, 1000, Slovenia

Keywords: nitroaromatic compounds, brown carbon, water soluble organic carbon, light absorption.

Presenting author email: frka@irb.hr

Despite the recent progress in understanding the formation and evolution of organic aerosols during atmospheric ageing, issues related to their impact on the atmosphere and the climate are only beginning to be understood. Brown carbon (BrC), as highly variable fraction of OA, is recognized as an important component of atmospheric light absorbing particulate matter. It has recently attracted much interest because of potentially large effects on the Earth's climate through a combination of direct effects on the transmission of radiation and indirect effects resulting from changes in cloud formation and microphysics. Herein, the water-soluble BrC (aqBrC) comprising aerosol light-absorbing water soluble organic compounds play a considerable role. There is growing evidence that aqBrC results from primary emissions and secondary aging processes (e.g. Hecobian *et al.*, 2010). Secondary transformations often involve nitrogen, thus brown secondary organic aerosols have been detected during photooxidation of different volatile aromatic precursors (e.g., toluene, benzene, or xylene) in the presence of NO<sub>x</sub>. It has been suggested that yellow-colored nitroaromatic compounds (NACs), in particular, abundant methylnitrocatechols (MNCs), are the major contributors to the Humic-like substances (HULIS) isolated from the water extracts of PM<sub>2.5</sub> (Claeys *et al.*, 2012). Moreover, semi-volatile MNCs are regarded as tracers of processed biomass-burning emissions as well as aged anthropogenic aerosols, whose (photo)transformation processes, including those in the atmospheric aqueous-phase, are only beginning to be understood (Iinuma *et al.*, 2010; Kroflič *et al.*, 2015; Frka *et al.*, 2016). Although even trace levels of organics could have a significant impact on the light absorption properties of atmospheric particles, little is known about the specific aqBrC constituents, such as NACs, and their size distribution as well as their (trans)formation mechanisms in the atmosphere.

Our comprehensive study aims to expand the understanding of aqBrC by investigating: (1) chemical characteristics of ambient size segregated WSOM and HULIS fraction including measurements of their light absorption properties by UV-Vis spectrometry and molecular level determination of target NACs (e.g. 4-nitrocatechol, 4NC; methyl-nitrocatechols, MNC; di- and nitrophenols, (D)NP; methyl nitrophenols, MNP; nitrosalicylic acids, NSA; nitroguaiacols, NG) by applying high performance liquid chromatography tandem mass spectrometry (HPLC-ESI-MS/MS) and (2)

aqueous-phase photolysis of model NACs as well as ambient HULIS extracts.

Ambient size segregated aerosol samples (0.038-15.6 μm aerodynamic diameters) comprise a one-year sample set collected in the urban background location of Ljubljana, Slovenia. Seasonal variations of NACs contribution to the optical properties of ambient aqBrC (represented by light absorption of the aerosol aqueous extract and HULIS fraction) have been measured. To complement these studies, NACs mass contributions to the aerosol water soluble organic (WSOC) and HULIS carbon (HULIS-C) content have been determined as well. The obtained data were correlated with those for levoglucosan as a tracer for biomass burning emissions. In addition, we will present results on aqueous-phase photolysis of model NACs and HULIS extracts under the simulated atmospheric conditions. Aging was performed in a custom-built reactor using a solar simulator, and online connected to a high performance liquid chromatography with diode array and mass spectrometric detection (HPLC-DAD-ESI-MS/MS).

This work was supported by the European Commission and the Croatian Ministry of Science, Education and Sports through Marie Curie FP7-PEOPLE-2011-COFUND, project NEWFELPRO and by the Slovenian Research Agency (Contract no. P1-0034-0140).

Hecobian, A., Zhang, X., Zheng, M., Frank, N., Edgerton, E. S. and Weber R. J. (2010) *Atmos. Chem. Phys.*, **10**, 5965-5977.

Claeys, M., Vermeylen, R., Yasmeen, F., Gomez-González, Y., Chi, X., Maenhaut, W., Mészáros, T. and Salma, I. (2012) *Environ. Chem.*, **9**, 273-284.

Iinuma, Y., Böge, R., Gräfe, R., and Herrmann, H. (2010) *Environ. Sci. Technol.* **44**(22) 8453-8459.

Kroflič, A., Grilc, M. and Grgić, I. (2015) *Sci. Rep.* **5**.

Frka, S., Šala, M., Kroflič, A., Huš, M., Čusak, A. and Grgić, I. (2016) *Environ. Sci. Technol.* **50**(11) 5526-35.

## Angular Scattering of the Sahara Dust Aerosol

Helmuth Horvath<sup>1</sup>, Lucas Alados Arboledas<sup>2</sup> and Francisco Jose Olmo Reyes<sup>2</sup>

<sup>1</sup>University of Vienna, Faculty of Physics, Aerosol Physics and Environmental Physics, A-1090 Vienna, Austria

<sup>2</sup>University of Granada, Department of Applied Physics, E-18071 Granada, Spain

Keywords: Light scattering, Asymmetry, Sahara, Phase function

Presenting author email: Helmuth.Horvath@univie.ac.at

Soil erosion aerosols can be transported considerable distances, the Sahara is one of the major sources on the world. In June 2016 the volume scattering function of the atmospheric aerosol has been measured in the Sierra Nevada, Spain, at an altitude of 2500 m, where Sahara dust intrusions happen many times. At the beginning moderate dust intrusion was observed (period 1), followed by period 2 with almost negligible influence by the Sahara aerosol, finally during period 3 a heavy load of Sahara aerosol was observed. In period 1 the aerosol scattering coefficient had an average value of  $51 \text{ Mm}^{-1}$ , corresponding to a visual range of 62 km. In period 2 the values were  $22 \text{ Mm}^{-1}$  and 118 km, whereas in period 3 the average scattering coefficient rose to  $72 \text{ Mm}^{-1}$  dropping the visibility to 47 km. Within the periods considerable variations occurred, but still the periods definitely can be distinguished. Figure 1 shows the scattering coefficient as a function of time.

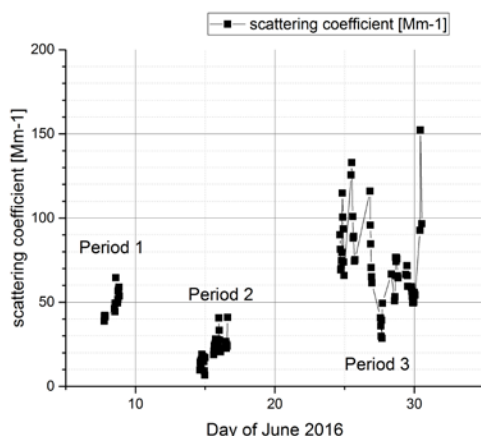


Figure 1: Measured scattering coefficient.

The scattering function in the three periods was different, average phase functions for the three periods can be seen in figure 2. It is evident, that the phase function, measured during the period which little influence by the Sahara dust, is more symmetric, the forward scattering is less and the backscattering is higher than for the Sahara aerosol. On the other hand the Sahara aerosol particles have a higher forward scatter, which is mainly caused by the larger size of the dust particles. The backscattering is considerably smaller which is mainly caused by the irregular shape of the dust particles. A considerable difference in the forward scattering occurs, e.g. at an angle of  $5.5^\circ$  the value of the phase function in period 3 is 1.6 times higher than in period 2.

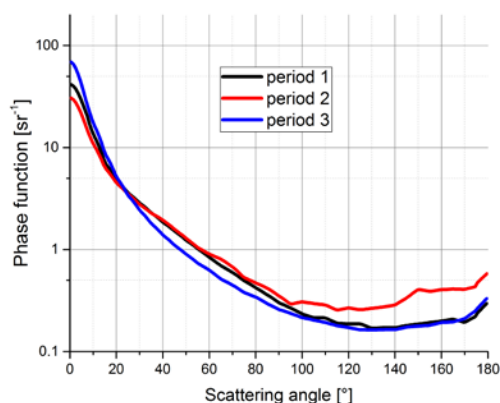


Figure 2: Average Phase Functions measured during the three periods. During Period 1 and 3 a strong influence by the Sahara aerosol was observed.

This is difficult to see, in figure 2, since the phase function varies by almost 3 orders of magnitudes. A better distinction is possible by comparing the asymmetry parameter and the backscattered fraction. The less asymmetric phase function has a smaller asymmetry parameter and a larger backscattered fraction. In figure each measurement is represented as a point in the (*asymmetry vs. backscattering*) plane. With a few exceptions Sahara and non-Sahara aerosols are clearly separated.

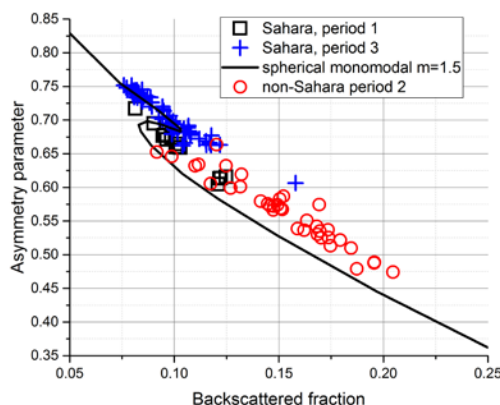


Figure 3: Data obtained with the polar nephelometer represented in the (*asymmetry vs backscattering*) space.

**Conclusion:** Using a newly developed polar nephelometer, soil erosion particles can easily be distinguished.

## Aerosol optical properties and carbon isotope analysis during Gosan Pollution Experiment (GoPoEx) 2014

S.-W. Kim<sup>1</sup>, C. Cho<sup>1</sup>, P. Sheridan<sup>2</sup>, Ö. Gustafsson<sup>3</sup>, A. Andersson<sup>3</sup>, W. Fang<sup>3</sup>, R. J. Park<sup>1</sup>, M. Lee<sup>4</sup>

<sup>1</sup>School of Earth and Environmental Sciences, Seoul National University, Seoul, 08826, Korea

<sup>2</sup>NOAA/ESRL Global Monitoring Division, Boulder, Colorado, 80305, USA

<sup>3</sup>Department of Applied Environmental Science, Stockholm University, Stockholm, 10691, Sweden

<sup>4</sup>Department of Earth and Environmental Science, Korea University, Seoul, 02841, Korea

Keywords: aerosol, scattering, absorption, carbon isotope

Presenting author email: sangwookim@snu.ac.kr

Located on the downwind side of China, Korea is simultaneously affected by anthropogenic fine pollutants emitted in the urban areas, and by wind-blown mineral dust from desert and dry regions in China (Kirillova et al., 2014). Especially in winter, a high concentration of pollutants and dust inflow into Gosan from China due to the increased usage of fossil/biomass fuels for house heating and fast synoptic flow (Kim et al., 2014). The carbonaceous composition of aerosols, which occupy a considerable fraction of fine particulate matter, depends on the origin of the air mass such as Northern China, Southern China, Northern of Korean peninsula and emission sources of aerosols. Therefore, to understand more certain characteristics of light-absorbing aerosols, the origin and source of aerosols should be considered.

In this study, we investigate the optical properties of dust and pollution aerosols and estimate the contribution of carbon sources from the carbon isotope analysis at Gosan Climate Observatory (GCO), Korea during Gosan Pollution Experiment 2014 (GoPoEx 2014; January 2014). Figure 1 shows time series of aerosol optical and physical properties at GCO during GoPoEx 2014. Mean value of aerosol scattering coefficient and absorption coefficient during GoPoEx 2014 were  $71 \pm 36 \text{ Mm}^{-1}$  and  $7 \pm 5 \text{ Mm}^{-1}$  at 550 nm, respectively.

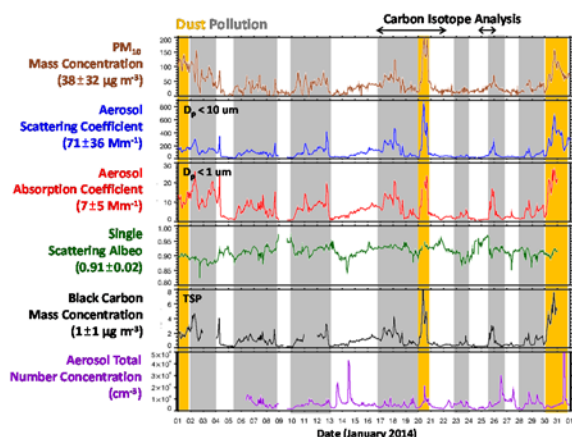


Figure 1. Time series of aerosol optical and physical properties during GoPoEx (January 2014). The pollution event is marked in grey and the dust events in yellow.

Values for scattering and absorption coefficient of pollution episodes were recorded as  $153 \pm 95 \text{ Mm}^{-1}$  and  $12 \pm 7 \text{ Mm}^{-1}$  at 550 nm. Therefore, single scattering Aerosol scattering coefficient and absorption coefficient during dust episodes were  $245 \pm 171 \text{ Mm}^{-1}$  and  $22 \pm 13 \text{ Mm}^{-1}$  at 550 nm, which were approximately 3.5 times greater than mean values during GoPoEx 2014. albedo of pollution episodes ( $0.92 \pm 0.02$ ) was slightly higher than those of dust episodes ( $0.90 \pm 0.03$ ). This is because that pollutant aerosols include more scattering fraction such as  $\text{SO}_4^{2-}$ , and  $\text{NO}_3^-$  in fine particulate matter emitted from industrial areas in the eastern coastal region of China while dust aerosols are transported from North China to Gosan. The radiocarbon ( $\Delta^{14}\text{C}$ ) data showed that fossil combustions contributed approximately  $66 \pm 7\%$  to elemental carbon (EC) aerosol in Gosan (Figure 2).

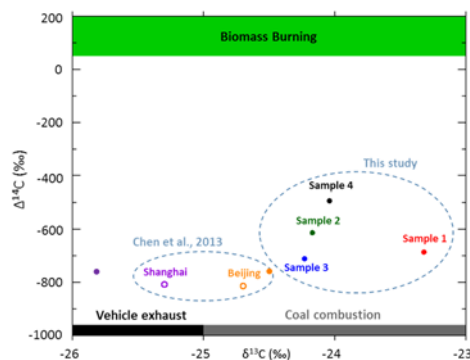


Figure 2. . Two-dimensional presentation of dual-isotope ( $\delta^{13}\text{C}$  vs.  $\Delta^{14}\text{C}$ ) signals for GoPoEx campaign compared to in China (Chen et al., 2013).

This work was supported by the Korea Ministry of Environment as “Climate Change Correspondence Program”.

Chen, B., Andersson, A., Lee M., Kirillova, E., Xiao, Q., Kruså, M., Shi, M., Hu, K., Lu, Z., Street, D. G., Du, K., and Gustafsson, Ö. (2013), *Environ. Sci. Technol.*, **47**, 9102–9108.

Kirillova, E., Andersson, A., Han, J., Lee, M., and Gustafsson, Ö. (2014), *Atmos. Chem. Phys.*, **14**, 1413–1422.

Kim, Y., Kim, S.-W., Yoon, S.-C., Kim, M.-H., Park, K. (2014), *Atmos. Environ.*, **85**, 9–17.

## Estimating contribution of brown carbon from multi-wavelength absorption measurements during summer and winter at an urban site

Jae-Myeong Yu, Yan Zhang and Seung Shik Park

Department of Environment and Energy Engineering, Chonnam National University, 77 Yongbong-Ro, Buk-ku, Gwangju 61186, Republic of Korea

Keywords: brown carbon, light absorption, HULIS, absorption Ångström exponent.

Presenting author email: yujaemyeong@gmail.com, park8162@chonnam.ac.kr

Ambient humic like substances (HULIS), which is a hydrophobic fraction of water-soluble organic carbon (WSOC), could influence the global direct radiative forcing of aerosols. A subclass of organic aerosols referred to as brown carbon (BrC) absorbs solar radiation in the near UV and visible region, and an example of BrC is HULIS. Despite its importance on environment and on climate forcing in particular, the absorption properties of BrC are poorly understood. In this study 24-hr PM<sub>2.5</sub> samples were collected at an urban site of Korea during summer and winter, and analyzed for determination of organic carbon (OC), elemental carbon (EC), WSOC, HULIS, and ionic species, to investigate possible sources and formation processes of HULIS. Moreover, real-time measurements of black carbon (BC) aerosols were made using a dual-spot multi-wavelength aethalometer (370, 470, 520, 590, 660, 880, 950 nm) at the same location to investigate light absorption properties of BrC aerosols.

Over the study period, average seasonal WSOC concentration was  $2.64 \pm 0.97$  (0.84–4.98) in summer and  $3.14 \pm 1.53$  (0.88–8.06)  $\mu\text{gC}/\text{m}^3$  in winter, respectively, contributing approximately 70.3% (56.2–84.1) and 63.3% (46.1–83.1) to OC concentrations. HULIS was on average  $1.31 \pm 0.48$  (0.52–2.59) in summer and  $1.85 \pm 0.81$  (0.54–4.26)  $\mu\text{gC}/\text{m}^3$  in winter, respectively, accounting for 49.6 and 60.0% of the respective WSOC (Figure 1). During summer, correlations of HULIS with EC ( $R^2=0.56$ ), oxalate ( $R^2=0.64$ ), and  $\text{K}^+$  ( $R^2=0.34$ ) suggest HULIS from traffic emissions and secondary formation, rather than from primary biomass burning. On the other hand, HULIS in winter was strongly associated with oxalate ( $R^2=0.85$ ) and  $\text{K}^+$  ( $R^2=0.83$ ), but not with EC ( $R^2=0.25$ ), suggesting the influence of biomass burning emissions and secondary organic aerosol formation to HULIS measured in winter.

The wavelength dependence of the aerosol absorption coefficients ( $b_{\text{abs}}$ ) is proportional to  $\lambda^{-\text{AAE}}$ , where  $\lambda$  is the wavelength and AAE is the absorption Ångström exponent. In this study, to obtain observational constraints from absorption measurements, a simple AAE model was applied to separate the contribution of BrC absorption from that of BC. With this attribution method, the  $\text{AAE}_{370-950\text{nm}}$  and  $\text{AAE}_{370-520\text{nm}}$  values were  $1.19 \pm 0.08$  and  $1.29 \pm 0.13$  in summer, and  $1.37 \pm 0.08$  and  $1.67 \pm 0.14$  in winter, respectively, indicating stronger influence

of biomass burning emissions in winter. However, the spectral dependence of estimated BrC absorption showed  $\text{AAE}_{370-660\text{nm}}$  values of 4.0 and 4.4 in summer and winter, respectively, which are lower than those from water extracts (WSOC and HULIS) of aerosol particles reported in other studies (Cheng *et al.*, 2016), indicating contribution of water-insoluble BrC to light absorption. The contribution of the aerosol light absorption from BrC at 370 nm to the total light absorption was 16.6% in summer and 29.3% in winter, respectively (Figure 2).

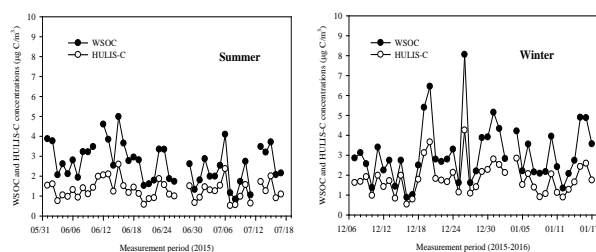


Figure 1. Temporal profiles of WSOC and HULIS concentrations in summer and winter periods.

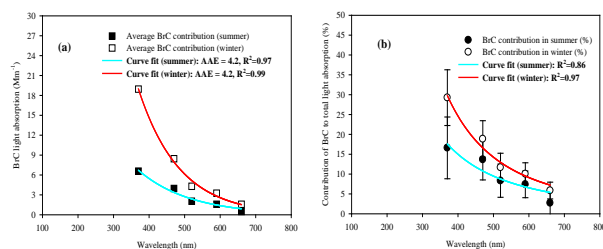


Figure 2. Estimated values of BrC AAE (a) and estimated contribution of BrC to total spectral absorption of aerosols in summer and winter (b).

This research was supported by Basic Science Research Programs through the National Research Foundation of Korea (NRF) funded by the Ministry of Education (NRF-2017R1A1A4A03000511).

Cheng, Y. *et al.* (2016) *Atmos. Environ.* **127**, 355–364.

## A long-term study of suburban aerosol optical properties based on CAPS PM<sub>ss</sub> monitor measurements

M.I. Gini<sup>1</sup>, P. Fetfatzis<sup>1</sup>, S. Vratolis<sup>1</sup> and K. Eleftheriadis<sup>1</sup>

<sup>1</sup>Institute of Nuclear & Radiological Sciences & Technology, Energy & Safety, National Centre of Scientific Research “Demokritos”, Ag. Paraskevi, 15310, Greece

Keywords: CAPS PM<sub>ss</sub>, single scattering albedo, absorption, scattering, extinction.  
Presenting author email: gini@ipta.demokritos.gr

Atmospheric aerosols influence the global radiation budget directly through scattering and absorbing of incoming and outgoing radiation. They act as cloud condensation nuclei, influencing cloud microphysical and radiative properties. The optical properties of atmospheric aerosol show a great spatial and temporal variability and are determined by multiple aerosol parameters (i.e. chemical composition, size, shape, concentration and mixing state). Although numerous studies have been performed and several instrumental techniques have been developed so far, large uncertainties remain in describing the optical properties of different aerosols, especially the aerosol absorption coefficient.

In this study, the optical properties of atmospheric aerosol were investigated using a CAPS PM<sub>ss</sub> monitor (Aerodyne), at operating wavelength of 630nm, that combines airborne particle extinction and scattering measurements (and thus single scattering albedo, SSA) on the same sample volume with rapid, real-time response (1s). The measurement campaign took place in a suburban area on the edge of Athens Metropolitan area, at the “DEM-GAW” monitoring station, located in a vegetated area at the grounds of N.C.S.R. “Demokritos”, from March 2015 to January 2016. In order to evaluate the possible measurement uncertainties and improve data reliability, a comparison between different instrument techniques (i.e. aethalometer, nephelometer) was performed for aerosols of different origin. Given that scattering measurements require correction for the truncation error, the particle number size distributions obtained by optical particle sizer (OPS TSI) were also analysed, whereas backward trajectory analysis was performed to characterise the transport pathways of air masses and identify the Sahara dust events and other major long-range transport influences.

First the correlation between the absorption measured by CAPS PM<sub>ss</sub> and a filter based instrument like the aethalometer was evaluated. Although, the two instruments were well correlated ( $R=0.76$ ), there was a factor of 54% between the two datasets. The seasonal variability of the daily cycle of absorption (Extinction minus Scattering) is presented in Figure 1 (a) and (b). For both seasons, a similar diurnal cycle in absorption was observed, with two local maxima occurring in the early morning and after sunset, as a result of the enhanced source emissions (i.e. traffic emissions) and the poor dispersion conditions during these hours of the day. However, in winter, higher absorption values were recorded due to variations in the emission sources (i.e.

residential heating including biomass burning,) and the meteorological conditions.

In Figure 2, the polar plots for (a) SSA and (b) absorption are presented. Increased absorption coefficients were associated with Westerly wind directions (urban area) and low wind speeds, implying that the observed levels were primarily attributed to local traffic and residential emission sources from the urban area of close proximity and also to local stagnation conditions. On the other, the highest SSA values were observed under North-Eastern wind, at high wind speed indicating influence from regional or longer range sources outside the urban area (i.e. aged aerosol, sulfates).

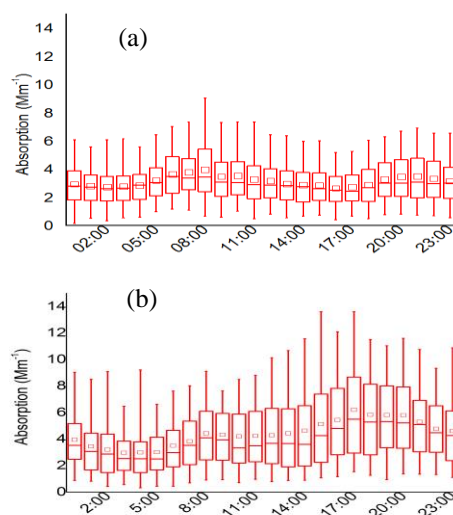


Figure 1. Seasonal variability of Absorption coefficient diurnal cycle measured by CAPS PM<sub>ss</sub> ((a): summer, (b): winter).

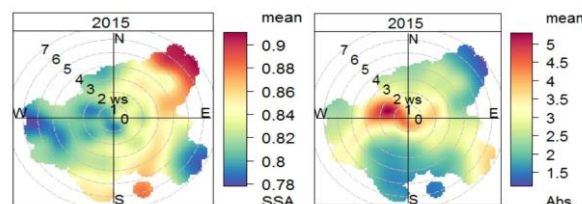


Figure 2. Bivariate polar plots for SSA and absorption coefficient measured by CAPS PM<sub>ss</sub>.

This work was supported by ENTEC FP7/REGPOT - 2012-2013-1 FP7, ID:316173)

## Measurements of the Real and Imaginary Components of the Refractive Index of Single Aerosol Particles

Rose E. Willoughby<sup>1</sup>, Michael I. Cotterell<sup>1</sup>, Antonio Valenzuela<sup>1</sup>, Bryan R. Bzdek<sup>1</sup>, Hongze Lin<sup>2</sup>, Andrew J. Orr-Ewing<sup>1</sup> and Jonathan P. Reid<sup>1</sup>

<sup>1</sup>School of Chemistry, University of Bristol, BS8 1TS, UK

<sup>2</sup>Department of Optical Engineering, Zhejiang University, Hangzhou 310058, China

Keywords: Refractive index, Cavity ring-down spectroscopy, Phase function, Bessel laser beam

Presenting author email: rose.willoughby@bristol.ac.uk

The interaction of atmospheric aerosols with radiation remains a significant source of uncertainty in modelling climate. Aerosols effect the climate directly by both scattering and absorbing solar and terrestrial radiation. This interaction is dependent on refractive index, which is made up of components that govern scattering,  $n$ , and absorption,  $k$ . The refractive index of an aerosol particle is determined by the composition and mixing state of the particle and wavelength of illumination. In this work, single hygroscopic aerosol particles have been studied at a number of wavelengths of illumination and at varied relative humidity ((RH), and therefore varied compositions) to provide accurate parameterisations of the optical properties of surrogates of atmospheric aerosol. We consider both inorganic and organic components and the mixing rules for treating the properties of highly complex mixtures.

Studying a single aerosol particle has the advantage of providing very accurate measurements of refractive index,  $\pm 0.1\%$  in  $n$ , compared to  $\sim \pm 1.4\%$  for a typical ensemble cavity ring-down spectroscopy (CRDS) measurement (by Mason *et al* (2012)). In this work, a single aerosol particle was optically trapped with a Bessel laser beam while the relative humidity surrounding the droplet was varied. The evolving extinction cross-section of the particle was measured with cavity ring-down spectroscopy while elastic light scattering was recorded.

$n_{405}$ ,  $n_{473}$  and  $n_{532}$  of binary aqueous inorganic and complex aqueous organic systems, of  $\sim 1$  to  $2\ \mu\text{m}$  in radius, have been studied. Combining measured  $n_\lambda$  with literature  $n_\lambda$  has enabled the behaviour of refractive index as a function of RH and wavelength to be modelled and parameterised for (aerosol composed of aqueous NaCl,  $\text{Na}_2\text{SO}_4$ ,  $\text{NaNO}_3$ ,  $\text{NH}_4\text{HSO}_4$  or  $(\text{NH}_4)_2\text{SO}_4$ ), providing the most extensive and precise parameterisation of  $n_\lambda$  to date. We will then present data that provides an assessment of the mixing rules for characterising the optical properties of complex multicomponent mixtures of inorganic and organic components. Finally, the weakly absorbing behaviour of aqueous aerosols in the near-infrared has been studied by intermittently irradiating a droplet with a near-infrared laser. The heating-induced size change for each droplet is precisely known, allowing the absorption,  $k$ , to be calculated.

In summary, we will use these single particle measurements to assess the accuracy of treatments of aerosol optical properties for aerosols spanning from simple binary inorganic mixtures to highly complex mixtures.

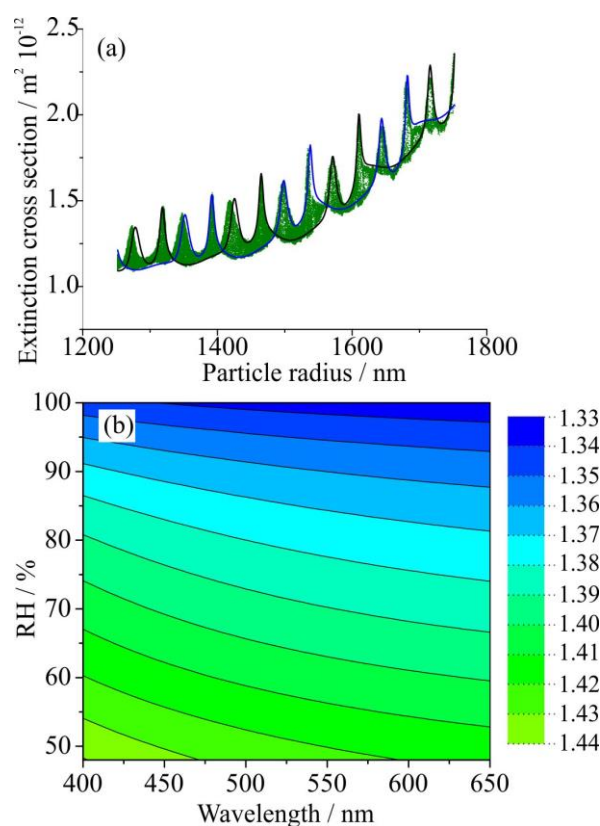


Figure 1 (a) Cavity ring-down spectrum of an aqueous NaCl aerosol particle, green points are the measured extinction cross section, black and blue lines are calculated from cavity standing wave Mie theory (Cotterell *et al* (2016)), (b) Parameterisation of refractive index (indicated in the key) in terms of illumination wavelength and relative humidity for aqueous NaCl.

This work is funded by the Natural Environment Research Council from the GW4+ DTP and the Aerosol Society in the form of the CN Davies Award.

Mason, B. J., King, S-J., Miles, R. E. H., Manfred, K. M., Rickards, A. M. J., Kim, J., Reid, J. P. and Orr-Ewing A. J. (2012) *J. Phys. Chem. A*, **116**, 8547-8556.  
Cotterell, M. I., Preston, T. C., Orr-Ewing A. J. and Reid, J. P. (2016) *Aerosol Sci. and Tech.*, **50**, 1077-1095

## Optical properties and PM concentration in air masses arriving at a high altitude location in the Mediterranean coast.

R. Castañer<sup>1</sup>, J.F. Nicolás<sup>1</sup>, M. Pandolfi<sup>2</sup>, M. Ealo<sup>2</sup>, S. Caballero<sup>1</sup>, N. Galindo<sup>1</sup>, J. Gil-Moltó<sup>1</sup>, C. Pastor<sup>1</sup>, M. Varea<sup>1</sup>, E. Yubero<sup>1</sup>, A. Alastuey<sup>2</sup> and J. Crespo<sup>1</sup>

<sup>1</sup>Atmospheric Pollution Laboratory (LCA-UMH), Miguel Hernández University, Elche, Spain.

<sup>2</sup>Institute of Environmental Assessment and Water Research (IDAEA-CSIC), Barcelona, Spain.

Keywords: mineral dust, light absorption coefficient, single scattering albedo, Angström exponents.

Presenting author email: [r.castaner@umh.es](mailto:r.castaner@umh.es)

Simultaneous measurements of PM and aerosol optical properties were performed from January 2014 to December 2015 at Mt. Aitana (38°39' N; 0°16' W; 1558 m a.s.l.). The sampling site is on the top of a mountain range located inland in the province of Alicante, in southeastern Spain.

Particle scattering ( $\sigma_{sp}$ : 10-171°) and hemispheric backscattering ( $\sigma_{bsp}$ : 90-171°) coefficients at three wavelengths (450, 525 and 635 nm) were measured with a LED-based integrating Nephelometer (model Aurora 3000, ECOTECH Pty Ltd, Knoxfield, Australia). Equivalent black carbon measurements were obtained at seven different wavelengths (370, 470, 520, 590, 660, 880 and 950 nm) using an Aethalometer (model AE31, Magee Scientific, USA). PM<sub>10</sub> and PM<sub>1</sub> mass fractions were obtained using a GRIMM (190) optical counter. PM gravimetric measurements were collected by means a high-volume sampler (DIGITEL with PM<sub>10</sub> cut-off inlet at 30 m<sup>3</sup>·h<sup>-1</sup>) and a low-volume sampler (LVS with PM<sub>1</sub> cut-off inlet at 2.3 m<sup>3</sup>·h<sup>-1</sup>). Back-trajectories daily classification was conducted by HYSPLIT model. Dust forecast models, NAAPS and BSC/DREAM8b were also used.

Air masses origin was classified in six sectors: AT (Atlantic), AN (North-Atlantic), EU (European), MED (Mediterranean), REG (Regional) and finally, NAF (North-African).

Table 1. Frequency of occurrence for each trajectory category and average values of the main meteorological parameters during 2014 and 2015.

Category	%	T	v	RH	P
AT/AN	53.4	8.4	5.9	72.9	526.5
EU/MED	10.3	9.3	4.7	67.7	73.3
REG	18.1	14.2	4.2	59.9	45.7
NAF	18.2	12.5	5.7	61.4	228.7
GLOBAL	100.0	10.3	5.4	67.8	874.2

T: (temperature °C); v: (wind speed m/s); RH (relative humidity %); P: (precipitation l/m<sup>2</sup>).

Clearly, Atlantic origin was the most common. On more than half days of the whole period (390 days ~53.4%) the air masses arriving at sampling site had this origin. PM<sub>10</sub> mean value was 13.1±0.6 µg·m<sup>-3</sup>, whereas PM<sub>1</sub> fraction registered 4.0±0.1 µg·m<sup>-3</sup>. PM<sub>1</sub>/PM<sub>10</sub> ratio recorded an average value of 0.41±0.01, which reflects a

certain preponderance of the coarse particles in the study area. Maxima values in summer and minima during winter time were exhibited by both fractions.

Mean values of optical properties were obtained:  $\sigma_{sp}$  (30.7±1.1 Mm<sup>-1</sup>),  $\sigma_{bsp}$  (3.9±0.1 Mm<sup>-1</sup>),  $\sigma_{ap}$  (2.4±0.1 Mm<sup>-1</sup>), BC (251.7±6.1 ng/m<sup>3</sup>), g (0.596±0.006), SAE (1.302±0.30), AAE (1.229±0.007) and SSA (0.900±0.004). Scattering coefficient ( $\sigma_{sp}$ ) mean value (30.7 Mm<sup>-1</sup>), was quite similar to those registered in stations located in the north of Spain: 25.4 Mm<sup>-1</sup> in Montsec-1570 m a.s.l (Pandolfi et al., 2014).

Scattering Angstrom exponent mean value, 1.302 indicates that although the scattering was in general determined by submicron particles, there was a certain contribution of coarse ones. The influence of NAF scenarios on  $\sigma_{sp}$  and  $\sigma_{bsp}$  was noticeable. During this category, scattering coefficient mean value 43.8 Mm<sup>-1</sup> was 30% higher than the mean value obtained for the whole period. It has been proved at sampling point that EC (elemental carbon) and OC (organic carbon) levels in summer are higher than in winter and that the relative EC concentration decrease between summer and winter is twice the one experimented by OC (Galindo et al., 2016).

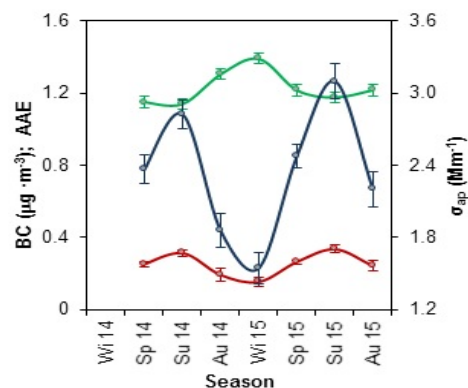


Figure 1: Seasonal evolution of  $\sigma_{ap}$ , BC and AAE during the study period.

This work was supported by the Spanish Ministry MINECO under the CGL2012-39623-C02-2 PRISMA-AITANA project. We would like to thank the Spanish Defense Ministry (EVA n. 5) for allowing access to its facilities.

Pandolfi, M., Ripoll, A., Alastuey, A., Querol, X., (2014) *Atmos. Chem. Phys.* **14**, 6443-6460.

Galindo, N., Yubero, E., Nicolás, J.F., Crespo, J., Soler, R. (2016) *Air. Qual. Res.* **16**, 530-541.

## Cirrus clouds observations at the Atmospheric Observatory ‘El Arenosillo’ (SW Iberian Peninsula) and their effects on the surface solar radiation

A. del Águila<sup>1</sup>, L. Gómez<sup>1</sup>, J.M. Vilaplana<sup>1</sup>, J.A. Adame<sup>1</sup>, M. Sorribas<sup>1</sup> and C. Córdoba-Jabonero<sup>1</sup>

<sup>1</sup>National Institute for Aerospace Technology, El Arenosillo Atmospheric Observatory, Mazagón-21130, Huelva, Spain

Keywords: Cirrus clouds, lidar, solar radiation.

Presenting author email: aguilapa@inta.es

Cirrus (Ci) clouds are involved in Climate Change concerns since they affect the radiative balance of the atmosphere. The degree of understanding of their climate implication is still low; however, Cirrus features are widely required in data assimilation by global climatic models, and the contribution of Ci-contrails formed from air traffic is still discussed.

A polarized Micro-Pulse Lidar (P-MPL), standard system within NASA/Micro Pulse Network (MPLNET, [mplnet.gsfc.nasa.gov](http://mplnet.gsfc.nasa.gov)), has been recently deployed at the El Arenosillo Atmospheric Observatory (ARN), located at mid-latitudes in the SW Iberian Peninsula (37.1°N 6.7°W, 40 m a.s.l.). It is inside of a natural protected environment near Doñana National Park and less than 1 km from the Atlantic coastline where flight routes frequently cross over this area. ARN is managed by the Spanish Institute for Aerospace Technology (INTA), and it is also a NASA/AERONET site. The INTA/P-MPL system has been used for the first time for Ci detection over that station in order to evaluate the radiative effects of Ci clouds. Several Ci case studies observed over ARN are examined, as reference for future long-term Ci observations. Their optical and macrophysical properties are retrieved, and used for radiative transfer simulations. Data are compared to the measured surface radiation levels and all-sky images simultaneously performed at the ARN station. In addition, results can contribute to validation purposes of the next ESA’s EarthCARE mission, whose scientific goal is related to the radiation-aerosol-cloud interactions.

The P-MPL model 4B (Sigma Space Corp., USA) is an elastic lidar with a highly-pulsed (2500 Hz) and low-energy ( $\sim 7 \mu\text{J}$ ) Nd:YLF laser at 532 nm, operational in full-time continuous mode (24/7), including polarization capabilities (Flynn *et al.*, 2007). Macrophysical and optical properties of Ci clouds have been retrieved using the procedure described in Córdoba-Jabonero *et al.* (2017). Both the top and base heights and thickness, the backscattering ratio profile (BSR, total-to-molecular backscattering coefficient ratio), the linear volume depolarization ratio ( $\delta^V$ ), the Ci Cloud Optical Depth (CCOD), and their Lidar Ratio (LR) are derived. Ci clouds are also classified according to their CCOD: sub-visual (svCi, CCOD < 0.03), semi-transparent (stCi, CCOD: 0.03-0.3) and opaque (opCi, CCOD > 0.3). Surface solar radiations, Global (G), Direct (D) and Diffuse (F) components together to Erythemal effective UV (UV-Ery), were simultaneously measured at ARN and simulated by a radiative transfer model (RTM) (pseudo-spherical SDISORT code, as

described in Dahlback and Stammes, 1991) under two scenarios: (1) No Ci clouds occurrence; and (2) presence of an homogeneous layer of Ci clouds.

First, the vertical features of different Ci layers (properties, heights) together to the temperatures found at those Ci altitudes are analysed. Figure 1 shows the BSR (R) and the LVDR ( $\delta^V$ ) for a case study occurred in autumn 2016. Second, the changes experienced in the different solar components on the surface under Ci cloud occurrence are evaluated.

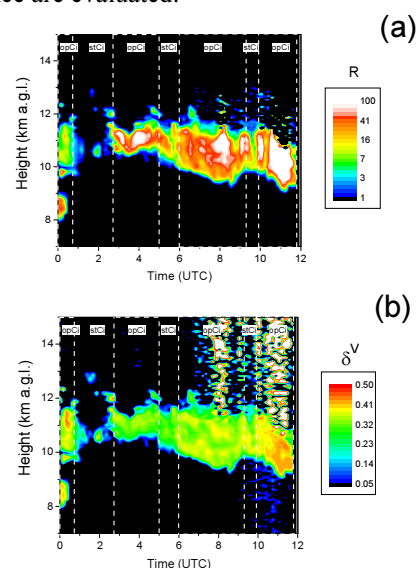


Figure 1. Temporal evolution of a Ci case observed over ARN in autumn 2016 in terms of (a) backscattering ratio (R), and (b) Linear Volume Depolarization Ratio ( $\delta^V$ ). Ci CCOD-type is also marked at the top.

This work was supported by the Spanish Ministerio de Economía y Competitividad (MINECO) under grants CGL2014-55230-R (AVATAR) and CGL2014-56255-C2-2-R (ICARO).

Córdoba-Jabonero *et al.* (2017) *Diversity on subtropical and polar cirrus clouds properties as derived from both ground-based lidars and CALIPSO/CALIOP measurements, Atmos. Res.*, **183**, 151-165.

Dahlback and Stammes (1991) *A new spherical model for computing the radiation field available for photolysis and heating at twilight, Planet Space Sci*, **39**, 671-683.

Flynn *et al.* (2007) *Novel polarization-sensitive micropulse lidar measurement technique, Optics Express*, **15** (6), 2785-2790.

## **Abstracts T205**

## Dynamics of single submicron aerosol particles measured by UV broadband light scattering and Raman spectroscopy

Grégory David, Kıvanç Esat and Ruth Signorell

Laboratory of Physical Chemistry, ETH Zurich, Vladimir-Prelog-Weg 2, CH-8093, Zurich, Switzerland

Keywords: Optical trapping, light scattering, Raman spectroscopy, efflorescence, deliquescence, photochemistry

Presenting author email: gregory.david@phys.chem.ethz.ch

Particle shape, size, refractive index, and chemical composition are key properties governing the interaction of aerosols with light and the surrounding atmosphere (Bohren and Huffman, 1983; Ghan and Schwartz, 2007; Laskin *et al.*, 2015). Single particle studies enable detailed investigations of how these properties are affected by atmospheric aging processes, such as evaporation, hygroscopic growth, phase transitions and photochemistry (Miles *et al.*, 2011; David *et al.*, 2016; Cremer *et al.*, 2016). There is considerable interest in the behavior of submicron-sized aerosol particles in the atmosphere due their enhanced aging kinetics, compared with micron-sized particles (David *et al.*, 2016; Cremer *et al.*, 2016). In this presentation, we report the first simultaneous measurements of the size, refractive index, and chemical composition of optically-trapped submicron particles. We use counter-propagating optical tweezers (CPT) to isolate a single particle in air, and combine UV broadband light-scattering (BLS) measurements with Raman spectroscopy to characterize the time evolution of the particle size, refractive index, and chemical composition. The BLS measurements provide refractive index data over the UV spectral range (from 320 to 700 nm) (David *et al.*, 2016), where such data are rare but urgently needed. This wavelength range is also crucial for sizing of submicron particles, with a lower limit of 300 nm radius. Raman spectra were collected from 200 to 3800  $\text{cm}^{-1}$ . Studies of single aqueous  $\text{K}_2\text{CO}_3$  and  $\text{NaCl}$  particles during efflorescence and deliquescence cycles show that efflorescence proceeds faster (typically < second) than deliquescence (typically several minutes) (manuscript in preparation). Using BLS, the kinetics of the efflorescence can be observed with a time resolution of 10 ms. This type of experiment will also help to improve our understanding of the photochemistry of single submicron droplets (David *et al.*, 2016).

Ghan, S. J. and Schwartz, S. E. (2007) *Bull. Am. Meteorol. Soc.* **88**, 1059-1083.

Laskin, A., Laskin, J. and Nizkorodov, S. A. (2015) *Chem. Rev.* **115**, 4335-4382.

Miles, R. E. H., Carruthers, A. E. and Reid, J. P. (2011) *Laser Photon. Rev.* **5**, 534-552.

This work was supported by the Swiss National Science Foundation (SNSF grant no. 200020\_159205) and ETH Zürich.

Bohren, C. F. and Huffman, D. R. (1983) *Absorption and Scattering of Light by Small Particles*, Wiley, New York.

Cremer, J. W., Thaler, K. M., Haisch, C. and Signorell, R. (2016) *Nat. Commun.* **7**, 10941.

David, G., Esat, K., Ritsch, I. and Signorell, R. (2016) *Phys. Chem. Chem. Phys.* **18**, 5477-5485.

## Seasonal variations of mass size distribution of carbon in atmospheric HULIS and WSOC for an urban background environment of Ljubljana, Slovenia

S. Frka<sup>1,2</sup>, I. Grgić<sup>1</sup>, J. Turšič<sup>3</sup>, M. I. Gini<sup>4</sup> and K. Eleftheriadis<sup>4</sup>

<sup>1</sup>Department of Analytical Chemistry, National Institute of Chemistry, Ljubljana, SI-1001, Slovenia

<sup>2</sup>Division for Marine and Environmental Research, Ruđer Bošković Institute, 10000 Zagreb, Croatia

<sup>3</sup>Environmental Agency of the Republic of Slovenia, 1000 Ljubljana, Slovenia

<sup>4</sup>Institute of Nuclear & Radiological Sciences & Technology, Energy & Safety, N.C.S.R. "Demokritos", 15341 Athens, Greece

Keywords: water-soluble organic carbon, humic-like substances, size distribution, biomass burning.

Presenting author email: irena.grgic@ki.si

Water-soluble organic fraction of atmospheric aerosols, usually quantified as water-soluble organic carbon (WSOC) represents a highly variable fraction (10 - 80%) of organic carbon in ambient aerosols, depending on season, location, time-of-day, and particle size. Particularly secondary organic aerosols (SOA) are associated with high levels of water-soluble organic fraction, consisting of oxidized and more soluble organic compounds, induced by photooxidation of anthropogenic or biogenic precursors (Pöschl, 2005; Ervens *et al.*, 2011).

One of the most important classes of water soluble organics extracted from atmospheric aerosols as well as isolated from fog and cloud waters has derived the term HUMic-Like Substances (HULIS) due to their physico-chemical similarities to that of natural humic matter (Graber and Rudich, 2006). Field experiments have observed HULIS in nearly all types of aerosol; the carbon fraction of HULIS (HULIS-C) in WSOC can be very variable, but generally constitutes 24-72% of WSOC (Zheng *et al.*, 2013). While size distribution of WSOC has been studied widely, the information on size distribution of HULIS is very limited (Salma *et al.*, 2013). In addition, very little is known on seasonal variations of HULIS in size-segregated ambient aerosols.

The present study is focused on the seasonal variations of size-resolved WSOC and HULIS-C in ambient aerosols collected by a ten-stage low-pressure Berner impactor at an urban background environment in Ljubljana, Slovenia. The obtained data were correlated with those of levoglucosan as a primary tracer for biomass burning emissions as well as with aerosol mass (PM) and total carbon (TC). Mass size distribution patterns of PM, WSOC and HULIS-C for all seasons, and also levoglucosan for winter and autumn were obtained as semi-smooth curves with characteristic modes. On the basis of the characteristics of HULIS-C in water soluble organic aerosol the possible sources and formation mechanisms will be discussed.

As shown in Figure 1 the mass size distribution of HULIS-C in winter was bimodal, with a clear ultrafine mode and a dominant accumulation mode with 97% contribution to the total HULIS-C concentration. For autumn, the distribution of HULIS-C consisted of three modes, and was nearly the same as for WSOC with almost the same MMADs (mass median aerodynamic diameters) and also the same contributions to each mode,

i.e. 7% to ultrafine, 83% to accumulation and 10% to coarse mode. The very similar size distributions of measured species (WSOC, HULIS-C, levoglucosan) indicate their common source, and since levoglucosan is a specific tracer for biomass burning we can conclude that biomass burning during colder seasons was the main contributor to both WSOC and HULIS-C in fine aerosols.

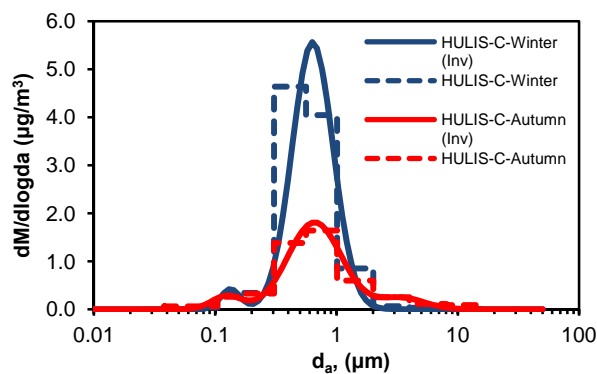


Figure 1. Mass size distributions of carbon in water-soluble humic-like substances (HULIS-C) in aerosols from an urban background site in Ljubljana, Slovenia for winter and autumn 2015.

-- Berner impactor data with mass concentration measured at every stage; — inverted size distributions by the Micron algorithm.

This work was supported by the European Commission and the Croatian Ministry of Science, Education and Sports through Marie Curie FP7-PEOPLE-2011-COFUND, project NEWFELPRO and by the Slovenian Research Agency (Contract no. P1-0034-0140).

Pöschl, U. (2005) *Angew. Chem. Int. Edit.* **44**, 7520-7540.

Ervens, B., Turpin, B.J. and Weber, R.J. (2011) *Atmos. Chem. Phys.* **11**, 11069-11102.

Graber, E. R. and Rudich, Y. (2006) *Atmos. Chem. Phys.* **6**, 729-753.

Zheng, G., He, K., Duan, F., Cheng, Y., Ma, Y. (2013) *Environ. Pollut.* **181**, 301-314.

Salma, I., Mészáros, T. and Maenhaut, W. (2013) *J. Aerosol Sci.* **56**, 53-60.

## Black Carbon and particle number concentrations from a large and uncontrolled combustion of a tire landfill

F. J. Gómez-Moreno<sup>1</sup>, B. Artíñano<sup>1</sup>, E. Díaz<sup>1</sup>, E. Alonso-Blanco<sup>1</sup>, E. Coz<sup>1</sup>, M. Becerril-Valle<sup>1</sup>,  
B. L. van Drooge<sup>2</sup>

<sup>1</sup> CIEMAT, Environment Department. Associated Unit to CSIC on Atmospheric Pollution, Madrid, Spain

<sup>2</sup> Institute of Environmental Assessment and Water Research, IDAEA-CSIC, 08034 Barcelona, Spain

Keywords: Black Carbon, particle number concentration, tire landfill.

Presenting author email: fj.gomez@ciemat.es

A very large and uncontrolled fire was declared in an abandoned tire landfill on 13 May 2016. This landfill was located in Seseña, a small town (21,500 inhabitants) 40 km South of Madrid. According to the available data, the landfill had over 100,000 tons of tires. National authorities estimated that the fire was extinct on 7 June.

Once the fire started, an emergency plan was activated including the assessment on how reducing the impact of emissions on the exposed population. The first line of buildings (El Quiñón, EQ) is located at 300 m distance of the tire landfill, becoming the most threaten community due to its proximity to the fire and prevailing winds.

Measurements for air quality were performed at the EQ School, located 700 m East of the tire landfill in a classroom approximately 3 meters high from 20 May to 3 June 2016. Particle number concentrations were measured by a TSI CPC3772 in the range of 10 nm and 1  $\mu\text{m}$  and a TSI CPC3775 instrument in the range of 4 nm and 1  $\mu\text{m}$ . Equivalent Black Carbon (eBC) concentrations were obtained by two aethalometers. A multi-wavelength aethalometer (Magee Sci. mod. AE33, Aerosol d.o.o) ( $\lambda = 370, 470, 520, 590, 660, 880,$  and  $950 \text{ nm}$ ) with a cut-off size of  $10 \mu\text{m}$  and a flow rate of  $5 \text{ Lmin}^{-1}$  was installed outside the EQ School. Data were recorded automatically every minute from 17 May to 17 June 2016. A Microaethalometer (microAeth® model AE51, Magee Scientific) at  $\lambda = 880\text{nm}$  and a cut-off size of  $2.5 \mu\text{m}$  was also used. The flow rate was  $0.1 \text{ Lmin}^{-1}$  and the sampling time 300 seconds. This last instrument was used to measure at several points around the experimental area in a dynamic pattern by moving it around and measuring at a mean adult height respiration level. These rounds lasted between 90 and 120 minutes, remaining between 5 and 15 minutes in every point, for a total length of 2 km.

The highest values obtained for both groups of instruments (CPC and aethalometers) coincided with the direct impact of the plume at the site, as the prevailing wind direction was from the tire landfill.

The particle number concentration measured outdoor the EQ School reached rather high ambient air values. During more than 60% of the measurement period the concentration of particles was always above  $1.0 \times 10^4 \text{ cm}^{-3}$ , with maximum hourly values of  $3.2 \times 10^5 \text{ particles cm}^{-3}$  on 28 May. These concentration levels are much higher than those recorded in urban areas like Madrid (Gómez-Moreno et al., 2011), even during winter pollution episodes, or Barcelona (Pérez et al., 2010). The observed values were closer to those

observed in industrial environments (Fernández-Camacho et al., 2012) due to the proximity to the emission sources.

The prevailing wind direction was the determining factor explaining the high concentrations observed in the transects performed with the Microaethalometer in EQ (Figure 1). Despite the fact that points 8 and 10 were protected by the surrounding buildings, the highest eBC concentrations were measured in these points when the plume directly impacted them. Similar behaviour was observed in the Magee aethalometer data outside the school.

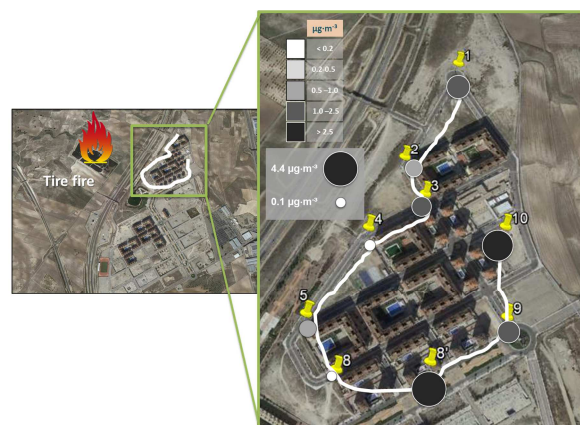


Figure 1. eBC measurements performed by the Magee AE51 on May 24 between 16:55 and 19:45. The values given are mean values of the measurement period, 5 to 15 minutes. The Magee AE33 was located in point 10.

This work was supported by the Spanish Ministry of Science and Innovation (PROACLIM Project CGL2014-52877-R).

Gómez-Moreno, F.J., Pujadas M., Plaza J., Rodríguez-Maroto J., Martínez-Lozano P. and Artíñano B. (2011) *Atmos. Environ.* **45**, 3169-3180.

Pérez, N., Pey J., Cusack M., Reche C., Querol X., Alastuey A. and Viana M. (2010) *Aerosol Sci. Tech.* **44**, 487-499.

Fernández-Camacho, R., Rodríguez S., De la Rosa J., de la Campa A. S., Alastuey A., Querol X., González-Castanedo Y., García-Orellana I. and Nava S. (2012) *Atmos. Environ.* **61**, 507-517.

## One year of on-line chemistry measurements of the non-refractory submicron aerosol at the Puy de Dome with an emphasis on air mass transport, free troposphere / boundary layer conditions, and organic aerosol sources

A. Farah<sup>1</sup>, E. Freney<sup>1</sup>, J. Nicolas<sup>1</sup>, M. Abboud<sup>2</sup>, W. Farah<sup>2</sup> and K. Sellegri<sup>1</sup>

<sup>1</sup> Laboratoire de Météorologie Physique, UMR6016, Université Clermont Auvergne-CNRS, 4 avenue Blaise Pascal, 63118, Aubière, France

<sup>2</sup> Unité de Recherche EGFEM, Faculté des Sciences, Université Saint Joseph, Beyrouth, Liban.

**Keywords:** Aerosol Mass Spectrometry, High altitude site, Long range transport, Boundary Layer/Free Troposphere.

Presenting author email: a.farah@opgc.univ-bpclermont.fr

Continuous chemical properties of non-refractory submicron (NR-PM<sub>1</sub>) aerosol particles were performed at the Puy-de-Dôme (PUY) research station (1465 m) from 01 April 2015 to 29 February 2016 using a time-of-flight aerosol chemical speciation monitor (ToF-ACSM) (Fig. 1) (Fröhlich et al., 2015). This instrument allows us to assess the changing chemical properties of the aerosol and how it is influenced by air mass type.

This work presents an overview of this year long data set, combining aerosol chemistry measurements with simultaneous measurements of aerosol size and optical properties.

Besides total mass concentrations, seasonal variations and relative species contributions during the different meteorological seasons, geographical origin and sources of organic aerosol (OA) are discussed. Results shows that the average mass concentrations of the non-refractory submicron particles ranged from 1  $\mu\text{g m}^{-3}$  up to 9  $\mu\text{g m}^{-3}$ . Highest nitrate and ammonium mass concentrations were measured during the winter and during periods when marine modified airmasses were arriving at the site, whereas highest concentrations of organic particles were measured during the summer and during periods when continental airmasses arrived at the site. OA source apportionment for each season was performed using positive matrix factorization to separate individual organic components contributing to the overall organic particle mass concentrations. Additionally, the data were divided into periods with free tropospheric (FT) conditions and periods with boundary layer (BL) influence, enabling the assessment of the composition for each.

Two cases of studies were chosen in both the winter and summer to study in more detailed the diurnal variations and the interaction of aerosol particles with gas-phase species.

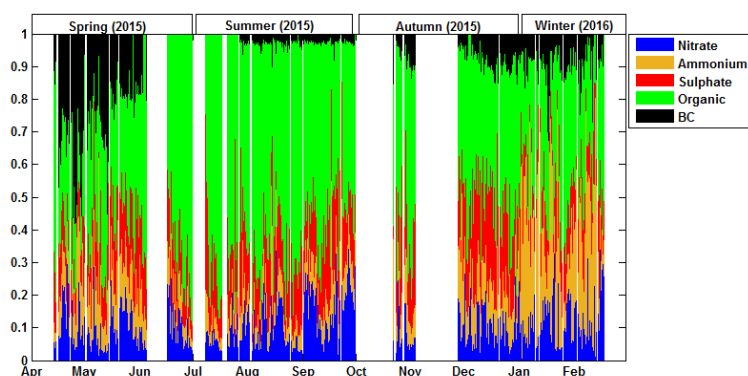


Figure 1. Time series of relative organic (green), sulfate (red), nitrate (blue), and ammonium (orange) contributions to the total PM<sub>1</sub> aerosol measured by the ToF-ACSM and the BC (black) concentration time series measured by the MAAP 5012 from April 2015 to February 2016.

This work was supported by the European Research Infrastructure for the observation of Aerosol, Clouds, and Trace gases (ACTRIS2) and the research council of the Saint Joseph University.

Fröhlich, R., Cubison, M. J., Slowik, J. G., Bukowiecki, N., Canonaco, F., Croteau, P. L., Gysel, M., Henne, S., Herrmann, E., Jayne, J. T., Steinbacher, M., Worsnop, D. R., Baltensperger, U. and Prévôt, A. S. H.: Fourteen months of on-line measurements of the non-refractory submicron aerosol at the Jungfraujoch (3580 m a.s.l.) – chemical composition, origins and organic aerosol sources, *Atmos Chem Phys*, 15(19), 11373–11398, doi:10.5194/acp-15-11373-2015, 2015.

## Light extinction estimates using the IMPROVE algorithm: The relevance of site-specific coefficients.

S. Valentini<sup>1</sup>, V. Bernardoni<sup>1</sup>, D. Massabò<sup>2</sup>, P. Prati<sup>2</sup>, G. Valli<sup>1</sup> and R. Vecchi<sup>1</sup>

<sup>1</sup>Department of Physics, Università degli Studi di Milano & INFN-Milan, Milan, 20133, Italy

<sup>2</sup>Department of Physics, University of Genoa & INFN-Genoa, Genoa, 16146, Italy

Keywords: light extinction, visibility, IMPROVE algorithm.

Presenting author email: sara.valentini@unimi.it

Atmospheric aerosol and gases affect visibility by scattering and absorbing the incoming radiation (Watson, 2002; Pitchford *et al.*, 2007). While the role of gases is relatively well understood, the effect of particulate matter (PM) is more complicated to be assessed since it depends on several factors such as particles size distribution and chemical composition as well as meteorological parameters (e.g. relative humidity – RH).

The U.S. Interagency Monitoring of Protected Visual Environments (IMPROVE) network proposed a method to retrieve atmospheric light extinction coefficient ( $b_{\text{ext}}$ ,  $\text{Mm}^{-1}$ ) in national parks from compositional and meteorological data (Malm *et al.*, 1994; Watson, 2002). The result of this approach (often called chemical light extinction) allows the evaluation of visibility indicators such as visual range (VR) via the Koschmieder equation  $\text{VR}=3.912/b_{\text{ext}}$ .

In this study we tailored the IMPROVE equation using site-specific dry mass extinction efficiencies and hygroscopic growth functions in order to obtain  $b_{\text{ext}}$  estimates which better reflect the typical atmospheric characteristics of the sampling site and period. The revised formulation was tested for the first time in the urban area of Milan, for two weeks during the winter season in 2015. Moreover, it was applied to a large and fully characterized dataset referred to  $\text{PM}_{10}$  samples collected in winter 2012.

Following the IMPROVE algorithm (Malm *et al.*, 1994; Watson, 2002; Pitchford *et al.*, 2007) the chemical light extinction equation used in this work was:

$b_{\text{ext}} = k_1 \times f_1(\text{RH}) \times [\text{AMSUL}] + k_2 \times f_2(\text{RH}) \times [\text{AMNIT}] + k_3 \times f_3(\text{RH}) \times [\text{OM}] + k_4 \times [\text{fine soil}] + b_{\text{ap}} + 0.60 \times [\text{coarse mass}] + 0.33 \times [\text{NO}_2] \text{ (ppb)} + \text{Rayleigh scattering}$ , where inputs are the concentrations of the five major PM components (ammonium sulphate - AMSUL, ammonium nitrate - AMNIT, organic matter - OM, fine soil, coarse mass) in  $\mu\text{g m}^{-3}$ ,  $\text{NO}_2$  concentration (in ppb), Rayleigh scattering by gases ( $\text{Mm}^{-1}$ ) and aerosol light absorption coefficient ( $b_{\text{ap}}$ ,  $\text{Mm}^{-1}$ ) measured with a home-made polar photometer on PTFE filters.

Dry mass extinction efficiencies ( $k_1$ - $k_4$ ,  $\text{m}^2 \text{g}^{-1}$ ) for every chemical component of interest were calculated considering size distributions measured in Milan (Vecchi *et al.*, 2012), particles densities and complex refractive indices (Watson, 2002). Furthermore, hygroscopic growth functions  $f_i(\text{RH})$ , defined as the ratios between ambient and dry aerosol scattering coefficients ( $b_{\text{sp}}$ ), were also calculated (using hygroscopic growth factors taken from the literature) and were applied to those PM components (AMSUL, AMNIT and OM), whose  $b_{\text{sp}}$  are enhanced by

their water uptake at medium-high RH values. It is worthy to note that in the original IMPROVE algorithm (Malm *et al.*, 1994; Watson, 2002) the hygroscopic growth function  $f(\text{RH})$  is calculated referring only to AMSUL hygroscopic properties and it is applied also to AMNIT, whereas OM is considered as non-hygroscopic.

Non-negligible discrepancies were found between tailored dry mass extinction efficiencies and the original IMPROVE ones. Furthermore, differences between calculated  $f_i(\text{RH})$  and IMPROVE hygroscopic growth function were found.

The methodology here described was applied to a  $\text{PM}_{10}$  dataset thus retrieving the extinction contribution given by the different  $\text{PM}_{10}$  components as well as by the major aerosol sources. Both methodological and experimental results will be shown in the presentation.

This work shows that – due to the large variability in size distributions and aerosol composition at sites with different characteristics (e.g. urban, industrial, rural) – it is advisable to calculate site-specific  $k_1$ - $k_4$  and  $f_i(\text{RH})$  coefficients instead of using the original IMPROVE ones, which refer to aerosol properties measured at U.S. national parks.

Malm, W.C., Sisler, J.F., Huffman, D., Eldred, R.A. and Cahill T.A. (1994) *J. Geophys. Res.* **99**, 1347-1370

Pitchford, M., Malm, W., Schichtel, B., Kumar, N., Lowenthal, D. and Hand, J. (2007) *J. Air & Waste Manage. Assoc.* **57**, 1326-1336.

Watson, J.G. (2002) *J. Air & Waste Manage. Assoc.* **52**, 628-713

Vecchi, R., Bernardoni, V., Bigi, A., Elser Fritsche, M., Fermo, P., Ghermandi, G., Piazzalunga, A., Gonzales Turrion, R., Urbani, M., Valli, G. (2012) *Ultrafine particles and  $\text{PM}_{10}$  measurements in a hot-spot pollution area: size distribution, mass closure and source apportionment. European Aerosol Conference EAC2012, Granada, 2-7 Sept. 2012*

## Combined Measurements of the Physicochemical, Optical and Dynamic Properties of Single Secondary Organic Aerosol (SOA) Particles

J. P. Reid<sup>1</sup>, G. Rovelli<sup>1</sup>, Y. C. Song<sup>1</sup>, K. L. Pereira<sup>2</sup>, J. F. Hamilton<sup>2</sup> and D. O. Topping<sup>3</sup>

<sup>1</sup>School of Chemistry, University of Bristol, BS8 1TS, UK

<sup>2</sup>Wolfson Atmospheric Chemistry Laboratories, Department of Chemistry, University of York, YO10 5DD, UK

<sup>3</sup>School of Earth, Atmospheric and Environmental Science, University of Manchester, M13 9PL, UK

Keywords: secondary organic aerosol, hygroscopicity, volatility, refractive index.

Presenting author email: chjpr@bristol.ac.uk

Secondary Organic Aerosols (SOA) formed from the atmospheric processing of Volatile Organic Components (VOCs) can account for a substantial fraction of the total aerosol mass (Fuzzi et al., 2015). Our understanding of the impact of SOA on atmospheric processes, such as cloud droplet formation and the interaction with solar radiation, can greatly benefit from an accurate characterisation of the physicochemical properties of the SOA and the dynamical processes that lead to their variation. In this work, we will present a single particle approach to *simultaneously characterise*: the equilibrium hygroscopic response of an SOA aerosol sample; the relative humidity (RH) dependence of the optical properties (refractive index, RI); the volatility distribution of semi-volatile organic components (SVOCs); and the kinetic factors regulating gas-particle partitioning of water and SVOCs.

In particular, we will present measurements of the properties for  $\alpha$ -pinene and toluene SOA extending over wide ranges in RH (<10 % to >99.5%) and temperature (-25 to 50 °C). SOA samples are generated in a photochemical flow reactor (300 L polyvinyl fluoride bag, controlled T and RH) from the oxidation of different VOCs precursors, such as  $\alpha$ -pinene and toluene. Known variable VOC, NO<sub>x</sub> and ozone concentrations are introduced in the chamber and UV irradiation is performed with an Hg pen-ray. SOA samples were collected with an electrical low pressure impactor, wrapped in aluminum foil and kept refrigerated at -20°C. SOA samples are fully extracted in a 1:1 water/ethanol mixture. Single charged SOA solution droplets are confined within an Electrodynamic Balance (EDB) in a N<sub>2</sub> gas flow with controlled temperature and RH. Each single confined droplet is illuminated by laser light (532 nm) and the resulting evolving light scattering pattern is collected and fitted with a library of Mie-Theory simulations (Cotterell et al., 2015) to monitor variations in the radius and the refractive index of the droplet.

The evaporation of single trapped SOA solution droplets can be observed at different RHs and temperatures. From the initial fast water evaporation (steep radius change in Figure 1, 20 °C) the equilibrium hygroscopic properties can be retrieved according to the comparative kinetics method described in Rovelli et al. (2016) up to RH>99.5 %). Secondly, a slower evaporative loss is observed afterwards and is due to the loss of SVOCs (see the inset in Figure 1). Long trapping experiments (up to >20000 s)

allow the observation of the kinetics of SVOCs evaporation at different temperatures and RHs. An increase in the refractive index can be observed over time as the water activity in the droplet changes (Figure 2, same droplets as Figure 1). A slower but significant change in refractive index arises during the slow evaporation as the composition of the droplet changes in time due to the loss of SVOCs. In addition, condensation/evaporation kinetics of water onto/from single SOA droplets can be observed following a fast step change in RH (< 0.5 s) with the aim of evaluating kinetics limitations to water diffusion in the condensed phase resulting from the likely formation of a viscous matrix at low RH and temperatures.

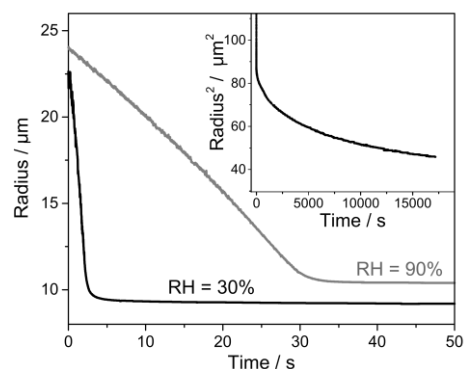


Figure 1. Evolution of radius of two SOA droplets evaporating in 90% and 30% RH (T=20 °C).

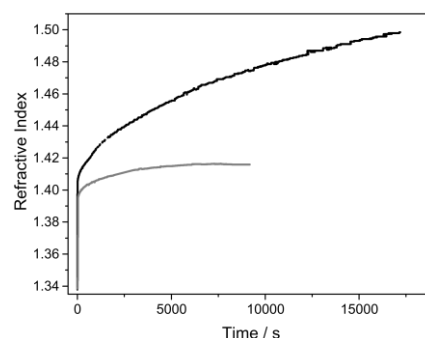


Figure 2. Evolution of refractive index of two SOA droplets evaporating in 90% and 30% RH (T=20 °C).

Cotterell et al., Phys. Chem. Chem. Phys. 17, 15843–15856 (2015).

Fuzzi et al., Atmos. Chem. Phys. 15, 8217–8299 (2015).

Rovelli et al., J. Phys. Chem. A 120, 4376–4388 (2016).

## Atmospheric aerosol and CCN properties in Dronning Maud Land, East Antarctica

A. Mangold<sup>1</sup>, Q. Laffineur<sup>1</sup>, H. De Backer<sup>1</sup>, V. De Bock<sup>1</sup>, A. Delcloo<sup>1</sup>, C. Hermans<sup>2</sup>, C. Gielen<sup>2</sup>, P. Herenz<sup>3</sup>, and H. Wex<sup>3</sup>

<sup>1</sup>Royal Meteorological Institute of Belgium, Brussels, Belgium; <sup>2</sup>Royal Belgium Institute for Space Aeronomy, Brussels, Belgium; <sup>3</sup>Leibniz Institute for tropospheric research, TROPOS, Leipzig, Germany

Keywords: Antarctica, atmospheric aerosol, aerosol optical properties, CCN

Presenting author email: alexander.mangold@meteo.be

Aerosols attenuate, scatter and absorb solar radiation, influencing in this way the temperature at the surface and within the atmosphere. Also, they influence the formation, properties and lifetime of clouds by acting as cloud condensation and ice nuclei. In this presentation, results of aerosol and cloud condensation nuclei (CCN) measurements will be shown with a focus on seasonality. Also, the influence of air mass origin will be analysed.

Since 2010, several complementary ground-based instruments for the monitoring of the composition of the Antarctic atmosphere and of the monitoring of meteorology, radiation, clouds, and precipitation have been operated at the Belgian Antarctic research station Princess Elisabeth. The station is situated about 180 km inland from the coast, near the Sør Rondane Mountains in Dronning Maud Land, East Antarctica (71.95° S, 23.35° E, 1390 m asl; Pattyn *et al.*; 2010). The station is inhabited from November until end of February.

Measured properties comprise aerosol size distribution, total aerosol number, total aerosol mass concentration, absorption coefficient and mass concentration of light-absorbing aerosols and total scattering coefficient. All instruments have been installed for continuous operation, including austral winters. Meteorological data come from an automatic weather station (Gorodetskaya *et al.*, 2013).

Besides these instruments, a sunphotometer (aeronet.gsfc.nasa.gov; 'Utsteinen') provides total aerosol optical depth (AOD) during austral summer since February 2009. In December 2015, a MAX-DOAS (multi-axis differential optical absorption spectroscopy) instrument has been installed. It enabled to retrieve the aerosol extinction and concentration of atmospheric trace gases in a few layers above the surface and their respective total column amounts. In addition, a cloud condensation nuclei counter (CCNc) has been operated in austral summers 2013/14, 2014/15, and 2015/16.

The mean mass concentration of light-absorbing particles is shown in Figure 1 (in ng/m<sup>3</sup>; at 660 nm) for years 2011 to 2016. Values peak during austral summer and are hardly above zero during winter. Respective values at 370 nm are consistently somewhat higher.

A Condensation Particle Counter measured aerosol total number concentration ( $N_{total}$ ) in the diameter range 3 to 3000 nm. Figure 2 shows data from December 2012 until April 2016.  $N_{total}$  showed a clear seasonal cycle with some hundreds of particles/cm<sup>3</sup> during austral summer and some tens of particles/cm<sup>3</sup> during winter. Mostly in summer,  $N_{total}$  increased to some thousands of particles/cm<sup>3</sup> during short periods (hours to one day).

Simultaneous measurements of  $N_{total}$ , size distribution (measured in 100 channels between 90 and 7000 nm) and CCN number ( $N_{CCN}$ ) revealed that then almost only the number of particles smaller than 90 nm increased.

The analysis of the hygroscopicity parameter derived from size distribution and  $N_{CCN}$  measurements showed a range between 0.5 and 1.2 at supersaturations of 0.1 %, with slight inter-annual variations. Mean values were 0.8 for summer 2013/14 and 0.9 for summer 2015/16.

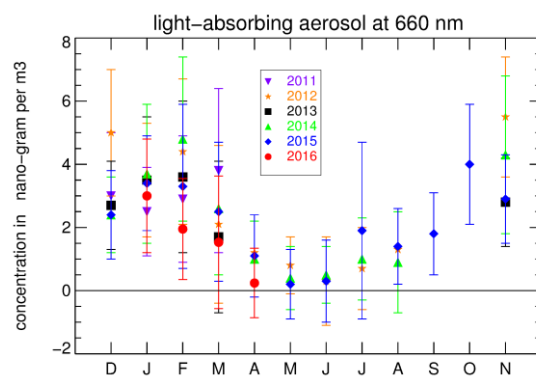


Figure 1: monthly means ( $\pm$  standard deviation) of mass concentration of light-absorbing aerosol

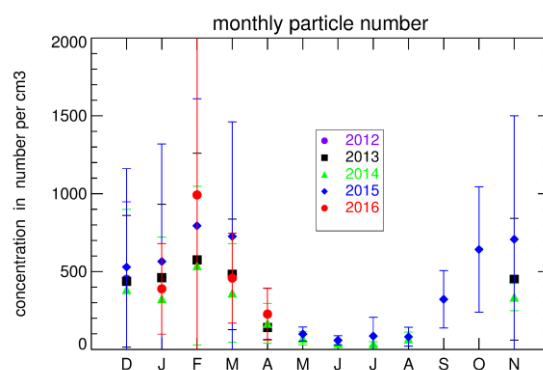


Figure 2: monthly means ( $\pm$  standard deviation) of total aerosol number concentration

This work was supported by the Belgian Federal Science Policy under grant BR/143/A2/AEROCLOUD.

Gorodetskaya, I. V., Van Lipzig, N. P. M., Van den Broeke, M. R., Mangold, A., Boot, W. and C. H. Reijmer (2013), *J. Geophys. Res. Atmos.*, **118**, doi:10.1002/jgrd.50177.

Pattyn, F., Matsuoka, K. and Berte, J. (2010), *Antarctic Science*, **22**(1), 79-85.

## Mass closure for particle size distribution measurements

H. Flentje<sup>1</sup> and B. Briel<sup>1</sup>

<sup>1</sup>Deutscher Wetterdienst DWD, Hohenpeißenberg, 82383, Germany

Keywords: size distribution, mass closure, quality assurance

Presenting author email: harald.flentje@dwd.de

Particle size distributions PSD based on unlike physical measurement principles may exhibit inconsistencies when the ambient aerosol differs from the standard particles used during calibrations. Namely, optical and aero-dynamical sizing depend on unrelated refractive and drag properties of particles, causing deviations between individual spectra. On longer term, however, they may compensate, a premise to certify techniques for bulk quantities like mass concentration PM. Actually, large discrepancies were found between size spectra from optical particle sizers (OPS) and scanning mobility particle sizers (SMPS), Wiedensohler et al. (2012), during inter-comparison experiments ([www.actris.eu](http://www.actris.eu)).

The consistency of PSD and the relation of their moments to other measurements of total number and PM constitute a primary quality control for size spectra. Here, data obtained with a GRIMM-OPC, a TROPOS-SMPS, a SHARP beta-absorption mass monitor (Thermo Sci.) and a condensation particle counter CPC (TSI) at the Global Atmosphere Watch (GAW) station Hohenpeißenberg are compared. The station is located on a hill in rural environment in Southern Germany, surrounded by grassland and forests, c.f. Flentje et al. (2015).

Preliminary results for mass-concentrations are summarized in table 1. They show that generally larger PM are inferred from combined SMPS and OPS spectra than observed with the SHARP instrument. Thereby, densities increasing from 1.6 – 2.6 g/cm<sup>3</sup> towards large particles have been used. Possible reasons for the deviations, like calibration, inlet, losses, volatility, particle density as well as corrections will be discussed. For this, we will also refer to comparisons between different mass concentration measurements, namely tapered element oscillation microbalance (TEOM/TEOM-FDMS) instruments and SHARP.

Table 1. Slope of linear fit and correlation of mass concentrations inferred from combined SMPS+OPS size distributions w.r.t. SHARP mass monitor, 2012-2016.

	Linear Fit	Correlation.
2012	1.27	0.8
2013	1.46	0.76
2014	1.47	0.82
2015	1.46	0.83
2016	(1.44)	(0.78)

The size ranges of SMPS (0.01 – 0.9  $\mu$ m) and OPS (0.25-30  $\mu$ m) overlap between 0.25 and 0.9  $\mu$ m (Fig. 1). After correction of the two lowest channels of

the OPS, the monthly median PSD match well in this size region. The OPS shows a stronger slope towards coarse particles. Individual spectra, however, deviate substantially from each other, depending on the type of aerosol.

Fig. 1 also illustrates that the contributions to the mass concentration from the coarse mode may be much higher than from the fine mode in case of Saharan dust events like around 20 December 2015. The accurate sizing thus is a critical prerequisite for correct mass assignments, particularly in case of absorbing or irregularly shaped particles.

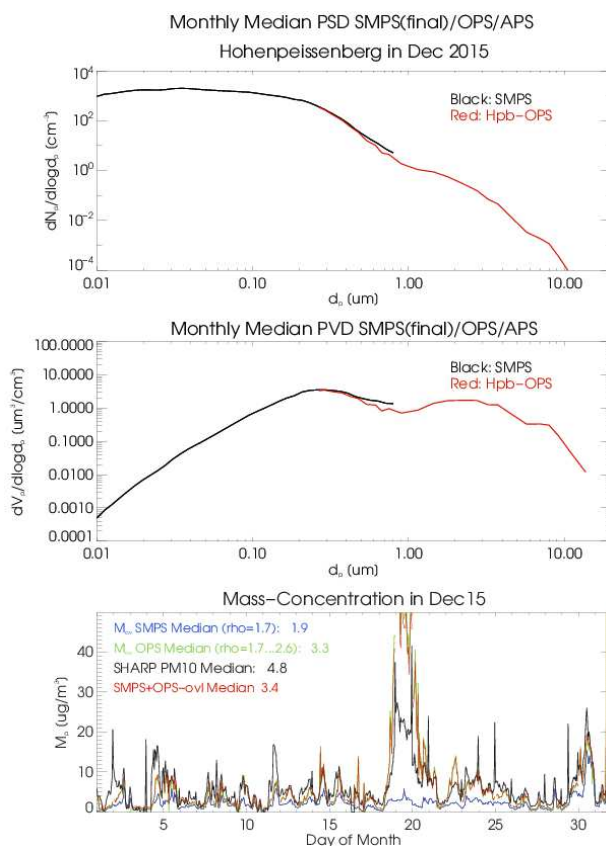


Figure 1. Monthly median size and volume distributions of  $dN/d\log d$  (top panel),  $dV/d\log d$  (mid-panel) and estimated mass concentrations (bottom) for Dec 2015.

Flentje et al., (2015), *Atmospheric Environment*, 109, 87-96.

Wiedensohler et al, (2012), *Atmos. Meas. Tech.*, **5**, 657–685.

## PROBING STRUCTURE AND CHEMICAL PROPERTIES OF FREESTANDING CLUSTERS WITH SYNCHROTRON RADIATION

N.L. Prisle<sup>1</sup>, J. Malila<sup>1,2</sup>, K. Jänkälä<sup>1</sup>, M. Patanen<sup>1</sup>, and M. Huttula<sup>1</sup>

<sup>1</sup>Nano and Molecular Systems Research Unit, University of Oulu, Oulu, 90014, Finland

<sup>2</sup>Department of Applied Physics, University of Eastern Finland, Kuopio, 70211, Finland

Keywords: Synchrotron radiation, free nanoclusters, surface structure, atmospheric composition.  
Presenting author email:Marko.Huttula@Oulu.fi

Despite intensive laboratory and field measurements, dating back over a century ago, molecular details of formation and growth of new atmospheric particles remain elusive. As changes in new particle formation and growth rates can affect global concentrations of cloud condensation nuclei, thus contributing to anthropogenic radiative forcing (Merikanto et al., 2009), a mechanistic understanding of these processes, including phase and surface properties of newly formed particles, is vital for reducing uncertainties in climate forecasts. Deductions based on indirect measurements have proven inconclusive (Kupiainen-Määttä et al., 2014), and recently there has been a surge towards measurements setups yielding molecular-level resolution of cluster properties.

Surfaces in particular are currently moving into the spotlight of the atmospheric science community. A suite of novel developments in methods originating from materials science now allow for highly surface sensitive chemical characterization of systems with increasing resemblance to atmospheric aerosols. Here, we present a custom-built experimental setup to produce and directly characterize chemical, structural, and phase-state properties of freestanding neutral multicomponent nanoclusters with well-defined composition, using synchrotron radiation based spectroscopy at the gas-phase endstation of the FinEstBeaMS beamline, MAX IV Laboratory. The unsurpassed brightness of the new MAX IV synchrotron light source has made feasible the use of powerful surface sensitive photoelectron spectroscopy techniques for samples of relatively low density, and in particular freestanding cluster beams of atmospherically relevant trace components.

The custom-built Multiuse Setup for Clusters Emission (MUSCLE) for producing and introducing freestanding nanoparticles to the synchrotron beam is shown in Figure 1. MUSCLE is our next generation cluster source based on the proven basic design of the Exchange Metal Cluster (EXMEC) source (Huttula et al., 2010). Both setups generate a continuously renewed beam of neutral clusters comprising a wide range of atomic, molecular or ionic components. MUSCLE and EXMEC share the same principles of operation. In the first stage, clusters are generated by letting a gas-phase substance or mixture pass through a converging-diverging nozzle into vacuum. In the second (pick-up) stage, the initially produced (host) clusters are doped with a controlled amount of some other substance to produce a mixed cluster. Taken to extreme, the initial host cluster can be completely converted to a cluster made up purely of the

dopant substance, which is referred to as the exchange method. Using this setup, we have generated clusters of e.g. aqueous alkali halides with controlled composition (Hautala et al., 2016) and semi-volatile atmospheric organics, like stearic acid (unpublished data). Using this setup, we have e.g. observed size-dependent structural phase transitions for CsBr clusters (Hautala et al., 2016).

The novelty of our approach lies in the combination of PES and other SR spectroscopic techniques that provide direct, genuine molecular level information, with cluster production capable of changing cluster properties (e.g. size and composition) in a systematic and controlled manner. This allows for additional degrees of freedom in experiments, to study how specific changes affect the overall cluster properties. To our knowledge, there are currently no or few setups capable of providing detailed information of the phase and mixing state of clusters in the full size range we are exploring, without relying on indirect estimations based e.g. nucleation theorems.

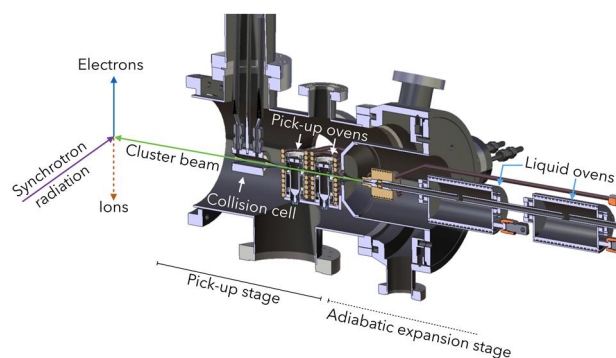


Figure 1. Main operational parts of next generation cluster source MUSCLE (Multiuse Setup for Clusters Emission).

This project has received funding from the European Research Council (ERC) under the European Union's Horizon 2020 research and innovation programme (grant agreement No 717022). The authors also acknowledge the financial contribution from the Academy of Finland.

Merikanto, J. *et al.* (2009). *Atmos. Chem. Phys.*, **9**, 8601-8616.

Kupiainen-Määttä, O., *et al.* (2014). *J. Aerosol Sci.*, **77**, 127-144.

Huttula, M. *et al.* (2010). *J. Electron Spectroscopy and Related Phenomena*, **181**, 145.

Hautala, L. *et al.* (2016). *Phys. Rev. B*, **95**, 45402.

## Heterogeneous Ice Nucleation from MD Simulations

M. Lbadaoui-Darvas<sup>1</sup>, S. Takahama<sup>1</sup>

<sup>1</sup>Atmospheric Particle Research Laboratory, EPFL, 1015 Lausanne, Switzerland  
Presenting author email: maria.lbadaoui-darvas@epfl.ch

Understanding how ice clouds are formed in the atmosphere is important for predicting the hydrologic cycle and radiative forcing in a changing climate system. Atmospheric aerosols provide surfaces which facilitate formation of ice particles from a supersaturated vapor phase, or supercooled aqueous droplet. However, our capability for prediction of heterogeneous ice nucleation in such systems are hindered by our lack of knowledge regarding detailed interfacial mechanisms of aerosol-water interactions. Furthermore, the morphology and composition of aerosol surfaces can be both diverse and complex on account of the various emission sources of particles, surface imperfections, and the subsequent transformations that occur within the photochemistry of the atmosphere.

In this work, we use molecular dynamics simulation to investigate the phenomena of ice nucleation on aerosol surfaces, as this computational technique is able to access the small physical length and time scales which are difficult to obtain otherwise by experimentation. We built a number of virtual surfaces which mimic those of atmospheric aerosols, and study their propensity for ice particle formation via different nucleation modes using this simulation tool to provide insight into underlying mechanisms that can form the basis of future models of heterogeneous ice nucleation.

We study in particular the free energy of deposition nucleation and the effect of the structure (lattice match) and chemical nature of the solid surface on CCN efficiency, from thermodynamic integration. We compare free energies immersion and deposition freezing, on pure and coated black carbon, mineral dust (SiO<sub>2</sub> and Al<sub>2</sub>O<sub>3</sub>). On the other hand we use metadynamics to obtain detailed information about the mechanism of ice crystal formation near the above mentioned solid surfaces in the immersion mode. This method proved to be equally successful in studying homogeneous and heterogeneous nucleation of ice and other crystals. By its nature, metadynamics is able to detect high dimensional subspaces of the phase space and thus can provide detailed information about the mechanism of ice nucleus formation. In other words choosing more than one collective variable for accelerating our simulation will

provide us with detailed free energy landscape that allows us to detect nucleation pathways and estimate their relative contribution to the total nucleation rate. The success story of this method is preceded by several recent studies. We adopted the use of the local Q6 and Q4 variables together with the potential energy to drive our simulations.

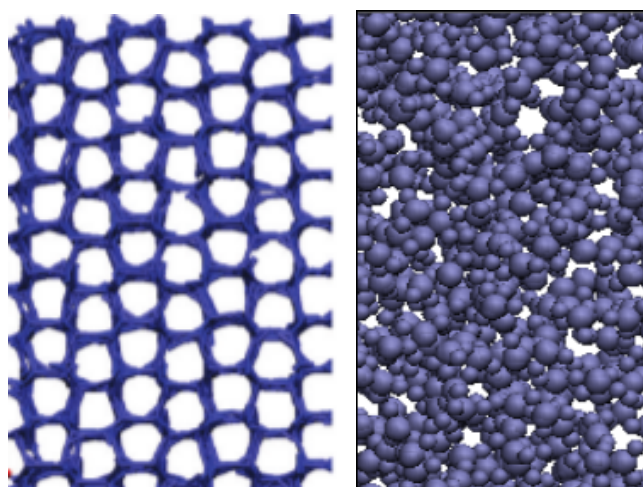


Figure 1. Illustration of hexagonal ice (left) and water (right) taken from MD simulations. The images were taken from Darvas et. al. *Langmuir*, (2012) And Darvas et. al. *J. Phys. Chem. C*, (2011) respectively

D.Quigley and P.M. Rodger, *J. Chem. Phys.*, (2008) **128**,154518.

D.Quigley and P.M. Rodger, *Mol. Sim.*, (2009) , **35** Inst Phys Publishing; Taylor and Francis.

Tribello G. et. al. *J. Chem. Theory Comput.*,DOI: 10.1021/acs.jctc.6b01073.

Sosso, G. C. et al. *Chem. Rev.*, (2016), **116** 7078–7116.

## Identifying the main sources of brown carbon in the atmosphere

I. El Haddad<sup>1</sup>, N. Kumar<sup>1</sup>, K. Daellenbach<sup>1</sup>, C. Bozzetti<sup>1</sup>, J. Corbin<sup>1</sup>, D. Massabò<sup>2</sup>, E. Brun<sup>1</sup>, A. Vlachou<sup>1</sup>, J. G. Slowik<sup>1</sup>, P. Prati<sup>2</sup>, U. Baltensperger<sup>1</sup>, J.-L. Jaffrezo<sup>3</sup>, G. Močnik<sup>4</sup>, M. Gysel<sup>1</sup> and A.S.H. Prevot<sup>1</sup>

<sup>1</sup>Laboratory of Atmospheric Chemistry, Paul Scherrer Institute, 5232, Villigen, Switzerland

<sup>2</sup>University of Genoa, Department of Physics, 33 Via Dodecaneso, 16146, Genova

<sup>3</sup>Laboratoire de Glaciologie et Géophysique de l'Environnement, CNRS/Université Grenoble Alpes, 54 Rue Molière, BP 96, 38402, St Martin d'Hères, France

<sup>4</sup>Aerosol d.o.o., Research and Development Department., Ljubljana, Slovenia

Keywords: brown carbon, sources, absorption.  
Presenting author email: imad.el-haddad@psi.ch

Atmospheric brown carbon (BrC) contributes significantly to aerosol absorption in the atmosphere, especially at lower wavelength. This fraction of the organic aerosol is composed of a large number of complex chromophores. The main processes by which these compounds are introduced in the atmosphere or formed through atmospheric oxidation remain virtually unknown and as a result, the contribution of BrC to atmospheric absorption is highly uncertain.

Here, using factorization techniques, we identify the main primary and secondary sources of water and methanol soluble BrC, at two urban sites in Switzerland over a yearly cycle. The same samples measured by UV/vis spectrometry for bulk absorption are analyzed using offline aerosol mass spectrometry for the identification of the main organic aerosol sources. The amount of humic-like substances on the samples was also determined. From these analyses, we will present estimated mass absorption cross-sections of different organic aerosol fractions, including primary biomass smoke, and wintertime and summer time secondary organic aerosol fractions (Figure 1).

We show that biomass burning, driving the concentration of humic-like substances, is the major source of BrC at both sites, during winter. In summer, the absorption due to brown carbon decreases significantly, suggesting that the organic aerosol, mostly related to SOA, is less absorbing. Through complementary smog chamber experiments, we investigate the optical properties of biomass burning emissions as a function of aging and assess the impact of BrC on the total absorption in different environments.

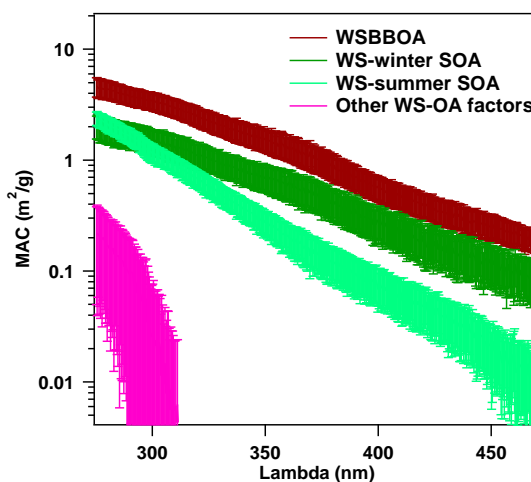


Figure 1. Comparison of the mass absorption cross-sections of the water soluble (WS) fractions from different sources that influence the organic aerosol at the two study sites. These sources include primary biomass burning, and wintertime and summer time secondary organic aerosols.

This work was supported by the Swiss Federal Office of Environment, Liechtenstein, Ostluft, the Cantons Basel, Graubünden, Thurgau.

## Particle number and elemental concentrations at the Mount Kenya Global Atmosphere Watch Station in Kenya

S. M. Gaita<sup>1</sup>, E. S. Thomson<sup>1</sup>, J. B. C. Pettersson<sup>1</sup>, J. Boman<sup>1</sup>, M. J. Gatari<sup>2</sup> and A. Andersson<sup>3</sup>

<sup>1</sup>Department of Chemistry and Molecular Biology, University of Gothenburg, Gothenburg, SE-412 96, Sweden

<sup>2</sup>Institute of Nuclear Science & Technology, University of Nairobi, Nairobi, 30197 00100, Kenya

<sup>3</sup>Department of Environmental Science and Analytical Chemistry, Stockholm University, Stockholm, SE-106 91, Sweden

Keywords: High altitude, Biomass burning, Free troposphere

Presenting author email: [Samuel.gaita@chem.gu.se](mailto:Samuel.gaita@chem.gu.se)

The Mount Kenya Global Atmosphere Watch station (3780 m a.s.l.) is a unique high altitude measurement station that provides exposure to both undisturbed free tropospheric air and to the locally influenced atmospheric boundary layer (Henne *et al.* 2008). Here we report on studies of the chemical and physical properties of airborne particles, including number and elemental concentrations of particulate matter (PM), sampled at the station located on the northwestern slopes of Mount Kenya.

Aerosol sampling was conducted from 14 August to 12 September 2015. Particle number concentrations were sampled using a Grimm dust monitor for optical particle counting. A dichotomous sampler was used to collect fine (PM<sub>2.5</sub> aerodynamic diameter less than 2.5 µm) and coarse (PM<sub>10</sub> aerodynamic diameter less than 10 µm) particles on filters and the collected samples were analysed using X-ray fluorescence elemental analysis. In addition, black carbon was characterized using reflectometry. A high volume sampler was used to collect PM<sub>2.5</sub> samples, which were analysed for both elemental and organic carbon.

On average, sulphur and black carbon dominated the detected elements in the fine mode for the sampling period. Sulphur had a mean concentration of 190±106 ng m<sup>-3</sup> and this accounted for approximately 40% of the measured elements' masses in the fine fraction. Black carbon contributed 170±83 ng m<sup>-3</sup> (≈ 35%). The coarse mode was dominated by iron and calcium with both elements accounting for approximately 74% of the measured elements' masses in the coarse fraction.

The mean concentration of the organic carbon was 1900±380 ng m<sup>-3</sup> and the elemental carbon had a mean concentration of 160±110 ng m<sup>-3</sup> in the sampled PM<sub>2.5</sub>. This highlights the influence of biomass burning for domestic purposes in the Mount Kenya region (Gatari *et al.* 2001, Gaita *et al.* 2014).

In addition to particle measurements various meteorological variables were monitored in real time. Combined the data exhibits modal variability between the daytime measurements, characterized by upslope winds and the station being within the atmospheric boundary layer, and the night time measurements characterized by downslope winds when the stabilizing

mixed layer leaves the station exposed to free tropospheric air. Here we discuss the observed diurnal cycling and identify how this cycle is linked to sources and source regions. Implications for air quality, particle transport and East Africa are also discussed.

This work is supported by the Swedish Research Councils, the Swedish Research Council Formas, the EU FP7-ENV-2013 BACCHUS project under Grant Agreement 603445, the International Science Programme-Uppsala, the Kenya Wildlife Service and the Kenya Meteorological Department.

Gaita, S. M., Boman, J., Gatari, M. J., Pettersson, J. B. C. and Janhäll, S. (2014). Source apportionment and seasonal variation of PM<sub>2.5</sub> in a Sub-Saharan African city: Nairobi, Kenya. *Atmos. Chem. Phys.* 14(18): 9977-9991. DOI: 10.5194/acp-14-9977-2014, Gatari, M. J., Boman, J. and Maina, D. M. (2001). Inorganic element concentrations in near surface aerosols sampled on the northwest slopes of Mount Kenya. *Atmospheric Environment* 35(34): 6015-6019. DOI: [http://dx.doi.org/10.1016/S1352-2310\(01\)00393-4](http://dx.doi.org/10.1016/S1352-2310(01)00393-4),

Henne, S., Junkermann, W., Kariuki, J. M., Aseyo, J. and Klausen, J. (2008). Mount Kenya Global Atmospheric Watch Station (MKN): Installation and Meteorology Characterization. *J. Appl. Meteorol. Clim.* 47(11): 2946-2962.

## Composition, sources apportionment and risk assessment of particulate organic matter at industrial, urban and forest areas of northern Algeria

S. Khedidji<sup>1,2\*</sup>, C. Balducci<sup>3</sup>, A. Cecinato<sup>3</sup>, M. Perilli<sup>3</sup> and N. Yassaa<sup>4</sup>

<sup>1</sup>Department of Organic Chemistry, University of Sciences and Technology Houari Boumediene (USTHB), Algiers, PhD, Algeria

<sup>2</sup>Department of Chemistry, University Akli Mohand Oulhadj of Bouira, Bouira, Algeria

<sup>3</sup>Istituto sull'Inquinamento Atmosferico, National Research Council (CNR), Roma, Italy

<sup>4</sup>Centre de Développement des Energies Renouvelable, Bouzaréah, Prof, Algeria

Keywords: PM<sub>10</sub>, n-alkanes, PAHs, sources apportionment

Presenting author email: [ksid83@gmail.com](mailto:ksid83@gmail.com)

The diel cycles of organic compounds enriched into particulate matter with aerodynamic diameter lesser than 10 µm (PM<sub>10</sub>) were determined between March and May 2014 in industrial, university and forested areas located at Bouira province, Northern of Algeria.

The net concentrations of *n*-alkanes, polycyclic aromatic hydrocarbons PAHs and highly-polar organic compounds HPOCs allowed to estimate the health risk associated to PM, while the normalized contents, which reached 53%, 7% and 40% for, respectively, provided insights about the kind of sources. In particular, the carbon preference index CPI and percentage of natural waxes (WNA) of *n*-alkanes allowed to discriminate the natural emission, while diagnostic ratios between concentrations of individual PAHs were applied to identify the main anthropogenic sources. According to them, PM<sub>10</sub> came out overall from road traffic and industrial manufacture.

The concentration of BaP remained below the WHO guideline value (1ng/m<sup>3</sup>) during the period of investigation, ranging from 0.02 to 0.27 ng/m<sup>3</sup> at all sites. In contrast, total carcinogenic power resulted relatively high in Bouira, overall with regard to employees and students. Finally, illicit substances such as Δ<sup>9</sup>-tetrahydrocannabinol THC (up to 0.19 ng/m<sup>3</sup>) were detected for the first time in Algeria.

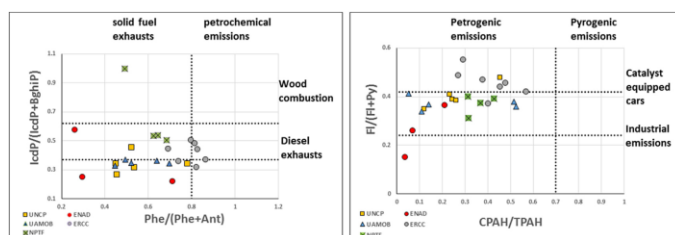


Fig. 2. Graphic illustration of the diagnostic ratios on the sources of PAHs emission

Funding for this study was provided by PhD training program of the Ministry of Higher Education and Scientific Research of Algeria (grant No. 04/KAAT/2014).

Khedidji, S., Ladj, R., Yassaa, N. (2013) A wintertime study of polycyclic aromatic hydrocarbons (PAHs) in indoor and outdoor air in a big student residence in Algiers, Algeria. *Environ. Sci. Pollut. Res.* **20**, 4906-4919.

Khedidji, S., Croes, K., Yassaa, N., Ladj, R., Denison, M.S., Baeyens, W., Elskens, M. (2015) Assessment of dioxin-like activity in PM<sub>10</sub> air samples from an industrial location in Algeria, using the DRE-CALUX bioassay. *Environ. Sci. Pollut. Res.* **584**, 1-4.

Cecinato, A., Balducci, C., Perilli, M. (2016) Illicit psychotropic substances in the air: the state-of-art. *Sci. Total. Environ.* **539**, 1-6.

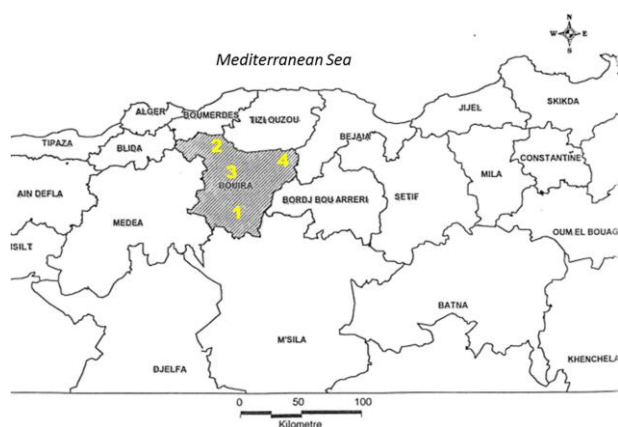


Fig. 1. Detailed geographical position of the sampling sites in the Bouira province.

## Aerosol Characterisation results from the South West Asian Aerosol-Monsoon Interactions (SWAAMI) aircraft experiment

J. Brooks<sup>1</sup>, H. Coe<sup>1</sup>, W. Morgan<sup>1</sup>, P. Williams<sup>1,2</sup>, J. Allan<sup>1,2</sup>, D. Liu<sup>1</sup>, S. Haslett<sup>1</sup>, S.K. Satheesh<sup>3</sup>, S. Suresh Babu<sup>4</sup>, A. Turner<sup>5</sup>

<sup>1</sup> Centre for Atmospheric Science, University of Manchester, UK.

<sup>2</sup> National Centre for Atmospheric Science, UK.

<sup>3</sup> The Indian Institute of Science (IISc).

<sup>4</sup> Space Physics Laboratory (SPL) of Vikram Sarabhai Space Centre (VSSC).

<sup>5</sup> The University of Reading, UK.

Keywords: characterisation, India, aircraft, distribution, sources.

Presenting author email: james.brooks-2@manchester.ac.uk

The Indian subcontinent is one of the most polluted regions in the world. Aerosol particles from various different sources build up and form a dense haze across the region. Aerosols can directly absorb/scatter incoming solar radiation, depending upon their composition, or indirectly reflect solar radiation by forming and interacting with cloud condensation nuclei (CCN). These impacts are thought to affect the water and radiative balance over India, influencing the monsoon circulation that occurs in the summer months. At the moment, the nature and magnitude of the aerosol impacts are poorly understood and constrained. Uncertainties lie in the vertical distribution, spatial distribution of various different aerosols and the relative contribution from different sources (Chakraborty et al, 2016).

The South West Asian Aerosol-Monsoon Interactions (SWAAMI) project, which occurred from June to July 2016, sought to address these uncertainties by carrying out an airborne experiment. Such experiment was on-board the UK Facility for Airborne Atmospheric Measurements (FAAM) BAe-146 research aircraft (pictured above). The field campaign conducted 22 flights in advance of the summer monsoon, and during the onset phase. The vertical and spatial extent of aerosols were studied across both Northern India (based out of Lucknow, in the Indo-Gangetic Plain) and in Southern India (based out of Bangalore). The campaign encompassed drier, desert-like regions in NW India, heavily polluted urban and industrial centres in the IGP and eastwards towards the Bay of Bengal, and the cleaner, yet heavily populated region around Bangalore in the south. Two aerosol instruments were operated by the University of Manchester on-board the aircraft; an Aerodyne Aerosol Mass Spectrometer (AMS) and a DMT Single Particle Soot Photometer (SP2).

Organics dominated the aerosol burden in the IGP aerosol haze, with sulphate a major contributor across the rest of N India. Bangalore had much lower

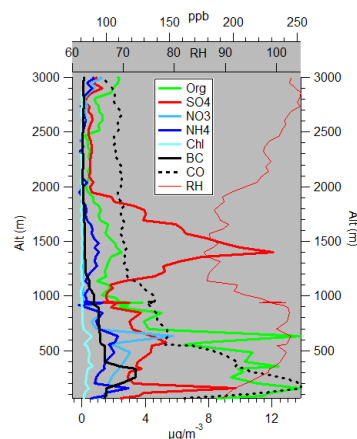


**Figure 1** Aerosol Profile out of Lucknow, N India, during flight B972 on 5<sup>th</sup> July 2016. Example of aerosol and thermodynamic structure.

aerosol concentrations, but organics contributed the most to the aerosol load in this region. Significant aerosol concentrations were observed up to altitudes of around 6km, with variations in this as the monsoon progresses. Organic aerosol dominated in the lower atmosphere up to ~2km, with elevated sulphate layers existing ~2-3km. Black carbon concentrations were greater in lower altitudes ~0-2km. PMF analysis results suggest three main factors contributing to the organic aerosol load (low-volatile oxidised OA (LV-OOA), hydrocarbon-like OA (HOA), and semi-volatile oxidised OA (SV-OOA)). Aerosol transport varies dependent on altitude, with long range transport of drier aerosol such as dust at higher altitudes, which changes through the monsoon onset.

Further observations will be presented and used to characterise the regional aerosol burden and its associated interactions with the monsoon.

This work was supported by the National Environmental Research Council (NERC) under grant NE/L002469/1.

*Reference:* Chakraborty, A., Gupta, T. and Tripathi, S. N. (2016) *Atmospheric Environment* **136** 144-155.

## Characterising Semivolatile Evaporation and Condensation to Understand the Partitioning of Secondary Organic Matter

Stephen Ingram<sup>\*1</sup>, Young Chul-Song<sup>1</sup>, David R. Glowacki<sup>1</sup>, David O. Topping<sup>2</sup>, and Jonathan P. Reid<sup>1</sup>

<sup>1</sup> School of Chemistry, University of Bristol

<sup>2</sup> School of Earth and Atmospheric Sciences, University of Manchester

Keywords: Secondary organic aerosol, viscosity, volatility, particle growth

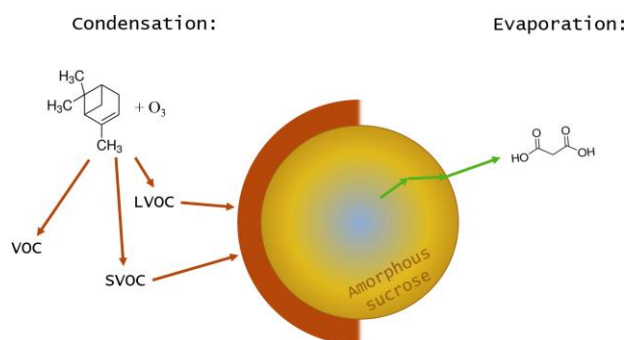
\*Presenting author email: s.ingram@bris.ac.uk

Recently, persuasive evidence has supported the existence of a moisture driven glass transition in secondary organic aerosol (SOA) particles<sup>1-3</sup> proceeding via the removal of water from the particle following a reduction in gas phase water activity. Physicochemically, this imparts kinetic limitations to both bulk phase diffusion and evaporation from the particle surface.<sup>4</sup> Therefore, it has been suggested that the ultraviscous or glassy state will substantially impede the partitioning of semi-volatile organic compounds (SVOCs) between the condensed and gaseous phases.<sup>5</sup> Although studies of diffusion in aerosols consisting of binary component mixtures have been extensive, we explore here the kinetics of mass transfer in aerosol of increasing complexity, consisting of many components of differing volatility and molecular size.

We will begin by presenting recent developments in assessing the coupled evaporation kinetics of water and an SVOC from benchmark ternary aerosol, where multiple chemical species volatilise in response to a step change in relative humidity. Particles are levitated in a standard optical tweezer instrument<sup>6</sup> and sized continuously by analysis of characteristic stimulated peaks in the Raman spectrum. Data analysis techniques have been developed that allow both diffusion coefficients and the semi-volatile effective vapour pressure to be simultaneously determined for the same particle. These allow the first direct determinations of diffusion constants of water in ternary component aerosol and studies of the kinetic factors that regulate SVOC partitioning. In particular, we will show how the diffusion kinetics of an SVOC, when compared with water, follow more closely the behaviour expected from the Stokes Einstein relationship, scaling with particle viscosity. It is also found that there is a significant influence of the conditioning history on the observed volatility suppression at low relative humidity. This is due to the fact that the precise radial composition at the point the measurement is made is a function of all sorption/desorption events the droplet has experienced previously.

Progressing from studies of low complexity, we then move to studies of the kinetics of evaporation and hygroscopic response for aerosol particles formed from a complex mixture of components but with well-defined heterogeneity. With reference to a numerical framework developed by Mai et. al.<sup>5</sup>, we suggest that viscosity may be crucial to the dynamic reversibility of condensation and evaporation of SVOCs. In particular, the kinetics of particle growth involving the gas phase ozonolysis of  $\alpha$ -

pinene have been studied. Oxidation products of varying volatility are produced which condense onto the surface of a dry (glassy) saccharide particle. The volatility and hygroscopic properties of these compounds are then estimated from the size response of the resultant droplet at varying RH. Separately, the evaporation of SVOCs from  $\alpha$ -pinene SOM has been studied in an electrodynamic balance, allowing a comparison of the volatility distributions of compounds formed over a range or gas phase conditions, and with a range of solubilities. We draw conclusions regarding the influence of these factors on the kinetics of gas-particle partitioning.



This work was funded by the Natural Environment Research Council (NERC), through the GW4+ doctoral training partnership.

### References

- Murray, B.J, *Atmos. Chem. and Phys.*, 2008, **8**, 5423–5433.
- Zobrist, B., Marcolli, C., Pedernera, D. A., and Koop, T., *Atmospheric Chemistry and Physics*, 2008, **8**, 5221–5244.
- Bateman, A. P., Bertram A. K. and Martin, S. T., *J. Phys. Chem. A*, 2015, **119**, 4386–4395.
- Yli-Juuti, T. et. al., Presented at the European Aerosol Conference, Tours, France, September 2016.
- Mai, H., M. Shiraiwa, M., Flagan R. C., and Seinfeld, J. H., *Environ. Sci. Technol.*, 2015, **49**, 11485–11491.
- Wills, J. B., Knox, K. J. and Reid, J. P., *Chem. Phys. Lett.*, 2009, **481**, 153–165.

## The effect of relative humidity and chemical composition on the evaporation of secondary organic aerosol particles

A. Buchholz<sup>1</sup>, C. Mohr<sup>2</sup>, A. Lambe<sup>3</sup>, C. Faiola<sup>1,4</sup>, E. Kari<sup>1</sup>, S.A. Nizkorodov<sup>1,5</sup>, A. Pajunoja<sup>1</sup>, O.-P. Tikkanen<sup>1</sup>, A. Ylisirniö<sup>1</sup>, D. Worsnop<sup>3</sup>, T. Yli-Juuti<sup>1</sup>, and A. Virtanen<sup>1</sup>

<sup>1</sup>Department of Applied Physics, University of Eastern Finland, Kuopio, Finland.

<sup>2</sup>Institute of Meteorology and Climate Research, Karlsruhe Institute of Technology, Karlsruhe, Germany.

<sup>3</sup>Center for Aerosol and Cloud Chemistry, Aerodyne Research Inc., Billerica, MA, USA.

<sup>4</sup>Department of Ecology and Evolutionary Biology, University of California Irvine, Irvine, CA, USA.

<sup>5</sup>Department of Chemistry, University of California Irvine, Irvine, CA, USA.

Keywords: secondary organic aerosol, volatility, evaporation, chemical composition.

Presenting author email: angela.buchholz@uef.fi

Secondary Organic Aerosol (SOA) is a major constituent of atmospheric aerosol and consists of a multitude of organic compounds with a range of physical and chemical properties, such as viscosity and volatility (Hallquist et al., 2009). The volatility and concentration of a compound will determine its partitioning between particle and gas phase. The Volatility Basis Set (VBS) groups compounds by saturation concentration (Donahue et al. 2006) and can be used in combination with equilibrium gas-particle partitioning theory to describe particle composition. In previous studies, slower than expected evaporation from VBS distributions was observed for  $\alpha$ -pinene particles (Vaden et al., 2011) which could be caused by physical limitations (e.g. mass transfer limitations in (semi)solid particles) or by chemical processes in the particle phase (e.g. oligomerization). It is therefore important to study the changes of the chemical composition of particles during evaporation to gain insights into the processes governing particle evaporation.

SOA with three different O:C ratios between 0.55 and 1.05 was generated from  $\alpha$ -pinene and a complex VOC mixture in a Potential Aerosol Mass reactor (PAM, Aerodyne Research Inc., Lambe et al., 2011) by varying the integrated oxidant exposure inside the reactor. A monodisperse size distribution (80nm) was selected with a nano-DMA operated with an open loop sheath flow system, thus also removing the majority of gas phase compounds. The monodisperse aerosol was either led directly to the measurement instruments or filled into a 100L stainless steel Residence Time Chamber (RTC) which was then closed off from all air flows. Samples were taken from the RTC in ~1h intervals to monitor changes in particle size and composition. Residence times of 0.5 – 10 h were achieved with this setup. The RH in the RTC was controlled by the RH of the nano-DMA sheath flow and was set to 0%, 40% or 80%.

The particle size was monitored with a Scanning Mobility Particle Sizer (SMPS) and the composition with a High Resolution Time-of-Flight Aerosol Mass Spectrometer (AMS, Aerodyne Inc.). In addition, a Filter Inlet for Gases and AEROSols (FIGAERO) coupled with a Chemical Ionization Time-of-Flight Mass Spectrometer (ToF-CIMS, Lee et al., 2014) provided

information on molecular composition as well as volatility of the compounds in the particle phase.

Particle evaporation was enhanced at higher RH but there was no change between 40% and 80% RH. We observed a strong dependency of evaporation on the initial particle composition, with lower volatility for particles with higher O:C ratios. During an evaporation experiment the O:C ratio remained constant. We use the detailed mass spectra from FIGAERO measurements to analyse the particle composition changes upon evaporation. SOA from complex VOC mixtures exhibits similar evaporation behaviour as particles from  $\alpha$ -pinene of similar O:C ratios.

In addition to chemical composition measurements, we analysed the observed evaporation behaviour using a kinetic evaporation model with emphasis on the mass transfer limitations inside the particles. A strong composition dependence in particle viscosity was observed.

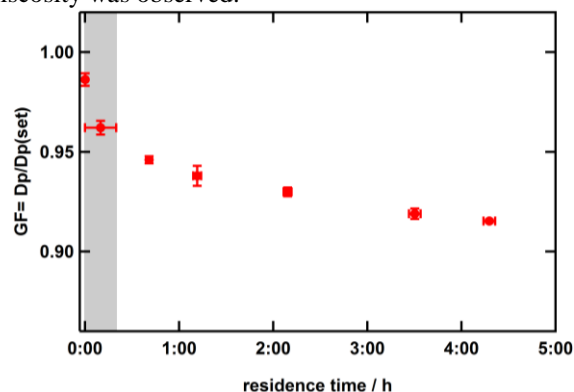


Figure 1. Results from a typical  $\alpha$ -pinene experiment. X-error bars are measurement intervals, y-error bars are 1 $\sigma$  standard deviations. Grey area: RTC filling.

This work was supported by the Academy of Finland (no. 272041, 259005 and 299544), the European Research Council (ERC Starting Grant 335478) and strategic funding from University of Eastern Finland.

Donahue et al. (2006), *EST*, **40**, 2635-2643.

Hallquist et al. (2009), *ACP*, **9**, 5155-5236.

Lambe et al. (2011), *AMT*, **4**, 445-461.

Lee et al. (2014), *EST*, **48**, 6309-6317.

Vaden et al. (2011), *PNAS*, **108**, 2190-2195.

## Characterization of secondary aerosols by cryo-TSEM-EDS: methodological development

S. Guilbaud, K. Deboudt, P. Flament and M. Fourmentin

Laboratoire de Physico-Chimie de l'Atmosphère (LPCA), Université du Littoral Côte d'Opale,  
189A Avenue Maurice Schumann, 59140 Dunkerque, France

Keywords: cryo-TSEM-EDS, semi-volatile compounds, single-particle analysis

Author email: sarah.guilbaud@univ-littoral.fr

Because of their impact on climate, biogeochemical cycles and human health (via inhalation and/or ingestion), the study of atmospheric aerosols has increased considerably in recent years.

The physical and chemical characteristics of primary particles can rapidly change after their emission, by gas condensation, aggregation or heterogeneous reaction. This is especially the case for industrial aerosols, generally released in the troposphere by high-temperature processes (e.g. for steelworks and metallurgy emissions) (Marris *et al.*, 2012). Thus, internal composition of these individual atmospheric particles turns rapidly into a complex mixture of primary and secondary phases.

Then this mixing state evolves with the aging of air masses, resulting in changes of chemical and physical properties of aerosols. When bulk analysis only gives the relative contribution of primary and secondary aerosols, individual particle analysis brings information of their mixing state. In this context, we challenge to describe the mixing state of secondary aerosols and its evolution by analytical microscopy (SEM-EDS), to better understand the aging processes of industrial particles.

Primary atmospheric components (calcite, soot, aluminosilicates, sodium chloride...) are relatively refractory and so stable under the electronic beam and the vacuum of the microscope. In the opposite, secondary components (ammonium nitrate or sulfate, semi-volatile organic compounds...) are rather instable and their study in conventional microscopy is very difficult. Indeed, the electron beam affects the particles very quickly and causes their destruction and evaporation in the chamber vacuum, avoiding the acquisition of EDS spectra or pictures (Figure 1). To prevent or limit this phenomenon called "beam damage", a cryo-stage could be used (Veghte *et al.*, 2014).

In this study, we developed a methodology for the cryo-TSEM-EDS analysis of semi-volatile particles with a diameter ranging from 100 nanometers to a few micrometers. For this purpose, a parametric study using model particles (NaCl, AlN, (NH<sub>4</sub>)<sub>2</sub>SO<sub>4</sub> and NH<sub>4</sub>NO<sub>3</sub>) was performed. Different parameters were considered as the beam acceleration voltage or the probe current. The influence of the spectral acquisition duration was also investigated. A parallel study was carried out on the best storage temperature (ambient, 4°C, -18°C) of samples and on the choice of the sampling substrate. The analysis

of particles sampled in the Dunkirk industrial and urban areas (France) allowed us to validate this methodology on real particles.

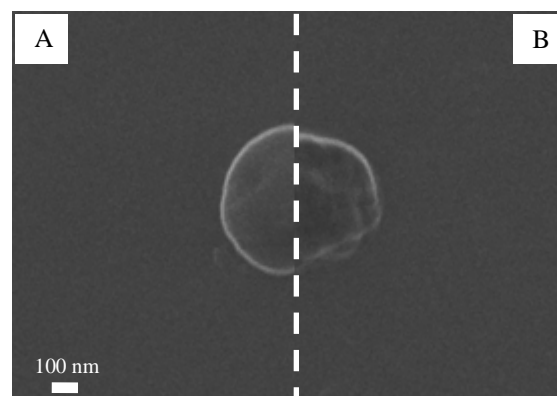


Figure 1. Ammonium sulfate particle (A) suffering from beam damage after observation duration of 5 seconds (B) at room temperature

To understand the evolution of the mixing state of primary and secondary components and the aging processes of industrial particles, samples were collected during a field campaign, at increasing distances from the emissions sources, in the south-west of Dunkirk. Then samples were analyzed using our cryo-TSEM-EDS methodology.

This work was supported by CaPPA (Chemical and Physical Properties of the Atmosphere) Project (ANR-10-LABX-005) funded by the French National Research Agency (ANR) through the PIA (Programme d'Investissement d'Avenir). The authors thank the "Hauts-de-France" Region, the "Ministère de l'Enseignement Supérieur et de la Recherche" and the European Fund for Regional Economic Development (FEDER), for their financial support (CPER Climibio).

Marris, H., Deboudt, K., Augustin, P., Flament, P., Blond, F., Fiani, E., Fourmentin, M. and Delbarre, H. (2012) *Sci. Total Environ.* **427-428**, 126-138.  
Veghte, D.P., Bittner, D.R. and Freedman, M.A. (2014) *Analytical Chemistry* **86**, 2436-2442

## Measured saturation vapour pressures of phenolic and nitro-aromatic compounds

<sup>1</sup>Thomas J Bannan, <sup>1</sup>A Murray Booth, <sup>1</sup>Benjamin T Jones, <sup>1</sup>Simon O'Meara, <sup>1</sup>Mark H Barley, <sup>3</sup>Ilona Riipinen, <sup>1</sup>Carl J. Percival, <sup>1,2</sup>David Topping.

<sup>1</sup> School of Earth, Environmental and Atmospheric Science, University of Manchester, Manchester, UK

<sup>2</sup> National Centre for Atmospheric Science, University of Manchester, Manchester, UK.

<sup>3</sup> Department of Environmental Science and Analytical Chemistry (ACES), Stockholm University, Stockholm, Sweden.

Presenting author email: Thomas.Bannan@Manchester.ac.uk

Aerosol particles are an important component of the Earth's atmosphere, effecting visibility, human health and climate on regional and global scales (Bilde et al., 2015). Mechanistic models attempt to predict the evolving composition and microphysics of aerosol populations through the use of fundamental properties of pure components and mixtures.

A critical parameter in this regard is the pure component equilibrium vapour pressure of the constituent molecules. Phenolic and nitro-aromatic compounds are extremely toxic components of atmospheric aerosol that are currently not well understood.

Here, solid and sub-cooled liquid state saturation vapour pressures of phenolic and nitro-aromatic compounds are measured using Knudsen Effusion Mass Spectrometry (KEMS) over a range of temperatures (298–318 K) (Booth et al., 2012). With a few exceptions, estimates produced from a wide range of estimation methods, in comparison to the measurements made here, are biased towards predicting saturation vapour pressures that are too high, by 5 to 6 orders of magnitude in some cases.

Basic partitioning theory comparisons indicate that overestimation of vapour pressures in such cases would cause us to expect these compounds to be present in the gas state, whereas measurements in this study suggest these phenolic and nitro-aromatic will partition into the condensed state for a wide range of ambient conditions if absorptive partitioning plays a dominant role (Figure 1).

The results of this study may support other studies quantifying the role of low volatility nitrogen containing organic compounds on aerosol growth and might impact therefore on attempts to resolve health impacts with specific chemical classes

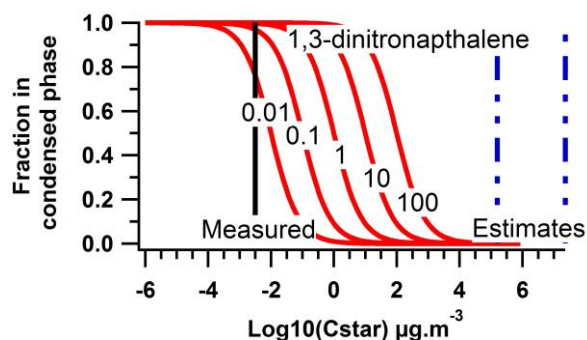


Figure 1: Fraction of 1,3-dinitronaphthalene in the condensed phase as a function of its volatility, represented by the  $C^*$  value (replicated from Valorso et al., 2011), for 5 existing condensed mass loadings [red lines, each value given in  $[mg.m^{-3}]$ ] against the measured volatility [solid black line] and range of estimates from predictive techniques [dashed blue lines].

This work was funded under NERC grants NE/M003531/1 and NE/J02175X/1

- Booth, A. M. et al., The role of ortho, meta, para isomerism in measured solid state and derived sub-cooled liquid vapour pressures of substituted benzoic acids. *RSC Advances*, 2012, 2(10), 4430-4443.
- Bilde, M. et al., Saturation vapor pressures and transition enthalpies of low-volatility organic molecules of atmospheric relevance: From dicarboxylic acids to complex mixtures. *Chemical reviews*, 2015, 115(10), pp.4115-4156
- Valorso, R., et al., Explicit modelling of SOA formation from  $\alpha$ -pinene photooxidation: sensitivity to vapour pressure estimation, *Atmos. Chem. Phys.*, 2011, 11, 6895-6910, doi:1.5194/acp-11-6895-20

## Comparison of atmospheric aerosol volatility at a rural site in Central Europe

L. Kubelová<sup>1,2</sup>, P. Vodička<sup>1</sup>, O. Makeš<sup>1,2</sup>, N. Zíková<sup>1</sup>, J. Ondráček<sup>1</sup>, J. Schwarz<sup>1</sup>, and V. Ždímal<sup>1</sup>

<sup>1</sup>Laboratory of Aerosol Chemistry and Physics, Institute of Chemical Process Fundamentals of the Czech Academy of Sciences, Prague, 165 02, Czech Republic

<sup>2</sup>Department of Environmental Studies, Faculty of Science, Charles University, Prague, 128 43, Czech Republic

Keywords: atmospheric aerosol, physical and chemical properties of aerosols, thermodenuder, volatility

Presenting author email: kubelova@icpf.cas.cz

Volatility is an important characteristic of atmospheric aerosols as it affects their origin, lifetime and removal. Accurate description of aerosol volatilities is important for models calculating condensation of semi-volatile species and it also enables better identification of aerosol sources (Wu et al., 2009). However, our understanding of volatilities of organic atmospheric aerosols and the related processes is still rather poor (Han et al., 2016).

To study aerosol volatility, we performed summer (17.6.2014-11.8.2014) and winter (9.1.2014-13.3.2014) measurement campaigns at a rural site Košetice (49°34' N, 15°05' E). The sampled aerosol was split into two branches, one thermodenuded (TD) and the other non-thermodenuded (NTD) followed by a 4-way valve that was switching every 10 minutes alternately to a Scanning Mobility Particle Sizer (TSI SMPS 3936) and aerosol mass spectrometer (c-ToF-AMS, Aerodyne). The thermodenuder (Aerodyne) (Huffman et al., 2009) was heated up to 140°C. These were the first measurement campaigns at a rural measurement site in the Czech Republic with the aerosol mass spectrometer. In parallel, we performed also a semi-online analysis of organic and elemental carbon (field OC/EC analyser, Sunset) and 24 hour sampling on filters (sequential low volume sampler, Leckel).

In this work, we focused mainly on differences between the thermodenuded and non-thermodenuded samples. The ratio of masses TD vs NTD for particular chemical compounds is shown in Fig.1 and Fig.2. The largest seasonal difference was observed at organic matter (TD/NTD ratio: summer 0.12; winter 0.3). This might be surprising as it suggests that winter sample that was influenced by domestic heating was less volatile as summer sample that was influenced by increased biogenic activity and higher solar radiation.

The measurement periods were divided into clusters according to the shape and origin of the relevant backward air mass trajectories. For each cluster we performed analysis of TD vs NTD concentration ratios for particular compounds and also for particular m/z of the organic mass. Moreover, the relatively high-time resolution of 1-minute of the AMS measurements enabled us to study the daily cycle in details and focus on particular peaks and their possible sources.

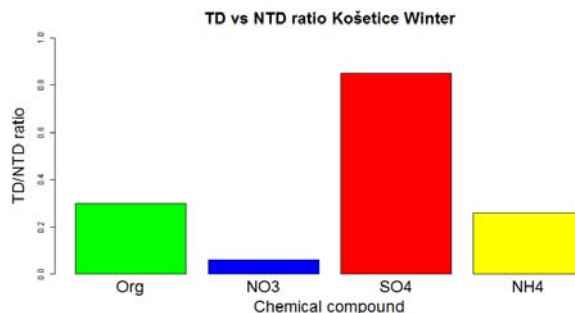


Fig.1: Ratio of thermodenuded and non-thermodenuded mass concentration of particular species measured by AMS. The data were measured during winter campaign at Košetice

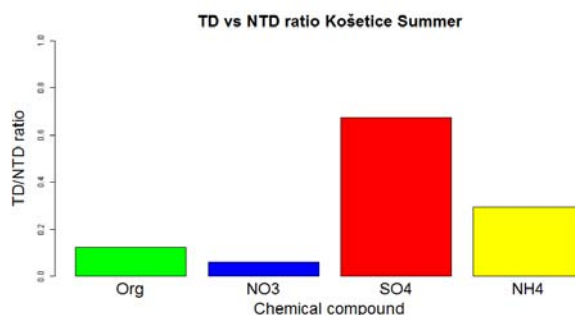


Fig.2: Ratio of thermodenuded and non-thermodenuded mass concentration of particular species measured by AMS. The data were measured during summer campaign at Košetice

This project has received funding from the European Union Horizon 2020 Research and Innovation Programme under Grant Agreement No. 654109, from the the Czech Science Foundation under project No. CSF P209/11/1342 and also from the Ministry of Education, Youth and Sports under project No. LM2015037.

Han, Z.; Xie, Z.; Wang, G.; Zhang, R.; Tao, J. (2016) *Atmos. Environ.* **124**, 186–198.

Huffman, J. A.; Docherty, K. S.; Mohr, C.; Cubison, M. J.; Ulbrich, I. M.; Ziemann, P. J.; Onasch, T. B.; Jimenez, J. L. (2009) *Environ. Sci. Technol.* **43** (14), 5351–5357.

Wu, Z., Poulain, L., Wehner, B., Wiedensohler, A., Herrmann, H. (2009) *J. Aerosol Sci.* **40**, 603–612.

## Relationship between Reactive Oxygen Species and Benzene Carboxylic Acids in the Coastal area during KORUS-AQ campaign

M.S. Bae<sup>1,5</sup>, Z.H. Shon<sup>2</sup>, T.H. Lee<sup>3</sup>, J.H. Jeong<sup>4</sup>, J.J. Schauer<sup>5</sup>

<sup>1</sup>Department of Environmental Engineering, Mokpo National University, Muan, 58554, Republic of Korea

<sup>2</sup>Department of Environmental Engineering, Dong-Eui University, 47340, Republic of Korea

<sup>3</sup>Department of Environmental Science, Hankuk University of Foreign Studies, Gyeonggi, 17035, Republic of Korea

<sup>4</sup>Department of Atmospheric Sciences, Pusan National University, Busan, 46241, Republic of Korea

<sup>5</sup>Department of Civil & Environmental Engineering, University of Wisconsin-Madison, Madison, 53705, USA

Keywords: ROS, WSOC, OC

Presenting author email: [minsbae@hotmail.com](mailto:minsbae@hotmail.com)

The aim of this study is to investigate the relationship between water-soluble organic & inorganic compounds ambient particulate matter (PM) and cellular redox activity. Ambient PM<sub>2.5</sub> samples were collected in between May 28 to June 20 of 2016 at a west coastal site, Anmyeon (36° 32'N; 126° 19'E, 45.7 m above sea level (ASL)) station in Republic of Korea during the KOREA-US Air Quality (KORUS-AQ) campaign.

Automatic 4 hr integrated samples collected for organic carbon (OC), water soluble organic carbon (WSOC), elemental carbon (EC), water soluble ions, and benzene carboxylic acids (BCA) analysis were collected on a 47-mm quartz fiber filter downstream of PM<sub>2.5</sub> cyclones that operated at flowrate of 92 lpm in medium volume samplers. The samplers was custom made (APM inc., Rep. Korea). Flow through the medium volume samplers were controlled using a mass flow controller (MFC). The influence of both long range transfer and different regional range transfers were determined by Advanced Research WRF version 3.4, which includes fully compressible nonhydrostatic equations with hydrostatic option and back trajectories. OC, EC, WSOC, and BCA were determined by SUNET carbon analyser, total organic carbon (TOC) analyser, liquid chromatography-mass spectrometry mass spectrometry (LC-MSMS), respectively. 24 hr integrated samples were collected for Reactive Oxygen Species (ROS) analysis. Total samples were analyzed for macrophage ROS activity. The macrophage ROS assay is a fluorogenic cell-based method to investigate the production of ROS in rat alveolar macrophages.

Correlation between ROS activity and different chemical components of PM was evaluated to identify the main drivers of PM toxicity. Results from this study illustrate that water-soluble species of PM play important roles in influencing potential cellular toxicity. Pairwise correlation scatterplots between the daily averaged ratio of WSOC to OC and EC to OC indicate that secondary productions can be highly associated with ROS. Trimestic acid in WSOC of ambient PM are highly correlated with ROS activity with  $r^2$  of 0.83. This study can provide the information of the toxicological contribution related to water-soluble compounds (i.e. aging productions) in ambient air.

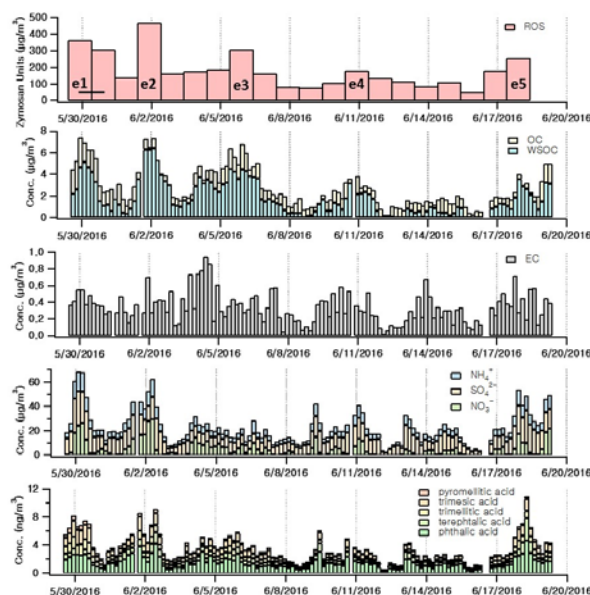


Fig. 1. Time series of ROS, OC, WSOC, ions, and BCA during the KORUS-AQ campaign.

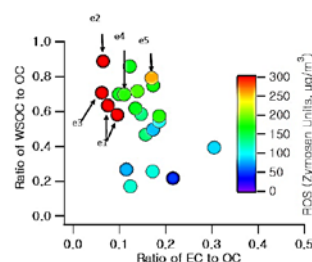


Fig. 2. Pairwise correlation scatterplots between the daily WSOC/OC and EC/OC colored by ROS.

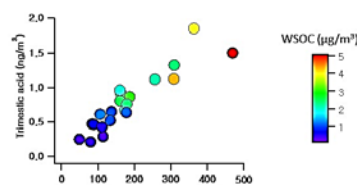


Fig. 3. Pairwise correlation scatterplots between the daily trimestic acid and ROS colored by WSOC.

We acknowledge the support by the National Research Foundation of Korea (NRF) (NRF-2015R1A2A1A10053971).

## Seasonal variability of submicronic aerosols in Romania

C. Marin<sup>1,2</sup>, L. Marmureanu<sup>1</sup> and J. Vasilescu<sup>1</sup>

<sup>1</sup>National Institute of Research and Development for Optoelectronics, Magurele, Romania

<sup>2</sup> University Politehnica of Bucharest, Faculty of Applied Sciences, Bucharest, Romania

Keywords: ACSM, Seasonal variability, Org.

Presenting author email: cristina.marin@inoe.ro

Aerosols play an important role in climatology studies, due to their direct and indirect effect on Earth radiative budget (IPCC, 2013).

In this study, a chemical aerosol assessment have been carried out at Magurele site (44.35°N, 26.03°E) for a two years period of interrupted measurements, which covers all seasons. The location is placed in the adjacent area of Romania's capital city, Bucharest. It is influenced by the urban activities (like intense traffic) and also by the actions carried out in the rural area, where agriculture and several small local industry, power plants represent the main activities.

The analysis is made with an Aerosol Chemical Speciation Monitor, which uses spectrometry techniques in order to retrieve mass concentration for five chemical species: organics (Org), sulphate (SO<sub>4</sub>), nitrate (NO<sub>3</sub>), ammonium (NH<sub>4</sub>) and chloride (Chl). For all the period analysed, the maximum concentrations have been: 76 µg m<sup>-3</sup> for Org, 13.4 µg m<sup>-3</sup> for NO<sub>3</sub> and 25.4 µg m<sup>-3</sup> for SO<sub>4</sub>, while NH<sub>4</sub> and Chl have reached a maximum value of 103 µg m<sup>-3</sup> and 12.8 µg m<sup>-3</sup> respectively. The percent for each species from the total average mass concentration and the period analysed are presented in table 1. For all the periods, Org represent the greater fraction of aerosol (around 50%), while NO<sub>3</sub> have seasonal variation, with greater concentration during autumn and winter. This variability can be explained by the nitrate chemistry, the ammonium nitrate salt exists in the aerosol phase under specific conditions, related with temperature and humidity (Seinfeld, 2006). That circumstances are accomplished during the cold season, when it is commonly to record mainly negative values, in the sample area, with some minimum value of -15° C. Even though the chloride do not have an evident seasonal variability, a small increasing during autumn can be related with some agricultural practices like manure burning.

Table 1. Average chemical composition in %.

Season	Org	SO <sub>4</sub>	NH <sub>4</sub>	NO <sub>3</sub>	Chl
Summer	58	18	18	7	1
Autumn	51	12	17	18	2
Winter	52	26	8	13	1
Spring	47	29	12	11	1

Diurnal trend of all the chemical species for the seasons analysed, is computed. Organics' diurnal trend variation with the season is shown in figure 1. The concentration is higher in the autumn than in the summer. One reason could be an increase in local

sources emissions because in autumn, the agriculture activities are intensified and a main source of aerosols represents the burning of agricultural waste. Organics concentrations have similar values in winter and spring. For all the seasons, a peak around 19 UTC (16 local time) is emphasized being related with traffic activity. This peak is correlated with the Bucharest ring road rush hour, the road being located very close to the site (1 km).

In this study, for evaluation of inorganic aerosol acidity, we have used the molar ratio between the molar concentration of cations and anions, method described by Hennigan et al. (2015). Low molar ratio corresponds to more acidic particles. Applying this method for all seasons, we highlight the presence of mainly acidic aerosols.

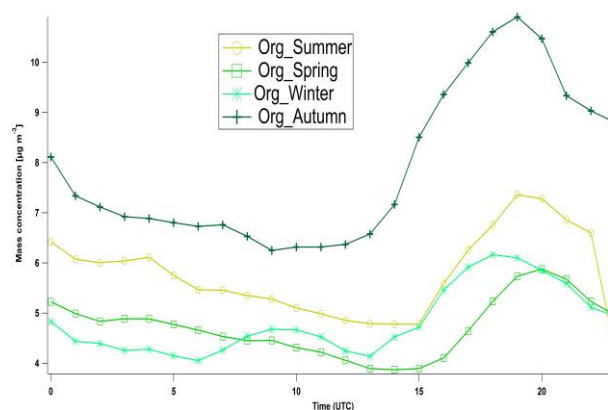


Figure 1. Org diurnal trend for all seasons.

A special interest, in this study, is given to acidic and non-acidic episodes, but also periods influenced by local sources (like traffic, local fires, heating during winter) or long range transport.

The research leading to these results has received funding from the European Union's Horizon 2020 Research and Innovation Programme, under Grant Agreement no 692014-ECARS; no 654109-ACTRIS 2 and from the National Core Program- PN 16 40 01 01.

IPCC (2013) Climate Change. *The Physical Science Basis*, Cambridge University Press.1535  
 Seinfeld, J. H., Pandis, S.N., (2006), John Wiley & Sons, Hoboken, New Jersey.  
 Hennigan, C. J., Izumi, J., Sullivan, A. P., Weber, R. J., and Nenes, A. (2015) *Atmos. Chem. Phys.* **15**, 2775–2790.

## Environmental Molecular Beam Studies of Water Interactions with Condensed Nopinone Surface

S. M. Johansson<sup>1</sup>, X. Kong<sup>1,2</sup>, E. S. Thomson<sup>1</sup>, and J. B. C. Pettersson<sup>1</sup>

<sup>1</sup>Dept. of Chemistry and Molecular Biology, Atmospheric Science, University of Gothenburg, Sweden.

<sup>2</sup>Laboratory of Environmental Chemistry, Department of Energy and Environment, Paul Scherrer Institute, Switzerland

Keywords: EMB method, surface uptake, desorption kinetics, organic aerosol  
Presenting author email: sofia.johansson@chem.gu.se

Naturally produced highly volatile organic compounds such as  $\beta$ -pinene are extensively emitted to the atmosphere by coniferous vegetation. Once in the atmosphere these compounds rapidly undergo gas phase oxidation, and thereby produce lower volatility compounds like nopinone. These lower volatility compounds may participate in new particle formation or condense on existing particles. The chemical composition as well as the physical properties of these organic surfaces will be influenced by water uptake, and thus alter the impact these aerosol particles may have on the climate.

In this study we present novel experimental observations of water interactions with nopinone surface employing the Environmental Molecular Beam (EMB) method (Johansson *et al.*, 2016). The EMB technique utilizes a molecular beam directed through vacuum onto a surface in a high-pressure chamber. The surface substrate can be coated with volatile compounds of interest, and the molecular flux of scattered or desorbed molecules from the surface is detected with mass spectrometry. The method enables studies of molecular level interactions at near ambient pressure, generating information about molecular collision dynamics, desorption kinetics, along with surface and bulk accommodation.

Here a condensed solid nopinone surface is investigated at a temperature of 200 K using pulses of water (D<sub>2</sub>O) molecules. The water molecules are directed onto the nopinone surface and the resulting molecular flux from the surface is detected over a wide range of scattering angles. The novel experimental results indicate that accommodation of water on the nopinone surface is close to unity after which a large fraction rapidly desorbs. Despite the seemingly hydrophobic properties of individual nopinone molecules, the efficient surface uptake is substantial on the time scale of the experiments. This work highlights the underlying molecular processes that govern interactions between water and the atmospherically relevant nopinone surface. Connections to and the implications for the behaviour of the large reservoir of atmospheric volatile biogenic compounds are discussed.

This work was supported by the Swedish Research Council.

Johansson S.M., Kong X.R., Papagiannakopoulos P., Thomson E.S., and Pettersson J.B.C., (2016)  
Submitted to: *Review of Scientific Instruments*

## Cloud droplet activation of black carbon particles containing organic coating

M. Dalirian<sup>1</sup>, A. Ylisirniö<sup>2</sup>, A. Buchholz<sup>2</sup>, A. Virtanen<sup>2</sup> and I. Riipinen<sup>1</sup>

<sup>1</sup>Department of Environmental Science and Analytical Chemistry, Stockholm University, Stockholm, SE-11418, Sweden

<sup>2</sup>Department of Applied Physics, University of Eastern Finland, Kuopio, 70210, Finland

Keywords: Black carbon, CCN, SMPS, AMS

Presenting author email: maryam.dalirian@aces.su.se

Atmospheric aerosol particles influence the climate indirectly by acting as cloud condensate nuclei (CCN) to form cloud droplets (Haywood and Boucher, 2000). Water-insoluble particles, which come from different natural (e.g. dust) and anthropogenic (e.g. black carbon and fumed silica) sources, form a significant fraction of atmospheric particles (Sorjamaa and Laaksonen, 2007; Sullivan et al., 2010). There are lots of studies about the CCN activation of completely soluble or insoluble particles, but mixed particles have been investigated less. However, real atmospheric aerosol particles often contain both water-soluble and water-insoluble substances. These particles can be formed, for instance, as originally insoluble particles are coated by soluble material during their aging in the atmosphere. The presence of such soluble materials on insoluble surfaces can affect water-particle interactions with implication to the CCN activity of these particles.

In this study, we investigated the CCN activity of the size-resolved water-insoluble black carbon BC (Regal Black 400R, Cabot Corporation) particles coated with some hygroscopic organic materials. The size of the BC cores were selected using a DMA (Differential Mobility Analyzer) in the range of 150-250 nm. Succinic acid, glutaric acid or levoglucosan which are organics with different solubilities in water were used to coat on the BC particles. A tube furnace was used to vaporize organic compounds and coat them on the BC particles. The CCN activation of the coated particles were measured using a single column CCN counter (CCNc, Droplet Measurement Technologies Inc.). SMPS (Scanning Mobility Particles Sizer, TSI Inc.) and AMS (Aerosol Mass Spectrometer, Aerodyne Research Inc.) measurements assisted us to gain a better insight into the shape and size of the produced coated particles (Fig. 1). The experimental results were compared to the theoretical calculations using the shell-and-core framework introduced by Kumar et al. (2011).

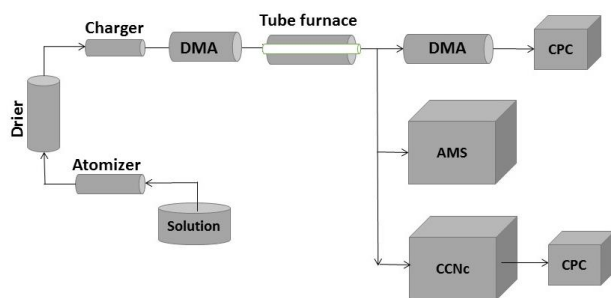


Figure 1: Schematic of the experimental set up

Figure 2 represents the CCN activation results of BC particles coated with different amount of levoglucosan. The electromobility diameter of the coated particles were derived from SMPS data while the aerodynamic diameters were extracted from AMS data analysis. Differences between these two diameters suggest that the BC particles are not spherical and formed as agglomerates. However, for the coated particles, the experimental critical supersaturations vs. electromobility and aerodynamic diameters are in good agreement with the theoretical calculations using shell-and-core model. Similar trends were also observed with the BC particles coated by other organics.

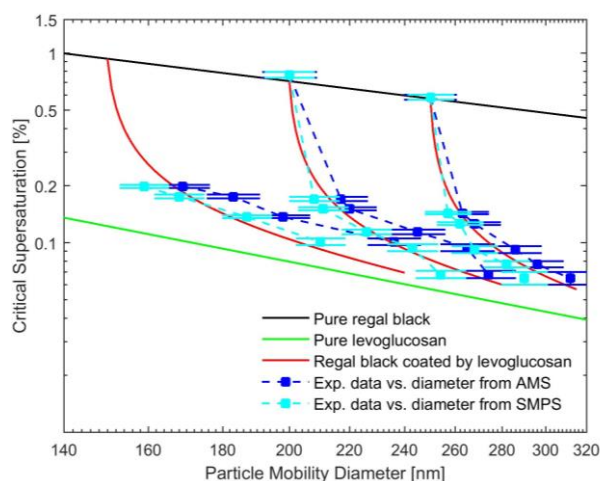


Figure 2: Critical supersaturation vs. dry particles mobility diameter for BC particles coated with levoglucosan.

Financial support from CRAICC is gratefully acknowledged.

Haywood, J. and Boucher, O (2000), *Rev. Geophys.*, 38(4), 513–543.

Henson (2007), *J. Geophys. Res.*, 112, D24S16, doi:10.1029/2007JD008549.

Kumar P., Sokolik I. N. and Nenes A. (2011), *Atmos. Chem. Phys.*, 11, 8661–8676.

Sorjamaa, R. and Laaksonen, A., *Atmos. Chem. Phys.*, (7), 6175–6180, 2007.

Sullivan, R. C., Moore, M. J. K., Petters, M. D., Kreidenweis, S. M., Qafoku, O., Laskin, A., Roberts, G. C. and Prather, K. a., *Aerosol Sci. Technol.*, 44(10), 830–846, doi:10.1080/02786826.2010.497514, 2010

## Could the diesel thermal power generators be a sulfate source of fine aerosol particles in the central Amazonian basin (ATTO)?

S. Carbone<sup>1</sup>, F. Coelho<sup>1</sup>, D. Moran<sup>2</sup>, J. Saturno<sup>2</sup>, B. Holanda<sup>2</sup>, C. Pöhlker<sup>2</sup>, W. Qiaoqiao<sup>2</sup>, M.O Andreae<sup>2</sup>, A. Medeiros<sup>3</sup>, R.A.F. de Souza<sup>3</sup>, S. Martin<sup>4</sup>, J. Brito<sup>5</sup>, L. Rizzo<sup>6</sup>, P. Schlag<sup>7</sup>, J.H. Barbosa<sup>7</sup> and P. Artaxo<sup>7</sup>

<sup>1</sup>Institute of Agrarian Sciences, Federal University of Uberlandia, Uberlandia, 38405-302, Brazil

<sup>2</sup>Multiphase Chemistry & Biogeochemistry Departments, Max Planck Institute for Chemistry, Mainz, Germany

<sup>3</sup>Department of Meteorology, Amazon State University, Manaus, Brazil

<sup>4</sup>School of Engineering and Applied Sciences, Harvard University, Cambridge, Massachusetts, USA

<sup>5</sup>Laboratory for Meteorological Physics, University Blaise Pascal, Clermont-Ferrand, France

<sup>6</sup>Department of Earth and Exact Sciences, Federal University of São Paulo, São Paulo, Brazil.

<sup>7</sup>Institute of Physics, University of São Paulo, São Paulo, Brazil.

Keywords: Amazon forest, power plants, sulfate.

Presenting author email: samara.carbone@ufu.br

The study of the chemical composition of aerosol particles in the Amazon forest is important to understand several processes involving the strong coupling between the atmosphere and the forest, as well as the PM<sub>1</sub> sources. For this reason submicron aerosol particles measurements were performed at the ATTO station, which is located about 150 km northeast of Manaus (Andreae et al., 2015). At ATTO station a unique online instrumentation set is operated continuously, such as the Aerosol chemical speciation monitor (ACSM, Aerodyne), and the Multiangle absorption photometer (MAAP, Thermo 5012). In this study, long-term measurements (near-real-time, ~30 minutes) of PM<sub>1</sub> chemical composition were investigated in this environment from July/2014 to December/2016 with focus on the sulfate mass concentrations.

During this period, sulfate mass concentrations varied from 0.1 to 3.8  $\mu\text{g m}^{-3}$  and comprised from 6% to 35% of the PM<sub>1</sub> mass concentration. Among the several PM<sub>1</sub> main sources under investigation, such as biomass burning organic aerosol, IEPOX-SOA, sea-salt and Sahara dust, none of them seem to fully explain the sulfate origin.

Most of the Brazilian north region is not connected to the main national electric power transmission line due to the physical barrier the Amazon forest imposes. Therefore, in order to fulfill the local demand, thermal power generation units are distributed over the northern region. For instance, at least 128 active units are located upwind of the ATTO station, according to the Brazilian Electricity Agency, Figure 1. Those units operate under power of 76–1500 kW discontinuously. That is, the amount of burned fuel can change significantly and abruptly according to the power demand. At least 83% of those units run on diesel and a smaller fraction on other fuels, such as biodiesel.

There are evidences that the thermal power plants that burn mostly fossil fuel in the surroundings of the city of Manaus are responsible for air pollution problems (Medeiros et al., 2017). In this study, we hypothesize that the diesel thermal power generation units upwind of ATTO station could be partly responsible for the reported sulfate mass concentrations at this station by emitting sulfur during the diesel burning process.

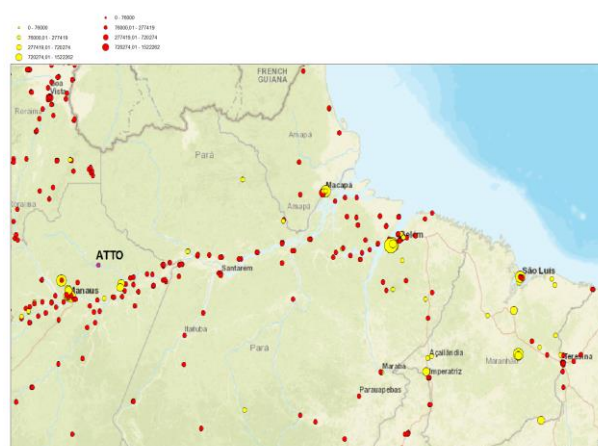


Figure 1. Power generation units inside the Amazon forest, ATTO station upwind. The size of the markers are proportional to the nominal power of each unit (W), and the colours refer to the fuel type, diesel (red) and others (yellow).

This work was supported by the Max Planck Society (MPG), Max Planck Graduate Center (MPGC), German Federal Ministry of Education and Research (BMBF contract 01LB1001A), the Brazilian Ministério da Ciência, Tecnologia e Inovação (MCTI/FINEP contract 01.11.01248.00) and São Paulo Research Foundation (FAPESP, process 2014/05238-8).

Andreae, M. O., et al. The Amazon Tall Tower Observatory (ATTO). (2015) Overview of pilot measurements on ecosystem ecology, meteorology, trace gases, and aerosols, *Atmos. Chem. Phys.*, **15**(18), 10723-10776.

Medeiros, A. S. S., Calderaro, G., Guimarães, P. C., Magalhaes, M. R., Morais, M. V. B., Rafee, S. A. A., Ribeiro, I. O., Andreoli, R. V., Martins, J. A., Martins, L. D., Martin, S. T. and Souza, R. A. F. (2017) Power Plant Fuel Switching and Air Quality in a Tropical Forested Environment, *Atmos. Chem. Phys. Discuss.*, 1-32.

## Stable carbon and nitrogen isotopic composition in fine aerosol at a Central European background station

P. Vodička<sup>1,2</sup>, K. Kawamura<sup>1</sup>, B. Kunwar<sup>1</sup>, J. Schwarz<sup>2</sup>

<sup>1</sup> Chubu Institute for Advanced Studies, Chubu University, Kasugai 487–8501, Japan

<sup>2</sup>Institute of Chemical Process Fundamentals of the CAS, Prague, 165 02, Czech Republic

Keywords:  $\delta^{15}\text{N}$ ,  $\delta^{13}\text{C}$ , isotope ratios, PM1, Central Europe

Presenting author email: vodicka@isc.chubu.ac.jp

Stable carbon ( $\delta^{13}\text{C}$ ) and nitrogen ( $\delta^{15}\text{N}$ ) isotope ratios were measured for total carbon (TC) and total nitrogen (TN) in PM1 aerosol collected from the Košetice rural background site (N49°35', E15°05', 534m a.s.l.; part of the EMEP, ACTRIS, and GAW networks) in Central Europe.

Fine aerosol (PM1) was sampled for 24 h every second day from September 27, 2013 to August 9, 2014 on pre-baked quartz fibre filters. With some sampling gaps, we collected more than 140 samples, which were subsequently analyzed by EA-IRMS (elemental analysis - isotope ratio mass spectrometry). Results of TC, TN and isotope ratios were used to study the seasonal changes in  $\delta^{15}\text{N}$  and  $\delta^{13}\text{C}$  and explore the possible processes associated with different isotopic ratios and various sources, by comparing the data with those from other locations (e.g. Kundu *et al.*, 2010; Paluvuri *et al.*, 2011).

Seasonal averages of  $\delta^{15}\text{N}$  for aerosol TN and  $\delta^{13}\text{C}$  for TC are shown in Fig. 1 and Fig. 2, respectively. The  $\delta^{15}\text{N}$  showed positive values in all season with the maximum enrichment of  $^{15}\text{N}$  in summer. A large variation of  $\delta^{15}\text{N}$  compared with other studies (e.g. Kunwar *et al.*, 2016) suggest bigger diversity of aerosol sources in Central Europe, especially in winter and summer, which is consistent with our previous studies on site (e.g. Vodička *et al.*, 2015).

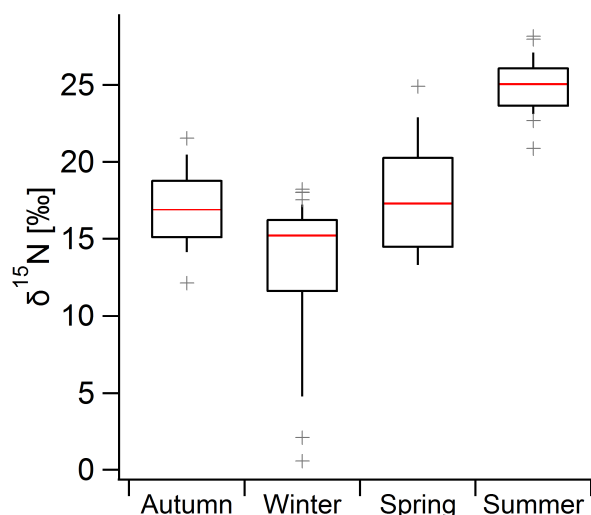


Fig. 1. Seasonal trend of  $\delta^{15}\text{N}$  in TN. The boxes indicate the 25<sup>th</sup> percentile (lower edge), median (red line), and 75<sup>th</sup> percentile (upper edge). The whiskers represent the 10<sup>th</sup> and 90<sup>th</sup> percentiles and crosses are outliers.

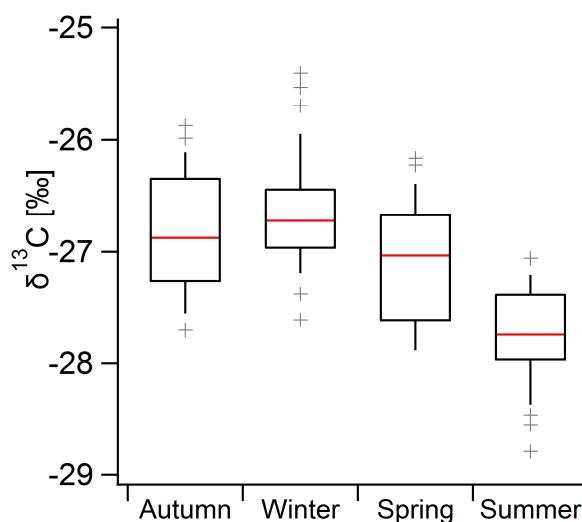


Fig. 2. Seasonal trend of  $\delta^{13}\text{C}$  in TC. The meaning of boxes is same like in Fig. 1.

Seasonal trend of  $\delta^{13}\text{C}$  in TC (Fig. 2) did not show a large variation with lower values compared to coastal aerosols (Kunwar *et al.* 2016). We found significantly lower  $\delta^{13}\text{C}$  values for summer, indicating a different source of carbon compared with other seasons. This is probably due to diverse sources of carbonaceous aerosols whose isotopic ratio is often overlaps (Gensch *et al.*, 2014).

Comparative analysis with supporting data from EC/OC, ions and meteorology can offer deeper insight for different isotope ratios, which will be discussed in detail during the presentation.

This conference contribution was supported by the the Japan Society for the Promotion of Science (JSPS) through Grant-in-Aid No. 24221001. We appreciate the financial support of JSPS fellowship to P. Vodička.

Gensch, I., Kiendler-Scharr, A., and Rudolph, J. (2014) *Int. J. Mass. Spec.* **365-366**, 206-221.

Kundu, S., Kawamura, K. and Lee, M. (2010) *J. Geophys. Res.* **115**, D20305.

Kunwar, B., Kawamura, K. and Zhu, C. (2016) *Atmos. Environ.* **131**, 243-253.

Pavuluri, C. M., Kawamura, K., Swaminathan, T. and Tachibana, E. (2011) *J. Geophys. Res.*, **116**, D18307,

Vodička, P., Schwarz, J., Cusack, M., Ždímal, V. (2015) *Sci. Total Environ.*, **518-519**, 424-433.

## Characteristics and formation of typical winter haze in Handan, one of the most polluted cities in China

S. Yang<sup>1</sup> F. K. Duan<sup>2</sup> and K. B. He<sup>3</sup>,

<sup>1</sup>School of Environment, Tsinghua University, Beijing 100084, China

<sup>2</sup>School of Environment, Tsinghua University, Beijing 100084, China

<sup>3</sup>School of Environment, Tsinghua University, Beijing 100084, China

Keywords: haze, secondary conversion, meteorological influence, heterogeneous reaction

Presenting author email: [yang-s16@mails.tsinghua.edu.cn](mailto:yang-s16@mails.tsinghua.edu.cn)

### Abstract review

The North China Plain (NCP) is one of the most severely polluted areas in China in terms of air quality (Duan et al., 2006). Handan, a city within the NCP region, is a typical city influenced by regional particulate matter (PM) pollution. One-year online field observation was carried out in 2015 in Handan with the aim of identifying the chemical composition and variations in PM<sub>2.5</sub>. Moreover, the concentration of aerosol precursors, meteorological factors, and secondary transformations are considered. The results demonstrate that the annual average PM<sub>2.5</sub> concentration in Handan is 122.35 μg m<sup>-3</sup>, approximately 2.5 times higher than the Chinese National Ambient Air Quality Standard (NAAQS) (35 μg m<sup>-3</sup>), and only 12 days were below the guideline. As expected, PM concentrations are highest in winter, especially in December.

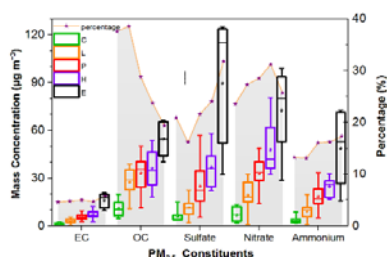


Fig.1 Concentrations and proportions of the five measured components at various daily pollution categories

For all the five-measured species commonly found in PM (nitrate, sulfate, ammonium, EC, and OC), nitrate and sulfate account for the largest proportion of PM<sub>2.5</sub>; during periods when the PM<sub>2.5</sub> concentration was below 400 μg m<sup>-3</sup>, nitrate dominates, while above this concentration, sulfate dominates. This is likely related to the nitrogen and sulfur oxidation ratios, which are in turn, especially the sulfur oxidation ratio, driven by high relative humidity (> 60%) (Sun et al., 2013). In addition,

haze events are driven by other meteorological conditions, wind speed and direction, where low wind speeds from the south and southwest enable pollutant accumulation, which are infrequently interspersed with brief periods with high wind speeds that promote pollutant dispersal.

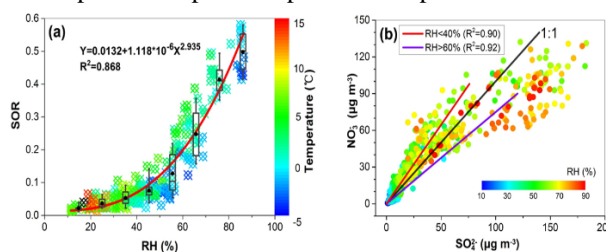


Fig. 2 SOR and RH color-mapped with temperature. (b) Correlation between NO<sub>3</sub><sup>-</sup> and SO<sub>4</sub><sup>2-</sup> color-mapped with RH.

Even though Handan is among the ten most polluted cities in China with regard to air pollution, few studies beyond model simulations have analyzed air pollutant concentrations in this city. Therefore, this study makes a significant contribution to understanding air pollution in Handan, which can further be used to improve our understanding of regional pollution in the highly populated North China Plain.

This work was supported by the National Science and Technology Program of China (grant numbers 2014BAC22B01 and 2016YFC0202700) and the National Natural Science Foundation of China (grant number 81571130090).

Duan, F.K., He, K.B., Ma, Y.L., Yang, F.M., Yu, X.C., Cadle, S.H., Chan, T., Mulawa, P.A., (2006) *Sci. Total Environ.* 355, 264-275.

Sun, Y.L., Wang, Z.F., Fu, P.Q., Jiang, Q., Yang, T., Li, J., Ge, X.L., (2013) *Atmos. Environ.* 77, 927-934.

## Local Vitrification of Water in Secondary Organic Aerosol

M. Lbadaoui-Darvas<sup>1</sup>, S. Takahama and M.N.D.S. Cordeiro<sup>3</sup>

<sup>1</sup>Atmospheric Particle and Research Laboratory, School of Architecture, Civil and Environmental Engineering, Swiss Federal Institute of Technology Lausanne (EPFL), CH-1015 Lausanne, Switzerland

<sup>2</sup>Atmospheric Particle and Research Laboratory, School of Architecture, Civil and Environmental Engineering, Swiss Federal Institute of Technology Lausanne (EPFL), CH-1015 Lausanne, Switzerland

<sup>3</sup>Department of Chemistry and Biochemistry, University of Porto, P-4169-007 Porto, Portugal

Keywords: alpha-pinene, molecular dynamics, SOA, molecular structure

Presenting author email: maria.lbadaoui-darvas@epfl.ch

A vast variety of organic compounds present in SOA can affect the state of water in the aerosol, eventually altering cloud condensation pathways, interactions, growth, reactivity and structure. (Lienhardt et al., 2015) The correct prediction of the physical state of SOA is thus a crucial question in atmospheric models, although to the large number organics makes it a difficult task. This study investigates molecular resolution structure of binary aqueous SOA searching for connections between the structure and solubility of the organic compounds and the physical state of water in the system.

In particular, we perform molecular dynamic simulations of the aqueous mixtures of major oxidation products of alpha-pinene. Some of the examined compounds are able to reduce the diffusion coefficient of water to as low as or lower than that in its glassy state. Further analysis reveals that this effect is reached by an interplay of solubility with lifetime and the number of hydrogen bonds formed by water either with other waters or with organics. Results concerning the structure emphasise that more soluble organic compounds form a mixture in which water is present in small clusters characterised by relatively high average local Steinhardt parameter and low coordination numbers. With the exception of one compound, a beta-peroxy derivative of pinonaldehyde, the addition of alpha-pinene oxidation products to water decreases the long-range order, as seen from the deviations of the first coordination shell from ideal tetrahedral arrangement as well as from the disappearance of the second peak of the oxygen-oxygen radial distribution functions. We conclude that alpha pinene oxidation product of medium and high solubility induce nanosegregation of the aqueous phase, resulting in smaller aqueous clusters whose physical state resembles the low density amorphous phase of water. We also develop a scoring function connecting the structure of the organic molecules to its efficacy to induce transition to glassy phase.

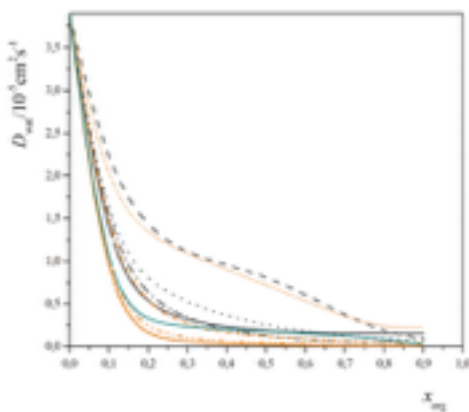


Figure 1. Diffusion coefficient of water as a function of organic concentration

Lienhard, D.M., Huisman, A.J., Krieger, U.K., Rudich, Y., Marcolli, C., Luo, B.P., Bones, D.L., Reid, J.P., Lambe, A.T., Canagaratna, M.R., Davidovits, P., Onasch, T.B., Worsnop, D.R., Steimer, S.S., Koop, T., Peter, T. (2015) *Atmos. Chem. Phys.*, **15**, 13599.

## Multistep phase transition in single optically-trapped aqueous aerosol particles

Kıvanç Esat, Grégory David, Theodoros Poulkas, Mikhael Shein and Ruth Signorell

Laboratory of Physical Chemistry, ETH Zurich, Vladimir-Prelog-Weg 2, CH-8093, Zurich, Switzerland

Keywords: Optical traps, light scattering, efflorescence, deliquescence

Presenting author email: kivanc.esat@phys.chem.ethz.ch

Aqueous aerosol particles enable us to prepare supersaturated samples upon drying, which eventually leads to efflorescence. Previous studies showed that an effloresced particle can become (semi-)solid amorphous or crystalline depending on the type of substance and the hydration-dehydration sequence it experiences (Mikhailov E. *et al.* 2009 and Ciobanu G.V. *et al.* 2010). Recently, Lee S. *et al.* (2016) demonstrated that the actual nucleation mechanism of supersaturated solutions can be a multiple pathway process, leading to the formation of solid particles with various structural properties. In this work, we study the efflorescence process of an optically-trapped, single aerosol droplet in the micron to submicron size range using light scattering methods.

We have recently demonstrated that ultraviolet broadband light scattering (BLS) is an accurate and precise technique to characterize the size, the refractive index, and the hygroscopic properties of individual spherical aerosol particles (David G. *et al.* 2016). Accurate sizing of a solid particle after efflorescence with BLS is a more challenging problem, since its shape can become irregular. However, we have found that the BLS spectrum recorded during efflorescence is still a very sensitive method to monitor the temporal changes a particle undergoes during efflorescence with high time-resolution ( $\sim 10$ ms). In this work, we observe multiple distinguishable steps during the transition using time resolved BLS measurements. Figure 1 shows the evolution of the BLS signal during efflorescence of a highly supersaturated aqueous  $K_2CO_3$  droplet at  $12.4 \pm 2\%$  relative humidity. The bottom panel classifies the different temporal features we observe for this model system. When the supersaturated droplet, feature  $\iota$ , starts to effloresce a spectral shift to feature  $\sigma$  is observed (see also top panel). This first spectral shift is followed by several further shifts ( $\sigma$  to  $\tau$ ,  $\tau$  to  $\sigma$ ;  $\sigma$  to  $\tau$ ,  $\tau$  to  $\sigma$ , and  $\sigma$  to  $\phi$ ). Intermediate features  $\sigma$  and  $\tau$  correspond to fast spectral fluctuations and slow drifting respectively. This process ends with feature  $\phi$ , where the particle becomes stable over an extended period of time (not shown). The steps and the intermediate regions can be studied with

very high temporal resolution. Repeated experiments show that each individual droplet exhibits a unique temporal behavior. In addition, structural differences between the dried particles are observed with Raman spectroscopy.

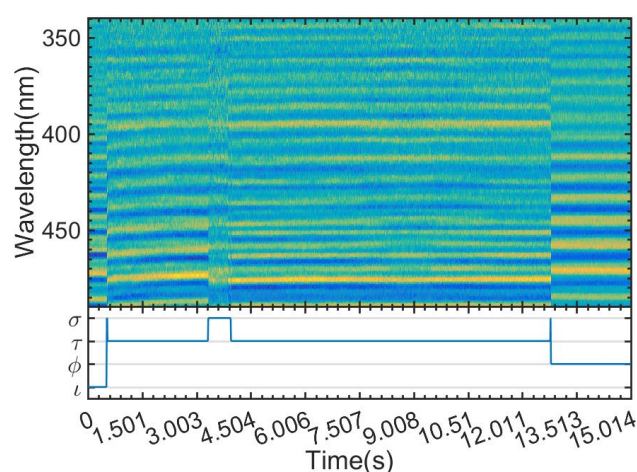


Figure 1. Evolution of the BLS signal of an efflorescing particle. In this color map image, blue means low and yellow means high intensity. The droplet radius before the phase transition is  $2160 \pm 80$  nm.

This work was supported by the Swiss National Science Foundation (SNSF grant no. 200020\_159205) and ETH Zürich.

Mikhailov E., Vlasenko S., Martin S. T., Koop T., Pöschl U., (2009), *Atmos. Chem. Phys.*, **9**, 9491–9522.

Lee S., Wi H. S., Jo W., Cho Y.C., Lee H. H., Jeong S., Kim Y., Lee G.W., (2016), *PNAS*, **113**, 13618–13623.

Ciobanu G.V., Marcolli C., Kreiger U. K., Zuend A. And Peter T., (2010), *J. Phys. Chem. A*, **114**, 9486–9495

David G., Esat K., Ritsch I. and Signorell R. (2016), *Phys. Chem. Chem. Phys.*, **18**, 5477–5485.

## Molecular dynamics simulation of the local structure and morphology of atmospheric nanoparticles

K.S. Karadima<sup>1,2</sup>, V.G. Mavrantzas<sup>1,2,3</sup> and S.N. Pandis<sup>1,2,4</sup>

<sup>1</sup>Department of Chemical Engineering, University of Patras, Patras, 26504, Greece

<sup>2</sup>Institute of Chemical Engineering Sciences, FORTH/ICE-HT, Patras, 26504, Greece

<sup>3</sup>Department of Mechanical and Process Engineering, ETH Zurich, Zurich, 8092, Zurich

<sup>4</sup>Department of Chemical Engineering, Carnegie Mellon University, Pittsburgh, 15213, USA

Keywords: molecular dynamics, nanoparticles, organic aerosol, morphology.

Presenting author email: kkaradima@chemeng.upatras.gr

The composition of atmospheric particles is complex and variable in space and time usually involving both inorganic and organic components as well as water, while thousands or tens of thousands of organic compounds remain unidentified. The morphology of these particles and their local structure and composition determines to a large extent their physical and chemical properties including rates of heterogeneous reactions, mass transfer rates of their components between the gas and particulate phases, equilibration timescales, etc. However, microstructures and phase configurations of airborne particles cannot be studied distinctly with typical experimental setups. Molecular dynamics simulations offer a potentially valuable alternative since they can provide significant insight into local morphologies and physicochemical properties.

In this work, we use molecular dynamics simulations to study multicomponent nanoparticles under atmospheric conditions and investigate the impact of humidity on particle composition and morphology at the nanoscale. Representative oxygenated and non-oxygenated organic compounds such as pinonic acid and n-triacontane are used to represent the organic fraction, while sulfate and ammonium ions as well as water molecules constitute the inorganic fraction. The gas phase is composed of nitrogen and oxygen molecules. An ensemble of six simulations is performed for a base case composition, where analysis revealed low standard mean error values for all calculated functions. A typical simulation, eg., for a system composed of 5000 atoms simulated for 60 ns in 8 CPUs, demands a two month computational time.

The molecular dynamics simulations provide information about the evolution of particle structure and density with time. The local concentration profiles of all species in the particle and the pair correlation functions as a function of distance from the center-of-mass of the particle can be used to study the simulated particle morphology. Pinonic acid molecules prefer to reside on the surface of the particle (Figure 1), especially when the water concentration in particle increases. However, the greater the organic mass fraction the deeper inside the particle the organic molecules can be traced, reaching even the core of the particle. Increasing the humidity or the organic mass fraction affects also the phase state of the particle and the mobility of its components. For example, the central part of the particle becomes less

solid-like and the mobility of all molecules and ions increases at higher relative humidity.

When the organic content of the particle is represented by n-alkanes, these tend to form a separate, well-organised structure at the surface of the particle. This is due to their hydrophobic character, which drives them away from the central part of the particle, where the inorganic species and most of the water prefer to be. This morphology renders organic molecules less mobile than inorganic species; on the other hand, it protects some of the alkane molecules from coming into contact with oxidizing agents. Lamellas formed by n-alkane molecules are observed in our simulations even when the particle contains oxygenated species (e.g., pinonic acid). In this case, however, pinonic acid molecules are found also at the interior of the particle, even close to its core. Still, a good fraction of both of these two types of organic molecules remains unreachable by radicals.

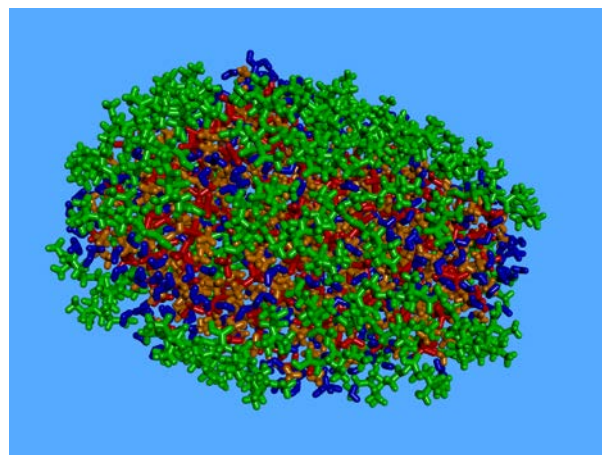


Figure 1. Snapshot of the predicted structure of a nanoparticle with a volume equivalent diameter of approximately 4.9 nm composed of 100 pinonic acid molecules (green), 200 sulfate ions (red), 400 ammonium ions (orange), and 400 water molecules (blue).

This work has been supported by the European Research Council Project “Atmospheric Organic Particulate Matter, Air Quality and Climate Change Studies” (ATMOPACS) (grant agreement 267099) and the U.S. National Science Foundation (grant agreement 1455244).

## Imaging molecular diffusion and iron oxidation reaction in organic aerosol particles

P. A. Alpert<sup>1</sup>, P. Corral Arroyo<sup>1</sup>, M. Ammann<sup>1</sup>, J. Dou<sup>2</sup>, U. Krieger<sup>2</sup>, S. S. Steimer<sup>3</sup>, J.-D. Förster<sup>4</sup>, F. Ditas<sup>4</sup>, C. Pöhlker<sup>4</sup>, S. Rossignol<sup>5</sup>, M. Passananti<sup>6</sup>, C. George<sup>7</sup>, B. Wang<sup>8</sup>, S. Zhang<sup>8</sup>, S. China<sup>9</sup>, A. Laskin<sup>9</sup>

<sup>1</sup>Laboratory of Environmental Chemistry, Paul Scherrer Institute, Villigen PSI, 5232, Switzerland

<sup>2</sup>Institute for Atmospheric and Climate Science, ETH Zurich, Zurich, 8092, Switzerland

<sup>3</sup>Department of Chemistry, University of Cambridge, Cambridge, CB2 1EW, England

<sup>4</sup>Biogeochemistry and Multiphase Chemistry Department, Max Planck Institute, Mainz, 55020, Germany

<sup>5</sup>Department of Chemistry, Aix-Marseille University, Marseille, 13284, France

<sup>6</sup>Department of Physics, University of Helsinki, Helsinki, 00100, Finland

<sup>7</sup>Université de Lyon 1 / CNRS, UMR5256, Institut de recherches sur la catalyse et l'environnement de Lyon, Villeurbanne, 69626, France

<sup>8</sup>State Key Laboratory of Marine Environmental Science, Xiamen University, Xiamen 361102, China

<sup>9</sup>Pacific Northwest National Laboratory, Richland, WA 99354, USA

Keywords: Multiphase Chemistry, Viscous Organic Aerosol, Iron Oxidation

Presenting author email: peter.alpert@psi.ch

Chemical reactions between gas phase oxidants and condensed phase organic aerosol particles may be limited due to exceptionally slow molecular diffusion. When organic matter is highly viscous, which typically occurs under cold and dry conditions, the distance a molecule can travel through an organic aerosol particle and then react during the particle lifetime may become quite short. We present a visualization and quantification of ozone molecular diffusion and reaction inside organic particles to oxidize inorganic materials, such as iron, at their core. This knowledge is applied to better understand how viscous organic matter can shield reactants in ambient atmospheric aerosol from oxidation. The degree to which organic matter in particles limits oxidant diffusion and reaction can affect iron oxidation state, which can impact the budget of HO<sub>2</sub> in the atmosphere and solubility of mineral nutrient deposition to the ocean.

The reaction of ozone with ferrous iron (Fe(II)) in mixed submicron Xanthan gum particles was spatially mapped on a 35x35 nm scale using scanning transmission X-ray microscopy coupled with near edge X-ray absorption fine structure spectroscopy (STXM/NEXAFS) in a temperature, T, and relative humidity, RH, controlled environmental cell at the PolLux beamline of the Swiss Light Source (SLS). Xanthan gum has multiple organic functionalities, is a surrogate for marine biogenic material rich in acidic-polysaccharides and it is gel-forming and polymerizable. Ozone exposed Fe(II) resulting in a transition to Fe(III) oxidation state. The STXM/NEXAFS technique is highly sensitive to the degree of oxidation at the Fe L-edge and the fraction of Fe(II),  $\alpha$ , can be derived from absorption at selected X-ray energies of 707.8 and 709.5 eV indicating Fe(II) and Fe(III), respectively.

At RH=80%, T=20 °C and 100 ppb of ozone, continued depletion of Fe(II) occurred from  $\alpha=0.7$  to 0.45 over a 2 hour exposure time. However, when RH was lowered to <10%,  $\alpha$  was maintained at its initial value of 0.7, even when ozone concentrations were increased to 300 ppb. Water is a known plasticizer (reduces viscosity when mixed) and Xanthan gum takes

up water even at subsaturated conditions. Thus, it is likely that Xanthan gum is highly viscous at low RH and prevents diffusion and reaction through the particle on spatial scales not accessible by STXM (i.e. <35 nm). At RH > 20%, gradients in  $\alpha$  were visualized as observed from a higher iron oxidation state at particle surfaces than in particle cores. Xanthan gum must transition from a glassy to a more semi-solid or liquid like state allowing for limited, but increasing molecular diffusion and reaction as RH increases.

Aerosol particles impacted by urban and marine environments were collected in the coastal South China Sea about 200 km offshore of the Guangzhou-Hong Kong urban district in the South China Sea and analyzed with STXM/NEXAFS for organic carbon and iron. The mixing state of organic carbon (OC), elemental carbon (EC, indicating the presence of soot), inorganic matter (In) were identified and mapped on thousands of single particles. The components OC and In was included in about 95% of all particles, which makes these the most common. Only 5% of particles were devoid of detectable organic material. All particles containing EC was associated with OC. Ferrous iron can be associated with EC and OC components, the latter being important as it can stabilize Fe(II) through organic ligands. Our analysis suggests that diffusion limitations can restrict oxidation reactions tending toward greater fractions of the more soluble and bioavailable Fe(II) compared with Fe(III). Thus, if Fe(II) is released into the atmosphere and transported to the ocean, moderate humidity (RH~50%) may be sufficient for reacto-diffusive limitations to persist preserving its oxidation state until deposition. This can impact predictions of nutrient iron deposition for use by marine algae and formation of Fe(III)-organic complexes, which form condensed phase radicals when exposed to sunlight. These data should aid in better understanding of aerosol chemistry and morphology in complex urban-marine environments. Furthermore, reacto-diffusive limitation should be considered important for accurate prediction of chemical aging, organic composition, toxicity, source apportionment and flux of atmospheric aerosol particles.

## Long-term observations of aerosol and cloud condensation nuclei concentrations in the Amazon rain forest and at a continental site with urban and rural influences

Oliver Lauer<sup>1</sup>, Mira L. Pöhlker<sup>1</sup>, Christopher Pöhlker<sup>1</sup>, Florian Ditas<sup>1</sup>, Thomas Klimach<sup>1</sup>, Isabella Hrabec de Angelis<sup>1</sup>, Alessandro Araújo<sup>2</sup>, Heinz G. Bingemer<sup>3</sup>, Joel Brito<sup>4,a</sup>, Samara Carbone<sup>4,b</sup>, Yafang Cheng<sup>1</sup>, Reiner Ditz<sup>1</sup>, Sachin S. Gunthe<sup>5</sup>, Jürgen Kesselmeier<sup>1</sup>, Tobias Könemann<sup>1</sup>, Jošt V. Lavrič<sup>6</sup>, Scot T. Martin<sup>7</sup>, Eugene Mikhailov<sup>8</sup>, Daniel Moran-Zuloaga<sup>1</sup>, Diana Rose<sup>3</sup>, Jorge Saturno<sup>1</sup>, Christiane Schulz<sup>1</sup>, Hang Su<sup>1</sup>, David Walter<sup>1</sup>, Jian Wang<sup>9</sup>, Stefan Wolff<sup>1,10</sup>, Henrique M. J. Barbosa<sup>4</sup>, Paulo Artaxo<sup>4</sup>, Joachim Curtius<sup>3</sup>, Meinrat O. Andreae<sup>1,11</sup>, and Ulrich Pöschl<sup>1</sup>

<sup>1</sup> Multiphase Chemistry & Biogeochemistry Departments, Max Planck Institute for Chemistry, Mainz, Germany.

<sup>2</sup> Empresa Brasileira de Pesquisa Agropecuária, Belém, PA, Brazil.

<sup>3</sup> Institute for Atmospheric and Environmental Research, Goethe University Frankfurt/Main, Germany.

<sup>4</sup> Institute of Physics, University of São Paulo, São Paulo, Brazil.

<sup>5</sup> Department of Civil Engineering, Indian Institute of Technology Madras, Chennai, India.

<sup>6</sup> Department of Biogeochemical Systems, Max Planck Institute for Biogeochemistry, Jena, Germany.

<sup>7</sup> School of Engineering and Applied Sciences, Harvard University, Cambridge, MA, USA.

<sup>8</sup> St. Petersburg State University, St. Petersburg, Russia.

<sup>9</sup> Biological, Environmental & Climate Sciences Dept., Brookhaven National Laboratory, Upton, NY USA.

<sup>10</sup> Instituto Nacional de Pesquisas da Amazonia (INPA), Manaus-AM, Brazil.

<sup>11</sup> Scripps Institution of Oceanography, University of California San Diego, La Jolla, CA USA.

<sup>a</sup> now at: Laboratory for Meteorological Physics, University Blaise Pascal, Clermont-Ferrand, France.

<sup>b</sup> now at: Federal University of Uberlândia, Uberlândia-MG, Brazil.

Keywords: CCN, Amazon rain forest, European semi-urban site, long-term study .  
Presenting author email: oliver.lauer@mpic.de

Size-resolved long-term measurements of atmospheric aerosol and cloud condensation nuclei (CCN) concentrations and hygroscopicity were conducted at the Taunus Observatory (TO) in central Europe close to the city of Frankfurt and the Taunus forest in Germany over two full seasonal cycle (July 2012 - April 2014). The analysis of this dataset is ongoing and will provide a climatology of CCN properties characteristic of a semi-urban/rural site in central Europe with different atmospheric conditions depending on the wind direction. The finding of this analysis will be compared with the results of the ATTO site, which is a remote central Amazonian rain forest site (Pöhlker et al. 2016; Andreae et al. 2015).

The particle hygroscopicity at the ATTO site exhibits a pronounced size dependence with lower values for the Aitken mode ( $\kappa_{\text{Ait}} = 0.14 \pm 0.03$ ), higher values for the accumulation mode ( $\kappa_{\text{Acc}} = 0.22 \pm 0.05$ ), and an overall mean value of  $\kappa_{\text{mean}} = 0.17 \pm 0.06$ , consistent with high fractions of organic aerosol. The hygroscopicity parameter,  $\kappa$ , exhibits remarkably little temporal variability: no pronounced diurnal cycles, only weak seasonal trends, and few short-term variations during long-range transport events. In contrast, the CCN number concentrations exhibit a pronounced seasonal cycle, tracking the pollution-related seasonality in total aerosol concentration. We find that the variability in the CCN concentrations in the central Amazon is mostly driven by aerosol particle number concentration and size distribution, while variations in aerosol hygroscopicity and chemical composition matter only during a few episodes.

Specifically, the hygroscopicity of the Aitken mode size range is a key aspect of our ongoing analysis.

This work was supported by the Max Planck Society (MPG), Max Planck Graduate Center (MPGC), German Federal Ministry of Education and Research (BMBWF contract 01LB1001A) and the Brazilian Ministério da Ciência, Tecnologia e Inovação (MCTI/FINEP contract 01.11.01248.00)

Andreae, M. O., Acevedo, O. C., Araújo, A., Artaxo, P., et al. (2015)

*The Amazon Tall Tower Observatory (ATTO): overview of pilot measurements on ecosystem ecology, meteorology, trace gases, and aerosols*, Atmos. Chem. Phys., 15, 10723-10776, 10.5194/acp-15-10723-2015.

Pöhlker, M. L., Pöhlker, C., Ditas, F., Klimach, T., et al. (2016)

*Long-term observations of cloud condensation nuclei in the Amazon rain forest – Part 1: Aerosol size distribution, hygroscopicity, and new model parametrizations for CCN prediction*, Atmos. Chem. Phys., 16, 15709-15740, 10.5194/acp-16-15709-2016

## Hygroscopic properties of different aerosol types at a suburban site (Madrid) in the Iberian Peninsula

E. Alonso-Blanco, F.J. Gómez-Moreno, M. Becerril-Valle, E. Coz, E. Díaz and B. Artíñano

Department of Environment, Center for Energy, Environmental and Technological Research (CIEMAT), Madrid, E-28040, Spain

Keywords: Aerosol Growth Factor, HTDMA, Aerosol Hygroscopicity  
Presenting author email: fj.gomez@ciemat.es

Aerosol–cloud interactions contribute to the largest uncertainty to estimate the aerosol effects on climate (IPCC, 2013). Absorption of water by aerosol particles may change the cloud characteristics in many ways such as altering their albedo, lifetime or precipitation efficiency.

The CIEMAT suburban measurement station (40° 27' 23.2" N, 03° 43' 32.3" E, altitude: ~650 m a.s.l.) is located in the north-west section of Madrid. Pollutants levels measured at the station, including aerosol particles, are mainly the result of traffic emissions in the city. Thus, the aerosol composition in the fine fraction is mainly carbonaceous material. Both the local and large scale meteorological features and, therefore, the atmospheric chemical processing of the aerosol are of special importance in this regard. This conditions the aerosol properties especially dependent on their composition as the hygroscopicity is.

Therefore, we study the changes in the hygroscopicity of different aerosol types measured during different meteorological situations: a Volcanic Ash Episode (VAE), a Local Polluted Episode (LPE) and a North Atlantic Episode (NAE). With this scope, information on the size-resolved hygroscopicity of ambient submicron particles (for dry particle sizes of 50, 80, 110, 190 and 265 nm conditioned at 90% RH) obtained using a custom-built Hygroscopic Tandem Differential Mobility Analyser (H-TDMA) (Nilsson et al., 2009) and on the chemical composition of non-refractory submicron aerosol (NR-PM<sub>1</sub>), ammonium, nitrate, sulphate, chloride and organics, determined with an Aerodyne Aerosol Chemical Speciation Monitor (ACSM) are used.

The probability density functions of the hygroscopic growth factor (PDF-GFs) presented structures with two groups of hygroscopic particles, less (LH) and more hygroscopic (MH) for all the episodes. However, the number fraction (NF) of the MH particles was larger for VAE (up to 0.8 for 265 nm particles) than for LPE and NAE, i.e. this last episode showed the largest NF values for MH particles (Fig. 1). This is evidenced in the mean hygroscopic growth factor (HGF<sub>mean</sub>) (Gysel et al., 2009) averaged for each episode. Values during VAE were much higher than during LPE and NAE. The HGF<sub>mean</sub> values found for 50 nm particles, ~1.2 for all the episodes, suggested a significant contribution of organics species traffic-related for this size.

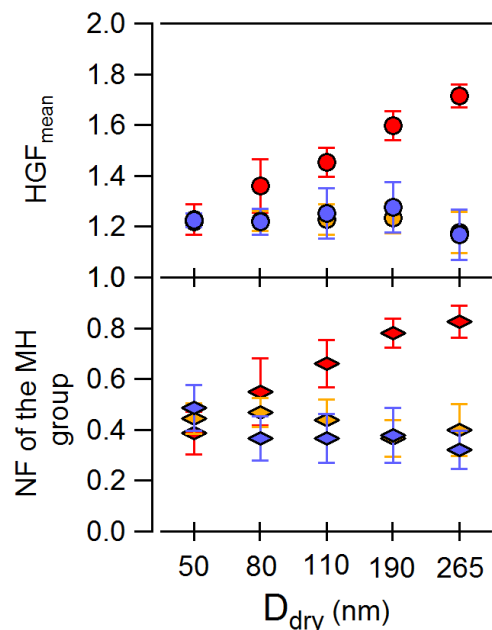


Figure 1. HGF<sub>mean</sub> and NF of the MH particles group for dry particle sizes of 50, 80, 110, 190 and 250 nm during the VAE (red), LPE (orange) and NAE (blue).

The hygroscopic growth was related with the inorganic species measured during the episodes. During VAE, sulphate corresponded to the 38±16% of the total aerosol mass, during the LPE nitrate was the 22±7% and during the NAE chloride was the possible responsible for the hygroscopicity observed. Organics were one of the main contributors to the NR-PM<sub>1</sub> during all episodes.

This work has been partially supported by the Spanish R&D Plan under PROACLIM Project (CGL2014-52877-R) and Madrid Regional Research Plan through TECNAIRE (P2013/MAE-2972). The authors are grateful to Martin Gysel for the development of TDMA<sub>fit</sub> algorithm to invert HTDMA data and allowing free use within the scientific community.

- IPCC (2013). The Physical Science Basis.  
Gysel, M., McFiggans, G. B., and Coe, H. (2009) *J. Aer. Sci.* **40**(2), 134-151.  
Nilsson, E., Swietlicki, E., Sjogren, S., Löndahl, J., Nyman, M., and Svenningsson, B. (2009) *Atmos. Meas. Tech.* **2**(1), 313-318.

## Volatility distribution of organic aerosol components using ambient and laboratory measurements

E. Karnezi<sup>1</sup>, E. Louvaris<sup>2,3</sup>, E. Kostenidou<sup>3</sup>, K. Florou<sup>2,3</sup> and S. N. Pandis<sup>1,2,3</sup>

<sup>1</sup>Department of Chemical Engineering, Carnegie Mellon University, Pittsburgh, 15213, USA

<sup>2</sup>Department of Chemical Engineering, University of Patras, Patras, 26504, Greece

<sup>3</sup>Institute of Chemical Engineering Sciences, FORTH/ICE-HT, 26504, Patras, Greece

Keywords: Volatility, thermodenuder, dilution

Presenting author email: ekarnezi@andrew.cmu.edu

Organic compounds represent a significant fraction of submicrometer atmospheric aerosol mass. Even if most of these compounds are semi-volatile at atmospheric concentration levels, the ambient organic aerosol volatility is quite uncertain. This work analyzes volatility measurements of organic aerosol and its components collected in several field and laboratory studies and synthesizes their results.

Measurements combining a thermodenuder (TD) and a High Resolution Time-of-Flight Aerosol Mass Spectrometer (HR-ToF-AMS) took place during summer 2009 and winter 2010 in Paris, France and during the winter of 2013 in the city of Athens. The Karnezi et al. (2014) volatility distribution algorithm is applied to these datasets in order to estimate the volatility of the organic aerosol (OA) and its components (determined using Positive Matrix Factorization) during the two campaigns.

Combining the O:C ratio and volatility distributions of the various factors, we integrated our results from both campaigns into the 2D-Volatility Basis Set. The factor locations agreed well with the location of factors proposed by Donahue et al. (2012), with the exception of the ELVOC components of most factors. The average O:C was not directly linked to the factor's volatility distribution.

The estimated vaporization enthalpies ( $\Delta H_{\text{vap}}$ ) for the different data sets were quite consistent with values around 100 kJ mol<sup>-1</sup>. The analysis of the measurements suggested low resistances to mass transfer in most cases. The estimated  $\Delta H_{\text{vap}}$  and accommodation coefficients for the biomass burning OA (BBOA) factor including their uncertainties are shown in Figure 1.

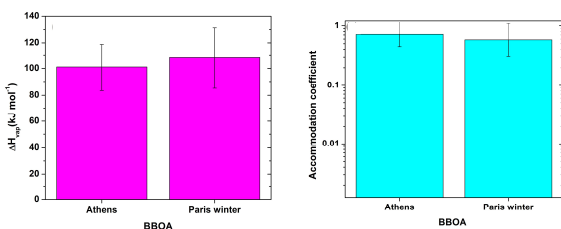


Figure 1. Comparison of estimated  $\Delta H_{\text{vap}}$  and accommodation coefficients for BBOA during the Athens and Paris winter campaigns.

Comparison of the OA volatility distributions requires scaling to the same concentration. Figure 2a shows a comparison between the volatility distributions of the cooking OA (COA) factors determined in the Athens

and Paris campaigns. The results indicate differences qualitatively consistent with the corresponding differences in the AMS spectra of the factors. On the other hand comparison of the COA volatility determined in Athens and the laboratory (meat charbroiling) after scaling to the same concentration suggest very similar volatility distributions (Figure 2b).

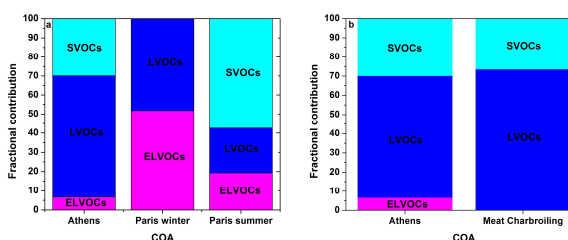


Figure 2. Comparison of the COA composition (a) between ambient COA in Athens and Paris campaigns (b) between the Athens winter COA and experimental COA from meat charbroiling experiments.

The uncertainties of the volatility distributions can be reduced by combining thermodenuder and isothermal dilution measurements as suggested by Karnezi et al. (2014). This approach, combining TD and isothermal dilution measurements, was tested in smog chamber experiments using OA produced during meat charbroiling. The use of isothermal dilution resulted in decrease of the uncertainty of the higher volatility components and of the estimated effective enthalpy of vaporization.

This work was supported by the FP7-IDEAS-ERC ATMOPACS project (Grant Agreement 267099) and the ARISTEIA action of the Operational Programme Education and Lifelong Learning and is co-funded by the European Social Fund (ESF) and national resources.

Donahue, N. M., Kroll, J. H., Pandis, S. N. and Robinson, A. L. (2012) A two-dimensional volatility basis set – Part 2: Diagnostics of organic-aerosol evolution, *Atmos. Chem. Phys.*, 12, 615–634.

Karnezi, E., Riipinen, I. and Pandis, S.N. (2014) Measuring the atmospheric organic aerosol volatility distribution, *Atmos. Meas. Tech.*, 7, 2953–2965.

## Hygroscopicity of dimethylamine-sulfuric acid nanoparticles

O.-P. Tikkanen<sup>1</sup>, O. Väisänen<sup>1</sup>, H. Wang<sup>1</sup>, E. Holopainen<sup>1</sup>, L. Hao<sup>1</sup>, A. Buchholz<sup>1</sup>, A. Pajunoja<sup>1</sup>, A. Virtanen<sup>1</sup> and T. Yli-Juuti<sup>1</sup>

<sup>1</sup>Department of Applied Physics, University of Eastern Finland, Kuopio, FI-70211, Finland

Keywords: Hygroscopicity, dimethylamine, nanoparticles, thermodynamics

Presenting author email: op.tikkanen@uef.fi

We have studied the hygroscopicity of aerosol particles that consist of mixtures of dimethylamine (DMA) and sulfuric acid (SA). Both sulfuric acid and dimethylamine have been observed in atmospheric particles (Sipilä *et al.*, 2010, Smith *et al.*, 2010).

The hygroscopic growth of the particles was measured with the nano hygroscopicity tandem differential mobility analyzer (nano-HTDMA) measurement system. The measured hygroscopicity was compared to theoretical values calculated with a state-of-the-art thermodynamic equilibrium model (E-AIM; Clegg *et al.*, 1998).

We prepared five aqueous DMA-SA solutions with molar DMA:SA ratios of 0.33:1, 0.5:1, 1:1, 1.5:1 and 2:1. The hygroscopicity measurements were carried out in four different relative humidities (RH) spanning from 0% to 80% and with four different dry particle diameters between 10 nm and 25 nm. The particles were produced by atomizing the aqueous solutions.

Table 1. DMA:SA ratios set in the atomization solution and measured with the AMS.

Atomization solution DMA:SA ratio [mol:mol]	AMS measured DMA:SA ratio [mol:mol]
0.5:1	1:1
1:1	1.7:1
2:1	1.95:1

In addition to the hygroscopicity measurements we also measured the compositions of the nanoparticles with an aerodyne high resolution time-of-flight aerosol mass spectrometer (AMS). The average aerodynamic diameter of the atomized particles measured with the AMS was approx. 300 nm. For the atomization solution DMA:SA ratios of 0.5:1, 1:1 and 2:1 the DMA:SA ratios measured with the AMS can be found in table 1. We found that the DMA:SA ratio of the particles measured with AMS differed from those predicted in preparing the aqueous solutions. Thus, the results were analyzed with respect to the AMS measured compositions.

Our results are summarized in figure 1 where the hygroscopic growth factor of particles with dry size of 15 nm is plotted as a function of the relative humidity. The hygroscopic growth factor is defined as  $GF = D_{wet}/D_{dry}$ , where  $D_{wet}$  is the diameter of the humidified particle.

The results show that the model underestimates the hygroscopic growth factor in all three studied compositions. Further, the relative difference between the measurements and the model increases as the

particles become more basic. The discrepancy increases with increasing RH.

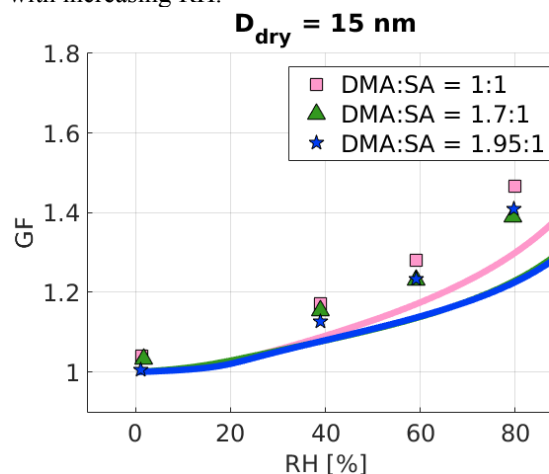


Figure 1. Measured (markers) and modelled (lines) hygroscopic growth factor ( $GF = D_{wet}/D_{dry}$ ) as a function of the RH. Different colors correspond to different particle compositions.

Our results hint, that the hygroscopicity of the dimethylamine containing aerosol particles might be underestimated in current models when the particle size is in order of few tens of nanometres. However, based on our analysis this relative difference is only 15% at maximum.

This work is supported by The Academy of Finland (272041, 259005, 299544), European Research Council (ERC Starting Grant 335478), University of Eastern Finland Doctoral Program in Environmental Physics, Health and Biology and strategic funding from the University of Eastern Finland.

### References

- Clegg, S. L., Brimblecombe, P., and Wexler, A. S. (1998) *J. Phys. Chem. A*, **102**, 2137-2154.
- Sipilä, M., Berndt, T., Petäjä, T., Brus, D., Vanhanen, J., Stratmann, F., Patokoski, J., Mauldin, R.L., Hyvärinen, A.-P., Lihavainen, H. and Kulmala, M., (2010) *Science* **327(5970)**, 1243-1246
- Smith, J. N., Barsanti, K. C., Friedli, H. R., Ehn, M., Kulmala, M., Collins, D. R., Scheckman, J., Williams, B. J. and McMurry, P. H. (2010). *Proc. Natl. Acad. Sci. U.S.A.* **107(15)**, 6634-6639

## On-road measurements of primary and secondary aerosol on European highways from the Baltic Sea to the Mediterranean

M. Dal Maso<sup>1</sup>, M. Olin<sup>1</sup>, J. Heikkilä<sup>1</sup>, P. Simonen<sup>1</sup>, A. Rostedt<sup>1</sup>, E. Saukko<sup>1\*</sup>, H. Kuuluvainen<sup>1</sup>, J. Kalliokoski<sup>1</sup>, O. Potila<sup>1</sup>, A. Järvinen<sup>1</sup>, M. Poikkimäki<sup>1</sup>, T. Rönkkö<sup>1</sup> and J. Keskinen<sup>1</sup>

<sup>1</sup> Laboratory of Physics, Tampere University of Technology, P.O. Box 692, 33101 Tampere, Finland

\* Now at PEGASOR Oy, Hatanpään valtatie 34, 33100 Tampere, Finland

Keywords: atmospheric aerosols, measurement, emissions, on-road measurement.

### Introduction

Motorways, while making up a minor fraction of roads in Europe, carry a disproportionately large amount of traffic (Eurostat, 2015). Measurements of vehicle emissions have shown that highway driving at high engine loads may cause above average emissions of both primary and secondary particulate matter (e.g. Simonen et al., 2016). These factors together make highways a significant source of air pollutants. Presently, comprehensive data of simultaneous primary and potential secondary aerosol mass measurements on motorways does not yet exist. Here, we present data from three trans-European measurement expeditions that were carried out on highways reaching from Southern Finland to the Mediterranean, covering in total close to 8'000 km of highways. This dataset elucidates the relative fractions of primary and secondary emissions for highway driving, as well as gives new insights on the particle number emissions for highway driving.

### Methods

The measurements we performed in 2015 and 2016 aboard the TUT Mobile measurement unit, an automatic- transmission Mercedes-Benz Sprinter van modified to accommodate high-quality aerosol and trace gas observation setups. The modifications included a stable electronic power supply, with a supplementary generator powered by the van engine, a lithium battery, a current regulation system and an inverter-charger allowing continuous operation while driving. In addition, the van is fitted with aerosol and gas sampling lines, instrument installation shelving, a GPS and weatherstation, and a temperature regulation system.

During the trans-European expeditions the instrumentation aboard the measurement unit consisted of aerosol size distribution instrumentation (Dekati ELPI), aerosol number concentration instrumentation (TSI and Airmodus CPC:s), trace gas detectors (CO<sub>2</sub>, NO<sub>x</sub>, O<sub>3</sub>), and a fast-response oxidation flow tube for the simulation the conversion of freshly emitted aerosol to photochemically aged aerosol (TUT Secondary Aerosol Reactor, TSAR). To bring the measured concentrations into the instrument's detection range, we used bridge dilution systems.

### Results and discussion

The route driven during the two expeditions is shown in Fig.1. Measurements were predominantly performed on highways, with the driving speed over 80 km/h.

The aerosol number concentrations were found to be clearly elevated in comparison to background. Motorway median number concentrations exceeded  $4 \cdot 10^4 \text{ cm}^{-3}$ . Using CO<sub>2</sub> data, we estimated average high-speed motorway driving number emission factors. Measurements using the TSAR showed that concentrations of potential secondary mass clearly exceeded the primary mass emissions.

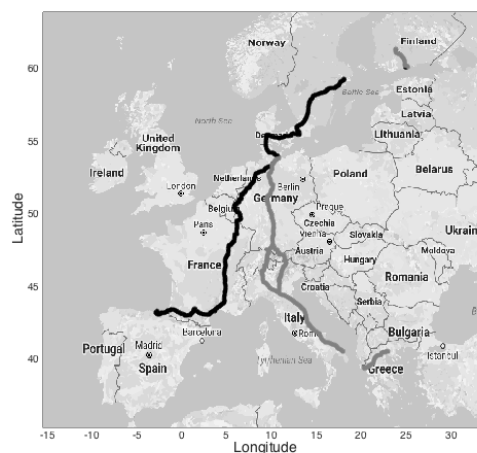


Figure 1. The routes driven during the expeditions

This work has been supported by the TUT Graduate School and the Maj and Tor Nessling Foundation.

Eurostat (2015): *Energy, transport and environment indicators*. Publications Office of the European Union, Luxembourg. doi: 10.2785/547816

Simonen, P. et al. (2016): A new oxidation flow reactor for measuring secondary aerosol formation of rapidly changing emission sources. *Atm. Meas. Tech. Discuss.*, 10.5194/amt-2016-300.

## Driving factors for aerosol variability in the foothills of central Himalayas

R.K. Hooda<sup>1,2</sup>, N. Kivekäs<sup>1</sup>, E. O'Connor<sup>1</sup>, M. Collaud-Coen<sup>3</sup>, J-P. Pietikäinen<sup>1</sup>, V. Vakkari<sup>1</sup>, J. Backman<sup>1</sup>, A.-P. Hyvärinen<sup>1</sup>, H. Lihavainen<sup>1</sup>

<sup>1</sup>Finnish Meteorological Institute, Helsinki, FI-00101, Finland

<sup>2</sup>The Energy and Resources Institute, IHC, New Delhi, 110003, India

<sup>3</sup>Federal office of Meteorology and Climatology, MeteoSwiss, Payerne, Switzerland

Keywords: Aerosol, driving factor, meteorology, long-range transport.

Presenting author email: niku.kivekas@fmi.fi

Despite of significant improvement atmospheric aerosols still pertain larger uncertainty than the greenhouse gases in the estimation of total radiative forcing (Forster et al., 2007). Yu et al. (2006 & 2009) presented that measurement-based estimate of globally averaged aerosol direct radiative forcing (DRF) is 55 – 80% greater than model-based estimates, and the discrepancy is even wider on regional scales and for the anthropogenic aerosols.

Multi-year continuous observations of aerosols significantly assist in analyzing trends, finding driving factors and validating computational simulations. In this study we have analyzed 10 years of continuous measurements of several aerosol variables and meteorological parameters between years 2005 and 2014 at Mukteshwar site in the foothills of Indian Himalayas.

The site (Fig 1) is located on a mountain ridge in the foothills of Indian Himalayas. The area is has a monsoon climate with most of the annual precipitation falling during the monsoon months (July and August).

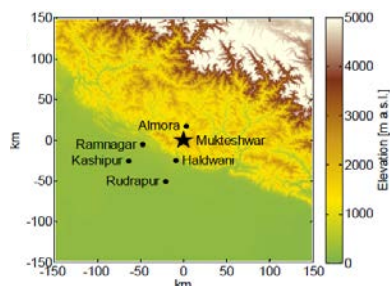


Figure 1. The orography near the Mukteshwar site and the major population centres close by.

The mixing of air from lower altitudes was associated to increased turbulence at the site, presented as wind speed variability and wind direction variability (Fig 2). There was more turbulence in day time, and the pattern of turbulence followed also the seasonal changes in sunrise and sunset times very well. A similar pattern was also found for water vapor concentration at the site.

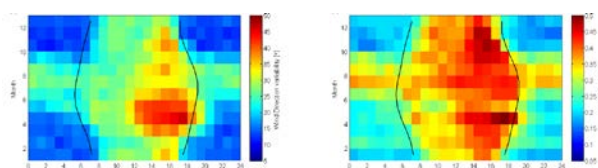


Figure 2. Wind direction variability (left) and wind speed variability (right) as function of time-of-day and month.

There was a clear diurnal cycle in all aerosol particle concentration parameters during all seasons apart for monsoon (Fig 3). All external aerosol parameters showed 1.5 – 2 times higher values during afternoon than during night time. This was linked to the diurnal pattern of turbulent mixing layer height, bringing polluted air from the valleys to the site. The aerosol internal properties did not show a clear diurnal cycle.

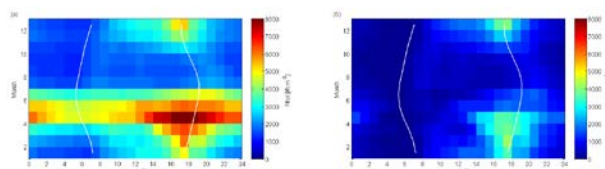


Figure 3. mean value and variability of particle number concentration as function of time-of-day and month.

The seasonal cycles of all external aerosol parameters were also very clear. Every year the monsoon rains removed most of the aerosol particles from the air. Then the aerosol concentration started to accumulate, showing a lower peak in the fall and a higher one in the pre-monsoon season. These peaks coincide with the crop-residue burning seasons and also with the dust-storm season in the spring. It is also clear that in spring the particle concentration parameters showed high values also at night, indication regional scale pollution. The winter months typically showed somewhat lower values, which could be explained by the lower mixing layer bringing less polluted air to the site.

In conclusion, we can state that the diurnal and seasonal meteorological cycles govern the aerosol concentrations at Mukteshwar so strongly that they hide other possible driving factors.

This work was supported by the Ministry of Foreign Affairs of Finland and Academy of Finland #264242.

Forster, P., et al. (2007) *Changes in atmospheric constituents and in radiative forcing, in Climate Change 2007, WG I, IPCC*: Cambridge Univ. Press.

Yu, H., et al. (2006), *Atmos. Chem. Phys.*, **6**, 613–666.

Yu, H., et al. (2009), *Remote sensing and in situ measurements of aerosol properties, burdens, and radiative forcing, in Atmospheric Aerosol Properties and Climate Impacts*, National Aeronautics and Space Administration, Washington, D. C., USA.

## Characterisation of propane-based CAST soot samples by combined vibrational spectroscopic and mass spectrometric studies

J. A. Noble<sup>1</sup>, L. Ngo<sup>1,2</sup>, A. R. Ikhenazene<sup>1</sup>, C. Irimiea<sup>1</sup>, G. Lefevre<sup>3</sup>, M. Vojkovic<sup>1</sup>, D. Duca<sup>1</sup>, S. Kenny<sup>1</sup>, C. Pirim<sup>1</sup>, Y. Carpentier<sup>1</sup>, B. Chazallon<sup>1</sup>, N. Nuns<sup>4</sup>, J. Yon<sup>3</sup>, E. Therssen<sup>2</sup>, and C. Focsa<sup>1</sup>

<sup>1</sup>Laboratoire de Physique des Lasers, Atomes et Molécules (PhLAM, UMR 8523 CNRS), Université de Lille, Lille, F-59000, France

<sup>2</sup>Laboratoire Physicochimie des Processus de Combustion et de l'Atmosphère (PC2A, UMR 8522 CNRS), Université de Lille, Lille, F-59000, France

<sup>3</sup>Complexe de Recherche Interprofessionnel en Aérothermochimie (CORIA, UMR 6614 CNRS, INSA Rouen, Uni. Rouen), Normandie Université, Rouen, F-76000, France

<sup>4</sup>Institut M.E. Chevreul (UMR 8207 CNRS), Université de Lille, Lille, F-59000, France

Keywords: soot, combustion aerosol, vibrational spectroscopy, mass spectrometry.

Presenting author email: jennifer.noble@univ-lille1.fr

Combustion soot is the most important anthropogenic source of solid aerosol particles. Soot particles can have a direct or indirect effect on climate that gives rise to important consequences for both atmospheric radiative forcing and cloud formation and lifetime, for example they might absorb solar radiation, heating the troposphere, or aid the formation of ice crystals, thereby producing reflective (i.e. cooling) ice clouds. Many studies have been conducted to characterise soot particles (Hoose *et al.* 2012). A better understanding of the role of combustion soots in atmospheric physicochemical processes can be obtained by investigating their composition and molecular structure.

In this study, we used micro-Raman and micro-Fourier Transform Infrared (FTIR) spectroscopies, in combination with Secondary Ion Time-of-Flight Mass Spectrometry (ToF-SIMS) and Two-step Laser (desorption/ionisation) Mass Spectrometry (L2MS), to characterise soot particles produced by a Combustion Aerosol Standard (CAST) burner supplied with various propane-air mixtures. In this work, two collections of exhaust material were made on quartz microfibre filters: a “front filter” (to collect particulate matter) and a second “back filter” covered with carbon black (to adsorb exhaust gases that passed through the front filter, following the principle of Faccineto *et al.* (2011)).

Micro-Raman and micro-FTIR spectroscopies are highly sensitive techniques which reveal the chemical composition of a soot via the vibrational modes of its composite molecules (Ess *et al.* 2016). In particular, the degree of aromaticity, determined by the relative abundance of polycyclic aromatic hydrocarbons (PAHs) in the soot, will determine its physicochemical properties. L2MS is also especially well adapted for PAH detection as it is possible to achieve a smooth desorption/ionisation step, thus avoiding post-ionisation fragmentation (Faccineto *et al.* 2011). In contrast, ToF-SIMS provides high sensitivity for both inorganic and organic species. Nevertheless, this technique has not, so far, been widely used in atmospheric environmental science (Cheng *et al.* 2014). Complementary high-resolution information is obtained on particular classes of molecules identified in the samples, including organosulfates, oxygenated/nitrogenated hydrocarbons, PAHs and heavy metals.

In our soot samples, the relative abundance and the mass distribution of PAHs is found to vary with operation point of the CAST burner (as has been previously

measured in various studies, including Parent *et al.* (2016)). Interestingly, the spectroscopic results also vary with the collection method of the soot, as is evident by comparing the distributions of the soot collected on the front and back filters, shown in Figure 1. Our combined mass spectrometry and vibrational spectroscopy studies suggest that this is a key factor in the successful extraction of spectral and compositional information, both in the laboratory and in factory tests.

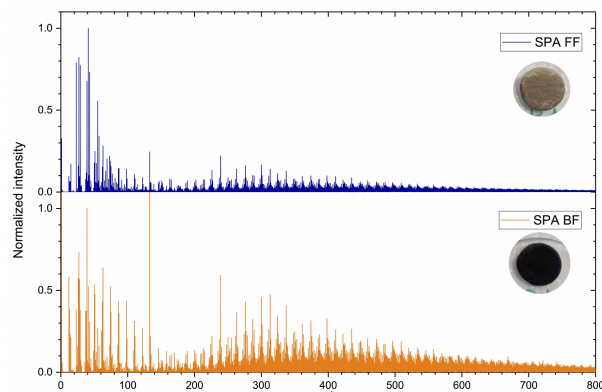


Figure 1. SIMS spectra of CAST SPA soot collected on front (blue) and back (orange) filters (details in text).

This work was supported by the French National Research Agency (ANR) through the PIA (Programme d'Investissement d'Avenir) under contract ANR-10-LABX-005 (CaPPA – Chemical and Physical Properties of the Atmosphere), the European Commission Horizon 2020 project PEMS4Nano, and the CLIMIBIO project via the Contrat de Plan Etat-Région of the Haut-de-France region.

Cheng, W. J., Weng, L. T., Li, Y. J., Lau, A., Chan, C., and Chan, C. M. (2014) *Surf. Interface Anal.* 46, 480-488.

Ess, M. N., Ferry, D., Kireeva, E. D., Niessner, R., Ouf, F.-X., and Ivleva, N. P. (2016) *Carbon* 105, 572-585.

Faccineto, A., Desgroux, P., Ziskind, M., Therssen, E., and Focsa, C. (2011) *Combust. Flame* 158, 227-239.

Hoose, C., and Möhler, O. (2012) *Atmos. Chem. Phys.* 12, 9817-9854.

Parent, P., Laffon, C., Marhaba, I., Ferry, D., Regier, T. Z., Ortega, I. K., Chazallon, B., Carpentier, Y., and Focsa, C. (2016) *Carbon* 101, 86-100.

## Characterization of the aging process of smoke observed over Austria using organic carbon mixing ratio

C. Talianu<sup>1,2</sup><sup>1</sup>*Institute of Meteorology, University of Natural Resources and Life Sciences, Vienna, Austria,*<sup>2</sup>*National Institute for R&D in Optoelectronics, Magurele, Romania*

Keywords: smoke, organic carbon, aerosol aging, lidar ratio.

Presenting author email: camelia.talianu@boku.ac.at

The smoke from anthropogenic and natural sources is considered to be a mixture of sulphates, black carbon (BC) and organic carbon (OC), see Solomon et al (2006). It is produced in two ways: emitted directly as particles into atmosphere (primary aerosols), or created in the atmosphere after chemical or physical transformations of precursor gases (secondary aerosols). Most of the smoke is in the optically active accumulation mode.

In this paper, a method to characterize the smoke aging process based on mixing ratio is presented. For this study we used MACCIII reanalysis data at 700 hPa level, related to OC, BC and Sulphate, for March – May 2014, for Vienna, Austria as reference site. Seven cases of smoke were identified, using a back-trajectories analysis based on Flexpart aerosol dispersion model, see Stohl et al (2005). The cases selected for this study are shown in Table 1.

Table 1. Cases of smoke over Vienna in Spring 2014.

Date	Hour	Source
22 March	00:00 UTC	Austria
2 April	12:00 UTC	North America
4 April	18:00 UTC	North America
8 April	18:00 UTC	Austria
14 April	12:00 UTC	North West Europe
29 April	18:00 UTC	South East Europe
7 May	06:00 UTC	North America

The microphysical properties for smoke compound calculated at 0 % relative humidity, are shown in Table 2.

Table 2. Microphysical properties for BC hydrophilic (BC1), BC hydrophobic (BC2), OC hydrophilic (OC1), OC hydrophobic (OC2), Sulphate (SU).

Spc	Sigma	Density [ $\mu\text{g}/\text{m}^3$ ]	Radius [ $\mu\text{m}$ ]	Reference
BC1	1.7	1.5	0.0118	Solomon et al (2006)
BC2	2.0	1.5	0.03	Solomon et al (2006)
OC1	2.0	1.7	0.06	Solomon et al (2006)
OC2	2.0	1.7	0.1	Solomon et al (2006)
SU	2.03	1.7	0.069	Koepke et al (1997)

The smoke aerosol is considered to have a small depolarization (less than 5%). The optical properties for

smoke were calculated using T-Matrix method for two wavelengths: 350 nm and 550 nm. The aging process was determined using two methods: ratio of OC mixing ratio to BC mixing ratio (OC/BC), respectively ratio of OC mixing ratio to total mixing ratio (OC/T). In order to estimate the aerosol ages, the result was compared with the ratio (RLR) of lidar ratio at 550 nm to lidar ratio at 350 nm, see Nicolae et al (2013).  $\text{RLR} < 1$  means fresh smoke and  $\text{RLR} \geq 1$  means aged smoke. The age of smoke is proportional to the growth of the RLR.

### Results

Figure 1 shows the comparison between RLR derived from optical parameters and the mixing ratios for each case analysed.

We obtained a good correlation between RLR and both methods. The results shows that the age of aerosols increases with increasing content of OC.

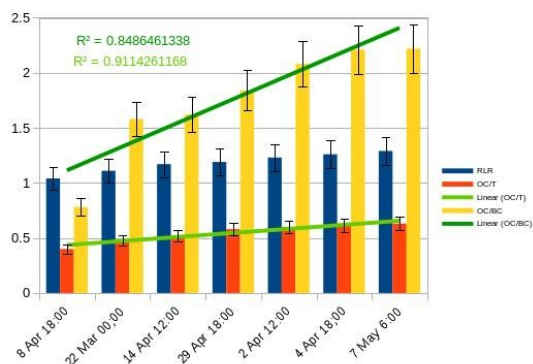


Figure 1. Comparison between RLR and OC/T and OC/BC.

This work is supported by Austrian Science Fund (FWF): project number M 2031 Meitner-Programm.

Solomon, F., Giorgi, F., and Liousse, C. (2006) *Tellus*, **58B**, 51–72

Stohl, A., Forster, C., Frank, A., Seibert, P., and Wotawa, G. (2005) *Atmos. Chem. Phys.*, **5**, 2461–2474

Koepke, P., M. Hess, I. Schult, and E.P. Shettle (1997), *Report No. 243*, Max-Planck-Institut für Meteorologie, Hamburg

Nicolae, D., Nemuc, A., Müller, D., Talianu, C., Vasilescu, J., Belegante L., and Kolgotin, A. (2013), *J. Geophys. Res.*, **118**, 2956–2965

## Typical winter haze pollution in Zibo, an industrial city in China: Characteristics, secondary formation, and regional contribution

Hui Li<sup>1</sup>, Fengkui Duan<sup>2</sup>, Kebin He<sup>3</sup>

<sup>1</sup> School of Environment, Tsinghua University, Beijing 100084, China

<sup>2</sup> School of Environment, Tsinghua University, Beijing 100084, China

<sup>3</sup> School of Environment, Tsinghua University, Beijing 100084, China

Keywords: Haze pollution, Heterogeneous process, Photochemical reaction, Regional transport  
li-h16@mails.tsinghua.edu.cn

### Abstract review

Heavy haze pollution occurs frequently in northern China, most critically in the Beijing-Tianjin-Hebei area (BTH). Zibo, an industrial city located in Shandong province, is often listed as one of the top ten most polluted cities in China, particularly in winter. However, no studies of haze in Zibo have been conducted, which limits the understanding of the source and formation of haze pollution in this area, as well as mutual effects with the BTH area. We carried out online and continuous integrated field observation of particulate matter in winter, from 11 to 25 January 2015.  $\text{SO}_4^{2-}$ ,  $\text{NO}_3^-$ , and  $\text{NH}_4^+$  (SIA) and organics were the main constituents of  $\text{PM}_{2.5}$ , contributing 59.4% and 33.6%, respectively. With the increasing severity of pollution, the contribution of SIA increased while that of organics decreased. Meteorological conditions play an important role in haze formation; high relative humidity (RH) and low wind speed increased both the accumulation of pollutants and the secondary transition from gas precursors (gas-particle phase partitioning). Since RH and the presence of  $\text{O}_3$  can indicate heterogeneous and photochemistry processes, respectively, we carried out correlation analysis and linear regression to identify their relative importance to the three main secondary species (sulfate, nitrate, and secondary organic carbon (SOC)). We found that the impact of RH is in the order of  $\text{SO}_4^{2-} > \text{NO}_3^- > \text{SOC}$ , while the impact of  $\text{O}_3$  is reversed, in the order of  $\text{SOC} > \text{NO}_3^- > \text{SO}_4^{2-}$ , indicating different effect of these factors on the secondary formation of main species in winter. Cluster analysis of backward trajectories showed that, during the observation period, six directional sources of air masses were identified, and more than 90% came from highly industrialized areas, indicating that regional transport from industrialized areas aggravates the haze pollution in Zibo. Inter-regional joint prevention and control is necessary to prevent further deterioration of the air quality.

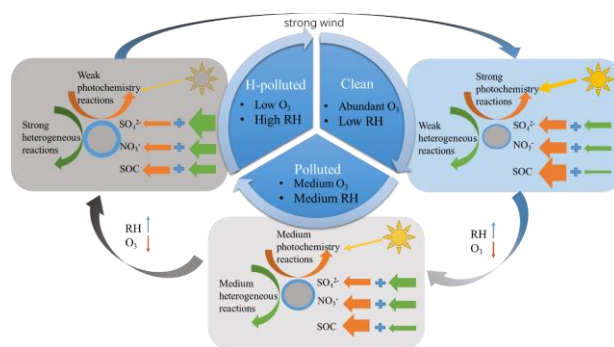


Figure 1. Conceptual model for the changes in photochemical and heterogeneous reactions during the evolution of pollution severity in winter. The thickness of each row denotes the level of relative importance for each corresponding process as shown in the below list\*.  
\*Symbol lists:

Relative importance	Least importance	Moderate importance	Very importance
Heterogeneous process	←	←	←
Photochemistry	←	←	←

This work was supported by the National Science and Technology Program of China (2014BAC22B01 and 2016YFC0202700), by the National Natural Science Foundation of China (81571130090).

Duan, F. K., He, K. B., Ma, Y. L., Ihozaki, T., Kawasaki, H., Arakawa, R., Kitayama, S., Tujimoto, K., Huang, T., Kimoto, T., Furutani, H., and Toyoda, M. (2016) *Environ Pollut*, 218, 289-296.

Sun, Y., Wang, Z., Fu, P., Jiang, Q., Yang, T., Li, J., and Ge, X. (2013a) *Atmospheric Environment*, 77, 927-934.

## **Abstracts T206**

## Tropospheric aerosol layers: homogeneity in vertical distribution of optical and microphysical characteristics

S.V. SamoiloVA, I.E. Penner, G.P. Kokhanenko, and Yu.S. Balin

Institute of Atmospheric Optics, 1, Academician Zuev Square, 634055 Tomsk, Russia

Keywords: tropospheric aerosol, microphysics, lidars, air mass advection.

Presenting author email: [penner@iao.ru](mailto:penner@iao.ru)

Relations between the vertical distribution of tropospheric aerosol and direction of air mass (AM) transport at different altitudes are studied, basing on the data of lidar observations in Tomsk (56°N, 85°W) [1]. Joint treatment of the data for 110 series of lidar measurements and modeling of the 10-day backward air mass trajectories showed that the height change in advection direction for 72% of cases does not occur more than once and takes place at the boundaries of the principal tropospheric layers - the boundary layer and middle troposphere. Sudden change of the lidar measured parameters is observed only in the transition from one layer to another. That indicates to a certain homogeneity in the aerosol composition within the layer.

### Direction of the air advection at different heights in the troposphere

In Western Siberia, the geometric characteristics of the main tropospheric layers have a clear seasonal dependence [2]. For total number of lidar observations mean values (standard deviation) of the upper border of the mixing layer, the boundary layer, the layers in the middle and upper troposphere are equal to 0.8 (0.2) km, 1.2 (0.3) km, 5.0 (0.7) km, 10.6 (0.6) km for cold period from October to March, and 1.7 (0.5) km, 2.5 (0.9) km, 6.2 (1.1) km, 11.3 (0.7) km for the warm period from April to September, respectively.

The troposphere conditions can be classified from the viewpoint of the transport direction change number (it is meant that air masses at different heights move with different velocity but by the same trajectories):

1. *monomodal type* – this type has no seasonal variations and amounts to 25% of all cases;
2. *bimodal type* – the direction changes one time, this type has no seasonal variations and amounts to 47%;
3. *multimodal type* – the direction changes more than one time, this type amounts to 11%;
4. *circulation type* – representative in the warm season, when the aerosol lifts to the upper layers and circulates over the Siberian territory, this type amounts to 17%.

### Results of the lidar data treatment

In the daytime, lidar measures backscatter coefficients (at 355, 532, 1064 nm) with a vertical resolution of 6 m, which allows to consider in detail the changes in tropospheric aerosol properties. At night, extinction coefficients at 355 + 387 and 532 + 607 nm with a resolution of 48 m can be determined in addition. The results of measurements in the nighttime on

30.05.2012 are presented below. Aerosol is transported in the boundary layer from Northern Europe, Atlantic ocean, Canada with a north-westerly direction; above there is a radical change to the south-westerly direction - from Kazakhstan, southern Europe and Mediterranean Sea. Variations of the total to Rayleigh scattering ratio are shown in Fig. 1.

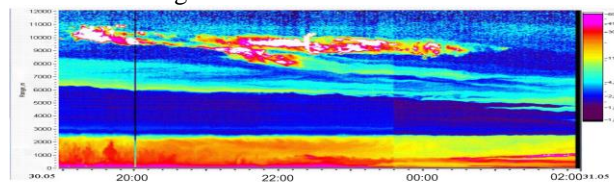


Figure 1. Spatial-temporal variations of the scattering ratio at 1064 nm, May 30, 2012.

Fig. 2 illustrates behavior of the optical and microphysical aerosol characteristics: backscatter at 1064 nm (left panel), lidar ratio at 355 and 532 nm (central left panel), Angstrom exponent (right center panel), and volume fraction and mean radius of fine particles (right panel). Between the layers aerosol characteristics change abruptly compared with less pronounced changes in their values inside the layer. High values for the northwest and low values for the south-west transport directions are displayed both for Angstrom exponent and in the contribution of fine particles; they are also seen in lidar ratio and mean radius.

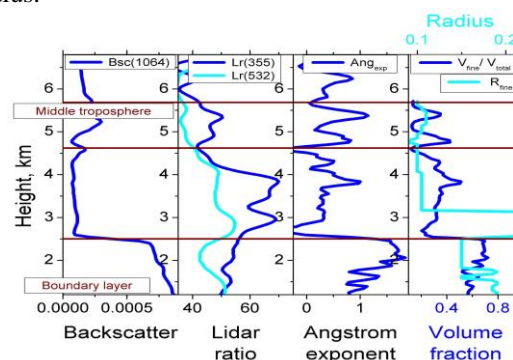


Figure 2. Stratification of 3-hour average aerosol parameters on May 30, 2012.

This work was supported in part by the Russian Foundation for Basic Research; grant N 16-48-700307.

Matvienko, G., et al. (2014) *International Journal of Remote Sensing* **35**, 5651–5676.

Arshinov, M., et al. (2006) *Atmos. Oceanic Opt.* **19**, 1062–1067.

## A new model to estimate aerosol optical depth from surface solar global and diffuse irradiance data

F. Filipitsch<sup>1</sup>, K. Behrens<sup>1</sup>, L. Doppler<sup>1</sup>

<sup>1</sup>Lindenberg Meteorological Observatory - Richard Assmann Observatory, German Meteorological Service, Lindenberg, 15848, Germany

Keywords: atmospheric aerosols, remote sensing, dust  
Presenting author email: Florian.Filipitsch@dwd.de

A strong increase of the aerosol optical depth (AOD) by Saharan dust is a well-known phenomena in Europe. Under certain weather conditions, dust emitted during strong sandstorms in the Sahara is transported over long distances and reach areas far north in central Europe. Such weather situation are still not well enough presented by numerical weather prediction models, which, in such situations, lead to huge errors in day-ahead forecasts of photovoltaic power production and generate huge financial losses. In March 2016, the PerduS (Photovoltaik ertragsreduktion durch Saharastaub) project was launched where the German Meteorological Service (DWD), the Karlsruhe Institute of Technology (KIT) and Meteocontrol are currently examining how dust affects the photovoltaic power production, with the goal to provide a better forecast during Saharan dust events in Europe.

As part of the project, a new algorithm is developed to estimate an effective AOD at certain spectral wavelengths to evaluate the Saharan-dust AOD prediction of the extended numerical weather prediction model ICON-ART. Additionally it is planned to use the algorithm as a radiative transfer model, which consider the radiative effects of dust and all other components in the atmosphere, to calculate the amount of solar energy reaching the surface under cloudless conditions for a given AOD prediction of ICON-ART.

As input for the AOD retrieval we use data from the DWD radiation measurement network. Each of the currently 26 stations is equipped with pyranometer instruments measuring the global and diffuse solar radiation at the surface. Under cloudless conditions, the incoming solar radiation is only affected by the atmospheric gases and aerosols. To estimate the AOD at certain spectral bands from the measured global and diffuse solar radiation at the surface, we developed an algorithm based on an optimal estimation approach, where we use LUT's as a forward model to reduce computational cost during the retrieval process. Based on results of prior studies, estimating the AOD from broadband ground based measurements under cloudless conditions, the main variables affecting the global and diffuse radiation at the surface are: sun position specified by sun zenith ( $sz$ ) and azimuth ( $azi$ ) angle, the atmospheric pressure at the surface ( $p$ ), gas absorption by water vapor ( $H_2O$ ), ozone ( $O_3$ ), nitrogen dioxide ( $NO_2$ ), the AOD, the effective

radius ( $R_{eff}$ ) and Single Scattering Albedo (SSA) of the aerosol.

$$G, D = LUT(sz,azi,p,H_2O,O_3,NO_2,AOD,R_{eff}, SSA)$$

With information about the sun position, pressure at station altitude, gas concentration and SSA from ancillary data sources, the two unknown variables AOD and  $R_{eff}$  will be retrieved in an iterative process by minimizing the error between measured and simulated radiation.

Figure 1 shows a result of a first study, using a multicoefficient approach to calculate a broadband AOD from direct broadband solar radiation measurements (Gueymard 1998), the AOD derived from AERONET sun photometer measurements and dust aerosol optical depth from the ICON-ART model during a Saharan dust event at the 19<sup>th</sup> of August 2012 at the DWD station Leipzig. The multicoefficient approach is limited to large spherical aerosol particles. As we can see in Figure1, the BAOD match the retrieved AOD for coarse particles from collocated AERONET measurements, but the fine mode can not be reproduced by this approach. The predicted dust AOD is also too low in this example.

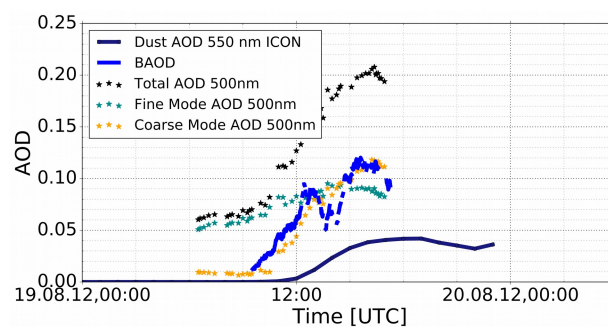


Figure 1. This is a comparison between theory and experimental data.

In our presentation we will focus on the new developed LUT based model and on results of case studies during Saharan dust events and comparisons between measurements and predictions of the ICON-ART model.

Gueymard, C.A. (1998) *J. Appl. Meteorol. Climatol.* 37 (4), 414-435.

## Remote sensing of atmospheric aerosol components based on sun-sky radiometer measurements

Y.S. Xie<sup>1</sup>, Z.Q. Li<sup>1</sup>, Y. Zhang<sup>1</sup> and D.H. Li<sup>1</sup>

<sup>1</sup>Institute of Remote Sensing and Digital Earth, Chinese Academy of Sciences, Beijing, 100101, China

Keywords: aerosol components, remote sensing, refractive indices, mixing model.

Presenting author email: xieys@radi.ac.cn

Aerosol has significant impacts on global climate change and air quality. Remote sensing is capable of detecting aerosol components in large spatial scale. In addition, it overcomes some problems of traditional chemical approaches, e.g., the non-contact and instantaneous detection of remote sensing can protect the natural status of ambient aerosol from mass loss or state alteration.

Some studies have developed the retrieval scheme of aerosol components from sun-sky radiometer measurements (Schuster *et al.*, 2005; Li *et al.*, 2013; van Beelen *et al.*, 2014). Based on these studies, we propose a comprehensive aerosol composition model that includes black carbon (BC), brown carbon (BrC), mineral dust (DU), particulate organic matters (POM), ammonia sulphate-like (AS), sea salt (SS) and aerosol water uptake (AW). Then the aerosol properties derived from remote sensing measurements are utilized to estimate these components.

We establish forward models for aerosol composition retrieval by using the joint information of light absorption, refractivity, particulate size and shape, which are individually provided by spectra imaginary part of refractive index (IRI), real part of refractive index (RRI), volume fraction ratio of fine to coarse mode and sphericity, as well as mixing states and hygroscopic growth of particles. The selection of a proper mixing model is one of the key step to derive aerosol components. In this study, we compare two effective medium approximations (EMAs), Maxwell-Garnett (MG) and Bruggeman (BR), with volume average (VA) mixing model. The results show that RRI calculated by MG, BR and VA are very close, while IRI derived by MG and BR is quite different from VA. Therefore, we select MG to model RRI and IRI in the forward model, taking its much faster computation speed than BR into account.

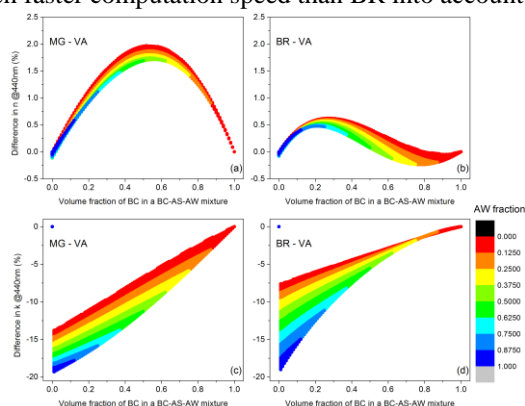


Figure 1. Differences in simulated refractive indices between EMAs and VA as components varying

Combining the refractive indices, size parameter and sphericity, we quantify the total deviation between simulation and observation by a cost function based on the least squares principle. The assumed volume fractions of components are inputs with each of them individually varying from 0 to 1. Searching for the minimum of the cost function yields the best modeling results, i.e., component volume fractions.

Figure 2 shows the volume fractions of aerosol components based on the sun-sky radiometer acquired during a campaign held in Huairou, Beijing, from October 2014 to January 2015. BC content is very low with average volume fraction of 1.24%. For most of the cases, DU takes up a major proportion in volume (larger than 60%). POM have noticeable variations with average volume fraction of 17.3%. The AS contents are relatively low, with about 70 percent of total retrievals smaller than 10%. The water uptake is primarily associated with AS and average volume fraction of AW is only 7.1%.

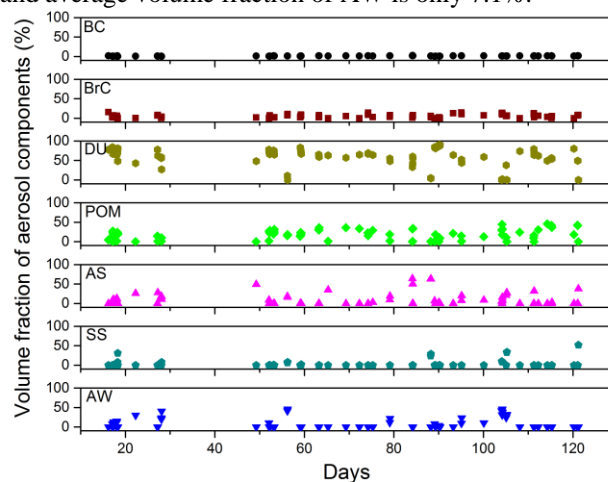


Figure 2. Retrieved columnar volume fraction of aerosol components during the campaign.

This work was supported by the National Natural Science Foundation of China (Grant No. 41501395).

Li, Z., Gu, X., Wang, L., Li, D., Xie, Y., Li, K., Dubovik, O., Schuster, G., Goloub, P., Zhang, Y., Li, L., Ma, Y. and Xu, H. (2013) *Atmos Chem Phys*, **13**, 10171-10183.

Schuster, G., Dubovik, O., Holben, B. and Clothiaux, E. (2005) *J Geophys Res-Atmos*, **110(D10)**, doi: 10.1029/2004jd004548.

van Beelen, A., Roelofs, G., Hasekamp, O., Henzing, J. and Rockmann, T. (2014) *Atmos Chem Phys*, **14(12)**, 5969-5987.

## Trends in MODIS and AERONET derived aerosol optical thickness over northern Europe

P. Glantz<sup>1</sup>, E. Freud<sup>1</sup>, C. Johansson<sup>1,2</sup> and M. Tesche<sup>3</sup>

<sup>1</sup>Department of Environmental Science and Analytical Chemistry, Stockholm University, Stockholm, Sweden

<sup>2</sup>SLB-analys, Environment and Health Administration, Stockholm, Sweden

<sup>3</sup>School of Physics, Astronomy and Mathematics, University of Hertfordshire, AL10 9AB Hatfield, 5 United Kingdom

Keywords: Trends in AOT, Satellite AOT retrievals, Validation of AOT

Presenting author email: paul.glantz@aces.su.se

### Introduction

Global warming is primarily a problem of too much carbon dioxide (CO<sub>2</sub>) in the atmosphere, which acts as a blanket, trapping heat and thus warming the planet. However, anthropogenic emissions of aerosols impact the Earth's radiation balance and climate as well (IPCC, 2013). Second to greenhouse gases, man-made aerosols have caused the largest anthropogenic forcing during the industrial era (Boucher et al., 2013). Characterizing global aerosol distribution and changes over time are necessary for understanding present climate conditions and future climate changes.

### Methods

In this study, 13 years of MODIS (MODerate resolution Imaging Spectroradiometer) Collections 5 and 6 (c005 and c006, respectively) Aqua and Terra aerosol retrievals have been combined with AERONET (AERosol ROBotic NETwork) ground-based sun-photometer observations to examine trends in aerosol optical thickness (AOT) over northern Europe for the months April – September. This results in 15,912 MODIS granules (each with a 2330 km-wide swath) for each of the two collections. By using MODIS Aqua and Terra observations combined over the investigation area (the latter satellite with overpasses earlier in the morning) means that the availability in AOTs increase significantly.

### Results and summary

For 1390 and 1085 daily coincident measurements against AERONET that were obtained for c005 and c006, respectively, MODIS AOT varied to 87% within the predicted uncertainty of one standard deviation of the retrieval over land. For the coastal site Gustav Dalen Tower, Sweden, larger deviations were however found for MODIS c005 and c006 (79 and 76%, respectively).

Since Baltic Sea provides substantially better statistical representation of AOT than the surrounding land support investigations of trends in AOT over specific marine regions. Figure 1 shows that negative trends with 1.2% and 0.92% per year in AOT were found for the southwestern Baltic Sea with MODIS c005 and c006, respectively. This is in line with results obtained at the AERONET Hamburg station (Figure 1). The strongest trend with -1.7% per year in AOT

derived from both MODIS c005 and AERONET was found for the central Poland area (not shown). MODIS Aqua and Terra c005 trends in AOT, derived from observations separated and combined over the northern Europe, are all statistically significant at the 95% confidence interval. The decrease in AOT over northern Europe are line with negative trends in PM<sub>2.5</sub> at five ground-based stations within the investigation area. A total decrease in MODIS Aqua/Terra c005 and Aqua c006 AOT is about 13-20% over the investigation period, which means a reduced cooling effect from the aerosols over northern Europe.

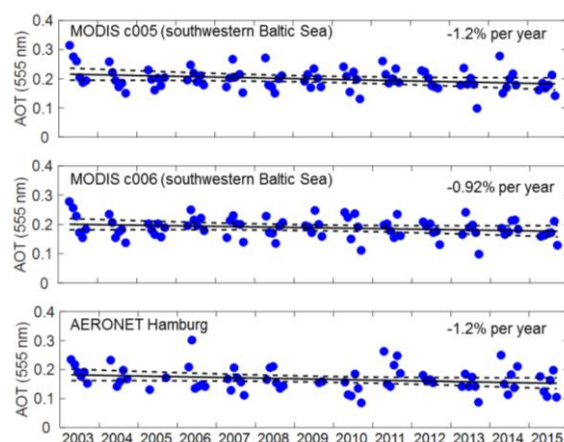


Figure 1. Time series of monthly mean AOT with respect to April – September. The dashed lines denote the 95% confidence interval.

This work was supported by Stockholm County Council.

Boucher et al. (2013), Working Group 1, IPCC, Cambridge University Press, 571-675

IPCC, 2013: *Climate Change 2013: The Physical Science Basis. Contribution of Working Group I to the Fifth Assessment Report of the Intergovernmental Panel on Climate Change* [Stocker, T.F., D. Qin, G.-K. Plattner, M. Tignor, S.K. Allen, J. Boschung, A. Nauels, Y. Xia, V. Bex and P.M. Midgley (eds.)]. Cambridge University Press, Cambridge, United Kingdom and New York, NY, USA, 1535 pp, doi:10.1017/CBO9781107415324.

## A European ceilometer and lidar network for aerosol profiling

W. Thomas<sup>1</sup>, I. Mattis<sup>1</sup>, F. Wagner<sup>1,2</sup>, M. Pattantyus-Abraham<sup>1</sup>, H. Flentje<sup>1</sup>

<sup>1</sup>Deutscher Wetterdienst (DWD), Meteorologisches Observatorium Hohenpeissenberg, D-82383 Hohenpeissenberg, Germany

<sup>2</sup>now at Karlsruhe Institute of Technology (KIT), Hermann-von-Helmholtz-Platz 1, 76344 Eggenstein-Leopoldshafen

Keywords: lidar, ceilometer, aerosol profile, aerosol backscatter, aerosol remote sensing  
Presenting author email: Werner.Thomas@dwd.de

Triggered by the eruptions of Eyjafjallajökull/Iceland in spring 2010, European Meteorological and Hydrological Services started to establish a European network for aerosol profiling based on Lidars and ceilometers. Nowadays ceilometers, e.g. the Vaisala CL51 and the Lufft CHM15K Nimbus, allow for the detection of aerosol layers in the atmosphere up to the tropopause region (Wiegner *et al* (2014)). Based on experience gained during the European COST action EG-CLIMET (ES0702) another two European consortia established in 2013 and continue the work on harmonizing national ceilometer networks with respect to routine operations, data exchange and data formats (E-PROFILE, see <http://www.eumetnet.eu/e-profile>) and harmonized aerosol profile retrievals (TO-PROF, COST ES1303, see <http://www.toprof.ima.cnr.it/>), actively supported by EARLINET, the European Aerosol Research Lidar Network. Such combined networks of ceilometers and advanced lidars systems have already shown their value for providing the four-dimensional aerosol distribution over larger areas (Pappalardo *et al* (2014)).

The Deutscher Wetterdienst (DWD) contributes to the European ceilometer network with its currently 100 CHM15K Nimbus instruments (as of January 2017), which are all connected to the Internet.

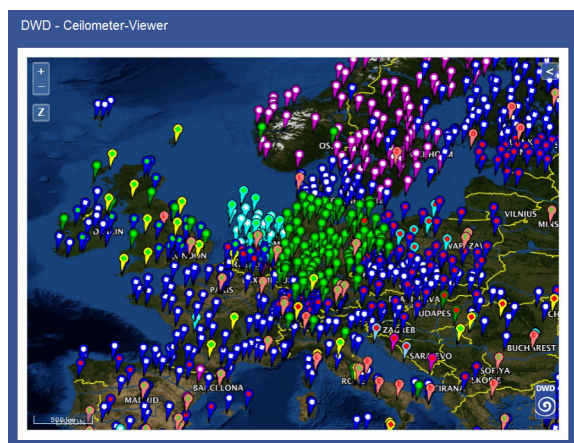


Figure 1: Lidars and ceilometers in Europe as provided by the ceilomap

The instruments provide freely available quick looks of the attenuated backscatter coefficient which can be accessed through the ceilomap web site hosted by DWD under [www.dwd.de/ceilomap](http://www.dwd.de/ceilomap). Computation of this physical quantity requires calibration of the instruments (see e.g. Wiegner and Geiß (2012); O'Connor *et al*

(2004)), which was jointly developed within TO-PROF mainly by DWD, MeteoSwiss, and the University of Reading/UK. Also firmware issues need to be analyzed and taken into account (see Kotthaus *et al* (2016)).

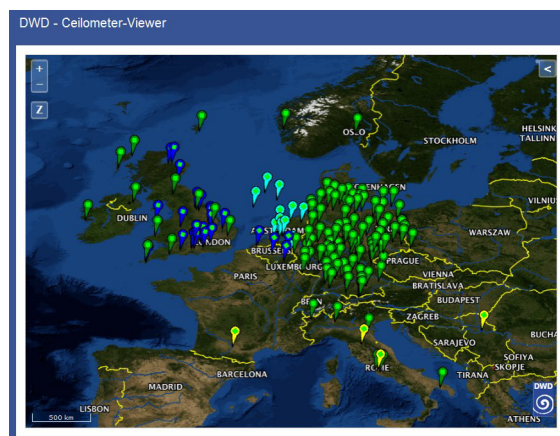


Figure 2: Lidars and ceilometers in Europe which provide quick looks and/or further information about the station and the instrument

Several Saharan dust episodes, biomass burning plumes from Canadian wild fires in 2013 and volcanic ash plumes (Eyjafjallajökull 2010) were tracked and analyzed in recent years and results will be shown. Moreover, data from the network are routinely used to validate model data from the COPERNICUS Atmospheric Monitoring Service (CAMS).

Kotthaus, S., O'Connor, E., Münkel, C., Charlton-Perez, C., Haefelin, M., Gabey, A.M. and Grimmond, C.S.B. (2016) *Atmos. Meas. Tech.* **9**, 3769-3791, doi:10.5194/amt-9-3769-2016.

O'Connor, E.J., Illingworth, A.J. and Hogan, R.J. (2004) *J. Atm. Oc. Tech.* **21**, 777-786.

Pappalardo, G., Amodeo, A., Apituley, A., Comeron, A., Freudenthaler, V., Linné, H., Ansmann, A., Bösenberg, J., D'Amico, G., Mattis, I., Mona, L., Wandinger, U., Amiridis, V., Alados-Arboledas, L., Nicolae, D. and Wiegner, M. (2014) *Atmos. Meas. Tech.* **7**, 2389–2409, doi:10.5194/amt-7-2389-2014.

Wiegner, M. and Geiß, A. (2012) *Atmos. Meas. Tech.* **5**, 1953–1964, doi:10.5194/amt-5-1953-2012.

Wiegner, M., Madonna, F., Biniotoglou, I., Forkel, R., Gasteiger, J., Geiß, A., Pappalardo, G., Schäfer, K. and Thomas, W. (2014) *Atmos. Meas. Tech.* **7**, 1979–2014, doi:10.5194/amt-7-1979-2014.

## Planetary boundary layer height influence on ground base aerosol concentrations

L. Marmureanu<sup>1</sup>, J. Vasilescu<sup>1</sup>, S. Andrei<sup>1</sup>, F. Toanca<sup>1</sup>, A. Dandocsi<sup>1</sup>, C. Marin<sup>1</sup>

<sup>1</sup>National Institute of Research and Development for Optoelectronics, Magurele, 077125, Romania

Keywords: submicronic aerosol, black carbon, planetary boundary layer high,

Presenting author email: mluminita@inoe.ro

Planetary boundary layer (PBL) plays an important role in local pollution and long range transport with significant impact on human health. The most important phenomena related to atmosphere-surface exchanges take place in the PBL. The aerosol concentrations are strongly related with PBL height evolution, highlighted by previous studies (Jiannong et al., 2013), diurnal cycle being evidenced mainly during summer and less pronounced during winter when temperature is lower and mostly negative.

The aerosol concentrations measured in a periurban area (Magurele, near Bucharest), for a long period of time from 2012 to 2016 (not continuously) revealed several important phenomena that can influence in a significant way the local aerosol concentrations. The most important is related with PBL height, cloud cover and in a lower proportion the atmospheric air masses changes with high visibility, due to the fact that these phenomena not occur very often.

In this study the PBL high was primarily derived from remote sensing instruments (ground based) LIDAR-multiwavelength, CEILOMETER and second from meteorological data, ECMWF .

The ratio of the two elastic range corrected signals channels from 1064 nm and the 532 nm, is used to determine the PBL height. For each of the profile's derivative, the negative and positive peaks are considered. The first smallest negative peak in RCS derivative ratio marks the PBL height. For large time series, each PBL height is compared to the previous one assuming a continuity function. (Belegante et al, 2014). For the Ceilometer CL31 mainly we retrieved cloud base using the almost the same principle based on magnitude of the return signal that provide information on the backscatter properties of the atmosphere.

The in-situ aerosol concentration was retrieved from compact time of flight aerosol mass spectrometer (Drewnick et al., 2005) (retrieve submicronic nonrefractory aerosols concentrations with high time resolution) (Marmureanu et al., 2016), Aerosol Chemical Speciation Monitor (retrieve concentration of submicronic nonrefractory aerosols with lower time resolution approx. 30'), and Aethalometer (filter base black carbon absorption measurements at 7 wavelengths).

Three main categories of correlative fluctuation between PBL height and aerosol concentration were identified. Regular diurnal variation of PBL height that evidenced an increasing of aerosol concentration with at least 2  $\mu\text{g}/\text{m}^3$  (fig. 1). Rare phenomena occurrence, like very low clouds formations around 200 meters, that is correlated

with the PBL height, and also to the increasing of aerosol concentration at ground (not shown).

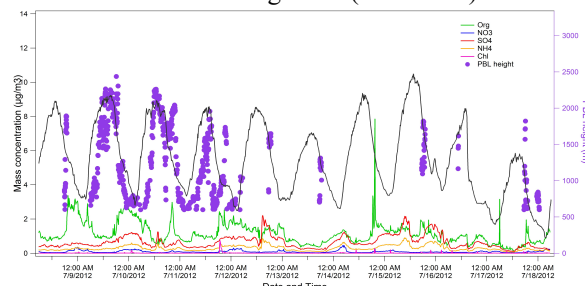


Figure 1 Temporal evolution of PBL height and in situ PM 1 concentrations

Low concentration of aerosols at ground, under 0.5  $\mu\text{g}/\text{m}^3$  (Fig.2) was depicted under special conditions when the visibility was really high (around 150 Km), the Carpathian Mountains being visible from Bucharest. The synoptic conditions underline the presence of polar influences, a rapid advection bringing the air masses from the north part to the S-E of Europe visible in the PBL height evolution and in meteorological parameters such as temperature and wind direction and intensity. The cold advection was caused by a frontal passage and the descendent airflow facilitate the decreasing of aerosols particles concentration, between 00-06 UTC.

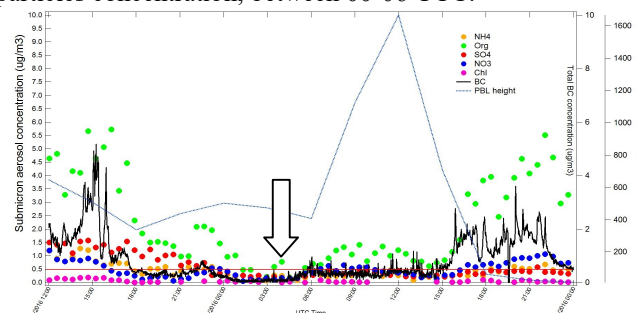


Figure 2 Mass loadings of aerosol species measured under clear sky condition

This work was supported by a grant of the Romanian ANCSI, CNCS/CCCDI - UEFISCDI, project number PN-III-P2-2.1-PED-2016-1300, within PNCDI III; the research leading to these results has received funding from the European Union's Horizon 2020 Research and Innovation Programme, under Grant Agreements no 692014 and 654109 (ACTRIS)

Jiannong et al., (2013) *Particuology*, 11, 34-40,

Drewnick, F., S.S. et al., (2005) *Aerosol Science and Technology*, 39:637-658,

Marmureanu et al., (2016) *Romanian Journal in Physics*, 61(9-10), 1635-1650.

Belegante, L et al., (2014) *C. Acta Geophys.*, 62, 276-289.

## Comparison of commercial lidars and ceilometers with advanced Raman lidars in the frame of INTERACT-II ACTRIS campaign

M. Rosoldi<sup>1</sup>, F. Madonna<sup>1</sup>, G. Pappalardo<sup>1</sup>, J. Vande Hey<sup>2</sup>, Y. Zheng<sup>3</sup> and VAISALA Team<sup>4</sup>

<sup>1</sup>Istituto di Metodologie per l'Analisi Ambientale (IMAA), Consiglio Nazionale delle Ricerche (CNR), Tito Scalo (PZ), I-85050, Italy

<sup>2</sup>Department of Physics and Astronomy, University of Leicester, Leicester, LE1 7RH, UK

<sup>3</sup>Sigma Space Corporation, Lanham, MD, 20706, USA

<sup>4</sup>VAISALA, Vantaa, 01670, Finland

Keywords: aerosol, remote sensing, lidar, ceilometer.

Presenting author email: [marco.rosoldi@imaa.cnr.it](mailto:marco.rosoldi@imaa.cnr.it)

The study of aerosol spatio-temporal distribution in troposphere is essential to improve our understanding of climate and air quality. For this purpose, global scale high resolution continuous measurements of tropospheric aerosols are needed. Advanced research lidars, because of their complexity and high cost, have limited geographical coverage and they are usually operated occasionally or during dedicated field campaigns. On the other hand, ground-based low-cost and low-maintenance remote sensing instruments, such as commercial automatic lidars and ceilometers, allow to obtain global coverage and high resolution. Therefore, it is very interesting for the scientific community to understand to which extent these instruments are able to provide reliable aerosol measurements and fill in the geographical gaps of existing networks of advanced lidars, like EARLINET (European Aerosol Research Lidar Network).

The INTERACT-II (INTERcomparison of Aerosol and Cloud Tracking) campaign, carried out at CIAO (CNR-IMAA Atmospheric Observatory) in Tito Scalo, Potenza, Italy (760 m a.s.l., 40.60 N, 15.72 E), aims to evaluate the performances of commercial automatic lidars and ceilometers for tropospheric aerosol profiling. The campaign has been performed in the period from July 2016 to January 2017 in the framework of ACTRIS-2 (Aerosols, Clouds, and Trace gases Research Infrastructure) H2020 research infrastructure project. Besides the commercial ceilometers operational at CIAO, the performance of a CL51 VAISALA ceilometer, a Campbell CS135 ceilometer and a Sigma Space mini-Micro Pulse Lidar (MPL) have been assessed, using the EARLINET multi-wavelength Raman lidars operative at CIAO as reference.

CIAO lidar signals have been processed using the EARLINET Single Calculus Chain, also with the aim to improve the data consistency and comparability (D'Amico et al., 2016; Mattis et al., 2016). In a first stage, the comparison between CIAO lidars and the mini-MPL has been focused on the signals collected by both the instruments, by comparing their range corrected signals, which are proportional to attenuated backscatter coefficient profiles. The performances of the CL51 and of the CS135 have been assessed by directly comparing their lidar-calibrated attenuated backscatter coefficient profiles with those of CIAO lidars, following a similar

approach used in the first INTERACT campaign (Madonna et al., 2015). All the time series considered in these comparisons refer to night time measurements. The profiles from all the instruments have been compared on a vertical resolution of 60 meters and using a temporal integration ranging between 1 and 2 hours.

A statistical analysis of simultaneous observations during the first half of the inter-comparison period, from July to September, has been performed to investigate the differences of the mini-MPL and ceilometers with respect to CIAO lidars. This analysis reveals that, among the considered devices, the mini-MPL shows the best performances with discrepancies limited to 10 % throughout the troposphere. Furthermore, in agreement with the outcome of INTERACT-I, ceilometers generally have fairly good performances in aerosol profiling in the lower troposphere, up to an altitude of about 2000 m above the ground, but they have limitations at higher altitudes, depending on the signal-to-noise ratio of each specific instrument.

The above preliminary analysis will be consolidated, by analyzing the cases collected in the period from October to December and comparing the mini-MPL and the CIAO lidar profiles of aerosol optical properties.

The ongoing data analysis will also assess the stability of the considered lidar technologies with respect to variation of working and environment temperature, aerosol loading and laser operations.

This work was supported by the European Commission for ACTRIS-2 in HORIZON 2020 research and innovation programme under grant agreement no. 654109. Sigma Space Corporation, Vaisala and Campbell Scientific are acknowledged for their contribution.

D'Amico, G., Amodeo, A., Mattis, I., Freudenthaler, V. and Pappalardo, G. (2016) *Atmos. Meas. Tech.*, 7, 1979–1997.

Mattis, I., D'Amico, G., Baars, H., Amodeo, A., Madonna, F. and Iarlori, M. (2016) *Atmos. Meas. Tech.*, 9, 3009–3029.

Madonna, F., Amato, F., Vande Hey, J. and Pappalardo, G. (2015) *Atmos. Meas. Tech.*, 8, 2207–2223.

## Mathematical simulation of brightness fields of reflected solar radiation: Influence of 3D cloud effects

T. B. Zhuravleva, I. M. Nasrtdinov, T. V. Russkova, Artyushina A.V., and A.N. Duchko

V.E. Zuev Institute of Atmospheric Optics SB RAS, Tomsk, Russia

Keywords: solar radiation, Monte Carlo method, isolated cloud, broken clouds, cloud 3D effects.

Presenting author email: ztb@iao.ru

To solve more correctly certain atmospheric remote sensing problems (retrieval of aerosol and cloud characteristics, improved interpretation of ground-based and satellite observations, cloud “screening” in solving inverse problems, etc.), spectral, spatial, and angular characteristics of the brightness fields of the cloudy atmosphere should be calculated taking into account its spatial inhomogeneity.

Spatial-angular characteristics of reflected solar radiation in broken clouds are simulated in the plane and spherical models of the atmosphere using statistical algorithms developed in the Institute of Atmospheric Optics SB RAS (package MATHART, Monte Carlo Codes for **TH**ree-Dimension**AI** Radiative Transfer). The spherical model of the atmosphere makes it possible to estimate the effect of the spatial inhomogeneity of the deterministic cloud realization on the radiation characteristics of the atmosphere for large viewing and solar zenith angles (larger than  $80^\circ$ ).

Cloud fields are constructed based on the model of Poisson point fluxes in space; clouds are approximated by inverted truncated paraboloids. A few modifications of the statistical algorithms, differing in the methods for simulating free path length and accounting for the molecular absorption ( $k$ -distribution method) are implemented. Results of cross-checks of the developed modifications and estimations of their efficiency are presented in (Zhuravleva et al., 2016, 2017).

With the appearance of an isolated cloud in the sky, the sky radiance is determined by the cloud presence/ absence on the line of sight (LS), shading of the LS by clouds/nonobscuration of direction “toward the Sun”, as well as by illumination of the LS by cloud reflected radiation. If the line of sight transects the cloud, the sky radiance may substantially exceed the clear-sky radiance, especially if the point of LS entry into the cloud is sunlit. Sky radiance decreases due to the effects of cloud shading of the line of sight and the observation point (OP) on the Earth’s surface. The cloud impact zone may exceed several-fold the horizontal cloud sizes and substantially increases with growing solar and detector zenith angles.

Then we considered several different cloud realizations for small and moderate cloud fractions ( $CF$ ). Considering the random character of the distribution of cloud elements (characteristic for the real atmosphere), the radiance for the specified illumination and observation conditions changes from one realization to another and, depending on the cloud configuration, may be either higher or lower than the clear-sky radiance. In

the cloud fields, in addition to the above-mentioned 3D effects of isolated cloud, there are also the effects of radiation interaction, i.e., mutual shading and the effects of multiple scattering between the clouds. The simulation results show that the specific features of broken cloud radiance field are mainly determined by cloud localization relative to two directions, i.e., the line of sight and direction “toward the Sun”. In this sense, for certain sensing geometries, the difference in sky radiance between realizations with different cloud fractions may be less than the variability range of reflected radiation within the same realization. The cloud realization influence on angular characteristics of radiance field is more strongly manifested in situations with a low  $CF$  because, as cloud amount grows, the uniform character of cloud distribution acts to smooth out the effects characteristic for isolated clouds.

Figure 1 presents the examples of two different cloud field realizations at cloud fraction  $CF = 2$  and the sky radiance changes in these realizations when the illumination conditions (solar azimuth  $\varphi_{Sun}$  and zenith  $\xi_{Sun}$  angles) vary.

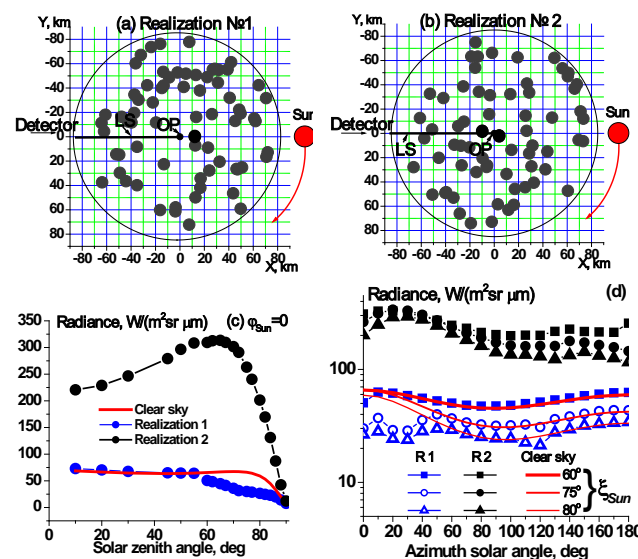


Figure 1. Cloud realizations and sky radiance for  $CF=2$  (viewing zenith angle –  $60^\circ$ ,  $\lambda=0.55 \mu\text{m}$ , cloud radius and thickness –  $5 \text{ km}$ , extinction coefficient –  $5 \text{ km}^{-1}$ )

This work was supported in part by RFBR (through the grant no. 16-01-00617-a) Zhuravleva, T.B. et.al (2016). *Proc. of SPIE*, **10035**, 1003-02. Zhuravleva, T.B. et.al (2017). *Atmos. Ocean. Opt.*, **30** (1), 103-110.

## Technique for Remote Sensing of Droplets of Sulfuric Acid in the Stratosphere

W. Sun<sup>1</sup>, G. Videen<sup>2</sup>, Y. Hu<sup>3</sup>, and R.R. Baize<sup>3</sup>

<sup>1</sup>Science Systems and Applications, Inc., Hampton, VA 23668, USA

<sup>2</sup>US Army Research Laboratory, Adelphi, MD 20782, USA

<sup>3</sup>NASA Langley Research Center, Hampton, VA 23681, USA

Keywords: Aerosol, remote sensing, droplets of sulfuric acid, stratosphere.

Presenting author email: wenbo.sun-1@nasa.gov

Stratospheric aerosols are mostly sulfuric acid droplets with diameters on the order of 0.1–1.0  $\mu\text{m}$ . The sulfur for the aerosols is either through direct injection from sulfur-rich volcanic eruptions, or from tropical injection of tropospheric air containing carbonyl sulphide (OCS), SO<sub>2</sub>, and sulfate particles. Stratospheric aerosols have significant impacts on the Earth's radiation balance for several years after volcanic eruptions. These particles may play a role in the nucleation of near tropopause cirrus, and thus indirectly affect radiation. Stratospheric aerosols also play important roles in the chemical, particularly ozone, balance of the stratosphere (Deshler 2008). However, due to their high altitude, small size and low optical thickness, the stratospheric droplets of sulfuric acid are difficult to detect with either in-situ or remote-sensing methods. In this presentation, we will introduce a limb polarimetric remote-sensing technique to measure these important particulates in the stratosphere.

### Technique for Detection of Sulfuric Acid Droplets

Sun et al. (2014) reported a novel method for detecting cloud particles in the atmosphere. A distinct feature in the angle of linear polarization (AOLP) of solar radiation that is backscattered from clouds can be used to detect clouds. The dominant backscattered electric field from the clear-sky Earth-atmosphere system is nearly parallel to the Earth surface. However, when clouds are present, this electric field can rotate significantly away from the parallel direction. Model results and satellite data both demonstrate that this polarization feature can be used to detect super-thin cirrus clouds having an optical depth of only  $\sim 0.06$  and super-thin liquid water clouds having an optical depth of only  $\sim 0.01$ . In this study, this method is applied to stratospheric acid droplet aerosols. We assume a limb detection of the stratosphere with a polarimeter facing along the direction of solar radiation. Using the radiative transfer model developed in Sun and Lukashin (2013), we simulated the backscattered solar light's AOLP from pure molecular atmosphere and the atmosphere including the stratospheric droplets of sulfuric acid with refractive index of  $m = 1.42 + 10^{-8}i$ . A bimodal lognormal size distribution (Davies 1974) with a modal size of 0.5  $\mu\text{m}$  is assumed for the acid droplets in this study. Figure 1(a) shows the backscattered light's AOLP from pure molecular atmosphere. Figure 1(b) shows the backscattered light's AOLP from the atmosphere with the stratospheric acid droplets. We can see the strong AOLP features of transparent droplets (Sun et al. 2014, 2015) in

Fig. 1(b). Therefore, using a polarimetric measurement in the limb detection of stratosphere, the stratospheric acid droplet aerosols can be reliably detected. To obtain the optical thickness of the aerosols along the limb sunlight direction, the method in Sun et al. (2015) can also readily be used.

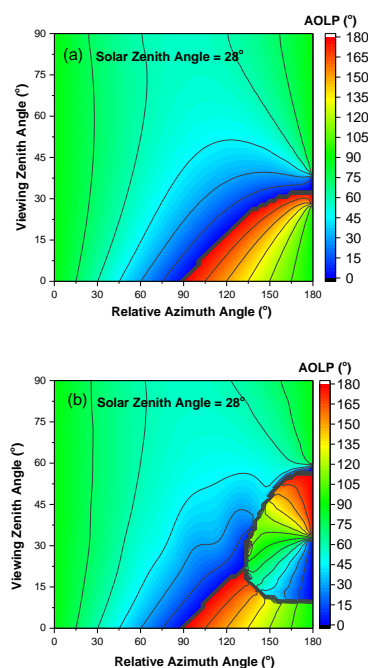


Figure 1. A comparison of backscattered light's AOLP from (a) purely molecular atmosphere and from (b) the atmosphere with the stratospheric acid droplets. The solar wavelength is 670 nm in this simulation.

This work was supported by the NASA CLARREO Science project.

### References

- Deshler, T. (2008) *Atmos. Res.* **90**, 223–232.
- Davies C. (1974) *Aerosol Sci.* **5**, 293–300.
- Sun, W., Videen, G., and Mishchenko, M. I. (2014) *Geophys. Res. Lett.* **41**, 688–693.
- Sun, W., Lukashin, C. (2013) *Atmos. Chem. Phys.* **13**, 10303–10324.
- Sun, W., Baize, R. R., Videen, G., Hu, Y., and Fu, Q. (2015) *Atmos. Chem. Phys.* **15**, 11909–11918.

## PathfinderTURB: an automatic boundary layer algorithm. Development, validation and application to study the impact on in-situ measurements at the Jungfrauoch

Y. Poltera<sup>1,3</sup>, G. Martucci<sup>1</sup>, M. Collaud Coen<sup>1</sup>, M. Hervo<sup>1</sup>, L. Emmenegger<sup>2</sup>, S. Henne<sup>2</sup>, D. Brunner<sup>2</sup> and A. Haefele<sup>1</sup>

<sup>1</sup> Federal Office of Meteorology and Climatology, MeteoSwiss, Payerne, Switzerland

<sup>2</sup> Swiss Federal Laboratories for Materials Science and Technology, Dübendorf, Switzerland

<sup>3</sup> Institute for Atmospheric and Climate Science, ETH Zurich, Zurich, Switzerland

Keywords: CBL, automatic detection, Jungfrauoch, ceilometer.

Presenting author email: Giovanni.martucci@meteoswiss.ch

**Abstract.** We present the development of the PathfinderTURB algorithm (de Bruine *et al.*, 2016; Poltera *et al.*, 2017) for the analysis of ceilometer backscatter data and the real-time detection of the vertical structure of the planetary boundary layer. Two typical aerosol layer heights are retrieved by PathfinderTURB: the Convective Boundary Layer (CBL) and the Continuous Aerosol Layer (CAL). PathfinderTURB combines the strengths of gradient- and variance-based methods and addresses the layer attribution problem by adopting a geodesic approach. The algorithm has been applied to one year of data measured by two CHM15k ceilometers operated at the Aerological Observatory of Payerne (491 m, a.s.l.) on the Swiss plateau, and at the Kleine Scheidegg (2061 m, a.s.l.) in the Swiss Alps. The retrieval of the CBL has been validated at Payerne using two reference methods: (1) manual detections of the CBL height performed by independent human experts using the ceilometer backscatter data of the year 2014; (2) values of CBL heights calculated using the Richardson's method from co-located radio sounding data. Based on the excellent agreement with the two reference methods, PathfinderTURB has been applied to the ceilometer data at the mountainous site of the Kleine Scheidegg for the period September 2014 till November 2015. At this site, the CHM15k is operated in a novel, tilted configuration at 19° zenith angle to probe the air next to the Sphinx Observatory (3580 m, a.s.l.) on the Jungfrauoch (JFJ). The boundary layer dynamics below the JFJ are shown in Fig. 1.

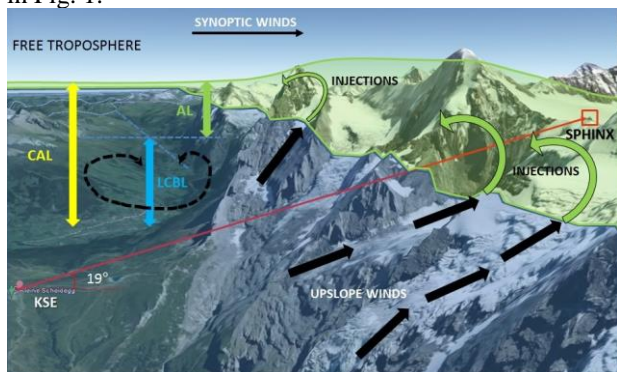
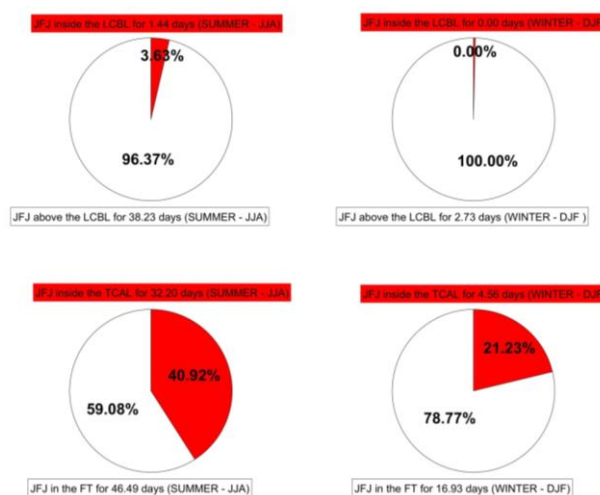


Figure 1. Schematic view of the daytime atmospheric structure and vertical pollution transport in below the JFJ. The red line shows the CHM15k line of sight towards the JFJ.

The analysis of the retrieved layers led to the following results: the CAL reaches the JFJ during 41% of the time in summer and during 21% of the time in winter for a total of 97 days during the two seasons. The season-averaged daily cycles show that the CBL height reaches the JFJ only during short periods (4% of the time) on 20 individual days in summer and never during winter (Figure 2).



Especially during summer the CBL and the CAL modify the air sampled in-situ at JFJ, resulting in an unequivocal dependence of the measured absorption coefficient on the height of both layers. This highlights the relevance of retrieving the height of CAL and CBL in mountainous regions.

This work has been financially supported by the SNF through ICOS-CH. The authors would further like to thank Nicolas Bukowiecki for giving access to JFJ aerosol measurement data.

Poltera, Y., Martucci, G., Collaud Coen, M., Hervo, M., Emmenegger, L., Henne, S., Brunner, D., and Haefele, A. (2017) *Atmos. Chem. Phys. Discuss.*, doi:10.5194/acp-2016-962, in review.

de Bruine, M., Apituley, A., Donovan, D., Klein Baltink, H., and de Haij, M. (2016) *Atmos. Meas. Tech. Discuss.*, doi:10.5194/amt-2016-327, in review.

## Analysis of aerosol optical and microphysical properties and radiative forcing estimates based on AERONET measurements at two sites of the Iberian Peninsula

A. J. Fernández<sup>1</sup>, F. Molero<sup>1</sup>, M. A. Revuelta<sup>2</sup>, P. Salvador<sup>1</sup>, M. Becerril-Valle<sup>1</sup>, E. Alonso-Blanco<sup>1</sup>, M. Barreiro<sup>1</sup>, E. Coz<sup>1</sup>, E. Díaz<sup>1</sup>, F. J. Gómez-Moreno<sup>1</sup>, L. Núñez<sup>1</sup>, M. Palacios<sup>1</sup>, B. Artíñano<sup>1</sup> and M. Pujadas<sup>1</sup>.

<sup>1</sup>Department of Environment, Centro de Investigaciones Energéticas, Medioambientales y Tecnológicas (CIEMAT). Avda Complutense, 40. Madrid, 28040. Spain.

<sup>2</sup>Agencia Estatal de Meteorología (AEMET). C/Leonardo Prieto Castro, 8, 28071. Spain.

Keywords: aerosols, optical and microphysical properties, radiative forcing estimates

Contact information: [alfonsojavier.fernandez@ciemat.es](mailto:alfonsojavier.fernandez@ciemat.es)

Atmospheric aerosols play an important role in the earth-atmosphere radiation budget by both scattering and absorbing solar radiation. Given their high spatial and temporal variability, they represent a high uncertain driver from the point of view of radiative forcing estimates. Depending on their optical and microphysical properties, aerosol can exert different effects on such radiative budget. For these reasons observational networks as AERONET (AERosol Robotic NETwork) (Holben et al., 1998) have been established over the globe to monitor continuously the aforementioned properties.

In the framework of PROACLIM spanish project we have analysed AERONET data obtained at two sites in Spain: Madrid (40°45 N, 3.72°W; 680 m above sea level (asl)) and La Coruña (43.36°N, 8.42°W; 67 m asl). The aim of the study is to characterize the radiative forcing and optical and microphysical properties of different type of aerosols at both stations to analyse their effects on the earth-atmosphere radiation budget and consequently on climate. In particular, significant differences between aerosols studied under Saharan dust events and typical aerosols observed at such stations are identified having considered such optical properties (see Figure 1).

Among others tasks, a 2D-cluster analysis has been performed, based on the Scattering Ångström Exponent (SAE) and Absorption Ångström Exponent (AAE). To do this we have used AERONET level 1.5 data (cloud screened data with pre and post calibrations) for the period 2012-2015. No level 2 data were used as aerosol optical properties at such level were scarce. Nevertheless, we have filtered AERONET level 1.5 data by the following criteria: AOD>0.2 and zenith angle>50° so as to avoid high uncertainty degree in the retrieval as other works have suggested previously when using this data level (1.5) (Valenzuela et al., 2015).

Additionally, we have corroborated this analysis through the quantification of the Saharan dust contribution at ground level. For that, backward trajectories by HYSPLIT model, study on aerosol model outputs such as SKIRON or BSC-DREAM, and verification from air quality monitoring networks have

been carried out. The methodology used, is based on the directive of European Commission for demonstration and subtraction of exceedance attributable to natural sources on ambient air quality and cleaner air (Querol et al., 2013).

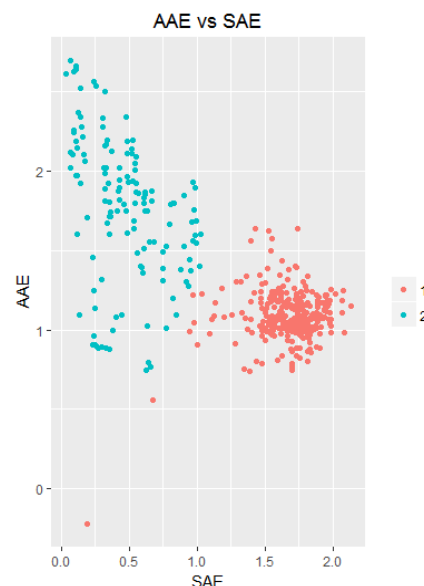


Figure 1. A 2D cluster analysis based on Scattering Ångström Exponent (SAE) and Absorption Ångström Exponent (AAE). Group 1 and 2 would stand for typical aerosol observed in the Madrid atmosphere and Saharan dust aerosols respectively in summer (2012-2015).

The research leading to these results has received funding from MICINN (Spanish Ministry of Science and Innovation) under project PROACLIM (CGL2014-52877-R). We thank AERONET and Juan Ramón Moreta González for their effort in establishing and maintaining the Madrid and La Coruña site.

Holben, B.N. et al. 1998. *Remote Sensing of Environment*, **66**, 1-16.

Querol, X. et al. 2013. *Procedimiento para la identificación de episodios naturales de PM10 y PM2.5, y la demostración de causa en lo referente a las superaciones del valor límite diario de PM10* Ed: Min. de Medio Ambiente, Medio Rural y Marino.

Valenzuela, A. et al. 2015. *Atmospheric Research*, **154**, 1-3.

## Ground-level PM<sub>2.5</sub> prediction using 3 km MODIS AOD over Tehran megacity

S. Sotoudeheian, M. Arhami and F. Azarmi

Department of Civil Engineering, Sharif University of Technology, Tehran, 11365, Iran

Keywords: PM<sub>2.5</sub>, AOD, MODIS, Linear mixed effect model.

Presenting author email: f.azarmi@mehr.sharif.edu

Remote sensing techniques have been used to provide estimation of Particulate Matter (PM) spatio-temporal variations and assess residents exposure levels. However, these techniques require improvements to provide reliable estimates with suitable coverage of PM particularly over polluted and variable urban environments (Tian and Chen (2010); Ghotbi *et al* (2016)). In order to enhance ground-level PM estimates, different types of models from simple linear regression to more complex nonlinear models which implement effective parameters besides satellite data such as meteorological and topographical parameters were used (Gupta and Christopher (2009); Sorek-Hamer *et al* (2013), Sotoudeheian and Arhami (2014)). However, most of previous studies were performed in regional scale with a coarse spatial resolution (10 km or more) (Gupta and Christopher (2009); Kloog *et al* (2011)) and very few number of investigations focused on local polluted urban areas with different mobile and stationary sources with fine resolution (Xie *et al* (2015)). In this study LME model was used in collaboration with various effective parameters to provide an accurate estimation of PM<sub>2.5</sub> over Tehran, the polluted capital of Iran, during a one year period. In order to overcome the intra-community variabilities in heavily polluted small environment and improve model performance in predicting ground-level PM<sub>2.5</sub>, adjusted Linear Mixed Effect (LME) model implementing proper inputs such as fine resolution Aerosol Optical Depth (AOD) product in fine resolution was used. In this model satellite-derived AOD with spatial resolution of 3 km from new collection of MODIS (collection 6 (C006) started in early 2014) which provided by NASA research team (Levy *et al* (2013)) was used. LME model consider the time-varying nature of effective parameters in models and could lead to significant improvement in predictive power of statistical models (Lee *et al* (2011)). This work is also the first attempt to estimate ground-level PM<sub>2.5</sub> over such polluted urban area of Tehran using new release of AOD with spatial resolution of 3 km.

Forward Stepwise Method (FSM) was used to obtain the optimal shape of model which had the best performance in predicting ground-level PM<sub>2.5</sub>. Initial shape of model was built with AOD variable as a random term and the other auxiliary parameters were added as a fixed term separately. The best model in this step was selected based on highest coefficient of determination ( $R^2$ ). This algorithm was repeated until all effective predictors were added to model. Finally, the best shape of model was selected between different steps using Akaike Information Criterion (AIC) statistics.

While in the final shape of LME model AOD was determined as the fixed and random variable, temperature, relative humidity, total cloud and planetary boundary layer height were used as the fixed parameters.

The results of model-fitting and cross-validation for the proposed LME model is represented in Figure 1 as the scatter plot between measured and predicted PM<sub>2.5</sub> during study period. The model could explain 72 and 57% variability of ground-level PM<sub>2.5</sub> during model-fitting and cross-validation, respectively. The corresponding RMSE and MAE were (8.5, 6.4)  $\mu\text{g}/\text{m}^3$  and (10.77, 7.6)  $\mu\text{g}/\text{m}^3$ , respectively. In general, LME model in collaboration with 3 km AOD product and meteorological variables was reliable in predicting ground-level PM<sub>2.5</sub>.

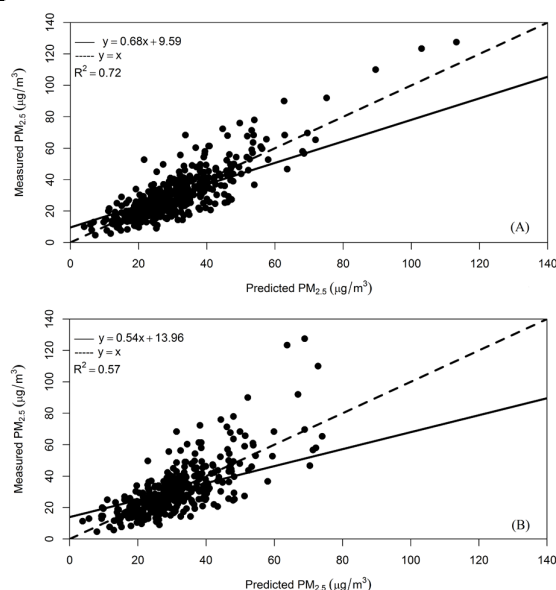


Figure 1. Scatter plots of predicted PM<sub>2.5</sub> versus observed PM<sub>2.5</sub> (A) model-fitting (B) cross-validation.

- Ghotbi, S., Sotoudeheian, S. and Arhami, M. (2016) *Atmos. Environ.* **141**, 333-346.
- Gupta, P. and Christopher, S. A. (2009) *J. Geophys. Res. Atmos.* **114**(D14).
- Kloog, I., Koutrakis, P., Coull, B. A., Lee, H. J. and Schwartz, J. (2011) *Atmos. Environ.* **45**, 6267-6275.
- Lee, H., Liu, Y., Coull, B., Schwartz, J. and Koutrakis, P. (2011) *Atmos. Chem. Phys.* **11**, 7991-8002.
- Levy, R., Mattoo, S., Munchak, L., Remer, L., Sayer, A. and Hsu, N. (2013) *Atmos. Meas. Tech. Discuss.* **6**, 159-259.
- Liu, Y., Franklin, M., Kahn, R. and Koutrakis, P. (2007) *Remote Sens. Environ.* **107**, 33-44.
- Sorek-Hamer, M., Strawa, A., Chatfield, R., Esswein, R., Cohen, A. and Broday, D. (2013) *Environ. Pollut.* **182**, 417-423.
- Sotoudeheian, S. and Arhami, M. (2014) *J. environ. health sci. eng.* **12**, 122.
- Tian, J. and Chen, D. (2010) *Remote Sens. Environ.* **114**, 221-229.
- Xie, Y., Wang, Y., Zhang, K., Dong, W., Lv, B. and Bai, Y. (2015) *Environ. Sci. Technol.* **49**, 12280-12288.

## Information content of lidar backscattering and extinction profiles with respect to the chemical composition of atmospheric aerosol

M. Kahnert<sup>1,2</sup> and E. Andersson<sup>2</sup>

<sup>1</sup>Research Department, Swedish Meteorological and Hydrological Institute, 601 76 Norrköping, Sweden

<sup>2</sup>Department of Earth and Space Science, Chalmers University of Technology, 412 96 Gothenburg, Sweden

Keywords: lidar, inverse modelling, data assimilation, chemical transport modelling

Presenting author email: michael.kahnert@smhi.se

Lidar observations of extinction and backscattering coefficients can provide information on the vertical distribution and abundance of atmospheric aerosol particles. But how much quantitative information about the particles' chemical composition can we really extract from the measurements? We investigate this question from the point of view of chemical data assimilation.

The problem of retrieving information about the chemical composition of aerosol particles from their optical properties is a highly under-constrained inverse problem. This raises the question how to best set up a chemical data assimilation system for lidar observations. If we simply allow all aerosol variables to be independently determined by the analysis algorithm (e.g. Liu et al., 2011) then this can result in the assimilation of measurement noise rather than signal. In some cases, the analysis result can even become worse than the a priori model estimate (e.g. Kahnert, 2009). Previous attempts to address this problem have relied on ad hoc assumptions about the information content of aerosol optical measurements. For instance, Benedetti et al. (2009) assimilated aerosol optical depth and allowed only the total aerosol mass concentration to be corrected by the analysis algorithm. Saide et al. (2013) used the aerosol mass concentrations per size bin as control variables in the analysis algorithm.

A disadvantage of ad hoc approaches is that one cannot be sure that one does not over-use the measurements (thus assimilating noise), nor that one fully exploits the information contained in the observations. Another disadvantage of ad hoc approaches is that the number of independent control variables is hard-coded. This severely limits the flexibility of such methods under varying conditions, such as varying numbers of observational parameters and wavelengths, and varying observation and background errors, all of which would effect the number of signal degrees of freedom of the measurements.

Here we apply methods of information and retrieval theory to analyse the information content of a set of measurements with respect to the chemical composition of aerosols. We construct a transformation of model-space into a new basis in which the model variables can be partitioned into signal-related and noise-

related components. We constrain our analysis algorithm to acting on the signal-related components only. In this way we automatise the choice of control variables for any set of observational parameters, thus maximising the amount of information extracted from the measurements, while avoiding the risk of assimilating noise.

The algorithm performance is investigated in a numerical test. We use our regional chemical transport model MATCH to produce two sets of aerosol fields, one generated with analysed meteorological data, and another set generated with 48h forecast data. The first is taken as a reference, while the second serves as a proxy for a background estimate. We generate synthetic observations of backscattering and extinction profiles by applying the observation operator to the reference results. The observations and the background estimate are analysed with a 3DVAR code.

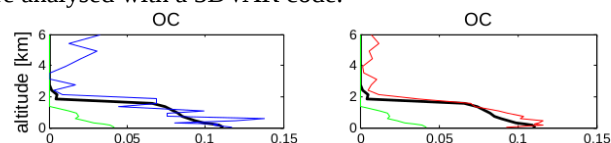


Figure 1. Comparison of reference (black), background (green), unconstrained (left blue) and constrained analysis (right red) for organic carbon.

The figure shows a comparison of the analysis with the reference and background profiles, in this case for organic carbon. The unconstrained analysis is shown on the left (blue line), the constrained one is shown on the right (red line). While the unconstrained approach produces noisy results and conspicuously high concentrations aloft, the constrained approach significantly alleviates such problems.

More information can be found in Kahnert and Andersson (2016).

Liu, Z. et al. (2011) *J. Geophys. Res.* **116**, D23206.

Kahnert, M. (2009) *Tellus* **61B**, 747-755.

Benedetti, A. et al. (2009) *J. Geophys. Res.* **114**, D13205.

Saide, P. E. et al. (2013) *Atmos. Chem. Phys.* **13**, 10425-10444.

Kahnert, M. and E. Andersson (2016) *Atmos. Chem. Phys. Discuss.* **16**, doi:10.5194/acp-2016-914.

## **Abstracts T207**

## Modelling of SOA markers: simulation through detailed mechanisms and validation by comparison with measurements. A new approach to understand SOA formation.

G.M. Lanzafame<sup>1,2</sup>, D. Srivastava<sup>1</sup>, N. Bonnaire<sup>3</sup>, F. Couvidat<sup>1</sup>, O. Favez<sup>1</sup>, B. Bessagnet<sup>1</sup> and A. Albinet<sup>1</sup>

<sup>1</sup>INERIS, Parc technologique ALATA, 60550 Verneuil en Halatte, France

<sup>2</sup>Sorbonne Universités, UPMC, 75252 PARIS cedex 05, France

<sup>3</sup>LSCE - UMR8212, CNRS-CEA-UVSQ, Gif-sur-Yvette, France

Keywords: Secondary Organic Aerosol, Tracers, Measurements, modelling.

Presenting author email: grazia-maria.Lanzafame-etudiant@ineris.fr

Secondary organic aerosol (SOA) is formed via the oxidation of both anthropogenic and biogenic gas-phase organic compounds and is a large and often dominant fraction of total OA (Kroll and Seinfeld, 2008). To assess the sources of secondary organic carbon, SOA “tracer” method related to specific precursors has been developed (Kleindienst et al., 2007). Due to the importance of SOA contribution on the total PM mass, it is necessary to develop atmospheric chemistry models that properly describe the formation of the SOA markers in the atmosphere in order to improve the understanding of SOA formation and to enhance air quality forecasts. In this context, the modelling approach developed has to be compared with data obtained through field measurements.

The aim of this work is to implement SOA tracer mechanisms inside the air quality model CHIMERE and to compare the model with field measurements results. This comparison gives an insight on the ability of the model to form SOA from specific precursors and on several processes (e.g. emissions, gas/particle partitioning).

Measurements of SOA markers were performed at SIRTA station, representing the suburban background air quality conditions of the Paris region (about 25 km SW from Paris city center). PM<sub>10</sub> samples were collected every third day all over the year 2015. SOA markers have been quantified using native standard compounds by LC/M-MS and/or GC/MS after derivatization with MSTFA+1% TMCS. SOA marker concentrations (Figure 1) were compared with the results of the model.

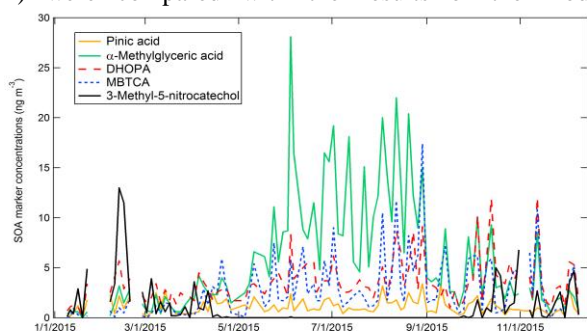


Figure 1. Annual trend of some SOA marker concentrations at SIRTA sampling site (2015).

The mechanisms describing the formation of the markers were introduced into the chemistry-transport model CHIMERE (Menut et al. 2013). Mechanisms for the formation of SOA markers were taken from the

Master Chemical Mechanism (MCM, NCAS, Universities of Leeds and York) otherwise, data were sought in the scientific literature. The gas phase mechanism simulation was performed using MELCHIOR2, the partitioning between particulate phase and gaseous phase was calculated using the thermodynamic model SOAP (Couvidat and Sartelet, 2015). Biogenic emissions were computed with MEGAN 2.1 algorithm (Guenther et al., 2012).

Simulated markers included both biogenic, (e.g; pinonic acid, pinic acid and MBTCA from  $\alpha$ -pinene oxidation), and anthropogenic (e.g. DHOPA and nitrophenols from toluene oxidation) precursors. An example of pinonic acid modelling over France for the year 2013 is shown on Figure 2.

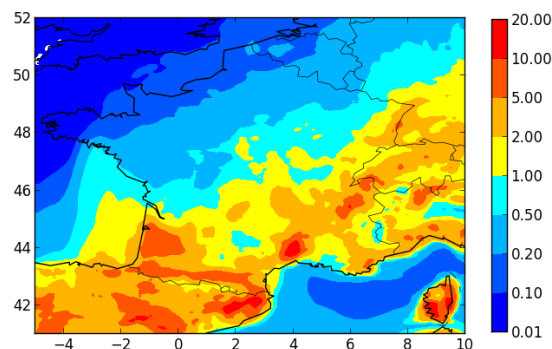


Figure 2. Map of distribution of pinonic acid ( $\text{ng m}^{-3}$ ) all over France in July 2013, simulated by CHIMERE.

### Acknowledgements

This work was supported by the French ministry of environment (MEEM) and by the FP7 ACTRIS and H2020 ACTRIS2 projects.

### References

- Couvidat F. and Sartelet, K. (2015) *Geosci Model Dev* 8, 1111-1138
- Kleindienst, T.E., Jaoui, M., Lewandowski, M., Offenberger, J.H., Lewis, C.W., Bhawe, P.V., and Edney, E.O. (2007). *Atmos. Environ.* 41, 8288–8300.
- Kroll, J.H., and Seinfeld, J.H. (2008). *Atmos. Environ.* 42, 3593–3624
- Menut, L., B. Bessagnet, D. Khvorostyanov, M. Beekmann, N. Blond, A. Colette, I. Coll, et al. (2013). *Geosci Model Dev* 6 (4): 981–1028.
- Guenther, A.B., Jiang, X., Heald, C.L., Sakulyanontvittaya, T., Duhl, T., Emmons, L.K., and Wang, X. (2012). *Geosci. Model Dev.* 5, 1471–1492

## Using Unmanned Air Vehicle to Verify the Air Quality Space Distribution Simulation at Toucheng Interchange near National Road No.5

S. Yu<sup>1</sup>, R.C.jhuang<sup>2</sup> and C.T. Chang<sup>2</sup>

<sup>1</sup>Department of Environmental Engineer, University of Taiwan, Ilan, 260, Taiwan

<sup>2</sup>Department of Environmental Engineer, University of Taiwan, Ilan, 260, Taiwan

Keywords: UAV, Caline4, traffic flow, rush hours, highway.

Presenting author email: ioioio7625@gmail.com

Recently, gaseous air pollution was the main efforts in environmental science were focused on. This type of pollution was regarded as most dangerous to human health. The objective of this study was to validate air quality forecast with Unmanned Aerial Vehicle (UAV) with PM<sub>2.5</sub>, CO sensor under the UAV, as shown in Figure 1.

The air quality will be predicted with a suitable model and local air quality monitoring data. It is well known that traffic jam is one of the main contributing sources to overall air pollution in the urban environment (Zhiqiang et al., 2000). The concentration of mobile sources traffic-related air pollutant exposure is simulated with using CALINE4. The concentration in Hsuehshan tunnel is simulated with Computational Fluid Dynamics fluid model (CFD). The differences of air quality between rush hours and normal traffic condition were also investigated.

The first step goes to collect local meteorological data, including ground and aerial, data of source by Taiwan's EPA. The emission rate of the sources is also estimated by Environmental Protection Agency. In addition, the traffic volume was supplied by Ministry of Transportation and Communications. To ensure the data of simulation, UAV and Tapered Element Oscillating Microbalance (TEOM) and high Volume detector to verification were used.

The spatial concentration was also estimated at high and low population density area. Different emission control strategies, such as adopting low emission vehicles, limiting the traffic flow, admitting the high passengers pass, were also assessed to improve air quality. According to the different kinds of road and air pollutant emission rate, the parameters of the model and meteorological conditions are necessary to be set to assess the incremental impact of the pollutant.

The predicted air quality depended on temporal and spatial variations. The results were incorporated into exposure assessment for comparing the data in ambient monitoring station and understanding the exposure of air pollutants. Traffic volume and pollutant emissions become higher during rush hours in weekend. The vehicle emissions rate depends on vehicle speed. In study, the average speed of 80 km/hr was used. The vehicles were subdivided into small passenger cars for personal use, business use of small passenger cars, gasoline passenger cars diesel passenger cars and buses.

Use of regional automotive pollutant emissions, different weather conditions can affect the analysis of the emissions caused by the scope and extent. The differences of concentration between modelling and experimental data have shown in Figure 2. The highest point was in the commuting times. The predict data is 3 times higher than others.



Figure 1. CO and PM<sub>2.5</sub> sensor of UAV

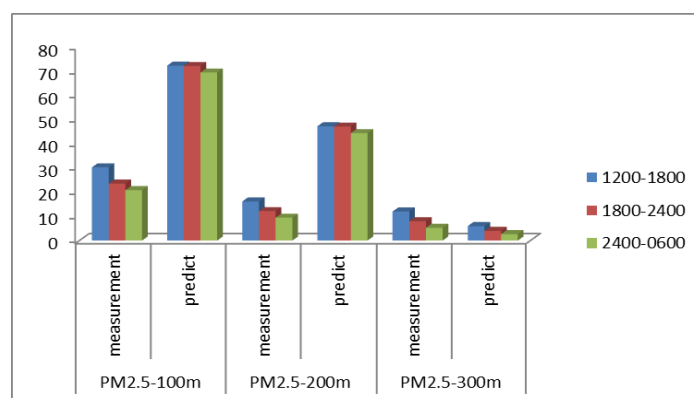


Figure 2. The comparison between modelling and experimental data.

Wang, J., DenBleyker, A., McDonald-Buller, E., Allen, D., Zhang, K. (2011) Modeling the chemical evolution of nitrogen oxides near roadways Atmospheric Environment 45 Pages 43- 52.

Jung, Y. R., Park, W. G., & Park, O. H. (2003). Pollution dispersion analysis using the puff model with numerical flow field data. Mechanics research communications, 30(4), 277-286.

## Seasonal variation of aerosol size distributions at the Puy de Dôme station with emphasis on free tropospheric conditions

A. Farah<sup>1</sup>, E. Freney<sup>1</sup>, A. Chauvigné<sup>1</sup>, J.L. Baray<sup>1,2</sup>, A. Colomb<sup>1,2</sup>, D. Hadad<sup>1</sup>, M. Abboud<sup>3</sup>, W. Farah<sup>3</sup> and K. Sellegri<sup>1</sup>

<sup>1</sup> Laboratoire de Météorologie Physique, UMR6016, Université Clermont Auvergne-CNRS, 4 avenue Blaise Pascal, 63118, Aubière, France

<sup>2</sup> Observatoire de Physique du Globe de Clermont Ferrand, UMS 833, Université Clermont Auvergne-CNRS, 4 avenue Blaise Pascal, 63178 Aubière, France

<sup>3</sup> Unité de Recherche EGFEM, Faculté des Sciences, Université Saint Joseph, Beyrouth, Liban.

Keywords: Aerosol size distribution, High altitude site, Long range transport, Boundary Layer/ Free Troposphere.

Presenting author email: a.farah@opgc.univ-bpclermont.fr

Aerosol particles have important direct and indirect impacts on the climate. Within the planetary Boundary layer (BL), these particles have a relatively short lifetime due to a large number of removal processes, e.g., rain, sedimentation, coagulation. Once aerosols are transported into the free troposphere (FT), their atmospheric lifetime increases significantly making them representative of large spatial areas. The physical and chemical properties of the FT aerosols are poorly characterized due to difficulties in performing high altitude measurements. In this work we use a one year data set of continuous measurements performed at the PUY (Puy de Dôme, 45°46' N, 2°57'E, 1465 m asl) global GAW station.

A methodology based on a combination of four methods (WCT, ECMWF, RADON-222, and NO<sub>x</sub>/CO), is applied to the PUY to identify when the site was in the FT or in the BL. This methodology allows us to study the differences in particle physical characteristics between the FT and the BL. In addition to aerosol size distribution measurements, we analyzed black carbon (BC) measurements and a range of different meteorological parameters. We observe that air masses sampled as BL have frequencies ranging from 50% in winter to 97% in summer. While concentrations of BC, Aitken and accumulation mode particles were higher in the BL than in the FT in winter and autumn, they were measured to be higher in the FT compared to BL in spring (Fig. 1(a, c and d)), indicating an eventual direct contamination of the FT by strong convective biomass burning events during this season. No significant difference between the BL and the FT concentrations was observed for the nucleation mode particles for all seasons, suggesting a continuous additional source of nucleation mode particles in the FT compared to the other aerosol size classes. Finally, coarse mode particles concentrations were found higher in the FT than in the BL during summer, and similar in the two atmospheric layers for the other seasons (Fig. 1(b)).

Airmass backtrajectories have been calculated for 96h for the period of March to December 2015 with the LACYTRAJ model in order to document the time spent of the sampled airmass in the FT since last contact with the BL.

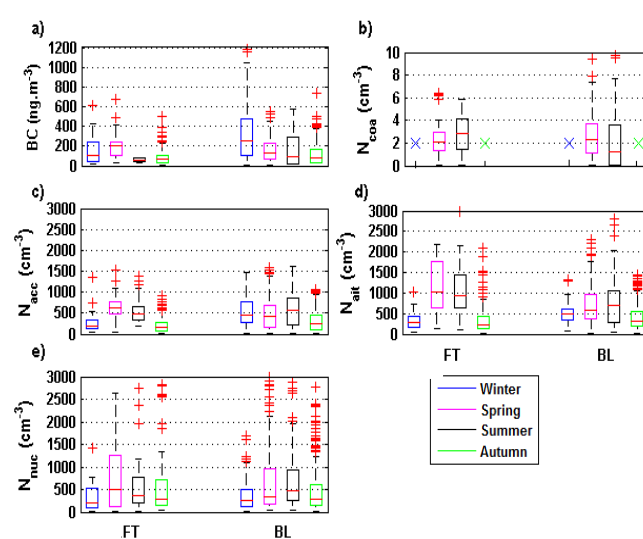


Figure 1. FT/BL variation of: **a)** BC, **b)** Coarse (coa) (>1  $\mu\text{m}$ ), **c)** Accumulation (acc) (100-300 nm), **d)** Aitken (ait) (40-80 nm), **e)** Nucleation (nuc) (10-20 nm), concentrations for the four seasons. Red line represents the median value, bottom and top sides of the boxes symbolize the 25<sup>th</sup> and 75<sup>th</sup> percentile respectively and the extremities of the black lines are the 10<sup>th</sup> and 90<sup>th</sup> percentile. Red Cross represents the outliers.

This work was supported by the European Research Infrastructure for the observation of Aerosol, Clouds, and Trace gases (ACTRIS2) and the research council of the Saint Joseph University.

## Aerosol particle dry deposition velocities above environmental substrates according to the diameter and the micrometeorological parameters : for the first time the "V" curve between 1.5 nm and 1 $\mu\text{m}$

G. Pellerin<sup>1,2</sup>, D. Maro<sup>1</sup>, E. Gehin<sup>2</sup>, D. Boulaud<sup>3</sup>, P. Laguionie<sup>1</sup>, D. Hébert<sup>1</sup>, O. Connan<sup>1</sup> and L. Solier<sup>1</sup>

<sup>1</sup>Institut de Radioprotection et de Sûreté Nucléaire (IRSN), PRP-ENV, SERIS, LRC, Cherbourg-Octeville, 50130, France

<sup>2</sup>Université Paris-Est, CERTES (EA 3481), UPEC, F-94010, Créteil, France

Institut de Radioprotection et de Sûreté Nucléaire (IRSN), PRP-ENV, Le Vésinet, 78116, France

Keywords: Aerosol, Eddy correlation, Dry deposition, Spectral analysis.

Presenting author email: geoffrey.pellerin@irsn.fr

Nuclear facilities introduce different types of radionuclides into the atmosphere in the form of gases and aerosols during chronic or accidental releases. These particles may be submitted to atmospheric dispersion, dry and wet deposition. The study of dry deposition based on the dry deposition velocity (dry deposition flux divided by an atmospheric concentration above the substrates) concept is a major issue concerning the impact of radionuclides on the population and the environment. Uncertainties on the dry deposition velocity values of submicronic particles are up to several orders of magnitude discrepancies according to the model used (Petroff *et al.*, 2008). Moreover there is no data for particle diameter under 10 nm. So, the aim of this study is to quantify dry deposition velocity according to the particles diameter and the atmospheric stability.

Dry deposition flux can be determined with different devices. We used 3 different methods to quantify the dry deposition velocities according to the particles diameter. (1): For particles around 1.5 nm we studied the dry deposition of free fraction of alpha particles of  $\text{Rn}^{222}$  decay products. The flux is calculated by the gradient method and so, we sample at two different heights. The sampling is made on diffusion screen at  $200 \text{ L}\cdot\text{min}^{-1}$  for catching particles under 1.5 nm and then the measure are carried by alpha spectrometry. (2) For particles between 2.5 nm and 1.2  $\mu\text{m}$  we used the eddy correlation method with a cospectral analysis (Damay *et al.*, 2009): the dry deposition flux is determined thanks to covariance between fluctuations of the vertical wind velocity and fluctuations of the atmospheric aerosol particle concentration during 30-minutes periods at high frequency. The aerosol particle concentration was measured by coupling two Condensation Particles Counters (CPC 3788, TSI, Inc.) for particle sizes between 2.5 and 14 nm (Twin CPC method) and for particle sizes between 7 nm and 1  $\mu\text{m}$ , an Electrical Low Pressure Impactor (ELPI, Dekati, Inc.) was used. The wind 3-component velocity was measured by an ultrasonic anemometer (Young 81000, Inc.). (3) The last method used is the direct deposition of fluorescein particles of 0.6  $\mu\text{m}$  on synthetic grass and the measurement are carrying on by a fluorimeter.

Four experimental campaigns were conducted on grassland in western France (near Poitiers) april 2015 and September 2016.

For the first time, the figure 1 shows dry deposition velocities normalized by friction velocities according to particles diameter and for the four sampling campaign. We can note that, even if the used different technics, all of the point are consistent and we can find the theoretical curve shape of dry deposition velocity with the effects of the three dry deposition mechanisms: Brownian diffusion, interception and impaction (Sehmel, 1980). Thus, the dry deposition velocity of ultrafine particles (nucleation mode) is essentially caused by Brownian diffusion.

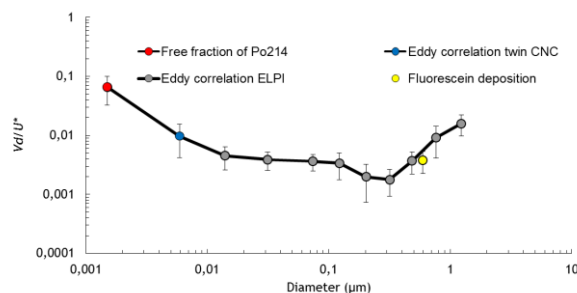


Figure 1: Dry deposition velocity ( $V_d$ ) normalized by the friction velocity ( $U^*$ ) averaged for the DEPECHEMOD 1 to 4 campaigns according to the particles diameter

We propose to present the all used methods and devices and then, to describe the results.

Petroff, A., Mailliat, A., Amielh, M., Anselmet, F., (2008). *Aerosol dry deposition on vegetative canopies. Part I: Review of present knowledge*. Atmospheric Environment 42, 3625-3653.

Damay, P.E., Maro, D., Coppalle, A., Lamaud, E., Connan, O., Hébert, D., Talbaut, M., Irvine, M. (2009), *Size-resolved eddy covariance measurements of fine particle vertical fluxes*, Journal of Aerosol Science 40, 1050-1058.

Sehmel, G.A. (1980). *Particle and gas dry deposition: A review*. Atmospheric Environment (1967), 14, 983-1011.

## Long-term monitoring of atmospheric radioactive aerosols in Prague, Czech Republic

M. Hýža, P. Rulík, H. Malá, V. Bečková, Z. Höglgye, E. Schlesingerová

National Radiation Protection Institute (SÚRO), Prague, 140 00, Czech Republic

Keywords: radioactivity, aerosol, radionuclides, atmosphere, seasonal variation

Presenting author email: miroslav.hyza@suro.cz

Atmospheric radioactive aerosols have been monitored in the Czech Republic, within the Radiation Monitoring Network, for over 30 years. This paper presents monitoring data from the site in Prague (50.06°N, 14.45°E, altitude 210 m) where low-level measurements of a wide range of radionuclides are performed. Radioactive aerosols are of special interest from radiation protection point of view, but they are also regarded as useful tracers of atmospheric processes.

Samples were collected using HVOL aerosol samplers (150-900 m<sup>3</sup>/h) equipped with polypropylene filters. Under normal conditions, the sample is collected for 3-7 days and later analyzed by gamma-ray spectrometry to determine the content of <sup>137</sup>Cs, <sup>7</sup>Be, <sup>22</sup>Na, <sup>210</sup>Pb and <sup>40</sup>K on the filter. In this measurement setup, no radiochemical pre-treatment is used and 6-day-long counting is usually performed using 150% HPGe detector.

Gamma spectrometric analysis is followed by a radiochemical separation in order to determine the concentration of <sup>90</sup>Sr, <sup>238</sup>Pu and <sup>239,240</sup>Pu in the quarterly combined filters. <sup>90</sup>Sr is determined destructively using the oxalate method. After the separation and ingrowth of the daughter product, <sup>90</sup>Y was counted by low-level proportional counter. By contrast, <sup>238</sup>Pu and <sup>239,240</sup>Pu is determined by co-precipitation, ion exchange and liquid-liquid extraction followed by electro-deposition and alpha spectrometry.

The resulting time series indicates that the present concentration of <sup>137</sup>Cs remains below the μBq/m<sup>3</sup> level. Another observation is that the time trend of <sup>137</sup>Cs consists of three periods, which can be described by three effective half-lives – 73 days for the period immediately after the Chernobyl accident, followed by the half-life of 1.37 years until 1993, and finally 22 years for the period 1993-2016 where resuspension dominates.

Statistical analyses show the presence of seasonality at the significance level of  $\alpha=0.05$  (the Kruskal-Wallis test) in all time series except for the <sup>90</sup>Sr. Cosmogenic radionuclides <sup>7</sup>Be and <sup>22</sup>Na show the strongest seasonality with maxima in June-July due to the stronger vertical mixing of the atmosphere in summer.

We have observed summer minima of <sup>40</sup>K and <sup>137</sup>Cs activity, which is driven mainly by resuspension as indicated by the strong correlation with dust content collected on the filter. Maximum or minimum concentration of <sup>210</sup>Pb is achieved in autumn, or spring respectively, which is probably caused by the difference in atmospheric vertical mixing, intensity of emanation from the soil and wet scavenging of the associated aerosol.

Since the oceanic production of <sup>210</sup>Pb is lower by approximately 2 orders of magnitude than the continental production, it is possible to make use of the different origins of <sup>210</sup>Pb and <sup>7</sup>Be to trace the oceanic and continental air masses. This was confirmed by the back trajectory analysis of air masses using the HYSPLIT model. (Stein, Draxler, et al. 2015)

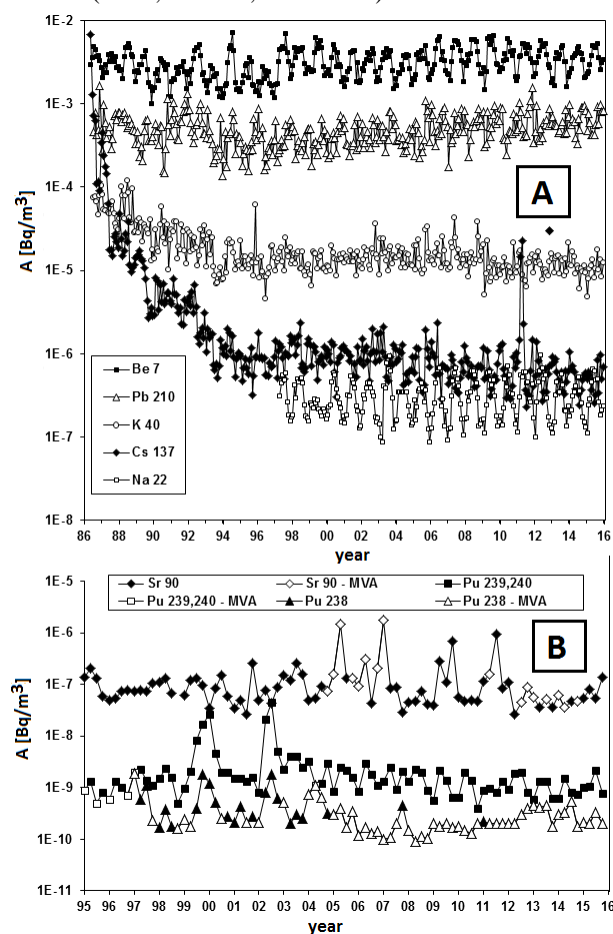


Figure 1 – Results of radioactive aerosol monitoring in Prague. A) Gamma-ray emitting radionuclides, B) Alpha/beta emitting radionuclides

The study was supported by the Ministry of the Interior of the Czech Republic MV-25972-53/OBVV-2010\_and by the State Office for Nuclear Safety with the use of the database of Radiation Monitoring Network “MonRaS”.

Stein, A.F., Draxler, R.R., Rolph, G.D., Stunder, B.J.B., Cohen, M.D., and Ngan, F., (2015). *NOAA's HYSPLIT atmospheric transport and dispersion modeling system*, Bull. Amer. Meteor. Soc., 96, 2059-2077, <http://dx.doi.org/10.1175/BAMS-D-14-00110.1>

## Data assimilation on dust forecast model using nighttime AOT retrieved from artificial neural network

S.-S. Lee<sup>1</sup>, B.J. Sohn<sup>2</sup>, H.C. Lee<sup>1</sup> and S.B. Ryoo<sup>1</sup>

<sup>1</sup>Environmental Meteorology Research Division, National Institute of Meteorological Sciences, Jeju, 63568, Korea

<sup>2</sup>School of Earth and Environmental Sciences, Seoul National University, Seoul, 08826, Korea

Keywords: Dust aerosol, MODIS, Aerosol optical thickness, Artificial neural network, Data assimilation

Presenting author email: sangsam.lee@korea.kr

The various infrared (IR) techniques of diagnosing the dust presence and intensity (so-called dust indices) are a useful tool for monitoring evolutionary features of dust storm. However, apart from a limitation of discontinuity between land and ocean and between daytime and nighttime, there appears a serious limitation that the dust indices are not physical quantities but qualitative indices in a lack of scalability. From this reason, an algorithm was developed to relate IR brightness temperatures (BTs) to VIS-based aerosol optical thickness (AOT) (Lee and Sohn, 2012). In doing so an artificial neural network (ANN) model approach was used to combine MODIS-measured infrared BTs with visible AOTs. For training the ANN model, IR BTs, surface type and geometrical information were used as inputs to predict MODIS-derived AOTs during the daytime when VIS-based AOTs are available. The training was done exclusively over dust-laid pixels during the spring (March - May) of 2006 over the East Asian domain (20°N-55°N, 90°E-145°E).

It should be noted that the obtained daytime AOTs from the ANN model are in good agreement with MODIS-derived AOTs, with a correlation coefficient of 0.77 over the analysis domain. A maximum correlation coefficient of 0.85 is found over “water bodies” type surface whereas a minimum correlation coefficient of 0.75 over the “barren” type surface. However, a weak correlation is found during the nighttime when derived AOTs are compared against AOTs from CALIPSO; the weak correlation has been known between MODIS-driven AOT and CALIPSO-driven AOT. Selected case study indicates that the developed ANN method appears to well capture evolutionary features of dust area at nighttime, suggesting that the model can be readily used for monitoring the dust movement. It is further suggested that more frequent AOT estimates due to the IR-based AOTs during the nighttime can provide benefits to the aerosol data assimilation, despite degraded quality in comparison to visible measurements.

A data assimilation (DA) system employing day and nighttime AOTs for the Asian Dust Aerosol Model (ADAM), the dust forecasting model operated by Korea Meteorological Administration (KMA), has been developed with an optimal interpolation (OI) method. Two Asian dust cases occurred in 5 – 9 April 2006 (CASE1) and 14 – 18 March 2009 (CASE2) were simulated using ADAM. To examine the impact of inclusion of IR-based AOTs in the data assimilation system on the forecasting, two experiments were performed with different assimilation cycles (i.e., DA1:

24 hour cycle with daytime only MODIS AOT, DA2: 12 hour cycle with additional IR-based AOT during the night). Besides a control (CTL) simulation with no data assimilation was performed. Simulations were validated by comparing with MODIS-derived AOT distributions as well as with ground-based Korean skyradiometer network (KSNET) observations of AOTs. It is found that both experiments (DA1, DA2) led to improved forecasting, but DA2 outperformed DA1. Results suggest that the ANN-based AOT contributes positively to the forecasting capability through more temporal coverage in the data assimilation.

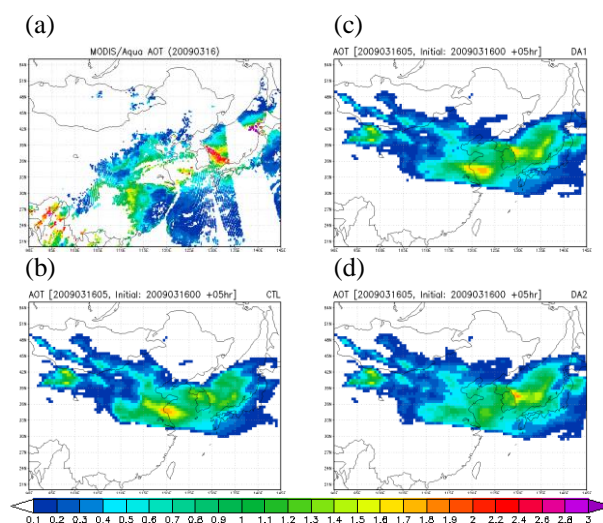


Figure 1. (a) Daytime AOT retrieval from MODIS/Aqua on 16 March 2009 and AOT at 05 UTC 16 March 2009 simulated by ADAM using (b) CTL, (c) DA1, (d) DA2. These simulation results are 5 hours-forecasting AOTs from at 00 UTC 16 March 2009.

This work was supported by a Grant (NIMS-2017-3100) funded by the National Institute of Meteorological Sciences (NIMS), the Korea Meteorological Administration (KMA).

Lee, S.-S. and Sohn, B.J. (2012) *J. Meteorol. Soc. Jpn.* **90**, 163-177.

## Improving CAMx with volatility basis set scheme for organic aerosol modelling: From chamber data to chemical transport model

J. Jiang<sup>1</sup>, S. Aksoyoglu<sup>1</sup>, G. Stefenelli<sup>1</sup>, G. Ciarelli<sup>2,3,1</sup>, U. Baltensperger<sup>1</sup>, I.EI. Haddad<sup>1</sup>, and A.S.H. Prevot<sup>1</sup>

<sup>1</sup> Laboratory of Atmospheric Chemistry, Paul Scherrer Institute, 5232, Villigen, Switzerland

<sup>2</sup> Laboratoire Inter-Universitaire des Systèmes Atmosphériques (LISA), UMR CNRS 7583, Université Paris Est Créteil et Université Paris Diderot, Institut Pierre Simon Laplace, Créteil, France

<sup>3</sup> Institut National de l'Environnement Industriel et des Risques, Parc Alata, 60550, Verneuil-en-Halatte, France

Keywords: chemical transport model, organic aerosol, volatility basis set, smog chamber.

Presenting author email: jianhui.jiang@psi.ch

Secondary organic aerosol (SOA) formed from oxidation of organic gases has been shown to dominate atmospheric particulate matter pollution worldwide. Modelling the formation and ongoing aging processes of SOA is still among the most challenging tasks due to its complicated sources, composition and chemical-physical properties. Traditional models tend to underestimate SOA substantially. One of the most important reasons is the potentially high but unaccounted for contribution of semi-volatile organics (SVOCs) and intermediate-volatility organics (IVOCs) to SOA formation. To better simulate oxidation processes of these precursors and organic aerosol (OA) components, the volatility basis set (VBS) approach has been implemented in chemical transport models (CTMs) like CAMx (Comprehensive Air quality Model with extensions) and CMAQ (Community Multiscale Air Quality) (Koo et al., 2014). Despite of its great potential, high uncertainties still remain. A recent study found distinct SOA formation characteristics between gasoline and diesel vehicles with or without diesel particle filter (Platt *et al.*, 2017); the SOA yield from residential biomass burning emissions may also vary significantly depending on the stove types and combustion conditions (Bruns *et al.*, 2017). All evidence highlights the importance to constantly update CTMs with the advanced knowledge from chamber studies.

Here, we constrained the parameters of a hybrid VBS-based box model using the most recent smog chamber data of biomass combustion and vehicles, and implemented them in CAMx to estimate the contributions of specific sources to the OA concentration in Europe. Chamber data of residential wood burning were retrieved from 14 smog chamber experiments under different temperatures, stove types, and hydroxyl (OH) radical exposure, while vehicle data covering new (Euro 5 gasoline and DPF-equipped diesel) and old vehicles operated at low and high temperature were obtained from Platt *et al.* (2017). The real-time measurements of OA concentration by high-resolution aerosol mass spectrometer (AMS) and non-traditional volatile organic compounds (NTVOC) by proton-transfer reaction mass spectrometer (PTR-ToF-MS) was adopted to constrain the model parameters, i.e. volatility distribution of primary emissions, NTVOC reaction rate, yields, and enthalpies of evaporation.

The simulated OA concentration under optimized parameter conditions of the box model demonstrated a good agreement with chamber data. As shown in Figure

1 for residential wood burning, we grouped the gas precursors into 6 compound classes, including furans, single-ring aromatics, polycyclic aromatic hydrocarbons (PAH), oxygenated aromatics, and organic compounds containing more or less than 6 carbon atoms. The simulated yields of compounds fit well with those of individual chamber experiments, and oxygenated aromatics present the highest contribution to residential wood burning SOA, with an average fraction of 36.1%.

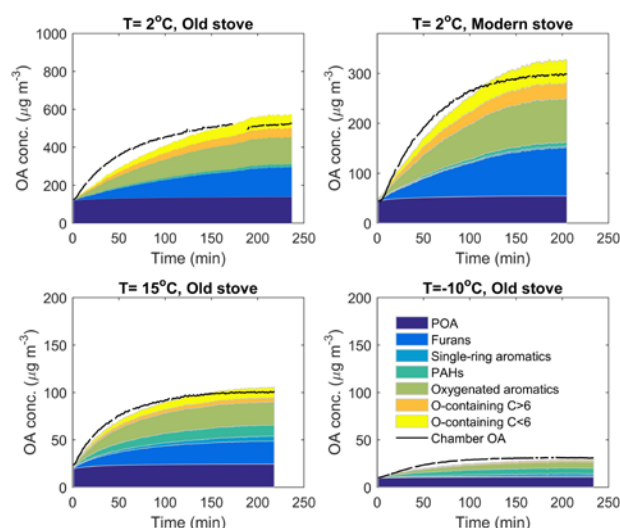


Figure 1. Contributions of major precursor compounds to secondary organic aerosol formation.

Based on the unprecedented results from the VBS box model study, we adapted the VBS module of CAMx v6.3 (Ramboll Environ, 2016) with the optimized parameters for different anthropogenic sources. Emission data was split into sub-categories of sources to enable simulation of OA under old and new technologies of gasoline and diesel vehicles, as well as biomass combustion. The updated model will be further validated by OA measurements from the ACSM network. By combining the cutting edge chamber experiments data with CTM, this study is expected to provide a benchmark for improving regional OA modelling worldwide.

Bruns, E.A., Slowik, J.G., Haddad, I.E., *et al.* (2017) *Atmos. Chem. Phys.* **17**, 705-720.

Koo, B., Knipping, E., and Yarwood, G. (2014) *Atmos. Environ.* **95**, 158-164.

Platt *et al.* (2017) *Submitted*.

## Melpitz Column Campaigns 2015 and 2017 – Detailed studies to characterize the vertical structure of the aerosol concentration and properties in the continental boundary layer under different conditions

B. Wehner<sup>1</sup>, S. Düsing<sup>1</sup>, T. Müller<sup>1</sup>, H. Baars<sup>1</sup>, J. Corbin<sup>2</sup>, M. Gysel<sup>2</sup>, N. Bukowiecki<sup>2</sup>, R. Käthner<sup>1</sup>, H. Siebert<sup>1</sup>  
and the Melpitz Team

<sup>1</sup>Leibniz Institute for Tropospheric Research (TROPOS), 04318 Leipzig, Germany

<sup>2</sup>Laboratory of Atmospheric Chemistry, Paul Scherrer Institute, Villigen PSI, Switzerland

Keywords: absorption, profiling, boundary layer

Presenting author email: birgit@tropos.de

The first Melpitz Column Campaign was performed from May 4 until July 10, 2015, while the second campaign took place between February 1 and March 10. During these periods a complex and complementary setup of aerosol and boundary layer measurements was installed at the TROPOS measurement site Melpitz. Besides a detailed aerosol characterization on ground and ground-based remote sensing, several platforms performing airborne measurements were applied during intensive periods to investigate the aerosol distribution in the whole column. The combination of several unmanned aerial systems (UAS), the helicopter-borne platform ACTOS (Airborne Cloud and Turbulence Observation System), research aircraft, and a tethered balloon within one campaign is unique and provides a dataset that is subject to ongoing investigations.

This work will focus mainly on vertical measurements or aerosol parameters such as particle number concentration and absorption and the comparison between summer and winter conditions.

### Measurements

The helicopter-borne platform ACTOS performed 13 2-hour flights between June 15 and 28, 2015 around Melpitz, the measurement site of TROPOS (40 km NE of Leipzig). During these flights measurements of the total particle number concentration  $N$ , number size distributions as well as particle absorption (450, 535, and 624 nm, STAP, Single Channel Three Color Absorption Photometer, Brechtel) under dry conditions ( $< 40\% rH$ ) were performed. During the winter campaign 2017 a tethered balloon was used to carry an isolated box with aerosol instrumentation. Here, again the STAP was used, complemented by a micro Aethalometer AE51 and an OPSS (GT-526, Met One Instruments) measuring aerosol particles larger than 300 nm. In addition, meteorological parameter were monitored continuously. Parallel to the flights the Raman lidar Polly<sup>XT</sup> performed continuous measurements over both campaigns.

### Results

Two case studies are shown in figure 1 presenting vertical profiles of selected parameters measured on June 25, 2015 and February 8, 2017 in Melpitz. During the first case clean marine air reached Melpitz causing low concentrations and low absorption coefficients. On February 8, easterly wind was dominating causing the

advection of polluted air from Eastern Europe followed by significantly higher absorption coefficients. The profile in February is measured by a tethered balloon and did not cover the same vertical range as the helicopter in June 2015.

A comparison of both cases illustrates nicely that not only ground-based measurements are influenced by long-range transport but also the boundary layer show much higher concentrations if continental air reaches the station. Here, the ground-based measurements are representative for the mixing layer, but this needs to be investigated for other cases.

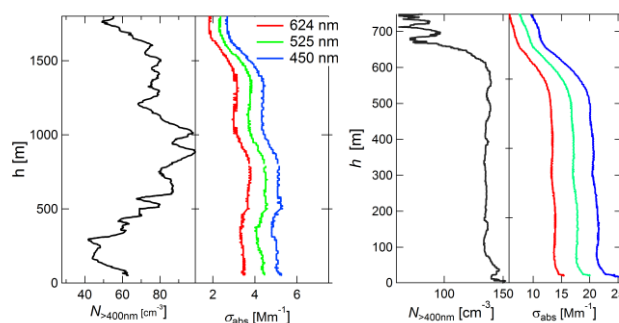


Figure 1: Vertical profiles of total particle number concentration  $> 400$  nm  $N_{>400\text{nm}}$  and particle absorption  $\sigma_{\text{abs}}$  at 450, 525, and 624 nm measured using ACTOS on June 25, 2015 at (left panel) and using a tethered balloon on February 8, 2017 (right panel) over Melpitz.

### Conclusions and Outlook

A detailed analysis of ACTOS and balloon measurements focussed mainly on the vertical distribution of absorbing aerosol is under progress. The most obvious result is that vertical profiles of aerosol concentration and aerosol absorption coefficient are mainly dominated by the air mass origin. Another important question will be under which conditions the ground-based measurements can be considered to be representative for the mixed layer. Furthermore, the vertical measurements will be compared with measurements and retrievals obtained by lidar in Melpitz during both campaigns. Long-term measurements on ground will be used to connect the profiles with ground and long-term variations.

## The simulation of the Dust Emission Rate from Jhuoshuei River

C.T. Wang<sup>1</sup>, T.H. Chiu<sup>1</sup>, Y.Y. Kao<sup>1</sup>, Y.H. Tseng<sup>1</sup>, S.J. Chen<sup>2</sup>, K.H. Chang<sup>3</sup> and W.Y. Lin<sup>1\*</sup>

<sup>1</sup>Institute of Environmental Engineering and Management, National Taipei University of Technology, Taipei 10608, Taiwan

<sup>2</sup>Department of Environmental Science and Engineering, National Pingtung University of Science and Technology, Pingtung 912, Taiwan

<sup>3</sup>Department and Graduate School of Safety Health and Environmental Engineering, National Yunlin University of Science and Technology, Yunlin 640, Taiwan

Keywords: Aerolian dust, Regression analysis, Simulate, AERMOD.

Presenting author email: wylin@ntut.edu.tw

The recent accretion in research attention to Aeolian dust has shown that dust transport systems operate in the river valley, and involve much larger quantities of sediment than was previously accumulated. Besides, the dust is also a major factor in the PM<sub>10</sub> through the natural production. Therefore, countries attach great importance to the prevention and control of dust (Margielewski et al., 2015).

The study area, the Jhuoshuei River is the longest river in the Taiwan, as shown in Figure 1. According to Aeolian dust events from 2012 to 2015, Used the TW-EPA air quality monitoring station data (ErLin & Lunbei) regresses analysis to derive the incremental concentration of dust emission rate estimation formula of the river.



Figure 1 Jhuoshuei River Basin and the air quality station location map.

Based on the multiple regression Eq. 1 and previous studies, the factors that affect the dust concentration, including wind speed, temperature and humidity are discussed. The records of four dust concentration events were selected. The first is to simulate the correlation between PM<sub>10</sub> concentration and relative humidity, the higher the relative humidity, the lower the PM<sub>10</sub> concentration. Then, the relationship between concentration and temperature is positive. Moreover, the wind speed from the riverbed to land increases, and the PM<sub>10</sub> concentration increases.

$$Y = \beta_0 + \beta_1 x_1 + \beta_2 x_2 + \varepsilon \quad (1)$$

where Y is dependent variable, x<sub>i</sub> is variable, β<sub>m</sub> is Regression coefficient and ε is Error. In combination with records of wind speed, temperature and relative humidity and PM<sub>10</sub> concentration by regression analysis is Eq. 2.

$$C = 39.52 \times WS + 1.94 \times \text{Temp} - 0.62 \times RH - 189.09 \quad (2)$$

where C is the incremental concentration caused by dust in the Jhuoshuei River, WS is the wind speed measured at Lunbei Station (m/s), Temp is the temperature at the Lunbei in Station (°C), and RH is the Lunbei's Relative

humidity of the station (%). The calculated incremental concentration is combined with the numerical model of Gaussian diffusion model to estimate the dust emission rate.

AERMOD began to become the preferred regulatory model of the Environmental Protection Agency in the United States in 2005, then officially became one of the United States Air Pollution regulatory models in 2006. Figure 2 shows the result of AERMOD combine with the emission rate of dust (Eq.2).

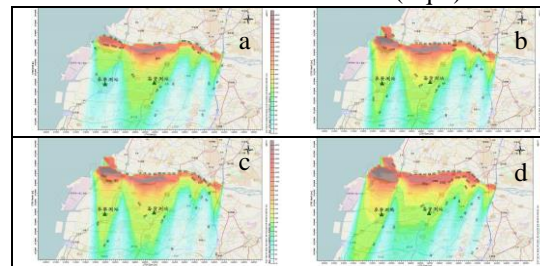


Figure 2 Dust graph by simulation  
(a) Sep-14-12, (b) Oct-25-13, (c) Jan-21-14,  
(d) Dec-7-15.

$$RE = \left| \frac{ADC - SDC}{ADC} \right| \times 100\% \quad (3)$$

where ADC is actual dust concentration, SDC is simulated dust concentration and RE is relative error.

The result of Eq. 3 is used to compare the difference between the regression equation by this study and Taiwan Data System (TEDS) Emission. Table 1 can be obtained that the calculation results and the TEDS are approximate the actual value, but the relative error rate in this study is better.

Table 1 The calculation results of the dust concentration value of Lunbei station

Date	PM <sub>10</sub>	This Study	Relative Error	TEDS	Relative Error
Sep-14-12	355	180	49%	160	66%
Oct-25-13	239	230	4%	190	33%
Jan-21-14	445	220	51%	190	64%
Dec-7-15	133	130	2%	70	62%

Margielewski, W., Krąpiec, M., Jankowski, L., Urban, J. and Zernitskaya, V. (2015). Quat. Int. 386: 212–225.

## Changes in sub-micron number size distributions at Czech rural and urban background stations in the last ten years

N. Zíková, J. Ondráček, Z. Wagner, V. Ždímal

Laboratory of Aerosol Chemistry and Physics, Institute of Chemical Process Fundamentals, Czech Academy of Sciences, Prague, 165 02, Czech Republic

Keywords: SMPS, long-term measurement, rural background urban background

Presenting author email: zdimal@icpf.cas.cz

In the Czech Republic, long-term sub-micron measurement has been set up simultaneously at two background stations, almost ten years ago. The first station is Prague-Suchdol, an urban background station that started in 11/2007, the second is Košetice observatory, a rural background station starting its measurement in 4/2008.

The Prague-Suchdol measurement originally consisted of a commercial Scanning Mobility Particle Sizer (3034 TSI SMPS, details in Římnáčová *et al.* 2011) until 11/2011. It was later upgraded at the TROPOS Institute to ACTRIS project (Aerosol, Clouds, and Trace gases Research Infrastructure Network) standards (Wiedensohler *et al.* 2012). New measurement started in 4/2012 and runs continuously with the exceptions of instrument calibrations etc. Size span, flows etc. can be found in Tab. 1.

The Košetice station is a professional meteorological station with multiple additional air quality measurements. The SMPS measurement was set up according to the EUSAAR/ACTRIS standards with the TROPOS-made SMPS system. Details about the measurement system can be found in (Zíková and Ždímal 2013), some information are also in the Tab. 1.

Table 1. Measurement details on Prague-Suchdol and Košetice SMPS systems.

	Prague	Košetice
dates	11/2007 - now	4/2008 - now
data availability		
size span [nm]	10 - 510	9 - 840
aerosol to sheath	1:4	1:5
flow [lpm]	$\pm 5\%$	$\pm 5\%$

To make both datasets comparable, the data evaluation was done in a similar way for both stations (with the exception of the first four years in Prague, where original measurement program was used). As the size spans of the two instruments are different, for comparison total number concentration of particles between 10 and 450 nm was used.

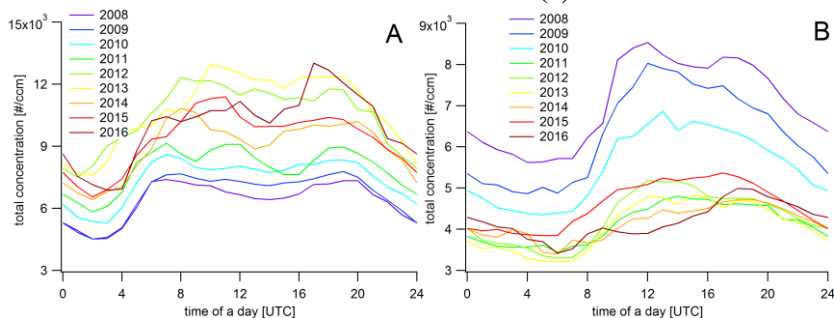


Figure 2. Daily cycles in Prague (A) and Košetice (B).

The preliminary results show the total number concentrations increased from 2011 to 2016 in Prague-Suchdol, while the concentrations were decreasing from 2008 to 2011 and later stayed stable in Košetice (Fig. 1).

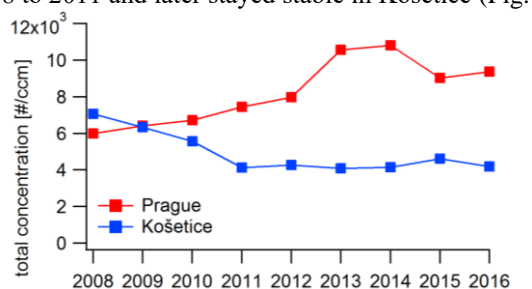


Figure 1. Total concentration from 10 to 450 nm from 2008 to 2016.

The daily cycles in Prague show two peaks, coinciding with the traffic, but from 2012, also a peak at midday, suggesting an increasing influence of new particle formation (NPF) events is evident. In Košetice, some influence of traffic pattern was observed at the beginning of the measurement, later the influence decreased (Fig. 2).

In this work, not only total concentrations are evaluated, but also particle number size distributions (PNSD) are compared in the last decade at the two stations, and possible explanations for the change in concentrations and PNSD changes are looked for. Additionally, also the change in the frequency and strength of the NPF events is evaluated.

Financial support from projects ACTRIS-2 H2020, num. 654109, and ACTRIS-CZ, MŠMT num. LM2015037 is gratefully acknowledged, as well as measurement support at the stations.

Římnáčová, D. *et al.* (2011) *Atmos. Res.* **101**: 539–52.

Wiedensohler, A. *et al.* (2012) *Atmos. Meas. Techniq.*

**5**(3): 657–85.

Zíková, N and Ždímal, V. (2013) *Aerosol Air Qual. Res.*

**13**(5): 1–11.

## Seasonal variation of organic compounds in PM<sub>2.5</sub> measured at Anmyeon Island, a background site in South Korea and major factors affecting their levels

Jong Sik Lee<sup>\*1</sup>, Eun Sil Kim<sup>2</sup>, Yong Pyo Kim<sup>3</sup>, Chang Hoon Jung<sup>4</sup>, Ji Yi Lee<sup>1,5</sup>

<sup>1</sup>Department of Renewable Energy Convergence, Chosun University, Gwangju 501-759, South Korea

<sup>2</sup>National Institute of Meteorological Sciences Anmyeondo Global Atmosphere Watch Station, Chungnam 32164, South Korea

<sup>3</sup>Department of Chemical Engineering and Materials Science, Ewha Womans University, Seoul 120-750, South Korea

<sup>4</sup>Department Health Management, Kyungin Women's College, Incheon 407-740, South Korea

<sup>5</sup>Department of Environmental Engineering, Chosun University, Gwangju 501-759, South Korea

Keywords: PM<sub>2.5</sub>, Individual organic compounds, background area, Northeast Asia, PM<sub>2.5</sub>

Presenting author email: [lys1313@gmail.com](mailto:lys1313@gmail.com)

Organic aerosols contain thousands of organic compounds and contribute to 20-90% of the total fine aerosol mass (Kanakidou et al., 2005). These organic aerosols originate from anthropogenic and natural (biogenic and geologic) sources and alter physical and chemical properties in the atmosphere depending on the atmospheric and meteorological condition. Organic aerosols have detrimental effects on human health as well as the environmental effects such as climate change, visibility. Also, the chemical composition in organic aerosol can be different depending on temporal and spatial distributions of organic aerosol, which can make different impact on the climate change and human health. Thus, understanding the characteristics of the organic compounds in organic aerosols and the contribution of various emission sources to the organic compounds in background area is necessary in order to assess their impact on climate change and human health.

Routine measurements of organic compounds were carried out at Anmyeon Island to understand temporal variation of organic compounds and their formation characteristics at background site. PM<sub>2.5</sub> sample were collected at Korea Global Watch Center located at Anmyeon Island in South Korea. Sampling was performed on every sixth day. A total of 59 samples were obtained during June 2015 and May 2016 using high volume air sampler with pre-baked quartz fiber filter. Filters were extracted using ultra sonicator with a mixture of dichloromethane and methanol (3:1, v/v) and the extracts were blown down to 0.5mL using a nitrogen evaporator (Turbo Vap II, caliper Life Sciences). About one hundred individual organic compounds in PM<sub>2.5</sub> at Anmyeon Island were identified and quantified using gas chromatography/mass spectrometry (GC/MS). Organic compounds analysed in the study were classified into five groups, polycyclic aromatic hydrocarbons (PAHs), n-alkanes, dicarboxylic acids (DCAs), n-alkanoic acids and sugars.

Seasonal patterns of organic compounds for five groups were different shown in Figure 1. PAHs and n-alkanes were highest in winter and lowest in summer. While, the concentration of dicarboxylic acids was highest in summer and lowest in winter. In this study, we will figure out the characteristics of organic compounds distributions in PM<sub>2.5</sub> at a background area through the correlation and

factor analysis of organic compounds with the other air pollutant and meteorological data.

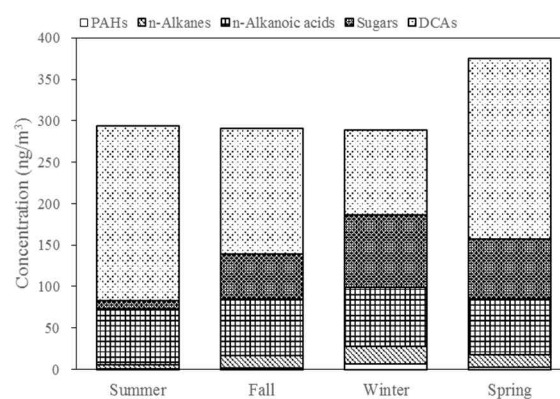


Figure 1. Seasonal variation of individual organic compounds during sampling periods.

This work was funded by the Korea Meteorological Administration Research and Development Program under Grant CATER2014-3190.

Kanakidou, M., Seinfeld, J. H., Pandis, S. N., Barnes, I., Dentener, F. J., Facchini, M. C., ... & Swietlicki, E. (2005). Organic aerosol and global climate modelling: a review. *Atmospheric Chemistry and Physics*, 5(4), 1053-1123.

## Potential impacts of electric vehicles on air quality in Taiwan

Nan Li<sup>1,2</sup>, Jen-Ping Chen<sup>2</sup> and I-Chun Tsai<sup>2,3</sup>

<sup>1</sup>School of Environmental Science and Engineering, Nanjing University of Information Science and Technology, Nanjing, 210044, China

<sup>2</sup>Department of Atmospheric Sciences, National Taiwan University, Taipei, 106, Taiwan

<sup>3</sup>Research Center of Environmental Changes, Academia Sinica, Taipei, 114, Taiwan

Keywords: Electric vehicle, Air quality, AQI, CMAQ.

Presenting author email: linan@nuist.edu.cn

Electric vehicles have been identified as a potential option for reducing air pollution, especially over urban areas. In this study, we used a regional air quality model to simulate gaseous and particulate pollutants in Taiwan, aiming at evaluating the prospective impacts of EV penetration on air quality. The simulations were parameterized using the best currently available emission inventories (TWEPA, 2015; Li et al., 2015), and the results were compared to the surface chemical measurements.

We assumed a 100% replacement of current light-duty vehicles in Taiwan. The burden of electricity supply (~58.1 billion kWh) was shifted to either coal-fired power plants or clean energy sources. With this ambitious EV penetration, CO, VOCs, NO<sub>x</sub> and PM<sub>2.5</sub> emissions in Taiwan from on-road sources would be reduced by 1500 (85%), 165 (79%), 33.9 (27%) and 7.2 (27%) Gg yr<sup>-1</sup>, respectively. On the other hand, electric sector NO<sub>x</sub> and SO<sub>2</sub> emissions would be increased by up to 20.3 (29%) and 12.9 (29%) Gg yr<sup>-1</sup> if all electricity were provided by thermal power plants. Overall, total emissions of most pollutants except for SO<sub>2</sub> (which increased by 11%) would be considerably reduced by EV penetration.

We further analyzed the consequent impacts of EV on the level of air quality. Replacement with EV would be effective in reducing annual mean surface concentrations of CO (by 260 ppb), VOCs (by 11.3 ppb), NO<sub>x</sub> (by 3.3 ppb) and PM<sub>2.5</sub> (by 2.1 μg m<sup>-3</sup>), while SO<sub>2</sub> would increase slightly (by 0.1 ppb). The large reductions tended to occur at times and places with high ambient concentrations. Greater benefits would clearly be attained if clean energy sources were fully encouraged. EV penetration would cause widespread reductions in annual average O<sub>3</sub> peak values (up to 7 ppb) across Taiwan, except for a slight increase (< 2 ppb) in downtown Taipei.

Further analysis suggests that EV penetration would tend to be of significant benefit to the mitigation of high pollution episodes. Calculated regional mean pollution episode days (AQI > 100) in Taiwan would be reduced by 7–9 d yr<sup>-1</sup> (11–15%), and the local reductions may reach 44 d yr<sup>-1</sup> in highly-polluted Taichung city. We found O<sub>3</sub> and PM<sub>2.5</sub> to be the main causes of air pollution, and attributed at least 70% of the improvements to O<sub>3</sub> reduction. Our findings are important for understanding the potential effects of EV on air quality, and can provide useful information to local governments for use in air pollution strategies.

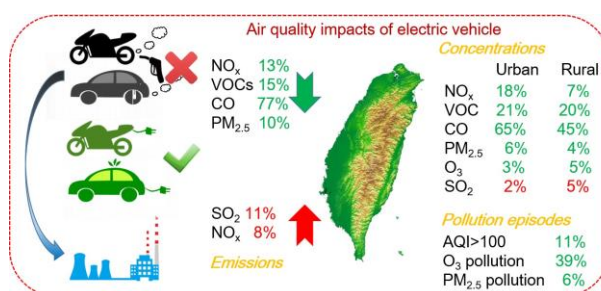


Figure 1. Air quality impacts of electric vehicle in Taiwan.

This work was supported by the Ministry of Science and Technology of Taiwan through Grants MOST-100-2119-M-002-023-MY5, MOST-103-2811-M-002-180 and MOST-104-2811-M-002-086, as well as the Nanjing University of Information Science and Technology Grant 2243141601065

Taiwan Environmental Protection Administration (TWEPA), 2015. Taiwan Emission Data System (TEDS), Version 8.1.

Li, M., Zhang, Q., Kurokawa, J., Woo, J.-H., He, K.B., Lu, Z., Ohara, T., Song, Y., Streets, D.G., Carmichael, G.R., Cheng, Y.F., Hong, C.P., Huo, H., Jiang, X.J., Kang, S.C., Liu, F., Su, H., Zheng, B., 2015. MIX: a mosaic Asian anthropogenic emission inventory for the MICS-Asia and the HTAP projects. *Atmos. Chem. Phys. Discuss.* 15 (23), 34813–34869

## Multivariate Analysis of Upwind SO<sub>2</sub> Emission Influences on Air Pollution in Rochester, NY

Fereshteh Emami,<sup>1</sup> Mauro Masiol,<sup>1</sup> Philip K. Hopke<sup>1,2</sup>

<sup>1</sup>Center for Air Resources Engineering and Science, Clarkson University, Potsdam, NY 13699, USA

<sup>2</sup>Department of Public Health Sciences, University of Rochester School of Medicine and Dentistry, Rochester, NY 14642, USA

Keywords: PM<sub>2.5</sub>, trends, sources, interventions

Presenting author email: phopke@clarkson.edu

There have been multiple changes to the air pollutant emissions affecting the northeastern United States since 2001. The monthly average PM<sub>2.5</sub> sulfate concentrations show a 65% decrease in Rochester, NY between 2001 and 2015. Husain et al. (1998) showed that the changes in the annual mean SO<sub>4</sub><sup>2-</sup> concentrations at Whiteface Mountain and Mayville, NY linearly followed changes in the SO<sub>2</sub> emissions in eight states upwind and contiguous with NYS. Data from other networks in the Northeast have reported similar results (Malm et al., 2011).

In this study, the relationships between SO<sub>4</sub><sup>2-</sup> concentrations and regional SO<sub>2</sub> emissions were investigated using air parcel back-trajectories to identify the likely source regions from which the air masses reach Rochester. PSCF plots (Figure 1) indicate the areas (U.S. and Canada) with high probabilities for different seasons and the entire period. Sixteen, fourteen and eleven states were identified for winter, transition, and summer seasons. All of the states were considered in the regression analysis of all seasons for the entire period 2001-2015.

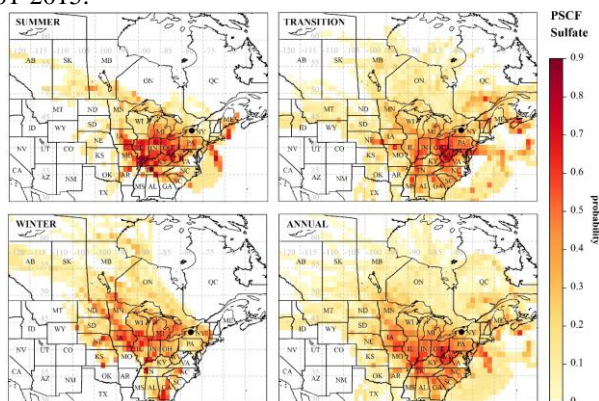


**Figure 1.** PSCF for different seasons and entire period.

The monthly mean SO<sub>4</sub><sup>2-</sup> concentrations generally follow the trend in regional SO<sub>2</sub> emissions with  $r = 0.70$  for all investigated states. This result indicates that changes have generally been homogeneous over the region and it is best to treat these emissions with a screening method. SO<sub>2</sub> emissions of each upwind state were screened using stepwise regressions to maximize correlations (Pearson's  $r$ ). The most important factors identified by the variable-screening process were SO<sub>2</sub> emissions from GA for winter, NC for transition, OH for summer and MI and NC for the entire period.

Considering the variability that may occur in meteorological conditions and the other likely sources of

SO<sub>4</sub><sup>2-</sup>, the trends of SO<sub>4</sub><sup>2-</sup> concentrations may have affected by systematic changes that are not reflected in the emissions data. For this reason, we included a dummy variable for year ( $T$ ) in multivariate regression as follows:

$$SO_4^{2-} = aT + b(SO_2)_1 + c(SO_2)_2 + \dots$$

where  $T=0, 1, 2, \dots$ , year and subscripts refer to regional aggregate SO<sub>2</sub> emissions for region  $i$ .

The parameters were estimated using multiple linear regression. The adjusted R<sup>2</sup> and root-mean-square error (RMSE) were used as measures of model performance. Another calculated parameter is selectivity ratio (SR) that provides a simple numerical assessment of the usefulness of each variable in a regression model. The larger the selectivity ratio, the more useful the given variables are for the prediction:

$$SR_i = \frac{v_{expl,i}}{v_{res,i}}, i = 1, 2, 3 \dots$$

where  $v_{expl,i}$  is explained variance by target projection and  $v_{res,i}$  is residual variance of each variable ( $i$ ).

For the winter and transition seasons, the best linear fit with SO<sub>4</sub><sup>2-</sup> concentration was obtained using Georgia and North Carolina emissions, respectively, with higher impact than the other probable changes (year variable). Looking more broadly over the upwind region, there is further influence of variables other than SO<sub>2</sub> emissions in the summer. A reasonable fit was obtained for SO<sub>4</sub><sup>2-</sup> concentrations in summer using both Ohio emissions and the dummy year variable. Enhanced photochemical activity during the summer produces higher SO<sub>2</sub> to SO<sub>4</sub><sup>2-</sup> conversion. The sulfate can then be transported over greater distances than SO<sub>2</sub>.

Considering the SR for the entire period, North Carolina has more effect than Michigan SO<sub>2</sub> emissions and the year dummy variable can be neglected. The model predictions are in good agreement with measurements across SO<sub>4</sub><sup>2-</sup> concentrations with  $R^2 \sim 0.7$ .

In summary, the relationships between PM<sub>2.5</sub> sulfate concentrations in Rochester NY and, regional SO<sub>2</sub> emissions has been estimated. The multiple linear regression models identified the main regional SO<sub>2</sub> source areas that result in the local sulfate concentrations.

Husain, L.; Dutkiewicz, V. A.; Das, M. (1998) *Geophys. Res. Lett.* **25**, 967–970.

Malm, W. C.; Schichtel, B. A.; Pitchford, M. L. (2011) *J. Air Waste Manag. Assoc.* **61**, 1131–1149.

## Changes of $^7\text{Be}$ concentrations in air observed during dust episodes, 2009-2015

J. Kusmierczyk-Michulec

CTBTO, Vienna International Centre, 1400 Vienna, Austria

Keywords: atmospheric aerosols, Beryllium-7, mineral dust, dry deposition

Presenting author email: [jolanta.kusmierczyk-michulec@ctbto.org](mailto:jolanta.kusmierczyk-michulec@ctbto.org)

Undeniably, the Sahara desert is the largest natural source for airborne mineral dust worldwide. With the increased number of satellites and development of satellite imagery it is possible to register massive sandstorms blowing off the northwest African desert, reaching over 1000 miles into the Atlantic.

Studies show that the most vigorous source for dust providing most of the mineral dust to the Amazon forest is the Bodélé depression in Northern Chad (Koren et al., 2006). Its main range of influence is included in the area between the Equator and the parallel  $30^{\circ}$  N, and two meridians  $80^{\circ}$  W and  $50^{\circ}$  E.

The effect of mineral dust is also noted by the monitoring stations belonging to the International Monitoring System (IMS) developed by the Comprehensive Nuclear-Test-Ban Treaty Organization (CTBTO). The IMS is a global system of monitoring stations, using four complementary technologies: seismic, hydroacoustic, infrasound and radionuclide, where the aim is a global monitoring of radioactive aerosols and radioactive noble gases, supported by atmospheric transport modelling.

Three of 80 radionuclide stations, located in the aforementioned area, are particularly influenced by dust events. These stations are: MRP43 ( $18^{\circ}\text{N}$ ,  $17^{\circ}\text{W}$ ) in Mauritania, KWP40 ( $29.3^{\circ}\text{N}$ ,  $47.9^{\circ}\text{E}$ ) in Kuwait and PAP50 ( $9^{\circ}\text{N}$ ,  $79.5^{\circ}\text{W}$ ) in Panama. Stations monitor various radioactive aerosols but the one that is measured on a daily basis by IMS particulate stations is  $^7\text{Be}$ .

Beryllium-7 ( $^7\text{Be}$ ) is one of the key radioactive isotopes originating from the interaction of cosmic rays with the terrestrial atmosphere.  $^7\text{Be}$  attaches predominantly to aerosol particles in the submicron size range (e.g. Ioannidou et al., 2005) and is removed from the atmosphere by dry and wet fallout (e.g. Kusmierczyk-Michulec et al., 2015).

This study investigates the influence of mineral dust on changes in  $^7\text{Be}$  concentrations in the atmosphere. For that purpose, data collected during 2009-2015 for the three aforementioned IMS radionuclide stations, were used.

To quantify the effect of dry deposition, data collected by three IMS stations affected by mineral dust were thoroughly analyzed.

To ensure that changes observed in  $^7\text{Be}$  concentrations are caused only by the mineral dust, for the further analysis only data collected during dry periods (no precipitation) and which originated over the Bodélé depression, as indicated by the analysis of air mass backward trajectories provided by a Lagrangian particle dispersion model FLEXPART (e.g. Stohl et al. 2005), were selected.

Considering that beryllium concentration at the beginning of the dust event is  $C(t_0)$  and at the end is  $C(t_1)$  the relative decrease  $\Delta C$  was defined as:

$$\Delta C = [(C(t_0) - C(t_1)) / C(t_0)] \times 100\% \quad (1)$$

The preliminary results indicate that the mean relative decrease in  $^7\text{Be}$  activity concentration caused by the 3-day long mineral dust event is about 13 %. In some cases this decrease can be much larger, up to 50%.

Ioannidou, A., Manolopoulou, M. and Papastefanou, C. (2005), *Appl. Radiat. Isot.* **63**, 277-284.

Koren, I., Kaufman, Y.I., et al., (2006), *Environ. Res. Lett.* **1**, doi:10.1088/1748-9326/1/1/014005

Kusmierczyk-Michulec, J., A. Gheddou and M. Nikkinen, (2015), *J. Environmental Radioactivity*, 144, 140-151.

Stohl, A., Forster, C., Frank, A., Seibert, P., and C.G. Wotawa, (2005), *Atmos. Chem. Phys.*, **5**, 2461-2474.

### Disclaimer

*The views expressed in this study are those of the authors and do not necessarily represent the views of the CTBTO Preparatory Commission.*

## Network Analysis of PM<sub>2.5</sub> Monitoring Data and Model Output for Alberta Using KZ Filtering and Hierarchical Clustering

J. Soares<sup>1</sup>, P.A. Makar<sup>1</sup>, A. Akingunola<sup>1</sup>, Y. Aklilu<sup>2</sup>

<sup>1</sup>Air Quality Modelling and Integration Section, Air Quality Research Division, Atmospheric Science and Technology Directorate, Science & Technology Branch, Environment and Climate Change Canada, Toronto, M3H 5T4, Canada

<sup>2</sup>Environmental Monitoring and Science Division, Alberta Environment and Parks, Edmonton, T5J 5C6, Canada

Keywords: air quality, particulate matter, network analysis, Canadian oil sands

Presenting author email: joana.soares@canada.ca

Network analysis is a powerful tool to deal with large-scale datasets by clustering the data on a basis of similarity. This methodology can be potentially helpful to assess the extent to which the monitoring network locations are representative of a larger region, and whether monitoring stations are in the best possible location to represent the scales associated with regional air quality model predictions. In order to better evaluate the effectiveness of a monitoring network, a combination of Kolmogorov-Zurbenko (KZ) filtering coupled with Hierarchical Clustering (HC), may be used to cross-compare station observations at different time scales (Solazzo and Galmarini, 2015). We describe here the current progress on the use of KZ filtering and HC of PM<sub>2.5</sub> monitoring data provided by Alberta Environment and Parks, and air quality modelling output from the Environment and Climate Change Canada's Global Environmental Multiscale - Modelling Air-quality and CHEMistry model (GEM-MACH, Moran *et al.*, 2010, Makar *et al.*, 2015), to optimize monitoring networks in the province of Alberta, including the Canadian oil sands.

The first stage of this work analyses the monitoring network data from August of 2013 through July of 2014, identifying station pairs which are potentially redundant, and pairs which may be representative of unique and very local conditions and/or may have instrumentation errors. The analysis shows the potential for the methodology to identify groups of stations with unique chemical signatures and/or sources of PM, e.g., stations located in and around the Canadian oil sands show a distinct cluster from other stations in the network, reflecting unique emissions sources at that location. Figure 1 shows an example PM<sub>2.5</sub> dendrogram station analysis (highly correlated pairs of stations branch from the others closer to the y-axis origin).

PM<sub>2.5</sub> simulation output for the same time period (Figure 2, GEM-MACH at 10km resolution nested to 2.5km) was then used as a proxy for the observations. Model output at station locations was analysed in the same manner as the observations, hence evaluating its use in monitoring network design.

In the final stage, the same methodology was applied to the model output, this time treating every model grid-square as a potential PM<sub>2.5</sub> monitoring station. The resulting clusters at specific levels of similarity may thus be used to generate "correlation maps"; i.e. maps of the simulation domain describing

sub-regions at each of which a single monitoring station would be expected to be representative, to a given level of correlation. These maps in turn could provide guidance for improvements to PM<sub>2.5</sub> monitoring network design.

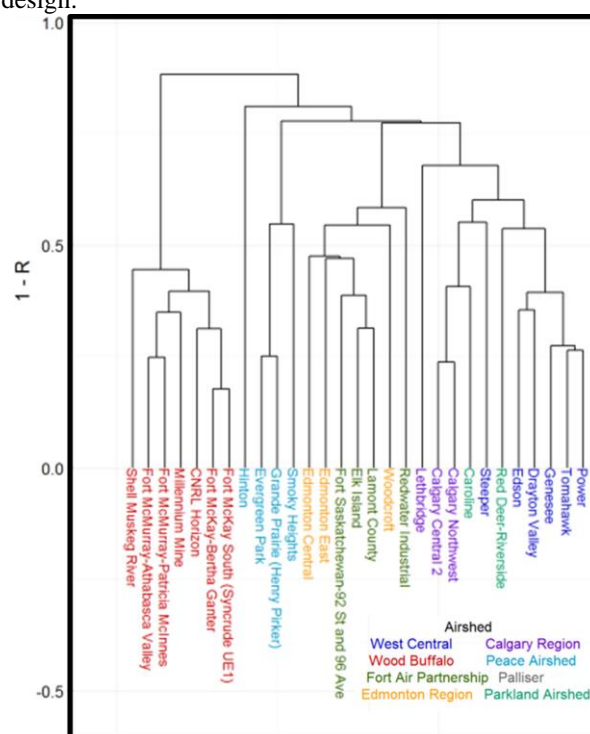


Figure 1. Hourly PM<sub>2.5</sub> observation dendrogram for monitoring stations in Alberta (oil sands stations in red).

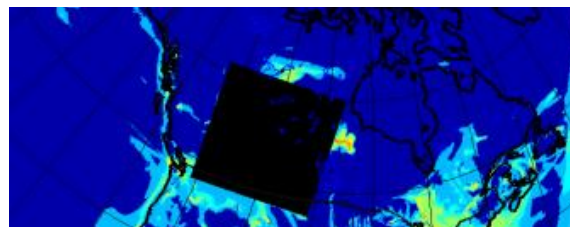


Figure 2. Continental and mesoscale (inset black region) model domains for GEM-MACH simulations.

Solazzo, E., and Galmarini, S., *Atm. Env.*, 112, 234-245, 2015.

Makar, P.A., et al., *Atm. Env.*, 115, 442-469, 2015.

Moran, M.D. *et al.*, (in) Steyn, D.G. and Rao, S.T. (Eds) *Air Pollution Modelling and its Application XX*, Springer, Dordrecht, 289-292, 2010.

## Investigating the nature and sources of non-water soluble sulfate sulfur in fine particles over a National Park in Central India

S. Kumar<sup>1</sup>, D. Shah<sup>2</sup>, R. Sunder Raman<sup>1,3</sup>

<sup>1</sup>Department of Earth and Environmental Sciences

<sup>2</sup>Department of Chemistry

<sup>3</sup>Centre for Research on Environmental and Sustainable Technologies

Indian Institute of Science Education and Research Bhopal

Bhopal By-pass Road, Bhauri, Bhopal – 462 066, Madhya Pradesh, INDIA

Keywords: water soluble sulfate (WSS), non-water soluble sulfate sulfur, total particulate sulfur (S), PM<sub>2.5</sub>  
Presenting author email: samresh@iiserb.ac.in

Sulfate aerosol is ubiquitous in the lower troposphere and is an important constituent of fine particles (PM<sub>2.5</sub>). Sulfate aerosol scatters visible light and influences cloud formation, thus affecting climate. In general, water soluble sulfate sulfur (WSS) is a major contributor (if not the only one) to total particle sulfur (S) and is estimated using the stoichiometric ratio of sulfur in sulfate. In this study, the relationships between PM<sub>2.5</sub>WSS and total S are examined. Ambient PM<sub>2.5</sub> particles over a National Park in Bhopal, Central India, were collected every other day between 01 January 2012 and 31 December 2013 on various filter substrates.

WSS was quantified using ion chromatography while total S was measured by ED-XRF. Key analysis parameters for total particle sulfur and sulfate sulfur are summarized in Table 1.

Table 1. Quality assurance parameters for total sulfur and sulfate sulfur

Analytes	Total particle Sulfur (S) ng	Sulfate Sulfur (WSS) ppb
Method detection limit	4.45	10
Repeatability(%) <sup>a</sup>	5	<10.5
Accuracy (%)	3 <sup>b</sup>	1 <sup>c</sup>

<sup>a</sup>10% of samples were analyzed as duplicate

<sup>b</sup>2% samples in a batch were NIST SRM 2783 #1132

<sup>c</sup>2% samples in a batch were check standard

A preliminary examination of the association between WSS and S (Fig. 1.) suggests the existence of significant amounts of non-WSS over the study location. Further, these relationships varied from season-to-season.

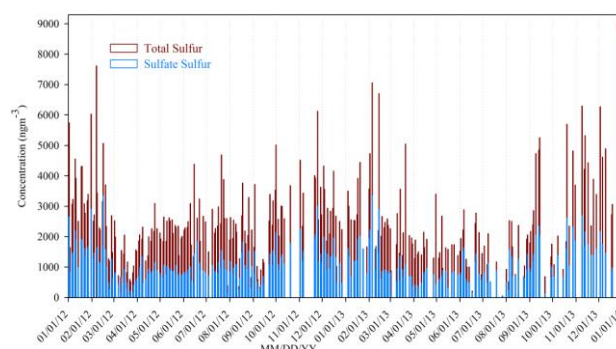


Fig.1. Temporal variability of total particle sulfur (brown) and sulfate sulfur (light blue) measured over national park in Bhopal between January 2012 and December 2013

This study will focus on identifying the nature and sources of non-WSS and its contribution to PM<sub>2.5</sub> at the study location

## Size resolved aerosols by the different regional influences in the West coastal Korea during KORUS-AQ campaign

M.S. Bae<sup>1</sup>, Z.H. Shon<sup>2</sup>, S.H. Oh<sup>1</sup>, T.H. Lee<sup>3</sup>, S.S. Park<sup>4</sup>, G.T. Park<sup>3</sup>

<sup>1</sup>Department of Environmental Engineering, Mokpo National University, Muan, 58554, Republic of Korea

<sup>2</sup>Department of Environmental Engineering, Dong-Eui University, 47340, Republic of Korea

<sup>3</sup>Department of Environmental Science, Hankuk University of Foreign Studies, Gyeonggi, 17035, Republic of Korea

<sup>4</sup>Department of Environment and Energy Engineering, Chonnam National University, Gwangju, 61186, Republic of Korea

Keywords: MOUDI, RTWC, size distribution.

Presenting author email: [minsbae@hotmail.com](mailto:minsbae@hotmail.com)

The measurements for size-resolved chemical compositions were conducted at a west coastal site in Republic of Korea during the KORUS-AQ campaign between May 28 to June 20, 2016. The clean background sampling site, Anmyeon (36° 32'N; 126° 19'E, 45.7 m above sea level (ASL)) station has been operated as a Global Atmosphere Watch supersite (GAWS) of World Meteorological Organization in Korea. The site receives both marine as well as continental air masses during different days according to the prevailing wind patterns.

The goal of this study is to characterize the size-resolved main chemical compositions (i.e. organic carbon (OC), water soluble organic carbon (WSOC), elemental carbon (EC), water soluble ions, and benzene carboxylic acids (BCA)) of aerosol particles at the West coastal Korea with the influence of different regional range transfers using a micro-orifice uniform deposit impactors (MOUDI). PM<sub>2.5</sub> mass, OC, EC, WSOC, and BCA were determined by SUNET carbon analyser, total organic carbon (TOC) analyser, liquid chromatography-mass spectrometry mass spectrometry (LC-MSMS). In addition, an optical particle sizer (OPS) (Model 3330, TSI Inc.) and Multi Angle Absorption Photometer (MAAP) (Model 5012, Thermo Fisher Scientific Inc.) were operated for sized resolved volume concentrations and black carbon (BC), respectively. The influence of different regional range transfers were determined by residence-time weighted concentrations (RTWC) analysis.

The five most abundant water-soluble species (in decreasing order) were chloride, sodium, non-sea salt (nss) sulfate, ammonium, and nitrate. During regional impact periods, sulfate and WSOC concentrations were enhanced as strongly as other species in the sub-micrometer stages. 1,2-benzene carboxylic acid is the most abundant compound in the sub micrometer stages as well. The size resolved the most abundant chemical properties in the region, comparison of different ionic balance approaches (i.e. size resolved ratio of NH<sub>4</sub><sup>+</sup> measured and NH<sub>4</sub><sup>+</sup> neutralized) and comparison of optical and chemical size distributions will be presented.

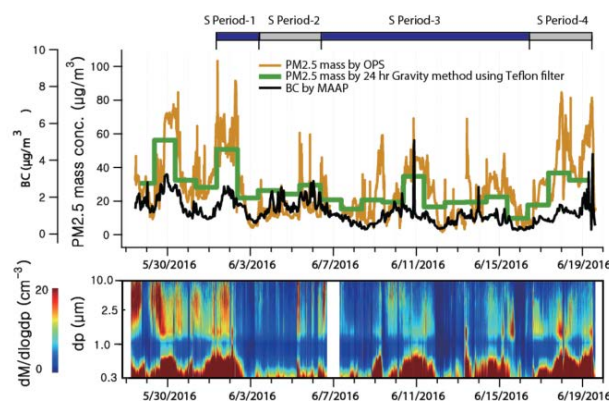


Fig. 1. Time series of PM mass and black carbon concentrations by OPS, gravity method, and MAAP.

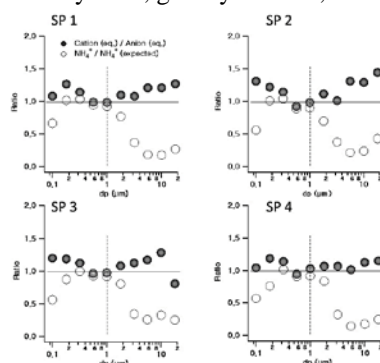


Fig. 2. Comparison of sized resolved ratios by two different ionic balance methods.

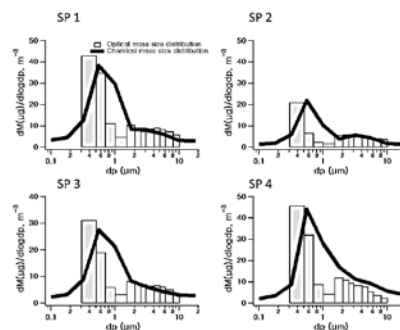


Fig. 3. Comparison of optical and chemical size distributions by OPS and MOUDI, respectively.

We acknowledge the support by the National Research Foundation of Korea (NRF) (NRF-2015R1A2A1A10053971).

## Assessing ventilation and air quality in real city blocks using LES

M. Kurppa<sup>1</sup>, A. Hellsten<sup>2</sup>, M. Auvinen<sup>1,2</sup> and L. Järvi<sup>1</sup>

<sup>1</sup>Department of Physics, University of Helsinki, Helsinki, 00014, Finland

<sup>2</sup>Finnish Meteorological Institute, Helsinki, 00101, Finland

Keywords: CFD, urban planning, ventilation, air pollution

Presenting author email: mona.kurppa@helsinki.fi

Urban areas worldwide suffer from decreased air quality owing to road traffic emissions in particular. Exposure to air pollutants has several detrimental health effects, which lead to a notable number of premature deaths every year. Transport of traffic-related air pollutants away from their sources is generally retarded in densely built areas due to buildings blocking the air flow that ventilates street canyons. Additionally, the presence of vegetation further complicates the flow pattern and pollutant dispersion. Therefore, a tool for simulating and predicting pollutant ventilation and air quality in real complex urban environments is vital for urban planning in order to plan healthy neighbourhoods.

One of the most promising methods for air quality modelling in actual city-blocks is the large-eddy simulation (LES), which resolves the three-dimensional turbulent fields of wind and scalar concentrations within the area of interest. This study applies a LES model PALM (Maronga *et al.*, 2015) which can be embedded with a Lagrangian stochastic particle model to study dispersion of inert and massless particles. In this case study, the ventilation of traffic-related emissions in the vicinity of a planned city boulevard in Helsinki (Kurppa *et al.*, 2017) was investigated. Simulations were conducted in four different city-block-design versions with varying orientation, height and structure of buildings (Figure 1) under two contrasting meteorological conditions. Lagrangian particles, representing traffic emissions, were released over streets with a release rate relative to the traffic rates. Additionally, the aerodynamic impact of street trees and surrounding vegetation on particle dispersion was taken into account. According to the results, variation in the building heights improves street canyon ventilation whereas the impact of smaller scale variation in building structure can be negligible. Moreover, street trees were shown to strongly modify the street canyon flow and dispersion.

Currently, the sectional aerosol module SALSA (Kokkola *et al.*, 2008) is being embedded to PALM in order to quantitatively simulate the concentration of the aerosol particles and their dynamic processes including deposition of air pollutant on plant leaves in urban areas. This high-resolution LES-based urban air quality model will be validated against point-measurements as well as mobile air pollution measurements conducted at pedestrian level in Helsinki. The development enables to quantitative study the impact of different planning solutions on the local air quality inside real street canyons

and courtyards. This tool provides new, essential information for urban planners and decision makers as well as for epidemiological studies related to air pollutant exposure.

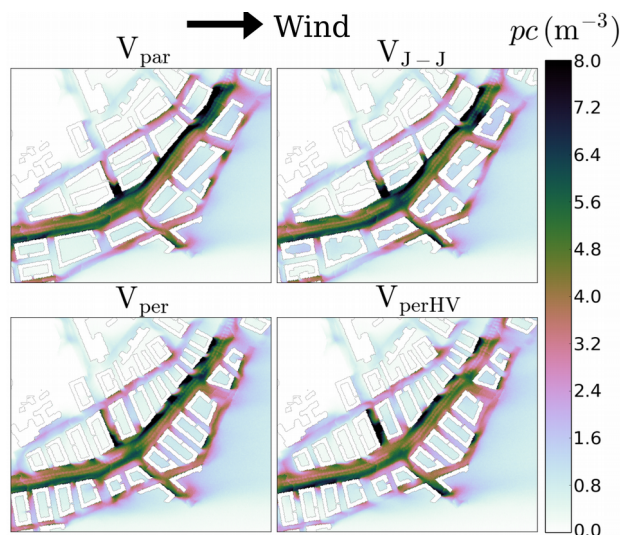


Figure 1. 40-minute mean concentration of inert particles  $pc$  ( $m^{-3}$ ) at 4 m above ground level in four different city-block designs. In  $V_{par}$  and  $V_{per}$  the building height is constant, whereas in  $V_{perHV}$  the height and in  $V_{J-J}$  the building structure varies, respectively. The wind is from south-west and the atmospheric boundary layer of 250 m is neutrally stratified. The simulations were conducted over a domain of 8.4 km<sup>2</sup> whereas the analysis area is 0.5 km<sup>2</sup>.

The study on ventilation of city blocks was commissioned and funded by the City Planning Department of the City of Helsinki. Further work is supported by the Doctoral Programme in Atmospheric Sciences (ATM-DP, University of Helsinki).

Kokkola, H. *et al.* (2008) *Atmos. Chem. Phys.* **8**, 2469-2483.

Kurppa, M., Hellsten, A., Auvinen, M., Vesala, T. and Järvi, L. (2017) In preparation to *Landscape Urban Plan.*

Maronga, B. *et al.* (2015) *Geosci. Model Dev.* **8**, 2515-2551.

## The topography contribution to the influence of the planetary boundary layer at high altitude stations

M. Collaud Coen<sup>1</sup>, E. Andrews<sup>2</sup> and D. Ruffieux<sup>1</sup>

<sup>1</sup> Federal office of Meteorology and Climatology, MeteoSwiss, Payerne, Switzerland

<sup>2</sup> University of Colorado, CIRES, Boulder, Colorado, 80305, USA

Keywords: High altitude stations, planetary boundary layer, topography.

Presenting author email: martine.collaudcoen@meteoswiss.ch

The long-term characterization of free troposphere (FT) aerosols usually relies on measurements at high altitude stations. The identification and analysis of these FT air masses is complicated by the planetary boundary layer (PBL) influence at the measuring sites. Several mechanisms can cause the upward movement of lower elevation air resulting in PBL-influenced sampling conditions, including thermally-driven valley wind and convection and advections from regional, meso-scale or long-range origin. The analysis of, for example, the aerosol and black carbon concentrations at many high altitude sites suggests that the station altitude is not the main parameter explaining the PBL influence. This study aims to characterize the topographical features around the high altitude stations in order to rank them as a function of the PBL influence due to thermal convection through an index called PBL-TopoIndex. Other important parameters such as the wind, the soil state and the synoptic weather conditions were not considered.

We analysed 41 high altitude stations representative of 5 continents and having an altitude range between 475 (ZEP) and 5352 m a.s.l. (CHC). The topography was taken from GTopo30 which has a horizontal grid spacing of 30 arc seconds corresponding to a spatial resolution between 928 m in the East/West direction at the equator and 598 m at 50° and constant (925 m) in the North/South direction.

The PBL-TopoIndex relies on the criteria that the PBL influence will be low if 1) the station is one of the highest point in the mountainous massif, 2) there is a large altitude difference between the station and the valleys, plateaux or the average domain elevation, 3) the slopes around the station are steep, and 4) the «drainage basin» for air convection is small. These principles are concretely implemented by the calculation of 5 parameters: the value of the hypsometric curve at the station altitude, the difference between the station altitude and the 50% of the hypsometric curve, the slope of the curve describing the station altitude minus the minimum altitude in a circular domain as a function of the domain radius, the mean gradient in elevation in the eight directions and the drainage basin for convection (calculated from the inverse topography). The geometrical mean of these five parameters determined from topographical features that are considered to enhance the PBL influence is called the PBL-TopoIndex. The PBL-TopoIndex allows ranking of the stations as a function of the PBL influence due to convection.

Fig. 1 shows the ranking of the stations as a function of the PBL-TopoIndex; higher PBL-TopoIndex

corresponds to stations with higher PBL influence. The first observation is that all islands have very low PBL-TopoIndex, whereas the stations in the Himalaya and the Tibetan plateau have high PBL-TopoIndex. Mount Pico in the Azores ranks as the station with the lowest PBL influence since it has the smallest area, the island has only one summit and the station is almost at the top of the summit. A similar environment is found at FWS. In contrast, PYR, the second highest station, lays at the foot of Mount Everest and at the confluence of several valleys leading to a high PBL-TopoIndex. Mussala (BEO, Bulgaria) and Mount Helmos (HAC, Greece) are both stations situated at the top of one of the highest mountains in the Balkan and the Peloponnese ranges, respectively, leading to PBL-TopoIndex similar to the islands.

The 5, 50 and 95 percentiles of aerosol parameters (absorption coefficient, scattering coefficient and/or number concentration) of 27 stations were analysed and correlation with the station altitude and the PBL-TopoIndex were calculated. The coefficient of determination ( $R^2$ ) is significantly higher for the PBL-TopoIndex ( $0.3 \pm 0.07$ ) than for the altitude ( $0.05 \pm 0.05$ ) for the minima (5 percentile) for all aerosol parameters, where the  $R^2$  error were calculated by 1000 bootstrapping iterations of removing 2 over the 27 stations.

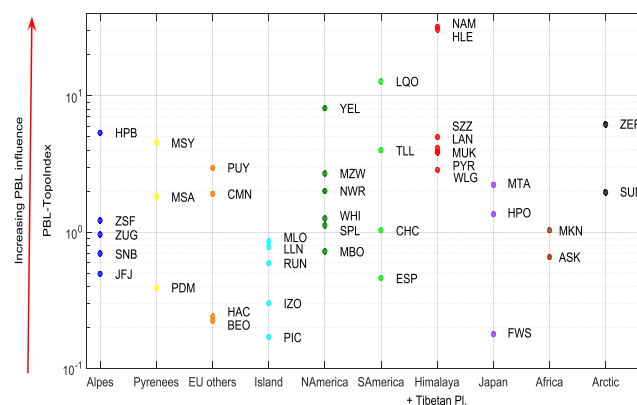


Figure 1. PBL-TopoIndex for 41 high altitude stations as a function of the mountain range or global regions

The data owners of the 27 stations (HPB, JFJ, SNB, ZSF, ZUG, CHC, PEV, TLL, MUK, NAM, PYR, IZO, LLN, MLO, PIC, MSA, MSY, PDM, MBO, NWR, SPL, WHI, BEO, CMN, PUY, SUM, WLG) who provided us with aerosol data and W. Schwanghart who developed TopoToolbox are greatly acknowledged.

## Long-term trends and spatio-temporal changes in atmospheric aerosols at Zugspitze

J. Sun<sup>1</sup>, M. Herrmann<sup>1</sup>, L. Ries<sup>2</sup>, W. Birmili<sup>3</sup> and A. Wiedensohler<sup>1</sup>

<sup>1</sup>Leibniz Institute for Tropospheric Research, Leipzig, 04318, Germany;

<sup>2</sup>German Federal Environment Agency (UBA), Platform Zugspitze, 82475, Germany;

<sup>3</sup>German Federal Environment Agency (UBA), Berlin, 14195, Germany

Keywords: long-term measurements, spatio-temporal variability, in-situ aerosol measurements.

Presenting author email: sun@tropos.de

Particle number concentration (PNC), particle number size distribution (PNSD), black carbon mass concentration (BC) and PM10 were continuously measured at the Umweltforschungsstation (UFS, Schneefernerhaus, Zugspitze, Germany). The aerosol measurements at UFS can be considered as representative for large part of Central Europe since UFS is located at an altitude where both polluted air from the boundary layer and less polluted air from the free troposphere can be investigated.

At UFS, polluted air from the lower troposphere was observed in warm season and less polluted air from the free troposphere was detected in cold season. The maximum monthly average concentrations in PNCs ( $N_{[20-100]}$ ,  $N_{[100-300]}$ ,  $N_{[300-800]}$ ) always occurred in the warm season.

A trend analysis method was used to determine the long-term trend in PNC and PNSD (Sen's Trend Analysis, see, e.g., Sen, 1968 and Birmili et al., 2015). Between 2007 and 2014, statistically sound negative trends were found in the PNCs, as shown in Table 1. The relative changes are between -2.1% / year in the nucleation mode ( $N_{[25-60]}$ ) and -3.5% / year in the accumulation mode ( $N_{[300-510]}$ ). A separation of the data set between day and night times, shows stronger decreases in daytime 12:00-16:00 UTC (-2.6 to -4.6% / year) than in the night 00:00-04:00 UTC (-1.9 to -2.7% / year).

Table 1. Temporal trend of particle number concentration 2007-2014, expressed as relative annual change.

	Relative slope (% / Year)	Relative CI (% / Year)
$N_{[25-60]}$	-2.10%	0.80%
$N_{[60-100]}$	-2.80%	1.60%
$N_{[100-300]}$	-3.00%	0.60%
$N_{[300-510]}$	-3.50%	1.30%
$N_{[25-510]}$	-2.90%	0.40%
$N_{CPC}$	-3.50%	0.50%

To detect the influence of local emission on the observed temporal trends, the trends in PNSD during weekday and weekend are investigated, as shown in Figure 1. Results suggest the reduction in PNC is due to the temporal changes in local sources around UFS. Changes in transported aerosol from lower boundary

layer might be another reason of the decrease in PNC. Based on the Radon method by Giemsa, the trends in PNC were calculated separately for the period when the air is from free troposphere and the period when UFS is within the boundary layer. Results show that downward trends in PNC are mainly affected by the air which is mixed up to UFS from lower boundary layers.

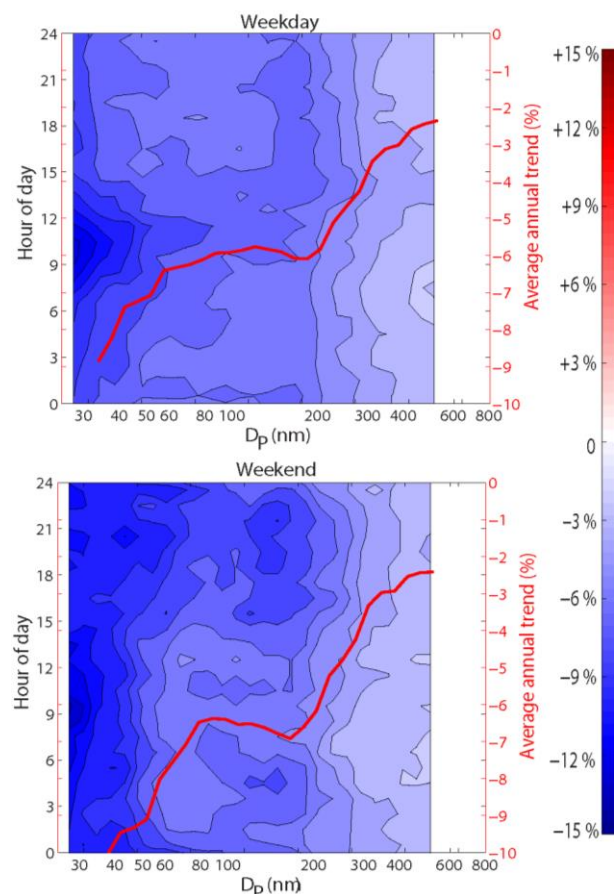


Figure 1. Temporal trends in PNSD during weekday and weekend from 2007 to 2014, expressed as relative annual change.

Sen, P. K. *Journal of the American Statistical Association*, 63(324), 1379-1389,1968.

Birmili, W., et al.. *Gefahrst. Reinh. Luft*, **75**(11/12), 2015.

## Comprehensive analysis of HYSPLIT model sensitivity to different meteorological input data

M. Reizer<sup>1</sup>, J.A.G. Orza<sup>2</sup> and K. Juda-Rezler<sup>1</sup>

<sup>1</sup>Faculty of Building Services, Hydro and Environmental Engineering, Warsaw University of Technology, Warsaw, 00653, Poland

<sup>2</sup>SCOLab, Física Aplicada, Universidad Miguel Hernández, Elche, 03202, Spain

Keywords: air mass back trajectories, HYSPLIT, meteorological input, k-means clustering.

Presenting author email: magdalena.reizer@is.pw.edu.pl

Analysis of air mass back trajectories is a method widely used for identification of atmospheric transport patterns, as well as of the origins and pathways of air pollution (e.g. Fleming *et al.*, 2012). Various methods of trajectory calculation have been developed, however, the accuracy of trajectory models always depends on variety of parameters, including the source of wind field data, wind field spatial resolution, trajectory type as well as the numerical integration scheme (Stohl, 1998). One of the models, which is most extensively used to generate trajectories backward in time at a given starting location, is the Hybrid Single-Particle Lagrangian Integrated Trajectory (HYSPLIT), developed by the National Oceanic and Atmospheric Administration (NOAA) Air Resources Laboratory (ARL) (Stein *et al.*, 2015).

The aim of the present work is to gain further insight into differences between the results of HYSPLIT model driven by different meteorological input data and to quantify the possible reasons responsible for the discrepancies. 4-day back trajectories starting at 8 sites representative of different environments (Fig. 1), at 200, 500, 1500 and 3000 m for period of 2014-2016 have been computed. The results of the model, forced by four commonly used meteorological data sets with different horizontal and vertical resolutions the NCEP/NCAR Reanalysis (2.5°), Global Data Assimilation System (GDAS) data (1° and 0.5°) and ECMWF ERA-Interim (0.5°) have been compared.

The results show significant differences between trajectories computed with the four meteorological datasets. Strong deviations from the average behaviour are studied in connection with meteorological parameters and studied site's locations. The average and median differences grow quadratically over time along the back trajectories independently from the type of site. Analysis of the results indicate a dependence with the starting height also a seasonal variation in the differences. Moreover, meteorological input data influence the number of clusters identified by k-means cluster analysis. Factors that might be responsible for these discrepancies have been identified.

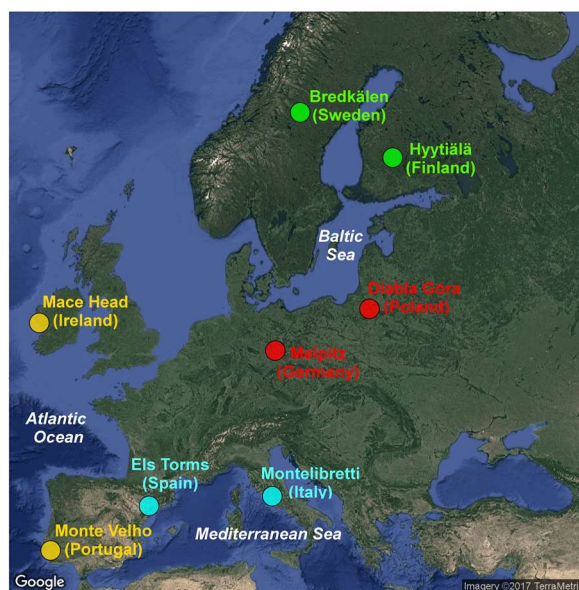


Figure 1. Location of the different types of sites: Scandinavian (green), continental (red), Mediterranean (blue), Atlantic (yellow).

This work was supported by the project financed by the Dean of Faculty of Building Services, Hydro and Environmental Engineering, Warsaw University of Technology. The authors also gratefully acknowledge the NOAA Air Resources Laboratory (ARL) for the provision of the HYSPLIT transport and dispersion model used in this publication.

- Fleming, Z.L., Monks, P.S. and Manning, A.J. (2012). Review: Untangling the influence of air-mass history in interpreting observed atmospheric composition. *Environ. Res.* **104-105**, 1-39.
- Stein, A.F., Draxler, R.R., Rolph, G.D., Stunder, B.J.B., Cohen, M.D. and Ngan, F. (2015). NOAA's HYSPLIT atmospheric transport and dispersion modeling system. *Bull. Amer. Meteor. Soc.* **96**, 2059-2077.
- Stohl, A. (1998). Computation, accuracy and applications of trajectories – a review and bibliography. *Atmos. Environ.* **32**, 947-966.

## Rapid nitrate-induced atmospheric ageing of diesel soot in wintertime urban plumes

A.C. Eriksson<sup>1,2</sup>, C. Wittbom<sup>1</sup>, P. Roldin<sup>1,3</sup>, M. Sporre<sup>4</sup>, E. Öström<sup>1,5</sup>, P. Nilsson<sup>2</sup>, J. Martinsson<sup>1,5</sup>, J. Rissler<sup>2</sup>, E.Z. Nordin<sup>2</sup>, B. Svenningsson<sup>1</sup>, J. H. Pagels<sup>2</sup>, E. Swietlicki<sup>1</sup>

<sup>1</sup>Division of Nuclear Physics, Lund University, Box 118, SE-22100, Lund, Sweden

<sup>2</sup>Ergonomics and Aerosol Technology, Lund University, Box 118, SE-22100, Lund, Sweden

<sup>3</sup>Department of Physics, University of Helsinki, P.O. Box 64, 00014, Helsinki, Finland

<sup>4</sup>Department of Geosciences, University of Oslo, Postboks 1022, Blindern, 0315 Oslo, Norway

<sup>5</sup>Centre for Environmental and Climate Research, Lund University, Box 118, SE-22100, Lund, Sweden

Keywords: Diesel soot, atmospheric ageing, ammonium nitrate, SP-AMS.

Presenting author email: [axel.eriksson@nuclear.lu.se](mailto:axel.eriksson@nuclear.lu.se)

Fresh and aged diesel soot particles have significantly different properties, resulting in different impacts on climate and human health – fresh diesel soot particles are highly aspherical and hydrophobic, while aged particles are spherical and hydrophilic. In addition to determining the intrinsic properties of diesel exhaust particles, ageing and its effect on water uptake also control the dispersion of diesel soot in the atmosphere.

We have therefore measured the physicochemical properties of diesel soot in urban and rural ambient air using soot particle aerosol mass spectrometry (SP-AMS) and auxiliary techniques. SP-AMS utilizes sizing based on low-pressure drag force and particle inertia. The measured vacuum aerodynamic diameter ( $D_{va}$ ) is sensitive to particle morphology as illustrated via the dynamic shape factor (DSF) in Figure 1. We have exploited the sensitivity towards particle shape to study soot transformation through field and laboratory experiments. Our experimental findings are underpinned by detailed simulations using the two-dimensional Lagrangian model ADCHEM.

The ambient measurements were conducted during wintertime, in the city and region of Copenhagen, Denmark. Roadside air from a busy street was sampled from December 26<sup>th</sup> 2011 to January 22<sup>nd</sup> 2012. The rural site Vavihill is part of the pan-European ACTRIS station network and is situated approximately 60 km North-East of the city of Copenhagen. SP-AMS data was acquired at Vavihill from January 10<sup>th</sup> to February 25<sup>th</sup>, 2013.

We have also studied diesel soot ageing under controlled conditions in the laboratory through smog chamber experiments. In the experiments, further described by Wittbom *et al* (2014), exhaust from an idling light-duty diesel powered Euro II vehicle were injected into a 6 m<sup>3</sup> smog chamber spiked with light aromatic SOA precursors.

Using back trajectory analysis (HYSPLIT4, Stein *et al.* 2015) we identified periods when the air-mass sampled at Vavihill had passed over Copenhagen upwind. Time-series analysis confirmed that recent urban emissions were present in the rural air during those periods. However, the soot containing particles present in the urban plumes were significantly larger than fresh diesel soot as measured in urban air. While fresh diesel soot has a mass mode around 100 nm ( $D_{va}$ ),

the urban plumes contained BC in the 200-400 nm range. This shows that during the transit from Copenhagen to Vavihill, which on average took 5 hours, transformed the soot into near spherical shapes.

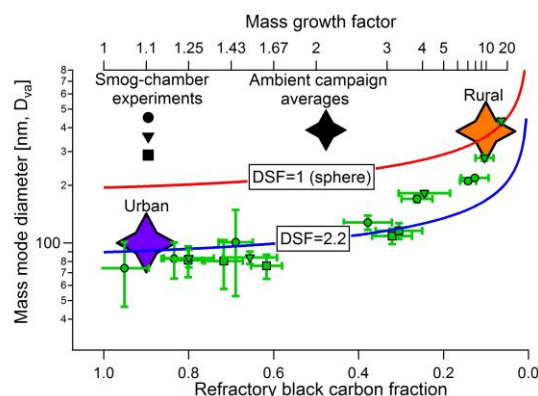


Figure 1. Comparison between smog chamber data and ambient campaign averages. Lines illustrate 1.2 fg BC particles with varied dynamic shape factor (DSF).

The mass spectra show that ammonium nitrate was abundant in the plumes. Ammonium nitrate, due to its ability to attract water, caused rapid atmospheric ageing of the diesel soot in the urban plumes. Our study shows that wintertime cold, humid ambient conditions with limited photochemistry can lead to fast soot ageing – more so than the dry intense photochemistry commonly investigated.

This work was supported by the Swedish research councils FORMAS and VR.

Stein, A. F.; Draxler, R. R.; Rolph, G. D.; Stunder, B. J. B.; Cohen, M. D.; Ngan, F. (2015). *Noaa's Hysplit Atmospheric Transport and Dispersion Modeling System*. *B Am Meteorol Soc* 96, (12), 2059-2077.

Wittbom, C.; Eriksson, A.C.; Rissler, J.; Carlsson, J. E.; Roldin, P.; Nordin, E. Z.; Nilsson, P. T.; Swietlicki, E.; Pagels, J. H.; Svenningsson, B. (2014). *Cloud droplet activity changes of soot aerosol upon smog chamber ageing*. *Atmos Chem Phys* 14, (18), 9831-9854.

## Tracking and tracing of aerosols using encapsulated DNA nanoparticles

R.N. Grass, J. Koch, C. A. Mora and W.J. Stark

<sup>1</sup>Department of Chemistry and Applied Biosciences, ETH Zurich, Zurich, 8093, Switzerland

Keywords: aerosol sampling, DNA, silica, analytics

Presenting author email: robert.grass@chem.ethz.ch

From an analytical perspective DNA is the molecule for which we have the most sensitive detection methods: Quantitative polymerase chain reaction (qPCR) is a molecular detection method available in many (biological/medical) research laboratories, which can not only detect the presence of single DNA molecules, but can also give information on the DNA sequence (by choice of PCR primers). So in order to detect aerosols in extreme dilutions it might be interesting to use DNA as an analytical handle. This could either be DNA, which is naturally present within the aerosol (e.g. from bioaerosols), or as presented below, the DNA could be intentionally added to the aerosol as analytical marker.

We have recently created DNA taggants, which consist of short DNA amplicons (ca. 100 base pairs) encapsulated within silica nanoparticles. (see Figure 1 and Paunescu et al. 2013). We have thereby shown, that the DNA encapsulated within the silica particles shows considerable stability towards temperature, biological decay and UV-radiation (Paunescu et al. 2014, Grass et al. 2015) and that the particles can be detected/counted on a single nanoparticle level (Paunescu et al. 2015). This technology thereby allows the tracking and tracing of polymers, fluids and foodstuff.

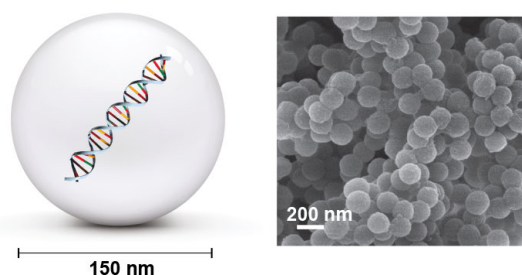


Figure 1. Schematic and electron microscopy image of DNA encapsulated within silica nanoparticles.

As a novel extension of this technology we now are also able to aerosolize the DNA encapsulates and use them as an aerosol tracer. Aside of laboratory based analytics (especially proof of quantitative detection) we will present data on using this technology in first field studies.

In a first study DNA encapsulates were utilized as a tracer for pesticides applied to an apple orchard. (Mora et al. 2016) The nanoparticles were mixed with the pesticide formulations, which were then sprayed onto the field by a commercial pesticide dispensing unit. Samples were collected from a total of 82 sampling locations and data analysis gave novel insights into pesticide drift, and pesticide delivery efficiency. (Figure 2)

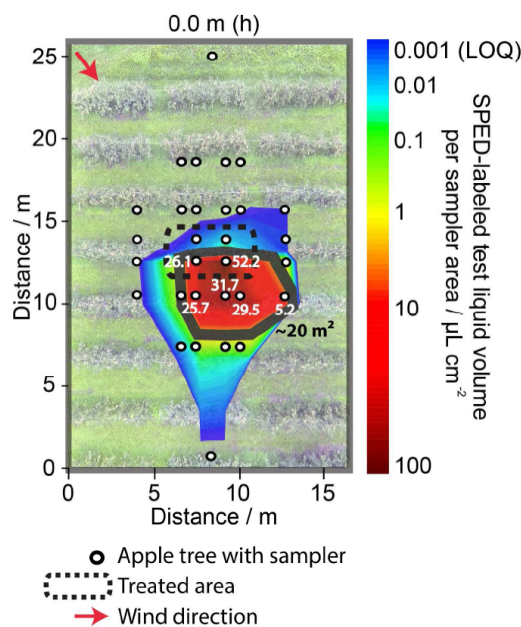


Figure 2. Pesticide drift quantified in an apple orchard via DNA encapsulated silica nanoparticles.

In a second field study nanoparticle dispersion comprising the DNA encapsulates were aerosolized and utilized to directly detect the transport of the aerosol in the environment over larger distances. For this various sampling protocols have been compared and will be discussed, and most recent data shows that this method is able to detect DNA tagged aerosols at low concentration ( $\text{ng}/\text{m}^3$ ). The data is presented and compared to established aerosol dispersion models.

We will additionally discuss strategies to detect these aerosols at  $\text{pg}/\text{m}^3$  levels and elaborate on the opportunities such novel analytical tools have for measuring the impact of anthropogenic aerosols.

Grass, R.N., Heckel, R., Puddu, M., Paunescu, D. and Stark, W.J. (2015), *Angew. Chem. Int. Ed.* **54**, 2552-2555.

Mora, C.A., Paunescu, D., Grass, R.N. and Stark, W.J. (2015) *Mol. Ecol. Resour.* **15**, 231-241.

Paunescu, D., Fuhrer, R. and Grass, R.N. (2013) *Angew. Chem. Int. Ed.* **52**, 4269-4272.

Paunescu, D., Mora, C.A., Puddu, M., Krumeich, F. and Grass, R.N. (2014) *J. Mater. Chem. B* **2**, 8504-8509.

Paunescu, D., Mora, C.A., Querci, L., Heckel, R., Puddu, M., Hattendorf, B., Günther, D. and Grass R.N. (2015) *ACS Nano* **9**, 9564-9572.

## **Current state and future of aerosol process parameterizations in air quality models**

Kirill Semeniuk<sup>1</sup>, Ashu Dastoor<sup>2</sup> and Kenjiro Toyota<sup>3</sup>

<sup>1</sup>Air Quality Research Division, Environment and Climate Change Canada, 2121 Route Transcanadienne, Dorval, QC H9P 1J3, Canada

<sup>2</sup>Air Quality Research Division, Environment and Climate Change Canada, 4905, Dufferin Street Toronto, ON M3H 5T4, Canada

Keywords: aerosol, parameterization, air quality models

Presenting author email: ashu.dastoor@canada.ca

Over the last two decades there has been significant improvement in laboratory and field data on aerosol properties and chemistry; however, air quality (AQ) and climate model intercomparisons demonstrate that aerosol related components have changed little since the late 1990s and early 2000s in models. The aerosol sub-model components which are still commonly used in AQ models are inorganic thermodynamics with the assumption of instantaneous equilibrium, binary nucleation based on classical nucleation theory, simple treatment of SOA (Secondary Organic Aerosol) formulations and internal mixing state formulations. Additionally, most AQ models do not include heterogeneous surface and condensed phase aerosol chemistry. In-cloud production of SOA via aqueous chemistry is not addressed as well. The treatment of SOA as a distinct process does not conform to the picture emerging from laboratory and field observations. Instead of just being a precursor to SOA, organic compounds are critical to new particle formation and growth. The implication of field studies is that pure inorganic secondary aerosols are not typical in the troposphere. There is actually no clear distinction between secondary organic and inorganic aerosols in the nucleation and accumulation modes. Organic compounds affect the deliquescence and efflorescence (crystallization) of inorganic compounds. To properly represent aerosol particle speciation requires three degrees of freedom which include size, mixing state representing the chemical composition and morphology representing the physical distribution of the chemical components. Numerically this is a challenging problem and most aerosol models only address the size distribution. It is common to assume that aerosols are internally mixed which avoids having to deal with mixing state and morphology. However, observational studies have demonstrated that aerosols have complex mixing states and morphology. Aerosol sub-models in climate models are typically of reduced complexity compared to AQ models. Recently there has been a trend towards more comprehensive treatment of aerosols in climate models in order to better capture direct and indirect aerosol effects. This is relevant to AQ modeling as well since it pertains to the proper representation of secondary inorganic and organic aerosol formation and growth and associated multi-phase chemistry. It is climate modeling that is spurring the move to more comprehensive process coupling but this benefits AQ

modeling and weather forecasting as well. The increased attention to submicron scale aerosol and its role in cloud evolution and health effects is spurring both process research and model development.

The issues noted above point to the need for an assessment of many of the key aerosol process parameterizations currently implemented in 3D models and addition of new ones; these include nucleation, thermodynamics, mixing state and multi-phase aerosol chemistry. These processes are important for the proper representation of new particle formation and aerosol impacts on air quality, climate change and health. Even though increasing the detail and accuracy of aerosol processes in models is computationally expensive, it is necessary given the current state of aerosol modeling and the fact that over the last decade there has been a substantial increase in computer power. Even without addressing the role of organic compounds there are improvements that can be made in terms of mixing state representation, nucleation, aerosol multi-phase chemistry and thermodynamics. This study identifies the current state of aerosol process sub-models, and provides recommendations for which aerosol processes can be reasonably improved in future 3D models based on new observations, field studies and aerosol parameterization development. The results of this will be presented at the conference. Manuscripts on this study are being submitted to a peer reviewed journal; therefore, the results of the study are not submitted in the abstract in accordance with the journal policy.

## **Abstracts T208**

## Fungal compositions in dry and wet deposition samples in Seoul, South Korea

C. An<sup>1</sup>, C. Woo<sup>1</sup>, S. Xu<sup>1</sup>, and N. Yamamoto<sup>1</sup>

<sup>1</sup>Department of Environmental Health Sciences, Seoul National University, Seoul, 08826, South Korea

Keywords: fungi, high-throughput sequencing, bioinformatics, bioaerosols

Presenting author email: nyamamoto@snu.ac.kr

Fungi are ubiquitously found in the environment, from which microscopic spores are released into the atmosphere. Globally, an estimated 28-50 Tg of fungal materials are emitted into the atmosphere each year (Elbert *et al.*, 2007; Heald and Spracklen, 2009), which are thought to be important from the contexts of human health as well as local and global climate systems.

Fungi are diverse with an estimated 1.5 million species (Hawksworth, 2001). Their taxonomic compositions and diversities in the atmosphere have been studied by DNA-based methods (Fröhlich-Nowoisky *et al.*, 2009) including high-throughput sequencing (Yamamoto *et al.*, 2012). However, knowledge is limited about fungal compositions and diversities of dry and wet depositions, which play important roles in global biogeochemical cycles. This study aimed at using high-throughput sequencing to explore fungal compositions and diversities in dry and wet deposition samples collected in Seoul, South Korea.

Dry and wet deposition samples were collected using an automatic dry and wet deposition sampler (Han *et al.*, 2016) on the roof (~20 m above ground) of the building of Seoul National University in South Korea (37°27'55.0"N; 126°57'17.7"E) from May to November 2015. DNA was extracted using a commercial extraction kit. Extracted DNA was PCR-amplified for the fungal internal transcribed spacer region and barcoded for massive parallel sequencing by Illumina MiSeq. The sequences produced were processed by bioinformatics tools such as FHiTHINGS (Dannemiller *et al.*, 2014).

Figure 1 shows relative abundances of fungal phyla detected from each of dry and wet deposition samples. Ascomycota was dominant in dry deposition samples with relative abundances ranging from 40% to 96%, whereas Basidiomycota was dominant in wet deposition samples with relative abundances ranging from 37% to 99%. At the genus rank, the five most abundant genera identified from dry deposition samples and respective mean relative abundances were *Cryptococcus* (28%), *Xenocylindrosporium* (14%), *Leptosphaerulina* (7.8%), *Microcyclospora* (2.1%), and *Perenniporia* (2.1%). The five most abundant genera identified from wet deposition samples were *Trametes* (44%), *Cryptococcus* (11%), *Phlebia* (4.3%), *Rhinochlamydia* (4.2%), and *Flammulina* (2.1%). *Trametes* is a genus of Basidiomycota and produces spore-bearing fruiting body (mushroom). A study indicated mushrooms act as nuclei for raindrops (Hassett *et al.*, 2015). The study reported here indicates *Trametes* as the most predominant genera that can act as ice and cloud condensation nuclei in the atmosphere in South Korea.

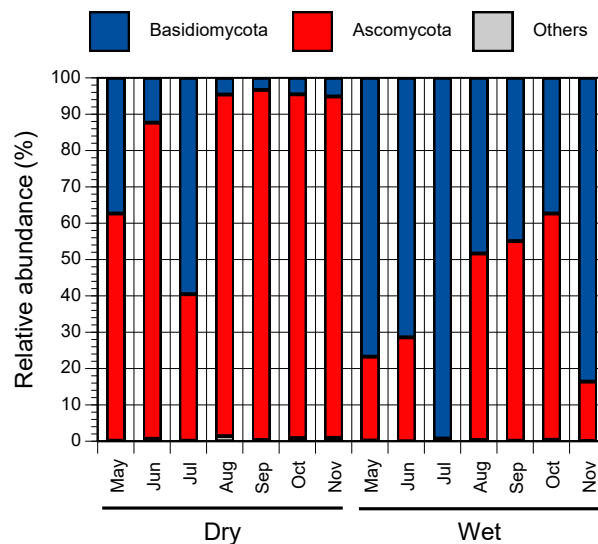


Figure 1. Fungal phylum-level compositions of dry and wet deposition samples in Seoul, South Korea.

This research was supported by the Basic Science Research Program through the National Research Foundation of Korea (2013R1A1A1004497).

- Dannemiller, K., Reeves, D., Bibby, K., Yamamoto, N., and Peccia, J. (2014) *J. Basic Microbiol.* **54**, 315-321.
- Elbert, W., Taylor, P.E., Andreae, M.O. and Pöschl, U. (2007) *Atmos. Chem. Phys.* **7**, 4569-4588.
- Fröhlich-Nowoisky, J., Pickersgill, D.A., Després, V.R., Pöschl, U. (2009) *Proc. Natl. Acad. Sci. USA* **106**, 12814-12819.
- Hawksworth, D.L. (2001) *Mycol. Res.* **105**, 1422-1432.
- Han, J.S., Seo, Y. S., Kim, M.K., Holsen, T.M., and Yi, S.M. (2016) *Atmos. Chem. Phys.* **16**, 7653-7662.
- Hassett, M.O., Fischer, M.W.F., and Money, N.P. (2015) *PLoS ONE* **10**, e0140407.
- Heald, C.L. and Spracklen, D.V. (2009) *Geophys. Res. Lett.* **36**, L09806.
- Yamamoto, N., Bibby, K., Qian, J., Hospodsky, D., Rismani-Yazdi, H., Nazaroff, W.W., Pecia, J. (2012) *ISME J.* **6**, 1801-1811.

## Assessment of total airborne microbes on hazy days in a typical semi-arid city of Northwest China

Yanpeng Li<sup>1,2\*</sup>, Zhengsheng Xie<sup>1</sup>, Rui Lu<sup>1</sup>, Wanxin Li<sup>1</sup>, Ying Song<sup>1</sup>

<sup>1</sup> School of Environmental Science and Engineering, Chang'an University, Xi'an 710054, P. R. China

<sup>2</sup> Key Laboratory of Subsurface Hydrology and Ecology in Arid Areas, Ministry of Education, Xi'an 710054, P.R.

China

Keywords: bioaerosols, microbes, concentration, haze.

Presenting author email: liyanp01@chd.edu.cn

Haze pollution which occurs frequently in northern and eastern China has caused both public and official concern in recent years. Numerous studies focused on the chemical composition in particulate matter (PM) during the haze events in Chinese cities, while little is known about biological fraction of PM in semi-arid region of China. In this study, to better understand the characteristics and potential risks of such biological aerosols, airborne microbial samples were collected using a bioaerosol sampler from Apr. 2016 to Jan. 2017 in Xi'an city, the largest semi-arid inland city of China. The concentration of total microbes was determined by epifluorescent stain approach. The emphases were on the concentration variation under different air quality conditions. Spearman correlation analysis was applied to examine the relationships of bioaerosols with meteorological parameters and air quality index (AQI). In addition, the back-trajectory model was also applied to determine the possible sources of airborne microbes.

The present results showed that concentration of total airborne microbes varied by season, as shown in Fig.1. The concentration of airborne total microbes was higher in autumn and winter, and lower in summer ( $2.27 \times 10^5 \text{CFU/m}^3$ ) and spring ( $2.82 \times 10^5 \text{CFU/m}^3$ ) with the highest concentrations observed in winter ( $7.52 \times 10^5 \text{CFU/m}^3$ ). The mean concentration of total airborne microbes on the hazy days and non-hazy days were  $5.79 \times 10^5 \text{CFU/m}^3$  and  $2.80 \times 10^5 \text{CFU/m}^3$ , respectively. Air quality index (AQI) had positive correlations with the total airborne microbes on the hazy days, suggesting that the concentration of airborne

microbes increased with increasing haze severity. The analysis of back-trajectories revealed that air mass arriving at Xi'an mostly came from the north and southwest direction while the total microbes were in the high level. In contrast, when the concentration of airborne total microbes was low, the air mass of Xi'an mainly came from the north and south direction. This finding suggested that the long distance transport of bioaerosols under certain conditions should be possible. The present results can provide basic data for hazard evaluation of bioaerosols on human health and for future determination of Chinese official standard of outdoor air quality.

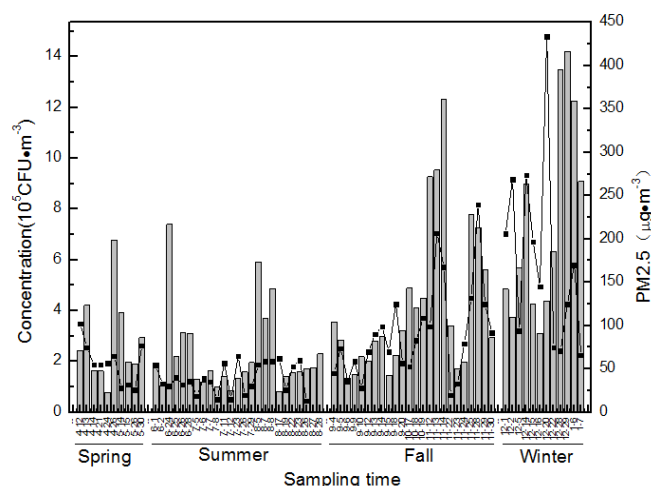


Figure.1. Concentration variation of airborne total microbes and  $\text{PM}_{2.5}$  during the sampling period in Xi'an City, China.

## Uptake of ozone on birch pollen grains

N. Visez<sup>1</sup>, C. Zhu<sup>1</sup>, J. Farah<sup>1,2</sup>, S. Gosselin<sup>1</sup>, M. Choël<sup>3</sup>, D. Petitprez<sup>1</sup>

<sup>1</sup>Univ. Lille, CNRS, UMR 8522, PC2A, F-59000 Lille, France

<sup>2</sup>Lebanese University, Faculty of Public Health (FSP III), Water & Environment Science, Tripoli, Lebanon

<sup>3</sup>Univ. Lille, CNRS, UMR 8516, LASIR, F-59000 Lille, France

Keywords: Allergy, Lipids, Chemical Composition, Bioaerosol.

Presenting author email: nicolas.visez@univ-lille.fr

Pollen grains are modified by air pollution (Sénéchal, 2015). The germination is generally decreased with pollutants exposure of the pollen. Polluted pollen has been shown, in many studies, to increase factors related to the severity of the allergen reaction (higher allergen content, higher IgE response with skin prick tests). The effects of air pollution on the lipid fraction of pollen are by far less documented. Pollen lipids are involved in pollen-stigma interaction (Piffanelli, 1998). Pollen lipids may also have adjuvant effects to the allergenic reaction (Traidl-Hoffmann, 2003). Lipids with double-bonds were detected on the pollen lipid fraction (Henricsson, 1996) and so, reaction with ozone could be expected both in anthers during dehiscence and during pollen wind-transportation in the atmosphere.

Birch pollen was harvested during pollination on trees in april 2016. Pollen was exposed *in vitro* to 115 ppb of ozone for 16 hrs. Pollen lipids were extracted with methylene chloride under sonication for 15 min and analysed by gas chromatography coupled to mass spectrometry. For the determination of uptake coefficient 5 mg of pollen were deposited on 47mm quartz-filter inside a filter holder. Loss of ozone on the birch pollen surface was determined by recording losses of gas-phase ozone during contact with those 5 mg of pollen.

Pollen lipids composition of birch pollen was modified by laboratory exposure to ozone. Most of the compounds were detected in both native and polluted pollen but ozone has changed the ratios. Mass concentrations of fatty acids and aldehydes were increased by ozone exposure and as expected, mass concentrations of alkenes were decreased. Criegee-like reactions can explain several changes observed in lipids consecutively to ozone exposure. The following reactions were written accordingly to the most abundant identified compounds in native pollen and, to their subsequent modification by ozone exposure.

Heptacosene + O<sub>3</sub> = Nonanal + Octadecanoic acid

Heptacosene + O<sub>3</sub> = Octadecanal + Nonanoic acid

Nonacosene + O<sub>3</sub> = Nonanal + Eicosanoic acid

Nonacosene + O<sub>3</sub> = Eicosanal + Nonanoic acid

Pentacosene + O<sub>3</sub> = Nonanal + Hexadecanoic acid

Tricosene + O<sub>3</sub> = Tetradecanal + Nonanoic acid

Thanks to the products identification, the double bond on alkenes could be located between the 9<sup>th</sup> and 10<sup>th</sup> carbon of linear chain.

Alcohols from C18 to C26 were also identified. A slight decrease of those compounds has been observed with ozone.

Alkanes were identified in pollen lipids but their distribution was not modified by ozone. The following compounds were identified: pentacosane, heptacosane, tricosane and nonacosane.

Most of the products from ozone reactivity were already observed in native pollen. One can infer that pollen lipids were already exposed to ozone prior to laboratory exposure. It is for instance difficult to compare exposure of pollen to ozone on trees, potentially for days, with the exposure of pollen while airborne during pollination. On trees, the exposure is longer but the pollen is protected by the anther. In atmosphere, pollen is directly exposed but for a shorter time. Uptake coefficient could be a tool to estimate both exposures.

As a first step toward this comparison, uptake coefficient was determined on birch pollen in the range of 10<sup>-5</sup>. Such a low value is not in favour of an important effect of ozone on birch pollen while airborne.

In order to examine the role of lipids in reactivity with ozone, pollen was defatted (washed with solvent prior to ozone exposure) and subsequently, the uptake was determined on this defatted pollen. The initial uptake was on the same order of magnitude on defatted pollen. However, the uptake of ozone was stopping more rapidly on defatted pollen. Less ozone has reacted on the surface of lipid-washed pollen.

This work is a contribution to the CPER research project CLIMIBIO. The authors thank the French Ministère de l'Enseignement Supérieur et de la Recherche, the Hauts de France Region and the European Funds for Regional Economical Development for their financial support to this project. The CaPPA project (Chemical and Physical Properties of the Atmosphere) is funded by the French National Research Agency (ANR) through the PIA (Programme d'Investissement d'Avenir) under contract ANR-11-LABX-005-01

Sénéchal H. et al. (2015) *The Scientific World Journal* **2015**, ID940243.

Piffanelli P. et al. (1998) *Sex Plant Reprod* **11**, 65-80

Traidl-Hoffmann C. et al. (2003) *Int Arch Allergy Immunol* **131**, 1-13.

Henricsson S. et al (1996) *Grana* **35**, 179-184.

## Real time characterization of bioaerosols emissions from green waste composting

Zaheer Ahmad Nasir<sup>1</sup> and Sean Tyrrel<sup>1</sup>

<sup>1</sup> School of Water, Energy and Environment, Cranfield University, Cranfield, MK43 0AL, UK

Keywords: Bioaerosols, Fluorescence, Emissions, Waste management

Presenting author email: [z.a.nasar@cranfield.ac.uk](mailto:z.a.nasar@cranfield.ac.uk)

The evidence base on public health risks associated with exposure to bioaerosols emissions from a growing number of waste management technologies such as green waste composting is limited. The knowledge on time varying emission factors and their determinants is critical to developing exposure estimates and supporting regulatory decisions. Real time detection and characterization of bioaerosols can overcome the challenges of existing detection methods to elucidate magnitude, nature and spatio-temporal characteristics of bioaerosols emissions over time.

The present investigation aims to use a novel fluorescence based bioaerosol sensor unit with highly resolved fluorescence intensity measurements (Spectral Intensity Bioaerosol Sensor (SIBS)) to detect and characterize bioaerosols in real time from green waste composting. The SIBS offers highly sensitive measurements of bioaerosols and provide a range of data (size, number, shape, and resolved emission fluorescence) on single particles in real time. It uses two excitation wavelengths (280 nm and 370 nm) and records fluorescence emission intensity from 288 nm-735 nm in 16 wavelength bands.

Four repeated measurements were made, on different days, at downwind of the source during daytime at a green waste composting facility with SIBS (Droplet Measurement Technologies, USA). Table 1 presents descriptive statistics on overall mean concentration of particles averaged from four repeated measurements.

Table 1. Summary of particle concentration at downwind of the source at a composting facility

	Mean	Maximum	Minimum	SD
<b>Number Concentration (#/cm<sup>3</sup>)</b>				
NT	2.49	4.29	1.31	1.31
NF	0.53	0.75	0.41	0.15
<b>Mass Concentration (µg/m<sup>3</sup>)</b>				
MT	9.41	24.83	2.79	10.33
MF	2.73	5.98	0.66	2.31
<b>Ratio</b>				
NF/NT	0.22	0.31	0.17	0.06
MF/MT	0.30	0.44	0.19	0.11

NT=Number of total Particles, NF= Number of fluorescent particles, MT=Mass of total Particles, MF= Mass of fluorescent particles, SD = Standard deviation

There was considerable variation in concentration of fluorescent particles over an operational day due to intermittent activities. Figure 1 shows the impact of various activities and wind direction on emissions at a composting site.

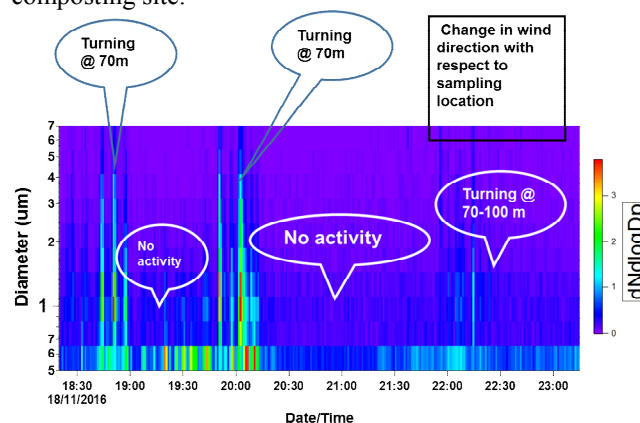


Figure 1. Representative number size concentration of fluorescent particles at downwind of the source at a green waste composting site

With reference to fluorescence emission spectra, an excitation emission matrix based on wavelength as a function of excitation can reveal significant information on nature of bioaerosols. During the present investigation, there were distinct spectral differences during activity (e.g. turning) and no activity periods. Assigning spectral response to biologically relevant fluorophores revealed that they were largely from coenzymes, structural biopolymers, secondary metabolites and pigments.

This study provides evidence that SIBS can quantify and characterize bioaerosols emissions from green waste composting facilities. Different real time data outputs from SIBS comprising of size segregated bioaerosols concentrations, morphology and resolved emission spectra overcomes the challenge of spot sampling and can aid an understanding of nature and temporal variability of bioaerosols emissions from green waste composting facilities. The findings have significant impact by way of informing planning and regulation of bioaerosols emissions from different industrial sources.

This work was supported by the Natural Environment Research Council [NE/M01163/1]. This award is made under the auspices of the Environmental Microbiology and Human Health programme. This work represents the views of the results and the research, and not the views of the funders.

## An inquiry on the potential uses of UV fluorescence for the detection of microorganisms in air, in suspension and on surface

Michaela Skulinova<sup>1,2</sup>, Geneviève Marchand<sup>1</sup>, Jean-François Gravel<sup>2</sup>, Jacques Lavoie<sup>1</sup>, Yves Cloutier<sup>1</sup>

<sup>1</sup>IRSST — Institut de recherche Robert Sauvé en santé et sécurité du travail

<sup>2</sup>INO-Institut National d'Optique

Keywords: fluorescence, microorganisms, bioaerosols, dust deposit

Presenting author email: cloutier.yves@irsst.qc.ca

This exploratory study aims to investigate the potential of fluorescence signals for the detection and the differentiation of microorganisms contained in bioaerosols or their deposits and relevant to Occupational Health and Safety. This study is also of concern for bioterrorism.

Two different excitation wavelengths were used to collect the fluorescence signal. The first one (266 nm) enables to obtain information concerning the composition of microorganisms and is therefore more relevant to identification (Pan 2015). The other (355 nm) is not specific to this purpose but allows the detection of biological material and the metabolic state of the microorganisms (Hill, 2009; Ho, 2002; Sivaprakasam, 2004, Hariston et coll., 1997). The fluorescence signatures of the following microorganisms were studied: *Staphylococcus epidermidis*, *Bacillus subtilis*, *Bacillus megaterium*, *Escherichia coli*, *Enterobacter cloacae*, *Cladosporium cladosporoides*, *Penicillium digitatum* and *Ulocladium chartarum*.

Works were focused on 1) pure and mixed suspensions of these microorganisms in order to mimic those that may be found in workplaces such as in biological cleaning fountain and cutting fluids, 2) surface deposits created by the deposition of aerosols in ventilation ducts, 3) localized deposits similar to dried droplets on stainless steel surfaces found in food industries, pharmaceutical industries and in hospitals, 4) bioaerosols.

Figure 1 shows the main UV fluorescence system that was installed in a hood or adapted for a Collision nebulizer depending on the purpose of the experiments.

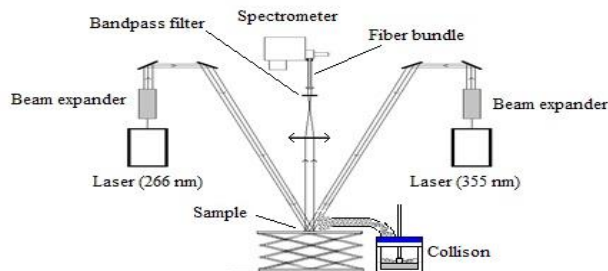


Figure 1 : UV fluorescence system

The position of fluorescence maxima (of bacteria, molds and their mixtures) measured with excitation wavelength at 266 nm seems to differ from specie to specie and can be used to distinguish them. With respect

to bacteria, the fluorescence maxima occur at higher wavelengths than fluorescence maxima of molds.

Mathematical analysis of fluorescence signal developed in this study is a new approach not reported in the literature. It highlights the important characteristics of the fluorescence signal that are hardly visible to the naked eye. This technique has shown that there are fundamental differences between fluorescence signals of Gram positive and Gram negative bacteria and therefore allows distinguishing these bacteria based on their fluorescence signature.

The fluorescence signals can also be used to identify and determine easily the amount of deposits on a surface, which is relevant to those that exist in the ventilation ducts.

Fluorescence signal of dipicolinic acid enables to identify easily the presence of bacterial spores in dust deposits. With regard to potential contamination, this substance is of a high interest and should be considered in fluorescence studies of microorganisms.

Fluorescence mainly the one produced with an excitation wavelength at 266 nm and the mathematical analysis used in this study have proven themselves to be of a special interest for identification of biomolecules and therefore of microorganisms in bioaerosols or deposits.

Hairston, P.P., Ho, J. and Quant, F.R. (1997) Design of an Instrument for Real-Time Detection of Bioaerosols Using Simultaneous Measurement of Particle Aerodynamic Size and Intrinsic Fluorescence. *Journal of Aerosol Science* 28(3): 471–482.

Hill, S.C., Mayo, M.W. and Chang R.K. (2009) Fluorescence of Bacteria, Pollens and Naturally Occurring Airborne Particles: Excitation/Emission Spectra. Army Research Laboratory.

Ho, J. (2002) Future of Biological Aerosol Detection. *Analytica Chimica Acta* 457(1): 125–148.

Pan, Y.L. (2015) Detection and characterization of biological and other organic-carbon aerosol particles in atmosphere using fluorescence, *Journal of Quantitative Spectroscopy & Radiative Transfer* 150, 12–35.

Sivaprakasam, V., Huston, A.L., Scotto, C. and Eversole J.D. (2004) Multiple UV Wavelength Excitation and Fluorescence of Bioaerosols. *Optics Express* 12(19): 4457.

## Sticking of particulate matter on airborne pollen

A. Ivanovsky<sup>1</sup>, N. Visez<sup>2</sup>, A. Roose<sup>1</sup> and M. Choël<sup>1</sup>

<sup>1</sup>Univ. Lille, CNRS, UMR 8516, LASIR, F-59000 Lille, France

<sup>2</sup>Univ. Lille, CNRS, UMR 8522, PC2A, F-59000 Lille, France

Keywords: bioaerosol, aeroallergen, pollen, particulate matter  
Presenting author email: marie.choel@univ-lille1.fr

The prevalence of allergic diseases related to pollen has increased over the last decades. Air pollution is suspected to enhance the risk of allergy (Sénéchal et al., 2015). Health effects of pollen are worsened in the case of co-exposure of pollen grains with particulate matter (PM) (Polosa, 2001). Modification of the biological and immunological properties of pollen may depend on the physical and chemical properties of particles attached to pollen. PM and pollen are monitored in mass and number concentrations, respectively. Yet the chemical nature of ambient PM is not regulated and even less frequently assessed when adhered on the surface of pollen. Few field studies were conducted with the aim to quantify particulate pollution on airborne pollen grains. Ribeiro et al. (2015) analyzed a total of 140 pollen grains of *Acer*, 123 of *Pinus* and 156 of *Platanus* collected in Porto and reported that the average number of particles per pollen was 16, 39 and 4 for *Acer*, *Pinus* and *Platanus*, respectively.

Birch pollen is highly allergenic and widespread in Europe. In this study, our aim was to explore the physical and chemical characteristics of particles sticking on the surface of birch pollen grains. Daily samplings of pollen were performed during the birch pollination period (March-April 2017) with a cascade impactor (Dekati® PM10). The impactor was set on the roof of a building at Lille University at 20 meters a.s.l. Particles were collected on carbon tape and were examined by low-vacuum scanning electron microscopy. X-ray elemental mappings of single pollen grains were performed to chemically classify particles adsorbed on the pollen surface. Number size distribution of ambient particles was recorded during sampling using an optical particle counter (Grimm® MiniWras).

For a specific day with a mean PM<sub>10</sub> mass concentration of 30 µg/m<sup>3</sup> lower than the daily limit value (50 µg/m<sup>3</sup>), our results show pollution of birch pollen by PM. Particles adhered to pollen were of different types comprising: carbonates, aluminosilicates, carbonaceous (soot, biogenic) heavy-metal rich particles and sea-salts. Among 128 birch pollen grains individually examined, over a third had particles stuck on their surface (Fig. 1). On average, a polluted birch pollen grain carried 2.7 particles on its surface. Our results highlight that for particles smaller than 0.2 µm or with a chemical contrast similar to that of pollen, counting and identification are uncertain.

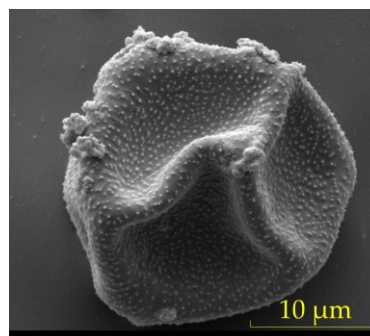


Figure 1. SEM image of PM adhering to a birch pollen grain.

This work is a contribution to the CPER research project CLIMIBIO. The authors thank the French Ministère de l'Enseignement Supérieur et de la Recherche, the Hauts de France Region and the European Funds for Regional Economic Development for their financial support to this project. The CaPPA project (Chemical and Physical Properties of the Atmosphere) is funded by the French National Research Agency (ANR) through the PIA (Programme d'Investissement d'Avenir) under contract ANR-11-LABX-005-01.

- Polosa, R. (2001) *Curr. Allergy Asthma Rep.* **1**, 102–107.  
Ribeiro H., Guimarães F., Duque L., Noronha F. (2015) *Env. Poll.* **206**, 7-16  
Sénéchal, H., Visez, N., Charpin, D., Shahali, Y., Peltre, G., Bioley, J.-P., Lhuissier, F., Couderc, R., Yamada, O., Malrat-Domenge, A., Pham Thi, N., Poncet, P., Sutra, J.-P. (2015) *Sci. World J.* **2015**, ID 940243.

## Potential pathogenicity of psychrotolerant yeasts isolated from atmospheric aerosols of Southwestern Siberia

I.S. Andreeva<sup>1</sup>, A.S. Safatov<sup>1</sup>, V.V. Morozova<sup>2</sup>, N.V. Tikunova<sup>2</sup>, I.V. Babkin<sup>2</sup>, G.A. Buryak<sup>1</sup>,  
E.K. Emelyanova<sup>1</sup>, E.N. Gorina<sup>1</sup>

<sup>1</sup>Dep. Biophysics and Ecological Researches, FBRI SRC VB “Vector” of Rospoterbnadzor, Koltsovo, Novosibirsk region, 630059, Russian Federation

<sup>2</sup>Dep. Molecular Microbiology, Institute of Chemical Biology and Fundamental Medicine SB RAS, Novosibirsk, 630090, Russian Federation

Keywords: atmosphere, bioaerosols, yeasts, biodiversity.

Presenting author email: [safatov@vector.nsc.ru](mailto:safatov@vector.nsc.ru)

Atmospheric bioaerosols comprising spores of plants, fungi, bacteria, viruses, protein macromolecules, waste products of microorganisms and particles with decaying remains of living organisms can cause or provoke allergic and infectious diseases and largely affect the state of the environment and human health.

Air sampling campaigns were carried out at 2 on-ground sites (settlements Klyuchi and Koltsovo of Novosibirsk region) and in the vicinity of Zavyalovo settlement at 8 altitudes from 500 to 7000 m in 2013-2016 years. The samples were sampled using liquid impingers with 50 ml of Hank's solution. Sampled air volumes were 1.5 m<sup>3</sup> for on-ground sites and 0.3 m<sup>3</sup> for altitude samples (Safatov, *et al.*, 2010).

Microorganisms culturability was studied in laboratory by seeding of impingers' liquid onto 5 different agarized culture media (Safatov, *et al.*, 2010). The seedings were incubated at temperatures 28-30 °C and 6-10 °C up to 20 days. Individual yeast colonies grown on agarized media were used for preparation of “pure” culture lines and subsequent morphological, biochemical and genetic analysis of these isolates.

Microbiological investigation of surface and altitude atmospheric air samples from Southwestern Siberia provided data including the amount and composition of isolated bacteria, yeasts and fungi. A special attention was paid to psychrotolerant yeasts found in atmospheric air aerosols at different altitudes and in different seasons. The percentages of yeasts in the studied samples were from 0 to 40 % for altitude samples and from 0 to 95 % in on-ground samples. It should be noted that numbers of colonies on the plates incubated at temperature 6-10 °C were more than numbers of colonies on the plates incubated at temperature 28-30 °C in more than 50 % cases. Besides, there were significant differences in microorganisms' biodiversity for the same sample seedings cultivated at different temperatures.

Viable yeast-like isolates were detected and classified under the genera *Bullera*, *Sporidiobolus*, *Aerobasidium*, *Cryptococcus*, *Sporobolomyces*, *Rhodotorula*, *Candida*, *Entyloma* and some others according to their phenotypic and genomic characteristics. Some of their species are within the groups of pathogenic and conventionally pathogenic microorganisms that are harmful for humans.

The temperature optimum of microorganisms' growth was shifted towards low temperatures for the majority of isolates. But there were some isolates, like *Rhodotorula ssp.* St-450, actively growing at the wide temperature range (from 6 up to 37 °C). This characteristic is related to pathogenic species of this genus usually. So the mentioned above strain may be related to potentially dangerous pathogenic microorganisms.

The distribution within phylogenetic groups correlated with the determined phenotypic characteristics of the corresponding genus, while the degree of similarity with the related species observed in the process of the phylogenetic tree construction was not always confirmed by the study of the phenotypic characteristics of the strains, which requires additional research for more exact identification of the isolated strains. Yeast-like fungi of the genera *Alternaria*, *Cladosporium*, *Penicillium*, *Mucor*, *Trichoderma*, *Fusarium* and *Aspergillus* at the concentrations from <1 to 5·10<sup>3</sup> cells/ml of the sample and actinomyces possessing hemolytic activity were also identified in atmospheric aerosols as possible pathogenic and allergenic agents.

Thus the conducted studies showed that there are many microorganisms in atmospheric aerosols displayed potential danger for humans as in on-ground atmospheric layer as in higher altitude layer at 500-7000 m.

These microorganisms may be really dangerous for humans when they are in the on-ground layer. The microorganisms in the layer 500-7000 m could be really dangerous for humans when they move down to the on-ground layer (possibly at long distances from the region where they were found) in case they will preserve its biological activity during their travel in atmosphere.

Safatov A.S., *et al.* (2010). In: *Aerosols – Science and Technology*. I. Agranovski (Ed.) Wiley – VCH, 407-454.

## UV-Vis Absorption Properties of Water Soluble HULIS in Ambient Aerosols: A study for IGP

Varun Kumar<sup>1</sup>, Anubha Goel<sup>1,2</sup>

<sup>1</sup>Department of Civil Engineering, Indian Institute of Technology, Kanpur, 208016, India

<sup>2</sup>APT, Center for Environmental Science and Engineering, Indian Institute of Technology, Kanpur, 208016, India

Keywords: HULIS, UV-Vis, Chromophore, IGP

Presenting author email: anubha@iitk.ac.in

Water Soluble HULIS is a very significant fraction of organic aerosols. HULIS can attenuate UV radiation influencing climate change, radiative budget of Earth and can influence human health as well. Structural and functional group studies of HULIS reveal a multitude of organic functional groups. The presence of these functional groups on a large carbon chain backbone give HULIS its chromophoric properties.

In present study we have tried to look into UV-Vis Absorption properties of water soluble HULIS on a Day-night basis. We collected 10 daytime samples and 10 night time samples of PM<sub>10</sub> by using a High Volume Sampler in the city of Kanpur located in central Part of Indo Gangetic Plains (IGP). The Water soluble HULIS was extracted using Solid Phase Extraction methodology (Varga et al., 2001). The extracted HULIS was re-dissolved in water and UV-Vis spectrum was obtained for each sample from 190 nm to 800 nm. The absorption values at wavelengths 254, 250, 365, 465 and 665 nm were separately determined for each sample and the absorption ratios E<sub>2</sub>/E<sub>3</sub> (250/365) and E<sub>4</sub>/E<sub>6</sub> (465/665) were calculated. The E<sub>4</sub>/E<sub>6</sub> (ratio of absorbance at wavelength 465 nm to 665 nm) is normally a measure of degree of Humification and molecular weight. E<sub>2</sub>/E<sub>3</sub> (absorbance at 250 nm and 365 nm) E<sub>2</sub>/E<sub>3</sub> inversely correlates with the Aromaticity and molecular weight of Humic substances. The E<sub>2</sub>/E<sub>3</sub> for 25 samples taken reveal that average day time E<sub>2</sub>/E<sub>3</sub> is higher with value **7.77 ± 1.06** as compared to **6.31 ± 1.47** of nighttime samples. This reveals the fact that Aromatic content and molecular weight of HULIS on an average is lesser at daytime as compared to nighttime and more HULIS exists as aliphatic species. The strong photo-oxidation may be attributed to lesser Aromaticity in HULIS at daytime samples. This is an indication of alteration of physical properties of HULIS during day and nighttime due to strong light absorbance at daytime which leads to formation of new species.

E<sub>4</sub>/E<sub>6</sub> Ratios were higher for Nighttime samples and lower for Daytime samples again showing a higher degree of Humification and longer molecular Chains in Night-time HULIS.

Absorption properties viz. absorption coefficient ( $b_{\text{abs},\lambda}$ ) and absorption Angstrom exponent (AAE) of HULIS in PM<sub>10</sub> samples were also calculated. The  $b_{\text{abs},365}$  varied from 7.3 to 20.3 ( $13.6 \pm 3.8 \text{ Mm}^{-1}$ ) and 19.2 to 43.1 ( $28.8 \pm 8.3 \text{ Mm}^{-1}$ ) during daytime and nighttime, respectively. The power fit of the spectrum gave AAE value of HULIS (at Kanpur; IGP); centering at  $4.9 \pm 1.4$  and  $5.1 \pm 1.3$  during daytime and nighttime, respectively.

These two values are identical as assessed from statistical two-tailed t-test [ $t = 0.33$ ;  $p > 0.05$ ]. This observation gives an indication that primary emissions might be dominating source of HULIS in IGP.

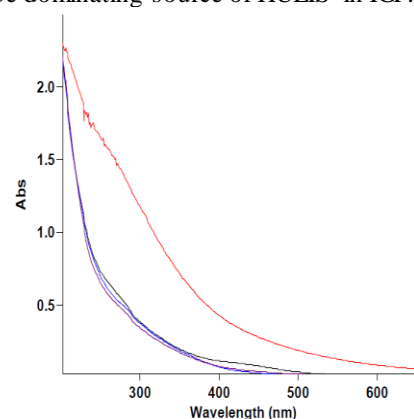


Fig1. UV-Vis Spectrum of HULIS and Sodium Salt of Humic acid (red)

This work was supported by the Internal Research funding of IIT Kanpur.

Varga, B., Kiss, G., Ganszky, I., Gelencser, A. and Krivacsy, Z.: *Isolation of water-soluble organic matter from atmospheric aerosol*, *Talanta*, 55, 561-572, 2001.

## Re-aerosolisation of biological aerosols from hot surfaces

K. Mirskaya, I.E. Agranovski

School of Engineering, Griffith, University, Brisbane, 4111 QLD, Australia

Keywords: bioaerosol, bioaerosol generation, hot surface

Presenting author email: [I.Agranovski@griffith.edu.au](mailto:I.Agranovski@griffith.edu.au)

In this study, the ability of droplet-surface collision to generate a viable bacterial aerosol has been investigated. The experiments were focused on the transition and film boiling regimes with the temperatures from 170 to 480°C. This temperature interval is extended around the Leidenfrost temperature of water, which is determined as 220°C (Baumeister et al., 1970) representing the fragment of the boiling curve that is characterised by the lowest heat transfer and, consequently presents the most favorable conditions for microbial survival.

Experiments were carried out with two common environmental bacterial strains; Gram-positive *Bacillus subtilis* (*B. subtilis*) and Gram-negative *Escherichia coli* (*E. coli*). A plastic funnel was strategically placed above the hot plate to ensure minimal escape of generated vapor-aerosol mixture during experiments achieving maximum possible microbial collection by the bioaerosol sampling equipment during experiments (Fig. 1). A round circular hole was drilled in the plastic funnel at a height of 90 mm above the hot surface in order to insert the tip of a micropipette for microbial suspension delivery to the hot surface. Two personal bubbler type bioaerosol samplers were used to collect bioaerosol, potentially generated on the hot surface. Standard microbial spread technique was employed for analysis of collecting liquid on completion of each experimental run.

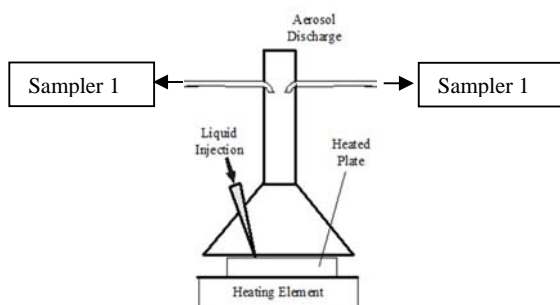


Figure 1. Experimental setup

Fig. 2 shows the bioaerosol recovery ratio as a function of the surface temperature. Both *B.subtilis* and *E.coli* demonstrated similar functional relationships between the surface temperature and bacterial aerosol concentration (Mirskaya and Agranovski, 2017). The temperature of 170°C was characterised by the lowest recovery ratio for both *B.subtilis* ( $1.2 \pm 0.5 \times 10^{-3}$ ) and *E.coli* ( $2.2 \pm 1.0 \times 10^{-4}$ ). Aerosolisation of microorganisms is likely occurred during the first few seconds after collision, when the surface was hot enough to maintain the boiling. The following cooling of the surface

accompanied by a slow evaporation of the droplet did not produce bubbles and unlikely was able to generate bioaerosols. The recovery ratios of both bacteria in aerosol increased with the temperature growth and reached their maximums at the temperature of 380°C for both *E.coli* ( $9.3 \pm 4.6 \times 10^{-3}$ ) and *B.subtilis* ( $3.8 \pm 1.1 \times 10^{-2}$ ).

At the temperature of 480°C the recovery ratio significantly decreased for *E.coli* as well as for *B.subtilis*. This allows for speculation that the loss of about 70% of the water droplet as a result of the levitating droplet formation (remained on the surface and not aerosolized) might have an effect on the aerosolisation of bacteria.

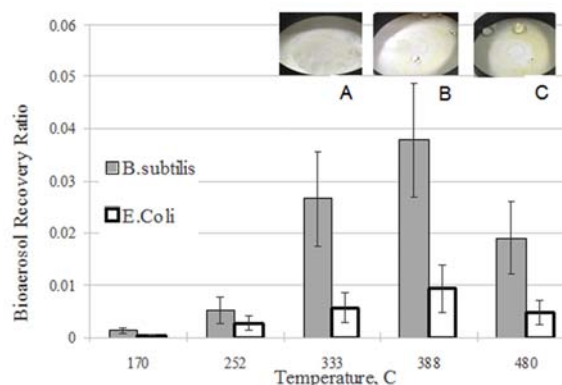


Figure 2. Microbial recovery

The processes of droplet-surface interaction are generally related to industrial procedures such as cooling of surfaces in metallurgical processes and combustion. However, it may have important applications in everyday life. Collision of contaminated water with the surface of hot rocks in a hot spa, steam generation in the iron-press, water cleaning of the hot barbecue facilities can potentially result in generation of viable biological aerosols. The results of this study demonstrate that water-surface interaction may be associated with establishment of viable bacterial aerosol when the water is contaminated with bacteria.

Baumeister, K.J., Simon, F.F., Henry, R.E. (1970). Role of the surface in the measurement of the Leidenfrost temperature, Augmentation Convective Heat Mass Transfer. ASME 91–101.

Mirskaya, K., Agranovski, I.E. Generation of bacterial aerosols by interaction of microbial suspension with hot surfaces. Journal of Aerosol Science. <http://dx.doi.org/10.1016/j.jaerosci.2017.02.001>.

## Characterization of the Chambre atmospheric simulation chamber

P. Prati<sup>1</sup>, E. Gatta<sup>2</sup>, P. Brotto<sup>3</sup>, D. Massabò<sup>1</sup>, F. Parodi<sup>4</sup>, A. Comite<sup>5</sup>, C. Costa<sup>5</sup>, J. F. Doussin<sup>6</sup>, P. Formenti<sup>6</sup>

<sup>1</sup>Department of Physics, University of Genoa and INFN, Genova, 16146, Italy

<sup>2</sup>Department of Physics, University of Genoa, Genova, 16146, Italy

<sup>3</sup>PM\_TEN srl, Genova, 16146, Italy

<sup>4</sup>INFN, Genova, 16146, Italy

<sup>5</sup>Department of Chemistry and industrial chemistry, Genova, 16146, Italy

<sup>6</sup>Laboratoire Interuniversitaire des Systèmes Atmosphériques (LISA), UMR7583, CNRS, Université Paris Est Créteil et Université Paris Diderot, Institut Pierre et Simon Laplace, Créteil, France

Keywords: bioaerosol, simulation chamber, eurochamp2020

Presenting author email: prati@ge.infn.it

ChAMBRé (Chamber for Aerosol Modelling and Bio-aerosol Research) is a stainless steel atmospheric simulation chamber (volume approximately 3 m<sup>3</sup>) recently installed at the National Institute of Nuclear Physics in Genoa (INFN-Genova, [www.ge.infn.it](http://www.ge.infn.it)) in collaboration with the Environmental Physics Laboratory at the Physics Department of Genoa University ([www.labfisa.ge.infn.it](http://www.labfisa.ge.infn.it)). ChAMBRé is one of the nodes of the EUROCHAMP2020 European network of atmospheric simulation chambers.

ChAMBRé (Figure 1) will be mainly devoted to bioaerosol studies with an experimental activity targeted to the assessment of the behavior of most common pathogens for humans and plants and to the analysis of the mechanisms controlling bacteria interactions with other aerosols and within the atmosphere. Subjects of investigations will be defined considering the most relevant pathogens for public health and identifying non-pathogenic bacteria with similar characteristics to allow for experiments in safe conditions. We have selected a reasonable number of different bacteria to cover the widest range of morphological features, belonging to phyla most commonly encountered in the atmosphere (e.g. Firmicutes, Proteobacteria and Actinobacteria) and taking into consideration their ability to produce endotoxins, spores and biofilm.

The first experiments will be performed on:

*Bacillus subtilis* (Phyla Firmicutes, rod-shaped, GRAM+, obligate aerobe with possible anaerobe phases, spore-forming)

*Pseudomonas syringae* (Phyla Proteobacteria, rod-shaped, GRAM-, highly pathogen for plants, common antimicrobial protection resistant)

*Streptomyces coelicolor* A3(2) (Phyla Actinobacteria, GRAM+, soil-dwelling, spore-forming, high similarity with several plants pathogens)

Microrganisms suspended in liquid solutions will be aerosolized through nebulization (Blaustein Atomizer – BLAM by CH-Technologies) and injected in ChAMBRé, where selected atmospheric conditions. Very promising results in this direction were obtained by the INFN-Genoa group and co-workers in a pilot experiment, performed at the CESAM facility thanks to the transnational access grant funded by Eurochamp-2 project, whose results have

been recently published (Brotto, 2015). Moreover another very interesting paper by Amato and co-workers (Amato, 2015) published nearly at the same time, reports the results of simulation chamber experiments performed at AIDA facility to investigate bacteria viability and ice nucleation activity.



Figure 1: the Chambre structure: a 7-stage Andersen impactor for bioaerosol collection is visible on the right side

The ChAMBRé set-up is going to be completed and its characterization (aerosol lifetime, wall losses, background levels, protocol for bioaerosol injection) is in progress. Results will be given at EAC focussing on the outcomes of the first experiments with bacteria.

This project/work has received funding from the European Union's Horizon 2020 research and innovation programme through the EUROCHAMP-2020 Infrastructure Activity under grant agreement No 730997

P. Brotto et al, *Aerobiologia*, 2015

P. Amato et al, *ACP*, 2015

## **Abstracts T209**

## Development of compound-specific carbon isotopic analysis for levoglucosan and its isomers, biomarkers of biomass burning

W. Wang and D.W. Han

Institute of Environmental Pollution and Health, University of Shanghai, Shanghai, 200444, China

Keywords: compound-specific carbon isotopic analysis; levoglucosan, mannosan and galactosan; biomarkers of biomass burning.

Presenting author email: wangwu@staff.shu.edu.cn

Biomass burning is an important source of atmospheric carbonaceous particulate matter, mainly exists in fine size fraction  $PM_{2.5}$ . It enhances the levels of ozone and other gases which impact air radiation balance and has effects on air quality, visibility, regional climate and human health. However, it is still uncertain including the source identification, the physical and chemical processes and the further evolution of combustion products, as well as the contributions of the type of burnt biomass to the organic carbon in the atmosphere.

It has been shown that changes in the stable carbon isotope ratios can be used as indicators of atmospheric processing of volatile organic compounds; for example, carbon isotope ratio measurements allow the calculation of the extent of photochemical processing of isoprene in the atmosphere. These data are valuable for obtaining insight into the atmospheric oxidation of isoprene and the loss processes in determining the atmospheric mixing ratios. Levoglucosan, as well as its isomers, is an prominent tracer for biomass burning due to its high concentration and stable physiochemical properties in the atmosphere.

Methylboronic acid (MBA) has been reported to determine natural  $^{13}C$  abundances of monosaccharides by derivatizing adjacent hydroxyl groups of monosaccharides followed by *N,O*-bis(trimethylsilyl)trifluoroacetamide (BSTFA) derivatization of the remaining single OH groups. Here, we develop a compound-specific carbon isotopic analysis for levoglucosan, mannosan and galactosan in order to investigate whether these anhydrosugars have source-specific isotopic signature and can provide fingerprints for the type of burnt biomass. MBA was used as the derivatization reagent prior to gas chromatography/combustion/isotope ratio mass spectrometry (GC/C/IRMS). The derivatizing C from the MBA reagent accounts for 29% of the analyte, but 70% in the trimethylsilyl (TMS) derivatives.

Figure 1 shows our first step results of successfully derivatization of anhydrosugars by MBA-BSTFA.

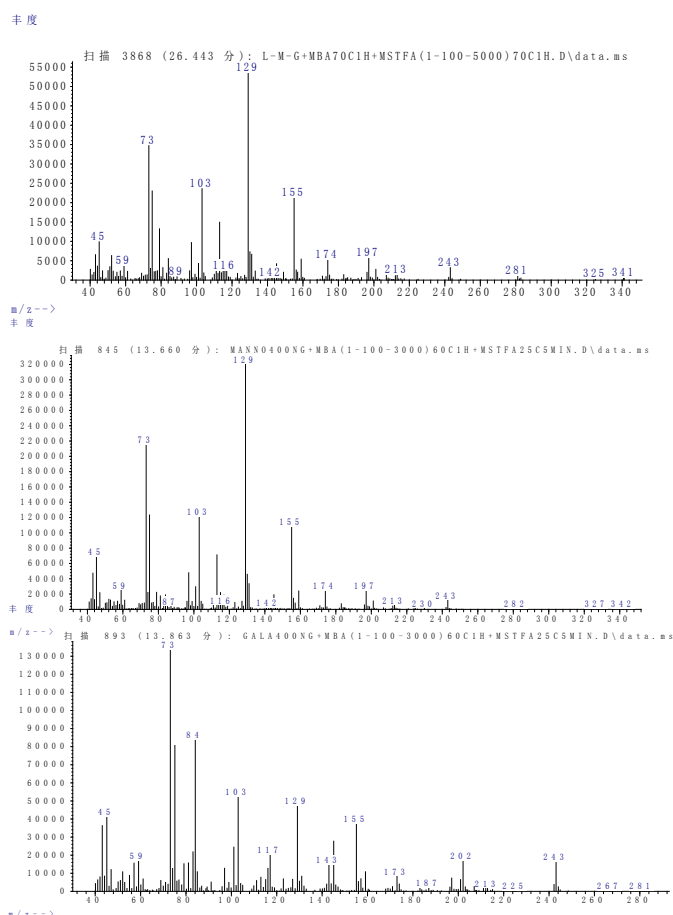


Figure 1. Mass spectra of MBA-BSTFA derivatives of levoglucosan (up), mannosan (middle) and galactosan (bottom)

This work was supported by the National Natural Science Foundation of China under grants 20877051, 2137707 and 41675123.

Gross, S. and Glaser, B. (2004) *Rapid Commun. Mass Spectrom.*, **18**, 2753–2764.

Qiang, L., Wang, W., Zhang, H.W., Wang, Y.J., Wang B., Bi, X.H. (2010) *Analy. Chem.*, **82**, 6764–6769.

Rudolph, J. and Czuba, E. (2000) *Geophys. Res. Lett.*, **27**, 3865–3868.

Van Dongen, B., Schouten, S., Damste, J. (2001) *Rapid Commun. Mass Spectrom.*, **15**, 496–500.

## Morphochemical characteristics and mixing state of long range transported wildfire particles at Ny-Ålesund (Svalbard Islands)

B. Moroni<sup>1</sup>, S. Crocchianti<sup>1</sup>, S. Becagli<sup>2</sup>, L. Caiazza<sup>2</sup>, R. Traversi<sup>2</sup>, R. Udisti<sup>2</sup>, M. Mazzola<sup>3</sup>, K. Markowicz<sup>4</sup>, C. Ritter<sup>5</sup>, T. Zielinski<sup>6</sup> and D. Cappelletti<sup>1</sup>

<sup>1</sup>Dipartimento di Chimica, Biologia e Biotecnologie, Università di Perugia, Perugia, I-06123, Italy

<sup>2</sup>Dipartimento di Chimica, Università di Firenze, Firenze, I-50019, Italy

<sup>3</sup>ISAC-CNR, Bologna, I-40129, Italy

<sup>4</sup>Institute of Geophysics, Faculty of Physics, University of Warsaw, Warsaw, 02-093, Poland

<sup>5</sup>Alfred Wegener Institute for Polar and Marine Research, Telegrafenberg A43, 14473 Potsdam, Germany

<sup>6</sup>Institute of Oceanology, Polish Academy of Sciences, Sopot, 81-712, Poland

Keywords: SEM-EDS; image analysis; aerosol sources; particle evolution.

Presenting author email: b.moroni@tiscali.it

Wildfires are an important variable of climate change in the Arctic as a source of particles which are able to modulate the radiative forcing in the atmosphere and the albedo properties of snow and ice exposed surfaces besides serving as large sources of cloud condensation nuclei (Spracklen *et al.*, 2011; Liu *et al.*, 2014). Recent studies on the mineral chemistry and geochemical signature of aerosols sampled at ground level and along vertical profiles at the scientific Polar base of Ny-Ålesund, Svalbard Islands (78°55'30"N 11°55'20"E), have shown a significant contribution of biomass burning forest fire on this area especially in summertime (Giardi *et al.*, 2016; Moroni *et al.*, 2016).

A prolonged and exceptionally intense air mass advection event transporting biomass burning aerosols generated in Alaska affected Ny-Ålesund in the mid of July, 2015. This study is focused on the morphochemical characteristics and mixing state of individual aerosol particles collected during the event. To this aim aerosol samples were collected on nucleopore polycarbonate membranes using a DEKATI 12-stage low volume impactor and analyzed by scanning electron microscopy (SEM) coupled with image analysis, 3D surface reconstruction and energy-dispersive X-ray microanalysis (SEM-EDS).

Results of SEM investigations depict a complex aerosol characterized by an external mixing between a main part of carbonaceous organic particles (tar balls – TBs - and organic particles - OPs), lower ammonium sulfate (AS) and minor potassium chloride (KC) and mineral dust (MD) amounts. The carbonaceous particles, in particular, are mostly in the accumulation mode size range with morphologies that range from spherical to slightly elongated. The organic particles show an internal mixing of low density organics and/or ammonium sulfate upon denser nuclei (Fig. 1).

Individual particle analyses were complemented by aerosol size distribution (Aerodynamic Particle Sizer, Scanning Mobility Particle Sizer) and optical (Particle Soot Absorption Photometer, nephelometer) measurements at ground level in order to retrieve the optical and radiative properties of the aerosol in the atmosphere and to predict the fate and behaviour of particles upon deposition at ground level.

Individual particle analyses were also compared with bulk chemical analyses on daily sampling filters and back-trajectory analyses of the air mass movement in order to enucleate distinct sources of the aerosol during the long range transport.

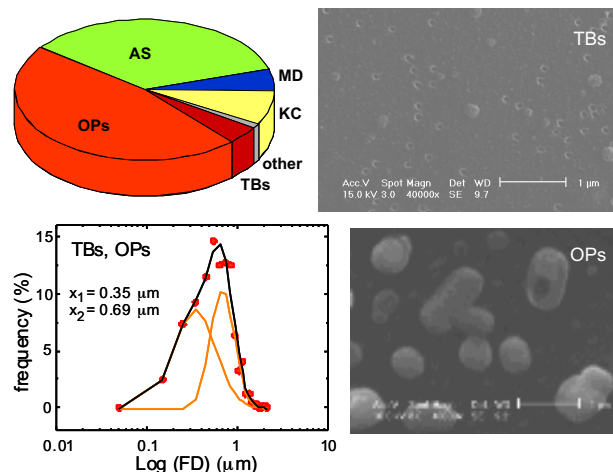


Figure 1. Relative abundance (% number) of the particles types, SEM micrographs and size distribution of TBs and OPs.

This study was carried out under the framework of the Italian research activities at the Dirigibile Italia-CNR base in Ny Alesund and has been supported by the University of Perugia.

Giardi, F., Becagli, S., Traversi, R., Frosini, D., Severi, M., Caiazza, L., Ancillotti, C., Cappelletti, D., Moroni, B., Grotti, M., et al. (2016) *Rend. Fis. Acc. Lincei* **27**, doi:10.1007/s12210-016-0529-3.

Liu, Y., Goodrick, S., Heilman, W. (2014) *Forest Ecol Manag* **317**, 80-96.

Moroni, B., Cappelletti, D., Ferrero, L., Crocchianti, S., Busetto, M., Mazzola, M., Becagli, S., Traversi, R., Udisti R. (2016) *Rend. Fis. Acc. Lincei* **27**, S115–S127.

Spracklen, D.V., Carslaw, K.S., Pöschl, U., Rap, A., Forster, P.M. (2011) *Atmos. Chem. Phys.* **11**, 9067–9087.

## Evaluation of a residential wood heating emissions abatement policy at local scale in a complex area, the Arve valley, France.

J. Allard<sup>1,2</sup>, F. Chevrier<sup>1,2</sup>, I. Ježek<sup>3</sup>, G. Močnik<sup>3,6</sup>, J.L. Besombes<sup>2</sup>, G. Brulfert<sup>4</sup>, J.P. Laurent<sup>1</sup>, and J.L. Jaffrezo<sup>1</sup>

<sup>1</sup>Université Grenoble Alpes-CNRS, IGE UMR5183, 38000 Grenoble, France

<sup>2</sup>Université Savoie Mont-Blanc, LCME, 73376 Le Bourget du Lac, France

<sup>3</sup>Aerosol d.o.o., 1000 Ljubljana, Slovenia

<sup>4</sup>Air Rhône-Alpes, Bron, France

<sup>6</sup>Josef Stefan Institute, 1000 Ljubljana, Slovenia

Keywords: Alpine valleys, temperature inversion, biomass burning, local meteorology

Presenting author email: julie.allard@univ-grenoble-alpes.fr

The sector of residential wood heating is the most contributor to particulate air pollution in the Arve valley during wintertime (Bonvalot *et al.*, 2016). Since 2013, a wide operation to renew the old residential wood appliances was launched. Presently, evaluations of this emission abatement policy with air quality models in this complex terrain are not enough satisfactory. Emissions of residential wood heating are among the most difficult to estimate because of the lack of local data and the large variability in the emission factors (EAA, 2013). Furthermore, the local meteorology, especially the high occurrence of temperature inversions in this area, have a large impact on the concentrations of particles and gaseous pollutants, and has not been correctly represented by meteorological model (Chemel *et al.*, 2016). To evaluate the efficiency of the abatement policy at local scale on air quality, continuous meteorological and chemical measurements were performed at three sites (Passy, Chamonix, Marnaz) of different typologies and urbanization levels located in the Arve valley, and data about renewed appliances were also collected.

At the studied sites, the contribution of biomass burning sources to the ambient PM<sub>10</sub> concentration levels was estimated from the continuous measurements of black carbon (eBC) performed with an Aethalometer AE33, coupled with the analysis of specific tracers of biomass burning (levoglucosan, Hulis...) on daily PM10 filter samples. Temperature inversions were investigated by temperature measurements along the slopes from measurements stations. These measurements used to characterize atmospheric vertical profiles were validated after being compared with aerosol lidar (WLS200S) and radiosounding measurements (Pacy *et al.*, 2016). Supplementary data from Meteo-France like wind, precipitation, snow depth were combined with the temperature of sensors in the slopes to classify meteorological conditions (cluster analysis). The collected data from old and new wood appliances allowed us to estimate emissions at dwelling scale (Air Rhône-Alpes inventory method).

Table 1. Emissions evolution of renewed wood appliances between 2013-2016 and located in a circle of a radius of 1 km near Passy station.

PM <sub>10</sub> emissions (kgPM <sub>10</sub> /an)	Winter 13-14	Winter 14-15	Winter 15-16
Circle (r= 1km)	2407 ± 121	1456 ± 91	495 ± 8

Considering the same meteorological conditions in wintertime, evolution of part of biomass burning on PM<sub>10</sub> concentrations is consistent with the evolution of PM<sub>10</sub> emissions estimated from data of renewed appliances close to Passy station. Additional wintertime measurements and data analysis at the 2 others sites (Chamonix, Marnaz) of the Arve valley will allow us to evaluate more rigorously the impact of wood appliances renew on the air quality in this area.

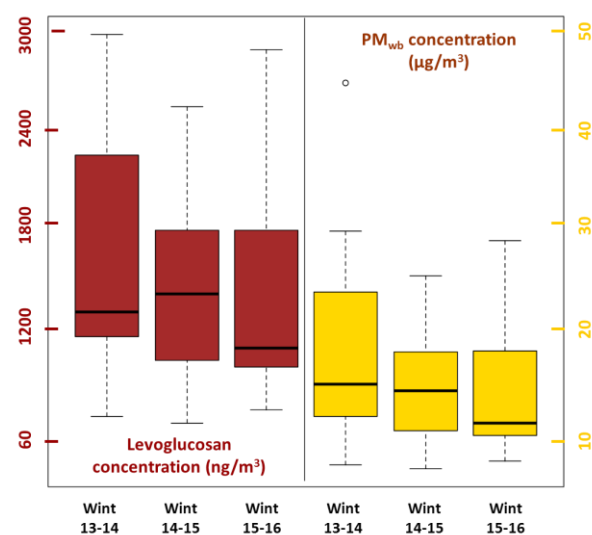


Figure 1. Evolution of levoglucosan and PMwb (wb: wood burning) concentrations in Passy for days without temperature inversions and with an average temperature ranging between -2 and 4°C (≈20 days/winter).

This work is supported by the Agency for the Environment and Energy Management (ADEME) with the DECOMBIO program (1362C0028).

Bonvalot L. *et al.* (2016) *Atmos. Chem. Phys.* **16**, 13753-13772.

EMEP/EAA air pollutant emission inventory guidebook (2013)

Chemel, C *et al.* (2016) *Atmos. Environ.* **128**, 208-215.

Pacy A. *et al.* (2016) *Pollution Atmosphérique*, 231-232.

## High PM<sub>1</sub> emissions from savannah and grassland fires in southern Africa

V. Vakkari<sup>1</sup>, J.P. Beukes<sup>2</sup>, K. Jaars<sup>2</sup>, M. Josipovic<sup>2</sup>, A.D. Venter<sup>2</sup> and P.G. van Zyl<sup>2</sup>

<sup>1</sup>Finnish Meteorological Institute, Research and Development, FI-00101 Helsinki, Finland.

<sup>2</sup>North-West University, Unit for Environmental Sciences and Management, 2520 Potchefstroom, South Africa.

Keywords: biomass burning, emission factor, secondary aerosol, savannah.

Presenting author email: ville.vakkari@fmi.fi

Open biomass burning (BB) is a major source of reactive trace gases and fine particles in the Earth's atmosphere. However, the emissions from wild fires and prescribed burns are highly variable depending on vegetation type and combustion phase of the fire (e.g. Janhäll *et al.*, 2010; Yokelson *et al.*, 2011), which poses a challenge for evaluating their effects on air quality and climate.

We investigated the emission factors and atmospheric evolution of BB smoke in southern Africa utilising continuous measurements at Welgegund, South Africa (26.57°S, 26.94°E, 1480 m above sea level) from 20 May 2010 to 31 December 2015. The measurements at Welgegund included among others aerosol particle number size distribution, CO<sub>2</sub>, CO, BC with a MAAP and basic meteorological parameters. Submicron particulate mass (PM<sub>1</sub>) was estimated from the number size distribution using a constant density of 1.5 g cm<sup>-3</sup>.

Using the methodology of Vakkari *et al.* (2014) we could identify 130 BB plumes over the nearly six year period. For 86 plumes the location of the fire could be identified from MODIS burnt area and/or SEVIRI fire radiative power observations. For these episodes – a total of 267 hours of in-plume sampling – we estimated the plume age based on local wind speed and direction (c.f. Vakkari *et al.*, 2014). For each 10-minute sample in the plumes the excess CO<sub>2</sub>, CO, BC and PM<sub>1</sub> (denoted with a Δ) were calculated.

For fresh plumes (age < 0.5 h) modified combustion efficiency (MCE) and PM<sub>1</sub> emission factor (EF<sub>PM1</sub>) were calculated following Yokelson *et al.* (2011). For aged BB smoke the ratio of flaming to smouldering was estimated from the ΔBC to ΔCO ratio: low ΔBC/ΔCO indicates smouldering combustion and high ΔBC/ΔCO designates flaming combustion. Combination of these parameters allowed us to investigate the effects of burning conditions and atmospheric transport on PM<sub>1</sub> mass in BB plumes, both in daylight and in the dark.

In good agreement with previous studies the EF<sub>PM1</sub> was found to be higher approximately factor of 3 for smouldering fires compared to flaming combustion (Figure 1a). Accounting for the MCE, the differences between savannah and grassland EF<sub>PM1</sub> were small.

Under daylight conditions fast secondary aerosol formation was observed in savannah and grassland fire plumes (Figure 1b). The secondary aerosol formation was faster in smouldering-dominated plumes; only the 20% most flaming observed plumes did not exhibit increase in the ΔPM<sub>1</sub> to ΔCO ratio in daylight conditions. In night-time plumes, whether flaming or smouldering, no change was observed in ΔPM<sub>1</sub>/ΔCO

during the first 3-5 hours, highlighting the role of photochemistry in secondary aerosol formation in BB smoke.

In conclusion, after only a few hours transport in daylight most of the PM<sub>1</sub> in savannah and grassland fire plumes is secondary aerosol. At this point the PM<sub>1</sub> yield can vary from 3 g kg<sup>-1</sup> for flaming combustion to > 30 g kg<sup>-1</sup> for smouldering plumes, where initial emissions are higher and also secondary aerosol formation is faster.

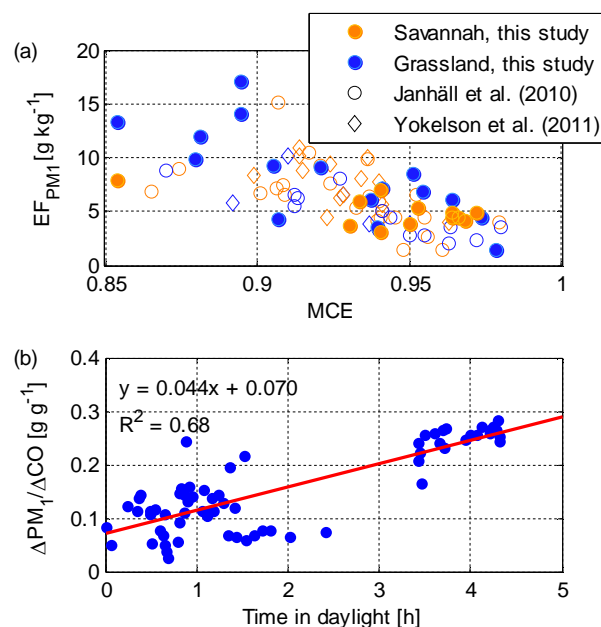


Figure 1. (a) EF<sub>PM1</sub> vs. MCE for fresh (< 0.5 h) savannah and grassland plumes. (b) Daytime temporal evolution of ΔPM<sub>1</sub>/ΔCO for smouldering combustion, i.e. for plumes with ΔBC/ΔCO ranging from 0.005 g g<sup>-1</sup> to 0.01 g g<sup>-1</sup>.

V. Vakkari is beneficiary of an AXA Research Fund postdoctoral grant. Financial support by North-West University (South Africa) is gratefully acknowledged.

Janhäll, S., Andreae, M. O. and Pöschl, U. (2010) *Atmos. Chem. Phys.*, **10**, 1427-1439.

Yokelson, R. J., Burling, I. R., Urbanski, S. P., Atlas, E. L., Adachi, K., Buseck, P. R., Wiedinmyer, C., Akagi, S. K., Toohey, D. W. and Wold, C. E. (2011) *Atmos. Chem. Phys.*, **11**, 6787-6808.

Vakkari, V., Kerminen, V.-M., Beukes, J. P., Tiitta, P., van Zyl, P. G., Josipovic, M., Venter, A. D., Jaars, K., Worsnop, D. R., Kulmala, M. and Laakso, L. (2014) *Geophys. Res. Lett.* **41**, 2644-2651.

## Emissions and short time scale processing of biomass burning examined at the FIREX lab intensive campaign

Ed Fortner<sup>1\*</sup>, Tim Onasch<sup>1</sup>, Leah Williams<sup>1</sup>, Manjula Canagaratna<sup>1</sup>, Wen Xu<sup>1</sup>, Phil Croteau<sup>1</sup>, Scott Herndon<sup>1</sup>, Rob Roscioli<sup>1</sup>, Tara Yacovitch<sup>1</sup>, Conner Daube<sup>1</sup>, Ben Werden<sup>2</sup>, Ezra Wood<sup>2</sup>, Berk Knighton<sup>3</sup>, Jathar Shantanu<sup>4</sup>, Liam Lewane<sup>4</sup>, Abril Galang<sup>4</sup>, Shiva Tarun<sup>4</sup>, Art Sedlacek<sup>5</sup>, John Jayne<sup>1</sup>, Doug Worsnop<sup>1</sup>

<sup>1</sup>Center for Aerosol and Cloud Chemistry, Aerodyne Research Incorporated, Billerica MA, USA

<sup>2</sup>Drexel University, Philadelphia PA, USA

<sup>3</sup>Montana State University, Bozeman MT, USA

<sup>4</sup>Colorado State University, Fort Collins CO, USA

<sup>5</sup>Brookhaven National Laboratory, Upton NY, USA

\*Corresponding Author: [efortner@aerodyne.com](mailto:efortner@aerodyne.com)

Keywords: biomass burning, VOC/nitrate oxidation, combustion, positive matrix factorization, aerosol mass spectrometry

The FIREX Fire Lab Intensive campaign conducted in the fall of 2016 at the USDA Fire Sciences Lab in Missoula, Montana focused on examining emissions and short time scale processing of biomass burning. A reaction chamber was constructed and the biomass burning emissions were directed into the chamber. A variety of controlled reactions were conducted by addition of UV, H<sub>2</sub>O<sub>2</sub>, O<sub>3</sub>, HONO, and NO<sub>x</sub> to the fire emissions in the chamber and the chamber was sampled for a period of 4-6 hours. Approximately 15 different fires were sampled with a variety of different fuels and different controlled reactions in the chamber (Table 1). The Aerodyne Mobile Laboratory (AML) sampled the chamber with a variety of gas phase and particulate phase measurements. Measurements were all on-line providing highly time resolved measurements on the order of seconds for CO, CO<sub>2</sub>, NO<sub>x</sub>, VOC's measured by PTRMS and other VOC's of interest measured by QCL in the gas phase. An iodide-adduct CIMS instrument with a Filter Inlet for Gases and AEROSols (FIGAERO) measured gas and particulate phase species of interest. Particle measurements were conducted with a broad suite of instrumentation including CPC, SMPS, SP2, Grimm OPC, TD-CAPS, E-CHAMP and L-ToF-SP-AMS measurements.

The newly constructed L-ToF-SP-AMS is similar to a conventional SP-AMS instrument but has a ToF chamber twice the length of a conventional HR-ToF-AMS allowing much higher mass resolution. The enhanced resolution allows an improved examination, relative to past studies, of the evolution of the nitrogen cycle during biomass burning. The evolution of particle size and chemical composition in the reaction chamber is examined. Figure 1 illustrates the difference in evolution that may occur depending on the reactions induced in the chamber. Positive Matrix Factorization (PMF) will be applied to the dataset providing different mass spectral signatures for different types of source fuels and oxidation reactions.

This study is part 1 of a combined study including on-line measurements of ambient wildfires with the AML.

Date	Fuel	Chamber Chemistry
7-Oct	Lodgepole Pine	HONO injection
8-Oct	Englemann Spruce Duff	HONO injection
10-Oct	Ponderosa Pine Litter	Lights Only
11-Oct	Douglas Fir Litter	O <sub>3</sub> Injection
12-Oct	Manzanita Clean	H <sub>2</sub> O <sub>2</sub>
13-Oct	Manzanita Dirty	N <sub>2</sub> O <sub>5</sub> Oxidation
14-Oct	Ponderosa Pine	HONO Injection
16-Oct	Ponderosa Pine	Nov HONO Mix Injection
17-Oct	Alpine Fir	N <sub>2</sub> O <sub>5</sub> Oxidation
18-Oct	Englemann Spruce	H <sub>2</sub> O <sub>2</sub>
19-Oct	Douglas Fir	N <sub>2</sub> O <sub>5</sub> Oxidation
20-Oct	Lodgepole Pine	HONO Low NO <sub>x</sub> injection
21-Oct	Sub Alpine Fir	O <sub>3</sub> Injection
22-Oct	Ponderosa Pine	N <sub>2</sub> O <sub>5</sub> Oxidation

Table 1; The fuel type sampled and the controlled reactions initiated for each fire examined with the chamber.

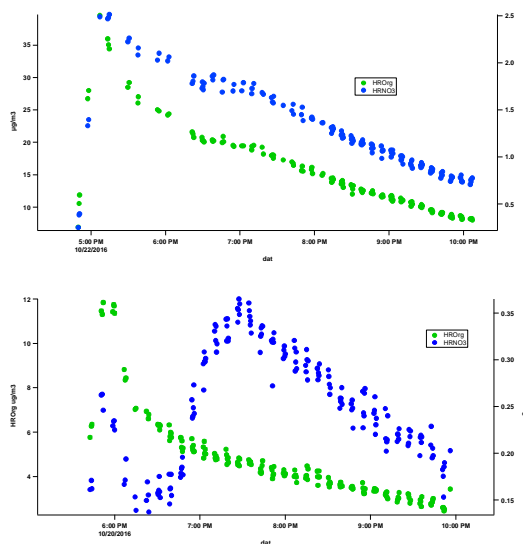


Figure 1; Chemical evolution of organic and nitrate signals obtained with L-ToF-SP-AMS is examined for NO<sub>3</sub> oxidation with NO<sub>x</sub> and O<sub>3</sub> addition (above) and NO<sub>x</sub> only addition (below).

This work was supported by NOAA Atmospheric Chemistry Carbon Cycle and Climate (AC4) NA16OAR4310104

## The contributions of coal, peat and wood burning to ambient PM<sub>2.5</sub>

J. Arndt, P.C. Buckley, I.P. O'Connor, E.J. McGillicuddy, P.C. Buckley, S. Hellebust, J.R. Sodeau, J.C. Wenger

Department of Chemistry and Environmental Research Institute, University College Cork, Ireland

Keywords: solid fuel burning, single particle mass spectrometry, source apportionment

Presenting author email: j.wenger@ucc.ie

During winter months, the levels of fine particulate matter (PM<sub>2.5</sub>) in many small rural towns across Ireland are often considerably higher than those in the cities (EPA, 2013). Although this air quality issue has been attributed to the residential burning of solid fuels, to date, there have been no formal studies to identify the sources of PM<sub>2.5</sub> at these locations. The objective of this work is therefore to identify and quantify the various sources of PM<sub>2.5</sub> in residential areas of small towns in Ireland.

Field measurements were made in three small towns (Killarney, Enniscorthy and Birr) during the winters of 2014-2015 and 2015-2016. An extensive range of instrumentation was deployed at the locations including a single particle mass spectrometer (ATOFMS, TSI model 3800), thermal-optical carbon analyser (Sunset Inc. model 3<sup>rd</sup> generation), TEOM and a 7-wavelength aethalometer (Model AE31, Magee Scientific) for characterisation of PM<sub>2.5</sub>.

At all three sites, a very strong diurnal variation in PM<sub>2.5</sub> mass concentration is observed, which shows a rapid increase during evening hours when local residents burn solid fuel in their homes for heating purposes. The total number of particles detected by ATOFMS shows a similar diurnal pattern. "Fingerprint" mass spectra available in the literature (Healy et al., 2010) have been used to assign the particles to different sources including traffic, coal burning, peat burning and wood burning. The number of counts per hour for each of the ATOFMS particle types has been converted to mass concentration using established scaling procedures (Healy et al., 2012). As an example, the diurnal profile for the particle types detected in Killarney is shown in Figure 1.

The results indicate that particles from combustion of all three fuel types were present in all three towns, with *Peat* particles accounting for 31%, 27% and 26% of PM<sub>2.5</sub> mass in Killarney, Enniscorthy and Birr respectively. *Wood* was the second dominant combustion source (17%, 21% and 23%), followed by *Coal* (16%, 17% and 5%). Combined particle classes which were confidently assigned to domestic solid fuel combustion contributed an estimated 72%, 82% and 60% of PM<sub>2.5</sub> (as measured by TEOM) in Killarney, Enniscorthy and Birr respectively.

The results of this study thus confirm that the contribution of solid fuel burning to PM<sub>2.5</sub> in these small towns is considerably higher than that observed in Cork city, where a value of around 50% was observed (Kourtchev et al., 2011; Dall'Osto et al., 2013). Furthermore, since all three solid fuels make a sizeable contribution, measures such as the proposed nationwide ban on bituminous coal may therefore only be partly

successful in reducing PM<sub>2.5</sub> concentrations. Future efforts to improve air quality in these towns, and others like them, will need to address how domestic residences are heated in general, rather than attempting to discourage use of one specific fuel.

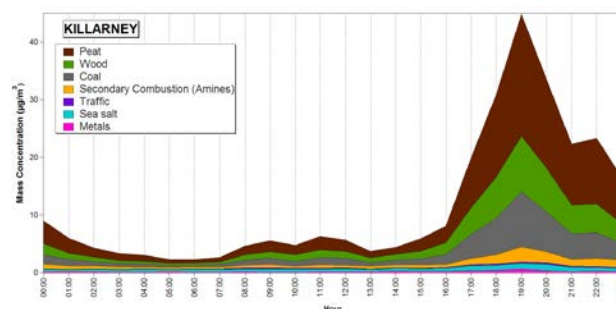


Figure 1. Diurnal profile of particle types (mass concentration) detected by ATOFMS in Killarney.

This research was supported by the Environmental Protection Agency and Department of Environment Community and Local Government in Ireland through the SAPHIRE project (2013-EH-MS.15).

- Dall'Osto, M., Ovadnevaite, J., Ceburnis, D., Martin, D., Healy, R.M., O'Connor, I.P., Kourtchev, I., Sodeau, J.R., Wenger, J.C., O'Dowd, C. (2013) *Atmos. Chem. Phys.* **13**, 4997-5015.
- EPA (2014) *Air Quality in Ireland 2013*, The Environmental Protection Agency, Ireland.
- Healy, R.M., Hellebust, S., Kourtchev, I., Allanic, A., O'Connor, I.P., Bell, J.M., Wenger, J.C., Sodeau, J.R. (2010) *Atmos. Chem. Phys.* **10**, 9593-9613.
- Healy, R.M., Sciare, J., Poulain, L., Kamili, K., Merkel, M., Müller, T., Wiedensohler, A., Eckhardt, S., Stohl, A., Sarda-Estève, R., McGillicuddy, E., O'Connor, I.P., Sodeau, J.R. & Wenger, J.C. (2012). *Atmos. Chem. Phys.* **12**, 1681–1700.
- Kourtchev, I., Hellebust, S., Bell, J.M., O'Connor, I.P., Healy, R.M., Allanic, A., Healy, D.A., Wenger, J.C., Sodeau, J.R. (2011) *Sci. Tot. Environ.*, **409**, 2143-2155.

## SOA Formation and Particle Characteristics in the Emissions from Biomass Cook Stoves Used in the Developing Countries

C. Andersen<sup>1</sup>, R. Lindgren<sup>2</sup>, R.L. Carvalho<sup>2</sup>, V.B. Malmberg<sup>1</sup>, E. Ahlberg<sup>3</sup>, N.G. López<sup>2</sup>, A.C. Eriksson<sup>1</sup>, T.B. Kristensen<sup>3</sup>, B. Svenningsson<sup>3</sup>, C. Boman<sup>2</sup> and J. Pagels<sup>1</sup>

<sup>1</sup>Ergonomics and Aerosol Technology, Lund University, SE-22100, Lund, Sweden

<sup>2</sup>Thermochemical Energy Conversion Laboratory, Umeå University, SE-90187, Umeå, Sweden

<sup>3</sup>Department of Physics, Lund University, SE-22100, Lund, Sweden

Keywords: cook stoves, atmospheric aging, biomass, SOA

Presenting author email: christina.andersen@design.lth.se

Air pollution poses a challenge to both health and climate. Globally around 7 million people die each year due to diseases caused by exposure to air pollution (WHO, 2012). UNICEF recently reported that 600 000 of these are children under the age of five and millions more suffer from respiratory diseases (Rees, 2016). Domestic burning of solid fuels for cooking and heating is a major contributor to these numbers. Detailed particle emission characteristics including effects of atmospheric processing is, however, largely missing for these types of stoves.

As part of The Salutary Umeå Study on Aerosols IN Biomass Cook Stove Emission (SUSTAINED), we studied the emissions from a number of biomass cook stoves and characterized fresh and aged aerosol particles using high resolution aerosol mass spectrometry (AMS).

Cook stoves of different technological advancement, were tested using an adjusted procedure of the standardised water boiling test. A range of wood logs and pelletized biomass fuels were used. Highly time-resolved analysis of transient emissions over the cooking cycle, was performed. Additionally full batch emissions were transferred to a 15 m<sup>3</sup> stainless steel chamber to investigate the impacts of atmospheric aging by passing the aerosol through an oxidation flow reactor (PAM [OH] ~ 1 × 10<sup>8</sup> molecules cm<sup>-3</sup> h<sup>-1</sup>). A SP-AMS (Onasch *et al.*, 2012) was used to measure the non-refractory and refractory particle composition including particle phase PAHs. A seven wavelength aethalometer was used to derive equivalent black carbon (BC) mass concentrations and Angstrom Exponents (AAE). SMPS, and DMS were used to study size distributions. Gas phase compounds were measured on-line by FTIR spectroscopy (major combustion gases) and FID (total hydrocarbons) as well as by Tenax tubes sampling for subsequent analysis of volatile organic compounds. Emission factors (EF; in units g/kg<sub>fuel</sub>) using common wood based fuels were calculated on the basis of AMS, aethalometer and CO<sub>2</sub> measurements.

We give preliminary results of BC and OA PM<sub>1</sub> EFs of the tested stoves based on 3-4 replicates using wood based fuels for each case. The highest EFs of 0.5 ± 0.3 and 1.2 ± 0.4 g/kg<sub>fuel</sub> for BC and OA (uncertainty given as ±1 std. dev. of the batch mean values), respectively, were attributed to the 3-stone fire. The rocket stove (using sticks) and a gasifier

stove (using pellets) have BC and OA EFs of 0.6 ± 0.3, 0.6 ± 0.7, 0.2 ± 0.1 and 0.1 ± 0.1 g/kg<sub>fuel</sub>, respectively. This indicates that the EFs, of carbonaceous aerosols decrease with increasing technological advancement of the stove i.e. more complete combustion. For comparison, a total PM emission factor for a conventional Swedish wood stove has been reported to be 0.8-1.6 g/kg dry fuel (Eriksson *et al.*, 2014), for which smoke is emitted to ambient air. The tested cook stoves will typically be applied indoors with no chimney and can therefore contribute to substantial indoor air pollution levels.

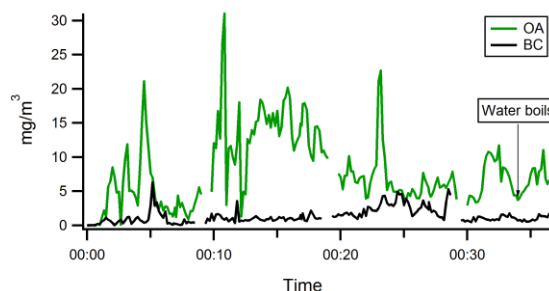


Figure 1. AMS transient measurement of organic aerosol (OA) and BC from a 3-stone fire batch. Fire initiated at t=0.

Aging of aerosols in the flow reactor at an OH exposure corresponding to atmospheric aging of 3 days (assuming a 24 h OH conc. of 1.5 × 10<sup>6</sup> molecules cm<sup>-3</sup>) resulted in an OA enhancement (OA<sub>enh</sub>) of a factor of 1.2 ± 0.3 and 1.6 ± 0.5 for the three stone and rocket stove, respectively. The OA<sub>enh</sub> is lower than reported for conventional wood stoves for heating. However, given the reported high global primary emissions from cook stoves, their SOA potential will most probably also make a substantial contribution to the global OA atmospheric loading.

This work was supported by the Swedish Research Council Formas.

Rees, N. (2016). Clear the air for children: the impact of air pollution on children (UNICEF).

Onasch, T.B. et al. (2012) *Aerosol Science and Technology*, 46(7), 804-817.

Eriksson, A. C. et al. (2014). *Environmental science & technology*, 48(12), 7143-7150.

## Regional Influence of Wildfires on Atmospheric Aerosol in the Western US and Insights into Emission and Aging of Biomass Burning Organic Aerosol

Q. Zhang<sup>1,2</sup>, S. Zhou<sup>1</sup>, S. Collier<sup>1</sup>, D. Jaffe<sup>3</sup>, J. Hee<sup>3</sup>, N. Wigder<sup>3</sup>, T. Onasch<sup>4</sup>, L. Kleinman<sup>5</sup>, A. Sedlacek<sup>5</sup>

<sup>1</sup>Department of Environmental Toxicology, University of California, Davis, USA

<sup>2</sup>Department of Environmental Science and Engineering, Fudan University, Shanghai, China

<sup>3</sup>School of Science and Technology, University of Washington, Bothell, USA

<sup>4</sup>Aerodyne Research Inc., Billerica, USA

<sup>5</sup>Brookhaven National Laboratory, Upton, USA

Keywords: Biomass burning emissions, organic aerosol, BBOA, AMS

Presenting author email: [dkwzhang@ucdavis.edu](mailto:dkwzhang@ucdavis.edu)

Biomass burning (BB) is one of the most important contributors to atmospheric aerosols on a global scale and wildfires are a large source of emissions that impact regional air quality and global climate. The environmental impacts of BB emissions are strongly correlated with the chemical, optical, and microphysical properties of BB aerosols, which are in turn dependent in a complex manner on fuel type, combustion phase, and atmospheric aging of emitted particles and gas species.

In this study, the regional and nearfield influences of wildfire emissions on ambient aerosol concentration and chemical properties in the Pacific Northwest region of the United States were studied using real-time measurements from a fixed ground site located in Central Oregon (~2700 m a.s.l.) as well as near their sources using an aircraft in summer 2013 during the DOE Biomass Burning Observation Project (BBOP) field campaign. Using an Aerodyne High Resolution Time-of-Flight Aerosol Mass Spectrometer (HR-ToF-AMS) coupled with a thermodenuder, we characterized the size resolved composition and volatility profiles of non-refractory submicron aerosol particles (NR-PM<sub>1</sub>) during periods affected by transported BB emissions. Episodes of high concentrations of NR-PM<sub>1</sub> were observed, during which organic aerosol (OA) dominated the PM composition along with elevated levels of anhydrosugar (e.g., levoglucosan). The regional characteristics of biomass burning aerosols were found to depend strongly on the modified combustion efficiency (MCE), an index of the combustion processes of a fire. Organic aerosol emissions had negative correlations with MCE, whereas the oxidation state of organic aerosol increased with MCE and plume aging (Collier *et al.*, 2016). Based on Positive Matrix Factorization (PMF) of the HR-AMS data, three types of BB organic aerosol (BBOA) were identified, including a fresh, semivolatile BBOA-1 (O/C = 0.35; 20% of OA mass) that correlated well with ammonium nitrate, an intermediately oxidized BBOA-2 (O/C = 0.60; 17% of OA mass), and a highly oxidized BBOA-3 (O/C = 1.06; 31% of OA mass) that showed very low volatility with only ~40% mass loss at 200°C. The remaining 32% of the OA mass was attributed to a BL-OOA (O/C = 0.69) representing oxygenated OA influenced by BL dynamics and a low-volatility oxygenated OA (LV-OOA; O/C =

1.09) representing regional free troposphere aerosol. The mass spectrum of BBOA-3 resembled that of LV-OOA and had negligible contributions from the HR-AMS BB tracer ions – C<sub>2</sub>H<sub>4</sub>O<sub>2</sub><sup>+</sup> (*m/z* = 60.021) and C<sub>3</sub>H<sub>5</sub>O<sub>2</sub><sup>+</sup> (*m/z* = 73.029). This finding highlights the possibility that the influence of BB emission could be underestimated in regional air masses where highly oxidized BBOA (e.g., BBOA-3) might be a significant aerosol component. We also examined OA chemical evolution for persistent BB plume events originating from a single fire source and found that longer solar radiation led to higher mass fraction of the chemically aged BBOA-2 and BBOA-3 and more oxidized aerosol. However, an analysis of the enhancement ratios of OA relative to CO (ΔOA/ΔCO) showed little difference between BB plumes transported primarily at night versus during the day, despite evidence of substantial chemical transformation in OA induced by photo-oxidation. These results indicate negligible net OA production in photochemically-aged wildfire plumes observed in this study, for which a possible reason is that SOA formation was almost entirely balanced by BBOA volatilization (Zhou *et al.*, 2016).

This work was supported by US Department of Energy (DOE) Atmospheric System Research (ASR) Program (DE-SC0014620 and DE-SC0007178).

### References

Collier, S., Zhou, S., Onasch, T., Jaffe, D., Kleinman, L., Sedlacek, A., Briggs, N., Hee, J., Fortner, E., Shilling, J. E., Worsnop, D., Yokelson, R. J., Parworth, C., Ge, X., Xu, J., Butterfield, Z., Chand, D., Dubey, M. K., Pekour, M., Springston, S., and Zhang, Q.: Regional influence of aerosol emissions from wildfires driven by combustion efficiency: Insights from the bbop campaign, *Environmental Science and Technology*, 50, 8613–8622, 10.1021/acs.est.6b01617, 2016.

Zhou, S., Collier, S., Jaffe, D. A., Briggs, N. L., Hee, J., Sedlacek, A. J., Kleinman, L., Onasch, T. B., and Zhang, Q.: Regional influence of wildfires on aerosol chemistry in the western us and insights into atmospheric aging of biomass burning organic aerosol, *Atmos. Chem. Phys.* (in press), 10.5194/acp-2016-823, 2016.

## Biomass burning fingerprint in Spain using ACSM

M.C. Minguillón<sup>1</sup>, A. Ripoll<sup>1</sup>, X. Querol<sup>1</sup>, A. Alastuey<sup>1</sup>

<sup>1</sup>Institute of Environmental Assessment and Water Research (IDAEA-CSIC), Barcelona, 08034, Spain

Keywords: biomass burning, factor profile, ACSM, air quality.

Presenting author email: mariacruz.minguillon@idaea.csic.es

Ambient aerosols presence in the atmosphere implies adverse effects on human health and influence on climate. Fine particulate matter (PM<sub>1</sub>, particles with an aerodynamic diameter <1 μm) composition may vary widely with location in terms of concentration and chemical composition, but it is known to be mainly comprised of secondary inorganic compounds and carbonaceous aerosols, the latter reaching up to 90% of the mass. One of the main sources of carbonaceous aerosols, whose impact also varies with location, is biomass burning.

Aerosol mass spectrometers have been widely used to address this issue, identifying and quantifying the contribution of biomass burning to the ambient organic aerosol (OA) concentration: BBOA (e.g. Cubison *et al.*, 2011). The mass spectral profile associated to BBOA is characterized by the enhanced signals at  $m/z$  60 and  $m/z$  73 from the ions C<sub>2</sub>H<sub>4</sub>O<sub>2</sub><sup>+</sup> and C<sub>3</sub>H<sub>5</sub>O<sub>2</sub><sup>+</sup> (e.g. Alfarra *et al.*, 2007). These signals arise from the presence of levoglucosan and similar species (mannosan, galactosan), resulting from the pyrolysis of cellulose. Despite these common tracers, the BBOA mass spectral profile may vary from site to site (e.g. Ng *et al.*, 2011; <http://cires1.colorado.edu/jimenez-group/AMSsd/>). The present work aims at characterizing the BBOA fingerprint at different urban and non-urban locations in Spain by using an Aerosol Chemical Speciation Monitory (ACSM, Aerodyne Research Inc.).

Five sampling campaigns were carried out using an ACSM for the identification and quantification of the BBOA at different sites of Spain. Two non-urban locations were studied: Montseny regional background site (Minguillón *et al.*, 2015) and Montsec continental background site (Ripoll *et al.*, 2015), both located in northeast Spain. Two big cities were selected as urban locations: Barcelona in northeast Spain, and Granada in south Spain. Finally, one small city in northeast Spain, highly influenced by biomass burning emissions, was also selected for the study: Manlleu (see Table 1).

Table 1. Sampling sites, type and sampling period.

Site	Type	Sampling period
Montsec	Continental	Jul 2011-Apr 2012
Montseny	Regional	Jun 2012-Jul 2013
Barcelona	Urban (big)	May 2014-May 2015
Granada	Urban (big)	Dec 2015-Feb 2016
Manlleu	Urban (small)	Dec 2016-Feb 2017

The organic mass spectral data matrix from the ACSM was used to carry out the source apportionment of OA applying Positive Matrix Factorization (PMF)

using the Multilinear Engine (ME-2) with the toolkit SoFi (Canonaco *et al.*, 2013).

All BBOA mass spectral profiles shared the aforementioned tracers at  $m/z$  60 and  $m/z$  73, whereas the degree of oxidation, traced by the intensity of the  $m/z$  44 peak, was different among sites. See example of the mass spectral profiles found at Montseny and Granada in Figure 1. While Montseny BBOA profile correspond to an intense wild fire episode, and was separated from the oxidized OA present during that episode; the Granada BBOA includes a non-negligible portion of oxidized material, as shown by the relatively high intensity of  $m/z$  44 signal.

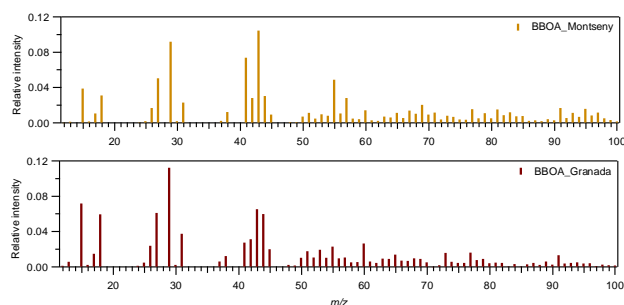


Figure 1. Mass spectral profiles of the BBOA sources found at Montseny and Granada.

This work was supported by the Spanish Ministry of Economy and Competitiveness and FEDER funds (CGL2012-39623-C02-1); the Spanish Ministry of Agriculture, Food and the Environment; the EU 7<sup>th</sup> Framework Programme through ACTRIS (grant agreement 262254); the H2020 through ACTRIS-2 (grant agreement 654109); the Andalusia Regional Government (project P12-RNM-2409); and the Generalitat de Catalunya (AGAUR 2014 SGR33). M.C. Minguillón acknowledges the Ramón y Cajal fellowship awarded by the Spanish Ministry of Economy, Industry and Competitiveness.

- Alfarra, M.R., Prevot, A.S.H., Szidat, S., *et al.* (2007) *Environ. Sci. Technol.* **41**, 5770-5777.
- Canonaco, F., Crippa, M., Slowik, J.G., *et al.* (2013) *Atmos. Meas. Tech.* **6**, 3649-3661.
- Cubison, M. J., Ortega, A. M., Hayes, P. L., *et al.* (2011) *Atmos. Chem. Phys.* **11**, 12049-12064.
- Minguillón, M.C., Ripoll, A., Pérez, N. *et al.* (2015) *Atmos. Chem. Phys.* **15**, 6379-6391.
- Ng, N.L., Canagaratna, M.R., Jimenez, J.L., *et al.* (2011) *Environ. Sci. Technol.* **45**, 910-916.
- Ripoll, A., Minguillón, M. C., Pey, J., *et al.* (2015) *Atmos. Chem. Phys.* **15**, 2935-2951.

## Measurement of the volatility distribution of emission factor from biomass burning

Y. Fujitani\*, K. Sato, A. Fushimi, K. Tanabe, Y. Kondo, Y. Morino, S. Kobayashi and A. Takami

National Institute for Environmental Studies, Tsukuba, Japan

Keywords: Volatility distribution, Primary organic aerosols, Dilution method, Emission factor  
Presenting author email: fujitani.yuji@nies.go.jp

The volatility distribution of emission factor (EF) (Donahue et al., 2006) for combustion sources is improving inventory of PM<sub>2.5</sub> and it enables air quality model to predict properly atmospheric organic aerosol concentrations (C<sub>OA</sub>). However, the data is shortage especially on characteristic sources in Asia. We measured emissions from combustions of rice straw and bare Japanese cherry branch (O.D. is less than 5 mm).

Experimental conditions were listed in Table 1. From modified combustion efficiency (MCE) and observation, the flaming burning was dominated. The burning material was set in the wood stove with covering a stainless steel hood. During burning process, exhaust was withdrawing from top surface of hood by the ejector (DI-1000, Dekati) and diluted exhaust was introduced into the 6-m<sup>3</sup> PFA chamber. Then, the diluted exhaust in the chamber was further diluted by FPS (Dekati) and distributed to online-instruments. As dilution air, particle- and HC- free clean dry air was used. Dilution ratios (DRs) of chamber air were controlled at ranging from 1 to 78. Temperature of sample air was kept at around 25 °C for any DRs.

Particles were measured by SP-AMS (Aerodyne) and SMPSs (TSI). Wall loss of particle in the chamber was corrected by decay of particle volume of SMPS data. SVOC in gas phase and VOC were measured by PTR-TOF (Ionicon). The fraction ( $X_p$ ) is the ratio of C<sub>OA</sub> to the total (SVOC in gas phase + C<sub>OA</sub>) concentration. SVOC in gas phase at DR = 1 was used the data of PTR-TOF at DR=1 and SVOC was regarded as the sum of concentration of organic species of saturation concentration (C\*) for log C\* = 0 to -2. SVOC in gas phase at a given DR was calculated as follow;

$$SVOC_{DR} = C_{OA,DR=1} / DR - C_{OA,DR} + SVOC_{DR=1} / DR$$

Figure 1 shows the relationship between C<sub>OA</sub> and  $X_p$  and that was used to determine EF of particle phase for log C\* = -4 to 4 according to Presto and Donahue (2006). The PTR-TOF data were used to derive gas phase for log C\* = 0 to 9 using relationship between molar mass and C\* of organic species. The particle phase in each volatility bin was calculated for partitioning theory. Then, data of PTR-TOF and SP-AMS was combined by comparing for the volatility bin that was overlapped range of particle phase (log C\* = 0 to 4). Finally, the relative distribution was obtained for log C\* = -2 to 6.

Figure 2 showed the distributions obtained in this study and wood burning (Grieshop et al. 2009) for reference. Volatility distributions and EF for rice straw were influenced by the water content. Distribution for branch burning was different from that for wood burning. This result indicated that experiments in various conditions are needed to obtain typical data.

Table 1 Experimental conditions. Water content in wet condition was 16.7 wt%. EF was determined from particle mass of Teflon filter sample for the chamber air.

	Amount of burned [g]	MCE	EF of particle phase [g/kg-dry weight]
Rice straw (Dry)	40	0.93	6.9
Rice straw (Wet)	47	0.89	12.6
Branch (Dry)	93	0.95	4.9

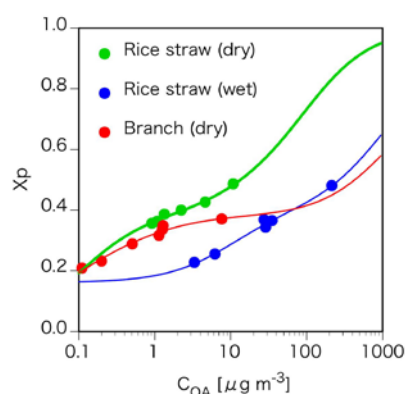


Figure 1 Fraction of particle phase and fitting data.

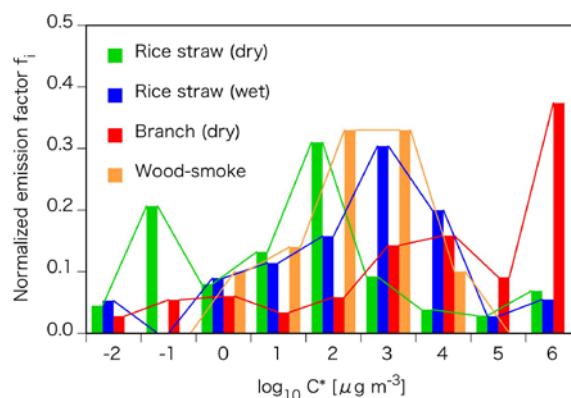


Figure 2. Volatility distribution of biomass burning determined by online-instruments.

### References

- Donahue N.M. et al. (2006) *Environ. Sci. Tech.* **40**, 2635-2643.  
Grieshop, A. P. et al. (2009) *Atmos. Chem. Phys.*, **9**, 1263-1277.  
Presto, A. A. and Donahue, N. M. (2006). *Environ. Sci. Tech.* **40**, 3536-3543.

### Acknowledgements

Part of this research was supported by the Environment Research and Technology Development Fund (5-1506) of the Ministry of the Environment, Japan.

## Near-field changes to the optical and chemical properties of biomass burning particles

T. B. Onasch<sup>1</sup>, J. Wormhoudt<sup>1</sup>, A. Sedlacek<sup>2</sup>, L. Kleinman<sup>2</sup>, E. Fortner<sup>1</sup>, J. Shilling<sup>3</sup>, M. Pekour<sup>3</sup>,  
D. Chand<sup>3</sup>, S. Collier<sup>4</sup>, Q. Zhang<sup>4</sup>, R. Yokelson<sup>5</sup>, K. Adachi<sup>6</sup>, P. Buseck<sup>7</sup>, L. Williams<sup>1</sup>, A. Freedman<sup>1</sup>

<sup>1</sup>Aerodyne Research, Inc., Billerica, MA

<sup>2</sup>Brookhaven National Laboratory, Upton, NY,

<sup>3</sup>Pacific Northwest National Laboratory, Pasco, WA

<sup>4</sup>University of California, Davis, CA

<sup>5</sup>University of Montana, Missoula, MT

<sup>6</sup>Meteorological Research Institute, Japan;

<sup>7</sup>Arizona State University, Tempe, AZ

Keywords: Biomass burning, aerosol chemistry, optical properties

Presenting author email: onasch@aerodyne.com

Rapid physical, chemical and optical changes in biomass burning particles were measured downwind (< 3 hours temporally) from wildland fires. The Biomass Burning Observation Project (BBOP), sponsored by the U.S. Department of Energy (DOE), involved the measurement of emissions from wildland fires in the Pacific Northwest and agricultural burns in the Central Southeastern United States observed from the DOE Gulfstream-1 airborne platform over a four month period in 2013.

Optical instrumentation included a CAPS PMex particle extinction monitor operating at 630 nm (Aerodyne Research), a photothermal interferometer (Brookhaven National Laboratory) measuring particle absorption at 632 nm and a 3 wavelength nephelometer (TSI). Information about the chemical evolution of the plumes was obtained primarily using a SP-AMS (Aerodyne Research) and a Single Particle Soot Photometer (SP2, Droplet Measurements).

The chemical composition of the particulate emissions were characterized in the context of the fire location, combustion conditions, and optical property measurements, including extinction and single scattering albedos. Figure 1a shows the chemical composition of organic aerosol was found to be rapidly changing as a function of downwind location, with oxygen to carbon ratios increasing as a result of atmospheric aging processes (e.g., dilution, photochemistry). The single scattering albedo, (SSA) of plume aerosols increases downwind (Figure 1b) as the ratio of total particle extinction to carbon monoxide concentration (a marker for the plume dilution) increases, a finding that is related to changes in organic aerosol chemistry.

This work focuses on the near-field observations from the BBOP study within the context of the recent results from Collier et al. (2016) and Shan et al. (2016) that looked in detail at the regional influences of the wildland fires in the Pacific Northwest measured from the Mt. Bachelor Observatory in central Oregon.

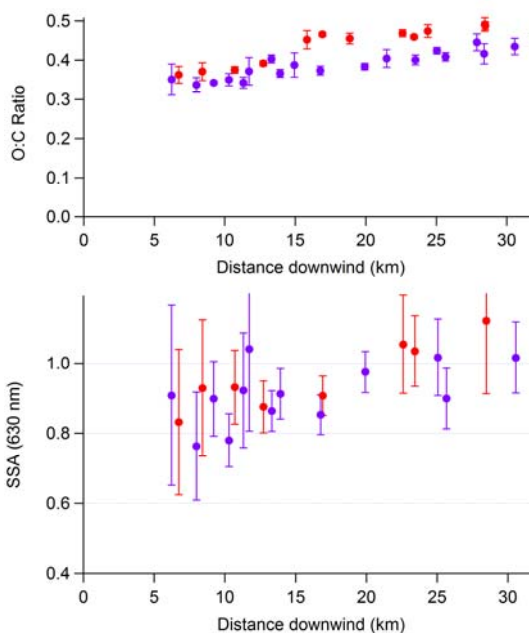


Figure 1. The measured changes in the O:C ratio and SSA (630 nm) of the biomass burning aerosol downwind of the Colockum Tarp wildland fire.

This work was supported by the Department of Energy ARM facility and Atmospheric Systems Research program.

Collier, S., Zhou, S., Onasch, T. B., *et al.* (2016) *Environ. Sci. Technol.* **50**, acs.est.6b01617.

Zhou, S., Collier, S., Jaffe, D. A., Briggs, N. L., Hee, J., Sedlacek III, A. J., Kleinman, L., Onasch, T. B., and Zhang, Q.: (2016) *Atmos. Chem. Phys. Discuss.*, doi:10.5194/acp-2016-823.

## Particle pollution from wood burning in mainland UK: a six-year national assessment

Anna Font<sup>(1)</sup>, David Green<sup>(1)</sup>, David Butterfield<sup>(2)</sup> and Gary W. Fuller<sup>(1)</sup>

<sup>1</sup>MRC-PHE Centre for Environment and Health, King's College London, SE1 9NH, UK

<sup>2</sup>National Physical Laboratory, Teddington, TW11 0LW, UK

Keywords: Urban aerosol, black carbon, wood / biomass burning.

Presenting author email: gary.fuller@kcl.ac.uk

### Introduction

Substantial growth in biomass combustion is anticipated due to policy initiatives aimed at increasing production of heating and electricity from renewable and low-carbon energy sources. These policies include the Renewable Heat Incentive, Feed-in Tariffs and the Merton Rule for on-site renewable heating in new buildings. A recent UK government survey (Walters, 2016) found that 7.5% of UK homes now burn wood.

There is concern that these changes might lead to increases in ambient particulate matter (PM) concentrations in the UK, especially from home heating. There is considerable uncertainty about the frequency of fire use, the balance between stoves and fireplaces and therefore the total emission. Earlier work in London found that the PM<sub>10</sub> from home wood burning in 2010 exceeded the PM<sub>10</sub> reductions from the first two phases of the London Low Emission Zone (Fuller et al 2014).

### Method

PM from wood burning was measured from the difference between the UV and IR absorption of airborne particles sampled by Aethalometers in Defra's UK automated black carbon measurement network. The study comprised 17 cities and 4 rural locations between 2009 and 2016. Wood burning was estimated using the Sandradewi et al (2008) method with coefficients from Fuller et al (2014).

### Results

As expected, PM from wood burning was greatest in winter and almost absent in summer. Concentrations were greatest in evenings and at weekends indicating residential combustion (Figure 1). The mean wintertime PM from wood burning varied between cities, from 0.2  $\mu\text{g m}^{-3}$  to 2.7  $\mu\text{g m}^{-3}$ . Most cities had a poor to moderate correlation between winter temperature and wood burning PM ( $R^2$ : 0.12 - 0.57). At one rural location,  $R^2$  was 0.76. Trends in wintertime wood burning over the seven winter's studied were either not significant or slightly downwards. The largest downward trend was 0.4  $\pm$  0.9  $\mu\text{g m}^{-3}$ .

### Conclusions

UK wood burning was 2 to 13% of winter PM<sub>10</sub> concentrations; and 3 to 17% of PM<sub>2.5</sub> (Figure 1). Greater concentrations during weekend evenings, when compared with weekdays, and the poor to moderate

correlation with temperature suggests that a large component of wood burning was decorative and that wood burning was not being used as primary heating.

No significant trend was seen. This might be due to the replacement of traditional fireplaces with lower emission wood stoves or milder windier winters at the end of the study period.

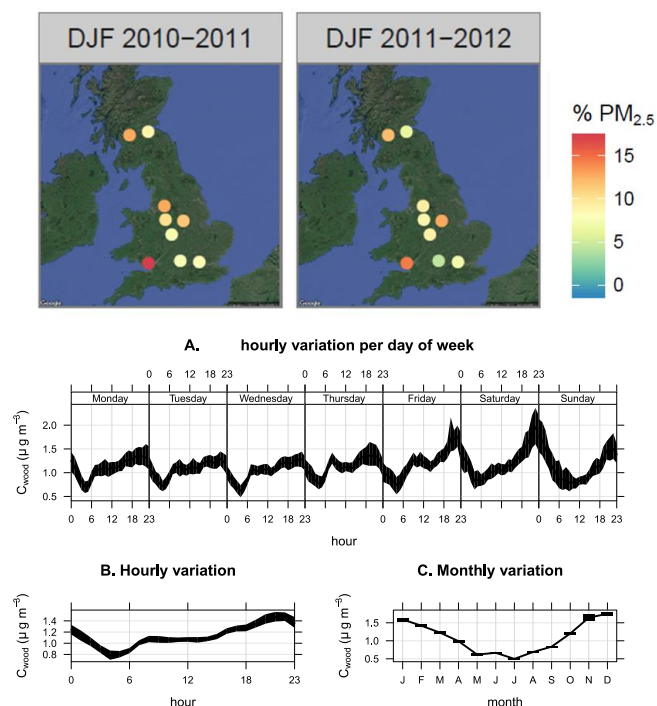


Figure 1. Upper panels show wintertime PM from wood burning as a percentage of PM<sub>2.5</sub>. Lower panels show PM from wood burning in Manchester averaged by hour, day and month.

### Acknowledgement

This work was funded by the UK Department for the Environment Food and Rural Affairs (Defra).

### References

- Fuller et al (2014). Atmos Env, 87,87-94.
- Sandradewi, et al. 2008. ES&T, 42(9), 3316-3323.
- Walters (2016), DECC, London.

## Identification of volatile organic compounds from small-scale wood combustion and their potential as secondary organic aerosol precursors

A. Hartikainen<sup>1</sup>, P. Tiitta<sup>1</sup>, P. Yli-Pirilä<sup>1</sup>, A. Leskinen<sup>2,3</sup>, M. Kortelainen<sup>1</sup>, J. Orasche<sup>4</sup>, R. Zimmermann<sup>4</sup>, J. Jokiniemi<sup>1</sup>, and O. Sippula<sup>1</sup>

<sup>1</sup>Department of Environmental and Biological Sciences, University of Eastern Finland, P.O. Box 1627, Kuopio, FI-70211, Finland

<sup>2</sup> Department of Applied Physics, University of Eastern Finland, Kuopio, FI-70211, Finland

<sup>3</sup>Finnish Meteorological Institute, P.O. Box 1627, FI-70211 Kuopio, Finland

<sup>4</sup>Joint Mass Spectrometry Centre, CMA-Comprehensive Molecular Analytics, Helmholtz Zentrum München, Neuherberg 85764, Germany

Keywords: atmospheric aging, volatile organic compounds, wood combustion, secondary organic aerosol  
Presenting author email: anni.hartikainen@uef.fi

Gaseous and particulate emissions from small scale wood combustion cause significant health and environmental effects. These effects are influenced by atmospheric reactions, which transform the initial fresh emission. During dark aging, i.e., when no sunlight is available, the reactions initiated by ozone (O<sub>3</sub>) or nitrate radicals (NO<sub>3</sub>) dominate the decay of volatile organic compounds (VOCs) and the formation of secondary organic aerosol (SOA). Photochemical aging, on other hand, consists primarily of reactions with hydroxyl radicals (OH) and O<sub>3</sub>, in addition to photolysis. While VOCs degrade, growth of SOA may increase the particulate emission.

We investigated both dark and photochemical aging of small scale wood combustion emission, and assessed the potential of emitted VOCs to act as precursors of SOA. To simulate the varying combustion conditions, modern logwood stove loaded with spruce logs was ignited with two distinct patterns, with slower ignition induced by larger kindling. Emission from the first batch was led to the 29m<sup>3</sup> smoke chamber (Leskinen et al. 2015), where the sample was exposed to ambient-like UV-light. In three out of the five experiments a four-hour dark aging period preceded the photochemical aging. The extent of photochemical aging was determined with decay of butanol-d<sub>9</sub> (Barnet et al. 2012) and reached up to 18 hours.

Gaseous and particulate phases in the chamber were extensively and continuously monitored with on- and offline instruments. VOCs were measured with a Proton-Transfer-Reactor Time-of-Flight Mass Spectrometer (PTR-ToF-MS). Compounds were identified based on ions' mass-to-charge-ratio (m/z), and grouped by chemical composition. Slower ignition emitted significantly larger concentrations of nearly all compounds: for example, the emissions of phenols, furans and aliphatic hydrocarbons increased by factors of 2.4, 2.6, and 2.4, respectively. In each case, the primary emission contained a substantial fraction of carbonyls and aromatic species, such as benzene and phenols. The SOA precursor potential was assessed based on literature, while an Aerosol Mass Spectrometer (AMS, Aerodyne Research Inc.) was used to measure the particulate-phase organic aerosol (OA) concentration and composition (Tiitta et al. 2016).

Dark aging decreased concentrations of particularly phenols, furans, and unsaturated aliphatic hydrocarbons (Figure 1). These compounds, along with

benzene, were likely to be the main precursors for the 63-75 % increase of OA during dark aging. Furthermore, dark aging caused formation of larger organic nitrogen compounds, e.g. C<sub>3</sub>H<sub>9</sub>NO, C<sub>3</sub>H<sub>7</sub>NO<sub>2</sub> and nitrophenols (C<sub>6</sub>H<sub>5</sub>NO<sub>3</sub>). Photochemical aging caused decrease in concentrations of most VOCs, excluding small carbonyls. OA was enhanced by 77-115%. The most important precursors for this SOA were aromatic hydrocarbons and phenols.

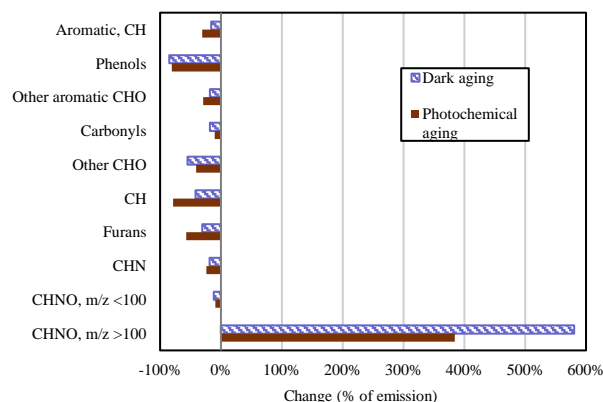


Figure 1. Change in mass concentration during dark and photochemical aging.

Comparison between slow and fast ignition showed similar relative changes of VOCs, but clearly larger absolute emission and SOA from slow ignition. This study provides new information on behaviour of VOCs and SOA precursors from small scale wood combustion, and demonstrates the distinct aging patterns in day- and night-time conditions. The VOCs emitted from small scale wood combustion were shown to transform rapidly in atmospheric conditions, with a variety of decaying compounds identified to contribute to SOA production.

This work was supported by Academy of Finland (Grant: 304459), Doctoral Programme in Environmental Physics, Health and Biology of University of Eastern Finland, and Helmholtz Virtual Institute of Complex Molecular Systems in Environmental Health (HICE).

Barnet et al. (2012) *Atmos. Meas. Tech.* **5**, 647-656.

Leskinen, A., et al. (2015) *Atmos. Meas. Tech.* **8**, 2267-2278.

Tiitta P. et al. (2016) *Atmos. Chem. Phys.*, **16**, 13251-13269.

## Chemical composition of emissions originating from biomass and municipal solid waste burning in a masonry heater

M. Bloss<sup>1</sup>, F. Mylläri<sup>2</sup>, M. Aurela<sup>1,2</sup>, M. Maasikmets<sup>3</sup>, H-L, Kupri<sup>3,4</sup>, K. Vainumäe<sup>3</sup>, P. Simonen<sup>2</sup>, L. Salo<sup>2</sup>, Ville Niemelä<sup>4</sup>, T. Rönkkö<sup>2</sup> and H. Timonen<sup>1</sup>

<sup>1</sup> Atmospheric Composition Research, Finnish Meteorological Institute, Helsinki, 00560, Finland

<sup>2</sup> Aerosol Physics, Faculty of Natural Sciences, Tampere University of Technology, Tampere, 33101, Finland

<sup>3</sup> Air Quality Management Department, Estonian Environmental Research Centre, Tallinn, 10617, Estonia

<sup>4</sup> Dekati Ltd, Tykkitie 1, Kangasala, Tampere, 36240, Finland

<sup>5</sup> Department of Environmental Engineering, Tallinn University of Technology, Tallinn, 19086, Estonia

Keywords: SP-AMS, PAM, SOA, BBOA

Presenting author email: matthew.bloss@fmi.fi

The volume of solid waste generated by cities is expected to be 2.2 billion tonnes by 2025 (Hoorweg *et al.*, 2012). Municipal solid waste (MSW) burning occurs in most countries and its emissions vary in composition depending on the waste being burned and burning conditions. MSW includes household wastes such as food waste, packaging, garden waste as well as industrial and commercial wastes (Wiedinmyer *et al.*, 2014). Management of this waste varies from country to country and for both developed and developing countries. However, in households MSW is often burned along with wood in order to get rid of waste and reduce fuel costs

Burning such wastes releases pollutants into the atmosphere. Burning pure wood releases mainly organic particulate matter into the atmosphere as well as black carbon which forms from the incomplete combustion of biomass. When MSW is added to fires other pollutants are released including toxic compounds such as Polychlorinated Dibenzodioxins/Dibenzofurans (PCDD/F's) (Wiedinmyer *et al.*, 2014).

In this study, pure wood logs or a combination of wood logs and normal household plastic waste were burnt in a fireplace. The fire was lit by the top down method which provides a higher heat from the start reducing the amount of unburnt emissions. After the fire had begun to die down, additional logs were added. The emissions were diluted using a double ejector diluter (Dekati Ltd) after being sampled from the flue gas. The emissions were analysed using a Soot Particle - Aerosol Mass Spectrometer (SP-AMS) (Aerodyne Research Inc) to gain information on the real time particulate mass concentration, chemical composition, size distribution as well as concentrations of refractory BC and some metals. In addition to chemical composition, physical properties (e.g. size distribution, number concentration) of submicron particles and trace gases were measured with a large variety of instruments. The secondary aerosol formation potential was studied using a PAM (Potential Aerosol Mass chamber, Aerodyne Research Inc) chamber which allowed simulation of the atmospheric aging of the emissions.

The aim of this study was to compare primary and secondary emissions originating from biomass burning and from the inclusion of MSW to biomass burning.

However, after analysing individual fragments it was found that the amount of oxidised compounds were increased after the PAM chamber. Many studies provide a variation in results concerning secondary production BBOA emissions (Ortega *et al.*, 2013). This variation can be affected by the type of fuel or its burning conditions which in our case were mostly flaming but also smouldering and ignition.

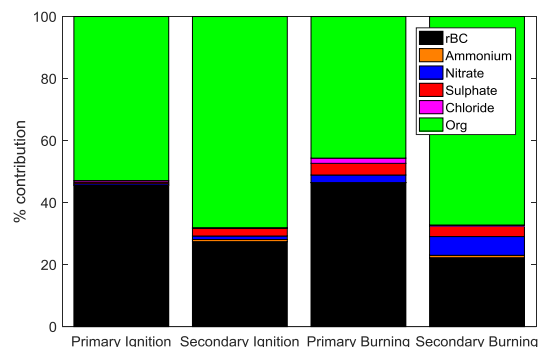


Figure 1. Contribution of inorganics, organics and BC for various measurement scenarios.

Figure 1 shows that during ignition, very little inorganics are present, especially for primary emissions which shows an almost equal distribution between BC and organics. During the burning phase inorganics increase, with a decrease in organics. Organics dominate secondary for both ignition and burning processes. However sulphates were also present, as well as an increase in nitrates during the burning process.

This work was supported by the Estonian Environmental Investment Centre project no. 10627

Hoorweg, D. & Bhada-Tata P. (2012) *What a Waste: A Global Review of Solid Waste Management*, Urban Development Series Knowledge Papers.

Ortega A.M., Day D.A., Cubison M.K., Brune W.H., Bon., de Gouw J.A. & Jimenez J.L. (2013) *Atmos. Chem. Phys.*, **13**, 11551-71.

Wiedinmyer C., Yokelson R.J. & Gullett B.K. (2014) *Environ Sci Technol*, **28**, 9523-30.

## Atmospheric lifetime of biomass burning organic markers: influence of vapor wall losses in smog chamber experiments

A. Bertrand<sup>1</sup>, G. Stefanelli<sup>2</sup>, E. Bruns<sup>2</sup>, S. Pieber<sup>2</sup>, B. Temime-Roussel<sup>1</sup>, A.S.H. Prevot<sup>2</sup>, J. Dommen<sup>2</sup>, J. Slowick<sup>2</sup>, H. Wortham<sup>1</sup>, N. Marchand<sup>1</sup> and I. El Haddad<sup>2</sup>

<sup>1</sup>Aix Marseille Univ, CNRS, LCE, Marseille, France.

<sup>2</sup>Laboratory of Atmospheric Chemistry, Paul Scherrer Institute, 5232, Villigen, Switzerland

Keywords: wood combustion, molecular marker, reactivity, smog chamber  
amelie.bertrand@etu.univ-amu.fr

Biomass burning is a predominant source of primary organic aerosol (POA) in numerous rural and urban sites across Europe. In winter, the reported contributions can reach values as high as 70 %.

Determining with accuracy the contribution of each source is an obligatory step for the implementation of relevant mitigation policies.

Molecular markers are widely used for source apportionment purposes. The chemical resolution from such data set allows for a finer discrimination between the sources. However, the method requires a variety of suitable markers that are specific to a source, or a group of sources and relatively stable in the atmosphere. The latter criteria is still very uncertain.

Levoglucosan is a well-known semi-volatile compound emitted by biomass burning. The concentration of levoglucosan found in the organic aerosol emitted by biomass burning can be significant, especially when it results from combustion of hard and soft type of wood. Initial studies showed levoglucosan was stable in the atmosphere (atmospheric lifetime  $\approx 8 - 10$  days) and as such was the marker of choice for biomass burning in source apportionment. However, recent experiments (Hennigan et al., 2010) conducted in a smog chamber determined a degradation rate of levoglucosan with hydroxyl radicals (OH) of  $1.1 \pm 0.5 \times 10^{-11} \text{ cm}^3 \text{ molec}^{-1} \text{ sec}^{-1}$ , corresponding to an average lifetime of 1.1 days, thus sparking discussion about the implication of its use in source apportionment studies. A potential effect could be the underestimation of the biomass burning contribution to the total PM.

Here, in experiments similar to Hennigan et al., we go further and attempt to retrieve the degradation rate for a variety of other markers emitted by biomass burning, including the isomers of levoglucosan, mannosan and galactosan, as well as a variety of methoxyphenols and PAHs. We also consider the recent development in our knowledge of the influence on measurements of losses by volatile and semi volatiles compounds to the Teflon® wall of the chamber.

The compounds originated from the combustion of beech wood in residential wood stoves. The particulate phase was injected along with the gaseous phase in the mobile smog chamber of the Paul Scherrer Institute (PSI). The PSI mobile smog chamber is a 7 m<sup>3</sup> flexible Teflon® bag. A set of forty UV lamps (1000 Watts) is installed. For the purpose of these experiments, relative humidity was kept at 50 %. The temperature within the chamber was set at 2 °C in order to simulate wintertime

conditions. After injection, the emissions were left static for 30 minutes. Photo-oxidation was then initiated and lasted for 4 to 5 hours under a continuous injection of a nitrous acid (HONO) mixture. A High Resolution – Time of Flight – Aerosol Mass Spectrometer (HR – ToF – AMS) provided the real time concentration of the organic aerosol. The chemical speciation of the organic aerosol was determined with a Thermal Desorption Aerosol Gas Chromatograph (TAG) coupled with an HR-ToF-AMS (TAG-AMS). The TAG-AMS permits the on-line collection and analysis of the aerosol at the molecular level, and with a time resolution within the order of less than an hour. The TAG-AMS used here allows the quantification of the most polar compounds with the implementation of an online derivatization step. Five to seven samples were collected and subsequently analyzed by TAG-AMS.

The numerous collected samples allow us to constrain the different variables implemented in a model to describe in a dynamic manner the different processes involved, including that of reactivity and wall losses, which drive the concentration of our compounds of interest in the condensed phase (Figure 1). The main variable to test for included the mass accommodation coefficient of particle, the loss rate by condensable vapor onto the Teflon® wall, the absorptive organic mass concentration of the wall, the saturation concentration of the compounds, and the rate constant with OH. We test over a large range each of these parameters to determine the best model to measured fits.

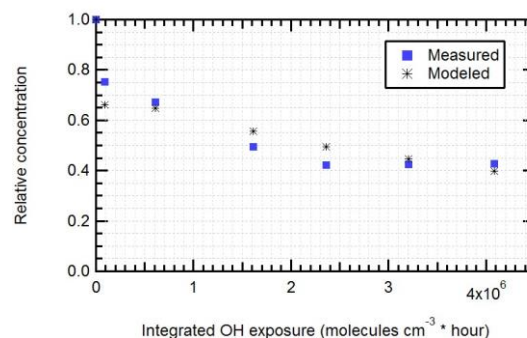


Figure 1. Modeled vs. measured relative concentration of levoglucosan in the particulate phase in the chamber.

Hennigan et al., 2010. Levoglucosan stability in biomass burning particles exposed to hydroxyl radicals: Levoglucosan stability in aerosol. *Geophys. Res. Lett.* 37

## The effects of biomass burning on fine aerosol acidity, liquid water content and nitrogen partitioning

A. Bougiatioti<sup>1,2</sup>, D. Paraskevopoulou<sup>3</sup>, I. Stavroulas<sup>2</sup>, R. Weber<sup>1</sup>, A. Nenes<sup>1,3,4,5</sup>, M. Kanakidou<sup>2</sup>, N. Mihalopoulos<sup>2,3</sup>

<sup>1</sup> School of Earth & Atmospheric Sciences, Georgia Institute of Technology, Atlanta, GA 30332, U.S.A.

<sup>2</sup> ECPL, Department of Chemistry, University of Crete, P.O. Box 2208, 71003 Heraklion, Greece

<sup>3</sup> IERSD, National Observatory of Athens, GR-15236, P. Penteli, Greece

<sup>4</sup> School of Chem. & Biomolecular Engineering, Georgia Institute of Technology, Atlanta, GA 30332, U.S.A.

<sup>5</sup> Institute of Chemical Engineering Sciences (ICE-HT), FORTH, Patras, Greece

Keywords: aerosols, water content, pH, biomass burning

Presenting author email: nmihalo@noa.gr

Aerosol acidity is an important property that influences many processes related to the aerosol chemical composition, gas-aerosol partitioning of semi-volatile species (Surratt et al. 2010) and the formation of secondary particulate matter. It is poorly constrained, mainly due to the fact that it varies considerably between different aerosol types, temperature, RH, atmospheric processing and may also change during transport. Among the various aerosol sources likely to influence aerosol acidity, biomass burning (BB) is one of the less understood, despite its significance on a regional and global scale.

Currently, the lack of a practical and accurate enough method to directly measure the pH of in-situ aerosol, leads to its indirect estimation via the combination of thermodynamic models with targeted experimental measurements. This study uses aerosol chemical composition measurements in conjunction with the ISORROPIA-II thermodynamic equilibrium model (Fountoukis and Nenes, 2007) to predict the aerosol pH for air masses in downtown Athens during winter 2013 in order to evaluate the influence of BB on aerosol acidity and water content. The real-time, quantitative measurements of the main aerosol constituents of submicron aerosol were provided by an Aerosol Chemical Speciation Monitor (ACSM) together with T and RH measured at the site.

As during wintertime the low temperatures favour the use of BB for domestic heating especially during night time, it was found to contribute significantly to increased organics concentration, particulate nitrates, chloride, potassium and black carbon (BC). The average value for total aerosol water was  $15.1 \pm 7.5 \mu\text{g m}^{-3}$  and  $8.5 \pm 3.1 \mu\text{g m}^{-3}$  for BB and non-BB days, respectively. The large difference in LWC is associated with the intense BB activities, contributing significant amounts of  $W_{\text{org}}$ , especially during nighttime.  $W_{\text{org}}$  exhibits a significant diurnal variability with morning and afternoon average mass concentrations being 10-15 times lower than nighttime ones. During daytime  $W_{\text{inorg}}$  appears to be the main component of particle water but during nighttime, the two components appear to have almost the same contribution, especially during no BB influence, which could be attributed to the higher concentration of organics during strong BB influence.

When investigating the fine aerosol acidity, the aerosol was generally acidic, with pH values during important BB influence being the highest ( $2.83 \pm 0.47$ ), while days with no BB influence exhibited lower pH values ( $2.08 \pm 0.23$ ). The reduced activity observed during strong BB influence is attributed to the concurrent presence of non-volatile cations, such as non-sea salt potassium and chloride, as well as the important excess of ammonium compared to sulfates. The lower pH values, in turn, favors the partitioning of the majority of nitrate and chloride to the aerosol phase.

These acidity effects of biomass burning can be also seen in regional and global scales, which could have significant implications for public health, climate and ecosystems.

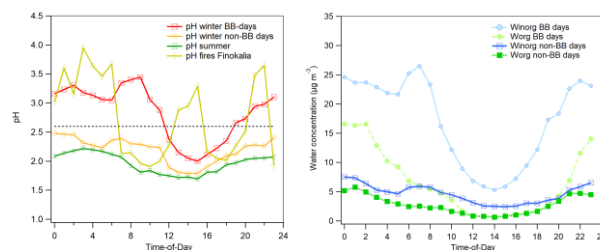


Figure 1. Diurnal profiles as hourly averages of predicted pH (left) and water components (right) BB and non-BB days.

The financial support by the European Union through the ACTRIS-2 Research Infrastructure Action under the Horizon 2020 research and innovation programme (Grant Agreement No 654109) is gratefully acknowledged. AN acknowledges support from the Georgia Power Faculty Scholar Chair and the Cullen-Peck Faculty Fellowship.

Fountoukis, C., and Nenes, A, *Atmos. Chem. Phys.*, **7**, 4639-4659, 2007.

Surratt, J. D., Chan, A. W., Eddingsaas, N. C., Chan, M., Loza, C. L., Kwan, A. J., Hersey, S. P., Flagan, R. C., Wennberg, P. O., and Seinfeld, J. H., *P. Natl. Acad. Sci. USA*, **107**, 6640–6645, 2010

## Extreme fire event over Siberia in summer 2012: radiative characteristics of aerosol

T. B. Zhuravleva<sup>1</sup>, D. M. Kabanov<sup>1</sup>, I. M. Nasrtdinov<sup>1</sup>, T. V. Russkova<sup>1</sup>, S. M. Sakerin<sup>1</sup>, A. Smirnov<sup>2,3</sup> and B.N. Holben<sup>3</sup>

<sup>1</sup>V.E. Zuev Institute of Atmospheric Optics SB RAS, Tomsk, Russia

<sup>2</sup>Science, Systems and Applications, Inc., Lanham, MD, USA

<sup>3</sup>NASA Goddard Space Flight Center, Greenbelt, MD, USA

Keywords: AERONET, 2012 Siberian extreme fire event, aerosol, optical and microphysical properties, diurnal radiative effects.

Presenting author email: ztb@iao.ru

Microphysical and optical properties of aerosol were studied during mega-fire event in summer 2012 over Siberia using ground-based measurements of spectral solar radiation at AERONET site in Tomsk and satellite observations. The data were analyzed using multiyear (2003-2013) measurements of aerosol characteristics under background conditions and for less intense fires, differing in burning biomass type, stage of fire, remoteness from observation site, etc. ("ordinary" smokes). In June – August 2012, the average aerosol optical depth (AOD, 500 nm) had been  $0.95 \pm 0.86$ , about a factor of 6 larger than background values ( $0.16 \pm 0.08$ ), and a factor of 2.5 larger than in "ordinary" smokes. The AOD values were extremely high on July 24-28 and reached 3-5. Comparison with satellite observations showed that ground-based measurements in the region of Tomsk not only reflect the local AOD features, but also are characteristic for the territory of the Western Siberia as a whole.

Single scattering albedo (SSA, 440 nm) in this period ranged from 0.91 to 0.99 with the average of  $\sim 0.96$  in the entire wavelength range of 440-1020 nm. The increase in absorptance of aerosol particles ( $SSA(440\text{ nm})=0.92$ ) and decrease in SSA with wavelength, observed in "ordinary" smokes, agree with the data of multiyear observations in analogous situations in boreal zone of USA and Canada (Figure 1).

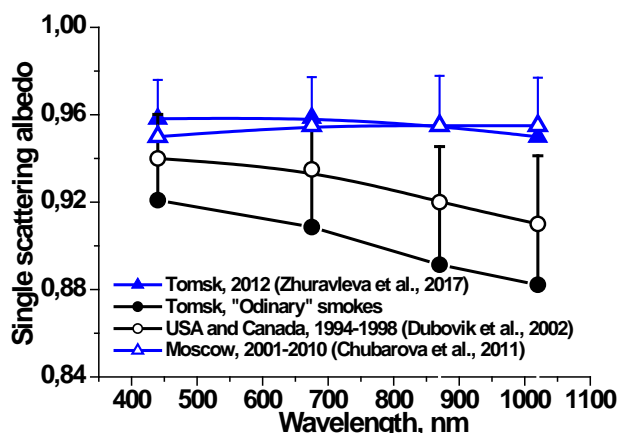


Figure 1. Average SSA for different periods and regions of observations

Volume aerosol size distribution in "extreme" and "ordinary" smokes had bimodal character with

significant prevalence of fine mode particles, but in summer 2012 the mean median radius and the width of the fine mode distribution somewhat increased. In contrast to data of multiyear observations, in summer 2012 an increase in the volume concentration and median radius of the coarse mode was observed with the growing AOD.

The calculations of the "average" radiative effects of smoke and background aerosol are presented. As compared to background conditions and "ordinary" smokes, under the extreme smoke conditions the cooling effect of aerosol considerably intensifies: direct radiative effects (DRE) at the bottom (BOA) and at the top of the atmosphere (TOA) are  $-13$ ,  $-35$ , and  $-60\text{ W m}^{-2}$  and  $-5$ ,  $-14$ , and  $-35\text{ W m}^{-2}$  respectively. The maximal values of DRE were observed on July 27 ( $AOD(500\text{ nm})=3.5$ ), when  $DRE(BOA)$  reached  $-150\text{ W m}^{-2}$ , while  $DRE(TOA)$  and  $DRE$  of the atmosphere were  $-75\text{ W m}^{-2}$ . During the fire event in summer 2012 direct radiative effect efficiency varied in range: at BOA - ( $-80, -40\text{ W m}^{-2}$ ), TOA - ( $-50, -20\text{ W m}^{-2}$ ) and in atmosphere - ( $-35, -20\text{ W m}^{-2}$ ) (Figure 2).

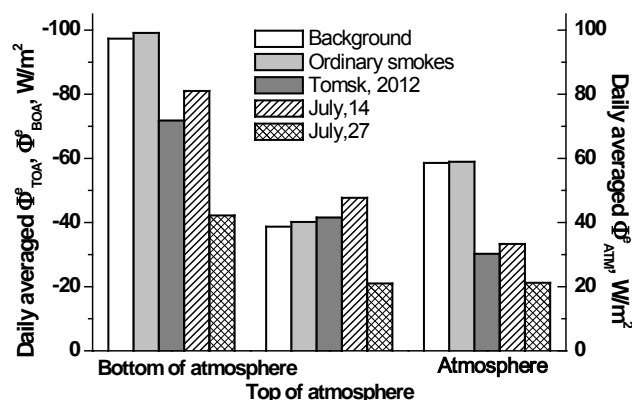


Figure 2. Radiative effects of aerosol under different atmospheric conditions.

Chubarova, N. et al. (2011). *Geography, Environment, Sustainability.*, **4** (1), 19–32.

Dubovik, O. et al. (2002). *J. Atmos. Sci.*, **59**, 590-608.

Zhuravleva T. et al. (2011). *Atmos. Meas. Tech.*, **10**, 179-198.

## Analysis of brown carbon organic species in primary and aged biomass-burning emissions under controlled conditions

V. Samburova<sup>1</sup>, D. Sengupta<sup>1</sup>, C. Bhattarai<sup>1</sup>, R.K. Chakrabarty<sup>2</sup>, A. Watts<sup>1</sup>, J. Connolly<sup>1</sup>, A. Khlystov<sup>1</sup>, and H. Moosmüller<sup>1</sup>

<sup>1</sup>Division of Atmospheric Sciences, Desert Research Institute, 2215 Raggio Parkway, Reno, NV 89512, USA

<sup>2</sup>Department of Energy, Environmental & Chemical Engineering, Washington University in St. Louis, Brookings Drive, St. Louis, MO 63130, USA

Keywords: biomass-burning, organic compounds, brown carbon.

Presenting author e-mail: [vera.samburova@dri.edu](mailto:vera.samburova@dri.edu)

Brown carbon (BrC) is an important contributor to light absorption properties of atmospheric aerosols in the blue and near-ultraviolet (UV) part of the spectrum. Several recent studies have shown that a significant portion of atmospheric BrC emissions are from biomass burning, in particular forest and peat fires. Although BrC is a recognized radiative forcing agent, there is still little known about chemical nature of this atmospheric organic fraction. No attempt has been made so far to quantitatively analyze the contribution of individual organic species and different compound classes, including Humic Like Substances (HULIS), polycyclic aromatic hydrocarbons (PAHs), and other water-soluble and non-water-soluble organic species, both primary and secondary, to light absorption. There is very little knowledge and large ambiguity regarding the contribution of PAHs to optical properties of organic carbon (OC) emitted from smoldering biomass combustion.

In the present study, five biomass fuels collected in different regions of the world (Russia, USA) were burned under controlled conditions (e.g., relative humidity, combustion efficiency, fuel-moisture content) at the Desert Research Institute Biomass Burning facility (Reno, NV, USA), “aged” in oxidation flow reactor (OFR), quantified for organic species (i.e. PAHs, HULIS), and analyzed for their optical properties.

Primary and aged combustion aerosols were collected on TIGF filters followed by XAD resin cartridges, extracted with different solvents, and analyzed for gas-phase (semi-volatile) and particle-phase organic species. Our gas chromatography mass spectrometry (GC-MS) analysis of 113 PAHs showed that PAHs contribute only 0.03-0.16% of biomass-burning BrC absorptivity and the most effective light absorbing PAHs are methylpyrenes, retene, methylfluoranthenes, perinaphthenone, and acenaphthalene (Samburova et al. 2016). Figures 1 and 2 show the distribution of different size PAHs between gas and particle phases. As was expected, light PAHs (two-ring PAHs) were dominant in the gas phase (92-98% of the total gas-phase PAH mass). Three and four-ring PAHs contribute most to the particle phase PAH mass (Figure 2). Detailed quantitative and spectrophotometric analyses on other organic species in

primary and aged biomass-burning emissions will be also presented.

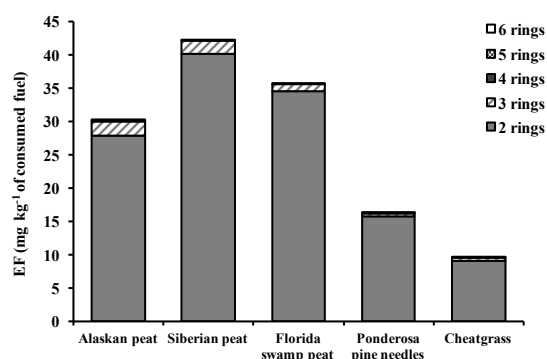


Figure 1. Emission factors of PAHs with different number of aromatic rings in gas-phase emissions.

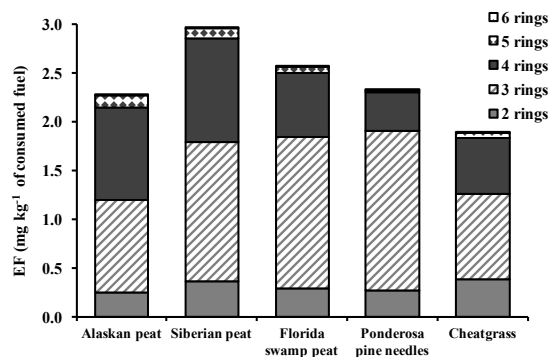


Figure 2. Emission factors of PAHs with different number of aromatic rings in particle-phase emissions.

This work was supported by the National Science Foundation (grant number AGS1544425) and NASA ROSES (grant number NNX15AI48G). We thank Dr. Anna Tsibar (Moscow State Lomonosov University, Moscow, Russia) for providing Siberian peat fuel and Anna Cunningham for technical assistance with organic chemical analysis.

Samburova, V., J. Connolly, M. Gyawali, R. L. N. Yatawelli, A. C. Watts, R. K. Chakrabarty, B. Zielinska, H. Moosmüller, and A. Khlystov. (2016) *Science Tot Environ.* **568**: 391-401.

## Influence of biomass burning from residential and district heating on local air quality assessed by mobile air pollutant measurements

F. Fachinger<sup>1</sup>, F. Drewnick<sup>1</sup> and S. Borrmann<sup>1,2</sup>

<sup>1</sup>Particle Chemistry Department, Max Planck Institute for Chemistry, D-55128 Mainz, Germany

<sup>2</sup>Institute of Physics of the Atmosphere, Johannes Gutenberg University, D-55128 Mainz, Germany

Keywords: biomass burning, residential heating, pollutant distribution, mobile measurement.

Presenting author email: fr.fachinger@mpic.de

Residential biomass burning is the most important source contributing to anthropogenic primary PM<sub>2.5</sub> emissions in Europe. While PM<sub>2.5</sub> emissions from traffic have steadily decreased over time, emissions from biomass burning have stagnated or even increased in recent years (Fuller *et al.*, 2013; EEA, 2016). One possible solution to this problem could be the installation of larger-scale biomass burning facilities instead of individual household devices for residential heating. Medium- and larger-scale biomass burning facilities show much better emission characteristics than small-scale installations due to better combustion conditions. Additionally, they can be much more cost-effectively equipped with efficient flue gas cleaning devices.

In this study, we investigate how biomass burning emissions from individual households and from medium-sized district heating facilities affect local air quality in two villages, namely St. Peter (Black Forest, Germany) and Ammertzwiller (Alsace, France). St. Peter with ~2500 inhabitants employs a 1.5 MW facility; Ammertzwiller (~400 inhabitants) runs a 400 kW facility. As additional contribution in both villages individual biomass burning occurs in residential areas. The influence of emissions from the district heating facilities, individual household combustion, and other local sources (especially traffic) compared to the background concentrations is investigated by means of mobile measurements using the mobile laboratory MoLa (Drewnick *et al.*, 2012). MoLa is based on a regular delivery vehicle equipped with an aerosol inlet system and various instruments measuring aerosol particle physical properties and chemical composition (e.g., PM<sub>1</sub>, particle number and size distribution, black carbon and non-refractory components of PM<sub>1</sub>) as well as several trace gases (e.g., NO<sub>x</sub>, CO<sub>2</sub>).

In the mapping experiments performed in this study, MoLa measured at very low driving speed in all roads in the respective village, providing spatially resolved pollutant distributions of the whole village area along the measurement track. In total, eight experiments during different times of the day were conducted in St. Peter and four in Ammertzwiller. Most measurements were executed in the heating season, but a few also in summertime for comparison.

From the measured pollutant concentrations along the tracks, maps of the pollutant distribution in the area are extrapolated (Fig. 1). The combination of such maps for various pollutants provides information on areas affected by emissions from different sources. For example, in the map of St. Peter shown in Fig. 1, an area

in the centre of the village (upper circle) is affected both by traffic emissions and biomass burning, while a purely residential area in the south of the village (lower circle) is most strongly affected by emissions from residential biomass burning. In contrast, in the vicinity and downwind of the district heating facility (marked with a star in Fig. 1), no enhancement of pollutants is observed. This demonstrates the advantage of district heating facilities over individual household biomass combustion for residential heating when considering local air quality.

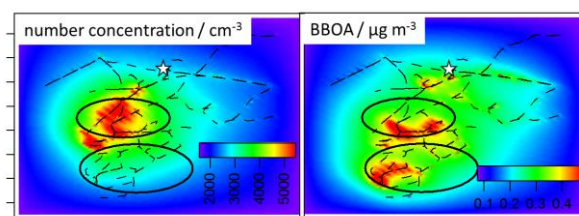


Figure 1. Pollutant distributions: Particle number concentration (left, mostly from traffic emissions) and BBOA (biomass burning organic aerosol, right).

For the areas identified to be affected by different sources, furthermore the concentration enhancement of the various pollutants with respect to the regional background (measured outside the village) is calculated. By this means, local and regional contributions to local pollutant concentrations can be separated for individual pollutants and for the various experiments under different conditions. This further helps in the assessment of influence of residential biomass burning (and other local sources) on local air quality, as opposed to regionally advected material.

This work was supported by the EU through its Interreg IV Program (Oberrhein, project C35 BIOCOMBUST; <http://www.biocomburst.eu>).

Drewnick, F., Böttger, T., von der Weiden-Reinmüller, S.-L., Zorn, S. R., Klimach, T., Schneider, J. and Borrmann, S. (2012) *Atmos. Meas. Tech.*, **5**, 1443-1457.

EEA (2016) *Air quality in Europe - 2016 report*, report no 28/2016.

Fuller, G.W., Sciare, J., Lutz, M., Moukhtar, S. and Wagener, S. (2013) *Atmos. Env.* **68**, 295-296.

## Organic speciation of gas and particle phase emissions from residential wood combustion

D. Bhattu<sup>1</sup>, G. Stefanelli<sup>1</sup>, P. Zotter<sup>2</sup>, J. Zhou<sup>1</sup>, T. Nussbaumer<sup>2</sup>, A. Bertrand<sup>3</sup>, N. Marchand<sup>3</sup>, B. Temime-Roussel<sup>3</sup>, U. Baltensperger<sup>1</sup>, J. G. Slowik<sup>1</sup>, A.S.H. Prevot<sup>1</sup>, I. El Haddad<sup>1</sup> and J. Dommen<sup>1</sup>

<sup>1</sup>Laboratory of Atmospheric Chemistry, Paul Scherrer Institute, 5232, Villigen, Switzerland

<sup>2</sup>CC Thermal Energy Systems & Technology, Bioenergy Research, Lucerne School of Engineering & Architecture, 6048, Horw, Switzerland

<sup>3</sup>Aix Marseille Univ, CNRS, LCE Marseille, France

Keywords: wood combustion, emission factor, aging, SOA, NMOGs

Presenting author email: deepika.bhattu@psi.ch

Biomass burning has increasingly been recognized as an important source of air pollution in the form of wild fires, crop residual burning and residential wood burning. The intense biomass burning emissions in combination with boundary layer dynamics in winter time makes this source the largest contributor of toxic products and particulate emissions (Schauer et al., 2001). Despite this, the emissions from residential wood burning are largely unregulated and least understood. Recent literature studies have also shown that large portion (~80%) of secondary organic aerosol (SOA) mass originates from non-traditional precursors not accounted for in models (Bruns et al., 2016). Current legislation limits the emission of particulate matter, but does not regulate the precursors potentially forming (SOA). Till date, the investigation of gas phase emissions from wood combustion and their SOA formation potential have largely focused on single combustion devices with limited operating conditions.

As both, primary emissions and SOA formation, is a strong function of device type, fuel load, type and operating conditions, we have performed a detailed chamber study investigating the gas-phase precursors and particle phase emissions from beech wood and pellets using seven types of combustion devices, namely:

1. Pellet boiler (15 kW) with advanced combustion technology at different combustion conditions: optimum, lack and high excess of oxygen,
2. Two-stage combustion logwood boiler (30 kW),
3. An industrial wood chip grate boiler (150 kW) at full and part load operation (100% and 30% power) with electrostatic precipitator,
4. Pellet stove with standard combustion technology (varying power output: 2-6 kW),
5. Single-stage combustion log wood stove (6 kW),
6. Two-stage combustion logwood stove (4.6 kW),
7. Two-stage combustion logwood stove (8 kW).

Using a potential aerosol mass reactor (PAM), the physical and chemical effects of different aging conditions were monitored with an SMPS, an Aethalometer, an HR-ToF-AMS, as well as a PTR-ToF-MS and other gas monitors. The short residence time in the reactor allowed a time resolved picture of SOA production potential and reduced wall losses. In general, significant SOA mass enhancement is

observed in high excess oxygen conditions compared to optimum and oxygen deprived combustion conditions (Figure 1). The highest non-methane organic gases (NMOGs) are emitted from the single-stage combustion logwood stove during cold start (start of each burn cycle) and the lowest in the burn out phase (end of each burn cycle). Despite of the comparable NMOGs with excess of O<sub>2</sub> conditions in pellet boiler, the percentage contribution in logwood stove emissions during flaming and burn out phase are largely occupied by SOA precursors (C>6) compared to the pellet boiler. Higher combustion temperatures and optimized combustion conditions (Air-to-fuel ratio of 1.5-2) in the industrial boiler (942-1027 °C) and the pellet boiler (589-852 °C) resulted in lower NMOGs and aged OA production. In addition, aged OA:POA ratios in the log wood stove have also been observed to be 6-27 times higher than in the pellet boiler depending on operating conditions (% O<sub>2</sub> content).

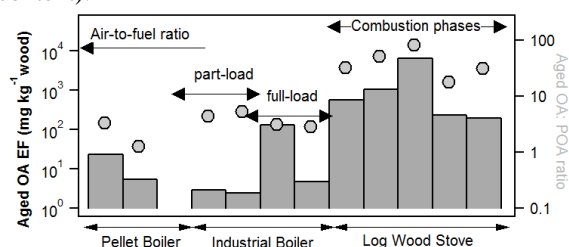


Figure 1: Aged OA emission factors (left axis) and Aged OA: POA ratios (right axis) for pellet boiler, industrial boiler and single stage combustion logwood stove under different operational conditions.

We aim to investigate the relationship between operational parameters of the combustion devices, and emissions composition and relative strength. Further, we also present the relationships between gas phase emissions and composition with their SOA formation potential to ascertain the contribution of residential wood burning to the total carbonaceous OA budget.

This work was supported by the Swiss National Science Foundation (NRP 70 “Energy Turnaround”)

Bruns, E. A., (2016) Sci. Reports, **6**, 27881.

Schauer J., (2001) Environ Sci. Technol. **35**, 1716-1728.

## Influence of the renewal of residential wood stoves on the PM biomass burning contribution in a French Alps valley.

A. Sylvestre<sup>1</sup>, B. Golly<sup>1</sup>, J.C. Francony<sup>1</sup>, C. Piot<sup>1</sup>, J.L. Jaffrezo<sup>2</sup>, A. Provent<sup>3</sup>, R. Vidaud<sup>3</sup>, H. Chanut<sup>3</sup>, G. Brulfert<sup>3</sup>, J.L. Besombes<sup>1</sup>,

<sup>1</sup>Université Savoie Mont Blanc, LCME, 73000 Chambéry, France

<sup>2</sup>Université Grenoble Alpes-CNRS, IGE UMR5001, 38402 St-Martin d'Hères, France

<sup>3</sup>Atmo Auvergne Rhône Alpes, 3 allée des Sorbiers, 69500 Bron, France

Keywords: PM10, biomass burning, Black Carbon, chemical speciation.

Presenting author email: Alexandre.sylvestre@univ-savoie.fr

In the last 10 past years, several studies showed the influence of biomass burning source (BB) on PM concentrations. In Alpine valley, BB is often the major PM source during winter (Favez et al., 2010). A program of exchanges of old stoves took place between 2012 and 2015 in the village of Lanslebourg (Maurienne valley) in order to reduce by 50% the wood-burning emissions in this area.

The aim of this study is to estimate the impact of these reductions emissions on both PM<sub>10</sub> atmospheric concentration and chemical composition. Measurement campaigns were conducted before, during and after the replacement of the wood stoves. Monitoring of PM<sub>10</sub>, O<sub>3</sub>, NO<sub>x</sub> and BC concentrations were performed using respectively TEOM-FDMS, two gas analysers and an aethalometer (AE31). The PM<sub>10</sub> chemical composition was investigated for major fraction (OC/EC and ions) and organic matter speciation, with 2 weeks daily samples per season (DA80, Digital). CMB (Chemical Mass Balance) was also performed to estimate the contribution of the biomass source in each season. In parallel, the model SIRANE, based on emission inventories and atmospheric dispersion, is used to model the PM<sub>10</sub> concentrations.

Results obtained do not show significant differences on PM<sub>10</sub> composition for the same season between campaigns. For the last campaign, PM<sub>10</sub> are dominated by OM representing 76%, 36% and 40% of the total PM<sub>10</sub> mass, respectively for the winter, the spring and the summer. EC represents between 8 and 2%, while SO<sub>4</sub><sup>2-</sup>, NH<sub>4</sub><sup>+</sup> and NO<sub>3</sub><sup>-</sup> represents respectively between 4 and 12%, 1 and 6% and 2 and 10%. However, even if no differences were observed for the major fractions between 2012/2014 and 2015/2017, some evolution of biomass burning markers was underlined. In 2015/2017, levoglucosan and its isomers accounted in average for 145 mg.g<sup>-1</sup><sub>OM</sub> and 147 mg.g<sup>-1</sup><sub>OM</sub> during respectively winter and spring. These values are lower than those obtained in 2012/2014, since value of 204 mg.g<sup>-1</sup><sub>OM</sub> in winter and 594 mg.g<sup>-1</sup><sub>OM</sub> in spring were obtained. According to these results, CMB allow to estimate a similar average contribution in winter for the BB source (representing 57% in 2013 and 54% in 2015 of the PM<sub>10</sub> concentrations). However, differences were observed for spring where the BB source represents, 13% in 2015 compared with 34% in 2013.

Aethalometer allowed to separate the BC from non-fossil source (exclusively biomass burning, BC<sub>wb</sub>) and fossil source (exclusively traffic, BC<sub>ff</sub>). Results recorded from November 2015 to January 2017 show a decreased of the BC concentrations especially compared to the 2012-2014 period. This behavior is mainly induced by a decrease of BC<sub>wb</sub>. These results are translated into a decrease of the BC<sub>wb</sub>/BC and BC<sub>wb</sub>/PM<sub>10</sub> ratio (Fig. 1.).

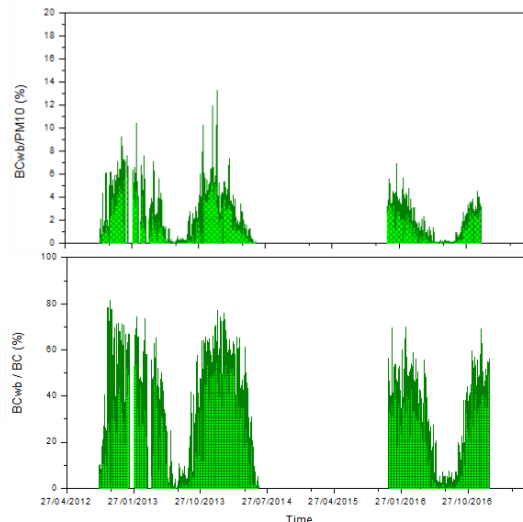


Figure 1: Evolution of BC<sub>wb</sub>/BC and BC<sub>wb</sub>/PM<sub>10</sub> ratio between Sep 2012 and Jun 2014 and between Nov 2015 and Jan 2017.

Thanks to an approach linking CMB and Aethalometer results, the average PM<sub>wb</sub> concentration is estimated from the BC<sub>wb</sub>. By this way the BB contribution on PM<sub>10</sub> concentration represents 55% in average for the cold periods of the years 2015/2017. These results will further be compared to the one obtained with the model SIRANE.

Favez, O., El Haddad, I., Piot, C., Boreave, A., Abidi, E., Marchand, N., Jaffrezo, J.L., Besombes, J.L., Personnaz, M.B., Sciare, J., Wortham, H., George, C., D'Anna, B. (2010) *Atmos. Chem. Phys.* **10**,

## Water-soluble dicarboxylic acids, oxocarboxylic acids and $\alpha$ -dicarbonyls in atmospheric aerosols during summer in central Alaska: an influence of biomass burning and biogenic sources

D.K. Deshmukh<sup>1,2</sup>, K. Kawamura<sup>1,2</sup>, M.M. Haque<sup>1,2</sup> and Y. Kim<sup>3</sup>

<sup>1</sup>Chubu Institute for Advanced Studies, Chubu University, Kasugai 487-8501, Japan

<sup>2</sup>Institute of Low Temperature Science, Hokkaido University, Sapporo 060-0819, Japan

<sup>3</sup>International Arctic Research Center, University of Alaska Fairbanks, Fairbanks 99775, USA

Keywords: Organic compounds, Biomass burning, Biogenic sources, Central Alaska.

Presenting author email: deshmukh@pop.lowtem.hokudai.ac.jp

Organic aerosols (OA) are abundant in the troposphere and crucial for air quality and climate (Kanakidou et al. 2005). OA are emitted directly into the atmosphere from primary sources and secondarily produced in the atmosphere by photooxidation of volatile organic compounds (VOCs) and unsaturated fatty acids (UFAs) followed by condensation on pre-existing particles. The photooxidation products are highly water-soluble and typically contain several types of functional groups, including carboxylic acids as well as keto and aldehyde groups.

Wildfire emissions in Alaska have increased over the few last decades relatively due to climate change effects and increase in temperature during summer in the boreal regions (Stocks et al. 2000; Grell et al. 2011). Wildfires burn huge areas nearly every summer and are a major agent of change in the boreal forest ecosystem. The largest and greatest number of wildfire occur in Alaska has a strong impact on air pollution from the local up to the hemisphere scale. Emissions of biogenic VOCs from the forested regions also make a considerable contribution to organic aerosol mass in central Alaska (Haque et al. 2016).

Total suspended particles (TSP) samples ( $n = 13$ ) were collected during summer season from June to September 2009 using pre-combusted quartz fiber filter and low volume air sampler at a flow rate of  $16.7 \text{ L min}^{-1}$  on the rooftop of the International Arctic Research Center (IARC) at University of Alaska Fairbanks campus ( $64.51^\circ\text{N}$  and  $147.51^\circ\text{W}$ ), Fairbanks, USA. The samples were measured for water-soluble dicarboxylic acids and related compounds, including oxocarboxylic acids ( $\text{C}_2$ - $\text{C}_9$ ) and  $\alpha$ -dicarbonyls using a gas chromatography (GC) equipped with flame ionization detector (FID) following a protocol described in Kawamura and Ikushima (1993), and Kawamura (1993). The samples were also measured for levoglucosan (LEVO) and 2-methylglyceric acid (2-MGA) using a GC-mass spectrometry (GC-MS) following a protocols described in Fu et al. (2010).

The molecular distribution of diacids showed a predominance of oxalic acid ( $\text{C}_2$ ) followed by succinic and malonic acid. Concentrations of  $\text{C}_2$  ranged from 50 to  $1088 \text{ ng m}^{-3}$  with an average of  $286 \text{ ng m}^{-3}$  in Alaska samples during the campaign. A predominance of  $\text{C}_2$  is likely due to that this diacid is the final product of photochemical oxidation reaction of several VOCs and UFAs of anthropogenic and biogenic origin. Azelaic ( $\text{C}_9$ )

and phthalic (Ph) acids are the next abundant diacids in Alaska aerosols. The abundant presence of  $\text{C}_9$  and Ph diacids suggests that TSP aerosols in central Alaska atmosphere have considerable influence of atmospheric processing of UFAs and aromatic hydrocarbons. We found that oxoacids showed a predominance of glyoxylic acid ( $\omega\text{C}_2$ ), whereas glyoxal (Gly) is more abundant than methylglyoxal (MeGly) in Alaska samples.

Strong correlations of concentration of  $\text{C}_2$  with concentrations of LEVO ( $r = 0.98$ ) and 2-MGA ( $r = 0.96$ ) suggest that oxalic acid was produced from biomass burning and biogenic sources in central Alaska during the campaign. The concentrations of most of the target diacids and related compounds also showed strong correlations with the concentrations of LEVO and 2-MGA during the campaign. Strong correlations of  $\text{C}_2$  diacid with saturated normal-chain diacids ( $\text{C}_3$ - $\text{C}_9$ :  $r = 0.91$ - $0.99$ ),  $\omega\text{C}_2$  ( $r = 0.99$ ), Gly ( $r = 0.99$ ), and MeGly ( $r = 0.99$ ) suggest that oxalic acid associated with TSP aerosols is produced from oxidation of higher homologous diacids,  $\omega\text{C}_2$ , Gly and MeGly in central Alaska. These results reveal that atmospheric processing of organic precursors derived from biomass burning and biogenic sources may control the water-soluble organic chemical composition of TSP aerosols in the atmosphere of central Alaska.

The authors acknowledge the financial support from the Japan Society for the Promotion of Science (JSPS) through Grant-in-Aid No. 24221001. We appreciate the financial support of a JSPS fellowship to D.K. Deshmukh.

Kawamura, K. (1993) *Anal. Chem.* **65**, 3505-3511.

Kawamura, K. and Ikushima, K. (1993) *Environ. Sci. Technol.* **27**, 2227-2235.

Stocks, B.J., Fosberg, M.A., Wotton, B.M., Lynham, T.J. and Ryan, K.C. (2000) *Ecol. Studies* **138**, 368-376.

Kanakidou, M. et al. (2005) *Atmos. Chem. Phys.* **5**, 1053-1123.

Fu, P.Q., Kawamura, K., Pavuluri, C.M., Swaminathan, T. and Chen, J. (2010) *Atmos. Chem. Phys.* **10**, 2663-2689.

Grell, G., Freitas, S.R., Stuefer, M. and Fast, J. (2011) *Atmos. Chem. Phys.* **11**, 5289-5303.

Haque, M.M., Kawamura, K. and Kim, Y. (2016) *Atmos. Environ.* **130**, 95-103.

## **Abstracts T210**

## Black carbon, carbon monoxide and carbon dioxide in the free troposphere at Helmos Hellenic Atmospheric Aerosol and Climate Change (HAC<sup>2</sup>) station in Greece

A-C. Kalogridis<sup>1</sup>, P. Fetfatzis<sup>1</sup>, O. Hermansen<sup>2</sup> and K. Eleftheriadis<sup>1</sup>

<sup>1</sup>Institute of Nuclear & Radiological Sciences & Technology, Energy & Safety, National Centre of Scientific Research “Demokritos”, Ag. Paraskevi, 15310, Greece

<sup>2</sup>Norwegian Institute for Air Research, 2027 Kjeller, Norway

Keywords: black carbon, carbon dioxide, free troposphere, PBL, Mediterranean

Presenting author email: akalogridi@ipta.demokritos.gr

HAC<sup>2</sup> observatory is one of the very few high-altitude atmospheric monitoring stations in Europe. It is situated in the Peloponnese peninsula in southern Greece at an elevation at 2340 m high. It is uniquely placed to study the free troposphere (FT) and characterise the background conditions of the Mediterranean Basin, a hot spot region of air pollution and climate change (Giorgi, 2006).

Continuous measurements of a number of aerosol parameters and greenhouse gases concentrations began in 2016. Here, the very first long-term measurements of black carbon, carbon monoxide and carbon dioxide are presented. Measurements of equivalent black carbon concentrations (eBC) were performed using an aethalometer (AE31 model, Magee Scientific Corp., Berkeley, CA 94703, USA), whereas a Picarro G2401 analyzer (Picarro Inc., CA, USA) was used to monitor CO and CO<sub>2</sub>. The goal of this analysis is to understand eBC, CO and CO<sub>2</sub> variability resulting from a complex combination of seasonal variations, long-range transport, local sources and planetary boundary layer (PBL) injections.

Time series of eBC, CO and CO<sub>2</sub> concentrations are illustrated in Figure 1 for two distinct events, representing two characteristic atmospheric regimes experienced at the station. On the top panel, we focus on the warmest days of the summer period, when daytime maxima of 20 to 25°C were recorded and when the boundary layer height was at its annual maximum (varying between 2000-2500 m according to ECMWF simulations). In those conditions, mixing from PBL and FT air masses is expected due to vertical transport of air masses by thermally-driven convection. During this event an enhancement in eBC and CO concentrations is observed, reaching up to 1500 ng.m<sup>-3</sup> and 0.20 ppm respectively, probably due to the influence of the PBL and to surface emissions. A negative correlation is observed between CO and CO<sub>2</sub> fluctuations suggesting that CO<sub>2</sub> depletion in PBL air by surface uptake can overshadow the enhancements due to the surface emissions. This behaviour has already been observed in the past in high altitude stations (McClure et al., 2016). During wintertime, as the boundary layer gets more shallow, HAC<sup>2</sup> station is exclusively in the free troposphere, thus, resulting in lower concentrations of CO and eBC. Specifically, with an average concentration of about 40 ng.m<sup>-3</sup>, eBC levels are a factor of ~8 lower compared to summertime. On the opposite, a rise in CO<sub>2</sub> concentrations is observed during wintertime that can be

explained by the CO<sub>2</sub> seasonal natural cycle in combination with enhancement of emissions from combustion processes. Further analysis of these preliminary results (analysis of back trajectories, identification of biomass burning events, aerosol scattering properties) will enable us to better understand the regional variations of CO<sub>2</sub>, CO and eBC within the Mediterranean basin.

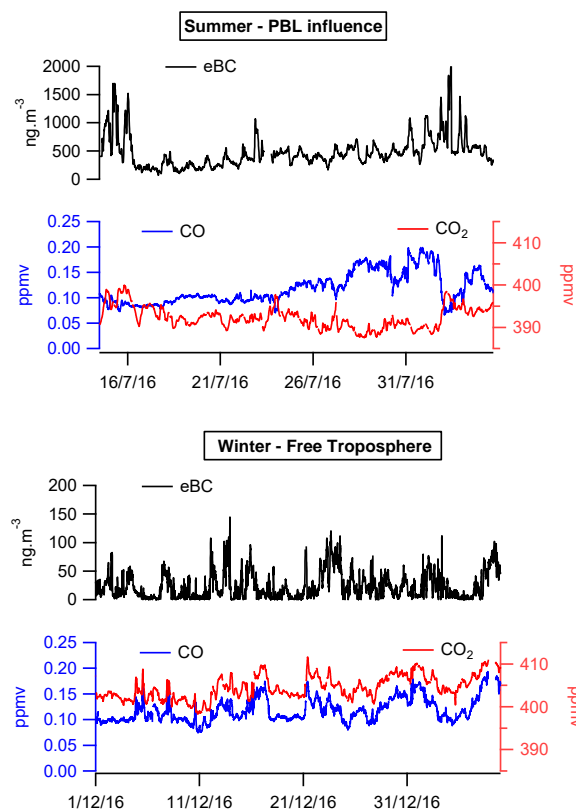


Figure 1. eBC, CO and CO<sub>2</sub> concentrations in summertime (top panel) and wintertime (bottom) in 2016

This work was supported by ENTEC FP7REGPOT - 2012-2013-1 FP7, ID:316173)

Giorgi, F.: Climate change hot-spots, *Geophys. Res. Lett.*, 33(8), L08707, doi:10.1029/2006GL025734, 2006.

McClure, C. D., Jaffe, D. A. and Gao, H.: Carbon Dioxide in the Free Troposphere and Boundary Layer at the Mt. Bachelor Observatory, *Aerosol Air Qual. Res.*, 16(3), 717–728, doi:10.4209/aaqr.2015.05.0323, 2016.

## Elucidating the composition of humic-like substances in the atmospheric aerosol via 2D liquid chromatographic fractionation and ultra-high resolution mass spectrometry

Tobias Spranger<sup>1</sup>, Dominik van Pinxteren<sup>1</sup>, Oliver Lechtenfeld<sup>2,3</sup>, Thorsten Reemtsma<sup>2</sup>, Hartmut Herrmann<sup>1</sup>  
<sup>1</sup>Atmospheric Chemistry Department (ACD), Leibniz-Institute for Tropospheric Research (TROPOS), Leipzig, 04318, Germany

<sup>2</sup>Department of Analytical Chemistry, Helmholtz Centre for Environmental Research (UFZ), Leipzig, 04318, Germany

<sup>3</sup>ProVIS – Centre for Chemical Microscopy, Helmholtz Centre for Environmental Research (UFZ), Leipzig, 04318, Germany

Keywords: HULIS, organic aerosol, liquid chromatography, FTICR-MS

Presenting author email: spranger@tropos.de

Atmospheric aerosol particles contain a large fraction of organic carbon (OC), which contributes up to 70% of the total particle mass (Kanakidou et al. 2005). OC plays an important role for cloud formation and the earth radiative budget, as it alters microphysical properties and the ability of particles to serve as cloud condensation nuclei (Kristensen et al. 2012). Moreover, it is expected to be involved in a wide range of human health issues (Mauderly and Chow 2008). Despite its importance, only a small fraction has been identified on a molecular level, due to the high complexity with thousands of substances. OC is dominated by a class of substances often referred as humic-like substances (HULIS), which contributes up to 80% of the water-soluble organic carbon (Zheng et al. 2013). Elucidating its composition is therefore crucial to understand aerosol properties and its roll on the cloud formation process. At the same time, the high complexity of the chemically unresolved mixture is challenging.

This work shows the development of an offline two-dimensional chromatographic method, combining size exclusion (SEC) and reverse-phased chromatography (RP-HPLC), for a detailed fractionation of aerosol particle extracts. The particle extracts are separated via optimized SEC into five fraction in molar mass ranges between 160-900 g/mol. Each fraction is separated further into eleven RP-HPLC fraction with calculated octanol/water partition coefficient of 0.2-3.3, utilizing a newly developed “spiked gradient” method. Heat maps of the UV-absorption at 254 nm illustrate the distribution of HULIS in the two-dimensional size-vs-polarity space (Figure 1). The distribution differs strongly depending on season and air mass input for a set of samples from Melpitz, a background station near Leipzig, Germany. In winter, the largest molecules with a relatively low polarity dominate the absorption properties, while in summer the smaller more polar ones dominate.

Additionally, the fractions were analysed by direct infusion ultra-high resolution electrospray ionisation Fourier transform ion cyclotron mass spectrometry (12T SolariX XR, Bruker Daltonics). The number of identified, unique molecular formulas increased by a factor of ~2.5 for the fractionated samples as compared to bulk samples, mainly due to a reduction of ion suppression in ESI and hence sensitivity enhancement of low concentration HULIS compounds (Noziere et al. 2015). Further, detailed information about the chemical composition are gained for each fraction. For later eluting

HPLC fractions, the hydrogen-to-carbon ratio increases, while the oxygen- and nitrogen-to-carbon ratios, as well as the carbon oxidation state, decreases. The sulphur-to-carbon ratio does not show differences within HPLC fractions. Preliminary results show a higher aromaticity, double bond equivalent and nitrogen-to-carbon ratio for the SEC fractions containing the largest molecules (>520 g/mol), possible explaining the high absorption of these fractions. The molecular diversity of the fractionated extracts will be discussed further in this work.

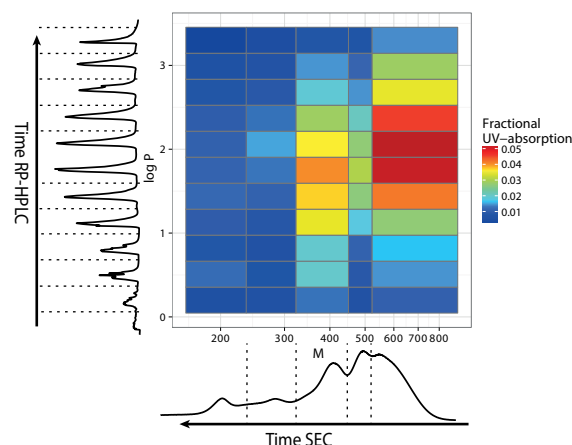


Figure 1. 2D heat map of an ambient filter sample, with the respective SEC chromatogram on the bottom and one RP-HPLC chromatogram on the left side. Dotted lines show the fraction limits.

The authors are grateful for using the analytical facilities of <sup>3</sup>ProVIS, which is supported by European regional Development Funds (EFRE – Europe funds Saxony) and the Helmholtz Association. This work was funded by the German Research Foundation (DFG) in the project HuCar as PI 1102/4-1 and HE 3086/28-1.

Kanakidou, M., et al. 2005. *Atmospheric Chemistry and Physics*, **5**: 1053-123.

Kristensen, T. B., et al. 2012. *Journal of Geophysical Research-Atmospheres*, **117**.

Mauderly, J. L., and J. C. Chow. 2008. *Inhalation Toxicology*, **20**: 257-88.

Noziere, B., et al. 2015. *Chemical Reviews*, **115**: 3919-83.

Zheng, G. J., et al. 2013. *Environmental Pollution*, **181**: 301-14.

## A New Method and Instrument for the Measurement of Carbonaceous Aerosols

M. Rigler<sup>1</sup>, L. Drinovec<sup>1,2</sup>, A. Vlachou<sup>3</sup>, G. Stefenelli<sup>3</sup>, J. G. Slowik<sup>3</sup>,  
A. S. H. Prévôt<sup>3</sup>, C. Hüglin<sup>4</sup>, A. D. A. Hansen<sup>5</sup> and G. Močnik<sup>1,2</sup>

<sup>1</sup>Aerosol d.o.o., Ljubljana, 1000, Slovenia

<sup>2</sup>Jozef Stefan Institute, Ljubljana, 1000, Slovenia

<sup>3</sup>Paul Scherrer Institute, Villigen, 5232, Switzerland

<sup>4</sup>EMPA, Dübendorf, 8600, Switzerland

<sup>5</sup>Magee Scientific Corp., Berkeley, CA 94704, USA

Keywords: total carbon analyzer, TC-BC method, carbonaceous aerosols  
Presenting author email: Martin.Rigler@aerosol.eu

Carbonaceous aerosols account for a large and often dominant fraction of fine particulate matter (PM<sub>2.5</sub>) and are extremely diverse. They impact air quality, visibility, the climate, cloud nucleation, the planetary radiation balance, and public health. The carbonaceous fractions are frequently separated into organic carbon (OC) and elemental carbon (EC) based on their volatility using thermal-optical methods. While the results for OC and especially EC concentrations vary significantly for different thermal evolution protocols (Bae, 2009), the total carbon (TC) concentration is very consistent between methods (Karanasiou, 2015).

To understand the formation and to perform source apportionment of carbonaceous aerosols, a highly time resolved online method to characterize them is needed. In this study we present a new real-time TC-BC method which combines an optical method for measuring black carbon (BC) by the Aethalometer AE33, and a thermal method for TC determination. This analysis is performed using the newly developed Total Carbon Analyzer (TCA). EC is calculated as  $b \cdot BC$ , where the proportionality  $b$  is region and/or site specific (Watson, 2005). The OC fraction is obtained from the difference TC - EC.

The Aethalometer measures the optical properties of carbonaceous aerosols collected on the filter and determines the real-time BC concentration (Hansen, 1982; Drinovec, 2015). The TCA operates on the principle of rapid combustion of PM collected on a quartz filter to create a pulse of combustion products which are converted to CO<sub>2</sub> and detected as a large transient increase above the CO<sub>2</sub> level in the ambient air used as carrier gas. Unlike most OC/EC instruments for the thermal analysis of carbonaceous aerosols, the TCA does not require special high purity gases or quartz glass components for its operation.

The TC-BC method with the new TC analyzer instrument was tested in campaigns during summer 2016 and winter 2017 in the city center of Zurich, Switzerland. The carbonaceous fraction of PM<sub>2.5</sub> was analyzed with the TCA in online mode with a time resolution as small as 20 minutes; Aethalometer data on a 1-minute timebase; and the OC/EC analysis of 24-h filters (Sunset, EUSAAR2). Part of both campaigns overlapped with ACSM and AMS measurements which

allowed us to obtain organic carbon concentrations with high time resolution (OC<sub>AMS</sub>).

The results from the summer campaign in Zurich (Figure 1) show good correlation between 24 h averages of BC and EC; and between TC<sub>OCEC</sub>=OC+EC, and normalized TC<sub>TCA</sub> determined by the new total carbon analyzer. OC<sub>AMS</sub> is lower than OC from the filter analysis as expected due to different size selection (PM<sub>2.5</sub> for filter samples and PM<sub>1</sub> for AMS).

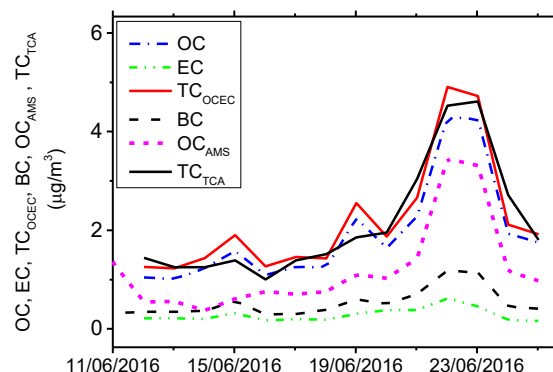


**Figure 1. Time series for aerosol carbon content using different methods: OC, EC, TC<sub>OCEC</sub> – EUSAAR2 thermal-optical method; BC – Aethalometer; OC<sub>AMS</sub> – AMS; TC<sub>TCA</sub> – new Total Carbon Analyzer.**

This work was financed in part by the EUROSTARS grant E!8296 TC-BC.

Bae et al. (2009), *Sci. Tot. Environ.* **407**, 5176-5183.

Drinovec et al. (2015), *Atmos. Meas. Tech.* **8**, 1965-1979.

Hansen et al. (1982), *Appl. Opt.* **21**, 3060-3062.

Karanasiou et al. (2015), *Atmos. Meas. Tech. Discuss.* **8**, 9649–9712.

Watson et al. (2005), *Aerosol Air Qual. Res.* **5**, 65–102.

## Black Carbon and Brown Carbon aerosols in Ireland

P.C. Buckley<sup>1</sup>, S. Hellebust<sup>1</sup>, J. Arndt<sup>1</sup>, I.P. O'Connor<sup>1</sup>, E.J. McGillicuddy<sup>1</sup>, E. Nicolosi<sup>2</sup>, G. Fuller<sup>2</sup>, J. Wenger<sup>1</sup>

<sup>1</sup> Department of Chemistry and Environmental Research Institute, University College Cork, Ireland

<sup>2</sup>Environmental Research Group, King's College London, London, SE1 9NH, UK

Keywords: Aethalometer, Black Carbon, Brown Carbon, Source Apportionment.

Presenting author email: paulbuckley@umail.ucc.ie

The measurement of Black Carbon (BC) using a 7 wavelength aethalometer has been shown to be an effective means of separating the contributions of fossil fuel combustion and biomass burning to particulate matter (PM) levels on continental Europe (Sandradewi et al. 2008). Particles emitted from these sources have differing absorption properties across the wavelength range 370 – 950 nm, with biomass burning absorbing more at the lower wavelengths due to the presence of more “Brown” Carbon within the particle (Andreae and Gelencsér 2006). The absorption coefficient ( $b_{\text{abs}}$ ) at different wavelengths is determined by the following relationship:

$$b_{\text{abs}} \propto \lambda^{-\alpha}$$

where  $\lambda$  is the wavelength and  $\alpha$  is the Ångström exponent, an absorption signature unique to each fuel type. Aethalometer measurements determine the absorption coefficients of ambient PM, which can be used to estimate the relative contributions of fossil fuel combustion and biomass burning to ambient PM levels. The absorption coefficients can also be used to calculate the  $\alpha$  value for the measured particles. This approach has been used in Europe to develop a model for source apportionment of BC particles (Favez et al. 2010).

In recent years, a series of field measurements have been carried out in small towns in Ireland and these campaigns have yielded results that are inconsistent with patterns observed in previous European studies. The patterns observed in Ireland show peaks in both morning and evening in the aethalometer channel most associated with fossil fuel combustion. However, these measurements did not match the observed levels of vehicular traffic during evening times.

The European studies report  $\alpha$  values of approximately 1 for fossil fuel combustion and 2 for biomass burning. However, the use of other types of fuel in Ireland and the UK, such as coal, peat and turf, make the estimates from this model much less reliable. Results from the field measurements confirm that the use of the standard model is not ideal in a multi-fuel environment like Ireland.

In addition to the field campaigns a series of combustion experiments have been carried out in

an effort to characterise the  $\alpha$  values unique for each fuel type commercially available in the area. The fuel types tested include wood, locally cut and dried turf, peat briquettes and coal products. The emissions were sampled directly from the flue of a domestic stove and real time measurements were made using a 7 wavelength aethalometer (Magee Scientific, model AE33).

The results gathered from these burning experiments highlight the different absorption properties of the emissions from the different fuel types. For example, the  $\alpha$  values observed for coal were significantly different to those observed for turf and peat (Figure 1). These values can be used to further develop a source apportionment model which will provide more accurate results for use in a multi-fuel environment such as Ireland, the UK or Eastern Europe.

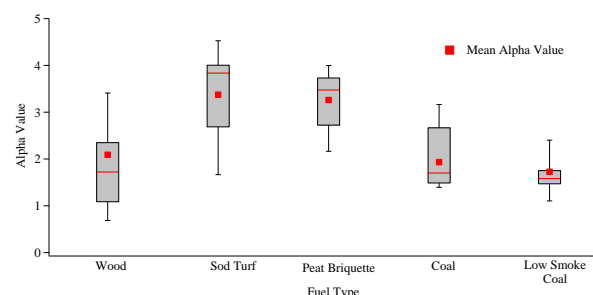


Figure 1. Alpha values for different fuel types tested during combustion experiments.

PB acknowledges support from the Irish Research Council through a Government of Ireland Postgraduate Scholarship (GOIPG/2015/3051). The SAPPHIRE project was supported by the Environmental Protection Agency and Department of Environment Community & Local Government in Ireland (2013-EH-MS.15).

Andrea, M.O. and Gelencsér, A. (2006) *Atmos. Chem. Phys.*, **6**, 3131–3148.

Favez, O. et al. (2010), *Atmos. Chem. Phys.*, **10**, 5295 – 5314.

Sandradewi, J. et al. (2008), *Atmos. Environ.*, **42**, 101–112.

## Correlation between black, elemental and organic carbon in urban and rural areas in the Iberian Peninsula

M. Becerril-Valle<sup>1</sup>, E. Coz<sup>1</sup>, A. S. H. Prévôt<sup>2</sup>, G. Močnik<sup>3,4</sup>, S. N. Pandis<sup>5,6,7</sup>, A. M. Sánchez de la Campa<sup>8,9</sup>, A. Alastuey<sup>10</sup> and B. Artíñano<sup>2</sup>

<sup>1</sup>CIEMAT, “Atmospheric Pollution 1”, Associated Unit to CSIC, Department of Environment, CIEMAT, Madrid, ES-28040, Spain

<sup>2</sup>Laboratory of Atmospheric Chemistry, Paul Scherrer Institute (PSI), Villigen-PSI, CH- 5232, Switzerland

<sup>3</sup>Aerosol d.o.o., Ljubljana, SI-1000, Slovenia

<sup>4</sup>Condensed Matter Physics Department, Jožef Stefan Institute, SI-1000 Ljubljana, Slovenia

<sup>5</sup>Institute of Chemical Engineering Sciences, ICE-HT, Patras, GR-26504, Greece

<sup>6</sup>Department of Chemical Engineering, University of Patras, Patras, GR-26504, Greece

<sup>7</sup>Department of Chemical Engineering, Carnegie Mellon University, Pittsburgh, PA-15213, USA

<sup>8</sup>Associated Unit CSIC-University of Huelva “Atmospheric Pollution”, Centre for Research in Sustainable Chemistry (CIQSO), University of Huelva, Huelva, ES-21071, Spain

<sup>9</sup>Department of Geology, Faculty of Experimental Sciences, University of Huelva, Huelva, ES-21071, Spain

<sup>10</sup>Institute of Environmental Assessment and Water Research (IDAEA-CSIC), Barcelona, ES-08034, Spain

Keywords: black carbon, elemental carbon, organic carbon.

Presenting author email: andre.prevot@psi.ch

Carbonaceous aerosols are one of the major components of atmospheric particle matter (PM). Organic carbon (OC) and elemental carbon (EC) or black carbon (BC) are the predominant components of this carbonaceous PM (Penner and Novakov, 1996). BC (or EC) is emitted during incomplete combustion of fossil fuels, biofuels, and biomass burning and it absorbs at all wavelengths of solar radiation (IPCC 2013).

The main purpose of this work was to study the correlations between eBC (equivalent BC, GAW/WMO, 2012), EC and OC in urban and rural areas in Spain. PM<sub>10</sub> eBC mass concentrations were measured using two multi-wavelength Aethalometers (Magee Sci. mod. AE33, Aerosol d.o.o) from December 22, 2014 to December 21, 2015. Ambient aerosol samples were collected on quartz-fiber filters for 24-h using Hi-Vol (30 m<sup>3</sup>·h<sup>-1</sup>) samplers. PM levels were determined by standard gravimetric procedures (UNE-EN 12341:1999). PM<sub>1</sub>, PM<sub>2.5</sub> and PM<sub>10</sub> inlets were used at the urban background site (CIEMAT, Madrid) from November 2014 to September 2015. PM<sub>2.5</sub> and PM<sub>10</sub> samples in the rural area (Villanueva del Arzobispo, Jaén) from November 2014 to June 2015. OC and EC concentrations were determined by a Thermal-Optical Transmittance (TOT) method (Sánchez de la Campa, 2009), adapted from Huntzicker (1982), using a Sunset Laboratory OCEC Analyzer and the EUSAAR2 temperature protocol (Cavalli, 2010).

Results showed that slopes and their standard errors of the linear regression through the origin between total eBC and EC mass concentrations in PM<sub>10</sub> were 2.15±0.23 in CIEMAT and 1.26±0.02 in Villanueva, they are consistent with results obtained in previous studies (Titos, 2017). Their corresponding correlation factors were 0.95 in CIEMAT and 0.99 in Villanueva.

OC/EC ratios at CIEMAT ranged from 1.0-5.4 in PM<sub>1</sub>, 1.5-5.2 in PM<sub>2.5</sub> and 1.5-5.5 in PM<sub>10</sub>, with the averages of 2.1±1.2, 3.0±1.3 and 3.3±1.7, respectively. In Villanueva, OC/EC ratios were in the range of 3.5-29.1 in PM<sub>2.5</sub> and 3.6-15.5 PM<sub>10</sub>. Their mean OC/EC ratios were 6.5±3.6 and 6.8±2.0, respectively. In the urban area, the ratios were similar to the reported in other studies, where

vehicular exhaust predominates (Schauer, 2002). The high ratios obtained in rural stations can be explained by the presence of local sources such as biomass burning combustion (Zhang, 2007). In Villanueva, the slopes and their standard errors of the linear regression between OC and EC were 5.4±0.3 in PM<sub>2.5</sub> and 5.4±0.2 in PM<sub>10</sub>, showing a high correlation both in PM<sub>2.5</sub> (R<sup>2</sup>=0.93) and PM<sub>10</sub> (R<sup>2</sup>=0.86). These results confirm that biomass burning processes and/or biogenic (both primary and secondary) had significant contributions to the aerosols in this area. The good correlation between OC and EC suggests they have common sources.

This work has been funded by the Spanish Ministry of Economy and Competitiveness (MINECO) through the FPI predoctoral research grant BES-2012-056545 and the MICROSOL (CGL2011-27020) and PROACLIM (CGL2014-52877R) projects. AEROCLIMA project (CIVP16A1811, Fundación Ramón Areces) and the Spanish Ministry of Agriculture, Food and Environment are also acknowledged as well as the Air Quality Service of Junta de Andalucía for their support in the experimental deployment and measurements.

Cavalli, F. et al. (2010) *Atmos. Meas. Tech.*, **3**, 79-89.

GAW/WMO (2012) “13th annual TFMM meeting, 17-19 April 2012, Gozo, Malta”.

Huntzicker, J.J. et al. (1982) *Particulate Carbon*. Springer US, Boston, MA, 79-88.

Na, K. et al. (2004) *Atmos. Environ.*, **38**, 1345-1355.

Penner, J.E. and Novakov, T. (1996) *J. Geophys. Res. Atmos.*, **101**, 19373–19378.

Putaud, J.P. et al. (2010) *Atmos. Environ.*, **44**, 1308-1320.

Sánchez de la Campa, A.M. et al. (2009) *Environ. Res.*, **109**, 671-681.

Schauer, et al. (2002) *Environ. Sci. Technol.*, **36**, 1169-1180.

Stocker, T. F. et al. (2013) *IPCC: Climate Change 2013*, Cambridge University Press.

Titos, G. et al. (2017) *Atmos. Environ.*, **114**, 19-31.

UNE-EN 12341: 1999 (1999).

Zhang, Y. et al. (2007) *J. Environ. Sci.*, **19**, 167-175.

## Calculation of photophoretic motion characteristics of fractal-like soot aggregates using the specialized aerosol solver

V.I. Gryazin, S.A. Beresnev

Institute of Natural Science and Mathematics, Ural Federal University, Ekaterinburg, 620083, Russia

Keywords: photophoresis, soot aerosol, fractal-like particles.

Presenting author email: gryazin.victor@mail.ru

Various applications of processes of radiation absorption and motion of soot particles are well-known under the numerous publications. Among them appreciable interest is caused by experimental and theoretical researches of the radiometric phenomena (thermo- and photophoresis) with carbonaceous aerosols well absorbing radiation practically in the all range of radiation wavelengths. Such investigations require numerous calculations; therefore specialized aerosol solver for a wide range of calculations related to the photophoretic motion of soot particles is developed. It is useful to keep the mathematical formalism used in model of homogeneous spheres (the general solution of fractal-like particle problem is extremely difficult).

The calculation of force and velocity of longitudinal radiometric photophoresis is based on the molecular-kinetic theory of this phenomenon (Beresnev et al, 1993). For calculations of optical characteristics for fractal-like particles it is possible to use methods of effective medium approximations (e.g., Chylek et al, 1988) and theoretical predictions for fractal-like soot particles by Mackowski (2006). It was revealed that the choice  $m = 1.764 + i0.570i$  for  $\lambda = 0.68 \mu\text{m}$  (the wavelength of the He-Ne laser) is optimum. Effective thermal conductivity of fractal-like soot particles can be calculated using the method offered for estimation of thermal properties of nanofluids with significantly enhanced thermal conductivity by the aggregation of nanoparticles into clusters (Evans et al, 2008).

The determined above characteristics are used in gas-kinetic calculations for photophoretic force and velocity. Reliability and accuracy of suggested model is necessary to estimate by comparison with adequate experimental and theoretical data. The experimental results of Karasev et al (2004) on photophoretic velocities of soot particles in nitrogen provide a unique opportunity to compare results. In experiment two groups of aggregates sizes distinctly differ: small particles at  $R_m \leq 0.5 \mu\text{m}$  and large particles  $R_m > 0.5 \mu\text{m}$  for which the mobility radius  $R_m$  was defined by various techniques at invariable fractal dimension  $D_f = 1.80$ .

On Fig. 1 the comparison of experimental photophoretic velocity  $U_{ph}$  with theoretical predictions at various estimations for a dimensionless heat-conductivity ratio  $\Lambda$  and optimum estimated other key parameters are presented. Photophoretic force and velocity extremely strongly depend on this ratio: the more the given ratio, the less value of radiometric effect. From comparison with experiment it becomes clear that the optimum value  $\Lambda$  is in an interval 70-110.

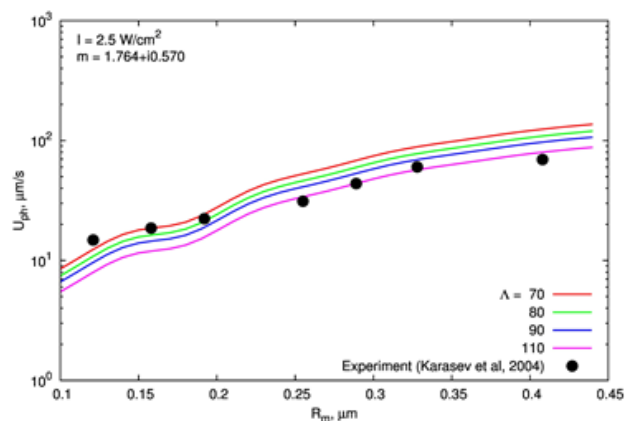


Figure 1. Dependence of the photophoretic velocity  $U_{ph}$  on the dimensionless heat-conductivity ratio  $\Lambda$ . Black circles – the group of aggregates with  $R_m \leq 0.5 \mu\text{m}$  from experiment (Karasev et al, 2004), lines – theory for spherical particles (Beresnev et al, 1993) with optimum estimated parameters.

It is obvious, that for the quantitative description of fractal-like aggregates photophoresis it is necessary to have a strict theoretical method for prediction of parameter  $\Lambda$  on the basis of knowledge of fractal dimension of the aggregate  $D_f$  and thermal characteristics of primary particles.

The analysis has shown that for a qualitative and quantitative explanation of photophoretic motion of aggregates it is possible to apply the well-developed theory for homogeneous spherical particles at correct treatment of key parameters.

This work was supported by the Ministry of Education and Science of the Russian Federation through the base part of the State task for high educational institutions (the research project #2189) and by the grant of President of Russian Federation for the state support of young Russian scientists MK-9289.2016.5.

Beresnev, S.A., Chernyak, V.G. and Fomyagin, G.A. (1993) *Phys. Fluids A* **5**(8), 2043-2052.

Chylek, P., Srivastava, V., Pinnick, R.G. and Wang R.T. (1988) *Appl. Opt.* **27**(12), 2396-2404.

Evans, W., Prasher, R., Fish, J. et al. (2008) *Int. J. Heat Mass Transfer* **51**, 1431-1438.

Karasev, V.V., Ivanova, N.A., Sadykova, A.R. et al. (2004) *J. Aerosol Sci.* **35**(3), 363-381.

Mackowski, D.W. (2006) *J. Quant. Spectr. Rad. Transfer* **100**, 237-249.

## Spatial and seasonal distribution of light absorbing carbonaceous aerosol

S. Gilardoni<sup>1</sup>, A. Marinoni<sup>1</sup>, P. Massoli<sup>2</sup>, S. Deiuili<sup>3</sup>, F. Migliorini<sup>3</sup>, V. Gianelle<sup>4</sup>, G. Lonati<sup>5</sup>, A. Malandrino<sup>5</sup>, S. Ozgen<sup>5</sup>, A. Freedman<sup>2</sup>

<sup>1</sup> Italian National Research Council ISAC, 40129 Bologna, Italy

<sup>2</sup> Aerodyne Research, Billerica, MA, USA

<sup>3</sup> Italian National Research Council ICMATE, 20125 Milan, Italy

<sup>4</sup> Regional Environmental Research Agency Lombardia, 20133 Milan, Italy

<sup>5</sup> Politecnico di Milano, 20133 Milan, Italy

Keywords: Black Carbon, Brown carbon, urban aerosol, rural aerosol

Presenting author email: [s.gilardoni@isac.cnr.it](mailto:s.gilardoni@isac.cnr.it)

Black carbon (BC) is an ubiquitous component of particulate matter produced from combustion processes. The World Health Organization (WHO) concluded that BC is a valuable indicator of health threat (WHO 2013). In addition, BC is a short-lived climate forcer (IPCC, 2013). The quantification of BC sources in urban and rural environment is mandatory for the implementation of effective air quality policy measures.

Two field experiments were performed in winter and summer 2016 in an urban and a rural site in the Milan area (Italy). The aim of the experiments was to investigate optical properties of carbonaceous aerosol, including BC and brown carbon (BrC). During the experiments, we deployed filter-based on-line optical measurements (nephelometer, aethalometer, and multi angle absorption photometer - MAAP) non-filter-based techniques (Cavity Attenuated Phase Shift spectroscopy - CAPS PM<sub>ssa</sub>, and Laser Induced Incandescence - LII), and off-line measurements of carbonaceous aerosol (thermo optical quantification of elemental/organic carbon, and visible spectrometer measurements of BrC).

BC concentrations measured by LII agrees with MAAP data, with a Pearson correlation coefficient ( $r^2$ ) larger than 0.91 (Figure 1). MAAP tends to underestimate BC concentration for values larger than 10  $\mu\text{g m}^{-3}$ , due to filter overloading effect (Hyvarinen et al., 2013).

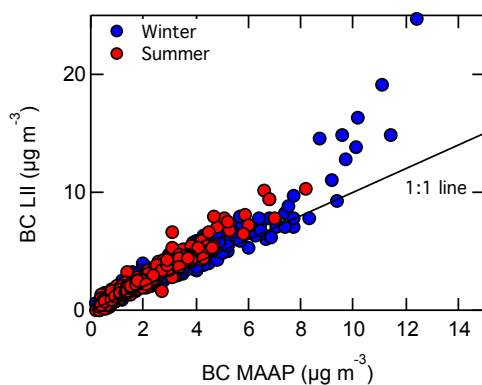


Figure 1. Comparison of BC concentrations measured by LII and MAAP in Milan urban area.

BC average concentrations were higher in winter and were comparable at the two sites, mainly due to

stagnant meteorological conditions (Table 1). BC mass absorption cross section (MAC) was estimated by the comparison of BC concentration and light absorption coefficients at 880 nm (Collaud-Coen et al., 2010). MAC did not show statistical significant differences among sites and seasons.

Season	Site	BC ( $\mu\text{g}/\text{m}^3$ )
Winter	Rural	2.5
Winter	Urban	3.8
Summer	Rural	0.5
Summer	Urban	2.0

Table 1. Average BC concentrations measured during the field experiments by LII.

Light absorption of water soluble BrC (at 365 nm) was negligible in summer, while it was comparable at the urban and rural sites in winter (3.2  $\text{Mm}^{-1}$  and 2.6  $\text{Mm}^{-1}$ , respectively). BrC in winter is mainly due to wood burning emissions. Thus, the similar values at the two sites indicate a broad impact of wood burning emissions at the basin scale.

In conclusion, the analysis of seasonal and spatial distribution of black carbon and brown carbon indicates that, in winter, rural concentrations of pollutants relevant for climate and health are similar to urban levels, suggesting that the impacts of anthropogenic emissions is not limited to urban environments.

The authors acknowledge Fondazione Cariplo (grant number 2015-1195) for founding the Black Cat project.

WHO (2013) REVIHAAP Tech. rep., European Centre for Environment and Health.

IPCC report (2013) Cambridge University Press, Cambridge, United Kingdom and New York, USA.

Hyvarinen A.P., Vakkari V., Laakso L., Hooda R. K., Sharma V. P., Panwar T. S., Beukes J. P., van Zyl P. G., Josipovic M., Garland R. M., Andreae M. O., Poschl U., Petzold A. (2013) *Atm. Meas. Tech.*, **6**, 81-90.

Collaud Coen M., Weingartner E., Apituley A., Ceburnis D., Fierz-Schmidhauser R., Flentje H., Henzing J.S., Jennings S.G., Moerman M., Petzold A., Schmid O., Baltensperger U. (2010) *Atm. Meas. Tech.*, **3**, 457-474

## Annual behavior of EBC size distribution in submicron aerosol in West Siberia

V. S. Kozlov, D.G. Chernov and M.V. Panchenko

V.E. Zuev Institute of Atmospheric Optics, Russian Academy of Sciences, Tomsk, Russia

Keywords: BC size distribution, annual behavior, submicron atmospheric aerosol, monitoring

Presenting author email: vkozlov@iao.ru

The improvement of radiative-climate models of the cloudless atmosphere depends significantly on the correct simulation of scattering and absorbing characteristics of aerosol (Bond *et al* 2013). The single scattering albedo (SSA) in the visible is an important optical parameter determining the radiative effects of aerosol and its role in the atmosphere as a cooling or heating factor. The value of SSA depends not only on the mass ratio of the absorbing and nonabsorbing matter, but also on the size distribution of the absorbing matter inside the submicron fraction of particles, which determines the aerosol forcing in the visible spectral region (Panchenko *et al* 2012).

Since 2014, the BC spectrometer is installed at the Aerosol Monitoring Station of the IAO SB RAS, and round-the-clock measurements of BC size distribution in the near-ground aerosol from 10 to 1000 nm had been started for the first time every 2 hours with one measurement cycle duration of 1.3 h. The diffusion method and BC spectrometer had been developed at the IAO SB RAS in cooperation with the IChKC SB RAS for measurement of the BC mass concentration and its size distribution in submicron particles (Kozlov *et al* 2016a). The method is based on the combination of a selector of particles (8-section diffusion battery of the grid type) (Reischl, 1991) and an *MDA-03* aethalometer (Kozlov *et al* 2016b) for measurements of the EBC concentrations at every section of the diffusion battery. The BC size distributions are determined from solution of the inverse problem (Cheng and Yeh, 1984). An iterative technique has been developed additionally for determination of the volume median diameter and a half-width in the approximation of unimodal lognormal distribution of absorbing matter.

The analysis of results of three-year monitoring of the BC size distribution in the near-ground aerosol has revealed stable regularities in the annual behavior of monthly average values of the BC volume median diameter  $D_m$ , nm and the distribution amplitude  $A_m$ ,  $\mu\text{m}^3/\text{cm}^3$ . The seasonal variability of these parameters for the unimodal lognormal size distribution includes a winter maximum and a summer minimum. Figure 1 shows the annual profile of  $D_m$  (vertical bars at the extremes of the curve are for the monthly average standard deviations SD). The estimates obtained have shown that the difference of the maxima and minima in the annual profile is statistically significant. The variability ranges for the diameter and the amplitude were  $D_m = 140\div 215$  nm (1.6 times) and  $A_m = 0.4\div 3.4$   $\mu\text{m}^3/\text{cm}^3$  (8.5 times). The half-width of the BC size distribution  $S = \ln\sigma_g$  varied within  $0.55\div 0.90$ . The form of the annual profile for this parameter is very unstable.

The dynamics of the volume median diameter  $D_m$  at the transition from winter to summer indicates the seasonal migration of BC over the size spectrum of submicron particles and demonstrates the decrease of the

BC coarseness in the warm season. The mentioned features are closely related to the influence of factors determining the generation and accumulation of BC and aerosol in surface air. The duration of heating period, contribution of traffic and the high frequency of temperature inversions in the lower troposphere of Siberia in winter also play an important role in dynamics of the aerosol and BC mass concentrations.

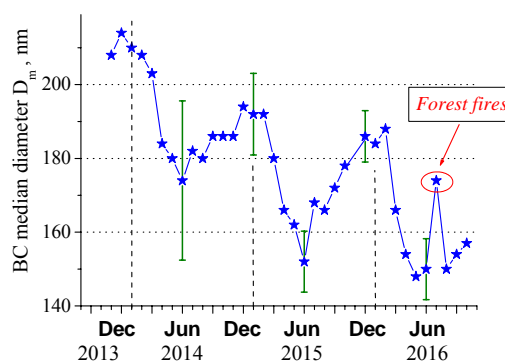


Figure 1. Annual behavior of the monthly averaged BC volume median diameter (and SD) in submicron aerosol

Measurements in July 2016 revealed the considerable impact of smokes from Siberian forest fires on the BC size distribution. The income of smoke plumes resulted in an increase of the monthly average value of the median diameter  $D_m$  from 150 to 175 nm (Fig. 1). At the same time, the diurnally average values of this parameter could achieve the level  $D_m \sim 200$  nm characteristic of the winter season.

As a conclusion from data of monitoring was revealed that the BC size distributions are characterized by stable seasonal dynamic that indicates the feasibility of parameterization of their annual behavior.

This work was supported by the Ministry of Education and Science of the Russian Federation (Agreement No. 14.604.21.0100 - ID RFMTFI60414X0100).

- Bond, T. C. et al. (2013). *J. Geophys. Res. Atmos.* **118**, 5380-5552.
- Cheng, Y. S., and Yeh, H. C. (1984). *Am. Ind. Hyg. Assoc. J.* **45**, 556-561.
- Kozlov, V.S., Shmargunov, V.P., Panchenko, M.V., Chernov, D.G., Kozlov, A.S., Malyshkin, S.B. (2016a). *Russian Physics Journal*. **58**,12,1804– 1810.
- Kozlov, V.S., Shmargunov, V.P., Panchenko, M.V. (2016b) *Proceedings of SPIE*. **10035**, 1003 30.
- Panchenko, M.V., Zhuravleva, T.B., Terpugova, S.A., Polkin, V.V., Kozlov, V.S. (2012). *Atmos. Meas. Tech.* **5**(7), 1513-1527
- Reischl, G.P., Majerovicz, A., Ankilov, A. et al. (1991). *J. Aerosol Sci.* **22**, 325-331.

## Correlation of temperature-resolved carbon fractions with individual organic compounds in PM<sub>2.5</sub> measured at a background site in South Korea

Yu Woon Chang<sup>1</sup>, Jong Sik Lee<sup>2</sup>, Eun Sil Kim<sup>3</sup>, Yong Pyo Kim<sup>4</sup>, Chang Hoon Jung<sup>5</sup>, Ji Yi Lee<sup>1,2\*</sup>

<sup>1</sup>Department of Environmental Engineering, Chosun University, South Korea,

<sup>2</sup>Department of Renewable Energy Convergence, Chosun University, South Korea,

<sup>3</sup>National Institute of Meteorological Sciences Anmyeondo Global Atmosphere Watch Station, Chungnam, South Korea.,

<sup>4</sup>Department of Chemical Engineering and Materials Science, Ewha Womans University, Seoul, South Korea,

<sup>5</sup>Department of Environmental Health, Kyungin Women's College, Incheon, South Korea.

Keywords: Anmyeon Island, Background site, NIOSH protocol, PM<sub>2.5</sub>, temperature-resolved fractions of OC and EC, WSOC, WISOC, HULIS-C, Individual organic compounds

Presenting author email: look412@naver.com, ljs1313@gmail.com, jsjili3@korea.kr, yong@ewha.ac.kr, jch@kiwu.ac.kr, yijiyi@gmail.com

Carbonaceous aerosol in PM<sub>2.5</sub> plays an important role in the atmosphere regard to regional and global climate change, visibility reductions and adverse health effects. Carbon fractions can be classified as Organic Carbon (OC) and Elementary Carbon (EC) by thermal-optical definition. Individual organic compounds in OC are mainly divided into 6 groups (polycyclic aromatic hydrocarbons, n-Alkanes, Hopanes, n-Alkanoic acids, Dicarboxylic acids and Sugars) according to characteristics of emission and formation.

Two major protocols for thermal-optical methods to classify OC and EC have been applied to atmospheric particulate matter, one is the IMPROVE protocol and the other is the NIOSH protocol. In the NIOSH protocol, OC can be divided by four OC fractions (OC1, OC2, OC3, and OC4 in a helium atmosphere at 310 °C, 475 °C, 615 °C, and 870 °C, respectively) and pyrolyzed-organic carbon (OP) was determined when transmitted laser light attained its original intensity after oxygen was added to the combustion atmosphere. And EC can be divided by six EC fractions (EC1, EC2, EC3, EC4, EC5 and EC6 in a 2% oxygen/98% helium atmosphere at 550°C, 625°C, 700°C, 775°C, 850°C and 870°C, respectively). The NIOSH protocol defined OC as OC1 + OC2 + OC3 + OC4 + OP and EC as EC1 + EC2 + EC3 + EC4 + EC5 + EC6 – OP, respectively.

Each temperature-resolved fraction of OC and EC has been reported to have different concentrations and distribution ratios by region and season, and different emission sources. Previous studies attempted the identification of source contributions of carbonaceous fractions using temperature-resolved carbon fractions and gasoline and diesel sources could be differentiated based on the abundance of individual temperature-resolved carbon fractions. Thus, understanding the characteristics of the temperature-resolved carbon fractions can be used to determine the specific source contribution of carbon fractions in PM<sub>2.5</sub>.

Organic speciation in PM<sub>2.5</sub> has been performed to use organic compounds as molecular markers for specific emission sources in the atmosphere based on the assumption that each molecular marker would originate from one unique source type. In this study, routine

measurements of OC and EC with organic compounds were carried out at Anmyeon Island which is a background area in Korea to understand the characteristics of carbon fractions in PM<sub>2.5</sub>, especially, the temperature-resolved OC and EC concentrations. Sampling was performed on every sixth day and a total of 59 samples were obtained during June 2015 and May 2016 using high volume air sampler with pre-baked quartz fiber filter. OC and EC were analyzed using the NIOSH protocol and organic compounds in PM<sub>2.5</sub> were identified and quantified using gas chromatography/mass spectrometry (GC/MS). Organic compounds analyzed in the study were classified into five groups, polycyclic aromatic hydrocarbons (PAHs), n-Alkanes, Dicarboxylic acids (DCAs), n-Alkanoic acids and Sugars. The OC1 and OP fractions were predominant in OC during cold season, while, the major fractions were OC1 and OC4 in summer. For EC, the major fractions were EC2 and EC3. We will figure out the formation characteristics of temperature-resolved OC and EC fractions through the correlation of temperature-resolved carbon fractions with the simultaneously analyzed individual organic compounds.

This work was funded by the Korea Meteorological Administration Research and Development Program under Grant CATER2014-3190.

Birch, M. E., and Cary, R. A. (1996). *Elemental Carbon-Based Method for Monitoring Occupational Exposures to Particulate Diesel Exhaust*, *Aerosol Sci. Technol.* 25:221–241.

Kim, E.; Hopke, P.K. *Improving Source Identification of Fine Particles in a Rural Northeastern U.S. Area Utilizing Temperature Resolved Carbon Fractions*; *J. Geophys. Res.* 2004, 109, D09204.

## Combined $^{14}\text{C}$ /AMS-PMF source apportionment during SOAS field campaign

M. Vonwiller<sup>1,2,3</sup>, G. Salazar<sup>1,3</sup>, W. W. Hu<sup>4,5</sup>, J.-L. Jimenez<sup>4,5</sup>, E. Edgerton<sup>6</sup>, S. L. Shaw<sup>7</sup>, A. S. H. Prevot<sup>8</sup>, S. Szidat<sup>1,3</sup>

<sup>1</sup>Department of Chemistry and Biochemistry, University of Bern, 3012 Bern, Switzerland.

<sup>2</sup>Laboratory of Radiochemistry, Paul Scherrer Institute, 5232 Villigen-PSI Switzerland.

<sup>3</sup>Oeschger Centre for Climate Change Research, University of Bern, 3012 Bern, Switzerland.

<sup>4</sup>Cooperative Institute for Research in Environmental Sciences, University of Colorado, Boulder, CO 80309, USA.

<sup>5</sup>Department of Chemistry & Biochemistry, University of Colorado, Boulder, CO 80309, USA

<sup>6</sup>Atmospheric Research and Analysis, Cary, NC 27513, USA.

<sup>7</sup>Environmental Sector, Electric Power Research Institute, Palo Alto, CA 94304, USA.

<sup>8</sup>Laboratory of Atmospheric Chemistry, Paul Scherrer Institute, 5232 Villigen-PSI, Switzerland.

Keywords: Carbonaceous aerosols, radiocarbon, AMS-PMF, SOA.

Presenting author email: [matthias.vonwiller@dcb.unibe.ch](mailto:matthias.vonwiller@dcb.unibe.ch)

The Southern Oxidant and Aerosol Study (SOAS) was a large field campaign during June-July 2013 in the southeast USA (Hu et al., 2015). Vast forested areas emitting large amounts of organic compounds and proximity to metropolitan areas present an ideal environment to investigate the influence of anthropogenic emissions like biomass burning on the biogenic secondary organic aerosol (SOA) formation. The main site of this study, located in rural Centreville AL, is equipped with meteorological monitoring devices and a wide variety of state-of-the-art analytical instruments. This project focusses on the source apportionment of the organic carbon (OC) fraction of ambient aerosol samples combining radiocarbon ( $^{14}\text{C}$ ) data with aerosol mass spectrometry positive matrix factorisation (AMS-PMF) (Zotter et al., 2014).

For  $^{14}\text{C}$  source apportionment, daily  $\text{PM}_{2.5}$  filters were analysed for the  $^{14}\text{C}$  levels in total carbon (TC) and elemental carbon (EC) by accelerator mass spectrometry. Sample preparation for EC isolation includes OC removal by water extraction and thermal removal of the retained water-insoluble OC using a thermal-optical OC/EC analyser (Sunset Laboratory) (Zhang et al., 2012). The remaining elemental carbon (EC) was combusted at  $760^\circ\text{C}$  in pure  $\text{O}_2$ . The evolved  $\text{CO}_2$  was guided to a gas inlet system, mixed with helium (Agrios et al., 2015) and measured with a Mini CARBON DATING System (MICADAS) (Szidat et al., 2014). The  $^{14}\text{C}$  content of the OC fraction was calculated for each day by isotopic mass balance (Fig. 1). Due to very low filter loading, samples were pooled for  $^{14}\text{C}$ -EC analysis over 1-4 days.

An AMS measured non-refractory organic and inorganic constituents in  $\text{PM}_1$  on site. PMF of the AMS mass spectra yielded 6 different factors: Biomass burning organic aerosol (BBOA), secondary organic carbon (SOC) formed through low volatility OC partitioning from isoprene (ISOPOOH-SOC), isoprene epoxydiols-derived SOC (IEPOX-SOC), low-oxidized oxygenated organic aerosol from biogenic sources (LO-OOAI), low-oxidized OOA from anthropogenic sources (LO-OOAII) and more-oxidized OOA (MO-OOA). For comparison of the two source apportionment methodologies, AMS-PMF

results were averaged over the same intervals as  $\text{PM}_{2.5}$  was sampled.

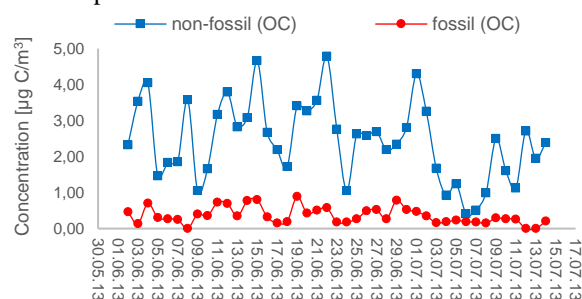


Fig. 1: Time series for the  $^{14}\text{C}$  source apportionment of OC in Centreville, AL.

A correlation analysis of results from both source apportionment techniques is performed. To gain more insight into the sources of SOA precursors, AMS-PMF results are combined with the results from the  $^{14}\text{C}$  source apportionment similar to the approach of Zotter et al. (2014). Statistically significant correlations between individual outcomes of both source apportionment approaches were found. From these, the fossil vs. non-fossil sources of SOA precursors are going to be discussed in detail.

All existing data on the  $^{14}\text{C}$  source apportionment confirm the expected high biogenic contribution at the Centreville site. OC measured offline by thermal optical reflectance (TOR, based on  $\text{PM}_{2.5}$ ) and measured online by AMS (based on  $\text{PM}_{2.5}$ ) are in overall acceptable agreement ( $r=0.81$ ), although an average ratio of  $\text{OC}_{\text{TOR}}/\text{OC}_{\text{AMS}}$  of  $\sim 1.4$  is observed.

Hu, W. W., et al. (2015), *Atmos. Chem. Phys.*, **15**, 11807-11833.

Zotter, P., et al. (2014), *J. Geophys. Res. Atmos.*, **119**, 6818-6835.

Zhang, Y.L. et al., (2012) *Atmos. Chem. Phys.*, **12** (22), 10841-10856.

Agrios, K., et al. (2015), *Nucl. Instr. Meth. B*, **361**, 288-293.

Szidat, S., et al. (2014), *Radiocarbon*, **56**, 561-566.

## Sector analysis of elemental and organic carbon (EC-OC) data from the Košetice Observatory (ACTRIS and EMEP site, Czech Republic)

M.Vana<sup>1</sup>, A.Holubová Šmejkalová<sup>1</sup>, E. Chalupníčková<sup>2</sup>

<sup>1</sup> Czech Hydrometeorological Institute, Kosetice Observatory, 394 22 Kosetice, Czech Republic

<sup>2</sup> Czech Hydrometeorological Institute, Central Laboratories, 143 06 Praha4, Czech Republic

Keywords: ACTRIS, elemental and organic carbon, air mass trajectories, Czech Republic  
Presenting author email: milan.vana@chmi.cz

Carbonaceous aerosol (TC) is a complex mixture of many organics (OC fraction) and elemental carbon (EC). EC is a product of anthropogenic activities, especially incomplete combustion of fossil fuels by transport, heating, power plants, wood and biomass burning and agriculture activities. EC could have larger health impact than other PM constituents (Cassee et al., 2013). Carbonaceous aerosols also play an important role in climate change (Boucher et al., 2013).

Regular EC-OC measurement has been implementing at the Košetice Observatory since February 2009 within the framework of EU-projects EUSAAR (European Supersites for Atmospheric Aerosol Research) and later ACTRIS (Aerosols, Clouds, and Trace gases Research Infrastructure Network) and ACTRIS-2.

Long-term air quality monitoring and research at Kosetice Observatory, operated by the Czech Hydrometeorological Institute (CHMI), has been carried out since 1988. The observatory is located in free area outside of settlement (49°35' N, 15°05' E, 534 m above sea level) and represents the Czech Republic in several international long-term monitoring programmes as EMEP (Co-operative Programme for Monitoring and Evaluation of Long-range Transmission of Air Pollutants in Europe), GAW (Global Atmosphere Watch) and International Co-operative Programme on Integrated Monitoring (ICP-IM) under the Convention of Long-Range Transport of Air Pollution (CLRTAP). Detailed information is available at (Vana et al., 2013)

Sampling frequency is every 6<sup>th</sup> day in fraction PM<sub>2.5</sub> on 2 quartz-fibre filters. Since October 2011 (within ACTRIS) the sampling on filters has been implementing behind the denuder catching the organic vapor. Amount of organic carbon (OC) on back quartz fiber filter represents positive artifact by measurement without denuder and negative artifact by measurements with denuder.

The analytical method is thermal-optical analysis. The samples are analyzed in CHMI Central Laboratories in Prague-Libuš using EC-OC Sunset Lab Dual Analyzer. Charring correction is made by laser transmission monitoring.

The mean annual concentration of total carbon in PM<sub>2.5</sub> in the period under review was 3,82 µg.m<sup>-3</sup>. The figure for elemental carbon (0,5 µg.m<sup>-3</sup>) represents the mean annual ratio of 13% on TC. EC-OC concentrations follow an annual course that reflects their emission levels, i.e. with maximums in winter and minimums in summer.

3D trajectories were used for sector analysis of measured EC-OC data (NILU, 2016).

Table 1. Mean concentration of EC, OC and TC according to classification of prevailing air masses (Košetice Observatory, 2009-2014).

	EC (µg/m <sup>3</sup> )	OC (µg/m <sup>3</sup> )	TC (µg/m <sup>3</sup> )	EC/TC (%)
N	0.47	3.39	3.86	12,1
NE	1.02	5,96	6.98	14,6
E	0.88	5.84	6,72	13.0
SE	0.68	4.44	5.12	13.2
S	0,55	3,98	4,51	12,2
SW	0,46	2,88	3,34	13,8
W	0,36	2,33	2,69	13,4
NW	0,31	2,34	2,65	11,7
total	0.50	3.32	3.82	13,0

The Table 1. shows that the highest concentrations of EC-OC are recorded in situations when air masses reach the territory of the Czech Republic from the north-eastern directions or the local air masses prevailing. On the other hand, the lowest concentrations are measured in the episodes, when the air masses have their origin from western directions. In winter time we found slightly increasing tendency in the concentrations from SE sector (EC 2,8 (µg/m<sup>3</sup>); OC 8,5(µg/m<sup>3</sup>). The difference between sectors is much larger in the cold period of the year. In the summer period the dominance of eastern sectors is not visible.

The research leading to these results has received funding from the project for support of national research infrastructure ACTRIS – participation of the Czech Republic (ACTRIS-CZ - LM2015037) – Ministry of Education, Youth and Sports of the Czech Republic

Cavalli, F., et al. 2016. A European aerosol phenomenology 4; harmonized concentrations of carbonaceous aerosol at 10 regional background sites across Europe. In press.

3D trajectories, [www.emep.int](http://www.emep.int). Kjeller, NILU (2016).

Vana, M., et al., 2013. Kosetice Observatory – 25 years. CHMU

## Characterizing the vertical presence of atmospheric black carbon in the Arctic during spring and summer

Hannes Schulz<sup>1</sup>, Marco Zanatta<sup>1</sup>, Andreas Herber<sup>1</sup> and Rüdiger Gerdes<sup>1</sup>

<sup>1</sup>Alfred Wegener Institute, Helmholtz Centre for Polar and Marine Research, Bremerhaven, 27570, Germany  
 Keywords: black carbon, single particle soot photometer, airborne measurements, Arctic atmosphere, transport.  
 Presenting author email: hschulz@awi.de

Albeit the role of black carbon as light absorbing aerosol and climate forcer is well recognized, especially in the Arctic, the uncertainty of its impact on the radiation budget is still considerable [AMAP, 2015]. This is caused, among other reasons, by the limited characterisation of the vertical distribution and seasonality of black carbon concentration and its properties. In order to better understand the spring and summer climatic impact of black carbon, the vertical distribution of refractory black carbon (rBC) concentration and particle diameter was quantified during spring 2014 and summer 2015 with two aircraft campaigns, as part of the NETCARE (Network on Climate and Aerosols: Addressing Key Uncertainties in Remote Canadian Environments) project. A single particle soot photometer was deployed on the research aircraft POLAR 6 during several flights conducted in the Western Arctic between about 65° and 83° North (Fig. 1).

During spring, the averaged rBC concentration ranged between 20 ng/m<sup>3</sup> and 30 ng/m<sup>3</sup>, almost one order of magnitude higher compared to summer, when mean concentration hardly exceeded 5 ng/m<sup>3</sup>. A decrease of rBC concentration with altitude was observed in spring, while rather constant rBC vertical presence was captured during summer. Furthermore, the rBC particle diameter undergo a dramatic shift from spring to summer, decreasing from 210 nm to 130 nm respectively. Although pollution events have been detected in the Canadian High Arctic (Alert and Eureka, Northwest Territories) and Sub-Arctic (Inuvik, Nunavut) during spring, its absolute rBC load and size distribution and altitude position were different. Sub-Arctic plumes were detected at higher altitudes and were characterized by wider vertical extend, higher rBC concentration and larger mean diameter compared to those encountered in the High Arctic.

The marked seasonality and spatial variability of the aforementioned BC properties might lead to a different impact of BC on the Arctic energy budget. Our work provides vertical, spatial and seasonal information of black carbon presence and characteristics in the Arctic, which will contribute to decrease the high uncertainty of radiative forcing and atmospheric warming estimations in the Arctic region [Samset et al., 2013].

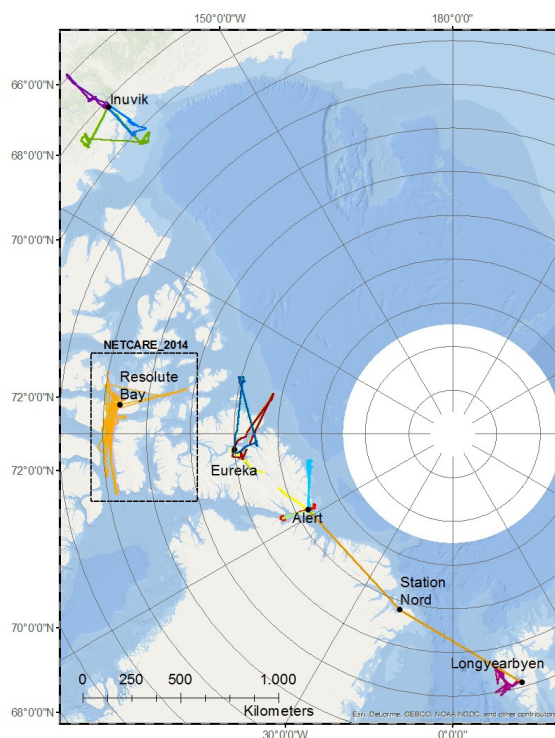


**Figure 1.** Map of the airfields and research stations from which measurement flights were operated during NETCARE 2014 (only Resolute/Lancaster Sound) and NETCARE 2015, traversing from Svalbard westward to the Alaskan boarder.

AMAP (2015). AMAP Assessment 2015: Black carbon and ozone as Arctic climate forcers. Samset, B. H., Myhre, G., Schulz, M., Balkanski, Y., Bauer, S., Bernsten, T. K., Bian, H., Bellouin, N., Diehl, T., Easter, R. C., Ghan, S. J., Iversen, T., Kinne, S., Kirkevåg, A., Lamarque, J.-F., Lin, G., Liu, X., Penner, J. E., Seland, Ø., Skeie, R. B., Stier, P., Takemura, T., Tsigaridis, K., and Zhang, K. (2013). Black carbon vertical profiles strongly affect its radiative forcing uncertainty. *Atmos. Chem. Phys.*, 13(5):2423–2434.

## Long-term trend of equivalent black carbon at different site types in Switzerland

Ch. Hueglin, A. Fischer, B. Schwarzenbach and L. Emmenegger

Empa, Swiss Federal Laboratories for Materials Science and Technology, Duebendorf, Switzerland

Keywords: traffic emissions, wood burning, aethalometer model, source apportionment.

Presenting author email: christoph.hueglin@empa.ch

Black carbon (BC) is one of the key constituents of atmospheric particulate matter and of high importance for air quality and climate change. Therefore, BC in PM<sub>2.5</sub> is measured at nine sites of the Swiss National Air Pollution Monitoring Network NABEL starting in 2007. Following the recommendations by Petzold *et al.* (2013), the light absorption of PM<sub>2.5</sub> is measured continuously by multi-angle absorption photometry or by using an aethalometer. Parallel to the light absorption measurements, elemental carbon in daily PM<sub>2.5</sub> samples is analysed using the thermal-optical method (TOT, EUSAAR-2 temperature protocol), allowing the determination of equivalent black carbon (EBC).

A trend analysis of the multi-year time series shows that EBC concentrations in Switzerland are clearly declining at all sites types (rural, suburban, urban and traffic sites). The annual changes are largest at the sites that are influenced by nearby road traffic emissions. The data analysis did not reveal regional differences in the temporal trends, although equivalent black carbon levels are generally higher south of the Alps compared to similar site types in the north.

At five of the sites, the light absorption of PM<sub>2.5</sub> is measured at multiple wavelengths. This allows the calculation of the contribution of traffic and wood burning emissions to total EBC since contributions from other sources of EBC can be neglected in Switzerland. The long-term trend of equivalent black carbon from traffic (EBC<sub>TR</sub>) and from wood burning emissions (EBC<sub>WB</sub>) has therefore been determined at those five sites using the methodology described in Zotter *et al.* (2016).

Figure 1 shows the monthly concentrations for EBC<sub>TR</sub> and EBC<sub>WB</sub> as well as the trend lines estimated from de-seasonalized data. EBC<sub>TR</sub> is significantly declining (95% confidence level) at all of the sites (note that at two of the sites single wavelength light absorption measurements have been replaced by multi-wavelength instruments only a few years ago). In contrast, the contributions from wood burning emissions remained constant during the past years at all of the sites. The negative temporal trend in total EBC is thus entirely due to declining contributions from internal combustion engines, i.e. mainly road traffic and some off-road vehicles and stationary diesel engines.

These observations illustrate a remarkable success of the measures taken to reduce black carbon emissions from road traffic and other engines, in particular the introduction of diesel particle filters. In contrast, little progress has been made for the reduction of black carbon emissions from wood burning appliances. As a consequence, the contribution from

wood burning emissions to total EBC has reached or even surpassed the traffic contribution at some locations, for example at a rural site in an alpine valley in Southern Switzerland (Fig. 1).

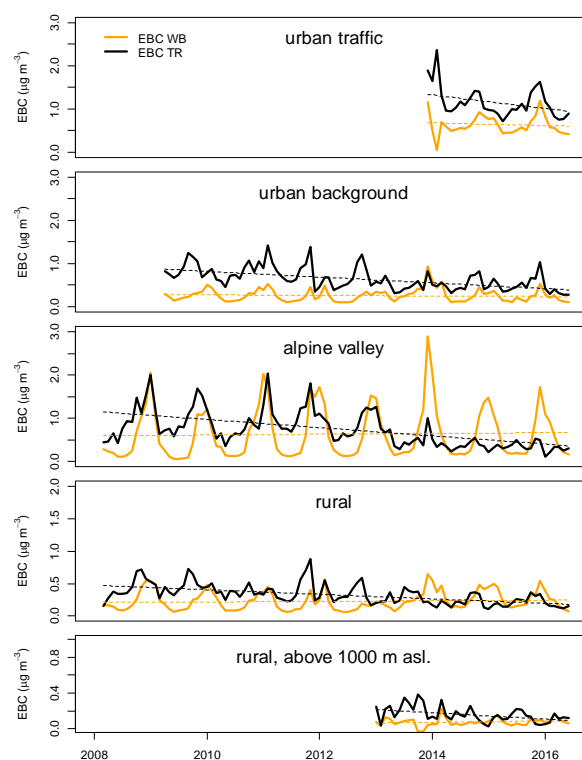


Figure 1. Time series of monthly equivalent black carbon from traffic (EBC<sub>TR</sub>) and from wood burning (EBC<sub>WB</sub>) at sites in Switzerland representing different environments. The broken lines indicate the corresponding linear trends.

This work was supported by the Swiss Federal Office for the Environment (FOEN) and the Competence Center Environment and Sustainability (CCES) through the project OPTIWARES.

Petzold, A., J. A. Ogren, M. Fiebig, P. Laj, S. M. Li, U. Baltensperger, T. Holzer-Popp, S. Kinne, G. Pappalardo, N. Sugimoto, C. Wehrli, A. Wiedensohler and X. Y. Zhang (2013). *Atmos. Chem. Phys.*, 13(16): 8365-8379.

Zotter, P., H. Herich, M. Gysel, I. El-Haddad, Y. Zhang, G. Močnik, C. Hüglin, U. Baltensperger, S. Szidat and A. S. H. Prévôt (2016). *Atmos. Chem. Phys. Discuss.*, doi:10.5194/acp-2016-621, in review.

## Multi Seasonal Functional Group Analysis by FT-IR Spectroscopy of Atmospheric Aerosol in Zurich

M. Reggente<sup>1</sup>, G. Ruggeri<sup>1</sup>, C. Hüglin<sup>2</sup>, and S. Takahama<sup>1</sup>

<sup>1</sup>Atmospheric Particle Research Laboratory, École Polytechnique Fédérale de Lausanne, Lausanne, Switzerland

<sup>2</sup>Empa, Swiss Federal Laboratories for Materials Science and Technology, Dübendorf, Switzerland

Keywords: Atmospheric aerosols, FT-IR, functional groups.

Presenting author email: matteo.reggente@epfl.ch

Atmospheric particulate matter (PM) has been associated with increased morbidity and mortality, reduced visibility, and is one of the least understood components of the climate system. Organic matter (OM) constitutes a substantial fraction (up to 80%) of PM (Lim and Turpin 2002), and its quantification and characterization can help in understanding the impact of atmospheric aerosol on health and climate. OM is a complex mixture of thousands of different organic molecules that vary in structure and physicochemical properties (Hamilton et al. 2004). The functional group (FG) representation simplifies the chemical analysis of OM by providing information about properties like volatility and hygroscopicity and can be used for overall organic matter and organic carbon (OC) quantifications, and its apportionment by source class (Russell et al., 2011).

We use the Fourier transform infrared (FT-IR) absorbance spectra of atmospheric aerosol (PM<sub>2.5</sub>) collected on Teflon filters to characterize the chemical composition of OM using the FG representation. Teflon filters are collected daily at the National Air Pollution Monitoring Network (NABEL) station in Zurich (Switzerland) from the 1<sup>st</sup> of April 2016 (until the 31<sup>st</sup> of March 2017). We processed the spectrum of each sample to correct the drift of the baseline and substrate interference using the method proposed by Kuzmiakova et al. (2016). We quantify the functional group composition of the ambient samples by fitting individual Gaussian line shapes (top panel in Fig. 1). We quantified alcohol COH, carboxylic COOH, alkane CH, carbonyl CO, and amine NH functional groups, as described in Takahama et al. (2013). We use the FT-IR spectra to apportion OM and FGs associated with traffic emission and wood burning using collocated measurements of black carbon (BC – light absorption of PM<sub>2.5</sub> measured at multiple wavelengths).

An example of FG study is shown in Fig. 1 for a sample collected in November 2016. The FG distribution shows that alkane CH accounts the 39% of the total OM. The significant contributions of alcohol and carboxylic acid (16% and 29% respectively) exemplifies the influence of processed aerosol from surrounding regions affecting the PM<sub>2.5</sub> in Zurich. Moreover, the high OM/OC ratio (2.01) with substantial contributions from alcohol, and carbonyl FGs are consistent with those found in biogenic or wood-burning samples (Russell et al., 2011). These sources have also been reported in previous studies of Zurich PM by carbon isotope analysis Szidat et al. (2004) and aerosol mass spectrometry (Canonaco et al., 2015).

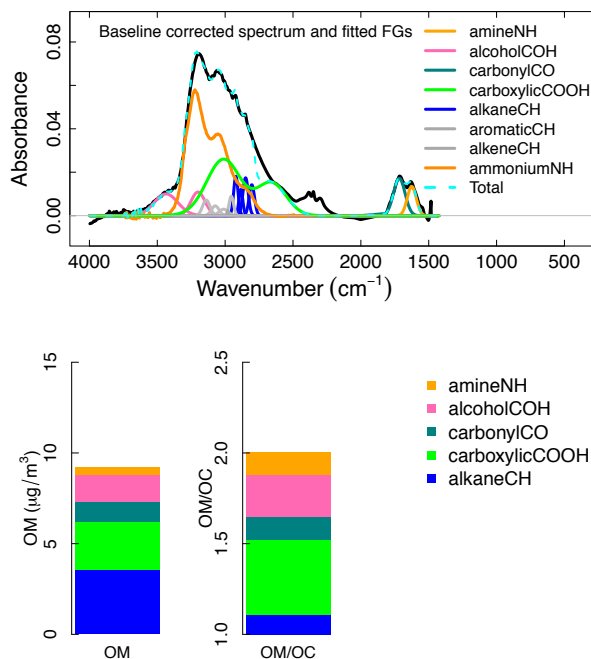


Figure 1. Example of FG analysis by FT-IR spectroscopy of atmospheric aerosol collected on one Teflon filter. Top panel: baseline corrected spectrum with fitted FGs. Bottom panel: FG contributions to total OM and their heteroatom contributions to the total OM/OC ratio (Takahama and Ruggeri, 2016).

The authors acknowledge funding from the Swiss Federal Office for the Environment (FOEN, P135-1008) and EPFL.

- Hamilton, J. F., et al., (2004), *Atmos. Chem. Phys.*, **4**, 1279-2004.
- Kuzmiakova, et al., (2016), *Atmos. Meas. Tech.*, **9**, 2615-2631.
- Lim, HJ., and Turpin, BJ., (2002) *Environ. Sci. Technol.*, **36**, 4489-96.
- Russell, L. M., et al., (2011), *P. Natl. Acad. Sci.*, **108**, 3516-3521.
- Szidat, S., et al., (2004), *Atmos Environ.*, **38**, 4035-4044.
- Canonaco, F., et al., (2015), *Atmos. Chem. Phys.*, **15**, 6993-7002.
- Takahama, S., et al., (2013), *Aerosol Sci. Technol.*, **47**, 310-325.
- Takahama, S. and Ruggeri, G., (2016), *Atmos. Chem. Phys. Discuss*, **2016**, 1–33.

## Ecotoxicity of humic-like substances

G. Kiss<sup>1</sup>, M. Gángó<sup>2</sup>, E. Horváth<sup>2</sup>, K. Imre<sup>1</sup> and N. Kováts<sup>2</sup>

<sup>1</sup>MTA-PE Air Chemistry Research Group, Veszprém, H-8200, Hungary

<sup>2</sup>Department of Environmental Science, University of Pannonia, Veszprém, H-8200, Hungary

Keywords: ecotoxicity, humic-like substances (HULIS), atmospheric aerosol

Presenting author email: kornelia@almos.uni-pannon.hu

Depending on the sampling site humic-like substances (HULIS) account for 30%-70% of the water-soluble organic fraction in atmospheric aerosol. Because of their abundance in atmospheric aerosol the physical, chemical, physico-chemical properties as well as the sources and formation processes of HULIS have been investigated thoroughly in the past 15-20 years (e.g. Graber and Rudich, 2006). However, it is not clear what effect humic-like substances – that can be released directly from biomass burning but also form and transform in the atmosphere – may have on living organisms.

In our study the ecotoxicity of humic-like substances isolated from rural aerosol and its relationship with chemical properties have been examined.

### Method

Sampling was carried out at K-puszta station, Hungary (46° 58' N, 19° 33' E, 126 m a.s.l.) between May 2014 and April 2015. Twenty four hour samples were collected on glass fibre filters (Ø=150 mm) with a Digital DHA-80 high volume sampler equipped with a PM2.5 inlet and operated at a flow rate of 30 m<sup>3</sup>h<sup>-1</sup>. Humic-like substances were isolated from the aqueous extracts of 24 samples using the method developed by Varga et al. (2001) and then analysed with UV spectrophotometry, fluorescence spectrometry and mass spectrometry (both with direct injection and following HPLC separation). The ecotoxicity of HULIS was characterized by a method based on the inhibition of the bioluminescence of *Vibrio fischeri* (ISO 21338:2010: Water quality - Kinetic determination of the inhibitory effects of sediment, other solids and colored samples on the light emission of *Vibrio fischeri* /kinetic luminescent bacteria test/) adapted to study aerosol particles (Kováts and Horváth, 2016).

### Results

First, the total carbon content of the isolated HULIS was determined then the carbon content was converted to HULIS mass (Kiss *et al.*, 2002) and compared to PM2.5 mass. The average atmospheric concentration of HULIS in PM2.5 aerosol was 1.4 and 2.9 ug m<sup>-3</sup> in summer and winter, respectively. The higher average concentration in winter may result both from higher emission and lower mixing height typical for the cold season. On average, HULIS accounted for 19% and 13% of PM2.5 mass in summer and winter, respectively.

The ecotoxicity tests gave different results for the summer and winter samples: HULIS isolated from the winter samples were found to be more toxic for the test organisms. EC<sub>50</sub> values obtained in our study were compared to literature data obtained with the same method and it was found that the ecotoxicity of HULIS isolated from summer samples was comparable to that of urban PM10 aerosol collected in summer. The ecotoxicity of HULIS isolated from winter samples exceeded that of urban PM10 aerosol collected in winter and approximated the ecotoxicity of Diesel particles.

This seasonal difference was observed also in the UV spectrophotometric and fluorescence spectrometric analyses. The specific UV absorbance (normalized to carbon content) of HULIS isolated from winter samples was greater and the spectrum looked somewhat different from that of the summer samples. The absorbance ratio E<sub>250</sub>/E<sub>365</sub> as well as the results of fluorescence spectrometric analyses indicated higher aromaticity of HULIS in the winter samples.

HPLC-MS analyses revealed the presence of nitrocatechol and its homologues in the winter samples. These compounds have been suggested in the literature as tracers of secondary aerosol related to biomass burning. These results agree well with earlier findings showing that at K-puszta the dominant source of the organic aerosol is biomass burning in wintertime.

By summarizing our results it can be presumed that the elevated ecotoxicity of HULIS in winter samples is connected to its higher aromaticity and the dominant source for these compounds is biomass burning.

### Acknowledgement

Ecotoxicity tests were accomplished with the support of the GINOP-2.3.2-15-2016-00017 project.

### References

- Graber, E.R., Rudich, Y. (2006) *Atmos. Chem. Phys.*, **6**, 729-753.
- Kiss, G., Varga, B., Galambos, I. and Ganszky, I. (2002) *J. Geophys. Res.* **107**, 8339-8346.
- Kováts, N., Horváth, E., (2016) *Luminescence*, **31/4**, 918-923.
- Varga, B., Kiss, G., Ganszky, I., Gelencsér, A., Krivácsy, Z. (2001) *Talanta*, **55/3**, 561-572.

**Seasonal variability of carbonaceous aerosols in South-East Italy**D. Cesari<sup>1</sup>, E. Merico<sup>1</sup>, A. Dinoi<sup>1</sup>, A. Marinoni<sup>2</sup>, P. Bonasoni<sup>2</sup>, and D. Contini<sup>1</sup><sup>1</sup> Istituto di Scienze dell'Atmosfera e del Clima, ISAC-CNR, S.P. Lecce-Monteroni km 1.2, 73100 Lecce, Italy<sup>2</sup> Istituto di Scienze dell'Atmosfera e del Clima, ISAC-CNR, 40129 Bologna, Italy

Keywords: organic carbon, elemental carbon, black carbon, temporal trend.

Presenting author email: d.cesari@isac.cnr.it

Organic (OC) and Elemental Carbon (EC) are important components of atmospheric aerosol particles that play a key role in climate system and affect human health. There is a lack of data reported for Southern Italy (Sandrini et al., 2014) and this work aims to fill this gap, focusing the attention on the long-term trends of OC and EC concentrations and on atmospheric processes and sources that influence this temporal variability. Measurements were taken at the Environmental-Climate Observatory of Lecce (SE Italy), regional station of the Global Atmosphere Watch program (GAW-WMO). The Observatory (40°20'8"N-18°07'28"E, 37 m a.s.l.) is located at about 4 km (SW) from the urban area of Lecce and can be classified as an urban background site. The site is located 30 km and 80 km from the most important industrial centers of the Apulia Region (Taranto and Brindisi) and is sometimes influenced by primary and secondary anthropogenic aerosol particles transported from these industrial settlements. A 3-years monitoring campaign has been performed between July 2013 and July 2016. Daily PM<sub>10</sub> and PM<sub>2.5</sub> samples were collected on quartz fiber filters (Whatmann, 47 mm in diameter) using an automatic sampler, that also provides aerosol mass measurement, based on the  $\beta$  attenuation method (SWAM 5A Dual Channel Monitor). The quartz fiber filters were thermally pre-treated in an oven at 700°C during 2 hours to remove possible organic contamination, and stored in a conditioned room (20°C and 50% RH) until the sampling. After sampling, all filters were stored at 4°C until the chemical analysis. From December 2014, simultaneous equivalent Black Carbon (eBC) concentrations (in PM<sub>10</sub> fraction) were measured using a Multi Angle Absorption Photometer (MAAP Thermoscientific, mod. 5012). Main meteorological parameters (ambient temperature, pressure, RH, wind direction and velocity) were also observed. From the whole PM dataset, a couple of samples PM<sub>10</sub>/PM<sub>2.5</sub> was taken every 3 day, in order to obtain a good statistical representation of the studied period, obtaining a subset of 722 PM samples (361 for PM<sub>10</sub> and 361 for PM<sub>2.5</sub>). These samples were analyzed by using a thermo-optical method with a Sunset Laboratory OC/EC analyzer, providing elemental and organic carbon concentrations. Punches of 1.0 cm<sup>2</sup> were cut from the filters and analyzed according to the NIOSH870 protocol. Results show average concentrations of 28.8  $\mu\text{g}/\text{m}^3$  for PM<sub>10</sub> and 17.5  $\mu\text{g}/\text{m}^3$  for PM<sub>2.5</sub>. In PM<sub>10</sub>, the average OC and EC concentrations were 5.4  $\mu\text{g}/\text{m}^3$  and 0.8  $\mu\text{g}/\text{m}^3$  respectively. In the fine fraction (PM<sub>2.5</sub>), the average OC and EC concentrations were 4.7  $\mu\text{g}/\text{m}^3$  and 0.6  $\mu\text{g}/\text{m}^3$  respectively. The OC/EC minimum ratio method was used, separating cold (autumn and winter) and warm (spring and summer) seasons, for estimating the

secondary organic carbon (SOC). SOC was mainly segregated in PM<sub>2.5</sub>, representing 53% - 75% of the total OC (Fig. 1a). The SOC seasonal variation shows higher concentrations during the cold months, because of the meteorological conditions favorable to secondary organics species formation. The EC was mainly present in PM<sub>2.5</sub> (Fig. 1b), with higher concentrations in cold months, because the stronger influence of combustion sources (biomass burning, domestic heating and road traffic) combined with the lower wintertime PBL. A subset of EC data was compared with eBC measurements, showing a good correlation ( $R^2=0.80$ ), however, eBC concentrations were often higher than EC concentrations. These differences could be explained by non-negligible presence of Brown Carbon (BrC), for example from biomass burning (Andreae and Gelencsér, 2006) and the assumption that the measured absorption coefficients by the MAAP is ascribed to eBC. This is in agreement with the biomass burning activities due to agricultural practices and domestic heating present in the studied area.

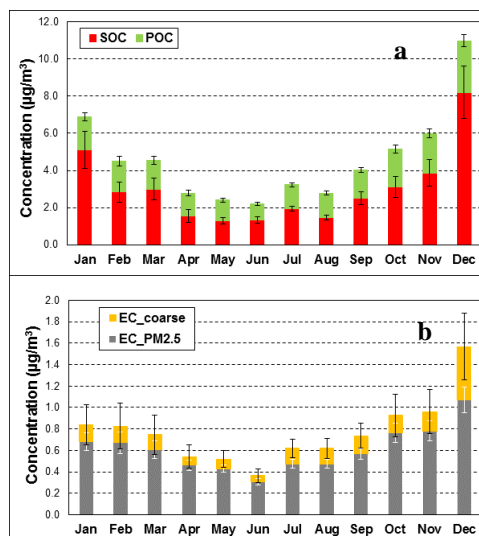


Figure 1. (a) SOC and POC in PM<sub>2.5</sub>; (b) EC in fine and coarse fraction (PM<sub>2.5-10</sub>).

Work supported by I-AMICA (Infrastructure of High Technology for Environmental and Climate Monitoring - PONa3\_00363) project funded by National Operational Program (PON) for "Research and Competitiveness 2007-2013" co-funded with European Regional Development Fund (ERDF) and National resources.

Sandrini, S., Fuzzi, S., Piazzalunga, A., et al. (2014) *Atmos. Environ.* **99**, 587-598.

Andreae, M.O. and Gelencsér, A. (2006) *Atmos. Chem. Phys.* **6**, 3131-3148.

## Highly Time Resolved Measurement of Atmospheric Elemental and Organic Carbon at a Typical Background Site in Central Europe

S. Mbengue<sup>1</sup>, M. Fusek<sup>2</sup>, J. Schwarz<sup>3</sup>, I. Holoubek<sup>1,4</sup>

<sup>1</sup>Global Change Research Institute of the CAS, Brno, 60300, Czech Republic

<sup>2</sup>Faculty of Electrical Engineering and Communication, Brno University of Technology, Brno, 61600, Czech Republic

<sup>3</sup>Institute of Chemical Process Fundamentals of the CAS, Prague, CZ-18000, Czech Republic

<sup>4</sup>Research Centre for Toxic Compounds in the Environment, Masaryk University, Brno, 62500, Czech Republic

Keywords: Organic carbon and elemental carbon, rural background, OC/EC ratio, OC-EC variability.

Presenting author email: [mbengue.s@czechglobe.cz](mailto:mbengue.s@czechglobe.cz)

Atmospheric organic (OC) and elemental (EC) carbon play an important role in atmospheric chemistry, climate change and public health. There have been relatively few studies dealing with atmospheric EC and OC in rural background sites which are less influenced by urban and industrial emissions. Nevertheless, measurements at background areas are important for understanding the transport and transformation characteristics of anthropogenic air pollutants, and their effects on various aspects of regional and global environment changes. In this study, we focus on variability of EC and OC concentrations (considering various day categories and seasons) from a rural background site which is representative for Central European rural areas.

The EC and OC in fine aerosols (PM<sub>2.5</sub>; smaller than 2.5 μm) were measured at the rural background atmospheric station (AS) in Křešín u Pacova (49°35'N, 15°05'E), which is a part of Košetice National Atmospheric Observatory, central Czech Republic. Measurements were performed from March 2013 to December 2016 at ground with a 4h time resolution using a field Semi-Continuous OCEC Aerosol Analyzer (Sunset Laboratory Inc., USA).

The mean EC and OC concentrations are comparable to those previously observed by Vodicka et al. (2015) at Košetice. During our observation period, EC and OC concentrations varied depending on the season with higher mean concentrations in winter ( $0.82 \pm 0.68$  and  $3.30 \pm 2.23 \mu\text{g}\cdot\text{m}^{-3}$  respectively) than in summer ( $0.34 \pm 0.18$  and  $2.30 \pm 1.15 \mu\text{g}\cdot\text{m}^{-3}$  respectively), which is likely related to higher energy consumption (residential heating, traffic) and unfavourable meteorological conditions (worse dispersion of pollutants) during winter. A high correlation ( $r^2 > 0.7$ ) between EC and OC observed in winter suggests that they were mainly controlled by similar sources and/or transported simultaneously to the receptor site. On the contrary, the weak correlation ( $r^2 = 0.3$ ) between them in summer suggests different sources and/or different transport characteristics of OC and EC. The OC/EC ratio has been examined for indication of possible sources of OC and EC at the AS Křešín. As expected for rural and background sites, the OC/EC ratio was most of the time (63%) larger than 4, suggesting that OC measured here was not only from direct emissions of particles from traffic combustion sources, but also produced by biomass burning and coal combustion or in the form of secondary

organic carbon (SOC) formed in the atmosphere by chemical reactions (Zhang et al., 2012). The obtained results show higher OC/EC ratio in summer ( $7.3 \pm 3.3$ ) than in winter ( $4.5 \pm 1.9$ ). In July, corresponding to the warmer period (the highest temperature) in the year, a peak of OC and OC/EC ratio was observed. These high OC/EC ratios could be explained by biogenic SOC formed during period of high photochemical activity. The diurnal variability of EC and OC was more pronounced in winter than in summer probably related to the larger influence of traffic emission during wintertime.

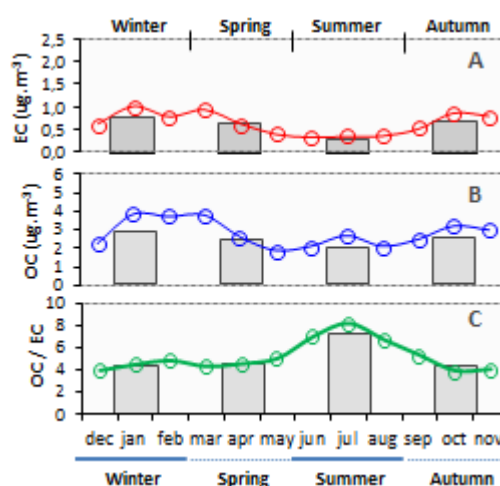


Figure 1: Monthly (line) and seasonal (bars) of EC (A) and OC (B) means concentrations and OC/EC ratio (C) at Křešín rural background station from 2013 to 2016.

This work has received funding from the European Union's Horizon 2020 research and innovation programme under grant agreement No. 654109, and from the project for support of national research infrastructure ACTRIS – participation of the Czech Republic (ACTRIS-CZ - LM2015037) – Ministry of Education, Youth and Sports of the Czech Republic.

Dvorská, A., Lammel, G., and Holoubek, I. (2009). *Atmos. Environ.*, **43**, 1280–1287.

Vodička P., Schwarz J., Cusack M., Ždímal V., 2015. *Sci. Total Environ.* **518**-519, 424-433.

Zhang, R., Tao, J., Ho, K.F., Shen, Z., Wang, G., Cao, J., Liu, S., Zhang, L., Lee, S.C. (2012). *Aerosol Air Qual. Res* **12**, 792–802.

## Photophoresis of fractal-like soot aggregates: new microphysical model and atmospheric applications

S.A. Beresnev, L.B. Kochneva, V.I. Gryazin, M.S. Vasiljeva

Institute of Natural Science and Mathematics, Ural Federal University, Ekaterinburg, 620083, Russia

Keywords: stratospheric aerosols, black carbon, fractal-like particles, photophoresis

Presenting author email: sergey.beresnev@urfu.ru

The theoretical description of photophoretic motion of soot aggregates, as a rule, is carried out for the model of homogeneous spherical particles without the necessary account of fractal-like structure of aggregates. This assumption can result not only in quantitative distinctions, but also to qualitative errors at the description of effects.

Nowadays, the theory of longitudinal radiometric photophoresis for spherical homogeneous particles by Beresnev *et al* (1993) has found confirmation in experiments with model macroscopic particles and real carbonaceous aerosols for a complete set of determining parameters. However, the most part of soot (black carbon) atmospheric particles have a fractal-like structure, and we can expect essential changes of thermal and optical characteristics of these aggregates in comparison with homogeneous spheres.

This report summarizes analysis and estimations of the photophoretic effects for soot atmospheric aerosols on the basis of new microphysical model by Beresnev *et al* (2014–2016). In new microphysical model the mathematical formalism used in model for homogeneous spheres by Beresnev *et al* (1993) is kept at correct treatment of key parameters. The correct estimation of effective density and effective heat conductivity of fractal-like aggregates as equivalent spheres can be successfully executed on the basis of “thermal” model by Evans *et al* (2008). On Fig. 1 the comparison of the new “photophoretic” theory for fractal-like particles with the unique experimental data by Karasev *et al* (2004) is presented.

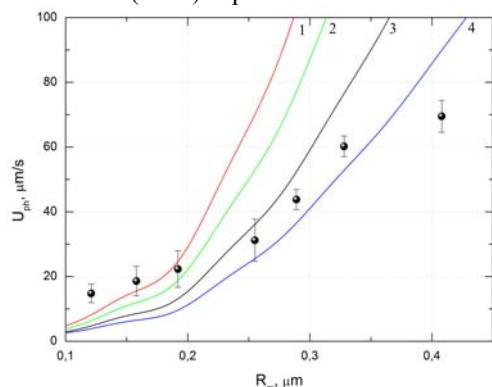


Figure 1. The comparison of the new theory for fractal-like soot aggregates with experiment by Karasev *et al* (2004). Black circles – experiment; 1 – FLP-theory for primary particles radius  $R_p=15$  nm; 2 – 20 nm; 3 – 30 nm; 4 – 40 nm. The heat conductivity of primary particles  $\lambda_a=80$  W/(mK), fractal dimension of aggregates  $D_f=1.80$ , light beam intensity  $I=2.5$  W/cm<sup>2</sup> (helium-neon laser with wavelength  $\lambda=0.68$   $\mu$ m).

The new model allows to carry out the estimations of photophoretic effects for soot aerosol in atmosphere similar with presented earlier by Beresnev *et al* (2012) for homogeneous spheres. The analysis of received results shows that for fractal-like soot particles the essential photophoretic effects in stratosphere are important: the essential photophoretic vertical velocities, excess of photophoretic forces over gravity, possibility of a levitation of particles at certain altitudes in the middle stratosphere (Fig. 2).

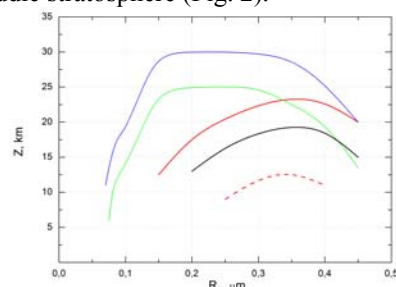


Figure 2. Altitudes of possible localization of soot particles in stationary equatorial atmosphere. Blue and green lines – homogeneous spheres at  $A=5$ ,  $\rho=0.165$  g/cm<sup>3</sup> and  $0.350$  g/cm<sup>3</sup>, correspondingly; red solid line – FLP-model at  $D_f=1.80$ ,  $\rho_a=2$  g/cm<sup>3</sup>;  $R_p=20$  nm,  $\lambda_a=50$  W/(mK); black solid line – the same, but  $\lambda_a=100$  W/(mK); red dash line –  $R_p=40$  nm,  $\lambda_a=50$  W/(mK).

This work was supported by the Ministry of Education and Science of the Russian Federation, the research project for UrFU #2189; and by the grant of President of Russian Federation for the state support of young Russian scientists #MK-9289.2016.5.

Beresnev, S.A., Chernyak, V.G. and Fomyagin, G.A. (1993) *Phys. Fluids A* **5**(8), 2043-2052.

Beresnev, S.A., Kochneva, L.B., Zhuravleva, T.B. and Firsov, K.M. (2012) *Atmos. Oceanic Opt.* **25**(4), 286-291.

Beresnev, S.A., Vasiljeva, M.S., Gryazin, V.I. and Kochneva, L.B. (2014) *Proc. SPIE* **9292**, paper 92920Z.

Beresnev, S.A., Vasiljeva, M.S., Gryazin, V.I. and Kochneva, L.B. (2015) *Proc. SPIE* **9680**, paper 96800W.

Beresnev, S.A., Vasiljeva, M.S., Gryazin, V.I. and Kochneva, L.B. (2016) *Proc. SPIE* **10035**, paper 10035-62.

Evans, W., Prasher, R., Fish, J. *et al.* (2008) *Int. J. Heat Mass Transfer* **51**, 1431-1438.

Karasev, V.V., Ivanova, N.A., Sadykova, A.R. *et al.* (2004) *J. Aerosol Sci.* **35**(3), 363-381.

## Calculating mass absorption cross-sections from elemental and organic carbon analysis

E.M.G. Nicolosi<sup>1,2</sup>, P. Quincey<sup>2</sup> and G.W. Fuller<sup>1</sup>

<sup>1</sup>MRC-HPA Centre for Environment and Health, School of Biomedical & Health Sciences, King's College London, SE1 9NH, UK

<sup>2</sup>Environment Division, National Physical Laboratory, Teddington, TW11 0LW, UK

Keywords: Pyrolysed carbon, ECOC analysis, optical attenuation, absorption cross section.

Presenting author email: eleonora.nicolosi@kcl.ac.uk

### Introduction

The Attenuation Versus Evolved Carbon (AVEC) plot is a new way to represent thermal- optical EC/OC analysis data. Unlike the thermogram, which is the usual method of presenting the analysis data, it provides information about the sample properties rather than the instantaneous instrument sensor status.

The plot can be used to refine the determination of organic carbon (OC) and elemental carbon (EC) split point; to investigate the optical properties of the particles; and to spot the occurrence of early evolution of EC during the inert phase.

### Method

A Sunset Laboratory Thermal-Optical Carbon Aerosol Analyser was used for the EC/OC analysis. 149 samples from three locations in the London area were analysed with two protocols, EUSAAR2 (Cavalli et al., 2010) and NIOSH-like Quartz (Birch and Cary, 1996). In the AVEC plot the accumulated carbon concentration (the integrated FID signal) is plotted against the attenuation ( $\ln(I_0/I)$  where  $I_0$  is the laser transmittance measured at the end of the analysis when all the carbonaceous compounds were desorbed), as the analysis proceeds, as shown in Figure 1.

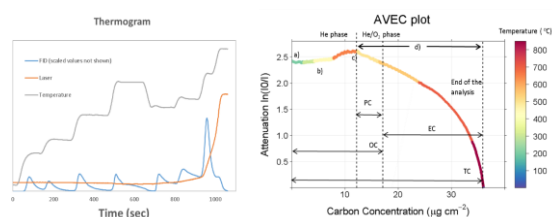


Figure 1. On the left is a thermogram and on the right the corresponding AVEC plot: the colours indicate the expected sample temperature, on the x-axis is the evolved carbon concentration ( $\mu\text{g} \cdot \text{cm}^{-2}$ ) and on the y-axis the attenuation ( $\ln(I_0/I)$ ).

### Results and discussion

The gradient of the AVEC plot curve in the oxygenated phase provides information about the mass absorption cross section ( $\sigma$ ) of the particles leaving the filter. This information will be a combination of the particles'  $\sigma$ , within-filter scattering effects, the effects of undetected scattered light, and shadowing effects, as for filter-based black carbon (BC) measurements.

The instrumental split point determination relies on either the pyrolysed carbon (PC) formed during the He-mode having the same  $\sigma$  as the native atmospheric EC, or all PC formed during the He-mode evolving completely from the filter before the native EC. Many results in the published literature demonstrate that neither of the assumptions is valid (Yu et al., 2002). Many studies claim that the  $\sigma$  of EC and PC is not the same and, in particular, PC has higher values (Subramanian et al., 2006).

We found out that although the Quartz protocol produced more additional attenuation than the EUSAAR2 protocol, the PC concentration ( $\mu\text{g} \cdot \text{cm}^{-2}$ ) calculated by the instrument was comparable. This suggests that the  $\sigma$  of the PC was higher in the Quartz samples than the EUSAAR samples.

We also measured the average apparent  $\sigma$  of the particles leaving the filter during the oxygenated phase (PC + EC), and found values comparable to the literature ( $30 \pm 6 \text{ m}^2 \cdot \text{g}^{-1}$  in rural samples,  $23 \pm 6 \text{ m}^2 \cdot \text{g}^{-1}$  in urban samples and  $12 \pm 3.5 \text{ m}^2 \cdot \text{g}^{-1}$  in roadside samples). To avoid the shadowing effect, we also measured  $\sigma$  for the particles leaving the filter at the end of the analysis. The  $\sigma$  values, which are expected to be a combination of inherent  $\sigma$  together with fixed instrumental factors, were consistent between the different sites and similar to the values found in literature for PC ( $45 \pm 10 \text{ m}^2 \cdot \text{g}^{-1}$  in rural samples,  $42 \pm 8 \text{ m}^2 \cdot \text{g}^{-1}$  in urban samples and  $35 \pm 14 \text{ m}^2 \cdot \text{g}^{-1}$  in roadside samples).

### Conclusion

The mass absorption cross section of PC was dependent on the protocol used, which may limit the use of PC as a source marker. Quantification of mass absorption cross sections in this way is highly relevant to black carbon measurement using filter-based methods.

### References

- Birch, M.E. and Cary, R.A. (1996). *AST* **25**(3), 221-241.
- Cavalli, F. et al., (2010) *AMT* **3** 79-89.
- Subramanian, R et al, 2006. *AST* **40**(10), 763-780.
- Yu, et al., 2002. *Environmental science & technology*, **36**, 754-761.

### Acknowledgements

This work is funded by the Engineering and Physical Sciences Research Council and by the National Physical Laboratory.

## Temporal variability and implications to estimates of black carbon radiative forcing over an ecologically sensitive zone in Central India

A K Paswan<sup>2</sup>, A Singh<sup>1</sup>, S Kumar<sup>1</sup>, R S Raman<sup>1,2</sup>

<sup>1</sup>Department of Earth and Environmental Sciences

<sup>2</sup>Centre for Research on Environmental and Sustainable Technologies  
Indian Institute of Science Education and Research Bhopal  
Bhopal By-pass Road, Bhauri, Bhopal – 462 066, Madhya Pradesh, INDIA

Keywords: black carbon, central india, mass absorption efficiency, ecological sensitive zone.  
Presenting author email: abhilashpaswan@gmail.com

It is now well recognized that black carbon (a component of aerosols that is similar but not identical to elemental carbon) is an important contributor to global warming, second only to CO<sub>2</sub>. However, the most popular methods for estimation of black carbon rely on accurate estimates of its mass absorption efficiency (MAE) to convert optical attenuation measurements to black carbon concentrations. Often a constant manufacturer specified MAE is used for this purposes. Recent literature has unequivocally established that MAE shows large spatio-temporal heterogeneities. This is so because MAE depends on emission sources, chemical composition, and mixing state of aerosols.

In this study, ambient PM<sub>2.5</sub> samples were collected over an ecologically sensitive zone (Van Vihar National Park) in Bhopal, Central India for two years (01 January, 2012 to 31 December, 2013). Samples were collected on Teflon, Nylon, and Tissue quartz filter substrates. Punches of quartz fibre filter were analysed for organic and elemental carbon (OC/EC) by a thermal-optical-transmittance/reflectance (TOT-TOR) analyser operating with a 632 nm laser diode. Teflon filters were also used to interdependently measure PM<sub>2.5</sub> attenuation (at 370 nm and 800 nm) by transmissometry. Site-specific mass absorption efficiency (MAE) for elemental carbon over the study site has been derived using a combination of measurements from the TOT/TOR analyser and transmissometer.

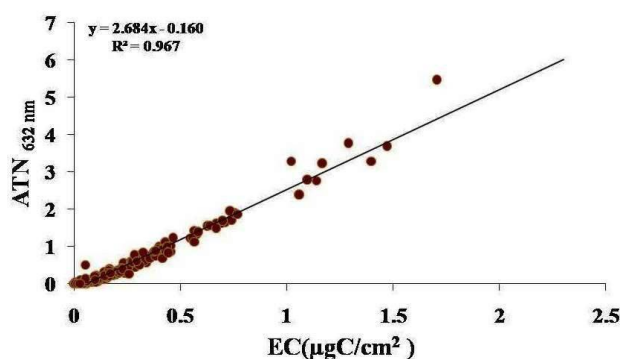


Figure 1. Correlation between attenuation at 632nm and Elemental carbon (EC).

Both measurements using TOT/TOR analyser and transmissometer are well correlated. An assessment of site-specific MAE values, its temporal variability and implications to black carbon radiative forcing will be discussed.

## Radiocarbon and AMS coupled source apportionment of carbonaceous aerosols in the Baltic region

A. Vlachou<sup>1</sup>, C. Bozzetti<sup>1</sup>, K.R. Daellenbach<sup>1</sup>, G.A. Salazar<sup>2</sup>, S. Szidat<sup>2</sup>, J.-L. Jaffrezo<sup>3</sup>, M. Elser<sup>1</sup>, M. Maasikmets<sup>4</sup>, V. Ulevicius<sup>5</sup>, U. Baltensperger<sup>1</sup>, I. El Haddad<sup>1</sup> and A.S.H. Prévôt<sup>1</sup>.

<sup>1</sup>Department of General Energy Research, Paul Scherrer Institut, Villigen PSI, CH-5232, Switzerland

<sup>2</sup>Department of Chemistry and Biochemistry & Oeschger Centre for Climate Change Research, University of Bern, 3012 Bern, Switzerland

<sup>3</sup>Université Grenoble Alpes, CNRS, IGE, 38000 Grenoble, France

<sup>4</sup>Estonian Environmental Research Center, Marja 4d, Tallinn, 10617, Estonia

<sup>5</sup>Department of Environmental Research, SRI Center for Physical Sciences and Technology, 02300 Vilnius, Lithuania

\*Presenting author email: [athanasia.vlachou@psi.ch](mailto:athanasia.vlachou@psi.ch)

Keywords: Source apportionment, <sup>14</sup>C analysis, Offline-AMS.

Carbonaceous aerosols represent a major fraction of the ambient particulate matter (PM) and significantly affect human health and climate. They are often classified into elemental carbon (EC) that is directly emitted into the atmosphere (primary) and organic carbon (OC) that may be either primary or formed in-situ (secondary) via the oxidation of volatile organic compounds from fossil and non-fossil sources.

Radiocarbon analysis provides an unequivocal separation between fossil and non-fossil sources by quantifying the <sup>14</sup>C content of the total carbon collected on ambient filter samples. At the same time, the analysis of aqueous filter extracts by the Aerodyne aerosol mass spectrometer (AMS) and the application of positive matrix factorization on the collected mass spectra have significantly enhanced our capability to identify the organic aerosol (OA) sources. The combination of such offline AMS (Daellenbach et al., 2016) and <sup>14</sup>C measurement techniques (Szidat et al., 2014) in comparison to each individual method provides a more robust source apportionment and a more profound investigation of the primary and secondary carbonaceous aerosols' origins.

Even though there have been a few reports on the chemical composition and sources of OA in the Baltic region, air quality studies are still scarce and so far none has used a combination of the techniques described above for datasets that cover large time periods. For example, in three different sites in Lithuania, Bozzetti et al. (2017) identified two oxygenated OA factors; however the fossil and non-fossil content of these factors, essential for the source apportionment, remains unknown. Moreover, in Tallinn and Tartu, Estonia, Elser et al. (2016) focused on the chemical composition and spatial distribution of OA with the use of a mobile platform for only a short period of time during March 2014.

While most of the studies performed in the Baltic region adopted online techniques for the OA characterisation only for short periods, little is known about the OA chemical composition and sources on a monthly or yearly basis. An example of long temporal evolution of the non-fossil fraction (fNF) of the total carbon for three sites in Estonia is shown in Figure 1. Here we will present a combined <sup>14</sup>C and offline AMS analysis of the OA at six locations in the Baltic region (Lithuania and Estonia), for the identification of the primary and secondary fossil and non-fossil sources of OA.

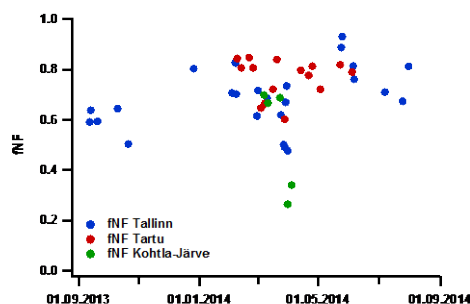


Figure 1. <sup>14</sup>C analysis (fNF) conducted on filter samples collected at three Estonian cities with the Mini Carbon Dating System (MICADAS).

This work is funded by the Swiss Federal Office for the Environment (FOEN) and the Estonian-Swiss cooperation program "Enforcement of the surveillance network of the Estonian air quality: Determination of origin of fine particles in Estonia".

Daellenbach, K.R., et al. (2016), *Atmos. Meas. Tech.* **9**, 23-39.

Bozzetti, C., et al. (2017), *Atmos. Chem. Phys.*, **17**, 117-141.

Elser, M., et al. (2016), *Atmos. Chem. Phys.*, **16**, 7117-7134.

Szidat, S., et al. (2014), *Radiocarbon*, **56**, 561-566.

## The mixing state of black carbon in Beijing during wintertime

Dantong Liu<sup>1</sup>, Rutambhara Joshi<sup>1</sup>, James Allan<sup>1</sup>, Hugh Coe<sup>1</sup>, Michael Flynn<sup>1</sup>, Jason Olfert<sup>2</sup>, Kurtis Broda<sup>2</sup>, Martin Irwin<sup>3</sup>, Pingqing Fu<sup>4</sup>, Yele Sun<sup>4</sup>, Xinlei Ge<sup>5</sup> and Junfeng Wang<sup>5</sup>

<sup>1</sup>Centre for Atmospheric Sciences, School of Earth and Environmental Sciences, University of Manchester, Manchester, UK

<sup>2</sup>Department of Mechanical Engineering, University of Alberta, Canada

<sup>3</sup>Cambustion Ltd, Cambridge, UK

<sup>4</sup>Institute of Atmospheric Physics, Chinese Academy of Sciences, Beijing, China

<sup>5</sup>School of Environmental Science and Engineering, Nanjing University of Information Science and Technology, Nanjing, China

Keywords: black carbon, mixing state.

Presenting author email: dantong.liu@manchester.ac.uk

Black carbon particles (BC) significantly contribute to warming effects in the atmosphere, altering climatic systems, and also pose significant health risks. These impacts are especially efficient at regional hotspots with high emissions of pollutants, such as in fast-developing megacities. These urban environments have the most population exposure, and improving the understanding of the sources and the processing of pollutants in these environments is critical in guiding policy making. Here we present the results of BC characterization in Beijing during the winter of 2016 (10<sup>th</sup> Nov-10<sup>th</sup> Dec), as part of a large joint UK-China field experiment. During this experiment, we successfully gathered 4 weeks of continuous measurements, including several severe pollution events in Beijing.

The mixing state of BC, which is how BC is associated with non-BC material (its coating) within a particle, is crucial to determine its lifetime in the atmosphere and also its optical properties. However precisely quantifying the BC mixing state has posed a challenge, in part due to complex particle morphology. We have applied morphology-independent measurements of BC mixing state on a single-particle basis throughout this experiment: mono-dispersed particle mass ( $M_p$ ) is selected using a Centrifugal Particle Mass Analyser (CPMA, Cambustion Ltd) and a single particle soot photometer (SP2, DMT inc.) was used downstream of the CPMA to measure the refractory BC mass ( $M_{rBC}$ ). The full scan of CPMA masses (21 mass bins covering most of  $M_p$ ) are performed every half hour, following polydispersed particles measured without running CPMA.

Figure 1 shows the preliminary results for one full scan. For monodispersed particles, there is significant fraction of particles with  $M_{rBC}$  lower than

$M_p$ , and the difference between  $M_p$  and  $M_{rBC}$  defines the coating mass. Higher  $M_{rBC}$  than  $M_p$  is due to multiply-charged particles passing through the CPMA. This set up will give the full picture of rBC and coating distributions, allowing a comprehensive examination of BC mixing state at each particle mass. By combining this system with measurements from an Aerodyne Soot Particle Aerosol Mass Spectrometer (SP-AMS), this information can also be linked to the BC sources and atmospheric processing within the city. These results will provide important information to understand the source distribution, emissions, lifetime, and optical properties of BC under complex environments in Beijing.

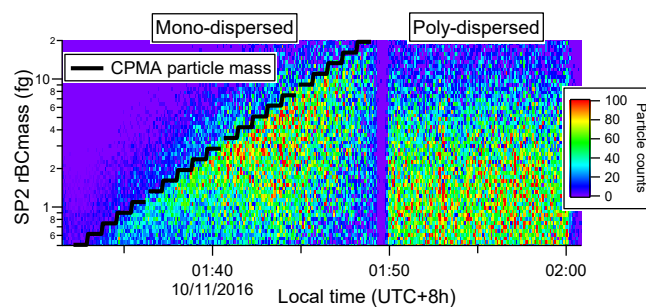


Figure 1. The example of one scan showing the CPMA-selected mono-dispersed and the following poly-dispersed rBC mass distributions.

This work was supported through the UK Natural Environment Research Council (NERC, reference NE/N007123/1).

## **Abstracts T211**

## Characterization of Biogenic Secondary Organic Aerosols in Malaysia Affected by Indonesian Peatland Fires

Y. Fujii<sup>1</sup>, S. Tohno<sup>2</sup> and M. Mahmud<sup>3</sup>

<sup>1</sup>Center for Environmental Science in Saitama, Kazo, 347-0115, Japan

<sup>2</sup>Department of Socio-Environmental Energy Science, Kyoto University, Kyoto, 606-8501, Japan

<sup>3</sup>Faculty of Social Sciences and Humanities, University Kebangsaan Malaysia, Bangi, 43600, Malaysia

Keywords: SOA, Biomass Burning, Haze, Peatland fire.

Presenting author email: fujii.yusuke.am@pref.saitama.lg.jp

During every dry season, peatland fires occur in Sumatra and Kalimantan islands, Indonesia. Due to the southwest monsoon season in Southeast Asia during this period, smoke particles and gases originating from Indonesian peatland fires travel to the west coast of Peninsular Malaysia, resulting in frequent transboundary haze pollution (Fujii *et al.*, 2015b). Recently, chemical characterization of Indonesian peatland fire aerosols with an emphasis on molecular markers of biomass burning at source in Sumatra Island and receptor sites in Malaysia was reported (Fujii *et al.*, 2015a,b,c). In this study, we characterized ambient total suspended particulates (TSP) with a focus on molecular markers of biogenic secondary organic aerosol (SOA) based on intensive ground-based field samplings in Malaysia during non-haze days and haze ones affected by peatland fires in Sumatra Island for the first time there.

The TSP samplings were conducted at a location in Bangi, Selangor, Malaysia from June 23 to July 8 in 2014. TSP samplings were conducted at the roof of a building in Universiti Kebangsaan Malaysia (~22 m above ground level, Latitude, Longitude: 2° 55' 41" N, 101° 46' 47" E). A high-volume air sampler was utilized to continuously collect TSP on quartz fiber filters for 18 hours (19:30–13:30 (+1 day) in local time) at a flow rate of 1.13 m<sup>3</sup> min<sup>-1</sup>. After sampling, solvent (a mixture of CH<sub>2</sub>Cl<sub>2</sub> and CH<sub>3</sub>OH)-extractable organic compounds regarding biogenic SOA tracers were quantified by gas chromatography/mass spectrometry. We determined  $\alpha/\beta$ -pinene, isoprene-, and sesquiterpene-SOA tracers in this study. Discussion of other chemical species such as water-soluble inorganic ions and molecular markers of biomass burning has been presented in our former report (Fujii *et al.*, 2015b).

During the sampling periods, the concentrations of 2-methylglyceric acid (2-MGA), 2-methyltetrols (2-MTL) and C<sub>5</sub>-alkene triols, which are isoprene-SOA tracers ranged from 4.7 to 21, 26 to 260, and 20 to 130 ng m<sup>-3</sup>, respectively. As shown in Fig. 1, significant difference in 2-MGA concentrations between the haze and non-haze samples was found in the quantified isoprene-SOA tracers. This result may indicate long-range transportation of peatland fire-induced smoke from Sumatra Island to Malaysia yielded 2-MGA, because 2-MGA is formed by photooxidation of isoprene under high-NO<sub>x</sub> conditions (Surratt *et al.*, 2010). The enhanced concentrations of 3-hydroxyglutaric acid (3-HGA) during the haze periods were also clearly observed as well as those of 2-MGA. Key role of NO<sub>x</sub> in the increase

level of 2-MGA during the haze periods can also be supported by the fact that 3-HGA is formed from UV-irradiated  $\alpha$ -pinene in the presence of NO<sub>x</sub> (Claeys *et al.*, 2007).

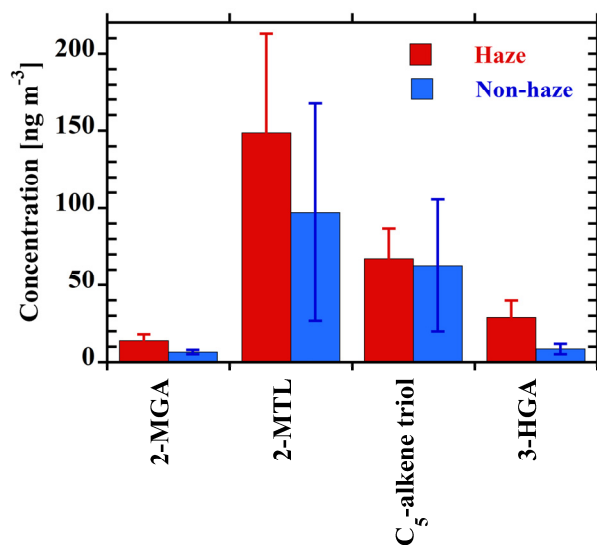


Figure 1. Comparison of average 2-MGA, 2-MTL, C<sub>5</sub>-alkene triol, and 3-HGA concentrations during the peatland fire-induced haze and non-haze periods.

### Acknowledgements

This work was supported by JSPS Kakenhi, grant numbers 15H02589 and 15J08153.

### References

- Claeys, M., Szmigielske, R., Kourtshev, I., van der Veken, P., Vermeylen, R., Maenhaut, W., Jaoui, M., Kleindienst, T., Lewandowski, M., Offenberg, J.H., and Edney, E.O. (2007) *Environ. Sci. Technol.* **41**, 1628–1634.
- Fujii, Y., Kawamoto, H., Tohno, S., Oda, M., Iriana, W., and Lestari, P. (2015a) *Atmos. Environ.* **110**, 1–7.
- Fujii, Y., Mahmud, M., Oda, M., Tohno, S., Matsumoto, J., and Mizohata, A. (2015b) *Aerosol Air Qual. Res.* **16**, 69–78.
- Fujii, Y., Tohno, S., Amil, N., Latif, M.T., Oda, M., Matsumoto, J., and Mizohata, A. (2015c) *Atmos. Chem. Phys.* **15**, 13319–13329.
- Surratt, J.D., Chan, A.W.H., Eddingsaas, N.C., Chan, M., Loza, C.L., Kwan, A.J., Hersey, S.P., Flagan, R.C., Wennberg, P.O., and Seinfeld, J.H. (2010) *Proc. Natl. Acad. Sci.* **107**, 6640–6645.

## Modelling the impact of viscosity on Secondary Organic Aerosols formation with the SOAP thermodynamic model inside a 3D air quality model

F. Couvidat<sup>1</sup>, Y. Kim<sup>2</sup> and K. Sartelet<sup>2</sup>

<sup>1</sup>INERIS, Institut National de l'Environnement Industriel et de Risques, Parc technologique ALATA,60550 Verneuil en Halatte, France

<sup>2</sup>CEREA, 6-8 avenue Blaise Pascal, Cité Descartes Champs-sur-Marne 77455 Marne la Vallée Cedex 2

Keywords: Secondary Organic Aerosol, Viscosity, 3D modelling.

Presenting author email: Florian.Couvidat@ineris.fr

Numerous studies (e.g. Virtanen et al., 2010) show that the partitioning between the gas and particle phases of Semi-Volatile Organic Compounds (SVOC) can differ significantly from thermodynamic equilibrium due to the high viscosity of the organic-phase. However, to our knowledge the impact of organic-phase viscosity on Secondary Organic Aerosol formation has never been investigated in 3D air quality models, which usually assume that organic aerosols are not viscous.

The impact of the particle viscosity on secondary organic aerosols (SOA) is studied here by coupling an air quality model to the Secondary Organic Aerosol Processor (SOAP Couvidat and Sartelet, 2015) thermodynamic model. SOAP can compute the partitioning of SVOC concentrations either by assuming thermodynamic equilibrium or by computing the dynamic evolution of concentrations according to the kinetics of condensation/evaporation and particle-phase diffusion (as a function of the organic-phase coefficient diffusion).

To compute the evolution of the SVOC partitioning, organic particles are separated into several layers with the external layer at the gas/particle interface and the internal layer at the center of the particle. To accurately solve the equations of diffusion of SVOCs inside particles, a high number of layers would be needed (around 100). However, this discretization would lead to a system that is too complex to be implemented in an air quality model. In SOAP, a simplified representation was designed to represent implicitly the diffusion of SVOC inside the particle with a low number of layers (between 2 and 5). A comparison between the explicit representation and the implicit representation of diffusion is shown in Figure 1.

SOAP was implemented in the 3D air quality model Polyphemus and SOA concentrations were simulated over Europe during July 2012. Concentrations were simulated assuming either that particles are not viscous (the condensation/evaporation is not limited by the diffusion inside the particle) or that particles are infinitely viscous (the diffusion inside the particle is very slow and compounds do not diffuse inside the particle).

Assuming infinitely viscous particles leads to a slight increase of SOA concentrations (SVOC concentrations in the particle phase). Less volatile

compounds appear to not be affected by the viscosity of particles, but the concentrations of more volatile compounds increased for viscous particles and could therefore exceed concentrations at equilibrium. Indeed, for volatile organic compounds, in the infinitely viscous simulation the compounds could condense even if the compounds would evaporate for a non-viscous aerosol.

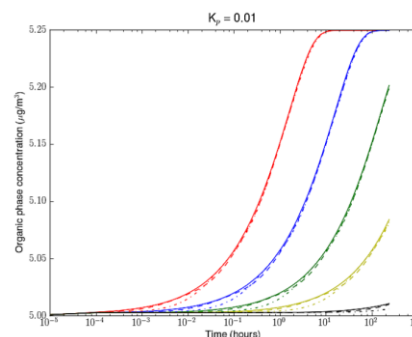


Figure 1. Comparison between the explicit representation (solid line) and the implicit representation (dotted line) of the organic-phase concentration of SVOC compound with a partitioning constant of 0.01  $\mu\text{g}/\text{m}^3$ .  $D_{\text{org}} = 10^{-19} \text{ m}^2 \text{ s}^{-1}$  (red),  $D_{\text{org}} = 10^{-20} \text{ m}^2 \text{ s}^{-1}$  (blue),  $D_{\text{org}} = 10^{-21} \text{ m}^2 \text{ s}^{-1}$  (green),  $D_{\text{org}} = 10^{-22} \text{ m}^2 \text{ s}^{-1}$  (yellow) and  $D_{\text{org}} = 10^{-24} \text{ m}^2 \text{ s}^{-1}$  (black)

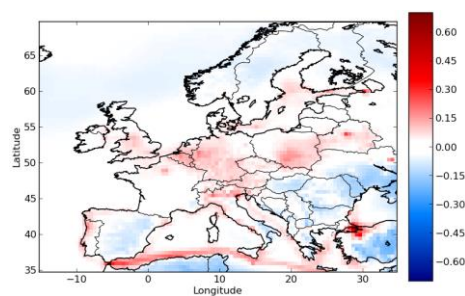


Figure 2. Differences in SOA concentration ( $\mu\text{g}/\text{m}^3$ ) between the infinitely viscous simulation and the non-viscous simulation.

### Bibliography

- Couvidat F. and Sartelet, K. (2015) *Geosci Model Dev* 8, 1111-1138
- Virtanen, A., Joutsensaari, J., Koop, T., Kannosto, J., YliPirilä, P., Leskinen, J., Mäkelä, J. M., Holopainen, J. K., Pöschl, U., Kulmala, M., Worsnop, D. R., and Laaksonen, A. (2010) *Nature* 467, 824-827

## Atmospheric evolution of primary and secondary organic aerosols: an explicit modeling of organic compound sources and sinks

M. Camredon<sup>1</sup>, G. Siour<sup>1</sup>, R. Valorso<sup>1</sup>, V. Lannuque<sup>1,2</sup>, B. Aumont<sup>1</sup>

<sup>1</sup>LISA UMR CNRS 7583, Universités Paris-Est Créteil and Paris Diderot, IPSL, 94010 Créteil, France.

<sup>2</sup>Institut National de l'Environnement Industriel et des Risques, 60550 Verneuil-en-Halatte, France.

Keywords: organic compounds, primary and secondary organic aerosol, modeling.

Presenting author email: marie.camredon@lisa.u-pec.fr

Fine particulate matter has a consequent impact on visibility, human health and climate. A large fraction of fine particles is organic, representing between 40 and 80% of the total mass (e.g. Jimenez *et al.*, 2009). This organic fraction can be directly emitted into the atmosphere (primary organic aerosol, POA) or formed by gas/particle partitioning of low volatility species produced during the oxidation of gaseous organic compounds (secondary organic aerosol, SOA). Organic aerosols are composed of hundreds of compounds having various chemical structures and spanning therefore a wide range of physico-chemical properties. However, the speciation and the concentration of individual species in organic aerosols remain largely unknown.

This study explores the speciation and the evolution of POA and SOA under various environmental conditions. The sources and sinks of gaseous and condensed organic compounds were represented explicitly in a box model for various locations and meteorological conditions. Anthropogenic emissions were built using the annual TNO (Netherlands Organization for Applied Scientific Research) inventory (Kuenen *et al.*, 2014). This inventory was coupled to the detailed speciation provided by Passant (2002) for non-methane volatile organic compounds and to the volatility distribution provided by Robinson *et al.* (2007) for less volatile organic species. Biogenic emissions were estimated using emissions potentials provided by MEGAN (Model of Emissions of Gases and Aerosol from Nature) (Guenther *et al.*, 2006). Emission of 183 anthropogenic and biogenic organic species were considered in the model.

Detailed oxidation chemical schemes for these emitted species were generated using GECKO-A (Generator for Explicit Chemistry and Kinetics of Organics in the Atmosphere) (Aumont *et al.*, 2005). The gas/particle partitioning of each organic compound was described by an absorption process following the Raoult's law and considering a homogeneous, ideal and inert condensed phase (Camredon *et al.*, 2007). The chemical schemes includes the formation of more than  $6 \times 10^5$  organic species and the gas/particle partitioning is considered for around  $1 \times 10^5$  of them. Deposition was represented in the model using the Wesley (1989) resistance parameterization with effective Henry's law constants estimated for all stable organic compounds using the Grohme (Raventos *et al.*, 2010) estimation method.

The reliability of the scenarios is evaluated comparing simulated results to NO<sub>2</sub> and O<sub>3</sub> observations available in the Airbase database (<http://acm.eionet.europa.eu/databases/airbase>). The simulations are used here to examine (i) the diurnal and seasonal variability of organic aerosol in various environments and (ii) the speciation of individual organic aerosol species.

Aumont, B., Szopa, S. and Madronich, S. (2005) *Atmos. Chem. Phys.* **5**, 2497-2517.

Camredon, M., Aumont, B., Lee-Taylor, J. and Madronich, S. (2007) *Atmos. Chem. Phys.* **7**, 5599-5610.

Guenther, A., Karl, T., Harley, P., Wiedinmyer, C., Palmer, P. I. and Geron, C. (2006) *Atmos. Chem. Phys.* **6**, 3181-3210.

Jimenez, L., Canagaratna, M. R., Donahue, N. M. et al. (2009), *Science* **326**, 1525-1529.

Kuenen, J.J.P., Visschedijk, J.H., Jozwicka, M. and Denier van der Gon, H. A. C. (2014) *Atmos. Chem. Phys.* **14**, 10963-10976.

Passant, N.R. (2002) *Speciation of uk emissions of nmvoc*, AEA Technology report.

Raventos-Duran, T., Camredon, M., Valorso, R., Mouchel-Vallon, C. and Aumont, B. (2010) *Atmos. Chem. Phys.* **10**, 7643-7654.

Robinson, A.L., Donahue, N.M., Shrivastava, M.K., Weitkamp, E.A., Sage, A.M., Grieshop, A.P., Lane, T.E., Pierce, J.R. and Pandis, S.N. (2007) *Science* **315**, 1259-1262.

Wesley, M.L. (1989) *Atmos. Env.* **23**, 1293-1304.

## Chemical ionization mass spectrometry as a probe for peroxy radical chemistry and SOA formation pathways

M. Ehn, C. Yan, O. Peräkylä, L. Quéléver, Q. Zha, M. P. Rissanen and M. Riva

Department of Physics, University of Helsinki, Helsinki, 00560, Finland

Keywords: Secondary organic aerosol, CIMS, highly oxidized molecules, volatile organic compounds  
Presenting author email: mikael.ehn@helsinki.fi

Secondary organic aerosol (SOA) is one of the largest contributors to sub-micron aerosol in the atmosphere (Jimenez *et al.*, 2009). The typical path to SOA goes via emissions of volatile organic compounds, their subsequent gas-phase oxidation to less volatile vapors, and condensation of these vapors onto aerosol particles. The amount of SOA formed as a function of emitted vapor is a key quantity which depends strongly on the environmental conditions, in addition to the chemical nature of the emitted molecules.

In the case of biogenic emissions, such as monoterpenes (C<sub>10</sub>H<sub>16</sub>), the oxidation process is primarily initiated by reactions with either ozone or the hydroxyl or nitrate radicals. The yield of SOA from these reactions have been the focus of many studies over the last decades, as monoterpenes have been found to be large contributors to atmospheric SOA. However, in addition to the initiation step of the oxidation, also the fate of the common peroxy radical (RO<sub>2</sub>) intermediates constitutes a critical branching step. These RO<sub>2</sub> can either undergo autoxidation (Crouse *et al.*, 2013; Ehn *et al.*, 2014) or terminate through bimolecular reactions with NO, HO<sub>2</sub> or other RO<sub>2</sub>. The combination of potential oxidants and termination steps produces a complex system even for a single VOC, when attempting to link such reactions to SOA formation. This is one of the reasons for the common discrepancies between chamber-derived SOA yields and the SOA loadings found in the atmosphere (Hallquist *et al.*, 2009).

Most SOA chamber studies try to target one or two of these pathways, but in the atmosphere, several of these pathways will be active over a diurnal cycle. Even under laboratory conditions it may be hard to restrict reactions to just one of these pathways. For example, alkene ozonolysis inevitably produces OH radicals, and NO<sub>x</sub> together with RO<sub>2</sub> can form large amounts of ozone. Therefore, it would be of great value to be able to identify the importance of each pathway at any given instance. We propose that nitrate-ion chemical ionization mass spectrometry (CIMS) can be one of the most efficient methods to probe the relative importance of these different pathways.

Nitrate CIMS (Jokinen *et al.*, 2012) has successfully been deployed to measure highly oxidized multifunctional (HOM) compounds from several biogenic VOCs in the laboratory (Jokinen *et al.*, 2015). Recently, using factor analysis, several types of atmospheric HOM very also identified in the boreal forest (Yan *et al.*, 2016), mainly resulting from monoterpenes. Several of these HOM types could clearly be linked to specific pathways (e.g. O<sub>3</sub>-

oxidation/RO<sub>2</sub>-termination or NO<sub>3</sub>-oxidation/RO<sub>2</sub>-termination) while for some only NO-termination could be deduced, with the oxidant remaining uncertain.

The basis for linking HOM with specific “oxidation pathways” using nitrate CIMS relies on several features of HOM and the CIMS instrument. First, the atmospheric lifetime of HOM from monoterpenes, typically containing seven or more O-atoms, is on the order of minutes. This means that the atmospheric oxidation pathways at any given time are reflected in the HOM distributions. Second, HOM are often detected as “monomers” and “dimers”, where the dimers contain roughly twice the C-atoms of the precursor VOC and have, through multiple studies, been confirmed to result from RO<sub>2</sub> + RO<sub>2</sub> reactions. If these dimers contain N-atoms, these are most likely the result of NO<sub>3</sub> oxidation. While lack of dimers and dominance of N-containing monomers (as is typical in the day-time boreal forest), suggests dominance of RO<sub>2</sub> + NO reactions. Finally, the nitrate CIMS is even capable of detecting some of the most highly oxidized peroxy radicals directly, lending additional support to the identification.

Through more detailed investigations of atmospheric HOM and SOA data, as well as targeted chamber studies, we are now taking this analysis one step further and aim to identify each of these oxidation pathways, and to ultimately link each pathway with a specific SOA yield for the most common biogenic VOC in the boreal forest. I will present an overview of these results and the ability of nitrate CIMS to determine the most important atmospheric oxidation pathways, with focus on the monoterpene  $\alpha$ -pinene. However, the ability to determine peroxy radical formation and termination pathways will certainly find application also for many other VOC.

This work was supported by the European Research Council (Grant 638703-COALA).

Ehn, M., *et al* (2014). *Nature*, **506**, 476-479.

Crouse, J., *et al* (2013). *J. Phys. Chem. Lett.*, 3513-3520.

Hallquist, M., *et al* (2009). *Atmos. Chem. Phys.*, **9**, 5155-5236.

Jimenez, J. L., *et al* (2009). *Science*, **326**, 1525-1529.

Jokinen, T., *et al* (2012). *Atmos. Chem. Phys.*, **12**, 4117-4125.

Jokinen, T., *et al* (2015). *Proc. Natl. Acad. Sci.*, **112**, 7123-7128.

Yan, C., *et al* (2016). *Atmos. Chem. Phys.*, **16**, 12715-12731.

## Using factor analysis methods in the analysis of PTR-MS data from herbivore induced plant volatile measurements

S. Mikkonen<sup>1</sup>, S. Isokääntä<sup>1</sup>, E. Kari<sup>1</sup>, A. Buchholz<sup>1</sup>, L.Q. Hao<sup>1</sup>, A. Virtanen<sup>1</sup> and C.L. Faiola<sup>1,2</sup>

<sup>1</sup> Department of Applied Physics, University of Eastern Finland, Kuopio, Finland

<sup>2</sup> Department of Ecology and Evolutionary Biology, University of California, Irvine, USA

Keywords: SOA, VOC, factor analysis, PTR-MS.

Presenting author email: santtu.mikkonen@uef.fi

Terrestrial plants are constantly emitting Volatile Organic Compounds (VOC). These emissions depend on plant-physiological conditions, and changes in these conditions could cause rapid alterations in emission dynamics. Herbivore induced plant volatiles (HIPVs), are a class of VOCs produced by plants mainly to provide direct and indirect protection against herbivores. Elevated HIPV emissions have been shown to induce secondary organic aerosol (SOA) formation and growth (e.g. Yli-Pirilä et al. 2016) and thus affect the climate on a regional scale (Joutsensaari et al. 2015).

We organized an intensive measurement campaign in our research facilities during summer 2015 in order to study HIPV emission dynamics, and subsequent SOA formation and growth. In the experiments, two Scots pine saplings were studied at the same time. One of them was exposed to four bark feeding pine weevils and the second one was a control plant. The experiment was repeated four times with different plants. The emitted compounds were monitored continuously before, during and after treatment by proton transfer reaction time-of-flight mass spectrometry (PTR-ToF-MS). Online measurements were supplemented with cartridge samples, which were analyzed offline via thermodesorption-gas chromatography-mass spectrometry (TD-GC-MS). SOA formation was monitored with a high resolution aerosol mass spectrometer (HR-AMS), and a scanning mobility particle sizer (SMPS).

The online monitoring techniques used in this study produce large sets of complex and highly detailed data on the chemical and physical quantities of the emissions. Multivariate statistical methods are developed to compress the information from a large number of observed variables to a small number of latent variables. Advantages of using these kind of methods for mass spectrometry data are well known. Positive Matrix Factorization (PMF), introduced by Paatero and Tapper (1994), is the de facto method of choice for the analysis of long time series of AMS data. Wyche et al. (2015) used principal component analysis (PCA), hierarchical cluster analysis (HCA) and positive least-squares discriminant analysis (PLS-DA) in the analysis of the large datasets produced in their smog chamber measurements. This inspired us to apply similar methodology to our HIPV and SOA formation data.

Different variations of PCA and factor analysis (FA) were tested on the PTR-MS measurement data. All mass signals differing significantly from the blank experiment were fed to the model. Best results were gained with FA using non-orthogonal rotation. Figure 1

shows a time series of three factors constructed from one of the four experiments. One of the factors (ML3) shows a clear diurnal cycle in the plant emissions with slightly elevated average concentration during the active feeding period of the weevils and sudden drop below the original level when the bugs were removed from the plant. ML2, on the other hand, shows significant increase after the weevils were put on the plant and quick recovery to the original level after they were removed. ML1 does not show drastic change within the experiment, there is only small elevation within the active feeding period, and thus it is believed to mostly consist of emissions that are not affected by this type of plant stress.

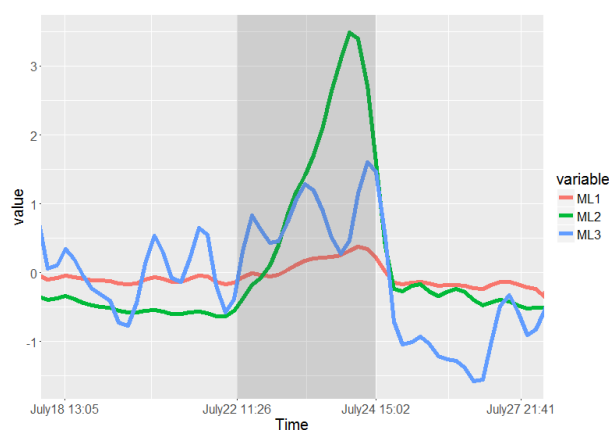


Figure 1. The three factors formed from the PTR-MS data of the second experiment. Shaded area indicates the active feeding time of the bark feeding pine weevils

In the other three experiments, similar patterns were detected and there seems to be a number of compounds that are assigning to the same factors in different cases. Identifying the compounds loading especially to ML2 and ML3 is ongoing process and will hopefully shed light to HIPV formation. These results will be used in the next phase of our study where we investigate the factors affecting SOA formation.

This work was supported by The Academy of Finland Centre of Excellence (grant no 272041) and European Research Council (ERC Starting Grant 335478).

Joutsensaari et al. *Atmos. Chem. Phys.*, 15, 12139-12157, 2015

Paatero and Tapper. *Environmetrics*, 5, 111-126, 1994.

Wyche et al. *Atmos. Chem. Phys.*, 15, 8077-8100, 2015.

Yli-Pirilä et al. *Environ.Sci.Technol.*, 50, 11501-11510, 2016

## Molecular composition of secondary organic aerosol during new particle formation and growth experiments at the CLOUD chamber

A. L. Vogel<sup>1,2</sup>, C. Zuth<sup>3</sup>, C. Yan<sup>4</sup>, J. B. Nowak<sup>5</sup>, J. Kirkby<sup>1,6</sup>, T. Hoffmann<sup>3</sup>, D. R. Worsnop<sup>4,5</sup>,  
and the CLOUD collaboration

<sup>1</sup>CERN, European Centre for Nuclear Research, Geneva, 1211, Switzerland

<sup>2</sup>Energy and Environment Research Division, Paul Scherrer Institute, Villigen, 5232, Switzerland

<sup>3</sup>Institute of Inorganic and Analytical Chemistry, Johannes Gutenberg-University Mainz, 55128, Germany

<sup>4</sup>Division of Atmospheric Science, Department of Physics, University of Helsinki, Helsinki, 00014, Finland

<sup>5</sup>Aerodyne Research Inc., Billerica, USA

<sup>6</sup>Institute for Atmospheric and Environmental Sciences, Goethe University, Frankfurt am Main, 60438, Germany

Keywords: SOA, Aerosol-CIMS, organonitrates, nucleation & particle growth.

Presenting author email: alexander.vogel@psi.ch

Predicting the number of particles which can serve as cloud condensation nuclei in the atmosphere is a major uncertainty in global climate models (IPCC, 2013). New particle formation (NPF) is one of the dominant sources of atmospheric particles, however, new particles need condensing vapours to grow into climatically relevant sizes. It has been (and still is) a challenge to measure the involved compounds that contribute to the condensing mass. Recently, it has been recognized that highly oxidized organic compounds are the major contributors to initial particle growth (Tröstl *et al.*, 2016), explaining why the condensation of inorganic compounds, such as sulphuric acid vapours, cannot explain observed growth rates in the ambient atmosphere. However, the mechanisms of VOC oxidation under atmospherically relevant conditions involving NO<sub>x</sub> and SO<sub>2</sub> chemistry remains highly uncertain. Recently, organic nitrates have received increased attention by means of ambient studies of organic aerosol composition (e.g. Kiendler-Scharr *et al.*, 2016). Identifying the chemical processes that govern new particle formation and growth is a prerequisite for global climate models to more accurately predict particle numbers from natural and anthropogenic emissions.

At the CLOUD experiment at CERN we studied new particle formation and particle growth from monoterpene oxidation at different atmospherically relevant mixing ratios of the precursor VOCs, NO<sub>x</sub> and SO<sub>2</sub>. Complementary particle phase composition measurements were implemented by the semi-online filter inlet for gases and aerosols (FIGAERO-CIMS, Lopez-Hilfiker *et al.*, 2014) using Iodide and Superoxide reagent ion chemistry. Particle filters were sampled for offline analysis by liquid chromatography coupled to electrospray ionization ultra-high resolution mass spectrometry (LC/ESI-HRMS). Thus, the chemical composition of the condensed phase was analysed by complementary approaches and the common features and discrepancies between the techniques will be demonstrated.

We found that thermal decomposition of oligomers is commonly observed during thermal desorption in the FIGAERO-CIMS. However, quantitative information of the fraction of monomeric

and dimeric oxidation products could be retrieved from the FIGAERO thermograms (intensity vs. temperature) and we found that stable oxidized dimers composed of carbon, hydrogen and oxygen (CHO-dimers) exhibit the lowest volatility. The formation of organic nitrates was observed under elevated NO<sub>x</sub> mixing ratios and the thermograms of organonitrate-dimers indicated that the nitrates showed higher volatility compared to the CHO-dimers. Reduced nucleation and growth rates were observed and we will link these observations to the direct measurement of volatility on the molecular level. Furthermore, mass closure between the FIGAERO-CIMS and a nano-SMPS was successful after correcting for gas-phase adsorption of ELVOCs onto the FIGAERO filter. The comparison to the offline LC-HRMS analysis confirmed the identities of the majority of CHO monomers and dimers observed by the FIGAERO-CIMS. However, a large fraction of organonitrates identified by FIGAERO-CIMS have so far not been detected by offline LC-HRMS. Possible explanations, such as hydrolysis of organic nitrates during sample preparation, or different ion chemistry in the electrospray ionization, will be discussed.

### Acknowledgements

This work was supported by the EC Seventh Framework Programme (Marie Curie Initial Training Network MC-ITN “CLOUD-TRAIN” no. 316662).

### References

- IPCC: Climate Change (2013) *The Physical Science Basis*, Cambridge University Press.
- Tröstl, J., *et al.* (2016) *nature* **533**, 527-531.
- Kiendler-Scharr, A., *et al.* (2016), *Geophys. Res. Lett.* **43**, 735–7744.
- Lopez-Hilfiker, F. D., Mohr, C., Ehn, M., Rubach, F., Kleist, E., Wildt, J., Mentel, T.F., Lutz, A., Hallquist, M., Worsnop, D.R. and Thornton, J.A. (2014) *Atmos. Meas. Tech.* **7**, 983-1001.

## Investigation of traffic related secondary aerosol formation in Helsinki city centre

K. Teinilä<sup>1</sup>, M. Aurela<sup>1</sup>, J. Niemi<sup>2</sup>, A. Kousa<sup>2</sup>, S. Saarikoski<sup>1</sup>, S. Carbone<sup>3</sup>, L. Kangas<sup>1</sup>, R. Hillamo<sup>1</sup> and H. Timonen<sup>1</sup>

<sup>1</sup>Finnish Meteorological Institute, Erik Palménin aukio 1, Helsinki, FIN-00560, Finland

<sup>2</sup>Helsinki Region Environmental Services Authority, Opastinsilta 6A, FIN-00520, Helsinki, Finland

<sup>3</sup>Federal University of Uberlândia, Uberlândia, Brazil

Keywords: PM<sub>1</sub>, organic aerosol, ACSM, traffic related aerosol.

Presenting author email: kimmo.teinila@fmi.fi

Aerosol chemical composition was measured with high time-resolution (app. 30 min) between March 19 and October 13, 2014 in Helsinki, Finland. Measurements were made at two measurement stations; a kerbside and an urban background station. Simultaneous measurements at the city centre and urban background stations gave the opportunity to explore the influence of traffic on PM<sub>1</sub> concentration and chemical composition.

The kerbside measurement site is located at a busy traffic environment in the city centre of Helsinki (Mannerheimintie 5) and the urban background station (SMEAR III) is located about 5 km northeast from Helsinki city centre. Composition of non-refractory submicron particles (NR-PM<sub>1</sub>: organics, sulphate, nitrate, ammonium and chloride) was measured continuously using two Aerosol Chemical Speciation Monitors (ACSM, Aerodyne Research Inc., Ng et al., 2011). Trace gases (NO, NO<sub>2</sub> and O<sub>3</sub>) were continuously measured at both stations. The sources and properties of organic aerosol (OA) were investigated by applying a multilinear engine algorithm (ME-2, Canonaco *et al.*, 2013) for organic mass spectra measured at both sites.

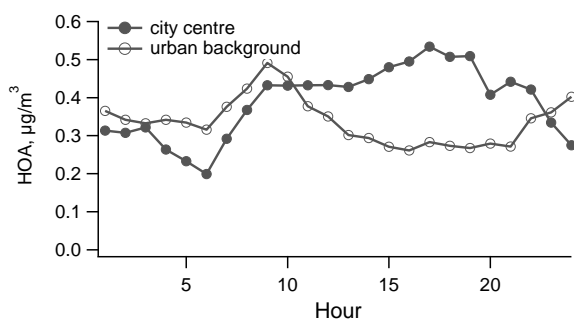


Figure 1. Diurnal cycles of HOA component at the city centre and urban background stations.

Concentration of hydrogen like organic aerosol (HOA) increased during morning hours at both stations (Figure 1) but stayed at higher level throughout the day only in Helsinki city centre. This indicates that SMEAR III is much less affected by motor vehicle emissions.

Concentration of semi-volatile oxygenated organic aerosol (SV-OOA) increased significantly in the afternoon and stayed high whole evening in Helsinki city centre, following the concentration trend of oxidant (O<sub>x</sub>=NO<sub>2</sub>+O<sub>3</sub>) (Figure 2).

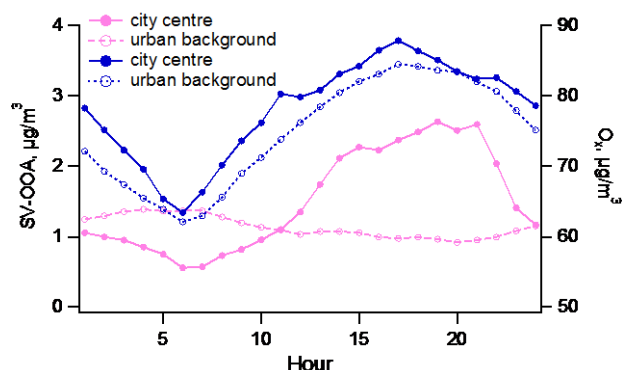


Figure 2. Diurnal cycles of SV-OOA component (pink) and oxidant concentration (O<sub>x</sub>=NO<sub>2</sub>+O<sub>3</sub>, dark blue) at the city centre and urban background stations

Concentration of SV-OOA did not show any increase at SMEAR III during afternoon and evening. The concentration of low-volatile oxygenated organic aerosol (LV-OOA) was also clearly higher in the city centre than at SMEAR III although its diurnal variations was flat at both sites. It seems that secondary organic aerosol is locally formed in Helsinki city centre and its formation is connected to motor vehicle emissions since no SV-OOA formation were observed at SMEAR III. The diurnal variation of SV-OOA indicates that its formation is a rapid process and is directly connected to the oxidative power of the surrounding atmosphere. The lack of similar kind of diurnal cycle for LV-OOA at both measurement sites indicates that its formation takes more time. LV-OOA is typically related to long range transported, aged aerosol. However its markedly higher concentrations in city centre may be related to additional local source. The slow oxidation of locally formed SV-OOA in Helsinki city centre could be this kind of source.

This work was funded by INKA-ILMA/EAKR (TEKES) and MMEA research programme.

Canonaco, F., Crippa, M., Slowik, J.G., Baltensperger, U. and Prévôt, A.S.H. (2013). *Atmos. Meas. Tech.*, 6, 3649-3661.

Ng, N. L., Herndon, S. C., Trimborn, A., Canagaratna, M. R., Croteau, P.L., Onasch, T. B., Sueper, D., Worsnop, D.R., Zhang, Q., Sun, Y.L. and Jayne, J.T. (2011). *Aerosol Sci. Technol.* 45:770-784.

## $\alpha$ -pinene SOA at low temperature: Influence of formation conditions on chemical composition and viscosity

W. Huang<sup>1</sup>, H. Saathoff<sup>1</sup>, K. H. Naumann<sup>1</sup>, A. Pajunoja<sup>2</sup>, A. Virtanen<sup>2</sup>, C. Mohr<sup>1</sup>

<sup>1</sup>Institute of Meteorology and Climate Research, Karlsruhe Institute of Technology, Eggenstein-Leopoldshafen, 76344, Germany

<sup>2</sup>Department of Applied Physics, University of Eastern Finland, Kuopio, 80101, Finland

Keywords:  $\alpha$ -pinene SOA, low temperature, chemical composition, viscosity

Presenting author email: wei.huang@kit.edu

Secondary organic aerosols (SOA) can be transported to or formed in the upper troposphere. Temperature (T) and relative humidity (RH) conditions representative of the upper troposphere, however, are rarely simulated in chamber studies, despite their potential importance for the phase state, morphology and chemical composition of SOA and thus their cloud formation potential (Zhang et al, 2015, Virtanen et al, 2010).

In order to simulate SOA uplifting, and to investigate the influence of atmospherically relevant temperature and humidity conditions on phase state, viscosity and chemical composition of  $\alpha$ -pinene SOA, we conducted two types of chamber experiments. For the first type of chamber experiment, SOA was produced directly in the AIDA simulation chamber (84.5 m<sup>3</sup>) at 223 K, 6 % RH (cold dry, CD) or 61 % RH (cold humid, CH); for the second type of chamber experiment (Wagner et al, 2017), SOA was first formed in the NAUA chamber (3.7 m<sup>3</sup>) at room temperature (296 K), <1 % or 21 % RH, and then transferred to the AIDA chamber kept at 223 K, 61 % RH (warm dry to cold humid, WDtoCH) or 30% RH (warm humid to cold humid, WHtoCH), respectively (Table 1). A Filter Inlet for Gases and AEROSols (FIGAERO) coupled to a high-resolution time-of-flight chemical ionization mass spectrometer (HR-ToF-CIMS) deploying iodide (I<sup>-</sup>) as the reagent ion was used for the chemical analysis of both gases and particles (Lopez-Hilfiker et al, 2014).

Table 1. Experimental conditions.

Exp. name	SOA position	T (K)	RH (%)
CH	AIDA	223	61
CD	AIDA	223	6
WDtoCH	NAUA→AIDA	296→223	<1→61
WHtoCH	NAUA→AIDA	296→223	21→30

Thermograms resulting from the thermal desorption of SOA particles deposited on the Teflon filter in the FIGAERO were analyzed. Single mode thermograms with signal maxima occurring at distinct desorption temperatures ( $T_{\max}$ ) are correlated with a compound's enthalpy of sublimation; multi-mode thermograms indicate contributions from isomers having different vapor pressures or decomposition of larger molecules (Lopez-Hilfiker et al, 2015). Significantly higher  $T_{\max}$  were observed in the sum thermograms for  $C_xH_yO_zI$  compounds of SOA formed at CD (91.5 °C)

and WHtoCH (71.7 °C) conditions compared to those at CH (53.5 °C) and WDtoCH (48.8 °C) conditions. Multi-mode desorption profiles for WHtoCH, CH and CD conditions were also witnessed (Fig. 1). The results suggest that SOA formed and evolved at WHtoCH, CH and CD conditions were more viscous than that at WDtoCH conditions, potentially resulting from high molecular weight organics and/or oligomers. Mass spectra comparison for these conditions support this conclusion.

The results provide insights into the influence of changing temperature and humidity conditions on chemical composition and viscosity of SOA during its formation and evolution in the atmosphere.

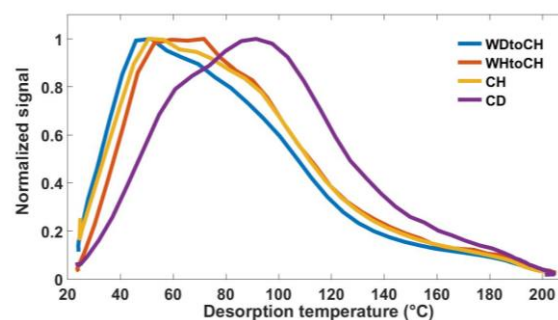


Figure 1. Sum thermograms for  $C_xH_yO_zI$  compounds at different experimental conditions.

This work was supported by the AIDA staff at KIT and the China Scholarship Council (CSC).

Zhang, X., et al. (2015) *Proc. Natl. Acad. Sci. U.S.A.* **112** (46):14168-14173.

Virtanen, A., et al. (2010) *Nature*. **467**, 824-827.

Wagner, R., et al. (2017) *J Geophys Res – Atmospheres*, under review.

Lopez-Hilfiker, F., et al. (2015) *Atmos. Chem. Phys.*, **15**, 7765-7776.

Lopez-Hilfiker, F., et al. (2014) *Atmos. Meas. Tech.*, **7**, 983-1001.

## Source apportionment of PM<sub>2.5</sub> by using organic and inorganic tracers in a suburban site of Turkey

A. Ar<sup>1</sup>, P. Ertürk Ar<sup>2</sup> and E.O. Gaga<sup>3</sup>

<sup>1</sup>Department of Food Engineering, Abant İzzet Baysal University, Bolu, 14280, Turkey

<sup>2</sup>Department of Environmental Engineering, Abant İzzet Baysal University, Bolu, 14280, Turkey

<sup>3</sup>Department of Environmental Engineering, Anadolu University, Eskişehir, 26090, Turkey

Keywords: PM<sub>2.5</sub>, PMF, PAHs, metals, n-alkanes.

Presenting author email: akifari@ibu.edu.tr

Atmospheric fine particulate matter (PM<sub>2.5</sub>) is an important air pollutant because of its adverse effects on human health, climate and visibility. PM<sub>2.5</sub> is a complex mixture emitted from natural and anthropogenic sources, which is mainly composed of organic compounds, elements and water soluble ions.

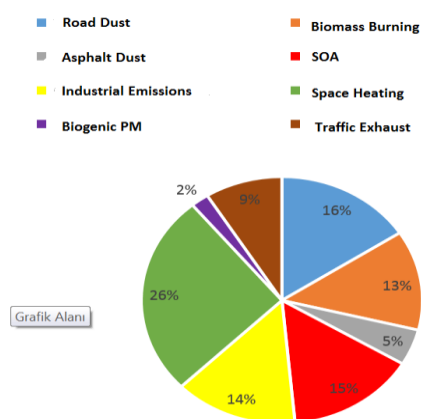
Secondary organic aerosols (SOA) are complex mixtures of organic compounds, Meteorology and predominant gas phase precursors are important parameters determining the composition of SOA. Quantification of the distribution of organic carbon into primary and secondary aerosol fractions has been difficult to accomplish because there is not a simple, direct analytical technique is available. However, indirect methods such as the carbon isotopic composition, organic to elemental carbon ratios and the use of chemical transport models have been applied to estimate the secondary organic carbon (SOC) formation in ambient fine PM.

Receptor models have been widely used for source apportionment of PM<sub>2.5</sub>. The most common receptor models can be categorized into univariate models such as chemical mass balance (CMB) and multivariate models such as principal components analysis (PCA), Positive matrix factorization (PMF) and UNMIX. Each model has its advantages and disadvantages, but all rely on the basic principles of mass balance. In comparison to the other models, PMF is well suited for longer time series studies and incorporates non-negativity constraints on the output, frequently resulting in a more physically interpretable result.

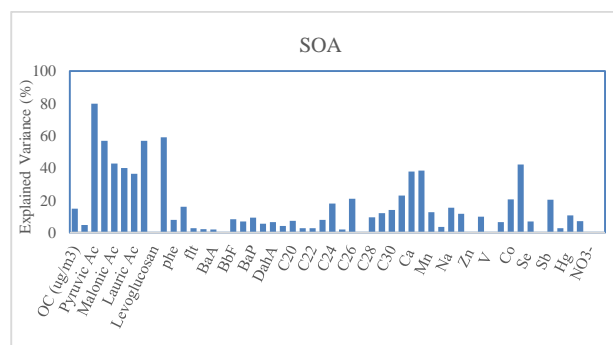
200 daily PM<sub>2.5</sub> samples were collected in 2014, in a suburban location of Eskişehir, Turkey by a high volume sampler (Thermo Scientific) on pre-fired quartz filters (Pall Corp.). All filters were analysed for OC and EC with the thermal-optical transmission technique (Birch and Cary, 1996). PAH, n-alkane and carboxylic acid concentrations were determined by ultrasonic extraction of filters by organic solvents followed by gas chromatography-mass spectrometry (GC-MS) analysis. Major and trace elements were analysed by inductively coupled plasma-tandem mass spectrometry (Agilent 8800 triple quad icp-ms) after microwave acid digestion by HNO<sub>3</sub>, HCl and HF mixture. Water soluble anions were analysed by ion chromatography after ultrasonic extraction in deionised water.

Elemental tracers were used to classify primary sources of fine PM while organic tracers like carboxylic acids used for SOA contribution, PAHs and EC for

primary combustion, n-alkanes for gasoline exhaust and vegetative detritus, and also levoglucosan for biomass burning.



Eight factors were determined by using organic and inorganic tracers. Secondary organic aerosol was seen to be the second most dominant contributor of fine PM just after space heating emissions.



This work was supported by the Scientific and Technological Research Council of Turkey under the grant of 113Y324 and The Committee of Scientific Research Projects of Anadolu University under the grant of 1107F127.

Birch, M. E., & Cary, R. A. (1996). *Aerosol Sci. Technol.* 25, 221-241.

Shrivastava, M.K., Subramanian, R., Rogge, W.F., Robinson, A.L. (2007). *Atmos. Environ.* 41, 9353-9369.

## Formation and contribution of highly oxidized organic molecules to the growth of new particles over the boreal forest

P. Roldin<sup>1,2</sup>, E. Öström<sup>2</sup>, D. Taipale<sup>3</sup>, N. Kivekäs<sup>4</sup>, M. Kulmala<sup>1</sup>, T. Kurtén<sup>5</sup>, M. Rissanen<sup>1</sup>, E. Swietlicki<sup>2</sup>, M. Ehn<sup>1</sup> and M. Boy<sup>1</sup>

<sup>1</sup>Department of Physics, University of Helsinki, P.O. Box 48, 00014 Helsinki, Finland

<sup>2</sup>Division of Nuclear Physics, Lund University, P.O. Box 118, 221 00 Lund, Sweden

<sup>3</sup>Department of Forest Sciences, University of Helsinki, P.O. Box 27, 00014 Helsinki, Finland

<sup>4</sup>Finnish Meteorological Institute, P.O. Box 503, 00101 Helsinki, Finland

<sup>5</sup>Department of Chemistry, University of Helsinki, P.O. Box 55, 00014 Helsinki, Finland

Keywords: ELVOC, autoxidation, secondary organic aerosol, oligomerization

Presenting author email: pontus.roldin@nuclear.lu.se

Field and laboratory experiments have identified large and rapid formation of highly oxidized organic molecules (HOM) (Ehn *et al.*, 2014), of which a fraction is extremely low-volatility organic compounds (ELVOC) (Kurtén *et al.*, 2016).

We have further developed the HOM monoterpene autoxidation mechanism proposed by Ehn *et al.* (2014) and coupled it to the Master Chemical Mechanism version 3.3.1 (MCMv3.3.1). The HOM formation mechanism comprises 770 reactions and 95 species. The gas-phase chemistry mechanism was implemented into the Aerosol Dynamics, gas- and particle-phase chemistry kinetic multilayer model for laboratory CHAMber studies (ADCHAM) (Roldin *et al.*, 2014) and the process-based chemistry transport models ADCHEM (Roldin *et al.*, 2011). We used different datasets to evaluate: (i) the HOM gas-phase formation mechanism, (ii) the potential role of HOM in new particle formation, (iii) their contribution to the activation and growth of new particles in the atmosphere (Öström, *et al.*, 2016) and (iv) how heterogeneous oligomer formation involving HOM may facilitate SOA formation.

The ADCHAM model was used to estimate the SOA formation during an  $\alpha$ -pinene ozonolysis, Ammonium Sulfate (AS) seed particle experiments in JPAC. ADCHAM considered condensation of all HOM species and other organic molecules with pure liquid saturation vapour pressures ( $p_0$ )  $< 10^{-2}$  Pa. The HOM  $p_0$  were either estimated with the functional group contribution method SIMPOL (Pankow and Asher, 2008) or based on detailed quantum-chemistry continuum solvent model COSMO-RS (Conductor-like Screening MOdel for Real Solvents) calculations (Kurtén *et al.*, 2016).  $p_0$  estimated with COSMO-RS are generally substantially higher than what is predicted by SIMPOL.

ADCHEM was operated as a 1D (vertical column) trajectory model along air mass trajectories reaching the measurement stations Pallas (67.97° N, 24.12° E) and Hyytiälä (61.85° N, 24.28° E). The model results were evaluated using measured particle properties and HOM gas-phase concentrations.

With the newly developed and constrained HOM formation mechanism ADCHEM captures the main features of the observed particle number size distribution

evolution during new particle formation events at the Pallas field station in northern Finland when the HOM  $p_0$  were estimated using SIMPOL, but underestimates the particle growth when using  $p_0$  based on COSMO-RS (Öström *et al.*, 2016). In this study we did not consider the contribution of heterogeneous oligomerization for the particle growth. According to the model results from Pallas, about 70 % of the nucleation model particle volume is SOA formed from HOM, 20 % from other VOC included in MCMv3.3.1 and 10 % from ammonium sulphate. We are currently performing similar ADCHEM model simulations for Hyytiälä during the spring 2014 where we will evaluate how sensitive the modelled activation and growth of new particles are to the HOM  $p_0$  and heterogeneous oligomerization. We will also test if heterogeneous oligomerization can further improve the agreement between the modelled and measured particle number size distributions during the simulated new particle formation events at Pallas.

This work was supported by the Cryosphere-atmosphere interactions in a changing Arctic climate – CRAICC the Swedish Research Council Formas, Project Nr. 2014-1445, the EU FP7 projects ACTRIS (Aerosols, Clouds, and Trace gases Research Infra Structure Network), the European Research Council (Grant 638703-COALA), eSTICC, the Swedish Strategic Research Program MERGE. The authors would like to thank Fredrik Söderberg for providing help to set up the model at the high performance-computing cluster Aurora, provided by the Swedish National Infrastructure for Computing (SNIC) center LUNARC.

Ehn, M. *et al.* (2014). *Nature*, 506, 476-479.

Jenkin, M. E. *et al.* (1997). *Atmos. Environ.*, 31, 81-104.

Kurtén T. *et al.*, (2016). *J. Phys. Chem. A*, 120, 2569-2582.

Pankow J. F. and Asher, W. E. (2008). *Atmos. Chem. Phys.*, 8, 2773-2796.

Roldin, P. *et al.* (2014). *Atmos. Chem. Phys.*, 14, 7953-7993.

Roldin, P. *et al.* (2011). *Atmos. Chem. Phys.*, 11, 5867-5896.

Öström, E. *et al.* (2016). *Atmos. Chem. Phys. Discuss.*, doi:10.5194/acp-2016-912, in review.

**Regional SOA modeling under consideration of HOMs**K. Gatzsche<sup>1</sup>, Y. Iinuma<sup>2</sup>, A. Tilgner<sup>1</sup>, T. Berndt<sup>1</sup>, L. Poulain<sup>1</sup>, and R. Wolke<sup>1</sup><sup>1</sup>Leibniz Institute for Tropospheric Research (TROPOS), Leipzig, 04318 Leipzig<sup>2</sup>Okinawa Institute of Science and Technology Graduate University (OIST), Okinawa, Japan

Keywords: Secondary organic aerosol (SOA), regional modeling, multiphase chemistry

Presenting author email: gatzsche@tropos.de

Secondary organic aerosol (SOA) is the major burden of the atmospheric organic particulate matter with about 140 – 910 TgC yr<sup>-1</sup> (Hallquist et al., 2009). SOA particles are formed via the oxidation of volatile organic carbons (VOCs), where the volatility of the formed OVOCs is lowered. Therefore, gaseous compounds are able to either nucleate to form new particles or condense on existing particles. The formation processes leading to SOA are very complex under natural conditions, because of a variety of gas-phase precursors, atmospheric degradation pathways and formed oxidation products. Up to now, atmospheric models often underpredict the SOA mass. Therefore, improved regional scale model implementations are necessary to achieve a better agreement between model predictions and field measurements.

Recently, highly oxidized multifunctional organic compounds (HOMs) were found in the gas phase from laboratory and field studies (Jokinen et al., 2015, Mutzel et al., 2015, Berndt et al., 2016a,b). From box model studies, it is known that HOMs are important for the early aerosol growth, however they are not yet considered in mechanisms applied in regional models.

The present study utilizes the state-of-the-art multiscale model system COSMO-MUSCAT (Wolke et al., 2012), which is qualified for process studies in local and regional areas. The established model system was enhanced by a kinetic partitioning approach (Zaveri et al., 2014) for the gas-to-particle transfer of OVOCs. The framework of the partitioning approach and the gas-phase mechanism were tested in a box model and evaluated with chamber studies, before implementing in the 3D model system COSMO-MUSCAT. Moreover, HOMs are implemented in the same way for the regional SOA modeling. 3D simulations were performed with an equilibrium partitioning and diffusion dependent partitioning approach, respectively.

The presentation will provide first 3D simulation results including comparisons with field measurements from the TROPOS field site Melpitz (51° 32' N, 12° 54' E, 87 m a.s.l.). Thereby, we will focus on two key issues influencing the SOA formation. Firstly, the increased SOA mass concentrations due to the consideration of HOMs from both isoprene and monoterpene oxidation (Fig. 1) is shown. Secondly, the influence of the particle phase diffusion coefficient on SOA formation will be presented, which is one of the key parameters in the newly implemented kinetic approach. The comparison of the equilibrium partitioning and diffusion dependent partitioning approaches reveals differences in the formed SOA mass.

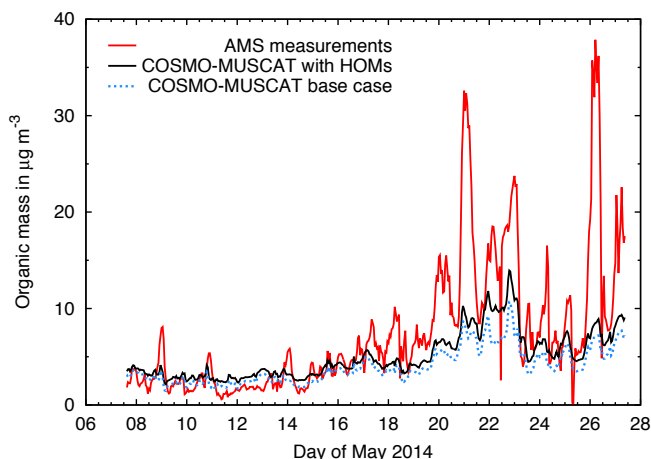


Figure 1. Time series of organic mass measured at the field site Melpitz. The red solid line shows Aerosol Mass Spectrometer (AMS) measurements; the black solid line marks the COSMO-MUSCAT simulation with considered HOMs from monoterpene oxidation and the blue dotted line depicts the simulation with the basic chemistry mechanism without HOMs.

**References:**

- Berndt, T., Richters, S., Jokinen, T., Hyttinen, N., Kurtén, T., Otkjær, R. V., Kjaergaard, H. G., Stratmann, F., Herrmann, H., Sipilä, M., Kulmala, M., and Ehn, M.: *Na. Commun.*, **7**, 2016a.
- Berndt, T., Hartmut Herrmann, Mikko Sipilä, and Markku Kulmala: *J. Phys. Chem. A*, 2016b
- Hallquist, M., Wenger, J. C., Baltensperger, U., et al. *Atmos. Chem. Phys.*, **9**, 5155 – 5236, 2009
- Jokinen, T., Sipilä, M., Richters, S., Kerminen, V.-M., Paasonen, P., Stratmann, F., Worsnop, D., Kulmala, M., Ehn, M., Herrmann, H., and Berndt, T.: *PNAS*, **112**, 7123 – 7128, 2015
- Mutzel, A., Poulain, L., Berndt, T., Iinuma, Y., Rodigast, M., Böge, O., Richters, S., Spindler, G., Sipilä, M., Jokinen, T., Kulmala, M., and Herrmann, H.: *Environ. Sci. Technol.*, **49**, 7754 – 7761, 2015
- Wolke, R., Schröder, W., Schrödner, R., and Renner, E.: *Atmos. Env.*, **53**, 110 – 130, 2012
- Zaveri, R. A., Easter, R. C., Shilling, J. E., and Seinfeld, J. H. (2014) *Atmos. Chem. Phys.*, **14**, 5153 – 5181, 2014

## Comparison of different methodologies used for the estimation of secondary organic carbon (SOC)

D. Srivastava<sup>1,2</sup>, O. Favez<sup>1</sup>, N. Bonnaire<sup>3</sup>, E. Perraudin<sup>2</sup>, V. Gros<sup>3</sup>, J.-L. Jaffrezo<sup>4</sup>, E. Villenave<sup>2</sup>, A. Albinet<sup>1</sup>

<sup>1</sup>INERIS, Parc Technologique Alata, BP 2, 60550 Verneuil-en-Halatte, France

<sup>2</sup>Université de Bordeaux, EPOC, UMR 5805 CNRS, 33405 Talence, France

<sup>3</sup>LSCE - UMR8212, CNRS-CEA-UVSQ, Gif-sur-Yvette, France

<sup>4</sup>UGA, CNRS, IGE, 38000 Grenoble, France

Keywords: SOA markers, SOC estimation, SOA tracer method, EC tracer method, WSOC, ACSM

Presenting author email: deepchandra.srivastava-etudiant@ineris.fr

A significant fraction of organic carbon (OC) is of secondary origin. The estimate of secondary organic carbon (SOC) is necessary for the implementation of air quality policy effectiveness. However, its evaluation still remains uncertain despite intensive efforts undertaken during the last decades to characterize and understand the chemistry leading to the formation of secondary organic aerosol (SOA). Though, there is still no direct way to separate secondary from primary organic aerosol fractions. Recent researches have used several methodologies to achieve this evaluation though the need of studies is still required to determine their associated variability and the consistency between the different methodologies.

The objective of this work is to estimate the contribution of SOC fraction to OA content by using various methodologies, and to evaluate and discuss the differences accounted in the apportionment and time evolution of SOC estimates. Measurements were conducted at the SIRTa atmospheric research observatory, representing the suburban background air quality conditions of the Paris area (about 25 km SW from Paris city center). PM<sub>10</sub> samples were collected every 4 hours over a period of intensive PM pollution events (PM > 50 µg m<sup>-3</sup> over several days) from 6 to 24, March 2015, concomitantly with online measurements, carried out using ACSM, Aethalometer 7λ, TEOM-FDMS, PTR-MS, NO<sub>x</sub> and O<sub>3</sub> analyzers. Following off-line sampled filter analyses, SOC were estimated using EC-, WSOC-, and SOA tracer-based methods, as well as using online data using positive matrix factorization (PMF) applied to ACSM data (Kleindienst et al. 2007; Sun et al. 2011; Turpin and Huntzicker 1995; Weber et al. 2007).

SOC estimates ranged from 19% to 51% of PM<sub>10</sub> OC during the campaign. SOA tracer method, which relies on the use of secondary species to account for SOC contribution from individual precursors, provided the lowest SOC estimate. For the first time, estimation of SOC concentrations from phenolic compounds (methylnitrocatechols (Iinuma et al. 2010)), known to account for a major fraction of SOA biomass burning (Bruns et al. 2016), has been investigated, showing a contribution of 60% to total SOC during the first part of the PM pollution event which reflects the predominance of local emissions and notably residential heating. The comparison of SOC estimates showed a similar time evolution profile to a certain extent (Figure 1). After

March 14<sup>th</sup>, high concentrations of secondary inorganic species such as NH<sub>4</sub>NO<sub>3</sub> and (NH<sub>4</sub>)<sub>2</sub>SO<sub>4</sub>, SOC results presented different temporal behavior. These results highlight the problem associated with the methods to apportion SOC in a polluted environment. Discussion will further focus on the photochemical origin of SOA, and cause for the noticeable change observed in the temporal behavior of SOC estimates according to the nature and origin of the PM during the pollution events. Information about the limitations and challenges associated to SOC estimations will also be discussed.

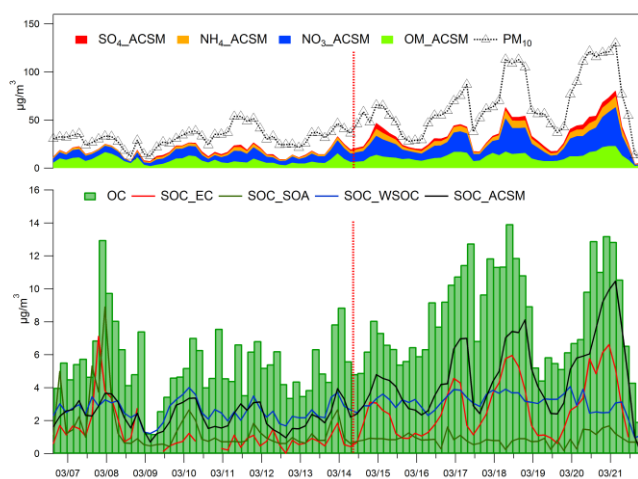


Figure 1. Temporal variation of SOC estimates and OC, along with the PM<sub>10</sub> chemical composition (obtained using ACSM data) identified at SIRTa (France) during an intense PM pollution event in March 2015.

### Acknowledgements

This work has notably been supported by the French ministry of environment (MEEM) and the French reference laboratory for air quality monitoring (LCSQA) as well as by the FP7 ACTRIS and H2020 ACTRIS2 Programmes.

### References

- Bruns, Emily A., et al. (2016), *Scientific reports*, 6, 27881.
- Iinuma, Y., et al. (2010), *Environmental Science & Technology*, 44, 8453-9.
- Kleindienst, Tadeusz E., et al. (2007), *Atmospheric Environment*, 41, 8288-300.
- Sun, Y. L., et al. (2011), *Atmos. Chem. Phys.*, 11, 1581-602.
- Turpin, Barbara J. and Huntzicker, James J. (1995), *Atmospheric Environment*, 29, 3527-44.
- Weber, Rodney J., et al. (2007), *Journal of Geophysical Research: Atmospheres*, 112, D13302.

## Influence of NH<sub>3</sub> on Secondary Organic Aerosols from the Ozonolysis and Photooxidation of $\alpha$ -Pinene in a Flow Reactor

Z.B. Babar<sup>1</sup>, J.-H. Park<sup>1,2</sup>, I.-J. Hwang<sup>3</sup>, and H.-J. Lim<sup>1</sup>

<sup>1</sup>Department of Environmental Engineering, Kyungpook National University, Daegu, 702-701, Korea

<sup>2</sup>Mass Spectrometry Research Center, Korea Basic Science Institute, Ochang, 363-883, Korea

<sup>3</sup>Department of Environmental Engineering, Daegu University, Gyeongsan, Gyeongbuk, 38453, Korea

Keywords: secondary organic aerosol,  $\alpha$ -pinene, NH<sub>3</sub>, flow reactor, optical properties.

Presenting author email: hylim@knu.ac.kr

Atmospheric aerosols play a key role in climate and human health. Organic aerosols comprise a large fraction of atmospheric aerosols (Kanakidou et al., 2005). A substantial fraction of fine organic particles consists of secondary organic aerosol (SOA) formed by atmospheric reactions of gaseous organics (Hallquist et al., 2009). Reduced nitrogen species (e.g., amino acids, amines, and ammonia) react with carbonyls to produce brown carbon that has a strong effect on climate via direct light absorption (Laskin et al., 2014).

This study presents detailed characterizations of a newly-developed flow reactor including: (1) residence time distribution measurements, (2) relative humidity (RH) and temperature control, and (3) OH radical exposure range (i.e., atmospheric aging time). Hydroxyl (OH) radical exposures ranged from  $8.20 \times 10^{10}$  to  $7.22 \times 10^{11}$  molecules cm<sup>-3</sup> (0.5 to 4.9 d of atmospheric aging). In this study, the effects of NH<sub>3</sub> gas on the secondary organic aerosol (SOA) formation of  $\alpha$ -pinene by dark ozonolysis and photooxidation were investigated using the newly-developed flow reactor. For both dark  $\alpha$ -pinene ozonolysis and photooxidation, higher SOA yields were observed in the presence of NH<sub>3</sub> than in the absence of NH<sub>3</sub>. At RH of ~50%, the SOA yield for ozonolysis and photooxidation in the presence of NH<sub>3</sub> increased by 23% and 15% relative to those in the absence of NH<sub>3</sub> (Figure 1). Similar effects were observed at lower and higher RH conditions. Fourier transform infrared spectroscopy analysis confirmed the presence of nitrogen-containing functional groups in SOA formed in the presence of NH<sub>3</sub> (Figure 2). The  $\alpha$ -pinene SOA formed in the presence of NH<sub>3</sub> showed higher absorption and fluorescence for UV-visible radiation than those formed in the absence of NH<sub>3</sub>.

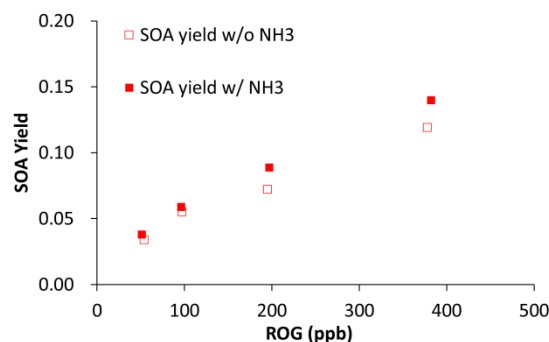


Figure 1. SOA yield as a function of  $\alpha$ -pinene concentrations at mid RH.

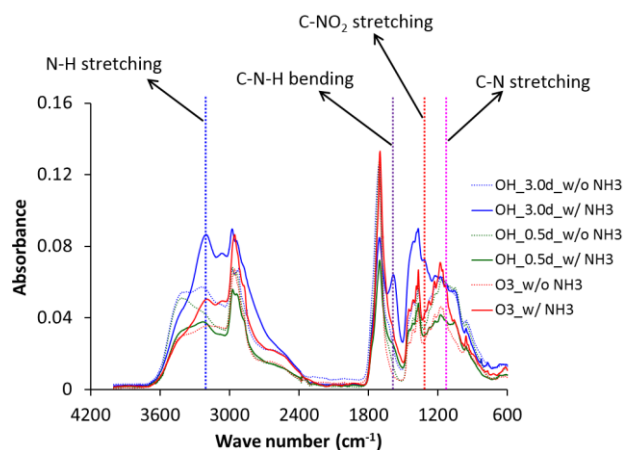


Figure 2. FTIR spectra of  $\alpha$ -pinene SOA formed from ozonolysis and photooxidation at the atmospheric aging time of 0.5 and 3 d with and without NH<sub>3</sub>.

This work was supported by the Korea Institute of Energy Technology Evaluation and Planning (KETEP) granted financial resource from the Ministry of Trade, Industry & Energy, Republic of Korea (No. 20142010201810) through POSCO E & C.

Hallquist, M., Wenger, J.C., Baltensperger, U., and et al., 2009. *The formation, properties and impact of secondary organic aerosol: current and emerging issues*. Atmos. Chem. Phys. 9, 5155–5236. doi:10.5194/acp-9-5155-2009.

Kanakidou, M., Seinfeld, J.H., Pandis, S.N., and et al., 2005. *Organic aerosol and global climate modelling: a review*. Atmos. Chem. Phys. 5, 1053–1123. doi:10.5194/acp-5-1053-2005.

Laskin, J., Laskin, A., Nizkorodov, S.A., Roach, P., Eckert, P., Gilles, M.K., Wang, B., Lee, H.J., Hu, Q., 2014. *Molecular selectivity of brown carbon chromophores*. Environ. Sci. Technol. 48, 12047–12055. doi:10.1021/es503432r.

## Characterization of gas phase emissions from residential coal combustion using proton transfer reaction time-of-flight mass spectrometry

F. Klein<sup>1</sup>, S.M. Pieber<sup>1</sup>, A. Bertrand<sup>2</sup>, H. Ni<sup>3</sup>, G. Stefanelli<sup>1</sup>, B. Temime-rousseau<sup>2</sup>, N. Marchand<sup>2</sup>, I. El-Haddad<sup>1</sup>, J. G. Slowik<sup>1</sup>, U. Baltensperger<sup>1</sup>, R. Huang<sup>1,3</sup>, A.S.H. Prévôt<sup>1</sup>

<sup>1</sup>Laboratory of Atmospheric Chemistry, Paul Scherrer Institute, Villigen, 5232, Switzerland

<sup>2</sup>Laboratoire Chimie Environnement, Aix Marseille Université, Marseille, 13331, France

<sup>3</sup>Key Lab of Aerosol Chemistry & Physics, Institute of Earth Environment, Chinese Academy of Sciences, Xi'an 710049, China

Keywords: VOC, PTRMS, coal combustion, aromatic hydrocarbon

Presenting author email: felix.klein@psi.ch

Residential coal combustion is acknowledged as an important source of ambient organic aerosol in Asia and Eastern Europe. However the chemical properties of the gas-phase emissions from residential coal combustion are mostly unknown. Identifying the gas phase precursors from coal combustion could help to better explain the extensive secondary aerosol formation observed in Chinese megacities.

The approach adopted for our study involves laboratory quantification of VOC emission factors from five different Chinese coals. Primary emissions from the three bituminous type and two anthracite type coals burned in a typical Chinese burner used for heating were analysed under controlled conditions after ~100 times dilution. A high resolution proton transfer time-of-flight mass spectrometer (PTR-ToF-MS) was used to quantify VOC emissions and to investigate their chemical composition. For the calculation of the emission factors we measured the total CO<sub>2</sub> emitted by the coals and then scaled the emissions by the carbon content of the coals.

Our measurements suggest that VOC emissions from residential coal combustion are mostly related to the ignition phase during which the coal is not properly burning. The VOC emissions drop to almost zero when the coal is in the stable flaming phase (Figure 1).

The VOC emissions from the bituminous type coals consist mainly of single ring aromatics and phenols which are formed by vaporisation from the coals (Figure 2). B3 emits more aromatics compared to B1 and B2 which can be explained by the different origin of the coals. About 80% of the emissions can be identified by PTR-ToF-MS measurements. The anthracite type coals emit more acids but the emission factors are negligible compared to the bituminous coals.

Our study indicates that oxidation of VOC precursors emitted by coal combustion could be a significant contributor to ambient secondary organic aerosol. By using only anthracite type coals the VOC emissions could be reduced to almost zero improving significantly the air quality in Chinese megacities.

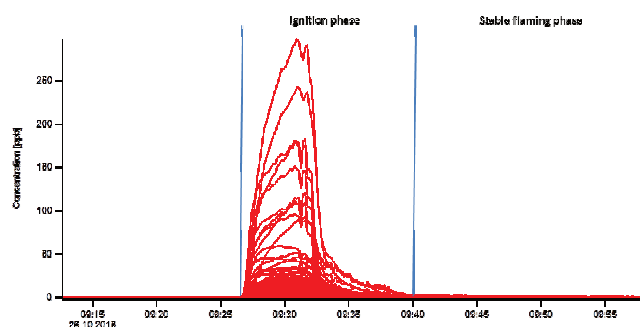


Figure 1. Time resolved VOC emissions from residential coal combustion

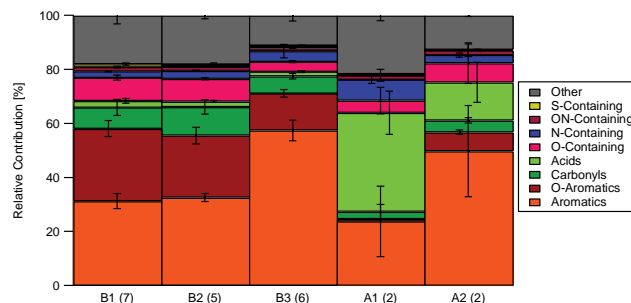


Figure 2. Chemical composition of non-methane VOC emitted by five different coals from China. B denotes bituminous coals, A anthracite coals.

This work was supported by the SNF as well as the Swiss Federal Office for the Environment.

## Secondary aerosol formation from shipping emissions

P. Simonen<sup>1</sup>, E. Saukko<sup>1,2</sup>, L. Ntziachristos<sup>1</sup>, K. Lehtoranta<sup>3</sup>, H. Timonen<sup>4</sup>, F. Mylläri<sup>1</sup>, T. Rönkkö<sup>1</sup>, P. Karjalainen<sup>1</sup>, J. Keskinen<sup>1</sup> and M. Dal Maso<sup>1</sup>

<sup>1</sup>Aerosol Physics, Faculty of Natural Sciences, Tampere University of Technology, Tampere, 33720, Finland

<sup>2</sup>Currently at: Pegasor Oy, Hatanpään valtatie 34C, Tampere, 33100, Finland

<sup>3</sup>VTT Technical Research Centre of Finland Ltd., Espoo, 02044, Finland

<sup>4</sup>Atmospheric Composition Research, Finnish Meteorological Institute, Helsinki, 00101, Finland

Keywords: marine exhaust, SOA, secondary aerosol

Presenting author email: pauli.simonen@tut.fi

The global contribution of shipping emissions to primary particle mass is approximately 1 Tg/year (Lack et al. 2009). In addition to primary particles, ship engines also emit precursor gases, which may condense onto particle phase as a result of atmospheric oxidation, thus forming secondary PM.

In this study, we measured both primary particle emissions and the secondary PM formation potential of a four-stroke four-cylinder medium speed diesel engine with a brake nominal power of 1640 kW. The exhaust was measured at 25 % and 75 % loads and using two different fuels, light fuel oil (LFO) and low sulphur grade (1% wt.) heavy fuel oil (HFO).

The secondary PM formation potential was measured with a Potential Aerosol Mass (PAM) flow through reactor, where the sample is exposed to high concentrations of oxidants. If the oxidation products of gaseous compounds are of low volatility, they will condense to particle phase to form secondary aerosol mass. This process mimics atmospheric oxidation, but takes place only within a couple of minutes instead of days in the atmosphere.

The size-distribution and chemical composition of primary and secondary aerosol particles were measured with an Electrical Low-Pressure Impactor (ELPI+), High-Resolution Low-Pressure cascade Impactor (HRLPI, Arffman et al. 2014) and Soot-Particle Aerosol Mass Spectrometer (SP-AMS).

We found that the secondary organic aerosol (SOA) formation potential of the exhaust was approximately 1 g kWh<sup>-1</sup> and did not vary strongly between fuels and loads. The mass of secondary PM is significant, especially when compared to primary PM mass emission rate of 0.06-0.65 g kWh<sup>-1</sup> (Ntziachristos et al. 2016).

In contrast to SOA formation potential, the inorganic fraction of secondary aerosol is strongly depended on fuel. HFO exhibited high sulphate aerosol formation potential, which was expected since the sulphur content of HFO is higher than that of LFO. LFO exhaust, in turn, produced ammonium nitrate in the PAM chamber.

The size-distributions of the aerosol aged in the PAM chamber are also different between the two fuels (Fig. 1). The higher sulphur content in HFO seems to promote nucleation, and thus the number concentration is higher in aged HFO exhaust than in aged LFO exhaust.

Even though the PAM chamber cannot fully

simulate the nucleation processes in the atmosphere, this observation may have atmospheric implications. If the HFO exhaust also exhibits stronger nucleation potential than LFO in the atmosphere, the choice of fuel may affect the amount of cloud condensation nuclei and therefore also the cloud formation, with climate implications.

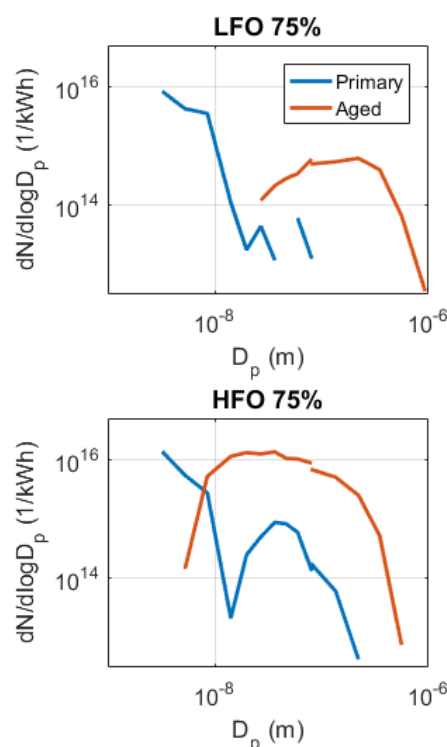


Figure 1. Number size-distributions of primary and aged aerosol at 75 % load. The distributions are combined of HRLPI and ELPI+ data.

This work was conducted in the framework of the HERE project funded by Tekes (the Finnish Funding Agency for Innovation). Pauli Simonen acknowledges Tampere University of Technology Graduate School.

Lack, D. et al. (2009) *J. Geophys. Res.* **114** D00F04, doi:10.1029/2008JD011300.

Arffman, A. et al. (2014) *J. Aerosol Sci.* **78** 97-109, <http://dx.doi.org/10.1016/j.jaerosci.2014.08.006>.

Ntziachristos, L. et al. (2016) *Fuel* **186** 456-465, <http://dx.doi.org/10.1016/j.fuel.2016.08.091>.

## Molecular Characterization of Biogenic SOA using online Extractive Electrospray Ionization Mass Spectrometry: On the fate of condensed phase ELVOC

F. D. Lopez-Hilfiker<sup>1</sup>, V. Pospisilova<sup>1</sup>, M. Xiao<sup>1</sup>, J. Dommen<sup>1</sup>, A. Prevot<sup>1</sup>, U. Baltensperger<sup>1</sup>, J. G. Slowik<sup>1</sup>

<sup>1</sup>Laboratory of Atmospheric Chemistry, Paul Scherrer Institute, Villigen PSI, 5232, Switzerland

Keywords: SOA, ESI, Oligomers, EESI-TOF, BSOA

Presenting author email: [felipe.lopez@psi.ch](mailto:felipe.lopez@psi.ch)

Recent measurements of the oxidation products from biogenic precursors by chemical ionization mass spectrometry (CIMS) have revealed a large source of extremely low volatility organic molecules (ELVOC) formed at high yield. These molecules can contribute to new particle formation and subsequent particle growth despite their low gas phase abundance. Semi-continuous measurements of aerosol composition and volatility measured by FIGAERO-CIMS from both chambers as well as temperate and boreal forests show that >50% of the total organic aerosol from biogenic sources has low or extremely low volatility. This finding is largely consistent with a significant source of secondary organic aerosol (SOA) formed from the condensation of initially low volatility organic vapors; however, the tendency of these molecules to undergo ionization-induced fragmentation and/or thermal decomposition has to date prevented their direct measurement.

As such, the fate of highly oxidized organics formed in the gas phase in the condensed phase remains an open question. If highly oxidized organic molecules undergo net fragmentation during particle phase processing the overall efficiency which low volatility gas phase organics form aerosol is significantly diminished. Alternatively, if intra-particle reactions lead to the efficient formation of dimers and higher order accretion products then the effective yield and persistence of ELVOC based SOA formation is greatly enhanced.

Here, we present the analysis from the first direct online measurements of individual organic aerosol components at atmospherically relevant particle mass loadings without thermal decomposition or ionization-induced fragmentation, using an extractive electrospray ionization time-of-flight mass spectrometer (EESI-TOF). We focus on the measurement of highly oxidized, low volatility organic molecules and oligomers, which are formed rapidly and in high yield from a variety of biogenic precursors (monoterpenes, sesquiterpenes, isoprene). We investigate the fate of highly oxidized gas phase organics in the particle phase and assess the degree that fragmentation and/or accretion reactions occur during particle ageing. To investigate these particle-phase formation and ageing mechanisms the EESI-TOF was deployed at the PSI atmospheric simulation chamber where biogenic precursor compounds were oxidized under a variety of conditions. We operate the chamber in both batch mode and continuous flow modes. Gas phase composition is measured online by CIMS and particle phase composition is monitored by the EESI-TOF and SMPS.

Figure 1 presents an example of one such experiment during the oxidation of  $\alpha$ -pinene by ozone, during which  $10 \mu\text{g m}^{-3}$  of SOA was formed. The figure shows an example of the level of molecular detail provided by the EESI-TOF, allowing for the first time, the ability to follow individual particle phase species. Our measurements utilizing the EESI-TOF and a variety of biogenic precursor molecules provide a new level of molecular insight that allows the direct assessment of particle phase oligomerization, fragmentation and intra-particle ageing reactions which influence SOA lifetime and response to atmospheric changes.

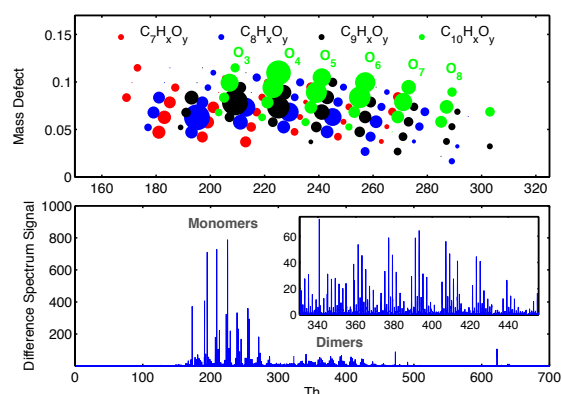


Figure 1. Bottom: Example mass spectra from the EESI-TOF highlighting the measurement of  $\alpha$ -pinene ozonolysis products. Top: Mass defect plot colored by carbon number highlighting a suite of compounds which comprise the monomer region of the mass spectrum.

This work was supported by the Swiss National Science Foundation (starting grant BSSGI0\_155846).

## Characterization of an Online Extractive Electrospray Ionization Time of Flight Mass Spectrometer (EESI-TOF): Application to Atmospheric Aerosol

F. D. Lopez-Hilfiker<sup>1</sup>, V. Pospisilova<sup>1</sup>, J. Dommen<sup>1</sup>, A. Prévôt<sup>1</sup>, U. Baltensperger<sup>1</sup>, Tofwerk AG<sup>2</sup>, J. G. Slowik<sup>1</sup>

<sup>1</sup>Laboratory of Atmospheric Chemistry, Paul Scherrer Institute, Villigen PSI, 5232, Switzerland

<sup>2</sup>Tofwerk AG, Thun, 3600, Switzerland

Keywords: SOA, ESI, Oligomers, SOA measurement,

Presenting author email: [felipe.lopez@psi.ch](mailto:felipe.lopez@psi.ch)

Thermal desorption of aerosol components for analysis is typical in most online aerosol sampling instruments (e.g. AMS, ATOFMS, SPLAT, PALMS). Most single particle instruments utilize simultaneous laser desorption/ionization, which is not quantitative due to matrix effects, while quantitative approaches like the AMS cause extensive thermal decomposition and fragmentation due to the high temperatures and hard ionization techniques used. While recent developments in semi-continuous measurements coupled to GC or soft ionization techniques like CIMS (e.g. TAG, SV-TAG, FIGAERO) have provided very useful tracer analysis on the ground and chambers, thermal decomposition during desorption even at low temperatures significantly changes measured aerosol composition. Key molecular information is lost, hindering mechanism development and source apportionment. Therefore there is a fundamental need in the atmospheric chemistry community for online, rapid response chemical characterization of atmospheric aerosol without artifacts from thermal decomposition.

To fill this gap in the measurement capabilities of the community, we describe the development of an online extractive electrospray time-of-flight mass spectrometer (EESI-TOF) for fast molecular analysis of aerosol organics without fragmentation or thermal desorption. This instrument couples an EESI inlet, recently developed at PSI, to a robust, commercially available high-resolution time of flight mass spectrometer. Briefly, the extractive electrospray instrument operating principle involves the collision of atmospheric aerosol with charged electrospray droplets. The soluble components are extracted into the electrospray droplet, and as the solvent from the electrospray evaporates, ion ejection by the coulomb explosion mechanism results in gas phase ions formed from the extracted aerosol. Therefore aerosol are ionized rapidly, and transferred into the gas phase without any need for heating.

The EESI-TOF provides rapid response (1Hz) measurements of highly oxidized organic species and oligomers with individual compound detection limits as low as  $1 \text{ ng m}^{-3}$  in 5 seconds, allowing for the simultaneous retrieval of molecular compositions for hundreds of compounds that comprise organic aerosol at high time resolution. Figure 1 shows an example of the level of detail this single instrument provides. An example mass spectrum collected at 1 Hz of  $5 \text{ ug m}^{-3}$  of SOA from the reaction of  $\alpha$ -pinene and ozone yields a suite of over 500 individual molecules (150 to 500+ Th)

which are detected by the EESI-TOF with excellent signal to noise even for oligomeric species which are clearly identifiable in the mass spectrum.

We present the detailed characterization of the EESI-TOF instrument and its application to atmospheric aerosol, both from chambers and ambient measurements. We discuss the instrument performance in the context of current aerosol measurement shortfalls, and potential applications of the instrument to the chemical speciation of organic aerosol at atmospherically relevant conditions.

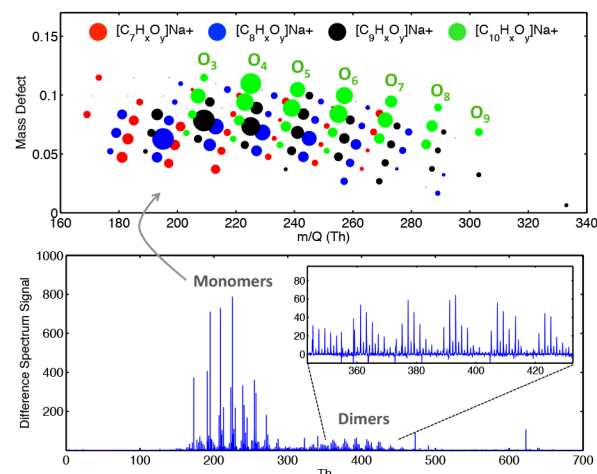


Figure 1. Bottom. A 5 second average mass spectrum collected from a flow tube reaction between  $\alpha$ -pinene and ozone. Organic aerosol was promptly produced with all mass contained in particles smaller than 50 nm. Inset. A region of the mass spectrum highlighting the formation of high molecular weight dimers either formed in the gas phase and rapidly partitioned to the condensed phase or formed via particle phase accretion reactions. Top. Mass defect plot showing chemical composition retrievals from a series of highly oxidized monomers detected in the particle phase by the EESI-TOF.

This work was supported by the Swiss National Science Foundation starting grant BSSGI0\_155846. We thank Markus Kalberer for useful discussions on the initial development of the EESI and Tofwerk AG for their help coupling the EESI to the TOFMS.

## Partitioning of SOA components during photochemical smog in Beijing and Hong Kong

Mattias Hallquist<sup>1</sup>, Michael Le Breton<sup>1</sup>, Anna Lutz<sup>1</sup>, Song Guo<sup>2</sup>, Jian Zhen Yu<sup>3</sup>, Åsa M Hallquist<sup>4</sup>, Ravi K. Pathak<sup>1</sup>, Qianyun Liu<sup>3</sup>, Chak K. Chan<sup>5</sup>, Yujue Wang<sup>2</sup>, Zhijun Wu<sup>2</sup>, and Min Hu<sup>2</sup>

<sup>1</sup> Department of Chemistry and Molecular Biology, University of Gothenburg, Gothenburg, Sweden

<sup>2</sup> State Key Joint Laboratory of Environmental Simulation and Pollution Control, College of Environmental Sciences and Engineering, Peking University, Beijing, China.

<sup>3</sup> Division of Environment, Hong Kong University of Science & Technology, Hong Kong, China

<sup>4</sup> IVL Swedish Environmental Research Institute, Gothenburg, Sweden

<sup>5</sup> School of Energy and Environment, City University of Hong Kong, Hong Kong

Keywords: SOA, Beijing, Hong Kong, Partitioning

Presenting author email: hallq@chem.gu.se

Secondary chemistry transforming primary pollutants is of high relevance for Chinese photochemical smog (Hallquist *et al.*, 2016). In particular, formation of O<sub>3</sub> and PM, including Secondary Organic Aerosols (SOA), are of major concern regarding impacts on health, climate and ecosystems. The atmospheric oxidation processes leading to SOA formation are complex and involves thousands of different compounds, both of biogenic and anthropogenic origin. Furthermore, for a thoroughly understanding both the gas and the particle phase need to be considered.

As part of an intercollaborative project to assess the photochemical smog in China, two major field campaigns were arranged in 2016: in Changping, Beijing during springtime and at HKUST, Hong Kong during the autumn. Alongside with other advanced instrumentations, a Time of Flight Chemical Ionisation Mass Spectrometer (ToF CIMS) utilising the Filter Inlet for Gases and AEROsols (FIGAERO) was used to chemically characterize the gas and the particle phase. (Lopez-Hilfiker *et al.*, 2014)

This specific instrument applies soft ionization limiting the fragmentation and one can usually identify molecular composition of hundreds of different parent molecules. In both Beijing and Hong Kong the ionization was done with iodide as the reagent ion, making it possible to specifically detect oxygenated compounds such as carboxylic acids, organic nitrates and sulphates as well as some inorganic compounds e.g. N<sub>2</sub>O<sub>5</sub>, ClNO<sub>2</sub>, and HONO.

For numerous compounds significant levels were detected in both the gas and particle phase enabling evaluation of partitioning and gas-to-particle transformation and its relationship to atmospheric conditions and estimated vapour pressures. Furthermore, the detection of molecular markers such as levoglucosan, C<sub>6</sub>H<sub>5</sub>NO<sub>3</sub>, C<sub>7</sub>H<sub>5</sub>SO<sub>4</sub>, C<sub>5</sub>H<sub>11</sub>SO<sub>7</sub>, C<sub>8</sub>H<sub>12</sub>O<sub>6</sub> can support source apportionment and atmospheric process description.

Figure 1 shows an example of gas and particle measurements of the time evolution of m/z corresponding to Pinic acid done at the Changping site outside Beijing during summer 2016.

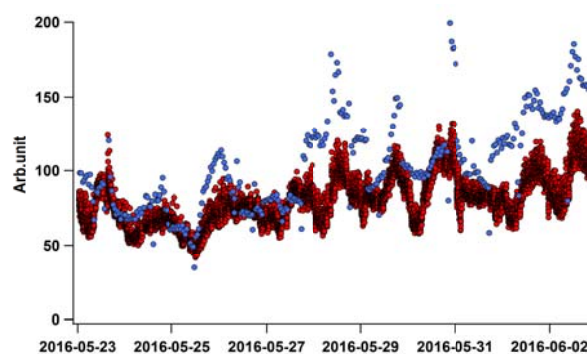


Figure 1. Time traces of signal related to particle (blue) and gas phase (red) pinic acid m/z during measurements at the Changping site

In order to further investigate atmospheric ageing/processing a portable laminar flow reactor (Go:PAM) was for selected periods utilized to oxidize the sampled air before characterisation with the ToF-CIMS-FIGAERO. These experiments were explorative but illustrated the potential of further formation of organic nitrates and sulfates in the observed air-masses.

The results of the measurements with the ToF-CIMS-FIGAERO are compared and evaluated in relation to data from other locations and complementary laboratory studies.

This work was supported by the Swedish Research Council (639-2013-6917); National Basic Research Program from Ministry of Science and Technology, China (2013CB228503); National Natural Science Foundation of China (91544214, 91544226) and Hong Kong Research Grants Council (C-5022-14 G).

Hallquist *et al.* (2016) *Photochemical smog in China: scientific challenges and implications for air-quality policies*, Natl Sci Rev, 2016, Vol. 3, No. 4

Lopez-Hilfiker *et al.*, (2014) *A novel method for online analysis of gas and particle composition: description and evaluation of a Filter Inlet for Gases and AEROsols (FIGAERO)*, Atmos. Meas. Tech.7(4), 983

## Gas phase composition and secondary organic aerosol formation from gasoline direct injection vehicles investigated in batch and flow reactors: cold-start emissions and the effect of a gasoline particle filter.

S.M. Pieber<sup>1</sup>, U. Baltensperger<sup>1</sup>, D. Bhattu<sup>1</sup>, E.A. Bruns<sup>1</sup>, P. Comte<sup>2</sup>, J. Czerwinski<sup>2</sup>, J. Dommen<sup>1</sup>, N. Heeb<sup>3</sup>, A. Keller<sup>4</sup>, F. Klein<sup>1</sup>, N.K. Kumar<sup>1</sup>, A.S.H. Prévôt<sup>1</sup>, J.G. Slowik<sup>1</sup>

<sup>1</sup>Paul Scherrer Institute, Laboratory of Atmospheric Chemistry, CH-5232 Villigen, Switzerland

<sup>2</sup>Bern University of Applied Sciences, CH-2560 Nidau, Switzerland

<sup>3</sup>Empa Material Science and Technology; CH-8600 Dübendorf, Switzerland

<sup>4</sup>University of Applied Sciences Northwestern Switzerland; CH-5210 Windisch, Switzerland

Keywords: SOA formation, SOA yield, gasoline particle filter, oxidation flow reactor, smog chamber, GDI

Presenting author email: simone.pieber@psi.ch

Vehicular pollution is a significant source of air pollution in many urban areas. Historically, diesel-fueled vehicles have been recognized as a significant source of primary fine particulate matter (PM), containing a significant fraction of black carbon (BC). Accordingly, the use of older-generation diesel vehicles is often restricted in cities and modern diesel vehicles are subject to stringent primary PM limits, which are met with both, oxidation catalysts and diesel particulate filters (DPFs). In contrast, gasoline fueled vehicles and especially gasoline direct injection (GDI) systems have been recognized only recently as significant source of primary PM, especially BC. In light of more stringent legislations, automobile manufacturers have recently considered equipping modern gasoline light-duty vehicles with gasoline particulate filters (GPFs) to reduce primary PM emissions. Although GPFs are likely to be similarly effective to DPFs in reducing primary emissions, recent research indicates that the dominant fraction of the total PM from modern GDIs is secondary, originating from gaseous precursors that are transformed in the atmosphere to form secondary organic aerosol (SOA). Those precursors are unlikely to be removed by GPF systems. Laboratory results are, however, missing. SOA formation of GDI vehicles (w/o GPFs) has been studied previously in atmospheric simulation chambers (SC). However, the SOA-forming precursors could not be unambiguously identified, in parts due to limitations of the applied techniques to study the non-methane organic compounds (NMOC) emitted, as well as the batch-style SC experiments, which limit the number of experiments practically.

Here, we investigate primary and secondary emissions from modern GDI vehicles, of which one is additionally equipped with a prototype GPF. Vehicles were tested on a chassis dynamometer during a modern regulatory driving cycle (WLTC) and the older low-load NEDC, under cold- and hot-started engine conditions. SOA formation was investigated through batch-style aging of collected emissions in the PSI mobile SC, and the potential aerosol mass (PAM) oxidation flow reactor (OFR). Further, time-resolved analysis of aged emissions during a driving cycle using the OFR was performed. Relevant SOA precursors were characterized by proton transfer reaction time-of-flight mass spectrometry (PTR). The SOA mass and its bulk chemical composition were characterized by aerosol mass spectrometry (AMS). An aethalometer was used to determine equivalent BC (eBC) concentrations.

GPF installation was found to greatly decrease primary PM through the near complete removal of eBC, but to have a complex and volatility-dependent effect on the minor primary organic aerosol (POA) fraction, and no detectable effect on NMOC emissions or SOA production (Fig.1). In all tests, overall NMOC and primary and secondary PM emissions were dominated by the engine cold start, i.e. before thermal activation of the catalytic after-treatment system (Fig.1-2). SOA formation in SC and OFR compared well in terms of SOA yields and bulk compositional properties such as O:C and H:C ratios. Effective SOA yield analysis shows that SOA production is predominantly explained by a small number of aromatic hydrocarbons (ArHC), based on a comparison with single substance SOA yields of toluene, *o*-xylene and 1,2,4-trimethylbenzene tested in our OFR.

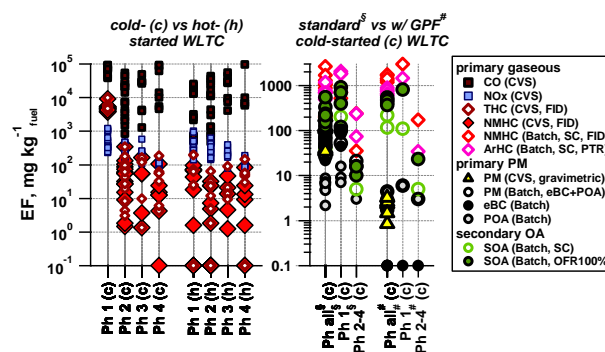


**Fig.1.** Emission factors (EF) of primary and secondary pollutants from constant volume sampler (CVS) and batch sampling (SC) from Phase 1 to 4 of a cold- and hot-started WLTC test. Total hydrocarbons (THC) and non-methane hydrocarbons (NMHC) were measured by flame ionization detection (FID). OFR100% denotes OFR operation at 100% UV power. Other abbreviations are explained in the text.

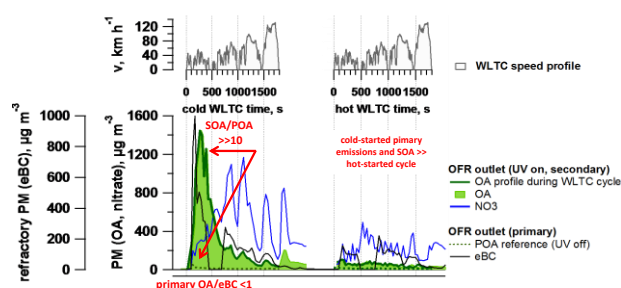


**Fig.2.** Time-resolved primary and secondary PM (SOA and nitrate (NO<sub>3</sub>) emissions profile.

This work was supported by the CCEM Project GasOMeP.

## Carboxylic acid oxidation products from limonene ozonolysis and their role in SOA formation

Julia Hammes<sup>1</sup>, Cameron Faxon<sup>1</sup>, Anna Lutz<sup>1</sup>, Ravi Kant Pathak<sup>1</sup>, Thomas Mentel<sup>1,2</sup>, Mattias Hallquist<sup>1</sup>

<sup>1</sup>Department of Chemistry and Molecular Biology, University of Gothenburg, Gothenburg, Sweden

<sup>2</sup>Institute of Energy and Climate Research, IEK-8: Troposphere, Forschungszentrum Jülich GmbH, Jülich, Germany

Keywords: Limonene, FIGAERO, CIMS, Carboxylic acids, SOA, MCM

Presenting author email: julia.hammes@chem.gu.se

### Introduction

Low vapor pressure products from the oxidation of volatile organic compounds (VOC) contribute significantly to atmospheric aerosol particle formation and growth (Hallquist et al., 2009). Limonene is a doubly unsaturated VOC which exhibits high reactivity in the presence of ozone and oxidation reactions can subsequently lead to the formation of secondary organic aerosol (SOA) in the atmosphere and indoor environments.

Carboxylic acids are one major class of products from limonene oxidation. They have been shown to play an important role in SOA formation due to their low vapor pressure (Salo et al., 2009). A previous modelling study assessed the relative contribution of carboxylic acids from limonene oxidation to SOA formation (Pathak et al., 2012). According to their model, limonene-ozonolysis produces significant amounts of carboxylic acids and the distribution is affected by changes of OH and ozone concentrations. Numerous carboxylic acids have been identified in this work, of which only a small fraction is currently incorporated in the MCM.

The aim of this study is to increase the understanding of the limonene-ozone system and to identify mechanisms that lead to carboxylic acid oxidation products.

### Material and Methods

Limonene has been oxidized in the Gothenburg Flow Reactor for Oxidation Studies at Low Temperatures (G-FROST) described in a previous study (Jonsson et al., 2008). In this study, limonene was added through a characterized diffusion source and concentrations were increased stepwise (15, 40, 150 ppb). Temperature (20°C), ozone concentrations (400, 1000 or 5000 ppb) and relative humidity (dry or 25% RH) were kept constant during the run of the experiments. Experiments were performed with and without 2-butanol as an OH scavenger.

The oxidation product distribution in the gas and particle phase was measured with an acetate High-Resolution Time-of-Flight Chemical Ionization Mass Spectrometer (HR-ToF-CIMS) coupled to a Filter Inlet for Gases and AEROSols (FIGAERO) (Lopez-Hilfiker et al., 2014) and analyzed for their chemical composition. SOA mass based on particle size distribution was derived with a Scanning Mobility Particle Sizer (SMPS).

### Results

Limonene has been oxidized in the presence of ozone under a variety of experimental conditions and monomer (C7-C10) and dimer (C14-C20) compounds with carboxylic acid functional groups were detected. The dimer compounds occurred almost exclusively in the particle phase. A total of 52 different C7-C10 species have been identified of which 37 have not been reported in previous studies. The known carboxylic acids contribute to 45-65% of the total C7-C10 signal. Carboxylic acid dimers from limonene ozonolysis have, to our knowledge, not been reported previously.

Chemical formulas of identified products as well as their distribution between the gas and particle phase and the dependence on different reaction conditions will be presented and reaction mechanism leading to the formation of these compounds will be proposed.

This work was supported by Formas (214-2010-1756) and is a contribution to the Swedish strategic research area Modelling the Regional and Global Earth system, MERGE.

Hallquist et al. (2009). *Atmos. Chem. Phys.* 9, 5155–5236

Salo et al. (2009). *J. Phys. Chem. A*, 114, 4586-4594

Pathak et al. (2012). *Environ. Sci. Technol.*, 46, 11660-11669

Jonsson et al. (2008), *Environ. Sci. Technol.*, 42, 5938–5944

Lopez-Hilfiker et al. (2014) *Atmos. Meas. Tech.*, 7, 983–1001

## **Abstracts T212**

## Wind dependence of sea-salt and non-sea-salt components in ambient aerosol in Niigata Plain during winter seasons

S. Ohara<sup>1,2</sup>, N. Kihara<sup>1</sup> and N. Murao<sup>2</sup>

<sup>1</sup>Central Research Institute of Electric Power Industry, Abiko, 270-1194, Japan  
<sup>2</sup>Graduate school of Engineering, Hokkaido University, Sapporo, 060-8628, Japan

Keywords: marine aerosol, sea salt, sulfate, winter monsoon.

Presenting author email: o-shin@criepi.denken.or.jp

Marine aerosol generation is strongly influenced by wind characters (O'Dowd and de Leeuw, 2007). In contrast to marine aerosol, for most airborne particulate and gas (e.g. sulfate, nitrate, and NO<sub>x</sub>), it has been reported that their concentrations reduce as wind speed increases (e.g. Jones *et al.*, 2010). In a coastal area of the Sea of Japan during winter season, ambient aerosols essentially consist of sea-salt and non-sea-salt components due to northwesterly winter monsoon off the Asian continent, which bring sea-salt aerosols emitted from the Sea of Japan as well as long-range transported air pollutants to this area. In this study, in order to examine the effect of wind on coastal aerosols, which indicate generation of sea-salt aerosol, and transport and dry deposition of sea-salt and non-sea-salt aerosols, wintertime measurements of sea-salt and non-sea-salt components in ambient aerosol were carried out in Niigata Plain, which locates in a coastal area of the Sea of Japan.

Field sampling of ambient aerosols was conducted at three sites in the Niigata Plain during winter of 2008 - 2016 (Figure 1). At each site, aerosol samples were collected every 6 hours on a 47 mm Teflon filter by using a ten-line low-volume sampler. The samples of the filter extract were analyzed for the species: NH<sub>4</sub><sup>+</sup>, Na<sup>+</sup>, K<sup>+</sup>, Mg<sup>2+</sup>, Ca<sup>2+</sup>, Cl<sup>-</sup>, NO<sub>3</sub><sup>-</sup> and SO<sub>4</sub><sup>2-</sup>. At the site B, aerodynamic particle spectrometer (APS) and size-segregated sampler were used for an additional field measurement during the winters of 2013 and 2015.



Figure 1. Location of the observation sites (A, B, and C) in Niigata Plain, Japan.

Differences in wind dependence between sea-salt and non-sea-salt components are observed (Figure 2). Under onshore wind condition, Na<sup>+</sup> concentration increased with wind speed, whereas nss-SO<sub>4</sub><sup>2-</sup> (non-sea-salt SO<sub>4</sub><sup>2-</sup>) concentration decreased with wind speed. The wind dependences of Na<sup>+</sup> and nss-SO<sub>4</sub><sup>2-</sup> concentrations in ambient air are consistent with the dependence in previous studies (e.g. Jones *et al.*, 2010). The slopes of Na<sup>+</sup> increase with onshore wind speed decreased with the distance from the sea (A>B>C).

Relationships between sea-salt and non-sea-salt aerosols concentrations and the distance from the sea under onshore wind condition are showed in Figure 3.

Na<sup>+</sup> concentration in ambient air increased with wind speed at the three sites, also decreased with the distance from the sea (A>B>C). Under relatively windy condition (>6 m s<sup>-1</sup>), Na<sup>+</sup> concentration decrease steeply from site A to sites B and C. In contrast, nss-SO<sub>4</sub><sup>2-</sup> concentration in ambient air appeared to be constant with the distance from the sea at the different wind speed levels.

The steeper decrease in Na<sup>+</sup> concentration under onshore windy condition would be attributed to coarse and giant sea-salt particles, which have greater dry deposition velocity, resulting greater fraction of sea-salt particle deposited during transport from site A to sites B and C. Relatively constant nss-SO<sub>4</sub><sup>2-</sup> concentration with the distance might be associated with smaller deposition velocity of particulate nss-SO<sub>4</sub><sup>2-</sup> (Diameter: ~ 0.1 – 1 μm) and well mixing of nss-SO<sub>4</sub><sup>2-</sup> during long-range transport.

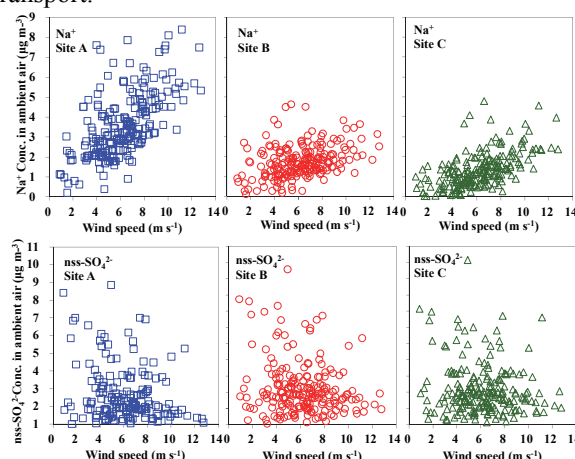


Figure 2. Relationships between Na<sup>+</sup> and nss-SO<sub>4</sub><sup>2-</sup> concentrations in ambient air and onshore wind speed (northwest) at the three sites (A, B, and C).

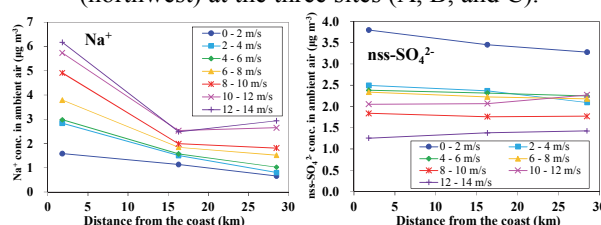


Figure 3. Relationships between Na<sup>+</sup> and nss-SO<sub>4</sub><sup>2-</sup> concentrations in ambient air and the distance from the coast under different onshore wind speed (northwest).

O'Dowd D., de Leeuw G. (2007) *Phil. Trans. R. Soc., A* **365**, 1753-1774.

Jones A. M., Harrison R. M., Baker J. (2010) *Atmos. Environ.*, **44**, 1682-1690.

## Overview of aerosol and trace gases measurements during the Antarctic Circumnavigation Expeditions 2016 - 2017

J. Schmale<sup>1</sup>, S. Henning<sup>2</sup>, A. Baccharini<sup>1</sup>, F. Tummon<sup>3</sup>, M. Hartman<sup>2</sup>, A. Welti<sup>2</sup>, J. Dommen<sup>1</sup>, F. Stratmann<sup>2</sup>, C. Bolas<sup>4</sup>, N. Harris<sup>5</sup>, D. Rosenfeld<sup>6</sup>, K. Carslaw<sup>7</sup>, M. Schnaiter<sup>8</sup>, A. Prévôt<sup>1</sup>, U. Baltensperger<sup>1</sup> and M. Gysel<sup>1</sup>

<sup>1</sup>Laboratory of Atmospheric Chemistry, Paul Scherrer Institute, Villigen 5232, Switzerland; <sup>2</sup>Department Experimental Aerosol and Cloud Microphysics, Leibniz Institute for Tropospheric Research, Leipzig, 04318, Germany; <sup>3</sup>Institute of Atmospheric and Climate Science, Federal Institute of Technology, ETHZ, Zurich, 8092, Switzerland; <sup>4</sup>Centre for Atmospheric Science, University of Cambridge, Cambridge, CB2 1EW, UK; <sup>5</sup>Centre for Atmospheric Informatics and Emissions Technology, University of Cranfield, Cranfield, MK 43 0AL, UK; <sup>6</sup>Institute of Earth Sciences, Hebrew University of Jerusalem, Jerusalem, 91904, Israel; <sup>7</sup>Institute for Climate and Atmospheric Sciences, University of Leeds, Leeds, LS2 9JT, UK; <sup>8</sup>Karlsruhe Institute of Technology, Institute for Meteorology and Climate Research, Eggenstein-Leopoldshafen, 76344, Germany

Keywords: Antarctica, aerosol, CCN  
Presenting author email: julia.schmale@psi.ch

Aerosol-cloud interactions are the least understood anthropogenic influence on climate change. A major cause of this limited understanding is the poorly quantified state of aerosols in the pristine preindustrial atmosphere, which defines the baseline against which anthropogenic effects are calculated. The uncertainty in aerosol induced radiative forcing ( $-0.55 \pm 0.7 \text{ W/m}^2$ ) is twice the uncertainty for  $\text{CO}_2$  ( $+1.68 \pm 0.35 \text{ W/m}^2$ ). In addition, models significantly underestimate cloud solar reflectance there, by as much as  $30 \text{ W m}^{-2}$  during summer. The poor representation of aerosol-cloud interactions is one of reason for the bias.

Here we present preliminary aerosol and trace gases data from the Antarctic Circumnavigation Expedition (ACE) that took place from December 2016 to March 2017 (see Figure 1 for the itinerary).

comprehensively characterize aerosol properties, their origin and interactions with clouds to validate satellite retrieval algorithms and to evaluate and constrain global climate models, in a region that still exhibits preindustrial-like aerosol conditions under certain circumstances.

Continuous measurements of the following parameters were performed during all three legs: particle number concentration and size distribution, aerosol chemical composition, cloud condensation and ice nuclei concentration, fluorescent particle concentration and traces gases concentrations (isoprene, CO,  $\text{CO}_2$ ,  $\text{CH}_4$ ) amongst other. Figure 2 provides a snapshot of preliminary data for the timer period at which the ship was anchored near Marion Island (see Figure 1). Air masses generally arrived from the island and concentrations of particles and cloud condensation nuclei were around 100 p/cc. During periods contaminated with the ship's exhaust gas particle concentrations as well as e.g. the  $\text{CO}_2$  mixing ratio increased significantly.



Figure 1. Itinerary of the Antarctic Circumnavigation Expedition (ACE) 2016 – 2017.

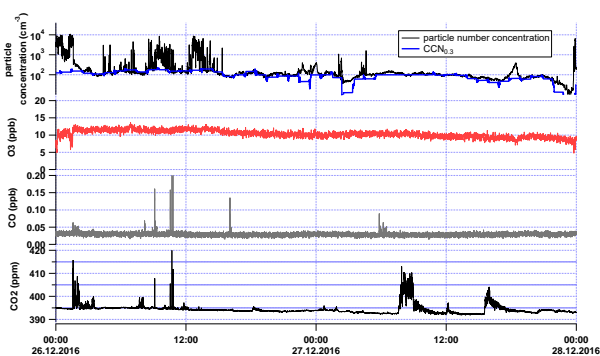


Figure 2. Preliminary time series of particle and cloud condensation nuclei concentrations as well as various trace gases while being at anchor at Marion Island during leg 1 (see Figure 1).

The objective of the project “Study of preindustrial-like-aerosol climate effects” (SPACE) was to

This project has received funding from EPFL, Swiss Polar Institute and from Ferring Pharmaceuticals.

## Marine bio-chemical variabilities and secondary organic aerosols over the Middle Adriatic area: Insight into organosulfur prevalence

A. Cvitešić<sup>1</sup>, A. Kroflič<sup>2</sup>, Z. Ljubešić<sup>3</sup>, M. Šala<sup>2</sup>, I. Grgić<sup>2</sup>, I. Ciglencečki<sup>1</sup> and S. Frka<sup>1</sup>

<sup>1</sup>Division for Marine and Environmental Research, Ruđer Bošković Institute, Zagreb, Croatia

<sup>2</sup>Department of Analytical Chemistry, National Institute of Chemistry, Ljubljana, Slovenia

<sup>3</sup>Department of Biology Faculty of Science, University of Zagreb, Zagreb, Croatia

Keywords: marine aerosols, secondary organic matter, organosulfur compounds, sea surface microlayer

Presenting author email: ana.cvitesic@irb.hr

As the oceans cover approximately 70% of the Earth's surface, marine aerosols are the most important natural aerosol system at the global level. Considerable influence of marine aerosols on the global radiative budget has been proven through their enhanced ability to act as cloud condensation nuclei (CCN) on which cloud droplets are formed. Marine organic aerosols, primarily emitted into the atmosphere via bubble bursting as well as formed through secondary processes, including oxidation of volatile organic compounds such as dimethyl sulfide (DMS), have been also shown to affect the chemistry of the marine environment (O'Dowd et al., 2015). Besides, marine-derived sulfate is thought to be the key precursor to marine organosulfur compounds (OS) serving as markers of multiphase chemical processes leading to SOA formation over the marine areas. However, mechanisms responsible for the SOA formation in the marine atmosphere are still not completely clarified (Surratt et al., 2008). Nevertheless, the sea surface microlayer (SML) being the very uppermost layer of the ocean at the air-sea interface, has a particular role in hindering a range of global dynamic exchange processes between the ocean and the atmosphere and serving as a medium for accumulation and transportation of marine organic matter (OM) up into the atmosphere (e.g. Engel and Galgani, 2016). Up to now, a relation between the chemical composition, physical-chemical properties and mechanisms responsible for SOA formation in the marine atmosphere are not completely understood, resulting in a significant uncertainty of marine SOA impact on the Earth's climate.

In this work, an interdisciplinary approach to determine a detail chemical composition of fine marine aerosols, with a special emphasis on OS constituents, during 1-year period at the Middle Adriatic Sea coastal area has been applied. A complex chemical approach, comprising ion chromatography, high temperature catalytic oxidation, inductively coupled plasma optical emission spectrometry, high pressure liquid chromatography-tandem mass spectrometry and electrochemistry, enabled the determination of parameters such as water soluble anions and cations, total and water soluble organic carbon, organosulfur and surfactant content. In order to provide a better insight into the possible sources of SOA over the marine atmosphere, the obtained results have been correlated and supported by the hydrological and biochemical data obtained for the marine SML and the underlying water

(~ 0.5 m depth) samples collected in parallel with fine aerosols. The results point out that during investigated period the formation of SOA components could be driven by the seasonality of marine biological productivity in the marine photic zone but also affected by the photochemical processing and local biomass burning events at the coastal Middle Adriatic area.

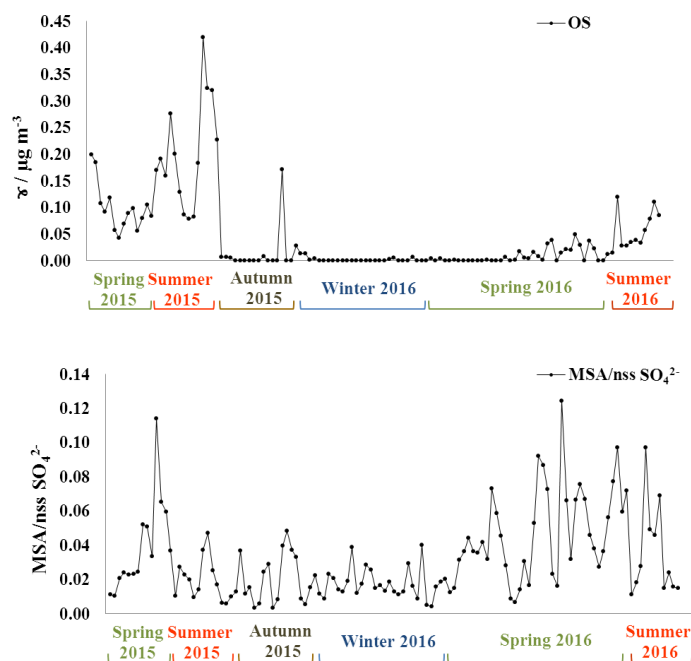


Figure 1. Seasonal variability of organosulfur content (OS) as well as the MSA/nss  $\text{SO}_4^{2-}$  ratio in fine aerosols collected at Middle Adriatic area.

This work was supported by the Croatian Science Foundation project "The Sulphur and Carbon dynamics in the Sea- and Fresh-water EnviRonment"; Croatian-Slovenian bilateral project "Estimating the role of marine biogenic organosulfur compounds in the formation and properties of atmospheric organic aerosols" (BI-HR/16-17-032), as well as by the Slovenian Research Agency (Contract no. P1-0034-0140).

O'Dowd, C. et al., (2015) *Sci. Rep.* **5**, 14883-14893.

Surratt, J.D. et al., (2008) *J. Phys. Chem.* **112** (36), 8345-8378.

Engel A. and Galgani L. (2016) *Biogeosciences* **13**, 989-1007.

## Latitudinal Distribution of Particulate MSA and MSA:nssSO<sub>4</sub> over the Atlantic using a Validated Quantification Method with HR-ToF-AMS

S. Huang<sup>1,2</sup>, L. Poulain<sup>2</sup>, D. van Pinxteren<sup>2</sup>, M. van Pinxteren<sup>2</sup>, Z. J. Wu<sup>3</sup>, H. Herrmann<sup>2</sup>,  
A. Wiedensohler<sup>2</sup>

<sup>1</sup> Institute for Environmental and Climate Research, Jinan University, Guangzhou, 511443, China

<sup>2</sup> Leibniz-Institute for Tropospheric Research, Leipzig, 04318, Germany

<sup>3</sup> College of Environment Sciences and Engineering, Peking University, Beijing, 100871, China

Keywords: marine aerosol, MSA, non-sea-salt sulfate, HR-ToF-AMS.

Presenting author email: shanhuang\_pku@163.com

The marine aerosol plays an important role in global climate regulation and marine biogenic system. Methanesulfonic acid (MSA) has been widely found in submicrometer marine aerosol particles, and has been used as a tracer for marine secondary organic aerosol (SOA). In the past, MSA was almost only detected by offline methods offering a time resolution from a few hours to days. Several modern techniques are of capacity to provide MSA information in high time resolution, such as High Resolution Time-of-Flight Aerosol Mass Spectrometer (HR-ToF-AMS). Nevertheless, MSA is not a default compound directly provided by HR-ToF-AMS, and the current quantification methods reported in the previous papers remain uncertainties. For this reason, the present study improves the MSA quantification method using HR-ToF-AMS and evaluates three previously published methods. With this validated quantification method, MSA mass concentrations derived from a unique dataset containing HR-ToF-AMS measurements on board the German research vessel Polarstern during 4 cruises over the Atlantic Ocean are investigated. These 4 research cruises were carried out in 2011 and 2012, covering spatial range from 53°S to 53°N over the Atlantic in two seasons (spring and autumn).

To quantify MSA by HR-ToF-AMS, the standard calibrations were performed using pure MSA aerosol particles. The standard MSA mass spectra were obtained accordingly. CH<sub>3</sub>SO<sub>2</sub><sup>+</sup> is selected as the key ion for MSA, and then the MSA mass concentration could be calculated with the key ion and the standard mass spectrum. To determine the RIE of MSA (RIE<sub>MSA</sub>), laboratory calibrations were carried out jointly using the AMS and a condensation particle counter (CPC, Model 3010, TSI Inc., USA). The present quantification method was directly applied to the AMS dataset during the Polarstern measurements. Then the resulting MSA mass concentration is compared to that obtained from parallel filter measurements. Excellent agreement is found (slope = 0.88, R<sup>2</sup> = 0.89), which validates the present method for ambient measurements. This comparison is much better than those using three previous methods, resulting in underestimations of 31 to 54% of MSA concentration.

With this new method, MSA mass concentrations were obtained during 4 North/South Atlantic. The spatial variation of the particulate MSA mass concentration as well as the MSA to non-sea-salt sulfate ratio (MSA:nssSO<sub>4</sub>) over the North/South Atlantic Ocean were determined for the first time. Figure 1 provides an

example of the latitudinal distribution of MSA mass concentration during the cruise in November 2012, with the background graph showing simultaneous mass concentration of chlorophyll-*a* (Chl-*a*). Seasonal variation of the MSA mass concentration was also observed, with higher values in spring (0.03 μg m<sup>-3</sup>) than in autumn (0.01 μg m<sup>-3</sup>). The measured MSA:nssSO<sub>4</sub> ratios oscillate within a range of 0.007 and 0.173, agreeing well with previous records in this region. But a seasonal pattern of MSA:nssSO<sub>4</sub> was not observed. A sharp increase in ratios between 30°S and 50°S in autumn might suggest a considerable contribution from biological sources due to low nitrate levels and marine air masses. However, in general anthropogenic sources show a ubiquitous and significant influence on aerosol particles in the MBL.

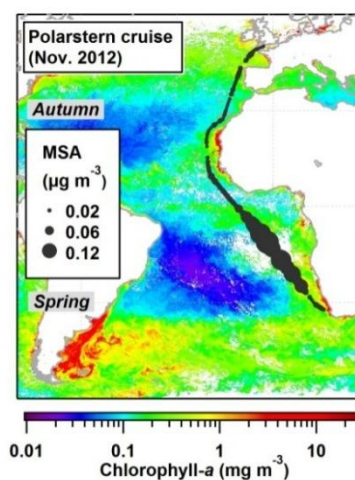


Figure 1. The latitude distribution of MSA mass concentration with Chl-*a* (background) during the Polarstern cruise in November 2012.

## Sources of cloud condensation nuclei over the Southern Ocean inferred from water uptake and volatility.

L. Cravigan<sup>1</sup>, J. Alroe<sup>1</sup>, B. Miljevic<sup>1</sup>, R. Humphries<sup>2</sup>, M. Keywood<sup>2</sup>, P. Selleck<sup>2</sup>, J. Ward<sup>2</sup>, A. Protat<sup>3</sup> and Z. Ristovski<sup>1</sup>

<sup>1</sup>International Laboratory for Air Quality and Health, Science and Engineering Faculty, Queensland University of Technology, Brisbane, Queensland, Australia.

<sup>2</sup>CSIRO Marine and Atmospheric Research, Aspendale, Victoria, Australia.

<sup>3</sup>Australian Bureau of Meteorology, Melbourne, Victoria, Australia.

Keywords: CCN, sea spray, hygroscopicity, Southern Ocean.

Presenting author email: [z.ristovski@qut.edu.au](mailto:z.ristovski@qut.edu.au)

Seasonal variations in cloud condensation nuclei (CCN) and cloud droplet number concentrations associated with biological activity have been observed over the Southern Ocean and have been linked to secondary sulfate and primary organic aerosol concentrations (McCoy *et al.*, 2015). Observational campaigns over the sparsely observed Southern Ocean are important to constrain the impact of aerosol cloud interactions on global radiative forcing and reduce the biases in modelled low to mid level clouds in this region (Bodas-Salcedo *et al.*, 2012).

In recent years QUT have contributed volatility and water uptake measurements to a number of remote marine aerosol investigations over the Southern Ocean using a novel Volatility and Hygroscopicity Tandem Differential Mobility Analyser (Johnson *et al.*, 2004). These projects include the Cold Water Trials of the RV-*Investigator* (CSIRO, Hobart) in January/February 2015, and the Clouds, Aerosols Precipitation, Radiation and Atmospheric Composition Over the Southern Ocean (CAPRICORN) project in March/April 2016 (RV-*Investigator*). Figure 1 shows the tracks for these two voyages.

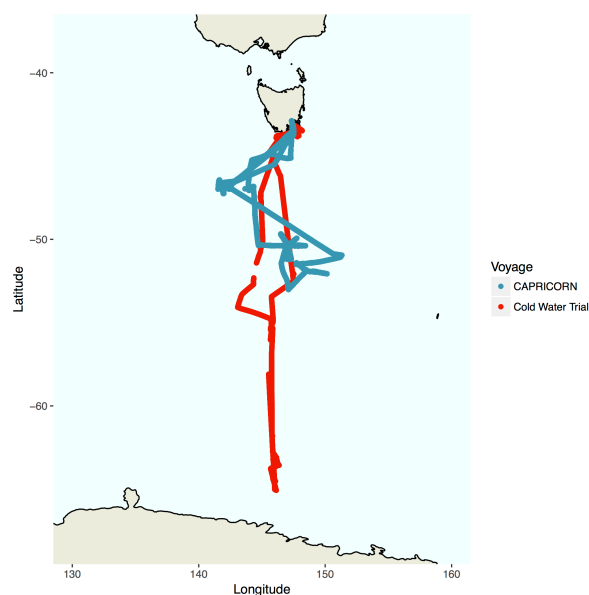


Figure 1. Voyage track for the Cold Water Trial of the RV-*Investigator* and the CAPRICORN projects.

This presentation will outline the marine aerosol species that contribute to CCN over the Southern Ocean

and the influence of atmospheric processing to CCN contributions. Hygroscopic growth factors and volatility have been used to identify contributions from SSA and secondary sulfate particles.

Summertime Southern Ocean aerosol concentrations at peak CCN sizes (<200 nm) are generally dominated by nss sulfates, formed via atmospheric processing of dimethyl sulfide (DMS). SSA is more transient, yet can significantly enhance CCN concentrations when present. During the CAPRICORN voyage the SSA mode contributed 32% to the particle number concentration at 100 nm on average, 12% at 40 nm and 44% at 150 nm. The nss sulfate mode contributed 45 to 73% to the overall number concentrations on average.

The organic enrichment of SSA at CCN sizes is poorly characterised and highly uncertain in the Southern Hemisphere. Size dependent organic SSA fractions were also calculated based on water uptake and volatility measurements, the influence of this seasonally varying enrichment on CCN will also be presented.

Detailed CCN source apportionment for the Cold-Water Trial and CAPRICORN will enhance the process understanding of aerosol-cloud interactions in this region and future modelling efforts.

This work was supported through an Australian Government Research Training Program Scholarship. The authors would like to acknowledge the assistance of the Australian Marine National Facility.

Bodas-Salcedo, A., Williams, K. D., Field, P. R., & Lock, A. P. (2012). *Journal of Climate*, 25(21), 7467–7486.

Johnson, G. R., Ristovski, Z., & Morawska, L. (2004). *Journal of Aerosol Science*, 35(4), 443–455.

McCoy, D. T., Burrows, S. M., Wood, R., Grosvenor, D. P., Elliott, S. M., Ma, P. L., *et al.* (2015). *Science Advances*, 1(6), e1500157. <http://doi.org/10.1126/sciadv.1500157>

## Investigation of aerosol optical and microphysical characteristics in the atmosphere of Kara and Barents Seas in summer and autumn of 2016

S.A. Terpigova<sup>1</sup>, P.N. Zenkova<sup>1</sup>, M.V. Panchenko<sup>1</sup>, V.V. Polkin<sup>1</sup>, D.G. Chernov<sup>1</sup>, D.M. Kabanov<sup>1</sup>, V.S. Kozlov<sup>1</sup>, V.P. Shmargunov<sup>1</sup>, S.M. Sakerin<sup>1</sup>, V.P. Shevchenko<sup>2</sup>, A.P. Lisitzin<sup>2</sup>, and N.V. Politova<sup>2</sup>

<sup>1</sup>V.E. Zuev Institute of Atmospheric Optics, 1, Ak. Zuev square, 634021, Tomsk, Russia

<sup>2</sup>P.P. Shirshov Institute of Oceanology, 36, Nakhimovskii ave., 117851, Moscow, Russia

Keywords: Arctic aerosols, black carbon, concentration, size distribution, optical depth

Presenting author email: swet@iao.ru

The results are presented of the study of spatial - temporal variability of the near-water aerosol and the spectral aerosol optical depth over Kara and Barents Seas in July till October 2016 (66 and 67-th cruises of RV "Akademik Mstislav Keldysh").

Measurements of the aerosol characteristics were carried out by means of the instrumentation complex consisting of nephelometer, optical particle counter, aethalometer and sun photometer. The following parameters were measured: number concentration of aerosol particles with diameter  $d > 0.3 \mu\text{m}$  ( $\text{PM}_{\text{total}}$ ) –  $N_A$ , their size distribution, mass concentration of equivalent black carbon  $M_{\text{BC}}$ , spectral aerosol optical depth  $\tau_A(\lambda)$ , and columnar water vapor  $W$ . About 1000 series of measurements of near-water aerosol were carried out in Barents Sea, and 1400 series in Kara Sea. Measurements by sun photometer were carried out under cloudless or partly cloudy conditions, totally 59 cycles (20 different days) of measurements in Kara Sea and 39 cycles (12 days) in Barents Sea.

Mean values of the measured parameters in Kara Sea are  $N_A = 10.9 \pm 31.3 \text{ cm}^{-3}$ ,  $M_{\text{BC}} = 0.105 \pm 0.264 \mu\text{g}\cdot\text{m}^{-3}$ ,  $\tau_A(0.55 \mu\text{m}) = 0.057 \pm 0.042$ , and  $W = 1.48 \pm 0.55 \text{ g}\cdot\text{cm}^{-2}$ . In Barents Sea, the mean values are  $N_A = 7.62 \pm 6.26 \text{ cm}^{-3}$ ,  $M_{\text{BC}} = 0.039 \pm 0.033 \mu\text{g}\cdot\text{m}^{-3}$ ,  $\tau_A(0.55 \mu\text{m}) = 0.073 \pm 0.06$ , and  $W = 1.16 \pm 0.40 \text{ g}\cdot\text{cm}^{-2}$ . The mean Angstrom exponents of the aerosol optical depth are  $0.46 \pm 0.30$  in Kara Sea and  $0.94 \pm 0.50$  in Barents Sea.

Figure 1 demonstrates the time series of the number concentration of aerosol particles ( $\text{PM}_{\text{total}}$ ) and mass concentration of black carbon, and Fig. 2 shows the time series of the aerosol optical depth.

In Kara Sea, the enhanced concentrations are observed near Gulf of Ob and Gulf of Enisey. Mean values in this region are  $N_A = 8.37 \pm 11.1 \text{ cm}^{-3}$  and  $M_{\text{BC}} = 0.167 \pm 0.111 \mu\text{g}\cdot\text{m}^{-3}$ . The most clean area is near the coast of Novaya Zemlya ( $N_A = 5.71 \pm 5.44 \text{ cm}^{-3}$  and  $M_{\text{BC}} = 0.103 \pm 0.149 \mu\text{g}\cdot\text{m}^{-3}$ ).

In Barents Sea, the greatest values of the mass concentration of black carbon are observed in the southern part, near the continent and exit from the White Sea, the smallest concentration is in western and northwestern regions. The areas of the enhanced aerosol number concentration ( $30 - 35 \text{ cm}^{-3}$ ) are near the west coast of Novaya Zemlya ( $72^\circ\text{N } 50^\circ\text{E}$ ,  $74^\circ\text{N } 55^\circ\text{E}$ ) and at the north of the central part of Barents Sea ( $76^\circ\text{N}$ ,  $35 - 45^\circ\text{E}$ ).

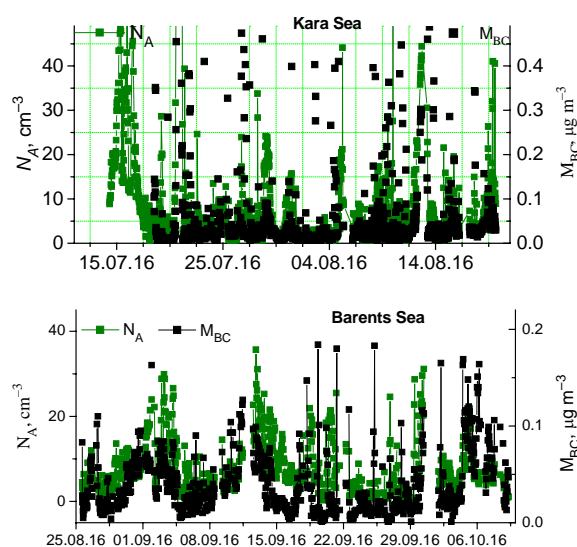


Figure 1. Time series of the concentrations of aerosol and black carbon

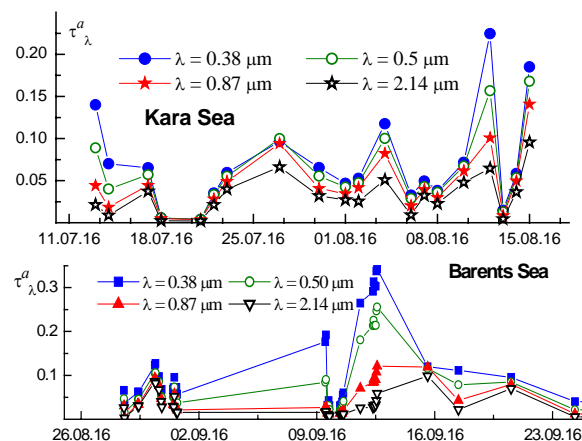


Figure 2. Time series of aerosol optical depth

The enhanced values of the aerosol optical depth also were observed near the west coast of Novaya Zemlya. Analysis of the satellite data (MODIS-Aqua) has shown that it was caused by remote transfer of smoke aerosol from wildfires in Baikal region.

The work was supported in part by Russian Science Foundation (measurements in Kara Sea under grant No. 14-50-00095 and measurements in Barents Sea under grant No. 14-27-00114) and Program of Presidium of Russian Academy of Sciences No. 32.

## Characteristics of High Aerosol Concentration Cases Measured at Vessel Gisang 1 over Yellow Sea during KORUS-AQ Campaign

Joo Wan Cha, Sang-Boom Ryoo, Beomchel Shin, Hee Choon Lee, Hee-Jung Ko,  
Yun Kyu Lim, Sang Sam Lee

Environmental meteorology Research Division, National Institute of Meteorological Science, Jeju, Rep. of Korea

Keywords: Asian dust, haze, KORUS-AQ

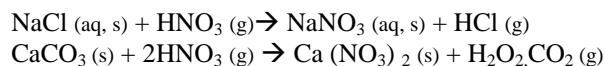
Presenting author email: jwcha@korea.kr

This study presents an analysis of aerosol measurements during the research vessel (Gisang 1) cruise of May-June 2016, in KORUS-AQ (Korea and USA - Air Quality) campaign with regard to aerosol mass concentration, size distribution, and chemical compositions. Aerosol mass concentration and size distribution were measured by PM<sub>10</sub> (beta-ray) analyzer and APS (Aerodynamic Particle Size). These aerosol mass and size observation data were used for a classification for cases such as Asian dust and haze over Yellow sea (Figure 1).

The aerosol chemical compositions were analysed by IC (Ion-Chromatograph), ICP-OES (Inductively Coupled Plasma Spectrophotometer), and ICP-MS (Inductively Coupled Plasma Mass Spectrometer). IC analysed cations (NH<sub>4</sub><sup>+</sup>, Na<sup>+</sup>, K<sup>+</sup>, Ca<sup>2+</sup>, Mg<sup>2+</sup>) and anions (SO<sub>4</sub><sup>2-</sup>, NO<sub>3</sub><sup>-</sup>, Cl<sup>-</sup>, F<sup>-</sup>, HCOO<sup>-</sup>, CH<sub>3</sub>COO<sup>-</sup>, CH<sub>3</sub>SO<sub>3</sub><sup>-</sup>). ICP-OES and ICP-MS analysed element compounds (20 species such as Al, Fe, Cu, Mg, Ti, and, Mn) after the measurement of suspended particles by PM<sub>10</sub> and PM<sub>2.5</sub> sampler over Yellow sea.

Analysis of air mass flow in this study showed that the ship was mainly influenced by Asian dust and haze from China and South Korea during the early part of its cruise. The typical marine-type aerosols dominated such as sea salt when the marine air mass influenced the cruise measurement. In Asian dust event, the air mass from Asian continental influenced the ship measurement and the maximum aerosol number concentration was showed around 8 μm in diameter during the early part of the event and around 3 μm in diameter during the later part of the event. In haze event, the air mass from China and South Korea continental influenced the ship measurement and the maximum aerosol number concentration was showed around 1 μm in diameter during the event.

According to the results of this chemical analysis, a large amount of NO<sub>3</sub><sup>-</sup> was observed in PM<sub>10</sub> when Asian dust was observed, which is considered to be an increase in volume concentration in coarse mode aerosols under the influence of the following reaction. (Tokuhiro et al, 2005)



NaNO<sub>3</sub>(aq, s) and Ca(NO<sub>3</sub>)<sub>2</sub> influence the coarse mode aerosols in Asian dust event over Yellow sea.,

The more detail information of chemical compounds of aerosol measurements over the sea during KORUS-AQ campaign will be presented in the conference.

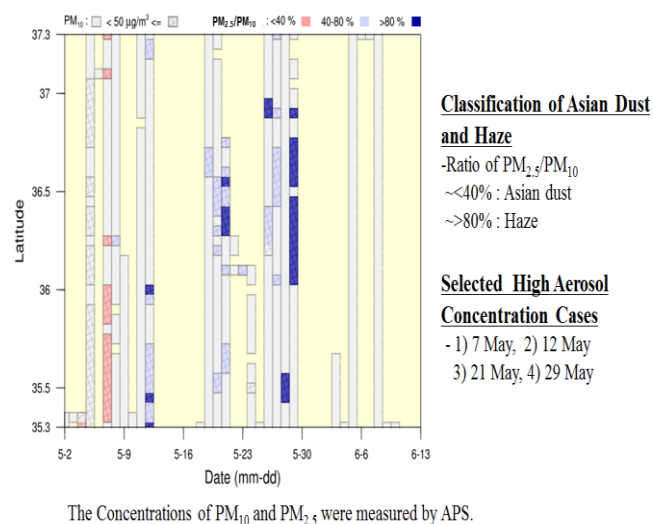


Figure 1. Classification of Asian dust and Haze by ratio of PM<sub>2.5</sub>/PM<sub>10</sub> with Latitude variation over the Yellow sea in 2016 during KORUS-AQ experiment.

### Acknowledgements

This work was supported by “Development and application of Technology for Weather forecast” project.

### Referene

Tokuhiro Nakamura, Kiyoshi Matsumoto, and Mitsuo Uematsu, (2005) *Atmospheric Environment*, **39**, 1749-1758.

## **Abstracts T213**

## The $^{40}\text{K}$ used as tracer of Saharan dust contributions

C. Dueñas<sup>1</sup>, E. Gordo<sup>1</sup>, E. Liger<sup>2</sup>, M. Cabello<sup>1</sup>, S. Cañete<sup>1</sup> and M. Pérez<sup>3</sup>

<sup>1</sup>Department of Applied Physics I, University of Málaga, Málaga, 29071, Spain

<sup>2</sup>Department of Applied Physics II, University of Málaga, Málaga, 29071, Spain

<sup>3</sup>Department of Radiology and Health Physics, University of Málaga, Málaga, 29071, Spain

Keywords:  $^{40}\text{K}$ , African dust outbreaks, PM10.

Presenting author email: mcdueñas@uma.es

A systematic 12-year analysis (January 2005-December 2016) of the concentration of radionuclides in bulk deposition and PM10 concentrations in ambient air has been performed to test the possible utility of  $^{40}\text{K}$  as tracer of mineral dust inputs of African origin in Málaga (4°28' 8"W; 36° 43'40"N). Samples of atmospheric deposition were collected monthly in an area of 1 m<sup>2</sup> using a collector that is a slightly tilted stainless steel tray and filling 25 or 50 L polyethylene vessels with bulk deposition. The radionuclide  $^{40}\text{K}$  appears approximately in 50% of the samples. Statistical analysis of the data, back-trajectory analysis and Dust Regional Atmospheric Model (DREAM) results were used to identify the diverse types of African dust outbreaks. The variation of the specific activity of  $^{40}\text{K}$  and PM10 with time were studied by time series analysis and seasonal patterns were identified, Figure 1. The monthly concentration of  $^{40}\text{K}$  in bulk deposition were in the range of 0.06-0.80 Bq/l with a monthly average of 0.21 Bq/l and exhibits maximum specific activities in summer and spring. The monthly concentration of PM10 ranged from 5 to 84  $\mu\text{g}/\text{m}^3$  with a monthly average of 30  $\mu\text{g}/\text{m}^3$ . The highest concentration of  $^{40}\text{K}$  and PM10 were recorded in October 2008 in connection with a very intense African dust outbreak (Cabello et al., 2012). The specific activity of  $^{40}\text{K}$  with meteorological variables, PM10 and number of intrusions were correlated showing good correlations mainly between  $^{40}\text{K}$ , PM10 and number of intrusions.

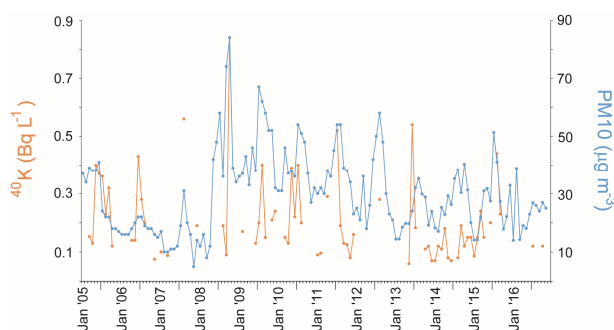


Figure 1. Temporal variations of  $^{40}\text{K}$  and PM10.

Cabello, M., Orza, J.A.G., Barrero, M.A., Gordo, E., Berasaluce, A., Cantón, L., Dueñas, C., Fernández, M.C., and Pérez, M. (2012) *J. Geophys. Res.* **117**, D11204.

## Physico-chemical transformation of Saharan dust particles by the city of Vienna – A combined chemical imaging approach

J. Ofner<sup>1</sup>, E. Eitenberger<sup>1</sup>, G. Friedbacher<sup>1</sup>, G. Schauer<sup>2</sup>, M. Greilinger<sup>2</sup>, H. Lohninger<sup>1</sup>, B. Lendl<sup>1</sup>, and A. Kasper-Giebl<sup>1</sup>

<sup>1</sup>Institute of Chemical Technologies and Analytics, Vienna University of Technology, Vienna, Austria

<sup>2</sup>Central Institute of Meteorology and Geodynamics (ZAMG), Vienna, Austria

Keywords: Saharan dust, chemical imaging, Sonnblick Observatory.

Presenting author email: johannes.ofner@tuwien.ac.at

Saharan dust events periodically occur in Europe and cause the transport of high amounts of desert sand from the Sahara into European cities and industrial areas. The mixing of ambient European air masses with these breakouts causes physico-chemical transformations of the Saharan dust particles, which provide a significant surface for heterogeneous atmospheric processes. By comparing Saharan dust aerosol, sampled at a background site (Sonnblick Observatory, 3106 m asl) with samples from a large city (Vienna), morphological as well as chemical differences of single particles become visible.

During a large Saharan dust event in Austria in spring 2016 (1<sup>st</sup> to 5<sup>th</sup> April), sampling was performed using Sioutas cascade impactors onto highly purified aluminium targets (Ofner et al., 2016) at the Sonnblick Observatory and in parallel in the city of Vienna. Aerosol particles from both locations in the range of 2.5 to 1  $\mu\text{m}$  aerodynamic diameter were analysed by scanning electron microscopy, combined with energy dispersive X-ray (EDX) imaging, and vibrational Raman micro-spectroscopic (RMS) imaging. All imaging techniques were applied to the same sample spot of 200x200  $\mu\text{m}$  and fused to a combined imaging dataset for subsequent multivariate analytics (Lohninger and Ofner, 2014; Ofner et al., 2015).

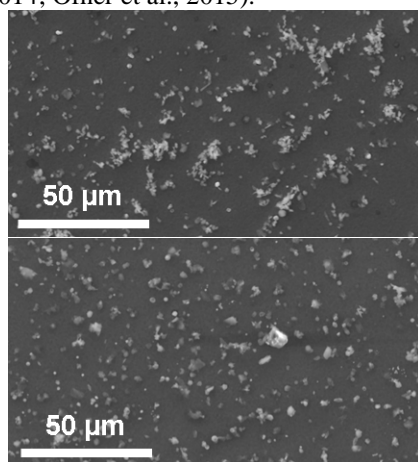


Figure 1. Electron microscopy of Saharan dust particles, sampled at the Mt. Sonnblick Observatory (upper image) and in the city of Vienna (lower image).

Electron microscopy (figure 1) of Saharan dust particles obtained from the two different sites unravels a significant change in morphology of the single particles, indicating that particles sampled in Vienna are strongly

influenced by the ambient conditions of this city. By analysing the combined chemical images of particles sampled at both sites, these ambient-caused transformation of particle morphology and chemical signature become visible (figure 2).

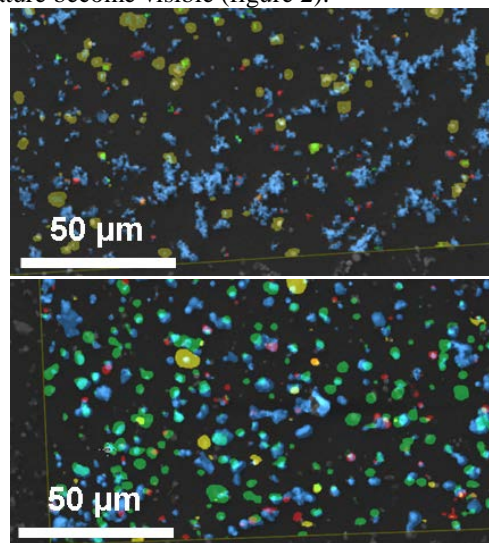


Figure 2. Image-based chemical analysis of a Saharan dust event, sampled on the Mt. Sonnblick Observatory (upper image) and in the city of Vienna (lower image): indicating silicates (blue), organic particles (yellow), soot (red) and inorganic salts (green).

This study will introduce the benefits of combined chemical images to analyse single particle features and discuss image-based results from the physico-chemical transformation of Saharan dust by ambient European air masses released by a city like Vienna.

This work was supported by the Hochschuljubiläumsstiftung of the City of Vienna under grant H-297306-2014.

Lohninger, H. and Ofner, J. (2014) *Spectrosc. Eur.*, **26**, 6–10.

Ofner, J., Kamilli, K. a., Eitenberger, E., Friedbacher, G., Lendl, B., Held, A. and Lohninger, H. (2015) *Anal. Chem.* **87**, 9413–9420.

Ofner, J., Kirschner, J., Eitenberger, E., Friedbacher, G., Kasper-Giebl, A., Lohninger, H., Eisenmenger-Sittner, C. and Lendl, B. (2016) *J. Microsc.*, doi:10.1111/jmi.12506.

## Relevance of wildfires on dust emissions via interaction with near-surface wind pattern

R. Wagner<sup>1</sup>, M. Jähn<sup>1</sup> and K. Schepanski<sup>1</sup>

<sup>1</sup>Leibniz Institute for Tropospheric Research (TROPOS), Permoserstr. 15, 04318 Leipzig, Germany

Keywords: mineral dust, emission, wildfire, LES modelling.

Presenting author email: robert.wagner@tropos.de

Mineral dust is a key player in the Earth system and shows diverse impacts on the radiation budget, cloud microphysics, marine and terrestrial ecosystems. Eventually, it also affects our modern way of life. Not only dust emissions from barren or unvegetated soil surfaces like deserts or uncultivated croplands are important sources of airborne mineral dust. Also, during fire events dust is entrained into the atmosphere and appears to contribute noteworthy to the atmospheric dust burden.

The underlying process, which drives dust entrainment during fires, is the so-called pyro-convection. The high temperatures in the center of a fire result in an upward motion of the heated air. Subsequently, air flows towards the fire replacing the rising air. The resulting accelerated winds are able to mobilize soil and dust particles up to a size of several millimeters, depending of both the size and the strength of the fire. Several measurements have shown that up to 80% of the mass fraction of the emitted particles during natural or prescribed fires is related to soil or dust particles (Meanhaut et al., 1996; Nisantzi et al., 2014). The particles are then mixed externally with the combustion aerosols into the convective updraft and were finally inject into altitudes above the planetary boundary layer where they can be distributed and transported over long distances by the atmospheric circulation.

To investigate the impacts of such fires on the near-surface wind pattern and the potential for dust emissions via exceeding typical threshold velocities, high resolving Large-Eddy Simulations (LES) with the All Scale Atmospheric Model (ASAM) were performed.

In the framework of this study, the influences of different fire properties (fire intensity, size, and shape) and different atmospheric conditions on the strength and extent of fire-related winds and finally their relevance for dust emissions were investigated by sensitivity studies.

Prescribed fires are omnipresent during dry seasons and pyro-convection is a mechanism entraining dust particles into boundary layer. As the quantity of dust emitted during fire events is still unclear, the results presented here will support the development of a parameterization of fire-related dust entrainment for meso-scale models. This will allow an estimation of such fire-related dust emissions on a continental scale and can finally reduce the uncertainty in the aerosol-climate feedback.

This work is part of the project “Dust at the interface – modelling and remote sensing” funded by the Leibniz Association.

Meanhaut, W., Salma, I., Cafmeyer, J., Annegarn, H. J., and Andreae, M. O. (1996): Regional atmospheric aerosol composition and sources in the eastern Transvaal, South Africa, and impact of biomass burning, *J. Geophys. Res.*, **101**, 23631-23650.

Nisantzi, A., Mamouri, R. E., Ansmann, A., and Hadjimitsis, D. (2014): Injection of mineral dust into the free troposphere during fire events observed with polarization lidar at Limassol, Cyprus, *Atmos. Chem. Phys.*, **14**, 12155-12165.

## Anomalous Si/Al Ratios in PM<sub>10</sub> and PM<sub>2.5</sub> Road Dust at Several Locations in India

Samiksha Shilpi<sup>1</sup>, and Sunder Raman Ramya<sup>1,2</sup>

<sup>1</sup>Department of Earth and Environmental Sciences

<sup>2</sup>Center for Research on Environment and Sustainable Technologies

Indian Institute of Science Education & Research Bhopal

Bhopal Bypass Road, Bhauri

Bhopal 462 066

Madhya Pradesh, INDIA

Keywords: Road dust; Si/Al; crust-air fractionation; anthropogenic sources

Presenting author email: shilpis@iiserb.ac.in

Across locations in the world, the mass of crustal dust accounts for nearly 30-40% PM<sub>10</sub> (particles with an aerodynamic diameter ≤10 μm) and 10-20% PM<sub>2.5</sub> (particles with an aerodynamic diameter ≤ 2.5 μm) mass, respectively.

The Si/Al ratio in road dust in both the size fraction (PM<sub>10</sub> and/or PM<sub>2.5</sub>) at several locations in India were examined and found to be unusually low (0.2-2.4, across size fractions and road dust types) in Delhi, Mumbai, Pune, and Bangalore. The anomalous Si/Al ratio in road dust could not be explained by known mechanisms. This study suggests that anthropogenic sources contribute Al to road dust. It further suggests that crust-air fractionation Si and Al occurs. These findings contradict popular assumptions about Al sources and fractionation, highlighting the need to revisit dust mass estimation using Al as a surrogate. This study also calls for an examination of anthropogenic inputs to “crustal aerosol”. Further, characterization of Si/Al ratio in road dust at locations in India and the influence of local geology/ geochemistry on it are especially important, if this ratio is to be used as an input to source apportionment and radiative transfer models.

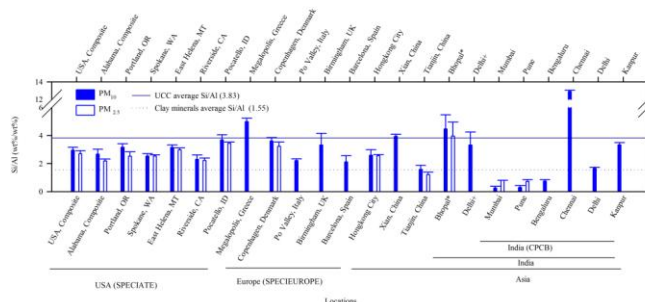


**Figure 1** .Si/Al ratios in paved road dust across different locations in the world  
(\*Data reported by Samiksha et al., 2016)

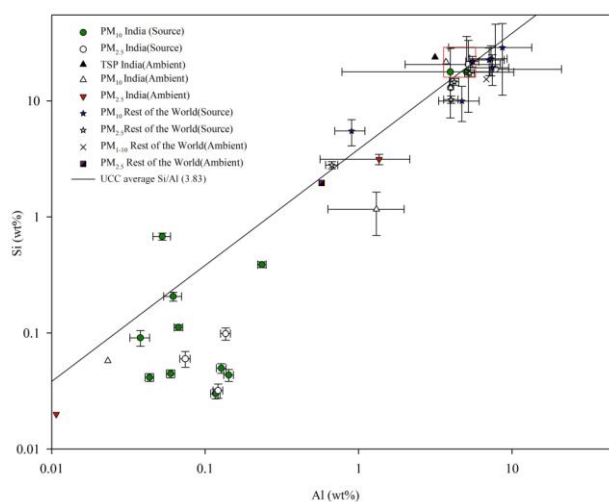


**Figure2.**Scatter plot of Si and Al abundance in source (road dust) and ambient aerosol samples across different size fractions (The rectangular box at the top right hand corner in the plot encloses measurements made at Bhopal, India and Kanpur, India).

In the light of the above results, we further intend to understand the mechanism of crust-air fractionation and change in mineral composition with changing size of the aerosol. We will use a nine stage Andersen aerosol impactor model TE 20-800 Anderson Sampler which will enable us to sample aerosol in nine size ranges (0.4-10 microns). We intend to see the mineral composition in different size fractions and explain the mechanism of crust-air fractionation occurrence.

### References:

Samiksha S. Sunder Raman R. Nirmalkar J. Kumar S. Sirvaiya R. (2016). PM10 and PM2.5 chemical source profiles with optical attenuation and health risk indicators of paved and unpaved road dust in Bhopal, India Environmental Pollution DOI: 10.1016/j.envpol.2016.11.067

## Road Dust of Venice (Italy) international airport: characterization and risk assessment

G. Valotto<sup>1</sup>, D. Zannoni<sup>1</sup>, G. Rampazzo<sup>1</sup>, F. Visin<sup>1</sup>, G. Formenton<sup>2</sup>, A. Gasparello<sup>2</sup>, D. Bassano<sup>3</sup>, S. Sollecito<sup>3</sup>

<sup>1</sup> Department of Environmental Sciences, Informatics and Statistics, Università Ca' Foscari Venezia, I-30123 Venezia, Italy

<sup>2</sup> Dipartimento Provinciale di Venezia, Agenzia Regionale per la Prevenzione e Protezione Ambientale del Veneto (ARPAV), I-30174 Mestre, Italy

<sup>3</sup> SAVE S.p.A., Marco Polo Venice airport viale G. Galilei 30/1, I-30173 Tessera-Venezia, Italy

Keywords: road dust, airport, airside, landside, risk assessment

Presenting author email: valotto@unive.it

Road dust is a non-exhaust source that can significantly contribute to atmospheric particulate by resuspension. Beside the issue of the overcoming of guidelines limits for the air quality, the characterization of this matrix is of crucially high interest for the inherent toxicity of resuspended particles, that can act as carriers of heavy metals and toxic-carcinogenic components.

In this work, Road dust collected in the Venice international airport (Fig. 1) is characterized with a multi-technique approach in order to identify the main pollutant sources and to highlight the differences between airside / landside places. Specifically, particle size distribution as well as elemental and molecular (polycyclic aromatic hydrocarbon - PAHs) composition of sub-samples most subjected to re-suspension process (characterized by particle size lower than 37  $\mu\text{m}$  and between 37-63  $\mu\text{m}$ ) were probed by laser diffraction analysis, Total Carbon (TC) analysis, High Performance Liquid Chromatography (HPLC), Inductively Coupled Plasma Optical Emission Spectroscopy (ICP-OES), and Inductively Coupled Plasma Mass Spectrometry (ICP-MS).

A preliminary risk assessment related to the exposure of inorganic and organic components is performed taking into account the following intake pathway: ingestion, dermal intake and inhalation of fugitive particles. The sampling site is a sensitive area due to the high number of workers and tourists which attend it. Indeed, it was the fourth busiest Italian airport in 2015 in terms of number of flights ( $\approx 82,000$ ) and the fifth in terms of number of passengers ( $\approx 8,800,000$ ) [Assaeroporti, 2016]. Moreover, the existing maintenance and extension builds [Marcopolodomani, 2016] promote the emission and the resuspension of fugitive dusts, placing this research a fundamental step for the protection of potential receptors.

Results confirm that road dust can be an important source of atmospheric particulate by re-suspension, and that it is also composed of particles originated by non-exhaust sources such as the brake, tire and road wear, and other local sources such as the activities related to construction sites and anti-icing safety procedures. Moreover, streets are the most polluted landside places; while road dust of airside area is significantly more concentrated in PAHs, Na, Al, Cu, Zn, Ag, Cd. Finally, as regards the risk assessment, the most critical pollutants (in concern order) are: As, BaP, Cr, Sb, BaA, and BbF.

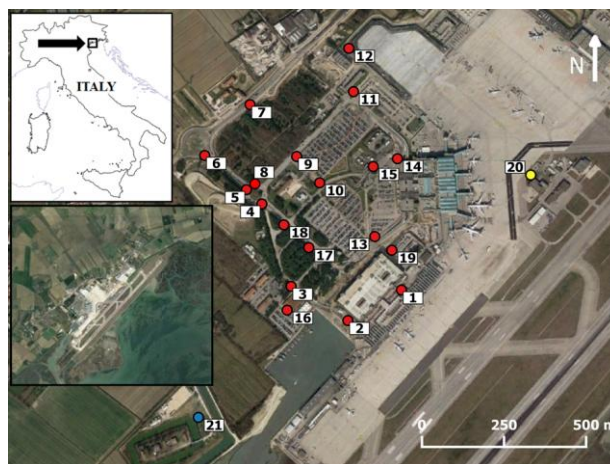


Figure 1. Sampling sites

Assaeroporti, 2016. Associazione Italiana Gestori Aeroporti. Available at: [http://www.assaeroporti.com/statistiche\\_201512/](http://www.assaeroporti.com/statistiche_201512/).

Marcopolodomani, 2016. Available at: <http://www.marcopolodomani.it/progetto/ampliament-o-aerostazione.html>

## New approach in airborne asbestos fibres identification, monitoring and source apportionment

P. Pokorná<sup>1</sup>, M. Klán<sup>1</sup>, D. Havlíček<sup>2</sup>, J. Plocek<sup>3</sup>, M. Racek<sup>4</sup>, J. Hovorka<sup>1</sup>

<sup>1</sup> Institute for Environmental Studies, Charles University, Benátská 2, 12801 Prague 2, Czech Republic

<sup>2</sup> Institute of Chemistry, Faculty of Science, Albertov 6, 12843 Prague 2, Czech Republic

<sup>3</sup> Institute of Inorganic Chemistry of the AS CR, v. v. i., 250 68 Řež u Prahy, Czech Republic

<sup>4</sup> Institute of Petrology and Structural Geology, Charles University, Albertov 6, 12843 Prague 2, Czech Republic

Keywords: actinolite/tremolite, rotating drum impactor, SEM EDX, X-ray powder diffraction.

Presenting author email: pokorna@natur.cuni.cz

Airborne asbestos fibres are, due to their fibrogenicity and carcinogenicity, subject to long-time monitoring and regulation. However, the high concentrations of asbestos fibres in the ambient air are still a hot topic in specific areas in Japan (Sakai et al., 2001) and USA (Harris et al., 2007; Sullivan, 2007; Larson et al., 2010). Since 2002 high concentrations of the airborne asbestos fibres have also been detected in the airshed of the Plzeň city, Czech Republic. The objective of presented study was to develop method for the asbestos minerals identification and highly-time resolved asbestos fibres monitoring to apportion asbestos sources within the airshed of Plzeň city.

First, in years 2010 and 2011, samples of stone aggregates for the construction/road works and airborne particulate matter (PM) with time resolution of 24h were collected in the quarry in the urban district Plzeň – Litice and at the six localities in the Pzeň city centre and analysed by X-Ray diffraction for the asbestos minerals. Than an intensive sampling campaigns of size-segregated PM with high time resolution of 30, 60 and 120 minutes were conducted from the 4<sup>th</sup> Apr to 14<sup>th</sup> May and from the 12<sup>th</sup> Aug to 9<sup>th</sup> Sep 2013 in Plzeň – Litice. The locality is situated at a suburban station nearby a stone quarry. Three/eight size fractions were sampled by a Davis Rotating-drum Uniform-size-cut Monitor (3/8 DRUM, DELTA Group UC-Davis) and analysed for the asbestos fibres numbers by scanning electron microscopy with energy dispersive X-ray spectroscopy (SEM, TESCAN-Vega; EDX, X-MAX 50, Oxford Instruments). Use of the 8/3DRUM with different integration time enable to optimize the continuous sampling method for critical fibre determination and counting by SEM EDX. Also hourly PM<sub>10</sub> PM<sub>2.5</sub> and PM<sub>1</sub> concentrations were measured by GRIMM (EDM 765). The wind speed (WS), wind direction (WD) and precipitation were also concurrently recorded.

The actinolite/tremolite proportionality in samples of the stone aggregates ranged between 0 and 23%. The highest portion was determined in the sample from the first layer of the Plzeň – Litice quarry. Therefore, usage of the aggregates from the quarry in the construction and road works led to elevated airborne asbestos fibres concertation in nearby localities. In the 24h PM samples from the city center actinolite/tremolite were reliably identified in 10 from 25 samples, i.e. in 40 % of the cases. From the intensive measurements in the urban district Plzeň – Litice the five samples were chosen for detailed

SEM EDX according to PM<sub>10</sub>, PM<sub>2.5-10</sub> and PM<sub>1-10</sub> concentrations and meteorological conditions (Tab. 1). The 8DRUM samples with integration time of 60/120 minutes were more suitable for the fibres detection and counting. The number of the critical actinolite/tremolite fibres increased with increasing PM<sub>10</sub>/PM<sub>1-10</sub> and PM<sub>10</sub>/PM<sub>2.5-10</sub> ratios, WS > 2 m.s<sup>-1</sup> and precipitation < 1 mm. The number of the critical actinolite/tremolite fibres was not dependent on the WD, thus the actinolite/tremolite fibres sources were omnipresent at the locality.

Table 1. Summary of detailed SEM EDX analysis for measured period 4<sup>th</sup> Apr to 14<sup>th</sup> May 2013 (samples 1-3) and 12<sup>th</sup> Aug to 9<sup>th</sup> Sept 2013 (samples 4-5)

Sample	Number of fibres on 1 mm <sup>2</sup>	Number of fibres in 1 m <sup>3</sup> air
1	32	282
2	10	57
3	28	126
4	4	79
5	20	120

The new proposed approach combines X-Ray diffraction analysis of stone aggregates/24h PM samples and SEM EDX of highly time resolved PM samples that enable to identify the asbestos minerals, to monitor the asbestos fibres with high time resolution and subsequently to apportion their sources.

This work was supported by the Environmental fund of Plzeň city

- Sakai, K., Hisanaga, N., Kohyama, N., Shibata, E., Takeuchi, Y. (2001) *Industrial Health* **39**, 132-140.  
 Harris, K.E., Bunker, K.L., Strohmeier, B.R., Hoch, R., Lee, R.J. (2007) In: Méndez-Vilas, A., Diaz, J., editors *Modern Research and Educational Topics in Microscopy*, vol. 2. Formatex Research Center, Badajoz, Spain. ISBN-13: 978-84-611-9420-9.  
 Larson, T.C., Vinicius, C., Bove, F.J. (2010) *J. Occup. Environ. Med.* **5**, 555-560.  
 Sullivan, P.A. (2007) *Environ. Health Persp.* **4**, 579-585.

## Estimation and dispersion modelling of particulate matter (PM<sub>10</sub>) emissions from the ceramics industry

J.B. Sousa<sup>1</sup>, A.J. Rossini<sup>1,2</sup> and S.A. Pozza<sup>2</sup>

<sup>1</sup> Environmental Company of the State of São Paulo, Limeira – SP, 13.483-132, Brazil

<sup>2</sup> School of Technology, University of Campinas, Limeira - SP, 13484-332, Brazil

Keywords: atmospheric pollution, ceramic cluster, emissions calculation, pollutant dispersion modelling.

Presenting author email: simone.pozza@ft.unicamp.br

The regional concentration of certain industries such as Santa Gertrudes (SP, Brazil) ceramic cluster, cause significant impacts on air quality due to the emission of gaseous fluoride and particulate matter (PM) into the atmosphere.

From the extraction of clay, which later goes through the natural processes of outdoor drying, transportation and processing to be used in the industry, particulates are emitted into the atmosphere.

Air quality monitoring data collected in Santa Gertrudes from 2014 to 2015, show that emissions frequently exceed WHO's daily limits of 50 µg/m<sup>3</sup> (Figure 1).

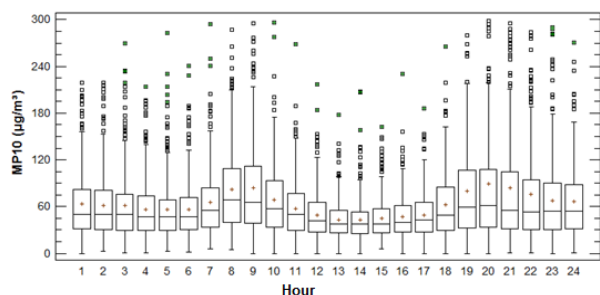


Figure 1 - Hourly monitoring data of PM<sub>10</sub> in the city of Santa Gertrudes (01/08/2014 to 31/07/2015)

Given that, a survey of the production stages of the ceramic industry was made in this work and the contribution of each phase to the emission of PM to the atmosphere was quantified.

The estimation of the potential emission of these activities was carried out using the equations and variables proposed by Monfort et al. (2011) and USEPA (1983). With this, the PM emissions of the ceramic pole were obtained (Table 1).

Table 1 - Emission factors obtained

Activity	Unity	Emission Factor
Handling in industry	g/ton	41,17
Clay mining and drying	g/(m <sup>2</sup> .day)	3,20 x 10 <sup>-5</sup>
Transportation on paved roads - loaded vehicle	g/VKT	3,60
Transportation on paved roads - empty vehicle	g/VKT	0,81
Transportation on unpaved roads - loaded vehicle	g/VKT	37,93
Transportation on unpaved roads - empty vehicle	g/VKT	25,03

g/VKT = grams per vehicle kilometer traveled

The PM emission estimation of the ceramic pole, together with the weather information obtained from monitoring stations in the region, were used in the AERMOD mathematical model of pollutant dispersion, which is widely used in the study of atmospheric pollutant dispersion.

The hourly cloud cover data, which is one of the main input data for the adopted dispersion model, were calculated using the relative air humidity information, with the methodology suggested by Zhao, Black and Baldwin (1997).

The output of such model shows that the obtained daily pollutant concentration has its dispersion affecting the urban area of the city of Santa Gertrudes with an initial concentration of 200 µg/m<sup>3</sup>, which later decays to 150 µg/m<sup>3</sup> in the urban area of Cordeirópolis and Rio Claro (Figure 2).

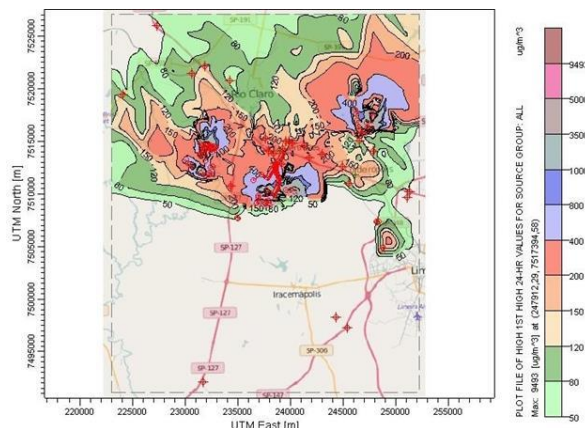


Figure 2 - Dispersion of PM<sub>10</sub> emissions from activities of the ceramic industries (maximum of 24 hours)

The results also showed that the outdoors clay drying process and mineral transportation significantly contribute to the air quality of the area.

Monfort, E et al. Diffuse PM10 emission factors associated with dust abatement Technologies in the ceramic industry. Atmos. Environ. Vol 45, p. 7286-7292, 2011.

USEPA (United States Environmental Protection Agency). An AP-42 update of open source fugitive dust emission. EPA-450/4-83-010, March 1983, 39p.

Zhao, Q., Black, T. L. e Baldwin, M., E. Implementation of the Cloud Prediction Scheme in the Eta Model at NCEP. Amer. Meteor. Soc., v. 12, p. 697-712. 1997..

## Long term flux of Saharan Dust to the Attica Region, Greece

K. Eleftheriadis, V. Vasilatou, M. Manousakas, M. Gini, E. Diapouli

Institute of Nuclear and Radiological Sciences & Technology, Energy and Safety, Environmental Radioactivity Laboratory, National Centre of Scientific Research "Demokritos", 15310 Ag. Paraskevi, Attiki, Greece

Keywords: surface flux; Sahara dust; elemental composition; deposition, mineral dust fraction

Presenting author email: [elefther@ipta.demokritos.gr](mailto:elefther@ipta.demokritos.gr)

Dust is primary aerosol arising from mechanical processes and may be generated either naturally or by anthropogenic activities. Natural dust occurs when wind blows over land surfaces, either producing or re-suspending particles, it is mainly coarse in size and dominated by mineral species (silicon, calcium, potassium, magnesium etc). On the other hand, anthropogenic dust may contain large quantities of carbon and several metals (copper, zinc, iron, magnesium, calcium etc.) contributing to ambient aerosol in both coarse and fine aerosol sizes (Athanasopoulou et al., 2010).

In this study, Particulate Matter (PM) samples, collected during two summer and two winter months over a long-term period (1984-2012) at a suburban site in Athens (Greece), were used in order to examine the connection between Sahara dust long range transport events and mass concentrations of the aerosol mineral component, as well as the relative abundance of specific crustal components. As a result, the average deposition flux of dust to the Aegean Sea around the Attica Region, during days with Sahara dust transport events, was calculated. The elemental concentration of aerosol samples was determined by means of ET-AAS, ED-XRF. Mineral dust was chemically reconstructed by using the elemental concentrations of the crustal species based on their common oxides. Two different air mass transport models (HYSPLIT and FLEXTRA) were used for the identification of the days with dust transport events.

The dust deposition velocity of the particles was calculated by using Stokes drag law, while the dust deposition flux was calculated taking into account the mean particle size of the aerosol coarse size fraction, which is dominated by the transported crustal component during Sahara dust intrusions. The deposition flux was calculated using a stoichiometrically derived mineral dust component based on the concentration of the mineral fraction of PM. For most of the years the deposition flux was higher in dry (summer) than in wet period (winter). The mineral dust contribution was higher in summer, when dry weather conditions prevail. The Ca/Fe ratio was examined for all years (fig. 1), since this ratio is often used for the identification of Saharan dust events. For the years 1996 and 1998 the Ca/Fe ratio indicates an influence by local urban generated dust. The dust deposition flux per day of a Sahara intrusion event varied from 61 –199  $\mu\text{g}/\text{m}^2$  with an average value of  $131 \pm 41 \mu\text{g}/\text{m}^2$ . The total dust deposition over the 4-month measuring period ranged from 237 to 2935  $\mu\text{g}/\text{m}^2$ . The periods we examine

in winter and summer may include only part of the sahara dust deposition affecting the marine environment annually. From intensive studies where the whole year was examined we can have a measure of the deposition occurring during the rest of the year for example during 2013 (Diapouli, et al, 2017)

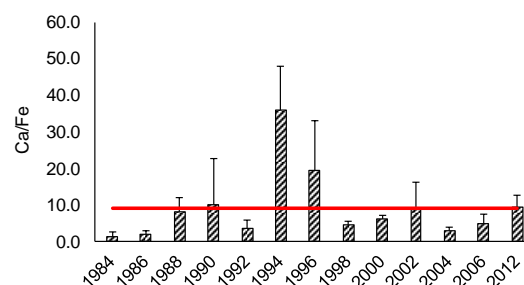


Figure 1: Average Ca/Fe ratio for the years 1984-2012

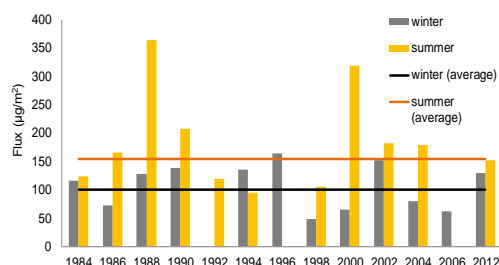


Figure 2. : 24h dust deposition flux in  $\mu\text{g}/\text{m}^2$  for the years 1984-2012 for winter (grey) and summer period (yellow).

This work was supported by ENTEC FP7REGPOT - 2012-2013-1 FP7, ID:316173)

Athanasopoulou, E., et al., 2010. "Implementation of Road and Soil Dust Emission Parameterizations in the Aerosol Model CAMx: Applications Over the Greater Athens Urban Area Affected by Natural Sources." *Journal of Geophysical Research Atmospheres* 115 (17).

Diapouli E., et al., (2016), "Airuse-life+: Estimation of natural source contributions to PM10 and PM2.5 concentration levels in Southern Europe. Implications to compliance with limit values", *Atmospheric Chemistry and Physics Discuss.*, doi:10.5194/acp-2016-781)

## **Abstracts T214**

## Calibration of Shortwave Radiometers in Brussels with an AOD rejection channel

S. Nevens<sup>1</sup>, A. Chevalier<sup>1</sup>, C. Conscience<sup>1</sup> and J. Amand<sup>1</sup>

<sup>1</sup>Section Absolute Radiometry, Royal Royal Meteorological Institute of Belgium, Brussels, 1180, Belgium.

Keywords: AOD, urban aerosols, field campaign, solar irradiance

Presenting author email: stijn.nevens@meteo.be

Shortwave radiometers are instruments designed to measure the solar irradiance. There are two basic categories of shortwave radiometers:

- Pyrheliometers are absolute radiometers which measure only the radiation coming directly from the sun. They have a narrow field of view designed to see only the sun disk. In a typical design, all solar radiation is absorbed in a cavity coated with a broad spectrum absorbing paint.

- Pyranometers are used for measurements of global radiation. By using an unshaded pyrometer we can measure direct solar radiation and diffuse radiation from the atmosphere and by using a shaded pyrometer we can measure diffuse radiation only. By subtracting the shaded and unshaded measurements we obtain direct solar radiation results. Pyranometers typically consist of a blackened thermopile detector protected by a glass dome.

Each five years the International Pyrheliometer Comparison (IPC) is hosted at PMOD/WRC, Davos, Switzerland in September/October. The World Radiometric Reference (WRR) is represented by six pyrheliometers which form the World Standard Group (WSG). During three weeks participants from all over the world can calibrate their reference pyrheliometers against the WRR. This is done by taking simultaneous solar measurements by both the WSG and the reference instruments by the participants. During these measurements, atmospheric conditions (including Aerosol Optical Depth, AOD) are monitored. In the end, a so called WRR factor is provided which has to be used as a scale to adjust the calibration of the reference pyrheliometer to be the same as the WRR. For each measurement the instantaneous WRR factor (= irradiance reference instrument / irradiance WSG) is given. See figure 1 for a set of simultaneous measurements.

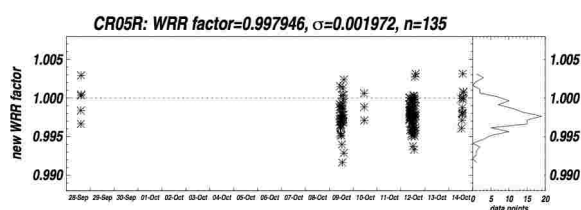


Figure 1: WRR factor (y scale) measurements for the RMIB CRO5R radiometer during the IPCXII during 3 weeks (x scale).

RMIB is a regional regional radiation centre which means that we are responsible to transfer the WRR calibration to all instruments in our region in order to ensure homogeneity of solar radiation measurements. To this end, in the spring of 2017 we are planning a calibration campaign for all interested parties. During 3 months, when weather conditions are favourable, the CRO5R radiometer calibrated during the IPCII will make solar measurements and its measurements will be disseminated. This allows parties interested in calibrating their instruments to either make measurements during the whole test campaign or set up their instruments on an ad hoc basis.

To make a reliable calibration, atmospheric conditions - including AOD - have to be taken into account. Even in the relatively clean conditions in Davos, aerosols can influence the calibration results. For instance (Finsterle, 2012) mentions a correction of the order of 0.1% due to an Saharan dust event during IPC-XI. So we expect the results in Brussels, a polluted urban area, to be severely influenced by aerosol peaks. To study this effect Brewer and Cimel based AOD measurements will be used as a rejection criterium (De Bock et al 2010). The rejection threshold is to be determined from results from previous IPC's and independently verified by comparing the calibration results during this campaign with AOD above and below the threshold. Our results will be used during the next IPC (XIII) for validation.

In this poster we present the results from the calibration campaign for various instruments and the influence of AOD on these results. Moreover we will assess the validity of applying the simple AOD rejection threshold proposed earlier.

This work was supported by the Solar Terrestrial Center of Excellence (STCE).

IPC-XII, WMO IOM Report No. 124, 2016

W. Finsterle, A. Fehlmann and W. Schmutz, *The 11th International Pyrheliometer Comparison and a Saharan Dust Event*, 2012

V. De Bock et al, *Aerosol Optical Depth measurements at 340 nm with a Brewer spectrophotometer and comparison with Cimel sunphotometer observations at Uccle, Belgium*, Atmos. Meas. Tech. Discuss., 3, 2743–2778, 2010.

## Evaluation of bioaccessible trace metal fractions in urban PM<sub>10</sub> samples collected near a ferroalloy plant

A. Hernández-Pellón<sup>1</sup>, S. Lanza<sup>1</sup>, C. Lasa<sup>1</sup> and I. Fernández-Olmo<sup>1</sup>

<sup>1</sup>Department of Chemical and Biomolecular Engineering, University of Cantabria, Santander, 39005, Spain

Keywords: bioaccessibility, PM<sub>10</sub>, trace metals, artificial lung fluids.

Presenting author email: ana.hernandez@unican.es

An accurate assessment of the potential toxicity of trace metals associated to particulate matter (PM), requires the evaluation of their bioaccessible fraction, instead of the common determination of the total metal content. In this regard, in the last years some works have focused on the study of trace metal bioaccessibility using simulated lung fluids as leaching agents (Mbengue et al., 2015). The present study aims to assess the pulmonary bioaccessibility of potentially toxic metals associated to PM<sub>10</sub> in the Region of Cantabria (northern Spain), in an urban area mainly influenced by the presence of a ferromanganese alloy plant.

An extensive PM<sub>10</sub> sampling campaign has been performed from January 2015 to January 2016 at CROS site (UTM, 30T, X = 431916, Y = 4807982), located at 850 m NNW from a ferroalloy plant. A total of 52 samples have been collected onto 150 mm quartz fiber filters (one filter per week). The 24h-PM<sub>10</sub> sampling has been carried out by means of a high volume sampler device (30 m<sup>3</sup>/h). After gravimetric determination, a quarter of each filter were subjected to microwave assisted acid digestion (HNO<sub>3</sub>:H<sub>2</sub>O<sub>2</sub> with a mixture of 8:2 ml) based on UNE-EN 14902:2006. Inductively coupled plasma mass spectrometry (ICP-MS) was then used to determine the total metal content of Mn, Fe and Zn. A total of 24 filters were selected for the assessment of trace metal bioaccessibility. Two simulated lung fluids were employed as leaching agents: Gamble's solution (pH=7.4) and artificial lysosomal fluid (ALF) (pH=4.5). The first is composed of inorganic salts, carbonates, chlorides and various metal phosphates and represents the human interstitial fluid of the deep lung. ALF is composed of a different salt solution and simulates the more acidic environment within the lung (Mukhtar and Limbeck, 2013). Once the remaining portions of the filters were cut into 6 equal pieces, each portion of the filter was introduced into a falcon tube and 30 ml of the simulated lung fluid were added (3 portions of each filter were used to assess the bioaccessible metal fraction with Gamble's solution and the other 3 with ALF, respectively). Leaching experiments were performed for 24h with a rotatory shaker (10 rpm). An incubator was used to maintain the temperature at 37°C. After the leaching test was performed, the samples were centrifuged at 4200 rpm for 10 minutes and filtered through 0.45 µm PP filters. Finally, the samples were acidified and stored at 4°C. Bioaccessible metal fraction analysis was performed by ICP-MS.

As Figure 1 shows, the bioaccessible fraction of Mn, Fe and Zn was always higher using ALF as the leaching agent. Mn solubility in Gamble's solution ranged

from 6.3% to 31.3%, with a mean value of 17.9%. The bioaccessible fraction of Fe and Zn were close to 0% in this fluid. On the contrary, Fe and Zn bioaccessibility increased using ALF as the extraction fluid. The bioaccessible fraction of Fe and Zn ranged from 35.4% to 94.6% (mean value=56.8%), and from 37.9% to 112% (mean value=73.5%), respectively. Finally, since the bioaccessible fraction of Mn was above 100% in all the samples, it can be assumed that ALF was capable of extracting the total content of this metal.

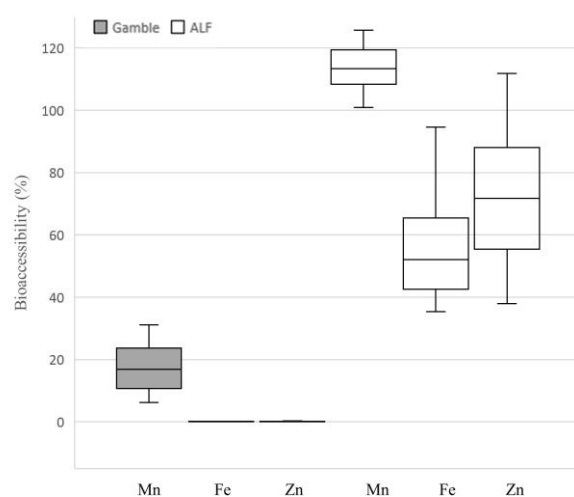


Figure 1: Bioaccessibility (%) of Mn, Fe and Zn associated to PM<sub>10</sub>. Leaching agents: Gamble's solution and ALF.

This work has been financially supported by the Spanish Ministry of Economy and Competitiveness (MINECO) through the Project CTM2013-43904R. Ana Hernández Pellón also thanks the Ministry of Economy and Competitiveness (MINECO) for the FPI grant awarded BES-2014-068790.

Mbengue, S., Alleman, L. Y. and Flament, P. (2015). *Bioaccessibility of trace elements in fine and ultrafine atmospheric particles in an industrial environment*. Environmental Geochemistry and Health, 37(5), 875-889.

Mukhtar, A. and Limbeck, A. (2013). *Recent developments in assessment of bio-accessible trace metal fractions in airborne particulate matter: A review*. Analytica Chimica Acta, 774, 11-25.

## Bias caused by water adsorption in hourly PM measurements

K. Imre, Á. Molnár and Gy. Kiss

MTA-PE Air Chemistry Research Group, University of Pannonia, Veszprém, 8200, Hungary

Keywords: water adsorption, PM10, bias

Presenting author email: [kornelia@almos.uni-pannon.hu](mailto:kornelia@almos.uni-pannon.hu)

### Introduction

Water vapour is the most significant condensable species in the atmosphere that may considerably distort standard PM measurements. Adsorbed water may be partly retained on the filter and particulates even at low relative humidities (called hysteresis). The magnitude of water retention strongly depends on the filter material as known for decades. Under unfavorable conditions daily PM measurements can be biased significantly by the interaction of water with the filter material and/or the aerosol particles collected.

### Instrumental and sampling

Sampling of aerosol for the gravimetric reference method was also carried out by a DIGITEL DHA-80 sampler run by the Hungarian Air Quality Network. The sampling site is an urban background monitoring station, located at the Marczell György Observatory of the Hungarian Meteorological Service in the south-eastern part of Budapest, Hungary. Sampling was performed in three campaigns focussing on different weather conditions.

The first campaign started on May 19, finished on June 1 and was characterized by low daily PM10 concentrations (between 18 and 28  $\mu\text{g m}^{-3}$ , average 21  $\mu\text{g m}^{-3}$ ) and mild spring weather (19.4 °C average temperature).

The second sampling period lasted from November 15 to 22 with PM10 values close to or even exceeding the daily PM10 threshold value set by the EU (50  $\mu\text{g m}^{-3}$ ) on 4 out of 7 days. This period was typical for late autumn with 6.12 °C average temperature.

The last campaign in 2016 was carried out from 13 to 19 December and elevated level of PM10 was recorded again (between 30 and 76  $\mu\text{g m}^{-3}$ , average 55  $\mu\text{g m}^{-3}$ ) in cold weather (-2.7 °C average temperature). The filters were conditioned till constant weight before and after sampling at RH=50% and RH<25% in an isolated measurement box then the filters were weighed in the RH controlled environment. In our experiments the mass measured at RH<25% was considered as dry mass.

### Results

With these experiments the error caused by the water content of the aerosol particles in the standard gravimetric measurement of the mass concentration of PM10 particles was determined. Despite the fact that 50% is the standard relative humidity for gravimetric

measurements and it is considered as a suitable condition for determining the dry aerosol mass, a non-negligible difference of aerosol mass at RH=50% and RH<25% was observed both in May and November (the processing of the filters collected in December is still in progress).

The amount of water reached 4.3% (average 1.7%) and 8% (average 6.0%) of the dry aerosol mass in spring and late autumn, respectively. These results clearly show that daily average PM10 concentration values obtained by the present standard method can be considerably distorted by water retained by particles at RH=50%. Based on these results it can be stated that conditioning of the filter before and after sampling at RH<25% gives more reliable PM10 concentrations than those obtained with the present standard method.

For the samples collected during the campaigns daily PM10 data obtained with the standard gravimetric method (GM, conditioning at RH=50%) have been compared to the official daily PM10 values derived from the particle monitor (BAM) data of the Hungarian Air Quality Network. In May the BAM/GM ratio ranged from 0.91 to 1.49 (average 1.20, RSD 18%) which means that the particle monitor working on the beta attenuation principle overestimates PM10 concentration by ca. 20% on average but with high fluctuations. By combining this result with that obtained from the gravimetric measurements at different RH values it can be concluded that daily PM10 concentrations derived from the particle monitor overestimated the “real” dry mass concentration by ca. 22% in May. In November the BAM/GM ratio ranged from 1.02 to 1.20 (average 1.08, RSD 5.4%) which indicates that the particle monitor overestimated PM10 concentration by ca. 8% in November but the deviation remained in a narrow range. (It must be noted that if the ratio of 1.20 obtained on November 16 was removed from the dataset then the results would be even more consistent and an average ratio of 1.06 with RSD of 2.3% would be obtained.)

Taking into account that the two methods apply different measuring principle, this deviation of 8% can be considered as a good agreement. However, as described above, the gravimetric results obtained at RH=50% overestimated the dry mass concentration by 6% on average in November. This means that daily PM10 concentrations derived from particle monitors overestimated the “real” dry mass concentration by ca. 14% in November.

### Acknowledgement

The financial support of the NKFI-113059 project is gratefully acknowledged.

## Oxidative potential of atmospheric aerosols collected at high air pollution site related to chemical composition: Krakow case study

K. Styszko<sup>1</sup>, M. Kistler<sup>2</sup>, L. Samek<sup>3</sup>, K. Szramowiat<sup>1</sup>, K. Kubisty<sup>1</sup>, A. Korzeniewska<sup>1</sup> and R. Rakoczy<sup>1</sup>, Anne Kasper-Giebl<sup>2</sup>

<sup>1</sup>Department of Coal Chemistry and Environmental Sciences, AGH University of Science and Technology, Krakow, Poland

<sup>2</sup>Institute of Chemical Technologies and Analytics, TU Wien, Vienna, 1060, Austria

<sup>3</sup>Department of Medical Physics and Biophysics, AGH University of Science and Technology, Krakow, Poland

Keywords: urban particulate matter oxidative properties, particle size.

Presenting author email: magdalena.kistler@tuwien.ac.at

Measurements of the oxidative potential (OP) of airborne particulate matter may be applied for the assessment of the health-based exposure by integrating various biologically relevant properties of particles. This study aimed at the determination of oxidative activity of two size fractions of particulate (PM<sub>2.5</sub> and PM<sub>10</sub>) using the ascorbic acid (AA) and reduced glutathione (GSH) assay.

Samples of PM were collected in Krakow, one of the most polluted cities in Poland, in the city centre. Samples were collected during wintertime, when heating sources used in residential areas have significant influence on the concentrations of particulate matter in the air. PM<sub>10</sub> and PM<sub>2.5</sub> concentrations varied from 8.9 to 92.5  $\mu\text{g}\cdot\text{m}^{-3}$ . The decrease of antioxidants concentration due to the interactions with particulate matter, the technique of HPLC/UV-Vis was applied. Samples were analysed following after 15, 30, 60 and 90 min of interactions between antioxidants and PM. Organic and elemental carbon concentrations were determined using a thermal-optical method. The concentration of the inorganic anions and cations were analysed with isocratic  $\text{Na}^+$ ,  $\text{K}^+$ ,  $\text{Mg}^{2+}$ ,  $\text{Ca}^{2+}$ ,  $\text{NH}_4^+$ ,  $\text{NO}_3^-$ ,  $\text{NO}_2^-$ ,  $\text{Cl}^-$ ,  $\text{SO}_4^{2-}$  ion chromatography. Concentrations of elements: Cl, K, Ca, Ti, V, Cr, Mn, Fe, Ni, Cu, Zn, Br, Sr, Rb, and Pb in PM<sub>10</sub> and PM<sub>2.5</sub> were analysed by means of a multifunctional energy dispersive X-ray fluorescence spectrometer.

Variations of gravimetrically measured concentrations of PM<sub>10</sub> and PM<sub>2.5</sub> and oxidative potential (OP) expressed as depletion of AA and GSH mass ( $\mu\text{g}$ ) over the 90 min incubation period per  $\text{m}^3$  are shown in Figure 1.  $\text{OP}_{\text{AA}}$  and  $\text{OP}_{\text{GSH}}$  measured for PM<sub>10</sub> varied from 14.50 to 65.27  $\mu\text{g}\cdot\text{m}^{-3}$  and from 6.00 to 39.5  $\mu\text{g}\cdot\text{m}^{-3}$ , respectively. For PM<sub>2.5</sub>,  $\text{OP}_{\text{AA}}$  and  $\text{OP}_{\text{GSH}}$  ranged between 2.1 and 81.7  $\mu\text{g}\cdot\text{m}^{-3}$  and between 37.0 and 132.0  $\mu\text{g}\cdot\text{m}^{-3}$ . PM<sub>2.5</sub> fraction performed the higher values of OP than PM<sub>10</sub>.  $\text{OP}_{\text{GSH}}$  was significantly higher for PM<sub>2.5</sub>. The significant correlation between oxidative stress and PM mass concentration was observed only for  $\text{OP}_{\text{AA}}$  and PM<sub>10</sub>. Furthermore, on the basis of correlation,  $\text{OP}_{\text{AA}}$  of PM<sub>10</sub> was significantly correlated with organic and elemental carbon as well as the following metals: Fe, Cr, Mn, Cu, Zn, Pb, Ti, V, Rb, Sr.  $\text{OP}_{\text{GSH}}$  of PM<sub>10</sub> differed in respect to their correlation with PM components, it was significantly correlated with OC, Pb and nitrite. The high correlation

between  $\text{OP}_{\text{AA}}$  of PM<sub>2.5</sub> and carbonaceous fraction, both OC and EC, between  $\text{OP}_{\text{GSH}}$  of PM<sub>2.5</sub> and EC and Ni were only observed.

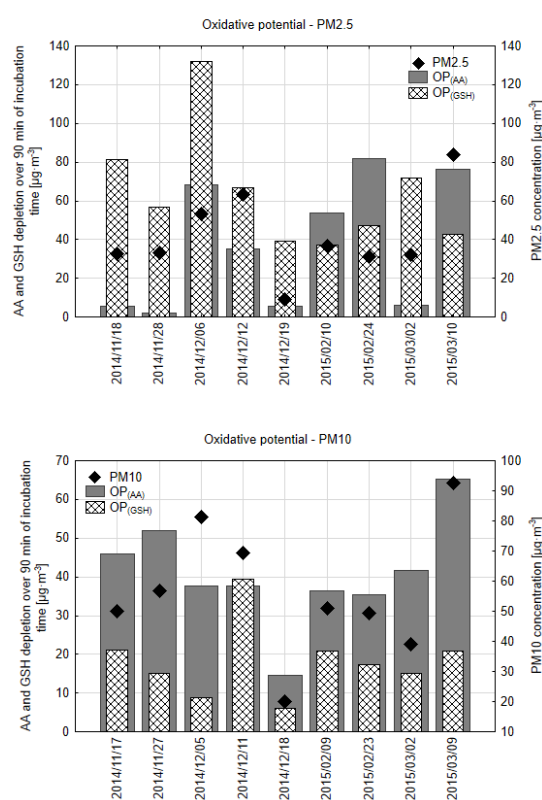


Figure 1. The variations of oxidative potential for ascorbic acid ( $\text{OP}_{\text{AA}}$ ) and glutathione ( $\text{OP}_{\text{GSH}}$ ) of PM<sub>10</sub> and PM<sub>2.5</sub> fractions and mass concentrations of PM<sub>10</sub> and PM<sub>2.5</sub>.

This work was financed by AGH University Grant no. 11.11.210.244. The infrastructure of the AGH Center of Energy in Krakow was applied for determination the concentration of ions. The authors acknowledge the financial support of OeaD and the Ministry of Science and Higher Education (Poland) within the framework of the project WTZ (Wissenschaftlich-Technische Zusammenarbeit), No. PL09/2015.

## Spatial distribution of particulate matter and its temporal evolution in a complex hot spot with influence in an urban park

F. J. Gómez-Moreno<sup>1,\*</sup>, B. Artñano<sup>1</sup>, E. Díaz Ramiro<sup>1</sup>, M. Barreiro<sup>1</sup>, S. Vardoulakis<sup>2</sup>, C. Dimitroulopoulou<sup>2</sup>, C. Yagüe<sup>3</sup>, G. Maqueda<sup>3</sup>, C. Román-Cascón<sup>4</sup>, M. Sastre<sup>3</sup> and R. Borge<sup>5</sup>

<sup>1</sup>Department of Environment, CIEMAT, Madrid, E-28040, Spain

<sup>2</sup>Environmental Change Department, Centre for Radiation, Chemical & Environmental Hazards, Public Health England, Chilton OX11 0RQ, UK

<sup>3</sup>Department of Geophysics and Meteorology, University Complutense of Madrid, Faculty of Physical Sciences, E-28040 Madrid, Spain

<sup>4</sup>Univ. Grenoble Alpes, CNRS, IRD, Grenoble INP, IGE, F-38000 Grenoble, France

<sup>5</sup>Department of Chemical and Environmental Engineering, Technical University of Madrid (UPM), E-28006 Madrid, Spain

Keywords: air quality, atmospheric aerosols, urban aerosols, PM<sub>x</sub>.

\*Presenting author email: fj.gomez@ciemat.es

The TECNAIRE project aims to diagnose the problems of air quality in urban environments, by developing new monitoring and modelling techniques to evaluate strategies for their management (Borge et al., 2016). Taking this into account, several field campaigns were carried out in two complex traffic hot spots (*Plaza de Fernández Ladreda*, FL, and *Escuelas Aguirre*, EA), in Madrid. The results obtained in EA are presented here. This location frequently experiences high pollution levels of particles and gases from traffic emissions. The site is located in the junction of two main streets (*Alcalá* street and *O'Donnell* street) in front of a very large park, *El Retiro* (118 hectares). This location allowed us to study the impact of trees and vegetation on urban air quality at local scale. A summer campaign was designed and performed from 15 June to 14 July 2016.

Several instruments were deployed in the study area. An Optical Particle Counter Grimm 1107 instrument (Grimm and Eatough, 2009) was installed inside the park, 30 m South of the park fence and at the roof of a 3 m high building. A second Grimm 365 was located close to the municipal monitoring station located in EA outside the park, both measuring PM<sub>10</sub>, PM<sub>2.5</sub> and PM<sub>1</sub> simultaneously. The instruments are marked with a G in Figure 1. A meteorological station was also set at this second location, providing, among others, turbulence parameters evaluated from a sonic anemometer. A TSI DustTrak DRX instrument (Tasić et al., 2012) was used to measure particulate matter (PM) levels at several points around the experimental area in a dynamic pattern, by walking with the instrument around the area and measuring at a mean adult height respiration level. These transects took between 15 and 30 minutes covering 1 km and 2 km length respectively. Additional measurements at specific spots, such as bus stops and traffic lights, were also made.

It was observed that the highest PM<sub>10</sub> values measured by the Grimm 1107 were between 20 June and 5 July, clearly influenced by a Saharan dust episode over the period 23 June-10 July. At the end of this period, some winds cleaned the lower troposphere, reducing surface PM<sub>10</sub> concentrations. The maximum 30-minute PM<sub>10</sub> values reached were around 130 µg/m<sup>3</sup>.

The DustTrak showed that the highest values were measured at the *Puerta de Alcalá* Square (left in Figure 1), a heavily trafficked area, with high intensity of (mostly diesel) buses.

The impact of vegetation was observed in the measurements of the 10<sup>th</sup> July (shown in Figure 1). The highest PM<sub>10</sub> values were obtained in the points close to the street, more directly affected by road traffic, while the lowest concentrations were measured inside the park, at around 300 meters from the park fence. In the points inside the park, the human activities could produce dust resuspension, increasing the concentrations, as it was observed i.e., during some gardening activities.

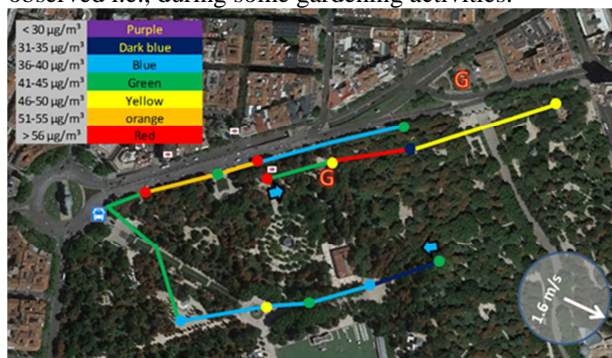


Figure 1. PM<sub>10</sub> concentrations measured for two representative transects inside *El Retiro* Park 10 July 2016 starting at 10:30 UTC. The Grimm instruments are marked with a G. The average wind speed and direction during that period are also included.

This work has been financed by Madrid Regional Research Plan through TECNAIRE (P2013/MAE-2972).

Borge, R., Narros, A., Artñano, B., Yagüe, C., Gómez-Moreno, F. J., de la Paz, D., Román-Cascón, C., Díaz, E., Maqueda, G., Sastre, M., Quaassdorff, C., Dimitroulopoulou, C. and Vardoulakis, S. (2016) *Atmos. Environ.*, 140, 432-445.

Grimm, H. and Eatough, D. J. (2009) *J. Air Waste Ma.*, 59, 101-107.

Tasić, V., Jovašević-Stojanović, M., Vardoulakis, S., Milošević, N., Kovačević, R. and Petrović, J. (2012) *Atmos. Environ.*, 54, 358-364.

## One year of aerosol size and black carbon measurements in Nanjing, China

A. Leskinen<sup>1,2</sup>, A. Ruuskanen<sup>1</sup>, D. Fang<sup>3</sup>, K. Kuuspallo<sup>4</sup>, P. Jalava<sup>4</sup>, Q. Wang<sup>3</sup>, C. Gu<sup>3</sup>, J. Jokiniemi<sup>4</sup>, M.-R. Hirvonen<sup>4</sup>, K.E.J. Lehtinen<sup>2,1</sup>, S. Romakkaniemi<sup>1</sup> and M. Komppula<sup>1</sup>

<sup>1</sup>Finnish Meteorological Institute, Yliopistoranta 1 F, 70210 Kuopio, Finland

<sup>2</sup>Department of Applied Physics, University of Eastern Finland, Yliopistoranta 1 F, 70210 Kuopio, Finland

<sup>3</sup>School of the Environment, Nanjing University, 163 Xianlin Ave., Nanjing, Jiangsu 210023, China

<sup>4</sup>Department of Environmental and Biological Sciences, University of Eastern Finland, Yliopistoranta 1 F, 70210 Kuopio, Finland

Keywords: black carbon, absorption, urban aerosol, China.

Presenting author email: ari.leskinen@fmi.fi

Aerosol size distribution and black carbon (BC) concentration were measured for one year (November 2014 – November 2015) at Nanjing University Xianlin campus on the rooftop of a five-floor building. The size distribution was measured in the range of 10 nm to 10  $\mu\text{m}$  with a TSI 3910 Nanoparticle Sizer (10–400 nm) and a TSI 3330 Optical Particle Sizer (0.3–10  $\mu\text{m}$ ). The BC concentration and aerosol light absorption coefficient were measured with a Magee Scientific AE-42 at seven wavelengths (370–950 nm) and corrected for artefacts due to filter loading and multiple scattering effects. The fraction of non-BC material contributing to the absorption coefficient was estimated based on the wavelength dependence of the absorption coefficient. Temperature, relative humidity, precipitation intensity and duration as well as wind speed and direction were measured with a Vaisala WXT520 weather station.

In this work we studied the behaviour of BC, non-BC absorbers (e.g., brown carbon), and particle size distributions in different meteorological situations, for example, wind blowing from different emission sources, as well as their seasonal and diurnal cycles. The measurements were also used to support toxicological and chemical analyses of filter samples collected in separate measurement campaigns at the same site. So far, the results from the first campaign have been published by Jalava *et al.* (2015).

During the measurement period the average (of hourly averages) and peak (99<sup>th</sup> percentile of hourly averages) concentrations were 14700 and 30700  $\text{cm}^{-3}$  for particle number, 80 and 244  $\mu\text{g m}^{-3}$  for  $\text{PM}_{10}$  mass, and 3.45 and 14.6  $\mu\text{g m}^{-3}$  for BC (at 880 nm). The overall average of BC-to- $\text{PM}_{10}$  ratio was 0.069.

The highest number and mass concentrations (of both  $\text{PM}_{10}$  and BC) were observed during southerly winds (Figure 1). There was also diurnal variation in the concentrations (Figure 2). The particle number concentration had two peaks every day: One at 6 am and the other at 6 pm. The BC concentration ([BC]), in turn, was at its highest in the night-time and lowest at around noon. The contribution of non-BC absorbers to the absorption coefficient was lowest in the early morning and highest in the evening (Figure 3).

From the results we conclude that the local traffic increases particle number and BC concentrations and that sunlight may play a role in the contribution of non-BC absorbers to the absorption coefficient. The non-BC absorber contribution was highest in the Northwest direction which may indicate biomass burning emission sources in this direction.

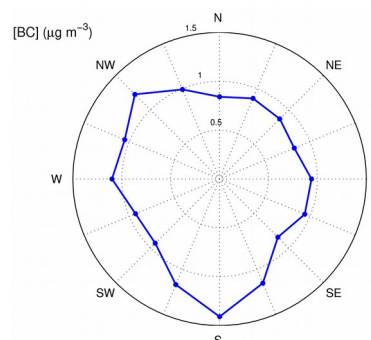


Figure 1. [BC] according to wind direction.

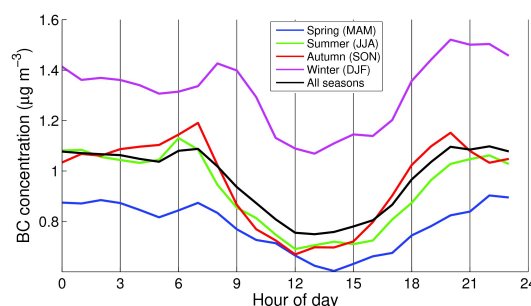


Figure 2. Diurnal and seasonal variation of [BC] concentration.

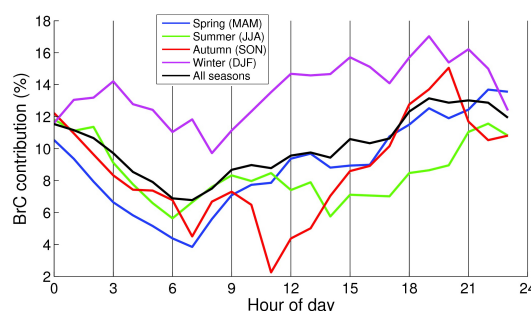


Figure 3. Diurnal and seasonal variation of the contribution of non-BC absorbers to the absorption coefficient.

This work was supported by the Academy of Finland under grant 278331 and the European Regional Development Fund.

Jalava, P.I., Wang, Q., Kuuspallo, K., Ruusunen, J., Hao, L., Fang, D., Väisänen, O., Ruuskanen, A., Sippula, O., Happonen, M.S., Uski, O., Kasurinen, S., Torvela, T., Koponen, H., Lehtinen, K.E.J., Komppula, M., Gu, C., Jokiniemi, J. and Hirvonen, M.-R. (2015) *Atmos. Environ.* **120**, 427-437.

## PM Emissions by Electric Cars

Helmuth Horvath<sup>1</sup>

<sup>1</sup>University of Vienna, Faculty of Physics, Aerosol Physics and Environmental Physics, A-1090 Vienna, Austria

Keywords: PM, Automotive, MPG, Power plant emissions

Presenting author email: Helmuth.Horvath@univie.ac.at

Electric cars frequently are advertised as zero emission vehicles. Cars cause PM by tailpipe emissions, tire wear, brake wear, road wear, and resuspension. Timmers and Achten (2016) give values for the different PM<sub>2.5</sub> emissions as 3, 3, 2, 3, and 12 milligrams per vehicle kilometer for tailpipe emissions, tire wear, brake wear, road wear, and resuspension respectively. For electric cars tailpipe and brake emissions are considered to be zero, but due to the additional weight of the battery, wear and resuspension emissions are higher, thus resulting in the same total emission as cars powered by internal combustion engines.

The electricity needed for charging the battery is supplied by power plants, which themselves emit particulate matter during operation. In the following the additional emission for charging batteries of electric cars are estimated.

The electricity consumption of electric cars is given by EPA, in analogy to gasoline powered cars, in MPGe (miles per gallon equivalent), with the energy equivalent of one gallon being 33.7 kWh. In Table 1 the energy consumption of various electric cars is given.

Vehicle	MPGe	kW/km
Chevrolet Spark EV	128/109	0.164/0.192
Chevrolet Volt	93	0.225
Fiat 500e	121/103	0.173/0.203
Kia Soul EV		0.181
Mini E	102/94	0.205/0.223
Smart ED	94/79	0.223/0.265
Tesla Model S 2015	101/102	0.207/0.205
Volkswagen e-Golf	126/110	0.166/0.190
Volkswagen e-Up	116	0.18

The first number in columns 2 and 3 is for city driving, the second for highway driving. In contrast to gasoline powered cars, the energy consumption per kilometer is less during city driving due to regenerative braking. Cars with a larger range have a higher energy consumption due to larger mass. On the average the power needed to drive one kilometer is 0.2 kWh.

Emission of power plants per vehicle kilometer can be estimated, using the power plant emission factors. When electricity is supplied exclusively by photovoltaic, wind, hydroelectric or nuclear power plants, the PM emissions for producing the energy, which is used for charging the batteries, are close to zero. But usually energy is supplied at least in part by thermal power plants.

Emission factors published by the Commission for Environmental Cooperation (2011) have been used for estimating the additional power plant PM<sub>2.5</sub> emission caused by electric cars. A few emission factors are shown in table 2 for power plants in North America.

	Average	Top10 plants	Remain	Highest	Fuel for highest
Canada	0.055	0.077	0.033	0.27	(natural gas)
USA	0.189	0.619	0.167	1.436	(coal)
Mexico	0.277	0.675	0.106	2.595	(oil)

An increase of the emission factors from North to south is evident. Depending on the age of the power plant, a large variety of emission factors exist.

With these emission factors the additional PM<sub>2.5</sub> emissions caused by an electric car can be calculated. An energy consumption of 0.2 kWh/km has been used, as already mentioned above. The results are shown in Table 3.

	Average	Top 10	Remaining	Highest
Canada	11	15.4	6.6	54
USA	37.8	123.8	33.4	287.2
Mexico	55.4	135	21.2	519

It is evident, that only clean power plants will emit about the same amount of PM<sub>2.5</sub> as modern cars with internal combustion engines. Whereas cars with internal combustion engines do not emit Sulfur compounds, power plants do so. The Sulfur Dioxide eventually is converted to Sulfates, which is an additional PM load. This must also be considered as PM emissions caused by electric cars.

**Conclusion:** The additional power plant PM emissions due to charging of batteries for electric cars cannot be neglected and must be included in the emissions of electric cars. Transmission losses and charging efficiency have not been included in this paper.

### References:

- Commission for Environmental Cooperation (2011): North American Power Plant Air Emissions, Montréal, Canada, 58 pp, ISBN 978-89700-009-7  
 Timmers V.R.J.H. and P.A.J. Achten (2016) Non-exhaust PM emissions from electric vehicles. *Atmospheric Environment* **134**, 10-17

## Very low emissions of airborne particulate pollutants measured from two municipal solid waste incineration plants in Switzerland

A. Setyan<sup>1,2</sup>, M. Patrick<sup>2</sup>, and J. Wang<sup>1,2</sup>

<sup>1</sup>Empa, Laboratory for Advanced Analytical Technologies, 8600 Dübendorf, Switzerland

<sup>2</sup>ETH Zürich, Institute of Environmental Engineering, 8093 Zürich, Switzerland

Keywords: municipal solid waste incineration, flue gas, aerosols, volatile organic compounds.

Presenting author email: ari.setyan@empa.ch

A field campaign has been performed in two municipal solid waste incineration plants in Switzerland, at Hinwil (ZH) and Giubiasco (TI). The aim was to measure particles at different locations of the abatement system and those released from the stacks into the atmosphere, in order to assess the efficiency of the abatement system and the environmental impact of these plants.

During this study, we measured the particle number concentration with a condensation particle counter (CPC), and the size distribution with a scanning mobility particle sizer (SMPS) and an aerodynamic particle sizer (APS). We also sampled particles on filters for subsequent analyses of the morphology, size and elemental composition with a scanning electron microscope coupled to an energy dispersive X-ray spectroscopy (SEM/EDX), and of water soluble anions by ion chromatography (IC). Finally, volatile organic compounds (VOCs) were sampled on adsorbing cartridges and analysed by thermal desorption gas chromatography/mass spectrometry (TD-GC/MS), and a portable gas analyser was used to monitor NO<sub>x</sub>, SO<sub>2</sub>, CO, CO<sub>2</sub>, and O<sub>2</sub>.

Both incineration plants were equipped with an electrostatic precipitator, a DeNO<sub>x</sub> system based on the selective catalytic reduction (SCR) technology, and bag-house filters. In addition to that, Giubiasco was equipped with a wet scrubber and Hinwil with a dry scrubber. At Giubiasco, measurements after the electrostatic precipitator were performed in two conditions, with the precipitator running and with one of the three units of the precipitator shut down.

The particle number concentration decreased significantly at two locations of the plants: at the electrostatic precipitator and the bag-house filters (Figure 1). The particle concentrations measured at the stacks were very low (< 100 #/cm<sup>3</sup>), stressing the efficiency of the abatement system of the two plants.

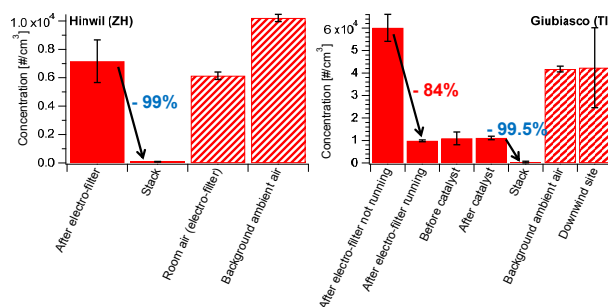


Figure 1. Average particle number concentrations measured at the different locations of the incineration plants. Solid bars correspond to measurements of the flue gas, while hatched bars correspond to ambient air.

Particles released from the stacks into the environment were compared to those collected at a downwind site. At the stacks, particles had a relatively uniform shape and size, and were possibly constituted of ammonium chloride salts (Figure 2b). We did not observe significant amounts of this type of particles at the near-field downwind site of Giubiasco (Figure 2c), and the concentration of chloride was rather low there, suggesting that the incineration plants released very limited amounts of particles to the surrounding areas.

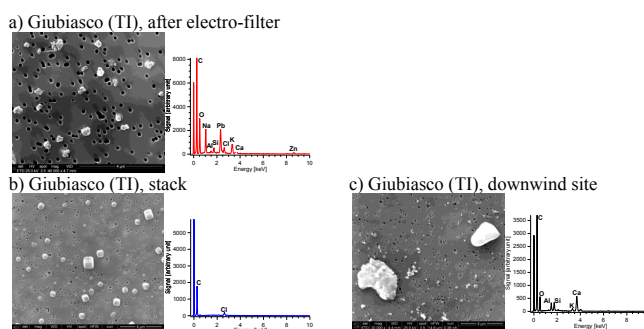


Figure 2. SEM images and EDX spectra from 3 different locations at Giubiasco (TI).

This work was supported by the Swiss Federal Office for the Environment (Bundesamt für Umwelt [BAFU]) and the Swiss Waste Industry Association (Verband der Betreiber Schweizerischer Abfallverwertungsanlagen [VBSA]).

## Summer-autumn air pollution in León (Spain): changes in the aerosol size distribution and effects on the respiratory tract

F. Oduber<sup>1</sup>, A. Castro<sup>1</sup>, A.I. Calvo<sup>1</sup>, C. Blanco-Alegre<sup>1</sup>, E. Alonso-Blanco<sup>2</sup>, P. Belmonte<sup>1</sup>, E. Coz<sup>2</sup>, A.S.H. Prévôt<sup>3</sup>, G. Močnik<sup>4,5</sup> and R. Fraile<sup>1</sup>

<sup>1</sup>Department of Physics, IMARENAB University of León, León, 24071, Spain

<sup>2</sup>Centre for Energy, Environment and Technology Research (CIEMAT), Department of the Environment, Madrid, Spain

<sup>3</sup>Laboratory of Atmospheric Chemistry, Paul Scherrer Institute, 5232 Villigen, Switzerland

<sup>4</sup>Research and Development Department, Aerosol d.o.o., 1000 Ljubljana, Slovenia

<sup>5</sup>Condensed Matter Physics Dept., Jožef Stefan Institute, 1000 Ljubljana, Slovenia

Keywords: aerosol concentration patterns, particle size distribution, respirable fraction, summer-autumn transition, traffic

Presenting author email: andre.prevot@psi.ch

In urban areas there are important sources of fine and ultrafine particles: traffic, industrial activity, residential wood and/or coal combustion, etc. León, Spain, is characterized by the absence of large emitting industries and the main source of particulate emissions is considered to be vehicular traffic during all the year. However, an important number of residential devices that use coal as fuel are still present, also natural gas and gasoil are used for heating and hot water during all the year. As a consequence, in autumn, winter and even spring there are remarkable emissions from this source. The aim of this study is to analyze the temporal variation of aerosol size distribution in León, Spain, from August to October 2012 in order to identify changes in the aerosol concentration associated with the summer-autumn transition. Furthermore, the influence of these aerosols in the respiratory tract by the study of inhalable, thoracic, respirable and tracheobronchial fractions was analyzed.

The aerosol sampling was carried out in the Secondary School IES Ordoño II, in the San Juan de Sahagún Avenue. The measuring probe was installed 1.5 m above the floor, directed towards a street. The study period comprises from 1th August to 23rd October, 2012. The particle number size distributions were measured using a passive cavity aerosol spectrometer probe (PCASP-X).

The total number of particle increased from August to October, ( $1000 \pm 600$  to  $1500 \pm 1000$  particles  $\text{cm}^{-3}$ , respectively) mainly due to smaller traffic intensity during summer holidays and the absence of heating emissions. Furthermore, in summer, a lower concentration of some elements was registered due to an increase in the boundary layer thickness that enhances dispersion.

The particle size distribution shows a bimodal profile, with a first fine or accumulation mode (Count Median Diameter  $\text{CMD} < 1 \mu\text{m}$ ) and a small fraction corresponding to a second fine mode or a coarse mode ( $\text{CMD} \geq 1 \mu\text{m}$ ). This last mode is less important because the particles concentration is less than one particle per cubic centimeter in this study. The monthly evolution of the particle numbers shows that 99% of the particles

have diameters less than  $0.5 \mu\text{m}$ , which may indicate that the main source of aerosol is road traffic. As summer progresses to autumn the number of particles of fine mode increases and the CMD decreases. There are more particles between 0600 and 1000 UTC and between 1700 and 1900 UTC, probably due to a greater presence of traffic in both hourly intervals. The number of particles  $N_t$  was higher on weekdays (between 700 and 1900 particles  $\text{cm}^{-3}$ ) than on weekends (between 800 and 1500 particles  $\text{cm}^{-3}$ ) (Figure 1).

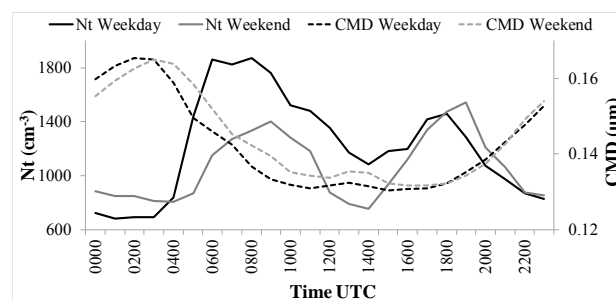


Figure 1. Hourly variation of the number of particles  $N_t$  and Count Median Diameter CMD.

The inhaled mass of aerosols was greater on August and September ( $41$  and  $45 \mu\text{g m}^{-3}$  respectively); and was greater on Thursday and Friday ( $45$  and  $53 \mu\text{g m}^{-3}$  respectively). The percentage of particles that does not traverse any non-ciliated airway and they reached the trachea and bronchi varied between 20% and 38%, with the lowest value in October. For the respirable fraction, in the high-risk population like children, elderly and weak people, the best month is August with  $6 \mu\text{g m}^{-3}$  and the worst is October with  $9 \mu\text{g m}^{-3}$  of particles that came to reach the alveolar zone.

This work was partially supported by the Spanish Ministry of Economy and Competitiveness: Grants TEC2014-57821-R, CGL2014-52556-R, co-financed with FEDER funds, and the grant BES-2015-074473 (acknowledged by F. Oduber), the University of León (Programa Propio 2015/00054/001). The authors are grateful to D. Baumgardner for his help with the code developed by Bohern and Huffman.

## Aerosol concentration during a thermal inversion followed by rain in northwestern Iberia

C. Blanco-Alegre<sup>1</sup>, A. Castro<sup>1</sup>, A.I. Calvo<sup>1</sup>, E. Alonso-Blanco<sup>2</sup>, F. Oduber<sup>1</sup>, E. Coz<sup>2</sup>, A.S.H. Prévôt<sup>3</sup>, G. Močnik<sup>4,5</sup> and R. Fraile<sup>1</sup>

<sup>1</sup>Department of Physics, IMARENAB University of León, 24071 León, Spain

<sup>2</sup>Centre for Energy, Environment and Technology Research (CIEMAT), Department of the Environment, Madrid, Spain

<sup>3</sup>Laboratory of Atmospheric Chemistry, Paul Scherrer Institute, 5232 Villigen, Switzerland

<sup>4</sup>Research and Development Department, Aerosol d.o.o., 1000 Ljubljana, Slovenia

<sup>5</sup>Condensed Matter Physics Dept., Jožef Stefan Institute, 1000 Ljubljana, Slovenia

Keywords: aerosols, pollution, precipitation, scavenging, thermal inversion

Presenting author email: grisa.mocnik@aerosol.eu, grisa.mocnik@ijs.si

Thermal inversion events, with high levels of atmospheric pollution, have become particularly important in recent years due to their effects on human health and natural environment. Additionally, in big cities there are restrictions to human activities (mainly traffic-related) when such events occur, affecting the economic activity and daily life of the population (Viard and Fu, 2015). The mixing height is the critical parameter governing vertical dispersion of the pollutants in the air because it determines the rate and the range of dispersion of substances formed or emitted near the ground (Gramsch et al., 2014). Thus, episodes of thermal inversion (frequent in winter) are usually related to the most serious pollution events. The weather conditions of thermal inversions cause the aerosol particles (mainly PM<sub>10</sub>) to be trapped under the atmospheric mixed layer. These conditions produce high concentrations of pollutants, often higher than World Health Organization (WHO) standards.

The aim of this study is to analyse the relationship between thermal inversions and the concentration of aerosol particles in León (Spain). For this purpose, a monitoring campaign was carried out at the university campus of León (42° 36' 50" N, 5° 33' 38" W, 846 m asl), located in Northwestern Iberia, with a Mediterranean Pluviseasonal-Oceanic bioclimate.

An event of thermal inversion was studied between 25<sup>th</sup> October 2016 and 2<sup>th</sup> November 2016. This period was characterized by the typical meteorological conditions of a thermal inversion: clear days with low wind speeds (maximum of 0.46 m/s), low pressures (maximum of 766.2 hPa) and large daily temperature ranges (between 9.8 and 19.8 °C).

The campaign involved different instruments: i) an optical particle counter (PCASP-X) for determining aerosol size distributions between 0.1 and 10 µm size in 31 channels; ii) a high resolution nanoparticle sizer (TSI-SMPS Model 3938) for the continuous monitoring of particle size distributions (between 14.3 and 661.2 nm in 107 channels); iii) an AE31 Aethalometer (Magee Scientific) for measuring Black Carbon (BC) concentration; iv) a laser disdrometer Thies LPM which registered raindrops between 0.125 and 8 mm size in 20

channels; v) a Davis Weather Station, used for continuously registering the temperature, humidity, wind speed and wind direction. To detect thermal inversion, we have used the radiosounding data from La Coruña, Santander and Madrid.

Preliminary results reveal a progressive increase (about 57%) in aerosols number concentration during the thermal inversion, mainly for Aitken mode (particles between 30 and 100 nm) with an increase of 63 %. In accumulation mode (particles larger than 100 nm) there was an increase of 49 %. In nucleation mode (particles less than 30 nm) there was an increase of 52 %. As a consequence, an 8% increase in the median particle size has been observed. BC values increased during the inversions by 33%. Furthermore, a change in air mass and a rain event (1.91 mm with a mean intensity of 0.38 mm/h, with raindrop sizes between 0.13 and 2.5 mm) occurred after the inversion and caused a decrease of 63% in the number of particles smaller than 1 µm. Besides, the rain event produced a decrease of 78% in BC values between before and after rain.

This work was partially supported by the Spanish Ministry of Economy and Competitiveness (Grant TEC2014-57821-R), the University of León (Programa Propio 2015/00054/001) and AERORAIN project (Ministry of Economy and Competitiveness, Grant CGL2014-52556-R, co-financed with FEDER funds). F. Oduber acknowledges the grant BES-2015-074473 from the Spanish Ministry of Economy and Competitiveness.

Gramsch, E., Cáceres, D., Oyola, P., Reyes, F., Vásquez, Y., Rubio, M.A. and Sánchez, G. (2014) Influence of surface and subsidence thermal inversion on PM<sub>2.5</sub> and black carbon concentration. *Atmos. Environ.* doi:10.1016/j.atmosenv.2014.08.066

Viard, V.B. and Fu, S. (2015) The effect of Beijing's driving restrictions on pollution and economic activity. *J. Public Econ.* 125, 98-115. doi:10.1016/j.jpubeco.2015.02.003

## Climate effects of urban aerosols

M.Zoran<sup>1</sup>, R.Savastru<sup>1</sup>, D.Savastru<sup>1</sup>, A.Dida<sup>2</sup>

<sup>1</sup>Environment Remote Sensing Dept, National Institute of R&D for Optoelectronics, Bucharest Magurele, 077125, Romania

<sup>2</sup>University Transylvania of Brasov

Keywords: urban aerosols, PM2.5 and PM10, meteorological parameters, climate, Bucharest.  
Presenting author email: maria@dnt.ro

Air pollution represents one of the most important driver affecting the Earth's energy balance and hydrological cycle, climate and human health. The current study presents a spatio-temporal analysis of the aerosol concentrations in relation with meteorological parameters in two size fractions (PM10 and PM2.5) in Bucharest metropolitan area. Both in-situ monitoring data as well as MODIS Terra/Aqua time-series satellite data for 2011 year provided useful tools for particle matter PM2.5 and PM10 monitoring. All these methods are important and complementary (Chudnovsky, 2014), (Hutchison, 2008). It was found that PM2.5 and PM10 aerosols exhibit their highest concentrations mostly in the central part of the town, due to road traffic as well as in the industrialized periurban areas. In addition to the local and regional anthropogenic PM sources, both the levels and composition of air PM depend on meteorological parameters (temperature, humidity, precipitation, winds etc.), and season of the year.

### Study area and data used

Study test area, Bucharest town placed in the South – Eastern part of Romania is one of the most crowded capital in Eastern Europe and maybe the most polluted. Economical development results in traffic increase (presently six times than 1990 year) as well as some periurban industries development, heavy metals sources (sometimes above the acceptable limits). The emission inventory includes 430 point sources due to residential heating, and area sources generated by the distribution of traffic emissions. Daily average particle matters concentrations PM10 and PM2.5 for Bucharest metropolitan area have been provided by 8 monitoring stations of Environmental Protection Agency. The C005 (version 5.1) Level 2 and Level 3 Terra MODIS AOD550 time-series satellite data for period 01/01/2011-31/12/2011 have been used. Meteorological variables (air temperature, relative humidity, atmospheric pressure) were provided by in-situ measurements. ORIGIN 8.0 and ENVI 5.0 software were used.

### Results

The predominant component in PM10 was PM2.5, as can be seen in Figure 1, which shows clear evidence that high mean PM10 and PM2.5 particle concentrations were observed in winter months, and low values in the summer months. Observational results

indicate yearly concentrations of PM2.5 and PM10 mean values respectively 35.96 and 40.91  $\mu\text{g m}^{-3}$ .

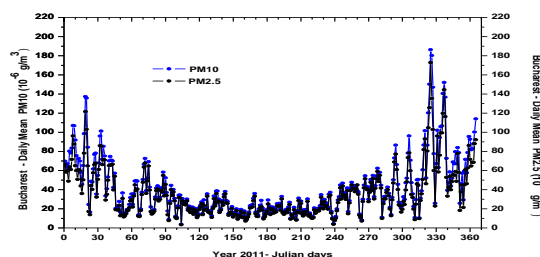


Figure 1. Daily mean PM10 and PM2.5 concentrations ( $\mu\text{g m}^{-3}$ ) during 2011 year in Bucharest test area

In spite of air quality improvements recorded in Bucharest metropolitan area in Romania between 1990 and 1997, still are recorded high levels of particulate matter (PM2.5 and PM10) and other pollutants concentrations. Figure 2 shows aerosol concentration map derived from MODIS Terra AOD550 (aerosol optical thickness) daily data. The results revealed a significant month-to-month variability in all AOD550 values, underlying the influence of varying aerosol load function of season. The AOD550 values (Level 3) lie in a wide range, as low as 0.2 up to 0.5. The influence of aerosol particles on climate, and how their properties are perturbed by anthropogenic activity, is one of the key uncertainties in climate change assessments.



Figure 2. Aerosol concentration map derived from MODIS Terra AOD550 over Bucharest area

This work was supported by Romanian National Authority for Scientific Research, NUCLEU Program under Contract 5N/2016 PN16 400101-02.

Chudnovsky A., Lyapustin A., Wang Y., Tang C., Schwartz J. Koutrakis P., (2014), *Cent. Eur. J. Geosci.* DOI: 10.2478/s13533-012-0145-4.  
Hutchison, K. D., Faruqui, S. J., & Smith, S. (2008). *Atmospheric Environment*, 42(3), 530–543.

## Mass Concentration and Health Risk Assessment of Toxic Trace Metals in Size-Segregated Airborne Particulate in Como, Northern Italy

S. Rovelli<sup>1</sup>, A. Cattaneo<sup>1</sup>, F. Borghi<sup>1</sup>, W. Nischkauer<sup>2</sup>, A. Limbeck<sup>2</sup> and D.M. Cavallo<sup>1</sup>

<sup>1</sup>Department of Science and High Technology, University of Insubria, Como, 22100, Italy

<sup>2</sup>Institute of Chemical Technologies and Analytics, TU Wien, Vienna, A-1060, Austria

Keywords: metal size-distribution, non-carcinogenic risk, cancer risk, heavy metals.

Presenting author email: sabrina.rovelli@uninsubria.it

As well documented in the scientific literature, the adverse effects of airborne particulate matter (PM) on human health are associated with its size and chemical composition (Harrison and Yin, 2000; Polichetti *et al.*, 2009). The presence and distribution of different toxic compounds among the various size fractions is of primary relevance in terms of health concern. Although PM is a complex and heterogeneous mixture of several substances, trace metals represent an important source of PM toxicity because of their toxic characteristics (Raashou-Nielsen *et al.*, 2016). Literature studies dealing with the metal characterization of size-segregated PM have been conducted worldwide in the last decade (Mbengue *et al.*, 2014; Malandrino *et al.*, 2016). Nevertheless, researches focused on the assessment of health risks associated with PM-bound toxic elements are few and even fewer are those studies concerning the health risk characterization of size-segregate PM.

In this study, the mass concentration of selected trace metals (Cr, Mn, Fe, Ni, Cu, Zn, Ba and Pb) was measured on an extended set of size-segregated PM samples collected during a long-term monitoring campaign at an urban background site in Como, Northern Italy. Results were subsequently used to evaluate the potential non-carcinogenic and carcinogenic risks for human health via the inhalation exposure route of those metals. The strength of the present work lies in the possibility to i) investigate how the selected elements are distributed in the airborne PM and ii) assess the contribution of the various PM fractions to the total PM<sub>2.5</sub> health risk.

Size-resolved aerosol particles were collected by means of a 13-stage Low Pressure Impactor (DLPI), equipped with high-purity polycarbonate filters. The sampling device was run once a week at 30 L min<sup>-1</sup> for 96h and weekly sampling campaigns were carried out from Monday to Friday morning, for a total of 10 monitored months (38 weekly sampling sessions). Minor and potentially toxic trace metals were then directly analyzed via laser ablation (LA) in combination with inductively coupled plasma-mass spectrometry (ICP-MS) with a novel measurement protocol specifically developed.

According to their size-distributions, the investigated elements could be roughly divided into three groups: I) metals mostly concentrated in the largest particles fraction, including Fe, Ba and Cu, with more than 70% in the PM<sub>1-2.5</sub> size range; II) metals showing higher contributions in the accumulation mode (PM<sub>0.1-1</sub>) (with more than 60% of the total PM<sub>2.5</sub> mass), including

Pb, Zn and Ni, with a clear peak between 0.3 and 0.6 µm (at least for Pb and Zn) and III) metals more spread throughout the size-distribution - without considering the lowest DLPI stages - with rather similar contributions for the smaller and coarser fractions to the total PM<sub>2.5</sub> (Cr and Mn).

Although based on the assumption that people living in the study area are chronically exposed to the average metal concentrations monitored during the whole campaign, the estimated hazard quotients for each element and the overall estimate for non-carcinogenic effects posed by all of the metals under investigations were always < 1, suggesting no significant risks for the exposed population. Aerosol particles > 0.3 µm seemed to play the major role in the characterization of the overall non-carcinogenic risk, whereas lower contribution were found for particles < 0.3 µm, with percentage contribution values decreasing with decreasing aerosol particle size. Moreover, also the estimated PM<sub>2.5</sub> carcinogenic risks (CR) for Ni and Cr were below or within the acceptable range established in terms of regulatory purposes for the general population (10<sup>-6</sup> or 10<sup>-5</sup>), thus indicating a negligible cancer risk for people living in the study area. The estimated CR for Ni was two orders of magnitude lower than the calculated CR for Cr, even though the higher contributions to the total PM<sub>2.5</sub>-CR for Ni were found to be mainly related to airborne particles that are able to more deeply penetrate into the human respiratory system.

Therefore, despite some assumptions or limitations, this type of researches could represent useful tools in epidemiological studies, providing innovative and alternative target with respect to the typical PM fractions (PM<sub>10</sub> or PM<sub>2.5</sub>) on which the epidemiological research is generally focused.

Harrison, R. and Yin, J. (2000) *Sci. Total Environ.* **249**, 85-101.

Polichetti, G., Cocco, S., Spinali, A., Trimarco, V. and Nunziata A. (2009) *Toxicology* **261**, 1-8.

Raashou-Nielsen *et al.* (2016) *Environ. Int.* **87**, 66-73.

Mbengue, S., Alleman, L.Y. and Flament, P. (2014) *Atmos. Environ.* **135**, 35-47.

Malandrino, M., Casazza, M., Abollino, O., Minero, C. and Maurino, V. (2016) *Chemosphere* **147**, 477-489.

## Highly Resolved Spatiotemporal Variability of Fine Particle Concentrations in an Urban Neighborhood

Y. Etzion, D.M. Broday

Faculty of Civil and Environmental Engineering, Technion - Israel Institute of Technology, Haifa, 3200003, Israel

Keywords: ambient fine NPC, continuous wavelet transform, spatiotemporal variability, urban air pollution.

Presenting author email: dbroday@technion.ac.il

Exposure to fine particles has been associated with a substantial burden of disease. Since adverse outcomes were reported even below  $10 \mu\text{g}\cdot\text{m}^{-3}$  of  $\text{PM}_{2.5}$ , studying the variability of fine and ultrafine (UF) particle concentrations in urban environments is important, since exposure variability is required to carry environmental epidemiology studies. Ambient concentrations of fine particles result from plethora of dynamic processes that occur at different spatiotemporal scales, including local and remote emissions, transport, aging, removal and transformation processes. We hypothesized that decomposing particle concentration records into using non-stationary methods can reveal the footprints of various processes at fine temporal scales while also spatially resolving local/short-term processes from regional phenomena.

Towards this goal, a network of relatively low-cost optical particle counters (OPCs) has been deployed in an urban residential neighborhood for six months. Five nodes were placed about 150-300 m from each other, measuring the number concentration of fine particles  $>0.5 \mu\text{m}$  in two size channels. The extremely long time-series (1 min sampling frequency) facilitated a frequency analysis for studying patterns that are typically hidden at different spatiotemporal scales within the particle concentration records. Specifically, we used a continuous wavelet decomposition (CWT) to resolve periodic cycles (e.g. diurnal patterns) and transient phenomena (e.g. synoptic events, local emissions).

The scale-dependent spatial variability in the study area, which can be extracted from the inter-nodal differences, was found to mostly appear in the high percentiles, and in the corresponding skewness, of the particle concentration distributions. For example, the overall inter-nodal normalized root mean squared error (NRMSE) of the measured particle concentrations was 19.5–33.6% when the nodes were deployed in the urban area but only 8-16% when the nodes were collocated in a central location in the study area. The increased variability during the deployment is clearly related to intra-neighborhood concentration variability, which is attributed to (spatiotemporal) variability in anthropogenic activity (commute, commerce), which can be partly assessed from high spatial resolution land use classification.

Applying a CWT, synoptic events (e.g. dust storms) and the diurnal cycle of the particle concentrations could be identified. In particular, short-

lived transient component at different time-scales are demonstrated in the wavelet scalogram (Figure 1). Based of the CWT decomposition, we reconstructed scale-specific particle concentration time series and analyzed them with respect to co-measured wind field characteristics.

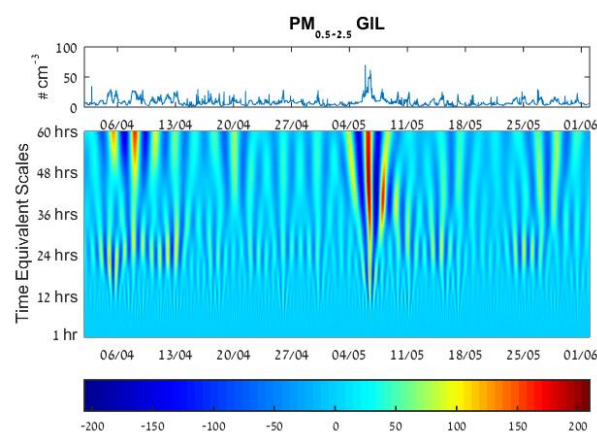


Figure 1. An example of a time series of fine particle number concentration measured at one of the urban measurement sites (code name GIL) during April-June 2014 (top) and its continuous wavelet decomposition (bottom). The color bar represents the magnitude of the wavelet coefficient at each decomposition level, which corresponds to a distinct time scale.

Based on such analysis, we could estimate the spatiotemporal variability of different contributions to the ambient fine particle levels in the study area, including local traffic and other human activities vs. long-range transport. Our results demonstrate that by using CWT it is possible to distinguish between inter and intra neighborhood contributions to observed fine particles.

This work was supported by the Technion Center of Excellence in Exposure Science and Environmental Health (TCEEH).

## Understanding of the chemical processes involving nitro- and oxy-PAHs in ambient air and evaluation of SOA PAH contribution on PM *via* annual and intensive field campaigns

A. Albinet<sup>1</sup>, S. Tomaz<sup>1,2</sup>, D. Srivastava<sup>1,2</sup>, G.M. Lanzafame<sup>1</sup>, O. Favez<sup>1</sup>, J.-L. Jaffrezo<sup>3</sup>, N. Bonnaire<sup>4</sup>, V. Gros<sup>4</sup>, L. Y. Alleman<sup>5</sup>, F. Lucarelli<sup>6</sup>, E. Perraudin<sup>2</sup>, E. Villenave<sup>2</sup>.

<sup>1</sup>INERIS, Parc Technologique Alata, BP 2, 60550 Verneuil-en-Halatte, France

<sup>2</sup>Université Bordeaux, EPOC-CNRS, UMR 5805, 33405 Talence, France

<sup>3</sup>UGA, CNRS, IGE, 38 000 Grenoble, France

<sup>4</sup>LSCE, UMR8212, CNRS-CEA-UVSQ, Gif-sur-Yvette, France

<sup>5</sup>IMT Lille-Douai, Univ. Lille, SAGE, 59000 Lille, France

<sup>6</sup>University of Florence, Dipartimento di Fisica Astronomia, 50019 Sesto Fiorentino, Italy

Keywords: PAH, OPAH, NPAH, Air quality, SOA, Source apportionment, PMF.

Presenting author email: alexandre.albinet@ineris.fr

Polycyclic aromatic hydrocarbons (PAHs) are ubiquitous compounds emitted by all combustion sources. They are of major health concern because of their carcinogenic, mutagenic and teratogenic properties and are therefore, regulated pollutants in ambient air. In the atmosphere, PAH oxidation through homogeneous and heterogeneous reactions may lead to the formation of oxy- and nitro-PAHs (Keyte et al., 2013). These latter species are also emitted concomitantly with PAHs during incomplete combustion processes. Oxy- and nitro-PAHs are potentially more toxic than their parent PAHs. The identification of the origins of oxy- and nitro-PAHs is challenging, due to the coexistence of their primary and/or secondary sources. These species are also of prime interest because they are, typically part of the secondary organic aerosol (SOA) generated from gaseous PAH oxidation, which is significant in urban environments (Chan et al., 2009).

The objective of this work is to better understand the chemical processes involved in the formation of nitro- and oxy-PAHs based on ambient air field observations, to better understand the sources of these toxic compounds and to identify specific molecules that could further be used as molecular markers of PAH oxidation and SOA formation.

Field measurements were performed over 1 year with samplings, every third day, of the gaseous and particulate (PM<sub>10</sub>) phases in Grenoble (2013) and at the SIRTA station (25 km SW from Paris city center) (2015). Intensive observations at SIRTA have been also performed with PM<sub>10</sub> samples collected every 4-hour during a period of severe PM pollution event (PM>50 µg m<sup>-3</sup> for several days) in March 2015, concomitantly with online measurements (e.g. ACSM, 7λ-Aethalometer).

The study of the occurrence of nitro-, -oxy and parent PAHs in the atmosphere, the seasonal and diurnal variations of their concentrations and substance patterns and the assessment of the cancer risk induced by these compounds have been performed. Based on these observations combined with literature knowledge and an extended aerosol chemical characterization, specific molecules of PAH oxidation have been identified

(Figure 1). These substances were then used in source-receptor models such as positive matrix factorization (PMF) to apportion the SOA contribution from PAH oxidation on PM<sub>10</sub> mass.

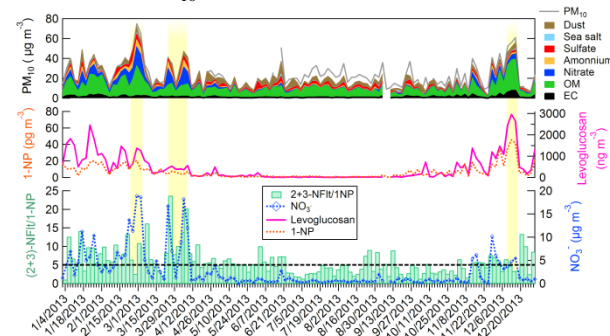


Figure 1. Annual trends of (2+3)-NFlt/1NP ratio, PM<sub>10</sub> chemical composition, nitrate, levoglucosan and 1-nitropyrene (1-NP) concentrations at Grenoble (2013).

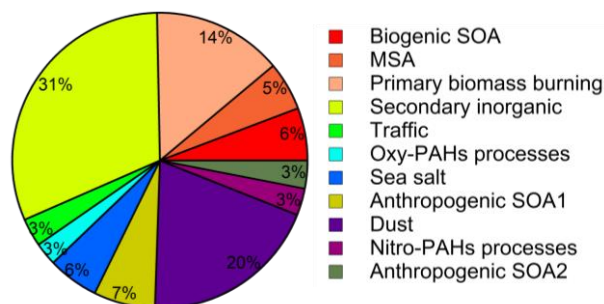


Figure 2. PM<sub>10</sub> source apportionment at SIRTA station in March 2015 (preliminary results).

### Acknowledgements

This work has been supported by the French ministry of environment (MEEM) and the French reference laboratory for air quality monitoring (LCSQA) as well as by the FP7 ACTRIS and H2020 ACTRIS2 programs.

### References

- Chan A.W.H. et al. (2009) *Atmos. Chem. Phys.*, **9**, 3049.  
Keyte, I. et al. (2013) *Chem. Soc. Rev.*, **42**, 9333.

## Online molecular-level characterization of submicrometer particulate organic matter in urban atmospheres and its application to source apportionment

Markus Müller<sup>1,2</sup>, Philipp Eichler<sup>2</sup>, Barbara D'Anna<sup>3</sup>, Wen Tan<sup>4</sup>, and Armin Wisthaler<sup>2,4</sup>

<sup>1</sup>Ionicon Analytik GmbH, Innsbruck, 6020, Austria

<sup>2</sup>Institut für Ionenphysik und Angewandte Physik, Universität Innsbruck, Innsbruck, 6020, Austria

<sup>3</sup>CNRS, UMR5256, IRCELYON, Institut de recherches sur la catalyse et l'environnement de Lyon, Villeurbanne, Université de Lyon, Lyon, 69626, France

<sup>4</sup>Department of Chemistry, University of Oslo, Oslo, 0371, Norway

Keywords: CHARON PTR-ToF-MS, urban organic aerosol, chemical composition.

Presenting author email: markus.mueller@ionicon.com

We applied a novel chemical analytical method for measuring submicrometer particulate organic matter (sub- $\mu\text{m}$  POM) in the urban atmospheres of Lyon (F), Valencia (E) and Innsbruck (A) during different seasonal periods. Proton-Transfer-Reaction Time-of-Flight Mass Spectrometry (PTR-ToF-MS; PTR-TOFMS 8000, Ionicon Analytik GmbH, Innsbruck, Austria) was used in combination with the "chemical analysis of aerosol online" (CHARON) inlet (Eichler et al., 2015) for measuring sub- $\mu\text{m}$  POM in an online and real-time manner, i.e. without filter pre-collection and at 1-min time resolution. Soft and quantitative ionization via  $\text{H}_3\text{O}^+$  ions yields molecular-level information (elemental composition) of organic analytes at single digit  $\text{ng m}^{-3}$  levels. Figure 1 depicts the average mass spectra generated by sub- $\mu\text{m}$  POM in Lyon, Valencia and Innsbruck.

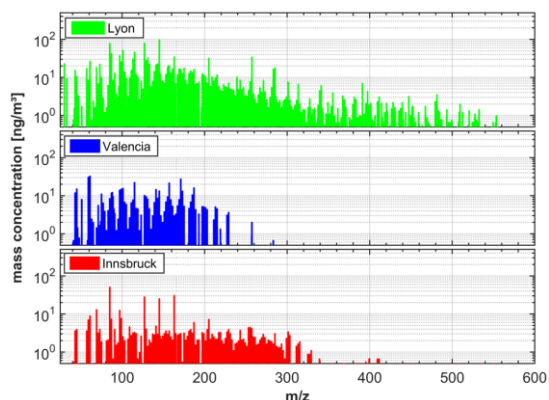


Figure 1. Average mass spectra generated by sub- $\mu\text{m}$  POM in Lyon (green; March 2015), Valencia (blue; June 2015) and Innsbruck (red; October 2015) as measured by CHARON PTR-ToF-MS.

Several molecular tracers including levoglucosan from fuelwood combustion, polycyclic aromatic hydrocarbons (PAHs) from vehicular traffic, nicotine from cigarette smoking, and monoterpene oxidation products derived from biogenic emissions were identified in the mass spectra and monitored in real-time.

The tracer information was used for interpreting positive matrix factorization (PMF) data allowing us to apportion

the sources of sub- $\mu\text{m}$  POM in the different urban environments.

Figure 2 shows the diurnal cycle of the total biomass burning organic aerosol (BBOA) and traffic primary organic aerosol (POA) PMF factors as obtained from the data measured in Innsbruck in October 2015. BBOA is elevated at night, with mean values of  $1.5 \mu\text{g m}^{-3}$  and low concentrations during the day. The traffic POA factor shows characteristic rush hour spikes during the morning and the evening. The bottom panel depicts the total PAH concentrations as apportioned to the biomass combustion and traffic source, respectively.

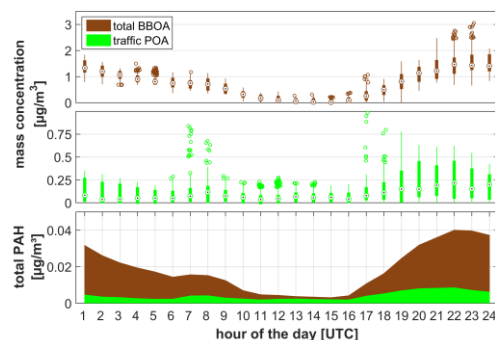


Figure 2. Diurnal cycle of the BBOA (brown; top panel) and traffic POA (green; middle panel) PMF factors as obtained from the data measured in Innsbruck in October 2015. The bottom panel depicts the total PAH concentrations as apportioned to the biomass combustion and traffic source, respectively.

This work was funded through the PIMMS ITN, which was supported by the European Commission's 7th Framework Programme under grant agreement number 287382.

Eichler, P., Müller, M., D'Anna, B., and Wisthaler, A. (2015) *Atmos. Meas. Tech.* **8**, 1353-1360.

## Aerosols Over Auckland

Guy Coulson, Gustavo Olivares, Sally Gray and Oliver Wilson

National Institute of Water and Atmospheric Research, Private Bag 99940, Auckland 1149, New Zealand

Keywords: Urban pollution, Aerosol processing, New Zealand

Presenting author email: [guy.coulson@niwa.co.nz](mailto:guy.coulson@niwa.co.nz)

Auckland, the largest city in New Zealand, is unique in being the largest city in the World to be almost completely surrounded by ocean and hence have no up or downwind sources of pollution. The city lies on a narrow isthmus between the Pacific Ocean and the Tasman Sea. Because of the lack of outside sources, average background concentrations of between 1000 and 4000 particles/cm<sup>3</sup> are common away from major sources with very steep concentration gradients approaching sources such as roads (Pattinson *et al* 2014).

New particle formation events were observed at an urban background site on four occasions during September 2012 (Coulson *et al* 2016). The form of the particle growth and the low background concentrations prior to the events suggests region-wide secondary formation. All events happened under windy conditions with wind from the SW. Under these conditions, the wind comes from open-ocean and across up to 20km of forested hills before encountering the urban plume of Auckland.

The Aerosol Tropospheric Chemistry in Urban Auckland (ATChU) experiment was carried out in order to investigate these new particle formation events and the processing of pollutants injected into clean air as they cross the Auckland isthmus. The experiment was a pilot study to investigate whether it is possible to track the changes in aerosols and aerosol precursors as they move from open-ocean (clean background) across the city (polluted) and out into ocean again. Measurements of aerosol size distribution, particle number concentration, BC, NO<sub>x</sub> and Ozone were made simultaneously at three points in Urban Auckland, one on the upwind urban edge, one in central Auckland and one on the downwind urban edge (Figure 1) for a period of approximately one month during March and April 2015.

Analysis of results to date indicates that region-wide events can be distinguished from local-source events and that the urban plume can be tracked across Auckland. This presentation will present a characterisation of Auckland's urban aerosol along with results from the ATChU campaign with an emphasis on aerosol processing in clean air.

This work was supported by NIWA under the Atmosphere Programme 4 Impacts of Air Pollutants. We acknowledge the assistance of Auckland Council, Halsey Drive School and the University of Auckland in providing monitoring sites.

Coulson, G., Olivares, G., Talbot, N. (2016) Aerosol Size Distributions in Auckland. *Air Quality and Climate Change* Volume 50 No.1. February 2016  
Pattinson, W., Longley, I., Kingham, S. (2014), *Atmospheric Environment* Volume 94, Pages 782-792

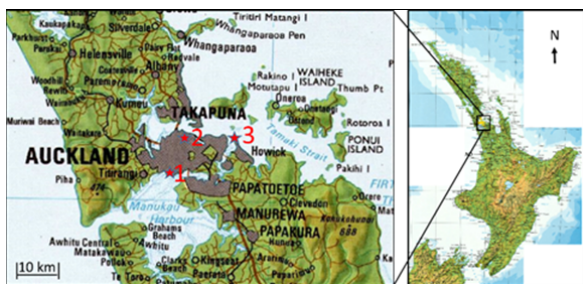


Figure 1. Three measurement locations in Auckland for the ATChU Campaign: 1) Halsey Drive School, 2) The University of Auckland, Health Sciences Building 3) Musick Point - Auckland Council air quality monitoring station

## Aerosol PSD and Optical Depth of Mega-agglomerations

R. MEZIANE and M. DIOURI

Atmospheric Physic Laboratory, University Mohammed 1st, Oujda, 60020, Morocco

Keywords: AERONET\*, aerosol optical depth, particle size distribution, sun-photometer

Presenting author email: [rajaemeziane@gmail.com](mailto:rajaemeziane@gmail.com)

The present study is devoted to the characterization of the particle size distribution evolution determined with the inversion problem resolution using data of aerosol optical depth (AOD) associated to sun-photometer measurements of AERONET network sites (Table 1).

The atmospheric evolution studies require the knowledge of physic-chemical characters tics of dominant gazes, but also those related to atmospheric aerosol. This latter constitute an important component in impacting the atmospheric evolution as well as the climate in regional and global change. The action of atmospheric aerosol on the radiative balance of the earth-atmosphere system can be directly (direct attenuation of solar radiation) or indirectly (attenuation of radiation through the liquid phase where aerosols has been served as condensation nuclei).

Aerosol optical parameters can be viewed in terms of volume particle size distribution in various regions and climates. In this work, results show that the coarse mode seems more important for Dhaka with an average radius around 3  $\mu\text{m}$  (Fig. 2). The fine mode is with significant amplitude for Taipei with an average radius around 0.2  $\mu\text{m}$  that indicate more influence of anthropogenic aerosol particularly on march (Fig. 1).

Table 1. Localizations of sites studies.

Sites	Latitude	Longitude	Elevation (m)
Taipei	25.03	121.5 E	26.0
Dhaka	23.72	90.39 E	34.0

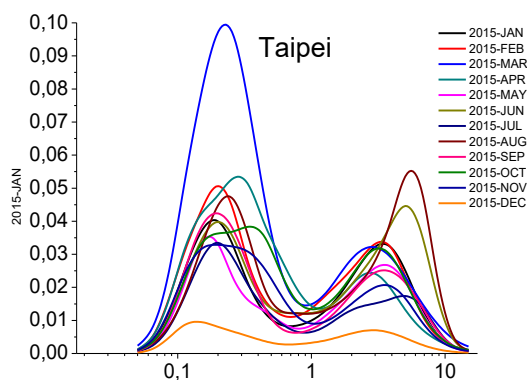


Figure 1. Monthly mean of PSD for Taipei

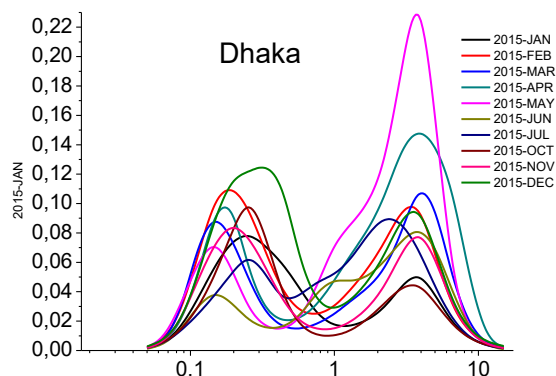


Figure 2. Monthly mean of PSD for Dhaka

The study of the aerosol optical depth show different aerosol type that dominate during different periods of the year with higher values on spring and summer. Results based on a spectral dependence indicate AOD with high values for small wavelengths and vice versa, except for the aerosol dominated by large particles, Dhaka case, a constancy of high values of AOD confirm the more visible ray attenuation and the observed lower visibility.

\* [www.aeronet.gsfc.nasa.gov](http://www.aeronet.gsfc.nasa.gov)

### References

- Diouri, M and Meziane, R. Global aerosol PSD of Urban Areas. *International Aerosol Conference, Bexico, Korea 2014.*
- Diouri, M and Meziane, R. Aerosol radiative forcing determined for large urban areas. *International Aerosol Conference, Bexico, Korea 2014.*
- Diouri, M and Meziane, R. Aerosol optical thickness observed on the world's top five cities. *International Aerosol Conference, Bexico, Korea 2014.*

### Acknowledgements

Kindly thanks to the AERONET/PHOTONS PI: Po-Hsiung Lin (Taipei) and B. Holben (Dhaka)

## Urban air quality monitoring in relation with <sup>222</sup>Rn at the surface level

M.Zoran, R.Savastru, D.Savastru,

Department of Satellite Remote Sensing, National Institute of R&D for Optoelectronics, Bucharest Magurele, 077125, Romania,

Keywords: air quality, radon, Bucharest, Romania.

Presenting author email: maria@dnt.ro

Radon (<sup>222</sup>Rn) is an important tracer of air masses dynamics for understanding the lower atmospheric mixing processes and air quality indices (AQI) monitoring, which potentially can improve exposure time estimates for use in epidemiological studies. This paper aims to explore trends of urban air quality in relation with surface time-series observation of radon (<sup>222</sup>Rn), ozone, particle matter (PM2.5, PM10), nitrogen dioxide (NO<sub>2</sub>), and sulphur dioxide (SO<sub>2</sub>) levels over year 2012 in Bucharest metropolitan zone in Romania. Have been analyzed correlation with main meteorological parameters recorded in the air near the ground.

### Results

The frequency distribution patterns of AQI and each target compound were evaluated for entire year using the relevant daily mean values (Figure 1). Figure 2 shows an autocorrelation between the temporal variation of daily mean ground level ozone concentrations and daily mean particle matter PM10 for the year 2012 for Bucharest test site. The changes recorded in the particulate matter PM2.5 and PM10 content are expected to affect considerably the photolysis of ozone and the rates of heterogeneous losses of ozone and its precursors. Also, increased temperatures during summer time may lead to increased biogenic isoprene emissions, strengthening the regional-scale ozone contribution.

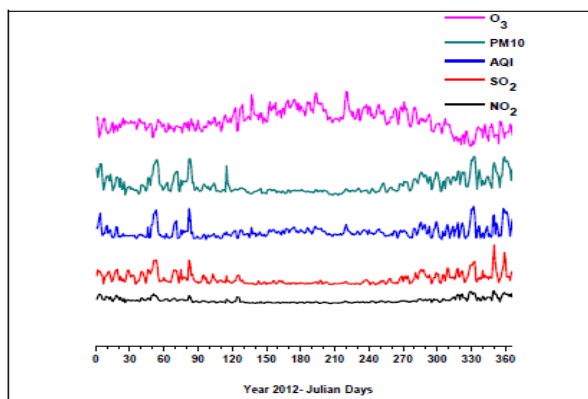


Figure 1. Daily mean variation of AQI, ozone, PM10, SO<sub>2</sub>, and NO<sub>2</sub> concentrations (µg/m<sup>3</sup>) during 2012 year in Bucharest test area

There is a positive correlation between radon in the air near the ground levels and AQI (Figure 3).

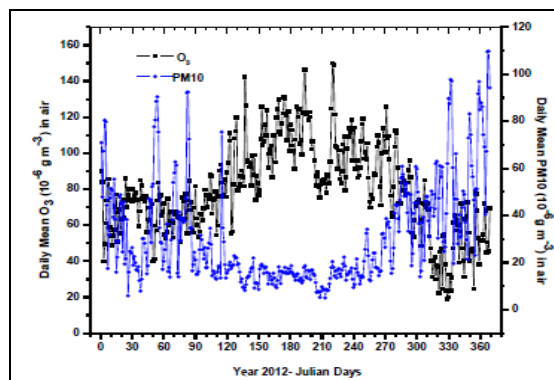


Figure 2. Daily mean PM10 and ozone concentrations (µg/m<sup>3</sup>) during 2012 year in Bucharest test area

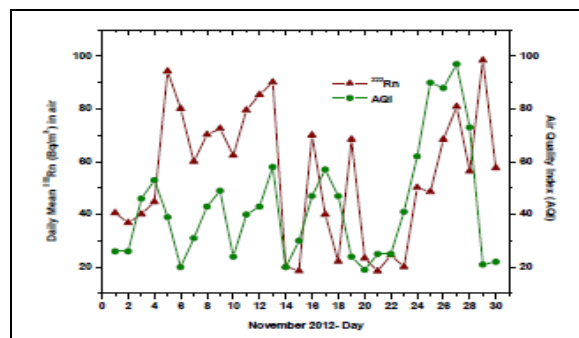


Figure 3. Daily mean <sup>222</sup>Rn and AQI during 2012 year in Bucharest test area

The difference of summer and winter values of radon in air concentration and AQI is attributed to meteorological variables influence (air temperature, relative humidity, pressure and wind intensity) and air masses stagnation (Zoran M. Et al, 2012 and 2016).

**Acknowledgements** This work was supported by Romanian National Authority for Scientific Research, Program NUCLEU Contract 5N/09.03.2016, under 16 40.01.01 research theme.

Zoran M., Savastru R., Savastru D., (2012), *Journal of Radioanalytical and Nuclear Chemistry* 293 (3): 877-888.

Zoran M., Savastru D., Dida A., (2016), *Journal of Radioanalytical and Nuclear Chemistry* DOI 10.1007/s10967-015-4681-5

## Association between surface temperature inversion and high PM<sub>2.5</sub> measured with an unmanned aerial vehicle

E. Gramsch<sup>1</sup>, C. Ayala<sup>1</sup> and A. Arellano<sup>2</sup>

<sup>1</sup>Department of Physics, University of Santiago de Chile, Santiago, Chile

<sup>2</sup>Department of Metallurgical Engineering, University of Santiago de Chile, Santiago, Chile

Keywords: temperature inversion, PM<sub>2.5</sub>, UAV.

Presenting author email: egramsch@gmail.com

### Abstract

The vertical distribution of temperature and PM<sub>2.5</sub> were measured with the aid of an unmanned aerial vehicle in a 2 month long campaign in Santiago de Chile. Simultaneously, the PM<sub>2.5</sub> and black carbon were measured at the surface. Measurements were performed during winter, when frequent temperature inversion occurs and very high levels of PM<sub>2.5</sub> are observed. At night, the top of the inversion layer is between 100 – 250 m and the bottom is between 0 and 80 m. Thus there is a very small layer for mixing of pollutants. PM<sub>2.5</sub> decreases very rapidly with height, reaching only ~ 10 µg/m<sup>3</sup> at 300 – 400 m.

### Introduction

Santiago de Chile is located in a valley enclosed by two mountain ranges, the Andes Mountains on the east and the coastal mountain range on the west. The city has 6,000,000 inhabitants and most of the economic activity of the country is located within its limits. In Santiago de Chile, during winter, the hills restrict wind speed and horizontal transport of pollutants. In addition, there are frequent temperature inversions that lead to stable atmospheric conditions which constrain vertical airflow. Thus, air quality is quite poor, especially during winter. The mixing layer height (MLH) is an important parameter characterizing the potential of the atmospheric boundary layer to take up emitted air pollutants (Tang et al. 2016). MLH defines the volume for the dilution of air pollutants emitted or formed near the surface and thus the near-surface pollutant concentrations.

### Results

In this work we have studied the vertical profile of PM<sub>2.5</sub>, temperature and relative humidity in the evening, once a day and correlated its results with ground measurements. Measurements were performed from May 30 until July 25, 2017 in a parking lot at the University of Santiago. Temperature and relative humidity were done with a HOBO datalogger and PM<sub>2.5</sub> was measured with an optical particle counter developed at the University. The counter was calibrated using a Teom PM<sub>2.5</sub> monitor located in the same place. The city has a mild slope, from 450 m.a.s.l. in the west to 850 m.a.s.l. in the east and the pollution characteristics in the lowest part are very different than the highest part of the city. The site is located in the western part of the city, where the thermal inversion is more severe and PM<sub>2.5</sub> levels are several times higher than the upper part of the city.

Measurements indicate that at night (8 – 10 pm) the top of the surface inversion reaches a height between 120 – 250 m and the base of the inversion reaches between 0 and 80 m. Thus pollutants emitted at night can mix in a layer that is at most 80 m height. Figure 1 shows PM<sub>2.5</sub> and temperature data taken in June 29, 2017 with the UAV in a day with strong surface temperature inversion and a mixing layer height reaching only about 70 m. PM<sub>2.5</sub> concentration in the ground is very high but decreases quickly with height, reaching only 10 µg/m<sup>3</sup> at 300 m.

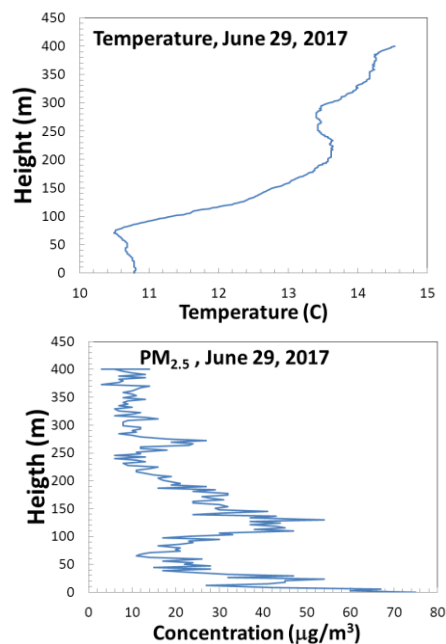


Figure 1. Temperature and PM<sub>2.5</sub> versus height measured with the UAV.

Data for other days also show a very rapid decrease of PM<sub>2.5</sub> when the temperature inversion is strong (such as figure 1). On days with little or no inversion, PM<sub>2.5</sub> does not decrease as rapidly.

This work was supported by the Fondecyt, Chile under grant N° 1151117.

Tang, G., J. Zhang, X. Zhu, T Song, C. Münkel, B. Hu, et al. Mixing layer height and its implications for air pollution over Beijing, China, *Atmos. Chem. Phys.*, 16, 2459–2475, 2016

## Air pollution by nanoparticles in 5D diagrams

L. Hejkrlik, H. Plachá and D. Richterová

Czech Hydrometeorological Institute, Branch office in Ústí nad Labem, Czech Republic

Keywords: nanoparticles, air pollution, meteorological conditions

Presenting author email: hejkrlik@chmi.cz

Number concentrations  $N$  of nanoparticles had been measured by SMPS in 3 channels (10–20 nm, 30–50 nm and 70–100 nm) with time resolution of one hour since June 2012 to December 2015 at a background urban site in Northern Bohemia (Hejkrlik, Plachá and Richterová, 2016). At nearly the same place hourly means of three meteorological elements were available (air temperature  $T_h$ , relative air humidity  $H_h$  and global radiation  $R_h$ ) alongside a complementary index of atmospheric pollution – mean hourly concentrations of  $SO_2$ .

The whole period of observations covered 1309 days, periodically involving all of the seasons of the year with no respect to weekdays or rush hours. Night hours ( $R_h=0$ ) were excluded even though they amounted to more than one half of available data.  $T_h$  varied between  $-11,2\text{ }^\circ\text{C}$  and  $36,1\text{ }^\circ\text{C}$ , for  $H_h$  it was between 21% and 100% and  $R_h$  reached its extremes between 0,2 and  $940,5\text{ W/m}^2$ . The maximum of mean concentration of  $SO_2$  was slightly over  $20\text{ }\mu\text{g/m}^3/\text{hour}$ . Resulting number of analyzed rows of 5 variables was approximately 14 000. The database was thoroughly checked for missing values which was extremely important especially for data measured by SMPS.

The nearly-continuous combinations of meteorological data were transformed into *three-dimensional* matrix where  $T_h$ ,  $H_h$  and  $R_h$  were assigned only few discrete values (48, 13 and 13 respectively). In the resulting 8112 cells of the 3D matrix mean concentrations of the modes of fine particles were calculated. To clarify the whole picture only the cells containing at least 15 values of  $N$  were taken into account. The results were displayed in the form of XYZ bubble graph, diameters of the spheres being the *fourth* dimension. Grapher™ 11 (Golden Software, LLC) allows for colouring of the bubbles regarding specific key, in this case one of four classes of mean hourly concentration of  $SO_2$  in corresponding cells. The colour of the spheres may be regarded as the *fifth* dimension.

The nucleation mode of nanoparticles (10–20 nm) demonstrate strong proliferation ( $N\sim 10^4/\text{cm}^3/\text{hour}$ ) under extreme both temperature and solar radiation while air moisture remains moderate. Against the expectations concentration of  $SO_2$  registered at the same time interval did not reach their maximum values (Fig. 1).

The overall picture changes for bigger particles (Fig. 2 and 3). Their concentrations are one order less, the maximum values show considerable affinity to low visibility and high humidity and the events with higher levels of  $SO_2$  are more frequent.

Hejkrlik L., Plachá H. and Richterová D. (2016). *UFP concentrations over some grids of paired meteorological data*. Abstract P2-AAS-AASP-220, EAC 2016, Tours, September 4–9, 2016.

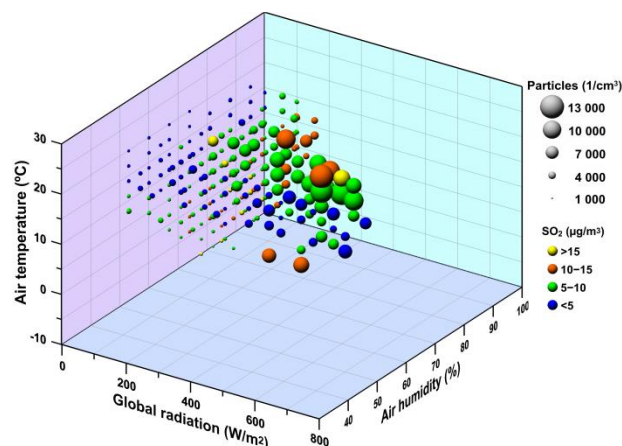


Figure 1. Number of 10–20 nm particles vs three meteorological elements and  $SO_2$  concentration (per hour)

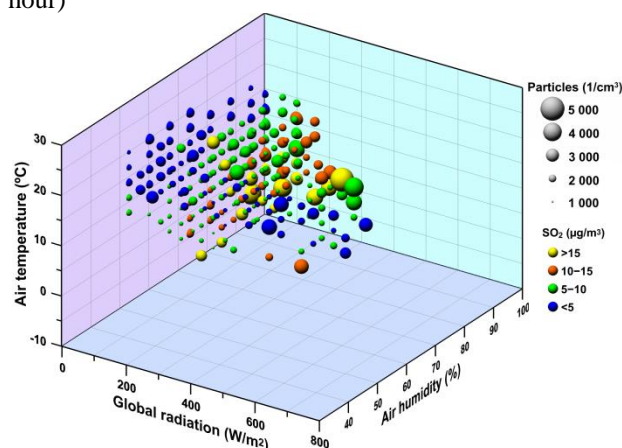


Figure 2. Number of 30–50 nm particles vs three meteorological elements and  $SO_2$  concentration (per hour)

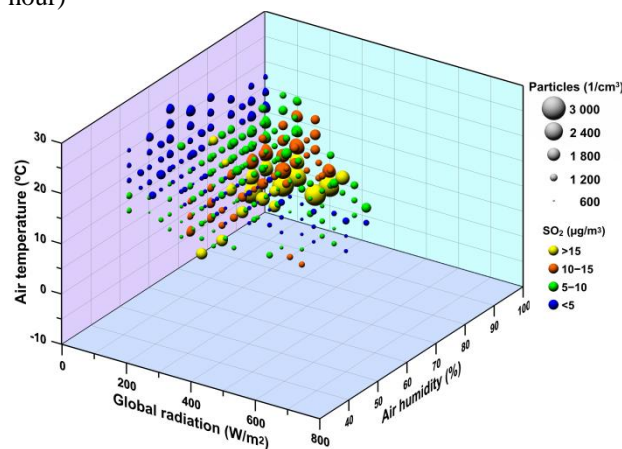


Figure 3. Number of 70–100 nm particles vs three meteorological elements and  $SO_2$  concentration (per hour)

## Estimation of airborne PM to total tire wear fraction under constant speed driving condition using a tire simulator

S.H. Lee<sup>1</sup> · K.B. Kim<sup>1</sup> · Y.R. Kim<sup>1</sup>

<sup>1</sup>Department of Engine Research, Korea Institute of Machinery and Materials, Daejeon, 305343, Rep. of Korea

Keywords: Tire simulator, Airborne PM, Tire wear, Constant speed driving, Fine particles.

Presenting author email: shlee@kimm.re.kr

Vehicles are one of the major sources of particulate matter (PM) in urban areas. There is increasing interest in the health effects of PM emissions associated with road traffic. Many related studies are underway to determine the characteristics of the particles emitted from various pollutants. Although many previous studies have focused on PM emitted from vehicle emissions, recent studies have shown that PM emitted from non-exhaust sources, such as road dust, tire wear particles, and brake wear particles occupies the same amount as PM emitted from the vehicle<sup>1</sup>.

In Korea, total amount of tire tread wear is reported to be more than 50,000 tons per year. However, there is no reliable data on the amount of airborne PM emissions (PM<sub>10</sub> and PM<sub>2.5</sub>) from tire wear that actually affect the human health. Although some of the previous studies have estimated the fraction of the amount of total tire wear on airborne PM emissions, experimental evidence is not reliable<sup>2</sup>.

The purpose of this study is to determine the fraction of tire wear to airborne PM emissions at least under constant speed driving conditions using a tire simulator. The fraction of the total tire wear on airborne PM emission varies depending on the driving conditions of the vehicle. Although the experiment is limited to the constant speed driving conditions in this stage, the experiment will be carried out under the acceleration, deceleration and tilting conditions in the future.

Table 1. Tested tires

Tire	Size	Tread wear	Speed
Tire A	205/55R16	440	80 km/h
Tire B	205/55R16	400	80 km/h
Tire C	205/55R16	400	80 km/h
Tire D	205/65R16	800	80 km/h

In this study, we estimated the fraction of the total tire wear on the airborne PM emissions using 4 different tires. All the experiments were conducted under constant speed of 80 km/h without acceleration or deceleration for 12 hours. Particle mass concentrations and particle mass size distributions were measured using size segregated cyclone (PM<sub>10</sub> and PM<sub>2.5</sub>), dusttrak and aerodynamic particle sizer (APS)

The experimental results showed that the fraction of total tire wear to PM<sub>10</sub> with no slip condition under constant speed condition ranged between 0.11~0.36% that was significantly underestimated compared to the previous study (8% for PM<sub>10</sub>, 1.2% for PM<sub>2.5</sub> according to the study of Luhana et al, 2004). This means that most tire wear could be occurred at acceleration or deceleration conditions.

Table 2. Fraction of the total tire wear on airborne PM emission according to tested tires

Tires	PM <sub>10</sub> Cyclone mass	PM <sub>2.5</sub> Cyclone mass	Tire wear	PM <sub>10</sub> / Tire wear	PM <sub>2.5</sub> / Tire wear	PM <sub>2.5</sub> / PM <sub>10</sub>
Tire A	610 µg	741 µg	6.1 g	0.22%	0.18%	0.82
Tire B	153 µg	124 µg	2.1 g	0.13%	0.11%	0.81
Tire C	544 µg	450 µg	2.7 g	0.36%	0.30%	0.83
Tire D	259 µg	209 µg	4.2 g	0.11%	0.09%	0.81

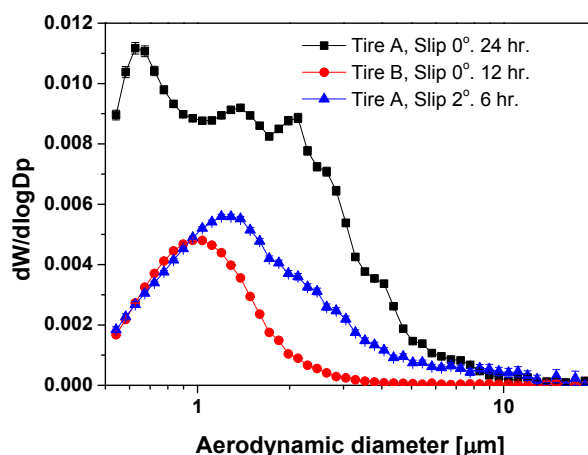


Figure 1. Mass size concentrations of tire wear particles.

This work was supported by the Center for Environmentally Friendly Vehicles (CEFV) under the project “Development of the global top tire for reduction of carbon dioxide and tire wear particles” through the Ministry of Environment, Rep. of Korea.

- 1) Dahl, A., Gharibi, A., Swietlicki, E., Gudmundsson, A., Bohgard, M., Ljungman, A., Blomqvist, G., Gustafsson, M., (2006) Traffic-generated emission of ultrafine particles from pavement-tire interface. *Atmospheric Environment*. Vol. **40**, pp. **1314-1323**.
- 2) Luhana, L., Sokhi, R., Warner, L., Mao, H., Boulter, P., McCrae, I., Wright, J., Reeves, N. and Osborn, D. (2004). Non-exhaust particulate measurements: results. Deliverable 8 of the European Commission DG TREN 5th Framework Particulates project.

## Daytime and nighttime concentrations of PM<sub>10</sub> and water-soluble ions at a traffic site in the western Mediterranean

N. Galindo, E. Yubero, J.F. Nicolás, M. Varea, R. Castañer, S. Caballero, J. Gil-Moltó, C. Pastor and J. Crespo

Atmospheric Pollution Laboratory (LCA-UMH), Miguel Hernández University, Elche, Spain

Keywords: PM<sub>10</sub>, water-soluble ions, diurnal variation, traffic.

Presenting author email: ngalindo@umh.es

PM<sub>10</sub> samples were collected during two sampling campaigns carried out in summer 2013 and winter 2014 at a traffic site in the urban center of Elche (southeastern Spain; Galindo and Yubero, 2017). Daytime sampling started at 8 a.m. and nighttime sampling at 10 p.m. The nocturnal period was selected to include the time interval with the minimum values of traffic volumes and solar radiation intensity. After gravimetric determination of PM<sub>10</sub> concentrations, samples were analyzed by ion chromatography to determine the concentrations of major anions (Cl<sup>-</sup>, SO<sub>4</sub><sup>2-</sup>, NO<sub>3</sub><sup>-</sup> and C<sub>2</sub>O<sub>4</sub><sup>2-</sup>) and cations (Na<sup>+</sup>, NH<sub>4</sub><sup>+</sup>, Mg<sup>2+</sup> and Ca<sup>2+</sup>).

The average daytime and nighttime concentrations of PM<sub>10</sub> and the analyzed ions calculated separately for summer and winter are presented in Table 1.

Table 1. Average daytime and nighttime concentrations (µg/m<sup>3</sup>) during the summer and winter campaigns.

	Summer		Winter	
	Day	Night	Day	Night
PM <sub>10</sub>	28.8	27.7	26.1*	20.6*
Cl <sup>-</sup>	0.87	1.26	1.31	1.43
NO <sub>3</sub> <sup>-</sup>	2.20*	3.08*	2.42	2.45
SO <sub>4</sub> <sup>2-</sup>	3.18	3.19	1.72	1.52
C <sub>2</sub> O <sub>4</sub> <sup>2-</sup>	0.20	0.21	0.17	0.19
Na <sup>+</sup>	0.77	0.84	0.61	0.71
NH <sub>4</sub> <sup>+</sup>	0.58	0.77	0.53	0.75
Mg <sup>2+</sup>	0.16	0.17	0.14	0.13
Ca <sup>2+</sup>	1.37	1.21	2.04*	1.11*

\*Daytime and nighttime average concentrations are statistically different at the 95% confidence level.

During summer, the only component showing statistically significant differences between day and night was nitrate, as previously observed in other urban environments (Vecchi *et al.*, 2009). This was due, on the one hand, to the higher decomposition rate of thermally unstable NH<sub>4</sub>NO<sub>3</sub> during daytime due to greater ambient temperatures. Besides that, the formation of particulate nitrate is favored at night, when relative humidity is high. This was confirmed by the high positive correlation coefficient between nitrate concentrations and relative humidity during nighttime (Fig. 1). The most likely pathway of nitrate formation during nighttime is the hydrolysis of N<sub>2</sub>O<sub>5</sub> (Pun and Seigneur, 2001).

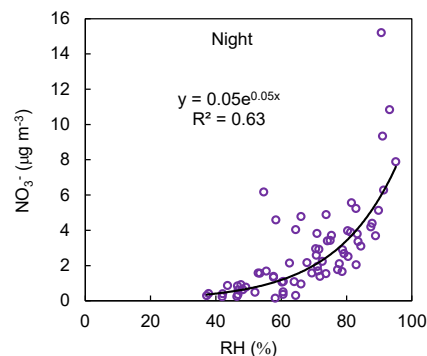
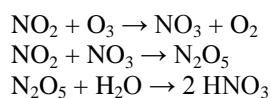


Figure 1. Relationship between nitrate concentrations and relative humidity during nighttime.

PM<sub>10</sub> concentrations only showed statistically significant differences between daytime and nighttime during winter. Taking into account that, of the analyzed species, only Ca<sup>2+</sup> (considered a tracer of dust resuspension) exhibited significantly lower levels during nighttime, the reduction in PM<sub>10</sub> concentrations registered during the nocturnal period in winter can be most likely attributed to a decrease in traffic flows. The variation of carbonate concentrations (estimated from the anion deficit) was similar to that of calcium (Fig. 2).

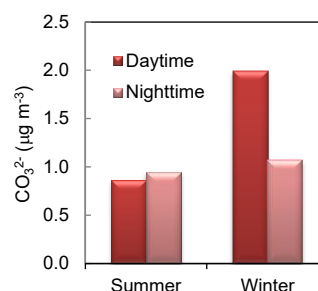


Figure 2. Average carbonate concentrations during the summer and winter campaigns.

This work was supported by the Spanish Ministry MINECO CGL2012-39623-C02-2 (PRISMA-AITANA) project.

Galindo, N. and Yubero, E. (2017) *Environ. Sci. Pollut. Res.* 24, 805-812.

Pun, B.K. and Seigneur, C. (2001). *Environ. Sci. Technol.* 35, 2979-2987

Vecchi, R., Bernardoni, V., Fermo, P., Lucarelli, F., Mazzei, F., Nava, S., Prati, P., Piazzalunga, A. and Valli, G. (2009) *Environ. Monit. Assess.* 154, 283-300.

## Metal concentrations in aerosols at a traffic site in Elche, southeastern Spain

N. Galindo, E. Yubero, J.F. Nicolás, M. Varea, R. Castañer, S. Caballero, J. Gil-Moltó, C. Pastor and J. Crespo

Atmospheric Pollution Laboratory (LCA-UMH), Miguel Hernández University, Elche, Spain

Keywords: metals, PM<sub>1</sub>, PM<sub>10</sub>, size distributions, traffic.

Presenting author email: ngalindo@umh.es

Between February 2015 and November 2016, PM<sub>1</sub> and PM<sub>10</sub> daily samples were collected three times a week at a traffic site in the city of Elche (southeastern Spain). The elemental composition of PM was determined by means of Energy Dispersive X-Ray Fluorescence (ED-XRF) using an ARL Quant'x Spectrometer (Thermo Fisher Scientific, UK).

Concentrations of PM and selected metals averaged for the whole study period are shown in Table 1.

Table 1. Mean concentrations of PM ( $\mu\text{g}/\text{m}^3$ ) and metals ( $\text{ng}/\text{m}^3$ ) in Elche.

	PM <sub>1</sub>		PM <sub>10</sub>	
	Mean	SD*	Mean	SD*
PM	11.9	5.2	25.9	12.6
As	2	2	2	2
Pb	2	4	3	5
Zn	15	6	26	13
V	4	3	7	7
Ni	5	2	9	3
Cr	4	2	9	10
Ba	11	10	28	30
K	75	82	187	193
Cu	6	2	16	5
Sr	3	2	8	4
Mn	5	3	13	10
Ti	7	7	24	37
Fe	96	75	386	314
Ca	303	316	1377	914

\*SD: standard deviation.

Calcium, a tracer of dust resuspension, was the most abundant element in PM<sub>10</sub>. Ca concentrations were higher than those reported for other Mediterranean urban areas (López *et al.*, 2005; Padoan *et al.*, 2016), probably because the climatic and geographic characteristics of the study region favor the resuspension of calcium-rich dust (Galindo *et al.*, 2017). In contrast, concentrations of other crustal elements, namely Fe, Mn and Sr, were lower than those found in previous studies (López *et al.*, 2005; Padoan *et al.*, 2016). The average concentration of nickel at the sampling site was high compared with the values documented by other researchers. Although this element is usually associated with oil combustion and industrial sources, the high Ni concentrations obtained in this study are likely due to a relevant contribution from soils. Similarly, vanadium concentrations were higher than the values found at larger urban areas (López *et al.*, 2005; Padoan *et al.*, 2016). A possible factor that could contribute to the measured concentrations of Ni and V is long range transport of aerosols from the Sahara desert. It has been previously reported that Saharan dust plumes

can carry anthropogenic pollutants emitted in the western Mediterranean basin and North Africa (Galindo *et al.*, 2017), contributing to increase Ni and V concentrations.

Trace metals associated with traffic, mainly Cu, Zn and Pb, showed concentrations significantly lower than those found at much more populated cities with higher traffic flows (López *et al.*, 2005; Padoan *et al.*, 2016).

The average distribution of metals between the submicron and coarse fractions is shown in Fig.1. As expected, crustal elements (Sr, Mn, Ti, Fe and Ca) were mainly distributed in the coarse fraction. Copper, which is also associated with mechanical processes such as brake wear and resuspension of road dust, was primarily found in the coarse fraction too. The size distribution of Ni (~55% associated with coarse particles) is consistent with mixed emissions from soils and anthropogenic sources. Regarding Zn, this element can be released from vehicle tire wear. Besides, it is considered a tracer of unleaded fuel and diesel combustion in motor vehicles. This explains its size distribution, which was slightly shifted to the submicron fraction (~60%). Trace elements mostly emitted by fossil fuel combustion, such as arsenic and lead, were associated to a greater extent with submicron particles.

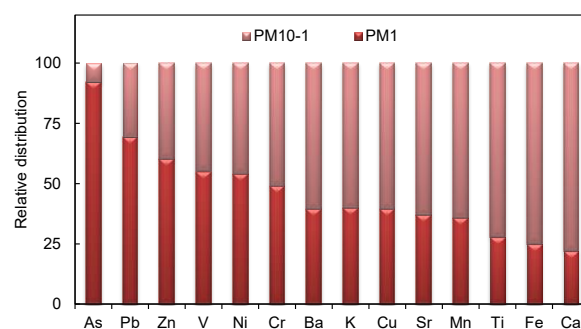


Figure 1. Relative distribution of elements between the submicron and coarse fractions.

This work was supported by the Spanish Ministry MINECO CGL2012-39623-C02-2 (PRISMA-AITANA) project.

Galindo, N., Yubero, E., Nicolás, J.F., Crespo, J., Varea, M. and Gil-Moltó, J. (2017) *Sci. Total Environ.*, In press (doi: 10.1016/j.scitotenv.2017.01.108).

López, J.M., Callén, M.S., Murillo, R., García, T., Navarro, M.V., de la Cruz, M.T. and Mastarl, M.A. (2005) *Environ. Res.* 99, 58-67.

Padoan, E., Malandrino, M., Giacomino, A., Grosa, M.M., Lollogrigida, F., Martini, S., and Abollino, O. (2016) *Chemosphere* 145, 495-505.

## Impact of residential wood combustion on benzo(a)pyrene and black carbon concentrations in the Helsinki metropolitan area, Finland

J.V. Niemi<sup>1</sup>, H. Hellén<sup>2</sup>, L. Kangas<sup>2</sup>, A. Kousa<sup>1</sup>, M. Vestenius<sup>2</sup>, K. Teinilä<sup>2</sup>, A. Karppinen<sup>2</sup>, J. Kukkonen<sup>2</sup>, H. Timonen<sup>2</sup>, T. Rönkkö<sup>3</sup> and L. Pirjola<sup>4</sup>

<sup>1</sup>Helsinki Region Environmental Services Authority, Helsinki, FI-00066 HSY, Finland

<sup>2</sup>Finnish Meteorological Institute, Helsinki, FI-00101, Finland

<sup>3</sup>Aerosol Physics, Faculty of Natural Sciences, Tampere University of Technology, Tampere, FI-33720, Finland

<sup>4</sup>Department of Technology, Metropolia University of Applied Sciences, FI-00180 Helsinki, Finland

Keywords: urban air quality, monitoring, emission inventory, dispersion modelling.

Presenting author email: jarkko.niemi@hsy.fi

Residential wood combustion (RWC) is a major source of fine particle (PM<sub>2.5</sub>) and black carbon (BC) emissions in Finland. The particle emissions of RWC also contain benzo(a)pyrene (BaP) that has been regarded as a marker of both the total and carcinogenic PAHs. RWC can significantly deteriorate air quality, especially in densely populated detached house areas in winter.

The main aim of this study is to quantitatively evaluate the impacts of RWC on the concentrations of BaP and BC in the Helsinki metropolitan area. We have conducted ambient air measurements during several years (2009-2015; Table 1), compiled a novel emission inventory and modelled atmospheric dispersion of BaP for selected years (Héllen et al., 2016). The measurements were performed at eight different suburban detached house areas (DH1-8), at three busy street canyons (SC1-3) and at an urban background site (UB). Furthermore, the contributions of RWC to BC concentrations were indicatively estimated with 7-wavelength aethalometer (AE33, Magee Scientific Corporation) at two sites (DH8 and SC3) in year 2016. The concentrations of levoglucosan, a source-specific tracer for biomass burning particles, were also measured and compared with the concurrently measured concentrations of BC and BaP.

The measured annual mean concentrations are shown in Table 1. The European Union target value for the annual mean BaP concentrations (1 ng m<sup>-3</sup>) was clearly exceeded in part of the suburban detached house areas. However, over most of the other urban areas, including the centre of Helsinki, the concentrations were below the target value. In the busy street canyons, the measured concentrations of BaP were at the same level as urban background, showing that the BaP emissions from traffic are negligible. The measured BaP concentrations were highly correlated with the measured levoglucosan concentrations at suburban detached house areas. The predicted annual mean concentrations (Fig. 1) agreed fairly well with the measured concentrations. Both measurements and modelling clearly indicated that RWC was the main local source of ambient air BaP in the Helsinki metropolitan area.

The measured annual mean BC concentrations were clearly highest in the busy street canyons (Table 1). In the detached house areas, the BC concentrations were also higher than those at urban background. Thus, traffic and RWC are both significant BC sources in the Helsinki metropolitan area. The quantitative evaluation of BC

source contributions will be presented using aethalometer and levoglucosan results.

Table 1. The annual mean concentrations at different sites in the Helsinki metropolitan area.

Site	Year(s)	BaP (ng m <sup>-3</sup> )	PM <sub>2.5</sub> (μg m <sup>-3</sup> )	BC (μg m <sup>-3</sup> )	NOx (μg m <sup>-3</sup> )
DH1	2009-2015	0.6	7.5	0.8*	21
DH2	2008	1.1	-	-	-
DH3	2011	1.2	10.4	-	21
DH4	2012	0.6	8.2	-	18
DH5	2013	0.4	7.1	-	13
DH6	2013	1.0	8.8	-	22
DH7	2014	1.0	10.8	0.8	19
DH8	2015	0.9	7.1	-	14
SC1	2007	0.3	-	-	76
SC2	2010	0.3	13.0	2.6	166
SC3	2015	0.2	8.0	1.4	108
UB	2007-2015	0.3	7.8	0.6**	28

\* year 2009 \*\*years 2012-2015

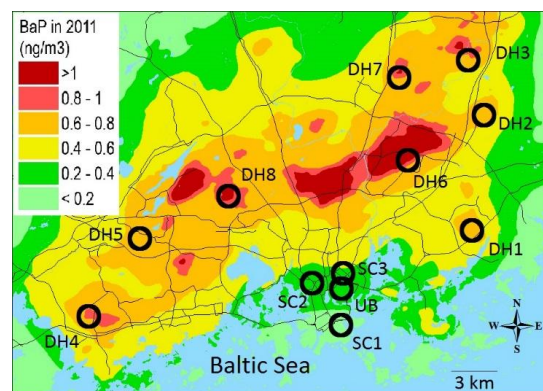


Figure 1. The predicted annual mean concentrations of BaP originated from RWC in the Helsinki metropolitan area in 2011. The main roads are shown for clarity.

This work has been supported by the Academy of Finland (grant no. 275608 and 266314), the Finnish Funding Agency for Innovation (MMEA research program) and the Nordforsk Nordic Programme on Health and Welfare (project no. 75007).

Hellén, H., Kangas, L., Kousa, A., Vestenius, M. Teinilä, K., Karppinen, A., Kukkonen, J. and J.V. Niemi (2016) *Atmos. Chem. Phys. Discuss.*, doi:10.5194/acp-2016-780.

**PM<sub>10</sub> and black carbon exposure during bicycle commuting: the effect of route selection**T. Siponen<sup>1</sup>, P. Tiittanen<sup>1</sup>, P. Taimisto<sup>1</sup>, A. Pulkinen<sup>1</sup>, P. Aarnio<sup>2</sup>, A. Kousa<sup>2</sup>, T. Yli-Tuomi<sup>1</sup>, J. Niemi<sup>2</sup> and T. Lanki<sup>1,3</sup><sup>1</sup>Department of Health Security, National Institute for Health and Welfare, Kuopio, FI-70701, Finland<sup>2</sup>Helsinki Region Environmental Services Authority, Helsinki, FI-00066, Finland<sup>3</sup>Institute of Public Health and Clinical Nutrition, University of Eastern Finland, Kuopio, FI-70211, FinlandKeywords: PM<sub>10</sub>, black carbon, ambient air pollution, exposure.

Presenting author email: taina.siponen@thl.fi

Road traffic is one of the main sources of particulate air pollution in urban areas. High exposures to traffic-related air pollution are often encountered during commuting. However, transportation mode and route have an influence on commuter's exposure. Our recent study suggests that bicyclists and bus passengers are more exposed to traffic-related air pollution than car drivers (Okokon *et al* 2017). In this study, we evaluated the difference in PM<sub>10</sub> (particles less than 10 µm in aerodynamic diameter) and black carbon (BC) exposure during cycling between more and less traffic-impacted routes.

Exposure measurements were conducted in Helsinki, Finland, during a two week field campaign in October/November 2016. Seven bicycling route pairs were selected for measurements. Air pollution measurements were conducted in the mornings and in the afternoons on weekdays during the field campaign. Measurements were done simultaneously on two bicycling routes, which had the same starting and end point and starting time. One route followed busy streets in traffic environments ('Traffic') and another, typically slightly longer route went through parks and more quiet streets ('Green'). Every route was biked back and forth at least two times both in the mornings and in the afternoons.

Photometric PM<sub>10</sub> concentrations were measured with TSI DustTrack DRX8533 and BC with Aethlabs microAeth AE51. PM<sub>10</sub> monitor was set at a 15 second time resolution and BC monitor at a 30 second time resolution. Both of these devices were placed in a backpack carried by researchers who rode the bike. A three-gear electric bicycle, Helkama Jopo Electro, was used. The Wilcoxon Signed-Rank test was used to compare the ratios of PM<sub>10</sub> and BC levels between traffic and non-traffic routes.

A total of 54 (62) pairs of one-way trips were included in the analyses for PM<sub>10</sub> (BC). Length of Traffic and Green routes ranged between 4.0-5.8 km and 4.8-6.6 km, respectively. Green routes were on average 0.8 km longer than Traffic routes, and bicycling of them took on average 1.5 minutes longer. For each trip the median of measured concentrations was calculated to represent a typical exposure level during a single trip.

Descriptive statistics for PM<sub>10</sub> and BC are presented in Table 1. PM<sub>10</sub> and BC levels were mostly higher on Traffic routes (65% and 95% of trip pairs, respectively). Exposure on Traffic routes was 6 %

higher for PM<sub>10</sub> and 36 % for BC compared to Green routes (Table 2).

In conclusion, these results showed slightly higher PM<sub>10</sub> and substantially higher BC levels on Traffic route than on Green route. More extensive information will be available after additional measurements in spring and summer 2017. The results of the study can be used in city planning for preparation of street network as well as to bicyclists for selecting routes.

Table 1. Descriptive statistics for exposure to PM<sub>10</sub> (particles <10 µm in diameter) and black carbon on different routes.

	N	Mean (SD)	Median (Min, Max)
<b>PM<sub>10</sub></b>			
<b>[µg/m<sup>3</sup>]</b>			
Traffic	54	19.4 (12.1)	17.5 (2.0, 49.5)
Green	54	18.0 (9.5)	16.0 (4.0, 43.0)
<b>Black carbon</b>			
<b>[µg/m<sup>3</sup>]</b>			
Traffic	62	1.5 (1.0)	1.3 (0.4, 0.5)
Green	62	1.1 (0.9)	0.8 (0.3, 0.4)

N=number of one-way trips, SD=standard deviation.

Table 2. Traffic route to Green route ratios of PM<sub>10</sub> (particles <10 µm in diameter) and black carbon exposures and number of measurements (N) included in analysis.

	N	Ratio	p-value
PM <sub>10</sub>	54	1.06	<.0001
Black carbon	62	1.36	<.0001

This work was supported by the Helsinki Region Environmental Services Authority.

Okokon, E.O., Yli-Tuomi, T., Turunen, A.W., Taimisto, P., Pennanen, A., Vouitsis, I., Samaras, Z., Voogt, M., Keuken, M. and Lanki, T. (2017) *Environ. Res.* **154**, 181-189.

## PM<sub>10</sub>, PM<sub>2.5</sub>, and PM<sub>10-2.5</sub> in the Po valley: variability, pattern and trend since 1998

A. Bigi, G. Ghermandi

Department of Engineering, “Enzo Ferrari”, University of Modena and Reggio Emilia, Modena, I-41125, Italy

Keywords: PM, trends, air quality

Presenting author email: alessandro.bigi@unimore.it

The stringent regulations on air quality standards and on anthropogenic emissions set by the European Commission lead to a continental improvement in air quality (EEA, 2016).

Nonetheless, the Po valley remains one of the few European regions with recurrent high concentration levels of atmospheric pollutants, both for particulate and gaseous compounds.

In order to assess pattern and variability in PM across the Po valley over 1998 – 2015, the time series of PM<sub>10</sub>, PM<sub>2.5</sub> and PM<sub>10-2.5</sub> from 41, 44 and 15 sites have been comprehensively investigated (Bigi and Ghermandi 2014, 2016).

PM<sub>2.5</sub> and PM<sub>10-2.5</sub> (PM<sub>10</sub>) series with a 7 (10) year or longer record have been analysed for long term trend in deseasonalized monthly means, annual quantiles and in monthly frequency distribution by robust statistical methods. A widespread and significant decreasing trend was observed at several sites for all size fractions, with the drop, up to a few percent per year, occurring mainly in winter for PM<sub>2.5</sub> and throughout the year for PM<sub>10</sub>.

To summarily estimate the impact of primary anthropogenic emissions, 3 different statistical methods have been applied to test for a significant weekly periodicity, yielding positive results for summer PM<sub>2.5</sub> and PM<sub>10</sub>, and for both summer and winter PM<sub>10-2.5</sub>.

As expected, hierarchical cluster analysis showed larger variability for PM<sub>10</sub> than for PM<sub>2.5</sub>, with larger PM split in five clusters over the valley, while the finer fraction only in 3. Two PM<sub>10</sub> clusters include the metropolitan area of Turin and Milan and their respective nearby sites, and the other three clusters gather northeast, northwest and central Po Valley sites respectively. On the contrary, PM<sub>2.5</sub> clusters divide the valley in a western, eastern and southern/Apennines foothill sector (Fig. 1).

Trends in primary and precursors emissions, in vehicular fleet details and in fuel sales have been

compared to the trends observed in atmospheric PM concentration. A significant basin-wide drop in emissions occurred for gaseous pollutants, contrarily to primary emissions of PM<sub>10</sub> and PM<sub>2.5</sub>, whose drop was lower and spatially restricted.

Overall the decrease in atmospheric PM<sub>2.5</sub> and PM<sub>10</sub> seems to originate from a drop in both primary emissions and in precursors of secondary inorganic aerosol emissions, largely ascribed to vehicular traffic.

Potentially, a recent increase in biomass burning emissions in winter and the modest decrease in NH<sub>3</sub> weaken an otherwise even larger drop in atmospheric concentrations.

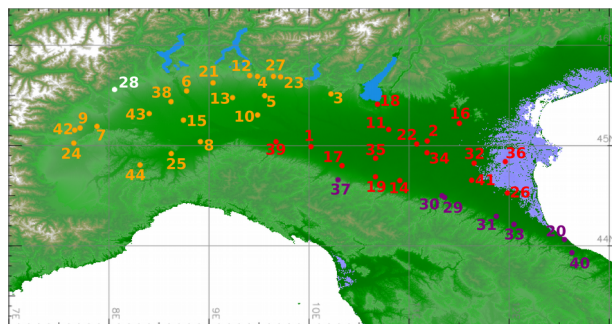


Figure 1. Result of the cluster analysis (partition around medoids + divisive algorithm). Sites within the same cluster have the same colour. Site 28 (Biella) resulted in an outlier and was not included in this classification.

EEA (2016) *Air quality in Europe — 2016 report*, European Environmental Agency.

Bigi, A. and Ghermandi, G. (2014) *Atmos. Chem. Phys.* **14**, 4895-4907.

Bigi, A. and Ghermandi, G. (2016) *Atmos. Chem. Phys.* **16**, 15777-15788.

## Characterization of PM<sub>2.5</sub> sources at Central European urban background site

K. Juda-Rezler<sup>1</sup>, M. Reizer<sup>1</sup>, J.A.G. Orza<sup>2</sup>, K. Maciejewska<sup>1</sup>, K. Klejnowski<sup>3</sup> and B. Błaszczak<sup>3</sup>

<sup>1</sup>Faculty of Building Services, Hydro and Environmental Engineering, Warsaw University of Technology, Warsaw, 00653, Poland

<sup>2</sup>SCOLab, Física Aplicada, Universidad Miguel Hernández, Elche, 03202, Spain

<sup>3</sup>Institute of Environmental Engineering, Polish Academy of Sciences, Zabrze, 41819, Poland

Keywords: urban air pollution, fine PM, elemental composition, PMF.

Presenting author email: katarzyna.juda-rezler@is.pw.edu.pl

Adverse health effects of atmospheric particulate matter (PM) has been studied intensively for many years (e.g. R ckerl *et al.*, 2011). PM<sub>2.5</sub> air pollution is among the leading causes of poor health and premature mortality worldwide. It is estimated that over 3 million premature deaths per year worldwide are attributable to outdoor PM<sub>2.5</sub> exposure (Giannadaki *et al.*, 2016), and according to the business-as-usual emission scenario the contribution of outdoor PM<sub>2.5</sub> air pollution to premature mortality will escalate up to 6.2 million by 2050 (Lelieveld *et al.*, 2015).

Ambient PM concentrations are routinely monitored worldwide. However, the measurements are often limited to the total mass concentrations of PM<sub>10</sub> and PM<sub>2.5</sub> without any information on the elemental composition of the aerosol particles, which is essential for the assessment of the influence of atmospheric aerosols on human health. Moreover, trace elements content in PM plays an important role in the identification of PM sources in order to develop air quality improvement strategies and Air Quality Plans.

The aim of present work is to analyse a full year profile of mass concentrations of PM<sub>2.5</sub> and its components at urban background site in Central Eastern Europe, as well as to identify emission sources and areas. Therefore, a dedicated long-term field campaign have been performed during the whole year 2016, for the first time in the centre of metropolitan area of Warsaw, Poland, with about 2 million inhabitants. Daily PM<sub>2.5</sub> samples were collected using low volume sampler and concentrations were determined by standard gravimetric measurement method according to the EN 14907 norm. For analyses of elemental and organic carbon content in PM<sub>2.5</sub>, thermal-optical method was used, while contents of 8 ions as well as major and trace elements (21) were determined by ion chromatography and inductively coupled plasma (ICP), respectively.

Source apportionment was carried out by the Positive Matrix Factorization (PMF) method, while cluster analysis of air mass back trajectories computed by HYSPLIT4 model (Stein *et al.*, 2015) was applied for identification of the probable PM<sub>2.5</sub> source locations. Seasonal and daily variation of the factors identified by PMF, as well as their dependence on air mass flows and local meteorological parameters have been studied. The causes of two PM<sub>2.5</sub> episodes in January exceeding 80  $\mu\text{g}/\text{m}^3$  (Fig. 1) have also been investigated.

Annual PM<sub>2.5</sub> level (18.86  $\mu\text{g}/\text{m}^3$ ) in Warsaw is lower, compared to other Polish urban sites (especially

in the South). Higher than in other cities contributions of OC and SIA in PM<sub>2.5</sub> (both ~30%), as well as high correlation between OC and SIA suggest an important role of long-range transport of air pollution in Warsaw. In the same time, higher content of As, Cd, Cr, Cu, Ga, Mn, Pb and Zn, compared to Southern European AIRUSE cities, indicate also local and regional influence of road traffic as well as of coal combustion in industrial and residential sources.

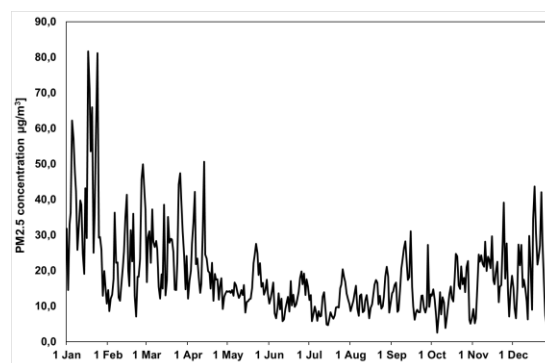


Figure 1. Daily PM<sub>2.5</sub> concentrations [ $\mu\text{g}/\text{m}^3$ ] in Warsaw in 2016.

This work was supported by the Polish National Science Centre under OPUS funding scheme 7th edition, Project no. UMO-2014/13/B/ST10/01096. The authors also gratefully acknowledge the NOAA Air Resources Laboratory (ARL) for the provision of the HYSPLIT transport and dispersion model used in this publication.

- Giannadaki, D., Lelieveld, J. and Pozzer, A. (2016). Implementing the US air quality standard for PM<sub>2.5</sub> worldwide can prevent millions of premature deaths per year. *Environ. Health* **15**:88, pp. 11.
- Lelieveld, J., Evans, J.S., Fnais, M., Giannadaki, D. and Pozzer, A. (2015). The contribution of outdoor air pollution sources to premature mortality on a global scale. *Nature* **525**, 367-371.
- R ckerl, R., Schneider, A., Breitner, S., Cyrys, J. and Peters, A. (2011). Health effects of particulate air pollution: A review of epidemiological evidence. *Inhal. Toxicol.* **23**, 555-592.
- Stein, A.F., Draxler, R.R., Rolph, G.D., Stunder, B.J.B., Cohen, M.D. and Ngan, F. (2015). NOAA's HYSPLIT atmospheric transport and dispersion modeling system. *Bull. Amer. Meteor. Soc.* **96**, 2059-2077.

## Land-use Regression Modelling of Ultrafine Particles, Soot, PM<sub>2.5</sub>, PM<sub>10</sub>, PM<sub>coarse</sub>, and Nitrogen Oxides in the Augsburg Region, Germany

J. Cyrus<sup>1,2</sup>, K. Wolf<sup>1</sup>, T. Hrciniková<sup>1,3</sup>, A. Schneider<sup>1</sup>, J. Gu<sup>2</sup>, T. Kusch<sup>2</sup>, A. Peters<sup>1</sup>

<sup>1</sup>Helmholtz Zentrum München - German Research Center for Environmental Health (GmbH), Institute of Epidemiology II, Neuherberg, 85764, Germany.

<sup>2</sup>Environmental Science Center, University of Augsburg, Augsburg, 86159, Germany

<sup>3</sup>Comenius University in Bratislava, Faculty of Natural Sciences, Department of Cartography, Geoinformatics and Remote Sensing, Bratislava, 84215, Slovakia

Keywords: Land-use regression, Ultrafine particles, Ozone, Particulate matter  
Presenting author email: cyrus@helmholtz-muenchen.de

In the recent past, land-use regression (LUR) modelling has become a popular method for estimating the small-scale variability of air pollution within cities. The developed models were then used for assessing outdoor pollution concentrations at the participants' residences in long-term epidemiological studies. However so far, only a few LUR models have been developed for ultrafine particles (UFP). In addition, most of them have used mobile or short-term measurements at several sites. Spatially resolved long-term monitoring campaigns for UFP have been used very rarely, because the appropriate monitoring devices are costly and require intensive maintenance. In this study, we developed LUR models to predict the spatial variability of air pollutants with a focus on particle number concentration (PNC) as indicator for UFP based on a long-term monitoring campaign.

As our study region was also part of the ESCAPE project (<http://www.escapeproject.eu>), LUR models have already been developed for PM<sub>10</sub>, PM<sub>coarse</sub>, PM<sub>2.5</sub>, soot (absorbance of PM filters, PM<sub>2.5</sub>abs), NO<sub>x</sub> and NO<sub>2</sub> (Beelen *et al* (2013), Eeftens *et al* (2012)). However, in ESCAPE the Augsburg area was combined with the Munich region, which exhibited generally higher air pollutant levels mainly due to a higher population and traffic density. Thus, with the new measurement campaign, we aimed to refine and update the existing LUR models for those pollutants and to compare the performances of the rather spread and heterogeneous ESCAPE models with the denser and more homogeneous models developed in this study.

Three bi-weekly measurements (reflecting the warm, cold and one intermediate season) of PNC, PM<sub>10</sub>, PM<sub>2.5</sub>, PM<sub>coarse</sub>, PM<sub>2.5</sub>abs, NO<sub>x</sub> and NO<sub>2</sub> were performed at 20 sites in 2014/15. Annual mean concentrations were calculated and adjusted for temporal variability by measurements from a reference urban background site. The development of the LUR models mainly followed the standardized ESCAPE approach using a supervised stepwise selection procedure. As geographic predictors we offered several traffic and land-use variables, elevation, population and building density. Models were validated using leave-one-out cross-validation.

In general, all LUR models performed well with the adjusted R<sup>2</sup> ranging from 68% (PM<sub>coarse</sub>) to 94% (NO<sub>2</sub>). The models consisted of four to seven predictors and contained at least one traffic predictor in a rather

small buffer, industry in the medium to distant vicinity and one predictor for green areas. For PNC, the adjusted model explained variance was high (R<sup>2</sup>=0.89). In general, the traffic-related air pollutants (PNC, PM<sub>2.5</sub>abs, NO<sub>2</sub>, and NO<sub>x</sub>) performed well with an adjusted LOOCV R<sup>2</sup> being less than 10% lower than the adjusted R<sup>2</sup>. For the mass fractions, the models were not as robust with the adjusted LOOCV R<sup>2</sup> being 12% (PM<sub>10</sub>, PM<sub>2.5</sub>) to 19% (PM<sub>coarse</sub>) lower than the adjusted R<sup>2</sup>.

Except for PM<sub>coarse</sub>, the explained variance was generally similar or higher for the new models compared to the ESCAPE models. Especially for NO<sub>2</sub>, the adjusted LOOCV R<sup>2</sup> increased from 66% to 89%. Whereas mainly traffic predictors were included in the ESCAPE model, the Augsburg model was dominated by industry and semi-natural areas in the rather distant neighbourhood (1-5km) which were completely missing in the ESCAPE model. As 75% of the ESCAPE measurement sites were located in the Munich area and only 25% in the Augsburg area, the ESCAPE model was partly dominated by Munich specific predictors. We assume that important predictors for Augsburg were not selected in the joint modelling due to the heterogeneous nature of the Munich-Augsburg area with a much higher building, population and traffic density in the Munich region leading to this difference in model performance.

The measured and predicted mean UFP concentrations were only moderately correlated with PM<sub>2.5</sub> (r<sub>measured</sub> = 0.58, r<sub>predicted</sub> = 0.64), but highly with NO<sub>x</sub> (r<sub>measured</sub> = r<sub>predicted</sub> = 0.91). The high correlations of PNC with NO<sub>x</sub> and with other traffic related pollutants indicate that traffic is one of the major sources for UFP in the Augsburg region.

This work was supported by intramural funding for Environmental Health projects of Helmholtz Zentrum München - German Research Center for Environmental Health (GmbH) and by the European Community's Seventh Framework Program (FP7/2007-2011) under grant agreement number 211250.

Beelen, R., Hoek, G., Vienneau, D., Eeftens, M., Dimakopoulou, K. et al. (2013), *Atmos. Environ.* **72**, 10-23.

Eeftens, M., Beelen, R., de Hoogh, K., Bellander, T., Cesaroni, G. et al. (2011) *Environ. Sci. Technol.* **46** (20), 11195-11205.

# On-line measurements of particle-bound reactive oxygen species (ROS) in Beijing

S. S. Steimer<sup>1</sup>, F. P. H. Wragg<sup>1</sup> and M. Kalberer<sup>1</sup>

<sup>1</sup>Department of Chemistry, University of Cambridge, Cambridge, CB2 1EW, United Kingdom

Keywords: ROS, field measurements, urban air pollution, particle toxicity.

Presenting author email: ss2349@cam.ac.uk

Reactive oxygen species (ROS), present in particles or generated by particle components upon deposition of particles in the human lung, are widely thought to be one of the main contributors to particle-related toxicity (e.g. Dellinger *et al*, 2001). However, there is so far only relatively little data available on their concentrations in ambient air, which makes it difficult to gauge their impact on air quality. Recent studies have shown that a large fraction of particle-bound ROS in secondary organic aerosol is relatively short-lived, with lifetimes of several minutes (e.g. Fuller *et al*, 2014). Traditional off-line sampling with high-volume samplers is therefore likely to severely underestimate ROS concentrations, showing the need for using on-line instrumentation.

We have recently developed a compact on-line instrument for the measurement of particle-bound ROS (OPROSI) (Wragg *et al*, 2016). To measure ROS concentrations, particles are continuously extracted and the extract is reacted with 2',7'-dichlorofluorescein (DCFH) in presence of horseradish peroxidase (HRP). This leads to formation of a fluorescent dye, which is detected spectroscopically. The instrument allows for up to 16 h of continuous measurement with a time resolution of  $\leq 12$  min and a limit of detection of 3.85 nmol [H<sub>2</sub>O<sub>2</sub>] equivalent per m<sup>3</sup> air.

For this study, we have used the OPROSI to continuously measure the concentration of particle-bound ROS in Beijing wintertime air during the first half of the Air Pollution and Human Health in a Developing Megacity (APHH-Beijing) campaign in November and December 2016. Measured ROS data are compared with other air pollution parameters such as total particulate mass, ozone and NO<sub>x</sub> as well as with meteorological measurements such as temperature and humidity. In addition, the wintertime ROS data will be compared to ROS measurements taken during the second half of the APMH-Beijing campaign in summer 2017 to investigate seasonal variations.

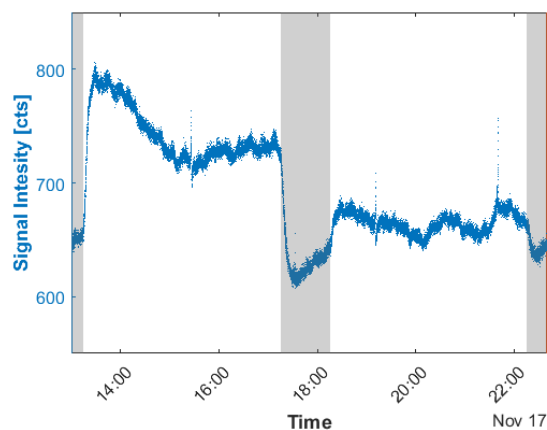


Figure 1. Raw data of ROS signal variation on 17<sup>th</sup> November 2016. Grey background denotes blank measurements.

This work was supported by an SNSF Early Postdoc.Mobility fellowship (project P2EZZP2\_162258).

Dellinger, B., Pryor, W. A., Cueto, R., Squadrito, G. L., Hegde, V. and Deutsch, W. A. (2001) *Chem. Res. Toxicol.* **14**, 1371–1377.

Fuller, S. J., Wragg, F. P. H., Nutter, J. and Kalberer, M. (2014) *Atmos. Environ.* **92**, 97–103.

Wragg, F. P. H., Fuller, S. J., Freshwater, R., Green, D. C., Kelly, F. J. and Kalberer, M. (2016) *Atmos. Meas. Tech.* **9**, 4891–4900.

## Seasonal and spatial differences of size-segregated trace elements in Turkey

P. Ertürk Arı<sup>1</sup>, A. Arı<sup>2</sup> and E.O. Gaga<sup>3</sup>

<sup>1</sup>Department of Environmental Engineering, Abant İzzet Baysal University, Bolu, 14280, Turkey

<sup>2</sup>Department of Food Engineering, Abant İzzet Baysal University, Bolu, 14280, Turkey

<sup>3</sup>Department of Environmental Engineering, Anadolu University, Eskişehir, 26090, Turkey

Keywords: PM2.5, trace metals, anions, ICP-MS

Presenting author email: [pelinn.erturkk@gmail.com](mailto:pelinn.erturkk@gmail.com)

Trace elements are important indicators of anthropogenic pollution. The effects of atmospheric aerosols are closely related to particle size and chemical content (Mészáros, 1999). Understanding the atmospheric aerosol size distribution is very important to understand health effects of the metal components, sources and transport mechanisms.

Daily size segregated particulate matter samples were collected during 10 days in summer and winter seasons in 2016, by a high volume air sampler (Thermo, USA) and 5 stage impactor system (TISCH model TE-235, USA) from two sampling stations Kütahya city (urban), and Tavşanlı province - Göbel district (rural) which are known to be affected by two thermal power plants and many other industries nearby.

The impactor system consisting of 5 stages and a back-up stage for size cutting. Polytetrafluoroethylene (PTFE) filters were used to collect particles on impactor plates (size fractions between 0.69-1.3; 1.3-2.1; 2.1-4.2; 4.2-10.2 and 10.2 < μm) and a back-up filter (below 0.69 μm).

Trace elements in size segregated atmospheric PM samples were analysed by using triple quadrupole ICP-MS (ICP-QQQ-MS) after microwave acid digestion.

Highest size-segregated PM concentrations were observed at urban samples in winter season (Figure 1).

Table 1. Average and standart derivations of trace elements.

Size (μm)	> 10.2	4.2 - 10.2	2.1 - 4.2	1.3 - 2.1	0.69 - 1.3	< 0.69
Concentration (μg m <sup>-3</sup> )	Avg ± Std.Dev	Avg ± Std.Dev	Avg ± Std.Dev	Avg ± Std.Dev	Avg ± Std.Dev	Avg ± Std.Dev
Kütahya Summer	4.7 ± 0.9	9.1 ± 1.7	5.2 ± 1.0	3.7 ± 0.7	4.2 ± 0.9	33.2 ± 8.6
Kütahya Winter	7.7 ± 3.0	15.2 ± 6.7	9.3 ± 3.8	9.5 ± 3.8	14.3 ± 5.7	58.3 ± 20.2
Göbel Summer	2.7 ± 1.3	5.0 ± 2.8	3.2 ± 1.3	2.4 ± 0.8	3.7 ± 1.6	28.9 ± 11.0
Göbel Winter	1.0 ± 0.6	2.7 ± 1.2	3.0 ± 1.1	5.9 ± 1.5	7.6 ± 2.7	26.2 ± 8.3

Crustal elements such as Mg, Al, Ti, V, Fe, Ca, Ga, Sr, Cs, La, Ce, Sm, Th and U were observed at higher concentrations in coarse mode particles in both stations. On the other hand, anthropogenic elements (Ge, As, Se, Cd, Sb and Pb ect.) were measured high concentrations in fine mode particles.

While investigating the seasonal changes of the crustal elements, as expected for the urban station, there was no declining trend in the summer season and a decreasing trend in the winter season (Figure 1).

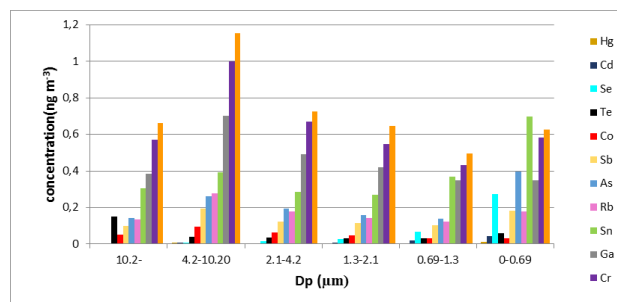


Figure 1. Urban station summer metal concentrations

Generally, in both stations the elements are distributed bimodal. The reason of formation of the first peak is the mixing of the rough ground dust, which is the main source for many elements, into the atmosphere due to wind and other turbulence factors. Contritely, particles released from anthropogenic sources, especially from combustion and from motor vehicle exhausts, are below 2.5 μm. The reason that anthropogenic elements also shown a second peak in coarse-mode particles is that the anthropogenic particles in the accumulation mode condense on the ground-based particles to form larger particles (Figure 2).

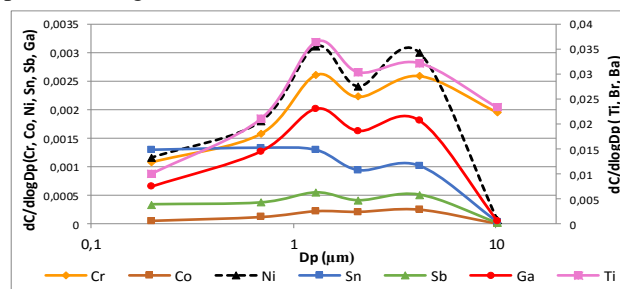


Figure 2. Urban station summer element concentration and size distribution

This work was supported by the Scientific and Technological Research Council of Turkey under the grant of 112Y305 and The Committee of Scientific Research Projects of Anadolu University under the grant of 1306F272.

Mészáros E. (1999). *Fundamentals of Atmospheric Aerosol Chemistry*. Akadémiai Kiado.

Perrone, M.G., Gualtieri, M., Consonni, V., Ferrero, L., Sangiorgi, G., Longhin, E., Ballabio, D., Bolzacchini, E. and Camatini, M. (2013). *Environmental Pollution*, 176, 215-227.

## Determination of Carbonaceous Aerosol Levels at two Different Stations in the Capital of Turkey, Ankara

P. Faramarzi<sup>1</sup>, S.Y. Aslanoglu<sup>1</sup>, F. Ozturk<sup>2</sup>, A.C. Saydam<sup>1</sup>, and G. Gullu<sup>1</sup>

<sup>1</sup>Department of Environmental Engineering, Hacettepe University, Ankara, 06800, Turkey

<sup>2</sup>Department of Environmental Engineering, Abant Izzet Baysal University, Bolu, 14030, Turkey

Keywords: Ankara, PM, EC, TC.

Presenting author email: yaslanoglu@hacettepe.edu.tr

It has been well reported in the literature that carbonaceous aerosols have significant contribution (~40-70 %) to the ambient particulate matter (Kanakidou *et al.*, 2005) and their impact on regional and global climate change (Boreddy *et al.*, 2017). There is still lack of information on the sources and levels of carbonaceous aerosols despite of their considerable contribution to air pollution.

Ankara is the capital and second biggest city of Turkey with a population about 4.6 million. Air pollution due to rapid urbanization and heavy traffic is one of the biggest environmental issues of this metropolitan. Turkish Ministry of Environment and Urbanization has been operated several stations in the city but the data are limited to PM mass, and priority gaseous pollutants such as SO<sub>2</sub>, NO<sub>x</sub> and O<sub>3</sub>. To our best knowledge, there is no reported data on the carbonaceous aerosols, their sources and levels for the city.

The objective of this study is to determine the levels of carbonaceous aerosols with aerodynamic diameter less than 2.5 μm (PM<sub>2.5</sub>) collected from one urban and one sub-urban station in Ankara. Sampling campaign was started in June 2016 and continued since then. Samples were collected by TECORA Skypost PM sampler on quartz fibre filters, which were conditioned at constant humidity (% 25-30) and temperature (25°C) both before and after analysis. A punch of collected samples (1.5 cm<sup>2</sup>) were analysed in terms of elemental carbon (EC), organic carbon (OC) and total carbon (TC=EC+OC) by using Sunset Lab (USA) thermal-optical aerosol analyser by using following the National Institute for Occupational Health and Safety (NIOSH) 870 protocol.

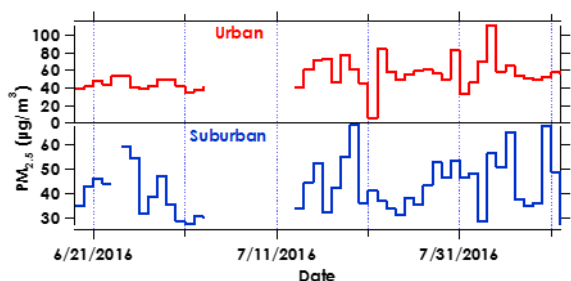


Figure 1. Temporal variation of PM<sub>2.5</sub> concentrations at two stations.

Temporal variation of PM<sub>2.5</sub> mass concentrations at two stations was depicted in Figure 1. Average PM<sub>2.5</sub> concentrations in urban and suburban stations were found

as 53.3±16.6 and 42.8±10.9 μg/m<sup>3</sup>, respectively, between June and August, 2016. The means of PM<sub>2.5</sub> concentrations are statistically different ( $p < 0.05$ ), implying the importance of urban pollution on air quality of the city.

The measured EC and TC concentrations of the samples collected at two stations during July 2016 were depicted in Figure 2. Whisker's bottom and top represent 10 and 90 %, box bottom and top represent 25 and 75 % of the data, respectively. In addition, red line and blue star within the box corresponding to median and mean concentrations, respectively.

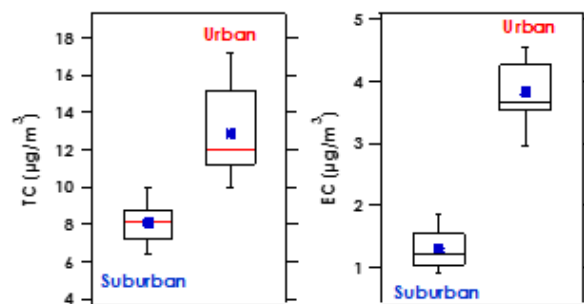


Figure 2. TC and EC concentrations measured at urban and sub-urban sites.

As it can be concluded from Figure 2, there is a statistically significant difference ( $p < 0.05$ ) in measured EC levels in urban and suburban stations. This is also true for TC concentrations. Based on the levels of carbonaceous aerosol concentrations, it can be concluded that levels of these pollutants are closely related with the degree of urbanization including traffic. Assessment of particle bound carbon concentrations with the more detailed chemical aerosol composition including metals, gaseous pollutants and meteorology will provide more comprehensive information about the degree of air quality and sources of these pollutants in the city.

This study was supported by Hacettepe University, Scientific Research Coordination Unit under grant FHD-2016-12903.

Boreddy, S.K.R., Kawamura, K., Okuzawa, K., Kanaya, Y., and Wang, Z. (2017) *Atmospheric Environment*, doi:10.1016/j.atmosenv.2017.01.042.

Kanakidou *et al.*, (2005) *Atmospheric Chemistry and Physics*. **5**, 1053-1123.

## Variability of traffic generated urban aerosols (PM<sub>10</sub>) in city street canyon: Riga (Latvia) case study

I. Steinberga<sup>1</sup>, A. Kanisceva<sup>1</sup>, L. Sustere<sup>1</sup>, J. Bikše Jr<sup>1</sup> and J. Kleperis<sup>2</sup>

<sup>1</sup>Faculty of Geography and Earth Sciences, University of Latvia, Riga, LV1004, Latvia

<sup>2</sup>Institute of Solid State Physics, University of Latvia, Riga, LV1063, Latvia

Keywords: urban aerosols, PM<sub>10</sub>, traffic, street canyon

Presenting author email: iveta.steinberga@lu.lv

Atmospheric aerosols can be solid, liquid, or a mixture of both and can contain a wide range of components, but most are believed to be mainly composed of an inorganic part, an organic part and associated water (Barley, McFiggans, 2010). The sources of PM are diverse and cover dust from soil and roads, diesel exhaust, combustion and industrial emissions, even bio-aerosols and ash from volcanic eruptions. Above mentioned PM may travel thousands of kilometres and life time vary from hours to several weeks (Gyan *et al.*, 2005; Wilkening *et al.*, 2000) Under some specific meteorological conditions PM concentrations could reach extremely high pollution levels exceeding national and international standards and levels leading to adverse health effects. Toxicity of PM mainly depends on their size and chemical composition (heavy metals, poly aromatic hydrocarbons - PAH) which is determined by specific sources (Brunekreef and Forsberg, 2005; Dickey, 2000). According to Kunzli *et al.* (2005) estimation adverse effect of air pollution in France, Switzerland and Austria leads for 40000 early deaths, more than 25000 new cases of adult bronchitis and more than 10 times more childhood bronchitis and even more than 16 million person-days of restricted activity.

Over the last decade's aerosol mass and composition changes have been detected almost at all monitoring stations in Latvia, but most of them in capital city (Riga). Preliminary assessment of annual concentrations show quite stable level at industrial, traffic and city background stations (see Figure 1), while detailed analysis indicate some tendency that specific individual effects leading to extremely high pollution episodes and over the years number of episodes have very strong increasing tendency.

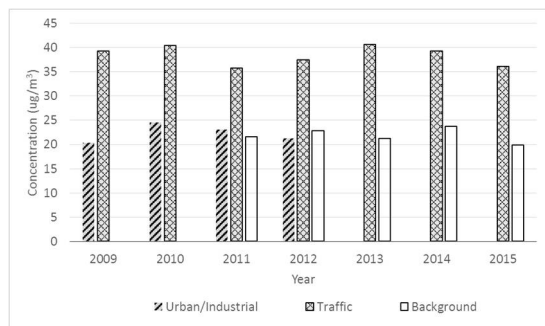


Figure 1. Annual mean concentrations of PM<sub>10</sub> in different monitoring stations in Riga.

This research covers following aspects of aerosol pollution in urban area: (1) trend analysis of historical measurements; (2) temporal (seasonal, weekly, diurnal) effect on aerosol concentrations as a result of recombination of direct source impact, specific meteorological and synoptic conditions; (3) detailed analysis (by using modelling tool OSPM - *Operational Street Pollution Model*) of traffic generated aerosols in street canyon on both sides; (4) development of different traffic flow scenarios; (5) modelling of ground-level (at 2m height) PM<sub>10</sub> and NO<sub>x</sub> concentrations for above mentioned traffic scenarios.

Some of the most interesting results showing very strong correlation between street maintenance activities and air pollution in street canyons. Figure 2 shows comparison of two meteorologically similar days. On January 22 the average daily value of PM<sub>10</sub> is 53.80ug/m<sup>3</sup> (exceedance of daily limit value), but during and after sanding activity (black square in the Figure 2) very stable and quite long high pollution episode is detected.

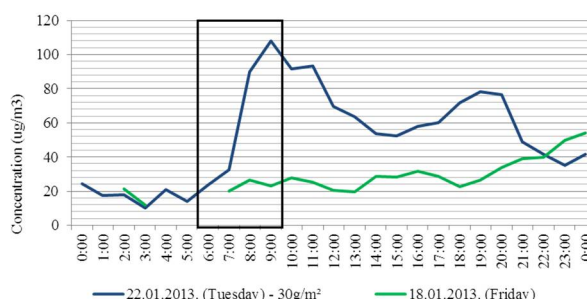


Figure 2. PM<sub>10</sub> concentrations (ug/m<sup>3</sup>) at street canyon with (blue)/without (green) sanding.

Barley, M.H., McFiggans, G. (2010) *Atmos. Chem. Phys.*, **10**, 749-767.

Brunekreef, B., Forsberg, B. (2005) *Eur Respir J*, **26**, 309-318.

Dickey, J.H. (2000) *Dis.-Mon.*, **46**, 566-589.

Gyan, K., Henry, W., Lucille, S., Laloo, A., Lamsec-Ebanke, C., McKay, R., *et al.* (2005) *Int. J. Biometeorol.*, **49**, 371-376.

Kunzli, N., Kaiser, R., Medina, S., Studnicka, M., Chanel, O., Fillinger, P. *et al.* (2005) *Lancet*, **356**, 795-801.

Wilkening, K.E., Barrie, L.A., Engle, M. (2000) *Science*, **290**, 65-7.

**Concentrations and gradients of traffic-derived metals in PM<sub>10</sub> and PM<sub>2.5</sub> near a major road**T. Yli-Tuomi<sup>1</sup>, P. Taimisto<sup>1</sup>, A. Pulkkinen<sup>1</sup>, J.V. Niemi<sup>2</sup>, A. Kousa<sup>2</sup> and T. Lanki<sup>1</sup><sup>1</sup>National Institute for Health and Welfare THL, PO Box 95, FI-70701 Kuopio, Finland<sup>2</sup>Helsinki Region Environmental Services Authority HSY, P.O. Box 100, FI-00066 HSY, Helsinki, Finland

Keywords: traffic emission, gradient, particulate matter, metal concentration.

Presenting author email: tarja.yli-tuomi@thl.fi

Traffic emissions are a significant source of particles in urban air. Due to the increased interest in health effects of airborne particles, the levels of several trace metals (Al, As, Ba, Ca, Cd, Co, Cr, Cu, Fe, K, Mg, Mn, Na, Ni, P, Pb, Sb, Si, Ti, V, Zn) in PM<sub>10</sub> and PM<sub>2.5</sub> were evaluated in atmospheric samples collected near a major road in the Helsinki region, Finland, in October-November 2012. During the measurements, the traffic intensity on the road was about 50 000 vehicles/day, (12% heavy duty vehicles). Six measurement containers were placed from 3.5 to 150 m distance from the road edge. At each site 48h filter samples were collected with Harvard impactors for gravimetric and metal analysis (extraction with nitric acid and hydrogen peroxide and analysis with ICPMS and ICP-OES).

Results from three 2-day periods are reported here. During period 1 and 2, the wind was nearly parallel with the road whereas during period 3, the wind was perpendicular to the road. The weather conditions during these periods are shown in Table 1.

The traffic-derived concentrations at the distances of 3.5, 10, 20, 40, and 80 m from the road edge were estimated by subtracting the concentration measured at 150 m. The gradient of these excess concentrations was drawn for each metal. The traffic-related concentrations at 3.5 m for those metals having clear decreasing gradient during all three periods are listed in Table 2. The highest metal concentrations in PM<sub>10</sub> were observed during perpendicular wind, while concentrations in PM<sub>2.5</sub> were higher when the wind carried particles along the road. Concentrations of traffic-related metals at the road edge were on average 6 and 4 times higher than those at 150 m distance for PM<sub>10</sub> and PM<sub>2.5</sub>, respectively.

Concentrations of the traffic-derived metals decreased relatively fast with increasing distance. At the distance of 10 m from the road edge, the concentrations in PM<sub>10</sub> were 61-86% and in PM<sub>2.5</sub> 68-97% of the 3.5 m concentration (Table 3). For Cu, Ba, Mn, Sb, and V in PM<sub>10</sub> the effect of traffic was close to zero at the distance of 80 m. The steepest decrease was observed for Cu in PM<sub>10</sub> and for Ba and Ca in PM<sub>2.5</sub>.

During the measurements, studded winter tires were used in cars and this likely affected the metal concentrations, especially Co in PM<sub>10</sub>. In addition, sand and salt were applied to roads to improve traction. Na in both PM<sub>10</sub> and PM<sub>2.5</sub> had decreasing gradient during measurement periods 1 and 2, but not during period 3. This suggests that NaCl was spread on the road when the temperature was close to the freezing point.

Table1. Weather conditions during the measurement periods.

Period	Temp (°C)	Wind Speed (m/s)	Wind Dir °	Calm (%)
1: 31.10.-2.11.	3.1	2.2	147	27
2: 7.-9.11.	1.3	1.9	276	40
3: 21.-23.11.	6.2	1.3	187	40

Table2. Excess concentration (ng/m<sup>3</sup>) of metals and PM<sub>10</sub> and PM<sub>2.5</sub> mass (µg/m<sup>3</sup>) at road edge compared to background during three measurement periods.

	PM10traf			PM2.5traf		
	1	2	3	1	2	3
Al	761	977	1219			
Ba	22	23	21	5.5	7.8	5.9
Ca	0.8	1.1	1.5	0.08	0.16	0.16
Co	0.6	1.0	1.3			
Cu	27	25	26	5.0	7.5	5.4
Fe	1484	1857	1954	265	328	296
K	0.14	0.20	0.24			
Mg	0.32	0.41	0.53	0.03	0.04	0.04
Mn	13	17	20	1.7	3.4	2.5
Sb	5.1	5.7	4.9	1.1	1.4	1.3
Si	526	619	821	142	222	163
Ti	62	87	105			
V	2.0	2.7	3.6			
PM	28	40	41	5.7	5.9	7.2

Table3. Gradients of traffic-derived PM<sub>10</sub> and PM<sub>2.5</sub> mass and metal concentrations.

Ratio	PM10traf		PM2.5traf	
	Mass (%)	Metals (%)	Mass (%)	Metals (%)
10m/3.5m	76	61 - 86	85	68 - 97
20m/3.5m	37	22 - 72	44	25 - 51
40m/3.5m	18	6 - 28	33	10 - 30
80m/3.5m	6	0 - 12	21	8 - 21

This work was supported by the intramural funding of THL and HSY.

## Study of Particulate Matter (PM) levels in São José dos Campos using a Generalized Linear Model (GLM)

D.C. Nogarotto<sup>1</sup> and S.A. Pozza<sup>1</sup>

<sup>1</sup>School of Technology, Campinas State University, Limeira, São Paulo, 13.483-132, Brazil

Keywords: PM<sub>10</sub>, air mass trajectories, HYSPLIT model, gamma distribution.

Presenting author email: simone.pozza@ft.unicamp.br

From the several factors that influence air pollution, Atmospheric Particulate Matter (APM) can be considered one of the most important. In this context, the comprehension of how APM relates to air masses may allow the identification of the emission sources of this pollutant, thus avoiding higher damages to health and the environment. Here, we studied PM<sub>10</sub>, in which particles have an aerodynamic diameter smaller than or equal to 10  $\mu\text{m}$ .

The main objective of this work was to identify which regions influenced the concentration of PM<sub>10</sub> at the city São José dos Campos (São Paulo, Brazil), according to air mass residence times. For this purpose, the time spent by incoming air masses over distinct residing regions was used as input of a Generalized Linear Model (GLM), while the daily concentration of PM<sub>10</sub> was used as the output. Specifically, the GLM was used with a gamma distribution.

Table 1. Region description (1-11) and statistical significance (5%).

Region	Description	Significance	% contribution
1	Local	Yes	31.7
2	Local	Yes	29.2
3	Local	Yes	5.6
4	Local/Atlantic	No	0.7
5	Atlantic	Yes	4.7
6	Continental	Yes	8.2
7	Atlantic	No	0.7
8	Regional/Continental	Yes	10.4
9	Continental	Yes	1.7
10	Continental	Yes	3.8
11	Pacific	Yes	3.2

Daily PM<sub>10</sub> concentration ( $\mu\text{g}/\text{m}^3$ ) data collected during seven months (Jun-Dez/2015) at São José dos Campos (SJC) station was used in this work. Such data was obtained from the QUALAR (Air Quality) database, available at CETESB's (Environmental Company of the State of São Paulo) website. This database provides hourly measurements of air quality parameters collected by São Paulo's (state) monitoring network.

The Hybrid Single-Particle Lagrangian Integrated Trajectory Model (HYSPLIT), provided by the National Oceanic and Atmospheric Administration (NOAA) Air Resources Laboratory (ARL), was used to obtain the trajectories of the air masses arriving in SJC. Three-day (72 hours) backward air mass trajectories arriving at SJC

(longitude:  $-45,9^\circ$  and latitude:  $-23,2^\circ$ ), at 500m above ground level (AGL) and always with a starting point for the calculations at 12:00 were considered.

According to the obtained trajectories, we defined 11 regions (Table 1, Figure 1) and verified the influence of each one on the PM<sub>10</sub> concentration level in SJC.

Some studies from the literature (Kavouras *et al*, 2013; Dimitriou and Kassomenos, 2014) used Multiple Linear Regression Model (MLRM) for the same purpose of this work. However, we propose the use of GLM with gamma distribution. The output of this model is always a positive number, which allows the improvement of the model according to the behaviour of output. Residual analysis was made and GLM presented more consistent results than MRLM.

Table 1 shows the percent of contribution to PM<sub>10</sub> from each region considered here. Notice that regions 1-3, which are very industrialized and contain several highways, have a contribution of about 66%. Marine Sources (regions 5 and 11) contributed around 8%. Regional and continental regions (6, 8, 9 and 10) have a contribution of around 24%, while regions 4 and 7 did not contribute to PM<sub>10</sub> concentration in SJC.

To conclude, GLM allowed the quantification of each region's contribution to PM<sub>10</sub> concentration in SJC, and the results indicated high influences of anthropogenic, mainly local sources.

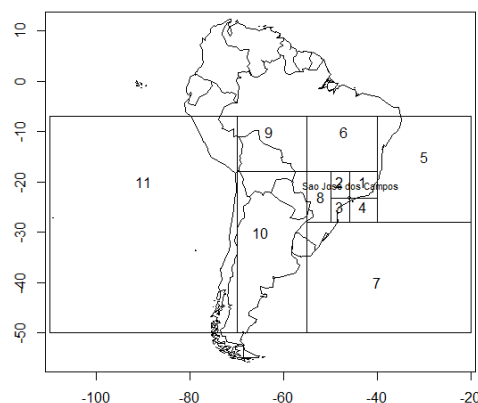


Figure 1. Regions of air mass residence in São José dos Campos

The authors would like to thank CAPES.

Dimitriou, K. and Kassomenos, P. (2014) *Atmos. Environ.* **98**, 648-654.

Kavouras, I.G., Lianou, M., Chalbot, M.C., Vei, I.C., Kotronarou, A., Hoek, G., Hameri, K. and Harrison, R.M. (2013) *Environ. Pollut.* **176**, 1-9.

## Nitro-monoaromatic compounds in urban aerosols of central and southeastern Europe: mass size distribution and solubility in simulated lung fluids

Z. Kitanovski<sup>1</sup>, G. Lammel<sup>1,2</sup>, R. Prokeš<sup>2</sup>, C. Samara<sup>3</sup>, P. Shahpoury<sup>1</sup> and A. Voliotis<sup>3</sup>

<sup>1</sup>Multiphase Chemistry Department, Max Planck Institute for Chemistry, Mainz, 55128, Germany

<sup>2</sup>Research Centre for Toxic Compounds in the Environment, Masaryk University, Brno, 625 00, Czech Republic

<sup>3</sup>Department of Chemistry, Aristotle University of Thessaloniki, Thessaloniki, 54124, Greece

Keywords: nitrocatechols, HULIS, bioaccessibility, PM toxicity.

Presenting author email: z.kitanovski@mpic.de

Biomass burning (BB) is one of the major sources of primary emitted particles in the atmosphere. It is also considered as a major primary source of atmospheric humic-like substances (HULIS, Zheng *et al.*, 2013). A significant part of HULIS is represented by lignin-derived aromatic compounds. Claeys *et al.* (2012) reported that 4-nitrocatechol (4-NC) and isomeric methyl-nitrocatechols are major constituents of HULIS extracted from PM<sub>2.5</sub> of BB aerosols. Nitrocatechols were recently measured in several studies world-wide (e.g. Kitanovski *et al.*, 2012; Kahnt *et al.*, 2013; Caumo *et al.*, 2016; Chow *et al.*, 2016).

Inhalation exposure towards particulate matter (PM) constituents is controlled by their mobilization into lung fluids. Related bioaccessibility studies have been mostly limited to inorganic PM constituents (Wiseman, 2015).

The mass size distribution of a number of nitro-monoaromatic compounds (NMACs, i.e. nitrocatechols, nitrosalicylic acids and nitrophenols) in size-segregated PM (PM<sub>10-7.2</sub>, PM<sub>7.2-3</sub>, PM<sub>3-1.5</sub>, PM<sub>1.5-0.95</sub>, PM<sub>0.95-0.49</sub> and PM<sub>0.49</sub>) collected in the cities of Mainz (MZ, Germany, urban area, ≈400000 inhabitants), Kladno (KL, Czech Republic, urban area, ≈70000 inh.), Ostrava (OS, Czech Republic, urban area, ≈400000 inh.) and Thessaloniki (TH, Greece, urban area, ≈800000 inh.) was determined. The substances were also measured in the gas-phase (sorption to polyurethane foam).

Concentrations of 12 NMACs in size-segregated PM samples were determined following Kitanovski *et al.* (2012). Their bioaccessibility was further investigated using simulated lung fluids (SLFs). For this purpose, the fine PM fractions (PM<sub>3-1.5</sub>, PM<sub>1.5-0.95</sub>, PM<sub>0.95-0.49</sub> and PM<sub>0.49</sub>) were leached in Gamble's solution and artificial lysosomal fluid (ALF) for 24 hours, at 37°C in the dark. The dissolved fraction of the nitro-compounds in the SLF leachates were subsequently solid-phase extracted and quantified (Kitanovski *et al.*, 2012).

Highest abundances are found for nitrocatechols (4-NC, 4-methyl-5-nitrocatechol, 3-methyl-5-nitrocatechol and 3-methyl-4-nitrocatechol) and nitrophenols (4-nitrophenol, 3-methyl-4-nitrophenol, 2-methyl-4-nitrophenol and 4-nitroguaiacol), i.e. 57-87% and 9-37% of total measured NMACs, respectively; while nitrosalicylic acids (3-nitro- and 5-nitrosalicylic acid) and dinitrophenols (2,4-dinitrophenol and 2-methyl-3,5-dinitrophenol) were less significant (1-15% and 0-1%, respectively). More than 95% of the PM<sub>10</sub> mass

concentration of 4-NC is found associated with PM<sub>3</sub>, independent of site and season (Figure 1). The solubility of NMACs in SLFs is investigated using poly-parameter linear free energy relationships (ppLFER), and its dependence on SLFs' pH value and PM size are quantified and discussed.

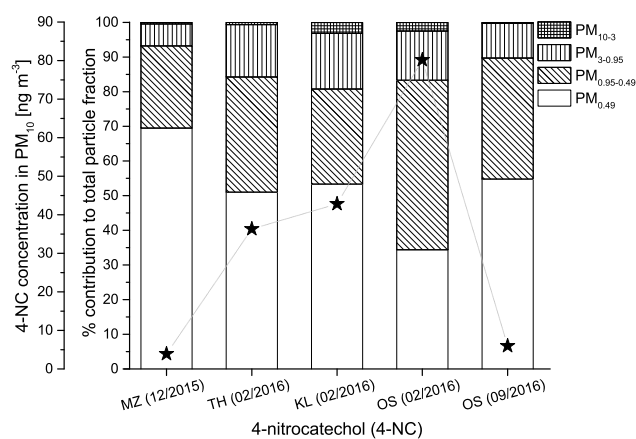


Figure 1. Mass size distributions of 4-nitrocatechols in urban PM<sub>10</sub>. Absolute concentrations are marked with asterisks.

We thank Ondřej Šáňka (MU) for onsite support. This work was supported by the Max Planck Society and the Czech Science Foundation (No. P503 16-11537S).

Caumo, S.E.S., Claeys, M., Maenhaut, W., Vermeylen, R., Behrouzi, S., Safi Shalamzari, M., Vasconcellos, P.C. (2016) *Atmos. Environ.* **145**, 272-279.

Chow, K.S., Huang, X.H.H., Yu, J.Z. (2016) *Environ. Chem.* **13**, 665-673.

Claeys, M., Vermeylen, R., Yasmeen, F., Gómez-González, Y., Chi, X., Maenhaut, W., Mészáros, T., Salma, I. (2012) *Environ. Chem.* **9**, 273-284.

Kahnt, A., Behrouzi, S., Vermeylen, R., Safi Shalamzari, M., Vercauteren, J., Roekens, E., Claeys, M., Maenhaut, W. (2013) *Atmos. Environ.* **81**, 561-568.

Kitanovski, Z., Grgić, I., Vermeylen, R., Claeys, M., Maenhaut, W. (2012) *J. Chromatogr. A* **1268**, 35-43.

Wiseman, C.L.S. (2015) *Anal. Chim. Acta* **877**, 9-18.

Zheng, G., He, K., Duan, F., Cheng, Y., Ma, Y. (2013) *Environ. Pollut.* **181**, 301-314.

## Insights into PM<sub>1</sub> during haze episodes in Beijing, China, using an aerosol mass spectrometer in a two-month winter field campaign 2016

S.H. Schmitt<sup>1</sup>, P.Schlag<sup>1,\*</sup>, G.Gkatzelis<sup>1</sup>, T. Hohaus<sup>1</sup>, Y. Wang<sup>2</sup>, D. Shang<sup>2</sup>, M. Hu<sup>2</sup>, K. Lu<sup>2</sup>,  
A. Wahner<sup>1</sup>, A. Kiendler-Scharr<sup>1</sup>

<sup>1</sup>Institute of Energy and Climate Research, IEK-8: Troposphere,  
Forschungszentrum Jülich GmbH, Jülich, Germany

<sup>2</sup>College of Environmental Science and Engineering, Peking University, Beijing, China  
\* now at: Institute of Physics, University of Sao Paulo, Sao Paulo, Brazil

Keywords: air pollution, China, AMS, PMF  
Presenting author email: [s.schmitt@fz-juelich.de](mailto:s.schmitt@fz-juelich.de)

Atmospheric aerosol impacts the climate system by absorbing and scattering light (direct aerosol effect) and by serving as cloud condensation nuclei (indirect aerosol effect). Furthermore, high atmospheric aerosol loadings are detrimental for human health.

Within the last decades aerosol mass concentrations have been observed to reach up to several  $\text{mg}\cdot\text{m}^{-3}$  in the eastern China plain, strongly influencing the air quality in densely populated areas and megacities like Beijing (Zhang et al 2015). Meteorological conditions have been shown to be a very critical parameter for the emergence of haze episodes and the subsequent cleaning of the air (Zhang et al 2016). As most of the studies were performed between spring and autumn there is still a lack of understanding of wintertime processes.

For this study particle and gas phase data have been collected at a rural site northeast of Beijing city ( $40^{\circ}24'31.4''\text{N}$   $116^{\circ}40'52.1''\text{E}$ ) in January and February 2016 within the framework of the University of Chinese Academy of science (UCAS) winter campaign of Beijing University and Forschungszentrum Jülich. This abstract focuses on the Aerodyne aerosol mass spectrometer (AMS) dataset.

The measurement period can be subdivided in two prevailing conditions. Firstly, periods with northerly winds, when air masses were very clean in respect to both gas- and particle phase only influenced by local sources from the closeby villages. Secondly, conditions of southerly winds, when haze was transported to the field station. During haze episodes PM<sub>1</sub> levels of up to  $350\mu\text{g}\cdot\text{m}^{-3}$  have been observed and the fraction of nitrate increased from 8% to 25%. This increase happened at the expense of organics which decreased from 68% to 44% while still being the largest contribution to PM<sub>1</sub> (see figure 1).

Application of unconstrained Positive Matrix Factorization (PMF) on the organic mass spectra showed contributions from coal-combustion identified by poliaromatic hydrocarbon (PAH) like mass spectra. In addition, a biomass burning factor, a hydrocarbon like factor and two oxidized organic aerosol factors (OOA) were identified. The coal combustion factor and the

hydrocarbon like factor were mainly found in local emissions during clean episodes while the oxidized factors showed highest contribution during haze conditions. Causes of the increase in OOA and nitrate during periods of haze will be discussed.

Understanding atmospheric chemistry under extremely polluted conditions is a major challenge to develop mitigation strategies. This study exhibits new insights into changes in aerosol composition for clean and haze episodes in rural Beijing during wintertime assisting to identify key processes.

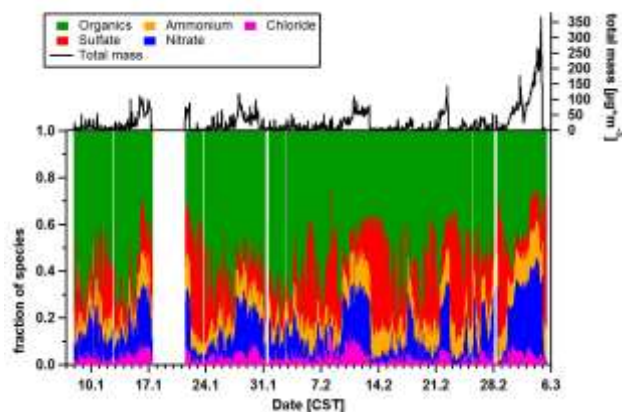


Figure 1: Total non-refractory PM<sub>1</sub> measured by AMS (upper panel) and species fractional contribution of the aerosol (lower panel). Note the increase of nitrate contribution with increasing total mass.

Zhang, R. Y.; Wang, G. H.; Guo, S.; Zarnora, M. L.; Ying, Q.; Lin, Y.; Wang, W. G.; Hu, M. & Wang, Y. (2015) *Formation of Urban Fine Particulate Matter* Chem. Rev., 115, 3803-3855

Zhang, Z.; Zhang, X.; Gong, D.; Kim, S. J.; Mao, R. & Zhao, X. (2016) *Possible influence of atmospheric circulations on winter haze pollution in the Beijing-Tianjin-Hebei region, northern China* Atmos. Chem. and Phys., 16, 561-571

## What is the mechanism behind new particle formation in highly polluted urban environments?

F. Bianchi<sup>1</sup>, L. Yao<sup>2</sup>, O. Garmash<sup>1</sup>, C. Yan<sup>1</sup>, J. Kontkanen<sup>1</sup>, H. Junninen<sup>1</sup>, S. Buenrostro Mazon<sup>1</sup>, M. Ehn<sup>1</sup>, M. Sipilä<sup>1</sup>, T. Petäjä<sup>1</sup>, M. Kulmala<sup>2</sup>, D.R. Worsnop<sup>1,3</sup> and L. Wang<sup>2,4</sup>

<sup>1</sup>Department of Physics, University of Helsinki, Helsinki, 00014, Finland

<sup>2</sup>Shanghai Key Laboratory of Atmospheric Particle Pollution and Prevention (LAP<sup>3</sup>), Department of Environmental Science & Engineering, Fudan University, Shanghai 200433, China

<sup>3</sup>Aerodyne Research, Inc., Billerica, MA 01821, USA

<sup>4</sup>Collaborative Innovation Center of Climate Change, Nanjing 210023, China

Keywords: Nucleation, Mass spectrometry, Megacity, Sulphuric acid.

Presenting author email: Federico.bianchi@helsinki.fi

Aerosol particles can influence climate directly and indirectly, and have an adverse impact on human health. Atmospheric nucleation of gas-phase precursors to clusters and then further to nanoparticles is the largest source of atmospheric aerosol particles (ref). This phenomenon is often referred to as New Particle Formation (NPF) and has been observed in numerous locations around the world, from the free troposphere (Bianchi *et al* 2016) to polluted urban cities (Xiao *et al* 2015).

Recently, several achievements have been reached regarding our understanding of nucleation; however, it is still unclear why NPF occurs more often than predicted in highly-polluted conditions, such as in Chinese megacities. A recent study has shown that this apparent discrepancy can be explained only if the molecular clusters are scavenged considerably less effectively than one would expect based on their collision rates with the pre-existing particles, or if they grow much faster in size than our current understanding allows (Kulmala *et al.*, 2017).

To improve our understanding in urban NPF, we performed a comprehensive measurement campaign in Shanghai, China, from December 2015 until February 2016. We used a nitrate-based Chemical Ionisation Atmospheric Pressure interface Time-Of-Flight (CI-API-TOF) mass spectrometer to determine the chemical composition of the neutral clusters and the concentration of low-volatility vapours, such as sulphuric acid and highly oxidised molecules (HOMs). Sub-3nm particles were measured using a Particle Size Magnifier (PSM). To measure the size distribution of aerosol particles and ions we used the Neutral Cluster and Air Ion Spectrometer (NAIS), Nano- and Long-Scanning mobility particle sizer (SMPS). The results of this intensive campaign have been coupled with long-term measurements of PSM, Nano- and Long-SMPS (March 2014 - March 2016).

We observed several NPF events taking place during sunny and relatively “clean” conditions. During the NPF event days, PM<sub>2.5</sub> was on average lower than during non-event days, although with a concentration still higher than 50 µg/m<sup>3</sup>. A high concentration (~10<sup>5</sup> cm<sup>-3</sup>) of sub-3nm particles was detected with the PSM during the nucleation event. Thereafter, larger particles

(4-63nm) were detected by the Nano-SMPS and the NAIS.

To complement the particle data, the mass spectrometer was able to determine the sulphuric acid and HOMs concentration during such events. Our results indicate that NPF in Shanghai is initially driven by sulphuric acid and amines followed by the condensational growth of anthropogenic HOMs.

Figure 1 shows an example of a NPF event measured at Fudan University in Shanghai. It is clear from the figure that a large number of particles (~2 × 10<sup>4</sup> cm<sup>-3</sup>) can easily reach a size of 50-60 nm in just a few hours.

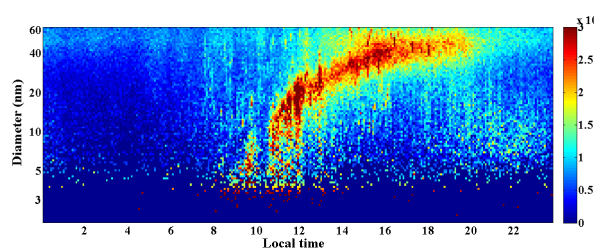


Figure 1. Example of a nucleation event measured by the Nano-SMPS in Fudan University, Shanghai.

This work was supported by the National Natural Science Foundation of China (No. 21222703, 21561130150, 41575113, & 91644213) and the Cyrus Tang Foundation (No. CTF-FD2014001). L.Wang thanks the Royal Society-Newton Advanced Fellowship (NA140106). This work was also partially funded by European Research Council (Grant 638703-COALA)

Bianchi, F., *et al.*, (2016) *Science* **6289**, 1109-1112.

Kulmala, M., Kerminen, V.M., Petäjä, T., Ding, A.J., Wang, L. (2017) *Faraday Discussion*, *In press*.

Xiao, S., *et al.*, (2015) *Atmos. Chem. Phys.* **15**, 1769-1781.

## Seasonal variation of urban coarse particles in Amman – Jordan

T. Hussein<sup>1</sup>, H. Juwhari<sup>1</sup> and M. Qaisi<sup>2</sup>

<sup>1</sup>University of Jordan, Faculty of Science, Department of Physics, Amman 11942, Jordan

<sup>2</sup>University of Jordan, Faculty of Science, Department of Geology, Amman 11942, Jordan

Keywords: Coarse, seasonal, urban

Presenting author email: t.hussein@ju.edu.jo

Urban aerosols have a complex dynamic behavior because they are a mixture of regionally transported aerosols and a wide range of locally emitted aerosols (Hussein *et al.*, 2014). Besides being externally mixed, their composition can vary depending on the source type, geographical region and state of development, and dynamic processes involved in their transformation.

The aerosol research in the Middle East and North Africa (MENA) region have been limited to PM concentrations, some gaseous pollutants, elemental and chemical analysis, long-range transport, mineral dust and dust episodes, and optical depth. Studies focused on particle number concentrations and the particle number size distributions are very rare in the MENA region. According to our knowledge, there is less than ten articles published about urban aerosols in Jordan.

The main objective of this study is to present, for the first time, the seasonal variation of coarse particle number and mass concentrations in the urban background atmosphere of Amman, Jordan. The analysis is based on long-term measurement of the particle number size distribution of particles in the diameter range 0.3–10  $\mu\text{m}$ .

those observed during the winter due to the fact that the boundary layer is deeper in the summer than in the winter.

This work was supported by Faculty of Academic Research at the University of Jordan and the Scientific Research Support Fund at the Ministry of Higher Education, Amman, Jordan.

Hussein, T., Mølgaard, B., Hannuniemi, H., Martikainen, J., Järvi, L., Wegner, T., Ripamonti, G., Weber, S., Vesala, T. and Hämeri, K. (2014) *Boreal Environment Research* 19, 1–20.

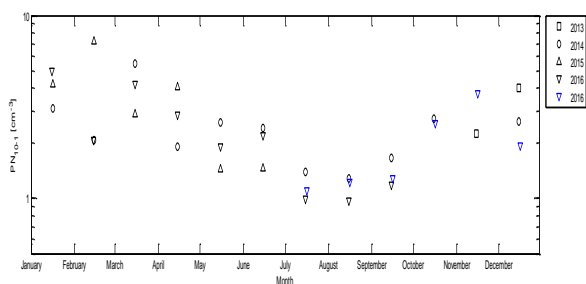


Figure 1. Monthly mean particle number concentration of coarse particles in Amman, Jordan.

Based on the monthly average (Figure 1), the concentrations showed a clear seasonal cycle with high concentrations during the winter (~8 particles/cm<sup>3</sup>, ~110  $\mu\text{g}/\text{m}^3$ , during February) and low concentrations during the summer (~1 particles/cm<sup>3</sup>, ~15  $\mu\text{g}/\text{m}^3$ , during July and August). These variations indicate that a part of the coarse particles is locally produce due to enhanced re-suspension of coarse particles from the arid regions in Jordan. During the summer season, the concentrations are lower than

## Measurements of the vertical distribution of the pollution in Paris (France) by the light aerosol counter LOAC on-board the tethered touristic balloon “OAG”

J.-B. Renard<sup>1</sup>, K. Léger<sup>2</sup>, Amélie Fritz<sup>2</sup>, J. Giacomoni<sup>3</sup>, B. Couté<sup>1</sup>, V. Duverger<sup>1</sup> and M. Jeannot<sup>1,4</sup>

<sup>1</sup> LPC2E-CNRS, Orléans, F-45000, France

<sup>2</sup> Airparif, Paris, F-75004, France

<sup>3</sup> Aerophile SAS, Paris, F-75015, France

<sup>4</sup> MeteoModem, Ury, F-77760, France

Keywords: Urban pollution, aerosol counter, balloon

Presenting author email: jean-baptiste.brenard@cnrs-orleans.fr

LOAC is a light aerosol counter/sizer operated at ground and under balloons, to determine the aerosol concentrations in 19 size classes between 0.2 and 100  $\mu\text{m}$ , and to estimate their main typology (carbonaceous particles, minerals particles, salts, droplets, Renard et al., 2016a,b). The counting can be converted in PM<sub>2.5</sub> and PM<sub>10</sub> mass concentrations, with an accuracy of about 20%.

LOAC has been operated since 2013 at the Observatoire Atmospherique Generali (OAG) tethered touristic balloon in the south-west of Paris, France (latitude 48.841°N, longitude 2.274°W; Figure 1). The measurements are continually performed at ground, and during the balloon flights up to an altitude of 300 m when the wind conditions are favourable.



Figure 1: The touristic tethered balloon “OAG” in Paris

The Paris region has recently encountered 4 strong pollution episodes, in December 2013, in March 2014, in March 2015, and in December 2016-January 2017. The retrieved LOAC mass concentrations at the OAG balloon are in good agreement with those of the air quality network Airparif (Renard et al., 2016c). The size distribution and the nature of the particles depend on the origin of the pollution (agricultural activities, industrial activities, transport, wood burning heating, Saharan dust plume). The winter episodes are usually dominated by the sub-micronic carbonaceous particles, while the Spring episodes are usually dominated by the micronic particles of different origins. Such measurements provide complementary information to the normative PM<sub>10</sub> mass concentrations for ambient air.

The balloon measurements allow us to determine the vertical evolution of the particles' concentrations. This evolution strongly depends on the meteorological conditions, with sometimes an inversion layer, and on the origin of the pollution (local sources vs. imported pollution or dust plume). Also, the respective contribution of particles in the 0.2-1  $\mu\text{m}$  range, 1-3  $\mu\text{m}$  range and 3-10  $\mu\text{m}$  range is strongly dependent on the origin of the pollution; typically the highest concentrations of sub-micronic particles were obtained during winter with primary carbonaceous pollution particles. Figure 2 presents an example for the 5 December 2016 event, which is characterized by the accumulation of carbonaceous particles for altitudes below 250 m.

The characteristics of the various pollution episodes are compared and discussed. Also, we present the interest of performing such kind of tethered balloon measurements in other cities.

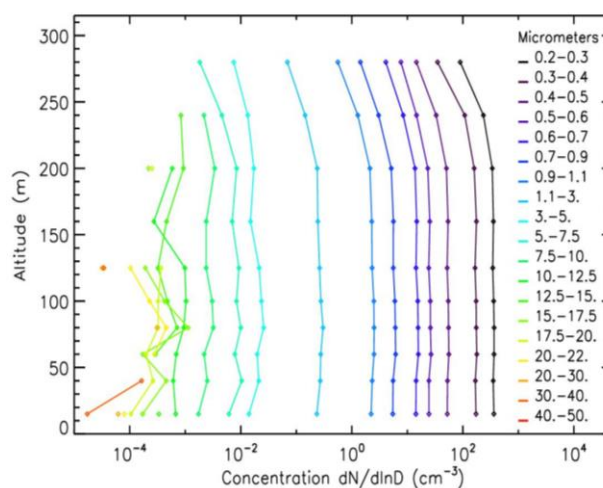


Figure 2: Evolution of particles concentrations with altitude during the 5 December 2016 pollution event

Renard et al. (2016a) *Atmos. Meas. Tech.*, **9**, 1721-1742.  
 Renard et al. (2016b), *Atmos. Meas. Tech.*, **9**, 3673-3686.  
 Renard, J.-B., Léger, K., Bernard, J.-F., Sciare, J., and Giacomoni, J. (2016c), *La météorologie*, **92**, 39-45.

## Determination of elemental composition of particulates in Antalya urban atmosphere

A.M. Tepe<sup>1</sup>, A. Zararsiz<sup>2</sup> and G. Doğan<sup>1</sup>

<sup>1</sup>Department of Environmental Engineering, Akdeniz University, Antalya, 07058, Turkey

<sup>2</sup>Saraykoy Nuclear Research and Training Center, Ankara, 06983, Turkey

Keywords: Eastern Mediterranean, air pollution, EDXRF, particulate matter.

Presenting author email: ahmettepe@akdeniz.edu.tr

Antalya is the Turkish Riviera located on Mediterranean coast of southwestern Turkey and it is one of the biggest cities in Turkey with a downtown population of over 2 million. Agriculture and tourism activities are the main source of income for Antalya. Even though the city suffers from air pollution in the downtown area especially during winter months.

To determine the levels of pollution, total of 169 particulate matter samples (PM<sub>2.5</sub>, PM<sub>2.5-10</sub>) were collected once in a two-day period in between July 2014 and July 2015. Samples were analyzed using an energy-dispersive X-ray fluorescence (EDXRF) for a total of 15 elements which are Na, Mg, Al, Si, S, K, Ca, Ti, V, Mn, Fe, Cu, Zn, As, Pb.

Statistical parameters were calculated for all measured elements in fine (PM<sub>2.5</sub>) and coarse (PM<sub>2.5-10</sub>) fraction. All elements concentrations are given in Table 1. Anthropogenic elements, such as S, As, Zn, Pb found in higher concentrations in the fine fraction. On the other hand, crustal elements, such as Ti, Ca, Al and Na were mostly abundant in the course fraction.

Table 1. Concentrations of elements in coarse and fine fraction (concentrations are in ng / m<sup>3</sup>).

Elements	Sample Number	Arithmetic Mean	
		Coarse	Fine
Na	169	326 ± 286	82 ± 78
Mg	169	233 ± 152	91 ± 97
Al	169	286 ± 288	78 ± 110
Si	169	803 ± 739	250 ± 298
S	164	387 ± 314	999 ± 809
K	169	170 ± 141	114 ± 72
Ca	169	2180 ± 1270	337 ± 215
Ti	168	43 ± 42	7,6 ± 8,9
V	164	2,1 ± 1,2	1 ± 0,9
Mn	161	13 ± 10	9 ± 8
Fe	151	295 ± 281	93 ± 75
Cu	144	6,4 ± 4,9	5,6 ± 5,4
Zn	168	17 ± 17	18 ± 24
As	129	0,4 ± 0,5	0,4 ± 0,4
Pb	159	11 ± 11	8,6 ± 8,5

To understand the concentration variations in time, monthly, seasonal and weekend/weekday changes were examined. For fine fraction higher concentrations, which are especially emitted from domestic heating, were observed in cold months. Course fractions concentrations are also significantly higher in cold months. Na concentrations is increasing especially in summer. The reason of that could be due to higher wind speeds blowing from the sea during hot months. As and Pb concentrations are similar in both fractions and increasing only in cold winter. This indicated that emissions from domestic heating are the most important source of As and Pb.

Enrichment Factors (EF) were determined for classify the measured elements as either natural or

anthropogenic. Crustal Enrichment Factors (EF<sub>C</sub>) and Marine Enrichment Factors (EF<sub>M</sub>) were calculated for the elements in fine and course fractions. Figure 1. and Figure 2. shows that results of crustal enrichment factor and marine enrichment factor, respectively.

EF<sub>C</sub> values of the Si, Fe, Na, Mg, Al, K and Ti elements in both particle fraction and values of Mn and V elements only in coarse fraction are determined less than 10.

EF<sub>M</sub> results were analyzed and EF<sub>M</sub>'s of all the measured elements are found higher than 10. This indicates, coarse fraction emissions which are from the marine are separated from the atmosphere in connection with gravity before it reached sampling area.

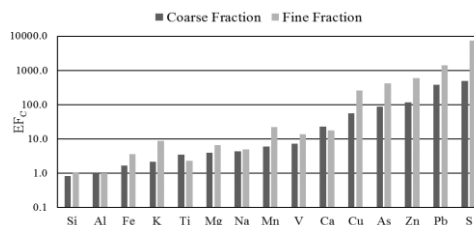


Figure 1. EF<sub>C</sub> values of the elements of the coarse and fine fractions.

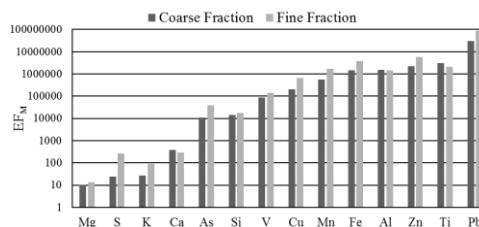


Figure 2. EF<sub>M</sub> values of the elements of the coarse and fine fractions.

This work was supported by the Akdeniz University Scientific Research Council, Project no. 2014.01.0102.002 and FYL-2014-194.

## Seasonal characteristics of fine and coarse mode aerosol particles over an urban region

Atar S. Pipal\*, T. A. Rajesh and S. Ramachandran

Space and Atmospheric Sciences Division, Physical Research Laboratory, Ahmedabad 380 009, India

**Keywords:** Size distribution,  $N_{\text{Fine}}$  and  $N_{\text{Coarse}}$ , effective radius, model, seasonal variations

Presenting author email\*: aspippal@gmail.com

### Abstract

The physical (size) and chemical (composition) properties of aerosols over urban regions exhibit wide variability as they are emitted from a variety of sources. Aerosol size distribution is one of the crucial physical properties that govern the aerosol interaction with atmospheric radiation, cloud formation, transport and deposition, and health effects at regional and global level. Therefore, the measurement of particle size distribution and its fine and coarse fractions are important to estimate their impact on climate (Wu et al., 2008).

Aerosol size distributions were measured using an Aerodynamic Particle Sizer (APS, Model 3321, TSI) during 2015 in Ahmedabad to characterize the fine and coarse aerosols along with their sources. Monthly mean size distribution (0.262- 9.575  $\mu\text{m}$ ) pattern was bimodal and number concentrations found to be highest in October (with a peak at  $\sim 0.40 \mu\text{m}$  and 500 particles per  $\text{cm}^{-3}$ ) followed by April. Seasonal analysis illustrates distinct behavior of aerosols between seasons indicating maximum peak in post-monsoon than pre-monsoon and winter while lower during monsoon period (Figure 1). The aerosol size distributions exhibit two peaks, one between 0.39 and 0.42  $\mu\text{m}$ , and between 1.41 and 1.71  $\mu\text{m}$  respectively. Mode radii and width of the lognormal size distributions did not show any significant seasonal variation.

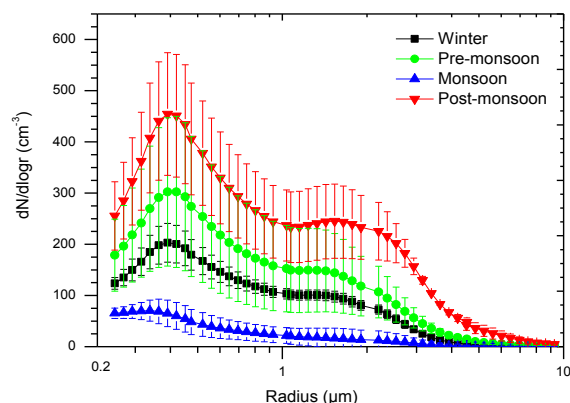


Figure: 1: Seasonal mean aerosol size distribution over Ahmedabad. Vertical bars represent  $\pm 1\sigma$  from the mean.

Diurnal variations in aerosol number concentrations were evident in particles of radius  $< 0.253 \mu\text{m}$  while in the higher radius range the diurnal variations were insignificant.

Contribution of  $N_{\text{fine}}$  (0.262-0.958  $\mu\text{m}$ ) and  $N_{\text{Coarse}}$  (1.070-9.575  $\mu\text{m}$ ) mode into total annual number concentration was  $\sim 66.5\%$  and  $\sim 33.5\%$ . Seasonal analysis inferred the highest level of fine and coarse particles in post-monsoon and lowest during monsoon. This study is important because systematic aerosol size distribution measurements on a continuous basis over urban regions are rare, as typically measurements have been made on campaign or event based mode.

### References

Wu, Z., Hu, M., Lin, P., Liu, S., Wehner, B., Wiedensohler, A., 2008. Particle number size distribution in the urban atmosphere of Beijing, China. *Atmospheric Environment*, 42, 7967-7980.

## **Abstracts T215**

## Exposure trends of PM<sub>2.5</sub> and Black Carbon sources in Gothenburg 1990-2011

P. Molnár<sup>1</sup>, D. Segersson<sup>2</sup>, L. Stockfelt<sup>1</sup> and G. Sallsten<sup>1</sup>

<sup>1</sup>Department of Occupational and Environmental Medicine, institute of Medicine, Sahlgrenska Academy, University of Gothenburg, Gothenburg, Sweden

<sup>2</sup>Swedish Meteorol & Hydrol Inst, S-60176 Norrköping, Sweden

Keywords: Exposure Assessment, Modelling, PM<sub>2.5</sub>, BC, Source Contribution

Presenting author email: peter.molnar@amm.gu.se

### Introduction

Air pollution is a known risk factor for cardio-pulmonary disease estimated to cause around half a million annual premature deaths in Europe (EEA, 2014). Particulate matter (PM) is thought to be the major contributor, but it is not known which sources and types of particles that are most responsible for the adverse health effects.

### Methods

The Swedish Meteorological & Hydrological Institute (SMHI) has modelled yearly mean PM<sub>2.5</sub> and Black Carbon (BC) levels in the greater Gothenburg area (96x112°km) for the years 1990, 2000, and 2011 in 50°m squares, as well as concentrations of major local PM<sub>2.5</sub> and BC sources: Traffic exhaust, traffic road wear, residential heating, shipping, and industry. The intermediate years was interpolated, adjusted for ventilation factor to take meteorological differences between years into account.

To assign exposure we have used two cohorts, the PPS-cohort and the GOT-MONICA-cohort (~9000 persons 1990), initially recruited to study predictors of cardiovascular disease. We collected data on residential addresses and assigned each individual yearly total and source-specific particulate exposures from the models.

### Results

There was a small reduction in total PM<sub>2.5</sub> concentrations. The yearly variation in long-range transported (LRT) PM<sub>2.5</sub> was the main cause of the variation between years with only a small reduction in the local contribution (Fig. 1). Of the specific local sources, we found a strong decrease in PM<sub>2.5</sub> from industrial sources around year 2000, and a smaller decrease from traffic exhaust and residential heating the last 10 years, while the other sources only changed marginally over time (Fig. 2).

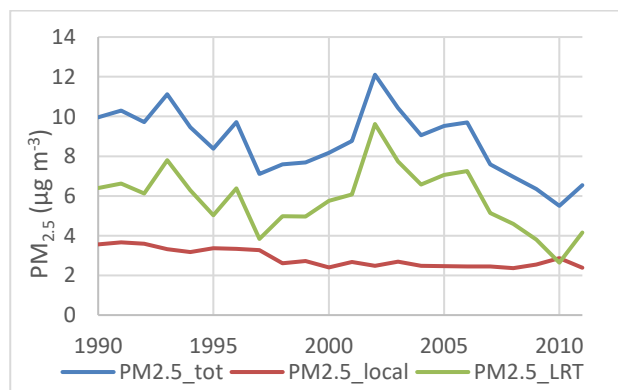


Fig. 1. Total, local and LRT, PM<sub>2.5</sub>, for 1990-2011.

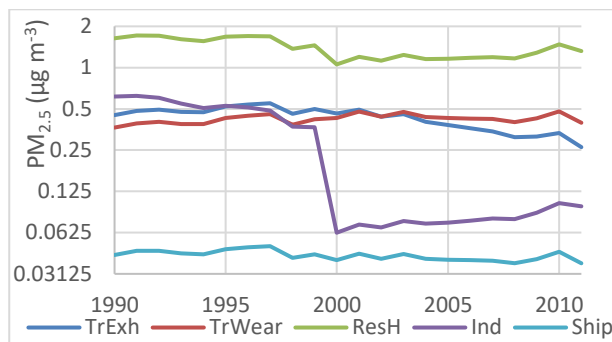


Fig. 2. Contribution from local PM<sub>2.5</sub> sources.

For BC, we found similar time trends as for PM<sub>2.5</sub>, with a small decrease in total locally produced BC. Strong decrease from industrial sources around the year 2000 was seen, a small decrease from traffic exhaust in the last 10 years, and generally lower contribution from residential heating in the second part of the study period compared to the first part (Fig. 3). The contribution from shipping increased over the period, but the absolute contribution to the population was small. The LRT contribution of BC was estimated to 0.2 ng m<sup>-3</sup> for the study period.

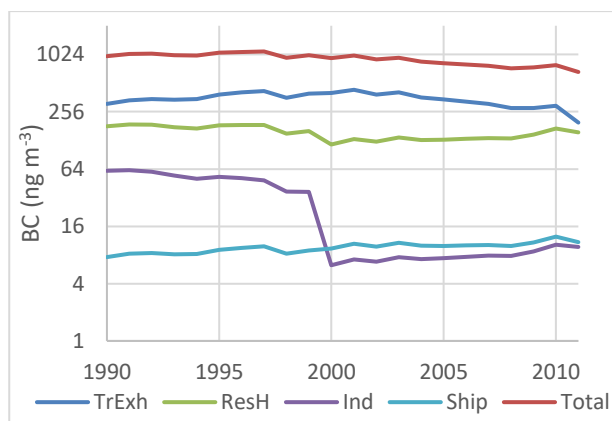


Fig. 3. Contribution from local BC sources.

### Conclusions

The changes in PM<sub>2.5</sub> concentration between years was driven by differences in LRT contribution. The reduction in locally produced PM<sub>2.5</sub> only influenced the total exposure marginally. For BC, the reduction of total BC was mainly driven by the reduction of the major local contributors, traffic exhaust and residential heating.

EEA 2014. Air quality in Europe - 2014 report. *European Environment Agency, Copenhagen*, EEA Report No 5/2014.

## Air quality in Ecuador: PM<sub>10</sub> characterization from 3 sites in the Amazon and Pacific Coast regions impacted by oil activities

F. Barraza<sup>1</sup>, G. Uzu<sup>2</sup>, E. Schreck<sup>1</sup>, H. Guyard<sup>2</sup>, A. Calas<sup>2</sup>, J.-L. Jaffrezo<sup>2</sup> and L. Maurice<sup>1</sup>

<sup>1</sup> Géosciences Environnement Toulouse (GET), Observatoire Midi Pyrénées, Université de Toulouse, CNRS, IRD, F- 31400 Toulouse, France

<sup>2</sup> IGE, Université Grenoble Alpes, CNRS, IRD, F-38000 Grenoble, France

Keywords: PM<sub>10</sub>, aerosols speciation, oil production, biomass burning, risk assessment  
fiorella.barraza@get.obs-mip.fr/ fiorella.barraza-castelo@univ-tlse3.fr

Crude oil reserves in Ecuador are essentially located in the Northeast Amazon region (NAR) whereas oil refining activities are developed along the Northern Pacific Coast (PC). During production, oil is extracted with formation water and gas and then separated in a central plant. On each drilling platform, waste gas is continuously burned in open flares, with basic emissions controls (San Sebastian and Hurtig, 2004). These practices still damage the environment and also represent a potential risk to inhabitants' health, who are exposed, by particles inhalation, to a cocktail of heavy metals and hydrocarbons (PAHs).

Literature dealing with aerosols chemical composition in Ecuador is dramatically poor. For that reason, two low-rate air samplers were installed in the NAR (Auca Sur and Shuara 9), close to open flares and one on the PC (Esmeraldas), in front of the National Refinery. Particulate matters (PM<sub>10</sub>) were collected monthly on quartz fiber filters, during two years (December 2014-December 2016).

Aerosol speciation was addressed by analyzing trace metals (ICP-MS), elementary and organic carbon OC/EC (thermal/optical analyzer), organic speciation (HPLC-PAD) and soluble species speciation (IC). PAHs contents were also measured (GC-MS). Oxidative potential of PM<sub>10</sub> was assessed by DTT assay in order to determine their ability to generate reactive oxygen species (ROS), which are key parameters to explain their biological effects.

Our results revealed that Mo and Ti present the highest concentrations of trace metals in PM<sub>10</sub> for the 3 sites, followed by Ba and Zn (in NAR) and Cr (in PC). No regulated metal exceeded PM<sub>10</sub> European or Ecuadorian regulations. The OC/EC ratios vary between 3 and 9 in the NAR and between 2 and 5 in the PC. Levoglucosan and Mannosan are the predominant monosaccharides, indicating that OC is mainly originated from biomass combustion episodes and soil biogenic emissions rather than oil activities. Soluble inorganic ions are dominated by sulphates, Na and K ions.

PM<sub>10</sub> mass balance, as already calculated by Chow et al. (2015) and Waked et al. (2014) formula, shows different source apportionment for the 3 sites (Figure 1). Organic matter (OM) is the main component in NAR whereas soil dust elements are the main elements recorded in PC. These first results tend to highlight the importance of agriculture practices, such as biomass burning or

deforestation, in the particles emission in the Northern Amazon.

Finally, DTT assay results show that aerosol chemical composition for each sampling area is able to induce different ROS quantities, indicating several potential damages for human health.

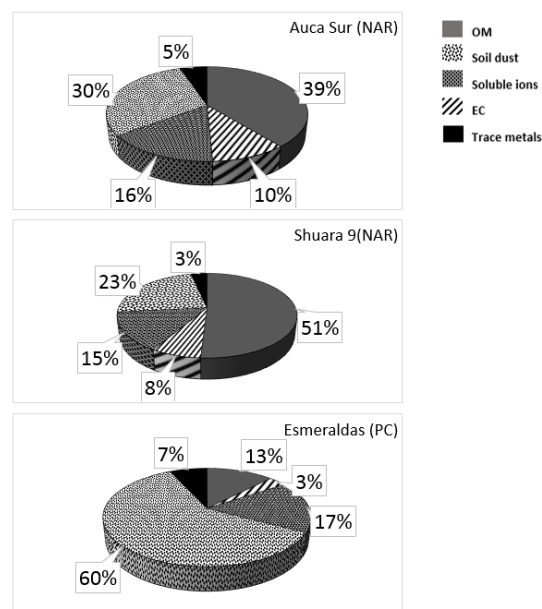


Figure 1. Chemical composition of PM<sub>10</sub> aerosols from 3 sampling sites in Ecuador

Further studies are however in progress to assess local population's exposure to the Heavy Metals-PAHs' cocktail.

The authors would like to thank the French National Agency of Research for the financial aid in the frame of the ANR-MONOIL Project N°ANR-13-SENV-0003-01

San Sebastián, M. and Hurtig, A.K. (2004). Pan Am J Public Health 15(3), 2004.

Chow, J.C., Lowenthal, D.H., Antony Chen, L.W., Wang, X. and Watson, J.G. (2015). Air Qual Atmos Health (2015)8:243-263.

Waked, A., Favez, O., Alleman, L.Y., Piot, C., Petit, J.-E., Delaunay, T., Verlinden, E., Golly, B., Besombes, J.-L., Jaffrezo, J.-L. and Leoz-Garziandia, E. (2014) Atmos. Chem. Phys., 14, 3325–3346, 2014

## Air quality planning and diesel vehicles: some surprises

T. Retny<sup>1</sup>, O. Klemm<sup>1</sup>, H. Hebbinghaus<sup>2</sup> and S. Wurzler<sup>2</sup>

<sup>1</sup>Institute of Landscape Ecology, Climatology, University of Münster, D-48249 Münster, Germany

<sup>2</sup>North Rhine-Westphalia State Agency for Nature, Environment, and Consumer Protection, Department of Air Quality Modelling, Anthropogenic Atmospheric Change, D-45133 Essen, Germany

Keywords: Urban air quality, modelling, diesel vehicles, PM<sub>10</sub>, NO<sub>2</sub>

Presenting author email: sabine.wurzler@lanuv.nrw.de

Road traffic is a main cause of air quality problems in cities all over the world. Despite years of air quality planning and a multitude of measures, air quality is still bad in busy street canyons and exceeds, e.g., the European annual average limit value for NO<sub>2</sub>.

For many years, it was expected that technical developments combined with stricter emission limit values for road vehicles would solve this problem, mainly with Euro 5 and 6 emissions standards. It was hoped that an increasing number of such modern vehicles would lead to a decrease of the NO<sub>x</sub> emissions and to compliance with the air quality limit values.

Yet, reality proved otherwise. Reductions in NO<sub>2</sub> concentrations were very weak (decrease of ~1-2 % NO<sub>2</sub> per year) over the last decade. If the decrease of nitrogen oxides continues to be that slow, limit value compliance for a majority of cases can be expected with some luck around 2030. This is far too late regarding European air quality regulations and the negative health effects of high NO<sub>2</sub> concentrations.

Differences between real driving emissions and the official test cycle emissions (NEDC) measurement were known to the experts for years. These are due to the NEDC taking into account only a small share of real life traffic situations and some other easings, e.g., no use of air conditioning and use of special tires. Therefore, emission models in general are based on real driving emission measurements. This poses a problem though when predicting air quality for future years and explains the high hopes on Euro 5 and 6.

With the so-called “Dieselgate” this problem became public news, escalated by the admission that some manufacturers not only used the existing loopholes but actively manipulated emission treatment to reach low levels during testing only. Fuelled by this, the idea of banning diesel vehicles from driving in cities was and is discussed publicly and controversially in different countries. Oslo has implemented such a ban for the first time in January 2017. Still, there is a lack of studies that investigate the actual effects on air quality in street canyons.

Aim of the present study is to estimate the possible reduction obtained by a ban of diesel vehicles of different Euro classes (Retny, 2016). A complete ban of diesel vehicles is not part of this study. The Immis<sup>Luft</sup> model (Diegmann, 2011) was used to calculate the NO<sub>2</sub> and PM<sub>10</sub> concentrations in four busy street canyons in North Rhine-Westphalia with different vehicle fleets. We distinguish the effects from the different road vehicle fleet members, such as e.g., passenger cars or heavy duty vehicles. The total number of vehicles was kept constant

for all the model calculations to avoid influences due to changes in the traffic flow. When omitting a certain Euro class, those vehicles were therefore replaced by increased numbers of vehicles from the other Euro classes.

Our model results show that air quality can be improved significantly by reducing the emission load caused by high emitting diesel vehicles, mostly with regard to NO<sub>2</sub> concentrations. Some vehicle types are much more promising in this regard than other. For example a ban of Euro 4 diesel vehicles leads only to a minor reduction of the NO<sub>2</sub> and PM<sub>10</sub> concentrations. The reason for this is that the Euro 4 vehicles are replaced mainly by Euro 5 vehicles and only by a low number of Euro 6 vehicles. Euro 5 vehicles emit in urban environments more NO<sub>x</sub> than Euro 4 vehicles do. This is compensated by the lower NO<sub>x</sub> emissions from Euro 6 vehicles. Therefore, the total effect is very low. Omitting Euro 4 and 5 diesel vehicles in the model calculations shows a much higher effect. Especially passenger cars and heavy duty vehicles are most promising with regard to improvements of the air quality. Owing to their low number compared to the number of passenger cars, light duty vehicles are of lesser relevance. Some of our findings are shown in Figure 1.

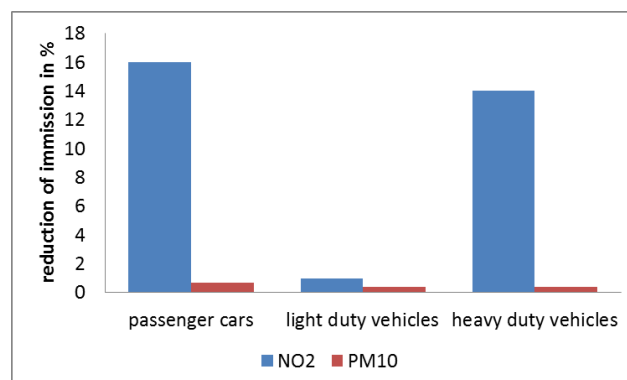


Figure 1. Model results for Friedrich-Ebert-Straße in Mönchengladbach: ban of Euro 4 and 5 diesel vehicles for passenger cars, light duty vehicles, and heavy duty vehicles. Effect on annual average NO<sub>2</sub> and PM<sub>10</sub> concentrations in %.

Retny, T. (2016) *Minderungspotenziale für NO<sub>2</sub> und PM<sub>10</sub> durch Fahrverbote für Dieselfahrzeuge in Umweltzonen*. Master thesis, University of Münster, 89pp.

Diegmann, V. (2011) *Immis<sup>em/luft/lärm</sup>, Handbuch*, IVU Umwelt GmbH, 175pp.

## Seasonal aerosol characteristics and sources at a rural site south in Beijing, China

Yang Hua<sup>1,2</sup>, Shuxiao Wang<sup>1,2</sup>, Jingkun Jiang<sup>1,2</sup>, Francesco Canonaco<sup>3</sup>, André S. H. Prévôt<sup>3</sup>, Wei Zhou<sup>1,2</sup>, Qingcheng Xu<sup>1,2</sup>, Xiaoxiao Li<sup>1,2</sup>, Baoxian Liu<sup>4</sup>

<sup>1</sup>State Key Joint Laboratory of Environment Simulation and Pollution Control, School of Environment, Tsinghua University, Beijing 100084, China.

<sup>2</sup>State Environmental Protection Key Laboratory of Sources and Control of Air Pollution Complex, Beijing 100084, China

<sup>3</sup>Laboratory of Atmospheric Chemistry, Paul Scherrer Institute, 5232 PSI Villigen, Switzerland

<sup>4</sup>Beijing Environmental Monitoring Center, Beijing 100048, China

Keywords: source apportionment, coal combustion, seasonal characteristics.

Presenting author email: huay13@mails.tsinghua.edu.cn

Air pollution in Beijing exhibited a remarkable spatial distribution characteristic of much higher concentration in south and lower concentration in north. Annual average PM<sub>2.5</sub> concentration of south sites was 30% higher than the whole city, while that of north sites was 32% lower (Beijing Municipal Environmental Protection Bureau, 2016). The much higher concentration in south was mainly resulted from two reasons. One is pollutants emissions is much higher in south of Beijing, especially in heating season. However, most researches were carried out at urban sites while pollution characteristics and sources in south of Beijing still lacks investigation, where residential coal combustion emission is high. In this study, we conducted continuous sampling in four seasons at a rural site southwest in Beijing. Pollution characteristics are investigated. A novel procedure of positive matrix factorization (PMF), the multi-linear engine (ME-2) algorithm is applied to ACSM OA spectra (Canonaco *et al* (2013)), providing an insight into pollution process in the most polluted area in Beijing.

The observation was conducted in four seasons (October 22<sup>nd</sup> to November 12<sup>th</sup>, 2014; March 30<sup>th</sup> to April 30<sup>th</sup>, 2015; August 11<sup>th</sup> to September 7<sup>th</sup>, 2015; December 5<sup>th</sup>, 2015 to January 7<sup>th</sup>, 2016) from 2014 to 2016. The sampling site was located at a rural site (Liulihe site, 116°2'E, 39°36'N) in the southwest in Beijing. The site is located on the border of Beijing and Hebei province. The district the site located in is most polluted in Beijing. The sampling height was 3m, on the roof of a one-storey sampling station 500m away from the traffic road. The sampling instruments include weather station (WXT520, VAISALA, Finland), gas pollutants monitors (API100/200/400E, Teledyne, USA) and PM<sub>2.5</sub>/PM<sub>10</sub> monitors (TEOM1405/1400a, Thermo Scientific, USA). ACSM was used to measure species including organic matter (OM), nitrate, sulfate, ammonium and chloride of NR-PM<sub>1</sub>.

Characteristics of sulfate and LVOOA in spring showed a significant regional transport impact. As to summer, photochemical reaction played a significant role in pollution. When it comes into autumn, SVOOA and nitrate contributed the most, indicating important contribution from local emission oxygenation. In winter season, pollution showed much more severe than other seasons. The severe pollution was resulted from the high

contribution of coal combustion, evidenced by the significant changes of pollution characteristics when entering into the heating period. The study also proved residential coal combustion for heating made a big difference on the much more severe pollution in rural area than urban area in Beijing. The combustion not only contributed high concentration of POA, but also sulfate and precursors such as NO<sub>2</sub>. More efforts must be put into the coal combustion emission control to reduce the pollution concentration in winter.

This work was supported by the MEP's Special Funds for Research on Public Welfare (201409002), Strategic Priority Research Program of the Chinese Academy of Sciences (XDB05020300), and National Natural Science Foundation of China (21625701 & 21521064). The authors also appreciate the support from Collaborative Innovation Center for Regional Environmental Quality.

Beijing Municipal Environmental Protection Bureau. (2016)

<http://www.bjepb.gov.cn/bjepb/resource/cms/2016/04/2016041514503583104.pdf>.

Canonaco, F., Crippa, M., Slowik, J.G., Baltensperger, U. and Prevot, A.S.H. (2013) *Atmospheric Measurement Techniques* **6**(12), 3649-3661.

## A chemometric approach to predict the contribution of ships to air pollution

H. Czech<sup>1</sup>, T. W. Adam<sup>2,3</sup>, B. Stengel<sup>4,5</sup>, M. Sklorz<sup>1</sup>, T. Streibel<sup>1,5</sup> and R. Zimmermann<sup>1,2,5</sup>

<sup>1</sup>Joint Mass Spectrometry Centre, Chair of Analytical Chemistry, University of Rostock, Dr.-Lorenz-Weg 1, 18059 Rostock, Germany

<sup>2</sup>Joint Mass Spectrometry Centre, Cooperation Group “Complex Molecular Analysis” (CMA), Helmholtz Zentrum München, Ingolstädter Landstrasse 1, 85764 Neuherberg, Germany

<sup>3</sup>Adviron Environmental Consulting, Hans-Unterleitner-Weg 10, 85354 Freising

<sup>4</sup>Department of Mechanical Engineering and Marine Technology, University of Rostock, Albert-Einstein-Straße 2, 18059 Rostock, Germany

<sup>5</sup>HICE – Helmholtz Virtual Institute of Complex Molecular Systems in Environmental Health ([www.hice-vi.eu](http://www.hice-vi.eu))

Keywords: HFO, MGO, PAH, SECA.

Presenting author email: [hendryk.czech@uni-rostock.de](mailto:hendryk.czech@uni-rostock.de)

Ship traffic is known to affect climate and human health globally. Since the introduction of sulphur emission control areas (SECA) for coastal waters and semi-enclosed seas of Europe and North America, the marine fuel consumption shifted from heavy fuel oil (HFO) to marine gas oil (MGO) as a lighter sulphur-reduced fraction of the crude oil refinery. Marker substances for ship emission, such as SO<sub>2</sub>, sulphate and the ratio of vanadium to nickel, are almost exclusively related to HFO and show lower abundances and ratios for MGO. Therefore, the discrimination between ship emissions and other combustion emission sources has been complicated (Bläsing, 2016). Since ship emissions are responsible for increased mortality in coastal areas with much ship traffic (Corbett et al., 2007), it is of interest to identify and quantify its contribution to ambient air pollution.

The primary volatile aromatic emissions of a bench-scale marine engine (maximum power of 80 kW), operated on HFO (2.3 % S) and MGO (0.08 % S) at different engine loads and fuel injection times were studied by laser-based time-of-flight mass spectrometry with resonance-enhanced multi-photon ionisation (REMPI) at 266 nm. REMPI refers to a soft ionisation technique with high selectivity for aromatic compounds (Boesl, 2000). Furthermore, the obtained spectra were combined with REMPI spectra from previously published studies of marine engines with HFO, wood stoves, diesel cars, gasoline cars and scooters to derive markers or latent variables suitable for ship emission identification and quantification. In a simulation, pseudo-randomly selected 5 % of the entire mass spectra of ship emissions were averaged, weighted from 0 to 1 in 0.1-steps ( $\phi$ , “ship contribution”) and combined with non-ship mass spectra weighted by 1 -  $\phi$ , leading to 1000 artificially-generated spectra of ambient air from known primary emission sources for every  $\phi$ .

First, ship and non-ship emissions were investigated for possible markers or discriminative m/z values by Kruskal-Wallis test and principal component analysis (PCA). Both techniques revealed that PAH with higher degree of alkylation are characteristic for ship emission of both fuels and less abundant in the non-ship emissions so that the emission classes are well-separated by the PCA scores. However, simple linear relations

between  $\phi$  and diagnostic ratios of two m/z with proper accuracy could not be observed.

On that account, a prediction model based on partial least-square (PLS) regression with two PLS components was generated for each fuel, i.e. for SECA and non-SECA, explaining 98 % of variance of  $\phi$ . Root mean squared prediction errors from 5- and 10-fold cross validation as well as an external test data set account for 0.033±0.001 in case of both fuels, characterising model validity and predictive power.

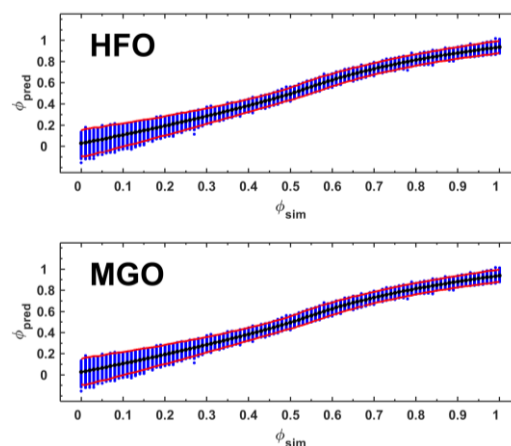


Figure 1. PLS regression models based on two PLS components for simulated and predicted  $\phi$  (blue), interval of the mean at 95 % confidence (black) as well as 3-fold standard deviation ( $3\sigma$ , red).

Based on  $3\sigma$  at  $\phi_{sim}$  of 0 and 1, quantitative results can be given between  $\phi_{sim}$  of 0.150 and 0.892 (HFO), and 0.152 and 0.895 (MGO) (Figure 1). In addition to the identification of ships running with MGO, this model might be able to detect HFO emission with exhaust after-treatment, which reduces sulphur and particle emissions, and support source apportionment.

This work was funded by the DACH-project “WooShi - Wood Combustion and Shipping” (grant ZI 764/5-1).

Bläsing, M., Kistler, M., & Lehndorff, E. (2016)

*Org. Geochem.*, **99**, 1-9.

Boesl, U. (2000) *J. Mass Spectrom.*, **35**, 289-304

Corbett, J. J., Winebrake, J. J., Green, et al. (2007)

*Environ. Sci. Technol.*, **41**(24), 8512-8518.

## Source apportionment of the organic fraction in the forest area

S. Byčėnkiėnė<sup>1</sup>, L. Krikščikas<sup>1</sup>, G. Mordas<sup>1</sup>, V. Dudoitis<sup>1</sup>, and V. Ulevicius<sup>1</sup>

<sup>1</sup>Department of Environmental Research, SRI Center for Physical Sciences and Technology, Vilnius, LT-02300, Lithuania

Keywords: source apportionment, organic aerosol, low-volatility OOA, semi-volatility OOA.

Presenting author email: steigvile.bycenkiene@ftmc.lt

Recent field and laboratory evidence indicates that the largest global source of organic aerosol (OA) in the atmosphere is derived from the oxidation of biogenic emissions. In many analyses, the oxygenated OA (OOA) can be further deconvolved into low-volatility OOA (LV-OOA) and semi-volatile OOA (SV-OOA). Differences in the mass spectra of these components are characterized in terms of the two main ions  $m/z$  44 ( $\text{CO}_2^+$ ) and  $m/z$  43 (mostly  $\text{C}_2\text{H}_3\text{O}^+$ ), which are used to identify the aging of OA components in the atmosphere (Fig. 1 (bottom)).

The aerosol chemical composition was measured by an Aerodyne aerosol chemical speciation monitor (ACSM, Ng et al., 2011). 1-h time resolution ACSM data were analysed to elucidate the PM<sub>1</sub> chemical composition using a graphical user interface SoFi (Paatero and Tapper, 1994), developed at PSI to perform a positive matrix factorization (PMF) source apportionment of the non-refractory organic aerosol mass spectra.

Organic aerosol spectra analysis (Fig. 1) was performed during a June month in Lithuania in forested environment of the South-East Baltic region. The area in research site is dominated by conifers. Enhancement of biogenic volatile organic compounds (BVOCs) (dominating by monoterpenes and isoprene) emissions from the forest due to abiotic stress (high temperature and solar radiation) was observed. However, the presence of abiotic stress (heat wave) changed the composition of the organic aerosol and as a result aerosol mass spectra. Positive matrix factorization was performed to understand the chemical characteristics of low-volatility OOA and semi-volatile OOA (Fig. 1). The background OA represented aged organic aerosol (with an intense signal of  $\text{CO}_2^+$  fragments) and a high degree of oxygenation O:C (>0.8). Our findings highlight the potential importance of gas-phase formation chemistry of stress induced new particle formation. We demonstrated that low-volatility vapours dominate the formation and growth of aerosol particles over forested regions. The low-volatility OOA component spectra have higher  $f_{44}$  (ratio of  $m/z$  44 to total signal in the component mass spectrum) and lower  $f_{43}$  (ratio of  $m/z$  43 to total signal in the component mass spectrum) than semi-volatile OOA.

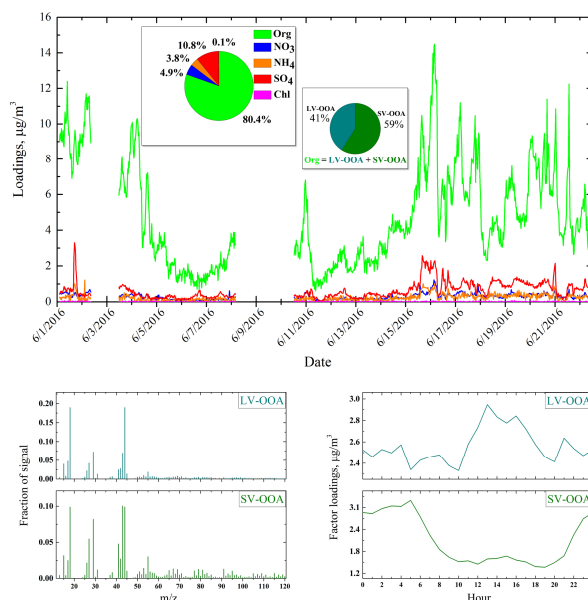


Figure 1. Upper: Average chemical composition and time series of NR-PM<sub>1</sub> OA for the entire study (relative contribution of NR-PM<sub>1</sub> chemical species (pie chart inside)). Bottom: time series of organic species (semivolatile oxygenated organic aerosol and low-volatility oxygenated organic aerosol) concentrations in June 2016.

This work was supported by the National Research Programme “Sustainability of agro-, forest and water ecosystems” project FOREstRESS (No. SIT-3/2015).

Ng, N. L., Herndon, S. C., Trimborn, A., Canagaratna, M. R., Croteau, P. L., Onasch, T. B., Sueper, D., Worsnop, D. R., Zhang, Q., Sun, Y. L., and Jayne, J. T. *Aerosol Sci. Tech.*, 45, 770–784, 2011.

Paatero, P. and Tapper, U. *Environmetrics*, 5, 111–126, 1994.

## Source apportionment of atmospheric particulate matter (PM<sub>10</sub>) using a constrained US-EPA-PMF5.0 model on different urban environments in France

D. Salameh<sup>1</sup>, O. Favez<sup>2</sup>, B. Golly<sup>1</sup>, J-L. Besombes<sup>3</sup>, L. Y. Alleman<sup>4</sup>, A. Albinet<sup>2</sup>, J-L. Jaffrezo<sup>1</sup>

<sup>1</sup>Université Grenoble Alpes-CNRS, IGE UMR5001, 38402 St-Martin d'Hères, France

<sup>2</sup>INERIS, DRC/CARA/CIME, 60550 Verneuil-en-Halatte, France

<sup>3</sup>Université Savoie Mont Blanc, LCME, 73376 Le Bourget du Lac, France

<sup>4</sup>IMT Lille Douai, Univ. Lille, SAGE, 59000 Lille, France

Keywords: particulate matter, harmonized source apportionment, constrained PMF, urban sites

Presenting author email: [dalia.salameh@univ-grenoble-alpes.fr](mailto:dalia.salameh@univ-grenoble-alpes.fr)

Particulate matter (PM) is one of the most studied atmospheric pollutant in urban areas due to particles adverse effects on human health (Pope et al., 2009). Intrinsic properties of PM (e.g. chemical composition and morphology) are directly linked to their origins. A harmonized and comprehensive apportionment study of PM sources in urban environments is extremely required to connect source contributions with PM concentration levels and then develop effective PM abatement strategies.

Multivariate receptor models such as Positive Matrix Factorization (PMF) are very useful and have been used worldwide for PM source apportionment (Viana et al., 2008). PMF uses a weighted least-squares fit and quantitatively determines source fingerprints (factors) and their contributions to the total PM mass. However, in many cases, it could be tricky to separate two factors that co-vary due to similar seasonal variations, making unclear the physical sense of the extracted factors. To address such issues of source collinearities, additional specific constraints are incorporated into the model (i.e. constrained PMF) based on user's external knowledge allowing better apportionment results.

In this work and within the framework of the SOURCES project, a harmonized source apportionment approach has been implemented and applied for the determination of PM<sub>10</sub> sources on a large number of sites (up to 20) of different typologies (e.g. urban background, industrial, traffic, rural and/or alpine sites) distributed all over France and previously investigated with annual or multiannual studies (2012-2016). A constrained PMF approach (using US-EPA PMF5.0 software) was applied to the comprehensive PM-offline chemical datasets (i.e. carbonaceous fraction, major ions, metals/trace elements, specific organic markers) in a harmonized way for all the investigated sites. Different types of specific chemical constraints from well-characterized sources were defined based on external knowledge and were imposed to some species in the PMF factor profiles. As an example, the contributions of the levoglucosan and mannosan, specific tracers of the biomass burning emissions, were pulled up maximally in the biomass burning factor profile resolved at Port de Bouc site (**Figure 1**) and were

set to zero in all other resolved PMF factors (e.g. vehicular emissions, biogenic emissions, etc...).

The different source categories contributing to ambient PM concentration levels were chemically characterized and quantified. Chemical profiles of the resolved common sources have been compared and give first time indication on the spatial variabilities of the source compositions, and their applicability as forcing factors in a fully constrained PMF.

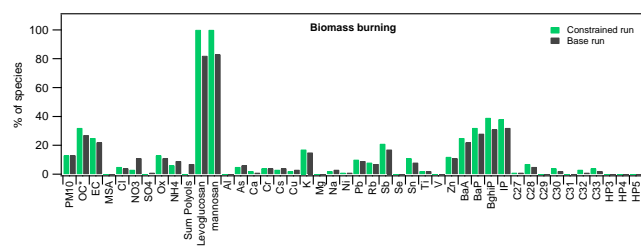


Figure 1. Example of the biomass burning factor (expressed in % of species) at Port de Bouc site for both base (grey) and constrained (green) PMF runs. The contributions of levoglucosan and mannosan were pulled up maximally in this factor.

The presentation will address the main points achieved with this program.

This work, including a postdoctoral grant for D Salameh, is funded by the French Ministry of Environment, Energy, and Sea (MEEM) through the Environment and Energy Management Agency (ADEME, contract 1462C0044 for the SOURCES program) and the national reference laboratory for air quality monitoring (LCSQA). The authors also gratefully acknowledge the funding by ANDRA of the program conducted at OPE by S Conil, and all dedicated staffs within the French regional monitoring networks for collecting the samples.

Pope, I. C., et al. (2009), *New England Journal of Medicine*, **360**(4), 376-386.

Viana, M., et al. (2008), *Journal of Aerosol Science*, **39**(10), 827-849.

## Extensive full-year source apportionment data analysis of organic aerosols

A. Tobler<sup>1</sup>, Y. Sosedova<sup>1</sup>, F. Canonaco<sup>1</sup>, A. Vlachou<sup>1</sup>, K. Dällenbach<sup>1</sup>, R. Fröhlich<sup>1</sup>, A. Prévôt<sup>1</sup> and U. Baltensperger<sup>1</sup>

<sup>1</sup>Laboratory of Atmospheric Chemistry, Paul Scherrer Institute, Villigen, Switzerland

Keywords: organic aerosol, positive matrix factorization, source apportionment.

Presenting author email: anna.tobler@psi.ch

Atmospheric aerosols are recognized to have adverse effects on climate (Carslaw et al., 2010), visibility (Watson, 2002) and human health (Peng et al., 2005). Therefore, the identification and source apportionment of those particles is of great importance. The Aerosol Chemical Speciation Monitor (ACSM, Aerodyne Research, Inc.) has been proven to be a robust instrument for long-term monitoring and characterization of the atmospheric particulate matter levels (Ng et al., 2010). Organic aerosol (OA) is further analyzed with Positive Matrix Factorization (PMF) (Paatero & Trapper, 1994). The main limitation of PMF is the assumption of constant factors. However, chemical fingerprints of OA factors may change due to meteorology or seasonality. To overcome this limitation, a small and rolling PMF window is moved over the dataset and allows the factor profiles to vary over time. This rolling module is part of the new SoFi interface (Canonaco et al., 2013) and is further described in Canonaco et al. (in prep.).

The rolling SoFi was applied to apportion OA sources in Magadino, Switzerland, based on one-year ACSM measurements (September 2013 to September 2014). The ACSM station in Magadino represents a rural site south of the Alps and is part of the Swiss National Air Pollution Monitoring Network (NABEL). To account for the varying chemical fingerprints of the aerosol factors during the year, PMF was run on a small window. Shifting the window on a daily basis allowed the OA factor profiles to adapt to the measured data. Resampled PMF runs with the bootstrap algorithm (Davison & Hinkley, 1997) applied on every window allowed the estimation of the statistical uncertainty of the PMF solution.

Seasonal PMF runs allowed establishing three main primary OA factors: traffic-related hydrocarbon-like HOA, biomass-burning BBOA and an amine-like local organic factor (LOA). The rolling mechanism was initialized constraining HOA, BBOA and LOA within the a-value approach. One up to two factors were left unconstrained to account for secondary OA sources. Rolling SoFi determined the number of oxygenated OA factors (OOA), based on the difference in fractions of the less and more oxygenated fragments in the OOA profiles.

The PMF runs resulting from the rolling PMF algorithm were post-analyzed using a set of criteria that defined the environmentally reasonable PMF runs. Such criteria could, for example, contain the Pearson correlation coefficients  $R^2$  between the factor solution and its corresponding tracer. The set of retained PMF

runs spans the so-called PMF solution. The variability within the a-value space and within the repeats can further be used to estimate the PMF uncertainty that contains both the rotational uncertainty and the statistical uncertainty. Fig. 1 shows the source apportionment result for the full-year analysis according to the procedure described above. For the future, further improvements of the rolling SoFi algorithm are planned: instead of a-value technique, the PMF input can be varied randomly to propagate the statistical model uncertainty to the PMF results. Instead of taking one “best” solution, we will decide for the cut-off of the group of “best” solutions.

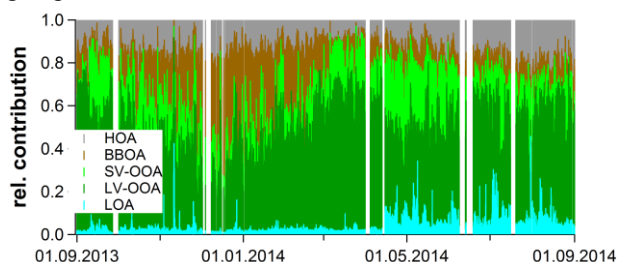


Figure 1. Full-year source apportionment of organic aerosols in Magadino 2013-2014

The ACSM measurements were supported by the Swiss Federal Office for the Environment (FOEN).

Canonaco, F., Crippa, M., Slowik, J. G., Baltensperger, U., & Prévôt, A. S. H. (2013). *Atmospheric Measurement Techniques*, **6**(12), 3649-3661.

Canonaco, F., Baltensperger, U., Prévôt, A. S. H., in prep.

Carslaw, K. S., Boucher, O., Spracklen, D. V., Mann, G. W., Rae, J. G. L., Woodward, S., & Kulmala, M. (2010). *Atmospheric Chemistry and Physics*, **10**(4), 1701-1737.

Davison, A. C., Hinkley, D. V. (1997). *Bootstrap methods and their application* (Vol. 1): Cambridge university press.

Ng, N. L., Canagaratna, M. R., Zhang, Q., Jimenez, J. L., Tian, J., Ulbrich, I. M., Worsnop, D. R. (2010). *Atmos. Chem. Phys.*, **10**(10), 4625-4641.

Paatero, P., Tapper, U. (1994). *Environmetrics*, **5**(2), 111-126.

Peng, R. D., Dominici, F., Pastor-Barriuso, R., Zeger, S. L., & Samet, J. M. (2005). *American Journal of Epidemiology*, **161**(6), 585-594.

Watson, J. G. (2002). *Journal of the Air & Waste Management Association*, **52**(6), 628-713.

## Seasonal Characterization of Organic Aerosol Sources and Composition Using Extractive Electrospray Ionization Time-of-flight Mass Spectrometry (EESI-TOF)

Lu Qi<sup>1,2</sup>, Alexander L. Vogel<sup>1</sup>, Sepideh Esmaeilrad<sup>1</sup>, Mindong Chen<sup>2</sup>, Xinlei Ge<sup>2</sup>, Urs Baltensperger<sup>1</sup>, Andre S. H. Prevot<sup>1</sup>, Jay G. Slowik<sup>1</sup>

<sup>1</sup>Laboratory of Atmospheric Chemistry, Paul Scherrer Institute, 5232 PSI Villigen, Switzerland

<sup>2</sup>Jiangsu Key Laboratory of Atmospheric Environment Monitoring and Pollution Control (AEMPC), Department of Environmental Science and Engineering, Nanjing University of Information Science & Technology, Nanjing 210044, China

Keywords: EESI-TOF, seasonal composition, source apportionment  
lu.qi@psi.ch

Organic aerosol (OA) has significant but highly uncertain effects on climate and human health. Online aerosol mass spectrometry (AMS), combined with statistical methods such as positive matrix factorization (PMF), have greatly advanced quantification of primary organic aerosol (POA) sources and total secondary organic aerosol (SOA) mass. However, such online measurements have two significant limitations: (1) AMS expense and operational requirements make impractical its use for long-term or spatially dense monitoring applications; and (2) the use of thermal vaporization and electron ionization yields extensive thermal decomposition and ionization-induced fragmentation, destroying chemical information needed for SOA source apportionment. PSI has overcome the first limitation through the development of a method for using online instrumentation to sample extracted and re-aerosolized material from filter samples routinely collected at ambient monitoring stations (Daellenbach et al., 2016, “offline-AMS”) and the second by development of a novel extractive electrospray ionization time-of-flight mass spectrometer (EESI-TOF).

The EESI-TOF provides mass spectra of the organic aerosol fraction with a linear response to mass and no thermal decomposition or ionization-induced fragmentation. Like the AMS, the EESI-TOF can be deployed in both laboratory and field settings, maximizing its utility for source apportionment. A continuously sampled aerosol flow intersects with a spray of charged droplets (50/50 water/methanol with 100 ppm NaI as a charge carrier) generated from a conventional electrospray source. OA components dissolve in the spray and pass through a heated capillary into vacuum, where the solvent evaporates. This increases the electrostatic repulsion of like charges, causing ejection of ions as sodium adducts, which are detected by time-of-flight mass spectrometry.

In this study, we analysed 86 filters collected at the NABEL monitoring station at Zürich-Kaserne, an urban background site. These filters were collected for 24 hours each, approximately every 4th day throughout 2013, then measured by adapting the offline-AMS method to EESI-TOF measurements. Figure 1 shows a yearly cycle of four selected ions: C<sub>6</sub>H<sub>10</sub>O<sub>5</sub> (levoglucosan and isomers), as well as C<sub>8</sub>H<sub>12</sub>O<sub>6</sub>, C<sub>9</sub>H<sub>12</sub>O<sub>5</sub>, and C<sub>8</sub>H<sub>10</sub>O<sub>6</sub>, which have all been observed in terpene oxidation products. C<sub>6</sub>H<sub>10</sub>O<sub>5</sub> is strongly elevated in

winter, while C<sub>9</sub>H<sub>12</sub>O<sub>5</sub> and C<sub>8</sub>H<sub>10</sub>O<sub>6</sub> peak during the summer months. These trends are consistent with previous studies identifying wood burning as a major source of wintertime OA in Zürich and terpene-derived biogenic SOA as a major summertime aerosol source in Central Europe. The time trend of C<sub>8</sub>H<sub>12</sub>O<sub>6</sub> is more difficult to interpret, as it correlates with terpene-related ions during the summer but levoglucosan during the winter. This is likely because C<sub>8</sub>H<sub>12</sub>O<sub>6</sub> can represent either 3-methyl-1,2,3-butanetricarboxylic acid (MBTCA) from terpene oxidation or hydroperoxides from the oxidation of phenolic compounds (Nakao et al., 2011; Yee et al., 2013), which are important precursors for SOA from wood burning (Bruns et al., 2016).

The complexity of the C<sub>8</sub>H<sub>12</sub>O<sub>6</sub> time series highlights the need for factor analysis of the offline EESI-TOF dataset. PMF analysis yields factors related to wood burning (POA and SOA) as well as biogenic SOA and local sources. The retrieved factors are analyzed in terms of their composition, correlation with marker ions, and relationship to offline-AMS factors retrieved over the same period.

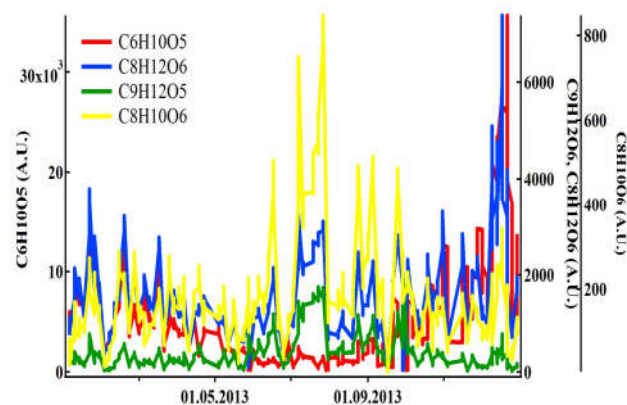


Figure 1. Yearly cycle of selected ions measured by the EESI-TOF

This work was supported by the Swiss National Science Foundation (starting grant BSSGI0\_155846) and BAFU.

Bruns et al. (2016) *Nature Sci. Rep.*, **6**, 27881.  
Daellenbach et al. (2016) *Atmos. Meas. Tech.*, **9**, 23-39.  
Nakao et al. (2011) *Atmos. Chem. Phys.*, **11**, 10649-10660.  
Yee et al. (2013) *Atmos. Chem. Phys.*, **13**, 8019-8043.

## Source apportionment of PM in Leipzig, Germany: From coarse to ultrafine particle size ranges

Dominik van Pinxteren<sup>1</sup>, Khandeh Wadinga Fomba<sup>1</sup>, Konrad Müller<sup>1</sup>, Gerald Spindler<sup>1</sup>, Gunter Löschau<sup>2</sup>, Andrea Hausmann<sup>2</sup> and Hartmut Herrmann<sup>1</sup>

<sup>1</sup> Leibniz-Institut für Troposphärenforschung (TROPOS), Atmospheric Chemistry Department (ACD), Permoserstr. 15, 04318 Leipzig, Germany

<sup>2</sup> Saxon State Office for Environment, Agriculture and Geology, Pillnitzer Platz 3, 01326 Dresden, Germany

Keywords: size-resolved aerosol particles, chemical composition, PMF, air quality.  
Presenting author email: dominik@tropos.de

A field campaign was conducted in 2013-2015 to chemically characterize aerosol particles and apportion their sources in five different size ranges, ranging from coarse to quasi-ultrafine particles. Forty-two size-resolved samples were taken using 5-stage Berner impactors at 4 sites in parallel (heavy traffic site, street-canyon kerbside, urban background, rural background) during summer and winter. All samples were analysed for inorganic ions, OC/EC, water-soluble organic carbon, trace metals and a variety of organic compounds including oxalate, monosaccharides, alkanes, PAHs and hopanes. Source apportionment was performed using Lenschow and macrotracer approaches as well as positive matrix factorisation (PMF). At a traffic site in the city centre of Leipzig, 50% of ultrafine mass concentration was found to be related to traffic emissions, while the urban and the regional background contribution was 20% and 30%, respectively, indicating a large reduction potential by local mitigation measures. Coarse particle mass concentration resulted to broadly the same extent, i.e. 1/3 each, from traffic, urban background and regional background sources. Accumulation mode particles showed highest absolute mass concentrations, 2/3 of which originated was imported from the regional background into the city centre and is thus difficult to control by local administrative actions.

PMF resolved a total of 11 sources: traffic exhaust, general traffic, coal combustion, biomass combustion, photochemistry, general secondary formation, cooking, fungal spores, urban dust, fresh sea/road salt and aged sea salt. Many of these were present in some of the particle size ranges only. PMF-derived mean source contributions agreed reasonably well with estimates from established macrotracer approaches, where available. In Figure 1, the relative contributions of the identified sources are shown for 3 impactor stages, i.e. 3 different particle size ranges (quasi-ultrafine, accumulation mode, coarse range) and all sites during different air mass regimes (season + air mass origin).

The quasi-ultrafine particle mass originated mainly from traffic (20-50%) and photochemistry (30-50%) in summer, while it was dominated by solid fuel (mainly biomass) combustion in winter (50-70%). For accumulation mode particles, two secondary sources typically contributed 40–90% to particle mass. In winter,

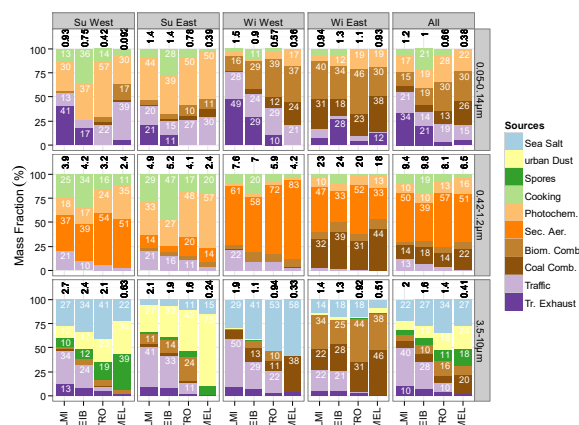


Figure 1. Mean source contributions (in percent of total mass concentration per particle size range) of quasi-ultrafine (upper row), accumulation mode (middle row) and coarse mode particles (lower row) during different seasons (Su=Summer, Wi= Winter) and air mass origins (West and East) and at the four different sites: LMI: traffic site in Leipzig city centre, EIB: mixed traffic/residential urban site, TRO: urban background at TROPOS institute, MEL: regional background site in Melpitz.

biomass and coal combustion contributions were up to ca. 25% and 45%, respectively. Main sources of coarse particles were diverse and included nearly all PMF-resolved ones depending on season and air mass origin. Source contributions to PM10 were determined from the sum of all impactor stages. Main sources were traffic (20-40% at kerbsides), photochemistry and secondary formation (30-60%), biomass combustion (10-15% in winter), and coal combustion (30-40% in winter with eastern air mass inflow).

A comparison with data from a previous campaign in the years 1999/2000 (Herrmann et al., 2006) indicated a strong reduction of traffic-related ultrafine particle mass and constituents concentrations (i.e. OC, EC, sulfate, alkanes, PAHs). EC traffic increments in ultrafine particles were less than 50% of the year 2000 ones, corroborating findings of other studies on the effectiveness of a low emission zone implemented in the city of Leipzig in 2011.

Herrmann, H., Brüggemann, E., Franck, U., Gnauk, T., Löschau, G., Müller, K., Plewka, A., Spindler, G., (2006), *J. Atmos. Chem.* **55**(2), 103-130.

## Source apportionment of ambient organic aerosol by online extractive electrospray ionization time-of-flight mass spectrometry (EESI-TOF)

G. Stefenelli<sup>1</sup>, F. D. Lopez-Hilfiker<sup>1</sup>, V. Pospisilova<sup>1</sup>, A. Vogel<sup>1</sup>, C. Hüglin<sup>2</sup>, U. Baltensperger<sup>1</sup>, A. S. H. Prévôt<sup>1</sup>, J. G. Slowik<sup>1</sup>.

<sup>1</sup>Laboratory of Atmospheric Chemistry, Paul Scherrer Institute, 5232, Villigen, Switzerland

<sup>2</sup>EMPA, Dübendorf 8600, Switzerland

Keywords: ambient aerosol, secondary organic aerosol, EESI-TOF

Presenting author email: [giulia.stefenelli@psi.ch](mailto:giulia.stefenelli@psi.ch)

Anthropogenic and biogenic emissions contain large amounts of volatile organic compounds (VOCs) which may undergo photochemical aging to yield secondary organic aerosol (SOA). The magnitude of SOA production from different sources remains highly uncertain, hindering estimates of the contribution of this source to the total ambient organic aerosol. Measurement techniques with high time resolution and chemical specificity are thus urgently needed, however, current methods suffer from thermal decomposition or ionization-induced fragmentation, which destroys the chemical information required for SOA source apportionment.

PSI has recently developed a novel extractive electrospray ionization time-of-flight mass spectrometer (EESI-TOF), which enables real-time chemical analysis of atmospheric particles without thermal decomposition or ionization-induced fragmentation (Lopez-Hilfiker et al., 2017). A stream of continuously sampled, suspended aerosol particles intersects with a highly charged spray (50/50 water/methanol with 100 ppm NaI) generated by a conventional electrospray probe. Organic compounds are rapidly extracted, ionized, and detected as sodium adducts.

We present results from the first field deployment of the EESI-TOF. Measurements were performed for one month during summer 2016 at a well characterized urban site in Zurich. Supporting measurements included proton transfer reaction time-of-flight mass spectrometer (PTR-TOF-MS) and a high resolution time-of-flight aerosol mass spectrometer (HR-ToF-AMS), as well as meteorological data and gas phase concentrations of specific tracers like NO<sub>x</sub> and SO<sub>2</sub> from the well-equipped National Air Pollution Monitoring Network (NABEL) station at the same measurement site.

Positive matrix factorization (PMF) analysis of EESI-TOF data yielded several organic aerosol factors related to primary and secondary emissions. Further, factors were separated according to different mass spectral fingerprints and aging processes. Some of the retrieved factors correlated strongly with reasonable counterparts from AMS PMF analysis, while others provide previously inaccessible insight into sources and ambient processing.

Figure 1 shows diurnal cycles of each OA factor, grouped as (a) primary OA; (b) SOA peaking during

daylight; and (c) SOA peaking at night. The primary factors include a cooking-related factor which includes long-chain fatty acids and levoglucosan (likely influenced by nearby open cooking activities), and an additional primary source showing high correlation with traffic and cigarette smoke emissions. The daytime factors are dominated by ions characteristic of monoterpene and sesquiterpene oxidation, with a lower contribution from aromatic oxidation products. Two nighttime SOA factors are observed, with one peaking overnight and one in the early morning. The first nighttime factor includes less oxygenated and more volatile terpene oxidation products, as well as organonitrates which are likely derived from NO<sub>3</sub> radical oxidation of monoterpenes. The factor peaking in the early morning contains the same signatures but also a stronger contribution from aromatic oxidation products, consistent with the onset of photochemistry.

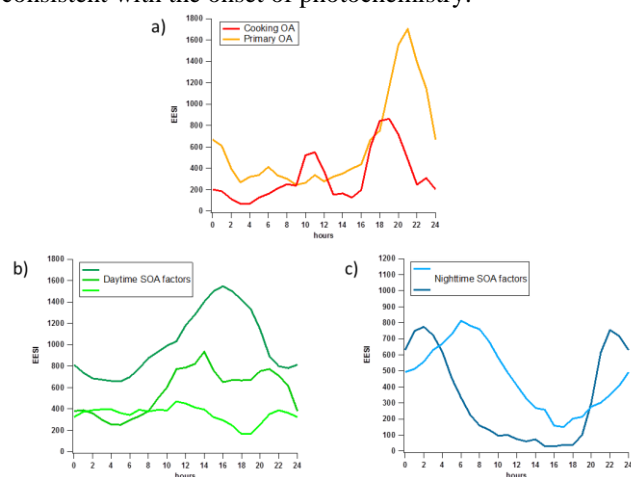


Figure 1. EESI-TOF organic aerosol factors: a) Diurnal patterns of primary organic aerosol factors, one of which is related to cooking emissions peaking at lunch and dinner time. b) Diurnal patterns of secondary organic aerosol factors peaking during daytime. c) Diurnal patterns of secondary organic aerosol factors peaking during night and early morning.

This work was supported by the Swiss National Science Foundation (starting grant BSSG10\_155846).

F. D. Lopez-Hilfiker et al., *in prep.* (2017).

## Sources of PM<sub>10</sub> at an urban air monitoring site in New South Wales, Australia

K. Larcombe<sup>1</sup>, R. Jayaratne<sup>1, 2</sup> and G. A. Ayoko<sup>1, 2</sup>

<sup>1</sup>International Laboratory for Air Quality and Health, School of Chemistry, Physics and Mechanical Engineering, Queensland University of Technology, Brisbane 4001, Australia

<sup>2</sup>Institute of Health and Biomedical Innovation, Queensland University of Technology, Brisbane, Australia

Keywords: 3-way PMF, PM<sub>10</sub>, source identification.

Presenting author email: g.ayoko@qut.edu.au

In this paper we describe the analysis of PM<sub>10</sub> data from an urban air monitoring site in New South Wales, Australia by the 3-way Positive Matrix Factorization (PMF) described by Paatero and Junnto (Paatero and Junnto, 2000), and used the preliminary results for source identification.

The 2-way PMF is widely used in the literature for source apportionment of chemical composition data (Friend et al. (2011)); particle size distribution data (Friend et al (2012)), aerosol mass spectrometric data (Crilley et al, (2013)), and gaseous, chemical, and particle size data (Zhou et al (2005)). However, with the exception of application of the 3-way PMF to the hourly concentrations of carbon monoxide (Paatero and Junnto, (2000)), in which the diurnal variation pattern of the resultant factor was used for source identification, 3 way PMF has rarely been used in the literature for source identification of a single air pollutant. The current study is part of our continuing exploration of the utility of 3-way PMF with the goal of generating information that could aid the understanding of the sources of particulate matter in an area, and facilitate the formulation of mitigating measures, particularly where chemical composition data and particle number concentration data are not available.

The air monitoring site used for the current study was located at Campbelltown, which is situated 50km South-West of Sydney's Central Business District and approximately 30kms from the Eastern Coast of Australia. The data employed consisted of hourly particulate matter (PM<sub>10</sub>), carbon monoxide (CO), ozone (O<sub>3</sub>), nitrogen oxides (NO, NO<sub>2</sub>, NO<sub>x</sub>), and sulphur dioxide (SO<sub>2</sub>) concentrations, and meteorological data, including relative humidity, visibility, temperature, wind direction, and wind speed.

After screening the data, which was collected from January 2014 to December 2015, for missing or incomplete days, a total of 56 days were excluded before subjecting the PM<sub>10</sub> data to 3-way PMF analysis. The best outcome for the analysis was deemed to be a four-factor solution, and a diurnal variation plot similar to that displayed as Figure 1 (where the two prominent peaks coincide with the peak vehicle traffic times), was constructed for each of these factors. Subsequent Pearson correlation of the PMF results with the concentrations of other gaseous pollutants and parameters measured at the site allowed the tentative assignment of the sources to be made.

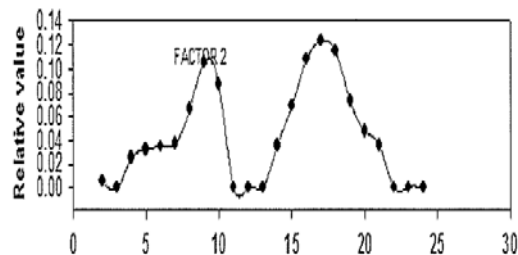


Figure 1: An example plot of the resolved diurnal variation plot.

Factor 1 was thought to be due to nucleation, factor 2 vehicle emissions, and factor 3 cooking. The appearance of the most prominent peak in the diurnal plot for factor 4 coincides with the time that the wind is from the direction of a land excavation company. Therefore this factor was assigned wind-blown particles.

Overall, the study demonstrates that the PM<sub>10</sub> data are stable enough for this type of analysis. The tentative sources also largely corroborate the results from similar studies performed on 2 air monitoring sites in South East Queensland, Australia. Further studies are needed to confirm the applicability of this procedure and of ME-2 to a wider range of similar data, and these are underway in our laboratory

### Acknowledgement

We wish to thank the Climate and Atmospheric Science Division of the Office of Environment and Heritage, Department of Planning and Environment, New South Wales, Australia for providing the data used for the study.

### References

- Crilley, L.R., Ayoko, G.A., and Morawska, L. (2013) *Anal. Chimica Acta*, **803**, 91-96.
- Friend, A., Ayoko, G. and Guo, H. (2012) *Sci. Total Environ. Res.* **409**, 719-737
- Friend, A., Ayoko, G., Jayaratne, R., Jamriska, M., Hopke, P. and Morawska, L. (2012) *Environ. Sci. Pollut. Res.* **19**, 2942-2950.
- Paatero, P and Junnto, S. (2000). *J.Chemometr.*, **14**:241-259.
- Zhou, L., Kim, E., Hopke, P.K., Stanier, C.D. and Pandis, S. (2004) *Aerosol Sci Technol.*, **38** (Suppl. 1), 118-132.
- Zhou, L., Kim, E., Hopke, P.K., Stanier, C.D. and Pandis, S. (2005) *J. Geophys. Res.* **110**, D07S19

## Aerosol chemical composition and spatial distribution in industrial areas using mobile aerosol mass spectrometry

M. Maasikmets<sup>1,2</sup>, M. Elser<sup>3</sup>, C. Bozzetti<sup>3</sup>, H. Keernik<sup>1</sup>, E. Teinemaa<sup>1</sup>, I. El-Haddad<sup>3</sup>, R. Richter<sup>3</sup>, J.G. Slowik<sup>3</sup>, U. Baltensperger<sup>3</sup>, and A.S.H. Prévôt<sup>3</sup>.

<sup>1</sup>Estonian Environmental Research Center, Marja 4d, Tallinn, 10617, Estonia

<sup>2</sup>Estonian University of Life Science (EULS), Institute of Agricultural and Environmental Sciences, Kreutzwaldi 5, 51014 Tartu, Estonia

<sup>3</sup>Department of General Energy Research, Paul Scherrer Institute, Villigen PSI, CH-5232, Switzerland

Keywords: source apportionment, AMS, industrial emissions

Presenting author email: marek.maasikmets@klab.ee

Atmospheric pollution is one of the salient issues in environmental health and particulate matter (PM) is an important factor influencing many environmental processes like climate change and adverse effects on health (Boucher et al., 2013). According to Belis et al. (2013) industrial sources are sometimes mixed with unidentified combustion sources or traffic. At the same time strict environmental legislation and regulations in Europe have been worked out for the industrial sources and thus helped to decrease some industrial emissions (like SO<sub>2</sub>) in developed countries. Nevertheless those restrictions at industrial level ensure mainly reductions for primary organic aerosol (POA), while secondary organic aerosol (SOA) remains often unregulated. This may lead to the underestimation of PM in emission inventories. Median relative contribution to PM from industrial sources in Europe is 15 ± 6%, which makes industrial sources the third most important contributor for PM<sub>2.5</sub> (Belis et al. 2013). While the PM levels and physicochemical properties of the particles are mostly well characterized in European urban areas, data are scarce for industrial sites, especially in the heavy industry areas.

The two biggest industrial towns in Estonia (Kohtla-Järve and Kiviõli) are located near important deposits of Estonian oil shale and main oil shale facilities are nearby, which are affecting directly the local and regional air quality. With the continuous decline of petroleum supplies, oil shale presents opportunities for supplying some of the fossil energy needs of the world in the years ahead. The resources of oil shale in the world are exceeding conventional oil resources by more than 50 %, which can make oil shale resources lucrative in the nearest future. Nowadays China has the highest production volumes of shale oil.

In this work we present the first detailed in-situ mass spectrometric measurements of air pollutants in Kohtla-Järve and Kiviõli. The measurements were performed using the Paul Scherrer Institute (PSI) mobile laboratory (Elser et al. 2016). The use of a high-resolution time-of-flight aerosol mass spectrometer (HR-ToF-AMS) with a novel PM<sub>2.5</sub> lens allowed for a detailed characterization of the NR-PM<sub>2.5</sub> fraction in the measurement areas. The spatial distributions of the sources of organic aerosols (OA), inorganic aerosols (nitrate (NO<sub>3</sub>), sulfate (SO<sub>4</sub>), ammonium (NH<sub>4</sub>), and

chloride (Cl)), equivalent black carbon (eBC) and some of the major gas-phase components (CO, CO<sub>2</sub> and CH<sub>4</sub>) were determined in the industrial areas.

The sources of OA were investigated using positive matrix factorization (PMF). Six sources were identified, including traffic (HOA), biomass burning (BBOA), two industrial sources (Industry 1 and 2), and two secondary factors (low-volatility and semi-volatile oxygenated OA).

Compared to regular urban areas, sulfate was found to have an enhanced contribution in the industrial areas and dominated the PM mass together with the organics. It has been shown in this work how the major part of this sulfate is produced from the two oil shale factories (oil shale burning and shale oil production) present in the area. The mass spectra of the two industrial factors exhibit similar patterns, with relatively high contribution of oxygenated fragments, compared to other primary sources. The separation of these two factors was only possible by the introduction of the SO<sub>4</sub> time series in the PMF analysis, as one of the identified industrial sources (Industry 1) was dominated by sulfate emissions, whereas the second industrial source (Industry 2) was dominated by emissions of organics.

Our results show that mobile measurements are a powerful technique for the spatial characterization of the major pollutants in urban areas.

This work was supported by the Estonian-Swiss cooperation program “Enforcement of the surveillance network of the Estonian air quality” and by the Swiss National Science Foundation (Starting Grant No. BSSGI0 155846 and IZERZ0 142146).

Belis et al. (2013). *Atmospheric Environment* **69**, 94-108.  
Boucher et al. (2013). *Climate Change* 2013. pp 571-658.  
Elser et al. (2016). *Atmos. Chem. Phys.* **16**, 7117-7134

## A PMF source apportionment study of redox-active metals in atmospheric fine particulate matter (PM<sub>2.5</sub>) in central Los Angeles using highly time-resolved measurements

M.H. Sowlat<sup>1</sup>, A.H. Mousavi<sup>1</sup>, C. Sioutas<sup>1</sup>

<sup>1</sup>Department of civil and Environmental Engineering, University of Southern California, Los Angeles, California, USA

Keywords: redox-active metals, source apportionment, PMF, Los Angeles.

Presenting author email: sioutas@usc.edu

In this work, we used a previously developed metal monitor (Dongbin et al. 20015) to measure the concentrations and diurnal variations of four important redox-active metals (i.e., Fe, Mn, Cr, and Cu) with a time resolution of 2 hr in central Los Angeles. Sampling was done over a relatively long period of time (i.e., June-August 2016, as the warm phase, and November 2016 through February 2017, as the cold phase), and then the Positive Matrix Factorization (PMF) model (ver. 5.0) was employed to apportion the sources that contribute to the concentrations of these important redox-active metals and PM<sub>2.5</sub> mass.

We also collected data for several important auxiliary parameters to help better identify the factors resolved by the PMF model. These parameters included particle volume and number size distribution profiles, gaseous pollutants concentrations, data for meteorological parameters, and traffic counts data. The final identification of the sources was done based on the diurnal variations of the four redox-active metals, diurnal variations for the contribution of each of the factors to total PM<sub>2.5</sub> concentrations, particle number and volume size distribution profiles, profiles of auxiliary variables.

The most physically applicable solution of the PMF model to the input data appeared to be the six-factor solution, with the factors being nucleation, traffic 1, traffic 2 (representing larger mode particles compared to traffic 1), urban background aerosol, secondary aerosol, and soil/road dust. Figure 1 demonstrates the relative contributions of each factor to the total PM<sub>2.5</sub> mass, Fe, Mn, Cr, and Cu concentrations.

As shown in Figure 1, secondary aerosol factor has the highest contribution (i.e., 44%) to the PM<sub>2.5</sub> mass, followed by traffic factors, urban background aerosol, and soil/road dust. The major contributors to the concentrations of Fe were traffic 2 and traffic 1, contributing to 37% and 33% of Fe concentrations, respectively. Moreover, traffic factors were also the major source of Cu, making up to 64% of Cu concentrations collectively. Furthermore, the diurnal variations of Fe and Cu concentrations, indicating peaks during morning and late afternoon/early evening traffic rush hours, suggested the major influence of vehicular emissions on Cu and Fe concentrations.

Urban background aerosol majorly contributed to Cr concentrations (40%), which could be attributed to Cr plating facilities as sources of Cr in the area. Mn, on the other hand, mostly comes from the soil/road dust factor, indicating the impact of wear debris tracers from traffic-related emissions. Results from this study are quite

consistent with earlier findings from previous works (e.e., Hasheminassab et al. 2014).

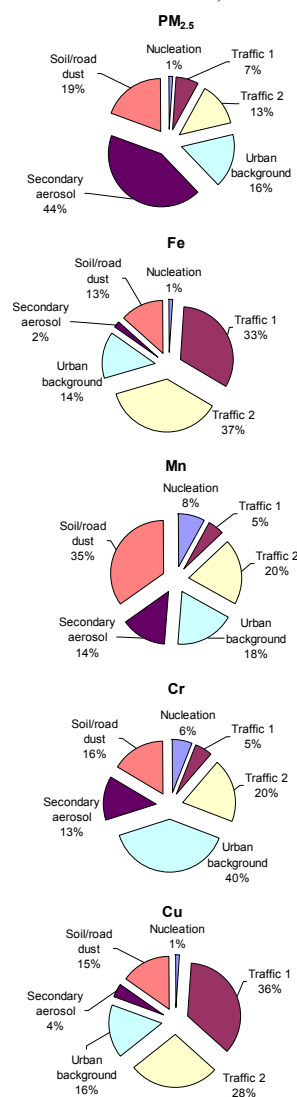


Figure 1. Relative contribution of each factor to the PM<sub>2.5</sub> and metal concentrations.

We thank the USC Viterbi School of Engineering's Ph.D. fellowship award for their support.

Wang, D., Sowlat, M.H., Shafer, M.M., Schauer, J.J., Sioutas, C. (2016) *Sci. Total Environ.* **565**, 123-131.  
 Hasheminassab, S., Daher, N., Saffari, A., Wang, D., Ostro, B.D., Sioutas, C. (2014) *Atmos Chem Phys* **14**, 12085-12097.



## Stable carbon isotope composition, sources and chemical processing of aerosol particles

A. Masalaite<sup>1</sup>, R. Holzinger<sup>2</sup>, A. Garbaras<sup>1</sup>, V. Remeikis<sup>1</sup>, T. Röckmann<sup>2</sup> and U. Dusek<sup>2,3</sup>

<sup>1</sup>Center for Physical Sciences and Technology, Vilnius, LT-02300, Lithuania

<sup>2</sup>IMAU, Utrecht University, Utrecht, the Netherlands

<sup>3</sup>Center for Isotope Research, Groningen University, Groningen, the Netherlands

Keywords: aerosol particles, carbon isotopic ratio, TD–PTR–MS.

Presenting author email: [agne.masalaite@ftmc.lt](mailto:agne.masalaite@ftmc.lt)

Carbonaceous particles are the important components of the atmospheric aerosol due to their direct effect on atmosphere, climate, and human health. Different approaches can be used to identify carbonaceous aerosol sources. The stable carbon isotopes can be used to get information about sources and processing of carbonaceous aerosol.

The main objective of this study is to present an overview of the works conducted using stable carbon isotope ratios, chemical composition and source apportionment for the aerosol samples (Masalaite et al., 2015, 2017).

The aerosol samples were collected at an urban (54°38' N, 25°18' E), coastal (55°55' N, 21°00' E) and forest (55°27' N, 26°00' E) site in Lithuania. Size segregated aerosol particles were collected with a micro-orifice uniform deposit impactor (MOUDI) in 11 size intervals ranging from 0.056 µm to 18 µm. PM<sub>1</sub> size fraction samples were collected on 150 mm diameter quartz microfiber filters (Whatman QM-A) using a high-volume (500 L/min) sampler "Digital DH-77" and on 47 mm diameter quartz filters with a low-volume (30 L/min) aerosol sampler.

The  $\delta^{13}\text{C}$  values of bulk total carbon ( $\delta^{13}\text{C}_{\text{TC}}$ ) were measured using an elemental analyser (Flash EA 1112) coupled to an isotope ratio mass spectrometer (Thermo Finnigan Delta Plus Advantage) (EA – IRMS). Isotopic composition of organic carbon was measured using a thermal-desorption isotope ratio mass spectrometry (IRMS) system (Dusek et al. 2013). Chemical composition was determined using the offline thermal-desorption proton-transfer-reaction mass spectrometry (TD–PTR–MS) setup consisted of an oven system coupled to the PTR–MS (Holzinger et al. 2010).

### Results

The study of size segregated carbonaceous particles suggested that two main sources represent the mixture observed in samples not taking into account certain regional differences and potential carbon fractionation in the particle phase. One of the sources dominated the production of fine particles (fossil fuel combustion), while the other source (continental non-fossil) was a dominant contributor of coarse particles (Masalaite et al., 2015).

The latest study revealed a clear distinction in source contribution between the more volatile OC fraction and the more refractory fraction. The less and more volatile particle fractions have quite different sources. According

to our source apportionment, the more volatile carbon fraction in the smallest particles is almost completely from fossil fuels, whereas the more refractory carbon fraction in the large size range is almost completely from biomass burning. The more refractory small particles and the less refractory large particles are roughly an even mix of these two sources.

Finally the results of the study by Masalaite et al., 2017 showed that carbon isotope analysis can potentially give insight into chemical processing of the carbonaceous aerosol. O/C ratio versus  $\delta^{13}\text{C}_{\text{OC}}$  values at separate desorption temperatures revealed positive correlation at low desorption temperatures and negative (or no) correlation at high desorption temperatures. We propose a hypothesis that the correlation might be due to oxidative processing of the aerosol particles.

Dusek, U., Meusinger, C., Oyama, B., Ramon, W., de Wilde, P., Holzinger, R., Röckmann, T., (2013) *J. Aerosol. Sci.* **66**, 72-82.

Holzinger, R., Williams, J., Herrmann, F., Lelieveld, J., Donahue, N., Röckmann, T., (2010) *Atmos. Chem. Phys.* **10**, 2257-2267.

Masalaite, A., Remeikis, V., Garbaras, A., Dudoitis, V., Ulevicius, V., Ceburnis, D. (2015) *Atmos. Res* **158–159**, 1-12.

Masalaite, A., Holzinger, R., Remeikis, V., Röckmann, T., Dusek, U. (2017) *Atmos. Environ.* **148**, 62-76.

## Composition, sources and long range contribution for PM<sub>2.5</sub> in Po valley urban background

A. Bigi<sup>1</sup>, A. Piazzalunga<sup>2</sup>, L. Pontoni<sup>3</sup>, G. Calzolari<sup>4</sup>, M. Giannoni<sup>4</sup>, F. Pirozzi<sup>3</sup>, G. Ghermandi<sup>1</sup>, S. Teggi<sup>1</sup>

<sup>1</sup>Dept of Engineering “Enzo Ferrari”, Università di Modena e Reggio Emilia, 41125 Modena, Italy

<sup>2</sup>Water and Life Lab, 24060 Entratico, Italy

<sup>3</sup>Dept of Civil, Building and Environmental Engineering, Università di Napoli, 80125 Napoli, Italy

<sup>4</sup>Dept of Physics and Astronomy, University of Florence and I.N.F.N., 50019 Sesto F.no, Italy

Keywords: PM<sub>2.5</sub>, PMF, Po valley

Presenting author email: alessandro.bigi@unimore.it

The Po valley experiences a strong anthropic pressure due to wide urban areas (e.g. Milan), intensive breeding, intensive agriculture and large manufacturing districts, along with topographic and meteorological conditions unfavourable to pollutant dispersion, making this region one with the worst air quality in Western Europe.

In order to complete a source apportionment study on PM<sub>2.5</sub> in urban background conditions representative of large part of the Po valley, daily samples have been collected in Modena by a standard European gravimetric sampler.

Samples have been collected in winter, between November 20th, 2013 and January 31st, 2014, and in summer, between July 1st and August 31st 2014. Daily filters have been punched and analysed for chemical composition of several species: soluble inorganic ions (NO<sub>3</sub><sup>-</sup>, SO<sub>4</sub><sup>2-</sup>, NH<sub>4</sub><sup>+</sup>, Cl<sup>-</sup>, Na<sup>+</sup>, Mg<sup>2+</sup>, Ca<sup>2+</sup>) have been determined by Ion Chromatography, Levoglucosan by HPAEC–PAD, Organic and Elemental Carbon by Laboratory OC-EC Aerosol Analyzer (Sunset Lab Inc.), 14 PAH by GC/MS and metals by ICP-MS (Al, Ti, V, Cr, Mn, Fe, Ni, Cu, Zn, As, Mo, Cd, Sn, Sb, Ba, Pb).

Secondary inorganic ions and carbon in organic fraction (OC) represent more than 40% and 25% of total mass. Correlation matrix showed a wide positive correlation among most metals, besides Vanadium; Magnesium and Calcium ions are anti-correlated to all other ions and to PM<sub>2.5</sub>, suggesting a crustal origin and larger presence in clean/fresh air masses. All PAHs are reciprocally correlated besides Phenanthrene.

The use of conditional bivariate probability functions (CBPF) highlighted the different contribution of closer sources to the observed concentration of gaseous and particulate pollutants. Peaks in tracers for traffic exhausts, biomass burning and brake wear are related to SW winds. Lower pollution conditions occur with NE winds (see NO<sub>x</sub> in Figure 1), besides for Ni and SO<sub>4</sub><sup>2-</sup> whose peaks are associated to these air masses.

Source apportionment of PM<sub>2.5</sub> have been performed by EPA PMF v.5.0 (base model + Fpeak rotation + Fpeak uncertainty by bootstrap). 6 sources have been identified: secondary nitrate, secondary sulphate, biomass burning, traffic exhausts, crustal material and resuspended dust + industry.

The contribution of biomass burning, showing the highest uncertainty among all factors, contributed to 14% (± 9%) to PM<sub>2.5</sub>. Crustal material profile, with a significant contribution only in summer, resulted in ~ 12% (± 2%) of total PM<sub>2.5</sub>. Inorganic secondary sources contributed around 40% to total PM<sub>2.5</sub> mass, according to the model. Contribution by traffic exhausts and resuspended dust+industry was estimated respectively in 30% (± 9%) and 2.4% (±1.6%).

Occasional trans-boundary pollution events have been investigated by statistical models applied to mean daily backtrajectories computed by HYSPLIT (meteorological data used: 0.5° GDAS; trajectory length: 36hrs; arrival height above ground level: 100 m).

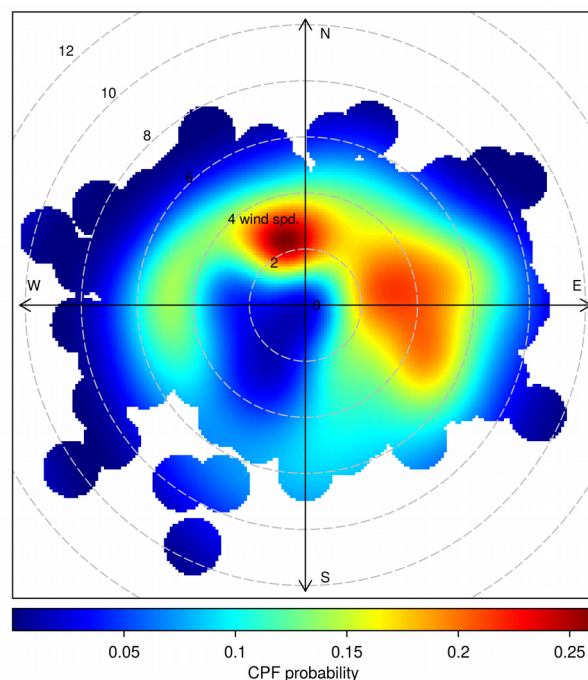


Figure 1. CBPF for hourly NO<sub>x</sub> below 30<sup>th</sup> quantile.

This work is supported by the Italian Ministero dell'Istruzione, dell'Università e della Ricerca (Project PRIN2010-11, 2010WLNFY2).

## Biogenic secondary organic aerosol relation to temperature depending tree stress emissions

K. Plauškaitė<sup>1</sup>, J. Pauraitė<sup>1</sup>, S. Byčėnienė<sup>1</sup>, A. Augustaitis<sup>2</sup>, V. Marozas<sup>2</sup> and V. Ulevičius<sup>1</sup>

<sup>1</sup>Department of Environmental Research, Center for Physical Sciences and Technology, Vilnius, LT-02300, Lithuania

<sup>2</sup>Department of Forest Science and Ecology, Aleksandras Stulginskis University, Kaunas, LT-53362, Lithuania

Keywords: organic, aerosol, biogenic, secondary.

Presenting author email: kristina.plauskaite@ftmc.lt

Atmospheric aerosols have a substantial impact on the global climate and human health. Biogenic secondary organic aerosols (B-SOA) constitute a significant part of the atmospheric aerosols (Han et al., 2014). B-SOA can be formed in the atmosphere upon oxidation of a number of biogenic volatile organic compounds (BVOC). Such ecosystem like forests are the main sources of the BVOCs and in the global scales, their emissions are higher than anthropogenic volatile organic compounds (VOC) (Misztal et al., 2015). Biogenic volatile organic compounds play a significant role in sustaining the oxidant balance of the lower layers of the atmosphere (McKinney et al., 2011).

In order to understand which B-SOA emissions from plants are related to the heat waves induced tree stress emissions, the chemical composition of aerosol particles in Lithuania in forested environment during 2013 – 2016 period were investigated. The real-time measurements of aerosol mass concentration were investigated at Rūgštelėškis, a rural environment. This site is located in the north-eastern part of Lithuania, in remote coniferous forested area. The measurements were performed applying an Aerosol Chemical Speciation Monitor (ACSM) (Ng et al., 2011). ACSM measures aerosol mass concentration and chemical composition of non-refractory submicron aerosol particles in real-time. It provides information about composition for particulate ammonium, nitrate, sulfate, chloride and organics. The instrument was calibrated using ammonium sulphate and ammonium nitrate.

### Results

The days with advection of clean air masses and dominant emissions of semi-volatile organic compounds were selected and divided into warm and cold periods (averaged daily temperature was equal to 17.4 °C and 6.9 °C, respectively). For clarification, the distinction of averaged mass spectrum during warm and cold periods was normalized (Figure 1). As the result, the signals of m/z 45 and 43 were more than 2.5 times higher during warm period than cold. Normalized distinction of m/z 26, 27, 37, 42, 53, 59, 65, 71, 73, 79, 82 was greater than 1.5 which indicates a great temperature dependency too. For selected days the submicronic forests organic aerosol mass (SFOM) analysis was performed. The SFOM concentration was 4 times greater during warm period than cold (4.7 and 1.2 µg/m<sup>3</sup>, respectively). Averaged diurnal plot of SFOM concentration showed the major

emissions during night time (from 20 to 8 h). Meanwhile SFOM concentration dependency on temperature was found to be increasing exponentially. Thus, a clear temperature dependency has been established for several m/z signals and SFOM concentration, which could lead to expanded understanding of the forest ecosystem.

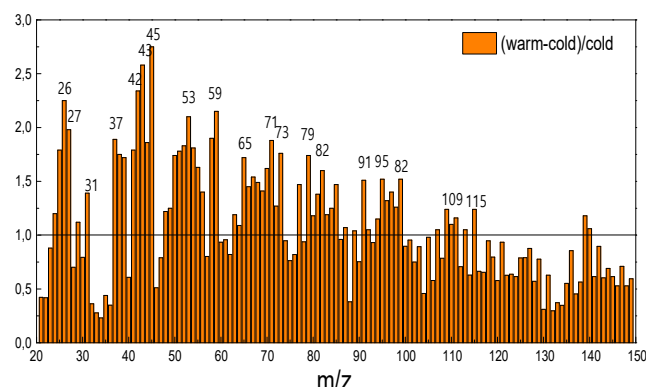


Figure 1. The normalized distinction of m/z of the averaged mass spectrum during warm and cold periods.

This work was supported by the National Research Programme “Sustainability of agro-, forest and water ecosystems” project FOREstRESS (No. SIT-3/2015).

Han, Y., Iwamoto, Y., Nakayama, T., Kawamura, K. and Mochida M. (2014) *J. Geophys. Res. Atmos.* **119**, 259–273.

Misztal, P., Hewitt, C.N., Wildt, J., Blande, J.D., Eller, A.S.D., Fares, S., Gentner, D.R., Gilman, J.B., Graus, M., Greenberg, J., Guenther, A., Hansel, A., Harley, P., Huang, M., Jardine, K., Karl, T., Kaser, L., Keutsch, F.N., Kiendler-Scharr, A., Kleist, E., Lerner, B.M., Li, T., Mak, J., Nölscher, A.C., Schnitzhofer, R., Sinha, V., Thornton, B., Warneke, C., Wegener, F., Werner, C., Williams, J., Worton, D.R., Yassaa, N. and Goldstein, A.H. (2015) *Scientific reports* **5**, 1–10.

McKinney, K.A., Lee, B.H., Vasta, A., Pho, T.V. and Munger, J.W. (2011) *Atmos. Chem. Phys.* **11**, 4807–4831.

Ng, N. L., Herndon, S. C., Trimborn, A., Canagaratna, M. R., Croteau, P. L., Onasch, T. B., Sueper, D., Worsnop, D. R., Zhang, Q., Sun, Y. L., and Jayne, J. T. (2011) *Aerosol Sci. Tech.* **45**, 770–784.

## Levels and Spatial Distribution of Metals in a Heavily Industrialized Region (Dilovası, Kocaeli) of Turkey

M.Keles<sup>1</sup>, B.Cetin<sup>2</sup>, S.Yurdakul<sup>3</sup> and F.Ozturk<sup>1</sup>

<sup>1</sup>Department of Environmental Engineering, Abant Izzet Baysal University, Bolu, 14030, Turkey

<sup>2</sup>Department of Environmental Engineering, Gebze Technical University, Kocaeli, 41400, Turkey

<sup>3</sup>Department of Environmental Engineering, Suleyman Demirel University, Isparta, 32260, Turkey

Keywords: metals, dry deposition flux, spatial distribution, heavy industry

Presenting author email: oztfatma@gmail.com

The status of water, soil and air quality strongly influence the environmental health all over the world. Though several air pollutants are of concern in terms of health, particulate matter is being considered as a proxy indicator of air pollution due to its significant health effects. According to a recent World Health Organization (WHO, 2017) report, air pollution in the Eastern Mediterranean Region is at alarming rate. It has been reported that annual average PM<sub>2.5</sub> levels are 2-11 times the WHO recommended levels. In addition, air pollution is responsible for one every tenth death in the Eastern Mediterranean Region.

Despite of the severity of the issue, there is not sufficient efforts have been put forward to determine the levels of PM pollution and parameters associated with it in the region. The objective of this study is to determine the levels and spatial distribution of metals deposited over the one of the heavily industrialized areas of Turkey, Dilovası, which is one of the districts of Kocaeli, is placed on the north-western part of Turkey and includes 185 small and medium size enterprises from 45 different sectors. To end these objectives, dry deposition plates as depicted in Figure 1 were located 23 different sites all over the region.



**Figure 1.** Dry deposition plate used during the field campaign

Pre-fired quartz filters were used over the plates to collect deposited PM. Due to the weather conditions, dry deposition samples were collected only in May, August and October 2015 during the field study. The collected samples were acid digested and analysed by using ICPMS in terms of metals from Li to U. The dry deposition fluxes found for the metals were ranged from

6.6±6.8 ng/m<sup>2</sup>/day for Pt to 15.3±11.8 ng/m<sup>2</sup>/day for Ca. For the metals listed by the USEPA as hazardous air pollutants (HAPs), the found dry deposition fluxes were tabulated in Table 1 below:

**Table 1.** Dry deposition fluxes of USEPA listed HAP metals (µg/m<sup>2</sup>/day)

	Avg	SD		Avg	SD
<b>Be</b>	0.039 ±	0.040	<b>Co</b>	2.31 ±	8.11
<b>Se</b>	0.078 ±	0.053	<b>Cr</b>	14 ±	15
<b>Hg</b>	0.088 ±	0.092	<b>Ni</b>	28 ±	18
<b>Cd</b>	0.42 ±	0.41	<b>Pb</b>	28 ±	93
<b>Sb</b>	0.48 ±	0.37	<b>Mn</b>	151 ±	130
<b>As</b>	1.01 ±	1.08			

Spatial distribution of measured metals was also evaluated in this study. Figure 2 depicted Pb distribution as an example.

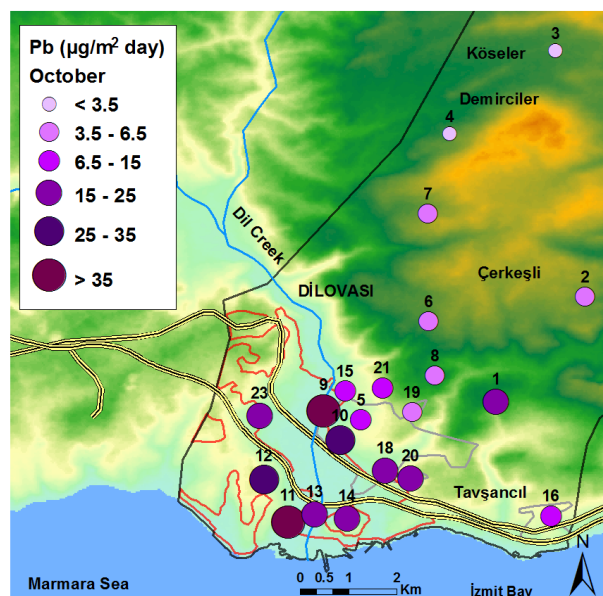


**Figure 2.** Spatial distribution of Pb during field campaign

This work was supported by the Turkish Scientific and Technological Research Council under grant 113Y500.

WHO, Regional Office for the Eastern Mediterranean, [www.emro.who.int](http://www.emro.who.int), last access date: 31/01/2017

## PM10 chemical composition and sources in the Central Mediterranean

G. Calzolari<sup>1</sup>, S. Becagli<sup>2</sup>, S. Nava<sup>1</sup>, F. Lucarelli<sup>1</sup>, M. Chiari<sup>1</sup>, M. Giannoni<sup>1</sup>, R. Traversi<sup>2</sup>, M. Severi<sup>2</sup>, M. Marconi<sup>2</sup>, R. Udisti<sup>2</sup>, A. di Sarra<sup>3</sup>, G. Pace<sup>3</sup>, D. Meloni<sup>3</sup>, C. Bommarito<sup>4</sup>, F. Monteleone<sup>4</sup>, F. Anello<sup>4</sup> and D. Sferlazzo<sup>5</sup>

<sup>1</sup> Department of Physics and Astronomy, University of Florence, and INFN-Florence, Sesto F.no, 50019, Italy

<sup>2</sup> Department of Chemistry, University of Florence, Sesto Fiorentino (Florence), 50019, Italy

<sup>3</sup> ENEA Laboratory for Observations and Analyses of Earth and Climate, Roma, 00123, Italy

<sup>4</sup> ENEA, Laboratory for Observations and Analyses of Earth and Climate, Palermo, 90139, Italy

<sup>5</sup> ENEA, Laboratory for Observations and Analyses of Earth and Climate, Lampedusa, 92010, Italy

Keywords: Aerosol sources, Mediterranean Basin, PM10, PMF.

Presenting author email: calzolari@fi.infn.it

The Mediterranean Basin has been identified as one of the “Hot-Spots” in future climate change projections; its atmosphere is affected by strong natural and anthropogenic aerosol emissions, as well as important climatic forcings. In order to study the atmosphere of this area, ENEA (Italian Agency for New Technologies, Energy and Sustainable Economic Development) set up the Station for Climate Observations on the island of Lampedusa (35.5° N, 12.6° E, 45 m a.s.l.). At the station, continuous observations of greenhouse gases, aerosol properties, total ozone, ultraviolet irradiance, and other climatic parameters are carried out. Furthermore, PM10 samples have been collected on a daily basis since 2004 to study also the chemical properties of the aerosol and to gain information on the aerosol sources and their contributions. Lampedusa island is a suitable site for the study of the interactions between atmospheric properties and climate as it is far from continental pollution sources (the nearest coast, in Tunisia, is more than 100 km away).

PM10 samples have been collected by means of two samplers on teflon and quartz filters in parallel. After mass gravimetric measurements, the aerosol chemical composition was measured using a wide set of analytical techniques. In particular, the ionic content was determined by Ion Chromatography (IC), the soluble metals by Inductively Coupled Plasma Atomic Emission Spectrometry (ICP-AES), the total (soluble + insoluble) elemental composition by Particle Induced X-ray Emission (PIXE), and the carbonaceous component (elemental and organic carbon, EC and OC) by Thermo-Optical Transmittance (TOT) analysis.

The present study was performed exploiting the data relative to the period 2012-2014. Despite the remoteness of the sampling site, several episodes with PM10 exceeding 100  $\mu\text{g}/\text{m}^3$  were observed (minima were found to be around 10  $\mu\text{g}/\text{m}^3$ ). In fig. 1, the measured PM10 concentrations are shown.

As concerns the chemical speciation, sea-salt and mineral dust contributions were estimated assuming the average composition of seawater and Earth's crust. Non-negligible secondary aerosol levels characterize the PM10 in Lampedusa. Moreover, for the first time for this sampling site, data on the carbonaceous fraction will be presented.

Source apportionment analysis was performed using the Positive Matrix Factorization model, using the EPA PMFv5 software. Several different sources were resolved, such as sea-salt, mineral dust, biogenic emissions, primary particulate ship emissions, secondary sulphate, secondary nitrate, and combustion emissions. Based on a literature approach (Becagli *et al.*, 2015), an estimation of the fraction of the total secondary sulphate originated from ship emissions was also derived. Large variations in absolute and relative contributions of the different sources were found, depending on the season and on transport episodes. Results were compared with speciation data and with the results obtained in a previous study based on the 2007-2008 data set (Calzolari *et al.*, 2015). It must be pointed out that measurements of carbonaceous species were not available at Lampedusa prior to 2011, therefore these is the first extensive data set shown for the site. The availability of EC/OC measurements allowed in this study a better and more comprehensive characterization of the PM10 sources.

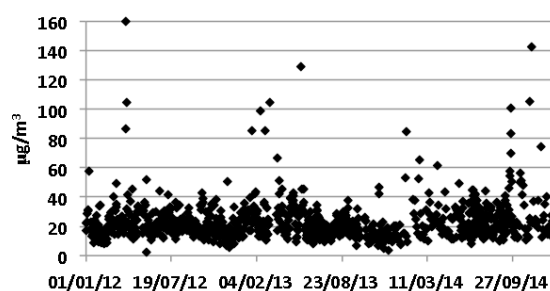


Figure 1. Measured PM10 concentrations in the years 2012-2014.

- G. Calzolari, S. Nava, F. Lucarelli, M. Chiari, M. Giannoni, S. Becagli, R. Traversi, M. Marconi, D. Frosini, M. Severi, R. Udisti, A. di Sarra, G. Pace, D. Meloni, C. Bommarito, F. Monteleone, F. Anello and D. M. Sferlazzo, (2015), *Atmos. Chem. Phys.* **15**, 13939-13955
- S. Becagli, F. Anello, C. Bommarito, F. Cassola, G. Calzolari, T. Di Iorio, A. di Sarra, J.-L. Gómez-Amo, F. Lucarelli, M. Marconi, D. Meloni, F. Monteleone, S. Nava, G. Pace, M. Severi, D.M. Sferlazzo, R. Traversi, and R. Udisti, *Atmos. Chem. Phys. Discuss.*, in review, 2016

## Chemical Composition and Source Apportionment of PM<sub>10</sub> in Port Talbot

D.C. Green<sup>1</sup>, Anna Font<sup>1</sup>, A.H. Tremper<sup>1</sup>, M. Priestman<sup>1</sup>, F. Canonaco<sup>2</sup>

<sup>1</sup>MRC HPA Centre for Environment and Health, King's College London, London, SE1 9NH, UK

<sup>2</sup>Laboratory of Atmospheric Chemistry, Paul Scherrer Institute, Villigen PSI, 5232, Switzerland

Keywords: Source apportionment, Steel works, PM<sub>10</sub>

Presenting author email: david.c.green@kcl.ac.uk

This study reports the chemical composition and multivariate receptor modelling results from a measurement campaign in Port Talbot and identifies key sources of PM<sub>10</sub> adjacent to the Tata steel complex. Port Talbot experiences PM<sub>10</sub> concentrations greater than those in the local area; these are linked to the major steel complex. This study aimed to identify the major sources of PM<sub>10</sub> using high time resolution measurement techniques. This is the first time that this equipment, capable of measuring a full range of organic, ionic, carbonaceous and element components of PM<sub>10</sub>, has been deployed at this location. Multivariate receptor modelling was used to differentiate sources of similar chemical composition from the steel complex as well as other urban and remote sources.

### Methods

Between the 14th Jan and 23rd Feb 2016, the aerosol components listed in Table 1 were measured in Port Talbot. Met, PM and gaseous measurements were taken from the adjacent measurement station. Source apportionment was undertaken by Positive Matrix Factorisation (PMF) using the SoFi Source Finder tool (Canonaco, Crippa et al. 2013). Missing PM<sub>10</sub> mass (the difference between the PM<sub>10</sub> mass and the sum of the measured chemical components) was attributed within the PMF algorithms (Larson, Covert et al. 2006).

Table 1: Instrument and aerosol components

Instrument	Aerosol components
Aerosol Chemical Speciation Monitor	Non-refractory organic (OC), SO <sub>4</sub> , NH <sub>4</sub> and NO <sub>3</sub>
Aethalometer	Black Carbon
XACT 625 (XRF)	As, Ba, Ca, Cd, Ce, Cl, Cr, Cu, Fe, K, Mn, Mo, Ni, Pb, Pt, S, Sb, Se, Si, Sr, Ti, V, Zn

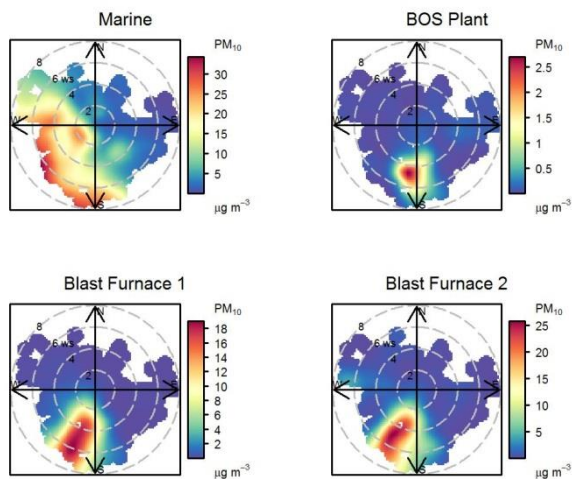


Figure 1: Bivariate polar plots of PM<sub>10</sub> sources

### Results

PMF outputs were configured to yield 1-10 sources. The optimum number was chosen based on the minimum model residuals and the correlation between factor time series. An 8 factor solution is chosen as the ideal.

To assign physically meaningful results to the factors, several analyses and additional sources of information were used, including the correlation with known source profiles and external measurement time series as well as a source direction consistent with known sources. The following sources names were subsequently assigned: Marine, Blast Furnace 1, Blast Furnace 2, Coke Ovens, Background, Solid Fuel Burning, Traffic and BOS Plant. Bivariate polar plots of the Marine, BOS Plant and the two Blast Furnace sources are shown in Figure 1. The contribution of marine aerosol was clearly important, contributing 44% to the mean PM<sub>10</sub> concentration, however by grouping the time series by PM<sub>10</sub> mass concentration the impact of the different sources on peak PM<sub>10</sub> concentrations can be identified; this analysis is shown in Figure 2. It is clear that emissions from the steel complex, notably the blast furnace and coke ovens, that were responsible for the peak concentrations; contributing >50% when PM<sub>10</sub> > 60 µg m<sup>-3</sup>.

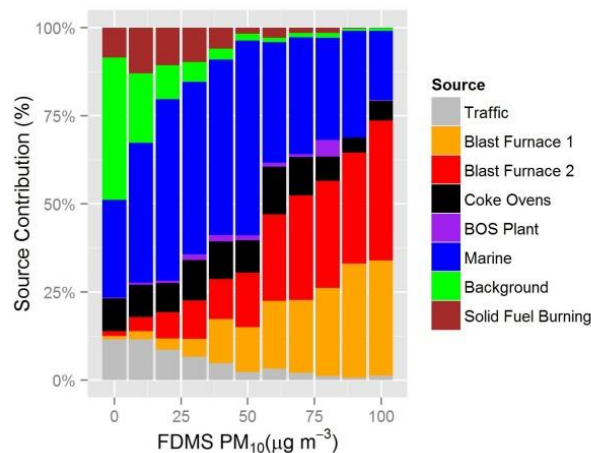


Figure 2: Source categories grouped by PM<sub>10</sub> mass

Canonaco, F., M. Crippa, J. G. Slowik, U. Baltensperger and A. S. H. Prévôt (2013). *Atmos. Meas. Tech.* 6(12): 3649-3661.

Larson, T. V., D. S. Covert, E. Kim, R. Elleman, A. B. Schreuder and T. Lumley (2006). *Journal of Geophysical Research: Atmospheres* 111(D10): n/a-n/a.

## Source apportionment of Arctic aerosol collected at Ny Ålesund – Svalbard Islands: Results from the 2015 campaign

G. Calzolari<sup>1</sup>, S. Nava<sup>1</sup>, M. Chiari<sup>1</sup>, F. Lucarelli<sup>1</sup>, M. Giannoni<sup>1</sup>, S. Becagli<sup>2</sup>, R. Traversi<sup>2</sup>, L. Caiazzo<sup>2</sup>, F. Giardi<sup>2</sup>,  
M. Severi<sup>2</sup>, M. Mazzola<sup>3</sup> and R. Udisti<sup>2</sup>

<sup>1</sup>Department of Physics and Astronomy, University of Florence and INFN, Sesto Fiorentino (FI), 50019, Italy

<sup>2</sup>Department of Chemistry "Ugo Schiff", University of Florence, Sesto Fiorentino (FI), 50019, Italy

<sup>3</sup>National Research Council, Institute of Atmospheric Sciences and Climate (CNR-ISAC), Bologna, 40129, Italy

Keywords: Arctic, PM10, elemental composition, aerosol sources.

Presenting author email: calzolari@fi.infn.it

Due to the present climate forcing, the Arctic is undergoing relevant variations of marine and coastal eco-systems, especially linked to ice extension and thickness. Arctic aerosol plays a relevant role in the complex climate-environment feedbacks, depending on many aerosol properties. In particular, both chemical composition and particle dimensions influence the interaction between particles and solar/terrestrial radiation, the cloud and fog formation (and their microphysical properties), the long-range transport processes and the deposition patterns.

Aerosol sampling was performed in the international research center of Ny Ålesund, at the Gruebadet laboratory (Udisti *et al* 2013). Ny Ålesund is located on a western fjord of Svalbard Islands, in a geographical position coinciding with the northernmost point influenced by the warm West Spitsbergen Current these islands, and thus it is an ideal site for the study of the interaction between the climate change and the atmosphere, ocean and land variations.

At Gruebadet, many instruments for the study of different aerosol properties are available thanks to the joint effort of different research groups, and samplings are ongoing since 2010 in the period March to September; in particular, in this work we will focus on the results gained by the analysis of daily PM10 samples collected during the 2015 campaign. Daily samples were collected on Teflon filters by means of a Tecora Skypost LV sampler.

Daily PM10 samples were analyzed for the ionic composition by Ion Chromatography (IC) and for metals and rare earth elements (REEs) by Inductively Coupled Plasma - Atomic Emission Spectroscopy (ICP-AES). Further, for the first time, daily samples were analyzed for the elemental composition by Particle Induced X-ray Emission (PIXE) analysis. PIXE is an almost unrivalled technique for the characterization of mineral dust, as it is sensitive to all the crustal elements (except O), included Si, which is usually not accurately quantifiable with other common chemical techniques: therefore, these data give new insight on the soil aerosol characterization.

The 2015 campaign was specially interested by biomass burning transport episodes from Northern America.

Data on PM10 concentrations and speciation will be shown. Further, the Positive Matrix Factorization (PMF) model was applied to the chemical data in order

to obtain the source apportionment of the PM10 at Ny Ålesund.

The logistic assistance of the Polar Support Unit of the CNR Department of Earth and Environment (POLARNET) is gratefully acknowledged.

Calzolari, G. *et al.* (2014). *Nucl. Instr. & Meth. B* **318**, 125–129

Udisti R. *et al.*, (2013). *Activity and preliminary results from the 2011 and 2012 field seasons at Ny Alesund in "Research Activity in Ny Alesund 2011-12"*. CNR Edizioni DTA/14-2013. ISSN 2239-5172, 53-68

## Quantifying the sources of air pollution in the Danube macro-region to support the development of abatement strategies

C. A. Belis<sup>1</sup>, E. Pisoni<sup>1</sup> and P. Thunis<sup>1</sup>

<sup>1</sup>European Commission, Joint Research Centre, Ispra, 21027, Italy

Keywords: source apportionment, PM, Danube macro-region

Presenting author email: claudio.belis@jrc.ec.europa.eu

Exceedances of PM<sub>10</sub> and precursor gases, such as NO<sub>2</sub> and SO<sub>2</sub>, have led to infringement procedures in almost all of the EU Member States of the Danube macro-region and some of them have been referred to court.

The SHERPA (Screening for High Emission Reduction Potential on Air), tool has been developed to identify the most efficient scale to act in a European context where a multi-level governance approach is needed (Thunis et al., 2016). SHERPA allows for a rapid exploration of potential improvements in air quality resulting from national/regional/local emission reduction measures.

An analysis was carried out to quantify the contribution made by different emission sources to PM<sub>2.5</sub> and the geographic areas from where the pollution originates. The SHERPA tool developed by the JRC was used to model PM<sub>2.5</sub> urban background concentrations in the main cities in the Danube macro-region: Bratislava, Budapest, Bucharest, Munich, Prague, Sofia, Vienna and Zagreb (Figure 1). The information was then integrated with the outcome of a previous source apportionment study combining receptor models and analysis of trajectories on Budapest, Sofia and Zagreb (Belis et al., 2015).



Figure 1. Geographical location of the cities considered in this study.

Average contributions by the main emission sources are as follows:

- i) agriculture accounts for a considerable share of PM<sub>2.5</sub> concentrations in cities: between 16 % and 32 % of urban PM<sub>2.5</sub> concentrations originates from agricultural activities.
- ii) energy production and industry also play an important role, with contributions ranging from 15 % to 30 % of the urban PM<sub>2.5</sub> concentrations.

iii) residential heating makes variable contributions throughout the Danube macro-region ranging from 10 % to 35 %.

iv) transport contributes between 10 % and 25 % playing a smaller but substantial role compared to the other sectors.

About one-quarter of the PM<sub>2.5</sub> fraction in Sofia and Zagreb originates from beyond the EU-28 boundaries or is of natural origin (Figure 2). On the contrary, reductions in local emissions could lead to sizeable improvements in Munich and Vienna with the main efforts focused on transport, energy/industry and residential heating.

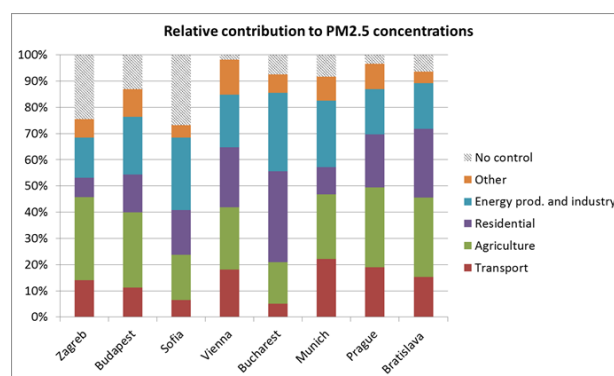


Figure 2. Reductions in the yearly PM<sub>2.5</sub> concentrations by reducing the emissions from different sources

Good agreement was observed between receptor models and SHERPA in the estimation of the contributions from remote areas in Sofia and Zagreb. Differences between the two approaches in the quantification of the biomass burning contributions were attributed to the limitations of the considered emission inventories.

Belis C., Georgieva E., Janos O., Sega K., Török S., Veleva B., Perrone M.G., Vratolis S., Pernigotti D., Eleftheriadis K. (2015) *A comparative analysis of the causes of air pollution in three cities of the Danube Region* EUR 27712 EN.

Thunis P., Degraeuwe B., Pisoni E., Ferrari F., Clappier A. (2016) On the design and assessment of regional air quality plans: The SHERPA approach, *Journal of Environmental Management*, Volume 183, Part 3, 952-958.

## Source Apportionment of PM<sub>2.5</sub> Mass and Optical Attenuation Over an Ecologically Sensitive Zone in Central India by Positive Matrix Factorization

J. Nirmalkar<sup>1</sup>, R. Sunder Raman<sup>1,2</sup> and Samresh Kumar<sup>1</sup>

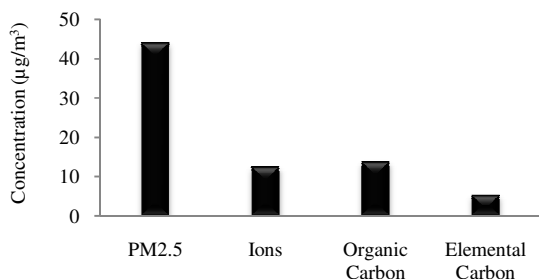
<sup>1</sup>Indian Institute of Science Education and Research, Earth and Environmental Sciences, Bhopal 462066, India

<sup>1,2</sup>Indian Institute of Science Education and Research, Center for Research on Environmental and Sustainable Technologies, Bhopal 462066, India

Keywords: PM<sub>2.5</sub> mass, Chemical characterization, Optical Attenuation, Positive Matrix Factorization

Presenting author email: j\_nirmalkar@yahoo.com

Atmospheric PM<sub>2.5</sub> samples (N=366) were collected over an ecologically sensitive zone (Van Vihar National Park) in Bhopal, Central India for two years (01 January, 2012 to 31 December, 2013). Samples were collected using three co-located Mini-Vol® samplers on Teflon, Nylon, and Quartz filter substrates. The aerosol was then chemically characterized for water-soluble inorganic ions, elements, and carbon fractions (elemental carbon and organic carbon) using ion chromatography, ED-XRF, and thermal-optical EC/OC analyzer, respectively. The mean mass concentration of PM<sub>2.5</sub>, ions, elemental carbon and organic carbon was found to be 44 µg/m<sup>3</sup>, 12.5 µg/m<sup>3</sup>, 5.3 µg/m<sup>3</sup> and 13.8 µg/m<sup>3</sup>, respectively. The major elements were S, Si, Al, K, Ca, Fe and Zn contributing to PM<sub>2.5</sub> mass at study site. The optical attenuation (at 370 nm and 880 nm) of PM<sub>2.5</sub> aerosols was also determined by optical transmissometry (OT-21). The application of Positive matrix factorization (PMF) to a combination of PM<sub>2.5</sub> mass, its ions, elements, carbon fractions, and optical attenuation and source apportionment of PM<sub>2.5</sub> using it will be discussed.



## Spatial and temporal aerosol elemental composition trends over Auckland, New Zealand

Talbot N<sup>1</sup>, Davy P<sup>2</sup>, Ancelet T<sup>2</sup>, Trompetter W<sup>2</sup>, Markwitz A<sup>2</sup>

<sup>1</sup>Air Quality Scientist, RIMU Auckland Council, 135 Albert Street, Auckland, New Zealand.

<sup>2</sup>GNS Science, Gracefield Rd, Gracefield 5010 Wellington, New Zealand

Keywords: Elemental Composition, PMF, Black Carbon, Emissions, Sulphate

Presenting author email: nick.talbot@aucklandcouncil.govt.nz

Identifying the composition and sources of air pollution is vital for effective air quality management and policy implementation. Airborne particles are composed of many elements and compounds from many different sources and, by analysing these components, the sources and their relative contributions to air pollution can be identified.

Here we present results of receptor modelling analysis of airborne particle samples collected at five ambient air quality monitoring sites across the Auckland Region from 2006 to 2013 (Figure 1). This represents the largest and most comprehensive source apportionment study undertaken in New Zealand to date.



**Figure 1** The location of the five air quality monitoring sites across Auckland.

The main objectives of the study were to:

- identify the sources contributing to elevated air pollution episodes;
- estimate the contribution of different particulate matter sources to ambient concentrations;
- distinguish between the contribution of home heating and motor vehicle emission sources;
- determine trends in source variability by season;

PM<sub>2.5</sub> and PM<sub>10</sub> size fractions were collected on filters over a 24-hour sampling period with samples taken every third day. The collected filters were examined using IBA, (PIXE, PESA, and PIGE) techniques (Trompetter *et al*, 2005). The subsequent PMF analysis of the sample sets identified five common source contributors to both PM<sub>2.5</sub> and PM<sub>10</sub>, these were; biomass burning; motor vehicles; secondary sulphate; marine aerosol; and crustal matter. At some sites, local industrial emissions were also identified but were found to be relatively minor contributors to particulate matter concentrations, indicative of the low number of industrial sites around Auckland. In contrast, shipping emissions were found to be impacting upon the Auckland CBD, identified by an SO<sub>2</sub>, nickel, and vanadium signature.

Average source contributions to PM<sub>2.5</sub> indicate that biomass burning and motor vehicle emissions are the predominant sources of PM<sub>2.5</sub> across all sites (Figure 2). Arsenic was also detected at several sites and associated with the biomass burning source; evidence of copper chrome arsenate treated timber being burnt for domestic heating. For the Takapuna and Queen Street sites, marine aerosol was also found to be a significant contributor.

For PM<sub>10</sub>, average source contributions show that marine aerosol and motor vehicle emissions are the predominant emission sources across all sites in Auckland. Motor vehicle contributions to PM<sub>10</sub> were significantly higher than for PM<sub>2.5</sub> due to the associated coarse particle road dust component (Figure 2).

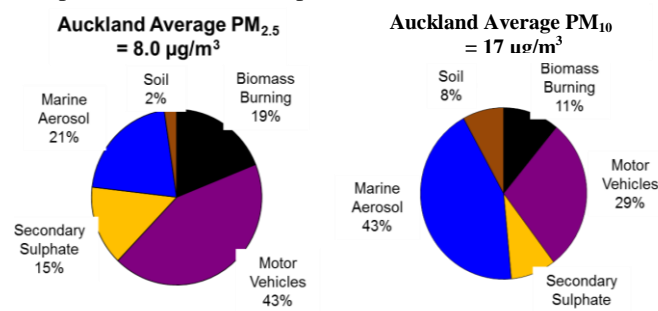


**Figure 2** Pan-Auckland average source contributions to PM<sub>2.5</sub> (left), and PM<sub>10</sub> (right).

The length of the dataset and regularity of filter collection has allowed long-term trends to be identified revealing interesting results. For example, statistically significant reduction in marine aerosol was observed. It is not currently known if this is a local, regional phenomenon and the cause is not yet understood. A significant reduction in sulphate emitted from road vehicles was also found. The reductions occur in downward step-changes which are closely correlated with the implementation of new statutory regulations reducing sulphur content in diesel. The results conclude that despite its advantageous geographical location for pollution dispersal, particulate matter sources in Auckland emits sufficient air pollutants to notably degrade air quality. Key results and implications will be described and discussed, along with comparisons with other major cities.

Trompetter, W., A. Markwitz and P. Davy, K. (2005). "Air particulate research capability at the New Zealand Ion Beam Analysis Facility using PIXE and IBA Techniques." *International Journal of PIXE* **15**(3&4): 249-255.

## Comprehensive source apportionment of long-term ACSM data

F. Canonaco<sup>a</sup>, A. Tobler<sup>a</sup>, K. Dällenbach<sup>a</sup>, C. Bozzetti<sup>a</sup>, J. G. Slowik<sup>a</sup>, I. El Haddad<sup>a</sup>, U. Baltensperger<sup>a</sup>, A.S.H. Prévôt<sup>a</sup>

<sup>a</sup>Laboratory of Atmospheric Chemistry, Paul Scherrer Institut, 5232 Villigen PSI, Switzerland

Keywords: AMS, PMF, ME2, ACSM

Presenting author email: francesco.canonaco@psi.ch

Long-term online monitoring with the aerosol chemical speciation monitor (ACSM, Aerodyne Research, Inc.) and subsequent source apportionment analysis (Paatero 1994) reveals major aerosol sources. This information is relevant e.g. for efficient political abatement strategies.

During the past decade, the positive matrix factorization algorithm (PMF, Paatero 1994), which represents multivariate time series as a linear combination of static factor profiles (source profiles) and their time-dependent contributions, has been extensively used for the source apportionment of organic aerosol (Zhang et al 2011). PMF results suffer from rotational ambiguity (Paatero et al 2002), i.e. multiple PMF results possess the same goodness of fit. Therefore, the PMF solution space requires a thorough investigation to retrieve environmentally reasonable solutions (Canonaco et al 2013). Past studies with constrained factor profiles of known sources, e.g. Lanz et al (2008), Canonaco et al (2013), Crippa et al (2014), performed only limited exploration of the rotational ambiguity of the PMF runs within the framework of the a-value approach.

Moreover, for long-term ambient aerosol studies the source profiles may evolve as a function of the seasons (Canonaco et al 2015). This change has to be addressed when performing long-term source apportionment (SA) studies.

In this study, we present a comprehensive SA analysis of ACSM data measured over more than one year in downtown Zurich with the source finder interface SoFi (Canonaco et al 2013). The following crucial aspects were considered during this study:

- time-dependent source profiles to capture the variability of the sources over the year
- intense exploration of the rotational ambiguity and assessment of the rotational uncertainty
- estimation of the statistical uncertainty for the PMF solution via resampling strategies e.g. using the bootstrap approach.

Previous investigation of this dataset (Canonaco et al 2015) resulted in three primary organic factors (POA) (traffic, cooking and biomass burning) and two secondary organic factors (semi-volatile oxygenated organic aerosol and a low-volatility oxygenated organic aerosol) (OOA) throughout the year with small variations for the POA profiles and larger variations for OOA.

A) is addressed by performing PMF on a small moving window and allowing the algorithm to best adapt to the current data.

For point B) independent variation of the a-value of the constrained primary factor profiles (traffic, cooking and biomass burning) are performed which create PMF runs represented by a large three-dimensional a-value matrix. The PMF runs are sorted based on a user-defined list of criteria, e.g. the correlation between time series of the traffic factor and traffic markers (NO<sub>x</sub>, black carbon), etc. The PMF runs fulfilling all criteria at the same time are retained and span the PMF solution. The repeats mainly due to the resampling strategy give an estimate of the statistical uncertainty of the OA sources (C).

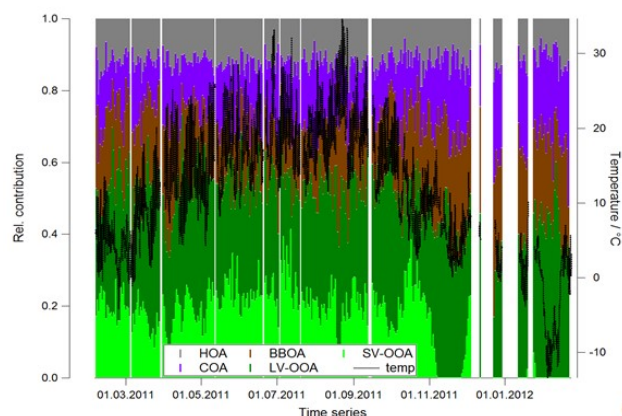


Fig. 1. Relative contribution of the five PMF factors over the year (left axis) including the temperature variation (right axis).

This work is supported by the Swiss Federal Office for the Environment (FOEN).

Canonaco, F. et al (2013) *AMT*, **6**, 3649-3661.

Canonaco F. et al (2015) *ACP*, **15**, 6993-7002.

Crippa, M. et al (2014) *ACP*, **14**, 6159-6176

Lanz, V. et al (2008) *EST*, **42**, 214-220

Paatero P. and Tapper U. (1994) *Environmetrics*, **5**, 111-126

Paatero, P. (1999) *J. Comp. Graph. Stat.*, **8**, 854-888.

Paatero, P. et al (2002) *Chemometr. Intell. Lab.*, **1**, 253-264

Paatero, P. et al (2014) *AMT*, **7**, 781-797

Zhang et al (2011) *Anal. Bioanal. Chem.*, **10**, 3045-3067

## Source Apportionment of Organic Aerosols in Lithuania using thermal desorption proton-transfer reaction mass spectrometry (TD-PTRMS)

Yandong Tong<sup>1</sup>, Daniel Steinfeld<sup>1</sup>, Carlo Bozzetti<sup>1</sup>, Rupert Holzinger<sup>2</sup>, Imad El Haddad<sup>1</sup>, Jay G. Slowik<sup>1</sup>, André S. H. Prévôt<sup>1</sup> and Urs Baltensperger<sup>1</sup>

<sup>1</sup>Laboratory of Atmospheric Chemistry, Paul Scherrer Institute (PSI), 5232 Villigen-PSI, Switzerland

<sup>2</sup>Institute for Marine and Atmospheric Research Utrecht, Utrecht University, the Netherlands

Keywords: Organic Aerosols, Source Apportionment, PTR-MS

Presenting author email: Yandong.Tong@psi.ch

Organic aerosols (OA) contribute a dominant fraction of the total aerosol mass (Jimenez *et al.*, 2009), however, the contribution of various sources to the total OA mass is still largely uncertain (Kanakidou *et al.*, 2005). The aerosol mass spectrometer (AMS) has been deployed in field studies to monitor the particle phase, providing fast, quantitative and size resolved aerosol characterisation in real time. Due to the high energy electron ionisation process in the AMS, extensive fragmentation of the organic components is common, preventing chemical characterisation at a molecular level. The proton transfer reaction time-of-flight mass spectrometer (PTR-TOF-MS) utilises a relatively soft ionisation by the proton transfer reaction, decreasing the amount of fragmentation observed and increasing the retained chemical information. Although traditionally used for gas-phase measurements, the PTR-TOF-MS has recently been coupled to an aerosol collector, which can then be heated under controlled conditions to desorb particle components (Holzinger *et al.*, 2010; Timkovsky *et al.*, 2015). This technique is well-suited for the analysis of ambient filter samples, which are routinely collected at monitoring locations around the world.

Here we use the TD-PTR-TOF-MS technique to analyse ambient PM<sub>1</sub> filter samples collected simultaneously at three sites in Lithuania from September 2013 to August 2014. These sites include urban (Vilnius), rural (Rugstelisikes) and coastal (Preila) areas. The TD-PTR-TOF-MS provides the volatility-dependent chemical composition of collected ambient organic aerosol. We conduct the first source apportionment analysis of offline PTR-MS data to quantify OA sources and compare these results to those of offline-AMS source apportionment (Bozzetti *et al.*, 2016).

Five factors were identified from the offline-PTR-MS source apportionment (Fig. 1). Biomass burning organic aerosols (BBOA), local organic aerosols (LOA) and summer organic aerosols (Summer OA) were clearly identified by their thermal desorption mass spectra and seasonal contributions, whereas two other organic aerosol factors (OA-1 and OA-2) could not be attributed yet according to our current references and tracers. The BBOA factor was identified by its clear seasonality with higher contributions during winter and lower during summer. The LOA factor was identified because among the three sites, this factor was overwhelmingly found in Vilnius during summer, whereas at the other two sites,

this factor only showed small contributions. Summer OA was dominant in summer at all sites, in contrast to the BBOA factor which was higher in winter. OA-1 had low volatility, with almost over 67% of the mass evaporating above 300°C. OA-2 was more volatile than OA-1, and was more abundant in Preila than at the other sites, also indicating that OA-2 is possibly related to the products of marine related sources/processes (hereafter this factor is called M-OA). The overall time series of the total resolved OA mass from the offline AMS and the offline TD-PTR-TOF-MS source apportionment results matched well in terms of temporal trend, with Pearson correlation coefficient of R=0.83, although with small discrepancies. In Vilnius 80% of the points of total OA time series were not statistically different within 3σ confidence interval of the AMS reference, while in Preila and Rugstelisikes, only 54.4 % and 65.6% of the points of total OA time series were in the 3σ confidence interval of the AMS reference.

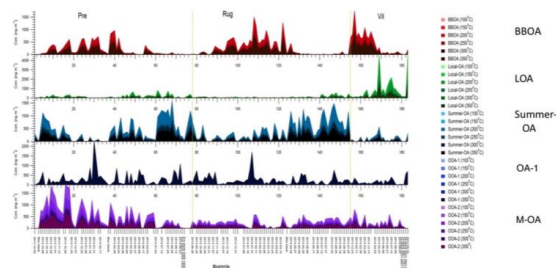


Figure 1. Temperature resolved time series of the five resolved factors. Light and dark colours indicate low and high desorption temperatures, respectively, for the PTR-MS measurements whereas dark colours indicate high temperature.

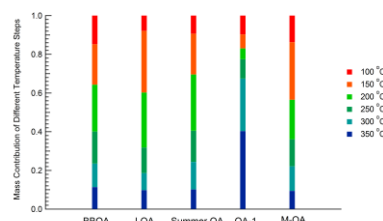


Figure 2. Mass Contribution in different temperature steps of the five resolved factors.

Holzinger *et al.* (2013), *Atmos. Chem. Phys.*, **13**, 10125–10141

Timkovsky *et al.* (2015), *J. Aerosol Sci.* **79**, 1–14.

## Assessment of the primary and secondary contributions from wood burning to the PM10 OC for a rural site in Belgium by making use of molecular markers and PMF

W. Maenhaut<sup>1</sup>, M. Claeys<sup>2</sup>, R. Vermeylen<sup>2</sup>, A. Kahnt<sup>2</sup> and J. Vercauteren<sup>3</sup>

<sup>1</sup>Department of Analytical Chemistry, Ghent University, Gent, BE-9000, Belgium

<sup>2</sup>Department of Pharmaceutical Sciences, University of Antwerp, Antwerpen, BE-2610, Belgium

<sup>3</sup>Flemish Environment Agency (VMM), Antwerpen, BE-2000, Belgium

Keywords: PM10, OC, wood burning, molecular markers, PMF.

Presenting author email: willy.maenhaut@ugent.be

From February 2010 to February 2011 PM10 aerosol samples were simultaneously taken every 4th day at a rural background site in Hamme, Flanders, Belgium. The site was expected to be particularly impacted by biomass burning. The samplings were done for 24 h and 47-mm diameter Pallflex® Tissuquartz™ 2500 QAT-UP filters were used. After sampling the PM10 mass concentration was determined by weighing; organic and elemental carbon (OC and EC) were measured by thermal-optical transmission analysis (Birch and Cary, 1996), the primary wood burning tracers levoglucosan (L), mannosan (M), and galactosan (G) were determined by means of gas chromatography / mass spectrometry (Maenhaut *et al.*, 2012) and other molecular markers were measured by liquid chromatography / mass spectrometry (Kahnt *et al.*, 2013). The latter markers were the resin acid dehydroabietic acid (DHAA), nitroaromatic compounds with molecular weights (MWs) of 139, 155, 169, and 183 (i.e., nitrophenols (NP; MW 139), 4-nitrocatechol (4-NC; MW 155), methyl-nitrocatechols (MNC; MW 169), and dimethyl-nitrocatechols (DMNC; MW 183)), and nitrooxy-organosulfates (NOS) with MW 295. The nitro-aromatic compounds are secondary tracers for wood burning, whereby the MNC are formed from the further oxidation of volatile organic compounds such as *m*-cresol (Iinuma *et al.*, 2010). The NOS are secondary compounds, which are formed from  $\alpha$ -pinene, and are likely attributable to both biogenic emissions and biomass burning (Kahnt *et al.*, 2013).

The data set with concentrations of the PM10 mass, OC, EC and 9 individual or summed molecular markers (i.e., L, M, G, DHAA, NP, 4-NC, MNC, DMNC and NOS) was subjected to receptor modeling by positive matrix factorization (PMF), using EPA PMF 5 (Norris *et al.*, 2014). A 4-factor solution was retained as final solution. The 4 factors (with their overall average percentage contributions to the experimentally measured PM10 mass) were primary wood burning (PWB; 16%), secondary wood burning related to the nitro-aromatic compounds (SWB-NA; 1.4%) NOS-related aerosol (NOS-A; 23%), and other carbonaceous aerosol (OCA; 51%). The key species (that is those with at least 30% of their mass attributed to the factor) were for PWB: OC, L, M, G, and DHAA; for SWB-NA: NP, 4-NC, MNC, and DMNC; for NOS-A: NOS; and for OCA: EC and OC. It is concluded that OCA originates from anthropogenic (non-wood burning) sources; PWB and SWB-NA are exclusively attributable to wood burning and NOS-A is likely from mixed sources. Fig. 1 shows the annual and seasonal mean concentrations of the experimental OC mass and of the OC in the 4 factors. Although the NOS

were poorly correlated with the primary and the nitro-aromatic secondary wood burning tracers (Kahnt *et al.*, 2013), it is noteworthy that NOS-A shows a similar seasonal pattern as PWB and SWB-NA, which suggests that it contains a substantial contribution from wood burning.

From scatter plots of the PMF-derived "wood burning" OC and PM (in each case sum of PWB, SWB-NA and NOS-A) versus levoglucosan, we arrive (by regression through the origin) at levoglucosan to "wood burning" OC and PM conversion factors of 6.7 and 29.3, respectively, whereby the  $R^2$  value for the regression of "wood burning" OC on levoglucosan was excellent (i.e., 0.95), but that for the regression of "wood burning" PM was rather poor (i.e., 0.48), so that the conversion factor of 29.3 should be treated with caution. For comparison, levoglucosan to wood burning OC and PM conversion factors of 9.7 and 22.6, respectively, were derived from a PMF analysis on data sets for four urban background sites in Flanders (Maenhaut *et al.*, 2016).

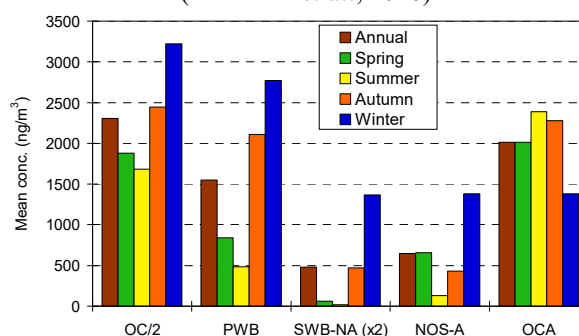


Figure 1. Annual and seasonal mean concentrations of the experimental OC mass and of the OC in the 4 factors.

- Birch, M.E. and Cary, R.C. (1996) *Aerosol Sci. Technol.* **25**, 221-241.
- Iinuma, Y., Böge, O., Grafe, R. and Herrmann, H. (2010) *Environ. Sci. Technol.* **44**, 8453-8459.
- Kahnt, A., Behrouzi, S., Vermeylen, R., Shalamzari, M.S., Vercauteren, J., Roekens, E., Claeys, M. and Maenhaut, W. (2013) *Atmos. Environ.* **81**, 561-568.
- Maenhaut, W., Vermeylen, R., Claeys, M., Vercauteren, J., Matheussen, C. and Roekens, E. (2012) *Sci. Total Environ.* **437**, 226-236.
- Maenhaut, W., Vermeylen, R., Claeys, M., Vercauteren, J., and Roekens, E. (2016) *Sci. Total Environ.* **562**, 550-560.
- Norris, G., Duvall, R., Brown, S. and Bai, S. (2014) *EPA Positive Matrix Factorization (PMF) 5.0 Fundamentals and User Guide*. U.S. EPA Office of Research and Development, Washington, DC 20460, EPA/600/R-14/108, April 2014; i-124.

## Air quality in a street canyon: particles and traffic composition

M. Almeida-Silva<sup>1\*</sup>, P. Baptista<sup>2</sup>, N. Canha<sup>1</sup>, T. Faria<sup>1</sup>, J. Lage<sup>1</sup>, A.V. Faria<sup>3</sup>, G. Duarte<sup>2</sup>, C. Alves<sup>4</sup>, S.M. Almeida<sup>1</sup>

<sup>1</sup>Centro de Ciências e Tecnologias Nucleares, Instituto Superior Técnico, Universidade de Lisboa, E.N. 10 ao km 139,7, 2695-066 Bobadela LRS, Portugal

<sup>2</sup>IN+, Center for Innovation, Technology and Policy Research - Instituto Superior Técnico, Universidade de Lisboa, Av. Rovisco Pais, 1 - 1049-001 Lisboa, Portugal

<sup>3</sup>LAETA, IDMEC, Instituto Superior Técnico, Universidade de Lisboa, Av. Rovisco Pais, 1 - 1049-001 Lisboa, Portugal

\* Presenting author email: marina@ctn.tecnico.ulisboa.pt

Combustion of fossil fuel in internal combustion engine vehicles is a major source of aerosol particles in a city. High pollution levels have been often observed in urban street canyons due to the increased traffic emissions and reduced natural ventilation (Voigtlander, et al., 2006).

Consequently, there is an increasing trend around the world with tightening emission control and larger scale of transport policy intervention in urban cities to control the traffic pollutants and reduce public health risks, such as the implementation of low emission zones and of congestion charging etc.

In this study, particles concentration, particles composition and traffic density were characterized in a characteristic street canyon in Portugal. The street canyon has a demographic density of 12 969 inh/km<sup>2</sup>, with 90% of residential population, 2 lanes for vehicles with a total extension of 1.2 km with 1 intersection with traffic lights (see Figure 1).

Sampling and measurement campaigns occurred in November 2016 using the following methodology:

1) PM10 and PM2.5 were sampled from 7 A.M. to 9 P.M. and 9 P.M. to 7 A.M. allowing the characterization of both periods of the day – rush-hour and non-rush-hour traffic, respectively.

2) For source apportionment analysis, using PMF, particles were analysed by a Thermal Optical technique for Organic Carbon (OC) and Elemental Carbon (EC) determination and by X-ray fluorescence (XRF) for element characterization.

3) PM10, PM4, PM2.5 and PM1 were measured continuously over the study period, as well as the meteorological conditions.

4) Traffic volumes were assessed by several volunteers for one representative working day, in the periods 7:30 to 9:30 A.M., 1:15 to 3:15 P.M. and 5:30 to 7:30 P.M., in order to obtain the peak and off-peak variations.

5) Simultaneously, a random sampling was performed to characterize the traffic composition, considering both vehicle type and vehicle age.

6) Furthermore, a vehicle equipped with a GPS, an OBD reader and a gas analyser passed by the street at least once per 15 min. This allowed characterizing vehicle dynamics variables such as average speed, idling time, etc.

These campaigns allowed characterizing the traffic and air quality status of the area and are part of a project named REMEDIO: Regenerating mixed-use MED urban communities congested by traffic through Innovative low carbon mobility sOolutions, part of Interreg MED Program and co-funded by ERDF.

This work was supported by the European Regional Development Fund (ERDF) through the Interreg Med project REMEDIO (Ref. 862). C2TN/IST authors gratefully acknowledge the FCT support through the UID/Multi/04349/2013 project. This work was also supported by FCT, through IDMEC, under LAETA, project UID/EMS/50022/2013, as well as from the IN+ Strategic Project UID/EEA/50009/2013.

Voigtlander, C J., Tuch, T., Birmili, W. and Wiedensohler, A. (2006) *Atmos. Chem. Phys.*, 6, 4275–4286.

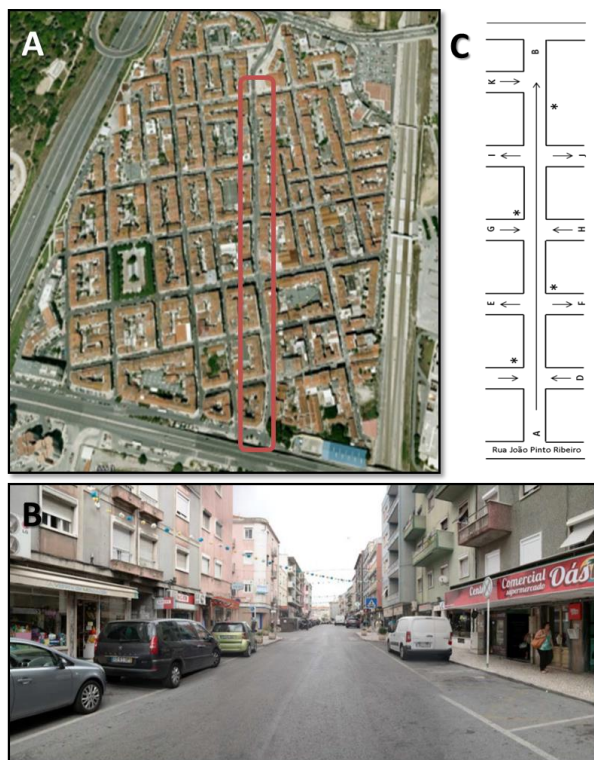


Figure 1. [A] Aerial view, [B] local view of the street canyon and [C] traffic intersections.

## **Influence of Intense secondary aerosol formation and long range transport on aerosol chemistry and properties in the Seoul Metropolitan Area during spring time: Results from KORUS-AQ**

Hwajin Kim<sup>1</sup> and Qi Zhang<sup>2</sup>

<sup>1</sup>Center for Environment, Health and Welfare Research, Korea Institute Science and Technology, Seoul, 136791, Korea

<sup>2</sup>Department of Environmental Toxicology, University of California, Davis, CA 95616, USA

Keywords: HR-ToF-AMS, Haze, sources, Seoul, Air quality.

Presenting author email: hjkim@kist.re.kr

Non-refractory submicrometer particulate matter (NR-PM<sub>1</sub>) was measured in the Seoul Metropolitan Area (SMA), Korea, using an Aerodyne high-resolution time-of-flight aerosol mass spectrometer (HR-ToF-AMS) from April 14 to June 15, 2016, as a part of the Korea-U.S. Air Quality Study (KORUS-AQ) campaign. This was the first highly time-resolved, real-time measurement study of springtime aerosol in SMA and the results reveal valuable insights into the sources and atmospheric processes that contribute to PM pollution in this region.

The average concentration of submicron aerosol (PM<sub>1</sub> = NR-PM<sub>1</sub> + black carbon (BC)) was 22.1 μg m<sup>-3</sup>, which was composed of 44% organics, 20% sulfate, 17% nitrate, and 12 % ammonium. Organics had an average atomic oxygen-to-carbon (O/C) ratio of 0.49 and an average organic mass-to-carbon (OM/OC) ratio of 1.82 (Canagaratna et al., 2015). The concentration and composition of PM<sub>1</sub> varied dynamically during this measurement period, due to the influences of different meteorological conditions, emission sources, and air mass origins. Four distinct sources of OA were identified via positive matrix factorization (PMF) analysis of the HR-ToF-AMS data (Zhang et al., 2011): vehicle emissions represented by a hydrocarbon like OA factor (HOA; O/C = 0.15; 17% of OA mass), cooking activities represented by a cooking OA factor (COA; O/C = 0.19; 22% of OA mass), and secondary organic aerosol (SOA) represented by a semi-volatile oxygenated OA factor (SV-OOA; O/C = 0.44; 27% of OA mass) and a low volatility oxygenated OA factor (LV-OOA; O/C = 0.91; 34% of OA mass).

Our results indicate that air quality in SMA during KORUS-AQ was influenced strongly by secondary aerosol formation with sulfate, nitrate, ammonium, SV-OOA, and LV-OOA together accounting for 76% of the PM<sub>1</sub> mass. Due to high temperature and elevated ozone concentrations, photochemical reactions during daytime promoted the formation of SV-OOA, LV-OOA and sulfate. In addition, aqueous-phase or heterogeneous reactions likely promoted efficient formation of nitrate whereas gas-to-particle partitioning processes appeared to have enhanced nighttime SV-OOA and nitrate formation. During a period of 4 days (from May 20 to May 23), LV-OOA was significantly enhanced and accounted for up to 41% of the PM<sub>1</sub> mass. Since this intense LV-OOA formation event was associated with large enhancement of VOCs (e.g., isoprene, toluene), high concentration of O<sub>x</sub> (= O<sub>3</sub> + NO<sub>2</sub>), strong solar radiation, and stagnant

conditions, it appeared to be related to local photochemical formation.

We also have investigated the formation and evolution mechanisms of severe haze episodes. Unlike the cases observed in winter when haze episodes were mainly caused by intense local emissions coupled with stagnant meteorological conditions, the spring haze events observed in this study appeared to be attributed by both regional and local factors. For example, episodes of long range transport of plumes were followed by calm meteorology conditions, which promoted the formation and accumulation of local secondary species, thus led to high concentrations of PM. Overall, our results indicate that PM pollutants in urban Korea originate from complex emission sources and atmospheric processes and that their concentrations and composition are controlled by various factors including meteorological conditions, local anthropogenic emissions, and upwind sources. Therefore, understanding the high aerosol pollution followed by efficient strategies to remove precursors are important to control the air pollution.

This work was supported by the Korea Institute of Science and Technology (KIST) and National Research Foundation of Korea (NRF) funded by the ministry of Science, ICT & Future Planning (2017R1A2B3004950)

Canagaratna, M.R., Jimenez, J.L., Kroll, J.H., Chen, Q., Kessler, S.H., Massoli, P., Hildebrandt Ruiz, L., Fortner, E., Williams, L.R., Wilson, K.R., Surratt, J.D., Donahue, N.M., Jayne, J.T., Worsnop, D.R., 2015. Elemental ratio measurements of organic compounds using aerosol mass spectrometry: characterization, improved calibration, and implications. *Atmospheric Chemistry and Physics* 15, 253-272.

Zhang, Q., Jimenez, J.L., Canagaratna, M.R., Ulbrich, I.M., Ng, N.L., Worsnop, D.R., Sun, Y., 2011. Understanding atmospheric organic aerosols via factor analysis of aerosol mass spectrometry: a review. *Analytical and bioanalytical chemistry* 401, 3045-3067.

## Source apportionment of water-soluble organic aerosols measured at an urban site

Geun-Hye Yu and Seungshik Park

Department of Environment and Energy Engineering, Chonnam National University, 77 Yongbong-Ro, Buk-ku, Gwangju 61186, Republic of Korea

Keywords: source apportionment, PM<sub>2.5</sub>, WSOC, HULIS, PMF

Presenting author email: fanygh@naver.com, park8162@chonnam.ac.kr

It has been reported that water-soluble organic carbon (WSOC) in the air is formed through atmospheric processing of volatile organic species, or emitted from biomass burning (BB) (Zhang *et al.*, 2010; Yu *et al.*, 2014; Park *et al.*, 2015). Many previous studies have indicated that it is important to conduct WSOC measurements to study secondary organic aerosol (SOA) and to quantify the contributions of primary and secondary OA because their contributions are an essential task to assess control strategies for ambient OA. The purpose of this study was to identify probable sources of WSOC and water-soluble humic-like substances (HULIS) in PM<sub>2.5</sub> and to estimate their quantitative contributions using a positive matrix factorization (PMF) model (US EPA PMF v5.0).

In this study 24-hr PM<sub>2.5</sub> samples were collected from November 2013 to October 2014 at an urban site of Gwangju, Korea, and then used to quantify the concentrations of OC, elemental carbon (EC), WSOC, HULIS, ionic species, and elemental constituents. HULIS was first separated using a hydrophilic-lipophilic balanced (HLB) solid phase extraction method and then quantified by total organic carbon analyzer. Approximately 30 elemental species were analyzed by an Energy Dispersive X-ray fluorescence spectrometry.

The dataset used for PMF analysis consisted of 160 samples and 32 chemical species, and results with six factors were selected as the optimum solutions of PM<sub>2.5</sub> data sets, providing physically realistic source profiles. The following sources were resolved; primary combustion emissions (fossil fuels), soil-related, crustal-related, BB and secondary nitrate, secondary sulfate, and industrial emissions. Results from the PMF analysis showed that predicted WSOC had a tight correlation with measured WSOC, with a slope of 0.98 and an R<sup>2</sup> of 0.88 (Figure 1). A similar relationship was also obtained for HULIS. The most dominant contributor of WSOC and HULIS was from BB + secondary nitrate related source, accounting for 50.7 and 62.4% of their concentrations, respectively (Figure 2). In addition, average contribution of SOA formation processes (secondary sulfate, BB and secondary nitrate related) to WSOC and HULIS was estimated to have 66.5 and 71.5%, respectively. Seasonally BB and secondary nitrate related source contributed 41.9 and 47.7% to WSOC and HULIS, respectively, with the higher fractions occurring in winter. On the other hand, the contribution of SOA to WSOC and HULIS

was estimated to be high in summer. It was found that the PMF model was useful to identify various sources of WSOC and HULIS species, and to apportion their quantitative contributions.

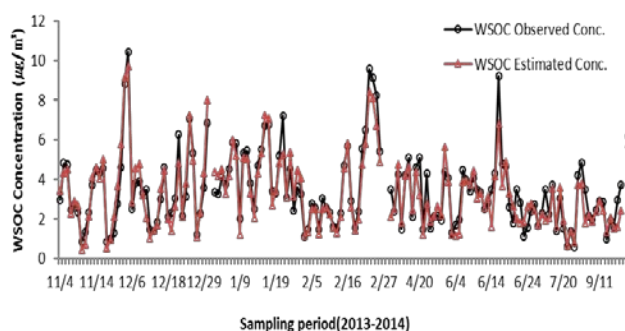


Figure 1. Temporal variation of measured and PMF-predicted WSOC concentrations

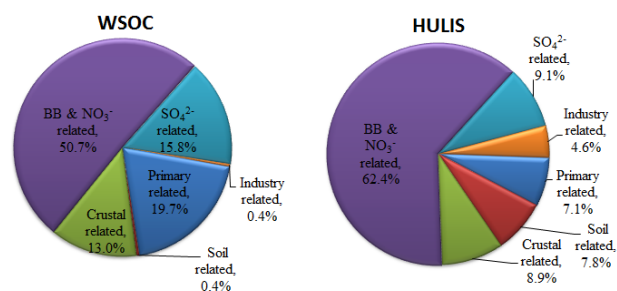


Figure 2. Contributions (%) of each source to measured WSOC and HULIS concentrations.

This research was supported by Basic Science Research Programs through the National Research Foundation of Korea (NRF) funded by the Ministry of Education (NRF-2014R1A1A4A01003896).

Zhang, X., Hecobian, A., Zheng, M., Frank, N.H. and Weber, R.J. (2010) *Atmos. Chem. Phys.* **10**, 6839-6853.

Yu, G.H., Cho, S.Y., Bae, M.S. and Park, S.S. (2014) *Environ. Sci. Proc. Imp.* **16**, 1726-1736.

Park, S.S., Cho, S.Y. and Bae, M.S. (2015) *Sci. Total Environ.* **533**, 410-421.

## Estimation of source apportionment for semi-continuous PM<sub>2.5</sub> data using the EPA-PMF at various air pollution monitoring Supersites in Korea

InJo Hwang<sup>1</sup>, Tae-Jung Lee<sup>2</sup>, Ho-Jin Lim<sup>3</sup>, and Seung-Muk Yi<sup>4</sup>

<sup>1</sup>Department of Environmental Engineering, Daegu University, Gyeongsan, Gyeongbuk, 38453, Korea

<sup>2</sup>Department of Environmental Engineering, Kyung Hee University, Yongin, Gyeonggi, 17104, Korea

<sup>3</sup>Department of Environmental Engineering, Kyungpook National University, Bukgu, Daegu, 41566, Korea

<sup>4</sup>Graduate School of Public Health, Seoul National University, Gwanak, Seoul, 08826, Korea

Keywords: hourly PM<sub>2.5</sub> samples, supersite, EPA-PMF model,  
Presenting author email: ihwang@daegu.ac.kr

Although there have been recently enforcement actions to meet national standards in Korea, the public continue to be concerned about the levels of air pollution. Drawing attention to environmental concerns, such issues have been a motive to activate environmental research along with technical, financial, and administrative investments. It also alerted people of the necessity to introduce and develop a comprehensive management system, which helps to minimize atmospheric pollution causing losses for individuals and industries alike. For these reasons, many countries recently have developed and carried out policies to control air pollutants, focusing their efforts on the establishment of new environmental guidelines as well as accurate evaluation of pollution sources. Accordingly, one of these efforts was to survey the physicochemical properties of atmospheric particulate matter (PM) and thereby, quantitatively understand to what extent the specific pollution sources affect the adjacent regional atmosphere (Yi and Hwang, 2014). The National Institute of Environmental Research of Korea has operated the six air pollution monitoring supersite in order to analyze the characteristics of the major regions atmospheric environment in relation to the long range transport of pollutants, Asian dust, PM, and ozone. In order to maintain and manage ambient air quality, it is necessary to identify sources and to apportion the ambient PM mass. To do so, receptor modeling has been developed that analyze various properties of the pollutants at the receptor site, and to evaluate the source contributions (Hwang and Hopke, 2006). The objective of this study was to estimate the PM<sub>2.5</sub> composition at the sampling sites by surveying concentration trends after analyzing the mass concentration of PM<sub>2.5</sub> samples, elements, ions, and carbon in PM<sub>2.5</sub>. The EPA-PMF model applied to identify the existing sources and apportionment of the PM mass to each source.

The hourly PM<sub>2.5</sub> samples were collected at Seoul, Ulsan, and Jeju Island air pollution monitoring supersites from January 2013 to December 2015 were analyzed. A total of 26280 samples (Seoul), 17520 samples (Ulsan), and 26280 samples (Jeju Island) were collected and 35 species (OC, EC, SO<sub>4</sub><sup>2-</sup>, NO<sub>3</sub><sup>-</sup>, Cl<sup>-</sup>, Na<sup>+</sup>, NH<sub>4</sub><sup>+</sup>, K<sup>+</sup>, Mg<sup>2+</sup>, Ca<sup>2+</sup>, As, Ba, Br, Ca, Cd, Co, Cr, Cu, Fe, Ga, Hg, K, Mn, Mo, Ni, Pb, Pd, S, Sb, Se, Si, Ta, Tl, V, and Zn) were analyzed by XRF (X-ray fluorescence spectroscopy; Xact-series 620, USA), IC (ion chromatography; URG-9000D, USA), and TOT (thermal optical transmittance; 4F-semi continuous field analyzer, USA) methods.

In the case of Seoul site, the PMF modelling identified ten sources such as secondary sulfate, secondary nitrate, mobile 1, mobile 2, oil combustion, roadway emission, industry, biomass burning, aged seasalt, and soil source, respectively. The source had highest effect on the ambient air quality, followed by secondary sulfate (24.5%), mobile 1 (23.9%), secondary nitrate (21.8%) source. This final results can be used to establish policies for air quality management in the future. More detailed results of source apportionment for PM<sub>2.5</sub> at various supersites will be presented.

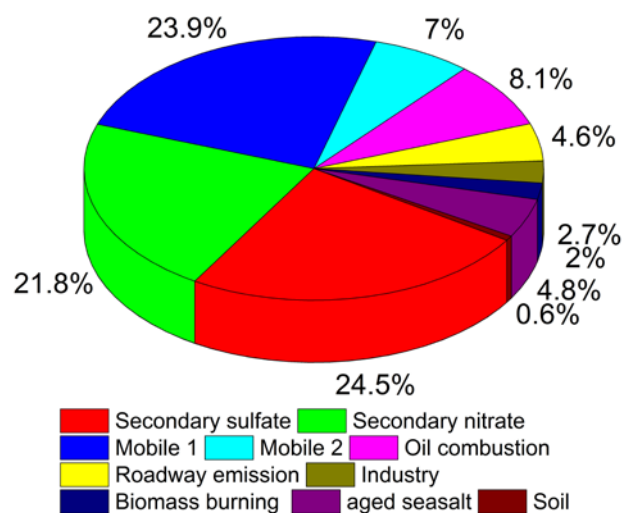


Fig. 1. Average source contributions of the identified sources to PM<sub>2.5</sub> concentrations at the Seoul site in 2013.

This research was supported by National Institute of Environmental Research (NIER).

Yi, S.M. and Hwang, I.J. (2014) Asian Journal of Atmospheric Environment 8(3), 115-125.

Hwang, I.J. and Hopke, P.K. (2006) J. Air and Waste Manage. Assoc. 56(9), 1287-1300.

## Organic Aerosol in Urban Air of China: Chemical Composition, Sources and Atmospheric Processes

R.-J. Huang<sup>1,2</sup>, Y. C. Wang<sup>1</sup>, Y. He<sup>1</sup>, R. Fröhliche<sup>2</sup>, F. Canonaco<sup>2</sup>, M. Elser<sup>2</sup>, K. R. Daellenbach<sup>2</sup>, I. El Haddad<sup>2</sup>, J. Slowik<sup>2</sup>, M. R. Canagaratna<sup>3</sup>, D. R. Worsnop<sup>3</sup>, A. S. H. Prévôt<sup>2</sup>, and J. J. Cao<sup>1</sup>

<sup>1</sup>Key Lab of Aerosol Chemistry and Physics, Institute of Earth Environment, Chinese Academy of Sciences, Xi'an, 710061, China

<sup>2</sup>Laboratory of Atmospheric Chemistry, Paul Scherrer Institute (PSI), 5232 Villigen, Switzerland

<sup>3</sup>Aerodyne Research, Inc., Billerica, MA, USA

Keywords: Haze pollution, Organic aerosol, Source apportionment, Atmospheric processes

Presenting author email: rujin.huang@ieecas.cn

Particulate air pollution in China is a serious environmental problem that is influencing visibility, air quality, regional and global climates and human health. Understanding of the chemical composition and sources of fine particulate matter, the mechanisms and atmospheric processes of substantial wintertime secondary aerosol production, and the constraint of sources and formation processes of secondary organic aerosol during haze pollution events are essential for effective mitigation of particulate pollution (Huang *et al.*, 2014).

Here, we present the results from recent field measurement campaigns in different Chinese cities. The non-refractory chemical composition was measured using an Aerodyne aerosol mass spectrometer. Black carbon was measured using an aethalometer, together with supporting measurements including gas-phase species and meteorological parameters. Filter samples were also collected and the organic markers were measured, including levoglucosan, organic acids, hopanes, and polycyclic aromatic hydrocarbons. The sources of organic aerosol were studied using a multi-linear engine (ME-2) receptor model (Canonaco *et al.*, 2013). Primary emission sources including vehicle emissions, biomass burning, coal combustion, cooking emissions and secondary organic aerosol factors including less oxidized oxygenated organic aerosol and more oxidized oxygenated organic aerosol were identified and quantified. The factors affecting the secondary organic aerosol formation were studied. Detailed results will be presented and discussed.

This work was supported by the National Natural Science Foundation of China (NSFC, Grant No. 41403110, No. 41673134, and No. 91644219)

Huang, R.-J., et al. (2014) *Nature* **514**, 218-222.

Canonaco, F., Crippa, M., Slowik, J. G., Baltensperger, U., Prévôt, A. S. H. (2013) *Atmos. Meas. Tech.*, **6**, 3649-3661.

## Long-term measurements of the chemistry and sources of submicron aerosols at SIRTa in Paris area, France

Y. Zhang<sup>1-3</sup>, O. Favez<sup>1</sup>, A. Albinet<sup>1</sup>, F. Canonaco<sup>4</sup>, F. Truong<sup>2</sup>, T. Amodeo<sup>1</sup>, A. Prevot<sup>4</sup>, J. Sciare<sup>3</sup>, V. Gros<sup>2</sup>

<sup>1</sup>INERIS, Verneuil en Halatte, 60550, France

<sup>2</sup>Laboratoire des Sciences du Climat et de l'Environnement, Gif sur Yvette, 91191, France

<sup>3</sup>The Cyprus Institute, Environment Energy and Water Research Center, Nicosia, Cyprus

<sup>4</sup>Paul Scherrer Institute, 5232 Villigen, Switzerland

Keywords: submicron aerosol, long-term measurements, organic aerosol, black carbon, sources, AuRo SoFi

Presenting author email: yunjiang.zhang-etudiant@ineris.fr

Atmospheric submicron aerosol particles ( $PM_{10}$ , aerodynamic diameter  $\leq 1 \mu m$ ) are of major concern for air quality.  $PM_{10}$  also have potential impacts upon global climate change and ecosystems. However, the impacts remain highly uncertain, mainly due to their complex chemical processes, various sources, and the interactions between meteorology and atmospheric aerosols. In the last decade, many studies have investigated the chemistry of atmospheric aerosols worldwide using online instrumentation. However, there is a lack of long-term ambient measurements (e.g.  $>5$  years) for a better understanding on the sources and formation mechanisms of  $PM_{10}$ . This is especially needed for policy makers to elaborate and evaluate efficient air pollution control strategies, and for modellers to validate and improve model simulations.

We have been performing multi-year in-situ measurements with real-time on-line instruments, including an Aerosol Chemical Speciation Monitor (ACSM) (Ng et al., 2011), and a 7-wavelength Aethalometer (Drinovec et al., 2015) at SIRTa station since mid-2011. These measurements are part of the European ACTRIS and ACTRIS-2 research programs. SIRTa is located about 25 km South-West of Paris city centre. The  $PM_{10}$  non-refractory chemical components (NR- $PM_{10}$ ), i.e., organic aerosol (OA), nitrate, sulphate, ammonium, and chloride, as well as black carbon (BC) were measured by the ACSM and Aethalometer, respectively. BC sources were identified using the Aethalometer model (Sandradewi et al. 2008). Positive matrix factorization (PMF) with the multi-linear engine (ME-2) was performed using the Source Finder (SoFi) (Canonaco et al., 2013) for OA source apportionment (e.g., Fig. 1). Finally, combining with the potential source contribution function (PSCF), we evaluated the possibility of geographical sources of  $PM_{10}$  at SIRTa.

We investigate the annual, seasonal, monthly, weekly (e.g., Fig. 1 and 2), and diurnal variations of various sources contributing to  $PM_{10}$  mass loadings, including primary sources (e.g., traffic and wood burning emissions) and secondary formation (from anthropogenic and biogenic related sources).

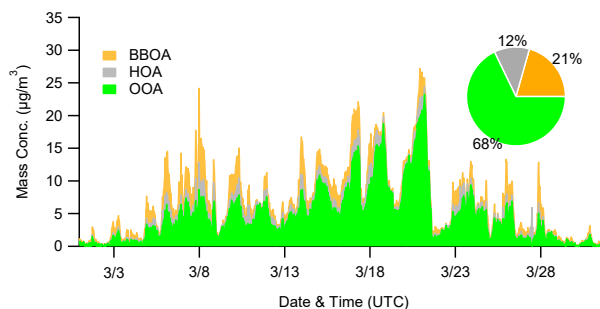


Figure 1. Time series of preliminarily PMF-resolved OA factors during March 2015. Pie chart shows show the average composition of OA.

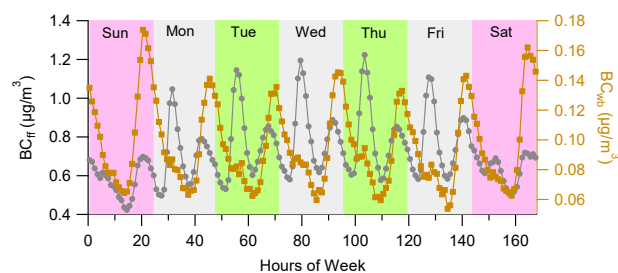


Figure 2. Weekly variations of different BC sources, i.e., fossil fuel ( $BC_{FF}$ ) and wood burning ( $BC_{WB}$ ) emissions.

This work has notably been supported by the FP7 ACTRIS and H2020 ACTRIS2 projects, the DIM-R2DS program, as well as by the French reference laboratory for air quality monitoring (LCSQA). Y. Z. acknowledges the PhD Scholarship from the China Scholarship Council (CSC).

Ng, N.L., Herdon, S.C., Trimborn, A. et al. (2011) *Aerosol Sci. Technol.*, 45, 780-794.

Drinovec1, L. Močnik1, G. Zotter, P. et al. (2015) *Atmos. Meas. Tech.* 8, 1965-1979.

Sandradewi, J., Prévôt, Andre S. H., Szidat, S. et al. (2008) *Environ. Sci. & Technol.*, 42, 3316-3323.

Canonaco, F., Crippa, M., Slowik, J. G. et al. (2013) *Atmos. Meas. Technol.*, 6, 3649-3661.

## Aerosol source apportionment in a European air pollution hot spot with both aerosol chemical composition and number size distribution

C. Leoni<sup>1</sup>, P. Pokorná<sup>1</sup>, M. Masiol<sup>2</sup>, J. Hovorka<sup>1</sup>, K. Křůmal<sup>3</sup>, Y Zhao<sup>4</sup>, S. Cliff<sup>4</sup>, P.K. Hopke<sup>2</sup>

<sup>1</sup>Institute for Environmental Studies, Faculty of Science, Charles University, Benátská 2, Prague 2, 128 01, CZ

<sup>2</sup>Center for Air Resources Engineering and Science, Clarkson University, Potsdam, NY 13699-5708, USA

<sup>3</sup>Institute of Analytical Chemistry of the AV CR, v. v. i., Veverí 967/97, 60200 Brno, CZ

<sup>4</sup>Air Quality Research Center, University of California, Davis, CA 95616, USA

Keywords: PM<sub>10</sub> and PM<sub>0.09-1.15</sub>, number size distribution, ultrafine particles, highly time resolved elemental composition

Presenting author email: leonic@natur.cuni.cz

Atmospheric aerosol particle concentrations continue to be above the European Union limit values in large part of the EU (EEA Report 2016). The Moravian-Silesian region in the Czech Republic represents one of the EU air pollution hot spots. Proper identification and quantification of the main PM sources is needed to improve the air quality. This is particularly challenging in Ostrava, due to the presence of several sources, some of them large and situated in the vicinity of the urban settlements.

The application of receptor models can be highly effective for the source apportionment. Receptor models analyse data matrices of aerosol chemical and physical characteristics of samples collected at a given locality, the receptor, to apportion their sources. Recently, the source apportionment started to focus not only on chemical composition, but on particle number size distribution (NSD) data. In fact, the toxicity of particles also depends on the particle size, not only on the chemical composition. The analysis of the chemical composition data is able to distinguish components contributing largely to particle mass, whereas the particle NSD data set is more effective for identifying components making an appreciable contribution to particle number. The chemical composition has been largely used in receptor modeling, while only few studies use particle NDS (Masiol et al., 2016, Sowlat et al., 2016, Beddows et al., 2015). The aim of this study is to make a comprehensive source apportionment in one of the most important air pollution hot spots in the EU, using receptor modeling on both particle chemical composition and number size distribution.

A monthly campaign was performed in winter 2014 in a residential district of Ostrava with a large metallurgy complex located 1.5 km south-west. Five-minute integration time particle number size distributions within the size ranges 14 nm – 10 µm (SMPS-3936L25 and APS-3321, TSI Inc.), gaseous pollutant and meteorological variables were registered. 2-h samples of size segregated PM was collected with a Davis Rotating-drum Uniform-size-cut Monitor (DELTA Group UC-Davis), in 8 size ranges, from 1.15 to 0.09 µm. The samples were analyzed for 24 elements with synchrotron X-ray fluorescence. Organic molecules in PM<sub>1</sub> (levoglucosan and homohopane) were measured with 24-hour time resolution (DHA-80 Digitel, GC-MS).

US EPS PMF model version 5 was used for source apportionment.

The preliminary results on mass chemical composition modeling showed five factors: coal combustion and secondary inorganic aerosol – S.I.A (39%), biomass burning (28%), re-suspended road dust (18%), raw iron production (9%) and sintering/steel production (6%). The preliminary results on spectra modeling show five factors associated with following modes: accumulation 1 (27%), accumulation 2 (10%), nanoparticles (31%), Aitken mode particles (28%), coarse particles (4%). The nanoparticles and the coarse particles have industrial origin, the accumulation 2 is related with coal combustion, the accumulation 1 with biomass burning. Contributions of the traffic and the long-range transport are still unclear.

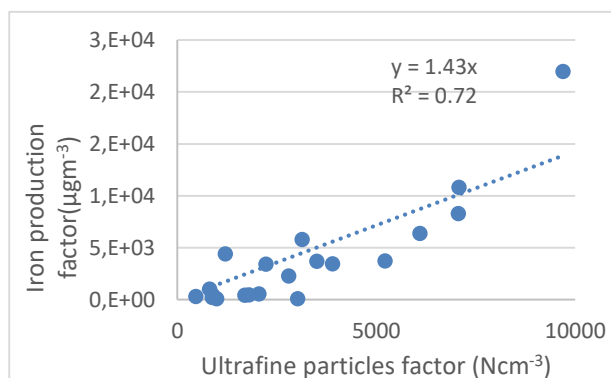


Figure 1. Linear regression of contributions of iron production factor vs daily average nanoparticles factor

In conclusion, the NSD modelling allows to resolve sources in the ultrafine size range, that is not possible with the aerosol particle mass concentration/chemical composition modelling alone. The two approaches appear to be complementary. The industry produces important source of ultrafine particles.

This work was supported by the Czech Grant Agency (P503/12/G147).

Masiol, M. et al., (2016) *Atmos. Env.* **139**, 57-74.

Sowlat, J. et al., (2010) *Atmos. Chem. Phys.* **16**, 4849-4866.

Beddows, D.C.S. et al., (2015) *Atmos. Chem. Phys.* **15**, 10107-10125.

## Size-segregated aerosol source apportionment by multistage cascade impactor samples collected at a pollution hot-spot area (Milan, Italy).

V. Bernardoni<sup>1</sup>, A. Bigi<sup>2</sup>, P. Fermo<sup>3</sup>, A. Piazzalunga<sup>3, #</sup>, G. Valli<sup>1</sup>, R. Vecchi<sup>1</sup>

<sup>1</sup>Department of Physics, Università degli Studi di Milano, and INFN, Milan, 20133, Italy

<sup>2</sup>Department of Mechanical and Civil Engineering, University of Modena and Reggio Emilia, Modena, 41125, Italy

<sup>3</sup>Department of Chemistry, Università degli Studi di Milano, Milan, 20133, Italy

<sup>#</sup>now at: Water&Life Lab, Entratico, 24060

Keywords: aerosol size distributions, chemical characterisation, size-segregated source apportionment  
Presenting author email: vera.bernardoni@unimi.it

Size distribution and chemical composition are the main parameters affecting aerosol effects at both local and global scale. Nevertheless, detailed information on the size segregated aerosol composition still lacks in the literature because it requires lot of man power and it is very time consuming when carried out using traditional instrumentation (multistage cascade impactors and laboratory analysis of the collected samples) or it requires very expensive on-line instrumentation (e.g. time-of-flight aerosol mass spectrometry).

Due to the importance of size-segregated composition in the evaluation of aerosol effects, it is also important to understand sources and processes leading to the measured concentrations in atmosphere, to develop a suitable and effective abatement strategy.

Hot-spot pollution areas are peculiar sites where source emissions and meteorological conditions foster particulate matter accumulation and very high aerosol concentrations are often registered. The Po Valley is one of the main hot-spot pollution areas in Europe, especially during wintertime.

In this work, a detailed physical and chemical characterisation of size segregated atmospheric aerosol in Milan urban area (Italy) was performed. This allowed the application of a 3-way source apportionment model for size-segregated source identification and apportionment.

Size segregated aerosol samples were collected using a Dekati-SDI cascade impactor (12 stages in the range 45nm-8.5µm) at an urban background station in Milan, Italy, during winter 2011-2012 (Elser Fritsche, 2012). Fourteen samplings were carried out with the cascade impactor, for a total of 168 samples available.

Samples were collected on polycarbonate membranes. Elemental composition (Si-Pb) was determined by Energy-Dispersive X-Ray Fluorescence, the main inorganic ions (nitrate, sulphate and ammonium) by ion chromatography (IC), and levoglucosan (marker for wood burning) by high-performance liquid chromatography coupled to pulsed amperometric detection. It is noteworthy that the detailed characterisation of size-segregated PM required the optimisation of the analytical techniques because of the small quantities of material to analyse and of the peculiarities of the PM deposits (Bernardoni et al., 2011a).

Ancillary information on atmospheric dispersion conditions was available by <sup>222</sup>Rn measurements and the main meteorological parameters (temperature, pressure, RH, solar radiation, wind speed and direction) were also monitored at the sampling site.

Results obtained for size-segregated samples were analysed using the MICRON inversion model aiming at the identification of the size-distribution modes for the different chemical components.

Size-segregated chemical composition and mass concentration temporal trends were used as input to perform a 3-way source apportionment (Ulbrich et al., 2012). A vector-matrix model (Tucker 1 model) was implemented: the measured data were reconstructed as the tensor product of a 2-D array representing source temporal trends and a 3-D matrix representing size-segregated source profiles. Multilinear Engine 2 (ME-2) was used to minimise the object function Q, represented by the sum of the squares of weighed residuals between measured and reconstructed data.

Physical-chemical characterisation of size-segregated samples and mode retrieval will be presented. Size segregated source apportionment results will be also shown and the obtained results will be discussed also in relation to previous source apportionment studies carried out in the area on PM10 (Bernardoni et al., 2011b) and PM1 sampling campaigns.

Bernardoni, V., Cuccia, E., Calzolari, G., Chiari, M., Lucarelli, F., Massabò, D., Nava, S., Prati, P., Valli, G., Vecchi, R. (2011a) *X-Ray Spectrom.*, **40**, 79–87

Bernardoni, V., Vecchi, R., Valli, G., Piazzalunga, A., Fermo, P. (2011b), *Sci. Total Environ.*, **409**, 4788-4795

Elser Fritsche M. (2012) Master Degree Thesis in Physics, Dept. of Physics, University of Milan.

Ulbrich, I. M., Canagaratna M. R., Cubison, M. J., Zhang, Q., Ng, N. L., Aiken, A. C., and Jimenez, J. L. (2012), *Atmos. Meas. Tech.*, **5**, 195–224

## Distinguishing source specific black carbon production from meteorologically driven temporal variability by means of $^{222}\text{Rn}$ tracer

A. Gregorič<sup>1</sup>, L. Drinovec<sup>2,3</sup>, I. Ježek<sup>2</sup>, J. Vaupotič<sup>3</sup>, L. Wang<sup>1</sup>, M. Mole<sup>1</sup>, S. Stanič<sup>1</sup> and G. Močnik<sup>2,3</sup>

<sup>1</sup>University of Nova Gorica, Nova Gorica, 5000, Slovenia

<sup>2</sup>Aerosol d.o.o., Ljubljana, 1000, Slovenia

<sup>3</sup>Jožef Stefan Institute, Ljubljana, 1000, Slovenia

Keywords: black carbon, source apportionment, radon, planetary boundary layer, lidar

Presenting author email: asta.gregoric@ung.si

Black carbon (BC), as a component of fine particulate matter in the atmosphere, causes undesirable health outcomes (WHO, 2012) and significantly influences the climate (Bond *et al.*, 2013). It is produced by incomplete combustion of carbonaceous fuels, mainly fossil fuel and biomass. BC is thus a good indicator of primary emissions. Atmospheric conditions play an important role in the magnitude and time evolution of atmospheric pollution. On diurnal timescales, the planetary boundary layer (PBL) evolution significantly influences the variability of black carbon concentrations. An alternative, recently used method for the assessment of PBL stability, is the use of naturally occurring noble radioactive gas radon ( $^{222}\text{Rn}$ ) (e.g. Chambers *et al.*, 2015). Its diurnal variation is governed by the dispersion within the PBL and therefore represents a reliable tracer for near surface atmospheric conditions, allowing the decoupling of meteorologically driven BC variation from the dynamics of the sources.

Several measurement campaigns have been carried out between 2012–2016 in Ljubljana, the capital of Slovenia, in order to evaluate the spatio-temporal heterogeneity of air pollution within the city and its surroundings, depending on contributions from main pollution sources and the meteorology. Ljubljana is located in a wide basin surrounded by hills in the central part of Slovenia. An additional measurement campaign was conducted in 2016 in the Vipava valley in western Slovenia, constrained by a mountain ridge and Karst plateau. Being just 30 km away from the coastal line, the weather in the valley is affected by both the sub-mediterranean and sub-alpine climate, leading to abrupt weather changes within the valley. At both locations, radon measurements have started in winter 2016/17. Additionally, LIDAR remote sensing provides accurate measurements of the PBL vertical structure and quantifies the relationship between radon concentrations and the mixing height. BC was measured using the Aethalometer model AE33. The Sandradewi (2008) model was used to apportion measured BC to traffic ( $BC_{\text{TR}}$ ) and biomass burning ( $BC_{\text{BB}}$ ).

The highest BC concentrations were found in urban traffic zones in the Ljubljana city center and near highways. Urban background stations are characterized by lower BC concentrations. Source apportionment of BC revealed different spatial and temporal patterns for the two sources. BC from traffic emissions prevails within the whole city and exhibits a large heterogeneity, with concentrations diminishing with increasing distance from the traffic sources. On the other hand, homogeneous

distribution of BC from biomass burning was observed within the whole city.

Although significantly less populated, BC concentrations in the Vipava valley reach similar levels as those in the Ljubljana basin, with higher diurnal variation of both sources. Traffic related BC prevails in the morning, whereas biomass burning contribution to BC is higher in the afternoon and evening.

Based on atmospheric radon measurements, significant atmospheric influence on the diurnal variation of BC can be clearly noticed in the Vipava valley, since both radon and BC mainly follow the same diurnal pattern, as seen from Figure 1. On the other hand, distinct peaks of BC, not in line with radon, are observed in the Ljubljana basin, indicating higher BC production in the capital city than in the Vipava valley, but with essentially similar consequences to the local air quality.

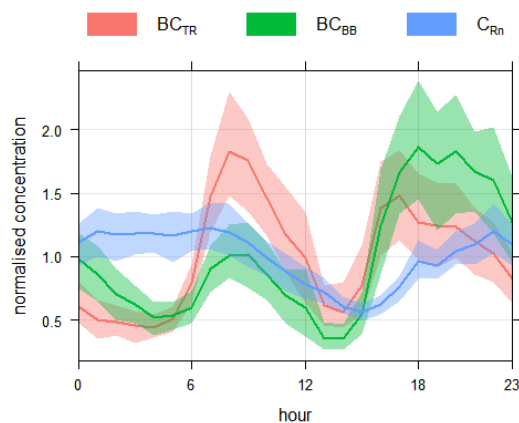


Figure 1. Normalised diurnal variation (mean and 95 % confidence interval in the mean, normalised to mean value) of black carbon from traffic ( $BC_{\text{TR}}$ ), biomass burning ( $BC_{\text{BB}}$ ) and radon concentration ( $C_{\text{Rn}}$ ) in the Vipava valley showing the controlling effect of PBL evolution observed by  $^{222}\text{Rn}$ .

This work was supported by JR-KROP grant 3211-11- 000519, JR-RK grant 3330-14-509063 and P1-0385 research program. We thank ARSO, Municipality of Ljubljana and Ames d.o.o for the use of their measurement sites.

Bond, T. C., *et al* (2013) *J. Geophys. Res. - Atmos.* **118**(11), 5380–5552.

Chambers, S. D., *et al* (2015) *Atmos. Chem. Phys.* **15**(3), 1175–1190.

Sandradewi, *et al* (2008) *Environ. Sci. Technol.* **42**, 3316–3323.

WHO (2012) *Health effects of Black Carbon*. The WHO European Centre for Environment and Health: Bonn.

## Near real time measurements and source apportionment of aerosol trace elements in Härkingen, Switzerland

P. Rai<sup>1</sup>, M. Furger<sup>1</sup>, J.G. Slowik<sup>1</sup>, F. Canonaco<sup>1</sup>, R. Fröhlich<sup>1</sup>, A.S.H. Prevot<sup>1</sup>, U. Baltensperger<sup>1</sup>

<sup>1</sup> Paul Scherrer Institute, Villigen PSI, Switzerland

Keywords: trace elements, source apportionment, fireworks, traffic emission

Presenting author email: Pragati.raï@psi.ch

Ambient aerosol is the complex mixture of solid and/or liquid particles suspended in the atmosphere. The identification and quantification of its sources has been proven very challenging. Highly time resolved and near real time measurement of trace elements add greater temporal variabilities to certain source apportionment analysis, which can assist in the identification of local anthropogenic sources such as traffic and industries. One of the most unusual anthropogenic activities that create notable air pollution is the display of fireworks to celebrate festivals. The chemical compositions of particles emitted by fireworks are generally metals (e.g. potassium, barium, copper), elemental carbon and secondary compounds (Kong *et al* 2015). Using one or two hour resolution metal data in receptor modelling analyses has proven to be very useful in the identification of local sources (Richard *et al* 2010; Visser *et al* 2015). Here we present the source apportionment of highly time resolved and near real time measurement of trace metals at Härkingen, Switzerland.

A field campaign was organized at the NABEL (Swiss Air Pollution Monitoring Network) station Härkingen next to a freeway for three weeks from 23 July to 13 August 2015, which included a firework episode on Swiss National Day (1 August). During the campaign PM<sub>10</sub> (particles with an aerodynamic diameter ≤ 10 μm) was sampled with 1-hour time resolution by an Xact® 625 ambient metals monitor. There are villages to the south and east of the site, and agricultural land immediately to the west and north as well as some industrial activities in southeast across the freeway. Sources were resolved using the multilinear engine (ME-2) implementation of positive matrix factorization (Paatero, 1999; Canonaco *et al* 2013).

First results are shown in Fig. 1. The ME-2 analysis identified seven emission sources at the sampling location. The time series for the fireworks factor is showing the highest peak (41 μg m<sup>-3</sup>) on 1 August at 2300 CEST which is a clear firework episode. The traffic related factor is strongly influenced by local traffic emission as shown by several peaks during morning and evening traffic peak hours while the resuspended dust factor is peaking during the day and decreased in the night time. The sea salt factor is having 1.1 μg m<sup>-3</sup> mass loading which is in good agreement with the Cl concentration during the non-firework period. The industrial factor is characterized by a number of episodic peaks, suggesting an industrial influence. The relative factor contributions are shown in Fig. 2. The highest contribution of the elements measured by the Xact was found to be the S-rich factor (35% of PM<sub>10</sub>) followed by resuspended dust (20%),

traffic related (16.5%), fireworks (13%), background dust (12%), sea salt (3%) and industrial (0.4%).

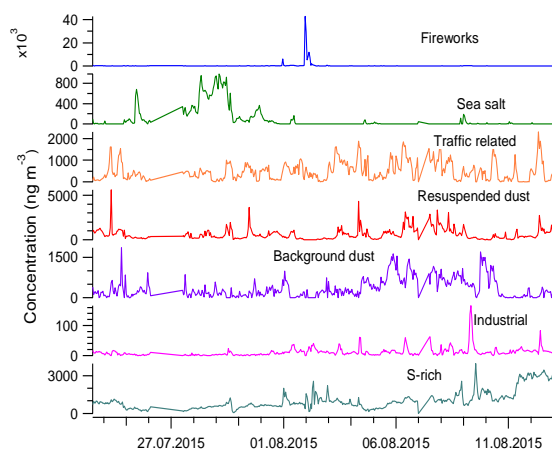


Figure 1. Source contributions (factor time series) for the ME-2 derived source factors at Härkingen, Switzerland.

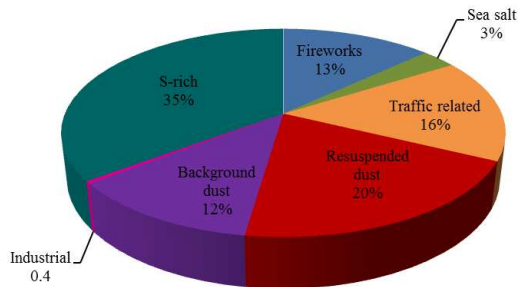


Figure 2. Relative contributions from different sources to the total PM<sub>10</sub> mass.

This project was supported by the Swiss Federal Office for the Environment (FOEN) and by the Swiss National Science Foundation (Grant 200021\_162448). The authors are grateful to María Cruz Minguillón, Christoph Hüglin (Empa), Krag Petterson (CES) and Varun Yadav (CES) for their help.

- Canonaco, F. *et al.* (2013) *Atmos. Meas. Tech.* **6**, 3649-3661.  
 Kong, S.F. *et al.* (2015) *Atmos. Chem. Phys.* **15**, 2167-2184.  
 Paatero, P. *et al.* (1999) *J. Comput. Graph. Stat.* **8**, 854-888.  
 Richard, A. *et al.* (2010) *Atmos. Meas. Tech.* **3**, 1473-1485.  
 Visser, S. *et al.* (2015) *Atmos. Chem. Phys.* **15**, 11291-11309.

## **Review on Source Apportionment of Fine Aerosol using Carbonaceous Constituents and Organic Molecular Markers: Case studies from India and South East Asia**

Lovleen Gupta<sup>1</sup>, Gazala Habib<sup>1</sup> and Ramya Sunder Raman<sup>2</sup>

<sup>1</sup>Department of Civil Engineering, Indian Institute of Technology, Delhi, 110 016, India

<sup>2</sup>Department of Earth and Environmental Sciences, Indian Institute of Science Education and Research, Bhopal, 462 066, India

Keywords: Carbonaceous aerosols, Molecular marker, Source apportionment, Black Carbon

Presenting author email: [lovleengupta@gmail.com](mailto:lovleengupta@gmail.com)

Fine aerosol (Diameter $\leq$ 2.5  $\mu$ m) is a complex and dynamic mixture of solid and liquid particles from natural and anthropogenic sources, which contains inorganic ions, metals, carbonaceous aerosol (black/elemental carbon and organic carbon) and complex organic compounds. The carbonaceous aerosol (CA) constitutes a significant portion (~20-70%) of PM<sub>2.5</sub>, and the complexity arises from temporal and spatial variation of anthropogenic sources. It has been found that presence of CA is responsible for a wide range of environmental problems, ranging from local issues (e.g. pollution toxicity) to global scale (e.g. climate change) leading to human health problems and food security. It has also been found that majority of the CA is from anthropogenic sources. So, if we know the sources well, we can adopt measures/strategies to control the CA emissions.

In South East Asia the field campaign (i.e. INDOEX, ACE-Asia) were conducted to understand the source of carbonaceous aerosol in this region. During INDOEX the ratio of carbonaceous components (organic carbon, elemental carbon) was used and fossil fuel combustion was thought to be dominant source of aerosol over India. However, at the same time the single particle analysis indicated the dominance aerosol from of biomass fuel combustion over India. Such approaches were debated and paved the need for detailed source apportionment studies in South Asian countries especially India and China. A recent study have shown a large discrepancies between satellite retrieved and climate model simulated absorbing aerosol optical depth over South Asia, indicating the inherent uncertainties in regional emission estimates. Therefore, it is suggested to strengthen the emission estimate by incorporating the information from source apportionment studies. It has also been emphasized to use Molecular Markers to resolve ambiguity in source apportionment of CA.

There are several techniques available to carry out the source apportionment. Source apportionment through receptor modelling is one of the widely used technique to quantify contribution of various sources. The technique uses the chemical profile of aerosol collected at receptor site. However, it is not well

understood if adding CA and MM as one of the components in receptor modelling strengthens the source apportionment ability or not. This paper will present the review on the source apportionment studies carried out in India and South east Asia and will critically analyse how the inclusion of CA organic MM have helped in improving our understanding of source contribution to atmospheric fine aerosol burden over South East Asia.

## A new approach for classifying airborne particles: A case study on the quantification of PM<sub>10</sub> from railway and road traffic in the Reuss valley (Canton of Uri, Switzerland)

J. Rausch<sup>1,2</sup>, T. Zünd<sup>1</sup>, D. Jaramillo Vogel<sup>1,2</sup>, R. Locher<sup>3</sup>, M. Meier<sup>1,2</sup> and K. Kammer<sup>4</sup>

<sup>1</sup>Particle Vision GmbH, c/o Fri Up, Annexe 2, Passage du Cardinal 11, Fribourg, 1700, Switzerland

<sup>2</sup>Department of Earth Sciences, University of Fribourg, Fribourg, 1700, Switzerland

<sup>3</sup>Institute of Data Analysis and Process Design (IDP), Zurich University of Applied Sciences (ZHAW), Winterthur, 8400, Switzerland

<sup>4</sup>Federal Office for the Environment (FOEN), Bern, 3003, Switzerland

Keywords: particle classifier, CCSEM, single particle analysis, PM<sub>10</sub>, traffic  
Presenting author email: juanita.rausch@particle-vision.ch

The MFM-U (Monitoring flankierende Massnahmen Umwelt) project was launched in 2003 by the Swiss authorities to monitor and control the environmental impact of freight traffic crossing the Swiss Alps. Within the frame of this project, the portion of PM<sub>10</sub> emitted from a specific highway and railway segment in the Alpine north-south axis (Altdorf, Reuss valley, Canton of Uri, Switzerland) was studied during September-November 2016. A new approach for the characterization, quantification and differentiation of primary particulate matter was tested. In addition, the lateral dispersion of the emitted pollutants was investigated. For this purpose, a transect consisting of two emission and two immission sites, located between the A2 highway and the AlpTransit railway line, was deployed. Passive and active sampling was performed during 4 weeks in sampling periods of one week. The coarse mode (PM<sub>2.5-10</sub>) was sampled passively on boron substrates with the Sigma-2 passive sampler. And the small particles (PM<sub>2.5</sub>) were collected actively on polycarbonate filters using the AirChek 3000 air pump system. Single particle analysis combining computer controlled scanning electron microscopy (CCSEM) and energy dispersive x-ray spectroscopy were performed on all collected samples. The morpho-chemical results were evaluated with a recently developed model based classifier, which enables the classification of airborne particles based on their chemical composition and size. Subsequently, the chemical fingerprints were compared to reference samples, and in the case of a positive match, they were assigned to a specific source (e.g. railway, road traffic, biogenic, geogenic etc).

The particle classifier allows to plot concentrations of each chemical class along transects (Figure 1), thus, facilitating the recognition of their emission point and dispersion trends. The transect measurements revealed that the coarse particles (PM<sub>2.5-10</sub>) from both sources (i.e. railway and road traffic), have a small contribution to the immission sites. However, the transport of the coarse fraction can be strongly influenced by specific meteorological parameters (e.g. high wind velocities in a prevalent direction).

On the other hand, PM<sub>2.5</sub> particles show a completely different transport behavior. They are finely dispersed in the air independently of the wind conditions. Thus, it can be generalized that PM<sub>2.5</sub>

particles measured away from the emitting source mainly represent a background concentration.

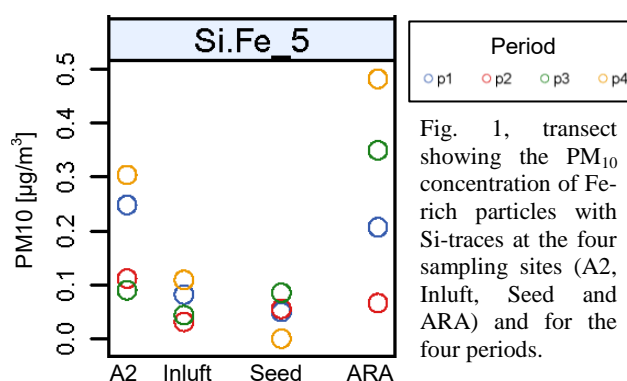


Fig. 1, transect showing the PM<sub>10</sub> concentration of Fe-rich particles with Si-traces at the four sampling sites (A2, Inluft, Seed and ARA) and for the four periods.

This study shows that the emissions of railway and road traffic are in part very similar (e.g. Fe-rich particles). However, road traffic emissions are by far more heterogeneous consisting of at least 47 different chemical subclasses. In Table 1 the most relevant groups emitted by railway and road traffic regarding the PM<sub>10</sub> mass measured in the studied segment, are summarized. The low concentration of brake wear emitted from the railway can be explained by the fact that the studied railway segment is lacking curves and inclination.

Table 1, PM<sub>10</sub> relevant chemical classes of railway and highway emissions

emission source	chem. composition	occurrence
<b>railway traffic</b>		
railway/wheel wear	Fe ± Si, Ca	very common
pantograph wear	Cu	rare
brake wear	Fe ± Cu, Zn	very rare
<b>road traffic</b>		
vehicle wear	Fe ± Si	very common
brake wear	Fe ± Cu, Zn, Ca, Cr, Al, Si, S	common
tire wear	C, Si, Ca, Al ± Na, K, Fe, S, Zn	common
soot agglomerates	C	very common

The PM<sub>10</sub> concentrations of primary particles emitted by the road and railway traffic obtained in this study are mainly dictated by the Fe-rich particles (13-52 % of measured PM<sub>10</sub>). In the case of road traffic, tire wear plays an additional important role (22-38 %).

## Source apportionment of particulate matter in a coal fired power plant area in Turkey

E.Can<sup>1</sup>, A. Arı<sup>1</sup>, G. Tuncel<sup>2</sup>, Eftade O.Gaga<sup>1</sup>

<sup>1</sup>Department of Environmental Engineering, Anadolu University, Eskişehir, 26555, Turkey

<sup>2</sup>Department of Environmental Engineering, Middle East Technical University, 6531, Ankara, Turkey

Keywords: Particulate matter, Trace elements, Chemical composition, Positive Matrix Factorization

Presenting author email: egaga@anadolu.edu.tr

Concentration of fine and coarse particulate matter (PM<sub>2.5</sub> and PM<sub>2.5-10</sub>) and associated trace elements were measured in urban and rural sites in a coal fired power plant area in Kütahya, Turkey, from March 2014 to September 2015. Daily fine and coarse particulate matter samples were collected by Gent Stack Filter Unit on nucleopore polycarbonate filters concurrently from two sites. Concentrations of 48 elements including Sulphur in PM samples determined by Inductively Coupled Plasma Mass Spectrometry (ICP-MS/MS).

The study area, Kütahya is a province in the Aegean region of Turkey, located in the inner western part of the Turkey. Coal is the most commonly used fuel for residential heating and industrial activities. The city is characterized as a thermal power plant city due to presence of three power plants. Shifting from coal to natural gas for space heating did not improve the air quality compared to neighboring cities. The major goal of the study is to investigate contribution of major pollution sources to ambient PM concentrations.

A preliminary air quality modelling, AERMOD was carried out to determine sampling site locations (Hacıoğlu *et al.*, 2016). Average PM<sub>10</sub> and PM<sub>2.5-10</sub> concentrations at the urban site (48 µg m<sup>-3</sup> and 20 µg m<sup>-3</sup>) were significantly higher than those at the rural sites (35 µg m<sup>-3</sup> and 16 µg m<sup>-3</sup>). Concentrations of most of the elements measured at urban site were also significantly higher than those at rural sites. Crustal elements were mostly measured in the coarse fraction in both sampling sites. Sulphur, Pb and Cd were mostly measured in fine fraction. Zn, As, Mo and Sb were found to be both in fine and coarse fractions. Elements of both anthropogenic and crustal origin was found to be mostly in both fractions. The effect of local meteorology (temperature, deposition, wind speed, wind direction, mixing height, and ventilation coefficient) on measured trace element concentrations were investigated. Short and long term variations of concentrations of elements were attributed to local meteorological parameters and variations in emission strength. The geographical locations of the local sources were identified by conditional probability function.

Source apportionment of PM<sub>2.5</sub> and associated components was accomplished by Positive matrix factorization (PMF) receptor modelling (Hopke *et al.*, 1997, Paatero and Hopke 2003, Polissar *et al.*, 1998). PMF model identified 8 principle sources for both stations. For urban station, factors and contributions are as follows: space heating (70%), thermal power plant (19%), industry (5%), oil combustion (2%), crustal (2%), traffic (1%), road dust (0.5%) and unidentified Zn factor (0.5%). For rural station, sources are as follows: space

heating (57%), thermal power plant 1 (17%), crustal 2 (9%), industry (9%), crustal 1 (6%), Zn (2%), traffic (0.7%) and thermal power plant 2 (0.2%).

In general, it can be concluded that sampling sites are under influence of local sources and space heating is the largest polluting source for both sampling sites.

This work was supported by the Anadolu University research Fund under grant 1306F272 and The Scientific and Technological Research Council of Turkey (TÜBİTAK) under grant 112Y305.

Hacıoğlu H.İ., Arı A., Özkan A., Elbir T., Tuncel G., Ozan O.D., Gaga E.O. (2016). Aerosol and Air Quality Research, 16, 1390-1402.

Hopke, P. K., Xie, Y., Raunemaa, T., Biegalski, S., Landsberger, S., Maenhaut, W., Artaxo, P. and Cohen, D. (1997). Aerosol Science and Technology, 27 (6), 726-735.

Paatero, P. and Hopke, P. K. (2003). Analytica Chimica Acta, 490 (1-2), 277-289.

Polissar, A. V., Hopke, P. K., Paatero, P., Malm, W. C. and Sisler, J. F. (1998). Journal of Geophysical Research: Atmospheres, 103 (D15), 19045-19057.

## Source apportionment of PM<sub>2.5</sub> observed at Daebu Island, Korea using air quality receptor models

S.H. Kim<sup>1</sup>, T.Y. Kim<sup>1</sup>, D.G. Park<sup>1</sup>, S.M. Yi<sup>1</sup> and J.B. Heo\*<sup>1</sup>

<sup>1</sup>Department of Environmental Health, School of Public Health, Seoul National University, Seoul, 151-742, Republic of Korea

Keywords: Receptor models, Source apportionment, PM<sub>2.5</sub>, Organic compounds.

Presenting author email: sunhyekim@snu.ac.kr

Daebu Island (126°35'E, 37°15'N) is a coastal region, which is located 40 km southwest of the center of Seoul. The site is also near Youn-heung coal fired power plant and Sihwa-Banwol industrial complex, South Korea. Exposure to ambient fine particles from coal fired power plants can be associated with health-related diseases (Laden *et al.*, 2000). With the growing concerns regarding the health effects of PM<sub>2.5</sub> from coal burning in the west coast of Korea, identifying sources of these areas has become greatly important. For this reason, this study evaluates source apportionments of ambient fine particles (PM<sub>2.5</sub>) in Daebu Island.

Samplers were installed on the roof of Daebu elementary school's official residence (126°34'E, 37°14'N, 12 m above ground) and 24-hour integrated PM<sub>2.5</sub> samples were collected from May 21, 2016 to November 1, 2016 at the sampling site. The major chemical species (organic and elemental carbon, ions and metals) as well as organic compounds (PAHs, n-Alkanes, n-Alkanoic acids, Dicarboxylic acids and Sugars) were analyzed.

Monthly average PM<sub>2.5</sub> mass concentration was highest in May ( $46.50 \pm 14.74 \mu\text{g m}^{-3}$ ) and lowest in July ( $19.00 \pm 12.73 \mu\text{g m}^{-3}$ ), which are late spring and summer season in Korea, respectively. Compared with PM<sub>2.5</sub> mass concentration results, chemical compositions of PM<sub>2.5</sub> show similar seasonal variation trends.

The results were used in positive matrix factorization (PMF) model and chemical mass balance (CMB) model. PMF results of PM<sub>2.5</sub> samples explain 9 contribution factors (Figure 1.), which are secondary sulfate (29.0%), mobile (22.0%), secondary nitrate (13.2%), oil combustion (10.1%), aged sea salt (7.9%), coal combustion (9.4%), soil (5.6%), non-ferrous smelter (1.7%) and industrial activities (1.1%).

We also performed CPF to show possible local source areas for each factor (Figure 2.) and applied PSCF to figure out long-range transport from source areas. CMB model results using organic molecular markers and comparison with other source apportionment results will be also discussed for the better understanding of main air pollution sources in Daebu Island.

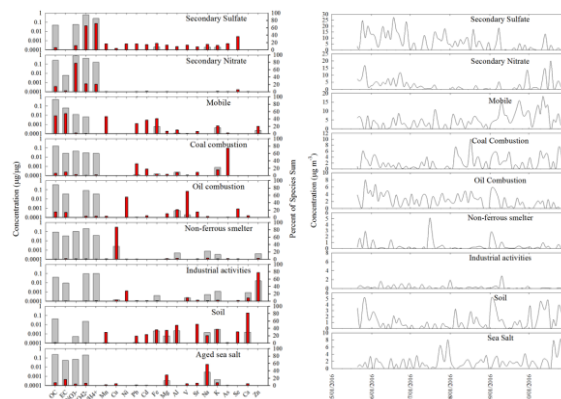


Figure 1. Source profiles and source contributions of the sampling area.

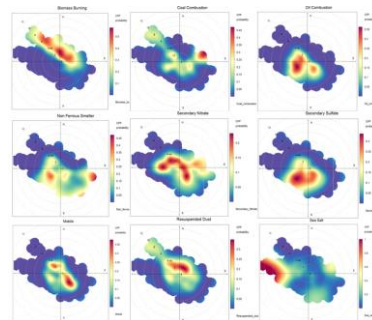


Figure 2. CPF analysis results for PM<sub>2.5</sub>

This work was supported by the BK21 PLUS (Brain Korea 21 Program for Leading Universities & Students) Project in 2017.

Laden, F., Neas, L. M., Dockery, D. W., & Schwartz, J. (2000) Association of fine particulate matter from different sources with daily mortality in six US cities. *Environmental health perspectives*, 108(10), 941.

## Chemical composition and source apportionment of PM<sub>2.5</sub> in Pohang, Korea

M.K Kim

Department of Environment & Resources, Research Institute of Industrial Science & Technology,  
Pohang, 790-330, Republic of Korea

Keywords: PM<sub>2.5</sub>, source apportionment, PMF, Pohang

Presenting author email: kimmk@rist.re.kr

PM<sub>2.5</sub> samples (n=120) were collected at an urban area of Pohang city which has iron and steel industrial complex for a year in 2011. The daily average concentrations of PM<sub>2.5</sub> except yellow dust event ranged from 3.4 to 67.6 ug/m<sup>3</sup>, with an annual average concentration of 26.9 ug/m<sup>3</sup>. The seasonal mean concentrations of PM<sub>2.5</sub> were 27.5 ug/m<sup>3</sup> (range: 16.8-43.2 ug/m<sup>3</sup>) in spring, 21.5 ug/m<sup>3</sup> (range: 3.4-45.9 ug/m<sup>3</sup>) in summer, 30.7 ug/m<sup>3</sup> (range: 13.2-66.7 ug/m<sup>3</sup>) in fall and 28.0 ug/m<sup>3</sup> (range: 11.8-67.6 ug/m<sup>3</sup>) in winter.

Table 1 shows the arithmetic mean, standard deviation and geometric mean for the measured species. The concentrations of anions (Cl<sup>-</sup>, NO<sub>3</sub><sup>-</sup> and SO<sub>4</sub><sup>2-</sup>) and cations (Na<sup>+</sup>, K<sup>+</sup>, Mg<sup>2+</sup>, Ca<sup>2+</sup> and NH<sub>4</sub><sup>+</sup>) were 10.7 ug/m<sup>3</sup> (39.9%) and 4.2 ug/m<sup>3</sup> (15.7%) respectively. The concentrations of OC and EC were 4.8 ug/m<sup>3</sup> (18.0%) and 2.2 ug/m<sup>3</sup> (8.1%) respectively.

Table 1. Summary for the PM<sub>2.5</sub> species concentrations (ug/m<sup>3</sup>) at an urban site during Apr. 2011 to Mar. 2012.

Species	A.M	S.D	G.M
PM <sub>2.5</sub>	26.881	14.095	23.089
Al	0.120	0.109	0.085
As	0.002	0.002	0.002
Cd	0.001	0.000	0.001
Cr	0.006	0.008	0.004
Cu	0.014	0.009	0.013
Fe	0.289	0.161	0.251
Mn	0.023	0.028	0.017
Ni	0.005	0.004	0.003
Pb	0.032	0.027	0.021
Ti	0.010	0.013	0.006
V	0.001	0.001	0.001
Zn	0.073	0.049	0.057
Na <sup>+</sup>	0.597	0.447	0.506
K <sup>+</sup>	0.260	0.196	0.197
Mg <sup>2+</sup>	0.059	0.037	0.052
Ca <sup>2+</sup>	0.276	0.187	0.236
Cl <sup>-</sup>	0.447	0.374	0.334
NO <sub>3</sub> <sup>-</sup>	3.505	3.093	2.518
SO <sub>4</sub> <sup>2-</sup>	6.766	4.107	5.604
NH <sub>4</sub> <sup>+</sup>	3.036	2.226	2.287
OC	4.832	2.015	4.117
EC	2.164	0.942	1.365

In this study, 22 chemical species were used for the PMF model and seven source factors were deduced. The first source profile is secondary sulfate which is primarily consisted of SO<sub>4</sub><sup>2-</sup> and NH<sub>4</sub><sup>+</sup>. The second source profile contains NO<sub>3</sub><sup>-</sup>, NH<sub>4</sub><sup>+</sup>, Ca<sup>2+</sup>, K<sup>+</sup> and Pb which implies secondary nitrate. The third source profile is interpreted as vehicle and road dust, characterized by OC, EC, SO<sub>4</sub><sup>2-</sup>, NO<sub>3</sub><sup>-</sup>, Al, As, P and Na<sup>+</sup>. The fourth source profile represents combustion process which includes OC, EC, SO<sub>4</sub><sup>2-</sup>, NO<sub>3</sub><sup>-</sup>, NH<sub>4</sub><sup>+</sup>, As, Fe, P, K<sup>+</sup> and Cl<sup>-</sup>. The fifth source profile is soil which contains OC, Al, Ti, Fe, P, K<sup>+</sup> and NH<sub>4</sub><sup>+</sup>. The sixth source profile comprises aged sea salt, characterised by Na<sup>+</sup>, K<sup>+</sup>, Fe, Al, SO<sub>4</sub><sup>2-</sup>, NO<sub>3</sub><sup>-</sup>, NH<sub>4</sub><sup>+</sup>, OC, EC. Sampling site is located at 500 m from seashore. Final source profile is the iron and steel industry. This source contains Fe, Mn, Zn, Cr, OC, EC, Ca<sup>2+</sup>, SO<sub>4</sub><sup>2-</sup>, NO<sub>3</sub><sup>-</sup>, NH<sub>4</sub><sup>+</sup> and Cl<sup>-</sup>.

Figure 1 represents the contributions from seven identified sources of PM<sub>2.5</sub> in Pohang. Secondary sulfate and nitrate related sources contributed 44.1% and 21.2% respectively. Pohang is the biggest city manufacturing iron and steel in Korea. The contribution from iron and steel source of PM<sub>2.5</sub> in Pohang is estimated at 4.7%.

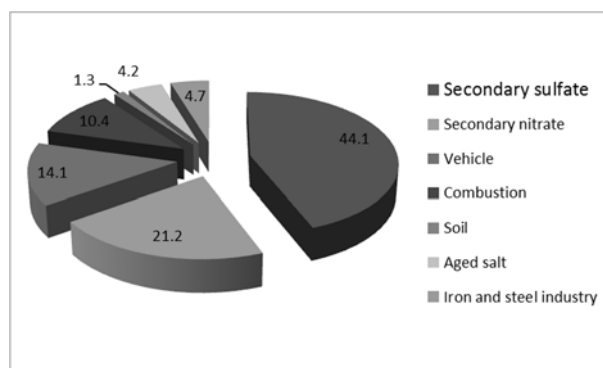


Figure 1. Contributions from the seventh identified sources of PM<sub>2.5</sub> in Pohang

Hwang IJ, Hopke PK. (2007) *Atmos. Environ.* 41(3), 506-518.

Choi JK, Heo JB, Ban SJ, Yi SM, Zoh KD (2013) *Science of the Total Environment* 447, 370-380

Liu G., Li J., Wu D., Xu H. (2015) *Particuology* 18, 135-143

## Identification of main PM<sub>2.5</sub> sources at a suburban site in Douai, Northern France

R. Roig, E. Perdrix, A. Chakraborty, L. Y. Alleman, B. Malet, B. Herbin, E. Tison and V. Riffault

IMT Lille Douai, Univ. Lille, SAGE - Département Sciences de l'Atmosphère et Génie de l'Environnement,  
59000 Lille, France

Keywords: SIA, MARGA, HR-ToF-AMS, source apportionment

Presenting author email: roger.roig@imt-lille-douai.fr

The French Hauts-the-France region is known to present high concentrations of atmospheric pollutants. Among them, fine particulate matter (PM<sub>2.5</sub>) exceedances occur mainly during cold periods and are often linked with increases of secondary inorganic aerosol (SIA) concentrations.

In north-western Europe specifically, semi-volatile ammonium nitrate may reach up to 27% of the PM<sub>2.5</sub> mass, with a higher contribution in winter when condensation processes associated to a low boundary layer are favored by cold temperatures (Putaud *et al.*, 2004).

SIA is not only formed at the local scale, but it can also be transported over long distances. Therefore, efforts should be aimed at better understanding the contributing sources throughout the year, with a special emphasis on winter, in order to implement efficient policies to reduce the levels of PM<sub>2.5</sub> and improve air quality.

In this context, a long-term field campaign aimed at determining the sources of PM<sub>2.5</sub> and their contributions at a suburban site in Douai, in the north of France, was carried out from August 2015 to July 2016.

During that period, hourly concentrations of 9 water-soluble ions (NO<sub>3</sub><sup>-</sup>, SO<sub>4</sub><sup>2-</sup>, NH<sub>4</sub><sup>+</sup>, Na<sup>+</sup>, K<sup>+</sup>, Ca<sup>2+</sup>, Mg<sup>2+</sup>, Cl<sup>-</sup>, C<sub>2</sub>O<sub>4</sub><sup>2-</sup>) and 5 precursor gases (NH<sub>3</sub>, SO<sub>2</sub>, HONO, HNO<sub>3</sub> and HCl) were determined continuously with a MARGA 1S (Monitor for AeRosols and GAses in ambient air) (ten Brink *et al.*, 2007). NO<sub>x</sub> were monitored every 15 minutes with a NOx 2000G monitor. A 2-wavelength (370 and 880 nm) aethalometer was used for the analysis of UV-absorbing aromatic compounds and near-infra-red absorbing compounds (black carbon) respectively, with a 5-min time resolution. The PM<sub>2.5</sub> total mass was measured by a Beta Attenuation Monitor (BAM-1020) every hour. Daily samples were collected on Teflon filters using a PARTISOL 2300 air sampler for elemental analysis. Meteorological parameters (temperature, relative humidity, pressure, wind speed and direction, precipitation) were also monitored on site.

Additional instruments were set up during a short intensive field campaign from February to March 2016 to better document particulate pollution in cold conditions. Complementary information on the chemical composition and size-distribution of non-refractory PM<sub>1</sub> aerosol, including NO<sub>3</sub><sup>-</sup>, SO<sub>4</sub><sup>2-</sup>, NH<sub>4</sub><sup>+</sup>, Cl<sup>-</sup> and organics was obtained by a HR-ToF-AMS (High Resolution-Time of Flight-Aerosol Mass Spectrometer) operated at a 5-min time step (DeCarlo *et al.*, 2006). A SMPS (Scanning Mobility Particle Sizer) was used to determine the

particle size distribution from 11.1 to 1083.3 nm with a time resolution of 5 minutes.

Source apportionment was applied using PMF (Positive Matrix Factorization) on different annual data sets. A total of 6 factors were found when the analysis was performed on the hourly-resolved 1-year-long dataset, including secondary nitrate, secondary sulfate, fresh marine, aged marine, dust resuspension and primary traffic. Source apportionment carried out on a daily-resolved dataset adding metals delivered comparable results and allowed for the determination of an additional industrial factor (smelter activity).

The daily variability of hourly PMF factors will be presented, as well as the analysis of their geographical origin through non-parametric wind regression (NWR) (Petit *et al.*, 2017) and concentration field maps (Seibert *et al.*, 1994) in order to distinguish between local and long-distance sources. Further investigation is ongoing related to the intensive field campaign on a combined database including the HR-ToF-AMS data, to study in more detail the different pollution sources and their contributions in winter.

This work is funded under the AACT-AIR (ADEME) program grant 1562C0011 and has also been supported by ARMINES. IMT Lille Douai participates in the CaPPA project, which is funded by the French National Research Agency (ANR) through the PIA (Programme d'Investissement d'Avenir) under contract ANR-11-LABX-0005-01, and in the CLIMIBIO project, both funded by the Regional Council "Hauts-de-France and the European Funds for Regional Economic Development (FEDER)".

- DeCarlo, P.F., Kimmel, J.R., Trimborn, A., Northway, M.J., Jayne, J.T., Aiken, A.C., Gonin, M. et al. (2006) *Anal. Chem.* **78**, 8281–8289.
- Petit, J.-E., Favez, O., Albinet, A., Canonaco, F. (2017) *Environ. Mod. Softw.* **88**, 183-187.
- Putaud, J.-P., Raes, F., Van Dingenen, R., Brüggemann, E., Facchini, M.-C., Decesari, S., Fuzzi, S. et al. (2004) *Atmos. Environ.* **38**, 2579-2595.
- Seibert, P., Kromp-Kolb, H., Baltensperger, U., Jost, D.T., Schwikowski, M. (1994) *Air Pollution Modelling and its Application X*, 595-596.
- ten Brink, H., Otjes, R., Jongejan, P., Slanina, S. (2007) *Atmos. Environ.* **41**, 2768-2679.

## PM10 characterization and source apportionment in Mt. Aitana

E. Yubero, N. Galindo, J.F. Nicolás, M. Varea, J. Gil-Molto, R. Castañer, S. Caballero, C. Pastor and J. Crespo

Department of Applied Physics, Miguel Hernández University, Avenida de la Universidad S/N, Elche, 03202 Spain

Keywords: regional background, PM<sub>10</sub>, source apportionment, PMF, African dust source

Presenting author email: eyubero@umh.es

Between March 2014 and September 2015, 160 daily PM<sub>10</sub> samples were collected at Mt. Aitana (38°39' N; 0°16' W; 1558 m a.s.l.) using a high-volume sampler (Digitel, 720 m<sup>3</sup>/day). Samples were analysed by ion chromatography, a thermal-optical method for evaluating the OC and EC content and XRF for metal determination.

The average PM<sub>10</sub> concentration recorded was 13.2 µg/m<sup>3</sup> demonstrating that it is clearly influenced by the impact of Saharan dust outbreaks. It is expected that this source will be identified as one of the most important contributors to the PM<sub>10</sub> mass.

In order to identify the sources that affect aerosol concentrations in this mountain background location an EPA PMF model was applied. Seven sources have been found to contribute to the concentration collected. The profiles of the sources are found in Figure 1

The first source is characterized by high EV of SO<sub>4</sub><sup>2-</sup>, Na<sup>+</sup>, Mg<sup>2+</sup> and Br suggesting that it consists mainly of aged marine aerosols. The highest values are obtained during the summer. The contribution of this source to PM<sub>10</sub> concentrations is important (28.8 %) due to the proximity of the site to the sea. Due to the high impact of anthropogenic activities on the Western Mediterranean Basin and the frequent recirculation of regional polluted air masses on the region, an interaction between natural and anthropogenic sources is expected.

The second and third sources are characterized by SO<sub>4</sub><sup>2-</sup> and NH<sub>4</sub><sup>+</sup> and NO<sub>3</sub><sup>-</sup> and NH<sub>4</sub><sup>+</sup>, respectively. Both sources represent secondary sulphates and nitrates. Their contributions are 15.4% and 3% respectively. In both sources OC is present, highlighting the presence of secondary organic compounds in this source. The low contribution of the nitrate source is due to the thermal decomposition of the ammonium nitrate and the dilution that takes place during the transport from the urban areas to the sampling site.

The sea salt factor typically accounts for 10% on a yearly average of the total PM<sub>10</sub> mass concentration. It is characterized by the presence of Na<sup>+</sup>, Cl<sup>-</sup>, and Mg<sup>2+</sup>. The ratio Na<sup>+</sup>/Mg<sup>2+</sup> is similar to that obtained in sea water.

The road dust factor is identified by the presence of Cu, Fe, K and Ca<sup>2+</sup> in the profile. This source contributes 6.2% to the PM<sub>10</sub> mass. Similar profiles of this factor are found in the literature (Amato, 2009).

The Saharan dust factor profile is mainly traced by the presence of crustal elements like Ca<sup>2+</sup>, K, Mn, Ti, Fe, Sr. The highest concentrations of this source are found to coincide with the arrival of dust from the north of Africa. This source accounts for the highest mass contribution at Aitana (34.3%).

Finally, the last source found is related with biomass burning. It is traced by elements like K<sup>+</sup>, OC and Zn. The contribution to the PM<sub>10</sub> mass is really low (2.3%). This factor represents both residential and agricultural burning.

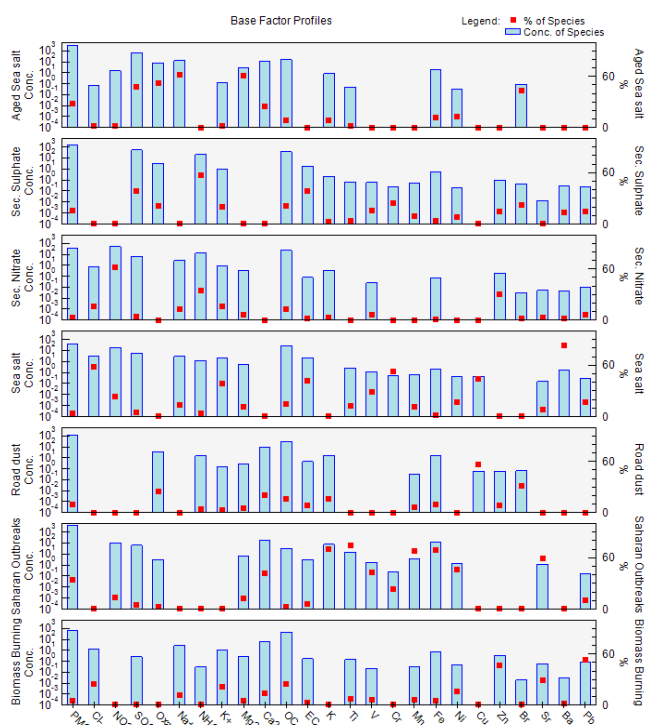


Figure 1: PMF profiles of the sources.

This work was supported by the Spanish Ministry MINECO CGL2012-39623-C02-2 (PRISMA-AITANA) project.

Amato F., Pandolfi M., Escrig A., Querol X., Alastuey A., Pey J., Perez N., Hopke P.K. (2009). *Atmos. Env.* 43, 2770-2780

## Organic aerosol source apportionment on long-term, spatially dense observation networks using 3 mass spectrometry techniques

K. R. Daellenbach<sup>1</sup>, I. El-Haddad<sup>1</sup>, I. Kourtev<sup>2,\*</sup>, G. Stefenelli<sup>1</sup>, C. Bozzetti<sup>1</sup>, A. Vlachou<sup>1</sup>, P. Fermo<sup>4</sup>, R. Gonzalez<sup>4</sup>, A. Piazzalunga<sup>3,\*\*</sup>, J. G. Slowik<sup>1</sup>, S. M. Luedin<sup>6,\*\*\*</sup>, V. Pflueger<sup>6</sup>, G. Vogel<sup>6</sup>, J.-L. Jaffrezo<sup>7</sup>, M. Kalberer<sup>4</sup>, U., Baltensperger<sup>1</sup>, A. S. H. Prévôt<sup>1</sup>

<sup>1</sup>Laboratory of Atmospheric Chemistry, Paul Scherrer Institute, CH-5232 Villigen, Switzerland

<sup>2</sup>Department of Chemistry, University of Cambridge, Cambridge CB2 1EW, U. K.

<sup>3</sup>University of Milano Bicocca, Department of Environmental Science, 20126 Milano, Italy

<sup>4</sup>University of Milan, Department of Chemistry, 20133, Milan, Italy

<sup>5</sup>ARPA Lombardia Regional Centre for Air quality Monitoring, 20122 Milan, Italy

<sup>6</sup>MABRITEC AG, Riehen, Switzerland

<sup>7</sup>Université Grenoble Alpes, CNRS, IGE, 38000 Grenoble, France

\* now at: University College Cork, Cork, Ireland

\*\* now at: Water and Soil Lab, 24060 Entratico, Italy

\*\*\* now at: University of Geneva, 1211 Geneva, Switzerland

Keywords: Aerosol mass spectrometer, FT-UHR MS, Source apportionment

Presenting author email: kaspar.daellenbach@psi.ch

Field deployments of the Aerosol Mass Spectrometer (AMS) have advanced the real-time measurement of organic aerosol (OA). Subsequent source apportionment quantifies the contribution of primary emission sources such as biomass burning (BBOA), traffic (HOA), cooking (COA) and secondary oxygenated OA (SOA). However, investigation of regional and seasonal differences by long-term systematic deployment of the AMS on a dense measurement network is impractical because of instrument cost and maintenance requirements. Moreover, the benefit of AMS data is restricted by the loss of chemical information caused by the fragmentation of the analyzed molecules. To overcome these limitations and in order to assess also the detailed chemical composition of coarse particulate matter (PM), we use an offline application of the HR-ToF AMS (oAMS, Daellenbach et al., 2016), a laser-desorption/ionization-ToF MS (LDI), and an ultrahigh resolution mass spectrometer (Orbitrap) for the analysis of conventional aerosol filters collected in central Europe.

We present oAMS measurements and source apportionment results of OA (smaller than 10  $\mu\text{m}$ ) at 9 stations in central Europe with different exposure characteristics for the entire year of 2013 (819 samples). We demonstrate that the dominant factors governing air quality can be region-specific, e.g. BBOA is strongly enhanced in alpine valleys relative to urban centers (oAMS, Fig. 1a). LDI results suggest that the elevated BBOA concentrations in the southern alpine valleys are mainly caused by more inefficient burning conditions. We observe the production of SOA in summer (SOOA), following the increase in biogenic emissions with temperature. The prominent contribution of compounds with an H/C of 1.5 observed for samples from Zurich collected during summer is consistent with SOA formation from biogenic precursors (Orbitrap, Fig. 1b). In winter, a SOA factor (WOOA) correlating with anthropogenic secondary inorganic species is dominant. While samples collected during winter in San Vittore are

similar to wood burning laboratory experiments. Differences in comparison to the samples collected in Zurich during winter point out the importance of other SOA precursors/formation pathways (Orbitrap, Fig. 1b). We will compare these results to health relevant compounds and present this thorough assessment of local and regional sources affecting air quality during winter and summer at the different sites.

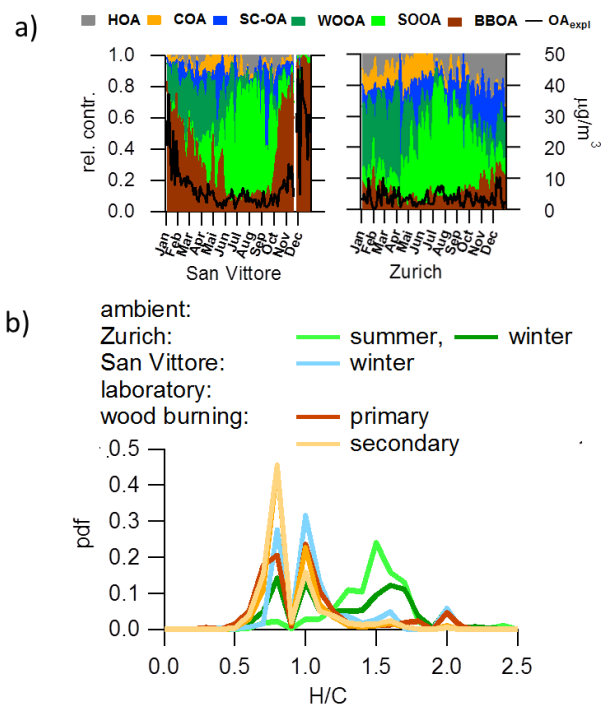


**Figure 1:** a) source apportionment results for 2 sites in central Europe (oAMS), b) H/C of OA from laboratory wood burning experiments and ambient OA in Zurich and San Vittore (Orbitrap).

This work was supported by the Swiss Federal Office of Environment, Liechtenstein, Ostluft, the Cantons Basel, Graubünden, Thurgau.

## Source apportionment analysis of rural background AMS data

O. Makeš<sup>1,2</sup>, P. Vodička<sup>1</sup>, J. Schwarz<sup>1</sup> and V. Ždímal<sup>1</sup>

<sup>1</sup>Institute of Chemical Process Fundamentals of CAS, v.v.i, Prague 6 - Suchbát, 165 02, Czech Republic

<sup>2</sup>Charles University in Prague, Faculty of Science, Institute for Environmental Studies, Albertov 6, 128 43, CZ

Keywords: AMS, source apportionment

Presenting author email: makes@icpf.cas.cz

During winter (9.1.-13.3.) and summer (17.6.-11.8.) 2014, two eight weeks long measuring campaigns were performed at the Košetice observatory, which is a rural background site connected to the national professional meteorological measurement network and it is placed in sparsely populated area in Central Europe (Zíková, 2013). Chemical composition and mass concentration was measured by Aerodyne Compact Time-of-Flight Aerosol Mass Spectrometer (AMS). The retrieved highly time resolved organic aerosol (OA) data were analyzed with using the SoFi graphical user interface which is developed by Paul Scherrer Institute (Canonaco *et al.* 2013) and is running under IGOR software (WaveMetrics). The preliminary results are presented in this abstract.

Organic aerosol data and error matrixes were trimmed and averaged to 30 min intervals and analyzed by positive matrix factorization (PMF) technique.

During summer season, we identified four factors whereas in winter season we identified just three factors. M/z profile of low-volatile oxygenated OA (LVOOA) factor, which was identified in both seasons, remains almost unchanged in both seasons. On the other hand the daily pattern (fig. 1, 2) of LVOOA looks different. It is caused by absence of semi-volatile oxygenated OA (SVOOA) factor in winter season because during winter measuring campaign were temperatures too low to distinguished SVOOA from LVOOA. In both periods we identified two mostly primary factors, hydrocarbon like OA (HOA) and biomass burning OA (BBOA). In both these factors profiles non- or low-oxidized ions prevail, but small amount of highly oxidized ions is also presented. The reason is that at the Košetice site there are almost no aerosol sources and all sampled aerosol travelled at least one kilometer from its source and became partly oxidized. HOA factor in winter probably originated not only from traffic, but also from coal burning. BBOA factor in both seasons is from wood and grass burning, in winter also from wood burning in local stoves.

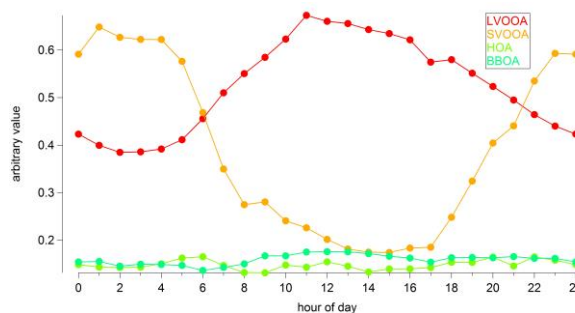


Figure 1. Averaged daily patterns for organic mass spectra during summer campaign.

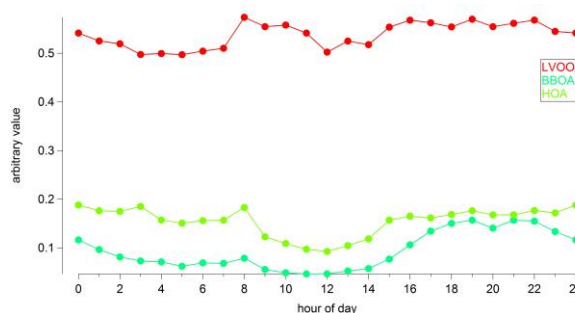


Figure 2. Averaged daily patterns for organic mass spectra during winter campaign.

### Acknowledgement:

Financial support by the ACTRIS - participation ČR, project MŠMT č. LM2015037 and by the EU Horizont 2020 project (no. 654109) is gratefully appreciated.

Canonaco F., et al. *SoFi, an IGOR-based interface for the efficient use of the generalized multilinear engine (ME-2) for the source apportionment: ME-2 application to aerosol mass spectrometer data*, Atmos. Meas. Tech. 6, 3649-3661 (2013).

Zíková N., *Long-Term Measurement of Aerosol Number Size Distributions at Rural Background Station Košetice*. Aerosol and Air Quality Research, 13: 1464–1474, 2013

## **Source apportionment of trace metals in a respirable size fraction of PM10, at an urban site of a South Asian Mega City**

Imran Shahid<sup>1</sup>, Muhammad Usman Alvi<sup>2,3</sup>, Khan Alam<sup>4</sup>, Muhammad Zeeshaan Shahid<sup>5</sup>, Farrukh Chishtie<sup>6</sup>

<sup>1</sup>*Institute of Space Technology, Islamabad, Pakistan*

<sup>2</sup>*Institute of Chemistry, University of the Punjab, Lahore 54590, Pakistan*

<sup>3</sup>*University of Education Lahore, Okara campus*

<sup>4</sup>*Department of Physics, University of Peshawar, Peshawar*

<sup>5</sup>*King Abdullah University of Science & Technology, Saudi Arabia*

<sup>6</sup>*Theoretical Research Institute Pakistan Academy of Sciences (TRIPAS), Islamabad*

Presenting author email: Imran.shahid@grel.ist.edu.pk

In the present study, elemental composition of PM10 and its corresponding source apportionment was conducted in the urban atmospheric of Karachi Metropolitan. The size segregated aerosol samples were collected on Quartz fiber filters using a high volume sampler during the months of March-April 2009. Trace elements such as Ni, Ba, Cd, Ca, Mg, Cr, Mn, Fe, Co, Cu, Sr and Ti were extracted by using 5% HNO<sub>3</sub> standard solution and Al, Pb, Zn, Se, P and S in 1% HNO<sub>3</sub> standard solution followed by analysis using ICP-AES spectrometer (Thermo Scientific USA, 6500 series). The PM10 concentration ranged from 255 µg/m<sup>3</sup> to 793 µg/m<sup>3</sup> with an average of 438 + 161µg/m<sup>3</sup>. Among the various elements analyzed, concentrations of Ca, Al and Fe were highest (> 10 000 ng/m<sup>3</sup>), followed by Mg and S (> 1000 ng/m<sup>3</sup>). Elements like Zn, P, Cu, Pb, Mn, Ti, Sr and Ba demonstrated medium concentrations (> 100 ng/m<sup>3</sup>), whereas lowest concentrations were measured for elements like Cr, Ni and Se (> 10 ng/m<sup>3</sup>). The Positive Matrix Factorization model identified five possible factors contributing towards PM10, including biomass burning, coal combustion, re-suspended road/soil dust, vehicular emission and industrial dust. A strong positive correlation (R<sup>2</sup> = 0.98) was observed between the model predicted PM10 mass and gravimetrically measured mass collected on filters. The contribution of different sources has been show in figure 1 and 2.

Figure-1 Contributions of identified sources to PM-10 mass at Karachi, Pakistan

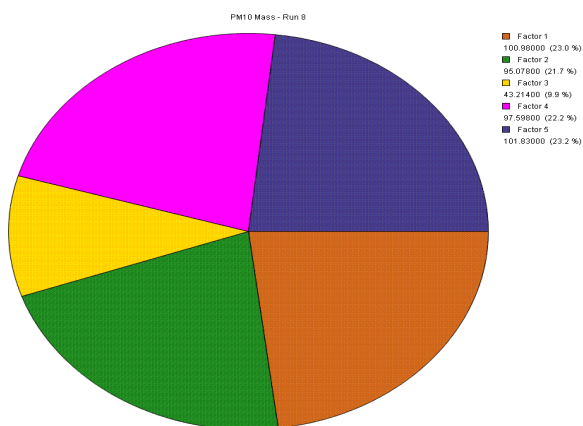
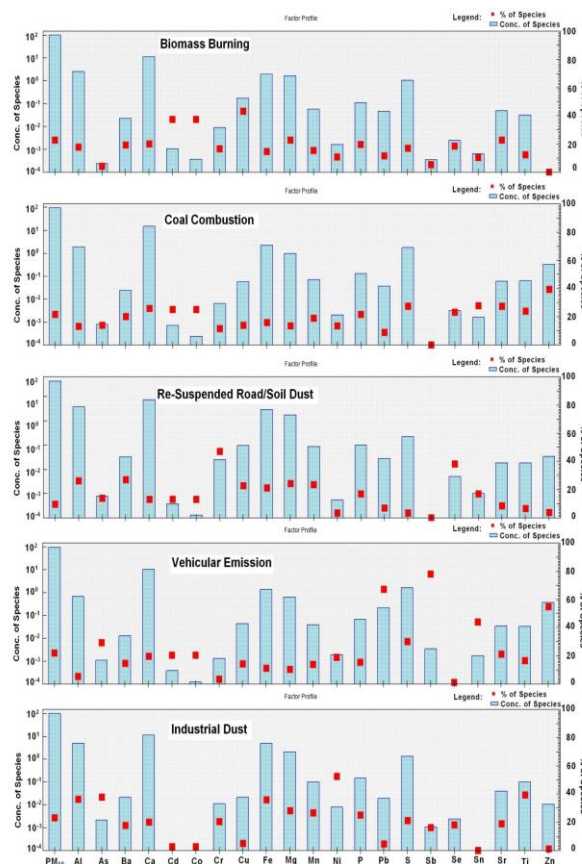


Figure-2: Trace metals in aerosols samples and their major sources at Karachi during March to April, 2009.

## The relationship between Black Carbon and Lung Deposited Surface Area in different urban environments in London

Erfan Abdollahei<sup>1</sup>, Tianye Zhu<sup>1</sup>, and Marc Stettler<sup>1</sup>

<sup>1</sup>Department of Civil and Environmental Engineering, Imperial College London, London, SW7 2AZ, UK

Keywords: Personal exposure, black carbon, lung deposited surface area.

Presenting author email: Tianye.zhu15@imperial.ac.uk

Black carbon (BC) and Lung Deposition Surface Area (LDSA) are two metrics by which ambient particulate matter (PM) concentrations are quantified and both are regarded as important indicators of the human health impacts of air pollution. In this study, we hypothesise that the comparison of LDSA to BC measurements could be used to give an indication of the source of the particles, by giving some further detail of their size distribution (ratio) and the proportion of black carbon (correlation). This study investigates the relationship of these two pollutants and how they are affected in different scenarios.

BC and LDSA are measured across four different locations to monitor personal exposure using Micro-Aethalometer (MicroAeth AE51, Aethlabs, United States) and Partector (Naneos Particles Solutions GmbH, Switzerland) respectively. Road side measurements in Central London (Marylebone), were collected along a designed route along of a range of roads with different traffic conditions (flow and density), at three different times through a day, including morning rush hour (7:30 to 9:30), lunch time (11:30 to 13:30) and evening rush hour (17:30 to 19:30). Measurements were also taken in the London underground system, close to the north perimeter fence of London Heathrow Airport, and in Hyde Park in Central London.

Plots of LDSA and BC measurements at each location are shown in Figure 1. The largest mean BC reading of 24.33  $\mu\text{g}/\text{m}^3$  was captured in the London Underground. This is likely due to the cross-sensitivity of the micro-aethalometer to iron particles generated by abrasion of the train brakes and wheels, and train tracks. Relatively low mean BC concentrations were measured at the other locations with 3.11  $\mu\text{g}/\text{m}^3$ , 2.15  $\mu\text{g}/\text{m}^3$  and 0.52  $\mu\text{g}/\text{m}^3$  recorded in Marylebone, at Heathrow and in Hyde Park, respectively. The highest mean LDSA measurement of 187.50  $\mu\text{m}^2/\text{cm}^3$  was obtained at Heathrow Airport.

The highest correlations between the LDSA and BC measurements were recorded in Marylebone Road and the London Underground, with correlation coefficients of 0.71 and 0.66 respectively. This indicates a significant proportion of the PM was measured by both instrument and suggests that LDSA could be used as a surrogate for BC, or vice versa.

The LDSA/BC ratios varied significantly at different sites. A high LDSA to BC ratio at Heathrow airport is indicative of a large number of small particles. A lower LDSA/BC ratio in the London Underground suggests that the measured particles were larger in size. The results of this could be used to distinguish sources of PM emissions using portable and relatively cheap instrumentation.

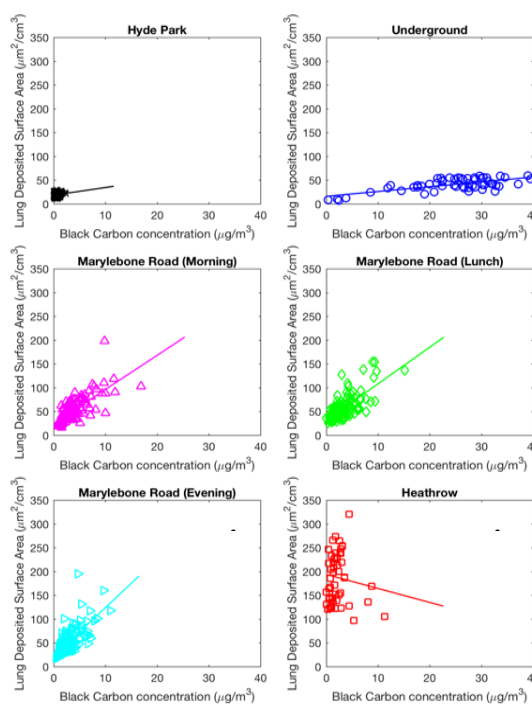


Figure 1: Plots of LDSA concentrations against BC concentrations with regression lines representing their ratio for different locations in London.

## **Abstracts T216**

## On abundance and potential sources of nitroaromatic compounds in size resolved ambient water soluble organic aerosols

S. Frka<sup>1,2</sup>, M. Šala<sup>1</sup>, J. Turšič<sup>3</sup> and I. Grgić<sup>1</sup>

<sup>1</sup>Department of Analytical Chemistry, National Institute of Chemistry, Ljubljana, 1000, Slovenia

<sup>2</sup>Division for marine and environmental research, Ruđer Bošković Institute, Zagreb, 10000, Croatia

<sup>3</sup>Environmental Agency of the Republic of Slovenia, Ljubljana, 1000, Slovenia

Keywords: nitroaromatic compounds, secondary organic aerosols, water soluble organic carbon, LC/ESI-MS/MS.

Presenting author email: frka@irb.hr

The (trans)formation, properties, and removal of organic particles remain one of the least understood aspects of atmospheric chemistry despite of their importance for both human health and climate change. Herein, nitrogen containing constituents of atmospheric organic aerosols (OA) associated with anthropogenic activities and biomass-burning (BB) have considerable role. To a large extent, understanding the processes involving organics in the atmosphere depends on how well these compounds are identified. Among the large number of unidentified organic compounds related to BB, nitroaromatic compounds (NACs) have drawn attention because of their UV light-absorbing ability being an important portion of brown carbon. Moreover, semi-volatile NACs as (methyl)nitrocatechols and nitroguaiacols are regarded as a significant fraction of organic aerosols, being secondary tracers of BB emissions as well as aged anthropogenic aerosols, whose (trans)formation and properties in the atmospheric waters are only beginning to be understood (Kitanovski *et al.*, 2019; Inuma *et al.*, 2010; Kroflič *et al.*, 2015; Frka *et al.*, 2016).

A comprehensive study on seasonal aerosol size-segregated (size range: 0.038-15.6  $\mu\text{m}$ ) water soluble organic matter (WSOM), with a focus on its specific NACs (e.g. 4-nitrocatechol; methyl nitrocatechols, (di)nitrophenols, methyl nitrophenols, nitrosalicylic acids, (di)nitroguaiacols, etc), through investigation of their molecular level speciation and quantification using LC/ESI-MS/MS will be presented. Identification and quantification of NACs in ambient PM<sub>2</sub> samples have been performed by using commercial but also by *de novo* synthesized authentic standards which structures were elucidated by combining high-resolution mass spectrometric (HRMS) data and NMR spectra. Abundance of a range of NACs, including 10 new, which have never been reported previously, will be presented. The obtained data were correlated with those for levoglucosan as well as with aerosol mass, total carbon, and carbon content in WSOM. On the basis of seasonal data collected at an urban background environment of Ljubljana, Slovenia, an insight into the ambient characteristics of NACs will be given. In addition a critical evaluation of their potential sources and transformation processes in the atmosphere will be discussed.

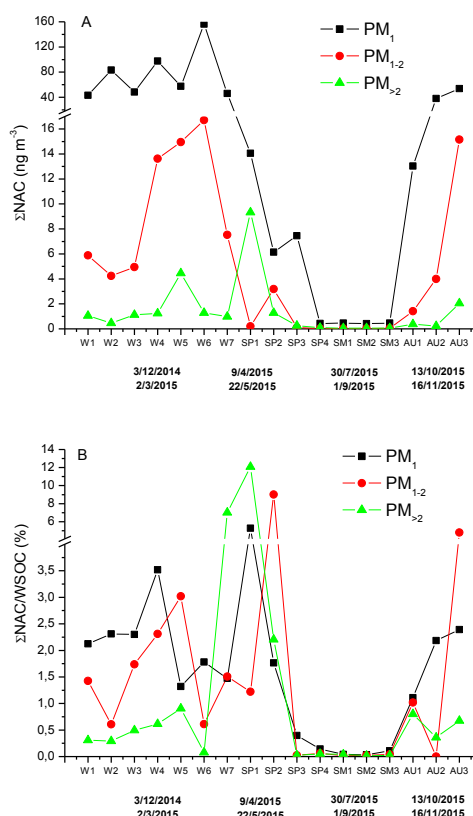


**Figure 1:** Seasonal variation of total NACs (A) and their percentage contribution to the WSOC (B) in different size fractions of water soluble organic aerosols from Ljubljana, Slovenia.

This work was supported by the European Commission and the Croatian Ministry of Science, Education and Sports through Marie Curie FP7-PEOPLE-2011-COFUND, project NEWFELPRO and by the Slovenian Research Agency (Contract no. P1-0034-0140).

Kitanovski, Z., Grgić, I., Vermeylen, R., Claeys, M., Maenhaut, W. (2012) *J. Chromatogr. A*, **1268**, 35-43.

Inuma, Y., et al (2010) *Environ. Sci. Technol.* **44**(22) 8453-8459.

Kroflič, A., et al. (2015) *Sci. Rep.* 5.

Frka, S., Šala, M., Kroflič, A., Huš, M., Čusak, A., Grgić, I. (2016) *Environ. Sci. Technol.* **50**(11) 5526-35.

## Sugar patterns in biomass burning emission samples – a link between burned and living biomass

M. Kistler, A. Kasper-Giebl

Institute of Chemical Technologies and Analytics, TU Wien, Vienna, 1060, Austria

Keywords: aerosols, saccharides, biomass burning, biogenic sources.

Presenting author email: magdalena.kistler@tuwien.ac.at

Many saccharides serve as markers for tracking biomass burning or vegetation. Anhydrosugars: levoglucosan (LG), and mannosan (MN), polyols: arabitol (AOL) and mannitol (MOL) and primary sugars: glucose (GLU) and fructose (FRU) can be here named (Caseiro et al., 2007 and literature cited therein).

Often atmospheric LG concentrations are in the same order of magnitude as polyols and primary sugars. During cold season or episodes of open fires they raise at least tenfold. In such samples LG contributes with 70-90% to “total sugars” and even total sugar mass can be used to estimate the biomass smoke contributions (Scaramboni et al., 2015). In contrast, the increase of sugars from biogenic sources (fungi, bacteria, soil biota, lichens) observed during periods of high vegetation activity is not as significant (about 2-5 times). Additionally, higher levels of polyols and/or primary sugars were reported also in parallel to biomass burning episodes, indicating that various biogenic particles may be co-emitted with biomass burning (Medeiros et al., 2006).

This shows that possible contributions of biomass combustions should be considered when assessing the biological activity using polyols and primary sugars.

In this study we compare the saccharides patterns in biomass burning emissions with those observed in the ambient atmosphere at different sites and during different seasons to answer the question how strong biomass burning influence the levels of biogenic markers.

The emission samples comprise PM<sub>10</sub> from combustion of various biomass types in small-scale residential stoves (n=140) and during open-burning experiments (n=30). Ambient air PM<sub>10</sub> samples were collected in years 2005 – 2015 and comprise 30 sites mainly in Austria.

Levoglucosan, mannosan, galactosan, xylitol, sorbitol, mannitol, arabitol, glucose, galactose, fructose, trehalose, cellobiose and sucrose were analysed in all samples after ultrasonic extraction of filter aliquots in Milli-Q water, though a number of analytes showed concentrations below the detection limit. High performance anion exchange chromatography coupled with pulsed amperometric detection (HPAE-PAD) according to Caseiro et al., (2007) or Iinuma et al., (2009) was applied.

In all emission samples two very strong correlation trends ( $R^2 \sim 0.9$ ) were observed between LG and MN with higher slope for softwood- and lower for hardwood combustion. The same trend (and slope characteristic rather for softwood) was found in ambient

samples collected during heating season in regions where biomass is a widely used fuel.

Simultaneously, in emission samples we found an evidence for a relation between LG with biogenic tracers: GLU, AOL, MOL. The relations were definitely less distinct, noticeable for part of samples and their slopes were  $\sim 100$  times lower than for LG vs. MN. Indications to similar relations were also noticed in ambient samples collected during winter, where active vegetation was not expected (Figure 1). While LG to MN ratio remained the same in emissions and ambient air ( $\sim 7$ ), the ratios between e.g. LG and GLU decreased from  $\sim 200$  in emissions to  $\sim 100$  in ambient air. Still an influence of biomass combustion on this compound cannot be neglected.

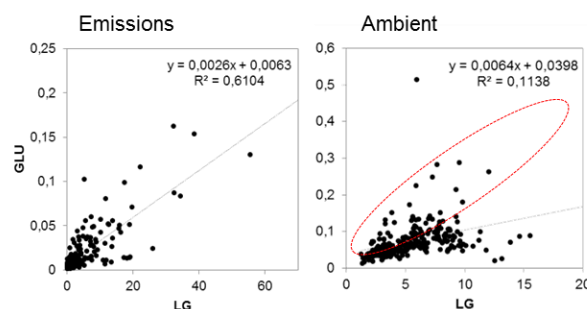


Figure 1. Relation between LG and GLU in emissions and in winter ambient PM. Scales represent the concentrations of sugars in extracts (ppm).

This work is based upon measurements conducted within a row of national projects: AQUELLA, AQUELLIS, FWF P20567-N19, PMInter conducted by group *Environmental Analytic*, TU Wiens between 2005- 2016. We thank the funding bodies and involved researchers.

Caseiro, A., Marr, I.L., Claves, M., Kasper-Giebl, A., Puxbaum, H., Pio, C.A. (2007) *J. Chrom. A* **1171**, 37-45.

Scaramboni, C., Urban, R.C., Lima-Souza, M., Nogueira, R.F.P., Cardoso, A.A., Allen, A.G., Campos, M.L.A.M. (2015) *Atmos. Environ.*, **100**, 185-192.

Medeiros, P. M., Conte, M.H., Weber, J.C., Simoneit, B.R.T. (2006) *Atmos. Environ.* **40**, 1694-1705.

Iinuma, Y., Engling, G., Puxbaum, H., Herrmann, H. (2009) *Atmos. Environ.* **43**, 1367-1371.

## Iron speciation of natural and anthropogenic atmospheric aerosols by X-ray Absorption Spectroscopy and selective leaching experiments

C. Petroselli<sup>1</sup>, B. Moroni<sup>1</sup>, S. Crocchianti<sup>1</sup>, R. Selvaggi<sup>1</sup>, F. Soggia<sup>2</sup>, M. Grotti<sup>2</sup>, F. d'Acapito<sup>3</sup> and D. Cappelletti<sup>1</sup>

<sup>1</sup>Dipartimento di Chimica, Biologia e Biotecnologie, Università degli Studi di Perugia, Perugia, 06123, Italy

<sup>2</sup>Dipartimento di Chimica e Chimica Industriale, Università degli Studi di Genova, Genova, 16146, Italy

<sup>3</sup>CNR-IOM-OGG c/o ESRF LISA CRG, Grenoble, F-38043, France

Keywords: EXAFS, Selective leaching experiments, Saharan dust, Steel production emissions.

Presenting author email: petrosellichia@gmail.com

Iron solubility is strictly connected with oxidation state and mineralogy in aerosols. Moreover, iron is an essential element as it acts as a micronutrient for many ecosystems, but it is also a strategic element in many anthropogenic processes. We decided to investigate the iron speciation in two different Fe-bearing aerosol types emitted from a natural and an anthropogenic aerosol sources. To this aim, we combined X-ray Absorption Spectroscopy (XAS) techniques with selective leaching experiments in order to obtain information on oxidation state, mineralogy and local structure of iron.

Specifically, we investigated long range transported Saharan dust (SH) sampled at a mid-altitude rural regional background site (Monte Martano, 1100m a.s.l.; Moroni *et al.* (2015)) during an extremely intense Saharan dust outbreak that occurred between November 30<sup>th</sup> and December 1<sup>st</sup> 2014, and freshly emitted steel production plant fumes (AST) collected inside the chimney stacks of a steel plant in the Terni city (Central Italy).

Both Extended X-ray Absorption Fine Structure (EXAFS) and X-ray absorption Near Edge Structure Spectroscopy (XANES) have been exploited (Figure 1). The Saharan dust sample is characterized by 6-fold coordinated Fe<sup>3+</sup> with bond distances compatible with both aluminosilicates (i.e. illite) and iron oxi(hydr)oxides (i.e. ferrihydrite). For the steel production emission sample, EXAFS results points towards a mixture of Fe<sup>2+</sup> and Fe<sup>3+</sup> in spinel structures with an excess of Fe<sup>3+</sup> with respect to the pure magnetite structure. While spinels are poorly soluble, iron contained in the aluminosilicate structure is more easily solubilised in natural conditions.

Leaching test results, reported in Table 1, show a general predominance of the residual insoluble fraction above the others. This fraction accounts for 69% of total iron in Saharan dust and for 93% in steel production emissions and it is associated to aluminosilicates and Fe-spinels, respectively.

Table 1. Leaching tests results on SH and AST samples.

	I(%)	II(%)	III(%)	IV(%)
SH	15	8	8	69
AST	4	2	1	93

(I) acid-labile, (II) reducible, (III) oxidizable, (IV) insoluble fraction

All these observations points towards a very little contribution from the oxides and hydroxides fraction (step II) to the total iron structure in both samples. This

is consistent with previous scanning electron microscopy analysis of urban aerosol samples in Terni by Moroni *et al.* (2013), who showed that iron oxi(hydr)oxides particles are rare and mainly associated to aluminosilicates particles.

The remarkable differences between the XAS results, combined with the distinct differences in the leaching tests allow to unambiguously distinguish the profile of the two aerosol sources. For the case of plant fumes, the present results are very important in itself because of the substantial lacking of similar detailed information in literature.

As an example of a preliminary application of the present experimental approach, the case of a mixed urban aerosol, collected in Terni during the Saharan dust intrusion of December 2014, was taken under consideration. The XAS spectrum of the mixed sample is very similar to the SH sample demonstrating that the iron local structure is mainly determined by the Saharan contribution. The leaching results, on the contrary, show that the mixing processes affect the overall solubility.

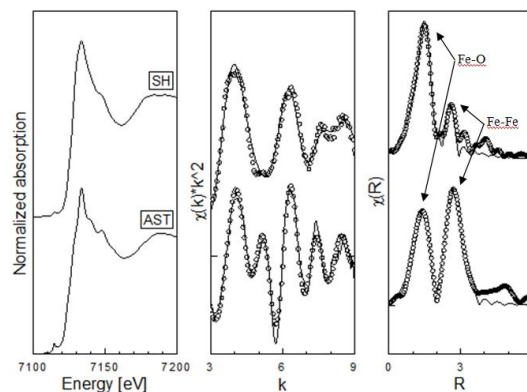


Figure 1. (a) XANES spectra, (b)  $k^2$  weighted EXAFS spectra and (c) relative Fourier transforms of SH and AST samples

This work was supported by the “Fondo Ricerca di Base 2015” of the University of Perugia.

Moroni, B., Castellini, S., Crocchianti, S., Piazzalunga, A., Fermo, P., Scardazza, F., Cappelletti, D. (2015) *Atmospheric Research*, **155**, 26-36.

Moroni, B., Cappelletti, D., Marmottini, F., Scardazza, F., Ferrero, L., Bolzacchini, E. (2013) *Rendiconti Lincei* **24**, 319-328

## Quantification of aliphatic amines in the aerosol particulate matter

A. Tinti<sup>1</sup>, L. Corbella<sup>1</sup>, P. Fermo<sup>1</sup>, C. Colombi<sup>2</sup>, E. Cuccia<sup>2</sup>, V. Gianelle<sup>2</sup>, S. Takahama<sup>3</sup>, S. Gilardoni<sup>4</sup>

<sup>1</sup>Dipartimento di Chimica, Università degli Studi di Milano, 20133 Milan, Italy

<sup>2</sup>ARPA Lombardy, 20159, Milan, Italy

<sup>3</sup>EPFL, CH-1015 Lausanne, Switzerland

<sup>4</sup>ISAC-CNR, 40129 Bologna, Italy

Keywords: amines, aerosol particulate matter, ion chromatography, agricultural emissions.

Presenting author email: alessandro.tinti@studenti.unimi.it

Amines are atmospherically-relevant organic compounds, being able to neutralize acids and to form toxic species. They are mainly present in the gaseous phase but they are partially converted into particulate phase after neutralization. The most common and abundant amines observed in particulate matter are aliphatic low-molecular-weight amines (Healy, 2015). More than one hundred of different molecules belong to this class; among them Ethyl-amine (EA), Methyl-amine (MA), Diethyl-amine (DEA), Trimethyl-amine (TMA) and Dimethyl-amine (DMA) are present with the highest concentrations. Till now different sources have been identified such as animal husbandry, agricultural activities, biomass burning, treatment of sewage and waste, combustion, industry, automobiles, cooking, tobacco smokes, composting operations and natural sources such as oceans, biodegradation of organic matter (that contains amino acids) and geologic sources (Ge, 2011). The class of methyl amines is the most common in the atmosphere and has the highest concentrations near major sources, with a total global emission of 285 Gg N year<sup>-1</sup>. TMA, the prevalent amine in the atmosphere, is estimated to have a global flux at approximately 170 Gg N year<sup>-1</sup>, which is the highest among all alkylamines. It's believed that the majority of this flux comes from animal husbandry activities (Ge, 2011; Schade, 1995).

The main object of this study is the analysis of aliphatic amines in PM<sub>10</sub> samples collected in one urban site in Milan and in two rural sites (Corte dei Cortesi - CDC and Schivenoglia), characterized by agricultural and zootechnical activities, and located in the southern part of Lombardy Region. Nitrogen organic species were first investigated by Fourier-Transform infrared spectrometry. Then, aliphatic amines were quantified by Ion Chromatography (IC) (VandenBoer, 2012).

After the set-up of the methodology, chromatography separation was achieved using a methanesulfonic acid (MSA) gradient elution on a Dionex CS17 column with conductivity suppressor (Dionex CSRS 500), which has allowed the quantification of the main cations as well.

The analytical results show higher concentration in the rural sites than at the urban one. In Milan the correlation of MA with K<sup>+</sup> and levoglucosan was observed in winter season, suggesting that one of the most important sources for this amine is biomass burning.

On the other hand, at the rural site we observed an increase in the DMA concentration (up to 36 ng/m<sup>3</sup>) in

early summer, likely due to the use of pesticides (indeed DMA is a component of pesticides). An increase of DMA has been observed in Milan both in early spring and in July. TMA concentration, mainly linked to husbandry activities, is higher at the rural sites. These preliminary results show that the concentration of single amine compounds can be higher than 100 ng m<sup>-3</sup> at rural sites. In addition, amines can potentially be significant markers to track the impact of agricultural emissions on air quality.

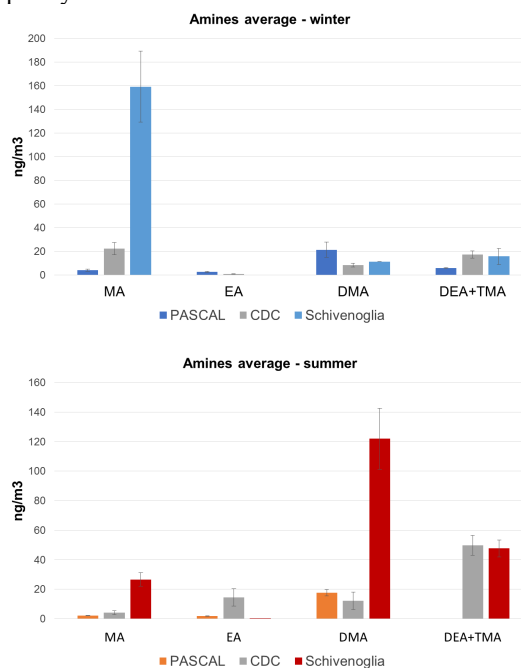


Figure 1. Average amines concentrations in the examined sites

Healy, R. M., Evans, G. J., Murphy, M., Sierau, B., Arndt, J., McGillicuddy E., O'Connor, I. P., Sodeau J. R., Wenger J. C., (2015) *Anal. Bioanal. Chem.* **407**, 5899-5909.

Ge, X., Wexler, A.S., Clegg, S.L., (2011) *Atmos. Environ.* **45**, 524-546.

Schade, G.W., Crutzen, P.J., J. (1995) *Atmos. Chem.* **22**, 319-346.

VandenBoer, T. C., Markovic, M. Z., Petroff, A., Czar, M. F., Bor-duas, N., and Murphy, J. G., (2012) *J. Chromatogr. A* **1252**, 74-83.

## Synthesis and high resolution mass spectrometry characterisation of peroxy pinic acids as a potential SOA markers

S. S. Steimer<sup>1</sup>, D. Pitton<sup>2</sup>, T. Hoffmann<sup>2</sup> and M. Kalberer<sup>1</sup>

<sup>1</sup>Department of Chemistry, University of Cambridge, Cambridge, CB2 1EW, United Kingdom

<sup>2</sup>Institute of Inorganic and Analytical Chemistry, Johannes Gutenberg University Mainz, Mainz, 55128, Germany

Keywords: mass spectrometry, ROS, peroxy acids, SOA markers

Presenting author email: ss2349@cam.ac.uk

A large number of epidemiological studies show that ambient aerosols are correlated with a wide range of respiratory and cardio-vascular diseases. While the particle components causing these negative health effects are not yet fully identified, reactive oxygen species (ROS) are thought to be a main contributor to the toxicity of particles in ambient air (e.g. Dellinger *et al.*, 2001). Peroxy acids are a subtype of ROS shown to be present in secondary organic aerosol (SOA) (e.g. Reinnig *et al.*, 2009). Recent studies also suggest that extremely low volatility organic compounds (ELVOCs), strongly involved in the initial stages of SOA formation, often contain peroxy acid functionalities (e.g. Rissanen *et al.*, 2014). This shows that peroxy acids are highly relevant atmospheric compounds.

While peroxy acids have been tentatively identified in aerosol particles, there are currently no standards available to verify these assignments. One of these tentatively identified peroxy acids is monoperoxy pinic acid, which is thought to form during  $\alpha$ -pinene oxidation (e.g. Reinnig *et al.*, 2009).

We have recently shown that LC-MS/MS can be used to distinguish between different carboxylic acids and their peroxy derivatives (Steimer *et al.*, in press). In the present study, we have synthesized and analysed diperoxy pinic acid and two monoperoxy pinic acid isomers to facilitate unambiguous identification of these compounds in SOA.

The analysis was performed using an Accela HPLC system with a T3 Atlantis C18 column coupled to an LTQ Orbitrap Velos mass spectrometer via electrospray interface. All measurements were taken in negative ionization mode.

A chromatogram of a mixture of pinic acid, two monoperoxy pinic acid isomers and diperoxy pinic acid is shown in figure 1, demonstrating the success of the synthesis and suitability of the chosen method. We will discuss the specific and characteristic fragmentation patterns of the synthesized pinic acid derivatives, highlighting similarities and differences in fragmentation behaviour compared to the previously analysed ROS & ELVOC proxies. The chromatographic separation and mass spectrometry fragmentation patterns (MS/MS) determined in this study will allow us to unambiguously identify peroxy pinic acids in  $\alpha$ -pinene SOA in future studies.

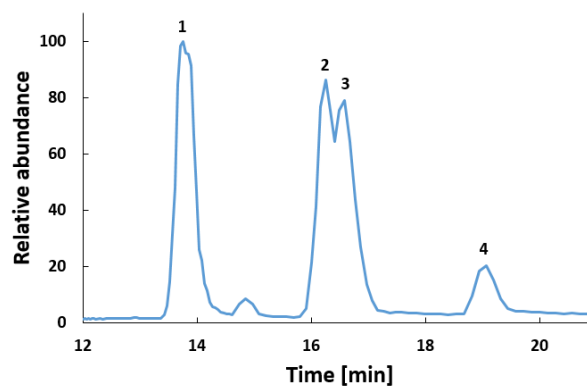


Figure 1. Separation of pinic acid (1), two monoperoxy pinic acid isomers (2, 3) and diperoxy pinic acid (4)

This work was supported by an SNSF Early Postdoc.Mobility fellowship (project P2EZZP\_162258).

Dellinger, B., Pryor, W. A., Cueto, R., Squadrito, G. L., Hegde, V. and Deutsch, W. A. (2001) *Chem. Res. Toxicol.* **14**, 1371–1377.

Reinnig, M., Warnke, J. and Hoffmann, T. (2009) *Rapid Commun. Mass Spectrom.* **23**, 1735-1741.

Rissanen, M. P., Kurtén, T., Sipilä, M., Thornton, J. A., Kangasluoma, J., Sarnela, N., Junninen, H., Jørgensen, S., Schallhart, S., Kajos, M. K., Taipale, R., Springer, M., Mentel, T. F., Ruuskanen, T., Petäjä, T., Worsnop, D. R., Kjaergaard, H. G. and Ehn, M. (2014) *J. Am. Chem. Soc.* **136**, 15596-15606.

Steimer, S. S., Kourtchev, I. and Kalberer, M. (in press) *Anal. Chem.*

## Submicron Organic Nitrate Particles in a Subtropical Forest

Christian Mark Salvador<sup>1\*</sup>, Charles C.-K. Chou<sup>1</sup>, H.-C. Cheung<sup>1</sup>, T.-T. Ho<sup>1</sup> and C.-Y. Tsai<sup>1</sup>

<sup>1</sup>Research Center for Environmental Changes, Academia Sinica, Taipei 11529, Taiwan

**Keywords:** Organonitrates, TD-PTR-TOF-MS, Anthropogenic tracer

Presenting author email: [cmgsalvador@gate.sinica.edu.tw](mailto:cmgsalvador@gate.sinica.edu.tw)

### Abstract

An important tracer of perturbation of human related activities in aerosols is the formation of organonitrate (ON) which is comprised of alkyl (ANs/RONO<sub>2</sub>) and peroxy nitrates (PNs/RO<sub>2</sub>NO<sub>2</sub>). This class of compounds, which are significant component of secondary organic aerosols are produced through the oxidation of the volatile organic compounds in the presence of anthropogenic NO<sub>x</sub> (NO + NO<sub>2</sub>).

Particle phase organonitrates of a subtropical experimental forest in central Taiwan were comprehensively studied using TD-PTR-TOF-MS during a field campaign from October to November 2015. The total mass concentration of organonitrates (ΣONs) was based on its fragmentation to NO<sub>2</sub><sup>+</sup> ion inside the drift tube of the PTR-MS. The degree of dissociation was probed using a standard isopropyl nitrate (IPN) and results indicated that 20% of IPN proceed to form NO<sub>2</sub><sup>+</sup>. The sum of the mixing ratios of ON observed in Xitou forest only contributed as much as 4% of the total organic matter which was way underestimated compared to the previous measurements of ONs which typically ranged between 20-40%. The most apparent rationale for such observation for our case was the elevated relative humidity, which averaged at 90%, during the campaign period. Controlled chamber studies indicated that organonitrates, particularly alkyl nitrates, dissociates to alcohol and nitric acid in aerosols at high R.H. conditions, particularly greater than 50% thereby significantly reducing the mixing ratio of ONs. The inverse relationship between the overall mass of organonitrate and relative humidity observed in this study validated such claim.

Other than relative humidity, a number of environmental factors showed moderate to strong association with organonitrates. The correlation of urban tracers, also measured by the TD-PTR-TOF-MS, with ONs indicated the influence of anthropogenic activities in the formation of organonitrates. The participation of ONs in particle growth was demonstrated through its relationship with nuclei mode particles (N100 nm) measured in Xitou forest

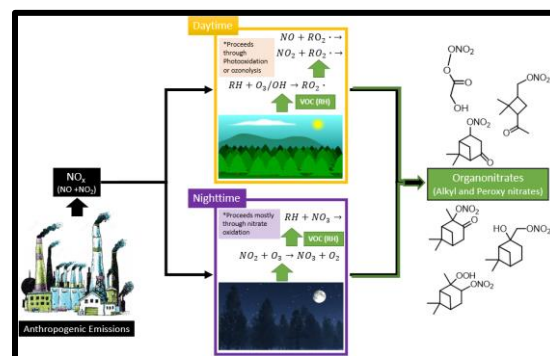


**Figure 1.** Mechanistic formation of organonitrates from anthropogenic NO<sub>x</sub> and biogenic hydrocarbons. Different dominant oxidation pattern exists during daytime and nighttime, thereby altering the chemical distributions of ONs during various time of the day.

Six major organonitrates were identified from the mass spectra but not at their unfragmented molecular form, rather at their respective RO<sup>+</sup> fragments. These compounds were moderately correlating with the total sum of mixing ratio of ONs thus confirming a nitrate moiety and suggesting the varying fragmentation rates of ONs to NO<sub>2</sub>. The most dominant organonitrate measured from Xitou forest was an oxidation product of isoprene, thus hinting the vital role such biogenic volatile organic compound in SOA formation in the experimental forest.

Aoki, N., S. Inomata, and H. Tanimoto (2007), Detection of C-1-C-5 alkyl nitrates by proton transfer reaction time-of-flight mass spectrometry, *International Journal of Mass Spectrometry*, 263(1), 12-21, doi:10.1016/j.ijms.2006.11.018

Holzinger, R., J. Williams, F. Herrmann, J. Lelieveld, N. M. Donahue, and T. Rockmann (2010b), *Aerosol analysis using a Thermal-Desorption Proton-Transfer-Reaction Mass Spectrometer (TD-PTR-MS): a new approach to study processing of organic aerosols*, *Atmospheric Chemistry and Physics*, 10(5), 2257-2267.

## Probing the chemical composition of fine ambient aerosol, rainwater and hailstone with UHPLC-MS technique. Is there anything in common?

P. Wach<sup>1</sup>, G. Spólnik<sup>2</sup>, K.J. Rudziński<sup>1</sup>, W. Danikiewicz<sup>2</sup>, K. Skotak<sup>3</sup> and R. Szmigielski<sup>1</sup>

<sup>1</sup>Laboratory of Environmental Chemistry, Institute of Physical Chemistry PAS, Warsaw, 01-224, Poland

<sup>2</sup>Mass Spectrometry Group, Institute of Organic Chemistry PAS, Warsaw, 01-224, Poland

<sup>3</sup>Institute of Environmental Protection, National Research Institute, Warsaw, 00-548, Poland

Keywords: secondary organic aerosol, organosulfates, rainwater, hailstone, aqueous phase SOA, mass spectrometry

Presenting author email: pwach@ichf.edu.pl

Atmospheric fine particulate matter with diameters up to 2.5  $\mu\text{m}$ , are especially important not only because of their impact on air quality, but what is considered to be more important, due to the fact that those airborne particles can easily penetrate the blood system and deteriorate the human (EEA, 2015). Over the past decade much research has been devoted to exploring the mechanisms underlying the formation and growth of aerosol in ambient air (Claeys, 2004).

In Poland there is a lack of studies dealing with the characterization of the composition of particles occurring in the air masses. In our research we mostly focus on the organosulfates, the polar fraction of secondary organic aerosol (SOA), formed from low molecular non-methane hydrocarbons with sulfuric acid, in major part from anthropogenic origin. The main low molecular non-methane hydrocarbon volatile organic compound (VOC) emitted by plants to the atmosphere at a very high rate of 600 TgC/year (Guenther, 2012) is isoprene (2-methyl-1,3-butadiene). As the most abundant VOC containing two conjugated double bonds in the structure, isoprene and its oxygenated derivatives such as methyl-vinyl ketone (but-3-en-2-one) and methacrolein (2-methylpropenal) are among the most important precursors of SOA.

The recognition of chemical composition and the origin of organosulfates is a very demanding task due to low concentration and complicated chemical composition of ambient aerosol samples. To meet this challenge we use ultra-high performance chromatography coupled with high resolution mass spectrometry. The results of our previous studies of the VOCs processing in the aqueous environment (Szmigielski, 2016; Rudziński, 2016) encouraged us to examine the composition of natural hydrometeors such as rain droplets, or hailstones. Even though the individual cases of natural water precipitations analysis have been reported in the literature (Altieri, 2009; Mazzoleni, 2010), to the best of our knowledge there is no research similar to ours with the use of UHPLC-MS methods.

The aim of this work was to compare the distribution of the organosulfates in ambient aerosol, rainwater and hailstone samples. The fine ambient aerosol was collected in the Diabla Gora field station (54°07'29.52"N; 22°02'17.08"E) during the 2014 summer campaign in Poland. This station is located in a densely forested and rural site of the Masurian region. The samples of rain were collected during the 2016 summer campaign in the Zielonka field station in Poland (53°40'00.1"N; 17°55'53.0"E), which is also considered as a rural site densely forested by conifer trees. The hailstone samples were gathered in 2016 during an intense summer storm episode in Warsaw, the capital city of Poland (52°13'52.2"N; 21°00'39.8"E). In contrast to Diabla

Gora and Zielonka, Warsaw is a typical urban area with the contribution of non-negligible green belt zones.

As an analytical tool an Aquity I-Class chromatograph coupled with the Synapt G2-S q-TOF type mass spectrometer was used for the analyses. In order to obtain the comparable analysis conditions a standard reversed-phase liquid chromatography with an extended bonding C-18 column was used. In our experiments the attention was given to organosulfates with molecular weights 215, 214, 212, 200, 184 and 153. Our recent results have revealed that these organosulfates are present in all examined samples, although at considerably variable relative abundance. This observation sheds new light into the mechanisms of the secondary organic aerosol formation in the atmosphere from isoprene and its related precursors.

Altieri, K.E. *et al.* (2009) *Atmos. Chem. Phys.* **9**, 2533-2542

Claeys, M. *et al.* (2004) *Science*, **303**, 1173-1176

EEA. *Air Quality in Europe – 2015 report*, (2015) ISBN: 978-92-9213-701-4-702-1, p.40

Guenther, A.B. (2012) *Geophys. Model Devel.* **5**, 1471-1492

Mazzoleni, L. R. *et al.* (2010) *Environ. Sci. Technol.* **44**, 3690-3697

Rudziński, K.J. *et al.* (2016), *Atmos. Environ.* **130**, 163-171

Szmigielski, R. (2016) *Atmos. Environ.* **130**, 14-22

## Organosulfates and other molecular tracers of secondary organic aerosols in Xi'an, China during summer and winter

M. Glasius<sup>1</sup>, L.S. Iversen<sup>1</sup>, A.M.K. Hansen<sup>1</sup> and R.-J. Huang<sup>2</sup>

<sup>1</sup>Department of Chemistry, Aarhus University, 8000 Aarhus C, Denmark

<sup>2</sup>Key Lab of Aerosol Chemistry and Physics, Institute of Earth Environment, Chinese Academy of Sciences, China

Keywords: organosulfates, secondary organic aerosols, molecular tracers.

Presenting author email: [glasius@chem.au.dk](mailto:glasius@chem.au.dk)

Organosulfates (OS) are formed via heterogeneous reactions of their organic precursors with newly formed, acidic sulphate aerosols (Surratt *et al.*, 2008; Riva *et al.*, 2016). Here we investigated occurrence and sources of OS during summer and winter in Xi'an, China (34.23°N, 108.88°E) with 8.6 million inhabitants. The region is affected by severe pollution events, dominated by secondary aerosols (Huang *et al.*, 2014).

Particles (PM<sub>2.5</sub>) were collected on quartz fibre filters using a high volume sampler. Particle filter samples were extracted and analyzed using an Ultra-High Performance Liquid Chromatograph coupled through an electrospray inlet to a quadrupole time-of-flight mass spectrometer (Hansen *et al.*, 2014). Organosulfates were identified using their characteristic MS fragments. Organosulfates were quantified using mannose sulfate, β-pinene OS and octyl sulfate. Other molecular tracers of SOA were quantified with authentic standards.

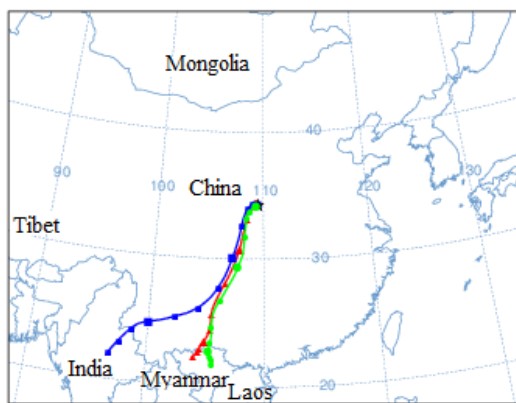


Figure 1. Typical pattern of air mass transport to Xi'an, China during summer campaign period (72h, calculated using HYSPLIT).

During summer, air masses were typically transported to Xi'an from forested, sub-/tropical regions south of the city (Fig. 1), while in winter air masses typically originated from arid, colder regions to the north. This change in transport patterns is clearly observed in the composition and levels of molecular tracers.

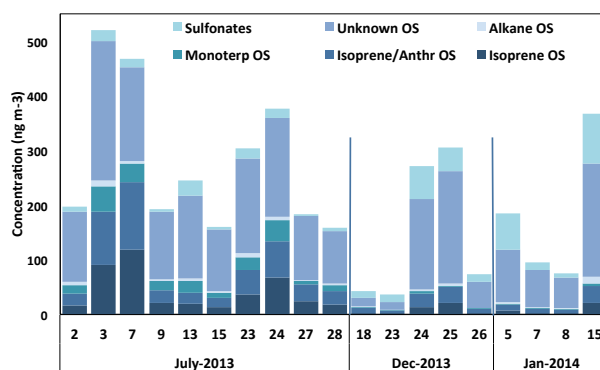


Figure 2. Estimated concentrations of organosulfates and organosulfonates in Xi'an, China.

Levels of OS derived from isoprene and monoterpenes were much higher in summer ( $65 \pm 49 \text{ ng m}^{-3}$ ) than in winter samples ( $11 \pm 9 \text{ ng m}^{-3}$ ) (Fig. 2). Molecular tracers of biogenic secondary organic aerosols (BSOA) showed the same pattern, probably due to long-range transport of aerosols.

A large number of previously unidentified OS were observed at high levels during both summer and winter. In contrast, the concentration of organic carbon (OC) was much higher during winter ( $37 \pm 17 \mu\text{g m}^{-3}$ ) than in summer ( $6.1 \pm 2.5 \mu\text{g m}^{-3}$ ), implying that other components than organosulfates dominate OC during winter in Xi'an.

The presentation will give an overview of the present knowledge of OS formation and levels globally. The results from Xi'an will be compared with previous studies of OS in differing environments from the Amazon to the Arctic, to identify key processes affecting the occurrence of OS in atmospheric aerosols.

This work was supported by the Danish Agency for Science, Technology and Innovation. The authors gratefully acknowledge the NOAA Air Resources Laboratory for the provision of the HYSPLIT transport model (<http://www.ready.noaa.gov>).

Hansen, A.M.K. *et al.* (2014) *Atmos. Chem. Phys.* **14**, 7807–7823.

Huang, R.-J. *et al.* (2014) *Nature*, **514**, 218–222.

Riva, M. *et al.* (2016) *Environ. Sci. Technol.* **50**, 5580–5588

Surratt, J.D. *et al.* (2008) *J Phys. Chem. A* **112**, 8345–8378.

## Organic markers and compounds in PM1 aerosol in urban and rural area in winter 2017

K. Krůmal, P. Mikuška, Z. Večeřa

Institute of Analytical Chemistry of the CAS, v. v. i., Veverí 97, 602 00 Brno, Czech Republic

Keywords: organic tracer, atmospheric aerosol, PM1.

Presenting author email: mikuska@iach.cz

Atmospheric particulate matter (PM) is known to play an important role in many environmental problems. During last years, much attention has been paid to the identification of emission sources of PM. To track the contributions of the main sources to composition of atmospheric aerosols, various source-specific organic tracers were analysed in collected PM (Krůmal *et al.*, 2010; Krůmal *et al.*, 2013; Krůmal *et al.*, 2015; Mikuška *et al.*, 2015).

Atmospheric aerosols in the size fraction PM1 were sampled over 24-h periods using a high-volume samplers (DHA-80, DHA-77, Digitel, 30 m<sup>3</sup>/h) on quartz filters during winter period of 2017 (18. 1. – 2. 2.) in parallel in two sites, Brno and Košetice (Figure 1). Brno, urban site, the second largest city in the Czech Republic with 370 thousand inhabitants, is an industrial, economical and political centre of Moravia, eastern part of the Czech Republic. Košetice, rural site, is classified as a background rural area and is located away from residential areas and also out of reach of a majority pollution sources.

Collected aerosols were analysed for monosaccharide anhydrides (MAs), resin acids (RAs), methoxyphenols (MPs), monosaccharides (MSs), disaccharides (DSs), sugar alcohols (SAs), alkanes, hopanes/steranes (H/S) and polyaromatic hydrocarbons (PAHs). Analysis of MAs, RAs, MPs, MSs, DSs and SAs included extraction of parts of filters with mixture dichloromethane/methanol (1:1 v/v) under ultrasonic agitation, derivatization of extracts with mixture of BSTFA + TMCS, dryness, redissolution in hexane and GC-MS analysis. Analysis of alkanes, H/S and PAHs included extraction of parts of filters with mixture of dichloromethane/hexane (1:1 v/v), fractionation on column with silicagel, dryness to 1 mL and GC-MS analysis.

Analysed compounds included:

- MAs: levoglucosan, mannosan and galactosan.
- RAs: abietic and dehydroabietic acid.
- MPs: vanillic and syringic acid, vanillin and syringol.
- MSs: xylose, fructose, galactose and glucose.
- DSs: sucrose and trehalose.
- SAs: arabitol, manitol, sorbitol and inositol.
- Alkanes: C8 – C40, pristane and phytane.
- H/S: 17 $\alpha$ (H),21 $\beta$ (H)-hopane, 22RS-17 $\alpha$ (H),21 $\beta$ (H)-homohopane, 17 $\alpha$ (H),21 $\beta$ (H)-norhopane and *aaa* (20R)-cholestane.
- PAHs: fluorene, phenanthrene, anthracene, fluoranthene, pyrene, retene, benzo[a]anthracene, chrysene, triphenylene, benzo[b+j+k]fluoranthene,

benzo[e]pyrene, benzo[a]pyrene, perylene, indeno[1,2,3-c,d]pyrene, dibenzo[a,h]anthracene benzo[g,h,i]perylene and picene.

Detailed results including mass concentrations of PM1 and comparison of analysed organic compounds in winter 2017 in Brno and Košetice will be presented.



Figure 1. Location of the sampling sites (Brno, Košetice) at the map of the Czech Republic.

This work was supported by Grant Agency of the Czech Republic under grant P503/12/G147 and by Institute of Analytical Chemistry of the CAS, v. v. i. under an Institutional research plan No. RVO:68081715.

- Krůmal, K., Mikuška, P., Vojtěšek, M., Večeřa, Z. (2010) *Atmos. Environ.* **44**, 5148-5155.
- Krůmal, K., Mikuška, P., Večeřa, Z. (2013) *Atmos. Environ.* **67**, 27-37.
- Krůmal, K., Mikuška, P., Večeřa, Z. (2015) *Atmos. Pollut. Res.* **6**, 917-927.
- Mikuška, P., Krůmal, K., Večeřa, Z. (2015) *Atmos. Environ.* **105**, 97-108.

## Molecular characterization of nanoparticles using Extractive Electrospray Ionisation Time-of-Flight Mass Spectrometry

V. Pospisilova<sup>1</sup>, F. D. Lopez-Hilfiker<sup>1</sup>, M. Xiao, O. Garmash<sup>2</sup>, A. Baccharini<sup>1</sup>, C. R. Hoyle<sup>1</sup>, A. S. H. Prévôt<sup>1</sup>, U. Baltensperger<sup>1</sup>, J. G. Slowik<sup>1</sup> and the CLOUD collaboration

<sup>1</sup>Laboratory of Atmospheric Chemistry, Paul Scherrer Institute, Villigen PSI, 5232, Switzerland

<sup>2</sup>Department of Physics, University of Helsinki

Keywords: Anthropogenic SOA, CLOUD, EESI-TOF

[Veronika.Pospisilova@psi.ch](mailto:Veronika.Pospisilova@psi.ch)

New particle formation (NPF) creates a significant fraction of the atmospheric particle number concentrations and is thought to be a source for up to half of the cloud condensation nuclei (CCN) on the global scale (Merikanto et al, 2009). Increasing the CCN number and so changing the cloud properties has a major influence on the Earth's radiative balance.

The growth of the nucleated particles to the CCN size is attributed to the condensation of low-volatility oxidation products from biogenic or anthropogenic precursors. The molecular identification of these oxidized species in the gas phase is nowadays possible using the chemical ionisation mass spectrometry (CIMS). However, the fate of these molecules in the particle phase remains unclear as currently no online instrumentation allows aerosol measurement on the molecular level without thermal decomposition and/or ionization-induced fragmentation.

Here, we present the first real-time chemical composition measurements of freshly nucleated particles using an extractive electrospray ionization time-of-flight mass spectrometer (EESI-TOF) developed at PSI (Lopez-Hilfiker et al., 2017). The measurements were performed at the CLOUD (Cosmics Leaving OUTdoor Droplets, (Kirkby et al, 2011)) chamber in the European Organization for Nuclear Research (CERN) as part of the CLOUD 11 campaign, focusing on nucleation in urban environments.

We show that the EESI-TOF enables fast analysis of organic molecules formed through the oxidation of anthropogenic precursors without thermal decomposition or fragmentation at final aerosol concentrations as low as  $\sim 100\text{ng/m}^3$ , common for CLOUD chamber experiments.

In Figure 1 we present a time evolution of 6 selected naphthalene photooxidation products in the particle phase monitored by the EESI-TOF. All species are detected in real time as sodium adducts. Their evolution follows the particle mass concentration measured by a variety of particle counters. These EESI-TOF mass spectra are compared with gas-phase spectra obtained by a nitrate CIMS. The latter is selective for highly oxidized molecules which are expected to partition to the particle phase. We observe similar molecular

patterns by both instruments, highlighting the partitioning activity of these compounds.

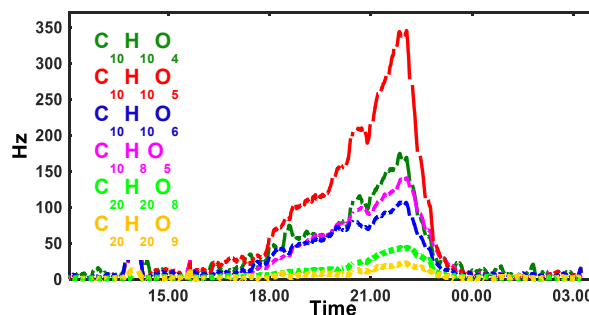


**Figure 1** EESI-TOF time series of selected species generated by oxidation of naphthalene in the CLOUD chamber.

In this presentation, we will focus on the evolution of these highly oxidized species in the gas and particle phase. We will use the CIMS data to calculate the net condensation flux of low-volatility compounds and estimate their concentration in the particle phase. The comparison of condensational flux and steady-state particle composition allows insight into particle phase reactions and therefore a direct assessment of oligomerization and fragmentation reactions in the particle phase.

This work was supported by the Swiss National Science Foundation (starting grant BSSGI0\_155846). We thank CERN for financial and technical support of the CLOUD project.

Merikanto, J., Spracklen, D., Mann, et al. (2009). Impact of nucleation on global CCN, *Atmos. Chem. Phys.*, **9**, 8601-8616.

Kirkby, J., Curtius, J., Almeida, J., et al. (2011). The role of sulfuric acid, ammonia and galactic cosmic rays in atmospheric aerosol nucleation, *Nature*, **476**, 429-433.

## Observation of synergies in secondary brown carbon formation from a monoterpene oxidation intermediate and dicarbonyls in aerosol mimicry experiments

C.J. Kampf<sup>1</sup>, S. Wittemann<sup>2</sup>, F. Kunkler<sup>2</sup>, A. Filippi<sup>2</sup>, T. Hoffmann<sup>2</sup><sup>1</sup>Institute of Organic Chemistry, University of Mainz, Mainz, 55128, Germany<sup>2</sup>Institute of Inorganic and Analytical Chemistry, University of Mainz, Mainz, 55128, Germany

Keywords: secondary brown carbon, dicarbonyls, imine pathway, HPLC-DAD, HPLC-HRMS.

Presenting author email: kampf@uni-mainz.de

Brown carbon (BrC) is a fraction of organic material in atmospheric particulates with a strong wavelength dependant absorption ( $\lambda^{-2} - \lambda^{-6}$ ), whereby absorption increases from visible to ultraviolet wavelengths (Laskin, 2015). Radiative forcing of BrC has been estimated to account for 27–70% of the black carbon (BC) forcing in a recent model study (Lin et al., 2014). BrC can originate from primary, i.e., primary organic aerosols (POA) emitted from biomass and biofuel combustion, and secondary sources (Laskin, 2015).

In previous studies, we observed the formation of nitrogen heterocycles (HetN) such as (bicyclic) imidazoles, pyrroles, (dihydro-)pyridines, and dipyrromethenes in bulk solution experiments mimicking the composition of atmospheric particles as shown in Fig. 1 (Kampf, 2012, 2016).

Only recently, Samy et al. (2013) found different HetN in ambient aerosols collected in the southeastern USA, e.g., hydroxypyridines, harmane, and norharmane. These HetN were attributed to biomass burning events in vicinity to the sampling site. Furthermore, imidazoles have been identified and quantified in ambient particulate matter in the absence of biomass burning (Teich, 2016), suggesting that the secondary processes discussed above are involved in the formation of light-absorbing species in the atmosphere.

In this study, we investigated potential synergies in mixed dicarbonyl solutions containing ammonium sulfate. We synthesized an intermediate product of the limonene ozonolysis, i.e., ketolimonaldehyde (KLA),

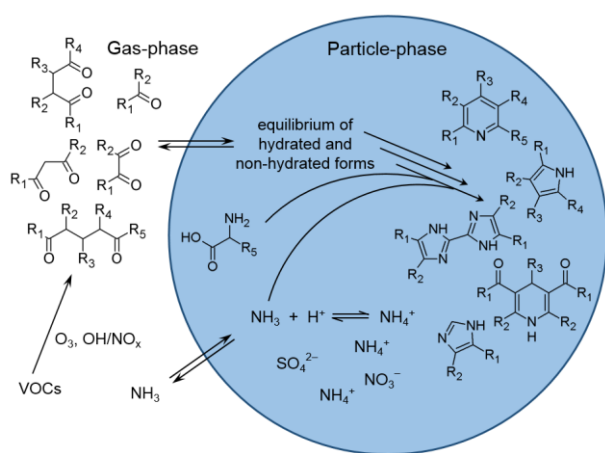


Fig. 1 Schematic overview of HetN formation in aqueous aerosol particles.

and mixed it with commercially available and atmospherically relevant carbonyl and dicarbonyl compounds such as acetaldehyde, glyoxal, and methylglyoxal. The temporal evolution of changes in absorption spectra, and concentrations of identified marker HetN were monitored using HPLC-DAD-MS, as well as HPLC-HRMS methods as outlined in Fig. 2.

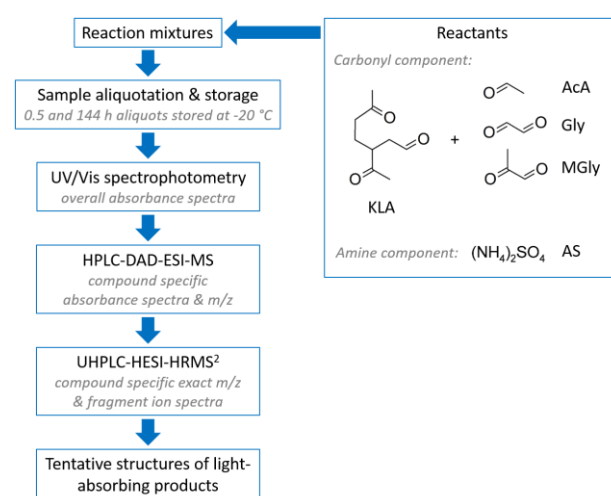


Fig. 2 Experimental and analytical procedure for the identification of potential synergistic products of KLA + acetaldehyde (AcA), glyoxal (Gly), and methylglyoxal (MGly) in ammonium sulfate (AS) solutions.

The German Research Foundation (DFG) under grant KA 4008/1-2 supported this work.

- Kampf, C.J., Jakob, R., and Hoffmann, T. (2012) *Atmos. Chem. Phys.*, **12**, 6323–6333
- Kampf, C.J., Filippi, A., Zuth, C., Hoffmann, T., Opatz, T. (2016) *Phys. Chem. Chem. Phys.*, **18**, 18353–18364
- Laskin, A., Laskin, J., and Nizkorodov, S.A. (2015) *Chem. Rev.*, **115**, 4335–4382
- Lin, G.X., Penner, J.E., Flanner, M.G., Sillman, S., Xu, L., and Zhou, C. (2014) *J. Geophys. Res.-Atmos.*, **119**, 7453–7476
- Teich, M., van Pinxteren, D., Kecorius, S., Wang, Z., and Herrmann, H. (2016) *Environ. Sci. Technol.*, **50**, 1166–1173

## Development of online Orbitrap mass spectrometry of organic aerosols: Applications for the identification of VOCs and SOA particle phase composition

C.Zuth<sup>1</sup>, A.Vogel<sup>2</sup>, S.Ockenfeld<sup>1</sup>, R. Huesmann<sup>1</sup>, T.Hoffmann<sup>1</sup>

<sup>1</sup>Institute of Inorganic and Analytical Chemistry, Johannes Gutenberg University, Mainz, 55128, Germany

<sup>2</sup>Laboratory for environmental chemistry & laboratory for atmospheric chemistry, Paul Scherrer Inst., Villigen, 5232, Switzerland

Keywords: molecular characterization, ultra-high resolution MS, Second. Organic Aerosol (SOA).

Presenting author email: zuth@uni-mainz.de

The emission of volatile organic compounds (VOCs) into the atmosphere, irrespective of biogenic or anthropogenic origin, acts as a well-established precursor for the formation of secondary organic aerosol (SOA). Particularly a detailed knowledge of the molecular composition of SOA is essential for elucidation of formation mechanisms (Zhang, 2015).

Providing high sensitivity and selectivity towards single chemical compounds, mass spectrometry (MS) is the most commonly applied technique for the chemical analysis of atmospheric aerosol particles (Farmer, 2010). Online mass spectrometry techniques avoid potential artefacts associated with offline analysis methods, such as evaporation and chemical reactions during long sample collection and analysis time periods (Pratt and Prather, 2012). One of the major advantages of online mass spectrometry is the ability to examine chemical changes in atmospheric environments in short timescales within seconds.

However, condensed phase reactions between inorganic (nitrate, sulfate and ammonium) and organic aerosol constituents, lead to the formation of low volatile irreversible products like monoterpene- and isoprene-derived organosulfates, nitrooxy organosulfates (Surratt et al., 2008) or organonitrates (Szmigielski, 2010). Due to the fact that these compounds consist of more than just C-, H-, and O-atoms, a high mass resolution is needed to determine the exact sum formula.

Furthermore another current research interest is the identification and correct determination of highly oxidized molecules (HOMs) which are able to contribute significantly to organic mass in tropospheric particles (Mutzel, 2015). Especially in the analysis of atmospheric aerosols at mass to charge ratios ( $m/z$ ) above 300 amu several compounds at the same nominal mass are basically possible whereby a high mass resolving power is needed to separate between two compounds.

Here we present the first coupled APCI-Orbitrap-MS<sup>2</sup>-technique for the online determination of SOA particle phase. This approach combines the high mass resolution ( $R=70.000$  at  $m/z$  200) and accuracy ( $<2$  ppm) of an QExactive Orbitrap mass analyser (Thermo Scientific, Germany), which enables the determination of the elemental composition by exact mass measurements, and the advantages of online measurement techniques.

As a soft ionization technique APCI provides information about the molecular mass by producing either  $[M-H]^-$  or  $[M+H]^+$  ions, depending on the polarity of the ion source. Additionally the QExactive mass

spectrometer allows MS<sup>2</sup> experiments for further structural elucidation of SOA products.

In this context, the presented technique was used in combination with a PTR-ToF-MS, for real-time identification of abiotic VOC production from authentic biogenic surfactants under ambient conditions.

Furthermore, the APCI-Orbitrap-MS<sup>2</sup>-technique allows the investigation of SOA derived organic molecules produced in environmental chamber experiments. First investigations on the formation of  $\alpha$ -pinene/O<sub>3</sub> oxidation products measured with varying relative humidities showed different molecular patterns within a mass scale of 0.3 amu which could only be observed with an appropriate mass resolution. According to these first experiences, real-time measurements of ambient organic aerosols are planned.

Farmer, D.K. and Jimenez, J.L. (2010) *Analytical Chemistry*. **82**, 7879-7884

Mutzel, A. et al. (2015) *Environ. Sci. Technol.* **49**, 7754-7761

Pratt and Prather (2012) *Mass Spectrometry Reviews*. **31**, 17-48

Surratt, J.D. et al., (2008) *J. Phys. Chem. A*. **112**, 8345-8378

Szmigielski et al., (2010) *Atmospheric Research*. **98**, 183-189

Zhang et al. (2015) *PNAS*. **112**, 14168-14173.

## Improving LC-MS methods for a detailed SOA characterization

G. Spolnik<sup>1</sup>, P. Wach<sup>2</sup>, K. Rudzinski<sup>2</sup>, K. Nestorowicz<sup>2</sup>, K. Skotak<sup>3</sup>, W. Danikiewicz<sup>1</sup> and R. Szmigielski<sup>2</sup>

<sup>1</sup>Institute of Organic Chemistry, Polish Academy of Sciences, Warsaw, 01-224, Poland

<sup>2</sup>Institute of Physical Chemistry, Polish Academy of Sciences, Warsaw, 01-224, Poland

<sup>3</sup>Institute of Environmental Protection, National Research Institute, Warsaw, 00-548, Poland

Keywords: aerosols, organosulfates, SOA, liquid chromatography, tandem mass spectrometry.

Presenting author email: grzegorz.spolnik@icho.edu.pl

The atmospheric aerosol is one of the most important object of recent studies. Significance of the molecular identification and quantitation of known compounds has been strongly emphasized among the crucial challenges in secondary organic aerosol research (Nozière, 2015). In previous years dozens of compounds such as MBTCA (Szmigielski, 2007) or 2-methyltetrol sulfates (Surratt, 2007) have been systematically pointed out as the markers of the SOA formation from  $\alpha$ -pinene or isoprene, respectively. In most recent years the structures of major isoprene derived organosulfates were proposed including the 2-methyltetrols sulfate ester (OS 216) cyclic hemiacetal of methyltrihydroxyaldehyde sulfate ester (OS 214) and methyl dihydroxylactone sulfate ester (OS 212) (Surratt, 2007; Hettiyadura, 2015) but many concomitant isomeric structures for these compounds do not allow the accurate identification. The occurrence of specific isomers as well as their number could not be established so far.

In this study we improved the chromatographic methods to make them more useful for the structural and quantitative analysis of the most polar fraction of SOA, especially organosulfates. We chose the UHPLC-MS/MS method and focus on two types of chromatographic techniques, C18 strengthened columns with 100% of aqueous mobile phase and HILIC that are complement and dedicated for the polar compounds analysis.

In our work we used Aquity I-Class liquid chromatograph (Waters) coupled with Synapt G2-S Q-ToF type mass spectrometer (Waters) that we used for structural studies. The spectrometer working parameters optimization for MS and MS/MS experiments highly improved the powerfulness of the technique regarding the detailed structural studies.

In RP-C18 chromatography most polar components of the SOA are in the stable ionic form in the common MS compatible buffers solution so their chromatographic behaviour does not change much according to the buffer type or acidic pH value. More significant role plays the column temperature and the peak resolution improved with increasing it. The most important factors in chromatographic resolving power on C18 column were injection matrix effect together with the sample solvent selection. The change of the standard sample solvent in the SOA analyses - methanol-water mixture - for the solvent with low organic solvent content shown dramatic improvement in peaks resolution, shape, separation, reduced ghost peaks and made this parameters volume injection independent. It

directly enhanced the intensity of the MS measurements and made more detailed studies possible.

The HILIC chromatography was used only as the supporting method for the most polar fraction analyses because of its low versatility with the respect for the compounds with very different polarity like SOA compound are.

Using the optimised methods we analysed the group of isoprene derived organosulfates OS 216, OS 214 and OS 212 in detail. We revealed the presence of four major isomers for OS 216, five for OS 213 and seven for OS 212 and it far more efficient analysis than those reported earlier. On the basis of the detailed MS/MS study we propose the structures of isomers corresponding to the specific chromatographic peaks.

The obtained results are easy reproducible in any LC-MS lab that can simplify the intercomparison of the results from aerosols researchers from around the world.

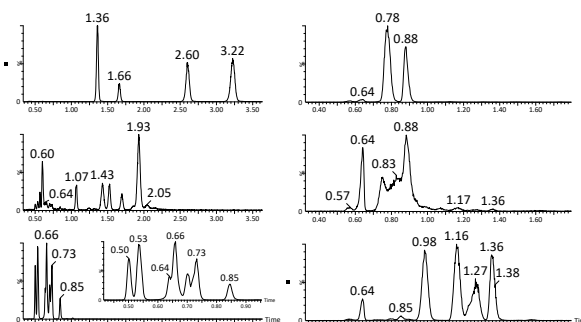


Figure 1. The separation of the compounds OS 216, OS 214 and OS 212 obtained with HILIC (left) and RP-C18 (right) methods

This work was supported by the National Science Center in Poland based on the decision UMO-2014/15/B/ST10/04276.

Nozière, B., M. Kalberer, et al. (2015) *Chemical Reviews* **115**(10), 3919-3983.

Surratt, J. D., M. Lewandowski, et al. (2007) *Environmental Science & Technology* **41**(15), 5363-5369.

Szmigielski, R., J. D. Surratt, et al. (2007) *Geophysical Research Letters* **34**, L2481

## Characterization of secondary organic aerosol sources using extractive electrospray time-of-flight mass spectrometry

J.G. Slowik<sup>1</sup>, F.D. Lopez-Hilfiker<sup>1</sup>, V. Pospisilova<sup>1</sup>, L. Qi<sup>1</sup>, G. Stefenelli<sup>1</sup>, Y. Tong<sup>1</sup>, A. Vogel<sup>1</sup>, U. Baltensperger<sup>1</sup>, A.S.H. Prévôt<sup>1</sup>

<sup>1</sup>Laboratory of Atmospheric Chemistry, Paul Scherrer Institute, Villigen PSI, 5232, Switzerland

Keywords: EESI-TOF, secondary organic aerosol

Presenting author email: jay.slowik@psi.ch

Organic aerosol (OA) is ubiquitous in the troposphere and significantly impacts climate and human health. Development of sound environmental policy requires quantitative links between OA and its sources, however, this has proven challenging due to the dominance of the secondary OA (SOA) fraction, formed by atmospheric reactions of emitted gases. Although online mass spectrometry has proven a powerful tool for interrogating OA composition, its ability to resolve SOA sources has been limited. This is in part due to the chemical composition of SOA, which is in large part comprised of highly functionalized, oxygenated organics, which readily decompose in response to heating (a required step in particle sampling for existing online instrumentation) and/or fragment in response to ionization.

To overcome these obstacles, we have developed a novel extractive electrospray ionization time-of-flight mass spectrometer (EESI-TOF) for the online measurement of organic aerosol composition. Aerosols are continuously sampled into the EESI-TOF and intersect with a highly charged spray generated by a conventional electrospray capillary. Organic molecules dissolve in the spray (methanol/water or acetonitrile/water with NaI as a charge carrier) and are detected as sodium adducts by time-of-flight mass spectrometry. The EESI-TOF provides a signal that is linear with mass, without the charge suppression or matrix artifacts affecting standard electrospray ionization systems, and with no fragmentation or thermal decomposition. The rapid response and high degree of chemical specificity of this field-deployable instrument make it a promising tool for SOA source apportionment.

As a first step towards identifying sources of ambient SOA, we investigate EESI-TOF mass spectra from SOA formed from the reaction of pure compounds that are known SOA precursors (e.g.  $\alpha$ -pinene, toluene, phenol, naphthalene, 1,2,4-trimethylbenzene), simple mixtures of these compounds, and real-world sources such as wood burning and vehicle emissions. SOA is generated by reacting these precursor gases with OH radicals in the PSI smog chamber and a potential aerosol mass (PAM) reactor.

Sample mass spectra for  $\alpha$ -pinene and toluene SOA are shown in Figure 1. Both spectra are dominated by highly oxygenated ions, but the  $\alpha$ -pinene SOA contains a prominent series of  $C_{10}H_{16}O_nNa^+$  ions, while the toluene SOA includes the  $C_7H_{10}O_nNa^+$  series. These ion series are directly linked to the precursor identity ( $C_{10}H_{16}$  for  $\alpha$ -pinene and  $C_7H_8$  for toluene). Similarly,

SOA from naphthalene ( $C_{10}H_8$ ) exhibits a strong  $C_{10}H_{10}O_nNa^+$  series. Although naphthalene and  $\alpha$ -pinene have the same carbon number, the lower H:C ratio of naphthalene is clearly preserved in the SOA products and allows the spectra from these precursors to be clearly distinguished.

Real-world SOA sources consist of complex mixtures of SOA precursors, rather than a single source, complicating separation. We investigate SOA from such sources over a range of reaction conditions and precursor concentrations. The degree to which EESI-TOF spectra of these sources are unique to each individual source is assessed, and the spectra utility for ambient source apportionment studies is evaluated.

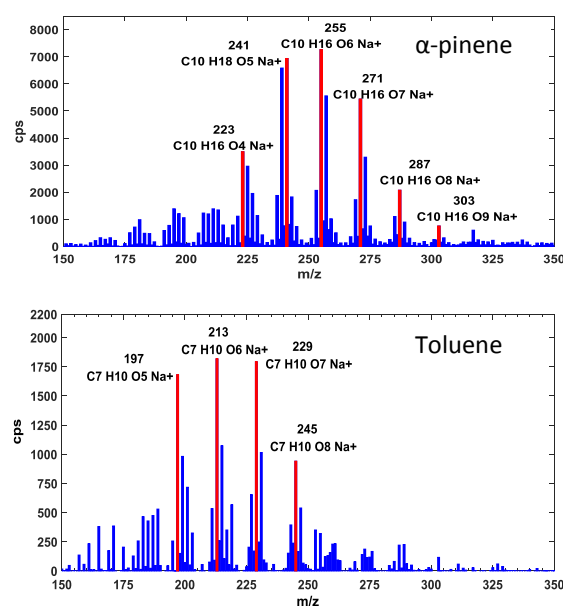


Figure 1. EESI-TOF mass spectra from the reaction of  $\alpha$ -pinene (top) and toluene (bottom) with OH radicals. Selected ions are labelled and marked in red.

This work was supported by the Swiss National Science Foundation (starting grant BSSG10\_155846).

## Molecular characterization of organosulfates in organic aerosol from European and Chinese cities by ultrahigh resolution mass spectrometry

Kai Wang<sup>1</sup>, Rujin Huang<sup>2</sup>, Christopher Kampf<sup>3</sup>, Yafang Cheng<sup>3</sup>, Ulrich Pöschl<sup>3</sup>, Thorsten Hoffmann<sup>1</sup>

<sup>1</sup>Institute of Inorganic and Analytical Chemistry, Johannes Gutenberg University, Mainz, 55128, Germany

<sup>2</sup>Institute of Earth Environment, Chinese Academy of Sciences, Xi'an, 710061, China

<sup>3</sup>Multiphase Chemistry Department, Max Plank Institute for Chemistry, Mainz, 55128, Germany

Keywords: organosulfates, organic aerosol, molecular composition, European and Chinese cities, ultrahigh resolution mass spectrometry,

Presenting author email: kaiwang1@uni-mainz.de

Organic aerosol (OA) constitutes a substantial fraction (20-90%) of submicrometer aerosol mass, playing an important role in air quality and human health. OA contains a variety of organic species, including hydrocarbons, alcohols, aldehydes, carboxylic acids and organosulfates (OS). Recent laboratory smog chamber and field campaign studies demonstrated that OS contributes a significant fraction in OA. Therefore, a better understanding of formation mechanism and molecular-level characterization of OS are important for assessing the effects of aerosol.

Over the past few years, ultrahigh resolution mass spectrometry (UHRMS) coupled with electrospray ionization (ESI) has been applied to characterize the complex organic mixtures in OA at the molecular level. Due to the high mass resolving power and high mass accuracy, the UHRMS techniques can detect thousands of individual organic aerosol components and provide their accurate chemical compositions for each analysis.

In this study, urban aerosol with particle diameter  $< 2.5 \mu\text{m}$  ( $\text{PM}_{2.5}$ ) was collected in Mainz, Germany and Beijing, China, respectively. Solvent mixture of acetonitrile and water was applied to extract the OS from the filter samples. The extracts were analyzed by Orbitrap (ESI-UHRMS) coupled with ultra-high-performance liquid chromatography (UHPLC) in both negative and the positive modes. The chemical composition difference of OS between the two cities have been discussed in detail.

This study was supported by the scholarship from Chinese Scholarship Council (CSC) and Max Plank Graduate Center with Johannes Gutenberg University of Mainz (MPGC).

Kroll, J. H.; Donahue, N. M.; Jimenez, J. L.; Kessler, S. H.; Canagaratna, M. R.; Wilson, K. R.; Altieri, K. E.; Mazzoleni, L. R.; Wozniak, A. S.; Bluhm, H.; Mysak, E. R.; Smith, J. D.; Kolb, C. E.; Worsnop, D. R. (2011) *Nat. Chem.* 3, (2), 133-139.

Tao, S.; Lu, X.; Levac, N.; Bateman, A. P.; Nguyen, T. B.; Bones, D. L.; Nizkorodov, S. A.; Laskin, J.; Laskin, A.; Yang, X. (2014) *Environ. Sci. Technol.* 48, (18), 10993-11001.

Lin, P.; Yu, J. Z.; Engling, G.; Kalberer, M. (2012) *Environ. Sci. Technol.* 46, (24), 13118-27.

Surratt, J. D.; Gomez-Gonzalez, Y.; Chan, A. W.; Vermeylen, R.; Shahgholl, M.; Kleindienst, T. E.; Jaoui, M.; Maenhaut, W.; Claeys, M.; Flagan, R. C.; Seinfeld, J. H. (2008) *J. Phys. Chem. A* 112, 8345-8378.

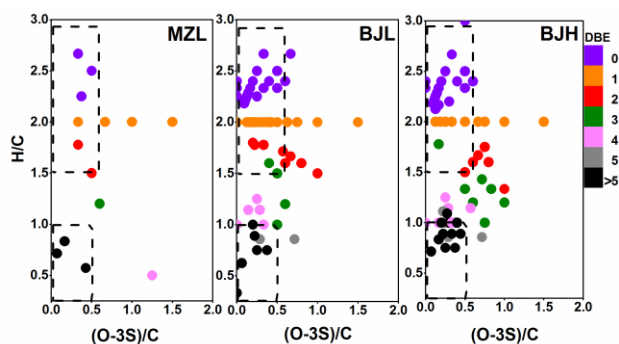


Figure 1. Van Krevelen diagrams constructed by plotting the H/C ratio against the (O-3S)/C ratio for CHOS species in Mainz low  $\text{PM}_{2.5}$  concentration (MZL), Beijing low  $\text{PM}_{2.5}$  concentration (BJL) and Beijing high  $\text{PM}_{2.5}$  concentration (BJH) samples. The color-coding denotes the DBE values.

## **Abstracts T217**

## Photochemistry of iron citrate in aerosol particles

P. Corral Arroyo<sup>1,2</sup>, P. A. Alpert<sup>2</sup>, J. Dou<sup>3</sup>, U. Krieger<sup>3</sup>, M. Ammann<sup>1</sup>

<sup>1</sup>Laboratory of Environmental Chemistry, Paul Scherrer Institute, PSI Villigen, 5232, Switzerland

<sup>2</sup>Department of Chemistry and Biochemistry, University of Bern, 3012, Bern, Switzerland

<sup>3</sup>Institute of Atmosphere and Climate, ETH Zurich, Zurich, 8092, Switzerland

Keywords: photochemistry, aerosol, aging  
Presenting author email: pablo.corral-arroyo@psi.ch

Photochemical reactions are driven by sunlight resulting in radical formation and reaction with other atmospheric compounds. Iron complexes are important species in indirect photochemical oxidation of organic compounds in atmospheric particles. Iron is emitted to the atmosphere from combustion, sea spray and windblown dust but frequently associated with organic materials emitted simultaneously or acquired from secondary organic aerosol formation. Ferric (Fe(III)) carboxylate complexes are an example of an atmospherically relevant iron-organic complex that absorbs light below about 500 nm followed by a ligand to metal charge transfer (LMCT) reaction. This results in the reduction of Fe(III) to Fe(II), oxidation of the carboxylate ligands and the formation of H<sub>2</sub>O<sub>2</sub>. The latter reoxidizes Fe(II) to Fe(III) closing a catalytic cycle (Fig. 1). This process represents an important sink of organic acids in the troposphere (Weller *et al.* (2013) and George *et al.* (2012)) and is potentially relevant as an aerosol aging process.

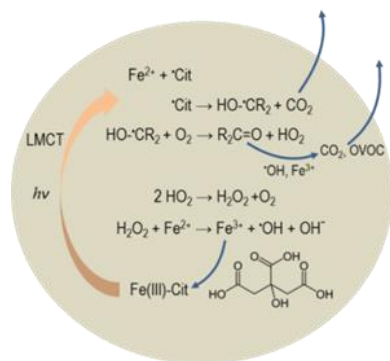


Figure 1. Catalytic mechanism of iron citrate complexes initiated by UV-VIS light, followed by decarboxylation of the ligand and later by re-oxidation of Fe(II) to Fe(III) that closes the cycle.

Photochemical reactions occurring within aerosol particles are difficult to quantify due to the small mass per particle and as a result, bulk samples are typically employed which allows for detailed photochemical information, but lacks insight on single particle composition. Therefore, we present a multi-method analysis of Fe-citrate photochemistry using aerosol and coated-wall flow tubes as well as scanning transmission X-ray microscopy coupled with near-edge X-ray absorption fine structure spectroscopy (STXM/NEXAFS).

Spatially resolved chemical structures of single aerosol particles as a function of photochemical exposure are quantified using the STXM/NEXAFS technique. Carbon functional group composition (Steimer *et al.* (2014)) and iron oxidation state (Moffet *et al.* (2012)) were mapped with 35x35 nm resolution with sub-micrometer sized particles.

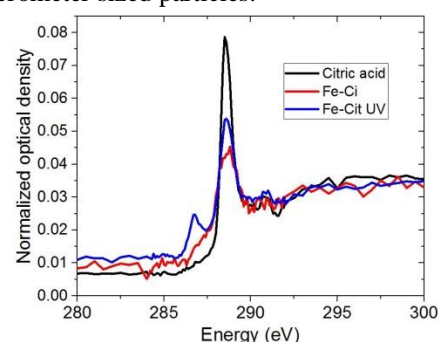


Figure 2. Individual particle absorption spectra of citric acid and iron citrate (Fe-Cit). UV exposure to iron citrate (Fe-Cit UV) lasted 2 hours under nitrogen in dry conditions. These spectra are normalized to their area from 280-320 eV.

After UV light exposure under dry N<sub>2</sub>, the fraction of Fe(III) remaining within aerosol particles decreased with a photochemical rate constant 0.08 s<sup>-1</sup> under the irradiation provided by our LED (375 nm, 350W/m<sup>2</sup>). After a longer exposure we observed a loss of the X-ray absorption signal at 288.6 eV (Figure 2) representative of carboxyl functionality, and an increase at 286.3 eV, characteristic of ketones. These results corroborate the suggested mechanism in the Figure 1 and the importance of these processes for aerosol aging. Further insight into this photochemistry will come from aerosol and coated flow tube experiments and offline product analysis at PSI (not shown).

This work was supported by the Swiss National Science Foundation under grant 163074.

Weller, C. *et al.*, Photochemistry and Photobiology A: Chemistry, 268, 24-36, 2013.

George, C. *et al.*, Topics in Current Chemistry, Springer Berlin Heidelberg (2012)

Steimer, S.S. *et al.*, Atmos. Chem. Phys., 2014, 14, 10761-10772.

Moffet R.C. *et al.*, Journal of Geophysical Research, VOL. 117, D07204, 2012

## Studies of Enhanced Chemical Reaction Rates and Photochemical Reactions in Dry Aerosol Droplets

Aleksandra Marsh<sup>1</sup> and Jonathan P. Reid<sup>1</sup><sup>1</sup>Department of Chemistry, University of Bristol, Bristol, BS8 1TS

Keywords: Reaction rates, kinetics, photochemistry, single droplet.

Presenting author email: aleksandra.marsh@bristol.ac.uk

Aerosol have a high surface to volume ratio and ambient aerosol composition continuously undergoes changes to functionality via oxidation, oligomerisation, volatilisation and changes to relative humidity (RH). However, most available studies measure bulk phase reaction rates, use electrospray ionisation and/or observe an ensemble of particles. Here we consider a single confined droplet where reaction chemistry is induced via dehydration (lowering RH) or illumination with a broadband light source. Recent literature suggests that aerosol phase chemistry occurs on timescales much faster than those observed in the same reactions conducted in the bulk. However, most examples consider a plume of charged droplets which are then analysed for product formation using mass spectrometry, Yan *et al* (2016). This is the first study of its kind that allows the interrogation of both product formation and reactant loss in the same single picolitre droplet in situ by Raman spectroscopy. We hope to provide mechanistic insights of the enhancement in reaction rate in aerosol through studying a single droplet.

Here we present work where a single uncharged droplet containing aqueous reactants is confined using an Aerosol Optical Tweezers, Wills *et al* (2009), product formation and changes to droplet composition is monitored via Raman Spectrometry. We observe that droplet phase esterification (condensation reaction) between glutaric acid and Carbitol can take place on the order of 100's of seconds, much faster reaction timescales than during bulk phase synthesis, where formation of dicarbitol glutarate requires reflux for 14-18 hours. In the aerosol phase the equilibrium of the esterification reaction is controlled using the gas phase RH and follows Le Chatelier's Principle, at low RH the equilibrium favours the formation of ester product and of water. This is shown in Figure 1 where the carbonyl peak shifts to a higher wavelength on drying.

Further, we confirm esterification using an atomiser set up, with tandem nafion dryers where the collected product is analysed using <sup>1</sup>H NMR, with evidence suggesting that smaller droplets lead to faster rates of reaction.

In a second class of reaction, we examine the reaction rates that occur in a photochemically driven reaction, again presenting data from single droplet measurements. Nitrate anions are prevalent in atmospheric aerosol and their photolysis leads to OH radical formation which influences a number of atmospheric processes, Scharko *et al* (2014). Here nitrate

photolysis is initiated via irradiation of aqueous sodium nitrate droplets with broadband light and reaction rates are determined via the observed loss of nitrate in the Raman spectra.

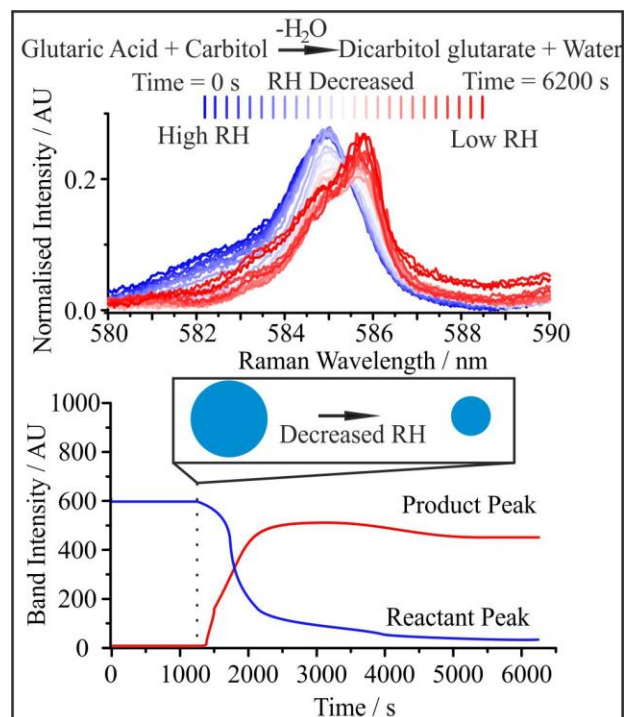


Figure 1: (upper) The carbonyl region (580-590 nm or 1600 – 1800  $\text{cm}^{-1}$ ) of an aqueous droplet containing a 3:1 carbitol/glutaric acid solution, an increase in carbonyl wavelength is observed when the RH is lowered from 80 – 0 % (blue – red). (lower) Band intensity of reactant (dicarboxylic acid) and product (ester) on RH change.

This work was funded by the EPSRC, through a DTA to Aleksandra Marsh.

Scharko, N. K., Berke, A. E. and Raff, J. D. (2014) *Environ. Sci. Technol.*, 48, 11991–12001

Wills, J. B., Knox, K. J. and Reid, J. P. (2009) *Chemical Physics Letters*, 481, 153-165

Yan, X., Bain, M. R. and Cooks, G. R. (2016) *Angewandte Chemie International Edition*, 55, 42, 12960-12972

## Condensed Phase Diffusivity Measurements of Volatile Organics in Levitated Viscous Aerosol Particles

S. Bastelberger<sup>1</sup>, U. Krieger<sup>1</sup>, B. Luo<sup>1</sup> and T. Peter<sup>1</sup>

<sup>1</sup>IAC ETH, ETH Zurich, Zurich, 8092, Switzerland

Keywords: SOA, VOC, condensed phase diffusion limitations, viscosity.

Presenting author email: sandra.bastelberger@env.ethz.ch

Field measurements indicate that atmospheric secondary organic aerosol (SOA) particles can be present in a highly viscous, glassy state (Virtanen *et al.*, 2010). This raises the question of how condensed phase diffusivities of water, oxidants and organic molecules are affected by cold and dry conditions when SOA is likely to be viscous. The influence of low water diffusivities in glassy aerosol particles has been widely studied, emphasizing possible kinetic limitations of hygroscopic growth and the plasticizing effect of water. In contrast, very little is known about diffusion limitations of organic molecules and oxidants in viscous matrices. These may influence atmospheric chemistry, aerosol morphology and gas-particle phase partitioning of complex mixtures with constituents of different volatility.

In this study, we quantify the diffusivity of a volatile organic in a viscous matrix. The evaporation of single particles generated from an aqueous solution of sucrose and small amounts of volatile tetraethylene glycol (PEG-4) is investigated in an electrodynamic balance at controlled humidity and temperature conditions. The evaporative loss of PEG-4 is determined using Mie resonance spectroscopy radius measurements. At high humidity, when no condensed phase diffusion limitations apply, the radius data is used to derive PEG-4 activity coefficients for the ternary system. At lower humidities, when the evaporation of PEG-4 is kinetically limited by condensed phase diffusion, the radius data is used in conjunction with a radially resolved diffusion model (based on the model of Zobrist *et al.*, 2011) to retrieve translational diffusion coefficients of PEG-4 as function of humidity and temperature.

A comparison of the experimentally determined diffusivities with viscosity estimates for the ternary system reveals a consistent breakdown of the Stokes-Einstein relationship at low humidities. This suggests that Stokes-Einstein, which is widely used to infer diffusivities from matrix viscosity data and the hydrodynamic radii of the diffusing molecules, is not adequate to predict diffusivities of volatile organics in viscous SOA.

The evaporation of PEG-4 shows a pronounced temperature and humidity dependence, the latter highlighting the plasticizing effect of water on viscous SOA. Evaporation is severely depressed for RH < 30%, corresponding to diffusivities < 10<sup>-14</sup> cm<sup>2</sup>/s at temperatures up to 15 °C. Our findings imply that atmospheric volatile organic compounds can be subject to severe diffusion limitations in glassy SOA.

Virtanen, A., Joutsensaari, J., Koop, T., Kannosto, J., Yli-Pirila, P., Leskinen, J., Makela, J. M., Holopainen, J. K., Poeschl, U., Kulmala, M., Worsnop, D. R., and Laaksonen, A. (2010) *Nature*, **467**, 824–827.

Zobrist, B., Soonsin, V., Luo, B. P., Krieger, U. K., Marcolli, C., Peter, T., and Koop, T. (2011) *Phys. Chem. Chem. Phys.*, **13**, 3514–3526.

## Feedbacks between microphysics and photochemical aging in viscous aerosol

Jing Dou<sup>1</sup>, Pablo Corral Arroyo<sup>2</sup>, Peter A. Alpert<sup>2</sup>, Markus Ammann<sup>2</sup>, Thomas Peter<sup>1</sup>, Ulrich K. Krieger<sup>1</sup>

<sup>1</sup>Institute for Atmospheric and Climate Science, ETH Zürich, Zürich, Switzerland

<sup>2</sup>Laboratory of Environmental Chemistry, Paul Scherrer Institute, 5232 Villigen PSI, Switzerland

Keywords: Fe-citrate complex, photochemistry, high viscosity

Presenting author email: [jing.dou@env.ethz.ch](mailto:jing.dou@env.ethz.ch)

Fe(III)-citrate complex photochemistry, which plays an important role in aerosol aging, especially in the lower troposphere, has been widely recognized in both solution and solid states. The complex can get excited by light below about 500 nm, inducing the oxidation of carboxylate ligands and the production of peroxides (e.g., OH•, HO<sub>2</sub>•), which will lead to more decarboxylation and oxygenated volatile organic compounds (OVOC) production, having a significant impact on the gas-particle partitioning. Recently, there is literature reporting that aqueous aerosol particles may attain highly viscous, semi-solid or even glassy physical states under a wide range of atmospheric conditions. However, systematic studies on the effect of high viscosity on photochemical processes are scarce.

In this research, mass and size changes of a single, aqueous Fe(III)-citrate/citric acid particle levitated in an electrodynamic balance (EDB) are tracked during photochemical processing. We have observed an overall

mass loss during photochemical processing due to evaporation of volatile (e.g., CO<sub>2</sub>) and semi-volatile (e.g., ketones) compounds. It is known that relative humidity and temperature strongly effects the viscosity of citric acid. Here we focus on the differences between the high and low viscosity cases by performing experiments at different relative humidities and temperatures. Low temperature and/or low relative humidity could result in reduced molecular mobility and low water content, which slows down the transport of products but can also affect chemical reaction rates (e.g., initial absorption process, charge and energy transfer). Meanwhile, a numerical model, which includes the equilibria of each component, main chemical reactions, and the transport of volatile and semi-volatile products, was developed to simulate the experimental data. It enables us to determine some of the crucial parameters like equilibrium constants, reaction rates and liquid phase diffusion coefficients by comparing model output with experimental data.

## Aqueous-phase reactivity of 1,2-dihydroxybenzenes (catechol) under nighttime atmospheric conditions

K. Vidović<sup>1</sup>, D. Lašič Jurković<sup>2</sup>, A. Kroflič<sup>1</sup>, S. Frka<sup>1,3</sup>, M. Šala<sup>1</sup>, and I. Grgić<sup>1</sup>

<sup>1</sup>Department of Analytical Chemistry, National Institute of Chemistry, 1000 Ljubljana, Slovenia

<sup>2</sup>Department of Catalysis and Chemical Reaction Engineering, National Institute of Chemistry, 1000 Ljubljana, Slovenia

<sup>3</sup>Division for Marine and Environmental Research, Ruđer Bošković Institute, 10000 Zagreb, Croatia

Keywords: aqueous-phase chemistry, aromatic nitration, methylcatechol, nitrite catalysis, brown carbon.

Presenting author email: kristijan.vidovic@ki.si

Secondary organic aerosols (SOA) constitute a significant proportion of ambient particulate matter and are well-known to have adverse effects on air quality and human health. SOA formed in the atmosphere and atmospheric brown carbon (BrC) as a significant SOA constituent represent key uncertainties in determining the impact of aerosols on climate, in part due to their complexity and continually changing composition. Besides, dynamic mechanisms of SOA formation and aging are poorly understood. It has been thought that SOA are formed from gas-phase oxidation followed by absorption of semi-volatile products into pre-existing particles (Pankow *et al.*, 1994). Recent studies have indicated that chemical processes in the atmospheric aqueous phase can also efficiently contribute to SOA formation (Volkamer *et al.*, 2007). Organic compounds in the atmospheric aqueous phase are oxidized to form low-volatile products which remain in the particle phase upon water evaporation (Blando and Turpin *et al.*, 2000).

Biomass burning (BB) is the major source of organic aerosol (OA) (Bond *et al.*, 2004); natural and anthropogenic BB emissions of aromatic hydrocarbons, thus contribute substantially to SOA precursors (Pillar *et al.*, 2015). Dihydroxybenzenes, such as catechol, are the most common gas-phase organic constituents of BB plumes (Veres *et al.*, 2010). Moreover, methyl, carbonyl, and nitro substituted catechol derivatives have also been found in cloud water and water extracts of ambient aerosol samples (Desyaterik *et al.*, 2013; Frka *et al.*, 2016).

We studied the kinetics of transformation of 3-methylcatechol (3MC) into its nitrated products under atmospherically relevant conditions. Laboratory experiments of 3MC nitration were performed in acidic aqueous solution (pH 4.5) in dark and in the presence of nitrite added as NaNO<sub>2</sub>. The influence of initial concentration of NaNO<sub>2</sub> and 3MC, oxygen presence, and pH was tested. 3MC and its main products, 3-methyl-5-nitrocatechol (3M5NC) and 3-methyl-4-nitrocatechol (3M4NC) were followed by use of a high pressure liquid chromatography (HPLC) equipped with a UV/vis diode array detector (DAD). Mechanism and kinetics of formation of ring-retaining nitration products were quantitatively explored by the kinetic model adopted from Kroflič *et al.* (2015). The results show that 3-methyl-*o*-quinone derived from the oxidation of 3MC by nitrous acid (HNO<sub>2</sub>) may participate in the conjugated addition reaction with nitrite ion.

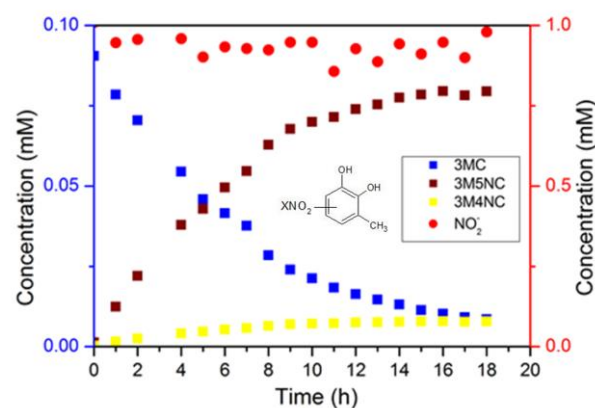


**Figure 1.** Experimental data of 0.1 mM 3MC nitration in acidic H<sub>2</sub>SO<sub>4</sub> solution (pH 4.5) at 25 °C in dark upon addition of 1 mM NaNO<sub>2</sub>.

This work was supported by the Slovenia Research Agency (Contract Nos. P1-0034 and P2-0152).

- Pankow, J. F. (1994) *Atmos. Environ.*, **28**(2), 189-193.  
 Volkamer, R., San Martini, F., Molina, L. T., Salcedo, D., Jimenez, J. L., & Molina, M. J. (2007) *Geophys. Res. Lett.*, **34**(19)  
 Blando, J. D., & Turpin, B. J. (2000) *Atmos. Environ.*, **34**(10), 1623-1632.  
 Bond, T. C., Streets, D. G., Yarber, K. F., Nelson, S. M., Woo, J-H. and Klimont Z. (2004) *J. Geophys. Res.* **109**, D14203, 1–43.  
 Pillar, E. A., Zhou, R., & Guzman, M. I. (2015) *J. Phys. Chem. A*, **119**(41), 10349-10359.  
 Veres, P., Roberts, J. M., Burling, I. R., Warneke, C., de Gouw, J., & Yokelson, R. J. (2010) *J. Geophys. Res.*, **115**(D23).  
 Frka, S., Šala, M., Kroflič, A., Huš, M., Čusak, A., & Grgić, I. (2016) *Environ. Sci. Technol.*, **50**(11), 5526-5535.  
 Desyaterik, Y., Sun, Y., Shen, X., Lee, T., Wang, X., Wang, T., & Collett, J. L. (2013) *J. Geophys. Res. Atmos.*, **118**(13), 7389-7399.  
 Kroflič, A., Grilc, M., & Grgić, I. (2015). *Environ. Sci. Technol.*, **49**(15), 9150-9158.

## Impact of aerosol acidity and liquid water content on nitrogen containing SOA species formed from $\alpha$ -pinene ozonolysis

L. Heikkinen<sup>1</sup>, M. Riva<sup>1</sup>, O. Peräkylä<sup>1</sup>, O. Garmash<sup>1</sup>, M. Äijälä<sup>1</sup>, E. Canaval<sup>2</sup>, L. Fischer<sup>2</sup>, A. Hansel<sup>2</sup>, L. Quéléver<sup>1</sup>, T. Petäjä<sup>1</sup>, D. Worsnop<sup>1,3</sup>, and M. Ehn<sup>1</sup>

<sup>1</sup>Department of Physics, University of Helsinki, Helsinki, 00560, Finland

<sup>2</sup>Institute for Ion Physics and Applied Physics, University of Innsbruck, Innsbruck, A-6020, Austria

<sup>3</sup>Aerodyne Research Inc., Billerica, MA 01821, USA

Keywords: AMS, FIGAERO, organic nitrates, multiphase chemistry

Presenting author email: liine.heikkinen@helsinki.fi

Atmospheric aerosols can be directly emitted to the atmosphere as particles or they can be formed from gas to particle phase transitions. The latter ones are called secondary aerosols. Secondary organic aerosol (SOA) accounts for a significant mass fraction of tropospheric aerosol particles and it originates from the oxidation of volatile organic compounds (VOCs).

The most abundant SOA precursors are isoprene and monoterpenes, such as  $\alpha$ -pinene. The formation of monoterpene-derived SOA has been well explained by oxidation reactions of monoterpenes leading to condensable low-volatility products (Ehn *et al.*, 2014). Such products could then condense onto aerosol surfaces and contribute to SOA formation. Isoprene-derived SOA, however, has been demonstrated to mainly form through acid-catalyzed reactive uptake of isoprene oxidation products (Surratt *et al.*, 2010), underlying that multiphase chemistry also plays an important role in SOA formation.

Atmospheric nitrogen oxides ( $\text{NO}_x$ ) react with peroxy radicals generated in the oxidation of VOCs, forming semi-volatile organic nitrates (ON) in the gas phase that can also significantly contribute to the SOA. Although, the lifetime of ON in the particle phase was recently estimated to be short, due to an efficient hydrolysis of these species (e.g. Lee *et al.*, 2016), a characterization of the products formed as well as the impacts of such processes in SOA formation and aging remain still poorly understood.

In this study, we investigate the importance of acid catalyzed hydrolysis and fate of organic nitrates formed from the ozonolysis of  $\alpha$ -pinene in the presence of  $\text{NO}_x$  and sulfate aerosol of varying acidity under different relative humidity (RH) conditions.

The measurements were conducted in a 2 m<sup>3</sup> Teflon chamber at room temperature. Three RH stages were chosen based on the literature: 1) under “dry” (non-humidified) conditions where the atomized neutral ammonium sulfate (AS) seed particles effloresce and ammonium bisulfate (ABS) has only minor aerosol liquid water content (ALW), 2) at 50% RH when the ALW is approximately equal in both seed types and 3) at 30% RH, when AS seed particles effloresce yet ABS particles still have moderate ALW. The chamber was operated in a steady state mode with a residence time of 50 minutes.  $\alpha$ -pinene, ozone, NO and seed aerosol particles (AS or ABS) were injected with a constant flow rate.

The chemical composition of aerosol particles was characterized with an Aerodyne Long Time-of-Flight

Aerosol Mass Spectrometer (L-ToF-AMS), which is similar to the AMS described previously, but it was carrying an extended ToF-chamber allowing a higher mass resolution. This facilitates better separation of N-containing compounds from other organics. Since the AMS uses flash vaporization (600°C) and a hard ionization technique (electron impact, 70 eV), particulate organic nitrates, for example, are mainly detected as  $\text{NO}^+$  fragments. However, also other N-containing fragments are formed, such as  $\text{C}_x\text{H}_y\text{N}_z^+$ . These fragments will be compared to ON standards.

More detailed chemical composition of the N-containing molecules was obtained with a Filter Inlet for Gases and AEROSOLS (FIGAERO; Lopez-Hilfiker *et al.*, 2014) mounted in front of a Long Time-of-Flight Iodide-Adduct Chemical-Ionization Mass Spectrometer (L-ToF-I-CIMS; Lee *et al.*, 2014). The FIGAERO collects the particles on a filter and heats the sample up to 200°C before introducing it to the CIMS.

In this presentation, the fate of organic nitrates under a wide range of acidities and ALW will be discussed. The abundance of  $\text{C}_x\text{H}_y\text{N}_z^+$  and  $\text{C}_x\text{H}_y\text{N}_z\text{O}_p^+$  fragments under these conditions, as well as the behavior of  $\text{NO}^+$  and  $\text{NO}_2^+$  ion fragments will be presented. In addition, a more detailed analysis of the level of functionalization as well as the evolution of the identified N-containing compounds under the different conditions will be discussed.

This work was supported by the European Research Council (Grant 638703-COALA).

Ehn, M. *et al.* (2014). A large source of low-volatility secondary organic aerosol. *Nature*, **506**, 476–479.

Lee, B. H. *et al.* (2014). An iodide-adduct high-resolution time-of-flight chemical-ionization mass spectrometer: application to atmospheric inorganic and organic compounds. *ES&T*, **48**, 6309–6317.

Lee, B. H. *et al.* (2016). Highly functionalized organic nitrates in the southeast United States: Contribution to secondary organic aerosol and reactive nitrogen budgets. *PNAS*, **113**, 1516–1521.

Lopez-Hilfiker, F. D. *et al.* (2014). A novel method for online analysis of gas and particle composition: description and evaluation of a Filter Inlet for Gases and AEROSOLS (FIGAERO). *AMT*, **7**, 983–1001.

Surratt, J. D. *et al.* (2010). Reactive intermediates revealed in secondary organic aerosol formation from isoprene. *PNAS*, **107**, 6640–6645.

## Impact of Particle Phase Chemistry on Nanoparticle Composition and Growth Rate

Murray Johnston, Peijun Tu, Yue Wu, Michael Apsokardu, Christopher Stangl, Justin Krasmonowitz

Department of Chemistry and Biochemistry, University of Delaware, Newark, Delaware, USA

Keywords: accretion reactions, biogenic secondary organic aerosol, siloxane secondary aerosol, particle growth model.

Presenting author email: mvj@udel.edu

The probability that a newly formed particle in the atmosphere ultimately serves as a cloud condensation nucleus (CCN) depends on the rate and mechanism of particle growth. The growth rate must exceed the loss rate in order to reach a climatically relevant size, and the mechanism by which the particle grows affects its chemical composition, morphology and therefore CCN activity. Small nanoparticles grow primarily by condensation of non-volatile compounds. Processes limited by the amount of available surface area, such as condensation, are favoured in small particles where the surface-to-volume ratio is high.

Particle phase chemistry has the potential to grow larger nanoparticles if it involves the reaction of semi-volatile reactants to form non-volatile products. Molecular partitioning from the gas phase to the particle phase provides a continuous source of reactant molecules to feed the reaction as it proceeds. Processes limited by the amount of available volume, such as particle phase chemistry, are favoured in larger particles where the surface-to-volume ratio is low.

This study assesses the impact of particle phase chemistry on nanoparticle growth and composition through a combination of experimental measurements and kinetic modelling. The results provide direct, molecular evidence for particle phase chemistry and show the impact on composition and growth rate of particles in the 20-100 nm size range.

Nanoparticle formation and growth are performed with a flow tube reactor. Reactants are fed into the flow tube where the point of mixing determines the reaction time. Particles exiting the reactor are size selected and analyzed with a variety of on- and off- line methods. Online elemental analysis is performed with the Nano Aerosol Mass Spectrometer (NAMS). [Klems and Johnston, 2013] Online molecular analysis is performed with Extractive Electrospray Ionization (EESI) [Horan et al., 2012] and/or Droplet Assisted Inlet Ionization (DAII) [Horan et al., 2017]. Offline molecular analysis is performed by collecting particles with a spot sampler (SS) followed by High Resolution Mass Spectrometry (HRMS) [Tu and Johnston, 2016].

The impact of accretion chemistry on particle growth and composition is illustrated in Figure 1 for SOA produced by  $\beta$ -pinene ozonolysis. In this experiment, size-selective particle analysis is performed for SOA produced at a specific time point in the reaction. The oligomer content relative to the total organic content is found to increase approximately linearly with increasing particle size. A linear increase is expected for a volume-limited process such as accretion

chemistry relative to a surface-limited process such as condensation.

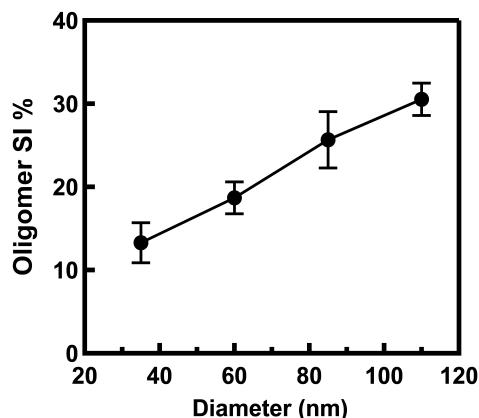


Figure 1: Percentage of total ion signal intensity from oligomers vs. particle diameter for  $\beta$ -pinene SOA.

Other examples will also be presented including dicarbonyl oligomerization and accretion chemistry associated secondary aerosol formation from siloxane oxidation, along with modelling the results. Together, these studies illustrate the potential impact that particle phase chemistry can have on nanoparticle growth and composition, and the particle size range (tens of nanometers) where this chemistry becomes important.

- Hall IV, W.A. and M.V. Johnston (2011) Oligomer Content of  $\alpha$ -Pinene Secondary Organic Aerosol, *Aerosol Science and Technology* **45**, 37-45.
- Horan, A.J., Y. Gao, W.A. Hall IV and M.V. Johnston (2012) Online Characterization of Particles and Gases with an Ambient Electrospray Ionization Source, *Analytical Chemistry* **21**, 9253-9258.
- Horan, A.J., M.J. Apsokardu and M.V. Johnston (2017) Droplet Assisted Inlet Ionization for Online Analysis of Airborne Nanoparticles, *Analytical Chemistry* **89**, 1059-1062.
- Klems, J.P. and M.V. Johnston (2013) Origin and Impact of Particle-to-Particle Variations in Composition Measurements with the Nano Aerosol Mass Spectrometer, *Analytical and Bioanalytical Chemistry* **405**, 6995-7003.
- Tu, P., W.A. Hall IV and M.V. Johnston (2016) Characterization of Highly Oxidized Molecules in Fresh and Aged Biogenic Secondary Organic Aerosol, *Analytical Chemistry* **88**, 4495-4501.

## Biogenic SOA: Chemistry, morphology, and cloud activation at lower to upper tropospheric conditions

C. Mohr<sup>1</sup>, W. Huang<sup>1</sup>, A. Pajunoja<sup>2</sup>, H. Saathoff<sup>1</sup>, A. Virtanen<sup>2</sup>, R. Wagner<sup>1</sup>

<sup>1</sup>Institute of Meteorology and Climate Research, Karlsruhe Institute of Technology, Eggenstein-Leopoldshafen, 76344, Germany

<sup>2</sup>Department of Applied Physics, University of Eastern Finland, Kuopio, 80101, Finland

Keywords: SOA, phase state, chemical composition, CIMS.

Presenting author email: claudia.mohr2@kit.edu

The potential of secondary organic aerosols (SOA) to influence climate via cloud formation has not been established conclusively. One of the many challenges hereby is the temporal and spatial gap between emissions of gaseous precursors, SOA formation, and potential cloud activation. During transport of SOA from the lower troposphere to the upper troposphere, temperature and relative humidity (RH) variations can induce changes in phase state and morphology of the particles, which in turn both influence and are influenced by the particles' chemical properties (Virtanen *et al.*, 2010, Bateman *et al.*, 2016). Little is known about such interactions.

To study the role of chemical composition and phase state on SOA - cloud interactions we performed chamber experiments in the temperature range 208-298 K. We used 2 simulation chambers at the Karlsruhe Institute of Technology (KIT).  $\alpha$ -pinene and limonene SOA was generated by ozonolysis in a 3.7 m<sup>3</sup> stainless steel chamber at room temperature and then transferred into the 84.5 m<sup>3</sup> aluminum chamber AIDA kept at temperatures between 298 and 208 K. For each temperature the RH in AIDA was then gradually increased from ~30% to ~95% followed by droplet or ice cloud formation induced by adiabatic expansion. OH was added to the AIDA chamber via reaction of O<sub>3</sub> with tetramethylethylene. Organic compounds in the gas and particle phases were measured with a Chemical Ionization Mass Spectrometer with a Filter Inlet for Gases and Aerosols (FIGAERO-CIMS) using I<sup>-</sup> as reagent ion (Lopez-Hilfiker *et al.*, 2014, Lee *et al.*, 2013). Viscosity of particles as a function of water uptake was investigated by the Aerosol Bounce Instrument (ABI, Pajunoja *et al.*, 2015).

We observed differences in chemical composition as well as water uptake behavior for organic particles under different temperature and humidity conditions. At room temperature, particle bounce measurements in the ABI indicated irreversible changes in the particles' hygroscopic behaviour with SOA aging (OH addition) and RH increase. At the same time, FIGAERO-CIMS particle-phase data showed a shift towards smaller, higher oxygenated compounds (Fig. 1). With SOA evolution at temperatures below 0°C, no such effects were observed.

The results show the importance of meteorological conditions during SOA processing on their physicochemical properties and consequently their climate effects via cloud formation. We will present

detailed chemical analysis of gas and particle phase components as a function of temperature, RH, and particle phase state and morphology.

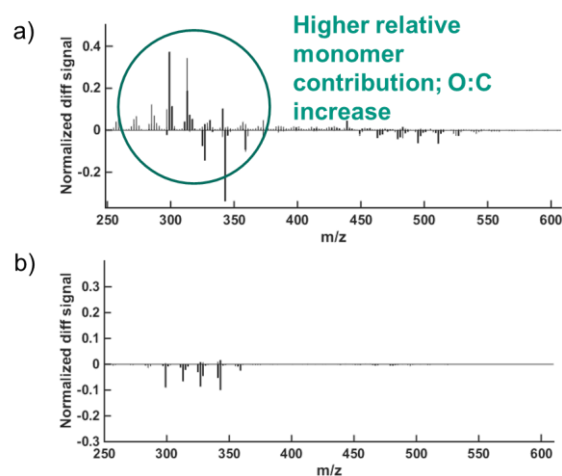


Figure 1. FIGAERO-CIMS difference spectra (after aging/RH increase – before aging/RH increase) at ambient temperature (a) and at 223 K (b).

Virtanen, A., *et al.* (2010) *Nature*, **467**, 824–827.

Bateman, A. P., *et al.* (2016) *Nature Geoscience*, **9**, 34–37.

Lopez-Hilfiker, F. *et al.* (2014) *Atmos. Meas. Tech.* **7**, 983–1001.

Lee, B. *et al.* (2013) *Environ. Sci. Technol.*, **48**, 6309–6317.

Pajunoja, A., *et al.* (2015) *Geophys. Res. Letter*, **42**, 3063–3068.

## Heterogeneous reactivity of pesticide-coated silica particles with OH radicals: influence of the humidity and the nature of particles

C. Mattei<sup>1</sup>, J. Socorro<sup>2</sup>, E. Quivet<sup>1</sup>, N. Marchand<sup>1</sup> and H. Wortham<sup>1</sup>

<sup>1</sup>Aix Marseille Univ, CNRS, Laboratoire de Chimie de l'Environnement, Marseille, France

<sup>2</sup>Department of multiphase chemistry, Max Planck institute for chemistry, Mainz, 55128, Germany

Keywords: Heterogeneous oxidation, kinetics, OH radicals, silica particles, humidity.

Presenting author email: coraline.mattei@etu.univ-amu.fr

Heterogeneous oxidation of semi-volatile organic compounds has an important role in atmospheric processes. Hydroxyl radicals (OH) are known to be one of the major agents for the degradation of atmospheric organic compounds. This work shows the influence of relative humidity on heterogeneous reactions of eight semi-volatile pesticides adsorbed on silica model particles, with OH radicals.

Experiments were realised in a laboratory set up. OH radicals were generated by reaction between ozone and 2,3-dimethyl-2-butene (DMB) and were measured thanks to m-xylene. Relative humidity level, temperature, oxidant concentration and air flow were maintained constant all along the experiments. Conditions were chosen to be as close as possible to real atmospheric conditions.

Current used pesticides (cyprodinil, deltamethrin, difenoconazole, fipronil, oxadiazon, pendimethalin, permethrin, tetraconazole) adsorbed on hydrophilic or hydrophobic silica particles were exposed to OH radicals at relative humidity levels varying from 0 % to 70 %. Second order kinetics constants were calculated. Whatever the experimental conditions, only four pesticides (cyprodinil, deltamethrin, pendimethalin and permethrin) reacted with OH radicals. For some of these degraded pesticides, relative humidity level influences the reactions kinetics.

In the case of deltamethrin adsorbed on hydrophilic silica particles, an increase in relative humidity increases the second order kinetics constants (Figure 1). Similarly, an increase in relative humidity decreases its half-life (half-lives calculated for  $1,5 \cdot 10^6$  molecule.cm<sup>-3</sup>, and exposure time of 12 hours). Results showed however that relative humidity does not always have the same influence on the degradation kinetics of semi-volatile organic compounds.

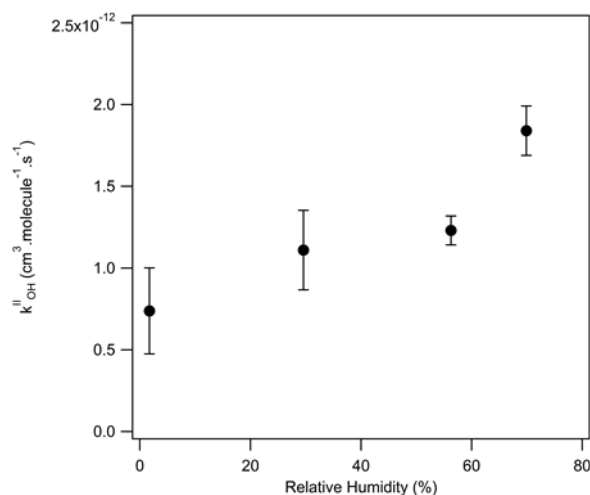


Figure 1. Relative humidity dependence of the kinetics of degradation of deltamethrin adsorbed on hydrophilic silica.

These results could help to have a better understanding of some heterogeneous chemistry processes happening in the atmosphere. They show that relative humidity is a parameter which should be considered when heterogeneous reaction are studied. In addition, this study reveals new aspects concerning the heterogeneous degradation of pesticides in the atmosphere, which is a topic of high environmental and human health concern.

This work was supported by the Ademe and the PACA Region, France.

## Effects of Particle Phase Water on the Heterogeneous OH Oxidation of Aqueous Organic Droplets

M.M. Chim<sup>1</sup>, C. Y. Chow<sup>1</sup>, J. F. Davies<sup>2</sup>, M. N. Chan<sup>1,3\*</sup>

<sup>1</sup>Earth System Science Programme, Faculty of Science, The Chinese University of Hong Kong, China

<sup>2</sup>Chemical Sciences Division, Lawrence Berkeley National Laboratory, Berkeley, USA

<sup>3</sup>The Institute of Environment, Energy and Sustainability, The Chinese University of Hong Kong, China

Keywords: heterogeneous oxidation, organic aerosol, relative humidity, viscosity.

Presenting author email: mnchan@cuhk.edu.hk

Organic aerosols can exist as aqueous droplets, with variable water content depending on their composition and environmental conditions (e.g. relative humidity (RH)). Recent laboratory studies have revealed that oxidation kinetics in highly concentrated droplets can be much slower from those in dilute solutions. However, it remains unclear whether the presence and amount of particle phase water affects the formation of reaction products physically and/or chemically.

In this work, we investigate the role of particle phase water on the heterogeneous chemistry of aqueous organic droplets consisting of 2-methylglutaric acid (2-MGA), measuring the reaction kinetics and the reaction products upon heterogeneous OH oxidation over a range of RH. An atmospheric pressure soft ionization source (Direct Analysis in Real Time, DART) coupled with a high-resolution mass spectrometer is used to obtain real-time molecular information of the reaction products. As shown in Figure 1, aerosol mass spectra show that the same reaction products are formed at all measured RH. At a given reaction extent of the parent 2-MGA, the aerosol composition is independent of RH. These results suggest the particle phase water does not alter reaction mechanisms significantly.

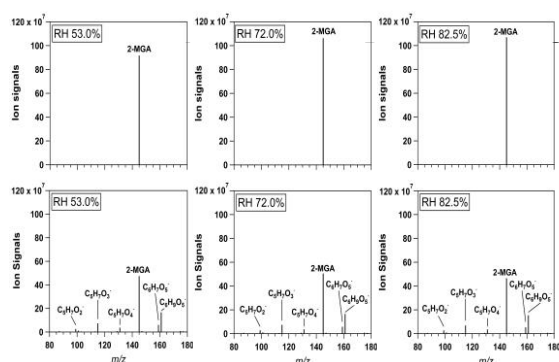


Figure 1: Aerosol mass spectra of the heterogeneous OH oxidation of 2-MGA aerosols at different relative humidity: (a) 53.0%, (b) 72.0% and (c) 82.5% before (upper row) and after (lower row) oxidation.

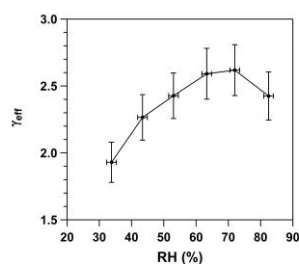


Figure 2: Effective OH uptake coefficient ( $\gamma_{\text{eff}}$ ) are plotted against different relative humidity, ranging from 33.8% to 82.5%, for the heterogeneous OH oxidation of 2-MGA aerosols.

Kinetic measurements, as shown in Figure 2, reveal that the effective OH uptake coefficient,  $\gamma_{\text{eff}}$ , decreases with decreasing RH below 72%. Isotopic exchange measurements performed using an aerosol optical tweezers reveal water diffusion coefficients in the 2-MGA droplets to be  $3.0 \times 10^{-13}$  to  $8.0 \times 10^{-13} \text{ m}^2 \text{ s}^{-1}$  over the RH range of 47% to 58%. These values are comparable to that of other viscous organic aerosols (e.g. citric acid), indicating that 2-MGA droplets are likely to be viscous at low humidity. Smaller  $\gamma_{\text{eff}}$  at low RH is likely attributed to the slower diffusion of reactants within the droplets. Overall, the observed relationship between the  $\gamma_{\text{eff}}$  and RH are likely attributed to changes in aerosol viscosity rather than changes in reaction mechanisms.

M. M. Chim, C. Y. Chow, and M. N. Chan are supported by the Direct Grant for Research (4053089) and One-Time Funding Allocation of Direct Grant (3132765), The Chinese University of Hong Kong. J. F. Davies is supported by the Department of Energy, Office of Science Early Career Award and the Director, Office of Energy Research, Office of Basic Energy Sciences, Chemical Sciences, Geosciences, and Biosciences Division of the U.S. Department of Energy under Contract No. DE-AC02-05CH11231.

## **Abstracts T302**

## A novel fully automated aerosol particle mass spectrometer combining laser ablation and flash vaporization techniques: Design and first aircraft measurements

A. Hünig<sup>1</sup>, O. Appel<sup>2</sup>, A.M. Batenburg<sup>1</sup>, A. Dragoneas<sup>1</sup>, S. Molleker<sup>2</sup> and S. Borrmann<sup>1,2</sup>

<sup>1</sup>Institute for Atmospheric Physics, Johannes Gutenberg University, Mainz, 55128, Germany

<sup>2</sup>Particle Chemistry Department, Max Planck Institute for Chemistry, Mainz, 55128, Germany

Keywords: Aerosol Mass Spectrometer (AMS), single particle laser ablation mass spectrometer.

Presenting author email: a.huenig@mpic.de

Important and largely unexplored aerosol features at tropical high altitudes are the Asian Tropopause Aerosol Layer (ATAL; Vernier *et al.*, 2011) and the “particle layer” near the tropical tropopause in Brazil, West Africa, and Northern Australia (Borrmann *et al.*, 2010). This is in particular the case for the particle chemical composition.

For the in-situ, online, direct reading chemical analysis of aerosol particles, two main types of (airborne) mass spectrometers currently exist. One uses a pulsed laser to vaporize and ionize submicron to micrometer sized single particles before injection into the mass spectrometer (e.g., Brands *et al.*, 2010). The other uses thermal vaporization and electron impact ionization (AMS; e.g. Drewnick *et al.*, 2005) to analyze small particle ensembles with sizes starting at 20 nm. The instrument we present here, the ERICA, is a “hybrid” instrument adopting both techniques to obtain complementary information (Figure 1).

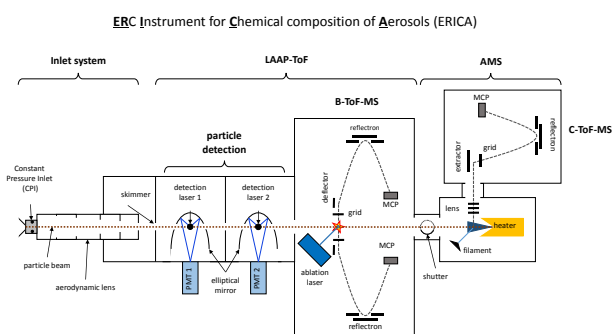


Figure 1. Instrument layout of ERICA.

After being focused by an aerodynamic lens the particles of around 80 nm to 2  $\mu\text{m}$  first enter a laser ablation mass spectrometer, which is a thorough in-house modification of the LAAPTOF by AeroMegt. Particles detected by two laser light scattering units are vaporized and ionized by a pulsed quadrupled Nd:YAG laser. The ions are then measured by a Bipolar Time-of-Flight Mass Spectrometer (B-ToF-MS). Particles too small for the laser detection or particles which are missed by the Nd:YAG ablation laser continue their travel “downstream” to the AMS-like segment of the instrument. Here they are flash-vaporized on a heated tungsten surface, ionized by electron impact with the resulting ions guided into a Compact Time-of-Flight MS (TOFWERK). The instrument was assembled to the required dimensions and automated for fully autonomous

operation on the single seated Russian M-55 “Geophysica” high altitude aircraft.

The first field deployment of ERICA took place in Kalamata, Greece, in August – September 2016. During this campaign a continuous data set with both ERICA components was successfully acquired covering altitudes from the ground up to 20 km. Figure 2 exemplifies the cation (A) and anion (B) spectrum of a single particle which shows typical soot-like fragments. It was sampled at approx. 17 km altitude during ERICA’s “maiden flight”. AMS time series of non-refractory compounds showed the dominant presence of organic and sulphate, as depicted in Figure 2C. This provides complementary information on the chemical composition and mixing state of the sampled aerosol particles within one single instrument, which is of value for a wide range of applications.

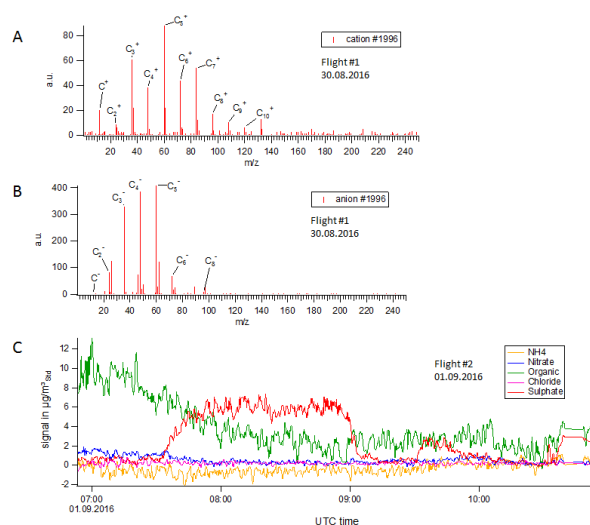


Figure 2. Example single particle mass spectrum and the AMS time series obtained during the second flight (C).

This work is supported by the ERC Advanced Research Grant No. 321040 of the EU’s Seventh Framework Programme.

Borrmann, S., *et al.* (2010), *Atmos. Chem. Phys.*, **10**, 5573–5592, doi:10.5194/acp-10-5573-2010

Brands, M., *et al.* (2011), *Aerosol Sci. Technol.*, **45**, 46–64, doi: 10.1080/02786826.2010.517813

Drewnick, F., *et al.* (2005), *Aerosol Sci. Technol.*, **39**, 637–658, doi: 10.1080/02786820500182040

Vernier, J.- *et al.* (2011), *Geophys. Res. Lett.*, **38**, L07804, doi:10.1029/2010GL046614

## Estimation of the ratio of aerosol to molecular backscattering by two closely disposed wavelengths using CuBr LIDAR sounding (510.6nm, 578.2nm)

I. V. Grigorov, D. V. Stoyanov and G. V. Kolarov

Institute of Electronics at Bulgarian Academy of Sciences, 1784-Sofia, Bulgaria

Keywords: remote sensing, lidar, aerosol backscatter coefficient

Presenting author email: [ivangr@ie.bas.bg](mailto:ivangr@ie.bas.bg)

In this work we continue our studies on a new algorithm of lidar data processing, developed in order to estimate the atmospheric backscatter ratio  $\beta_a(h)/\beta_m(h)$  (aerosol to molecular backscatter coefficients), using data of lidar sounding at two closely disposed wavelengths  $\lambda_1=510.6$  nm and  $\lambda_2=578.2$  nm of a CuBr-laser. The spectral distance between these wavelengths provides well-distinguished molecular scattering signals. On the other hand both wavelengths are too close to accept similarity in the aerosol scattering conditions in the first order of approximation. Both lidar channels have similar technical parameters (as overlapping functions, photon detector sensitivity, optical transmission, etc.). They provide similar behaviour of the output signal levels for the detected wavelengths.

The developed mathematical apparatus is based on calculating the ratio  $R(h)$  of both attenuated lidar signal profiles, but normalized respectively by the values of lidar signal from the near region (at  $h = h_0$ ).

$$R(h) = \left[ \frac{S_{\lambda_2}(h)}{S_{\lambda_2}^0(h_0)} \right] / \left[ \frac{S_{\lambda_1}(h)}{S_{\lambda_1}^0(h_0)} \right]$$

Having in mind that  $S_{\lambda_{1,2}} = C_{1,2} [\beta_{a_{1,2}}(h) + \beta_{m_{1,2}}(h)] T_{1,2}(h)$ , (where the indexes 1 and 2 correspond to  $\lambda_1$  and  $\lambda_2$ ) we show in this study a transformation of the ratio  $R(h)$  to display its dependency from three parameters: the ratio of the transparency of the atmosphere  $F(h) \sim [T_2(h)/T_1(h)]$ , the ratio of aerosol backscatter coefficients  $\mu(k) \sim \beta_{a_2}(h)/\beta_{a_1}(h) \sim (\lambda_1/\lambda_2)^k$  and the ratio of molecular backscatter coefficients  $\alpha \sim \beta_{m_2}/\beta_{m_1}$ , measured for both laser wavelength. Finally an analytical equation is issued for to calculate the atmospheric backscatter ratio  $\frac{\beta_{a_1}(h)}{\beta_{m_1}(h)} = \frac{R(h) - \alpha F(h)}{\mu(k)F(h) - R(h)}$ .

Further in this work is performed a comparison with backscatter ratio profiles, calculated by using real data of lidar measurements and widely applicable in practice inversion method of Klett-Fernald. In the comparison the coefficient  $\mu(k)$  was used as variable parameter. According to the literature data, for different

types of aerosol the factor  $k$  can vary within the range  $0.57 \leq k \leq 1.8$ . Correspondingly  $\mu(k)$  takes values within the range from 1 to 0.8. We calculated the atmospheric backscatter ratio  $\beta_a(h)/\beta_m(h)$  by the proposed method at different values of  $\mu(k)$  to see how it coincides with the backscatter ratio determined by applying Klett-Fernald method for to calculate atmospheric backscatter coefficient. In Figure 1 we presented the results of such comparison for the data of lidar measurement made on August 18, 2014. It is evident that, at altitudes above 3 km, the coincidence between the backscatter ratio profiles, calculated by the two methods was quite good.

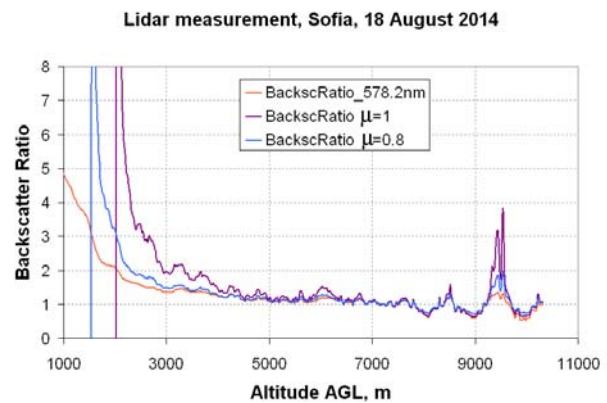


Figure 1. Comparison of the atmospheric backscatter ratio profiles, calculated by two methods.

The results of this analysis of experimental data demonstrated the opportunity to detect and process lidar signal profiles at two closely disposed wavelengths in order to determine atmospheric aerosol backscatter coefficient profile, skipping the use of Klett-Fernald inversion procedure.

This study has received funding from the European Union's Horizon 2020 research and innovation programme under grant agreement No 654109 (ACTRIS-2 project).

## In-situ characterization of aerosol nanoparticles at close-to-ambient conditions by small angle x-ray scattering (SAXS)

Paulus S. Bauer<sup>1</sup>, H. Amenitsch<sup>2</sup> and Paul M. Winkler<sup>1</sup>

<sup>1</sup> Faculty of Physics, University of Vienna, 1090 Vienna, Austria

<sup>2</sup> Institute of Inorganic Chemistry, Graz University of Technology, 8010 Graz, Austria

Keywords: in-situ, nanoparticle characterization, SAXS, helium.

Presenting author email: paulus.bauer@univie.ac.at

A main task in aerosol science is the measurement of airborne particles. Especially the analysis of nanoparticles in the range between 1nm to 50nm requires particular attention, since they cannot be observed with visible light anymore. To determine the size and number concentration of aerosol nanoparticles Differential Mobility Particle Sizer (DMPS) and Condensation Particle Counter (CPC) are mostly used. A common drawback of these techniques is that they extract the aerosol particles from their original environment. Thereby, nanoparticles can get modified or get lost e.g. by wall collisions inside the instrument, which can affect the measured size distribution and concentration (Wang et al., 2002).

Hence, an in-situ measurement technique can overcome these shortcomings of the conventional aerosol instruments. Small-angle X-ray scattering (SAXS) is capable to measure in-situ particle size distribution in the nanometer range and has already been applied in nucleation studies with extremely high nanoparticle concentrations of  $\sim 10^{12}/\text{cc}$  and carrier gas pressures  $\sim 2$  kPa (Laksmono et al., 2011). In order to compare the in-situ SAXS results to the DMPS and CPC measurements it is important to choose system settings as close to ambient conditions as possible.

Here we report experiments conducted at the SAXS beamline at the Elettra synchrotron near Trieste. We have chosen this beamline due to high beam intensity and the available experience on aerosol studies in flow tubes (Jungnikl et al., 2011). To provide a representative environment a flow tube operated under ambient pressure, temperature and particle concentrations was used. Figure 1 shows a schematic of the flow tube setup at the ELETTRA synchrotron.

The scattered intensity depends on the electron density of the particles. Therefore tungsten particles with a high electron density were used and generated by a hot-wire-generator. A critical issue for SAXS experiments is the background scattering signal originating from air. The background is almost as large as the signal from the tungsten particles. This was resolved by the use of helium as carrier gas. The advantage of helium is the operation under ambient conditions (temperature, pressure), which allows the usage of modified state-of-the-art aerosol instruments like CPC and DMPS system.

Due to the low background of helium and the high electron density of tungsten particles we obtained defined signals from aerosol SAXS measurements. Thereby a comparison between in-situ results to conventional measurement techniques can be achieved.

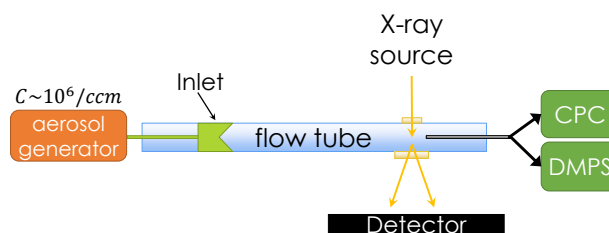


Figure 1. Schematic of the setup at the SAXS beamline at ELETTRA synchrotron near Trieste.

This work was supported by the European Research Council under the European Community's Seventh Framework Programme (FP7/2007-2013) / ERC grant agreement No. 616075.

Laksmono, H. et al. (2011). *Phys. Chem. Chem. Phys.* 13, 5855.

Jungnikl, K., et al. (2011). *Aerosol Sci. Technol.* 45, 7, 805.

Wang, J. et al. (2002). *J. Aerosol Sci.* 33, 6, 843

## The effect of sheath flow rate on the particle trajectory inside an optical cavity with direct flow configuration

Haneol Lee<sup>1</sup>, Young-Su Jeong<sup>2</sup>, Kibong Choi<sup>2</sup> and Weon Gyu Shin<sup>1</sup>

<sup>1</sup>Department of Mechanical Engineering, Chungnam National University, Daejeon, 34134, South Korea

<sup>2</sup>Agency for Defense Development, Daejeon, 34186, South Korea

Keywords: sheath flow, particle residence time, particle tracking, computational fluid dynamics.

Presenting author email: wgshin@cnu.ac.kr

Airborne microorganisms such as viruses, bacteria, and fungal spores can cause harmful health effects for people and the major size of these particles is known to be 1 - 10  $\mu\text{m}$  (Primmerman 2000; Kim *et al.* 2013; Kang *et al.* 2014). Since these particles are barely detectable by human senses, it is essential to develop a device that can measure these particles quickly and accurately. It is important to optimize the internal flow path for the development of such equipment, but there is not much research related to it.

In this study, we performed numerical simulations to optimize flow field around nozzles inside an optical cavity when the direct flow configuration was used. Also we numerically investigated the effect of sheath flow rate on the performance parameters such as particle residence time, particle beam width, particles loss rate by obtaining particle trajectories of 1 to 10  $\mu\text{m}$ .

In the present study, 3-dimensional steady state numerical simulations have been carried out with the commercial Computational Fluid Dynamics (CFD) code ANSYS Fluent 15.0 solver. In our simulations, the  $Re$  at the exit of the upper nozzle was greater than 2000 and thus turbulent flow was assumed. In order to describe turbulent flow field, we used the realizable  $k$ - $\epsilon$  turbulence model. After calculating the flow field, Discrete Phase Model (DPM) in Fluent was used to calculate particle trajectories. Also, in order to investigate the dispersion of particles caused by turbulence in exit of the upper nozzle, the stochastic tracking model called Discrete Random Walk (DRW) model was used.

Figure 1 shows velocity flow field in the measurement region. The flow around the nozzle dispersed into the chamber when sheath flow was not used. In contrast, when sheath flow was used, sheath flow prevent aerosol flow from dispersing inside the chamber.

In summary, we conducted numerical simulation to investigate the effects of sheath flow on the particle in order to optimize flow field around nozzles inside an optical cavity when direct flow configuration is applied. Simulation results show the particle loss rate and the residence time of particles can change according to the sheath flow rate. Therefore, in the design of particle detection devices, it is important to consider the influence of the sheath flow using numerical simulations.

This work was supported by Agency for Defense Development under the contract UD140072ID.

Kang, J. S., Lee, K. S., Kim, S. S., Bae, G.-N., Jung, J. H. (2014). *Lab Chip* **14**,244-251.

Kim, K.-H., Jahan, S. A., Kabir, E. (2013). *Environ. Int.* **59**, 41-52.

Primmerman, C. A. (2000). *Linc. Lab. J.* **12**, 3-32.

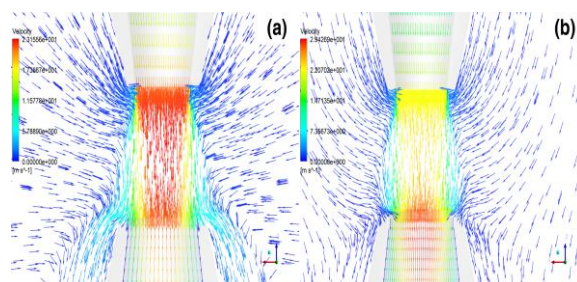


Figure 1. Velocity flow field inside the measurement region: (a) without sheath flow (b) with sheath flow.

## Generation of Monodisperse Particles Using Inkjet Aerosol Generator

Woo Jin Shin<sup>1</sup>, Haneol Lee<sup>1</sup>, Young-Su Jeong<sup>2</sup>, Kibong Choi<sup>2</sup> and Weon Gyu Shin<sup>1</sup>

<sup>1</sup>Department of Mechanical Engineering, Chungnam National University, Daejeon, 34134, South Korea

<sup>2</sup>Agency for Defense Development, Daejeon, 34186, South Korea

Keywords: inkjet aerosol generator, Polystyrene latex (PSL), Drying module, Aerosol

Presenting author email: wgshin@cnu.ac.kr

As biological detection instruments become more sophisticated, there is need for more sophisticated and advanced aerosol generator to test those instruments. The inkjet technology has been used to generate highly monodisperse aerosol particles with the size range from sub-micrometer to super-micrometer. Inkjet technology has advantages for controlling droplet size and droplet generation rate precisely (Iida et al. 2014).

In previous studies, the mass concentration of the solute in the solution was adjusted to control the size of the generated aerosol particles in inkjet aerosol generator (Bottiger et al. 1988; Iida et al. 2014). Particle concentration in an aqueous suspension does not need to be adjusted precisely. It is difficult to know beforehand what solute (or particle) concentration in the aqueous suspension exactly generates the size seen by the particle sizing instrument.

In this study, we aimed to control the size of generated aerosol particles by adjusting waveform parameters instead of adjusting the mass concentration of the solution (Shin et al. 2015). The inkjet aerosol generator consists of an inkjet nozzle system and a drying module. The inkjet nozzle system was used to generate size controlled inkjet droplets and the drying module was developed to rapidly turn droplets into fully dried aerosol particles. Figure 1 shows inkjet system which used in our experiment.

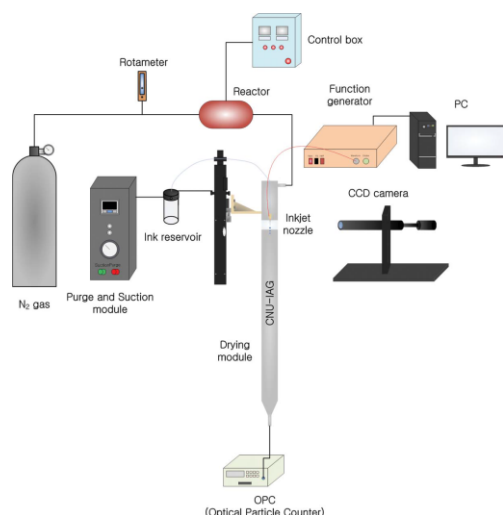


Figure 1. Schematic diagram of experiment set-up.

When droplets have the size range of 30 to 70  $\mu\text{m}$  in diameter, aerosol particles with the size range of 3.5 to 7.1  $\mu\text{m}$  were generated after the drying process.

We controlled the particle size easily within a factor of two by adjusting rising/falling time and voltages of an actuating waveform. Generated particles were shown to have a narrow particle size distribution. Figure 2 shows the particle size distribution after evaporation of droplets with the initial size of 65  $\mu\text{m}$  droplets. After complete evaporation, about 4  $\mu\text{m}$  monodisperse particles were generated.

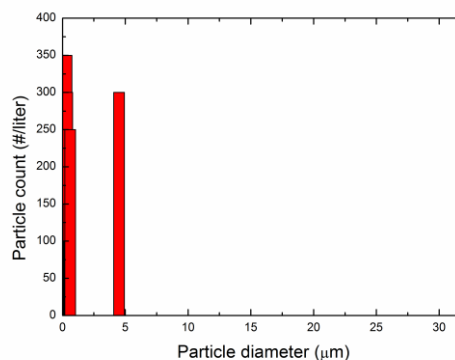


Figure 2. Particle size distribution after evaporation of 65  $\mu\text{m}$  size droplet

In summary, inkjet aerosol generator was developed to generate monodisperse aerosol particles in the size range from 2.5 to 7.0  $\mu\text{m}$ . The particle generation efficiency was measured to be 45 – 95 %.

This work was supported by Agency for Defense Development (ADD-13-02-06-03)

Bottiger, J. R., Deluca, P. J., Stuebing, E. W., and Vanreenen, D. R. (1998) *J. Aerosol Sci.* **29**, 965–966.  
Iida, K., Sakurai, H., Saito, K., and Ehara, K. (2014) *Aerosol Sci. Technol.* **48**, 789–802.  
W. J. Shin, Y. S. Jeong, K. Choi, W. G. Shin (2015). *Aerosol Sci. Technol.* **49**, 1256-1262.

## Coupling of an electrodynamic balance with mass spectrometry as a platform for atmospheric chemistry research

A.W. Birdsall<sup>1</sup>, U.K. Krieger<sup>2</sup> and F.N. Keutsch<sup>1,3</sup>

<sup>1</sup>Department of Chemistry and Chemical Biology, Harvard University, Cambridge, MA, 02138, U.S.A.

<sup>2</sup>Institute for Atmospheric and Climate Science, ETH Zürich, Zürich, CH-8092, Switzerland

<sup>3</sup>School of Engineering and Applied Sciences, Harvard University, Cambridge, MA, 02138, U.S.A.

Keywords: atmospheric chemistry, electrodynamic balance, mass spectrometry, instrument development

Presenting author email: abirdsall@g.harvard.edu

The use of a droplet levitation device, such as an electrodynamic balance (EDB), to suspend single aerosol droplets in a laboratory setting is an attractive platform for performing atmospheric chemistry research. Laboratory control of aerosol composition allows isolation and careful study of particular physical or chemical processes of interest. Stably trapping a droplet enables tracking the changes of a single droplet on the timescale of an aerosol particle's multiday lifetime in the atmosphere. The use of a suspended aerosol particle allows for a more realistic look at the interplay of chemical and physical processes that can govern such processes as multiphase reactions, phase partitioning, or surface-mediated reactions, compared to laboratory experiments performed in the bulk condensed phase.

Considerable atmospherically-relevant research with levitated droplets has been conducted using optical detection techniques (e.g., Krieger *et al.*, 2012). However, coupling a droplet levitation instrument with an analytical technique with better specificity at identifying individual chemical components is necessary to study more chemically complex systems. Mass spectrometry is an attractive analytical technique in this respect. Previous attempts to couple a trapped droplet to mass spectrometry in an online fashion have been limited, and focused on acoustic levitation of the droplet (Crawford *et al.*, 2016; Warschat *et al.*, 2015; Westphall *et al.*, 2008).

In this work, an EDB has been coupled with a commercial time-of-flight mass spectrometer and custom-built ionization source as a platform for atmospheric chemistry research. A charged droplet (typical size 5-10  $\mu\text{m}$ ) is injected into the EDB using a commercial inkjet printer cartridge. The droplet is levitated for an arbitrarily long amount of time in an electric field within the trap, surrounded by a gas phase whose composition, including relative humidity, can be controlled. Once it is time for the droplet to be analysed, a combination of gas flow and modification to the electric field transfers the droplet to an ionization region, within which analyte molecules are volatilized on a heated surface and ionized with a corona discharge, and subsequently enter the mass spectrometer for analysis. The sensitivity of this technique is more than sufficient for mass spectral analysis of a single particle in this size range (Figure 1). The temporal evolution of an aerosol particle of a particular composition is determined by analysing a series of particles of the same composition

that reside in the trap for a varying amount of time before mass spectrometric analysis, in a boxcar fashion.

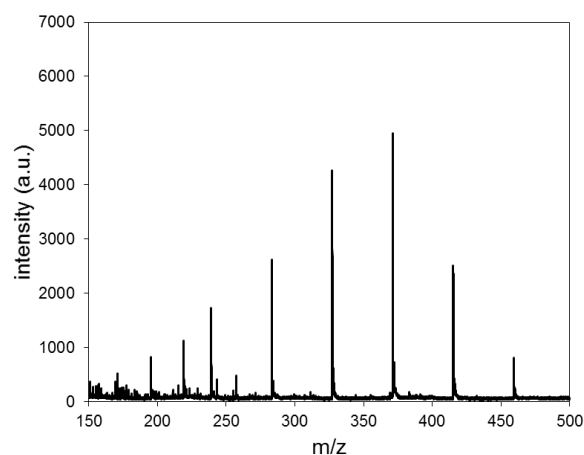


Figure 1. Sample mass spectrum of a single particle generated from a solution of polyethylene glycol-400 in water (30 wt. %) and ionized with the custom-built ionization source.

The analytical characteristics of this system have been determined. The utility of this system has been demonstrated with an experiment in which the differential gas-phase loss timescales have been measured for a droplet containing a family of model compounds.

Crawford, E., Esen, C. and Volmer, D. (2016) *Anal. Chem.* **88**, 8396–8403.

Krieger, U., Marcolli, C. and Reid, J. (2012) *Chem. Soc. Rev.* **41**, 6631–6662.

Warschat, C., Stindt, A., Panne, U. and Riedel, J. (2015) *Anal. Chem.* **87**, 8323–8327.

Westphall, M., Jorabchi, K. and Smith, L. (2008) *Anal. Chem.* **80**, 5847–5853.

## Design and Performance of a Commercially Available Tandem Drift Tube Ion Mobility Spectrometer and Fast Response Condensation Particle Counter

D.R. Oberreit<sup>1</sup>, D.T. Buckley<sup>2</sup> and C.J. Hogan<sup>2</sup>

<sup>1</sup>Kanomax FMT, Inc., White Bear Lake, MN, 55110, USA

<sup>2</sup>Department of Mechanical Engineering, University of Minnesota, Minneapolis, MN 55455, USA

Keywords: instrumentation, electrical mobility, condensation particle counter, aerosol measurement.

Presenting author email: derek.oberreit@kanomaxfmt.com

Electrical mobility based measurements of aerosol particle size distributions at atmospheric pressures have historically utilized devices that spatially distribute aerosol particles based on their electrical mobility (e.g. differential mobility analyzers). These devices are designed such that aerosol particles of a given electrical mobility follow a prescribed trajectory within the device where the termination location consists of a flow conduit (Knutson & Whitby 1975), an electrode (Biskos et al. 2005), or an optical inspection volume (Kulkarni & Wang 2006). The electrical mobility resolution for devices utilizing spatial separation is limited by the ratio of aerosol flow to separation gas flow as well as the sensor area (in the case of electrode and optical terminations). Additionally, the resolution of these devices degrades with decreasing particle size due to the increased diffusivity of small particles. Drift tube type ion mobility devices are able to achieve high resolution discrimination of electrical mobilities with size independent diffusion broadening; however, these devices have typically been applied to measurement of large molecules at concentrations above what is found in typical aerosols. These limitations have been addressed in the development of a drift tube ion mobility spectrometer which utilizes an aspirating condensation particle counter to overcome the concentration limits of typical electrode based drift tube spectrometer detectors. This work describes the design and performance of a commercially available drift tube ion mobility spectrometer system for aerosol particle size distribution measurements.

The Drift Tube Ion Mobility Spectrometer (DTIMS) for aerosol analysis described here consists of a Kanomax Model 3670 Drift Tube (see Figure 1), and a Kanomax Model 3650 fast condensation particle counter (CPC).

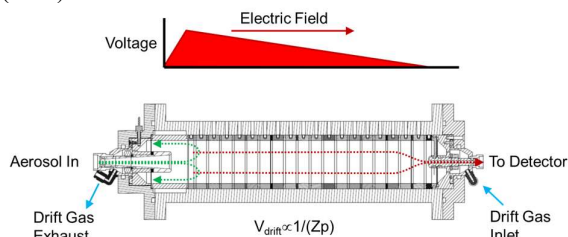


Figure 1: Drift Tube Ion Mobility Spectrometer Schematic

Prior to analysis, the electric field is disabled allowing particles to advectively enter a defined aerosol sample volume. At the start of the analysis, an axial electric field is applied and charged particles traverse the drift cell at a

velocity proportional to their electrical mobility,  $Zp$ . The particle concentration at the end of the drift region is measured by a CPC. The particle size distribution can then be calculated from the particle concentration relative to the onset of the electric field.

The theoretical resolution,  $Zp/\Delta Zp$ , of the DTIMS is primarily driven by the ratio of drift length to axial aerosol sample volume length. For the drift tube described here the length ratio is  $\sim 20$ , which is typically much higher than the mobility distribution width for species within an aerosol particle size distribution. The theoretical resolution is reduced with increased drift times due to diffusion broadening as well as the velocity distribution of the counter flow drift gas (which is required to define the aerosol sample volume). Therefore, it is advantageous to utilize high electric fields to minimize drift times.

The shortest practical drift time for a DTIMS (for a given electrical mobility) is limited by the time constant of the CPC. For this system, a fast CPC was developed with a time constant near 20 ms, which minimizes detector driven temporal smearing (see Figure 2).

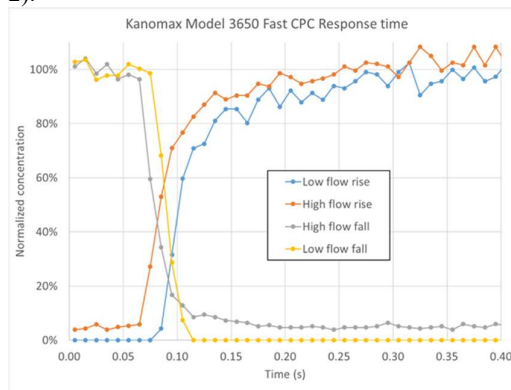


Figure 2: Fast CPC response times

Additionally, the Model 3650 CPC is designed with a 50% detection efficiency near 1.9 nm to capitalize on the benefits of the DTIMS technology for small particle analysis.

Biskos, G., Reavell, K. & Collings, N. (2005) *Aerosol Science and Technology* 39:527-541.

Knutson, E. O. & Whitby, K. T. (1975) *Journal of Aerosol Science* 6:443-451.

Kulkarni, P. & Wang, J. (2006) *Journal of Aerosol Science* 37:1303-1325.

## The PINQ: A novel instrument for the rapid quantification of PM oxidative potential

R.A. Brown<sup>1</sup>, S. Stevanovic<sup>1</sup>, N.K. Gali<sup>2</sup>, Z. Ning<sup>2</sup>, Z. Ristovski<sup>1</sup>

<sup>1</sup>International Laboratory for Air Health and Quality, Queensland University of Technology, Brisbane, 4001, Australia

<sup>2</sup>School of Energy and Environment, City University of Hong Kong, Kowloon, Hong Kong SAR

Keywords: oxidative potential, reactive oxygen species, profluorescent nitroxide

Presenting author email: reece.brown@hdr.qut.edu.au

Worldwide, the WHO has found atmospheric pollution responsible for more than 7 million premature deaths each year. A large contributor to this increased mortality is atmospheric particulate matter (PM), with PM being linked to lung cancer, cardiovascular disease, and lung disease. A proposed mechanism to explain this link is oxidative stress (Ristovski et al. 2012), wherein PM generated through combustion processes introduce a group of free radicals known as reactive oxygen species (ROS) to cells when inhaled. These ROS impede cell function creating oxidative stress, which can lead to inflammation and cell death.

To investigate this hypothesis, instrumentation to accurately measure the ROS content (oxidative potential) of PM is essential. The ideal system should be: sensitive to a wide range of species; collect ultrafine PM with high efficiency; and collect and measure rapidly. Several systems have been developed to address this, using both commercially available and in-house designed instrumentation coupled with either the DCFH-DA or DTT probes (Fuller et al. 2014). These systems are limited in effectiveness by probe reaction times, time resolution, sensitivity, and ease of use. The purpose of this research is to create a superior novel instrument to continuously collect ultrafine PM for ROS quantification using the BPEAnit profluorescent nitroxide probe (Stevanovic et al. 2012).

The particle into nitroxide quencher (PINQ) is an instrument which collects PM into a solution of BPEAnit in dimethyl sulfoxide (DMSO) for oxidative potential measurements; independent of particle size and solubility. The design is a steam collection device, in which the sample aerosol is mixed with water vapour to create a supersaturated mixture. Ultrafine particles in this mixture undergo condensational growth, growing them to a size at which they can be efficiently collected. The grown particles are continuously collected directly into a standing liquid vortex of BPEAnit in DMSO, regardless of particle solubility. This is possible due to a novel solvent-resistant Teflon-aluminium composite vortex collector, which is based on a design previously described in literature (Orsini et al. 2008). The collected sample is continuously removed from the base of the vortex collector.



Figure 1. 3D Rendering of the PINQ System

Laboratory testing of the PINQ indicates that it is capable of collecting insoluble ultrafine PM into solution for oxidative potential analysis with a very high efficiency. The sample reaction with the BPEAnit probe is diffusion limited; therefore the sample liquid exiting the vortex collector is fully reacted and ready for fluorescence analysis. This rapid high efficiency sample collection and analysis minimizes potential underestimations, and provides the potential for real-time applications when coupled with a flow through fluorimeter.

Data will be presented on: size dependent collection efficiencies; measurements of diesel emissions for different fuels and engine load conditions; and continuous diurnal profiles of ambient ROS concentrations.

Fuller, S.J. et al., 2014. Comparison of on-line and off-line methods to quantify reactive oxygen species (ROS) in atmospheric aerosols. *Atmospheric Environment*, 92, pp.97–103.

Orsini, D. a. et al., 2008. A Water Cyclone to Preserve Insoluble Aerosols in Liquid Flow - An Interface to Flow Cytometry to Detect Airborne Nucleic Acid. *Aerosol Science and Technology*, 42(5), pp.343–356.

Ristovski, Z.D. et al., 2012. Respiratory health effects of diesel particulate matter. *Respirology (Carlton, Vic.)*, 17(2), pp.201–212.

Stevanovic, S. et al., 2012. The use of a nitroxide probe in DMSO to capture free radicals in particulate pollution. *European Journal of Organic Chemistry*, (30), pp.5908–5912.

## Smart Air Quality Network, the measurement network for the future

V. Ziegler<sup>1</sup>, Michael Beigl<sup>2</sup>, Matthias Budde<sup>2</sup>, Josef Cyrus<sup>3</sup>, Stefan Emeis<sup>4</sup>, Thomas Gratza<sup>7</sup>, Hans Grimm<sup>6</sup>, M. Pesch<sup>1</sup>, Andreas Philipp<sup>5</sup>, Till Riedel<sup>2</sup>, Klaus Schäfer<sup>4</sup>, Jürgen Schnelle-Kreis<sup>3</sup>

<sup>1</sup> GRIMM Aerosol Technik Ainring GmbH & CO.KG, Germany; <sup>2</sup> Karlsruhe Institute of Technology, TECO; <sup>3</sup> German Research Center for Environmental Health, Helmholtz Zentrum München (HMGU); <sup>4</sup> Karlsruhe Institute of Technology, Institute of Meteorology and Climate Research, Department Atmospheric Environmental Research, (IMK-IFU); <sup>5</sup> Institute of Geography, University of Augsburg; <sup>6</sup> Aerosol Akademie,e.V.; <sup>7</sup> Umweltamt, Stadt Augsburg

Keywords: Alternative Measurement Network, Instrumentation, Low Cost Sensor, Algorithm  
Presenting author email: vz@grimm-aerosol.com

Air Quality and with this, subjective and health related life quality, is one of the biggest topics of modern cities and developing countries in our time. For many regions and cities it is difficult to take action regarding air quality in mobility, residential or working areas, because there is no fine-meshed and profound database available for making right decisions in time.

Although the required basic data as well as the measurement principles would be available, a proper platform for connection, combination and evaluation of measurement data to get profound decisions is still missing.

SmartAirQualityNetwork shall be a very pragmatic and data driven attempt in which all available data will be combined with mobile measurements to an integrated measurement strategy for the first time. With the connection and combination of open data sources as meteorological data as well as research data about air pollution levels, city development plans, remote sensing data about influencing factors as mixing layer heights, comprehensive coverage with ultra-low-cost-Sensors, “scientific scouts”, demand-oriented usage of UAVs together with methods of real-time-modelling and analyzing, a new measurement and analyzing concept will be developed.



**Fig.1:** Different measurement technologies and air pollution sources will be combined via a new platform and modelling concept using efficient algorithms getting valuable information to develop valuable measures against pollution levels.

In the test region of Augsburg (Bavaria, Germany), the intension is, to establish a prototype of a measurement network 2.0 using IoT-Methods and analytics of big data that will be able to be scaled and multiplied to any other region.

The main target is to give new real time information that can be used for several in-time actions and measures based on air pollution levels as alternative routing in navigation systems. High polluted zones and traffic control activities in order to reduce traffic and pollution levels as well as to inform people via mobile apps about pollution levels will be given and recommendations for actions and valuable information for clean air strategies will be developed.



**Fig.2:** Based on a central Data Cloud, important information will be available for navigation systems, traffic control systems or apps to inform the public in-time.

Beside a broad awareness of possible influencing factors to the public as well as for decision makers, it will provide a broad database for controlling an increased individual mobility, alternative mobility concepts and development of new traffic control systems.

### References & pictures

GRIMM Aerosol Ainring GmbH & CO.KG, Wikimedia Commons, University of Augsburg, KIT-TECO, Open Street Map, World Air Quality

### Project Partners:



### Founding:



## A state of the art device for continuous unattended measurements of ultrafine particles

M. Pesch<sup>1</sup>, V. Ziegler<sup>2</sup>, F. Tettich<sup>2</sup>, W. Frenzel<sup>3</sup>

<sup>1</sup> Grimm Aerosol Technik Pouch GmbH, Germany

<sup>2</sup> Grimm Aerosol Technik Ainring GmbH, Germany

<sup>3</sup> Technical University of Berlin, Department of Environmental Chemistry

Keywords: Ultrafine Particles, UFP, Environmental CPC, Air quality network, source apportionment, hot-spot measurements  
Presenting author email: mp@grimm-aerosol.com

Although ultrafine particles account only for a little share in the total mass concentration, they are under a cloud of being harmful to health. For this reason an additional monitoring of this particle fractions' exposure is absolutely required. Due to strong gradients in time and space, the measurements of ultrafine particles should be carried out unattended and continuously with high time resolution of seconds and at different measurement sites as rural background, outskirts of the city, urban background and at traffic and industrial sites (hot-spot measurements).

Grimm has been developed a state of the art device to measure ambient exposures of ultrafine particles with high temporal resolution (1 second). The main components of the system are a special environmental Condensation Particle Counter (CPC,  $d_{50} = 7 \text{ nm}$ ), a well-established Nafion drying system and an air conditioned mini-shelter (figure 1).

This new device EDM465-UFP is absolutely qualified for continuous measurements (24/7) of ultrafine particle exposures at different pollution levels from 0 to approx.  $2 \cdot 10^5 \text{ particles/cm}^3$ . It has been performed for long term unattended measurements with low service requirements, maintenance at the device is needed only once per months.



Figure 1: The GRIMM EDM465-UFP for unattended continuous ultrafine particle measurements, outside view (left) and inside view (right)

Counting efficiency, dryer performances and particle losses in the inlet pipe have been characterized comprehensively.

Figure 2 shows the determination of ultrafine particles at hot-spot conditions whereas figure 3 shows the measurement device observing urban background concentrations of ultrafine particles at the tropospheric

research platform at the department of environmental chemistry, TU-Berlin



Figure 2: Unattended continuous hot-spot measurements with the EDM465-UFP



Figure 3: Measurements of urban background levels of ultrafine particles at the tropospheric research platform of the department of environmental chemistry, Technical University of Berlin

### References

- [1] Review of evidence on health aspects of air pollution – REVIHAAP project: final technical report. Hrsg.: World Health Organization, Regional Office Europe, Kopenhagen, Dänemark (2013)
- [2] Birmili, W., Rückerl, R., Hoffman, W., Weinmayer, G., Schins, R., Kuhlbusch T.A.J., Vogel, A., Weber, K., Franck, U., Cyrys, J., Peters, A.: Ultrafeine Partikel in der Außenluft: Perspektiven zur Aufklärung ihrer Gesundheitseffekte. Gefahrstoffe Reinhaltung der Luft 74 (2014) Nr. 11/12.
- [3] Peters, A.; Wichmann, H. E.; Tuch, T.; Heinrich, J.; Heyder, J.: Respiratory effects are associated with the number of ultrafine particles. Am. J. Respir. Crit. Care Med. 155, Nr. 4, (1997) S.1376-1383

## New Developments in Single Particle Measurements of Black Carbon and Bioaerosols

A.R. Attwood<sup>1</sup>, H Schulz<sup>2</sup>, G. Granger<sup>1</sup>, M. Zanatta<sup>2</sup>, A.B. Herber<sup>2</sup>, M. Mahin<sup>1</sup>, D. Baker<sup>1</sup>, G.L. Kok<sup>1</sup> and R. Gerdes<sup>2</sup>

<sup>1</sup>Droplet Measurement Technologies, Longmont, Colorado 80503, USA

<sup>2</sup>Alfred Wegener Institute, Helmholtz Centre for Polar and Marine Research, Bremerhaven, 27568, Germany

Keywords: black carbon, bioaerosol, optical properties, incandescence.

Presenting author email: aattwood@dropletmeasurement.com

Accurate measurements of particle concentration, composition and temporal and spatial variability are essential for estimating their radiative effects in the atmosphere. Here, we present two new single particle instruments for the measurement of black carbon and bioaerosols. These particles are ubiquitous in the atmosphere and can directly effect the Earth's radiative balance by absorbing and scattering solar radiation.

### Black Carbon-SP2-XR

Black carbon aerosol is emitted by combustion processes and plays a major role in climate forcing by absorbing solar radiation and re-radiating the energy as heat. Single particle measurements of black carbon have been developed previously but were not ideal for use in long term monitoring due to their large size and complexity of the data analysis. We have developed a new instrument, the SP2-XR, that uses the same physical principles as existing technologies but with a smaller footprint, easier data analysis and extended size range.

The SP2-XR discriminates between scattering and absorbing particles based on their interaction with a high powered Nd:YAG laser beam (Figure 1a). The signal received by the incandescence and scattering detectors can be used to calculate particle mass, size and number concentration.

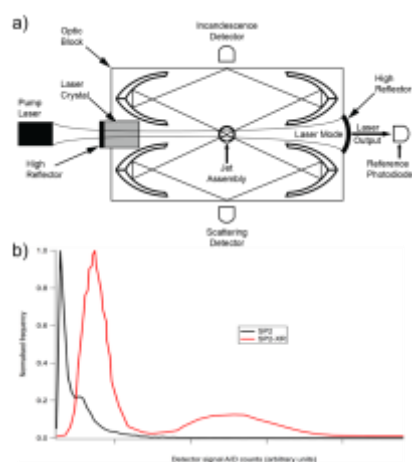


Figure 1. a) Optical layout of the SP2-XR. b) Comparison of peak height histograms of the SP2 and SP2-XR for 56 nm Aquadag particles.

Previous techniques were also limited by the smallest black carbon particle size that was detectable

(70 nm). Advances in the optical design and electronics allows for detection of particles down to 50 nm (Figure 1b).

### Bioaerosol-WIBS-NEO

Bioaerosols are an important class of atmospheric particles due to their potential impacts on air quality, climate, ecology and human health. Traditional culture based methods and manual cell-counting techniques for measuring bioaerosols provide poor temporal resolution and require significant time post-collection. Here we present data using an improved, online, automated single particle instrument to measure bioaerosol in both indoor and outdoor environments.

The Wideband Integrated Bioaerosol Sensor with New Electronics Option (WIBS-NEO) provides highly sensitive measurements of pollen, mold and other bioaerosols. It uses a UV xenon source to excite fluorescence in individual particles at particular wavebands. The optical layout of the NEO is modelled after a similar instrument (WIBS-4A, Figure 2) but improved electronics allows for more robust sampling and larger particle size range.

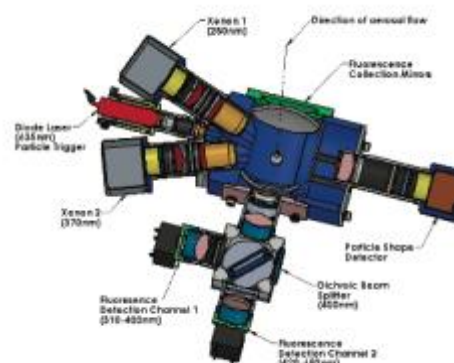


Figure 2. Optical layout of the WIBS-NEO.

## Novel concept of ion counting based upon aerosol technology

B. Gorbunov

ANCON Technologies, CIC, University of Kent, University Rd., Canterbury, Kent CT2 7FG, UK

Keywords: nanoparticles, single ion counting, particle generator, integrated charge particle extractor, Faraday cup.

Presenting author email: [boris.gorbunov@naneum.com](mailto:boris.gorbunov@naneum.com)

Single ion detection is accomplished by employing a novel detection principle: tagging of ions. Instead of amplification of a weak electric signal from the Faraday cup here we enlarge every ion by attaching to it an electrically neutral tagging nanoparticle or simply tag. This creates a mixture of electrically charged (by ions) tags and neutral tags. Charged tags containing ions then separated from the neutral tags with an electric field and counted individually by an Optical Particle Counter (OPC) or a Condensation Particle Counter (CPC).

It is important that tagging objects should be considerably larger than molecular ions to be individually detectable by an OPC or CPC. This implies a size limit on the tag radius  $R_t > 20$  nm. The optimal radius range for tags therefore is 20 nm to 300 nm.

In addition, tags should be electrically neutral. This excluded tag formation methods based upon dispersion of bulk material into nano-objects, e.g. nebulization of liquids. Homogeneous nucleation of liquid or solid particles from a gas phase is a preferable method of generating tags (Gorbunov, 1999). In practice multi-component nucleation is employed to generate neutral tags because it is more efficient (Gorbunov, 2001).

Molecular ions are tagged in a purposely designed tagging chamber. Collisions of ions with tags are mainly controlled by the Brownian diffusion that is enhanced by turbulent diffusion. The concentration of tags in the tagging chamber should be much greater than the sample ion concentration to sustain tagging probability ( $P_t$ ) close to 1. For this volume of the tagging chamber ( $V_{tc}$ ) should be sufficiently high to satisfy inequality (1)

$$e^{-f_c \frac{V_{tc}}{Q}} \ll 1 \quad (1)$$

Here  $f_c$  is the ion-tag collision frequency (see for example Lushnikov and Kulmala, 2004) and  $Q$  is the flow rate through the tagging chamber. Thus in the tagging chamber a mixture of charged tags that collided with ions and neutral tags is formed.

Each charged tag has the same properties as the original neutral tag except for electrical mobility. Therefore, electrically charged tags can be separated from the neutral tags in an electric field. For this two parallel adjacent laminar flows are formed in the extraction chamber: the sample flow from the tagging chamber and a clean air flow without ions and tags generated by a separate pump. When a suitable strength electric field across the flows is applied charged tags from the sample flow are moved into the clean air flow. Therefore, the clean air flow coming out of the extraction chamber contains only charged tags. These tags are individually counted with an OPC or CPC. The number of charged tags is equal to the number of ions (subject to expression 1) hence readings from the OPC/CPC delivers number of ions in the sample flow. Thus number of ions is counted without employing the Faraday cup and measuring an electric current. The design of this device is described by Gorbunov *et al.* (2017).

The number of ions in a sample is equal to the OPC/CPC tag counts only if each tag is charged with a single elementary charge. For this the number of tags should be much greater than the number of ions in a sample.

This technology is based on a direct counting measuring method that counts number of charged objects and therefore does not require calibration providing that the tagging efficiency and ionised tag extraction efficiency is close to 100%.

Lushnikov A. A. and Kulmala M. (2004) *Phys. Rev. E*, **70**, 046413.

Gorbunov B. (1999) *J. Chem. Phys.* **110**, 10035.

Gorbunov B. (2001) Atmospheric aerosol formation. *J. Chem. Phys.* **115**, 2641-51.

Gorbunov B., Burton M., Steer B., Ion S. and Hughes M. (2017) Design of ion counter device. *Proceedings of EAC2017*.

## Applications of individual ion counting

B. Gorbunov, G. Hyatt-Gipson, M. Burton, B. Steer and R. Muir

ANCON Technologies, CIC, University of Kent, University Rd., Canterbury, Kent CT2 7FG, UK

Keywords: ionisation, clusters, ion counting, particles trace analysis.

Presenting author email: [boris.gorbunov@naneum.com](mailto:boris.gorbunov@naneum.com)

The Airborne Object Counting (AOC) method enables counting of clusters, nano-objects molecules as well as ions and electrons. For this an ionization means should be added to the AOC set-up (Gorbunov *et al.*, 2017). A  $^{241}\text{Am}$  ionization chamber (Steer *et al.* 2012) was added in front of the set-up. Any ionizing source generates in the air a number of different ions, e.g.  $^{241}\text{Am}$   $\alpha$ -emitter produces  $\text{O}_2^-$  and  $\text{H}_3\text{O}^+$  based ions. To count molecules of certain kind an ion filter is required to select ions of interests. A Differential Mobility Spectrometer (DMS) ion filter was placed between the ionization chamber and the tagging chamber. The filter enables one to scan the ion mobility parameter and record mobility spectra as a function of the compensation voltage (CV) similar to DMA. Therefore, only ions of chosen mobility could pass through the ion filter to the AOC set-up. With the ionization chamber and the ion filter, several molecules have been detected including cocaine, trinitrotoluene, iso-propanol and acetone. The latter two are typical VOC metabolites often found as *in vivo* and also *in vitro* samples and identified as possible biomarkers of some pathological conditions.

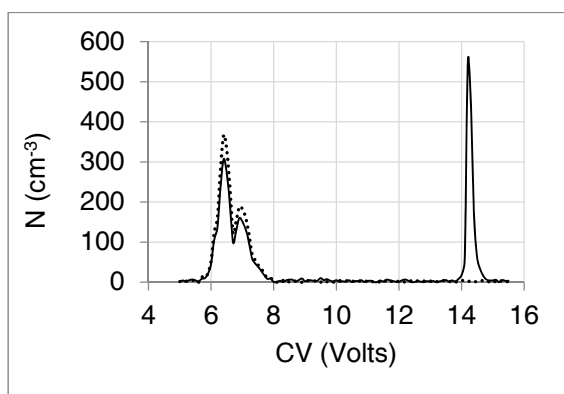


Figure 1. AOC counts vs. compensation voltage of the ion filter. Clean air containing traces of acetone was introduced into the set-up according to (Gorbunov *et al.*, 2017). The background signal from the clean air is indicated with a dashed line, while the signal from air with acetone is shown with solid line.

To confirm the detection capability of the AOC method a reference method is needed. Unfortunately, there are no methods available to generate and to quantify such low concentrations of ionized molecules in the air which this method is capable of measuring (down to hundreds and tens of molecules per  $\text{cm}^3$ ). The detection capability of the AOC method was evaluated assuming that for ultra-low concentrations the ion losses are equal to losses for larger concentrations. The concentration measured in tests was down to hundreds of ionized molecules per  $\text{cm}^3$ , e.g. 560 per  $\text{cm}^3$  for acetone (Fig. 1). This level of concentration was obtained with a double enclosed permeation tubes. A signal of 15 molecules per  $\text{cm}^3$  could be reliably detected with 3:1 signal noise ratio. The minimal detection level for this signal/noise level would be 15 molecules per  $\text{cm}^3$ .

The AOC method is confirmed to be able to count individual ionized molecules. This is also sufficient to monitor VOC metabolites emitted by single cells and single cell bacteria making it potentially possible to detect cancer and other biomarkers at earlier stages.

The AOC breakthrough in sensitivity of charge detection opens new horizons in many areas. For example, one such application of IIT could be detection of high energy cosmic ray particles with energy above  $10^{16}$  eV. Therefore, AOC can be employed to detect and possibly identify ionizing radiation for security and other applications. It is anticipated that this concept opens doors for advances in detection sensitivity in chemistry, biology, medicine and physics.

Steer B., Gorbunov B., Rowles J. and Green D. (2012) *J. Chem. Phys.* **136**, 054704-8.

Gorbunov B (2017) Novel concept of ion counting based upon aerosol technology. *Proceedings of EAC2017.*

## Improved Understanding of HGPMs Collection of Airborne Particles

M.-D. Cheng<sup>1</sup>, P. Cable-Dunlap<sup>2</sup> and S.L. Allman<sup>3</sup>

<sup>1</sup>Environmental Sciences Division, <sup>2</sup>Global Security Directorate, and <sup>3</sup>BioScience Division

Keywords: aerosol, high-gradient magnetic, permanent magnet, paramagnetics.

Presenting author email: chengmd@ornl.gov

Environmental monitoring and sample collection using magnetic force is gaining popularity in recent years. The collection applications span a wide range from microbial samples, medical treatment and air pollution particles. Most if not all the magnetic collection methods are electromagnetic-based collectors; we had developed a collector based on the high-gradient permanent magnetic separation (HGPMs) principle using fabricated permanent magnets. The initial performance of the HGPMs collector was evaluated experimentally using laboratory-generated particles of varying magnetic susceptibility (Cheng et al., 2014) without knowing *a priori* the magnet performance and particle removal behavior within the system. The collector was found to have nearly 100% of collection efficiency for paramagnetic and ferromagnetic particles greater than 40nm of the electrical mobility diameter, which was significant in environmental sampling application. Ongoing research reveals some interesting phenomena about the configuration of permanent magnets initially conceptualized in the prototype collector presented in Cheng et al. (2014). The permanent magnet orientation therefore magnetic field orientation, magnetic insulator, and material property all play a role in determining the performance of the collector. We have been successful in using the COMSOL<sup>®</sup> multiphysics software to investigate the effect of magnetic force on particle collection in our system and validate the model prediction by the experimental data, recently. For example, the simulated volume magnetic field strength (B) of one of the three identical stages shown in Figure 2 was found to be close to the measured field strength, within the experimental uncertainty in Figure 1 (one of the three peaks) of  $\pm 20\%$ . The uncertainty was attributed to the measurement using a hand-held 3D Hall probe; a measurement apparatus has since been constructed and the repeated measurements gave an uncertainty within  $\pm 10\%$ . Also, note that the B curves in Figure 1 has fat tails; we believe this was likely to be due to the averaging of B in all three dimensions while numerical simulation did not duplicate the 3-dimensional measurements. One of the key findings in this intercomparison between experimental and theoretical results was that the calculated maximal B value was found to be at the location where two identical poles

facing each other, which is consistent with the experimental data. This indicates the physics in the model produces consistent results as the observations. Use the array of three-stacked HGPMs units in the prototype enables a cascade trapping of particles and ensures the high collection efficiency for small particles in a very small footprint. The success also implies that the device can likely be operated for a long time without an external power.

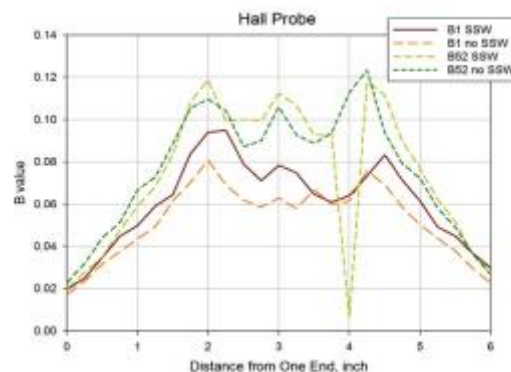


Figure 1. Measured Magnetic Field Strength

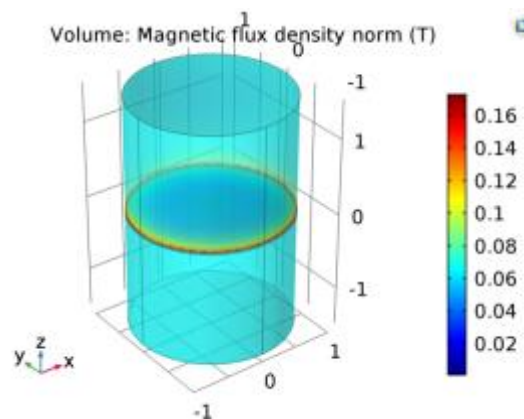


Figure 2. Simulated Magnetic Field Strength

This work was supported by the National Nuclear Security Administration of the U.S. Department of Energy.

### References:

- Cheng, M.-D., S.L. Allman, G.M. Ludtka, and L.R. Avens (2014) *J Aerosol Sci.*, 77: 1-9.
- Cheng, M.-D., G.M. Ludtka, and L.R. Avens (2016) High-Gradient Permanent Magnet Apparatus and Its Use in Particle Collection, US Patent #9,387,486, July 12.

## The Effect of Temperature and Humidity on the Performance of Low-Cost PM Sensors

Xiaoting Liu, Adrien Mabon, Akwasi Bonsu Asumadusakyi, Mandana Mazaheri,  
Rohan Jayaratne, Matthew Dunbabin and Lidia Morawska

International Laboratory for Air Quality and Health,  
Queensland University of Technology, Brisbane 4001, QLD, Australia

Keywords: Low-cost sensors, Aerosols, Atmospheric Pollution

Presenting author email: x65.liu@hdr.qut.edu.au

Due to the rapid advances in technology, low cost air monitoring sensors are becoming increasingly available in the market. These sensors are being used in numerous applications such as personal sampling and the investigation of spatial distribution of air pollution. While most of these devices respond to the level of concentration of the pollutants, there are many questions regarding the accuracy of the values that the sensors are capable of reporting (Lewis and Edwards, 2016). In addition, there are concerns regarding the effects of external factors such as temperature and humidity on the performance of these devices.

This study was carried out, in particular, to assess the effect of these two parameters on the performance of two commonly available low-cost particle mass sensors, the Sharp GP2Y1010AUOF (Wang et al., 2015) and the Shinyei PPD42NS (Austin et al., 2015). Both these sensors operate on the principle of light scattering. They do not report the PM values directly but provide a voltage output that is related to the PM<sub>2.5</sub> concentration.

The sensors were placed within a laboratory chamber and exposed to ambient aerosols under controlled conditions. At fixed PM concentrations, the output of each sensor showed a large coefficient of variation, so that the individual fluctuations at ambient concentration were relatively high. The air temperature was increased with an electrical heater from room temperature to 60°C and the relative humidity was increased up to 100% by inserting moist tissue paper or steam from a boiler into the chamber. Care was taken to ensure that neither of these methods introduced any particles into the chamber.

Figure 1 shows the voltage output of the two devices as a function of air temperature at a fixed PM<sub>2.5</sub> value of  $5 \pm 1 \mu\text{g m}^{-3}$ . While the Shinyei was relatively resilient to temperature changes ( $R^2=0.07$ ), the output of the Sharp showed a marked increase with temperature ( $0.8 \mu\text{V } ^\circ\text{C}^{-1}$  at  $R^2=0.46$ ).

Figure 2 shows the voltage output of the two devices as a function of relative humidity at a fixed PM<sub>2.5</sub> value of  $5 \pm 1 \mu\text{g m}^{-3}$ . Interestingly, both sensor outputs remained relatively constant within the expected uncertainty until the relative humidity reached about 75%. Beyond this value, the outputs increased significantly.

Our results show that both these sensors cannot be expected to provide reliable PM data when the atmospheric relative humidity exceeds 75%. This is of concern as such values of relative humidity are

commonly exceeded in many locations around the world, especially at night and during the early morning hours.

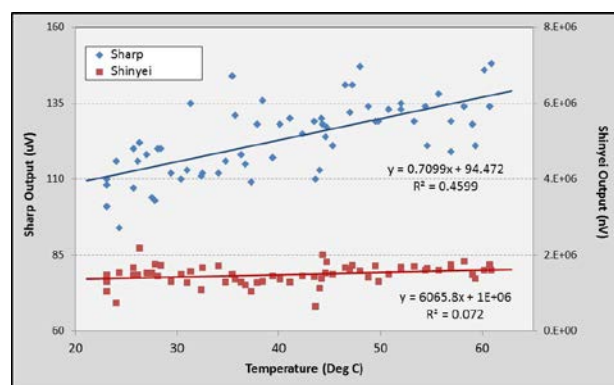


Figure 1. The voltage output of the two sensors as a function of air temperature at a fixed PM<sub>2.5</sub> concentration.

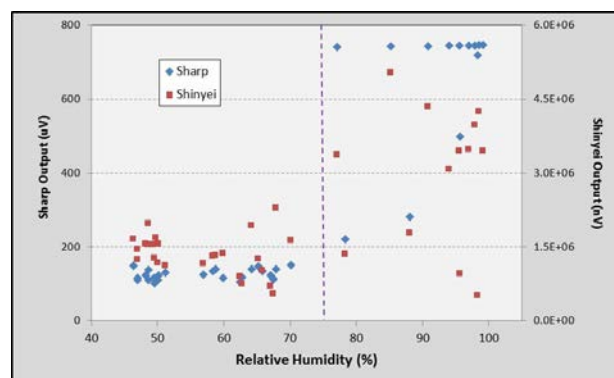


Figure 2. The voltage output of the two sensors as a function of relative humidity at a fixed PM<sub>2.5</sub> concentration.

Austin, E., Novosselov, I., Seto, E., Yost, M.G. (2015). Laboratory evaluation of the Shinyei PPD42NS low-cost particulate matter sensor. *PLOS One*. <http://dx.doi.org/10.1371/journal.pone.0137789>.

Lewis, A., Edwards, P. (2016). Validate personal air pollution sensors. *Nature*. 535, 29-31.

Wang, Y., Li, J., Jing, H., Zhang, Q., Jiang, J., Biswas, P. L. (2015). Laboratory evaluation and calibration of three low-cost particle sensors for particulate matter measurement. *Aerosol Sci. Technol.* 49, 1063-1077.

## Photoionization Sensor: Method for Detecting Ultrafine Particle Surface Area, Size and Concentration in Continuous Flow

R.T. Nishida\*, A.M. Boies and S. Hochgreb

Department of Engineering, University of Cambridge, Cambridge, CB2 1PZ, UK  
 Keywords: Ultrafine particles, Photocharging, Detection, Modelling, UV irradiation

\*Presenting author email: rn359@cam.ac.uk

Direct ultraviolet (UV) photoionization is a method of electrically charging aerosol nanoparticles distinct from the conventional diffusion charging mechanism which relies on the collision of particles and ions. Photoionization yields significantly higher charging efficiencies than diffusion based methods for some nanoparticle materials over a range of particle sizes. The increased charging, material dependency, and collision free charging mechanism provide opportunities for improvements in sensing, capture and control of aerosol nanoparticles.

In direct particle photoionization, aerosol particles emit electrons and become positively charged to multiple charge states by absorbing ultraviolet photons of sufficient energy. In this work, an experimental photoionization chamber is outfitted with a low strength electric field (of order 10 V/cm) in order to capture ions, reduce recombination, and increase the particle charge state in a continuous flow of aerosol nanoparticles. The electric field enables measurement of two distinct currents: the first from capturing ions generated during photoionization, and the second from the remaining charged particles as seen in Fig. 1.

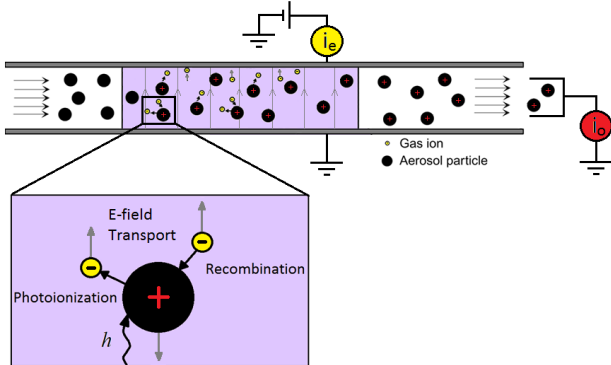


Figure 1 – Diagram of particle photoionization sensor. Highly mobile ions and some charge particles are transported and captured in the electric field yielding an electrode current. Remaining charged particles yield outlet current.

The measured currents are in the first instance proportional to the concentration,  $N$ , and the photoelectrically active surface area  $d_p^2$  as seen in Fig. 2 giving a real-time measure of total particle surface area. By increasing the strength of the electric field, more particles are captured during the photoionization process affecting both the electrode current  $i_e$  and  $i_o$ . The electric field strength is used as a parameter for distinct

measurement states and the resulting electrical currents are used to obtain information on the size and concentration of aerosol nanoparticles.

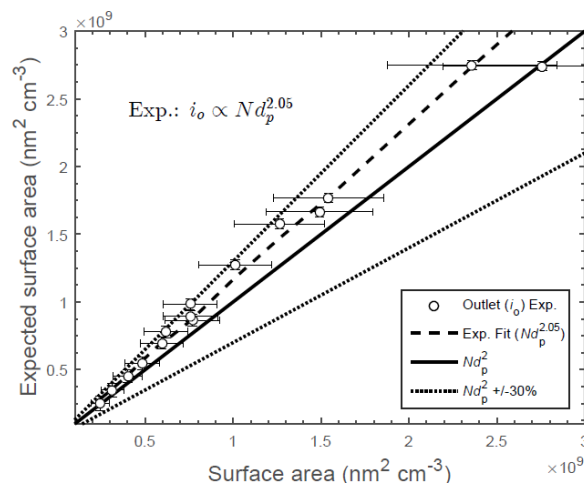


Figure 2 - Photoelectrically active surface area estimates as a function of measured particle surface area (SMPS) for soot nanoparticles (25-80 nm,  $9 \times 10^4$ - $1.1 \times 10^6$  cm<sup>-3</sup>).

Experimental data is obtained for photoionization of a range of particle materials, sizes and concentrations in continuous flow including soot, silver, and gold nanoparticles. Results are compared with those from a 3D computational fluid dynamics model which includes equations for particle and ion flow, photocharging, recombination, diffusional wall losses and electric field transport.<sup>1</sup> The photocharging theory is evaluated for the applicability of its experimental constants, including a single empirical constant and a particle work function for each material to account for photoionization. The effect of particle morphology on the signal yield is analyzed by sintering agglomerated particles and measuring the change in photoelectrically active surface.

The method of detecting particle size and concentration parameters is evaluated in terms of experimental uncertainty and applicability in a commercial low-cost, environmental monitoring device for ultrafines.

<sup>1</sup>R. Nishida, A. Boies, S. Hochgreb. Journal of Applied Physics, 2017, 121(2).

## Towards accurate determination of aerosol transport parameters in microgravity

A. Vedernikov<sup>1</sup>, D. Balapanov<sup>1</sup> and S. Beresnev<sup>2</sup>

<sup>1</sup>Microgravity Research Centre, Universite Libre de Bruxelles, Brussels, 1050, Belgium

<sup>2</sup>Institute of Natural Science and Mathematics, Ural Federal University, 620083, Ekaterinburg, Russia

Keywords: microgravity, thermophoresis, photophoresis, instrumentation.

Presenting author email: [avederni@ulb.ac.be](mailto:avederni@ulb.ac.be)

Aerosol transport parameters are widely used in science and technology. The number of publications quickly increases. Only those dealing with thermophoresis exceeded 400 in 2016, growing quicker than exponentially since the year 2000. Brownian random walk, motion of simple-shaped particles in gravity, in electrostatic and magnetic fields, are well defined. A vast variety of other types of motion is much less accurately defined, often in a limited region of parameters, various models and experimental results are far from being consistent. It is true even for the most extensively investigated transport phenomena – thermophoresis and photophoresis, not to say about diffusio-phoresis, gravito-photophoresis, and various other types of particle motion driven by physicochemical transformation and accommodation peculiarities on the particle-gas interface. Suffice it to say, that the formula of Talbot et al (1955) is still used in most computational software packages and even in theoretical papers. This formula is an interpolation with a very limited theoretical background and it is proved to be inconsistent with the reality in a wide range of parameters. There is a strong need in high quality experimental data on particle transport properties with vivid interest to expand the scope for non-isometric particles, agglomerates, dense clouds.

Microgravity is the most favorable condition to get accurate measurements of aerosol transport properties. The advantages of microgravity were admitted since long ago. Particularly, microgravity suppresses particle sedimentation, gravity driven convection; it facilitates accurate measurements at  $Kn < 10^{-1}$ , i.e. very big particles, and  $Kn > 10$ , i.e. very small particles and/or rarefied gases. Existing experimental microgravity-related results are isolated and cannot be treated as reference.

In the framework of the European Space Agency project Interaction in Space and Atmospheric Particle Systems (Blum et al, 2008), we developed and tested a Cloud Manipulation System (Vedernikov et al, 2012) that we consider as a prototype of equipment for such work. The system is based on the use of thermophoresis and gas flow that does not introduce additional particle-particle forces. The system configuration is close to an octopole electrodynamic balance (Zheng et al, 2001). The trapping regime allows growing gigantic agglomerates consisting of millions of initially micron-sized particles, figure 1. The system is able to levitate the cloud, and to scan the cloud through the observation field, a function similar to an automated motorized table. Slow pressure variation in the chamber along with on-going particle/cloud levitation, allows to choose the Knudsen number and to make

repetitive measurements on the same particle(s) in the range  $10^{-3} < Kn < 10^3$ .

In microgravity, there is no particular difficulty in handling big particles of high density materials and high thermal conductivity. Such aerosol systems are of great interest in direct investigation of the “negative thermophoresis”. In 2005, thermophoretic motion of 50-80 micrometer copper particles ( $Kn \approx 2 \cdot 10^{-3}$ ) was investigated in short duration microgravity at Bremen drop tower. Thermal stress slip flow was proven to be the leading motion mechanism. Current technologies provide at least ten times increase of the accuracy, i.e. better than  $10^{-4}$  with respect to the velocity in free-molecular regime.

To conclude, it is now feasible to get benchmark data of aerosol transport properties, making reference measurements in microgravity for most wide range of precisely known Knudsen number, thermal conductivity ratio and accommodation properties. Contrary to the current practice, fitting parameters should be excluded from interpreting the data. There exist all necessary components to tackle the problem, which is still complicated, will require substantial efforts and cooperative work on theoretical and experimental fields.

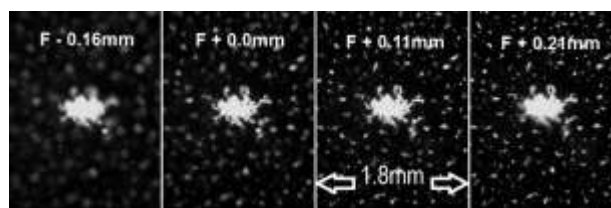


Figure 1. Scanning of a cluster grown by forced agglomeration in the drop tower experiment.

ESA PRODEX program, the Belgian Federal Science Policy Office, ZARM Drop Tower Operation and Service Company Ltd. are greatly acknowledged.

Talbot, L., Cheng, R. K., Schefer, R. W., & Willis, D. R. (1980) *J. Fluid Mech*, **101** (pt 4), 737-758.

Blum, J., Levasseur-Regourd, A.C., Muñoz, O., Slobodrian, R.J., Vedernikov, A. (2008) *Europhysics News* **39**, 27-29.

Vedernikov, A., Freuville, N., Balapanov, D., Cecere, A. (2012) *Proc. 63<sup>rd</sup> International Astronautical Congress*, IAC, 777-787.

Zheng, F., Qu, X., Davis, E.J. (2001) *Rev. Sci. Instrum*, **72**(8), pp. 3380-3385

## Use of the Aerodynamic Aerosol Classifier (AAC) for evaluation of aerosol microphysical and optical properties.

J.D. Allan<sup>1,2</sup>, D. Liu<sup>1</sup>, M.R. Alfarra<sup>1,2</sup>, P.I. Williams<sup>1,2</sup>

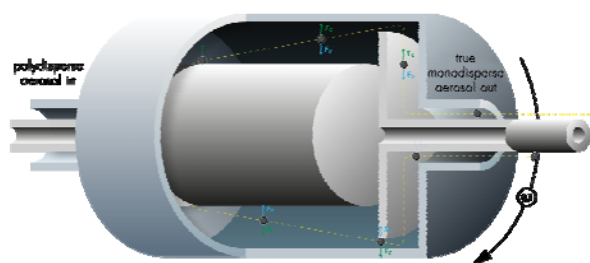
<sup>1</sup>School of Earth, Atmospheric & Environmental Sciences, the University of Manchester, M13 9PL, UK

<sup>2</sup>National Centre for Atmospheric Science, the University of Manchester, M13 9PL, UK

Keywords: AAC, photoacoustic, classification, black carbon, optical properties

Presenting author email: james.allan@manchester.ac.uk

The Aerodynamic Aerosol Classifier (AAC) is a new instrument produced by Cambustion Ltd. (Tavakoli et al., 2014). It uses two concentric cylinders and selects particles according to their migration through a particle-free sheath gas in a similar manner to a Differential Mobility Analyser (DMA). However, by rotating the column and using centrifugal rather than electrostatic forces, they are selected according to their aerodynamic, rather than mobility diameter.



A major feature of this instrument is the lack of a requirement for electrostatic charging prior to selection, as is the case with DMAs and mass selectors such as the Centrifugal Particle Mass Analyser (CPMA) and Aerosol Particle Mass analyser (APM). The benefits of this are twofold:

1. Elimination of multiply charged and uncharged particles
2. No reliance on the charging efficiency of the particle size

The use of the instrument in series with another scanning size classification instrument can be used to infer particle microphysical data, as was shown by Tavakoli and Olfert (2014), who used a scanning mobility particle sizer (SMPS). In addition to this, here also show additional methodologies such as using a scanning CPMA with an electrometer as a detector to deliver a similar data product.

One particularly exciting application is the use of this instrument to classify particles prior to measurement of their optical properties, such that size-resolved optical properties can be evaluated. While Liu et al. (2017) evaluated monodisperse NIR properties, visible optical properties were limited to the bulk. Previous experiments using classification by electro-mobility or mass selection have been confounded by the presence of uncharged or multiply charged particles. While methods exist to exclude their influence, it is far more desirable to eliminate these entirely. Furthermore, with photoacoustic instruments employing a single-pass cell such as the

DMT Photoacoustic Soot Spectrometer (PASS) (Arnott et al., 1999), signal-to-noise is limited, so it is highly desirable that a classifier delivers as high a throughput as possible.

Here we present our first laboratory test data of AAC classification followed by evaluation by other microphysical and optical instruments, including the CPMA, SMPS, PASS and Aerodyne Cavity Attenuated Phase Shift Particulate Matter Single Scattering Albedo (CAPS  $PM_{SSA}$ ) (Onasch et al., 2015). Particles tested include atomiser-generated soot analogues and particles from a light duty diesel engine dynamometer rig.

**Acknowledgements.** This work was supported by the National Centre for Atmospheric Science (NCAS).

### References

- Arnott, W. P., Moosmuller, H., Rogers, C. F., Jin, T. F., and Bruch, R.: Photoacoustic spectrometer for measuring light absorption by aerosol: instrument description, *Atmos. Environ.*, 33, 2845-2852, 1999.
- Liu, D. T., Whitehead, J., Alfarra, M. R., Reyes-Villegas, E., Spracklen, D. V., Reddington, C. L., Kong, S. F., Williams, P. I., Ting, Y. C., Haslett, S., Taylor, J. W., Flynn, M. J., Morgan, W. T., McFiggans, G., Coe, H., and Allan, J. D.: Black-carbon absorption enhancement in the atmosphere determined by particle mixing state, *Nat Geosci*, 10, 184-188, 10.1038/NNGEO2901, 2017.
- Onasch, T. B., Massoli, P., Keegan, P. L., Hills, F. B., Bacon, F. W., and Freedman, A.: Single Scattering Albedo Monitor for Airborne Particulates, *Aerosol Sci. Technol.*, 49, 267-279, 10.1080/02786826.2015.1022248, 2015.
- Tavakoli, F., and Olfert, J. S.: Determination of particle mass, effective density, mass-mobility exponent, and dynamic shape factor using an aerodynamic aerosol classifier and a differential mobility analyzer in tandem, *J. Aerosol. Sci.*, 75, 35-42, 10.1016/j.jaerosci.2014.04.010, 2014.
- Tavakoli, F., Symonds, J. P. R., and Olfert, J. S.: Generation of a Monodisperse Size-Classified Aerosol Independent of Particle Charge, *Aerosol Sci. Technol.*, 48, I-Iv, 10.1080/02786826.2013.877121, 2014.

## Extending the use of 1nm-Growth Enhancers to a wider range of CPCs

A.F. Zerrath<sup>1</sup>, J.H.T. Scheckman<sup>1</sup>, J. Spielvogel<sup>2</sup>, and A.J. Tiwari<sup>1</sup>

<sup>1</sup> TSI Incorporated, Shoreview, Minnesota, 55126, USA

<sup>2</sup> TSI GmbH, 52068 Aachen, Germany

Keywords: nanoparticles, instrumentation, particle nucleation, SMPS

Presenting author email: axel.zerrath@tsi.com

In recent years, nano-aerosol measurements were extended down to 1 nm, bridging the gap between conventional particle and ion/cluster mass spectroscopic measurements. Particle measurements in this size range are valuable for researchers investigating nucleation (Jiang *et al*, 2011, Zhao *et al*, 2011), nanoparticle synthesis (Dahlkötter *et al*, 2016), and combustion (Alanen *et al*, 2015).

Initially, only particle counting was extended down to 1 nm (Iida *et al*, 2009) with the use of a growth enhancer preceding the standard Condensation Particle Counter (CPC). This nano growth enhancer utilizes Diethylene glycol (DEG) to grow particles large enough to be counted by the succeeding Butanol-based condensation particle counter. Such a CPC was then also used in a typical SMPS system along with a TSI Model 3085 nano-DMA (Jiang *et al*, 2011).

In 2016, the first fully integrated commercially available SMPS system capable of measuring size distributions down to 1nm (TSI 3938E77) was released. This system combines an Electrostatic Classifier (TSI Model 3082), DMA (TSI Model 3086 1nm-DMA) optimized for performance down to 1nm, DEG-based Nano Enhancer (TSI Model 3777) and CPC (TSI Model 3772).

Although the majority of SMPS systems operate with a Butanol-based CPC, a significant number of systems are configured with Water-based CPCs (WCPCs). In this study, the compatibility of alternate CPCs with the 1 nm SMPS system was tested using an alternate Butanol and a water-based CPC. Test aerosol was generated by vaporizing NaCl in a 430 °C tube furnace (Scheibel and Porstendorfer, 1983). Aerosol was not preclassified prior to measurement by the SMPS. A flow equalizer was used to allow the Nano Enhancer to operate at its design flow rate.

Figure 1 shows size distribution measurements made by the 1 nm SMPS system in its standard configuration, and while using a water-based CPC. Size distributions measured by the standard system and by the alternate systems agreed on average integrated number concentration by 6-10%; this value compares very favourably with a previous large study of side-by-side SMPS performance (Kaminski *et al*, 2013) which used a particle size distribution peaking at ~ 40 nm. A similar degree of agreement was found between the standard configuration and a configuration using a non-standard Butanol-CPC.

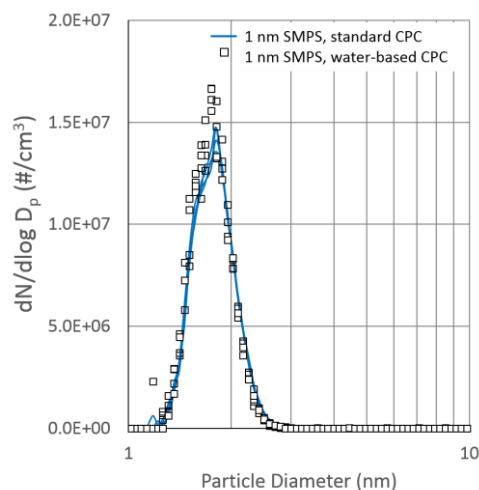


Figure 1. NaCl aerosol distributions as measured by a 1 nm SMPS, using both the standard Butanol-based CPC and a water-based CPC.

The results of this study describe the conditions under which the Nano Enhancer, model 3777, can be used with other Butanol- and water-based CPC models.

- Alanen, J. *et al*, (2015), *Fuel* **162**, 155-161.
- Dahlkötter, F., Krinke, T., Tritscher, T., Bischof, O.F., Kykal, C., Werner, A., Weber, A., Spielvogel, J. (2016), *NOSA Symposium*.
- Iida, K., Stolzenburg, M.R., McMurry, P.H. (2009) *Aeros. Sci. Tech.* **43**, 81-96
- Jiang, J., Chen, M., Kuang, C., Attoui, M., McMurry, P.H. (2011) *Aeros. Sci. Tech.* **45**, 510-521.
- Jiang, J., Zhao, J., Chen, M., Eisele, F.L., Scheckman, J., Williams, B.J., Kuang, C., McMurry, P.H. (2011) *Aeros. Sci. Tech.* **45**, ii-v.
- Kaminski, H., Kuhlbusch, T.A.J., Rath, S., Götz, U., Sprenger, M., Wels, D., Polloczek, J., Bachmann, V., Dziurawitz, N., Kiesling, H.-J., Schwiigelshohn, A., Monz, C., Dahmann, D., Asbach, C. (2013) *J. Aeros. Sci.* **57**, 156-178.
- Scheibel, H. G., & Porstendorfer, J. (1983). *J. Aeros. Sci.* 113-126
- Zhao, J., Smith, J.N., Eisele, F.L., Chen, M., Kuang, C., McMurry, P.H. (2011) *Atmos. Chem. Phys.* **11**, 10823-10836.

## Offline Validation of the New ‘Total Carbon Analyzer’

M. Rigler<sup>1</sup>, L. Drinovec<sup>1,2</sup>, A. Vlachou<sup>3</sup>, A. S. H. Prévôt<sup>3</sup>, C. Hüglin<sup>4</sup>,  
A. D. A. Hansen<sup>5</sup>, J.-L. Jaffrezo<sup>6</sup> and G. Močnik<sup>1,2</sup>

<sup>1</sup>Aerosol d.o.o., Ljubljana, 1000, Slovenia

<sup>2</sup>Jozef Stefan Institute, Ljubljana, 1000, Slovenia

<sup>3</sup>Paul Scherrer Institute, Villigen, 5232, Switzerland

<sup>4</sup>EMPA, Dübendorf, 8600, Switzerland

<sup>5</sup>Magee Scientific Corp., Berkeley, CA 94704, USA

<sup>6</sup>Université Grenoble Alpes, CNRS, IGE, 38000 Grenoble, France

Keywords: total carbon analyzer, TC-BC method, carbonaceous aerosols

Presenting author email: [Martin.Rigler@aerosol.eu](mailto:Martin.Rigler@aerosol.eu)

Carbonaceous material often dominates the composition of fine particulate matter (PM<sub>2.5</sub>). Carbonaceous aerosols impact air quality, visibility, the climate, cloud nucleation, the planetary radiation balance, and public health. The carbonaceous fractions are often described as “organic carbon” (OC) and “elemental carbon” (EC), based on their volatility using thermal-optical methods (prEN 16909). However, the diversity and heterogeneity of this material presents challenges for analysis and attribution. While the OC and especially EC concentrations determined in this way vary significantly between different thermal protocols (Bae, 2009), the total carbon (TC) concentration is very consistent and method independent (Karanasiou, 2015).

The new TC-BC method (Rigler, 2017) combines an optical method for measuring black carbon (BC) by the Aethalometer (Hansen, 1982; Drinovec 2015), and a thermal method for TC determination. The newly developed Total Carbon Analyzer (TCA) uses a conceptually simple method and produces highly time resolved data. The TCA collects the PM on a quartz-fiber filter and then combusts it very rapidly using ambient air as the carrier gas. This creates a CO<sub>2</sub> pulse which is readily detected as a large transient increase above the ambient CO<sub>2</sub> level. In contrast to conventional OC/EC analyzers, the new TCA method measures TC on the quartz filter without the need for special high purity gases, quartz glass components or specially-prepared catalysts. The TCA can operate in both online and offline modes.

The first step in the validation of the online TC-BC method is to compare the offline analysis of samples relative to the standardized OC/EC method (prEN 16909). The experiments were performed by analyzing (1) a series of different sucrose concentrations deposited on the quartz filters; (2) high EC content synthetic aerosols produced by controlled combustion, collected on quartz filters; and (3) 24-h. samples of ambient PM, collected by a high-volume PM<sub>2.5</sub> sampler during a winter campaign in 2013 and 2014 at Magadino (Switzerland). The offline-mode TCA analyses of filter punches were compared with laboratory analysis results from two OC/EC instruments using the EUSAAR-2 protocol at two different laboratories.

Figure 1 shows the inter-comparison result. The high values of the correlation coefficients confirm the performance of the TC method in comparison to conventional OC/EC analyzers. The differences between analyzers can be explained in terms of the differences in calibrations and the sample composition.

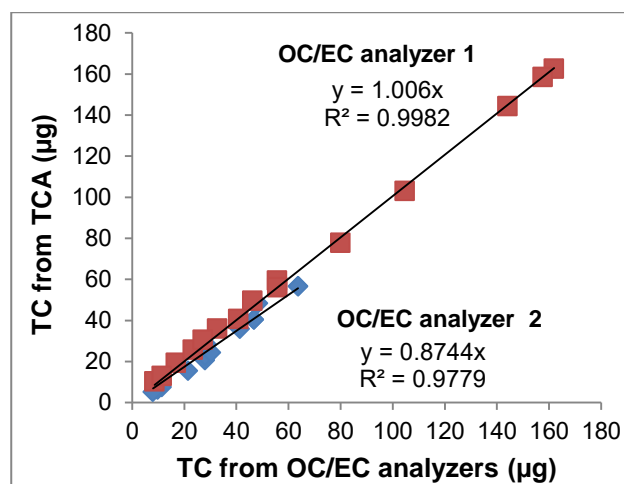


**Figure 1.** Comparison of new Total Carbon Analyzer with two different standard OC/EC instruments.

This work was financed in part by the EUROSTARS grant E!8296 TC-BC.

### References

- Bae et al. (2009), *Sci. Tot. Environ.* **407**, 5176-5183.  
 Drinovec et al. (2015), *Atmos. Meas. Tech.*, **8**, 1965-1979.  
 Hansen et al. (1982), *Appl. Opt.* **21**, 3060-3062.  
 Karanasiou et al. (2015), *Atmos. Meas. Tech. Discuss.* **8**, 9649–9712.  
 prEN 16909:2015, Ambient air - Measurement of elemental carbon (EC) and organic carbon (OC) deposited on filters, DIN, Duesseldorf.  
 Rigler et al. (2017), submitted, **T210N1a8**, EAC 2017.

## Formation of the new approaches for detection and radiation control of technogenic aerosols in conditions of improvement of cleaning technologies of a radioactive gas-aerosol emissions.

A.G. Tsovanov<sup>1</sup>, A.E. Karev<sup>1</sup>, D.E. Fertman<sup>2</sup>, N.V. Tsoy<sup>2</sup>, C.B. Chebushov<sup>3</sup>

<sup>1</sup> SRC FMBC of FMBA Russia, Moscow, Russia

<sup>2</sup> JSC “SNIIP”, Moscow, Russia

<sup>3</sup> JSC “Atomenergomash”, Moscow, Russia

Keywords: new instrumentation, radioactive, gas-aerosol, monitoring, minimum detectable activity

Presenting author email: karev17@gmail.com

There is shown as improving cleaning technologies of radioactive gas-aerosol emissions is connected inevitably with appearing of new criteria of radiation cleanness of air environment. As consequence new approaches and instruments appear for verification of these criteria. The way which science-technic society is passing in this direction in connection with rapid development of nano-industry is a striking confirmation of this.

Conception of Achievable Limit (Absolute) of Radiation Cleanness is suggested which is based on next important points:

Exposure levels due to radioactive emissions should be lower of established limits and on the reasonably achievable low level (General provisions of the safety of nuclear power stations NO-001-15 p.1.2.3).

Minimum detectable activity (MDA) or detection limit - the radioactivity which, if present in a sample, produces a counting rate that will be detected (i.e. considered to be above background) with a certain level of confidence. (IAEA2007 glossary safety rad. protection 2007).

In this way MDA could be new criteria of radiation cleanness in the area below reasonably achievable control levels.

Complex for monitoring gas-aerosol ratio and particle-size distribution of radioactive gas-aerosol mixtures described earlier (Rizin, 2015) is suggested as an instrument for preparation of aerosol samples and verification of these samples on compliance to established levels. This complex is the universal instrument for solving such class of tasks for different facilities and hazardous factors including radioactive ruthenium compounds and UF<sub>6</sub>.

In this case calibration of measuring devices is suggested to conduct using manufactured Special Aerosol Standards (SAS) (Ruzer, 2005).

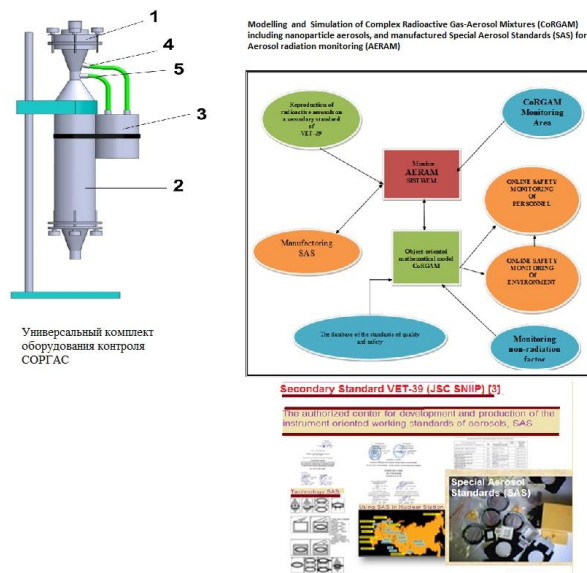


Figure 1 Modeling and Simulation of Complex Radioactive Gas-Aerosol Mixtures (CoRGAM) including nanoparticle aerosols, and manufactured Special Aerosol Standards (SAS) for Aerosol radiation monitoring (AERAM)

A.I. Rizin, D.E. Fertman, S.B. Chebushov, A.E. Karev, A.G. Tsovanov, N.V. Tsoy, S.M. Shinkarev. The 2015 European Aerosol Conference EAC 2015, Materials on CD

L.S. Ruzer, D.E. Fertman, A.I. Rizin and all (2005), Radioactive aerosol standards. AEROSOLS HANDBOOK, CRC PRESS

## **Abstracts T303**

## Influence of Dilution Stage on Measurements of Particle Emissions of a Small Scale Biomass Boiler

I.V Dyakov<sup>1</sup>, B. Bergmans<sup>1</sup>, F. Idczak<sup>1</sup>, H. Breulet<sup>2</sup>

<sup>1</sup> Cellule Emissions Atmosphériques, Institut Scientifique de Service Public (ISSEP), Liège, 4000, Belgium

<sup>2</sup> Accidental Risk Department, Institut Scientifique de Service Public (ISSEP), Liège, 4000, Belgium

Keywords: particle emission, dilution devices, pellet boiler, biomass combustion.

Presenting author email: i.dyakov@issep.be

Sampling particles in the flue gas of biomass combustion appliances usually implies a stage of dilution. Many of the existing analysers require the flue gas dilution because of different reasons e.g. the high particle concentration, the elevated flue gas temperature and the high moisture content surpassing the analysers' limits. A variety of portable or stationary systems exists providing the partial or complete dilution of the sample.

The purpose of this work was to measure the number concentrations and size distributions of the particles emitted from small scale biomass boiler using different dilution systems and evaluate the effect of the dilution system on the measurements.

In this study a 40 kW pellet boiler set in laboratory conditions was adopted as a source of relatively constant particle emissions.

Three portable dilution systems were used: a Palas VKL-10E one stage ejector dilutor with the predetermined degree of dilution, a Dekati ejector dilutor with the variable degree of dilution and a Venacontra two stage dilutor, consisting of a porous tube and an ejector stage also with the variable degree of dilution. A complete dilution tunnel built according to the Method-5G was implemented in this study as well. The dilution ratio was controlled by measuring the carbon dioxide concentrations in the raw gas and in the diluted samples.

The components of the gas emission were measured simultaneously using Gasetm DX4000 FTIR and Horiba PG-300 gas analysers.

The particle concentrations were measured in real time by an ELPI+ analyser in a range of aerodynamic diameters between 0.006 and 10  $\mu\text{m}$ . The results are represented in Fig. 1 as average curves of all measurements with different dilution ratios (DR). Error bars are calculated as standard deviations over those measurements. The data from different dilution devices are distinguished by the line colour, the dilution ratios are shown in brackets.

The total concentrations of particles measured with portable devices were within the range from  $1.5 \times 10^8$  to  $3.0 \times 10^8$  particles per  $\text{cm}^{-3}$ . The results obtained by the Venacontra dilutor are systematically higher than others, with an approximate factor of two. The distributions of particles are qualitatively similar, indicating no specific effects influencing the conversion of the particles in each dilution system.

The measurements in a complete dilution tunnel demonstrate that the total particle concentration is lower, around  $1.2 \times 10^8$  particles per  $\text{cm}^{-3}$ . Qualitatively the particle size distribution is also different with the

maximum shifted towards bigger diameters. This is most likely due to the different conditions to which the flue gas is exposed, i.e. the temperature and residence time inside the dilution devices that affect the formation of particles.

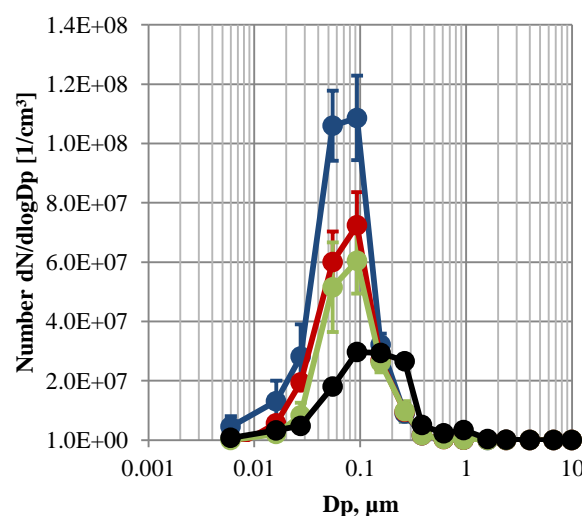


Figure 1. The particle size distribution measured by different dilution devices. Blue line – Venacontra dilutor (DR 39-102); red line – Palas VKL-10E dilutor (DR 12); green line – Decati dilutor (DR 12-91); black line – complete dilution tunnel (DR 11).

During the real life operation the boiler automatically switches between full and low power regimes to keep the water temperature constant. The particle concentrations in the full power regime are always higher than those in the low power regime. However, it is demonstrated that during the low power regime the particle emissions have elevated values if normalised to the produced energy. The particle size distributions of the both power regimes are similar. The low power regime also influences the gas emission, for example concentrations of carbon monoxide are increased, indicating the reduced quality of combustion during this approach of the exploitation of the biomass combustion devices.

Walloon Government supported this work through the Moerman funds. Authors are grateful to the European Regional Development Fund (ERDF/EFRO), project no. P12-05 EMOVO.

## **Characterizations of Black Carbon Produced from a MiniCAST Soot Generator over a Wide Range of Setpoints**

F. Liu<sup>1</sup>, M. Saffaripour<sup>1</sup> and, K.A. Thomson<sup>1</sup> and G.J. Smallwood<sup>1</sup>

<sup>1</sup>Measurement Science and Standards, National Research Council, Ottawa, Ontario, Canada, K1A 0R6

Keywords: miniCAST soot, filter based methods, optically based methods, mass concentration

Presenting author email: Fengshan.liu@nrc-cnrc.gc.ca

Emissions of black carbon generated during incomplete combustion of fossil fuels from various combustion systems, such as vehicles, aero-engines, and gas turbine combustors, have been identified to be harmful to humans and a major global warming contributor just after carbon dioxide. Development of reliable, sensitive, and real-time measurement capabilities of black carbon mass concentration is critical to assess the effectiveness of new black carbon emission mitigation strategies and to provide the required metrology needs for potential regulations on black carbon emissions. Such requirements can only be met by optically based black carbon measurement methods. However, optical methods are dependent on the optical properties of the black carbon particles, which in turn vary with several parameters of the particles, such as primary and aggregate sizes, coating of the particles by non- or weakly-absorbing organic materials, the relative contents of organic carbon (OC) and elemental carbon (EC), and the carbon atom orders. Since different optical methods of black carbon mass concentration measurement utilize different working principles, it is expected that they may respond differently to changes in the particle properties.

To understand how the changes in black carbon properties affect the mass concentration measurements by different optically based instruments, it is necessary to fully characterize the black carbon over a wide range of size (primary particle and aggregate), mass concentrations, and EC/OC ratios. In this study, two series of measurements of black carbon generated from a miniCAST soot generator over a wide range of setpoints were conducted using cavity attenuated phase shift (CAPS) particulate matter monitor (operated at 660 nm), photoacoustic extinctions (PAX) (operated at 870 nm), photoacoustic soot spectrometer, three wavelength (PASS-3) (operated at 405, 532, and 781 nm), laser-induced incandescence (LII 300), a 7-wavelength aethalometer, and a scanning mobility particle sizer (SMPS). In addition, filter samplings of black carbon particles were also collected for thermal optical analysis (TOA) to obtain the EC and OC contents and to provide benchmark mass concentration, for Raman spectroscopy analysis for carbon atom orders, and for transmission electron microscope (TEM) analysis for particle morphology. One series of measurements was carried out without a catalytic stripper (CS) and the other was conducted with a CS.

The preliminary results indicate that there is fairly good agreement between the mass concentrations measured by LII, PAX, CAPS, and the aethalometer at most of the miniCAST setpoints. However, PASS-3 measured lower aerosol absorption coefficients than CAPS and PAX (with conversion to the same wavelength in the comparison). The filter samples are currently being analyzed and the results will be available soon. It is expected that the results obtained in this study will help to improve our understanding of relationship between the mass concentration measurement uncertainties of different optical instruments and the black carbon properties (morphology, carbon atom orders, and EC/OC ratio).

## Field comparison of instruments for measurement of air pollutants

F. Borghi<sup>1</sup>, A. Spinazzè<sup>1</sup>, G. Fanti<sup>1</sup>, L. Del Buono<sup>1</sup>, D. Campagnolo<sup>1</sup>, S. Rovelli<sup>1</sup>, A. Cattaneo<sup>1</sup>, D.M. Cavallo<sup>1</sup>

<sup>1</sup>Department of Science and High Technology, University of Insubria, Como, 22100, Italy

Keywords: PM concentration, gravimetric analysis, intercomparison, direct reading instrument

Presenting author email: f.borghi2@uninsubria.it

It is well known that particulate matter (PM) can cause different adverse effects on human health (Brook *et al.*, 2010). Recently, scientific attention has moved towards PM and ultrafine particles (UFP) exposure in urban population, also highlighting the inadequacy of current air quality monitor approaches, due to limitations regarding these kind of stations (such as poor spatial and temporal resolution). Different kind of monitoring instruments have yet to be evaluated, especially on field.

The aim of this study was to compare the use of co-located real-time devices and gravimetric samplers to measure UFP and size-fractionated PM mass concentrations.

Paired direct-reading devices and gravimetric samplers were used to measure different PM fraction (Table 1) during N = 16 monitoring session, under different meteorological scenarios. The monitoring campaign were performed during the winter period, in an urban background station placed in Como (Northern Italy). In order to acquire several meteorological data, an external and co-located weather station was also used.

UFP and PM concentrations measurement were analyzed using linear regression analysis, separately for each PM fraction; the performance of instruments were tested evaluating linear regression outcomes following criteria defined by Watson *et al.* (1998).

Table 1. Instrument and related PM size-fraction used in field campaign (Pho: Photometer; PCIS: Personal Cascade Impactor Samplers; CPC: condensation Particle counter; DSC: miniaturized diffusion charger).

Direct Reading	
Instrument	PM fraction
DSC	UFP
CPC	UFP
Pho#1	PM <sub>1</sub> , PM <sub>2.5</sub> , PM <sub>5</sub> , PM <sub>10</sub> , TSP
Pho#2	PM <sub>1</sub> , PM <sub>2.5</sub> , PM <sub>4</sub> , PM <sub>10</sub> , TSP
Pho#3	PM <sub>2.5</sub>
Filter-based	
Instrument	PM fraction
Harvard Impactor	PM <sub>2.5</sub>
PCIS	(PM <sub>0.25</sub> ; PM <sub>0.5</sub> ) PM <sub>1</sub> , PM <sub>2.5</sub> , PM <sub>10</sub>
PCIS-modified	PM <sub>2.5</sub> , PM <sub>10</sub>
Pho#3 (gravimetric)	PM <sub>2.5</sub>

Results showed that the UFP concentrations measured using CPC were overestimated compared with the DSC, showing an absolute deviation that appeared to increase with the UFP concentration. Although these two devices

could be classified as comparable, relevant differences in the performance were observed. Regarding measurement of size fractionated PM, the comparison of different direct-reading devices generally indicated an over-estimation of two of the tested instruments, with respect to the third one, used as reference. However, the comparison of light-scattering devices with filter-based samplers indicated that direct-reading devices tend both to over-estimate or under-estimate the mean PM concentrations with respect to the corresponding gravimetric analysis. Besides, the comparison of different filter-based samplers showed that the observed over-estimation error increased with increasing PM concentration levels. However, the good level of agreement between the investigated methods allowed them to be classified as comparable, although they cannot be characterized as having reciprocal predictability.

Among the considered meteorological parameters, only ambient relative humidity was correlated with the absolute error resulting from the comparison of direct-reading vs. filter-based techniques, as well as among different filter-based samplers for the same PM fraction.

In conclusion, despite a general good level of comparability, relevant absolute errors were identified among different measurement and sampling techniques, which outlines the need of standardized protocols and harmonized performance evaluation criteria for existing devices, in order to ensure the obtaining of accurate results.

Brook, R. D., Rajagopalan, S., Pope, C.A., Brook, J. R., Bhatnagar, A., Diez-Roux, A. V. et al. (2010) *Circulation* **121**, 2331-2378.

Watson, J.C., Chow, J.C. And Moosmuller, H. (1998) *Guidance for using continuous monitoring in PM<sub>2.5</sub> monitoring networks*. U.S. Environmental Protection Agency, Office of Air Quality Planning and Standards Research Triangle Park, NC 27711. EPA-454/R-98-012, 1998.

## Comparison of aerosol chemical characterization techniques utilizing a PTR-ToF-MS: A study of biogenic SOA formation and aging

G. Gkatzelis<sup>1</sup>, P. Eichler<sup>2</sup>, T. Hohaus<sup>1</sup>, M. Müller<sup>2</sup>, P. Schlag<sup>1†</sup>, S. Schmitt<sup>1</sup>, R. Tillmann<sup>1</sup>, Kang-Ming Xu<sup>3</sup>, R. Holzinger<sup>3</sup>, A. Wisthaler<sup>2</sup>, A. Kiendler-Scharr<sup>1</sup>

<sup>1</sup>Institut für Energie und Klimaforschung – Troposphäre (IEK-8), Forschungszentrum Jülich GmbH, Jülich, Germany

<sup>2</sup>Institut für Ionenphysik und Angewandte Physik, Universität Innsbruck, Innsbruck, Austria

<sup>3</sup>Institute for Marine and Atmospheric research Utrecht, Princetonplein 5, 3584 CC, Utrecht, The Netherlands

<sup>†</sup>Now at: Institute of Physics, University of Sao Paulo, Sao Paulo, Brazil

Keywords: Aerosol chemical characterization techniques, PTR-ToF-MS, biogenic SOA.

Presenting author email: [g.gkatzelis@fz-juelich.de](mailto:g.gkatzelis@fz-juelich.de)

Atmospheric organic aerosols (OA), a major contributor to the submicrometer particulate matter (PM<sub>1</sub>), play a key role in climate change and air quality. OA are either directly emitted through e.g. combustion processes (primary OA, POA) or formed through the oxidation of volatile organic compounds (secondary OA, SOA). SOA constitute a major fraction of OA (Jimenez et al 2009) with biogenic VOC oxidation products controlling their global contribution. A detailed understanding of biogenic SOA (BSOA) formation and aging still remains a challenge. In order to better quantify and chemically characterize BSOA, new on-line and semi on-line measurement techniques have been established.

In this framework, a comparison of three different aerosol chemical characterization techniques has been performed to study BSOA formation and aging. The aerosol collection module (ACM, Hohaus et al 2010), the chemical analysis of aerosol on-line (CHARON, Eichler et al 2015) and the collection thermal desorption unit (TD, Holzinger et al 2010) are different inlets utilizing a PTR-ToF-MS as detector. These techniques were deployed in a set of chamber experiments at the atmosphere simulation chamber SAPHIR to investigate the SOA formation and aging from the ozonolysis of  $\beta$ -pinene, limonene and real plant emissions. SAPHIR-PLUS, a newly constructed plant chamber, was used to obtain real plant emissions (Scots pine) into SAPHIR. The composition of fresh and photochemically aged SOA was investigated in detail using the above compound specific techniques in addition to HR-ToF-AMS and SMPS.

Comparison of the individual instruments to an SMPS showed recovery rates between 20 and 80%, independent of the identity of the monoterpene oxidized. Further comparison with a focus on the different family characteristics (oxygen content, carbon content, molecular weight) showed that the PTR-ToF-MS conditions (drift tube voltage) play a key role in the fragmentation patterns with increasing recovery rates of organic mass for reduced fragmentation, as seen in Fig. 1. A detailed analysis of the volatility of the different family groups and the individual compounds has been

performed. Tracers from each monoterpene system as well as the real plant emissions were identified and will be presented.

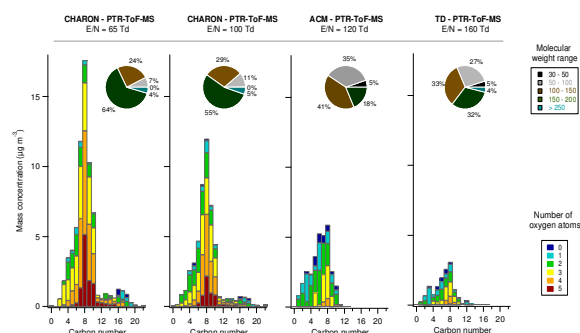


Figure 1. Comparison of the aerosol chemical characterization techniques utilizing a PTR-ToF-MS based on their chemical formula, molecular weight and operating conditions.

This work is supported by the EC's 7th Framework Program under Grant Agreement Number 287382 (Marie Curie Training Network PIMMS) and by the Helmholtz President's Fund (Backfeed).

Eichler, P., (2015) *A novel inlet system for online chemical analysis of semi-volatile submicron particulate matter*, Atmos. Meas. Tech., **8**, 1353–1360.

Hohaus, T., (2010) *A new aerosol collector for quasi on-line analysis of particulate organic matter: the Aerosol Collection Module (ACM) and first applications with a GC/MS-FID*, Atmos. Meas. Tech., **3**(5), 1423-1436.

Holzinger, R., (2010) *Aerosol analysis using a Thermal-Desorption Proton-Transfer-Reaction Mass Spectrometer (TD-PTR-MS): a new approach to study processing of organic aerosols*, Atmos. Chem. Phys., **10**, 2257–2267.

Jimenez, J. L., (2009) *Evolution of Organic Aerosols in the Atmosphere*, Science, **326**, 1525-1529.

## Quantification of Black Carbon on filters of different Station types in Austria via transmissiometer measurements

*Marion Greilinger*<sup>1,2</sup>, *L. Drinovec*<sup>3,4</sup>, *G. Močnik*<sup>3,4</sup>, *G. Schauer*<sup>1</sup>, *A. Kasper-Giebl*<sup>2</sup>

<sup>1</sup>Central Institute for Meteorology and Geodynamics (ZAMG), Vienna, 1190, Austria

<sup>2</sup>Technical University of Vienna, Institute of Chemical Technologies and Analytic, Vienna, 1060, Austria

<sup>3</sup>Aerosol d.o.o., Ljubljana, 1000, Slovenia

<sup>4</sup>J. Stefan Institute, Ljubljana, 1000, Slovenia

Keywords: transmissiometer, Black Carbon (BC), filter loading effect, attenuation

Presenting author email: marion.greilinger@zamg.ac.at

Black Carbon (BC), a common tracer for combustion emissions, exhibits high optical absorption across the visible part of the optical spectrum. Therefore, optical methods can be used for either online or offline determination of aerosol BC concentrations. The most common online measurement setup is the Aethalometer, whereas a common setup for offline measurement of e.g. filters from different stations is via the thermo-optical method described by Ahmed *et al.* (2009). The big disadvantage of this thermo-optical method is, that it is very time consuming and filters of other materials than quartz fiber cannot be measured directly. We tested optical transmissiometer measurements (OT-21, Magee Scientific) for the quantification of BC on quartz fiber filters of different station types.

The OT-21 measures the transmission of light through a particle-loaded filter at 880 nm and 370 nm. The attenuation ( $ATN = -\ln(I/I_0)$ ), where  $I$  and  $I_0$  are the respective transmission intensities through the loaded and unloaded filter, is assumed to be proportional to the BC content loaded on the filter. All filter-based optical methods exhibit the filter loading effect, causing a non-linear relationship between BC concentration and attenuation, especially for highly loaded filters. Hence, measurements have to be compensated for this loading effect.

We compare two methods for the filter loading effect compensation and evaluation of transmissiometer data for quartz fiber filters of three different station types in Austria. One approach from Virkkula *et al.* (2007) assuming that the empirical derived correction function for Aethalometer data is of the same form as for the Particle Soot Absorption Photometer (referred as logarithmic method) and one approach from Drinovec *et al.* (2015) using the dual-spot loading effect compensation algorithm (referred as linear method).

Both methods allow calculations of the filter loading effect, the mass absorption cross section ( $\sigma_{abs}$ ) as well as the mass attenuation cross section ( $\sigma_{att}$ ) and the Angström exponent ( $\alpha$ ). We evaluated quartz fiber filters of several urban, rural and background stations and compare the results for  $k$ ,  $\sigma_{abs}$ ,  $\sigma_{att}$  and  $\alpha$ . Additionally we tried to adopt this method for glass fiber filters.

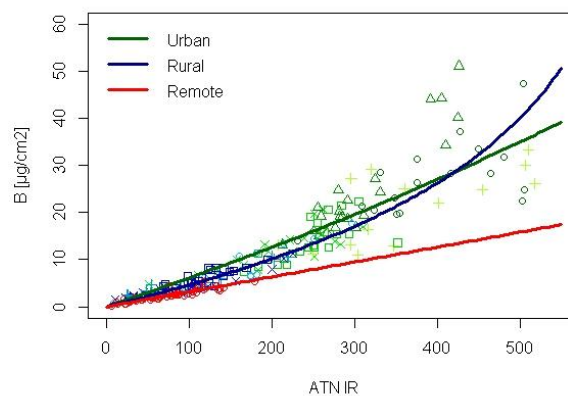


Figure 1. Attenuation measured via transmissiometer vs. thermo-optically measured EC surface density for three different station types (urban, rural and remote). A non-linear relationship is observed due to the filter loading effect, which is mostly pronounced for rural station due to coating of aged aerosol.

This work was supported by the Austrian Research Promotion Agency FFG as well as from Aerosol d.o.o.

Ahmed, T., Dutkiewicz, V.A., Shareef, A., Tuncel, G., Tuncel, S., Husain, L. (2009) *Measurement of black carbon (BC) by an optical method and a thermal-optical method: Intercomparison for four sites*. Atmos. Environ. 43, 6305–6311.

Drinovec, L., Močnik, G., Zotter, P., Prévôt, A.S.H., Ruckstuhl, C., Coz, E., Rupakheti, M., Sciare, J., Müller, T., Wiedensohler, A., Hansen, A.D.A. (2015). *The “dual-spot” Aethalometer: an improved measurement of aerosol black carbon with real-time loading compensation*. Atmospheric Meas. Tech. 8, 1965–1979.

Virkkula, A., Mäkelä, T., Hillamo, R., Yli-Tuomi, T., Hirsikko, A., Hämeri, K., Koponen, I.K. (2007) *A Simple Procedure for Correcting Loading Effects of Aethalometer Data*. J. Air Waste Manag. Assoc. 57, 1214–1222.

## Evaluation of semi-continuous OCEC analyzer performance with the EUSAAR2 protocol

A. Karanasiou<sup>1</sup>, P. Panteliadis<sup>2</sup>, M.C. Minguillón<sup>1</sup>, M. Pandolfi<sup>1</sup>, N. Perez<sup>1</sup>, G. Titos<sup>1</sup>, and A. Alastuey<sup>1</sup>

<sup>1</sup> Institute of Environmental Assessment and Water Research, IDAEA-CSIC, C/ Jordi Girona 18-26, Barcelona, Spain

<sup>2</sup> GGD, Department of Air Quality, Public Health Service Amsterdam, 1018WT, the Netherlands

Keywords: thermal-optical analysis, black carbon, elemental carbon, organic carbon

Presenting author email: angeliki.karanasiou@idaea.csic.es

The European Committee of Standardization (CEN), has recently adopted EUSAAR2 as the reference temperature protocol to be used when performing the offline, thermal-optical/transmittance (TOT) Organic (OC) and Elemental Carbon (EC) analysis (CEN/TC 264/WG 35 prEN16909:2016). The application of the reference protocol in the semi-continuous Sunset OCEC analyser and the comparison with other methods, eg. Black Carbon (BC) from absorption measurements can provide an insight on their comparability and evaluate the high-time resolution concentrations of carbonaceous aerosol. A Field OCEC analyzer (Sunset Laboratory Inc.) was installed at the urban monitoring site Palau Reial in Barcelona and at the rural monitoring station Montseny, Spain. Online analysis of TOT-OCEC in PM<sub>2.5</sub>, were compared with offline TOT-OCEC applying the EUSAAR2 temperature protocol. EC measurements with the Field OCEC Analyzer were compared with BC from a MAAP 5012 (Thermo Scientific) and an aethalometer, model AE33 (Magee Scientific) (PM<sub>2.5</sub>). Further, offline chemical composition (PM<sub>1</sub>, PM<sub>2.5</sub> and PM<sub>10</sub>) and Aerosol Chemical Speciation Monitor (ACSM) data (PM<sub>1</sub>) were available for comparison.

A very good agreement was observed between the offline and online EC measurements ( $R^2=0.9$ ). However, the offline OC concentrations were constantly higher than the online concentrations due to the positive sampling artefacts of the offline measurements. In fact, this difference was higher for the offline measurements obtained by a low volume PM<sub>2.5</sub> sampler (DERENDA) where the positive artefacts are expected to be higher than in the high volume sampler (MCV). BC measurements obtained by the aethalometer were in good agreement with EC concentrations of the semi-continuous OCEC analyser (Figure 1) and also with the optical EC directly determined every minute, operating as an aethalometer in this respect. OC online measurements were correlated with the organic aerosol (OA) concentrations calculated from the ACSM data resulting in OA/OC ratio equal to 2.3 (Figure 2). Further tests were conducted to explore the performance of the semi-continuous analyser during intense African dust and biomass burning events. This exercise provides an insight on the comparison of the online OCEC analysis method with the offline, reference method at two challenging environments, an urban site dominated by road traffic emissions and a rural site dominated by biogenic emissions.

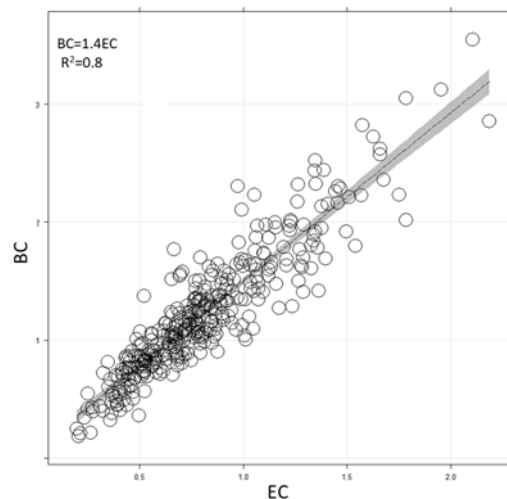


Figure 1. Comparison between BC data obtained from the aethalometer (880nm) and EC data of the semi-continuous OCEC analyser ( $\mu\text{g}/\text{m}^3$ ) at the Palau Reial site

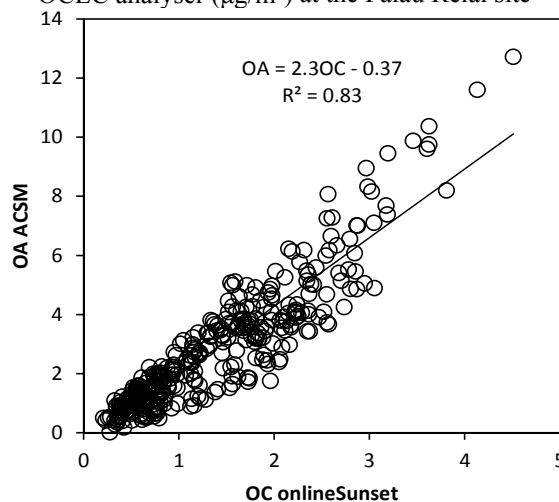


Figure 2. Correlation of OA concentrations ( $\mu\text{g}/\text{m}^3$ ) as obtained by the ACSM and OC ( $\mu\text{g}/\text{m}^3$ ) of the semi-continuous OCEC analyser at the Montseny site

This work was partially supported by ACTRIS-2 Trans-National Access TNA grant “Evaluation of semi-continuous OCEC analyzer performance with the EUSAAR2 protocol” SCOPE. A. Karanasiou, M. Pandolfi and M.C. Minguillón are funded by Ramón y Cajal Fellowships (RYC-2014-16885, RYC-2013-14036, RYC-2015-18458) awarded by the Spanish Ministry of Economy and Competitiveness cofounded by the European Social Fund.

## Comparison between remote sensing and airborne in-situ measurements using drones

Dimitra Mamali<sup>1</sup>, Eleni Marinou<sup>2,3</sup>, Michael Pikridas<sup>4</sup>, Ioannis Biniotoglou<sup>2,5</sup>, Panagiotis Kokkalis<sup>2</sup>, Aleksandra Tsekeri<sup>2</sup>, Michael Kottas<sup>2</sup>, Vasilis Amiridis<sup>2</sup>, Jean Sciare<sup>4</sup>, Christos Keleshis<sup>4</sup>, Ronny Engelmann<sup>6</sup>, Albert Ansmann<sup>6</sup>, Herman W J Russchenberg<sup>1</sup>, George Biskos<sup>1,4</sup>

<sup>1</sup>Department of Geoscience and Remote Sensing, Delft University of Technology, Delft, The Netherlands

<sup>2</sup>Institute for Astronomy, Astrophysics, Space Applications and Remote Sensing, National Observatory of Athens, Greece

<sup>3</sup>Department of Physics, Aristotle University of Thessaloniki, Thessaloniki, Greece

<sup>4</sup>The Cyprus Institute, Energy, Environment and Water Research Centre, Nicosia, Cyprus

<sup>5</sup>National Institute for R&D in Optoelectronics, Ilfov, Romania

<sup>6</sup>Leibniz Institute for Tropospheric Research, Leipzig, Germany

Keywords: dust mass concentration, lidar, drones

Presenting author email: D.Mamali@tudelft.nl

Vertical profiles of the aerosol mass concentration derived from light detection and ranging (lidar) observations were compared to airborne optical particle counter (OPC MetOne; Model 212) measurements during the INUIT-BACCHUS-ACTRIS campaign. The campaign took place in April 2016 and its main focus was the study of aerosol dust particles. During the campaign a Polly-XT Raman lidar located at Nicosia (35°.08' N, 33°.22' E), Cyprus, was used to provide round-the-clock vertical profiles of aerosol optical properties. Simultaneously the vertical size distribution profile, measured by an Optical particle counter, was monitored using drones during the first morning hours of seven selected events within the campaign. The flights were performed 30 km westerly at Orounda (35°.10' N, 33°.09' E), Cyprus, reaching altitudes of 2.5 km a.s.l, making these measurements ideal for comparison with the lidar data.

The polarization lidar photometer networking method (POLIPHON) was used for the estimation of the fine (non-dust dominated) and coarse (dust dominated) mode in the aerosol mass concentration profiles. This method uses as input the particle backscatter coefficient and the linear particle depolarization profiles of the lidar at 532 nm wavelength in order to derive the aerosol mass concentration. The first step in this approach makes use of the lidar observations to separate the backscatter and extinction contributions of the weakly depolarizing non-dust aerosol components from the contributions of the strongly depolarizing dust particles, under the assumption of an externally mixed two-component aerosol. In the second step, sun photometer measurements of aerosol optical thickness (AOT) and volume concentration are used to calculate the associated concentrations from the extinction coefficients retrieved from the lidar. The estimated aerosol volume concentrations were converted into mass concentrations with an assumption for the bulk aerosol density (2.6 g

cm<sup>-3</sup> for dust particles), and compared with the OPC measurements.

Our results show very good agreement between the aerosol mass concentrations derived from the airborne in-situ measurements with the UAVs and the remote sensing observations (cf. Fig.1). For the case study analyzed, which is a dust event that took place on 15 April 2016, the correlation coefficient between the air-borne OPC and the lidar measurements was found to be 0.9, whereas all the values from the UAV measurements lie within the uncertainty limits of the mass concentration derived by POLIPHON (40%).

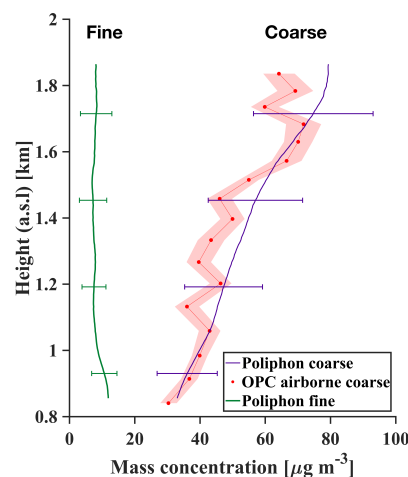


Figure 1. Mass concentration profiles for dust (coarse) and non-dust (fine) particles derived from the POLIPHON method (green and blue line, respectively), and coarse-mode particles measured by the OPC (red circles). The shaded area around the OPC measurements and the error bars in the lidar observations represents the uncertainties of the measurements.

### Acknowledgements

This project received funding from the European Union's Seventh Framework Program (FP7) project BACCHUS under grant agreement no. 603445, and the European Union's Horizon 2020 research and innovation program ACTRIS-2 under grant agreement No 654109.

## **Abstracts T304**

## A Miniature Curved Plate Mobility Classifier

Da-Ren Chen<sup>1</sup> and Qiaoling Liu<sup>1</sup>

<sup>1</sup>Particle Laboratory, Department of Mechanical and Nuclear Engineering,  
Virginia Commonwealth University, Richmond, USA

Keywords: ultrafine particles, mini-plate MC, particle electrical mobility  
Presenting author email: dchen@vcu.edu

Recent studies has evidenced that the increased exposure to ultrafine particles (UFPs) are particularly relevant to the increasing morbidity and mortality of human beings, especially for children, elders and people having lung diseases (Hoek et al. 2002; Peters et al. 2004; Delfino et al. 2005; 2010; Oberdörster et al. 2005; Bräuner et al. 2007; Shah et al. 2008; Li et al. 2010; Stewart et al. 2010). People in the communities in the close proximity to heavy traffic, highways, and combustion sources, e.g., coal-fired powerplants, have high chance of the UFP exposure. It is therefore important to monitor the presence and size distribution of near-ground (or surface) UFPs. Because of high diffusivity of UFPs, multiple ultrafine particle sizers are in need for near-ground, spatial size distribution measurement of UFPs. Sizers based on the particle electrical mobility have been applied in aerosol community for measuring the size distribution of sub-micrometer particles. An electrical mobility classifier is required in a particle electrical monbility sizer for sizing particles. Miniature particle mobility classifiers have been developed for miniature and cost-effective UFP sizers. Among various configurations, the classifiers in the parallel-plate configuration provide a uniform electric field in the size classification zone. They are also easy for machining and maintenance. To widen the measurable particle size range, an extended particle classification length in classifiers is required when the rates of flows are fixed, resulting in the increase of the final package of UFP sizers. A curved mobility classifier was proposed in this study to keep the final package of UFP sizers in bay while broadening the measurable particle size range.

The prototype curved mobility classifier, shown in Figure 1, is constructed by two coaxially aligned cylinders (having both ends sealed) with a circular spacing. In the prototype, a DC electrical field is established in the spacing between two cylinders to classify particles. Both polydisperse aerosol and clean sheath flows are introduced in the classification region via the inlets of aerosol and sheath flows. Both flows travelled downstream in the circumferential direction and exited from the outlet(s), depending on the operational modes. The prototype design enables three operational modes, i.e., precipitator (without the use of sheath flow); electrical mobility analyser (EAA; with the use of sheath flow and one outlet); and differential mobility analyser (DMA; with the use of sheath flow and two onlets). The performances of the prototype operated in the precipitator and EAA modes were evaluated at various flowrate conditions via the use of DMA-classified particles. As an

example, Figure 2 shows the transfer functions of prototype at different tested particle sizes, operated at the EAA mode with aerosol and sheath flows of 0.3 lpm and 1.5 lpm, respectively. The transfer functions at different tested particle sizes are merged as one when plotted them via normalized voltage as abscissa. The above data shows the successful operation of this prototype. The detail result of this study will be presented in the conference.

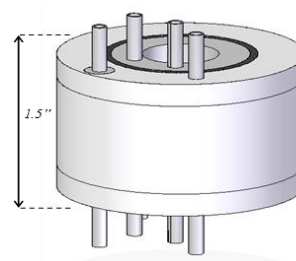


Figure 1. Schematic diagram of studied miniature curved plate mobility classifier

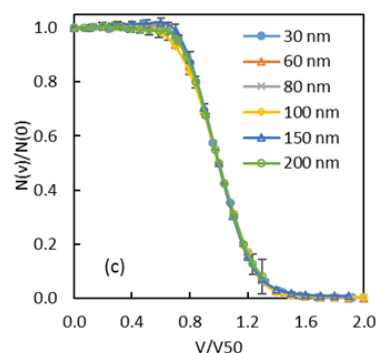


Figure 2. Transfer function of the prototype at different particle sizes when operated at the EAA mode (aerosol flow: 0.3 lpm and sheath flow 1.5 lpm)

This work was financially supported by USEPA under the grant contract #83513201.

Conflict of Interest: Chen holds a licensed intellectual property entitled as “Miniaturized Ultrafine Particle Sizer and Monitor”, which is similar in name but unrelated in configuration to this project

## PoCAMon –“All in one “ Personal Online Continuous Air monitor , Gamma Dose Meter and Gas warner

T. Streil and V. Oeser

SARAD GmbH, Wiesbadner Str.10, 01159 Dresden

Keywords: Aerosol Sampler, Radioactiv aerosols, Alpha, Beta, Gammas Spectrometry Presenting author email: [Streil@sarad.de](mailto:Streil@sarad.de)

The PoCAMon combines a very compact design with a high flow rate and long battery life. Its size and weight are still acceptable for carrying by one person.

The unit measures long-lived aerosols as well as short-lived Radon/Thoron daughters by alpha spectroscopy and beta counting. The radioactive aerosols and particles are collected on the surface of a high resolution membrane filter. The alpha and beta decays on the filter are measured by a high-end semiconductor radiation detector (400 mm<sup>2</sup>). This allows a perfect separation of the different decay products.

Fig 1 show a filter spectra of radon decay products and fig 2 show Po 210 aerosols, which was used to simulate Pu 239 aerosols. Natural Uranium aerosols are shown in fig 3 and by a special algorithm the device can decide in the dose conversion factor for the dose estimation. If only natural Uranium is in the spectra the device use for the personal warning the dose conversion factor for Uranium, which is 10 times less, than for Plutonium or Thorium aerosols.

The increased pump rate (more than 3 l/ min) is suitable for lower detection limits. The low noise rotary van pump is processor controlled and guarantees a constant flow rate over the whole measuring time. A sensor measures permanently the pressure drop on the filter in order to recognize an exhausted or perforated filter instantly.

With the 3.8 Ah NiMH battery pack the PoCAMon achieves an operation time of more than 30 hours.

The quality control is a main issue of any radiation measurement. Therefore the PoCAMon records a complete alpha spectrum for each measured value. This allows the monitoring of the device's perfect operation in each moment of the measurement.

Optional can be integrated a 10 cm<sup>3</sup> LaBr Scintillator coupled with a Silicon Photo Multiplier as high sensitive Gamma Dose meter including nuclide Identification by an Energy resolution of 4 %.

There are options for additional sensors for carbon monoxide and combustible gases as needed in underground mines to warn the staff and switch off the device in case of dangerous explosive concentrations.

All measured data are stored in a 2GB memory card and can be accessed with a PC or laptop via a USB interface. Data transmission and device control can also be done via wireless ZigBee network or via a server for stationary operation with network access. A barometric pressure sensor and a GPS receiver are further optional features of the device.

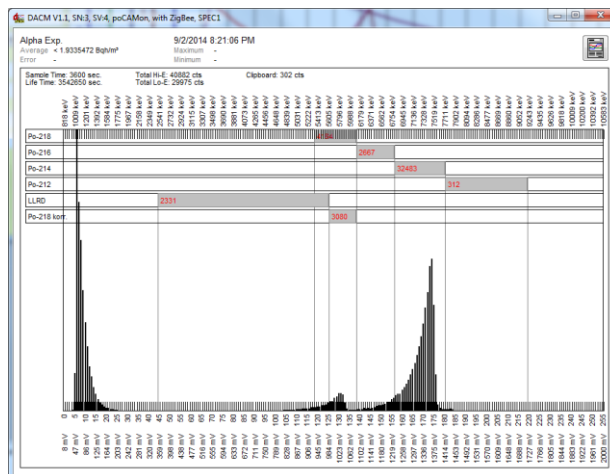


Fig 1 filter spectra of radon decay products

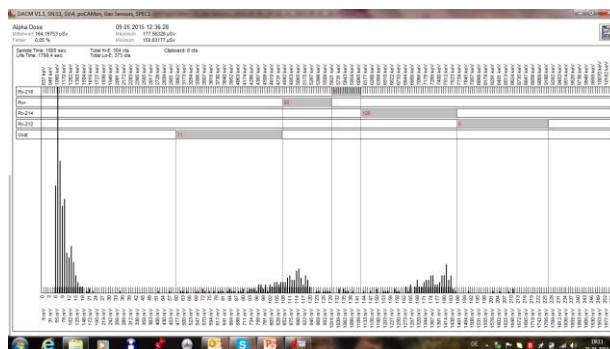


Fig 2 filter spectra of Po210 aerosols ( simulation for Pu239)

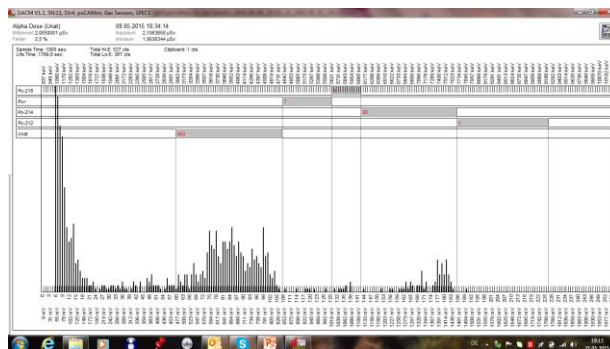


Fig 3 filter spectra of natural Uran aerosols

## Developments in personal and mobile monitors: a survey

F. Borghi<sup>1</sup>, A. Spinazzè<sup>1</sup>, D. Campagnolo<sup>1</sup>, L. Del Buono<sup>1</sup>, S. Rovelli<sup>1</sup>, A. Cattaneo<sup>1</sup>, D.M. Cavallo<sup>1</sup>

<sup>1</sup>Department of Science and High Technology, University of Insubria, Como, 22100, Italy

Keywords: portable monitoring, sensor network, air pollution, miniaturized sensors

Presenting author email: f.borghi2@uninsubria.it

Today it is well known that air quality has a huge impact on the quality of life, causing adverse effects on human health, on environmental and on the economy (Fishbain *et al.*, 2017). Air quality monitoring is required by national and international regulation and contemplate the use of monitoring stations to assess environmental exposure (Velasco *et al.*, 2016). Commonly used equipment are characterized by high costs (for purchasing and for maintenance) and can provide accurate data only for a restricted area. Accurate measurements conducted at adequate spatio-temporal scales are essential for air pollution monitoring and exposure assessment studies, especially in heterogeneous environments, such as urban environments, characterized by different emission sources (Antonić *et al.*, 2016). In recent years, different kind of mobile and miniaturized monitors (MMMs) for air pollutants have been developed (Duvall *et al.*, 2016; Dye *et al.*, 2016). These instruments are commonly low-cost, easy to use, portable and able to provide high spatial and temporal density and resolution and they are becoming increasingly important in community and individual exposure assessment monitoring (Castell *et al.*, 2015).

This study aims to provide information on the current knowledge about the use of MMMs for air pollutants in exposure assessment studies. Original articles and reviews identified in principal databases of scientific literature by means of an appropriate query of search were considered for this survey. The global aim was to realize an overview of the state-of-the-science, with particular concern on the main problems related to the issue of exposure assessment. Furthermore, key issues and some identified priorities derived from direct on-field experiences, related to the use of MMMs in the field of exposure assessment are discussed.

In order to identify and collect studies that used these kind of innovative sensors, a systematic review was performed; we consulted three different databases (Pubmed, Scopus and ISI web of knowledge) using an appropriate query of search, which arranged pertinent search terms regarding for example air quality, wearable and low-cost sensor and participatory network. Proper research outcomes were identified and selected following inclusion/exclusion criteria. We finally considered only articles provide information about on-field studies performed with MMMs, regarding environmental pollution (no restriction about kind of pollutants).

The number of articles analysed by year of publication increase over time, both as regards total articles actually considered in the review, both as regards the total number of articles (with no inclusion/exclusion criteria).

Results shows clearly how three developments in personal monitoring may be able to change the way to communicate and share scientific data (Guevara *et al.*, 2012). The first implementation concerns the integration of personal monitors with Global Position System (GPS). Use of GPS is becoming increasing due to the possibility to acquire geo-referred data and to understand pollution patterns and hotspots. It is now well known how geo-referred data, characterized by high spatial resolution may define more accurately human exposure than stationary monitors. The second and the third implementations concern the data communication and transfer via wireless and related web or smartphone applications. Several authors highlighted how Wireless Communication Module could simplify the use and transfer of data, removing technical and physical barriers. Furthermore, data transferred via Wireless can be easily use and shown to users using a web/smartphone interface, helping to increase scientific interest of the citizens to air pollution.

The integrated use of air pollution miniaturized and low-cost system, GPS, wireless communication and a user friendly interface web/smartphone can provide benefits to society, incrementing the awareness and the data sharing process between citizen and scientist (Guevara *et al.*, 2012). In conclusion MMMs, due to their characteristics could be applied in high-quality, low-cost, high-sensitivity exposure assessment studies, as well as to improve effective monitoring networks. In addition, one of the most interesting developments is the development of miniaturized instruments for participatory and ubiquitous monitoring strategies (Carminati *et al.*, 2017).

- Antonić, A., Marjanović, M., Pripuzić, K., Podnar Žarko I. (2016) *Future Gener. Comput. Syst.* **56**, 607-622.
- Carminati, M., Ferrari, G., Sampietro, M. (2017) *Measurement* **101**, 250-256.
- Castell, N., Kobernus, M., Liu, H.Y., Schneider, P., Lahoz, W. *et al.* (2015) *Urban Climate* **14**, 370-382.
- Duvall, R.M., Long, R.W., Beaver, M.R., Kronmiller, K.G., Wheeler, M.L., Szykman, J.J. (2016) *Sensor* **16**, 1698.
- Dye, T., Graham, A., Hafner, H. (2016) *EM* **66**, 1-5.
- Fishbain, B., Lerner, U., Castell, N., Cole-Hunter, T., Popoola, O., *et al.* (2017) *Sci. Total Environ* **575**, 639-648.
- Guevara, J., Barrero, F., Vargas, E., Becerra, J., Toral S. (2012) *IET Intell. Transp. Sy.* **6**, 177-186.
- Velasco, A., Ferrero, R., Gandino, F., Montrucchio, B., Rebaudengo, M. (2016) *Sensor* **16**, 710.

## A miniature particle counter (LOAC) under meteorological balloons for the study of the temporal and spatial variability of stratospheric aerosols

D.Vignelles<sup>1\*</sup>, J.-B.Renard<sup>1</sup>, G.Berthet<sup>1</sup>, F.Dulac<sup>2</sup>, F. Jégou<sup>1</sup>, L. Rieger<sup>3</sup>, A. Bourassa<sup>3</sup>, J.-P. Vernier<sup>4,5</sup>, G. Taha<sup>6,7</sup>, S. Khaykin<sup>8</sup>, T. Lurton<sup>1</sup>, B. Couté<sup>1</sup>, V. Duverger<sup>1</sup>

<sup>1</sup> LPC2E/CNRS/University of Orléans, 3A Avenue de la recherche scientifique, 45071 Orléans

<sup>2</sup> LSCE-CEA/IPSL, University of Paris Saclay, CEA Saclay 701, 91191 Gif-sur-Yvette, France

<sup>3</sup> Institute of Space and Atmospheric Studies, University of Saskatchewan, Saskatoon, Canada

<sup>4</sup> Science Systems and Applications Inc., Hampton, USA

<sup>5</sup> NASA Langley Research Center, USA

<sup>6</sup> Universities Space Research Association, Greenbelt, MD, USA

<sup>7</sup> NASA Goddard Space Flight Center, Greenbelt, MD, USA

<sup>8</sup> LATMOS, CNRS, University of Versailles St Quentin, Guyancourt, France

Keywords: Aerosol counter, Stratosphere, Balloon

\*Presenting author email: damien.vignelles@cnrs-orleans.fr

The study of the stratospheric aerosols is important for our understanding of the terrestrial radiative budget. Stratospheric aerosols play also an important role on the spatial and temporal distribution of the gas species in atmosphere through heterogeneous processes. In order to characterise the local variations of the stratospheric aerosol content, we have performed one hundred meteorological balloon profiles (Vignelles et al. 2016) carrying a new miniature aerosol counter called LOAC (Light Optical Aerosol Counter). This strategy has allowed us to produce a dataset of aerosol profiles up to 30 km over France with a frequency of 2 profiles per month over 3 years.

The LOAC particle counter has been designed for balloon-borne tropospheric studies (Renard et al. 2016). Its metrological performance in stratosphere has been characterised regarding the dependence on atmospheric pressure, inner temperature, cosmic rays and low concentration of particles. Tests in laboratories and on-board have shown that the principal limitation of the utilisation of LOAC in stratosphere is introduced by the temperature variations and by the influence of cosmic rays. A detection threshold has been determined in the laboratory to be of 1 particule.cm<sup>-3</sup> in term of concentration which also limits the use of LOAC in the stratosphere where aerosol concentrations during volcanic quiescent periods may be lower than this limit.

Inter-comparisons between two LOAC under meteorological balloons and between a LOAC and another aerosol counter have revealed good performances and have allowed us to discuss the LOAC limitations in term of measurement reproducibility. Also these results have raised questions about the current hypothesis used by other teams concerning stratospheric aerosol properties.

At last, we have compared our LOAC dataset with three satellite records (OSIRIS, CALIOP and OMPS), a ground-based lidar (lidar OHP) and a model output (WACCM) over France. Comparative results have revealed good agreement between the various datasets up to 25 km (Figure 2 – Vignelles 2016). Above 25 km, data differ significantly.

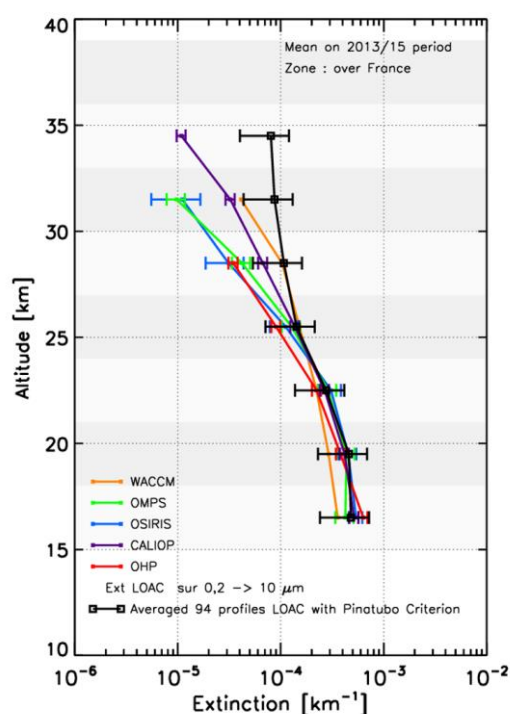


Figure 2. Comparative satellites, model, ground lidar and LOAC extinctions averaged over 3 km bands over France for the 2013-2016 period.

### References:

- Renard et al. (2016) *LOAC: a small aerosol optical sounter/sizer for ground-based and balloon measurements* AMT. 9, 1721-1742. doi:10.5194/amt-9-1724-2016
- Vignelles et al. (2016) *Balloon-borne measurement of the aerosol size distribution from an Icelandic flood basalt eruption.* EPSL. 453, 252-259. doi:10.2016/j.epsl.2016308.027
- Vignelles (2016) *Caractérisation des performances du nouveau mini compteur de particule LOAC embarqué sous ballon météorologique : application à l'étude de la variabilité spatiale et temporelle des aérosols de la haute troposphère et de la stratosphère* – PhD thesis

## Optofluidic Surface-Enhanced Raman Spectroscopy (SERS) Platform for Airborne Bacteria Particles

Jae Hee Jung

Center for Environment, Health and Welfare Research, Korea Institute of Science and Technology (KIST),  
Seongbuk-gu, Seoul 02792, Republic of Korea

Keywords: Raman Spectroscopy, Real-time Sampling, Bioaerosol, Microchannel  
Presenting author email: jaehee@kist.re.kr

As indoor air quality (IAQ) management has become an important issue in modern society, there is a great deal of research interest in the presence of bioaerosols, which are airborne particulate matter of biological origin, in relation to their adverse health effects (Goyer, 2001; Nazaroff, 2014). Bioaerosols such as virus, bacteria and fungi are the primary components of atmospheric aerosols. Their size distribution ranges from 20 nm to 100  $\mu\text{m}$  which is easy to be aerosolized into air. Due to their low settling velocities, they are suspended in air for a long time. Therefore, for active disease control and to minimize bioaerosol exposure risk, there is a requirement for effective bioaerosol monitoring systems, including continuous bioaerosol sampling and rapid analysis (Jung and Lee, 2013; Fraser et al., 2009; Agranovski et al., 2004).

To date, several methods to detect bioaerosols have been proposed. Polymerase chain reaction (PCR) techniques have been used extensively to detect sampled airborne microbes because PCR can provide a highly quantitative analysis. However, these techniques are not adequate for real-time detection because they take >1 h to analyze the microbes. Although antibody-based detection methods have been used due to their sensitivity, additional pre-treatment processes are necessary to transfer bioaerosols from an airborne to a colloidal state. Thus, they cannot guarantee continuity for an integrated “ $\mu$ -total analysis system”. One of the most used real-time detection techniques with an air-based platform exploits the auto-fluorescence of microorganisms by exerting UV light on them. Although this technique allows continuous real-time monitoring of bioaerosols directly, it suffers from low fluorescent intensity, leading to poor signal to noise ratio, low detection limit, and the requirement for precise optical systems for measurements.

In this study, we present the optofluidic surface-enhanced raman spectroscopy (SERS) platform which consists of novel bioaerosol sampling technique based on inertial microfluidics with two-phase continuous flow, and *in situ* measurement of particle raman scattering spectra. This two-phase fluid, sampling air and collecting liquid, stably forms a stratified flow in the simple curved-microfluidic channel composed of one curve with an angle of 180°, three inlets, and two outlets in a single microchip. The collecting liquid including silver colloid covers the outer wall of the channel during bioaerosol sampling. For collection, the particles are transferred from air to the liquid phase by centrifugal

and drag forces by passing fluids through the curved region. The cut-off diameter of particle collection was selected controlling the air flow velocity (microfluidic air flow of 1.2 L/min showed a particle collection efficiency of ~98% at a particle diameter of 1  $\mu\text{m}$ ), and continuous enriched particle sampling was possible for real-time SERS measurement to identify sampled particle.

Our results indicated that the developed system represents a significant step forward as an inexpensive, simple, portable and continuous bioaerosol monitor based on the optofluidic platform.

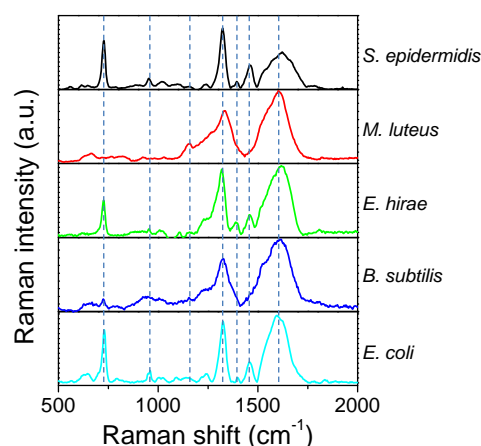


Figure 1. Various Raman spectra from airborne bacteria measured by the optofluidic SERS platform

This research was supported by the KIST Institutional Program. This research was also supported in part by the Ministry of Land, Infrastructure, and Transport (16RTRP-B082501-03) and the Ministry of Environment (2016000160008), Republic of Korea.

Galton, E., Tovey, M. Mclaws and Rawlinson, W. D. (2011) *J. Infection*, **62**, 1-13.

Goyer, N. *Bioaerosols in the Workplace: Evaluation, Control and Prevention Guide: Technical Guide*, Montreal: IRSST, (2001).

Nazaroff, W. (2014) *Indoor Air*, **26**, 61-78.

Jung, J. H. and Lee, J. E. (2013) *J. Aerosol Sci.*, **65**, 101-110.

Fraser, C. et al. (2009) *Science*, **324**, 1557-1561.

Agranovski, I. E. et al. (2004) *Atmos. Environ.*, **38**, 3879-3884.

## A New PAHs and BC Monitor for Automatic Routine Monitoring of Urban Ambient Aerosol

C. Carbone<sup>1</sup>, E. Cozzani<sup>1</sup>, S. Zampolli<sup>2</sup>, M.G. Pietrogrande<sup>3</sup>, A. Poggi<sup>1,2</sup>, S. Fuzzi<sup>1,4</sup> and S. Decesari<sup>4</sup>

<sup>1</sup>Proambiente S.c.r.l., CNR Research Area, Bologna, Italy

<sup>2</sup>Institute of Microelectronics and Microsystems, Italian National Research Council, Bologna, Italy

<sup>3</sup>Terra&AcquaTech, University of Ferrara, Ferrara, Italy

<sup>4</sup>Institute of Atmospheric Sciences and Climate, Italian National Research Council, Bologna, Italy

Keywords: PM monitoring, urban aerosol sources, PAHs, BC, MEMs.

Presenting author email: c.carbone@consorzioproambiente.it

In the frame of the POR-FESR 2014-2020 Programme of Emilia Romagna Region (Italy), we are developing and here presenting a low cost, automatic and small-sized instrument to monitor near-real time particulate black carbon (BC) and polycyclic aromatic hydrocarbons (PAHs) in urban ambient air.

This new monitor reflects the most recent innovative trend for air quality monitoring: the strengthening of the traditional monitoring networks with low cost, small-sized and automatic sensors, able to produce high flows of real time data and send them to the administrations or directly to citizens. This kind of unconventional monitoring systems – i.e. fast, low cost, automatic and real time vs low time resolution, bulky, more expensive and non-automatic (or automatic but not quantitative) - are revolutionizing both the amount of available data and their application.

PAHs and BC are co-emitted from the same combustion sources (e.g. traffic, residential heating), exerting relevant effects on global warming and human health. The availability of big real time data of these two key source specific aerosol chemical components, in combination with smart tools to convert rough data into simple and easily readable information, can allow European Municipalities and Environmental Agencies to assess risks of emission scenarios and vulnerability of the different urban districts, so supporting them in the development of joint strategies for the mitigation of climate change and the improvement of air quality.

The innovative character of the proposed device lies in two main technology features: 1) Integration of BC (multi-wavelengths Aethalometer) and PAHs (Gas Chromatography system) measurements; 2) The core technology for online PAHs measurements. The step beyond the conventional devices used for the determination of particulate-bound PAHs is provided by the implementation of Micro-Electro-Mechanical-Systems (MEMs) fabrication technology to realize an innovative sensing device, capable to overcome the high cost of the current sampling procedures and off-line laboratory analyses. Such small-sized and portable device is so suitable to be integrated in air quality monitoring networks, thus obtaining automatic measurements characterized by an improved spatial and time resolution (2-3 hours, compared to the typical 12/24 hours of the conventional methods). It permits to identify more precisely risk situations due to air pollution that can be

associated with daily cycles (peak hours), transport events, intermittent and specific sources.

Results from laboratory test validated the feasibility of the measurement chain for automatic PAHs quantitative analysis: Aerosol Sampling; Thermal Desorption; Gas Chromatography System with PID detector. Figure 1 shows, as an example, a chromatogram obtained by spiking on filter a 16 PAHs mix at concentrations comparable to real ambient conditions.

Here we present the concept of the instrument and the potentiality of possible applications by exhibiting results of its deployment in a real environment.

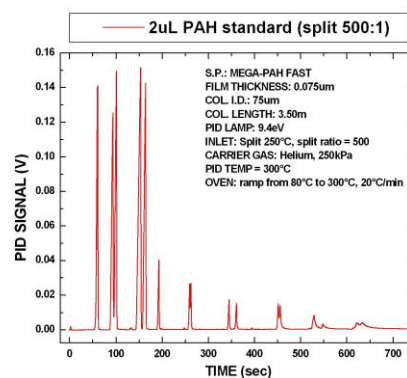


Figure 1. Example of results from laboratory test to validate the feasibility of the measurement chain for automatic PAHs analysis.

This work was supported by the “Programma Operativo Regionale Fondo Europeo Sviluppo Regionale (POR-FESR)” 2014-2020 <http://www.regione.emilia-romagna.it/fesr/por-fesr/>.

## Miniaturized aerosol instruments for unmanned aerial vehicles

F.J. Brechtel<sup>1</sup>, M. Ramstrom<sup>2</sup>, A.B. Corless<sup>1</sup> and T.S. Bates<sup>3</sup>

<sup>1</sup>Brechtel Mfg. Inc., 1789 Addison Way, Hayward, CA 94544 U.S.A.

<sup>2</sup>Hugo Tillquist AB, Box 1120, SE-164 22 KISTA, Sweden

<sup>3</sup>NOAA PMEL, 7600 Sand Point Way NE, Seattle, WA 98115 U.S.A.

Keywords: UAV, miniaturized instruments, aerosol measurements

Presenting author email: [fredj@brechtel.com](mailto:fredj@brechtel.com)

More routine measurements of the aerosol direct and indirect effects on climate are required to reduce the uncertainties in model predictions of climate change. One possibility for providing measurements over broader spatial and temporal scales is to deploy miniaturized instruments on-board unmanned aerial vehicles (UAVs). UAVs can provide information near the Earth's surface as well as important vertical profile information in the atmosphere. Networks of UAVs could provide near global coverage of climate-relevant information that could be used to better constrain climate models.

Scientists and engineers at Brechtel Mfg. have been working on various miniaturized instrument modules over the last 8 years that can be deployed on-board medium-sized UAVs. These include a Mixing-based Condensation Particle Counter (Model 9403, MCPC), a Single-channel Tri-color Absorption Photometer (Model 9406, STAP), an eight-channel filter sampler (Model 9401, FILT), an optical particle counter (Model 9405, mOPC), a wind and turbulence probe (Model 9402, GUST), a miniature scanning electrical mobility sizer system (Model 9404, mSEMS) and a Base Module (Model 9400, BaseM) for system integration. An isokinetic inlet system has also been developed for small UAV platforms. The typical dimensions of the modules are between 5 and 15 cm with weights between 0.2 and 4 kg.

The MCPC, STAP and FILT modules have been simultaneously deployed on-board two Manta UAVs over the Arctic by NOAA in 2011 and 2015 (Bates *et al.*, 2013). Based in Svalbard, approximately 20 flights with 80 flight hours were completed during the two campaigns. The MCPC and STAP have also been deployed on UAVs during field studies in Germany and Greece. The mOPC, mSEMS and mGUST modules are currently under development.

Example vertical profiles of the aerosol light absorption coefficient as well as the total aerosol number concentration for particles larger than 8 nm diameter are shown in Fig. 1 for one of the Svalbard flights in 2011. The red arrows denote atmospheric temperature inversions that correspond with a local maximum in the number concentration near 1000 m and elevated concentrations above 1700 m attributed to long-range transport. Real-time communication of measured parameters to the ground station allowed changes to be made to the on-going flight pattern to capture interesting ambient aerosol features.

A brief review of the size, weight, power and other specifications of the various modules will be presented. Results from intercomparison studies between the UAV

devices and traditional benchtop instruments will be shown. A measurement framework is proposed where observations from ground site networks, UAV vertical profiles and satellite overpasses are synchronized to better constrain satellite retrievals and, eventually, climate models. Key limitations with respect to current UAV-deployable measurements are discussed, including in-cloud sampling and observations of detailed aerosol radiative properties that can be directly compared to remotely-sensed parameters from satellites.

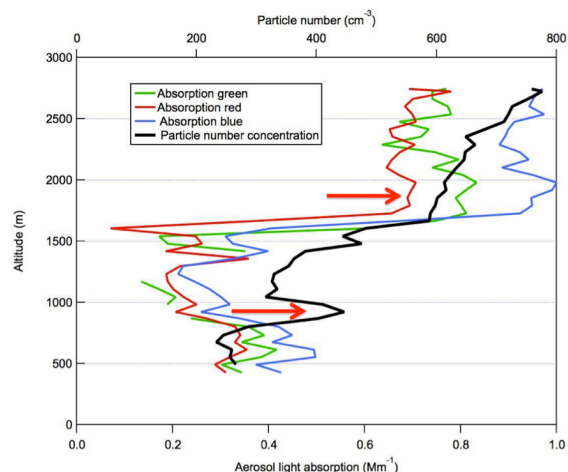


Figure 1. Example vertical profiles of aerosol light absorption coefficient (red, green & blue wavelengths) and total number concentration (black) over Svalbard, Norway (Bates *et al.*, 2013).

This work was supported by the US NSF, NOAA and DOE under various SBIR Grants.

T.S. Bates, P.K. Quinn, J.E. Johnson, A. Corless, F.J. Brechtel, S.E. Stalin, C. Meinig, and J. Burkhardt (2013). Measurements of atmospheric aerosol vertical distributions above Svalbard, Norway using unmanned aerial systems (UAS). *Atmospheric Measurement Techniques*, 6: 2115-2120, doi:10.5194/amt-6-2115-2013.

## Low-cost and Lightweight Instruments for Probing Physicochemical Properties of Aerosol Particles

G. Biskos<sup>1,2</sup>, K. Barmounis<sup>1</sup>, S. Bezantakos<sup>3</sup>, and A. Maisser<sup>1</sup>

<sup>1</sup>Energy Environment and Water Research Center, The Cyprus Institute, Nicosia 2121, Cyprus

<sup>4</sup>Faculty of Civil Engineering and Geosciences, Delft University of Technology, Delft 2628-CN, The Netherlands

<sup>2</sup>Maison de la Recherche en Environnement Industriel 2 (MREI2), Université du Littoral Côte d'Opale, 59140, Dunkerque,

Keywords: Aerosol Measurements, Size Distributions, Volatility, Hygroscopicity

Presenting author email: [g.biskos@cyi.ac.cy](mailto:g.biskos@cyi.ac.cy); [g.biskos@tudelft.nl](mailto:g.biskos@tudelft.nl)

Probing the physicochemical properties of airborne particles such as their concentration, size, volatility and hygroscopicity is key for understanding their environmental impacts (McMurry, 2000). Although a wide number of instruments is currently available for measuring those properties, the associated high cost and complexity limits their use in dense monitoring networks as well as on highly mobile platforms (e.g., drones).

Recent developments in our lab have shown that instruments such as the Differential Mobility Analyzer (DMA) can be manufactured in a simple and cost-effective way using mold casting or 3D printing (Barmounis et al. 2016). What is more, using tubular precipitators made out of Electrostatic Dissipative Materials can result in extremely inexpensive and efficient Particle Size Segregators (PSSs; Bezantakos et al. 2015). In this work we demonstrate that by combining such cost-effective tools one can make instruments for probing a number of aerosol particle properties. To prove the concept we have built and tested a versatile system consisting of a 3D printed DMA, a PSS and two mini CPCs (cf. Figure 1), to measure the size distribution, the volatility and the hygroscopicity of aerosol particles.

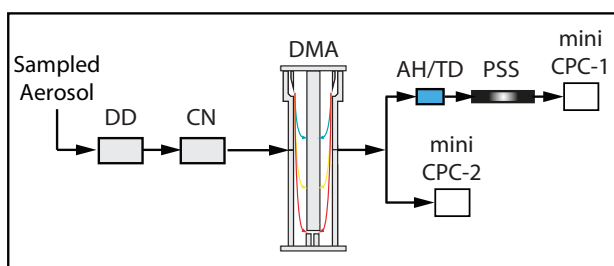


**Figure 1.** Cost-effective systems for measuring the particle size distribution as well as the hygroscopicity and volatility of aerosol particles. The system consists of a Diffusion Drier (DD), a Charge Neutralizer (CN) a 3D-printed DMA, an Aerosol Humidifier/Thermal Denuder (AH/TH), a Particle Size Segregator (PSS) and two mini CPCs.

As demonstrated in Figure 2, the system can determine the hygroscopic behavior (i.e., both potential phase transitions and hygroscopic growth) as well as the volatility of aerosol particles, with the results being of similar quality with those from state-of-the-art tandem DMA systems. Considering their low manufacturing cost, and simplicity (i.e., avoiding a sheath flow system for in the PSS), systems similar to those described here can be

employed in dense air quality monitoring networks and mobile platforms thereby providing sufficient density of information. This, in turn, can allow us to understand the evolution of aerosol particles in the atmospheric environment and therefore their impacts on human health and climate.

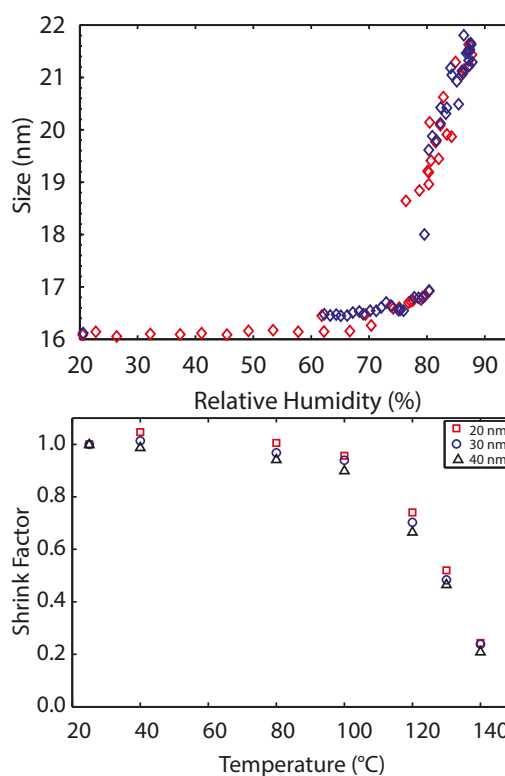


**Figure 2.** Hygroscopicity (top) and volatility (bottom) of laboratory-generated particles using the cost-effective system shown in Figure 1.

### References

- McMurry, P. H. (2000), *Atmos. Environ.*, 34:1959–1999.  
 Barmounis, K., A. Maisser, A. Schmidt-Ott, and G. Biskos (2016) *Aerosol Sci. Technol.*, 50, ii-v.  
 S.Bezantakos, L. Huang, K. Barmounis, M. Attoui, A. Schmidt-Ott, and G. Biskos (2015), *Aerosol Sci. Technol.*, 49, iv-vi.

## A Low-Cost Optical Instrument for estimating the contribution of Waste-to-Energy plants to the local PM2.5

M. Del Guasta<sup>1</sup>

<sup>1</sup>Institute of Applied Optics CNR, Sesto Fiorentino, 50019, Italy  
 Keywords: PM2.5, optical sensor, combustion aerosols, WtE plants  
 massimo.delguasta@ino.it

Recent epidemiological studies evidenced the primary importance of PM2.5 and ozone in causing lung diseases, including cancer, in EU states (Beelen *et al.*, 2013). The development of new methods for monitoring PM2.5 is thus challenging in our countries.

In the case of waste-to-energy (WtE) plants, the perception of danger for health could be acute. On the other side, the chronic shortage in the budget of local environmental agencies (especially in Mediterranean countries) inevitably leads to a lack of monitoring around most of those sources.

A low-cost, automatic device for the continuous monitoring of PM2.5 and wind direction is described. Its test in small networks, set around WtE plants, is also presented. The fast response of the device and its capability of detecting the direction of arrival of PM makes possible the estimation of the contribution of WtE plants to the local PM2.5 concentrations.

The instrument was developed around the photometric smoke sensor SHARP GP2Y1010, already identified as potentially useful in PM monitoring by Budde *et al.*, 2012. GP2Y1010 is sensitive enough for measuring PM2.5 concentrations near to background (5  $\mu\text{g}/\text{m}^3$ ), but its output is temperature-dependent and requires proper calibrations and a proper driving for using it as an outdoor PM2.5 measuring tool.

The GP2Y1010 was interfaced with a specifically designed PIC18 (Microchip) controller board. The board manages the GP2Y1010 sensor, a GPS-GPRS module, house-keeping, temperature, and humidity sensors. A low-cost wind direction sensor, based on Hall effect, was also designed and implemented. GP2Y1010 data averaged every 5 minutes are converted to PM2.5 units through temperature-dependent calibration functions. PM2.5 data are stored together with meteo and housekeeping data on SD card and eventually transmitted to a server via GPRS in real time. The calibration data and measurement settings (specific for each device) are also stored into the SD.

The instrument can operate without line-power by means of solar panels. In such a case, a power-management software adapts the measurement rate to the battery status. The degradation of the sensor due to deposition of dirt is automatically monitored every week.

The whole electronics, including GP2Y1010, is calibrated in two phases. The calibration of the sensor output in terms of PM2.5 is obtained by comparing the averaged, analog output of the sensor with the PM2.5 measured by means of a Grimm OPC 1.109, assuming a density of 1.4  $\text{g}/\text{cc}$  for the aerosols. Combustion aerosols of different origin were tested for calibration, including

paper pyrolysis, oil and PVC combustion. Paper pyrolysis was selected for calibration: the smoke chamber is filled with combustion aerosols and a continuous measurement of GP2Y1010 and Grimm 1.109 is performed with 1-minute resolution, following the decay of PM. The second calibration, for temperature drift, was performed inside a thermal chamber with a saw-tooth thermal cycle ( $-10^\circ\text{C}$  to  $+50^\circ\text{C}$ ), in order to measure the temperature-dependency of the PM2.5 data. Each calibration was carried out simultaneously on eight prototypes at a time.

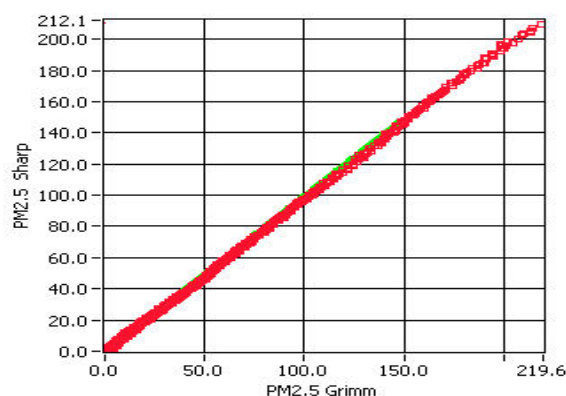


Figure 1. PM2.5 Calibration curve of a prototype.

Three prototypes were tested in the field at Prato (Italy), placed 300 m around a WtE plant, between Nov. 2015 and Apr. 2016. The angular distribution of PM2.5 with wind direction was obtained.

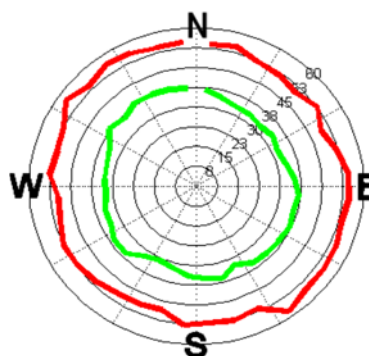


Figure 2. Four months of PM2.5 [ $\mu\text{g}/\text{m}^3$ ] data (Prato, Italy) plotted as distributions with wind direction: averages (green), 98<sup>o</sup> percentiles (red)

Beelen, R. *et al.* (2013) *The Lancet*, Vol. 383, **9919**, 785 – 795

Budde, M., Busse, M., Beigl, M. (2012) *Ninth Int. Conf. on Networked Sensing (INSS)*, 2012, 1-4.

## **Abstracts T305**

## Dekati Diluter characterization in the 1-20 nm particle size range

J. Vanhanen<sup>1</sup>, M. Svedberg<sup>1</sup>, E. Miettinen<sup>1</sup>, J.-P. Salo<sup>1</sup>, and M. Väkevä<sup>1</sup>

<sup>1</sup>Airmodus Ltd., Erik Palménin aukio 1, 00560 Helsinki, Finland.

Keywords: dilution, particle number, ultrafine particle, cluster.

Presenting author email: [joonas.vanhanen@airmodus.com](mailto:joonas.vanhanen@airmodus.com)

One of the main advantages of condensation particle counters is the sensitivity (McMurry, 2000). The ability to detect individual particles is important in many applications. A CPC can be used as single particle detector usually up to about  $10^4$  #/cm<sup>3</sup>, after which coincidence starts to be an issue ( $> 10\%$  of the signal). Using dilution allows one to measure with single particle detection mode and hence get more precise measurements. For the smallest aerosol particles and clusters of molecules, dilution is not trivial due to diffusional losses to the walls of the diluter. In the recent years CPC technology, and also the calibration methods have been developed and the lowest cut-off diameters are now pushed to the 1 nm size range (Vanhanen et al. 2011, Jiang et al. 2011, Kangasluoma et al. 2015). This creates a need for a diluter design suitable also for these smallest clusters. In this study, we characterized the Dekati ejector diluter (Dekati Diluter), in the particle size range of 1-20 nm in diameter.

Two different measurement setups were used in this study; a Hauke DMA – setup and a high flow DMA – setup. With the Hauke DMA a tube furnace with nitrogen as carrier gas was used to produce silver nanoparticles and an Americium neutralizer was used to achieve the charge equilibrium before the DMA. The particle diameter size range measured with this setup was from 4.1 to 20 nm. The CPC cut-off curves were taken into account within the whole size range when analyzing the data. With the high flow DMA (SEADM, HalfMini) a hot wire generator with NiCr – wire and HEPA filtered compressed air as a carrier gas was used to produce nanoparticles. The size range was from 1.2 to 4 nm. The hot wire generator produces so called self-charged particles and thus no additional neutralizer / charger was used (Kangasluoma et al. 2013). An aerosol electrometer was used as a reference instrument and Airmodus A11 nano Condensation Nucleus Counter (nCNC) was used as the detector after Dekati Diluter. Measured pressure difference between the inlet of the ejector and the outlet of the ejector was about 20 mbars and the dilution factor according to the data sheet is about 9. By comparing the concentrations of a reference instrument and the instrument after the Dekati Diluter, so called particle number concentration reduction factor (PCRf) can be calculated. This factor contains both the dilution and the particle losses inside the diluter.

In figure 1, the particle number concentration reduction factor (PCRf) and the estimated particle losses are presented. The PCRf above 10 nm is relatively constant

with mean value of 9.31. This is well in line with the factory calibration. The PCRf increases towards the smallest particle size measured in this study (44.4 at 1.2 nm). We assume that this is due to diffusional losses inside the diluter. If the mean dilution factor above 10 nm (9.31) is taken into account, the particle losses for 1.2 nm clusters inside the Dekati Diluter are 79 %. This is still quite reasonable when considering the high diffusivity of such small clusters. Already at 1.9 nm the losses are 43%. Based on these results the Dekati Diluter can well be combined with Airmodus nCNC, provided the particle number concentration reduction factor as a function of particle size is included in data inversion.

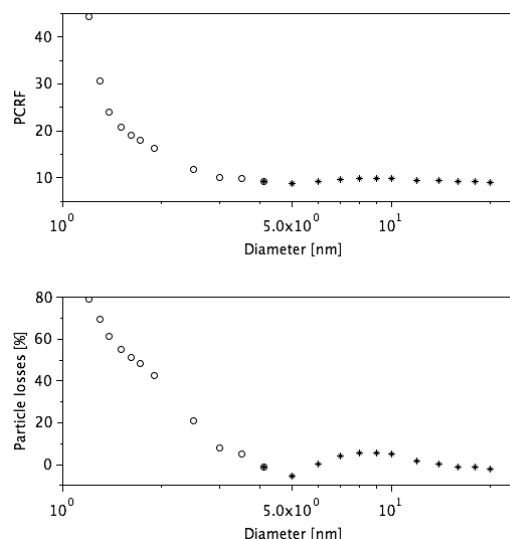


Figure 1. Particle number concentration reduction factor (upper) and the estimated particle losses (lower) as a function of particle diameter. Circles are measured using the high flow DMA setup and the stars are measured using the Hauke DMA setup.

This study was supported by Dekati Oy.

- McMurry, P. (2000) *Aerosol Science and Technology*, 33:297-322.
- Vanhanen, J. et al. (2011) *Aerosol Science and Technology*, 45:4, 533-542.
- Jiang, J. et al. (2011) *Aerosol Science and Technology* 45:4, 510-521.
- Kangasluoma, J. et al. (2015) *Aerosol Science and Technology*, 49:8, 674-681.
- Kangasluoma et al. (2013) *Aerosol Science and Technology*, 47:5, 556-563.

**Characterization of the boosted 3776 butanol TSI CPC as detector in the sub 2 nm range.  
Activation of sub 2 nm with butanol vapors.**

Michel ATTOUI

LISA, Université Paris Est & Université Paris Diderot  
CNRS UMR-7583 Paris France.

Keywords : CPC, detection efficiency, nanoparticles,

Boosted butanol laminar sheathed condensers CPCs have (Kuang2012) demonstrated their ability to detect sub 3 nm with acceptable detection efficiency although lower than mixing cpc with di ethylene glycol as working fluid. In the other hand Kangasluoma et al. 2015 have showed that unsheathed condensers butanol CPCs are able to detect particles down to 1 nm. So if unsheathed condenser can detect particles of 1 nm why not the sheathed condenser CPC design? The abilities of this CPC in terms of flowrates control (sheath and capillary) are used to study the activation (or no activation) of THABr and TBABr monomer by lowering the aerosol losses in the capillary and working at the limit or threshold of the homogeneous nucleation. The presentation gives the effect of the flowrate in the capillary on the detection efficiency for different temperatures difference  $\Delta T$ s between the saturator and condenser until the limit of the homogeneous nucleation. The figures 1 and 2 below give the inverse mobility spectra of TBABr (tetrabutylammonium bromide) with flowrates of 50 cc/min 70 cc/min in the capillary at the limit of the homogeneous nucleation and respectively in the condenser. The figures 3 and 4 give the results with THABr (tetraheptylammonium bromide) in the same with 50 et 70 cc/min aerosol flowrate in the capillary at the limit of the homogeneous nucleation always.

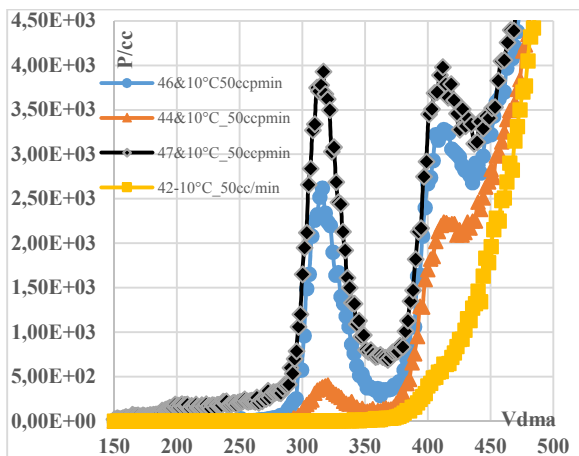


Figure 1  
TBABr with 50 cc/min in the capillary

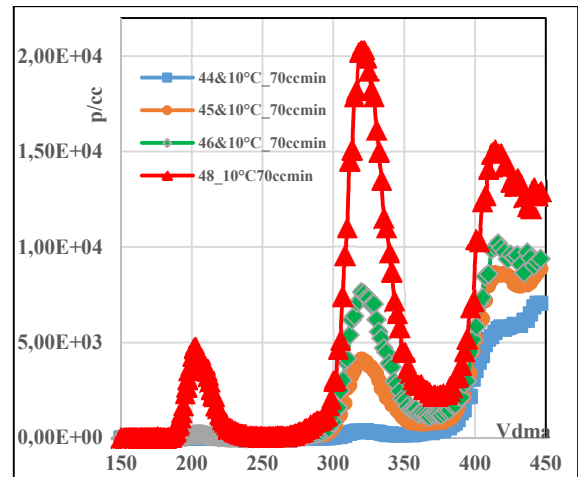


Figure 2

TBABr with 70 cc/min in the capillary

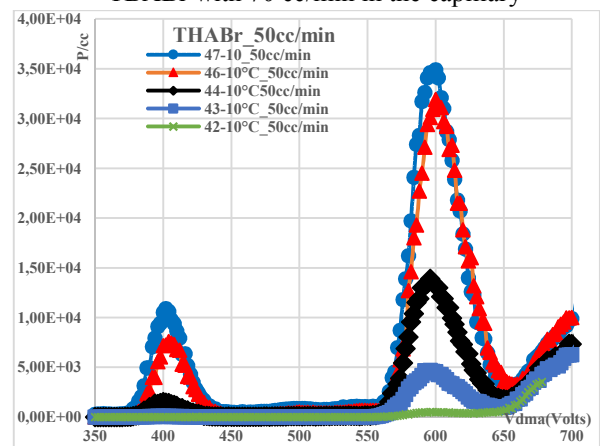


Figure 3

THABr with 50cc/min in the capillary

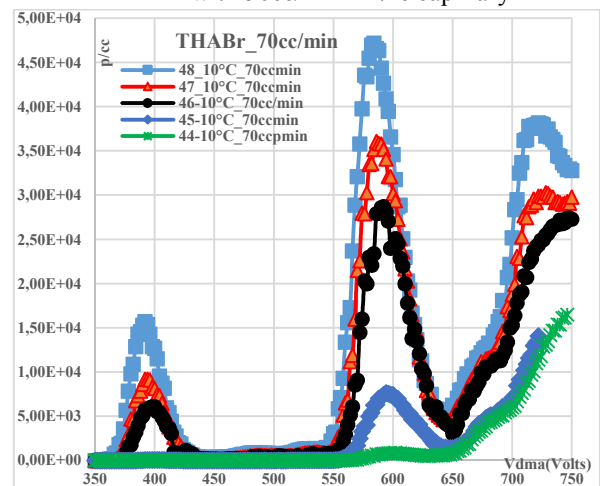


Figure 4

THABr with 70 cc/min in the capillary

References:

- Kuang,C et al. (2012): Aerosol Science and Technology, 46:3, 309-315.
- Kangasluoma et al. (2015) : Aerosol Science and Technology, 46:3, 309-315.

The author thanks TSI Inc. for providing the 3776 butanol CPC.

## How to compare the efficiency of different air disinfection devices

A.S. Safatov<sup>1</sup>, V.G. Akimkin<sup>2,3</sup>, G.A. Buryak<sup>1</sup>, A.V. Nagolkin<sup>4</sup>, G.V. Shuvalov<sup>5</sup>, D.A. Trubitsin<sup>5</sup>, V.A. Vechkanov<sup>1</sup>

<sup>1</sup>Department of Biophysics and Ecological Researches, FBRI SRC VB "Vector" of Rospoterbnadzor, Koltsovo, Novosibirsk region, 630059, Russian Federation

<sup>2</sup>FRBI Research Institute of Disinfectology of Rospoterbnadzor, Moscow, 117246, Russian Federation

<sup>3</sup>I.M. Sechenov First Moscow State Medical University, Moscow, 119991, Russian Federation

<sup>4</sup>«Potok-Inter», Co. Ltd., Moscow, 115162, Russian Federation

<sup>5</sup>«Aeroservis», Co. Ltd., Novosibirsk, 630099, Russian Federation

<sup>6</sup>Federal State Unitary Enterprise "SNIIM", Novosibirsk, 630004, Russian Federation

Keywords: bioaerosols, air disinfection device, disinfection efficiency.

Presenting author email: [safatov@vector.nsc.ru](mailto:safatov@vector.nsc.ru)

The creation of appropriate conditions in premises with high purity requirements is impossible without special preparation of air medium. For many productions, it is most critical to ensure aseptic conditions. Therefore, bioaerosol removal from indoor air is an urgent task. Currently, the market offers a wide variety of flow through type air disinfectors, which are tested for filtration efficiency according to the available standards (see AHAM, 2002), based on the CADR (Clear Air Delivery Rate) value. However, the CADR value does not say anything about the inactivation of microorganisms that have passed through disinfectors, which results in the reduction of the concentration of viable microorganisms at the device outlet not only due to the retention of particles in the device.

The authors presented substantiation report (Vechkanov, V.A., *et al.*, 2016) on the necessity of common procedure and efficiency criteria for air disinfection devices (ADD) of flow through type.

The analysis of literature and own data allow us to formulate criteria for estimation of ADD efficiency.

According to our point of view, a natural measure of the efficiency of aerosol disinfection by the test device  $E_b$  is the ratio of the concentrations of viable microorganisms at the device output  $C_{b,out}$  and inlet  $C_{b,in}$ :

$$E_b = 100 * (1 - C_{b,in} / C_{b,out}), \% \quad (1)$$

Very important ADD's efficiency characteristic is filtration efficiency  $E_m$ . The relationship based on the ratio of aerosol mass concentrations at the device output ( $C_{m,out}$ ) and inlet ( $C_{m,in}$ ) is proposed:

$$E_m = 100 * (1 - C_{m,in} / C_{m,out}), \% \quad (2)$$

It should be noticed that device filtration efficiency is estimated using counter aerosol concentrations for the most penetrating aerosol particle (for HEPA-filters this diameter usually is approximately 200 – 300 nm). But efficient filtration of microorganisms containing particles (having diameters of several micrometers) is important for ADD really. It is assumed usually than microorganisms are distributed uniformly in particles volume. In this case one particle with diameter of 3  $\mu\text{m}$  which may contains many microorganisms has the same mass as  $10^3$  particles with diameter of 3 nm which contains no microorganism. It is clear that one big particle will not be noticeable in aerosol particles count size distribution but as soon as it contains many microorganisms the efficiency of air

disinfection may be low. So ADD filtration efficiency should be characterized by aerosol mass concentrations.

One can calculate efficiency of microorganisms passing through ADD inactivation  $E_i$  from formulas (1) and (2):

$$E_i = 100 * (1 - (1 - E_b / 100) / (1 - E_m / 100)), \% \quad (3)$$

The  $E_i$  value shows percentage of microorganisms which lost their viability during passing through ADD out of all microorganisms passed AAD.

While the proportion of the total number of aerosol particles that passed through the device only weakly depends on indoor temperature and relative humidity (except for their extreme values), for viable microorganisms such dependencies can be very sharp. In addition, even at fixed temperature and relative humidity, various microorganisms differently respond to inactivating factors inside the device such as ozone and air ions concentrations, UV-radiation, the gas phase composition, the composition of aerosol containing microorganisms, etc.

Obviously, it is correct to compare the efficiencies of air disinfection by different devices only on condition of identical microorganisms aerosolized from the same material (liquid or dry) under identical microclimatic conditions. In all other cases, the comparison of the efficiencies of air disinfection by various devices will be incorrect. So there is a need for collectively choice of test microorganisms' strains list (including at least a pair of bacteria, a pair of viruses, and a pair of fungi) and fixing constant microclimatic conditions for all experiments in different laboratories.

Association of Home Appliance Manufacturers (AHAM):  
Standard Test Procedure ANSI/AHAM AC-1 (2002)  
AHAM.

Vechkanov, V.A., *et al.* (2016) *Abstracts European Aerosol Conference 2016, Tours, France, Sept. 4-9, 2016. P2-AAS-AAP-126.*

## A mass-based calibration technique for the high time resolution XACT 625 X-ray Fluorescence monitor

Anja H Tremper<sup>1</sup>, Tsai-Chia Chung<sup>2</sup> and David C Green<sup>1</sup>

<sup>1</sup>MRC HPA Centre for Environment and Health, King's College London, London, SE1 9NH, UK

<sup>2</sup>Department of Earth Sciences, Royal Holloway, University of London, Egham, TW20 0EX, UK

Keywords: generated particles, XRF, calibration check

Presenting author email: anja.tremper@kcl.ac.uk

The Cooper Environmental Services XACT 625 monitor is designed to measure a suite of elements in near real time and has been successfully deployed in three UK campaigns (Hamad et al. 2016, Font et al. 2017, Font et al. 2017).

It is calibrated using thin film standards, which is an established method but has various limitations. Thin film standards are much higher in concentration than most ambient samples, the element mix of the standard might not be representative of the particle mix found in the environment and the collection properties on a filter might also differ (Indresand et al., 2013). An alternative laboratory, and potentially field deployable, calibration method was tested to address these issues.

In this independent, mass-based, calibration technique the XACT was assessed using generated particles in the laboratory. Ammonium sulphate ( $\text{NH}_3\text{SO}_4$ ), potassium chloride (KCl) and zinc acetate ( $\text{Zn}(\text{O}_2\text{CCH}_3)_2$ ) were dissolved in deionised water to obtain a range of standard solutions which span the ambient concentration range. Wet particles were produced from these solutions in an aerosol generator and passed through premature driers to reduce the relative humidity to approximately 40%. The flow was isokinetically split in a flow splitter (TSI 3708) and sampled by Tapered Element Oscillating Microbalance (TEOM), Scanning Mobility Particle Sizer (TSI SMPS 3080) and the XACT 625; HEPA filtered make-up air was provided where necessary.

The mass measured by the TEOM was compared to the calculated mass using the elemental concentration measured by the XACT. The SMPS was used to give information of the size distribution found in the aerosol.

The mass concentration of S, Cl, K and Zn as measured by the XACT were used to calculate the total  $\text{NH}_3\text{SO}_4$ , KCl and  $\text{Zn}(\text{O}_2\text{CCH}_3)_2$  concentrations deposited. These calculated masses were compared to the mass measured with the TEOM using RMA regression. Results are shown in Table 1 and Figure 1.

**Table 1: RMA regression results**

Element	Slope	Intercept	R2
$\text{NH}_3\text{SO}_4$	0.93 (0.84-1.02)	6.75 (1.56-11.45)	0.95***
KCl*	1.04 (0.92-1.17)	3.42 (-7.53-13.17)	0.93***
KCl**	0.95 (0.92-0.99)	6.04 (3.37-8.62)	0.99***
$\text{Zn}(\text{O}_2\text{CCH}_3)_2$	1.03 (0.99-1.06)	1.94 (1.06-2.79)	0.99***

\* calculated using Cl, \*\* calculated using K

TEOM and XACT results compare well in all cases and slopes are not significantly different from the 1:1 line for all comparisons, except KCl when it was calculated from K and was significantly less than 1.

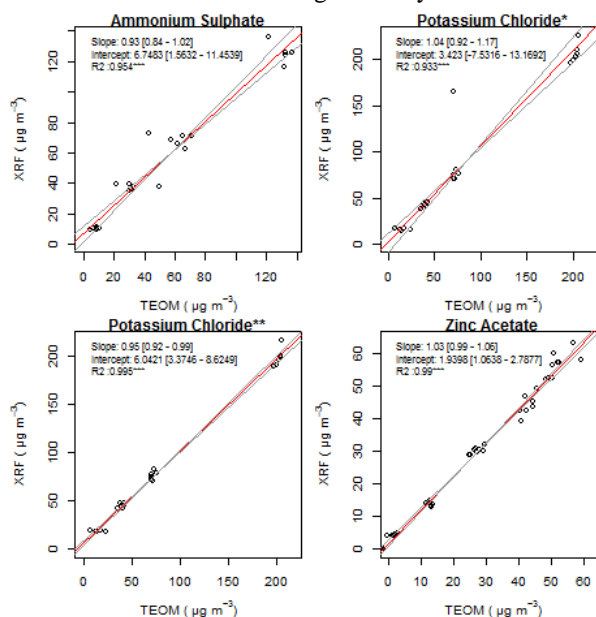


**Figure 1: RMA regression**

Table 2 shows the elemental concentrations of the standards measured with the XACT compared to the concentration range encountered in the field.

Overall the calibration using generated particles offers a valid alternative to thin film standards. The calibrations were carried out using single salt solutions and further experiment will include using mixed solutions to represent a more complex particle mix.

**Table 2: Element standard concentration range and field concentrations (ng/m<sup>3</sup>)**

Element	Measured Standard Range	Measured Field Median	Measured Field Max
S	548 - 6902	559	10800
Cl	1526 - 20846	725	21240
K	1942 - 22102	122	4021
Zn	287 - 3806	26	6863

Font et al., *Identifying Key Sources of Emissions of Problem Pollutants in Wales - Pontardawe Report*, 2017  
 Font et al., *Identifying Key Sources of Emissions of Problem Pollutants in Wales - Port Talbot*, 2017  
 Hamad et al., *Air Qual Atmos Health*, 2016, 9  
 Indresand et al., *X-Ray Spectrom*, 2013, 42

## Performance evaluation of the sizing capabilities of a new diffusion charging based particle sensor

L. Salo<sup>1</sup>, J. Gao<sup>2</sup>, S. Saari<sup>1</sup>, E. Saukko<sup>3</sup>, K. Janka<sup>3</sup>, T. Rönkkö<sup>1</sup>, J. Keskinen<sup>1</sup>

<sup>1</sup>Aerosol Physics, Faculty of Natural Sciences, Tampere University of Technology, 33720 Tampere, Finland

<sup>2</sup>State Key Laboratory of Environmental Criteria and Risk Assessment, Chinese Research Academy of Environmental Sciences, Beijing 100012, China

<sup>3</sup>Pegasor Oy, 33100 Tampere, Finland

Keywords: diffusion charger, particle sensor, particle size detection

Presenting author email: laura.salo@tut.fi

Monitoring indoor and outdoor particle concentrations is a continuing concern. Many electrical particle sensors output a quantity termed lung deposited surface area concentration, but with new technological advances (Saukko, 2016), the more familiar quantities, mass and number concentration, can also be obtained.

Charged particles' mobilities in an electrical field decrease with increased size. Pegasor's Air Quality Indoor sensor (AQI) uses this fact in order to determine the size of the particles it measures. It employs a trap—similar to the ion traps found in many electrical aerosol measurement instruments—to remove a portion of the particles. By varying the trap strength, the sensor is able to determine the trap voltage that removes precisely 50 % of the particles,  $U_{50}$ . Through calibration, a relationship between  $U_{50}$  and particle size  $d_p$  is established. The particle size is then used in calculations of the number and mass concentrations. In this work, the AQI is calibrated and its performance tested through measurements with a test aerosol in a laboratory setting and indoor and outdoor air measurements in Beijing.

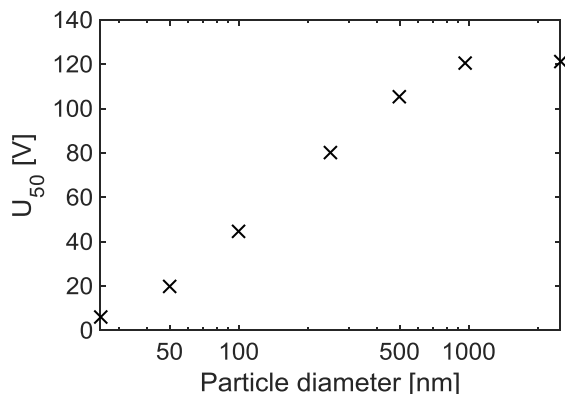


Figure 1: Trap voltage required to remove half of measured particles as a function of particle diameter.

Figure 1 shows the trap voltage found to remove 50 % of particles at each particle size from 25 nm to 2500 nm. For the particles up to 500 nm the required voltage increases, while it is practically the same for the two largest sizes (1  $\mu\text{m}$  and 2.5  $\mu\text{m}$ ), as particle mobility reaches a minimum. This suggests an upper limit on the size of particles, which can be characterized this way. Fortunately, smaller particles are often of greater interest.

Table 1 displays results from laboratory measurements with a unimodal test aerosol with large number concentrations and small particles. The test aerosol mimics particle size distributions found in diesel-

motor emission measurements. Results for AQI are compared to a scanning mobility particle sizer (SMPS). These results show that the sensor correctly determines the size of particles between diameters of 16 nm to 21 nm, to an accuracy of 20 %.

Table 1: Comparison of measured count median diameter for SMPS and AQI in a laboratory setting.

CMD SMPS [nm]	CMD AQI [nm]	Error [%]
7,1	13,7	+93,0
8,45	13,7	+61,1
10,78	14,0	+29,5
13,4	13,9	-3,9
16,1	13,3	-17,5
18,1	15,9	-12,3
20,1	18,8	-6,6
21,7	21,2	-2,4

In Beijing, the AQI sensor was tested for a 2-week duration in indoor measurements, and a short period in outdoor measurements. Measurements from outdoor air with an SMPS recorded a count median diameter of 68 nm as the average for a 7-hour measurement, while the AQI sensor recorded a value of 232 nm. The discrepancy is likely to have been caused by the sensor using a width for the particle size distribution that is different to the one observed. The distributions in Beijing measured with the SMPS were very wide and often contained two modes while the AQI sensor is calibrated to a narrower width of  $\sigma_g = 1.88$ .

Overall, the sensor performed well, in both the laboratory measurements and the field measurements. There is a challenge regarding the determination of the CMD in environments that have distribution width different to the one used by the sensor. Although the sensor is marketed for indoor use, it showed potential for use in emission measurements as well.

This work received funding from Tekes project GCLL: Finnish-Chinese Green ICT R&D&I Living Lab for Energy Efficient, Clean and Safe Environments. The authors would like to thank the Chinese Research Academy of Environmental Sciences for cooperation on the Beijing measurements.

Saukko, E., Salo, L., Rönkkö, T., Janka, K. & Keskinen, J. (2016). Dynamic cutpoint switching of mobility analyzer for improved aerosol characterization, *European Aerosol Conference*, 4.9-9.9.2016.

## Quantitative feature extraction for calibration of aerosol FT-IR spectra

S. Takahama<sup>1</sup>, M. Reggente<sup>1</sup>, G. Ruggeri<sup>1</sup>, A. T. Weakley<sup>2</sup>, A. M. Dillner<sup>2</sup>

<sup>1</sup>Atmospheric Particle Research Laboratory, École Polytechnique Fédérale de Lausanne (EPFL), Lausanne, CH

<sup>2</sup>Air Quality Research Center, University of California – Davis, Davis, California, USA

Keywords: Atmospheric aerosols, FT-IR, functional groups.

Presenting author email: satoshi.takahama@epfl.ch

Vibrational modes of functional groups in chemically complex molecular mixtures generate information-rich Fourier Transform Infrared (FT-IR) spectra. These spectra can be used for quantitative prediction of a multitude of substances in particulate matter (PM), provided that appropriate calibration models are developed for each substance. Calibration models that extract the relevant features from the spectra can be developed using laboratory standards or collocated ambient measurements, though some caution must be applied when extrapolating to new samples outside of the chemical domain of training set samples. Wavelength selection schemes integrated into the model building process can additionally reveal the most important vibrational modes associated with substances for which such calibration models can be developed. In this presentation, we review the state-of-the-art pertaining to the selection of statistical algorithms and samples used for model training, and provide an assessment regarding their performance. Quantification of organic functional group abundances and organic and elemental carbon (OC and EC, respectively) concentrations equivalent to thermal optical reflectance (TOR) measurements on Teflon filters are provided as primary examples.

First, we describe challenges for removing substrate and other interferences from the analyte signal. Explicit baseline correction approaches (Kuzmiakova et al. 2016) are compared with those which implicitly account for baseline effects in the calibration model (Reggente et al., 2016). Second, we contrast the peak-parameter representation (Takahama et al., 2013) and multivariate regression techniques (Ruthenburg et al., 2014), for apportioning regions of the FT-IR spectrum to contributions from different vibrational modes. The two methods are compared in terms of their physical constraints, interpretability, and training sample requirements. Third, we compare algorithms for wavelength selection and describe the impact of reducing the number of variables on prediction accuracy and interpretive capability, particularly for the molecular substructures which are strongly associated with the complex entities of TOR-equivalent OC and EC (Takahama et al., 2016).

In addition, we summarize methods for determining the suitability of available calibration models for application to new samples. This procedure follows from evaluation of spectral similarity in the feature space of the calibration model (Reggente et al., 2016). Finally, an outlook on future developments in FT-IR analysis is presented.

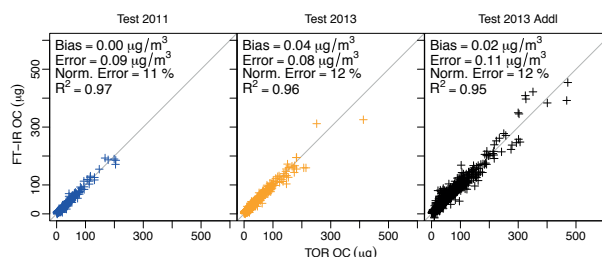


Figure 1. Example of TOR-equivalent OC predicted by a calibration model developed using 523 samples from seven sites in the IMPROVE monitoring network from 2011. Left panel: predicted values for the same seven sites in 2011. Middle panel: predicted values for the same sites in 2013. Right panel: predicted values for 11 additional sites in 2013 (using the same calibration model).

This work was supported by Swiss National Science Foundation (200021\_143298), EPFL, and the U.S. EPA and IMPROVE programs (National Park Service cooperative agreement P11AC91045).

Kuzmiakova, A.; Dillner, A. M. & Takahama, S.: An automated baseline correction protocol for infrared spectra of atmospheric aerosols collected on polytetrafluoroethylene (Teflon) filters, *Atmospheric Measurement Techniques*, 2016, 9, 2615-2631, doi:10.5194/amt-9-2615-2016.

Reggente, M.; Dillner, A. M. & Takahama, S.: Predicting ambient aerosol thermal-optical reflectance (TOR) measurements from infrared spectra: extending the predictions to different years and different sites *Atmospheric Measurement Techniques*, 2016, 9, 441-454, doi: 10.5194/amt-9-441-2016.

Ruthenburg, T. C.; Perlin, P. C.; Liu, V.; McDade, C. E. & Dillner, A. M.: Determination of organic matter and organic matter to organic carbon ratios by infrared spectroscopy with application to selected sites in the IMPROVE network, *Atmospheric Environment*, 2014, 86, 47-57, doi:10.1016/j.atmosenv.2013.12.034.

Takahama, S.; Johnson, A. & Russell, L. M.: Quantification of Carboxylic and Carbonyl Functional Groups in Organic Aerosol Infrared Absorbance Spectra, *Aerosol Science and Technology*, 2013, 47, 310-325, doi: 10.1080/02786826.2012.752065.

Takahama, S.; Ruggeri, G. & Dillner, A. M.: Analysis of functional groups in atmospheric aerosols by infrared spectroscopy: sparse methods for statistical selection of relevant absorption bands, *Atmospheric Measurement Techniques*, 2016, 9, 3429-3454, doi: 10.5194/amt-9-3429-2016.

## **Abstracts T306**

## Development of Carbonaceous Particulate Matter Analyser

Y.D. Kim, J.H. Kang, M.E. Kim, J.Y. Lee, J.S. Jung, S. Lee

Center for Gas Analysis, Korea Research Institute of Standards and Science, Daejeon, 34113, Republic of Korea

Keywords: particulate matter, organic carbon, elemental carbon, thermal optical method

Presenting author email: [ydkim@kriss.re.kr](mailto:ydkim@kriss.re.kr)

Carbonaceous particulate matter (PM) is one of major components of ambient PM and generally classified into organic carbon (OC) and elemental carbon (EC) by thermal optical analysis. The method uses differences in thermal and optical properties between organic PM and elemental PM for analytical separation. In this study, a new OC/EC analyser (KRISS OCEC analyser) is developed based on the thermal optical method. The performance of the new OC/EC analyser was evaluated by comparing OC and EC results with those of a commercial analyser. Prior to the performance evaluation, both analysers were calibrated with the same sucrose standard solutions. The performance evaluation was conducted with both standards and ambient PM<sub>2.5</sub> samples. For the standards, as shown in Figure 1, results from both analysers agrees well with an excellent linearity. For ambient PM<sub>2.5</sub> samples, results are compared for total carbon (TC), OC, and EC (Figure 2). Preliminary results from both analysers typically agrees well within the reported uncertainties. TC results agree within 3% while OC and EC results are within 6% and 7%, respectively. More performance tests will be conducted to fully evaluate the new OCEC analyser in the future.

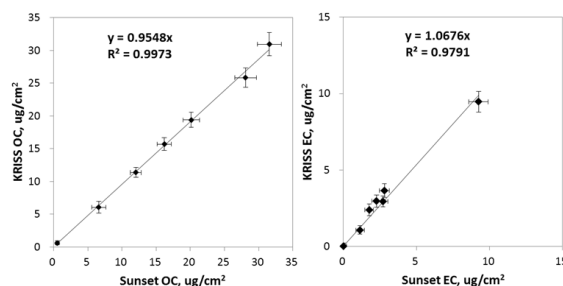


Figure 2b. Comparisons for OC and EC.

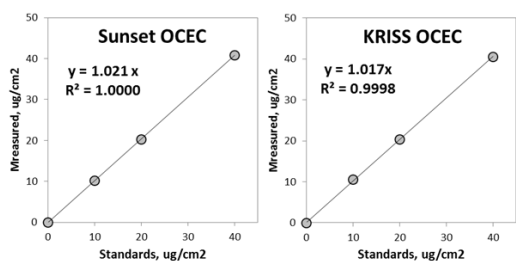


Figure 1. Performance evaluation with sucrose standards.

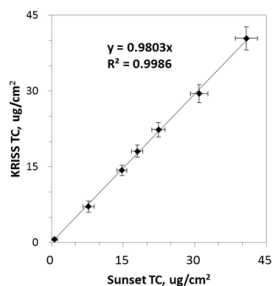


Figure 2a. Comparisons for TC

## Measurement of the Number Concentration of Nanoparticles in Suspensions using Electropray Sources

G. B. Baur, F. Lüönd and K. Vasilatou

Laboratory of Particles and Aerosols, Federal Institute of Metrology METAS, Bern-Wabern, CH-3003, Switzerland

Keywords: Electropray, Nanoparticles, Colloidal suspensions, Characterization, Concentration.

Presenting author email: konstantina.vasilatou@metas.ch

Colloidal nanoparticles (NPs) find important applications in industry and research, among others in the fields of clinical chemistry, diagnostics, therapeutics, consumer products and food packaging. Two of the properties that influence the most the performance of the nanomaterials are the physical size and number concentration of the NPs. However, because of the great diversity of NPs there is currently no method available that can be universally applied for the accurate and simultaneous measurement of both.

Electropray differential mobility analysis (ES-DMA) is a method that enables high-resolution measurements of the size distribution of NPs, however, transport losses and the lack of sample-specific calibration standards have prevented so far a direct implementation of the method for the measurement of the absolute number concentration of NPs in colloids. In 2011 Li *et al.* presented a novel approach towards this direction by combining ES-DMA with a statistical analysis of droplet-induced oligomer formation to calculate the NP concentration in suspension. This method relies on the evaluation of the droplet size generated by the ES source and is an elegant way to avoid characterization of particle losses during measurement. As such, it does not provide any information on the transfer efficiency of the electropray nor the parameters that affect its performance.

The goals of this study were the following: 1) to investigate the parameters that influence the performance of the ES and quantify its transfer efficiency under various conditions, 2) to validate ES-DMA as a simple, accurate and broadly applicable method for measuring the number concentration of engineered NPs in colloids based on the use of reference suspensions, 3) to provide accurate particle size distribution measurements down to 10 nm with minimal sample preparation even in the presence of salt residues and additives.

To this end, we coupled an ES to a liquid flow meter (for the accurate measurement of suspension flow rates) and combined it with a temperature-controlled flow reactor, a differential mobility analyzer (DMA) and a condensation particle counter (CPC). The measuring efficiency of the system was examined for the first time systematically under a wide range of experimental conditions. Using reference suspensions, such as spherical monodisperse Au-, SiO<sub>2</sub>- and polymer-NPs, (synthesized and characterized especially for the project 14IND12 EMPIR-Innanopart by our partner institutes) we found that the transfer efficiency of the ES depends strongly on

the suspension flow rate, the NP size and composition and can vary from <10% to >70%. Moreover, combining thermal treatment of the aerosol at elevated temperatures (Tsai *et al.*, 2013) together with a careful adjustment of the suspension flow rate we were able to accurately measure the NP size distribution down to 10 nm avoiding centrifugation (and its deleterious effects) that would otherwise be necessary for the removal of the organic/inorganic salts and additives.

We have thus demonstrated a fast, accurate and easy-to-use method for the measurement of particle size distribution and number concentration in suspensions. The present method relies on the use of reference suspensions and can be applied to NPs of a large size and material range. Moreover, we believe our results could shed light on the mechanisms of aerosol losses in the ES, provide practical guidelines on how to optimise its transfer efficiency and assist instrument manufacturers in improving the instrument's design. In the near future we are planning to extend our investigation to binary mixtures and non-spherical nanoparticles.

This work is part of the 14IND12 Innanopart project funded by the European Union through the European Metrology Programme for Innovation and Research (EMPIR).

Li, M., Guha, S., Zangmeister, R., Tarlov, M. J. and Zachariah M. R. (2011) *Langmuir* **27**, 14732-14739.

Tsai, D-H., DelRio, F. W., Pettibone J. M., Linn, P.-A., Tan, J., Zachariah M. R. and Hackley, V. A. (2013) *Langmuir* **29**, 11267-11274.

## The accuracy of commercial pulsed LII compared with reference rBC mass in laboratory and field measurements

J.-F. Yuan<sup>1</sup>, J. C. Corbin<sup>1</sup>, R. L. Modini<sup>1</sup>, M. Zanatta<sup>2</sup>, T. Müller<sup>3</sup> and M. Gysel<sup>1</sup>

<sup>1</sup>Laboratory of Atmospheric Chemistry, Paul Scherrer Institut, PSI Villigen 5232, Switzerland

<sup>2</sup> Helmholtz Center for Polar and Marine Research, Alfred Wegener Institute, Bremerhaven 27570, Germany

<sup>3</sup> Leibniz Institute for Tropospheric Research, Leipzig 04318, Germany

Keywords: Laser-induced incandescence, refractory black carbon, APM, Black carbon mass measurement, SP2  
Presenting author email: Jinfeng.Yuan@psi.ch

Laser-induced incandescence (LII) is a powerful in-situ method for refractory black carbon (rBC) mass quantification. Currently there are two commercial LII instruments (Michelsen *et al.*, 2015). One is a continuous wave LII system (“SP2”: Single Particle Soot Photometer, Droplet Measurement Technologies, CO, USA), which heats single particles to their sublimation point (~4400K) (Schwarz *et al.*, 2006). The consequent peak incandescence is proportional to the rBC mass. The other instrument is a pulsed LII system (“LII-300”, Artium Inc., CA, USA), which heats rBC particle ensembles to temperatures below their sublimation temperature (3400-3800K) (Artium Inc., 2015). The consequent incandescence (given fixed emissivity and temperature) is proportional to the rBC mass. The time-resolved temperature is measured by a two-colour pyrometry (Snelling *et al.*, 2005) when the pulsed LII is in its normal operation mode.

SP2 and pulsed LII have different advantages. The SP2 provides detailed, particle-resolved information including single-particle rBC mass, core size distributions and mixing state. The pulsed LII provides rBC mass concentration, though the data can be used to estimate average primary particle sizes from cooling rates. The pulsed LII also benefits from a very wide detection range ( $1 \mu\text{g m}^{-3}$ - $20 \text{g m}^{-3}$ ) and is more suited to routine monitoring. The lower limit of quantification of the pulsed LII has recently been pushed down to an atmospherically relevant level ( $\sim 0.05$ - $0.2 \mu\text{g m}^{-3}$ ) with the introduction of a new high-sensitivity mode (HS). For the analysis of data recorded in HS mode, the temperature reached by the incandescing BC is assumed to be the same as that inferred from two-colour pyrometry during the last previous normal mode measurement.

This study aims at assessing the performance of the commercial pulsed LII instrument in both its normal and new HS mode and uses laboratory and field measurements to answer the following research questions: What is the limit of detection for each mode? Do the HS and normal mode measurements agree? Do measured rBC mass concentrations in each mode agree with a reference measurement? Does the level of disagreement or agreement depend on BC type (fullerene soot, CAST soot and Aquadag), mass concentration and/or BC particle size?

In our experiments, the reference rBC mass is that from the SP2 referenced to an APM (Aerosol Particle

Mass Analyzer), i.e. the SP2 was specifically calibrated to each BC type using the APM.

The current outcomes from the lab studies are as follows: a) The rBC mass concentration detection limits of the normal and HS modes of the pulsed LII are 0.5 and  $0.06 \mu\text{g m}^{-3}$ , respectively; b) HS mode measurements agree with normal mode measurement to within ~10% for pure rBC. However, this small uncertainty only applies if the colour temperature has been determined with normal mode measurements of the same BC type; c) Large discrepancies exist between pulsed LII and SP2-APM reference rBC measurements. The size of the discrepancy depends mainly on BC type, rBC mass concentration and to a lesser extent on size distribution. HS and normal mode measurements are a factor of 2-12 and 2-16 larger than reference mass concentrations, respectively, for different BC type and mass concentrations. The discrepancy for each BC type decreases with increasing mobility size. Therefore, we recommend careful use of pulsed LII results, including cross-calibration against a reference rBC measurement.

In ongoing field experiments, we are also addressing the following additional questions: Do the HS and normal mode measurements agree for ambient rBC? Are pulsed LII rBC measurements sensitive to coating around the rBC cores? How well do ambient pulsed LII and APM-SP2 reference measurements agree?

This work is supported by the ERC under grant ERC-CoG-615922-BLACARAT, the European Union Seventh Framework Programme (FP7/2007-2013) under grant agreement n° 262254 and the European Union Horizon 2020 research and innovation programme under grant agreement No 654109.

Artium Inc, CA, USA. (2015) *AC-LII Manual*.

Schwarz et al., (2006) *J. Geophys. Res.* **111**, D16207.

Michelsen H. A., Schulz, C., Smallwood, G. J and Will, S. (2015) *Progress. Energy. Combust. Sci.* **51**, 2-48.

Snelling, D. R., Smallwood, G. J., Liu, F., Gulder, O. L and Bachalo, W. D. (2005) *Applied Optics* **44**, 6773-3785.

## Intercomparison of Condensation Particle Counters challenged by various nanoaerosols in the range 6 – 460 nm

S. Bau<sup>1</sup>, R. Payet<sup>1</sup> and O. Witschger<sup>1</sup>

<sup>1</sup>Laboratory of Aerosol Metrology, Institut National de Recherche et de Sécurité (INRS), Vandœuvre les Nancy, F-54519, France

Keywords: CPC, intercomparison, number size distribution, hydrophobicity.

Presenting author email: sebastien.bau@inrs.fr

Strategies for measuring occupational exposure to aerosols of nanomaterials highlight the use of techniques for measuring airborne particles number concentration as well as their number size distribution, e.g. Methner et al. (2012), Witschger et al. (2012). Number concentration is the most frequent characteristic used for airborne nanoparticle monitoring, task emission classification, or protective equipment performance evaluation against nanoparticles. European standards are currently in the process of being published on CPC (CEN, 2017) or their implementation as part of a strategy (CEN, 2015) to assess exposure to airborne nanomaterials. Consequently, providing data on how instruments behave regarding a set of aerosols is of interest when the potential for occupational exposure is being evaluated.

This study aim is to compare the number concentration of airborne particles reported by 8 different models of Condensation Particle Counters (CPC) with regards to a reference, freshly calibrated, CPC (Grimm, model 5.403). Among them, 3 are handheld models (TSI model 3007, 2 TSI model 8525 P-Trak), while the 5 others are stationary CPC. The latter include butanol-based CPC (TSI models 3776 and 3772-CEN) as well as water-based CPC (TSI model 3786, 2 TSI model 3787).

Polydisperse test aerosols with modal diameters between 6 and 460 nm were produced either by electro-erosion (PALAS GFG 1000) or by nebulization (PALAS AGK 2000, home-built Laskin-type generator). Non-hydrophobic aerosols consisted of metal-based particles (Ti, C, Al, Cu, Ag), as well as nebulized suspensions (SiO<sub>2</sub>), while hydrophobic particles consisted of DEHS as well as alkanes (*n*-C<sub>13</sub> to *n*-C<sub>20</sub>). Overall, 375 different conditions were investigated to represent a wide range of aerosols potentially encountered in workplaces. The range of number concentrations provided by the reference CPC was  $5 \cdot 10^2 - 4 \cdot 10^5 \text{ cm}^{-3}$ .

To highlight the possible effect of particle counting efficiency on the total concentration reported by the different CPC, 40% of the test aerosols presented a modal diameter below 40 nm. Considering the performance of P-Trak, Figure 1 clearly shows that their sensitivity to the mode of the aerosols measured, presenting ratios for the case of smaller particles significantly different from those observed for larger particles. This is also observed for TSI model 3007, but to a lesser extent.

Besides, the influence of particle hydrophobicity for water-based CPC was investigated through the generation of ~ 100 hydrophobic test aerosols. Contrary

to butanol-based CPC TSI model 3776, Figure 2 highlights a significant effect of particle hydrophobicity on the response of CPC TSI model 3787.

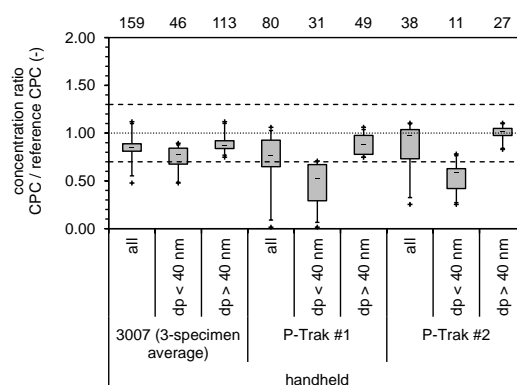


Figure 1. Boxplot of the concentration ratios between handheld CPC under study and reference CPC.

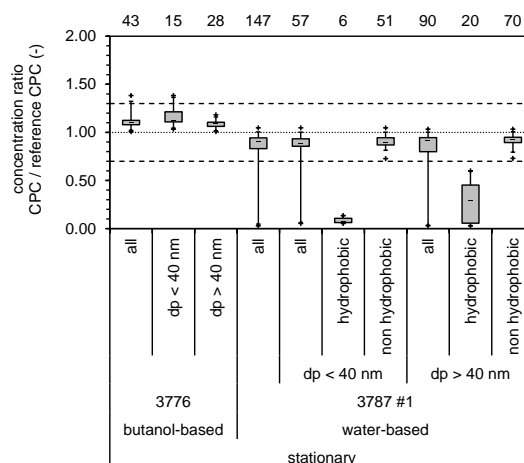


Figure 2. Boxplot of the concentration ratios between stationary CPC under study and reference CPC.

- CEN (2015). Workplace exposure - Assessment of inhalation exposure to nano-objects and their agglomerates and aggregates - Complementary element.
- CEN (2017). Workplace exposure - Characterization of ultrafine aerosols/nanoaerosols - Determination of number concentration using condensation particle counters, prEN 16897.
- Methner M., Beaucham C., Crawford C., Hodson L. and Geraci C. (2012) *J. Occup. Environ. Hyg.*, **9**, 543-555.
- Witschger O., Le Bihan O., Reynier M., Durand C., Marchetto A. and Zimmermann E. (2012). *Hyg. Sécurité Travail*, **226**, 41-55.

## An Improved Well Impactor Ninety-Six (WINS) as the PM<sub>2.5</sub> sampling inlet

T.C. Le and C.J. Tsai\*

Institute of Environmental Engineering, National Chiao Tung University, Hsinchu City, 30010, Taiwan

Keywords: WINS, PM<sub>2.5</sub>, impactor, particle overloading

Presenting author email: cuc004.ev03g@nctu.edu.tw

The Well Impactor Ninety-Six (WINS) is designated as the inlet for USEPA PM<sub>2.5</sub> FRM (Federal Reference Method) samplers (Peter *et al.*, 2001). The WINS with the cutoff diameter ( $d_{pa50}$ ) of 2.48  $\mu\text{m}$  and geometric standard deviation (GSD) of 1.18 is a single-jet, round-nozzle inertial impactor. It consists of an upper housing containing a nozzle and a lower housing supporting an impaction well. The well, which contains a 37 mm glass fiber (GF) soaked with 1 ml mineral oil as the substrate, is used to minimize particle overloading and subsequent particle bounce-off. However, like other impactors, WINS still has the particle overloading problem which affects  $d_{pa50}$  and sampled PM<sub>2.5</sub> concentrations (Kenny *et al.*, 2000; Vanderpool *et al.*, 2001). Therefore, its impaction well needs to be replaced every five 24-hr sampling days to avoid particle overloading and achieve sampling accuracy (USEPA, 1998).

This study developed a novel modified WINS (M-WINS) which uses water to wash the impaction substrate clean continuously to eliminate the particle bounce and particle overloading effects, and extend the service life of the impactor without the need of impaction well cleaning and replacement of the oil-soaked GF filter. The M-WINS uses a wetted GF filter as the substrate through which a 0.8 mm hole is drilled at the centre as shown in Fig. 1. Deionized water flow is injected continuously upward at a flow rate of 0.3 ml/min by using a syringe pump to wash off deposited particles from the substrate. Washed water is drained off by using another syringe pump through a hole drilled at the edge of the well.

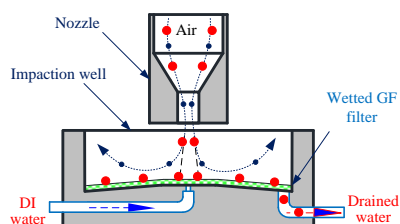


Figure 1. Schematic diagram of the impaction well of the M-WINS.

The laboratory test showed that  $d_{pa50}$  of the WINS decreased from 2.44 to 2.05  $\mu\text{m}$  while  $d_{pa50}$  of the M-WINS only varied slightly from 2.44 to 2.49  $\mu\text{m}$  in 0 to 6 mg range of loaded particle mass. The trend of the decrease in  $d_{pa50}$  of the WINS was similar to the results in previous studies (Kenny *et al.*, 2000; Vanderpool *et al.*, 2001).

The field test results shown in Fig. 2 indicated that the WINS without regular replacement of the well under-sampled PM<sub>2.5</sub> concentration compared to the VSCC (Very Sharp Cut Cyclone) with the sampling bias

increasing from -3.0 to -5.7% (day 1 to day 5), -9.0 to -17.1% (day 6 to day 11, if the sampling biases of ~30% at day 9 and day 11 were removed since low PM<sub>2.5</sub> concentrations were sampled) and -15.7 to -21.3% (day 12 to day 17). During the period, the PM<sub>2.5</sub>/PM<sub>10</sub> ratio was  $0.62 \pm 0.19$  and the measured PM<sub>2.5</sub> concentration range of the VSCC was 3.7–33.5  $\mu\text{g}/\text{m}^3$ . The deposited particles mound was observed on the WINS substrate at the end of sampling. The cutoff diameter of the WINS was shifted downward from 2.48 to 2.12  $\mu\text{m}$  as the estimated loaded mass was increased to 4.1 mg after 17 sampling days.

The sampling biases of the novel M-WINS were  $< \pm 3.6\%$  for PM<sub>2.5</sub>  $> 7.1 \mu\text{g}/\text{m}^3$  (day 1 to 8 and 11 to 17) and  $< -6.4\%$  for PM<sub>2.5</sub>  $< 4.6 \mu\text{g}/\text{m}^3$  (day 9 and 10). The cutoff diameter of the M-WINS only shifted from 2.46 to 2.51  $\mu\text{m}$ , which falls well in the range of the USEPA requirement of  $2.5 \pm 0.2 \mu\text{m}$  (USEPA, 2001). No particles piled up on the substrate were observed after 17 continuous sampling days. It is expected that the current M-WINS can be used as a PM<sub>2.5</sub> inlet for continuous unattended sampling for a long time with a very good sampling accuracy.

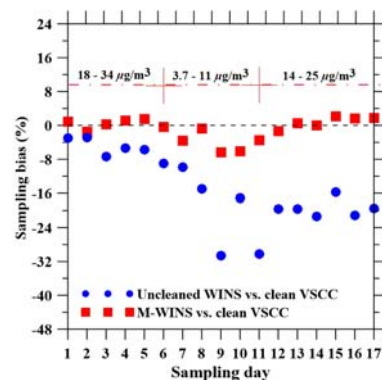


Figure 2. Sampling bias of the WINS and the M-WINS using the VSCC as the reference.

The final support of this work by the Taiwan Ministry of Science and Technology via the contracts MOST 105-2622-8-009-007-TE4 and MOST 105-2221-E-009-005-MY3 is gratefully acknowledged.

Peters, T. M, Vanderpool, R. W., and Wiener, R. W. (2001) *Aerosol Sci. Technol.*, 34, 389-397.

Kenny, L. C., Gussman, R., and Meyer, M. (2000). *Aerosol Sci. Technol.*, 38, 15-22.

Vanderpool, R. W; Peters, T. M; Natarajan, S.; Gemmill, D. B.; Wiener, R. W. (2001) *Aerosol Sci. Technol.*, 34, 444-456.

USEPA, (1998), Volume II, Part II, Section 2.12.

USEPA, (2001), Subpt. F, Table F-1.

## Evaluation of cost effective and lightweight optical particle counters for measuring the size of atmospheric particles with unmanned aerial vehicles

F. Schmidt-Ott<sup>1,3</sup>, S. Bezantakos<sup>2</sup>, N. Surawski<sup>3</sup> and G. Biskos<sup>3,4</sup>

<sup>1</sup>Maastricht Science Programme, Maastricht University, 6211 KW Maastricht, The Netherlands.

<sup>2</sup>Maison de la Recherche en Environnement Industriel 2 (MREI2), Université du Littoral Côte d'Opale, 59140, Dunkerque, France

<sup>3</sup>Energy Environment and Water Research Center, The Cyprus Institute, Nicosia 1645, Cyprus

<sup>4</sup>Faculty of Civil Engineering and Geosciences, Delft University of Technology, Delft 2628-CN, The Netherlands

Keywords: Aerosol Measurement, Particle Sizer, Instrumentation, OPC

Presenting author email: [f.schmidt-ott@student.maastrichtuniversity.nl](mailto:f.schmidt-ott@student.maastrichtuniversity.nl); [g.biskos@tudelft.nl](mailto:g.biskos@tudelft.nl)

Measuring the size and concentration of aerosol particles suspended in the breathing air is highly required to understand their environmental and health impacts (McMurry, 2000). Optical particle counters (OPCs), that are capable of measuring the size distribution of particles above 0.4  $\mu\text{m}$ , are widely used for this reason. Although OPCs are in general compact and portable instruments, they are relatively expensive to obtain (i.e., of the order of a few thousand Euros). Recent developments, however, have led to significantly lowering their cost and further miniaturizing them, without compromising their performance (Sousan et al., 2016), opening the way for increasing the temporal and spatial resolution of aerosol measurements. In addition, the miniaturized and low-cost OPCs provide an attractive technology for conducting aerosol size distribution measurements with unmanned aerial vehicles (UAVs), which is an elegant way of obtaining 3D maps of the atmospheric column in a systematic and cost-effective way.

In this work we tested two lightweight and cost effective OPCs (Alphasense Model OPC-N2), at various temperatures and pressures, resembling the conditions that the instruments will encounter onboard UAVs. In brief, the sizing accuracy and detection efficiency of the OPCs was evaluated using polystyrene latex (PSL) spheres having sizes from 0.8 to 10  $\mu\text{m}$ , at room conditions initially and later at temperatures and pressures ranging from 23 down to  $-5^\circ\text{C}$  and from 1.0 to 0.7 atm, respectively. PSL particles of various standard sizes, which were produced via atomization, were dried using a silica diffusion drier before entering a cylindrical chamber (1.4-m in length and 0.4-m in diameter) carried by a flow of 4 lpm (cf. fig. 1).

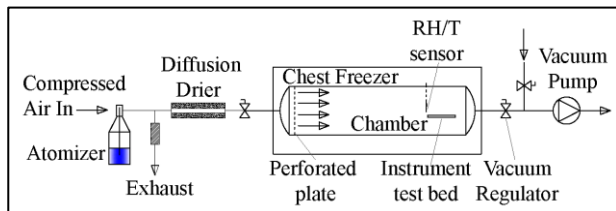


**Fig.1.** Experimental setup for testing the lightweight/cost-effective OPCs.

Table 1 shows the geometric mean diameters (GMDs)

calculated by fitting a lognormal distribution to the measurements, versus the nominal size of PSL particles at room conditions (i.e.,  $23^\circ\text{C}$  and 1 atm.). The performance (i.e., sizing accuracy and stability), when measuring 0.8  $\mu\text{m}$  PSL spheres of all OPCs at lower temperatures and pressures is depicted in Fig.2. The sizing accuracy was good under all tested conditions, with the exception of a random deviation of one of the sensors under low temperature conditions.

These results indicate that miniaturized OPCs tested in this work can be used onboard UAVs, but their reliability should be further investigated and improved.

**Table 1:** Measured GMDs at room conditions.

PSL Size ( $\mu\text{m}$ )	GMD ( $\mu\text{m}$ ) Alphasense OPC-N2 #1	GMD ( $\mu\text{m}$ ) Alphasense OPC-N2 #2
0.8	0.78	0.78
1.0	1.04	1.04
2.5	2.53	2.53
5.1	5.12	5.11
7.2	7.07	6.89
10.2	9.99	9.99

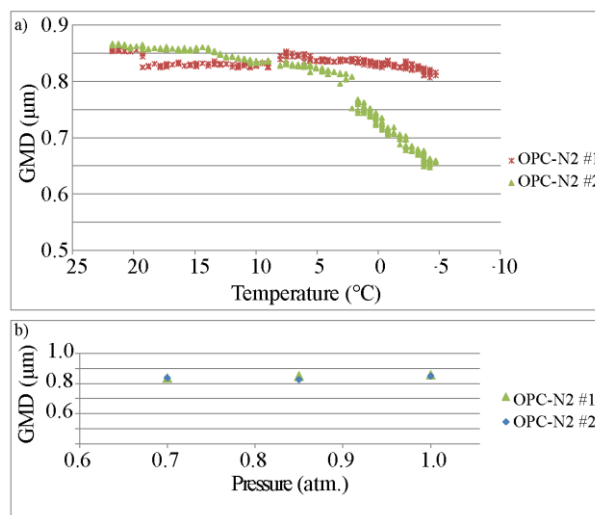


**Fig. 2.** Measured GMD by all OPCs at lower temperatures (a) and pressures (b), using 0.8  $\mu\text{m}$  PSL spheres.

### References

- McMurry, P. H. (2000), Atmos. Environ., 34:1959–1999.  
 Sousan, S., Koehler, K., Hallett, L., Peters, T. M. (2016) Aerosol. Sci. Tech., 50, 1352-1365.

## Evaluation of atomic force microscopy measurements of small regular and non-regular particles using Gwyddion software

J. Šperka<sup>1</sup>, M. Havlíček<sup>1</sup>, M. Valtr<sup>1</sup>, D. Nečas<sup>2</sup>, P. Klapetek<sup>1</sup>

<sup>1</sup>Department of primary nanometrology and technical length, Czech Metrology Institute, Brno, Okružní 31, 638 00, Czech Republic

<sup>2</sup>RG Plasma Technologies, CEITEC - Central European Institute of Technology, Masaryk University, Purkyňova 123, 612 00 Brno, Czech Republic

Keywords: Gwyddion software, atomic force microscopy, nanoparticles

Presenting author email: jsperka@cmi.cz

Within techniques of aerosol particles measurements, atomic force microscopy (AFM) has been already employed for microanalysis of individual collected particles and for estimation of particle size distributions using suitable software. Overview of AFM applications in the area of aerosol particles measurements can be found e.g. in (Kulkarni, 2011, pages 222-223).

AFM measurements are not very often used for characterization of solid state aerosol particles because other techniques, such as light scattering for determination of approximate particle size distribution in optical particle counters, are usually more suitable for their routine large-scale evaluation. However, when we consider individual aerosol particles and their more precise characterization, then AFM, along with competitive techniques such as light microscopy, electron microscopy or secondary ion mass spectrometry is the right choice for individual solid state particles evaluation. In some cases, AFM can be even the most accessible solution to gain information about shape of solid aerosol particles. One (more exotic) example for all is employment of AFM measuring devices for in situ measurements of extraterrestrial dust and soil particles at the nano-meter scale in the case of extraterrestrial NASA/Phoenix (Contreras-Torres, 2010) or ESA/MIDAS-Rosetta missions. The second one brought us AFM topographic images of selected dust particles with sizes of one micrometer to a few tens of micrometers with a variety of morphologies (Bentley, 2016). AFM data obtained by Rosetta spacecraft were processed in Gwyddion open source software (<http://gwyddion.net/>), which we use for the evaluation of particles throughout this contribution as well (Nečas, 2012).

For isolated nanoparticles on flat substrates is AFM or other scanning probe microscopy measurement relatively easy task. However, in real situations, for nanoparticles on rough substrates or for nanoparticles that are not isolated, is the situation more complicated and therefore many questions arise from the point of particle analysis in AFM image processing software (Klapetek, 2011).

The aim of this work is to investigate the influence of particles shape on the measurement uncertainty of nanoparticle parameters with respect to measurement conditions, i.e. the substrate roughness and particle agglomeration. We present real AFM measurements (see Figure 1 with topographic image of some closely packed particles with a diameter of one

micrometer with corresponding extracted height profile) and numerical modelling of particles with various morphologies together with simulation of particle deposition on the surface, creation of virtual AFM images by tip-sample convolution and data analysis using Gwyddion software. Particles were measured using Bruker Dimension Icon atomic force microscope with ScanAsyst imaging mode in air.

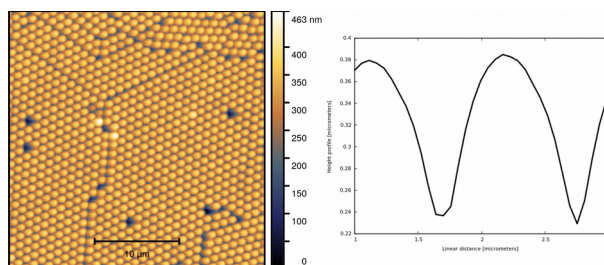


Figure 1: (on the left) Dense packed polymer microspheres with diameter of one micrometer as measured by AFM, (on the right) corresponding height profile extracted from AFM data.

This work was supported by project no. 17601404 “Měření nepravidelných nanočástic” financed by Czech Metrology Institute.

(Kulkarni, 2011) Kulkarni, P., Baron, P. A., & Willeke, K. (Eds.). (2011). *Aerosol measurement: principles, techniques, and applications*. John Wiley & Sons.

(Contreras-Torres, 2010) Contreras-Torres, F. F., Basiuk, E. V., & Rodríguez-Galván, A. (2010). Atomic Force Microscopy of Extraterrestrial Samples. *Journal of Advanced Microscopy Research*, 5(3), 159-176.

(Bentley, 2016) Bentley, M. S., Schmied, R., Mannel, T., Torkar, K., Jeszenszky, H., Romstedt, J., & Koeberl, C. (2016). Aggregate dust particles at comet 67P/Churyumov-Gerasimenko. *Nature*, 537(7618), 73-75.

(Nečas, 2012) D. Nečas and P. Klapetek, “Gwyddion: an open-source software for spm data analysis,” *Open Physics*, vol. 10, no. 1, pp. 181-188, 2012.

(Klapetek, 2011) Klapetek, P., Valtr, M., Nečas, D., Salyk, O., & Dzik, P. (2011). Atomic force microscopy analysis of nanoparticles in non-ideal conditions. *Nanoscale research letters*, 6(1), 514.

## Intercomparison of a personal CPC and different conventional CPCs

Christof Asbach<sup>1\*</sup>, André Schmitz<sup>2</sup>, Frank Schmidt<sup>2</sup>, Christian Monz<sup>3</sup>, Ana Maria Todea<sup>1</sup>

<sup>1</sup> Institut für Energie- und Umwelttechnik e.V. (IUTA), Duisburg, Germany

<sup>2</sup> University Duisburg-Essen, Duisburg, Germany

<sup>3</sup> Institut für Gefahrstoffforschung (IGF), Bochum, Germany

Keywords: Condensation Particle Counter, Personal Exposure, Particle Number Concentration, Water CPC

\*Presenting author email: asbach@iuta.dee

Condensation particle counters (CPCs) are commonly used to measure the number concentration of airborne submicron particles with sizes down to a few nanometers. Except for a few handheld versions, most of the available CPCs are rather large, mains-operated instruments. Only recently, the first personal CPC (PUFP C100), that can be carried on a belt or in a backpack, independent of its orientation, was introduced by Enmont LLC (New Richmond, OH, USA, Ryan et al., 2015). The personal CPC uses water as working fluid and can measure particles with sizes down to 4.5 nm and concentrations up to 200,000 1/cm<sup>3</sup>. Its battery and water reservoir allow for approximately 6 h continuous operation.

In an intercomparison study, we compared the response of the PUFP C100 with other conventional and static CPCs, namely a butanol based ultrafine particle counter (TSI model 3776), used as reference, a general purpose water based CPC (TSI model 3787) and two old butanol based TSI CPCs (model 3022 and 3025A). All CPCs were simultaneously challenged with identical test aerosols of different particle sizes, morphologies, materials and concentrations (Asbach et al., 2017a). The study comprehended two phases. The test aerosols in the first phase included hydrophilic NaCl particles with modal diameters of 35 nm and 92 nm, moderately hydrophobic carbon particles with a modal diameter of 82 nm and highly hydrophobic DEHS particles with modal diameters of 111 nm and 233 nm. The different levels of hydrophobicity were chosen to investigate whether this particle property has an effect on the detection efficiency of the water based personal and static CPCs.

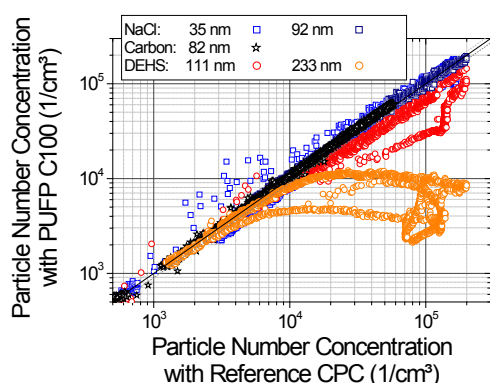


Figure 1: Number concentration measured with PUFP C100 vs. reference CPC (TSI model 3776; Asbach et al., 2017b)

As Figure 1 shows, number concentrations of NaCl and carbon particles measured with the PUFP C100 agreed mostly within  $\pm 10\%$  with those measured with the butanol based CPC model 3776 (TSI). In contrast highly hydrophobic DEHS particles with 233 nm modal diameter were drastically underreported because of insufficient water condensation onto the particle surfaces, whereas the deviation was lower for 111 nm DEHS particles. The reason for the difference between the two different sizes of DEHS particles is likely due to the fact that the DEHS was diluted with isopropyl alcohol (IPA) prior to dispersion to produce the smaller particles. It is assumed that the IPA did not fully evaporate, impurifying the DEHS and thus facilitating water condensation. The same effect has been observed for the static water CPC, whereas all butanol CPCs remained unaffected. Both old butanol CPCs continuously underestimated the particle number concentrations, independent of the particle material. In the second phase, very small NaCl particles with modal diameters of 5.4 nm, 13.6 nm and 25.2 nm and narrow size distributions ( $1.27 \leq \sigma_g \leq 1.40$ ) were used to scrutinize the lower size detection limit of the CPCs. The results showed that the PUFP C100 had nearly 50% detection efficiency at 5.4 nm, which then slowly increased to reach 100% at 25.2 nm, whereas the TSI water based CPC already showed 100% detection efficiency at 5.4 nm. The old UCPC (TSI model 3025A) reached its maximum detection efficiency also already at 5.4 nm, whereas the CPC model 3022 showed a detection efficiency of approximately 30% at 5.4 nm, 55% at 13.6 nm and 70% at 25.2 nm. The latter value is comparable with the underestimation of this CPC observed during measurements with larger particles.

### Acknowledgement

The IGF-project 18314N of the research association "Umwelttechnik" is funded by the German Federal Ministry for Economy and Energy (BMWi) via AiF within the framework of the program for the promotion of industrial cooperative research and development (IGF) based on a decision by the German Bundestag. Additional funding has been received from the nanoIndEx project, which has been funded under the frame of SIINN, the ERA-NET for a Safe Implementation of Innovative Nanoscience and Nanotechnology

### References

- C. Asbach et al., *Aerosol Air Qual. Res.* 2017 (accepted)
- C. Asbach et al., *Sci. Total Environ.* 2017 (revision submitted)
- P. Ryan et al., *Sci. Total Environ.*, 508: 366-373, 2015.

## Calculation Model to Simulate the Performance of a Diffusion Size Classifier Sensor for Nanoparticle Characterisation

S. Gerkens, L. Cachón

Testo SE & Co. KGaA, Celsiusstrasse 2, 79822 Titisee-Neustadt, Germany

Keywords: Diffusion Charging, DiSC, performance, simulation.

Presenting author email: SGERkens@testo.de

The diffusion charging (DC) measuring principle to characterize nanoparticles is earning a great acceptance in several applications due to its versatility, high performance and robustness as well as user friendly maintenance.

Applications like personal exposure (Rivas, 2014), occupational health and safety (Kaminski, 2015) or ambient air monitoring (Hudda, 2016) are typical fields where the diffusion charging has demonstrated its effectiveness. Moreover, the trend to measure particle emissions in different vehicle categories for type approval and technical inspection with portable instrumentation (Gallus, 2014) has motivated the introduction of diffusion charging in this field as well. All these very diverse applications benefit from the comparatively insensitivity of diffusion charging to varying particle morphology or surface chemistry.

This unique feature enables a new and powerful approach: the accurate simulation of a real sensor's physical response for nearly every type of particulate, especially for non-ideal polydisperse particle size distributions encountered in most experimental situations. Figure 1 gives an example for the performance evaluation of a Testo DC-based sensor (DiSC).

Thus, diffusion charger based technology can be easily adapted to even complex particle compositions using minimal resources.

This paper presents the simulation concept, method validation by experimental laboratory results as well as its feasibility for relevant case studies.

Rivas et al. (2014), "Child exposure to indoor and outdoor air pollutants in schools in Barcelona, Spain", *Environment International*, **69**, 200-212.

Kaminski et al. (2015), "Measurements of Nanoscale TiO<sub>2</sub> and Al<sub>2</sub>O<sub>3</sub> in Industrial Workplace Environments – Methodology and Results", *Aerosol and Air Quality Research*, **15**, 129–141.

Hudda, N., Fruin, SA. (2016), "International Airport Impacts to Air Quality: Size and Related Properties of Large Increases in Ultrafine Particle Number Concentrations", *Environ. Sci. Technol.*, **Apr 5;50(7)**, 3362-70.

Gallus et al. (2014), "On-road particle number measurements using a portable emission measurement system (PEMS)", *Atmospheric Environment*, **124**, 37-45.

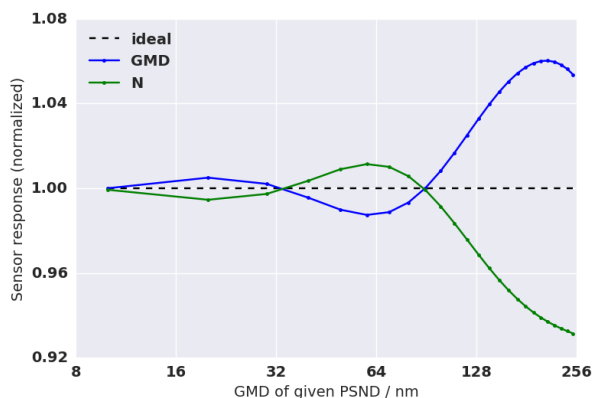


Figure 1. Simulated sensor response when challenged with polydisperse PSNDs (here: unimodal lognormal) with varied GMD and fixed GSD (=1,7), normalized to input PSND's parameters.

## Accuracy and Reproducibility of Fast Mobility Size Spectrometers over 10 years

J.P.R. Symonds and M. Irwin

Cambustion, J6 The Paddocks, 347 Cherry Hinton Road, Cambridge CB1 8DH

Keywords: size distribution, particle electrical mobility, metrology

Presenting author email: mirwin@cambustion.com

Fast response particle mobility sizers, such as the Cambustion DMS500 (Reavell *et al.*, 2002) and the TSI EEPs / FMPS have been commercially available for around 15 years. Compared with a Scanning Mobility Particle Sizer (SMPS), these instruments trade spectral resolution and absolute accuracy for a fast time response (up to 200 ms  $T_{10-90\%}$ ). Some initial studies (e.g. Ikeda and Iwakiri, 2006), showed that early examples of these instruments were not as accurate as established methods of sizing, and instrument consistency/repeatability was rather variable.

In response to these studies, a traceable calibration using aerosol sizing and number standards was introduced for the DMS500 (Symonds and Reavell, 2006). Recognising that soot agglomerates gain more charge in a corona charger compared with “compact” (near spherical) particles, separate calibrations were produced for soot and compact particles, via different data inversion matrices (Symonds and Reavell, 2006).

The calibration standards used for the DMS500 are a Differential Mobility Analyser (DMA) for particle diameter, and a standard aerosol electrometer for particle number (Symonds, 2010). For larger compact particles, Polystyrene Latex (PSL) standard sizes spheres are used.

In recent years, instruments such as the DMS500 have become more widely adopted, in particular for automotive emission measurements, where rapidly changing aerosols necessitate a fast time response. Indeed, in order to pinpoint the exact temporal source of emissions spikes, these instruments are frequently used as a faster response surrogate for homologation metrics, e.g. solid particle number in Europe. Given the need for comparability in this application, high accuracy and reproducibility are paramount.

As it is a decade since traceable calibrations for compact and soot aerosols were pioneered for the DMS500, we here present a statistical analysis of the full corpus of instrument calibrations undertaken in that time.

### Results

Figure 1 shows a year-to-year comparison between DMA sizing and DMS500 sizing using 100 nm NaCl particles. Data shows continuous improvements in consistency and accuracy. Note that the DMS500 underwent a major hardware revision in 2009 to the “MkII” version, which the data shows gave a step improvement in the consistency of the instrument. Figure 2 shows an equivalent comparison of the number concentration compared with an aerosol electrometer. Dotted lines indicate internal quality control standards.

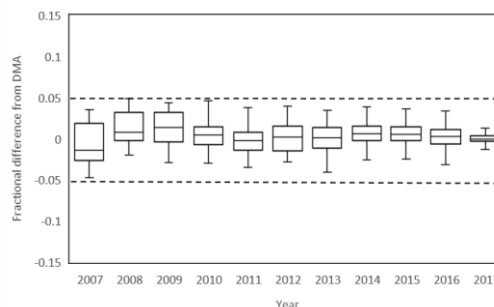


Figure 1. Fractional difference between DMA and DMS500 sizing, 100 nm NaCl particles (compact matrix)

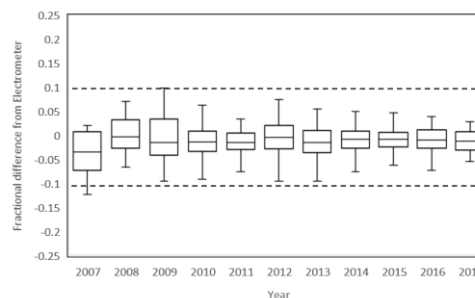


Figure 2. Fractional difference between standard electrometer and DMS500 number concentration, 100 nm NaCl particles (compact matrix)

Data will also be presented showing the performance at a range of particle sizes, and for soot aerosols using the agglomerate calibration matrix.

- Reavell, K., Hands, T., & Collings, N. (2002). *A Fast Response Particulate Spectrometer for Combustion Aerosols*. SAE Technical Paper, 2002-01-2714
- Ikeda, T. and Iwakiri, Y. (2006) *JCAP II Cross Check Tests on High-Speed Particle Sizing Instruments*. 10<sup>th</sup> ETH Conference on Combustion Generated Nanoparticles
- Symonds, J.P.R. and Reavell, K.St.J. (2006). *Calibration Of A Differential Mobility Spectrometer*. European Aerosol Conference, Salzburg T02A034
- Symonds, J.P.R. (2010) *Calibration of Fast Response Differential Mobility Spectrometers*, Metrology of Airborne Nanoparticles, Standardisation and Applications, National Physical Laboratory, London

## **Abstracts T307**

## Direct measurement of the dependence of photoacoustic signal upon droplet size

J.W. Cremer<sup>1</sup>, P.A. Covert<sup>1</sup>, E. Parmentier<sup>1</sup> and R. Signorell<sup>1</sup>

<sup>1</sup>Laboratory of Physical Chemistry, ETH Zürich, Zürich, CH-8093, Switzerland

Keywords: optical trap, single-droplet, absorption spectroscopy, heat transfer

Presenting author email: johannes.cremer@phys.chem.ethz.ch

It has been well established that the interaction of light with atmospheric aerosols has a large impact on Earth's climate. However, uncertainties in the magnitude of the aerosol impact remain large, due in part to broad distributions of aerosol size, composition, and chemical reactivity. The task of constraining this effect falls in part to increased and better field measurements of aerosol absorption. To this end, aerosol photoacoustic spectroscopy has emerged as an accurate and precise, field-deployable method for determination of aerosol absorption. Within a narrow particle size distribution, the photoacoustic response from the aerosol phase scales linearly with aerosol number density. Yet, theoretical considerations indicate that particle heating and evaporation during the photoacoustic process could damp the measured response (Raspet et al., 2003; Murphy, 2009), which implies that the response will *not* scale linearly with increases in particle absorbance cross-section that result from increases in droplet size. To date, these effects of particle heating and evaporation upon the photoacoustic response have not been experimentally quantified.

Here, we present the first measurements of the droplet-size-dependence of the photoacoustic response obtained from single-phase, spherical droplets. Collected using our single-droplet photoacoustic spectrometer (Cremer et al., 2016), these data allow us to explore the heating and evaporation effects mentioned above. Measurements were made of a simple model system consisting of droplets of dye-containing tetraethylene glycol. As expected, our results show a significant nonlinearity between the magnitude of the photoacoustic signal ( $|S|$ ) and the absorption cross section calculated by Mie theory especially for particles with a radius larger than 1  $\mu\text{m}$ . This is accompanied by a changing phase shift ( $\varphi_s$ ) between the excitation laser and the generated signal that is also size dependent. Both these effects can be explained by local heat transfer processes at the surface of the particle and have been predicted theoretically by Raspet et al. (2003) and Murphy (2009).

The results here give an experimental confirmation of the theoretical framework, improving confidence in photoacoustic absorption measurements of fine soot aerosols and opening up the possibility to correct photoacoustic field and laboratory measurements for the bias experienced when measuring the absorption of larger aerosol particles.

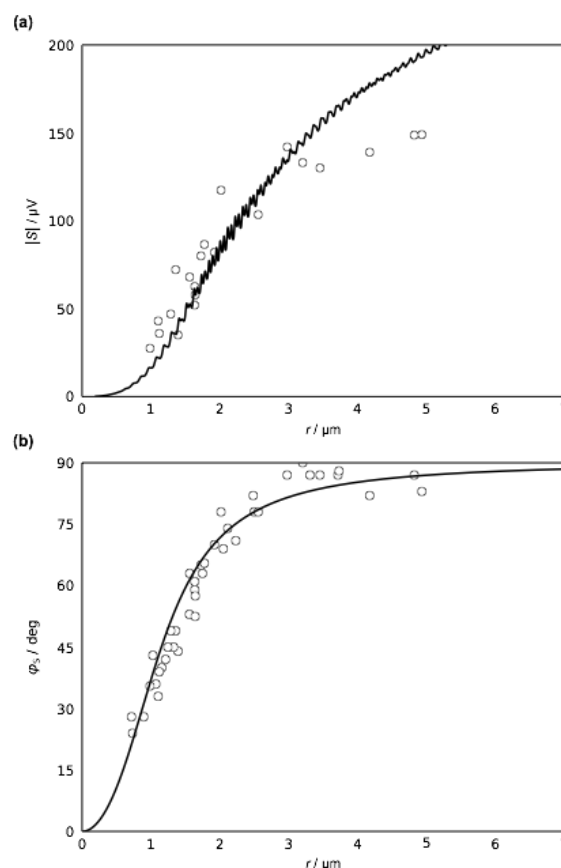


Figure 1: Magnitude (a) and phase-shift (b) of the droplet (radius,  $r$ ) photoacoustic response (dots) overlaid with theoretical response (lines) based on Murphy (2009) and Raspet et al. (2003).

This work was supported by the Swiss National Science Foundation (SNF Project No. 200020\_159205) and ETH Zürich.

Cremer, J.W., Thaler K.M., Haisch, C., and Signorell, R. (2016) *Nature Comm.* **7**, 10941.

Murphy, D.M. (2009) *Aerosol Sci. Tech.* **43**, 356–363.

Raspet, R., Slaton, W.V., Arnott, W.P., and Moosmüller, H. (2003) *J. Atm. Ocean. Tech.* **20**, 685–694.

## Mapping Aerosol Concentrations in the Port of Newcastle with a scanning lidar

Y. Zheng and J. Fisher<sup>1</sup>  
H. Bridgman<sup>2</sup>

<sup>1</sup>Sigma Space Corporation, Lanham, USA,

<sup>2</sup>School of Environmental and Life Sciences, University of Newcastle, Newcastle, Australia

Keywords: Scanning lidar, mapping, aerosol transportation

Presenting author email: yzheng@sigmaspace.com

Aerosols play an important role in the global climate, air pollution and aviation transportation. In the recent years, aerosol lidar has been routinely used to remotely monitor aerosol concentration and air pollution (Welton, 2001) When pointing the laser beam horizontally and scan through a designated area, the emissions and transportation of the local aerosol can be dynamically tracked and mapped (T.Y. He, 2012).

Mini Micro Pulse Lidar (MiniMPL) is a miniature aerosol lidar designed by Sigma Space Corporation. It is capable of measuring aerosol up to 15km. A scanner capable of scanning the whole hemisphere is mounted on the top of the lidar's weatherproof enclosure.

A scanning MiniMPL was set up at Fort Scratchley of the port of Newcastle (NSW is on the east coast of Australia) by Pacific Environment Limited. The lidar scanned from a grain terminal to Stockton Bridge, which covered a 70° sector (Fig 1). The Port of Newcastle is the largest bulk shipping port on the east coast of Australia and the world's leading coal export port (161 MT/y in 2016). There is also an Orica chemical plant on Kooragang island which emits aerosols and gases of various kinds. Our goal was to map the aerosol emission in this region and study their transportation pattern.



Fig. 1 The scan map of the port of Newcastle.

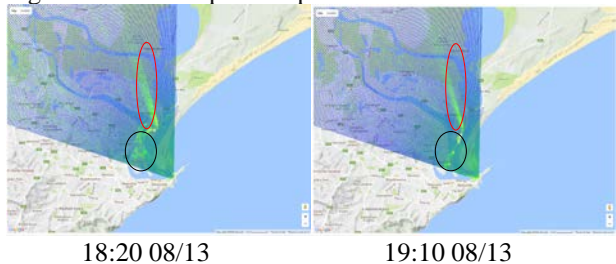


Fig. 2 Plumes from the Orica chemical plant.

We set the scan plan so that the average time for each line of sight is 20s. The angular resolution is 0.5 degree. A complete section scan takes about 50 minutes.

The scan plan was carried out between 08/12/2016 and 08/18/2016. During this period, multiple burst of emission and their transportation paths was uncovered by the MiniMPL. At 18:20 on 08/13 there was significant burst of plume from ORICA. The plume was partly blown away towards the north (Red circles in Fig.2). The major part of the plume drifted southeast towards the lidar and eventually towards the ocean (black circles).

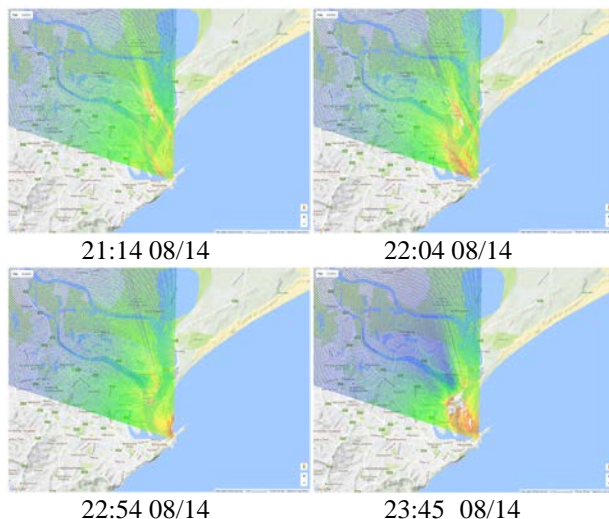


Fig. 3 Mixed plume from Orica and a ship.

On 08/14 there was another burst of gas plume from ORICA starting from noon. In addition, at about 21:14, there were multiple bands of additional plumes which indicates a common origin somewhere in the ocean. At 22:54, the source of the plume showed up in the port near the lidar. At 23:45, the core of the plume continued its journey towards the Stockton Bridge. The source of this transporting plume was most likely a ship.

The lidar scan has proved to be an effective aerosol plume mapping tool. More data are being analysed, including 3D volume scan and potential comparison with data from in situ instruments.

Welton, E. J., Campbell, J. R., Spinhirne, J. D., and Scott, V. S., (2001), *Proc. SPIE*, 4153, 151-158  
He, T.-Y. et al (2012), *Atmos. Meas. Tech.*, 5, 891-900

## Measurements of vapour pressure using the Union College Electrodynamic Balance

P. Kotowitz<sup>1</sup>, U.K. Krieger,<sup>2</sup> U. Weers,<sup>2</sup> A.T. Novak<sup>1</sup>, C. Porat<sup>3</sup> and A.J. Huisman<sup>1</sup>

<sup>1</sup>Department of Chemistry, Union College, Schenectady, NY, 12308, USA

<sup>2</sup>Institute for Atmosphere and Climate, ETH Zürich, Zürich, CH

<sup>3</sup>Department of Mechanical Engineering, Union College, Schenectady, NY, 12308, USA

Keywords: vapour-liquid equilibrium, vapour pressure, single-particle measurements

Presenting author email: huismana@union.edu

Vapour pressure and the enthalpy of vaporization are key parameters in calculations of gas-particle partitioning. However, measurements of vapour pressures of Low- or Semi-Volatile Organic Compounds (L-/SVOC) are difficult to perform. Even the well-studied system of substituted dicarboxylic acids shows that when measurements are available from multiple techniques, they often disagree (c.f. Bilde *et al.* 2015). For many compounds, only one measurement of vapour pressure is available (or no direct measurements of vapour pressure at ambient temperature are available) making it difficult to evaluate the accuracy of models of partitioning for these compounds.

We present measurements of vapour pressures of several compounds from the Union College ElectroDynamic Balance (EDB). Here, morphology dependent resonance spectroscopy (e.g., Zardini *et al.* 2006, Soonsin *et al.* 2010, Huisman *et al.* 2013) is used to determine the vapour pressure of a compound at a variety of relative humidities, allowing for accurate determination of the pure component vapour pressure at that temperature. The measurements are repeated at a variety of temperatures and plotted according to the van't Hoff equation

$$\ln \frac{p_2^\circ}{p_1^\circ} = -\frac{\Delta_{\text{vap}}H^\ominus}{R} \left( \frac{1}{T_2} - \frac{1}{T_1} \right)$$

where  $p^\circ$  are the pure component vapour pressures,  $\Delta_{\text{vap}}H^\ominus$  is the enthalpy of vaporization, and  $T$  are absolute temperatures. An example of such data are shown in Figure 1 for the compound 2-methylsuccinic acid, allowing for determination of both the pure component vapour pressure at 25°C and the enthalpy of vaporization about that temperature.

The Union College EDB employs a double-ring design similar to that used at ETH Zürich, but with a different containment vessel and flow pattern, along with a vapour delivery system that allows dew points up to 30 °C to be achieved within the EDB. The improved flow pattern and ability to reach elevated dew points improves the characterization of LVOC by extending the range of humidities available at the elevated temperatures needed to observe evaporation of these compounds. Measurements on several validation samples, including polyethylene glycols (PEG-3 through PEG-7) and dicarboxylic acids will be presented, along with new measurements of substituted dicarboxylic acids and other compounds of interest to atmospheric science.

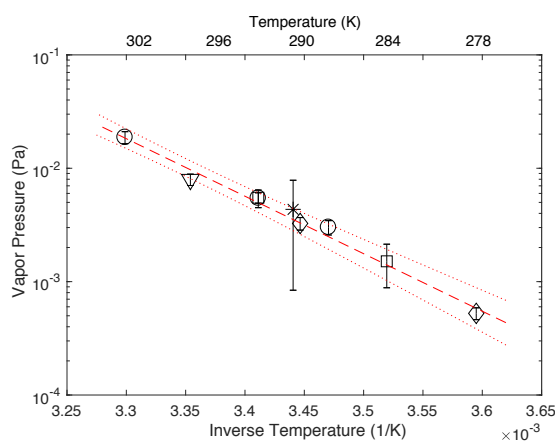


Figure 1. Vapour pressure of 2-methylsuccinic acid measured in the Union College EDB. Different symbols indicate measurements derived from independent particles. Dashed line indicates fit to the van't Hoff equation; dotted lines indicate 2σ bounds.

This work was supported by the Union College Faculty Research Fund, Undergraduate Research Fund, and Presidential Green Grants. Construction of the Union College Electrodynamic Balance was supported in part by the United States National Science Foundation US NSF International Research Fellowship Program IRFP#1006117 and American Chemical Society Petroleum Research Fund (ACS PRF #54592-UNI6). Any opinions, findings, and conclusions or recommendations expressed in this material are those of the authors and do not necessarily reflect the views of the US National Science Foundation. Acknowledgement is made to the Donors of the American Chemical Society for the partial support of this work.

### References:

- Bilde, *et al. Chem. Rev.*, **2015**, *115* (10), pp 4115–4156
- Huisman, Krieger, Zuend, Marcolli, & Peter. *Atmos. Chem. Phys.* **2013**, *13*, pp. 6647-6662
- Soonsin, Zardini, Marcolli, Zuend, & Peter. *Atmos. Chem. Phys.*, **2010**, *10*, pp. 11753-11767
- Zardini, Krieger, & Marcolli. *Optics Express*, **2015**, *14* (15), pp. 6951-6962

## Multi-instrument intercomparison of aerosol light absorption coefficient measurements

D. Massabò<sup>1</sup>, J. Perim de Faria<sup>2</sup>, V. Bernardoni<sup>3</sup>, U. Bundke<sup>2</sup>, P. Prati<sup>1</sup>, G. Valli<sup>3</sup>, R. Vecchi<sup>3</sup> and A. Petzold<sup>2</sup>

<sup>1</sup>Dept. of Physics, University of Genoa & INFN, Via Dodecaneso 33, 16146, Genoa, Italy

<sup>2</sup>Forschungszentrum Jülich GmbH, IEK-8, 52425 Jülich, Germany

<sup>3</sup>Dept. of Physics, Università degli Studi di Milano & INFN Via Celoria 16, 20133, Milano, Italy

Keywords: Optical properties, Light Absorption, Instrument Intercomparison

Presenting author email: Massabo@ge.infn.it

Atmospheric aerosols can alter the global radiation budget by aerosol-radiation and aerosol-clouds interaction. Currently, a high uncertainty still affects the quantification of the aerosol effects on Earth radiation budget. In this frame, optical absorption properties of aerosol are of peculiar interest because they are still barely known and are contributors to the global warming potential of atmospheric aerosols.

Important sources of light absorbing aerosol are fossil fuel combustion and wood/biomass burning. They both emit light absorbing carbonaceous species: black carbon (BC) – a strongly absorbing species whose imaginary part of the refraction index is independent on the wavelength ( $\lambda$ ) – and brown carbon (BrC, mainly from wood/biomass burning), which is less absorbing than BC but has an enhanced absorbing behaviour at short  $\lambda$ . Thus, the  $\lambda$ -resolved characterization of the aerosol absorbing properties is of major importance to support environmental and health protection policies.

One of the most widespread instruments for the on-line determination of the aerosol absorption coefficient ( $b_{\text{abs}}$ ) is the Multi-Angle Absorption Photometer (MAAP) (Petzold & Schöllner, 2004). It measures continuously both the light transmitted and scattered in the forward and back hemispheres by aerosol deposited on a glass-fiber filter, allowing the reconstruction of the scattering phase function on the whole scattering plane by assumptions on its shape. This allows to effectively remove the cross-sensitivity to aerosol scattering components and filter loading effects (Müller et al., 2011). The  $b_{\text{abs}}$  of atmospheric aerosol is inferred by applying the radiative transfer model developed by Hänel (1994). This approach does not require a posteriori data treatment, as in the case of attenuation measurements, where also information about scattering is needed (e.g. Collaud Coen et al., 2010): such corrections are typically composition dependent and prevent real-time accurate source apportionment. The main drawback of this instrument is that the information is provided at one  $\lambda$  only (637 nm), not allowing to distinguish different absorbing components.

Off-line multi- $\lambda$  devices were recently developed to perform filter-based measurements of  $b_{\text{abs}}$  at the University of Genoa (Multi-Wavelength Absorbance Analyser - MWAA) (Massabò et al., 2013) and at the University of Milan (polar photometer – PP\_UniMI) (Vecchi et al., 2014). The MWAA is based on the MAAP technology for the scattering phase function reconstruction, but it has the great advantage to operate at 5- $\lambda$  in the range 375-850 nm. PP\_UniMI is a 4- $\lambda$  device (range 405-780nm), and has the peculiarity to measure the scattering phase function with 0.4° resolution in the

range 0-173° instead of reconstructing it from measurements at fixed angles, thus allowing to measure aerosol collected virtually on any kind of substrate.

An extensive intercomparison campaign was designed in collaboration with Forschungszentrum Jülich. For this campaign, ambient aerosol was sampled on filters in parallel to on-line aerosol optical properties measurement devices – both well established and newly developed (as listed in Table 1) at the meteorological tower measurement facilities at Jülich, Germany. Three different filter media were used: Quartz-fiber, PTFE and polycarbonate, in order to evaluate possible effects due to sampling artefacts. A test campaign was conducted in November/December 2016 and the preliminary result of the instrument intercomparison between the TAP (Tricolor Absorption Photometer) and the MWAA is shown in Figure 1 as example. We will report on the final intercomparison over a 3-weeks campaign done in January/February 2017. With this set-up we will be able to determine the MWAA and PP\_UniMI performances in comparison to other measurements methods, taking into account the aerosol load, aerosol characteristics and meteorological characteristics for the sampling period.

Table 1. List of instruments used for the optical closure study

Instrument	Manufacturer	Measured Property	$\lambda$ (nm)
CAPS PM <sub>SSA</sub>	Aerodyne	Ext. + Scat. Coef.	630
Aurora 4000	EcoTech	Scat. Coef.	635, 525 and 450
PSAP	Radianc Research	Abs. Coef.	660, 530 and 467
TAP	Brechtel	Abs. Coef.	652, 528, 467

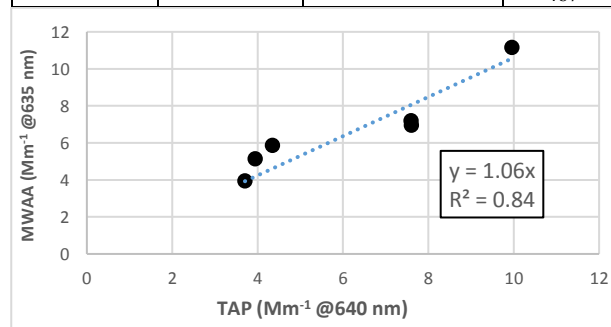


Figure 1. Preliminary result of the instruments intercomparison. test campaign.

### References:

- Petzold & Schöllner, (2004). *J. of Aerosol. Sci.*, **35**, 421-441.  
 Hänel, (1994). *Applied Optics*, **33**, 7187-7199.  
 Massabò et al., (2013), *J. of Aerosol Science*, **60**, 34-46.  
 Vecchi et al., (2014), *J. of Aerosol Science*, **70**, 15-25  
 Collaud Coen et al, (2010). *Atmos. Meas. Tech.* **3**, 457 – 474.  
 Müller et al, (2011). *Atmos. Meas. Tech.* **4**, 245 - 268.

## Enhanced particle size analysis using polarization scattering method

Qiaolin Xie<sup>1,2</sup>, Nan Zeng<sup>1,2</sup>, Sirui Chen<sup>1,2</sup>, Hui Ma<sup>1,2</sup>

1Shenzhen Key Laboratory for Minimal Invasive Medical Technologies, Institute of Optical Imaging and Sensing, Graduate School at Shenzhen, Tsinghua University, Shenzhen 518055, China

2Department of Physics, Tsinghua University, Beijing 100084, China

Keywords: particle size, aerosol monitoring, polarization scattering, Mueller matrix

Presenting author email: zengnan@sz.tsinghua.edu.cn

In china, due to the worsening air pollution, there has been growing interests in applying some new techniques and methods to offer potential characterization on physical and chemical composition of suspended aerosols in recent years [1]. Among various techniques, optical measurements show their advantages of local detection, fast response and portable operation. Especially optical scattering methods based on an angle distribution of light scattered by aerosols have demonstrated the capability of on-line counting of particles with different sizes and optical properties [2].

However, in our field measurements, we found that the size analysis only based on the scattering intensity will not work properly in the case of a possible particle agglomeration in the detection area in a heavily polluted environment. The detected signals from a dense distribution of fine particles can be wrongly considered as a bigger particle. Focusing on this problem, this paper presents an improved aerosol monitoring system using polarization scattering measurement. Optical polarization methods have been used in remote sensing systems applied in atmospheric applications [3]. It is convenient to upgrade a non-polarization instrument to a polarization version by adding a polarization state generator (PSG) and a polarization state analyser (PSA). With the additional polarization characters, such as degree of polarization (DOP) and Mueller matrix elements, we can improve the performance and enhance the capability of traditional optical aerosol analysis.

In our studies, we employ a polarization sensitive Monte Carlo simulation program developed by our lab to simulate the scattering process and the corresponding polarization change by various suspended particles, and then we can extract a suitable character from the Mueller matrix of a scattered aerosol by the incident light to distinguish the above mentioned fine particles. As shown in Fig.1, the simulations indicate the similar scattering intensity and the possible mistake between a group of dense fine particles and a single big particle. Also it can be seen that the new polarization character is sensitive to particle size and independent of concentration, which shows the potential of the polarization detection to correct the aerosol size analysis using optical scattering measurements.

Fig.2 presents our experimental schedule including our synchronous four channel polarization analyser and the generator for an incident circular polarized light.

Fig.3 shows our experimental results from fine particles with two sizes. The results also show the

feasibility of the new polarization character and support the improvement of the on-line evaluation of particle size using our polarization scattering monitoring system.

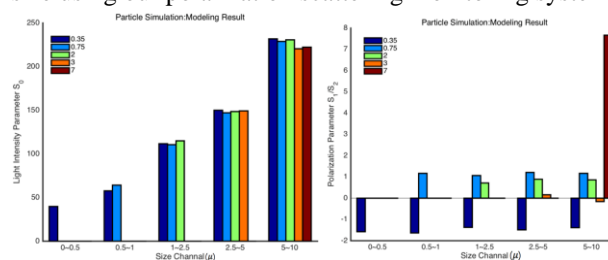


Figure 1. Simulation results of intensity index and polarization index for various particle concentrations

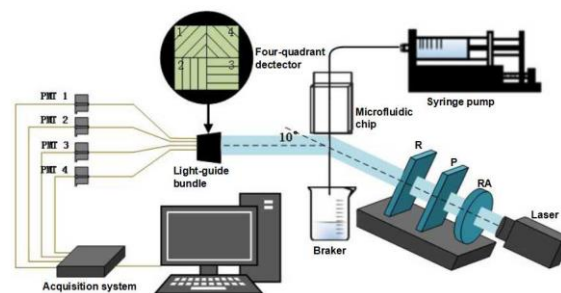


Figure 2. Experimental schedule of our polarization scattering particle size monitoring

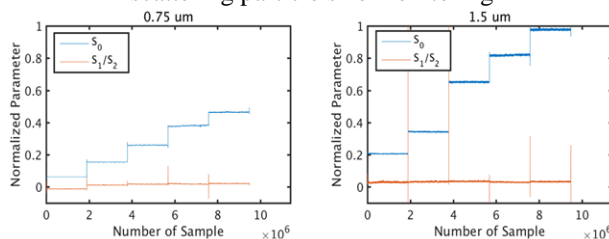


Figure 3. Comparison of experimental results between non-polarization intensity and our polarization character

This work was supported by National Natural Science Foundation of China (NSFC) (41475125); and The National Key Research and Development Program of China (2016YFC0208600, 2016YFF0103000)

[1] J. K. Zhang, Y. Sun, etc., *ATMOS CHEM PHYS* 14,2887-2903 (2014).

[2] P. H. McMurry, *ATMOS ENVIRON* 34, 1959-1999 (2000).

[3] Kirk Knobelspiesse, Brian Cairns, etc., *Opt. Express* 20, 21457-21484 (2012).

## Characterisation of the filter loading effect in various filter materials

L. Drinovec<sup>1,2</sup>, T. Müller<sup>3</sup>, A. Wiedensohler<sup>3</sup>, G. Močnik<sup>1,2</sup>

<sup>1</sup> Aerosol d.o.o., Ljubljana, 1000, Slovenia

<sup>2</sup> Jozef Stefan Institute, Ljubljana, 1000, Slovenia

<sup>3</sup> Leibniz Institute for Tropospheric Research, Leipzig, 04318, Germany

Keywords: filter photometer, Aethalometer, filter loading effect

Presenting author email: luka.drinovec@aerosol.eu

Filter-based absorption photometers are widely used for the measurement of the particle light absorption coefficient. These instruments measure optical attenuation of light passing the fibrous filter while it is loaded by the particles from the air stream, resulting in sensitive measurements of particle light absorption at several wavelengths and at high time resolution.

Optical properties of particles caught in the filter matrix depend on particle depth distribution within the filter matrix and the distribution of light in the filter (Müller et al. 2014). The most important parameter controlling the sensitivity of the filter photometer is the multiple scattering parameter  $C$  (Weingartner et al., 2003), the parameter describing the enhancement of the probability of absorption of light due to the particles embedded in the filter. The value of parameter  $C$  depends on the filter material, particle size, and possibly the presence of scattering aerosols.

Filter photometers are prone to the filter loading effect (FLE), which describes the variation of photometer response (its sensitivity) on the amount of the particles collected on the filter (Virkkula et al., 2007; Collaud Coen et al., 2010; Hyvärinen et al., 2013). FLE varies between different filter materials in magnitude and its dependence on the loading of the spot, parametrized as the reduction of the instrumental sensitivity on the attenuation of light ( $ATN$ ) measured by the filter photometer (Weingartner et al., 2003; Virkkula et al., 2007; Virkkula, 2010; Drinovec et al., 2015). FLE also depends on the aerosol properties such as the particle number size distribution and the thickness of particle coating with non-absorbing material (Drinovec et al., 2016).

We have analysed FLE in Aethalometer model AE33 (Magee Scientific, USA; Aerosol d.o.o., Slovenia) using different filter tapes including Pallflex T60 and TX40 materials. We assumed that multiple scattering, parametrized by  $C$ , can be treated separately from FLE. FLE was measured for different laboratory generated aerosols. Aerosol particle mixtures with different number size distributions and single scattering albedos were generated using a CAST burner (Jing, Switzerland) for absorbing particles and an atomizer with ammonium sulphate solution for scattering particles. Particle light extinction and scattering coefficients were measured using a CAPS PMex (Aerodyne research, USA) and an integrating nephelometer Aurora 4000 (Ecotech, Australia). Particle light absorption obtained from the Aethalometer was

compared to the one calculated by subtracting the light scattering from light extinction coefficient measured by the CAPS. The particle number size distribution was measured by a custom made mobility particle size spectrometer (TROPOS, Germany).

Our results show that filter-based absorption photometers response depends strongly on both filter type and aerosol particle properties. The intercept of the instrumental response vs.  $ATN$  was used to determine the multiple scattering parameter  $C$ . FLE in T60 follows a linear dependence on attenuation. (Figure 1). For TX40 we observed non-linearity of the FLE curve which is most pronounced for bigger soot particles.

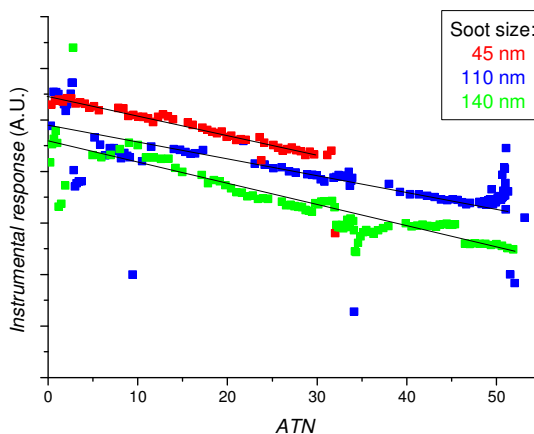


Figure 1. Instrumental response as a function of attenuation ( $ATN$ ) for soot particles of different size.

This research is part of a project that has received funding from the European Union's Horizon 2020 research and innovation programme under ACTRIS-2 grant agreement No 654109.

Collaud Coen et al. (2010) *Atmos. Meas. Tech.*, **3**, 457–474.

Drinovec et al. (2015) *Atmos. Meas. Tech.*, **8**, 1965–1979.

Drinovec et al. (2016) *Atmos. Meas. Tech. Discuss.*

Hyvärinen et al. (2013) *Atmos. Meas. Tech.*, **6**, 81–90.

Müller et al. (2014) *Atmos. Meas. Tech.*, **7**, 4049–4070.

Virkkula et al. (2007) *J. Air Waste Manage.*, **57**, 1214–1222.

Virkkula (2010) *Aerosol Sci. Technol.*, **44**: 8, 706–712.

Weingartner et al. (2003) *J. Aerosol Sci.*, **34**, 1445–1463.

## Helmos Hellenic Atmospheric Aerosol and Climate Change station first measurements of Saharan Dust Events

P. Fetfatzis<sup>1</sup>, S. Vratolis<sup>1</sup>, V. Vasilatou<sup>1</sup>, and K. Eleftheriadis<sup>1</sup>

<sup>1</sup> Institute of Nuclear & Radiological Sciences & Technology, Energy & Safety,  
Environmental Radioactivity Laboratory,

National Center of Scientific Research 'Demokritos', 15310 Ag. Paraskevi Attiki, Greece.

Keywords: coarse particles, African dust transport, long range transport models, Saharan dust events

Presenting author email: prodomos.fetfatzis@ipta.demokritos.gr

The Helmos Hellenic Atmospheric Aerosol and Climate Change station (HAC)<sup>2</sup> is a new high altitude station in Greece, part of the NCSR 'Demokritos' Environmental Radioactivity Laboratory. The regular measurements of atmospheric aerosols parameters and concentrations of climate gases, started at the end of 2015. The name (HAC)<sup>2</sup> is taken from the Helmos mountain, on which the station has been built, at the northern Peloponnese, at Neraidorachi peak 2340 m ASL. It is the only station at high altitude for atmospheric research in the region of the eastern Mediterranean and aims to study physical-chemical characteristics of aerosols and climate gases.

Through the Mediterranean, Sahara Dust Events (SDE) are frequent and have a large impact on aerosol optical properties in the region. The fig.1 presents the 4 days back trajectories of a characteristic SDE for the (HAC)<sup>2</sup> station, and it has been obtained from the online platform of NOAA HYSPLIT MODEL, backward trajectories ending at 01:00 UTC, 01 Mar 2016, CDC1 meteorological data. The Skiron model (reanalysis data) has been used as the expected SDE in the city of Athens for comparisons to the (HAC)<sup>2</sup> measurements.

Table 1. Comparison between measured from TV OPC parameter measured at (HAC)<sup>2</sup> and the Skiron model dust prediction reanalysis.

Month	Measured number of SDE	Predicted number of SDE
January	2	2
February	2	2
March	3	3
April	2	2
May	3	3
June	4	3

Optical Particle Counter (OPC) measurements PM<sub>10</sub> are conducted at the (HAC)<sup>2</sup> station on a continuous basis. For measurements during the first six months of 2016 the aerosol parameter Total Volume (TV) have been derived figure 2. The TV is calculated from the size distribution, but the contribution on SDE to the TV is mainly from the coarse particles, as Marconi M. et al mentioned. The relationship among the above parameter has been investigated for identifying SDE at the table 1, and at the figure 2.

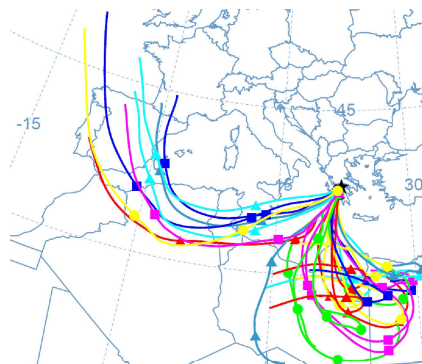


Figure 1. A characteristic SDE for the (HAC)<sup>2</sup> station NOAA HYSPLIT MODEL 4 days Backward trajectories ending at 01:00 UTC 01 Mar 2016, CDC1 Meteorological Data.

The TV parameter shows very good agreement with the Skiron model predictions for SDE. Other aerosol SDE indicative parameter will be further investigated for the (HAC)<sup>2</sup> station, such as Coarse Volume (CV) parameter, CV/TV scattering and SSA angstrom exponents, PM concentrations, using algorithms like M. Collaud Coen et al.

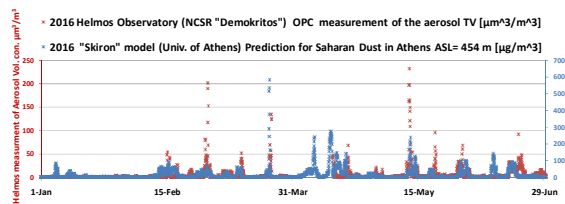


Figure 2. Measurements of the aerosol TV [ $\mu\text{m}^3/\text{m}^3$ ] versus "Skiron" model prediction for Saharan Dust [ $\mu\text{g}/\text{m}^3$ ]

This work was supported by ENTEC FP7REGPOT - 2012-2013-1 FP7, ID:316173)

Marconi M. et al., Atmos. Chem. Phys. Discuss., 13, 21259–21299, 2013.

M. Collaud Coen et al., Atmos. Chem Phys., 4, 2465–2480, 2004.

## A sensor for reliable in-situ detection of volcanic ash in the presence of cloud particles

E. Weingartner<sup>1</sup>, Z. Jurányi<sup>1\*</sup>, D. Egli<sup>1</sup>, B. Neining<sup>2,3</sup> and H. Burtscher<sup>1</sup>

<sup>1</sup> University of Applied Sciences Northwestern Switzerland, CH-5210 Windisch, Switzerland

<sup>2</sup> METAIR AG, Airfield LSZN, CH-8915 Hausen am Albis, Switzerland

<sup>3</sup> Zurich University of Applied Sciences, CH-8401 Winterthur, Switzerland

\* now at: Alfred-Wegener-Institut (AWI), Bremerhaven, Germany

Presenting author email: ernest.weingartner@fhnw.ch

A volcanic eruption emits a significant amount of hazardous ash particles into the air. If the eruption is strong enough, the volcanic ash plume can reach high altitudes and can be a serious security risk for airplanes.

We have developed a new prototype aerosol sensor for the reliable detection of volcanic ash. The envisaged application is the employment of this new technique on-board of passenger aircraft. It allows in-situ monitoring of the airplane's exposure to volcanic ash.

The challenge of this development is the requirement that the sensor can distinguish cloud droplets (or ice crystals) from the hazardous refractory ash particles. At aviation altitudes, water droplets and ice crystals are often present in the particle size region of the ash (1–20 micrometer) and their concentrations can reach the same concentrations that are considered as the limits of the different volcanic ash contamination zones. Therefore, it is crucial that the sensor can differentiate between volcanic ash and water or ice particles.

The measurement principle of our instrument, called DUWAS (Dual Wavelength Ash Sensor), is based on the detection of scattered light from individual particles outside of the airplane cabin through a glass window. The desired component-specific particle differentiation (ash vs. water) is achieved with two lasers operating at different wavelengths, e.g. at 660 nm (Vis) and 2750 nm (infrared, IR). Jurányi *et al.* (2015) have shown that the unique behavior of the refractive index of water at the IR wavelength allows distinguishing hydrometeors from other aerosol particles (such as volcanic ash).

The new volcanic ash detector was first carefully tested in the laboratory with various test aerosols and micrometer-sized water droplets. Then, ground-based outdoor measurements were conducted and the instrument response to mineral dust (a surrogate for volcanic ash) and natural cloud droplets (and ice crystals) was investigated. The instrument was also tested in summer 2016 on-board of the research aircraft METAIR-DIMO (Fig 1).



Figure 1: The measurement pod (left) with the DUWAS below the wing of the METAIR research aircraft (right)

The flights lasted between one and three hours. Fig 2 presents ~3 minutes of exemplary data collected during a flight through thin edges of a natural cloud.

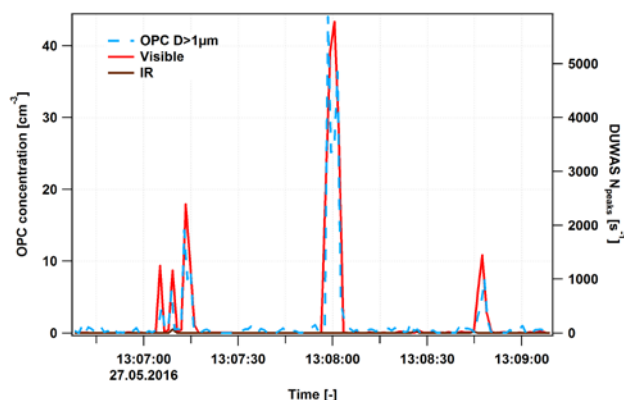


Figure 2: Airborne measurements through edges of a natural cloud. The particle count rates from the DUWAS (Vis, IR) are compared to an optical particle counter (OPC) which was also integrated in the measurement pod of the airplane. The presence of cloud particles are clearly seen in elevated OPC concentrations as well as in higher count rates in the visible channel of the DUWAS.

As expected, the cloud particles do not change the DUWAS IR count rates. The IR count rates are much lower ( $<10 \text{ min}^{-1}$ ) and are correlated (not shown) with the concentration of refractory particles (e.g. dust and ash) in the super-micrometer size range.

A detailed analysis of the airborne measurements shows that the DUWAS can discriminate cloud particles from other aerosols in the ambient atmosphere. With some assumptions on the physical and optical properties of volcanic ash, the DUWAS is able to detect critical ash concentrations (e.g.  $2 \text{ mg/m}^3$ ) without being affected by the presence of cloud droplets or ice crystals.

Based on all these tests we plan to further develop the sensor. These next steps should be done in collaboration with an industrial partner, interested in commercializing the instrument. A patent application has been filed. More detailed information on this method is found in Jurányi *et al.* (2015) and Weingartner *et al.* (2016).

Jurányi, Z. et al. (2015), *Atmos. Meas. Tech.*, 8(12), 5213-5222, doi:10.5194/amt-8-5213-2015.

Weingartner, E. et al. (2016), *IEEE Metrol. Aerosp.*, 19-24. doi:10.1109/MetroAeroSpace.2016.7573179.

## Measurement of physical and optical properties of aerosol particles in urban environment

A. Nagy<sup>1</sup>, A. Czitrovsky<sup>1</sup>, A. Kerekes<sup>1</sup>, W.W. Szymanski<sup>2</sup>

<sup>1</sup>Wigner Research Centre for Physics, H-1121 Budapest, Konkoly Thege M. st. 29-33. Hungary

<sup>2</sup>Faculty of Physics, University of Vienna, A-1090 Vienna, Boltzmannngasse 5, Austria

Keywords: size distribution, refractive index, urban aerosol.

Presenting author email: nagy.attila@wigner.mta.hu

A new optical method based on elastic light scattering on single particles was developed for the determination of different physical properties of aerosol particles suspended in the ambient air (Szymanski *et al.*, 2002). Comprehensive numerical analysis and laboratory tests were performed to study the reliability of the method (Nagy *et al.*, 2006). A mobile prototype instrument was built so that we can study the method in field measurement campaigns and compare the results with other devices. In a recent publication, we presented some of our results focusing on the measurement of the imaginary part of the complex refractive index which is related to the absorption of the particles (Nagy *et al.*, 2016).

Two longer measurement campaigns had been carried out and the results are summarized here. The investigated size range was limited to 0.6 – 5 µm due to the capabilities of the prototype instrument, which must be considered during the interpretation of the data.



Figure 1. The mobile environmental laboratory during a measurement campaign in Budapest.

The mobile prototype instrument was engaged in a container and in a mobile aerosol laboratory among different commercial aerosol instrumentation during a measurement campaigns in Budapest. The aim of the campaigns was to test the instrument in longer measurement series and to find the proper data evaluation method to present the results. We have extracted and presented the number concentration and the absorbing fraction of particles (absorbing - imaginary refractive index are larger than 0.1) from the data. The counting efficiency and the obtained size distribution was very

comparable with the results of other commercially available instruments. The variations of the distributions clearly indicate the different composition of the particle ensemble and there is also correlation with weather conditions

Time series of different parameters (concentrations, refractive index, size parameters, absorbing fraction and average absorption of the absorbing fraction of the aerosol particles) were calculated and used for the interpretation by considering the actual meteorological conditions. E.g. from the data sets, it is evident that most of the absorbing particles are in the smaller size range (below 1 micron), and the larger absorbing particles have different characteristics. On table 1. daily averages of the concentrations, absorption fractions and average absorptions (imag. refractive indices) are presented at different times on the same location.

Table 1. Sample measurement data from a campaign in Budapest.

Location and date	Concentration [particles/litre]	Absorbing fraction [%]	Absorption of the absorbing fraction
Location 1.	1644	34.6	0.55
Location 2.	2508	10	0.39
Loc. 1. Date 1.	1097	13.3	0.43
Loc. 1. Date 2.	1064	40.3	0.58
Loc. 1. Date 3.	4616	41.4	0.6
Loc. 1. Date 4.	429	33.7	0.5

This work was supported by the Hungarian TÉT\_10-1-2011-0725 project.

Szymanski, W.W., Nagy, A., Czitrovsky, A., Jani, P. (2002). A new method for the simultaneous measurement of aerosol particle size, complex refractive index and particle density, *Measurement Science and Technology*, 13, 303-307.

Nagy, A., Szymanski, W.W., Golczewski, A., Gál, P., Czitrovsky, A. (2007) Numerical and experimental study of the performance of the Dual Wavelength Optical Particle Spectrometer (DWOPS) (2007), *Journal of Aerosol Science*, vol. 38 issue 4. pp. 467-478.

Nagy A. et al., Real-time determination of absorptivity of ambient particles in urban aerosol in Budapest, Hungary, *Aerosol and Air Quality Research*, Vol. 16, pp. 1-10. (2016)

## Revival of an old method with new techniques: In-situ measurement of aerosol light absorption using photothermal interferometry

B. Visser, A. Meier, S. Sjogren, D. Egli, P. Steigmeier, H. Burtscher and E. Weingartner

University of Applied Sciences Northwestern Switzerland, CH-5210 Windisch, Switzerland

Presenting author emails: bradley.visser@fhnw.ch; ernest.weingartner@fhnw.ch

### Background

The precise measurement of light absorbing particles in the air is important both for its role in climate change and as a measure of combustion products associated with health effects. Routine monitors (i.e. multi angle absorption photometers, aethalometers and particle absorption photometers) determine the absorption of particulate matter collected on a fibrous filter. These methods require various corrections (e.g. Weingartner *et al.*, 2003) which are often handled with large generic correction factors.

Other techniques measure aerosol light absorption while the particles are airborne and are therefore not affected by the filter substrate. An advantage of these in-situ methods is that they can be used to calibrate and validate routine monitors because they can be calibrated using gases with known light absorption. Unfortunately, existing in-situ absorption instruments are neither practical nor sensitive enough for ambient air concentrations.

### Experimental method

We are currently developing a new reference instrument to precisely measure aerosol light absorption to be used in the laboratory and the field. The in-situ technique is based on photothermal interferometry (PTI). The application of PTI to measure aerosol absorption was demonstrated two decades ago (e.g. Moosmüller and Arnott, 1996; Sedlacek, 2006). We believe that this promising technique has the potential to deliver more precise and accurate data with a fairly robust and simple tool based on first physical principles.

Our PTI prototype consists of a folded Jamin interferometer (Figure 1). The aerosol light absorption is measured by heating particles with pulses of light of a defined wavelength. The absorbed energy is transferred to the surrounding air lowering its density and changing the refractive index. This causes a phase shift  $\Delta\phi$  between a reference beam and the sample beam with the aerosol and pulsed light. To achieve a high (and linear) sensitivity, the relative path lengths of the two beams of the interferometer are continuously adjusted such that the system is in quadrature, i.e. the light intensities at both photo-detectors remain essentially equal.

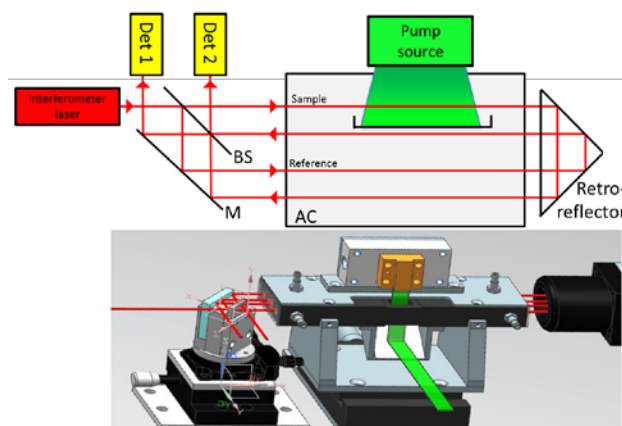


Figure 1: A PTI configuration that is currently exploited. A beam splitter (BS) first separates and then recombines the sample and reference beams. All components (BS, mirror (M) and retroreflector) are commercially available. The technical drawing below shows the whole optical setup with assembled aerosol chamber (AC) and the pump light (green).

### Achievements and challenges

Our current interferometer setup adjusts the path length continuously to keep the system in quadrature. It has a lower detection limit (DL) of about  $\Delta\phi = 1 \mu\text{rad}$  (1-minute time resolution) and the DL is determined by external noise and vibrations. This value is a factor of  $>100$  higher than the theoretical detection limit and thus has the potential to be further lowered.

The challenge of this development is to find an efficient and practical method to heat up the aerosol with a well-defined light source. We are currently exploring the following possibilities:

- 1) Employment of a pump laser collinear with interferometry laser using dielectric mirrors. Advantage: high pumping efficiency (estimated DL:  $< 10 \text{ ng m}^{-3} \text{ eBC}$ ). Disadvantage: difficult to adjust and offset caused by photothermal effects in common optical components.
- 2) Transverse excitation using lasers, high power LED arrays or diode laser arrays (as shown in Figure 1). Advantage: simple setup, smaller offset. Disadvantage: lower pumping efficiency (estimated DL:  $100 \text{ ng m}^{-3} \text{ eBC}$ ).

Moosmüller, H., and W. P. Arnott (1996), *Optics Letters*, 21(6), 438-440.

Sedlacek, A.J. (2006) *Rev. Sci. Instrum.* **77**, 064903.

Weingartner, E. et al. (2003), *J. Aerosol Sci.*, 34(10), 1445-1463.

## Study of the wavelength dependence of the optical depth for estimation the aerosol contamination of the atmosphere

A. Nagy<sup>1,2</sup>, A. Czitrovsky<sup>1,2</sup>, A. Kerekes<sup>1</sup>, Sz. Kugler<sup>1</sup>

<sup>1</sup>Wigner Research Centre for Physics, Institute for Solid State Physics and Optics,  
Konkoly Thege Miklós st. 29-33., 1121 Budapest, Hungary

<sup>2</sup>Envi-Tech Scientific Technical Development and Environmental Ltd.,  
Konkoly Thege M. st. 29-33., 1121 Budapest, Hungary

Keywords: remote sensing, radiation measurement, size distribution, extinction coefficient

Presenting author email: nagy.attila@wigner.mta.hu

The optical depth expresses the quantity of light removed from a beam by absorption or scattering during its path through the atmosphere. The relationship between the aerosol contamination of the atmosphere and wavelength dependence of the optical depth and extinction coefficient has been studied theoretically than experimentally by a number of groups (King *et al.* 1978, Liu *et al.* 1999, Schmid *et al.* 1997 *etc.*). From spectral attenuation measurements, the size distribution and the concentration of aerosol can be determined.

Our aim was to develop a multi channel radiometer for the measurement of the extinction coefficient at different wavelengths. The system consists of a three channels detection system with wide spectral range (from UV to IR) in which the selection of the wavelengths can be made using narrow band filters. The central wavelength of the filters was fitted to the characteristic spectral lines corresponding to certain materials.

The system has three detection channels. Two of them has narrow band interference filter holder, for selecting the proper wavelengths. In the third detection channel the incoming light is reflecting from four mirrors which have high reflectivity only in a narrow band around a certain UV line. These four mirrors increase the wavelength selectivity by four orders of magnitudes. So, this device combine the benefits of the UV radiometer and a wide range spectrometer for the determination of the wavelength dependence of the extinction coefficient.

In addition to the commonly used data retrieval process for the determination of the size distribution and concentration of atmospheric aerosols (King *et al.* 1978), an evaluation method based on the ratio of the signals obtained in different channels is introduced. This method is independent of the absolute intensity which is varying with the cloud density or meteorological conditions.

After the calibration of the device we made several measurement campaigns at different optical conditions. The measurement results are under evaluation.



Figure 1. The multichannel radiometer device

This work was supported by the Hungarian Research and Development Office.

King, M. D., Byrne, D. M., Herman, B. M., and Reagan, J. A. (1978). Aerosol size distributions obtained by inversion of spectral optical depth measurements. *J. Atmos. Sci.* 35:2153-2167.

Liu Y, Arnott W.P., Hallett H., (1999) Particle size distribution retrieval from multispectral optical depth: influences of particle non-sphericity and refractive index, *J. Geophys. Res.*, 104, 31753-31762.

Schmid, B., Matzler, C., Heimo, A., Kampfer, N., (1997) Retrieval of optical depth and particle size distribution of tropospheric and stratospheric aerosols by means of Sun photometry, *Geoscience and Remote Sensing, IEEE Transactions on Volume 35, Issue 1, 172 – 182.*

Xin-peng Tian, Lin Sun, Retrieval of aerosol optical depth over Arid Areas from MODIS data, *Atmosphere* 2016, 7(10) 134.

Goody, R., Principles of Atmospheric Physics and Chemistry, Oxford University Press, New York, 1995. Radiative transfer

## **Abstracts T308**

## Electrochemical oxidation of RBk5 with using graphene/TiO<sub>2</sub> composite electrode

J.Y. Li<sup>1</sup>, J.M. Hong<sup>1</sup> and C.T. Chang<sup>2</sup>

<sup>1</sup>Department of Environmental Science and Engineering, Huaqiao University, Xiamen, Xiamen361021, China

<sup>2</sup>Department of Environmental Engineering, National ILAN University, I-Lan 26047, Taiwan

Keywords: Graphene/TiO<sub>2</sub>, Electrochemical oxidation, RBk5

Presenting author email: jinyanlee@foxmail.com

Dye wastewater has the characteristics of large amount of water, high content of organic matter, high chroma, complex composition and bio-refractory. The homobifunctional dye Reactive Black 5 (RBk5) is a member of a class of azo dyes, which is widely used in textile industry. Electrochemical advanced oxidation processes (EAOPs) are able of treating toxic organic wastewater effectively without secondary pollution.

In this study, we successfully prepared graphene/TiO<sub>2</sub> (GN/TiO<sub>2</sub>) composite electrode to degrade RBk5 by electrochemical oxidation. Graphene oxide (GO) was prepared first by a modified Hummers' method with using graphite as the raw material. Then, GO and TiO<sub>2</sub> were mixed into suspension with different mass ratio (1:4, 1:1 and 4:1) under ultrasonic condition, which transferred into stainless steel high pressure reactor to form GN/TiO<sub>2</sub> electrode. Polyvinylidene fluoride (PVDF) was uniformly mixed in an appropriate amount of N,N-dimethyl-acetamide (DMAC) as adhesive agent to help the prepared materials loaded on the conductive carbon cloth. The diagram of Field Emission Scanning Electron Microscope (FESEM) of GN/TiO<sub>2</sub> composite electrode is shown in Figure 1. It can be seen from the figure that the GO had been reduced and combined with TiO<sub>2</sub> to obtain large specific surface area. It reveals that the material we prepared can provide more active sites (Cao et al., 2017).

At the same time, the active carbon electrode was prepared as working electrode (WE) with same loading method to compare the removal performance under RBk5 concentration of 10 ppm. In addition, the permeates at certain reaction time intervals were determined at the wavelength of 600nm with UV spectrophotometer, as shown in the Figure 2. Electrochemical measurements were performed with using a conventional three-electrode cell and a multifunctional polarimeter (China). An Ag/AgCl and a copper wire electrode were served as the reference electrode (RE) and auxiliary electrode (CE). As shown in Figure 2, all material electrodes achieved more than 90% RBk5 removal efficiency. Comparing with the active carbon electrode, the GN/TiO<sub>2</sub> electrode presented better removal performance for RBk5 treatment. Furthermore, the GN/TiO<sub>2</sub> electrode prepared by GO:TiO<sub>2</sub> with mass ratio 1:1 had the best electrocatalytic performance. It results from that the graphene has an excellent conductivity and TiO<sub>2</sub> is a common photocatalyst which can provide h<sup>+</sup>. Therefore, it maybe play a better synergistic role in this mass ratio (Yilong et al., 2017).

The Fourier-transform Infrared Spectroscopy (FT-IR) was employed to study the function groups of electrodes. The removal performance were assessed under different conditions, such as initial pH (3.0, 6.6 and 10.0), initial RBk5 concentration (5, 10, 15 and 20ppm) and applied current (6.6, 10.0, 13.5 and 17.5 mA). In addition, the operational parameters influencing the electrochemical degradation of RBk5 with electrode were optimized under the initial pH of 6.55, initial RBk5 concentration (C<sub>0</sub>) of 10ppm and applied current of 10 mA. Furthermore, the electrocatalytic performances of different GN/TiO<sub>2</sub> composite electrodes for RBk5 removal were also assessed.

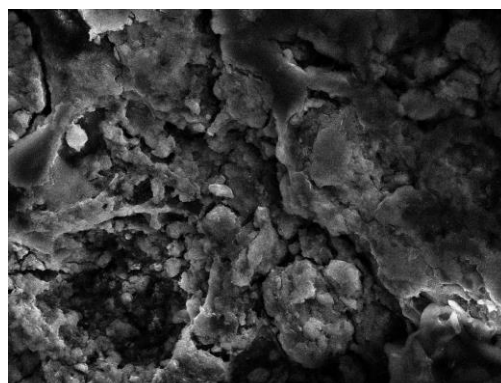


Figure 1. FESEM of GN/TiO<sub>2</sub> (GO:TiO<sub>2</sub> = 1:4)

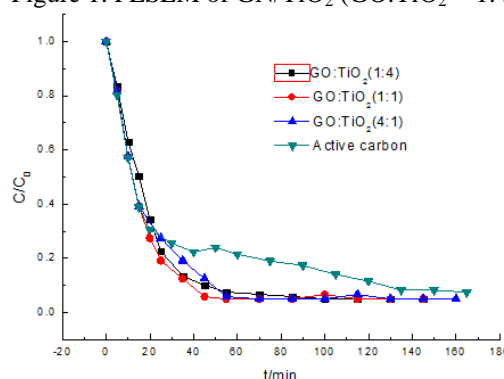


Figure 2. C/C<sub>0</sub> of electrochemical reactors packed with different electrodes (C<sub>0</sub>=10ppm, pH=6.6, applied current=10mA)

Cao, Y., Xia, Y., Jianhua, C., Huade, Z., Yuancai, C.(2017) *Applied Catalysis B:Environmental*. 200,673-680.

Yilong, Y., Yongli, L., Jinshu, W., Junshu, W., Di, H., Qier, A. (2017) *Journal of Alloys and Compounds*. 699, 47-56.

## Development and Characterization of a 3D Printed Precipitator for Aerosol Nanoparticle Segregation

Athina Avgousta Floutsi<sup>1</sup>, Spyros Bezantakos<sup>2,3</sup>, Nicholas Surawski<sup>3</sup> and George Biskos<sup>1,3</sup>

<sup>1</sup>Faculty of Civil Engineering and Geosciences, Delft University of Technology, Delft 2628 CN, the Netherlands

<sup>2</sup>Maison de la Recherche en Environnement Industriel 2 (MREI2), Université du Littoral Côte d'Opale, 59140, Dunkerque, France

<sup>3</sup>Energy, Environment, and Water Research Center, The Cyprus Institute, Nicosia 2121, Cyprus

Keywords: aerosol precipitator, 3D print, nanoparticle segregation, relative penetration efficiency

Presenting author email: [A.A.Floutsi@student.tudelft.nl](mailto:A.A.Floutsi@student.tudelft.nl), [g.biskos@cyi.ac.cy](mailto:g.biskos@cyi.ac.cy)

In a recent study, Bezantakos et. al. (2015), provided a simple and cost-effective method for aerosol nanoparticle segregation. In this method, particle size segregation is achieved by employing tubes composed by Electrostatic Dissipative Materials (EDMs). By applying a positive potential difference along the tube, an electric field with a radial and an axial component is created. This causes not only a deceleration of the incoming particles of the same polarity charged, but also their removal via electrostatic deposition. As the study results indicate, EDM tubes can be considered as a combination of Diffusion Batteries (DBs) and electrostatic precipitators. In contrast with the low portability of DMAs, due to their size and weight, EDM tubes are compact and light weighted, thus may be used in applications where portability is the major priority.

Based on these principles and aiming to investigate the effects of geometry on the relative penetration efficiency, we designed and 3D printed a conical precipitator (Fig.1). This precipitator was printed using Z-ABS (Acrylonitrile Butadiene Styrene, plastic), with medium hardness and elasticity and high impact strength. Both mechanical and chemical treatment were applicable for this type of material. Conductivity was achieved after applying a graphite based spray to the desirable surfaces of the precipitator.

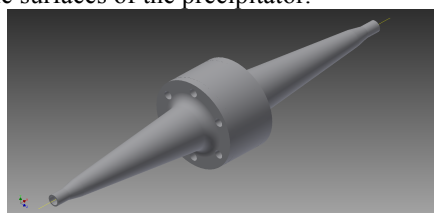


Fig. 1: 3D printed conical precipitator.

Metal rings were attached to the conical precipitator for grounding the inlet and the outlet, and a metallic nail was attached at the intermediate part for applying a high voltage. Initially, the aerosol concentration at 0 V was measured. Then a potential difference was applied to the intermediate part and the aerosol concentration was measured after 100 s in order to avoid transitional phenomena (i.e., avoiding particles that were already in the tube, but not at its inlet, to be subjected to the electric field). The applied potential difference ranged from 20 to 3000 V depending on the aerosol size of our sample. By following this procedure

we were able to calculate the relative penetration efficiency  $P_r$ , according to (Bezantakos et al., 2015):

$$P_r(V) = 1 - \frac{N(0) - N(V)}{N(0)} = \frac{N(V)}{N(0)}$$

where  $N(0)$  and  $N(V)$  are the average particle number concentration measured over 30 s by the ultrafine Condensation Particle Counter (uCPC) when zero and V volts were applied respectively.

Figure 2 shows the measured relative penetration efficiency of particles having electrical mobility diameters from 20 to 80 nm that pass through the conical precipitator. As the results in Fig.2 indicate, when the applied potential difference is fixed, the relative penetration of the particles increases logarithmically with their size, resulting in steeper curves as the particle size decreases. Also, larger particles require a higher potential difference between the intermediate part and the two ends in order to decrease their relative penetration efficiency.

The conical precipitator that was developed here can be considered as an effective and compact electrostatic precipitator due to its ability to size segregation charged aerosol nanoparticles. The selection of the aerosol size for the conical precipitator can be made not only by adjusting the flow rate as in DBs but also by adjusting the potential difference along its surface, which is much more practical. Other advantages that make this device highly attractive for deploying on board the UAVs, are its compact size and light weight.

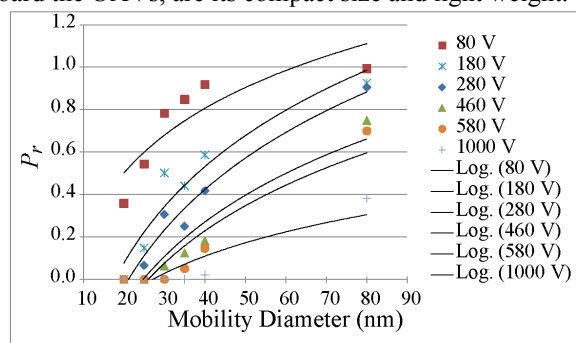


Fig. 2: Relative penetration efficiency ( $P_r$ ) of monodisperse particles having electrical mobility diameters ranging from 20 to 80 nm, through the conical precipitator.

### References

Bezantakos, S., Huang, L., Barmounis, K., Attoui, M., Schmidt-Ott, A., & Biskos, G. (2015). *Aerosol Science and Technology*, 49(1), iv-vi.

## Approaching the resolving power of SEADM's DMA P5 to its theoretical limit

Amo-Gonzalez Mario<sup>1</sup>, Juan Fernandez de la Mora<sup>2</sup>

<sup>1</sup>SEADM, Parque Tecnológico de Boecillo 205, Valladolid, Spain

<sup>2</sup>Mechanical Engineering Department, Yale University, New Haven, Connecticut 06520-8286, USA

Keywords: DMA, resolving power, laminarizers, prelaminarizers.

Presenting author email: juan.delamora@yale.edu

**Introduction:** SEADM's planar DMA P5, which operates at supercritical Reynolds numbers, has demonstrated over recent years its capability for high resolving power. Working with Reynolds numbers of  $1 \times 10^5$  and with THA<sup>+</sup> ion ( $1 \text{ cm}^2/\text{V/s}$ ) as calibration standard, its resolving power was 70-80. This resolving power is remarkably good; however it is still far from the theoretical value, limited by Brownian diffusion. In this work we improved the laminarization stage of DMA P5 and we used two DMA blowers in series to increase the Reynolds number in the separation channel. The results returned resolving powers as high as 110, much closer to the theoretical limit.

**Methods:** We used SEADM's P5-G DMA, with critical dimensions collected in Table 1. This DMA, allows the classification of charged nano-particles and ions with sizes comprising between 0 and 4 nm. The DMA combines a horizontal laminar flow of gas with a vertical electric field between two parallel plates, such that ions of different mobilities penetrating through a slit in the upper plate opening out into a fan shape as they drift towards the other plate, whereby only a small range of mobilities is sampled through a second slit in the lower plate and transmitted to the ion detector (electrometer or mass spectrometer).

Table 1. Critical dimensions (mm) of SEADM's P5-G DMA

	$W_{\text{DMA}}^a$	$H_{\text{DMA}}^b$	$L_{\text{DMA}}^c$	$W_{\text{slit}}^d$	$L_{\text{slit}}^e$
Inlet	17	10	40	0.6	7
Outlet	14.9	10		0.17	6.5

<sup>a</sup>Channel width. <sup>b</sup>Channel height. <sup>c</sup>Channel length. <sup>d</sup>Slit width. <sup>e</sup>Slit length.

The outlet slit of this DMA allows monodisperse sample flows ( $q_s$ ) of 10 liters per minute, without choked flow in the slit. The maximum ( $q_s$ ) tested in this work was 5 l/min. The three laminarizers located just before the DMA nozzle have been redesigned to avoid small steps that might lead to periodic vortex shedding. Two new pre-laminarizer screens are placed before the DMA drift gas inlet to dampen upstream turbulence. These prelaminarizers improve substantially the resolving power in the absence of steps between the three DMA laminarizers. The ionization source was SEADM's nano-ESI. The solution used in this test is formed of tetraheptylammonium bromide (THABr) 1 mM in methanol / water 9:1. The DMA blowers used were Domel model 792.3.265-852, with 1100 watts of power. One blower alone and two blowers in series were tested.

Following the blower stages an intercooler reduced the air temperature to near ambient levels. The electrometer used was SEADM's LYNX E11. This is a low noise and ultrafast electrometer (Fernandez de la Mora, 2017).

**Results:** The first five groups of points (from left to right) in Figure 1 correspond to only one DMA blower configuration working at 6000 rpm ( $36 \text{ V}^{1/2}$ ), 9000 ( $46 \text{ V}^{1/2}$ ), 12000 ( $54 \text{ V}^{1/2}$ ), 15000 ( $61 \text{ V}^{1/2}$ ), 18000 ( $69 \text{ V}^{1/2}$ ). The last group of points placed in ( $74 \text{ V}^{1/2}$ ), corresponds to two DMA blowers working in series at full power.

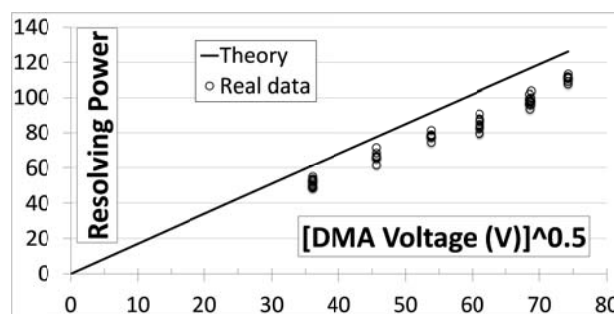


Figure 1. Resolving power as a function of the square root of the DMA voltage. Circles: Experimental data. Continuous line: Theoretical resolution considering only Brownian diffusion as limiting factor. Monodisperse sample flow rate / slit length: 0.31 liters/min/mm.

The maximum Reynolds number reached in the separation channel with the two blowers working in series was approximately  $1.3 \times 10^5$  (based on a characteristic length of 10 mm, a kinematic viscosity  $\nu = 1.69 \cdot 10^{-5} \text{ m}^2/\text{s}$  for air at  $40^\circ \text{C}$  and a fluid velocity of 219 m/s). The resolving power average working with two DMA blowers in series was 111, whereas working with only one DMA blower the resolving power average was 98. Experimental resolving powers obtained are quite close to the theoretical ones, only limited by Brownian diffusion.

**Conclusions:** Planar DMAs are able to reach resolving powers of 110 operating at Reynolds number of  $1.3 \times 10^5$ . Its high transmission, resolution and duty cycle make the DMA the ideal instrument for IMS-MS studies.

Fernandez de la Mora, Perez-Lorenzo L.J., Arranz G., Amo-Gonzalez M., Burtscher H. (2017) *Fast high-resolution nanoDMA measurements with a 25 ms response time electrometer*, accepted for publication in *Aerosol Science and Technology*.

## Measurement of Atmospheric Charged Particle during a Lightning Event by AEMSA

Hong-Ku Lee<sup>1</sup> and Kang-HoAhn<sup>2</sup>

<sup>1</sup>Department of Mechanical Engineering, Hanyang University, Seoul, 04763, R. of Korea

<sup>2</sup>Department of Mechanical Engineering, Hanyang University, Ansan, 15588, R. of Korea

Keywords: Atmospheric particle charging, Charging polarity reversal, Lightning effect

Presenting author email: khahn@hanyang.ac.kr

There have been numerous research reports on atmospheric aerosol effect on climate, visibility, human health and so on. Charged atmospheric particles may also affect human health because the deposition of charged particles in human lungs is enhanced compared to that of uncharged particles (Fews, et al., 1999). Atmospheric aerosol charging is caused mainly by cosmic rays and/or natural radioactive material decay. Because the ionization process generates well-balanced ion pairs, positive and negative ions in the air are at almost the same concentrations. The atmospheric aerosol electrical charge is therefore usually neutral. To measure the charging characteristics of the atmospheric aerosol, we used the aerosol electrical mobility spectrum analyzer (AEMSA) devised by Ahn and Chung (2010). The AEMSA can detect the electrical mobility spectrum of charged single particles in the nano-meter size range, regardless of their polarity, without electrical scanning. We measured the particle charge polarity distribution in the atmosphere during a lightning event at ground level. We found that the 80 – 200 nm particle charge balance during a lightning event was skewed either to the positive or the negative. Furthermore, the particle charge polarity changed very rapidly (within a few minutes) from negative to positive or vice versa. As a result, we found that when the ground is polarized by thunder cloud, the number of particle charged by opposite polarity increases near the ground..

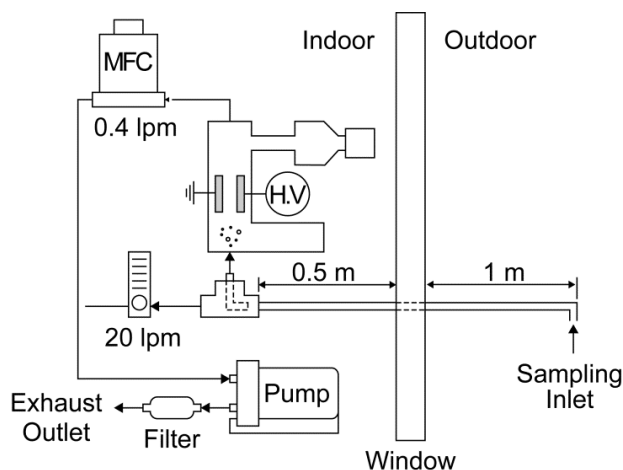


Figure 1. Schematic of atmospheric particle sampling and measurement system.

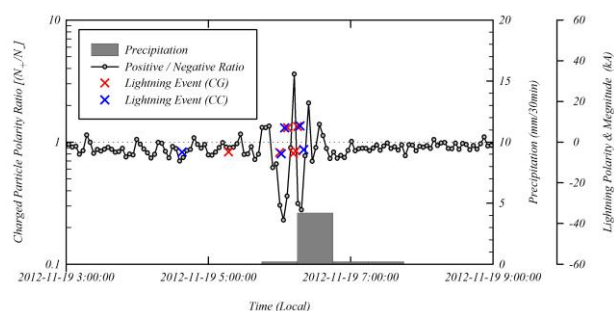


Figure 2. The charged particle polarity ratio ( $N_+ / N_-$ ) during lightning event.

Ahn, K. H., & Chung, H. (2010) *Journal of Aerosol Science*, 41, 344-351.

Fews, et al. (1999) *Int. J. Radiat. Biol.*, 75 (12), 1523-1531,

## Expanded size range of high-resolution nanoDMAs by improving the sample flow injection at the aerosol inlet slit.

J. Fernandez de la Mora<sup>1</sup>

<sup>1</sup> Yale University, Mechanical Engineering Department, New Haven, CT 06520

Keywords: Differential Mobility Analyzer; inlet slit; Flow instability; Mixing layer; nanoparticles; Size range.  
Presenting author email: juan.delamora@yale.edu

High-resolution DMAs requiring hundreds of lit/min of sheath gas flow  $Q$  to classify 1 nm particles have not been previously examined and optimized under the modest  $Q$  values (tens of lit/min) needed to classify particles well above 10 nm. Here we study the resolving power  $\mathcal{R}$  ( $1/\mathcal{R}$  =FWHM= relative width of the transfer function at half Maximum) of the Halfmini DMA, at sample flow rates  $q > 1$  lit/min. The charge-reduced electro sprayed ovalbumin protein used as test aerosol has an accurately determinable Gaussian mobility distribution, which limits the measurable  $\mathcal{R}$  to at most 25-30. Non-ideal DMA response can however be precisely probed by comparing measured peak widths with the convolution of the protein's mobility distribution with the triangular Knutson-Whitby distribution associated to the finite  $q/Q$  ratio. For the unmodified Halfmini DMA (m series),  $\mathcal{R}$  departs considerably from ideal at  $q/Q$  values as modest as 2% (Figure 1).

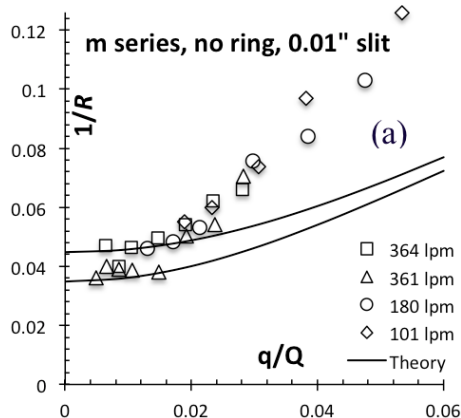


Figure 1. Full width at half maximum (FWHM) for ovalbumin ions as a function of the aerosol to sheath gas flow rate  $q/Q$ , showing flow nonidealities for  $q/Q > 2\%$ .

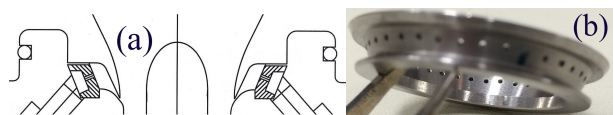


Figure 2: (a) placement of perforated ring ensuring axisymmetric entry of the sample gas into the separation region of the DMA. (b) Image of a ring with 24 perforations 0.02" in diameter.

The nonideal response in Figure 1 reveals a problem with the aerosol inlet flow, which is not removed by increasing or decreasing the slit height, nor by

reorienting axially the sample flow as it merges with the sheath gas. By introducing a ring with many perforations upstream of the inlet slit, which favors a more symmetric distribution of the sample flow over the slit perimeter (Figure 2),  $\mathcal{R}$  values close to ideal are approached with  $q/Q$  ratios as large as 6-12% (Figure 3).

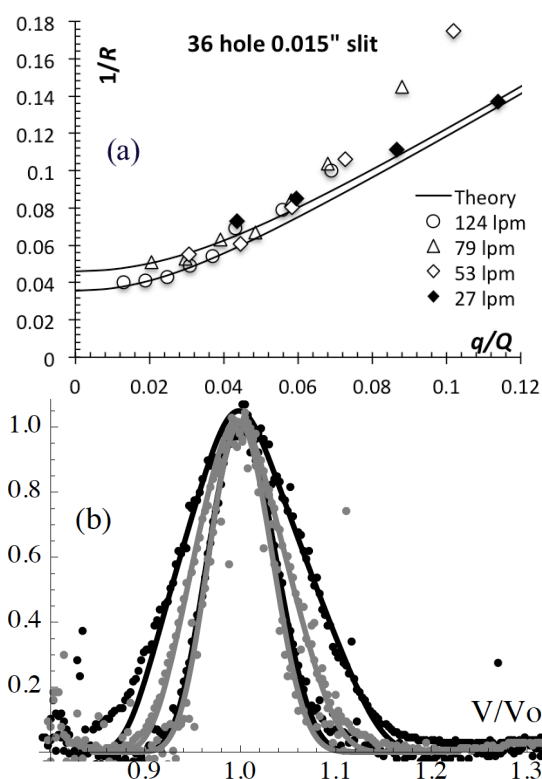


Figure 3: DMA response at modest sheath gas flow rates, achieving essentially ideal response at  $Q=27$  L/min at all sample flows investigated. (a) Peak widths FWHM. (b) Peak structures for the series at  $Q=27$  L/min (gray, black, gray, black at increasing  $q$ ) compared to theoretical convolution.

Conclusions: Symmetrization of the inlet aerosol flow permits achieving ideal performance at unusually small  $Q$  values. This enables classifying particles larger than 30 nm in an instrument designed to have its peak performance with 1-4 nm particles.

## **Abstracts T309**

## Real-time measurement of PM<sub>2.5</sub> size distribution using a Lab-made 11-stage Electrical Low Pressure Impactor

Jangseop Han<sup>1</sup>, Joohee Seo<sup>1</sup>, Junho Hyun<sup>2</sup> and Junggho Hwang<sup>1,2</sup>

<sup>1</sup>Department of Mechanical Engineering, Yonsei University, Seoul, 03722, Republic of Korea

<sup>2</sup>Graduate program of Clean Technology, Yonsei University, Seoul, 03722, Republic of Korea

Keywords : electrical low pressure impactor, collection efficiency, corona discharge.

Presenting author email: hanjangseop@yonsei.ac.kr

In recent years, increasing public concern regarding air quality has led to the development of efficient aerosol-monitoring techniques. Real-time aerosol number concentration can be measured by using optical and electrical methods. The optical method typically uses light-scattering technology. However, for particles smaller than approximately 0.3  $\mu\text{m}$ , the light-scattering intensity drops very rapidly.

Commercially available particle-detection systems based on electrical methods have been widely used. The scanning mobility particle sizer (SMPS) has excellent size resolution, but needs almost 3 minutes to perform even a single measurement. The electrical low pressure impactor (ELPI) has a time resolution (1 second) for measuring transient size distributions of ambient and indoor aerosol particles. The ELPI has wide particle size range based on aerodynamic diameter.

The ELPI is composed of a particle charger, a cascade impactor, and a multichannel electrometer. By passing through the particle charger, incoming particles are charged by ions. The charged particles are then classified in the cascade impactor by their inertia. Each impactor stage is insulated from each other. The multichannel electrometer at each stage measures the charges carried by the collected particles. Marjamaeki et al. (2000) evaluated the performance of the commercial ELPI and compared with the SMPS results.

In this study a wire-to-rod-type corona charger serves as the particle charger. The average charge number and penetration of particle are experimentally determined. The charging efficiency of the particle is intimately related with the resolution of the ELPI. In this study, 11-stages are divided into 2 channels (first channel: 2.5 $\mu\text{m}$  ~ 250nm, second channel: 250nm ~ 10nm) and applied two different chargers. Carbon brush ionizer is serially connected to the charger at the second channel to enhance charging efficiency for nano-particles. Figure 1 show the schematic of an 11 stage electrical low pressure impactor. The 11-stage cascade impactor is designed based on the procedure described by Hillamo and Kauppinen (1991), and it's performance is evaluated using polystyrene latex (PSL) particles.

To measure the charges carried by particles, we use a lab-made electrometer that can measure 1 fA using a three stage amplifier circuit. The performance of the lab-made electrometer is compared with a commercial electrometer (Keithly 6517B). Additionally, a network module is attached to ELPI, so that users can communicate ELPI with a remote network system (smartphone, internet).

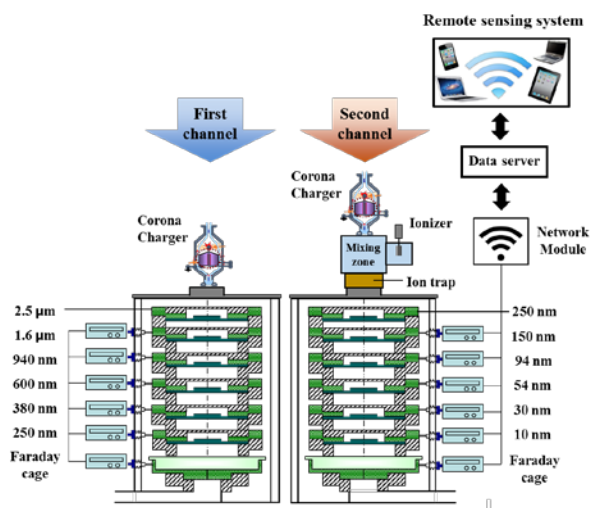


Figure 1. Schematic of an 11-stage electrical low pressure impactor.

After evaluating each stage of the impactor, the size distributions of the test particles are estimated using the data inversion algorithm (Park et al. (2009)) and compared with the data measured by the TSI SMPS and Dekati ELPI. The results obtained from the data inversion algorithm, with currents measured by the impactor, match well with the TSI SMPS and Dekati ELPI data.

This subject is supported by Korea Ministry of Environment (MOE) as "the Technologies for Responding to Atmospheric Environment Policies Program".

- R. E. Hillamo, E. I. Kauppinen, On the performance of the Berner low pressure impactor, *Aerosol Sci. Tech.*, 1991, 14, pp.33-47.
- M. Marjamaeki, J. Keskinen, D. R. Chen, D. Y. H. Pui, Performance evaluation of the electrical low-pressure impactor (ELPI), *J. Aerosol Science*, 2000, 31, pp. 249-261.
- D. Park, S. Kim, M. An, J. Hwang, Real-time Measurement of the Size Distribution of Diesel Exhaust Particles using a Portable 4-stage Electrical Low Pressure Impactor, *Part. Part. Syst. Charact.*, 2009, 26, 179–186.

## **Abstracts T310**

## Fate of atmospheric clusters inside a mass spectrometer (CI-API-TOF)

M. Passananti, M.P. Rissanen, C. Yan, X.C. He, J. Kangasluoma, F. Bianchi, H. Junninen, M. Ehn and H. Vehkamäki

Department of Physics, University of Helsinki, Helsinki, 00014, Finland

Keywords: cluster, sulfuric acid, ammonia, CI-API-TOF.

Presenting author email: monica.passananti@helsinki.fi

Atmospheric aerosol particles have an important impact on climate, air quality and human health. Nevertheless the processes for the formation and growth of new particles in the atmosphere are still poorly understood. The first steps in new particles formation involve atmospheric clusters, therefore the knowledge of their chemical composition and stability is crucial to understand the factors and the conditions that lead to new particles formation. In the last years the development of high-resolution mass spectrometers has led to important discoveries about the chemical composition of the species that are involved in the new particle formation. The Chemical Ionization Atmospheric Pressure interface Time Of Flight mass spectrometer (CI-API-TOF), indeed, is able to detect the elemental composition of many atmospheric clusters at ambient low concentration (Jokinen *et al.*, 2012). Although CI-API-TOF can supply significant information about atmospheric clusters, data interpretation should be considered carefully. Clusters are less stable aggregates compared to molecules, hence they can undergo transformations inside a mass spectrometer easier than molecules. The chemical ionization process, the low pressure and the energetic collisions inside the instrument could lead to fragmentation and/or evaporation of molecules from clusters. It has been already shown that theoretical models predict a higher cluster concentration than the measured concentration (Olenius *et al.*, 2013). This discrepancy could be due to the cluster fragmentation process inside the instrument, which is significantly affected by the tuning of the instrument.

Although the fragmentation of clusters inside the CI-API-TOF is known, a systematic study has not been carried out until now. In this work, we investigated the fate of sulfuric acid-ammonia clusters inside the CI-API-TOF. It has been shown that sulfuric acid clusters with ammonia (or amines) are directly involved in new particles formation (Vehkamäki and Riipinen, 2012), therefore it is essential to correctly determine their composition and concentration in the atmosphere.

The experiments are carried out in the laboratory where sulfuric acid-ammonia clusters are produced and then analysed by CI-API-TOF. The tuning of the instrument is systematically changed to evaluate its effect on clusters detection. Clusters, after the charging process, are guided inside the atmospheric pressure interface through a series of three vacuum chambers before arriving to the time of flight mass spectrometer (Figure 1). The pressure decreases between successive chambers until arriving to  $10^{-6}$  mbar in the mass spectrometer. In the first two chambers (SSQ and BSQ) the ions are guided through quadrupoles (Quad1 and Quad2), in the last chamber (PB)

several lenses focus the ions. The fragmentation of clusters may happen mainly in the first chamber (SSQ) where the pressure is relatively high ( $\sim 2$  mbar). Here, the charged clusters are accelerated by an electric field and they can produce energetic collisions with neutral molecules.

In the first part of this study the effects of the voltages applied in the three chambers will be evaluated separately and successively more voltages will be changed at the same time in order to evaluate the overall effect. The first results show a more significant fragmentation when high voltages are applied to Quad1 and Quad2, and also the voltage difference between the SSQ and BSQ chamber seems to have an important impact on cluster fragmentation.

This work will be useful to correctly determine the concentration and composition of sulfuric acid-ammonia clusters in the atmosphere and it lays the foundation for developing a theoretical model to describe and predict the fate of clusters inside the CI-API-TOF.

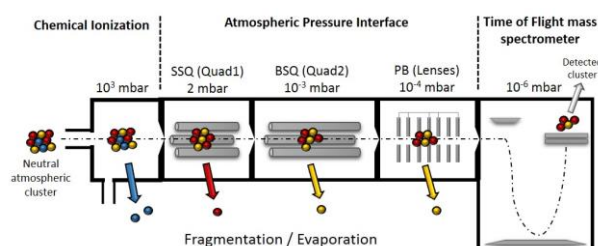


Figure 1. Schematic representation of the CI-API-TOF and possible transformation of atmospheric clusters inside the instrument.

This work was supported by the European Research Council project 692891-DAMOCLES.

Jokinen, T., Sipilä, M., Junninen, H., Ehn, M., Lönn, G., Hakala, J., Petäjä, T., Mauldin III, R. L., Kulmala, M. and Worsnop, D. R. (2012) *Atmos. Chem. Phys.* **12**, 4117-4125.

Olenius, T., Schobesberger, S., Kupiainen-Määttä, O., Franchin, A., Junninen, H., Ortega, I.K., Kurtén, T., Loukonen, V., Worsnop, D.R., Kulmala, M. and Vehkamäki, H. (2013) *Faraday Discuss.* **165**, 75-89.

Vehkamäki, H. and Riipinen, I. (2012) *Chem. Soc. Rev.* **41**, 5160-5173.

## Time-Resolved Characterization of Organic Nitrogen in Particulate Matter: An Investigation into Beijing's Air Quality

S.J. Swift<sup>1</sup>, W. Dixon<sup>1</sup>, R.E. Dunmore<sup>1</sup>, N.J. Farren<sup>1</sup>, F. Squires<sup>1</sup>, K.L. Pereira<sup>1</sup>, J.D. Lee<sup>1</sup> and J.F. Hamilton<sup>1</sup>

<sup>1</sup>WACL, Department of Chemistry, University of York, York, YO10 5DD, UK

Keywords: Beijing, Particulate Matter, Organic Nitrogen, Nitrogen Chemiluminescence Detection.

Presenting author email: ss1375@york.ac.uk

With *ca.* 22 million inhabitants living in Beijing under involuntary exposure and substantial evidence that adverse health effects are strongly correlated with poor air quality, the investigation into the chemical composition and concentration of constituents in the ambient atmosphere in megacities, such as Beijing, is a crucial field of study<sup>1</sup>. Particulate matter (PM) is known to be ubiquitous in areas of poor air quality, of which anthropogenic emissions provide a significant contribution<sup>2</sup>. Exposure to high PM loadings has been strongly correlated with impaired lung function, respiratory diseases and premature mortality<sup>3</sup>. It is widely known that organic nitrogen (ON) compounds are especially toxic and carcinogenic, and increasing evidence has suggested that ON contributes significantly to PM<sup>4</sup>. ON is known to be emitted into the atmosphere anthropogenically through a wide range of combustion sources, but most of the observed ON is formed through gas-phase oxidation processes leading to secondary organic aerosol formation<sup>2</sup>.

Few studies have yet investigated ON content in China, creating wide scope for future research development in this field. Nitrogen chemiluminescence detection is a highly selective and sensitive technique for the detection of ON compounds in ambient particulate matter. When coupled with comprehensive two-dimensional gas chromatography, the identification of hundreds of ON compounds is possible. The use of two different stationary phases (Figure 1) allows species to be separated by two physical properties (*i.e.* boiling point and polarity), significantly increasing resolution and providing a characteristic chemical space where compounds of similar chemical speciation are grouped, aiding in the identification of unknown compounds. Due to the low concentration of ON within PM, detection of ON is challenging and has been left relatively untouched. To the best of our knowledge, very few studies have used this novel technique and no previous use has been undertaken in China.

Here, for the first time, we provide highly time-resolved chemical characterization of ON compounds in Beijing's PM. PM samples were collected at the Institute of Atmospheric Physics in Beijing, China (39°97'40.0"N 116°37'10.0"E), as a part of the Sources and Emissions of Air Pollutants in Beijing (AIR-POLL) project during October to December 2016 (winter) and May to June 2017 (summer). The sampling site is approximately 9 km from the center of Beijing, located in a mainly residential area between the 3<sup>rd</sup> (100 meters north) and 4<sup>th</sup> (400 meters east) ring road. PM samples were collected onto preconditioned quartz fiber filters (Whatman, UK) using

a HiVol sampler (Ecotech 3000, Australia) with a size selective inlet of PM<sub>2.5</sub>. Highly-time resolved PM samples were collected during daytime hours (*e.g.* 08:00 – 18:00); one to three-hour sampling duration dependent on PM concentrations. Filter samples were dissolved into ethyl acetate, extracted using pressurized liquid extraction (ASE 350, Dionex, CA) and analyzed using comprehensive two-dimensional gas chromatography (Agilent 7890, CA) coupled to a nitrogen chemiluminescence detector (Agilent 255, CA) (GC×GC-NCD). An extensive library consisting of over 100 ON compounds (an extent not exhibited by previous studies<sup>4,5</sup>) has been built, allowing rapid identification of a vast range of ON compounds (*i.e.* nitroalkanes, nitrosamines, alkanenitriles, nitrophenols, nitroalkenes, alkenenitriles, nitro-PAHs, amides, amines, nitramines, and nitroaromatics) in China's PM. This library coupled with the highly sensitive detection capabilities of the NCD, will allow for a considerable number of ON compounds to be identified. The temporal evolutions of these species will be compared with meteorological data, providing greater insights into the sources and chemical transformations of ON. The lifetime cancer risk from exposure to these species in Beijing's PM will be determined.

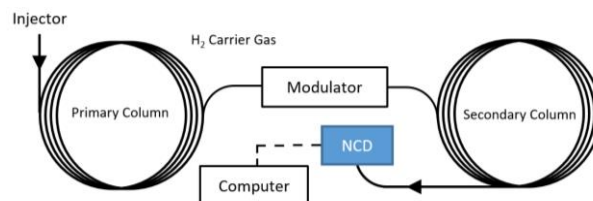


Figure 1. Schematic of GC×GC-NCD.

This work was supported by the Natural Environmental Research Council under NE/L002574/1.

- Hou, Q., An, X., Tao, Y. and Sun, Z. (2016) *Sci. Total Environ.* **563-564**, 557-565.
- Zhang, Q., Duan, F., He, K., Ma, Y., Li, H., Kimoto, T. and Zhang, A. (2015) *Front. Environ. Sci. Eng.* **9**, 1004-1014.
- Pope III, C. A. and Dockery, D. D. (2006) *J. Air Waste Manage. Assoc.* **56**, 709-742.
- Farren, N. J., Ramírez, N., Lee, J. D., Finessi, E., Lewis, A. C. and Hamilton, J. F. (2015) *Environ. Sci. Technol.* **49**, 9648-9656.
- Özel, M. Z., Ward, M. W., Hamilton, J. F., Lewis, A. C., Raventos-Duran, T. and Harrison, R. M. (2010) *Aerosol Sci. Technol.* **44**, 109-116.

## Chemical image-based determination of particle size and chemical composition – Towards image-based particle quantification

J. Ofner<sup>1</sup>, E. Eitenberger<sup>1</sup>, G. Friedbacher<sup>1</sup>, H. Lohninger<sup>1</sup>, B. Lendl<sup>1</sup>, and A. Kasper-Giebl<sup>1</sup>

<sup>1</sup>Institute of Chemical Technologies and Analytics, Vienna University of Technology, Vienna, Austria

Keywords: chemical imaging, quantification, particle size distribution

Presenting author email: johannes.ofner@tuwien.ac.at

The determination of aerosol size distributions for a number of chemical elements or compounds and the simultaneous determination of mass concentrations is a tricky task – especially if chemical species are present, which cannot be analysed by a single technique.

Chemical imaging of precipitated particles with different techniques allows an image-based determination of the chemical composition of the particulate matter (Ofner et al., 2015). Aerosol particles were sampled using a Sioutas cascade impactor. Stage B with the size range of 2.5 to 1  $\mu\text{m}$  aerodynamic diameter was analysed by scanning electron microscopy, combined with energy dispersive X-ray (EDX) imaging, and vibrational Raman micro-spectroscopic (RMS) imaging. All imaging techniques were applied to the same sample spot of 200x200  $\mu\text{m}$  and fused to a combined imaging dataset for subsequent multivariate analytics (Lohninger and Ofner, 2014; Ofner et al., 2015). After image-based chemical identification of single species (demonstrated for  $\text{NaNO}_3$  in figure 1), the related images were analysed by a particle finder software and the particle size distribution was obtained (figure 2).

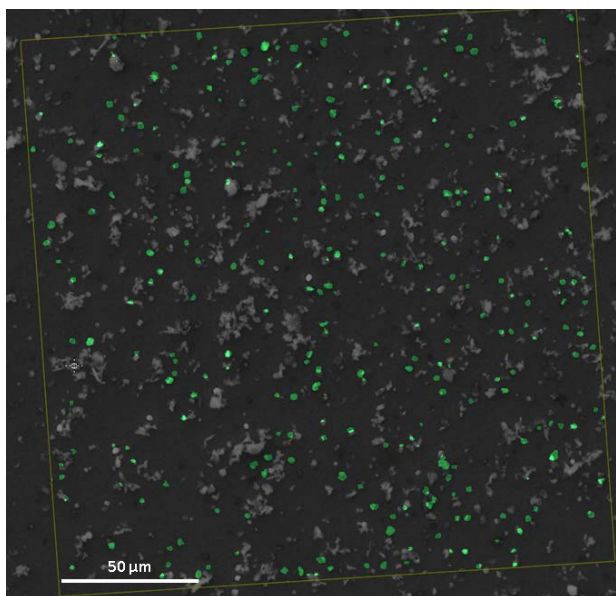


Figure 1. Combined chemical image of  $\text{NaNO}_3$  particles (green).

In the given example (Figures 1 and 2), 260 particles with diameters between 0.5 and 3  $\mu\text{m}$  were extracted from the imaging dataset. The obtained particle size distribution is in excellent agreement with the expected impactor stage (1 – 2.5  $\mu\text{m}$  aerodynamic diameters). By calculating the particle volumes based on

the 2D projection an overall volume of 704  $\mu\text{m}^3$  was obtained, resulting in an overall measured particle mass of 1.59 ng on the sample spot of 200x200  $\mu\text{m}$ .

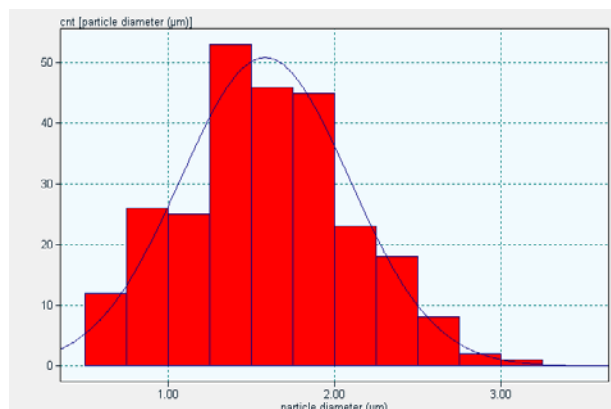


Figure 2. Particle size-number distribution of  $\text{NaNO}_3$  particles obtained from chemical image in figure 1.

This study will introduce image-based determination of particle size distributions and calculation of precipitated particle masses, based on morphological and chemical images. The selection of the sampling spot as well as the sampling substrate will be discussed as well as species- and morphology related effects on the quality of the size distribution. First attempts towards image-based quantification will be made and correlated to established methods.

This work was supported by the Hochschuljubiläumstiftung of the City of Vienna under grant H-297306-2014.

Lohninger, H. and Ofner, J. (2014) *Spectrosc. Eur.*, **26**, 6–10.

Ofner, J., Kamilli, K. a., Eitenberger, E., Friedbacher, G., Lendl, B., Held, A. and Lohninger, H. (2015) *Anal. Chem.* **87**, 9413–9420.

## Development of a mobile observation platform for air quality monitoring

X.G. Chi<sup>1</sup>, Z. Xu<sup>1</sup>, L.F. Zheng<sup>1</sup>, C.J. Zhu<sup>2</sup>, and A.J. Ding<sup>1</sup>

<sup>1</sup>School of atmospheric sciences, Nanjing University, 210023, China

<sup>2</sup>Kunshan Yangchen Langu Environment Institute LTD., 215334, China

Keywords: mobile observation platform, aerosol, trace gas, transport model.

Presenting author email: Xuguang.chi@nju.edu.cn

In recent years, mobile observation platforms capable of resolving air pollutant concentrations in real time has been used worldwide to evaluate in situ emissions, local air quality trends, and air pollutant exposure (Brantley et al., 2014). Mobile monitoring is often chosen over other methods for its ability to efficiently obtain data at a high spatial resolution, which normally cannot be obtained from currently existing stationary monitoring sites. Since the beginning of 2016, within the framework of Chinese national key research and development plan, Nanjing University (NJU) and Kunshan Yangchen Langu Environment Institute have been developing a mobile platform equipped with real-time instrumentation for air quality monitoring. The mobile platform was designed to achieve the following main functions: 1) In situ and high-precision monitoring of the atmospheric aerosols and key gas pollutants, which include chemical composition, physical properties, and vertical profile; 2) Real time data QA/QC, data analysis, data integration and storage; 3) a navigation platform based on Euler air quality forecast model (WRF-Chem) and Lagrangian traceability model (WRF-FLEXPART) for the real-time reverse tracing and prediction of air mass. In this poster we present the design and fabrication of the mobile platform and the preliminary results from a test run conducted during 2016 G20 Hangzhou summit period in Kunshan, China.

As shown in Figure 1, the mobile platform comprised of a 13 meters long trailer, which consists of three independent working compartments: A: Control and data processing compartment; B: Routine measurements compartment (extendable design); C: mass spectrometry and Lidar compartment.

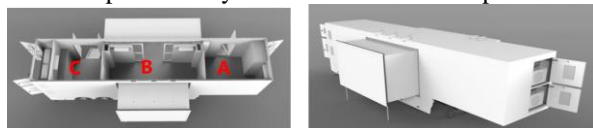


Figure 1. Design layout of the mobile platform.

The mobile platform was equipped with a wide range state-of-the-art air pollutant measurement instrumentations. The instruments currently on board the mobile platform were summarized in Table 1. Other equipment, such as Scanning Mobility Particle Sizer (SMPS), Aerosol particle sizer (APS) and meteorological instruments can also be incorporated.

Brantley, H. L. et al. (2014): Mobile air monitoring data-processing strategies and effects, *Atmos. Meas. Tech.*, 7, 2169–2183, 2014

Table 1. Instrumentation on board the mobile platform

	Parameter	Principle	Instruments
G A S	O <sub>3</sub>	UV Absorption	T400, API, USA
	SO <sub>2</sub>	UV Fluorescence	T100, API, USA
	CO	IR Absorption	T300U, API, USA
	NO, NO <sub>2</sub> , NO <sub>x</sub>	Chemiluminescence	T200, API, USA
	VOC	PTR TOF MS	PTR-TOF 1000, IONICON, Austria
A E R O S O L	PM <sub>2.5</sub> chemical composition and size distribution	SPA-MS	SPA-MS 0515, Hexin mass spectrometry, China
	PM <sub>2.5</sub> mass	nephelometric/radiometric	SHARP-5030, Thermo Fisher Scientific, USA
	PM <sub>10</sub> mass	nephelometric/radiometric	SHARP-5030, Thermo Fisher Scientific, USA
	Scattering, backscattering	Nephelometer	Aurora 3000, Ecotech, Australian
	Absorption	absorption	MAAP-5012, Thermo Fisher Scientific, USA
	Vertical profile	High power Lidar	AGHJ-I, Wuxi CAS photonics, China



Figure 2. Instrument installation in July 2016 (left); mobile platform during G20 summit campaign (right).

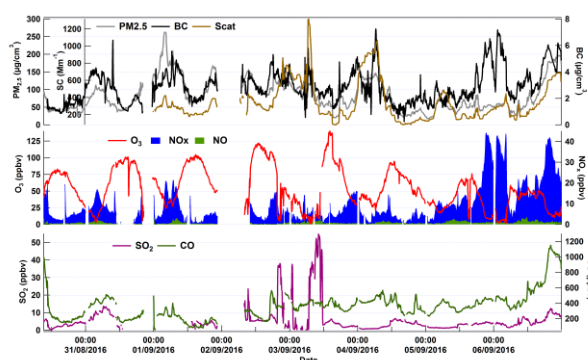


Figure 3. Preliminary results from mobile platform observation during 2016 G20 summit campaign.

This work was funded by Kunshan Yangchen Langu Environment Institute, LTD.

## A new on-line single particle laser mass spectrometer for detection of both, polyaromatic hydrocarbons and inorganic constituents from the same individual particles

J. Passig<sup>1</sup>, J. Schade<sup>1</sup>, M. Fuchs<sup>1</sup>, M. Oster<sup>1</sup>, C. Jäger<sup>2</sup>, M. Sklorz<sup>1</sup> and R. Zimmermann<sup>1</sup>

<sup>1</sup>Joint Mass Spectrometry Centre of University of Rostock and Helmholtz-Zentrum München and Virtual Institute HICE-Aerosol and Health, Chair of Analytical Chemistry, University of Rostock, 18051 Rostock, Germany

<sup>2</sup>Astrophysics and Cluster Physics Group, University Jena, 07745 Jena, Germany

Presenting author email: ralf.zimmermann@uni-rostock.de

Anthropogenic aerosol particles play a significant role in the earth climate and evoke substantial public health effects. For sampled aerosol particulate matter (PM), in-depth chemical analysis approaches are available. However, they can neither resolve the high temporal variability of ambient aerosols nor reveal physico-chemical properties of a larger number of individual particles. In contrast, few on-line approaches for a fast and direct chemical analysis of ambient aerosols have been successfully developed, namely the Aerosol Mass Spectrometer (AMS, Aerodyne) which is capable to obtain chemical information on non-refractory compounds of size-selected particles ( $< 0.1\text{--}10\ \mu\text{m}$ ) and various Aerosol Time-of-Flight-MS (AToF) based method. Only the latter technology features real single particle (SP) analysis, which is a prerequisite for differentiation between internally and externally mixed particle ensembles. The mixing state is a crucial parameter for the understanding of ambient aerosols and its biological effects (WHO, 2016; Oeder et al., 2015). The AToF methods base on aerodynamic acceleration of particles into the vacuum of a ToF mass analyser, particle-sizing by laser velocimetry and Laser Desorption/Ionization (LDI) of SP with a triggered single laser pulse in the ion source. Typically, positive and negative inorganic ions, cluster ions as well as fragments of carbonaceous compounds are detectable in the SP MS. The MS signature can be used for classification of the particles or quantification of fractions. However, organic signals usually are not obtained. Recently, multi-step laser photo-ionization approaches for the matrix-effect free detection of health-relevant polycyclic aromatic hydrocarbons (PAHs) bound on individual particles were developed (Bente et al., 2009). Herein, the single particles are heated in the ion source by an IR-pulse ( $\text{CO}_2$ -laser,  $10.6\ \mu\text{m}$ ), evaporating absorbed molecules from the particle surface. Few  $\mu\text{s}$  later, the plume is hit by an UV-pulse (KrF-laser,  $248\ \text{nm}$ ) that selectively ionizes the PAH via Resonance-Enhanced Multiphoton Ionization (REMPI).

In the new approach (Fig. 1a,b), the latter technique is extended by a third laser pulse (ArF-laser,  $193\ \text{nm}$ ) that targets on the LDI analysis of residual core of the same particle after the LD/REMPI PAH-measurement. Differentiation between the surface/core ions is enabled by fast field inversion of the ion source between the REMPI- and LDI pulses, resulting in opposite acceleration and detection of the ions in the dual ToF-mass analyser (see Fig. 1b/3). With this technique, both the surface PAH-content and the inorganic substances of the particles core from the very same individual airborne particle of known size are characterised. Fig. 1c shows an example for the

simultaneous LD/REMPI-MS and LDI-MS characterisation of the same wood combustion particle of  $1.2\ \mu\text{m}$  diameter. The blue LDI mass spectrum (Fig. 1c) depicts typical inorganic ions from wood ash ( $\text{Na}^+$ ,  $\text{K}^+$ ,  $\text{Fe}^+$ ) while other signals are carbonaceous fragments and carbon clusters (soot component). The red LD/REMPI mass spectrum (Fig. 1c) shows the PAH-signature of the same particle. The prominent peak at  $234\ m/z$  is assignable to retene (biomarker for coniferous wood combustion), other signals are originated by (alkylated) PAH, such as pyrene ( $202\ m/z$ ) or benzo[a]pyrene ( $252\ m/z$ ).

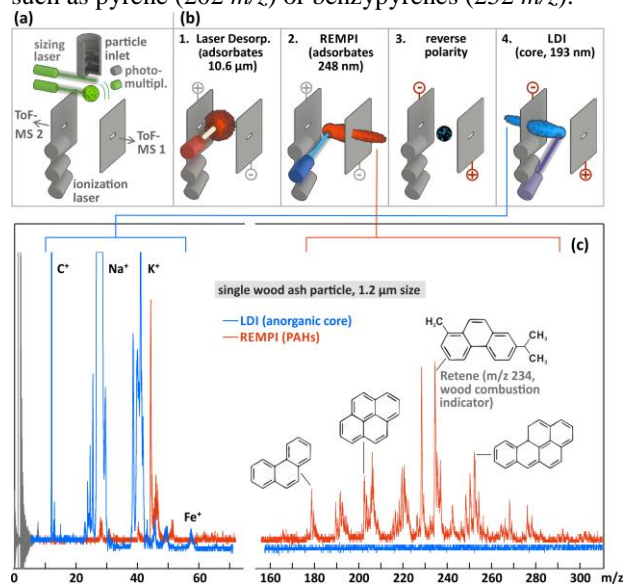


Figure 1: (a) Multi-step AToF-principle: Individual particles are aerodynamically accelerated and sized via laser velocimetry. When reaching the dual ToF MS analyser ion source, the laser ionization sequence (b) is triggered: 1. The targeted particle is heated by an IR-pulse. 2. The plume of desorbed PAH is selectively ionized and analyzed in one leg of the dual ToF MS analyser. 3. Fast TOF ion source polarity inversion after the formed PAH-ions have left the ion source region. 4. A LDI-laser pulse hits the core and positive ions of the inorganic compounds (elements, carbon clusters from soot) are detected in the opposite TOF leg. (c) Resulting REMPI (red) and LDI (blue) mass spectra from a single airborne wood ash particle.

In conclusion, the new single particle MS-method allows a better classification of particles (and differentiation of internal/external mixtures) as well as a semi-quantification of the highly health-relevant PAH compound class.

This work was supported by the German Science Foundation (DFG) and Helmholtz Association (HGF/HICE).

WHO report (2016), Ambient Air Pollution

S. Oeder et al., PLoS ONE 10 (6) (2015)

M. Bente et al., Anal. Chem. 80 23, 8991-9004 (2008)

## An Aerosol-icpTOF: Direct Measurement of Trace Multi-Elements for Ambient Aerosol

H. Hagino<sup>1</sup>, M. Tanner<sup>2</sup>, O. Borovinskaya<sup>2</sup>, H. Hikita<sup>3</sup>, A. Shimono<sup>3</sup>, Y. Mizuno<sup>4</sup>

<sup>1</sup>Japan Automobile Research Institute (JARI), Tsukuba, Ibaraki, Japan

<sup>2</sup>Tofwerk AG, Thun, Switzerland

<sup>3</sup>Shoreline Science Research, Tokyo, Japan

<sup>4</sup>Horiba, Ltd. Biwako Factory, Shiga, , Japan

Keywords: ICP-TOFMS, Aerosol Mass Spectrometry, Metal, Real-time Measurement.

Presenting author email: hhagino@jari.or.jp

Inductively coupled plasma mass spectrometry (ICP-MS) is widely used when rapid and sensitive detection for a wide range of elements of airborne particles is required in many situations, such as the monitoring of the ambient particulate matter (PM), emission sources, and the clean room air for semiconductor manufacture processes. In analysis by ICP-MS, the airborne particles are usually collected on filters and elemental analysis is carried out through pre-processing on the resultant sample, as well known as off-line analysis. This off-line analysis using ICP-MS takes time for a day or a few days, and reduces the time resolution about the behaviour of particle concentration.

For on-line and real-time analysis of aerosol samples using ICP-MS, the gas exchange devices (GED) which followed by the replacement of air with argon and transported to the ICP-MS is need to be equipped due to sustaining the plasma (Nishiguchi *et al.*, 2008). The bulk aerosol sample were produced by a GED with ICP-QMS that exchanges the gas molecules from air to Ar the resulting gas-converted air sample can be introduced directly into the ICP-MS instrument. However, the ICP-MS used a quadrupole mass spectrometer (ICP-QMS), a detailed study on the signal fine structure with scanning-based mass spectrometers but no simultaneous multi-element measurement was possible. In order to further improve time resolution of the ICP-QMS and to extend its capabilities to determine single particle information, ICP-MS equipped with the Time-of-Flight Aerosol Mass Spectrometer (ICP-TOFMS) was developed recently (e.g. Martine and Günther, 2008) and provided commercially (icpTOF, Tofwerk).

This study describes a direct trace multi-elemental aerosol measurement in which an icpTOF (Aerosol-icpTOF) has been equipped with a GED (GEDIII, J-Science Laboratory). This Aerosol-icpTOF is the real-time, field-deployable, aerosol mass spectrometer that is capable of directly distinguishing the elemental composition of ions having the same nominal mass and will be described the more details in elsewhere (Hagino *et al.*, *In-preparation*).

Figure 1 shows a comparison between the trace elements in ambient PM<sub>2.5</sub> measured by the Aerosol-icpTOF and the Continuous Particulate Monitor with X-ray Fluorescence (XRF) (Model PX375, HORIBA). The icpTOF and XRF are a fundamentally different instruments. However, the high degree of correlation as trace element concentrations increase and decrease during the 1-h time or more high time resolution and the quantitative ability of the Aerosol-icpTOF.

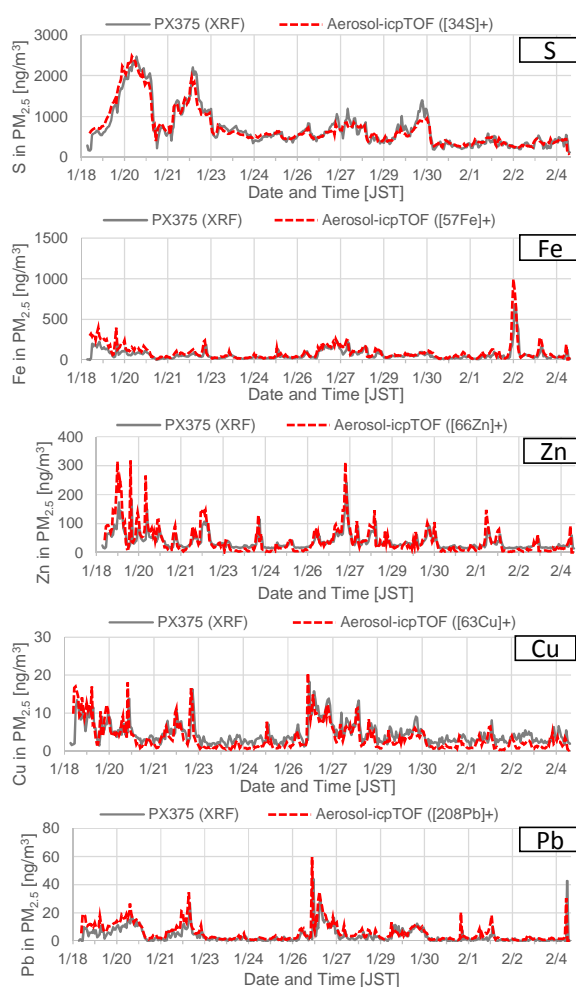


Figure 1. Comparison of the Aerosol-icpTOF trace element 1-h averaged concentration with the PX375 XRF analyser for the online PM<sub>2.5</sub> composition measurements during the 2017 Tsukuba field campaign.

This research was supported by the Environment Research and Technology Development Fund (5-1605) of the Ministry of the Environment, Japan.

Nishiguchi, K., *et al.* (2008). Real-Time Multi-Element Monitoring of Airborne Particulate Matter using ICP-MS Instrument Equipped with Gas Converter Apparatus. *J. Anal. Atom. Spectrom.*, 23:1125–1129.  
 Tanner M, Günther D., A new ICP-TOFMS. Measurement and readout of mass spectra with 30 micros time resolution, applied to in-torch LA-ICP-MS., *Anal Bioanal Chem.* 2008 Jun;391(4):1211-20.

## Highly selective formaldehyde detection with microporous membranes for indoor air quality monitoring

A.T. Güntner, S. Abegg, K. Wegner and S.E. Pratsinis

Particle Technology Laboratory, Department of Mechanical and Process Engineering, ETH Zürich, Sonneggstrasse 3, CH-8092 Zürich, Switzerland

Keywords: Formaldehyde, indoor air quality monitoring, microporous membranes

Presenting author email: sabegg@student.ethz.ch

Certain volatile organic compounds present in aerosols are potentially hazardous for human health. Formaldehyde (FA), for instance, is proposed as a tracer for indoor air quality monitoring due to its carcinogenic nature (Salthammer, 2010). The recommended exposure limit should not exceed 100 ppb (Salthammer, 2010) challenging portable devices in terms of *sensitivity* and *selectivity*. Chemo-resistive metal-oxide sensors made by flame spray pyrolysis (FSP) are quite attractive as they can detect sufficiently low FA levels, offer fast response and recovery times and can be produced cost-effectively (Güntner, 2016). However, they *lack selectivity* to FA.

Here, we propose a modular sensor system that overcomes this limitation by placing a highly selective membrane for aerosol pre-separation upstream of a highly sensitive chemo-resistive sensor. The membrane consists of a supported microporous membrane that is hydrothermally grown in a stainless steel autoclave (Fig. 1a). The resulting membrane is coin-type with a diameter of 16 mm (Fig. 1b). The micropore sizes are comparable to the molecular dimensions of volatile compounds (Davis, 2002), thus, ideal for a pre-separation of the gas mixture. They are widely applied in catalysis (Frei, 2006) and large-scale molecular separations (Kuznicki, 2001). FSP-made SnO<sub>2</sub> nanoparticles, that are deposited on sensor substrates via thermophoresis (Fig. 1c), form a highly porous film which is used as detector (Güntner, 2016). These detectors are wire-bonded onto a chip carrier for the integration into the electric circuit (Fig. 1d).

This modular system exhibits excellent selectivity to carcinogenic formaldehyde over ethanol, ammonia, acetone and isoprene (all > 100) at realistic 50% relative humidity. Moreover, relevant formaldehyde concentrations down to 30 ppb are *selectively* detected with a high signal-to-noise ratio (> 70), despite significantly higher interfering gas levels. Response times below 10 min are sufficiently fast considering recommended formaldehyde exposure time guidelines (Salthammer, 2010). This modular membrane-sensor concept can be tailored to target other pollutants and may constitute a new class of highly sensitive and selective detection systems for indoor air quality monitoring.

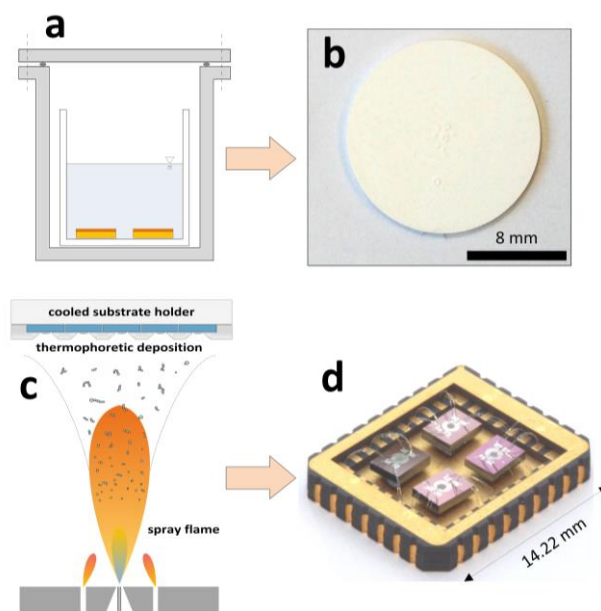


Figure 1. (a) Microporous membranes are hydrothermally grown on supports and (b) are of coin-type shape with a diameter of 16 mm. (c) Sensors are produced by flame spray pyrolysis and (d) are bonded onto a chip carrier for electrical integration. Placing the membrane upstream the sensor result in a highly selective formaldehyde detection system.

This work was supported by the Swiss National Science Foundation (Nr. 200021\_159763/1).

Davis, M. E. (2002) *Nature* **417** (6891), 813-821.

Frei, H. (2006) *Science* **313** (5785), 309-310.

Güntner, A. T., Koren, V., Chikkadi, K., Righettoni, M. and Pratsinis, S. E. (2016) *ACS Sensors* **1** (5), 528-535.

Kuznicki, S. M., Bell, V. A., Nair, S., Hillhouse, H. W., Jacobinas, R. M., Braunbarth, C. M., Toby, B. H. and Tsapatsis, M. (2001) *Nature* **412** (6848), 720-724.

Salthammer, T., Mentese, S. and Marutzky, R. (2010) *Chem Rev* **110** (4), 2536-2572.

## Development of a detection method to determine alcohols and carboxylic acids in aerosol particles using in-situ silylation and aerosol mass spectrometry

M. Weloe<sup>1</sup>, S. Morat<sup>1</sup>, T. Hoffmann<sup>1</sup>

<sup>1</sup>Institute of Inorganic and Analytical Chemistry, University of Mainz, Mainz, 55128, Germany

Keywords: aerosol mass spectrometry, silylation, in-situ derivatization.

Presenting author email: maweloe@uni-mainz.de

Atmospheric aerosols have an important impact on climate and human health. They interact with solar radiation directly or indirectly as cloud condensation nuclei. Due to their small sizes they can enter deeply the human breathing system. For a better understanding of this influences the chemical composition has to be determined. (Pöschl, 2005)

The aerosol mass spectrometer (AMS) of Aerodyne Research Inc. is a frequently used online instrument to determine the composition of aerosol particles within a range between 35 and 1500 nm diameter. After entering the AMS the particles are vaporized at 600 °C and ionized by electron impact, whereby the formed ions strongly fragment and are finally analysed by a Time-of-Flight mass spectrometer (ToF-MS). (DeCarlo *et al.*, 2006) Inorganic species like nitrate, sulphate or ammonium can be qualitatively and quantitatively analysed. Due to the high resolution of ToF-MS the elemental composition of the organic bulk aerosol can also be determined but since all compounds are vaporized, ionized and fragmented at the same time, information about single organic components or functional groups cannot easily be obtained.

In this project a method was developed to detect alcohols and carboxylic acids in aerosol particles using the AMS. To do so the aerosol particles are mixed with gaseous N-methyl-N-(trimethylsilyl) trifluoroacetamide (MSTFA) in a flowtube reactor, where MSTFA condenses onto the particle and reacts with alcohols and carboxylic acids to trimethylsilyl ethers and -esters, respectively (figure 1). The products can be identified through carbon-silicon (CSi) containing fragments, whereby the trimethylsilyl ion (TMS,  $[\text{C}_3\text{H}_9\text{Si}]^+$  at  $m/z$  73) is characteristic for all these products.

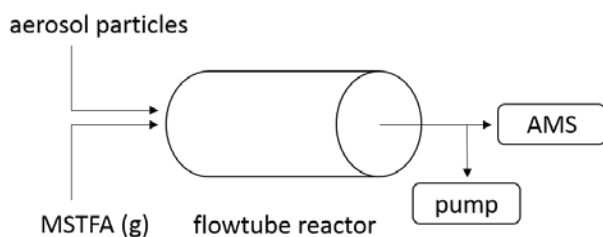


Figure 1. Principle set-up of the in-situ silylation.

The first results have shown that this method is already useful to determine the concentration in solutions which are pneumatically atomised to an aerosol (figure 2).

To estimate the yield of the reaction aerosols of atomised solutions containing presilylated compounds were analysed.

Ozonolysis experiments of  $\alpha$ -pinene have shown that ions of certain derivatized aerosol species were detected so that not only information about the bulk organic aerosol could be obtained but also information about single components (figure 3).

At measurements of outdoor aerosols a reaction of MSTFA with organic species could be detected and distinguished from the reaction with water.

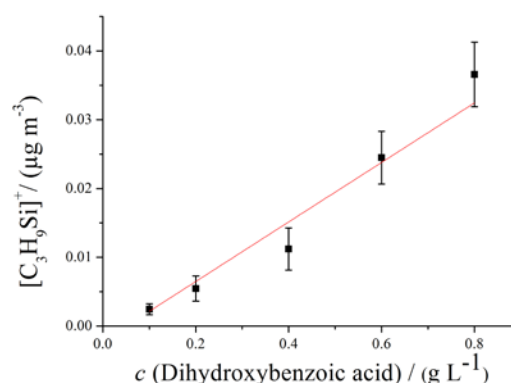


Figure 2. Linear relationship between the detected signal of the TMS ion and the concentration of 3,5 dihydroxybenzoic acid in methanolic solution.

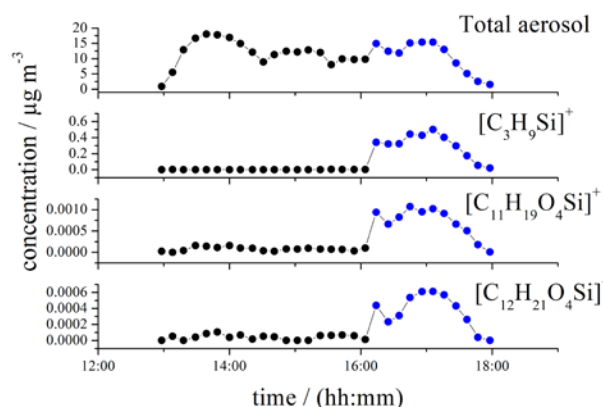


Figure 3. Time series of the concentrations of the total aerosol, the TMS ion,  $[\text{C}_{11}\text{H}_{19}\text{O}_4\text{Si}]^+$  and  $[\text{C}_{12}\text{H}_{21}\text{O}_4\text{Si}]^+$ . The time, when the particles were mixed with MSTFA are colored in blue. The last two ions correspond to the silylation of pinic acid and 10-hydroxy pinonic acid, respectively which are two known products from the oxidation of  $\alpha$ -pinene with ozone.

Pöschl, U. (2005) *Angew. Chem. Int. Ed.* **44**, 7520 – 7540.

De Carlo *et al* (2006) *Anal. Chem.* **78**, 8281-8289.

## Can chemical biomarkers help discriminating environmental microbial species?

Sonia García-Alcega<sup>1\*</sup>, Sean Tyrrel<sup>1</sup> and Frederic Coulon<sup>1</sup>

<sup>1</sup>School of Water, Energy and Environment, University of Cranfield, Cranfield, MK43 0AL, UK

Keywords: bioaerosols, chemical markers, outdoor environments, air quality

\*Presenting author email: s.garciaalcega@cranfield.ac.uk

Occupational activities involving high levels of biological material such as wastewater treatment plants, biowaste facilities, animal farms and agriculture are of great concern for workers as respiratory diseases are potentially linked to continuous exposure to bioaerosols (O'Connor et al. 2015).

Given the limitations of cell culturing techniques for bioaerosol studies, we explore the feasibility of using microbial chemical markers such as phospholipid fatty acids (PLFAs) and microbial volatile organic compounds (MVOCs) to identify and quantify microorganisms in air. PLFAs are present in cell membranes of living organisms and are indicators of microbial biomass, community composition and stress. MVOCs are side-products produced during the secondary metabolism of moulds, fungi and bacteria. MVOCs classification is diverse comprising chemical groups such as alcohols, aldehydes, alkanes, esters, ethers, furans, aromatic compounds, ketones, organic acids, organosulfur compounds and terpenes.

### Materials and methods

Air samples were collected from three contrasting locations in Colchester, UK: a farm, a recreational park and a compost facility. PLFAs were collected via filtration with polycarbonate filters (25L min<sup>-1</sup> during 1h). Filters were solvent extracted and PLFAs were analysed by GC-FID. Cell densities were calculated from PLFAs concentrations using the following conversion factors: bacteria contain 100 μmol of PLFAs g<sup>-1</sup> (dry weight), and 1g of bacteria is equivalent to 2.0 × 10<sup>12</sup> cells (Keinänen et al. 2002). MVOCs were collected with thermal desorption tubes (TD) coated with tenax and carbotrap 50/50 (v/v). Sampling was done during 30 min at 100 ml min<sup>-1</sup> flow rate.

### Results

MVOCs profiles were different from the 3 different environments. In the park the most predominant group of MVOCs were aromatic compounds (80%), whereas in the compost facility were furans (40%). In the farm there were 3 dominant MVOC groups: alcohols (24%), aldehydes (26%) and alkanes (21%) (Fig 1).

Cell densities calculated from PLFAs analysis resulted in 3.2 × 10<sup>5</sup> in the farm, 2.3 × 10<sup>5</sup> in the compost facility and 2.7 × 10<sup>5</sup> in the recreational park (Fig 2).

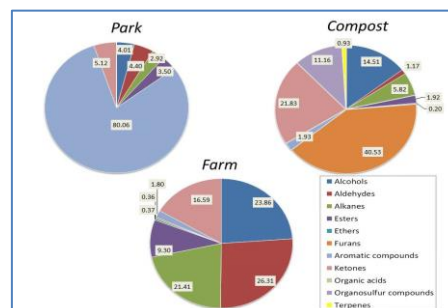


Figure 1. MVOCs distribution in three contrasting sites, a park, a compost facility and a farm in Colchester.

There was a good correlation between total MVOCs concentration (ng m<sup>-3</sup>) and cell density between the 3 sites (R<sup>2</sup>=0.98) suggesting that MVOCs are good indicators of microbial concentration in air.

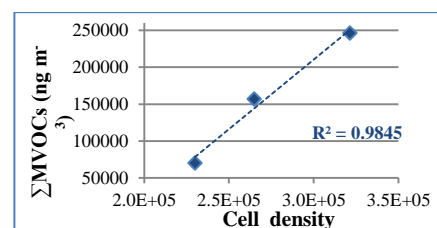


Figure 2. Correlation between total concentration of MVOCs (ng m<sup>-3</sup>) and cell densities from outdoor environments.

### Conclusion

Chemical biomarkers such as PLFAs and MVOCs can be used to characterise microbial communities from outdoor air. There are MVOCs that also have anthropogenic origin and therefore more research needs to be done in order to discriminate MVOCs from VOCs.

This work was supported by the UK Natural Environment Research Council (NERC) through the Environmental Microbiology and Human Health Programme (Grant reference NE/M010961/1).

Keinänen, M.M. et al., 2002. The Microbial Community Structure of Drinking Water Biofilms Can Be Affected by Phosphorus Availability. *Applied and Environmental Microbiology*. **68**,434–439.

O'Connor, D.J., Daly, S.M. & Sodeau, J.R., 2015. On-line monitoring of airborne bioaerosols released from a composting/green waste site. *Waste Management*, **42**, 25-30.

## A Novel Field Reversal - Surface Ionization Detector for Characterization of Biomass Burning and Sea Salt Aerosols

D. Gall, C. Nejman and J.B.C. Pettersson

Atmospheric Science, Department of Chemistry and Molecular Biology, University of Gothenburg, Gothenburg, SE-412 96, Sweden

Keywords: sodium, potassium, biofuel, marine aerosol.

Presenting author email: dan.gall@gu.se

The chemical composition of suspended particles in air indicates their origin and their potential effects on atmospheric processes, climate and health. The main focus of the present study is aerosol particles containing alkali metal compounds, including sea salt particles and potassium-rich particles produced during biomass combustion.

The Atmospheric Science Group at University of Gothenburg has developed several aerosol instruments based on surface ionization (SI) technique, including Alkali Aerosol Mass Spectrometers (Svane *et al.*, 2009) and simple surface ionization detector (SID) setups that operate at ambient pressure (Jäglid *et al.*, 1996). We have shown that submicron alkali salt particles give rise to ion pulses in contact with a hot platinum filament in air. The alkali content in individual aerosol particles is ionized by SI on the hot filament, and the emitted ions diffuse to a closely situated collector where they are detected as a current. The ionization probability may approach 100% for elements with low ionization potentials (IP's), while species with high IP's are not detected. The method may therefore provide sensitive and selective measurements of individual aerosol particles containing alkali salts.

The aim of this project is to further develop the surface ionization technique that operates at atmospheric pressure. Specific goals are to develop the method to distinguish between K- and Na-containing particles and to provide quantitative measurements over a wide particle size range.

Earlier work has shown that rapid electric field reversal (FR) may be used to investigate the desorption kinetics of alkali atoms on metals in air (Hagström *et al.*, 2000). We herein combine the FR methodology with a SID instrument and describe a new FR-SID that may be used to determine the mass concentration of potassium and sodium in aerosol particles. Rapid reversal of the electric field outside the hot filament in the SID allows us to distinguish between Na and K based on differences in their desorption kinetics on a hot platinum surface. Results from laboratory studies with size-selected alkali salt particles are presented, including particles containing KCl, NaCl, K<sub>2</sub>SO<sub>4</sub>, Na<sub>2</sub>SO<sub>4</sub>, KNO<sub>3</sub> and NaNO<sub>3</sub>. The response of the instrument is evaluated depending on key parameters including particle composition, filament temperature, filament voltage and gas flow rate through the instrument.

We conclude that the new method provides quantitative alkali mass concentration measurements in the particle size range 20 – 1000 nm. In contrast, an earlier version of the ambient pressure SID instrument

measures the number concentration of particles larger than approx. 200 nm, and cannot distinguish between Na and K. We note that the two modes of operation may be combined, and the SID can be optimized to simultaneously measure the mass concentration of Na and K, and the total particle number concentration.

The FR-SID instrument has been applied in field measurements with the aim to characterize ambient biomass burning and sea salt particles, and the obtained results are compared with meteorological conditions and air mass back trajectories.

### Acknowledgements

We thank Benny Lönn and Torbjörn Gustavsson for technical support during the project. The Swedish Energy Agency is acknowledged for financial support.

Hagström, M, Engvall, K and Pettersson J.B.C.

Desorption kinetics at atmospheric pressure: alkali metal ion emission from hot platinum surfaces. (2000) *J. Phys. Chem. B* **104**, 4457.

Jäglid, U., Olsson, J.G. and Pettersson, J.B.C. Detection of sodium and potassium salt particles using surface ionization at atmospheric pressure. (1996) *J. Aerosol Sci.* **27**, 967.

Svane, M, Gustafsson, T.L., Kovacevik, B. Noda, J., Andersson, P.U., Nilsson, E.D., and Pettersson, J.B.C. On-line chemical analysis of individual alkali-containing aerosol particles by surface ionization combined with time-of-flight mass spectrometry. (2009) *Aerosol Sci. Technol.* **43**, 653-661.

## ACMCC (Aerosol Chemical Monitor Calibration Center): Results from the 2016 ACTRIS intercomparison exercises

E.Freney<sup>1</sup>, Favez<sup>2</sup>, O., Gros<sup>3</sup>, V., Sciare<sup>4</sup>, J., Amedeo<sup>2</sup>, T, Trong<sup>3</sup>, F., Jayne<sup>5</sup>, J., Croteau<sup>5</sup>, P., Williams<sup>5</sup>, L, Canagaratna<sup>5</sup>, S., Lambe<sup>5</sup>, A., S., Cubison<sup>6</sup>, M. and all intercomparison participants.

<sup>1</sup>Laboratoire de Météorologie Physique, CNRS-Université Blaise Pascal, Clermont Ferrand, 63117, France

<sup>2</sup>INERIS Verneuil-en-Halatte, 60550, France

<sup>3</sup>Laboratoire des Sciences du Climat et de l'Environnement, CNRS-CEA-UVSQ, 91 191, Gif-sur-Yvette, France

<sup>4</sup>The Cyprus Institute, Environment Energy and Water Research Center, Nicosia, Cyprus

<sup>5</sup>Aerodyne Research, Inc., Billerica, Massachusetts, USA

<sup>6</sup>Tofwerk AG, Thun, Switzerland

Keywords: ACSM, calibration, ACTRIS

Presenting author email: valerie.gros@lsce.ipsl.fr

The Aerosol Chemical Speciation Monitor (ACSM, *Aerodyne Res. Inc.*) has been installed in a growing number of supersites around the world for long-term monitoring of the submicron aerosol chemical composition. In Europe, most of these ACSM measurements are part of the European research infrastructure for aerosol, clouds, and trace gases (ACTRIS, <http://www.actris.eu>). Coordinated efforts to ensure that measurement are comparable from one site to another, and that all instruments follow recommended standard operating procedures are essential for the data quality of these networks.

Within ACTRIS, selected expertise centers offer training and calibration of the instruments used in the network. The Aerosol Chemical Monitor Calibration Centre (ACMCC) is dedicated to online aerosol chemical monitors, with a first ACSM intercomparison/calibration campaign performed in 2013 (Crenn et al, 2014; Frohlich et al., 2014). In 2016, a second large ACTRIS campaign involved 15 quadrupole ACSMs and 6 of the newer ToF-ACSM devices. In this work, we present the results obtained from this 2016 intercomparison, focusing on new calibration procedures and on the influence of artefacts recently identified for aerosol mass spectrometer measurements (Pieber et al., 2016). These new procedures result in a significant improvement in the agreement between the Quad-ACSM instruments (Fig. 1).

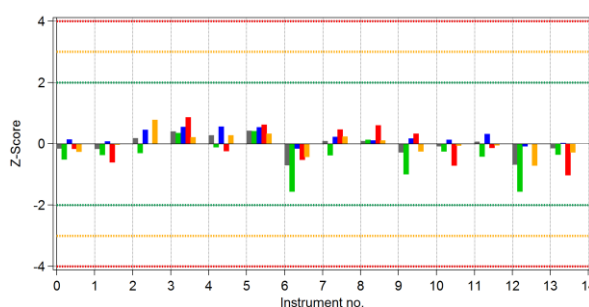


**Figure 1. Z –score analysis of each species measured by the Quad ACSM for the 15 instruments participating in the intercomparison.**

Results obtained by the 6 ToF-ACSM devices also allow for the first time extensive comparison of these instruments (Fig. 2), showing consistency between them as well as with data measured from the conventional quadrupole ACSM

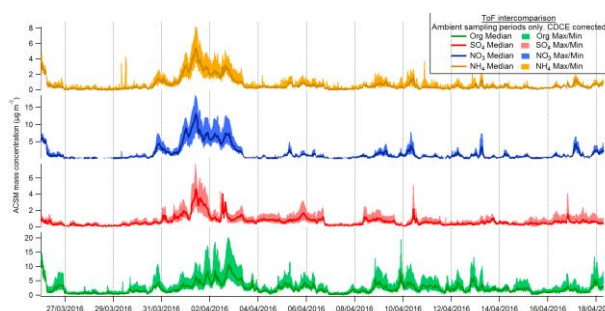


**Figure 2 Time series comparison of the 6 ToF-ACSM instruments over a two week period.**

## Bipolar reference spectra of atmospherically relevant single particles by laser ablation aerosol particle time-of-flight mass spectrometry

X. Shen, R. Ramisetty, W. Huang, C. Mohr, and H. Saathoff

Institute of Meteorology and Climate Research, Karlsruhe Institute of Technology, Hermann-von-Helmholtz-Platz 1, 76344 Eggenstein-Leopoldshafen, Germany

Keywords: single particle mass spectrometry, laser ablation, reference spectra, overall detection efficiency  
Presenting author email: xiaoli.shen@kit.edu

Single particle mass spectrometry has been a tool in atmospheric sciences for almost half a century. The identification of the chemical composition and mixing state of individual aerosol particles greatly helps in elucidating their impacts on human health, visibility, ecosystem, and climate (Canagaratna et al., 2007; Murphy, 2007). The only currently commercially available single particle mass spectrometer is the laser ablation aerosol particles time-of-flight mass spectrometer (LAAPTOF, Aeromeg GmbH). The overall detection efficiency (ODE) of this instrument for spherical polystyrene latex (PSL) particles of physical diameter (dp) between 350 and 800 nm has previously been reported as ~0.15% to ~2.2% (Gemayel et al., 2016; Marsden et al., 2016). The ODE of other particles with different morphologies have not been defined yet. In addition, there is a lack of LAAPTOF reference spectra available to the user, which would help greatly in the interpretation of especially ambient data.

We present LAAPTOF ODE for PSL with physical diameters of 200 to 2000 nm, as well as ammonium nitrate ( $\text{NH}_4\text{NO}_3$ ) and sodium chloride (NaCl) particles in the size range of 300 to 1000 nm.

Furthermore, we show reference mass spectra for different laboratory generated particles, e.g.,  $\text{NH}_4\text{NO}_3$ , NaCl,  $\text{K}_2\text{SO}_4$ , secondary organic aerosols (SOA), and some mixtures of them. Our results show that aerosol particles with internal mixtures can result in spectra with new clusters of ions, rather than simply a combination of the spectra from single component particles (c.f. Fig. 1). The reference spectra will be discussed as a function of particle size, shape, and laser power. An example of field data interpretation based on reference spectra will be given. The aim is to provide other users with references for comparison and ambient data interpretation. In the near future we plan to make the reference spectra publicly available on a database.

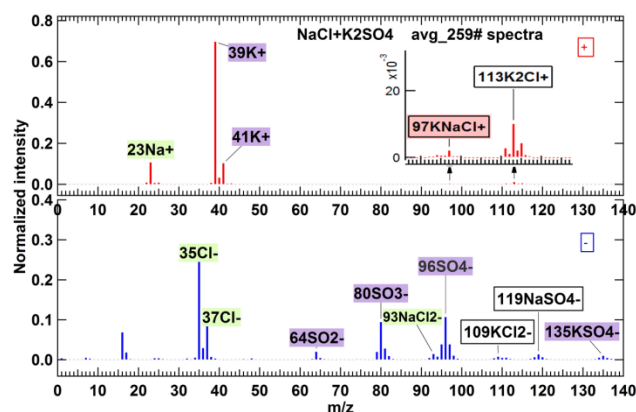


Figure 1. Average mass spectra for particles of internal mixtures of NaCl and  $\text{K}_2\text{SO}_4$ . Green labels represent the fragments arising also from pure NaCl particles; purple labels represent the fragments arising also from pure  $\text{K}_2\text{SO}_4$  particles; box labels represent the fragments from particles with internal mixtures of both salts.

Canagaratna et al. (2007) *Mass. Spectrom. Rev.* 26, 185–222.

Gemayel et al. (2016) *Atmos. Meas. Tech.* 9, 1947–1959.

Marsden et al. (2016) *Atmos. Meas. Tech. Discuss.*, doi:10.5194/amt-2016-150.

Murphy et al. (2007) *Mass. Spectrom. Rev.* 26, 150–165.

## NOVEL FTIR ONLINE METHOD FOR E-CIGARETTE AEROSOL CHARACTERIZATION

F. Radtke<sup>1</sup>, R. Monni<sup>1</sup>, A. Susz<sup>1</sup>, A. Stoop<sup>1</sup>, J. Verbeeck<sup>1</sup> and S. Maeder<sup>1</sup>

<sup>1</sup>PMI R&D, Philip Morris Products S.A., CH-2000 Neuchâtel, Switzerland  
(Part of Philip Morris International group of companies)

Keywords: Infrared Spectroscopy, Puff-by-Puff Aerosol Characterization, Online Chemical Quantification.  
Presenting author email: Falk.Radtke@pmi.com

The global electronic cigarettes (e-cig) market and product variety has been steeply increasing in the last decade (466 brands in Jan. 2014 and more than 2 million users worldwide). (Cressey, 2014) Nowadays, the users are almost 3 million and they are expected to continue growing over the next years. In this context, being able to screen and assess a large portfolio of e-cigarettes and e-liquids is fundamental, thus implying a strong need for rapid aerosol characterization methods as an alternative to the classical, time consuming aerosol collection and offline analysis methods. For this purpose an online puff-by-puff liquid aerosol characterization method has been developed to quantify key e-cigarette aerosol constituents using Fourier Transformed Infrared (FTIR) spectroscopy.

The experimental setup is composed of three main parts: 1) a programmable single syringe aerosol generation pump, 2) a transfer section with a heated pump and heated tubes, and 3) a Gasmeter™ FTIR spectrometer.

Since the used FTIR system is designed for the analysis of gaseous chemicals, liquid droplet aerosols, like e-cigarette aerosols, need to be fully transferred into gas phase. This is realized by conveying the generated aerosol through a heated sampling system for FTIR analysis at 180°C. At the same time the sample is also diluted in a stream of dry nitrogen, in order to have sufficient sample volume to fill the 0.4 L measuring chamber in the FTIR.

After verification of the FTIR instrument calibration for chemicals of interest, the setup has been tested with calibration gases (e.g. CO) for the puff-by-puff application instead of using aerosols. We could demonstrate that the system delivers a linear response for the dynamic measurement over a broad range of concentrations, spanning from low ppm up to 100s ppm in case of CO.

In a first comparative study, aerosols generated from different liquid compositions were investigated using a commercially available e-cigarette. All e-cigarette aerosols were generated in accordance with the Coresta recommended e-cig smoking protocol, namely 55 mL drawn with a rectangular puff profile during 3 seconds and drawing one puff every 30 seconds (CORESTA-N°81, 2015). The measured overall IR spectral response of the aerosol mixture was deconvoluted and matched online with reference calibration spectra in order to obtain the concentration in µg/L for water, propylene glycol (PG), glycerol, and nicotine with a time resolution of 2 sample points per second.

The FTIR results were benchmarked against (i) liquid formulation (mass ratios) (ii) classical aerosol collection on filter followed by GC/Karl Fischer analysis

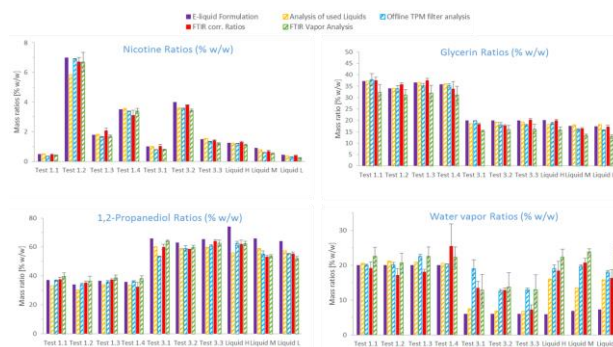


Figure 1. Benchmark of the presented online method with classical offline methods for the quantification of water, nicotine, glycerol and PG.

of the filter extract (yields/50 puffs) (iii) e-cig device mass loss, as shown in Figure 1.

After calibrating the setup for the puff-to-puff aerosol dynamic response the FTIR results showed a very good agreement with the liquid formulation data and the analysis results from classical aerosol collection on filter. The observed deviation of the water results could be explained with the water uptake of the e-liquid in particular for liquid mixtures starting with low water content.

The results of this study demonstrate that the developed method allows a simple and fast in-depth e-cigarette performance assessment on a puff-by-puff basis. The method is further capable to quantify secondary aerosol constituents like e.g. carbonyls. Decomposition products from glycerol and/or PG, like carbonyls, usually result from overheating of the e-liquid during aerosol generation either due to a uncontrolled heating process or during end of liquid situations. FTIR results related to carbonyls are shown in a separate publication.

CORESTA-No. 81 - Routine Analytical Machine for E-Cigarette Aerosol Generation and Collection - Definitions and Standard Conditions (2015).

Cressey, D. (2014). E-cigarettes: The lingering questions. *Nature*, 513, 24-26. doi: 10.1038/513024a

## **Abstracts T311**

## Measurements of Size Distribution and Mass Concentration of Fine Particles from a Stack of a Coal-Fired Power Plant in Korea

Bangwoo Han<sup>1</sup>, Hak-Joon Kim<sup>1</sup>, Chang Gyu Woo<sup>1</sup>, Yong-Jin Kim<sup>1</sup>, and Sung-Nam Chun<sup>2</sup>

<sup>1</sup>Environmental and Energy Systems Research Division, Korea Institute of Machinery and Materials, Daejeon, 34103, Korea

<sup>2</sup>Clean Combustion Group, Clean Power Generation Laboratory, KEPSCO Research Institute, Daejeon, 34056, Korea

Keywords: PM10, PM2.5, size, stack, coal-fired

Presenting author email: bhan@kimm.re.kr

Fine particles have been recognized as the most serious pollutants in Korea due to the local frequent high concentrations larger than  $50 \mu\text{g}/\text{m}^3$  for PM10 or  $25 \mu\text{g}/\text{m}^3$  for PM2.5. Coal-fired power plants are known main sources of fine particles and precursor gases such as SOx and NOx. However, particles from coal-fired power plants are monitored as total suspended particulates (TSP). It is important to understand the contributions of coal-fired power plants not to TSP but to PM10 or PM2.5 from the perspective of adverse health effects. In this work, particle size distributions and mass concentrations were measured at the same time of the primary fine particles from a stack of a coal-fired power plant and the PM10 and PM2.5 converted from the size distributions were compared to those from weight-based measurements.

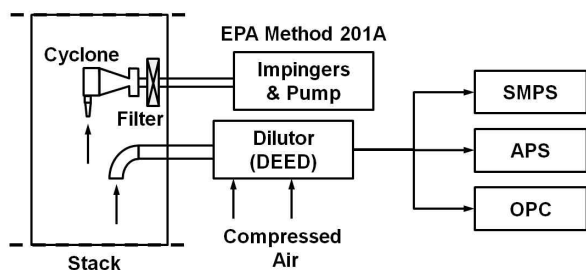


Figure 1. Experimental setup for PM measurements from a stack of a coal-fired power plant

Measurements were conducted at a stack of a 500 MW coal-fired power plant which burns bituminous coal in Korea. Figure 1 shows the experimental setup. Particles sampled from a stack were diluted with a dilutor system (DEED, Dekati, Finland) with a dilution ratio of 108 and then measured by three kinds of size measurement systems such as SMPS (Model 3936, TSI, USA), APS (Model 3321, TSI, USA) and OPC (Model 1.109, GRIMM, Germany). PM10 and PM2.5 were also measured by weighing filters with the standard method, EPA 201A. Sampling probes from the stack to measurement systems were heated by a line heater with a temperature controller.

Figure 2 shows size distributions of particles emitted from a stack of a coal-fired power plant with SMPS, APS and OPC systems. Total number concentrations were in an order of  $10^5$  particles/ $\text{cm}^3$  after consideration of dilution ratio, which were just similar to

those in high density of vehicular traffic areas (Schneider et al., 2015). Two peaks corresponding to nuclei and accumulation modes were detected and nuclei mode particles were unstable but accumulation ones ( $\sim 100 \text{ nm}$ ) were very stable with time. Large difference of size distributions acquired by the APS and OPC were found at the size range larger than  $0.5 \mu\text{m}$ . PM10 and PM2.5 obtained by the weight-based EPA 201A method were  $1.6$  and  $1.1 \text{ mg}/\text{m}^3$ , respectively, which were 8.0 and 5.8 times higher than those converted from the size distributions of OPC when particle density was assumed as  $1.2 \text{ g}/\text{cm}^3$  (that is,  $0.20$  and  $0.19 \text{ mg}/\text{m}^3$ , respectively). Particle losses during sampling and dilution in the size range larger than  $0.5 \mu\text{m}$  probably result in the big differences in size distributions and PM10, PM2.5 mass concentrations, which indicates that new sampling and dilution systems with little particle losses should be accompanied by the size measurement systems to accurately measure the fine particles emitted from the stacks of coal-fired power plants.

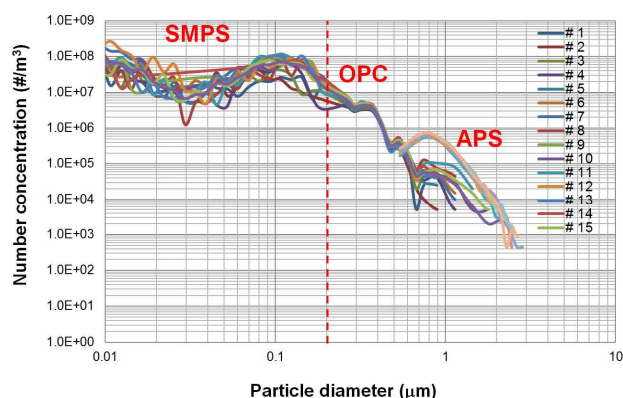


Figure 2. Particle size distributions measured by three measurement systems, SMPS, APS and OPC.

This research was supported by the Korea Institute of Energy Technology Evaluation and Planning (KETEP) grant funded by the Korea government Ministry of Trade, Industry and Energy.

Schneider, I. L., Teixeira, E.C., Oliveira, L.F.S. and Wiegand, F. (2015). *Atmos. Pollut. Res.*, **6**, 877-885.

## Raman microspectroscopic analysis of soot samples from wood combustion: Influences of aging

A.C.Wiesheu<sup>1</sup>, A. Hartikainen<sup>2</sup>, O.Sippula<sup>2</sup>, M. Ihalainen<sup>2</sup>, H. Lamberg<sup>2</sup>, J. Jokiniemi<sup>2</sup>, R. Niessner<sup>1</sup>, and N.P.Ivleva<sup>1</sup>

<sup>1</sup>Institute of Hydrochemistry, Chair of Analytical Chemistry, Technical University of Munich, Marchioninstr. 17, D-81377 Munich, Germany

<sup>2</sup>University of Eastern Finland, Department of Environmental and Biological Sciences, Fine Particle and Aerosol Technology Laboratory, P.O. Box 1627, FIN-70211 Kuopio, Finland

Keywords: soot, structure, aging, oxidation, Raman microspectroscopy (RM)  
Presenting author email: natalia.ivleva@ch.tum.de

Aerosol generated by combustion sources has a significant influence on atmospheric chemistry, Earth's climate and human health. Therefore, the detailed physicochemical characterization of combustion particulate matter (PM) is crucial for an understanding of its impact on the environment. Especially in the winter months, PM emitted by biomass burning (mainly wood combustion) is a major PM source in central Europe. Moreover, the identification and quantification of aging effects which take place in the atmosphere after the emission of PM are essential.

There exist several methods, which are available for the characterization of the molecular and crystalline structures in soot. These are high-resolution transmission electron microscopy (HRTEM), X-ray photoelectron spectroscopy (XPS), X-ray absorption near edge structure (XANES), Infrared (IR) spectroscopy and Raman microspectroscopy (RM) (Ivleva *et al.* 2007). RM is a nondestructive noncontact method, which is based on the inelastic scattering of light, and enables a chemical analysis with a spatial resolution down to 1  $\mu\text{m}$ . This method provides us information on the soot structure (including disordered graphitic and amorphous carbon) and associated reactivity (Schmid *et al.* 2011, Ess *et al.* 2016).

In this contribution we focus on RM analysis of structural changes occurring during soot aging in the atmosphere. Several experiments on aging of wood combustion exhaust were performed, including different wood types and stoves. Aerosol aging was simulated in a photochemical flow tube aging reactor (PEAR, Ihalainen, 2016). Our results show that photochemical aging, dominated by OH-radical driven reactions, is changing the soot nanostructure. While the Raman spectra of soot treated with only ozone show no changes (see Figure 1 top), the application of both UV light-induced OH-radical exposure together with ozone resulted in a decrease of the intensity of the D(defect)-peak around 1350  $\text{cm}^{-1}$  compared to the G(graphite)-peak around 1600  $\text{cm}^{-1}$  (see Figure 1 bottom). This can be attributed to a change in the soot nanostructure (Ferrari and Robertson 2000). During aging the ordered structures became disordered and less graphitic. Moreover, we could detect no influence of wood type or used stove on the aging.

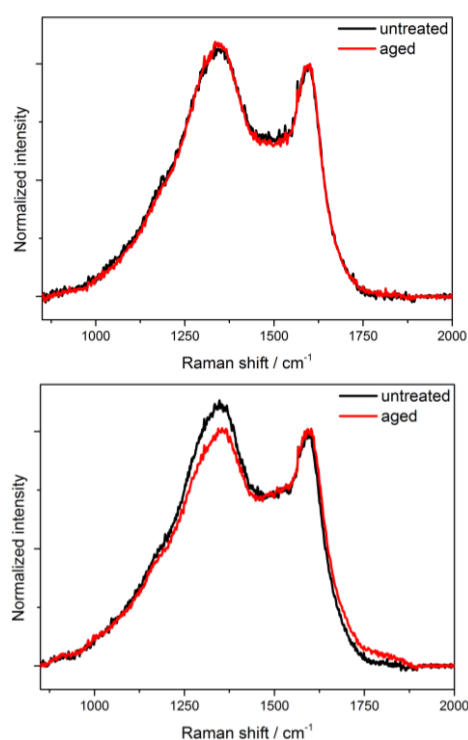


Figure 1. Raman spectra of soot samples from two different stoves after ozonolysis (top) and photochemical aging (combination of OH-radicals, ozone and UV light). Unaged samples are shown in black, while aged samples are shown in red.

- Ess, M., Ferry, D., Kireeva, E., Niessner, R., Ouf, F.-X. & Ivleva, N.P., *Carbon*, 105, 572-585.
- Ferrari, A.C., Robertson, J. (2000), *Phys. Rev. B*, 2000, 61, 14095-14107.
- Ihalainen, M., Tiitta, P., Kortelainen, M., Sklorz, M., Stengel, B., Müller, L., Kohlmeier V., Jakobi, G., Hartikainen, A., Streibel, T., Zimmermann, R., Jokiniemi, J., Sippula, O., *Abstract in the European Aerosol Conference 2016*, Tours, 4-9.9.2016.
- Ivleva, N.P., McKeon, U., Niessner, R. and Pöschl, U. (2007) *Aerosol Sci. Tech.* 41, 655-671.
- Schmid, J., Grob, B., Niessner, R. and Ivleva, N.P. (2011) *Anal. Chem.* 83, 1173-1179.

## Half-mini DMA modification for high temperature aerosols and evaluation on various combustion exhausts

M. Amo<sup>1</sup>, C. Barrios<sup>1</sup>, J.C. del Castillo<sup>1</sup>, J.F. de la Mora<sup>2</sup>, A.G. Konstandopoulos<sup>3,4</sup>, P. Baltzopoulou<sup>3</sup> and N.D. Vlachos<sup>3</sup>

<sup>1</sup> SEADM S.L., Parque Tecnológico de Boecillo 205, 47151 Valladolid, Spain

<sup>2</sup> Mechanical Engineering Dept., Yale University, New Haven, CT 06520-8286, U.S.A.

<sup>3</sup> Aerosol & Particle Technology Lab. CPERI/CERTH, Themi 57001, Greece

<sup>4</sup> Dept. of Chemical Eng., Aristotle Univ. of Thessaloniki, P.O. Box 1517, Thessaloniki 54006, Greece

Keywords: Half-mini DMA, sub-23nm particle emissions, high temperature aerosol analysis.

Presenting author e-mail: [juan.delamora@yale.edu](mailto:juan.delamora@yale.edu)

The reliable measurement and understanding of particles emitted by road vehicle engines below the currently adopted 23 nm size cut-off is now under intense study in an effort to derive future European legislation on particle emissions, as recommended by the JRC Science and Policy Report (Giechaskiel and Martini, 2014). Here we present the modification of a nano-DMA for better compatibility with exhaust aerosols and the subsequent evaluation of measurement capability improvements obtained on various engine exhaust streams. In particular, it is shown that the modified DMA facilitates the size-specific analysis of sub-23 nm exhaust aerosols especially at low solid particle concentrations, up to now challenging or inaccessible to analysis due to the extensive sample conditioning required to avoid artifacts.

The Half-Mini DMA (HM-DMA) is a Differential Mobility Analyzer operating at supercritical Reynolds numbers typically able to classify 1 to 15 nm particles with high resolution. Recently, the HM-DMA was extended to particle diameters up to 30 nm (de la Mora, 2017) fully covering the 1 – 23 nm particle size range of interest. Also, motivated by application to engine emissions, such an extended range HM-DMA has been successfully upgraded for improved compatibility with exhaust gas temperatures, mainly by use of a heat-tolerant semiconducting glass tube in the path from the inner electrode (held at high voltage) to the grounded outlet, yielding a device capable of high classification efficiency at sample temperatures approaching 200 °C.

The HM-DMA temperature is maintained by insulating it thermally from the environment while controlling the sheath gas temperature by methods previously developed at SEADM S.L.. The evaluation of the developed HM-DMA is performed on numerous streams of hot combustion exhaust. Laboratory exhaust streams are generated by custom operation of the Combustion Aerosol Standard (Matter Eng.) soot generator. Additionally, the HM-DMA is evaluated with exhaust from automobile internal combustion engines (Diesel and gasoline direct injection) at various degrees of exhaust sample pre-conditioning, from raw exhaust sampling up to standard conditioning protocols and including the variable use of a catalytic stripper for removal of sulphur and hydrocarbon compounds. The high temperature HM-DMA is benchmarked against cold (up to 50 °C) sample aerosol classifiers in terms of resolving power and output concentration of classified particles.

The higher DMA working temperature allows for reduction of the exhaust sample pre-conditioning (sorptive/catalytic cleaning, hot dilution) normally required to avoid artifacts from condensable exhaust species. Downstream instrumentation compatible with higher temperatures can directly benefit from higher concentrations of classified solid particles, especially significant for composition analysis, by using total sample dilution factors nearly an order of magnitude lower than those normally required by vehicle emission evaluation protocols. Downstream particle instruments that require a colder aerosol sample still benefit from reduced dilution (required hot pre-dilution is partly supplanted by the DMA sheath flow contribution) as well as from reduced thermophoretic losses from the diluter and HM-DMA.

The new HM-DMA (Fig. 1) has been found to facilitate size-specific analysis of 1 – 30 nm exhaust particulate, complementing established sub-23 nm particle emissions measurements while also allowing the study of engine emission phenomena previously inaccessible due to size-classified particle quantities being below instrument measurement thresholds.

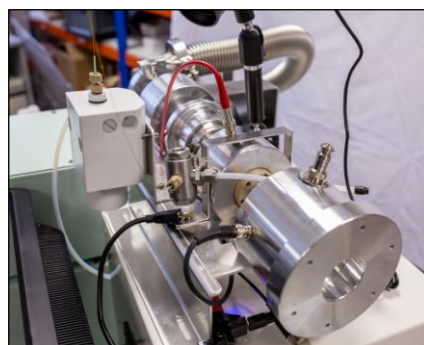


Figure 1. The high temperature capable half-mini DMA.

This work has received support from the “Horizon 2020” E.U. Framework Programme, through the SUREAL-23 project (Grant Agreement 724136).

Giechaskiel B., Martini G. (2014), *JRC Science and Policy Report*: “Review on engine exhaust sub-23 nm particles”, Joint Research Centre.

Fernandez de la Mora J. (2017) Expanded size range of high-resolution nanoDMAs by improving the sample flow injection at the aerosol inlet slit, *J. Aerosol Sci.*, under review.

## Assessment of a propane diffusion flame generator (CAST) as a reference aerosol generator in the sub-23 nm range

E. Daskalos<sup>1</sup>, A. Melas<sup>1</sup>, P. Baltzopoulou<sup>1</sup>, A.G. Konstandopoulos<sup>1,2</sup>

<sup>1</sup>Aerosol & Particle Technology Laboratory, CERTH/CPERI, P.O. Box 60361, 57001, Thessaloniki, Greece

<sup>2</sup>Department of Chemical Engineering, Aristotle University, PO. Box 1517, 54006, Thessaloniki, Greece

Keywords: sub-23nm particles, soot aggregates, volatile matter

Presenting author email: emdaskal@cperi.certh.gr

Concerns on negative effects of vehicle emissions, drove many countries to introduce emission standards. Existing European legislation regulates solid particles number according to the guidelines of the Particle Measurement Programme (PMP), not taking into account the sub-23 nm fraction of the exhaust emissions due to size related inherent difficulties that lead to measurement uncertainties (Giechaskiel et al. 2008). However, as recommended by the JRC Science and Policy Report (Giechaskiel and Martini, 2014), there is an urgent need for an updated version of the regulations that would take into consideration sub-23 nm particles by further reducing the cut-off particle size limit. Towards this target, research efforts focus on robust sampling and measuring in the sub-23 nm particle size range.

In order to validate experimental measurement and sampling setups a reference aerosol is needed to generate particles in the size range of interest in a consistent and repeatable way. Specifically, in the automotive sector the use of a propane diffusion flame soot generator (Combustion Aerosol Standard, CAST) can be of value due to its ability to generate repeatable soot particle distributions. A characterization of solid soot particles from CAST has been presented in (Konstandopoulos et al. 2011). However, recent studies show that CAST-generated particles may contain volatile fraction under specific operation conditions. These findings question the applicability of CAST in several applications, e.g. as a solid particle generator (Mamakos et al., 2013).

Herein, we will study the volatile fraction and the structure of CAST-generated particles for particle sizes used in the current PMP but also in the sub-23 nm region. More specifically, the particle size distribution of CAST-generated particles is altered by controlling the flow of a mixing gas (N<sub>2</sub>) that dilutes the fuel (propane). Figure 1 shows particle size distributions of CAST-generated particles that have been obtained in the sub-23 nm region. Particles with mean mobility diameter in the range of 10-100 nm are generated and their size distribution is measured with Scanning Mobility Particle Sizer (SMPS) by using a long DMA (TSI 3081) for larger sizes and a nano-DMA (TSI, 3085) for sub-23 nm particles. The volatile fraction of CAST-generated particles is measured by thermo-gravimetric analysis of filtered samples under nitrogen. Microstructural analysis is performed by applying two different approaches; Transmission Electron Microscopy (TEM) image analysis and tandem mobility-aerodynamic diameter measurements (Baltzopoulou et al., 2012). The particle collection on TEM grids is done with an in-house developed thermophoretic sampler

(Konstandopoulos et al. 2011). Finally, particle losses and possible volatile material evaporation are both numerically and experimentally studied by passing the CAST-generated particles through a PMP-compliant Volatile Particle Remover.

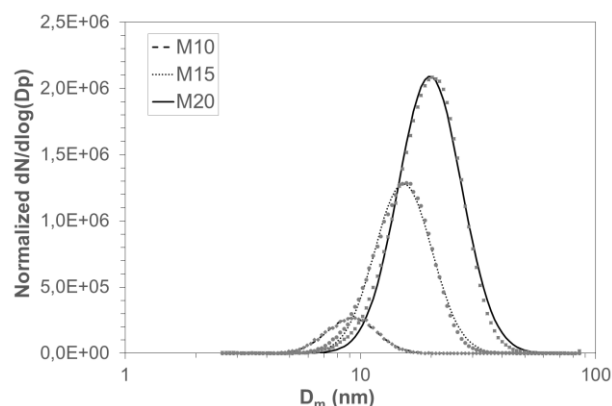


Figure 1. CAST distributions with mean diameters of 10 nm, 15 nm and 20nm.

This work was supported by the Horizon 2020 E.U. Framework Programme, through the SUREAL-23 project (Grant Agreement 724136).

- Giechaskiel, B., Dilara, P., and Andersson, J. (2008), *Aerosol Sci. Technol.* **42**, 528–543.
- Giechaskiel B., Martini G. (2014), *JRC Science and Policy Report*: “Review on engine exhaust sub-23 nm particles”, Joint Research Centre.
- Konstandopoulos, A. G., Daskalos, E., and Vlachos, N. (2011), *15th ETH-Conference on Combustion Generated Nanoparticles*, June 26–29, Zurich, Switzerland.
- Mamakos A., Khalek I., Giannelli R. and Spears M. (2013), *Aerosol Sci. Technol.* **47**, 927-936.
- Baltzopoulou P., Kostoglou M., Papaioannou E. and Konstandopoulos A. (2012), *European Aerosol Conference EAC 2012*, EAC-2012-P074, September 2-7, Granada, Spain.

## FATCAT: a new characterization method for particulate emissions from wood burning appliances

A. Keller, D. Egli, P. Steigmeier, H. Burtscher

Institute for Aerosol and Sensor Technology, University of Applied Sciences Northwestern-Switzerland, 5210 Windisch, Switzerland

Keywords: SOA (Second. Organic Aerosols), Wood Combustion, Emissions, Measurement (characterization), Total Carbon.

Presenting author email: alejandro.keller@fhnw.ch

Biomass burning is a major contributor to environmental particulate matter pollution that should be contemplated by emission control legislation. However, existing standards are based on total particulate matter (PM) without differentiation by chemical composition or particle size. This is not ideal since neither combustion efficiency nor toxic potential are well reflected by this approach. Legislation also neglects the potential for the formation of secondary organic aerosol (SOA), which is one of the most important atmospheric pollutants in Europe (Denier van der Gon et al., 2015). As a consequence, policy decisions for improving air quality may not achieve the desired results unless they are based on a more appropriate standard.

We propose an alternative metric that incorporates recent scientific results and is compatible with type-approval testing as well as field measurements (Keller and Burtscher, 2017). In short, we produce SOA by aging emissions in the micro smog chamber (MSC; Keller and Burtscher, 2012) and quantify the emissions using particle-bound total carbon (TC) analysis.

We will present the FAsT Thermal CARbon Total-izer (FATCAT), our semi-online device developed for this task. The device collects a sample on a filter and heats it rapidly, within 50 seconds, to 800°C under an oxidizing atmosphere. Further oxidation of carbonaceous material is achieved by a catalyzer located downstream of the heating unit. Total carbon detection is done by means of a CO<sub>2</sub> measurement. Fast heating allows an analysis time under 2 minutes (see fig. 1).

We present emission data from a variety of wood-burning devices, including automatic as well as batch operated installation. We will compare emission factors, calculated from our TC measurements, against standard gravimetric measurements and thermal-optical analysis data. Our TC data comprises measurements performed on raw as well as aged emissions in order to show how SOA increases the emission factor. We will show that the combination of aging and TC analysis is a feasible and practical alternative for characterization of wood-burning appliances.

This research was supported by the Swiss Federal Office for Energy (SFOE), the Swiss Federal Office for the Environment (FOEN) and the OPTIWARES project of the Competence Center Energy and Mobility (CCEM) from the ETH Zurich.

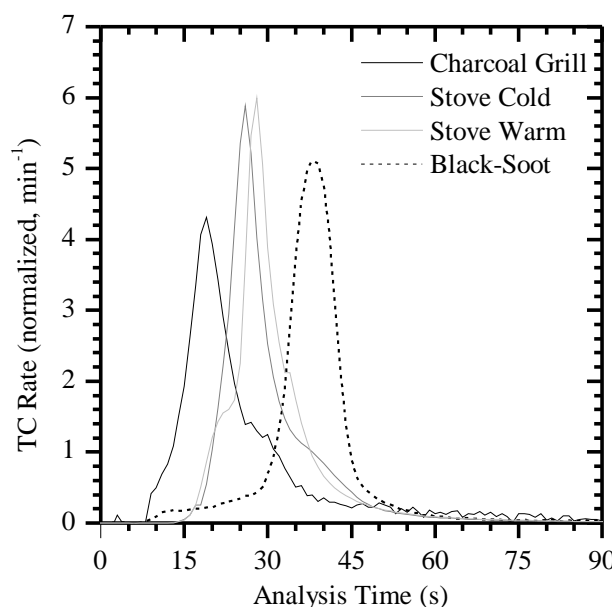


Figure 1: Examples of the total carbon analysis cycle performed for raw emissions (i.e. not aged in the MSC) for two different biomass burning appliances and a CAST (Jing Ltd, Switzerland) black-soot sample. The charcoal grill is a commercial batch-operated appliance that uses a ventilator to achieve better combustion. The curves from the log-wood batch-operated stove correspond to cold-start and warm-start combustion-cycles. Time zero marks the start of the 50 seconds filter heating. The curves show the time-resolved total carbon rate normalized to an area of one. The total carbon emissions for these measurements are TC = 3, 62, and 33 mg/m<sub>STP</sub><sup>3</sup> at 13% O<sub>2</sub> for the grill, stove cold, and stove warm respectively. Peaks appearing to the left of the graph correspond to more volatile material whereas the CAST signal, consisting almost exclusively of refractory black carbon, appears later in time when the filter temperature is closer to the final temperature of 800°C.

Denier van der Gon, H. A. C. *et al.* (2015). *Atmos. Chem. Phys.*, 15(11):6503–6519.

Keller, A. and Burtscher, H. (2012). *J. Aerosol Sci.*, 49(0):9 – 20.

Keller, A. and Burtscher, H. (2017). Manuscript submitted to *J. Aerosol Sci.*

## Ambient pressure particle mass spectrometry for inline detection of nanoparticle growth in flame reactors

Samer Suleiman<sup>1\*</sup>, Sebastian Kluge<sup>1</sup>, Christof Schulz<sup>1,2</sup> and Hartmut Wiggers<sup>1,2\*</sup>

<sup>1</sup>Institute for Combustion and Gas Dynamics – Reactive Fluids (IVG), University of Duisburg-Essen, Duisburg, Germany

<sup>2</sup>Center for Nanointegration Duisburg-Essen (CENIDE), University of Duisburg-Essen, Duisburg, Germany

Keywords: Mass Spectrometry, Molecular Beam, Inline Detection.

Presenting author email: samer.suleiman@uni-due.de

Inline characterization of nanoparticle formation with particle mass spectrometry (PMS) is well established to investigate the evolution of particle size and particle size distribution during low pressure nanoparticle synthesis. It is commonly used to determine the influence of process conditions (temperature, precursor concentration, pressure) on particle growth. The method is based on a high vacuum nozzle/skimmer molecular beam sampling and is equipped with a deflection unit and an off-axis Faraday cup detector to measure deflected, energy-filtered currents of charged particles. Due to limitations in pressure drop, the conventional two-stage vacuum system is limited to sampling from low-pressure reactors (< 100 mbar abs.). There are only few reports on molecular-beam mass spectrometry (MBMS) of particles from atmospheric-pressure systems, mostly used for the investigation of sooting flames (Grotheer, 2011).

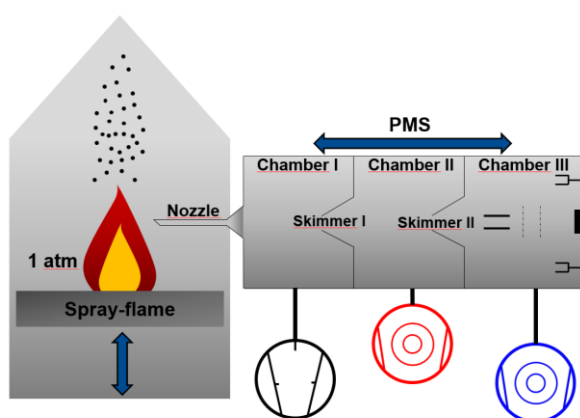


Figure 1. Sketch of the newly developed PMS.

In this study we present a newly developed PMS that can be operated at atmospheric pressure. It contains an additional dilution chamber operated at about 50 mbar in front of the first expansion chamber (chamber I) to connect the PMS to reactors working at atmosphere (Figure 1) Chamber I allows sampling and dilution of particle, thus preserving the particles' properties by adding inert gases. After a very short residence time of about a few  $\mu$ s within this first chamber, the diluted aerosol is sampled via the commonly used two-stage nozzle/skimmer system (chamber II and III).

As molecular beam sampling requires high vacuum conditions, suitable nozzle orifices and pumping capacities have to be chosen while preventing nozzle clogging. Based on calculations, nozzle diameters of 0.69

and 0.49 mm were selected for chamber I and II, respectively. From Figure 2 it is obvious that the pressure in the analysis chamber III is independent from chamber I and II and thus allows for molecular beam sampling. This enables operation of the PMS within a wide pressure range up to atmospheric pressure.

The nanoparticle sampling rate can be tuned by adjusting the pressure in chamber I, either using dilution gases or reducing the pumping power. As the setup is mounted on a two-way positioning unit, it allows for a spatially resolved investigation of the particle formation in gas-phase reactors. Results concerning the investigation of nanoparticles from sooting flames as well as from a spray-flame nanoparticle reactor, both operated at ambient pressure, will be discussed.

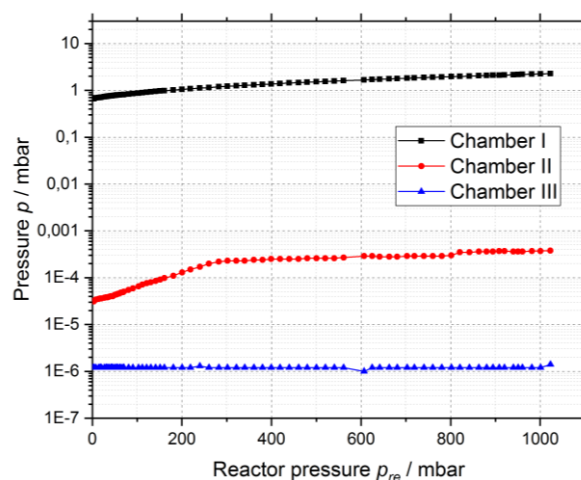


Figure 2. Pressure correlations of the several pressure stages dependent of the operated reactor chamber as inlet pressure.

Grotheer, H.-H., Wolf, K. (2011) *Photoionization mass spectrometry for the investigation of combustion generated nascent nanoparticles and their relation to laser induced incandescence*, Appl. Phys. B 104, 367-383

## Laser-based techniques applicability for soot particles detection and analyses: soot particles nucleation into laboratory flames

C. Irimiea<sup>1,2</sup>, A. Faccinetto<sup>2</sup>, Y. Carpentier<sup>1</sup>, I. K. Ortega<sup>3</sup>, E. Therssen<sup>2</sup>, C. Focsa<sup>1</sup>

<sup>1</sup> Univ. Lille, CNRS, UMR 8523 - PhLAM - Physique des Lasers Atomes et Molécules, F-59000 Lille, France

<sup>2</sup> Univ. Lille, CNRS, UMR 8522 - PC2A - Physicochimie des Processus de Combustion et de l'Atmosphère, F-59000 Lille, France

<sup>3</sup>Onera-The French Aerospace Lab, F-91761 Palaiseau, France

Keywords: soot, optical properties, mass spectrometry, laboratory flame

Presenting author email: cornelia.irimiea@univ-lille1.fr

Soot particles released into the atmosphere after incomplete combustion are potentially rich in adsorbed volatile organic compounds that play an important role in defining their physical and chemical properties.

This work details the results of measurements on soot generated by laboratory methane diffusion flames by coupling in-situ and ex-situ techniques. Our research has a main objective: implementation of laboratory techniques used for the identification of the mechanisms involved in soot particles nucleation.

Within this framework, in-situ laser based techniques as laser induced incandescence/fluorescence (LII-LIF) and Raman scattering are used for the detection of soot particles and their precursors. In parallel, ex-situ laser two-step mass spectrometry (L2MS), secondary ions mass spectrometry (SIMS) and absorption spectroscopy are used for the chemical characterization of soot particles. Ex-situ measurements (Raman, mass spectrometry) required the development of a dedicated sampling system for the deposition of particles on silicon wafers/quartz fiber filters directly from the flame.

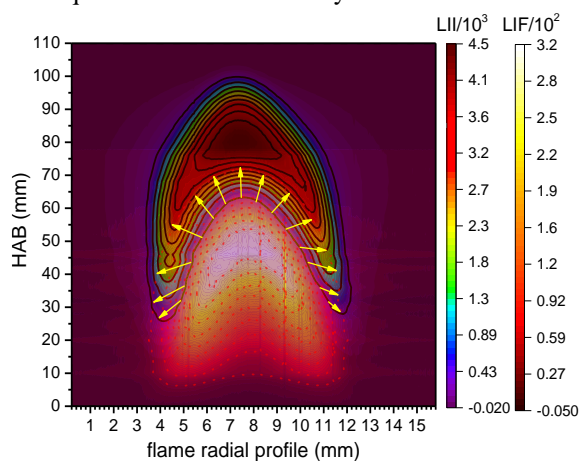


Figure 1. 2D flame cartography obtained by LII-LIF. LII shows the position of soot nanoparticles (top of the cartography) while LIF reveals the soot precursors in the gas phase (bottom of the cartography).

The impact of our results is manifold. LII/LIF measurements show a stratified distribution of soot particles (LII) and large organic molecules (LIF, mostly polyaromatic hydrocarbons PAHs) as shown in Fig. 1. The knowledge of the optical emission properties of soot is critical for their correct detection and quantification: in particular, our results point out to a change of the soot

refractive index absorption function  $E(m_\lambda)$ , in emission, with the height above the burner (HAB), which is most probably related to the organic content of soot particles.

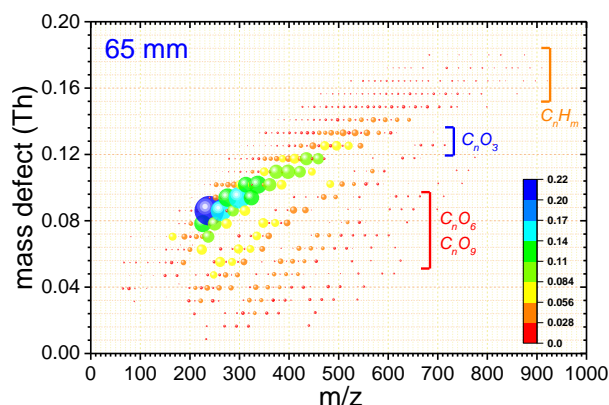


Figure 2. Mass defect plot obtained from SIMS measurements, representative of particulate matter sampled at 65 mm HAB (soot inception zone) from the centreline of the methane diffusion flame. The colour/size of the points is direct proportional with the integrated area of the specific masses divided by the total ion counts.

The complex chemical composition of the soot surface obtained from mass spectrometry data allows the chemical characterization (identification) of fluorophores and soot particles previously detected with in-situ techniques. Mass spectrometry results show that PAHs and oxy-PAHs are main components of the phase adsorbed on the soot surface, and that their surface concentrations evolve with the HAB. In particular, a region of high interest from this flame is the soot zone inception, (yellow arrows in Fig. 1), in which the transition from the gas to the particulate phase occurs. The mass defect of molecules identified with SIMS in the nucleation zone is shown in Fig. 2, and permits to capture important chemical information about the combustion compounds involved in soot particles formation.

The applicability of our techniques is extended to aerosol soot samples thus allowing the validation of our measurements to external combustion sources.

This work was supported by the LABEX CaPPA (Chemical and Physical Properties of the Atmosphere) under the contract ANR-10-LBX-005 and by the CPER CLIMIBIO (Hauts de France Region and European Funds for Regional Economic Development).

## Chemical characterisation of particulate matter from different emission sources with thermal and laser desorption atmospheric pressure photo ionisation ultra-high resolution mass spectrometry

C.P. Ruger<sup>1</sup>, A. Neumann<sup>1</sup>, M. Sklorz<sup>1</sup> and R. Zimmermann<sup>1,2,3</sup>

<sup>1</sup> Chair of Analytical Chemistry, University of Rostock, 18051 Rostock, Germany

<sup>2</sup> HICE – Helmholtz Virtual Institute of Complex Molecular Systems in Environmental Health – Aerosols and Health, www.hice-vi.eu

<sup>3</sup> Cooperation Group Comprehensive Molecular Analytics, Helmholtz Zentrum Munchen, 85764 Neuherberg, Germany

Keywords: combustion aerosol, mass spectrometry, ship diesel, atmospheric pressure ionisation.

Presenting author email: christopher.rueger@uni-rostock.de

The comprehensive chemical characterisation of combustion aerosol is still a challenging task for analytical instrumentation. Nonetheless, mass spectrometric (MS) techniques have been at the forefront, such as aerosol mass spectrometer (AMS), proton transfer reaction (PTR) and photo ionisation mass spectrometer (PI-MS) for the online analysis as well as MS coupled chromatography for offline analysis. High resolution mass spectrometry (HR-MS) equipped with atmospheric pressure ionisation techniques enables detailed insights into complex organic mixtures on the molecular level (Nizkorodov, 2011). Recently, we applied gas chromatography coupled to HR-MS (Schwemer, 2015) as well as laser desorption ionisation (Ruger, 2015) for the characterisation of ship diesel particulate matter (Streibel, 2016).

In this study we present a combined thermal and laser desorption atmospheric pressure photo ionisation source hyphenated to HR-MS (FT-ICR MS) (Figure 1). Particulate matter (PM) samples generated via impactor sampling can be placed directly in-source without further treatment. This aspect avoids common extraction problems, e.g. contaminants. The sample can be heated with a defined heating rate or desorbed at once applying laser desorption (435 nm 3 W laser diode). Evolved species are ionized via a photo ionisation lamp. Ions are transferred into the mass spectrometer and temperature resolved high resolution mass spectra are obtained. PM was sampled from different emission sources, such as a ship diesel engine, a log wood stove and a gasoline car engine.

The setup, both thermal desorption and laser desorption, was evaluated with standard substances and standard mixtures. For the approach towards complex mixtures, several petroleum samples such as diesel fuel, marine gas oil, and heavy fuel oil as well as their derived combustion aerosols were analysed. Laser desorption parameters, e.g. laser diode energy, focus and irradiation time, were varied. Too high energy lead to decomposition, whereas to low energy reveal low signal-to-noise ratios. TD shows a simulated distillation-like behaviour for the mixture's compounds which means that the average mass over charge ratio was shifted to higher values for higher temperatures (up to  $m/z$  600) and is therefore capable for analysing volatile and semi-volatile components. Especially for combustion aerosol samples, 35 °C are not sufficient for evaporating all organics adsorbed

on the particulate matter. However, it could be shown that LD exhibits species with higher  $m/z$ . For the investigation of aerosol received from heavy petroleum combustion, the higher end of the distribution is accessible, which is not feasible with the thermal desorption.

In summary, we present a novel ionisation source especially designed for particulate matter characterisation. Thermal as well as laser desorption are shown. Both concepts can be applied complementary, whereas the thermal desorption is suited for volatile and semi-volatile species whereas laser desorption is capable of evaporating high boiling point compounds. Capabilities and proof-of-principle measurements were conducted. Various particulate matter samples from different emission sources were investigated.

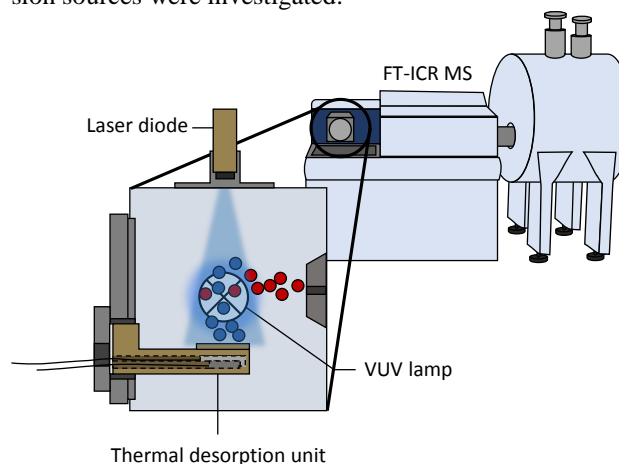


Figure 1. Scheme and photograph image of the utilized setup for thermal and laser desorption.

Funding by the Helmholtz Foundation for the HICE virtual institute is gratefully acknowledged.

Schwemer T. et al. (2015) *Analytical chemistry*, **87**, 11957-11961

Ruger C. P., et al. (2015) *Analytical and bioanalytical chemistry*, **20**, 5923-5937

Streibel T. et al. (2016) *Environmental science and pollution research international*, DOI: 10.1007/s11356-016-6724-z

Nizkorodov, S. A.; Laskin, J.; Laskin, A. *Phys. Chem. Chem. Phys.* **2011**, DOI: 10.1039/c0cp02032j

## Variation of nanostructure of laboratory generated soot aerosols with particle size

R. Dastanpour<sup>1</sup>, S. Rogak<sup>1</sup>, K. Thomson<sup>2</sup>, J. Olfert<sup>3</sup>

<sup>1</sup>Department of Mechanical Engineering, University of British Columbia, Vancouver, V6T 1Z4, Canada

<sup>2</sup>Measurement Science and Standards, National Research Council, Ottawa, Ontario, Canada

<sup>3</sup>Department of Mechanical Engineering, University of Alberta, Edmonton, Alberta, Canada

Keywords: soot, nanostructure, HRTEM, graphitization

Presenting author email: r.dastanpour@alumni.ubc.ca

Investigation of the morphology of black carbon particles by high resolution transmission electron microscopy (HRTEM) and Raman spectroscopy provides insight into the internal structure and graphitization of these particles. Properties of soot particles, including their interaction with optical rays, are highly influenced by their nanostructure.

For decades, mass-specific absorption cross section (MAC) of soot has been assumed to be independent of its size and mass. However, our recent investigation (Dastanpour, 2016) has showed that the MAC number increases substantially with the particle mass (Figure 1).

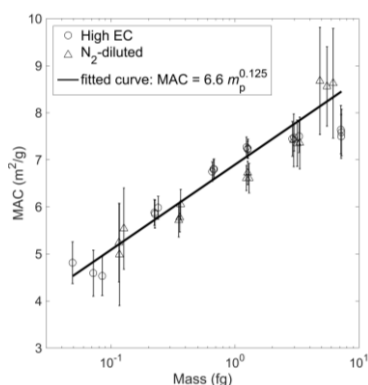


Figure 1: MAC versus particle mass. Error bars are the standard deviations of the MAC measurements. High EC and N<sub>2</sub>-diluted at two different operating conditions.

Considering this along with the correlation between the primary particle and aggregate diameters (Dastanpour & Rogak, 2014) it may be speculated that the small and large particles have different nanostructure and may have different levels of graphitization. This is consistent with the hypothesis that the aggregates are mainly formed in microscopic scales; after which particles with different formation, growth, and oxidation histories are mixed to form the ensemble emissions.

Here, we investigate the internal structure of the size-classified particles by Raman spectroscopy and HRTEM analysis.

To this end, particles were generated at two operating conditions similar to our previous study: combustion of CH<sub>4</sub> (labelled as High EC), and CH<sub>4</sub> and N<sub>2</sub> mixtures (labelled as N<sub>2</sub>-diluted), within a laminar inverted diffusion flame. Size-classified soot samples at mobility-equivalent diameters of 125 nm, 250 nm, and 300 nm were collected on 300-mesh Lacy grids from Ted Pella and preheated quartz filters for HRTEM and Raman spectroscopy, respectively.

The measured Raman spectra was fitted by 4 Lorentzian-shaped bands (G, D1, D2, and D4) and one Gaussian-shaped band (D3). Our results show that the ratio of average intensities of all D bands to the G band increase substantially with the particle size. G band represents crystalline graphitic structures consisted of sp<sup>2</sup>-bonded carbon atoms in unreactive basal planes, while D bands represent defects of the graphitic crystallites and amorphous carbon. This confirms that the larger particles are more graphitic.

An open-source image processing program was developed for the analysis of the images produced by the HRTEM. A combination of histogram equalization, Gaussian lowpass filter, top-hat transformation, binarization, and morphological opening and closing were used to enhance the quality of the images and accuracy of the image processing. As a new feature, the new algorithm enables fully automated measurement of the separation distance of fringes. To this end, each fringe is split into small linear-shaped segments and population density of the separation distances are measured with respect to these segments. A sample HRTEM image taken for this study and fringes detected in a portion of it are illustrated in Figure 2.

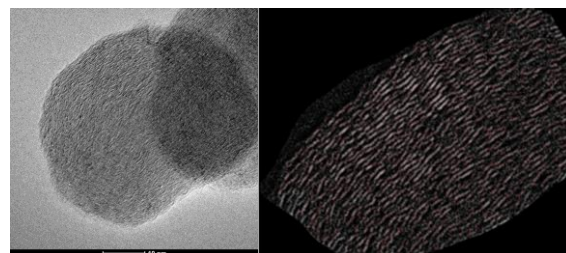


Figure 2: Sample HRTEM image (left), and detected fringes (right).

Average and distribution of length, tortuosity, and separation distance of the polycyclic aromatic hydrocarbon (PAH) layers were calculated for particles of different sizes. This information provides insight into the formation and growth histories of these particles and can be used for the assessment of the graphitization level of these particles.

Dastanpour, R. and Rogak, S. (2014) *Observations of a Correlation between Primary Particle and Aggregate Size for Soot Particles*, *Aerosol Sci. Technol.* 48 (10), 1043-1049

Dastanpour, R. (2017) *Characterization of primary particle size variation and its influence on measurable properties of aerosol soot* (Doctoral dissertation, University of British Columbia)

## Characterization of brake wear particle emitted from passenger car brake system

H. Hagino <sup>1</sup><sup>1</sup>Japan Automobile Research Institute (JARI), Tsukuba, Ibaraki, JapanKeywords: Non-Exhaust Emission, Brake Abrasion, Metal, Oxygenated Organic Aerosol.  
Presenting author email: hhagino@jari.or.jp

Particulate matter (PM) in the atmosphere is an important component of air pollution that can cause adverse health effects. PM comprises a complex mixture of components derived from different sources, with motor vehicle emissions being one of the most important sources in urban areas. PM originating from motor vehicles is categorized based on two main sources: exhaust emissions (e.g., vehicle tailpipe emissions) that represent PM resulting from incomplete fuel combustion and lubricant volatilization during the combustion processes; and non-exhaust emissions created through brake, tire, and general vehicle wear processes and through the resuspension of road wear particles (Thorpe and Harrison, 2008). Several studies using road tunnels and/or roadside environments have shown that automotive brake abrasion dust (hereafter called brake wear particles) is an important source of PM originating from motor vehicles. Specifically, brake wear particles are estimated to contribute 16–55% of non-exhaust traffic-related PM<sub>10</sub> (particles up to 10 μm in size, which pertain to the 50% cut-off aerodynamic diameter) emissions. Temporal patterns of brake wear particles in PM<sub>2.5</sub> emissions have been shown to exhibit periodic behavior, with two peaks coinciding with rush-hour traffic in street canyon traffic road tests and at an urban background site. Considering the increasingly strict controls on vehicle exhaust emissions, the relative contribution of brake wear particles will become increasingly important in the consideration of total traffic-related PM emissions. Furthermore, several toxicological studies have suggested that metallic brake wear particles damage tight junctions within the mechanisms that involve oxidative stress; therefore, the important point is not only the particle mass, but also the particle quality (e.g. chemical composition and biological effect). Using actual vehicles and/or roadway tests may result in PM samples that are contaminated by re-entrained road dust and/or tire wear particles. To determine the emission factors and chemical compositions of brake wear particles from brake pads and rotors (or lining and drum) without contamination, which is important for toxicological testing of the particle-weighted emission factor, it is better to use a brake wear particle dynamometer with an enclosing chamber and a constant-volume sampling system.

In this study, a brake wear dynamometer with a constant-volume sampling system was developed to measure driving distance-based mass emission factors of airborne brake wear particulate matter (PM). Brake wear particle emission factors from non-asbestos organic (NAO) and Low Steel (LS) friction material (pads) used in a brake assembly were determined for one passenger car under transient driving cycles using the tailpipe emission test method. Real-time monitoring were

demonstrated brake wear particle components and gaseous species emissions under urban city driving cycles. The levels of observed airborne brake wear particle emissions for PM<sub>10</sub> were 0.04–1.4 mg/km/vehicle for NAO frictions and 2.9–8.1 mg/km/vehicle for LS frictions.

Organic and sulfur components were found in the non-refractory submicron particle phase (NP-PM<sub>1</sub>) using a Time-of-Flight Aerosol Mass Spectrometer (ToF-AMS) (Figure 1), indicating that they originated from organics in the NAO friction materials. The O/C and H/C ratios of the organic compounds were 0.68 and 1.62, respectively. Although the organics from brake wear particles were primary organic aerosols (POAs), higher oxidative components we also observed, in contrast with the NAO brake materials (e.g., O/C 0.11 and H/C 1 for a monomer phenol resin and O/C 0.14, and H/C 0.57 for a monomer aramid fiber) and tailpipe emissions (e.g., O/C/0.03 and H/C 2 for gasoline and diesel exhausts). There were similar oxidation levels for secondary organic aerosols (SOAs; e.g., O/C 0.68 and H/C 1.27 for toluene-derived SOAs). These results indicate that the NAO friction particles changed to oxygenated organic particles during the abrasion process.

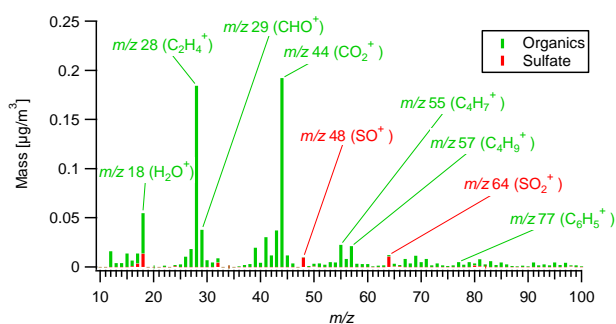


Figure 1. Aerosol mass spectra of organic (green) and sulfate (red) brake wear particles.

## References

- Hagino et al., Airborne brake wear particle emission due to braking and accelerating, *Wear*, Volumes 334–335, 15 July 2015, Pages 44–48, doi:10.1016/j.wear.2015.04.012
- Hagino et al., Laboratory testing of airborne brake wear particle emissions using a dynamometer system under urban city driving cycles, *Atmospheric Environment*, Volume 131, April 2016, Pages 269–278, doi:10.1016/j.atmosenv.2016.02.014
- Hagino, Measurement of Brake Wear Particle Emissions using a Dynamometer System under Urban City Driving Cycles, <https://wiki.unece.org/display/trans/PMP+43rd+Session>

## **Abstracts T312**

## How to measure volatile substances in various size classes of UFP

H. Plachá, M. Bitter, P. Goll and J. Kufel

Czech Hydrometeorological Institute, Branch Office Ústí nad Labem, Czech Republic

Keywords: UFP, SMPS, nucleation mode, thermodenuder.

Presenting author email: placha@chmi.cz

Number concentration of ultra-fine particles in the range of 10–800 nm has been measured by SMPS at the station in Ústí nad Labem since the year 2012. The ultra-fine particles have been divided into seven size classes (10–20 nm, 20–30 nm, 30–50 nm, 50–70 nm, 70–100 nm, 100–200 nm and 200–800 nm).

After the process of verification the results have been passed on to the Air quality pollution database of the Czech Republic (ISKO) and to the European database ACTRIS.

In the process of the measurement and evaluation of the number of particles in each of the size classes we have registered a high proportion of nanoparticles in the modes from 10 to 30 nm, especially during summer. In winter the number of these particles was also rather high, but the bulk of particles is generally higher in this season which means that the increase in the proportion of small particles is not that remarkable. Production of these particles was caused mainly by the condensation of the atmospheric gases or by the emissions resulting from high temperature processes (nucleation mode).

In the Ústí region plentiful sources of volatile substances can be found, such as lignite thermal power plants or various forms of chemical industry. These substances are often carriers of odour both in the immediate state and after a number of interactions. In order to understand the matter we decided to install another SMPS nearby the sources of air pollution. Additionally both of the analysers were retrofitted with thermodenuder, which is used in alternating mode measurements (5-minute measurements with and without thermodenuder) at the stations in Ústí nad Labem and Lom (a locality in close proximity to power stations and chemical factories in North Bohemian coal basin).

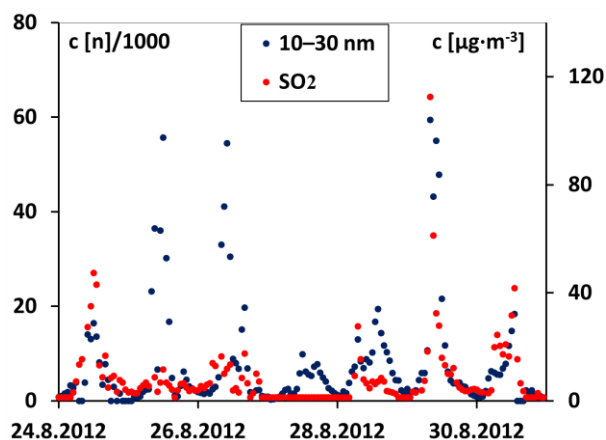


Figure 1. The course of concentration of SO<sub>2</sub> and UFP (10–30 nm) in the summer season.

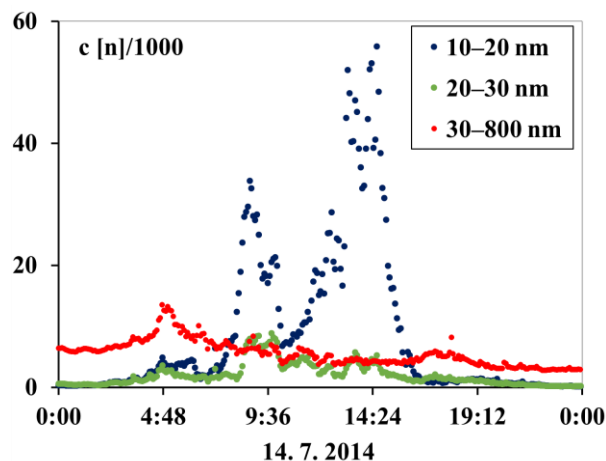


Figure 2. The course of concentration of UFP in July 2014.

The results of measurements from previous Project Cil 3 are given in figures 1. and 2. The new measurement are part of the Project border cooperation Cil 2 SN-CZ 2014-2020 Hallo Nachbar. Ahoj sousede. The title of this Project is "OdCom: Objectification of complaints about odour in the Ore Mountains and in the Usti region". Implementation and funding of this project is enabled by Development Bank of Saxony (SAB), and is controlled by the Saxon State Ministry of the Environment and Agriculture. The implementation period of this project is planned from 1.4. 2016 to 31. 3. 2018 and the sustainability period of the project should be five years after the handover of the Final Report of the project. At least during this period the measurements at both stations will be carried on and the data will be available for the ACTRIS database.

This paper is supported by Cil 2 and ACTRIS CZ.

Schladitz A., Leníček J., Beneš I., Kováč M., Skorkovský J., Soukup A., Jandlová J., Poulain L., Plachá H., Löschau G., and Wiedensohler A. (2015) *Air quality in the German-Czech border region: A focus on harmful fractions of PM and ultrafine particles*, Atmospheric Environment, 122, 236–249.

Hejkrlik L., Plachá H. and Richterová D. (2016) *UFP concentrations over some grids of paired meteorological data*, Abstract P2-AAS-AASP-220, EAC 2016, Tours, September 4–9, 2016.

## Development of a dual-wavelength thermo-optical transmittance analyser: characterization and first results

D. Massabò<sup>1</sup>, A. Altomari<sup>1</sup>, V. Bernardoni<sup>2</sup>, G. Valli<sup>2</sup>, R. Vecchi<sup>2</sup> and P. Prati<sup>1</sup>

<sup>1</sup>Dept. of Physics, University of Genoa & INFN, Via Dodecaneso 33, 16146, Genoa, Italy

<sup>2</sup>Dept. of Physics, Università degli Studi di Milano & INFN Via Celoria 16, 20133, Milano, Italy

Keywords: Carbonaceous Aerosol, Thermo-optical Analysis, EC and OC separation, Light Absorption

Presenting author email: Massabo@ge.infn.it

Carbonaceous aerosol (CA) plays an important role in many different issues ranging from human health to global climate change. It mainly consists of organic carbon (OC) and elemental carbon (EC) although a minor fraction of carbonate carbon could be also present. Thermal-optical methods (TOT/TOR) are presently the most widespread approach to OC/EC speciation. Despite their popularity, there is still a disagreement among the results, especially for what concerns EC as different thermal protocols can be used. In fact, the pyrolysis occurring during the analysis can heavily affect OC/EC separation, depending on PM composition in addition to the used protocol. The main hypothesis at the basis of the technique relies on the optical properties of EC and OC: while EC is strongly light absorbing, OC is generally transparent in the visible range. However, a fraction of light-absorbing OC exists: the Brown Carbon (BrC) (Andreae and Gelencsér, 2006). The presence in the sample of BrC can shift the split point since it is slightly absorbing also @ 635nm, the typical laser wavelength used in this technique (Chen et al., 2015).

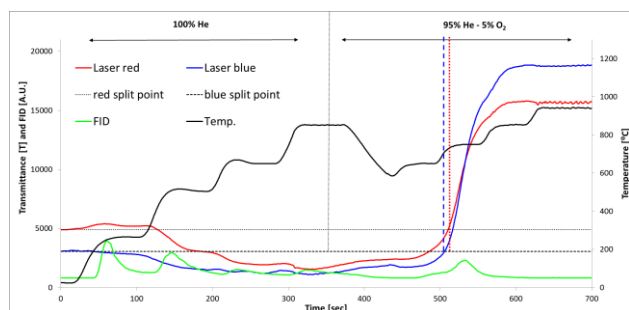


**Figure 1:** TOT analysis performed with both 635 and 405 nm lasers showing the identification of two distinct split points (and consequently of two different EC and OC repartitions).

At the Physics Department of the University of Genoa, a Sunset EC/OC analyser unit has been modified in order to monitor the optical transmittance during the thermo-optical analysis at two different wavelengths: 635 nm (the original wavelength of the instrument) and 405 nm (Fig.1). The additional use of the 405 nm transmittance measurement provides valuable information about the composition of the sample as well as on the pyrolytic carbon formation, both able to affect the instrumental “split point” (i.e. the moment of the analysis in which the laser transmittance is back to its starting value, thus defining EC/OC separation).

We present here the new instrument set-up, providing its full characterization with “synthetic”

samples (i.e. mixtures of sucrose, graphitic carbon, and pure scattering particles). Moreover, we show also the results obtained analysing at 2- $\lambda$  - with both NIOSH and EUSAAR\_2 protocols - real PM samples collected in very different conditions (i.e. summer-winter) and sites (ranging from urban to rural/mountain).

Furthermore, we have recently introduced a new possibility, based on the apportionment of the absorption coefficient ( $b_{abs}$ ) of particle-loaded filters, for correcting the thermo-optical analysis of PM samples (Massabò et al, 2016), an example in Fig.2. The apportionment is based on the optical analysis performed by the Multi-Wavelength Absorbance Analyser (MWAA), an instrument developed at the Physics Department of the University of Genoa (Massabò et al., 2015). The apportionment method uses the information gathered at five different wavelengths in a renewed and upgraded version of the approach usually referred to as Aethalometer model (Sandradewi et al., 2008).

We present here also the results of the thermo-optical analysis correction (Massabò et al., 2016) applied to the dual- $\lambda$  analysis, which lead to a better homogeneity between the results obtained with different thermal protocols.

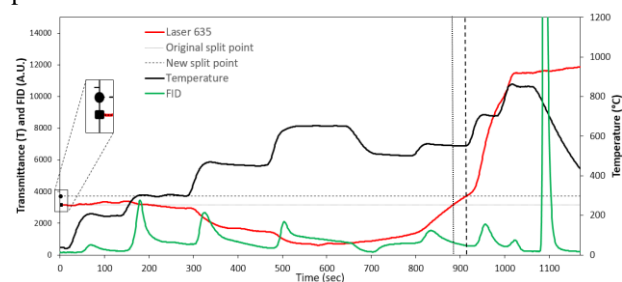


**Figure 2:** Example thermogram showing the original split point –square dot (i.e. non-corrected for BrC presence)- and the new split point – round dot (i.e. corrected for BrC presence). The new split point is rightmost of the original one leading to a new EC/OC separation.

This work was supported by INFN, under the grants MANIA and DEPOTMASS, and by Amministrazione Provinciale di Genova.

### References:

- Andreae, MO, and Gelencsér, A. (2006). *Atm. Chem. and Phys.*, **6**, 3131-3148.
- Chen et al., (2015), *Atmos. Meas. Tech.*, **8**, 451-461.
- Massabò et al., (2015), *Atmospheric Environ.* **60**, 34-46.
- Sandradewi et al., (2008), *Environ. Sci. Technol.*, **42**, 3316-3323
- Massabò et al., (2016), *Atmospheric Environ.* **125**, 119-125.

## Determining the connection between hygroscopicity and semi-volatile composition

J. Alroe<sup>1</sup>, Z. Ristovski<sup>1</sup>, B. Miljevic<sup>1</sup>, L. Cravigan<sup>1</sup> and G. Johnson<sup>1</sup>

<sup>1</sup>International Laboratory for Air Quality and Health, Science and Engineering Faculty, Queensland University of Technology, Brisbane, 4001, Australia.

Keywords: aerosol, hygroscopicity, composition, volatility

Presenting author email: j.alroe@qut.edu.au

The health- and climate-related effects of aerosols are significantly influenced by aerosol hygroscopicity. This property is affected by chemical composition and many models have been developed to link the two parameters. These efforts have been inhibited by the complexity of organic compounds present in most atmospheric aerosol. Semi-volatile compounds present the biggest challenge as they are highly dynamic, readily undergoing chemical changes and partitioning between the gas and particle phase.

In numerous studies, this semi-volatile component has been removed using thermal separation or isothermal dilution, to investigate its effects on hygroscopicity. In most cases, this same separation was not applied to supporting compositional measurements, preventing direct chemical characterisation of the semi-volatile component. These methods have offered limited agreement regarding the hygroscopic contribution of different aerosol species (Villani et al., 2013).

Recently, Cerully et al. (2015) and Hildebrandt Ruiz et al. (2015) used an aerosol mass spectrometer (AMS) and a cloud condensation nuclei counter (CCNc) to examine hygroscopic and compositional changes following removal of the semi-volatile component. They confirmed that hygroscopic contributions cannot be sufficiently constrained by volatility, but attempts to parameterise with respect to composition had inconsistent results, highlighting the need for further investigation.

In this study, an alternative real-time sampling system has been developed which couples a volatility and hygroscopicity tandem differential mobility analyzer (VH-TDMA) to an AMS. A schematic is shown in Figure 1. The VH-TDMA provides direct volume fraction measurements of the semi-volatile component, allows investigation of size-dependent variations, and reveals hygroscopic differences in externally mixed aerosol samples.

To characterize this system, it was used to sample secondary organic aerosol (SOA) formed on ammonium sulfate seed particles. Preliminary data, shown in Figure 2, clearly demonstrate hygroscopic changes at 90%RH resulting from removal of organic- and sulfate-related aerosol mass at 120°C. The system has also been put to use in the 2016 Reef to Rainforest campaign in coastal northern Queensland and in baseline Southern Ocean measurements at Cape Grim in 2015, and these results will be presented.

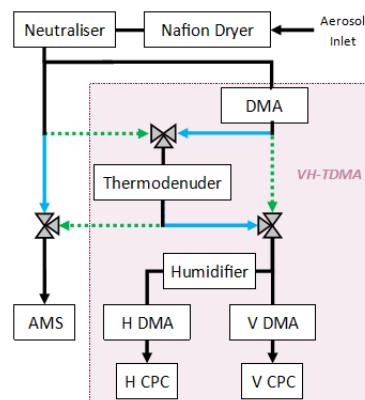


Figure 1. The integrated sampling system. Automated valves allow each instrument to cycle between heated and unheated aerosol (blue and green flow paths).

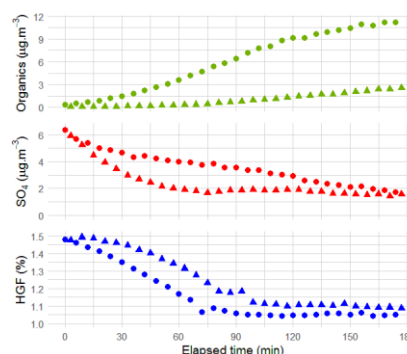


Figure 2. Hygroscopic and chemical properties of heated (triangles) and unheated (circles) aerosol during chamber-generated growth of SOA.

This work was supported through an Australian Government Research Training Program Scholarship and by the Marine National Facility.

Cerully, K. M., A. Bougiatioti, J. R. Hite, Jr., H. Guo, L. Xu, N. L. Ng, . . . A. Nenes (2015), *Atmos. Chem. Phys.* **15**, 8679-8694.

Hildebrandt Ruiz, L., A. L. Paciga, K. M. Cerully, A. Nenes, N. M. Donahue and S. N. Pandis (2015), *Atmos. Chem. Phys.* **15**, 8301-8313.

Villani, P., K. Sellegri, M. Monier and P. Laj (2013), *Atmos. Environ.* **79**, 129-137.

## Setup of an interface for operation of IAGOS (In-service Aircraft Global Observing System) CORE instruments onboard the IAGOS CARIBIC platform.

U. Bundke<sup>1</sup>, M. Berg<sup>1</sup>, H. Franke<sup>2</sup>, A. Zahn<sup>3</sup>, H. Boenisch<sup>3</sup>, J. Perim de Faria<sup>1</sup>, F. Berkes<sup>1</sup> and A. Petzold<sup>1</sup>

<sup>1</sup>Institute for Energy and Climate, IEK8, Forschungszentrum Jülich GmbH, Jülich, D-52428, Germany

<sup>2</sup>enviscope GmbH, Frankfurt, D-60489, Germany

<sup>3</sup>Karlsruhe Institute of Technology, Karlsruhe, Germany

Keywords: IAGOS, CARIBIC, global measurements

Presenting author email: u.bundke@fz-juelich.de

The European Research Infrastructure IAGOS (In-service Aircraft for a Global Observing System; [www.iagos.org](http://www.iagos.org)) responds to the increasing requests for long-term, routine in-situ observational data by using commercial passenger aircraft as measurement platforms.

The infrastructure is built from two complementary approaches: The “CORE” component comprises the implementation and operation of autonomous instruments installed on up to 20 long-range aircraft of international airlines for continuous measurements of important reactive gases and greenhouse gases, as well as aerosol particles, dust and cloud particles. The fully automated instruments are designed for operation aboard the aircraft in unattended mode for several months and the data are transmitted automatically.

The complementary “CARIBIC” component consists of the monthly deployment of a cargo container equipped with instrumentation for a larger suite of components. The CARIBIC container has equipment for measuring ozone, carbon monoxide, nitrogen oxides, water vapor and airborne particles. Furthermore the container is equipped with a system for collecting air samples. These air samples are analyzed in the laboratory. For each sample measurements for more than 40 trace gases including CFC's prohibited by the Montreal protocol, and all greenhouse gases are performed.

The Interface described in this work is designed to host one of IAGOS CORE (Package2) instruments. Available are:

- P2a, P2b, measuring NO<sub>y</sub> and NO<sub>x</sub>
- P2c, measuring the aerosol size-distribution (0.25 μm... 2.5μm), the total- and the non-volatile particle core number concentration
- P2d, greenhouse gases CO<sub>2</sub>, CO, H<sub>2</sub>O and CH<sub>4</sub>
- P2e, aerosol optical properties and size-distribution (0.25 μm ... 2.5μm)

The Interface has provisions for gas supply, butanol working liquid, connections to the chemical- and an aerosol inlet line as well as provides the connectivity to the CARIBIC master computer defining the different measurement phases see Figure 1.

Introducing the IAGOS CORE interface in the CARIBIC container will allow closure studies between both suits of in-situ instruments in the near future, thus generating excellent opportunities for QA/QC studies. Up to now the only way to compare these instruments outside the lab is to find occasional events with time and spatial colocations of the IAGOS CARIBIC aircraft with the IAGOS CORE fleet.

Within the certification documents of the interface an envelope is defined for operating optional P2-instruments. The instruments have to fulfill certain criteria like EMI- and vibration tests as well as power consumption and weight. The CARIBIC platform will be ideal for first airborne tests for future P2-instruments until they are certified under the very restrictive rules for IAGOS CORE operation.

The interface was integrated in November 2016 in the CARIBIC container. The certification is under way as part of the next CARIBIC container revisions scheduled in late spring 2017.

ntainer is scheduled late spring 2017.

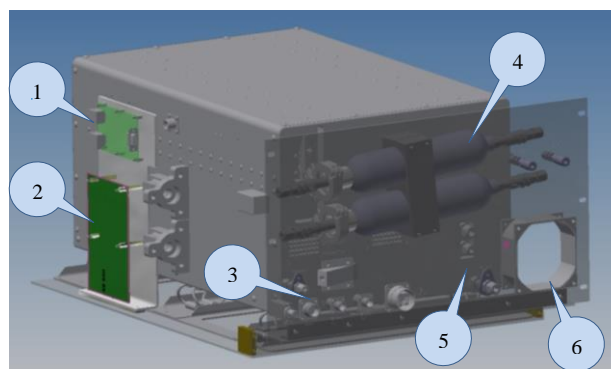


Figure 1. IAGOS CORE Interface: 1) communication module, 2) data-acquisition, 3) electrical provisions, 4) Butanol- supply and -waste reservoir cylinder, 6) ventilation duct

### Acknowledgements

Parts of this work were funded by the Federal Ministry of Education and Research, Germany, in IAGOS D (Grant Agreement No. 01LK1301A).

## Identification and quantification of ambient cigarette-related aerosol using online aerosol mass spectrometry

C. Struckmeier<sup>1</sup>, P. Faber<sup>1</sup>, F. Fachinger<sup>1</sup>, F. Drewnick<sup>1</sup>, and S. Borrmann<sup>1,2</sup>

<sup>1</sup>Particle Chemistry Department, Max Planck Institute for Chemistry, Mainz, 55128, Germany

<sup>2</sup>Institute for Atmospheric Physics, Johannes Gutenberg University, Mainz, 55128, Germany

Keywords: cigarette smoke, AMS, PMF, marker peaks.

Presenting author email: frank.drewnick@mpic.de

Emissions from cigarette smoking ubiquitously contribute to the urban ambient aerosol load and consist of a well-defined mixture of organic and inorganic aerosol components. Rogge *et al.* (1994) estimated the urban background concentration of cigarette-related organic aerosol to be about one percent of total PM<sub>1</sub>.

While various types of sub-micron organic aerosols associated with different types of sources are frequently identified in online aerosol mass spectrometer (AMS) data, cigarette-smoking organic aerosols (CSOA) are typically not found. Only in a few measurements CSOA was identified in AMS data, i.e. in a football stadium (Faber *et al.*, 2013) and in measurements contaminated by emissions from nearby smokers (Fröhlich *et al.*, 2015; Struckmeier *et al.*, 2016).

Here we present a detailed assessment of the suitability of AMS measurements for the identification and quantification of ambient cigarette-related organic aerosol using field and laboratory data. For this purpose, the applicability of both positive matrix factorization (PMF) of ambient organic aerosol spectra as well as of individual marker ion signals are investigated.

CSOA mass spectra identified from ambient aerosol measurements by applying PMF or in laboratory measurements are dominated by C<sub>n</sub>H<sub>2n-1</sub><sup>+</sup> and C<sub>n</sub>H<sub>2n+1</sub><sup>+</sup> ions (Fig. 1), and are very similar to mass spectra of cooking-related organic aerosol (COA). The most striking difference between mass spectra from these two types of sources is the appearance of strong signals at *m/z* 42 and 84 in the mass spectra of CSOA.

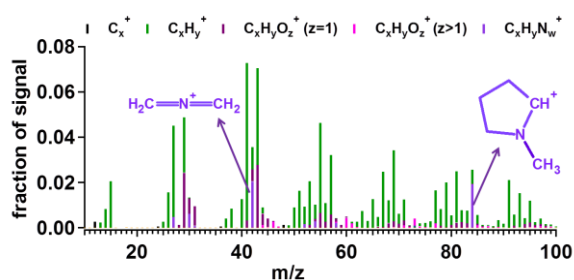


Figure 1. CSOA mass spectrum with marker peaks and associated marker ions (Struckmeier *et al.*, 2016).

These signals were identified as C<sub>2</sub>H<sub>4</sub>N<sup>+</sup> (*m/z* 42) and C<sub>5</sub>H<sub>10</sub>N<sup>+</sup> (*m/z* 84), fragmentation products of the nicotine molecule and thus potential marker ions for CSOA. C<sub>5</sub>H<sub>10</sub>N<sup>+</sup> was found to be the more robust marker for this type of organic aerosol because it is more specific for nicotine, compared to C<sub>2</sub>H<sub>4</sub>N<sup>+</sup>, which also

results from other parent molecules. In Fig. 2, diurnal patterns of CSOA measured at a site in central Rome (Struckmeier *et al.*, 2016) are shown. Good agreement between patterns determined using PMF and from the marker ion was found.

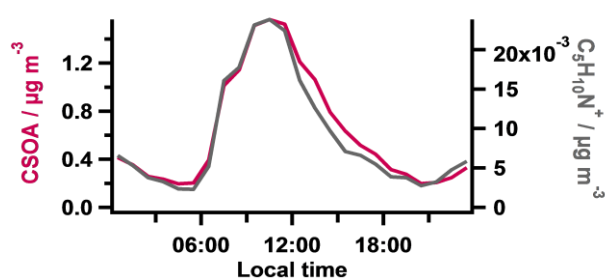


Figure 2. Diurnal patterns of CSOA, determined using PMF, and the marker ion at *m/z* 84 (Struckmeier *et al.*, 2016).

Due to interferences with other ions at *m/z* 84, which mainly are associated with primary aerosol types (COA and hydrocarbon-like OA, HOA), CSOA concentrations must be at least 10% of total primary organic aerosol, i.e. ~2.5% of PM<sub>1</sub>, to be detectable using this marker and the current setup. Thus identification of CSOA in ambient aerosol just using this marker is only possible if the measurements are performed close to the emission points. CSOA detection limits for PMF-based identification and the influence of mass spectral resolution are also discussed as well as variability of observed CSOA mass spectra.

This work was supported by internal funds of MPI for Chemistry, Particle Chemistry Department. We thank F. Barnaba, F. Costabile, L. Di Liberto, and G.P. Gobbi for support during the field measurements in central Rome.

Faber, P., Drewnick, F., Veres, P.R., Williams, J., and Borrmann, S. (2013) *Atmos. Environ.* **77**, 1043-1051.  
 Fröhlich, R., Cubison, M.J., Slowik, J.G., Bukowiecki, N., Canonaco, F., Croteau, P.L., Gysel, M., Henne, S., Herrmann, E., Jayne, J.T., Steinbacher, M., Worsnop, D.R., Baltensperger, U., and Prévôt, A.S.H. (2015) *Atmos. Chem. Phys.* **15**, 11373-11398.  
 Rogge, W.F., Hildemann, L.M., Mazurek, M.A., and Cass, G.R. (1994) *Env. Sci. Technol.* **28**, 1375-1388.  
 Struckmeier, C., Drewnick, F., Fachinger, F., Gobbi, G.P., and Borrmann, S. (2016) *Atmos. Chem. Phys.* **16**, 15277-15299.

## **Abstracts T313**

## Factors influenced and variable interactions of Particulate Matter (PM<sub>10</sub>) Concentrations at An Industrial Cities in Peninsular Malaysia

N.Z. Yahaya<sup>1</sup> and Z.F. Ibrahim<sup>2</sup>

<sup>1</sup>School of Ocean Engineering, University Malaysia Terengganu, Kuala Terengganu, 21030, MALAYSIA

<sup>2</sup>Researcher, <sup>1</sup>School of Ocean Engineering, University Malaysia Terengganu, Kuala Terengganu, 21030, MALAYSIA

Keywords: Stochastic Boosted Regression Trees, Algorithm, Particles, Pollutant interactions.

Presenting author email: [nzaitun@umt.edu.my](mailto:nzaitun@umt.edu.my)

This paper investigated the use of boosted regression trees (BRTs) to draw an inference about weekend and weekday particulate matter (PM<sub>10</sub>) concentrations at two selected industrial areas in Malaysia. A total of 122,706 hourly PM<sub>10</sub> concentrations, gases and meteorological data were gathered for the year 2000 to 2013 from the Klang (CA011) and Perai (CA003) air quality monitoring. The comprehensive R Software (R Development, 2016) and its packages were used to perform this analysis temporally and an advanced artificial Intelligent Approach Stochastic Boosted Regression Trees were first developed by Friedman in 2001 and adding the stochastic element in the algorithm in 2002 (Friedman, 2002). An hourly PM<sub>10</sub> data were used as a response variable and nitric oxide (NO), Nitrogen Dioxide (NO<sub>2</sub>), Sulphur Dioxide (SO<sub>2</sub>) and Carbon Monoxide (CO) and meteorological parameters as explanatory variables. Recent research has demonstrated that a Boosted Regression Trees (BRT) model with stochasticity can be used to obtain the best model (Carlaw, 2009) that can deal with a high level of complexity and large datasets and yield substantial outcomes (Yahaya, 2013, Yahaya *et al.*, 2016; Suleiman *et al.*, 2016). Figure 1 demonstrates diurnal plots for weekend and weekdays trend for this entire study.

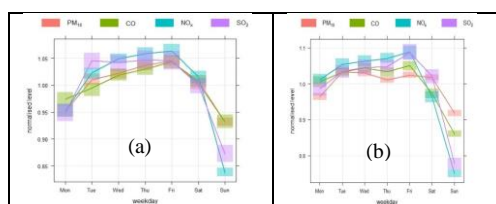


Figure 1. Daily mean of weekday trends for a) Klang station and b) Perai station.

The particles BRT algorithm model was constructed from multiple regression tree models, and the ‘best iteration’ of BRT model was performed by optimizing prediction performance. Using the number of trees between 2,000–7,600, learning rate of 0.05, and interaction depth of 5 were found to be the best setting for developing the PM<sub>10</sub> boosting model. The performance of the boosting models were assessed, and the fraction of predictions within two factor (FAC2), coefficient of determination (R<sup>2</sup>) and the index of agreement (IOA) of the model developed for weekend and weekday are 0.71 and 0.72 for CA011 and 0.51 and 0.52 for CA002 weekend and weekday respectively which within acceptable range. The FAC2 of all stations were found between 0.90 and 0.95 which range are acceptable for model performance.

Further investigated were performed to identify the interaction between parameters by using an artificial

intelligent technique with stochastic approach Boosted Regression Trees (BRT). Consistently, it was found that highest factor that influenced PM<sub>10</sub> was CO (30.28 %) gas and followed by temperature (16.81%) and wind direction (16.4%). This can be link to the location of these chosen station is co-inside closed to an arterial road that link this cities to the other, whereby a lot of motor vehicles the source emission strength due to city development were the highest influence to the Perai station. The Friedman’s H-Statistic (Friedman and Popescu, 2005) was used to assess the strength of variable interactions between gases. Strong H-Index were found for CA011 day time of 0.4 compared to only 0.3 during weekend at CA011 stations as shown in **Figure 2**.

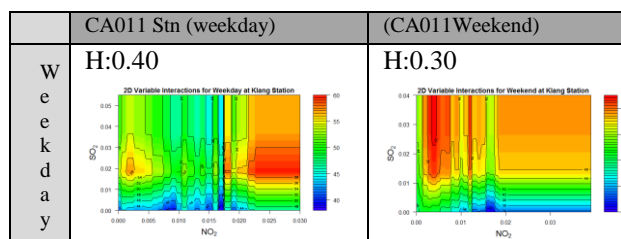


Figure 2. Two-ways variables interactions of SO<sub>2</sub> and NO<sub>2</sub> to fitted PM<sub>10</sub> concentration

Results showed that the model developed was within the acceptable range and could be used to understand particles formation and identify important parameters that influence the for estimating particles concentration during weekday and weekend data and this can be applied to other datasets.

### References.

- Carlaw, D. C. & Taylor, P. J. 2009. Analysis of air pollution data at a mixed source location using boosted regression trees. *Atmospheric Environment*, 43, 3563-3570.
- Friedman, J.H. (2002). Stochastic gradient boosting. *Computational Statistics & Data Analysis*, 38, 367-378.
- Friedman, J.H. and Popescu, B.E. (2005). “Predictive Learning via Rule Ensembles.” Section 8.1
- R Core Team (2016). R: A language and environment for statistical computing. R Foundation for Statistical Computing, Vienna, Aus.
- Suleiman, A., Tight, M.R. & Quinn, A.D. (2016). *Journal of Env. Model Assess.* 21: 731. doi:10.1007/s10666-016-9507-5
- Yahaya, N. Z., Tate, J. E. & Tight, M. R. (2011). Analysing Roadside Particle Number Concentrations using Boosted Regression Trees (BRT). *In: The European Aerosol Conference, EAC 2011, 5- 9 September 2011* 2011 The University of Manchester, UK.
- Yahaya (2013). Temporal and Spatial Variations of Ultra-fine Particles in the Urban Env. PhD Thesis of University of Leeds, UK.
- Yahaya, N.Z (2013) Noor Zaitun Yahaya, Nurul Adyani Ghazali, Sabri Ahmad, Mohammad Akmal Mohammad Asri, Zul Fahdli Ibrahim, Nor Azam Ramli (2017). Analysis of Daytime and Nighttime Ground Level Ozone Concentrations Using Boosted Regression Tree Technique. *Journal of Environment Asia*, 10(1) pp: 118-129

## Spatial and temporal variation of haze in the Yangtze River Delta region from 1961 to 2015

Rui Han<sup>1</sup>, Shuxiao Wang<sup>2,3</sup> and Jiandong Wang<sup>2</sup>

<sup>1</sup> National Meteorological Information Center, China Meteorological Administration, Beijing 100081, China

<sup>2</sup> State Key Joint Laboratory of Environment Simulation and Pollution Control, School of Environment, Tsinghua University, Beijing 100084, China

<sup>3</sup> State Environmental Protection Key Laboratory of Sources and Control of Air Pollution Complex, Beijing 100084, China

Keywords: Yangtze River Delta (YRD), Haze, Spatial-temporal variation, Meteorological factors.

Presenting author email: hanr@cma.gov.cn

In recent years, the haze weather in the Yangtze River Delta region (YRD) has been increasingly severe, which has become one of the key problems restricting the sustainable development of the YRD. The meteorological conditions play an important role in the formation of haze. Therefore, analysing the temporal and spatial distribution of haze and the impacts of meteorological factors is important to understand the haze formation mechanism. The results of this study will provide scientific basis for regional air pollution control in the YRD region.

In this study, data quality control and quality assessment of haze weather in YRD were conducted. Based on the calculation, the interannual, inter-decadal trend of haze days, temporal and spatial distribution of haze weather in the YRD were analysed using Mann-Kendall method and sliding T-test method. In addition, the meteorological factors influencing the formation of haze were studied using correlation analysis of haze weather phenomena, surface and upper air meteorological factors, and air pollutant concentrations, under six types of topography.

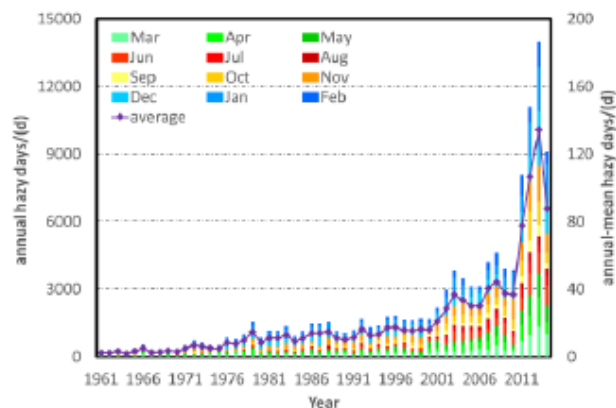


Fig.1 Annual-sum hazy days and annual-average hazy days of 104 stations in YRD, 1961-2015.

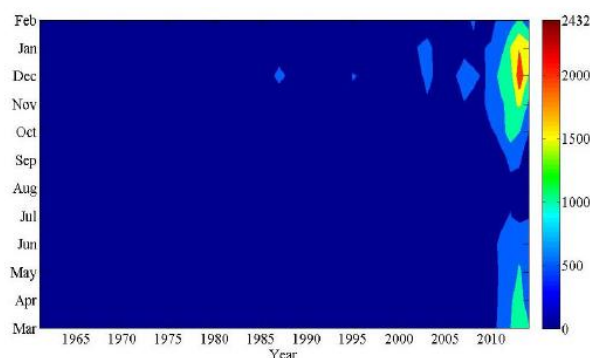


Fig.2 The seasonal change of hazy days in YRD, 1961-2015.

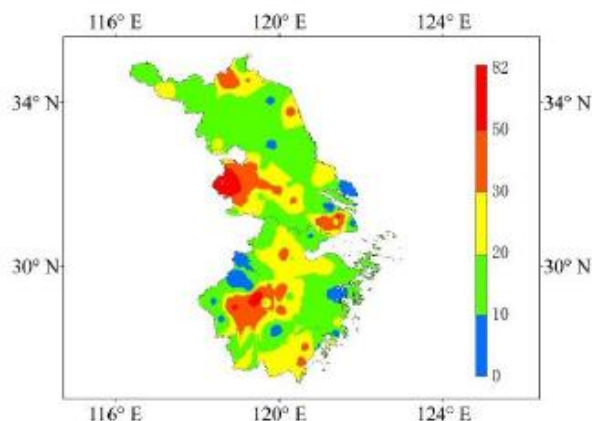


Fig.3 Spatial distribution of average hazy days in YRD.

The results show that the number of haze days in YRD have increased from 1961 to 2015, and the average haze days during 1961-2015 are about 21 days (Fig.1). The main reason for the interannual growth of haze days is the increase of anthropogenic pollutant emissions. Winter had the highest haze occurrence frequency in the YRD. The haze days gradually increase from September to December and next January, then it gradually decreases from March. Meanwhile, the haze coverage is also increasing in the YRD (Fig.2). The spatial distribution of haze in Jiangsu Province and Shanghai has been expanding to the whole provinces. The "isolated points" in Zhejiang province are increasing gradually (Fig.3).

## Multivariate study for examining influence of physical and operational properties of urban railway system on subway air quality

M.J. Kim<sup>1</sup>, J.W. Park<sup>2</sup>, J.S. Sim<sup>2</sup>, D.S. Moon<sup>3</sup> and D.S. Park<sup>1</sup>

<sup>1</sup>Transportation Environmental Research Team, Korea Railroad Research Institute, Uiwang, 16105, Korea

<sup>2</sup>R&D Center System Team, Seoul Metro, Seoul, 04806, Korea

<sup>3</sup>Green Transport and Logistics Institute, Korea Railroad Research Institute, Uiwang, 16105, Korea

Keywords: Urban railway system, Particulate matter (PM), Principal component analysis (PCA), Multivariate analysis of variance (MANOVA).

Presenting author email: mjkim88@krri.re.kr

Urban railway system has been considered an air quality hot spot, since a large portion of the urban railway system are constructed underground and air pollutants are originated from internal sources (Kim *et al.*, 2014). An objective of this study is to investigate an influence of physical and operational properties of the urban railway system on particulate matters (PM<sub>10</sub>, PM<sub>2.5</sub> and PM<sub>1.0</sub>) inside platform and railway tunnel based on multivariate statistical analyses.

First, to examine whether the physical and operational properties of railway system affect the PM concentrations, multivariate analysis of variance (MANOVA) that analyses differences among group-data means is carried out (Kim *et al.*, 2012). As the physical variables, length, depth and minimum curve radius of the railway tunnel are used. As the operational variable, the number of railroad cars that stops at each of the stations is used. It should be noted that there are two types of the railroad car operation: one is a general subway which stops at every stations, and the other is an express subway which stops at only a few crowded stations. For the MANOVA, one-day PM concentration data obtained at the platform and railway tunnel is divided into several populations depending on the physical and operational properties. Then, the significant differences of the average PM concentrations among these populations are examined.

Later, to investigate correlation and dependence between the railway system property variables and PM concentrations inside the platform and tunnel, principal component analysis (PCA) is used. The PCA is a dimensionality reduction technique that extracts essential information from multivariate data (Kim *et al.*, 2012). Since the property variables which affect the platform and tunnel PM concentrations are different, the PCA is respectively applied on the platform data and tunnel data. As input variables for analysing tunnel data, (1) tunnel properties, (2) PM<sub>10</sub>, PM<sub>2.5</sub> and PM<sub>1.0</sub> concentrations in the tunnel, (3) PM<sub>10</sub>, PM<sub>2.5</sub> and PM<sub>1.0</sub> concentrations at the platform connecting to tunnel entrance (namely, pre-platform PMs) and (4) PM<sub>10</sub> concentration in outdoor air are used. The pre-platform PMs are taken to consider a piston effect which pushes the PM-containing air from the platform to tunnel by motion of railroad cars. Furthermore, since the outdoor PM<sub>10</sub> is flowed into the tunnel through ventilation, it is used as the input variable.

Table 1 shows MANOVA result from a subway line No. 9 in Korea. Null hypothesis for the MANOVA

is that there is no significant difference of the average PM concentrations depending on the physical and operational properties. The MANOVA rejects the null hypothesis, if *p*-statistic of the data is lower than significance level of 0.05. The result indicates that the tunnel length and the number of railroad cars stopping at each station has significant influence on the tunnel and platform PM concentrations, respectively.

Table 1. MANOVA results for examining influences of the railway system properties on PM concentrations.

	Tunnel length	Tunnel depth	Tunnel radius	Stopped subway No.
<i>p</i> -statistic	0.002	0.91	0.49	0.0002

Figure 1 shows a loading plot obtained for the tunnel data using PCA. In general, clustered variables in the loading plot represent the variables that have strong dependence. Since one cluster containing the tunnel and pre-platform PM concentrations is remarkably observed in Figure 1, it infers the piston effect which pushes the PM-containing air from the platform to tunnel would be a major variable affecting the tunnel PM concentrations.

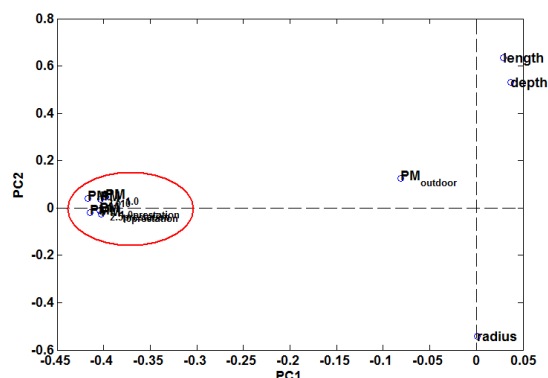


Figure 1. Loading plot of the tunnel data.

This research was supported by a grant from the Railway Technology Research Project of the Ministry of Land Infrastructure and Transport (17RTRP-B082486-04).

Kim, M., SankaraRao, B., Kang O., Kim, J. and Yoo, C. (2012), *Energy and Building* **46**, 48-55.

Kim, M., Liu, H., Kim, J.T. and Yoo, C. (2014) *J. Hazard. Mater.* **278**, 124-133.

## Predicting indoor PM<sub>10</sub> using artificial neural network at subway station, Seoul, Korea.

Sechan Park<sup>1,2</sup>, Minhae Kim<sup>1,2</sup>, Hyeong-Gyu Namgung<sup>2</sup>, Sung-Joon Bae<sup>3</sup> and Soon-Bark Kwon<sup>1,2\*</sup>

<sup>1</sup>Railway System Engineering, University of Science and Technology (UST), Uiwang, 16105 Korea

<sup>2</sup>Transportation Environmental Research Team, Korea Railroad Research Institute (KRRI), Uiwang, 16105 Korea

<sup>3</sup>Seoul Metro Urban Railway R&D Center, Seoul, Korea

Keywords: artificial neural network, PM10, subway station, underground, IAQ

Presenting author email: sechani@krri.re.kr

This study predicts after 1hour indoor PM<sub>10</sub> (PM<sub>10\_in</sub>) on selected subway stations using input variables such as outdoor PM<sub>10</sub> (PM<sub>10\_out</sub>), subway Frequency (SF), and information on ventilation operation ratio (VR) using artificial neural network (ANN). ANN has been widely used to predict complex environmental processes. ANN model predicts PM<sub>10\_in</sub> using input variables of one hour previous data. We hope that this predictive tool could provide an effective ventilation strategy of underground station preventing passengers from exposure of PM<sub>10</sub>.

This study analyzed the PM<sub>10</sub> measured hourly on a platform in six selected major underground subway transfer stations (A1, A2, B1, B2, C1 and C2) in Seoul. Official data on the air pollution monitoring network and the roadside monitoring network near (within 2.9 km) each underground subway station (www.airkorea.or.kr) were obtained as PM<sub>10\_out</sub> of our study. SF was collected from public notice at each station and VR is steady operation everyday as turn on at 7 a.m. and turn off at 10 p.m. As shown in Figure1, we adopted variables such as PM<sub>10\_out</sub>(t), VR(t), SF(t) and PM<sub>10\_in</sub>(t) to predict PM<sub>10\_in</sub>(t+1).

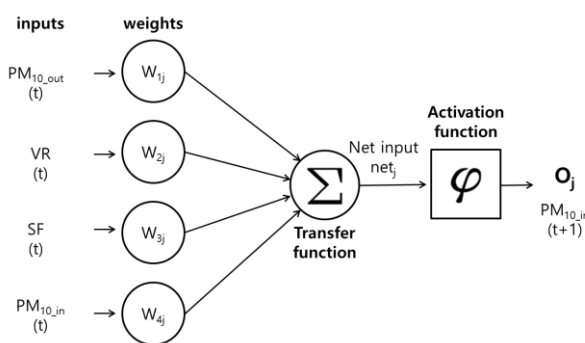


Fig 1. Structure of the ANN used in this study.

Figure 2 shows the distribution of predicted PM<sub>10\_in</sub> and measured PM<sub>10\_in</sub> at each station. The predicted PM<sub>10\_in</sub> showed a slope of less than 1.0 (0.66~0.80) for all six stations. The average correlation coefficient was 0.74 (0.67~0.80). The correlation coefficient for stations A2 and B1 was the highest at 0.8, while the correlation coefficient of station B2 was the lowest, at 0.67.

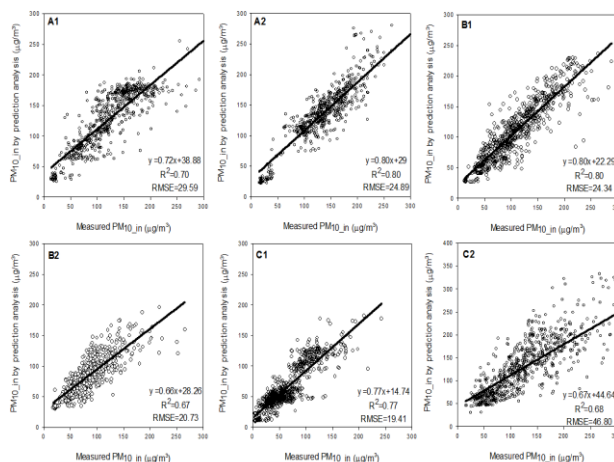


Fig 2. Correlation between measured PM<sub>10\_in</sub> and predicted PM<sub>10\_in</sub> using ANN.

This work was supported by the Railway Technology Development Program ((16RTRPB067918-04) funded Korea Ministry of Land, Infrastructure and Transport (MOLIT).

Kwon, S., Jeong, W., Park, D., Kim, K., Cho, K. (2015) *Journal of Hazardous Materials*. **297** 295-303  
 Moreno, T., Pérez, N., Rechea, C., Martins, V., Miguel, E., Capdevila, M., Centelles, S., Minguión, M., Amato, F., Alastuey, A., Querol, X. (2014). *Atmospheric Environment*. **92** 461–468  
 Park, S., Kim, M., Kim, M., Namgung, H., Kim, K., Cho, K., Kwon, S.-B. (2016) *Journal of Hazardous Materials*. Submitted

## Spatial Variability of PM<sub>2.5</sub> in New Delhi, India

P. Pant<sup>1</sup>, S. Guttikunda<sup>2</sup>, M. Kumar<sup>3</sup>, J.L. Matawle<sup>4</sup>, S. Kushwaha<sup>5</sup>, S. Pervez<sup>4</sup> and R.E.Peltier<sup>1</sup>

<sup>1</sup>Department of Environmental Health Sciences, University of Massachusetts, Amherst, MA 01003, USA

<sup>2</sup>Department of Atmospheric Sciences, Desert Research Institute, Reno, NV, USA

<sup>3</sup>Institute of Environment and Sustainable Development, Banaras Hindu University, Uttar Pradesh 221005, India

<sup>4</sup>Pt Ravishankar Shukla University, Raipur, Chhattisgarh 492010, India

<sup>5</sup>Chhatrapati Shivaji Institute of Technology, Durg, Chhattisgarh 491001, India

Keywords: PM<sub>2.5</sub>, Delhi, chemical composition

Presenting author email: pallavipant@umass.edu

Delhi, India has been shown to have fine and coarse particulate matter (PM) concentrations exceeding the Indian 24-hr ambient air quality standards. Despite the poor air quality, only a limited amount of data are available on trends of PM in Indian cities, and there is a gap in our understanding of spatiotemporal patterns of air pollutants. There is limited understanding of spatial variability in source contributions, their strengths, and temporal trends since most studies have focused on a limited number of sampling locations. Lack of information on spatial heterogeneity of PM<sub>2.5</sub> and its constituents can lead to misclassification of population exposure. This issue has special relevance in Delhi, and other large cities in Asia and Africa where population densities are often very high, and people are exposed to poor air quality all year round.

The aim of this study was to determine spatial heterogeneity in PM<sub>2.5</sub> concentrations across the Greater Delhi region. Two different approaches were used for this: first, PM<sub>2.5</sub> monitoring was conducted across 16 sites in the region in September 2015, and 24h integrated filter samples (Teflon and quartz) were collected at a range of locations for a period of one or two days. Filter samples were analysed for elements (ED-XRF) and carbon (Sunset OC-EC Analyser). Second, using hourly real-time PM<sub>2.5</sub> data (2013-2016) from five monitoring stations, spatial and temporal trends were assessed to establish diurnal and seasonal patterns. For the real-time data, the quality of the data was assessed, and any suspicious data was removed before analysis. Data analysis was conducted using Microsoft Excel 2010 and R (version 3.2.4, R-project.org).

Results from the sampling campaign indicated significant spatial variability, both for PM<sub>2.5</sub> and the chemical components. Average PM<sub>2.5</sub> concentration during the sampling campaign was observed to be  $58.5 \pm 23.8 \mu\text{g}/\text{m}^3$  across the sampling sites. Concentrations of PM<sub>2.5</sub>, and specific constituents tend to be higher closer to pollution hotspots, and areas near specific sources.

Based on the real-time data from regulatory monitors, 24h average PM<sub>2.5</sub> concentrations across the monitoring stations exceeded  $100 \mu\text{g}/\text{m}^3$ , with the highest average concentration observed at Anand Vihar, a high-traffic site ( $165 \mu\text{g}/\text{m}^3$ ) (Figure 1). Seasonal differences in PM<sub>2.5</sub> concentrations are stark, and concentrations are typically 1.5-3 times higher in winter compared to summer. Similar to the field campaign, the concentrations were observed to be higher at locations

with specific sources. Diurnal trends for PM<sub>2.5</sub> were observed to vary across the sites, but the lowest concentrations were observed during the afternoon across all sites.

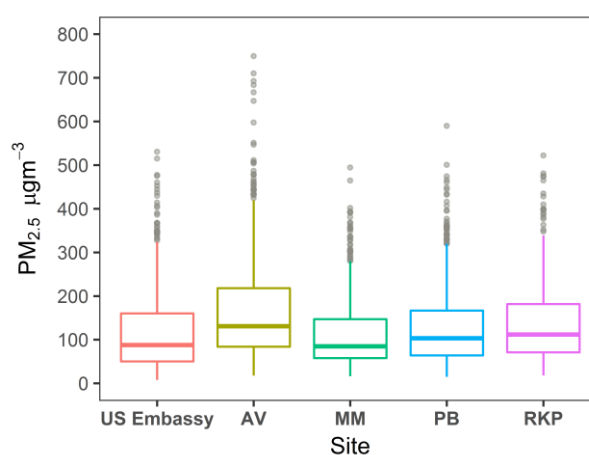


Figure 1. Average 24h PM<sub>2.5</sub> concentrations based on real-time monitoring data for five stations across Delhi.

A national air quality monitoring network focused on PM speciation, complemented by construction of a detailed emission inventory and source modelling, could be the first step towards understanding spatiotemporal as well as regional variability in PM composition in India. It is also crucial to perform regular QA/QC checks on the data, as well as the instruments in order to ensure consistency and comparability of results.

Authors would like to acknowledge financial support from Climate and Health Research Network (USA) and thank Dr. Gazala Habib and her team at IIT-Delhi for their help with the IIT-Delhi (central) sampling set-up. We would also like to thank Dr. Judith C. Chow (DRI, USA) for access to instruments.

## Mineral-oil-spread agar plates do not enhance the efficiency of the viable Andersen cascade impactor for measurement of size distribution of airborne fungi

P. Duquenne, X. Simon, V. Koehler, and C. Coulais

Department of pollutant metrology-Institut National de Recherche et de Sécurité (INRS), Vandœuvre-lès Nancy, 54500, France

Keywords: bioaerosol, fungi, size distribution, waste sorting  
[philippe.duquenne@inrs.fr](mailto:philippe.duquenne@inrs.fr)

Measurements of the size distribution of airborne microorganisms (SDAM) provide helpful data for occupational hygiene. The viable Andersen cascade impactor (ACI) collects microorganisms on agar media and is one of the mostly used techniques to assess SDAM at occupational settings. However, the ACI suffers from limits due to overloading of agar media, impaction stress, desiccation effects, particle bounce, and microbial embedding in agar. As a consequence, the ACI often underestimates microbial load and is limited to measurements in low contamination environments. Previous studies reported substantial enhancement of the biological collection efficiencies of the ACI by using mineral-oil-spread agar plates (Xu *et al.*, 2013). These improvements remain to be tested in broad conditions.

The aim of the study was to evaluate (1) the usefulness of the viable ACI for SDAM measurements in waste sorting plants and (2) the effect of mineral-oil-spread plates on SDAM.

The SDAM was studied in a waste sorting plant (WSP) treating household waste in France. Samples were collected at different times during the year in a grinding area (GA) and in two sorting cabins where cardboards (SCC) and plastics (SCP) are manually separated from other waste. Two types of experiments were carried out. For the first set of experiments (SET-A), 48 side by side samplings were performed in the SCC with 2 stages viable ACI; one was mounted with plastic Petri dishes filled with 20 ml of MEA and one mounted with plastic Petri dishes containing 20 mL of MEA layered with 100 µl of mineral oil (Viatrap®, SKC, France). Duration of sampling was from 15 to 120 seconds. For the second set of experiments (SET-B), 25 samples were collected in the SCC, SCP and GA with the 6 stages viable ACI mounted with glass Petri dishes filled with 37 ml of MEA. Duration of sampling was from 10 to 60 seconds. ACI samplers operated at 28.3 L/min. After sampling, Petri dishes were packed in a cold box and transported to the INRS laboratory and incubated in the day. Petri dishes were incubated at 25°C for five days and the grown fungal colonies were counted. The positive-hole correction was applied for establishing the concentration of airborne fungi (Macher, 1989).

Results from SET-A experiments revealed that the investigated bioaerosol was dominated by fungal particles collected on the ACI stage with a 0.95 µm cut-off point. Five of the Petri dishes were not countable due to overloading. The analysis of data showed no effect of

layering the MEA medium with mineral oil on fungal concentrations calculated from the two stages of the sampler (figure 1) as well as on the distribution of fungal particles on the stages.

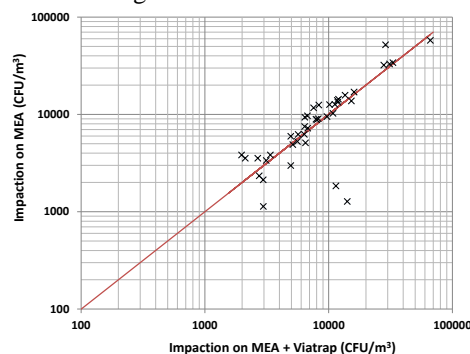


Figure 1: Effect of layering the MEA medium with mineral oil on fungal concentrations calculated from the two stages of the ACI sampler.

Results from SET-B experiments showed that 20% of ACI samples were not countable due to overloading forcing very short duration of sampling. The microbial median aerodynamic diameter was from 1.8 to 3.5 µm for GA samples, from 3.2 to 3.4 µm for SCC samples and from 2.6 to 4.1 µm for SCP samples. The SDAM vary from a sampling day to another with a dominant mode generally between 1.5 and 3.5 µm (figure 2).

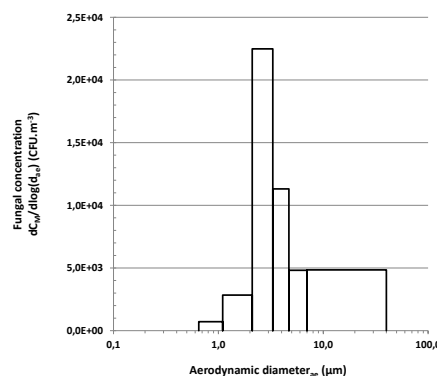


Figure 2: Example of size distribution of airborne fungi measured in the grinding area of the WSP.

We concluded that the ACI is not totally adapted to WSP and that mineral oil did not affect particles bounds and blow-off in our study.

Xu Z., *et al.*, (2013). PloS one 8:e56896.  
 Macher, J.M. (1989). Aihaj 50:561-568.

## **Abstracts T314**

## Development of an Integrated Exposure – Dose Management Tool for Reduction of Particulate Matter in Air: Overview of the LIFE Index-Air Project

S.M. Almeida<sup>1</sup>, M.Almeida-Silva<sup>1</sup>, N.Canha<sup>1</sup>, T. Faria<sup>1</sup>, K. Eleftheriadis<sup>2</sup>, E. Diapouli<sup>2</sup>, V. Galifianakis<sup>2</sup>, A. Miranda<sup>3</sup>, J. Ferreira<sup>3</sup>, O. Hänninen<sup>4</sup>, M. Lazaridis<sup>5</sup>

<sup>1</sup>Centro de Ciências e Tecnologias Nucleares (C<sup>2</sup>TN), Instituto Superior Técnico, Universidade de Lisboa, Estrada Nacional 10, ao km 139.7, 2695-066 Bobadela-LRS, Portugal

<sup>2</sup>ERL, Institute of Nuclear and Radiological Science & Technology, Energy & Safety, NCSR Demokritos 15310, Attiki, Greece

<sup>3</sup>Centre for Environment and Marine Studies (CESAM), University of Aveiro, 3810-193 Aveiro, Portugal

<sup>4</sup>Department of Health Protection, National Institute for Health and Welfare, PO Box 95, 70701 Kuopio, Finland

<sup>5</sup>Department of Environmental Engineering, Technical University of Crete, Chania, Polytechnioupolis, 73100, Greece

Keywords: particulate matter, exposure, health effects, decision support tool.

Presenting author email: smarta@ctn.tecnico.ulisboa.pt

Airborne Particulate Matter (PM) is a complex mixture of microscopic particles derived from anthropogenic and natural sources. It is still a major environmental problem in several EU countries, while new evidence regarding its detrimental impact on human health has emerged.

There is a great deal of improvement with respect to emission control strategies of anthropogenic emission in European urban areas. However, the quantitative result of these changes in actual human exposure for specific toxic particle compounds is largely unknown with respect to each one of the emission sources and therefore the definition of the effective strategies can be jeopardized.

This brings us to the considerable importance of assessing the personal integrated exposure to air suspended particles mixtures of chemical compounds as it is the key determinant of the dose received by an individual and thus directly influences the health impacts, which is the ultimate objective of the air quality management strategies.

Measuring of the outdoor air levels and trends of pollutants at fixed ambient air quality monitoring sites together with modelling outdoor air concentrations with dispersion and chemical transport models has been the traditional way of evaluating urban air quality and estimating the needs of air pollution abatement programs. The potential of harmful health effects of air pollution has been estimated by comparing these levels to air quality guidelines and with health outcomes. However, this logic has been changed by a number of recent developments in scientific knowledge. Poor correlations have been found between ambient PM concentrations and personal exposure and therefore this approach fails to account for all components of exposure. Since people spend 90-95% of their time indoors, individual's exposure to PM is dominated by indoor air pollution, which is partly outdoor air pollution that has penetrated indoors and partly pollution from indoor sources. However, data available for risk assessment of indoor air pollution are scarce and often insufficient. Information is available for the indoor air concentrations of some well-known pollutants, but is lacking for others whose effects are unclear such as the

chemical components of indoor PM that are currently poorly characterized.

The main objective of the LIFE Index-Air project ([www.lifeindexair.net](http://www.lifeindexair.net)) is to incorporate a database of outdoor and indoor air quality and a package of models to develop an innovative and versatile policy tool that will establish a relation between population exposure to mixtures of PM compounds, health effects and emission sources. This will be a cost effectiveness management tool for local, regional and national policy makers that will be used to quantitatively evaluate the impacts of policies on specific human exposure levels as well as plan new ones.

More specifically the LIFE Index-Air project has the following objectives:

1. Development and implementation of an innovative method aiming at a versatile and long term decision making tool in the hands of the authorities;
2. Creation of an available, accessible, comparable and interoperable database on chemical constituents of PM<sub>2.5</sub> and PM<sub>10</sub> sampled indoors and outdoors of EU cities;
3. Development of an exposure assessment system and an operational platform for particulate matter dose calculation to be incorporated in the tool;
4. Identification of the health endpoints associated with the exposure to PM;
5. Determination of the emission sources contribution to the human exposure to PM and evaluation of control strategies capable of underpinning the sustainable development of expected changes anticipating climate change and long term changes in the atmosphere;
6. Consolidate the knowledge base to assist authorities to implement the "Thematic Strategy on Air Pollution" and to formulate air quality action plans.

This work was supported by the European Community through the project LIFE Index-Air (LIFE15 ENV/PT/000674). C2TN/IST authors gratefully acknowledge the FCT support to the UID/Multi/04349/2013 project.

## **Abstracts T315**

## Sampling artefacts from biomass burning aerosol collected at three sites in Indochina

Chung-Te Lee<sup>1\*</sup>, Charles C.-K. Chou<sup>2</sup>, Shao-En Sun<sup>1</sup>, Zhong-Ting Chuang<sup>1</sup>, and Neng-Huei Lin<sup>3</sup>

<sup>1</sup>Graduate Institute of Environmental Engineering, National Central University, Taoyuan, 320, Taiwan

<sup>2</sup>Research Center for Environmental Changes, Academia Sinica, Taipei, 115, Taiwan

<sup>3</sup>Department of Atmospheric Sciences, National Central University, Taoyuan, 320, Taiwan

Keywords: sampling artefacts, biomass burning aerosol, mountain aerosol.

Presenting author email: ctlee@cc.ncu.edu.tw

Aerosol sampling artefacts for species of water-soluble inorganic ions (WSIIs) and organic carbon (OC) has been an issue since early days (Eatough et al., 1990; Pierson et al., 1980). Among them,  $\text{NO}_3^-$ ,  $\text{Cl}^-$ , and OC are subject to volatilization loss (negative artefacts). On the other hand, the adsorption of organic vapor by quartz filter plays a role in making positive artefact. The sampling artefacts can be ranged from -80% for volatilization and +50% for filter adsorption (Eatough et al., 1990; Turpin et al., 1994). Although numerous studies reported measuring artefacts at various places during years, sampling artefacts varied by site substantially. The observation of sampling artefacts at some specific sites is still worthwhile to report. This study collected aerosol during extensive biomass burning seasons at Suthep Mountain (SMT, 98°53'E, 18°48'N, 1396 m a.s.l) in 2010, Doi Ang Khang (DAK, 99°05'E, 19°03'N, 1536 m a.s.l) from 2013 to 2015, and Son La (103°54'E, 21°20'N, 675 m a.s.l) in 2011.

$\text{PM}_{2.5}$  (aerodynamic cut diameter equal to or less than 2.5  $\mu\text{m}$ ) were collected using collocated R&P ChemComb Model 3500 Speciation Sampling Cartridges (formerly Rupprecht & Patashnick Co.; now Thermo Fisher Scientific Co, Inc.) supported by tripods. For the collection of WSIIs, honeycomb denuders were installed to denude interfering gases followed by a three-filter series firstly with a Teflon filter (R2PJ047Teflo, PALL Life Sciences, Inc.) then a nylon filter (Gelman Science, Inc.) followed by citric acid coated quartz fiber filter (TISSUQUARTZ 2500QATUP, PALL Life Sciences, Inc.). Similarly, a three-filter series using quartz fiber filters was for carbonaceous aerosol collection.

Figure 1 shows that volatilized  $\text{NO}_3^-$  varied with corrected  $\text{NO}_3^-$  (retained plus volatilized  $\text{NO}_3^-$ ) verifying the relationship of volatilized  $\text{NO}_3^-$  with aerosol  $\text{NO}_3^-$  ( $R^2$  values of linear correlation ranged from 0.44 to 0.91 for various sites). The relationship may scatter with high levels of corrected  $\text{NO}_3^-$ , however; no upper limit appeared. The fractions of volatilized  $\text{NO}_3^-$  over corrected  $\text{NO}_3^-$  at different sites varied from 39% to 61%. Meanwhile, volatilized  $\text{Cl}^-$  were even with better linear correlations with the corrected  $\text{Cl}^-$  ( $R^2$  values ranged from 0.68 to 0.93 for different sites) and the fractions of volatilized  $\text{Cl}^-$  over corrected  $\text{Cl}^-$  at the sampling sites varied from 69% to 80%.

Figure 2 shows positive artefacts are more abundant than negative artefacts during aerosol collection. As the sampling sites are located in mountains, natural organic vapour emitted from trees needs to consider during mountain aerosol collection.

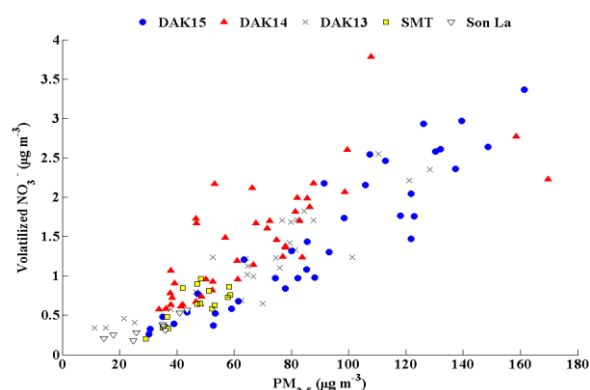


Figure 1. Volatilized  $\text{NO}_3^-$  versus corrected  $\text{NO}_3^-$  (retained plus volatilized  $\text{NO}_3^-$ ) of  $\text{PM}_{2.5}$  collected at the three sites in different times.

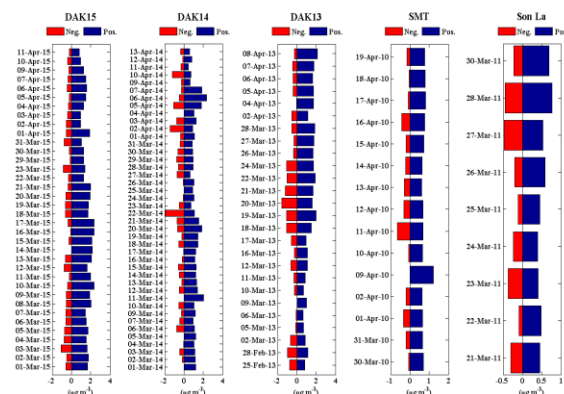


Figure 2. Positive and negative artefacts during  $\text{PM}_{2.5}$  collection for OC at the three sites in different times.

This work was supported by Ministry of Science and Technology in Taiwan under grant MOST 105-2119-M-008-015.

Eatough, D.J., Aghdaie, N., Cottam, M., Gammon, T., Hansen, L.D., Lewis, E.A., Farber, R.J., 1990. In: Mathai, C.V. (Ed.), *Transaction of Visibility and Fine Particles*. Air and Waste Management Association, Pittsburgh, PA, pp. 146-156.

Pierson W. R., Brachaczek W. W., Korniskit T. J., Truex T. J., Butler J. W., 1980. *J. Air Pollut. Control Ass* 30. 30-34.

Turpin, B.J., Hering, S.V., Hutzicker, J.J., 1994. *Atmos. Environ.* **28**, 3061-3071.

## Development of an isokinetic sampling probe appropriate for high-speed flow conditions

N.G. Heo<sup>1</sup>, J.H. Lim<sup>1</sup>, K.H. Ahn<sup>2</sup> and S.J. Yook<sup>1,\*</sup>

<sup>1</sup>School of Mechanical Engineering, Hanyang University, Seoul, 04763, Republic of Korea

<sup>2</sup>Department of Mechanical Engineering, Hanyang University, Ansan, 15588, Republic of Korea

Keywords: sampling probe, isokinetic sampling, high-speed flow.

\*Corresponding author email: ysjnuri@hanyang.ac.kr

Fine and ultrafine dusts make great impact on environment and human body. In order to forecast the concentration of fine and ultrafine dusts, PM<sub>2.5</sub> concentration is measured at many observation stations. However, due to the fact that the measurements are conducted at fixed locations of the observation stations, the boundary conditions for forecasting are insufficient and the accuracy of forecasting is unsatisfactory. Therefore, in order to enhance the accuracy of forecasting, it is needed to obtain a lot more boundary conditions by measuring PM<sub>10</sub> concentrations using vehicles such as cars, trains, and unmanned aerial vehicles. As a result, an efficient isokinetic sampling probe needs to be developed to accurately measure PM<sub>10</sub> concentrations in high-speed flow conditions. In this study, an isokinetic sampling probe was developed and the aspiration ratio of the sampling probe was numerically and experimentally investigated.

A commercial CFD code, ANSYS FLUENT *Release* 14.5, was used to numerically estimate the aspiration ratio of the isokinetic sampling probe. The flow was assumed to be steady, turbulent, and incompressible. For the simulation of turbulent flow, the standard  $k-\epsilon$  turbulence model was used. Freestream air velocity was varied in the range between 8.9 m/s and 21 m/s. Discrete Phase Models (DPM), provided in the FLUENT code, was used to calculate particle trajectories. For validating the present study's numerical approach, a shrouded probe was first considered. Figure 1 shows the comparison of the aspiration ratio of the shrouded probe between the experimental data of Chandra (1992) and the numerical results of the present study for the freestream airflow velocity of 75 km/h. As shown in Figure 1, the agreement was good and therefore the present numerical approach was validated to correctly predict the aspiration ratio of the shrouded probe.

As the next step, an isokinetic sampling probe was newly designed in the present study, and the aspiration ratio of the newly designed sampling probe was predicted using the validated numerical approach. Figure 2 compares the aspiration ratio between the present study's newly designed sampling probe and the existing shrouded probe, for the freestream airflow velocity of 75 km/h. As shown in Figure 2, the isokinetic sampling probe developed in the present study was anticipated to show the aspiration ratios very close to 1.0, meaning that the isokinetic sampling is possible in the tested particle size range. The aspiration ratio of the newly designed isokinetic sampling probe was also determined by experimental means.

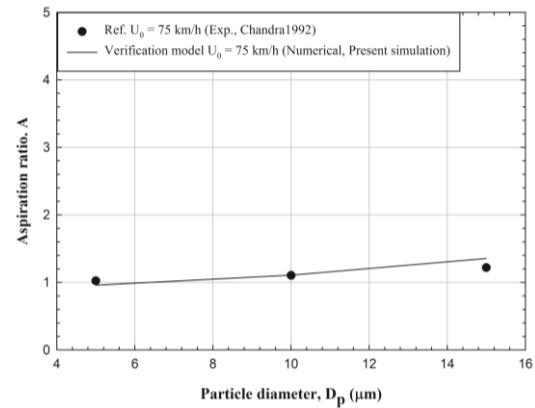


Figure 1. Comparison of the aspiration ratio of the shrouded probe between the experimental data of Chandra (1992) and the numerical results of the present study, for the freestream airflow velocity of 75 km/h.

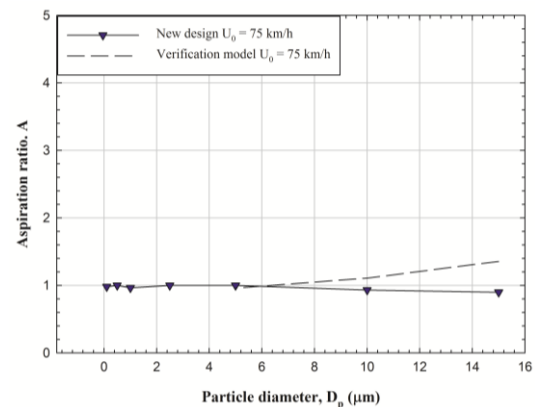


Figure 2. Comparison of the aspiration ratio between the isokinetic sampling probe developed in the present study and the existing shrouded probe, for the freestream airflow velocity of 75 km/h.

This research was supported by R&D Center for Green Patrol Technologies through the R&D for Global Top Environmental Technologies funded by Ministry of Environment, Republic of Korea (MOE).

Chadra, S. (1992) *Experimental investigation into operational characteristics of a Shrouded probe for aerosol sampling*, PhD Thesis, Texas A&M Univ.

## Atmospheric cluster analysis by tandem DMA-MS

M. Passananti<sup>1</sup>, J. Kangasluoma<sup>1</sup>, M. Attoui<sup>2</sup> and H. Vehkamäki<sup>1</sup>

<sup>1</sup>Department of Physics, University of Helsinki, Helsinki, 00014, Finland

<sup>2</sup>LISA, University Paris Est Creteil, Creteil, 94010, France

Keywords: APi-TOF, clusters, DMA, sulfuric acid.

Presenting author email: monica.passananti@helsinki.fi

The development of instruments to improve measurements is a non-stop process that is fundamental in order to increase the knowledge in environmental science. However, the characterization of the instruments is a crucial point to correctly interpret the experimental data. In atmospheric science the analysis of particles, clusters and molecules should be done carefully, artefacts and phenomena such as wall loss, should be always considered and taken into account.

In the last years the development of Mass Spectrometers (MS) as the Atmospheric Pressure interface Time Of Flight (APi-TOF) has led to a better knowledge of the composition of molecular aggregates (clusters) that lead to the formation of new particles in atmosphere. It has been shown that these clusters could undergo transformations (fragmentation and/or evaporation) inside the instrument due to the low pressure and energetic collisions (Kürten *et al.*, 2014; Olenius *et al.*, 2013). We decided to carry out a systematic study on the fate of clusters inside the APi-TOF, but evaluating these transformation on each cluster could be very challenging. Therefore we decided to combine the APi-TOF with a high resolution Differential Mobility Analyser (DMA). The DMA classifies charged particles (and clusters) as a function of their electrical mobility, hence with this instrument is possible to measure the clusters size and separate them based on their size. Combining these two instruments we can select only one cluster size and inject it into the APi-TOF. In this way we can have the powerful combination between a separation and a characterization technique. Injecting into the APi-TOF only a mono-mobile size ions distribution it is easier to understand the fate of clusters inside the instrument because only one kind of clusters is studied at a time.

We analysed sulfuric acid and sulfuric acid-amine clusters and we produced them by electrospray ionization. The different concentrations and molar ratios between sulfuric acid and amine were tested to obtain a suitable cluster size distribution and to evaluate these effects on cluster formation. The tuning of the APi-TOF was systematically changed to study its impact of cluster fragmentation inside the APi section. This latter is made by three vacuum chambers (SSQ, BSQ and PB) where an electric field is applied to guide the ions through the APi. In total, 27 voltages and 2 radio frequencies are applied to APi-TOF, most of which can be changed to optimize the results as a function of the specific application of the instrument. In this work we evaluated the effects of the voltages applied to SSB, BSQ and PB chambers without changing the radio frequencies.

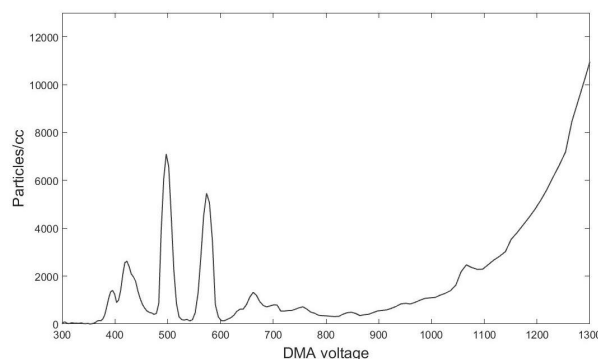


Figure 1. Differential mobility spectrum of sulfuric acid (100mM) and dimethylamine (50mM) solution in water/methanol 1/1 v/v. The spectrum is recorded in negative polarity.

The first results are very promising, the differential mobility spectra of sulfuric acid and sulfuric acid-amine clusters showed sharp peaks (Figure 1) with a suitable intensity to obtain a clear signal in the APi-TOF. Moreover, we observed a fragmentation of clusters when high voltages are applied to the APi section, and in general the tuning of the instrument showed a strong impact on cluster detection (sensitivity, resolution, fragmentation, etc.). In conclusion, the use of the tandem DMA-MS could allow a better characterization of the APi-TOF and could give useful data for develop a model to predict the fate of clusters inside the mass spectrometer.

This work was supported by the European Research Council project 692891-DAMOCLES.

Kürten, A., Jokinen, T., Simon, M., Sipilä, M., Sarnela, N., Junninen, H., Adamov, A., Almeida, J., Amorim, A., Bianchi, F., Breitenlechner, M., Dommen, J., Donahue, N.M., Duplissy, J., Ehrhart, S., Flagan, R.C., Franchin, A., Hakala, J., Hansel, A., Heinritzi, M., Hutterli, M., Kangasluoma, J., Kirkby, J., Laaksonen, A., Lehtipalo, K., Leiminger, M., Makhmutov, V., Mathot, S., Onnela, A., Petäjä, T., Praplan, A.P., Riccobono, F., Rissanen, M.P., Rondo, L., Schobesberger, S., Seinfeld, J.H., Steiner, G., Tomé, A., Tröstl, J., Winkler, P.M., Williamson, C., Wimmer, D., Yei, P., Baltensperger, U., Carslaw, K.S., Kulmala, M., Worsnop, D.R. and Curtius, J. (2014) *PNAS* **111**, 15019-15024.

Olenius, T., Schobesberger, S. Kupiainen-Määttä, O., Franchin, A., Junninen, H., Ortega, I.K., Kurtén, T., Loukonen, V., Worsnop, D.R., Kulmala, M. and Vehkamäki, H. (2013) *Faraday Discuss.* **165**, 75–89.

## Aerosol trapping, optimization and characterization for comparative in-vitro assessment of combustible and heat-non burn platforms.

Didier Goedertier, Ignacio Gonzalez Suarez, Gregory Vuillaume, Julia Hoeng and Manuel C Peitsch  
PMI R&D, Philip Morris Products S.A., Quai Jeanrenaud 5, CH-2000 Neuchâtel, Switzerland (Part of Philip Morris International group of companies).

Keywords: cigarette smoke, smoke fractions

Presenting author email: didier.goedertier@pmi.com

There are more than 6000 chemical constituents present in cigarette smoke (CS), many of which are known/suspected to be toxicants or carcinogens. Public health authorities have classified some of those smoke constituents as likely causes of smoking-related diseases such as lung cancer, heart disease and emphysema. In vitro toxicological assessment is an integral part of the safety assessment program to evaluate cytotoxicity, genotoxicity as well as mechanistic endpoints of aerosol fractions. This can be challenging as most cellular models cannot be exposed directly; the smoke/aerosol needs to be collected in a biocompatible solvent, which can then be applied to the cells. Moreover, given the chemical complexity of smoke/aerosols, it is unlikely that all constituents are trapped efficiently in a given solvent and thus, cells will only be exposed to a fraction of the constituents. Also, there are many variables that can influence fraction composition, which can make the interpretation of bioassays readouts difficult.

Here, we performed a detailed chemical characterization of the smoke of the reference cigarette (3R4F) and the aerosol of the Tobacco Heating System version 2.2 (THS2.2), which is a candidate Modified Risk Tobacco Product (MRTP) that utilizes an electronically controlled heating system to heat and not burn tobacco. Three different fractions were generated: an aqueous extract (AE) generated by bubbling mainstream 3R4F smoke or THS2.2 aerosol through Phosphate Buffered Saline (PBS); total particulate matter (TPM); and gas-vapour phase (GVP, the substance that passes through the filter during TPM collection). In addition, we provide an example on how the different parameters influencing the composition of the THS2.2 AE fraction can be optimized to ensure reproducibility of in vitro toxicology studies.

The levels of 25 analytes, covering 8 chemical classes, determined by the Analytisch-Biologisches Forschungslabor GmbH (ABF), were measured in AE, TPM and GVP from both items. The levels of 8 carbonyls were measured in GVP and AE. The results showed substantial differences in chemical classes between test items and fractions. Analyte concentrations were generally lower in THS2.2 compared with the respective 3R4F fraction. In both items, TPM was enriched in acid derivatives, whereas GVP was enriched in carbonyl compounds and AE showed a more mixed profile, particularly in the case of THS2.2.

Optimization of smoke/aerosol collection requires to balance between a minimized deviation from ideal trapping behaviour and maximized constituent concentrations. Here, we used an Optimal Total puff

Volume (OTPV) approach to optimize THS2.2 aerosol collection in PBS (AE fraction). Trapping efficiency was monitored by measuring the levels of 8 carbonyls. Eight experimental variables were investigated. Four experimental variables (test item number, trapping solvent volume, trapping temperature and sample collection point) showed a higher impact in trapping efficiency and influenced the concentration of all 8 carbonyls. In particular, the use of 4 test items in a larger solvent volume (40ml) using an ice-cold impinger and collecting the aerosol after the aerosol generation pump resulted in higher carbonyl concentrations (Figure 1).

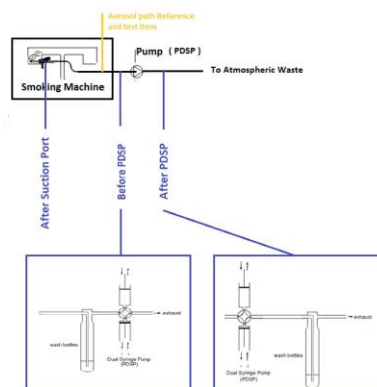


Figure 1: AE fraction collection set-up and sample collection points

Taken together, our research results showed that no individual fraction is by itself able to recapitulate the chemical complexity of CS. This observation is particularly relevant in the context of in vitro toxicological assessment of tobacco products, because different biological effects are to be expected based on the type of fraction chosen for a particular study. Consequently, depending on the aim of the study, the right aerosol fraction(s) has to be chosen.

Moreover, we showed that the OTPV approach is useful to optimize trapping efficiency in the AE fraction, thus increasing the reproducibility.

## **Abstracts T401**

## Rapid disease screening and monitoring from exhaled breath with portable sensor arrays

N.J Pineau, A.T. Güntner and S.E. Pratsinis

Particle Technology Laboratory, Department of Mechanical and Process Engineering, ETH Zürich, Sonneggstrasse 3, CH-8092 Zürich, Switzerland

Keywords: Sensor array, flame aerosol-made sensors, breath analysis, diabetes, kidney failure

Presenting author email: pineau@student.ethz.ch

The real-time monitoring of acetone, ammonia and ethanol from human breath could enable completely non-invasive disease detection already in an early stage or real time therapy progress monitoring. This, because those analytes are distinct breath markers for kidney failure with 4880 ppb ammonia compared to healthy 960 ppb (Davies, 1997) and diabetes 1710 ppb acetone instead of 760 ppb (Deng, 2004). Simultaneous measurement of acetone and ethanol may enable even noninvasive blood glucose monitoring (Galassetti, 2005).

Currently, mass spectrometry-based methods are used for performing breath analysis, but such devices are bulky, expensive and need trained personnel. For portable breath analyzers, however, especially nanostructured metal-oxides based gas sensors are promising due to their small and inexpensive design (Güntner, 2016a) that could be provided to a widespread population. Furthermore, such sensors have already been explored intensively for their ppb sensitivity to reducing and oxidizing gases. Nevertheless, the challenge remains to measure breath markers selectively and accurately in the complex gas mixture of human breath.

The olfactory detection system of mammals overcomes this challenge by a broad number of sensing receptors and subsequent analysis for combinatorial selectivity. Therefore, one bioinspired approach is to combining multiple sensors with different selectivity to an array and applying statistical methods (Güntner, 2016b) for the correct quantification of multiple analytes in a gas mixture.

Here, we present a highly sensitive sensor array for the selective and accurate measurement of acetone, ethanol, and ammonia in gas mixtures at breath relevant concentrations. The array is based on flame aerosol made sensing films that are patterned precisely on 500  $\mu\text{m}$  designated areas on micromachined Si-wafer chips. Each sensing film consists of specially tailored nanoparticles that feature distinct selectivity characteristics to the target breath markers.

The so created array was tested in simulated breath consisting of acetone, ammonia, and ethanol at breath-relevant concentrations. Subsequent multivariate linear regression allowed the precise prediction of the analyte concentrations. In fact, acetone (Fig. 1a), ethanol (Fig. 1b) and ammonia (Fig. 1c) were predicted with average errors of 48, 235, and 28 ppb for acetone, ammonia, and ethanol, respectively.

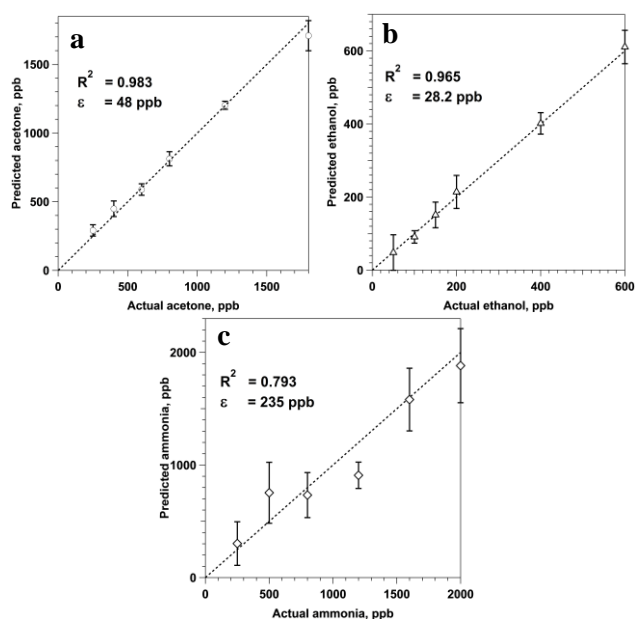


Figure 1. Predicted analyte concentration over the actual for (a) acetone, (b) ethanol and (c) ammonia in simulated breath. The small average prediction errors allow accurate differentiation between healthy and diseased breath.

In conclusion, a flame aerosol based sensor array was developed resulting in excellent sensing performance with high accuracy in simulated breath. This array shows high potential as an easy, inexpensive, portable, and non-invasive breath analyzer for the early stage detection of diabetes or kidney failure for widespread populations, or allows a personal treatment-monitoring in real time.

This work was supported by the Swiss National Science Foundation (grant Nr. 200021\_159763/1).

Davies, S., Spanel, P. and Smith, D. (2010) *Kidney Int.* **52** (1), 223-228.

Deng, C., Zhang, J., Yu, X., Zhang, W. and Zhang, X. (2004) *J Chromatogr B*, **810** (2), 269-275.

Galassetti, P.R., Novak, B., Nemet, D., Rose-Gottron, C., Cooper, D.M., Meinardi, S., Newcomb, R. Zaldivar, F. and Blake, D.R. (2005) *Diabetes Technol. Ther.* **7** (1), 115-23.

Güntner, A. T., Pineau, N. J., Chie, D., Krumeich, F. and Pratsinis, S. E. (2016a) *J. Mater. Chem. B*, **4**, 5358-5366.

Güntner, A.T., Koren, V., Chikkadi, K., Righettoni, M. and Pratsinis, S.E. (2016b) *ACS Sens.* **1**, 528-535.

## Investigation of Electrostatic Behaviour of Dry Powder Inhaled Formulations

M. Jetzer<sup>1,2</sup>, B. Morrical<sup>1</sup>

<sup>1</sup>Novartis Pharma AG – Global Drug Development, Novartis Campus, Lichtstrasse 35, 4056 Basel, Switzerland

<sup>2</sup>Department of Pharmaceutical Sciences, University of Basel, Klingelbergstrasse 50, 4056 Basel, Switzerland

Keywords: Dry Powder Inhaler (DPI), Electrostatic Charge, Inhaler Device, Aerosol Performance.

Presenting author email: martin.jetzer@novartis.com

Dry powder inhalers (DPIs) are well established for delivering pharmaceutical aerosols to the lungs. They commonly consist of large carrier particles and micronized drug particles. Carrier surface modifications with force control agents such as magnesium stearate (MgSt) have been reported to alter the performance of DPI formulations (Thalberg, 2016). Extensive research has been conducted on aerosol characteristics of DPIs such as particle size and mass output, but their electrostatic properties are only poorly studied (Hinds, 1999). Static electrification showed to have a significant effect on inhaler function, separation of drug from carrier particles and lung deposition (Murtomaa, 2002).

In this study, the electrostatic behaviour of DPI formulations was investigated. The aim was to generate insights in electrostatic charge generation during capsule spinning in the inhalation device (i.e. unit dose capsule inhaler) and its effect on the aerosol performance. The dynamic electrostatic emitted dose (DEED) of an aerosol when actuated from different DPI formulations containing fluticasone propionate (FP) was monitored in real-time using a dynamic Faraday cage connected to a charge measuring unit electrometer (JCI 178). The *in vitro* aerosol performance was assessed with Single Particle Aerosol Mass Spectrometry (SPAMS).

Measurements of the DEED show that there is a significant difference in electrostatic charge between the different formulations tested and also between the two devices used in this study (Figure 1 and 2). The titanium device shows an overall reduction in electrostatic charge for the MgSt blends and a shift from negative to positive overall charge for the untreated blend with the difference in device contact material. This drop in charge indicates a significant amount of charge in the powder is from triboelectrification in the device itself.

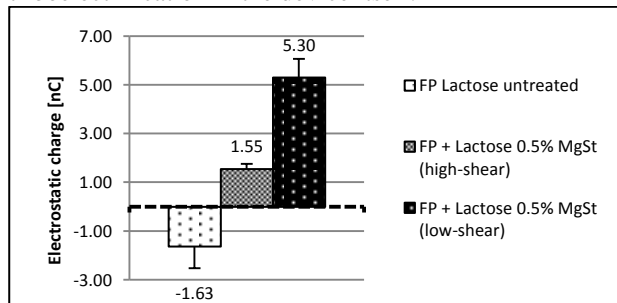


Figure 1. DEED measurement with standard Breezhaler® device (n=5 capsules)

The results agree with those previously observed in literature where particles are charging up in the manufacturing process or in capsule spinning during actuation (Kwok, 2008).

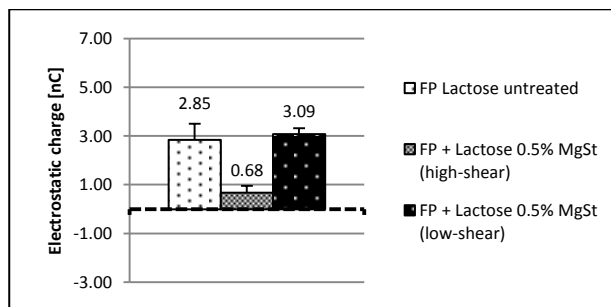


Figure 2. DEED measurement with grounded titanium device (n=5 capsules)

In addition to contacts with the inhaler surface, charged particles also contact each other. Small particles tend to adhere to inhaler surfaces more than larger ones. This might result in reduced amount of released drug (Pu, 2009).

The SPAMS results show an increase in aerosol performance when using a titanium device compared to the standard Breezhaler® device (Figure 3). This trend could be observed for all tested blends (data not shown).

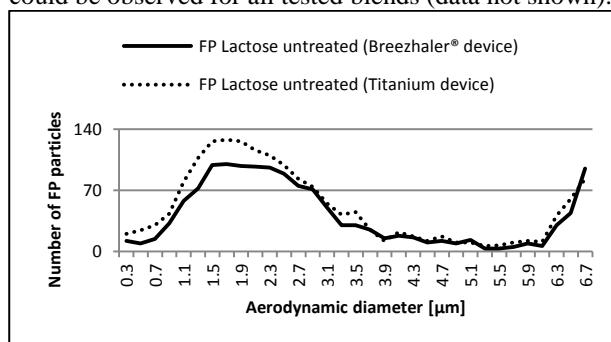


Figure 3. Aerodynamic particle size distribution (APSD) of Fluticasone propionate (FP) obtained by SPAMS.

The study demonstrated that the aerosol performance and to a certain degree device deposition are influenced by the material properties and grounding of the device. By partially dissipating electrostatic charges from the device surface using the titanium device, a lower device deposition and therefore a higher number of emitted FP particles was observed. We suggest that it is probably the electrostatic charge of FP acquired by triboelectrification during actuation that is affecting device deposition and has a high impact on aerosol performance.

Thalberg, K. et al. (2016) *Int J Pharm* 504:27-38.

Hinds, WC. (1999) *Aerosol Tech.* Wiley, NY, 191–192.

Murtomaa, M. et al. (2003) *J Electrostatics* 58:197-207.

Kwok, PC. et al. (2008) *Pharm Res* 25:277-288.

Pu, Y. et al. (2009) *J Pharm Sci*, 98:2412-2421.

## Aerosol-made E-nose for selective formaldehyde detection in breath screening of lung cancer and air quality monitoring

A.T. Güntner<sup>1</sup>, V. Koren<sup>1</sup>, K. Chikkadi<sup>2</sup>, M. Righettoni<sup>1</sup> and S.E. Pratsinis<sup>1</sup>

<sup>1</sup>Particle Technology Laboratory & <sup>2</sup>Chair in Micro and Nanosystems, Department of Mechanical and Process Engineering, ETH Zürich, Sonneggstrasse 3, CH-8092 Zürich, Switzerland

Keywords: Formaldehyde, lung cancer, breath analysis, air quality monitoring, E-nose, flame spray pyrolysis  
Presenting author email: Andreas.Guentner@ptl.mavt.ethz.ch

Formaldehyde (FA) is a potential marker for lung cancer detection simply from breath (Fuchs 2010) and a carcinogenic indoor air pollutant (Salthammer 2010). Its typical concentrations are below 100 ppb posing a *sensitivity* and *selectivity* challenge to portable sensors.

Inexpensive, portable and simple-in-use gas sensors based on nanostructured metal-oxides (MOx) are quite attractive (Güntner 2016a, Güntner 2016b). They can detect low FA levels with fast response time and a compact design. To address the selectivity challenge, a viable option is to combine broadly sensitive but differently selective sensors in arrays, so-called electronic noses (E-nose). (Persaud 1982) Statistical response analysis is achieve combinatorial *selectivity*.

Here, we present a highly sensitive, selective and compact electronic nose (E-nose) for real-time quantification of FA at realistic conditions. (Güntner 2016c) The E-nose consists of four nanostructured and highly porous Pt-, Si-, Pd- and Ti:SnO<sub>2</sub> sensing films directly and precisely deposited onto silicon wafer-based microsubstrates by flame spray pyrolysis (Figure 1).

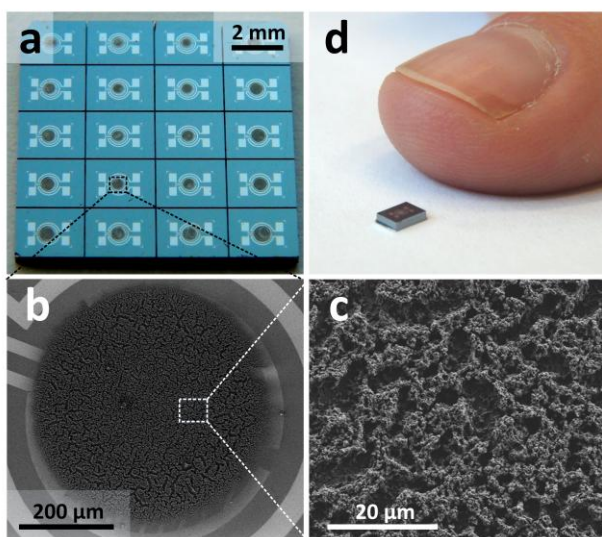


Figure 1. (a) Sensor package with flame-made Si:SnO<sub>2</sub> patterns. SEM confirms (b) the accurate sensing film deposition onto interdigitated electrodes and indicates (c) the porous film architecture favorable for gas sensing.

The constituent sensors can detect FA down to 3 ppb at breath-realistic 90% relative humidity (Figure 2a). Each dopant induces different analyte selectivity enabling *selective* detection of FA in gas mixtures by multivariate linear regression (Figure 2b). In simulated breath (FA

with higher acetone, NH<sub>3</sub> and ethanol), FA is detected with an average error  $\leq 9$  ppb using the present E-nose and overcoming selectivity issues of single sensors. This device could facilitate easy screening of lung cancer patients and monitoring of indoor FA levels.

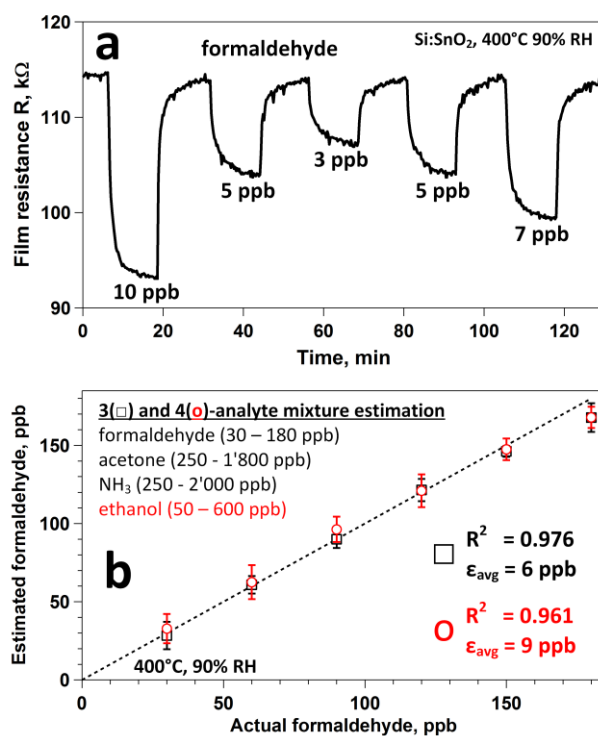


Figure 2. (a) Film resistance of a Si:SnO<sub>2</sub> (400 °C, 90% RH) sensor upon exposure to 10, 7, 5 and 3 ppb of FA. (b) E-nose estimation of FA in 3- & 4-analyte mixtures.

This work was supported by the Swiss National Science Foundation (Nr. 200021\_159763/1).

Fuchs, P., Loeseke, C., Schubert, J. K. and Miekisch, W. (2010) *Int. J. Cancer* **126** (11), 2663-2670.

Güntner, A.T., Pineau, N. J., Chie, D., Krumeich, F. and Pratsinis, S.E. (2016a) *J. Mater. Chem. B* **4**, 5358-5366.

Güntner, A.T., Righettoni, M. and Pratsinis, S.E. (2016b) *Sens. Actuators B* **223**, 266-273.

Güntner, A.T., Koren, V., Chikkadi, K., Righettoni, M. and Pratsinis, S.E. (2016b) *ACS Sens.* **1**, 528-535.

Persaud, K. and Dodd, G. (1982) *Nature* **299** (5881), 352-355.

Salthammer, T., Mentese, S. and Marutzky, R. (2010) *Chem. Rev.* **110** (4), 2536-2572.

## Charting the human airways with airborne nanoparticles, AiDA

J. Jakobsson<sup>1</sup>, H. L. Aaltonen<sup>2</sup>, P. Wollmer<sup>2</sup> and J. Löndahl<sup>1</sup>

<sup>1</sup>Div. of Ergonomics and Aerosol Technology (EAT), Lund University, 221 00, Lund, Sweden

<sup>2</sup>Dept. of Translational Medicine, Lund University, 205 02, Malmö, Sweden

Keywords: Lung deposition, nanoparticles, diagnostics, Airspace Dimension Assessment, AiDA

### Introduction

Airspace Dimension Assessment (AiDA) is a technique to assess airspace dimensions in the distal lung by measuring the lung deposition of inhaled nanoparticles (Löndahl et al. 2017, Jakobsson et al. 2016). Nanoparticles deposit in the lungs almost exclusively by diffusion, and the average diffusion distances, corresponding to airspace dimensions in the lung, can be inferred by measuring the half-life time of inhaled nanoparticles (Löndahl et al. 2017). In addition to the particle half-life time, the particle deposition at residence time 0 s in the lung (estimated from extrapolation) may provide further medically relevant information about the lung. The primary suggested application for the AiDA technique is as a diagnostic technique for respiratory disease.

The aim of this work was to investigate the capabilities of the AiDA technique to estimate airspace dimensions at different volumetric lung depths in healthy human subjects, and how they compare to well-established lung models.

### Methods

AiDA measurements were performed with 50 nm polystyrene latex nanospheres on breath samples with an upper sample front at 700 mL – 4500 mL volumetric lung depth, using a setup described in detail elsewhere (Jakobsson et al. 2016). Particle half-life was determined by curve-fitting of data for breath holding times (5-20 s) corresponding to aerosol residence times in the lung ranging from 6-23 s. The airspace dimensions were estimated using the relation described by Löndahl et al. 2017:  $r = 2.89\sqrt{Dt_{1/2}}$ , where  $r$  is the radius of the hypothetical airspace,  $t_{1/2}$  is the particle half-life and  $D$  is the particle diffusion coefficient. Measurements were performed on one healthy male subject (as a pilot study for a planned more extensive study).

### Results

The measured airspace dimensions, assessed with the AiDA technique compare well to the values from established lung models, from anatomical dead-space to the distal lung. The airspace dimensions between volumetric lung depths from 1000-4500 mL were on average  $.25 \pm .01$  mm, which corresponds to the expected values for the respiratory zone of the lung.

The estimated particle recovery at 0 s residence time (from extrapolation) was found to be strongly dependent on volumetric sample depth, and may reflect particle losses in the conducting airways.

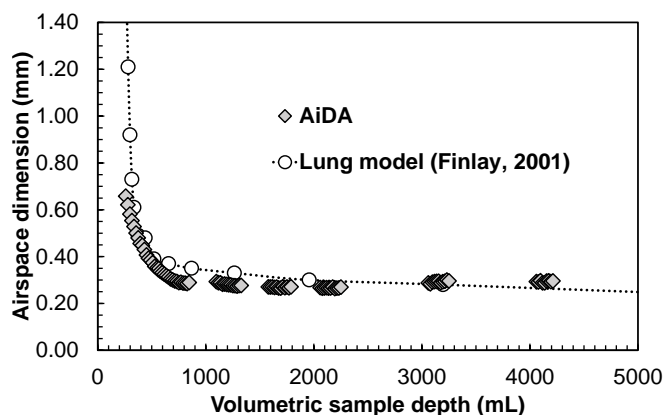


**Figure 1.** The airspace dimension ( $r$ ) at sample depths ranging from  $\approx 200$  - 4500 mL, assessed by the AiDA technique, compared to lung model.

Some measurement artefacts caused by smearing of the exhaled sample in the sample collector was observed and managed by truncation of the measured data.

### Conclusion

Airspace dimensions measured with the AiDA technique are close to the expected values from established lung models at sample depths ranging from anatomical dead-space to the distal lung. The interval 1000-2500 mL volumetric lung depth seems to be ideal for assessing airspace dimensions of the distal lung, and suitable for diagnostic applications, such as detection and quantification of lung emphysema. The significance of the estimated particle recovery at 0 s residence time remains to be studied further.

This work was supported by Swedish Research Council, Vinnova, EU EuroNanoMed, The Swedish Heart and Lung Foundation, the Crafoord foundation and the Sten K Johnsson foundation.

Löndahl, J., J. Jakobsson, D. Broday, H. Aaltonen and P. Wollmer (2016). Do nanoparticles provide a new opportunity for diagnosis of distal airspace disease? *Int J of Nanomed* 2017; 12: 41–51.

Jakobsson, J., J. Hedlund, J. Kumlin, P. Wollmer and J. Löndahl (2016). A new method for measuring lung deposition efficiency of airborne nanoparticles in a single breath. *Sci Rep* 6: 36147.

Finlay, W. H. (2001). *The Mechanics of Inhaled Pharmaceutical Aerosols* (p. 98). London: Academic Press.

## Numerical analysis of the effect of pulsating airflow on the nebulized aerosols in a patient-specific human nasal cavity

A. Farnoud<sup>1</sup>, X.G. Cui<sup>2</sup>, I. Baumann<sup>3</sup> and E. Gutheil<sup>1</sup>

<sup>1</sup>Interdisciplinary Center for Scientific Computing, Heidelberg University, Heidelberg, 69120, Germany

<sup>2</sup>Lawrence Berkeley National Laboratory, Berkley, CA, 94720, USA

<sup>3</sup>Department of Otorhinolaryngology, Head and Neck Surgery, Medical Center of the Heidelberg University, Heidelberg, 69120, Germany

Keywords: Particle deposition, nasal cavity, nebulized aerosol, pulsating airflow.

Presenting author email: ali.farnoud@iwr.uni-heidelberg.de

Chronic rhinosinusitis (CRS) is a common upper respiratory disease, which is defined as the inflammation of the nasal and paranasal cavity for the duration of more than 12 weeks (Fokkens *et al.*, 2012). The prevalence of the CRS disorder in Europe is 10.9% (Hastan *et al.*, 2011). Nasal drug delivery into the sinuses is a promising approach for the treatment of CRS patients. However, the common nasal pump sprays are not efficiently transporting the medication to the sinuses. Möller *et al.* (2009) experimentally showed that the use of a pulsating airflow could improve the delivery of the aerosols into the posterior regions of the sinuses. The present numerical study investigates the dispersion and deposition of micro-particles carried by a pulsating airflow into a patient-specific human nasal airway. Large eddy simulations with the Smagorinsky sub-grid scale model are used to study the flow with an inhalation flow rate of 7.5 L/min for both a steady and a pulsating airflow with a frequency of 45 Hz. 10,000 mono-disperse particles with a diameter of 10  $\mu\text{m}$  are uniformly injected at the nostrils. After a real process time of 1 s the particles have left the pharynx or they stick on the wall. A numerical time step of  $10^{-5}$  s is chosen, which satisfies the stability conditions. The numerical computations are performed on the high-performance computer of bwForCluster MLS&WISO Production using 256 processors, which take about 30 hours for the steady airflow and 45 hours for the pulsating airflow on a mesh with 15 million grid cells.

The left part of the Figure 1 illustrates the streamlines of the gas velocity and the right part shows the deposition pattern of the particles for the steady inhalation. Complex swirling is observed in the vestibule, the nasal valve, and the nasopharynx, directly

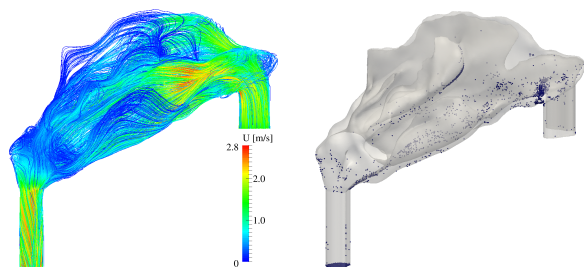


Figure 1. Streamlines of the gas velocity (left) and deposition pattern of the particles (right) for a steady inhalation rate of 7.5 L/min.

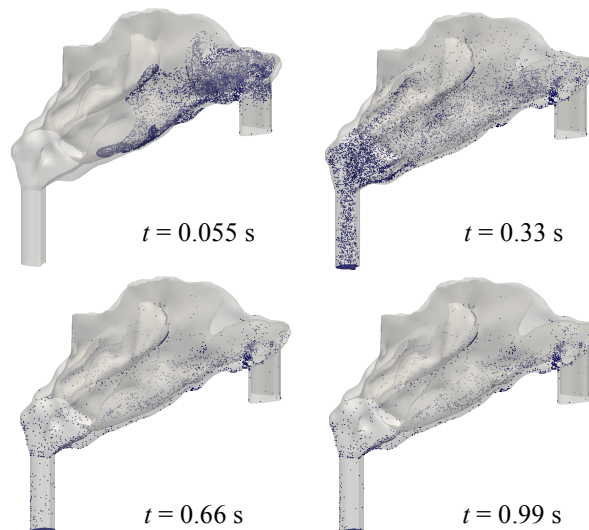


Figure 2. Temporal evolution of the particles for the pulsating airflow.

affecting the dispersion and deposition of the particles. The results show vortices after the nasal valve and the anterior part of the olfactory region, which may be the reason for low particle deposition in the olfactory region. The particles tend to deposit in the nasal valve and the nasopharynx, where there is a change in the flow direction. The pulsating airflow shows an increase in deposition efficiency of the aerosols. Figure 2 provides the evolution of the particles carried by a pulsating airflow. The aerosols are more dispersed and penetrate deeper into the posterior regions and the meatuses where the connections to the sinuses reside.

Financial support of the German Research Foundation (DFG) through HGS MathComp is gratefully acknowledged. The simulations were performed at bwForCluster MLS-WISO, which is supported by the state of Baden-Württemberg through bwHPC and the DFG.

Fokkens, W.J., Lund, V.J., Mullol, J., Bachert, C., Alobid, I., *et al.* (2012) *Rhinol Suppl.* **23**, 1-298.  
 Hastan, D., Fokkens, W.J., Bachert, C., Newson, R.B., Bislimovska, J., *et al.* (2011) *Allergy*. **66**, 1216-1223.  
 Möller, W., Schuschnig, U., Meyer, G., Haussinger, K., Keller, M., Junge-Hulsing, B. and Mentzel, H. (2009) *Rhinology* **47**, 405-412.

## Aerosol-assisted synthesis of large-pore mesoporous silica nanoparticles as drug carriers for controlled release applications

M. Shaban<sup>1</sup>, J. Poostforooshan<sup>1</sup>, S. Reiser<sup>2</sup>, M. Türk<sup>2</sup> and A.P. Weber<sup>1</sup>

<sup>1</sup>Institute of Particle Technology, Technical University of Clausthal, Clausthal-Zellerfeld, D-38678, Germany

<sup>2</sup>Institute for Technical Thermodynamics and Refrigeration, Karlsruhe Institute of Technology (KIT), Engler-Bunte-Ring 21, D-76131 Karlsruhe, Germany

Keywords: Aerosol-assisted, Mesoporous silica, Spray drying, ibuprofen, supercritical fluids.

Presenting author email: masoom.shaban@tu-clausthal.de

Aerosol-assisted spray pyrolysis has been used as a facile aerosol route to obtain large-pore mesoporous silica microspheres using simple inorganic salts as a pore template and colloidal SiO<sub>2</sub> as building blocks [1]. Significantly, this approach avoids the need for any calcination process and porous particles with high-purity can be produced. The effect of the addition of salt (NaNO<sub>3</sub>+LiNO<sub>3</sub>) to the silica suspension (Köstrosol 2040AS, 40 wt %) on particle morphology, surface area and pore size was characterized by SEM (Gemini, Zeiss), TEM (JEM-2100, JEOL) and ASAP (Accelerated Surface Area and Porosimetry System 2020, micromeritics). The textural parameters of mesoporous silica particles with salt (MS-1) before and after washing by water and silica particles without salt (MS-0) are illustrated in Table 1.

Table 1. Textural parameters of MS-1 and MS-0.

Sample	Salt/SiO <sub>2</sub> molar ratio	S <sub>BET</sub> (m <sup>2</sup> g <sup>-1</sup> )	V <sub>p</sub> (cm <sup>3</sup> g <sup>-1</sup> )	D <sub>p</sub> (nm)
Unwashed MS-1	1:1	9	0.06	21
Washed MS-1	1:1	130	0.67	20
MS-0	0:1	131	0.23	6

\*S<sub>BET</sub> is the BET specific surface area; V<sub>p</sub> is the total pore volume; D<sub>p</sub> is the average pore diameter calculated from adsorption branches of isotherms using the BJH method.

It was observed that both samples display Type IV N<sub>2</sub> Isotherms (Figure 1), which are characteristic of mesoporous materials [2].

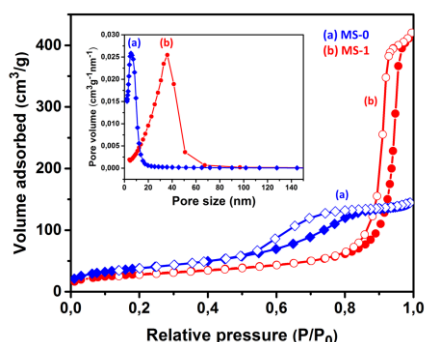


Figure 1. Nitrogen adsorption-desorption isotherms and pore size distributions (inset) of MS-0 and MS-1 (open symbols, desorption; solid symbols, adsorption).

TEM analyses were used to study the formation of the mesopores structure and the topology of the resulting materials. As shown in Figure 2a and b, porosity was not observed in the MS-1 before exposure to the water, it can be concluded that salt is responsible to induce

porosity in the structure. Furthermore, TEM images of MS-1 particles clearly illustrated the presence of the porous structure in the interior of the particles with spherical morphology. The successful formation of porous silica microsphere is also confirmed by SEM images (Figure 3).

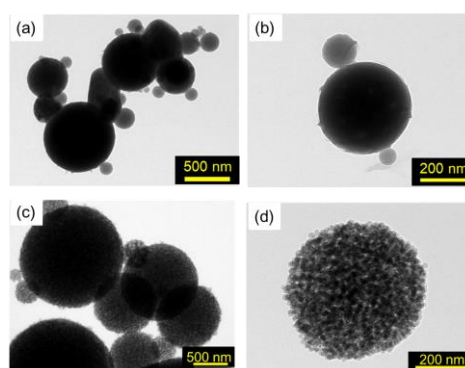


Figure 2. TEM images of unwashed MS-1 (a, b), and washed MS-1 (c, d).

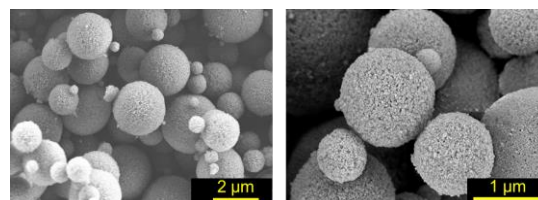


Figure 3. SEM images of washed MS-1.

Mesoporous materials such as e.g. MS-1 can be used as promising carrier materials for poorly water-soluble drugs such as racemic ibuprofen. Ibuprofen is often prescribed to treat e.g. arthritis, fever and pains, however its dissolution rate and therewith bioavailability is limited. Therefore, as a first approach, ibuprofen has been deposited onto MS-1 applying the so-called Controlled Particle Deposition process [3]. This process is a suitable and innovative method for the preparation of dissolution enhancing solid dosage forms without using any additional auxiliary materials. Our first preliminary results show that high drug loadings (>10wt%) can be achieved. Thus, part of our ongoing work will be to investigate the loading of additional new carriers and the dissolution behavior of drug-loaded materials like MS-1.

[1] C. Panatarani, I.W. Lenggoro, K. Okuyama, J. Nanoparticle Res. 5, 47-53 (2003)

[2] J. Poostforooshan, A. P. Weber, ACS Appl. Mater. Interfaces 8, 21731-21741 (2016)

[3] S. Reiser, M. Sun, M. Johannsen, M. Türk, J. Supercrit. Fluids, (2017) <http://dx.doi.org/10.1016/j.supflu.2017.02.015>

## **Abstracts T402**

## Generation of a fungal consortium: impact of analytic tools on biodiversity analysis

J. Degois<sup>1</sup>, X. Simon<sup>1</sup>, C. Bontemps<sup>2</sup>, P. Leblond<sup>2</sup>, P. Duquenne<sup>1</sup>

<sup>1</sup>Department of pollutant metrology-Institut National de Recherche et de Sécurité (INRS), Vandœuvre-lès Nancy, 54500, France

<sup>2</sup>Laboratoire, Laboratoire de Génétique et Microbiologie, UMR INRA 1128 IFR 110, Université de Lorraine, France

Keywords: bioaerosol, moulds, biodiversity  
jodelle.degois@inrs.fr

The biodiversity in bioaerosols is an important issue to investigate for a better understanding of occupational risks due to exposure to airborne particles. The methods used for studying biodiversity include morphology methods, molecular biology or biochemical techniques. While providing different information about the composition of bioaerosols, these methods have specific advantages and limits. High-throughput sequencing followed by bioinformatics analysis is presented as a powerful tool for biodiversity studies that overcome the main drawbacks of the culture-based method. However, these molecular methods may lead to erroneous measurements of microbial composition of complex environmental bioaerosols due to biases that were insufficiently investigated.

In the present study, we used bioaerosols with a known microbial composition and produced in laboratory conditions to investigate such biases. The aim was study the effect of 1) the DNA extraction kit; 2) the target gene for sequencing; 3) the method used for sequences assignment on results from biodiversity measurements in bioaerosols.

The complex fungal bioaerosol was generated from a liquid culture prepared with four different moulds species (*Aspergillus niger*, *Cladosporium cladosporoides*, *Penicillium brevicompactum* and *Wallemia sebi*). The bioaerosols were aerosolized using a bubbling generator (Simon et al. 2011). Aerosolised moulds were collected by filtration of the air through polycarbonate membrane (0.8 µm) using closed-face cassette (Millipore, France), at 2 L/min and for one hour. DNA extraction was performed using the two commercial kits, FastDNA<sup>®</sup>SPIN kit for soil (MP Biomedicals, USA) and PowerSoil<sup>®</sup> DNA isolation kit (MOBio, USA). Then, two genetic targets (18S and ITS2) were sequenced by an external provider (INRA Transfert, France) using Illumina<sup>®</sup> technology. Sequences were cleaned using Mothur software (Schloss et al. 2009). Assignment of 18S sequences was done using BLAST (Basic Local Alignment Search Tool) algorithm with NCBI database. ITS2 sequences were identified using BLAST algorithm or another algorithm executed in Mothur. Cultivable molds were identified according to macroscopic and microscopic criteria. Fungal biodiversity obtained thank that the different methods was compared.

Results show that the MP Biomedicals kit was the only one allowing the extraction a sufficient amount of DNA for sequencing (>3 ng/µL). This demonstrates

that DNA extraction is a crucial step when studying biodiversity by high-throughput sequencing.

Three fungal genera among the four ones composing the initial liquid culture were observed in the generated bioaerosols when biodiversity was assessed by identification of cultured fungi (figure 1). Indeed, *Wallemia sebi*, a small spore size (1-2 µm of diameter) and slow growing fungi, was not observed on the Petri dishes in the experimental conditions. At the opposite, when biodiversity was assessed by the molecular method, *W. sebi* accounted for near 60% of the sequences regardless the target gene and the algorithm used for the sequence assignment. For the other fungi, the proportion of each genus was dependent on the method used. *Aspergillus niger* was weakly detected by sequencing (near 0.10%), may be due to the bad efficiency of DNA extraction for this specie. Furthermore, data from sequencing revealed the occurrence of unidentified sequences at the genus rank, sequences assigned to other fungi and also to plants or animals for the 18S (which is a eukaryota genetic target and can detect all DNA of plants, animals, Fungi or protozoa). These results were not expected and may indicate errors due to sequencing or assignment.

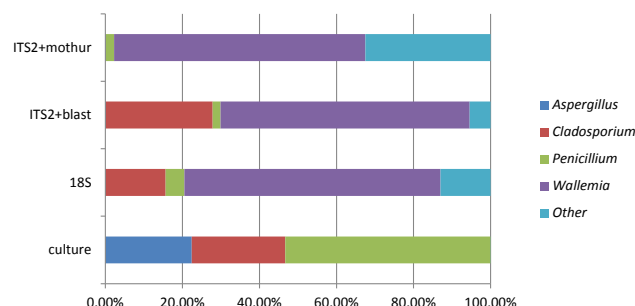


Figure 1: Proportion of the four aerosolized moulds according to several analysis methods

The study shows that results from biodiversity investigations are strongly depending on the analysis method used. In our case, using the MPBio kit for DNA extraction, ITS2 sequencing and BLAST assignment provided results that were the closest to those expected ones. Further studies are required to evaluate the impact of these findings when considering of biodiversity in complex and unknown environments.

Schloss, Patrick D., et al. (2009), App. and Enviro. Microb., 75 (23), 7537-7541.

Simon, Xavier, et al. (2011), J. Aerosol Sci., 42 (8), 517-31.

## Inactivation of Bacterial Activity in the Circulation Water of Wet Electrostatic Precipitator as Home Air Purifier

Chang Gyu Woo, Bangwoo Han, Hak-Joon Kim, Yong-Jin Kim

Environmental and Energy Systems Research Division, Korea Institute of Machinery and Materials, Daejeon, 34103, Korea

Keywords: antimicrobial, air filter, wet ESP

Presenting author email: yjkim@kimm.re.kr

People have much interest in the air quality. The risk of fine particles and contagious bio aerosols to human health become widely known to people. As the time to stay crowded places such as a hospital, a day-care centre is increasing, the exposure to such threat is also increasing.

An air purifier with humidifier function is chosen to customers because it can be used for both functions. However, its air purifying ability is quite low compared to conventional mechanical air purifier. A wet electrostatic precipitator (ESP) is developed for industrial huge facility. Recently, small wet ESP for home is developed as technology is developed. Water is required to run a wet ESP. The water management is important to maintain air purification as in a filter type air purifier. The secondary contamination can occur without a proper replacement. To suppress such problem, caution is needed when we use disinfectants. The use of improper chemicals such as PHMG, PGH can cause even death as in the recent event in Korea.

To circumvent such risk, bactericidal effects without harmful chemicals are prepared in this study. Air ions from carbon microfiber ionizer (Han, 2015), grapefruit seed extract (GSE) as natural product (Woo, 2015), and non-thermal plasma (NTP) were used to inactivate bacterial activity. Air ions are generated inside the ESP. Dust particles containing bacteria are charged and those charging process can inactivate bacteria. GSE are used widely to disinfect organic foods. Bacteria can foster in the circulation water of the ESP. A few drops of GSE can be added to the circulation water. NTP can be generated by applying proper electric field between metallic electrodes in the water. That plasma can effectively inactivate bacterial activity in the water. Here, we compared those disinfecting method. *Staphylococcus aureus* (KTCT 1621) was used as test strain. We assumed *S. aureus* can be cultivated in the water. Cultivated *S. aureus* with nutrient broth was poured in the circulation water. The water runs in the wet ESP and was sampled to find out the change of bacterial concentration in the water.

All methods were effective to reduce the concentration of the viable bacteria compared to the control case. Normalize survival rate (%) was determined as CFU numbers compared to control CFU numbers. Figure 1 shows the bactericidal effect was in order: GSE, NTP, and air ion. To exclude ozone effect, the measurement was done as in Figure 2.

This research can be used to improve the indoor air quality with relatively low cost. We used wet ESP,

and it naturally can be used as a humidifier. This approach can be applied to elevate the indoor air quality with ease by suppressing bacterial activity in the circulation water.

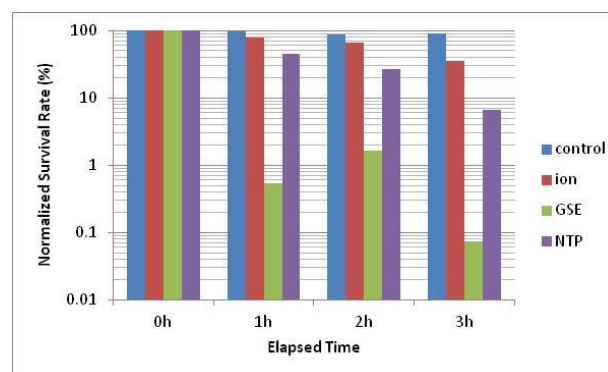


Figure 1. Normalized survival rate with respect to disinfection method.

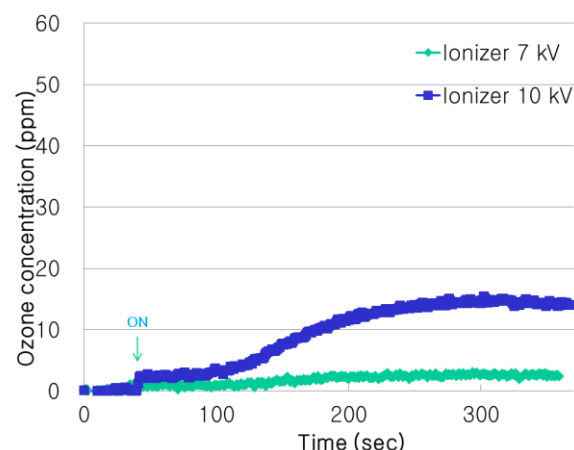


Figure 2. Ozone measurement results with respect to the electric voltage to the carbon microfiber ionizer.

This work was primarily supported by the Eco-Innovation Project operated by the Korea Ministry of the Environment, and partially by a General Research Fund (NK205B) from the Korea Institute of Machinery and Materials.

Han, B., Kang, J.-S., Kim, H.-J., Woo, C.-G., and Kim, Y.-J. (2015) *Aerosol Air Qual. Res.*, **15**, 1035-1044  
 Woo, C.-G., Kang, J.-S., Kim, H.-J., and Han, B. (2015) *Aerosol Sci. Technol.*, **49**, 611-619

## Accurately assessing the viability dynamics of infectious species in aerosol using next generation technology

M. Otero-Fernandez, A.E. Haddrell and J.P. Reid  
 School of Chemistry, University of Bristol, Bristol, BS8 1TS, UK  
 Keywords: Bioaerosol, longevity, instrumentation development.  
 Presenting author email: j.p.reid@bristol.ac.uk

Bioaerosol are defined as aerosol that either contain, or were emitted from, a living organism. Some of the organisms that are commonly found in bioaerosol include viruses, bacteria and spores. The study of bioaerosol is challenging for several reasons. Firstly, there remain all the challenges associated with standard aerosol experiments (small sample size, broad concentration ranges), with the additional difficulty of studying the variability presented by living organisms (population variation, complex chemical composition). The conventional methodologies, based on analytical approaches developed in the 1950s and 1960s, have limitations. These include uncertainties at each stage of the method, including at droplet generation (impact of aerosolisation on viability, quantifying number of species *per droplet*), droplet suspension (avoiding wall loss, interaction with contaminants, exposure to known concentrations of oxidants, light etc.) and final analysis (sampling inefficiency). Thus, many fundamental questions about the dynamics of bacteria and viruses in the aerosol phase remain to be answered. For example, it is unknown if the absolute number of bacteria in a droplet has an effect on the longevity of the bacteria in the droplet.

The application of a next generation bioaerosol generation/levitation/sampling analytical technique that couples droplet on demand technology with AC trap levitation will be reported, referred to as the Controlled Electrodynamic Levitation and Extraction of Bioaerosol onto a Substrate (CELEBS) technique. With this approach, a population of aerosol particles containing microorganisms can be produced and levitated (in a highly-controlled environment) with known chemical and biological composition (Figure 1). The use of a droplet on demand dispenser to produce the aerosol significantly reduces the volume of starting solution required for an experiment from millilitres to microlitres, decreasing costs and increase in experimental safety. Through manipulating the electric field in the AC trap, the population of the droplets can be extracted onto a substrate where the overall health and infectivity of the species in the droplet can then be measured off-line. The level of control over the bioaerosol that can be achieved and the information that can be gained is unique and potentially significant when compared with conventional technology.

The overall utility of this approach will be presented. Systems to be described include: changes in longevity of bacteria in a droplet as a function of (A) relative humidity (e.g. Fig. 2), (B) particle composition,

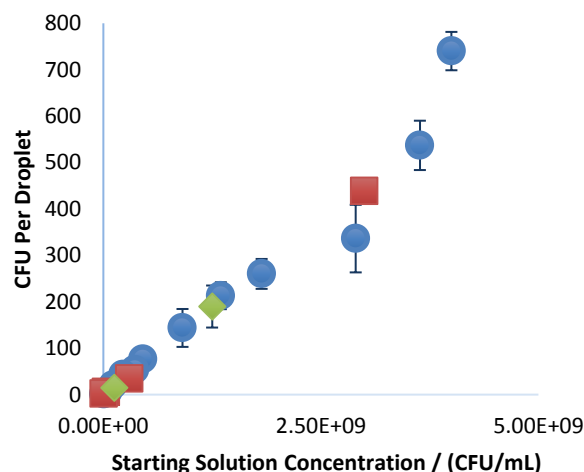


Figure 1. Absolute number of microscopic species per droplet produced by a droplet dispenser as a function of the solution starting concentration. Squares, BG Spores; Diamonds, E. coli MRE162; Circles, FluoSpheres.

(C) the number of species per particle, and (D) chemical composition of the droplet itself. Species longevity in an aerosol droplet is routinely described by a half-life. Given the gentle mechanism by which we produce the aerosol, we do not see this form of decay. Thus using this next generation technology to probe bioaerosol gives a better insight into how these species actually behave in the environment, and will enable us to address some of the fundamental questions regarding bioaerosol.

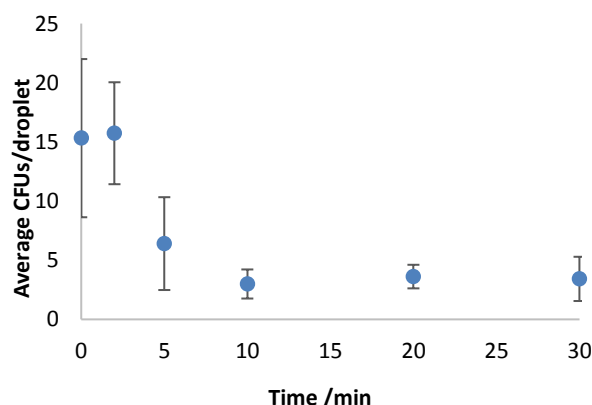


Figure 2. Time-dependence of number of E. coli MRE162 CFU per droplet in a relative humidity of ~30%.

*Acknowledgements:* We thank Dr. R. Thomas (DSTL-Porton Down) for helpful discussions.

## Aerobiological study in Southeast Spain: Olea vs Ole e1

M. Varea<sup>1</sup>, S. Martínez-Perez<sup>2</sup>, E. Flores<sup>3</sup>, V. Soriano<sup>4</sup>, J. Fernández<sup>4</sup>, J. Gil-Moltó<sup>1</sup>, N. Galindo<sup>1</sup>, E. Yubero<sup>1</sup>, J.F. Nicolás<sup>1</sup>, S. Caballero<sup>1</sup>, R. Castañer<sup>1</sup>, C. Pastor<sup>1</sup>, J. Crespo<sup>1</sup>

<sup>1</sup>Department of Applied Physics, Miguel Hernández University, Elche, 03202, Spain.

<sup>2</sup>Pharmacy Section, Elche University Hospital, Elche, 03203, Spain.

<sup>3</sup>Clinical Analysis Section. San Juan University Hospital, Alicante, 03550, Spain.

<sup>4</sup>Allergy Section. Alicante University Hospital, Alicante, 03010, Spain,

Keywords: Pollen, allergens, Olea, Ole e1, PM10, back trajectories.

Presenting author email: [montse.varea@umh.es](mailto:montse.varea@umh.es)

Pollen count is an essential work-tool for allergists, since it allows to confirm or identify the different types of pollens that cause pollinosis in each of the geographical areas. However, different studies have confirmed the presence of allergenic activity outside the pollination period, suggesting that the pollutant count does not include the total allergen exposure. This also points to that there are other sources of allergens, such as atmospheric aerosol, in addition to the pollen grain, that may constitute a relevant allergenic load (Sánchez *et al*, 2005).

Allergenic particles are within the breathable size range, and can penetrate deep into the airway and cause asthma attacks (D'Amato *et al*, 2000). However, little is known about its prevalence in the atmosphere, its geographic and temporal variation and its detailed chemical composition.

The city of Elche is located in the southeast of Spain, with a drier and less rainy climate than in the rest of the Mediterranean coast, registering an atypical pollinic calendar within the Mediterranean area. Due to this, the population of Elche is exposed to non-severe concentration of allergenic pollen from February to July, and cheno-amaranthaceae, olea and grass pollens are the most important causes of rhinitis and asthma (Fernández *et al*, 1998).

This work is focused on quantifying the presence of Oleaceae allergenic activity in the atmosphere of Elche, establishing their relationships with the respective atmospheric pollen grain counts and assessing the influence of weather variables on allergens, during the period between March and July 2010.

To characterize pollen counts, classical Burkard collector were used. Meanwhile, for the aeroallergens load (Ole e1), twenty-four hours samples of PM10 were collected on quart fibre filters by means of low volume samplers. Pollen identification was conducted by expert technicians and was based on comparison with reference slides and photographs, following the instructions of the Aerobiology Committee of the Spanish Society of Allergology and Clinical Immunology. Allergens were quantified by immunological techniques after extraction of the samples.

The pollination period of the olive tree began in late April and ended in July, with the majority recorded during May, while the maximum concentrations of Ole e1 was reached in June (Figure 1).

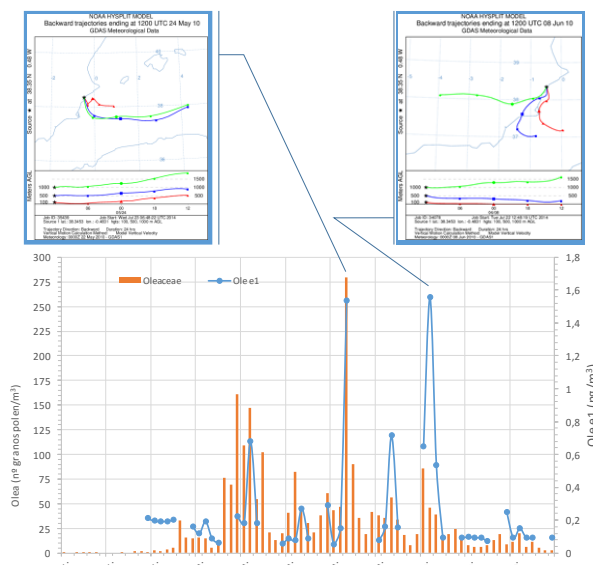


Figure 1. Ole e1 and Oleaceae daily concentrations in 2010 in Elche, with back trajectories for the two maximum peaks.

The study of olive pollen grains and Ole e1 allergen levels shows that the presence of light intensity precipitations reduces the presence of pollen in the air, and on the contrary, substantially increases the concentration of allergen due to the pollen rupture by rehydration. On the other hand, the backtrajectories obtained using the atmospheric model HYSPLIT, confirm the influence of the air mass contributions coming from other regions of Spain, where the olive tree are grown, increasing both the count of Oleaceae and Ole e1 allergen (Figure 1).

This work was supported by the Ministerio de Educación y Ciencia under the CGL2007-63326 (DAPASE) project and the Carlos III Institute by research grants RD 12/013/017 (Research Network of Adverse Drugs and Allergens Reactions -RIRAAF).

D'Amato, G., Liccardi, G. and D'Amato, M. (2000) *J. Invest. Allergol. Clin. Immunol.* **10**, 33-39.

Fernández, J., García, F., Esteban, A. and Miralles, A. (1998) *Rev. Esp. Alergol. Inmunol. Clin.* **13**, 88-91.

Sánchez, J.A., Brandao, R., Lopes, L. and Galan, C. (2005) *J. Invest. Allergol. Clin. Immunol.* **15**, 112-116.

## Commuters exposure to airborne microorganisms in the Barcelona subway system

T. Moreno<sup>1</sup>, X. Triadó-Margarit<sup>2</sup>, M. Veillette<sup>3</sup>, C. Duchaine<sup>3</sup>, M. Talbot<sup>3</sup>, M. C. Minguillón<sup>1</sup>, V. Martins<sup>1</sup>, F. Amato<sup>1</sup>, E. de Miguel<sup>4</sup> and E. O. Casamayor<sup>2</sup>

<sup>1</sup> Inst. Environmental Assessment and Water Research (IDAEA-CSIC), 08034 Barcelona, Spain

<sup>2</sup> Centre for Advanced Studies of Blanes (CEAB), Spanish Research Council (CSIC), 17300 Blanes, Spain

<sup>3</sup> Centre de Recherche de l'Institut Universitaire de Cardiologie et de Pneumologie de Québec, Québec, Canada

<sup>4</sup> Transports Metropolitans de Barcelona, TMB Santa Eulalia, 08902 L'Hospitalet de Llobregat, Spain

Keywords: bioaerosol, indoor air quality, airborne bacterial community, subway system.

Presenting author email: teresa.moreno@idaea.csic.es

With the increase in knowledge on health problems associated with air pollution, air quality in public places has become an issue of concern for public health. Hence, the interest in bioaerosols (the fraction of aerosols of biological origin) has increased, as they may have infectious, allergenic, or toxic properties. Given the fact that nearly 200 cities around the world have subway networks which are used by >100 million people every day, a confined and crowded place where the transmission of respiratory diseases could be facilitated, there is surprisingly little information published on subway aerial microbiological burdens. Moreover, many of these studies have used culture-dependent approaches, despite the fact that only a small fraction of the actual microbial content (<1%) can be identified with such techniques. We examined for the first time the bioaerosols (including pathogenic microorganisms-*Aspergillus fumigatus*, influenza viruses, and rhinoviruses), inside trains and on platforms and lobbies, in the Barcelona (Spain) subway system.

Trains from 6 lines and 4 subway stations were selected to take air samples. All trains are equipped with an air conditioning (A/C) system (windows impossible to open) that works continuously throughout the year maintaining a comfortable temperature (with higher intensity on summer). Over a 4-month period extending from 18/11/2013 to 11/02/14, a total of 54 air samples were collected at an average interval of one per week. Samples were collected at 1m above the ground using a Coriolis®µ (Bertin Technologies, Montigny-le Bretonneux, France), in 15 ml of PBS (phosphate buffered solution), at a rate of 200 L/min for 10 minutes (details are shown in Triadó *et al.*, 2017).

*Influenza A & B* were detected in a number of samples: 30 out of 54 for influenza A and 26 out of 54 for influenza B. On average, the concentrations of influenza A were higher than those for influenza B, being  $2.66 \times 10^2$  and  $1.82 \times 10^2$  genomes/m<sup>3</sup>, respectively. We did not observe differences according to the setting of the A/C system or between different stations. *Rhinovirus* was seldom detected during the study.

*Bacterial load* was higher than the values reported by target microorganisms, as expected. The concentrations ranged from  $1.07 \times 10^3$  and  $3.29 \times 10^6$  equivalent *E. coli* genomes/m<sup>3</sup> of air. Bacterial communities did not present significant differences in composition and structure among compartments (inside train -AC or non-AC-, platform or lobby, Fig. 1).

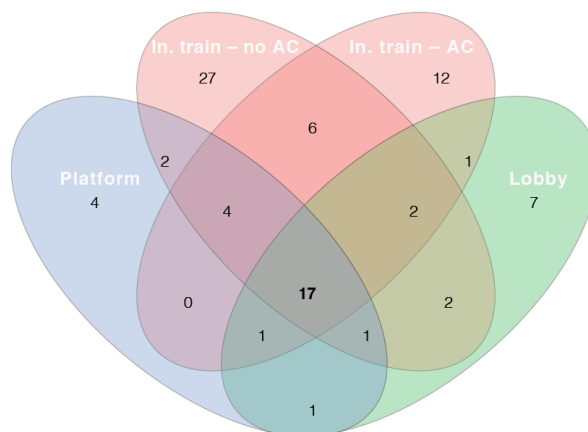


Figure 1. Venn diagram showing taxon overlap between different compartments in the Barcelona subway system (Triadó *et al.*, 2017).

The results show low overall bioaerosol concentrations for the targeted microbial populations, and that the commuters are not the main source generating bioaerosols in the subway system, largely dominated by a limited number of taxa, with *Methylobacterium* being the most abundant. The degree of overlap observed for airborne bacterial communities seems to be probably related to the prevalence of abiotic factors, favoured by pollutants from outdoor sources, night-time maintenance activities (facilitators), and moreover biofouling in A/C.

Considering the low proportion of human-related microbiota in our sequence dataset, we conclude that only one minor part of the bioaerosols can be related to potentially pathogenic bacteria, thus there is not an important biological exposure in the studied environments.

This study was supported by the Spanish Ministry MINECO and FEDER funds (METRO CGL2012-33066; DISPERSAL 829/2013OAPN), the EU 7th Framework Programme (FP7/2007-2013, Grant agreement no. 315760 (HEXACOMM), and the IMPROVE LIFE Project (LIFE13 ENV/ES/000263).

Triadó-Margarit *et al.* (2017). *Indoor Air*. doi: 10.1111/ina.12343.

## Pollen calendar: Airborne pollen in Southeastern Spain (Alicante).

M. Varea<sup>1</sup>, E. Flores<sup>2</sup>, V. Soriano<sup>3</sup>, J. Fernández<sup>3</sup>, J. Gil-Moltó<sup>1</sup>, N. Galindo<sup>1</sup>,  
E. Yubero<sup>1</sup>, J.F. Nicolás<sup>1</sup>, S. Caballero<sup>1</sup>, R. Castañer<sup>1</sup>, C. Pastor<sup>1</sup>, J. Crespo<sup>1</sup>

<sup>1</sup>Department of Applied Physics, Miguel Hernández University, Elche, 03202, Spain.

<sup>2</sup>Clinical Analysis Section. San Juan University Hospital, Alicante, 03550, Spain.

<sup>3</sup>Allergy Section. Alicante University Hospital, Alicante, 03010, Spain,

Keywords: Pollen calendar, Airborne pollen, Southeastern Spain, Mediterranean weather

Presenting author email: [montse.varea@umh.es](mailto:montse.varea@umh.es)

Pollinosis has a marked clinical impact worldwide. Aerobiological research is essential in order to chart the behaviour of airborne allergens over the year; the data obtained are valuable both to allergists for planning treatments and to allergy sufferers for planning their work and recreational activities.

Pollen calendars, defined as graphs summarising the annual dynamics of major airborne pollen types in a given location (Belmonte and Roure, 2002), are of particular interest since they provide readily accessible visual information on the various airborne pollen types occurring in the course of the year.

Pollen calendars have already been published in several cities in Spain, but very little in the Valencian Community. This region has a typical Mediterranean climate, with mild temperatures and very low rainfall, making it one of the areas of national and international tourist interest. This work is focused on Alicante, the second urban nucleus of the Valencian Community, in order to trace the seasonal behaviour of different types of pollen.

A Hirst-type volumetric spore trap was used for aerobiological sampling over a six-year period (2010–2015). Sampling and data analysis were performed in accordance with the standard protocol drawn up by the Spanish Aerobiology Network, and the minimum recommendations of the European Aeroallergen Network (EAN) (Galán *et al* 2014).

Pollen types accounting for at least 2% of the total pollen count were analysed in this work. These species are representative of the pollen spectrum in Alicante, providing a clear view of pollen to which local residents are exposed.

The types of pollens with the highest contribution to the total pollen count observed in Alicante were: Cupresaceae (27.1%), *Pinus* (14.9%), *Quercus* (13.5%) and *Olea* (12.7%), Poaceae (5%), Palmaceae (4.8%), Chenopodiaceae-Amaranthaceae (4%) and Urticaceae (3.8%), as shown in Figure 1.

The use of a range of ornamental species in the design of urban green spaces has undoubtedly influenced the pollen spectrum in the city. Hence, the maximum contribution was obtained for Cupresaceae (cypress trees), widely used as fences in parks and gardens. On the other hand, *Pinus* and *Quercus* are the predominant trees in the mountains of the Alicante province.

Palmaceae had a much greater contribution than that registered in other areas of Spain, due to the proximity

of the city to the largest extension of palm tree gardens in Europe (Chofre *et al* 2016).

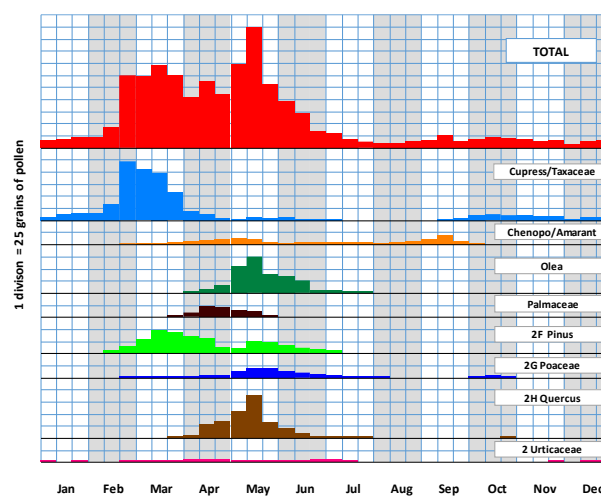


Figure 1. Pollen calendar of Alicante (2010-2015).

*Olea* and Poaceae are considered the most allergenic pollen types in Spain. However, the prevalence of positive skin prick tests among monosensitized patients in the study area is 53% for *Olea*, and only 5% for Poaceae. In contrast, there is a higher prevalence of Chenopodiaceae (32%, *Salsola Kali*) and Urticaceae (7%, *Parietaria*) (Fernández *et al* 2015). The reasons are: (1) the semiarid climate that favours the growth of these species, and (2) the existence of different areas of wasteland, on which grass grows, that could generate a longer pollen season.

This work was supported by the Carlos III Institute by research grants RD 12/013/017 (Research Network of Adverse Drugs and Allergens Reactions -RIRAAF).

Belmonte, J. and Roure, J.M. (2002) *Polinosis: Polen y alergia*, A.L. Valero & A. Cadahía (Ed.).

Chofre, C., Gil-Moltó, J., Galindo, N., Varea, M. and Caballero, S. (2016) *Environ. Monit. Assess.* **188**, 509-519.

Fernández, J., Flores, E., Varea, M., Soriano, V. and Gonzalez P. (2015) *Asian Pac. J. Allergy Immunol.* **33**, 196-202.

Galán, C., Smith, M., Thibaudon, M., Frenguelli, G., Oteros, J., Gehrig, R., Berger, *et al* (2014) *Aerobiología* **30**, 385–395.

## Ambient air BioPMs originated from different sources and their effects on innate immune responses

Dingyu Liu<sup>1</sup>, Rob Mariman<sup>2</sup>, Miriam E. Gerlofs-Nijland<sup>2</sup>, Gert Folkerts<sup>3</sup>, John F. Boere<sup>2</sup>, Jos J.E. Reijnders<sup>4</sup>, Flemming R. Cassee<sup>1,2</sup>, Elena Pinelli<sup>2</sup>

<sup>1</sup> Institute for Risk Assessment Sciences (IRAS), Utrecht University, Utrecht, 3508 TC, Netherlands

<sup>2</sup> Centre for Environment Health, National Institute for Public Health and the Environment (RIVM), Bilthoven, 3720 BA, Netherlands

<sup>3</sup> Department of Pharmacology and Pathophysiology, Utrecht Institute for Pharmaceutical Sciences, Utrecht University, Utrecht, 3508 TC, The Netherlands

<sup>4</sup> Department of Mechanical Engineering, Technology University Eindhoven (TU/e), Eindhoven, 5600 MB, Netherlands

Keywords: Particulate matter, microorganism, livestock, biodiesel, innate immune.

Presenting author email: dingyu.liu@rivm.nl

Studies indicate that asthma patients have enhanced responsiveness to ambient particulate matter (PM) (Brunekreef *et al* 2002, Pope *et al* 2009). BioPM is a suspension of particles containing living microorganisms or parts thereof released in air. However, to what extent such effects are different for BioPM obtained from different sources remains unclear. The aim of this study is to investigate whether size-resolved BioPM originating from livestock and diesel exhaust engine triggers the activation of innate immune cells.

Coarse (2.5-10  $\mu\text{m}$ ), fine (< 2.5  $\mu\text{m}$ ) and quasi ultrafine BioPM (qUF < 0.18  $\mu\text{m}$ ) were collected from a chicken farm using the versatile aerosol concentration enrichment system (VACES). The fine+UF fraction of diesel (containing 20% or 50% biodiesel) exhaust particles (DEP) were collected from diesel engine also using the VACES. Human embryonic kidney, HEK-Blue cells, expressing different Toll-like receptors (TLR 2, 3, 4, 5, 7, 8 and 9) and mononuclear macrophages (MM6) cell line were exposed to increasing concentration of BioPM from these two sites (farm: 3.125-6.25-12.5-25-50-100  $\mu\text{g}/\text{ml}$ ; DEP: 2.5-5-10-20-40  $\mu\text{g}/\text{ml}$ ). The levels of secreted embryonic alkaline phosphatase (SEAP) and cytokines (Tumor Necrosis Factor- $\alpha$ , TNF- $\alpha$ ; Interleukin-6, IL-6; Interleukin-8, IL-8) were measured indicating TLR and MM6 activation. TLR antagonists were used to examine whether BioPM activates MM6 via a TLR ligand.

For HEK-Blue cells, only TLR2 and TLR4 were activated by BioPM from livestock, but not by DEP. For MM6 cells, BioPM samples from livestock induced a concentration-dependent increase in cytokine levels, whereas DEP did not induce any significant increase. The ultrafine and fine+UF fractions of BioPM from livestock induced a higher cytokine response than the coarse fraction of BioPM samples from livestock. Blocking experiments indicate that the cytokine production by MM6 cells upon stimulation with livestock BioPM is TLR4 and TLR2 dependent.

These findings indicate that BioPM from livestock can trigger inflammatory response of innate immune cells. To understand how BioPM activate innate immune cells is crucial for the future research on the relationship between BioPM (and the components

thereof) and respiratory symptoms. For example, asthma which is could be triggered by BioPM is expected to increase in the next two decennia, resulting in expenditures up to 900 million euros per year in the Netherlands.

This work was supported by the Dutch Ministry for Public Health and the Environment under grant S/121012/01.

Brunekreef B., Holgate ST. (2002): *Air pollution and health*. 360:1233-1242

Pope A, Ezzati M., and Dockery W. (2009): *Fine-Particulate Air Pollution and Life Expectancy in the United States*. N Engl J Med, 360: 376-386

## The effect of passive air sampling parameters on determining the aerosol microbial composition and abundance

N. Grydaki, C. Whitby and I. Colbeck

School of Biological Sciences, University of Essex, Colchester, Essex, CO4 3SQ, UK.

Keywords: bioaerosols, passive sampling, petri dishes, quantitative PCR, high-throughput DNA sequencing

Presenting author email: ngrydaki@essex.ac.uk

Passive sampling approaches have been used as an alternative method for determining the microbial aerosol composition and abundance in the indoor environment (Frankel et al., 2012; Würtz et al., 2005). The use of suspended empty petri dishes (no media or adhesives) as passive air samplers (Fig. 1), introduced by Adams et al. (2013), has been adopted from many studies recently, representing a convenient, cost-effective and discrete method for time-integrated bioaerosol collection.

Although studies have utilized the settling dish method in indoor studies for durations ranging from 4 weeks up to 2.5 months, no standardised settled particle sampling protocol is currently available making difficult the cross-comparison of molecular results between studies. Moreover, it has not been demonstrated what is the difference in the microbial content of settled particles collected on an elevated surface, compared to the traditional approach of settled dust typically collected from indoor surfaces, e.g. a shelf, using swabs. Additionally, there is no information regarding the assessment of this long-term passive sampling method in terms of representing the actual exposure to the airborne load, in comparison with the most commonly used active bioaerosol collection of snapshot samples.

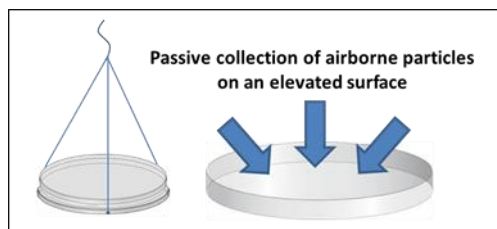


Figure 1. Schematic representation of a suspended petri dish used for bioaerosol passive sampling.

In this study we aimed to address these questions by assessing the microbial communities in settled particles over known time periods. Triplicates of sterile, empty petri dishes were installed in an office environment and left for a duration of 3 months. Each plate was placed on a petri dish lid, and was hung from the ceiling at a height of 230 cm above the floor, using nylon monofilament fishing line. Moreover, sterile petri dishes were also left on an indoor surface, at a height of 116 cm. Petri dishes were left open to allow particles to settle on their surface and were capped, using a new sterile lid, collected and stored at -20 °C at the end of every week for the first month, and at the end of every second week for the next two months. A triplicate of filter samples (47 mm nuclepore polycarbonate track-

etched, 0.4 µm pore size) was also collected at 28 L/min, for duration of 3 hours, at the same day that plates were collected.

The surface of petri dishes was wiped using nylon flocked swabs moistened with sterile PBS buffer. The tip of the swab was then cut directly into a tube containing lysing beads and DNA was extracted using a phenol-based protocol. Samples are going to be analysed using quantitative PCR (qPCR) for evaluation of the microbial abundance and will be processed for high-throughput sequencing of 16S rRNA and ITS1 region on Illumina Miseq platform for determination of the bacterial and fungal diversity. Results could contribute to the establishment of an appropriate sampling protocol for assessing the indoor exposure to biological particles.

This work is supported by the E.U. 7th framework program HEXACOMM FP7/2007-2013 (N° 315760).

Adams, R.I., Miletto, M., Taylor, J.W., Bruns, T.D., (2013). Dispersal in microbes: fungi in indoor air are dominated by outdoor air and show dispersal limitation at short distances. *The ISME journal*, 7(7), 1262-1273

Frankel, M., Timm, M., Hansen, E.W., Madsen, A.M., (2012). Comparison of sampling methods for the assessment of indoor microbial exposure. *Indoor Air*, 22(5), 405-14.

Würtz, H., Sigsgaard, T., Valbjørn, O., Doekes, G., Meyer, H.W., (2005). The dustfall collector - a simple passive tool for long-term collection of airborne dust: a project under the Danish Mould in Buildings program (DAMIB). *Indoor Air*, 15, 33-40.

## Investigation of Bioaerosol Characterization on a Global Scale using Automobile Air Conditioning Filter

J. Li<sup>1</sup> and M.S. Yao<sup>1</sup>

<sup>1</sup>College of Environmental Sciences and Engineering, Peking University, Beijing, 100871, China

Keywords: automobile air conditioning filter, bioaerosol, microbiota, allergen, size distribution

Presenting author email: 1301111588@pku.edu.cn

Bioaerosols have different characteristics in different regions and pose various effects on atmospheric processes, micro-ecology and human health. Therefore, the study of bioaerosol characteristics on a global scale is of great significance for better understandings on global effects caused by bioaerosols. Nevertheless, it is less feasible to get atmospheric particulate matter (PM) samples across the world uniformly by using existing sampling methods. Here, automobile air conditioning filters, which could reduce in-vehicle particle levels by filtering out atmospheric PMs, were selected as the outdoor PM sample providers. By now, automobile air conditioning (AC) filter dust samples were collected from 117 automobiles distributed in 15 different geographical locations in China (CN), Korea (KR), India (IN), Singapore (SG), Indonesia (ID), the United States of America (US), France (FR), Germany (DE), Switzerland (CH) and South Africa (ZA). Similarities and differences between the present novel sampling method and other traditional impinger samplers were compared by identifying the dominant culturable bacterial genus.

Biological contents (culturable bacteria and fungi, total bacteria, bacterial community structure and allergens) in dust samples were studied using culturing, real-time quantitative PCR detecting (qPCR) system, high-throughput gene sequence and enzyme linked immunosorbent assay (ELISA) methods. Normalized size distributions (dN/dLogDp) of aerosolized dust samples were directly monitored using an ultraviolet aerodynamic particle sizer (UVAPS). Preliminary work showed that regardless of locations, automobile AC filter dust samples were found to contain different levels of culturable bacteria and fungi (from 370 to 12 894 CFU/mg and from 4 to 421 CFU/mg separately), total bacteria (from 22 289 to 1 252 261 #/mg) and allergens (from 0.022 to 12.817 ng/mg). All the peak concentrations of aerosolized dust samples from different locations laid between 1-2  $\mu$ m. Bacterial community richness, diversity and structure were varied in different cities. Bacterial genera of *Corynebacterium*, *Albirhodobacter*, *Sphingomonas*, *Burkholderia* and *Brevundimonas* were dominant in most cities except Johannesburg, South Africa.

## Dominant pathogens detected in exhaled breath using a novel Loop-Mediated Isothermal Amplification based protocol

Yunhao Zheng<sup>1</sup>, Xiaoguang Li<sup>2</sup>, Maosheng Yao<sup>1\*</sup> and Jie Xu<sup>2</sup>

<sup>1</sup>State Key Joint Laboratory of Environmental Simulation and Pollution Control, College of Environmental Sciences and Engineering, Peking University, Beijing, 100871, China

<sup>2</sup>Department of Infectious Diseases, Peking University Third Hospital, Peking University, Beijing, 100191, China

Keywords: Pathogens, Exhaled breath, Throat swabs, LAMP, bioaerosol  
Presenting author email: zyh224@pku.edu.cn

Respiratory infection causes a tremendous toll on humans worldwide every year. It is very important for patients to be diagnosed accurately and rapidly as they need effective and appropriate drugs in adequate doses. However, point-of-care diagnostic methods are significantly lacking at the bedside. Here, we investigated a rapid and non-invasive pathogen diagnosis method using Loop Mediated Isothermal Amplification (LAMP) to multiplexing detection of common respiratory pathogens from human exhaled breath samples and throat swabs. And then we analyzed the dominant pathogen of respiratory disease.

Exhaled breath specimens were collected using a previously developed and commercialized exhaled breath collection tool( Figure1) from human subjects with respiratory infection symptoms at Peking University 3rd Hospital. The pathogens to be detected included *Streptococcus pneumoniae*, *Staphylococcus aureus*, *Methicillin-resistant Staphylococcus aureus*, *E. coli*, *Klebsiella pneumoniae*, *Pseudomonas aeruginosa*, *Acinetobacter baumannii*, *Stenotrophomonas maltophilia*, *Haemophilus influenzae*, *Legionella pneumophila*, *M. Pneumonia*, *Chlamydia pneumonia*, and *M. tuberculosis*.

Results showed that LAMP can be used together with the exhaled breath collection tool for detecting breath-borne pathogens. For four out of fifteen patients, *E. coli* and *P. aeruginosa* was detected, while for one subject both MRSA and *E. coli* were detected from the exhaled breath samples. For throat swabs samples, we have detected pathogens from 25 out of total 65 samples, and

the dominant pathogen was *H. influenzae*, of which the positive rate was 50%. Here, depending on the initial pathogen load in the sample, the entire procedure only takes 20-40 min to complete for a respiratory infection diagnosis.



Figure 1 The exhaled breath samples collection device

### Acknowledgements

This study was supported by the National Natural Science Foundation of China (Grants 21477003, 21277007, and 41121004) and Ministry of Education (Grant 20130001110044).

## The bioaerosol bacterial microbiome at urban, agricultural, and industrial sites: Exposure, size fraction and composition.

R.M.W. Ferguson, A.J. Dumbrell, C. Whitby and I. Colbeck

School of Biological Sciences, University of Essex, Colchester, CO4 3SQ, UK

Key words: Bioaerosols, Human Health, Next-Generation Sequencing, qPCR, Environmental Microbiology  
Presenting author email: rmwfer@essex.ac.uk

### T402 – Bioaerosols and allergens (IEH, AA, IND)

Understanding the identities, distribution and abundance of airborne microorganisms remains in its infancy. Meanwhile, the impact from emissions of these microorganisms on local air quality is a growing concern for public health. We investigated the bioaerosol bacterial microbiome at urban, rural, and industrial sites using qPCR and next generation sequencing (NGS). Thus, we were able to determine which bacterial pathogens were present and also their abundance. As smaller particles penetrate further into the lungs, and represent a greater health risk, we also investigated the community structure recovered from different particle size fractions. **Bioaerosol collection:** Bioaerosol samples were collected in the winter and summer at 10 UK sites comprising 3 urban, 3 agricultural, and 4 industrial locations (Table 1). 390 samples (36 per site) were collected over 6 hours at each site, representing one of the most comprehensive assessments of bioaerosols in these environments to date.

Table 1. Sampling locations.

Location	London	Colchester	Milton Keynes
Urban	Park	Park	Park
Agricultural	Farm	Farm	Farm
Industrial	MBT*	composting site	WWTP** (x2 sites)

\* MBT = mechanical biological treatment plant

\*\* WWTP = waste water treatment plant

**Bioaerosol bacterial abundance.** Industrial sites had significantly higher concentrations of bacterial bioaerosols, with  $6.5 \pm 0.7 \log_{10}$  16S rRNA copies  $m^{-3}$  air, compared with  $4.9 \pm 1$  and  $5.3 \pm 0.8 \log_{10}$  16S rRNA copies  $m^{-3}$  air for agricultural and urban respectively ( $p = 0.046$ ) (Figure 1).

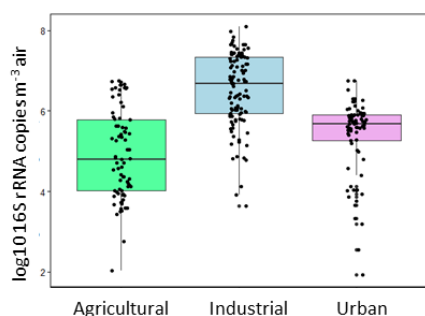


Figure 1. Bacterial concentration at urban, agricultural, and industrial sites ( $n = 81$ ).

Within industrial sites, compost and MBT facilities had the highest concentrations (Figure 2). With

$7.4 \pm 0.3$  and  $6.9 \pm 0.6 \log_{10}$  16S rRNA copies  $m^{-3}$  air for compost and MBT respectively, compared with  $5.9 \pm 0.7$  and  $5.7 \pm 0.6 \log_{10}$  16S rRNA copies  $m^{-3}$  air respectively for a large and small WWTP (Figure 2).

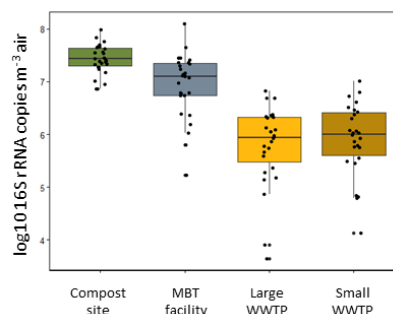


Figure 2. Bacterial concentration at industrial sites. ( $n = 27$ ).

**Size fraction.** The size-fraction data at the compost site showed that the highest bacterial abundances were in the largest ( $>7\mu m$ ) size class, with a decrease with smaller particle size from  $4.2 \pm 0.3$  to  $3 \pm 0.4 \log_{10}$  16S rRNA copies  $m^{-3}$  air (figure 3). PCR-DGGE analysis showed that the community structure also varied between the size classes, with a decrease in diversity from  $>50$  to  $<35$  OTUs between the largest and smallest size fractions.

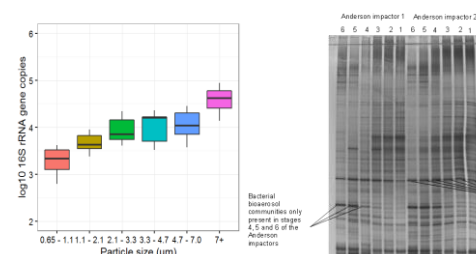


Figure 3. Left, bacterial abundance in different size fractions ( $n = 6$ ). Right PCR-DGGE fingerprint showing size fractionated bioaerosol samples. Sampler 1: lanes 1-6 sampler 2: 7-12, numbers 1-6 indicate the size stage.

**Conclusions.** These data provide evidence of variability in outdoor microbiomes and highlights the need to monitor a range of sites. Due to the ability of smaller particles to penetrate the respiratory system more deeply, they represent a greater human health risk. Our data shows variation in concentration and diversity between size fractions, indicating more attention needs to be paid to size fractionated data. NGS is being used to identify specific pathogens in the samples.

This work was supported by NERC (NE/M010813/1) and the British Aerosol Society.

## Automatic pollen monitoring: towards an operational system

B. Crouzy<sup>1</sup>, B. Clot<sup>1</sup>, T. Konzelmann<sup>1</sup> and B. Calpini<sup>1</sup>

<sup>1</sup>Federal Office of Meteorology and Climatology MeteoSwiss, Payerne, 1530, Switzerland

Keywords: pollen, automatic monitoring, optical methods, real time.

Presenting author email: benoit.crouzy@meteoswiss.ch

A dramatic increase in the prevalence of pollen allergy triggered the development of pollen monitoring networks over the last decades of the 20th Century, responding to the new needs for information. Monitoring data are used for the prevention, diagnosis and therapy and as a basis for forecasting. The current limitation of pollen information is the state of the monitoring technology: the widely used Hirst-trap and manual microscope counting method is very reliable, but suffers from two drawbacks: a delayed data availability and a resolution mostly limited to average daily values. Thus, a major challenge in pollen monitoring is to automatically produce real-time data for timely information and precise forecasting. In this direction, we present the results of the 2015 and 2016 validation campaigns of a new air-flow cytometer performed at MeteoSwiss, Payerne (Switzerland).

The Plair PA-300 is an air-flow (bio-)aerosol cytometer using time-resolved laser scattering and induced fluorescence (Crouzy *et al.*, 2016). Pollen concentrations obtained from this automatic monitoring device were compared to reference manual measurements performed in the same way as current operational measurements at MeteoSwiss. We used four criteria for the evaluation of the automatic system: reliability (1), ability to count (2) and identify (3) different pollen taxa and ability to count other aerosols than pollen (4).

A prerequisite for bioaerosol identification is the correct determination of aerosol physical properties (size, shape and emission spectrum). Testing this was the first natural step of device validation. As a second step, basing on the raw optical parameters produced by the detector, we developed supervised learning algorithms (support vector machines and neural networks) for pollen taxa identification. Having gained insight into the identification capabilities of the device, we could finally move to the pre-operational test of the device, where the automatic counts were compared to reference manual counts performed in parallel. Manual and automatic counts were in very good agreement for total pollen (Figure 1) and several pollen taxa. The results of the 2015 pollen season could be confirmed and further extended to additional taxa in 2016, when the concentrations of the most relevant allergenic pollen taxa could be followed. The automatic device showed a good reliability over the two seasons, comparable to the reference Hirst-type manual detector.

One essential advantage of the tested device is the high sampling obtained in real-time: the hourly values of pollen concentration from the automatic device have the same degree of statistical significance as the daily values of the reference manual counts. The tested system could

thus provide in real time information on exposure peaks, beyond the traditional daily averages obtained with a delay (typically one to nine days) from manual networks. Real-time data based on a statistically valid sample size could benefit patients (information on current exposure levels), doctors (information on sub-daily peaks) and forecasters (forecast based on timely information, assimilation in dispersion models).

In parallel to this effort specific to pollen, this air flow cytometer is currently tested for its ability to identify and count other types of aerosols, such as spores, particulate pollutants and PM (collaboration between Plair SA, the Swiss Federal Office for Environment and MeteoSwiss).

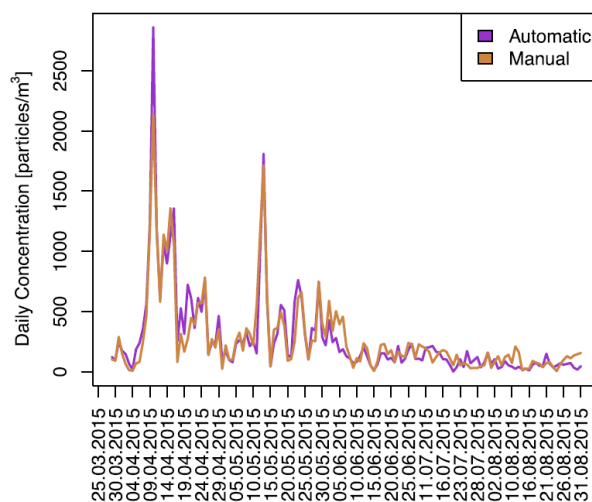


Figure 1. Comparison between automatic (Plair PA-300) and manual (Hirst method) total pollen counts. Pearson correlation coefficient  $R = 0.95$ .

Crouzy, B., Stella, M., Konzelmann, T., Calpini, B., Clot, B. (2016) *Atmospheric Environment* **140**, 202-212.

## **A novel co-culture model of alveolar macrophage and epithelial cells to investigate immune responses to bioaerosol components**

Shagun Khera <sup>1</sup>, Vikram Sharma <sup>1</sup>, Sean F. Tyrrel <sup>2</sup>, Zaheer A. Nasir <sup>2</sup> Tony L. Gladding <sup>3</sup>, Catherine A. Rolph <sup>3</sup>, Enda T. Hayes <sup>4</sup>, Ben Williams <sup>4</sup>, Alan Bennett <sup>5</sup>, Gyuri Fejer <sup>1</sup>, Simon K. Jackson <sup>1</sup>

<sup>1</sup> School of Biomedical and Healthcare Sciences, Plymouth University, Plymouth, UK

<sup>2</sup> School of Energy, Environment and Agrifood, Cranfield University, Cranfield University, Cranfield, Bedfordshire, UK

<sup>3</sup> The Open University, Walton Hall, Milton Keynes

<sup>4</sup> Air Quality Management Resource Centre, Faculty of Environment and Technology, University of the West of England, Bristol, BS16 1QY

<sup>5</sup> Public Health England, Porton Down

Keywords- alveolar macrophages, endotoxin, bioaerosol

Presenting Author email: shagun.khera@plymouth.ac.uk

Bioaerosol particles containing bacteria and fungi and their molecular components such as endotoxin and glucan, are associated with adverse effects on human health and airborne transmission of infections. To assess the health risks associated with bioaerosol emissions, appropriate technology to determine exposure-response relationships and aid in the development of regulatory frameworks is required. Cell-based biosensors have been recognized as potential leaders in the next generation of functional biosensing as they provide rapid and useful information on physiological responses to a variety of bioactive analytes. Alveolar macrophages (AM) are the first line of defence against airborne environmental microbes. Recently, we described a novel, continuously growing, non-transformed, model of lung AMs (MPI cells), a first in the field (Fejer et al, 2013). This robust system provides an excellent new model for AMs without restricted availability.

We have developed a co-culture of alveolar macrophages (MPI cells) and alveolar epithelial cells (MLE-12) as these cell types play critical roles in development of lung injury. The co-cultured cells were stimulated with different concentrations of endotoxin, glucan and cockroach and dust mite allergens. The unique inflammatory/molecular signatures in response to stimulation were determined by cutting-edge techniques including mass spectrometry and Luminex multiplex assay as well as ELISA and RT-PCRs. The results from these experiments suggest that co-cultures of the two cell types synergistically produce factors that induce a strong

immune response, an effect not observed with monocultures of either cell type. The results provide insight into the mechanisms of airway damage from bioaerosol components and strongly support the potential of this model to study the impact of bioaerosol generated from industries such as large-scale composting, on human health. Moreover, advancement of such a model will allow the future development of high throughput and potentially 'in-field' use of cell-based biosensors.

### References-

Fejer G, Wegner MD, Györy , Cohen I, Engelhard P, Voronov E, Manke T, Ruzsics Z, Dölken L, Prazeres da Costa O, Branzk N, Huber M, Prasse A, Schneider R, Apte RN, Galanos C, Freudenberg MA.(2013). *Proc Natl Acad Sci U S A*. 11; 110 (24), 2191-8

## Biophysical characterisation of pathogen containing aerosols

E. Pfrommer<sup>1,2,3</sup>, T. Gutmans<sup>3</sup>, C. Dreier<sup>1</sup>, R. Reimer<sup>1</sup>, C. Schneider<sup>1</sup>, G. Gabriel<sup>1</sup>, K. Schepanski<sup>2</sup> and U. E. Schaible<sup>3</sup>

<sup>1</sup>Heinrich Pette Institute, Leibniz Institute for Experimental Virology Hamburg, 20251, Germany

<sup>2</sup>Leibniz Institute for Tropospheric Research (TROPOS), Leipzig, 04318, Germany

<sup>3</sup>Research Center Borstel, Leibniz Center for Medicine and Bioscience, Borstel, 23845, Germany

Keywords: bioaerosols, airborne transmission, infection

Presenting author email: elisabeth.pfrommer@hpi.uni-hamburg.de

Infectious airway pathogens can be transmitted both via direct contact and airborne routes. Airborne infection is defined as transmission of pathogens through the air, from infected to sentinel host and is mainly influenced by two factors. I) the aerobiology of pathogen containing aerosols, which facilitates airborne transmission, is defined by size and other physicochemical characteristics of the aerosol (Fernstrom and Goldblatt, 2013); II) the pathogen induced pathology, which is based on microbial virulence and inflammatory host responses, enables expelling of pathogens as aerosol droplets (Jones and Brosseau, 2015). Prominent airborne pathogens are *Mycobacterium tuberculosis* and influenza A virus, which both cause respiratory infections and are transmitted via the airborne route from human to human. A better understanding of physicochemical properties and airborne transmission modalities of pathogen containing aerosol particles and the required pathology will enable us to better define risks of infection, to improve protocols to protect risk groups like health workers or house hold contacts and, ultimately, to develop prevention measures for pathogen shedding.

Even though it is well established that influenza A virus and *Mycobacterium tuberculosis* can transmit by respiratory droplets, little is known about the actual composition of pathogen containing aerosols. We therefore employed imaging of aerosol-containing particles by transmission electron microscopy and atomic force microscopy to get a unique insight into aerosol composition. For size separation, we use the Andersen Impinger, which consists of 8 stages, through which air is consistently sucked (Andersen, 1958). Dependent on the flow-velocity of the aerosol, which is determined by their size and density, aerosols will settle on different levels, so that bigger aerosols will settle earlier than smaller, allowing a rough size range separation of airborne particles. Additionally to the Andersen Impinger, a dynamic light scattering based method was used to specify the aerosol sizes. This combination of methods allows for a unique insight into aerosol transmission, *in vitro* and *in vivo*.

Besides size, also mass density of pathogens will influence their airborne behavior and thereof their residence time in the air flow. The mass density of influenza A virus was primary described at 1.18 g/cm<sup>3</sup> (Wang et al, 2010). With our methods we were able to reproduce that value and also determine the mass density of one mycobacterium at 1.23 g/cm<sup>3</sup>.

For both, influenza A virus and *Mycobacterium tuberculosis*, a strong influence of relative humidity on their airborne transmission was described before, without understanding underlying mechanisms (Lowen et al, 2007, Ko et al, 2000). Using Atomic Force Microscopy, we are able to examine properties of single pathogens under different humidity conditions and define their hygroscopicity. We found that both mycobacteria and influenza A viruses are highly hygroscopic.

By defining size, surface properties, morphology and physicochemistry including hygroscopicity and mass density of pathogen containing aerosols first *in vitro* and then *in vivo*, this study will enhance our understanding of airborne transmission properties in general and specifically for influenza A Virus and *Mycobacterium tuberculosis*. Ultimately, the retrieved aerosol characteristics will be implemented in the atmosphere-aerosol model COSMO-MUSCAT and used to assess the dispersion of pathogen containing aerosols in a natural atmospheric environment.

### References

- Fernstrom, A. & Goldblatt, M. Aerobiology and Its Role in the Transmission of Infectious Diseases. *J. Pathog.* **2013**, 13 (2012).
- Jones, R. M. & Brosseau, L. M. Aerosol Transmission of Infectious Disease. *J. Occup. Environ. Med.* **57**, 501–508 (2015).
- Andersen A (US ACC. New Sampler for the Collection, Sizing, and Enumeration of Viable Airborne Particles. 1958;(904).
- Wang, S. *et al.* Label-free imaging, detection, and mass measurement of single viruses by surface plasmon resonance. *Proc. Natl. Acad. Sci.* **107**, 16028–16–32 (2010).
- Lowen, A. C., Mubareka, S., Steel, J. & Palese, P. Influenza virus transmission is dependent on relative humidity and temperature. *PLoS Pathog.* **3**, 1470–1476 (2007).
- Ko, G., First, M. W. & Burge, H. a. Influence of relative humidity on particle size and UV sensitivity of *Serratia marcescens* and *Mycobacterium bovis* BCG aerosols. *Tuber. Lung Dis.* **80**, 217–228 (2000).

## Characteristics of Aerosol Suspension in a Rotating Drum

W.R. Ke<sup>1</sup>, C.W. Lin<sup>1</sup>, S.H. Huang<sup>1</sup>, W.C. Lee<sup>2</sup>, Y.M. Kou<sup>3</sup>, and C.C. Chen<sup>2</sup>

<sup>1</sup>Institute of Occupational Medicine and Industrial Hygiene, National Taiwan University, Taipei, 10055, Taiwan

<sup>2</sup>Institute of Environmental Health, National Taiwan University, Taipei, 10055, Taiwan

<sup>3</sup>Department of Occupational Safety and Health, Chung Hwa University of Medical Technology, Tainan, 717 Taiwan

Keywords: Aerosol generation, Suspension time, Rotating drum.

Presenting author email: kuoyumei@yahoo.com.tw

The survival of airborne pathogen in the environment is a critical factor in successful transmission of infection via the airborne route. Although there have been many publications study the effect of environmental parameters on the survival of bioaerosol, the results were difficult to compare due to great difference in methodologies (Asgharian and Moss, 1992; Paez-Rubio and Peccia, 2005 ). Therefore, the aim of this work was to build a simple and robust system for retaining particles in air-borne state for prolonged periods. Subsequently, long-term effects of environmental conditions on air-borne microorganisms could be studied and compared.

In the present study, a rotating drum composed of cylinder chamber route on a horizontal axis with gravity in the vertical direction was chosen because it is inexpensive and easy-to-operate. The dimension of the chamber was 29cm in diameter and 59 cm in length. In order to evaluate the performance of the rotating drum for particle levitation, potassium sodium tartrate (PST) solid particles, generated by an ultrasonic atomizer (Model8700-120MS, Sonotek Corp.), were used as surrogate aerosols. The particle size distributions and number concentrations were measured with an aerodynamic particle sizer (APS model 3321, TSI Inc.). Accordingly, the decay constants of particle number concentration as a function of particle size and rotating rate were determined. The experimental results were compared to a mathematical model for the prediction of optimal rotation rate resulting in maximum levitation time.

In the static chamber, the trajectory of the particles is downward due to gravitational settling. When centrifugal forces are added, air-borne particles adopt a spiral trajectory thereby significantly enhancing the path length to be travelled by each particle before coming into contact with the chamber wall. The results revealed that decay constant increased with increasing particle size at different rotating rates. Moreover, all size ranges of particles had longest suspension time at 5 rpm: the 1- and 5- $\mu$ m particles spent 24 and 2.5 hours reaching 5% of initial concentration, respectively. Conversely, the 5- $\mu$ m particles took 4 minute at 0 rpm. However, the suspension time which was calculated by theoretical model was longer than experimental data, and the distinctions need for further discussion.

This work was supported by the Ministry of Science and Technology, Taiwan, under grant MOST 105-3011-F-273-001.

Asgharian, B. and Moss, O. R. (1992) *Aerosol Science and Technology* 17:263-277.

Facile, N., Barbeau, B., Prévost, M., Koudjonou, B. (2000) *Water Research* 34:3238-3246.

Paez-Rubio, T. and Peccia, J. (2005) *Journal of Environmental Engineering* 131:512-517.

## Experimental set-up for studies of viability of aerosolized model organisms for infectious diseases

M. Alsved<sup>1</sup>, T. Šantl-Temkiv<sup>2</sup>, S. Holm<sup>3</sup>, T. Svensson<sup>1</sup>, P. Medstrand<sup>4</sup>, A. Widell<sup>4</sup>, M. Bohgard<sup>1</sup>, J. Löndahl<sup>1</sup>.

<sup>1</sup>Department of Design Sciences, Lund University, Lund, Sweden

<sup>2</sup>Department of Physics and astronomy, Aarhus University, Denmark

<sup>3</sup>Helmholtz Centre Potsdam, GFZ German Research Centre for Geosciences, Potsdam, Germany

<sup>4</sup>Department of Medicine, Lund University, Lund, Sweden

Keywords: Bioaerosols, Norovirus, airborne diseases, *Pseudomonas syringae*

### Introduction

Airborne pathogenic microorganisms are among major causes of infectious diseases globally. Nevertheless, the understanding of airborne transmission of bacteria and viruses between hosts is limited and often overseen in disease prevention. Especially in hospitals, where there are immunocompromised patients, airborne spreading of disease is a threat. An outbreak of disease at a hospital ward causes major stress on the health care, resulting in reduced staff because of infected personnel and increased workload because of ill patients.

In this study, we have developed a set-up for looking at the effect of aerosolization on survival of microorganisms. The aim is to understand what conditions that make airborne microorganisms maintain their viability, and thus potential to cause infections.

### Methods

The set-up for experimental analysis of aerosolized model organisms is schematically illustrated in Figure 1. Two models for infectious diseases were tested: murine norovirus, MNV, a cultivable model virus for human norovirus and a plant pathogen bacterial species, *Pseudomonas syringae*. A suspension of bacteria in 0.1% NaCl solution or virus in growth medium was aerosolized into a 1 m long stainless steel pipe and diluted with particle free air. The experiment was carried out with two aerosol generators: sparging liquid aerosol generator (SLAG, CH Technologies) at 14 l/min (30 l/min dilution) and an atomizer (model 3076, TSI) at 1.8 l/min (12.5 l/min dilution). The aerosol was collected into a BioSampler impinger (SKC) with 20 ml 0.1% NaCl (*P. syringae*) or phosphate buffered saline (MNV) at 12.5 l/min during

30 minutes. The size distribution was monitored with a scanning mobility particle sizer (SMPS, design: Lund University) and an aerodynamic particle sizer (APS, model 3321, TSI).

The amount of collected *P. syringae* and MNV in the Biosampler was evaluated using flow cytometry and quantitative polymerase chain reaction (qPCR), respectively. In addition, viability after aerosolization was assessed with LIVE/DEAD® *bac*Light Viability and counting kit (ThermoFisher) for *P. syringae* and with a technique that measures replicating minus RNA for MNV. Minus RNA qPCR specifically detects minus RNA, which is only present inside cells during replication, while mature MNV particles contain only positive RNA.

### Results and Conclusion

The set-up and methodology was successfully used to assess the viability of model organisms after aerosolization. *P. syringae* had  $40 \pm 10\%$  survival after aerosolization with SLAG. We were able to detect replicating MNV with the minus RNA qPCR after aerosolization with the atomizer, but results are not yet quantitative.

Using our aerosolization setup in combination with the state-of-the-art molecular and single-cell techniques, such as minus RNA qPCR and flow cytometry, allows us to obtain detailed information on how the viability of airborne microorganisms is affected by the environment. Our future aim is to investigate environmental factors that support viability of airborne microorganisms and thus spreading of infectious pathogens through air.

This work was supported by FORMAS (project 2014-1460) and AFA Insurance.

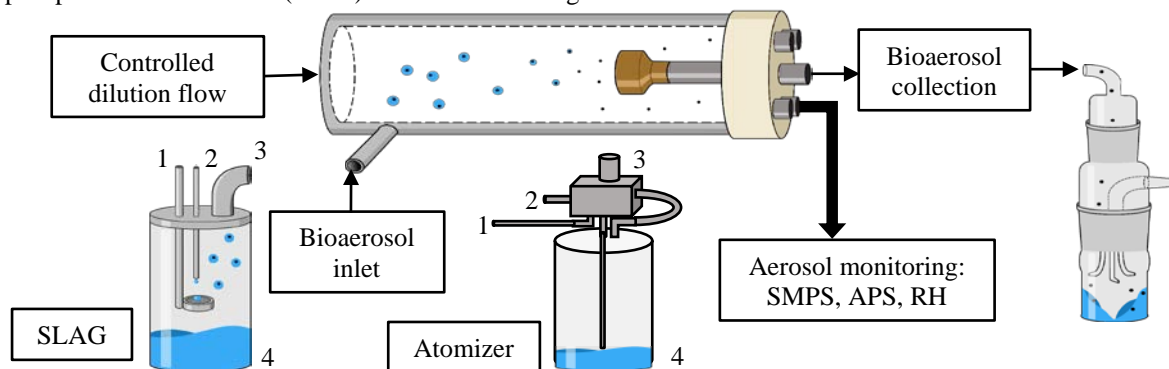


Figure 1: Schematic view of the experimental setup for aerosolization and collection of bioaerosols. Number explanation: 1. Pressurized air inlet, 2. Microorganisms solution inlet, 3. Bioaerosol outlet (connected to bioaerosol inlet), 4. Waste solution.

## Bioaerosol Capture via Passive Technique: Design and Performance of Rutgers Electrostatic Passive Sampler (REPS)

J. Therkorn<sup>1,2</sup>, J. Scheinbeim<sup>3</sup>, and G. Mainelis<sup>3,\*</sup>

<sup>1</sup>Asymmetric Operations Sector, Johns Hopkins University, Applied Physics Laboratory, Laurel, MD, USA;

<sup>2</sup>Department of Environ. Sciences, Rutgers, The State University of New Jersey, New Brunswick, NJ, USA;

<sup>3</sup>Department of Chemical and Biochemical Engineering, Rutgers, The State University of New Jersey, Piscataway, NJ, USA.

Keywords: passive sampling, bioaerosols, ferroelectric polymers

Presenting author email: [mainelis@rutgers.edu](mailto:mainelis@rutgers.edu)

Passive sampling of airborne particles has multiple advantages over active sampling methods: no power or pumps are needed, low cost, usable over broad spatiotemporal scales, and amenable to the creation of massively distributed sampling networks.

Here, we report on the design, development and field testing of a passive bioaerosol sampler. Rutgers Electrostatic Passive Sampler (REPS) uses parallel layers of a polarized, ferroelectric polymer (polyvinylidene fluoride, PVDF)<sup>1</sup>. PVDF has been permanently polarized by application of an external electric field, and we have shown that it enhances electrostatic capture of microorganism-sized particles from 15 nm to >5000 nm.

Field testing was conducted in four 10-day-long outdoor campaigns in highly varied environmental conditions (-2 to 33°C, 17 to 98% RH). Collection efficiencies of REPS were compared to those of an active control sampler (Button Aerosol Samplers) and passive control samplers (PTFE settling filters and agar settling plates). Total bacteria and fungi were counted by Acridine Orange staining/microscopy each day for the Button Samplers and at the end of each field campaign for passive samplers. Culturable bacteria and fungi were determined daily by plating aliquots of extracted Button Sampler filter suspension and via agar settling plates, and at the end of campaigns for passive samplers.

Compared to passive PTFE filters, REPS enhanced passive capture of total microorganisms by 7-fold. REPS also collected 65% of the culturable bacteria of the active Button Samplers. Since the Button Samplers operated at 4 L/min, REPS had an equivalent sampling flow rate of 2.6 L/min and 1.2 L/min for culturable bacteria, and total bacteria and fungi, respectively. These results suggest that REPS passively collects a similar number of microorganisms as an active sampler over long sampling durations, especially for culturable bacteria. Capture of culturable bacteria is likely enhanced by better preservation of their culturability in the absence of a desiccating flow rate. These results suggest that our newly developed passive sampler is an effective bioaerosol sampling tool. Since the device is small (fits in a standard 50 mL centrifuge tube) and lightweight (~ 50g), it has a

variety of potential applications, including sampling in flood-damaged homes, monitoring aeroallergen patterns and assessing the presence of airborne microorganisms over broad spatial scales. Future tests will include indoor testing and development of a personal sampler prototype.

### References

1. Therkorn, J.; Thomas, N.; Calderón, L.; Scheinbeim, J.; Mainelis, G., Design and development of a passive bioaerosol sampler using polarized ferroelectric polymer film. *Journal of Aerosol Science* **2017**, *105*, 128-144.

### Acknowledgement

This work was supported by the United States Environmental Protection Agency's STAR (Science to Achieve Results) Graduate Fellowship [FP-91760601-0], and the Air and Waste Management Association's Milton Feldstein Memorial Scholarship for Air Quality Research. This work was also supported by the NIH-NIEHS funded Center for Environmental Exposure and Disease, P30 ES005022.

## Continuing Development of Electrostatic Precipitator for Bioaerosols with high Concentration Rate

T. Han and G. Mainelis\*

<sup>1</sup>Department of Environmental Sciences, Rutgers, The State University of New Jersey  
14 College Farm Rd. New Brunswick, NJ 08901, USA

Keywords: Bioaerosol, collection efficiency, electrostatic precipitator, concentration rate  
Presenting author email: [mainelis@rutgers.edu](mailto:mainelis@rutgers.edu)

We recently developed an electrostatic collector for bioaerosols, where biological particles are electrostatically deposited onto a narrow electrode covered by a hydrophobic substance and then removed and collected by rolling water droplets (20 or 40 microliter) to achieve high sample concentration rate [1-3]. As part of further development of this technology, we designed a field-deployable version of the electrostatic precipitator with the superhydrophobic surface (FDEPSS), which consists of two combined half-cylinder collection chambers and an integrated control box [4]. The collector is made of a static dissipative material, and each collection chamber features a 3.2 mm wide collection electrode. The round top part of each chamber contains eight carbon fiber ionizers arranged in two lines of four. The collected particles are removed by a 20  $\mu$ L rolling water droplet. Sampler's components were integrated into a control box.

The FDEPSS was tested with two bacterial species, *Bacillus atrophaeus* and *Pseudomonas fluorescens* bacteria, and one fungal spore, *Penicillium chrysogenum* for 10 and 60 min collection times and showed collection efficiency of  $\sim 70\%$  at a sampling flow rate of 20 L/min. The use of a collecting water droplet of 20  $\mu$ L per collection chamber achieved sample concentration rates approaching  $0.5 \times 10^6/\text{min}$ . The FDEPSS was also tested against BioSampler (SKC Inc., Eighty Four, PA) and Button aerosol sampler (SKC Inc.) when sampling bioaerosols outdoors for 60 min. The samples were characterized based on the total airborne adenosine triphosphate (ATP) concentration, which was reported as relative luminescence units (RLU). The FDEPSS detected  $5.1 \times 10^5 \text{ RLU}/\text{m}^3$ , while the BioSampler and the Button sampler showed  $4.1 \times 10^5 \text{ RLU}/\text{m}^3$  and  $8.7 \times 10^5 \text{ RLU}/\text{m}^3$ , respectively. Since ATP analysis can be performed with small sample volumes, and the FDEPSS captures particles into 20  $\mu$ L of liquid, resulting in a high concentration rate, we showed that this sampler could detect the presence of airborne microorganisms 40 $\times$  faster than the BioSampler or Button aerosol sampler. This FDEPSS feature could be integrated into bioaerosol detection systems, particularly when concentrations are low and time is critical.

We are currently working on the next iteration of the FDEPSS, which will have higher concentration rates even further (up to  $1\text{-}2 \times 10^6/\text{min}$ ) and improve preservation of microorganism viability, culturability and DNA integrity. The sampler is being redesigned into a two-stage

electrostatic collector to address deficiencies of the current single-stage collector. In the new design, a novel wire-to-wire type ionizer will effectively charge the incoming bioaerosol particles while producing very low ozone concentrations ( $\sim 10$  ppb), thus addressing an issue common with electrostatic collectors. The collection chamber is being redesigned to capture particles on four collection electrodes simultaneously - a feature that will allow multiple analyses of the collected bioaerosol to gain more information about its properties. The resulting new field-deployable sampler will be able to operate for up to 8 hours, and the entire collected sample will be concentrated in one droplet (e.g., 20  $\mu$ L). Since the sampler is an open channel collector and the charger requires low current ( $<0.001 - 0.01$  mA), it will have low power consumption and will be powered by batteries or solar array for outdoor applications. These features will make the sampler easy to deploy for various studies.

### References

1. Han, T., H.R. An, and G. Mainelis, *Performance of an Electrostatic Precipitator with Superhydrophobic Surface when Collecting Airborne Bacteria*. Aerosol Science and Technology, 2010. **44**(5): p. 339-348.
2. Han, T., D. Fennell, and G. Mainelis, *Development and Optimization of the Electrostatic Precipitator with Superhydrophobic Surface (EPSS) Mark II for Collection of Bioaerosols*. Aerosol Science and Technology, 2015. **49**: p. 210-219.
3. Han, T. and G. Mainelis, *Design and development of an electrostatic sampler for bioaerosols with high concentration rate*. Journal of Aerosol Science, 2008. **39**(12): p. 1066-1078.
4. Han, T., et al., *Design and evaluation of the field-deployable electrostatic precipitator with superhydrophobic surface (FDEPSS) with high concentration rate*. Aerosol and Air Quality Research, 2015. **15**(6): p. 2397-2408.

### Acknowledgement

The Centers for Disease Control / National Institute for Occupational Safety and Health (USA) grants R21-OH008656, R01-OH009783, and 2R01-OH009783.

## **Abstracts T403**

## ***In vitro* dosimetric and cytotoxic assessment of a commercially available tobacco heating product (THP) versus a reference cigarette**

J Adamson, T Jaunky, S Santopietro, A Terry, D Thorne, D Breheny, M Gaça  
 Research & Development, British American Tobacco, Southampton, SO15 8TL, UK

Keywords: Tobacco heating product, THP, *in vitro*, exposure systems, cytotoxicity, dosimetry  
 Corresponding author email: [jason\\_adamson@bat.com](mailto:jason_adamson@bat.com)

In the past decade, the awareness and usage of electronic cigarettes has increased exponentially; tobacco heating products (THPs) are less well known but are beginning to establish themselves with consumers in certain markets. Both e-cigarettes and THPs are being offered to the consumer as harm reduction alternatives to cigarette smoking, with these products delivering nicotine via inhaled aerosols with vastly different chemical profiles compared to traditional combusted tobacco. In this study, the aerosol from a new commercially available THP (**Figure 1**) was assessed *in vitro*, comparing the cytotoxicity of a continuous lung cell line after exposure to cigarette smoke and THP aerosol.

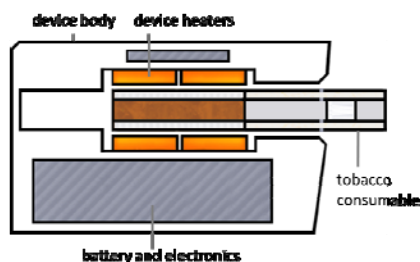


**Figure 1.** The THP assessed in this study

A range of biologically relevant aerosol dilutions were generated using the Borgwaldt RM20S Smoking Machine. The aerosol was delivered to *in vitro* exposure chambers housing H292 lung cell lines at the air liquid interface. After a 60-minute exposure (Health Canada smoking regime) lung cells received a 24-hr recovery period. Thereafter, cell viability was assessed by the Neutral Red Uptake assay (NRU)<sup>1</sup>.

Cell culture media in the base of each exposure chamber (25 ml DMEM) was retained post-exposure for nicotine quantification. The purpose herein was to enable post-exposure cell viability data to be presented as a function of exposed nicotine (a marker common in both aerosols) rather than arbitrary ratio dilutions of aerosol with air. Exposed media samples of 1 ml were spiked with d<sub>4</sub>-nicotine standard (10 ng/ml) and analysed via liquid chromatography mass spectrometry (UPLC-MS/MS)<sup>2</sup>.

The dose response of nicotine in the exposed media was established for each product. Cigarette smoke being more concentrated, the biological dilution range selected was greater compared to THP, ranging 1:20 – 1:10000 for the cigarette and 1:2 – 1:200 for the THP (aerosol:air, v:v) (**Figure 2**).

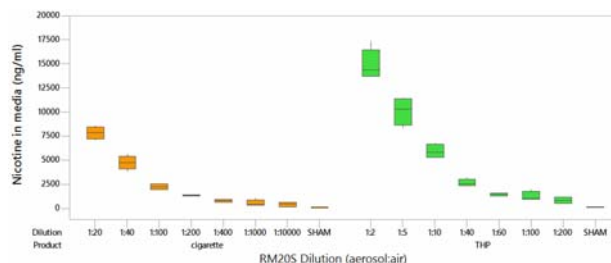


**Figure 2.** Nicotine in media after 1-hr exposure (n=4)

Cytotoxicity was presented against aerosol dilutions (**Figure 3A**), and media nicotine concentration (**Figure 3B**) to make more appropriate product exposure comparisons. Cell viability was calculated as a percentage of the air (SHAM) control in each case (n=4/dilution).

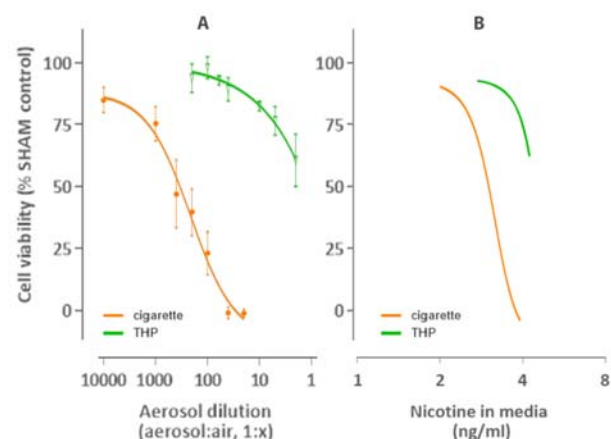


**Figure 3.** Cytotoxicity after 1-hr aerosol exposure versus dilution [A] and media nicotine concentration [B]

Our data demonstrate that the *in vitro* cytotoxic response from a cigarette and THP are significantly different, with the observed frameshift in the THP response clearly indicative of reduced effect. As well as dosimetry data clearly demonstrating cellular exposure, this enables the comparative biological response to be presented against exposed nicotine, and can put such data into wider context of other nicotine delivery products. These *in vitro* data, along with emission chemistries and aerosol characterisation, provide a solid foundation for clinical assessment of our new tobacco heating products.

1. Azzopardi D et al., 2016. Electronic cigarette aerosol induces significantly less cytotoxicity than tobacco smoke. *Tox. Mech. and Met.* 26:6:477-491
2. Adamson J et al., 2016. Application of dosimetry tools for the assessment of e-cigarette aerosol and cigarette smoke generated on two different *in vitro* exposure systems. *Chem. Cent. J.* 10:74

## Neutralization of Aerosolized Spores by Combustion Products of Powdered Materials: Effect of Exposure Time

S.A. Grinshpun<sup>1</sup>, W. Nakpan<sup>1</sup>, M. Yermakov<sup>1</sup>, R. Indugula<sup>1</sup>, T. Reponen<sup>1</sup>, E. L. Dreizin<sup>2</sup>, M. Schoenitz<sup>2</sup>

<sup>1</sup>Center for Health-Related Aerosol Studies, University of Cincinnati, Cincinnati, Ohio, USA

<sup>2</sup>Department of Chemical, Biological, and Pharmaceutical Engineering, New Jersey Institute of Technology, Newark, New Jersey, USA

Keywords: bioaerosol, combustion, neutralization, exposure time.

Presenting author email: sergey.grinshpun@uc.edu

Highly pathogenic bio-agents may be aerosolized in the event of explosion or fire in a bio-weapon facility. If the facility is targeted, a fraction of microorganisms (e.g., stress-resistant bacterial spores such as *Bacillus anthracis*) may survive the high temperatures and exposure to chemicals. This scenario would represent a major threat. In the frameworks of the bio-agent defeat program, novel reactive materials are being developed to neutralize (i.e. inactivate) viable bio-agents during their release to the atmosphere. In this effort, we used a state-of-the-art laboratory facility for evaluating the biocidal effects of combustion products of various reactive powders, which were prepared using high-energy mechanical milling. Most of the tested materials are capable of retaining substantial quantities of iodine stabilized in the metal matrix and released upon their heating and ignition.

The objective of this research was to determine inactivation factor (IF) as a function of exposure time ( $\tau$ ) for *Bacillus thuringiensis* kurstaki (Btk) spores, a well-established surrogate of *B. anthracis*. The IF value was determined by measuring the concentrations of exposed and non-exposed viable spores. The spores dispersed in a dry airflow were exposed over different time intervals (approximately, 0.1–2.0 s) to hydrocarbon flames seeded with different reactive powders. The exposure occurred in a temperature-controlled environment. The following materials were tested: Al, Al·I<sub>2</sub>, Al·B·I<sub>2</sub>, Mg, and Mg·B·I<sub>2</sub>. Composite materials were prepared with specific weight ratios. The tests were also performed with unseeded hydrocarbon flame.

The IF data are presented in Fig. 1 for two characteristic air temperatures ( $T_{\text{air}}$ ) of the exposure chamber: the lower one was chosen to be below and the higher to be above the iodine boiling point ( $T_{\text{I-boiling}} \approx 184$  °C). At a lower temperature, the trends were similar for all materials: IF exponentially increased as the exposure time increased. The similarity of IF data obtained for unseeded flame, Al and Al·I<sub>2</sub>, suggests that the inactivation effect in this case is primarily driven by the heat stress and not by the chemical interaction between the aerosolized spores and combustion products. The same is true for the three other materials (Mg, Al·B·I<sub>2</sub>, and Mg·B·I<sub>2</sub>), except for the slope, which is steeper suggesting a more sensitive dependence of IF on the exposure time for these materials. Given that at  $T_{\text{air}} \approx 170$  °C the iodine released from combustion of iodine-containing materials does not remain in the gaseous phase, essentially no advantage can be taken from its

biocidal qualities. Under this condition, magnesium oxide and boron released during combustion may have a measurable chemical contribution to the spore inactivation effect, in addition to the thermal effect.

The data obtained at  $T_{\text{air}} > T_{\text{I-boiling}}$  point to a complex kinetic interaction between the thermal and chemical inactivation effects. Combustion of the iodine-containing materials produced a powerful spore inactivation when the temperature was sufficiently high to allow taking a full advantage from the gaseous iodine.

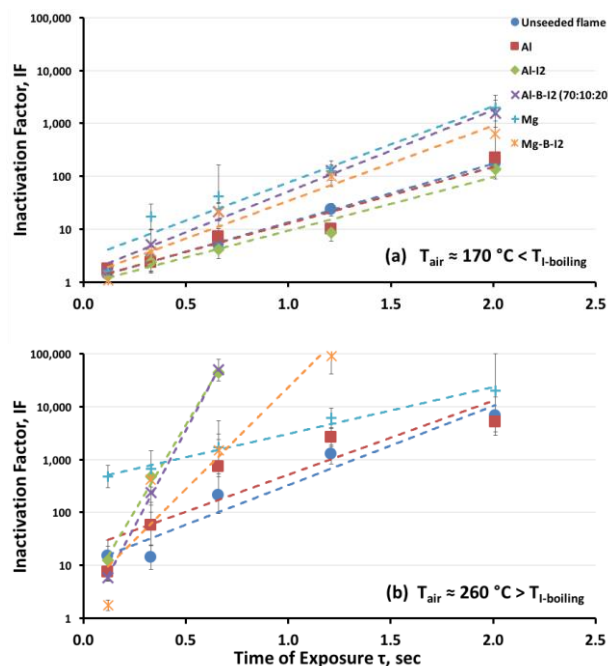


Figure 1. IF as a function of  $\tau$  for the aerosolized Btk spores at two different temperature conditions (a) and (b)

The data collected in this study help establish hypotheses related to the biological response of airborne microorganisms to exposure to different biocidal materials. We believe that the heat-induced stress is capable of damaging the spore protein coats and affect the spore outer membrane, cortex, and inner membrane; this, in turn, enhances the penetration of biocidal chemical products. The study provides a foundation for selecting materials for the neutralization of viable airborne spores under specific exposure conditions.

This research was funded by the U.S. Defense Threat Reduction Agency (DTRA). The authors are grateful for this support.

## Ecotoxicological assessment of guaiacol and its nitrated derivatives

A. Kroflič<sup>1</sup>, M. Pflieger<sup>2</sup>, M. Debeljak<sup>1</sup> and K. Vogel-Mikuš<sup>3,4</sup>

<sup>1</sup>Department of Analytical Chemistry, National Institute of Chemistry, Ljubljana, SI-1000, Slovenia

<sup>2</sup>Laboratory for Environmental Research, University of Nova Gorica, Nova Gorica, SI-5000, Slovenia

<sup>3</sup>Department of Biology, Biotechnical Faculty, University of Ljubljana, Ljubljana, SI-1000, Slovenia

<sup>4</sup>Jožef Stefan Institute, Ljubljana, SI-1000, Slovenia

Keywords: biomass burning, nitroguaiacol, *V. fischeri* acute toxicity, plant toxicology.

Presenting author email: ana.kroflic@ki.si

Guaiacol (2-methoxyphenol, GUA) is the main component of the most abundant natural aromatic polymer lignin. Its analogues have already been determined in the tropospheric gaseous, aqueous, and particulate phases, in surface rivers and even in drinking water. The most important source of GUA and its analogues in the environment is wooden biomass burning (Stockwell *et al.*, 2015), besides biogenic emissions (Misztal *et al.*, 2015) and local industrial sewages (Michalowicz *et al.*, 2011). As European Environmental Agency and other regulatory agencies recognize both particulate matter (PM) and volatile organic compounds (VOC) as harmful for human health, aromatic GUA is also believed potentially toxic for living organisms. Analogously to nitrophenols, known environmental toxicants, mostly secondarily formed nitroguaiacols (NG) are thought to be even more ecotoxic than their precursor compound. These atmospheric pollutants are deposited onto the Earth's surface by dry deposition or precipitation. If deposited by snow or dry particles, GUA and NG can accumulate on the surface and are only washed in the ground by rain or when the snow melts, which can result in high concentration of toxicants locally. However, no toxicological data for GUA or NG have been reported to date.

We represent the first ecotoxicological study of GUA and its nitrated derivatives. Acute toxicities of four atmospheric pollutants, GUA, 4-nitroguaiacol (4NG), 6-nitroguaiacol (6NG), and dinitroguaiacol (DNG), and their mixtures were first determined by a bioluminescent *V. fischeri* assay (Pflieger and Kroflič, 2017). Individual EC<sub>50</sub> values (effective concentration of the chemical that caused 50% luminescence reduction) and modes of action are shown in Table 1. All compounds are considered as harmful or slightly toxic according to the European Directive 93/67/EEC and U.S. EPA toxicity classification, respectively. The toxicity of the investigated compounds can be considered concentration additive.

Table 1. Effective concentrations EC<sub>50</sub> (mg L<sup>-1</sup>) after 30-min incubation with *V. fischeri* and toxicity classification according to Verhaar scheme (modified).

	GUA	4NG	6NG	DNG
EC <sub>50</sub>	100	23	37	17.4
Class	I: Baseline toxicity	IV: Respiratory uncouplers		

As further toxicological testing is needed to prove the predicted modes of action and considering that organisms of different trophic levels could respond stronger to an exposure to the compounds of interest, we also present the first results of an ongoing study on the plant toxicity. Maize and sunflower plants were grown in nutrient solutions containing investigated pollutants and exhibited growth inhibition towards nontoxic control. The uptake of aromatics by shoots during the treatment was followed by high performance liquid chromatography (HPLC) and demonstrated a decreasing affinity of plants towards the aromatic compounds with increasing number of nitro groups on the aromatic ring (Figure 1). Simultaneously, DNG inhibited the plant growth the most. After the treatment, the roots were freeze dried and the water extracts analysed for their chemical composition by HPLC.

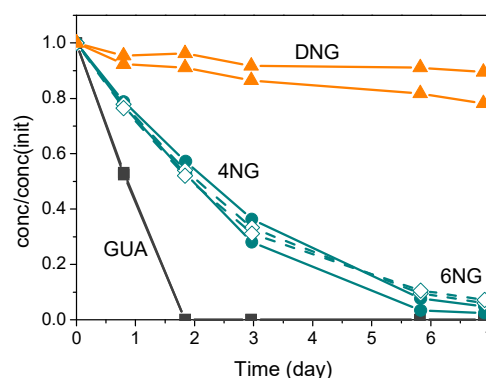


Figure 1. Pollutant concentration decrease in nutrient solution during the treatment.

This work was supported by the Slovenian Research Agency (Contract No. P1-0034).

Pflieger, M. and Kroflič, A. (2017) *submitted for publication*.

Michalowicz, J., Stufka-Olczyk, J., Milczarek, A. and Michniewicz M. (2011) *Environmental Science and Pollution Research* **18**, 1174-1183.

Misztal, P.K. *et al* (2015) *Scientific Reports* **5**, 10.

Stockwell, C.E., Veres, P.R., Williams, J. and Yokelson, R.J. (2015) *Atmospheric Chemistry and Physics* **15**, 845-865.

## Mechanisms of toxicity of particulate emissions produced by different gasoline and alternative fuels in human lung cells

H. Libalova<sup>1</sup>, M. Vojtisek-Lom<sup>2</sup>, J. Klema<sup>3</sup>, M. Machala<sup>4</sup> and J. Topinka<sup>1</sup>

<sup>1</sup>Department of Genetic Toxicology and Nanotoxicology, Institute of Experimental Medicine CAS, Prague, Czech Republic

<sup>2</sup>Center of Vehicles for Sustainable Mobility, Czech Technical University in Prague, Czech Republic

<sup>3</sup>Department of Cybernetics, Czech Technical University in Prague, Czech Republic

<sup>4</sup>Department of Chemistry and Toxicology, Veterinary Research Institute, Brno, Czech Republic

Keywords: gasoline emissions, organic extracts, toxicity, gene expression profiling  
libalova@biomed.cas.cz

The toxic effects of gasoline exhaust particles are far less studied comparing to diesel emissions despite their massive production by passenger cars and substantial contribution to the air pollution. Here we examine toxicity of organic compounds bound on exhaust particles from conventional and alternative gasoline fuels using a direct injection spark ignition (DISI) engine.

Mixtures of organic compounds were extracted from particulate emission produced by four different fuels: conventional gasoline fuel (E 0), blend of gasoline fuel with 15% of ethanol (E15), blend of gasoline fuel with 25% of i-butanol (i-BUT 25) and blend of gasoline fuel and 25% n-butanol (n-BUT 25). Human lung epithelial cells (BEAS-2B) representing a model of the target organ were exposed for 4 and 24h to organic extracts of gasoline exhaust particles (GEP extracts) to investigate the adverse effects and compare their toxic potencies. In order to reveal global changes on molecular level, gene expression profiling was performed using microarray technique (Illumina Human HT-12 v4 BeadChips). Significantly deregulated genes and modulated pathways were identified using differential gene expression analysis and gene set enrichment analysis.

Four hour exposure resulted in numerous genes deregulated in response to each GEP extract. n-BUT 25 altered expression of the highest total number of genes including up- and downregulated (451) while other extracts were less efficient concerning the gene numbers (E 0 – 261, E 15 – 251, i-BUT 25 – 220; Figure 1A).

56 genes were common for all treatments. Gene set enrichment analysis revealed a list of pathways that were significantly overrepresented across the genes. The list involves processes and pathways related to DNA damage response, SREBP signaling, senescence and autophagy, plasminogen activation and blood coagulation, cell-cell

junction and adhesion, regulation of ECM components or metabolism of lipids and steroids or DNA damage response. Several priority genes such as SERPINB2, PLAT, F3, HMGCR, HMGCS1, INSIG1, IL24, IL1B, CDH1, CDH2 and others contributing to single or multiple processes were identified and selected for further validation.

Upon 24h exposure, numbers of deregulated genes were more consistent across all treatments, we found 319, 271, 402 and 342 genes modulated in response to the exposure of E 0, E 15, i-BUT 25 and n-BUT 25 extracts, respectively (Figure 1B). However, less genes (40) were found as commonly deregulated for all treatments. Interestingly, pathway analysis identified the only pathway “Alanine, aspartate and glutamate metabolism” to be significantly overrepresented among these common genes. However, several common priority deregulated genes such as CYP1A1, ALDH3A1, GADD45A, IL1A, TNFAIP8L3 or HMGCS1 further indicate possible modulation of other processes such as metabolism of polycyclic organic compounds, detoxification of toxic products, DNA damage response and growth arrest, immune response and metabolism of lipids and steroids. In contrast to 4h exposure, long term exposure to diverse GEP extracts induced more distinctive gene expression patterns.

Our results indicate substantial differences in toxic effects and consequent molecular responses in BEAS-2B cells upon exposure to different GEP extracts, possibly due to differences in chemical composition of gasoline exhaust particles.

This work was supported by the Ministry of Education, Youth and Sports of the Czech Republic under the projects no. LM2015073 (Research Infrastructure NanoEnviCz) and LO1508 (NANOGEN), and Czech Science Foundation (CENATOX P503/12/G147).

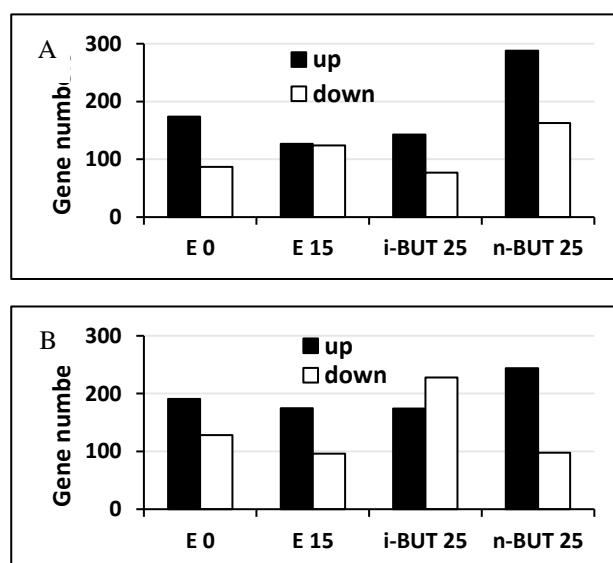


Figure 1. Numbers of significantly deregulated genes upon A) 4h and B) 24h exposure.

## Brake wear (nano)particles: physico-chemical characterization and effects on airway epithelial cells.

C. Puisney<sup>1,2</sup>, E. Oikonomou<sup>2</sup>, S. Nowak<sup>3</sup>, A. Chevillot-Biraud<sup>3</sup>, JF. Berret<sup>2</sup>, A. Baeza-Squiban<sup>1</sup>

<sup>1</sup>Lab Molecular and Cellular Responses to Xenobiotics UMMR-CNRS 8251, Univ Paris Diderot, Paris, France

<sup>2</sup>MSC, CNRS UMR 7057, Univ Paris Diderot, Paris, France

<sup>3</sup>ITODYS, UMR CNRS 7086, Univ Paris Diderot, Paris, France

Keywords: nanosize, metals, cytotoxicity, inflammation, oxidative stress

Presenting author email: [baeza@univ-paris-diderot.fr](mailto:baeza@univ-paris-diderot.fr)

### Introduction

Epidemiologic studies have shown that ambient particulate matter exposure (PM) is associated to an increase of health effects such as pulmonary and cardiovascular mortality. PM concentration is highly dependent on traffic that is one of the most important source of ambient anthropogenic PM in urban areas. Toxicity and health outcomes induced by vehicle exhaust such as Diesel are well documented, whereas those induced by brake wear particles exposure have been rarely studied. However, brake wear dust has been shown to represent the most important source of non-exhaust traffic related particles (55%). It is a heterogeneous mixture including a nanosized fraction and a majority of metallic compounds.

Our purpose was to isolate and characterize brake wear nanoparticles in order to assess their potential toxic effects. The respiratory tract being the main route of exposure to airborne particles, nanoparticles were studied on a human bronchial epithelial cell line: Calu-3.

### Methods

Brake wear dusts (BWD) were recovered from brake test bench or entire vehicles. A full characterization of brake wear dust was done by thermogravimetric analysis, X-fluorescence and scanning electron microscopy. Fractionation by filtration was performed to recover the nanosize fraction (BWNP) that was characterised by dynamic light scattering, transmission electron microscopy coupled to X-ray dispersive energy.

Calu-3 cells were exposed to BWP and its nanosize fraction (BWNP) for 4h or 24h from 1 to 100  $\mu\text{g}/\text{cm}^2$ . Different endpoints were studied (i) cell viability by WST-1 assay measuring mitochondrial activity (ii) production of reactive oxygen species by a fluorescent probe (H<sub>2</sub>DCF-DA) (iii) pro-inflammatory response by measuring the release of Interleukin-6 cytokine by ELISA.

### Results

BWD showed a low carbonaceous but high metal content (Iron and copper being the major one), and a large size distribution. The nanosize fraction recovered by filtration of the BWD suspension represented 26% by

mass of BWD. It contains negatively charged nanoparticles of a hydrodynamic diameter around 200 nm. TEM-EDX revealed a large diversity of shape of nanoparticles mainly composed of iron and copper and exhibit a size distribution centred on 80 nm.

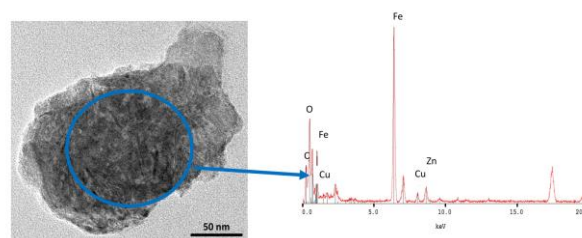


Figure 1 : Brake wear nanoparticle

BWD induced a dose-dependent cytotoxicity on Calu-3 cells being significant from 1  $\mu\text{g}/\text{cm}^2$  and producing a decrease of 79% of viability at 100  $\mu\text{g}/\text{cm}^2$ . By contrast BWNP exhibited more limited cytotoxicity reaching only 35% loss of viability at 100  $\mu\text{g}/\text{cm}^2$ . This cytotoxicity is associated to ROS production after 4 hrs of exposure to both types of particles from 50  $\mu\text{g}/\text{cm}^2$ . BWD induced a significant and consistent release of IL-6 whereas BWNP induced only a very slight effect.

### Conclusion

In conclusion, we isolated the nanosize fraction of BWP that represented a significant mass in BWP and transition metals content. Toxicity studies reveals that although both types of particles induced intracellular production, only the BWP induced cytotoxicity and a consistent cytokine release.

This study is funded by “DIM Nano-K – Région Ile-de-France”.

**Pro-inflammatory Effects of PM<sub>2.5</sub> from Beijing Winter Haze: Revealing the Role of Individual External and Internal Microbiome**

Fangxia Shen<sup>1,2</sup>, Fobang Liu<sup>2</sup>, Xiangyu Zhang<sup>3</sup>, Jing Li<sup>3</sup>, Kira Ziegler<sup>2</sup>, Ting Zhang<sup>3</sup>, Tianle Zhu<sup>1</sup>, Manabu Shiraiwa<sup>4</sup>, Maosheng Yao<sup>3</sup>, Haijie Tong<sup>2</sup>, Kurt Lucas<sup>2</sup>, Ulrich Pöschl<sup>2</sup>

<sup>1</sup>School of Space and Environment, Beihang University, Beijing, 100191, China

<sup>2</sup>Multiphase Chemistry Department, Max Planck Institute for Chemistry, Mainz, 55128, Germany

<sup>3</sup>College of Environmental Sciences and Engineering, Peking University, Beijing, 100871, China

<sup>4</sup>Department of Chemistry, University of California, Irvine, California, 92697-2025, USA.

Keywords: PM<sub>2.5</sub>, inflammation, oxidative stress, microbiome, LPS

Presenting author email: fxshen@buaa.edu.cn

China has experienced frequent serious haze episodes in recent years, which accordingly has led to increasing number of studies regarding its formation mechanisms. On the other hand, the public is becoming more concerned about the health impact of the haze problems. Oxidative stress and inflammation is generally accepted mechanism by which air pollutants cause adverse health effects. However, the molecular level mechanism is far away from clear. Human microbiome, which composes 10 times more microorganisms than our own cells, has gained increasing attention in its roles in people's health. In particular, components from our resident microbiome, i.e., lipopolysaccharide (LPS), play an important role in regulating immune homeostasis. This study aims to investigate the potential synergistic role of air pollutants and microbial components, and relevant results could further shed new light on the understanding of the mechanism.

Particulate matters smaller than 2.5  $\mu\text{m}$  (PM<sub>2.5</sub>) collected in Beijing during 2016 winter haze period were used to stimulate THP-1-derived macrophages. The cellular immune response was evaluated by measuring the cytokine production, including IL-1 $\beta$ , IL-8, TNF and IL-6. To simulate the internal body microenvironment exposure, elevated LPS of different concentrations together with PM<sub>2.5</sub> water extractions was applied to study the cellular response. No toxicity was detected when 10  $\mu\text{g}/\text{ml}$  PM<sub>2.5</sub> water extractions were given to the macrophages. The pro-inflammatory immune effect of PM<sub>2.5</sub> collected on days of different pollution levels varies, however, it was not induced by the cytotoxicity. Characterization results of PM<sub>2.5</sub> indicated that this discrepancy in cellular inflammatory response was attributed to particle-borne LPS and metal levels (Fe and Ni). Furthermore, the pro-inflammatory cytokine secretion was augmented when macrophages were stimulated with PM<sub>2.5</sub> in the presence of elevated lipopolysaccharide (LPS). Samples collected from heavily polluted episodes show stronger enhancing pro-inflammatory effects when 100  $\text{pg}/\text{ml}$  LPS was applied. Whereas, the enhancing effect was weak in the presence of either 1 or 10  $\text{pg}/\text{ml}$  LPS. PCR array assay results suggest that oxidative stress plays vital role in the magnifying effects of PM<sub>2.5</sub>. Knowing the body internal microenvironment can be of great importance to evaluating the PM<sub>2.5</sub> health effects. The results obtained here provide an evidence about the synergistic effects of PM<sub>2.5</sub> and microbial LPS. Overall, this study highlights the importance of studying roles of human microbial

structures, especially respiratory microbiome, when unraveling the underlying mechanism at cellular and molecular level.

## **Abstracts T404**

## A temperature and humidity controlled air-liquid interface for cell culture exposition based on high-efficiency electrostatic deposition

H. Wiegand<sup>1</sup>, K. Fetsch<sup>1</sup>, J. Meyer<sup>1</sup> and G. Kasper<sup>1</sup>

<sup>1</sup>Institut of Mechanical Process Engineering and Mechanics – Gas Particle Systems, Karlsruhe Institute of Technology (KIT), Karlsruhe, 76131, Germany

Keywords: air-liquid interface, electrostatic cross flow precipitator, temperature and humidity controlled system, precise deposition rates onto cell cultures

Presenting author email: harald.wiegand@kit.edu

The air-liquid interface (ALI) provides a realistic in-vitro exposure scenario for the deposition of inhalable nanoparticles onto cell cultures for toxicological, pharmaceutical and environmental research. It is hence necessary to regularly provide a sufficient particle dose within an acceptable time while achieving the required separation of nanoparticles from the carrier gas. For this purpose a cross-flow ALI precipitator capable of exposing cultured human lung cells to nanoparticles is presented. It is based on an early state precipitator which used a specially developed conductivity measurement to characterize particle deposition rates described in [1].

### Experimental

In Figure 1A schematic of the inlet and the deposition zone is shown. Three gas flows are fed into the ALI precipitator. The aerosol flow consists of polydisperse sodium chloride particles (20-520 nm) which is used as a surrogate aerosol for deposition rate measurements.

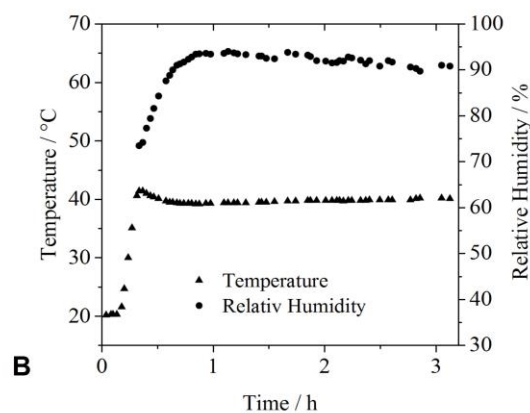
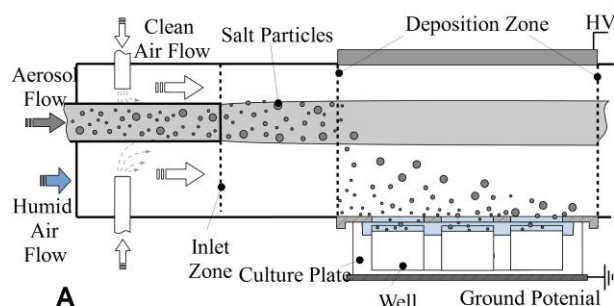


Figure 1. A: Schematic of the precipitator. B: Temperature and humidity stability over time, Position of the measurements was the precipitator inlet.

It is generated by dispersing an aqueous solution into air and it is unipolar charged. The humidified flow has a relative humidity of 85 to 95 % to provide suitable conditions for cell culture experiments. In order to guarantee laminar flow conditions and to provide a sheathed airflow a third flow of clean air is used. All three flows have a temperature 40 °C. Temperature and humidity of the flows as well as the conditions within the precipitator are controlled. The particles are deposited in an electrostatic field (1 to 3 kV/cm) directly into the wells crossing the clean and the humid air flow (Figure 1A). As the conductivity of the liquid in each well changes proportionally to the quantity of deposited salt the deposition rates can be determined [1].

### Results

Tests of the temperature and humidity control were successfully performed and the results are given in Figure 1b. After 30 minutes the required range of relative humidity is reached and stable process parameters are achieved after 60 minutes. Once the temperature and humidity stability is reached the set-up keeps the flow rates, temperatures and humidity's at a constant level. First results of particle deposition characterization indicate a deposition efficiency of about 40 % of the introduced particle mass in the cell culture wells without any optimization.

### Conclusion

Humidity and temperature control of an electrostatic ALI precipitator are possible and suitable conditions for cell culture experiments can be provided. To run deposition rate experiments with monodisperse aerosols higher deposition rate are required in the next step. The aim is a precipitator, for which the particle deposition rate can be calculated as a function of particle size and operating conditions.

1. Wiegand, H., Meyer, J., and G. Kasper, (2015) *An electrical conductivity based method of determining the particle deposition rate in air-liquid interface devices*. Toxicology in Vitro, Volume 29, Issue 5, 1100-1106

***In vitro* dosimetry and bioimaging with aerosol-made  $\text{YVO}_4:\text{Eu}^{3+},\text{Bi}^{3+}$  nanophosphors**Anastasia Spyrogianni<sup>1</sup>, Peter G. Tiefenboeck<sup>2</sup>, Frank Krumeich<sup>1</sup>, Jean-Christophe Leroux<sup>2</sup>, Sotiris E. Pratsinis<sup>1</sup>, Georgios A. Sotiriou<sup>3</sup><sup>1</sup>Department of Mechanical and Process Engineering, ETH Zurich, Zurich, 8092, Switzerland<sup>2</sup>Department of Chemistry and Applied Biosciences, ETH Zurich, Zurich, 8093, Switzerland<sup>3</sup>Department of Microbiology, Tumor and Cell Biology, Karolinska Institutet, Solna, 17177, SwedenKeywords: nanotechnology, fluorescence microscopy, *in vitro*, cells.

Presenting author email: spyrogianni@ptl.mavt.ethz.ch

Luminescent rare-earth-based inorganic nanoparticles (nanophosphors) are promising bioimaging agents due to their high photostability, sharp emission bands and relatively low toxicity (Escudero *et al.*, 2016a). Flame aerosol technology provides a scalable (Mueller *et al.*, 2003) and highly reproducible (Strobel & Pratsinis, 2007) process for production of such nanophosphors (e.g.  $\text{Y}_2\text{O}_3:\text{Eu}^{3+},\text{Tb}^{3+}$ ) with precise control of their composition and properties (Sotiriou *et al.*, 2011; Sotiriou *et al.*, 2012). Nanophosphors that can be excited in the near-ultraviolet and visible region, such as  $\text{YVO}_4:\text{Eu}^{3+},\text{Bi}^{3+}$  (Takeshita *et al.*, 2008), provide a useful tool for bioimaging (Escudero *et al.*, 2016b) and *in vitro* dosimetry (Halamoda-Kenzaoui *et al.*, 2015) studies using conventional fluorescence microscopes.

Here,  $\text{YVO}_4:\text{Eu}^{3+},\text{Bi}^{3+}$  nanophosphors are made by flame spray pyrolysis. The optimal Bi content for maximum red-shift of their excitation band edge towards the visible region is identified through systematic experiments. The nanophosphors with the optimal composition are highly crystalline and appear bright red under a conventional fluorescence microscope. Their photostability during dynamic imaging of HeLa cells *in vitro* is confirmed, contrary to commercial fluorescent (organic-dye labeled)  $\text{SiO}_2$  nanoparticles that exhibit 50% photobleaching within 3.5 h (Fig. 1).

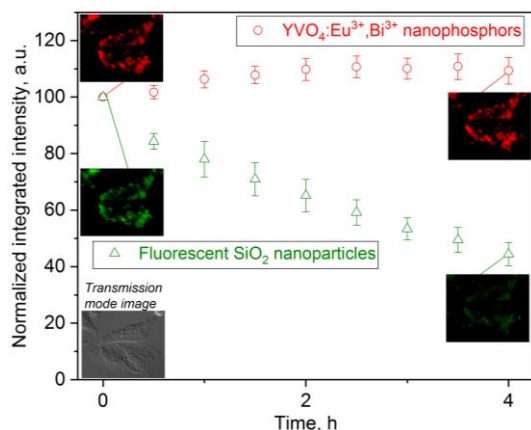


Figure 1. Dynamic fluorescence microscopy imaging of HeLa cells co-incubated with  $\text{YVO}_4:\text{Eu}^{3+},\text{Bi}^{3+}$  nanophosphors and fluorescent  $\text{SiO}_2$  nanoparticles. The fluorescence intensity of images corresponding to  $\text{YVO}_4:\text{Eu}^{3+},\text{Bi}^{3+}$  is stable with time (circles and red images), while that for fluorescent  $\text{SiO}_2$  decreases down to 50% within 3.5 h (triangles and green images). The corresponding optical microscopy image in transmission mode at 0 h is also shown.

Furthermore, the deposition rate of these nanophosphors is measured by optical absorption spectroscopy, indicating slower deposition rate in serum-containing than serum-free cell culture medium, consistent with previous studies for different nanomaterials (Allouni *et al.*, 2009; Spyrogianni *et al.*, 2016). This is also confirmed *in vitro* by monitoring the fluorescence intensity of images of HeLa cells after incubation with nanophosphor suspensions in the presence and absence of serum for various time points (Halamoda-Kenzaoui *et al.*, 2015).

This work was supported by the Swiss National Science Foundation (no. 200020-146176) and the European Research Council (FP7/2007–2013, no. 247283).

- Allouni, Z.E., Cimpan, M.R., Hol, P.J., Skodvin, T., & Gjerdet, N.R. (2009) *Coll. Surf. B* **68**, 83-87.
- Escudero, A., Carrillo-Carrion, C., Zyuzin, M.V., & Parak, W.J. (2016a) *Topics Curr. Chem.* **374**.
- Escudero, A., Carrillo-Carrion, C., Zyuzin, M.V., Ashraf, S., Hartmann, R., Nunez, N.O., Ocana, M., & Parak, W.J. (2016b) *Nanoscale* **8**, 12221-12236.
- Halamoda-Kenzaoui, B., Ceridono, M., Colpo, P., Valsesia, A., Urban, P., Ojea-Jimenez, I., Gioria, S., Gilliland, D., Rossi, F., & Kinsner-Ovaskainen, A. (2015) *PLOS ONE* **10**, e0141593.
- Mueller, R., Madler, L., & Pratsinis, S.E. (2003) *Chem. Eng. Sci.* **58**, 1969-1976.
- Sotiriou, G.A., Schneider, M., & Pratsinis, S.E. (2011) *J. Phys. Chem. C* **115**, 1084-1089.
- Sotiriou, G.A., Franco, D., Poulidakos, D., & Ferrari, A. (2012) *ACS Nano* **6**, 3888-3897.
- Spyrogianni, A., Herrmann, I.K., Lucas, M.S., Leroux, J.C., & Sotiriou, G.A. (2016) *Nanomedicine (Lond.)* **11**, 2483-2496.
- Strobel, R., & Pratsinis, S.E. (2007) *J. Mater. Chem.* **17**, 4743-4756.
- Takeshita, S., Isobe, T., & Niikura, S. (2008) *J. Lumin.* **128**, 1515-1522.

## Particle mass monitoring by Quartz Crystal Microbalance using electrostatic deposition enhancement

S. Mühlhopt<sup>1</sup>, C. Schlager<sup>1,2</sup>, T. Krebs<sup>2</sup>, M. Berger<sup>2</sup> and H.-R. Paur<sup>1</sup>

<sup>1</sup>Institute for Technical Chemistry, Karlsruhe Institute of Technology, Karlsruhe, 76021, Germany

<sup>2</sup>Vitrocell Systems GmbH, Waldkirch, 79183, Germany

Keywords: quartz crystal microbalance (QCM), dosimetry, toxicity testing

Presenting author email: Sonja.muelhopt@kit.edu

Investigating ultrafine particles and airborne nanomaterials regarding their lung toxic potential the Air Liquid Interface (ALI) exposure of lung cell cultures towards aerosols and subsequent determination of biological endpoints is the method of choice (Paur et al., 2011). The knowledge of the exact relevant *in-vitro* dose (RID) is essential to determine the dose-response relationship of the inhalable aerosol (Mühlhopt et al., 2016a). Due to the low mass of these particles and the complex geometry of the ALI exposure chambers, established measurement methods such as SMPS or gravimetric analysis reach their limitations.

To determine the deposited mass, quartz crystal microbalance (QCM) was developed as online monitoring tool (Mühlhopt et al., 2009). Deposited mass can be detected online under normal diffusional conditions by measuring the difference of frequency (Sauerbrey, 1959). The QCM sensor is located at the same position cells are located in a regular experiment at the air liquid interface to measure the mass deposited by diffusional deposition. To evaluate the effects of less toxic compounds or to reduce time of exposure an electrostatic field between cells and aerosol inlet is needed. Under these conditions, detection of deposited mass by QCM is not possible.

A novel QCM is developed in which the potential for the electrical field is applied to the exit of the aerosol inlet (Mühlhopt et al., 2016b). The inlet tubing by itself is grounded but a mesh contacted to a high voltage supply is located at the exit of the inlet (Figure 1).

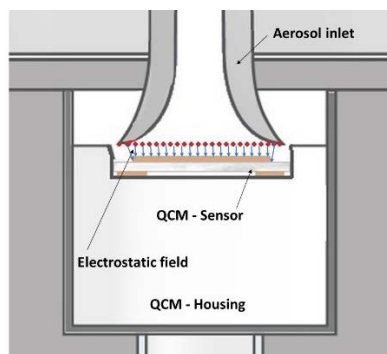


Figure 1 Scheme of the Quartz Crystal Microbalance (QCM) exposed to the aerosol streaming in via the aerosol inlet and deposited on the sensor surface due to electrostatic forces.

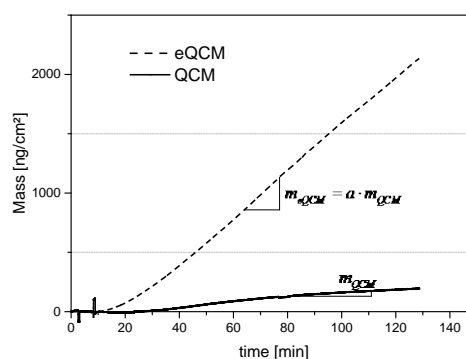


Figure 2. Fluorescein sodium mass loading signal of quartz crystal microbalances using diffusional deposition (compact) and electrostatic deposition (dotted).

Figure 2 compares the signals monitored with the two types of QCM sensors: the compact curve shows the linear mass loading by diffusional deposition with the gradient  $m_{QCM}$ . For the electrostatic enhanced deposition of particles on the sensor of the linear dotted curve shows the gradient  $m_{eQCM}$  with the increase factor  $a$ . The increase factor  $a$  reaches values of up to 30 depending on the charge distribution of the aerosol and is discussed for standard aerosols as well as for combustion aerosol of a biomass burner.

The financial support by the KIT Innovation Fund is gratefully appreciated. We thank Ms. Sonja Schaaf for the technical assistance.

Mühlhopt, S., Diabaté, S., Krebs, T., Weiss, C., and Paur, H.R. (2009). *Journal of Physics: Conference Series*, 170, S.012008/1-4.

Mühlhopt, S., Dilger, M., Diabaté, S., Schlager, C., Krebs, T., Zimmermann, R., Buters, J., Oeder, S., Wäscher, T., Weiss, C., and Paur, H.-R. (2016a). *Journal of Aerosol Science*, 96, pp. 38–55

Mühlhopt, S., Schlager, C., Paur, H.R. (2016b) *DE 10 2014 118 846 B4*

Paur, H.-R., Cassee, F.R., Teeguarden, J., Fissan, H., Diabate, S., Aufderheide, M., Kreyling, W.G., Hänninen, O., Kasper, G., Riediker, M., Rothen-Rutishauser, B., and Schmid, O. (2011). *Journal of Aerosol Science*, 42, pp. 668–692.

Sauerbrey, G. (1959). *Zeitschrift für Physik*, 155, pp. 206–222.

## Efficiency, variability and control of aerosol sampling and deposition in the Vitrocell® 24/48 trumpet unit

A.K. Kuczaj<sup>1,2</sup>, F. Lucci<sup>1</sup>

<sup>1</sup>Philip Morris International R&D, Philip Morris Products S.A. (part of Philip Morris International group of companies), Switzerland

<sup>2</sup>Multiscale Modeling and Simulation, Applied Mathematics, University of Twente, The Netherlands

Keywords: deposition, in-vitro, computational fluid dynamics

Presenting author email: arkadiusz.kuczaj@pmi.com

Modern system toxicology approaches deploy in vitro studies in order to understand impact of substances on tissue cultures in a controlled conditions. In order to expose biological samples to flowing aerosol sophisticated exposure systems as for example Vitrocell 24/48 are used (Kuczaj *et al* 2016). Both the flow and thermodynamical conditions in such systems are controlled in order to deliver aerosols in reliable, repeatable and reproducible way. The flowing aerosol is always affected due to locally changing flow conditions, residence time, and deposition effects. We computationally investigate leading mechanisms of aerosol deposition and their efficiency in the wells where the biological inserts are exposed.

Aerosols may deposit mainly by means of inertial impaction, gravitational settling, and diffusion. The importance of each of these mechanisms depends on the particle size as well as on the flow conditions. We investigate characteristics flow scales and importance of deposition mechanisms in the actual 3D geometry of the Vitrocell trumpet unit. We adopt a sectional, compressible, internally mixed aerosol model for the description of the transport and evolution of a polydisperse aerosol (Frederix *et al* 2017). This model was shown to give accurate predictions for non-isokinetic aerosol sampling, driven by inertial particles drift. The model was also extended to include particles diffusion based on the Stokes-Einstein Brownian diffusivity model. Developed wall boundary conditions to capture the deposition flux due to gravitation, Brownian motion and inertial drift were separately validated using bent pipe deposition experiments.

The aerosol particles in the trumpet deposition unit, spanning a large size particle diameter range ( $1\text{ nm} < d < 5\ \mu\text{m}$ ), deposit with a size-dependent deposition efficiency  $\eta$  (Fig.1). For the increasing residence time (decreasing flow rate), the deposition efficiency is larger as particles have more time to sediment. From the presented deposition efficiency data, the effective deposition efficiency for polydisperse non-evolving aerosol with known distribution can be computed being the weighted average of efficiencies over the span of aerosol sizes. It is important to realize that in the operational regime of the system, deposition of particles within 200 nm to 5  $\mu\text{m}$  does not depend on the flow rate. In this aerosol size regime it is purely dictated by the gravitational force (as shown in Fig.2). For particles smaller than 200 nm the diffusion effects starting to play

a role and deposition is related to the residence time of particles over the deposition plate.

We investigate influence of potential variable conditions in the system on the aerosol deposition, i.e., flow rate, distance to the deposition plate, and density of particles. We extend our study to evolving aerosols taking advantage of developed model.

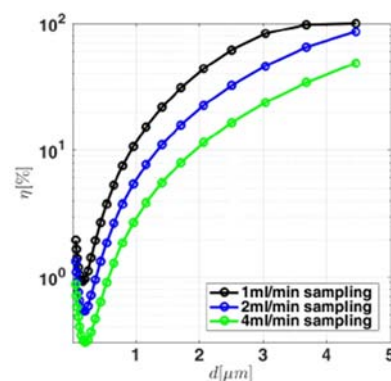


Figure 1. Predictions of the Vitrocell trumpet deposition efficiency for 1.0 (black), 2.0 (blue) and 4.0 (green) ml/min sampling flow rate.

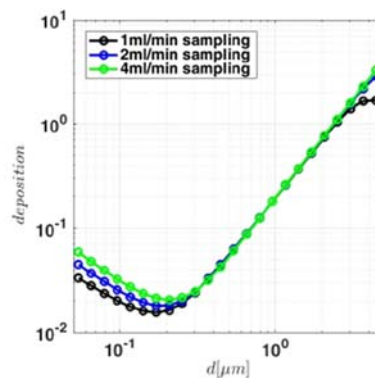


Figure 2. Deposition flux of on the tissue inserts for three investigated flow rates.

Kuczaj, A.K. et al. (2016), *Aerosol flow in the Vitrocell 24/48 exposure system: flow mixing and aerosol coalescence*. Applied In Vitro Toxicology, 2(3):165–174  
 Frederix, E.M.A. et al. (2017), *Application of the characteristics-based sectional method to spatially varying aerosol formation and transport*. J. Aerosol Sc., 104:123-140

The research presented in this work was funded by Philip Morris Products S.A. (part of Philip Morris International group of companies).

## **Abstracts T406**

## Oxidative potential of water-soluble fractions of PM<sub>2.5</sub> and PM<sub>10</sub> in South-eastern Italy during advection of African dust

D. Chirizzi<sup>1</sup>, D. Cesari<sup>1</sup>, M.R. Guascito<sup>1,2</sup>, A. Dinoui<sup>1</sup>,  
L. Giotta<sup>2</sup>, A. Donateo<sup>1</sup>, and D. Contini<sup>1</sup>

<sup>1</sup> Istituto di Scienze dell'Atmosfera e del Clima, ISAC-CNR, S.P. Lecce-Monteroni km 1.2, 73100 Lecce, Italy

<sup>2</sup> Department of Biological and Environmental Sciences and Technologies, University of Salento, Lecce, 73100, Italy

Keywords: oxidative potential, DTT assay, particulate matter, Saharan dust

Presenting author email: d.contini@isac.cnr.it

Several studies showed that atmospheric particulate matter (PM) has adverse effects on human health although the exact mechanisms of toxicity are still not completely understood (Pope et al, 2009). Reactive oxygen species (ROS) either transported on particles or catalytically generated by particles through redox reactions are suspected to cause injurious cellular responses (Bates et al., 2015) suggesting that oxidative potential (OP) of PM could be an useful indicator for potential health effects. The contribution of different sources to OP has been object of several studies, however, detailed analyses of the oxidative potential of PM during Saharan dust outbreaks (SDO) are not yet available. This work was specifically performed to fill this gap evaluating the OP of water-soluble PM<sub>2.5</sub> and PM<sub>10</sub>, using the DTT assay, comparing results obtained during SDO events with those referring to average particles concentrations and those referring to samples having high carbon content due to relevant contributions from combustion sources (mainly road traffic and biomass burning). Measurements were taken at the Environmental-Climate Observatory of Lecce (Southern Italy, 40°20'8"N-18°07'28"E, 37 m asl), regional station of the Global Atmosphere Watch (GAW) network.

Daily samples were collected on quartz filters (pre-fired at 700 °C for 2 h) using a low-volume (2.3 m<sup>3</sup>/h) dual channel sampler (SWAM, Fai Instruments). Sixty samples (30 of PM<sub>2.5</sub> and 30 of PM<sub>10</sub>) were selected and divided in three groups: a standard group having OC and EC comparable with the long-term average values; a group having high OC and EC concentrations; and a group representing SDO cases. A punch (1.0 cm<sup>2</sup>) was obtained from each sample and it was used for the determination of organic (OC) and elemental carbon (EC) via thermo-optical method using a Sunset OC/EC Analyser following the NIOSH-870 protocol. Water-soluble content was extracted from 1/4 of each filter in 15 mL of deionized water (DI, Milli-Q; >18 MΩ). The extracts were used for the DTT assay performed following Cho et al. (2005). The rate of DTT consumption ( $\delta_{DTT}$ , pmol/min) was used to determine the OP as DTT activity normalised in terms of sampled volume (V) as  $DTT_V = \frac{\delta_{DTT} - \delta_{blank}}{V}$  or in terms of collected aerosol mass (M) as  $DTT_M = \frac{\delta_{DTT} - \delta_{blank}}{M}$ . The two points of view are not equivalent because the OP is dependent on the collected mass.  $DTT_M$  represents an intrinsic property of particles linked to sources, while  $DTT_V$  depends on emission rates

and dilutions and characterizes the human exposure to particles at a specific site.

Results show that  $DTT_V$  increases in samples having a high carbon content due to significant contributions of combustion sources (mainly road traffic and biomass burning). This happens for both fractions PM<sub>2.5</sub> and PM<sub>10</sub>, however, the oxidative potential of coarse particles (PM<sub>2.5-10</sub>) is lower than that of fine particles (PM<sub>2.5</sub>). The  $DTT_V$  of Saharan dust particles is not different from the average  $DTT_V$  of aerosol in this area and it is lower than that of particles having a high carbon content (Fig. 1). The mass-normalized  $DTT_M$  is larger, on average, for PM<sub>2.5</sub> compared to PM<sub>10</sub>. The maximum relative difference for the two size fractions was observed during SDO events showing that dust transported from Africa have a low  $DTT_M$ . Results suggest that  $OP_{DTT}$  could be a good quantitative indicator, to be used in addition to mass concentration, to investigate air quality in zones subjected to advection of natural sources such as Saharan dust.

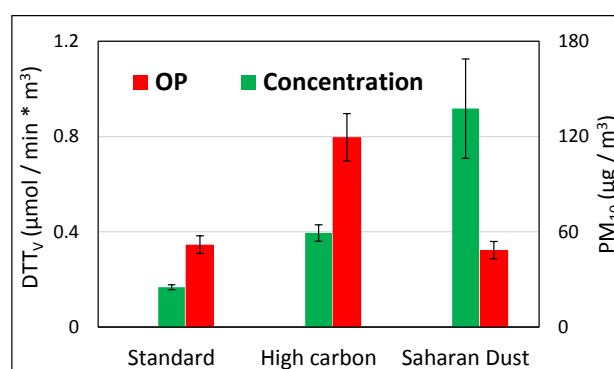


Figure 1. Comparison of  $DTT_V$  and concentrations in the three groups of samples for PM<sub>10</sub>.

Work supported by I-AMICA (Infrastructure of High Technology for Environmental and Climate Monitoring - PONa3\_00363) project funded by National Operational Program (PON) for "Research and Competitiveness 2007-2013" co-funded with European Regional Development Fund (ERDF) and National resources.

Cho, A.K., Sioutas, C., Miguel, A.H., Kumagai, Y., et al. (2005) *Environ. Res.* **99**, 40-47.

Bates, J.T., Weber, R.J., Abrams, J., Verma, et al. (2015) *Environ. Sci. Technol.* **49**, 13605-13612.

Pope, C.A., M. Ezzati, D.W. Dockery, (2009) *N. Engl. J. Med.* **360**, 376-386.

## Ambient sources and health effects of reactive oxygen species - PM 2.5 characteristics and effects to normal and diseased airway epithelia

Z. Leni<sup>1</sup>, L.E.Cassagnes<sup>2</sup>, J. Dommen<sup>2</sup>, I. El Haddad<sup>2</sup>, and M. Geiser<sup>1</sup>

<sup>1</sup>Institute of Anatomy, University of Bern, 3012 Bern, Switzerland

<sup>2</sup>Laboratory of Atmospheric Chemistry, Paul Scherrer Institute, 5232 Villigen, Switzerland

Keywords: air liquid interface, oxidant/antioxidant imbalance, particulate matter, reactive oxygen species

Presenting author email: zaira.leni@ana.unibe.ch

Long-term exposure to ambient levels of fine particulate matter (PM) has been clearly associated with adverse respiratory effects and increased mortality from cardiovascular diseases. PM with aerodynamic diameters  $\leq 2.5 \mu\text{m}$ , which mainly originates from combustion processes, are considered particularly toxic. Despite the acknowledged harmful consequences caused by air pollution, the interaction of particles with the inner surface of the lungs is only partially known (Künzi *et al.*, 2013). The aim of this project is to elucidate the relationship between PM and adverse effects of reactive oxygen species (ROS) production to normal and diseased human airway epithelia. ROS production leading to oxidative stress plays a key role in the biological response of lung cells. Thus, it is of a great interest to extensively examine the ROS formation and the oxidant/antioxidant imbalance in the primary target of inhaled particles, i.e. the airway epithelium (Manke *et al.*, 2013; Dunnick *et al.*, 2015). We applied several chemical compounds representative for different aerosol constituents to the air-liquid interface (ALI) of fully differentiated human bronchial epithelial cell cultures (HBEC). These were hydrogen peroxide ( $\text{H}_2\text{O}_2$ ), a powerful oxidizing agent present as a gas in the air and representative of organic peroxides in the particle phase, 1,4-naphthoquinone (1,4-NQ), a polycyclic aromatic quinone found in ambient particles, and vanadium (applied as  $\text{V}_2\text{O}_5$ ), a metal emitted from anthropogenic sources. Furthermore, cells were exposed to aqueous filter extracts collected during winter and summer in a rural area (San Vittore, Switzerland, 2013). Cell cultures were exposed to various doses of these compounds and of the filter extracts for 1, 6 and 24 h, and cellular responses were measured thereafter (Table 1).

Parameters assessed included cytotoxicity (release of lactate dehydrogenase, LDH from damaged cells), release of (pro)inflammatory mediators and endogenous and exogenous ROS production. Biological molecules released in the lining fluid will be assessed by the implementation of new mass-spectrometric techniques (e.g. using ESI ion mobility mass spectrometer and Orbitrap mass spectrometer) (Zhang X. *et al.*, 2014). Furthermore, gene expression (GeneGlobe analysis) of selected pathways leading to inflammation, DNA damage, apoptosis and senescence response was evaluated. Preliminary results show a dose and time dependent increase of cytotoxicity for all the compounds and filter extracts examined. Further analyses unraveling the pro-inflammatory response and the effects of ROS generated by these compounds are ongoing.

This work was supported by the Swiss National Science Foundation grant CR32I3\_166325

Künzi L., Peter Mertes P., Schneider S., Jeannet N., Menzi C., Dommen J., Kalberer U., Geiser M. (2013). *Atmos Environ*, **68**, 143-150.

Manke, A., Wang, L. & Rojanasakul, Y. (2013). *Biomed Res Int*.

Dunnick KM., Pillai R., Pisane KL., Stefaniak AB., Sabolsky EM., Leonard SS. (2015). *Biol Trace Elem. Res*, **166**(1), 96-107.

Zhang X., Knochenmuss R., Siems WF., Liu W., Graf S., Hill HH Jr. (2014) *Anal Chem.*, **86**(3):1661-70

	Conc_#1 ( $\mu\text{g}/\text{cm}^2$ )	Conc_#2 ( $\mu\text{g}/\text{cm}^2$ )	Conc_#3 ( $\mu\text{g}/\text{cm}^2$ )	Conc_#4 ( $\mu\text{g}/\text{cm}^2$ )
$\text{H}_2\text{O}_2$	50 (48mM)	10 (9.6mM)	1 (960 $\mu\text{M}$ )	0.1 (96 $\mu\text{M}$ )
1,4-NQ	50 (10.43mM)	10 (2.86mM)	1 (200.86 $\mu\text{M}$ )	0.1 (20.86 $\mu\text{M}$ )
$\text{V}_2\text{O}_5$	10 (18mM)	1 (1.8mM)	0.1 (180 $\mu\text{M}$ )	0.01 (18 $\mu\text{M}$ )
Filter summer	2	0.6	0.1	-
Filter winter	2	0.6	0.1	-

**Table 1. Doses of  $\text{H}_2\text{O}_2$ , 1,4-NQ and  $\text{V}_2\text{O}_5$  applied to HBEC:** Cell cultures on Transwell® inserts of  $0.33 \text{ cm}^2$  growth area were treated with 10  $\mu\text{l}$  for  $\text{H}_2\text{O}_2$ , 1,4-NQ and  $\text{V}_2\text{O}_5$  and 50  $\mu\text{l}$  for the filter extracts.

## Important sources and chemical species of ambient fine particles related to adverse health effects

Jongbae Heo<sup>1,\*</sup> and Seung-Muk Yi<sup>1,2</sup>

<sup>1</sup>*Institute of Health and Environment, School of Public Health, Seoul National University, Seoul, 08826, Republic of Korea*

<sup>2</sup>*Department of Environmental Health, School of Public Health, Seoul National University, Seoul, 08826, Republic of Korea*

Keywords: Fine particles, case cross-over study, emergency room visits, real time measurements, source apportionment

Presenting author email: [jongbae heo@gmail.com](mailto:jongbae heo@gmail.com)

Although many epidemiological studies have reported that exposure to ambient fine particulate matter (PM<sub>2.5</sub>) has been linked to increases in mortality and morbidity health outcomes, the key question of which chemical species and sources of PM<sub>2.5</sub> are most harmful to public health remains unanswered in the air pollution research area. This study was designed to address the key question with evaluating the risks of exposure to chemical species and source-specific PM<sub>2.5</sub> mass on morbidity (Heo et al., 2014).

Hourly measurements of PM<sub>2.5</sub> mass and its major chemical species, including organic carbon, elemental carbon, ions, and trace elements, were observed from January 1 to December 31, 2013 at the Korea PM<sub>2.5</sub> supersite in Seoul and the results were used in a positive matrix factorization to estimate source contributions to PM<sub>2.5</sub> mass. Nine sources, including secondary sulfate, secondary nitrate, mobile, biomass burning, roadway emission, industry, oil combustion, soil, and aged sea salt, were identified and secondary inorganic aerosol factors (i.e. secondary sulfate, and secondary nitrate) were the dominant sources contributing to 40% of the total PM<sub>2.5</sub> mass in the study region.

In order to evaluate the risks of exposure to chemical species and sources of PM<sub>2.5</sub> on morbidity, emergency room visits for cardiovascular disease and respiratory disease were considered. Hourly health outcomes were compared with hourly measurements of the PM<sub>2.5</sub> chemical species and sources using a poisson generalized linear model incorporating natural splines, as well as time-stratified case-crossover design. The PM<sub>2.5</sub> mass and several chemical components, such as organic carbon, elemental carbon, zinc, and potassium, were strongly associated with morbidity. Source-apportioned PM<sub>2.5</sub> mass derived from biomass burning, and mobile sources, was significantly associated with cardiovascular and respiratory diseases. The findings represent that local combustion may be particularly

important contributor to PM<sub>2.5</sub>, leading to adverse human health effects.

This work was supported by NRF-2014R1A2A2A04007801 through the National Research Foundation of Korea (NRF) and NIER-0571A-20160005 through the Korea National Institute of Environmental Research (NIER).

Heo J., Schauer J., Yi O., Peak D., Kim H., and Yi S., (2014). *Epidemiology*, 25: 379-388.

**ULTRAFINE PARTICLES FROM BIOMASS BURNING: CHEMICAL COMPOSITION AND BIOLOGICAL EFFECTS FROM A LABORATORY STUDY AND AMBIENT AIR MEASUREMENTS IN NORTHERN ITALY.**

R. Vecchi<sup>1</sup>, S. Becagli<sup>2</sup>, V. Bernardoni<sup>1</sup>, D. Caruso<sup>3</sup>, L. Corbella<sup>4</sup>, E. Corsini<sup>3</sup>, M. Dell'Acqua<sup>1</sup>, P. Fermo<sup>4</sup>, C.L. Galli<sup>3</sup>, G. Lonati<sup>5</sup>, L. Marabini<sup>3</sup>, M. Marinovich<sup>3</sup>, S. Ozgen<sup>5</sup>, A. Papale<sup>3</sup>, S. Signorini<sup>6</sup>, R. Tardivo<sup>5</sup>, and G. Valli<sup>1</sup>

<sup>1</sup>Department of Physics, Università degli Studi di Milano, Milan, 20133, Italy

<sup>2</sup>Department of Chemistry, Università degli Studi di Firenze, Sesto Fiorentino, 50019, Italy

<sup>3</sup>Department of Pharmacological and Biomolecular Sciences, Università degli Studi di Milano, Milan, 20133 Italy

<sup>4</sup>Department of Chemistry, Università degli Studi di Milano, Milan, 20133, Italy

<sup>5</sup>Politecnico di Milano, Milan, 20133, Italy

<sup>6</sup>LEAP Energy and Environment Laboratory, Piacenza, 29121, Italy

Keywords: UFP, composition, biomass burning, toxicology.

Presenting author email: roberta.vecchi@unimi.it

This work is part of a collaborative project called TOBICUP (TOxicity of BIomass Combustion generated Ultrafine Particles) aiming at providing the composition of ultrafine particles (UFPs) emitted by wood combustion and elucidating the related toxicity.

In the Po Valley, which is one of the continental hot-spots for air quality, wood combustion gives a significant contribution to observed high PM concentration as well as to organic pollutants with a strong toxicological impact, such as Polycyclic Aromatic Hydrocarbons (PAHs) and dioxins.

TOBICUP project aimed at verifying the toxicological responses of the samples collected both directly from residential wood combustion emissions under burning cycles reflecting real-life situations and in ambient air at a sampling site where biomass burning for residential heating is widely used. As for the laboratory tests, two commercial residential solid biomass room heaters (one automatically stoked and one manually fed appliance) were tested in the Laboratory for Energy and Environment of Piacenza (LEAP) facility. In the project two ambient monitoring campaigns were carried out in summer and winter periods at an alpine town in Northern Italy, where wood burning is largely diffused for domestic heating in winter.

Both in laboratory and ambient samples UFPs composition was analysed for elements, ions, total carbon, polycyclic aromatic hydrocarbons (PAHs) and for biological activity.

The induction of the pro-inflammatory cytokine interleukin-8 (IL-8) by UFPs was investigated in two human cells lines (A549 and THP-1) and in human peripheral blood leukocytes. In addition, UFP-induced oxidative stress and genotoxicity were investigated in A549 cells. Effects were compared to traffic-emitted particles (DEP).

Compositional differences were observed for pellets and wood UFP samples, where high TC levels characterise the wood log combustion and potassium

salts are dominant in every pellet sample. Crucial aspects determining the UFP composition in the wood stove experiments are critical situations in terms of available oxygen whereas for the automatically controlled pellets stove local situations (e.g. hindered air-fuel mixing due to heaps of pellets on the burner pot) determine the emission levels and composition. Wood samples contain more potentially carcinogenic PAHs with respect to pellets samples. (Ozgen et al., 2017)

Ambient air UFPs were able to stimulate an inflammatory response, as shown by the release of IL-8 in several cellular models, including peripheral blood leukocytes. It is noteworthy that summer UFPs were more active in inducing IL-8 release compared to winter UFPs in both cells lines, but the release was overall similar to the one observed with DEP. Opposite to the inflammatory effect, genotoxic effects induced by UFPs sampled during wintertime were higher than those induced by UFPs sampled during summertime, indicating that seasonal differences in UFPs composition differently affected biological responses. The presence of PAHs and transition metals in ambient air UFPs is likely to contribute to the genotoxicity observed in A549 cells in this study. (Corsini et al., 2017; Corsini et al., submitted).

This work was supported by Fondazione Cariplo (TOBICUP project, Ref. 2013-1040).

Corsini E, Ozgen S, Papale A, Galbiati V, Lonati G, Fermo P, Corbella L, Valli G, Bernardoni V, Dell'Acqua M, Becagli S, Caruso D, Vecchi R, Galli CL, Marinovich M (2017) *Toxicol Letters* **266**, 74–84

Ozgen S, Becagli S, Bernardoni, Caserini S, Caruso D, Corbella L, Dell'Acqua M, Fermo P, Gonzalez R, Lonati G, Signorini R, Tardivo R, Tosi E, Valli G, Vecchi R, Marinovich M (2017). *Atmos Environ* **150**, 87-97

## Detection of air pollution-related biomarkers of exposure and harm in urine of travellers between Germany and China

Xiao Wu<sup>1,2,3</sup>, Jutta Lintelmann<sup>1,2</sup>, Sophie Klingbeil<sup>3</sup>, Jie Li<sup>4</sup>, Ralf Zimmermann<sup>\*1,2,3</sup>

<sup>1</sup> Cooperation Group Comprehensive Molecular Analytics, Helmholtz Zentrum Muenchen - German Research Centre for Environmental Health GmbH, Neuherberg, D-85764, Germany

<sup>2</sup> HICE - Helmholtz Virtual Institute of Complex Molecular Systems in Environmental Health: Aerosol and Health, Neuherberg, D-85764, Germany

<sup>3</sup> Chair Analytical Chemistry, Institute of Chemistry, University of Rostock, Rostock, D-18051, Germany

<sup>4</sup> Department of Environmental Health, Shandong University, Jinan, 250012, China

Keywords: Air pollution, oxidative stress, PAH, 8-hydroxy-2'-deoxyguanosine, malondialdehyde.

Presenting author email: xiao.wu@helmholtz-muenchen.de

**Introduction:** Over the last few decades, China had notable success in terms of economic growth, as well as booming transportation and industry. However, these changes are accompanied by worse air quality such as extremely high concentration of PM<sub>2.5</sub> (particulate matter with an aerodynamic diameter below 2.5 µm), which is caused by fossil fuel and biomass combustion (Chan and Yao, 2008). They can be inhaled and accumulated in the bronchus and pulmonary alveolar surfaces, inducing the formation of reactive oxygen species (ROS) such as peroxides, superoxide, hydroxyl radical, and singlet oxygen. These species disturb the natural oxidative stress balance by attacking macromolecules, such as phospholipids, proteins, and DNA (Risom *et al.*, 2005, Pardo *et al.*, 2015). The influence of acute exposures to PM<sub>2.5</sub> on the concentrations of biomarkers of exposure and oxidative stress should be investigated. For this purpose urine samples from 9 individuals travelling from Germany to China were collected and analysed before and after the travel period in a pilot study. Furthermore the exposure was evaluated via the PM<sub>2.5</sub> concentrations at the whereabouts of the subjects.

**Materials and methods:** Robust LC and LC-MS/MS methods were established for the determination of biomarkers. 8-hydroxy-2'-deoxyguanosine, malondialdehyde, F<sub>2a</sub>-isoprostanes were analysed with LC-MS/MS (API3000, AB Sciex) with electrospray ionization (ESI). Hydroxylated polycyclic aromatic hydrocarbons were analysed on an HPLC-system with integrated solid phase extraction1 (HPLC-FLD, Ultimate 3000, Dionex). 9 volunteers travelled from Germany (mean daily concentration of PM<sub>2.5</sub>: 21 µg/m<sup>3</sup>) to China (mean daily concentration of PM<sub>2.5</sub>: 108 µg/m<sup>3</sup>). Urine samples were collected before and after the trip.

**Results:** In samples collected after return to Germany, the median concentrations of oxidative stress biomarkers were observed to be higher than in samples collected before leaving Germany. Decreasing trends were observed in the sequences of samples collected after return in the following weeks. (Figure 1) Correlations were found between the PM<sub>2.5</sub> exposure and excreted oxidative stress biomarkers.

**Conclusion:** Travellers are ideal models for PM pollution induced biomarker and acute health effects

study. Exposure to PM pollution can cause oxidative stress and damage. Further work can be conducted to include more biomarkers. The large amount of travellers and the non-invasive sampling (urine) renders the approach to be easily extended to larger epidemiological and biological studies.

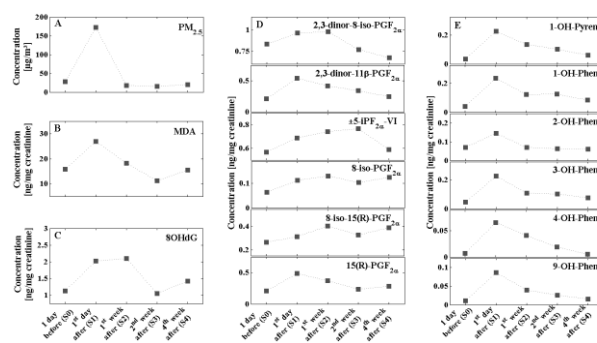


Figure 1. Time trend curves for the median concentration values of PM<sub>2.5</sub> and biomarkers.

This work is in the framework of “Cooperative Health Research in the Augsburg Region” and “Helmholtz Virtual Institute of Complex Molecular Systems in Environmental Health - HICE”, which was funded by Intramural Funding for Environmental Health Projects of Helmholtz Zentrum München - German Research Centre for Environmental Health, Germany and the Impulse and Networking Funds (INF) of the Helmholtz Association (HGF), Germany.

Chan, C.K. & Yao, X., 2008. Air pollution in mega cities in China. *Atmospheric Environment*, 42, 1-42.  
 Pardo, M., Shafer, M.M., Rudich, A., Schauer, J.J. & Rudich, Y., 2015. Single Exposure to near Roadway Particulate Matter Leads to Confined Inflammatory and Defense Responses: Possible Role of Metals. *Environ Sci Technol*, 49, 8777-85.  
 Risom, L., Moller, P. & Loft, S., 2005. Oxidative stress-induced DNA damage by particulate air pollution. *Mutat Res*, 592, 119-37.

## Water Disinfection by Antimicrobial Fibrous Material Produced by Aerosol Filtration

Manju Bhamidipati<sup>1</sup>, Sarah Adam<sup>2</sup>, Marco Valenti<sup>1</sup>, Patricia Kooyman<sup>2</sup>, Andreas Schmidt-Ott<sup>1</sup>

<sup>1</sup>Department of Chemical Engineering, Technical University of Delft, 2628BX, Netherlands

<sup>2</sup>Department of Chemical Engineering, University of Cape Town, 7701, South Africa

Keywords: Water disinfection, antimicrobial, Textile Nanofinishing

Presenting author email: A.S.M.Bhamidipati@student.tudelft.nl

With the rapid outbreak of various contagious diseases caused by multi-resistant antimicrobials, the concept of smart textile Nanofinishing is gaining momentum. Nanosized particulate antibacterial agents exhibit a high surface-to-volume ratio, which leads to a high antibacterial efficiency (Kim, Kuk et al. 2007). Out of the very many available antimicrobial agents, metallic nanoparticles, especially silver, exhibit an extreme antimicrobial activity not only towards bacteria but also other classes of microorganisms (Jeong, Hwang et al. 2005). On the example of a glass fibre filter we show in the present study that the aerosol process for textile nanofinishing introduced by Feng et al., 2015 can be applied to produce an antibacterial agent for water disinfection. The fibrous material is loaded with nanoparticles by an aerosol filtration process. The water disinfection test we carried out could also be considered as a measure of the antimicrobial effect of aerosol-treated textile garments.

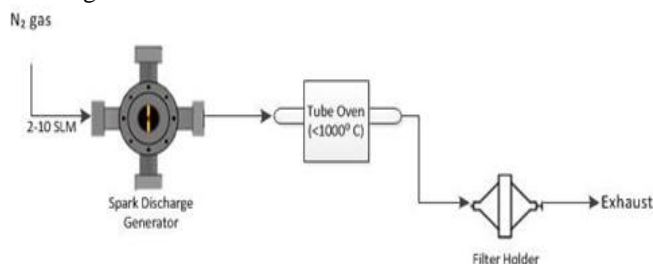


Figure 1. Schematic of the synthesis and deposition of silver nanoparticles.

Ultrapure nanoparticles are synthesized by spark discharge. (Schwyn, Garwin et al. 1988) An inert gas is passed through the spark generator followed by a tube oven and then through the fibrous material (filter). The mean sizes and the degree of agglomeration (singlets or agglomerates) are controlled by the conditions in the generator. Typically, agglomerates, essentially smaller than 10 nm, consisting of ca. 5 nm primary particles are formed. These agglomerates coalesce to form round particles in the tube oven. Having diameters essentially below 10 nm, the particles are transported to the fibers mainly by diffusion, where they stick.

Experiments were conducted on a non-wild type *Escherichia coli* strain (DH5 $\alpha$ ) in phosphate buffered saline (PBS). Nanoparticles deposited on the filters are added to the flasks containing this mixture. A time-kill curve was determined by carrying out a cell count at different times. As seen in fig. 2, the antibacterial activity is very effective, and faster death of bacteria is obtained for the high-surface-area agglomerates (without oven) in

comparison with the coalesced ones. Antimicrobial activity of size selected particles and alloyed particles (spark mixing by using electrodes of different materials) are under study for further optimization.

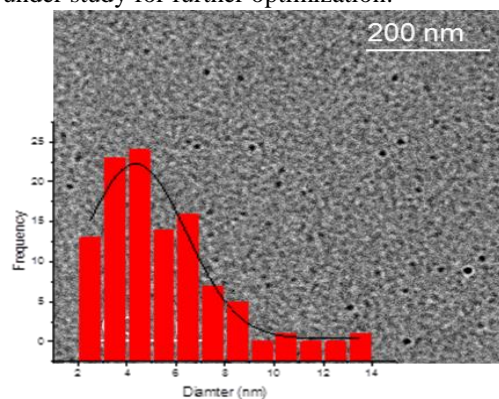


Figure 2. Electron micrograph of Ag singlet nanoparticles produced by spark ablation and size distribution

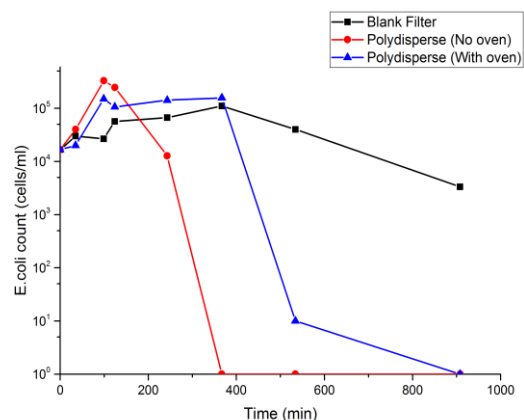


Figure 3. Time-Kill curve of *E. coli* against silver nanoparticles.

Jeong, S. H., Y. H. Hwang and S. C. Yi (2005). "Antibacterial properties of padded PP/PE nonwovens incorporating nano-sized silver colloids." *Journal of Materials Science* **40**(20): 5413-5418.

Kim, J. S., E. Kuk, K. N. Yu, J.-H. Kim, S. J. Park, H. J. Lee, S. H. Kim, Y. K. Park, Y. H. Park and C.-Y. Hwang (2007). "Antimicrobial effects of silver nanoparticles." *Nanomedicine: Nanotechnology, Biology and Medicine* **3**(1): 95-101.

Schwyn, S., E. Garwin and A. Schmidt-Ott (1988). "Aerosol generation by spark discharge." *Journal of Aerosol Science* **19**(5): 639-642.

## A study of aerosol concentration and composition on cardiovascular illness at a semi urban site in Delhi

Avdesh Bhardawaj<sup>1</sup>, Nisar Ali Baig<sup>1</sup>, Gazala Habib\*<sup>1</sup> and Sandeep Singh<sup>2</sup>

<sup>1</sup>Department of Civil Engineering, Indian Institute of Technology Delhi, Hauz Khas, New Delhi-110016, India

<sup>2</sup>Department of Cardiology, All India Institute of Medical Sciences Delhi, New Delhi-110029, India

Keywords: aerosol, cardiovascular illness, arrhythmia, PM<sub>2.5</sub>, Delhi

Presenting author email: gazala@civil.iitd.ac.in

Air Pollution is increasingly been linked to various human illnesses including respiratory and cardiovascular diseases (CVD) (Arnold, 2014). Delhi has been consistently ranked high among the most air polluted cities of the world, hence exposing its inhabitants towards health crisis. This study reports the effect of aerosol [PM<sub>2.5</sub> and ultrafine particles (UFP, D<sub>p</sub>≤100 nm)] concentrations and composition on cardiovascular illness among people in Delhi.

The case cross over study was carried out at the Indian Institute of Technology (IIT) Delhi campus which is a semi urban location in Delhi. Case in present study is the onset or triggering of abnormality in cardiovascular related parameters due to aerosol inhalation during the working hours of the volunteer as security guards. The volunteer were recruited through a detailed health, dietary and pollution exposure questionnaire. Only participants who were working in IIT Delhi for at least more than one year, were non-smokers, non-alcohol drinkers and not on any kind of medication were recruited for the study. Sixty two volunteer were monitored till Dec 2016 and repetitively assessed 1-3 times, therefore total sample size was 120. The sampling was carried out at the five gates of the IIT Delhi campus at which the subjects (security guards) did their duties for 8 hours each in 3 rotating shifts. The location was ideal as the subjects were exposed continuously to traffic generated smoke and other aerosol including re-suspended particles from the roads. The mass and number concentration of PM<sub>2.5</sub> and UFP, were measured using portable Wide Range Aerosol Spectrometer (Mini WRAS-1371, GRIMM, Germany) whereas the PM<sub>2.5</sub> collected on quartz fibre filters using a 4 stage Sioutas cascade impactor (SKC, Inc. USA) were analysed for elemental carbon (EC) and organic carbon (OC). On each day of sampling, the blood pressure (BP), saturation of peripheral oxygen (sPO<sub>2</sub>) and pulse rate of participants were measured using BP meter, and pulse oximeter. In case of any abnormal reading indicating sickness, the sampling for that participant was not carried out. The participants were tagged with ECG hollers for 8 hours duration and an activity chart was provided to the participants to record for any abnormal activity that can affect the ECG like running or emotional distress during the sampling period. ECG software was used to extract HRV pattern of each subject. The input from cardiologist was taken to identify and confirm HRV. The information on emotional distress, rigorous physical activities were taken from activity diary. The time of happening of such

events were noted, the ECG pattern corresponding to that duration was treated as noise and removed from further analysis. After removing the noise the HRV was analysed against particle number and mass concentration obtained at one minute interval from real time Mini-WRAS. The PM<sub>2.5</sub>, EC and OC mass concentration were also linked with ECG patterns to identify the link between aerosol mass, and composition with irregularity in cardiovascular parameters leading to arrhythmia diseases in consultation with a cardiologist of All Indian Institute of Medical Sciences (AIIMS) Delhi.

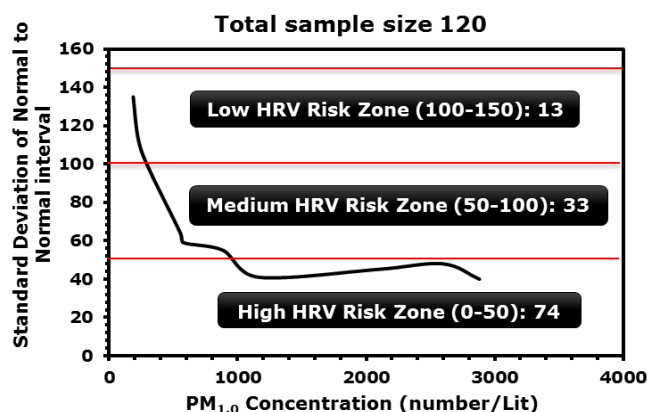


Figure 1. Variation of SDNN with UFP concentration

The results showed a pattern link between standard deviation between normal to normal bit interval (SDNN an indicator of HRV and arrhythmia) with aerosol concentration. The more the aerosol concentration. Importantly, UFP (aerodynamic diameter ≤1.0 μm) showed a clear evidence of influencing HRV. At number concentration 300-3000 particle per lit 107 out of 120 samples lied in medium and high risk zone (SDNN 0-100) probably indicating arrhythmia cases (Figure 1). Further, the link between composition and ECG parameters will be discussed. For validation of results study with a bigger sample size and for longer time needs be carried out.

**Acknowledgements:** This work was supported by IIT Delhi and the SERB, Department of Science and Technology (DST), Government of India.

### References:

Arnold, Carrie. "Disease burdens associated with PM<sub>2.5</sub> exposure: how a new model provided global estimates." *Environmental health perspectives* 122, no. 4 (2014): A111.

## Winter smog in Poland, is it a real hazard to health?

M. Kowalska<sup>1</sup>, J.E. Zejda<sup>1</sup>

<sup>1</sup>Department of Epidemiology, School of Medicine in Katowice, Medical University of Silesia, 40-752 Katowice, Poland

Keywords: PM2.5, daily mortality and hospitalization

Presenting author email: mkowalska@sum.edu.pl

Relationship between daily worsening of ambient air quality and health consequences is well documented. It's been over 60 years since the London smog, although in Europe have been taken many corrective actions there are still regions where each year concentrations of air pollutants (including fine dust) permanently exceed accepted limit values.

Poland is a country where the main source of obtaining energy remains coal burning. Each winter season daily concentrations of dust and sulphur dioxide sharply increase especially during favourable meteorological condition. The major problem is related to individual heating. Figure 1 shows typical course of both pollutants levels measured in one of the Polish cities located in Silesian voivodeship, Katowice. Figure 2 presents daily average of wind speed and temperature of ambient air in the same period and place.

Previous studies conducted at the Department of Epidemiology indicated the existence of the relationship between daily ambient air pollution and mortality due to respiratory diseases in population living in the study region (Kowalska, 2016). Table 1 presents relative risk of daily mortality in older population, in response to an increase of PM2.5 concentration.

Table 1. Relative risk of death due to respiratory diseases in Silesia inhabitants related to an increase of PM2.5 concentration by 10 µg/m<sup>3</sup>, period 2000-2005

Period of moving average PM2.5 concentration (day)	RR in older Silesians (+ 65 years)	
	Average	95% CI
1	1.001	0.991-1.010
3	1.008	0.997-1.019
5	1.015	1.003-1.028
7	1.021	1.006-1.036
14	1.034	1.014-1.053
30	1.035	1.010-1.061

Recent smog episode allows to re-analysis daily changes in specific mortality and morbidity due to respiratory diseases eg. bronchitis, pneumonia, influenza, asthma exacerbation and total respiratory diseases (January 2017). Health related data are provides from the registry of the National Health Fund in Katowice, data of aerosanitary situation was obtained from the State Inspectorate of Environmental Protection in Katowice.

Data analysis in progress ans to results are important particularly that the issue of smog and its health consequences are subject of enormous public health concern. The lack of current epidemiological evidences hampers the process of risk management and risk

communication process via media. Residents expect the necessary corrective actions, without the involvement of experts and government authorities and also the society it will not be possible.

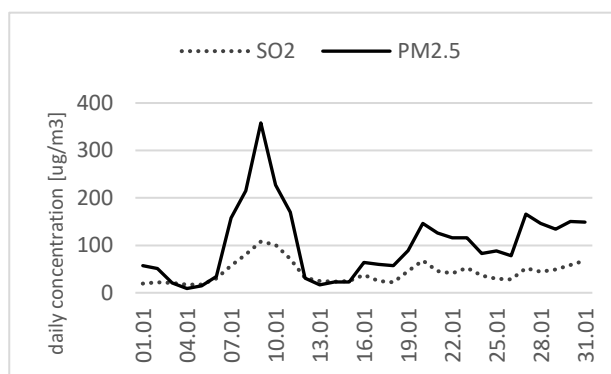


Figure 1. Daily concentration of PM2.5 and sulphur dioxide in Katowice, January 2017.

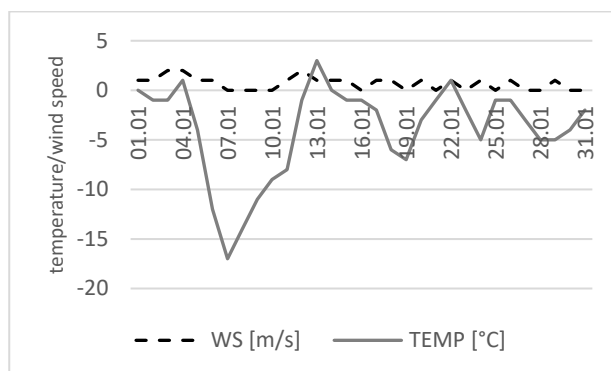


Figure 2. Meteorological parameters in Katowice, January 2017 (wind speed, temperature of ambient air)

This work was supported by the Medical University of Silesia statutory research under grant KNW-1-069/K/6/0.

Kowalska, M. (2016) *Relationship between quality of ambient air and respiratory diseases in Polish population*, Billerica WitPress:201-210

State Inspectorate of Environmental Protection in Katowice (2017) <http://powietrze.katowice.wios.gov.pl/dane-pomiarowe>

## Association between reactive oxygen species formation with environmental persistent free radicals and transition metals in PM<sub>2.5</sub> in Beijing

Fobang Liu<sup>1\*</sup>, Fangxia Shen<sup>2, 1</sup>, Maosheng Yao<sup>3</sup>, Xiangyu Zhang<sup>3</sup>, Jing Li<sup>3</sup>, Ting Zhang<sup>3</sup>, Kurt Lucas<sup>1</sup>, Manabu Shiraiwa<sup>4</sup>, Ulrich Pöschl<sup>1</sup>, and Haijie Tong<sup>1</sup>

<sup>1</sup>Multiphase Chemistry Department, Max Planck Institute for Chemistry, Mainz, 55128, Germany

<sup>2</sup>School of Space and Environment, Beihang University, Beijing, 100191, China

<sup>3</sup>College of Environmental Sciences and Engineering, Peking University, Beijing, 100871, China

<sup>4</sup>Department of Chemistry, University of California, Irvine, California 92697-2025, USA.

Keywords: reactive oxygen species, environmental persistent free radicals, transition metals, PM<sub>2.5</sub>, Beijing  
Presenting author email: fobang.liu@mpic.de

Reactive oxygen species (ROS) play a central role in the adverse health effects of atmospheric particulate matter (PM, Pöschl and Shiraiwa 2015). Previous studies have shown that environmental persistent free radicals (EPFRs), organic peroxides, and transition metals in PM could generate substantial amount of ROS (Gehling et al., 2014; Charrier et al., 2014; Tong et al., 2016; Arangio et al., 2016; Fang et al., 2016). Beijing, one of the global megacities, has been suffering from severe PM<sub>2.5</sub> pollution. Exploring the dependence of reactive oxygen species formation on the abundance of EPFRs and transition metals in PM<sub>2.5</sub> is the key to understand the influence of PM<sub>2.5</sub> on public health in Beijing.

In this study, the concentrations of transition metals, particle-bound EPFRs, and ROS formed in phosphate buffer solutions (pH=7.4) of PM<sub>2.5</sub> at an urban site (Peking University) of Beijing, were quantified using ICP-MS and electron paramagnetic resonance (EPR) spectroscopy. In addition, the dose-dependent ROS yields of PM<sub>2.5</sub> in respiratory tract were calculated using the Multiple Path Particle Dosimetry (MPPD) model (Asgharian et al., 2001).

Fig. 1 shows the temporal evolution of the abundance of transition metals, particle-bound EPFRs, and total radical yields in daily PM<sub>2.5</sub> samples. The yield of radicals was in positive correlation with the concentration of transition metals but showed no clear correlation with the abundance of EPFRs, indicating a significant role of Fenton-like reactions involving iron ions and organics. Moreover, the EPR measurements showed that hydroxyl radicals were the dominant radical species formed in the extracts, which accounted for 16-80% of total radical yields, followed by carbon-centered organic radicals (14-69%), oxygen-centered organic radicals (2-10%), and superoxide radicals (0-7%). Our calculation results based on the MPPD model indicate that ROS have the highest deposition flux in the upper respiratory tract for adults with a mean value of  $1.4 \times 10^{11}$  spins/ $\mu\text{g}$ , but for children and infants, more ROS could be deposited in tracheobronchial and pulmonary regions.

Overall, our results indicate that transition metals could play a vital role in the ROS generation by urban fine particulate matter under physiologically relevant conditions and thereby may pose a public health hazard in the Anthropocene.

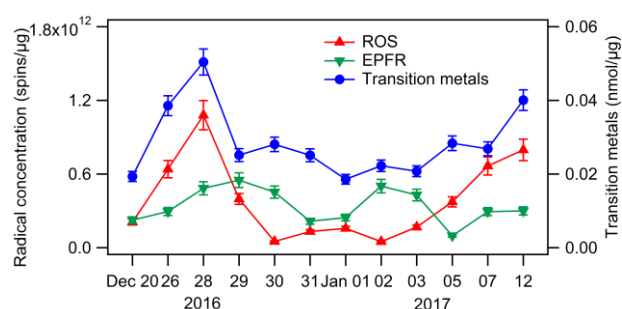


Fig. 1. Time series of the abundance of EPFRs, transition metals, and radical yields in extracts of PM<sub>2.5</sub>.

### Acknowledgement

This work was funded by the Max Planck Society. We acknowledge the technical support in ICP-MS analysis by Steve Galer, Siegfried Herrmann, and Reimund Jotter from Max Planck Institute for Chemistry.

Arangio, A. M., Tong, H., Socorro, J., Pöschl, U., & Shiraiwa, M. (2016) *Atmos. Chem. Phys.*, 16(20), 13105-13119.

Asgharian B, Hofmann W, Bergmann R. (2001) *Aerosol Sci Technol.* 34, 332-339.

Charrier, J. G., McFall, A. S., Richards-Henderson, N. K., and Anastasio, C. (2014) *Environ. Sci. Technol.*, 48, 7010-7017.

Fang, T., Verma, V., Bates, J. T., Abrams, J., Klein, M., Strickland, M. J., Sarnat, S. E., Chang, H. H., Mulholland, J. A., and Tolbert, P. E. (2016) *Atmos. Chem. Phys.*, 16, 3865-3879.

Gehling, W., Khachatryan, L., & Dellinger, B. (2014) *Environ. Sci. Technol.*, 48(8), 4266.

Pöschl, U., and Shiraiwa, M. (2015) *Chem. Rev.*, 115, 4440-4475.

Tong, H., Arangio, A. M., Lakey, P. S., Berkemeier, T., Liu, F., Kampf, C. J., Brune, W. H., Pöschl, U., & Shiraiwa, M. (2016) *Atmos. Chem. Phys.*, 16(3), 1761-1771.

## Development of a multilevel regression model to analyze the association between eye diseases and air pollutants (PM<sub>10</sub>, PM<sub>2.5</sub>, NO<sub>2</sub>, SO<sub>2</sub>, O<sub>3</sub>)

S.-J. Park<sup>1</sup>, S. Han<sup>2</sup>, J.-S. Youn<sup>2</sup>, J. Seo<sup>3</sup> and K.-J. Jeon<sup>2</sup>

<sup>1</sup>Department of Industrial & Management Engineering, Myongji University, Yongin, Gyeonggi-do, 17058, Republic of Korea

<sup>2</sup>Department of Environmental Engineering, Inha University, Incheon, 22212, Republic of Korea

<sup>3</sup>Department of Ophthalmology, Dongtan Sacred Heart Hospital, Hallym University, Hwaseong, Gyeonggi-do, 18450, Republic of Korea

Keywords: Fine particles, Air Pollution, Eye Disease, Multilevel Regression  
Presenting author email: sonmupsj@mju.ac.kr

Recently, many studies have been conducted on the relationship between air pollutants and respiratory diseases. However, the relationship between eye diseases and air pollutants has not been actively researched compared to the studies with respiratory diseases. Most studies have focused on identifying the presence or absence of associations by analyzing correlations between air pollutants and eye diseases. The objective of developing a multilevel regression model is to provide a more systematic and accurate prediction by taking into account the patient's characteristics (age, sex, etc.) and other environmental characteristics (temperature, humidity, etc.).

In regression analysis, unlike correlation analysis, it has the advantage of showing the relation between the incidence of eye disease and other factors as a mathematical prediction model. In multilevel regression, hierarchical structure, the relationship between independent and dependent variables can be better explained than the general regression model.

In this study, the relationship between air pollutants and the number of patients tends to change depending on the characteristics of the patients. Therefore, the characteristics of the patient are high-level independent variables that determine the degree of association, and the amount or concentration of pollutants is a low-level independent variable that determines the direct association. Based on data from the National Health Insurance Corporation, this multilevel regression model used the number of patients with various ocular diseases such as keratitis conjunctivitis as a dependent variable based on the data of the eye patients who were treated at the medical institutions in Seoul. And the amount and concentration of air pollutants and patient characteristics were used as independent variables.

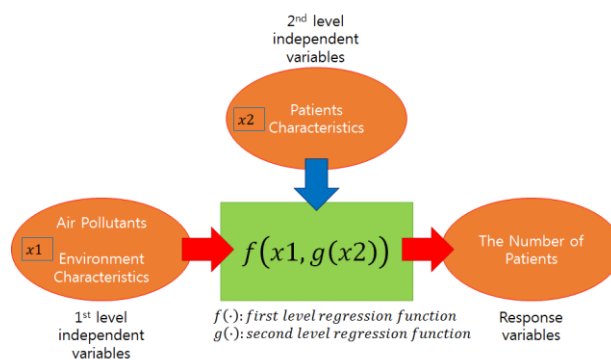


Figure 1. Schematic diagram of multilevel regression model.

This work was supported by funded by the Korea Ministry of Environment (MOE) as “the Environmental Health Action Program (2016001360005).”

Gelman, A. and Hill, J., (2007) *Data Analysis Using Regression and Multilevel/Hierarchical Models*, Cambridge University press, New York.

Hong, J., Zhong, T., Li, H., Xu, J., Ye, X., Mu, Z., Lu, Y., Mashaghi, A., Zhou, Y., Tan, M., Li, Q., Sun, X., Liu, Z., and Xu, J. (2016) *Scientific reports*, **6**.

## Estimation of pulmonary toxicity of nanomaterials following subacute inhalation

Yasuo Morimoto<sup>1</sup>, Hiroto Izumi<sup>1</sup>, Yukiko Yoshiura<sup>1</sup>, Yuri Fujisawa<sup>1</sup>, Taisuke Tomonaga<sup>1</sup>, Takako Oyabu<sup>1</sup>, Takami Okada<sup>1</sup>, Toshihiko Myojo<sup>1</sup>, Manabu Shimada<sup>2</sup>, Masaru Kubo<sup>2</sup>

<sup>1</sup> University of Occupational and Environmental Health, Japan, Kitakyushu, 807-8555, Japan

<sup>2</sup> Hiroshima University, Higashi-Hiroshima, 739-8511, Japan

Keywords: nanomaterial, pulmonary toxicity, inhalation, inflammation.

Presenting author email: yasuo@med.uoeh-u.ac.jp

The objective of this experiment is whether or not pulmonary toxicity of nanomaterials can be estimated following subacute inhalation. We performed 4 week's inhalation studies using four type of nanomaterials in rats, nickel oxide (NiO), titanium dioxide (TiO<sub>2</sub>), cerium dioxide (CeO<sub>2</sub>), and zinc oxide (ZnO). As the experimental condition, concentration of each nanomaterial was proximately 2 mg/m<sup>3</sup> in chamber, and exposure periods was 4 weeks (6 hours/day, 5 days/week).

Table 1. Concentration of nanomaterials in each exposure chamber

Nanomaterials	Concentration
NiO	1.65 ± 0.2 mg/m <sup>3</sup>
CeO <sub>2</sub>	2.09 ± 0.29 mg/m <sup>3</sup>
TiO <sub>2</sub>	1.84 ± 0.74 mg/m <sup>3</sup>
ZnO	2.11 ± 0.45 mg/m <sup>3</sup>

Cell analysis and chemokines in bronchoalveolar lavage fluid (BALF) were analyzed at 3 days, 1month and 3 months after end of exposure.

Inhalation of NiO and CeO<sub>2</sub>, materials with high toxicity among nanomaterials, increased in neutrophil number and percentage of neutrophil in BALF, on the other hand TiO<sub>2</sub> and ZnO, materials with low toxicity among nanomaterials, did not.

Concentration of cytokine-induced neutrophil chemoattractant (CINC)-1 and 2, representative chemokines for neutrophil, in BALF were upregulated by NiO and CeO<sub>2</sub>, and by no TiO<sub>2</sub> and ZnO. Data of lactate dehydrogenase (LDH), marker of lung injury, and heme oxygenase (HO)-1, marker of reactive oxygen species (ROS) in BALF show similar tendency to CINC. Taken together we suggested that under this experimental condition, subacute inhalation studies may be useful for estimation of pulmonary toxicity of nanomaterials.

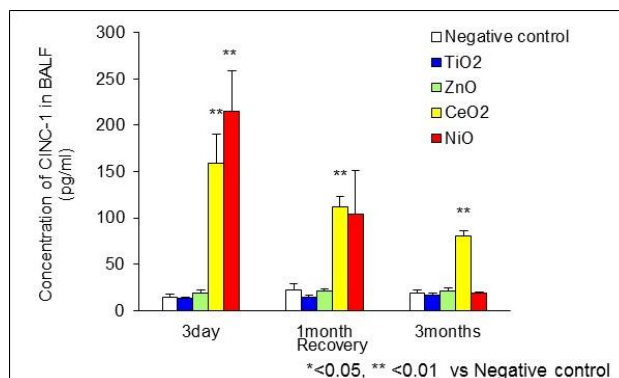


Figure 1 Concentration of CINC-1 in BALF

Table 2. Summary of inhalation study

Endpoint	Inhalation			
	TiO <sub>2</sub>	ZnO	CeO <sub>2</sub>	NiO
Neutrophil number in BALF	→	→	↑	↑→
Percentage of neutrophil in BALF	→	→	↑	↑→
LDH release in BALF	→	→	↑	↑
CINC-1 in BALF	→	→	↑	↑
HO-1 in BALF	→	→	↑	↑
Pathological finding	→	→	↑	↑

### Acknowledgment

This work is partially supported by "Development of innovative methodology for safety assessment of industrial nanomaterials" by Ministry of Economy, Trade and Industry (METI) of Japan.

Morimoto, Y., Izumi, H., and Kuroda, E. (2014) *J. Immunol. Res.* 2014:962871.

## Reactive oxygen species (ROS) formation mechanism: links between in situ ambient measurements and laboratory aging experiments of different emission sources

J. Zhou<sup>1</sup>, M. Elser<sup>1</sup>, G. Stefenelli<sup>1</sup>, P. Zotter<sup>2</sup>, M. Krapf<sup>1</sup>, E.A. Bruns<sup>1</sup>, R. Fröhlich<sup>1</sup>, J. G. Slowik<sup>1</sup>, T. Nussbaumer<sup>2</sup>, M. Geiser<sup>3</sup>, U. Baltensperger<sup>1</sup>, R. Huang<sup>1</sup>, A.S.H. Prevot<sup>1</sup>, I. El Haddad<sup>1</sup> & J. Dommen<sup>1</sup>

<sup>1</sup>Laboratory of Atmospheric Chemistry, Paul Scherrer Institute, 5232, Villigen, Switzerland

<sup>2</sup>Bioenergy Research Group, Lucerne School of Engineering & Architecture, 6048, Horw, Switzerland

<sup>3</sup>Institute of Anatomy, University of Bern, 3012, Bern, Switzerland

Keywords: reactive oxygen species, particle sources, ambient aerosols, ROS closure

Presenting author email: [Jun.zhou@psi.ch](mailto:Jun.zhou@psi.ch)

Oxidative stress is an imbalance between the production of reactive oxygen species (ROS) and the body's antioxidant defense. The oxidative potential (OP) of aerosols to induce oxidative stress when inhaled is usually characterized by a-cellular assays in the particulate mass (PM). The formation of ROS is linked to sources of atmospheric PM (Bates et al., 2015) is especially related to the oxygenated organic aerosol fraction (OOA) in different types of particles (Stevanovic et al., 2013), and is most consistently linked with more oxidized OOA (MO\_OOA) (Verma et al., 2015).

In this study, a 2',7'-dichlorofluorescein (DCFH) based assay was employed for the on-line quantification of the ROS content in the water-soluble fraction of PM generated from different sources. These sources included primary and secondary organic aerosols from biogenic as well as anthropogenic emissions. Additionally, ROS in ambient PM in two contrasted locations, Beijing (China) and Bern (Switzerland), were measured. Results show that ROS content is variable in different organic aerosols (OA).

The contributions of the sources to ROS are analyzed by source apportionment and multiple linear regression, one part of the results is shown in Figure 1. Further, the ROS content attributed to the different ambient OA sources is compared with that obtained from different laboratory-Characterized sources of OA, and a ROS closure is also done by the different sources

of ambient OA. These studies are then used to infer the formation mechanisms of ROS in different ambient locations.

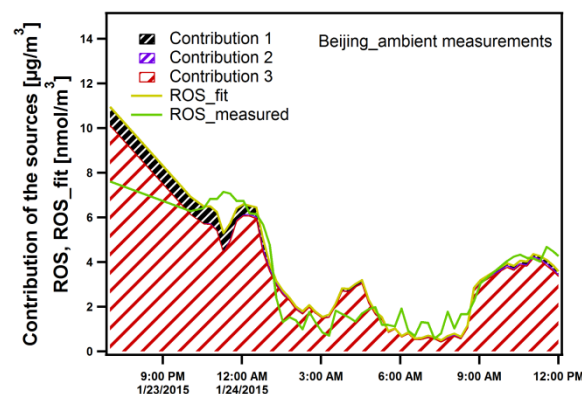


Figure 1: The contributions of the OA sources to ROS. Contribution 1, 2 and 3 represent cooking emissions, biomass burning emissions and OOA emissions, respectively.

This work was supported by the Swiss National Science Foundation (NRP 70 "Energy Turnaround") and the China Scholarship Council (CSC).

Bates, J. T., et al. (2015) *Environ. Sci. Technol.*, 49, 13605-13612.

Stevanovic, S., et al. (2013) *Environ. Sci. Technol.*, 47, 7655-7662.

Verma, V., et al. (2015) *Environ. Sci. Technol.*, 49, 4646-4656.

Wragg, F. P. H., et al. (2016) *Atmos. Meas. Tech.*, 9, 4891-4900.

## Air pollution epidemiology and regional differences in concentration-response relationships

O. Hänninen, I. Rumrich and A. Asikainen

National Institute for Health and Welfare (THL), Department of Health Protection, P.O. Box 95, 70701 Kuopio, Finland

Keywords: PM<sub>2.5</sub>, concentration-exposure relationship, toxicity, infiltration

Presenting author email: [otto.hanninen@thl.fi](mailto:otto.hanninen@thl.fi)

Ambient aerosols (measured as PM) are one of the most studied risk factors in environmental epidemiology of this millennium. Epidemiological evidence is backed with large body of toxicological understanding of the mechanisms. Exposure processes involve both indoor and outdoor environments and are modified by time- and physical activity. In the human domain, intake, uptake, and dose can be defined and actually required based on the presumption that actual biological responses to the pollution particles and molecules are the causal factors leading to the health impacts.

Particles originating from different sources such as road dust, combustion generated particles, sea salt etc. or generated in the atmosphere from gaseous precursors have chemically diverse composition. Aerosol processes create accumulation mode particles that are mixtures from many sources. Less studied but equally obvious health impact modifying factors would be particle size, infiltration, time-activity and population differences.

In this paper we (i) reanalyze selected epidemiological evidence on possible regional patterns in concentration-response (C-R) relationships; and (ii) discuss their interpretation and possible causes and (iii) links to the aerosol science.

**Methods.** To test to what extent the apparent differences in epidemiological hazard ratios could be explained (or attributed) the building stock properties we reanalysed the natural all-cause mortality data from the large European ESCAPE study (Beelen et al., 2014). Seven Nordic, seven Central European and five South European cohorts were analyzed for association between population PM<sub>2.5</sub> exposures and all cause natural mortality. We supplemented original random effects model of Beelen et al. (2014) for all twenty studies (HR 1.07, 95%CI 1.02-1.13 per 5 µg m<sup>-3</sup> of PM<sub>2.5</sub>) by calculating similar estimates for the Nordic, Central European and Southern European countries.

**Results.** A climatologically/regionally grouped re-analysis of hazard ratios observed in the recent European ESCAPE cohort compilation study on natural cause mortality by dividing the original cohorts into similar regions produced pooled random effects estimates and compared the relative differences in the regional hazard ratio increments (HRI) after subtracting the background risk (HRI = HR-1), we see that the Central European value (7%) is 1.75 times higher than the Nordic one, and Southern European value (12%) even 3 times higher, respectively (Table 1).

**Discussion:** When looking at the widely overlapping confidence intervals of both the original cohort studies, but also the pooled estimates, it is evident that even the best currently available European epidemiological data is not able to confirm – or to deny

– the existence of regional differences in C-R relationships for PM<sub>2.5</sub>.

Table 1. Pooled regional hazard ratios for Europe from random effects model for natural mortality indicate a trend, but it does not reach statistical significance.

Cohorts	n	Cohort size	Hazard ratio (95% CI) per 5 µg m <sup>-3</sup> of PM <sub>2.5</sub>
Northern Europe	7	82 672	1.04 (0.92-1.18)
Central Europe	7	202 882	1.07 (1.01-1.14) **
Southern Europe	5	36 599	1.12 (0.92-1.38)
<b>All</b>	<b>19</b>	<b>322 159</b>	<b>1.07 (1.02-1.13) **</b>

It has been shown that infiltration factors differ by regions. As the analysis of infiltration factors for the three regions yielded only 10-15% differences, there may well be other factors playing a role.

Accounting for that the infiltration coefficient trend actually should be partly compensated, or diluted, by outdoor (and potentially traffic) time-activity, it makes clear that as such these tentative analyses leave well room for suggest that there are also other regional factors, such as differences in the particle size distribution (better infiltration or respiratory tract deposition of particles in Southern parts of Europe) or larger toxicity of the particles that could e.g. be related with multiple pollutants, such as oxidative radicals commonly found in higher concentrations towards the Mediterranean region.

This work has been supported by Academy of Finland Contract 285672 (BATMAN); Nordic Programme on Health and Welfare project #75007 (Nordic WelfAir) and EU LIFE+ INDEX AIR. This paper aims at improving the interaction of ambient epidemiology and the aerosol society.

### References

- Beelen B, et al. 2014. Effects of long-term exposure to air pollution on natural-cause mortality: an analysis of 22 European cohorts within the multicenter ESCAPE project. *Lancet*;383:785-795.
- Hänninen O, Rumrich I, Asikainen A, 2017. Estimating health effects of indoor exposures to outdoor particles: Considerations for regional differences. (tentative)

## Molecular biological effects and toxicity of combustion aerosol emissions on air/liquid-interface exposed human and murine lung cells

R.Zimmermann<sup>1,11</sup>, T.G.Dittmar<sup>2,11</sup>, T.Kanashova<sup>2,11</sup>, J.Buters<sup>3,11</sup>, S.Öder<sup>3,11</sup>, A.Huber<sup>3,11</sup>, H.Paur<sup>4,11</sup>, S.Müllhopt<sup>4</sup>, M.Dilger<sup>4,11</sup>, C.Weiß<sup>4,11</sup>, B.Buchholz<sup>11</sup>, B.Stengel<sup>5,11</sup>, K.Hiller<sup>7,11</sup>, S.C.Sapccariu<sup>7,11</sup>, K.A.BeruBe<sup>8,11</sup>, A.J.Wlodarczyk<sup>8,11</sup>, B.Michalke<sup>9</sup>, T.Krebs<sup>10,11</sup>, M.Kelbg<sup>5,11</sup>, J.Tiggesbäumker<sup>5,11</sup>, T.Streibel<sup>1</sup>, E.Karg<sup>1</sup>, S.Scholtes<sup>1,11</sup>, J.Schnelle-Kreis<sup>1</sup>, J.Lintelmann<sup>1</sup>, M.Sklorz<sup>1</sup>, S.Klingbeil<sup>1,11</sup>, J.Orasche<sup>1</sup>, L.Müller<sup>1,11</sup>, A.Rheda<sup>1</sup>, J.Passig<sup>1,11</sup>, T.Gröger<sup>1</sup>, G.Abbaszade<sup>1</sup>, S.Smita<sup>5,11</sup>, J.Orasche<sup>1,11</sup>, O.Uski<sup>6</sup>, P.Jalava<sup>6</sup>, M.Happo<sup>6</sup>, A.Hartikainen<sup>6</sup>, H.Lamberg<sup>6</sup>, M.-R.Hirvonen<sup>6,11</sup>, S.Kasurinen<sup>6</sup>, O.Sippula<sup>6,11</sup>, J.Jokiniemi<sup>6,11</sup> and further HICE co-workers

<sup>1</sup>Joint Mass Spectrometry Centre, Rostock University (Analyt. Chem.) & Helmholtz Zentrum München (HMGU/CMA), Germany, D; <sup>2</sup>MDC, Berlin, D; <sup>3</sup>ZAUM, Technical University Munich, D; <sup>4</sup>KIT (ITC/ITG), Karlsruhe, D; <sup>5</sup>University of Rostock (Inst. of Piston Machines/Int. Combust. Engines & Inst. of Physics & Chair of Systems Biology), D; <sup>6</sup>University Eastern Finland-Kuopio; <sup>7</sup>Uni Luxemburg; <sup>8</sup>Cardiff University, UK; <sup>9</sup>HMGU, D; <sup>10</sup>Vitrocell GmbH, Waldkirch, D; <sup>11</sup>HICE – Helmholtz Virtual Institute of Complex Molecular Systems in Environmental Health-Aerosols and Health, [www.hice-vi.eu](http://www.hice-vi.eu)

Keywords: combustion emissions, human lung cell & animal exposure, air-liquid-interface, health effects, omics  
Presenting author email: [ralf.zimmermann@helmholtz-muenchen.de](mailto:ralf.zimmermann@helmholtz-muenchen.de) or [ralf.zimmermann@uni-rostock.de](mailto:ralf.zimmermann@uni-rostock.de)

It is known that combustion aerosol emissions are important for public health. In the framework of the Virtual Helmholtz Institute-HICE, the physical and chemical properties of various combustion emissions as well as their biological effects on lung cells were thoroughly investigated and jointly analysed. For addressing the biological activity and the toxicity of the different combustion aerosols, human and murine lung cell cultures were exposed to diluted combustion exhaust fumes by the modern air-liquid interface (ALI)-exposure technology. The ALI-approach allows a very realistic lung cell exposure by simulation the situation in the lung. After 4h exposure the biological response of the exposed lung cells are analysed by a comprehensive multi-omics molecular biological effect-characterisation on the transcriptomic, proteomic and metabolomic level. Up to now emissions of wood combustion, ship engines, small diesel engines and car gasoline engines were investigated. For wood combustion experiments emissions from a masonry heater and a metal stove (beech, birch, spruce and pine log wood) as well as a state of the art pellet burner (soft wood pellets) were used. Shipping emissions were generated on a test-bed ship diesel engine, running either on common heavy fuel oil (HFO) or distilled diesel fuel (DF). A small diesel engine for land based mobile application was included as well. Finally a modern car engine operated with gasoline (E10) and ethanol (E85) was investigated. Two special field deployable ALI-exposure-station systems and a mobile S2-biological laboratory were set up and applied for this study. The ALI-exposure station is now commercially available (Vitrocell GmbH). Human alveolar basal epithelial cells (A549, BEAS2B and primary cells) as well as murine macrophages (RAW) were ALI-exposed to freshly diluted combustion aerosols. The cellular effects were then comprehensively characterized (viability, cytotoxicology, multi-omics molecular-biological effects monitoring) and put in context with the chemical and physical aerosol data. The HICE concept is summarized in the literature [1]. The overall cellular response of the combustion aerosols (i.e. the regulation strength on the different ‘omics-levels) was compared at a similar aerosol dilution (in most cases 1:40). The dilution/dose of 1:40 (1:100 for HFO) was

selected to be below a measurable direct cytotoxicity after the 4h ALI exposure (LDH release- or viability-assay). Figure 1 puts the overall cellular response, measured by the transcriptomic regulation strength (i.e. the concentration changes of m-RNA copies in the cells) of exposed cell with respect to reference experiments in context to the deposited combustion aerosol PM mass.

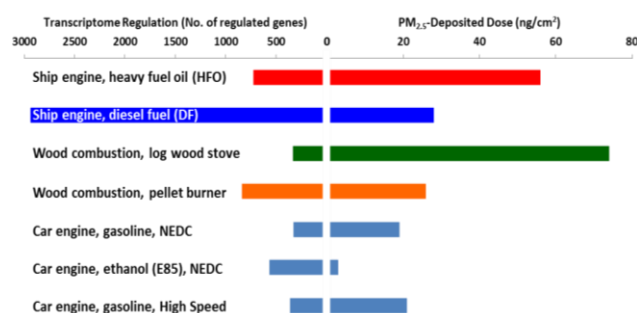


Figure 1: Particle deposition dose (right, measured as deposited PM-mass per surface unit) and overall biological effects strengths (left, measured as the total number of m-RNA transcripts with a fold change larger than  $\log_2(1.5)$ ) in human lung cells for different ALI-cell exposure experiments with 1:40 diluted combustion aerosols (1:100 for HFO).

The figure depicts that the overall biological response-strength differed considerably for different aerosol sources and is not well correlated with the deposited PM mass. This is pointing to large differences in the relative toxicity of the aerosol emissions from different combustion sources and fuel types. The latter finding is supported by the detailed analyses of the activated cellular response pathways (GO-term analysis), depicting regulation of pathways such as pro-inflammatory signalling, xenobiotic metabolism, phagocytosis or oxidative stress. The obtained holistic molecular biological results demonstrate the complexity of PM-induced biological effects. The results obtained with the cell cultures have been compared to simultaneously performed animal exposure experiments (BL6 mice) on e.g. the omics-level. Furthermore the direct combustion emission exposure experiments have been accompanied also by simulated atmospheric aging experiments (UV-aging in flow tube)

## Investigation of Spatial and Temporal and Genotoxicity and Cytotoxicity of Atmospheric Particles Collected from Kutahya

Gonca CAKMAK DEMIRCIGIL<sup>1</sup>, Esra EMERCE<sup>1</sup>, Pelin ERTURK<sup>2</sup>, Akif ARI<sup>2</sup>, Roel SCHINS<sup>3</sup>, Sema BURGAZ<sup>1</sup> and Eftade O. GAGA<sup>2</sup>

<sup>1</sup>Gazi University, Faculty of Pharmacy, Toxicology Department, Ankara, Turkey

<sup>2</sup>Anadolu University, Faculty of Engineering, Department of Environmental Engineering, Eskişehir, Turkey

<sup>3</sup>IUF-Leibniz Research Institute for Environmental Medicine, Duesseldorf, Germany

Keywords: PM<sub>2.5</sub>, comet assay, environment, in vitro toxicity.

Presenting author email: goncacad@gmail.com

The International Agency for Research on Cancer (IARC), has classified outdoor air pollution as carcinogenic to humans (Group 1) (IARC, 2013). The attempt to understand the human health effects of air pollutants especially for Particulate Matter (PM) is increasing. The research is mostly related with the environmental exposures either in industrial or urban areas. The study area, Kütahya is a province in the Aegean region of Turkey, located in the inner western part of the Turkey. Coal is the most commonly used fuel for residential heating and industrial activities. The city is characterized as a thermal power plant city due to presence of three power plants. Shifting from coal to natural gas for space heating did not improve the air quality compared to neighboring cities.

The daily PM<sub>2.5</sub> samples were collected on the nucleophore filters for one year from two stations namely Kütahya (urban) and Göbel (rural, thermal power plant region). For each station parallel days in summer (8 days) and winter (7 days) were chosen. The aim was to determine in vitro genotoxicity by use of Comet Assay and cytotoxicity by use of trypan blue (TB), WST-1 and Lactate Dehydrogenase (LDH) tests. The cell line was human lung cancer epithelial cell line (A549 cells). 50 µg/mL PM concentration and 24 h incubation duration were used for Comet and TB assays for each 30 PM samples. The lyophilization of the samples was carried out according to Wessel *et al.* study (Wessel *et al.*, 2010).

The cell viability was higher than 70% for all of the PM samples for 50 µg/mL. The genotoxicity was found to be increased against to the negative control for each of the PM samples ( $p > 0.05$ ). Only one of the PM sample from Kütahya in winter showed statistically significant genotoxicity vs. Göbel winter sample in the same day ( $p < 0.05$ ).

There was no seasonal difference among the Kütahya and Göbel stations when total winter samples and total summer samples of the stations were compared ( $p > 0.05$ ).

PM genotoxicity in Kütahya was found to be higher than that of Göbel when the summer and winter data of each station was combined ( $p > 0.05$ ).

Since the amount of the PM samples were not enough to determine the cytotoxicity by using WST-1 and LDH assays separately for each 30 PM samples, the PM suspensions were pooled for each season and each station after genotoxicity assays were finished. Accordingly, the viability for both of the assays was decreased below 70% - 80% for concentrations higher than 100 µg/ml for each of the season and station. The lowest viability was determined in Kütahya station for winter season.

Environmental PM has a complex composition showing spatial and temporal changes. So that the present study could contribute to the toxicity determination of PM<sub>2.5</sub> toxicity from two different stations and seasons. We could not find clear differences among the samples however samples from urban station were shown to be more genotoxic and cytotoxic in winter which could be the representing the traffic and residential heating sources.

This work was supported by TUBITAK-112Y305 and Anadolu University-BAP-1306F272 grants.

International Agency for Research on Cancer (2014). *IARC Monographs on the Evaluation of Carcinogenic Risks to Humans*: vol. 109, Outdoor Air Pollution. Lyon, France: IARC.

Wessels A1, Birmili W, Albrecht C, Hellack B, Jermann E, Wick G, Harrison RM, Schins RP. (2010) *Environ Sci Technol.* **1;44(9)**:3539-45.

## In-vitro cytotoxicity of nanoparticles and condensable compounds from biomass combustion determined by a simple sampling method

P. Zotter<sup>1</sup>, S. Richard<sup>2</sup>, M. Egli<sup>2</sup> and T. Nussbaumer<sup>1</sup>

<sup>1</sup>Bioenergy Research Group, Lucerne School of Engineering and Architecture, Horw, 6048, Switzerland

<sup>2</sup>Institute for Medical Engineering, Lucerne School of Engineering and Architecture, Hergiswil, 6052, Switzerland

Keywords: wood combustion, health effects, in vitro, emissions

Presenting author email: peter.zotter@hslu.ch

Energy wood utilisation is expected to significantly increase within the next years in order to replace fossil fuels (Thees et al., 2013). However, biomass combustion contributes to air pollution, especially with inhalable particulate matter (PM), which induces adverse health effects (Kocbach Bolling et al., 2009). The current air pollution control legislation considers emission limits on filterable solid PM in the hot flue gas only. Health effects of condensable organic compounds (COC) and potential secondary organic aerosols are usually not directly measured and rarely investigated. Furthermore, experimental methods to investigate health effects of emissions in the stack applied so far are complex and costly. Hence information available on health effects from flue gases is scarce and limited to a small number of specific applications.

Therefore, an economic and less complex method for the collection and subsequent in vitro cell analysis of solid PM and COC in hot flue gases from biomass combustion was developed. For this purpose, sampling methods US-EPA-5H and VDI-2066 were adapted. Hot flue gases were passed through impingers which are cooled to 5°C. The rapid cooling induces the condensation of mainly COC, into the impinger fillings. Subsequently, human epithelial lung cells H187 were exposed to these liquids and the cell viability (PI staining method) was analysed. Two parallel sampling trains were applied: one with a filter upstream of the impingers to determine the cytotoxicity of COC only and one without a filter to determine the cell viability of COC and solid PM.

Table 1. Investigated combustion devices and conditions.

Combustion device	Combustion conditions
Pellet boiler (15 kW)	Optimum, lack and high excess of O <sub>2</sub>
Log wood stove (6 kW)	Cold start, flaming, warm start Dry and wet wood
Grate boiler (150 kW)	Full and part load Going to standby from part load
Log wood boiler (30 kW)	Cold start, stationary, lack of O <sub>2</sub>

To characterise the sampling procedures and subsequent cell analyses, the influence of different parameters (e.g., blanks, different sampling liquids) were investigated. Furthermore, different combustion devices

and conditions were compared (Table 1). In addition to the cell analysis, a detailed characterisation of the flue gas (particle size distribution, PM mass, O<sub>2</sub>, CO, NO<sub>x</sub>, CH<sub>4</sub>, total hydrocarbons) is carried out.

Results indicate that the proposed method is capable to assess cytotoxicity of COC. Furthermore, the method reveals significant differences (several orders of magnitude) in cell viability of flue gases from the investigated combustion devices and conditions (Figure 1). The highest cytotoxicity is found during the warm start in the log wood stove and low cytotoxicity occurs in the pellet boiler operated at optimum conditions while the industrial wood chip grate boiler reveals no detectable cytotoxicity (Figure 1). No difference in cell viability between samples containing COC only and COC plus solid PM was found indicating the high health relevance of COC.

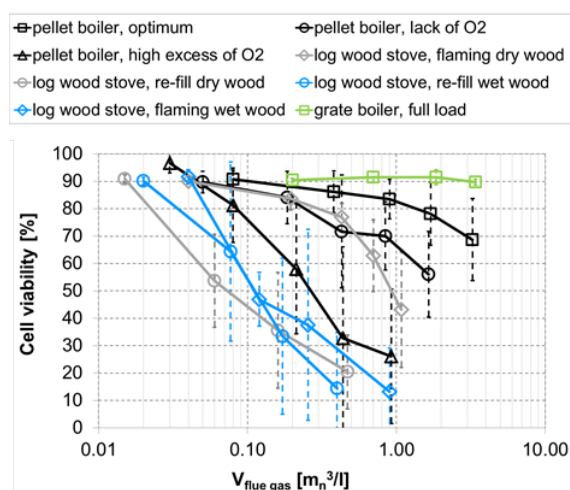


Figure 1. Cell viability of selected combustion devices and conditions as function of the sampled flue gas volume ( $V_{\text{flue gas}}$ , normalised to 13% O<sub>2</sub>).

This work was supported by the Swiss Federal Office for the Environment.

Thees, O., E. Kaufmann, R. Lemm, and A. Bürgi (2013) Schweizerische Zeitschrift für Forstwesen, 164(12): p. 351-364.

Kocbach Bolling, A., J. Pagels, K. Yttri, L. Barregard, G. Sallsten, P. Schwarze and C. Boman (2009) *Part. Fibre Tox.* 6(1), 29.

## A statistical analysis of brown haze events, surface air pollutants, and hospital admissions in Auckland, New Zealand

Talbot NP<sup>b\*</sup>, Scarfe J<sup>a</sup>, Dirks KN<sup>a</sup>, Salmond JA<sup>c</sup>, Marshall R<sup>c</sup>

<sup>a</sup>School of Population Health, University of Auckland, Private Bag 92019, Auckland, New Zealand

<sup>b</sup>Auckland Council, 135 Albert Street, Auckland, New Zealand

<sup>c</sup>School of Environment, University of Auckland, Private Bag 92019, Auckland, New Zealand

Keywords: Brown haze, Air pollutants, Epidemiology, Respiratory health.

Presenting author email: nick.talbot@aucklandcouncil.govt.nz

### Background

This paper reports on the relationships between brown haze events, surface air pollution, and respiratory hospital admissions in Auckland, New Zealand. Research has consistently linked poor air quality with numerous adverse health outcomes. Moreover, epidemiological results have indicated increased susceptibility to air pollution from certain population groups such as the young and the elderly.

### Study area

Auckland is located on an isthmus at the northern end of New Zealand's North Island with a population of over 1.3 million. Its isolated and exposed geographical position allows Auckland favorable conditions for low background pollution levels. Despite this, brown haze events sometimes occur over Auckland during cool winter mornings (Figure 1). On average, there were eight brown haze days in each winter season from 2001 to 2011 with a large interannual variability.

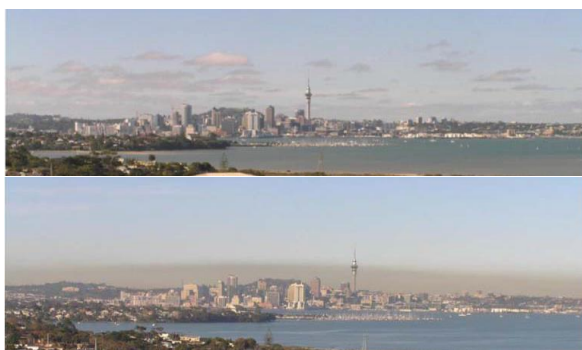


Figure 1 Examples of Auckland CBD on a clear morning (Top) and a brown haze morning (Below).

### Air pollution and climate data

The former Auckland Regional Council (now Auckland Council) provided daily mean NO, NO<sub>2</sub>, CO, and PM<sub>10</sub> measurements that were collected from a permanent monitoring site with data covering the period 2001 to 2011 (for some of the pollutants). The monitoring site is located within the Auckland urban airshed. The surface meteorological measurements (temperature (in °C) and relative humidity (in %), were obtained from the Auckland Airport weather station.

### Hospital admissions data

Auckland District Health Board's catchment area for the hospital admissions data for this study was 457,000 people and covers an area of approximately 150 km<sup>2</sup>.

Hospital admissions data were obtained from the New Zealand Ministry of Health and consisted of admissions to hospital within the Auckland District Health Board catchment with a primary diagnosis based on the International Classification of Diseases 10<sup>th</sup> Revision (ICD10) diseases of the respiratory system (J00-99) over the period of 2001-2011 inclusive.

### Statistical methodology

Spearman rank correlation coefficients were calculated for the four pollutants measured at the site to gain an understanding of how the pollutants concentrations are related. The log relative risk for each pollutant was estimated. The percentage increase in hospital admissions with 95% confidence intervals was calculated per unit increase in pollutant concentration. The log relative risk for a brown haze day was estimated to measure the percentage increase associated with a brown haze day.

### Results

Increases in hospital admissions were associated with haze events for all age groups, however, with differing lag periods. CO, NO and NO<sub>2</sub> were significantly correlated with respiratory hospital admissions with an 11-day lag period for the 0–14 year age group, and a 5–7 lag period for ages 65+. A 3-day lag period was found for the 15–64 age group for CO, NO and PM<sub>10</sub>. When directly assessing hospital admission and brown haze events, significant increases in admissions were found. A lag period of 5 days was recorded for the 0–14 and 65+ groups, and an 11-day lag for the 15–64 categories.

### Conclusions

The results provide the first statistical link between Auckland brown haze events, surface air pollution and respiratory health. The results empower medical institutions and practitioners to observe Auckland brown haze and be alerted to likely increases in respiratory admissions over the days ahead, with both resource management and medical care benefits.

## Development of eye exposure characteristic chamber for the identification of environmental disease caused by fine particles

Sunah Yoon<sup>1</sup>, Sehyun Han<sup>2</sup>, Ki-Joon Jeon<sup>2</sup> and Soonjo Kwon<sup>1</sup>

<sup>1</sup>Department of Biological Engineering, Inha University, Incheon, 22212, Republic of Korea

<sup>2</sup>Department of Environmental Engineering, Inha University, Incheon, 22212, Republic of Korea

Keywords: ocular diseases, particulate matter (PM), cell viability, inflammatory responses, oxidative stress  
Presenting author email: soonjo.kwon@inha.ac.kr

Particulate matters (PMs) possess the potential to induce acute and chronic health issues upon daily exposure. Ocular surface, which is exposed to the atmosphere, is vulnerable to the risk from air pollutants. However, the studies on the effects of PM on ocular diseases have not been elucidated.

We studied the influence of PM components on human conjunctival epithelial cells. Collected PM samples were classified into aerodynamic diameter and solubility. We analyzed cellular cytotoxicity, inflammatory response, and oxidative stress following exposure of conjunctival epithelial cells to collected PMs in the range of 0.1-100 µg/ml. Results showed that different size and solubility of PM samples induced different level of damage on conjunctival cell viability, inflammatory response, and oxidative stress.

This work was supported by funded by the Korea Ministry of Environment (MOE) as “the Environmental Health Action Program (2016001360005)”.

Patel, H., Eo, S., & Kwon, S. (2011) *Toxicology Letters*, **200**, 124-131.

Xiang, P., He, R. W., Han, Y. H., Sun, H. J., Cui, X. Y., & Ma, L. Q. (2016) *Environment International*, **89-90**, 30-37.

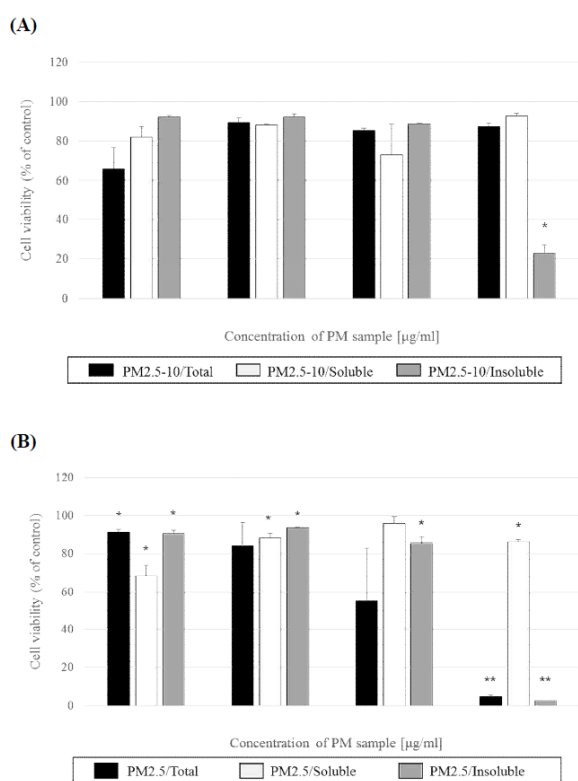


Figure 1. Effect of particulate matter samples on cell viability in cultured conjunctival epithelial cells after 24hr exposure at the concentration of 0.1-100 µg/ml. Each particulate matter samples, (A) PM2.5-10 and (B) PM2.5 were tested.

## The oxidative potential of subway PM<sub>2.5</sub>

T. Moreno<sup>1</sup>, F. Kelly<sup>2</sup>, C. Dunster<sup>2</sup>, A. Oliete<sup>2</sup>, V. Martins<sup>1</sup>, C. Reche<sup>1</sup>, M.C. Minguillón<sup>1</sup>, F. Amato<sup>1</sup>, M. Capdevila<sup>3</sup>, E. de Miguel<sup>3</sup> and X. Querol<sup>1</sup>

<sup>1</sup> Inst. Environmental Assessment and Water Research (IDAEA-CSIC), 08034 Barcelona, Spain

<sup>2</sup> MRC-PHE Centre for Environmental Health, King's College London, London, United Kingdom

<sup>3</sup> Transports Metropolitans de Barcelona, TMB Santa Eulalia, 08902 L'Hospitalet de Llobregat, Spain

Keywords: toxicity, PM chemistry, subway air quality, airborne metals.

Presenting author email: teresa.moreno@idaea.csic.es

Numerous studies have shown negative health effects related to exposure to PM concentrations. However, considering mass concentration alone is not necessarily enough as it ignores sources, constituents, and biologic activity of PM, so that current knowledge does not allow precise quantification of the health effects of individual PM components. The capacity of inhaled particles to generate reactive oxygen species (ROS), or free radicals, at the air–lung interface has been suggested to trigger oxidative stress, leading to adverse health effects. The oxidative potential (OP), defined as a measure of the capacity of PM to oxidize target molecules, has been proposed as a measure related to biological responses to PM exposure, and thus could be more informative than PM mass alone as it integrates biologically relevant properties, like size, surface and chemical PM composition. The effects of subway PM on oxidative stress and ROS activity in alveolar macrophage cells have been previously considered in relationship to PM shape, size, surface area and/or chemical constituents, but results show little clarity on whether subway PM is relatively more toxic than outdoor PM highly influenced by road traffic (see refs in Moreno *et al.*, 2017).

To investigate the toxic effects of PM<sub>2.5</sub> subway particles the OP of 36 samples collected in 6 stations in the Barcelona subway system was determined using the validated respiratory tract-lining fluid model that measures the degree to which PM can oxidize 3 antioxidants found at the surface of the lung, ascorbate (AA), urate (UA) and reduced glutathione (GSH). Stations were selected with different designs to obtain a range of PM sample characteristics, including a platform with screen doors (PSDs). In 2 stations sampling was undertaken measuring differences in days after night-time works (ballast addition/rail change) to see any influences in the platforms air quality the following day.

Average PM<sub>2.5</sub> mass concentrations ranged from 31 µg/m<sup>3</sup> in the PSDs station to 102 µg/m<sup>3</sup> in a platform after night-time works (ballast addition). Chemical compositions show high concentrations of Fe, TC, Ba, Cu, Mn, Zn and Cr, all characteristic of the subway environment and sourced from rail tracks, wheels, catenaries, brake pads and pantographs. The results indicate that the OP of subway PM samples is not obviously related to variations in PM<sub>2.5</sub> concentrations. On the other hand OP values were highly significantly correlated for both AA and GSH when considering both mass and volume (Table 1). Our data suggest a possible link between OP (AA and GSH) and some elemental

concentrations, especially Cu, As and perhaps Sb. Cu concentrations in these samples are related to the wear of brake pads and the electrical supply (catenary and pantographs). In stations in subway line 4 Cu is emitted by the lateral brakes used by trains (which are the richest in Cu of all 4 types of brakes used), and the Cu pantographs that are still used in this line. Other metals present in raised concentrations, such as Fe or Cr, do not show correlation with OP values in any of the stations. In fact a highly significant negative correlation was found with OP<sup>AA</sup>/µg, which would be consistent with the low OP of hematite and magnetite, the most common Fe compounds in the subway environment. Encouragingly, lowest OP<sup>TOT</sup>/m<sup>3</sup> values were found at the subway station with PSDs coinciding with improved air quality and reduced OP of ambient PM<sub>2.5</sub>.

This study was supported by the Spanish Ministry MINECO - FEDER funds (METRO CGL2012-33066), IMPROVE LIFE (LIFE13ENV/ES/000263), EU 7<sup>th</sup> Framework Programme (FP7/2007-2013, grant 315760 HEXACOMM), National Institute for Health Research Health Protection Research Unit (NIHR HPRU).

Moreno *et al.* (2017). *Atmos. Environ.* **148**, 230-238.

Table 1. Spearman test values (ρ) for all variables considered. \*\* p<0.01, \* p<0.05.

	OP <sup>AA</sup> /µg	OP <sup>GSH</sup> /µg	OP <sup>AA</sup> /m <sup>3</sup>	OP <sup>GSH</sup> /m <sup>3</sup>
OP <sup>GSH</sup> /µg	0,62**			
OP <sup>GSH</sup> /m <sup>3</sup>			0,77**	
PM <sub>2.5</sub>	-0,61**	-0,24**	0,54**	0,52**
Al	-0,04	-0,15	0,00	-0,23
Ca	-0,10	-0,07	-0,29	-0,32
K	-0,16	-0,19	-0,29	-0,27
Fe	-0,56**	-0,14	0,07	0,25
V	0,08	-0,14	-0,05	-0,18
Ni	-0,05	-0,10	0,02	-0,04
As	0,14	0,38*	0,32*	0,36*
Sr	-0,45*	-0,30	0,19	0,03
Cd	0,33*	0,22	-0,09	-0,03
Sn	0,33	0,36*	0,09	0,07
Sb	0,29	0,59**	0,00	0,35
La	0,38*	0,48**	0,16	0,19
Pb	0,48**	0,42*	-0,08	-0,09
Ti	-0,13	-0,06	0,20	0,03
Cr	-0,51**	-0,11	-0,08	0,22
Mn	-0,46**	-0,03	0,13	0,34*
Cu	0,29	0,69**	0,42*	0,64**
Zn	0,09	0,28	0,29	0,33*
Ba	-0,15	-0,04	0,42*	0,21
TC	0,25	0,22	0,09	-0,06

## Development of eye exposure characteristic chamber for the identification of environmental disease caused by fine particles

S. Han<sup>1</sup>, J.-S. Yi<sup>1</sup>, J.-S. Youn<sup>1</sup>, H.-S. Lee<sup>2</sup>, J. Seo<sup>3</sup> and K.-J. Jeon<sup>1</sup>

<sup>1</sup>Department of Environmental Engineering, Inha University, Incheon, 22212, Republic of Korea

<sup>2</sup>Department of Ophthalmology, Seoul St. Mary's Hospital, The Catholic University of Korea, Seoul, 06591, Republic of Korea

<sup>3</sup>Department of Ophthalmology, Dongtan Sacred Heart Hospital, Hallym University, Hwaseong, Gyeonggi-do, 18450, Republic of Korea

Keywords: PM<sub>10</sub> & PM<sub>2.5</sub>, Environmental eye disease, Exposure chamber, *In-vivo* study  
Presenting author email: ecoshian@gmail.com

An environmental disease is a disease that occurs due to environmental factors such as physical, chemical, and biological factors, and it is recognized that there is a correlation between environmentally harmful factors and disease through epidemiological investigation. Among them, environmental eye diseases are diseases caused by atmospheric environmental factors such as yellow dust and fine particles, and they cause dry eye syndrome and allergic conjunctivitis. Recent studies have shown that the incidence of environmental eye disease tends to increase gradually, but most of the studies are mainly based on statistical analysis using correlation analysis between pollutants and eye diseases. In the case of respiratory diseases, nonclinical studies using animal test chambers as well as statistical analysis have been performed. The purpose of this study is to investigate the effect of air pollutants on ocular diseases using animal test chambers (OECD Guideline 403/412, EPA OPPTS 870.1300.) to identify the mechanism and biomarker of environmental eye diseases.

The conventional ophthalmic toxicity assessment method is an eye dropping method, which is different from actual exposure. To compensate for this, a chamber-based eye disease model is constructed similar to the exposure method. Fine particles (PM<sub>10</sub>, PM<sub>2.5</sub>) should be concentrated in the eye and external exposure (respiratory, skin) should be minimized. The restraint equipment restricts the movement of the test animal and exposes only the eye area. The separate test space into clean/dirty zones supply clean air from the clean zone to breathe, and supply air containing fine dust in the dirty zone to shut down the external factors of the test. The uniform flow of the clean/dirty zone was confirmed by the flow analysis inside the test chamber.

Brush type particle generator (ISO 19601) is applied to the generation and supply of fine particles, and a dilution rate of up to 25 times was achieved by mass flow controller (MFC) and peristaltic pump. Exposure & breeding cage is controlled by temperature and humidity using a thermo-hygrostat, and cages suitable for AAALAC are selected for breeding and general management. The chamber system developed in this study is made according to the GLP test equipment validation procedure and all procedures and results are documented and verified to be suitable for animal experiments.

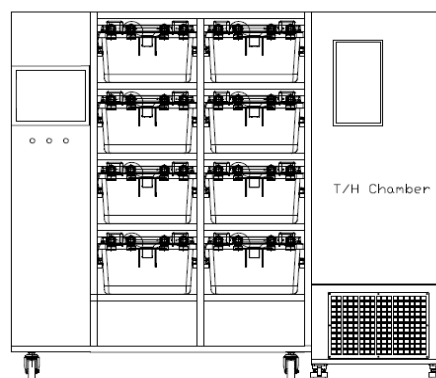


Figure 1. Schematic diagram of eye exposure test chamber for the toxicity evaluation by fine particles.

This work was supported by funded by the Korea Ministry of Environment (MOE) as “the Environmental Health Action Program (2016001360005).”

- Ko, S. B. (2012) *J Korean Med Assoc.*, 55(3), 212-213  
Chien, L. C., Lien, Y. J., Yang, C. H., & Yu, H. L. (2014) *PloS one*, 9(10), e109175.  
Galor, A., Kumar, N., Feuer, W., & Lee, D. J. (2014) *Ophthalmology*, 121(4), 972-973.

## Toxicity of wood smoke particles in human lung epithelial cells: the role of PAHs, soot and zinc

M. Dilger<sup>1</sup>, J. Orasche<sup>2</sup>, C. Schlager<sup>3</sup>, S. Mühlhopt<sup>3</sup>, R. Zimmermann<sup>2</sup>, H.-R. Paur<sup>3</sup>, S. Diabaté<sup>1</sup>, C. Weiss<sup>1</sup>

<sup>1</sup>Institute of Toxicology and Genetics, Karlsruhe Institute of Technology, Eggenstein-Leopoldshafen, Germany

<sup>2</sup>Joint Mass Spectrometry Centre, Rostock University & Helmholtz Zentrum München, Rostock/Munich, Germany

<sup>3</sup>Institute for Technical Chemistry, Karlsruhe Institute of Technology, Eggenstein-Leopoldshafen, Germany

Keywords: wood smoke, air-liquid-interface, polycyclic aromatic hydrocarbons, soot, metals.

Presenting author email: dilger@kit.edu

The health impact of emissions from domestic burning of biomass and coal is estimated to contribute to over 4 million premature deaths per year worldwide. Wood is the main fuel source for biomass combustion and the shift towards renewable energy sources will further increase emissions from wood combustion even in developed countries. However, little is known about the constituents of wood smoke and biological mechanisms responsible for adverse health effects.

We exposed human A549 and BEAS-2B lung epithelial cells to freshly generated wood smoke at the air-liquid-interface (ALI) using a continuous flow exposure system. Toxicity at ALI was compared to submerged exposure with collected wood smoke particles (WSP). To address critical constituents of WSP, we exposed A549 cells under submerged conditions individually to benzo[a]pyrene (B[a]P), carbon black nanoparticles (CB14, Printex 90®) and zinc oxide nanoparticles (ZnO) to represent the polycyclic aromatic hydrocarbons (PAHs), soot and metal fraction of WSP, respectively.

At the ALI, in both cell lines, the 1:10 diluted wood smoke did not induce cell death. However, enhancing the particle dose by use of an electrostatic field, led to an increase of toxicity, while this method had no effect on cells when exposed to clean air.

Under submerged conditions, even particle doses greatly exceeding the toxic dose at the ALI provoked no signs of acute toxicity. However, WSP induced formation of cellular reactive oxygen species (ROS) as well as a response to bioavailable PAHs. We thus tested the contribution of B[a]P, ZnO and CB14 to the observed effects of WSP.

ZnO and CB14 were able to induce ROS formation in cells, measured as enhanced H<sub>2</sub>DCF oxidation. However, the magnitude of the effects differed considerably. ZnO increased ROS formation only at high concentrations, which are well beyond the levels of Zn present in the tested WSP samples. CB14, however, potently induced H<sub>2</sub>DCF oxidation, in comparable magnitude to WSP when EC content is used as dose metric. Of note, augmented ROS formation by WSP or CB14 did not trigger an adaptive anti-oxidative stress response in A549 cells, evidenced by a lack of heme oxygenase-1 up-regulation at the protein and mRNA level.

As expected, the PAH response induced by WSP could be mimicked by B[a]P. Strikingly, PAHs adsorbed to WSPs were even more potent in activating target gene

expression than B[a]P individually applied in suspension. As PAHs are adsorbed on the particle surface, particles might serve as a vehicle to deliver PAHs to the cell either due to particle sedimentation and/or increasing PAH uptake via a “trojan horse” mechanism, where particles act as carriers for PAHs.

In conclusion, this study demonstrates cytotoxicity of WSP specifically at the air-liquid-interface. Mechanistic investigations employing classical submerged cell culture methods indicated a critical role of soot, metals and especially PAHs in hazardous effects of WSP (Figure 1). As metabolic activation of PAHs is critically linked to genotoxicity, mutagenesis and carcinogenesis, the effect of WSPs on these endpoints needs to be critically evaluated in the future. Furthermore, a systematic comparison of toxicological responses at the ALI and in conventional cell culture systems is warranted and needs to be scrutinized in animal studies.

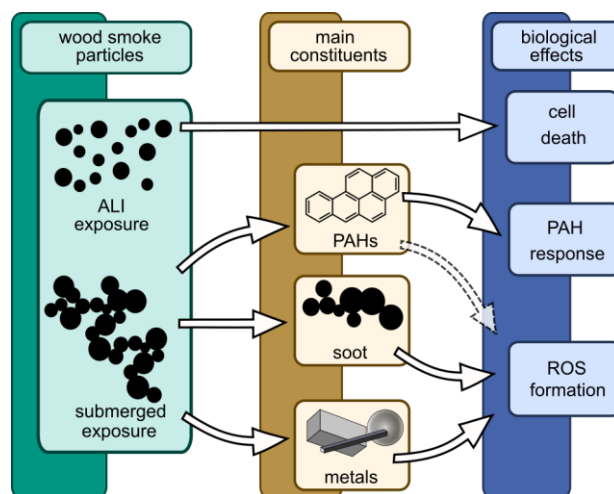


Figure 1. WSP lead to cell death at the air-liquid-interface and induce ROS formation as well as a strong PAH response under submerged conditions. These effects can be mimicked by individual substances representing the PAH, metal and soot fraction of WSPs.

This work was supported by the Helmholtz Virtual Institute for Complex Molecular System in Environmental Health—Aerosols and Health (HICE, www.hice-vi.eu).

## Multi-model assessment of health impacts of air pollution in Europe in frame of the AQMEII model intercomparison project

U. Im1\*, J. Brandt1, C. Geels1, K.M. Hansen1, J.H. Christensen1, M.S. Andersen1, E. Solazzo2, U. Alyuz3, A. Balzarini4, R. Baro5, R. Bellasio6, R. Bianconi6, J. Bieser7, A. Colette8, G. Curci9, A. Farrow10, J. Flemming11, A. Fraser12, P. Jimenez-Guerrero5, N. Kitwiroon13, G. Pirovano4, L. Pozzoli3,a, M. Prank14, R. Rose12, R. Sokhi10, P. Tuccella9, A. Unal3, M.G. Vivanco15, G. Yardwood16, C. Hogrefe17, S. Galmarini2

<sup>1</sup> Aarhus University, Department of Environmental Science, 4000 Roskilde, Denmark

Keywords: multi-model ensemble, AQMEII, health impact assessment, premature death.

Presenting author email: ulas@envs.au.dk

According to the World Health Organization (WHO), air pollution is now the world's largest single environmental health risk. Chemistry and transport models (CTMs) are useful tools to calculate the concentrations of health-related pollutants taking into account the non-linearities in the chemistry and the complex interactions between meteorology and chemistry. However, CTMs include different chemical and aerosol schemes that introduce differences in the representation of the processes. These uncertainties are introduced into the health impact estimates using output from these different CTMs. Multi-model (MM) ensembles can be useful to minimize these uncertainties introduced by the individual CTMs.

In the present study, the simulated surface concentrations of health related air pollutants ( $\text{CO}$ ,  $\text{O}_3$ ,  $\text{SO}_2$  and  $\text{PM}_{2.5}$ ) for the year 2010 from twelve modelling groups participating in the AQMEII (Air Quality Model Evaluation International Initiative) exercise, serve as input to the Economic Valuation of Air Pollution model (EVA: Brandt et al., 2013), in order to calculate the impacts of these pollutants on human health, using exposure response functions from WHO, and the associated external costs in Europe. In addition, the impacts of a 20% global emission reduction scenario on the human health and associated costs have been calculated.

The AQMEII project attempts to bring together modellers from both sides of the Atlantic Ocean to perform joint regional model experiments using common boundary conditions, and emissions with a specific focus on regional modelling domains over Europe and North America (Galmarini et al., 2017). AQMEII Phase 3 (AQMEII3) is devoted to performing joint modelling experiments with HTAP2.

The MM mean and standard deviations from the twelve-model ensemble for different health outcomes are presented in Table 1. Results show that in Europe, the MM mean number of premature deaths due to air pollution is calculated to be  $\sim 400\,000 \pm 100\,000$ , that agrees with the WHO estimate of 482 000. Estimated health impacts among different models can vary up to a factor of 3.  $\text{PM}_{2.5}$  is calculated to be the major pollutant affecting the health impacts and the differences in models regarding the treatment of aerosol composition, physics and dynamics is a key factor. The geographical distribution of the total premature death in 2010 as calculated by the MM mean is presented in Figure 1.

Table 1. MM mean health outcomes of air pollution

Health Outcomes	MM Mean	MM StDev
Chronic Bronchitis (CB)	358 000	93 000
Respiratory Hospital Admissions (RHA)	22 000	6 000
Cerebrovascular Hospital Admissions (CHA)	46 000	12 000
Congestive Heart Failure (CHF)	31 000	7 000
Lung Cancer (LC)	55 000	14 000
Premature Death (PD)	412 000	102 000
Infant mortality (IM)	401	104

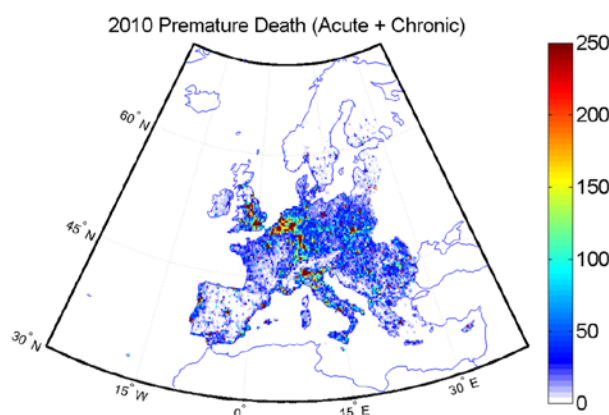


Figure 1. This is a comparison between theory and experimental data.

The total MM mean costs due to health impacts of air pollution are estimated to be 400 billion € in Europe. Finally, the scenario with a 20% reduction in global anthropogenic emissions leads to a decrease of 18% of all health outcomes.

This work is funded by NordForsk under the Nordic Programme on Health and Welfare, Project #75007.

Brandt et al., 2013. *Atmos. Chem. Phys.*, 13, 7725-7746.  
Galmarini et al., 2017. *Atmos. Chem. Phys.*, 13, 7725-7746.

## On lung anti-oxidant depletion as a measure of oxidative potential for ambient fine particles: predictive indicator of cellular stress.

B. Crobeddu<sup>1</sup>, J. Sciare<sup>2,3</sup>, J. Deweirdt<sup>4</sup>, I. Baudrimont<sup>4</sup>, A. Baeza-Squiban<sup>1</sup>

<sup>1</sup> Lab Molecular and Cellular Responses to Xenobiotics, UMR-CNRS 8251, Univ Paris Diderot, Paris, France

<sup>2</sup> Laboratory of climate and environment sciences, CEA-CNRS, Centre de Saclay, France

<sup>3</sup> Energy Environment Water Research Center (EEWRC), The Cyprus Institute, Nicosia, Cyprus

<sup>4</sup> CRCTB, INSERM U1045, Univ Bordeaux, France

Keywords: PM<sub>2.5</sub>, inflammation, airway epithelial cells, endothelial cells

Presenting author email: [baeza@univ-paris-diderot.fr](mailto:baeza@univ-paris-diderot.fr)

### Introduction

Particulate air pollution remains a major issue for public health. Considering the chemical complexity of ambient particles (PM), the determination of their intrinsic oxidative potential (OP) is more and more often proposed as additional indicator to the EU regulated PM mass concentration in order to better infer PM toxicity. This is supported by the mechanisms of PM toxicity which are related to their ability to induce an oxidative stress in cells.

Our objective was to compare several acellular assays to assess OP of different ambient PM<sub>2.5</sub> samples as well as to investigate their cellular effects induced in human pulmonary epithelial and endothelial cells in order to determine which OP assay is the most predictive of toxicity. One OP assays was further performed on 2-week PM<sub>2.5</sub> samples collected at contrasted sites.

### Methods

Acellular and cellular assays were performed with PM<sub>2.5</sub> filters sampled during two campaigns targeted on two combustion sources of high toxicity: traffic and domestic wood burning. PM<sub>2.5</sub> sampled for OP and biological assays were recovered from Teflon filters by sonication. For the 2-week PM<sub>2.5</sub> time series, OP assays were directly performed on filters. Chemical analysis comprise major ions, OC, EC, carbohydrates (incl. levoglucosan), metals and polyaromatic hydrocarbons (PAH).

OP was characterized using different acellular assays: the consumption of dithiothreitol (DTT), a reducing agent, the scission of plasmid DNA, the depletion of lung antioxidants (ascorbic acid (AA) and glutathione (GSH)) and oxidation of the dichlorofluorescein probe.

The human bronchial epithelial cell line (NCI-H292) and human pulmonary artery endothelial cells (HPAEC) were exposed for 4 or 24 h to particles from 1 to 10  $\mu\text{g}/\text{cm}^2$ . Oxidative stress was evaluated by measuring intracellular ROS production using the DCFH-DA probe and by studying the mRNA expression of antioxidant enzymes (Heme oxygenase 1 (HO-1)). The induction of a pro-inflammatory response was characterized by measuring the mRNA expression of cytokines (IL-6, IL-8, TNF $\alpha$ ).

### Results

Correlation analyses between the different OP assays and cellular responses induced in the two cell types allowed us to select the antioxidant (ascorbate and glutathione) depletion assay as the best OP reference assay. This assay was further used in real-world conditions on daily filter sampling at 2 sites of interest: ("close to traffic" and "regional background"). An exhaustive chemical analysis (PM, major ions, elemental/organic carbon, metals, PAH, carbohydrates) associated with a statistical analysis (source apportionment) to quantify PM sources related to traffic and biomass combustion has highlighted that PM<sub>2.5</sub> collected at the traffic site exhibited a higher PO (figure below).

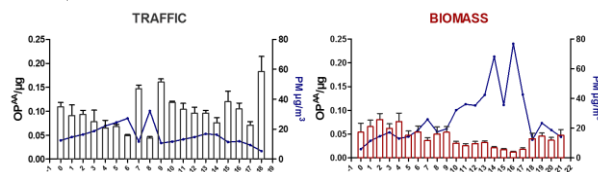


Figure: Daily variations of the OP measured by the AA antioxidant depletion assay in the two different sites. The line corresponds to PM in  $\mu\text{g}/\text{m}^3$ .

### Conclusion

In conclusion, this study has demonstrated that the OP assessment of PM<sub>2.5</sub> measured by the depletion of antioxidants naturally present in the lung lining fluid is predictive of the cellular effects induced in human pulmonary epithelial and endothelial cells. This OP assay proved to be sensitive enough to exhibit a significant daily variability within a specific site. Its application at larger scale in operational networks should increase our knowledge on sources/chemical compounds controlling OP in fine aerosols.

*This work was supported by the French Environment and Energy Management Agency (ADEME: convention n° 1262C0037) in the context of the call for research proposals of the national research program for environmental and occupational health (PNREST) 2012 of ANSES (French Agency for Food, Environmental and Occupational Health & Safety) under grant n° 2012-2-013, project "POTOX".*

## Comparison of the pro-inflammatory effects of size-segregated particles sampled in different sites in Africa (Abidjan in Cote D'Ivoire and Cotonou in Benin).

M. Tran<sup>1</sup>, J. Adon<sup>2</sup>, C. Liousse<sup>2</sup>, A. Baeza-Squiban<sup>1</sup>, V. Yoboué<sup>3</sup>, A. Akpo<sup>4</sup>, C. Galy-Locaux<sup>2</sup>, C. Chiron<sup>2</sup>, E. Gardrat<sup>1</sup>, J.F. Léon<sup>1</sup>

<sup>1</sup>Lab Molecular and Cellular Responses to Xenobiotics, UMR-CNRS 8251, Univ Paris Diderot, Paris, France

<sup>2</sup>Laboratoire d'Aérogologie UMR-CNR 5560, Univ Toulouse 3-Paul Sabatier-UPS, Toulouse, France

<sup>3</sup>Université Félix Houphouët Boigny, Laboratoire de Physique de l'Atmosphère et de la mécanique des fluides, Abidjan, Cote d'Ivoire

<sup>4</sup> Université d'Abomey calavy, Bénin

Keywords: ambient particles, cytotoxicity, inflammation, airway epithelial cells

Presenting author email: [baeza@univ-paris-diderot.fr](mailto:baeza@univ-paris-diderot.fr)

### Introduction

The involvement of particulate matter (PM) in cardiorespiratory diseases is now well established in developed countries whereas in developing areas such as Africa with a high level of specific pollution, PM pollution and its effects are less studied. Health effects result mainly from the lung inflammation, an early outcome triggered by PM inhalation. The fine and ultrafine fractions of the aerosol are considered as the more prone to induce biological effects due to their ability to reach the distal lung together with specific compositions including transition metals and organic compounds. In vitro studies using relevant target cells of inhaled particles are suitable models to investigate the mechanisms of toxicity of PM and to compare their reactivity according to the size and composition.

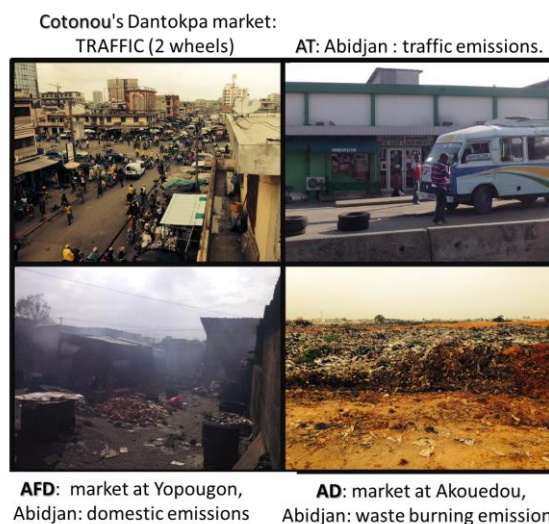
Our objective was to characterize and compare the biological reactivity of urban African aerosols from different sites on human bronchial epithelial cells in order to identify toxic sources and to determine if the toxicity is differentially associated to specific sizes and chemistry aerosol according to the sites. This study is a contribution to the WP2-DACCIWA FP7 program with the aim to characterize particulate pollution on domestic fire site, traffic sites and waste burning site of two West-African capitals.

### Methods

Particles were sampled in the dry (January 2016) and the wet season (July 2016) on 3 consecutive days for 3 hrs. Four sites were chosen including 3 in Abidjan (Cote d'Ivoire) to investigate different sources such as domestic fires, waste burning and traffic which was also investigated in Cotonou (Benin).

For biological studies, particles were sampled using five stages DGI impactors equipped with nuclepore filters running at 70L/min whereas for chemical studies, quartz and Teflon filters were used to measure mass, carbon (black carbon, organic carbon and total carbon) and ions analysis respectively. The coarse (C: >2.5-1 $\mu$ m), fine (F:<1-0.2 $\mu$ m) and ultrafine (UF: <0.2 $\mu$ m) particles were removed from filters by sonication in culture medium for further dilution to do cell exposure.

NCI-H292 cell line was used as a model of human bronchial epithelial cell. Cells were exposed to particles for 24h at 1, 5 and 10  $\mu$ g/cm<sup>2</sup>.



Different endpoints were studied (i) cell viability by WST-1 assay measuring mitochondrial activity (ii) pro-inflammatory response by measuring the release of Interleukin-6 (IL-6) and IL-8 cytokines by ELISA.

### Results

PM mass measured for all the sites was generally higher than WHO norms. Organic carbon and dust particles are the two more important contributors for the ultra-fine and fine particle sizes with more organic carbon in Abidjan and dust particles in Cotonou respectively.

In the range of concentrations used, no or limited cytotoxicity was observed. By contrast we observed that whatever the season, particles from domestic fires were the most reactive inducing significant IL-6 and IL-8 release. Samples from the dry season were more reactive than those of the wet season. In addition, the UF fraction appears as the most reactive one, size fractions being compared at isomass.

A tentative cross-analysis between physico-chemical and toxicological results will be proposed in order to conclude on the link between aerosol size differentiated composition and inflammation markers for the main combustion sources prevailing in South West Africa during dry and wet seasons.

This study is funded by "DACCIWA".

## Effects of short-term exposure to particulate matter on cognitive performance

M. A. Shehab<sup>1</sup> and F. D. Pope<sup>1</sup>

<sup>1</sup>School of Geography, Earth and Environmental Sciences, University of Birmingham, Birmingham, B15 2TT, UK

Presenting author email: [mas247@student.bham.ac.uk](mailto:mas247@student.bham.ac.uk)

### Background

Particulate matter (PM) air pollution is one of the major contributors of morbidity and mortality in the modern world, with well-documented short- and long-term health effects (Brunekreef *et al* 2005). There are far fewer studies investigating the effect of PM upon cognitive performance, and in particular, there are only a limited number of studies investigating the short-term effects of exposure upon cognitive effects.

### Methodology

Two distinct cohort experiments were performed with each cohort comprised of 30 healthy adult volunteers. Each experiment tested the cognitive ability of their respective cohorts under conditions of elevated PM exposure and clean conditions. The high exposure conditions in the first experiment were generated from burning candles, which is a well-known source of PM. The second cohort underwent cognitive assessment just after commuting in which they were subjected to urban levels of air pollution, which includes PM, and after sitting in a low exposure setting.

The PM mass concentration for the candle burning experiment was measured using an Optical Particle Sizer (TSI, 3330). No PM measurements were made during the commuting experiment but it is well known that PM concentrations are higher in urban outdoor environments compared to indoor environments with no local significant PM source.

Three cognitive tests used to assess cognitive performance: A. Mini-Mental State Examination (MMSE), B. Stroop color and word test - adult version, and C. Ruff 2 and 7 Selective Attention Test. The subjects filled a questionnaire, that included enquiries about confounding factors that may affect cognition and hence their test performance. Confounding factors included exposure to noise, caffeine consumption and emotional state.

### Results

For both the candle burning and commuting experiments, a decline in short-term cognitive performance was observed in the mini-mental state examination (MMSE) test, which is used for global assessment of individual's cognitive functioning. Additionally, the commuting experiment showed a short-term cognitive decline in the Ruff 2 and 7 test for selective attention in terms of automatic detection speed. There is some evidence that confounding factors, including emotional state (i.e. fatigue), and

sleeping (not feeling refreshed the morning of taking the test), may have also affected the performance of the subjects.

### Conclusions

This is the first study that investigates human exposure to airborne pollutants and its effect on short-term cognitive performance on healthy adults, considering confounding factors. The study presents strong evidence that short-term exposure to PM from commuting and from candle burning can reduce the individual's cognitive function. The duplication of this result in both the candle burning and commuting experiments provides solid evidence that short-term exposure to PM<sub>2.5</sub> can cause cognitive impairment.

This work was supported by the government of Kuwait.

Brunekreef, B., Janssen, N. A. H., De Hartog, J. J., Oldenwening, M., Meliefste, K., Hoek, G., Lanki, T., Timonen, K. L., Vallius, M., Pekkanen, J. & Van Grieken, R. 2005. *Personal, indoor, and outdoor exposures to PM<sub>2.5</sub> and its components for groups of cardiovascular patients in Amsterdam and Helsinki*. Research report (Health Effects Institute), 1-70; discussion 71-9.

## **Abstracts T407**

## Lung deposition model of airborne multi-walled carbon nanotubes for inhalation exposure assessment

Y.K. Bahk<sup>1,2</sup>, P. Sachinidou<sup>1,2</sup>, E. Gitsis<sup>1</sup> and J. Wang<sup>1,2</sup>

<sup>1</sup> Institute of Environmental Engineering, ETH Zurich, 8093 Zurich, Switzerland

<sup>2</sup> Laboratory of Advanced Analytical Technologies, EMPA, 8600 Dübendorf, Switzerland

Keywords: airborne CNT, lung deposition model, exposure assessment.

Presenting author email: ykbahk@ifu.baug.ethz.ch

Aerosol deposition in the human airway is significant not only in occupational health, but also in pharmaceutical research for drug delivery to the deep part of the lung. Airborne particle depositions have been estimated either empirically or numerically, however, due to ethical reasons, investigations are limited to laboratory animal tests. For this reason, a number of studies have been published regarding developments of deposition models for particles in the human airway. Yeh and Schum (1980) have developed the model of human lung airways and the model led to the accurate prediction of regional particle deposition in the lung. A multiple path model for particle depositions in the rat lung has been developed by Anjilvel and Asgharian (1995), and they have extended the model to the particle deposition in the human lung (Asgharian et al., 2010). They also showed the models for deposition of inhaled fibrous particles such as asbestos in both rat and human lung (Asgharian and Yu, 1988; Asgharian and Anjilvel, 1998). Ding et al. (1997) revised Asgharian's model and proposed combined deposition of impaction and interception of fibers in the nasal region.

Carbon nanotubes (CNTs) possess a cylindrical shape with a high aspect ratio as asbestos fibers. Thus toxicological concerns on CNTs lead to interests in CNT deposition in the human lung. Several studies showed that CNTs have cytotoxicity and causes inflammations in the lung cells. Furthermore, CNTs have a potential toxicity effect on lung cancers (Ma-Hock et al., 2009). Recent studies have presented numerical calculations of CNT deposition in the lung using different deposition models. For instance, Sturm (2014) introduced the theoretical approach for a risk assessment of carbon nanotubes in the human alveoli by employing the model using aerodynamic diameter. On the other hand, Erderly et al. (2013) used a mouse model to assess the workplace exposure of CNTs for an inhalation toxicological study. For an empirical estimation of inhaled CNTs, Su and Cheng (2015) used a human respiratory tract replica and obtained the local deposition fraction of CNTs in the airways in the lung. Existing studies regarding model calculation of CNT deposition have considered CNTs as a single standing cylindrical particle in the models.

However, recent studies presented that CNTs can exist in a form of either singly standing tubes or agglomerates, or a mixture of both. Therefore, the agglomerate's properties need to be taken into account in the lung deposition model. For example, the relationship between the fraction of agglomerates within a CNT population and the mobility diameter of the CNTs was obtained by the SEM analysis and shown in Figure 1.

Airborne CNTs were collected and a number of images have been taken by SEM and agglomerated and single standing CNTs counted by the image analyzing software (ImageJ). The data were fitted to the exponential line as shown in Figure 1 to define the relationship between the mobility size and the fraction of agglomerated and single standing CNTs. The obtained relationship was applied in the lung deposition model, which included revised models of previous studies. Different breathing scenarios were considered in the model and sphere model was also revised in order to compare with the present model. The developed model can also be applied in the lung deposition model for nanoparticle agglomerates.

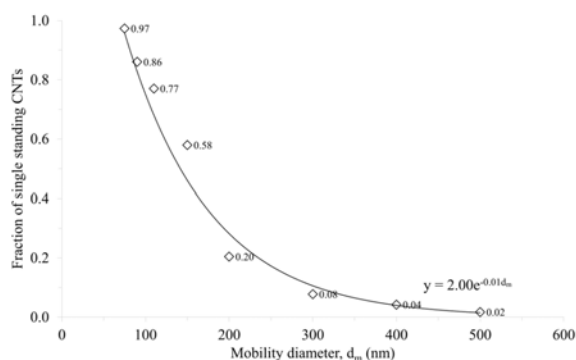


Figure 1. Fraction of single standing CNTs as a function of the classified mobility diameters. The fitting shows the relation between single standing CNT fractions and mobility sizes.

- Yeh, H.C. and Schum, G.M. (1980) *Bull. Math. Biol.* **42**, 461-480.
- Anjilvel, S. and Ascharian, B. (1995) *Fundam. Appl. Toxicol.* **28(1)**, 41-50.
- Asgharian, B., Hofmann, W. and Bergmann, R. (2010) *Aerosol Sci. Technol.* **34(4)**, 332-339.
- Asgharian, B and Yu, C.P. (1998) *J. Aerosol Medicine* **1(1)**, 37.
- Ding, J.Y., Yu, C.P., Zhang, L. and Chen, Y.K. (1997) *Aerosol Sci. Tech.* **26(5)**, 403-414.
- Ma-Hock, L., Treumann, S., Strauss, V., F. (2009) *Toxicol. Sci.* **112**, 468-481.
- Sturm, R. (2014) *SOP Transactions of Nano-technology* **1**, 21-31.
- Erdely, A., Dahm, M., Chen, B.T. et al. (2013) *Part. Fibre Toxicol.* **10**, 53.
- Su, W.C. and Cheng, Y.S. (2015) *J. Aerosol Sci.* **79**, 72-85.

## Computational Modeling to Predict Regional Deposition of Inhaled E-cigarette Aerosols within the Respiratory Tract

A.A. Rostami<sup>1</sup>, B. Asgharian<sup>2</sup>, O. Price<sup>2</sup>, and Y.B. Pithawalla<sup>1</sup>

<sup>1</sup> Altria Client Services LLC, Center for Research and Technology, Richmond, VA, USA

<sup>2</sup> Applied Research Associates, Inc. Arlington Division, Raleigh, NC, USA

Keywords: e-cigarette, aerosol dosimetry, deposition model, respiratory tract, computational model, electronic nicotine delivery systems.

Presenting author email: ali.a.rostami@altria.com

Standard particle dosimetry models developed for estimating respiratory tract deposition of environmental aerosols, do not account for the complex phenomena such as coagulation, hygroscopic growth, volatility of chemicals within the aerosol, etc. Such models are for solid particles with no phase change. If directly applied to cigarette smoke or aerosols generated by use of Electronic Nicotine Delivery Systems (ENDS), these models would result in inaccurate predictions.

In addition, aerosols generated by ENDS are different from aerosols generated from cigarette smoke in multiple ways, including the number of chemical constituents and their physicochemical properties. While cigarette smoke consists of many constituents that may potentially be generated by chemical reactions at high temperatures, ENDS aerosol is most likely generated through direct vaporization of an e-liquid formulation. Most e-liquids predominantly contain propylene glycol (PG), glycerol, water, nicotine and small amounts of flavors. As the liquid is heated, it undergoes phase change, and most of the resulting vapor mixture condenses into liquid particles. The primary composition of the aerosol (vapor and droplets) is similar to the e-liquid composition on a mass basis. Thus the aerosol is made of constituents that are volatile and hygroscopic.

The dynamics of ENDS aerosol after inhalation into the highly humid respiratory airways is also different from that of cigarette smoke. Not only that volatile compounds such as PG and nicotine rapidly vaporize, due to mixing with inhaled air and existing air in the lungs, but also the composition of liquid particles undergo changes due to moisture uptake. Hence the regional deposition pattern of ENDS aerosol in the respiratory tract is expected to be different from the deposition pattern of aerosols generated by cigarette smoking.

An ENDS aerosol inhaled by users is typically partitioned between particle and vapor phases. For exposure assessment, it is important to estimate simultaneous deposition of inhaled particles and vapors in the airways from the oral cavity to the pulmonary region. The dynamic nature of the inhaled ENDS aerosol makes it extremely difficult to experimentally measure its partitioning and deposition in real time. A dosimetry model previously developed for inhalation of smoke from combustible cigarettes was extended to inhaled

ENDS aerosols by including specific mechanisms, parameters, and physicochemical properties. Multi-constituent aerosol puffs containing PG, glycerol, water, and nicotine were used to predict the deposition of these chemicals throughout the respiratory tract. In the puffing regimen the model includes: puff withdrawal, mouth-hold, mixing of the dilution air with the puff, puff inhalation, lung hold and puff exhalation. The aerosol undergoes simultaneous coagulation and phase change, which changes droplet composition, size distribution, and in turn respiratory tract deposition. Material transport, concentration, and deposition of each chemical in the respiratory tract were calculated from the mathematical solution of the convection diffusion equations. Deposition of each ENDS aerosol constituent in the anterior portion of the oral cavity and in the distal airways of the tracheobronchial airways and pulmonary region, were estimated under a variety of use conditions.

Figure 1 shows an example of modeling results for the regional deposition fraction of inhaled aerosol from a prototype cigalike ENDS device, under a set of defined use conditions. The y-axis refers to the fraction of inhaled PG, glycerol and nicotine in both vapor and particulate phases that are deposited. Results from this dosimetry model can be used as inputs to a physiologically based pharmacokinetic model (PBPK) to estimate the distribution of nicotine in the body and the relevant internal exposure. Exposure predictions using computational models can be key components of the overall risk assessment for ENDS.

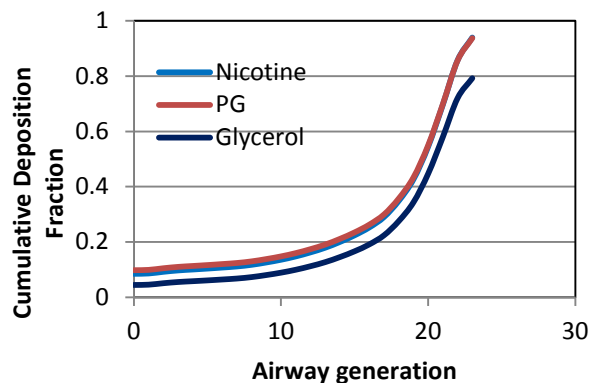


Figure 1. Modeling predictions for regional deposition fractions of inhaled aerosol from a prototype cigalike ENDS device, under a set of defined use conditions.

## Particle deposition in the lung of mothers and their children in residential environments

A. Stamatelopoulou<sup>1,2</sup>, M. Pilou<sup>3</sup>, C. Housiadis<sup>3</sup>, D.N. Asimakopoulos<sup>2</sup>, D. Sarigiannis<sup>4</sup> and T. Maggos<sup>1</sup>

<sup>1</sup> Environmental Research Laboratory, NCSR “Demokritos”, 15310 Agia Paraskevi, Greece

<sup>2</sup> Department of Applied Physics, Faculty of Physics, University of Athens, Athens, Greece

<sup>3</sup> Thermal Hydraulics & Multiphase Flow Laboratory, NCSR “Demokritos”, 15310 Agia Paraskevi, Greece

<sup>4</sup> Environmental Engineering Laboratory, Aristotle University of Thessaloniki, Greece

Keywords: residential environment, children, lung deposition, aerosol dynamics modelling

Presenting author email: mina.stam@ipta.demokritos.gr

Nowadays, the modern way of human life has led to their increasing exposure to residential indoor air pollutants, which has been associated with several adverse health effects. Especially young children comprise a vulnerable subpopulation, as they spend the largest part of their time indoors and their respiratory system is under development. Particulate matter (PM) constitute a principal component of residential indoor air pollution and have been linked with both acute effects, such as irritation in the skin, eyes, nose and throat and upper airways, and chronic health effects including asthma and cardiac disease (Zabonetti et al 2000, Miller et al 2007). For this reason, special attention has been paid recently, in order for their concentrations in residential environments where young children live to be determined.

In this context, a pilot study was conducted in Athens, with the aim to assess the indoor air quality in 25 homes, where young children under of 3 years of age lived. PM concentrations were measured in the main living area of each household for 1 week, using both the Grimm 1.108 (14 size channels, 1 minute time interval) and the Dylus 1700 (2 size channels, 1 minute time interval), a low cost particle sensor.

On the other hand, deposition of inhaled airborne particles in the respiratory tract is related to both the physical properties of the particles and the anatomical and physiological characteristics of respiration. The deposited particles can be cleared by biological processes, transported in one or more parts of the body or retained at the deposition site. Thus, exposure characterization and estimation of NPs intake, translocation and clearance are equally important for the assessment of their potential health impacts.

In the present study the data from PM exposure in the homes are combined with two numerical models to estimate PM doses in the human respiratory tract (HRT) and adjacent tissues. In particular, a one-dimensional computational model that describes transport and deposition of particles in the HRT and takes into account particle and lung dynamics (Mitsakou et al., 2005, 2007a,b) is combined with a compartmental, mathematical model that describes PM clearance from and retention at the alveolar region of the lungs and translocation to interstitium and hilar lymph nodes over time (Tran et al.,1999).

The lung deposition (Figure 1) here was calculated for the average weekly PM concentration for both the mothers and their children, discriminating between night (sleep) and day (active) periods. Next the PM daily dose in the alveolar region is introduced to the clearance/translocation model and the PM burden at the alveoli, interstitium and hilar lymph nodes is calculated over a 5 year period.

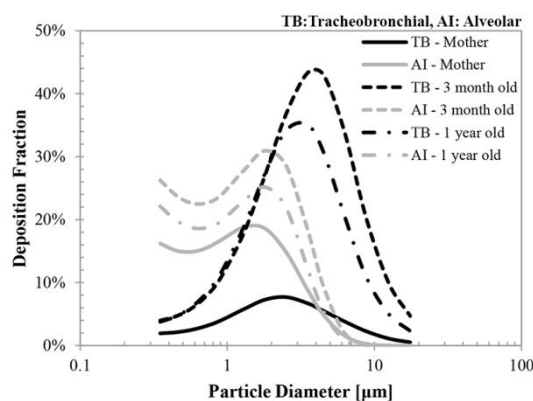


Figure 1. Particle deposition fraction in different regions of the respiratory tract for light activity.

This work was supported by project HEALS [grant agreement No 603946] of the European Commission (FP7).

- Miller, K.A, Siscovick, D.S, Sheppard, L, et al., (2007) Long-term exposure to air pollution and incidence of cardiovascular events in woman. *N. Engl. J. Med.* 356, 447-458.
- Mitsakou, C., Helmis, C., & Housiadas, C. (2005) *J. Aerosol Sci.* 36, 75-94.
- Mitsakou, C., Housiadas, C., Eleutheriadis, K., Vratolis, S., Helmis, C., & Asimakopoulos, D. (2007a) *Indoor Air* 17, 143-152.
- Mitsakou, C, Mitrakos, D., Neofytou, P., & Housiadas, C. (2007b) *J. Aerosol Medicine* 20, 519-529.
- Tran, C.L., Jones, A.D., Cullen, R.T. and Donaldson, K. (1999) *Inhal Toxicol* 11,1059–1076.
- Zanobetti, A., Schwartz, J., & Dockery, D. W. (2000) *Environ Health Perspect* 108, 1071-1077.

## Anthropometry and Anatomy Based Tools for Generation of Personalized Human Respiratory Model for Aerosol Inhalation Exposure Simulations

A. Przekwas<sup>1</sup>, A. Zhou<sup>1</sup>, R. Kannan<sup>1</sup>, and P. Segars<sup>2</sup>

<sup>1</sup>CFD Research Corporation, Huntsville AL, 35806, USA.

<sup>2</sup>Ravin Advanced Imaging Laboratories, Department of Radiology, Duke University, Durham, NC 27705, USA

Keywords: lung imaging, anthropometry, lung anatomy, airway morphology, inhalation exposure, aerosol deposition, multiscale modeling

Presenting author email: [Andrzej.przekwas@cfdr.com](mailto:Andrzej.przekwas@cfdr.com)

High fidelity computational modeling of inhalation aerosol exposure and respiratory drug delivery has been accepted as a standard practice in toxicology and pharmacology. Computational fluid dynamics (CFD) models of respiration, aerosol inhalation and deposition require high-resolution 3D anatomical geometry models of human lung parenchyma and airways. There are several lung models with various resolutions of major airways but relatively few whole lung models. Most of them have been developed for a specific subject anatomy. This paper presents a novel computational framework for the generation of subject specific human 4D lung anatomic geometry model based on human anthropometric data. The framework consists of four main components: 1) generation of a 3D anatomical geometry of a human skin from a set of anthropometric measurements using principal component analysis (PCA), 2) generation of the lung lobes and main airways based on PCA tools calibrated on medical imaging data, 3) generation of arbitrary resolution airway tree “filling” the lobes using a stochastic model, and 4) generation of the lung respiratory tidal dynamics model using subject specific spirometry data or 4D medical imaging. The framework can be used to generate lung models for multiscale simulations of respiratory aerosol exposures using either 4D CFD high fidelity simulations or reduced order models on mobile computing platforms.

The starting point in the current framework is the subject specific basic anthropometric measurements, height and weight as a minimum. More data improves the model accuracy. The framework uses a PCA based algorithm, calibrated and validated on large data sets of 3D human skin scans, to generate subject specific skin anatomic geometry model. To generate subject specific lung lobes and main airways we use a similar PCA algorithm to correlate the critical anatomical thoracic parameters with the lung anatomy principal components. The algorithm is calibrated on the XCAT database of whole body CT scans with a detailed resolution of lung geometry and respiratory motions [Segras et al. 2010]. This module generates the accurate 3D anatomic geometry of both lung lobes and main airways including the trachea and 3 to 4 generations of the bronchial tree. Figure 1 presents a snapshot of the framework GUI used to generate human body anatomy from anthropometric measurements and subject specific lung lobe models.

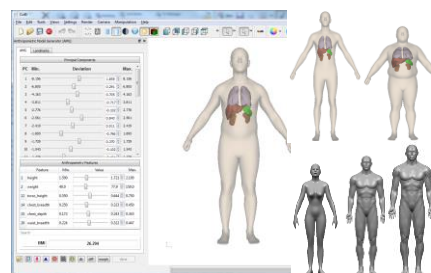


Figure 1. GUI for generation of personalized human body anatomy and the respiratory anatomy models

Because current CT imaging does not provide detailed tracheal-bronchial wall surface anatomy, we use an anatomical template of the airways (nose/mouth to bronchi) to morph it to the surface of the CT imaged airways. In the final step, we use a stochastic optimization algorithm and respiratory physiology constraints to “propagate” the respiratory tree beyond the image generated tree. Figure 2 shows the subject specific integrated whole lung model, geometry of the upper airway and the virtual terminal alveoli. The model has been used to simulate aerosol deposition, mucociliary and transmucosal transport [Kannan 2017]. The paper will present several examples of lung models for aerosol toxicology and pharmacology applications.

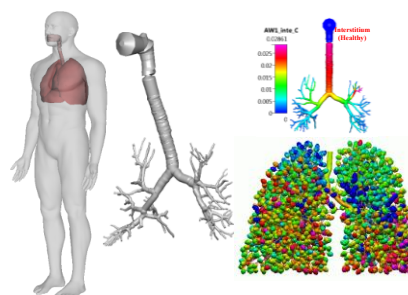


Figure 2. Subject specific lung, major airways and virtual terminal alveoli model.

Segars WP, Sturgeon G, et al. (2010) 4D XCAT phantom for multimodality imaging research. *Med Phys.* 37(9):4902-15.

Kannan R, Chen ZJ, Singh N, Przekwas AJ, et al (2017) A quasi-3D wire approach to model pulmonary airflow in human airways. *Int. J. Num. Meth. Biomed Eng.* In print

## Method for processing cascade impactor data to estimate activity of radioactive aerosol particles deposited in different regions of human respiratory tract.

A.E. Karev, A.G. Tsovyanov, S.M. Shinkarev  
SRC FMBC of FMBA Russia, Moscow, Russia

Keywords: radioactive aerosol, impactor, aerosol deposition, AMAD, respiratory tract

Presenting author email: karev17@gmail.com

Regional deposition of aerosols into human respiratory tract cannot be divided strictly on the definite size fractions. It makes difficult modeling aerosol deposition into respiratory tract using an impactor. There is shown that Andresen Cascade Impactor (ACI) cannot serve adequately as a model of aerosol deposition into human respiratory tract despite declared characteristics. Method for processing cascade impactor data is required for solving mentioned task.

Method suggested allows estimate activity particle-size distribution through different regions of a respiratory tract in the range of applicability of term “aerodynamic diameter”. It’s especially actual in case of multimodal particle-size distributions as approximation by unimodal log-normal function is not quite correct.

Comparison a dependencies of the percentage of deposited aerosol particles calculated by suggested method, on activity median aerodynamic diameter (AMAD), shows fairly good agreement with analogic dependences from ICRP 66 Publication (reference worker, light exercise). Relative error of suggested method varies from 0,1% to 26% within AMAD values from 0,2  $\mu\text{m}$  to 10  $\mu\text{m}$ . Maximum values of relative error were obtained for AMAD 0,1  $\mu\text{m}$  – from 27,2% for BB region (bronchi) till 38,9% for bb region (bronchioles). Probably it’s tied with small number of stages for sampling submicron aerosol particles in construction of considered impactor (Tsovyanov, 2014).

According to experimental data (Dorrian, 1995) particles size distributions on work places of the nuclear facilities are characterized basically by AMAD values from 1 to 10  $\mu\text{m}$  and partially by AMAD from 0,1 to 1  $\mu\text{m}$ . Hence it could be considered that within mentioned AMAD ranges percentage of deposited aerosol particles calculated by suggested method using special impactor (Tsovyanov, 2014) within relative errors is in good agreement with data from ICRP 66 Publication (ICRP, 1994).

In general any impactor model could be used. Increasing number of stages will make final result closer to ICRP 66 data.

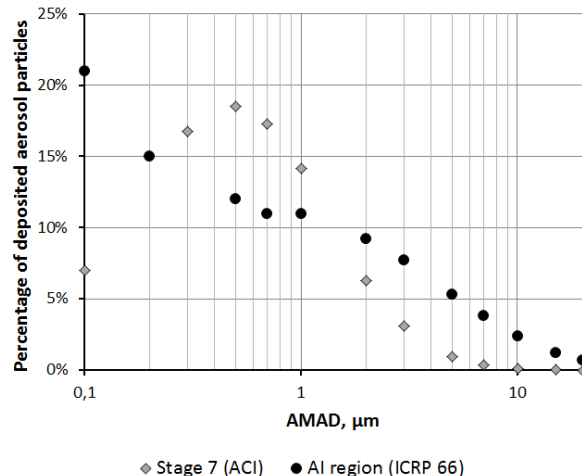


Figure 1 Comparison dependencies of the percentage of deposited aerosol particles on AMAD for stage № 7 ACI and for AI region (alveoli) from ICRP 66 Publication

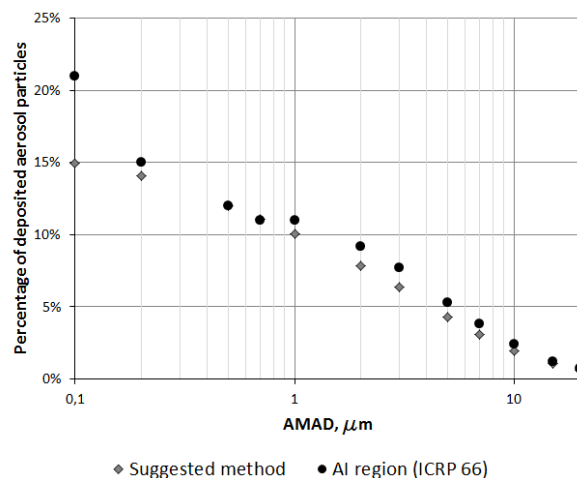


Figure 2 Comparison dependencies of the percentage of deposited aerosol particles on AMAD, calculated by suggested method, and for AI region (alveoli) from ICRP 66 Publication

Tsovyanov A.G., Karev A.E. (2014) Patent RU 2509375: Impactor-phantom of the human respiratory tract

Dorrian M.D. (1995) Radiat. Prot. Dosimetry. - V. 60. - N 2. - P.119-133.

Human Respiratory Tract Model for Radiological Protection / ICRP Publication 66. Ann. ICRP 24 (1-3). – 1994.

## **Abstracts T408**

## Combined source and health risk apportionment approach to develop an emission reduction plan for PM<sub>2.5</sub> in the Sha-Lu area, Taiwan

H.T. Hsu<sup>1</sup>, L.H. Young<sup>2</sup>, B.F. Hwang<sup>2</sup>, M.Y. Lin<sup>3</sup>, C.N. Chen<sup>2</sup>, Y.C. Chen<sup>4</sup>, P.J. Tsai<sup>3</sup>

<sup>1</sup>Department of Health Risk Management, China Medical University, Taichung, 404, Taiwan

<sup>2</sup>Department of Occupational Safety and Health, China Medical University, Taichung, 404, Taiwan

<sup>3</sup>Department of Environmental and Occupational Health, National Cheng-Kung University, Tainan, 701, Taiwan

<sup>4</sup>Environmental Health Research Center, National Health Research Institute, Miaoli, 350, Taiwan

Keywords: PM<sub>2.5</sub>, metal composition, electric arc furnace, positive matrix factorization.

Presenting author email: hthsu@mail.cmu.edu.tw

PM<sub>2.5</sub> refers to fine particulate matter whose aerodynamic diameter is less than 2.5 μm. Because of its small particle size, PM<sub>2.5</sub> can be transmitted not only to the gas exchange site of the lungs (Pinkerton et al., 2000), but can also penetrate through the barriers in the lungs and enter the circulatory system, after which it can be distributed to other organs in the body (Feng et al., 2016). Therefore, the impact of PM<sub>2.5</sub> on human health is an important research topic.

Recently study has indicated that the same increase in concentration of 10 μg/m<sup>3</sup> of PM<sub>2.5</sub> in different areas and in different seasons within the same area will have varying degree of negative effects on health (Franklin et al., 2008). Overall, it is probable that only measuring PM<sub>2.5</sub> mass concentrations may not provide a full explanation of its toxicity and health effects (Hopke et al., 2006; Schaumann et al., 2004). Based on epidemiological and toxicological studies, the health effects of PM<sub>2.5</sub> have a high degree of correlation with the metal composition of PM<sub>2.5</sub> (Hamad et al., 2016).

In this study, sampling activities over the course of approximately one year were completed in Sha-Lu region, Taichung city. We combined the techniques of receptor modeling and human health risk assessment to develop the best strategy to reduce the health impacts of PM<sub>2.5</sub>. According to the results of PMF modeling, there are five sources contributing to PM<sub>2.5</sub> emissions in the Sha-Lu region. The order of these sources in their contribution to PM<sub>2.5</sub> emissions is: steel industry > residual oil combustion > road dust and traffic > coal-fired power plant > glass production industry. According to the results of the human health risk assessment, the contribution to cancer risk from the various PM<sub>2.5</sub> emission sources is: road dust and traffic > coal-fired power plant > residual oil combustion > glass production industry > steel industry. The main substance contributing to cancer risk is As, and the secondary one is Cr<sup>+6</sup>. In order to reduce the potential cancer risk to local residents, it is recommended that the power plant use coal with a lower content of As and Cr so as to control and reduce the emission of these two elements and the associated cancer risks. The results of this research show that solely controlling the overall concentration of PM<sub>2.5</sub> would not be sufficient and would not likely reduce the health risks. An analysis of the degree to which emission sources contribute to health risks is feasible and also provides important information

for further decision-making. Therefore, the approach used herein is a method that can be widely used for future environmental management.

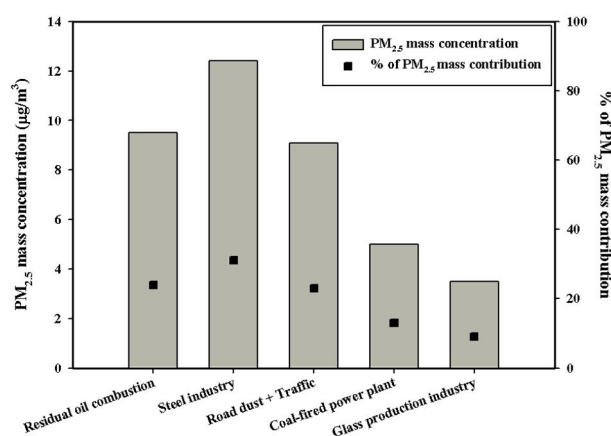


Figure 1. PM<sub>2.5</sub> concentration and percentage contribution from five emission sources obtained by PMF simulation in this study.

This work was supported by the National Health Research Institute under grant EH-102-SP08.

Feng, S., Gao, D., Liao, F., Zhou, F., Wang, X. (2016) *Ecotox. Environ. Safe.* **128**, 67-74.

Franklin, M., Koutrakis, P., Schwartz, J. (2008) *Epidemiology* **19**, 680-689.

Hamad, S.H., Schauer, J.J., Antkiewicz, D.S., Shafer, M.M., Kadhim, A.K.H. (2016) *Sci. Total Environ.* **543**, 739-745.

Hopke, P.K., Ito, K., Mar, T., Christensen, W.F., Eatough, D.J., Henry, R.C., Kim, E., Laden, F., Lall, R., Larson, T.V., Liu, H., Neas, L., Pinto, J., Stölzel, M., Suh, H., Paatero, P., Thurston, G.D. (2006) *J. Exp. Sci. Environ. Epidemiol.* **16**, 275-286..

Schaumann, F., Borm, P.J.A., Herbrich, A., Knoch, J., Pitz, M., Schins, R.P.F., Luettig, B., Hohlfeld, J.M., Heinrich, J., Krug, N. (2004) *Am. J. Respir. Crit. Care Med.* **170**, 898-903..

## Nanoparticle stability and size as important factors in nano-TiO<sub>2</sub> toxicity in macrophage-like cells.

J. Sikorova<sup>1</sup>, T. Brzicova<sup>1</sup>, A. Milcova<sup>1</sup>, K. Vrbova<sup>1</sup>, J. Klema<sup>2</sup>, P. Pikal<sup>3</sup>, J. Topinka<sup>1</sup> and P. Rossner<sup>1</sup>

<sup>1</sup>Department of Genetic Toxicology and Nanotoxicology, Institute of Experimental Medicine CAS, Prague, 142 20, Czech Republic

<sup>2</sup>Department of Computer Science, Czech Technical University, Prague, 121 35, Czech Republic

<sup>3</sup>Precheza, Prerov, 751 52, Czech Republic

Keywords: Nanomaterial, TiO<sub>2</sub>, cytotoxicity, macrophages  
jitka.stolcpartova@biomed.cas.cz

OECD identified TiO<sub>2</sub> NPs as one of priority manufactured nanomaterials for toxicology and risk assessment so as to avoid adverse effects from the use of this material (OECD 2010).

Toxicity of TiO<sub>2</sub> NMs relies on characteristics of NMs such as shape, size, crystal structure, zeta potential, aggregation and agglomeration tendency, surface characteristics and coatings. However, their influence to toxicity remains unclear due to ambiguous results from different studies (Shi et al., 2013). In vivo studies revealed target organs (spleen and liver) and macrophages seem to be target cells as they have to cope with engulfed TiO<sub>2</sub> NMs load.

The presented study measured the cytotoxic effect without photoactivation of fourteen divers TiO<sub>2</sub> NMs on human monocytic cell lines THP-1 differentiated into macrophage-like cells.

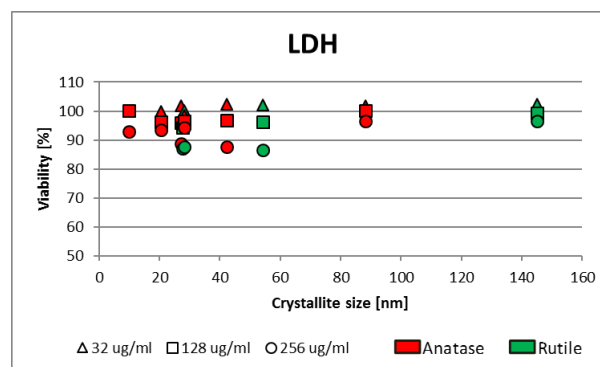
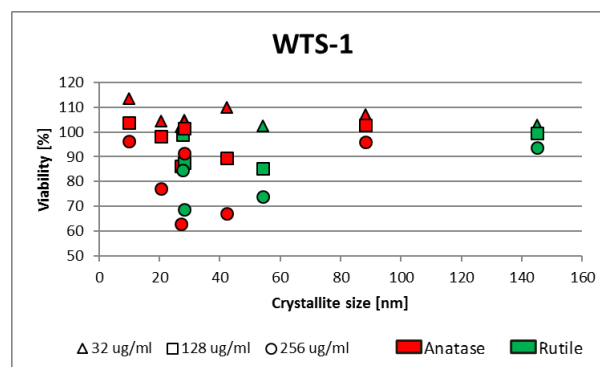
A set of NM consists of 5 variants of anatase and 5 variants of rutile nanoparticles differing in their diameter (from 3 to 165 nm), 3 variants of anatase high aspect ratio nanomaterials of different widths and lengths and one silicon coated (hydrophobic) rutile particles. TiO<sub>2</sub> samples were characterized in the powder form using following methods: x-ray diffraction, thermogravimetric analysis and Brunauer Emmet Teller measurements. Following dispersion, the size distribution in water and cell culture medium and zeta potential in cell culture medium were measured by dynamic light scattering.

Three cytotoxicity assays were used: MTS, WTS-1, and LDH. For all nanomaterials, three independent repetitions were carried out.

Over all, cytotoxicity of all NMs was low even at the highest concentration of 256 µg/ml. The viability did not decrease below 60% for WTS-1 and MST assays and 80% for the LDH assay. Despite low toxicity, polydispersity index, besides concentration, was identified as the important cytotoxic factor. More stable suspension led to higher cytotoxicity.

Crystal size seemed to have also an influence. There is visible a nonlinear shape for crystalline size and cytotoxicity relationship with the highest toxicity between 20-60 nm (Fig. 1). Nonlinear relationship was also shown in Chang review (2013) who concluded that the highest toxicity occurred within particles with diameter between 10-40 nm. Zhang et al. (2012) found TiO<sub>2</sub> NPs with diameter 21 ± 3nm more toxic for mouse macrophages cells than 12 ± 2 nm and 98 ± 20 nm. Increase cytotoxicity

in given diameter size range would give an answer to inconsistent findings at size and cytotoxicity relationship.



Figures 1, Cytotoxicity assays based on 2 different mechanism showed similar nonlinear relation between crystallite size and viability.

The authors acknowledge the assistance provided by the Research Infrastructure NanoEnviCz, supported by the Ministry of Education, Youth and Sports (MEYS) of the Czech Republic under Project No. LM2015073, and CENATOX (GACR P503/12/G147) and NANOGEN (MEYS LO1508) projects.

OECD (2010) Series on the Safety of Manufactured Nanomaterials No. 27. ENV/JM/MONO/2010/46.

Shi, H., Magaye, R., Castranova V. and Zhao J. (2013) *Part Fibre Toxicol.*, 10:15.

Chang, X., Zhang, Y., Tang, M. and Wang, B. (2013) *Nanoscale Res. Lett.*, 8:51.

Zhang, J., Song, W., Guo, J., Zhang, J., Sun, Z., Li, L., Ding, F. and Gao M. (2012) *Toxicol. Ind. Health*; 29(6): 523–533.

## Effect of nanoparticles on oxidative stress and intracellular calcium signaling in pulmonary artery endothelial cells in physiological and pathological conditions

J. Deweirdt<sup>1</sup>, J.F. Quignard<sup>1</sup>, C. Guibert<sup>1</sup>, J.P. Savineau<sup>1</sup> and I. Baudrimont<sup>1</sup>  
<sup>1</sup>CRCTB, INSERM U1045, Univ Bordeaux, F-33076 Bordeaux, France

**Keywords:** nanoparticles, pulmonary artery endothelial cells, calcium signaling, stretch-activated channels, oxidative stress, pulmonary hypertension

Presenting author email : Juliette.deweirdt@u-bordeaux.fr

### Introduction

Many epidemiological studies have revealed the involvement of nanoparticles (NP) in increasing of respiratory and cardiovascular mortality and morbidity. It has been shown in humans, a correlation between exposure to nanoparticles and an increase in pulmonary arterial pressure. The pulmonary circulation could be one of the primary targets of inhaled particles and people with pulmonary hypertension (PH) could be a population at risk. Despite the main role of calcium signaling and oxidative stress in the pathogenesis of this disease, the effect of particulate pollution on these cellular targets is poorly described. In this context, the objectives of this study are to evaluate, on human pulmonary vascular cells, under no stretch or cyclic mechanical stretch that mimic wall pressure found in PH, the effects of nanoparticles (black carbon) on the biological responses such as calcium signaling and oxidative stress in physiological and pathological conditions.

### Methods

Human Pulmonary Artery Endothelial Cells (HPAEC) are cultured in physiological (0% to 5% stretching and normoxia: 21% O<sub>2</sub>) and pathological conditions that mimic the PH (stretch system: 30 cycles/min, 15% stretching and hypoxia: 1% O<sub>2</sub>), using STREX®, B-bridge International system. HPAEC cells are exposed for 4h or 24h to carbon black-FW2 NP from 5 to 15 µg/cm<sup>2</sup>. Different endpoints are studied (i) production of reactive oxygen species by a fluorescent probe (H<sub>2</sub>DCF-DA), MitoSOX probe and electronic paramagnetic resonance (EPR), (ii) calcium signaling using the fluorescent indicator dye Fluo-4, Rhod2 and confocal microscopy analysis.

### Results

In HPAEC, a 4h-exposure to FW2-NP (5 - 15 µg.cm<sup>2</sup>) induced a concentration-dependent increase of intracellular ROS levels, mainly a cytoplasmic and a mitochondrial increase of superoxide anion level. In addition, after a 24h-exposure to HPAEC, FW2-NP attenuated, in a concentration-dependent manner, the ATP (10<sup>-5</sup>M)-induced increase in intracellular calcium ion level ([Ca<sup>2+</sup>]<sub>i</sub>) (fig1).

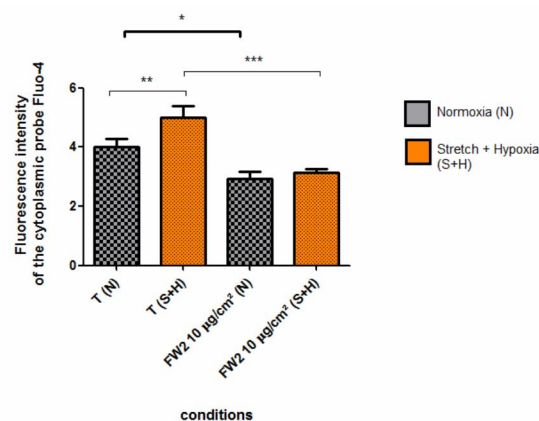


**Figure 1: Intracellular [Ca<sup>2+</sup>]<sub>i</sub> (ATP response) in normal and pathological conditions.**

A 24h-exposure to FW2 NP (10 µg/cm<sup>2</sup>), induced a modification of the intracellular Ca<sup>2+</sup> level. These modifications appear to be more significant in pathological condition. Indeed, there is a significantly decrease for the ATP response: 28% p<0.05 (\*) in normoxia condition, against a very significantly decrease in stretch and hypoxia condition 37.2% p<0.001 (\*\*\*). T means control.

When cells are treated with both FW2 NP and thapsigargin (known to deplete endoplasmic reticulum Ca<sup>2+</sup> stores), we show a significant decrease of the calcium response as compared to control cells suggesting an effect of these particles on the intracellular calcium release from the endoplasmic reticulum.

A 1h-pretreatment with polyethylene glycol (PEG)-superoxide dismutase (300 U/ml) and polyethylene glycol (PEG)-catalase (600 U/ml), significantly decreases the modifications of intracellular Ca<sup>2+</sup> level induced by FW2 NP. Thus, the perturbation of intracellular calcium homeostasis induced by particles seems also to be correlated to oxidative stress.

### Conclusion

In conclusion, the present study shows that, in HPAEC, carbon-black FW2-NP (i) produces different reactive oxygen species (ii) impairs calcium homeostasis. In conditions that mimic PH, the perturbation of intracellular calcium homeostasis induced by nanoparticles could be correlated to a deterioration of the endoplasmic reticulum stocks and to oxidative stress.

*This work was supported by the Fondation pour la Recherche Médicale (FRM).*

## Pulmonary effects of silver nanowires with different length in instillation study

T. Oyabu, Y. Morimoto, Y. Yoshiura and T. Myojo

Institute of Industrial and Ecological Sciences, University of Occupational and Environmental Health, Japan, Kitakyushu, 807-8555, Japan

Keywords: silver nanowire, instillation, inflammation

Presenting author email: [toyabu@med.uoeh-u.ac.jp](mailto:toyabu@med.uoeh-u.ac.jp)

Recently, many kinds of nanomaterials have been developed and in production. Nanowires with thin and long shape are one of them and their health effects are concerned because of their shape like asbestos. We performed the intratracheal instillation study of silver nanowires with different length and investigate the effects of wire lengths on lung.

We made the short nanowires from silver nanowire (Novarials Co., diameter: 70nm, length: 45micrometer, suspended in water) by ultrasonic methods. The original nanowires (long nanowire) and the created nanowires (short nanowire) are the same diameter with different length and same concentration. These two were diluted with sterile distilled water and 0.5mg/0.4ml each were instilled into Wistar male rat lung through their trachea. As control only distilled water were instilled. The scanning electron microscope images of both nanowires were shown in Fig. 1. At 3 days after the instillation, their lung weight, total cell counts and neutrophil number and lactate dehydrogenase concentration in bronchoalveolar lavage fluid (BALF) from the each 5 rats of 3 groups were compared.

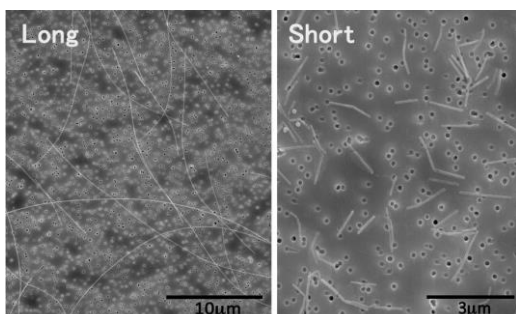


Fig.1 Scanning electron microscope images of long and short nanowires.

The recovered cells in BALF of lung instilled long nanowires were shown in Fig. 2. Many neutrophils were induced and long nanowires were seen to be phagocytized.

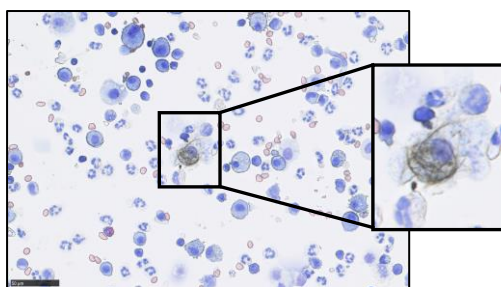


Fig. 2 Long nanowires inside the recovered cells in BALF.

The lung weights and total cell count (TCC), neutrophil numbers (PMN) in BALF of each groups at 3days after the instillation were shown in Fig. 3. Those indicators of pulmonary effect of lung instilled both nanowires were extremely increased compared with control group.

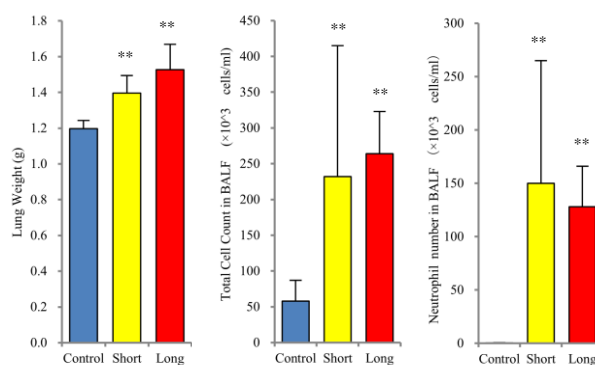


Fig.3 Lung weight, and TCC, PMN in BALF at 3 days after the instillation. (\*\*:  $P < 0.01$ )

Hereafter, time-dependent change of those indicators and also histopathological changes of lung after the instillation will be examined.

This work was supported by JSPS KAKENHI Grant Number 15K08789 of Japan.

## Characterization of the air-liquid interface cell exposure (ALICE-CLOUD) system for in-vitro toxicological studies of engineered nanomaterials (ENMs)

Yaobo Ding<sup>1,2</sup>, Patrick Weindl<sup>1,2,3</sup>, Clara Wimmer<sup>1,2,3</sup>, Paula Mayer<sup>1,2</sup>, Tobias Krebs<sup>3</sup> and Otmar Schmid<sup>1,2</sup>

<sup>1</sup>Institute of Lung Biology and Disease, Helmholtz Zentrum München, 85764 Neuherberg, Germany

<sup>2</sup>Comprehensive Pneumology Center - Member of the German Center for Lung Research (DZL),  
81377 Munich, Germany

<sup>3</sup>VITROCELL Systems GmbH, 79183 Waldkirch, Germany

Keywords: nanoparticle, aerosol exposure, air-liquid interface, in-vitro, toxicology.

Presenting author email: yaobo.ding@helmholtz-muenchen.de

Engineered nanomaterials (ENMs), despite their unique physico-chemical properties for advanced applications compared to conventional materials, have been found to bear potential adverse effects on human health (Geiser and Kreyling, 2010). In inhalation toxicology studies, cell exposure to ENM aerosols under air-liquid interface cell culture conditions provides a more physiologically-relevant platform to investigate their toxic effects as compared to the traditional submerged cell culture systems (Paur et al., 2011).

In this study, we characterized the performance of the VITROCELL® CLOUD 6/6 system (6-well; VITROCELL Systems, Germany) for aerosolized delivery of ENMs to air-liquid interface cells. The system is equipped with a vibrating membrane nebulizer (Aeroneb Pro, Aerogen, Ireland) which generates aerosol droplets from a liquid suspension containing ENMs. As described by Lenz *et al* (2014) in the VITROCELL CLOUD system the aerosol droplets form a dense cloud, which utilizes cloud dynamics to rapidly (within 3 min) fill the exposure chamber, to uniformly mix the aerosol by circulating in vortices and to finally sediment spatially uniform onto the transwell inserts containing the cells. A quartz crystal microbalance (QCM) is integrated (corner position) to monitor the cell-deposited dose.

A fluorescein solution was nebulized to investigate the uniformity and efficiency of aerosol deposition into the inserts. The mean deposition factor in the inserts was 0.67 with an insert-insert variability of 11.3% (Figure 1). The QCM received a slightly lower (-18.9%) dose than the inserts. Subsequently, titanium dioxide (TiO<sub>2</sub>) nanoparticle suspensions of varied concentrations were nebulized and the mass doses measured by the QCM were compared to the values predicted from Figure 1. The actual dose measured by the QCM was significantly lower than predicted (-19% and -40% for 1 and 5 mg/ml TiO<sub>2</sub> suspension, respectively) indicating that some of the TiO<sub>2</sub> may have been retained by the nebulizer (Figure 2).

Our preliminary results show that the VITROCELL-CLOUD system can be used to deliver high ENM dose rates (<1000 ng/cm<sup>2</sup>/min) uniformly (<12% insert-insert variability) and efficiently (< 19% delivery efficiency) to cells cultured at the air-liquid interface. The cell-delivered ENM dose can be measured accurately with an integrated QCM. Next, different ENM suspensions (TiO<sub>2</sub>, ZnO, CNTs, etc.) of varied

concentrations will be tested to investigate how material type and suspension properties affect aerosol delivery. Cell cultures will be used to characterize the toxic effects of these ENMs on lung epithelial cells.

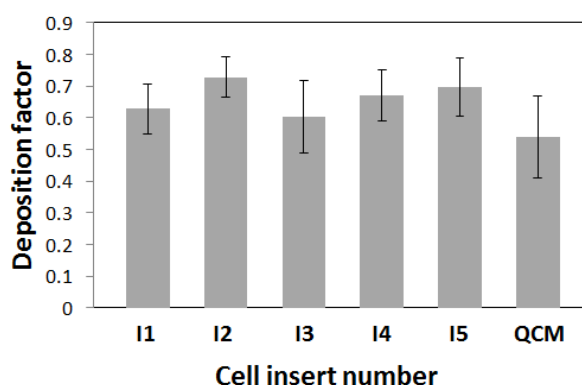


Figure 1 Deposition factor (area-scaled deposition efficiency) of the five different inserts and the QCM

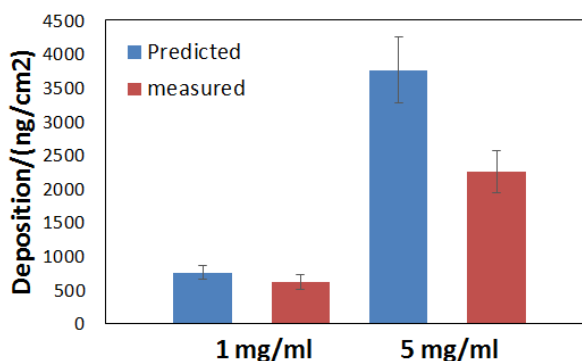


Figure 2 Measured deposition mass versus calculated numbers using different suspension concentrations

This work was supported by the EU SmartNanoTox project (grant number: 686098).

Marianne Geiser, M. and Kreyling, W.G. (2010) *Part Fibre Toxicol.* 2010 Jan 20;7:2.

Paur H, Cassee FR, et al., Schmid, O., (2011) *J. Aerosol Sci.* 42: 668–692.

Lenz, A.-G., Stoeger, T., et al., Schmid, O., (2014) *Am. J. Resp. Cell Mol. Biol.*, 51, 526–535.

## Dosimetric considerations for designing toxicological studies with aerosolized nanoparticles: On the role of dose metric and tissue-delivered dose

Otmar Schmid<sup>1,2</sup>

<sup>1</sup>Institute of Lung Biology and Disease, Helmholtz Zentrum München, 85764 Neuherberg, Germany

<sup>2</sup>Comprehensive Pneumology Center - Member of the German Center for Lung Research (DZL), 81377 Munich, Germany

Keywords: nanoparticle, aerosol exposure, air-liquid interface, in-vitro, toxicology.

Presenting author email: yaobo.ding@helmholtz-muenchen.de

Aerosolized delivery of biopersistent nanoparticles (NPs) to animals (*in vivo*) or cell-based (*in vitro*) models of the lung is a technological challenge, which typically requires an interdisciplinary approach involving aerosol scientists and biologists/toxicologists. For translation of preclinical NP toxicity data into risk assessment it is expected that not only exposure levels, but tissue-delivered dose play an important role. Hence, for designing nanotoxicological experiments in terms of *required aerosol concentration* and *expected exposure time* accurate information on the toxicologically most relevant dose metric, the tissue-delivered dose and the expected toxicologically relevant dose range are essential.

In this talk, guidance on these issues is provided. In particular an overview of typically required dose ranges for the onset of toxicological effects for both *in vitro* and *in vivo* toxicity studies is presented and put into perspective of realistic exposure scenarios such as urban and occupational environments (Paur et al., 2011).

Insight on the toxicologically most relevant dose metric is provided based on a meta-analysis of nine *in vivo* studies on particle-induced, acute pulmonary toxicity in animal models (mouse, rat) encompassing five different types of nanomaterials (polystyrene, titanium dioxide, carbonaceous materials, transition metal oxides (Co, Ni, Zn) and hydrothermally synthesized  $\alpha$ -quartz with a wide range of primary particle diameters (9-535 nm) and mass-specific BET surface areas (6-800 m<sup>2</sup>/g). The acute influx of inflammatory cells (polymorphonuclear neutrophils, PMNs) into the lungs 24h after intratracheal instillation of NPs was chosen as toxicological endpoint for acute lung inflammation. The toxicological data were investigated with respect to various dose metrics, namely (primary) particle number, joint length, BET and geometric surface area, volume and mass (Schmid and Stoeger, 2016).

Surface area is identified as the biologically most relevant dose metric for spherical NPs explaining about 80% of the observed variability in acute pulmonary toxicity ( $R^2 = 0.77$ ). Moreover, using surface area as the dose metric allows identification of material-based toxicity classes independent of particle size. Typical materials without intrinsic toxicity – so called low-solubility, low-toxicity (LSLT) materials - show low surface-specific toxicity with an EC<sub>50</sub> of 175 cm<sup>2</sup>/g-lung (ca. 0.05 cm<sup>2</sup>/cm<sup>2</sup>-lung), where EC<sub>50</sub> represents the dose inducing 50% of the maximum effect (here: 30% PMN)

(Figure 1). On the other hand, some transition metal oxides (here: Co, Ni, Zn) display a 12-fold enhanced surface-specific toxicity compared to LSLT particles (EC<sub>50</sub> = 15 cm<sup>2</sup>/g-lung; data not shown in Figure 1).

This analysis implies that surface-related modes of action are driving acute pulmonary toxicity for the types of NPs investigated here. The relevance of other dose metrics such as number and volume is acknowledged for other modes of action, namely fiber-induced toxicity and extremely high particle lung burden (overload conditions), respectively.

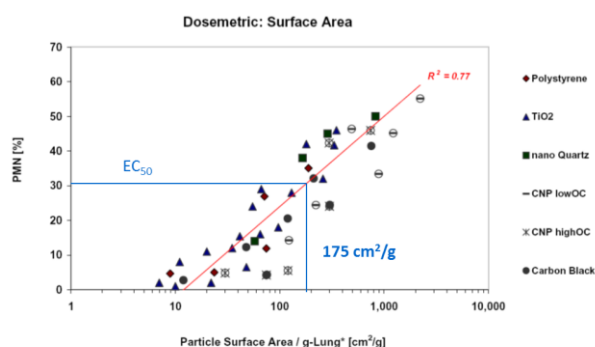


Figure 1: Acute pulmonary toxicity (PMN influx into the lung) scales well with surface area dose of NPs delivered to the lung even for different types of material.

For designing nanotoxicological experiments, first the adequate dose metric needs to be identified (often surface area), then the expected/available aerosol exposure concentration has to be converted into tissue-delivered dose rate and finally the typical onset dose for toxicological response has to be targeted. It is generally found that significantly higher tissue-delivered surface area doses are required for cell-based *in vitro* toxicological studies (1–10 cm<sup>2</sup>/cm<sup>2</sup>-cells) as compared to *in vivo* studies (0.05 cm<sup>2</sup>/cm<sup>2</sup>-lung) for LSLT materials. This needs to be taken into account when designing nanotoxicological studies.

This work was supported by the EU SmartNanoTox project (grant number: 686098).

Paur H, Cassee FR, et al., Schmid, O., (2011), *J. Aerosol Sci.* 42: 668–692.

Schmid, O., Stoeger, T., (2016), *J. Aerosol Sci.*, 99, 133–143, 2016

## **Abstracts T409**

## Generation of copper and copper oxide nanoparticles for exposure studies by MOCVD

P. Moravec<sup>1</sup>, J. Schwarz<sup>1</sup>, P. Vodička<sup>1</sup>, J. Kupčík<sup>2</sup> and J. Švehla<sup>1</sup>

<sup>1</sup>Laboratory of Aerosol Chemistry and Physics, Institute of Chemical Process Fundamentals of the CAS, v.v.i., Prague, 16502, Czech Republic

<sup>2</sup>Centre of Instrumental Techniques, Institute of Inorganic Chemistry of the CAS, v.v.i., Husinec-Řež, 25068, Czech Republic

Keywords: exposure studies, MOCVD, nanoparticle characterization, nanoparticle generation.

Presenting author email: moravec@icpf.cas.cz

Particles containing copper are frequently emitted into the atmosphere therefore they can be easily inhaled. Even though they were found highly toxic, Karlsson *et al.* (2008), in vivo studies of their toxicity are still rather rare. Cu/Cu<sub>2</sub>O/CuO nanoparticles (NPs) can be synthesized from copper acetylacetonate (CuAA), Nasibulin *et al.* (2005), however, the long lasting generation has not yet been studied. In this work we tested a method of long lasting generation of copper and copper oxide NPs by pyrolysis and oxidation of CuAA.

Experiments were performed in an externally heated work tube with i.d. 25 mm and 1 m long heated zone. A stream of nitrogen carrier gas, saturated by precursor vapour in a saturator ( $Q_S$ ), was fed into the reactor, where it was mixed either with a stream of nitrogen (pyrolysis) or a mixture of nitrogen and air (oxidation). A stream of NPs laden gas ( $Q_R$ ) was diluted in the outlet part of the work tube by a diluting stream ( $Q_{Dil}$ ) of nitrogen (pyrolysis) or air (oxidation). The particle production was studied in dependence on reactor ( $T_R$ ) and saturator temperature ( $T_S$ ), and on flowrates  $Q_S$ ,  $Q_R$  and  $Q_{Dil}$ , and NPs production was monitored using SMPS (TSI model 3936L75). Samples for NPs characterization were deposited onto TEM grids, using a nanometer aerosol sampler (TSI model 3089) and on cellulose, quartz, Zefluor and Sterlitech Ag filters. The particle characteristics were studied using HRTEM (JEOL 3010), energy dispersive spectroscopy (INCA/Oxford connected to JEOL 3010), inductively coupled plasma – optical emission spectrometry (Agilent 4200 MP-AES), elemental and organic carbon analysis (EC/OC, Model 4, Sunset Laboratory) and X-ray diffraction (Bruker D8 Discover diffractometer).

Two experimental campaigns with total duration 102 (pyrolysis, see Fig. 1) and 104 h (oxidation) were carried out. The particle production was studied in the range of  $T_R$ : 500-700 °C,  $T_S$ : 120-134 °C,  $Q_R$ : 800-1500 cm<sup>3</sup>/min,  $Q_S$ : 80-300 cm<sup>3</sup>/min and  $Q_{Dil}$ : 1500-2200 cm<sup>3</sup>/min. Even though both NPs production, and NPs characteristic obtained by pyrolysis and oxidation differ somewhat, both methods provide experimental conditions favourite for exposure experiments. For pyrolysis, the generation of NPs at  $T_R$  700 °C provides production rate sufficiently high (up to 4000 µg/m<sup>3</sup>, i.e. 12 µg/min) and can be further increased by an increase of  $T_S$  or/and  $Q_S$ , and it is stable at steady state conditions for sufficiently long time. The primary particle size is very small (5-15 nm), so that they have very high surface area, which is the biologically most effective matrix for

acute nanoparticle toxicity in the lung, Schmid and Stoeger (2016). The NPs also have well-defined characteristic; the content of Cu in NPs is 73 wt. %, predominantly in the form of metallic Cu, and they contain only 9 wt. % of total carbon (TC). For oxidation, the optimal  $T_R$  was identified as 600 °C, but the differences against 700 °C were small. The NPs production rate was smaller (up to 2000 µg/m<sup>3</sup>, i.e. 6 µg/min), primary NPs size was bigger (20-30 nm), so that the NPs surface area was smaller than that at pyrolysis. But they have perfectly defined composition: 74 wt. % of Cu in the form of copper oxide (CuO), and practically zero content of OC (<1 wt. %).

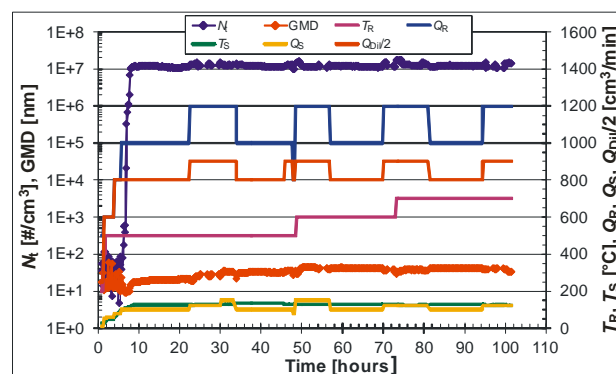


Figure 1. Number concentration ( $N_t$ ) and geometric mean diameter (GMD) of Cu/Cu<sub>2</sub>O NPs generated by pyrolysis at various experimental conditions.

Follow-up exposure experiments are being performed at the Institute of Analytical Chemistry of the CAS, v.v.i. (Večeřa *et al.*, 2011).

This work was supported by the Czech Science Foundation under grant P503/12/G147. XRD analyses were performed by Mgr. Anna Kallistová, Geological Institute of the CAS, v.v.i.

- Karlsson H. L., Cronholm P., Gustafsson J. and Möller L. (2008) *Chem. Res. Toxicol.* **21**, 1726-1732.  
 Nasibulin A.G., Shurygina L.I. and Kauppinen E.I. (2005) *Colloid J.* **67**, 5-25.  
 Schmid O. and Stoeger T. (2016), *J. Aerosol Sci.*, **99**, 133-143.  
 Večeřa Z., Mikuška P., Moravec P., Smolík J. (2011) *Proc. 3<sup>rd</sup> Int. Conf. Nanocon*, 21.-23.9.2011, Brno, Czech Republic, pp 652-654.

## Comparison of four acellular methods for measuring the Oxidative Potential of PM collected in five French cities.

Aude Calas<sup>1</sup>, Gaëlle Uzu<sup>1</sup>, Ana Oliete<sup>2</sup>, Christina Dunster<sup>2</sup>, Frank J. Kelly<sup>2</sup>, Jean M.F. Martins<sup>1</sup>, Stephan Houdier<sup>1</sup>, Celine Begorre<sup>1</sup>, Samuel Weber<sup>1</sup> and Jean-Luc Jaffrezo<sup>1</sup>

<sup>1</sup>IGE, UMR 5001, Institut des Géosciences de l'environnement, CS 40 700, 38 058 Grenoble Cedex 9

<sup>2</sup>MRC-PHE Center for Environmental and Health, King's College London, SE1 9NH London, UK

Keywords: aerosol, health, proxy PM- health

Presenting author email: [aude.calas@univ-grenoble-alpes.fr](mailto:aude.calas@univ-grenoble-alpes.fr)

Exposure to ambient PM and adverse health outcomes have long been associated by epidemiological studies (Pope, 1996). This can be attributed, in part, to the oxidative stress induced by reactive oxygen species produced by PM (Knaapen, 2004). Oxidative potential (OP) of PM is increasingly studied as a relevant metric for health impact (instead of PM mass concentration) (Ayres, 2008). As a result, in the last decade assays have been developed to quantify the oxidative potential of aerosols (Salvi and Holgate, 1999, Hedayat, 2015). Among all these new approaches, acellular assays, besides being non-invasive, have the advantages of being fast, easy to organize, relatively inexpensive compared to cellular tests, and they can be automated.

Different measurement methods for OP were sometimes associated and compared with PM mass and PM composition. However, these studies mainly compared OP results with a few classical PM constituents (EC, OC, metals, PAH) and the studies were mostly conducted across a few days or months. Moreover in such assays, particles were usually extracted with methanol or Milli-Q water which are unrepresentative of physiological conditions. Here, an improvement in the OP assay which takes into account lung bioaccessibility by using a solution (Gamble + DPPC solution) that mimics more closely the lung fluid composition was realized. Several acellular assays have been carried out using a Gamble + DPPC solution as extraction solution (when compatible with the assay). Further, OP measurements were carried out across a full year (one sample every three days with exceptions) and extensive PM composition was available (> 160 species analyzed) for each samples. To the best of our knowledge, all of this provides a quite unique dataset and improves the knowledge of the relationship between OP and PM chemical composition.

OP<sub>DTT</sub> and OP<sub>AA</sub> were measured on PM from 5 different locations (French cities of Nice, Grenoble, Chamonix, Passy and Marnaz) using the Gamble + DPPC extraction solution. OP<sub>RTLF</sub> (OP<sub>GSH</sub> and OP<sub>AA</sub>) measurements, performed at King's College London, were also conducted in the samples from the Arve valley (i.e. Chamonix, Passy and Marnaz). Finally, OP<sub>ESR</sub> measurements were performed on some samples from Chamonix and Passy.

Regarding the use of a solution better mimicking the lung fluid solution, our results show that, even if the difference is not statistically significant, PM OP<sub>DTT</sub> is always overestimated when Milli-Q water is

used as the solution of extraction in comparison with extraction realized in Gamble + DPPC solutions. Our results for the different OP measurement methods and the diverse locations show seasonal amplitude of the OP values varying according to the OP assay and the location. For Chamonix, correlations of the OP assays with specific chemical species were found (EC, OC, levoglucosan, metals, PAH) which are stronger during the cold period. Correlations were also found between OP<sub>DTT</sub>, OP<sub>AA</sub> and OP<sub>RTLF</sub> when PM concentrations were high (cold period).

Further statistical works will be presented on the influence of the chemical composition of PM on the OP metric. As the OP series are coupled with full PM composition, a PMF was applied in order to determine the sources of the aerosols on these sites. Then the OP variations were compared to the dynamics of the sources to infer the role of each sources in the total OP we observed. This allows us to give a first approximation of the main OP sources in this region. The comparison of the different OP measurements methods will also be discussed.

This work was supported by the INSU LEFE-CHAT 2015-2018 program and by ADEME (Primequal Decombio project 2014-2018 1362C0028). IGE is part of Labex OSUG@2020 (ANR LABX56).

Ayres, J. G. (2008) *Evaluating the Toxicity of Airborne Particulate Matter and Nanoparticles by Measuring Oxidative Stress Potential — A Workshop Report and Consensus Statement*. Inhalation Toxicology, 20, 75–99.

Hedayat, F. (2015) *Review - Evaluation of the Molecular Assays for Measuring the Oxidative Potential of Particulate Matter*. Chemical Industry & Chemical Engineering Quarterly 21 (1): 201–10.

Knaapen, A. M. (2004). *Inhaled Particles and Lung cancer. Part A: Mechanisms*. International Journal of Cancer, 109, 799–809.

Pope III, C.A. (1996). *Adverse Health Effects of Air Pollutants in a Nonsmoking Population*. Toxicology, 111, 149–55.

Salvi, S. and Holgate, S. T. (1999). *Mechanisms of Particulate Matter Toxicity*. Clinical and Experimental Allergy. 29, 1187–94.

## Particle deposition efficiency in respiratory tract cast models

D.J. Hsu<sup>1</sup> H.Y. Lin<sup>2</sup> Y.M. Sun<sup>3</sup>

<sup>1</sup>Department of Safety, Health and Environmental Engineering, National Kaohsiung First University of Science and Technology, Kaohsiung 811, Taiwan

<sup>2</sup>Department of Occupational Safety and Health, Chang-Jung Christian University, Tainan 711, Taiwan

<sup>3</sup>Department of Digital Design and Information Management, Chung-Hwa University of Medical Technology, Tainan 717, Taiwan

Keywords: deposition efficiency, regional deposition, nanoparticles

Presenting author email:hsuderjen@nkfust.edu.tw

The removal efficiency of inhaled particles in the nasal region have been performed in the past, either replicate casts or human volunteers. However, most of those studies were primarily based on a limited number of white male subjects (Kim and Hu, 2006). Kesavanathan and Swift (1998) pointed out that nasal anatomic and dimensional factor are important in determining the amount of deposition in the nasal passage. Studies indicated that Taiwanese have a shorter craniofacial depth and longer craniofacial width than Americans, and Chinese workers have shorter face length, longer face width and smaller nose protrusion than Americans (Yu et al., 1996). These facial differences are likely to affect the anatomical structure of the upper respiratory tract and, consequently, the characteristics of particle deposition in this region between the two ethnic groups. Thus, it is important to conduct particle deposition experiments to explore the possible difference between the two ethnic groups.

Three Taiwanese (subjects A~C) and two Caucasian adults (subjects D~E) were recruited to obtain the computed tomography (CT) scans of their respiratory tract extending from the nostril to trachea. The images of the CT scans were stored in DICOM file (Digital Imaging and COmmunications in Medicine) to build the 3D computer model using the Mimics and 3 Matic software package (Materialise, Leuven, Belgium). Then, based on the 3D computer models, the airway models were constructed with epoxy by a rapid prototyping machine. Figure 1 shows one of the models, which includes nasal cavity, nasopharyngeal and trachea, constructed and employed in the deposition experiments. The human respiratory flow rates of 5, 10, 15, and 20 LPM were used to represent different human workload. The particle sizes for the study ranged from 20 to 500 nm and a Scanning Mobility Particle Sizer (SMPS) (TSI Inc., Shoreview, MN, USA) was used to measure the particle sizes and number concentrations.

The results obtained from the respiratory flow rate of 15 LPM were shown as an example in Figure 2. As shown, the trend of deposition efficiency in nano-sized ranges conforms with the published data, i.e., deposition efficiency first decreases with the increasing particle sizes and, after 100 nm, increases with the increasing particle sizes. Additionally, deposition efficiency from Taiwanese is greater than that of from Caucasians for about 5%. Regarding regional deposition, all five models showed the same trend, i.e., nasal cavity



Figure 1. Replicate cast of the upper respiratory tract with separated nasal cavity, nasopharyngeal and trachea

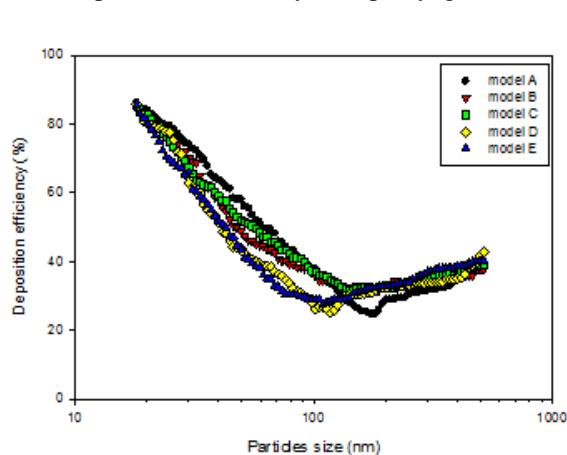


Figure 2. Particle deposition efficiency of Taiwanese (subjects A~C) and Caucasians (subjects D and E).

is with the highest deposition efficiency and trachea the lowest. The efficiency difference in the nasal cavity between Taiwanese and Caucasians can be as high as 7.1%. This constraint of this work is that the number of subjects is limited.

The work concludes that more subjects in both ethnic groups are needed and ICRP should be modified according to ethnic groups.

This work was financially supported by the National Science Council, Taiwan under NSC102-2221-E-327-001.

Kesavanathan, J. and Swift, D.L. (1998) *Aerosol Sci. Technol.* 28, 457-463.

Kim, C., and Hu, S.C. (2006) *J. Appl. Physiol.* 101, 401-412.

Yu, C.Y., Yeh, W.Y., Yang, Y.X., and Chang, P.H. (1996) *J. Occup. Safety Health* (in Chinese). 4, 31-46.

## A novel device based on thermophoresis for cell exposure at the air-liquid interface

M. Ihalainen<sup>1</sup>, P. Jalava<sup>2</sup>, T. Ihanola<sup>2</sup>, K. Kuuspallo<sup>1</sup>, M-R. Hirvonen<sup>2</sup>, J. Jokiniemi<sup>1</sup>  
University of Eastern Finland, Department of Environmental and Biological Sciences,  
P.O. Box 1627, FI-70211 Kuopio, Finland

<sup>1</sup>Fine Particle and Aerosol Technology Laboratory

<sup>2</sup>Inhalation Toxicology Laboratory

Keywords: Air Liquid Interface, toxicity, aerosol, nanoparticle.

Presenting author email: jorma.jokiniemi@uef.fi

Inhalation exposure is the main route causing health effects by the air pollutants. Air-liquid interface (ALI) in-vitro exposure mimics most realistically real life conditions. In ALI devices it is crucial to know the dose for the cells accurately. The dose from inhaled particles is determined by particle size and concentration at the air-liquid interface. The most important natural deposition mechanisms at the air-liquid interface are interception, impaction, gravitational settling and diffusion. However, diffusion is strongly dependent on particle size (Comouth et al., 2013) and thus dose determination becomes difficult. Also deposition by diffusion is very inefficient for particles larger than about 10 nm. Hence it is not possible to get high enough dose for toxicological studies by diffusion in most applications. Deposition by thermophoresis does not depend much on particle size up to several hundred nanometers. Thus from various initial size distributions it is fairly easy to determine the deposited amount of particles by thermophoresis (Broßell et al., 2013).

We have designed a novel ALI device where it is easy to control flow rates, temperature and relative humidity. Deposition of various nanoparticles has been determined by collecting particles on foils for subsequent microscopic analysis. The aerosols were characterized with the scanning mobility particle sizer (SMPS) prior the ALI device. A model describing the deposition of the ALI device was constructed and validated with the experimental results. The results show (Fig 1.) that the online data (SMPS) estimated quite well the size distribution of the deposited particles (SEM).

Our ALI device shows several advantages compared to existing commercial devices as high deposition efficiency, uniform deposition over the whole cell area, reliable determination of the exposure dosage and possibilities to select parameters without compromising the well-being and viability of the target cells. So far the ALI device has been used to expose cells with silver and zinc oxide nanoparticles and wood smoke.

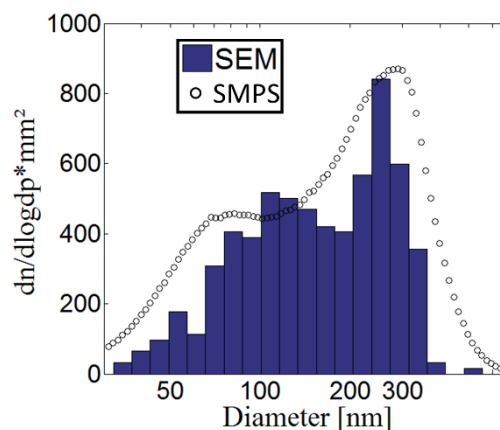


Figure 1. The number size distributions of the silver particles measured prior the deposition with a scanning mobility particle and after the deposition from the deposition surface with electron microscopy.

The results from the toxicity analysis of sub 1 $\mu$ m emission aerosol and gas experiments and the good viability of the cells in zero experiments indicate, that even higher, more realistic dilution ratios can be used in ALI experiments with Termo-Device, and still get toxicological responses.

Comouth, A., Saathoff, H., Naumann, K.-H., Muelhopt, S., Paur, H.-R., Leisner, T. *Modelling and measurement of particle deposition for cell exposure at the air-liquid interface (2013) Journal of Aerosol Science, 63, pp. 103-114.*

Broßell, D., Tröller, S., Dziurawitz, N., Plitzko, S., Linsel, G., Asbach, C., Azong-Wara, N., Fissan, H., Schmidt-Ott, A. *A thermal precipitator for the deposition of airborne nanoparticles onto living cells-Rationale and development (2013) Journal of Aerosol Science, 63, pp. 75-86.*

## Wood-smoke Inhalation Exposures from Traditional Hunting Practices in a First Nations Community

P. Pant<sup>1</sup>, R. J. Moriarity<sup>2</sup>, M. Wilton<sup>2</sup>, E.N. Liberda<sup>3</sup>, L.J. Tsuji<sup>2</sup>, and R.E.Peltier<sup>1</sup>

<sup>1</sup>Department of Environmental Health Sciences, University of Massachusetts, Amherst, MA 01003, USA

<sup>2</sup>Department of Physical and Environmental Sciences, University of Toronto Scarborough, Ontario, Canada  
M1C 1A4

<sup>3</sup>School of Occupational and Public Health, Ryerson University, Toronto, Ontario  
M5B 2K3, Canada

Keywords: PM<sub>2.5</sub>, Inhalation exposure, indoor air quality, woodsmoke

Presenting author email: pallavipant@umass.edu

Exposure to wood smoke, a dynamic mixture of gases and particles, has been associated with adverse respiratory health effects (Naeher et al., 2007). Such exposure is a significant health risk for tribal populations who participate in seasonal subsistence hunting for game where wood burning is an integral part of this culturally-relevant activity. To participate in these events, entire families travel to remote wilderness hunting camps, and wood is used as an energy source for cooking and heating. In addition, game meat is smoked in specially constructed teepees with limited ventilation. The objective of this study was to measure indoor air quality in tents used for subsistence hunting activities in a population of Native North American hunters by characterizing wood-smoke aerosol components through personal and microenvironment sampling.

Indoor air was monitored for black carbon (BC) and fine particulate matter (PM<sub>2.5</sub>) using a microAethalometer (AE51, AethLabs, USA), and a portable nephelometer (pDR 1500). Time-integrated samples were also collected using Teflon and quartz filters, and chemical speciation (ions, metals and carbon) was conducted using standardized protocols. Carbon monoxide (CO) and temperature of the woodstove were also measured during the study period. The study protocol was reviewed and approved by the Institutional Review Boards at the University of Massachusetts, Amherst (USA), the University of Toronto (Canada), and Ryerson University, Toronto (Canada), as well as Tribal representatives.

Average indoor PM<sub>2.5</sub> and BC concentrations were significantly higher during meat smoking compared to the in-cabin concentrations.

A strong correlation was observed between OC and EC during both phases (hunting and meat smoking), but the concentrations were several fold higher for the meat smoking phase (Figure 1). For short periods of time, concentrations as high as 1000 µg/m<sup>3</sup> were observed for PM<sub>2.5</sub>, and 300-500 µg/m<sup>3</sup> for BC. Average BC concentrations (6.5 µg/m<sup>3</sup>) during meat smoking were at levels much higher than typical concentrations observed in indoor environments in North America.

Overall, indoor levels of PM<sub>2.5</sub> and BC were found to be very high during meat smoking, and considering that this is a seasonal activity, can pose a serious risk to respiratory health of this population. This also indicates that other communities can face similar risks, especially in cases where similar cultural activities are followed.

Interventions such as better designed stoves and/or venting structures and use of propane space heaters were tested and data analysis is currently underway.

This study was funded through a US EPA STAR grant # R835605. This abstract's contents are solely the responsibility of the authors and do not necessarily represent the official views of the US EPA. Further, US EPA does not endorse the purchase of any commercial products or services mentioned in the abstract. We would also like to thank all the participants for their help in sample collection and Randa Kallin and Sevan Dulgarian at UMass Amherst for assistance with sample analysis.

Naeher, L.P., Brauer, M., Lipsett, M., Zelikoff, J.T., Simpson, C.D., Koenig, J.Q. and Smith, K.R. (2007) *Inhal. Toxicol.* **19**(1), 67-106.

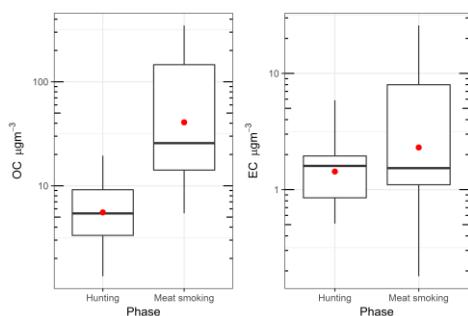


Figure 1. Comparison of organic carbon (OC) and elemental carbon (EC) concentrations during hunting and meat smoking phases.

## Effect of inhaled PbO nanoparticles on mice organs after long-term exposition

Mikuška P.<sup>1</sup>, Večeřa Z.<sup>1</sup>, Buchtová M.<sup>2,3</sup>, Dumková J.<sup>4</sup>, Putnová B.<sup>2</sup>, Dočekal B.<sup>1</sup>, Čapka L.<sup>1</sup>, Coufalík P.<sup>1</sup>, Křůmal K.<sup>1</sup>, Fictum P.<sup>5</sup>, Hampl A.<sup>4</sup>

- <sup>1</sup> Institute of Analytical Chemistry, v.v.i., The Czech Academy of Sciences, Veveří 97, Brno, Czech Republic
- <sup>2</sup> Institute of Animal Physiology and Genetics, v.v.i., The Czech Academy of Sciences, Brno, Czech Republic
- <sup>3</sup> Department of Animal Physiology and Immunology, Faculty of Science, Masaryk University, Brno, Czech Republic
- <sup>4</sup> Department of Histology and Embryology, Faculty of Medicine, Masaryk University, Brno, Czech Republic
- <sup>5</sup> Department of Pathological Morphology and Parasitology, Faculty of Veterinary Medicine, University of Veterinary and Pharmaceutical Sciences, Brno, Czech Republic

Keywords: nanoparticles, lead oxide, inhalation, toxicity.  
Presenting author email: mikuska@iach.cz

Nanoparticles of various chemistries and sizes are becoming a reality in many industrial applications. As a result, there is an increasing need for understanding the adverse effects that nanoparticles may have on human and animal health.

Lead (Pb) can enter the human body mainly by direct inhalation of particles. Outdoor sources of exposure could be traffic road, power plants, industry, and other combustion sources. Indoor sources such as painting the walls or cigarette smoking including second hand tobacco smoke can also significantly contribute to the Pb exposure. PbO nanoparticles are important materials for industry. The key applications of lead oxide nanoparticles are magnetic resonance imaging and magnetic nanoparticles for data storage.

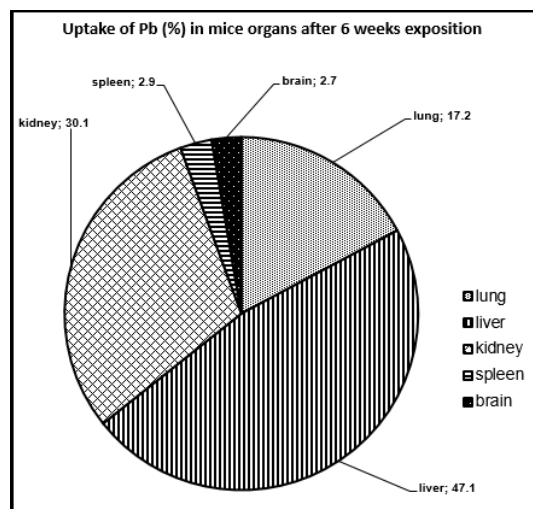
Since nanoparticles containing lead (Pb) represent a serious issue for human health, lead oxide (PbO) nanoparticles were chosen for the evaluation in our study. The study aims on expansion of the understanding of PbO nanoparticle fate upon their entry into lungs of mice due to inhalation of PbO nanoparticles, with the main focus on the changes that the nanoparticles may cause to target tissue structure.

PbO nanoparticles were synthesized continuously by direct evaporation of Pb (at the temperature of 830 °C) from melted lead inside a hot wall tube flow reactor. Released Pb vapours were transported by nitrogen stream through the flow reactor and subsequently condensed to form Pb nanoparticles. At the output from the reactor, Pb nanoparticles were mixed with air and Pb was oxidized by oxygen to PbO nanoparticles. The size distribution of generated nanoparticles was monitored by SMPS.

Adult female mice were continuously exposed to the PbO nanoparticles (number concentration of  $1.23 \times 10^6$  particles/cm<sup>3</sup>, mode 25.9 nm, geometric mean diameter 25.9 nm, mass concentration of 121.7 µg PbO/m<sup>3</sup>) for 6 weeks (24 hrs/day, 7 days/week). In parallel, control animals were exposed to the same air as the experimental group just without nanoparticles supplement. At the end of exposure, mice organs (lung, liver, kidney, brain and spleen) were collected for chemical, biochemical, histological and electron microscopical analyses.

Inhalation of PbO nanoparticles results in their accumulation not only in the organ of entry, the lungs, but they were also transported by blood to other organs causing serious damage at tissue as well as at cellular level. The exposure to high doses of such nanoparticles leads to complex symptoms affecting the entire body.

Figure 1. Uptake of Pb (%) in mice organs after 6 weeks inhalation exposition.



This work was supported by Grant Agency of the Czech Republic under grant No. P503/12/G147 and by Institute of Analytical Chemistry of the ASCR, v. v. i. under an Institutional research plan No. RVO:68081715.

## Aerosol emission and human health effects from cleaning spray use studied in an exposure chamber

K. Lovén<sup>1</sup>, C. Isaxon<sup>1</sup>, J. Nielsen<sup>2</sup>, E. Assarsson<sup>2</sup>, P. Tallving<sup>2</sup> and A. Gudmundsson<sup>1</sup>

<sup>1</sup>Ergonomics and Aerosol Technology, Lund University, Lund, SE-22100, Sweden

<sup>2</sup>Occupational and Environmental Medicine, Lund University, Lund, SE-22185, Sweden

Keywords: cleaning product, spray, human exposure, health effects.

Presenting author email: [karin.loven@design.lth.se](mailto:karin.loven@design.lth.se)

Cleaning workers belong to a large occupational group, which are exposed to many risk factors, including high physical workload and handling of chemical products. Documented risks for professional cleaners include musculoskeletal disorders as well as the development of different respiratory symptoms (Unge *et al.*, 2007; Lillienberg *et al.*, 2013). Spray is a cleaning method with the advantage of easy use and even and precise dosage. A survey conducted within this study confirmed that spray cleaning products are used by about 78 % of Swedish professional cleaning workers. Our survey also showed that almost half of those using cleaning sprays experience self-reported symptoms due to this use. There are some studies (e.g. Zock *et al.*, 2007) linking the use of cleaning sprays to the development of new-onset asthma as well as other respiratory symptoms. However, no human exposure study have been conducted until now in order to understand how the cleaning spray aerosols affect the user.

### Method

A human exposure study was conducted in a 21,6 m<sup>3</sup> stainless steel chamber with controlled temperature, relative humidity (RH) and air exchange rate (AER). 19 volunteers; 11 female cleaning workers and 8 young females as controls, participated. The chamber was furnished as a bathroom and was cleaned using three different cleaning methods (three exposures) during three different days. The cleaning methods included A: zero exposure with only microfiber cloths, B: cleaning chemicals applied as foam, C: cleaning chemicals applied as spray. During the exposures, the temperature was about 22 °C, the RH 30 % and the AER 0.9 h<sup>-1</sup>.

Particle concentrations and size distributions (in the size range 0.5-20 µm) were measured in the chamber using an Aerodynamic Particle Sizer (model 3321, TSI Inc., USA). A Condensation Particle Counter (model 3010, TSI Inc., USA) was used to measure the particle concentration in the size range 0.01-1 µm and a VelociCalc (model 9565-P, probe 986, TSI Inc., USA) was used to measure the total VOC concentrations in the chamber.

Before and after each exposure day the volunteers went through biological sampling, including blood sample, nasal lavage and exhaled condensate. Spirometry, peak nasal inspiratory flow (PNIF) and tear film break up time (BUT) were measured and the subjects also filled in self-assessment questionnaires.

### Results and conclusions

During spray exposure (C) a clear increase in particle concentration (0.5-20 µm) can be seen (Figure 1) while cleaning. Foam exposure (B) gave rise to a small increase compared to the zero exposure (A). The particle concentration (0.01-1 µm) also increased some during exposure C and B, but the concentration was generally low; below 500 particles/cm<sup>3</sup>. A slight difference between exposure C and B was also observed in the VOC measurements.

With the results from this study, we can conclude that foam might be better than spray as an application method of cleaning solution, at least from an aerosol exposure perspective. The results from the medical analysis will be available later this year and will give an answer to how the different cleaning methods affect the user.

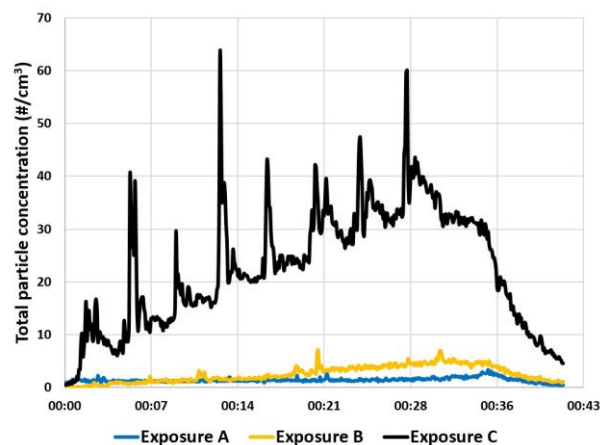


Figure 1. Total particle concentration (#/cm<sup>3</sup>) measured with an APS (0.5-20 µm). Comparison between the three different types of exposures, A: zero exposure with only microfiber cloths, B: cleaning chemicals applied as foam, C: cleaning chemicals applied as spray.

This work was supported by Swedish AFA Insurance.

Lillienberg *et al.* (2013) *Annals of Occupational Hygiene* **57**(4):482-492.

Unge *et al.* (2007) *International Archives of Occupational and Environmental Health* **81**:209-220.

Zock *et al.* (2007) *American Journal of Respiratory and Critical Care Medicine* **176**:735-741.

## **Abstracts T410**

## Aerosol Particles (0.3-10 $\mu\text{m}$ ) inside a Workshop Area

A.Maragkidou<sup>1</sup>, O. Jaghbeir<sup>2</sup>, K. Hämeri<sup>1</sup> and T. Hussein<sup>2</sup>

<sup>1</sup>University of Helsinki, Department of Physics, P.O.Box 64, FI-00014, Helsinki, Finland

<sup>2</sup>The University of Jordan, Department of Physics, Amman 11942, Jordan

Keywords: particulate matter, indoor air quality, emission rate, loss rate.

Presenting author email: [androniki.maragkidou@helsinki.fi](mailto:androniki.maragkidou@helsinki.fi)

A large amount of scientific studies has been focused on particulate matter (PM) and more specifically on PM<sub>10</sub> and PM<sub>2.5</sub> since they are associated with serious human health effects, such as health implications mainly on children's heart and their respiratory system, asthma, cardiovascular disease, pulmonary inflammation, lung cancer, even death (Brunekreef and Forsberg, 2005; Pope *et al.*, 2006; Sangiorgi *et al.*, 2013).

So far, most of the researches focused on measuring the particle mass and number concentration of the coarse and fine particles, respectively (Tran *et al.*, 2012; Voliotis *et al.*, 2014; Slezakova *et al.*, 2015). In order to fill this gap, the main purpose of this study is to assess the exposure to large particles (PM<sub>10</sub>) inside a workshop area of an educational building (Department of Physics, the University of Jordan), as well as study, report and illustrate the particle number concentration of the coarse (1-10  $\mu\text{m}$ ) and the particle mass concentration of the fine fraction (0.3-1  $\mu\text{m}$ ) from 31<sup>st</sup> of March until 6<sup>th</sup> of April 2015. Furthermore, we applied a simple indoor aerosol model in order to estimate the emission and loss rate of aerosol particles within the measured size range inside the workshop area

Our results indicated that during workdays, the highest mean and median PN<sub>1-10</sub> (PM<sub>1-10</sub>) and PN<sub>0.3-1</sub> (PM<sub>0.3-1</sub>) concentrations were observed during the operation of the welding machine followed by the activity of iron welding without the use of the exhaust fan and the running of the exhaust fan afterwards. On the other hand, the maxima PN<sub>1-10</sub> (PM<sub>1-10</sub>) and PN<sub>0.3-1</sub> (PM<sub>0.3-1</sub>) concentrations were detected when iron welding took place, and later the operation of the exhaust fan and the activity of iron sorting/drilling occurred. During the weekend, PN<sub>1-10</sub> (PM<sub>1-10</sub>) varied between 0.28-0.82 cm<sup>-3</sup> (1.09-12.77  $\mu\text{g}/\text{m}^3$ ), while PN<sub>0.3-1</sub> (PM<sub>0.3-1</sub>) ranged between 12.51-64.04 cm<sup>-3</sup> (0.43-2.27  $\mu\text{g}/\text{m}^3$ ) (Figures 1 and 2).

When the workshop area was open and occupied, the (average) particle number loss rate for fine particles fluctuated from 0.24±0.01 to 2.01±0.07 h<sup>-1</sup> and for coarse particles from 0.35±0.01 to 2.11±0.05 h<sup>-1</sup>. Furthermore, the (average) particle number emission rate for the coarse and the fine fraction ranged from 75-1008 particles/h×cm<sup>-3</sup> and 5.74×10<sup>4</sup>-9.31×10<sup>4</sup> particles/h×cm<sup>-3</sup>, respectively.

We believe that the extraordinary variation in the PM and PN concentration between fine and coarse particles during the occurrence of the activities could be due to the ventilation rate of the room and the time spent there as well as to the effect of occupancy of the workshop area. However, the type of the activities themselves could have also played a significant role.

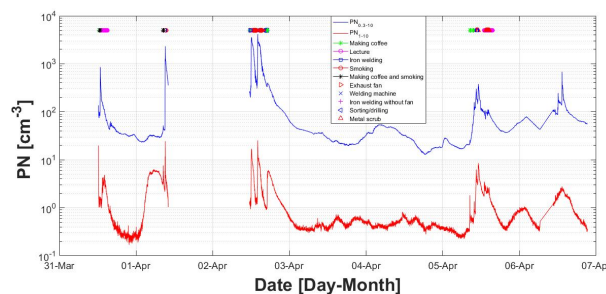


Figure 1. Particle number concentrations (Time series based on 1-minute resolution).

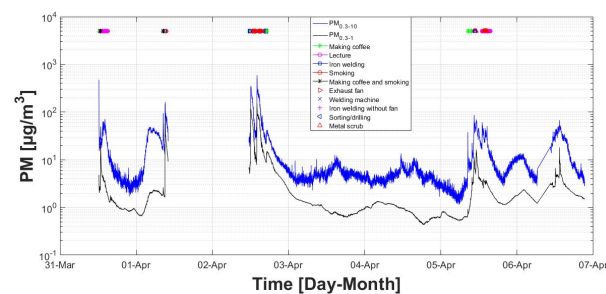


Figure 2. Particle mass concentrations (Time series based on 1-minute resolution).

This study was supported by the European Commission (FP7-PEOPLE-2012-ITN) Marie Curie ITN (HEXACOMM, project no. 315760), the Deanship of Academic Research at the University of Jordan and the Academy of Finland Centre of Excellence (grant no. 272041). We would like to thank the occupants of the workshop areas from where we conducted the experiment; they were very cooperative.

- Brunekreef, B. and Forsberg, B. (2005) *Eur. Respir. J.* **26**, 309–318.
- Pope, C.A., Young, B., Dockery, D. (2006) *J. Air. Waste Manage. Assoc.* **56**, 709–742.
- Tran, D.T., Alleman, L.Y., Coddeville, P., Galloo, J.C. (2012) *Atmos. Environ.* **54**, 250–259.
- Sangiorgi, G., Ferrero, L., Ferrini, B.S., Lo Porto, C., Perrone, M.G., Zangrando, R., Gambaro, A., Lazzati, Z., Bolzacchini, E. (2013) *Atmos. Environ.* **65**, 205–214.
- Voliotis, A., Bezantakos, S., Giamarelou, M., Valenti, M., Kumar, P., Biskos, G. (2014) *Environ. Sci. Process Impacts.* **16**, 1489-1494.
- Slezakova, K., Texeira, C., Morais, S., Pereira, M.do C. (2015) *J. Toxicol. Environ. Health. Part A.* **78**, 886-896.

## Investigating Indoor Air Quality of a Shooting Range

S.Y. Aslanoglu<sup>1</sup>, F. Ozturk<sup>2</sup>, and G. Gullu<sup>1</sup>

<sup>1</sup>Department of Environmental Engineering, Hacettepe University, Ankara, 06800, Turkey

<sup>2</sup>Department of Environmental Engineering, Abant Izzet Baysal University, Bolu, 14030, Turkey

Keywords: Shooting range, PM, EC/OC, metal.

Presenting author email: yaslanoglu@hacettepe.edu.tr

Shooting is among the nine sports branches, which have formed the first modern Olympic Games has held in Athens in 1896. Becoming a skilled shooter needs long training time, intensive labour, accuracy, precision, high stability, and focus. A professional shooting athlete shots millions of actual pellets or cartridges throughout her/his sports life from the age about 13. Particularly at indoor shooting ranges, this can cause a high rate of gunshot residue exposure specifically lead, other metals and their by-products.

The objective of this study is to determine both metals and total carbon (TC) of a world cup standard shooting range's ambient air during small bore rifle and pistol competitions, which are officially held by Turkish Shooting and Hunting Federation. To this end, particulate matter samples with aerodynamic diameter less than 10  $\mu\text{m}$  ( $\text{PM}_{10}$ ) were collected by TECORA Skypost PM sampler on quartz fibre filters. Collected filter samples were conditioned at constant temperature (25°C) and humidity (25%) before and after sampling to calculate PM mass. In order to prevent the carbon loss, filter samples were stored at -18°C both before and after sampling process till analysis. A punch of collected samples (1.5  $\text{cm}^2$ ) were analysed in terms of elemental carbon (EC), organic carbon (OC) and TC (EC+OC) by Sunset Lab (USA) thermal-optical aerosol analyser by following the National Institute for Occupational Health and Safety (NIOSH) 870 protocol. Average  $\text{PM}_{10}$ , OC, EC, and TC concentrations were found as  $28.71 \pm 8.88$ ,  $4.74 \pm 0.55$ ,  $0.25 \pm 0.09$ ,  $4.99 \pm 1.59$   $\mu\text{g}/\text{m}^3$ , respectively. Even though the same type of 0.22 calibre (5.6 mm) RWS R 50<sup>®</sup> rim fire cartridges were used for the rifle and pistol shots, the released  $\text{PM}_{10}$  and carbon concentrations from pistol shots were found to be 1.5 times higher than that from rifle shots as given in Table 1.

Table 1.  $\text{PM}_{10}$ , EC, OC, and TC concentration values (01 and 02-days rifle and 03-day pistol competitions).

Day	$\text{PM}_{10}$ ( $\mu\text{g}/\text{m}^3$ )		OC ( $\mu\text{g}/\text{m}^3$ )		EC ( $\mu\text{g}/\text{m}^3$ )		TC ( $\mu\text{g}/\text{m}^3$ )	
	avg	std	avg	std	avg	std	avg	std
01	25.44	4.02	0.53	0.20	0.04	4.24	0.31	
02	21.93	3.72	0.53	0.19	0.04	3.92	0.29	
03	38.76	6.47	0.60	0.35	0.05	6.82	0.44	

Only 01-day rifle  $\text{PM}_{10}$  sample was analysed by non-destructive Wavelength Dispersive X-ray Fluorescence Spectrometer (WDXRF) in terms of metals including lead. Obtained results were used to calculate crustal enrichment factors ( $\text{EF}_c$ ), shown in Figure 1, by

taking Al as reference element in order to identify the contribution of gunshot residue (Mason, 1996). Calculated  $\text{EF}_c$  values revealed that S, Zn and Pb were highly enriched in the shooting range's ambient air implying not only Pb but also Zn and S were the metals released to indoor at elevated concentrations during shooting.

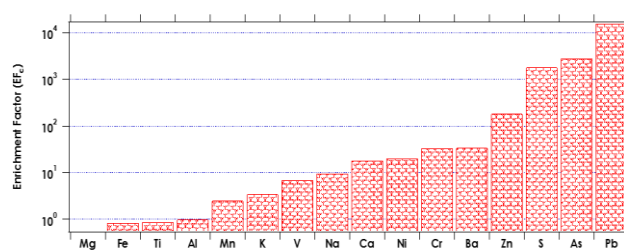


Figure 1. Calculated crustal enrichment factor values for each element determined in 01-day rifle sample.

In addition to crustal enrichment factors, mass per shot values were calculated in order to derive competition specific emission factors (SF) based on the rifle and pistol shot numbers (Table 2). In compliance with the PM, EC, OC, and TC concentrations released from the shots, pistol SF values are approximately 3.5 times higher than that from the rifle SF values, which further implies that this variation comes out mainly from the shorter barrel length of pistols as compared to rifle barrels. Short barrels can cause early and wide dispersion of gunshot residue within the fire line, which accordingly increase exposure levels of pistol shooters relative to rifle shooters.

Table 2. Competition specific  $\text{PM}_{10}$ , EC, OC, and TC emission factors.

Gun Type	$\text{SF}_{\text{PM}}$ ( $\mu\text{g}/\text{shot}$ )	$\text{SF}_{\text{OC}}$ ( $\mu\text{g}/\text{shot}$ )	$\text{SF}_{\text{EC}}$ ( $\mu\text{g}/\text{shot}$ )	$\text{SF}_{\text{TC}}$ ( $\mu\text{g}/\text{shot}$ )
Rifle	0.1074	0.0194	0.0010	0.0204
Pistol	0.3030	0.0537	0.0029	0.0566

Mason, B., (1996) *Principles of Geochemistry*, 3<sup>rd</sup> Edition, John Wiley & Sons.

## Ultrafine particle emissions in the ceramic industry: determinants of release and impact on worker exposure

M. Viana<sup>1</sup>, C. Ribalta<sup>1</sup>, A. Salmatonidis<sup>1</sup>, M.C. Minguillón<sup>1</sup>, X. Querol<sup>1</sup>, A. S. Fonseca<sup>1</sup>, A. López-Lilao<sup>2</sup>, V. Sanfélix<sup>2</sup>, P. Carpio<sup>2</sup>, E. Monfort<sup>2</sup>, C. Estepa<sup>3</sup>, C. Borrell<sup>3</sup>, G.F. de la Fuente<sup>3</sup>

<sup>1</sup>IDAEA-CSIC, Barcelona, Spain

<sup>2</sup>ITC, Castellón, Spain

<sup>3</sup>ICMA, Zaragoza, Spain

Keywords: ultrafine particles, nanoparticles, exposure, indoor air, occupational exposure, emissions.

Presenting author email: mar.viana@idaea.csic.es

Process-generated ultrafine particles (UFPs) are unintentionally emitted into workplace air during high-energy industrial process (mainly thermal or mechanical) [1,2]. They may be primary or secondary in nature and, in contrast to engineered nanoparticles, they are characterised by their non-specific and highly variable chemical composition and morphology. Because of their high-energy nature, industrial ceramic processes have the potential for occupational exposure to this type of health hazardous airborne particles [3].

In this work we monitored UFP release and its impact on occupational exposure in industrial settings during different types of processes frequently used in the ceramic industry. These included laser-based tile sintering, conventional sintering, tile ablation to produce engravings, physical vapour deposition (PVD), and inkjet printing with engineered nanoparticle pigments. The high-energy nature of several of these processes implies a significant potential for unintentional UFP and nanoparticle release, which has so far not been characterised under real-world conditions. The work was carried out in two pilot plants (laboratory and industrial scale), and in real-world industrial settings. Special attention was paid to new particle formation processes and their dependence on process variables such as temperature or tile chemical composition. After release and exposure characterisation, emission factors were quantified in the laboratory by means of dustiness tests using a rotating drum. Finally, exposure models such as Stoffenmanager will be applied for comparison with the experimental data.

Particle concentrations in the range 5 nm – 10 µm were monitored at the emission sources, in the worker breathing zones and in indoor background air. Whenever possible, outdoor measurements were also carried out. The metrics monitored were particle number concentration (N; between 4-1000 nm, CPC, DiscMini), particle size distribution (10-420 nm, NanoScan), particle mass concentration (PM<sub>10</sub>, PM<sub>2.5</sub>, PM<sub>1</sub>, Dusttrak DRX, Grimm 1107), and black carbon (BC, Magee AE51). Offline techniques such as transmission electron microscopy (TEM) and Energy-Dispersive X-ray (EDX) spectroscopy were used for particles collected on Au TEM grids using a cassette and a portable SKC Leland pump (3 lpm). Additionally, major and trace elements on particle collected on polycarbonate filter substrates were determined by inductively coupled plasma mass

spectrometry (ICP-MS) and atomic emission spectroscopy (ICP-AES).

Results evidenced significantly high UFP emissions and impact on exposure during several of the processes studied: tile sintering (with exposure concentrations >10<sup>5</sup> cm<sup>-3</sup>), tile ablation (>10<sup>4</sup> cm<sup>-3</sup>), and plasma spraying (>10<sup>6</sup> cm<sup>-3</sup>, Fig. 1). Mean particle diameters ranged between 18-260 nm. Other processes such as PVD or inkjet printing did not result in statistically significant UFP emissions. New particle formation events (nucleation) were detected during tile sintering, whereas UFPs were mainly primary during ablation. The main parameters controlling UFP emissions were identified as process temperature and raw tile chemical composition. When transported towards the breathing zone, particles increased in diameter (e.g., from 20 nm to 38 nm). Emission factors quantified by means of dustiness tests were compared with UFP concentrations measured in the workplaces. Our results evidence the need for risk assessments and strategies to minimise occupational exposures to UFPs in the ceramic industrial sector.

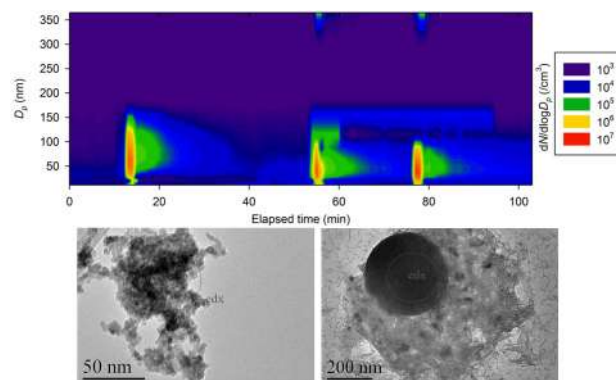


Figure 1. UFP concentrations and size distribution during plasma spraying; UFPs by TEM-EDX.

This work was supported by ERANET-SIINN project CERASAFE ([www.cerasafe.eu](http://www.cerasafe.eu), ID: 16) and national project PREDEXPIN (CGL2015-66777-C2-1-R).

- [1] Koponen et al., 2011. J. Exposure Sci. 21, 408-418.
- [2] Broekhuizen, P., et al., 2012. J. Nanoparticle Res. 14, 1–25.
- [3] Voliotis A, et al., 2014. Environ Sci Process Impacts, 16(6), 1489-1494.

## Unit operations at WEEE plastics recycling line as a sources of ultrafine particles and microparticles

E. Hroncová<sup>1</sup>, J. Ladomerský<sup>1</sup>

<sup>1</sup>Department of Environmental Management, Matej Bel University, Banská Bystrica, 974 01, Slovakia

Keywords: ultrafine particles, microparticles, working environment, plastics, WEEE.

Presenting author email: emilia.hroncova@umb.sk

The presented article is focused on the protection of air quality in the working environment in the mechanical recycling of plastics from waste electrical and electronic equipment (WEEE). Its aim is to map the concentration of ultrafine particles (UFP) and microparticles (MP) in the workplace air through the mechanical recycling of plastics from WEEE and to determine equipment's and locations that are sources of dust exposure. Information about the exact location where these particles are leaking is the basis for finding secondary measures to reduce dust, even in the case of modern lines. Another objective of dust measurement was to answer the question, whether emissions of UFP are released also in the case of mechanical operations of plastics recycling. The third aim of the research was to verify, if recycling of the plastic waste is considered also as the source of UFP a MP fugitive emissions in the outdoor air, which is spread out through the open gate of the recycling hall. We started from the knowledge that the amount of plastic waste is growing across the world and it is necessary to increase the proportion recycled. Suitably designed measures for recycling of plastics can also improve competitiveness and create new economic activities and jobs (COM, 2013). It can be estimated that growth of WEEE is three times faster than the average growth of municipal solid waste (Cossu, 2013). In Slovakia, the proportion of plastic recycling is increasing intensively. E.g. production of plastic packaging (category 150102) between 2005 to 2013 increased from 21,470 t to almost 46,000 t and separately collected plastics (category 200139) from 9,350 t to 24,000 t. There is high capacity recycling equipment for mechanical (crushing, grinding, separation) plastic waste recycling. Material recovery of separately collected waste plastics in category 150102 between 2005-2013 increased from about 12,500 t to almost 30,000 t and waste category 200139 from about 2,500 t to 18,500 t.

Whilst increasing the recycling of plastics, it is necessary to responsibly address the issue of dust in the working environment, particularly in the recycling of plastics from WEEE. UFP a MP number concentration was measured using the analysers: Optical particle Sizer 3330 and NanoScan SMPS nanoparticle Sizer 3919 from TSI Incorporated, in a hall with a modern line for the mechanical recycling of plastics from WEEE for 2 days during the summer season of 2016 and 2 days during the winter season of 2017. The analysers were placed at a distance of 1.5 to 3.0 metres from potential sources of UFP and MP. The values of UFP (10 – 100 nm) number concentrations found were in the range approximately of 25,000 to 50,000 #.cm<sup>-3</sup> (10 minutes on average). In

ambient air (10 m from the external walls of the hall), UFP number concentration was 8,340 #.cm<sup>-3</sup>. MP (0.1 – 10 µm) number concentrations were in the range of 2,500 to 3,800 #.cm<sup>-3</sup>. MP (0.3 – 10 µm) number concentrations were in the range of 290 to 410 #.cm<sup>-3</sup>. The mass concentrations of micro particles (0.1 – 10 µm) (at fixed density of 1 g.cm<sup>-3</sup>) ranged from 310 to 1,410 µg.m<sup>-3</sup> and in outdoor air 54 µg.m<sup>-3</sup>. These findings suggest that the biggest source of UFP and MP emissions is undersized fibre filter of silos for separated plastics from dry separation line and emptying of plastic debris from dry separation line into the open container. The surprising finding is that that the biggest source of UFP and MP emissions is also the extruder.

This work was supported by the Slovak Grant Agency VEGA under contract No. VEGA 1/0547/15.

COM (2013) *Green paper. On a European strategy on plastic waste in the environment.* European Commission. Brussels, 7.3.2013.

Cossu, R. (2013) *Waste Manage*, **33**, 497-498.

## On the equivalence between mass-specific surface area of powders and their aerosols and proposal of a new dustiness index for bulk nanomaterials

C. Dazon<sup>1</sup>, O. Witschger<sup>1</sup>, S. Bau<sup>1</sup>, R. Payet<sup>1</sup>, V. Fierro<sup>2</sup>, K.A. Jensen<sup>3</sup>,  
E. Jankowska<sup>4</sup>, D. Bard<sup>5</sup>, I. Tuinman<sup>6</sup> and P. Llewellyn<sup>7</sup>

<sup>1</sup>Aerosol Metrology Laboratory, Institut National de Recherche et de Sécurité (INRS), Vandœuvre, France

<sup>2</sup>Institut Jean Lamour - UMR CNRS 7198, Epinal, France

<sup>3</sup>The Danish Nanosafety Centre, National Research Centre for the Working Environment (NRCWE), Copenhagen, Denmark

<sup>4</sup>Central Institute for Labour Protection - National Research Institute (CIOP-PIB), Warsaw, Poland

<sup>5</sup>Health and Safety Laboratory (HSL), Buxton, UK

<sup>6</sup>TNO Quality of Life, Food & Chemical Risk Analysis, Zeist, The Netherlands

<sup>7</sup>Laboratoire MADIREL - CNRS UMR 7246, Marseille, France

Keywords: nanomaterial, powder, dustiness, surface area.

Presenting author email: claire.dazon@inrs.fr

Surface area is more and more highlighted as one of the biologically most effective dose metric for pulmonary toxicity of low-solubility, low-toxicity (LSLT) nanomaterials (NIOSH, 2011; Schmid & Stoeger, 2016). On the other hand, the dustiness of a powder is an increasingly important determinant in control banding tools to evaluate and control the risk of exposure to nanomaterials in powder form (Liguori *et al.*, 2016). However, there is currently no dustiness index that would be based on the surface area metric and thus complement the mass- and number-based indexes. The main reason why such criterion is still missing relies in the question of the equivalence between the mass-specific surface area of powders ( $SSA_{\text{Powder}}$ ) and the mass-specific surface area of particles after aerosolization ( $SSA_{\text{Aerosol}}$ ) remains unclear.

In that context, the objective in this work was to investigate the equivalence between  $SSA_{\text{Powder}}$  and  $SSA_{\text{Aerosol}}$ , and eventually propose a new dustiness index for powder.

Five nanomaterials in powder form covering a wide range of  $SSA_{\text{Powder}}$  were chosen and characterized in terms of particle sizes (Table 1). The Small Rotating Drum (SRD) (Jensen *et al.*, 2016), in which the aerosol is generated by the repeated drops of a powder sample, was used to produce aerosolized particle samples.

Table 1. Size characteristics of the nanomaterials.

	Powder			Aerosol
	XRD	BET	Laser Diffraction	ELPI
	$d_{\text{XRD}}$ (nm)	$d_{\text{BET}}$ (nm)	$d_{50, V}$ (LD) ( $\mu\text{m}$ )	$d_{a, \text{mode}}$ ( $\mu\text{m}$ )
TiO <sub>2</sub> (b)	21	31	1.0	2.0
TiO <sub>2</sub> (d)	7	5	1.3	1.7
BaSO <sub>4</sub> (b)	26	41	13	1.6
SiO <sub>2</sub> (a)	n/a	9	4.1	1.6
SiO <sub>2</sub> (b)		5	11.1	0.9

To collect the aerosolized samples for subsequent  $N_2$  adsorption analysis by the BET method, a specific protocol using the Aero Select instrument (Ancon) was developed. In this work, the same surface area analysis technique (by  $N_2$  adsorption) was kept here to measure

$SSA_{\text{Powder}}$  and  $SSA_{\text{Aerosol}}$ . Figure 1 shows the data obtained in this work as well as that of a previous work (Bau *et al.*, 2010) where  $SSA$  of aerosolized particles was based on analyzing transmission electron microscopy (TEM).

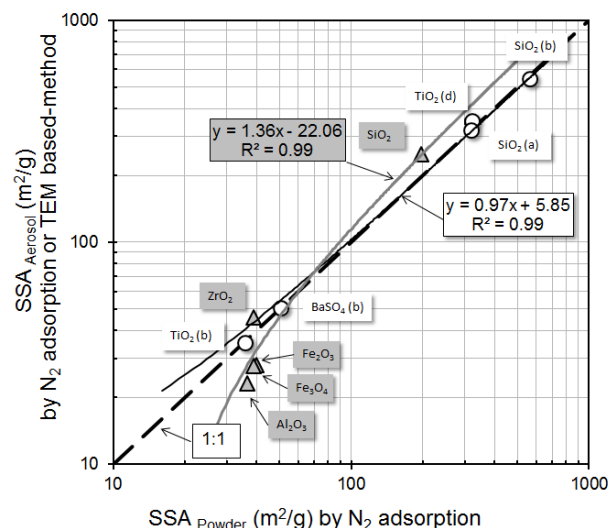


Figure 1. Comparison of  $SSA_{\text{Aerosol}}$  with  $SSA_{\text{Powder}}$ . Gray triangles: data from (Bau *et al.*, 2010). White disks: data obtained in this work, presented w/ 1 SD.

On the basis of these results, the equivalence between  $SSA_{\text{Powder}}$  and  $SSA_{\text{Aerosol}}$  can be validated in the context of pure nanomaterials and for aerosols released by a low energy generation process. A new dustiness index, surface-based, is therefore proposed.

This work is supported by the European Commission, as part of mandate M/461 'Nanotechnologies'.

Bau, S., Witschger, O., Gensdarmes, F., Rastoix, O., Thomas, D. (2010), *Powder Technol.*, **200** (3),190-201.

Liguori, B., Hansen, S.F., Baun, A., Jensen, K.A. (2016) *NanoImpact*, **2**, 1-17

NIOSH (2011), Publication No. 2011-160.

Jensen, K.A., Levin, M., Witschger, O. (2016) In: R. Tantra (Ed.) *Nanomaterial Characterization - An Introduction*; Wiley & Sons, pp.209-230.

Schmid, O., Stoeger, T. (2016), *J Aerosol Sci.*, **99**, 133-143.

## Characteristics of Nanoparticle and Hazardous Air Pollutants (HAPs) in Three-dimensional (3D) Printing Center

J.-S. Youn, E. Han, S. Han, Y.-W. Jung and K.-J. Jeon

Department of Environmental Engineering, Inha University, Incheon, 22212, Republic of Korea

Keywords: 3d printing, nanoparticle, indoor air quality, HAPs.

Presenting author email: yjs9855@gmail.com

The original purpose of three dimensional (3D) printers was to create the prototypes before launching the product. However, in recent years, the scope of use of 3D printers has expanded to various fields such as medical, education, and industry. The 3D printers are expected to emit toxic gases and particulate matter (PM) because it melts filaments at high temperature over 200°C to make samples. However, there is not much research on air pollutants emitted from 3D printing operation and their impacts on human health, and recent studies have mostly focused on estimation of air pollutants emission rate (Afshar-Mohajer, 2015; Stephens 2013). In this study, we analyzed physicochemical properties of nanoparticles and gaseous species emitted from fused filament fabrication (FFF) type 3D printers (FINEBOT and Delta Robot) which have the same type of feed stock filaments such as polylactic acid (PLA). Measurements were performed at the Inha University 3D printing center.

With the exception of the sampling tool and instruments and 3D printers, the center was empty during the sampling time and we turned off the ventilation system to reduce interruption of background emissions. We used three FINEBOT and two Delta Robot to measure air pollutants emission. Variety of instruments such as scanning mobility particle sizer (SMPS), optical particle counter (OPC), personal particle sampler with TEM grid, and gas sampler were used. Four distinct measurement periods over total 3h were considered: 1) background measurements, 2) one Delta Robot operation, 3) two Delta Robot operation, 4) two Delta Robot and three FINEBOT operations.

At the beginning of each sampling phase, new particle formation was detected in a size range of less than 20 nm and enhanced as number of operating 3D printers increased. Also, there was second peak between 70 and 100 nm which was explained by the agglomerates of the new formed particles, directly emitted large size particles, and single particle growth. To analyze the shapes and chemical properties of nanoparticle, transmission electron microscopy (TEM) coupled with energy-dispersive X-ray spectroscopy (EDS) was used, and the results showed mean primary particle size was 22.98 nm which corresponds to the number size distribution results. The particles were round shape and most of them agglomerated (Figure 1). The chemical properties of nanoparticle exhibited enhancement of silicon (Si) and sulfur (S) during 3D printing operation. Of the 45 gaseous species analyzed, 16 of them were considered as hazardous air pollutants (HAPs), known to be

carcinogens or cause serious health effects. This study points to the need for future work to understand the direct health impacts of air pollutants emitted from 3D printing.

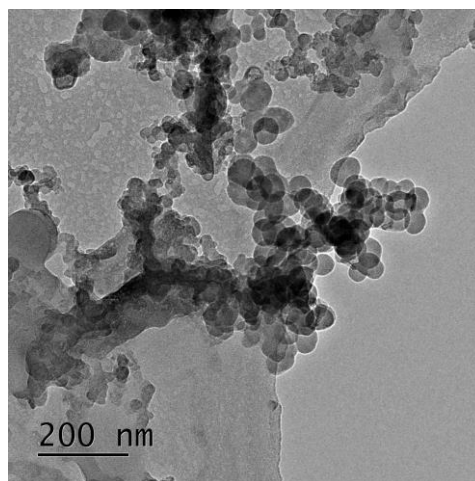


Figure 1. Particle shape of 3D printing operation collected by a TEM grid with personal sampler.

This work was supported by funded by the Korea Ministry of Environment (MOE) as “the Environmental Health Action Program (2016001360005).”

Afshar-Mohajer, N., Wu, C., Ladun, T., Rajon, D. and Huang, Y. (2015), *Build Environ*  
Stephens, B., Azimi, P., Orch, Z. and Ramos, T. (2013) *Atmos. Environ.*

## Characteristics of nano-sized wear particles in subway tunnels

Y.I. Lee<sup>1,2</sup>, K.M. Choi<sup>1,2</sup>, D.G. Kim<sup>3</sup>, W.D. Kim<sup>3</sup>, S.J. Bae<sup>4</sup>, T.S. Kim<sup>2</sup> and D.S Park<sup>1,\*</sup>

<sup>1</sup>Transportation Environmental Research Team, Korea Railroad Research Institute, Uiwang City, Korea

<sup>2</sup>Department of Mechanical Engineering, Sungkyunkwan University, Suwon, Korea

<sup>3</sup> Environmental Management Division, Daegu Metropolitan Transit Corporation, Daegu, Korea

<sup>4</sup>R&D Center, Seoul Metro, Seoul, Korea

Keywords: nano particle, brake system, wear particle

Presenting author email: freego83@krii.re.kr

Subway is one of the major means of transportation system in south korea. Recently, the concerns and interests about particulate matter (PM) were increasing, for it causes many diseases such as conjunctivitis, rhinitis, respiratory disease, and lung cancer. Accumulated PM can be found in closed facilities such as subway systems which commonly used by citizens and passengers stayed for long periods of time. Almost all of subway tunnel is placed in underground. Moreover, the installation of platform screen door (PSD) separates the platform from the subway tunnels which causes the accumulation of PM. These particles are generated by friction between brake pad and rail, wheel and rail, pantograph and electric wire which generates wear particles. It is accumulated in subway tunnel and blown by wind of cabin and this could cause health risk to the passengers. Indoor Air Quality (IAQ) in subway tunnel is needed to manage for health.

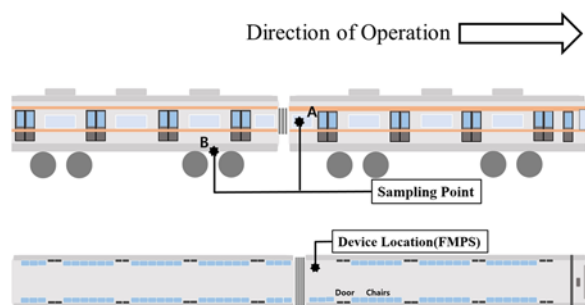


Figure 1. Schematic of experiment setup

The purpose of this study was to determine concentration and size distribution of PM when the subway was at operation. Two Fast Mobility Particle Sizer (FMPS) were used for the collection of fine PM for this study. The devices were installed in the cabin while inlet tubes were put outside through window and under cabin near brake pads to compare characteristic of Fine PM at window and under cabin. Daegu subway Line 1 was measured from Sulhwamyungkok to Ansim and the real-time at each station were recorded by hand.

As the result, we can find the nanoparticles was emitted when the brake system is used under cabin. it is because of sliding between wheel and rail.

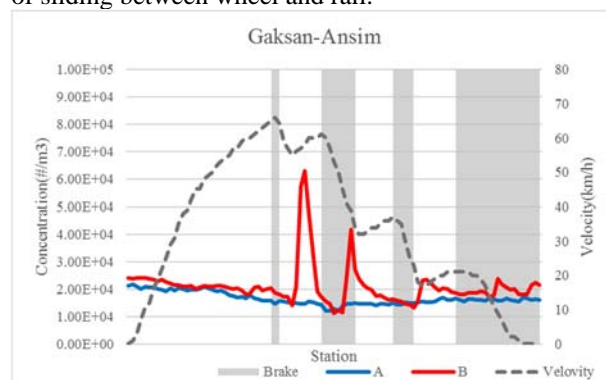


Figure 2. The number concentration of nano particles each site

### Acknowledgements

This research was supported by a grant from the Railway Technology Research Project of the Ministry of Land Infrastructure and Transport(16RTRP-B082486-03).

## Aerosol particle release at finishing of dental composites

L. Ondrackova<sup>1</sup>, P. Bradna<sup>2</sup>, V. Zdimal<sup>1</sup> and D. Pelclova<sup>3</sup>

<sup>1</sup>Laboratory of Aerosols Chemistry and Physics, Institute of Chemical Process Fundamentals of the CAS, v.v.i., Prague, 165 02, Czech Republic

<sup>2</sup>School of Dental Medicine, First Faculty of Medicine, Charles University and General University Hospital in Prague, Prague, 121 08, Czech Republic

<sup>3</sup>Department of Occupational Medicine, First Faculty of Medicine, Charles University and General University Hospital in Prague, Prague, 121 08, Czech Republic

Keywords: aerosol particles, grinding, dental composites.

Presenting author email: ondrackova@icpf.cas.cz

Newly developed dental composite materials contain increased concentrations of filler particles of the nanometer size to produce materials with high mechanical and wear resistance, improved polishability and long-lasting gloss. With nanocomposites, however, a question arises on possible health risk caused by filler nanoparticles released during finishing and polishing nanocomposite restorations in dental offices. As data in the current literature (Bogdan *et al.*, 2014, Van Landuyt *et al.*, 2012 and Van Landuyt *et al.*, 2014) are conflicting, our study was focused on detailed characterization of aerosol particles released during grinding nanocomposites Filtek Ultimate and Estelite Sigma Quick by diamond and tungsten carbide bladed burs. The results were compared with the aerosol particle distributions obtained from a composite Charisma reinforced with micrometer size filler particles and an unfilled resin.

Experiments were performed in a closed experimental room (2.0 × 1.3 × 2.5 m) where the electrical micromotor, control unit and particle spectrometers were situated, and the operator ground the specimens surface. Aerosol particle concentration and size distribution were measured by two different on-line spectrometers SMPS 3936 (Scanning Mobility Particle Sizer) and APS 3321 (Aerodynamic Particle Sizer). For each experiment a new bur was used and grinding was done without water cooling. Start time of the grinding was synchronized with the beginning of particle size scanning that took 120 s. After grinding, the operator remained in the experimental chamber during the next 3 or 5 scans, depending on the time evolution of particle concentration.

Control measurements of particle concentrations by SMPS and APS inside the experimental cabinet together with the operator, micromotor and handpiece with a fixed diamond bur rotating at 150 000 rpm showed no increase in background concentrations of aerosol particles. Subsequent measurements revealed that aerosol generated by grinding the composites and also unfilled resin using round medium diamond bur and bladed carbide finisher running at 100 000 and 150 000 rpm respectively, contained particles of two discrete size ranges – nanoparticles and microparticles. Particle number size distributions recorded 30 seconds after the end of grinding by round medium diamond bur are depicted in Fig. 1. APS particle number size distributions were recalculated to mobility diameters and particle concentrations corrected by subtraction of particle

background concentrations. Points represent experimental data, with lines representing fit by lognormal model.

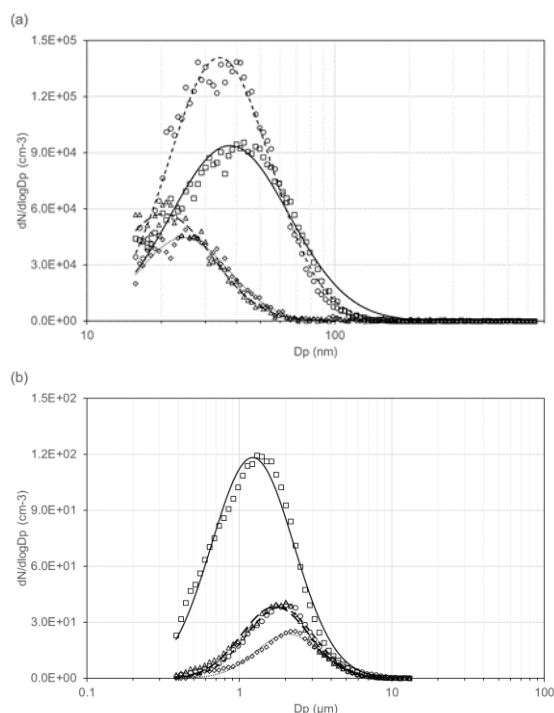


Figure 1. Particle number size distribution measured by: a) SMPS and b) APS after grinding Filtek Ultimate (□), Estelite Sigma Quick (Δ), Charisma (○) and unfilled resin (◇) by round medium diamond bur.

This work was supported by the Charles University in Prague project P28/1LF/6.

Bogdan, A., Buckett, M.I., Japuntich, D.A. (2014) *J. Occup. Environ. Hyg.* **11** (7), 415-426.

Van Landuyt, K.L., Yoshihara, K., Geebelen, B., Peumans, M., Godderis, L., Hoet, P., Van Meerbeek, B. (2012) *Dent. Mater.* **28** (11), 1162-1170.

Van Landuyt, K.L., Hellack, B., Van Meerbeek, B., Peumans, M., Hoet, P., Wiemann, M., Kuhlbusch, T.A., Asbach, C. (2014) *Acta Biomater.* **10** (1), 365-374.

## Aerosol behavior at the Museum of “Last Supper” of Leonardo Da Vinci: secondary formation and volatilization

L. Ferrero<sup>1,\*</sup>, G. Močnik<sup>2,3</sup>, C. Rostagno<sup>4</sup>, A. Proto<sup>5</sup>, C. Pironti<sup>5</sup>, R. Cucciniello<sup>5</sup>, O. Motta<sup>5</sup>, C. Rizzi<sup>1</sup> and E. Bolzacchini<sup>1</sup>

<sup>1</sup>Department of Earth and Environmental Sciences, University of Milano-Bicocca, Piazza della Scienza 1, 20126, Milan, Italy.

<sup>2</sup>Aerosol d.o.o., Kamniška 41, SI-1000 Ljubljana, Slovenia.

<sup>3</sup>Department of Condensed Matter Physics, Jozef Stefan Institute, SI-1000 Ljubljana, Slovenia

<sup>4</sup>Director of Cenacolo Vinciano and Cappella Espiatoria, Polo Museale Regionale della Lombardia, Palazzo Arese Litta, Corso Magenta 24, 20123 Milano.

<sup>5</sup>Dipartimento di Chimica e Biologia, Università degli Studi di Salerno  
Via Giovanni Paolo II 132, 84084, Fisciano (SA), Italy.

Keywords: Aerosol dynamic, indoor, Last Supper, Secondary aerosol, volatilization

\*Presenting author email: [luca.ferrero@unimib.it](mailto:luca.ferrero@unimib.it)

Atmospheric particles can affect cultural heritage, especially the most fragile, such as the Last Supper of Leonardo da Vinci. The Leonardo's paint is protected by a filtering system that allows to maintain the indoor average particulate matter concentration around  $3 \mu\text{g m}^{-3}$ . Previous indoor studies in the Last Supper museum allowed to study the indoor/outdoor penetration of particulate matter and the main sources, but still uncertainty concerning the particles dynamics still persist<sup>[1]</sup>.

In order to shed light on the indoor particles behaviour, the museum was set-up with a combination of: 1) Aethalometer (AE-33, Magee Scientific, 7- $\lambda$ ), 2) condensation particle counters (TSI 3787), 3) an optical particle counters (Grimm 1.107), 4) a low volume sampler (Mega system) 5) a custom developed rotating impactor, 6) a  $\text{NO}_x$ - $\text{NH}_3$  detector (Environment spa) and 7) passive and active  $\text{CO}_2$  sampler (Aquadria srl).

One year of data (March 2016-February 2016) were collected at 1 min time resolution using the real time instrumentation.

Particles concentrations reached a low level as reported in previous studies<sup>[1]</sup>. However, high time resolution data allowed to determine the diurnal cycle of particle concentration. During night, the total number concentration reached a value of  $20.7 \pm 0.1 \text{ cm}^{-3}$  (BC was  $8 \pm 1 \text{ ng m}^{-3}$ ) and then increased with visitors up to  $167.8 \pm 3.3 \text{ cm}^{-3}$  (BC was  $37 \pm 4 \text{ ng m}^{-3}$ ). Using the apportionment of particle concentration based on N/BC ratio<sup>[3]</sup> the diurnal cycle of primary and secondary particles was obtained (Figure 1). It clearly shows a secondary particles peak in the afternoon (up to  $300 \text{ m}^{-3}$ ). This peak can be related to a  $\text{NH}_3$  peak observed at the same time: the  $\text{NH}_3$  concentration peaks in the afternoon reaching a double concentration than that observed during night-time.

Actually, the filtering system of the museum does not treat the  $\text{NH}_3$  that can accumulate inside it. Moreover,

the chemical composition of collected PM samples showed a mass fraction of  $\text{NH}_4\text{NO}_3$  of 7% inside the museum that, compared with the external value of 30% highlighted the volatilization and decomposition of  $\text{NH}_4\text{NO}_3$ . The presence of ammonia became a driver of new particle formation.

In this respect a deeper analysis of gas-phase chemistry is in progress.

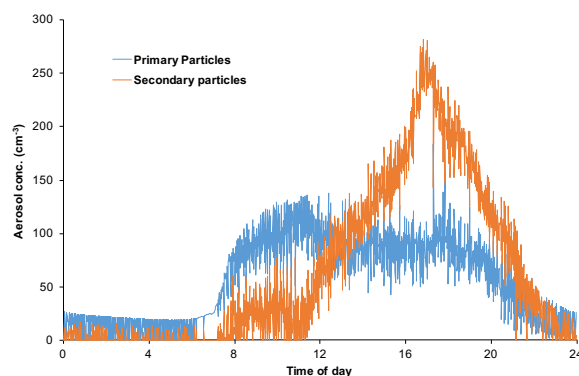


Figure 1. Diurnal behaviour of primary and secondary particles during the opening days of Cenacolo Vinciano.

### References:

- [1] Daher et al., Environ. Sci. Technol., 2011, 45 (24), pp 10344–10353.
- [2] Gasparini F., Stolfi G., Il Cenacolo Vinciano: impiantistica e microclima all'interno del Refettorio., 2014.
- [3] Reche et al., Atmos. Chem. Phys., 11, 6207–6227, 2011

## Combining NSAM and CPC concentrations to determine airborne nanoparticle count mode diameter: application to a set of six workplace aerosols

S. Bau<sup>1</sup> and O. Witschger<sup>1</sup>

<sup>1</sup>Laboratory of Aerosol Metrology, Institut National de Recherche et de Sécurité (INRS), Vandœuvre les Nancy, F-54519, France

Keywords: CPC, NSAM, count median diameter, workplace aerosols.

Presenting author email: sebastien.bau@inrs.fr

Because nanomaterials have been increasingly developed and used in many technology and industry sectors over the last 20 years, increasing numbers of workers are likely to be exposed to airborne nanoparticles. In addition, the question of the nanomaterial characteristics that should be assessed in epidemiological studies remains open. Thus, assessing occupational exposure to airborne nanoparticles shall not only rely on mass concentration and chemical composition; key parameters, such as particle size, have to be included in measurement strategies.

We previously (Bau et al., 2013) proposed a methodology to estimate the count median diameter of an aerosol based on the simultaneous size-integrated measurement of two particle concentrations, lung-deposited surface area and number, thanks to field-portable, commercially available aerosol instruments (NSAM/CPC combination), associated with the Geometric Standard Deviation (GSD) of the aerosol. Indeed, in the absence of size-resolved instruments, this approach can be used as a screening tool to detect the presence of nanoparticles.

In this study, the field-applicability of the method was tested through six sets of experimental data stemming from workplace measurement campaigns where different materials (TiO<sub>2</sub>, SiO<sub>2</sub>, Ag, MWCNT) were produced and handled, covering a range of modal diameters between 30 and 320 nm; the latter data measured with an ELPI were used as reference. Data were taken considering spherical particles with unit density; no further specific data treatment was applied. Although particle density influences the number concentration in each channel of the ELPI, data recently published by Charvet et al. (2015) for thermal metal spraying aerosols show that the modal diameter is almost constant (roughly  $\pm 20\%$ ), whatever the particle density considered in ELPI data post-treatment. The GSD of the workplace aerosol being unknown, a typical value of 1.8 was considered according to different authors (Harris & Maricq, 2001; Maynard, 2003; Park et al., 2009).

The six different sets of experimental data stemming from workplace measurement campaigns are: (1, 2) aerosols measured in a plant that produces both pigment grade TiO<sub>2</sub> and nano-TiO<sub>2</sub> as powders during bagging operations, (3) aerosols emitted during discharging bags of nano-TiO<sub>2</sub> powder into an industrial funnel for further incorporation into cosmetic products, (4) aerosols measured in a research laboratory during dry sandpapering of a reactor producing nanocomposite thin films embedded with Ag nanoparticles, (5) aerosols

released during automated extrusion of a polymer containing MWCNT and (6) aerosols released in a workshop producing photocatalytic media made of amorphous silica fibres felt with TiO<sub>2</sub>.

Accounting for the presence of the cyclone upstream the NSAM, only the submicron mode of the ELPI number size distribution is considered. The count mode diameter derived from the NSAM/CPC combination are compared to the modal diameters stemming from the number size distributions from ELPI measurements in Figure 1.

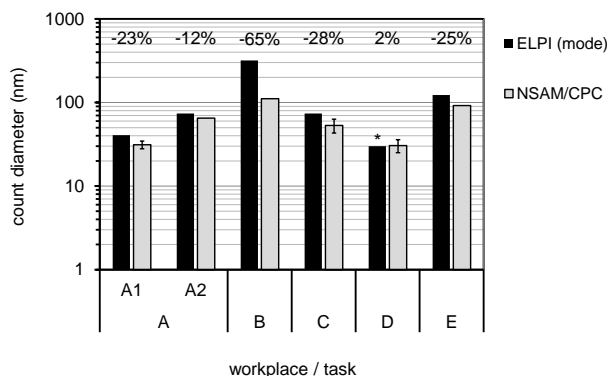


Figure 1. Comparison between the CMD based on the NSAM/CPC approach and the reference modal diameter taken from ELPI number size distribution. The star symbol (\*) corresponds to a modal aerodynamic diameter likely below 30 nm. Indications given on top correspond to the relative deviation between both approaches.

Assuming the GSD of the aerosols to be 1.8, the count mode diameters stemming from combined NSAM/CPC were found to be in the same order of magnitude as ELPI reference data; this finding suggests the possible field-applicability of the approach.

- Bau S., Witschger O., Gensdarmes F., & Thomas D. (2013). *J. Nanopart. Res.*, **15**, 2104.
- Charvet A., Bau S., Bémer D., & Thomas D. (2015). *Aerosol Sci. Technol.*, **49**, 1263-1270.
- Harris S.J., & Maricq M. (2001). *Aerosol Sci. Technol.*, **32**, 749-764.
- Maynard A.D. (2003). *Ann. Occup. Hyg.*, **47**, 123-144.
- Park J.Y., Raynor P.C., Maynard A.D., Eberly L.E., & Ramachandran G. (2009). *Atmos. Environ.*, **43**, 502-509.

## Characterization of fine and ultrafine particles emitted from hardwood processing

J. Gu<sup>1</sup>, I. Kirsch<sup>1</sup>, T. Schripp<sup>1,\*</sup>, F. Froning<sup>2</sup>, D. Berthold<sup>2</sup> and T. Salthammer<sup>1</sup>

<sup>1</sup>Department of Material Analysis and Indoor Chemistry, Fraunhofer WKI, Braunschweig, 38108, Germany

<sup>2</sup>Department of Technology for Wood-Based Materials, Fraunhofer WKI, Braunschweig, 38108, Germany

\* Current affiliation at Institute of Combustion Technology, German Aerospace Center, Stuttgart, 70569, Germany

Keywords: wood dust, ultrafine particles, occupational exposure, wood processing

Presenting author email: [jianwei.gu@wki.fraunhofer.de](mailto:jianwei.gu@wki.fraunhofer.de)

Wood dust, especially hardwood dust, has been known to cause health problems and cancers in workers (IARC 1995). The occupational wood dust concentration is normally regulated by a limit value, i.e., the mass concentration of particles at the work place ( $5 \text{ mg/m}^3$  in EU). However, little is known about the chemical composition and size distribution of dust emitted from processing of wood. Also an urgent need is the determination of the emission of ultrafine particles (UFPs, diameter  $<100 \text{ nm}$ ), which has little mass concentration but great number and surface area concentration and is overlooked by the mass-based limit values. The chemical composition and size distribution of the wood dust emission from different wood processing procedures is necessary to better evaluate the health risks of wood dust and to help policymakers & industry to improve the air quality in the wood processing environment.

In this study, we measured the dust emitted from a whole hardwood processing procedure and their chemical composition and physical properties (size distribution  $5.6 \text{ nm}$ – $10 \text{ }\mu\text{m}$ ). The measurement consists of two parts. First, we measured the dust/particles emitted from trail wood processing on a pilot plant scale at WKI. The instruments used to process the woods are the same as in wood industry. The procedures include chopping, sawing, chipping, screening, drying, fiberizing and pressing of several hardwood species and a pine wood. Second, the measurement will be repeated at two wood plants (one sawmill and one wood-based panel manufacturer). Finally, human exposure to the wood dust will be modelled combining the measured aerosol size distribution and a Human Respiratory Tract Model (ICRP 1994) to evaluate the real occupational exposure and risks. UFPs were measured by a Fast Mobility Particle Sizer (FMPS, model 3091, TSI, USA) which covers a size range of  $5.6$  to  $560 \text{ nm}$ . Fine particles were measured by a Laser Aerosol Spectrometer (LAS, model 1.108, GRIMM, Germany) and by an Optical Particle Sizer (OPS, model 3300, TSI, USA) as well.  $\text{PM}_{10}$  and  $\text{PM}_{2.5}$  samples were collected on filters by low volume samplers (model LVS 3.1, Derenda, Germany). In addition, cascade impactor (model DLPI<sup>+</sup>, Dekati, Finland) was used to sample size-segregated dust (in 14 stages) between in  $16 \text{ nm}$  and  $10 \text{ }\mu\text{m}$  for chemical composition analysis.

Figure 1 shows the particle mass size distribution (measured by cascade impactor) during the trial chipping. The majority of particle mass is distributed around  $10 \text{ }\mu\text{m}$ . A second peak was found in the accumulation mode of  $200\text{--}300 \text{ nm}$ . Note that each processing lasted for only a few minutes, while the

sampling time of cascade impactor was 3 hours covering periods before and after processing and breaks in between. The concentrations in real industrial production are expected to be higher.

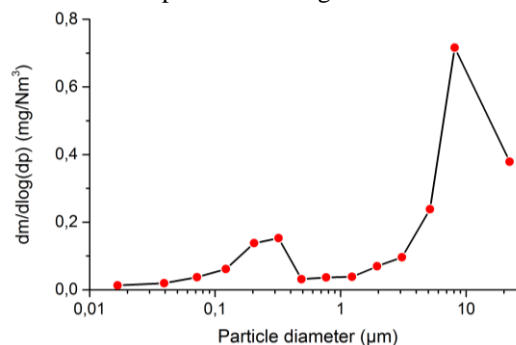


Figure 1. Particle mass size distribution (measured by cascade impactor) during trail chipping processing.

Figure 2 shows the particle number size distribution (measured by FMPS) of chipping different woods at peak number concentrations (thus to minimize the influence of other sources). Very high number concentrations were observed ( $1.1 \times 10^6$  –  $4.8 \times 10^6 \text{ p/cm}^3$ ). It is also found that the majority of particle numbers is in the ultrafine range ( $<100 \text{ nm}$ ).

Further results will be presented at the conference.

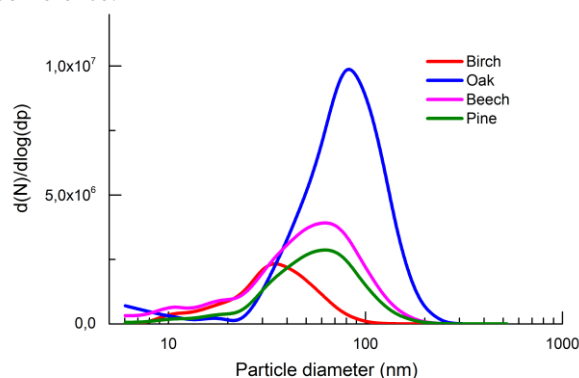


Figure 2. Particle number size distribution (at peak concentration) of chipping of different woods.

The work was funded by Federal Ministry of Food and Agriculture (Germany) through Agency for Renewable Resources (FNR) under grant number 22007113.

IARC (1995) *IARC Monographs on the Evaluation of Carcinogenic Risks to Humans - Wood Dust and Formaldehyde*, WHO, Lyon.

ICRP (1994) *Human Respiratory Tract Model for Radiological Protection*, ICRP publication 66, Ann. ICRP 24.

## Analysis of Incense burning in a temple and its health impacts: A study of Kanpur

Anubha Goel<sup>1</sup>, Om prakash Choudhary<sup>2</sup>, Radhika Mundra<sup>3</sup>

<sup>1</sup>Department of Civil Engineering, Indian Institute of Technology, Kanpur, 208016, India

<sup>2</sup>Environment Engineering and Management Program, Indian Institute of Technology, Kanpur, 208016, India

<sup>3</sup>Department of Civil Engineering, Indian Institute of Technology, Kanpur, 208016, India

Keywords: Incense, PAHs, bioreactivity, health risk

Presenting author email:anubha@iitk.ac.in

Religious ceremonies and rituals constitute a major activity in many parts of India, with people visiting temples on a regular basis. Incense burning, in the form of dhoop, camphor, oil-lamps, and incense sticks, is frequently performed inside temple premises. Exposure to air pollutants emitted from these can have both acute and chronic effects on temple visitors. The study was carried out on a popular temple in Kanpur city, India to study the incense emissions on three major and five normal days. Major Day is a special day for worship in a week at that temple and a large number of people visit the temple. All other days in a week are considered as normal day. Incense sticks are the primary source of incense emission in the temple. Real time air samples for pollutants in particle phase were collected by running the Micro Orifice Uniform Deposit Impactor (MOUDI) and Optical Particle Counter (OPC). The measured PM load from these samples ranged from 227.83 to 833.12 $\mu\text{g}/\text{m}^3$  in PM<sub>1</sub> and 282.02 to 971.56 $\mu\text{g}/\text{m}^3$  in PM<sub>10</sub>.

Incense sticks of five different brands, commonly used in the temple, were analyzed. Carbon, hydrogen and nitrogen contents for incense material fall in the approximate range of 41 - 49 %, 3.0-5.8 % and 5.6-7.4 % respectively. As expected the ratio for ash are much lower: 3.6-13.6 %, 0.1-1.0 %, and 0.99-2.26 % for C, H, and N, respectively. It was observed that the carbon, hydrogen and nitrogen have higher values for all 3 elements compare to incense material.

The levels of PAHs were determined on particles by MOUDI. Filters from MOUDI for 2 major (BD-2, BD-4) and one minor day (BD-5) were analyzed for PAHs.

SAMPLING DAY	$\Sigma$ PAH observed( $\mu\text{g}/\text{m}^3$ )
2	7333.63
4	8103.09
5	6292.91

More than 50% PAHs occurred on ultrafine particles (with contribution higher on major days) followed by coarse and fine particles. 11 out of 12 PAHs were detected on all days in which Pyrene (Pyr) and Benzo-k-Fluoranthene was comparatively higher and Benzo-a-Fluoranthene (BaF) was the lowest. 5 out of 12 have been found to be carcinogenic which are benzo[a]anthracene (BaA), chrysene (Chr), benzo[b]fluoranthene (BbF), benzo[k]fluoranthene

(BkF), indeno[1,2,3-cd]pyrene (INP) and benzo[g,h,i]perylene[B(ghi)P]. Risk assessment is performed for both particulate matter as well as PAHs. The maximum probability of getting cancer due to exposure to PAHs and PM<sub>2.5</sub> over 70 years period, were estimated to have BaP<sub>eq</sub> = 1295.67 ng/m<sup>3</sup> and PM<sub>2.5</sub> = 986.11 $\mu\text{g}/\text{m}^3$  respectively.

**Incremental Life Time Risk Assessment (ILCR)** for PPAHs was calculated by ILCR was calculated for the exposure to BaP<sub>eq</sub> concentration. The highest and lowest BaP<sub>eq</sub> was observed on for age group 16-21 year and 51-61 year. This can be very dangerous from the health point of view as it has potential to cause cancer in human. Given the adverse effects of these pollutants, especially PAHs and the fine fraction of particulate matter, it is important to evaluate the risk caused by these harmful substances on the large number of visitors. The results suggest that long-term exposure to the highly polluted temple environment can have both acute and chronic consequences. The C/H ratio and the particle bound PAHs are similar to the studies in Taiwan (T.T. Yang et al. 2017). These particle bound PAH are biologically active and hence increasing the production of proinflammatory mediator. Also, the high C/H ratio indicates high bioreactivity. The results obtained from our study indicate coherence with the Taiwan studies and we suggest further study in this direction.

Tzu-Ting Yang, Su-Chen Ho, Lu-Te Chuang, Hsiao-Chi Chuang, Ya-Ting Li, Jyun-Jie Wu, *Characterization of particulate-phase polycyclic aromatic hydrocarbons emitted from incense burning and their bioreactivity in RAW264.7 macrophage*, Environmental Pollution 220 (2017) 1190e1198

## Real-time Number Size Distributions of Particles Released from Stick Incense Burning

Ying I. Tsai<sup>1</sup>, Natthawadee Chantrawichaikun<sup>1</sup> and Su-Ching Kuo<sup>2</sup>

<sup>1</sup> Department of Environmental Engineering & Science, Chia Nan University of Pharmacy & Science, Tainan City 71710, Taiwan

<sup>2</sup> Department of Medicinal Chemistry, Chia Nan University of Pharmacy & Science, Tainan City 71710, Taiwan

Keywords: incense stick burning; particulate number; particulate mass; size distribution

Presenting author email: mtsaiyi@mail.cnu.edu.tw (Y.I. Tsai)

Indoor particulate matter (PM) is emitted from many sources, such as cooking, smoke, and hair spray. Among them, incense burning is also a significant source of PM emission. Moreover, PM consists of carbons, inorganic salts, and other components (Tsai et al., 2010). Several studies have investigated PM emitted during incense burning; however, real-time particle size distribution are still lacking. In the study, PM emitted during incense stick burning were monitored to identify the real-time PM size distributions (number, surface area, and mass) of incense sticks from Thailand and Taiwan (TH and TW, respectively).

Twenty types of incense sticks from Thailand and Taiwan were selected in this study. A burning test was conducted in a 0.325-m<sup>3</sup> operation chamber by using a NanoSMPS (NanoScan SMPS Nanoparticle Sizer; model 3910, TSI Inc., USA) and an Optical Particle Sizer (model 3330, TSI Inc., USA) to collect PM during real-time burning and for 2 hours postburning.

The particle number, surface area, and mass size distributions of TH and TW during burning and postburning are shown in Fig. 1. As shown in Fig. 1 (left), the average particle number size distribution (PN) was higher for TW than for TH; however, both had the same pattern. The peak of particles emitted from TH during burning and postburning was 106.0 nm, with a Dp50% of 114.0 nm, and 222.1 nm, with a Dp50% of 232.4 nm, respectively. However, the peak of particles emitted from TW during burning and postburning was 106.0 nm, with a Dp50% of 109.3 nm, and 207.7 nm, with a Dp50% of 212.7 nm, respectively. The results indicated that the peak of particles emitted from TH was higher than that of particles emitted from TW during postburning, whereas the peak of particles emitted from TH and TW during burning was similar.

PS was slightly larger during burning than during postburning. The peak of particles emitted from TH during burning and postburning was 194.2 nm, with a Dp50% of 215.2 nm, and 465.3 nm, with a Dp50% of 499.3 nm, respectively. Therefore, during both burning and postburning, the peak of particles emitted from TW was higher than that of particles emitted from TH.

As revealed in Fig. 1 (right), the average particle mass size distribution of particles emitted from TH was slightly higher during postburning than during burning. Moreover, the particle mass emitted from TW was higher during burning than during postburning. The peak mode of particles emitted from TH during burning and postburning was 465.3 nm, with a Dp50% of 436.3 nm, and 497.7 nm, with a Dp50% of 547.5 nm, respectively. However, the peak mode of particles emitted from TW during burning and postburning was 532.3 nm, with a Dp50% of 540.2 nm, and 608.9 nm, with a Dp50% of 625.1 nm, respectively. Thus, during both burning and postburning, the peak mode of particles emitted from TW was higher than that of particles emitted from TH.

The highest PN was identified in accumulation I mode during both burning and postburning (in Fig. 2). The second highest PN was discovered in Aitken mode during burning for TH and TW. By contrast, the second highest PN was found in accumulation III mode during postburning for TH and TW. Moreover, during postburning, PN increased in the accumulation modes (I, II, and III). Ultrafine particles were emitted in the nuclei and Aitken modes, accounting for 44.44% and 47.69% of particle emissions from TH and TW during burning. This finding showed that more ultrafine particles were emitted from TW than from TH. Thus, TW may exert more harmful effects on human health than TH.

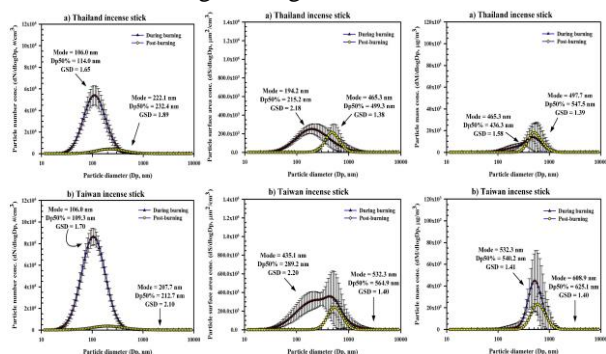


Fig. 1. Average particle number (left), particle surface area (center) and particle mass (right) size distribution during burning and postburning.

As illustrated in Fig. 1 (center), the average particle surface area size distribution (PS) was larger for TW than for TH; however, both exhibited the same

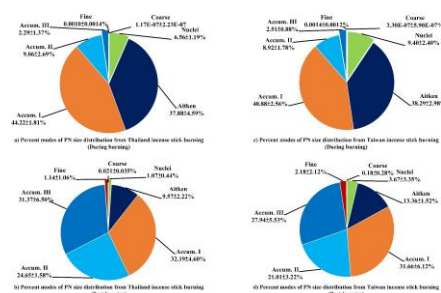


Fig. 2. Percent modes of particle number size distribution of Thailand and Taiwan incense sticks.

This work was supported by the Ministry of Science and Technology, Taiwan, under the grants MOST 102-2221-E-041-003-MY3 and MOST 105-2221-E-041-003-MY3.

Tsai, Y.I., Wu, P.-L., Hsu, Y.-T. and Yang, C.-R., (2010) *Atmos. Environ.* **44**, 3708-3718.

## Chemical characterization of fine particulate matter emitted from incense stick burning

Su-Ching Kuo<sup>1</sup>, Ying I. Tsai<sup>2</sup> and Natthawadee Chantrawichaikun<sup>2</sup>

<sup>1</sup> Department of Medicinal Chemistry, Chia Nan University of Pharmacy & Science, Tainan City 71710, Taiwan

<sup>2</sup> Department of Environmental Engineering & Science, Chia Nan University of Pharmacy & Science, Tainan City 71710, Taiwan

<sup>2</sup> Keywords: incense stick burning, chemical compositions, levoglucosan, sugar alcohol

Presenting author email: suching@mail.cnu.edu.tw (S.-C. Kuo)

Incense sticks are widely used for aromatherapy, worshipping deities, and religious ceremonies, particularly in temples, shrines, churches, and residences (indoor air) in Taiwan and Thailand. However, many studies have shown that fine particles emitted from incense stick burning may exert harmful effects on human health.

In this study, 20 types of incense sticks selected from Thailand and Taiwan were used for the chemical characterization of the emitted fine particles. A Personal Environmental Monitor sampling device (PM<sub>2.5</sub>, MSP Inc.) was used to collect fine particles emitted from incense stick burning. Ion chromatography was used to analyze the chemical composition of fine particles and ash, including saccharides (sugars, sugar alcohols, and anhydrosugars) and inorganic salts (anions and cations). The concentration of particulate matter with a diameter of 2.5 μm or less (PM<sub>2.5</sub>) emitted from incense stick burning was measured to compare the PM<sub>2.5</sub> emission rate between Thailand and Taiwan incense sticks (hereafter denoted as TH and TW, respectively).

Figure 1 shows the mass percent of the total chemical compositions of PM<sub>2.5</sub> emitted from TH and TW. The compositions of TH and TW were 39.17% ± 19.92% and 45.06% ± 13.78% for others, 38.23% ± 23.27% and 28.74% ± 7.64% for element carbon (EC), and 20.15% ± 11.41% and 24.36% ± 7.23% for organic carbon (OC, including undetermined OC, anhydrosugars, total sugar alcohols, and total sugars), respectively.

The percentage of total sugars in PM<sub>2.5</sub> mass was 0.19% ± 0.17% for TH and 0.28% ± 0.17% for TW, implying that TW emitted more total sugars than TH. For both TH and TW, mannose was the most abundant sugar species (0.097 ± 0.084 mg g<sup>-1</sup> PM<sub>2.5</sub> for TH and 0.23 ± 0.15 mg g<sup>-1</sup> PM<sub>2.5</sub> for TW), followed by glucose and galactose. Mannose-yielding carbohydrates are often found in hardwood. Thus, mannose was higher in TW than in TH, indicating that TW is probably made from hardwood.

The percentage of sugar alcohols in PM<sub>2.5</sub> mass was 0.48% ± 0.42% for TH and 0.77% ± 0.25% for TW,

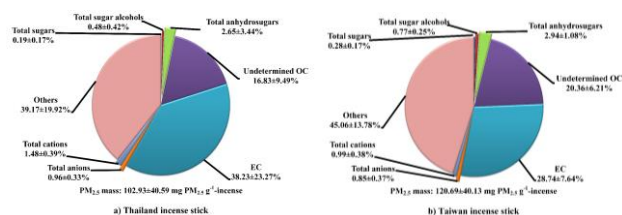


Fig. 1 Percentage of chemical composition in PM<sub>2.5</sub> mass emitted from Thailand and Taiwan incense stick burning.

implying that TW emitted more sugar alcohols than TH. Chemical composition of PM<sub>2.5</sub> is shown in Table 1. For TH, glycerol was the most abundant sugar alcohol (0.18 ± 0.16 mg g<sup>-1</sup> PM<sub>2.5</sub>), followed by arabitol and xylitol. By contrast, for TW, xylitol was the most abundant component (0.37 ± 0.23 mg g<sup>-1</sup> PM<sub>2.5</sub>), followed by glycerol and arabitol. Xylitol is often found in hardwood and is directly emitted from hemicellulose (Tsai et al., 2010). Xylitol is considered a potential marker of incense stick burning.

The percentage of anhydrosugars in PM<sub>2.5</sub> mass was 2.65% ± 3.44% for TH and 2.94% ± 1.08% for TW, implying that TW emitted more anhydrosugars than TH. In addition, for both TH and TW, levoglucosan was the most abundant anhydrosugar (2.46 ± 3.18 mg g<sup>-1</sup> PM<sub>2.5</sub> for TH and 3.11 ± 1.07 mg g<sup>-1</sup> PM<sub>2.5</sub> for TW), followed by mannosan. Levoglucosan is a major organic compound found in wood burning smoke and is considered a marker of wood or biomass combustion.

The percentage of total inorganic salts in PM<sub>2.5</sub> mass was higher for TH than for TW. Moreover, for both TH and TW, K<sup>+</sup>, Cl<sup>-</sup>, and PO<sub>4</sub><sup>3-</sup> were the most abundant inorganic species in this study. By contrast, a previous study found that SO<sub>4</sub><sup>2-</sup>, NO<sub>3</sub><sup>-</sup>, and NH<sub>4</sub><sup>+</sup> were the most abundant inorganic salts in atmospheric aerosols. This finding indicates that inorganic salts are different between atmospheric aerosol and PM<sub>2.5</sub> emitted from incense stick burning. Moreover, K<sup>+</sup> was reported to be the most abundant inorganic species in agricultural burning and is considered a favorable marker of vegetative burning. Thus, in this study, K<sup>+</sup> is considered a marker of incense stick burning.

Table 1. Specific and major chemical compounds (mg species g<sup>-1</sup>-PM<sub>2.5</sub>) of PM<sub>2.5</sub> emitted from Thailand and Taiwan incense sticks.

Compound	Thailand incense sticks (TH)	Taiwan incense sticks (TW)
Mannose	0.097±0.084	0.23±0.15
Glycerol	0.18±0.16	0.13±0.063
Xylitol	0.076±0.10	0.37±0.23
Arabitol	0.16±0.13	0.13±0.080
Levoglucosan	2.46±3.18	3.11±1.07
Chloride	0.65±0.33	0.63±0.44
Phosphate	0.14±0.14	0.15±0.038
Potassium	1.33±0.34	1.04±0.40

This work was supported by the Ministry of Science and Technology, Taiwan, under the grants MOST 102-2221-E-041-003-MY3 and MOST 104-2221-E-041-001-MY2.

Tsai, Y.I., Wu, P.-L., Hsu, Y.-T. and Yang, C.-R., (2010) *Atmos. Environ.* **44**, 3708-3718.

## **Abstracts T411**

## Fate of aerosolized Nanoparticles: The influence of surface active substances on lung deposition and respiratory effects (NANOaers)

L. Hillemann<sup>1</sup>, D. Göhler<sup>1</sup>, Sandra Wagener<sup>2</sup>, Claudia Cascio<sup>2</sup>, Jutta Tentschert<sup>2</sup>, Emilia Visileanu<sup>3</sup>, Helfried Steiner<sup>4</sup>, Günter Brenn<sup>4</sup>, Blanca Suarez<sup>5</sup>, Joseph D. Brain<sup>6</sup>, and M. Stintz<sup>1</sup>

<sup>1</sup>Institute of Process Engineering and Environmental Technology, TU Dresden, 01062 Dresden, Germany

<sup>2</sup>Federal Institute for Risk Assessment (BfR), 10589 Berlin, Germany

<sup>3</sup>National Research and Development Institute for Textile and Leather (INCDTP), 030508 Bucharest, Romania

<sup>4</sup>Institute of Fluid Mechanics and Heat Transfer, TU Graz, 8010 Graz, Austria

<sup>5</sup>Fundación Gaiker, 48170 Zamudio, Spain

<sup>6</sup>Harvard School of Public Health, Boston, MA 02115, USA

Keywords: spray application, particle release, fate, exposure assessment

Presenting author email: Lars.Hillemann@tu-dresden.de

The occurrence of manufactured nanomaterials (MNM) is steadily increasing, also in applications affecting the everyday life of consumers and the public in general. Two prominent types of MNMs, often used and relevant for inhalative uptake are nano-Ag and nano-CeO<sub>2</sub>. They are relatively inexpensive and produced in much larger volumes than exotic nanomaterials, such as fullerenes and quantum dots. Nano-Ag is often used in materials like medical supplies, cosmetics and textiles for its bacterial inhibiting properties. Compared to the bulk material, the large surface area per unit enhances the release of silver ions. Several studies have shown adverse health effects on living cells exposed to nano-Ag.

Primarily, nano-structured CeO<sub>2</sub> as an ideal UV absorber is often added to lacquers and wood preservative coatings to improve their UV stability. CeO<sub>2</sub> belongs to the group of respirable granular bio-durable particles.

Inhalation is the most relevant route of uptake for MNM. During exposition, MNM are exposed towards specific chemical surroundings. In general, aerosolized MNM do not enter body barriers in their pristine form. When used in the form of sprayed products, MNM are released into the air in droplets. For this kind of application, the fate of the MNM depends on the composition of the liquid and on mechanical influences in the spraying process.

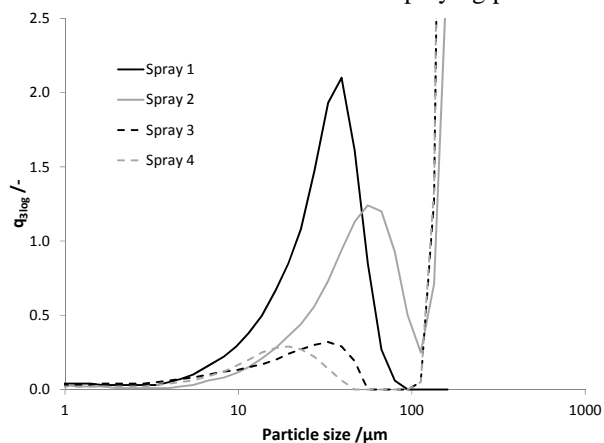


Figure 1. Size distribution of droplets generated by spray application employing different liquid compositions.

During inhalative exposition, MNM are exposed towards specific chemical surroundings as e.g. cellular surface molecules of airway epithelium. Within these different environments, particles can change their properties for example by agglomeration and dissolution.

Chemical matrices may have the potential to avoid MNM agglomeration which may lead to smaller particle sizes and different toxicity compared to the materials tested in existing studies on inhalative toxicity of MNM. If products contain MNM, it cannot be excluded that MNM are also airborne in the nanometer size range, potentially facilitating uptake into the human lung. For this process also the change of particle properties during their airborne state is crucial.

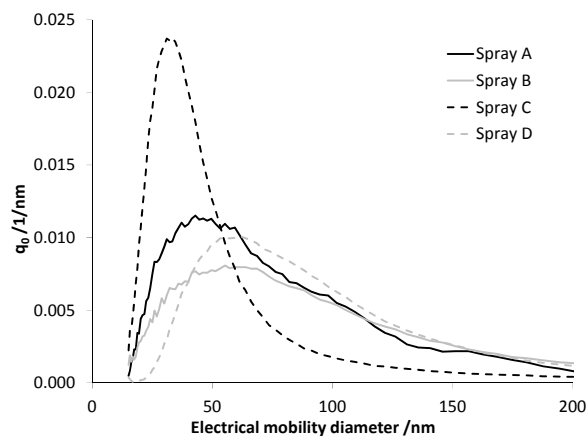


Figure 2. Size distribution of particles resulting from drying of droplets generated by spray application: Most of the particles are smaller than 100 nm.

The contribution presents the actual state of knowledge of the project. It discusses the size distribution of particles released by spray application in different scenarios of spray processes.

This work is supported by the German Federal Ministry of Education and Research.

## Evaluation of mobile air purifiers under real conditions

S. Schumacher<sup>1</sup>, M. Küpper<sup>1</sup>, D. Spiegelhoff<sup>1</sup>, U. Schneiderwind<sup>1</sup>, H. Finger<sup>1</sup>, and C. Asbach<sup>1</sup>

<sup>1</sup> Institut für Energie- und Umwelttechnik e.V. (IUTA), 47229 Duisburg, Germany

Keywords: air purifier, particle filtration, comparison between test and real conditions

Presenting author email: schumacher@iuta.de

Over the last years, air pollution has more and more moved into the focus of public attention. This not only concerns atmospheric pollution, but also the indoor air quality, which can be deteriorated either by infiltration from outside or by indoor sources (e.g., smoking, cooking or candles). Since people in industrial nations spent most of their time inside buildings, the latter is of special importance. A way to improve the indoor air quality is to use mobile air purifiers. Such devices use a fan to draw the polluted air through a filter and release the purified air back to the room so that the concentration of the pollutants decreases exponentially with time.

There are various national standards to test mobile air purifiers. Most of them classify the cleaning performance using the clean air delivery rate (CADR), which describes the flow rate of clean air delivered by the air purifier. It is determined by measuring the temporal decay rate of an initial pollution concentration in a closed room while the air purifier is running. However, such standardized tests are always conducted in test chambers without furnishings and with good air mixing (Finger 2015). In contrast, in occupied rooms the flow and hence the pollutant dispersion can be much more complex so that deviations might be expected.

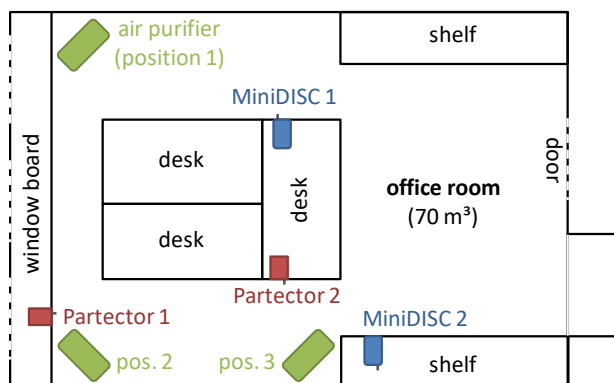


Figure 1. Sketch of the office room with the positions of the portable particle monitors (Partector and MiniDiSC) and different locations of the air purifier.

To address this question, we first determined the nominal CADR of an air purifier according to the Chinese standard GB/T 18801, i.e. in a 30 m<sup>3</sup> test chamber using cigarette smoke as test aerosol. The CADR was evaluated for both number concentration and lung deposited surface area (LDSA) concentration. Afterwards, the air purifier was operated in an occupied office room with a volume of about 70 m<sup>3</sup>. As test aerosol we provided an initial concentration of the natural outdoor aerosol by shortly opening a window. To measure the local CADR,

four portable particle monitors based on diffusion charging (MiniDiSC and Partector) were located at different positions in the room. The devices measure the LDSA concentration, which might be a more relevant measure concerning human health effects of the pollutants. The portable particle monitors have been checked before in the standardized test chamber to show the same CADR if exposed to the same conditions. The LDSA concentration decay was measured with the instruments in the office room and hence the effectiveness of the air purifier for different positions within the room determined.

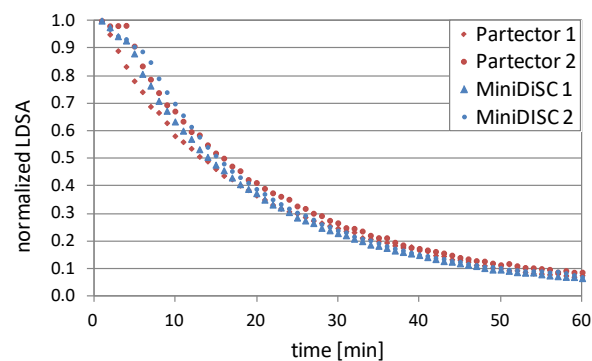


Figure 2. Exponential decay of the LDSA in the office room measured by portable particle monitors located at four different positions.

In the office room, the four portable devices showed similar decay curves at different positions (see Fig. 2), indicating that the air purifier homogeneously distributed the cleaned air within the room. As next step, we changed the position of the air purifier to test to what extent this influences the cleaning efficiency throughout the room. Also here, we did not observe significant deviations. However, we found first evidences that the CADR in the office room is slightly smaller than measured in the standardized test chamber. Results from the different measurements will be presented and different factors such as the particle size distribution of the test aerosol, the characteristics of the measurement devices, unknown particle sources or infiltration from outside discussed, as they might explain the observed deviations.

Finger, H. et al. (2015): *Gefahrstoffe - Reinhalt. Luft* **75** 497.

## Exposure estimation by propagation modelling based on experimental determined airborne particle release data from nanostructured materials

D. Göhler<sup>1</sup>, R. Gritzki<sup>2</sup>, M. Rösler<sup>2</sup>, C. Felsmann<sup>2</sup> and M. Stintz<sup>1</sup>

<sup>1</sup> Research Group Mechanical Process Engineering, Institute of Process Engineering and Environmental Technology, Technische Universität Dresden, D-01062 Dresden, Germany

<sup>2</sup> Chair of Building Energy Systems and Heat Supply, Institute of Power Engineering, Technische Universität Dresden, D-01062 Dresden, Germany

Keywords: propagation modelling, exposure estimation, particle release, nanostructured materials, EHS.  
Presenting author email: [daniel.goehler@tu-dresden.de](mailto:daniel.goehler@tu-dresden.de)

The exposure is in addition to the substance-specific hazard-profile the basis to perform an overall risk assessment on nanostructured materials. Exposure describes in this context the state of dispersion (i.e. concentration and size) at the entrance to the subject of protection (i.e. at the breathing zone of consumer/worker), which originates from release (i.e. state of dispersion at source) due to transport (e.g. dilution) and transformation (e.g. coagulation) processes. Nowadays, numerous release and exposure studies concerning the handling of nanostructured materials are available. Both kinds of studies differ in their advantages and disadvantages (e.g. reality near, accuracy, resolution or reproducibility). However, there is still a gap to estimate exposure levels based on release data.

In order to start with filling the gap, exposure estimation was performed using experimental determined particle release data (Vorbau 2009, Göhler & Stintz 2014 and Göhler et al. 2016) and propagation modelling (cf. Gritzki et al. 2003, Knopp et al. 2005, Gritzki et al. 2009) within a 5 m x 6 m x 3 m = 90 m<sup>3</sup> model room, which contains a door, a triple part window, a heated floor, a work bench and a consumer/worker (cf. Göhler et al. 2017). Aerosol propagation was modelled for 15 propagation scenarios based on three different release scenarios (i.e. dry wiping, sanding, spraying) at three different release locations and four different ventilation scenarios (i.e. natural ventilation by door slit infiltration at 0.5 h<sup>-1</sup>, natural ventilation by a pivot-hung window at 1.5 h<sup>-1</sup>, two types of technical ventilation at 8.0 h<sup>-1</sup>). To estimate both nearfield and farfield exposure, two sensors (S1, S2) were used to observe the aerosol condition in the breathing zone (1.6 m) before the person or respectively on the left-hand side of the wall behind the person.

Results have shown that the level of exposure depends fundamentally on the combination of release scenario, ventilation scenario and the positioning of the worker/consumer (i.e. distance to source and position within the flow field). For example, the ratio between the number of released particles to the number of inhaled particles, which can be seen as a kind of dilution factor, varied overall exposure scenarios between  $3.9 \cdot 10^2$  and  $1.7 \cdot 10^7$ . Interestingly, it could be observed that convective flow structures based on personal heat can cause particle availability in the breathing zone.

The presentation will give more detailed information on the chosen scenarios, assumptions, simplifications and

specifications as well as on number- and mass-weighted results for exposure, inhalation and regional deposition in the human airways, which were deduced from the data of propagation modelling.

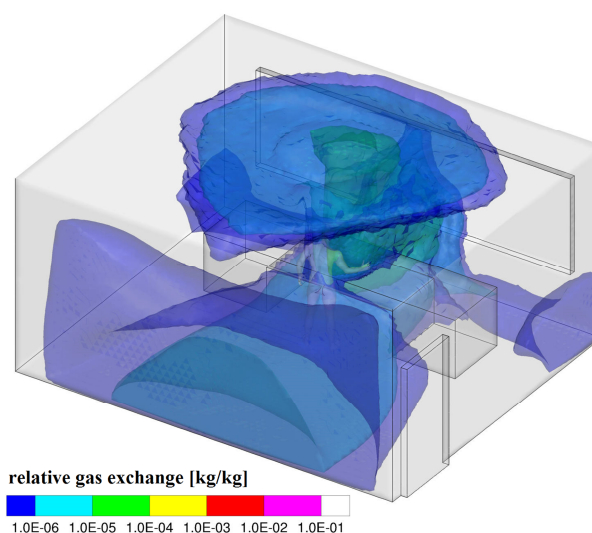


Figure 1. Aerosol propagation (at 135 s) based on sanding (duration of 60 s) of a workpiece located on the workbench and natural ventilation by pivot-hung window (1.5 h<sup>-1</sup>); isosurface-visualisation.

This work was supported by the German Paint Industry Association (VdL e.V., Frankfurt/Main, Germany).

Göhler, D., Stintz, M., Rommert, A. and Eichstädt, D. (2016) *Farbe und Lack*, **121**, 142-149.

Göhler, D. and Stintz, M. (2014) *J. Nanopart. Res.*, **16**, 2520.

Göhler, D., Gritzki, R., Stintz, M., Feldmann, C. and Rösler, M. (2017) *J. Phys.: Conf. Ser.*, in review.

Gritzki, R., Richter, W. and Rösler, M. (2003) *Int. J. Vent.*, **1**, 33-39.

Gritzki, R., Peschk, A., Richter W. and Rösler, M. (2009) *Bauphysik*, **31**, 51-55.

Knopp, T., Lube, G., Gritzki, R. and Rösler, M. et al. (2005) *Comput. Method. Appl. M.*, **194**, 3797-3816.

Vorbau, M., Hillemann, L. and Stintz, M. (2009) *J. Aerosol Sci.* **40**, 209-217.

## Experimental Determination of the air and surfaces Transfer Coefficients of Exhaled Droplets in a Classroom

G. Da<sup>1</sup>, E. Géhin<sup>1</sup>, S. Delaby<sup>2</sup>, S. Ritoux<sup>2</sup>, T.L. Ha<sup>2</sup>, E. Robine<sup>2</sup>

<sup>1</sup>University Paris-Est, CERTES, Créteil, 94000, France

<sup>2</sup>CSTB, Department of Health and Comfort, Champs/Marne, 77447, France

Keywords: Exhaled-droplets, Particle-Transfer, Emission-rate, Indoor-Environment.

Presenting author email: guillaume.da@u-pec.fr

A significant amount of work using numerical simulations has been carried out on the dispersion of exhaled particles for different types of indoor environments (Nicas *et al.*, 2005; Chen *et al.*, 2014). A program was proposed to study the environmental determinants of viral exposure by both experimental and numerical methods. Using a fluorescent-tracer based technique (Da *et al.*, 2015), this abstract presents the experimental determination of the emission rate of exhaled droplets in a room, as well as their transfer to surface and to air, since, after evaporation, the residues may remain airborne for prolonged periods (Xie *et al.*, 2009).

Based on the physical parameters of an oropharyngeal emission, a test bench for the generation of monodisperse droplets ( $d_d = 22$  or  $40 \mu\text{m}$ ) was used in this study. The droplet generator used a liquid solution of water and sodium fluorescein. The mass concentration of fluorescein simulated the salts concentration in the saliva. The generated monodisperse droplets were then transported in a moist air jet ( $33^\circ\text{C}$ ) with similar conditions as at the outlet of the mouth, and ultimately released continuously at the source opening in an experimental classroom ( $90 \text{ m}^3$ ) where droplets were subjected to evaporation. The size distribution of the airborne residues (non-porous spherical particle of dry fluorescein,  $\rho_m = 1.540 \text{ kg}\cdot\text{m}^{-3}$ ) were measured in real time using an aerodynamic particle sizer spectrometer. The transfer coefficients of the generated particles from the source to surface and from the source to air were obtained. The particle number concentration change in the room was obtained using the mass balance equation. The total mean emission rate ( $q$ ) between the beginning and the end of the source emission was then calculated.

Assuming homogeneous particle number concentration ( $\text{cm}^{-3}$ ) in the room, no particle emission source (after the generation), and no condensation or coagulation process, the concentration at a given size followed an exponential decay (figure 1).

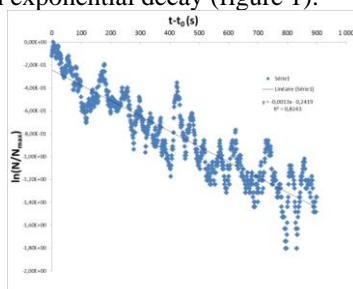


Figure 1: Particle decay during one trial conducted in the classroom

Using the particle decay curve (figure 1),  $k$  was obtained experimentally. Table 1 shows the purification rates obtained for 3 different trials conducted with “ $22 \mu\text{m}$ ” droplets.

Table 1. Purification rates ( $k$ ). Estimation of the mean emission rate ( $q$ ) in the classroom

Trials	Theoretical purification rate ( $\text{s}^{-1}$ )	Measured purification rate ( $\text{s}^{-1}$ )	Emission rate ( $\text{s}^{-1}$ )
1	0.00090	0.00133	$3.91 \times 10^4$
2	0.00086	0.00134	$5.56 \times 10^4$
3	0.00081	0.00128	$2.80 \times 10^4$

The measured purification rates systematically overestimate the theoretical purification rates. However, these differences were not exceeded 40%. The mean emission rate was ( $4.09 \times 10^4$ )  $\text{s}^{-1}$  and  $M_{mes}$  was in a range 2.2-5.9 mg. In the case of the generation of « $22 \mu\text{m}$ » droplets, the results showed that the mean transfer coefficient from the source to the surface ( $\tau_s = 1.4 \pm 0.3$  %) was 10 times higher than the mean transfer coefficient from the source to air ( $\tau_{skc} = 0.23 \pm 0.12$  %). We observed the same tendency for the generation of « $40 \mu\text{m}$ » droplets, with  $\tau_s = (2.1 \pm 1.3$  %) and  $\tau_{skc} = (0.07 \pm 0.03$  %) respectively.

Using a fluorescent-tracer based technique, the size distribution of the droplet residues (dry fluorescein) was studied and showed that it was possible to determine the transfer coefficients of droplets to surface as well as the transfer coefficient to air efficiently. This study was conducted in the frame of the French national research program on air-quality entitled “Study of Environmental determinants of viral exposure”, and funded by the French Ministry of Ecology, Sustainable Development and Energy.

### References

- Chen, C., Lin, C.H., Jiang, Z., Chen, Q. (2014). *Indoor Air Journal* **24**, 580–591.
- Da, G., Géhin, E., Ben-Othmane, M., Havet, M., Sollicc, C., Motzkus, C. (2015) *Environ Sci Pollut Res Int* **22**, 4873-80.
- Nicas, M., Nazaroff, W.W. and Hubbard, A. (2005) *J Occup Environ Hyg* **2**, 143-154
- Xie, X., Li, Y., Sun, H.Q and Liu, L. (2009). *Journal of the Royal Society Interface* **6**, 703-714.

## **Abstracts T412**

## Advanced air ventilation strategy based on predicted indoor particulate matter level for underground subway station

Soon-Bark Kwon<sup>1,2\*</sup>, Minhae Kim<sup>1,2</sup>, Sechan Park<sup>1,2</sup>, Hyeong-Gyu Namgung<sup>1</sup>, Tae-Suk Oh<sup>3</sup>

<sup>1</sup>Railway System Engineering, University of Science and Technology (UST), Uiwang, 16105 Korea

<sup>2</sup>Transportation Environmental Research Team, Korea Railroad Research Institute (KRII), Uiwang, 16105 Korea

<sup>3</sup>Seoul Metro Urban Railway R&D Center, Seoul, Korea

Keywords: air ventilation strategy, particulate matter (PM), subway station, underground, IAQ

Presenting author email: sbkwon@krii.re.kr

We have monitored indoor air quality of six selected underground subway stations and presented a multivariate correlation between measured variables (Kwon et al., 2015) and prediction method using artificial neural network (ANN) model (Park et al., 2016). Based on our previous results, prediction of particulate matters less than 10  $\mu\text{m}$  ( $\text{PM}_{10}$ ) was enabled using input variables of public-open data such as outdoor air pollution, traffic information and etc. which can be downloaded from governmental website. In this study, we validated the prediction model using measured data set of one subway station (Nov 2016 to Jan 2017) and conducted air ventilation simulation based on the validated model.

Multi-regression model and ANN model were adopted to predict the indoor  $\text{PM}_{10}$  and correlations of 0.894 and 0.858 were obtained compared to measured data as shown in Figure 1.

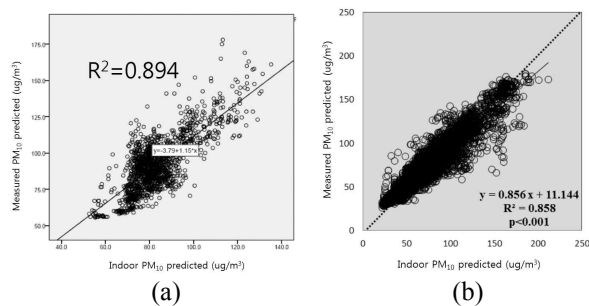


Fig 1. Correlation analysis between predicted and measure  $\text{PM}_{10}$  by (a) multi-regression model and (b) ANN method.

Based on indoor  $\text{PM}_{10}$  prediction model, we set up ventilation strategy keeping  $\text{PM}_{10}$  level of underground station maintained under the regal regulation or target level. Air ventilation strategy initiated by comparing predicted indoor  $\text{PM}_{10}$  with the regal regulation (150  $\mu\text{g}/\text{m}^3$ ) or management target level (100  $\mu\text{g}/\text{m}^3$  or less). At second step, predicted outdoor  $\text{PM}_{10}$  was compared to determine air introduction or not (i.e., supplying fresh air only when lower  $\text{PM}_{10}$  than indoor). We also considered indoor  $\text{CO}_2$  level not to over the regal regulation value of 1,000 ppm. Total of 8 ventilation steps including NV(normal vent), EV(eco vent), ZV(zero vent), and RC(recirculation) modes. Figure 2 shows the time-dependent air ventilation modes applied to one day of Jan 2017. We tried 3 different strategies depending on target  $\text{PM}_{10}$  value, i.e., enforced outdoor standard (50  $\mu\text{g}/\text{m}^3$ ),

current standards, and enforced indoor standard (100  $\mu\text{g}/\text{m}^3$ ) and found efficient ventilation method depending on outdoor and indoor  $\text{PM}_{10}$  level. In addition, energy consumption was calculated for different ventilation strategy.

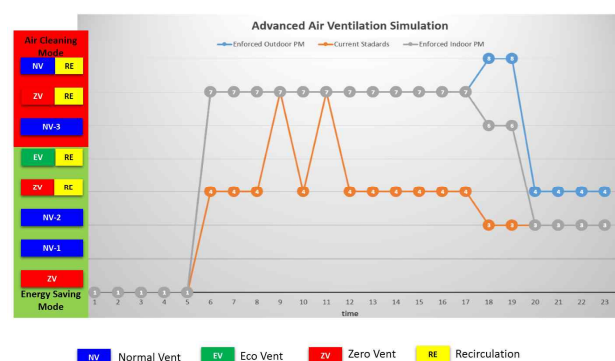


Fig 2. Air ventilation strategies and time-dependent simulation for underground station based on predicted  $\text{PM}_{10}$  level.

This work was supported by the Railway Technology Development Program (16RTRPB067918-04) funded Korea Ministry of Land, Infrastructure and Transport (MOLIT).

Kwon, S.-B., Jeong, W., Park, D., Kim, K., Cho, K. (2015) *Journal of Hazardous Materials*. 297 295-303

Park, S., Kim, M., Kim, M., Namgung, H., Kim, K., Cho, K., Kwon, S.-B. (2016) *Journal of Hazardous Materials*. Submitted

## Particle indoor to outdoor ratio separated into chemical components in an occupied residence

Y. Omelekhina<sup>1,2</sup>, A. Eriksson<sup>1,3</sup>, P.T. Nilsson<sup>1</sup>, J. Pagels<sup>1</sup>, and A. Wierzbicka<sup>1</sup>

<sup>1</sup>Ergonomics and Aerosol Technology, Lund University, 221 00, Lund, Sweden

<sup>2</sup>Department of Environmental Technology, Kaunas University of Technology, 442 49, Kaunas, Lithuania

<sup>3</sup>Nuclear Physics Department, Lund University, 221 00, Lund, Sweden

Keywords: AMS, chemical composition, I/O ratio

Presenting author email: aneta.wierzbicka@design.lth.se

### Introduction

Considering that on average in developed countries we spend about 65% of our time in private homes, understanding the exposures in homes is of utmost importance. Aerosol concentrations indoors come from indoor sources, infiltrate from outdoors and can be formed from precursors both of indoor and outdoor origin. Several characteristics and processes influence the properties of aerosols indoors, among them: active indoor sources (presence of occupants), outdoor aerosol characteristics, change of chemical composition upon infiltration (from outdoors to indoors), size dependent penetration from outdoors, ventilation, tightness of the building envelope and deposition (Morawska et al., 2013). In this study, we aimed to investigate the differences in chemical composition between aerosols indoors and outdoors. We report preliminary results for 14-days period.

### Methods

Indoor and outdoor measurements were performed in an occupied residence in Malmö, Sweden. The residence was naturally ventilated four-bedroom apartment (117 m<sup>2</sup>), located in a three-store concrete building surrounded by a green zone.

Time-of-Flight Aerosol Mass Spectrometer (AMS, DeCarlo et al., 2006) was used to measure particle mass loadings and size-resolved mass distributions of indoor and outdoor organic, sulphate and nitrate. Automatically switching valve alternated between indoor and outdoor lines with the time resolution of 20 and 10 minutes, respectively. Both sampling lines were mounted at the ground floor level and led to the basement where the aerosol was dried and measured by AMS. Calculated residence time of the particles in line was 1.5 minutes. Indoor sampling line was heated and insulated, additional carrier flow was used to lower the residence time.

### Conclusions

Indoor to outdoor (I/O) ratios were calculated to investigate differences in chemical composition of particles inside and outside. I/O ratio for organics accounted to 5.6, for nitrate 0.2, for sulphate 0.5, and for ammonium 0.2.

The I/O ratio for organic species was high due to the contribution from indoor sources. Figure 1, illustrates elevated particle mass concentrations during occupancy period when cooking activities took

place such as – frying and baking, followed by candle burning. During non-occupancy period organics loadings were low indoors - a few µg/m<sup>3</sup>.

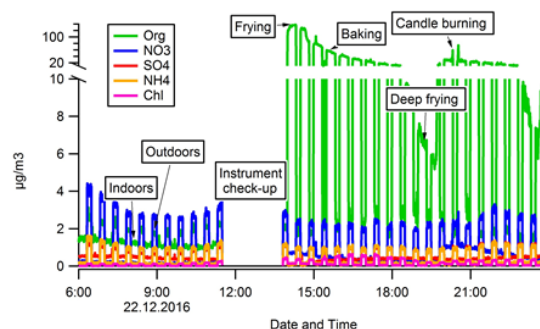


Figure 1. Aerosol mass concentrations during non-occupancy (6:00-11:00) and occupancy (14:00-24:00) periods inside and outside of the residence.

The nitrate I/O ratio was the lowest because of its evaporation indoors i.e. dissociation of ammonium nitrate particles into gases (nitric acid and ammonia) due to higher temperature and lower relative humidity compared to outdoors. The weather conditions varied during the measurement period with T outdoors from -8.8 to 9.7 °C and RH from 32 to 100 %. Indoors, T ranged from 20.2 to 25 °C and RH from 19 to 63 %. Low value I/O ratio for non-volatile sulphate can be explained by dominating outdoor sources and reflects reduced infiltration.

In general, the differences in chemical composition of particles found indoors and outdoors becomes apparent from the results. Levels of organics in indoor environments were mainly influenced by indoor sources, thus these should not be neglected when considering possible health effects.

This work was financed by the Swedish Research Council FORMAS (Project Dnr 942-2015-1029)

Morawska, L. (2013) *Indoor aerosols: from Personal exposure to risk assessment. Indoor Air*, **23**, 462–487.

DeCarlo, P.F., (2006). *Field-Deployable, High - Resolution, Time-of-Flight Aerosol Mass Spectrometer. Anal. Chem.* **78**, 8281-8289.

## O/I aerosol particle transformation

J. Ondráček<sup>1</sup>, N. Talbot<sup>1</sup>, L. Kubelová<sup>1,2</sup>, O. Makeš<sup>1,2</sup>, M. Cusack<sup>1</sup>, J. Schwarz<sup>1</sup>, P. Vodička<sup>1</sup>, N. Zíková<sup>1</sup>, V. Ždímal<sup>1</sup>

<sup>1</sup>Institute of Chemical Process Fundamentals of the CAS, Prague, 165 02, Czech Republic

<sup>2</sup>Department of Environmental Studies, Faculty of Science, Charles University, Prague, 128 43, Czech Republic

Keywords: I/O, aerosol transformation, size distribution, chemical composition.

Presenting author email: ondracek@icpf.cas.cz

In developed countries, people typically spend over 80% of their daily time indoors (Leung and Drakaki, 2015). Therefore, the adverse health effects are strongly correlated with the exposure to indoor particles (Hussein et al., 2006). The indoor environment is usually highly influenced by the indoor sources (cooking, smoking, heating). Nevertheless, the indoor aerosol size and composition follow that outdoors in the absence of indoor sources. While penetrating indoors, the originally outdoor particles may undergo several physical and chemical changes.

We have conducted two indoor/outdoor campaigns in an unoccupied apartment during summer and winter. One of the aims of these measurements was to assess the changes to aerosol particles during and after their migration from outdoors to indoors. Aerosol number size distribution as well as chemical composition was measured indoors and outdoors to obtain I/O ratios. From these ratios, changes in particle size and physicochemical characteristics indoors could be identified in relation to the chemical composition outdoors, as well as physical parameters such as wind speed, temperature, and RH.

The measurement was conducted in an empty apartment in the campus of the Institute of Chemical Process Fundamentals during summer 2014 (from 16<sup>th</sup> August to 8<sup>th</sup> September and during winter 2015 (from 5<sup>th</sup> to 24<sup>th</sup> February). The instruments were located in one of the bedrooms, while kitchen was designated as an indoor sampling room. The measurement was performed using the same length of tubing for indoor and outdoor sampling. Switching between indoor and outdoor was accomplished using automated electromagnetic valve. The set of the instruments included SMPS (3936, TSI), c-TOF AMS (Aerodyne Research), field EC/OC analyser (Sunset Laboratory), Berner Low Pressure Impactor (Hauke) and Low Volume Samplers. The measurement set-up allowed for analysis of size distribution and chemical composition with relatively high time resolution – sampling of the online instruments was set to 5 minutes, and at the same time detailed chemical analysis using the integral samples from BLPI and LVS. The measurement was complemented using meteorological data from monitoring station of Czech Hydrometeorological Institute located inside the campus of ICPF as well. The data analysis included only periods when no indoor sources were present. Also different ventilation scenarios were included in this study (windows and door closed, microventilation, windows and door closed with running offline instruments in the sampling room).

The overall PNCs for summer and winter were

similar despite seasonal differences in sources and sinks acting to increase and reduce PNC during specific periods of the day. Size-resolved PNC exemplified these differences, exhibiting afternoon increases during summer (secondary organic aerosol and NPF) and early evening increases (home heating and low mixing layers) during winter. Indoors, a dominant broad mode between 70 and 100 nm was found. Smaller modes were considerably less defined indoors than outdoors, which was attributed to the ultrafine particles diffusing onto building surfaces.

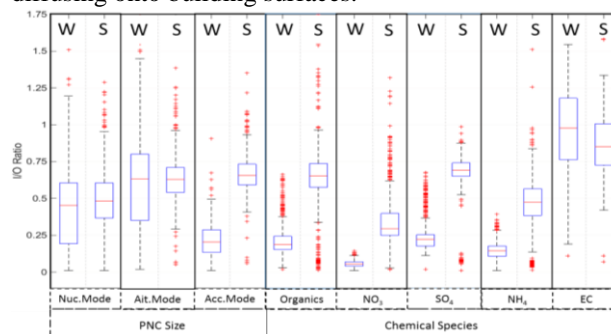


Figure 1. I/O ratio for PNC (SMPS) and PM<sub>1</sub> chemical composition (AMS and EC/OC); W - winter, S - summer; red line - median, the box - 25<sup>th</sup> and 75<sup>th</sup> percentiles; whiskers - 5<sup>th</sup> and 95<sup>th</sup> percentiles; crosses - outliers.

A substantial reduction in indoor mass concentration was observed for all aerosol chemical species during the winter phase of the study, which could not be fully accounted for particle drying. A decrease in I/O ratios of between 34–38% for all of the species during the winter was attributed to physical factors affecting all species rather than chemical processes acting upon each chemical species individually. The analysis of the data using Spearman rank statistical tests identified negative correlation of wind speed with indoor concentrations for all the species.

This work was supported by the European Union Seventh Framework Programme (FP7/2007–2013) under grant agreement No 315760 HEXACOMM, by European Union's Horizon 2020 research and innovation programme under grant agreement No 654109 and by Ministry of Education, Youth and Sports of the Czech Republic under grant agreement No LM2015037.

Hussein, T., Glytsos, T., Ondráček, J., Dohányosová, P., Ždímal, V., Hämeri, K., Lazaridis, M., Smolík, J. and Kulmala, M. (2006) *Atmos. Environ.* **40**, 4285–4307.  
Leung, D.Y.C. and Drakaki, E. (2015). *Front. Environ. Sci.* **2**, 1–7.

## Indoor to outdoor ratio of black carbon concentrations in occupied residences

A. Wierzbicka<sup>1</sup>, S. Lucciola<sup>2</sup>, Y. Omelekhina<sup>3</sup>, P.T Nilsson<sup>1</sup> and A. Gudmundsson<sup>1</sup>

<sup>1</sup>Ergonomics and Aerosol Technology, Lund University, Lund, 221 00, Sweden

<sup>2</sup>Department of Mechanical Engineering, University of Cassino and Southern Lazio, Cassino, 43 03043, Italy

<sup>3</sup>Department of Environmental Technology, Kaunas University of Technology, 442 49, Kaunas, Lithuania

Keywords: EC, indoor air quality, outdoor pollution

Presenting author email: aneta.wierzbicka@design.lth.se

Epidemiological studies confirm association of negative health effects with exposure to black carbon (BC). BC is also of concern as a carrier of chemicals to human lungs due to large surface area and adsorption properties. BC is emitted from variety of combustion sources that originate from both outdoors (e.g. diesel exhaust) and indoors (e.g. candles burning, cooking) (Isaxon, et al 2015). Pollution control measures focus mainly on outdoor concentrations whereas control of indoor levels seem to be neglected despite the fact that we spend on average 90% of our time in indoor environments. The aim of this study was to assess the differences in BC concentrations inside and outside occupied residences during weeklong real time measurements in four residences.

BC concentrations were measured simultaneously indoors and outside of four occupied residences using two microAeth<sup>®</sup> AE51 (AethLabs, USA) instruments. Measurements inside and outside lasted at least seven consecutive days in each residence. MicroAeth<sup>®</sup> AE51 enables real-time measurements of BC with 1 min resolution. MicroAeth<sup>®</sup> measures the transmission of infrared (IR) light (880 nm) through the aerosol sample collected on a filter filter. The accumulation of particles on the filter over time increases the absorbance, which is calculated relative to a reference cell. The attenuation IR is then transferred to mass concentration of black carbon (Cheng and Lin, 2013). Preliminary results from four residences are presented here. Residences comprised: one mechanically ventilated apartment, one naturally ventilated apartment, and two detached single family houses with natural ventilation. All residences were placed in urban area in southern Sweden.

Indoor to outdoor (I/O) ratios were used to compare differences in concentrations of BC in occupied residences. I/O ratios were calculated on the basis of average concentrations during the entire measurement period. I/O ratios of BC concentrations for studied residences ranged from 0.7 to 1.2. I/O ratio was greater than 1 only for one residence. Average I/O ratio for four residences was 0.8. The highest concentrations of BC were reached indoors accounting to 6.5 and 5.7  $\mu\text{g}/\text{m}^3$ , while maximum concentrations measured outdoors in the same residences reached 5.4 and 3.2  $\mu\text{g}/\text{m}^3$  respectively.

In Figure 1 differences between indoor and outdoor BC concentrations in one of the residences are presented. Higher peaks of BC indoors illustrate clear contribution of indoor sources to measured concentrations indoors, as these peaks do not coincide or show time-delayed pattern with concentrations outdoors. Time-delayed pattern is typically observed in naturally ventilated residences.

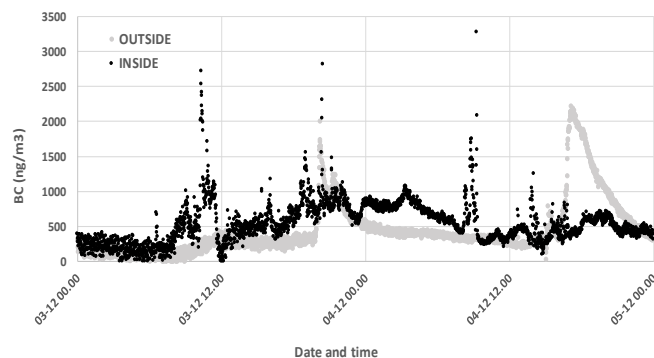


Figure 1. Differences in BC concentrations inside and outside of occupied residence.

In general, average concentrations of BC were lower indoors than outdoors with an exception for one residence where the opposite was observed. Lower concentrations indoors in comparison to outdoors suggest that control measures focused on outdoor pollution control measures should be the main way to minimise exposure indoors to BC. However, the analysis of time resolved data revealed clear and significant contribution of indoor sources to measured BC concentrations indoors, therefore measures to control emissions indoors should be also considered.

This work was financed by the Swedish Research Council FORMAS (Project Dnr 942-2015-1029).

Cheng, Y.-H., Lin, M.-H. (2013). *Aerosol Air Qual. Res.* 13, 1853-1863.

Isaxon, C., et al. (2015). *Atmospheric Environment*, 106, 458-466.

## **Abstracts T413**

## Prediction and quantification of emissions and workers exposure during ceramic industrial processes

C. Ribalta<sup>1</sup>, M. Viana<sup>1</sup>, M.C. Minguillón<sup>1</sup>, A. López-Lilao<sup>2</sup>, S. Estupiñá<sup>2</sup>, E. Monfort<sup>2</sup>

<sup>1</sup> Institute of Environmental Assessment and Water Research, Barcelona, 08034, Spain

<sup>2</sup> Instituto de Tecnología Cerámica, Castellón, 12006, Spain

Keywords: workers exposure, prediction of emissions, ceramic industry, dustiness.

Presenting author email: carla.ribalta@idaea.csic.es

Indoor air quality, especially in occupational environments, still suffers from major knowledge gaps despite humans spending most of our lifetime indoors. In general, industrial environments represent complex exposure scenarios difficult to standardize as there are a great variety of sources, materials and processes. The case of the ceramic sector is a potential case of study as during the manufacturing cycle (handling, materials preparation, bag filling, tiles production or cleaning processes, among others) a wide variety of powdered materials with different characteristics and chemical compositions are used. These materials can penetrate in the human respiratory tract with the possibility to cause respiratory-related illnesses.

In this regard, it is important to determine workers exposure as well as to understand particle emission patterns in order to establish efficient risk management measures with the final objective to reduce workplace exposure.

The main objectives of the present work are (1) to determine workers exposure to micro- and nano-sized particles in different processes of the ceramic industry with the final goal to contribute on workers exposure prevention (2) to assess the performance of standard laboratory-scale emission tests by comparison with real-world exposure measurements.

In order to achieve our objectives, workers exposure was assessed during different common processes in the ceramic industry: handling, milling and bag filling. The instrumentation used included: Condensation Particle Counter (CPC), DiSCmini, NanoScan, DUSTtrak, Optical particle counter (Grimm), and cassettes for particle collection for subsequent TEM analyses. The dustiness tests were carried out using the drop method.

Workers exposure during material milling with a pendular mill was assessed. Seven materials with different particle shape and size were studied and milling was carried out using low and high, usually used, energy conditions. Results of workers exposure to PM<sub>10</sub> are shown in Figure 1. Bars marked with an asterisk denote a statistically significant increase with respect to the background (BG) values for each material.

Relations between workers exposure, materials used and applied energy to the process were assessed. As shown in Fig.1 workers exposure to PM<sub>10</sub> can highly vary depending on the material used. Besides, for most of them, high energy conditions showed higher workers exposure than low energy conditions.

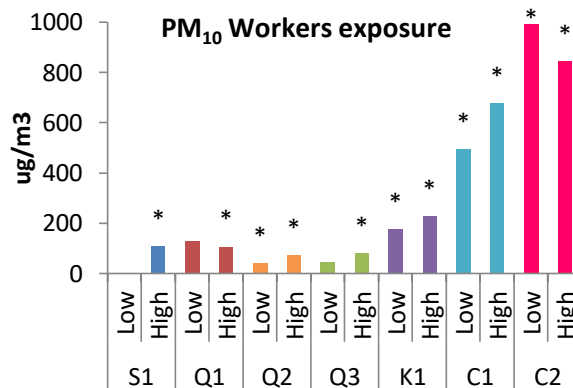


Figure 1. Workers exposure to PM<sub>10</sub> during a milling operation when using 7 different materials and with low and high energy milling conditions.

On the other side, in Figure 2, as an example, the inhalable fraction for the dustiness test of three of the studied materials is shown. Dustiness can increase or decrease after milling for a given material (López-Lilao *et al* 2016). Hence, in order to assess if the differences in the exposure levels can be justified by the dustiness of the processed material, relations of workers' exposure with dustiness laboratory test were assessed.

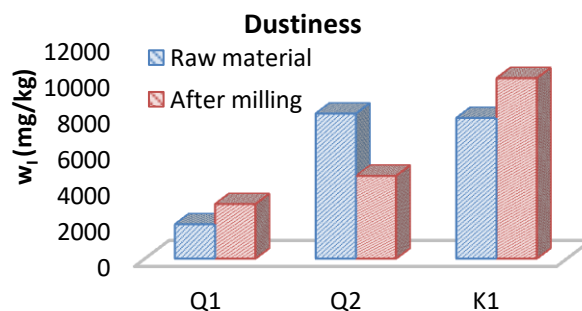


Figure 2. Dustiness test (inhalable fraction) for three of the studied materials before and after the milling process.

This work was supported by the Spanish Ministry of Science and Innovation CGL2015-66777-C2-1-R.

López-Lilao, A., Escrig, A., Orts, M.J., Mallol, G., Monfort, E. (2016) Journal of occupational and environmental hygiene 11, 817-828.

## Application of secondary nanoelectrospray ionization ultrahigh resolution mass spectrometry (nanoSESI-UHRMS) for detecting exhaled particles in real time

X. Li<sup>1,2</sup>, D.D. Jin<sup>1,2</sup> and L. Huang<sup>1,2</sup>

<sup>1</sup>Institute of Mass Spectrometer and Atmospheric Environment, Jinan University.

<sup>2</sup>Guangdong Provincial Engineering Research Center for on-line source apportionment system of air pollution.

Keywords: endogenous particles, exhaled breath, secondary electro spray ionization, ultrahigh resolution MS.

Presenting author email: tamylee@jnu.edu.cn

Exhaled particles in human breath (EBPs) has aroused increasing concern due to its potential in respiratory disease diagnosis, monitoring environmental exposure, *etc.* Up to now there are many analytical techniques reported for detecting the size and/or chemical composition of EBPs or condensate of EBPs (Löndahl *et al.*, 2014), which mainly include scanning or fast mobility particle sizer (DMPS, SMPS and FMPS), optical particle counter (OPC), condensation nuclei counter (CNC), time-of-flight secondary ion mass spectrometry (TOF-SIMS), inductively coupled plasma mass spectrometry (ICP-MS) and high performance liquid chromatography mass spectrometry (HPLC-MS). Recently, the online real-time detection of submicrometer aerosol particles by using extractive/secondary electro spray ionization mass spectrometry has been successfully demonstrated over the range of 3–600  $\mu\text{g}/\text{m}^3$  by Gallimore and Kalberer (2013).

In this study, the application of a secondary nanoelectrospray ionization source coupled with a ultrahigh resolution ( $R$  120,000–140,000) mass spectrometer (nanoSESI-UHRMS) for the facile detection of EBPs was tentatively explored. Four non-smoking healthy subjects with normal lung function participated in the experiments. The subject inhaled room air and the exhaled breath sample was delivered to the nanoSESI source (Figure 1).

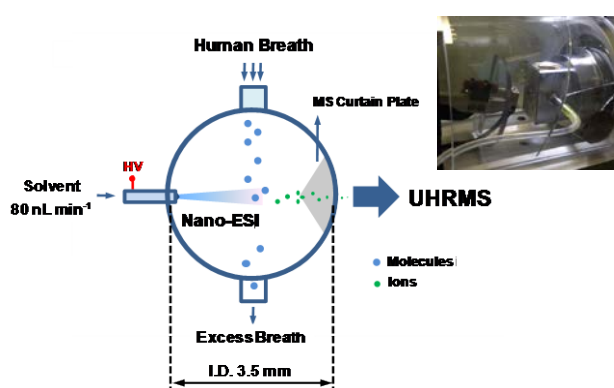


Figure 1. Schematic of nanoSESI source; insert shows the photo of the source.

Non-volatile species such as silicate ( $m/z$  94.9798) and phosphate ( $m/z$  96.9687) were found for all four subjects (Figure 2) (Li *et al.*, 2016), and they are very likely from the EBPs rather than the gas phase. One of sources of these EPBs is related with the rupture of a liquid bridge of the lung lining fluid during the

reopening of a collapsed terminal airway. In addition, there was an increasing trend in signal intensity during each single breath for both silicate and phosphate. This may be because the ratio of smaller particles in the exhaled breath increases during the exhalation. Moreover, several organic acids have also been observed, including  $m/z$  227.2010 (C14:0),  $m/z$  213.1853 (C13:0) and  $m/z$  199.1696 (C12:0) while an increase was present for  $m/z$  185.1381 (C10:0)  $m/z$  171.1381 (C10:0),  $m/z$  157.1223 (C9:0),  $m/z$  143.1066 (C8:0).

In the follow-up work, the method will be further investigated with more subjects involved, in order to have a better understanding of the detection of EBPs.

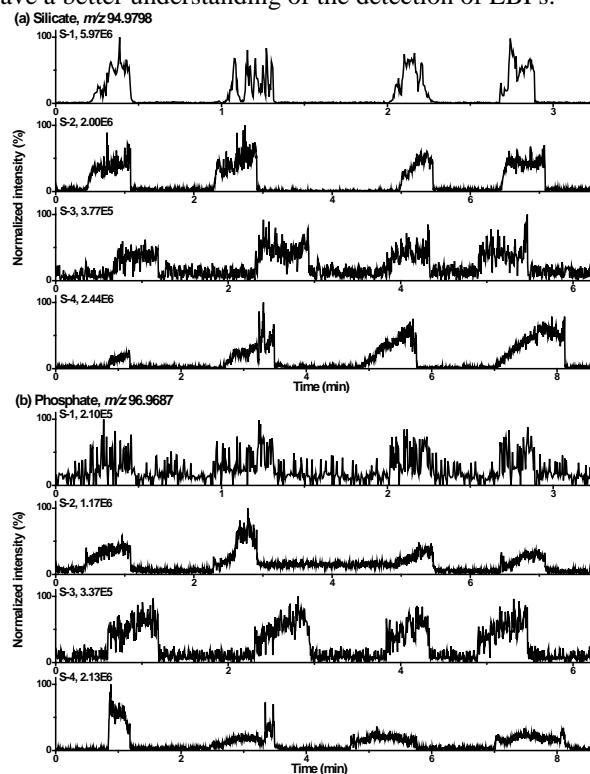


Figure 2. Four replicate detection of (a) silicate and (b) phosphate in exhaled breath of four subjects (S-1–S-4).

This work was supported by the National Natural Science Foundation of China (No. 91543117).

Gallimore, P.J., Kalberer, M. (2013) *Environ. Sci. Technol.* **47**, 7324–7331.

Löndahl, J., Möller, W., Pagels, J.H., *et al.* (2014) *J. Aerosol Med. Pulm. Drug Deliv.* **4**, 229–254.

Li, X., Huang, L., Zhu, H., *et al.* (2016) *Rapid. Commun. Mass Spectrom.* **31**, 301–308.

## Aerosol Monitoring for a Rapid Detection of the Respirator Performance Failure

S.A. Grinshpun, J. Corey, B. Wu, M. Yermakov, Y. Liu

<sup>1</sup>Center for Health-Related Aerosol Studies, University of Cincinnati, Cincinnati, Ohio, USA

Keywords: bioaerosol, combustion, neutralization, exposure time.

Presenting author email: sergey.grinshpun@uc.edu

Some elastomeric respirators (e.g., half-mask and full-mask) are designed to provide a high protection level, which translates to a rather low penetration, P (often  $P < 1\%$ ). The integrity of a respirator seal or filter cartridge may be compromised during actual use (e.g., when a respirator is worn by workers engaged in strenuous activity). Currently, there are no methods available to monitor possible leakage in real time and alert the respirator wearer at a workplace when the seal has been breached. In this effort, we developed and evaluated a novel low-cost wearable Respirator Seal Integrity Monitor (ReSIM), which is capable of rapidly detecting the respirator performance failure at a workplace. The main idea behind this development is that super-micrometer particles, which are present in most of occupational air environments, are too large to penetrate inside a properly working elastomeric respirator in measurable quantities (earlier studies showed  $P < 0.01\%$  for these particles) while their penetration would increase substantially if the seal fails.

The ReSIM prototype developed in this pilot study utilized an aerosol particle sensor (PPD60PV-T2, Shinyei, Kobe, Japan). Modifications were made towards developing the detection and enumeration capabilities for aerosol particles inside an operating respirator. The most important modification is the inclusion of an air pump to replace the PPD60PV-T2's built in resistor to heat air for convective flow. The prototype was exposed to different aerosol compositions and concentrations. Super-micrometer monodisperse Polystyrene Latex (PSL) microspheres as well as sub-micrometer NaCl particles were generated by a Collision nebulizer; sub-micrometer combustion particles were also generated by a burning wood stick. These three were used as challenge aerosols. An optical dust monitor (1.108, Grimm Technologies Inc., Ainring, Germany) was used in parallel to the tested sensor to assess the speed of the sensor's response, functional sensitivity and accuracy. The latter are important for testing the ReSIM on a respirator-wearing manikin in an exposure chamber to ensure that the ReSIM does not interfere with the respirator function and adequately detects a variety of seal failures. The aerosol concentrations were monitored inside and outside the respirator to examine the sensor response to different intermittent controlled seal failures.

The ReSIM was shown to provide reasonable responsiveness to super-micrometer PSL particles and sub-micrometer combustion particles. Figure 1 presents a lab calibration of the PPD60PV-T2 for particles of  $0.5 - 1.6 \mu\text{m}$  based on average readings taken at 30-s intervals. A linear fit with an  $R^2 = 0.7925$  was obtained between data generated by the ReSIM and the Grimm

monitor. Observations from calibration and other testing point to noise and unreliable detection at levels below  $500 \text{ particles/cm}^3$ . The response speed of the sensor is very high, but limited by the need to average particle detection time over an interval to generate a stable result.

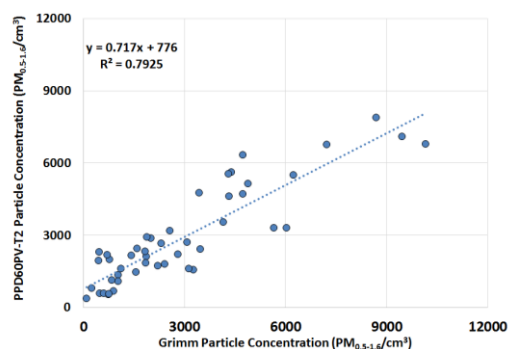


Figure 1. PPD60PV-T2 vs. Grimm monitor.

The ReSIM was connected to an elastomeric respirator with a solenoid control valve simulating a leak. Figure 2 shows the concentration as measured with the sensor (red line) and a rolling average concentration (green line) calculated while ignoring intervals with detected leaks. Across the top of the chart are purple diamonds for correctly detected leaks, blue triangles for correctly detected lack of leaks, a red square indicating incorrect leak detections and brown circles for undetected leaks. Across multiple tests, the ReSIM has correctly identified 101/105 intervals with good seals and 28/32 intervals with leaks.

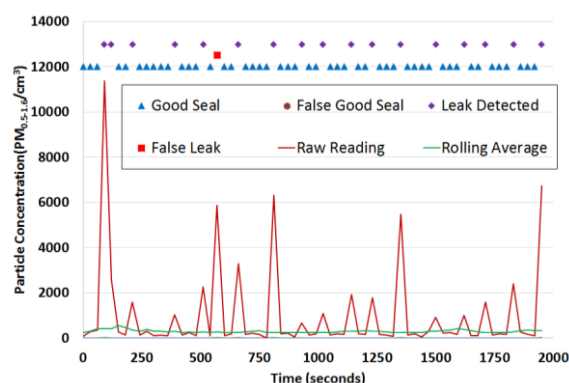


Figure 2. Preliminary PPD60PV-T2 leak detection results.

To conclude, the ReSIM does not interfere with the respirator function and can adequately detect various seal failures in real time. This in-respirator aerosol monitor allows alerting a wearer in case of a sudden increase in inhalation exposure due to the seal failure.

This research was funded by the Ohio Bureau of Workers Compensation.

## Energy efficiency, comfort and indoor air quality in ClimACT schools

S.M. Almeida<sup>1</sup>, V. Manteigas<sup>1</sup>, J. Lage<sup>1</sup>, M.Almeida-Silva<sup>1</sup>, N.Canha<sup>1</sup>, C. Pina<sup>1</sup>, C. Mafra<sup>2</sup>, R. Rato<sup>2</sup>

<sup>1</sup>Centro de Ciências e Tecnologias Nucleares (C<sup>2</sup>TN), Instituto Superior Técnico, Universidade de Lisboa, Estrada Nacional 10, ao km 139.7, 2695-066 Bobadela-LRS, Portugal

<sup>2</sup>Instituto de Soldadura e Qualidade, Av. Prof. Dr. Cavaco Silva, nº 33, 2740-120 Porto Salvo, Portugal

Keywords: Indoor air quality, comfort, energy efficiency, schools  
Presenting author email: smarta@ctn.tecnico.ulisboa.pt

The application of energy efficiency and indoor air quality measures in the schools' buildings is fundamental. Educational sector's buildings consume a significant amount of the total energy consumed across Europe. They represent more than 12% of the consumption of the tertiary building sector accounting for an estimated 15Mtoe annually. Energy bills are typically the second largest expenditure category for schools. Therefore it is imperative for schools to reduce energy-related expenditures, but without affecting students' health, comfort and performance. Children spend most of their time indoors, and a great part is at the school. Beyond the fact that children are particularly vulnerable to indoor air pollution, scientific evidence shows that exposure to poor indoor air quality can cause or contribute towards short and long-term health problems including asthma, allergic reactions and respiratory tract infections and reduce the productivity (Annesi-Maesano et al., 2013; Daisey et al., 2003).

The main objective of the Interreg Sudoe project ClimACT ([www.climact.net](http://www.climact.net)) is to promote the transition to a low carbon economy in schools. To this end, ClimACT is developing and implementing tools and methodologies to support schools managers and, not less important, students in the identification of intelligent solutions that consider energy efficiency, respect for the environment, private and external costs, financial support mechanisms and human behaviours. The ClimACT solutions are being validated in real-life conditions in 35 pilot schools from Portugal, Spain, France and Gibraltar.

This paper will present the work developed in six ClimACT schools located in Lisbon and Loures, where detailed Energy Audits were performed. Moreover, indoor air quality and comfort parameters were examined for the purpose of assessing levels of volatile organic compounds, aldehydes, PM2.5, PM10, CO<sub>2</sub>, CO, temperature and relative humidity and potential sources. Ventilation rates were derived from CO<sub>2</sub> (Canha et al., 2013).

The survey revealed the main parameters affecting the overall performance of the investigated buildings. The problematic building envelope, the improper control of heating and lighting systems, and the lack of interest concerning the efficiency of such buildings were the main factors in the reported efficiency. Despite the existing indoor air quality legislation in Portugal, results showed that it is rather difficult to achieve its requirements, especially those

regarding to CO<sub>2</sub> and PM10 concentrations, as the operating profile, the high occupation density, the lack of intelligent ventilation systems and controls and the occupants' behaviours, in most cases, complicate its practical application. Higher CO<sub>2</sub> levels were observed during students' activities inside the classrooms and lower concentrations were associated with the non-occupied periods. CO<sub>2</sub> average and maximum concentrations measured during occupancy were 2800 mg/m<sup>3</sup> and 12000 mg/m<sup>3</sup>, respectively. The observed values exceeded the CO<sub>2</sub> limit value established by the Portuguese Legislation (2250 mg/m<sup>3</sup>) indicating insufficient ventilation in classrooms. PM10 concentration during the occupied period varied between 3.0 and 430 µg/m<sup>3</sup> (average - 27 µg/m<sup>3</sup>) and frequently exceeded the national limit value for this pollutant (50 µg/m<sup>3</sup>). The ratio between PM10 concentrations measured during the occupied and non-occupied periods was 1.5 showing that occupancy, through re-suspension of previously deposited particles and possible particle generation, influences the indoor levels of airborne particles. The lowest PM10 concentrations (with an average of 18 µg/m<sup>3</sup>) were measured in the only building dedicated to higher education which is also the only one to have HVAC systems with filtration of outside air.

After the evaluation of energy, comfort and indoor air quality performance, this work identified and evaluated a package of measures that promote sustainability to the schools, and ensure a comfortable and healthy environment for educational purposes.

This work was supported by the European Regional Development Fund (ERDF) through the Interreg Sudoe project ClimACT – Acting for the transition to a low carbon economy in schools – development of support tools (SOE1/P3/P0429). C<sup>2</sup>TN/IST authors gratefully acknowledge the Fundação para a Ciência e Tecnologia support to the UID/Multi/04349/2013 project.

Annesi-Maesano, I., Baiz, N., Banerjee, S., Rudnai, P., Rive, S. (2013) *Journal of Toxicology and Environmental Health-Part B-Critical Reviews* **16**, 491-550.

Daisey, J.M., Angell, W.J., Apte, M.G. (2003) *Indoor Air* **13**, 53-64.

Canha, N., Almeida, S.M., Freitas, M.C., Taubel, M., Hanninen, O. (2013) *Journal of Toxicology and Environmental Health-Part A-Current Issues* **76**, 400-408.

## Sampling and analysis of bitumen fumes: comparison of German and French methods

B. Sutter<sup>1</sup>, E. Pelletier<sup>1</sup>, M. Blaskowitz<sup>2</sup>, C. Ravera<sup>1</sup>, C. Stolze<sup>3</sup>, C. Reim<sup>4</sup>, E. Langlois<sup>1</sup>, D. Breuer<sup>2</sup>

<sup>1</sup>French National Research and Safety Institute for the Prevention of Occupational Accidents and Diseases (INRS), Vandoeuvre les Nancy Cedex, 54519, France

<sup>2</sup>Institute for Occupational Safety and Health of the German Social Accident Insurance (IFA), 53757 Sankt Augustin, Germany

<sup>3</sup>BG BAU - Berufsgenossenschaft der Bauwirtschaft, Gebersdorfer Straße 67 90449 Nürnberg

<sup>4</sup>BG BAU - Berufsgenossenschaft der Bauwirtschaft, Landsberger Straße 309 80687 München

Keywords: Bitumen, Fumes, Personal samplers, performances.

Presenting author email: benjamin.sutter@inrs.fr

In Europe, no consensus exists on a method that samples and analyses bitumen fumes on road constructions sites, essentially for historical and practices reasons. As the bitumen fumes are considered as semi-volatile aerosol, the particulate and vapours fractions have to be sampled simultaneously, due to the strong interaction between those two phases (Dragan et al. 2015). Thus, different samplers' design (GGP (Breuer 2008) vs 37 mm cassette + XAD-2 sorbent tube (INRS 2015), extraction solvents (tetrachloroethylene vs n-heptane), and analytical techniques (FT-IR vs GC-FID) were preconized leading to theoretically different results. Starting from that point, the Institute for Occupational Safety and Health of the German Social Accident Insurance (IFA) and the French National Research and Safety Institute for the Prevention of Occupational Accidents and Diseases (INRS) wanted to compare their methods to correlate them to each other.

The comparison study was conducted into two steps: laboratory and workplace assays. During the laboratory assays, a bitumen fume generation system developed at INRS (Sutter et al. 2016) was used to simultaneously expose 6 IFA and 6 INRS samplers to controlled fumes. Organic matter from bitumen fumes was analysed by the methods and the masse was determined on each collection substrates and compared. It was found that the GGP samples 9 % more fumes than the INRS system due to a better sampling efficiency of the inhalable fraction. Terchloroethylene extracted 9 % and 29 % more mass than the n-heptane did on filter and XAD-2 sorbent bed respectively. It was also highlighted that the sensitivity of the FT-IR and FID was different in function of the substrate analysed. This is a new fact that was not identified previously. But globally, when the masses quantified on filters and XAD-2 beds are summed giving the total organic mass concentration of fumes, there is a strong correlation between the methods.

Workplace assays confirmed the laboratory correlation between the methods even if dramatically different environmental conditions were encountered during those assays (Figure 1). Thus this equation:  $C_{IFA} = 1,7646 C_{INRS} \pm 0,39$  should be applied to convert IFA quantifications to INRS ones and vice versa.

This work confirmed, with laboratory and field assays, some observations on the sampling performances of the samplers used by the IFA n°6305-1 and INRS MetroPol M-2 methods. This work also identified different performances of the analytical methods in

function of the particulate or vapour fraction collected on the collection substrates. But considered globally, the total quantifications of the IFA and INRS methods were strongly correlated.

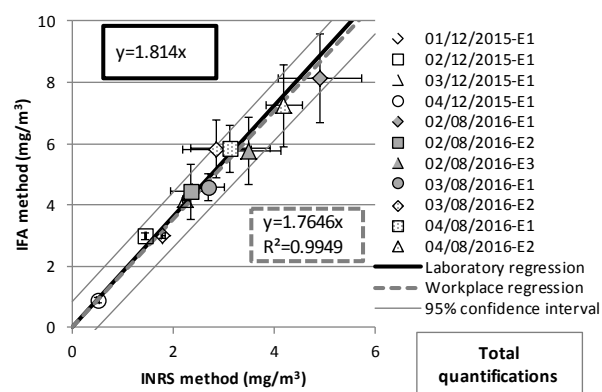


Figure 1. Comparison of the concentrations determined by IFA n°6305-1 and INRS MetroPol M-2 methods for field measurements.

- Breuer D. (2008) *Bitumen (Daempfe und Aeerosole, Mineralöl-Standard)*. BGIA Method 6305-1 Berlin, Erich Schmidt. BGIA Working Folder.
- Dragan GC, Breuer D, Blaskowitz M, Karg E, Schnelle-Kreis J, Arteaga-Salas JM, Nordsieck H, Zimmermann R. (2015) *An evaluation of the "GGP" personal samplers under semi-volatile aerosols: sampling losses and their implication on occupational risk assessment*. Environ Sci Process Impacts; vol. 17, p. 270-7; DOI: 10.1039/c4em00468j.
- INRS. (2015) *MetroPol method M-2 : Fumées de bitume par chromatographie en phase gazeuse - Bitumen fumes by gaseous chromatography*. DOI: 10.13140/RG.2.1.2017.9684.
- Sutter B, Pelletier E, Ravera C, Langlois E. (2016) *Performances of a Bitumen Fume and Condensate Generation System for Sampling Method Development*. Journal of Environmental Protection; vol. 07, p. 973-84; DOI: 10.4236/jep.2016.77086.

## Inhaled particle number concentration of subway users in Seoul, Korea

Minhae Kim<sup>1,2</sup>, Sechan Park<sup>1,2</sup>, Hyeong-Gyu Namgung<sup>2</sup>, Seung-won Ryu<sup>3</sup>, Chul-hoy Heo<sup>3</sup>, Myung-chul Jung<sup>3</sup> and Soon-Bark Kwon<sup>1,2\*</sup>

<sup>1</sup>Railway System Engineering, University of Science and Technology (UST), Uiwang, 16105 Korea

<sup>2</sup>Transportation Environmental Research Team, Korea Railroad Research Institute (KRRI), Uiwang, 16105 Korea

<sup>3</sup>Eum engineering Co., Seoul, Korea

Keywords: inhalation, particulate matter (PM), subway environment, exposure

Presenting author email: minhaekim@krri.re.kr

In order to evaluate the indoor air quality, both particle mass and number concentrations are used. Particle number concentration is dominated by the smallest particles, those which contribute nearly negligibly to particle mass concentration. While larger particles can be filtered out of inhaled air by nasal mucosa and upper airway, fine particles have been found all the way down to the bronchioles and alveoli (Londahl et al, 2006). It would be better to conduct an analysis using the particle number concentration instead of mass concentration when evaluating the relationship between particulate matter and health. The main objective of this paper is to initiate a profound shift in the ways of human body risk assessment of the subway users.

Two transfer stations in Seoul, Korea with the greatest number of users were selected for this study. We measured the particle number concentration according to particle size. The size and concentration of PM were monitored using an optical particle sizer (OPS; TSI, Model 3330, USA) and a Nanoscan SMPS (TSI, Model 3910, USA). Measurements were taken at four locations as the tester moved around: outdoors (A), the concourse (B), the platform (C) and inside the train (D) as shown in Figure 1.

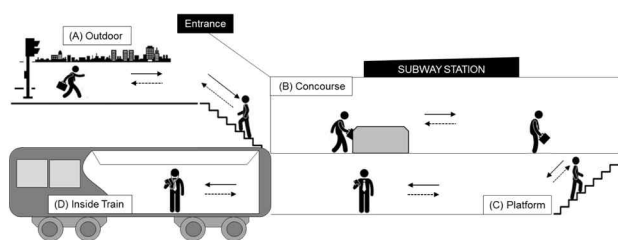


Figure 1. Route of subway users in this study

It should be pointed out that the analysis of inhaled PM number concentration and inhalation rate were used to assess the hazards to the health of subway users. This study used its own measurement results and the average inhalation rate of adults according to activity patterns (EPA, 2011). There was a marked contrast between the particles size  $0.3 \mu\text{m}$  or less and  $1 \sim 10 \mu\text{m}$ .

In case of particles size  $0.3 \mu\text{m}$  or less, 64% of them was inhaled at outdoor, 30% at concourse and 6% on the platform. For particles sized  $1 \sim 10 \mu\text{m}$ , most (59%) were inhaled in the train while only 23% were inhaled outdoors.

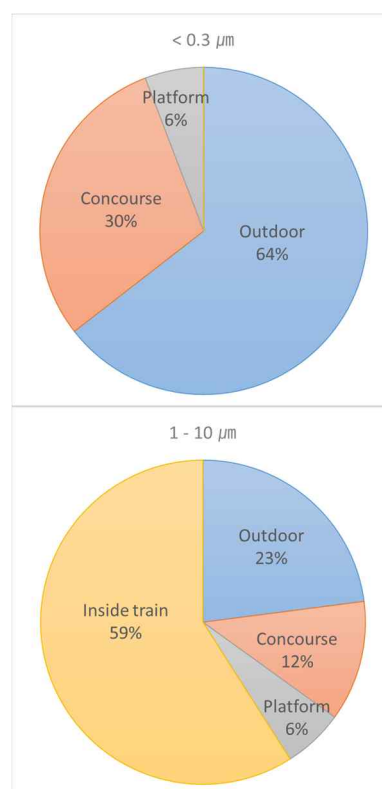


Figure 2. Location of inhaled particle number concentration ratio in two size groups; (a)  $0.3 \mu\text{m}$  or less and (b)  $1 \sim 10 \mu\text{m}$

This research was supported by a grant (16RTRP-B074139-04) from the Railway Technology R&D Program funded by Ministry of Land, Infrastructure and Transport of Korean government.

Londahl, J., Pagels, J., Swietlichi, E., Zhou, J., Ketzel, M., Massling, A., Bohgard, M. (2006) *Aerosol Science*. **37**, 1152-1163

U.S. EPA. (2011) Exposure Factors Handbook 2011 Edition (Final). U.S. Environmental Protection Agency, Washington, DC, EPA/600/R-09/052F

## Source measurements directional and distance evaluation

A.C.Ø. Jensen<sup>1</sup>, A.B. Blume<sup>1,2</sup>, M. Dal Maso<sup>3</sup>, O.J. Nielsen<sup>4</sup>, T. Rosenørn<sup>4</sup>, I.K.K. Koponen<sup>1</sup>

<sup>1</sup>The National Research Centre for the Working Environment, Copenhagen, 2100, Denmark

<sup>2</sup>Technical University of Denmark, Kgs. Lyngby, 2800, Denmark

<sup>3</sup>Tampere University of Technology, Tampere, FI-33101, Finland

<sup>4</sup>Department of Chemistry, University of Copenhagen, Copenhagen, 2100, Denmark

Keywords: Source measurements, Modelling, Chamber studies, aerosol dispersion, occupational health

Presenting author email: alj@nrcwe.dk

Near field/far field modelling of aerosol dispersions takes into account a source to determine the magnitude of the dispersion of aerosols. In occupational settings this source strength is often measured by aerosol instruments or estimated based on mass of material used and directly applied in the model (Koivisto *et al.*, 2014). However, if the measurement of the source is not considered carefully the output from the model can lead to wrong conclusions.

In occupational settings it is not always possible to make a direct on-line measurement of the source and determinations have to be made at a point removed from the direct source, while monitoring workers (Jensen *et al.*, 2015). We show here how position and distance from a source affects the particle concentrations, using TiO<sub>2</sub> dispersed by a brush particle generator. The source strength was monitored using FMPS, SMPS, CPC, and ELPI. The position of the source outlet was varied using seven different positions relative to the measurement position throughout the experiment.

Results show high dependability on the distance and direction of the source flow. Figure 1 shows the relative position on the X and Y axis of the source measurement point and the outlet of the brush generator which were always kept on the same Z axis plane. The total number concentration plot measured by the FMPS is shown in Figure 2. It shows that the concentration measured with the source directly below the measurement position and pointing towards the measurement inlet is around two orders of magnitude higher than for the source outlet pointing away from the measurement position when comparing maximum concentrations.

Using the source strengths for modelling of the indoor occupational concentrations and exposure assessment, leads to results that are different and depends on which of the source measurements is used. Using the lowest source strength concentration instead of the higher source concentrations, underestimates the

exposure and can lead to misleading conclusions when used in modelling. Therefore care should be taken when determining the source measurement position with respect to distance, orientation, and dilution between source and sampling point. In addition, the flow direction between the measurement point and the source outlet should be considered.

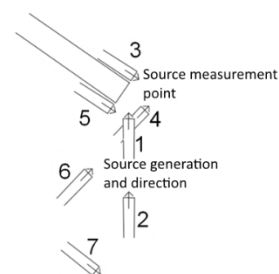


Figure 1, the seven source positions and direction compared to the source measurement point.

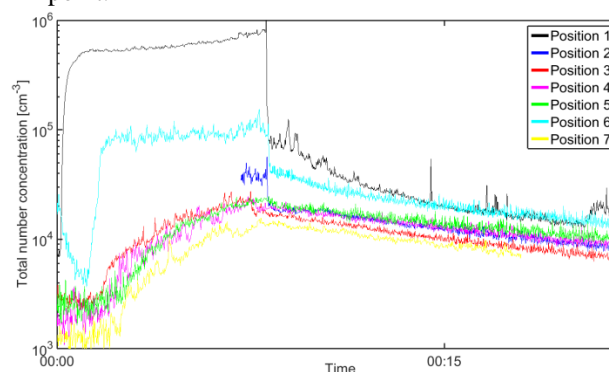


Figure 2, Total number concentrations as measured by the FMPS.

Koivisto, A.J., Jensen, A.C.Ø., Levin, M., Kling, K.I., Dal Maso, M., Nielsen, S.H., Jensen, K.A., and Koponen, I.K. (2014) *Environmental Science Processes & Impacts*, 17, 62-73.

Jensen, A.C.Ø., Levin, M., Koivisto, A.J., Saber, A.T., Kling, K.I., and Koponen, I.K. (2015) *Aerosol and Air Quality Research*, 15, 1906-1916.

## Comparative assessment of children's personal exposure to particle number concentrations at schools in Australia, Italy and Bhutan

L. Morawska<sup>1,\*</sup>, M. Mazaheri<sup>1,2</sup>, G. Buonanno<sup>3</sup>, S. Clifford<sup>1,4</sup>, F. Fuoco<sup>3</sup>, T. Wangchuk<sup>5</sup>

<sup>1</sup>International Laboratory for Air Quality and Health, Institute for Health and Biomedical Innovation, Queensland University of Technology, Brisbane, Australia

<sup>2</sup>Climate and Atmospheric Research, NSW Office of Environment and Heritage, Sydney, Australia

<sup>3</sup>University of Cassino and Southern Lazio, Cassino, Italy

<sup>4</sup>Mathematical Sciences School, Queensland University of Technology, Brisbane, Australia

<sup>5</sup>Department of Environmental Science, Sherubtse College, Royal University of Bhutan, Trashigang, Bhutan

Keywords: Ultrafine particles, personal exposure, school children, comparative assessment

Presenting author email: l.morawska@qut.edu.au

This work aimed to assess how different children's exposures at schools are in different countries. For this purpose, the measured children's personal exposure to ultrafine particle number concentration (PNC) during a school day was compared and apportioned according to the time spent in classrooms as a proportion of the total school-based exposure, and proportion of total daily exposure in two cities located in developed countries, Brisbane, Australia and Cassino, Italy, and rural areas of a developing country, Trashigang District in Bhutan. Brisbane and Cassino have similar sources of air pollution (traffic emissions) but different urban characteristics; Brisbane is spread over larger area but with lower population density than Cassino. Biomass burning is the main source of air pollution and PNC in rural Bhutan, with much lower population density, and traffic than Brisbane and Cassino.

The analysis incorporated time-series of school hours and total 24-hour PNC, along with the corresponding activity diary data and activity patterns for 118 school children in Australia, 49 in Italy and 46 in Bhutan. The proportion of children's daily exposure received inside the classroom during teaching times is given by  $p_{in} = \bar{c}_{in}t_{in} / \sum_{k \in D} \bar{c}_k t_k$ , where  $\bar{c}_{in}t_{in}$  correspond to the mean PNC in when in the classroom and time spent in the classroom,  $\bar{c}_k$  is the mean PNC during school hours only or total 24-hours and  $t_k$  is the corresponding amount of time spent,  $D$  (Buonanno et al., 2012, Mazaheri et al., 2014, Wangchuk et al., 2015).

The derived proportions of children's personal exposure in school classrooms during the school hours only and total 24 hours showed significant differences between the three study areas (Figure 1a,b).

Most of the students in Cassino spent almost the entire school time in the classrooms, resulting in the proportion of school exposure in the classroom being close to 1 (0.95). Students in Brisbane spent a significant part of the school day inside the classroom (0.69), but not the whole day, as in Cassino. By contrast, students in Bhutan spent only ~30% of their school time in the classroom, and hence their corresponding indoor exposure is much lower than that of children in Brisbane and Cassino (0.39) (Figure 1a). Exposure in classrooms as a proportion of total 24 hours was similar for children in Cassino and Brisbane, but slightly higher in Cassino. Bhutanese children were exposed to much higher ambient and home PNC than children in the two other cities, due to biomass burning for cooking and heating, which is why school indoor exposure as a proportion of daily exposure was the lowest (around 0.05) (Figure 1b).

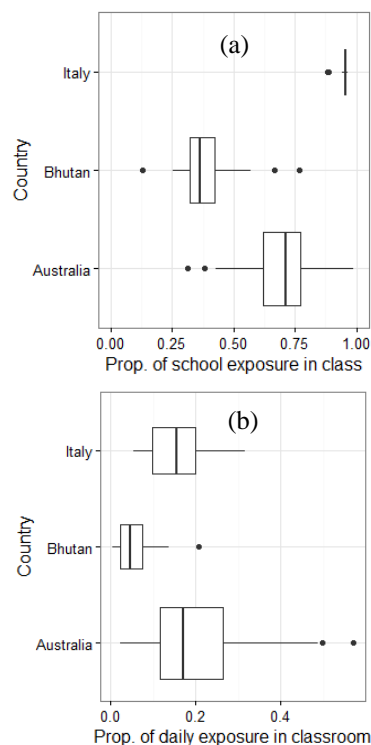


Figure 1. Boxplots of children's average personal exposure during school hours only (a) and the total 24 hours (b) in the three study areas.

The preliminary assessment of the results shows the notable differences between the PNC exposures that children receive in each country. The results have applications in exposure assessments to ultrafine particle concentrations and air quality management at schools.

This work was supported by the 2013 IHBI Collaborative Research Development Grant, ARC, QLD DTMR and QLD DETE (Linkage Grant LP0990134); Royal University of Bhutan (Grantno.RER/SCRG/2012/842).

Buonanno, G., S. Marini, L. Morawska and F. C. Fuoco (2012). *STOTEN* 438(0): 271-277.

Mazaheri, M., S. Clifford, R. Jayaratne, M. A. Megat Mokhtar, F. Fuoco, G. Buonanno and L. Morawska (2014). *Env Sci & Tech* 48(1): 113-120.

Wangchuk, T., M. Mazaheri, S. Clifford, M. R. Dudzinska, C. He, G. Buonanno and L. Morawska (2015). *Env Res* 140(0): 691-698.

## Assessment of traffic-related emissions on exposure to particles at schools

M. Mazaheri<sup>1,2,\*</sup>, C Reche<sup>3</sup>, I Rivas<sup>3,4</sup>, M Álvarez-Pedrerol<sup>4</sup>, M Viana<sup>3</sup>, A Alastuey<sup>3</sup>, J Sunyer<sup>4</sup>, L Crilley<sup>5</sup>, X Querol<sup>3</sup>, L Morawska<sup>2</sup>

<sup>1</sup>Climate and Atmospheric Research, NSW Office of Environment and Heritage, Sydney, Australia

<sup>2</sup>International Laboratory for Air Quality and Health, Institute for Health and Biomedical Innovation, Queensland University of Technology, Brisbane, Australia

<sup>3</sup>Institute of Environmental Assessment and Water Research, Spanish National Research Council, Barcelona, Spain

<sup>4</sup>Centre for Research in Environmental Epidemiology, Barcelona, Spain

<sup>5</sup>School of Geography, Earth and Environmental Sciences, University of Birmingham, Birmingham, UK

Keywords: ambient particles, schools, urban characteristics, high insulation regions

Presenting author email: mandana.mazaheri@environment.nsw.gov.au

This work presents a comparative assessment of the impact of local traffic on ambient particle number concentrations (PNC) at schools in Brisbane, Australia and Barcelona, Spain. The cities are of similar climate but differ in various urban characteristics.

We used the available measured times-series of ambient PNC, NO<sub>x</sub>, NO<sub>2</sub>, and elemental carbon (EC) during the Ultrafine Particles from Traffic Emissions and Children's Health: UPTECH project conducted at 25 primary schools ([www.qut.edu.au/research/research-projects/uptech](http://www.qut.edu.au/research/research-projects/uptech)) in Brisbane, Australia and BRain dEvelopment and Air polluTion ultrafine particles in scHool ChildrEn: BREATHE project conducted at 39 primary schools in Barcelona, Spain ([www.creal.cat/projectebreathe](http://www.creal.cat/projectebreathe)).

Particle exposure was defined as the hourly averaged PNC over 24 hours for each participating school. In order to compare the impact of traffic on ambient PNC at schools, average PNC during school hours were calculated along with corresponding NO<sub>x</sub> concentrations for the UPTECH and NO<sub>2</sub> concentrations for the BREATHE (NO<sub>2</sub> concentrations were not available for all the UPTECH schools). PNC, NO<sub>x</sub>, NO<sub>2</sub> and EC were used as proxies for traffic related emissions (Wang et al. 2013). Schools were then classified as high and low traffic; HT and LT. Full details on the method is described by (Mazaheri et al. 2016). Figure 1 presents PNC daily cycles at HT and LT in Brisbane and Barcelona, where high PNC were associated to peak traffic times in Barcelona, whereas peak PNC was during mid-day for Brisbane schools

Indicators of traffic related emissions (PNC and EC) PNC and EC at BREATHE schools were significantly higher than UPTECH. Average PNCs were significantly higher at high traffic school than the classified low traffic ones in Barcelona. The difference in PNCs between high and low traffic in Brisbane schools was not significant. The ratios of ambient PNC and EC at BREATHE to UPTECH for high traffic schools were 2.6 and 2.5, respectively. For low traffic schools, the PNC and EC ratios were 1.6 and 2.1, respectively.

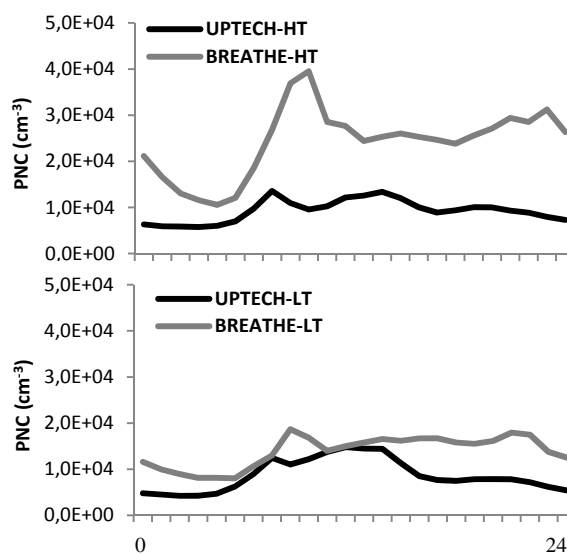


Figure 1. PNC daily cycles in HT and LT schools

These results demonstrate that the impact of local traffic on ambient particles was more pronounced in Barcelona than Brisbane. The differences between the HT schools and fractional analysis of the PNC daily cycles suggest that the main driver of the ambient PNC in Brisbane was a combination of background conditions as well as local and distant sources, rather than the immediate traffic, which was the case for Barcelona. We are now analysing the impacts of specific urban characteristics, to quantify their contribution in modifying local city PNC concentrations.

Mandana Mazaheri was supported by the 2015 Endeavour Fellowship, funded by Australian Government-Department of Education; UPTECH by the Australian Research Council Linkage Grant LP0990134; BREATHE by the European Research Council Advanced Grant 268479.

Wang, M., R. Beelen, X. Basagana, T. Becker, et al. (2013) *Environ Sci Tech* 47(9): 4357-4364.

Mazaheri, M., C. Reche, I. Rivas, L. R. Crilley, et al. (2016) *Env Int* 88: 142-149.

## **Abstracts T414**

## Hourly land-use regression model using data collected with low-cost PM monitors

Mauro Masiol<sup>1</sup>, Naděžda Zíková<sup>1,2</sup>, Andrea R. Ferro<sup>3</sup>, Philip K. Hopke<sup>1,4</sup>, David C. Chalupa,<sup>5</sup> David Q. Rich<sup>4</sup>

<sup>1</sup> Center for Air Resources Engineering and Science, Clarkson University, Potsdam, NY, United States

<sup>2</sup> Institute for Environmental Studies, Faculty of Science, Charles University, Prague, Czech Republic

<sup>3</sup> Dept. Civil and Environmental Engineering, Clarkson University, Potsdam, NY, United States

<sup>4</sup> Dept. of Public Health Sciences, University of Rochester Medical Center, Rochester, NY, United States

<sup>5</sup> Dept. of Environmental Medicine, University of Rochester Medical Center, Rochester, NY, United States

Presenting author email: philip\_hopke@urmc.rochester.edu

In U.S., air quality is monitored using fixed air quality stations operated in routine monitoring networks managed by state, local, and tribal agencies. Generally, one or few urban background stations are deployed within major cities and aim to: (i) assess the city wide air pollution for regulatory compliance purposes and (ii) estimate the average population exposure.

However, air pollution can exhibit high spatial and temporal variability within an urban area due to the locations and strengths of local sources, the population density, and effects of street canyons, complex terrain, urban heat island, and meteorology. Thus, the spatial and temporal coverage of common monitoring networks is likely insufficient to capture the variability required by accurate exposure and epidemiological studies.

The recent development of low-cost PM monitors provides the potential for increased the spatial/temporal resolution of urban air monitoring. Those monitors have sufficiently low prices that a large number of sampling points can be deployed over the urban area. However, low-cost monitors are not built to meet rigid performance standards of regulatory monitors. Most low-cost PM monitors are based on light scattering, i.e. they detect larger particles depending on the wavelength, and provide a signal indicative of the PM mass concentrations. As a consequence, they have known limitations (Holstius *et al*, 2014; Kumar *et al*, 2015). In addition, although the use of a large number of low-cost monitors may help with spatial and temporal resolution compared to conventional monitoring networks, small-scale variability of PM can still unmeasured.

Among the approaches available to model the local-scale, intra-urban air quality variations, land-use regression (LUR) models incorporate monitoring data at different locations across the study area with a set of predictor variables derived from geographic information systems (GIS). Predictors may include the location and density of potential sources, traffic distributions, population density, land use, physical geography and climate.

This study aims to model the urban-scale variability of PM across the Monroe County, New York, and takes advantage of the synergy between the application of advanced LUR models and spatially resolved PM data measured with low-cost monitors. The ambient concentration of PM was measured at 23 sites using low-cost monitors (Airviz Inc. Speck<sup>TM</sup>) during the 2015/16 heating season (Dec-Mar). Data were handled according to the results of our prior evaluation studies

with reference instruments (Manikonda *et al*, 2016; Zíková *et al*, 2017) to provide a robust, reliable dataset with 1 h time resolution. Corrected data were then used as part of the input for a deletion/substitution/addition LUR approach (Su *et al*, 2015). Raster surfaces were developed for a series of predictors potentially related to the PM levels, including number of bedroom, fireplaces, kitchens, property value, property year built, road type and railways densities, road traffic intensity, elevation and percent of various land cover data features. Circular buffers were calculated around the 23 sampling sites with radii ranging from 50 m to 5000 m (50 m steps) and predictor statistics were computed for each buffer. In addition, concentrations of common air pollutants (CO, NO, NO<sub>2</sub>, NO<sub>y</sub>, SO<sub>2</sub>, O<sub>3</sub>, PM<sub>2.5</sub>, BC, Delta-C) and weather variables (air temp., RH, pressure) measured at reference sites were included as independent variables.

Since PM levels may quickly change in time within urban areas, following traffic fluxes (e.g., rush hours), human habits (e.g., energy demand, need for domestic heating, etc.), meteorology, actinic fluxes, and mixing layer dynamics, the model was run over the whole dataset as well as over each hour of the day.

Preliminary results showed that the model is able to explain between 0.55 and 0.65 of the variances of the original datasets. Statistically significant predictors selected by the model changed during the hours of the day according to the more likely emission sources present in the study area.

This work was supported by the New York State Energy Research and Development Authority under agreement 63040.

Holstius, D.M., Pillarisetti, A., Smith, K. R., Seto, E. (2014) *Atmos. Meas. Tech.* **7**, 1121–1131.

Kumar, P., Morawska, L., Martani, C., Biskos, G., Neophytou, M., Di Sabatino, S. Britter, R. (2015) *Environ. Int.* **75**, 199–205.

Manikonda, A., Zíková, N., Hopke, P.K., Ferro, A.R. (2016) *J. Aerosol Sci.* **102**, 29–40.

Su, J.G., Hopke, P.K., Tian, Y., Baldwin, N., Thurston, S.W., Evans, K., Rich, D.Q. (2015) *Atmos. Environ.* **122**, 477–483.

Zíková, N., Hopke, P.K., Ferro, A.R. (2017) *J. Aerosol Sci.* **105**, 24–34.

## **Abstracts T417**

## Effect of the supply air supporting the shaping of exhaust air during processing of nanomaterials

T. Jankowski<sup>1</sup>

<sup>1</sup>Department of Chemical, Aerosol and Biological Hazards, Central Institute for Labour Protection – National Research Institute, 00-701 Warsaw, Poland

Keywords: nanoparticles, trace gases, grinding, ventilation

Presenting author email: tojan@ciop.pl

According to the Machinery Directive 2006/42/EC should be taken actions to eliminate or reduce the risk of air pollutants at source emissions. Elimination or reduction exposure to harmful dust generated in the production process it should be implemented through the use of effective devices for capture dust directly from the emission sources and air distribution to prevent the spread of pollutants in the workspace (Lee et al., 2007).

Local exhaust ventilation in the form of nozzles, hoods is the most effective way of ensuring good air quality in the workplace for example, the welding process or the processing of nanomaterials (ISO/TS 12901-2, 2014). The task of the local exhaust ventilation is to capture air pollutants directly at the source of the emission and prevent their spread in the working rooms. The key to high efficiency of capture of air pollutants is proper cooperation between local and general ventilation.

The article presents the results of studies which aim was to demonstrate the effect of the application of the supply air supporting the shaping of the exhaust air flow during the processing of stainless steel coated with (or without) a layer of silver nanoparticles nanomaterials. A study was performed in different variants of supporting of exhaust ventilation.

Table 1. Test configurations of emission source and ventilation.

Type of process	Speed	Size of abrasive material	Type of ventilation	Exhaust air flow rate
Dual disc grinder	1360 min <sup>-1</sup>	ø 250 mm	nozzle	224 ± 0.79 m <sup>3</sup> /h

Parameters enabling both assessment of pollutants emission from machines and assessment of working effectiveness of capture systems of pollutants are determined with the use of three measurement methods: smoke flow visualization, anemometric methods with using multipoint system of Testo thermo anemometers (Testo AG, Germany) and pollutants concentration methods (a spectrophotometer OPS meter model 3330 (TSI, USA) and condensation particle counter CPC model 3775 (TSI, USA).

The results of size distribution, number and mass concentrations of particles were compared with the results of velocity and turbulence intensity of the air surrounding the emission source using a supply and exhaust ventilation. The results of tests at different type of grinding are shown in figures 1, 2 and 3.

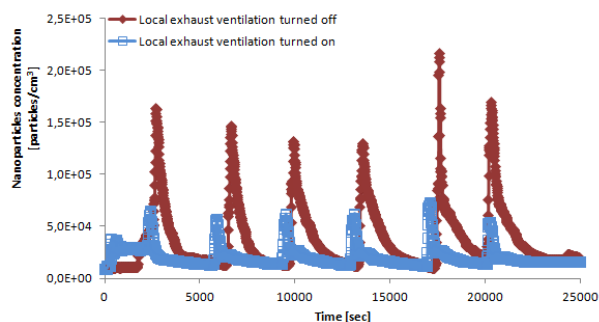


Figure 1. Number pollutant concentration carried out in machining of steel with and without nanoparticles.

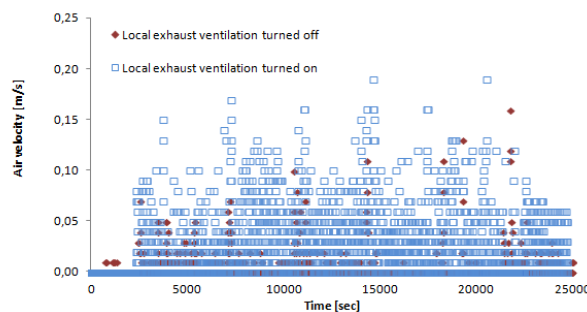


Figure 2. Air velocity distribution in the emission source.

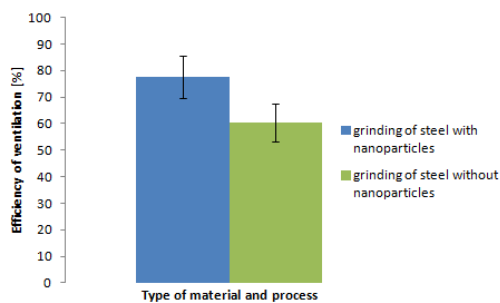


Figure 3. Comparison between efficiency ventilation of grinding of steel with and without nanoparticles.

This paper has been based on the results of a research task I-53/TSB carried out within the scope of the statutory activity of the Central Institute for Labour Protection – National Research Institute supported by the Ministry of Science and Higher Education.

Lee, M. and McClellan, W. (2007) *J. Nanopart. Res.*, 9, 127–136.

ISO/TS 12901-2:2014 Nanotechnologies — Occupational risk management applied to engineered nanomaterials. Part 2.

## Development of Cool and Clean Air Motorcycle Helmets

A.L. Jian<sup>1</sup>, S.H. Huang<sup>1</sup>, W.C. Lee<sup>2</sup>, Y.M. Kou<sup>3</sup>, and C.C. Chen<sup>2</sup>

<sup>1</sup>Institute of Occupational Medicine and Industrial Hygiene, National Taiwan University, Taipei, 10055, Taiwan

<sup>2</sup>Institute of Environmental Health, National Taiwan University, Taipei, 10055, Taiwan

<sup>3</sup>Department of Occupational Safety and Health, Chung Hwa University of Medical Technology, Tainan, Taiwan

Keywords: Aerosol filtration, PM<sub>2.5</sub>, Mobile source, Air supplied helmet.

Presenting author email: r05841001@ntu.edu.tw

According to a recent Taiwan EPA report, PM<sub>2.5</sub> concentration emitted from motorcycle tailpipes could exceed 730 µg/m<sup>3</sup>, depending on the brand and the model. When idling at traffic lights, motorcyclists could be exposed to PM<sub>2.5</sub> of up to 460 µg/m<sup>3</sup>. Motorcyclists are exposed to significantly higher PM<sub>2.5</sub> than others. The aim of this study was to design a full faced helmet (FFH) that provides clean air and cool temperature inside the helmet to decrease particle exposure and increase comfort for motorcyclists.

A commercial FFH was modified to generate cool and clean air in a way similar to the powered-air-purified-respirator commonly used in industrial settings. Three different clean air supply locations (A: upper rear of the head, B: zygomatic side, and C: lower chin) were designed in this study. A small wind tunnel was used to simulate the turbulence that motorcyclists might encounter while riding on the road. The operating parameters included: the supply air flow rate to the helmet (Q<sub>s</sub>), the velocity in the wind tunnel (U<sub>0</sub>) and breathing flow rate which is a combination of tidal volume (V<sub>t</sub>) and breathing frequency (f). To minimize infiltration of aerosol outside the helmet into the breathing zone, the FFH was tightly sealed with a windjammer or a long neckerchief. A condensation particle counter was used to measure particle number concentrations both inside (C<sub>in</sub>) and outside (C<sub>out</sub>) the FFH, where the measurements were used to calculate the protection factor (PF= C<sub>out</sub> / C<sub>in</sub>).

Results showed that the PF of the FFH increased with increasing Q<sub>s</sub>, but decreased with increasing wind speed and breathing flow rate. At breathing flow rate of 7.5 L/min with the FFH sealed using windjammer, PF increased from 1 to 500 as Q<sub>s</sub> increased from 0 to 50 L/min under calm air condition with air supply at location A. Meanwhile, the PF decreased from 500 to 3 when wind speed increased from calm air to 5 m/s. When Q<sub>s</sub> was 40 L/min, the particle concentration decreased by 96.6 % with air supply at location A (PF=29). For location B, the particle concentration decrease was 99.8 % (PF=514). There was 86.3 % reduction in particle concentration at location C (PF=7). Besides, the PF of the FFH increased with using a neckerchief that seals tightly around the neck. In addition, temperature decreased 3 °C when Q<sub>s</sub> was 93 L/min with air supply at location A.

In conclusion, applying a higher Q<sub>s</sub> and/or using an adjustable visor that sealed tightly around the neck would achieve a higher level of protection. This study demonstrated the feasibility of incorporating clean and cool air systems into the helmet. The designed Cool and Clean Air Motorcycle Helmet could decrease particle exposure, improve comfort of the helmet for motorcyclists. The by product is the stronger incentives to use full face helmet to improve the effectiveness of protection and safety.

This work was supported by the Ministry of Science and Technology, Taiwan under grant MOST 105-3011-F-002-008.

Lung, S.-C. (2006) *Epidemiology* 17(6), S54.

Yu, W.Y., Chen, C.Y., Chiu, W.T., Lin, M.R., (2011) *Int J Epidemiol* 40(3) 794-803.

Tan, F.L. and Fok S.C. (2006) *Applied Thermal Engineering* 26(17-18) 2067-2072.

## Investigation of nano-particle exposure by spray coating processes

U. Uhrner<sup>1</sup>, Q. Ye<sup>2</sup>, T. Nöst<sup>1</sup>, O. Tiedje<sup>2</sup>, P.J. Sturm<sup>1</sup> and J. Laloy

<sup>1</sup>Traffic & Environment, IVT, Graz University of Technology, Graz, 8010, Austria

<sup>2</sup>Department of coating systems and painting technology, Fraunhofer IPA, Stuttgart, 70569, Germany

<sup>3</sup>Department of Pharmacy, Namur Nanosafety Centre, Namur, 5000, Belgium

Keywords: manufactured nanomaterial, atomization, paint overspray, nano-particle exposure.

Presenting author email: uhrner@ivt.tugraz.at

The increasing application of manufactured nanomaterials (MNM) in industrial products requires knowledge about environmental and human safety. MNM are an important component of paint materials. In spray coating processes, a large fraction of paint overspray remains and may pose potential health risks.

Within the joint transnational research project (NanoGeCo) detailed investigations on the generation and fate of nanoparticles by atomization processes in spray coating are carried out. Finally, toxicological studies using a whole body exposure model will be carried out to evaluate the potential risk of human exposure. This work presents measurements of particle size distributions (PSD) and concentrations as well as chemical characterisation in paint overspray. Two different main paint materials, water borne and solvent borne paints, both with and without MNM were atomized using an industrial spray gun and different spray rates within a professional spray booth.

Two main arrangements of the spray target, spray direction and inlet positions were developed (Fig. 1). Overspray PSD were measured at various sampling positions using a Scanning Mobility Particle Sizer (SMPS) and in some experiments an Electrical Low Pressure Impactor (ELPI). In addition, a particle sampling system using impactors and small gold plates was developed for subsequent substance analysis by laser scanning microscopy (LSM) and scanning electron microscope (SEM) and energy dispersive x-ray spectroscopy (EDX).

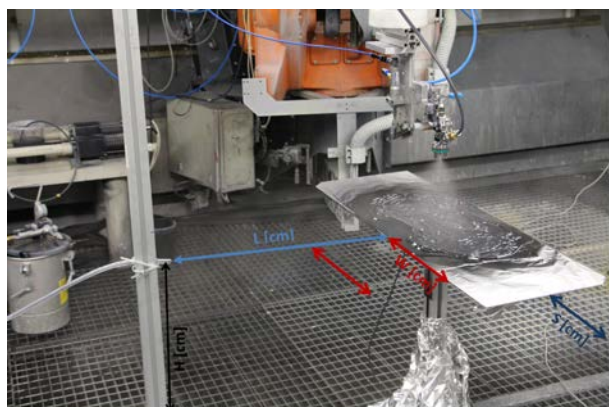


Figure 1. Arrangement of spray application and sampling position definition.

Based on numerous experiments we conclude that coatings are strong nano-particle sources. The main parameters impacting upon nano-particle exposures are

the dilution/ventilation conditions in spray booths and the paint type. High nano-particles concentrations were measured during atomization of solvent borne coatings (Fig 2, top). Over one order of magnitude lower concentrations were measured during atomization of water borne coatings (Fig 2, bottom). Further important parameters are the duration of the spray application and to a lesser extent the MNM within the paint matrix and the amount of paint sprayed. The measured size distributions and aerosol probe sampling and subsequent analysis by LSM and SEM/EDX indicate that high particle numbers due to MNM may be suppressed by solution within liquid phase larger sized nano-particles.

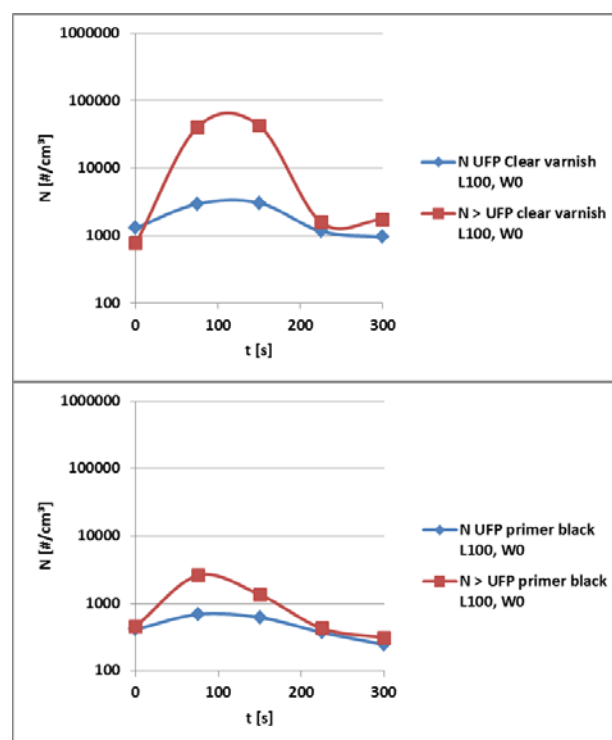


Figure 2. Time series for ultrafine number concentrations (N UFP blue line) and total number of particles in the range of 100 to 600 nm (N > UFP red line) for solvent borne coating (top) and water borne coating (bottom).

This work is supported by ERA-NET SIINN on “Safe Implementation of Innovative Nanoscience and Nanotechnology”.

## **Abstracts T501**

## **Long term aerosol aging under atmospherically relevant conditions in a CSTR-like aerosol tank.**

F. Friebel<sup>1</sup>, P. Lobo<sup>2</sup>, S.D. van Dusseldorp<sup>1</sup>, E. Mühlhofer<sup>1</sup>, and A. A. Mensah<sup>1</sup>

<sup>1</sup> ETH Zurich, Institute for Atmospheric and Climate Science, Zurich, Switzerland

<sup>2</sup> Center of Excellence for Aerospace Particulate Emissions Reduction Research, Missouri University of Science and Technology, Rolla, Missouri, USA

Keywords: CSTR, aerosol aging, soot aging, ambient conditions

Presenting author email: franz.friebel@env.ethz.ch

Aerosol particles which are emitted into the atmosphere are exposed to different reactants and therefore change their properties. The average atmospheric lifetime ranges from several hours to more than a week. Experimental approaches which investigate the occurring changes in aerosol particle properties should ideally cover this time scale. Generally, there are two approaches to achieve/mimic these time frames. One, the concentration of reactants, e.g. Ozone or OH-radicals can be increased to trigger faster reaction rates. Two, larger aerosol tanks can be constructed to extend the observation time. Both approaches imply their specific challenges. Treating aerosols with high concentrations of oxidants bears the risk that atmospheric processes are not represented well. Extending the observation time by extending the tank volume is often technically and financially limited.

Here we present a new concept which decouples long observation times from high chamber volumes thereby allowing for low reactants concentrations and low aerosol flows.

Generally, aerosol tanks get filled once and provide a flow of aged aerosol until the reservoir is exploited. In contrary to that, the CSTR-like aerosol tank is continuously filled with fresh aerosol and provides a constant sample flow over an unlimited time scale after the tank reached its steady state. The sample flow does not consist of uniform aerosol particles but aerosol particles at different aging stages. Nevertheless, statistical challenges in subsequent data analysis can be disentangled by incorporation of the well-defined aerosol age distribution.

In Summer 2016 we conducted a lab campaign at ETH Zurich successfully applying the CSTR-like aerosol tank concept. Size selected soot particles were exposed to different ozone concentrations (0-200 ppb) and different levels of humidity (0-80%) in a 3 m<sup>3</sup> stainless steel tank. The setup allowed observing changes in the CCN-activity of soot particles throughout an ageing period of up to 12 h.

## **Abstracts T502**

## Multilayer particle resuspension in a turbulent boundary layer

Sofia Eirini Chatoutsidou<sup>1</sup>, Yannis Drossinos<sup>2</sup> and Mihalis Lazaridis<sup>1</sup>

<sup>1</sup>School of Environmental Engineering, Technical University of Crete, 73100 Chania, Greece

<sup>2</sup>European Commission, Joint Research Centre (JRC), I-21027 Ispra (VA), Italy

Keywords: multilayer, resuspension, kinetics

Presenting author email: schatoutsidou@yahoo.gr

Multilayer particle resuspension involves particle detachment and suspension to the air from complex, multilayer, possibly fractal-like particle deposits. As such, resuspension depends strongly on the particle position within the layer, and thereby on the morphology of the deposit. Unlike monolayer resuspension, different kinetics apply at different layers thus the resuspension rate depends on the layer position.

The present model considered an idealized description of the deposit where  $k$  layers of identical particles were stacked on top of each other. The total number of particles was considered the same in each layer and interactions were assumed only between particles at different layers (inter-layer interactions): within-layer (intra-layer) interactions were neglected. Inter-layer interactions may be between particles or between particles and the surface. The fraction of remaining particles in each layer was determined using Friess and Yadigaroglu (2001) kinetics:

$$\frac{dp_i}{dt} = -Jp_i \text{ for } i = 1$$

$$\frac{dp_i}{dt} = -Jp_i \left[ 1 - \frac{p_{i-1}}{p_i} \right] \text{ for } i \geq 2$$

where,  $p_i$  is the fraction of remaining particles in layer  $i$  at time  $t$  and  $J$  is the single-particle resuspension rate constant.  $J$  was obtained by a kinetic force-balance approach for the bound particle (Chatoutsidou et al., 2016).

Figure 1 shows the fraction of particles remaining within different layers for the same single-particle resuspension rate  $J$  (only particle-particle interactions, no particle-surface interactions), but characterized by different kinetics. At low exposure times, the difference between the layers is significant as a result of the particle position within the deposit; however, as exposure time increases the fraction of remaining particles in all layers approaches a steady-state condition where resuspension occurs at a rate equal to  $J$ . Moreover, the results indicate that after  $10^3$  s exposure to the flow, all layers result at nearly the same remaining mass on the surface, where higher friction (removal force) is required to detach more particles.

The resuspension rate was evaluated using the fractional resuspension rate  $\Lambda(t)$ , i.e., the rate of decrease of the fraction of particles remaining within a layer. Figure 2 presents the evolution of  $\Lambda(t)$  for a 3-layer deposit. Accordingly, two regimes may be identified: a short-term regime ( $<10^{-2}$  s) characterized by different rates at different layers and a long-term regime ( $>10^{-2}$  s) where  $\Lambda(t)$  attains a similar value for all layers. The present results confirm the  $1/t$  power law in the long term regime, where  $\Lambda(t)$  decreases linearly with time. In

addition, in the short-term regime  $\Lambda(t)$  is lower for higher layer number (closest to the surface). This finding is directly associated with easier particle detachment from the top layer due to unobstructed space from above.

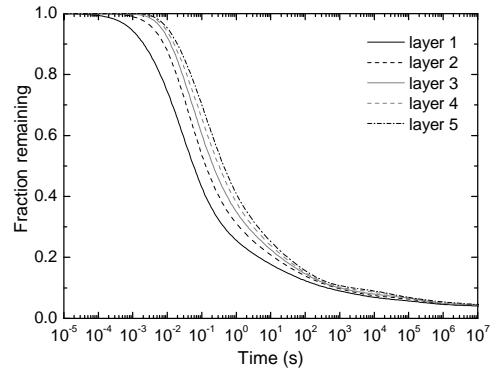


Figure 1: Fraction of particles remaining in the first 5 layers of a 6-layer deposit for  $50 \mu\text{m}$  stainless steel particles on a stainless steel surface at friction  $0.5 \text{ m/s}$ .

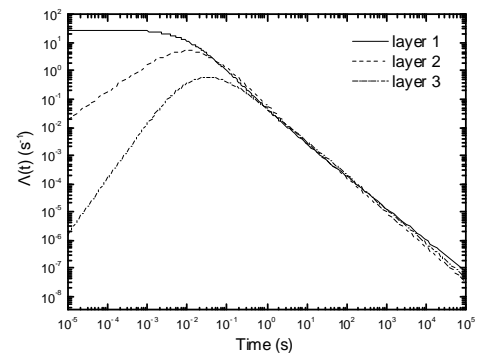


Figure 2: Fractional resuspension rate versus time for a three-layer deposit of  $50 \mu\text{m}$  stainless steel particles on a stainless steel surface at friction velocity  $0.5 \text{ m/s}$ .

The present study evaluated particle resuspension in multilayer deposits. Two regimes were identified: a short-term regime where different behavior was found as a result of the particle position in the deposit and a long-term regime where similar results were obtained for all layers.

This work was supported by the European Union 7<sup>th</sup> framework program HEXACOMM FP7/2007-2013 under grant agreement N° 315760.

Chatoutsidou, S.E., Drossinos, Y., Tørseth, K. and Lazaridis, M. (2016) *J. Adhes. Sci. Technol.* **31**, 817-843.  
 Friess, H. and Yadigaroglu, G. (2001) *Nucl. Sci. Eng* **138**, 161-176.

## **Sedimentation Effect of Finely Dispersed Aerosol in Tubes in Shock-Wave and Shock-Free Modes**

D.A. Gubaidullin, R.G. Zaripov and L.A. Tkachenko

Institute of Mechanics and Engineering, Kazan Science Center, Russian Academy of Sciences,  
Kazan, 420111, Russia

Keywords: aerosol, coagulation and sedimentation, drift particles, oscillations.  
Presenting author email: damirgubaidullin@gmail.com

In the present work, sedimentation of a finely dispersed aerosol and dynamics of particles are considered in tubes with various geometry on the end near to resonant frequencies.

Experimental investigations of oscillations of aerosol were carried out for different length of tubes in a shock-wave mode ( $\Delta P \sim 0.1$  bar), in a shock-free wave mode ( $\Delta P \sim 0.01$  bar) and at the transition to shock-wave mode ( $\Delta P \sim 0.04$  bar) near to subharmonic and fundamental resonances. Di-ethyl-hexyl-sebacate  $C_{26}H_{50}O_4$  was used as the working fluid to generate aerosol. The majority of droplets have the geometric diameter  $0.863 \mu m$ . Number concentration of drops for all experiments monotonously decreases in due to course and with growth of the excitation frequency. In the case of a closed tube, this process is defined by the coagulation of aerosol and sedimentation of droplets on the tube walls. In an open tube, the discharge of aerosol to the environment is observed in addition to the coagulation of aerosol and sedimentation of droplets on the tube walls. It has been found that a decrease in the tube length and increase of the amplitude of displacement piston, result in a decrease in the sedimentation time of aerosol. The dependences of sedimentation time of aerosol on the excitation frequency have non-monotonic character with a minimum on a resonance both in open and in the closed tubes. It is established, that presence of a flange slows down process of the aerosol sedimentation. Reduction of internal diameter of a flange to increase in a sedimentation time of aerosol which attains the maximum value for a case of a closed tube. In so doing, the sedimentation time of aerosol in the case of an open tube is reduced by a factor of two and more compared to this time in a closed tube. The sedimentation time of the aerosol in the closed tube at the shock-free mode and in the transition to shock-wave mode (for small amplitudes of displacement piston) is up to 5 times less, than at a natural sedimentation. In an open tube, natural sedimentation lasts up to 12 times more slowly, than in the shock-free mode and lasts up to 18 times more slowly than in the transition to shock-wave mode. The sedimentation time of the aerosol differs by 1.5 times in the shock-free mode and at the transition to shock-wave mode with almost identical exaltation amplitude.

To study the mechanism of coagulation of the aerosol and the forces acting on the droplets and particles of aerosol in the wave field in the tube, the dynamics of single particles is considered. Dynamics of a single particle with various physical and geometrical

parameters is experimentally investigated at the longitudinal oscillations gas in closed and open tubes in a shock-wave mode. Along an axis of a tube the particle moves from the closed (open) end to the piston, near to a wall – to the return side, making longitudinal oscillations with increase in the oscillations swing that is caused by acoustic streaming. In a radial direction, the oscillating particle moves from an axis to a wall of the tube up to a boundary point. Outside of a tube, the particle moves from the open end to an exterior wave field practically without oscillations with nonlinear increase of coordinate from time. It is revealed, that the increase in lengths of a tube and excitation frequency of gas in up to - resonant modes gives in growth of an oscillations swing of a particle and increase of its average velocity. Nonmonotonic character for dependence of oscillations swing and average velocity of a spherical particle from excitation frequency of gas is detected. At approach to a resonance oscillations swing and average velocity are incremented, attain the maximum value on a resonance frequency and decrease behind a resonance. Effect of a weight and diameter of a particle on its oscillations swing and average velocity is investigated. Shift of a curve maximum for dependence of a particle average velocity from oscillation frequency aside magnifications of frequency is shown at increase of a weight or diameter of a particle.

The process of the particle drift over time in different sections of the tube and the external wave field at different frequencies and amplitudes of excitation of the gas in the shock-free wave mode is experimentally investigated. A particle placed near the open end of tube begins to move to the piston under the influence of the internal wave field. Its oscillating motion with amplitude and frequency is significantly lower than amplitude and frequency of oscillations of the gas due to friction of the fishing line and the weight of the particle. The particle is placed outside the tube close to the open end moves in an external wave field. Noticeable oscillations of a particle were not observed. Dependence of distance on time is linear. Increase the amplitude of excitation of the gas increases the amplitude of oscillations and average velocity of the particle. The position of the particle, placed inside the tube in the vicinity of the open end, wherein the particle oscillates harmonically with no drift in any direction along the axis is revealed.

The study was performed by a grant from the Russian Science Foundation (project No.15-11-10016).

## The liquid phase aerosol particle evaporation under the dry gas blow

M.P. Anisimov<sup>1,3,4</sup>, V.I. Terekhov<sup>2</sup>, P.K. Hopke<sup>1,3</sup> and N.E. Shishkin<sup>1,2</sup>

<sup>1</sup>Aerosol Technologies Laboratory, Novosibirsk State Technical University, Novosibirsk, 630073, Russia.

<sup>2</sup>Institute of Thermophysics, Siberian Branch of the Russian Academy of Sciences, Novosibirsk, 630090, Russia

<sup>3</sup>Clarkson University, Potsdam, 13699, USA.

<sup>4</sup>Nanoaerosol Research Lab, Technological Design Institute of Scientific Instrument Engineer, Siberian Branch of the Russian Academy of Sciences, Novosibirsk, 630058, Russia.

Keywords: liquid aerosol, particle evaporation, nucleation rate, binary liquid.

Presenting author email: anisimovmp@mail.ru

It was shown by the multiple and systematic researches, that temperature of the liquid aerosol particle surfaces for the various liquids are non-uniform [1, 2 et al.]. The non-uniform surface temperatures are resulted by the internal droplet processes which are independent in some interval of the blowing gas velocities. We did not found in the scientific literature the reason for the non-uniform temperature distribution on the droplet surfaces. The thermographic measurements show that non-uniform temperature distribution on the droplets surfaces is initiated by the spontaneous local centers of the vapor nucleation which can be seen as dots with the decreased temperatures. Set up was created in the present research for the empirical vapor nucleation studies on the evaporated droplets which were hooked within the dry gas flow. The boiling centres number and their appearance dynamics were detected by the infrared imager under brand Thermo Tracer TH7102MV. A transition to a steady state regime can be detected for a single droplet, when near the same number of the boiling centres can be seen per the unit of time within a range of the monitoring system view. The vapor nucleation rates were measured for the droplets of various single liquids and some water solutions.

A driving force is appeared to reach a vapor-liquid equilibrium when a droplet is blown by the dry gas. The liquid evaporation process gets stronger when vapor is removing from the near droplet vicinity. The fields of fluctuations are appeared on the droplet surface and the local boiling (or vapor production) can be seen time to time. Boiling makes the local cooling, from other side, due the evaporation heat consumption from surroundings. A thermal imaging reveals easily the areas with decreased temperature on a droplet surface. These areas can be attributed to the boiling events in the liquid under investigation.

The droplets by diameters from 1.5 to 2 mm were hanged within the dry or low saturated gas flow. Gas (air) was saturated by water vapor less than 2 % in case of water droplets research. The air flow velocity was in the interval from 1 to 5 m/s and temperature ~ 20 0C in that case. The basic elements of the research set-up are shown in Fig. 1. The temperature distributions on the evaporated droplet surfaces of water and water solutions were measured using thermography. The temperature measurements accuracy was not less 0,2 °C. Digital presentation of the object image gives the ability to define quantitatively the droplet size and its volume drifts against the time. The integral evaporation intensity on the liquid – vapor interfacial surface as well as heat-

mass transfer coefficients along the interfacial boundary were calculated using the droplet volume drifts against the time. Details of the data development is presented in article [1]. A regular shape of droplets is presented on the thermographic images shown in Fig. 2. The droplets surface temperature image was varicoloured as a rule.

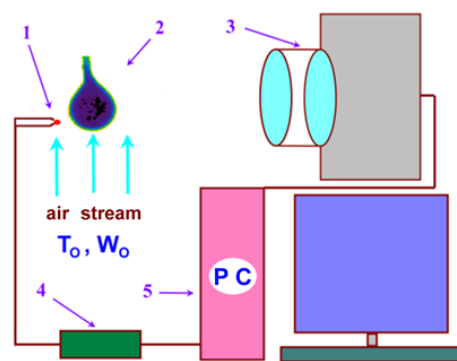


Figure 1. Schematic presentation of the system for a droplet evaporation monitoring.

1 – a thermocouple; 2 – the hooked droplet of a tested liquid; 3 – an infrared imager with a microscope attachment; 4 – a thermocouple signal digitizer and an intermediate memory set; 5 – Computer.

The temperature stains are appeared spontaneously. The water droplets with the time scale step of 5 second are shown in Fig. 2. It can be seen the considerable temperature irregularity even for not too far ranged points. The droplet surface temperatures at the nearly located crosses are different considerably.

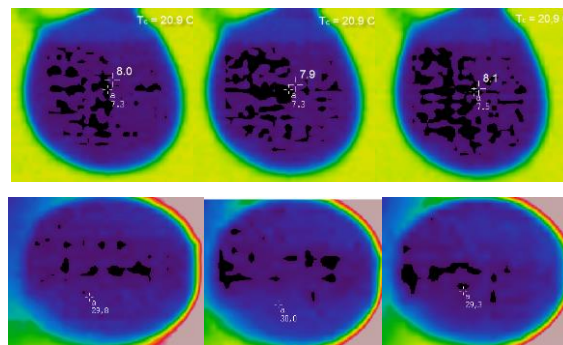


Figure 2. The water droplet images with 5 sec. time interval each other.

The gas-flow temperatures are equal to 20,9 °C (upper level) and 80 °C (down one).

The temperature distribution on the droplet surfaces of acetone, methanol, ethanol and their water solutions were approximately the same. The evaporation intensity was characterized by the droplet diameters changing and it is presented in Fig. 3. The air flow velocity was near 1.5 m/s under temperature 23°C. The bigger quantity of ethanol leads more intensive droplet evaporation as can be seen in Fig. 3.

The measuring system had no ability a single boiling event monitoring, due that the number of the boiling events was defined by the decreased temperature areas on the thermal imaging pictures of a droplet.

It seems intuitively that all boiling events are generated at the upper layer of each droplet. The dipper levels of droplet are smoothing the geometrical and thermodynamic disturbances in the upper level. The special evaluations of the radial temperature gradients were not provided on the present stage of research. The boiling centre distribution was assumed uniform along the droplet surfaces. As the nucleation volume the droplet cover, where the nucleation events can be well detected by infrared imager, is taken.

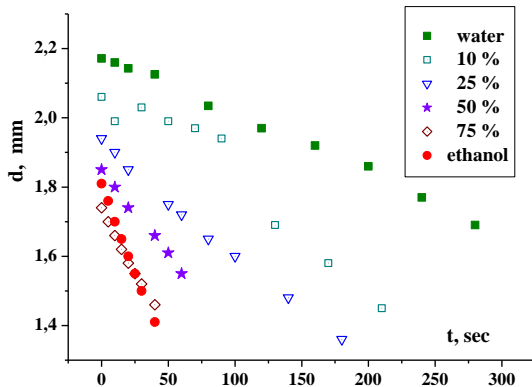


Figure 3. The droplet's diameters (d) variation on time (t) for the water – ethanol solutions.

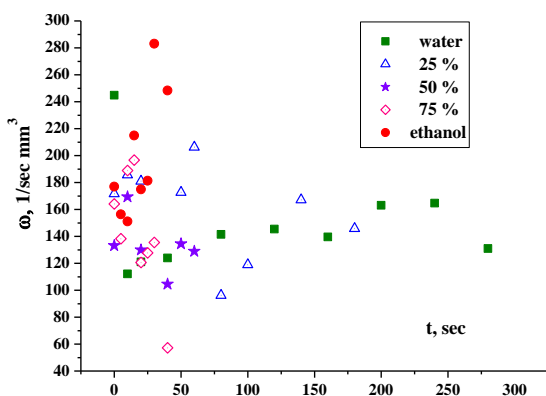


Figure 4. The liquid nucleation rates,  $\omega$ , on time (t) for water-ethanol systems.

An equation  $\omega = N \cdot k / (\tau \cdot V)$  was taken for the nucleation rate calculation, where  $\omega$  is the nucleation rate (i. e. the number of nucleation events per unit volume per unit time). Number of nucleation events was defined for the part of the droplet image (field of vision), which was exposed by an infrared imager with a microscope

attachment in the time interval  $\tau = 0,25$  sec.  $k$  is shape factor to calculate the total number of the nucleation events along the whole droplet surface. A field of vision is less than total droplet surface, thus its value is more than unity.  $\tau^\circ$  is the time interval for a single image exposition.  $V$  is the boiling volume, which is equal to the droplet surface times the height of the droplet nucleating cover. We suppose that the height is equal to two image pixels approximately. We hope to get more accurate estimation of that height.

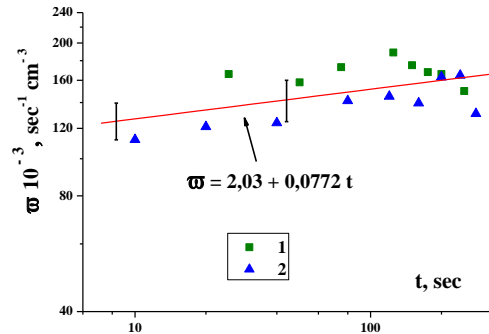


Figure 5. The boiling nucleation rate on the water droplet surface blown by dry air.

Red line is averaged data from two experimental sets.

Results of the droplet diameter and the nucleation rate measurements on the droplet surfaces are presented in Fig. 3 and Fig. 4. Relatively big standard deviation (10%) is the result of small statistics of the boiling events and subjective (operator dependent) fixation of the low temperature areas. We hope to get better statistics and objective (automatic) count of the nucleation event centers in future experiments.

The average nucleation rates for water droplets by diameter of  $\sim 2$  mm and the air velocity near 1.5 m/c at the nucleation temperature 24 °C is presented in Fig. 5 for two series of measurements. Standard deviation which was calculated jointly for both series is 10%. As one can see in Fig. 5. The nucleation rate is growing with time slightly. We think that these data have the qualitatively agreement with hand book [3]. It is known for the present time that the nucleation rate data collected from the different measuring systems have several orders of magnitude difference. For example data on the nucleation rates collected using the static and flow diffusion chamber [4] are deviated each other up to 3-4 orders of magnitude and the flow diffusion chamber data are deviating from the adiabatic expansion two-piston chamber results [5].

It is supposed, that suggested measuring scheme gives ability to measure the nucleation rate on the liquid droplets surfaces which can be blown by dry gas for the first time. The measuring scheme development has potential to create the new method for quantitative measurements of the liquid nucleation rate on the droplet surfaces which are located in the dry gas atmosphere. However it would be inconsistently to compare the nucleation rate data which a collected using the different measuring schemes. We need to find the consistent set of the axiomatic statements for the vapor – gas nucleation

to get the set-up independent data and then expend that experience for liquid and solid phase nucleation.

This work was supported by grant of the Russian Ministry of Science and Education under Contract № 14.Z50.31.0041 which is issued at February 13th of 2017 (MA&PH). Authors, (TV&ShN) acknowledge the Russian Academy of Sciences (RAS) for financial support through the DEMMPC Program, as well as Integration program of Siberian Division RAS and the grant № 26 of National Academy of Science, Belarus.

Terekhov V.I., Terekhov V.V., Shishkin N.E., Bi K.Ch. Inzh.(2010) *Phys. Zh. (in Russian)*. **5**. 829-836.

Terekhov V.I., Shishkin N.E. (2012) *Letters JTP (in Russian)*. **38**, 1. 51-57.

Skripov V.P., Sinitsin E.N. (1980) *Moscow: Atomizdat*. 209.

Brus, D., Hyvarinen, A. Zdimal, V. and Lihavainen H. (2005). *J. Chem. Phys.* **122**. 214506.

Anisimov, M.P., Hameri, K., Kulmala, M. (1994) *J. Aerosol Sci.* **25(1)**. 23-32.

## Semiempirical design of the nucleation rate surfaces

M.P. Anisimov and O.O. Petrova-Bogdanova

Aerosol Technologies Laboratory, Novosibirsk State Technical University, Novosibirsk, 630073, Russia.  
Nanoaerosol Research Lab, Technological Design Institute of Scientific Instrument Engineer, Siberian Branch of  
the Russian Academy of Sciences, Novosibirsk, 630058, Russia.

Keywords: nucleation, nucleation rate surfaces, phase diagrams, axiomatic statements.

Presenting author email: anisimovmp@mail.ru

### Introduction

Classical nucleation theory has developed considerably over the last century. There have been many theoretical attempts to simulate clusters through the use of the intermolecular potentials and to describe nucleation with simple models, created by simplifying real systems [1]. It is well known that very simple models (e.g., an ideal gas) do not consider the possibility of a phase transition, and complicate models often generate mathematical problems that are difficult to solve. Researchers dealing in nucleation have made a considerable breakthrough in theory and the development of experiments. Experiments on nucleation are very laborintensive and, as a rule, expensive. The greatest success was achieved in empirical studies on the nucleation of supersaturated vapors and strained (superheated) liquids. The available data on the nucleation parameters are presenting the islands in the full region of possible conditions for nucleation which are located in the interval from critical conditions to the limit of absolute zero temperature. There is correspondence between the experimental values of the nucleation rates in supersaturated vapor and the predictions of modern theories only for a limited number of empirical data [2]. At present, it is theoretically possible to obtain only slopes close to those of experimental isotherms of the nucleation rates, but in this case to the temperature trends of the theoretical and empirical results are different. To get correspondence of theory and experiment, linear corrections are introduced into the theoretical expressions for nucleation rates [3]. Such corrections make the theory parametric and do not guarantee that it will correspond to reality outside of the empirical data according to which normalization was performed. The limited volume of the experimental data and their disagreement with the theoretical results stimulates the search for new ideas to describe real fields of the nucleation rates. It is reasonable to consider the perspective for the recently formulated concept which is based on the semiempirical design of nucleation rate surfaces over  $p$ - $T$  phase equilibrium diagrams, where  $p$  is pressure and  $T$  is temperature [2]. The use of phase equilibrium diagrams allows us to bind of them with the nucleation rate surface with good enough accuracy. The available empirical values of the nucleation rates determine the slope of linearized nucleation rate surfaces. Such an approach gives hope of obtaining exact data for the interval of the nucleation temperature and the supersaturation of vapors that cannot be provided by any experiment. We believe that semiempirical designs

of nucleation rate surfaces will soon become an effective instrument to solve many industrial and scientific nucleation problems. The research presents the results of semiempirical design for systems with monotropic polymorphic phase transformations.

### Axiomatic Statements

Thermodynamics considers systems consisting of a large number of particles that can exchange energy and matter with the surrounding medium. It is well known that a change in the parameters of the state of the system (e.g., pressure and temperature) can move the system from one phase state to another. Phase changes are accompanied by the breaking of the first derivative of thermodynamic potential of system on pressure, temperature etc. These intense parameters are associated with phase transitions of the first order, while the second derivatives are breaking during phase transitions of the second one. When there is a phase transition of the second order, a new phase appears in the result of fluctuations in a sample. The correlation radius of the fluctuations is rising to the sample size when the system approaches the temperature of phase transition. As a result, the phase transition occurs within the whole volume of the sample. It is easy to recognize that nucleation is impossible during a phase transition of the second order. In addition, the amount of the initial metastable phase in a system with weak deviation from the equilibrium state can be insufficient to create of a new phase. It is obvious that regions of the metastable phase states are represented by the fields on the phase diagrams which are located between the binodal and spinodal conditions. The possibility of continuing the phase equilibrium line beyond the triple point cannot be doubted, as can be seen on example of the metastable equilibria of water vapors over their supercooled liquid phase, which are published in many reference books. It is reasonable to assume that the phase equilibrium lines (including the regions of unstable equilibria) can be taken as the lines of the zero nucleation rates. Nucleation rate surfaces  $J(p, T)$  [2] can be constructed over the phase equilibrium diagrams in the  $p$ - $T$  axes. Using the results from [5–8], we can formulate the following set of axiomatic statements:

1. Phase equilibrium lines can be continued in the region of the existence of another, stable phase (these lines represent the unstable equilibrium of phases in the region of the third (stable) phase).
2. Phase equilibria lines correspond to the lines of the zero nucleation rates.



multiple triple points can be designed easily following the example which is shown in the present consideration. Fig. 2 represents a simplified example of the enantiotropic phase state diagram for the example of vapor-condensate equilibria, which is similar topologically to the phase diagram for sulfur. Melting lines are omitted in the present consideration to make images simpler.

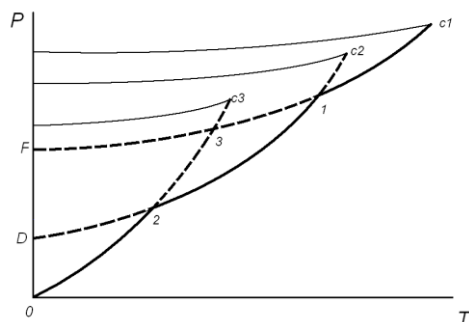


Figure 2. The enantiotropic phase state diagram.

The diagram involves two triple points for the phase states in equilibrium (points 1 and 3) and one additional (metastable) triple point (designated by 2) for the unstable phases. The essential data to design the nucleation rate surface involves both the stable and metastable equilibria for vapor-condensed states of matter in this case. The spinodal line for each phase can be calculated using the equation of phase states. It is simply postulated in the present research the existing of critical points for each pair of vapor-condensate equilibria.

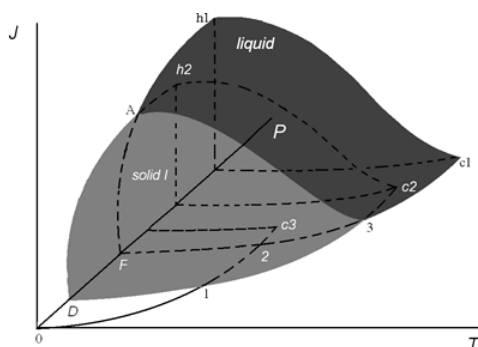


Figure 3. The Nucleation rate surfaces for liquid and solid I phases.

The vapor-liquid critical point is well established. It is assumed that for each single nucleation rate surface, the available experimental nucleation rate values can be collected. The resulting nucleation rate surfaces are presented as sums of the nucleation rates for each phase, which are available for the given conditions. It is obvious that topology for each single nucleation rate surface in Fig. 4 is similar to that shown in Fig. 1 for liquid and solid embryo nucleation. When other triple points are included (see Fig. 3), additional nucleation rate surfaces are generated. In the same way, the nucleation rate surfaces (light grey and grey colors) can

be developed over the triple points for solid I, solid II (*etc* in the common case) and vapor phases in Fig. 4. A multifold nucleation rate surface can be observed in which each phase its own nucleation rate surface that can be detected experimentally using the algorithm by Anisimova et al. [10].

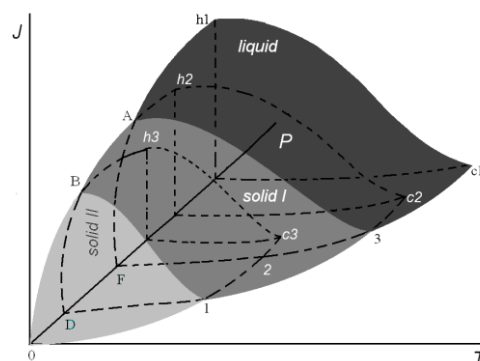


Figure 4. Three fold nucleation rate surface over the enantiotropic phase state diagram with three triple points

Fig. 4 can be used to clarify the sequence order of new phase embryos generation. The existence of the multifold nucleation rate surfaces at any triple point is carefully proven in articles [5, 10] suggesting that the surface topologies in Fig. 5 qualitatively true and applicable for the present prove the formation kinetics of different phases.

Research is supported by grant of the Russian Ministry of Science and Education under Contract № 14.Z50.31.0041 which is issued at February 13th of 2017.

Reiss, H. in: Hale, B. and Kulmala, M. (Eds.) (2000), *Nucleation and Atmospheric Aerosols*, AIP, Melville, NY, p. 181-196.

Anisimov, M. P. (2003) *Russian Chemical Reviews*, **72**, 591.

Wolk, J., Strey, R., and Wyslouzil, B. E., *Nucleation and Atmospheric Aerosols*, Ed. by M. Kasahara and M. Kulmala (Kyoto Univ. Press, Kyoto, 2004), 101–107.

Gibbs, J.W. *The Collected Works*, 1: Thermodynamics (Longman, Green, New York, 1928; Gostekhizdat, Moscow, 1950).

Anisimov, M. P., Hopke, P. K., and Buznik, V. M. (2007) *Doklady Physical Chemistry*, **417** (1), 297-300.

Anisimov, M. P., Hopke, P. K., Rasmussen, D. H., Shandakov, S. D., and Pinaev, V. A. (1998), *Journal of Chemical Physics*, **109**, 1435.

Anisimov, M. P. (1990), *Journal of Aerosol Science*, **21** (1), 23.

Anisimov, M. P., Fominykh, E. G., Akimov, S. V., and Trilis A. V. (2010), *Russian Journal of Physical Chemistry*, **84** (3), 364-369.

Anisimov, M.P., Hopke, P.K. (2001), *Journal of Physical Chemistry B*, **105**, 11817-11822.

Anisimova, L. Hopke, P.K., Terry, J. (2001), *Journal of Chemical Physics*, **114** (22), 9852-9855.

## A large eddy simulation of particle removal in a room-sized differentially heat cavity

A. Dehbi, J. Kalilainen, T. Lind

Laboratory for Thermal-hydraulics, Paul Scherrer Institut, Villigen, 5234, Switzerland

Keywords: Deposition, Natural convection, CFD, Euler-Lagrange.

Presenting author email: abdel.dehbi@psi.ch

Particle removal within an enclosure with predominant turbulent free convection flows is of great importance in many industrial, environmental and medical applications. It is therefore essential that trustworthy analytical tools be developed to predict the deposition behavior as well as lifetimes of airborne particles in such flows to plan alleviating or mitigating counter-measures.

Recent experiments (Kalilainen *et al.*, 2016) and accompanying CFD simulations (Dehbi *et al.*, 2017) have been conducted to investigate particle-laden flows in a 0.7 m in side cubical differentially heat cavity (DHC) at Rayleigh (Ra) number  $10^9$ , and have both shown that micron-sized particles are removed at rates considerably faster than those predicted by the simple stirred settling model (Hinds, 1999).

In this work, we extend the simulations to a hypothetical cubical room-sized DHC with side 3.25 m and temperature differential of 36 K between the vertical hot and cold walls, resulting in a Ra number of  $10^{11}$ .

A well-resolved Large Eddy Simulation (LES) with 8 million cells is first conducted to compute the turbulent air flow field inside the DHC. Once statistically stationary conditions are reached, spherical particles with AMMD's between 0.5  $\mu\text{m}$  and 10  $\mu\text{m}$  are released uniformly in the domain and tracked in Lagrangian manner for 1700 s.  $10^5$  particles are used for each bin size. The forces applied to particles are drag, gravity and thermophoresis. The simulations are conducted according to CFD best practice guidelines to minimize numerical errors.

The results indicate that turbulent velocity magnitudes are large enough in the whole domain to overcome the gravity force of the largest aerosol considered (10  $\mu\text{m}$ ), and thus all particles are entrained by the flow field, albeit not always perfectly.

For all sizes, it is found that the particle airborne concentration remains uniform in space while decaying exponentially with time. It is thus fitting to compare the calculated decay rates with those predicted by the stirred settling model which results in a decay constant given by  $L/(\tau_p g)$ ,  $L$  being the room height,  $\tau_p$  the aerosol relaxation time and  $g$  the gravity acceleration.

The predicted decay constants are displayed in Figure 1 for Ra  $10^{11}$ . For comparison purposes, the previous computational and experimental results at Ra  $10^9$  are also shown. Results at Ra  $10^{11}$  confirm and amplify previous findings at Ra  $10^9$ , namely, that stirred settling model matches the LES results for intermediate to larger particles, i.e. in the range of 4-10  $\mu\text{m}$ , but the discrepancy grows as particle size decreases. For particles with diameters 2.0  $\mu\text{m}$  and below, the decay constants are roughly independent of particle inertia, and

for the smallest particle with diameter 0.5  $\mu\text{m}$ , the decay constant predicted by the stirred settling model is a factor 20 larger than the LES value. The intermediate-to-large particles (4-10  $\mu\text{m}$ ) deposit predominantly on the bottom wall. Gravity thus is the overriding force responsible for the removal of the larger particles. As particle size decreases, the deposition fraction on other walls increases, and even tops that of the bottom wall for the smaller particles (2  $\mu\text{m}$  and below), as turbulent dispersion and thermophoresis dominate aerosol transport to the boundaries.

In separate LES computations under the same Ra number, we show that decreasing the temperature differential by a factor 10 causes the LES curve to shift towards that of the stirred settling model.

In conclusion, high fidelity LES computations indicate that when significant turbulent free convection currents are present in enclosures, as the AMMD decreases towards the micron size range, particles are removed at rates increasingly faster than those predicted by the simple stirred settling model. This is principally due to the increased importance of turbulent diffusion and thermophoresis as particles become smaller. While such findings are intuitively expected, the contribution of this work is to provide quantitative measures for the observed trends in particle deposition rates.

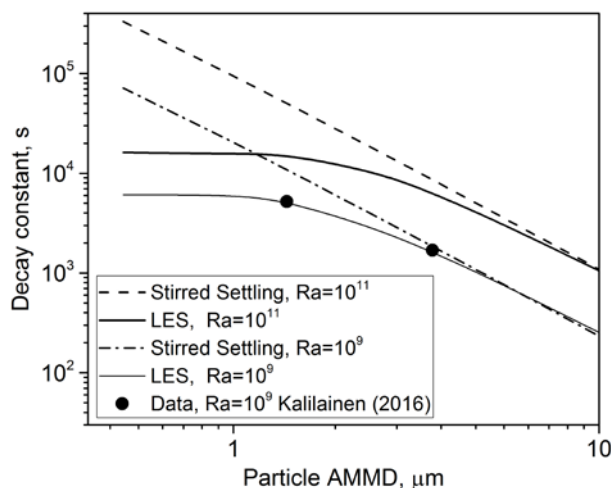


Figure 1. Decay constants versus AMMD for different Rayleigh numbers

Kalilainen, J., Rantanen, P., Lind, T., Dehbi, A. (2016)

*J. Aerosol Sci.* **100**, 73-87.

Dehbi, A., Kalilainen, J., Lind, T., Auvinen, A. (2017)

*J. Aerosol Sci.* **103**, 67-82.

Hinds, W.C. (1999) *Aerosol technology*, John Wiley & Sons, Inc.

## Using Dynamic Meshes to Evaluate Transparent Electrode Performance

Ali Mohamadi Nasrabadi, Jangseop Han, and Jungho Hwang\*

Department of Mechanical Engineering, Yonsei University, Seoul, 03722, Republic of Korea

Keywords: Transparent electrode, Printing, Dynamic Mesh, Ansys Fluent

\*Corresponding author: hwangjh@yonsei.ac.kr

Presenting author email: a.mohamadi@yonsei.ac.kr

Transparent electrodes (TEs) structured of metal grid with periodic metal lines have been widely used in many applications recently. Optical transmittance and electrical sheet resistance are in constant competition together being functions of pitch distance. Increasing the grid pitch distance leads to increase the transmittance but also increase sheet resistance.

This study is in the following of our previous study [Park et al. (2015)] which experimentally studied the effect of deposition charged particle over a transparent electrode pre-patterned with silver grid (width 18  $\mu\text{m}$ , thickness 360 nm, pitch 500  $\mu\text{m}$ ) to increase the performance of TEs. These numerical simulations are performed using a discrete phase model (DPM) module that is available in a commercial CFD based solver, ANSYS Fluent 14. To extend the ability of software, to simulate electric field and deposition patterns, some codes (user defined function (UDF)) was added. In the following, after validation of our results with Park et al. (2015), the effect of different pitch distances and duration of particle depositions over TEs were numerically investigate.

Park et al. (2015) reported that After 3 minutes of EAD with silver nanoparticles, grid thickness increased from 360 nm to 587 nm, resulting in decreasing TE sheet resistance about 3.78 times, while transmittance was kept constant. For given grid width of 18  $\mu\text{m}$ , Park et al. (2015) considered only one metal grid pitch (500  $\mu\text{m}$ ) and also 3 minutes EAD printing process. Due to time consuming and cost of experimental process, numerical study can be an effective tool for considering and studying wider range of variables such as more number of metal grid pitches and EAD printing time to evaluate performance and determine proper condition. In the following, the effect of deposition charged particle for different pitch distances, 125  $\mu\text{m}$ , 250  $\mu\text{m}$ , 500  $\mu\text{m}$ , 1000  $\mu\text{m}$ , and 2000  $\mu\text{m}$ , was calculated to evaluate transparent electrode.

Our results showed that by increasing duration of particle printing over pre-patterned transparent electrodes it is possible to overcome high resistivity even by increasing pitch distance. In this case the transparency was 89% and sheet resistivity was 12.32  $\Omega$ . Sq-1 which after 10 minutes atomization of charged particles resulting in decreased TE sheet resistance to 0.214  $\Omega$ . Sq-1. Therefore, the factor of  $\delta_{DC}/\delta_{op}$  changed from 420 to 13500 for pitch distance of 2000  $\mu\text{m}$  after 1 min and 10 min ,respectively, printing charged particles. However, the  $\delta_{DC}/\delta_{op}$  was 900 and 12300 afre 1 min

and 10 min printing, respectively, for pitch distance of 125  $\mu\text{m}$ .

Figure 1 shows that increasing height could overcome the high resistivity and increased the factor of  $\delta_{DC}/\delta_{op}$  for transparent electrode for pitch distance of 2000  $\mu\text{m}$ . The factor of  $\delta_{DC}/\delta_{op}$  for pitch distance of 2000  $\mu\text{m}$  after 1 min printing was 420 while this number for pitch distance of 125  $\mu\text{m}$  was 1550. After 10 minutes printing, this number for transparent electrode with pitch distance of 2000  $\mu\text{m}$  became 13500 which is higher than  $\delta_{DC}/\delta_{op}$  transparent electrode with pitch distance of 125  $\mu\text{m}$ .

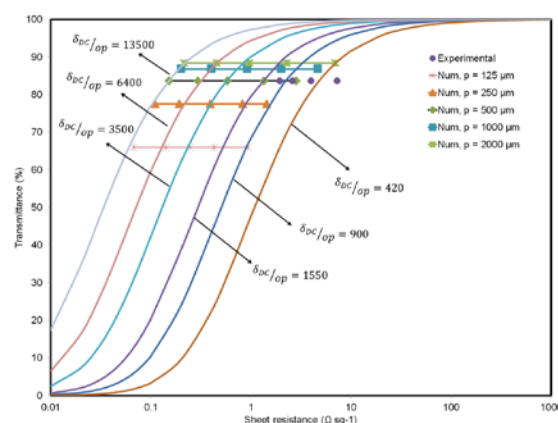


Figure 1. Plot of transmittance (at 550 nm) as a function of sheet resistance.

This research was supported by Basic Science Research Program through the National Research Foundation of Korea (NRF) funded by the Ministry of Science, ICT and future Planning (NRF-2015R1A2A1A01003890).

Park, K. T., Park, J., Park, J. W., & Hwang, J. (2015). Maskless, site-selective, nanoaerosol deposition via electro-aerodynamic jet to enhance the performance of flexible Ag-grid transparent electrodes. RSC Advances,5(56), 44847-44852.

## Experimental Study on Effect of External Disturbance on a Carbon Fiber Particle Settlement

Jiang Lin and Lei Jiang

Zhejiang University of Science and Technology, Hangzhou, 310023, China

Keywords: Fiber particle settlement, Aspect ratio, disturbance quantity, rotational speed  
Presenting author email: linjiang@zust.edu.cn

The settlement law of carbon fiber with different length to diameter ratio is studied. The morphology of the carbon fiber was recorded by a high-speed camera. It is found that (1) the fiber deposition in the water is gradually from the vertical direction to the horizontal direction, and eventually stabilized. (2) with the same amount of disturbance, the initial rotation rate decreases with the increase of the aspect ratio, and reaches the maximum value when  $n=50r/min$  reaches  $4.2r/min$ . (3) with the increase of the ratio of length to diameter of the fiber, the initial rotation rate decreases. And the change of the rotation angle tends to be linear. The greater the disturbance is, the shorter the fiber rotation rate reaches 0. Figure 1 shows the dynamics of aerosol fiber particles under the three ratios of length to diameter.

Z Liang , C Zhou, et al .Numerical simulation of non-isothermal planar contraction flow of polymer melts .Polym. Mater. Sci. & Eng ., 2013, 19(1):15-19 .

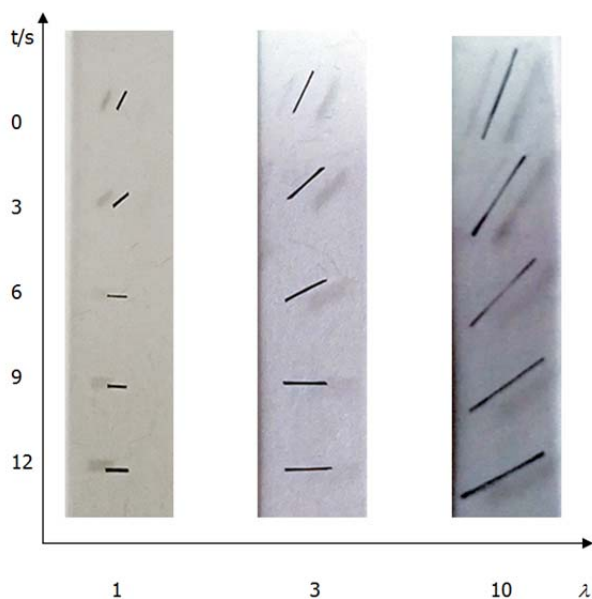


Figure 1 Dynamics of fiber particles under the different ratio of length to diameter

This work was supported by the National Foundation of Science China under grant NO.51376162.

Y Wei ,J Chen., et al .Leonov viscoelastic constitutive model and evaluation of model parameters. Polym .Mater .Sci.& Eng ., 2014 , 20(4):18-22 .

## Features of reflection of acoustic waves from the boundary or layer of aerosol

D.A. Gubaidullin, D.D. Gubaidullina and Yu.V. Fedorov

Department of Continuum Mechanics, Institute of Mechanics and Engineering KazSC RAS, Kazan, 420111, Russia

Keywords: acoustic waves, aerosol, interface, layer, reflection and transmission coefficients.

Presenting author email: kopperfildd@yandex.ru

The inclined incidence of the acoustic wave on a layer of gas-droplet mixture of finite thickness is theoretically investigated. In the case of the incidence of the low-frequency acoustic wave to interface between the pure gas and aerosol the basic laws of reflection and transmission of a wave are established. This circumstance allows us to evaluate the transmission and reflection coefficients, depending on the volume content of inclusions and the angle of incidence of the acoustic wave. In particular, for the interface between pure gas and aerosol analytical expressions of the critical angle of wave incidence at which reflection coefficient becomes zero are obtained, i.e. thus there is a complete passage of the acoustic wave through the interface. These expressions allowed to establish that when the wave falls from the gas-droplet mixture into clean gas border, then at angles of incidence higher than  $24.5^\circ$  reflection coefficient will never be zero, but if the wave falls from the clean gas side to the border of aerosol, zero value of the reflection coefficient is possible for any non-zero angles of incidence and volume content of inclusions. These conclusions were valid not only for the border, but also for a layer of gas-droplet mixture of finite thickness.

Based on the results of calculations of the acoustic wave reflection from the layer of aerosol of finite thickness relation between the wavelength and the thickness of the layer, at which the reflection coefficient possesses the extreme value values are established. Fig. 1 clearly illustrates confirm of this fact. It is established that the increase of the angle of incidence of the acoustic wave on the boundary or layer of aerosol causes: first, either to increase or to decrease of the reflection coefficient at low frequencies, and second, to appearance of additional minima depending on the reflection coefficient from frequency of disturbances related to the difference of speed of sound and density of the medium (Fig. 2). Intervals the angle of incidence at which these minima appear are found. The results of this theory, in the special case of normal incidence of the wave are in good agreement with theoretical data of other authors.

Main investigations on this subject are reflected in works of Gumerov et al. (1988), Nigmatulin and Gubaidullin (2000), Ishii and Matsuhisa (1983), Shagapov and Sarapulova (2014).

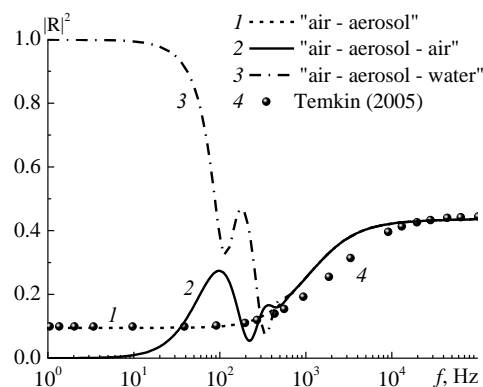


Figure 1. The results of calculations of reflection coefficient for mediums.

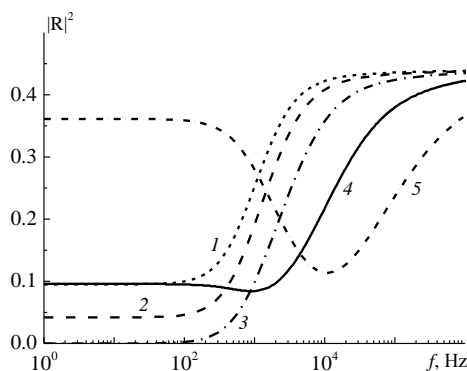


Figure 2. The results of calculations of reflection coefficient at different angles of incidence of a wave on the air side: 1 - 5 –  $0^\circ$ ,  $39^\circ$ ,  $60^\circ$ ,  $75^\circ$ ,  $83^\circ$ .

The study was carried out with the support of the Russian Scientific Foundation (project No. 15-11-10016).

Gumerov, N.A., Ivandaev A.I. and Nigmatulin, R.I. (1988) *J. Fluid Mech.* **193**, 53-74.

Gubaidullin, D.A. and Nigmatulin, R.I. (2000) *Int. J. Multiphase Flow.* **26**, 207-228.

Ishii, R. and Matsuhisa, H. (1983) *J. Fluid Mech.* **130**, 259-277.

Gubaidullin, D.A., Gubaidullina, D.D. and Fedorov Yu.V. (2013) *Abstract of European Aerosol Conference*, Prague.

Temkin, S. (2005) *Suspension acoustics: an introduction to the physics of suspensions*, Cambridge University Press.

Shagapov, V.Sh. and Sarapulova, V.V. (2014) *Izv. Atmospheric and Oceanic Physics.* **50**, 602-609.

## Acoustic waves in multifractional aerosols with heat and mass transfer

D.A. Gubaidullin<sup>1</sup>, E.A. Teregulova<sup>1</sup>

<sup>1</sup>IME KazSC RAS, Kazan, 420111, Russia

Keywords: aerosol, acoustic waves, interphase heat and mass transfer

Presenting author email: teregulova@inbox.ru

Investigation of the acoustics and wave dynamics of multiphase media is of a significant interest due to wide dissemination of such media in nature and their application in practice [Nigmatulin, R.I (1991), Temkin S. (2005), Gubaidullin D.A.(1998)]. Previously it has been studied particularity of propagation of acoustic waves in two fractional aerosols [Zink J.W. and Delsasso L.P.(1958), Gubaidullin D.A., Nikiforov A.A. Utkina E.A.(2011)]. The goal of this study is to investigate propagation of acoustic waves in multifractional aerosols with particles of different materials and sizes, and drops of the same type with heat and mass transfer.

For considered media the mathematical model is presented, the dispersion equation is received, and dispersion curves are calculated. Influence parameters of a disperse phase on dissipation and dispersion of acoustical waves are analyzed. Comparison with experiment is carried out.

Dependencies of the relative sound velocity and attenuation decrement on wavelength from the dimensionless oscillation frequency for the three fractional mixture of air with particles of aluminum and sand, and drop of water are built (Fig. 1 and 2). The graphs show that with the increase of mass content of the particles the dispersion of the sound velocity and dissipation of waves increase.

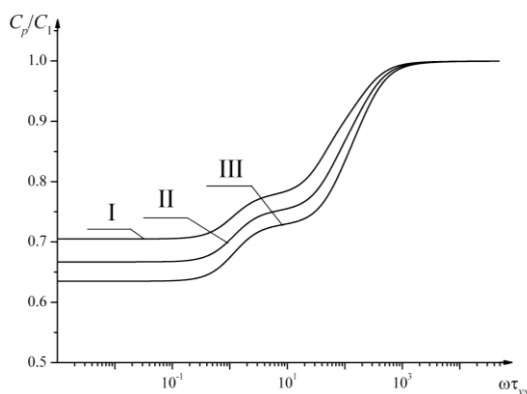


Figure 1. Dependence of the relative sound velocity on the dimensionless oscillation frequency for the mixture of air with particles of aluminum, sand and drop of water at various mass concentration of the disperse phase (I:  $m = 0.3$  ( $m_a = 0.1, m_s = 0.1, m_l = 0.1$ ), II:  $m = 0.5$  ( $m_a = 0.1, m_s = 0.2, m_l = 0.2$ ), III:  $m = 0.7$  ( $m_a = 0.2, m_s = 0.3, m_l = 0.2$ ))

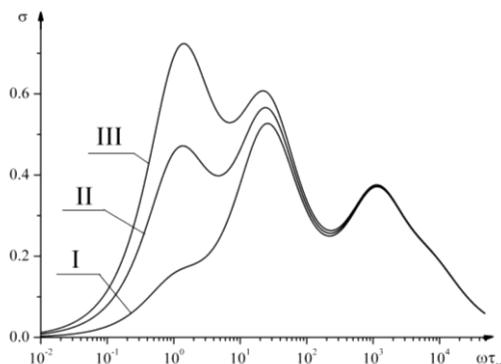


Figure 2. Dependence of the attenuation decrement on wavelength from the dimensionless oscillation frequency for the mixture of air with particles of aluminum, sand and drop of water at various mass concentration of the disperse phase (I:  $m = 0.3$  ( $m_a = 0.1, m_s = 0.1, m_l = 0.1$ ), II:  $m = 0.5$  ( $m_a = 0.1, m_s = 0.2, m_l = 0.2$ ), III:  $m = 0.7$  ( $m_a = 0.2, m_s = 0.3, m_l = 0.2$ ))

Accounting of three fraction composition and the difference in the thermophysical properties of fractions lead to an emergence of the characteristic inflections for dependence of the relative speed of sound (Fig. 1), as well as to the emergence of three local maximum for the dependence of the attenuation decrement on wavelength (Fig. 2) on the frequency inversely proportional to the characteristic relaxation times of the respective phases velocity.

The study was performed by a grant from the Russian Science Foundation (project No. 15-11-10016).

Nigmatulin, R.I., Dynamics of Multiphase Media, Vol. 1,2, Hemisphere.-1991.

Temkin S. Suspension acoustics: An introduction to the physics of suspension – Cambridge University Press, 2005. – 398p.

Gubaidullin D.A. Dynamics of twophase gas-vapor-droplet media. Kazan: Kazan mathematical society, 1998. 153 c.

Zink J.W. and Delsasso L.P. Attenuation and Dispersion of Sound by Solid Particles Suspended in a Gas // J. Acoust. Soc. Am. 30. 765-771 (1958)

Gubaidullin D.A., Nikiforov A.A., Utkina E.A Acoustic waves in two-fraction mixtures of gas with vapor, droplets and solid particles of different materials and sizes in the presence of phase transitions // Fluid Dynamics. 2011 . T. 46. № 1. C. 72-79.

## Temporally resolved measurements of heavy, rigid fibre translation and rotation in nearly homogeneous isotropic turbulence

L. Sabban, A. Cohen and R. van Hout<sup>1</sup>

<sup>1</sup>Faculty of Mechanical Engineering, Technion-Israel Institute of Technology, Haifa, 32000, Israel

Keywords: isotropic turbulence, particle/fluid flows.

Presenting author email: lilsab@technion.ac.il

The interaction between fibres and turbulence is important in both industrial and environmental application. Therefore, time resolved, planar particle image velocimetry (TR-PIV) and two-orthogonal view, digital holographic cinematography were used to measure fibre flow interaction and 3D fibre trajectories and orientation dynamics in near homogeneous isotropic air turbulence (HIT).

The fibres were imaged from two orthogonal directions by digital holographic cinematography at an acquisition rate of 2 kHz, about five times higher than the Kolmogorov frequency. The Taylor micro-scale Reynolds number was  $Re_\lambda \approx 130$ , and the spatial resolution  $17 \mu\text{m}/\text{pix}$ . The volume of interest, i.e. the intersection of the two orthogonal views, was about  $17 \times 17 \times 17 \text{ mm}^3$  located at the centre of the turbulence chamber. In addition to the holography, planar time-resolved PIV measurements were performed in order to characterize the flow characteristics, estimate the TKE dissipation rate,  $\varepsilon$ , and study fibre alignment with the flow. The acquisition frequency was 3 kHz, about six times the Kolmogorov frequency. Using a long working distance microscopic lens, a FOV of  $6.3 \times 12.6 \text{ mm}^2$  was obtained leading to a spatial resolution comparable to the Kolmogorov length scale. The Kolmogorov length scale,  $\eta_k$ , describes the size of the smallest, dissipative scales of turbulence.

Two sets of nylon fibres having nominal lengths,  $L=0.5\text{mm}$  (about 3 times the Kolmogorov length scale), and diameters of  $D=13.7$  (*dtex*1.7) and  $19.1\mu\text{m}$  (*dtex*3.3), were released in a turbulence chamber at a volume fraction of  $2 \times 10^{-6}$ . The ratio of fibre length to the Kolmogorov length scale was 2.8. The fibre Stokes numbers were 1.35 and 2.44, respectively. Eight woofers mounted on the chamber's corners generated HIT. Here, for the first time, the effect of fibre inertia on particle-turbulence coupling was measured in HIT.

As a result of increased inertia, PDF's of fluctuating fibre translational velocities were narrower than the ones of the air. While fibre orientations in the cameras' frame of reference were random as a result of the strong turbulence, it was shown that fibres align with the flow to minimize drag.

PDF's of fibre in-plane and polar angle rotation rates based on the holography measurements and normalized by their respective rms values, deviated from a normal distribution but collapsed for both *dtex* values. Results shown in Figure 1, present the normalized mean squared rotation rate,  $\langle \dot{p}_i \dot{p}_i \rangle / (\varepsilon/\nu)$ , ( $\dot{p}_i$  denotes the fibre rotation rate and  $\nu$  is the kinematic fluid viscosity) as a function of the aspect ratio,  $\beta=L/D$ , together with DNS, results for naturally buoyant fibres (Parsa *et al*, 2012),

clearly indicated that inertia reduced the mean squared fibre rotation rate. The present results were in excellent agreement with recent DNS by Zhao *et al* (2015) that considered the effect of inertia on fibre rotation rates at the center of a turbulent channel flow. To the best of our knowledge, these are the first experiments that quantified the effect of inertia on the normalized, mean squared fibre rotation rate in near HIT.

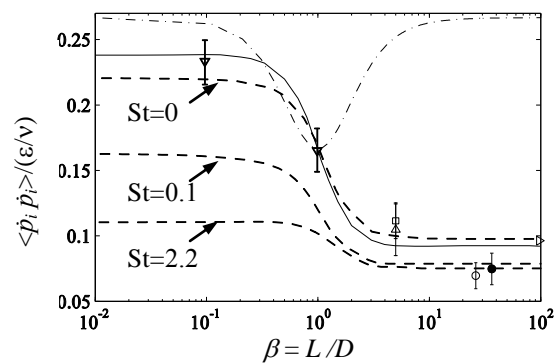


Figure 1. Normalized, mean squared particle rotation rate versus aspect ratio. Literature results (neutrally buoyant particles): (Solid line) DNS at  $Re_\lambda=180$  by Parsa *et al* (2012); (dash dot) Eq. (12); DNS at  $\triangleright Re_\lambda=53.3, L/\eta_k < 10, \beta \rightarrow \infty$  by Shin and Koch (2005); (dashed lines) DNS by Zhao *et al* (2015); Experiments at  $\triangle Re_\lambda=160$ ,  $\square Re_\lambda=244$  by Parsa *et al* (2012), and  $\nabla Re_\lambda=91$  by Marcus *et al* (2014); Present results (inertial fibres):  $\bullet$  *dtex*1.7,  $\circ$  *dtex*3.3.

This work was supported in part by the Edmund J. Safra Philanthropic Foundation, the Wolfson Family Charitable Trust, the Technion Fund for Promotion of Research and the Israel Science Foundation under grant no. 915/10. We also acknowledge the support of EU COST Action FP1005.

Marcus, G. G., Parsa, S., Kramel, S., Ni, R. and Voth, G. (2014) *New J. Phys.* **16**, 102001. Doi:10.1088/1367-2630/16/10/102001.

Parsa, S., Calzavarini, E., Toschi, F. and Voth, G. A. (2012) *Phys. Rev. Lett.* **109**, 134501.

Shin, M. and Koch, D. L. (2005) *J. Fluid Mech.* **540**, 143–173.

Zhao, L., Challabotla, N. R., Andersson, H. I. and Variano, E. A. (2015) *Phys. Rev. Lett.* **115**, 244501.

## **AeroSolved: Eulerian computational platform for polydisperse aerosol transport, evolution and deposition**

E.M.A. Frederix<sup>1</sup>, F. Lucci<sup>2</sup>, M. Nordlund<sup>2</sup>, B.J. Geurts<sup>1</sup> and A.K. Kuczaj<sup>2,1</sup>

<sup>1</sup> Multiscale Modeling and Simulation, Applied Mathematics, University of Twente, The Netherlands

<sup>2</sup> Philip Morris International R&D, Philip Morris Products S.A.

(part of Philip Morris International group of companies), Switzerland

Keywords: CFD, aerosol, Euler-Euler, polydisperse, phase change, multi-species

Presenting author email: arkadiusz.kuczaj@pmi.com

An aerosol is defined as a colloidal system of small solid particles or liquid droplets suspended in a gas. Aerosols are present in numerous natural and industrial processes, e.g., cloud formation, fuel dispersion in combustion chambers, spray painting and cooling, inhalation and many more. The dynamics of aerosols including their transport, evolution and deposition follows complex physical phenomena regulating the interaction between the carrier and the dispersed phases and behavior of each phase.

We have developed AeroSolved (<http://www.aerosolved.com>) - a computational code for simulations of multi-species aerosol flows in a multiphase coupled framework based on the OpenFOAM computational platform. The code was developed to study flows with aerosols including their generation via nucleation process through their transport, evolution and finally deposition. The implemented aerosol physics is applicable to a wide range of practical applications, including the development of aerosol generators, inhalation devices, validation of aerosol delivery systems for *in vivo* inhalation studies and *in vitro* sciences, as well as for atmospheric sciences.

In this computational package the Eulerian framework is adopted with discretized sectional (for arbitrary shaped size distribution, [1]) and two-moment (for log-normal size distribution, [2]) aerosol dynamics with gas and liquid phases modelled as continuous fields including temperature and phase changes and density variations. The multispecies aerosol dynamics is mathematically described by a system of multiphase transport equations with various source terms. The presented computational framework was developed as described in details in [3].

The source terms present in the transport equations account for aerosol processes such as nucleation, condensation/evaporation and coagulation. The present flux term can be considered as the total flux of droplets drifting away from the mixture due to diffusion, drag and gravity forces in the Eulerian context. The transport equations for the mass fractions for each gas and liquid phases are consistently solved with the global mass conservation equation. The droplet distribution is resolved with a sectional method where the droplet size domain is divided into adjoining sections. To each section a representative droplet mass is assigned and a corresponding droplet number per unit of

mixture mass. The governing equations and the related submodels are implemented in the extended pressure implicit with splitting of operator (PISO) algorithm used for aerosol dynamics. Multispecies nucleation is modelled following the classical nucleation theory. For the multispecies evaporation/condensation all species components are treated independently assuming dilute flow regime. Polydisperse coalescence effects are also captured. For the particle/droplets drift velocity the model assumes the Stokes drag. The particle/droplets Brownian diffusion coefficient is modelled using the Stokes-Einstein equation.

In addition, special boundary conditions have been developed to better capture deposition on realistic often complex computational grids. For the inertia/sedimentation mechanism, a Lagrangian sub-grid model boundary treatment approach is used to predict the inertial droplet velocity for the particles approaching the wall. Deposition due to diffusion process assumes perfectly absorbing conditions at the wall. Models for film formation and evaporation are under development. More detailed and complete overview of the models, their implementation and validation can be found in [3].

AeroSolved was jointly developed between Philip Morris International R&D (PMI R&D) and the Department of Applied Mathematics at the University of Twente (UT), The Netherlands. The code is heavily used in the context of *in vitro* toxicological inhalation studies and characterization of novel aerosol exposure systems used in modern system toxicology approaches. AeroSolved is available as Git repository via <http://www.aerosolved.com> as the open source code under the GNU General Public License 3.0.

The research presented in this work was funded by Philip Morris Products S.A. (part of Philip Morris International group of companies).

[1] Frederix, E., Stanic, M., Kuczaj, A.K., Nordlund, M. and Geurts, B.J. (2016) *Characteristics-based sectional modelling of aerosol nucleation and condensation*, *J. Comput. Phys.*, 326, 499-515.

[2] Winkelmann, C., Kuczaj, A.K., Nordlund, M. and Geurts, B.J. (2017) *Simulation of aerosol formation due to rapid cooling of multispecies vapors*, *J Eng Math*, doi: 10.1007/s10665-017-9918-6.

[3] E. Frederix, E. (2016) *Eulerian modelling of aerosol dynamics*. PhD Thesis, University of Twente.

## **Abstracts T503**

## Effective dielectric permeability of a monolayer of precipitated metal aerosol

V.V. Maksimenko<sup>1,4</sup>, V.A. Zagaynov<sup>1,4</sup>, A.S. Smoliyanskiy<sup>2,4</sup>, I.E. Agranovski<sup>3</sup>

<sup>1</sup>National Research Nuclear University MEPhI ( Moscow Engineering Physics Institute), 31, Kashirskoe shosse, 115409, Moscow, Russia

<sup>2</sup>D. Mendeleev University of Chemical Technology of Russia, 9, Miusskaya square, 125047, Moscow,

<sup>3</sup>School of Engineering, Griffith, University, Brisbane, 4111 QLD, Australia

<sup>4</sup>Karpov Institute of Physical Chemistry, 105064 Moscow, Russia

Keywords: aerosol, localization, nanoparticle, scattering.

Presenting author email: [I.Agranovski@griffith.edu.au](mailto:I.Agranovski@griffith.edu.au)

Island metal films obtained by deposition of aerosol particles on dielectric substrate are widely used in modern plasmonic sensing. Introduction of effective dielectric permeability  $\bar{\epsilon}$  is the common way to describe these systems.

There are at least two objections to this approach. First, existing effective medium theories (EMT) are derived not for monolayer of particles, but for unbounded three-dimensional system of heterogeneities, and their applicability to monolayer is not proven (Bohren and Huffman, 1998). Moreover, these approximations predict appearance of imaginary part of  $\bar{\epsilon}$  and the effective absorption even in a system of absolutely nonabsorbing particles. This mysterious absorption causes the main claims to EMT in spite of their successful applicability to description of many physical properties of heterogeneous systems.

Here, we show how correctly to introduce  $\bar{\epsilon}$  for a monolayer of particles. Besides, the above mentioned paradox related to mysterious absorption is also solved - we have possibility to explain appearance of the imaginary part of  $\bar{\epsilon}$ . Its appearance relates to the light localization in a system of particles.

The reason of the localization is the specific interference effects existing even in a random system of nonabsorbing particles. The localization relates to loops on the photon trajectory. Every closed loop can be passed by two alternate ways, clockwise and counterclockwise. The phase shift for both processes is the same. So, the corresponding probability amplitudes interfere constructively. Therefore, probability of a loop generation abnormally increases. Increased return probability stimulates generation of new loops and so on. This self-supporting process reduces to the photon localization.

Effective dielectric permeability  $\bar{\epsilon}$  is solution of the following simple equation

$$\frac{\bar{\epsilon} - 1}{3\bar{\epsilon}} = f \frac{\epsilon - \bar{\epsilon}}{\epsilon + 2\bar{\epsilon}} \Pi(\xi), \text{ where}$$

$\Pi(\xi) = (1 - \xi^2)[\theta(\xi + 1) - \theta(\xi - 1)]$ ,  $f$  is the packing factor,  $\xi = z/R$ ,  $R$  is the particle radius,  $z$  is the coordinate in the direction across the film,  $\epsilon$  is the dielectric permeability of metal,  $\theta$  is the unit step function. Dependence of  $\text{Re}\bar{\epsilon}$  and  $\text{Im}\bar{\epsilon}$  on  $\xi$  and

$\text{Im}\bar{\epsilon}$  on frequency at different values of  $\xi$  is presented in Figs.1-2.

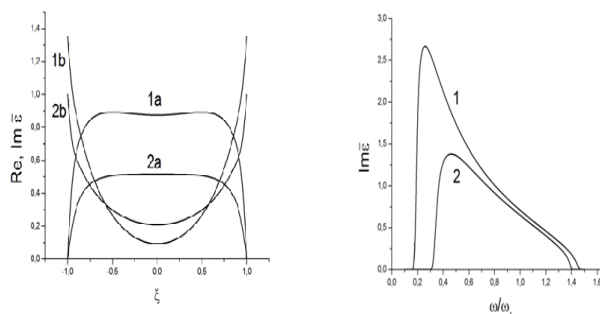


Fig.1. Dependence of real (1b and 2b) and imaginary parts (1a and 2a) of  $\bar{\epsilon}$  on transverse coordinate. Packing factor  $f = 0.5$ , the curves 1 correspond  $\omega/\omega_1 = 0.9$ , the curves 2 correspond  $\omega/\omega_1 = 1.2$ ,  $\omega_1$  is the frequency of dipole surface plasmon in spherical metal particle.

Fig.2. Frequency dependence of imaginary part of  $\bar{\epsilon}$  on two film slices. Curve 1 -  $\xi = 0.3$ , curve 2 -  $\xi = 0.8$ .

Packing factor  $f = 0.5$ .

In contrast to three-dimensional packing of particles, the effective dielectric permeability of island film  $\bar{\epsilon}$  is a function of transverse coordinate  $z$ . In other words, we deal with a range  $\bar{\epsilon}(z)$ . However, this does not diminish the role of last. A possibility to introduce this value simplifies essentially a calculation of basic electrodynamics characteristics of the films, which are determined by simple integrals containing  $\bar{\epsilon}(z)$  (Maksimenko et al, 2017). The main feature of the film electromagnetic response is resonance increase of cross sections in vicinity of the dipole plasmon frequency.

This work was supported by RSCF (No. 14-03-00507 and No.14-07-00025).

Bohren, C.F., Huffman, D.R., Absorption and Scattering of Light by small particles (Wiley, New York, 1998).

Maksimenko, V.V., Zagaynov, V. A., Smoliyanskiy A.S., Agranovski, I.E., Effective dielectric permeability of island metal films: Light scattering and absorption, Thin Solid Films, v. 621, p. 84-90, 2017.

## Absorption efficiency of particulate and gaseous aerosol constituents at aqueous surfaces

Sandro Steiner, Pierrick Diana, Eric Dossin, Philippe Guy, Gregory Vuillaume, Athanasios Kondylis, Shoaib Majeed, Stefan Frentzel, Julia Hoeng

Philip Morris International R&D, Philip Morris Products S.A. (part of Philip Morris International group of companies)

Absorption of components present in inhaled aerosols into body fluids and tissues is an important determinant of net exposure in humans. The kinetics with which particles and gaseous aerosol constituents absorb into fluids and tissues of the respiratory tract tissue may vary widely, depending on their distribution in the lung and their physicochemical properties. Slow kinetics of an abundant aerosol constituent may decrease its net exposure, while fast kinetics of trace constituent may result in a considerably increased exposure rate compared to the composition of the native aerosol. Similar considerations need to be taken into account when testing the effect of aerosols in *in vitro* exposure setups.

With the aim of gaining more insight into how an applied aerosol translates into a delivered dose of individual components to cells exposed in the Vitrocell<sup>®</sup>24/48 system, we determined the absorption of various constituents from cigarette smoke into an aqueous matrix used as a surrogate for the liquid lining of the respiratory tract lumen. As test aerosol, we used whole smoke (WS) generated from 3R4F reference cigarettes (University of Kentucky) smoked under the Health Canada intense smoking regime.

In 12 to 15 independent experimental repetitions, 3R4F WS was bubbled through N,N-dimethylformamide (DMF) at -50°C. WS composition was subsequently determined by analyzing the DMF samples by gas and liquid chromatography coupled to mass spectrometric detection. In three separate, independent experimental repetitions, small volumes of phosphate buffered saline (PBS) were exposed to WS in the Vitrocell<sup>®</sup>24/48 aerosol exposure system at 37°C. The PBS was collected and analyzed for smoke constituents that were trapped from WS during exposure using the same analytical methods. More than 60 smoke constituents including alkanes and alkenes, polyaromatic hydrocarbons (e.g. benzo[a]pyrene), nitrosamines (e.g. N-nitrosonornicotine), alkaloids (e.g. nicotine), furans (e.g. 2-methylfuran), thiols (e.g. thiophene), ketones (e.g. diacetyl), and carbonyl compounds (e.g. acrolein) were detected in all generated DMF samples. Based on their concentration in WS and PBS the fraction of constituents present in WS that was absorbed by PBS during the exposure, i.e., the constituents' absorption efficiencies, were calculated.

The absorption efficiencies of different constituents varied by orders of magnitude, with the result that, as an example, the relative contribution of the ketone diacetyl

to the overall detected smoke constituents was more than two-fold higher in the PBS samples than in WS, whereas in contrast, the relative contribution of naphthalene to the overall detected smoke constituents was more than 40-fold lower in the PBS samples as compared to the WS.

As preclinical toxicity testing is among the first steps in the development of new inhalation products, the demand for efficient and dosimetrically accurate aerosol-to-cell delivery systems is increasing in the community. Recently, the accuracy of the Vitrocell 24/48 delivery system has been assessed (Steiner et al.; Majeed et al.; Adamson et al.). Here we extended the assessment towards PBS absorbed (trapped) constituents, upon smoke exposure in the Vitrocell 24/48. The findings emphasize that for an evaluation of the biological impact of an aerosol, monitoring the absorption of individual constituents to test system (cellular) surfaces is of equal importance as determining the chemical composition of the aerosol. Furthermore, *in vitro* absorption studies as presented here may also allow building a solid knowledge base for estimating *in vivo* absorption and thereby *in vivo* dose delivery.

### References:

- Adamson, J., et al., An inter-machine comparison of tobacco smoke particle deposition *in vitro* from six independent smoke exposure systems. *Toxicology in Vitro*, 2014. 28(7): p. 1320-1328.
- Majeed, S., et al., Characterization of the Vitrocell<sup>®</sup> 24/48 *in vitro* aerosol exposure system using mainstream cigarette smoke. *Chemistry Central Journal*, 2014. 8(1): p. 62.
- Steiner, S., et al., A new fluorescence-based method for characterizing *in vitro* aerosol exposure systems. *Toxicology in Vitro*, 2017. 38: p. 150-158.

## **Abstracts T504**

## Modeling and simulation of electrostatically charged particle dynamics in the inflow and transition area of cabin air filter media

C. Schober<sup>1</sup>, D. Keerl<sup>2</sup>, M. Lehmann<sup>3</sup> and M. Mehl<sup>4</sup>

<sup>1</sup>Graduate School of Excellence advanced Manufacturing Engineering (GSaME), University of Stuttgart, Stuttgart, 70569, Germany

<sup>2</sup>MANN+HUMMEL Innenraumfilter GmbH & Co. KG, Himmelkron, 95502, Germany

<sup>3</sup>MANN+HUMMEL GmbH, Ludwigsburg, 71636, Germany

<sup>4</sup>Institute for Parallel and Distributed Systems (IPVS), University of Stuttgart, Stuttgart, 70569, Germany

Keywords: Particle Dynamics, Simulation, Four-Way Coupling, Electrostatic Interactions.

Presenting author email: carolin.schober@gsame.uni-stuttgart.de

Cabin air filters are applied to prevent small particles such as pollen, fine dust and soot amongst others from being transferred into the interior (cabin) of a vehicle. The filter media often make use of the so called electret effect as means for achieving high filtration efficiency at low pressure drop. Thereby, electrostatic filtration effects are supplemented to the well-known mechanical collision mechanisms (such as inertia, diffusion, etc.). Besides the interference of several fiber-particle interactions (Coulombic attraction/repulsion, induced dipolar forces, image charge effects) particle-particle interactions potentially play an important role. However, this effect is completely neglected in previous research studies due to the high degree of complexity. The objective of this work is to determine the effect of particle-particle forces and whether a simplified approach is justifiable.

### Four-way coupling for enhanced particle simulations

In this work, we present a detailed investigation of the particle motion in the inflow area and transition areas of the filter media. For a precise description of the underlying physical procedures, the simulation is based on a four-way coupling. This approach takes into account the reciprocal influence between the fluid flow and the particle motion as well as the interactions between single electrostatically charged particles.

The software package ESPResSo (Arnold *et al.*, 2013) used in this work provides a powerful tool for this four-way coupling. Based on a molecular dynamic approach the software offers the advantage of applying efficient algorithms for the modeling of electrostatic interactions. Particle-particle interactions on a molecular level are expressed by means of the potential  $U(r)$ , which depends on the distance  $r$  between two particles. The most important representatives regarding the potential interactions of aerosol particles are Lennard-Jones, harmonic bonding and predominantly the long-ranged Coulomb potential. In order to emulate the air flow, the molecular dynamic simulation is coupled with a Lattice-Boltzmann fluid.

The first part of this work deals with the simulation of particle dynamics in a flow field representing the inlet of the filter medium. The mutual interference of particles with varying characteristics in a periodic domain is simulated. Particle collisions lead to

bonds which keep the particles together due to adherence forces (Jimenez, 2013). The various potentials lead to particle movements until force equilibrium is achieved. Different particle concentrations and charge intensities result in different degrees of agglomeration.

In the second step the flow of the balanced particle concentrations or agglomerates entering the fibrous structure of a filter medium is analyzed. The transition to the filter medium is simplified as single fibers or single pores, respectively. Due to the sudden increase of the flow velocity, as shown in figure 1, the equilibrium is disturbed and particles rearrange. The movement of agglomerates and possible impacts with fibers are simulated with a focus on the influence of the fully coupled system on the collection efficiency of the filter medium.

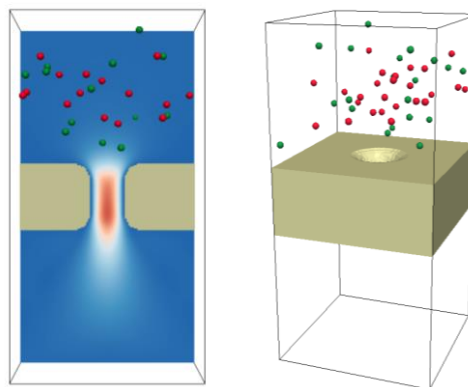


Figure 1. Positively and negatively charged particles in the transition area to a single pore. In addition to the three-dimensional view of the scenario (right), a slice plot of the air flow field is shown (left).

Arnold A., Lenz O., Kesselheim S., Weeber R., Fahrenberger F., Roehm D., Košován P. and Holm C. (2013) *ESPResSo 3.1: Molecular Dynamic Software for Coarse-Grained Models*, Lecture Notes in Computational Science and Engineering.

Jiménez J.F.C. (2013) *Particle agglomeration in flow modelled with molecular dynamics coupled to a thermal Lattice-Boltzmann code*, Task Quarterly

## Stokes-Brinkman model of fluid flow through porous body of arbitrary shape

R.F. Mardanov<sup>1</sup>, S.K. Zaripov<sup>1</sup>, V.F. Sharafutdinov<sup>1</sup>, S.J. Dunnett<sup>2</sup>

<sup>1</sup>Kazan Federal University, Kazan, 420008, Russia

<sup>2</sup>Loughborough University, Loughborough, LE11 3TU, UK

Keywords: aerosol filtration, porous body, Stokes flow, Brinkman equation, boundary element method

Presenting author email: renat.mardanov@kpfu.ru

Fully or partially porous bodies can be used as aerosol filter elements. To evaluate the capture efficiency for porous elements, the fluid flow in an ordered or random packing of porous elements must be calculated. Corresponding models approximating a circular Kuwabara cell model for a porous circular cylinder were developed by Stechkina (1979), Kirsh (2006), Mardanov et al (2016). In this work the problem formulation and results of the study of fluid flow past an arbitrary shaped porous body in a rectangular periodic cell are presented.

Let us consider the two-dimensional flow of an incompressible viscous fluid through a porous body with constant permeability  $k$  in a periodic rectangular cell. The typical size  $R_c$  of the porous element and the velocity  $U$  are selected as the length and velocity scales. The computational domain  $\Omega$  consists of a homogeneous area  $\Omega^e$  of the external flow and a porous medium  $\Omega^i$  of the internal flow inside the body. Denote the periodic cell porosity by  $\varepsilon = 1 - \pi / (4h_1h_2)$  (fig. 1).

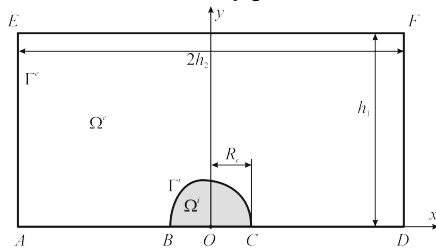


Figure 1. Calculation domain

The external flow in the area  $\Omega^e$  is described in the Stokes flow approximation. The flow stream function  $\psi^e(x, y)$  satisfies the biharmonic equation

$$\Delta^2 \psi^e = 0.$$

On the boundaries  $AE, DF$  the periodic conditions are set

$$\psi^e(-h_2, y) = \psi^e(h_2, y), \quad \psi^{e'}(-h_2, y) = -\psi^{e'}(h_2, y),$$

$$\omega^e(-h_2, y) = \omega^e(h_2, y), \quad \omega^{e'}(-h_2, y) = -\omega^{e'}(h_2, y),$$

where  $\omega^e = -\Delta \psi^e$  is the vorticity (a prime denotes differentiation with respect to the outward normal to the boundary). On the boundary  $EF: \psi^e = h_1, \quad \omega^e = 0$ .

On the axis-lines  $AB$  and  $CD$  the symmetry conditions hold:  $\psi^e = 0, \quad \omega^e = 0$ .

In the porous domain  $\Omega^i$  the flow is described within the Brinkman model. The stream function  $\psi^i(x, y)$  of the fluid flow inside the body satisfies the Brinkman equation ( $S = R_c / \sqrt{k}$ )

$$\Delta^2 \psi^i - S^2 \Delta \psi^i = 0.$$

The symmetry conditions are taken on the line  $BOC: \psi^i = 0, \quad \omega^i = 0$ . On the boundary  $BC$  between the free space and the porous medium the conditions of equality of velocity vectors, pressure and tangential stresses are taken. Considering the flow stream function and vorticity these are written as:

$$\psi^e = \psi^i, \quad \psi^{e'} = \psi^{i'}, \quad \omega^{e'} = S^2 \psi^{i'} + \omega^{i'}, \quad \omega^e = \omega^i.$$

The boundary element method (BEM) is used to solve the above boundary value problem. Due to the form of the boundary conditions taken the method described can be used to solve the problem of fluid flow through a porous body of arbitrary shape. The method was tested for the case of a porous circular cylinder of unity radius. Comparison of the streamlines and gas capture coefficient  $Q = \psi(0, 1)$  obtained by the BEM and by CFD ANSYS/FLUENT calculations are shown in figs. 2, 3, where good agreement is shown. The results of parametrical studies of porous element of various shapes will be presented at the conference.

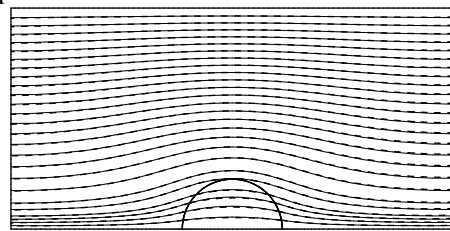


Figure 2. Fluid flow streamlines at  $S = 3, \varepsilon = 0.96$ .

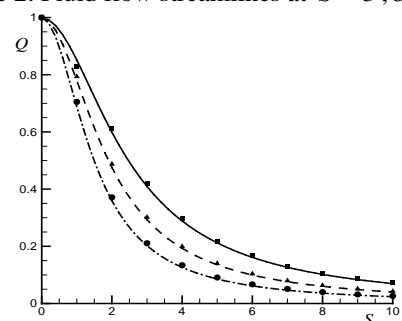


Figure 3. The dependence  $Q(S)$  for various porosity ( $\varepsilon = 0.9; 0.96; 0.99$  – solid, dashed and dash-dotted lines, ANSYS/FLUENT – symbols).

This work is supported by the Russian Government Program of Competitive Growth of Kazan Federal University, RFBR grants № 15-01-06135, 16-51-10024.

Stechkina, I.B. (1979) *Fluid Dyn.* **14**(6), 912–915.

Kirsch, V.A. (2006) *Theor Found Chem Eng* **40**(5), 465–471.

Mardanov, R.F., Dunnett, S.J. and Zaripov, S.K. (2016) *Eng Anal Bound Elem* **68**, 54–62.

## Study on the penetration of silver nanowires passing through polyester filters

Seoungho Lim<sup>1</sup>, Haneol Lee<sup>1</sup>, Hyunseol Park<sup>2</sup> and Weon Gyu Shin<sup>1</sup>

<sup>1</sup>Department of Mechanical Engineering, Chungnam National University, Daejeon, 34134, South Korea

<sup>2</sup>High Efficiency and Clean Energy Research Division, Korea Institute of Energy Research, Daejeon, 34129, South Korea

Keywords: silver nanowire, filtration, polyester filter, mobility diameter

Presenting author email: wgshin@cnu.ac.kr

Particles with a high aspect ratio such nanowires have a wide range of industrial applications. However, since those particles may be harmful to human health, filtration of nanoparticles with a high aspect ratio has been investigated (Ji et al. 2012; Wang and Otani 2012). The orientation angle of particles acts as an important variable to predict the collection efficiency by interception of fibrous particles.

There have been numerical studies on the penetration of fibrous particles and nanowires through a fiber filter or screen filter. In simulation the orientation angle and shape of a fibrous particle and geometric characteristics of the filter were considered. However, up to now, filtration of nanowires through commercial fibrous filters has not been investigated.

In this study we aimed to find out whether the single fiber theory considering the effect of interception of diffusing particles can be applied to predict the penetration of particles with a high aspect ratio through commercial filters. In this study, the theoretical, numerical, and experiment studies were carried out regarding the penetration of silver nanowires through two types of polyester filters: the screen filter and the fibrous filter. The silver nanowires were classified using DMA in the size range of 200 nm to 400 nm as the mobility diameter increased by 50 nm.

In the experiments, we used the screen filter with a regular array of filter fibers and the fibrous filter with an irregular array of filter fibers.

The orientation angles of silver nanowires passing through the single layer and multi-layers of polyester filter were obtained by fitting experimental data. In cases of single layer, the orientation angle of silver nanowires passing through the screen filter is very close to the average orientation angle of 40° reported by Wang et al. (2011) and in the range from 33° to 51° reported by Son et al. (2014). Seto et al. (2010) show that the orientation angle for the case of the fibrous filter with relatively low solidity is close to 40°. However, in our experiments for the case of the fibrous filter with relatively high solidity, the orientation angle is in the range from 70° to 80°

Also, we experimentally investigated the penetration of silver nanowires through the multiple layers of both screen and fibrous filters. The orientation angle of nanowires passing through the multiple layers for both the screen and the fibrous filters is smaller than the orientation angle of nanowires passing through the single layer. Numerical predictions for the penetration of silver nanowires passing through single polyester filter and 5 layers of screen filter were carried out using

orientation. Figure 1 shows penetration of silver nanowires through 5 layers of screen filter.

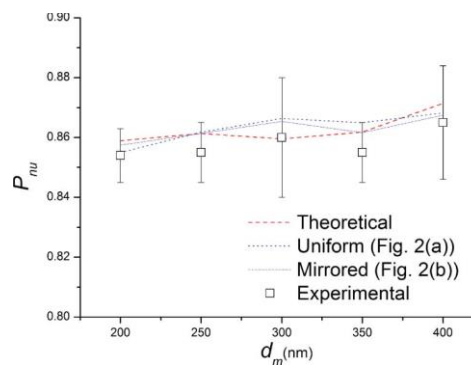


Figure 1. Penetration of silver nanowires through 5 layers of screen filter.

Numerical prediction results show good agreement with experimental data and theoretical prediction. Our results show that the three-dimensional numerical models for the prediction of penetration of silver nanowires are effective when the filter fiber diameter, solidity and thickness of filter are known.

This work was conducted under the framework of Research and Development Program of the Korea Institute of Energy Research (KIER) (B6-2440).

- Ji, Z., Wang, X., Zhang, H., Lin, S., Meng, H., Sun, B., Gorge, S., Xia, T., Nel, A. E., and Zink, J. I. (2012) *ACS Nano* **6**, 5366–5380.
- Wang, C., and Otani, Y. (2012) *Ind. Engineering Chem. Res.* **52**, 5–17.
- Wang, J., Kim, S. C., and Pui, D. Y. H. (2011) *J. Nanopart. Res.* **13**, 4565–4573.
- Seto, T., Furukawa, T., Otani, Y., Uchida, K., and Endo, S. (2010) *Aerosol Sci. Technol.* **44**, 734–740.
- Son, M., Park, H., Park, M., Wang, J., and Shin, W. G. (2014) *Aerosol Sci. Technol.* **48**, 480–488.

## Nanodroplets oil separation in fibrous filters modified by aerogel

Ł. Werner<sup>1</sup>, A. Jackiewicz<sup>1</sup>, J. Gac<sup>1</sup>, B. Nowak<sup>1</sup> and M. Bojarska<sup>1,2</sup>

<sup>1</sup> Faculty of Chemical and Process Engineering, Warsaw University of Technology, Warsaw, 00-645, Poland

<sup>2</sup> Lehrstuhl für Technische Chemie II, Universität Duisburg-Essen, Essen 45117, Germany

Keywords: filtration, fibrous filters, melt-blown, aerogel modification.

Presenting author email: l.werner@ichip.pw.edu.pl

In recent years we could observe the rapid growth in the use of novel technologies in many industries, in healthcare, agriculture and in many automotive applications. Unfortunately, it is related to the appearance of significant amount of liquid aerosols and oil mists. The use of filters allows to reduce or even eliminate droplets from airstream which could deposit in human respiratory system and causing diseases such as asthma, allergy, pneumonia, bronchitis or even cancer. Moreover, filters are used in ventilation systems to ensure protection against contamination, which can lead to irregularities in its operation and damage its individual components.

One of the most effective and commonly used method to remove oil droplets from the air is filtration in fibrous filters made by the melt-blown technique. Researchers are looking for fiber surface modification methods that would increase the effectiveness of such materials or give them new properties (Cheikh R. et al. 2002). Generally, they could be divided into chemical and physicochemical methods. Chemical methods rely on performing changes in the chemical composition of the surface, while physicochemical ones influence the surface morphology, i.e. texture or roughness (Zielińska and Halacheva 2011).

The aim of this study was to enhance the filtration efficiency by modification of polymer nonwovens using aerogel spheres. Aerogels are organosilicon structures, synthesized in two step sol-gel process. They are highly porous solid materials with very low density (and hence low weight) and good thermal insulation. Due to its hierarchic porosity (in micro- and nanoscale), aerogels are highly effective as sorbents, used to absorb oils and other mineral and organic liquids. Aerogels with methyltrimethoxysilane (MTMS) used as a precursor have hydrophobic, oleophilic and oil-sorptive properties (Yun et al. 2014 and Rao et al. 2006). For the above reasons they have been chosen to carry out the modification of made by us melt-blown fibers.

The filters were modified with different ratio of MTMS to methanol. For the observation of fibers surface the high resolution scanning electron microscope was applied (see Figure 1). Both unmodified and modified filters were tested with the highest class tests bench from Palas company. It was checked how these fabrics separate oil nano- and submicron droplets of diethylhexyl sebacate (DEHS) from air.

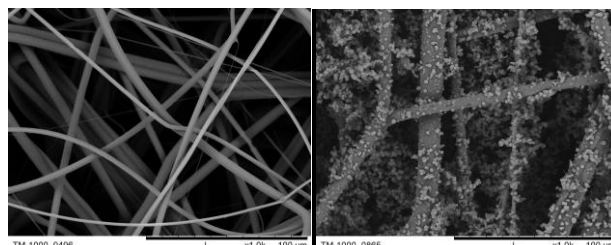


Figure 1. SEM pictures of filtering materials: unmodified (left side), modified with aerogel in 1:15 ratio (right side)

Results below shown (see Figure 2) that for all samples with aerogel filtration efficiency increased as compared to raw material (reference filter). Moreover, due to the advanced test bench we received data for a wide range of droplet diameters from 20 nm to 2 μm, which allows to determine the most penetrating particle size (MPPS).

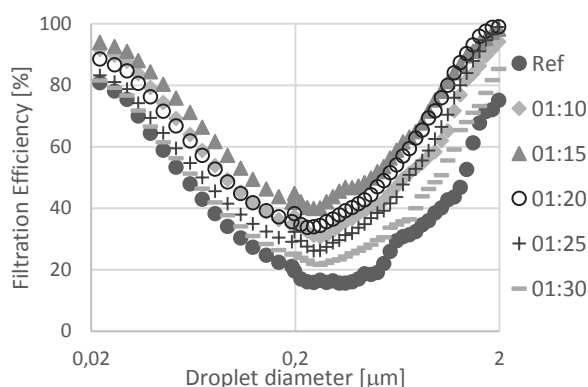


Figure 2. Fractional efficiency of reference filter (Ref) and aerogel modified filtering materials at different MTMS:methanol ratios

This work was supported by NCBiR project “Oil removal from gas and liquid streams thanks to filter media modified by aerogel” LIDER/011/L6/14/NCBR/2015.

Cheikh R., Askeland P., Schalek R. and Drzal L. (2002) *J. Adhesion Sci. Tech.* **16**, 1651-1668.

Rao A.V., Bhagat S. D., Hirashima H., Pajonk G. M. (2006) *J. Coll. and Int. Sc.* **300**, 279-285.

Yun S., Luo H. and Gao Y. (2014) *RSC Adv.* **4**, 4535-4542.

Zielińska D. and Halacheva S. (2011), *Techniczne Wyroby Włókiennicze.* **1:2**, 16-20.

## Particle removal efficiency of commercial air purifiers by particulate matter (PM)

S. Yun<sup>1</sup> and Y. Seo<sup>2</sup>

<sup>1</sup>Yonsei Institute of Green Technology, Yonsei University, Seoul, 03722, Republic of Korea

<sup>2</sup>Department of Mechanical Engineering, Kumoh National Institute of Technology, Gumi, 39177, Republic of Korea

Keywords: removal efficiency, PM, HEPA.

Presenting author email: yjseo@kumoh.ac.kr

Air ventilation is more effective way than air purifiers in terms of enhancement of indoor air quality, but it is not always possible due to outdoor weather conditions such as rain and dust storm, etc. As an alternative, use of residential air purifiers is significantly increased. Its performance is very important as it has a direct relationship with person's life.

Fine particulate matter was used to verify removal efficiency of several commercial air purifiers in this study. Tests were conducted in a wind tunnel and 0.3  $\mu\text{m}$  polystyrene latex beads were used. All air purifiers contain pre-filter and high-efficiency particulate air (HEPA) filter.

The removal efficiency is calculated as below:

$$\eta = 1 - \frac{C_a}{C_b}$$

where,  $C_a$  and  $C_b$  are after and before concentrations for after and before air purifiers, respectively. The removal efficiency was  $0.95 \pm 0.03$  that was lower than commonly known efficiency with a HEPA filter.

In addition, field tests were conducted in and out of ten households for six days. During the tests, particulate matters were verified inside and outside. Air purifiers were on for first three days and they were off for the next three days. All other ventilation systems were off during the test. Table 1 shows test conditions for five of ten households.

Both  $\text{PM}_{2.5}$  and  $\text{PM}_{10}$  were verified. Averaged indoor  $\text{PM}_{2.5}$  concentration without air purifiers was about  $62 \mu\text{g}/\text{m}^3$  and the concentration decreased to  $31 \mu\text{g}/\text{m}^3$ . Averaged outdoor  $\text{PM}_{2.5}$  concentration was approximately  $40 \mu\text{g}/\text{m}^3$  for all six days. After P-test ( $p < 0.05$ ), operation of air purifiers makes significant differences in the indoor  $\text{PM}_{2.5}$  concentration. In case of  $\text{PM}_{10}$ , similar results with  $\text{PM}_{2.5}$  case were obtained. Averaged indoor  $\text{PM}_{10}$  concentration was decreased from about 94 to  $50 \mu\text{g}/\text{m}^3$  which shows statistically difference.

The above results clearly demonstrated the effectiveness of air purifiers in terms of enhancement of indoor air quality.

More experiments will be conducted by using bacteria and mold and the results will be described during the session in EAC 2017.

**Table 1.** Descriptions of the tested houses.

Home	Building stories	House size, $\text{m}^2$	Room size, $\text{m}^2$
1	15	108.9	8.9
2	5	79.2	8.9
3	18	79.2	10.6
4	15	105.6	15.5
4	25	89.1	15.2

Grinshpun, S. A., Mainelis, G., Trunov, M., Adhikari, A., Reponen, T. and Willeke, K. (2005) *Indoor air* **15(4)**, 235-245.

Hutton, G., E. Rehfuess, and F. Tediosi. (2007) *Energy for Sustainable Development* **11(4)**, 34-43.

Mølgaard, B., Koivisto, A. J., Hussein, T. and Hämeri, K. (2014) *Aerosol Science and Technology* **48(4)**, 409-417.

Yu, I. T. S., H. Qiu, X. Wang, L. Tian, and L. A. Tse. (2013) *International Journal of Cardiology* **168 (3)**, 2831-2836.

## Simultaneous removal of soot and NO<sub>x</sub> from biomass boiler fumes over catalytic sintered filter.

G. Tesquet<sup>1</sup>, A. Villot<sup>1</sup>, A. Guyon<sup>2</sup>, F. Tresse<sup>3</sup>, L. Le Coq<sup>1</sup>.

<sup>1</sup> Ecole des Mines de Nantes, GEPEA UMR CNRS 6144, 4 rue Alfred Kastler, BP 20722, 44307 Nantes cedex 03, France

<sup>2</sup> Sintertech, Le pont-de-Claix, 38800, France

<sup>3</sup> Prodec Metal-STI Group, Mérignac, 33700, France

Keywords: catalytic filter, emission, NO<sub>x</sub> Soot.

Author: Guillaume.Tesquet@mines-nantes.fr

Because of the global warming, due to the high greenhouse gases emission, and the limited resources of fossil fuels, the worldwide concern for the energy production from biomass combustion, has strongly enhanced. However, biomass combustion plant generates lot of pollutants too (PM<sub>2.5</sub> / PM<sub>10</sub>, nitrogen and sulfur oxide, heavy metals, ...). Soot and NO<sub>x</sub> (NO and NO<sub>2</sub>), which from industrial small-scale boiler, are pollutants focused in this project. Since Directive 2010/75/EU of January 2014, the control of soot and NO<sub>x</sub> emissions is more stringent, due to their harmful effects on the human health and environment, only for high power plants. However, in a near future, this will be extended on smaller biomass boiler (< 4 MWh).

Soot is carbonaceous aggregates with a size from 10-100 nm in aerodynamic diameter. They are emitted when the combustion is uncompleted, which are mainly due to combustion conditions poor in O<sub>2</sub>. At the exhaust of combustion room, emitted particles are generally trapped by two different devices: inertial filtration (cyclone(s)) for the largest (PM<sub>10</sub>) and then, porous filter media for the smallest (PM<sub>2.5</sub>). There are several kind of filter media, as bag filter and rigid filter mainly, which of various nature in function of their composition (ceramic, metallic), structure (fibrous, sintered ...) (Heidenreich *et al.* 2013).

The most widely used technique for removing of only NO<sub>x</sub> is the Selective Catalytic Reduction (SCR) over V<sub>2</sub>O<sub>5</sub>-WO<sub>3</sub> (MoO<sub>3</sub>)/TiO<sub>2</sub> with NH<sub>3</sub>, as reducing agent, and in excess of O<sub>2</sub>. However, this SCR unit has to be located at the upstream particles filtration system, because it's efficient at a temperature range of 330°C to 400°C, and this brings such problems as dust deposition on catalyst (Yang *et al.* 2011). Several studies have been performed over transition metals oxide from Fe, Cu, Co and Ni supported on high specific surface materials in order to reduce NO<sub>x</sub> at lower temperature (< 300°C).

The aim of this work is to remove simultaneously soot and NO<sub>x</sub> from small-scale biomass boiler, thanks to a copper alloys functionalized sintered filters. The filter media (disc) are prepared by Sintertech industry and the functionalization by PRODEC METAL society and/or Ecole des Mines de Nantes. In order to be competitive with DeNO<sub>x</sub> system existing, the NO<sub>x</sub> conversion as to reach about 30-40%, but without reducing agent and at lower temperature than currently.

Media filters are tested on an experimental pilot, which allows simulating fumes from biomass boiler. Test conditions are chosen to be the closest of real condition of a flue gas treatment located after cyclones,

*i.e.* temperature between 200 and 300°C, 7% in O<sub>2</sub>, NO<sub>x</sub> concentration of 220 ppm and 4E+08 part/cm<sup>3</sup> of soot with a mode around 0.1µm. Test duration is of 1h.

The main challenge in this work is to find a catalyst able to reduce NO<sub>x</sub> at low temperature. Results presented are NO<sub>x</sub> conversion average by 10 minutes range. In a first time, two types of metallic deposition (Cu, Ni) and two types of support oxidation, thermally and chemically, to form copper oxide CuO have been studied at different temperatures and with or without particles to observe their influence. Experiments show a better NO<sub>x</sub> conversion, in the first 10 min, for a Cu deposition than Ni with 2.7 and 1.3% respectively. Support oxidation treatment doesn't reveal an important influence about NO<sub>x</sub> conversion, so the thermal oxidation is favorised because this is cheaper. In the Figure 1, after the 10 first minutes, NO<sub>x</sub> is near to zero because the media filter is undersized compared to the flow used in test. This condition are chosen in order to quickly saturated the filter and do measurement in 1 day. Soot influence isn't well determined with these tests. This could come from the interaction with the different type of catalysts, as described by Yoshida *et al.* (1989).

In a second time, the parameters, which have obtained better results, are combined to optimize the NO<sub>x</sub> conversion. By consequent, the support is thermally oxidized and metallic copper deposition is performed. Others oxidized media filter are prepared with doping elements, as potassium or iron. All these tests are not carried out still. But, the K doped filter show a NO<sub>x</sub> conversion of 17% in the first 10 min, and around 10% for the test remaining (Figure 1). This no expensive filter is a promising solution.

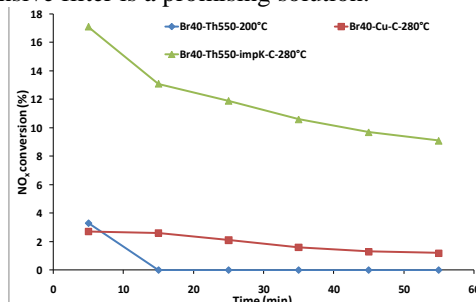


Figure 1: NO<sub>x</sub> conversion as a function of time

This work is supported by Agence de l'environnement et de la maîtrise de l'énergie (ADEME).

1 Heidenreich, S. (2013), Fuel, 104, 83-94.

2 Yang, S, Wang, Li, J, Yan, N, Ma, L, Chang, M, (2011), Appl Catal B : Environ. 110 71-80.

3 Yoshida, K, Makino, S, Sumiya, S, Muramatsu, G, Helferich, R, (1989) SAE Paper. 892046.

## Cleaning efficiency and aging of electret filters in mobile air purifiers

S. Schumacher<sup>1</sup>, D. Spiegelhoff<sup>1</sup>, U. Schneiderwind<sup>1</sup>, H. Finger<sup>1</sup>, and C. Asbach<sup>1</sup>

<sup>1</sup>Institut für Energie- und Umwelttechnik e.V. (IUTA), 47229 Duisburg, Germany

Keywords: air purifiers, electret filters, particle size dependence, filter aging

Presenting author email: schumacher@iuta.de

Air pollution is a growing problem, especially in metropolitan areas. This not only concerns atmospheric pollution, but also the indoor air quality, which can be deteriorated either by infiltration from outside or by indoor sources (e.g., smoking, cooking or candles). Since people in industrial nations spent most of their time inside buildings, the latter is of special importance. A way to improve the indoor air quality is to use mobile air purifiers. Such devices use a fan to draw the polluted air through a filter and release the purified air back to the room so that the concentration of the pollutants decreases exponentially with time. In the study presented here, fibrous electret filters were used.

There are various national standards to test mobile air purifiers. Most of them rate the cleaning performance using the clean air delivery rate (CADR), which describes the flow rate of clean air delivered by the air purifier. The CADR ideally equals the product of the filtration efficiency and the volumetric flow rate of the device. It can be determined for both particulate and gaseous pollutants. Concerning particles, most standards determine the CADR value integrated over a particle size range from 0.3 to 10  $\mu\text{m}$ . However, relevant indoor aerosols as well as the cigarette smoke used for the standardized CADR tests mainly consist of much smaller particles and contain only few particles larger than 0.3  $\mu\text{m}$  (see Fig. 1). Therefore, the question arises whether such CADR measurements yield a praxis-oriented measure.

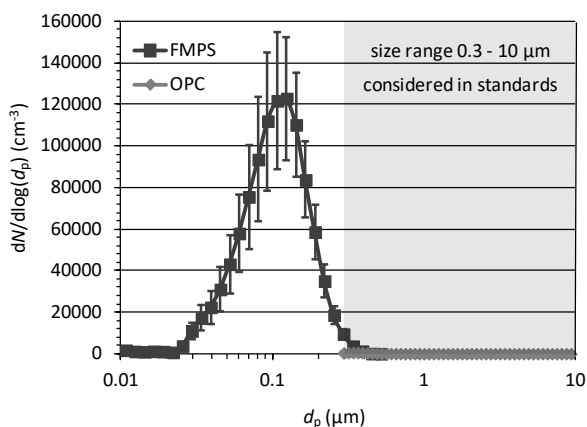


Figure 1. Cigarette aerosol used for CADR tests. The size range considered in most standards is indicated.

To address this question, we investigated the size-dependent CADR for particles between 0.03 to 0.6  $\mu\text{m}$  with a fast mobility particle sizer (FMPS) and an optical particle counter (OPC). As shown in Fig. 2, the CADR drops with decreasing particle size. This means that recent standards strongly overestimate the cleaning efficiency with respect to relevant indoor aerosols such as cigarette smoke if considering only particles larger than 0.3  $\mu\text{m}$ .

ciency with respect to relevant indoor aerosols such as cigarette smoke if considering only particles larger than 0.3  $\mu\text{m}$ .

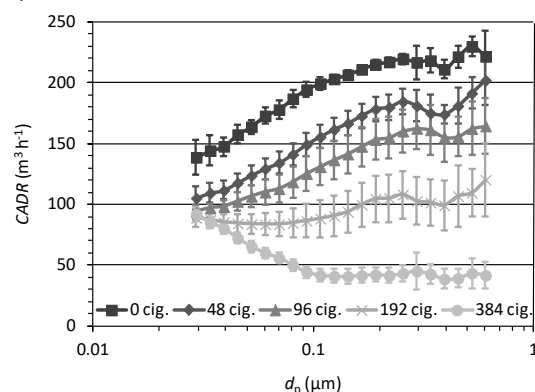


Figure 2. CADR as a function of particle size after aging with the indicated number of cigarettes.

Furthermore, it is known that the efficiency of electret filters can drastically degrade with time (Finger 2015) due to exposure to particles, gases or humidity. We developed a method to reproducibly age the filters in order to evaluate their long-term stability: The air purifier continuously runs in a 25  $\text{m}^3$  room, in which cigarettes are burned in steps of 12 at the same time. Fig. 2 shows the size-fractionated CADR after aging with the indicated number of cigarettes. Whereas the CADR after aging with 384 cigarettes drops only by about 33% for 0.03  $\mu\text{m}$  particles, it more drastically decreases by more than a factor of 4 for 0.6  $\mu\text{m}$  particles. We explain this effect by the strong size dependence of the electrostatic contribution to the total filtration efficiency (Schumacher 2017). We furthermore compare the results to aging with 48 cigarettes at the same time in a 3  $\text{m}^3$  cube as proposed by a recent Chinese standard and find a very distinct aging behaviour. This shows that for a praxis-oriented rating of the long-term stability the considered particle size range and the conditions of aging are of great importance.

The IGF project 19145 N was funded via the German Federation of Industrial Research Associations (AiF) within the programme to support industrial collective research (IGF) by the German Federal Ministry for Economic Affairs and Energy (BMWi) based on a decision of the German Bundestag.

Finger, H. et al. (2015): *Gefahrstoffe - Reinhalt. Luft* **75** 497.

Schumacher, S. et al. (2017): submitted to *Chem. Eng. Technol.*

## Collection of polyamide nanofibers on PTFE foam coated filter

Han-Bin Kim<sup>1,2</sup>, Ki Bong Lee<sup>2</sup>, Sang-Joon Cho<sup>3</sup>, and Myong-Hwa Lee<sup>1,\*</sup>

<sup>1</sup>Thermochemical Energy System R&D Group, Korea Institute of Industrial Technology, Republic of Korea

<sup>2</sup>Department of Chemical and Biological Engineering, Korea University, Republic of Korea

<sup>3</sup>Changmyoung Industry LTD., Republic of Korea

Keywords: Nanofiber, Bag filter, Polyamide polymer, Electrospinning.

Presenting author email: hbbunny89@kitech.re.kr

Bag house is generally used to remove particulate matters exhausted from various combustors. Bag filter is the most important component to determine the collection performance of a bag house. PTFE foam coated filter tolerable to relatively high temperature was developed in our recent study (Park et al (2010)). However, the filter has still a large pore size more than  $10\ \mu\text{m}$ , which results in low collection efficiency. Therefore, we attempted to decrease the pore size by collecting nanofibers made of a polyamide polymer on the PTFE foam coated filter in this study.

Electrospinning process using a twin fluid nozzle was employed to produce polyamide nanofibers. Polyamide solution was prepared by melting a polyamide polymer in a lithium chloride (LiCl) added dimethylformamide (DMF). Figure 1 shows the experimental setup to produce nanofibers using electrospinning. The solution was injected through a syringe nozzle under a certain electric field. Fiber diameter depended on several operating parameters, i.e. solution concentration, electric field, tip to collector distance, flowrate of compressed air. The effects of the operating parameters on the fiber diameter and morphology were observed by a scanning electron microscope (SEM). Figure 2 is a SEM image of the PTFE foam coated filter covered with polyamide nanofibers. We could clearly see the polyamide nanofibers distributed on the PTFE foam coated filter. In addition, the change in collection efficiency, pressure drop and filter cleaning efficiency were investigated and discussed in terms of a fiber diameter and a fiber loading on the filter surface.

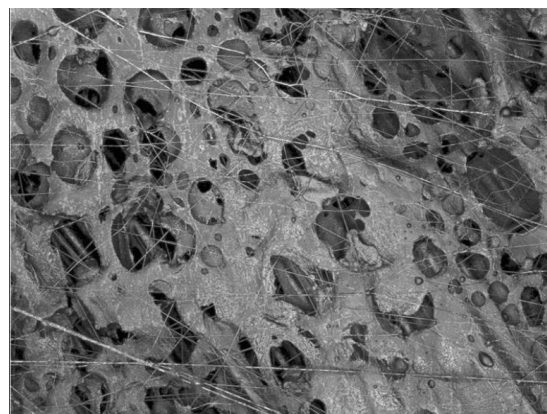


Figure 2. Surface morphology of a PTFE foam coated filter covered with polyamide nanofibers.

This work was supported by the Gyeonggi-Do R&D program under grant D161670.

Park, B. -H.; Lee, M. -H.; Kim, S. -B.; Kim, G. -S.; Jo, Y. -M. (2010) Journal of the Air & Waste Management Association, 60, 137-141.

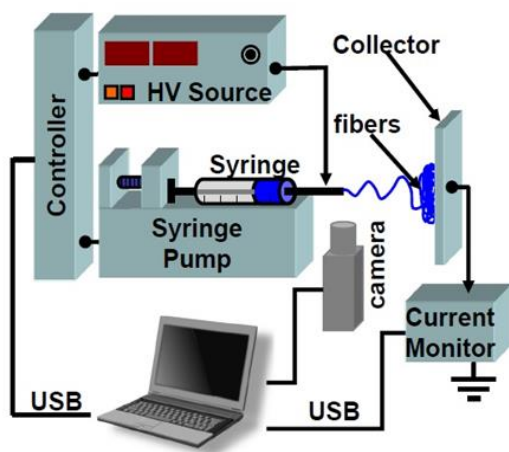


Figure 1. Experimental setup for electrospinning.

## Efficiency of air filters for general ventilation and gas turbines in humid environments

Frank Schmidt<sup>1</sup>, Thomas Engelke<sup>2</sup>, Claudia König<sup>1</sup>, Eckhard Däuber<sup>2</sup>, Christof Asbach<sup>2\*</sup> and Stefan Haep<sup>2</sup>

<sup>1</sup>University Duisburg-Essen, Nanoparticle Process Technology, Duisburg, Germany

<sup>2</sup>Institut für Energie- und Umwelttechnik e. V. (IUTA), Duisburg, Germany

Keywords: filter efficiency, HVAC, gas turbine intake, humid environment.

\*Presenting author email: asbach@iuta.de

### Introduction and Methodologies

Current filter testing standards provide rather non-specific guidelines for the climatic conditions in the test channel:

- DIN EN 779:2012  
Room air or outside air; no information about the temperature; relative humidity should be < 75%
- ASHRAE 52.2-2012  
Temperature 10°C to 38°C; rel. humidity 45% ±10%

Although humidity levels are >70% most of the year in many real environments, standard tests are performed at lower humidity. During normal operation, condensed humidity (fog), sea spray or rain may deposit on the filters, especially in gas turbine intake systems in coastal regions and with offshore locations of gas turbines. In such cases, crystalline salt particles or salt dissolved in water droplets are transported with the air and may reach the turbine blades if not properly filtered out (Loud and Slaterpryce, 1991). As a result, fouling and corrosion can lead to a reduction of the performance and/or of the life-time of the gas turbine. Due to the good water solubility of sea salt, water that passes through the filter may also wash off already deposited particles and transport them into the turbine (Schroth and Cagna, 2008). All of these effects are not taken into account in the abovementioned standards for filter testing.

Therefore, some first systematic attempts were carried out to indicate the effect of high humidity on pressure drop during the exposure to different dusts, as well as the influence of water droplets on the pressure drop. Furthermore, fractional separation efficiencies were measured for relevant operating conditions.

### Results and Discussion

The influence of humidity on the pressure drop and efficiency of used and unused filter was examined. Figure 1 shows the pressure drop as a function of relative humidity. The humidity was repeatedly ramped from 50% to 90% and back to 50%. The pressure drop of the unused filter (class E10) shows no dependence on humidity (blue curve).

An identical filter had been installed in a gas turbine intake system and was removed after 13,000 operating hours before it was tested in the lab. The increase of humidity to values of 90% caused an increase of the pressure drop of around 37 Pa (red curve). Reducing the humidity back to values of 50% again decreased the pressure drop, however, only to values 6 Pa higher than the original value.

Fractional separation efficiencies were determined at the four marked points. Figure 2 shows the corresponding curves. The efficiency at low humidity (dark green curve) decreased significantly after humidity treatment (dark blue curve). Lowering the humidity caused an increase of fractional separation efficiency (light green curve). Re-increasing humidity decreases the efficiency again (light blue curve).

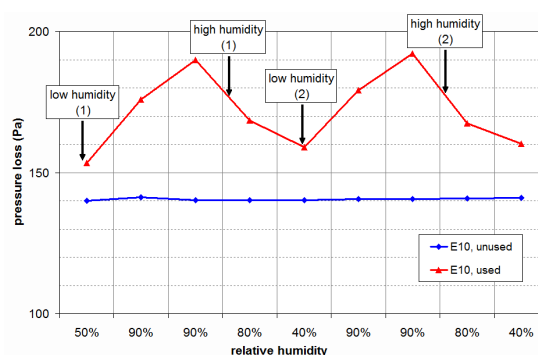


Figure 1. Pressure loss of used and unused filters (class E10).

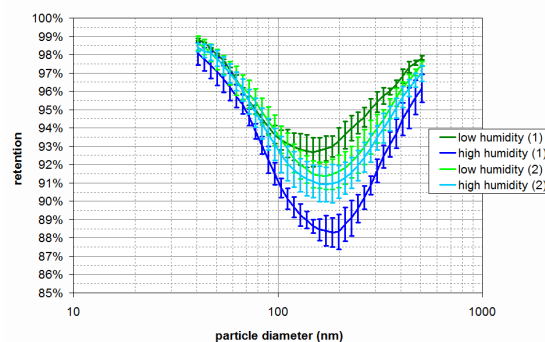


Figure 2. Fractional separation efficiencies of an used filter (class E10) at different humidity.

### Acknowledgement

The project (no. 18292 N) is supported by the Federal Ministry of Economic Affairs and Energy on the basis of a decision by the German Bundestag within the scope of the Industrial Collective Research (IGF) via AiF.

Loud, R. L. and A. A. Slaterpryce, A. A. (1991) *Gas Turbine Inlet Air Treatment*; Schenectady, General Electric Company publication, New York

T. Schroth, T. and Cagna, M. (2008) in *Proc. of GT2008, Gas Turbine Technical Congress & Exposition*, Berlin

## Filtration performance of particle filters for general ventilation aged in real life or loaded with ASHRAE or A2 test dust in the lab

Frank Schmidt<sup>2</sup>, Thomas Engelke<sup>1</sup>, Achim Breidenbach<sup>2</sup>, Christof Asbach<sup>1\*</sup>

<sup>1</sup> *Institut für Energie- und Umwelttechnik e.V. (IUTA), Duisburg, Germany*

<sup>2</sup> *University Duisburg-Essen, Duisburg, Germany*

Keywords: filtration, ASHRAE, test dust, DIN EN 779, HVAC.

\*Presenting author email: [asbach@iuta.de](mailto:asbach@iuta.de)

### Introduction and Methodologies

The first test standards for measuring the performance of air filters for general ventilation were introduced more than 40 years ago. The basic design of the test rig and the test procedures of DIN EN 779:2012 have been developed in 2009. The most important change from the previous version is the introduction of minimum efficiencies for filter classes F7 to F9, which is the lowest value among the initial efficiency, the lowest efficiency throughout the loading procedure of the test and the efficiency of the discharged filter. The latter is evaluated from a media sample treated with isopropanol (IPA) and is the most important criterion for synthetic filters.

However the practical relevance of data (also for filters made of glass fibres) derived from lab testing is still an open question, because it is unclear to what degree the performance of filters used for general ventilation in real life can be predicted from these tests.

In the present study we investigated the pressure drop and efficiency of HVAC bag filters (glass fibres) during loading with test dust ASHRAE and A2 or aged in real air conditioning systems at a flow rate of 3,400 m<sup>3</sup>/h:

- Fine filters (classes F7 up to F9; glass fibre filters) have been installed in regular ventilation systems, removed after 3 to 21 months, tested in the lab and installed again.
- Filters of the same lot were artificially aged by loading with ASHRAE- or A2-dust.
- The lab tests were performed at defined conditions (50% relative humidity and 20°C).
- In accordance with EN 779 DEHS (DiEthylHexylSebacate) was used to measure the efficiencies of 0.4 µm particles.
- Pressure drop and filter efficiencies (retention of particles) were measured for new, regularly used and artificially aged filters. The results were compared.

### Results and Discussion

**Fig. 1** indicates that the increase of pressure drop for fine filters using ASHRAE loading dust is much higher than found in real life, so the results of  $\Delta p$ -measurements are not comparable due to the different properties of the test dust and the particles contained in ambient air.

ASHRAE test dust consists of: 72% fine dust A2 (SiO<sub>2</sub>), 23% carbon black and 5% cotton linters. The last-mentioned ingredient does not enter into the filter due to

its size but instead forms a layer on the front filter surface, so the fine depth filters behave like a surface filters with higher pressure drop and higher filter efficiency.

In contrast, loading with A2-dust fits the real life application very well.

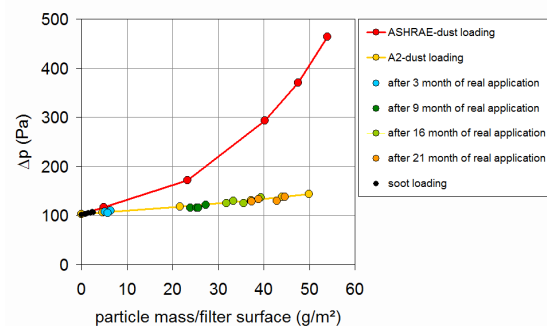


Figure 1. Increase of pressure drop with dust loading: ASHRAE- and A2-dust vs. real life application.

**Fig. 2** shows the retentions of 0.4 µm DEHS particles. Glass fibre filters showed only little increase in particle retention with increasing particle mass on the filter.

Loading filters with ASHRAE dust led to unrealistically high pressure drop for all investigated kinds of media.

Using only A2 gave much lower values of retention, which are more comparable to real life applications.

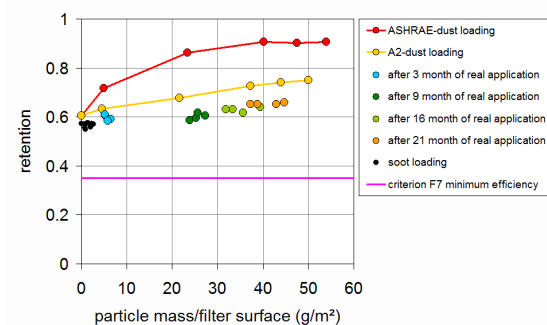


Figure 2. Retention of 0.4 µm particles: ASHRAE, A2-dust and real life loading.

### ACKNOWLEDGEMENT

The IGF-project 17659 N of the research association “Umwelttechnik“ is funded by the German Federal Ministry for Economy and Energy (BMWi) via AiF within the framework of the program for the promotion of industrial cooperative research and development (IGF) based on a decision by the German Bundestag.

## Nanoparticle filtration efficiency of HVAC filters and their media

Christof Asbach<sup>1\*</sup>, Wolfgang Mölter-Siemens<sup>1</sup>, André Schmitz<sup>2</sup>, Frank Schmidt<sup>2</sup>, Ana Maria Todea<sup>1</sup>

<sup>1</sup> Institut für Energie- und Umwelttechnik e.V. (IUTA), Duisburg, Germany

<sup>2</sup> University Duisburg-Essen, Duisburg, Germany

Keywords: filtration, nanoparticles, HVAC, ULPA, HEPA

\*Presenting author email: asbach@iuta.dee

Airborne nanoparticles are ubiquitous in ambient and indoor air. Various studies have shown that nanoparticles can penetrate deep into the human lung and cause adverse health effects. Especially in urban areas, a large fraction of nanoparticles stem from industry and traffic exhaust and may enter indoor environments through HVAC systems. In order to protect humans in indoor environments from exposure to nanoparticles, they have to be efficiently removed by the HVAC filters.

Typically, the number concentration of nanoparticles in the (urban) air is orders of magnitude higher than the concentration of micron sized particles. Still, current standards for the evaluation of HVAC filters (e. g. EN 779) only prescribe the determination of the filtration efficiency at a particle size of 0.4  $\mu\text{m}$ . It is known that the filtration efficiency increases for particle sizes below the most penetrating particle size (MPPS), which typically is between around 100 and 300 nm. High upstream nanoparticle concentrations are therefore required in order to produce statistically secured data downstream of the filter. In the present work, we use a flame aerosol generator (Monsé et al., 2014), which feeds directly into a test rig according to EN779 to produce nanoscale NaCl test aerosols. An aqueous NaCl solution is fed into an hydrogen-oxygen flame via a two component jet, where the NaCl evaporates. Upon cooling downstream of the flame, the vapour nucleates and forms small particles. Due to the immediate dilution inside the EN779 test rig, the particles remain small (modal diameters between 5 nm and 25 nm, depending on settings) with very high concentrations of  $10^7$   $1/\text{cm}^3$  and above and low geometric standard deviations. By feeding the aerosol into the test rig via an extension tube, the modal diameter of the test aerosol can be increased to approximately 65 nm (see Figure 1).

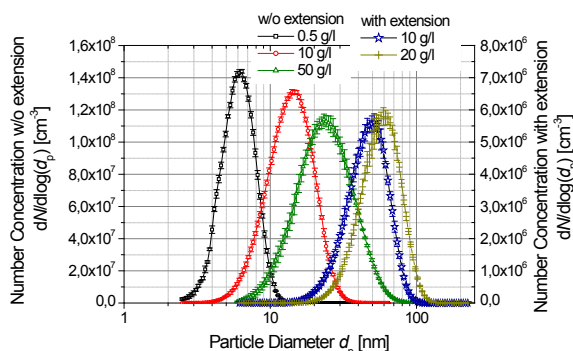


Figure 1: Size distributions of NaCl aerosols in EN 779 test rig, injected with and without extension tube

In the present work, we investigated the efficiency of assembled full size HVAC filter cassettes with a typical cross section of 600 mm x 600 mm and flow rates of several thousands of cubic meters per hour. The efficiency of the filters for particle sizes up to approximately 40 nm were tested using the aforementioned flame aerosol generator, whereas polydisperse DEHS aerosols were used for the larger particles. An example for the fractional deposition efficiency measured with this method is shown in Figure 2.

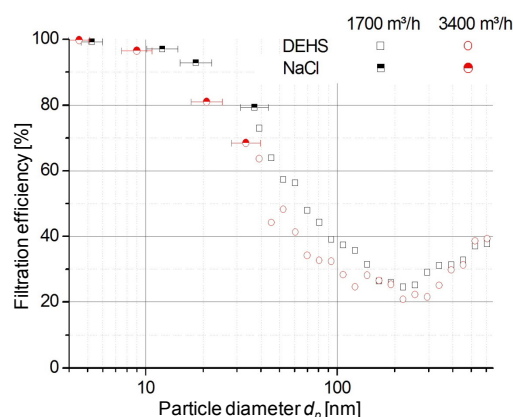


Figure 2: Example for the fractional collection efficiency of a full scale HVAC filter for particle sizes between 5 nm and 600 nm

Besides measurements on full size filter cassettes, the efficiency of the exact same media that were used to build the cassettes was measured as well. One of the goals of the research is to point out whether cross-reading from media tests to the performance of filter cartridges is valid.

The experimental procedure, measurement strategy and experimental results for the fractional collection efficiency of filter media and cassettes down to 5 nm will be presented.

### Reference

C. Monsé et al., *Aerosol Sci. Technol.* **48**: 418-426.

### ACKNOWLEDGEMENT

The IGF-project 18314N of the research association “Umwelttechnik“ is funded by the German Federal Ministry for Economy and Energy (BMWi) via AiF within the framework of the program for the promotion of industrial cooperative research and development (IGF) based on a decision by the German Bundestag.

## **Abstracts T505**

## Random fragmentation of linear chains

L. Isella<sup>1</sup>, A.D. Melas<sup>2</sup>, A.G. Konstandopoulos<sup>2,3</sup> and Y. Drossinos<sup>4</sup>

<sup>1</sup>European Commission, Joint Research Centre, Brussels, Belgium

<sup>2</sup>Aerosol and Particle Technology Laboratory, Centre for Research and Technology Hellas, Thessaloniki, Greece

<sup>3</sup>Department of Chemical Engineering, Aristotle University, Thessaloniki, Greece

<sup>4</sup>European Commission, Joint Research Centre, Ispra, Italy

Keywords: Random fragmentation, monomer chains.

Presenting author email: amelas@cperi.certh.gr

The study of the dynamic behaviour of straight chains provides insights into the dynamics of more complex structures, like fractal-like agglomerates, and it allows the comparison of analytical results with numerical simulations. Furthermore, chains may be considered simple models of nanotubes and nanofibers (straight chains) or biological macromolecules (flexible chains). Whereas the mobility of straight chains has been extensively studied, their agglomeration and, more importantly, their fragmentation properties have not been investigated as thoroughly.

Herein, we analyze the fragment-size distribution of a linear chain upon random, multiple bond (link) removal (breakage). Consider a chain composed of  $N+1$  monomers connected via  $N$  links. Fragmentation occurs by randomly removing  $n \leq N$  bonds ( $n$  cuts). Equivalently, a bond is removed randomly and the process is repeated  $n$  times. This random fragmentation of a discrete chain is related to an occupancy problem on how to distribute  $N+1$  balls into  $n+1$  baskets under the constraint that no basket remain empty (Feller, 1968). The joint probability that fragments of size  $s_i$  ( $i=1, \dots, n+1$ ) are generated after  $n$  cuts is

$$P(S_1 = s_1, \dots, S_{n+1} = s_{n+1}) = 1 / \binom{N}{n},$$

where the denominator is a binomial coefficient. In particular, the fragment-size distribution after one cut is uniform,  $1/N$ . In general, after  $n$  cuts the probability that a fragment of size  $s$  is formed is

$$P(S_1 = s) = \binom{N-s}{n-1} / \binom{N}{n}, s = 1, \dots, N-n+1.$$

A related problem is to determine the average size of the largest (smallest) fragment after  $n$  simultaneous cuts (an order statistics problem, as the segments are ordered according to their size). If the discrete nature of the chain is neglected, this problem may be mapped into the division of the  $[0,1]$  interval (after proper normalization) into  $n+1$  subintervals, the location of the cuts being chosen from a uniform distribution (David and Nagaraja, 2003). It can be shown that in this continuum version the expectation value of the smallest segment is  $1/(n+1)^2$ , with  $n+1$  the number of subintervals ( $n$  cuts), whereas the expectation value of the largest

segment is  $H(n+1)/(n+1)$  where  $H(n)$  is the  $n$ -th harmonic number (e.g.,  $H(1)=1$ ,  $H(2)=3/2$ ,  $H(3)=11/6$ ). Figure 1 shows the predicted (analytically) average size (length) of the largest segment (first order statistics) of a 100-monomer discrete chain as a function of number of cuts (bonds removed), and the analytical predictions for the division of its continuum analogue (division of a segment). The large  $n$  approximation to the harmonic number (continuum interval) is also plotted: as shown the asymptotic approximation is surprisingly accurate even for small  $n$ .

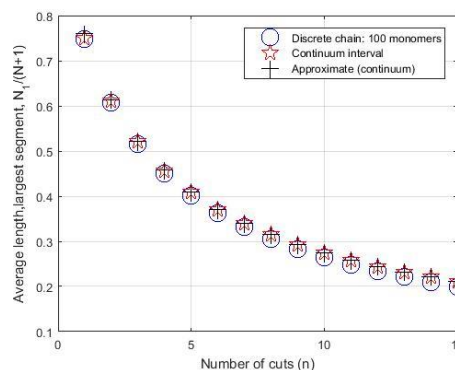


Figure 1. First order statistics (average size, length, of the largest fragment after  $n$  simultaneous cuts): discrete case (chain, numerical simulations), analytic approximation, and continuum limit (division of a segment).

The uniform fragment-size distribution of a singly and randomly broken monomer chain should be contrasted to the U-shaped distribution of a randomly broken fractal-like agglomerate. Numerical simulations suggest that upon randomly breaking a bond in, e.g., DLCA agglomerates the fragment-size distribution peaks at single monomers and  $N-1$  clusters (the distribution is symmetric). Namely, single-bond, random fragmentation of fractal-like agglomerates favors, on average, the generation of monomers (and  $(N-1)$ -mers). As the fractal dimension decreases the fragment probability distribution tends to become uniform, i.e., it approaches the distribution of a uniformly, singly fragmented chain.

Feller, W. (1968) *An introduction to probability theory and its applications*, 3<sup>rd</sup> edn., John Wiley & Sons.

David, H.A. and Nagaraja, H.N. (2003) *Order statistics*, 3<sup>rd</sup> edn., John Wiley & Sons.

## Towards a coarse-grained model of nano-particle agglomeration

M.Smiljanic<sup>1</sup>, A.Kronenburg<sup>1</sup>, R.Weeber<sup>2</sup> and C. Holm<sup>2</sup>

<sup>1</sup>Institute of Combustion Technology, University of Stuttgart, Stuttgart, 70174, Germany

<sup>2</sup>Institute for Computational Physics, University of Stuttgart, Stuttgart, 70569, Germany

Keywords: soot, nano-particles, collision, aggregates.

Presenting author email: milena.smiljanic@itv.uni-stuttgart.de

The agglomeration of nano-particles is of growing importance in many industrial applications, such as particle flame synthesis and spray-drying, where the structure of the agglomerates strongly affects final product characteristics. Detailed models use Langevin Dynamics to track the movement of each particle and compute particle collisions and particle-particle interactions individually (see e.g. Isella and Drossinos, 2010). More recent work investigates the influence of turbulent motion on aggregates' growth and the resulting aggregate morphology (Inci *et al.*, 2017). Numerical simulations were, however, limited to rather low numbers of particles (up to 4 million particles) and rather dense particle loadings. This limited the statistics and prevented long simulation times.

The simulation of larger systems will require some simplifications of the modelling process. Here, we develop a coarse-graining approach for the agglomeration of nano-particles and clusters, covering both primary particles of the size of few nanometers to agglomerates that are several orders of magnitude larger. Coarse-graining involves the replacement of parts of the clusters by "representative" particles of (representative) ellipsoidal shape. This is illustrated in Fig. 1.

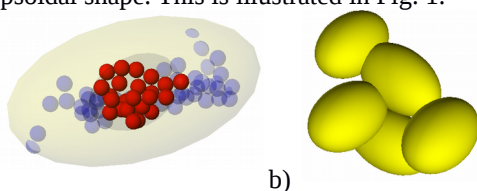


Figure 1: (a) A "representative" ellipsoidal particle containing a cluster and (b) clustering of ellipsoids using the new collision detection mechanism.

The agglomerate's morphology is usually characterized by the number of particles ( $N$ ), radius of gyration ( $R_g$ ) and fractal dimension ( $D_f$ ). These characteristics need to be "inherited" by the coarse-grained particles and determined the size and axes lengths of the representative ellipsoid. A new algorithm has been implemented to identify clusters during code execution. The agglomerates can then be replaced by the coarse-grained particles if agglomerates reach a certain size. The ellipsoid collision detection mechanism cannot be based on single particle collision algorithms but we use here a zero Gay-Berne potential (Berardi *et al.* 1995).

In addition to size and orientation, the coarse-graining requires modelling of directional drag forces

and specific collision probabilities. Due to the sparse nature of agglomerates, two ellipsoids that envelop their respective agglomerates could intersect, but the agglomerates that they represent would not necessarily touch and stick. The collision probability is a function of compactness of the underlying aggregates and of the overlap of the two ellipsoids. Figure 2 shows collision probabilities for different agglomerates. These probabilities decrease as the clusters' center-to-center distances increase. For more compact clusters ( $D_f=2.1$ ), the probability of collision reaches 50% when the clusters' centers of mass are separated by 8 primary particle diameters while more sparse clusters ( $D_f=1.6$ ) require a distance of less than 6 diameters. These sticking probabilities are computed for a wide range of aggregate sizes and morphologies and present new properties for the coarse-grained particles such that a realistic collision frequency can be approximated for agglomerates containing many hundreds of primary particles.

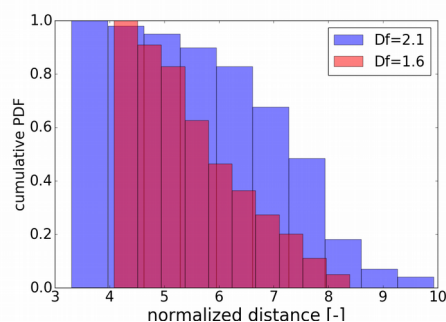


Figure 2. Comparison of cumulative PDF's of the sticking probability for similar clusters, plotted over the normalized center-to-center distance.

This work was supported by the Deutsche Forschungsgemeinschaft (DFG) as part of the Collaborative Research Center (SFB) 716-A8, held by University of Stuttgart.

Isella, L., Drossinos, Y., 2010, Phys. Rev. E 82:011404.

Inci, G., Kronenburg, A., Weeber, R., Pflüger, D. 2017. Flow, Turbulence and Combustion, DOI:10.1007/s10494-016-9797-3.

Berardi, R., Fava, C., Zannoni, C. 1995. Chemical Physics Letters 236 (462-468).

## A New Mechanism of Ultrafine Particle Generation during Concrete Fracture

Lidia Morawska<sup>1</sup>, Prashant Kumar<sup>2</sup>, Nassib Jabbour<sup>1</sup>, Rohan Jayaratne<sup>1</sup>, Graham Johnson<sup>1</sup>, Joel Alroe<sup>1</sup>, Erik Uhde<sup>3</sup>, Tunga Salthammer<sup>3</sup>, Luke Cravigan<sup>1</sup> and Ehsan Faghghi<sup>1</sup>

<sup>1</sup>International Laboratory for Air Quality and Health, Queensland University of Technology, Brisbane, Australia.

<sup>2</sup>Department of Civil and Environmental Engineering and Environmental Flow (EnFlo) Research Centre, Faculty of Engineering and Physical Sciences, University of Surrey, Guildford GU2 7XH, United Kingdom.

<sup>3</sup>Fraunhofer WKI, Department of Material Analysis and Indoor Chemistry, 38108 Braunschweig, Germany

Keywords: Ultrafine particles, concrete, airborne dust, urban pollution

Presenting author email: l.morawska@qut.edu.au

**Introduction.** The production of dust during construction activities have a significant impact on the air quality of urban environments, particularly in the growing number of megacities in the world. While it is known that the fracture and crushing of concrete gives rise to large quantities of dust, it is not that well known that this process also produces ultrafine particles. Kumar et al (2012) observed that over 90% of the particles by number produced during concrete recycling activities were in the ultrafine size range. This is of concern as these small particles can penetrate deeper into the human lungs and therefore have a greater impact on health than coarser particles (Oberdorster et al., 2005). In this study, for the first time, we propose a new mechanism for the production of such ultrafine particles as a result of concrete fracture, based on evaporation and subsequent condensation of volatile chemicals at the fracture site.

**Methods.** We carried out a series of laboratory studies in order to investigate the nature and origin of these ultrafine particles. These experiments were conducted within a 1 m<sup>3</sup> chamber. Concrete samples were fractured on the floor of the chamber. Particle size distributions were measured with a scanning mobility particle sizer (SMPS) in the size range 5-300 nm. An inlet dust filter prevented coarse dust from entering the sampling tube. Particles in selected size ranges were passed through a Volatility Tandem Differential Mobility Analyser (VTDMA) to study their volatility and composition (Johnson et al., 2005). The concrete samples were placed on a wooden support on the base of the box and struck several times with a heavy hammer until a sufficiently high ultrafine particle number concentration was obtained. The monitoring equipment was placed outside the chamber with the sample air being continuously drawn out of the chamber for analysis.

**Results.** When the concrete was struck without fracture, no ultrafine particle production was seen. In contrast, significantly large ultrafine number concentrations were observed only when the concrete fractured. The average count median diameter (CMD) of the particles that were so produced was 37 nm. Fig 1 shows typical SMPS scans of the particle size distribution obtained from one concrete sample. The VTDMA experiments showed that the ultrafine particles were almost totally volatile. Fig 2 shows the average of 4 typical VTDMA scans for the same concrete sample as Fig 1. The characteristic

volatilisation temperature is observed to be approximately 80 °C.

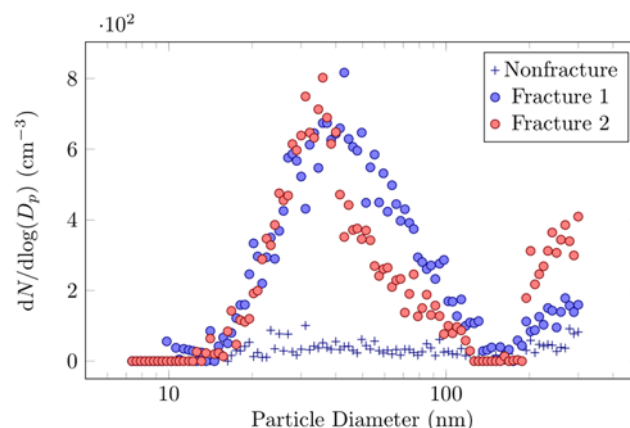


Fig 1: The ultrafine particle number size distributions obtained in two separate experiments soon after the concrete sample was fractured with approximately ten blows of the hammer in a period of 60s. Also shown is the particle size distribution of a nonfracture experiment.

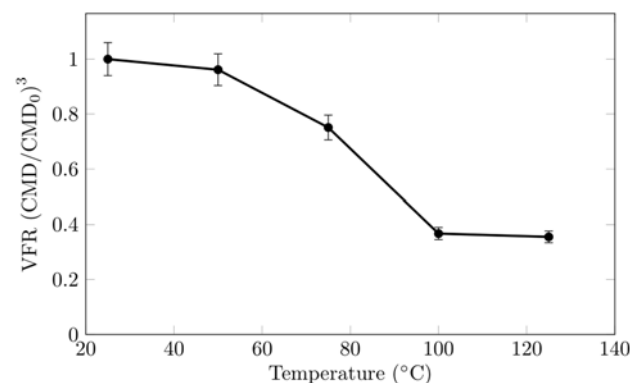


Fig 2: The average results of a VTDMA experiment on the particles shown in Fig 1. The volume fraction remaining is the ratio of (CMD/CMDmax)<sup>3</sup>.

**Conclusions.** We confirmed that ultrafine particles are produced only when concrete is fractured and that these particles are volatile at a temperatures greater than 80°C. We propose a new mechanism, that these secondary particles are formed by the condensation of volatiles rather than mechanical fracturing of the concrete.

Kumar, P.; Mulheron, M.; Som, C., *Journal of Nanoparticle Research* (2012), 14, 1-14.

Oberdorster, G., Oberdorster, E., Oberdorester, J. *Nanotoxicology: Environ Health Persp.* (2005), 823-839, 113.

## **Abstracts T506**

## Electron scattering in water clusters, water droplets, and liquid bulk water

S. Hartweg, B. L. Yoder, D. Luckhaus, and R. Signorell

Laboratory of Physical Chemistry, ETH Zürich, Zürich, Switzerland

Keywords: Photoelectron spectroscopy, photoelectron anisotropy, electron mean free path, vacuum ultraviolet light.

Presenting author email: Sebastian.hartweg@phys.chem.ethz.ch

Molecular clusters, liquid droplets, and aerosol particles are ubiquitous in the Earth's atmosphere. Via absorption and scattering of sunlight, they influence the local weather as well as the climate on a global scale. In addition to these physical processes, aerosol particles can promote chemical reactions, for example electron-induced reactions. Electron transport properties play a crucial role in this context. The present contribution is devoted to a better fundamental understanding of electron scattering processes in water clusters, water droplets, and liquid bulk water at electron kinetic energies below a few ten electronvolts.

Neutral water clusters and aerosol droplets are ionized with vacuum ultraviolet (VUV) light at photon energies below 35 eV and the electronic and electron scattering properties are probed with angle-resolved photoelectron spectroscopy (West *et al.* 2013, Yoder *et al.* 2013, Hartweg *et al.* 2016, Signorell *et al.* 2016). The experimental data is analysed with a detailed electron scattering model (Signorell *et al.* 2016, Luckhaus *et al.* 2017).

We present the first cluster size-resolved measurements of angle-resolved photoelectron spectra of neutral water clusters (H<sub>2</sub>O)<sub>n</sub> with 1 ≤ n ≤ 20 in the valence electronic region (Hartweg *et al.* 2016). These photoelectron photoion double imaging coincidence spectra (i<sup>2</sup>PEPICO) were collected at the DELICIOUS III spectrometer (Garcia *et al.*, 2013) at the DESIRS VUV beamline at SOLEIL synchrotron. Within the photon energy range of 12.5 to 35 eV we observe a rapid decrease of the photoelectron anisotropy for the 1b<sub>1</sub> and 3a<sub>1</sub> orbital up to a cluster size of 5-6 molecules, and convergence of the anisotropy for larger clusters. This indicates that photoionization of water clusters is readily described by a short-range scattering potential given by 5-6 molecules. This size of 5-6 molecules coincides with the smallest cluster sizes for which 3 dimensional H-bond structures become more stable than planar ring structures.

For larger (H<sub>2</sub>O)<sub>n</sub> clusters with up to 1000 molecules per cluster, coincidence measurements are no longer feasible. As in this size range clusters of similar size have almost identical electronic properties, detailed knowledge of the individual cluster size is not essential here. Information about the average cluster size, however, is still needed, and we obtain it via the sodium doping technique (Schläppi *et al.*, 2014). We use a table top VUV light source for photoionization in combination with an imaging photoelectron spectrometer (West *et al.*, 2013, Yoder *et al.*, 2013, Signorell *et al.* 2016). We compare the results for larger clusters with

corresponding results for liquid water droplets (Signorell *et al.* 2016). In contrast to the situation for small clusters, the electron scattering properties of the larger clusters and droplets are strongly-influenced by inelastic and elastic scattering during electron transport through the cluster or droplet.

Finally, we report predictions for photoelectron anisotropies of liquid bulk water from our detailed electron scattering model (Signorell *et al.* 2016, Luckhaus *et al.* 2017). The predictions for liquid bulk water agree reasonably well with experimental liquid jet data (Faubel *et al.* 2012). Again, scattering properties in the liquid bulk are found to be strongly influenced by inelastic and elastic scattering during electron transport.

West A. H. C., Yoder B. L., Signorell R. (2013) *J. Chem. Phys. A*, **117**, 13326-13335

Yoder B. L., West A. H. C., Schläppi B., Chasovskikh E., Signorell R. (2013) *J. Chem. Phys.* **138**, 044202

Hartweg S., Yoder B. L., Garcia G. A., Nahon L., Signorell R., (2016), arXiv:1612.02338

Signorell R., Goldmann M., Yoder B. L., Bodi. A., Chasovskikh E., Lang L., Luckhaus D., (2016) *Chem. Phys. Lett.* **658**, 1-6

Luckhaus D., Yamamoto Y., Suzuki T., Signorell R., submitted 2016

Garcia G. A., de Miranda B. K. C., Tia M., Daly S., Nahon L. (2013) *Rev. Sci. Instrum.*, **84**, 820-825

Schläppi B., Ferreiro J. J., Litman J. H., Signorell R., (2014) *Int. J. Mass. Spectrom.*, **372**, 13-21

Faubel M., Siefertmann K. R., Liu Y., Abel B., (2012), *Acc. Chem. Res.*, **45**, 120-130

## Liquid-liquid phase separation in several types of secondary organic materials free of inorganic salts

M. Song<sup>1,2</sup>, P. F. Liu<sup>3</sup>, S. T. Martin<sup>3,4</sup>, A. K. Bertram<sup>2</sup>

<sup>1</sup>Department of Earth and Environmental Sciences, Chonbuk National University, Jeollabuk-do, 54896, Republic of Korea

<sup>2</sup>Department of Chemistry, University of British Columbia, Vancouver, BC, V6T 1Z1, Canada

<sup>3</sup>John A. Paulson School of Engineering and Applied Sciences, Harvard University, Cambridge, Massachusetts 02138, USA

<sup>4</sup>Department of Earth and Planetary Sciences, Harvard University, Cambridge, Massachusetts 02138, USA

Keywords: liquid-liquid phase separation, secondary organic materials, relative humidity.

Presenting author email: mijung.song@jbnu.ac.kr

Particles consisting of secondary organic materials (SOMs) are ubiquitous in the atmosphere. To predict the role of these particles in climate, visibility, and atmospheric chemistry, information on the phase states of the particles is important. However, the phase states of the SOMs are still poorly understood.

Recently, Renbaum-Wolff et al. (2016) showed that liquid-liquid phase separation (LLPS) occurs at high relative humidity (RH) (~95 - 100 %) in  $\alpha$ -pinene-derived SOM free of inorganic salts. In addition, they showed using a thermodynamic modelling that the presence of LLPS at high RH modifies changes the cloud condensation nuclei (CCN) properties of the SOM particles. Most recently, Rastak et al. (2017) showed that isoprene-derived SOM particles do not undergo LLPS during RH cycles. They also used these observations together with thermodynamic modelling and showed the hygroscopic properties of biogenic organic aerosol in the laboratory and the field.

Herein we expand on these initial findings by investigating LLPS in several types of SOM particles free of inorganic salts. SOM particles were generated by the ozonolysis of  $\beta$ -caryophyllene, ozonolysis of limonene, and photo-oxidation of toluene with the particle mass concentrations ranging from  $15 \mu\text{g}\cdot\text{m}^{-3}$  to  $7000 \mu\text{g}\cdot\text{m}^{-3}$ . LLPS was investigated during RH cycling using a temperature and RH controlled flow-cell coupled to an optical microscope.

SOM particles. Figure 1 presents examples of optical images of the  $\beta$ -caryophyllene-derived SOM and limonene-derived SOM particles upon moistening (Song et al., 2017). LLPS is observed at 91.5 % RH for the  $\beta$ -caryophyllene-derived SOM particle and at 95.3 % RH for the limonene-derived SOM particle. However, LLPS was not observed in the toluene-derived SOM particles for the particle mass concentrations of  $80 \mu\text{g}\cdot\text{m}^{-3}$  to  $1000 \mu\text{g}\cdot\text{m}^{-3}$ . The presence and absence of LLPS in SOM particles may help explain the difference between the hygroscopic parameter,  $k$ , of SOM particles measured above and below water saturation. Moreover, the results should be considered when predicting the CCN properties of SOM particles in the atmosphere. Detailed results from this study will be presented

This work was supported by the NRF grant funded by the Korea Government (MSIP) (2016R1C1B1009243).

Rastak, N. et al. (2017) *Geophys. Res. Lett.*, submitted, 2017.

Renbaum-Wolff et al. (2016) *Atmos. Chem. Phys.*, **16**, 7969-7979, 10.5194/acp-16-7969-2016.

Song et al. (2017) *Atmos. Chem. Phys.*, to be submitted.

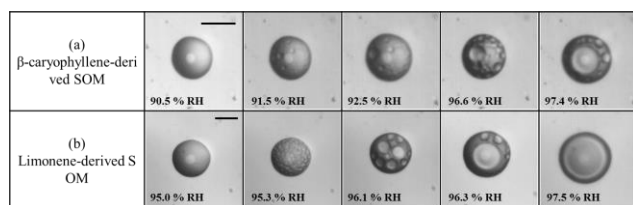


Figure 1. Optical images for liquid-liquid phase separation in SOM particles with increasing RH. Size bar is  $20 \mu\text{m}$ . The images are taken from Song et al. (2017).

Humidity cycles were performed with supermicron SOM particles at 290 K. During humidity cycles, LLPS was observed at greater than ~95 % RH in the  $\beta$ -caryophyllene-derived SOM and limonene-derived

## Settling rate of nanosized fractal-like agglomerates by Brownian dynamic simulations accounting for rotational dynamics

Anastasia Spyrogianni,<sup>1</sup> Katerina S. Karadima,<sup>2,3</sup> Eirini Goudeli,<sup>1</sup> Vlasis G. Mavrantzas,<sup>1-3</sup> Sotiris E. Pratsinis<sup>1</sup>

<sup>1</sup>Department of Mechanical and Process Engineering, ETH Zurich, Zurich, 8092, Switzerland

<sup>2</sup>Department of Chemical Engineering, University of Patras, Patras, 26504, Greece

<sup>3</sup>FORTH-ICE/HT, Patras, 26504, Greece

Keywords: diffusion coefficient tensor, mobility diameter, settling rate, polydispersity.

Presenting author email: spyrogianni@ptl.mavt.ethz.ch

The settling rate of nanoparticles is of current interest for *in vitro* dosimetry in nanotoxicology and nanomedicine studies (Cohen *et al.*, 2015) as well as for the stability of nanofluids (Ghadimi *et al.*, 2011). Measuring the settling rate  $u_s$  of individual nanosized particles/agglomerates is not trivial, contrary to millimeter-sized (or larger) spheres (Masliyah & Polikar, 1980) and agglomerates (Binder *et al.*, 2009) that can be easily tracked in a settling column. Therefore, the agglomerate  $u_s$  is often calculated with analytical expressions that are modifications of the Stokes' law settling rate equation (DeLoid *et al.*, 2015; Liu *et al.*, 2015).

Here, a Brownian dynamics algorithm is developed and employed to study the settling rate of fractal-like SiO<sub>2</sub> agglomerates in water, accounting for their rotational dynamics (Ilie *et al.*, 2014) through the use of a Cartesian vector to track nanoparticle orientation (Evensen *et al.*, 2008) and their inherent anisotropic diffusivity (de la Torre *et al.*, 2007). The code addresses single, rigid, fractal-like agglomerates under gravity in the regime of low Reynolds numbers, in the absence of van der Waals interactions with the solvent molecules. The employed agglomerates are generated by a discrete element modeling method (Goudeli *et al.*, 2015) and have mass fractal dimension  $D_f$  of  $1.80 \pm 0.01$ , close to that of the aerosol-made, fumed SiO<sub>2</sub> (Martin *et al.*, 1986). The translational and rotational diffusion coefficient tensors of the SiO<sub>2</sub> agglomerates are calculated with HYDRO++ (de la Torre *et al.*, 2007) and used to obtain their mobility diameter  $d_m$ . The obtained  $d_m$  is in excellent agreement with that from scaling laws for fractal-like agglomerates from the literature (Dastanpour & Rogak, 2016; Sorensen, 2011).

For given  $d_m$ , the agglomerate settling rate  $u_s$  increases with increasing primary particle diameter for agglomerates consisting of monodisperse primary particles PPs. The agglomerate  $u_s$  increases also with increasing PP polydispersity, for constant average primary particle diameter and agglomerate  $d_m$  (Fig. 1). This highlights that the commonly-made assumption of monodisperse PPs (DeLoid *et al.*, 2015; Liu *et al.*, 2015) can lead to underestimation of the agglomerate  $u_s$ . No effect of the agglomerate relative shape anisotropy on the  $u_s$  is observed.

This work was supported by the Swiss National Science Foundation (no. 200020-146176) and the European Research Council (FP7/2007–2013, no. 247283).

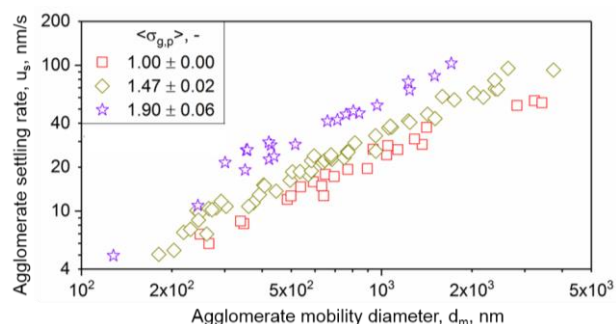


Figure 1. Settling rate  $u_s$  in water of SiO<sub>2</sub> agglomerates consisting of polydisperse primary particles with average geometric mean primary particle diameter of  $\sim 30$  nm and varying average geometric standard deviation  $\langle \sigma_{g,p} \rangle$  as function of  $d_m$ .

- Binder, C., Hartig, M.A.J., & Peukert, W. (2009) *J. Colloid Interf. Sci.* **331**, 243-250.
- Cohen, J.M., DeLoid, G.M., & Demokritou, P. (2015) *Nanomedicine (Lond.)* **10**, 3015-3032.
- Dastanpour, R., & Rogak, S.N. (2016) *J. Aerosol Sci.* **94**, 22-32.
- de la Torre, J.G., Echenique, G.D., & Ortega, A. (2007) *J. Phys. Chem. B* **111**, 955-961.
- DeLoid, G.M., Cohen, J.M., Pyrgiotakis, G., Pirela, S.V., Pal, A., Liu, J.Y., Srebric, J., & Demokritou, P. (2015) *Part. Fibre Toxicol.* **12**, 32.
- Evensen, T.R., Naess, S.N., & Elgsaeter, A. (2008) *Macromol. Theory Simul.* **17**, 403-409.
- Ghadimi, A., Saidur, R., & Metselaar, H.S.C. (2011) *Int. J. Heat Mass. Tran.* **54**, 4051-4068.
- Goudeli, E., Eggersdorfer, M.L., & Pratsinis, S.E. (2015) *Langmuir* **31**, 1320-1327.
- Ilie, I.M., den Otter, W.K., & Briels, W.J. (2014) *J. Chem. Phys.* **141**.
- Liu, R., Liu, H.H., Ji, Z.X., Chang, C.H., Xia, T., Nel, A.E., & Cohen, Y. (2015) *ACS Nano* **9**, 9303-9313.
- Martin, J.E., Schaefer, D.W., & Hurd, A.J. (1986) *Phys. Rev. A* **33**, 3540-3543.
- Masliyah, J.H., & Polikar, M. (1980) *Can. J. Chem. Eng.* **58**, 299-302.
- Sorensen, C.M. (2011) *Aerosol Sci. Tech.* **45**, 765-779.

## **Abstracts T507**

## Formation rate of charged nanoparticles and ion balance

X. Chen<sup>1</sup>, V.-M. Kerminen<sup>1</sup>, J. Paatero<sup>2</sup>, P. Paasonen<sup>1</sup>, H. E. Manninen<sup>1,3</sup>, T. Petäjä<sup>1</sup> and M. Kulmala<sup>1</sup>

<sup>1</sup>Department of Physics, University of Helsinki, P.O. Box 64, FI-00014 Helsinki, Finland

<sup>2</sup>Finnish Meteorological Institute, Observation services, P.O. Box 503, 00101 Helsinki, Finland

<sup>3</sup>CERN, CH-1211 Geneva, Switzerland

Keywords: ionising radiation, air ions, ion balance, ion formation rate.

Presenting author email: xuemeng.chen@helsinki.fi

Air ions are airborne charge carriers in the atmosphere (e.g. Hirsikko et al., 2011). Their motions in the Earth-atmosphere electric field give rise to the electrical conductivity of air (Harrison, 2001). The study of the air conductivity lays the foundation of the atmospheric electricity discipline, where the original interest in air ions manifests itself (Israël, 1970). During the development of the atmospheric electricity discipline, there emerged the relation of air ions to the formation of cloud droplets (Wilson, 1895, 1899). These observations promoted the attraction of air ions in the atmospheric aerosol study.

Ionising radiation produces primary air ions via ionisation of air molecules. These initial charge carriers undergo a series of dynamic processes, including both chemical reactions and physical transformations. In the end, a fraction of primary ions can pass their electric charges to more stable air ions, including cluster ions and charged aerosol particles, which can be detected by modern instrumentation (e.g. Chen et al., 2016). Based upon the theoretical understanding of air ion formation from ionising radiation, mathematical models have been proposed to describe the ion balance between the ion production rate/ionisation rate ( $I$ ) and measured air ion concentrations (Harrison, 2001; Israël, 1970; Tammet et al., 2006). These models are typically built on a quasi-steady state assumption.

For the study of atmospheric aerosols, the topic of new particle formation (NPF) is of primary importance, because the NPF process supplements aerosol particles in the air (Poschl, 2005). Air ions are known to participate in NPF (Kulmala & Kerminen, 2008). The NPF process involving air ions is typically characterised by the formation rate of charged particles in a certain measurable size range ( $J$ ) (Kulmala et al., 2012). The formula for the  $J$  determination originates from the balance equation of ion concentration to its root (Kulmala et al., 2004).

Apparently,  $J$  and  $I$  share the same origin. However,  $I$  takes typically a value of about  $10 \text{ cm}^{-3} \text{ s}^{-1}$  (Chen et al., 2016; Harrison & Carslaw, 2003), whereas  $J$  is usually found in the range of  $0.01\text{--}1 \text{ cm}^{-3} \text{ s}^{-1}$  (Nieminen et al., 2011). In this work, the ion balance concept is reviewed to investigate the connection between  $I$  and  $J$ . By a term-to-term comparison of  $I$  and  $J$  determination approaches, we aim to consolidate the theoretical framework for air ion study from both the atmospheric electricity and atmospheric aerosol disciplines.

With an updated ion balance theory, the feasibility for an ion closure auditing is assessed based on ambient measurement data collected from the SMEAR II station located in a boreal forest in southern Finland. Moreover, the validity and reliability of the parameters used in the balance equation are evaluated with an emphasis on the identification of the future needs for parameterisation.

This work was supported by the Academy of Finland Centre of Excellence (project no. 272041 and 1118615) and the European Union's Horizon 2020 research and innovation programme under grant agreement No 654109. Xuemeng Chen acknowledges the Doctoral Programme in Atmospheric Sciences (ATM-DP, University of Helsinki) for financial support.

- Chen, X., et al. (2016). *Atmospheric Chemistry and Physics*, **16**(22), 14297-14315. doi: 10.5194/acp-16-14297-2016
- Harrison, R. G. (2001). *Atmospheric electricity and cloud microphysics*. Paper presented at the European Physical Society Workshop on Ion-Aerosol-Cloud Interactions, CERN, Geneva.
- Harrison, R. G., & Carslaw, K. S. (2003). *Rev. Geophys.*, **41**(3), art-no. 1012. doi: 10.1029/2002rg000114
- Hirsikko, A., et al. (2011). *Atmos. Chem. Phys.*, **11**(2), 767-798. doi: 10.5194/acp-11-767-2011
- Israël, H. (1970). *Atmospheric electricity, Vol. I* (Vol. 1). Jerusalem: Israel Program for Scientific Translations.
- Kulmala, M., & Kerminen, V.-M. (2008). *Atmospheric Research*, **90**(2-4), 132-150. doi: 10.1016/j.atmosres.2008.01.005
- Kulmala, M., et al. (2012). *Nat. Protoc.*, **7**(9), 1651-1667. doi: 10.1038/nprot.2012.091
- Kulmala, M., et al. (2004). *Journal of Aerosol Science*, **35**(2), 143-176. doi: 10.1016/j.jaerosci.2003.10.003
- Nieminen, T., et al. (2011). *Atmospheric Chemistry and Physics*, **11**(7), 3393-3402. doi: 10.5194/acp-11-3393-2011
- Poschl, U. (2005). *Angew Chem Int Ed Engl*, **44**(46), 7520-7540. doi: 10.1002/anie.200501122
- Tammet, H., Hörrak, U., Laakso, L., & Kulmala, M. (2006). *Atmos. Chem. Phys.*, **6**, 3377-3390.
- Wilson, C. T. R. (1895). *Proc. R. Soc. Lond.*, **59**, 338-339.
- Wilson, C. T. R. (1899). *Philos. T. R. Soc. Lond., Series A*, **192**, 403-453.

## Self-organization of spark-produced atomic clusters on a carbon film TEM grid.

B.R. Keijzers<sup>1</sup>, J. Feng<sup>2</sup>, M. Valenti<sup>1</sup>, G. Biskos<sup>3</sup>, A. Schmidt-Ott<sup>1</sup>

<sup>1</sup>Faculty of Applied Sciences, Delft University of Technology, NL-2600GA Delft, Netherlands

<sup>2</sup>Faculty of Mathematics and Natural Sciences, University of Leiden, NL-2333 CC Leiden, Netherlands

<sup>3</sup>The Energy Environment and Water Research Center, The Cyprus Institute, Nicosia 2121, Cyprus

Keywords: atomic clusters, self-organization, Surface functionalization  
baskeijzers@gmail.com

We found that Au atomic cluster deposition from the aerosol phase onto smooth substrates leads to an interesting self-organization effect. During a specific phase, patches of rather dense particle coverage occur, in which there is no particle-particle coalescence (fig. 2 b). A similar phenomenon and similar patterns have been observed earlier by Wanner et al., (2006) in a vacuum deposition experiment. Such structures are of technological interest, e.g. for surface functionalization in catalysis, nanooptics or nanoelectronics.

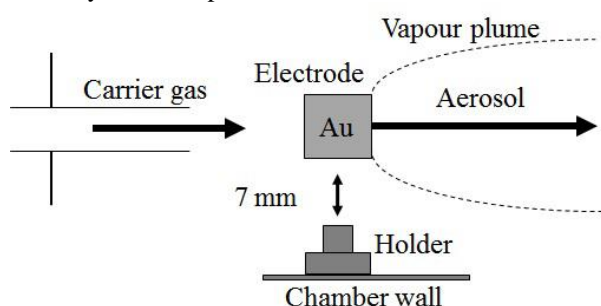


**Figure 1.** Set-up for producing and immobilizing atomic clusters. The Au electrodes are perpendicular to the plane, and the carrier gas flow. The TEM grid is placed onto the holder.

We produce atomic clusters by atmospheric-pressure spark discharge between 2 Au electrodes in N<sub>2</sub> (see Maisser et al., 20) and immobilize them by diffusional deposition onto a TEM grid in close proximity to the spark (fig. 1). Inspired by the mechanisms proposed by Wanner et al., our interpretation of the patterns observed on TEM micrographs (fig. 2) with growing deposition time are as follows:

- Atomic clusters deposit on the substrate. Only those larger than 1 nm are visible.
- A layer (“carpet”) with a thickness of a few atomic layers forms from the small atomic clusters as they become denser. This carpet (grey patch) continuously shrinks, as it is consumed by adding material onto the larger clusters, an Ostwald ripening phenomenon. We ignore the large particles (ca. 10 nm) in this interpretation, assuming that they have formed in the gas phase by recirculation of some of the spark-emitted plume in the chamber.
- While the particles coarsen, the carpet shrinks, which pulls the particles closer to each other until they are in very close proximity, forming agglomerates of fractal-like structure.
- Under further deposition, the agglomerates do coalesce. Upon annealing, they would form round units.

While most of the phenomena observed can be explained with the driving force of energy minimalization, the phenomenon of temporarily maintaining gaps between closely-spaced primary units in fig. 2 b and c is surprising.

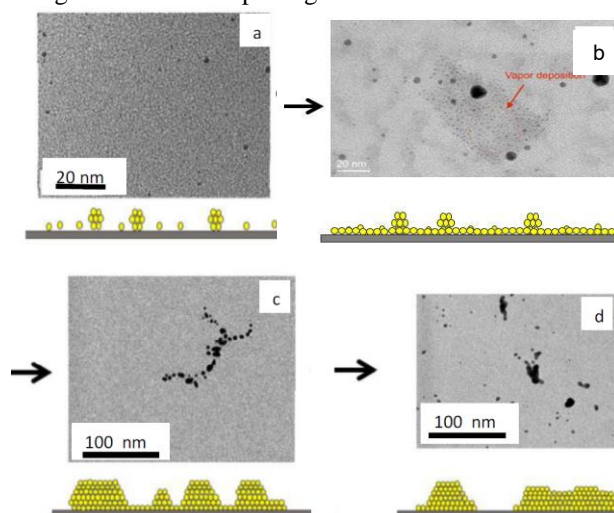


**Figure 2.** Evolution of particle structures on a TEM grid during deposition of atomic clusters during 1s (a), 5s (b), 8s (c) and 60s (d). Fig. 2b is adapted from Feng (2016). Although the position of the TEM grid was different with respect to fig. 1 here (8mm downstream of the spark), the analogy with Wanner et al. (2016), indicates that it fits into the series.

The mean particle size on the substrate grows with the deposition time. Especially the structure shown in fig. 2b can be of special interest for catalysis, if it is “frozen” through the use of materials with a higher melting point than Au. The results presented here demonstrate that such structures, formerly produced in a vacuum system, can also be obtained by an aerosol-based process at 1 bar, which allows a much more cost-effective production.

Wanner, M., Werner, R., Gerthsen, D., *Dynamics of gold clusters on amorphous carbon films induced by annealing in a transmission electron microscope*, Surface Science 600, 632 (2006).

Feng, J., *Scalable Spark Ablation Synthesis of Nanoparticles : Fundamental Considerations and Application in Textile Nanofinishing* (doctoral thesis, Delft University of Technology (2016)

Maisser, A., Barmounis, K.; Attoui, M. B.; Biskos, G.; Schmidt-Ott, A. *Atomic Cluster Generation with an Atmospheric Pressure Spark Discharge Generator*, Aerosol Science and Technology 10, 886-894 (2016).

## Water Vapour Nucleation on Solid Aerosol Particles by Molecular Dynamics

Donguk Suh and Kenji Yasuoka

Department of Mechanical Engineering, Keio University, Yokohama, 223-8522, Japan

Keywords: water adsorption, heterogeneous nucleation, molecular dynamics.

Presenting author email: suh@mech.keio.ac.jp

Aerosols grow from precursor particles that have various shapes in the atmosphere through heterogeneous nucleation. In this study, molecular dynamics (MD) was used to directly examine the vapour-to-liquid growth rate of aerosols that start from spheres or cubes. The growth rate is defined as the number of vapour molecules that attach on the seed surface over time over surface area. Previous studies using argon have proven the existence of a shape effect, namely curvature effect by comparing the growth rate of spherical and cubic nanoparticles (Suh and Yasuoka 2011; Suh and Yasuoka 2012). Water vapour is used in this study because it is an important topic because solid particles in the atmosphere directly influence air quality. Seed particles with various shapes and sizes were inserted into multiple supersaturated water vapour systems. The objective is to find how the shape of particles from gas emissions will affect heterogeneous nucleation. A constant number, volume, temperature ensemble was used. Two different seed configurations (sphere and cube) made of aluminium were investigated. Three different sizes were tested for each shape. The Yasuoka-Matsumoto method was used to calculate how quickly condensation occurs on the particle surface. Previous studies have shown that though the different shapes have similar surface areas, condensation is faster for the cube by several factors. The result for water vapour is different, however, with monatomic vapour systems. The source of the discrepancy is from the different adsorption characteristics

The difference between vapour condensation of monatomic molecules and water was compared to the same type of solid seed as shown in Fig. 1. There were only van der Waals interactions between the seed molecules and the vapour. The supersaturation ratio of the ambient vapour was varied, but it did not have a significant effect on the condensation rate. Faster spreading and thus a layer-by-layer growth for monatomic vapour was seen, whereas water droplets that coagulated with the seed maintained its overall structure on the surface. In summary, depending on the vapour-vapour affinity and vapour-seed affinity, the rate of the liquid spreading on the seed surface changed.

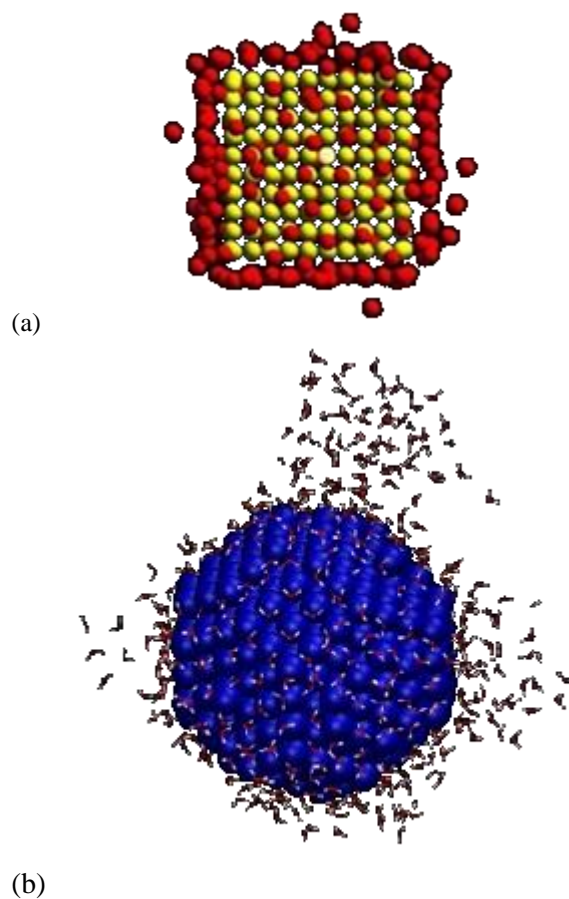


Figure 1. Snapshots of vapour adsorption on solid seed for (a) argon (b) water.

This work was supported by the Mizuho Foundation for the Promotion of Science.

Suh, D. and Yasuoka, K. (2011) *J. Phys. Chem. B* **115**, 10631-10645

Suh, D. and Yasuoka, K. (2012) *J. Phys. Chem. B* **116**, 14637-14649.

## Direct Observation of Cluster Size Distributions during Nucleation and Growth in Laval Expansions

M. Lippe, S. Chakrabarty, J.J. Ferreiro and R. Signorell<sup>1</sup>

<sup>1</sup>Laboratory of Physical Chemistry, ETH Zürich, Vladimir-Prelog Weg 2, 8093 Zürich, Switzerland

Keywords: Nucleation, Cluster growth, Laval nozzle, Photoionization, Mass spectrometry.

Presenting author email: martina.lippe@phys.chem.ethz.ch

We have recently (Ferreiro 2015, Ferreiro 2016) reported on fundamental studies of condensation of propane gas in the uniform (constant pressure and temperature) postnozzle flow of Laval nozzles. The neutral clusters are ionized by soft single photon ionization using vacuum ultraviolet light and detected by time-of-flight mass spectrometry with high dynamic range. This experimental setup allows cluster formation and detection under controlled conditions which is crucial to investigate nucleation and growth at the molecular level. The whole process, from the nucleation to the growth to molecular aggregates of sizes of several nanometers (~10 nm in diameter), can be monitored at the molecular level with a time-resolution of ~3  $\mu$ s. We record mass spectra at chosen times, pressures and temperatures which allows us to determine directly the critical nucleus size range as well as determine kinetics and possible mechanisms of cluster-size specific growth. A typical nucleation experiment for propane is shown in Figure 1. The onset of nucleation is observed as a sharp increase of the maximal cluster size  $n_{\max}$  with increasing supersaturation.

Here, we demonstrate results on homogeneous gas phase nucleation of propane and toluene as well as systematic results on growth processes for propane, toluene (Figure 2 (Chakrabarty 2017)) and water clusters. Additionally, we discuss how information about size, composition, and abundance of individual molecular clusters provides unique experimental data for comparison with ongoing molecular-level simulations.

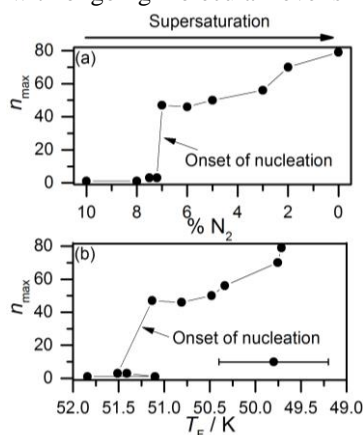


Figure 1. Modified from (Ferreiro 2016). Typical result for a nucleation experiment for propane. The maximal cluster size  $n_{\max}$  detected in the mass spectra is shown as a function of the (a) nitrogen concentration %  $N_2$  and (b)

Laval postnozzle flow temperature  $T_F$ . The steep increase of  $n_{\max}$  with increasing supersaturation is attributed to the onset of nucleation.

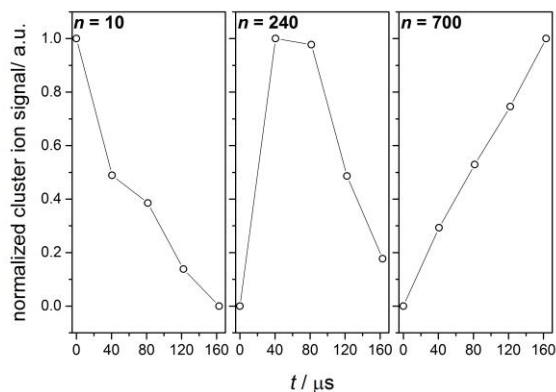


Figure 2. Modified from (Chakrabarty 2017). Typical results for a growth experiment for toluene. The evolution of the cluster abundance is shown for three different cluster sizes  $n$  as a function of the reaction time  $t$ . The three cluster sizes are chosen to illustrate the different time dependences observed in our experiment.

This work was supported by the Swiss National Science Foundation (SNF Project No. 200020\_159205).

Ferreiro, J.J., Gartmann, T.E., Schläppi, B. and Signorell, R. (2015) *Z. Phys. Chem.* **229**(10-12), 1765-1780.

Ferreiro J.J., Chakrabarty S., Schläppi B. and Signorell R. (2016) *J. Chem. Phys.* **145**, 211907-1-21907-10.

Chakrabarty S., Ferreiro J.J., Lippe M. and Signorell R. (2017) *manuscript in preparation*.

## Determination of the cesium chloride nanodrops surface tension from experiments on the vapor nucleation

S.A. Trubachev<sup>1,2</sup>, S.V. Valiulin<sup>1</sup>, A.M. Baklanov<sup>1</sup>, V.V. Karasev<sup>1</sup>, A.A. Onischuk<sup>1,2</sup>, S.V. Vosel<sup>1,2</sup>

<sup>1</sup>Voevodsky Institute of Chemical Kinetics and Combustion SB RAS, Novosibirsk, 630090, Russia

<sup>2</sup>Novosibirsk State University, Novosibirsk, 630090, Russia

Key words: nucleation, nanoparticles, nanodrop, cesium chloride, surface tension.

Presenting author email: [valiulin@kinetics.nsc.ru](mailto:valiulin@kinetics.nsc.ru)

Based on experiments on vapor nucleation and rigorous equation for the nucleation rate (Vosel *et al.*, 2013), we have shown that the surface tension  $\sigma$  of the critical nuclei (nanodrops) may significantly differ (Fig. 1) from that of the flat surface  $\sigma_\infty$  for the same substance. In particular, for metals (Ag, Cs, Li, Mg, Zn, Bi) this difference may be 30 - 100%. On the other hand, for the substances with non-metallic bond, (sulfur, water and ibuprofen) the surface tension of the critical nucleus and flat surface are almost equal (Onischuk *et al.*, 2016). To understand the influence of the chemical bond types on the value of relationships  $\sigma/\sigma_\infty$  is necessary to determine the surface tension of the critical nucleus of the substance with third type of the chemical bond (ionic bond). For that in the present work was studied homogeneous nucleation of the cesium chloride vapor.

To this end a laminar flow nucleation chamber was used. The concentration and size distribution of the outgoing aerosol particles were analyzed by an Automatic Diffusion Battery (ADB) coupled with a condensation nucleus counter. The nucleation volume was evaluated by the "supersaturation cut-off" method. The region of aerosol formation was localized by the 90 degree light scattering approach.

To calculate the critical nucleus surface tension numerical simulation of vapor to particles conversion was carried out. Simulation was based on the experimental results: outlet particles size and concentration, evaluated nucleation volume, temperature field into the nucleation chamber, mean vapor mass flow along the axial coordinate of the chamber.

As a result the nucleation rate was determined to be  $3 \cdot 10^9 \text{ cm}^{-3} \text{ s}^{-1}$  for the supersaturation  $1.6 \cdot 10^8$  and nucleation temperature 600 K. The surface tension  $\sigma_S$  of the cesium chloride critical nucleus was calculated to be 143 mN/m for the radius of the surface of tension 0.39 nm. This value of surface tension exceeds by 35% the surface tension  $\sigma_\infty$  for flat cesium chloride interface. Such a high deviation of  $\sigma_S$  from  $\sigma_\infty$  is in agreement with the assumption that the surface tension for substance with metal and ionic bond elements is strong dependent of curvature.

*The reported study was funded by RFBR according to the research project №16-33-00012 mol\_a.*

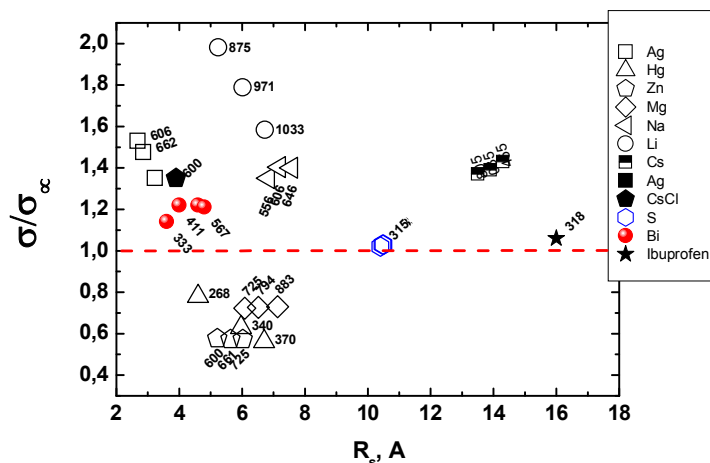


Figure 1. The ratio  $\sigma_S/\sigma_\infty$  for different elements. The nucleation temperature is shown for each point.

Vosel S.V., Onischuk A.A., Purtov P.A., Tolstikova T.G. (2013). "Classical Nucleation Theory: Account of dependence of the surface tension on curvature and translation-rotation correction factor," in *Aerosols Handbook. Measurement, Dosimetry, and Health Effects*, edited by L. S. Ruzer and N. H. Harley. CRC Press, Taylor & Francis Group: New York.

Onischuk A.A., Valiulin S.V., Vosel S.V., Karasev V.V., Zelik V.D., Baklanov A.M. Surface tension of sulfur nanoparticles as determined from homogeneous nucleation experiments // *Journal of Aerosol Science*. (2016). V. 97. P. 1-21.

## Molecular understanding of atmospheric new particle formation from sulfuric acid and diamines

J. Elm

Department of Physics, University of Helsinki, Helsinki, FI-00014, Finland

Keywords: Nucleation, Quantum Chemistry, Diamines and Clusters.

Presenting author email: jonas.elm@helsinki.fi

### Introduction

It is widely known that atmospheric bases, such as ammonia and dimethylamine, are important stabilizers of sulfuric acid clusters and promote new particle formation. The work by Almeida *et al.* (Nature 2013) showed that ppt levels of dimethylamine was able to enhance new particle formation rates more than three orders of magnitude compared to ammonia and was sufficient to explain new particle formation events observed in the ambient atmosphere.

Recent field campaigns performed by Jen *et al.*, (Geophys. Res. Lett., 2016) showed that atmospheric diamines can be equally as abundant as monoamines (dimethylamine and trimethylamine). At a site at Jefferson Street in Atlanta, diamine concentrations was even found to exceed monoamines by a factor of 3. As diamines are more basic than monoamines, they could have the potential to form new particles at even lower concentrations than monoamines.

Here we present the molecular interaction between the primary nucleation precursor  $\text{H}_2\text{SO}_4$  and diamines.

### Model systems

As a representative diamine we have chosen to study 1,4-diaminobutane (see Figure 1), better known as putrescine (put). Putrescine is a foul smelling diamine which is emitted into the atmosphere by breakdown of amino acids in dead organic material.

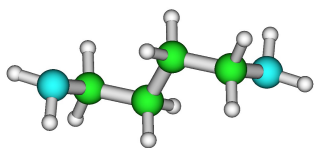


**Figure 1:** The molecular structure of putrescine. Green = carbon, blue = nitrogen and white = hydrogen

We study the cluster formation between sulfuric acid and putrescine to establish the role of diamines in atmospheric new particle formation. As a comparison we also study the corresponding clusters consisting of sulfuric acid and ammonia/dimethylamine.

### Computational Methodology

We utilize density functional theory ( $\omega\text{B97X-D/6-31+G(d,p)}$ ) to obtain the molecular structure and

vibrational frequencies of the clusters. We thoroughly sample the configurational space using a semiempirically guided sampling technique in order to obtain the best minimum cluster structures. To improve the energy of the structures we utilize a high level DLPNO-CCSD(T) method. An example of the largest cluster consisting of four sulfuric acid molecules and four putrescine molecules is shown in Figure 2.

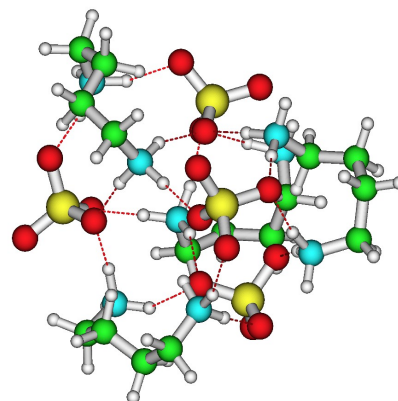


**Figure 2:** The molecular structure of the  $(\text{H}_2\text{SO}_4)_4(\text{put})_4$  cluster. Yellow = sulfur, green = carbon, blue = nitrogen and white = hydrogen

We calculate the formation free energies of the obtained clusters and use the values to obtain atmospheric new particle formation rates using the Atmospheric Cluster Dynamics Code (ACDC). Furthermore, using ACDC we examine the growth paths of the clusters in order to obtain a detailed mechanism of how the particles are formed.

### Conclusions

From our calculations the following important trends can be established:

- Putrescine significantly enhances the new particle formation rate compared to ammonia and dimethylamine.
- Ammonia and dimethylamine can at most stabilize two sulfuric acid molecules.
- A single putrescine molecule is able to stabilize sulfuric acid clusters with at least up to four sulfuric acid molecules.

## First results from the Antarctic Circumnavigation Expedition: New particle formation and its chemistry over the Sub Antarctic Ocean

A. Baccharini<sup>1</sup>, J. Schmale<sup>1</sup>, S. Henning<sup>2</sup>, F. Tummon<sup>3</sup>, M. Hartmann<sup>2</sup>, A. Welti<sup>2</sup>, F. Stratmann<sup>2</sup>,  
N. Harris<sup>4</sup>, A. Prévôt<sup>1</sup>, M. Gysel<sup>1</sup>, U. Baltensperger<sup>1</sup> and J. Dommen<sup>1</sup>

<sup>1</sup>Laboratory of Atmospheric Chemistry, Paul Scherrer Institute, Villigen 5232, Switzerland;

<sup>2</sup>Department Experimental Aerosol and Cloud Microphysics, Leibniz Institute for Tropospheric Research, Leipzig, 04318, Germany;

<sup>3</sup>Institute of Atmospheric and Climate Science, Federal Institute of Technology, ETHZ, Zurich, 8092, Switzerland;

<sup>4</sup>Centre for Atmospheric Informatics and Emissions Technology, University of Cranfield, Cranfield, UK

Keywords: Antarctica, aerosol, new particle formation, trace gases, API-TOF.

Presenting author email: andrea.baccharini@psi.ch

Aerosols have a major impact on our climate, they scatter and absorb solar radiation and take part in cloud formation processes through acting as cloud condensation or ice nuclei. Among the various climate forcings aerosols account for the largest fraction of uncertainty in the overall radiative forcing balance (IPCC 2013). One of the main reasons is the lack of a proper characterization of the preindustrial aerosol-cloud interactions which form a baseline against which present day anthropogenic aerosol cloud forcing is calculated.

With this contribution we will present first results from the “Study of preindustrial-like aerosol climate effects” (SPACE) project that took place from December 2016 to March 2017 as part of the Antarctic Circumnavigation Expedition (ACE) (see Figure 1). ACE explores one of the few places on Earth that can still reveal information about the preindustrial atmosphere. We will focus in particular on new particle formation (NPF) events in the Sub-Antarctic Ocean, addressing two open and highly relevant questions in terms of aerosol-climate interactions:

1) Which are the molecular pathways involved in NPF over the open ocean? Recently it has been showed that iodide plays a central role over coastal environments through the sequential addition of iodic acid to the cluster formation (Sipilä et al., 2016). However, it is not clear whether this mechanism may occur also over the open ocean.

2) How intense could NPF events have been in the pristine pre-industrial atmosphere, and which mechanisms governed the process? Ion-induced nucleation from biogenic organic precursors has been proven to be a potentially important mechanism by which particles are produced without anthropogenic pollutants (Kirkby et al., 2016).

A proper characterization of NPF over the pristine Sub-Antarctic Ocean will significantly improve our understanding of the pre-industrial atmosphere and will provide new insight into the available particle production mechanisms that may occur without anthropogenic pollution.

In order to address these questions, the first stages of NPF have been investigated using an atmospheric pressure interface time-of-flight mass spectrometer (API-

TOF) (Junninen et al., 2010) and a neutral cluster and air ion spectrometer (NAIS). Those instruments were deployed on board of the Akademik Tryoshnikov icebreaker during the ACE expedition for leg 2 and leg 3 (see Figure 1), in addition to several other instruments (e.g., particle counters, an aerosol mass spectrometer, trace gas monitors, cloud condensation particle counter). The API-TOF has been used to measure both the chemical composition of ions, naturally present in the atmosphere, and neutral particles by means of a chemical ionization source (CI-API-TOF, Jokinen et al., 2012).

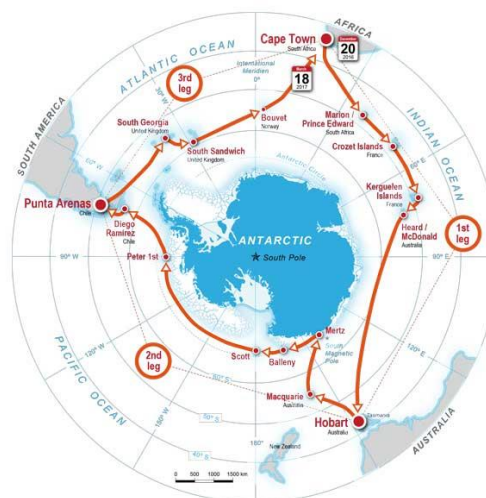


Figure 1. Antarctic Circumnavigation Expedition Itinerary.

This work was supported by the Swiss National Science Foundation, EPFL, the Swiss Polar Institute and the ACE foundation.

IPCC (2013). Intergovernmental Panel on Climate Change, Climate Change 2013: The Scientific Basis. Cambridge University Press.

Sipilä M. et al. (2016). *Nature* 537, 532-534.

Kirkby J. et al. (2016). *Nature* 533, 521-526.

Junninen, H., et al. (2010) *Atmos. Meas. Tech.* 3(4), 1039-1053.

Jokinen, T., et al. (2012) *Atmos. Chem. Phys.* 12, (9), 4117-4125.

## **Abstracts T508**

## Formation and light absorption properties of black and brown carbon aerosol particles co-emitted from combustion in flames

Ravi Kant Pathak<sup>1</sup>, Xiangyu Pei<sup>1</sup>, Mattias Hallquist<sup>1</sup>, Evert Ljungström<sup>1</sup>, Song Guo<sup>2</sup>, Joakim H. Pagels<sup>3</sup>, Neil M. Donahue<sup>4</sup>, Birgitta Svenningsson<sup>5</sup>, Axel C. Eriksson<sup>5</sup>

<sup>1</sup>Atmospheric Science, Department of Chemistry and Molecular Biology, University of Gothenburg, Gothenburg, 41296, Sweden

<sup>2</sup>State Key Joint Laboratory of Environmental Simulation and Pollution Control, College of Environmental Sciences and Engineering, Peking University, Beijing, 100871, China

<sup>3</sup>Ergonomics and Aerosol Technology, Lund University, Lund, 22100, Sweden

<sup>4</sup>Center for Atmospheric Particle Studies, Carnegie Mellon University, Pittsburgh, 15213, Pennsylvania, US

<sup>5</sup>Division of nuclear physics, Department of Physics, Lund University, Lund, 22100, Sweden

Keywords: MAC, BrC, AAE, BC, flames

Presenting author email: [ravikant@chem.gu.se](mailto:ravikant@chem.gu.se)

Light absorbing carbon (LAC) particles include black carbon (BC) and light absorbing organic carbon (OC) – also called “brown carbon” (BrC) (Bond, 2001). BC is well-known for its warming effects on the atmosphere; however, the light absorptivity of BrC is not represented in climate models as it largely remains poorly understood. The “brown carbon” (BrC) in the atmosphere is thought to be present in the form of both primary (POA) and secondary organic aerosol (SOA) (Kirchstetter *et al.* 2004; Lack *et al.* 2012). However their sources, formation, transformation, and properties largely remain poorly understood.

In this study, optical and morphological properties of combustion aerosol particles generated from propane fuelled premixed-diffusion flames under three different settings (one setting leading to internally mixed and two settings leading to externally mixed) were studied using state of the instruments including Photo Acoustic Soot Spectrometer with three wavelength (PASS-3) and Differential Mobility Analyzer (DMA) integrated in a set up with Aerosol Particle Mass (APM) analyzer and a Condensation Particle Counter (CPC), i.e. DMA-APM-CPC system. These distinctly different flames generated soot particles of BC and OC mixtures and their size distribution, effective density, dynamic shape factors and size resolved mass absorption cross-section (MAC) of both BC and OC were characterized.

The effective density of BC particles exhibited strong inverse size dependence, while the dynamic shape factor generally showed direct size dependence in both internally as well as externally mixed soot particles. The mixing state apparently did influence the morphological properties of soot. Most interesting and astonishing finding of this study was significantly high MAC values ( $2\text{--}5\text{ m}^2\text{ g}^{-1}$ ) of primary OC i.e. BrC, which in fact were in a comparable range of MAC values of strongly light absorbing BC particles at 405 nm as shown in Figure 1. The presence of this strongly light absorbing BrC fraction is hypothesized to be co-produced with BC due to incomplete combustion of fuel in the flames. The imaginary refractive index of BrC ( $k_{org}$ , the fundamental parameter determining the particle's absorptivity) was quantified from MAC values for OC and showed very

strong wavelength-dependence with larger values at small wavelength range. The analyses of light absorption of size-resolved soot particles containing BC and OC using Ångström Absorption Exponent (AAE) – a parameter of relative light absorption by particles at two different wavelengths (*e.g. here, 405 nm & 781 nm*), indicating that BrC was produced in all three flame settings. The MAC values of organics were observed to be significantly influenced by flame settings, i.e. premixing and diffusion air flows, which we hypothesize to depend on the molecular composition of the BrC, larger MAC indicates higher degree of conjugation of aromatic rings in the composition.

These findings if extended to emission of primary BrC due to incomplete combustion processes can be hypothesized to have significant implications from the perspective of radiative forcing of BrC aerosol on the planet.

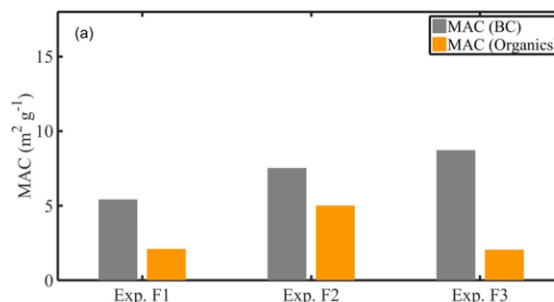


Figure 1: Mass absorption cross section (MAC) of pure BC and Organics, i.e. BrC in three flames at 405 nm,

Financial support by the Swedish Environmental Research Council (FORMAS: 2011-9791-19556-89) is gratefully acknowledged.

Bond, T.C.(2001) *Geophys. Res. Lett.*, 28, 21, 4075-4078

Kirchstetter, T.W. *et al.*(2004) *J. Geophys. Res.:Atmos.* 109(D21)

Lack, D.A. *et al.*(2012) *Proc. Nat. Acad. Sci.* 109, 37, 14802-14807

## “Morphology and Optical Properties of Mixed Aerosol Particles”

Mehmouh M.Fard <sup>(1)</sup>, Ulrich Krieger <sup>(1)</sup>, Yinon Rudich <sup>(2)</sup>, Claudia Marcolli <sup>(1)</sup>, and Thomas Peter <sup>(1)</sup>

(1) Institute for Atmospheric and Climate Science, ETH Zurich, Universitätsstrasse 16,8092, Zurich, Switzerland.

(2) Department of Environmental Sciences, Weizmann Institute, Rehovot, 76100, Israel

Keywords: LLPS, core-shell morphology, EDB, absorption efficiency, mie-code modelling.

Presenting author email: mford@env.ethz.ch

Experiments and modeling studies have shown that deliquesced aerosols can exist not only as one-phase system containing organics, inorganic salts and water, but often as two-phase systems consisting of a predominantly organic and a predominantly inorganic aqueous phase <sup>(1,2)</sup>. Recent laboratory studies conducted with model mixtures representing tropospheric aerosols <sup>(1,2,3)</sup>, secondary organic aerosol (SOA) from smog chamber experiments <sup>(4)</sup>, and field measurements <sup>(5)</sup> suggest that liquid-liquid phase separations (LLPS) is indeed a common phenomenon in mixed organic/ inorganic particles.

During LLPS, particles may adopt different morphologies mainly core-shell and partially engulfed. A core-shell configuration will have consequences for heterogeneous chemistry and hygroscopicity and as a result will alter the optical properties of the particles in particular for organic phases containing absorbing molecules, e.g. brown carbon.

The primary objective of this project is to establish a method for investigating the morphology of mixed inorganic and absorbing organic compounds of atmospheric relevance and study their radiative properties before, during, and after phase transitions mainly during LLPS. This will be the first study looking into the radiative effect of LLPS in detail.

Our ternary model system consist of ammonium sulfate (AS)/ Polyethylene Glycol (PEG)/ and water (H<sub>2</sub>O). Carminic acid (CA) was added as a proxy for an absorbing organic compound to the system. The behavior of single droplets of above ternary mixture was monitored during relative humidity (RH) cycles using optical microscopy. The same ternary mixture particle was levitated in an electrodynamic balance (EDB) and the change in its absorption properties was measured at varying RH.

In addition, Mie-code modeling is used to predict the absorption efficiency of the same ternary system and the result will be compared with the data obtained from EDB experiment. We also intend to determine the occurrence of LLPS in accumulation-sized particles and the change in their absorption using a cavity ring down aerosol spectrometer. If LLPS alters the absorptive properties of the suggested model aerosols significantly, absorption measurements of accumulation mode particles of the same composition would allow proving that LLPS indeed occurs in particles of accumulation mode size. Up to now LLPS has not been studied for particles in this size range.

### References:

1. Bertram, et al. *Atmos. Chem & Phys*, 11(21), 10995-11006, 2011.
2. Krieger, et al. *Chemical Society Reviews*, 41(19), 6631-6662, 2012
3. Song, M. et al. *Geophys Res Lett*, 39(19), 2012b
4. Smith et al. *Atmos Chem & Phys*, 12(20), 9613- 9628, 2012.
5. You, Y. et al. *Proceedings of the National Academy of Sciences*, 109(33), 13188-13193, 2012.

## Absorption coefficient spectral behaviour of laser-heated carbonaceous nanoparticles

F. Migliorini, S. De Iuliis, R. Dondè, G. Zizak

CNR-ICMATE, Institute of Condensed Matter Chemistry and Technologies for Energy

Keywords: carbonaceous nanoparticles, absorption properties, laser-induced incandescence

Presenting author email: francesca.migliorini@cnr.it

Laser-induced incandescence (LII) technique is widely used for Black Carbon (BC) measurements and involves heating particles with a high-power laser pulse. Laser heating of soot has been proved to significantly affect the particles internal structure (Vander Wal, 1999) and to promote the formation of new particles as a result of a vaporization effect (Michelsen, 2007). In addition, recently, the possibility of a permanent or reversible change in the optical properties of laser-heated soot particles has been considered and investigated, since this change might affect the LII signals and should be accounted for in the interpretation of the data (Thomson, 2011). Although, this issue is far from being solved and more detailed studies are needed to understand the impact of the variation of soot optical properties on LII measurements.

The aim of the present work is to investigate the effect of rapid laser heating on soot nanoparticles absorption properties. To this purpose wavelength-resolved extinction measurements of cold and laser-heated soot particles were performed in the visible spectral region. Cold soot particles of different age and maturity were produced by Nitrogen-quenched diffusion flames. The spectral behavior of soot absorption properties was explored at the LII prompt signal, when particles reach the maximum temperature, and few tenths of second after the laser pulse, when particles are already cooled down to the surrounding environment temperature. In particular, measurements were performed at three laser fluences: 1.3 mJ/mm<sup>2</sup> (low fluence, LF), 2.6 mJ/mm<sup>2</sup> (medium fluence, MF) 4 mJ/mm<sup>2</sup> (high fluence, HF), respectively. In this way the particles were heated to different temperature values, in a range between 3000 and 4000 K.

Figure 1 shows the spectral behavior of cold and heated carbonaceous nanoparticles at the LII peak signal.

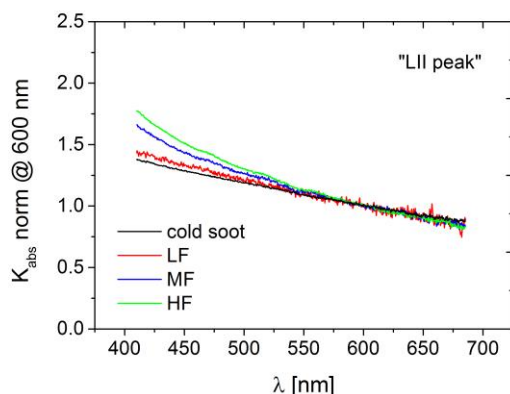


Figure 1. Absorption coefficient spectral behavior of cold and laser-heated particles at the LII peak.

A significant variation of the absorption coefficient of the laser-heated soot nanoparticles compared to the absorption coefficient of the non-heated ones can be observed. In particular, while above 550 nm the spectra tend to flatten, for lower wavelengths a significant increase of the absorption coefficient is detected for the heated soot nanoparticles.

A similar behavior was observed also few tenths of a second after the laser irradiation. Therefore it is reasonable to assume that permanent modifications occur under laser irradiation.

Finally, a nonlinear fitting of the absorption coefficient curves was performed in order to obtain the dispersion coefficient or Ångström exponent,  $\alpha$ , which is a useful quantity to assess the wavelength dependence of the aerosol optical properties. A dispersion coefficient of almost 1 was obtained for cold soot particles, which is in good agreement with the value reported in the literature. Surprisingly, an increase in the  $\alpha$  value was observed during and after the laser heating. More work is needed to assess the reasons for such a behavior.

Since the optical properties of soot particles were proved to strongly change during and after laser heating in relation to the entity of the heating process, it is mandatory to take into account such a variation when performing LII measurements and data interpretation.

The authors acknowledge Ministero dello Sviluppo Economico for founding this research activity.

Vander Wal, R.D. (1999) Carbon **37**, 231-239.

Michelsen, H.A Tivanski, A.V.; Gilles, M.K.; van Poppel, L.H.; Dansson, M:A.; Buseck, P.R. (2007) Appl. Opt. **49**, 959-977.

Thomson, K.A.; Geigle, K.P.; Köhler, M.; Smallwood, G.J.; Snelling, D.R. (2011) Appl. Phys. B: Laser and Optics **104**, 307-319.